REPORT DOCUMENTATION PAGE

Form Approved OMB No. 0704-0188

Public reporting burden for this collection of information is estimated to average 1 hour per response, including the time for reviewing instructions, searching existing data sources, gathering and maintaining the data needed, and completing and reviewing the collection of information. Send comments regarding this burden estimate or any other aspect of this collection of information, including suggestions for reducing the burden, to Department of Defense, Washington Headquarters Services, Directorate for Information Operations and Reports (0704-0188), 1215 Jefferson Davis Highway, Suite 1204, Arlington, VA 22202-4302. Respondents should be aware that notwithstanding any other provision of law, no person shall be subject to any penalty for failing to comply with a collection of information if it does not display a currently valid OMB control number.
PLEASE DO NOT RETURN YOUR FORM TO THE ABOVE ADDRESS.

1. REPORT DATE *(DD-MM-YYYY)*	2. REPORT TYPE	3. DATES COVERED *(From – To)*
27-11-2006	Conference Proceedings	16 October 2006 - 20 October 2006

4. TITLE AND SUBTITLE

Biological Effects of Electromagnetic Fields

5a. CONTRACT NUMBER
FA8655-07-1-5026

5b. GRANT NUMBER

5c. PROGRAM ELEMENT NUMBER

6. AUTHOR(S)

Conference Committee

5d. PROJECT NUMBER

5d. TASK NUMBER

5e. WORK UNIT NUMBER

7. PERFORMING ORGANIZATION NAME(S) AND ADDRESS(ES)

University of Ioannina
Panepistimioupolis
IOANNINA GR45110
Greece

8. PERFORMING ORGANIZATION REPORT NUMBER

N/A

9. SPONSORING/MONITORING AGENCY NAME(S) AND ADDRESS(ES)

EOARD
PSC 821 BOX 14
FPO AE 09421-0014

10. SPONSOR/MONITOR'S ACRONYM(S)

11. SPONSOR/MONITOR'S REPORT NUMBER(S)
CSP 07-5026

12. DISTRIBUTION/AVAILABILITY STATEMENT

Approved for public release; distribution is unlimited. (approval given by local Public Affairs Office)

13. SUPPLEMENTARY NOTES

14. ABSTRACT

The Final Proceedings for Biological Effects of Electromagnetic Fields, 16 October 2006 - 20 October 2006

15. SUBJECT TERMS

Biology, Radio Frequency Safety and Health

16. SECURITY CLASSIFICATION OF:			17. LIMITATION OF ABSTRACT	18, NUMBER OF PAGES	19a. NAME OF RESPONSIBLE PERSON
a. REPORT	b. ABSTRACT	c. THIS PAGE			ROBERT N. KANG, Lt Col, USAF
UNCLAS	UNCLAS	UNCLAS	UL	1510	**19b. TELEPHONE NUMBER** *(Include area code)* +44 (0)20 7514 4437

EMF EFFECTS ON MICROCIRCULATORY SYSTEM

CHIYOJI OHKUBO

RAD, WORLD HEALTH ORGANIZATION, GENEVA CH1211, SWITERLAND

Abstract

The speaker reviews the importance of studying the effects of electromagnetic fields on microcirculatory system, especially in respect of possibility that vasculature may have direct and indirect role in interaction of static magnetic fields. It outlines the physiological importance of microcirculation and relatively new methods of evaluation technique in vivo and explains in details the local and/or whole body exposure effects of static magnetic field with range of 0.3–180 mT, power frequency electromagnetic fields with range of 0.1-30 mT and microwaves at 1.5 GHz with range 0.08 - 8 W/kg brain average SARs on microcirculatory systems in different tissues in experimental animals.

Introduction

The circulatory system is the transport system of the organism that supplies O_2, ions, hormones, and substances absorbed from the gastrointestinal tract to the tissues, and returns CO_2 to the lungs and other products of metabolism to the liver and kidneys. It also has a central role in the regulation of body temperature, and the distribution of the hormones and other agents that regulate tissue and cell function. The principal function of microcirculation is exchanging physiological substances between blood and tissues, and the compensatory adjustments should contribute to the efficacy of the exchange process: lumen dimensions, length, tortuosity, diameter of branch ratios, vascular density, wall thickness, vessel diameter (vasomotion), blood flow velocity, blood viscosity, intramicrovascular hematocrit, leukocyte-endothelial cell interaction and others.

Microcirculation consists of structurally and functionally differentiated small blood vessels: small muscular arteries, arterioles, metarterioles, capillaries, postcapillary venules, venules, and lymphatic capillaries. In the cutaneous microvascular beds, the connection between the arterioles and the venules is made by some thoroughfare channels including capillaries or arteriolar-venular shunts. In most vascular beds, the precapillary resistance vessels are responsible for the largest function of the resistance in a vascular bed, and hence are the major components that influence regional hemodynamics and total peripheral resistance. Smooth muscle cells are found in all of these except the blood capillaries and lymphatic capillaries. The blood capillary wall is composed of a single layer of endothelial cells. The lymphatic capillaries are composed of endothelium-lined vessels similar to blood capillaries. Fluid and protein that have extravasated from the blood capillaries partially enter the lymphatic capillaries and are transported via the lymphatic system back to the blood vascular system. Postcapillary venules play an important role in fluid and cellular exchange and are the major site of leukocyte migration into tissue spaces.

Rhythmical and spontaneous changes in both the diameter of arterioles and the volume and velocity of blood flow due to constriction and dilation of the vascular smooth muscle are known as vasomotion (1). The quantitative description of spontaneous arteriolar vasomotion requires data on frequency, amplitude, diameter, and branching order of the vessels observed. Fluid absorbed into lymphatic capillaries is passively transported through dynamic changes due to arteriolar vasomotion in cutaneous tissue. Frequency and amplitude of spontaneous vasomotion could play an important role in disease. In microangiopathies, lymphedema, and essential hypertension, altered patterns of arteriolar vasomotion could constitute an additional pathogenetic factor (2). Extracellular control of the smooth muscle cells is exerted through neurogenic, hormonal, local and myogenic mechanisms (3).

For evaluating EMF exposure effects on microcirculatory system, various microcirculatory preparations, e.g., rabbit ear chamber (REC) (4), dorsal skin fold chamber (DSC) in mice (5) and cranial window (CW) in mice and rats (6-7), have been used to observe and analyze microcirculation in our group. These preparations allow non-invasive, continuous measurement of hemodynamics, blood velocity, angiogenesis, metabolites, e.g., pH and pO2, transport of molecules and particles, and cell to cell interactions in vivo (8).

Static fields

The REC offers the advantage of superior optical quality. Due to the longer duration of an individual measurement, we have exclusively utilized REC to investigate the effects of SMFs on microcirculation using microphotoelectric plethysmography (MPPG) monitoring system. REC is a round-table chamber made of acryl resin for disk with an observing table and three holding pillars, a sustaining ring, and a glass window. The

methods for installation of REC and its availability to the bioelectromagnetic research have been published in detail (9-12). Blood Pressures (BPs) in a central artery contralateral to that of an ear lobe having the REC, fixed on the stage of the microscope, were monitored by a BP monitoring system.

1. Local exposure on the ear lobe to SMF (1.0 mT, 10 min) in conscious rabbits
Experimental Procedures: The SMF of 1.0 mT were generated by a C-shaped electromagnet device. An animal set on the observing stage of a microscope, laid prone in a holder without anesthesia. An intact central artery of the ear lobe fixed on an observing stage of the microscope was applied to analyzing the temporal changes of microcirculation in MPPG monitoring system. Two experimental procedures were randomly categorized: (1) sham exposure (CTL) and SMF exposure (SMF). MPPG profiles including DC levels and amplitudes of MPPG and/or BPs just before (pre-) exposure were compared with those during exposure and post-exposure.
Results: SMFs had a biphasic effect upon the microcirculatory system; when the vascular tone was low, the SMF induced vasoconstriction, and when it was high, the SMF induced vasodilation (9).

2. Whole-body exposure to SMF (5.5 mT, 30 min) in conscious rabbits
Experimental Procedures: The SMFs of 5.5 mT (Bmax) were generated by a doughnut-shaped annular electromagnet device. A rabbit in a holder was placed into the annular electromagnets. The measured magnetic flux densities were 5.0–5.5 mT in the trunk, 0.5–4.0 mT in the head, 1.0–4.0 mT in the throat, and<1.0 mT in the ear lobe, respectively. Two experimental procedures were randomly categorized: sham exposure (CTL) and SMF exposure (SMF). These values pre-exposure were compared with those during exposure and post-exposure.
Results: Comparing SMF with CTL, there were no significant changes in MPPG values throughout the experiment. For BPs, comparing SMF with CTL, there were no significant changes throughout the experimental period (13).

3. Local exposure on the ear lobe to SMF (1.0 mT, 10 min) in pharmacologically treated rabbits with REC
This study is attempted to demonstrate the vasoconstrictor effect as well as the vasodilating effect by local exposure on the cutaneous microcirculation within a REC under pharmacologically modified vascular tone. Based on the hypothesized effects, nor-adrenaline (NA) and acetylcholine (ACh) were chosen to enhance and reduce the vascular tone pharmacologically.
Experimental Procedures: Cutaneous microcirculation of REC exposed to SMF was studied under pharmacological treatment using MPPG method. NA and ACh were used for increase sympathetically and decrease parasympathetically in vascular tone, respectively.
Results: The temporal changes of MPPG profiles during and after exposure were quantitatively analyzed. In NA group, the vasoconstriction with reduced vasomotion was observed throughout the experimental period. In NA+SMF group, the vasoconstrictor effects with reduced vasomotion followed by NA infusion were significantly reduced. In contrast, in ACh group, the vasodilation with increased vasomotion was observed throughout the experimental period. In ACh+SMF group, however, the vasodilator effect with increased vasomotion followed by ACh infusion were significantly reduced. In mean amplitudes of MPPG between ACh+SMF and ACh groups, there were significant differences for up to 60 min after cessation of SMF exposure. In CTL group, there were no significant changes throughout the experimental period (11).

4. Local exposure on the ear lobe to SMF (1.0 mT, 30 min) in pharmacologically treated rabbits without REC
The purpose of this study is to elucidate the hypothesized homeostatic effects of SMF on BPs, and to show that it can alter the microcirculation in a cutaneous tissue and hence modify the BPs. This study was designed to investigate the effects of SMF on a Ca^{2+} channel blocker, nicardipine (NIC)-induced hypotension as well as a nitric oxide synthase (NOS) inhibitor, Nx-nitro-L-arginine methyl ester (L-NAME)- induced hypertension.
Experimental Procedures: The effects of SMF on BPs in rabbits were investigated under pharmacological treatment. Hypotensive and vasodilator actions were induced by NIC. Hypertensive and vasoconstrictor actions were induced by L-NAME.
Results: In NIC alone, the acute and intense vasodilation with increased vasomotion resulting in increases of both MPPG parameters was observed. In SMF + NIC, by contrast, the vasodilating effect with increased vasomotion following NIC injection was reduced. In mean amplitude between SMF+NIC and NIC, there was a significant difference during SMF exposure. In L-NAME alone, 10 min after L-NAME infusion, the vasoconstriction resulting in decreases of mean DC level was observed. In SMF + L-NAME, by contrast, the vasoconstrictor effect following L-NAME infusion was reduced. In mean amplitude between SMF + L-NAME and L-NAME, however, there were no significant differences throughout the experimental period. In NIC alone, BPs decreased from baseline immediately after NIC injection. In contrast, in SMF + NIC, the reduction of BPs was suppressed. In L-NAME alone, BPs gradually increased from baseline after L-NAME infusion. In contrast, in SMF + L-NAME, the elevation of BPs was suppressed during exposure and post-exposure (14).

5. Local exposure on the neck or pelvic to SMF (1.0-5.5 mT, 30 min) in pharmacologically treated rabbits
Experimental Procedures: Magnetic flux densities were up to 5.5 mT and the spatial magnetic gradient peaked in neck (carotid sinus baroreceptor) region at the level of 0.06 mT/mm. The duration of exposure was 30 min and the effects on BP were investigated up to 100 min post-exposure. BPs were pharmacologically modulated by norepinephrine (NE)-induced hypertension as well as an L-type voltage-gated Ca^{2+} channel blocker, nicardipine (NIC)-induced hypotension. Baroreflex sensitivity (BRS) was estimated from invasive recordings of systolic BP and pulse interval.
Results: Neck exposure to 5.5 mT significantly attenuated the pharmacologically induced vasoconstriction or vasodilation, and subsequently suppressed the increase or decrease in BP compared with sham exposure. In contrast, pelvic exposure to 5.5 mT did not significantly antagonized NE-elevated BP or NIC-reduced BP. The neck exposure to 5.5 mT has a biphasic and restorative effect on vascular tone and BP acting to normalize the tone and BP. The neck exposure to 5.5 mT caused a significant increase in BRS in NE-elevated BP compared with sham exposure. The buffering effects of the SMF on increased hemodynamic variability under NE-induced high vascular tone and NIC-induced low vascular tone might be, in part, dependent on baroreflex pathways, which could modulate NE-mediated response in conjunction with Ca^{2+} dynamics (15).

6. Whole-body exposure to SMFs (0.3, 1.0, and 10.0 mT, 10 min) in anesthetized mice
This study was designed to investigate the effects of SMFs for modulating the muscle capillary mirocirculation under pentobarbital-induced hypnosis.
Experimental Procedures: SMFs were generated by a C-shaped electromagnet device. Muscle capillary microcirculation of mice exposed to SMFs (0.3, 1.0, and 10.0 mT, 10 min) was studied under pentobarbital anesthesia. FITC-labeled dextran was used for an in vivo fluorescent plasma marker of the muscle capillaries.
Results: Significant increases of the peak blood velocities by SMFs of at least 1.0 mT were observed, whereas those of the mean blood velocities were not. In CTL or SMF exposure at 0.3 mT, on the other hand, there were no significant changes throughout the experimental period within either of the peak blood velocities (16).

7. Whole-body exposure to SMF (10 or 25 mT, 12 weeks) in reserpine-induced hypotensive rats
This study investigated the interrelated antihypotensive effects of static magnetic fields (SMF) and plasma catecholamine levels in reserpine-induced hypotensive Wistar-Kyoto rats.
Experimental Procedures: Seven-week-old male rats were exposed to two different ranges of SMF intensities, 3.0-10 mT (Bmax) or 7.5-25 mT (Bmax) for 12 weeks. Six experimental groups of 10 animals each were examined: (1) no exposure with intraperitoneal (ip) saline injection (sham exposed control); (2) 10 mT SMF exposure with ip saline injection (10 mT); (3) 25 mT SMF exposure with ip saline injection (25 mT); (4) no exposure with ip reserpine injection (RES); (5) 10 mT SMF exposure with ip reserpine injection (10 mT + RES); (6) 25 mT SMF exposure with ip reserpine injection (25 mT + RES). Reserpine (5 mg/kg) was administered three times a week for 12 weeks, and 18 h after each injection, arterial blood pressure (BP), heart rate, skin blood flow, plasma nitric oxide metabolites, plasma catecholamine levels, and behavioural parameters of a functional observational battery (FOB) were monitored.
Results: The reserpine idministration significantly decreased BP, reduced plasma norepinephrine (NE), increased the FOB hunched posture score and decreased the number of rearing events in the RES group, compared with the respective age-matched control group. Exposure to 25 mT, but not 10 mT, for 2-12 weeks significantly prevented the reserpine-induced decrease of BP in the 25 mT + RES group compared with the respective RES group. Moreover, exposure to 25 mT for 5 weeks partially suppressed the reserpine-induced NE reduction, but did not bring about a complete reversal of reserpine effects. NE levels for the 25 mT + RES group for 5 weeks were significantly higher compared with the RES group, but still lower compared with the control group. In addition, the FOB hunched posture score for the 25 mT + RES group was significantly lower and the number of rearing events was higher compared with the RES group, but these behavioural parameters did not revert to control levels. There were no significant differences in any of the physiological or behavioural parameters measured between the 10 mT + RES and RES groups, nor between the two different SMF groups and the control group (17).

8. Whole-body exposure to SMF (5.5 mT, 30 min) in pharmacologically induced hypertensive rabbits
The purpose of our study is to elucidate the hypothesized hypotensive or antipressor effects of SMFs, and to show that it can alter the microcirculation in a cutaneous tissue and hence normalize the BPs. More particularly, this study was designed to investigate the effects of SMF on pharmacologically induced hypertension via NA-mediated increases in sympathetic nerve activity, or a NOS inhibitor in vascular endothelial cells and/or neurons.
Experimental Procedures: Hypertensive and vasoconstrictor conditions were induced by NA or a NOS inhibitor, L-NAME. As a preliminary intensity-finding experiment using SMFs ranging 1.0–50.0 mT in NA-induced hypertension, whole-body exposure to SMFs under 5.5 mT did not significantly induce antipressor effects.

Results: In NA alone, just after NA infusion, the acute and intense vasoconstriction resulting in reduction of mean DC level of MPPG was observed. In SMF + NA, by contrast, the vasoconstrictor effect following NA infusion was antagonized. In L-NAME alone, the vasoconstriction resulting in decreases of mean DC level was observed. In SMF+L-NAME, the vasoconstrictor effect following L-NAME infusion was reduced. Comparing mean amplitude of MPPG between SMF+L-NAME and L-NAME; however, there were no significant differences throughout the experimental period. In NA alone, BPs increased from baseline after NA infusion. In contrast, in SMF + NA, the elevation of BPs was antagonized and hypotension was induced. After withdrawal of SMFs, there were significant differences between SMF+NA and NA in BPs. In L-NAME alone, BPs increased from baseline after L-NAME infusion. In contrast, in SMF + L-NAME, the elevation of BPs was suppressed during exposure and post-exposure. For plasma vasoactive substances, comparing between NA and SMF + NA in pre- and post-exposure, there were no significant changes in any catecholamines, angiotensin II and aldosterone levels (13).

9. Whole-body exposure to SMF (1, 5, 10 and 25 mT, 12 weeks) for genetically hypertensive rats
The purpose of our study is to elucidate the hypothesized antipressor effects of SMFs with mT levels on a genetically hypertensive animal.
Experimental Procedures 1: A SMF exposure device was composed of a pair of rectangular magnetic plates (strontium-ferrite) externally placed in parallel. Four types of SMF exposure devices with different magnetic flux densities were used. The mean flux densities in the center of a cage were ranging from 3.0 to 10.0 mT (Bmax) here referred to as SMF 10 mT and ranging from 8.0 to 25.0mT(Bmax) as SMF 25mT. Effects of SMFs on development of hypertension were investigated using young male stroke-resistant spontaneously hypertensive rats (SHRs) beginning at 7 weeks of age. SHRs were randomly assigned to two different exposure groups or an unexposed group. A rat in a cage with magnetic plates was exposed to either SMF continuously for 12 weeks, except during the short period of measuring BPs and heart rate and blood sampling. The BPs and heart rate in each rat were determined weekly using tail-cuff method.
Results 1: The changes of systolic BP with continuous exposure to either SMF for 12 weeks and with crossover exposure to SMF 25 mT for 6 weeks were indicated, as compared with sham exposed group. The rats exposed to SMFs displayed suppression and retardation in the development of systolic BP during 2–9 weeks. However, at least 1 week after crossover exposure for 6 weeks, significant differences between systolic BP disappeared. Similar suppressions of development of hypertension exposed to SMFs also occurred in diastolic BP during 5–6 weeks in SMF 10 mT and during 3–6 weeks in SMF 25 mT. Moreover, antipressor effects on mean BP were observed during 3–5 weeks in both SMFs. Exposure to SMFs for 5 weeks significantly reduced the concentrations of plasma angiotensin II and plasma aldosterone concentration, as compared with sham exposed group. There were no detectable effects of SMFs on the other measured vasoactive substances (renin activity, angiotensin I, arginine vasopressin and angiotensin I-converting enzyme concentrations) (18).
Experimental Procedures 2: Seven-week-old SHRs were exposed to three different ranges of SMF intensity, ranging from 0.3 to 1.0 mT (Bmax) here referred to as SMF 1 mT, ranging from 1.5 to 5.0 mT (Bmax) here referred to as SMF 5 mT, for 12 weeks and sham exposure. Arterial BP, hear rate, skin blood flow and plasma NO metabolites (NOx) and plasma cathecholamine levels were monitored.
Results 2: SMF 5 mT, but not SMA 1 mT, significantly suppressed and retarded the early stage development of hypertension for several week, compared with the age matched, unexposed (sham exposed) control. Exposure to 5 mT resulted in reduced plasma NOx concentrations together with lower level of anigiotensin II and alsosteron in SHR (19).

10. Local-body exposure on the baroreceptor region to SMF (180 mT, 6 and 14 weeks) in genetically hypertensive rats
The purpose of our study is to elucidate the hypothesized antipressor effects of SMFs with mT levels on SHRs special regard to exposure region to the baroreceptor.
Experimental Procedures: This study investigated the combined effects of a moderate intensity SMF and a Ca^{2+}channel blocker, nicardipine in stroke-resistant SHRs. A disc-shaped permanent magnet or a dummy magnet was implanted in the vicinity adjacent to the left carotid sinus baroreceptor region in the neck of each rat. Five-week-old male rats were exposed to SMF intensity up to 180 mT (Bmax) with a peak spatial gradient of 133 mT/mm for 14 weeks. Four experimental groups of 14 animals each were examined: (1) sham exposure with intraperitoneal (ip) saline injection (control); (2) SMF exposure with ip saline injection (SMF); (3) sham exposure with ip nicardipine injection (NIC); (4) SMF exposure with ip nicardipine injection (SMF+NIC). Nicardipine (2 mg/kg ip) was administered three times a week for 14 weeks, and then 15 min after each injection, arterial blood pressure (BP), heart rate (HR), baroreflex sensitivity (BRS), skin blood flow (SBF), skin blood velocity (SBV), plasma nitric oxide (NO) metabolites (NOx), plasma catecholamine levels and behavioural parameters of a functional observational battery were monitored.

Results: The action of nicardipine significantly decreased BP, and increased HR, SBF, SBV, plasma epinephrine and nor-epinephrine in the NIC group compared with the control respective age-matched group without changing plasma NOx levels. Neck exposure to SMF alone for 5–8 weeks significantly suppressed or retarded the development of hypertension together with increased BRS in SMF group. Furthermore, the exposure to SMF for 1–8 weeks significantly promoted the nicardipine-induced BP decrease in the SMF+NIC group compared with the respective NIC group. Moreover, the SMF induced a significant increase in plasma NOx in the nicardipine induced hypotension. There were no significant differences in any of the physiological or behavioural parameters measured between the SMF+NIC and the NIC groups, nor between the SMF and the control groups (20-21).

Summary of Static Field Effects

Microcirculation and BPs were modulated by SMFs with mT levels in pharmacologically treated animals and genetically hypertensive animals. By contrast, these physiological parameters were not changed by SMFs in normal animals. Appreciable minimum level for modulating microcirculation and BPs was 1.0 mT in pharmacologically treated animals. For the minimum exposure duration of 1.0 mT, it took 10 min to change microcirculation and 30 min to modulate BPs in these animals. To induce antipressor effects of SMFs on pharmacologically induced hypertensive animals, the whole-body exposure to SMF of 5.5 mT for 30 min was needed. To induce antipressor effects of SMFs on genetically hypertensive animals, whole-body exposure to SMFs of 5.0 mT for at least 2 weeks was required.

The effects of SMFs in the mT range were mediated by antagonizing the action of biochemical substances, there by inducing homeostatic effects biphasically:

1. Suppression of an adrenergic neurotransmitter, NA-induced vasoconstriction, and hypertension
2. Suppression of a cholinergic neurotransmitter, ACh-induced vasodilation
3. Suppression of reserpine-induced hypotension and bradykinesia.
4. Suppression of an anesthetic agent, pentobarbital-induced decrease in the peak blood velocities
5. Suppression of a Ca2+ channel blocker, nicardipine-induced vasodilation and hypotension
6. Suppression of a NOS inhibitor, L-NAME-induced vasoconstriction and hypertension
7. Suppression of early BP elevation via inhibition of elevation of vasopressor hormones, Ang II and Ald
8. Suppression of delay BP elevation via the NO pathway and hormonal regulatory systems
9. Enhancement of nicardipine-induced antipressor effects in SHRs which partially related to NOx activity

The effects of SMFs with mT levels on microcirculation and BPs obtained from different mammals would be used in possible explanation for the therapeutic effects on many ischemic diseases related to dysfunction in circulation and microcirculation. Furthermore, the SMFs might exert regulatory effects on BPs.

ELF EMFs

1. Whole body exposure effects to threshold levels of 50 Hz EMFs (0.3-30 mT, 30 min or 15 days) in mice

Whole body exposure effects to threshold levels of 50 Hz electromagnetic fields (3.0, 10.0, 30.0 mT for acute exposure and 0.3, 1.0, 3.0 mT for subchronic exposure) on intramicrovascular behaviour of leukocytes in the cutaneous microcirculation was evaluated by newly developed dorsal skin fold chamber (DSC) technique in mice under conscious conditions. The results indicated that the exposure intensity at 3.0 mT is a threshold level for increasing leukocyte adhesion to the endothelial walls. Effects of 50Hz electromagnetic fields (EMF) exposure on leukocyte are mainly performed *in vitro*, however, little information of these is available *in vivo* experiments. In order to investigate the acute and subchronic exposure effects of threshold levels of 50Hz EMF on leukocyte behaviour *in vivo* system, we measured the behaviour of intra-microvascular leukocytes in the cutaneous microcirculation in mice.

Experimental Procedures: Male mice (BALB/c) having the DSC were subjected to intravital-microscopic study. We have developed the DSC with non-metal materials of Duracon resin, which could not be physically affected by EMF exposure. For visualization of intra-microvascular leukocytes, fluorescent dye (rhodamine 6G; 0.3mg/kg, iv) was injected. The numbers of leukocyte rolling or adhering to the venular walls were measured by confocal laser microscopy and recorded into VCR and analyzed from the images. The magnetic flux densities used for the acute exposure (30 minutes) were controlled at 3, 10, 30 mT at the centre of animal body(n=10 each), respectively. For subchronic exposure study, mice were divided into 4 groups (n=10 each), i.e., exposure group with 50 Hz EMF at 0.3, 1.0 and 3.0 mT and control group with sham exposure. The 50Hz EMF exposure was intermittently performed everyday from 16:00 to 12:00(20hours/day) for 15 days. Plasma cytokine (IL-1β, TNF-α) concentration was measured by ELISA.

Results: Acute Effects (3, 10, 30 mT, 30 min): A tendency to increase the adherent cell count of leukocytes due to the 50 Hz EMF exposure toward higher magnetic field intensity was recognized. Following the exposure at 30 mT, the counts of adherent cell was significantly higher than those obtained before exposure. Subchronic Effects (0.3, 1.0 and 3.0 mT, 15 days): Following subchronic exposure to 50Hz EMF, no significant changes in arteriolar blood flow velocity and diameter were noticed in both groups, however, statistically significant

increases($p<0.05$) in adherent leukocyte counts at 3.0 mT were noticed. There was no change in IL-1β and TNF-α plasma levels between before and after exposures in any group. No noticeable changes in the adherent cell counts were observed between before and after sham exposures in the control group.
Conclusion: The results indicated that 50 Hz EMF exposure may influence cell to cell interaction between venular endothelial cells and leukocytes. Previous observations using human monocyte in *in vitro* system indicated that changes in cytokine profile of monocyte were induced by exposures of 50 Hz EMF. We hypothesize that 50 Hz EMF exposure effects on leukocyte and endothelial cell interaction due to change in cytokine levels, however, IL-1β and TNF-α may not be involved in this phenomenon (5, 22-23).

2. Whole body exposure effects to 50Hz EMFs (3mT, 15 days) on mammary tumour proliferation in mice
The tumor vasculature consists of both vessels recruited from the pre-existing network from the angiogenic response of host vessels to cancer cells. In the process of cancer promotion, angiogenesis is one of the key issues to proliferate their cells into host tissue. We have intravital-microscopically found that 50Hz electromagnetic fields(EMF) as well as static magnetic field exposure(>1mT) might modify the microvascular tone in rabbits under conscious conditions. If 50Hz EMF can affect on hemodynamic parameters of pre-existing microvasulature, 50Hz EMF may also affect on tumor vasculature or angiogenic process, hence, growth rate of tumor cells which implanted into the animals.
Experimental Procedures: Mammary tumour cells (MMT06562: MMT) were grafted into DSC. The area occupied by tumour tissue within a DSC was measured by PC image analysis with NIH image. Mice were divided into 2 groups (n=10-12 each), i.e., exposure group with 50 Hz EMF at 3 mT and control group with sham exposure. The 50Hz EMF exposure was intermittently performed everyday (22hours/day) for 15 days. Bood vessel diameter, blood flow velocity, adherent leukocyte counts to venular wall were evaluated by comparison between these values of pre- and post-exposure within group, or these of exposure group and control group.
Results: After MMT grafting, almost one week required to initiate the angiogenic response. During 2 weeks' whole body exposure to 3 mT, 50 Hz EMF, successive changes of angiogenesis including vascular density and growth of the tumor were compared with non-exposed control animals. The area occupied by tumor tissue within DSCs of the exposure group is smaller than its control group, however, no significant difference was found between them.
Conclusion: The results indicated that 50 Hz EMF exposure at 3 mT induced no effects on the mammary tumour cell proliferation in tumour bearing animals (24).

3. Whole body exposure effects to 50Hz EMFs (3mT, 15 days) with or without transient magnetic fields (7.4 kHz with 50 msec, 162 μT) on brain tumour proliferation in SCID mice
This study evaluates whole body exposure effects to ELF-EMF with transient magnetic field on the implanted brain tumour growth and tumour microcirculation within a mice cranial window (CW).
Experimental Procedures: Male SCID (Severe combined immuno-deficiency) mice were used in this study. One week after installation of CW, the window was opened and a small piece of human glioma U87 tissue which grown in source mouse was implanted into the centre of CW. Then, mice were divided into two groups: exposure and sham group. In exposure group, mice were subchronically exposed to combination of 50 Hz EMF with repetitive transient magnetic fields (1 burst/s, 7.4 kHz waves with duration of 50 msec and peak magnet density of 162 μT) for 15 days (15 hours/day: 7 p.m. to 10 a.m.) following tumour implantation. During and after the exposure, we measured the size of tumour, microcirculatory parameters of angiogenic vessels in the growing tumour by real-time confocal microscopy, and vascular permeability of rhodamine-labelled albumin using a photon counting system.
Results: Although tumour size increased markedly following implantation, tumour growth did not show any significant difference between the exposure group and control group. Tumour angiogenesis was also induced inside and around the tumour tissue, however, ELF-EMF with transient magnetic fields did not affect any of the microcirculatory parameters of these angiogenic vessels, for instance, vascular density, mean diameter and branched numbers of vessels.
Conclusion: No possible pathophysiological effect in the brain tumour microcirculation can be induced by the subchronic and combined exposures of 50 Hz (3 mT) and transient magnetic fields. The growth rate of implanted brain tumour tissue was not also affected by the present exposure conditions (6).

4. Whole body exposure effects to ELF EMFs (10, 16 and 50 Hz, 28 mT, 10 min) on cutaneous microcirculation in mice
Experimental Procedures: Three different ELF EMFs, e.g., 10, 16 and 50 Hz, were used in this study. Following caudal vein injection of FITC-dextran 250 kDa, the microvasculature (initial arteriole diameter of 45–80 μm), was examined by intravital microscopy and video images were recorded. Measurements of blood vessel diameter within a DSC were continuously monitored for 33 min including pre-, during and post- exposure of ELF-EMF

and every 389 ms blood vessel diameter were calculated.
Results: During and post-exposure to 16 Hz EMF, arteriolar diameters increased significantly compared with the pre-exposure period, and the changes were larger during post-exposure. No noticeable changes in arteriolar diameters were obtained from exposure to sham, 10 Hz and 50 Hz EMFs.
Conclusion: This study indicates that frequency specific interation may be evoked by ELF EMF (16 Hz), however, further research is needed to confirm this phenomenon (25).

RF EMFs
Local exposure to 1.5 GHz RF-EMF (0.08 - 35 W/kg brain average SARs, 10, 50, 80 min or 4 weeks) in rats

There is little information are available about the exposure effects of EMF on cerebral microcirculation. In this study we developed a cranial window method for evaluating the exposure effects of EMF on the BBB function, hemodynamics of pial microcirculation and behaviour of intramicrovascular leukocytes by using an intravital microscopy in rats.
Experimental Procedures 1: In the monopole antenna experiment, the exposure system consisted of a small anechoic chamber and a monopole antenna. The head of each rat was positioned toward the central antenna and was locally exposed to 1,439MHz electromagnetic near-field TDMA (time division multiple access) signal for PDC (Personal Digital Cellular, Japanese cellular telephone standard) system. The degree of intensity of RF exposure was controlled by mean specific absorption rate (SAR) of the brain. The SAR values were 1, 4, and 8 W/kg for acute effect experiment, and 4 W/kg for sub-chronic effect experiment, respectively. The EMF exposure duration was 10 minutes for the acute exposure experiment and was 60 minutes everyday, 5 days a week for 4 weeks for the subchronic exposure experiment. The pial microcirculation including vascular diameters, plasma velocities, leukocyte behaviour and BBB-function within the cranial window was investigated by a fluorescence microscope equipped with an SIT camera.
Results 1: Acute Exposure Experiment: The values in the diameters and maxmal plasma velocity of the pial venule of pre- and post-exposures did not significantly differ from each other for any SARs tested. Corresponding to the increase in SAR, the number of rolling leukocytes on the venular endothelia tended to decrease, however, no significant differences were recognized between the values for pre- and post-exposures. No extravasation of two kinds of fluorescence dyes, FITC-Dx (MW: 250,000) and sodium-fluorescein (MW: 376), from the pial venule was noticed due to any SARs. Subchronic Exposure Experiment: The values in the diameters and maxmal plasma velocity of the pial venule of pre- and post-exposures did not significantly change. No significant differences were recognized between the values for pre- and post-exposures in vascular diameters, plasma velocities and adherent leukocyte counts. No extravasation of the two kinds of fluorescence dyes from the pial venule was noticed (7).
Experimental Procedures 2: In the loop antenna experiment, the head of rat was positioned 2mm under the loop antenna and was locally exposed to 1,439MHz electromagnetic near-field TDMA signal for PDC system. The degree of intensity of EMF exposure was controlled by average specific absorption rate (SAR) of the brain at 0.2, 2.0, and 7.5W/kg for acute effect experiment, and 2 W/kg for subchronic effect experiment, respectively. Other experimental procedures were same with the monopole antenna experiment mentioned above.
Results 2: Acute Effect Experiment: No significant differences were recognized between the values for pre- and post-exposures in maximal plasma velocities and adherent leukocyte counts. No extravasation of two kinds of fluorescent dyes, FITC-Dx and sodium-fluorescein, from the pial venule was noticed due to any SARs. Sub-chronic Effect Experiment: The infection of piamater, the regeneration of dura mater and the serpiginous change of vessel were not observed within a cranial window of each group throughout the experiment. There was no significant difference in the maximal plasma velocity of the pial venule of each group at 4th week. No extravasation of two kinds of fluorescence dyes, FITC-Dx and sodium-fluorescein, from the pial venule was noticed in any group (7).
Experimental Procedures 3: Rat's head was locally exposed to 1,457MHz electromagnetic near-field TDMA (time division multiple access) signal for PDC (Personal Digital Cellular, Japanese cellular telephone standard) systems by an "8"-shaped loop antenna placed 4 mm upward to the cranial window. RF-EMF exposure intensity was maintained at an averaged SAR (2.0W/kg) in parietal targeted area. During 80 min experimental period including 50 min RF-EMF exposure, three microcirculatory parameters (BBB-function, plasma velocities and vessel diameters) in pial venules were measured every 10 min, and the results were compared between those of RF and Sham groups. Other experimental procedures were same with the monopole antenna experiment mentioned above.
Results 3: No statistical changes were observed between RF group and Sham group in any microcirculatory parameters (26).
Experimental Procedures 4: Possible adverse health effects of radiofrequency electromagnetic field (RFEMF) exposure during mobile phone uses on the developing brain in children are one of the important public health issues. The aim of the present study is to investigate whether RF-EMF exposure induces transient effects on

brain microcirculation being observed only during RF-EMF radiation period in juvenile rats. As juvenile and adult rats, we used 4 and 8 weeks male Sprague-Dawley rats, respectively. Both juvenile and adult rats were divided into two groups: RF group was exposed to RF-EMF and Sham group was not exposed to any RF-EMF. Other experimental procedures were same with the "8"-shaped loop antenna experiment mentioned above.
Results 4: We succeeded to directly observe pial microcirculation through the cranial windows during RF-EMF exposure in juvenile rats. In 4 weeks juvenile rats, no changes in any of the three microcirculatory parameters were elicited by the RF-EMF exposure. No statistical changes were recognized between RF group and Sham group. These negative effects obtained from RF-EMF exposure in juvenile rats were also confirmed in 8 weeks adult rats. No transient effects of RF-EMF exposure on the brain microcirculation in either juvenile or adult rats were recognized (27).
Conclusion: These results from acute and subchronic exposure to RF EMF suggested that no noticeable changes in the cerebral microcirculatory parameters, at least on BBB-function, plasma velocities or vessel diameters, in either juvenile or adult rats under present exposure conditions.

There is an importance of understanding the effects of magnetic fields on microcirculatory system. It may have direct and indirect role in interaction of magnetic fields with different tissues. The results from our studies could be useful in applying them for microcirculatory disorders. In addition, results obtained from exposure to ELF and RF EMFs failed to show any changes in microcirculatory system except for leukocyte and endothelial cell interaction. Levels of EMFs used in our studies are very higher than the international exposure guidelines. These animal studies can contribute to evaluate possible health risks of EMFs.

Acknowledgements
All the studies were performed at Department of Environmental Health (former Department of Physiological Hygiene), National Institute of Public Health, Japan from which I have retired in March 2004. I sincerely express my greatest appreciations to all members of the Department.

References
1. Asano M, Branemark PI. Microphotoelectric plethysmography using a titanium chamber in man. In: Harders H, ed. Advances in Microcirculation. Vol.4. Basel: S. Karger, 1972:131–160.
2. Funk W, Intaglietta M. Spontaneous arteriolar vasomotion. In: Messemer K, Hammersen F, eds. Progress in applied microcirculation. Vol. 3. Basel: Karger, 1983:66–82.
3. Mulvany MJ. Functional characteristics of vascular smooth muscle. In: Messemer K, Hammersen F, eds. Progress in applied microcirculation. Vol. 3. Basel: Karger, 1983:4–18.
4. Asano M, Yoshida K, Tatai K. Microphotoelectric plethysmography using a rabbit ear chamber. J Appl Physiol. 1965; 20:1056–1062.
5. Ushiyama A, Yamada S, Ohkubo C. Microcirculatory parameters measured in subcutaneous tissue of the mouse using a novel dorsal skinfold chamber. Microvascular Research. 2004; 68:147– 152
6. Ushiyama A, Masuda H, Ohkubo C. Effects of subchronic exposure to extremely low frequency electromagnetic fields on the cranial microcirculation in the brain tumor bearing mouse. Abstract book of 25th Annual Meeting of the Bioelectromagnetics Society. 2003: 89.
7. Masuda H, Hirota S, Ushiyama A, Wake K, Watanabe S, Taki M, Ohkubo C. In vivo evaluation of exposure effects to radio-frequency electromagnetic fields on the cerebral circulation in rats. Abstract book of the Blood-Brain Barrier (BBB) Workshop of COST281-Potential health implications from mobile communication systems; 2003 Nov 2-6; Reisensburg: Germany; 2003. p.28-29.
8. Jain RK. The Eugene M. Landis Award Lecture 1996. Delivery of molecular and cellular medicine to solid tumors. Microcirculation. 1997; 4:1–23.
9. Ohkubo C, Xu S. Acute effects of static magnetic fields on cutaneous microcirculation in rabbits. In Vivo. 1997; 11:221–225.
10. Xu S, Okano H, Ohkubo C. Subchronic effects of static magnetic fields on cutaneous microcirculation in rabbits. In Vivo. 1998; 12:383–389.
11. Okano H, Gmitrov J, Ohkubo C. Biphasic effects of static magnetic fields on cutaneous microcirculation in rabbits. Bioelectromagnetics. 1999; 20:161–171.
12. Gmitrov J, Ohkubo C, Okano H. Effect of 0.25 T static magnetic field on microcirculation in rabbits. Bioelectromagnetics. 2002; 23:224–229.
13. Okano H, Ohkubo C. Anti-pressor effects of whole-body exposure to static magnetic field on pharmacologically induced hypertension in conscious rabbits. Bioelectromagnetics. 2003; 24: 139-147
14. Okano H, Ohkubo C. Modulatory effects of static magnetic fields on blood pressure in rabbits. Bioelectromagnetics. 2001; 22:408–418.
15. Okano H, Ohkubo C. Effects of neck exposure to 5.5mT static magnetic field on pharmacologically modulated blood pressure in conscious rabbits. Bioelectromagnetics. 2005; 26:469–480.

16. Xu S, Okano H, Ohkubo C. Acute effects of whole-body exposure to static magnetic fields and 50-Hz electromagnetic fields on muscle microcirculation in anesthetized mice. Bioelectrochemistry. 2000; 53:127–135.
17. Okano H, Ohkubo C. Effects of 25 mT static magnetic fields on blood pressure in reserpine-induced hypotensive Whiter-Kyoto rats. Bioelectromagnetics. 2005; 26:36-48.
18. Okano H, Ohkubo C. Effects of static magnetic fields on plasma levels of angiotensin II and aldosterone associated with arterial blood pressure in genetically hypertensive rats. Bioelectromagnetics. 2003; 24:403-412.
19. Okano H, Masuda H, Ohkubo C. Decreased plasma levels of nitric oxide metabolites, angiotensin II, and aldosterone in spontaneously hypertensive rats exposed to 5 mT static magnetic field. Bioelectromagnetics. 2005; 26:161-172.
20. Okano H, Ohkubo C. Exposure to a moderate intensity static magnetic field enhances the hypotensive effect of a calcium channel blocker in spontaneously hypertensive rats. Bioelectromagnetics. 2005; 26:611-23.
21. Okano H, Ohkubo C. Elevated plasma nitric oxide metabolites in hypertension: synergistic vasodepressor effects of a static magnetic field and nicardipine in spontaneously hypertensive rats. Clin Hemorheol Microcirc. 2006; 34:303-308.
22 Ushiyama A, Ohkubo C. Acute effects of low-frequency electromagnetic fields on leukocyte-endothelial interaction in vivo. In vivo. 2004; 18:125-132
23. Ushiyama A, Masuda H, Hirota S, Ohkubo C. Subchronic effects on leukocyte-endothelial interactions in mice by whole body exposure to extremely low frequency electromagnetic fields in vivo. In vivo. 2004; 18: 425-432.
24. Ushiyama A, Ohkubo C. Effects of whole body exposure to 50 Hz electromagnetic fields on the microcirculatory system and the proliferative process of mammary tumor cells in mice. EBEA 2001 (5th International Congress of the European Bio Electromagnetics Association), Helsinki, 2001: 46-48.
25. Traikov L, Ushiyama A, Lawlor G, Sasaki R, Ohkubo C. Subcutaneous arteriolar vasomotion changes during and after ELF-EMF exposure in mice *in vivo.* The Environmentalist. 2005; 25: 93–101.
26. Masuda H, Ushiyama A, Hirota S, Watanabe H, Wake K, Watanabe S, Yamanaka Y, Taki M, Ohkubo C. Real-time measurement of brain microcirculation during RF-EMF exposure using an ‘‘8’’-shaped loop antenna. In: Abstract book of the 28th General Assembly of International Union of Radio Science; 2005 Oct 23-29; New Delhi, India. 2005. K03.5 (097) in CD-ROM.
27. Masuda H, Ushiyama A, Takahashi Y, Hirota S, Tanaka S, Kawai H, Wake K, Watanabe S, Taki M, Ohkubo C. No transient effects of RF-EMF exposure on the brain microcirculation in either juvenile or adult rats. Abstract book of 28th Annual Meeting of the Bioelectromagnetics Society. 2006: 104.

SUPPRESSION OF NO PRODUCTION IN MACROPHAGES BY ELF ELECTRO-STIMULATION

MUNEYOSHI KAGAWA, TOSHIYUKI SHIMOOKA, YUJI KURACHI and KOICHI SHIMIZU

GRADUATE SCHOOL OF INFORMATION SCIENCE AND TECHNOLOGY, HOKKAIDO UNIVERSITY

Abstract

We have pursued the possibility to control immune functions by ELF electro-stimulation. As the first step, the effect of electro-stimulation on the NO producing ability of macrophages was examined. The decrease of NO production due to the electro-stimulation was observed with statistical significance. To elucidate the mechanism of this phenomenon, the amount of the NO synthesizing enzyme was measured. The measurement showed the decrease in the emergence of the enzyme with statistical significance, as well. These facts suggested that the ELF electro-stimulation suppressed the emergence of the NO synthesizing enzyme and that the amount of NO production was consequently decreased by the electro-stimulation. To analyse the association between the amount of the NO synthesizing enzyme and the amount of NO production, the dose-response of this effect was investigated by changing the electric current density of the electro-stimulation. The rates of the decrease in NO synthesizing enzyme and the NO production were found to be very close. These results showed that the change in the NO synthesizing enzyme is closely involved in the mechanism of the suppression of NO production by electro-stimulation. This suggested the feasibility to control the immune function by applying electro-stimulation from outside the body.

Introduction

The influence of ELF electromagnetic field on various physiological functions has been reported, and much study has been conducted mainly from the view point of adverse effects. On the other hand, there is a clinical application such as therapeutic instruments using ELF electric field. With the view towards the immune control by ELF electric field exposure, we have studied the effect of electro-stimulation on cell functions. Macrophages play important roles in a human immune system. We have examined the effect of electro-stimulation on the phagocytic activity and the active oxygen production ability of macrophages. Through this study, it has been found that the both activities are suppressed by the capacitively coupled electro-stimulation[1,2]. The electric current induced in the suspension of cells was in the similar order to that induced in the human body with the therapeutic instrument of electric field exposure.

In the current study, we have examined the effect of electro-stimulation on the production capacity of nitric oxide (NO). The NO is a kind of the same radicals as the active oxygen and is produced in the immune function of a macrophage. The NO is produced to kill bacteria but can destroy normal cells when produced excessively. Moreover, it reacts with the active oxygen and becomes the peroxynitrite ($ONOO^-$). The $ONOO^-$ is more toxic and damages normal cells. Therefore, if we can control the NO production, it will contribute to the prevention and the treatment of various diseases. We have examined this possibility by the ELF electro-stimulation in vitro.

Materials and Methods

macrophage preparation

Peritoneal exudate macrophages were used in all the experiments. The thioglycollate medium (4.05%, 2 ml) was injected in the peritoneal cavity of a normal mouse (Std:ddy, female, 7-11weeks). After 3 or 4 days, the cells were harvested from the mouse abdomen. Then, macrophages were collected from the cells in the established method. [3] We prepared the cell culture solution (RPMI 1640 with L-Glutamine , Sodium Bicarbonate and 10%Fetal Bovine Serum: RPMI 1640, hereafter) with 0.5×10^5IU penicillin G potassium and 50mg streptomycin sulfate added. The collected macrophages were suspended in the cell culture solution to make the cell density of 2×10^6cells/ml. When electro-stimulation was applied to the cells, the IFN-γ(10U/ml) and the LPS(1μg/ml) were added as stimulants to both the stimulation group and sham group.

electrostimulation system

The macrophage cells were stimulated by the electric current in the container insulated electrically from the electrodes to simulate the condition of electro-stimulation from outside the human body. Figure 1 shows the structure of the sample container.

Two plane electrodes were kept parallel with 3 mm distance by a plexiglass separator. The electrodes were square cupper plates (24mm×24mm×6mm top and 32mm×32mm×6mm bottom). The top electrode was insulated with a 0.15 mm thick cover-glass, and the bottom one with 0.10 mm thick silicone film. The outline of the electrostimulation system is shown in Fig.2. Two electrodes were connected to a high-voltage power source through a noise filter. As the power source, the power supply of a commercial apparatus for the electric field therapy was used (Healthtron , Hakuju Inst. Health Science, maximum supply voltage 10kV). A sinusoidal AC signal of 50Hz was supplied to the apparatus with a waveform generator to make the high-voltage with the sinusoidal waveform of 50Hz. In the experiment, the cell suspension was placed in the container, and electro-stimulation was applied in a CO_2 incubator (38ºC, $CO_2$5%). The cell suspension of the sham group was kept in another incubator of the same condition.

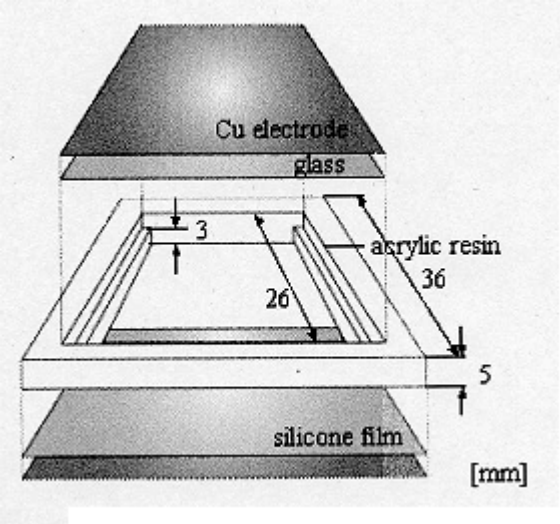

Fig.1 Sample container

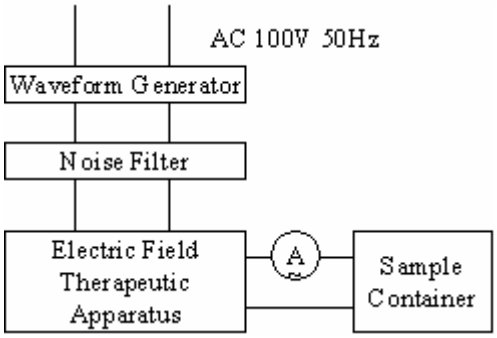

Fig.2 Schematic diagram of electro-stimulation system.

Effect on NO production

We stimulated macrophages in the suspension with IFN-γ and LPS, and applied the electro-stimulation for the exposure group. The sham group was treated in the same way except connecting to the power source. The amount of NO produced outside the cell was measured as fluorescent intensity (495nm excitation and 515nm emission) using fluorescent reagent Diaminofluorescein-2(DAF-2) for the NO detection.

Macrophages were collected in the established method, and washed three times with Hanks' Balanced Salt Solution (HBSS) in centrifugation (400G) for 5 minutes. Then, they were suspended in the culture liquid RPMI 1640 again, and the electro-stimulation (50Hz, 35μA/cm^2, 16h) was applied. After the electro-stimulation, the macrophages were washed with HBSS in centrifugation, and cultured in HBSS suspension with DAF-2(10μM) and L-arginine(1mM) two hours without electro-stimulation. After the two hour culturing, the supernatant part was separated in centrifugation. With a fluorescent photometer, the fluorescent spectrum of the supernatant was measured. The supernatant of the sham group was collected in the same process except for the electro-stimulation, and the fluorescent spectrum was measured in the same way as the stimulation group.

Figure 3 shows an example of the measured result. The abscissa is the wavelength and the ordinate is the fluorescent intensity. The wavelength of the intensity peak was around 515 nm in both cases. There was no significant change in the shape of the spectrum, but 30% decrease in the intensity was observed in the stimulation group. This suggest the suppression of NO production by the electro-stimulation. The same experiments were repeated nine times. Figure 4 shows the reduction ratios of the fluorescent intensity between the stimulation and the sham groups. In all the nine cases, the fluorescent intensity was decreased by the electro-stimulation. The p-value of the paired-t test was 1.79×10^{-2}, which suggested the suppression of NO production by the electro-stimulation with a statistical significance.

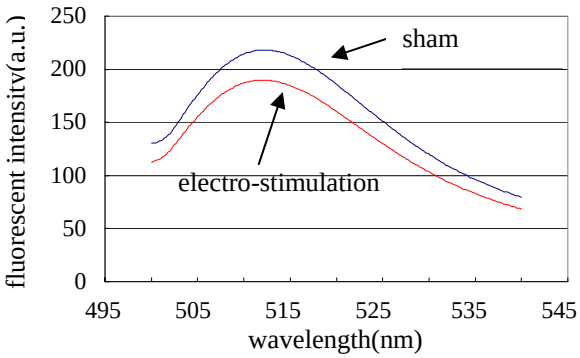

Fig3. Example of measured NO production by fluorescence spectroscopy.

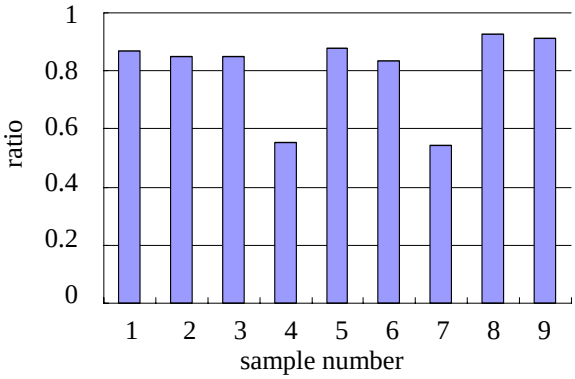

Fig.4 Suppression of NO production.

Effect on iNOS expression

NO is synthesized in a macrophage by the inducible nitric oxide synthase (iNOS). To elucidate the mechanism of the suppression in the NO production, the effect of the electro-stimulation on the iNOS expression was examined. The amount of the iNOS expression was evaluated by measuring the fluorescent intensity in the indirect immunity fluorescent method. [5, 6]

In the same way as the one mentioned above, macrophages were collected, separated into two groups, and electro-stimulation (50Hz, 35μA/cm^2, 16h) was applied to the stimulation group. After the electro-stimulation, the macrophages were collected in the centrifugation. With 70% ethanol, the cell membrane was processed to enhance its permeation. After three times centrifugation (400G, 5 minutes), macrophages were suspended in HBSS. We added the rabbit anti-iNOS antibody (BD Biosciences) and kept it in a shaker bath at 4 ºC in 30 minutes. Then we added 20μg/ml of the FITC tagged hircine anti-rabbit Ig antibody (MP Biomedicals Inc.) and kept it in the shaker bath. Finally, we fixed the suspension with 1% paraformaldehyde, and measured the fluorescent intensity with a flow cytometer (FACS Calibur Becton Dickinson and Company).

Figure 5 shows an example of the results. The abscissa is the fluorescent intensity in an arbitrary unit, and the ordinate is the number of the cell. The broken line in the figure shows the average intensity of all the cells. The average values were 79 and 65 for the sham (a) and the stimulation (b) cases, respectively. This result showed the decrease in iNOS expression by the electro-stimulation. The same experiments were repeated eleven times. Figure 6 shows the ratio of the average intensity between the simulation and the sham cases. As shown in the figure, the decrease in fluorescent intensity was observed in all the eleven trials. The p-value of the paired-t test was 5.52×10^{-5}. This suggested that the iNOS expression was suppressed by the electro-stimulation with statistical significance.

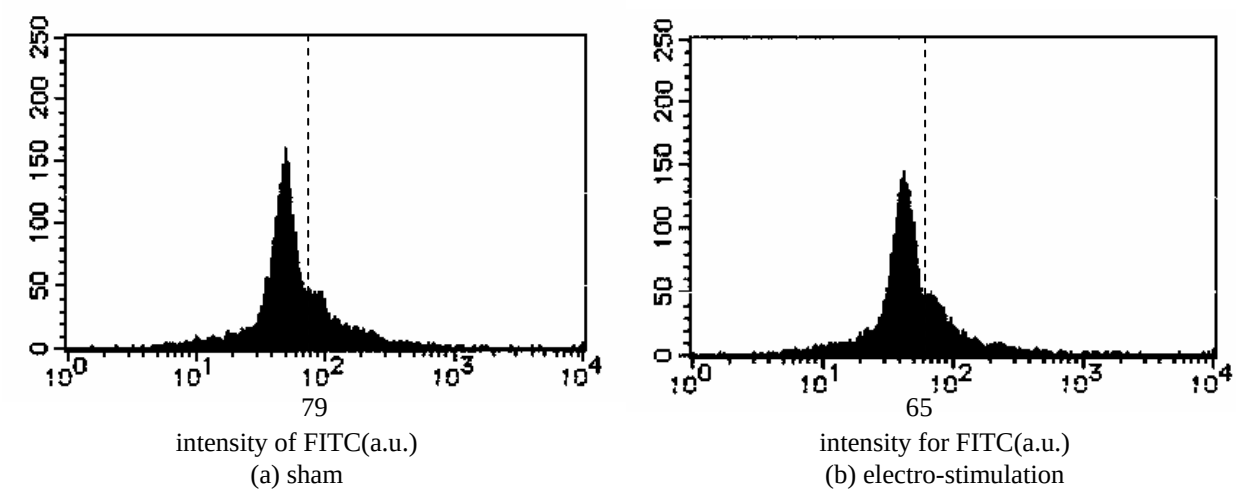

Fig.5 Example of measured iNOS expression by fluorescence spectroscopy.

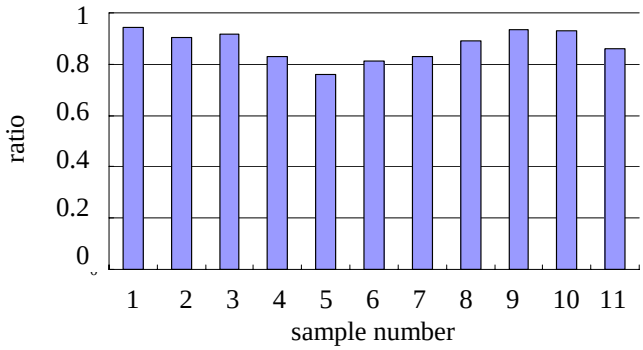

Fig.6 Suppression of iNOS expression.

Analysis of dose-response

As the first step of quantitative evaluation, the dose-response of these phenomena was analysed. In experiments, the amounts of the NO production and the iNOS expression in different current densities (0.35μA/cm^2, 0.675μA/cm^2, 3.5Aμ/cm^2) were measured. After the electro-stimulation in 16 hours, the cell suspension was divided into two. One was used for the measurement of the NO production, and another is for that of iNOS expression. Figure 7 shows the results of the measurements. The abscissa is the current density and the ordinate is the fluorescent intensity normalized by that of the sham case. The number of repeated measurements were 4, 6 and 4 for the cases of 0.35μA/cm^2 , 0.675μA/cm^2 and 3.5μA/cm^2, respectively. The result of 35μA/cm^2 case was added, in which the numbers of the repeated experiments were 11 and 9 for NO and iNOS cases, respectively.

With the current density of 0.35μA/cm^2, we could not observe apparent decrease in either of the NO or the iNOS. With 0.675μA/cm^2, about 5% decrease was observed. With the current density of more than 3.5μA/cm^2, more than 15% decrease was observed. In both of the NO and the iNOS, the threshold of the suppression seems to exist between 0.35μA/cm^2 and 3.5μA/cm^2. The similar characteristics in the dose-response strongly suggested the close correlation between the suppression of iNOS expression and that of NO production.

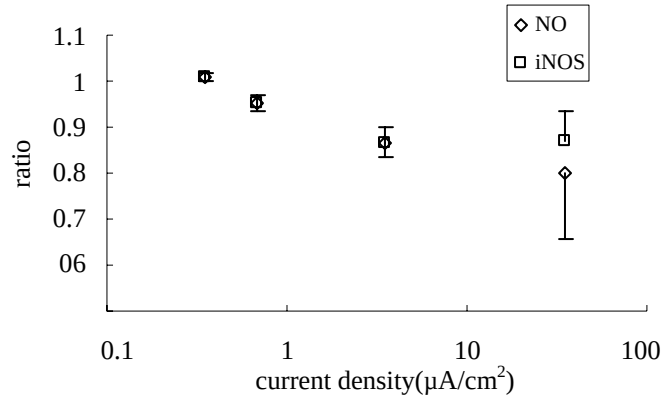

Fig.7 Analysis of NO and iNOS suppression effect by electro-stimulation.

Discussion

In the in-vitro experiments, it was found that the NO production is significantly suppressed by the ELF electro-stimulation. This suggested the possibility to control the functions of macrophages by the electro-stimulation applied from outside the body using the apparatus for the electric field therapy. Since a macrophage plays an important role in the first stage of the immune response, the electro-stimulation can influence the entire immune reaction. For example, we can expect the relief from the following diseases. They include the chronic inflammation and the autoimmune diseases caused by an excessive immune response. We can also expect the relief from the endotoxin shock due to the excessive NO production, the etiologic vasodilation, the cardio-vascular ischemia, the cerebral hemorrhage and the cancers. Moreover, we have confirmed the suppression of the active oxygen production by the electro-stimulation.[2] Therefore, we can also expect the control of $ONOO^-$

production which shows high cell-toxicity.

However, the finding of this study is only the result of in-vitro experiments using macrophages. We need further investigation to confirm this effect with human macrophages, and the investigation on this effect in-vivo where other kinds of cells are closely interacted. Yoshikawa and his co-workers reported the increase of NO production in the liver when LPS (2 mg/kg) was administered by abdominal injection and the magnetic field (60Hz, 0.1mT) was exposed in 5.5 hours. The current density induced by this magnetic field inside the body is estimated at $1.1\times10^{-8}A/cm^2$. This result is opposite to our result. It seems that the direct comparison between these two cases is not appropriate, since the object cell and the current density is greatly different among them.

Besides this, there have been few reports on the effect of ELF electromagnetic fields on the NO production, and little has been known on its mechanism. We consider that the arginine metabolism, iNOS activity and iNOS expression are closely associated with the decrease in the NO production. To investigate this mechanism, we have compared the amounts of NO production and the iNOS expression.

Figure 7 shows the coincidence in the reduction ratio of fluorescent intensity between NO and iNOS by the same electro-stimulation. This result suggests that the electro-stimulation affects the NO production through iNOS expression. The signal transmission pathway for the iNOS expression is stimulated by LPS and IFN-γ through receptors on a cell membrane. As the result, a transcription factor is activated and the iNOS is transcribed. In our study, the electro-stimulation was applied from the beginning when we started the stimulation with LPS and IFN-γ. Therefore, it is most plausible that the electro-stimulation affects this process.

However, the following possibility cannot be neglected. In the peritoneal exudate cells used in this study, about 10% cells were not macrophages. Since these non-macrophage cells can affect the signal transmission pathway of the NO production, they might influence the mechanism of the suppression of the NO production. Therefore, we have to examine this point in the experiment using the pure macrophage cells separated from other cells.

In our experiment, the threshold of the effect was found between $0.35\mu A/cm$ and $3.5\mu A/cm^2$. In the study for the biological effects of ELF electromagnetic fields, the minimum threshold of magnetic field exposure has been reported. [7] According to the report, the threshold current density for the characteristic change in tissues and cells was in the order of $10mA/m^2$ or $1\mu A/cm^2$. Though this threshold is for the electric current induced by magnetic field, it is very close to our result in which the electric current was induced by the electric field.

Conclusion

With the view toward the control of immune functions by ELF electric field exposure, the effect of the electro-stimulation on the NO production of macrophages was examined in vitro. The decrease of NO production due to the electro-stimulation was observed with statistical significance. In experiments, it was found that the expression of NO synthesizing enzyme or iNOS was suppressed in the same rate as NO in the electro-stimulation. Further investigation is required to ascertain this mechanism of NO suppression and to verify the feasibility of the immune control by electro-stimulation.

Reference

[1] I. Fujii, T. Shimooka, Y. Morita and K. Shimizu, "Experimantal verification for the effect of capacitively coupled electrostimulation on macrophage's endocytosis," Tec. Report IEICE., MBE2001-101, pp.97-102,2002.(in Japanese)

[2] Takeshi Tatebe, Toshiyuki Shimooka, Muneyoshi Kagawa, Koichi Shimizu, "Effect of ELF electrostimulation on reactive oxygen generation of macrophage", Tec. Report IEICE, MBE2003-131, pp.13-18, 2004.(in Japanese)

[3] Stohlman SA, Frelinger JA, Weiner LP. Resistance to fatal central nervous system disease by mouse hepatitis virus, strain JHM. II Adherent cell-mediated protection. J Immunol., 124(4):1733-9, 1980.

[4] Wataru Yoshida, Minori Ogawa, Yuko Furuoya, Yu Igarashi, Rumi Sato, Akiko Hayashi, Kazuya Hirano, Masatoshi Beppu, "Effect of Estrogenic Compounds on Superoxide and Nitric Oxide Production by Activated Macrophages Assessed by Sensitive Microplate Assays", Journal of Health Science, 48(5), pp.455-459, 2002.

[5] Oh-Deog KWON, Chang-Yeol YIM, Kyu-Shik JEONG, Kyu-Yong JUNG, John R. McGREGOR, Neil R.BASTIAN Wolfram R. SAMLOWSKI, "Suppression of Cytokine-Inducible Nitric Oxide Synthesis During Intraperitoneal Meth A Tumor Growth" , J Vet Med Sci., 66, pp.357-365, 2004.

[6] Wolfram E. Samlowski, Jhon R. McGregor, Gregory J. Litton, "Liver Sequestration of Murine Lymphokine Activated Killer Cells Is Mediated by Carbohydrate-specific Receptor", Regional immunology Vol.2, pp.254-265, 1989.

[7] ICNIRP Guidelines : "Guidelines for limiting exposure to time-varying electric, magnetic, and electromagnetic fields(up to 300GHz)", Health Physics, Vol.74, No.4, pp494-522.1998.

[8] Yoshikawa T, Tanigawa M, Tanigawa T, Imai A, Hongo H, Kondo M, "Enhancement of nitric oxide generation by low frequency electromagnetic field" , Pathophysiology, pp.131-135, Jul;7(2), 2000.

THE ANALYSIS OF VARIOUS APPROACHES TO ASSESSMENT OF SPATIALLY HETEROGENEOUS EMF EXPOSURE IN THE WORKPLACE

JOLANTA KARPOWICZ, PATRYK ZRADZIŃSKI, KRZYSZTOF GRYZ, MARCIN MOLENDA

CENTRAL INSTITUTE FOR LABOUR PROTECTION – NATIONAL RESEARCH INSTITUTE, LABORATORY OF ELECTROMAGNETIC HAZARDS WARSZAWA, POLAND, e-mail: jokar@ciop.pl

Abstract

The subject of presented investigations is a spatial distribution of electromagnetic field (EMF) in the workplace, in the vicinity of dielectric heaters where worker's exposure occurs. Detailed spatial distribution of *E*-field in the vicinity of 4 dielectric heaters of various constructions was measured and taken as reference data: 2 dielectric heaters of low emitted field (1 not shielded and 1 shielded) and 2 dielectric heaters of high emitted field (1 not shielded and 1 shielded). Numerical simulations of EMF emitted by numerical model of such devices were carried out with the use of specialized software packages for EMF simulations based on various numerical methods. The comparative analysis of various principles for limitation on workers' exposure to spatially heterogeneous EMF was taken into consideration (EC Directive, IEEE, IEC and EN standards, Polish occupational regulation and standards). The results of measurements and numerical modeling of worker's exposure were discussed, as well as the discussion concerning the worker's protection level corresponding to the use of various spatial averaging protocols while exposure assessment. The obtained results have proved the practical usefulness of various calculations methods for intermediate frequency EMF exposure assessment. The use of the Protection Level Factor, defined by authors for the analysis of the protection level associated with various exposure assessment protocols has been demonstrated at the example of a detailed analysis of electric field from dielectric heaters and its various assessment methods. For example, following the comparison of exposure assessment rules from IEEE standards, EC Directive and Polish regulations - IEEE rules, which seems to be the most liberal for 1 MHz, become to be the most restrictive for the frequency of 27 MHz.

Keywords: EMF exposure, exposure assessment, measurements, numerical calculations, dielectric heaters

1. Introduction

Electromagnetic field's (EMF's) exposure assessment can be required for various purposes, like occupational safety and health (OSH) engineering, epidemiological studies of EMF-exposed groups, environmental monitoring. For all of those purposes, EMF exposure assessment adequate to the real exposure level is the crucial step towards appropriate risk assessment. The highest requirements concerning detailed EMF exposure assessment come from the legislations concerning mandatory control of occupational or environmental EMF exposure. The highest influence on the legislative rules concerning EMF in particular countries come from European Directive 2004/40/EC, ICNIRP's guidelines and IEEE standards. There are also many national regulations implementing various additional rules concerning the protecting of workers against EMF overexposure.

The provisions of the Directive 2004/40/EC are based on the ICNIRP's guidelines in which the limit values of external measures of EMF exposure refer to the electromagnetic fields spatially averaged over the human body. Up to now, it is a lack of European Standards (EN) from CENELEC, harmonized with the Directive 2004/40/EC and focused on details of measurement's procedures and assessment of workers exposure. Various examples of procedures for spatial averaging of electromagnetic fields affecting human body were taken from the existing standards in order to analyze the possible practical consequences of various approaches to solving this problem. Analyzed procedures may be considered as a possible statement for future harmonized standards.

The assessment of the EMF exposure while hand-operating of the dielectric heaters is exactly a practical example of the above-mentioned problems. Dielectric heater's operation involves putting sticking/gluing components from thermoplastic foil between electrodes (upper – powered and lower - grounded) and switching

on the RF power (usually of the frequency of 27 MHz). In the case of manual operation, the worker is sitting or standing in front of the device, in the distance of 30 – 50 cm from the electrodes.

During the heating process, the worker is exposed to a spatially heterogeneous field of high electric field strength and relatively weak magnetic component. Usually, it is a sinusoidal time-varying field. Theses exposure conditions cause that protocol for EMF hazard's assessment should include the real characteristic of exposure and that exposure effects in the worker's body depend on the spatial distribution of the exposure. Such effects are well illustrated by differences in results of calculation of *SAR*, which are shown on figure 1 and in table 1. The calculations were done with a homogeneous model of worker's body, in a sitting position, grounded and exposed to electric fields from the model of dielectric heater or in spatially uniform (homogeneous), vertically polarized field. Both fields are of the same field strength at reference point located in vertical axe of torso of the body model, at height of powered electrode of a dielectric heater. The calculations results of *SAR* values were normalized by the whole body SAR (taken as 100%) in worker's body exposed to an uniform field, because such exposure scenario is usually taken for calculations of relation between external (*E* field) and internal (*SAR*) limitations for permissible EMF exposure.

a) b)

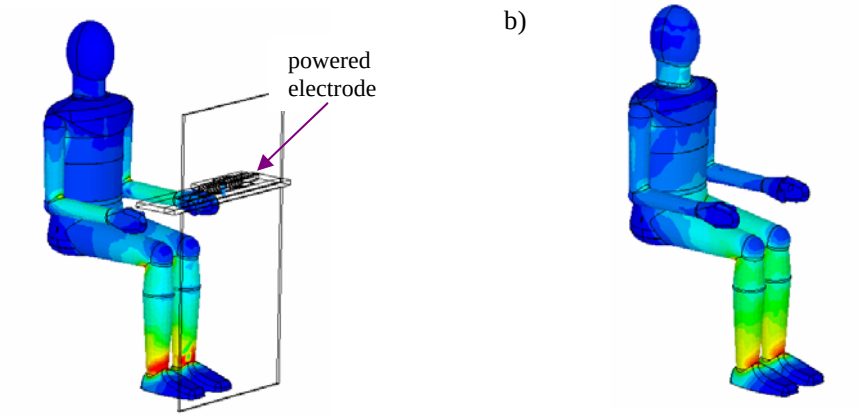

Fig 1. *SAR* distribution in homogeneous grounded model of sitting worker exposed to EMF: a) in front of dielectric heater; b) in vertically polarized uniform field

Table 1.
Results of *SAR* calculations for homogeneous grounded model of sitting worker

	SAR, relative value, %	
	exposure from dielectric heater	exposure in vertically polarized uniform field
SAR - max (10g) local value in the body model	170	1350
SAR - value averaged over whole body	14	100

However, the spatial distribution of *SAR* calculated for both cases is rather comparable with the highest exposure effects localized in ankles, the absolute level of *SAR* values are app. 10-fold higher in the case of uniform field exposure. Various approaches to assessment of spatially heterogeneous EMF exposure in the workplace, where exposure conditions are similar to that in the vicinity of dielectric heaters, were analysed. Exposure limitations and exposure assessment protocols fixed by the EC Directive, EN, IEC, IEEE standards and occupational regulation and standards established in Poland, were taken into consideration.

2. European Directive 2004/40/EC and European Standards

European Directive 2004/40/EC on minimum health and safety requirements regarding the exposure of workers to the risk arising from electromagnetic fields (EMFs) was established in 2004 as the 18th individual Directive within the meaning of Article 16(1) of Framework Directive 89/391/EEC [1]. The EMF's Directive requires that employers undertake risk/exposure assessments using detailed procedures from harmonized European Standards given by the European Committee for Electrotechnical Standardisation (CENELEC), which have not been published yet. This Directive specifies the minimum requirements, thus giving Member States the option of

maintaining or adopting more favorable provisions for the protection of workers, in particular the fixing of lower values for the action values or the exposure limit values for electromagnetic fields. The implementation of this Directive should not serve to justify any regression in relation to the situation which already prevails in each Member State.

The Member States should implement the provisions of the Directive into national legislation by April 2008 and should consider them as minimal requirements against occupational risks due to exposure to EMFs. Detailed comparative analysis of protection levels coming from the Directive's provisions and provisions of existing national regulations and existing national and international standards is very impeded because of the lack of above mentioned European Standards. From the formal point of view, until harmonized European standards from CENELEC cover all relevant assessment, measurement and calculation situations, worker's EMF exposure assessment may be carried out in accordance with other, e.g. national scientifically-based standards and guidelines. Such practice is not guaranteeing that results of exposure assessment carried out according to various protocols will provide comparable conclusions concerning the level of EMF hazard in the workplace.

2.1. EMF exposure limitations established by Directive 2004/40/EC

The employer shall assess and, if necessary, measure and/or calculate the levels of EMFs to which workers are exposed. According to the obligations arising out of the Directive, workers shall not be exposed above the exposure limit values in any event. Additionally, action values were defined for testing and assessing environmental conditions in the workplace. On the basis of the assessment of the levels of EMF, if the action values (external measures as: electric field strength, E, and magnetic field strength, H, in the workplace) are exceeded, the employer shall assess and, if necessary, calculate whether the exposure limit values (internal measures of maximum permissible exposure effects in exposed worker's body as: induced current density, J, and specific energy absorption rate SAR) are exceeded.

The action values are obtained from the exposure limit values according to the rationale presented in ICNIRP's guidelines [3]. External measures are provided strictly as an aid for practical exposure assessments, to determine whether the internal measures are likely to be exceeded. Overexposure concluded from EMF measurements in the workplace do not guarantee that limit values are exceeded in exposed body.

The limit values for electric field strength from the intermediate frequency range are presented within frequency ranges from table 2. The same values were mentioned in the ICNIRP's guidelines, as reference values.

Table 2.
The exposure limitations referring to external measures of the EMF exposure (unperturbed RMS values) - action values from the Directive 2004/40/EC

Frequency range	Electric field strength, E [V/m]
0.82 kHz - 1 MHz	610
1 – 10 MHz	$610/f$
10 – 400 MHz	61

f - frequency in MHz

As these values were calculated for the frequencies above 100 kHz to protect against the thermal effect inside the exposed body, electric field from the workplace should be spatially - and time - averaged for the analysis of the compliance with the internal measures' limitations. Currently, there is a lack of European exposure standards harmonized with above mentioned directive. Protocols from existing product standard concerning the analysis of compliance with ICNIRP's guidelines for general public exposure assessment, obligatory for testing products emitting EMF before entrance to European market (emission product standard), can be considered as a possible source of the protocol for the analysis of compliance with the Directive's provisions.

2.2. Spatial averaging from the EN/IEC product standards

The method of spatially averaging of the results of measurements of EMF is presented in the European standard EN 50357 [2] and IEC Standard 62369-1 [4] for testing the compliance with reference values (external measures published by ICNIRP). Following the provisions of these standards, the torso is the most appropriate part of the body to be assessed and the grid from Figure 2 should be used. The position of the grid in relation to the unit

under test can vary according to the typical usage of the EMFs emitting unit, e.g. the height *Z* should be modified for the assessment of a sitting person exposure. The layout and dimensions of the grid shall remain identical.
For assessment referring to the EMF exposure of torso, the EMF's spatial distribution should be measured in 45 grid points. The result of the arithmetic average of the measured *E* values should be compared with the limit value from ICNIRP's guidelines. In the exceptional cases where the exposure is predominately to the head, then the grid located in a position referring to the head must be used.

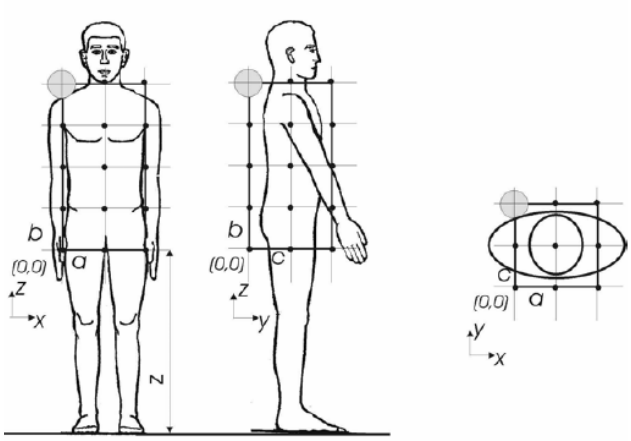

Fig. 2. Torso measurement grid for spatially averaged measurements according to EN 50357 or IEC 62369-1 (normative dimensions: a, b, c = 15 cm; Z = 85 cm)

3. EMF exposure limitations and assessment by IEEE standards

IEEE Std C95.1-2005[5] provides the recommendations to minimize aversive or painful electro stimulation in the frequency range of 3 kHz to 5 MHz and to protect against adverse heating in the frequency range of 100 kHz to 300 GHz similar to ICNIRP's rationale. The recommendations are expressed in the terms of basic restrictions (BRs) and maximum permissible exposure (MPE) values. The BRs are limits on fields induced in the body, specific absorption rate (SAR), and current density. The MPEs are derived from the BRs. The MPE values for electric field strength from the intermediate frequency range are presented within frequency ranges from table 3.

Table 3.
Electric field maximum permissible values (MPE) from IEEE STd C95.1-2005

Frequency range	Electric field strength, *E* [V/m]
3 kHz – 1 MHz	1842
1 – 30 MHz	1842/*f*
30 – 100 MHz	61.4

f - frequency in MHz

For spatially heterogeneous exposures, the mean values of the incidental fields should be obtained by spatially averaging the squares of the field strengths. The IEEE Std C95.3-2002 [6] standard provides details concerning exposure assessment protocol for testing compliance with IEEE Std C95.1-2005 provisions.

3.2. Spatial averaging from the IEEE exposure assessment standard

According to IEEE Std C95.3-2002 [6], for the measurement of electric or magnetic fields, carried out for the assessment of the whole-body exposure, spatial averaging of the measurement's results means the root mean square of the field over an area equivalent to the vertical cross section of the adult human body. The spatial average can be measured by scanning (with a suitable measurement probe) a planar area equivalent to the area occupied by a standing adult human (projected area). In the majority of cases, a simple vertical, linear scan of the fields over a 2 m height through the center of the projected area will be sufficient. IEEE document doesn't describe details how to do spatial averaging.

4. Workers EMF exposure limitations and assessment standards in Poland

The occupational safety and health (OSH) legislation in Poland concerns, among others, ambient environmental factors, electromagnetic fields at workplace. Regulations concerning occupational exposure to EMF of 0 Hz - 300 GHz frequency range have been in force since 1972 in Poland as mandatory legislation (current ed. - PL Journal of Laws 217/2002, item 1833 [8]). Regulations are periodically revised and, if necessary, updated under the umbrella of Interdepartmental Commission for Maximum Admissible Concentrations and Intensities for Agents Harmful to Health in the Working Environment, which is the scientific advisory body established by the Prime Minister of the Polish Government.

The main base for all EMF regulations in Poland was taken from the thresholds of thermal and nerve excitation effects, similarly to ICNIRP's approach implemented by the Directive 2004/40/EC. As periodical assessment of EMF exposure level in the workplace is mandatory in Poland, the regulations refer directly to external measures only (*E*, *H*). The internal measures (*J*, *SAR*) were not directly introduced into published regulations since there is no possibility to measure them in real conditions. However, the permissible internal measures of exposure effects defined by ICNIRP's guidelines (EC Directive) and IEEE Standards were used as an important contribution to theoretical rationale for the level of prohibited exposure to EMF's of various frequencies, drafted as scientific background for above mentioned national legislation.

Following the above-mentioned regulation and Polish Standard, the strength of electric and magnetic fields (*E*, *H*), the frequency of these fields (*f*) and workers' exposure duration (*t* and exposure factor *W*), should be taken into consideration for occupational EMF exposure assessment. The main provisions include:

- high exposure - Workers without protective clothes should not have been allowed to access to the area of EMF higher than the level of prohibited exposure (table 4) – the exposure level harmonized with the permissible internal measures from ICNIRP/EC Directive.

- medium exposure - The range of exposure level of permissible EMF exposure duration shorter than 8 hours. In the case that both electric and magnetic fields are relatively high, the exposure factor defining the permissible exposure duration is the sum of components from both fields of the frequency up to 3 GHz. The 8-hours permissible exposure level is the equivalent for ICNIRP/EC Directive external measures' limitation (table 4).

Table 4.
Electric field strength – exposure limitation established in Poland (external measures)

Frequency range	Electric field strength, *E* [V/m]	
	prohibited exposure	8 hours exposure
1 kHz < $f \leq$ 3 MHz	1000	100
3 MHz < $f \leq$ 15 MHz	3000/f	300/f
15 MHz < $f \leq$ 150 MHz	200	20

f - frequency in MHz

4.1. Protocol from the Polish Standard PN-T-06580 for workers exposure assessment

Polish Standards determine the protocols how to do EMF measurements and workers exposure assessment (PN-T-06580:2002, revised in 2002 [7]). Worker's exposure assessment should be performed on the results of spot measurements of RMS value of electric and/or magnetic field strength. The maximum value over the worker's body position in the workplace should be considered for testing the compliance of EMF exposure condition with OSH regulations. In practice, it is usually the maximum value of measured electric or magnetic field strength in the vertical axis of worker's body, up to 2 m height.

5. Method

The EMF exposure of workers can be evaluated following the results of calculations in the case when for a particular workplace the exposure assessment on the basis of EMF measurements is not adequate. Such situations occur when EMF's distribution is highly heterogeneous, a worker operates close to the field source or his body is in contact with it. Such exposure assessment needs appropriate modeling of EMF source - for

assessment considering external measures and additionally appropriate modeling of workers body - for assessment considering internal measures limitation.
The subject taken for the investigations presented has been a spatial distribution of electric field in the workplace in the vicinity of dielectric heaters where worker's exposure occur.
A detailed spatial distribution of *E*-field in the vicinity of 4 dielectric heaters of various construction was executed: 2 dielectric heaters of low level of emitted field - 1 not shielded (M-m1) and 1 shielded (M-m2); 2 dielectric heaters of high level of emitted field - 1 not shielded (M-d1) and 1 shielded (M-d2). Measurements were done by RMS value meter with isotropic probe. Three dimensional components (X, Y and Z) of electric field strength have been recorded online using notebook computer. The recording system is shown on figure 3. A measuring probe was placed in succeeding appointed points along measuring lines. The registration of only one single pulse was done at each measurement point.

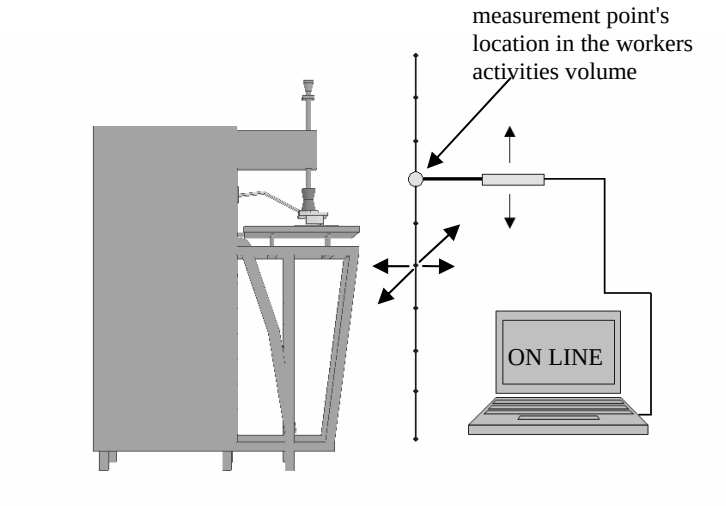

Fig. 3. Online registration system used for EMF measurement for data – acquisition in the vicinity of real dielectric heater.

Numerical simulations were carried out with the use of specialized software packages for EMF simulations based on various numerical methods:
- OPERA 3D v. 8.7 (Vector Fields Ltd, United Kingdom) – specialized for finite element method – FEM
- CST MICROWAVE and EM STUDIO (CST – Computer Simulation Technology - Germany) - specialized for finite integration technique – FIT.

The geometrical model of dielectric heater is shown in figure 4. EMF's source for this numerical modeling was created by powered electrode of 1 kV electrical potential.

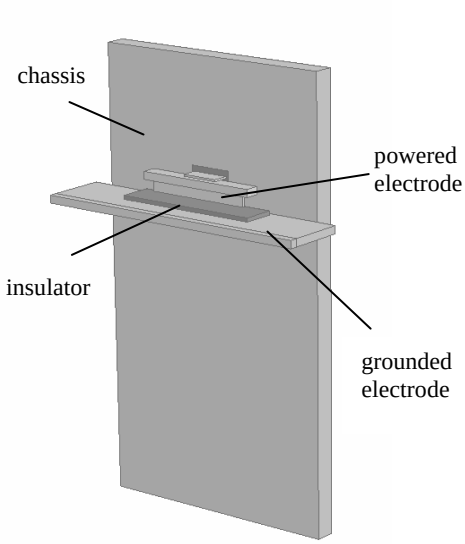

Fig. 4. Geometrical model of dielectric heater.

6. Results

Spatial distribution of *E* field in the vicinity of dielectric heater obtained from calculations and measurements have been averaged over the volume of worker's torso (following EN/IEC standards' protocol) and over the vertical axis of workers body position (following IEEE standard protocol). Averaging of measurements results have been carried out on the base of maximum values registered from each welding pulses. The results were presented in fig. 5 as values relative to the maximum value over the workers body which is taken for exposure assessment following the protocol established by Polish Standard PN-T-06580. Bars representing various measurements result's averaging are labeled in figure 5 as M-m1; M-m2; M-d1 and M-d2 (with above mentioned meaning). Bars representing averaging of calculation's results are labeled as follow: C-s1 - from Opera software, C-s2 - from CST MW and C-s3 - CST EM.

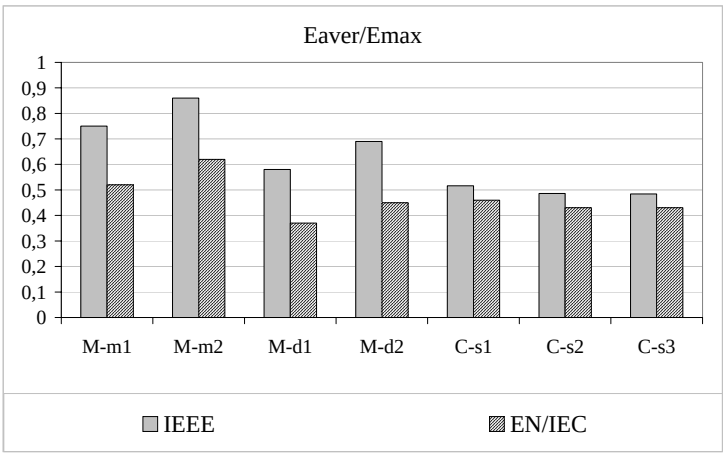

Fig. 5. Spatial averaging over the workplace the *E*-field from dielectric heaters

The data concerning *E*-field spatial distribution, obtained from simulations with the use of very simple model of EMF source and various software, averaged over the workers body presented the similar relation to maximum value of *E* field at workplace (0.43-0.51) as the ratio observed among the measurement results from real workplace (0.35-0.85). Thanks to this fact, obtained results of calculations suggest that various numerical simulations' methods could be acceptable for calculations executing for the assessment of intermediate frequency EMF occupational exposure. Very simple models of EMF source can be also accepted, but "calibration" of the calculation results has to be done by the comparison with measurement results to obtained confirmation concerning the absolute values of exposure level (*E*-field).

For a deeper analysis of the practical consequences of the use of various exposure assessment protocols and limit values, the protection level coefficient can be consider. Protection Level Factor (PLF) can be define as the ratio of the exposure estimator taken for exposure assessment on the basis of particular exposure assessment protocols (e.g. various spatial averaging protocols above mentioned), divided by exposure limitation harmonized with this protocol (e.g. E field averaged following the protocol from IEEE C95.3 divided by limit value fixed by IEEE C95.1). With such definition, PLF of higher value correspond to the more restrictive exposure assessment rules, or in other word, higher protection level.

The practical usefulness of the analysis of various exposure assessment rules with the use of PLF value can be show at the example of electric fields of spatial distribution like in the vicinity of dielectric heaters and maximum value at the axis of worker's torso of 1000 V/m, assessed following the limit values from tables 2-4. The field taken for the analysis can be described by max value of 1000 V/m, value averaged following IEEE rules of 700 V/m and value averaged following EN/IEC rules of 500 V/m. For such values, in the case of electric field of frequency of 1 MHz, PLF values are: for the exposure assessment rules established by the European Directive and EN/IEC standards – PLF(EC, 1MHz) = 0.8; for exposure assessment rules established by IEEE standards – PLF(IEEE, 1MHz) = 0.4 and for exposure assessment rules established in Poland as the threshold of prohibited exposure – PLF(PL, 1MHz) = 1. In the case of electric field of 27 MHz PLF values have different order: PLF(EC, 27MHz) = 8; PLF(IEEE, 27MHz) = 10; PLF(PL, 27MHz) = 5 – IEEE rules, which seems to be the most liberal for 1 MHz, become to be the most restrictive for the frequency of 27 MHz.

7. Conclusion

These investigations can support the work on methods of numerical simulations for the routine assessment of worker's exposure to EMF from intermediate frequency range. There is relatively a wide gap of experience of "numerical" assessment of worker's exposure to EMF from intermediate frequency range in comparison with the huge amount of data concerning power frequency and microwave.
The selection of geometry of EMF source's models, as well as the selection of numerical simulations methods can significantly influence on the level of obtained results, however the relative spatial distribution of E-field could be similar.
Presented methodology of analysis of the protection level which is associated with various exposure assessment protocols can be use for detailed comparative analysis of various exposure limitation standards, legislation or guidelines. The overall analysis should consider not only the spatial averaging of incidental fields but also rules of time-averaging of non-continuous exposure, calibration of measurement devices for non-sinusoidal fields, etc. components of exposure assessment protocols.

Acknowledgment
This paper has been prepared within the investigations supported by the State Committee for Scientific Research and Ministry of Economy, Labour and Social Policy of Poland (grant 1.A.02).

References

[1] Directive 2004/40/EC of the European Parliament and of the Council of 29 April 2004 on the minimum health and safety requirements regarding the exposure of workers to the risks arising from physical agents (electromagnetic fields) (18th individual Directive within the meaning of Article 16(1) of Directive 89/391/EEC), O.J. nr L-184 of 24 May 2004.
[2] EN 50357:2001 Evaluation of human exposure to electromagnetic fields from devices used in Electronic Article Surveillance (EAS), Radio Frequency Identification (RFID) and similar applications.
[3] ICNIRP *Guidelines for Limiting Exposure to Time-Varying Electric, Magnetic, and Electromagnetic Fields (up to 300 GHz)*, Health Physics, vol. 74, No. 4 (April), 494-522, 1998.
[4] IEC Draft 62369-1. Evaluation of human exposure to electromagnetic fields from Short Range Devices (SRDs) in various applications over the frequency range 0-300 GHz. Part 1: Fields produced by devices used for Electronic Article Surveillance, Radio Frequency Identification and similar systems (September 2004).
[5] IEEE Std C95.1-2005, Standard for Safety Levels with Respect to Human Exposure to Radio Frequency Electromagnetic Fields, 3 kHz to 300 GHz. Published by the Institute of Electrical and Electronics Engineers, New York, USA, 2006.
[6] IEEE Std C95.3-2002 Recommended Practice for Measurements and Computations of Radio Frequency Electromagnetic Fields With Respect to Human Exposure to Such Fields, 100 kHz–300 GHz. Published by the Institute of Electrical and Electronics Engineers, New York, USA, 2002.
[7] Polish Standard PN-T-06580:2002. Labour protection in electromagnetic fields and radiation of the frequency range from 0 Hz to 300 GHz. Part 1: Terminology. Part 3. Methods of measurement and evaluation of the field on the work stands (in Polish).
[8] Regulation of the Minister of Labour and Social Policy, Permissible occupational conditions, Journal of Laws 217/2002, item 1833 (in Polish).

ACTIVE SUPPRESSION OF AN INDUSTRIAL FREQUENCY ELECTROMAGNETIC FIELD (EMF): THE PRACTICAL REALIZATION

A.SHENKMAN, N. SONKIN, E. NEEMAN, V. KAMENSKY,
R. ZEMAH

HOLON INSTITUTE OF TECHNOLOGY,
52 GOLOMB ST., P.O.B. 305, HOLON 58102, ISRAEL

ABSTRACT

The present work deals with the active suppression of an electromagnetic field (EMF) of complicated multi-circuit transmission lines and its practical realization. This research is the continuation of a previous one [1], in which more simple case of only one (single) transmission line EMF was investigated and a method of its suppression proposed.

In double circuit transmission systems, for instance, the EMF has an elliptic space-time characteristic, as the big and small axes of the ellipse can be approximately of the same lengths.

The active suppression of an EMF in such cases can be carried out by means of two loops installed in parallel to the transmission lines having independent automatic control of the currents in each loop.

The method of calculating the EMF of the transmission system and of the loops and the computer program for performing such calculations, have been developed in this work. Based on these calculations, loop parameters and their arrangement in space may be determined.

As a result of the research, a practical application (pilot installation- see the pictures) of the suppression of EMF, induced by a high voltage (160kV) double transmission line in an office building of an industrial zone of the city of Rosh Haayin has been performed. Two loops located along the protected office have been installed and activated by a control system. The experimental results of such protection were in very good agreement with the theoretical predictions. The electromagnetic field in various points of the protected office has been reduced 3-10 times, so that the suppressed EMF became less than the permissible value.

INTRODUCTION

In the previous research [1] it was shown that the space-time characteristic of the EMF of a single transmission line has very narrow elliptic form. It was also shown that the suppression of such EMF could be done by using a single loop, whose space-time characteristic is a straight line. The suppression is achieved when the parameters of the loop (its ampere-turns and position in the space) are chosen in such a way that its straight-line-characteristic coincides with the big axis of the elliptic-characteristic of the transmission line EMF and equals it in length. The two EMF's of the line and the loop of course have to be of opposite phases.

ELECTROMAGNETIC FIELD GENERATED BY A COMPLICATED POWER LINE

Let us now analyze a double-circuit transmission line having any phase sequence. Fig. 1 shows such a line going in parallel to a four story building.

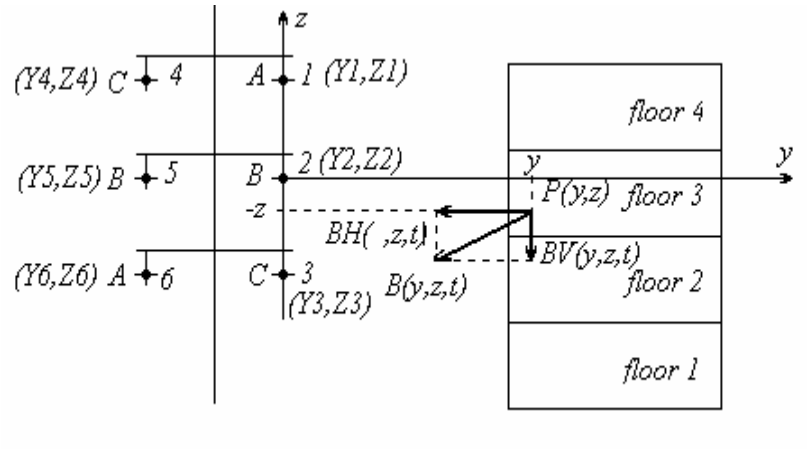

Fig.1 Three-phase double-circuit power line and a protected building

Let $P(y,z)$ be the point, where we wish to calculate the magnetic field (the point of observation), where y, z are the coordinates of the point of observation. (In this case the observation point is located on the third floor).

In accordance to the Biot-Savart law the magnetic flux density produced by an infinite conductor is:

$$B(y,z,t)=\frac{\mu_0}{2\pi}\frac{I_m\sin(\omega t-\alpha)}{R(y,z)} \tag{1}$$

where μ_0 is the magnetic permeability of air, $I_m\sin(\omega t-a)$ is the current carried by the conductor and $R_i(x,z)$ is the distance from *i*-phase to the point of observation.

$$R_i(y,z)=\sqrt{(y_i(y)^2+(z_i(z))^2}\,, \tag{2}$$

where $y_i=y-Y_i$, $z_i(z)=z-Z_i$ and Y_i *and* Z_i are coordinates of an *i*-phase.

Then the vertical and horizontal components of EMF are defined by the expressions:

$$\begin{aligned} BV_i(y,z,t)&=B_i(y,z,t)\frac{y_i(y)}{R_i(y,z)}\\ BH_i(y,z,t)&=B_i(y,z,t)\frac{z_i(z)}{R_i(y,z)} \end{aligned} \tag{3}$$

The sum of the vertical and horizontal components at point $P(y,z)$ for a three-phase double-circuit line is given by:

$$\begin{aligned} BV(y,z,t)&=\sum_{i=1}^{6}BH_i(y,z,t)\\ BH(y,z,t)&=\sum_{i=1}^{6}BH_i(y,z,t) \end{aligned} \tag{4}$$

With the vertical and horizontal components (4) the space-time characteristic of the transmission lines EMF is built and shown in Fig.2. As can be seen, the obtained ellipse is pretty wide so that the successful suppression of EMF by use of only one loop cannot be achieved.

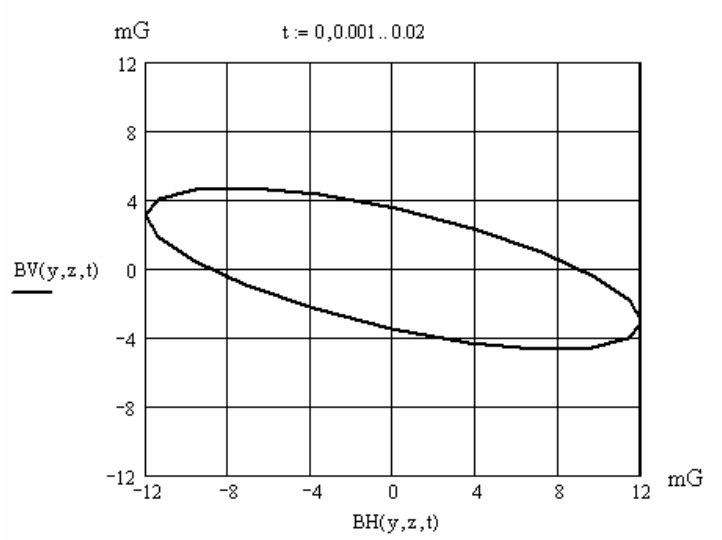

Fig. 2 An elliptic characteristic of EMF

In Fig.3 the above two components (4) are shown as functions of the distance from the office wall, parallel to the transmission lines, along the *y*-axes, and in Fig. 4 they are shown along the *z*-axis from the floor up to the ceiling. The origin of these coordinates is located at the point of the location of the sensor, which activates the control system).

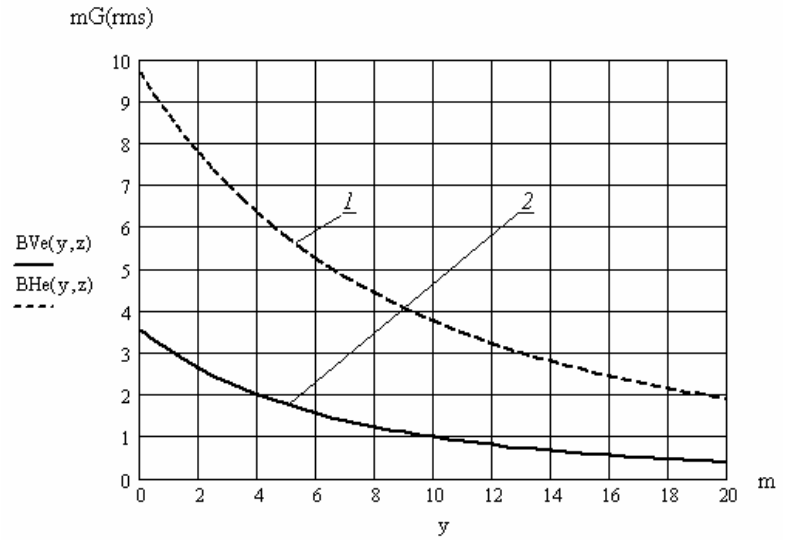

Fig. 3 Effective values of transmission lines' EMF inside the office: 1-horisontal, 2-vertical components

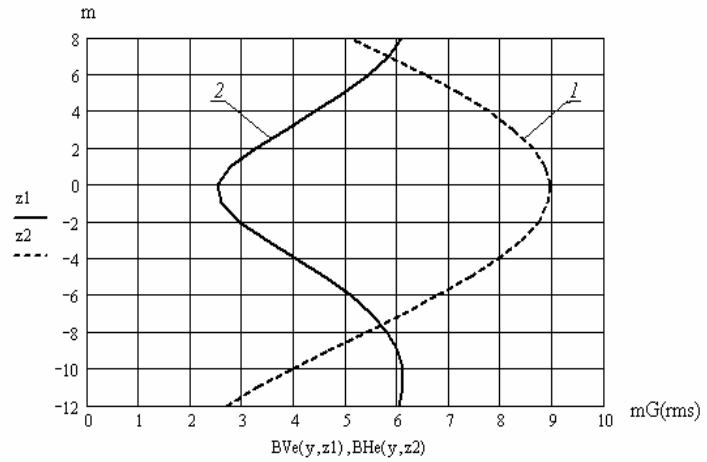

Fig. 4 Effective values of transmission lines' EMF in the office versus height: 1-horisontal, 2-vertical components

Both components of the EMF, of course, can be measured and compared with the one computed and, if the line currents and the phase sequences are presented by their actual values, the computed values (Figs 3 and 4) should be in agreement with the measured ones. Now, being sure that the picture of the EMF is correct we can design the compensation loops.

ELECTROMAGNETIC FIELD GENERATED BY COMPENSATING LOOPS

Since the EMF of a two-circuit transmission system is expressed by the wide ellipse, as is mentioned above, the suppression of such a field should be performed by means of two perpendicular loops, as shown in Fig. 5. In this case the protected area is the office of ECTEL Company. (The position of the sensor, whish activates the automatic control system, is indicated by ©)

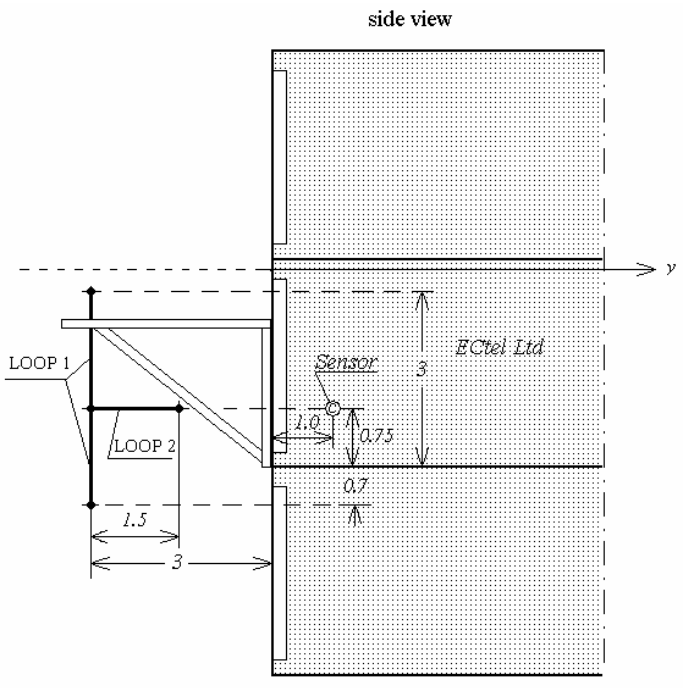

Fig. 5 The position of the protecting loops

The EMF of these loops is calculated as a sum of the vertical and horizontal components of all four lines:

$$BV_l(y,z,t) = \sum_{i=1}^{4} BV_{li}(y,z,t)$$
$$BH_l(y,z,t) = \sum_{i=1}^{4} BH_{li}(y,z,t) \qquad (5)$$

The suppressed field $(BVs(y,z,t),\ BHs(y,z,t))$ is then obtained as a sum of the vertical and horizontal components of the transmission line system $(BV(y,z,t),\ BH(y,z,t))$ and the loop system $(BVl(y,z,t),\ BHl(y,z,t))$:

$$BVs(y,z,t) = BV(y,z,t) + BVl(y,z,t)$$
$$BHs(y,z,t) = BH(y,z,t) + BHl(y,z,t) \qquad (6)$$

As it was already mentioned, the vertical loop (loop 1) should be positioned in such a way that its characteristic (line 2 in Fig. 6a) will coincide with the big axes of the ellipse (line 1 in Fig. 6a). The resulting EMF is also shown in Fig. 6a as line 3, which actually is an ellipse, but due to the relatively small scale looks as a line. Then the horizontal loop (loop 2) is designed and positioned in such a way that its characteristic (line 2 in Fig. 6b) coincides with the small axis of the original ellipse (line 1 in Fig. 6a). Note that this small axes after the first compensation turns into the big one, as shown in Fig. 6b (1). (Also note that line 3 in Fig. 6a now looks like an ellipse in Fig. 6b due to the larger scale). After the second compensation (by loop 2) the resulting EMF is suppressed up to the very small ellipse (3), which again looks like a straight line.

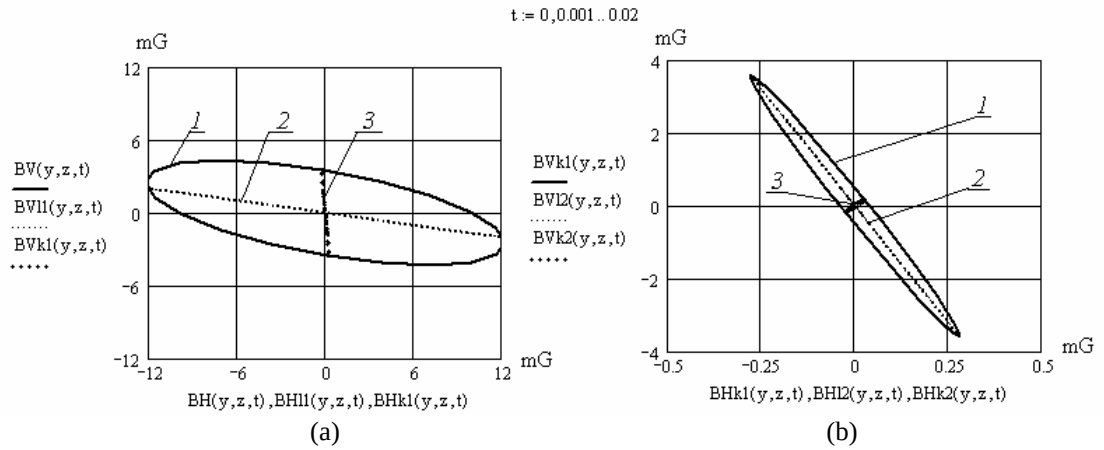

(a) (b)

Fig. 6 The field characteristics of the transmission lines (1) and the loops (2 and 3)

The resulting curves of the suppressed field (curves 1) and the curves of the original field (curves 2) are shown in Fig.7a and b. It should be mentioned that the minimum point of the suppressed EMF is at the position of the sensor. Therefore, by choosing this position we can influence the distribution of the suppressed field along the office/home.

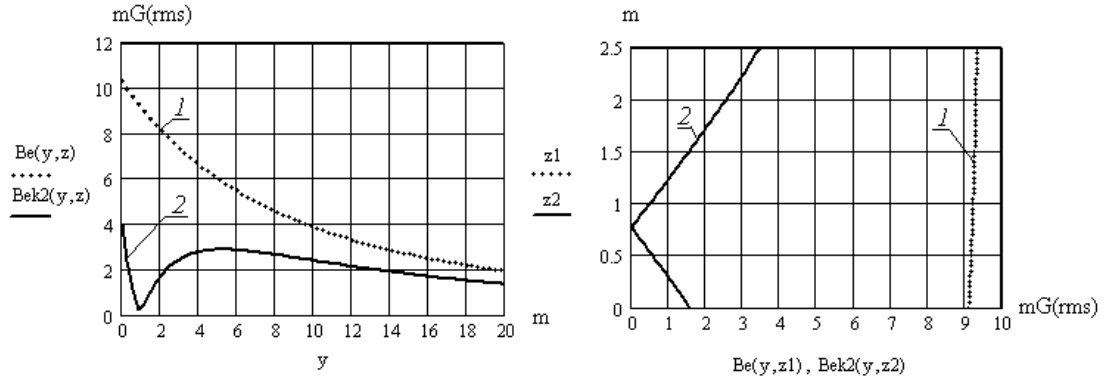

(a) (b)

Fig. 7 The EMF distribution inside the office: versus the distance from the wall (a) and the height (b) (1-original field, 2-suppressed field)

PRACTICAL REALIZATION

For checking and proving the proposed method of EMF suppression an experimental sample of a suppressing system to protect an office (of ECTEL Company in Rosh Haain) was projected and installed. The front of the office building and the loop installation is shown in Fig. 8. The same installation as seen from the corner of the building and the transmission line are shown in Fig.9.

The resulting curves of the suppressed EMF along the protected office along with the original EMF (before the compensation) are shown in Fig. 10a and b: the calculated curves (a) and measured (b). As can be seen, there is a good agreement between the theoretical and practical results. The remaining EMF inside the office does not exceed 2.5mG, which is the required norm [3].

Fig. 8 The picture of the protecting loops in the front of the building

Fig. 9 The picture of the protecting loops and the transmission lines from the corner of the building

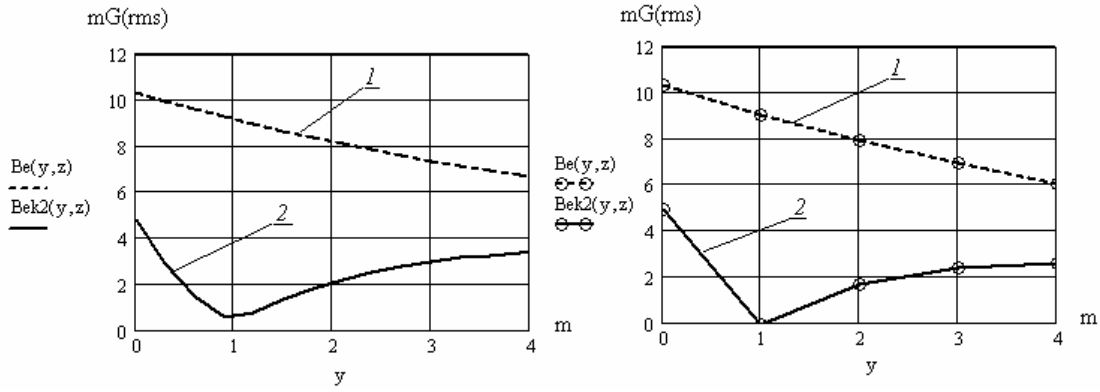

(a) (b)

Fig. 10 The resulting curves of the EMF: calculated (a) and measured (b) (1-original field, 2-suppressed field)

SUMMARY

The method of active suppression of the EMF induced by a complicated system of high voltage, large power transmission lines is developed and practically performed.

It is shown that in such cases the protecting system comprises two compensating loops, which should be arranged in space perpendicularly to each other, usually one lies in the vertical plane and the second one in the horizontal plane.

The pilot installation, based on the proposed method, was performed and tested on one of the offices in the building, located near to a high voltage transmission system.

The pilot performances are very successful: the original EMF has been suppressed 3-7 times, so that the remaining EMF is of 2-2.5mG, which is required the norm.

REFERENSCES

[1] A. Schenkman, N. Sonkin V.Kamensy“ Transmission lines as a source of industrial frequency electromagnetic field (EMF) radiation and a device for its active suppression”, *Proceedings of 3-th International Workshop Biological effects of EMFs*, pp. 593-599, 4-8 October2004, Kos, Greece.

[2] A. Schenkman, N. Sonkin V.Kamensy“ Active protection from electromagnetic field hazards of a high voltage power line” *HAIT Journal of Science and Engineering B, Volume 2, Issues 1-2*, pp. 254-265, 2005 Holon Academic Institute of Technology, Israel.

[3] “ELF Electromagnetic Fields and the Risk of Cancer” *Documents of the NRPB*, Volume 12, No 1, 2001

MEASUREMENT OF THE MAGNETIC FIELD AND INDUCED VOLTAGE IN 217Hz COMPONENT AND ITS HARMONICS DUE TO THE CELL PHONE

M. LAK
YOUNG RESEARCHERS CLUB, ISLAMIC AZAD UNIVERSITY, SCIENCE AND RESEARCH BRANCH, TEHRAN, IRAN
mahdilak@yahoo.com

M. KAVIANI MOGHADAM
DEPARTMENT OF MEDICAL PHYSICS, TARBIAT MODARES UNIVERSITY, TEHRAN, IRAN
kaviani_mm@yahoo.com

M. JANAHMADI
DEPARTMENT OF PHYSIOLOGY, SHAHEED BEHESHTI MEDICAL SCIENCES, TEHRAN, IRAN
mjanahmadi@yahoo.com

S.M.P. FIROOZABADI
DEPARTMENT OF MEDICAL PHYSICS, TARBIAT MODARES UNIVERSITY, TEHRAN, IRAN
pourmir@modares.ac.ir

Abstract

The quick growth of mobile communication has led to investigate the possible adverse effects on public health. It spite of security regulation norm for public exposure by governments from different country all around the world, the current controversy lies now on the possibility that the ELF could produce biological non-thermal effects. Nowadays some scientists are concerned about the possible impact of ELF fields of mobile phone. Magnetic ELF component are mainly generated by supply current in the phone.

In order to achieve a practical conclusion about sensitivity of nervous system to cell phone, the magnetic flux density in 217Hz and its harmonics from cell phone battery current were measured and these data will be used for stable magnetic field coil that made electrically for studying the effects of environmental ELF fields on bioelectric activity of nerve cell.

For measuring ELF fields of cell phone resulted from battery current, an on-made search coil was provided and calibrated precisely under several experimental conditions. Using Fast Fourier Transform (TNM-DSO Software) the power spectrum of induced voltage in search coil was analyzed and the amplitudes of 217Hz and its harmonics were extracted, considering the difference between induced voltage in search coil and magnetic

flux density of cell phone in 217Hz component and its harmonics, we measured a range of power variation in different times of the day.

The results of this study suggest that, ELF B-field of cell phone was not the same in different points. These findings emphasize the need for caution and regard all variations of power range during the different time of the day when biological effect of magnetic fields from cell phone is studied. To reach windowing effect, we must consider the physical characteristics of fundamental component wave (217Hz) and its harmonics produced by mobile phone accurately near to real one in exposure system.

Keywords: Mobile phone, ELF magnetic fields, 217Hz

Introduction

Modern technology offers powerful tools to stimulate a range of benefits for society, in addition to economic development. However, technological progress in the broadest sense has always been associated with hazards and risks [1].

Radio frequency transmitted by digital GSM telephones in the 900MHz band (890-915MHz) belongs to the "heating" category of the frequency spectrum. Hand-held digital mobile phones generate pulsed magnetic fields resulted from battery current, they transmit information in burst of microwaves and operate in one of the eight time slots, i.e. sending the information to the base station in 0.577 ms bursts with 217 bursts per second. This pulsed magnetic field (MF) of extremely low frequency (ELF) mainly include 217Hz (pulse their harmonics and subharmonics) [2]. It is quite possible that living organism have two- fold sensitivity to the pulsed GSM signal, to both the microwave carrier and lower frequency pulsing “time division multiple access”(TDMA)[3]. Besides a large number of researches which have been focused on high frequency components much less attention has been paid on the low frequency pulsed magnetic fields associated with pulsed battery current characteristic for GSM-type mobile phone [4,5,6,7,8,9,10,11].

The pulsed ELF-MF in mobile phone signals could exert influence on biological systems through non-thermal effects and this ELF emission is itself capable of causing significant biological effects [4]. In contrast to heating, which relies on an organism’s ability to absorb energy from irradiating field, the possibility of non-thermal effects arises from an “oscillatory similitude” between the radiation and living organism to respond to low-intensity pulsed via its ability to recognize certain frequency characteristics of that radiation, in fact non-thermal effects are non-linear [3].

The existence of specific amplitude and frequency values at which the response of the object was more pronounced. The sensitivity of the biological systems to weak MF has been described elsewhere, mainly in respect to the dependence of bioeffects on the amplitude or the frequency of the applied fields. More and more studies have suggested that for non-ionizing radiation cannot be applied the principle of ionizing radiation when the increase of the dose enhance the effects [12].

Thus in this paper we monitored the environment intensities of magnetic field emitted by one model of digital cell phone to settle the experimental conditions in order to reproduce the pattern of waves of mobile phones in a configuration closer to real condition.

These ranges of intensities will be used for studying the effects of environmental ELF battery’s fields on bioelectrical activities of nerve cell.

Material and Methods

The assessment ELF fields of GSM mobile phones requires a search coil, according to Faraday's induction law the variable magnetic field induces a voltage in wire winding. The average diameter of on-made search coil was 5mm with 500 turns wire with 0-260kHz frequency response. For RF immunity the probe was shielded with aluminum foil.

To obtain calibration factor, the search coil was exposed with known magnetic field. It was done with a system when an accurately known current with 217Hz frequency was injected through the circular coil (drived by known signal). The flux density of magnetic field was measured by a hand-held digital magnetic field meter (TES 1394, Electronic Electrical Corp.).

The calibration factor (μT/mV) was the ratio between flux density (B) and induced voltage in search coil that measured with the analog oscilloscope (Topward 7046A).

For scanning the surface B-field (flux density) distribution on the back side of the mobile phone a 10×10mm grid (Figure 1), in a way that the search coil was situated 4mm far from battery surface, was used. With considering the surface of battery we had 15 points on the back side of phone and we measured induced voltage in three axes in different times of the day in each points. The amplified induced voltage (root mean square) in search coil was measured with digital oscilloscope (DSO, TNM Electronics). By using Fast Fourier Transform (FFT) method (TNM-DSO software), the power spectrum of induced voltage was analyzed and the power of 217Hz component and its harmonics were extracted and saved in computer. Then, the B-field in 217Hz calculated with calibration factor.

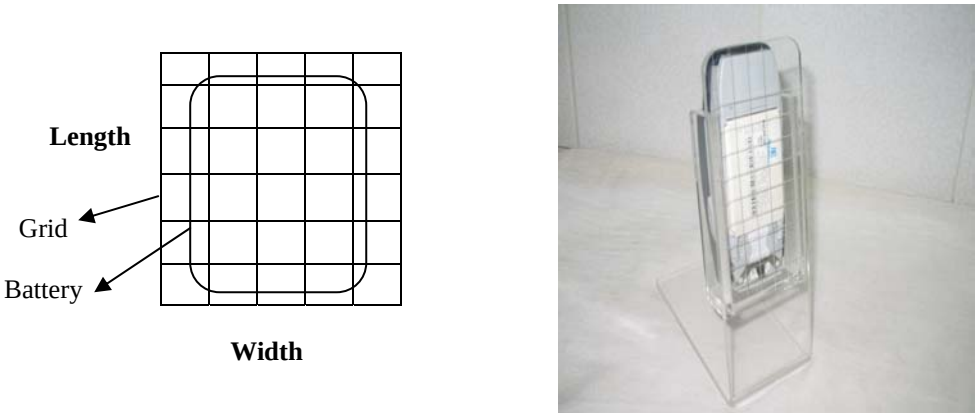

Figure 1- 10×10mm grid for scanning B-field of mobile phone

Results

Ten experiments were carried to calculate calibration factor. The magnetic flux densities in 6 cm far from the circular coil were measured with digital magnetic field meter and induced voltage in search coil measured with the analog oscilloscope. According to the ratio B/V, where B is the B-field of circular coil and V is the induced voltage in the search coil, we calculated the calibration factor (Figure 2). The calibration factor was 51.57 μT/mV with .997 regression coefficient.

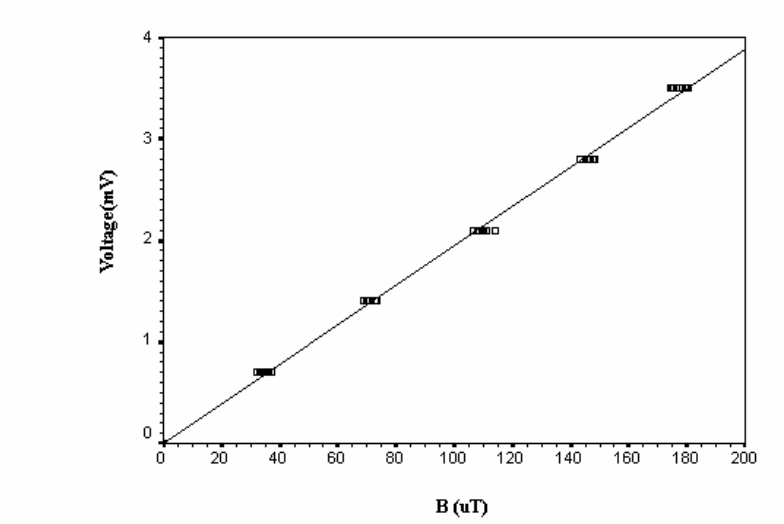

Figure 2- Measured magnetic flux density (B) and induced voltage (V) at 6 cm far from the circular coil

The induced voltages (rms) in 217Hz component of the sum vector of all three axes ($Bs=\sqrt{B_x^2+B_y^2+B_z^2}$) in different times of day in 15 points on the back side of phone were measured (Table 1). The measured induced voltage waveform is shown in Figure 2. It consists of pulses train. The duration of pulse is 0.577ms and the repetition interval is 4.61ms that are the same of sending information to the base station with 217 Hz (Figure 3).

Table 1-The sum vector of three axes of induced voltage in 217Hz in different times of day

Induced Voltage (rms in mV)	Maximum	Minimum	Average
Morning	2.77	0.25	1.39
Afternoon	1.62	0.19	0.80
Evening	2.09	0.23	0.81

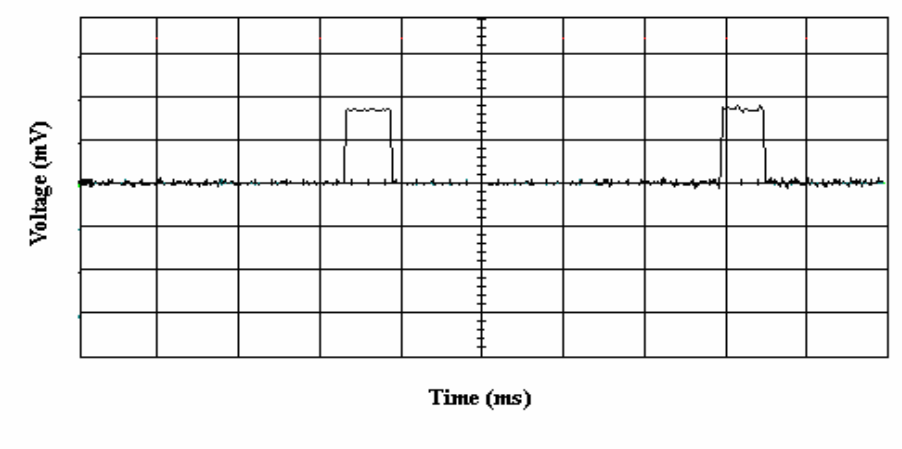

Figure 3: Induced voltage waveform in 217 Hz

The power spectrum of induced voltage was analyzed by Fast Fourier Transform (FFT) method and the amplitude of induced voltage in 217Hz and its harmonics were extracted (Table 2)(Figure 4).

Table 2- The sum vector of three axes of induced voltage in 433Hz and 650 Hz in different times of day

Induced Voltage (rms in mV)		**Maximum**	**Minimum**	**Average**
433Hz	Morning	2.57	0.24	1.31
	Afternoon	1.54	0.13	0.74
	Evening	1.99	0.22	0.77
650Hz	Morning	2.24	0.19	1.10
	Afternoon	1.21	0.07	0.61
	Evening	1.68	0.18	0.64

B-field distribution on back side of mobile phone is the result of the surface scan with 4mm distance between the phone's surface and search coil. The distribution pictures show the 217 Hz component of sum vector of all three axes of induce voltage(rms) times calibration factor (MATLAB software, version6.5, the Math Works Inc.)

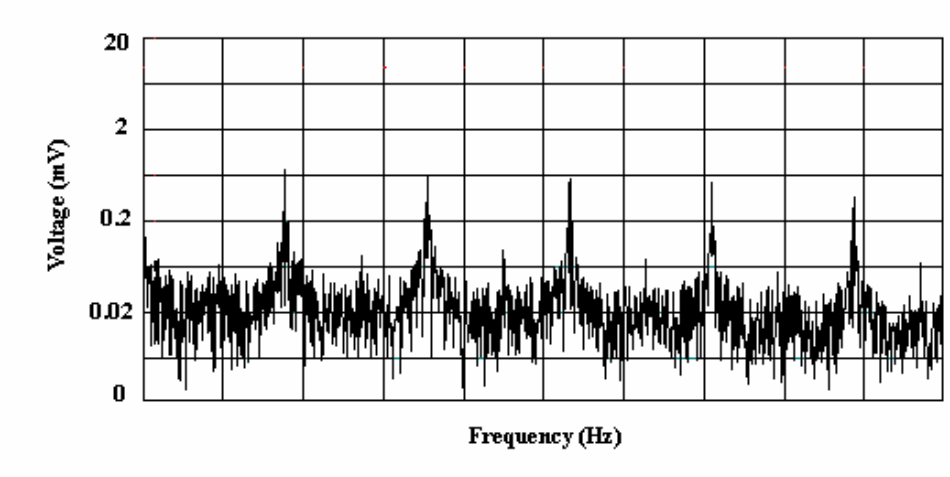

Figure 4- The power spectrum of induced voltage in 217 Hz and its harmonics

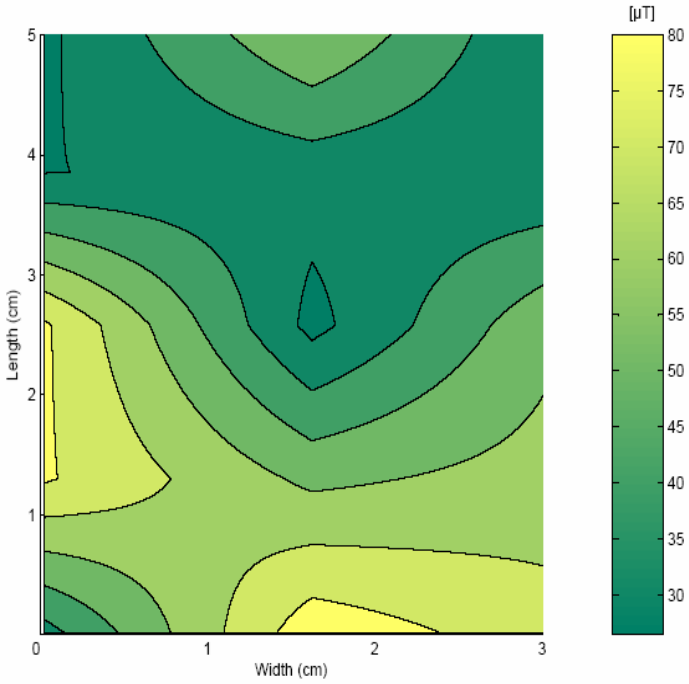

Figure 5- B-field distribution on back side of mobile phone

Discussion and Conclusion

The obtained results clearly show that the amplitude of induced voltage (rms) in 217 Hz and its harmonics considerably varies in different points of handset's battery back side. In this study, the results of changing magnetic fields from battery phone are not new and our research outputs were similar to the other works [5].

In addition to the other works we measured the B-fields in different parts of the day (Morning, Afternoon and Evening) according to network jam. So, we obtained a power range of induced voltage from 0.07 to 2.77 mV and B-fields between 26.40μT to 86.52μT. We had done our experiments in Iran workplace.

Furthermore the relative powers of two main harmonics to fundamental component were 94% and 78%.

As it may be interesting to know that all early publication made a link between "windows" and information transfer it is better to consider a range of intensities. So, for reasonable approach to the ELF "windows" problem we must consider a range of parameters such as magnetic flux density (amplitude) or frequency. In this way it appears reasonable to claim the existence of "window effect".

Besides considering the rage of intensities, it should be stressed that for biological studying of mobile phone, according to the power spectrum analysis, we must consider the intensities of higher harmonics of fundamental component, in addition to 217Hz signals, in ELF exposure systems.

To properly assess the validity of any experimental results demonstrating cell phone bioeffects, it is necessary to understand the mechanism by which these effects may occur.

Further investigation is on the way to settle the experimental condition in order to reproduce the pattern of the waves of mobile phones in a configuration closer to real one and examining the effects of low-frequency component of mobile phone on nervous system.

References

[1] WHO. WHO hand book on establishing a dialogue on risks from electromagnetic fields. World Health Organization, Geneva, Switzerland, 1992.

[2] Tuor M., Ebert S., Schuderer J., Kuster N. Assessment of ELF exposure from GSM handsets and development of an optimized RF/ELF exposure set up for studies of human volunteers. Bag Reg. No. 2.23.02-18 /02.001778. Final Report 2005.

[3] Gandhi OP., Kang G. Some present problems and proposed experimental phantom for SAR compliance testing of cellular telephones at 835 and 1900 MHz. Phys Med Biol 47:1501-1518; 2002.

[4] Hyland G.J. Physics and biology of mobile telephony. The Lancet 356: 1833- 36; 2000.

[5] Kuster N., Kastle R., Schmid T. Dosimetric evaluation of handheld mobile communications equipment with known precision. IEICE Trans E80-A (5):1-8; 1997.

[6] Jokela K., Puranen L., Sihvonen A.P. Assessment of the magnetic field exposure due to the battery current of digital mobile phones. Health Physics. 86(1): 56-66; 2004.

[7] Azenza M.J., Del Moral A. Cell membrane biochemistry and neurobiological approach to biomagnetism. Prog. Neurobiol. 44: 517-601; 1994.
[8] Cranfield C., Wieser H.G., Madan J., Dobson J.AL. Preliminary evaluation of nanoscale biogenic magnetite-based ferromagnetic transduction mechanisms for mobile phone bioeffects. IEEE Transactions on nanobioscience. 2(1): 40-43; 2003.
[9] Ilvonen S., Sihvonen A-P., Käkkäinen K., Sarvas J. Numerical assessment of induced ELF currents in the human head due to the battery current of a digital mobile phone. Bioelectromagnetics 26:648-656; 2005.
[10] Linde T., Mild K.H. Measurement of low frequency magnetic fields from digital cellular telephones. Bioelectromagnetics 18: 184-186;1997.
[11] Pedersen G.F, Andersen J.B. RF and ELF exposure from cellular phone handsets: TDMA and CDMA systems. Radiation Protection Dosimetry 83(1-2): 131-138; 1999.
[12] Marko S.M. Myosin phosphrylation –A plausible tool for studying “Biological window”. 3rd International Workshop “Biological Effects of Electromagnetic Fields, 2004. Oct 4-8; Kos, Greece.p.1-9.

AN INVESTIGATION OF THE DEPENDENCE BETWEEN MAXIMUM LEVEL OF OUTPUT POWER MOBILE PHONE AND RECEIVING LEVEL

NIKOLAY TODOROV ATANASOV[1], GABRIELA LACHEZAROVA ATANASOVA[2]

[1]DEPARTMENT OF WIRELESS COMMUNICATIONS AND BROADCASTING, HIGHER COLLEGE OF TELECOMMUNICATIONS AND POSTS, 1 "ACAD. STEFAN MLADENOV" STR., 1700 SOFIA, BULGARIA, e-mail: natanasov@hctp.acad.bg
[2]DEPARTMENT OF TELECOMMUNICATION TECHNOLOGIES, HIGHER COLLEGE OF TELECOMMUNICATIONS AND POSTS, 1 "ACAD. STEFAN MLADENOV" STR., 1700 SOFIA, BULGARIA, e-mail: ghristova@hctp.acad.bg

Abstract
RF power control is used to minimize the transmit power required by the mobile or base station subsystem while still maintaining the quality of the radio links. By minimizing the transmit power levels, interference among co-channel users can be reduced.

For circuit-switched services in GSM system, the mobile is commanded by the base station to change its power level. The base station directs this process with the help of the uplink receiving level and quality measurements.

In this paper we consider dependence between maximum output power level of GSM mobile phone and receiving level.

The measurements were performed with GSM mobile phones, which used service software in the networks of the three PLMNs (Public Land Mobile Network) in Bulgaria.

Our results indicate the receiving levels in those the GSM mobile phone transmit with maximum output power.

Introduction
The adaptive power control allows the mobile station (MS) to increases or decreases output power level for provides of reliable communications. It also decreases interference with other co-channels users and, through dense frequency reuse, improves spectral efficiency, while maintaining an adequate communications quality and facilities a reduction in power consumption, which is particularly important in hand-held MSs. And not the lastly place decrease of the output power level provides to decrease of absorbing energy (decrease of Specific Absorption Rate SAR) in the head of a user, which is particularly important for the users of mobile phones.

The power control procedure is accomplished by during a call (when the MS is in Traffic CHannel – TCH) and it controls from base station (BS). Output power level of MS for GSM900 can be reduced in 15^{th} steps from 33dBm (2W) to 5dBm (3.2mW) and each step is 2dBm [1].

The adaptive power control procedures rely on measurements of the received RF signal strength (RXLEV), the received signal quality (RXQUAL) [2].

RXLEV is evaluated by measuring the received level of the broadcast control channel (BCCH) carrier, which is continuously transmitted by the BS on all time slots of the B frame in Fig. 1 and without variations of the RF level. An MS measures the received signal level from the serving cell and from the BSs in all adjacent cells by tuning and listening to their BCCH carriers. The root mean squared level of the received signal is measured over a dynamic range of -103dBm to -41dBm for intervals of one slow associated control channel (SACCH) multiframe (480 ms). The RXLEV parameters are then coded into 6-bit words for transmission to the serving BS via the SACCH.

RXQUAL is estimated by measuring the bit error rate (BER) before channel decoding, using the Viterbi channel equalizer's metrics and/or those of Viterbi convolutional decoder [3]. Eight values of RXQUAL span the logarithmically scaled BER range of 0.2% to 12.8% before channel decoding.

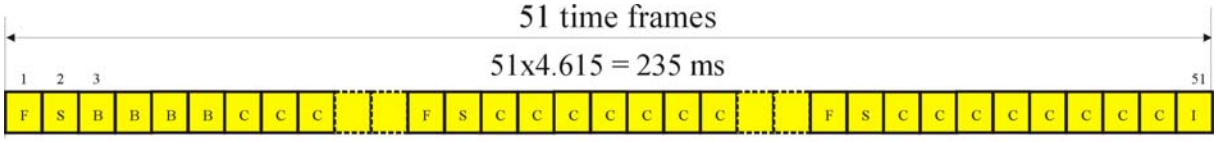

F: Frequency Control Channel;
S: Synchronisation CHannel;
B: Broadcast Control CHannel;
C: Common Control CHannel (Access Grant/Paging CHannel);
I: Idle Frame

Figure 1. Multiframe 51 in GSM system

The adaptive power control is based on RXLEV and RXQUAL measurements. In every SACCH multiframe the BS compares the RXLEV readings reported by the MS, or obtained by the base station, with set thresholds. The exact strategy for RF power control is determined by the network operator with the aim of providing an adequate quality of service for speech and data transmissions while keeping interferences low.

Most of the investigations were performed to determinate transmission levels of BSs [4, 5], but a small amount of investigations are performed to determinate output power levels of MS in real operating conditions [6]. That's provoking us to set following aims.

Aims of the investigation

1. Estimation of the received levels (RXLEVs) in those output power level (TXLEV) of the mobile station is 33 dBm (2 W) for GSM900 for every one PLMNs Bulgarian operator.
2. Estimation of output power levels (TXLEVs) of the mobile station on occupation of different logical channels during a call in the GSM900.

Schema of the investigation

For achieved of the traced aims were measured receiving levels of the BCCH carrier (RXLEVs) and TCH carrier (RXLEV_TCHs), quality of a receiving signal (RXQUAL), output power levels of the mobile phone (TXLEVs) and absolutely distance between mobile phone and base station (DISTANCE).

The investigation was performed using two mobile phones type NSE-1 and service software for network monitoring.

The measurement was made whit that set up:

1. The both mobile stations were connected to a personal computer through interface cables for observing and reading the values of the RXLEVs, RXLEV_TCHs, TXLEVs, RXQUALs, and DISTANCEs in the radio interface by service software for network monitoring;
2. For elimination of the influence from operator's hand and head on the values of the measurement parameters, the both mobile phones were raised from the ground surface of 1.5 meters on the set ups and the set ups were placed at distance with radius 5 meters of the operator.

The schema of the measurements:

1. The measurements were performed in the three points displayed in Fig. 2, marked like point A, point B, and point C (the point C is farthest away from the base station). These points are in outskirts whit hilly relief and trees.
2. The values of RXLEV, RXLEV_TCH, TXLEV, RXQUAL and DISTANCE were measured in every one of the three points in two deference days, for the three network operators.
3. The measurements were realized by making ten originated calls from the one mobile station and reading of RXLEV_TCH, TXLEV, RXQUAL, and DISTANCE, and the second mobile station continuously measured the level of the BCCH carrier (RXLEV). Every originated call was with period of sixty seconds, and the reading of the values on measurement parameters was made of every five seconds.
4. There were measurements carried out in the two accidentally selected points in the urban area. In the every one of these points were made ten originated calls and measurements of RXLEV, RXLEV_TCH, TXLEV, RXQUAL, and DISTANCE by the pointing above schema. The aim is to compare values of parameters from points in the urban area, when the mobile station and subscriber are too close to base station (some hundred meters) to values of parameters from points in the thinly populated places, when the mobile station and subscriber are too far away from base station (some kilometres).
5. For every one of the network operator the output power levels of the mobile station on occupation of different logical channels during an originated call was determinate. The logical channels in GSM

system during an originated call are occupy as following [7]:

BCCH/CCCH	Broadcast Control CHannel/ Common Control CHannel	
RACH	Random Access CHannel	**Start a call**
AGCH	Access Grant CHannel	
SDCCH	Stand-alone Dedicated CHannel	
TCH	Traffic CHannel	
…	…	**…**
TCH	Traffic CHannel	**Stop a call**
BCCH/CCCH	Broadcast Control CHannel/ Common Control CHannel	

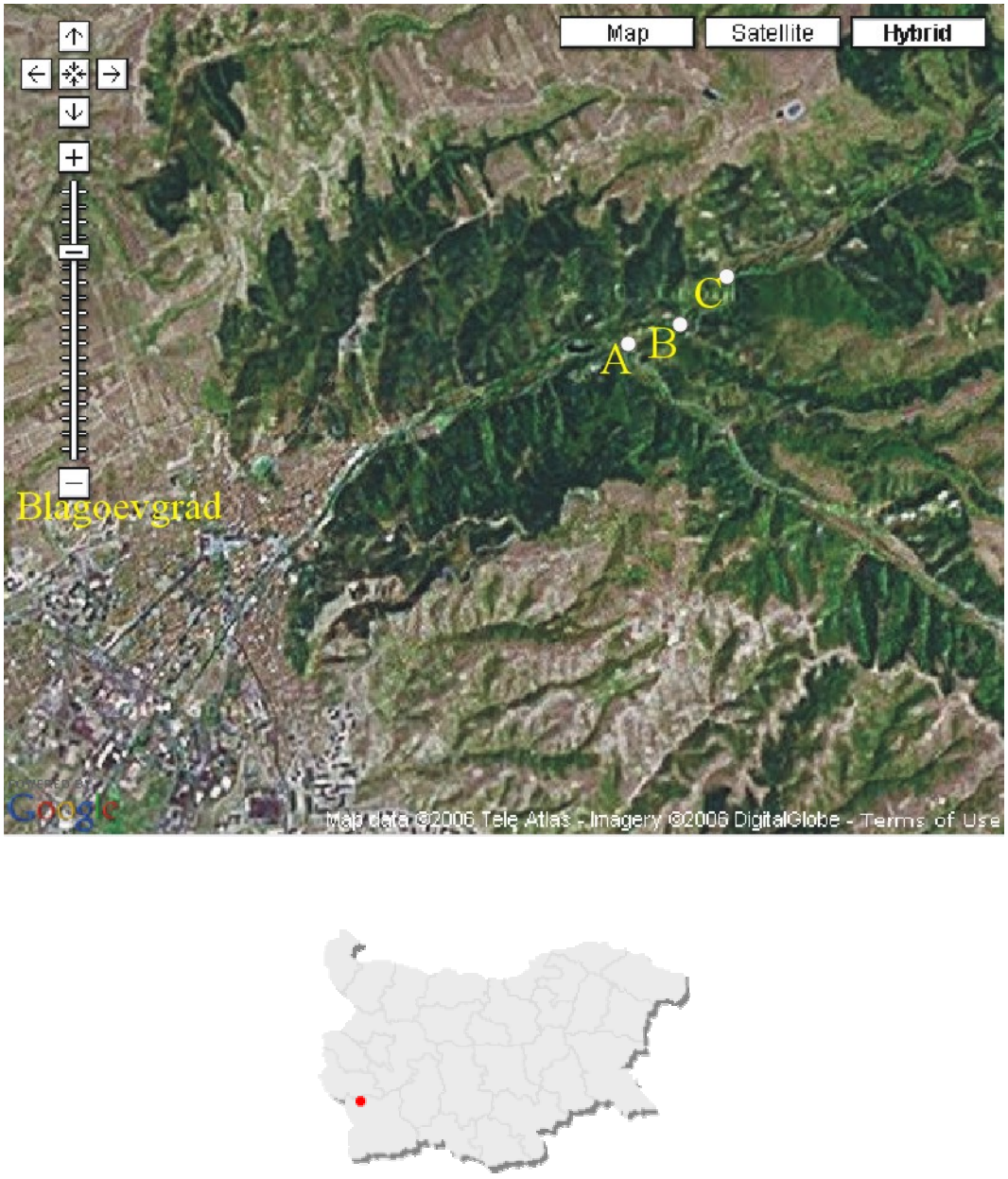

Figure 2. Placement of the points of measurements in outskirts with hilly relief and trees.

Figure 3. Placement of the first point of measurements in urban area.

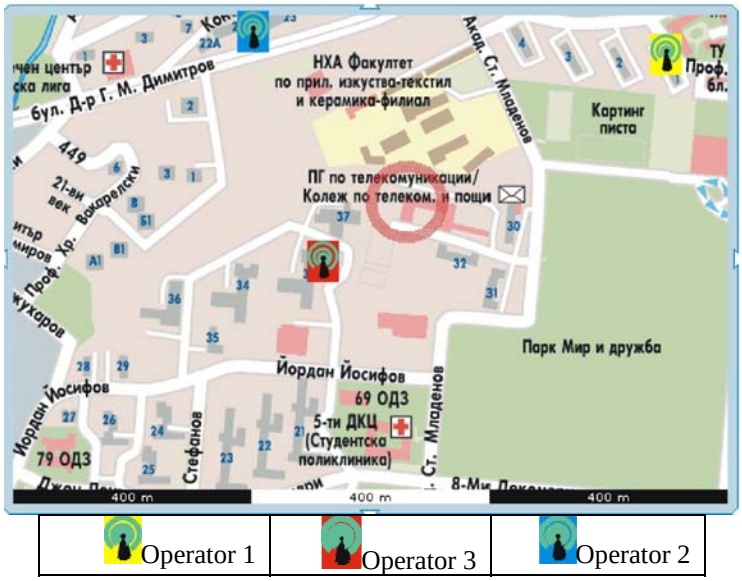

Figure 4. Placement of the second point of measurements in urban area.

Results

The results of the measurements are displayed of Figs. 5…19.

"Pointing" assessments for showing of the uncertainty of the measurement were determinate [8]. "Directed" assessment of statistical moments of the investigated accidental value and more specific – of the mathematical expectation $\hat{m}_x$ and dispersion $\hat{\sigma}_x^2$ [9] were performed.

The point assessments of performed n (where n=10) independent measurements with registration implementations $x_1, x_2, \ldots, x_i, \ldots, x_n$ of the accidental value X is as following:

$$\hat{m}_x = \frac{1}{n}\sum_{i=1}^{n} x_i \,, \hat{\sigma}_x^2 = \frac{n}{n-1}\left[\frac{1}{n}\sum\left(x_i\right)^2 - \hat{m}_x^2\right] \qquad (1)$$

The root mean squared deviation $\hat{\sigma}_x$ was evaluated.

The "interval" assessments for specific cases displayed of Figs. 8(a, b), 9(a, b), and 10(a, b) were determinate on the base of the "pointing" assessments of $\hat{m}_x$ and $\hat{\sigma}_x$ by (1).

THE DEPENDENCE BETWEEN MAXIMUM LEVEL OF OUTPUT POWER MOBILE PHONE AND RECEIVING LEVEL

The half-magnitude of the confidential interval $\varepsilon = \frac{I_{m_x}}{2}$ and confidential boundaries were determinate, as following:

$$m_1 = \hat{m}_x - \frac{\hat{\sigma}_x}{\sqrt{n}} A',\ m_2 = \hat{m}_x + \frac{\hat{\sigma}_x}{\sqrt{n}} A', \qquad (2)$$

where $A' = 1.960$ with $p_I = 0{,}95$.

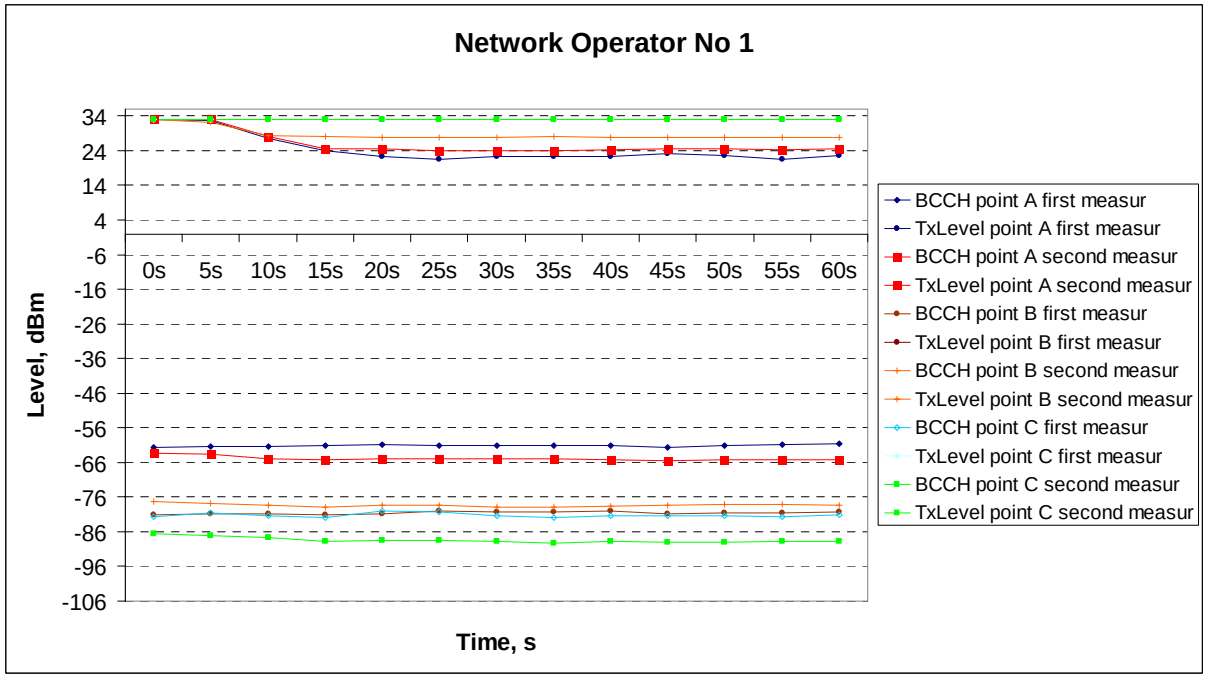

Figure 5. Dependence between RXLEV and TXLEV of MS in the time, for Network Operator 1.

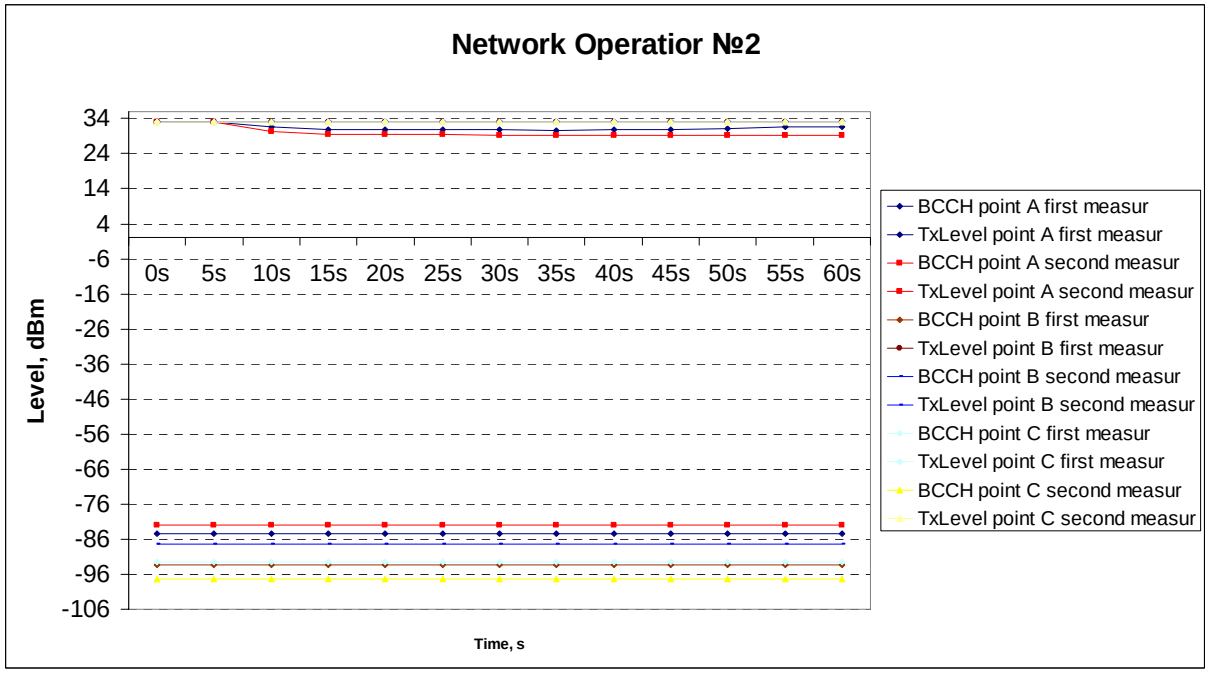

Figure 6. Dependence between RXLEV and TXLEV of MS in the time, for Network Operator 2.

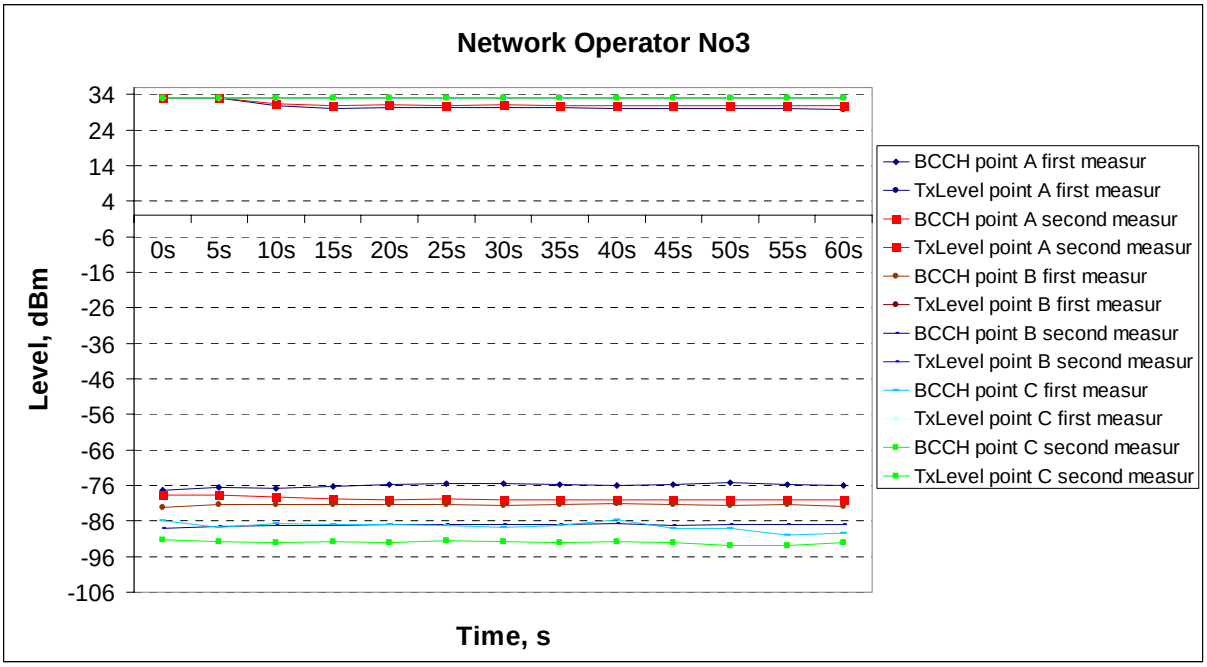

Figure 7. Dependence between RXLEV and TXLEV of MS in the time, for Network Operator 3.

From the results displayed of Fig. 5 can be seen the two boundary cases for network operator 1 – *TxLevel point B second measure* and *TxLevel point C first measure*. In the first case TxLevels of MS are very close to the maximum levels. In the second case TxLevels of MS are always 33dBm; its RXLEVs are highest from another cases in those TxLevel is also always 33dBm. These two cases correspond of two points from Fig. 2. The values measured in these two cases and two points are displayed graphically in Figs. 8(a, b).

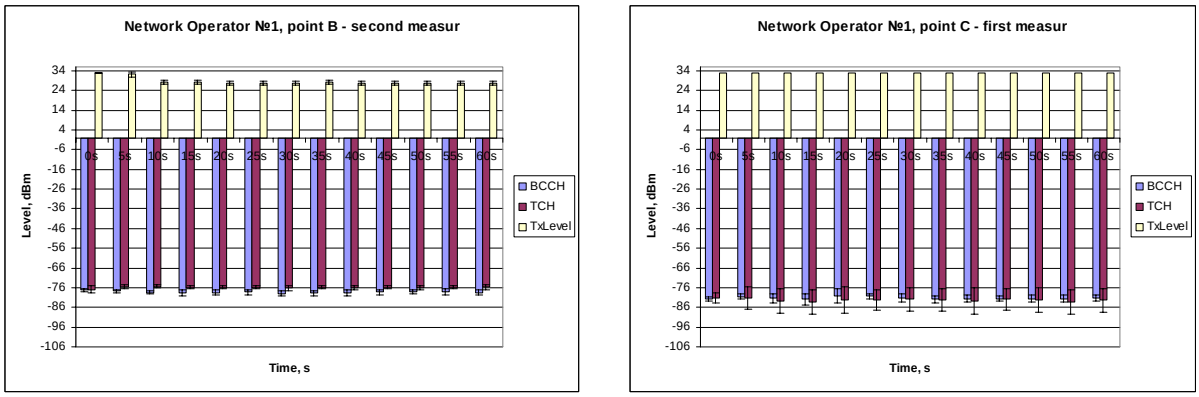

(a) **(b)**

Figure 8. Presentation of average data of RXLEV, RXLEV_TCH, and TXLEV for Network Operator 1 in points indicated in Fig. 2: **(a)** point B; **(b)** point C.

In Table 1 and Table 2 are presented: confidential boundaries m_1 and m_2 of confidential interval I_{m_x}; the error ε (a half-magnitude of confidential interval) by n=130 independent measurements and confidential stochastic p_I=0.95. The results presented in Table 1 and Table 2 corresponded to the results from Figs. 8(a, b) respectively.

Table 1

	BCCH	TxLevel
m_1	-78.598	28.272
m_2	-78.084	29.069
ε	0.257	0.398

Table 2

	BCCH	TxLevel
m_1	-81.608	33.000
m_2	-80.930	33.000
ε	0.339	0.000

From the results displayed of Fig. 6 can be seen the two boundary cases for network operator 2 – *TxLevel point A first measure* and *TxLevel point B second measure*. In the first case TxLevels of MS are very close to the maximum levels. In the second case TxLevels of MS are always 33dBm; its RXLEVs are highest from another cases in those TxLevel is also always 33dBm. These two cases correspond of two points from Fig. 2. The values measured in these two cases and two points are displayed graphically in Figs. 9(a, b), respectively.

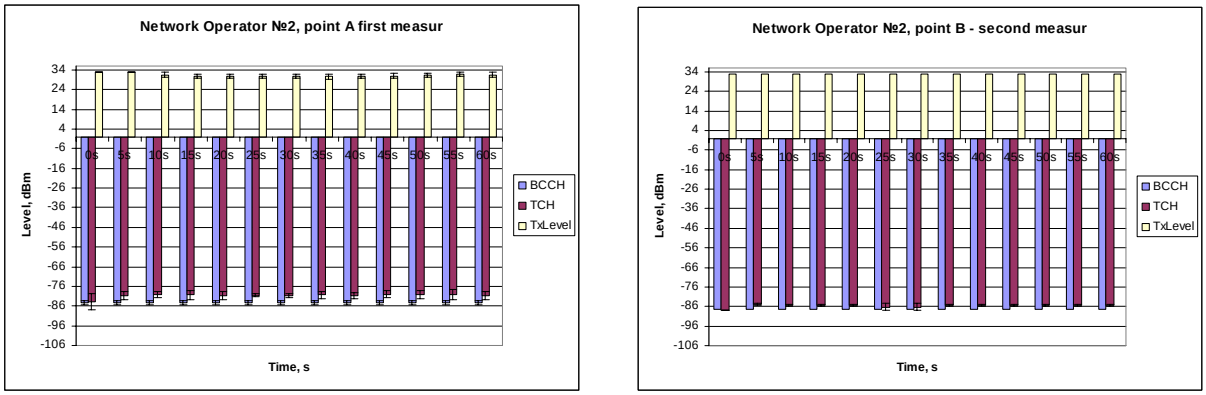

(a) **(b)**

Figure 9. Presentation of average data of RXLEV, RXLEV_TCH, and TXLEV for Network Operator 2 in points indicated in Fig. 2: **(a)** point A; **(b)** point B.

In Table 3 and Table 4 are presented: confidential boundaries m_1 and m_2 of confidential interval I_{m_x}; the error ε by n=130 independent measurements and confidential stochastic p_I=0.95. The results presented in Table 3 and Table 4 corresponded to the results from Figs. 9(a, b) respectively.

Table 3

	BCCH	TxLevel
m_1	-81.115	31.217
m_2	- 80.347	31.647
ε	0.384	0.214

Table 4

	BCCH	TxLevel
m_1	-85.878	33.000
m_2	-85.276	33.000
ε	0.339	0.000

From the results displayed of Fig. 7 can be seen the two boundary cases for network operator 3 – *TxLevel point A second measure* and *TxLevel point B first measure*. In the first case TxLevels of MS are very close to the maximum levels. In the second case TxLevels of MS are always 33dBm; its RXLEVs are highest from another cases in those TxLevel is also always 33dBm. These two cases correspond of two points from Fig. 2. The values measured in these two cases and two points are displayed graphically in Figs. 10(a, b), respectively.

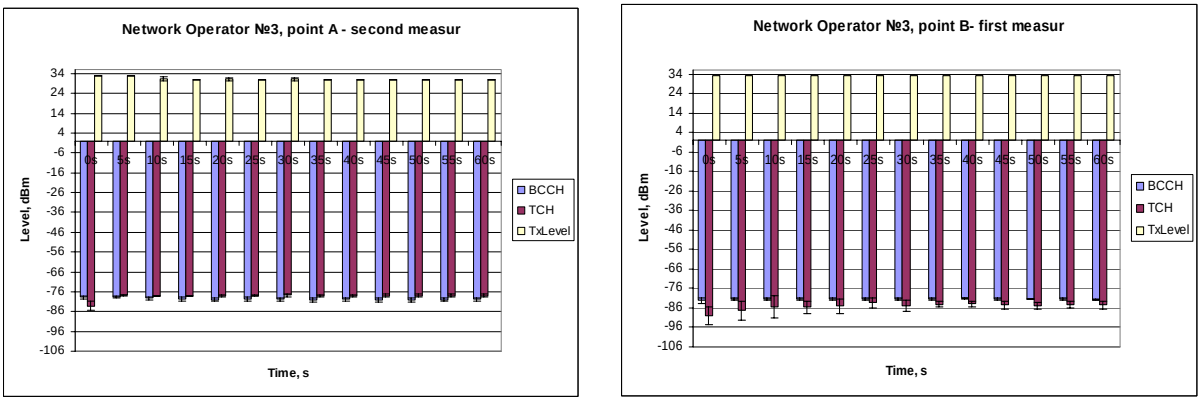

(a) **(b)**

Figure 10. Presentation of average data of RXLEV, RXLEV_TCH, and TXLEV for Network Operator 3 in points indicated in Fig. 2: **(a)** point A; **(b)** point B.

In Table 5 and Table 6 are presented: confidential boundaries m_1 and m_2 of confidential interval I_{m_x}; the error ε by n=130 independent measurements and confidential stochastic p_I=0.95. The results presented in Table 5 and Table 6 corresponded to the results from Fig. 10(a, b) respectively.

Table 5

	BCCH	TxLevel
m_1	-79.876	31.235
m_2	- 79.557	31.503
ε	0.157	0.134

Table 6

	BCCH	TxLevel
m_1	-81.600	33.000
m_2	- 81.345	33.000
ε	0.128	0.000

The received data in course of the present investigation (Figs. 5…10; Tables 1…6) showed that received level RXLEV in that output power level TXLEV of the mobile station is 33dBm for:

- Network operator 1 is approximate: - 81dBm;
- Network operator 2 is approximate: - 85dBm;
- Network operator 3 is approximate: - 81dBm.

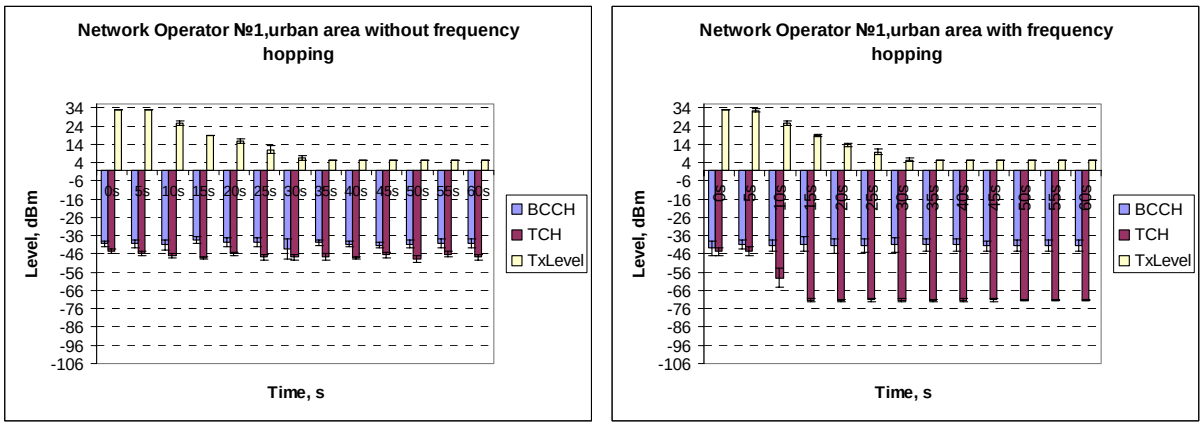

(a) **(b)**

Figure 11. Presentation of average data of RXLEV, RXLEV_TCH, and TXLEV for Network Operator 1 in points indicated in Fig. 3: **(a)** without frequency hoping; **(b)** with frequency hoping.

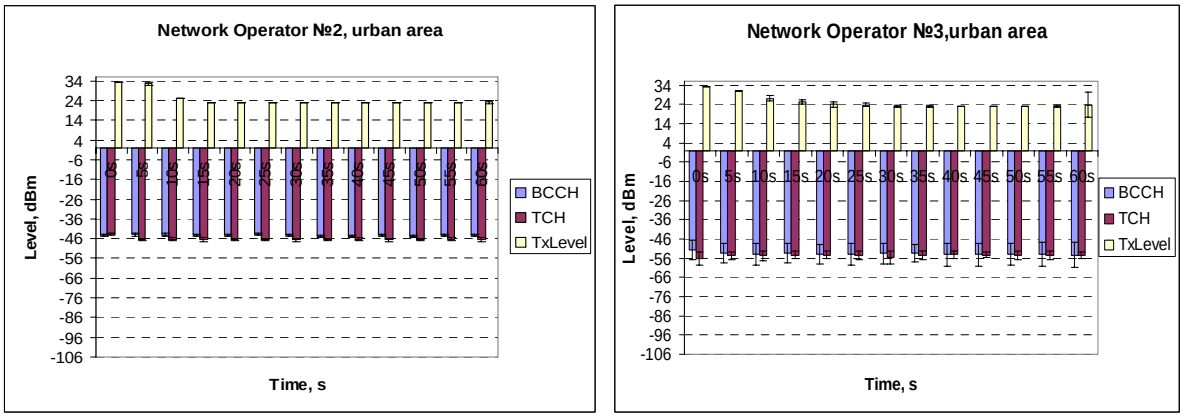

(a) **(b)**

Figure 12. Presentation of average data of RXLEV, RXLEV_TCH, and TXLEV in points indicated in Fig. 3: **(a)** for network operator 2; **(b)** for network operator 3.

Analysis of the data from Figs. 11 and 12 showed that in the urban area output power level of the MS decrease during a call. The boundaries of the lowest output power levels of the MS are different, from 5dBm for network operator 1 to 23dBm for network operators 2 and 3. Based on these results can be seen, that values of the received levels of BCCH carrier for network operators are between -54dBm …-40dBm. Therefore, BSs of the operators are equally distant from the point of measurement. In the same time the alterations of output power level of the MS are different for the network operators. The different strategies for RF power control of the network operators are confirm from these results.

Adaptive power control of MS for the network operators starts after initial 10 seconds (see Figs. 8(a), 9(a), 10(a), 11, and 12). The reason for this is that during these seconds MS occupied controls channels; it is confirmed form the results illustrated of Fig. 13.

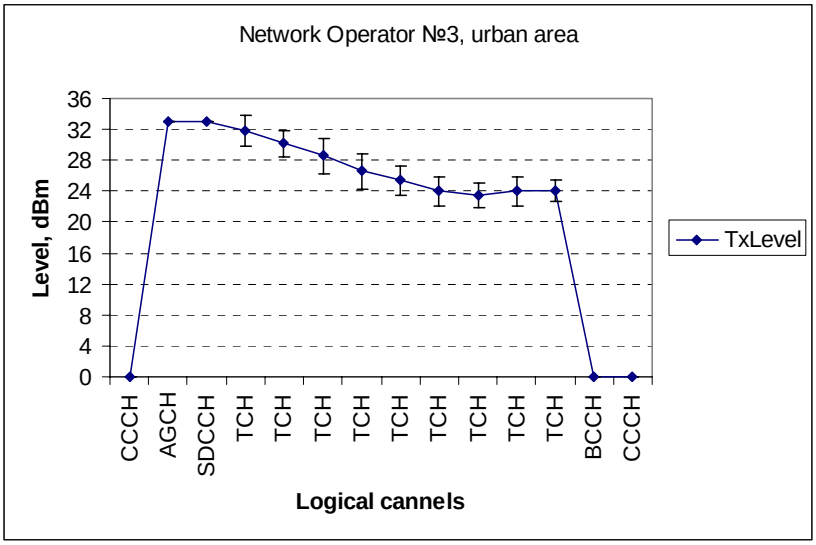

Figure 13. Presentation of average data of TXLEV in points indicated in Fig. 4.

In Fig. 11(a) TCH and BCCH channels using the same carrier, and have similar levels.

In Fig. 11(b) the TCH carrier is different from the BCCH carrier. In this case received level of TCH carrier is lower than level of BCCH carrier, it's mean that transmission power of BS is lower compared with the case from Fig. 11(a).

Summary

On the basic of the results of measurements of RXLEV, RXLEV_TCH, TXLEV, RXQUAL, and DISTANCE in the three points from Fig. 2 were established average value on the received levels RXLEVs in those output power level TXLEV of the mobile station is 33dBm (2W). Therefore, the received values (RXLEV ≈ - 85dBm …-81dBm) can be used to provide a reference levels.

These results can be applied to found the areas (points) in those output power level TXLEV of the mobile station is 33dBm (2W).

The results from the investigation demonstrated that adaptive power control of MS depended on level of BCCH carrier, but not of the level of TCH carrier (see Figs. 11(a, b)).

The results received via measurements in real operating conditions can be useful for further *in Vitro* and *in Vivo* investigations for the influence of the GSM mobile phones on the man.

Finally, according to reference from [10] to necessary to determine a complex of hygienic requirements to a mobile telephone, allowing the subscriber to realize the right of a voluntary choice of a comprehensible risk level and according by the World Health Organization recommendations to subscriber can be suggest: 1. During the first 10 seconds the mobile phone transmitted with maximum power 2 Watts, therefore, in this time the mobile phone must be distant from subscriber's head; 2. When the bars displaying receiving level strength of the mobile phone display are smaller from the maximum number, then the mobile phone will be transmit with maximum power during a call.

References

[1] N. Atanasov, "An Investigation of Adjusting Output Power Transmitter in Mobile Station for GSM900," *Telecom*, pp388-394, October, 2004.

[2] L. Hanzo, P. Sherriman, and J. Streit, *Wireless Video Communications Second to Third Generation Systems and Beyond*. New York: IEEE Press, 2001.

[3] R Steele and L. Hanzo, eds., *Mobile Radio Communications*. New York: IEEE Press-John Wiley, 2nd ed., 1999.

[4] Base Stations & wireless networks: Expose and helth consequences, *WHO*, Geneva, 15-16 June 2005.

[5] L. Guliani and B. Francesco, "The monitoring of BTS in Italy shows lower environmental limits are achievable" *Mobile communication and health: medical, biological and social problems*, pp. 89-90, September 2004.

[6] M. Wuschek, "Investigations into the power control of a GSM mobile phone under real operating conditions," *FGF Newsletter*, vol. 1, pp. 40-50, April 2005.

[7] G. Atanasova, "An Investigation of Signaling in Air Interface for GSM900," *Telecom*, pp327-333, October, 2004.

[8] H. Radev and V. Bogoev, *Uncertainty of the result of the measurement*. Sofia: Softtrade, 2001.
[9] E. Ferdinandov and B. Patchedgieva, *Stochastic and Statistics methods in the Communications.* Sofia: Ciela, 2005.
[10] Somov, "Ecological and technical characteristics of mobile communication networks," *Mobile communication and health: medical, biological and social problems*, pp. 119-120, September 2004.

STRESS HORMONE REACTIVITY IN MEDICAL STAFF EXPOSED TO ELECTROMAGNETIC RADIATION

MICHEL ISRAEL, KATIA VANGELOVA, DESIMIRA VELKOVA, MICHAELA IVANOVA

NATIONAL CENTER OF PUBLIC HEALTH PROTECTION,
15 ACAD. IVAN GESHOV BLVD., 1431 SOFIA, BULGARIA

Abstract

The **aim** of the investigation was to study the effect of electromagnetic radiation (EMR) on stress hormone reactivity of medical staff in physiotherapies. The excretion rates of stress hormones cortisol, adrenaline and noradrenaline were followed during morning shift in 15 female physiotherapists using RIA kits and a spectrofluorimetric method. The mean number of treatments with EMR emitting devices per month and the emission of each device was followed. A control group of nurses, matched by age, sex and work task was followed. The psychosocial factors were followed and showed no differences between the two groups. Significantly higher excretion rates of cortisol ($F_{(1,69)} = 7.171$, $p = 0.009$), adrenaline ($F_{(1,69)} = 7.869$, $p = 0.007$) and noradrenaline ($F_{(1,69)} = 10.643$, $p = 0.002$) with the studied physiotherapists in comparison with the control group of nurses was found. In conclusion, our data showed that EMR influenced stress hormone reactivity of medical staff in physiotherapies.

Key words: Cortisol, adrenaline, noradrenaline, medical staff, EMR exposure.

Introduction

Stress at work and work related changes in health and well being of the medical staff have been subject to growing concern in recent years (Deane et al. 2002, Elfering et al. 2002, Fujiwara et al. 2004). Little is known about stress at work of the medical staff in physiotherapies, exposed to some common for the medical staff stressors as risk of infections, emotional load of dealing with patients, heavy lifting, exposure to chemicals, but also some specific stressors as the exposure to electromagnetic radiation (EMR) from different devices as equipment for microwave and high frequency diathermy, pulsed magnets, d'Arsonvale devices, optical sources (UV, IR and visible), lasers etc.

Several studies investigated the effects of radiofrequency EMR emitted from GSM, broadcasting and TV transmitters on hypothalamic-pituitary adrenal axis and sympathetic adrenomedullary system. Mann et al. (1998) studied several endocrine parameters in humans exposed at night to a low level (0.2 W/m^2) radiofrequency field from GSM at 900 MHz and found a transient 1 hour increase in cortisol during the first hour of the exposure. Radon et al. (2001) failed to find an effect of low level pulsed radiofrequency EMR (carrier frequency 900 MHz, pulsed frequency 217 Hz, average power flux density of 1 W/m^2) on the salivary cortisol. Our earlier data (Vangelova et al. 2002) showed a trend for increase in 11-oxycorticosteroid (11-OCS) excretion rates in operators, working under low-level radiofrequency EMR. Next our study (Vangelova and Israel 2005) showed dose-effect relationship in the excretion of stress hormones and radiofrequency EMR. There are no data for the effect of EMR on stress hormone reactivity in medical staff in the physiotherapies, exposed to high level EMR, but for very short periods of time.

The **aim** of the investigation was to study the effect of EMR on stress hormone reactivity of medical staff in physiotherapies.

The study is a part of complex investigation of health risk in medical staff exposed to EMR.

Material and methods

Subjects

We investigated 15 female physiotherapetists, aged 49.5 ± 7.4 years with average length of service 26.4 ± 7.7 years, working in 4 hospital physiotherapies in Sofia. A control group of nurses, matched by age up to three years, work organization and having similar job task was studied. The control group was of mean age 48.9 ± 6.9 years and length of service 25.8 ± 7.3 years. All the investigated subjects worked fast-rotating two-shift system:

morning shifts (7:30 a. m- 2:00 p.m) and afternoon shifts (1:30 - 08:00 p.m). The investigated subjects have signed informed consent for participation in the study.

EMR exposure and confounding physical factors
EMR exposure
The method for EMR exposure assessment is presented in details elsewhere /9/. In general, the method is based on the following:
Parameters for exposure assessment
In order to establish unified conditions for exposure assessment for different frequencies (over the overall frequency range) we apply a general unified indicator associated with the energetic irradiation dose, according to the ICNIRP Guidelines /8/, ACGIH TLVs /15/, and the Bulgarian National Standards /1,2/.

Conditions for applying the wave impedance
We can consider a prevailingly directed flow at distances from the emitter to the object not shorter than 6 wavelengths and an entirely homogeneous flow of electromagnetic energy – at about 100 wavelengths. In the far field the conductivity of the medium is proportional to the squared distance from the emitter. At approaching it the value of this quantity increases proportionally to the volume between the emitter and the object, reaching maximum through areas obtained along the main diagonal of the volume. This reflects on an undefined value of the wave impedance.

Dimensions of values related to energy load
The energy load of the human organism is defined for three cases as a derived quantity of energy falling at external irradiation: $\boldsymbol{W_E = E^2.T,\ (V/m)^2.h}$, $\boldsymbol{W_H = H^2.T,\ (A/m)^2.h}$ and $\boldsymbol{W_S = S.T,\ \mu W/cm^2.h}$, based on dispersed energy per unit time on human body during the official working shift. Measurable quantities are used – intensities and power density according to the distance from the generator to the measuring device and the respective frequency range of the single photon.
As ***SAR*** is introduced by the dimension of base metabolism of an adult man (175 cm/70 kg) the dimension of ***SA*** is the dimension of ***SAR*** by the time.
The two types of quantities - $\boldsymbol{W_E}$, $\boldsymbol{W_H}$ and $\boldsymbol{W_S}$ on the one side, and ***SAR, SA*** on the other do not differ substantially in conditions of air equivalent environment and a human body situated in it.
SAR is introduced through Human Equivalent Antenna. If the respective effective area is $\boldsymbol{A_e}$, then through relationships between the dimensions of the quantities ***W*** and ***SA*** following by the definition for power and from the way of determining human body exposure, the quantity ***W*** corresponds to whole body value of ***SA*** at constant body weight and unchanging mean conductivity of the tissue, standardized to the effective exposure area $\boldsymbol{A_e}$. The magnitude of the latter on its part depends on the mutual orientation of a standing person and the intensity of the falling electric field ***E***.
The measurable quantity in all cases is the same – ***E [V/m].*** Consequently $\boldsymbol{W_E}$ will incorporate the definition of ***SA*** and vice versa.

Determination of the exposure duration
We divide the time of being in the working environment with NIR into two sets of intervals for exposure duration: real exposure time at work with a device $\boldsymbol{T_{app}}$ ***[h]***, and a total duration of the working shift ***T [h]***. The difference between them is so called "void time" when there is no real exposure.
We use the method of the "chronometer scenario" because the void time has no equipartitioned averaged evaluation. The duration time is introduced by the number of devices and the number of patients serviced by the individual.

Measurement method
The method is unified as far as three parts of its nature are unified: Equipment; Distances to the particular device, mandatory for the measurement – 6 distances depending on the frequency range; list with the mandatory restrictions to the behavior of the physicist/engineer, performing the measurement.
The major characteristics of the method are the 6 mandatory distances to the different types of generators determined depending on the frequency range of the radiation. They conform to two conditions: Requirements for measurement in the far and near field zones; Requirements for determination of ***SAR*** in different cases of electromagnetic energy falling on a standing human.

General relationships for assessment of individual exposure
The dose is a function of the squared mean measured intensity and can be presented by the ***SAR*** quantity.
Our calculation formulation is based on the vision of the averaged dose: the dose (calculated with the actual measured values of the field and exposure time) multiplied by the mean geometric value of the partial doses on

the distance from the physician/nurse to the patient r_1 and the dose of the same to another characteristic distance (one of the cited – r_i, i ≠ 1). Thus a characterizing quantity is obtained which is a non-dimensional growing sum $\overline{D}$:

$$\overline{D} \approx \sum \frac{1}{q} \sqrt{D(r_1)} \sqrt{D(r_{i\neq 1})}$$

Here $1/q$ is a non-dimensional quantity – ratio.
The squared field strength (E^2) used for the dose assessment is equal to the product of the measured intensity of the field at distance r_1 and the sum of weighed intensities of the other 5 distances.
The method allows, at unified measurements, the elaboration of individual exposure assessment for each person in physiotherapy through calculations depending on the number of devices, number of patients and the actual configuration of the ward.
SAR is calculated for the relevant frequency directly through the calculated dose multiplied by the individual's mass:
$SAR = D.m + B(f) + C$,
where m is the mass of the exposed person; B is a frequency -depending ratio, and C is a constant.
The method was used for assessment of the exposure in several physiotherapy units. Assessment of the exposure in several physiotherapy units by devices is shown on Table 1. Calculating the relative values for the whole frequency range in the studied physiotherapies the obtained quota is much larger than 1.

Table 1

Frequency	Devices	Calculated parameter	Basic restriction
≤ 2 kHz	Magnets	j ≈ 0,28 – 0,31 A/m^2	j ≤ 2 mA/m^2
≤ 2 kHz	Interferentz	j ≈ 0.69 mA/m^2	j ≤ 2 mA/m^2
f ≤ 2.5 MHz	UHF generator for ultrasound therapy	j ≈ 3.8 mA/m^2	j ≤ 2 mA/m2
≤ 100 kHz	Diadynamik (Bulgaria)	j ≈ 0.15 mA/m^2	j ≤ 1 A/m^2
≤ 100 kHz	Galvanostat	j ≈ 0.15 mA/m^2	j ≤ 1 A/m^2
150 ÷ 300 kHz	D'Arsonval	SAR ≤ 0.4 W/kg	0,4 W/kg
27,12 MHz	UHF devices	SAR = 3,71 – 9,78 W/kg	0,4 W/kg
2450 MHz	Medical radar	SAR = 0,31 – 5,3 W/kg	0,4 W/kg whole body 20 W/kg for limbs 10 W/kg for head

Light sources (polychromatic) - restrictions according to ACGIH (2004):
IR: S ≤ 1.8.t$^{-3/4}$ W/cm^2 (for cornea and lens)
IR: S ≤ 0.6/α W/cm^2.sr (for retina protection)
IR (with blue light filter – B1): 1 μW/cm^2, and : t_{max} ≤ 10 (mJ/cm^2)/S(W/cm^2)
UV and visible light: t_{max} ≤ 0.003 (J/cm^2)/S (W/cm^2)

Quartz (UVB-1, UVB, UVA, Visible: S ≈ 17.6 mW/cm^2
Solux Infrarouge, without filters: S ≈ 286.1 mW/cm^2
Solux Infrarouge, with filter B1: S ≈ 4.9 mW/cm^2

Noise and microclimate
The noise and microclimate were followed, too, and were within hygienic norms with no differences between the groups.

The psychosocial factors
The psychosocial factors were assessed by the questionnaire "My job", based on checklists, containing five subscales (Kompier et al. 1994). The working condition scale contains items about work posture, lighting, noise, vibrations, temperature, humidity, flow, dust, odours, etc. The job content scale sums eighteen items as a monotony, tasks, requiring intense concentration, time pressure, work organization, etc.). The job control scale (ten items) includes questions about novelties at work, ability to influence the pace, methods of work, promotion, etc. The work related social support scale sums ten items: five ones concerning support from coworkers and five from supervisors. Health complaints scale is the sum of sixteen items.

The excretion rates of stress hormones
The excretion rates of stress hormones were followed during the morning shift (7:30 – 14:00). The following

three periods were studied: early morning (6:30 – 8:30), second period (8:30 – 11:00) and third period (11:00 – 13:30). The urine aliquids were stored at –20°C and the subsamples for catecholamine assay were acidified to pH 3 with 6N HCL prior refrigeration. Urine free cortisol was assessed by radioimmunological kit (Orion Diagnostica, Espoo, Finland): interassay CV 5.2, 5.2, 6.1 % for low, mean and high value urine samples. The catecholamines adrenaline and noradrenaline were measured with spectrofluorimetric method (Vangelova 2000).

Statistics

The time-of-day variations of the studied stress hormones were analyzed for the effect of radiofrequency EMR exposure and time-of-day by tests of between-subjects effects (SPSS). Variation analysis (one-way ANOVA) and correlation analysis were used to calculate the psychosocial factors and the relationships between the studied variables.

Results

Our data show no significant differences of psychosocial factors between the exposed and control group (Table 2). The studied physiotherapists and control group of nurses had a feeling of strain at work and emotional load of dealing with patients, increased risk of infections, heavy lifting and work tasks, requiring concentration. The working conditions were described as moderate, but the physiotherapists found the lighting unsatisfactory. The number of psychosomatic complaints were comparatively high with both studied groups, slightly higher with the physiotherapists in comparison to the control group of nurses. The main psychosomatic complaints were musculoskeletal disorders (pain in the back, bones and muscles), numbness and/or timbling sensation in the limbs, physical and mental exhaustion, fatigue, dizziness, etc.

Table 2.
The psychosocial factors in exposed to EMR physiotherapists and control group

Scales/Groups	Maximal scores	Physiotherapists	Control group (nurses)
Working conditions	17	7.1 ± 3.0	7.1 ± 9.8
Work content	16	5.4 ± 3.2	7.0 ± 3.2
Control	10	2.9 ± 2.02	5.3 ± 1.8
Social support	10	2.3 ± 1.9	2.6 ± 2.4
Psychosomatic complains	16	9.4 ± 3.3	8.9 ± 2.7

Significantly higher excretion of cortisol with the physiotherapists in comparison to the control group of nurses (Figure 1) was found ($F_{(1,69)} = 7.171$, $p = 0.009$). The excretion rates of cortisol followed the typical diurnal rhythm with highly significant time-of-day variations ($F_{(2,69)} = 12.231$, $p = 0.000$).

The adrenaline excretion rates (Figure 2) were significantly higher in the studied physiotherapists in comparison to the control group of nurses ($F_{(1,69)} = 7.869$, $p = 0.007$). Also, significantly higher excretion rates of noradrenaline (Figure 3) with the physiotherapists in comparison to the nurses ($F_{(1,69)} = 10.643$, $p = 0.002$) were found. The time-of-day variations of adrenaline and noradrenaline were not significant.

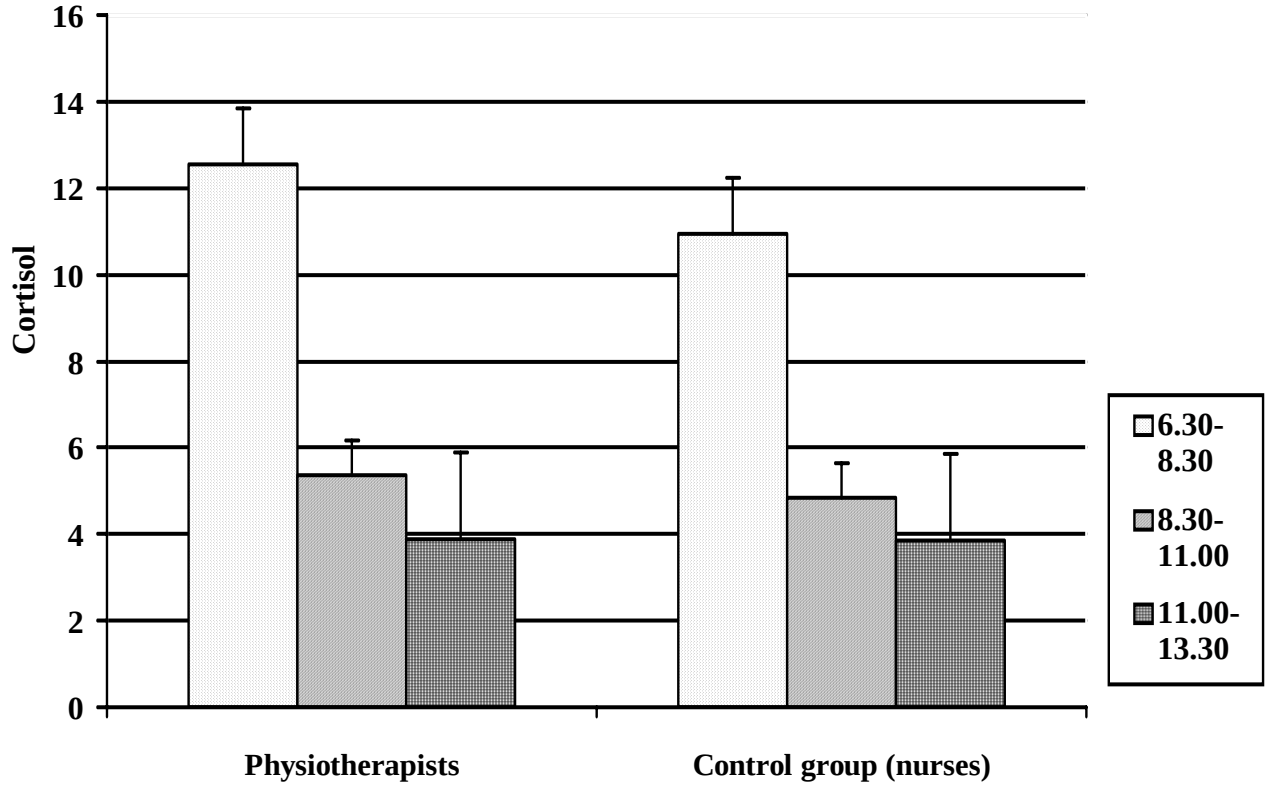

Figure 1. The excretion rates of cortisol in physiotherapists exposed to EMR and control group.

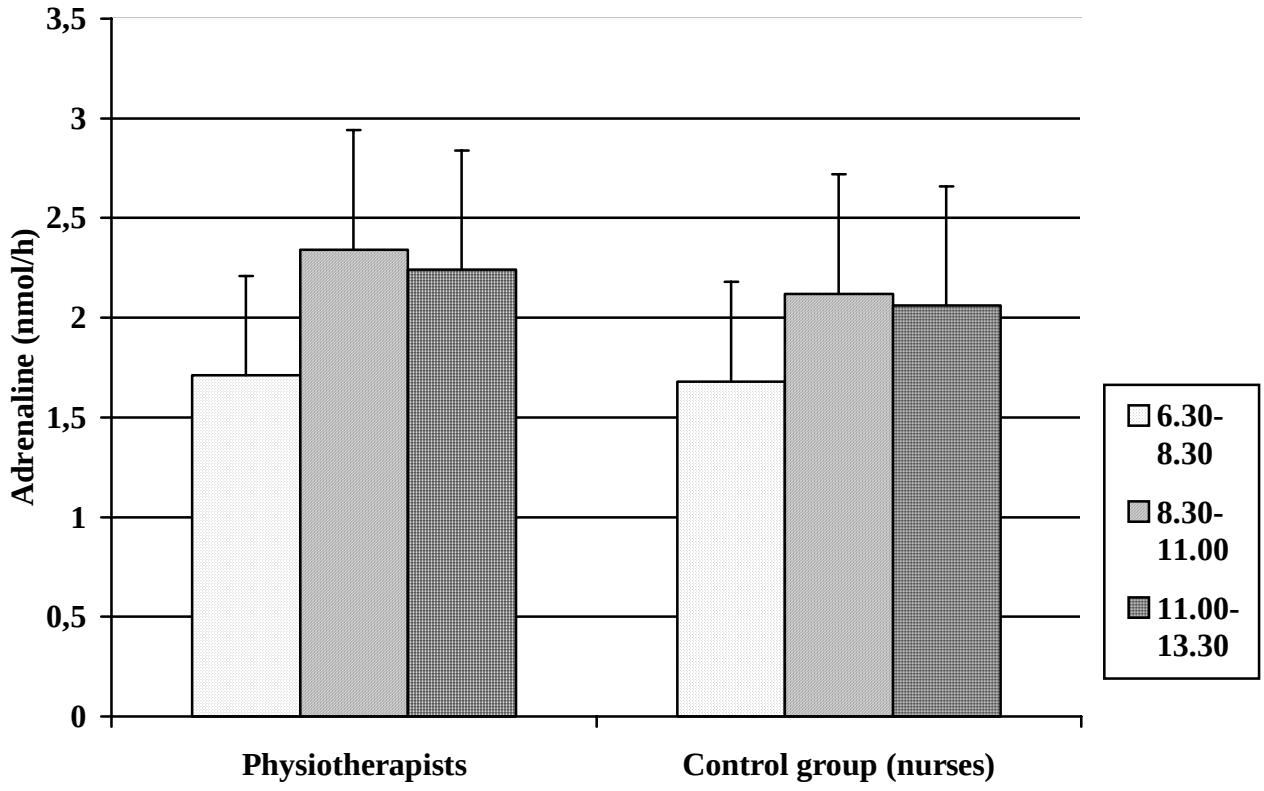

Figure 2. The excretion rates of adrenaline in physiotherapists exposed to EMR and control group.

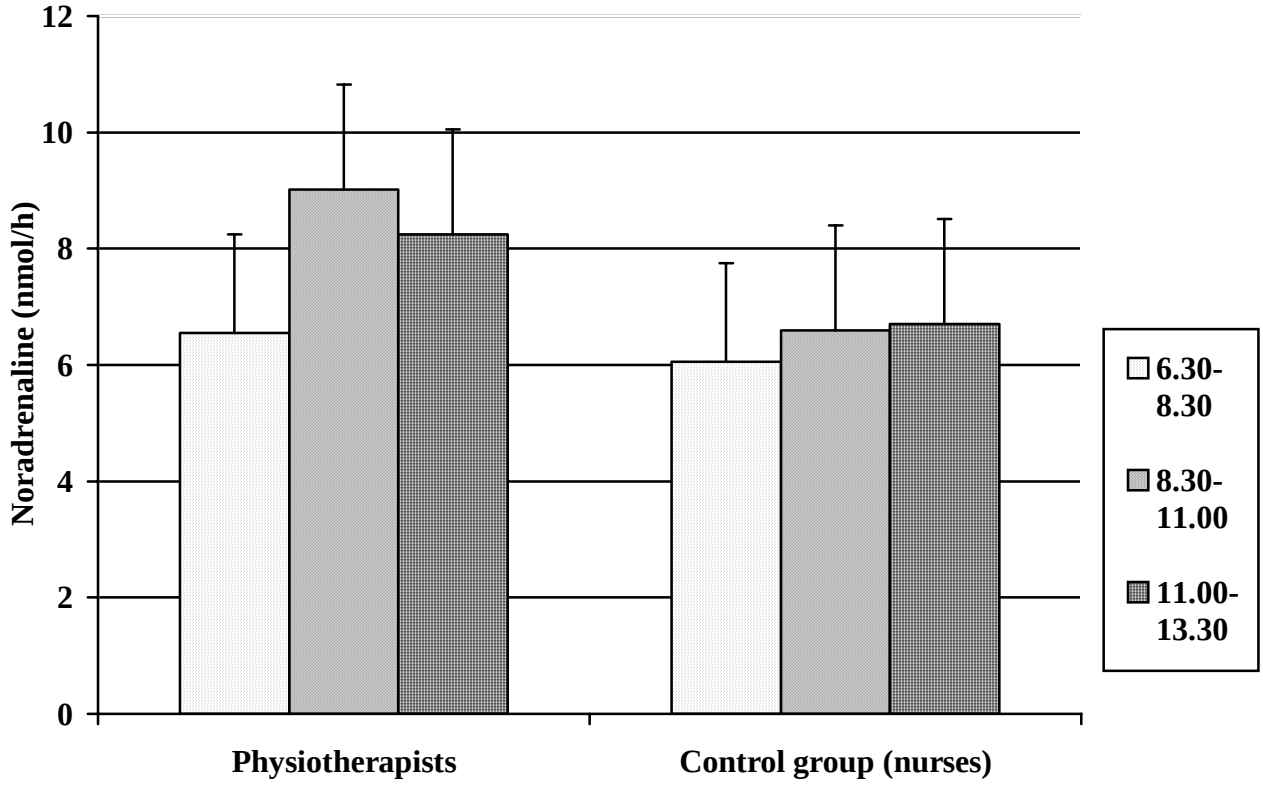

Figure 3. The excretion rates of noradrenaline in physiotherapists exposed to EMR and control group.

Discussion

Our data show significant effect of non-ionising radiation on the excretion rates of stress hormones during the working day. The work conditions, work content, work control and psychosocial support showed no significant differences between the exposed and control group. No acute incidents and changes in the task requirements among the groups during the period of the study were registered. The number of treatments in the studied physiotherapies did not exceed the number of treatment by the studied control group of nurses. The studied physiotherapist had no complains concerning the EMR emissions and were not aware of the level of the exposure during the study.

The present study confirmed our previous data (Vangelova et al. 2002, Vangelova and Israel 2005) for effect of EMR exposure on stress hormones reactivity, with the highest effect on noradrenaline excretion rates. The stress hormones are important biomarkers for allostatic load (McEwen 1998, Chrousos 2000, Tsigos and Chrouos 2002) and the long term effects of increased secretion of stress hormones are associated with health implications. The effects of catecholamines on the cardiovascular function are well known. The excessive and sustained cortisol secretion has been for long associated with depression, osteoporosis, immunosuppression and the entire spectrum of the metabolic syndrome (Fraser et al. 1999, Rosmond et al 1998).

Summing up, significantly higher excretion rates of stress hormones with the medical staff under EMR exposure in physiotherapies were found. As outlined above, the chronic elevation of stress hormones may be associated with health implications. Reduction of EMR exposure in physiotherapies both by technical solutions and limiting the time of exposure should be encouraged.

References

1. Bulgarian National Standard 14425 –90. Labour protection. Electromagnetic fields – radiofrequency range. Admissible values and requirements for control (in Bulgarian).
2. Bulgarian National Standard 17137-90. Labour protection. Electromagnetic fields – microwave range. Admissible values and requirements for control (in Bulgarian).
3. Chrousos, G.P. The role of stress and the hypothalamic-pituitary-adrenal axis in the pathogenesis of metabolic syndrome: neuroendocrine and target tissue-related causes. Intern. J. Obesity 2000; 24 (Suppl. 2): S50-5.
4. Deane R, Chummun H, Prashad D. Differences in the urinary stress hormones in male and female nurses at different ages. Journal of Adv. Nurs. 2002; 37 (3): 304-310.
5. Elfering A, Grebner S, Semmer NK, Gerber H. Time control, catecholamines and back pain among young nurses. Scandinavian Journal of Work and Environmental Health 2002; 28 (6): 386-393.
6. Fraser, R., Ingram, M.C., Anderson, N., Morrison, C., Davies, E., Connell, J.M.C. Cortisol effects on body mass, blood pressure, and cholesterol in general population. Hypertension 1999; 3: 1374-8.
7. Fujiwara K, Tsukishima E, Kasai S, Masuchi A, Tsuts A, Kawakami N, Miyake H, Kishi R. Urinary catecholamines and salivary cortisol on workdays and days off in relation to job strain among female health providers. Scandinavian Journal of Work and Environmental Health 2004; 30, 2, 129-138.
8. ICNIRP. Guidelines for limiting exposure to time-varying electric, magnetic and electromagnetic fields (up to 300 GHz). Health Physics 1998; 74(4): 494–522.
9. Israel, M., Tschobanoff, P. Exposure to non-ionizing radiation of personnel in physiotherapies. In: Bioelectromagnetics. S. N. Ayropetyan and M. S. Markov (eds.), Springer Press, 2006: pp.367-376
10. Kompier M, Levi L. Stress at work: causes, effects and prevention. A guide for small and medium sized enterprises. European Foundation for Improvement of Living and Working Conditions. 1994, Geneva.
11. Mann K, Wadner P, Brunn G, Hassan F, Hiemke C, Roschke J. Effects of pulsed high frequency electromagnetic fields on the neuroeudocrine system. Neuroendocrinol 1998; 67: 139-44.
12. McEwen BS. Protective and demaging effects of stress mediators. New England Journal of Medinine 1998: 338(3): 171-179.
13. Randon K, Parera D, Rose D–M, Jung D, Vollrath L. No effects of pulsed radiofrequency electromagnetic fields on melatonin, cortisol and selected markers of the immune system in men. Bioelectromag 2001; 22: 280-7.
14. Rosmond, R., Dallman, M.F., Bjorntorp, P. Stress related cortisol secretion in men: Relationships with abdominal obesity and endocrine, metabolic and hemodinamic abnormalities. J. Clin Endocrinol. Metab. 1998; 83: 1853-1859.
15. Threshold Limit Values for Chemical Substances and Physical Agents & Biol. Exp. Indices, ACGIH, Signature Publications, 2004.
16. Tsigos C, Chrousos GP. Hypothalamic-pituitary-adrenal axis, neuroendocrine factors and stress. Journal of Psychosomatic Medicine, 2002; 53 (4): 865-871.
17. Vangelova K. Method for assessment of catecholamines adrenaline and noradrenaline in urine. In: Methods for Investigations in Hygiene. National Center of Hygiene, Medical Ecology and Nutrition, Sofia, 2000; 2:

2-4 (in Bulgarian).
18. Vangelova K., Israel M., Mihailov S. The effects of low level radiofrequency electomagnetic radiation on the excretion rates of stress hormones in operators during 24 hour shifts. Centr. Eur. J. Public Health 2002; 10, 23-27.
19. Vangelova K., Israel M. Variations of melatonin and stress hormones under extended shifts and radiofrequency electromagnetic radiation. Rev. Environ. Health 2005, 20 (2): 151-161.

EFFECTS OF ELF-EMF EXPOSURE ON BODY WEIGHT GAIN, HAEMOPOIESIS AND MAMMARY CARCINOGENESIS IN BALB/c and BALB NeuT MICE.

IEZZI M.[1,4], FELICETTI P.[1,4], BORGIA L.[1,4], PANNELLINI T.[1,4], MARIGGIO' M.A.[2,4], PIETRANGELO A.[2,4], MEZZETTI A.[3,4], CUCCURULLO F.[4], FANO' G.[2,4], MUSIANI P.[1,4]

[1] IMMUNO-ONCOLOGY LAB, [2] CELL PHYSIOLOGY LAB, [3] ATHEROSCLEROSIS LAB, [4]AGING RESEARCH CENTER, G. d'ANNUNZIO UNIVERSITY FOUNDATION, VIA COLLE DELL'ARA, 66013 CHIETI, ITALY.

ABSTRACT

Several epidemiological studies have pointed to a positive correlation between Extremely Low Frequency ElectroMagnetic Fields (ELF-EMFs) exposure and the incidence of haematological or solid tumors. To better clarify its effects on haemopoiesis and cancer development, we exposed to continuous and intermittent ELF-EMF young and adult BALB/c mice or inbred BALB Neu T mice: the latter constitute a transgenic model of HER-2-dependent mammary carcinogenesis. We monitored the body weight trend and studied haemopoietic lineages and mature immune cells in bone marrow and lymphoid organs by morphologic and FACS analysis.

In young but not in adult male and female BALB/c mice there was a transient decrease of body weight and a decrease in bone marrow and splenic myelopoietic cells, whereas there were no haematological differences between treated and control young or adult BALB NeuT mice, probably because of the cancer-driven haematological dysregulation. Histological and Whole Mount grading showed that ELF-EMF do not influence mammary carcinogenesis.

This study demonstrates that ELF-EMF produce a biological stress that affects growth. Healthy subjects are able to both adapt to and compensate it. Further in vivo studies are needed to determine the consequences of ELF-EMFs exposure combined with other known stress factors.

INTRODUCTION

There is a large body of epidemiological evidence in favour of a significant positive correlation between exposure to magnetic fields and the risk of cancer [1, 2, 3, 4, 5] and the International Agency for Research on Cancer (IARC) has classified extremely low frequency electro) magnetic fields (ELF-EMF) as possible sources of human cancer [6]. Subsequent in vitro, in vivo and epidemiological studies, however, have not yet substantiated this correlation and its extent.

Carcinogenesis is a complex process and ELF-EMFs could be involved in any of its steps [7]. They do not induce direct DNA damage in vitro, but may synergize with compounds that induce DNA modification [8]. It has been shown, for example, that ELF-EMFs exposure co-promotes the rat mammary tumors induced by 7,12-dimethylbenz[a]anthracene (DMBA) [9, 10].

The central role of the immune system in the natural history of carcinogenesis makes it essential to determine the immunological consequences of exposure to ELF-EMFs. Some studies show that ELF-EMFs have no effect on or do not suppress the immune system, whereas others have found proliferative effects. Exposure of murine bone marrow cells to a magnetic field causes proliferation and differentiation/reduction of the granulocyte-macrophage progenitor, whereas its effect on the proliferation of stromal stem cells proliferation is not clear [11]. Leukopenia and neutropenia have been observed in mice after long exposure to ELF-EMFs [12]. In another report, ELF-EMFs had no effect on the cytotoxic activities of NK and LAK cells, nor on the production of IFN-γ, TNF-α, IL-2 and IL-10 production by human PBMC [13].

These discrepancies can readily be assigned to the use of dissimilar cell systems, mouse models, magnetic flux

densities, and exposure units and periods.
The present study set out to determine whether a striking relationship exists between carcinogenesis and exposure to ELF-EMF, and how far the immune system is affected.
A pair of Helmholtz coils was used to deliver variable, homogeneous, sine-wave AC magnetic fields at 50 Hz with an intensity of 0.5-1.0 mT. The apparatus comprises plastic cages in which the animals are exposed to the ELF-EMFs and is located in an insulated room with the control animals outside the EMF area (see appendix- Instrument).
BALB/c and BALB NeuT mice were employed. BALB/c is one of the most frequently used inbred strains owing to its good breeding performance and long reproductive lifespan. It is particularly well known for the production of plasmacytomas on injection of mineral oil and widely used for studies on lymphoma.
BALB-neuT are transgenic for the rat transforming HER-2/neu oncogene [14, 15]. Its transforming mutated form under the transcriptional control of a mammary tumour virus causes fast and aggressive mammary carcinogenesis. Tumours become spontaneously evident after the progression of tumorigenesis and their relationship with the surrounding tissues is preserved. Reproduction of the development of autologous tumours, the occurrence of invasion and metastasis, and the presence of an intact immune system are other key features of these genetically modified mice [16]. At 10 weeks of age, they display advanced cancerization, especially around the nipple where the side buds become in situ carcinomas and an increasing number of hyperplastic foci form along the mammary tree. The in situ carcinomas become invasive between the 15th and the 20th week and metastasize after the 30th week [17].
Our experiment was designed to answer the following questions.

Initially:
* Whether ELF-EMFs influence the growth and the haemopoietic system of BALB/c and BALB NeuT mice
* Whether male and female animals are equally responsive
* Whether young and adult animals are equally responsive
Subsequently:
* Whether the effects were transient or persistent
* Whether a dose-response relation or a threshold value for the ELF-EMF intensity is apparent
* Whether continuous and intermittent (night-time only) exposure exert the same effects

Lastly the effect of ELF-EMFs effect on mammary carcinogenesis in BALB NeuT mice was investigated.

Mice were randomised as explained in the Appendix. Briefly, groups of female and male BALB/c and female BALB-neuT were exposed continuously and intermittently to ELF-EMF at 0.5 or 1mT at 6 weeks of age (young mice) and 10 weeks of age (adult mice).
Animal body weight was recorded at the beginning of the experiment and every 15 days.
After 4 and 12 weeks from the beginning of the exposure mice were sacrificed and primary and secondary lymphoid organs were analyzed by histology, immunohistochemistry and flow cytometry.
Tumour burden in BALB neuT mice was assessed by Whole Mount analysis, histology and immunohistochemistry.

Since no differences were evident between 0,5 and 1 mT ELF-EMF exposure, only data referring to 0,5 mT will be shown below.

ELF-EMFs slow down the body weight gain of young, but not of adult BALB/c mice.
Young male and female BALB/c mice were treated for 12 weeks. The controls were housed in the same room. Their body weight was recorded at the beginning of the experiment and every 15 days.
After 4 weeks of exposure, a significant decrease in body weight was observed in both continuously and intermittently treated mice (Fig.1, 2). This was made up later.

ELF-EMF EXPOSURE AFFECTS BODY WEIGHT GAIN AND HAEMOPOIESIS IN YOUNG BALB/C MICE.

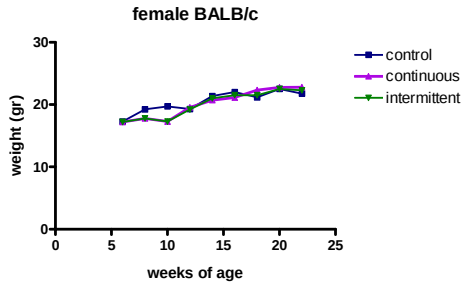

Fig.1

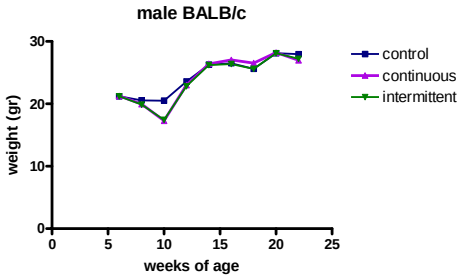

Fig.2

There was no comparable decrease in the adult animals.

ELF-EMFs impaired bone marrow myelopoiesis and splenic lymphoid compartment in the young BALB/c mice.

Several bone marrow and spleen alterations were found after 4 weeks' exposure.
No comparable changes were noted in the adult animals.

Bone marrow haemopoiesis.
Morphometrical analysis of cytological bone marrow samples showed that myeloid progenitors were reduced in both continuously and intermittently exposed mice (Tab 1). Myelocytes are large cells with specific granules in the cytoplasm and an indented nucleus, usually
displaced from the center. Metamyelocytes are similar to the myelocyte stage except that they are smaller and demonstrate a deeply indented, kidney shaped nucleus. In spite of the reduction in the total myeloid compartment (see Segmented cells in Tab 1), the ratio between mature neutrophils and immature myelocytes was normal (data not shown). The decrease of segmented cells was coupled with a relative increment in the proportion of red cells and lymphocytes. However the bone marrow cellularity was normal, as well as the differentiation in all the lineages, so neither maturative blocks nor dysplasia were evident.

Table 1. Bone marrow cell count in 10 week old mice.

	Controls	**Intermittent ELF-EMFs exposure**	**Continous ELF-EMFs exposure**
Myeloid Immature Cells	13 ± 3.1*	8 ± 3.1†	7± 4.1†
Segmented cells	33 ± 9.1	23 ± 8†	24 ± 7.1
Erythroid Cells	45 ± 7.3	54 ± 10.6†	53 ± 11.6
Lymphoid Cells	12 ± 5.1	18 ± 3.1	16± 6

*The values (mean ± SD from 16 mice per group) are expressed as cell percentages
†Significantly different values (a: p≤ 0.001) from those of WT littermates

Histological and immunohistochemical analysis of lymphoid organs.
The volume of the spleens of treated and untreated mice was determined from the following formula: "(transverse diameter)2 * longitudinal diameter/transverse diameter". No differences were found (data not shown). No splenomegaly or other macroscopic pathological aspects were observed.
Despite their normal size, the spleens of treated mice revealed a reduction in the white pulp area (Tab. 2).

Table 2. Extension of the white pulp in the H&E stained spleens.

	Controls	**Intermittent ELF-EMFs exposure**	**Continous ELF-EMFs exposure**
White pulp	52 ± 1.1*	46 ± 2°	43 ± 3°

*The values (mean ± SD from 16 mice per group) are expressed as the percentage of the area occupied by
White pulp area [%= (White pulp area*100)/total spleen area].
° Significantly different values (P≤0.01) from those of WT littermates.

The same results were obtained when we correlated the CD4, CD8 and B220 positive areas with the total spleen area, showing that the reduction involved all the lymphoid subsets.
No architectural nor cytopathological alterations were observed in the lymphoid (black arrows) or haemopoietic (green arrows) compartments. (Fig.4)

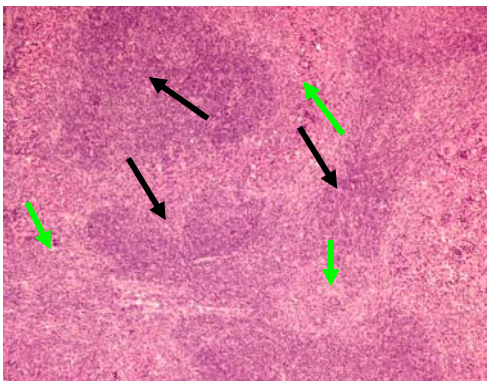

Fig. 4

The percentages of the CD4, CD8 and B220 positive areas in the lymph nodes did not differ in the treated and untreated mice.

The effects of ELF-EMFs exposure on the immune system are reversible.
Bone marrow and spleen samples were collected from the treated and untreated BALB/c mice after 12 weeks. The haematological parameter values of treated mice are not significantly different with respect to the controls. Count of bone marrow cells on cytological smears shown a normalization in percentage of myeloid compartments and quantitation of white pulp area percentage in the spleen showed no differences between experimental groups (data not shown).
FACS analysis of spleen and bone marrow from 18-week-old mice.
To obtain a clearer picture of any slight effects of ELF-EMF, at the end of the treatment we performed FACS analysis of bone marrow and spleen cells at the 18th week of age; a statistically significant reduction in CD11b+ granulocyte and monocyte lineages was observed in the male (Fig. 5, 6), but not the female mice.

ELF-EMF EXPOSURE AFFECTS BODY WEIGHT GAIN AND HAEMOPOIESIS IN YOUNG BALB/C MICE.

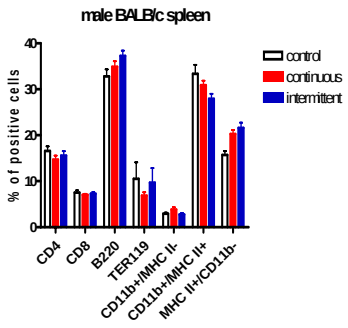

Fig 5

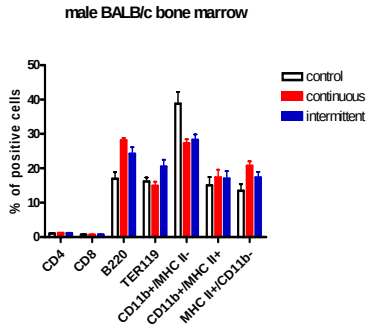

Fig 6

ELF-EMFs slow down the body weight gain of young but not of adult BALB/neuT mice.
Young and adult female BALB/neuT mice were exposed the same ELF-EMF for 12 weeks.
After 4 weeks, a slight decrease in body weight was observed in both continuously and intermittently treated young mice. This was made up later.

ELF-EMFs exposure does not affect bone marrow myelopoiesis and splenic lymphoid compartment in young and adult female BALB/neuT mice.
As for BALB/c mice we analyzed hematological parameters as well as the structure of hematopoietic and lymphoid organs. A progressive increase in the number of monocytes and granulocytes was found in the peripheral blood of BALB/neuT mice after 4 and 12 weeks of exposure. Cytological examination of bone marrow smears revealed a predominance of segmented cells when compared to treated or untreated BALB/c mice (Table 3, compare to Table 1), coupled with a relative decrease in the proportion of red cells and lymphocytes.

Table 3 Bone marrow counts in 12-week-old BALB/neuT mice.

	Controls	**Discontinous ELF-EMFs treated mice**	**Continous ELF-EMFs treated mice**
Myeloid Immature Cells	20 ± 4.1*	21 ± 6.1	24± 3.1
Segmented cells	42 ± 9.1	47 ± 3	39 ± 5.1
Erythroid Cells	35 ± 7.3	36 ± 10.6	33 ± 11.6
Lymphoid Cells	10 ± 6.0	12 ± 9.2	14± 4.0

At 18 weeks of age, FACS analysis of the spleen and bone marrow revealed a pronounced increase of CD11b+ granulocyte and monocyte lineages in all treated and untreated BALBneuT mice when compared to BALB/c mice. All the alterations were proportional to the tumor burden and not to the treatment.

ELF-EMF exposure does not modify the occurrence and progression of BALB-neuT mammary tumors.
To assess the effects of ELF-EMFs exposure on tumor occurrence and progression, mammary glands of control and treated mice were analysed by Whole Mount preparation, histology and immunohistochemistry.
Fig 7 and 9 show representative whole mount pictures of the inguinal mammary gland from a control (a), a continuously (b) and an intermittently (c) exposed BALB Neu T mouse at 10 and 18 weeks of age. Fig 8 and 10 show their respective histological aspects.
These pictures show that ELF –EMS exposure didn't modify the occurrence, the progression or the histological features of the HER-2 dependent tumors.

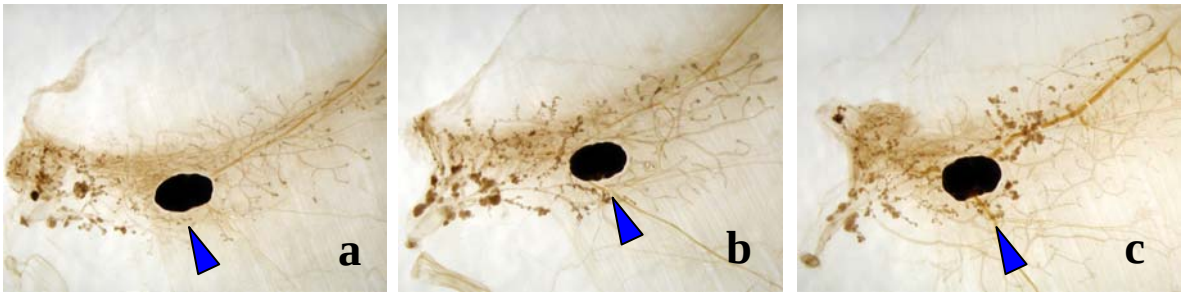

Fig 7

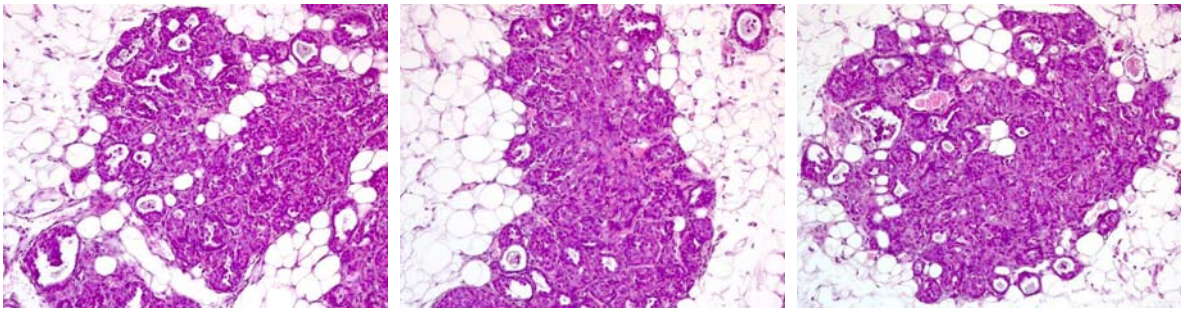

Fig 8

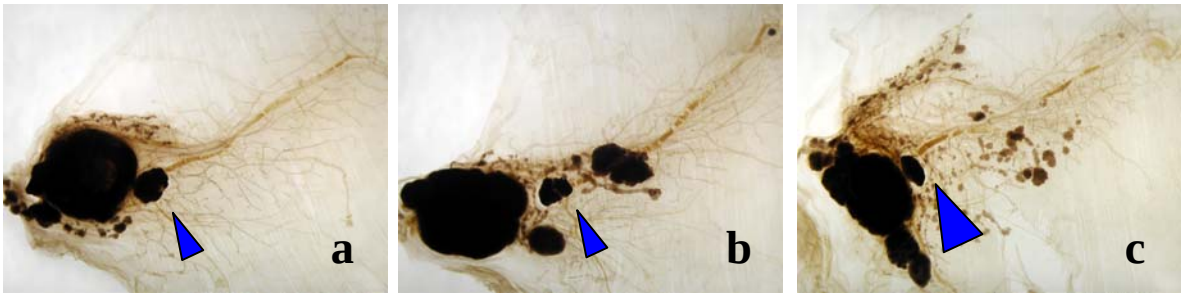

Fig 9

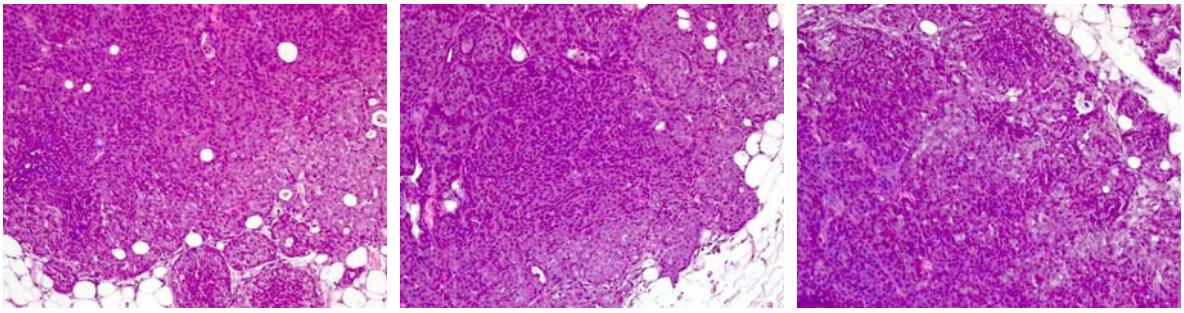

Fig 10

ELF-EMF EXPOSURE AFFECTS BODY WEIGHT GAIN AND HAEMOPOIESIS IN YOUNG BALB/C MICE.

SUMMARY

This study was performed on a large number of animals (a total of 720 mice) with an innovative dedicated generator of ELF-EMF to answer the following questions:

* Whether ELF-EMFs influence the growth and the haemopoietic system of BALB/c mice
* Whether male and female animals are equally responsive
* Whether young and adult animals are equally responsive

Our results clearly indicate that ELF-EMF exposure slow down the body weight gain and alter the haemopoietic system of young, but not of adult BALB/c mice resulting more effective on male compared to female animals.

Subsequently we wondered:

* Whether these effects are transient or persistent
* Whether a dose-response relation or a threshold value for the ELF-EMF intensity is apparent
* Whether continuous and intermittent (night-time only) exposure exert the same effects

Interestingly we found that after the first 12 weeks of exposition gain loss and alterations of spleen and bone marrow cell count were almost completely recovered persisting only a reduction of granulocyte and monocyte lineages in the male mice exposed from the young age.
We were not able to find a dose-response relation or a threshold value for the ELF-EMF intensity nor a difference between continuous and intermittent exposure.

Lastly the effect of ELF-EMF exposure on BALB NeuT mice growth, hemopoietic system and mammary carcinogenesis was investigated.

Only a slight loss of weight during the first month of treatment was reproduced in the BALB NeuT system. Spleen and bone marrow cell count as well as tumoral occurrence and growth appeared not to be influenced by ELF-EMF exposition probably because of the aggressiveness of this model of mammary cancerogenesis and of cancer-driven haematological dysregulation.

This study demonstrates that ELF-EMF produce a biological stress that affects weight gain and haemopoiesis of growing mammalian organisms. Healthy subjects are able to both adapt to and compensate it. Further studies are requested to elucidate the role of oncosuppressors or repair systems in this scenario.

ACKNOWLEDGMENTS

This study was supported by grants from the Italian Ministry of Environment and Territorial Protection (5377/2002/SIAR, 5378/2002/SIAR, DSA/2004/0026779, DSA/2004/0026778)

REFERENCES

[1**]** Sandler DP, *Recent studies in leukemia epidemiology.* Curr Opin Oncol, 7(1):12-18, 1995
[2] Gurney JP et al, *Extremely low frequency electromagnetic fields (EMF) and brain cancer in adults and children: review and comment.* Neuro-oncol. 1(3):212-20, 1999
[3] McBride ML et al, *Power-frequency electric and magnetic fields and risk of childhood leukemia in Canada.* Am J Epidemiol, 149(9):831-42, 1999
[4] Shuz JP et al, *Residential magnetic fields as a risk factor for childhood acute leukaemia: results from a German population-based case-control study.* Int J Cancer. 91(5):728-35, 2001
[5] Kliukiene J et al, *Residential and occupational exposures to 50-Hz magnetic fields and breast cancer in women: a population-based study.* Am J Epidemiol, 159(9):852-61, 2004

[6] Mild KH et al, *Occupational Carcinogens: ELF MFs.* Environmental Health Perspective, vol.113 (11), 2005
[7] Juutilinen J et al, *Possible Cocarcinogenic effects of ELF electromagnetic fields may require repeated long-term interaction with known carcinogenic factors.* Bioelectromagnetics, 21:122-128, 2000
[8] Scassellati Sfarzolini G et al, *Evaluation of genotoxic effects in cell exposed in vitro to extremely-low frequency electromagnetic fields.* Ann. Ig, 16(1-2): 321-340, 2004

[9] Baum A et al, *A histopathological study on alterations in DMBA-induced mammary carcinogenesis in rats with 50Hz, 100 muT magnetic field exposure.* Carcinogenesis, 16, 119-125, 1995
[10] Thun-Battersby S et al, *Exposure of Sprangue-Dawley rats to 50-Hertz, 100-μTesla magnetic field for 27weeks facilitates mammary tumorigenesis in the 7,12-dimethylbenz[a]-anthracene model of breast cancer.* Cancer Research, 59, 3627-2633, 1999
[11] Van Den Heuvel R et al, *Haemopoietic cell proliferation in murine bone marrow cells exposed to extreme low frequency (ELF) electromagnetic fields.* Toxicology in vitro, 15, 351-355, 2001
[12] Bonhomme-Faivre L et al, *Alterations of biological parameters in mice chronologically exposed to low-frequency (50Hz) electromagnetic fields.* Life Sciences, 62 (14): 1271-1280, 1998
[13] Ikeda K et al, *No effects of extremely low frequency magnetic fields found on the cytotoxic activities and cytokine production of human peripheral blood mononuclear cells in vitro.* Bioelectromagnetics, 24: 21-31, 2003
[14] Muller WJ et al, *Single-step induction of mammary adenocarcinoma in transgenic mice bearing the activated c-neu oncogene.* Cell, 54: 105-115, 1988
[15] Stern DF et al, *p185, a product of the neu proto-oncogene, is a receptorlike protein associated with tyrosine kinase activity.* Mol Cell Biol, 6: 1729-1740, 1986
[16] Finn OJ et al, *Prophylactic cancer vaccine.* Curr Opin Immunol, 14: 172-177, 2002
[17] Pannellini T et al, *Immunobiology of her-2/neu transgenic mice.* Breast Dis., 20:33-42, 2004.

APPENDIX

Instrument. The 50Hz electromagnetic fields were generated by a pair of Helmholtz coils. This device was planned and built to deliver variable, homogeneous, sine-wave alternate current magnetic fields with 50 Hz frequency and intensities ranging between 0.1-1.0 mT±2%. The pair of Helmholtz coils, (r=630mm, distance between coils=700mm), parallel to the ground and producing homogeneous magnetic field over the specified volume-under-test corresponding to the plastic cage in which where the animals to be exposed, were located in an isolated room containing also the control animals out of the electromagnetic fields exposure area. The coils were connected to a power supply Elgar Electronics (mod. CW 2501P) and were used to generate 0.1-1.0mT ELF for long time animal exposure (up to 16 weeks).

The Helmholtz coils connected to the power supply

Mice.
Female and male Balb-c and Balb-neuT mice transgenic for the activated rat *neu* oncogene have been generated in our laboratories.
Four-week old females were routinely screened for the transgene by PCR, as previously described ([ ]Muller Cell 1988).
120 male,120 female BALB/c and 120 BALB-neuT mice entered the study at 6 and 10 weeks of age. Each group of 120 mice was divided into 3 groups of 40 mice: control group, intermittently exposed group and continuously exposed group. Mice exposed intermittently were exposed during the night only (active period of mice). Half of the

mice were selected for the sacrifice after 4 weeks of exposition. The remaining 20 mice were sacrificed after 12 weeks of treatment. GraphPad Software was used to secure uniform randomization.
All the procedure was repeated twice for the experiments with 0,5mT and 1mT intensity ELF-EMF.

Analysis of body weight trend

Mice were weighted before they entered the study and start the exposition to the ELF-EMF. The body weight was checked each 15 days and the body weight trend was plotted and analyzed by GraphPad.

Blood and bone marrow smear

Peripheral blood was collected via intra-cardiac extraction.
Bone marrow was flushed from femur and tibia and suspended in PBS 1X. A small drop of blood or bone marrow suspension is placed on the surface of a clean glass slide near the end. An edge of the spreader slide is placed on the first slide to the left of the drop of blood and is pulled to the edge of the drop. When the smear was completely dried, it was stained by May-Grunwald Giemsa.

Histology and Immunohistochemisty

For histologic evaluation, tissue samples were fixed in 10% neutral-buffered Formalin, embedded in paraffin, sectioned at 4 µm, and stained with H&E. For immunohistochemistry, paraffin-embedded or acetone-fixed cryostat sections were immunostained with anti-p185 (clone C-18) (Santa Cruz Biotechnology), anti-proliferative cell nuclear Ag (PCNA) (clone PC10) (DakoCytomation), anti-endothelial cells (CD31, PECAM-1, clone MEC13.3) (BD Pharmingen), anti-Mac-1 (CD11b/CD18, clone M1/70.5), anti-CD8 (Ly/T2, clone YT5 169.4) and anti-CD4 (LT34, clone YT5.191.1.2; all from Sera-Lab, Crawley Down, Sussex, United Kingdom), or anti-CD11c (clone N418; Chemicon International Inc., Temecula, CA), anti-CD45R/B220 (clone RA3-6B2; all from PharMingen, San Diego, CA),Abs. After washing, sections were overlaid with biotinylated goat-anti-rat and anti-rabbit Ig (Vector Laboratories) for 30 min. Unbound Ig was removed by washing, and slides were incubated with avidin-biotin complex /alkaline phosphatase (DakoCytomation). To quantify germinal centers (GC), each spleen was transversely dissected into four segments from which semiserial sections were obtained. The GC in the total area of each section were counted. Morphologic studies were conducted independently by three pathologists in a blind fashion.

Whole mount and image analysis

Whole mounts of all mammary glands were done as indicated in http://ccm.ucdavis.edu/tgmouse/HistoLab/wholmt1.htm. Digital images were acquired by dividing the whole mount of each gland into 10 quadrants. Ten points were randomly chosen on the duct surface in each quadrant and the corresponding lesions were measured. All lesions with a diameter >150 µm on the same quadrant were counted. Images of whole-mount preparations were taken with a Nikon Coolpix 950 digital camera (Nital Spa, Turin, Italy) mounted on a stereoscopic Leica MZ 6 microscope (Leica Microsystems, Milan, Italy). A 0.63 objective were used to obtain images with a total magnification of x630 and a resolution of 1,600 x 1,200 pixels. Images were acquired within Adobe Photoshop version 6.0 graphic software (Adobe Systems, San Jose, CA). Glands larger than a single imaging area were captured by photographing contiguous microscopic fields in a raster pattern. Each captured image was merged using the layer technique in Adobe Photoshop to form a single composite image for analysis. Spatial calibration was determined by photographing a 1 mm stage using the same parameters as those for image capturing of whole-mount preparations. The distance drawn on the 1 mm calibration image was divided by 1,000 to find the number of pixels per micrometer. In each image, 100 discrete points were randomly chosen on the duct surface and lesion widths in micrometer were measured perpendicular to duct direction. Points with no lesion were ranked as zero. Lesion measurements were recorded on an Excel spreadsheet and mean and SE were calculated for each treatment group. Statistics were obtained with a two-tailed Student's *t* test.

Flow Cytometry

Single cell suspensions of bone marrow and spleen were prepared. The cells were washed in PBS with 1%FCS (staining buffer). Aliquots of $0.5-1.0\times10^6$ cells were then stained for 30 min on ice with monoclonal antibodies conjugated with fluorescein isothiocyanate (FITC) or phycoerythrin (PE). The antibodies used in these experiments included reagents specific for: B220 (CD45R), TER-119, CD4, CD8α, MHC-classII (all antibodies were purchased from Miltenyi). Cells were washed once in staining buffer and multicolor flow-cytometric analysis was done with a FACScan (Becton-Dickinson). A minimum of 10 000 events were acquired and the data was analyzed using CellQuest software. Statistics were obtained with two-tailed Student's t test.

SUPPRESSION OF NO PRODUCTION IN MACROPHAGES BY ELF ELECTRO-STIMULATION

MUNEYOSHI KAGAWA, TOSHIYUKI SHIMOOKA, YUJI KURACHI and KOICHI SHIMIZU

GRADUATE SCHOOL OF INFORMATION SCIENCE AND TECHNOLOGY, HOKKAIDO UNIVERSITY

Abstract

We have pursued the possibility to control immune functions by ELF electro-stimulation. As the first step, the effect of electro-stimulation on the NO producing ability of macrophages was examined. The decrease of NO production due to the electro-stimulation was observed with statistical significance. To elucidate the mechanism of this phenomenon, the amount of the NO synthesizing enzyme was measured. The measurement showed the decrease in the emergence of the enzyme with statistical significance, as well. These facts suggested that the ELF electro-stimulation suppressed the emergence of the NO synthesizing enzyme and that the amount of NO production was consequently decreased by the electro-stimulation. To analyse the association between the amount of the NO synthesizing enzyme and the amount of NO production, the dose-response of this effect was investigated by changing the electric current density of the electro-stimulation. The rates of the decrease in NO synthesizing enzyme and the NO production were found to be very close. These results showed that the change in the NO synthesizing enzyme is closely involved in the mechanism of the suppression of NO production by electro-stimulation. This suggested the feasibility to control the immune function by applying electro-stimulation from outside the body.

Introduction

The influence of ELF electromagnetic field on various physiological functions has been reported, and much study has been conducted mainly from the view point of adverse effects. On the other hand, there is a clinical application such as therapeutic instruments using ELF electric field. With the view towards the immune control by ELF electric field exposure, we have studied the effect of electro-stimulation on cell functions. Macrophages play important roles in a human immune system. We have examined the effect of electro-stimulation on the phagocytic activity and the active oxygen production ability of macrophages. Through this study, it has been found that the both activities are suppressed by the capacitively coupled electro-stimulation[1,2]. The electric current induced in the suspension of cells was in the similar order to that induced in the human body with the therapeutic instrument of electric field exposure.

In the current study, we have examined the effect of electro-stimulation on the production capacity of nitric oxide (NO). The NO is a kind of the same radicals as the active oxygen and is produced in the immune function of a macrophage. The NO is produced to kill bacteria but can destroy normal cells when produced excessively. Moreover, it reacts with the active oxygen and becomes the peroxynitrite ($ONOO^-$). The $ONOO^-$ is more toxic and damages normal cells. Therefore, if we can control the NO production, it will contribute to the prevention and the treatment of various diseases. We have examined this possibility by the ELF electro-stimulation in vitro.

Materials and Methods

macrophage preparation

Peritoneal exudate macrophages were used in all the experiments. The thioglycollate medium (4.05%, 2 ml) was injected in the peritoneal cavity of a normal mouse (Std:ddy, female, 7-11weeks). After 3 or 4 days, the cells were harvested from the mouse abdomen. Then, macrophages were collected from the cells in the established method. [3] We prepared the cell culture solution (RPMI 1640 with L-Glutamine , Sodium Bicarbonate and 10%Fetal Bovine Serum: RPMI 1640, hereafter) with 0.5×10^5IU penicillin G potassium and 50mg streptomycin sulfate added. The collected macrophages were suspended in the cell culture solution to make the cell density of 2×10^6cells/ml. When electro-stimulation was applied to the cells, the IFN-γ(10U/ml) and the LPS(1μg/ml) were added as stimulants to both the stimulation group and sham group.

electrostimulation system

The macrophage cells were stimulated by the electric current in the container insulated electrically from the electrodes to simulate the condition of electro-stimulation from outside the human body. Figure 1 shows the structure of the sample container.

Two plane electrodes were kept parallel with 3 mm distance by a plexiglass separator. The electrodes were square cupper plates (24mm×24mm×6mm top and 32mm×32mm×6mm bottom). The top electrode was insulated with a 0.15 mm thick cover-glass, and the bottom one with 0.10 mm thick silicone film. The outline of the electrostimulation system is shown in Fig.2. Two electrodes were connected to a high-voltage power source through a noise filter. As the power source, the power supply of a commercial apparatus for the electric field therapy was used (Healthtron , Hakuju Inst. Health Science, maximum supply voltage 10kV). A sinusoidal AC signal of 50Hz was supplied to the apparatus with a waveform generator to make the high-voltage with the sinusoidal waveform of 50Hz. In the experiment, the cell suspension was placed in the container, and electro-stimulation was applied in a CO_2 incubator (38ºC, $CO_2$5%). The cell suspension of the sham group was kept in another incubator of the same condition.

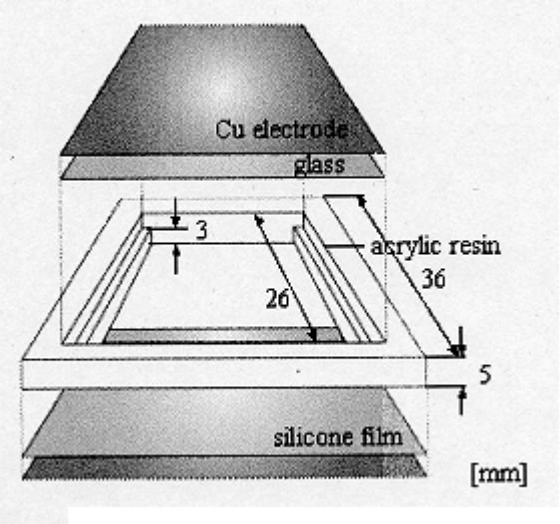

Fig.1 Sample container

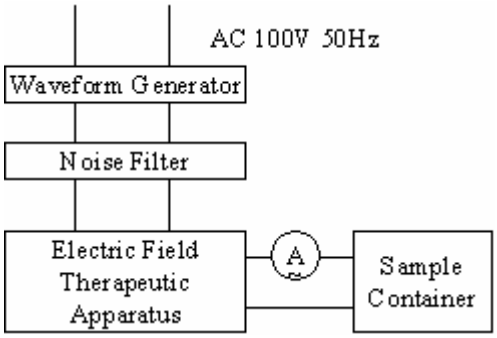

Fig.2 Schematic diagram of electro-stimulation system.

Effect on NO production

We stimulated macrophages in the suspension with IFN-γ and LPS, and applied the electro-stimulation for the exposure group. The sham group was treated in the same way except connecting to the power source. The amount of NO produced outside the cell was measured as fluorescent intensity (495nm excitation and 515nm emission) using fluorescent reagent Diaminofluorescein-2(DAF-2) for the NO detection.

Macrophages were collected in the established method, and washed three times with Hanks' Balanced Salt Solution (HBSS) in centrifugation (400G) for 5 minutes. Then, they were suspended in the culture liquid RPMI 1640 again, and the electro-stimulation (50Hz, 35μA/cm^2, 16h) was applied. After the electro-stimulation, the macrophages were washed with HBSS in centrifugation, and cultured in HBSS suspension with DAF-2(10μM) and L-arginine(1mM) two hours without electro-stimulation. After the two hour culturing, the supernatant part was separated in centrifugation. With a fluorescent photometer, the fluorescent spectrum of the supernatant was measured. The supernatant of the sham group was collected in the same process except for the electro-stimulation, and the fluorescent spectrum was measured in the same way as the stimulation group.

Figure 3 shows an example of the measured result. The abscissa is the wavelength and the ordinate is the fluorescent intensity. The wavelength of the intensity peak was around 515 nm in both cases. There was no significant change in the shape of the spectrum, but 30% decrease in the intensity was observed in the stimulation group. This suggest the suppression of NO production by the electro-stimulation. The same experiments were repeated nine times. Figure 4 shows the reduction ratios of the fluorescent intensity between the stimulation and the sham groups. In all the nine cases, the fluorescent intensity was decreased by the electro-stimulation. The p-value of the paired-t test was 1.79×10^{-2}, which suggested the suppression of NO production by the electro-stimulation with a statistical significance.

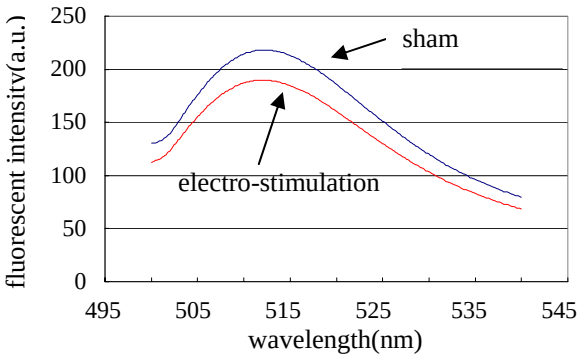

Fig3. Example of measured NO production by fluorescence spectroscopy.

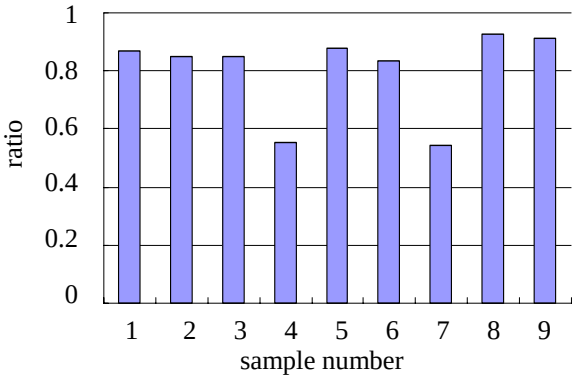

Fig.4 Suppression of NO production.

Effect on iNOS expression

NO is synthesized in a macrophage by the inducible nitric oxide synthase (iNOS). To elucidate the mechanism of the suppression in the NO production, the effect of the electro-stimulation on the iNOS expression was examined. The amount of the iNOS expression was evaluated by measuring the fluorescent intensity in the indirect immunity fluorescent method. [5, 6]

In the same way as the one mentioned above, macrophages were collected, separated into two groups, and electro-stimulation (50Hz, 35μA/cm^2, 16h) was applied to the stimulation group. After the electro-stimulation, the macrophages were collected in the centrifugation. With 70% ethanol, the cell membrane was processed to enhance its permeation. After three times centrifugation (400G, 5 minutes), macrophages were suspended in HBSS. We added the rabbit anti-iNOS antibody (BD Biosciences) and kept it in a shaker bath at 4 ºC in 30 minutes. Then we added 20μg/ml of the FITC tagged hircine anti-rabbit Ig antibody (MP Biomedicals Inc.) and kept it in the shaker bath. Finally, we fixed the suspension with 1% paraformaldehyde, and measured the fluorescent intensity with a flow cytometer (FACS Calibur Becton Dickinson and Company).

Figure 5 shows an example of the results. The abscissa is the fluorescent intensity in an arbitrary unit, and the ordinate is the number of the cell. The broken line in the figure shows the average intensity of all the cells. The average values were 79 and 65 for the sham (a) and the stimulation (b) cases, respectively. This result showed the decrease in iNOS expression by the electro-stimulation. The same experiments were repeated eleven times. Figure 6 shows the ratio of the average intensity between the simulation and the sham cases. As shown in the figure, the decrease in fluorescent intensity was observed in all the eleven trials. The p-value of the paired-t test was 5.52×10^{-5}. This suggested that the iNOS expression was suppressed by the electro-stimulation with statistical significance.

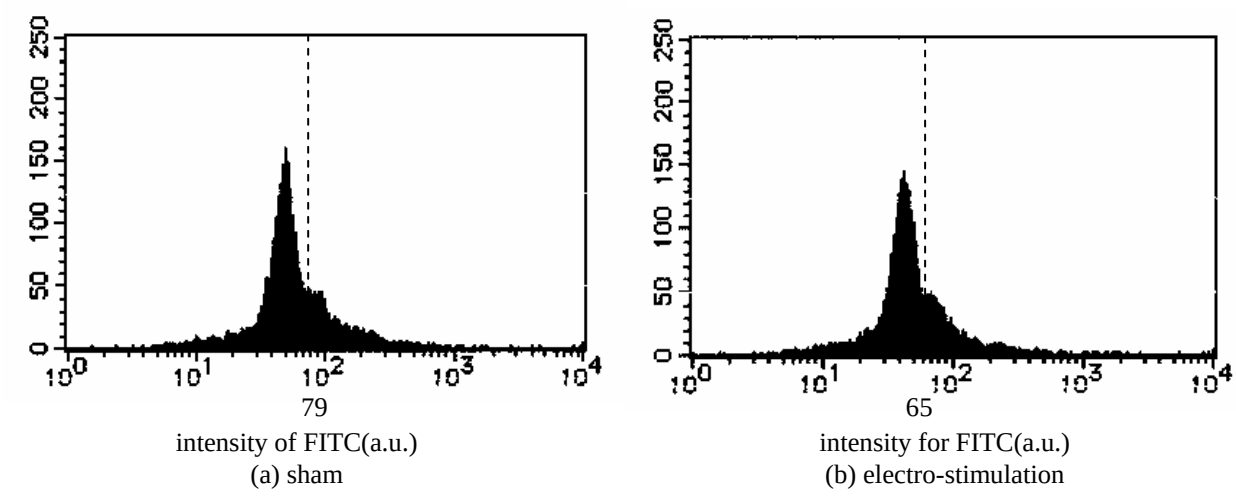

Fig.5 Example of measured iNOS expression by fluorescence spectroscopy.

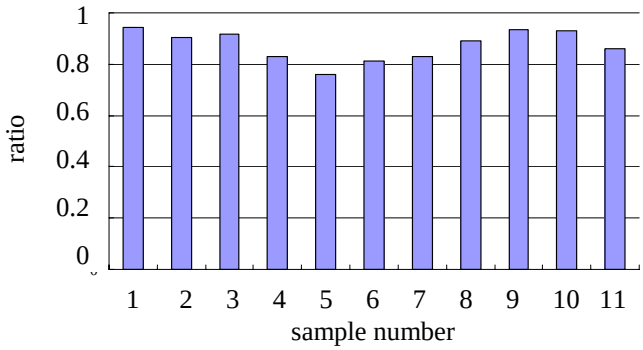

Fig.6 Suppression of iNOS expression.

Analysis of dose-response

As the first step of quantitative evaluation, the dose-response of these phenomena was analysed. In experiments, the amounts of the NO production and the iNOS expression in different current densities (0.35μA/cm^2, 0.675μA/cm^2, 3.5Aμ/cm^2) were measured. After the electro-stimulation in 16 hours, the cell suspension was divided into two. One was used for the measurement of the NO production, and another is for that of iNOS expression. Figure 7 shows the results of the measurements. The abscissa is the current density and the ordinate is the fluorescent intensity normalized by that of the sham case. The number of repeated measurements were 4, 6 and 4 for the cases of 0.35μA/cm^2 , 0.675μA/cm^2 and 3.5μA/cm^2, respectively. The result of 35μA/cm^2 case was added, in which the numbers of the repeated experiments were 11 and 9 for NO and iNOS cases, respectively.

With the current density of 0.35μA/cm^2, we could not observe apparent decrease in either of the NO or the iNOS. With 0.675μA/cm^2, about 5% decrease was observed. With the current density of more than 3.5μA/cm^2, more than 15% decrease was observed. In both of the NO and the iNOS, the threshold of the suppression seems to exist between 0.35μA/cm^2 and 3.5μA/cm^2. The similar characteristics in the dose-response strongly suggested the close correlation between the suppression of iNOS expression and that of NO production.

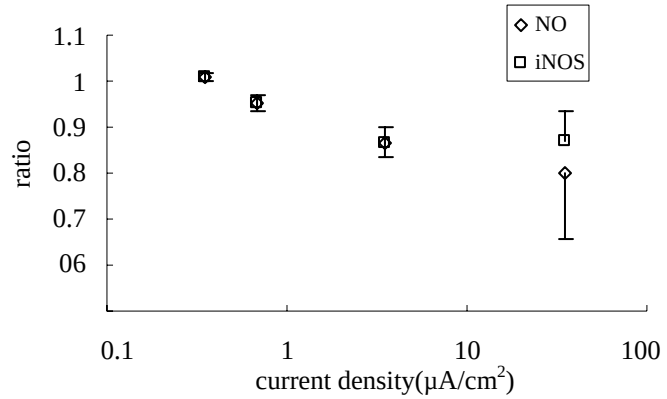

Fig.7 Analysis of NO and iNOS suppression effect by electro-stimulation.

Discussion

In the in-vitro experiments, it was found that the NO production is significantly suppressed by the ELF electro-stimulation. This suggested the possibility to control the functions of macrophages by the electro-stimulation applied from outside the body using the apparatus for the electric field therapy. Since a macrophage plays an important role in the first stage of the immune response, the electro-stimulation can influence the entire immune reaction. For example, we can expect the relief from the following diseases. They include the chronic inflammation and the autoimmune diseases caused by an excessive immune response. We can also expect the relief from the endotoxin shock due to the excessive NO production, the etiologic vasodilation, the cardio-vascular ischemia, the cerebral hemorrhage and the cancers. Moreover, we have confirmed the suppression of the active oxygen production by the electro-stimulation.[2] Therefore, we can also expect the control of $ONOO^-$

production which shows high cell-toxicity.

However, the finding of this study is only the result of in-vitro experiments using macrophages. We need further investigation to confirm this effect with human macrophages, and the investigation on this effect in-vivo where other kinds of cells are closely interacted. Yoshikawa and his co-workers reported the increase of NO production in the liver when LPS (2 mg/kg) was administered by abdominal injection and the magnetic field (60Hz, 0.1mT) was exposed in 5.5 hours. The current density induced by this magnetic field inside the body is estimated at $1.1\times10^{-8}A/cm^2$. This result is opposite to our result. It seems that the direct comparison between these two cases is not appropriate, since the object cell and the current density is greatly different among them.

Besides this, there have been few reports on the effect of ELF electromagnetic fields on the NO production, and little has been known on its mechanism. We consider that the arginine metabolism, iNOS activity and iNOS expression are closely associated with the decrease in the NO production. To investigate this mechanism, we have compared the amounts of NO production and the iNOS expression.

Figure 7 shows the coincidence in the reduction ratio of fluorescent intensity between NO and iNOS by the same electro-stimulation. This result suggests that the electro-stimulation affects the NO production through iNOS expression. The signal transmission pathway for the iNOS expression is stimulated by LPS and IFN-γ through receptors on a cell membrane. As the result, a transcription factor is activated and the iNOS is transcribed. In our study, the electro-stimulation was applied from the beginning when we started the stimulation with LPS and IFN-γ. Therefore, it is most plausible that the electro-stimulation affects this process.

However, the following possibility cannot be neglected. In the peritoneal exudate cells used in this study, about 10% cells were not macrophages. Since these non-macrophage cells can affect the signal transmission pathway of the NO production, they might influence the mechanism of the suppression of the NO production. Therefore, we have to examine this point in the experiment using the pure macrophage cells separated from other cells.

In our experiment, the threshold of the effect was found between $0.35\mu A/cm$ and $3.5\mu A/cm^2$. In the study for the biological effects of ELF electromagnetic fields, the minimum threshold of magnetic field exposure has been reported. [7] According to the report, the threshold current density for the characteristic change in tissues and cells was in the order of $10mA/m^2$ or $1\mu A/cm^2$. Though this threshold is for the electric current induced by magnetic field, it is very close to our result in which the electric current was induced by the electric field.

Conclusion

With the view toward the control of immune functions by ELF electric field exposure, the effect of the electro-stimulation on the NO production of macrophages was examined in vitro. The decrease of NO production due to the electro-stimulation was observed with statistical significance. In experiments, it was found that the expression of NO synthesizing enzyme or iNOS was suppressed in the same rate as NO in the electro-stimulation. Further investigation is required to ascertain this mechanism of NO suppression and to verify the feasibility of the immune control by electro-stimulation.

Reference

[1] I. Fujii, T. Shimooka, Y. Morita and K. Shimizu, "Experimantal verification for the effect of capacitively coupled electrostimulation on macrophage's endocytosis," Tec. Report IEICE., MBE2001-101, pp.97-102,2002.(in Japanese)

[2] Takeshi Tatebe, Toshiyuki Shimooka, Muneyoshi Kagawa, Koichi Shimizu, "Effect of ELF electrostimulation on reactive oxygen generation of macrophage", Tec. Report IEICE, MBE2003-131, pp.13-18, 2004.(in Japanese)

[3] Stohlman SA, Frelinger JA, Weiner LP. Resistance to fatal central nervous system disease by mouse hepatitis virus, strain JHM. II Adherent cell-mediated protection. J Immunol., 124(4):1733-9, 1980.

[4] Wataru Yoshida, Minori Ogawa, Yuko Furuoya, Yu Igarashi, Rumi Sato, Akiko Hayashi, Kazuya Hirano, Masatoshi Beppu, "Effect of Estrogenic Compounds on Superoxide and Nitric Oxide Production by Activated Macrophages Assessed by Sensitive Microplate Assays", Journal of Health Science, 48(5), pp.455-459, 2002.

[5] Oh-Deog KWON, Chang-Yeol YIM, Kyu-Shik JEONG, Kyu-Yong JUNG, John R. McGREGOR, Neil R.BASTIAN Wolfram R. SAMLOWSKI, "Suppression of Cytokine-Inducible Nitric Oxide Synthesis During Intraperitoneal Meth A Tumor Growth" , J Vet Med Sci., 66, pp.357-365, 2004.

[6] Wolfram E. Samlowski, Jhon R. McGregor, Gregory J. Litton, "Liver Sequestration of Murine Lymphokine Activated Killer Cells Is Mediated by Carbohydrate-specific Receptor", Regional immunology Vol.2, pp.254-265, 1989.

[7] ICNIRP Guidelines : "Guidelines for limiting exposure to time-varying electric, magnetic, and electromagnetic fields(up to 300GHz)", Health Physics, Vol.74, No.4, pp494-522.1998.

[8] Yoshikawa T, Tanigawa M, Tanigawa T, Imai A, Hongo H, Kondo M, "Enhancement of nitric oxide generation by low frequency electromagnetic field" , Pathophysiology, pp.131-135, Jul;7(2), 2000.

IMMUNE STIMULATION IN FISH AND FARM ANIMALS THROUGH WEAK LOW FREQUENCY ELECTROMAGNETIC FIELDS: A. HYPOTHESIS

J.J.M. Cuppen[1], H.K. Parmentier[2], H.F.J. Savelkoul[2]

1: Immunent BV, 2: Wageningen University, The Netherlands

Abstract

A hypothesis is proposed how LF EMF treatment can stimulate an immune response, based on recent insights in immunology. Danger signals have been shown in the last decade to be an essential factor in the coordinated response of the immune system to pathogens. We hypothesize that the EMF treatment induces mild stress to cells in the body, which then produce danger signals for the immune system. In this way EMF treatment takes the place of multiplying pathogens and the damage these cause in the triggering of an immune response.

Introduction

Immunent has developed a signal for advancing and elevating the immune response to pathogens (multiple LF components, 0.1-50 µT, 30 minutes per day) which we have tested at various experimental conditions. Pilot findings with this signal (proprietary, but available for research purposes) were presented at the 2004 Kos meeting (Cuppen and Vink 2004). In subsequent experiments with carp, goldfish and chickens significant and often strong effects of immune stimulation have been observed. The effects include: 40% increased oxidative burst of isolated phagocyting cells ($p<0.001$), 60% decreased mortality in infected fish ($p<0.001$), 5% decreased feed consumption for equal growth in chicken ($p<0.05$) comparable to the use of preventive antibiotics and 40% decreased intestinal lesions in chicken ($p<0.01$) due to Eimeria infections. These results are reported in detail at this conference in one presentation and two posters.

In this paper we take the liberty to hypothesize about the observed strong responses of the immune system of this broad range of animals. The hypothesis regards the possible mechanism of action and attempts to answer the question how such weak, short duration EMF signals can induce an effective immune response.

Hypothesis

During last decade in immunology a hypothesis has been developed that immune response is not only due to the presence of non-self cells but also needs the presence of promoters (e.g. Matzinger 2002, Kapsenberg 2003, Shi et al 2003). This holds in particular for the innate immune response to pathogens not earlier encountered. Such promoters are called “danger” signals. An example might be Heat Shock Proteins (prime examples of cell response to injury or insult), as well as Interferon, Interleukins and other cytokines. Danger signals are formed when cells get stressed or damaged, and this is “presumed by the cells” to be caused by harmful pathogens. The idea behind the view is that strange DNA that does not cause damage, such as a foetus or food, does not and should not trigger an immune response. Support for this view has been obtained from the new approach to transplants that originated from it: after surgery the transplant organ contains lots of danger signals due to the cell damage caused by surgery or the trauma of the donor. Flushing of the transplant organ, which eliminates danger signals from the organ tissue, led to an enormous decrease in rejection reactions from the receiving patient. With this technique, a strong reduction in immune suppressing medication could be achieved.
In immunology other factors besides damage due to pathogens have been identified that stimulate the production of danger signals, such as stress or shock from salt, cold or heat. See Engelsma, Hougee and Nap (2003), and Huising, Guichelaar and Hoek (2003).

The danger signal hypothesis can be schematically represented as in Figure 1.

Figure 1. Matzinger Hypothesis

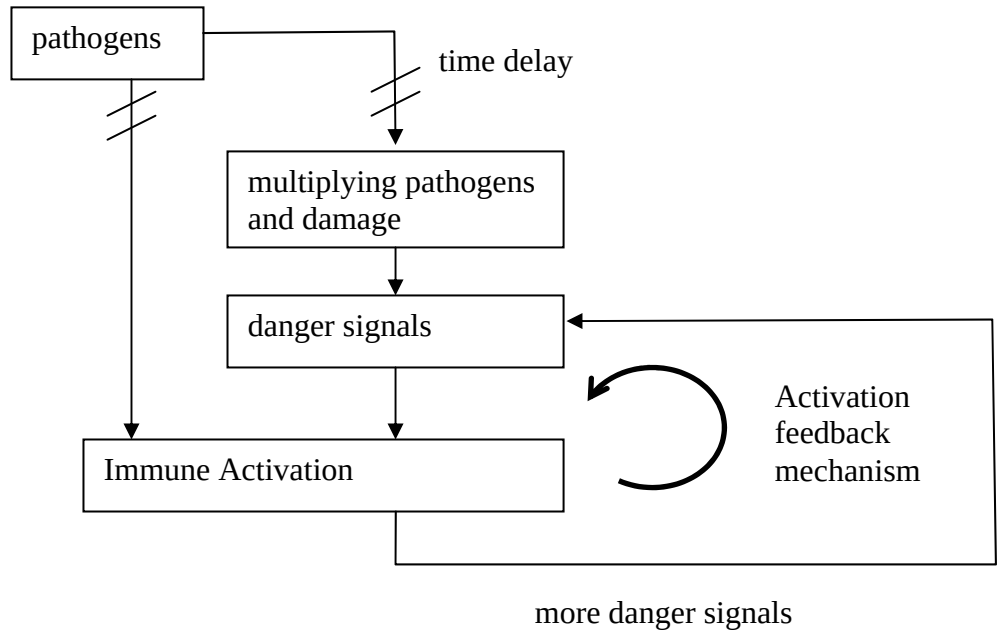

Several authors (see Blank, Khorkova, and Goodman 1992, Goodman, Blank and Lin 1994, Blank, Lin and Goodman 1995, Simkó and Mattsson (2004), Monselise, Parola and Kost 2003, de Bruyn and de Jager 1994, Mevissen, Haussler, Szamel, Emmendorffer, Thun-Battersby and Loscher 1998, Markov, Nindl, Hazlewood and Cuppen 2006) discussing the effects initiated by various EMF signals have demonstrated the production of cytokines, increased immune parameters and stress effects and concluded that EMF causes stress at the cellular level and that this leads to production of cytokines and consequently biological response, including immune response. This has led Mattson and Simkó (2004) to formulate a hypothesis that proposes a mechanism for immune activation due to short term EMF exposure (see Figure 2) and a mechanism for cell damage due to long term EMF exposure.

Fig 2. Simkó and Mattsson hypothesis

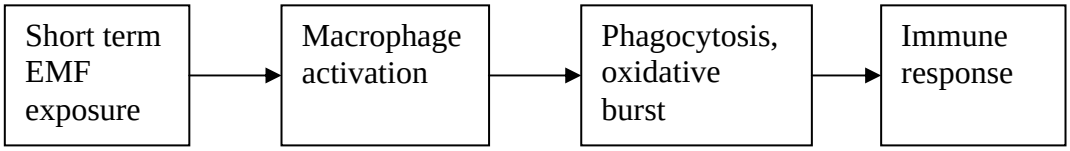

Based on published theoretical and experimental studies, as well as our own experience we propose a hypothesis, that combines and extends the views quoted, by

a) the observation that an immune response is a self stimulating process, at least in the initial stages. Macrophages become activated under the influence of danger signals, and thus have a higher statistical chance and a lower expected time until they actually encounter and recognise pathogens. Once this happens they themselves produce cytokines that increase the immune response etcetera
b) the observation that for chronic infection apparently the feedback cycle stated in a) does not gain sufficient momentum for the infection to reach acute phase
c) the observation that for new infections a more active and alert immune system will start the feedback

loop in a) earlier, thus slowing down the multiplication of pathogens and reducing damage.

Therefore we propose an extended hypothesis which can be schematically represented as in Figure 3.

Figure 3. Our Hypothesis

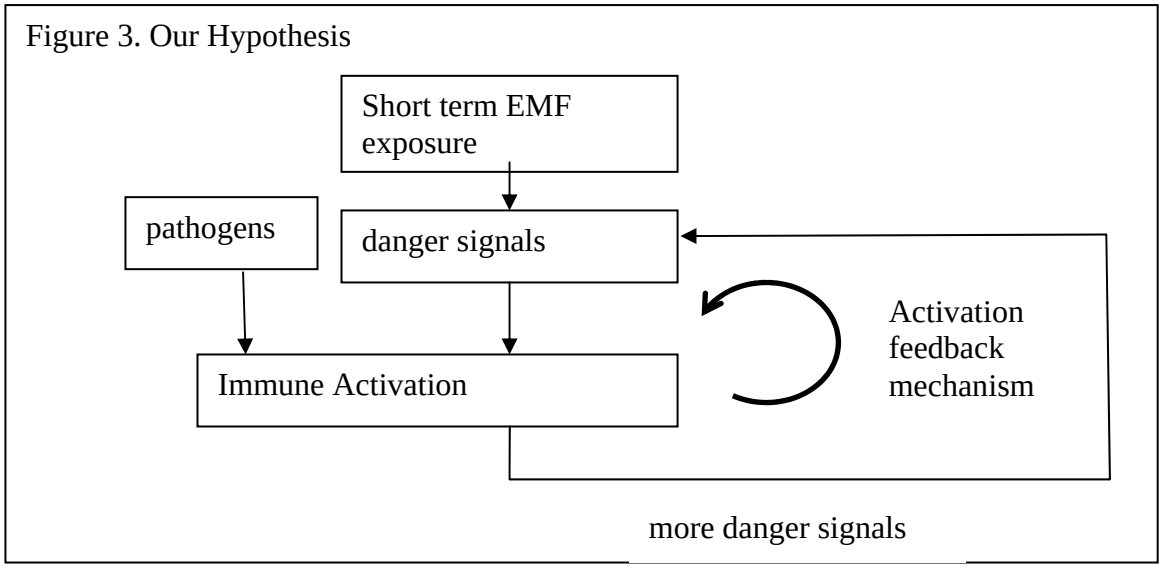

The core of the proposed Hypothesis is that short term LF EMF exposure, possibly repeated, can produce danger signals that can trigger the immune system activation feedback mechanism in the presence of pathogens. As such the EMF induced danger signals take the place of the danger signals that would be produced by multiplying pathogens and the damage they cause to cells and tissues. In this way a timely EMF treatment can avoid the delay given by the time it takes for enough damage to occur and danger signals to be produced in a normal disease development. Thus the immune response to pathogens can be advanced in time and damage and a well developed pathogen attack can be avoided.

In our own in vivo experiments (Cuppen et al. 2004, 2006c, 2006d) we have observed immune stimulation effects after repeated exposures of 30 minutes per day. There is evidence in literature and there are anecdotal indications that continuous exposure to EMF leads first to increased immune parameters, but later to decreased immune parameters, which can be interpreted as exhaustion (Mevissen et al. 1998, Jager et al. 2004).

References

Blank M., Khorkova O. and Goodman, R. (1992): Changes in polypeptide distribution stimulated by different levels of electromagnetic and thermal stress. Bioelectrochem. Bioenerg. 33, 109-114, 1992

Blank M., Lin H. and Goodman, R. (1995) Increased expression of heat shock genes in cells exposed to 60 Hz electromagnetic fields. Mol. Biol. Cell 6, 466a, 1995.

Monselise E. B.-I., Parola A.H., Kost D. (2003): Low-frequency electromagnetic fields induce a stress effect upon higher plants, as evident by the universal stress signal, alanine. Biochem Biophys Res Commun. 2003 Mar 7;302(2):427-34.

Bruyn L. de, de Jager L. (1994) Electric field exposure and evidence of stress in mice. Environ Res. 1994 Apr;65(1):149-60.

Cossarizza A., Angioni S.,Petraglia F., Genazzani A. R., Monti D., Capri M., Bersani F., Cadossi R. and Franceschi C. (1993) Exposure To Low Frequency Pulsed Electromagnetic Fields Increases Interleukin-1 And Interleukin-6 Production By Human Peripheral Blood Mononuclear Cells. Exp Cell Res 204(2):385-387 1993

Cuppen J.J.M. and Vink A. (2004): Effects of ELF exposure on weight and immune parameters in young turkey broilers, 3rd Intl workshop on Biological Effects of EMFs, Kos, 2004, p 1203.

Cuppen J.J.M, Wiegertjes G.F., Geervliet J., Smink W., Beynen A.C., Elmusharaf M.A. and Grooten H.N.A. (2006b): Immune Stimulation In Fish And Farm Animals Through Weak Low Frequency Electromagnetic Fields, B. Experiments, this proceedings.

Cuppen J.J.M., Wiegertjes G.F., Molenaar M., Geervliet J., Smink W. (2006c): Immune Stimulation In Fish And Fish Immune Cells Through Weak Low Frequency Electromagnetic Fields With Variable Field Strength, this proceedings

Cuppen J.J.M., Beynen A.C., Elmusharaf M.A., Grooten H.N.A. and Smink W. (2006d): Immune Stimulation In Chicken Broilers Through Weak Low Frequency Electromagnetic Fields With Coccidia Infection, this proceedings

Engelsma M.Y., Hougee S., Nap D. et al. (2003) Multiple acute temperature stress affects leucocyte populations and antibody responses in common carp, Cyprinus carpio L, Fish Shellfish Immunol, 15 (5), 397-410

Goodman R., Blank M., Lin H. et al. (1994) Increased levels of hsp70 transcripts induced when cells are exposed to low frequency electromagnetic fields, Bioelectrochemistry and Bioenergetics, 33 (2), 115.

Huising M.O., Guichelaar T., Hoek C. et al. (2003) Increased efficacy of immersion vaccination in fish with hyperosmotic pretreatment, Vaccine, 21 (27-30), 4178-93.

Jager L. de, Bruyn L. de (2004) Long-term Effects of Time Varying Extremely Low Frequency Magnetic Fields, 3rd Intl workshop on Biological Effects of EMFs, Kos, 2004, p 573.

Kapsenberg M.L. (2003): Dendritic-cell control of pathogen-driven T-cell polarization. Nature Rev Immunol 2003;3:984-93.

Markov M.S., Nindl G., Hazlewood C.F. and Cuppen J.J.M. (2006) Interactions between electromagnetic fields and immune system: possible mechanism for pain control. In: S.N. Ayrapetryan and M.S. Markov (eds.), Bioelectromagnetics, Springer 2006, pp 213-225.

Matzinger P. (2002): The danger model: a renewed sense of self. Science 2002;296:301-5.

Mevissen M., Haussler M., Szamel M., Emmendorffer A., Thun-Battersby S. and Loscher W. (1998). Complex Effects of Long Term 50 Hz Magnetic Field Exposure In Vivo on Immune Functions In Female Sprague - Dawley Rats Depend on Duration of Exposure. Bioelectromagnetics 19:259-270.

Shi Y., Evans J.E., Rock K.L. (2003): Molecular identification of a danger signal that alerts the immune system to dying cells. Nature 2003;516-21.

Simkó, M. and Mattsson M.O. (2004): Extremely low frequency electromagnetic fields as effectors of cellular responses in vitro: possible immune cell activation. J. Cell. Biochem. 93:83-92, 2004.

IMMUNE STIMULATION IN FISH AND FARM ANIMALS THROUGH WEAK LOW FREQUENCY ELECTROMAGNETIC FIELDS: B. EXPERIMENTS

J.J.M. Cuppen[1], G.F. Wiegertjes[2], J. Geervliet[3], W. Smink[3], M.A. Elmusharaf[4], A.C. Beynen[4], H.N.A. Grooten[3]

1: Immunent BV, 2: Wageningen University, 3: FIS BV, 4: Utrecht University, The Netherlands

Abstract

Most of the publications in the bioelectromagnetics are related to animal/human studies, very few to effects of magnetic fields on plants and practically no studies were performed on small farm animals and fish. Our goal is to examine how properly selected magnetic fields can decrease the potential of development of infectious diseases in farm animals.

Experimental results presented and discussed here are set up to (indirectly) test the hypothesis that low frequency electromagnetic field (LF EMF) treatment can stimulate an immune response through the creation of danger signals which are necessary to trigger an immune reaction in the presence of pathogens.

The reported cell experiments show that the treatment stimulates oxygen burst in phagocytes which supports the notion that danger signals are indeed formed. Experiments with goldfish demonstrate a large decrease of mortality caused by infectious disease (gill parasites and accompanying microbial infections). This result is consistent with the idea that the exposure to EMF increases the strength of the immune reaction, so that a larger percentage of animals sufficiently combats the disease early enough to prevent disease to develop and that these animals are therefore able to return to health. Finally experiments with chicken broilers with coccidia infection, induced after starting the EMF treatment, show both less intestine damage due to the disease and a better growth to feed ratio. This demonstrates the effectiveness of the treatment in prevention of disease: the results indicate that, in the presence of pathogens, a self stimulating immune response originates sooner and more strongly than without the EMF treatment. An infection is then counteracted earlier, with less opportunity for pathogens to multiply and to cause damage.

All results combined support our hypothesis that the Immunent LF EMF treatment induces the formation of cytokines (danger signals) that put the immune system in a state of higher alertness and activity.

Introduction

In aquaculture and farming, infectious disease is one of the biggest, if not the biggest problem and challenge, economically as well as in terms of animal welfare and environmental pressure. "Disease is the biggest single impediment to aquaculture development," said Rohana Subasinghe, Senior Fisheries Research Officer at the United Nations' Food and Agriculture Organization (FAO). Total damage in aquaculture of infectious disease is estimated at $9 billion yearly. In Ecuador in 1999 70% of the crop of farmed shrimp was lost due to a single virus infection that led to a national crisis and a loss of 150.000 jobs.

For chicken farmers infectious diseases form the biggest problem they face. Economically, for animal welfare, environmentally and for acceptance in the market and in society. Preventive antibiotics have been used not only to prevent infectious disease, but also as a growth promoter. The antibiotic use could prevent or eliminate infectious disease at an early stage, before the pathogens strongly multiply in the animals and the animals have to spend substantial energy to combat the disease. In general 5 to 10% decrease of feed necessary to support equal growth could be achieved with preventive antibiotics. However, preventive antibiotics have been banned in Europe from animal feed since 2006, with similar developments in other countries, because of development of microbial resistance related to humans. Therefore the agriculture and aquaculture sectors are urgently searching for other disease inhibitors to substitute antibiotics.

Environmentally, infectious disease causes a lot of pressure: by the chemicals and pharmaceuticals used, by the pathogens that multiply in farms and increase disease pressure on the surrounding wildlife, and by the pressure on aqua farmers to abandon farms with disease and start new farms in nature areas.

It has been shown that various EMF signals are capable of influencing the immune system (Markov, Nindl, Hazlewood, Cuppen, 2006).

Immunent has developed an EMF signal for advancing and elevating the immune response to pathogens (multiple LF components, 0.1-50 µT, 30 minutes per day) which have been tested at various experimental conditions. Pilot findings with this signal (proprietary, but available for research purposes) were presented at the 2004 Kos meeting (Cuppen and Vink 2004).
In immunology during the last decade the view has been developed that an immune reaction to pathogens needs promoters to be present in addition to the presence of pathogens (or other non-self cells) (Matzinger 2004).
In a companion paper at this conference (Cuppen et al. 2006a) the hypothesis was proposed that the enhanced immune reaction observed after LF EMF treatment is due to the fact that LF EMF induces the formation of such (a level of) danger signals, cytokines such as heat shock proteins (HSP's), Interferon, Interleukins, that an immune response can occur earlier and/or stronger than without the treatment. The treatment triggers the self-sustaining feedback mechanism in the immune reaction which otherwise would occur much later, when pathogens significantly multiplied and caused more damage.

Figure 1. Our Hypothesis (Cuppen et al., 2006)

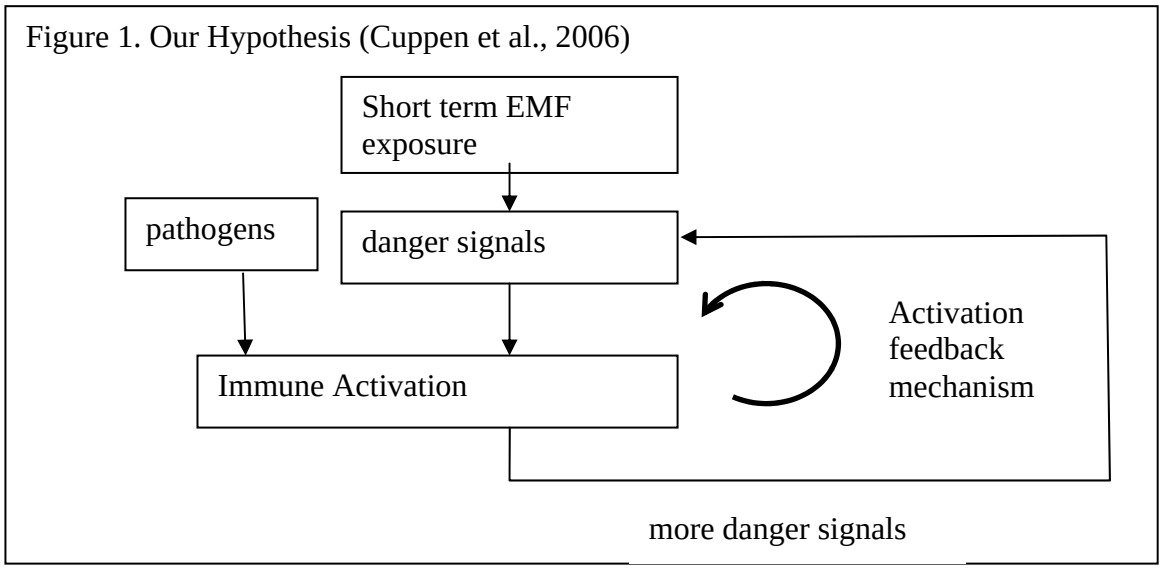

Materials and results

This paper describes three different types of experiments conducted with the Immunent signal applied with different configurations on the subjects of research. For that reason the paper is written in three section describing the methods and results, followed by a discussion section.

In vitro cell experiments

Phagocytes (Macrophages and dendrites) from Carp were isolated as described in (Cuppen et al. 2006c, which also contains detailed descriptions of the other materials and methods) and stimulated in the different ways as described below. Oxygen burst was measured with a NBT assay as a measure of immune activity. and in vitro subjected to the treatment.
In 20 runs 48 samples each were divided over six test groups. Three groups had no chemical pre-stimulation (called negative), three (called positive) received chemical pre-stimulation with 10 µl 0.01 µg/µl PMA (Phorbol 12-myristate 13-acetate). Pairs of groups were formed (a positive and a negative). One pair was exposed for 30 minutes to sham: called control, one to a signal with 5 µT field strength: called low, and one to a signal with 1.5 mT field strength: called medium as indicated in Table 1.

Table 1. Summary of the in vitro experiment setup

	No EMF treatment	EMF treatment with field strength	
	Control	5 µ Tesla	1.5 m Tesla
No chemical pre-stimulation	negative control	negative low	negative medium
Pre-stimulation with PMA	positive contr	positive low	positive medium

In each run the 48 samples are taken from a single fish and therefore the oxygen burst activity numbers in different test groups of that same run can be compared to each other. However for different runs different fish are used and the cells of one fish may show large differences in their baseline reactivity and activation capacity to the cells of another fish. Therefore the absolute numbers between different runs are not comparable. This complication can be overcome by normalizing all data to the average negative control value in each run, and positive EMF data to the positive control.

Six out of 20 runs were discarded on the (sole) basis that positive control average did not exceed negative control average by more than 50%. This means that cell preparation must be considered to have failed.

The Oxygen burst was increased in 12 out of 14 cases after 5 µT treatment (see Figure 2), and in 11 out of 14 cases after 1.5 mT treatment. With pre stimulation with PMA, oxygen burst was further increased in 9 out of 14 cases at 5 µT, and in 12 out of 14 cases at 1.5 mT.

Figure 2.

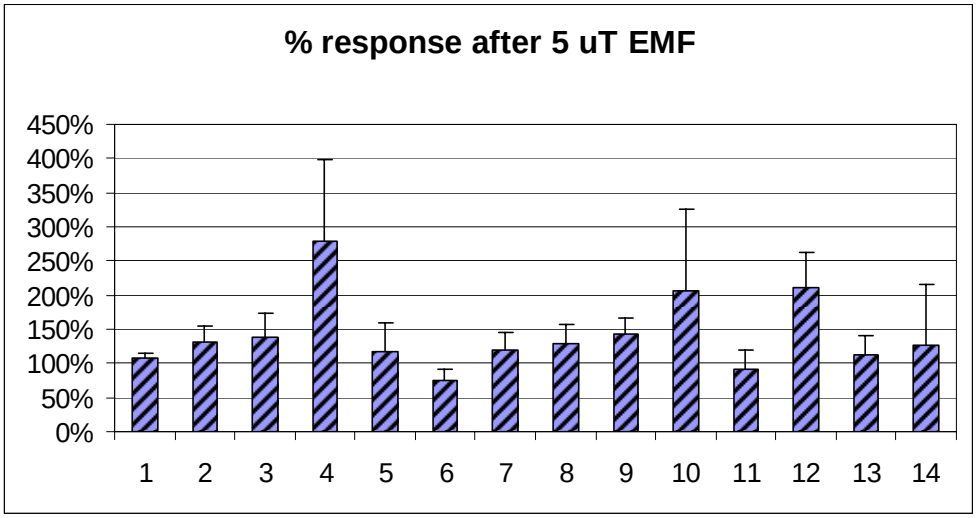

All results together are summarized in Table 2.

Table 2. Summary in vitro results, averaged over all runs (Average % increase in oxygen burst.)

	No EMF treatment	EMF treatment with field strength	
	control	5 µ Tesla	1.5 m Tesla
no chemical pre-stimulation	negative control = 100%	142 %	133 %
pre-stimulation with PMA	positive control = 276% of negative control	118% of positive control	122% of positive control

Statistical analysis (ANOVA) was carried out with SAS via a meta-analysis of the 14 datasets. A significant ($p<0.0001$) increase by EMF on the response of the exposed cells was found. As can be seen in Figure 2, the numbers given in Table 2 are averages of strongly varying results. It cannot therefore be concluded that the effect is stronger at 5 µT than at 1.5 mT or vice versa, but rather that the effects may be of the same order of magnitude at these two field strengths.

A second point we wish to make is that a treatment at or below 5 µT is in the practice of farm applications (large areas and volumes to be treated) much easier and less costly to achieve than at 1.5 mT.

The data achieved at 1.5 mT are in line with those reported for 50 Hz, sinusoidal, 1 mT fields in murine and human macrophages by Simkó, Droste, Kriehuber and Weiss 2001 and Lupke, Rollwitz and Simkó 2004.

In vivo experiments with diseased goldfish

To evaluate the potential of LF EMF to prevent or decrease the infections caused by ecto parasites (gill parasites) such as *dactylogyrus/ gyrodactylus, trichodina, chilodinella* and *costia* a series of 4 experiments was executed using fantail goldfish (*Carrassius auratus spp*.). Infection with those parasites occurs consistently at the grower and increases during storage, packing and international transport due to crowding. This and

subsequent secondary bacterial infections cause high mortality if not treated. The progress of the diseases can be measured by daily counting and removing from the tank any dead fish over a period of a few weeks. In the reported experiments, running 3 or 4 weeks, fish are divided over 12 to 20 tanks per experiment. Each tank is an experimental unit, and these are divided over a control group (usually 4 tanks) and test groups (usually 4, sometimes 2 tanks each) that are exposed to different EMF treatments, always for 30 minutes per day. In the early experiments we used 12 fish per tank, which was increased first to 21 and then to 30 fish per tank in order to increase the statistical power of the experiments once it became clear that this is feasible.

Tanks are exposed to uniform, vertical AC electromagnetic fields, with a (proprietary) Immunent signal consisting of several components with base frequencies between 100 and 10.000 Hz. The treatment is given daily for 30 minutes in each tank, by an automated Immunent signal generator that continuously monitors current output that was calibrated to magnetic field strength. For a detailed discussion of materials and methods, and more data, see (Cuppen et al. 2006c) in these proceedings.

The treatment is aimed at boosting the fish immune defense and, thereby, decreasing the mortality. The experiment is powerful because large numbers of animals can be used and the measurement is easy and accurate. For example, results in Figure 3 account for a total of 336 fish in the experiment, 84 in control and 252 in the six experimental series.

In experiments 1 and 2 (see Cuppen 2006c) mortality after 17 days was decreased by LF EMF from 52% ± 14% untreated to 19% ± 10%, and from 52% ± 8% untreated to 26% ± 19%. Moreover the intermediate day values had a comparable ratio to the end values so that the quoted standard deviations probably strongly underestimate statistical significance. In these experiments there were 8 control tanks and 15 experimental tanks at 5 μT with 12 fish initially each.

Next, experiments were performed at different field strengths. Figure 3 shows the typical mortality curves in an experiment with 4 control tanks and 2 experimental tanks per field strength with 21 fish initially per tank.

Figure 3 Mortality with treatment on different field strength levels

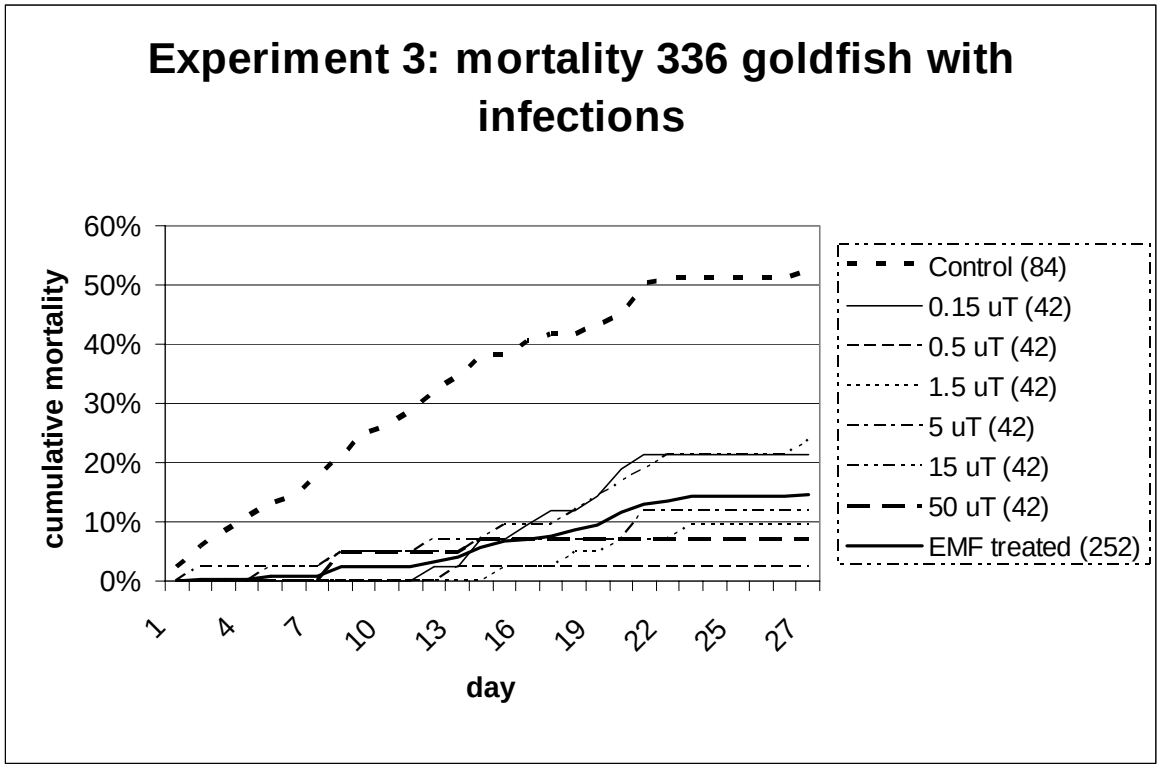

At only two replicates per field strength these results indicate that the treatment is effective in the whole window of field strength between 0.15 and 50 μT (and probably beyond). The average line of all treated tanks (solid, thick) corresponds very well, or is even better than the results of experiments 1 and 2. Together they show that a surprisingly strong improvement of the survival of these fish with this disease can be achieved with this form of EMF.

Because of its interest for practical application in farming and aquaculture, we investigated further at the lower field strength level. Since these field strengths cannot be reliably produced directly in our setup (too low

voltages, too low currents, and therefore too high electronic noise levels) this was done using the stray fields of our coils around tubs at 5 µT. These are solenoid coils which produce the desired field, sufficiently uniform, at 50 cm, 100 cm and 120 cm distance from the (outside) of the coil. Figure 4 gives the results.

Figure 4. Treatment results at extremely low field strengths.

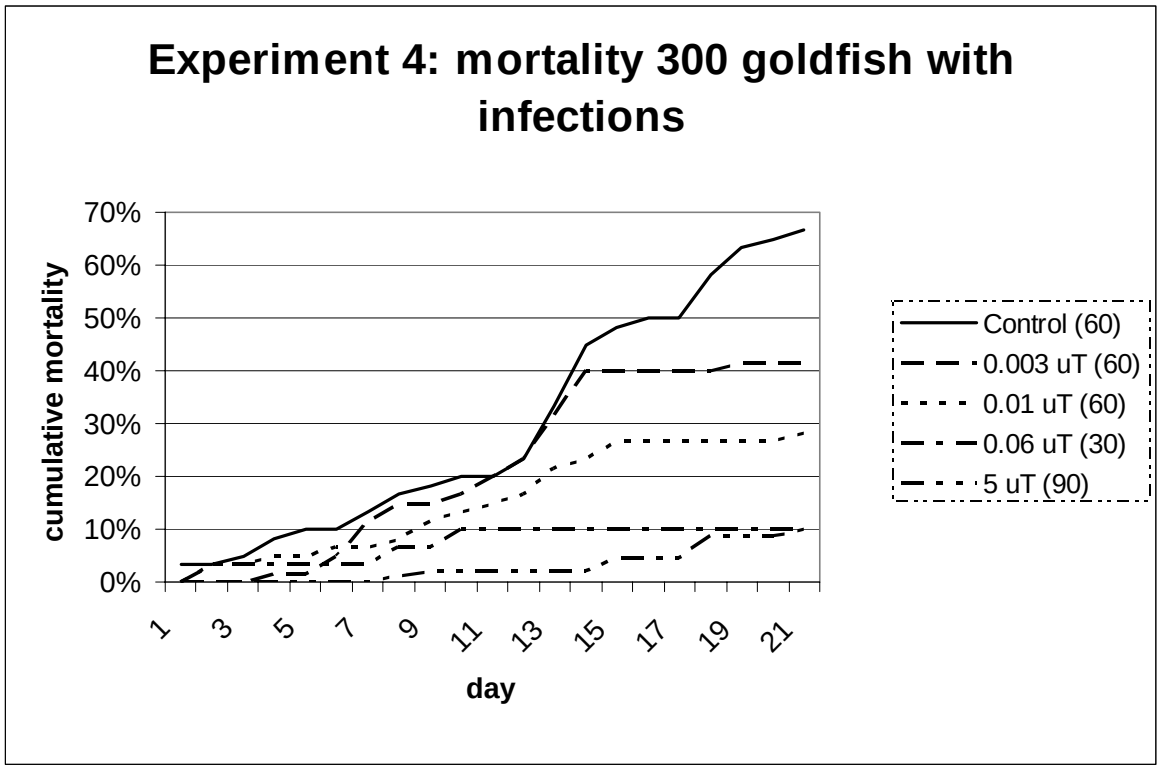

A dose response pattern is visible between 0.003 and 0.06 µT with the latter value delivering a result not far from our reference value of 5 µT.

The results obtained demonstrate that the treatment with EMF drastically reduced the mortality in fish that is due to above-mentioned parasites and secondary microbial infections. These results indicate that even in strongly diseased fish the stimulation with LF EMF mobilizes the immune system for fighting the invaders possibly because it puts the immune system in a higher state of activity, thus giving it a better chance of fighting the disease.

The dose response values given in Figure 4 indicate that some effect of the treatment remains even at field strengths as low as 3 nT. Therefore in experiments large distances must be maintained between control tanks and experimental tanks, so that the stray fields are below 1 nT or less.

This observation raises questions for the experimental setups with sham controls. The field cancellation between the opposing currents in the sham coils must be extremely good. It can be doubted if the required cancellation is ever reached in practice.

Using Helmholtz pairs of coils should also be surrounded with careful measurements of the stray fields, which can be substantial.

In vivo experiments with chicken broilers, exposed to infection pressure from coccidia parasites

A universal infection in fattening chicken is coccidiosis, with *Eimeria* parasites that live and explosively multiply in a particular part of the intestines of a particular host for each *Eimeria* specie. Number of studies has suggested that the immune response to *Eimeria* infection among other is mediated through the release of cytokines. Breed et al. (1997) reported that chicken peripheral blood leucocytes of *E. tenella* infected chickens produce interferon-γ after in vitro re-stimulation. Moreover, it has been shown that treatment chickens with interferon-γ preceding infection with *E. acervulina* decrease the negative effect of infection on weight gain (Lowenthal et al., 1997).

For the three subsequent experiments 192, 288 and 272 one-day old female broilers (Ross 308) were purchased from the hatchery. On day of arrival, they are wing-banded, weighed and randomly housed in wire-floor, suspended cages. Each cage is provided with thick foil and litter. Under the floor of each cage a 16-loop coil was located to deliver LF EMF for 30 minutes per day to chicken within the cage. No attempt was made to create a

uniform field since in a preliminary experiment it was determined that effective field strengths lie between 0.1µT and 50 µT. Moreover the practical application that is our goal will also not allow complete uniformity of the field strengths. The field strength (rms) in the middle of the cage was set at 6,5 micro Tesla, measured with an F.W.Bell 5180 Tesla meter. Dosimetry control during the experiment was ensured by constantly monitoring the (rms) current through the coil. The applied signal was designed by Immunent, which contains several LF components with frequencies between 100 and 10.000 Hz.
In the experiment 1, infection pressure was provided with Campylobacter jejuni on day 6, in the experiment 2 high level infection pressure was given on day 15 with Coccidia, containing a controlled mixture of different Eimeria species, and in experiment 3, a low level of the same infection pressure was given at day 15. Detailed information about materials and methods, as well as more data, are provided in (Cuppen et al. 2006d this proceedings).
It has been common practice (now illegal) to include preventive antibiotics in chicken feed in order to fight potential infection. This caused infections to be suppressed from the start, so keeping the chicken healthy they will properly develop and gain weight. This is usually estimate in what is called “feed conversion”, the number of kilograms of feed required for 1 kilogram of growth of the animal. To determine whether EMF could replace preventive antibiotics by providing enhanced immune response as a preventive measure, the feed uptake and growth were carefully measured per cage during the experiment, and corrected for the number of chickens actually present every day.

At the end of the growing cycle chickens were normally slaughtered and intestines evaluated for lesions as caused by the infection in a blind setup.

The results obtained are given in Tables 3 and 4.

Table 3: Feed conversion of broilers (kg feed consumed / kg weight increase).

	Negative control	Positive control	EMF no infection	EMF w infection
Experiment 1	1.78 ± 0.02	1.73 ± 0.04	not in experiment	1.61± 0.03*
Experiment 2	1.58 ± 0.04	1.63 ± 0.04	1.57 ± 0.05	1.52 ± 0.06 *
Experiment 3	1.83 ± 0.03	1.84 ± 0.05	1.73 ± 0.03*	1.72 ± 0.03*

∗ significant ($p<0.05$) vs. the relevant control

Feed conversion for the EMF treated groups was significantly improved in 4 out of 5 cases compared with non-treated groups. This result indicates that this EMF treatment has a similar effect as preventive antibiotics on feed conversion in the chickens. Of course this could be the result of an as yet unknown effect of EMF, but we consider it likely that the mechanism is through an enhanced immune competence of the chicken, and that therefore these results support our hypothesis.

Economically, these results are important as well, since 10 points feed conversion translate into a cost reduction of about 5 euro cents per chicken.

In experiment 3, we could also measure (blind) the damage of the infection in terms of lesions in the chicken intestines. The results are shown in Table 4.

Table 4: Mean lesion scores of intestines in chicken broilers after Coccidiosis infection at day 16.

	Control		EMF	
	- cocc	+ cocc	- cocc	+ cocc
E. acervulina				
day 21	0.44 ± 0.22	2.44 ± 0.15	0.44 ± 0.18	2.00 ± 0.16*
day 29	1.06 ± 0.27	1.69 ± 0.09	0.31 ± 0.13*	1.50 ± 0.15*
day 36	1.38 ± 0.26	1.75 ± 0.19	0.94 ± 0.24*	1.22 ± 0.10*
E. maxima				
day 21	0.13 ± 0.08	2.25 ± 0.19	0.06 ± 0.06*	1.67 ± 0.13*
day 29	0.56 ± 0.20	1.63 ± 0.08	0.00 ± 0.00*	1.33 ± 0.21*
day 36	1.50 ± 0.38	2.10 ± 0.12	0.50 ± 0.25*	1.22 ± 0.21*
E. tenella				
day 21	0.13 ± 0.08	1.50 ± 0.09	0.06 ± 0.06	1.42 ± 0.11
day 29	0.19 ± 0.09	1.31 ± 0.13	0.06 ± 0.06*	1.00 ± 0.11*
day 36	0.56 ± 0.15	1.42 ± 0.15	0.13 ± 0.08*	1.17 ± 0.11*

The reductions in pathology after EMF treatment are significant in all measurements more than 5 days after infection showing less damage due to the disease and therefore indicating a better immune response with EMF treatment.

Discussion and conclusions

The in vitro and in vivo results clearly indicate that LF EMF treatment induces an enhanced immune response. It is not clear at present what the exact mechanism is of this EMF stimulation. In (Markov et al. 2006) we discussed that one of the key players of the immune system (T-lymphocytes) has a very specific response to EMF stimulation: react only when lymphocytes are activated. “Activation” means that the immune system gets the signal that some thing wrong is coming or going on. Then lymphocytes would be in high state of alert, ready to react. In Fig. 1, it is suggested that EMF stimulation and pathogens actually in combination trigger the immune system, giving it the signal that something “wrong” is indeed coming..

Moving from biology to fish and chicken farming, the results reported have extraordinary importance: by helping the immune system to handle infections in fish tanks, ponds or chicken barns, the LF EMF stimulation drastically reduces mortality and increases the efficiency of feed conversion. This is even more important since the preventive antibiotics are being banned for further application as feed supplement in the EU and other countries.

An additional advantage of the LF EMF stimulation reported on in this study is that it is achieved with a very low magnetic flux density which is a) economically and technically feasible in large areas and b) makes it unlikely that adverse effects would be initiated by this EMF stimulation.

All results above were obtained at levels less than 6.5 µT field strength (except one in vitro series at 1.5 mT) and in the one case tested, the effects were maintained even to a level of 0.006 µT. At these levels a direct effect on the pathogens is highly unlikely and the effect can only take place though resonance and the triggering of a system ready to react. A comparison might be made with a car stopping for a red light. No sufficient amount of energy was transferred to make any meaningful change in the process of the driving car. Nevertheless the signal was detected and a response generated that causes the car to stop. Likewise the minute signal required to generate the effects reported indicates that a physiological process was triggered that was waiting to go off.

In summary, our in vitro results indicate that the Immunent signal indeed increases immune activity on cell level and that ROS production is increased causing oxygen stress at cell level. The in vivo experiments show a) reduced mortality and b) increased growth and reduced pathology after LF EMF treatment. The effects are strong, up to being actually relevant for animal management in farms. The effects measured support the hypothesis that LF EMF creates stress at cell level that can trigger an immune response that sustains itself after the immune system becomes active enough to attack a sufficient number of pathogens.

References

Breed D.G., Dorrestein J., Schetters T. P., Waart L. V., Rijke E., and Vermeulen A. N.. (1997). Peripheral blood lymphocytes from Eimeria infected chicken produce gamma-interferon after stimulation in vitro. Parasite Immunol. 19:127-135.

Cuppen J.J.M. and Vink A. (2004): Effects of ELF exposure on weight and immune parameters in young turkey broilers, 3rd Intl workshop on Biological Effects of EMFs, Kos, 2004, p 1203.

Cuppen J.J.M., Parmentier H.K. and Savelkoul H.F.J. (2006a): Immune Stimulation In Fish And Farm Animals Through Weak Low Frequency Electromagnetic Fields, A. Hypothesis, this proceedings.

Cuppen J.J.M., Wiegertjes G.F., Molenaar M., Geervliet J., Smink W. (2006c): Immune Stimulation In Fish And Fish Immune Cells Through Weak Low Frequency Electromagnetic Fields With Variable Field Strength, this proceedings

Cuppen J.J.M., Beynen A.C., Elmusharaf M.A., Grooten H.N.A. and Smink W. (2006d): Immune Stimulation In Chicken Broilers Through Weak Low Frequency Electromagnetic Fields With Coccidia Infection, this proceedings

Lowenthal J.W., York J.J.,. ŎNeill T.E, Rhodes S., Prowse S. J., Strom D.G., and Digby M.R.. (1997). In vivo effects of chicken interferon-gamma during infection with Eimeria. J. Interferon Cytokine Res. 17:551-558.

Lupke M., Rollwitz J. and Simkó M. (2004) 50 Hz magnetic fields induce reactive oxigen intermediates in human monocytes and in Mono Mac 6 cells. Free Radic. Res. 38, 985-993

Markov M., Nindl G., Hazlewood C., Cuppen J. (2006) Interactions between electromagnetic fields and immune system: Possible mechanism for pain control. In: Ayrapetyan S and Markov M (eds.) Bioelectromagnetics: Current concepts. Springer, Dordrecht, The Netherlands. 213-226

Matzinger P. (2002): The danger model: a renewed sense of self. Science 2002;296:301-5.

Maxey B.W and Page R.K., (1977) Efficacy of lincomycin feed medication for the control of necrotic enteritis in broiler-type chickens. Poult Sci., 56: 1909-13.

Simkó M., Droste S., Kriehuber R. and Weiss D.G. (2001): Stimulation of phagocytosis in murine macrophages by 50 Hz electromagnetic fields. Eur. J. Cell Biol. 80, 562-566

PULSED ELECTROMAGNETIC FIELDS EFFECTS ON MEMBRANE PARAMETERS OF ATTACHED CELLS IN CULTURE

MIHAELA G. MOISESCU[1,4], EUGENIA KOVACS[1], TUDOR SAVOPOL[1], IRINA STOIAN[2], PHILIPPE LEVEQUE[3], LLUIS M MIR[4]

[1] BIOPHYSICS AND CELL BIOTECHNOLOGY DEPT., "CAROL DAVILA" MEDICAL UNIVERSITY, BUCHAREST, ROMANIA, MMOISESC@UNIVERMED-CDGM.RO

[2] BIOCHEMISTRY DEPT., "CAROL DAVILA" MEDICAL UNIVERSITY, BUCHAREST, ROMANIA

[3] XLIM, UMR 6615 CNRS -UNIVERSITE DE LIMOGES, FRANCE, LEVEQUE@UNILIM.FR

[4]UMR 8121 CNRS, INSTITUT GUSTAVE-ROUSSY, VILLEJUIF, FRANCE, LUISMIR@IGR.FR

Abstract

The effects of pulsed electromagnetic fields (EMFs) were studied on processes and parameters of cell membrane of B16 metastatic murine melanoma cells and DC-3F transformed Chinese hamster lung fibroblasts. The fluid phase endocytosis were quantified on attached cultured cell under EMFs exposure.

The pulsed EMFs used were trains of low amplitude 900 MHz EMFs at a 217Hz envelope frequency, 580µs pulse duration, for times up to 30 minutes. Cells grown on Petri dishes were exposed at subconfluence using a wire-patch antenna or a TEM antenna. Endocytosis is critical for cellular functions like nutrition, signaling, transmembrane transport or surface area control. Fluid phase endocytosis is one main type of endocytosis corresponding to the liquid media engulfment in intracytoplasmic vesicles (endosomes) formed on the inner cell surface. Fluid phase endocytosis can be monitored by the Lucifer Yellow (LY, a fluorescent non diffusible dye) uptake and we previously showed that exposure of the cells to GSM microwaves significantly increases LY uptake in the absence of a temeperature increase. The results here reported confirm and extend our previous observations. Indeed, we confirm that GSM microwaves increase LY uptake using another exposure system, a TEM irradiation antenna. Using known inhibitors of endocytotic pathways, we have identified, among the various cellular mechanisms resulting in external molecules engulfment, the mechanism that is actually affected by the exposure to the EMFs. Indeed, our data show that only the clathrin-dependent pathway is perturbed by the EMFs pulses while the potocytosis is not affected.

Introduction

Endocytosis is one of the basic cellular mechanisms participating to molecule exchange between the cell and its environment. Various ways of endocytosis mediate essential cell processes among which: extracellular molecules incorporation, membrane renewal and surface area control, antigen presentation, membrane receptor expression, etc. [1]. In the fluid phase endocytosis and the receptor mediated endocytosis, vesicles are constantly formed on the inner surface of the membrane and correspond to the absorption of extracellular medium into intracytoplasmic vesicles (endosomes). They detach in the cytoplasm and fuse with other internal cellular vesicles. The cytoplasmic surface of these vesicles is covered by a specialized protein, the chlatrin. Pinocytosis is another related endocytosis process in which the vesicles also detach from the cell membrane even though they are not covered by the chlatrin. Membrane area is restored by exocytosis, which corresponds to the fusion of internal vesicles to the plasma membrane. In the potocytosis, the vesicles (termed caveolae, and surrounded by a protein known as caveolin) formed at the inner cell surface do not detach but allow for active transport of molecules towards the cell inside. Apart from these general endocytotic pathways, specialized cells possess specialized endocytotic functions like the phagocytosis of the macrophages.

We previously showed that the incorporation of the Lucifer Yellow, a non permeant molecule that enter normal cells only by endocytosis, was increased under pulsed electromagnetic fields exposure (EMFs) using a standardised wire-patch antenna (Fig. 1). Here we confirm the increase in endocytosis using another exposure system, a TEM irradiation antenna. Moreover we have identified, among the various cellular mechanisms resulting in external molecules engulfment, the mechanism that was actually affected by the EMFs exposure.

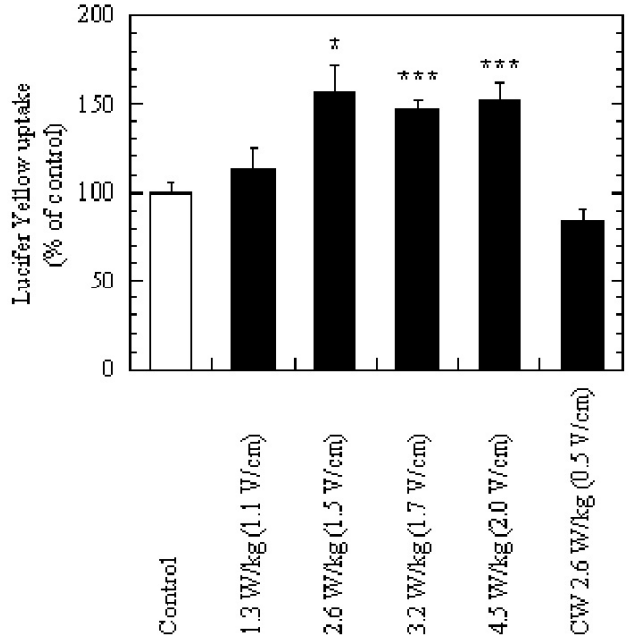

Fig.1. Increase of LY uptake by B16F1 cells after 10min of incubation at 30°C, caused by GSM-EMFs exposure to various SAR into the wire-patch antenna. CW: exposure to EMFs without 217Hz modulation. Values in brackets: peak electric field intensities of the EMFs electric component. 100% correspond to $(9\pm2.2)x10^6$ LY molecules by cell. Unpaired Student's t-test: * $p<0.05$, ** $p<0.01$, *** $p<0.001$ (from [2]).

Materials and methods

Wire-patch antenna experimental set-up The experimental exposure system is described in figure 2.

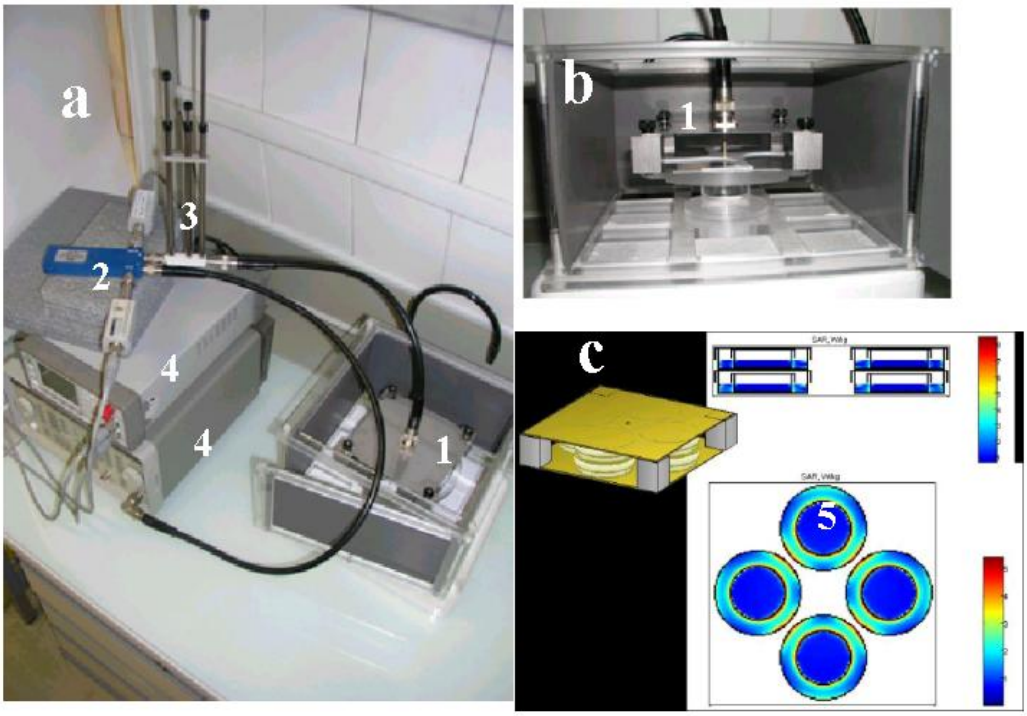

Fig.2**a** and 2**b**. **1** - wire-patch antenna, **2** - bidirectional coupler for forward and reflected power monitoring, **3** - impedance matcher, **4** – wattmeters;

Fig.2**c**. Modelling of field homogeneity in 4 samples exposed to GSM-EMFs: **5** - 35mm Petri dishes with attached cells in culture in 50mm Petri dishes with water.

TEM antenna experimental set-up The experimental exposure system is described in figure 3.

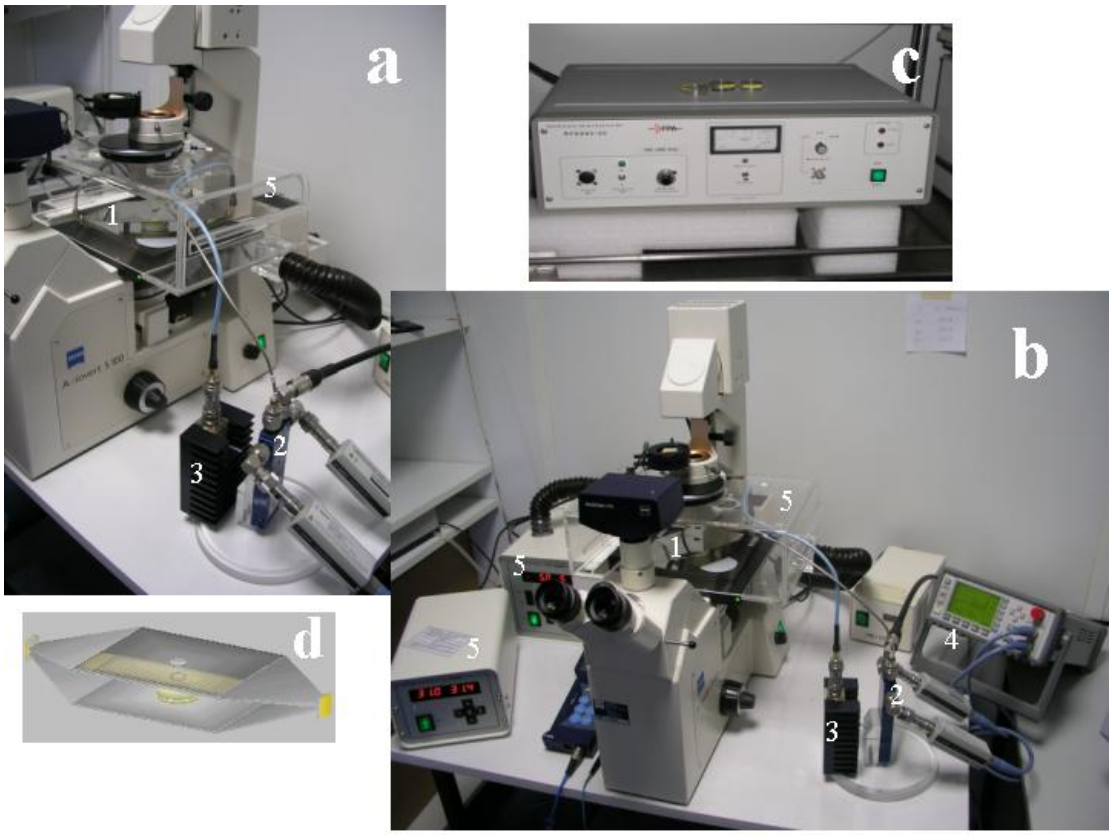

Fig.3**a** and 3**b**. **1** - TEM antenna, **2** - bidirectional coupler for forward and reflected power monitoring, **3** – 50Ω load, **4** - wattmeter **5 –** temperature, CO_2 and humidity control systems;
Fig. 3**c**. 900 MHz CW / GSM generator of adjustable powers;
Fig.3**d**. Modelling of TEM antenna with 35mm Petri dish with attached cells in culture to be exposed to GSM-EMFs.

Cells
F10 or F1 metastatic B16 murine melanoma cells and DC-3F transformed Chinese hamster lung fibroblasts were used. They were cultured at 37°C, 5% CO_2, in Eagle MEM (Gibco) supplemented with 10% foetal calf serum (Life Technologies), 100 units/ml of penicillin and 100 µg/ml of streptomycin (Gibco).
Exposure to EMFs
Two kinds of EMFs waves were used: (i) pulsed waves (GSM-EMF because they correspond to the EMFs delivered by the GSM mobile phones) consisting in 580µs-long square pulses delivered with a low frequency envelope at 217 Hz and with a high-frequency carrier sine wave at 900 MHz ; (ii) continuous wave (CW-EMF) consisting in a high-frequency sine wave at 900 MHz.
The signal generator RF S 900-60 (RFPA, Bordeaux,France) was delivering these two kinds of signals at adjustable powers ranging from 1 to 7 W (mean incident powers) for GSM-EMF and from 1 to 56 W for CW (mean or peak incident powers being identical for the CW-EMF).
EMFs in vitro exposure devices were a wire-patch or a TEM antennas.
Into the TEM antenna a single 35mmPetri dish with cells attached to was placed in the middle of the antenna.
Into the wire-patch antenna four Petri dishes were simultaneously exposed. Each 35mm Petri dish with the cultured cells was placed inside a 50mm Petri dish, used as a sample holder and both dishes were placed above another 50mm Petri dish. Both 50mm Petri dishes were containing water in order to preserve the same depth of the medium volume and the dielectric properties continuity. Therefore, a fair homogeneity of the EMF was achieved for the whole of the cells reducing the edge effects at the periphery of the 35mm dish [5].
For all experiments, cells were subjected to either EMFs exposure or sham exposure, under identical experimental conditions, in particular regarding to the location of the dishes in the wire-patch / TEM antennas and the location of the antennas in the incubator.

Media temperature was measured immediately before and after each exposure, using a digital thermometer and no significant rise in temperature was found at the powers used in the experiments, in agreement with the theoretical calculations.
Exposures were characterized by the **SAR** (Specific Absorption Rate) or power density absorbed by cell unit mass: SAR = $\sigma E^2/\rho$, [SAR] = W/Kg with **E** = local electric field intensity, **σ** = electric conductivity and **ρ** = absorbing material density.

Endocytosis rate determination

The endocytosis rate was quantified by the accumulation of Lucifer Yellow (LY, Sigma), a non diffusible fluorescent dye. 24h before the experiment, the cells were seeded into 35mm Petri dishes in order to have a cell monolayer in exponential growth at the time of exposure. Cells were incubated for various time durations (ranging from 10 to 30 min) with 2 ml of culture medium containing 2 mM LY, in the presence or the absence of the applied EMFs. The incubations and EMFs exposures were done at 30°C. Immediately after the incubation, the cells were rapidly washed three times with 3 ml of NaCl 0.09%, trypsinized (Trypsin-EDTA 0.05%, Gibco), centrifuged (1000rpm, 10min, room temperature) and the cellular pellets resuspended in 1ml H_2O. Then, the cell suspension was sonicated 2x15s, at 100 W, on ice or chemically lysed. (Promega Lysis Reagent kit). The total fluorescence was measured using a spectrofluorometer (SFM 25, Kontron Instruments) at excitation and, respectively, emission wavelengths of 423 and 536 nm. The baseline was obtained for cells not exposed to the fluorescent dye. 20µl of cellular lysis was used for protein dosage (MicroBCA Protein Assay kit, Pierce).
For the experiments with endocytosis inhibitors, before the EMF exposure, the cells were incubated for 30 min at 37°C with Chlorpromazine Hydrochloride (Sigma) or Filipin III from Streptomyces filipinensis (Sigma). The two chemicals were also present into the media during the EMF exposure.
Viability of the cells incubated with 15µM Chlorpromazine or 1µg/ml Filipine III was 90 to 95%.of the viability of the controls (data not shown).

Results

The cells in the TEM antenna were exposed to SARs of 2.7 W/kg and 5 W/kg for 20 minutes. Indeed from previous work using the wire-patch antenna and the same cells, we knew that the exposed B16-F1 melanoma cells could display an increased dye uptake compared to the control cells after incubations times as short as 10min and we also knew that exposure to SARs between 0.6 and 1.3 W/kg had no significant effect on LY uptake while exposure to SARs between 2.6 and 4.5 W/kg significantly increased the LY uptake. Above an apparent threshold value under which no effect was detected, the increase of the fluorescent dye uptake was independent of the delivered GSM-EMF power, with a constant increase of approximately 1.5-fold with respect to control cells incubated under the same conditions but in the absence of the EMF exposure.
Cell viability after cells exposure to EMFs in the TEM antenna was similar to the viability in the controls (data not shown).
The results of cells exposure to GSM microwaves in the TEM antenna are reported in figure 4. Experiment was repeated 8 times, including each time an exposed and an unexposed Petri dish. As for the exposure in the wire-patch antenna, an statistically significant increase in the LY uptake was detected when cells were exposed at 5 W/kg ($p<0.05$, paired t-Student's test). No significant increase was detected at 2.7 W/kg, a SAR value close to the threshold in the wire-patch antenna exposure system. These results confirm thus our previous observations.

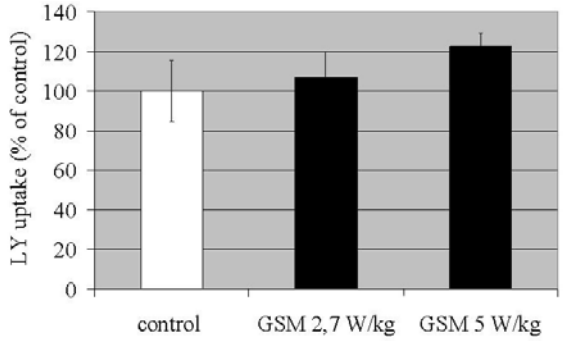

Fig.4. Increase of LY uptake by B16F10 cells after 20min of incubation at 30°C, caused by GSM-EMFs exposure to various SAR (2.7 and 5 W/kg) into the TEM antenna. 100% correspond to (19.8± 3.04)x10^6 LY molecules by cell. Each value is the average of 8 samples ± SD.

To determine whether the increased LY uptake is due to a increase in classical endocytosis (mediated by the chlatrin coated vesicles) or by potocytosis (mediated by the caveolin coated vesicles), the cells were preincubated with drugs selectively inhibiting these two endocytotic pathways: We used chlorpromazine that is a known inhibitor of the clathrin-dependent pathway [3], and Filipin III that is a known inhibitor of the potocytosis, that is of the caveolae-dependent pathway [4]. Results are reported in figures 5 and 6. Exposures were performed in the wire-patch antenna exposure system because several Petri dishes can be simultaneously exposed and because our previous experience using this exposure system.

Figure 5 shows that chlorpromazine slightly decreased LY uptake in the control unexposed cells. More interesting, chlorpromazine completely blocked the increase in LY uptake provoked by the exposure of the cells to the GSM microwaves. This results that the LY uptake pathway stimulated by the GSM microwaves is a chlatrin dependent pathway.

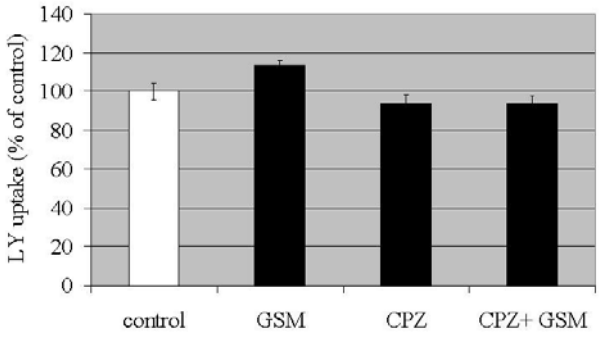

Fig.5. LY uptake by B16F10 cells after 20min of incubation at 30°C, in the presence or not of GSM-EMFs pulses and/or 15µM chlorpromazine (CPZ). GSM-EMFs exposure of 3.2W/kg SAR into the wire-patch antenna. Each value is the average of 8 samples ± SD.

Figure 6 shows that an increased endocytosis rate under EMFs exposure was still detected in the filipin III-treated cells. Thus the inhibition of the caveolin dependent pathway does not prevent the stimulation of the LY uptake by the GSM microwaves, suggesting that only the clathrin-dependent pathway is perturbed by the EMFs pulses.

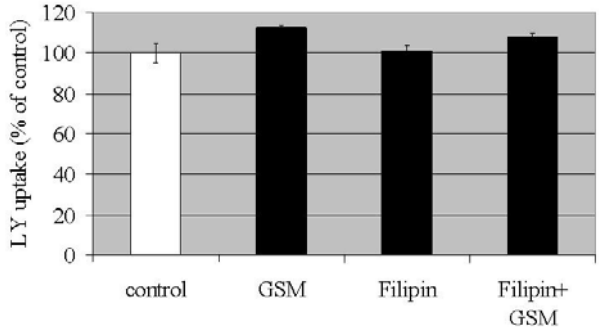

Fig.6. LY uptake by B16F10 cells after 20min of incubation at 30°C, in the presence or not of GSM-EMFs pulses and/or 1µg/ml filipin III. GSM-EMFs exposure of 3.2W/kg SAR into the wire-patch antenna. Each value is the average of 8 samples ± SD.

Summary
The results here reported confirm and extend our previous observations [2]. Indeed, we confirm that GSM microwaves increase LY uptake using another exposure system, a TEM irradiation antenna. Results are similar to those obtained using the wire-patch antenna even though significant increase at a SAR of 2.6 W/kg was detected with the wire-patch antenna and no significant increase was detected at a SAR of 2.7 W/kg with the TEM antenna. Indeed, these SAR values result mainly from models of energy deposition in the two exposure systems, approximately validated by measurements of temperature increase. Precision of both the models and of the measurements does not allow precise comparisons between the two exposure systems. At a SAR of 5 W/kg with the TEM antenna there is a statistically significant increase in the LY uptake. In the experiments here reported, the LY uptake increase in the cells exposed to the GSM microwaves was lower than 1.5 times the uptake in the control cells but this increase was still statistically significant.
The effects of the GSM microwaves on the endocytosis (LY uptake) are also confirmed by the effects of the two inhibitors used. Indeed, one of the two molecules tested actually inhibited the increase in LY uptake, while the other not. This excludes a non-specific effect of the addition of a chemical in the incubation medium. Simultaneously, the inhibition provoked by a known inhibitor of one of the endocytosis pathways confirms our previous observations and conclusions, namely that the exposure of the cells to the GSM microwaves affects the endocytosis pathways.
Moreover we have identified, among the various cellular mechanisms resulting in external molecules engulfment, the mechanism that is actually affected by the exposure to the EMFs. Indeed, our data demonstrate that only the clathrin-dependent pathway is perturbed by the EMFs pulses. Thus the potocytosis is not affected, while the classical endocytosis is actually modified by the cell exposure to the GSM microwaves.

Acknowledgements
Nous remercions le Conseil Scientifique de l'ACI "effets biologiques de la radiotéléphonie mobile" et le ministère chargé de la recherché qui a finance ce projet, ainsi que les opérateurs de téléphonie mobile qui ont complété ce financement en concertation avec le Conseil Scientifique de l'ACI et le ministère chargé de la recherche. We also thank M.A. Verjus for technical assistance and the Romanian Ministry of Research for grant CEEX n° 67/2005 to Pr E. Kovacs.

References
[1] Alberts B.; Johnson A.; Lewis J.; Raff M.; Roberts K.; Walter P., *Molecular Biology of the Cell*, 4th edition, Garland Publishing, New York, **2002**, 711-766;
[2] Mahrour N.; Pologea-Moraru R.; Moisescu M.G.; Orlowski S.; Leveque P.; Mir L.M., In-vitro increase of the fluid phase endocytosis induced by pulsed radiofrequency electromagnetic fields : importance of the electric field component, *Biochim. Biophys Acta*, **2005**, *1668*, 126-137;
[3] S. B. Sieczkarski, G. R. Whittaker, Dissecting virus entry via endocytosis, *J. Gen. Virology*,**2002,** *83*, 1535 – 1545;
[4] P.A.Orlandi, P.H. Fishman**,** Filipin-dependent inhibition of cholera toxin: evidence for toxin internalisation and activation through caveolae-like domains, *J.Cell Biol.*, **1998**, *141* ,905-915;
[5] L. Laval, P. Leveque, A new in vitro exposure device for the mobile frequency of 900 MHz, *Bioelectromagnetics*, **2000**, *21*, 255– 263.

TEM CELL IN BIOMEDICAL EXPERIMENTS

TOMASZ DLUGOSZ, HUBERT TRZASKA

WROCLAW UNIVERSITY OF TECHNOLOGY,
INSTITUTE OF TELECOMMUNICATIONS, TELEINFORMATICS & ACOUSTICS
WYBRZEZE WYSPIANSKIEGO 27, 50-370 WROCLAW, POLAND
tomasz.dlugosz@pwr.wroc.pl, hubert.trzaska@pwr.wroc.pl

Abstract

This paper deals with application of Transverse ElectroMagnetic (TEM) cell as an exposure system in technical and biomedical studies. In many publications is described problem of influence of an object upon the electromagnetic field (EMF) distribution inside a exposure system while inverse effect - influence of exposure system on tested object is overlooked. The problem plays primary role if a correlation between investigations carried out in an enclosure (eg TEM cell) and that in the free space is looked for.

Introduction

TEM cell was proposed by Myron L. Crawford in 1970 [3] as a new way of establishing standard, uniform EMF in a shielded environment and until now it is one of the most frequently applied EMF standard and exposure system. TEM cell is based on the idea that a TEM wave propagates inside a transmission line. Inside can be immersed an object that susceptibility to the EMF is tested. It is used for probes' calibration, electromagnetic compatibility and biomedical investigations (Fig. 1). The reasons of such popularity of TEM cell are its advantages: quite homogeneous EMF distribution inside the cell, similar to plane wave, wide frequency range, field intensity independent from frequency, simple EMF intensity estimations, etc.

However, "in the pot of honey is a spoon of a ter". Even not to mention the mutual interactions between the cell and object tested in it, these are: nonideal EMF distribution, moreover disturbed by the object, limited volume of the cell and the volume decrease with frequency increase, problems with larger objects testing in wide frequency range, etc. The former are discussed then while the latter are illustrated bellow. A concept of the homogeneity improvement by the way of covering the cell walls with a dielectric material is shown in Fig. 2. An approach to the frequency range widening is presented in Fig. 3. The slots limit tangential currents and, as a result, higher modes in the cell.

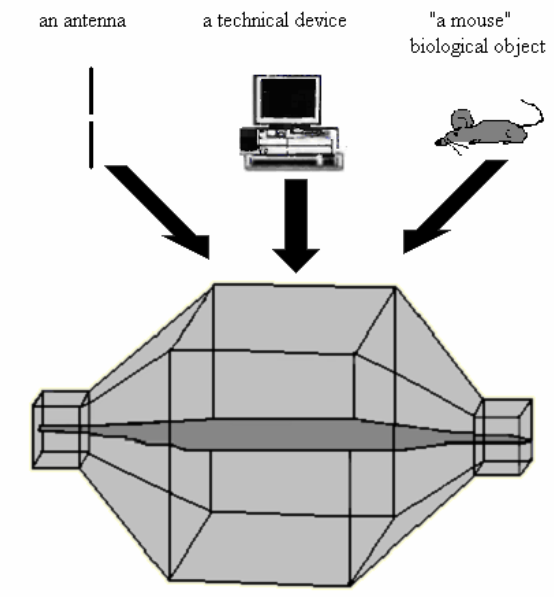

Fig. 1. A different way of using TEM cell.

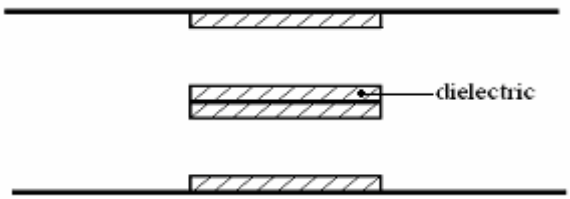

Fig. 2. Dielectric sheets in a cell.

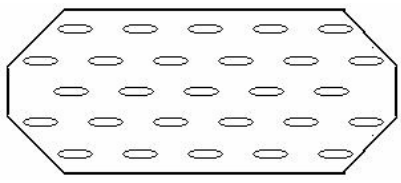

Fig. 3. A center conductor of a TEM cell.

What are the feelings of an antenna inside a cell?

Before we start our considerations related to biomedical experiments we would like to remind a problem of antenna's calibration in the cell, it would illustrate the role of mirror reflections phenomenon and then our way to farther considerations.

The answer to the question in the title is: due to infinite large number of mirror reflections (Fig. 5) the single antenna feels as an element of antenna system. If consider a cell without side walls, as in Fig. 1, and take into account only two plates, as shown in Fig. 4, the input reactance of a short dipole antenna X_i is expressed by:

$$X_i = X_{11} - \Delta X = X_{11} - 2\sum_{i=2}^{\infty}(-1)^{i-1} X_{1i} \tag{1}$$

where: X_{11} – input reactance of the antenna in free space, ΔX – input reactance change due to a mutual couplings, X_{1i} - mutual reactance of the antenna and its i-th mirror reflection.

Presence of the mirror reflections, and their result ΔX, leads to a calibration error δ in relation to the free space conditions, the error we'll formulate in the form:

$$\delta = \frac{\Delta X}{X_i}. \tag{2}$$

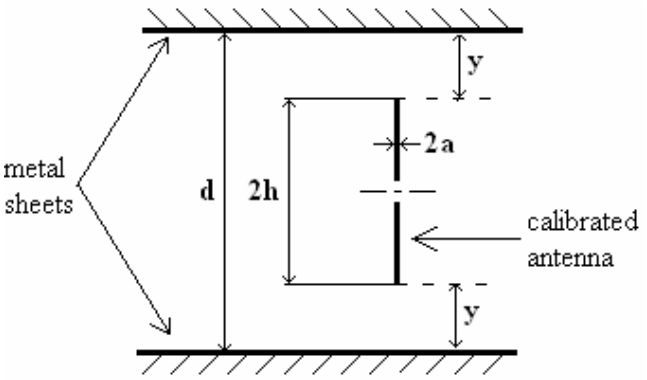

Fig. 4. Geometry of calibration.

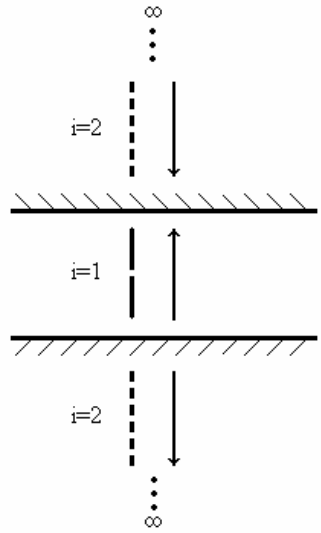

Fig. 5. Mirror reflections caused by metal sheets.

The input reactance of the antenna as well as the mutual reactances of the antenna and its mirror reflections is a function of its slenderness ratio. The slenderness ratio is a function of the relation of the antenna's length (2h) to diameter of it's arm (2a). Calculated runs of the error δ versus b/2h for h/a = 30, 300 and 1000 are shown in Fig. 6 [9]. In the estimations the plates were assumed infinitely large and perfectly conducting. The case while h/a=30 was reestimated on analytical and numerical way [4]. Results are presented in Fig. 7.

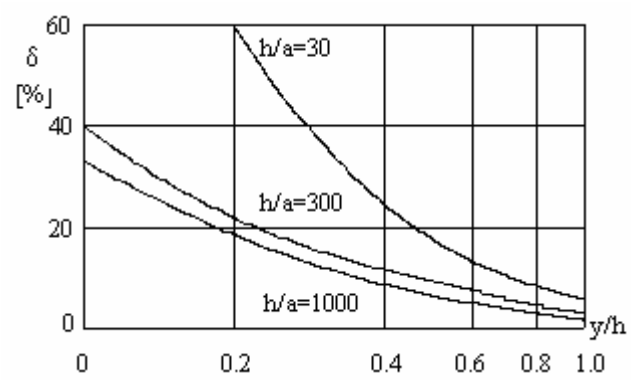

Fig. 6. Error δ versus y/h as a function of slenderness

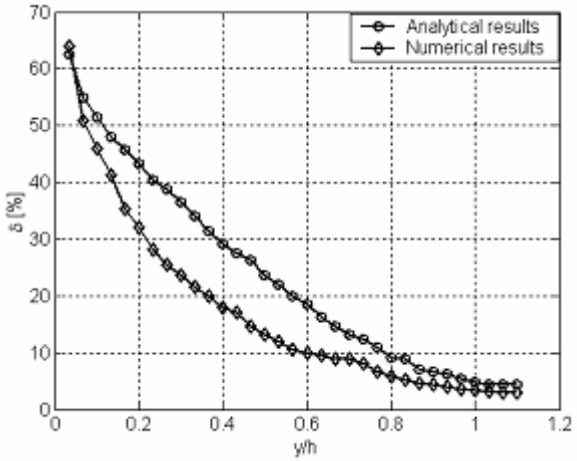

Fig. 7. Error δ versus y/h for h/a=30.

ratio.

The above considerations allow several conclusions:

- real error of calibration is remarkably limited by presence at the input of a probe a capacitive divider,
- the phenomenon is of deterministic character and appropriate correction factors may be used to eliminate the error discussed,
- if the phenomenon exists in the presented case of an antenna calibration, a similar phenomenon should exist while in the cell any other material medium is immersed,
- if in the case of antennas a correction factor may improve accuracy of calibration similar approach should exist in the case of the medium investigations in order to find a way to refer the exposure conditions (and results of measurements) in the cell to that in the free space.

Numerical methods in biomedical dosimetry

An estimation of EMF energy absorption in any case may be done on the ground of the Maxwell equations solution. Unfortunately, analytical solutions are known only for the simplest structures. Even above presented estimations of input impedance of a dipole antenna required an assumption of it's perfect conductivity and sinusoidal current distribution along the antenna. The assumption may be accepted only for very thin structures. What to say about biological media where not only shapes may be arbitrary ones but the electrical parameters of the media are different for different tissues, organs and even parameters of the same tissues may be different depending upon a history of their donator. These limitations have lead, not only at our field, to necessity to use substitutional methods, i.e.: numerical ones. Along with the computer technology development and computers availability more and more sophisticated numerical methods and models were worked out.

The above is well illustrated by development of models applied in numerical dosimetry. In Fig. 7 are presented different models of a mouse (Fig. 7a). The oldest ones are spheroidal (Fig. 7b) [11] and cube (Fig. 7c) models. Follows them (Fig. 7d) a block model, containing of several cages, that allows bit better representations of the mouse's shapes and different electrical parameters. Now the most sophisticated model allows almost ideal reflection of investigated animal.

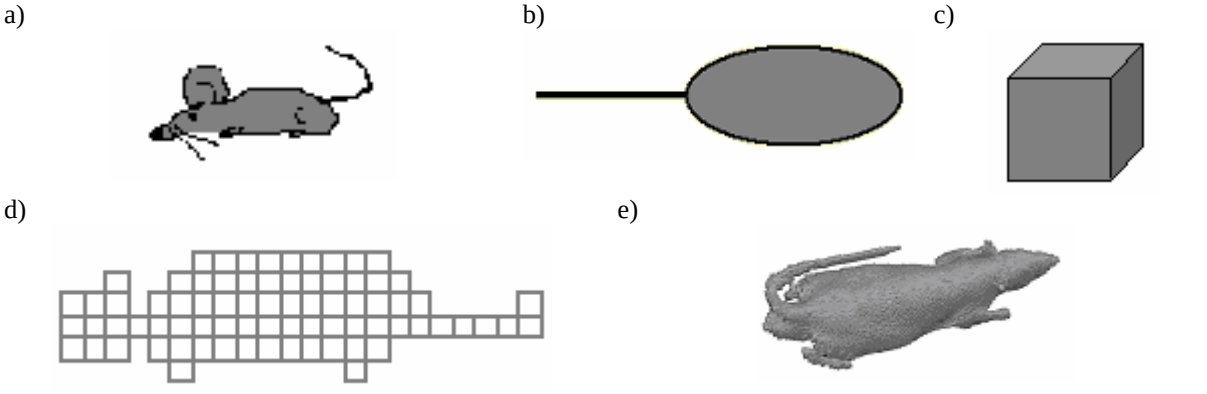

Fig. 7. Models of a mouse: a) real object, b) spheroidal model, c) cube model, d) block model, e) voxel model.

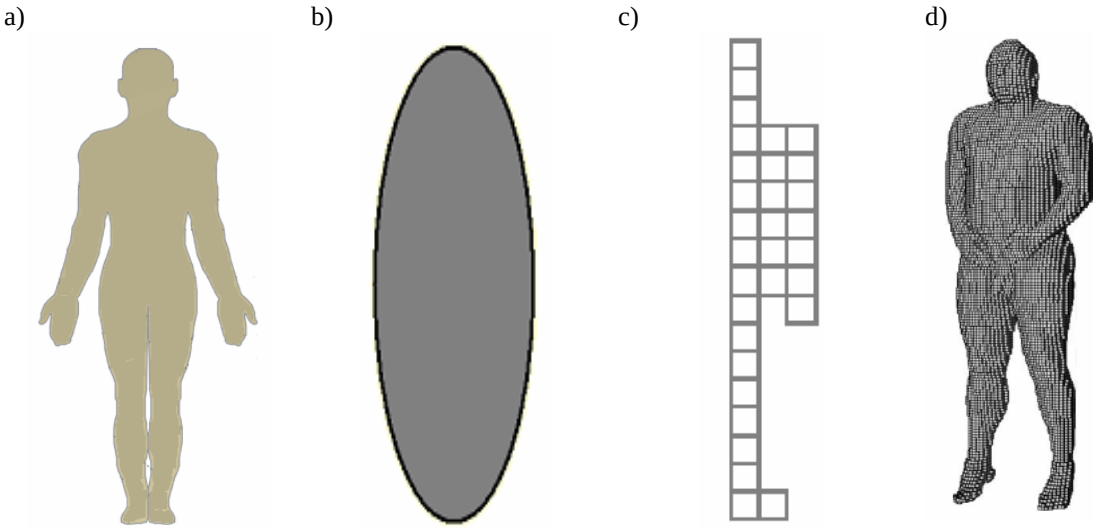

Fig. 8. Models of a man: a) real object, b) spheroidal model, c) block model, d) voxel model.

Similar development, as regards as a model of the man, is presented in Fig. 8 [6] [7] [8] [10]. We may only remind here that homogeneous spheroidal and block models were applied in analytical studies, block model of a man was proposed by Guy and Johnson [10] and the most sophisticated "millimeter resolution" model of a man was developed by Gandhi [7].

It is evident that more sophisticated models require more sophisticated hard- and software. Both of them were not fully available to the authors. Thus, our estimations are limited to the use of rather simple codes (Maxwell SV [1], Fidelity [15]) and a possibility to use them in quite simple computers, as well as simple homogeneous or block models. With no regard to it our aim was not to strictly analyse presented phenomena, but only focus an attention of researchers upon the scale of the problem. From this point of view accepted tools and methods are fully correct and make it possible to present limitations in the exposure systems use and what is the most important, precautions in biomedical (and not only) experiments should be done.

In below presented estimations electrical parameters of animals and men were taken from [5] [6].

Biological object in a TEM cell

Studies of the effect discussed have been initiated by the authors [4]. The way of thinking was as follows: if a conducting medium close to an antenna is able to affect it's input impedance, the same phenomenon should exist in the case of any arbitrary medium. A twofold question was here formulated: what does it mean "an input impedance of a mouse" and "a mutual impedance of the mouse and it's mirror reflection", if an answer to the questions exists at all!

At the first step a cube model of a mouse immersed inside a TEM cell was studied. We assumed that the influence of the cell upon the object should be reflected by the power absorbed in it. The power is:

$$P_{abs} = 0.5\sigma \int_V |E|^2 dV \,, \tag{3}$$

where: P_{abs} – power absorbed by the object, σ – absorber conductivity, E – electric field intensity within the object, V - volume of the object.

Analysed homogeneous lossy model, in the form of a cube of side h = 1.5 cm, conductivity σ = 1 S/m and ε_r = 80, was immersed between two parallel, perfectly conducting plates of sizes 20x20 cm and E-field was kept constant: E = 1 V/m. Results of estimations are shown in Fig. 9. If dimensions of tested object are quite small (d>>h) P_{abs} approaches the value in the free space. However, while the object is large, as compare to d, the power may be remarkable different. The latter case has nothing common with results obtained in the free space. If distance between plates increases (ratio d/h increases) than power absorbed decreases and that means the committed error decreases.

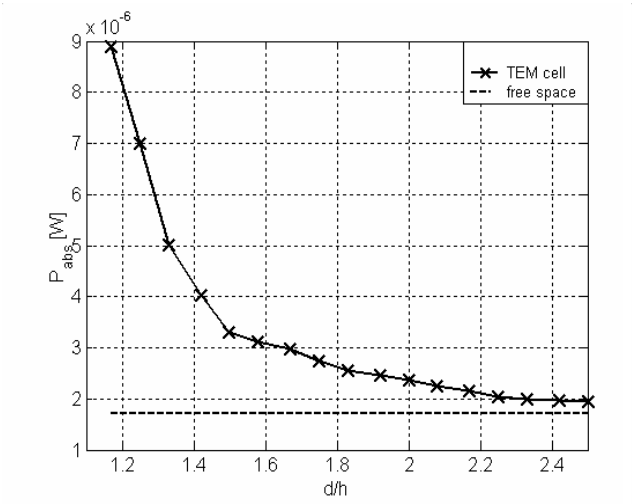

Fig. 9. Absorbed power by examined cube.

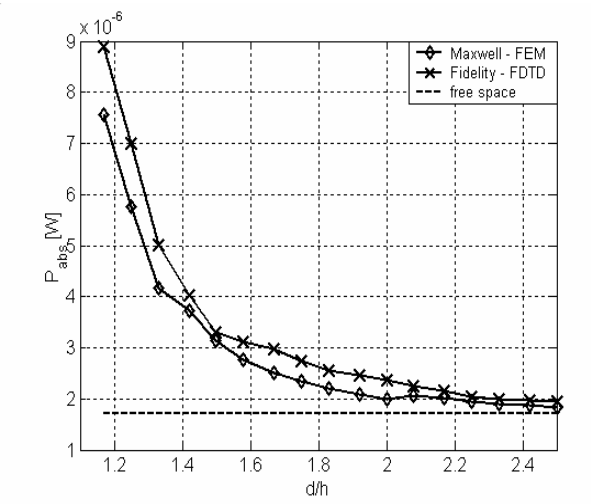

Fig. 10. Comparison of results obtained with different numerical methods.

Similar results are obtained for more complicated model (Fig. 7d) of a mouse - block model (Fig. 11) that was made of 76 cube pieces of side 1 cm. The tissue values are the same as above.

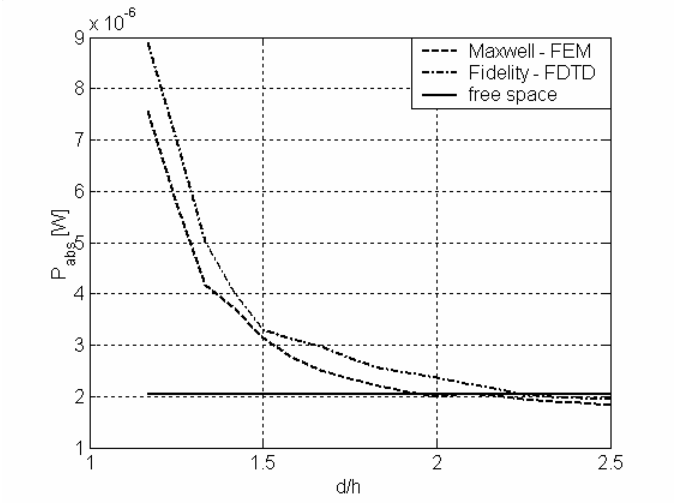

Fig. 11. Results of absorbed power by block model of a mouse.

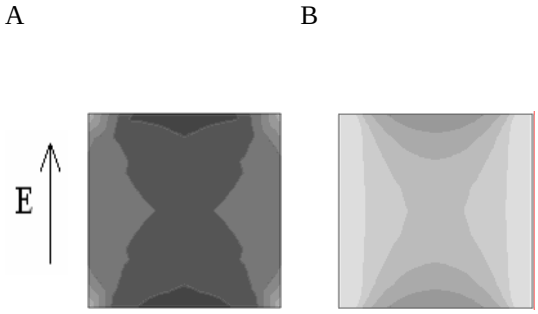

Fig. 12. Results of estimations of the E-field distribution: a) f = 100 MHz, b) f = 1 GHz.

In traditional approach, in biomedical investigations is assumed that the power absorbed within tested object is distributed homogeneously. It is not always acceptable. Lets analyse single object exposed in a TEM cell, in conditions while the proximity effects may be neglected. Results of estimations of the E-field distribution within the homogeneous cube, as described above, for two frequencies are shown in Fig. 12. Of course similar situations is for model of a man (Fig. 13). It is necessary to remind here that absorbed power, and the SAR, are proportional to E^2, that makes that their distribution inside the model is more inhomogeneous as compare to E one, shown in the figures.

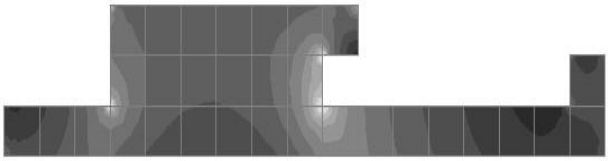

Fig. 13. Electric field inside model of a man.

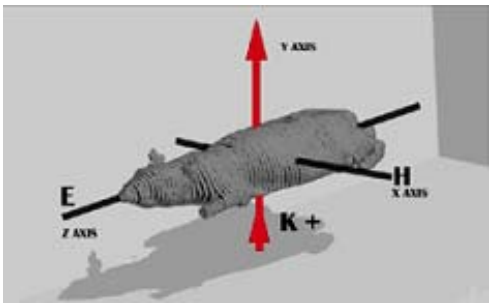

Fig. 14. Location a mouse in relation to vectors [12].

Even in the free space conditions electric field distribution inside a model is non-homogeneous, as a result can be observed fact that each of the organs absorb different power. Results of SAR, for voxel model of a rat that orientation is defined by the incident field vectors (Fig. 14), are shown in Fig. 15. The model was processed in the far-field conditions at frequency 450 MHz.

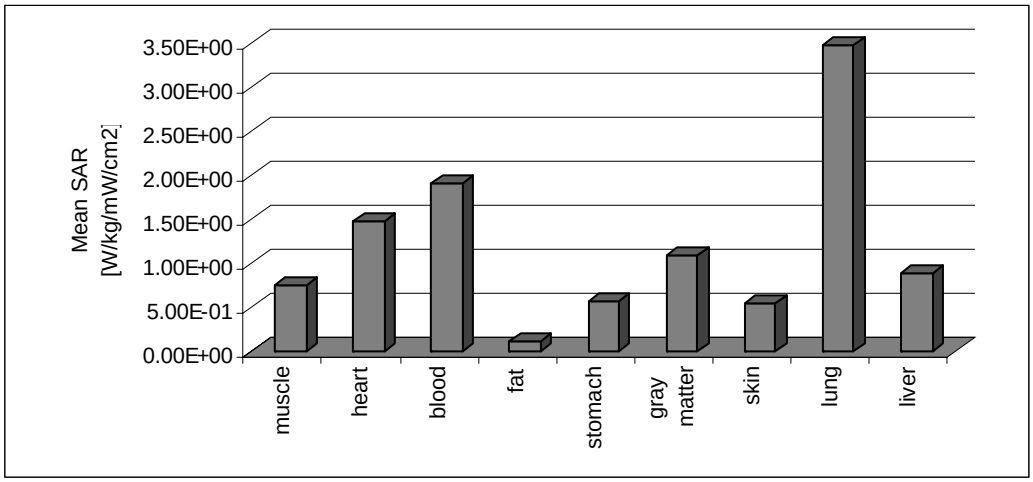

Fig. 15. SAR calculated for different organs in a one-millimetre rat model.

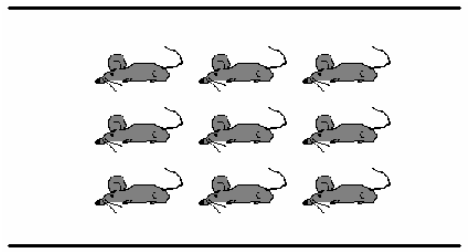

Fig. 16. TEM cell with n examined objects.

A typical condition, in biomedical investigations, is simultaneous exposure in a cell more than one object, sometimes the objects occupy whole volume of the cell. Let's consider the cell while exposed several objects in it, as shown in Fig. 16. In standard approach the power absorbed in the cell (P_{abs}) is calculated as difference of the input and the output power: P_{in} and P_{out} respectively:

$$P_{abs} = P_{in} - P_{out}\,. \tag{4}$$

Then, the power absorbed by i-th animal is calculated dividing the above by number of objects (n):

$$P_i = \frac{P_{abs}}{n}\,. \tag{5}$$

There is no proof that powers absorbed by animals are identical. A few simulations were done to illustrate the statement. Firstly we considered the case where two mice were placed inside a TEM cell (Fig. 17a). One of them is placed in the center of the exposure system and the other in the center between the first one and the wall of the system. Similarly to above estimations the mice are represented here by cubes (5x5x5 cm) that parameters are: $\sigma = 0.84$ and $\varepsilon_r = 80$. E-field intensity is constant and equals 1 V/m. Results, presented in Fig. 17b, confirm our doubts and show a magnitude of exposure estimation error while formula (5) is in use, in the worst conditions the power absorbed by mouse 2 is twice as much as power absorbed by mouse 1.

a) b)

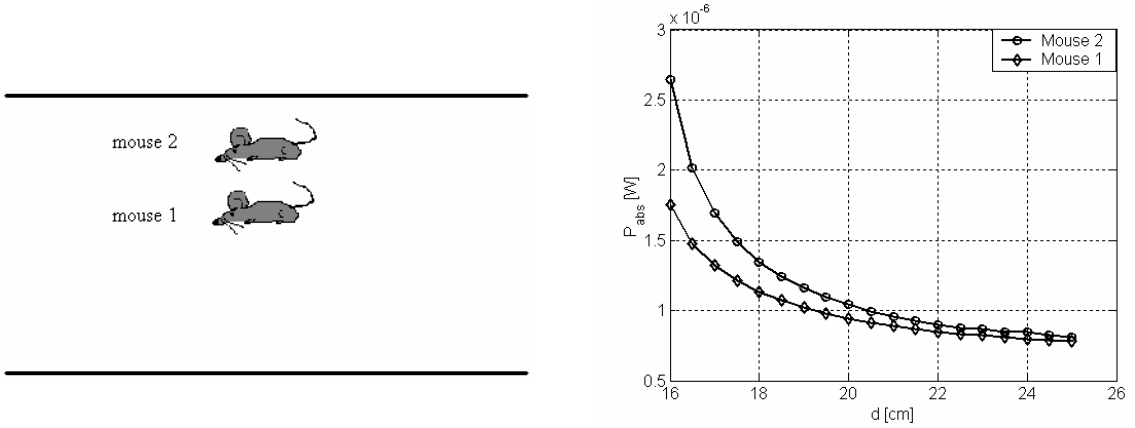

Fig. 17. Powers absorbed by two mice placed in TEM cell: a) model, b) results of calculations.

a) b)

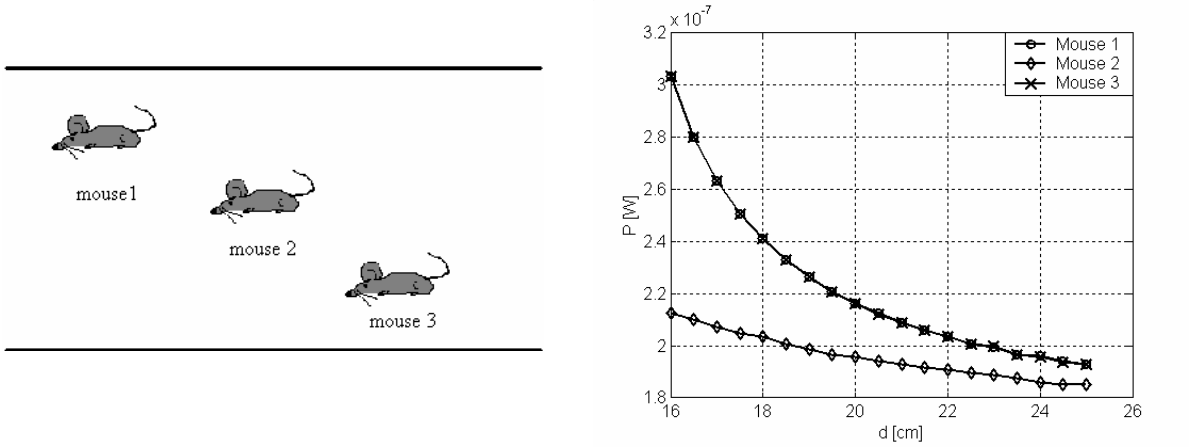

Fig. 18. Powers absorbed by three mice placed in TEM cell: a) model, b) results of calculations.

Similar effect exists in different space configuration of mice, like shown in Fig. 18. In this case the power absorbed by mouse 1 and 3 may be two times bigger than power absorbed by mouse 2. Again can be said that an assumption of identical power absorption in each examined object in discussed exposure system is not appropriate and it may lead to remarkable errors in experiments carried out in the conditions.

Conclusion

The paper discusses role of an affect, caused upon a tested object, by an exposure system due to existence of mirror reflections of the object in the walls of the system. The problem has never been considered before. The authors were inspired to start investigations in the field by estimations and experiments with the use of antennas in EMF measurements in close proximity of conducting objects or while the antennas were calibrated within a TEM cell or waveguide.

The question: what does it mean "input impedance of a mouse" remains unanswered, however, results of estimations, presented in the paper, show essential role of the phenomenon, especially in biomedical investigations while many animals are simultaneously exposed in an exposure system. Apart from different power absorbed by separate objects the absorbed power distribution within them is not homogeneous - especially at higher frequencies, even in the plane wave conditions.

Although the estimations were done for a TEM cell, their results are valid for any case while the discussed effect exists (waveguide, any conductivity media). Presented approach may allow to estimate a role of the phenomenon in any case and a possibility to refer results of exposure to the free space conditions.

Presented results lead to question:

- what is accuracy of biomedical investigations if do not take into account different exposure levels of different animals and even different their organs and tissues?
- what a way may be summarized very precise formulation of protection standards based upon such experiments?

References

[1] Ansoft, *„Maxwell 2D SV"*, simulation software for high performance electronic design http://www.ansoft.com.

[2] Chen Kun-Mu, Guru B.S., Nyquist D.P., *„Quantification and Measurement of Induced Fields Inside Finite Biological Bodies"*, Biological Effects of Electromagnetic Waves, USN/URSI Annual Meeting, Boulder, Colorado, October 20-23, 1975, pp. 19-43.

[3] Crawford M.L., *„Generation of Standard EM Fields Using TEM Transmission Cells"*, IEEE Trans. on Electromagnetic Compatibility, Vol. EMC-16, No. 4, 1974, pp. 189-195.

[4] Dlugosz T., Trzaska H., *„Mutual Interactions in EMF Dosimetry"*, International Conference and COST 281 Workshop on Emerging EMF-Technologies, Potential Sensitive Groups and Health, Graz, Austria, 20-21 April, 2006, (CD Proceedings).

[5] Federal Communications Commision, *„Tissue Dielectric Properties"*, http://www.fcc.gov/cgi-bin/dielec.sh.

[6] Gajšek P., Hurt W.D., Ziriax J.M., Mason P.A., *„Parametric Dependence of SAR on Permittivity Values in a Man Model"*, IEEE Trans. On Biomedical Engineering, Vol. 48, No. 10, October 2001, pp. 1169-1177.

[7] Gandhi O.P., Okoniewski M., *„Computation of Electromagnetic Fields in the Human Body"*, XXVIIth URSI GA, Maastricht, Netherlands, 17-24 August, 2002, (CD Proceedings).

[8] Gandhi O.P., Sedigh K., Beck G.S., *„Distribution of Electromagnetic Energy Deposition in Models of a Man with Frequencies Near Resonance"*, Biological Effects of Electromagnetic Waves, USN/URSI Annual Meeting, Boulder, Colorado, October 20-23, 1975, pp. 44-67.

[9] Grudzinski E. Trzaska H., *„EMF Probes Calibration in a Waveguide"*, IEEE Trans. On Instrumentation and Measurement, Vol. 50, No. 5, October 2001, pp. 1244-1247.

[10] Guy A.W., Johnson C.C., Lin J.C., Emery A.F., Kraining K.K., *„Electromagnetic power deposition in man exposed to HF fields and the associated thermal and physiologic consequences"*, USAF School of Aerospace Medicine, Brooks Air Force Base, Texas, Report SAM-TR-73-13, December 1973.

[11] Leicher-Preka A., Ho H.A., *„Dependence of Total and Distributed Absorbed Microwave Energy Upon Size and Orientation of Rat Phantoms in Waveguide"*, Biological Effects of Electromagnetic Waves, USN/URSI Annual Meeting, Boulder, Colorado, October 20-23, 1975, pp. 158-168.

[12] Luebbers R., Kunz K., *„FDTD99"*, ftp://starview.brooks.af.mil/

[13] United States Air Force Research Laboratory, *„EMF Dosimetry Research"*, http://www.brooks.af.mil/AFRL/HED/hedr/dosimetry.html.

[14] United States National Library of Medicine, National Institutes of Health, *„The Visible Human Project"*, http://www.nlm.nih.gov/research/visible/visible_human.html.

[15] Zeland Software, *„Fidelity”*, Electromagnetic Simulation and Electronic Design Automation, http://www.zeland.com .

ALTERATIONS IN HEMOLYSIS AFTER *IN VITRO* EXPOSURE OF HUMAN ERYTHROCYTES TO GSM900 ELECTROMAGNETIC FIELD

M. KOUZMANOVA[1], G. ATANASOVA[2], N. ATANASOV[3], S. TASHEVA[1]

[1]*Department of Biophysics and Radiobiology, Biological Faculty, Sofia University, 8 Dragan Tzankov blvd., 1164 Sofia, Bulgaria, e-mail* mkouzmanova@yahoo.com
[2]*Department of Telecommunication Technologies, e-mail* ghristova@hctp.acad.bg
[3]*Department of Wireless Communications and Broadcasting, e-mail* natanasov@hctp.acad.bg
Higher College of Telecommunications and Posts, 1 Acad. Stefan Mladenov str., 1700 Sofia, Bulgaria

Abstract

During the last decade the sources of radiofrequency electromagnetic (RF EM) radiation increased enormously both in residential and occupational environment. The study of the biological effects of RF EM radiation could contribute to better understanding of the possible health hazards. This study was designed to investigate the changes in hemolysis after *in vitro* exposure of human erythrocytes to GSM900 electromagnetic field (EMF).

Erythrocyte suspensions with two different cell concentrations (hematocrit 20% and 40 %) were exposed to EM radiation from GSM mobile phone (carrier frequency 902 MHz, 2 W output power in pulse) for 20 min. Alterations in haemolysis were registered 0, 10, 20, 30, 40, 50 and 60 min after the treatment. Hemolysis was determined by measuring the absorbance of hemoglobin at 413 nm in the supernatant obtained by centrifuging the suspensions. Hemolysis was expressed as a hemoglobin concentration.

Our data indicated statistically significant decrease in the hemoglobin level in irradiated suspensions. The GSM900 EMF exposure probably stabilized erythrocyte membrane and caused reduction in the hemolysis depending on the suspension water content (hematocrit) and on the time elapsed after irradiation.

Introduction

During the last decade the sources of radiofrequency electromagnetic (RF EM) radiation increased enormously both in residential and occupational environment. More and more people are exposed to EM radiation not only at work, but also at home. Particularly digital GSM (Global System Mobile) phones are biologically active, especially those with short, helical antennae [19]. To explore if the influence of mobile telephone is really hazardous for the human health, it is necessary to elucidate interaction mechanisms of electromagnetic field (EMF) with biological systems.

The study of the biological effects of RF EM radiation could contribute to better understanding of the possible health hazards. Research on the potential influence of EMF on living organisms and humans is performed at all different organization levels of organisms: from population studies via studies of individuals (humans and animals), cells and tissues (of humans, animals and plants; of unicellular organisms and bacteria) to the lowest, molecular level. Interaction mechanisms of low level EMF with biological systems are not clearly identified. Identifying them could help to find potential field targets in living material.

Reports from *in vitro* research indicate that low level high frequency fields may alter membrane structural and functional properties that trigger cellular responses. It was hypothesized that the cell membrane may be susceptible to low level high frequency fields, especially when these fields are amplitude modulated at extremely low frequencies [20]. There are abundant data on the effects of weak physical signals on cell functional activity. However cell targets for these signals are not established yet. Since water is the main component of biological systems and all metabolic processes take place in aqueous medium it was supposed that the minor changes in the physico-chemical properties of water could significant modify cell functional activity. The data about the effect of EMF on water specific electrical conductivity and wheat sprouting serve as an additional evidence for the hypothesis according to which the EMF-induced water structure changing is an important pathway through which the biological effect of EMF is realized [6].

Evidences for directly non-thermal interaction with living systems are obtained after investigation of the RF EMF effects on the membrane permeability [2, 15]. These effects have not been explained by integral heating of the samples. Some other mechanisms such as formation of local temperature gradients in membrane-water interface or existence of hot spots in the system should be considered [11]. Changes in the ion transport and in the osmotic fragility are considered as an indicator for alterations in the erythrocyte membrane [1, 13]. Structural alterations were found out under the action of microwaves in membranes of granulocytes [22], erythrocytes [8],

melanoma cells (B-16 melanoma) [17]. Investigations of influence of EMF on the cation transport, membrane structure and fluidity show direct interactions of the field with specific membrane macromolecules or macromolecule complexes, which very often lead to global changes in the membrane properties. Considering the frequency dependence of the effects, different models for interaction of high frequency EMF energy and membrane components were submitted. The model about absorption of EM energy from water, bounded to biomolecules, is most likely [4, 14].

Microwaves could initiate chemically important events, i.e. configurational changes, e.g. multiple transitions between closely spaced vibratory states at successively higher energy levels. In the 10^8– 10^{11}-Hz range, mono-water rotation occurs. Water-lattice vibrations (quasi-rotational or vibratory motions) may be important in the labialization of the primary and secondary structure of the biopolymers in the frequency range of 10^{11} – 10^{14} Hz. Other researchers believe bound water has a principal dispersion region in the range of 3×10^8 – 2×10^9 Hz [16].

The cell membrane, nervous cells and DNA molecules are considered in literature as most probably acceptors of microwave (MW) radiation. Cell activity and viability depend on the state of the cell membrane. Because of its unique bioelectrochemical properties the cell membrane is considered as primary acceptor of microwave radiation. A number of studies of EMF bioeffects have been performed on native and model membranes and substantial changes in membrane dielectric properties and membrane transport were reported.

Erythrocyte membrane is often used as a model membrane in investigating the structure and the functions of the biological membranes as well as in studying the influence of different physical and chemical factors on the membranes.

This study was designed to estimate the effects of GSM900 EMF *in vitro* exposure of human erythrocytes on hemoglobin release, their dependence on the suspension water content and on the time elapsed after irradiation.

Materials and methods

Erythrocyte concentrates were obtained from the National Center of Hematology and Transfusiology. Red blood cells were washed three times in 0.155 M NaCl (2000×g for 10 min). After the last centrifugation suspensions were diluted to final cell concentration – hematocrit 20% or 40%.

The exposure was performed by GSM mobile phone type NSM-3, which was connected to a personal computer through an interface cable. The mobile phone was programmed via special software to emit carrier frequency 902 MHz (60^{th} uplink channel of GSM900). The signal included standard GSM modulation. GSM signal was pulsed. The duration of the pulses was 577μs that corresponded to one time slot of TDMA frame. The TDMA frame in GSM systems has a duration 4.615 milliseconds (Fig. 1). Discontinuous transmission mode (DTX) was off during all exposures. Mobile phone pulse output power was 2 W.

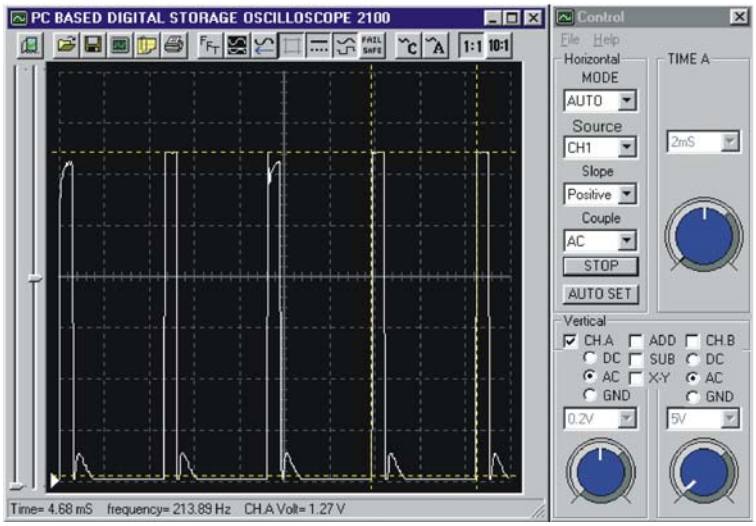

Figure 1. The emitted GSM signal, measured into mobile phone control circuit of the power amplifier.

Two milliliters of erythrocyte suspensions with different water content (hematocrit 20% or 40%) were transferred into two petri dishes (3 mm depth). One of them were control, another were exposed at 2 cm distance from the side of the mobile phone helical antenna. The exposure was 20 minutes. For eliminating of the influence of operator's hand on exposure conditions mobile phone was raised from the floor of 1 meter of the set up. The mobile phone and exposed erythrocyte suspensions were placed in the free space.

Alterations in hemolysis were registered 0, 10, 20, 30, 40, 50 and 60 min after the treatment. At given time intervals, 80 μl of the suspensions (control and irradiated) were transferred to 1.3 ml 0.155 M NaCl in Eppendorf

tubes and centrifuged at 10000rpm for 10s in a centrifuge MLW TH21. Hemolysis was determined by measuring the absorbance of hemoglobin in the supernatant at 413 nm. Hemolysis was expressed as a hemoglobin concentration (μM), calculated as follows:

$C = E\ V_2/\varepsilon\ l\ V_1$

where: C – hemoglobin concentration; E – absorbance of the supernatant at 413 nm; ε – molar extinction coefficient, for hemoglobin at λ = 413 nm ε = 120000 M^{-1} cm^{-1}; l – length of the optical way (1 cm), V_1 – volume of added erythrocytes, V_2 – final volume.

The presented data are average and standard deviations of 8 measurement of the released hemoglobin quantity for each term. The Student *t*-test was used to estimate the statistically significant differences between the experimental samples.

Results and discussion

During the study of hemolysis in the process of blood aging we observed an increase of the quantity of the released hemoglobin with the increase of the time of blood storage. After the construction of the graphics *hemoglobin / days after blood taken* for control samples it was found that the values of the released hemoglobin between 2nd and 10th days were close (Fig. 2, 3). In the latest terms the quantity of the released hemoglobin was about 5 times more than at early terms. Because of the great differences in the quantity of the released hemoglobin, averaging of the results from spontaneous hemolysis before and after 10th day of blood storage would result in large standard deviations and would mask effects of the investigated factor. Experiments related to influence of different factors on the hemolysis should be made in the first 10 days of *in vitro* storage of the blood.

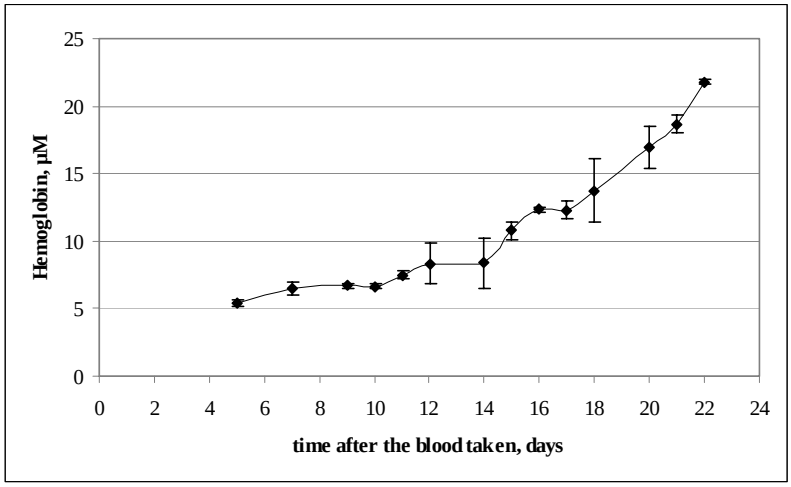

Figure 2. Quantity released hemoglobin from human erythrocytes in the process of *in vitro* blood aging (control, hematocrit 20%).

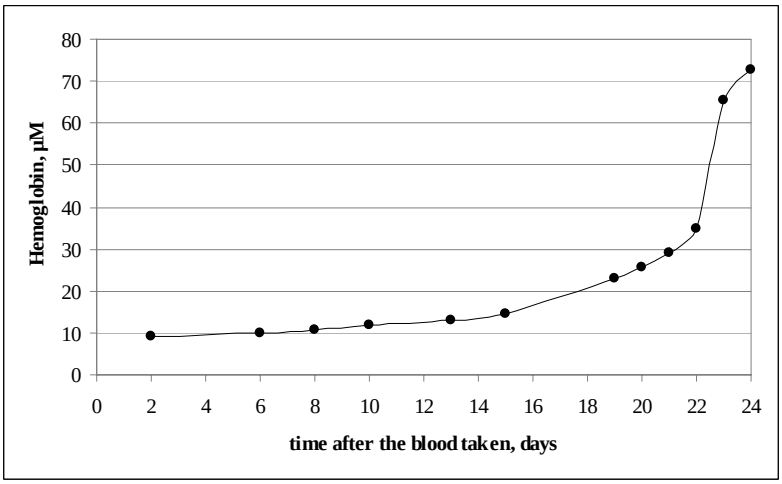

Figure 3. Quantity released hemoglobin from human erythrocytes in the process of *in vitro* blood aging (control, hematocrit 40%).

Represented data about the effects of GSM900 EMF (Figs 4, 5) are the averages and standard deviations of the values of released hemoglobin obtained in the first 10 days after the blood taken.

During the study of the hemolysis, we observed that the amount of the released hemoglobin increased with the time elapsed after the exposure to EMF both in the control and exposed erythrocytes. The differences between control and exposed cells are bigger at the beginning of the term of the blood storage at two studied hematorcits.

From the beginning of post exposure period to 60th min after irradiation the amount of released hemoglobin increased about two times in the erythrocyte suspensions with hematocrit 20%. There were no statistical significant alterations in irradiated erythrocytes immediately after termination of the exposure. Effects of EMF appeared 10 min after exposure and differences retains 30 min. There were no significant differences in the later terms (Fig. 4).

The *in vitro* exposure of erythrocyte suspensions with hematocrit 40% with GSM900 EMF for 20 min caused statistically significant decrease of the hemolysis (about 10-15%) compared to the control in all investigated terms (Fig. 5). Differences between control and exposed erythrocyte suspensions were more strongly expressed in suspensions with hematocrit 40%, which is close to physiological one (Table 1).

The obtained results showed that the EMF induces more significant changes in the suspensions with the lower water content (hematocrit 40%). These results contradict our previous results about the effects of 24 GHz MW *in vitro* exposure of human erythrocytes, where the most significant changes in erythrocyte electrophoretic mobility were observed in the suspensions with higher water content (hematocrit 20%) [12]. It is probably because the water content is of no importance in the realization of the effects of EMF on living organisms at this lower frequency (902 MHz). The decrease of the hemolysis is probably due to some stabilization of erythrocyte membrane after the irradiation with GSM900 EMF as a result of the field influence.

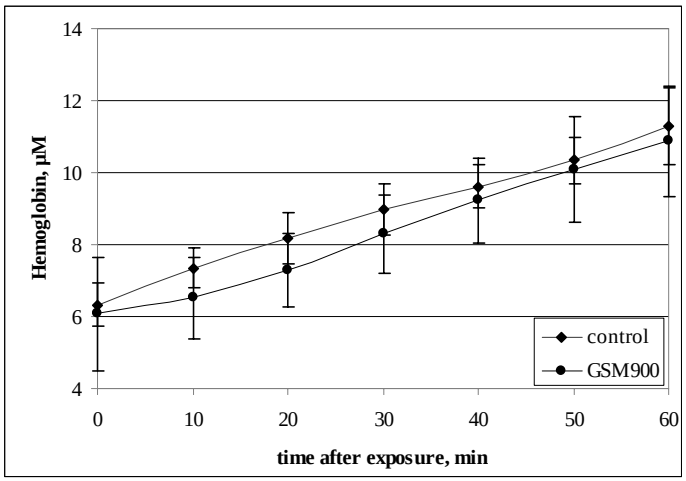

Figure 4. Quantity released hemoglobin from human erythrocytes after 20 min *in vitro* exposure to GSM900 EMF of the suspensions with hematocrit 20%.

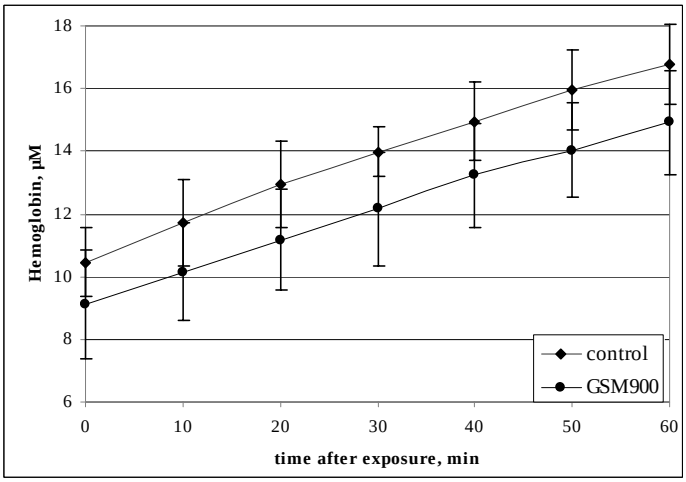

Figure 5. Quantity released hemoglobin from human erythrocytes after 20 min *in vitro* exposure to GSM900 EMF of the suspensions with hematocrit 40%.

Table 1. Rated decrease of the spontaneous hemolysis (compared to the control) and statistical significance of the differences between control and exposed to GSM900 EMF erythrocyte suspensions with hematocrit 20% and 40%.

Time after exposure, min	**Hemolysis decrease compared to the control, %**		**Statistical significance (p)**	
	Hematocrit 20%	Hematocrit 40%	Hematocrit 20%	Hematocrit 40%
0	4	15	-	0.99
10	10	13	0.98	0.99
20	11	14	0.99	0.99
30	8	14	0.95	0.999
40	10	11	-	0.99
50	3	12	-	0.999
60	3	11	-	0.999

These results are in consent with some authors. Microwave *in vitro* exposure (2.45 GHz, pulsed, power flux density: 5 mW/cm², exposure duration: 20 min, SAR: 400 μW/g) significantly decreased spontaneous hemolysis of human erythrocytes at 42°C, but had no effect at 37°C or 48°C [9]. Some authors find no effects of high frequency EMF on hemolysis. Heating erythrocytes to 43°C for 10 min with microwaves (2.45 GHz, CW, exposure duration: 15 min, SAR: 91 mW/g) or hot air did not significantly increase hemolysis, compared with hemolysis at 4°C. Hemolysis of cells coated with concanavalin A-luminol-bovine serum albumin and heated to 43°C for 10 min by use of microwaves or hot air was significantly greater than that of controls at 4°C [10]. Possible nonthermal effects of 434 MHz microwave radiation (CW, exposure duration: 6 h, electric field strength: 15 V/cm, power flux density: 100 – 600 mW/cm², time of investigation: after exposure) on human blood should be investigated *in vitro* [5]. Plasma levels of hemoglobin and sodium and potassium ions serve as an indicator of haemolysis, caused by an increased membrane fragility. Indicated by the measurements no increased membrane fragility was observed, which could be clearly assigned to nonthermal effects.

Our results contradict the results of another authors, who state that exposure to high frequency EMF increases hemolysis. Cleary et al. investigated the effects of RF irradiation (10, 50, and 100 MHz, CW, exposure duration: 2 h, electric field strength: 1; 4,5; 9 V/cm) on cation permeability and hemolysis of rabbit erythrocytes *in vitro*. Potassium and sodium release were not altered by exposure. Hemoglobin release as an indicator for hemolysis was statistically significant increased at 50 and 100 MHz at field strength of 9 V/cm. The mechanism of the observed hemolytic effect is unknown [3]. Low intensity radiation from mobile phones leads to release of hemoglobin from red blood cells and accumulation of the hemoglobin in the body could result in heart diseases or kidney stones [7]. It was found that 2.45 GHz irradiation induces a significant hemoglobin loss due to transient permeabilisation of irradiated erythrocytes rather than to their lysis [18]. The microwave induced hemoglobin loss by irradiated erythrocytes is up to 80% of the spontaneous hemoglobin loss by the controls. The rate of the increase of hemoglobin loss with increasing power density was found to be highly dependent on the initial level of spontaneous hemolysis. It seems that the membrane is as more sensitive to the radiation power as it was leaker at the start. Kinetics of hemolysis degree at three different power densities was studied. At low power densities (0.8 and 1.36 mW/cm^2) there is a quasi-linear increase of hemolysis degree with time of irradiation. At higher density (5 mW/cm^2) this tendency seems to reverse after first 10 hours of irradiation. The only reasonable explanation for this seems to be that the spontaneous hemoglobin loss of controls increases faster than that of the exposed samples. It appears like long-term irradiation would exert a protective action against spontaneous hemolysis caused by cells ageing. This observation is paralleled by the results of kinetic measurements of the osmotic resistance of irradiated erythrocytes, which show a progressive increase of the osmotic resistance with time of irradiation at exposures to 5 mW/cm^2. Sajin et al. studied the effects of long-term exposure of human blood to 2.45 GHz irradiation at athermal power densities (CW, exposure duration: 60 h (84 h kinetic measurements), power flux density: 10 mW/cm², max value (50 W/m², 25 W/m², 10 W/m², 5 W/m², 2.5 W/m², 1 W/m², 0.5 W/m², 0.25 W/m²)) [21]. A significant increase of the hemoglobin loss by irradiated erythrocytes as well as a strong dependence of the rate of the increase of hemoglobin loss on the initial level of spontaneous hemolysis were revealed. It was found that at low power densities, the hemolysis degree increases quasi-linearily with the exposure time, while at higher density (5 mW/cm²), this tendency is reversed after first 10 h of irradiation. Long-term irradiation seems to exert a protective effect against spontaneous hemolysis caused by blood ageing. The osmotic fragility test performed on samples exposed to 5 mW/cm² at different

irradiation times showed that the osmotic resistance increased in time, reaching a maximum at the end of irradiation (60 h), while the osmotic resistance of the controls was constant.

The data about the effects of EMF on hemolysis in available literature are contradictory. More research and additional methods are necessary to decide these contradictions and to explain the mechanisms of low level RF EMF interaction with erythrocyte membrane.

Summary

Our data indicate statistically significant decrease in the hemoglobin level in irradiated suspensions. The 900 MHz EMF exposure probably stabilized erythrocyte membrane and caused reduction in the hemolysis that depended on the suspension water content (hematocrit) and on the time elapsed after irradiation.

References

1. Baranski S., Szmigielski S., Moneta J., 1974, Effect of MW irradiation *in vitro* on cell membrane permeability, in: *Biological Effects and Health Hazards of Microwave Radiation*, P. Czerski, K. Ostrowski, C. Silverman, et al. (Eds.), Polish Medical Publishers, Warsaw, Poland, p. 173–177.
2. Cleary S.F., F. Garber, L.M. Liu, 1982, Effects of X-band MW exposure on rabbit erythrocytes, *Bioelectromagnetics*, 3: 453–466.
3. Cleary S.F., L.M. Liu, F. Garber, 1985, Erythrocyte hemolysis by radiofrequency fields, *Bioelectromagnetics*, 6 (3): 313–322 (*www.emf-portal.de*).
4. Cleary S.F., L.M. Liu, G. Cao, 1989, Functional alternation of mammalian cells by direct high frequency electromagnetic field interactions, in: *Charge and Field Effects in Biosystems-2*, M.J. Allen, S.F. Cleary, F.M. Hawkridge (Eds.), Plenum Press, N.Y., p. 211–221.
5. Dunscombe P.B., K. Gammampila, N.W. Ramsey, 1983, A search for nonthermal effects of 434 MHz microwave radiation on whole human blood, *Radiat Res*, 96 (2): 235–250 (www.emf-portal.de).
6. Hakobyan S., N. Baghdasaryan, A. Amyan, S. Ayrapetyan, 2001, The effect of EMF on water specific electrical conductivity and wheat sprouting, in: *Proceedings of WHO Meeting on EMF Biological Effects and Standard Harmonization in Asia and Okeania, Seul, Korea*, p.123.
7. Harris S., 1999, Now mobiles give you kidney damage, http://emfacts.com
8. Ismailov, E., 1987, Biophysical effects of VHF radiation, Moscow, p.84 (*in Russian*)
9. Kiel J.L., D.N. Erwin, 1984, Microwave and thermal interactions with oxidative hemolysis, *Physiol Chem Phys Med NMR*, 16 (4): 317–323 (*www.emf-portal.de*).
10. Kiel J.L., D.N. Erwin, 1986, Physiologic aging of mature porcine erythrocytes: effects of various metabolites, antimetabolites, and physical stressors, *Am J Vet Res*; 47 (10): 2155–2160 (*www.emf-portal.de*).
11. Kim Yu.A., Yu.V. Kim, B.S. Fomenko, E.L. Holmuhamedov, I.G. Akoev, 1989, Effects of microwave radiation on inducable ion transport of rat erythrocytes, in: *Charge and Field Effects in Biosystems – 2*, M.J. Allen, S.F. Cleary, F.M. Hawkridge (Eds), Plenum Press, New York and London, p. 223–232.
12. Kouzmanova M., M. Hristova, 2004, Effects of *in vitro* microwave exposure on electrophoretic mobility of human erythrocytes, *Annuaire de l'Universite de Sofia* (*10eme session scientifique, Sofia'03*), 96(4): 221–227.
13. Kovacs E., T. Savopol and A. Dinu, 1997, Lower Power Microwave Effects On Erythrocytes Membranes, in: *Abstract Book of II World Congress for Electricity and Magnetism in Biology and Medicine, Bologna, Italy*, p. 259.
14. Litvinov G.S., N.Ya. Gridina, G.I. Dovbeshko, et al., 1994, Millimeter wave effect on blood plasma solution, *Electro- and Magnetobiology*, 13(2): 167–174.
15. Liu L.M., F.G. Nickless, S.F. Cleary, 1979, Effects of microwave radiation on erythrocyte membranes, *Radio Sci*, 14: 109–115.
16. NCRP Reports №86, 1986, Biological Effects and Exposure Criteria for Radiofrequency Electromagnetic Fields, Recommendations of the National Council on Radiation Protection and Measurements (NCRPM), Bethesda, MD.
17. Phelan A.M., D.G. Lange, H.A. Kues, G.A. Lutty, 1992, Modification of membrane fluidity in melanin-containing cells by low-level MW radiation, *Bioelectromagnetics*, 13: 131–146.
18. Pologea-Moraru R., E. Kovacs, T. Savopol and A. Dinu, 1997, Lower power microwaves effects on erythrocytes membranes, in: *Abstract Book of II World Congress for Electricity and Magnetism in Biology and Medicine, Bologna, Italy*, p.259.
19. Prastalo R., G. Tesanovic, S. Sukalo, 2003, Mechanism of mobile phone radiation acting on biological systems, *TELSIKS, Serbia and Montenegro, Nis*, p. 675–678.
20. Repacholy M.H., 2001, Review of health effects and gaps in knowledge, in: *Proceedings of WHO Meeting on EMF Biological Effects and Standard Harmonization in Asia and Okeania, Seul, Korea*, 33–42.
21. Sajin G., E. Kovacs, R.P. Moraru, T. Savopol, M. Sajin, 2000, Cell membrane permeabilization of human erythrocytes by athermal 2450-MHz microwave radiation, *IEEE Trans Microwave Theory Tech*; 48 (11): 2072–2075 (*www.emf-portal.de*).
22. Szmigielski S., 1975, Effect of 10 cm (3 GHz) electromagnetic radiation (microwaves) on granulocytes *in vitro*, *Annals NY Acad Sci*, 247: 275–281.

ANALYTICAL METHOD FOR HUMAN EXPOSURE ASSESSMENT TO SHORT RANGE DEVICES

DINA SIMUNIC AND DAMIR ZRNO

UNIVERSITY OF ZAGREB, FACULTY OF ELECTRICAL ENGINEERING AND COMPUTING, UNSKA 3, HR-10000 ZAGREB, CROATIA

Abstract

Electromagnetic dosimetry and exposimetry quantify electromagnetic fields inside and outside of the biological material, i.e., human body, respectively. They are primarily used for evaluation of human exposures due to various devices generating electromagnetic fields. The both: dosimetry and exposimetry have their bases in experimental and/or numerical methods. In this paper a proposed new formula for a *SAR* of short-range radio-frequency devices in multiple reflection environment has been developed. The involved scenario assumed semi-infinite plane with properties of homogeneous muscle. The shown results indicate that a reliable human exposure assessment in the indoor environment requires an application of deterministic numerical methods, capable of calculation of multiple reflection conditions, such as ray-tracing.

Introduction

Dosimetry and exposimetry of high-frequency fields have been investigated for a number of years in variously shaped object, like the prolate spheres [1] and spheres [2]. The dipole-type normal excitation has been studied in the semi-infinite slab [3], even under near-field conditions [4]. Human body in vicinity of wireless communications devices acts as a disturbing element of wireless communications systems performance [5]. On the other hand, biological effects of electromagnetic fields are being investigated also for a number of years [6]. Some numerical techniques, which are excellent tools for a calculation of deposited electromagnetic energy in the human body, like FDTD, are being extensively used throughout years [7]. Insofar, the attention has been mostly focused to cellular telephony. The constant development of new wireless technologies introduces presence of wireless technologies in the total human environment, which further complicates calculations of deposited electromagnetic energy. This paper presents an analytically developed SAR formula for multiple reflections conditions, natural to indoor environment.

Oblique incidence of plane wave

Let us suppose that tissue is a homogeneous material, so that it acts like a semi-infinite plane to the impinging

electromagnetic wave. The considered technology is in the ISM frequency range of short range devices (SRD), i.e., ISM part at 2.5 GHz. Analytical formulas have been derived for *SAR* of the SRD base stations. The SRD technology usually uses half-wave antennas, which allows us to conclude that all the calculations related to human exposure to SRD base stations have to be performed for far-field propagation conditions. For a plane wave travelling in air (Fig. 1), induced SAR at a planar interface air/tissue is defined by tissue mass density ρ, tissue conductivity σ, tissue impedance (Z_t) and power density in the tissue (S_t):

$$SAR = \frac{\sigma}{\rho}\left(S_t Z_t\right) \tag{1}$$

Fig. 1 shows a vertically polarized EM wave impinging obliquely the air/tissue interface. Air is characterized by μ_0, ε_0; tissue by μ_0, ε_r, σ.

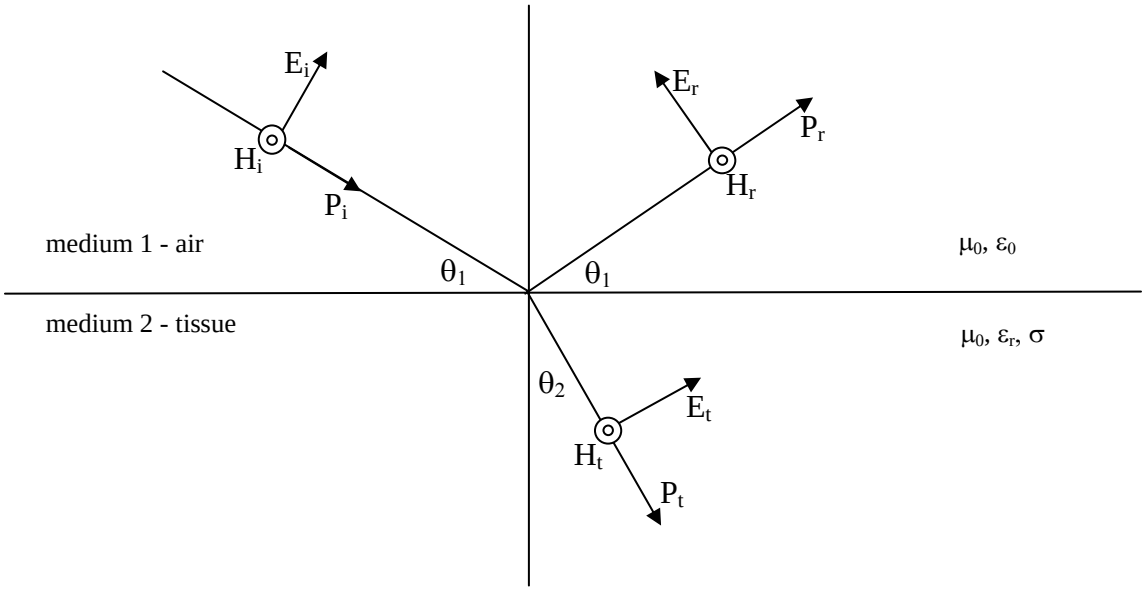

Fig. 1 Oblique incidence of a vertically polarized wave

Transmitted power density in the tissue (S_t) is defined as a difference of the incident (S_{inc}) and reflected (S_{refl}) power density:

$$S_t = S_{inc} - S_{refl} \tag{2}$$

The transmitted power density, S_t, is at the air-tissue interface defined in terms of S_{inc} by a reflection coefficient Γ:

$$S_t = S_{inc}\left(1 - |\Gamma|^2\right) \tag{3}$$

SAR is defined at the air-tissue interface as:

$$SAR = \frac{\sigma}{\rho} S_{inc} Z_t \left(1 - |\Gamma|^2\right) \tag{4}$$

Tissue impedance, Z_t, is for the plane wave exposure defined by tissue conductivity, σ, tissue permittivity, ε_r, tissue permeability, μ_0 and angular frequency, ω:

$$Z_t = \sqrt{\frac{\mu_0}{\varepsilon_r \varepsilon_0 - j\frac{\sigma}{\omega}}} \tag{5}$$

Reflection coefficient depends on a wave polarization. For a vertically polarized wave impinging obliquely tissue, Γ_v, is defined by an incident angle (θ_1), free space permittivity ε_0, tissue conductivity σ, tissue permittivity ε_r, and angular frequency, ω:

$$\Gamma_v = \frac{\sin\Theta_1 \left(\varepsilon_r - j\frac{\sigma}{\omega\varepsilon_0}\right) - \sqrt{\left(\varepsilon_r - j\frac{\sigma}{\omega\varepsilon_0}\right) - \cos^2\Theta_1}}{\sin\Theta_1 \left(\varepsilon_r - j\frac{\sigma}{\omega\varepsilon_0}\right) + \sqrt{\left(\varepsilon_r - j\frac{\sigma}{\omega\varepsilon_0}\right) - \cos^2\Theta_1}} \tag{6a}$$

Reflection coefficient for horizontal polarization Γ_h is slightly differently defined:

$$\Gamma_h = \frac{\sin\Theta_1 - \sqrt{\left(\varepsilon_r - j\frac{\sigma}{\omega\varepsilon_0}\right) - \cos^2\Theta_1}}{\sin\Theta_1 + \sqrt{\left(\varepsilon_r - j\frac{\sigma}{\omega\varepsilon_0}\right) - \cos^2\Theta_1}} \tag{6b}$$

The graphs for the both reflection coefficients, depending on the incident angle, are given in Fig. 2.

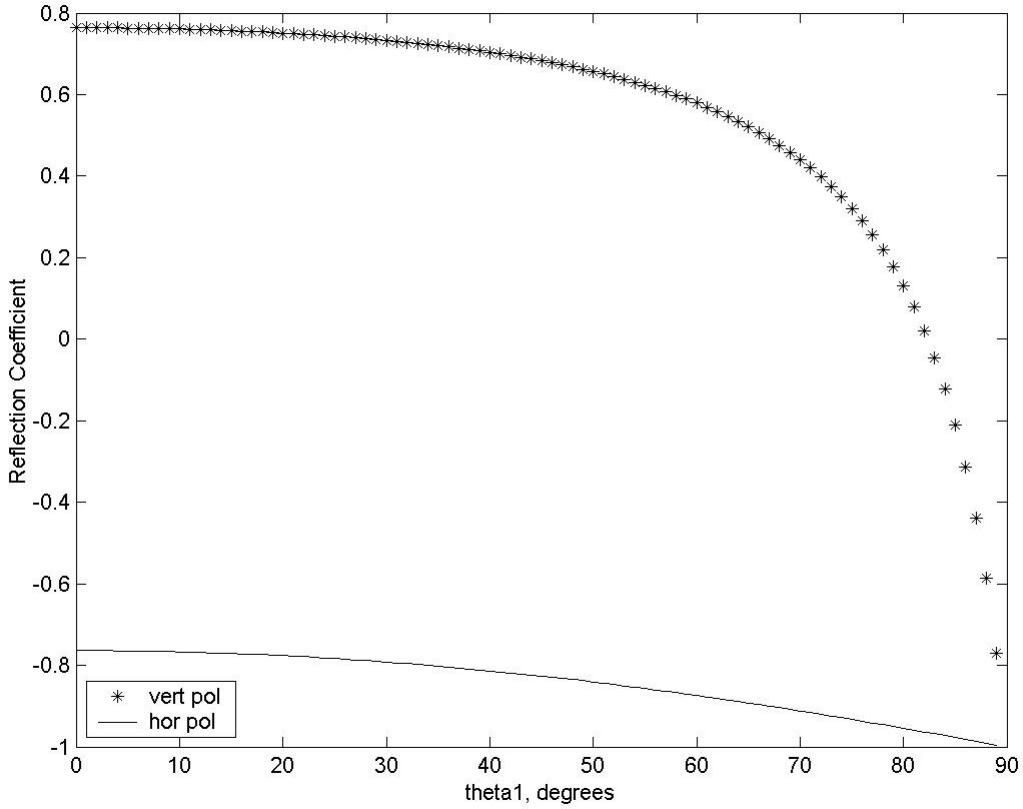

Fig. 2 Calculated reflection coefficient for vertically and horizontally polarized impinging wave

SAR in the tissue for a vertically polarized wave is defined as:

$$SAR_{\mathrm{v}} = \frac{\sigma}{\rho}\left(S_{\mathrm{inc}} \frac{\omega\mu_0}{\sqrt{\sigma^2 + \left(\omega\varepsilon_{\mathrm{r}}\varepsilon_0\right)^2}} \left(1 - \left| \frac{\sin\Theta_1 \left(\varepsilon_{\mathrm{r}} - j\frac{\sigma}{\omega\varepsilon_0} \right) - \sqrt{\left(\varepsilon_{\mathrm{r}} - j\frac{\sigma}{\omega\varepsilon_0} \right) - \cos^2\Theta_1}}{\sin\Theta_1 \left(\varepsilon_{\mathrm{r}} - j\frac{\sigma}{\omega\varepsilon_0} \right) + \sqrt{\left(\varepsilon_{\mathrm{r}} - j\frac{\sigma}{\omega\varepsilon_0} \right) - \cos^2\Theta_1}} \right|^2 \right) \right) \quad (7a)$$

For a horizontally polarized wave *SAR* in the tissue is defined as:

$$SAR_{\mathrm{h}} = \frac{\sigma}{\rho}\left(S_{\mathrm{inc}} \frac{\omega\mu_0}{\sqrt{\sigma^2 + \left(\omega\varepsilon_{\mathrm{r}}\varepsilon_0\right)^2}} \left(1 - \left| \frac{\sin\Theta_1 - \sqrt{\left(\varepsilon_{\mathrm{r}} - j\frac{\sigma}{\omega\varepsilon_0} \right) - \cos^2\Theta_1}}{\sin\Theta_1 + \sqrt{\left(\varepsilon_{\mathrm{r}} - j\frac{\sigma}{\omega\varepsilon_0} \right) - \cos^2\Theta_1}} \right|^2 \right) \right) \quad (7b)$$

Fig. 3 shows calculated surface *SAR* in dependence of impinging angle, θ_1, with used electrical parameters in the 2.45 MHz frequency band for the homogeneous all-muscle model (ε_{2r} = 53.57, σ_2 = 1.81 S/m, and ρ = 1040 kg/m^3) for the both polarizations.

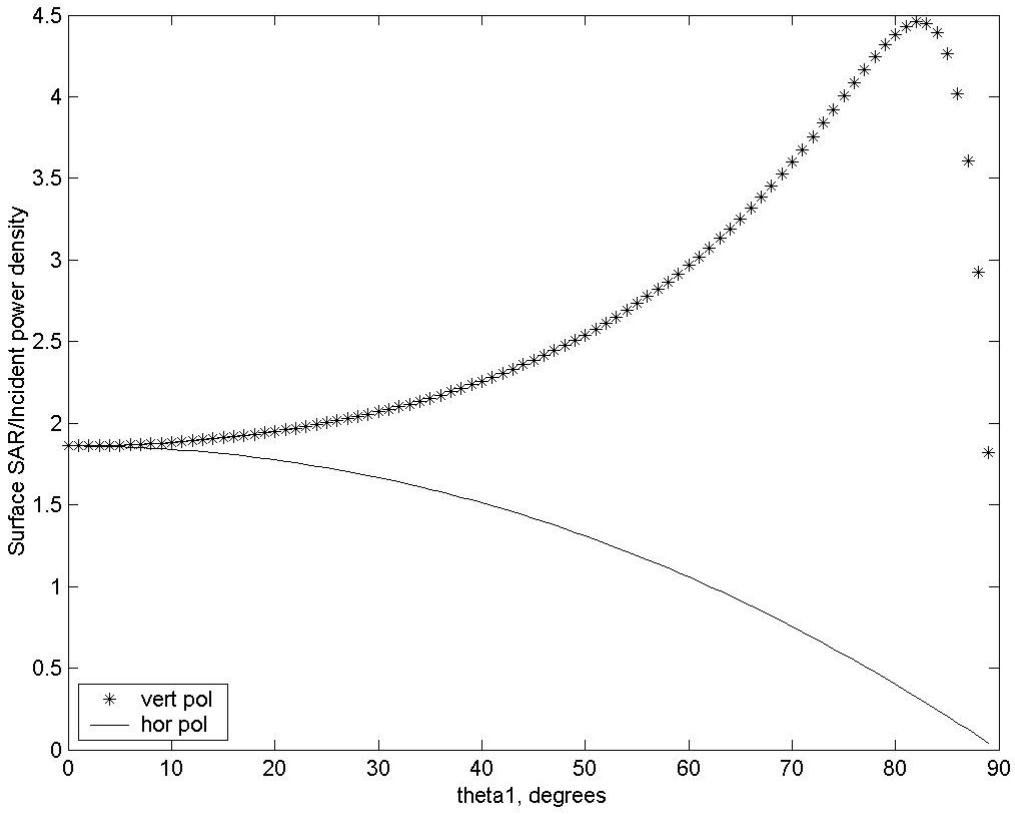

Fig. 3 Calculated ratio of surface *SAR* and incident power density in dependence of vertically and horizontally polarized obliquely impinging angle, θ_1, at 2.45 GHz, with electrical properties of homogeneous all-muscle model

The results indicate that for a range of incident angles the ratio of surface *SAR* and incident power density depends highly on the polarization and on angle of incidence.

Multiple oblique incidence of plane waves

In the case of multiple reflections environment, where all reflected and transmitted components have a general arrangement and thus statistical phase difference, it is necessary to define a position of human body in the indoor space. Fig. 4 depicts a situation with only one barrier (e.g., a wall), which is placed at a distance ζ from the human being.

Even under these very especial and simplified circumstances (only one perfectly conducting wall), the analytical calculation of the reflected components of electric field is quite complex. The reflected field is calculated from a number of reflected components, i.e., the first reflection E_{1r}, the second reflection E_{2r},... the n-th reflection E_{nr}, by using incident field (E_0), reflection (Γ) and transmission coefficient (T), as given by Eqs. (8a-n).

$$E_{1r} = E_0 \Gamma e^{j\omega t} \tag{8a}$$

$$E_{2r} = E_0 T\Gamma' T' e^{j(\omega t-\zeta)} \tag{8b}$$

$$E_{3r} = E_0 T\Gamma'^3 T' e^{j(\omega t-2\zeta)} \tag{8c}$$

…

$$E_{nr} = E_0 T\Gamma'^{(2n-3)} T' e^{j(\omega t-(n-1)\zeta)} \tag{8n}$$

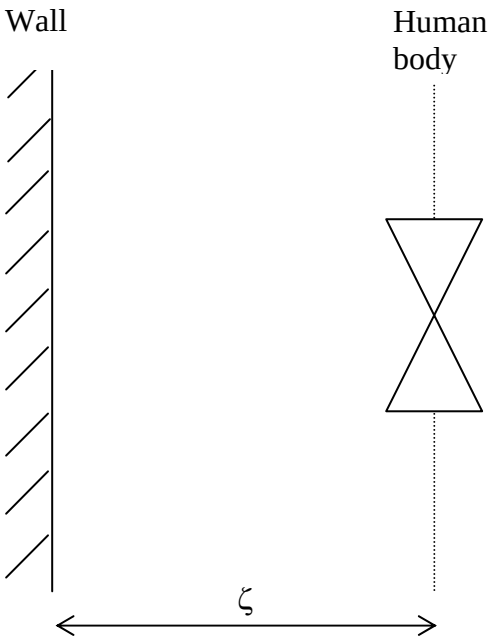

Fig. 4 Human body in a reflective environment with only one wall

Reflection and transmission coefficient depend on polarization and incidence angles. Reflection coefficient for vertically polarized field is given by:

$$\Gamma_{vm} = \Gamma_{1v} \frac{\left(\omega\varepsilon_0\left(\varepsilon_r - \cos^2\Theta_1\right) - j\sigma\right)\left(1-\Gamma_{1v}^2 t_d^2 t_s\right) - t_d^2 t_s \sin^2\Theta_1\left(1-\Gamma_{1v}^2\right)}{\left(\omega\varepsilon_r\varepsilon_0 - j\sigma\right)\cos^2\Theta_t\left(1-\Gamma_{1v}^2 t_d^2 t_s\right)} \qquad (9a)$$

Reflection coefficient for horizontally polarized field is defined as:

$$\Gamma_{hm} = \frac{\Gamma_{1h}\left(1-t_d^2 t_s\right)}{1-\Gamma_{1h}^2 t_d^2 t_s} \qquad (9b)$$

Fig. 5 shows reflection coefficients for the multiple incidence of waves of the both polarizations.

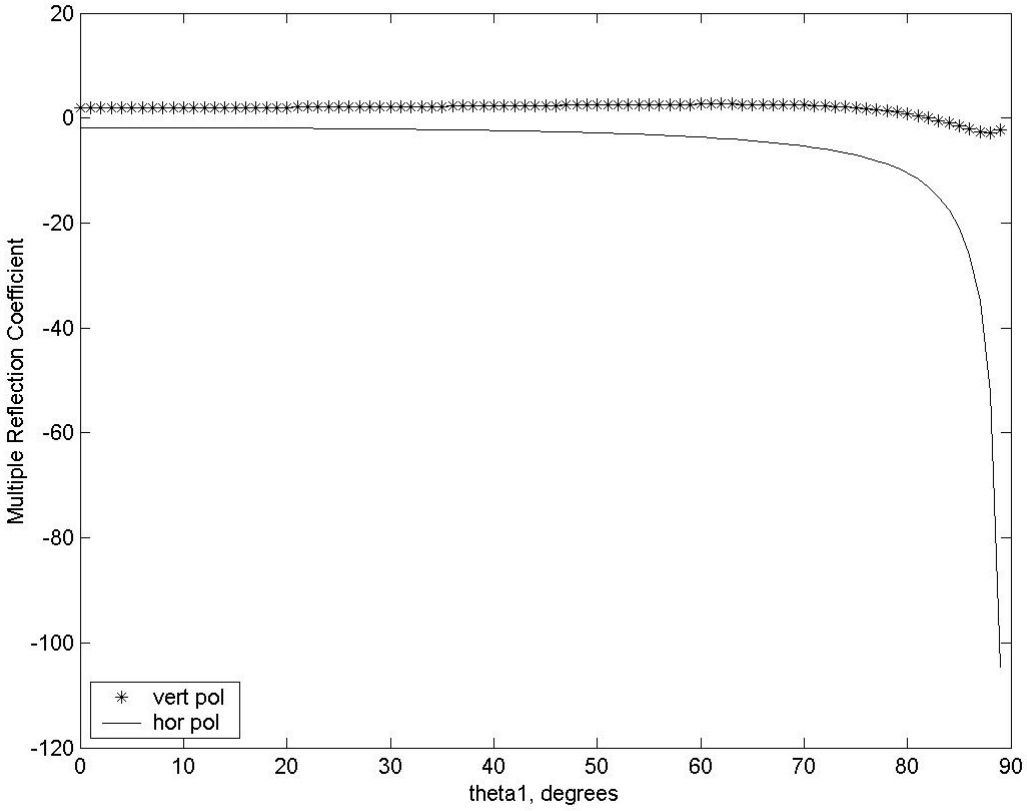

Fig. 5 Calculated reflection coefficient for multiple incidence of vertically and horizontally polarized wave

Results of application of relation (4) for *SAR* with the reflection coefficient of multiple reflection of electromagnetic waves (9a) and (9b) are shown in Fig. 6.

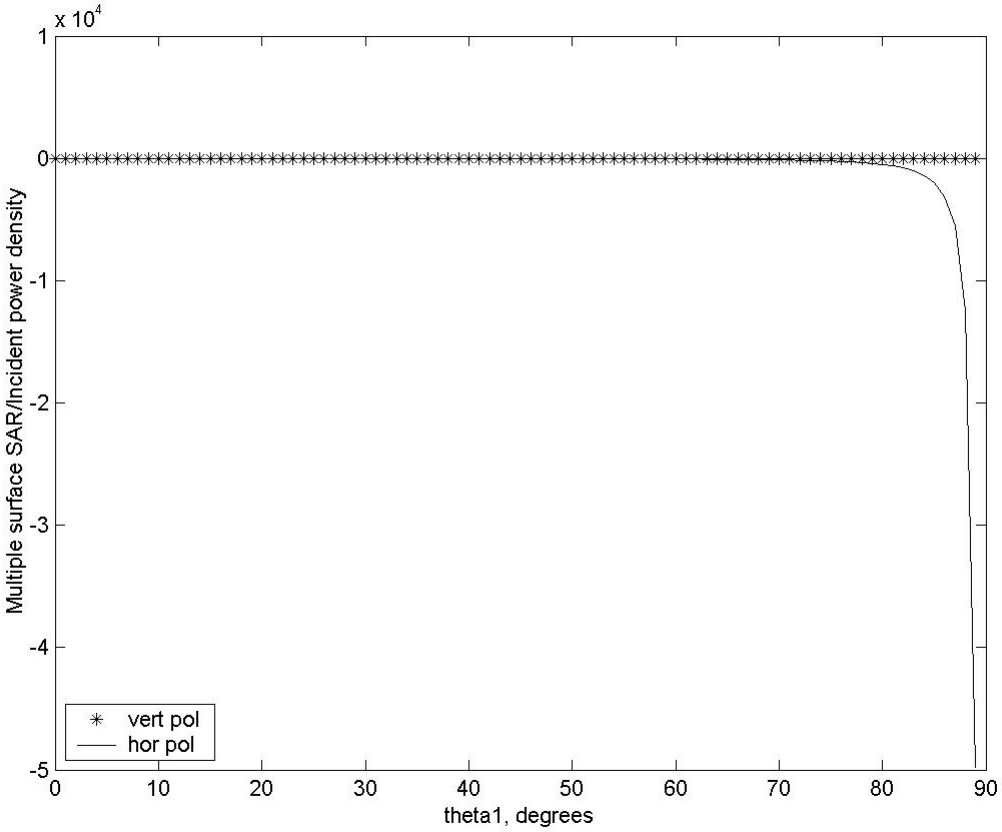

Fig. 6 Calculated ratio of surface *SAR* and incident power density in dependence of incident angle θ_1 of vertically and horizontally polarized obliquely impinging wave at 2.45 GHz, with electrical properties of homogeneous all-muscle model, for multiple reflection

The results on Fig. 6. show that for a range of incident angles the surface *SAR* is equal to incident power density except for horizontal polarization for angles higher than approximately 75 degrees.

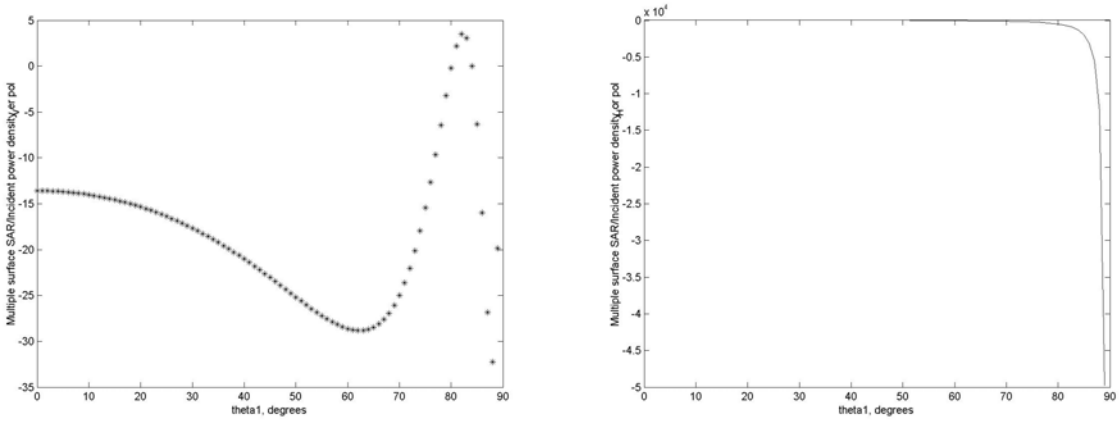

a. b.

Fig. 7 Calculated ratio of surface *SAR* and incident power density in dependence of incident angle θ_1 of vertically (a) and horizontally (b) polarized obliquely impinging wave at 2.45 GHz, with electrical properties of homogeneous all-muscle model, for multiple reflection

Further inspection into the calculated results shows that there are differences in calculation of *SAR* for vertically polarized wave, following the reflection coefficient, where it can happen that for some angles (e.g., 82 degrees) the value of total *SAR* is up to 3.5 times higher than for the normal incidence.

These results show that for the relevant *SAR* calculation as many reflections as possible have to be taken into account. Also, it if utmost importance to realize that calculation of normal incidence of electromagnetic fields does not indicate the so-called “worst-case” *SAR*.

Summary

The formula for *SAR* has been developed under the conditions of multiple reflections in a semi-infinite plane with electrical properties of homogeneous all-muscle model. The calculated results show that at certain incidence angles the *SAR* values for vertically polarized wave can be up to 3.5 times higher than for the normal incidence. Thus, if is of importance for *SAR* calculation in multiple reflective environment, such as indoor, to take into account as many reflected rays as possible. This can be performed by introducing numerical methods, such as ray-tracing [9],[10].

References

[1] Iskander MF, Barber PW, Durney CH, Massoudi H. 1980. Irradiation of prolate spheroidal models of humans in the near field of a short electric dipole. IEEE Trans. on MTT. 28(7):801-807

[2] Kritikos HN, Schwan HP.1972. Hot spots generated in conducting spheres by electromagnetic waves and biological implications. IEEE Trans. Biomed. Eng., 19:53-58.

[3] Chatterjee I, Gandhi OP, Hagmann MJ, Riazi A. 1980. Plane-wave spectrum approach for the calculation of electromagnetic absorption under near-field exposure conditions. Bioelectromagnetics, 1:363-377.

[4] Kuster N, Balzano Q. 1992. Energy absorption mechanism by biological bodies in the near field of dipole antennas above 300 MHz. *IEEE Trans Vehicular Technol*, 41(1):17-23.

[5] Ziri-Castro KI, Scanlon WG, Evans NE. 2004. Indoor Radio Channel Characterization and Modeling for a 5.2-GHz Bodyworn Receiver. *IEEE Antennas and Wireless Propagation Letters*, 3:219-22.

[6] Radiofrequency Radiation Dosimetry Handbook, Fourth Edition, *USAF School of Aerospace Medicine, Aerospace Medical Division (AFSC), Brooks Air Force Base*, October 1986.

[7] Kunz KS, Luebbers RJ. The finite difference time domain method for electromagnetics, CRC Press, Boca Raton, FL, 1993.

[8] Sullivan DM, Borup DT, Gandhi OP. 1987. Use of the finite-difference time-domain method in calculating EM absorption in human tissues. *IEEE Trans. Biomed. Eng.*, 34:148–57.

[9] Zrno D, Šimunić D. 2003. Matrix Based Ray-Tracing Model for Indoor Propagation, ICECOM 2003. Dubrovnik, pp. 221-224

[10]Simunic D, Zrno D. A Novel Method for Electromagnetic Dosimetry Related to Human Exposure from Short-Range Devices. Submitted to Journal for Ecodynamics.

FULFILLING THE OCCUPATIONAL HEALTH TRAINING REQUIREMENTS OF EU DIRECTIVE 2004/40/EC

MICHAEL BANGAY
Radhaz Consulting Pty Ltd
Suite 5, 8 Clay Drive, Doncaster, Victoria 31 Australia
michael@radhaz.com.au

Abstract

This paper addresses the application of the European Union Directive 2004/40/EC in respect to worker information and training. The Directive has placed obligations on employers to protect their workers from risks to their health and safety arising from their workplace exposure to electromagnetic fields. Employers are required to meet particular health and safety requirements that include exposure assessment and worker training. This paper sets out an approach that achieves the employee training and information objectives described in Article 6 of Directive 2004/40/EC. An overview of training material provided in Australia by the author of this paper to meet similar requirements to Article 6 is presented.

Introduction

Governments around the world are reacting to the growing concerns over exposure to electromagnetic fields. While much of the concern has centred around the public's exposure to magnetic fields around high voltage power lines, mobile telephone emissions and radiated signals from telecommunications towers, there are new endeavours to address worker safety. Hazards associated with high-level exposure to radiofrequency (RF) fields have been well understood for many years. While the issue of injuries resulting from radiated low frequency fields like those around electrical power infrastructure is less clear, injuries caused by radiated RF fields and associated currents is quite clear and requires a response to protect both the employee and employer. The understanding about RF hazards and the way it can cause heating and burns extends back into the early days of radio use. Safety standards to guard against the heating effects of RF radiation have been in place for almost fifty years. The current preoccupation over possible athermal health effects alleged to be caused by exposure to levels of RF below the ICNIRP limits has possibly come at the expense of a more appropriate response to known RF hazards that need to be controlled.

During the mid 1980's Australia's government owned national telecommunications company faced a major occupational health and safety crisis with maintenance and installation staff refusing to climb masts/towers for fear that they may be physically harmed by the RFR radiation. The company responded by initiating a well-resourced hazard management program that included a hazard assessment and staff training. The training program has been continually refined over the past 20 years to produce training that establishes safe working procedures for all RF workers. This paper provides an outline of the training program conducted by Radhaz Consulting Pty Ltd over the past eight years.

Employers have an obligation to carryout an assessment of RF exposure levels around devices that emit RF radiation to determine if there is a risk that must be managed. Generally, a potential hazard is defined as an exposure situation that allows a worker to be exposed to levels that are in excess of the exposure limit values described in the Annex of Directive 2004/40/EC which were obtained from the ICNIRP guidelines ICNIRP7/99. These values are described as the occupational exposure limits and do not apply to members of the public. It is assumed that exposed workers have an intelligent awareness of the hazard and have their exposure controlled as a consequence of good engineering design, safe work procedures and training.

The initial assessment of the hazard by the employer to determine compliance or otherwise forms the basis of the measures needed to control the hazard. Depending on the circumstances, the assessment may be either performed by calculation or by measurement. Measurement is generally preferred for

frequencies below 110 MHz due re-radiation situations and the need to determine touch or induced current levels. The hazard assessment will determine the critical issues of frequency, applicable limit units and exclusion distance boundaries. For this reason the assessment should be performed by organisations with proven competences with accreditation from a suitable body. The accreditation requirements should ensure that the procedures, tools, instrumentation and personnel are of a sufficient standard to make certain that the assessment is credible.

Once an employer has established the possibility of a hazard there is an "duty of care" or obligation to control the hazard and apply the hierarchy of control these are:

- Elimination
- Substitution
- Isolation
- Engineering controls
- Administrative procedures
- Protective clothing and equipment

Concurrent with of the control the hazard is the education of the employees so that when they work with potentially high levels of RF radiation they may intelligently apply safe work procedures. In summary, the training of workers should cover the following topics:

- The properties of radiofrequency radiation
- The biological effects
- The safety standards that provide protection
- Clear presentation of the areas of high exposure in the worker's workplace
- Safe work procedures
- The characteristics of an RF source that effect exposure

Properties of Radiofrequency radiation

Most workers do not have an adequate understanding of the properties of RF radiation. It is neither practical nor necessary to give workers a comprehensive or scientific understanding of RF radiation. However, it is appropriate to describe the relevant properties that may cause health effects and remove the misunderstanding that can cause unnecessary worry and disruption to the workplace. Some of the fundamental properties that need to addressed are:

- RF radiation is part of the electromagnetic spectrum
- RF fields are energy waves composed of electric and magnetic fields that can be modulated
- The waves are described by their frequency/wavelength and intensity
- RF radiation is part of the non-ionising spectrum and not like the ionising part of the spectrum that includes x-rays, gamma rays and UV light
- RF radiation is not the same as power frequency magnetic fields
- Is more similar to IR light in that the main known effect is heating

Biological effects

The knowledge regarding the known short-term effects about RF radiation is well established. This knowledge should have a direct bearing on the work practices of employees who are exposed to it during the course of their employment. The WHO has identified three known effects where there is an extensive body of scientific evidence to support their existence. These effects are: tissue heating by various mechanisms, neuro-stimulatory and acoustic. When describing these effects it is important to point out the influence of frequency showing that the level of absorption and the effect are related to frequency.

The neuro-stimulatory effect that is caused by the induced RF currents in tissue stimulating the nerves and causing an involuntary reaction is limited to frequencies of about 100 kHz and is more related to those workers who work with induction heaters.

The acoustic effect is a particular phenomenon that manifests itself as a clicking or buzzing in then ears when the exposed person is subjected to high power pulsed microwave fields like those around radar antenna. While this is an established phenomenon, it is quite rare to encounter the exposure situation that generates this effect.

Of greater importance are the heating effects which can range from cataracts, burns and heat exhaustion. It is this particular effect where most importance should be directed as it is relevant to most

workers who are employed in the field of radio communications and broadcasting along with manufacturing industries that use RF welding and drying equipment. The more serious injuries that generally occur are a consequence of high limb or contact currents that cause burns or nerve damage. High currents are generally through physical contact with a reradiating metal objects or live conductors/antenna elements. There are many documented cases where RF welder operators have received bad burns that require medical involvement. Similarly, workers who work around high power MF, HF and VHF broadcast antennas have received bad burns though contacting live conductors and reradiating guy wires.

While the more serious injuries occur as a result of contact currents, whole body heating can occur as a result of being in a strong ambient field like that around a HF broadcast antenna. The heating effects will be felt as either a localised heating more commonly in the ankles and lower leg or as a core temperature rise in the body that if allowed to continue would result in heat exhaustion.

While many workers express the concern that RF exposure may lead to male fertility effects, eye damage and cancer induction, it is important that the training puts these concerns in their proper perspective and alleviate unnecessary worry. It would require extremely high levels of sustained exposure that is well above the ICNIRP limits to cause eye damage and short-term fertility effects. There is no substantiated scientific evidence that RF causes cancer.

An important part of training is to raise the issue of medical implants that may be either metal rods as in the case of bone breakages or active devices like pacemakers. In these circumstances workers are advised to speak with medical specialist before working in areas that have high fields. Similarly, the issue of pregnancy needs to be addressed. Some authorities consider the unborn child for purposes of the exposure limits to be a member of the general public that consequently requires the mother to restrict her exposure to the general public limits. Should this approach be taken it would be necessary for pregnant workers to notify their employer with the intention of ensuring that their work place exposure does not exceed the general public limits.

Safety standards

Article 6 of the EU Directive requires workers to be provided with information about “the values and concepts of the exposure limit values and action values”. This component of the training creates a potential challenge for workers in the various industries using RF radiation. Quite often workers do not have an educational background or familiarity with the units of measurement that would otherwise enable them to understand the measurement terms. While it is simple to present a table with exposure frequencies and related limit values it is necessary to provide an explanation for the concepts. The key points to present are:

- Exposure limit values which ICNIRP calls Basic Restrictions which relate to power density at the skin’s surface, energy and current densities in the body which are not easily measured. Although important at a theoretical level, exposure limit values need not be taught in much depth.
- Action values are described by ICNIRP as Reference Levels and are the units of measurement for the physical quantities of electric and magnetic field strength, equivalent plane wave power density, contact current and induced limb current. Measurement of these quantities will determine compliance with the limits. A clearer understanding of action values needs to be given to those workers participating in training.

A successful method used by the author when conveying the concepts of action values is to build on knowledge of common every-day experience. This method includes using the analogy of radiated heat from an electrical radiator and the use of a domestic microwave oven to heat food. This allows more complex and less familiar concepts to be built on the knowledge of familiar and readily understood experiences.

Clear presentation of exposure areas in the worker’s workplace

A further requirement of the Directive is that workers receive the results of the exposure assessment. This requirement logically seeks to provide the worker with an understanding of where the areas of non-compliant exposure occur so that they may avoid those areas. The adoption of a common reporting format of hazard zones greatly simplifies this aspect worker information. A common graphical presentation that is gaining worldwide acceptance and is standard practice in Australia is to show site/building plans marked with two colours. The colour yellow depicts areas where the exposure

levels exceed the time averaged ICNIRP general public limits but are less than the occupation exposure limits. The colour red on the drawing shows the areas where the time averaged exposure levels are in excess of the occupational exposure limits. The use of simplified colour coded scale drawings enables workers to understand the hazardous areas without having to interpret units of measurement. Employers who provide a graphical presentation of hazard areas will fulfil their requirement to assess/map exposure areas and also provide the necessary hazard assessment information to their workers.

Australia has developed a standard reporting format for identifying RF hazard zones around transmitting antennas. The assessment report is known as a radio communications site management book (RCSMB) and finds its major use with radio systems that enable calculation of the exposure levels based on antenna gain/aperture and input power. The RCSMB is also suitable for use where exposure levels are determined by measurement and its format allows its use for industrial applications of RF. The RCSMB is the one document that addresses all of RF safety issues related to a particular site. The RCSMB contains the following sections:

1. **Site Contact Details -** *who should be contacted when any information is required*
2. **Site RF EME Diagrams –** *plan and elevation drawings showing exclusion zones*
3. **Site Access Control** - *Access Control Procedure - RF Hazard Warning Signs Installed - Special Requirements / Local Rules*
4. **Equipment Installed at this Site -** *Summary of Physical Equipment Installed - Equipment List*
5. **Site Specific Documents –** *Photographs – additional measurements*
6. **Safe Work Procedure –** *The procedures that need to be followed to ensure a safe workplace*
7. **Additional Information Sources –** *generic RF hazard information – web based information etc*

Safe work procedures

Every worker whose duties require them to access areas of RF exposure that exceed the ICNIRP general public limits need to have a written set of understandable safe work procedures. The procedures can be generic and applicable for all RF workplaces. The procedures should include:

- Read the site safety documentation (RCSMB)
- All workers accessing the area must be trained
- All workers entering the area must be authorized
- Obey all warning signs
- Assume all RF sources/antennas are active
- Have transmitters/sources locked out/disconnected before working on them
- Do not pass in front of the radiating faces of antennas, always pass behind/below
- Use personal RF monitors (PPE) when working around transmitting antennas or unfamiliar antennas. Note: specific training is a prerequisite for correct use

The characteristics of an RF source that effect exposure

The majority of sites will not have sufficient documentation to identify the hazard zones and it will be up to the worker to conduct their job safety analysis (JSA). Training needs to provide a basic understanding of the properties and characteristics of RF transmitting sources/antennas. This will enable workers to enter a site and generally determine where potential hazard zones exist. An important part of this training is to educate workers about transmitting antennas. The training material on antennas should not be at an engineering level or involve complex mathematics. Rather, it should focus on the physical differences that allow antennas to be defined to be either omni directional or directional with the emphasis on where potential hazard zones exist. A brief introduction to the calculation of radiated power flux levels should be given with attention being given to the three variables in the equation. The variables of gain, power and distance from the source should be explained in sufficient detail to enable the worker to see how these variables may effect their exposure.

Summary

Training for workers who work around RF transmitting sources is essential for their safety. It is possible to pitch the training material at an educational level that captures the majority of workers. The use of graphical materials (power point slides) and analogies from every day life will help most workers meet the training objectives. Wherever possible, workers should be encouraged to discuss their experiences and draw on their knowledge during group discussions. The training should not be delivered as a lecture; preferably, the training should be presented as small group training.

The training can be delivered in less than one day (4 – 6 hr) and should be accompanied by a comprehensive set of training notes. The training objectives need to be clearly stated with a written assessment conducted at the conclusion of training. A certificate should be issued if the assessment indicates correct understanding of the material.

Where possible the material should be accredited by an external educational/advisory organisation. The person conducting the training should be able to demonstrate an in depth knowledge of the material and have obtained formal training qualifications.

Acknowledgements

Australian Centre for RF Bioeffects Research: Specification of Key Learning Objectives for Training on RF EME Awareness & Operating Procedures.

TRANSPARENCY FORUM - A RISK COMMUNICATION PROJECT IN SWEDEN

L. Mjönes and Lena Hyrke

Swedish Radiation Protection Authority
SE-171 16 Stockholm, Sweden

Abstract

The roll-out of the third generation system for mobile telephony has been fast in Sweden. The decision to build the UMTS system, 3G, was taken in 1999. In spring 2006 the population coverage for the system was over 90 percent. The rapid launching has created concern and opposition among parts of the general population. During 2004 and 2005 the Swedish Radiation Protection Authority, SSI, has arranged the "Transparency Forum", TF, a series of three open seminars regarding the 3G roll-out where all stakeholders were involved: authorities, industry and NGO:s, including interest groups. The basis for TF is a risk communication model (RISCOM) for delicate situations. A key element in TF is that all stakeholders are involved on equal terms in the planning and realization of the project. The three seminars covered: Roles and responsibilities of the different organisations, The scientific basis for risk assessment and Risk management and precautionary principles. An independent evaluation company evaluated the project. The conclusion was that TF had offered an arena for stakeholders to meet and that the dialogue had been valuable. The evaluators pointed out that it is the responsibility of SSI to carry on working in the transparent way opened up by the TF.

Recent Risk Communication Activities in Sweden

The Swedish Radiation Protection Authority, SSI, is the competent authority for radiation protection in Sweden, both for ionising and non-ionising radiation. During 2004 and 2005 SSI has made special efforts to inform and educate the public and the municipalities as well as arranging other kinds of dialogue-projects concerning mobile telephony and health.

In 2004 a series of six regional one-day training courses, "Mobile telephony and health", was organised by SSI and the National Board of Health and Welfare. The training course was offered to all Swedish municipalities. Altogether more than 300 regional and municipal employees and politicians attended the courses. The response from the attendants has been very positive.

Early the same year SSI took the initiative to a network of experts on mobile telephony and health in the five Nordic countries: Denmark, Finland, Iceland, Norway and Sweden. The work in this group resulted in a common position paper "Mobile Telephony and Health" (1). In short the Nordic authorities pointed out that there is no scientific evidence for adverse health effects from mobile telecommunication systems, but that some scientific uncertainty and knowledge gaps could justify a precautionary attitude regarding the use of handsets for mobile telephony.

During 2004 and 2005 SSI, arranged the "Transparency Forum for mobile telephone systems", TF, a series of three open seminars regarding the 3G roll-out where all stakeholders were involved: authorities, industry and NGO:s, including interest groups. The basis for TF was a risk communication model (RISCOM) for delicate situations. A key element in the RISCOM model is that all stakeholders are involved on equal terms in the planning and realization of the project. The three seminars in TF covered: Roles and responsibilities of the different organisations, The scientific basis for risk assessment and Risk management and precautionary principles.

This paper describes the Transparency Forum in more detail.

The process of defining the project

The roll-out of the third generation system for mobile telephony has been fast in Sweden. The decision to build the UMTS system was taken in 1999. The licences for the operators were distributed in 2000. In spring 2006 the population coverage for the system exceeded 90 percent in Sweden. The rapid launching has created considerable concern and opposition among certain parts of the general population. The media coverage of the

3G issue has been intensive. Interest groups have been active in the resistance towards the launching of the new system and sabotage against masts carrying UMTS base stations has occurred. Also, individuals that have reported a variety of health problems that they relate to exposure to electromagnetic fields have argued that the authorities have neglected their problems. The debate at the municipal level has been intensive, involving local civil servants as well as local politicians. The building of masts has been appealed in court etc. SSI and other central authorities, have received critical views concerning the authorities' role in the controversy on new mobile phone technologies. One reason for this is the perceived technocratic approach that is no longer accepted. The need for a dialogue was obvious.

The RISCOM model of transparency

For more than 15 years, SSI has been working with risk communication in the nuclear waste arena, trying to achieve a better dialogue between different stakeholders. Using this risk communication experience and methodology, SSI has been co-financier in the development of a communication model for dialogue in different areas of complex issues of society – RISCOM (from RISkCOMmunication). One suggestion of the RISCOM approach is to create an arena for dialogue and discussion for concerned parties (2,3,4).

Decisions on certain complex issues, for instance regarding nuclear waste management, involve both scientific/technical and value-laden parts. If this is evident, transparent, both to the public and the decision-makers the decisions taken will generally improve in quality. It is also important that all parties understand the roles and responsibilities of the different stakeholders.

According to the RISCOM model, appropriate procedures must be created in which the decision-makers and the public can validate claims of:

- Truth (technical-scientific issues: Is this true? Are we doing things right?
- Legitimacy (normative issues: What is fair, acceptable, legitimate)
- Authenticity (trust, no hidden agendas, personal integrity and organisational identity)

These are the three corner-stones (often illustrated as a triangle) in the RISCOM concept, they are equally important and interconnected.

It is seldom possible for the public to understand the scientific and technical issues in detail, or for the different scientists and experts to understand the details of each other's disciplines. Therefore, appropriate decision processes must be created; allowing the public to judge whether they can trust different scientists and experts. The public, and other stakeholders, must have the opportunity to evaluate the trustworthiness and authenticity of all parties involved. An important and useful tool to evaluate Truth, Legitimacy and Authenticity is the concept of "stretching". Stretching usually means that critical questions are raised from different perspectives and answered. All involved parties must allow themselves to be stretched. Public participation is essential for transparency and a satisfactory public involvement is not possible without transparency. The media is also important in a transparent process. Experienced journalists are vital for stretching scientists, experts and authorities but must also allow themselves to be stretched.

The RISCOM concept has been successfully applied in the nuclear waste management discussions in Sweden.

Transparency Forum

During 2004 SSI initiated a dialogue project outline on the launching of the third generation of mobile telephony, the "Transparency Forum for mobile telephone systems". The aim of this project was to improve the dialogue and transparency in society regarding electromagnetic fields, focusing on new mobile telephone systems, and to increase the mutual understanding of different stakeholders' roles and value judgements, so that different discussions will be addressed in the right arenas (political, technical, municipal etc.).

All kinds of relevant stakeholders have taken part in the project; authorities, industry and NGO:s, including interest groups. All were given the opportunity to express their opinions and ideas since a key element in RISCOM is that all stakeholders are involved on equal terms in the planning and realization of the project.

The reference group

A reference group was created, with a broad representation of the relevant stakeholders. The reference group did, at a series of regular meetings, take decisions on defining the process, program, timetable, meeting places, etc. A requirement for the Transparency Forum concept was that the project was to be defined and decided by this reference group, and not by SSI alone. The RISCOM principles were used all the way as the structure for

dialogue. Swedish authorities financed the project and SSI was the project manager, also using consultant experts.

A number of preparatory meetings were held to define the need for a dialogue process, starting with representatives from two municipalities experiencing a debate concerning the implementation of new mobile phone technologies. The municipal interest was very high, leading to widened meetings with other stakeholders, also approving the initiative (other authorities, municipal representatives, industry, NGO:s etc.). Therefore, a reference group with a broad range of stakeholders was established to define the Transparency Forum project. A project outline was created, that has been updated and accepted by the reference group, along with a formal agreement specifying the conditions for participating.

Organisations represented in the reference group:
Authorities

Swedish Radiation Protection Authority
National Board of Health and Welfare
National Electrical Safety Board
Swedish Work Environment Authority
National Post and Telecom Agency
National Institute of Public Health
Swedish Emergency Management Agency
Stockholm County Council (Medical expertise)
Nacka and Södertälje municipalities

Industry
Ericsson
MTB (Organises manufacturers and dealers of mobile phones)
Tele2 (Network operator)
TeliaSonera (Network operator)
Vodafone (Network operator)

NGO's
TCO Development (Labelling of mobile phones and other electronic products)
Vågbrytaren, Swedish for Breakwater (Interest group fighting unhealthy electromagnetic radiation)
FEB, Swedish Association for the Electro hypersensitive

Three interactive seminars

During the project preparation it was decided that three seminars should be organised where it would be possible for all stakeholders to state their true opinions and be questioned on their views by all others. The reference group decided on the following themes for the three seminars:

Seminar 1 - The roles and arenas of the different stakeholders
This first seminar was held late in 2004 and about thirty people attended. The seminar gave a description of the historical evolution of the new mobile telephone systems, focusing on decisions in political, technical, and economical areas that have led to the present situation.

To create a dialogue people have to meet, and be given the opportunity to understand other stakeholders' roles and responsibilities. Several Swedish national authorities are more or less involved when it comes to the question of UMTS, and the roles and interactions of these are not always easily understood. Therefore, a description of the interaction between different stakeholders and arenas was designed. Representatives for the involved authorities, industrial companies and NGOs gave accounts of their different views on the mobile telephone issue. A Member of Parliament representing the Green party presented that party's view.

After the presentations a number of interesting questions that had appeared during the day were discussed in working groups. Some of the questions were.

- How can Society take better care of people who claim to be electro hypersensivive?
- How can the precautionary principle be applied to mobile telephony?
- Who has the responsibility for weighing risk against benefits of new techniques?

- How should anecdotic reports and personal experiences be taken into account in the risk estimation process?

The discussion in the groups were loud and vivid, but were held in a good mood.

Seminar 2 - The research basis for the risk estimation

The second seminar was held for two days early in 2005 and about sixty people attended. The scope of the seminar was to discuss the research in the area of radiofrequency electromagnetic fields and health as a basis for the risk estimation for mobile telephony.

Risk evaluation and judgment is not a strictly technical and scientific issue, values also plays a very important role. It is important to understand how we, as individuals, perceive risks and makes personal risk judgments. The second seminar was therefore planned with a broad framing where the themes of discussion were:

- Radiation – physical and biological facts and risk estimations for electromagnetic fields
- Risk estimation concerning mobile telephone systems
- Different methods for risk estimation
- The basis for SSI´s risk estimation and regulations for electromagnetic fields
- The situation for individuals who find themselves hyper-sensitive to electromagnetic fields

Among the participating scientists were Anders Ahlbom and Maria Feychting from the Karolinska group, Lennart Hardell from Örebro University, Jacob Eberhardt from Lund University (the Salford-Persson group) and Igor Belyaev from Stockholm University. Lars-Erik Holm, director general of SSI presented the authority's risk estimation for exposure from mobile phones and from base stations. Representatives for the industry and the interest organisations presented their respective views on the risks. The discussions and stretching after the presentations were intensive and sometimes rather aggressive

Also at the second seminar discussions in working groups were an important part. The group discussions were held at the end of the first day. A specific scope this time was that the groups should present questions that could be used for the stretching the next day. Four groups were formed:

1. Research on health risks from base stations and antennas
2. Research on electrical hypersensitivity
3. Risk estimation procedures
4. Research, methodology and evaluation

The working groups were successful in formulating a number of relevant questions for the stretching.

Seminar 3 - Precautionary principles and exposure limits

The third and last seminar, also for two days, was held in spring 2005 and about a hundred people attended. The scope of this seminar was to discuss precautionary principles and exposure limits as applied to mobile telephony.

Precautionary principles are used in many different areas and there are many different interpretations on the practical use and consequences. The precautionary principles relate of course to the use of exposure limits for electromagnetic fields. Themes to discuss were:

- Legal aspects of exposure limits and the precautionary principle (EU and national legislation)
- Exposure limits for electromagnetic fields
- Different interpretations and practical implications

The seminar began with a very interesting presentation on the background and the legal aspects of the precautionary principle by Annika Nilsson, legal expert from Lund University. Maila Hietanen, vice chairman of ICNIRP (Internation Commission on Non-Ionizing Radiation Protection) presented ICNIRP's work and the 1998 guidelines. Igor Belyaev gave an account of the guidelines from RNCNIRP, the Russian commission on non-ionizing radiation protection. The proposal from the WHO EMF Project for a Precautionary Framework, was

also presented. The second day concluded with a panel discussion focussed on exposure limits and how to apply the precautionary principle.

At the beginning of the second day the Swedish minister of the environment, Lena Sommestad, gave the Government's view on precautionary principles and exposure limits applied to mobile telephony. Lars-Erik Holm gave an account of the scientific basis of SSI:s risk estimation and exposure limits. He also presented the role of SSI:s international expert group on electromagnetic fields (5). After that other central Swedish authorities involved in mobile telephony: the National Board of Health and Welfare, the National Electrical Safety Board and the Swedish Work Environment Authority gave their views on the risk estimation.

A representative from Stockholm municipality discussed the rights of those who claim to be electrically hypersensitive and the industry and the NGOs in turn presented their views on the risk estimation. The second day of the seminar concluded with a questioning of some of the speakers and a panel discussion.

The evaluation of the project

To investigate whether the aim of the project was fulfilled, an evaluation was made by an external company specialised in evaluations of different authorities dialogue projects. The evaluation method that was used included different kinds of interviews and telephone questionnaires. Special care was taken to make sure that as many of the project's participants as possible took part in the evaluation. It was also important for the credibility of the evaluation that personal opinions should be taken into consideration and analysed. A special focus was therefore put on subjective impressions of both the project's accomplishment as well as the effects of the project.

The evaluation clearly shows that the majority of the participants have the distinct opinion that the project has resulted in an improved dialogue of the UMTS issue. The project has contributed to that the stakeholders have been sitting at the same table actually meeting each other's different opinions and views in a way that not had occurred in Sweden prior this project. There have also been different forms of learning and a new forum for dialogue has been created. Due to the meeting between different stakeholders with different opinions and values there has been an increased understanding for other stakeholders' roles and values. The project did not have as an aim to reach consensus (6).

The final report

During the entire project the documentation of the process has been of the greatest importance. Some parts of the seminars have also been recorded to make sure that all aspects of the interesting discussions were not lost in mere notes. It was stated already in the beginning of the project that the documentation would result in a final report. The idea was that this report would try to capture the very essence of the Transparency Forum; the dialogue itself. The report is being written not only for the participants of the project but also for all those who did not have the opportunity to participate in the project, of for example geographic reasons. The report is expected to be released in the autumn of 2006.

How is the dialogue continued?

Originally there was an ambition to continue the dialogue of Transparency Forum in a more permanent way, as a regular part of the work of SSI and other stakeholders. But in December 2005 the project was concluded and the reference group resolved. The evaluation points out that it is important to continue the dialogue. The question is how. For this there are no readymade plans as of today, but SSI is determined to continue the work that has been started. SSI has the intention to summon the stakeholders regularly to discuss different aspects of electromagnetic fields and health in order to maintain the dialogue.

References

(1) Mobile telephony and Health – A common approach for the Nordic competent authorities. http://www.ssi.se/news/newsEntire.asp?ID=114&MenueType=5&menu2=Press

(2) R. Espejo and T.Gill The systematic roles of SKI and SSI in the Swedish nuclear waste management system, SSI Report 98:02, RISCOM pilot study, Stockholm 1998.

(3) K. Andersson (Ed), Review/decide and inquiry/decide- Two approaches to decision making, SSI Report 98:03, RISCOM pilot study, Stockholm 1998.

(4) K. Andersson, R. Espejo, C.-O. Wene, Building Channels for Transparent Risk Assessment, SSI Report 98:04, Final Report RISCOM pilot Project, Stockholm 1998.

(5) Reports from SSI:s International Independent Expert Group on Electromagnetic Fields 2003 and 2004, SSI Rapport 2005:01.

(6) P. Salino, S. Faugert, K. Eduards, H. Segerpalm, Transparensforum, An evaluation of the Transparency Forum project (in Swedish), Faugert & Co, 2006.

EFFECTS OF THE STATIC MAGNETIC FIELD GENERATED BY 0.5 T MRI UNIT ON HUMAN CD4$^+$ T CELLS ACTIVATION PATTERNS.

CARMELA LA MENDOLA[1], ANTONIO LO CASTO[2], SERGIO SALERNO[2], GIUSEPPE MAMONE[2], NADIA CACCAMO[1], ROBERTO LAGALLA[2]

[1]Dipartimento di Biopatologia - Università degli Studi di Palermo
[2]Sezione di Scienze radiologiche - Dipartimento di Biotecnologie mediche e Medicina legale - Università degli Studi di Palermo

Abstract

The aim of this study was to investigate the effects of a 0.5 T static magnetic field (SMF) of a MRI clinical unit on human CD4$^+$ T cell lines in terms of cytokines content, expression of surface markers, cell proliferation. Cells were sorted by immunomagnetic beads from peripheral blood mononuclear cells (PBMC). Cells were cultured in complete medium and split into 2 groups of samples, one to be exposed and the other one as control. After 2 hrs of exposure to the SMF at 37°C, cells were stimulated or non stimulated with a mitogen, and incubated for 48 and 72 hrs. After 48 hrs of incubation it was observed in exposed CD4$^+$ T cell lines: a decrease of IFN-γ production assayed by ELISA technique, a decrease of IFN-γ content, cell proliferation, expression of CD25 an activation surface marker- assayed by flow cytometry. After 72 hrs of incubation these effects were no statistically significant. This observation indicates that magnetic fields could have temporarily biological effects on T lymphocytes and that lymphocytes represent a sensitive model for the studying and understanding of the effects of magnetic fields on the immune system.

Introduction

The influence of static magnetic field (SMF) on biological systems has been a topic of considerable interest for many years [1-2]. We have previously demonstrated that SMF can influence the release of cytokines and intracellular calcium by human CD4$^+$ T cell lines [3-6]. Immune system cells represent a sensitive model for the study and understanding of immunophysiological effects of the SMF [7]. The aim of this study was to investigate the effects of a 0.5 T SMF of a MRI clinical unit on human CD4$^+$ T cell lines on cytokines content, expression of surface markers, cell proliferation.

Materials and methods

Peripheral blood mononuclear cells (PBMC) were isolated from heparinized blood by centrifugation on Ficoll-Hypaque (Pharmacia, Uppsala, Sweden). Cells were maintained in RPMI-1640 (Gibco, Grand Island, NY) supplemented with 10% heat-inactivated pooled human AB$^+$ serum, 2mM L-glutamine, 20mM HEPES, 100 U/ml penicillin, 100 μg/ml streptomycin, 5 x 10^{-5} M 2-mercaptoethanol and 150 IU/ ml rIL-2. CD4$^+$ T lymphocytes were sorted by immunomagnetic beads, using an anti-CD4 specific monoclonal antibody (mAb) and CD4$^+$ T cells were then expanded *in vitro* in IL-2/CM supplemented with a purified mitogen, phytohemagglutinin, PHA (Leucoagglutinin, 0,5 μg/ml, Sigma, St. Louis, USA) and irradiated (30 Gy from a Caesium source) allogeneic feeder cells (PBL and Epstein Barr Virus-B cells at a ratio of 10/1). Cells were maintained for 2 weeks without restimulation prior to functional analysis. Purity of the CD4$^+$ T cells was assessed by two colours flow cytometry. PE-conjugated anti-CD3 mAb was used with FITC-conjugated anti-CD4 (mAb Becton Dickinson, San Jose, CA). The cells were analysed by FACScan flow cytometer (Becton Dickinson, Mountain View, CA). This T cells expansion procedure, using PHA and allogeneic stimulation, induces expansion of virtually all CD4$^+$ T cells and does not introduce any bias in the T cell repertoire. Cell culture was split into two groups of samples, one to be exposed and the other one as control to be kept under isothermal conditions for the whole time of the experiment, before the exposure to the SMF. After 2 hrs of exposure to the SMF, cells were stimulated with PHA, employed at a 0.5 μg/ml suboptimal concentration. After 48 hrs and 72 hrs of cell culture, CD4$^+$ T cells were collected and incubated at 37°C for 48 hrs and 72 hrs. A superconducting MRI unit (Vectra, GE Medical Systems, Milwaukee, WI, USA) commonly employed for clinical examinations was the source of the 0.5 T SMF. A specific device for keeping the cell samples at 37° C was used; it was constituted by a thermostated water bath in which a plexiglass tube holder with the tubes

containing cell samples were placed before their introduction within the gantry of the MRI unit. The experiment was repeated twice in different days. Intracellular staining was used to determine the IFN-γ intracellular concentration at the single-cell level both on exposed and sham exposed cell samples, before and after exposure to the SMF. Staining for intracellular nuclear antigen was performed by incubation of fixed permeabilized cells with FITC-labelled anti-Ki67 antibody and/or with PE-labelled anti-CD25 antibody (Becton Dickinson). After two more washes in PBS 1% FCS, the cells were analysed by FACScan flow cytometer (Becton Dickinson). Viable lymphocytes were gated by forward and side scatter and analysis was performed on 100.000 acquired events for each sample. Cells were harvested and fixed with 4% (w/v) paraformaldehyde in PBS for 10 m at room temperature. Fixed cells were suspended and washed twice with permeabilization buffer containing 0.1% saponin (Sigma-Aldrich, Milano, Italy), 1% heat-inactivated FCS, and 0.1% NaN_3 in PBS. The permeabilized cells were then incubated in the presence of saponin with FITC-coniugated anti-IFN-γ , anti-Ki67 and anti-CD25 (Sigma-Aldrich, Milano, Italy) for 1 h at ice temperature. After two more washes in PBS 1% FCS, the cells were analysed by FACScan flow cytometer (Becton Dickinson, Mountain View, CA). Viable lymphocytes were gated by forward and side scatter and analysis was performed on 100,000 acquired events for each sample. The IFN-γ, CD25 expression and Ki67 concentration were monitored by single excitation flow-cytometer technique. The fluorescence was recorded at 490 nm excitation and 520 nm emission.

Results

In $CD4^+$ T cell lines exposed for 2 hrs to a 0.5 T SMF, after 48 hrs of *in vitro* culture, there was a decreased IFN-γ intracellular content and expression of CD25 surface marker with respect to sham exposed cells, that was enhanced in cells stimulated with PHA (Tab. 1, 2). The exposure also caused a decrease of the rate of proliferation of $CD4^+$ T cell lines in exposed cells with respect to sham exposed, stimulated and not stimulated with PHA, as demonstrated by typical FACS intracellular analysis of Ki67 expression (Fig. 1). After 72 hrs of exposure there were not significant differences of the above parameters analysed between the exposed and sham-exposed cells.

Discussion

In this study we investigated the bioeffects of the SMF on the intracellular content of IFN-γ, CD25 marker expression and cell proliferation, using an homogeneous cell population of human $CD4^+$ T cell lines. IFN-γ cytokine is a highly versatile homodimeric protein that plays an essential role in cell mediated immune responses to viral and mycobacterial infections [8]. The IFN-γ gene is located on chromosome 12 and codes for a 17 kDa protein, which then undergoes posttranslational glycolysis converting the IFN-γ to a 20-25 kDa glycoprotein. IFN-γ is produced by NK cells, dendritic cells, cytotoxic T cells, Th0 cells and Th1 cells. IFN-γ directs several immunoregulatory mechanisms that enhance the cytokine's function and increases the production of MHC class I and II, which in turn increase the likelihood that the infected cell will be recognized as such. Moreover, FACS analysis for CD25 expression, which is expressed as an early membrane marker of T cell activation, in exposed and sham exposed cells, treated and not treated with PHA, shows lower expression of CD25 marker surface in exposed cells. Furthermore, we evaluated the cells proliferation by the expression of Ki-67 protein. The Ki-67 protein is present during all active phases of the cell cycle (G1, S, G2 and mitosis), but is absent from resting cells (G0) and therefore it is an excellent marker for determining the so-called growth fraction of a given population. Although the functional role of Ki-67 protein during cell proliferation is unknown, it is unquestionable that Ki-67 protein expression and cell proliferation are closely linked. During the interphase, this antigen can be exclusively detected within the nucleus, whereas in mitosis most of the protein is relocated to the surface of the chromosomes [9]. In this paper, after 48 hrs of *in vitro* culture, a significant decrease of intracellular content of IFN-γ, CD25 expression and cell proliferation was observed in $CD4^+$ T cells exposed for 2 hrs to the 0.5 T SMF of a MRI clinical unit with respect to sham exposed cells, stimulated and not stimulated with PHA. However, after 72 hrs of exposure there were not significant differences of the above parameters analysed between the exposed and sham-exposed cells. These results indicate that $CD4^+$ T cell lines are a target population of SMF, and that the inhibitory effect of the latter is reversible.

References

1. Hong FT. Magnetic field effects on biomolecules, cells, and living organisms. Biosystems 1995; 36, 187–229.
2. Rosen AD. Mechanism of action of moderate-intensity static magnetic fields on biological systems. Cell Biochem Biophys 2003; 39, 163–173.
3. La Mendola C, Lo Casto A, Salerno S, Mamone G, Caccamo N, De Maria M. Effect of the static magnetic fields generated by 0.5 T MRI unit on intracellular calcium concentration and IFN-γ release of human CD4+ T cells. Proceedings Biological effects of EMFs – 3rd International Workshop, 4-8 October, Kos, Greece, 2004: 367-370.

4. Aldinucci C, Pessina F. Pulsed electromagnetic fields enhance the induction of cytokines by peripheral blood mononuclear cells challenged with phytohemagglutinin. Bioelectromagnetics 1998;19:445-51.
5. Salerno S, Lo Casto A, Caccamo N, D'Anna C, De Maria M, Lagalla R, Scola L, Cardinale AE. Static magnetic field generated by a 0.5T MRI unit affects in vitro expression of activation markers and interleukin release in human peripheral blood mononuclear cells (PBMC). Int J Radiat Biol 1999; 75: 457-463.
6. Salerno S, La Mendola C, Lo Casto A, Mamone G, Caccamo N, Cardinale AE, Salerno A. Reversible effect of MR and ELF magnetic fields (0.5 T and 0.5 mT) on human lymphocyte activation patterns. Int J Radiat Biol 2006; 82:77-85.
7. Cadossi R, Bersani F, Cossarizza A, Zucchini P, Emilia G, Torelli G, Franceschi C. Lymphocytes and low-frequency electromagnetic fields. FASEB J. 1992; 6:2667-74.
8. Suzue K, Asai T, Takeuchi T, Koyasu S. In vivo role of IFN-gamma produced by antigen-presenting cells in early host defense against intracellular pathogens. Eur J Immunol. 2003; 33:2666-75.
9. Ikeda K, Shinmura Y, Mizoe H, Yoshizama H, Yoshida A, Kanao S, Sumitani H, Hasebe S, Motomura T, Yamakawa T, Mizuno F, Otaka Y, Hirose H. No effects of extremely low frequency magnetic fields found on cytotoxic activities and cytokine production of human peripheral blood mononuclear cells in vitro. Bioelectromagnetics 2003, 24: 21-31.

Fig.1. FACS intracellular analysis of $CD4^+$ T cells exposed in vitro for 2 hrs to a 0.5 T SMF, stained with antibody anti-ki67 FITC conjugated.

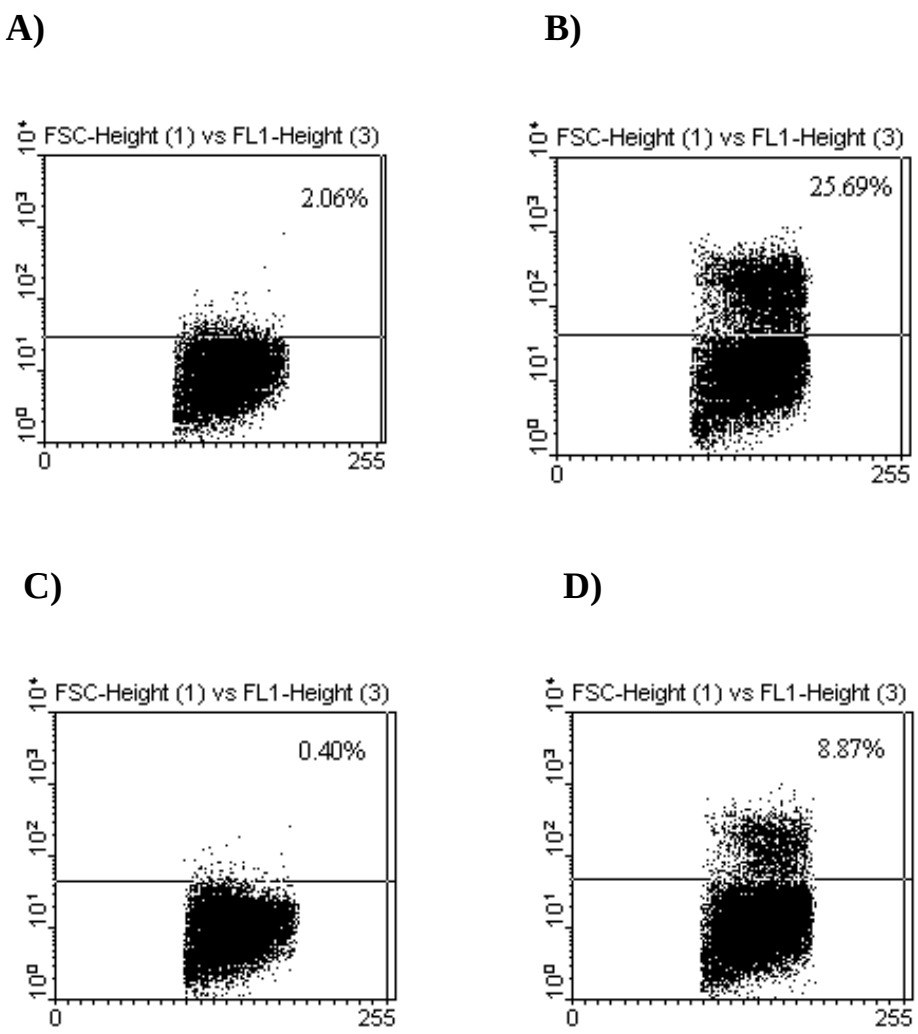

A) Control: $CD4^+$ T cells in complete medium.

B) Control : $CD4^+$ T cells stimulated with PHA.

C) Exposed cells: $CD4^+$ T cells in complete medium.

D) Exposed cells: $CD4^+$ T cells stimulated with PHA.

Table 1. Assay of intracellular IFN-γ of $CD4^+$ T cells exposed in vitro for 2 hrs to a 0.5 T SMF.

Samples		Sham-exposed	Exposed
%IFN-γ^+CD4^+			
48 h at 37 °C	5	2.4 ± 2.5	1.5 ± 1.3
48 h at 37 °C,PHA	5	3.6 ± 2.8	2.4 ± 2.1

Table 2. Expression of surface activation marker on the membrane of $CD4^+$ T cells exposed in vitro for 2 hrs to a 0.5 T SMF.

Samples		Sham-exposed	Exposed
% $CD25^+CD4^+$			
48 h at 37 °C	5	4.2 ± 2.8	3.1 ± 1.7
48 h at 37 °C,PHA	5	9.0 ± 4.5	6.7 ± 2.6

INFLUECE OF ELECTROMAGNETIC FIELD EXPOSURE ON THE GROWTH OF OCIMUM BASILICUM AND ITS ESSENTIAL OIL

FAEZEH GHANATI[1], ELHAM RAJABBEIGI[1,2], PARVIZ ABDOLMALEKI[1]

[1]DEPT. BIOL. FAC. SCI. TARBIAT MODARES UNIV (TMU), POB:14115-175, TEHRAN IRAN

[2]YOUNG RESEARCHERS CLUB IN AZAD ISLAMIC UNIVERSITY, POB14515-775

Abstract

The effect of electeromagnetic field (1 kHz, square wave) on the growth and essential oils of sweet basil (Ocimum basilicum) was studied. The plants in vegetative growth phase were discontinuously exposed to the electeromagnetic field for 6 days, each 5 hours. The results showed decrease of the growth of shoots of treated plants compared to the control group. The activity of polyphenol oxidase was increased by the treatment, whereas the amount of volatiles, in particular of methyl chavicol was decreased. It can be suggested from the results that electeromagnetic field exposure of basil caused metabolism pathway shifted from producing essential oil to the synthesis of other metablites.

Introduction

Interaction between cells and extraneously applied electromagnetic fields (EMFs) have been investigated over last years and many of them have focused on their influence on the growth of organism (Hirano et al., 1998; Davis 1996). However, investigations, dealing with effect of EMF on the performance are scarce and the possible mechanism of he effects of electromagnetic fields on the cells are yet to be elucidated (Panagopoulos et al. 2002).

According to a simple hypothesis an oscillating, external electric field, by exerting an oscillating force on the free ions on both sides of the cell membranes can give a false signal for gating channels that leads in turn to disordering the membrane and therefore the whole cell function (Panagopoulos et al. 2002). Any slight membrane structure disturbance could potentially lead to detectable physiological and biochemical effect. In plants it has been shown that exposure to EMF can alter the metabolism of certain amino acids e.g., asparagines, glutamine, alanine and GABA (Ben-Izak Monselise et al. 2003).

The present study the effect of EMF on the growth, the quality and the quantity of essential oils of sweet basil (Ocimum basilicum), a plant of high economic value was studied.

Seeds of sweet basil were cultivated in a soil containing sand-clay and humus (2:1) and grown at 27 ± 2 ºC and 16 h photoperiodic with a photosynthetic photon flux of 58 μmol m^{-2} s^{-1} at the plant level. Micro- and micronutrients and physical parameters of the soil are shown in Table 1.

A locally designed electromagnetic wave generator capable to generate different wave shape including sinusoidal, triangular and quadratic, was used. This system could generate EMF in the range of 0.1HZ– 10 KHZ with a continuous fine control in stable conditions. It was consisted of two vertical coils each 28 turns of 0.3 mm copper wire rounded around a quadratic frame of 48 × 34 cm. One coil oriented in vertical plane (XOZ) with pointing vector in horizontal direction (anti parallel with the gravity) while the other coil oriented in horizontal plane (XOY) with pointing vector in vertical direction (perpendicular with the gravity). Impedance of each coil was 8 ohm. The maximum consuming power of the system was 9 watt controlled by a fine analog controller. The calibration of system was performed at three different frequency (50, 300 and 1000 HZ) in the center of the chamber. The consuming power was 8 watt at 1kHZ in which the average electric and magnetic strength were 96/3± 4.8(kV/m) and 984± 43(mA/m), respectively. A digital thermal sensor was used to control the temperature inside the chamber during the exposure. While the sample were exposed to the defined EMF, the control samples were placed in the same conditions (i.e., the same temperature, humidity and light intensity), but far enough from the apparatus, being shielded from possible exposure. The plants in vegetative growth phase were discontinuously exposed to the aforesaid EMF for 6 days, each 5 hours. After the period of exposure, plants were gathered and kept at –80 ^{0}C until used for biochemical and analysis. The rate of growth as well as the ratio of fresh weight to dry weight of

the samples before and after the treatment were measured (Table 2). Statistical analysis was done by SPSS and t-test and the differences were considered significant at the level of $p \leq 0.05$.

Polyphenol oxidase (PPO) was extracted from homogenized cells in freshly prepared 100 mM Na-phosphate buffer (pH 6.8) followed by centrifugation at 15,000 × g for 20 min (Kahn 1975). Aliquots of supernatant were added to 100 nM Na-phosphate buffer (pH 6.5) and freshly prepared 4-methylcatecol at a final concentration of 0.02 M. The increase in absorbance at 410 nm per min per mg protein content of the homogenate was the expression of Enzyme activity.

The essential oils were extracted from 50 g (dry weight) of shoot samples by steam-distillation for 3h using a Clevenger type apparatus and were analyzed by GC and GC-MS.

Analytical gas chromatography was carried out in a GC-9A (Shimadzu, Tokyo, Japan) equipped with a DB-5 fused silica column (30 m×0.25 mm, film thickness 0.25 µm, J & W scientific corporation). Oven temperature was held at 60 ºC for 5 minute and then programmed to 210 ºC at a rate of 3 ºC/min. Injector and detector (FID) temperature were 270 ºC; helium was used as carrier gas with a linear velocity of 32 cm/s. Percentages were calculated by area normalization method without the use of response factor correction. The retention indices were calculated for all compounds using a homologous series of n-alkanes.

GC-MS analysis was carried out on a GC-MS system (Varian 3400, USA) equipped with a DB-5 fused silica column (30 m × 0.25 mm, film thickness 0.25 µm, J & W scientific corporation); Oven temperature program was 50 º - 60 ºC at a rate of 3 ºC/min. Transfer line temperature 270 ºC, carrier gas helium with a linear velocity of 31.5 cm/s, split ratio 1/60, ionizing energy 70 ev, scan time 1 sec, mass range 40-300 amu.

The constituents were identified by comparison of their mass spectra with those in a computer library (LIBR-TR and Wiley5 lib.) or with authentic compounds. The identifications were confirmed by comparison of their Retention indices in table 3, either with those of authentic compounds or with data in the literature.

The result showed that the growth of the plants treated with EMF was decreased compared to that of the control group, whereas the ratio of fresh weight to dry weight of increased with EMF-exposed plants were higher than those of the control ones (Table 2).

There activity of PPO of EMF-exposed plants was also significantly higher than that of the control plants (Fig.1).

In comparison to control plants, the amount of the total volatiles of EMF-exposed plants was reduced. The major components of the essential oils of both control and EMF-treated plants were methylchavicol, nerol and geraniol, however the amount of methylchavicol was significantly enhanced by exposing to EMF (Table 3).

Table1. Characteristics of the soil in which the plants were cultivated.

Soil parameters [a]									
pH	EC(dsm^{-1})	%O.C	%Total N	P(ppm)	K(ppm)	Mn(mg/kg)	Fe(mg/kg)	Cu(mg/kg)	Zn(mg/kg)
7.6	4.85	1.79	0.153	52.4	670	13	12.4	0.94	3

Table 2. Effect of EMF on the growth and water content of *Ocimum basilicum*

	Ctrl	EMF
Net Growth (mm)	77.0±0.05	45.0 ±0.1
FW/DW	13.7±0.01	14.3±0.03*

Data are means of three independent experiments in triplicate ± SD, n=3. Asterisk refer to as statistically significant difference at the level of $p \leq 0.05$, by Student t.Test.

Table 3. Percentage of volatile compounds identified in the oil of *Ocimum basilicum* before and after treatment with EMF

Compound	%Eos	
	Control plants	EMF–exposed plants
α-pinene	0.23	0.33
myrcene	0.37	0.40
α-phellandrene	0.15	0.30
α-terpinene	0.11	0.23
limonene	trace	0.23
(E)- β-ocimene	0.44	0.45
trance linalool oxide	trace	-
(E)- β-ocimene	0.82	0.98
linalool	0.20	0.36
neo-allo-ocimene	0.20	0.17
cis-menth-2-en-1-ol	0.37	0.45
borneol	0.32	0.43
methyl chavicol	34.06	42.25
neral	0.16	-
nerol	28.80	19.03
geraniol	27.79	24.53
α-copaene	0.21	-
β-cubebene	0.29	0.66
β-caryophyllene	2.42	1.89
β-sesquiphellandrene	0.82	-
α-humulene	0.43	1.76
spathulenol	1.88	1.19
caryophylleneoxide	0.81	0.28

Retention indices on DB-5 capillary column , t= trace (≤ 0.05%)

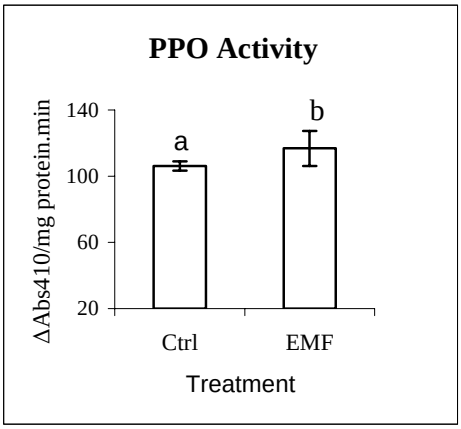

Fig 1. Effect of electromagnetic field on the activity of PPO of shoot of *Ocimum basilicum*. Data are means ± SD, n= 3, signs with different letters indicate significant differences at p≤0.05 according to t-Test.

EFFECT OF EMF ON ESSENTIAL OILS OF BASILE

Summary

The mechanism of the effect of EMF on plant metabolism is still unclear. However, it has been suggested that the production or enhancement of free radicals (Scott, 1993) and ferrous ions (Miyakoshi, 2005), ion change and mass resonance are involved in the adverse effects of EMF on the growth and metabolism of plants.

Decrease of growth can be resulted from damage DNA, proteins, cellular membranes and mutiple genes (Da Silva et al., 2000; Sahebjamie et al. 2006).

Polyphenol oxidase is responsible for tissue browning of raw fruits and vegetables (Mathew & Parpia 1971), which has been found in most higher plants. PPO is a bifunctional enzyme that hydroxylates monophenols to O-diphenols, the only specific reaction catalysed by this enzyme (cresolase or monophenolase) and also oxidizes self generated O-diphenols to the corresponding o-quinon (catecholase or diphenolase) (Gowda & Paul, 2002). Most phenolics that are oxidized by PPO, are intermediates or derivatives of the shikmate and phenyl propanoids pathway. In the present study the increase of the activity of PPO in EMF-exposed basils was not accompanied by an increased production of essential oils. From the results presented here it can be suggested that in EMF-treated plants the activity of PPO shifted from producing essential oil to the synthesis of other metabolites like quinines. Interestingly, despite to the reduction of the of total essential oil content in EMF-treated plants, the amount of methyl chavicol, a main medicinal volatile of basil increased by EMF. Taking all together, the results presented by this study suggest that EMF can be applied as a useful tool to manipulate the metabolism of medicinal plants in order to obtain more desired components.

References

Ben-Izak Monselise E., Parola AH., Kost D. 2003. Low-frequency electromagnetic fields induce a stress effect upon higher plants, as evident by the universal stress signal, alanin, BBRC, 302: 427-434.

Da Silva RL, Albano F., dos Santos LRL, Tavares AD, Felzenszwalb I. 2000. The effect of electromagnetic field exposure on the formation of DNA lesions. Redox Report, 5(5): 299-301.

Davies MS. 1996. Effects of 60 Hz Electromagnetic Fields on early growth in three plant species and replication of previous results. 17: 154-161.

Ghanati F., Morita A. & Yokota H. 2002. Induction of suberin and increase of lignin content by excess Boron in tobacco cells. Soil Sci. Plant Nutr. 48(3):357-364.

Gowda LR. & Paul B. 2002. Diphenol activation of the monophenolase and diphenolase activities of field bean (*Dolichos lablab*) polyphenol oxidase. Journal of Agricultural and Food Chemistry 50: 1608-1614.

Hirano M., Ohta A. and Abe K. 1998. Magnetic field effects on photosynthesis and growth of the Cyanobacterium *Spirulina platensis*. Journal of Fermentation and Bioengineering 86(3):313-316. Kahn V. 1975. Polyphenol oxidase activity and browning of tree Avocado varieties . J. Sci. Food. Agric. 26:1319-1324.

Mathew A.G.H.A.B., Parpia .1971. Food browning as a polyphenol reaction . Adv. Food Res. 19: 75-145.

Miyakoshi J. 2005. Effects of static magnetic fields at the cellular level . Progress in Biophysics and Molecular Biology 87:213-223.

Panagopoulos D., Karabarbounis A & Margaritis LH. 2002. Mechanism for action of electromagnetic fields on cell. Biochemical and Biophysiological Research Communications 298:95-102.

Sahebjamei H., Abdolmaleki P. and Ghanati F. 2006. Effects of static magnetic field on the oxidant enzymes activities of suspension-cultured tobacco cells, Bioelectromagnetics, in press.

Scott G., Free Radicals provide a mechanism for EMFs to promote cancer, In Electromagnetic News, Dec., 1992 (It was then republished in Open Forum on Health (prev. Hauora), Spring 1993.

BIOEFFECTS OF EXTREMELY LOW FREQUENCY ELECTROMAGNETIC FIELDS IN THE LIGHT OF NONEQUILIBRIUM THERMODYNAMICS LAWS

Yulia Chukova

Russian People's Academy of Science, Krasnopresnenskiy Ecological Fund, Malaya Gruzinskaya St. 6 – 42, 123242, Moscow, Russian Federation
Electronic address: y.chukova@mtu-net.ru

Abstract

It is found that reasons for a poor replicability of the nonthermal bioeffects of electromagnetic fields of the extremely low frequency (50-60Hz) have the fundamental basis, revealed by the thermodynamic theory of systems under the Rayleigh-Jeans radiation. It is shown the difference between the Rayleigh-Jeans region and the Wien region of electromagnetic radiation from the viewpoint of energy conversion. The rules and conditions of the good replicability of medical and biological experimental results are formulated.

1. Introduction

The discussion of the electromagnetic fields of extremely low frequency (50-60 Hz) effects on health had began in 1979 with the report by Wertheimer and Leeper [1], who noted that the incidence of cancer was much more in children living in houses where electromagnetic fields exposure was presumed to be higher than usual. This report has given rise to important problem because the exposure of increasingly larger human populations to higher mean levels of extremely low frequency electromagnetic fields is an outcome of the electrification of residential and commercial buildings, particularly in the well-developed countries of the world. The intensity of these man-made fields is substantially more than the ambient nature electric and magnetic fields. Later many epidemiological studies have been published concerning the effects of electromagnetic fields on health, mainly on possible carcinogenic effects. One part reported presence of an association between field exposure and human cancer (leukemia), brain tumor and breast cancer [2,3], but the second part had not found this association. The experimental researches both in vitro and in vivo in this sphere were conflicting too. And may be, that the findings of effects absence are more frequent [4]. So great length of this discussion shows the complication and importance of the problem. Prof. R. Reiter called this situation the Cheshire cat phenomenon [5].

Similar situation was presented in [6] and is connected with bioeffects under microwave radiation. To be more specific, we can say with reasonable confidence that in the present-day a matter of microwave region is more dramatic, as the some scientists do not study the nonthermal bioeffects since they are sure that they do not exist, while the others (Russian) scientists cure many illnesses (cancer etc) on these effects basis.

This conflicting situation may be changed for the better, if the experimentalists use the advances in the nonequilibrium thermodynamics of systems under electromagnetic radiation [7]. This theory shows that the large field of phenomena which were before considered as independent ones, follows a general law of nonequilibrium thermodynamics. This law governs the phenomena of conversion of electromagnetic radiation energy into electrical work, chemical bonds energy and luminescence. It is valid for living and inorganic systems. The qualitative and quantitative validity of this theory was tested in solar cells and it allowed to calculate the dependence of entropy generation rate on absorbed power of radiation due to the irreversibility of a process. This theory is useful in understanding the various aspects of human vision, protozoa photomovement, photosynthesis of plants, nonthermal bioeffects of radiofrequency radiation and other processes. The aim of this paper is to show the reasons of the Cheshire cat phenomenon existence.

2. The thermodynamic law of the isothermal processes under electromagnetic radiation

As it is known [8], the efficiency η of the isothermal conversion of electromagnetic energy into Helmholtz free energy F in open thermodynamic systems is defined as

$$\eta = \Delta F / \Delta W_a \qquad (1)$$

where ΔF is the change of the Helmholtz free energy of the products at the outlet from the system in relation to Helmholtz free energy of the reactants at the inlet of the open thermodynamic system and ΔW_a is the electromagnetic radiation energy, absorbed by the system. If $\Delta F > 0$, we have the endergonic process and if $\Delta F < 0$, we have the exergonic process.

In line with the first and second laws of nonequilibrium thermodynamics for the steady state of a system we have the relation [7]

$$\eta = 1 - T (\dot{S}_a + \dot{S}_i) / \dot{W}_a \qquad (2)$$

where T is the temperature of the system, $\dot{W}_a$ is the absorbed power, $\dot{S}_a$ is the flux of entropy of electromagnetic radiation absorbed by the system, $\dot{S}_i$ is the entropy generation rate as a result of the thermodynamic irreversibility of the process.

Usually in work concerning isothermal process, the thermodynamic method is used to analyse only the limiting efficiency η^* obtained from Eq. (2) under assumption of thermodynamic reversibility of the process, i.e. with the condition $\dot{S}_i = 0$ [9]. Then

$$\eta^* = 1 - T \dot{S}_a / \dot{W}_a \qquad (3)$$

We can find η^* for nonequilibrium electromagnetic radiation with arbitrary spectral characteristics, using follow equations

$$\dot{W}_a = \int E_\nu d\nu \qquad (4)$$

$$\dot{S}_a = 2\pi k c^{-2} \int \nu^2 [(1+\rho) \ln(1+\rho) - \rho \ln\rho] d\nu \qquad (5)$$

$$\rho = c^2 E_\nu / 2\pi h \nu^3 \qquad (6)$$

where k is the Boltzmann constant, h is the Planck constant, c is the speed of light, ν and E_ν are the frequency and the spectral density of absorbed radiation power respectively.

The analyse of Eq. (3) with Eqs. (4 – 6) shows that there are two regions of energy conversion, where the dependence of the η^* on absorbed power $\dot{W}_a$ is quite different because of the ρ may be both more and less than unity [6, 10].

For the $\rho >> 1$ we have

$$\dot{S}_a = 2\pi k c^{-2} \int (1 + \ln\rho) \nu^2 d\nu \qquad (7)$$

and for $\rho << 1$

$$\dot{S}_a = 2\pi k c^{-2} \int \rho (1 - \ln\rho) \nu^2 d\nu \qquad (8)$$

The region, which corresponds to the $\rho << 1$, is the Wien region and the other one, which corresponds to the $\rho >> 1$, is the Rayleigh-Jeans region. These regions are known to experimentalists as the regions, where $h\nu >> kT$ (the Wien region) and $h\nu << kT$ (the Rayleigh-Jeans region). It should be substituted the corresponding values in to Eq. (6) to be certain that is the case.

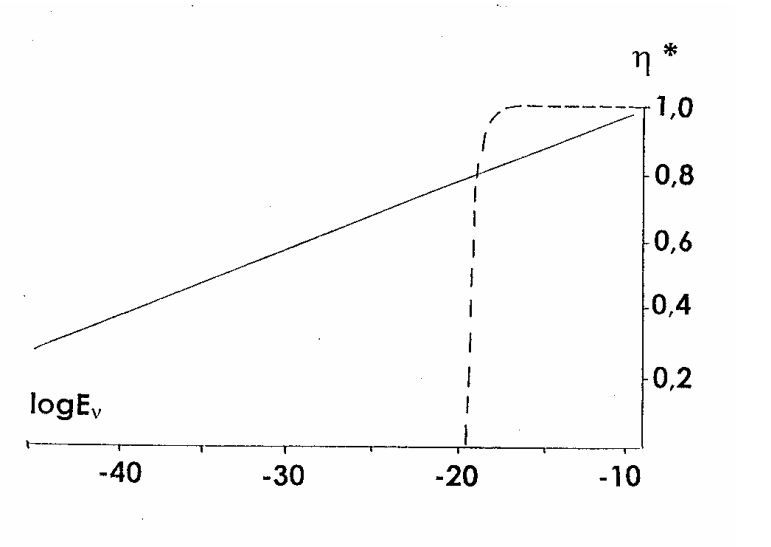

Fig. 1. Dependence of limit efficiency η^* on logarithm of absorbed power spectral density E_ν for the Wien region (solid line) and for the Rayleigh-Jeans region (dotted line). E_ν is measured in J/cm^2.

The upper limit of the η^* is equal to 1 in both the Wien region and the Rayleigh-Jeans one, but the dependence η^* on absorbed power (or the spectral density E_ν) is different. It is slow in the Wien region, where the limit efficiency and absorbed power $\dot{W}_a$ (or E_ν) have the logarithmic relationship. The dependence η^* on E_ν in semilogarithmic coordinates is the straight line, and the interval of E_ν, where the η^* takes the values from zero to unity, is very large (solid line in Fig. 1). In the Rayleigh-Jeans region the η^* dependence on the absorbed power $\dot{W}_a$ (or E_ν) is very strong until it flattens out on a plateau, where $\eta^* = 1$. The thermodynamic limit efficiency varies from 0 to 0.9 with a tenfold increase in E_ν (dotted curve in Fig. 1). Both these curves have the point, where $\eta^* = 0$ and exergonic process is balanced out by endergonic one. The geometry place of these points is defined by [10]

$$c^2 E_\nu^0 = 2\pi k T \nu^2 [(1 + \rho_0) \ln (1 + \rho_0) - \rho_0 \ln\rho_0] \qquad (9)$$

where the E_ν^0 is the spectral density of absorbed radiation and the ρ_0 is the function of distribution at the point $\eta^* = 0$. But the thermodynamic limit efficiency is of no interest for experimentalists.

The real efficiency η of irreversible process may be of interest to them. It is known that the entropy generation rate $\dot{S}_i$ rises at first linearly [7, 11]

$$\dot{S}_i = \alpha \dot{W}_a \qquad (10)$$

where α is constant. One should take into account, the linear changing of the entropy generation rate does not change the form of η^* dependence on E_v , but leads to a parallel shift of the whole curve of η^* along the logarithm absorbed power axis in the Rayleigh-Jeans region and along the η axis in the Wien region [6]. This shift changes the position of the endergonic and exergonic compensation point.

Allowance for nonlinear irreversibility of real process leads to a decrease of η sometimes up to zero in both regions [11].

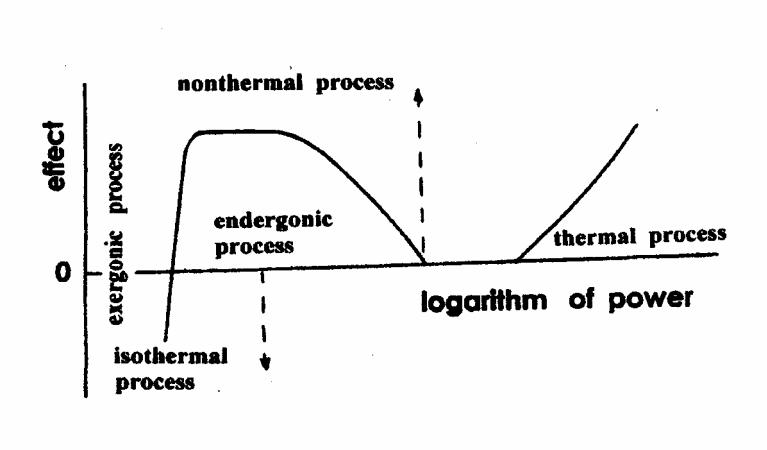

Fig. 2 . Position of isothermal, nonthermal and thermal process in the line of logarithm of absorbed power (Rayleigh-Jeans region).

In the final analysis the η dependence on the absorbed power is complicate. Fig.2 gives it over a wide range of the absorbed power for the Rayleigh-Jeans region. Fig.2 shows different processes (isothermal exergonic process, isothermal endergonic one, nonthermal endergonic one, thermal one) and different dependences (increase, decrease and the lack of any dependence). As is known from experiment [12] the interval of endergonic process may be small (power windowing). Fig. 2 demonstrates the very complicate situation for bioeffect study in the Rayleigh-Jeans region.

The analyse of experimental results on bioeffects of extremely low frequency electromagnetic fields shows that experimentalists study the different ranges of the exciting power, and this is true that they have the different results, including the absence of any effects [4]. The up-to-date experimental results will allow in the future to define the boundary of different processes under the Rayleigh-Jeans radiation in different living systems. Then the general situation will be not like the Cheshire cat.

3. The influence of individual properties of subjects

The Rayleigh-Jeans region has many differences from the Wien one, sending the experimentalists in search of a new apparatus for the experiments. But they must search the new methods of research too, if they want to have the good replicability of the results. The fact is that the role of individual properties of living subject is different in the Wien and in the Rayleigh-Jeans regions.

The indicator of individual properties is the entropy generation rate ${}^0\dot{S}_i$ at the point of endergonic and exergonic processes balance in the real experiments. This point is very known in photosynthesis of green leaves and is called a compensation point. It is studying for human vision processes too. The experimental results for this point allows to calculate the entropy generation rate ${}^0\dot{S}_i$ at this point. In the null point of the real process the dissipative term is equal to the thermodynamic limit efficiency

$$1 - T\,{}^0\dot{S}_a / {}^0\dot{W}a = T\,{}^0\dot{S}_i / {}^0\dot{W}a \qquad (11)$$

and the value of $^{0}\dot{S}_{i}$ may be calculated. The entropy generation rate $^{0}\dot{S}_{i}$ is own characteristic of every individual and can change as a function of internal conditions, for example as age. For the group of individuals with different $^{0}S_{i}$ there are the family of curves $\eta = \eta (E_v)$. In Wien region (Fig. 3a) this family permits to find the average value of endergonic effect in ensemble. In Rayleigh-Jeans region the situation is more complicate (Fig. 3b). Averaging over the ensemble gives the zero result as a rule because of the endergonic and exergonic processes are the opposite ones, and averaging over the small group gives the chance result. This is (and will be always) the reason of poor replicability of the experimental results in conditions of low-level of excitation. Knowledge of thermodynamic theory allows to reduce the extent of poor replicability.

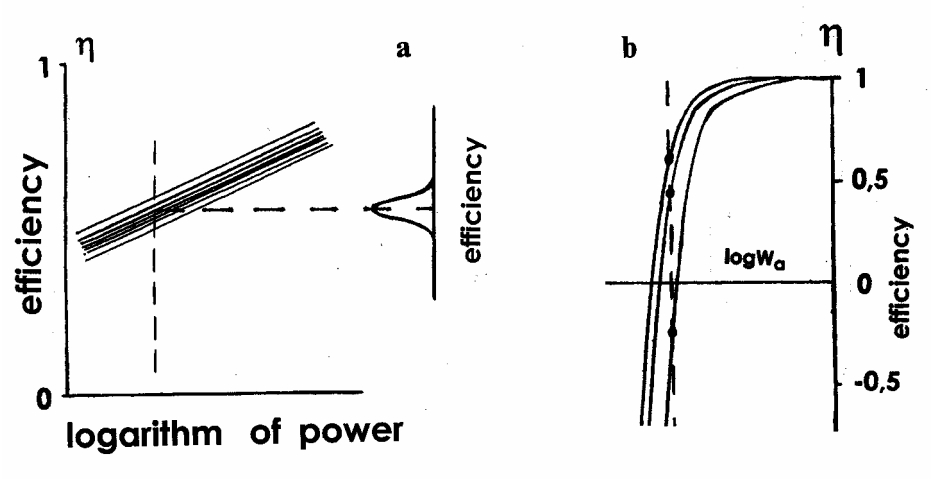

Fig. 3. The different role of the number of objects in experiment under the Wien (a) and the Rayleigh-Jeans radiation (b).

The phenomenon of poor replicability near the boundary of endergonic and exergonic processes depends on the sharpness of $\eta = \eta (E_v)$ dependence. This phenomenon is small in Wien region and would be taken into account by Gauss distribution (the inset in right part of Fig. 3a). This factor is great in Rayleigh-Jeans region. In this region the individual properties of subject are the main ones.

I think that the up-to-date figurative popular expression “the Cheshire cat phenomenon” may be in the future the strict scientific term, indicating that the experimentalist studies the initial stage of endergonic effect under Rayleigh-Jeans radiation without the selection of endergonic and exergonic processes. The selection of these processes allows to save from the Cheshire cat phenomenon.

4. Conclusion

Key features of energy conversion in Rayleigh-Jeans region are sharp dependence of efficiency on power and sharp change-over from exergonic process to endergonic one. On the basis of the thermodynamic theory it is thought that the Cheshire cat phenomenon will be seen in pilot studies of bioeffects under other frequencies of Rayleigh-Jeans region and will cloud the work of experimentalists. However the study of nonequilibrium thermodynamics allows them to understand the situation and reduce to zero (or minimum) the Cheshire cat phenomenon. May be, that the experimentalists, who works in the sphere of extremely low frequency, will be more well than the researchers of microwaves, where the microbiological researches are necessarily associated with the ensemble averaging. In such experiment only the experimentalist of extra class can see the effect.

As known, there is the melatonin synthesis reaction, which is the very good object for study. It enables to clear the influence of electromagnetic fields on the processes in animals and human. Melatonin synthesis will be used as a promoter in solution of discussed problem [13].

5. Acknowledgement

of the financial support from the Research and Writing Initiative of the Program on Global Security and Sustainability of the John D. and Catherine T. MacArthur Foundation

References

1. N. Wertheimer, E. Leeper, Electrical wiring configuration and childhood cancer. American Journal of Epidemiology, 109, 272 - 284 (1979).

2. D.A. Savitz, D.P. Loomis, Magnetic field exposure in relation to leukemia and brain cancer mortality among electric utility workers. American Journal of Epidemiology, 141, 123 (1995)

3. A. Ahlbom, M. Feychting, M. Koskenvuo, Electromagnetic fields and childhood cancer. Lancet, **342**, 1295 (1993)

4. H. Takebe, T. Shiga, M. Kato, E. Masada, Biological and health effects from exposure to power-line frequency electromagnetic fields. Confirmation of absence of any effects at environmental field strengths (Ohmsha, IOS press, 2001).

5. Reiter R. J. An assessment of the bioeffects induced by power-line frequency electromagnetic fields - Modern Radio Science, ed. By M.A. Stuchly. Oxford University Press, 1999, pp. 287 -307

6. Yu.P. Chukova. - Reasons of poor replicability of nonthermal bioefects by millimeter waves - Bioelectrochemistry and bioenergetics, 1999, v.48, p.349 - 353

7. Yu.P. Chukova, Advances in nonequilibrium thermodynamics of the systems under electromagnetic radiation (Khrizostom, Moscow, 2001, ISBN 5-7508-0285-X).

[8] L.N.M. Duysens - In *The photochemical apparatus. Its structure and function.* Brookhaven symp. in biology. (Upton -N.Y., 1959).

9. P.T.Landsberg , G.Tonge - Thermodynamic energy conversion efficiencies.- J. Appl. Phys. 1980, v.51, N7, p.R1 - R20

10.Chukova Yu.P. Effective non-equilibrium radiation temperature (Weinstein temperature) and fundamental thermodynamic prohibition of endergonic reactions.- Russian Journal of Physical Chemistry, 1990,v.64,p.16-19

11. Chukova Yu.P. Energetic and informational interactions in terms of thermodynamics.-Biophysics, 1992, v.37, N 5, p.889-893

12. W.R.Adey,- Frequency and Power Windowing in Tissue Interaction with Weak Electromagnetic Fields, - Proceedings of the IEEE, 1980, v.68, N1, p.119

13. Reiter R.J. Melatonin aspects of exposure to low frequency electric and magnetic fields – In: Advances in electromagnetic fields in living systems, ed. By J.C. Lin . Plenum Press, N.Y.,1997, v.2, pp 1-27

USE OF A MODEL ORGANISM FOR AN ESTIMATION OF ACTION OF THE PHYSICAL FACTORS OF VIDEODISPLAY TERMINALS

VOYCHUK S.I., GROMOZOVA E.N., PODGORSKIY V.S.
INSTITUTE OF MICROBIOLOGY AND VIROLOGY OF NAS OF UKRAINE
UKRAINE, KIEV, 03143, ZABOLOTNY STR., 154,
E-MAIL: VOYCHUK@SERV.IMV.KIEV.UA

Abstract

It is very important to understand whether the electric and magnetic fields generated by video display terminals (VDT) are capable to influence on the living organisms. The effect of VDT (17" computer monitor with cathode-ray tube) was studied on viability of *S. cerevisiae* cells, which is the model organism for studying of eukaryotes. The capacity of electric field at the 4 cm distance to the display was 6.4±3.57 V/m, 4.8±2.04 V/m at 30-40 cm, 0.1±0.02 V/m at 100 cm, and zero at 200 cm. Experimental samples were settled on the distance 4, 40 and 250 cm opposite to the central point of the monitor. Some samples were additionally treated with nystatin (20 μg/10^6 cells) just after exposure. Viability was determined by the colony forming units.

Exposure of the yeast cells to the VDT radiation only did not change their viability. Same time exposed cells showed much grater sensitivity to the nystatin than the control ones. Effect depended on the distance to the computer monitor and the time of exposure.

These results suggests that physical factors of VDT cause some changes in the yeast cells, which reduce their viability at the presence of the strong stress factors, such as nystatin.

Introduction

The problem of an overload of environment with anthropogenic electromagnetic fields (EMFs) grows together with development of scientific and technical progress and introduction of the newest electrical engineering devices. Anthropogenic EMFs, changing a natural electromagnetic background, can result in the origin of a number of disturbances at cellular, subcellular and molecular levels that reflects in the different diseases (cancers tumors, leukemia, dermatitises, mental decline, and so on) [4, 16]. Researches in this field carried out in the different laboratories of the world behind several directions depending on the frequency characteristics of EMFs. Special attention given to influence on the user of radiation emitted from video display terminals (in particular monitors of computers and TV sets) [3, 12]. Except for a mental fatigue, aggression and depression [16], work with video display terminals (VDT) influences a physiologic state of the user's organism changing frequency of heart rhythms, reducing concentration of melatonin in saliva and increasing maintenance in urine of 8-hydroxydeoxyguanosine, and also the number of leucocytes multiplying in a blood [7, 9, 14]. For today, VDT is possible to consider as a risk factor, which increases probability of origin of disease of skeletal-muscular and visual systems [13], skin [2, 10, 15] and reproductive system [11, 12]. In the publications, which generalize the new data on EMFs effects, absence of unique mind is marked in relation to the mechanisms of EMFs action on living objects. This results in the constant revision and perfection of the already established norms of allowable radiation on the living organism [8].

The situation arisen in the given direction of researches closely linked to absence of the biological system-indicator adequate to revealing of harmful effect of VDT on an organism. Multicellular organisms, because of complexity of their structure, not are able to be the sensors of EMFs action that is why attention of scientists aimed on the use as biosensors of separate cultures of human cells [6] or most studied microorganisms [1]. Microscopic biological objects are more conservative in the reactions to action of any factor, and that is why can be used as indicators of the negative/positive influence of EMFs. There are some rather simple and convenient microscopic modeling systems for research of various processes occurring in the eukaryotic cells, in particular cells of yeast *Saccharomyces cerevisiae* and *Schizosaccharomyces pombe* [5].

Studying of EMFs effects with eukaryotic modeling microorganisms will allow to use them as sensory/indicators systems for analysis of the radiation effects from different household devices (computers, mobile phones, the microwave-ovens, and so on) and accordingly to prevent originating the majority of the problems linked to the action of EMFs on the living organism.

The purpose of work was studying the reaction of the yeast *Saccharomyces cerevisiae* cells on the influence of emission of video display terminals.

Materials and methods.

Yeast *Saccharomyces cerevisiae* Y-517 from Ukrainian collection of microorganism at the Institute of Microbiology and Virology of NAS of Ukraine were used for studying. The culture of yeasts was preliminary cultivated on agar medium at 28 ^{o}C during 24 h, and then washed off with sterile distilled water, filtered through cotton wool for the separation of pieces of medium and diluted to 10^9 cells/ml (OD_{540} = 0,75). Cells were held in the distilled water in order to stop the process of division and accordingly to provide the condition of the work with the same organisms. The optical density of cell suspension measured on a wavelength 540±10 nm in a cuvette with optical way 3 mm.

Received cell suspension divided in equal amounts (5 ml) into the 20 ml glass vials. The vials placed (a) in metallic boxes – for shielding of EMFs and (b) simply in glass vial – for shielding of UV-radiation only.

The source of the electromagnetic fields was 17"-monitor with the cathode-ray tube SAMTRON 75E. The monitor was disposed on a wooden-table on 42 cm higher than system block. The screen of monitor was white-color with maximal brightness and contrast. For studying the influence of physical factors generated by VDT on the yeast cells, the diagrams of electromagnetic emission from the computer monitor were analyzed. Measurements carried out with a dosimeter of intensity of an electromagnetic field – NFM 1, in a range 60 kHz – 350 MHz. The readings were taken at 4, 40, 100 and 250 cm from a surface of the screen and walls of monitors. The exposed samples placed on distance 4, 40 and 250 cm to the center of monitor. Irradiation carried out at the room temperature of 24.5±0.5 ^{o}C and day light during maximum 24 h. Cell suspension periodically mixed.

Viability of the exposed and unexposed yeasts cells was determined by the colony forming units in absence and in presence of the fungicidal antibiotic nystatin. Nystatin (2-3 mg) was dissolved in 1 ml of dimethylis sulfoxidum and sterile distilled water added to the necessary volume to receive final concentration of 20 μg of nystatin in 1 ml of solution. This solution used for further researches.

Initially and after 3, 6 and 24 hours yeasts cells from each vial used for determination of viability and sensitivity to the fungicidal antibiotic nystatin. For this purpose 0.1 ml of cells added to 9.9 ml of the sterile distilled water or to 9.9 ml of water containing 20 μg/ml of nystatin getting the concentration of 10^6 cells/ml and mixed it during 10 min. After that, the series of dilutions was done and concentrations 10^3 and 10^2 cells/ml received. From these solutions, 0.1 ml added to the Petri dishes with agar and placed in a thermostat at 28 ^{o}C. The colonies counting and data analyses were done after 72 h.

Results and discussion.

Analysis of the yeast *Saccharomyces cerevisiae* viability in the distilled water showed that cells keep during a long time (more than 24 hours) in a wide range of temperatures (20 – 28 ^{o}C) stable physiologic state. Necessary to notice, that the opportunity of use of only water medium without admixtures is very important as, at first, simplifies process of carrying out of researches and, secondly, minimizes influence of additional physical and chemical factors, which take place at presence in medium of free ions.

As well as in previous our researches [17, 18] at optimum for yeast *Saccharomyces cerevisiae* conditions of an external environment (temperature, pH, and so on) action of EMFs generated by VDT did not reflect on standard parameters of the growth processes. Microscopy also has not given an opportunity to find any differences between the exposed and control samples.

Same times in the presence of the strong stress-factor, such as fungicidal antibiotic, the negative consequences of electromagnetic emission from the VDT were seen. The data concerning vitality of *Saccharomyces cerevisiae* cells at the presence of nystatin shown in Table 1.

Table 1. Percent of viable cells of *Saccharomyces cerevisiae* Y-517 in the presence of nystatin (20 μg/10^6 cells) and in dependence on the distance to the monitor and time of exposure
Values are the mean±SD from the minimum three separate experiments.

Time of an exposition, h	Distance to the monitor, cm			The control
	4	40	250	
0	-	-	-	28±9,9
3	4±2,8	14,8±6,7	25±9,9	28±9,9
6	12±1,2	42,5±5,3	40±2,2	55±7,3
24	29±29,7	22±4,2	45,5±3,5	25±9,9

The maximum of activity of an antibiotic and accordingly a minimum of a resistance of the cells were observed at minimal (4 cm) distance from the center of the monitor. After three hours nystatin suppressed growth of 70 % of cells in the control, and in the exposed samples – 96 %, 85 % and 75 % accordingly on the distance 4, 40 and 250 cm. After 6 and 24 hours these parameters reduced that, probably, testifies to increase of stability of cells to action of the external stress-factors of the physical and chemical nature.

It is necessary to note, that after 6 hours in control samples observed substantial increase (on 20 %) of viable cells. The cause of such phenomenon can be in change of some properties of the yeast cells. For example, the stay of living organisms in the distilled water results in decrease of permeability of cytoplasm membranes and cellular walls with the purpose of not allow an efflux of the intracellular compounds. It, in turn, complicates process of penetration and probability of attachment of polyene antibiotic to the molecules of cytoplasm membranes.

After 24 hours, vitality of cells in the controls diminished up to initial parameters while in the exposed samples remained at high level. This can testify to the presence of differences in character of flowing of intracellular processes in the exposed and unexposed yeast cells, what clearly recognized under action of the strong stress-factor such as fungicidal antibiotic.

Table 2. Doses of radiation in a range 60 kHz – 350 MHz from the SAMTRON 75E monitor with cathode-ray tube, V/m

Values are the means.

Distance from VDT, cm	Screen	Left side	Right side	Top side	Back side
4	6,4	15	9	3	7
40	4,5	2	3	3	7
100	0,1	0,5	0,5	0,5	0,5
250	0	0	0	0	0

The ability of cells to survive under action of an antibiotic is in direct dependence on the distance to the display. The data in Table 2 present doses of radiation received for the monitor with cathode-ray tube SAMTRON 75E used during experiments. Seen, that the intensity of EMFs in the same manner significantly decreased with the distance. Both these facts may suggest that electric fields generated by VDT may play a key role in the influence on the biological objects. It is very important to note that on the distances of 200 and 250 cm from the screen of the display the intensity of EMFs in the range 60 kHz – 350 MHz are equal zero, but biological action of VDT emission still obvious.

Summary

EMFs generated by VDT had the negative influence on the modeling organism *Saccharomyces cerevisiae* that especially seen in the presence of the stress-factor (antibiotic nystatin). Cells of *S. cerevisiae* Y-517 provides unique tools for understanding environmental effects on cellular systems and can be biological sensors at development of the bioanalytical systems for analyses of bioeffects from different electromagnetic devises such as computers, TV sets, mobile phones, microwave ovens and so on.

Other microorganisms may also be sensible to the action of the electromagnetic fields generated with different laboratory or industrial equipments. Therefore, during work with microbiological objects it is necessary to take into account and eliminate the possible influencing of emissions from VDT for avoidance of errors at the estimation of results of researches or during biotechnological processes.

References

1. Parkhomenko I.M., Zarubina A.P., Romanova N.A. et al., Perspectives of the microorganisms' use as biosensors of the low doses of ionizing radiation, *Moscow University Herald, Biology Ser. 16.*, No.2, 2001, pp. 33-40.
2. Aminian O., Mansoori P., Sharifian A. et al., The relationship between Video Display Terminals (VDTs) usage and dermatologic manifestations: a cross sectional study, *BMC Dermatol.*, Vol.5, No.1, 2005, pp. 1-3.

3. Eriksson N., Hoog J., Mild K.H. et al., The psychosocial work environment and skin symptoms among visual display terminal workers: a case referent study, *Int. J. Epidemiol*., Vol.26, No.6, 1997, pp. 1250-1257.
4. Feychting M., Ahlbom A., Kheifets L., EMF and health, *Annu. Rev. Public. Health*., Vol.26, 2005, pp. 165-189.
5. Forsburg S.L., The yeasts *Saccharomyces cerevisiae* and *Schizosaccharomyces pombe*: models for cell biology research, *Gravit. Space Biol. Bull*., Vol.18, No.2, 2005, pp. 3-9.
6. Guisasola C., Desco M., Millan O. et al., Biological dosimetry of magnetic resonance imaging, *J. Magn. Reson. Imaging.*, Vol.15, No.5, 2002, pp. 584-590.
7. Higuchi S., Motohashi Y., Liu Y. et al., Effects of VDT tasks with a bright display at night on melatonin, core temperature, heart rate, and sleepiness, *J. Appl. Physiol.*, Vol.94, No.5, 2003, pp. 1773-1776.
8. Hill D.L., McLeish K., Keevil S.F., Impact of electromagnetic field exposure limits in Europe: is the future of interventional MRI safe? *Acad. Radiol.*, Vol.12, No.9, 2005, pp. 1135-1142.
9. Ishihara I., Ikushima M., Horikawa J. et al., A very low level of magnetic field exposure does not affect a participant's mental fatigue and stress as much as VDT work, *J. UOEH*., Vol.27, No.1, 2005, pp. 25-40.
10. Liden C., Wahlberg J.E., Work with video display terminals among office employees. V. Dermatologic factors, *Scand. J. Work. Environ. Health*., Vol.11, No.6, 1985, pp. 489-493.
11. Marcus M., McChesney R., Golden A., Landrigan P., Video display terminals and miscarriage, *J. Am. Med. Womens Assoc*., Vol.55, No.2, 2000, pp. 84-88.
12. Shaw G.M., Adverse human reproductive outcomes and electromagnetic fields: a brief summary of the epidemiologic literature, *Bioelectromagnetics*., Vol.5, 2001, pp. 5-18.
13. Signorelli C., Lepratto M., Summa A., Management of the visual risk in VDT workers and the role of the occupational physician, *Ann. Ig*., Vol.17, No.6, 2005, pp. 573-584.
14. Takahashi K., Sasaki H., Saito T. et al., Combined effects of working environmental conditions in VDT work, *Ergonomics*., Vol.44, No.5, 2001, pp. 562-570.
15. Tamez Gonzalez S., Ortiz-Hernandez L., Martinez-Alcantara S., Mendez-Ramirez I., Risks and health problems caused by the use of video terminals, *Salud. Publica Mex*., Vol.45, No.3, 2003, pp. 171-180.
16. Travers P.H., Stanton B.A., Office workers and video display terminals: physical, psychological and ergonomic factors, *AAOHN J*., Vol.50, No.11, 2002, pp. 489-493.
17. Voychuk S.I., Gromozova E.N., Lytvyn P.M., Podgorskiy V.S., Changes of surface properties of yeast cell wall under exposure of electromagnetic field (40.68 MHz) and action of nystatin, *The Environmentalist*, Vol.25, 2005. pp. 139-144.
18. Voychuk S.I., Gromozova E.N., Podgorskiy V.S., Effect of EMF (40,68 MHz) on the sensitivity to stress-factors, *Proceedings: 3rd International Workshop "Biological Effects of EMFs", Kos, Greece, 4 - 8 October 2004*, Vol.2, pp. 799 - 804.

INVESTIGATION INTO THE EFFECTS OF 900MHZ ELECTROMAGNETIC RADIATION ON MESENCHYMAL STEM CELLS.

E.F.ANDREWS (1), A.T. BARKER (2), G.G. COOK (1), L. COULTON (3), W. LIU (1), A. SCUTT(4)

(1) DEPT. OF ELECTRONIC & ELECTRICAL ENGINEERING, UNIVERSITY OF SHEFFIELD, SHEFFIELD, U.K.
(2) DEPT. MEDICAL PHYSICS & CLINICAL ENGINEERING, ROYAL HALLAMSHIRE HOSPITAL, SHEFFIELD, U.K.
(3) BONE BIOLOGY GROUP, UNVERSITY OF SHEFFIELD MEDICAL SCHOOL, SHEFFIELD, U.K.
(4) KROTO RESEARCH INSTITUTE, UNVERSITY OF SHEFFIELD, SHEFFIELD U.K.

ABSTRACT

The controversy over the safety of mobile phones and their base stations continues despite many years of study into the non-thermal interactions of radio frequency electromagnetic fields (RF-EMF) with biological tissue. This study exposes rat mesenchymal stem cells (MSC) to RF-EMF in a Crawford TEM cell at 900MHz. A robust dosimetric analysis of the exposure system is performed to determine the configuration which will optimise system efficiency, minimise heating and provide the most uniform specific absorption rate (SAR) across the cell monolayer. Data from exposure of MSC to continuous wave, GSM and intermittent (5mins on/ 10mins off) 900MHz RF-EMF is presented. SAR levels are all below the 2 W/kg ICNIRP guidelines for public exposure. Recruitment, proliferation and differentiation of MSC are measured using the CFU-f assay under osteogenic (bone stimulating) conditions. No effect is observed. Additionally, hydrogen peroxide is used as a model of oxidative stress in order to determine if GSM 900MHz RF-EMF is a cofactor in stressing cells. Again, no effect is observed on MSC recruitment, proliferation or differentiation into bone.

INTRODUCTION

There is continuing widespread debate concerning the possible biological effects of radio frequency electromagnetic fields (RF-EMF) emitted by mobile phones [1]. In-vitro studies are useful because they provide a simplified biological model that allows the exposure parameters to be more precisely defined and controlled compared with in-vivo exposure. This paper presents dosimetric analysis of a Crawford TEM cell [2] at 900MHz using finite difference time domain (FDTD) modelling, to determine the optimum dish separation and height off the septum, and level of culture medium so as to maximise both the power deposited and its uniformity in a monolayer of mesenchymal stem cells (MSC) in the bottom of each culture dish. A similar system has previously been used by the authors to expose human leukocytes in suspension [3]. Specific absorption rates (SAR) are calculated in the ~1mm layer of culture medium at the dish bottom using both in-house [4] and commercial SEMCAD [5] software, with subsequent experimentation based on the results using the fibroblastic-colony forming units (CFU-f) assay to quantify any effects on stem cell recruitment, proliferation and differentiation.

Exposures using continuous wave (CW), GSM type bursts and intermittent carrier (5 mins on / 10mins off) were performed at 900MHz, whilst maintaining a constant ambient temperature of 37°C. In order to ascertain if such non-thermal RF-EMF could also act as a co-factor in causing an effect, a common in-vitro model of oxidative stress was used. Hydrogen peroxide (H_2O_2) is an oxidative agent, known to cause stress to cells, and a concentration of this was added to the cells, sufficient to affect them with no RF-EMF applied whilst at the same time not killing them all.

Materials and Methods

RF Equipment

Briefly, the exposure system in Fig.1 utilises a GSM handset in engineering test mode as a source, which is then amplified and routed through a travelling wave TEM cell. Environmental control is achieved by placing the TEM cell inside an incubator which maintains 95% humidity, 37°C, and 5% CO_2, and real time thermal monitoring of internal TEM cell temperature is provided by a fluoroptic thermometer. To expose at higher SAR values non-thermally the system needs to deliver high efficiency, measured in W/kg per W of input power, while minimising the thermal load. Air fans are therefore attached to the TEM cell at its tapered ends to increase cooling. A second identical TEM cell provides sham exposure for control purposes.

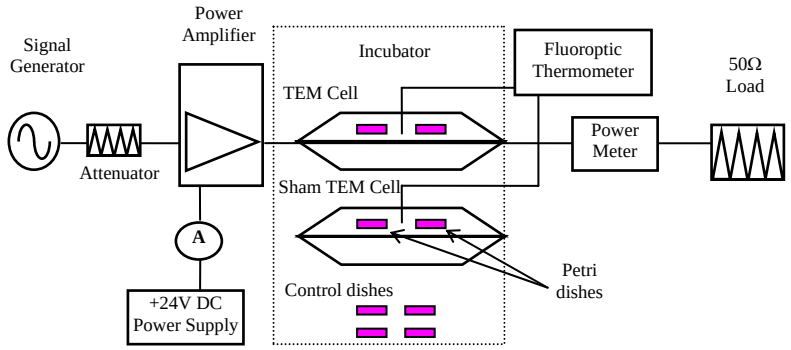

Figure 1: Schematic of Exposure system.

Fibroblastic Colony Forming Unit Assay

The fibroblastic colony forming unit (CFU-f) assay is a cell culture model which uses primary bone marrow seeded at low density. The low density seeding allows the cells to form colonies without contact inhibition. Each colony is assumed to grow in isolation from the others, and be derived from a single MSC, and the number of colonies is a measure of the number of colony forming units present in the original bone marrow cell suspension therefore. This MSC proliferates and differentiates depending on the stimulus [7] which can be chemical or physical. The colonies are then sequentially stained for alkaline phosphatase, calcium and collagen, which are all markers of osteogenic differentiation.

Primary BMSC were extracted from the femur and tibia of adult Wistar rats. Bone marrow was extracted using the method published in [7]. Briefly, the leg bones were removed and the bone marrow extracted and re-suspended in 1ml of Dulbecco's Minimum Essential Medium (DMEM) to create a single cell suspension. Cells from all bones were then pooled and 10ml supplemented DMEM per bone was added to create primary bone marrow suspension. The supplements added to the DMEM were 10% Serum Supreme, 1% Ultraglutamine, 1% Penicillin/Streptomycin and osteogenic stimuli, 50µg/ml ascorbic acid and 10^{-8}M dexamethasone.

The primary bone marrow suspension was used to seed the 90mm Petri dishes at a density of 1.2×10^6 cells, in 10ml supplemented DMEM. RF-EMF exposure was for five 3-hour periods over 5 consecutive days, after which the medium was changed, and thereafter twice a week. Cells were then cultured for a total of 16 days, after which the plates were washed in PBS and fixed with cold 70% industrial methylated spirits (IMS). After fixing, they were immediately histochemically stained for alkaline phosphatase (APase) activity, and then sequentially for calcium-positive, collagen-positive and total colonies. After each staining, the cultures were digitally photographed and the subsequent photographs processed to allow for automatic analysis. The images were then analyzed using Bioimage ''Intelligent Quantifier'' image analysis software [8]. The software counts the colony number and calculates each colony area. This data was subsequently analyzed using SPSS for significance testing using the ANOVA test at $p < 0.05$.

As a result of the dosimetric analysis (see results section), the required medium height in the Petri dishes had to be 10mm (60ml medium) instead of the standard 2-3mm (10ml medium). However, this amount of fluid above the monolayer hinders the gas exchange between the monolayer and atmosphere, causing hypoxia and cell death. In order to comply with the dosimetric analysis therefore, the extra 50ml of medium was added for the duration of the RF exposure and the hour-long temperature equalization pre-exposure period. Immediately after RF-EMF exposure, this extra medium was then removed from each dish and stored separately at 4°C overnight until the next exposure the following day, when it was returned to the same dish. This is because it has been shown that non-adherent cells in the medium are crucial to MSC recruitment and proliferation [7]. After the initial five days exposure however, this extra medium was no longer used. To control for the effect of the extra medium, a set of dishes were placed outside the TEM cells with 10ml of medium, in contrast to the dishes inside the exposed and sham exposed cells which contained 60ml.

The protocol for co-exposure of the MSC to GSM modulated RF-EMF and H_2O_2 was the same as for exposure to RF-EMF alone, with the following modifications. A third control group was added, where MSC were exposed to H_2O_2 alone, outside of the TEM cell, and a concentration of 10^{-5}M H_2O_2 was added to the MSC immediately before placing them in the TEM cells.

Results

Dosimetric analysis

The aim of the dosimetry analysis was to optimise the system to give high SAR efficiency and uniformity. The use of both in-house and commercially available SEMCAD FDTD code provides valuable control data for accuracy assessments, and also expedites analysis since the in-house code runs on a Unix super-cluster rather than the standard Windows PC, which our version of SEMCAD is configured for (although a Unix version is available). Uniformity can be quantified as the ratio of standard deviation of SAR to the mean (%SD), and is calculated for the bottom layer of voxels in a dish. Acceptable uniformity is 30% SD or less [6]. No software currently available can realistically grid to the micrometer scale (the thickness of the monolayer), however a grid size as small as 0.3mm is possible with reasonable simulation time in SEMCAD, which is better than the resolution achieved using physical measurements. It is assumed for the purposes of dosimetry that the SAR in this bottom layer of voxels is representative of the SAR in the monolayer. The volume of medium in the tissue culture dish affects the SAR uniformity and efficiency, as does its distance from the septum, as shown in Fig.2 for 1V peak excitation of the TEM cell. Here our in-house FDTD code has been used to calculate the SAR in the bottom 1mm layer of medium contained within a 90x18mm circular dish with a lid. The SAR clearly increases with medium height (h) and elevation above the septum (z), with bigger changes observed at higher medium levels, whereas the variation of uniformity with elevation converges towards a standard trend as the medium height increases. A medium level of h = 10mm was therefore chosen, at z = 5mm off the septum. A smaller elevation of z = 1mm would have provided the best uniformity of exposure, but with a reduced mean SAR. However, the CFU-f assay requires medium heights of 3mm or less in order to allow adequate oxygen diffusion to the stem cells. This would reduce the SAR by about 10dB and degrade the uniformity, so the medium height was temporarily increased to 10mm for the duration of the planned exposure (3 hours plus 1 hour warm up time) as mentioned previously.

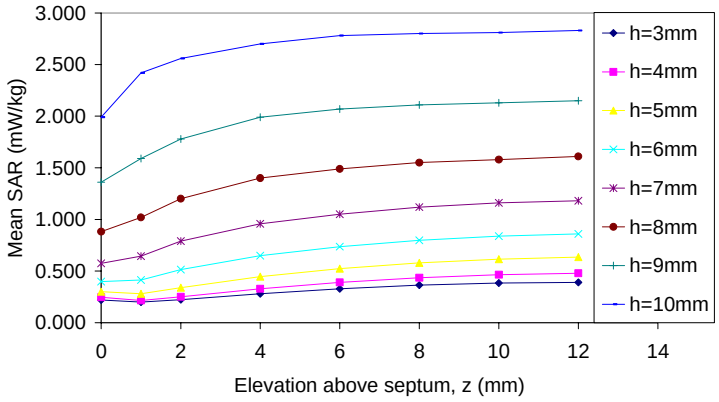

(a)

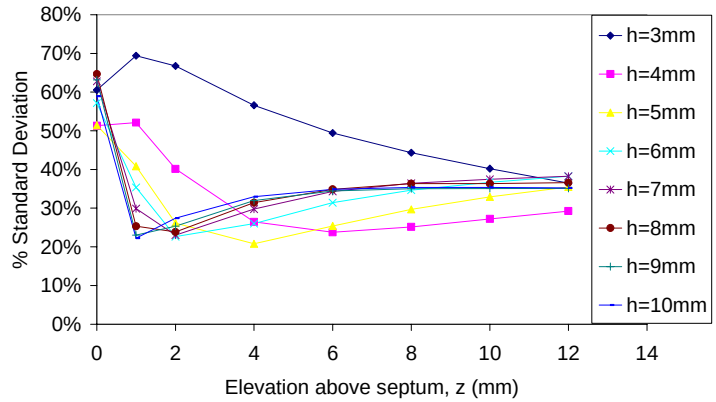

(b)

Figure 2: Variation of (a) mean SAR and (b) SAR uniformity in bottom layer of culture medium as a function of dish elevation (z) for various medium heights (h).

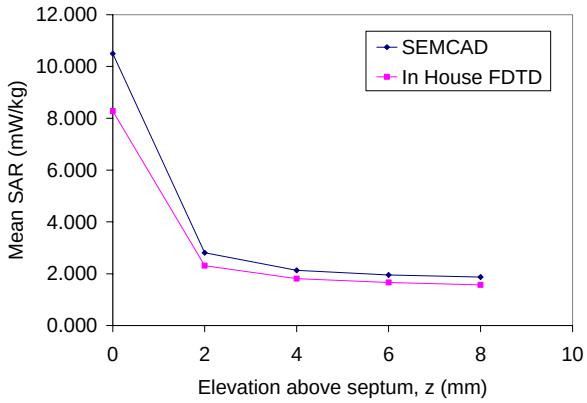

Figure 3: Comparison of in-house FDTD code and SEMCAD. Mean SAR for the whole medium volume varying with elevation above septum (h=10mm).

To increase the number of samples exposed simultaneously, two dishes were used, and SEMCAD was now employed to further refine the dosimetry and to investigate the effect of separation between the dishes on SAR and uniformity. As seen in Fig.3 our in-house and SEMCAD code agree reasonably well for a control example. Fig.4 shows the field interacting with the dishes to produce both dissimilar and non-uniform SAR distributions in the bottom layers. Increasing the separation reduces the coupling

and makes the distributions more alike, but edge effects from the tapered ends of the TEM cell begin to influence the uniformity at the furthest separation. The best uniformity is found at a separation of s = 50mm, where the mean SAR's in the bottom layers and their %SD's are similar, which allows the dishes to be treated almost identically. The CFU-f assay uses imaging software to analyse the colony formation of MSC, which excludes the outer 1mm of the dish bottom as the imaging process produces artefacts here. If this area is not taken into account the SAR values are slightly higher than those in Fig.4, with mean = 2.61 mW/kg, %SD = 31.9% for dish 1 and mean = 2.58 mW/kg, %SD = 32.7% for dish 2. The effective SAR efficiency is ~1.0 W/kg per Watt of TEM cell input power.

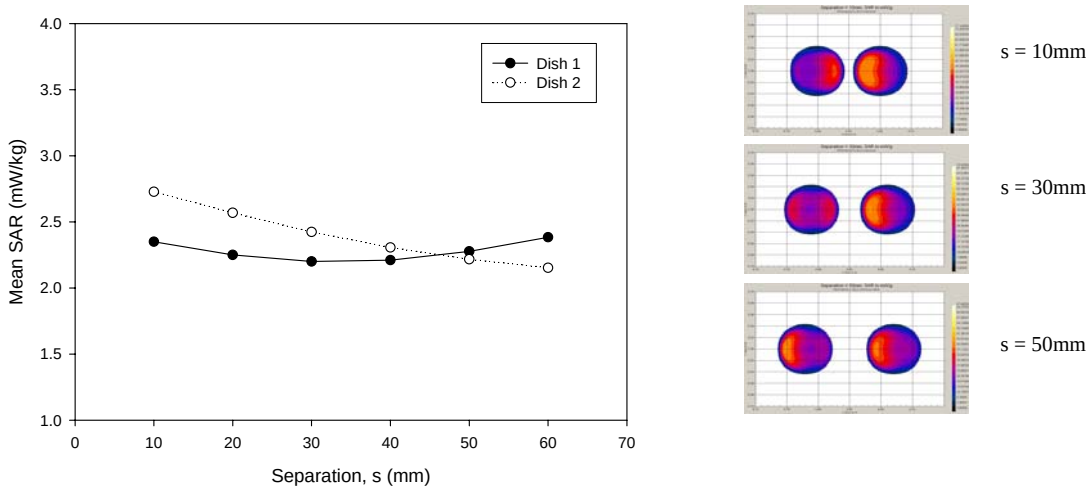

Figure 4: Variation of mean SAR in bottom layer of medium for 2 dishes as a function of separation (s) (h = 10mm, z = 5mm), with example SAR contrast plots shown at s = 10mm, 30mm and 50mm.

Biological Results

Having determined the optimum elevation, medium level and separation for the two dishes, MSC were then exposed to 900MHZ CW, GSM and intermittent CW (5mins on/10mins off) RF-EMF. Averaged SAR values were 1.6 W/kg for CW, 1.6W/kg for GSM and 0.9W/kg during the on period for the intermittent exposure (further work is planned with a higher SAR for the intermittent exposure scheme). After consecutive histochemical staining and image analysis, colony numbers and areas were calculated, and are shown in Figs.5-7.

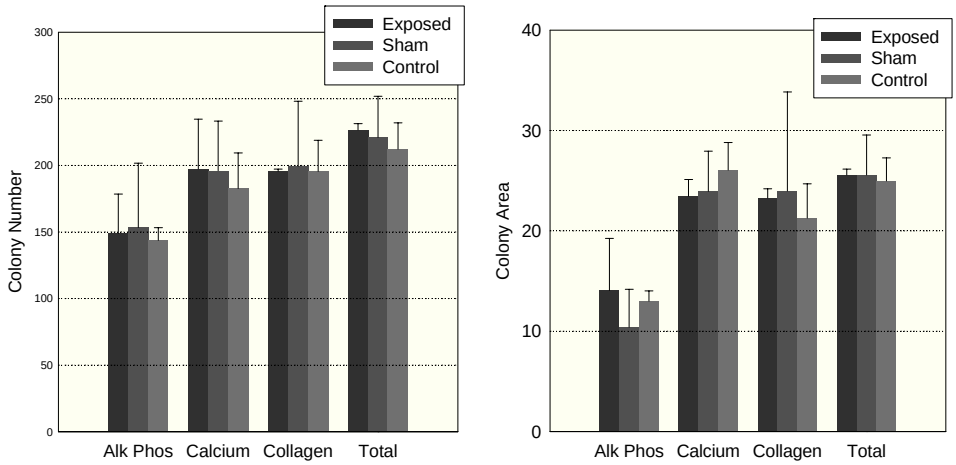

Figure 5: Colony number and area for a representative CW 900MHz RF-EMF exposure. (n = 3 or 4)

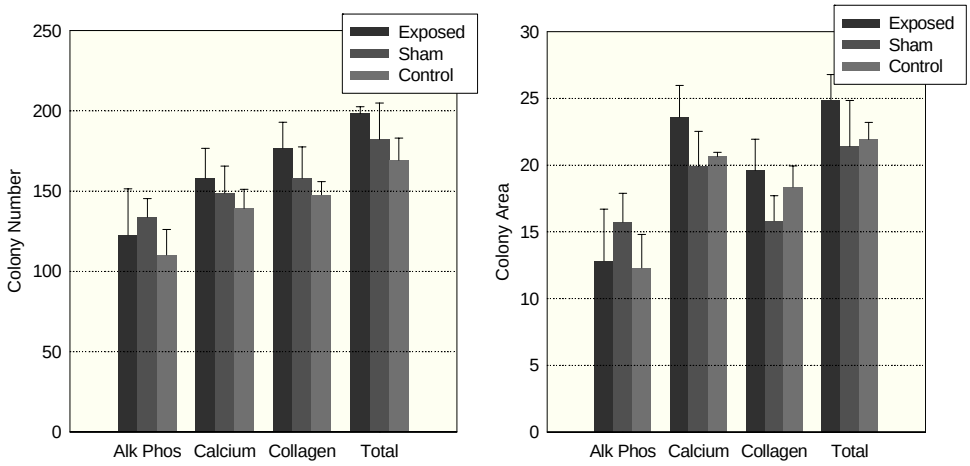

Figure 6: Colony number and area for a representative GSM 900MHz RF-EMF exposure (n = 4)

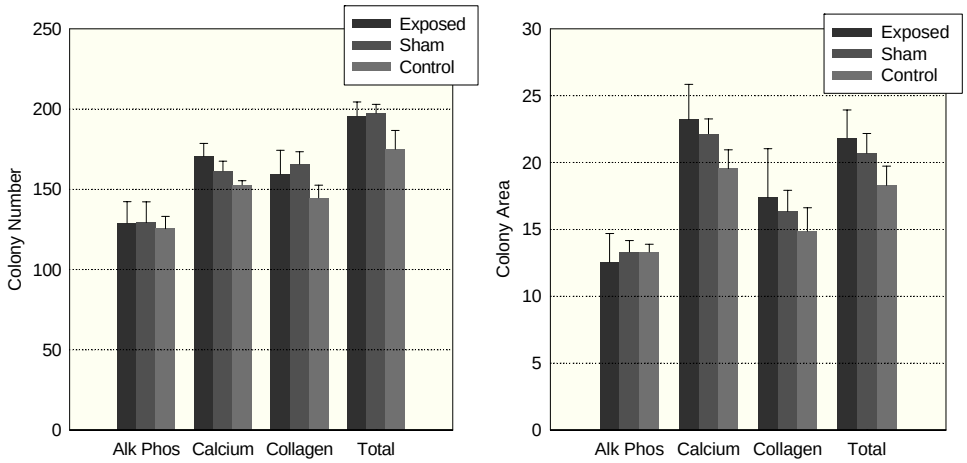

Figure 7: Colony number and area for a representative intermittent 900MHz RF-EMF exposure (n = 4).

Effect of simultaneous oxidative stressing by hydrogen peroxide

MSC were then co-exposed to 900MHz GSM RF-EMF at an averaged SAR of 1.6W/kg and to 10^{-5}M H_2O_2 in the same optimized configuration, and the results are shown in Fig.8.

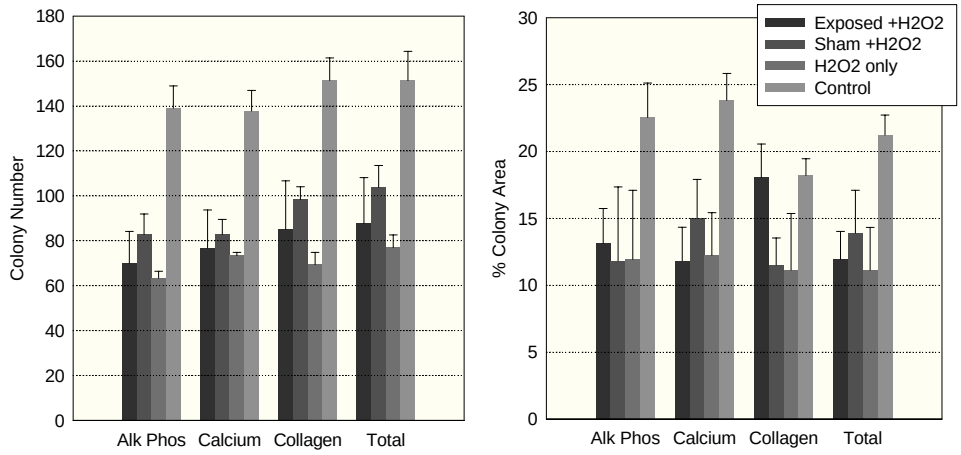

Figure 8: Colony number and area for a representative co-exposure of 900MHz GSM RF-EMF and H_2O_2 exposure (n = 4).

Discussion

Generally no significant differences in colony numbers or areas between exposed and sham exposed MSC are evident in Figs.5-7, although there does appear to be borderline differences in colony numbers between some controls and sham exposed MSC in Fig.7. This is to be expected, given the difference in conditions between these groups. Generally, in the control group, the colony number is slightly reduced, and the colony area slightly smaller. This suggests that the extra handling and medium levels of the exposed and sham groups could be affecting both the recruitment and the proliferation of the MSC. This is probably due to them receiving higher amounts of growth factors from the larger volume of medium. Another behavioural difference was seen in the distribution of the colonies; in the control group the colonies tended to be in the middle of the dish, whereas they were more evenly spread in the exposed and sham groups. This is likely to be due to moving the dishes in and out of the TEM cell, as well as stirring when the extra medium is added.

Diem et al, [10] used intermittent exposure to show that 1800MHz RF-EMFs could cause DNA breakages in both cultured human diploid fibroblasts and cultured rat granulosa cells at non-thermal levels after 16 hours continuous exposure (SAR =1.2 and 2 W/kg). Our experiments exposed MSC to daily 3 hour periods of intermittent RF-EMF for 5 consecutive days, at an SAR of 0.9 W/kg but found no significant effects. As the SAR levels for the data shown here is lower than that of [10], further exposures are ongoing at higher SAR's. While caution is required in comparing different frequencies, different cell types, and the responses of cultured and primary cells, this does suggest that a long continuous exposure is required to induce any effect, rather than an equivalent cumulative exposure.

Oxidative stress is known to play a role in stem cell differentiation [11]. It has been shown that there are interactions between oxidative stress levels and the ability of the stem cells to proliferate, and that antioxidants can increase the total number of cells. Stolzing and Scutt [11] showed that H_2O_2 reduces both alkaline phosphatase expression and total colony number. As expected, in our experiments H_2O_2 alone generally significantly reduced MSC number, as well as their proliferation, as shown by the reduced colony numbers and sizes in Fig.8. This also helps corroborate the assaying procedure itself.
Co-exposure with RF-EMF generally showed no additional effects compared with sham exposure, although some significant differences were again observed between H_2O_2 MSC colony numbers outside and inside the TEM cells. Finally it is worth noting the anomalous significant differential collagen area of H_2O_2 stressed MSC when exposed to GSM compared to sham exposure, although no conclusions may be drawn from this one result.

SUMMARY

A dosimetric analysis has been performed using a TEM cell based exposure system for in-vitro stem cell cultures, with subsequent experimentation based on the results. Optimal positioning and filling of the cell culture Petri dishes for maximum mean SAR and uniformity in the stem cell monolayer was calculated using both in-house and commercial FDTD modelling software. MSC recruitment, proliferation and differentiation were not affected by CW, GSM or intermittent CW exposure to 900MHz RF-EMF, even when the MSC were co-exposed with H_2O_2.

ACKNOWLEDGEMENTS

We would like to thank Dr A. Stolzing for her help in the preparation of this manuscript.

REFERENCES

[1] W. Stewart, "Mobile phones and Health", *Report of Independent Expert Group on Mobile Phones, NRPB*, 2000.
[2] H.B. Lim et al., "Effect of 900 MHz Electromagnetic Fields on Nonthermal Induction of Heat-Shock Proteins in Human Leukocytes", *Radiation Research*, Vol.163, pp. 45-52, 2005.
[3] E.F. Andrews, et al., "Investigation of SAR Uniformity in TEM Cell Exposed Culture Media", *Proceedings of Technical Seminar on Antenna Measurements and SAR (AMS 2004)*, pp.71-74, 2004.
[4] H.B. Lim et al, "FDTD design of RF dosimetry apparatus to quantify the effects of near fields from mobile handsets on stress response mechanisms of human whole blood", *International Journal of Numerical Modelling-Electronic Networks Devices and Fields*, Vol.15, pp. 562-577, 2002

[5] SPEAG, Zurich, Switzerland.
[6] N. Kuster and F. Schonborn, “Recommended minimal requirements and development guidelines for exposure setups of bio-experiments addressing the health risk concern of wireless communications” *Bioelectromagnetics* Vol.21, pp.508-514, 2000.
[7] A. Scutt, L. Reading, N. Scutt, and K. Still, "Mineralizing Fibroblast-Colony-Forming Assays," in *Bone Research Protocols*, vol. 80, Methods in Molecular Medicine, M. H. Helfrich and S. H. Ralston, Eds. Totowa, NJ: Humana Press Inc., 2003, pp. 29-40.
[8] K. Dobson, L. Reading, and A. Scutt, "A Cost-Effective Method for the Automatic Quantitative Analysis of Fibroblastic Colony-Forming Units," *Calcified Tissue International*, vol. 65, pp. 166-172, 1999.
[9] A. Scutt and P. Bertram, "Bone Marrow Cells Are Targets for the Anabolic Actions of Prostaglandin E2 on Bone: Induction of a Transition from Nonadherent to Adherent Osteoblast Precursors," *Journal of Bone and Mineral Research*, vol. 10, pp. 474-487, 1995.
[10] E. Diem, C. Schwarz, F. Adlkofer, O.Jahn, H. Rudiger, “Non-thermal DNA breakage by mobile-phone radiation (1800 MHz) in human fibroblasts and in transformed GFSH-R17 rat granulosa cells in vitro,” *Mutation Research* Vol.583, pp. 178-83, 2005.
[11] A. Stolzing and A. Scutt, “Effect of reduced culture temperature on antioxidant defences of mesenchymal stem cells”, *Free Radical Biology and Medicine*, Vol. 41, pp.326-338, 2006.

BIOPHYSICAL STUDIES OF LIGHT INTERACTION WITH MEMBRANE MODEL SYSTEMS BASED ON CHLOROPHYLL a

LAURA TUGULEA

Faculty of Physics - University of Bucharest
P.O.Box MG-11, Bucharest-Magurele, 077125 ROMANIA

Abstract

The interaction of light energy with plants results in the most important process on earth: the photosynthesis. Biophysical studies on membrane model systems bring relevant insights for *in vivo* primary reactions in photosynthetic membranes. Liposomes with chlorophyll *a* are biomembrane models, providing a hydrophobic environment for chlorophyll *a*, the major pigment in photosynthesis. The spectral features of chlorophyll *a* allow its use as sensor for physical properties of liposomes and for specific molecular interactions in the liposome bilayer. Supported lipid bilayers (SLB) can be obtained by deposition of liposomes on solid surfaces, using different supports. This new approach provides access to basic aspects of membrane biophysics and represents the basis for developing different applications. The objective of our work was to obtain SLB with chlorophyll *a* and to use chlorophyll as a marker in biophysical studies on these structures. Specific interactions occurring inside the lipid membranes, exposed to light (in the visible range of electromagnetic radiation) have been studied, using the strong absorption and emission of chlorophyll *a*. The most interesting application of SLB with chlorophyll *a* is represented by devices for light energy conversion, mimicking photosynthesis. Photovoltaic devices based on chlorophyll *a* are presented.

Introduction

Liposomes are phospholipidic vesicles which enclose an aqueous volume. They have been under extensive investigation for more than 20 years as carriers for the improved delivery of a broad spectrum of agents: chemotherapeutic agents, imaging agents, antigens, chelating compounds, hemoglobin and cofactors, lipids and genetic material [1]. Liposomes can be prepared so that they can entrap certain quantities of materials both within their aqueous compartment and within the membrane.

The value of liposomes as membrane model systems derives from the fact that they can be prepared of natural constituents and the liposome membrane forms a bilayer structure which is almost identical to the lipid portion of the natural cell membranes. The similarity between liposomes and natural membranes can be increased by chemical modification of the liposome membrane and can be exploited in different applications, both *in vivo* and *in vitro*, mimicking successfully the behaviour of natural membranes. Apart from their chemical constituents, which determine such properties as membrane fluidity, charge density and permeability, liposomes can be characterized by their size and shape. They can range in size from ~ 25 nm to 1000 nm or greater, which equals the dimensions of a living cell. Alternatively, liposomes can be prepared of entirely artificial components, chosen for their improved chemical properties.

The liposomes with chlorophyll a (Chla) are excellent models for biomembranes, specifically for photosynthetic membranes and are successfully used to study the influence of different agents on the bilayer structure at molecular level [2-5]. Chlorophyll a is a “valuable” molecule, but insufficiently exploited in biotechnological applications. The strong visible absorption and fluorescence of Chla allow its use as a sensor for the interactions at molecular level and as a fluorescence marker. It has been shown that Chla has also radioprotective, antimutagenic and anticarcinogenic activities. Chlorophyll's antioxidant

properties could be partly responsible for its protective effects in natural and artificial structures.

The deposition of liposomes on solid surfaces, by different techniques, conducted to a new approach: supported lipid bilayers (SLB) [6-8]. This new approach provides access to basic aspects of membrane biophysics and molecular ordering and may constitute a strategy for developing biotechnological applications [9].

Because it turns out that liposomes of diferent size require completely different methods of manufacture and because different applications demand the use of liposomes within particular size, an objective of our work was to prove that the spectral features of Chl*a* allow its use as a sensor for physical properties of liposomes (size, shape, molecular dynamics).

The main objective of the present work was to obtain stable Chla-liposomes and supported Chl-lipid membranes and to characterize the structures by using Chla as a marker and molecular sensor. Using the strong absorption and emission of chlorophyll *a*, specific interactions occurring inside the lipid membranes, exposed to light (in the visible range of electromagnetic radiation) have been studied. A particular application of SLB with chlorophyll *a* was developed by manufacturing devices for light energy conversion, mimicking the primary act in photosynthesis (separation of charges under the light irradiation).

Materials and Methods

Chl a - Liposomes preparation procedure

Chla- liposomes were prepared using the thin-film hydration method. The lipid and Chla were dissolved in chloroform, with Chla/lipid molar ratio varying from 1/100 to 1/10. Different types of thin films were obtained, by vacuum evaporation, using different lipids: ß-stearoyl-oleoyl L-phosphatidylcholine (SOPC), dimyristoyl phosphatidylcholine (DMPC), dioleoyl phosphatidylcholine (DOPC) or soybean lecithin. Chla was prepared from fresh spinach leaves by Strain&Svec method and checked for purity (absorption and fluorescence in VIS). The hydration (2 hours) of the lipid-Chla film was done by adding phosphate buffer, pH in the range: 6.2 - 7.6, in a rotary evaporator (BIOBLOCK SCIENTIFIC – Heildolph 94200, 60–90 rpm). Multilamellar vesicles (MLV) were obtained by mechanical dispersion (VIBRAX stirrer, 200rpm) of the hydrated films (30'). Intermediate unilamellar vesicles (IUV) or small unilamellar vesicles (SUV) were obtained from the multilamellar liposomes by using the exposure to ultrasonic in a bath (Branson 1210), above lipid Tc, for variable periods. For obtaining a homogenous population of liposomes, the suspension was collected after a centrifugation at 100000 g for 1 h.

Formation of supported lipid membranes

Chla-SLB have been obtained by adsorption method. A drop of Chla-SUVs suspended in phosphate buffer was spread on different solid supports: Silicon wafers and semitransparent SnO_2 or ITO glass. Chla-SLBs are formed by spontaneous deposition of Chla - SUVs.

Chla-SLBs on n-dopped silicon wafers have been covered by a semitransparent gold electrode (1.5 mm2 measurable area). Thus a photovoltaic device, sandwich type, was manufactured.

Spectral measurements

The optical absorption spectra were obtained on a double beam UV - VIS spectrophotometer Lambda 2S Perkin Elmer & PECSS software. A computer assisted Aminco Bowman was used for recording the fluorescence spectra. A front face geometry, on Perkin Elmer LS 55 fluorometer, was used for measuring the fluorescence, collected at 45^o from the solid support.

Photo-electrical measurements

The irradiation of Chla- liposomes in suspension was done by using a halogen lamp (650 W), a convergent lens and a water filter (5 cm thick). The photovoltaic devices were illuminated, within the visible range of the electromagnetic spectrum, by using a halogen lamp and a grating monochromator (Oriel). For the electrical measurements (photocurrents) a dedicated software and a Keithley 6517 electrometer were used.

Results and discussions

Characterisation of Chla - liposomes by light absorption in VIS

The liposomes will scatter light in the visible range of the electromagnetic spectrum, if their dimension is in the range of the respective wavelengths. Typical diameters for MLVs range between 100nm and 1000nm, each vesicle consisting of five or more concentric lamellae. Typical dimensions for SUVs are 15 nm (pure egg lecithin liposome in normal saline) or 25 nm (for DPPC liposomes). IUVs have

the order of magnitude around 100nm, according to R.R.C. New [1].

In order to do a rapid estimation of the size of the lipid vesicles, the absorption changes in the VIS spectra of Chl a were monitored and some spectral criteria were established. Inspecting the absorption spectrum of Chla in different liposomes, presented in Figure 1, major differences can be observed as regarding the base line (background) of the spectra. The main absorption bands of Chla (Soret band and red band) are present in the spectrum and confirm the localisation of the porphyrin ring of chl*a* at the lipid-water interface in the vicinity of polar lipid heads (the red band is shifted to longer wavelengths as comparing with solution, i.e. 670 nm).

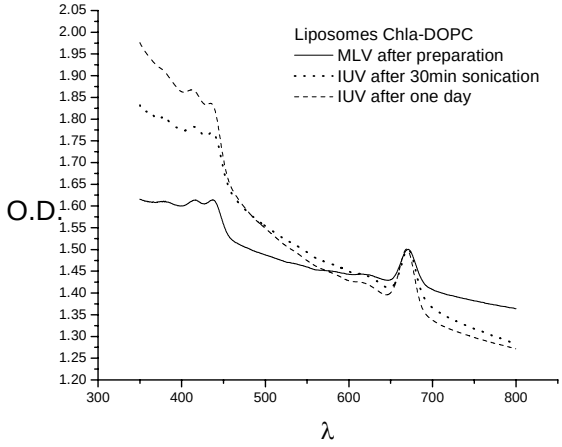

Figure 1. Absorption spectra of Chla liposomes

A $1/\lambda^4$ dependence of the baseline was observed in VIS absorption spectra of the Chl*a*-unilamellar vesicles (SUV or IUV), suggesting that the size of the vesicles is small enough to act as point sources of scattered light. And it was observed that smaller liposomes scatter shorter wavelengths (blue) more intensely, while larger liposomes scatter long (red) wavelengths. It is the case of Rayleigh scattering, applying to particles with a radius less than the wavelength of light / 20 ($R < \lambda/20$) [10]. The increase of the background scattering observed in the stability studies can be explained by the aggregation or fusion of the vesicles. The larger vesicles formed by aggregation strongly scatter light in comparison with the non-aggregated vesicles obtained after sonication.

Assuming a Rayleigh scattering, the over-estimated absorbances values can be corrected for the

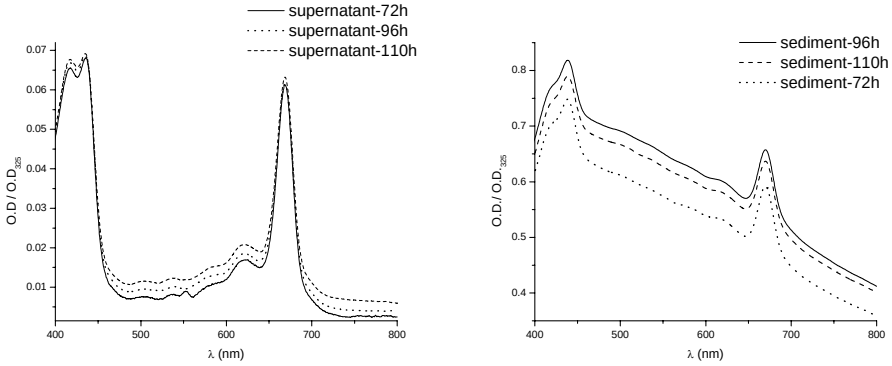

Figure 2. Corrected spectra of Chla liposomes in suspension, after centrifugation

contribution of light scattering on the basis of the OD measured at 325nm, where the scattering is the sole contributor to the O.D. (11):

$$(OD_{\lambda})_{corrected} = (OD_{\lambda})_{measured} - (OD_{325})_{measured} \times (325/\lambda)^4$$

In Figure 2 the corrected spectra are presented for 2 cases: supernatant and sediment, obtained after the centrifugation of Chla-liposomes. The suspension of Chla-liposomes (SUVs) was manufactured as described above, by sonicating the MLVs. By ultracentrifugation, the remained large vesicles are deposited on the bottom of the tube and a homogenous population of liposomes remains in the supernatant. The correction by the above formula of the absorption spectra works very well in the case of the supernatant, but does not correct the base line in the case of the sediment. As a conclusion, the average diameter of the liposomes in the homogenous population is around 60 nm.

Therefore, the spectral analysis of Chl a- liposomes, using the spectral properties of Chla, leads to a rapid monitoring of the liposome preparation. The Chla-liposomes prepared as described above are unilamellar and have diameters in the range 40-100 nm. The nature of lipids and pH value of the buffer are influencing the dimension of liposomes. The neutral pH values proved to be the best as concerning the stability of liposomes [12].

The influence of the lipid nature on Chla –liposome was also investigated. Figure 3 presents the normalized absorption spectra (corrected for the baseline) of Chla- IUVs, obtained by using different lipids. The background absorption is depending on the lipid nature. The difference between DMPC and DOPC is the presence of unsaturated acyl chains in the case of DOPC, thus providing a different environment for Chla in the lipid bilayer. This explains the lower background and therefore the smaller dimension of the DOPC liposomes.

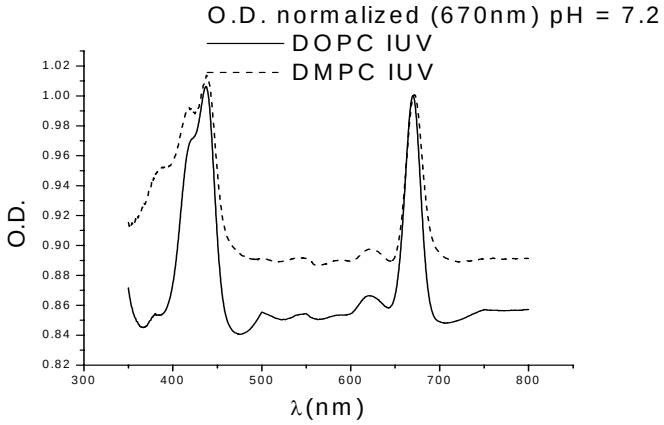

Figure 3. Absorption spectra of Chla- IUVs

Stability studies on liposomes with Chl a were performed by monitoring the changes in the Chl a spectra for different factors. The photooxidation of Chl a was monitored by comparing the absorbance ratio in the Soret band $O.D._{438}/O.D._{416}$. A correlation between Chl a oxidation and lipid oxidation was also observed by performing VIS and UV spectroscopy on the lipids - Figure 4.

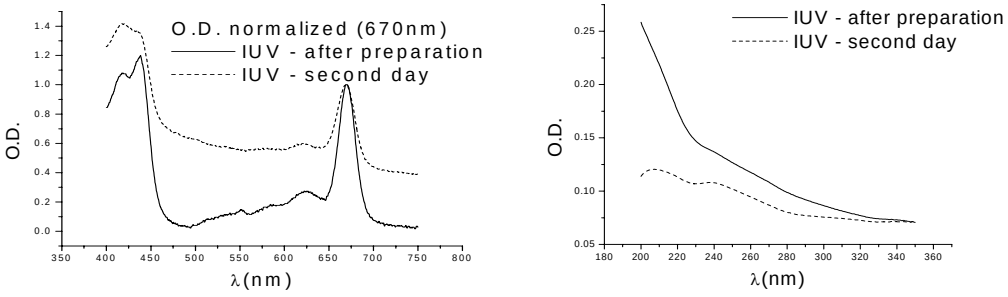

(a) (b)

Figure 4. Absorption spectra of Chla - IUVs in VIS (a) and UV (b)

Light effect on liposomes with Chl a

In order to monitor the effect of light on Chla incorporated in liposomes as compared with Chla in solution (ethanol, polar solvent), aliquots of 4 ml suspension of Chla- liposomes were irradiated using a halogen lamp (white light). In order to prevent heating of the solution and consequences, a water filter was interposed between the sample and lamp. The irradiated cuvette was monitored by measuring the absorption spectrum, every 10 minutes. For comparison, Chla in ethanol solution (the same concentration as in the liposomes) was irradiated and monitored in the same conditions.
The combined effect of oxygen and illumination on the exposed liposomes was monitored by 2 spectral criteria: the ratio of absorbance in the Soret band of Chla (OD 438/ OD 416) and photobleaching % (at the maximum in red, 670 nm). The results are presented in Figure 5, for two cases: pH= 6.2 and pH= 7.35. In both cases, the photoxidation of Chla is pleading for the fact that Chla is photobleached by a slower rate when incorporated in the lipid bilayer.

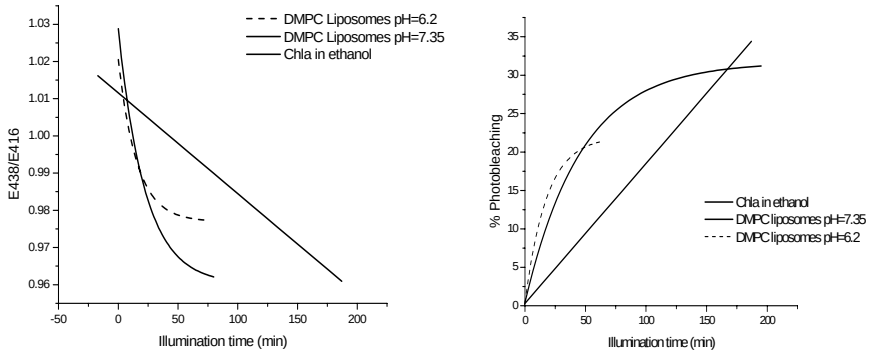

Figure 5. Dependence of spectral parameters upon illumination time

Formation of Chl a-supported lipid membranes:

The deposition of liposomes on solid surface was accomplished by the adsorption technique. Different events could take place in the process of unilamellar vesicles adsorption on the surface [9]:

- interaction of vesicles with other vesicles and with the substrate
- fusion and rupture of vesicles/ rupture of individual vesicles
- transformation of surface bound vesicles in a continuous supported lipid bilayer.

The concentration quenching of Chla fluorescence, in a suspension of Chla-SUVs, as presented in Figure 6,

could be explained by two possible mechanisms: transfer of energy or formation of molecular non-fluorescent Chla aggregates. The second mechanism could be considered in the case of liposome fusion or rupture of vesicles: Chla inserted in the lipid bilayer achieves more freedom to self-aggregate in fused or ruptured liposome membranes. Following this result, the optimum concentration for liposome adsorption was estimated.

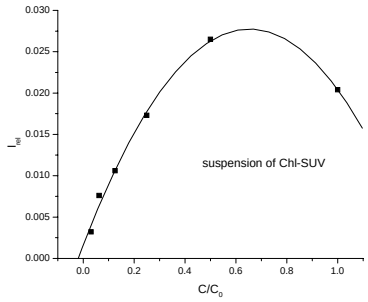

Figure 6. The dependence of Chla fluorescence on concentration, in a suspension of Chla-SUVs (λexc= 430 nm, λem= 680 nm)

To monitor the adsorption of Chla-liposomes on solid supports, the Chla absorption and emission properties have been used. In figure 7, the absorption spectra of Chla both in liposome suspension and on ITO covered by Chla-SLB are represented. The spectra are very similar. The red maximum is at 670 nm in both spectra, leading to the conclusion that after deposition on the solid support, Chla remains in the same environment as in the liposomes, i.e. with the porphyrin ring in the vicinity of lipid polar groups.

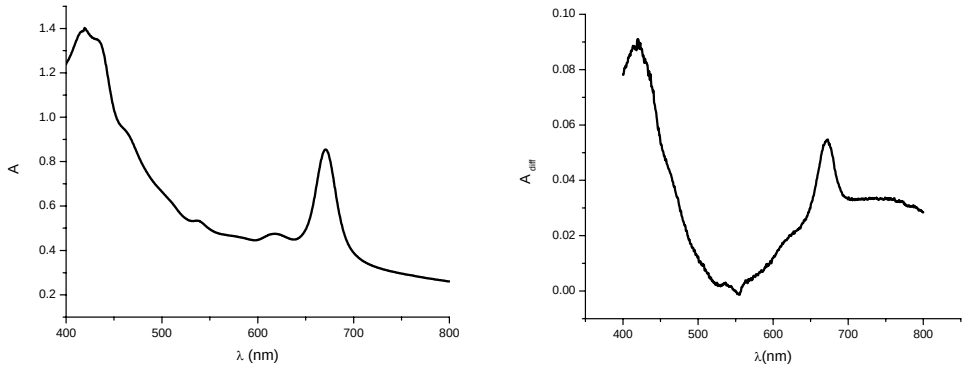

A. B.

Figure 7. Absorption spectra in VIS range

(A) Chla-SUVs in suspension, (B) Chla-SLB on ITO (ITO absorption was extracted graphically)

Also the emission spectra of Chla-liposome in suspension as compared with the Chla-SLB on silicon wafer, presented in Figure 8, are sustaining the above conclusion, that Chla is keeping the place in the lipid bilayer when liposomes are spread on the solid support surface.

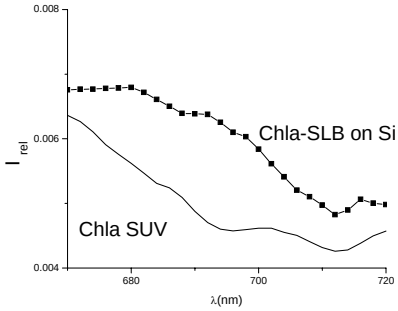

Figure 8. Emission spectra of Chla in SUVs and in BLS on Silicon wafer

(λexc= 430 nm)

Sensitization process at chlorophyll/Si hetero-junction

As already mentioned in the introduction, SLBs are envisaged as useful new structures for different biotechnological applications. By manufacturing a photovoltaic device, based on Chla-SLB deposited on Si wafer, some promising preliminary results have been obtained. The action spectrum presented in figure 9 (the photocurrent plotted as function of the wavelength of the illumination light) is pleading for an effect of sensitization at Chlorophyll/Si hetero-junction.

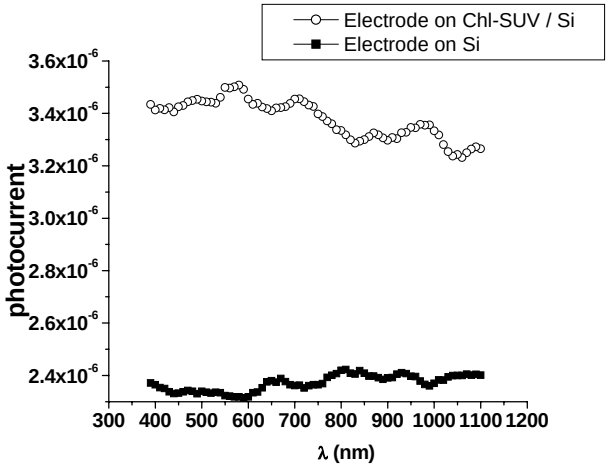

Figure 9. Action spectrum of the sandwich type cell (Si/Chla-SLB/Au)

Summary

Chlorophyll a incorporated in the liposome lipid bilayer was used to monitor the formation of both Chl- liposomes and supported Chl-lipid membranes.

The strong visible absorption and fluorescence of Chlorophyll a allow its use as a sensor for the interactions at molecular level and as a fluorescence marker.

Spectral criteria have been developed in order to monitor the size and shape of Chla-liposomes, the oxidation state of the components and for studying the effect of irradiation with light (VIS range).

Interaction of Chla with light and the Chla absorbance and fluorescence properties were successfully used to monitor the supported lipid membranes on ITO and Si substrate.

Preliminary photo-electrical measurements are pleading for successful utilization of supported Chl lipid membranes in building up photovoltaic devices using Chl a as a photo- sensitisation factor.

Acknowledgement

The Romanian National Council of Research in Higher Education (CNCSIS grant No.1148, theme 30 A/2006) and the Romanian Ministry of Education and Research (CEEX program, Contract 67/2005) are acknowledged for the financial support. The Perkin Elmer fluorescence equipment was purchased by a donation offered by the Department of Biophysical Chemistry, University of Bielefeld, Germany (Professor Dr. Eberhard Neumann). The author would like to thank to Adrian Enache and Andreia Popa (former master students) for their contribution to this work.

References

1. R.R.C. New (editor) "Liposomes - a practical approach"(1990), IRL at Oxford University Press
2. V.A. Nadtochenko et al. (1993) J.Photochem.Photobiol.B:Biol. **18**, 221
3. Laura Tugulea, Simona Pascanu (1996) Romanian Journal of Biophysics **6**, no.1-2, 1
4. Marcela Barbinta Patrascu, Manuela Voinea, Laura Tugulea (2003) Analele Universitatii din Bucuresti, Fizica, **LII**, 35
5. Barbanta-Patrascu Marcela, Tugulea Laura (2005) Romanian Journal of Physics **50**, Nos. 9-10
6. J.T.Groves, N.Ulman, P.S.Cremer, S.G.Boxer (1998), Langmuir **14**, 3347
7. N.Bergstrand, K.Edwards (2001) Langmuir 17, 3245
8. E. Reimhult, F.Hook, B.Kasemo (2002) J.Chem.Phys.**117**, no.16, 7401
9. R.P.Richter, J.Lai Kee Him, A. Brisson (2003) Materials today, November, 32
10. W. J. Moore "Physical Chemistry" Longmans Green and Co. Ltd., London (1962), pp. 761-763
11. O. Bittner et al. (2002) Chemistry and Physics of Lipids **114**, 81
12. Laura Tugulea, I.M. Iacovache (2002) W. Mejbaum-Katzenellenbogen's Molecular Biology Seminars "Liposomes, From Models to Applications", Wrocław/Piechowice by Szklarska Poręba, Poland, May 26-29, 2002

THE EFFECT OF TERAHERTZ RADIATION OF A FREE ELECTRON LASER ON THE LYOPHLIZED SAMPLES OF OX SERUM ALBUMIN

N.L.LAVRIK, E.M.NEMOVA

INSTITUTE OF CHEMICAL KINETICS AND COMBUSTION SBRAS, NOVOSIBIRSK, RUSSIA

lavrik@ns.kinetics.nsc.ru

The lyophilized samples of ox serum albumin (OSA) were IR irradiated at λ = 120 -140 mkm by a free electron laser of a power of 130-280 mw. The analysis of IR absorption spectra indicates a decrease in both the optical density of the bands of characteristic frequencies (2700 - 3100 cm^{-1}) and the value of background determined by scattering intensity. The analysis of UV absorption spectra indicates a decrease in the optical density of irradiated samples at λ = 270 nm as compared with the non-irradiated ones. The thermal heating of samples caused an increase in the scattering of IR spectra and no changes of absorption value in the region of characteristic frequencies and UV absorption spectra. The influence of terahertz radiation was did`t observed for water solution of OSA. The observed laser effects are interpreted in the framework of the hypothesis of the existence of photochemical destruction, laser swelling and ablation.

Introduction

Studying the influence of interaction between electromagnetic terahertzian radiation, THz (70 - 240mkm), and bioobjects is actual because of a feasible effect of this radiation on their functioning and structure [1-2]. However, the total number of works devoted to this problem is rather small [3]. A direct study on the interaction between terahertzian radiation and biomolecules is presented in a limited number of works [4-8]. Thus, in [5] it is shown that the irradiation of horse-radish DNA molecules, lysocyme and peroxidase leads to soft ablation under free electron laser irradiation (λ =100-200 mkm, pulse duration 50 pc, frequency 5,6 MHz, mean power 200 W). The existence of soft ablation is assigned to the fact [7] that the irradiated protein partially preserves a functional activity.

It is concluded then [8] that the irradiation of the lyophilized preparation of ox serous albumin (OSA) causes changes (deformation) in a secondary structure. In this work, a pulse laser with a generation wavelength of 90 mkm and a pulse energy of 5 mJ was used. The values of doses were varied from 0.2 to 3 J. This information was extracted from changes of the fluorescence properties of the probe whose interaction with an OSA molecule was dependent on the irradiation dose obtained by the OSA molecule. The deformation of substance structure under laser pulse can be followed by swelling and ablation [9]. Thus, according to [9] the action of laser radiation is likely to lead to the swelling of OSA samples.

The swelling (the formation of tubercles at the irradiated surface), i.e., the deformation of object macrostructure, can actually cause direct changes in the electron characteristics of the OSA molecule. Thus, of interest is to observe changes in the IR and UV absorption spectra of OSA samples under terahertzian radiation because these spectra contain direct information on the electron properties of the molecule under study. The goal of the present work is to compare the IR and UV absorption spectra of OSA samples before and after THZ irradiation.

Materials and Methods.

The lyophilized OSA preparation of the firm «PPP» was used without repurification. The starting preparation was represented by 3 mm flat plates. The samples were irradiated in teflon (fluoroplast) cells. The thickness of the windows was 3 mm. The sample irradiated (the preparation was preliminarily grinded in an agate mortar) was spread throughout a window with 50 mkm cylindrical cavities of a diameter of 30 mm.

A free electron laser (FEL) [10] produced terahertzian radiation with the parameters λ = 130-140 mkm, a pulse duration of 50 ps, a frequency of 5,6 MHz, and a mean power of 200 mW. The time of irradiation was 3, 6 and 9 min which corresponded to doses of 36, 72, and 108 J, respectively. The power was controlled by an power meter IMO-2. The laser beam half-width was 8 mm.

The thermal heating was realized by locating a cell in a thermostat at a given temperature under irradiation of a thermal gun. The heating temperature was measured using a differential thermocouple. The samples were heated to 55^0C.

The IR spectra of irradiated and test samples were analyzed in the cells used for irradiation. A Fourier-spectrometer ("Bruker") was employed for analysis. The UV spectra of irradiated and test samples were analyzed using aqueous OSA solutions whose concentration was 1mg/ml. The solutions were prepared by dissolving the weighted portions of irradiated and non-irradiated OSA powders in deionized water. The UV absorption spectra were obtained using a "Hewlette-Packard" spectrometer.

Results and discussion

Figure1a shows the IR absorption spectrum of albumin powder (control). The range of characteristic frequencies from 2700 to 3500 cm^{-1} is determined by the stretching vibrations of CH, NH and OH groups [11]. Figure1b shows the IR absorption spectrum of albumin powder after a 3 min irradiation by the FEL at λ = 130 mkm and with a power of 200 mW. A comparison of these spectra indicates a decrease in the intensities of both the background at 2800 cm^{-1} and the lines of characteristic frequencies at 2930 cm^{-1}. Note that the value of the absorption of the structurized spectrum region changes in proportion to the change in the background absorption. Heating the samples by either air convection in a thermostat or the directed stream of hot air from a heat gun with a temperature up to 55^{o}C causes another change in the IR absorption spectra, i.e., the background intensity increases and that of specific bands remains unchanged. Thus, the action of FEL radiation and the thermal heating of OSA samples lead to changes in the IR spectra with different signs. It is concluded then that the nature of changes in absorption spectra is quite different. The difference between the absorption spectra of the starting sample and the irradiated one depends on the time of irradiation (dose).

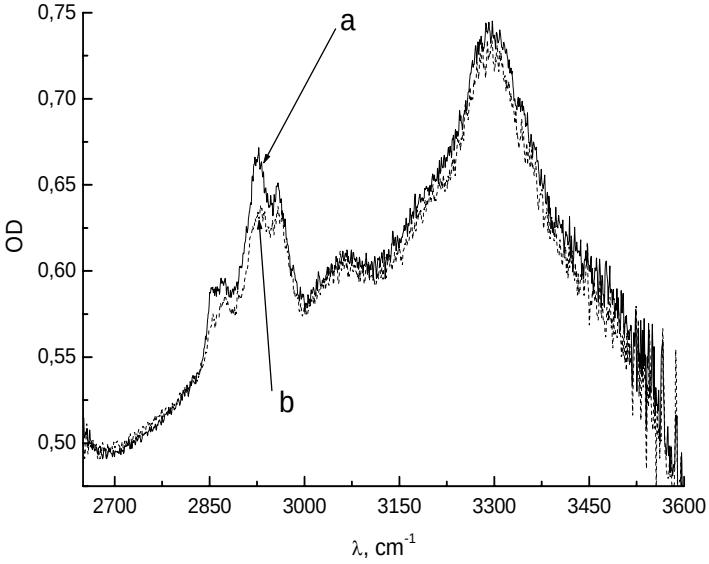

Fig.1. IR spectra of OSA before (a) and after (b) irradiation.

Both the increase in the intensity of background absorption, determined by cell absorption and sample scattering, and the absence of changes in the intensity in the area of absorption of CH, NH, and OH vibrations under heating can be assigned to either the appearance of fractures in the sample or the subdivision of the granules of laminar OSA. In this case, the background intensity is sure to increase and the intensity of the structurized spectrum region will remain constant because the concentration of characteristic groups remains unchanged.

A decrease in the absorption intensity of the background and the structurized spectrum region under FEL irradiation can be assigned to the fact that under irradiation a considerable heating causes carbonization, agglomeration, etc. Such “burning” or “agglomeration” can cause a decrease in the number of reflecting surfaces. In addition, the process of “agglomeration” can decrease the number of CH, NH, and OH groups if initial molecules are destructed and the products are formed in which a fraction of molecules containing the given structural fragments is smaller. This chemical process is e.g., well known for the process of humus-formation where chemical transformations in soil cause an increase of C/H, N/C ratios in time. An increase in the values of these ratios testifies to the increase in the aroma of the systems studied [12]. When the process of “burning” prevails in the effect of the decrease of OSA sample absorption, the presence of oxygen will be of major importance because the samples were irradiated from which oxygen was not removed. Therefore, it is interesting to perform experiments on THz irradiation of OSA samples in an oxygen-free medium.

Note that a feasible effect of conglomeration is in agreement with the concepts of the existence of the effect of laser ablation in the system under study. Indeed, since irradiation was performed in a closed volume, the possible products of ablation whose structure is sure to differ from the initial ones, remain in the same volume and can lead to a change in absorption spectra. As for the effect of laser swelling (the swelling of the irradiated sample surface at the irradiation site) which precedes laser ablation, it is also possible because the OSA powder is a set of laminar structures at the surface of which the swelling effect can be observed. However, our method of recording the effects of irradiation fails to reveal the manifestations of swelling because these cause no

changes in the value of absorption of both a substrate and the structurized part of the spectrum. Finally, the swelling can be absolutely absent because in our experiments the pulse energy and the dose substantially exceed those in [8].

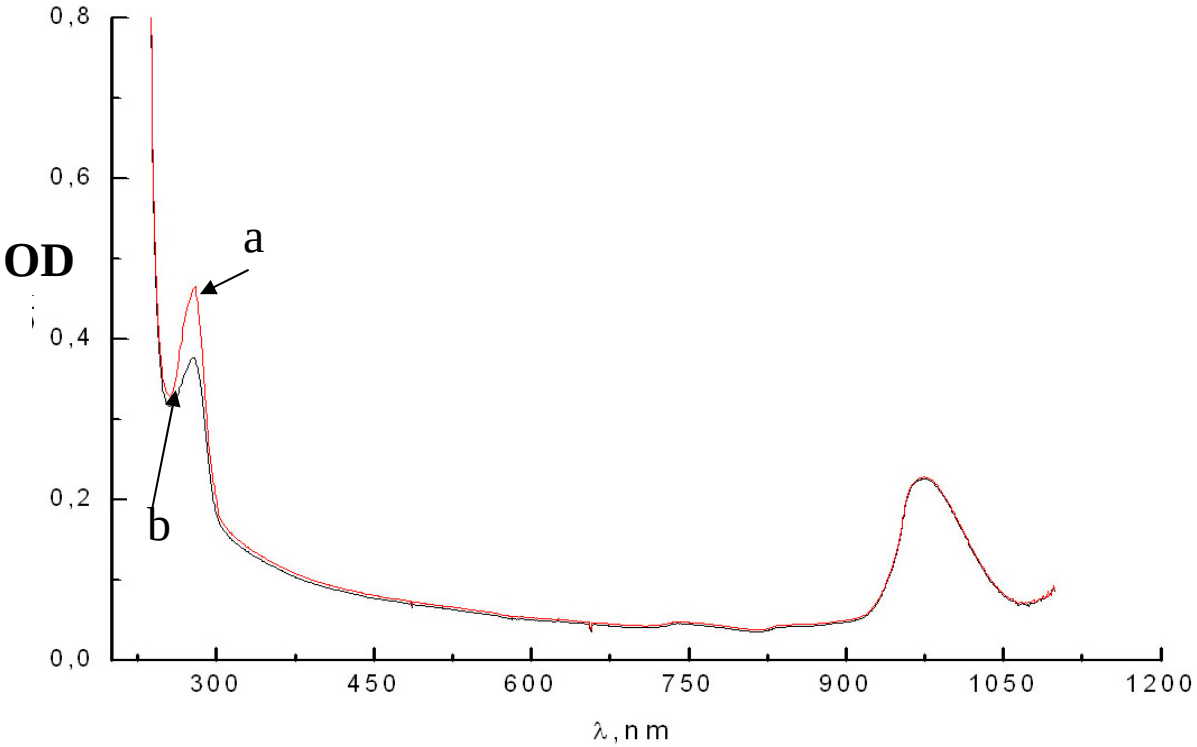

Fig.2. Electronic absorption spectra of OSA samples before (a) and after (b) irradiation.

Assumption of the effect of "agglomeration" accompanied by a significant chemical destruction of the initial structure of OSA molecule is confirmed by the effect of a decrease in the intensity of the UV spectrum absorption of the OSA molecule after irradiation (fig.2). As follows from the figure, after irradiation, the absorption intensity of the sample decreases by about 40%. This testifies to a decrease in the number of structural groups determining a characteristic "protein" absorption at λ = 270 nm. The tests performed using the thermally heated OSA samples indicate the absence of any changes in the UV absorption spectra.

Thus, the terahertzian radiation with a wavelength of 130 mkm and a power of 200 mW leads to the observed changes in the UV and IR absorption spectra that are opposite in their directivity to the influence of thermal heating. The changes in absorption spectra are likely to be due to the destruction of initial molecules.

References

1. C.F.Blackman, M.C.Surles, S.C.Bename. // Biol. Effects of Electromagnetic Waves, 1976, **1**, 406-413.
2. M.Zhengyu. // Infrared Phys., 1989, **29**, 631-636.
3. V.I.Fedorov, S.S.Popova, A.N.Pisarchik. // Intern. J. Infrared and Millimeter Waves. 2003, **24(8)**, 1235–1252.
4. D.D.Dlott, M.D.Fayer. // IEEEJ.Quantum Electron, 1991, **27**, 2697-2713.
5. A.Xie, A.F.G.Meer, W.Hoff, R.H.Austin.// Phys.Rev.Lett., 2002, **88**, 018102/1-4.
6. S.A.Ilyina, G.F.Bakaushina, V.I.Gaiduk, A.M.Hrapko, N.B.Zinovieva. // Biofizika, 1979, **24(3)**, 513 - 518 (in Russian).
7. A.K.Petrov, A.S.Kozlov, M.B.Taraban, T.N.Goryachkovskaya, S.B.Malishkin, V.M.Popik, S.E.Peltek. // Dokladi Akademii Nauk, 2005, **404(5),** 698-700 (in Russian).
8. V.M.Govorun, V.E.Tretiakov, N,N.Tulyukov, V.B.Fleurov, A.I.Demin, A.Yu.Volkov, V.A.Batanov, A.B.Kapitanov. // Infrared and Millimeter Waves, 1991,**12**, 1469-1474.
9. A.Yu.Malishev, N.M.Bituyrin.// Quntum Electronics, 2005, **35(9)**, 825-830 (in Russian).
10. V.P.Bolotin, D.A.Kairan, B.A.Knyazev et al. Status of Novosibirsk free electron laser and First Experiments with High Power Terahertz Radiation. Preprint of Institute of Nuclear Physik. Novosibirsk, 2004.
11. K.Nakamoto. // Infrared spectra of inorganic and coordination compounds. John Wiley & Sons, Inc., New York, London, 1965.
12. N.L.Lavrik, M.I.Dergacheva, E.I.Kovaleva. // Chemistry of stable development, 2000, **8**, 815-821.
13. A.Malyshev, N.Bityurin. // Appl. Phys. 2004, **A 79**, 1175-1179.

THE ROLE OF THE OPTICAL VISUAL SYSTEM IN RECOGNIZING THE THIRD DIMENSION OF THE OPTICAL IMAGE

Medhat ElMessiery and Manal M. Awad

Department of Engineering Mathematics and Physics Faculty of Engineering

Cairo University, Cairo Egypt

Abstract

Against the popular believe that the acute visual recognition takes place at the fovea this work examines the possible focusing effect of the visual system as a whole in the formation of clear image on the retina as a whole . Accordingly the image is affected by the curvature of the retina, the gradient of the index of refraction of the lens and other media as well as the curvature of the retina itself. The present approach utilizes the ray tracing technique to track the image at different levels until it reaches the curved surface of the retina. The results confirm that it is possible to have a focused image on considerable area of the retina. Also it gives a reasonable explanation to the third dimension recognition.

Introduction

The eye is the most efficient image system. The visual system in man is capable of reducing the dimensions of the external world to almost 0.3 % of its original size without losing acuity, resolution and sharpness of the formed image. It is so adjustable to distance so that it deals with objects that are large and small, far and near and bright and dull. It differentiates colours within the visible spectrum. the system is in a continuous process of adjusting its parameters to focus objects at different distances on the retina (accommodation), thus the refractive power of the lens increases for focusing a near object upon the retina. Most importantly it is capable of recognizing the third dimension of the perceived world.

Over the years, A number of models were introduced in order to explain the remarkable abilities of this system . Most of the classical approaches deal with the paraxial properties of image formation on the retina.

For example, the paraxial schematic eye is highly approximative and serves only in obtaining some parameters such as the equivalent power , the position of the cardinal points, the retinal image size , magnification factor. This model simplifies many mathematical difficulties and overlooks the problems of media inhomogeneity; geometrical considerations and the effect of the curved shape retina on image reception.

Rosenblum et al.[1] introduced a defined model of the human eye by including a inhomogeneous crystalline lens with a purely radial gradient index of refraction. The model has the same basic elements that Blaker[2] used and consists of a corneal refracting surface with a radius of 7.8 mm, an aqueous chamber that is 3.6 mm thick, and has an index 1.336. The crystalline is composed of an anterior thin lens of radius 10.0 mm with an index of 1.386, a radial gradient of a central index of 1.406 and an edge index of 1.375, and a posterior thin lens of radius 6.0 mm and an index of 1.386.

The index of refraction distribution within the radial gradient takes the form.

$$n(y)=n_0\left(1\pm\frac{V^2}{2}y^2\right)$$

Which describes a quadratic change in refractive index from a central value of n_0. The magnitude of the coefficient V depicts the type of gradient index lens being used. Rosenblum et al [3] used a value for V^2 of $41.58m^{-2}$. They found that the focal length, measured from the posterior of the crystalline lens, is 16.55 mm. This posterior focal length compares favourably with the 16.51 mm value that Blaker[2] obtained using both an axial and a radial gradient in his model of the eye.

Despite the difficulties in introducing a mathematical description to the different refracting surfaces of the system, Al-Ahdali and ElMessiery[3] introduced a model of the human eye for which they take into consideration the laminated nature of lens fibres. The thickness of each lamina is 0.0056 mm; thus lens comprises 300 eccentric lenses of minute dimensions. The index gradient of the lens is such that the index of refraction increases exponentially from the lens core to its peripheral zone. The radius of anterior and posterior group decreases exponentially from the pole toward the core.

The laminated lens model offers a plausible explanation to the image formation which is not only compressed but completely focused on a curved surface of the retina. The acuity of the image is usually examined by the spot diagram which is a plot of intersection points of rays from an object point with an image plane. The spot diagram is constructed by using finite ray tracing for all rays that emerge from the object and reach their final destination on the image plane. This diagram is very effectively in studying firstly, the distribution of light intensity on the image plane of a luminous object. Secondly, The imaging features, the possible defects, and limitations of an optical system.

The merit function is related to the image quality. The optimum form of image formation may be achieved by minimizing the merit function. Most commonly used merit functions are the RMS blur circle radius, the wave aberration function, and the sum of squares of the aberration coefficients.

It is based on determination of the central coordinates of the intersection of rays with the image plane. The RMS blur circle radius gives a measure of the transverse aberration among other optical defects of the system. In order to obtain reliable values for RMS blur circle radius, one needs to trace several hundred rays, uniformly distributed over the entrance pupil, through the optical system.

The least square deviation is given as :

$$(RMS)^2=\frac{1}{N}\sum_{I}^{N}\left[(X(I)-<X(I)>)^2+(Y(I)-<Y(I)>)^2\right]$$

Where X(I) and Y(I) are the coordinates of intersection of the ray at the image plane.

$<X(I)>$ and $<Y(I)>$ represent the average coordinates of the ray intercepting the image plane.

They are the result of tracing N rays passing through equal areas in the entrance pupil.

$$<X(I)>=\frac{1}{N}\sum_{I}^{N}X(I) \quad \text{and} \quad <Y(I)>=\frac{1}{N}\sum_{I}^{N}Y(I)$$

Al Ahadali [4] used caustic surfaces as a merit function and optimized the caustic points towards an Gaussian focal point. In this case the lens parameters are varied by a certain procedure.

Pomerantzeff et al [5] have introduced an eye model based on the wide angle of light entrance to the eye which was based on finding the square root of the distance between the Gaussian focal point and the caustic Kortez and Handelman[6] discussed the mechanism of eye accommodation and produced a simple model explaining the effect of such accommodation on image formation.

Manal and Essam[7] have used this model to examine the demagnification power of the eye for near and far vision they found that the image rotates and demagnifies as it formed on the curved retina.

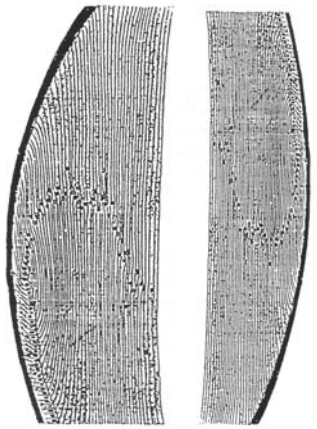

Figure1, the laminated distribution of the human lens

THE MODEL:

Since the dimensions of human eye are large in comparison to the visible wave length (λ = 4000 to 7000 A°, Iris diameter = 4 mm), the geometrical optics approach is applicable. In this work we use the laminated lens model, which was described previously and proved its accuracy and reliability in connection with the main parameters of

the visual system. This model is based mainly on the following:

1. The lens is not a homogenous medium, but in fact, there are many zones of optical discontinuity within it and they vary both in refractive index and in radius of curvature as shown if figure(1). In the absence of accurate information about the number of these zones or their curvature. This variation in the index of refraction is dealt with by assuming an exponential increase of the lens index of refraction from the core to the peripheral. The surfaces of both the cornea and the lens deviate from being spherical to ellipsoidal. The lens thickness varies as the lens changes from unaccommodated to the accommodated modes. Accordingly the image is formed with extra features that are it is compressed by an average value from 0.3 to 7 %. The radius of curvature R of the surfaces of the cornea and the lens ; are expressed mathematically as rotationally symmetric aspherical surface so that

$$x^2 + y^2 + (1+Q)z^2 - 2zR = 0$$

The degree of asphericity are examined by varying Q in order to give the optimum acuity of the image on the retina.

2. Vector ray-tracing technique is employed to study the optical characteristics of the system. Both paraxial and marginal rays are simulated, by considering 400 rays (which are equally distributed on the cornea) emerging from each point of the source and they were all traced through the system until they strike the retina. The angles of incidence vary from 0° to ± 20° and the maximum iris entrance radius was taken as 2mm.
3. Computer simulation technique studied the visual system under accommodation and unaccommodating modes also far and near objects were studied.
4. The constants introduced in this model, were obtained under the optimal conditions of; focusing the images on the curved surface of the retina; Minimum radius of the blur circle and caustic surface and finally minimal spherical aberration.
5. The spot diagram is constructed by using finite ray tracing for all rays that emerge from the object and reach their final destination on the image plane. This diagram is used in studying firstly, the distribution of light intensity on the image plane of a luminous object. Secondly, the imaging features, the possible defects, and limitations of an optical system.

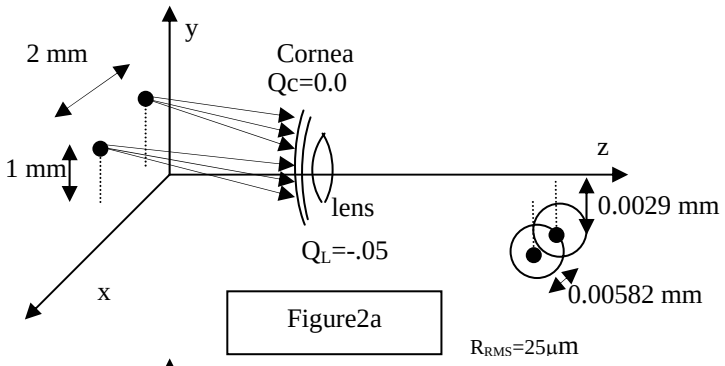

Figure2a

R_{RMS}=25μm

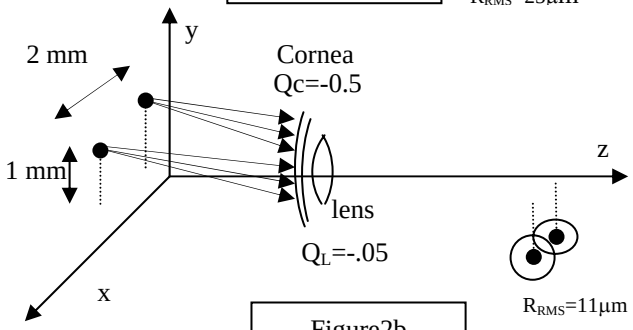

Figure2b

R_{RMS}=11μm

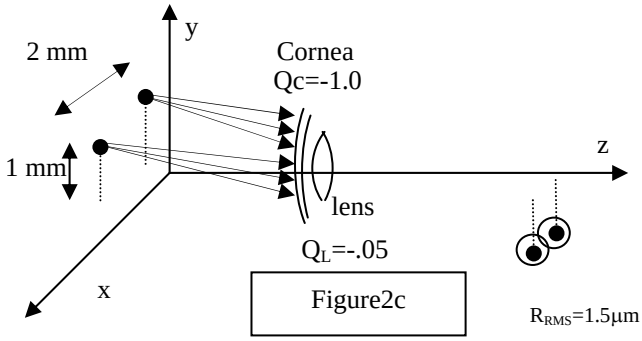

Figure2c

R_{RMS}=1.5μm

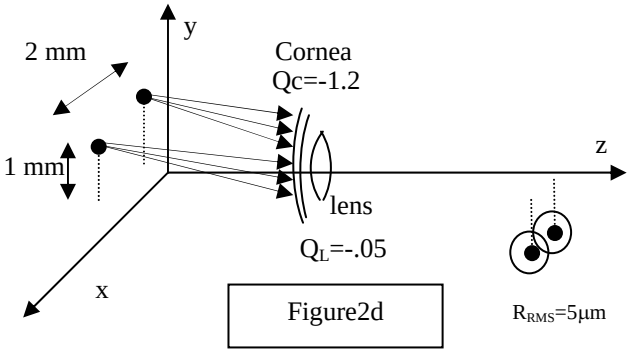

Figure2d

R_{RMS}=5μm

RESULTS:

Figure(2) represents the variations of RMS of the blur radius with lens asphericity for different values of both the cornea Q_c and the lens Q_L. Here, the object is considered at far vision, i.e. the incident rays are parallel to the optical axis and uniformly distributed at the entrance grid placed in front of the cornea.

A four hundred incident rays are used to construct the image of two point objects

(2 mm apart and height 1 mm); as they received on the retina. These objects are considered at far vision.
Figures (2a,b,c and d) show the variation of RMS value of the radius of the blur circle of the image point at the retina for different values of cornea asphericity represents; lens asphericity is kept constant at a value of -0.5.
It is clear that the cornea asphericity plays a dominate factor of the image acuity and there is a critical value of Q_C of -1.0 at which the blur circle has a minimum rms radius.
In order to examine the effect of the complicity of the eye in comparison with other optical system the image of a cube in the near vision is first received on a plane Figure(3a) and the second on the curved surface of the retina Figure(3b).

In the first case the projection of the cube is demagnified square that hide the far edges LKMN behind but in the second case the projection of the same object is firstly subjected to different demagnification factor that exhibits the all sides of the cube with different location. Secondly the straight edges are focused and curved and thirdly the image rotates with respect to the object with an angle that is proportional to the axial distance.

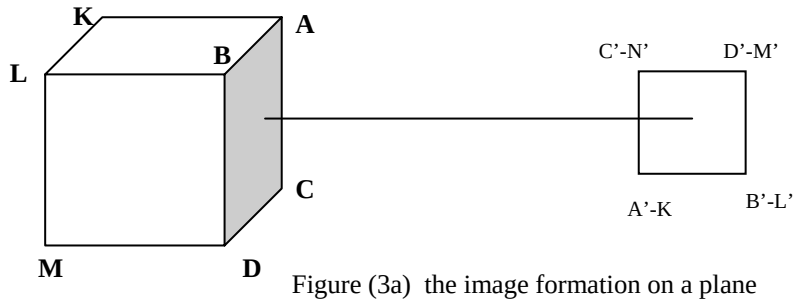

Figure (3a) the image formation on a plane

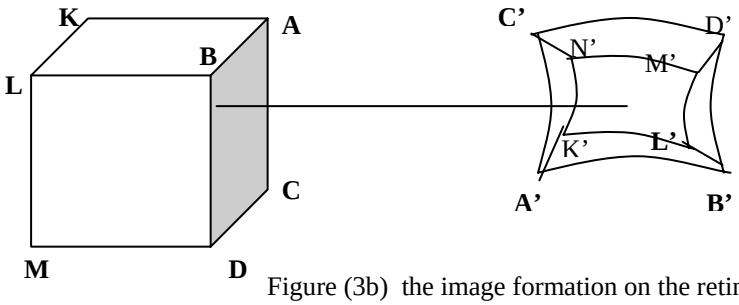

Figure (3b) the image formation on the retina

Figure (3) comparison between the image formation on a plane and on the curved retina

DISCUSION AND CONCLUSION

The present investigation aimed at producing a complete model to the image formation at the retina of human eye. The model suggests that:
1-The cornea acts as a very powerful converging lens. The aqueous humour has a refractive index differing slightly from the corneal substance, thus the posterior surface has a negligible refractive power. The focusing depends on the cornea curvature of lens surfaces curvature and the gradients of the lens index of refraction. Thus the asphericity of the system plays a strong role in the perfection of the eye as an optical system.

2- There is a linear dependence between corneal asphericity and lens asphericity that gives the optimum sharpness conditions as illustrated in figure(1).

3-The fovea is less than one half a millimetres (less than 500 micrometers) in diameter, which means that maximum visual acuity occurs in only 3 degrees of the visual field. Outside this fovea area the visual acuity is reduced five to tenfold, and it becomes progressively poorer as the periphery is approached.
The image blur circle of a point source could have a rms radius in the order of 5 micrometers. While the average diameter of cones in the fovea (the central part of the retina where vision is most highly developed), is approximately 1.5 micrometers. a person can distinguish two separate points if their centres lie approximately 2 micrometers apart on the retina, which is slightly greater than the width of a single cone in the fovea.

4- The blur circles for objects at far vision do not affect the image. However as the size of the object decreases the image itself as a whole lies within a very small area on the retina (in the order of 2 cones) so that it will not be recognized in full details. For bigger object the resolution improves and the blur circle does not seriously damage the details of the object. As the object comes nearer to the eye the problems of aberration appears more seriously.

6- The demagnification factor for far vision is almost constant ($0.29 \pm 0.003\%$) which means that all images will be demagnified equally irrespective of their geometry as long as they are in the far vision region.
For Near vision (object distance $\leq$ 25 cm). The demagnification factor is almost constant (6.8) for small object height up to 50 mm. But decreases linearly for object height greater than 50 mm.

The variation of lens height is not the main factor affecting the accommodation process but also the shape of the lens (lens asphericity) changes during accommodation in order to obtain the maximum sharpness of the image.

7- The accommodation process does not affect the demagnification factor where it is almost the same for both accommodated and unaccommodated lens. So the accommodation process affects only the sharpness of the image but not the size of the image.
8- The perception of the 3D of the image is not an absolutely mental process. But it is done by the variation of demagnification factor with the axial distance.

REFERENCES

1-Rosenblum, W, M., Blacker, J, W, & Block, M, G, "Matrix method for the evaluation of lens systems with radial gradient-index elements", *Am. J. Optomet.Physiol. Opt,* Vol 65, 1988, pp 661-665.

2-Blaker, J, W, "Toward an adaptive model of the human eye", *J.Opt.Soc.Am*., Vol 70, 1980, pp 220-223.

3-AL-Ahdali, E, H, & EI-Messiery, M, A, "Examination of the effect of the fibrous structure of a lens on the optical characteristics of the human eye: a computer simulated model", *Applied Optics*, Vol. 34, No. 25, 1995, pp 5738-5745.

4-AL-Ahdali, E, H, "Optimization of three and four-element lens systems by minimizing the caustic merit function" PhD. Thesis, Birmingham, ALABAMA, 1989, pp 27-3 5.

5- Pomerantzeff, 0, Pankratov, M, & Dufault P, " Wide-Angle optical model of the eye", *Am.J. Of. Optom. & Physio. Optics*, Vol 61, No. 3, 1984, pp 166-176.

6- Kortez, J, F, & Handelman, G, H, "model of the accommodative mechanism 'in the human eye", *Vision Res*., Vol 22, 1982, pp 917-927.

7-Manal , M and Essam G,"3Dcompressed image recognition and variable magnification power of the human vision system" 4th IEEE International Midwest Symposium",-ISBN 0-7803-8294-3/04, pp356-360 .

8-EI-Messiery, M, A, & Gomaa, E, "A computer model for the visual system of the eye", *Proc. ICEMP* , Vol1, 1998 pp 298-304.

CALCULATIONS OF OCULAR HEATING DUE TO COMMUNICATIONS HANDSETS

PETER WAINWRIGHT

HEALTH PROTECTION AGENCY, RADIATION PROTECTION DIVISION, CHILTON, DIDCOT, OXFORDSHIRE OX11 0RQ, UK

Exposure standards for radiofrequency radiation are framed in terms of acceptable specific energy absorption rate (SAR) in order to limit temperature rises in the body. The eye lens is particularly sensitive due to the lack of perfusion and limited capacity for repair. This work combines the FDTD method (for SAR computations) and finite element method (for thermal computations). A comparison is made between use of an isolated eye model, with convective boundary conditions, and a full head model. The resolution of the model is insufficient to describe the actual blood flow distribution at the choroid. However, an "equivalent perfusion rate" is used which is chosen to match the convective heat transfer coefficient used in other models. Calculations were made for exposure to a wireless handset with a monopole antenna at 380, 900 and 1800MHz, and with a helical antenna at 380MHz. A range of antenna positions was considered. Despite the range of different exposures, a consistent relationship was found between temperature rise in the eye, SAR averaged over the eye, and the 10g average SAR which is subject to restriction in ICNIRP guidelines.

Introduction

Recent years have seen a rapid increase in the use of personal wireless communications devices such as mobile phones. Unlike other sources of radiofrequency and microwave radiation, these are used in close proximity to the head. These sources can produce exposures which approach national or international safety guidelines (ICNIRP 1998, NRPB 2004, IEEE 2005) and therefore require fairly detailed safety assessment.

Over the past few years several authors (van Leeuwen *et al* 1999, Wainwright 2000, Bernardi *et al* 2000, Gandhi *et al* 2001, Hirata and Shiozawa 2003) have computed the temperature rises in the brain expected during use of a GSM mobile phone. In view of the high blood perfusion rate in the brain, temperature rises are likely to remain well within safe limits, indeed considerably less than the normal diurnal variation of brain temperatures.

The eye is more susceptible than most other organs to damage by microwave radiation. It lacks an internal blood supply, so that it is prone to the appearance of hot spots in the central regions (Hirata 2005). Furthermore, the lens has a limited capacity for repair, and the accumulation of cellular debris can lead to a loss of transparency. Animal experiments (Guy *et al* 1975) have shown the induction of cataracts with acute high level exposure.

Many models of the eye, for humans and other species, have been constructed over the years (Lagendijk 1982, Scott 1988a,b). Modelling the anatomy of the eye itself is relatively straightforward. However, a critical factor in the temperature calculation is the blood flow in the vessels surrounding the eye, particularly in the choroid, which has a dense network of vessels supplying the retina.

A new combined electromagnetic and thermal model of the human head has been developed at HPA. This model combines a finite difference time domain electromagnetic model with 2mm resolution and a finite element thermal model with 1mm resolution in the eye.

The aim of this study is to clarify the relationship between specific energy absorption rate (SAR) and temperature rises in the eye, and to determine whether the present basic restriction on SAR, recommended by ICNIRP, gives adequate protection against possible adverse effects such as cataract. To this end the new model has been used to compare the SAR and temperature rises due to radiation from antennas and handsets at frequencies produced by several widely used types of communication handset. The three frequencies studied

here are 380MHz (used by the Terrestrial Trunked Radio system, TETRA), 900MHz and 1800MHz (used by GSM mobile phones). The model has also been used to study the differences between two alternative antenna types, the monopole and helix.

Some older studies (Lagendijk 1982, Scott 1988a,b) have used a model of the eye in isolation from the head, and a boundary condition at the surface to take into account all heat losses to blood in the choroid and surroundings. The parameters of this boundary condition were chosen to fit temperature data obtained by measurement in the rabbit eye. In order to transfer this information to the full head model, an "equivalent" blood perfusion rate has been estimated for the layer of elements surrounding the eye. This perfusion rate produces a heat transfer approximately equivalent to that in the older truncated models.

Methods

The SAR in the head was calculated using the finite difference time domain (FDTD) technique implemented by a computer program developed at HPA and previously used to calculate SAR from TETRA exposures (Dimbylow *et al*, 2003). This technique uses a segmented voxel (VOlume piXEL) dataset to describe the human anatomy. The body is divided into a regular 3D array of hexahedral cells, and the tissue type of each cell is described by an integer code in the range 0 — 255. This tissue code is used as an index into several arrays which contain the electromagnetic and physical properties for each tissue, for example the density, permittivity and conductivity. Each program run is performed for one frequency. Prior to the run, the permittivity and conductivity at that frequency is calculated for each tissue. This is done using a 4-Cole-Cole model (Gabriel 1996). The open boundary was simulated using the "Perfectly Matched Layer" technique (Berenger 1994) using a 6-cell PML layer and a minimum 5-cell air gap between this and the nearest object.

The original voxel dataset of the head was derived from an MRI scan of an adult male. After initial segmentation as described in (Dimbylow and Mann 1994), a number of additional adjustments were made to correct shortcomings in the data acquisition and automatic tissue segmentation. For example, some voxels on the surface of the head had been erroneously labeled as CSF, and some inside the brain labeled as muscle. The original dataset did not distinguish the cartilage in the nose, and the eyes were half-closed. The original dataset did not show the orbital fat between the optic nerve and the orbital muscles; this region appeared as solid muscle.

The resolution of the original voxel dataset was 1 mm. However, in view of the large number of calculations to be performed it was found that a lower resolution of 2 mm was more appropriate for the majority of SAR calculations. Therefore, the dataset was resampled to the lower resolution using a simple voting algorithm to determine which of the 8 voxel tissue types would be assigned to the larger cube. In the course of this procedure the thin layer of skin covering the head was eroded in places. A subsequent automated procedure ensured a uniform 2 mm (1 voxel) covering of skin over the entire head.

For the thermal calculations a finite element technique was used, since this allows for non-uniform meshing and better conformance to curved interfaces (such as the surface of the eyeball). In this case accuracy of anatomical modeling far from the source is not critical, while the the structures of the eye must be represented in detail. The finite element mesh was derived by an automated procedure (Wainwright 1999) from the voxel dataset used for the SAR calculations. The SAR from the FDTD code was interpolated onto the finite element mesh in the following way: If an element lay entirely within one voxel, the SAR for that voxel was assigned to the element. If an element spanned several voxels, a simple numerical quadrature procedure was applied to integrate the power density over the element and derive the equivalent SAR.

The heat flow was modeled using the bioheat equation (Pennes 1948):

$$\rho c \frac{\partial T}{\partial t} = \nabla.(k \nabla T) + \rho S - \rho \rho_b c_b \omega (T - T_b) \quad (1)$$

together with the boundary conditions

$$k \frac{\partial T}{\partial n} = -(h_r + h_c)(T - T_{amb}) \quad (2)$$

where ρ, c, k and ω are respectively the density, specific heat, thermal conductivity and blood perfusion rate, T is the temperature and S the SAR. The suffices "b" and "amb" indicate the parameters of blood and the ambient temperature. The radiative and convective heat transfer coefficients h_r and h_c may vary over the surface of the body. However, in this work it has been assumed that the total value h is 20 W kg^{-1} for the cornea (Lagendijk 1982) and 8 W kg^{-1} elsewhere. In this paper all results are shown for the steady state, $\partial T/\partial t=0$.

Choroidal blood flow

Although a very thin layer, the choroid has a particularly high blood perfusion rate, which is necessary to supply the oxygen demands of the retina. This has a significant impact on the temperature distribution in the posterior chamber of the eye. The actual value and distribution of choroidal blood flow in humans is still a matter of debate. Many papers have used a model of the eye in isolation from the head, and a boundary condition at the surface to take into account all heat losses to blood in the choroid and surroundings (Lagendijk 1982, Scott 1988a,b). More recently, the value of the heat transfer coefficient has been questioned. It is not clear whether the extrapolation from rabbit to human models is valid. The anesthesia used in the original study may have had a significant effect on the measured blood flow (Kojima *et al* 2004).

Despite these shortcomings, the isolated eye models have been widely used, and a definitive improvement on this approach has not yet been forthcoming. Therefore the model in this study has been designed to replicate as closely as possible the effect of the choroid in the older models, while adding a complete model of the head. By examining simple analytical models of planar layers or concentric spheres it is possible to derive an "equivalent perfusion" for the choroid which replicates the heat loss of the older models in the simplest cases. This is then applied to the realistic SAR distribution in the whole head model.

First consider the steady-state one-dimensional bioheat transfer problem with two regions: region 1 the "choroid" ($0<x<d$), and region 2 the "head" ($x>d$). Assume a known heat flux F incident from the left at the interface $x=0$. In each region the temperature rise ΔT can be expressed as a sum of exponentials:

$$\Delta T(x) = A_i \exp(\alpha_i x) + B_i \exp(-\alpha_i x) \tag{3}$$

where in each region $i=1,2$

$$\alpha_i = \sqrt{\frac{\rho_b c_b \rho_i \omega_i}{k_i}} \tag{4}$$

The coefficients A_i and B_i can then be obtained using the continuity of temperature and heat flux at the tissue interfaces. Note that in the "infinite" region $x>d$ the solution cannot have an exponentially increasing part, so it is necessary that $A_2=0$. When this is done, we have a relationship between heat flux F and $\Delta T(0)$:

$$h = \frac{F}{\Delta T(0)} = k_1\alpha_1 \frac{k_1\alpha_1 \sinh(\alpha_1 d) + k_2\alpha_2 \cosh(\alpha_1 d)}{k_1\alpha_1 \cosh(\alpha_1 d) + k_2\alpha_2 \sinh(\alpha_1 d)} \tag{5}$$

Assume the rest of the "head" contains tissue of very low perfusion, so $\alpha_2 \approx 0$. Then in order to generate a heat transfer coefficient of h=65 W m^{-1} ºC^{-1} (Lagendijk 1982) it is necessary to set α_1=341 m^{-1}, or ω_1=16.3 ml kg^{-1} s^{-1}. If the "head" contains tissue similar to fat, ω_2=0.467 ml kg^{-1} s^{-1} (Duck 1990, Appendix A). Then α_1 must have a somewhat smaller value of 284 m^{-1}.

It is possible to derive a similar analytical solution for a more realistic spherical model of the eye, where the "eye" is the region $r<a$ and the "choroid" is $a<r<a+d$. In this case

$$h = \frac{k_1}{a} \frac{(k_1\alpha_1^2 a + k_2\alpha_2)\sinh(\alpha_1 d) + (k_2\alpha_1\alpha_2 a + k_1\alpha_1)\cosh(\alpha_1 d)}{k_1\alpha_1 \cosh(\alpha_1 d) + k_2\alpha_2 \sinh(\alpha_1 d)} \tag{6}$$

Interestingly, the change from planar to spherical geometry has a major effect on the heat transfer coefficient. For an eye of radius 1.25 cm surrounded by fat, this predicts h=67 W m^{-1} ºC^{-1} *even when* $\alpha_1=0$. This means that the coefficient proposed by Lagendijk (1982), 65 W m^{-1} ºC^{-1}, could be entirely accounted for by a sufficiently large volume of relatively low-perfusion material surrounding the eye. Since the surroundings include higher-perfusion tissues such as muscle and brain, and the choroid itself, it seems likely that the true value of the effective h is considerably higher than this.

As a control value, this paper uses a blood perfusion rate of 16.3 ml kg^{-1} s^{-1} in the choroid. Using the simple spherical model in Equation (6), this corresponds to h=130 W m^{-1} ºC^{-1}, a value which is twice that used in Lagendijk's rabbit model. The sensitivity of the results to this parameter has been investigated by either doubling, or eliminating entirely, the blood flow to the choroid.

Results

First, several computations were made to validate different aspects of the method. The basic configuration was a monopole, radiating at 380 MHz, on top of a metal box. This is a simplified representation of the Motorola MTP700 TETRA handset (Dimbylow *et al* 2003). As a worst-case scenario the handset model was placed as close as possible to the eye in a vertical orientation.

There was some concern initially that the 5-cell (1cm) air gap between the objects and the PML layer might not be sufficient for adequate accuracy in the FDTD calculations. Therefore one typical calculation was performed with both a 5-cell and a 10-cell gap. However, the resulting change in the computed SAR averages was found to be less than 1%. It was therefore concluded that the 5-cell gap was indeed adequate for the present study.

Some comparisons were done to investigate the effect of the improvements made to the segmentation of the anatomical model. The original model contained muscle in place of the cartilage of the nose and the orbital fat behind the eyeball. Inserting the orbital fat had relatively little impact. The maximum change in temperature was

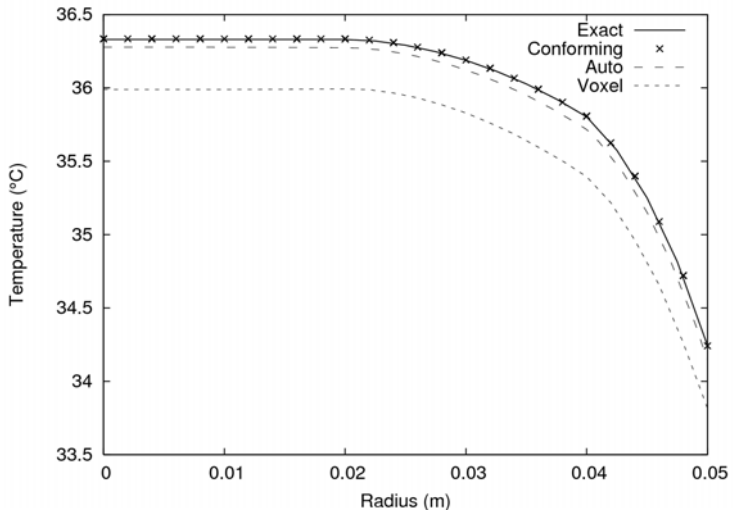

Figure 1: Finite element and exact solution for temperature in a sphere

about 10% of the peak temperature rise in the eye. A similar result was found for the cartilage.

The finite element thermal method was validated by comparison with the exact solutions derived by Durkee *et al* (1990) for spherical shell models. A uniform SAR of 1 W kg^{-1} was injected into a homogeneous sphere of muscle-equivalent material with a radius of 5 cm. The arterial blood temperature was 37ºC, the ambient temperature was 20 ºC and the convective heat transfer coefficient *h* at the surface was 8 W m^{-1} $ºC^{-1}$. Several finite element meshes were created to model this sphere. These meshes each had a nominal resolution of 2 mm. However, one (the "conforming mesh") was chosen to conform as closely as possible to the spherical boundary. The others were created by the automeshing procedure (Wainwright 1999) and by simply subdividing a mesh of cubical voxels. The latter meshes do not have a continuous normal vector at the surface, and as a result the surface area is somewhat greater than that of the real sphere. This causes a slight overestimate of heat loss from the surface, and slightly lower predicted temperatures as seen in .

A range of different thermal models were compared, ranging from a simple analytic solution with a spherical "eye", to a finite-element solution in an anatomically realistic head. This comparison shows the effects of the factors which are included at each stage of development of a realistic model. The differences between each model and the next can be explained, and this provides some reassurance that the final finite-element calculation correctly implements the model. Each model was applied to a test case consisting of a uniform SAR, 1 W kg^{-1}, applied within the eye alone. For each model, the maximum and minimum ΔT within the eyeball was calculated. The maximum occurs at or near the centre of the eyeball, and the minimum at the periphery.

The successive models were:

1. A homogeneous spherical "eye", of 26mm diameter. A constant convective heat transfer coefficient h=65 W m^{-2} $ºC^{-1}$ was assumed at the surface (Lagendijk 1982). This model was solved using the analytic method (Durkee *et al* 1990).
2. A finite element model containing the eye tissues only, extracted from the full head model, with the same constant *h*.
3. The same model as in 2, but using a different coefficient h= 20 W m^{-2} $ºC^{-1}$ on the cornea (Lagendijk 1982).
4. The complete head model, with SAR in the eye alone, with no special blood supply to the choroid.

5. The complete head model, with SAR in the eye alone, using the equivalent choroidal blood flow suggested above.

The results are shown in Table 1.

	Min. ΔT (°C)	***Max. ΔT (°C)***
1. Spherical	0.067	0.114
2. Isolated eye, constant *h*	0.046	0.110
3. Isolated eye, variable *h*	0.060	0.135
4. Eye in head	0.063	0.137
5. Eye in head, choroidal BF	0.031	0.102

Table 1: Comparison of eye models

Good agreement is seen between the maximum temperature rise in models 1 and 2. Errors are due to the finite element discretization, as discussed above. The greatest discrepancy arises in those areas of the eye surface where the staircasing effect is most noticeable. The difference between models 2 and 3 arises from the reduction of the heat transfer coefficient at the cornea. The temperature profile is now asymmetric, with the maximum being located toward the anterior part of the eye.

The agreement between models 3 and 4 is at first sight the most surprising feature of these calculations, because model 4 contains no special blood supply for the choroid. However, this result does agree with the argument made in the previous section. There it was shown that the fatty tissue surrounding the eye has a sufficient blood flow to generate an effective heat transfer coefficient of 67 W m^{-1} $^oC^{-1}$, nearly equal to the value used in the isolated eye models. Figure 2 shows the maximum and minimum ΔT in the eye for a range of choroidal blood perfusion. The central value, in particular, is relatively insensitive to this value. The difference between the central and peripheral temperature is almost constant because there is a constant thermal resistance between the centre and periphery; this cannot be eliminated however large the choroidal perfusion.

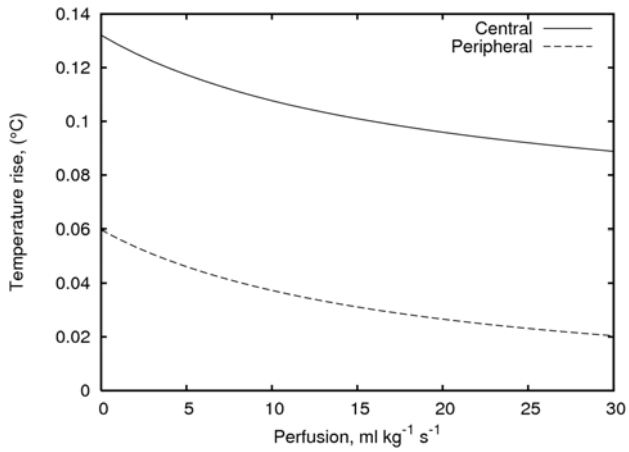

Figure 2: Effect of choroidal perfusion on ΔT

Figure 3 shows the TETRA handset placed as close as possible to the eye; the antenna feed point is 2.4 cm from the surface of the eye. Only the metallic parts of the antenna and handset are shown here. The handset is covered with a plastic casing and this prevents it from being moved any closer to the eye. In the following figures, this position is used as the origin for displacements of the antenna. The length of the monopole is about 3λ/16, where λ is the free-space wavelength. As seen from the figures this leads to quite a long and unwieldy antenna at the TETRA frequency, 380MHz. A more compact design uses a helical antenna (Dimbylow *et al* 2003). The temperature and SAR quoted here have been calculated for an antenna input power normalized to 1W. In order to study the effect of frequency on the temperature distribution, calculations were also performed using appropriately scaled monopole antennas at the GSM frequencies, 900 and 1800MHz, mounted on the same metal box.

Figure 4 and Figure 5 show the relative SAR profiles for the TETRA monopole handset located at 2.4 cm and at

8.4 cm. The greyscale values are not to the same scale. In Figure 4 the maximum (white) represents 4 W kg^{-1}, while in Figure 5 it represents 1 W kg^{-1}. It can be seen here that when the handset is held well away from the face the maximum SAR occurs not in the eye but in superficial structures such as the nose. Also, for a distant source, the SAR distribution in the eye becomes much more uniform, since the penetration depth at 380MHz is comparable to the eye size.

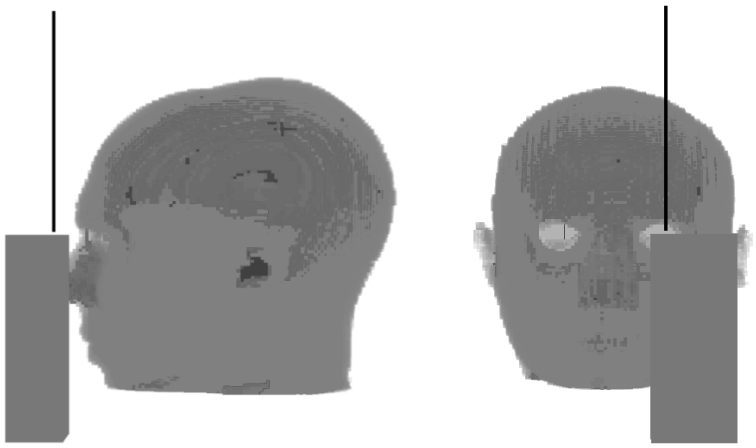

Figure 3: TETRA handset close to eye

Figure 4: TETRA at 2.4cm

Figure 5: TETRA at 8.4cm

An investigation was made into the relative contributions made to the temperature rise by the SAR inside and outside the eye. A plot of temperature rise along the central AP axis of the eye (Figure 6) shows heat conduction from outside the eyeball accounts for about 40% of the temperature rise in the lens. A detailed examination of the SAR and temperature profiles (not shown) has been done and reveals that this heat comes mainly from the orbital muscles above and below the eye.

Figure 7 shows the temperature rise along the central axis of the eye for various values of the choroidal perfusion rate. The middle curve is for the control value; the other curves show ΔT for the case of no perfusion or of double perfusion. As previously seen in Figure 2, it is apparent that increments in the perfusion rate become successively less effective, and in fact that ΔT for the lens converges to a nonzero value.

Figure 8 shows the central axis temperature rises for TETRA monopole and helical antennas, and GSM900 and GSM1800 monopole antennas (with appropriately scaled size) mounted on the same metal box. The profiles are very similar. The main difference arises from the fact that the penetration depth is smaller at 1800MHz, and therefore in this case the temperature rise is noticeably more peaked in the anterior part of the eye.

Table 2 summarises the SAR averages and temperature rises obtained for three frequencies, two antenna types and two values of the antenna-eye distance. The ICNIRP basic restriction (ICNIRP 1998) is framed in terms of the maximum SAR average over any 10g of tissue in the head. However, also listed is the average over the eye alone, which has been calculated by other authors (Hirata 2005). The maximum ΔT is always found near the posterior pole of the lens. For sufficiently small values of SAR and ΔT, thermoregulatory changes to blood flow are negligible and the relationship between these quantities is therfore linear. The slope of this linear curve is

also shown in the table, using both the ICNIRP SAR average and the eye averaged SAR.

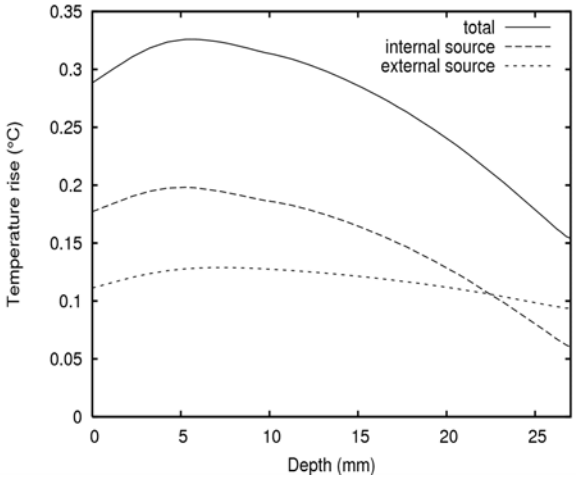

Figure 6: Contribution of internal and external SAR to ΔT

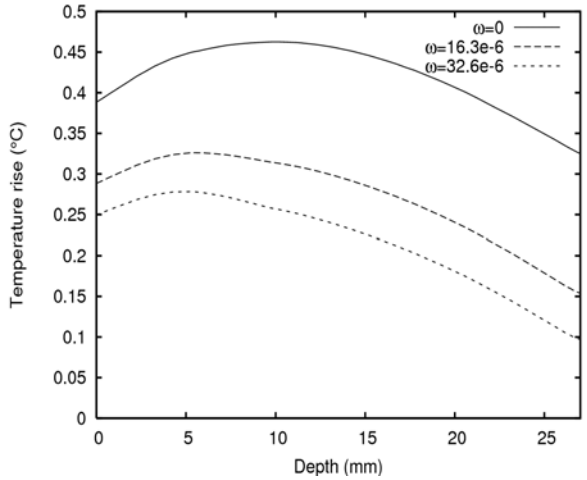

Figure 7: ΔT for various values of choroidal perfusion rate

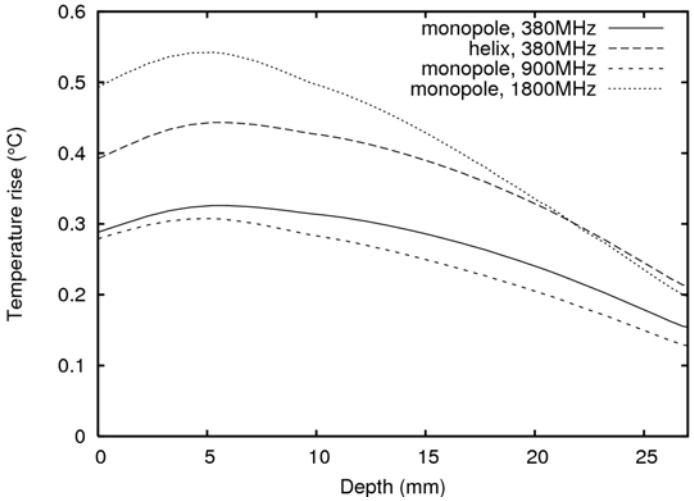

Figure 8: Temperature rises for various antenna types and frequencies

	SAR_{eye} (W kg^{-1}, ~10g)	SAR_{head} (W kg^{-1}, 10g)	Max. ΔT(eye) (°C)	$\frac{\Delta T}{SAR_{eye}}$	$\frac{\Delta T}{SAR_{head}}$
Monopole, 380MHz, 24mm	1.73	2.95	0.33	0.19	0.11
Monopole, 380MHz, 84mm	0.42	0.85	0.077	0.18	0.09
Helix, 380MHz, 24mm	2.35	3.97	0.44	0.19	0.11
Helix, 380MHz, 84mm	0.51	1.04	0.09	0.18	0.09
Monopole, 900MHz, 24mm	1.65	2.71	0.31	0.19	0.11
Monopole, 900MHz, 84mm	0.09	0.55	0.017	0.18	0.03
Monopole, 1800MHz, 24mm	2.97	4.00	0.55	0.19	0.14
Monopole, 1800MHz, 84mm	0.24	0.70	0.043	0.18	0.06

Table 2: Temperature rise and SAR summary

When the eye-averaged SAR is 10W kg^{-1}, the temperature rise in the eye is generally greater than 1°C but less than 2°C. However, when the ICNIRP occupational exposure restriction is respected (10W kg^{-1} in the head), the temperature rise in the eye is limited to about 1°C for all the TETRA exposures. However, it might reach 1.4°C if an antenna at 1800MHz were held very close to the eye.

Summary

These calculations have shown that the temperature rise in the eye is due not only to the energy directly absorbed by the eye tissues, but also by heat conduction from adjacent tissues which also absorb significant energy from the electromagnetic field. In some cases, about 40% of the temperature rise in the lens can be attributed to conduction from tissues outside the eye. Some studies have cited the SAR average over the eye as a predictor of thermal effect. This is because the mass of the eye is similar to the 10g averaging mass specified by ICNIRP. However, the present results show that the absorption in the orbital muscles must also be taken into account.

Under most circumstances the SAR average over the eye is substantially lower than the maximum SAR average in the head. Then, if the ICNIRP occupational exposure restriction is followed (10 W kg^{-1} in the head), the temperature rise in the eye is generally less than about 1ºC . However, at 1800MHz, it is theoretically possible to place an antenna very close to the eye and to produce larger temperature rises in the anterior part of the eye. However, this is still below the threshold which has been determined for cataractogenesis under acute exposures.

References

Berenger J. P. (1994), A perfectly matched layer for the absorption of electromagnetic wave, *J. Comput. Phys.* **114**, 185–200.

Bernardi P., Cavagnaro M,. Pisa S. & Piuzzi E. (2000). Specific absorption rate and temperature increases in the head of a cellular-phone user. I*EEE Trans. Microw. Theory Tech.*, **48**(7), 1118 – 1126.

Dimbylow P. J. & Mann S. M. (1994), SAR calculations in an anatomically realistic model of the head for mobile communication transceivers at 900 MHz and 1.8 GHz, *Phys. Med. Biol.* **39**, 1537–53.

Dimbylow P., Khalid M. & Mann S. (2003), Assessment of specific energy absorption rate (SAR) in the head from a TETRA handset, *Phys. Med. Biol.* **48**, 3911–3926.

Duck F. A. (1990), *Physical Properties of Tissue*, Academic Press.

Durkee J. R. Jr., Antich P. P. & Lee C. E. (1990), Exact solutions to the multiregion time-dependent bioheat equation. I: Solution development, *Phys. Med. Biol.* **35**(7), 847–867.

Gabriel S., Lau R. W. & Gabriel C. (1996), The dielectric properties of biological tissues: 3. Parametric models for the dielectric spectrum of tissue, *Phys. Med. Biol.* **41**, 2271–2293.

Guy A. W., Lin J. C., Kramar P. O. & Emery A. F. (1975), Effect of 2450-MHz radiation on the rabbit eye, *IEEE Trans. Microw. Theory Tech.* **MTT-23**(6), 492–498..

Gandhi O.P., Li Q.-X. & Kang G (2001). Temperature rise for the human head for cellular telephones and for peak SARs prescribed in safety guidelines. *IEEE Trans. Microw. Theory Tech.* **49**(9), 1607 – 1613.

Hirata A. (2005), Temperature increase in human eyes due to near-field and far-field exposures at 900 MHz, 1.5 GHz, and 1.9 GHz, *IEEE Trans. Electromag. Compat.* **47**(1), 68–76.

Hirata A. & Shiozawa T. (2003) , Correlation of maximum temperature increase and peak SAR in the human head due to handset antennas, *IEEE Trans. Microw. Theory Tech.* **51**(7), 1834 – 1841.

ICNIRP (1998). Guildelines for limiting exposure to time-varying electric, magnetic, and electromagnetic fields (up to 300 GHz). *Health Phys.* **74**, 494-522.

IEEE (2005). Standard for Safety Levels with Respect to Human Exposure to Radio Frequency Electromagnetic Fields, 3 kHz to 300 GHz. Std C95.1 – 2005.

Kojima M., Hata I., Wake K., Watanabe S., Yamanaka Y., Kamimura Y., Taki M., Sasaki K. (2004). Influence of Anesthesia on Ocular Effects and Temperature in Rabbit Eyes Exposed to Microwaves. Bioelectromagnetics **25**, 228-233.

Lagendijk J. J. (1982), A mathematical model to calculate temperature distributions in human and rabbit eyes during hyperthermic treatment, *Phys. Med. Biol.* **27**(11), 1301–1311.

NRPB (2004). Advice on limiting exposure to electromagnetic fields (0 – 300 GHz). *Documents of the NRPB,* **15**(4).

Pennes H. H. (1948), Analysis of tissue and arterial blood temperature in the resting human forearm, *J. Appl. Physiol.* **1**, 93–122.

Scott J. A. (1988a), A finite element model of heat transport in the human eye, *Phys. Med. Biol.* **33**(2), 227–241.

Scott J. A. (1988b), The Computation of Temperature Rises in the Human Eye Induced by Infrared Radiation. *Phys. Med. Biol.* **33**(2), 242–257.

van Leeuwen G. M. J., Lagendijk J. J. W., van Leersum G. J. A. M., Zwamborn A. P. M., Hornsleth S. N. & Kotte A. N. T. J. (1999), Calculation of change in brain temperatures due to exposure to a mobile phone. *Phys. Med. Biol.* **44**, 2367–2379.

Wainwright P. R. (1999), Localized specific absorption rate calculations in a realistic phantom leg at 1–30 MHz using a finite element method, *Phys. Med. Biol.* **44**, 1041–1052.

Wainwright P. R. (2000), Thermal effects of radiation from cellular telephones, *Phys. Med. Biol.* **45**, 2363–2372.

NUMERICAL EVALUATION OF EXTERNAL ELECTROMAGNETIC FIELDS INFLUENCE ON BRAIN ELECTRICAL ACTIVITY

Marina Rezinkina
National Technique University "KPI", Frunze st., 21, Kharkov 61002, Ukraine,
e-mail: marinar@kpi.kharkov.ua

Eleonora Bydianskaya
Kharkov Scientific Research Institute of Hygiene of Labour and Industrial Diseases
Trinklera st., 6, 61022, Kharkov, Ukraine

Anatoliy Shcherba
Institute of Electrodynamics, avenue Pobedy, 56, Kiev, Ukraine

Abstract

Hodgkin-Huxley model, describing generation of action potentials in the nerve cell membranes has been used for appreciation of the possible EMF influence mechanisms on the brain own electric activity. The carried calculations have shown that at simultaneous passing through a nerve cell of action potentials and external ac, suppression of the own excitation pulses is possible starting from the certain level of the external current value, which depends on its frequency. To avoid such suppression of action potentials, their levels may be increased relatively minimum limit level. It may be supposed that brain "tunes up" its work at presence of external ac, increasing amplitudes of its own excitation signals so that their suppression does not occur. It is possible also that this "tuning" acts some time after external EMF removing while brain adapts again to its absence, as it is observed in experiment.

1. Introduction.

There are studies connected with influence of electromagnetic fields (EMF) on the activity of cerebrum of animals (see for instance [1]) and people (see for instance [2-5]). As it is shown in these works, low frequency or amplitude modulated radio-frequency EMF of the defined strength and frequency may influence bioelectrical activity of mammals' cerebrum. It is expressed in changes observed by means of electroencephalography (EEG) [1-5]. However, literature data on the character of the EMF influence are discrepant. Thus, it is mentioned about blocking of cerebrum bioelectrical activity upon action of magnetic field with 10 Hz frequency and 0.1 мТл stress [4]. At the same time it is shown in [2] that influence of the magnetic field with frequency f=0-500 Hz and 0.2 мТл magnetic field stress was expressed in increase of the potential levels, registered by EEG after lifting of the exposure. It is shown in [3] that magnetic fields of 60 Hz frequency and 1 Ga stress cause reliable change of EEG of people after lifting of the exposure.

As it is shown in [6], heterogeneity of the electrical properties of cortex tissues and, in particular presence of the intercellular fluid, leads to low frequency filtration of electromagnetic field. As a result, EEG has only low frequency components. It is possible that the answer of the cerebrum neurons to the influence of radio-frequency electromagnetic fields is suppressed also by the low frequency filter, which serves cerebrum intercellular fluid, so it is not registered by EEG. However, influence on the people's EEG of high frequency electromagnetic fields in the limited time diapason $t < 300$ ms after lifting of the exposure has been fixed [5].

The purpose of this work is estimation of the parameters of electrical processes in the membrane of a brain neuron for evaluation of the limit levels of current density, induced as a result of external EMF application, which do not influence own bioelectric processes, occurring at normal cortex operation in absence of an external EMF. To understand the mechanism of EMF influence on the own electrical activity of cerebrum, it is suggested to use simple, but demonstrative Hodgkin-Huxley model [7], describing passage of bioelectric pulses through the neuron membrane.

2. Evaluation of the neuron membrane charges and potentials at external current flow.

Let's consider influence of the external EMF on the cellular level. The author of [8] has made estimation of Q_R – charge density of the cell membrane: $Q_R=V_m \cdot C_m$, where $C_m=10^{-2}$ F/m^2 - specific membrane capacitance, V_m=-60 mV - resting potential of the membrane: $Q_R \sim 6 \cdot 10^{-4}$ K/m^2. Let's evaluate Q_p – value of the charge density in brain tissues at flowing in them of the normalized, for instance in [9], permitted level of current density J_p=10 mA/m^2 at f ≤ 1000 Hz: $|Q_p|=|J_p|/\omega$. For industrial frequency 50 Hz $|Q_p| \sim 0.3 \cdot 10^{-4}$ K/m^2, i.e. makes up about 5 % from Q_R. For lower frequencies, for instance 10 Hz, as in the experiments described in [1,2], $|Q_p|$ is even greater: $|Q_p| \sim 0.16 \cdot 10^{-3}$ K/m^2, i.e. makes up nearly 27 % from Q_R. Such a change of charge may influence own electrical processes, occurring at cerebrum functioning.

Let's perform evaluative calculations of the levels of potential, appearing in intercellular medium and membrane of a nervous cell at flowing in the cerebrum tissues of the very low frequency (f ≤ 1000 Hz) current with the density J^{ext}=10 mA/m^2, equal to the permitted level. It is necessary to take into account that an external current J^{ext} passes both through the membrane and through the nucleus of the cell. Let's consider that specific conductivity of the intercellular fluid does not exceed $\gamma_i \sim 0{,}03 – 0{,}1$ См at frequencies f ≤ 100 Hz (see for instance [10]). Then G_i^* - conductivity of the intercellular medium corresponding to the unit area, makes up: $G_i^*=G_i/S=\gamma_i \cdot S/(L \cdot S) \sim 10^4$ S/m^2 (at L~10^{-5} m - transverse size of a cell, S – the area of a cell). At the same time, capacitive conductivity of a membrane, corresponding to a unit area at frequency, for instance 10 Hz, is equal to: $\omega \cdot C_m^* = \omega \cdot C_m/S \sim 0{,}6$ S/m^2. So, at outside current J^{ext} flowing, Ohm's law for a cell membrane and intercellular medium may be expressed as follows, taking into account that $G_i^* >> \omega \cdot C_m^*$:

$$U = I^{ext} \cdot [1/(\omega \cdot C_m)+1/G_i] = I^{ext} \cdot S \cdot [1/(\omega \cdot C_m \cdot S)+1/(G_m \cdot S)] = J^{ext} \cdot [1/(\omega \cdot C_m^*)+1/G_i^*] \sim J^{ext}/(\omega \cdot C_m^*) \sim 16 \text{ мВ},$$

where I^{ext} – external current.

Thus, at very low frequencies of the external current flowing through a cell, the main drop of voltage is in its membrane (see [8] also). So, at flowing of the induced by external sources current with density 10 mA/m^2, which is normalized as permitted, drop of voltage in a membrane may reach 16 mV at f=10 Hz and about 3 mV at f=50 Hz.

The same result may be obtained at evaluation of the field problem. In 1D approach: $J_i=J_m=J^{ext}$ (where J_i - current density in the intercellular medium; J_m - current density in the cell membrane) and $J_i=\gamma_i \cdot E_i$; $J_m=j \cdot \omega \cdot \varepsilon \cdot \varepsilon_0 \cdot E_m$ (where E_i - electric field stress in the intercellular medium, E_m - electric field stress in the cell membrane, ε=81). From this $\gamma \cdot |E_i|=\varepsilon \cdot \varepsilon_0 \cdot \omega \cdot |E_m|$. For very low frequencies $E_m >> E_i$, thus for f=10 Hz and γ_i =0.1 S/m:

$$|E_m| = |E_i| \cdot [\gamma_i/(\varepsilon \cdot \varepsilon_0 \cdot \omega)] \sim |E_i| \cdot 0.2 \cdot 10^7. \quad (1)$$

General fall of voltage in a cell:

$$U_c = d_m \cdot |E_m| + d_i \cdot |E_i|, \quad (2)$$

where d_i - thickness of a cell ($d_i \sim 10^{-5}$ м); d_m - membrane thickness ($d_m \sim 10^{-8}$ м).

Substituting (1) in (2), we get: $U_c = |E_m| \cdot (10^{-8}+10^{-5} \cdot 5 \cdot 10^{-7})$, thence $E_m \cdot d_m \sim U_c$. As a result we get:

$$U_m \sim U_c \sim [J^{ext}/(\varepsilon \cdot \varepsilon_0 \cdot \omega)] \cdot d_m,$$

where U_m- voltage drop in a membrane,

that at f=10 Hz gives $U_m \sim 16$ mV.

Considering that this value has the same order as, for instance potential difference, caused by the presence of K^+ ions inside a cell, $E_K \sim$ -12 mV (see for instance [11]), such change of the membrane potential may cause change of its conductivity to K^+ ions.

3. Calculations with the help of Hodgkin-Huxley model.

Let's use the known Hodgkin-Huxley model [7] describing electric processes in the membrane of neuron (see fig. 1). The equivalent electrical circuit of a patch of the axon membrane is shown in fig. 2.

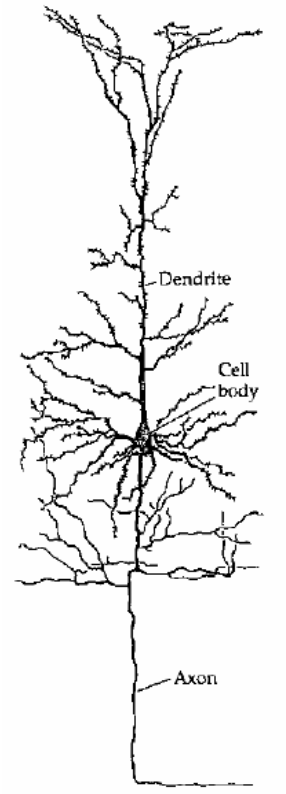

Fig. 1. A real neuron.

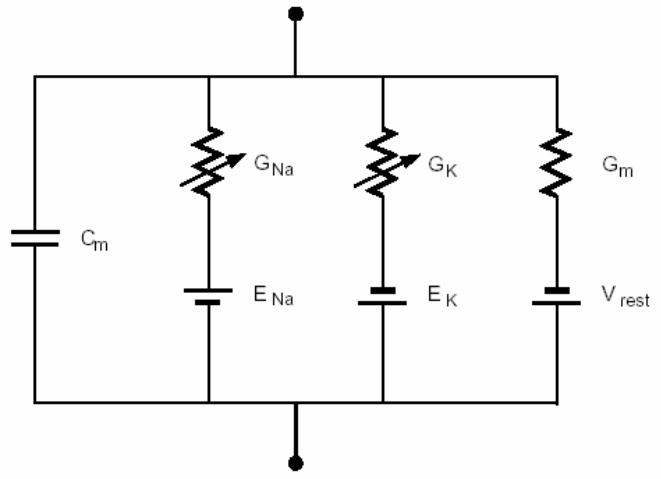

Fig. 2. Equivalent electrical circuit of a patch of axon.

It is known that high concentration of potassium ions as well as low concentration of sodium and chlorine ions exists inside a neuron cell in the state of rest. The membrane of a cell performs the role of a barrier, preventing ions penetration from the intercellular medium inside a cell and vice versa. The rest potential E_m settles in a cell membrane as a consequence of presence on its both sides of different concentration of Na^+ and K^+ ions. If it is considered that membrane potential V is equal to 0 in the rest state, $E_K \sim -12$ mV, $E_{Na} \sim 115$ mV, $E_{rest} \sim 10.613$ mV, $G_m \sim 3$ Sm/m^2, $C_m \sim 10^{-2}$ F/m (see for instance [11]), where E_K - potential difference, connected with presence of potassium ions inside a cell; E_{Na} - potential difference, connected with presence of sodium ions inside a cell; E_{rest} – value, chosen by calculations, which provides equality to zero of the membrane

potential in the rest mode; G_K - conductivity of a unit area to K^+ ions; G_{Na} - conductivity of a unit area to Na^+ ions; G_m – leak conductivity of a unit area; C_m - membrane capacity of a unit area (see fig. 2).

Let's take into account presence in the equivalent circuit of a cell of the additional current sources, imitating current of axon excitation, as well as current, running in cortex at application of an external EMF. As all quantities in the equivalent scheme are expressed as specific values, we suppose that external source is characterized by density J^{ext} and frequency f, and the source of axon excitation current is characterized by density J^{ax} and duration τ^{ax}.

It is supposed in Hodgkin-Huxley model that full current through a membrane consists of a capacitive current, as well as conductivity currents of K^+, Na^+ ions and leak current through active resistance of a membrane. Nonlinear dependencies of the conductivities to K^+ and Na^+ ions relatively the value of the membrane voltage V are entered in this model. These dependencies assume that transition from non-conducting state of a membrane to its conducting state occurs at certain voltage on the membrane. According to Hodgkin-Huxley model, this transition complies with the first-order kinetics. The equation of such transition for K^+ ions may be written down as follows:

$$\frac{dn}{dt} = \phi(T) \cdot [\alpha_n(V) \cdot (1 - n) - \beta_n(V) \cdot n], \tag{3}$$

where $\phi(t) = 3^{(T-6.3)/10}$ - coefficient depending on the temperature; T - temperature in the Celsius degrees; $\alpha_n(V)$, $\beta_n(V)$ - coefficients depending on the voltage level.

Specific conductivity to potassium ions G_K is supposed to be equal to $G_K = \overline{G}_K \cdot n^4$ ($\overline{G}_K$ =36 mS/cm^2), and coefficients $\alpha_n(V)$, $\beta_n(V)$ are written as follows:

$$\alpha_n(V) = \frac{10 - V}{100 \cdot \{\exp[(10 - V)/10] - 1\}}; \qquad \beta_n(V) = 0.125 \cdot \exp(-V/80),$$

where V - in millivolt.

Specific conductivity to sodium ions G_{Na} is written in the form $G_{Na} = \overline{G}_{Na} \cdot m^3 \cdot h$ ($\overline{G}_{Na}$ =120 mS/cm^2), and it is supposed also that transition from m condition to (m-1) condition and from h to (h-1) condition also complies with the first-order kinetics:

$$\frac{dm}{dt} = \phi(T) \cdot [\alpha_m(V) \cdot (1 - m) - \beta_m(V) \cdot m]; \tag{4}$$

$$\frac{dh}{dt} = \phi(T) \cdot [\alpha_h(V) \cdot (1 - h) - \beta_h(V) \cdot h], \tag{5}$$

where $\alpha_m(V)$, $\beta_m(V)$, $\alpha_h(V)$, $\beta_h(V)$ - coefficients depending on the voltage level.

Coefficients $\alpha_m(V)$, $\beta_m(V)$, $\alpha_h(V)$, $\beta_h(V)$ are written as follows:

$$\alpha_m(V) = \frac{25 - V}{10 \cdot \{\exp[(25 - V)/10] - 1\}}; \qquad \beta_m(V) = 4 \cdot \exp(-V/18);$$

$$\alpha_h(V) = 0.07 \cdot \exp(-V/20); \qquad \beta_h(V) = \frac{1}{\exp[(30 - V)/10] + 1},$$

where V - in millivolt.

Let's write down the equation for all current densities, flowing through a membrane (equivalent scheme is shown in fig. 2):

$$C_m \cdot \frac{dV}{dt} = \overline{G}_{Na} \cdot m^3 \cdot h \cdot (E_{Na} - V) + \overline{G}_K \cdot n^4 \cdot (E_K - V) + G_m \cdot (V_{rest} - V) + J^{ext} + J^{ax}. \tag{6}$$

Let's replace derivatives in the expressions (3)-(6) by their differential analogues and express volumes of the sought functions at the time step t for T=6.3^0 C as follows:

$$n_t = \frac{n_{t-\Delta t} + \alpha_n(V_t)\cdot\Delta t}{1+\Delta t\cdot[\alpha_n(V_t)+\beta_n(V_t)]};\ m_t = \frac{m_{t-\Delta t} + \alpha_m(V_t)\cdot\Delta t}{1+\Delta t\cdot[\alpha_m(V_t)+\beta_m(V_t)]};$$

$$h_t = \frac{h_{t-\Delta t} + \alpha_h(V_t)\cdot\Delta t}{1+\Delta t\cdot[\alpha_h(V_t)+\beta_h(V_t)]};\ V_t = \frac{V_{t-\Delta t}\cdot C_m/\Delta t + \overline{G}_{Na}\cdot m^3\cdot h\cdot E_{Na} + \overline{G}_K\cdot n^4\cdot E_K + G_m\cdot V_{rest} + J^{ext}(t) + J^{ax}}{C_m/\Delta t + \overline{G}_{Na}\cdot m^3\cdot h + \overline{G}_K\cdot n^4 + G_m},$$

where Δt [ms] - step in time domain; C_m [μF/cm^2]; J^{ext}, J^{ax} [μA/cm^2]; $\overline{G}_K$, $\overline{G}_{Na}$ [mS/cm^2]; V [mV].

The obtained system of nonlinear equations was solved by the iterative method in each time step. The value of Δt was chosen equal to 0.01 ms.

An example of the calculated axon membrane voltage at application to it of the excitation current with density J^{ax}_{min} = 14 μA/cm^2 and duration τ^{ax} = 0.5 ms is shown in fig. 3.

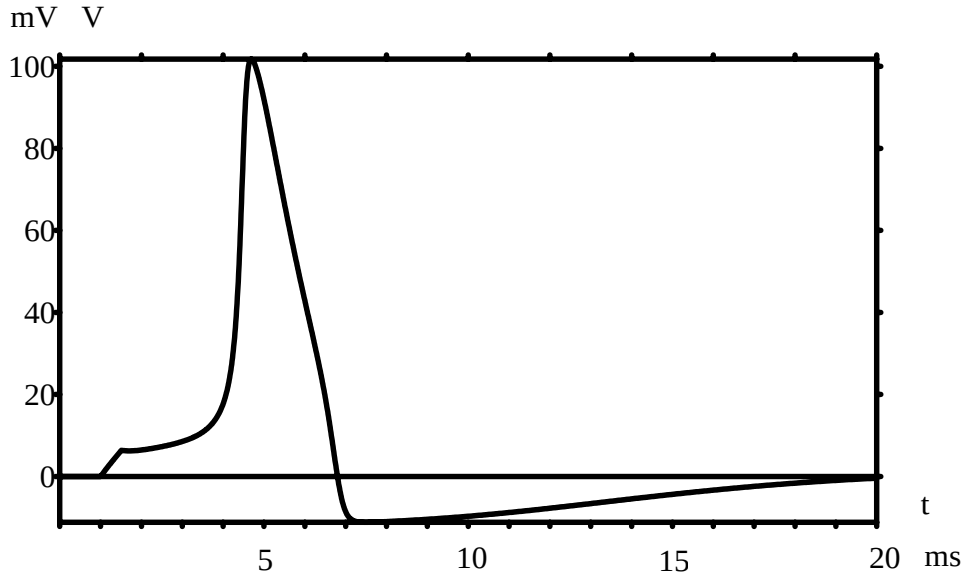

Fig. 3.

The calculated dependencies of n, m, h change in time domain for this case are presented in fig. 4.

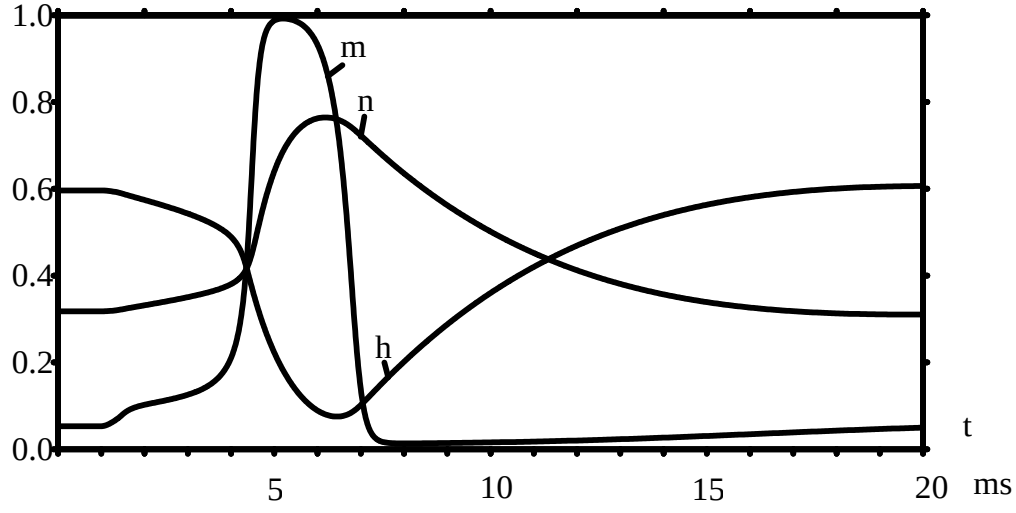

Fig. 4.

It is known that excitation potentials with certain periodicity are generated in an axon at application of an external dc. The same phenomenon is present also at application of an external ac. The calculated boundary levels of the external currents densities J^{ext}_{lim1} and J^{ext}_{lim2}, such that presence of an external field does not cause appearance of induced excitation potentials in an axon if $J^{ext} < J^{ext}_{lim1}$, but potentials with certain periodicity depending on J^{ext} value are generated in an axon if $J^{ext} > J^{ext}_{lim2}$ are presented in the table for different frequencies. Generation of a single induced excitation pulse or a transition stage occurs at $J^{ext}_{lim1} < J^{ext} < J^{ext}_{lim2}$.

Table.

f [Hz]	J^{ext}_{lim1} [mA/m^2]	J^{ext}_{lim2} [mA/m^2]
10	50	60
30	20	25
50	15	20
100	20	30
1000	65	70

Calculated changes in time domain of the potentials in the neutron's membrane at application of the external current of 10 Hz frequency with the amplitude 60 mA/m^2 and 100 mA/m^2 are presented in fig. 5 and 6 correspondingly.

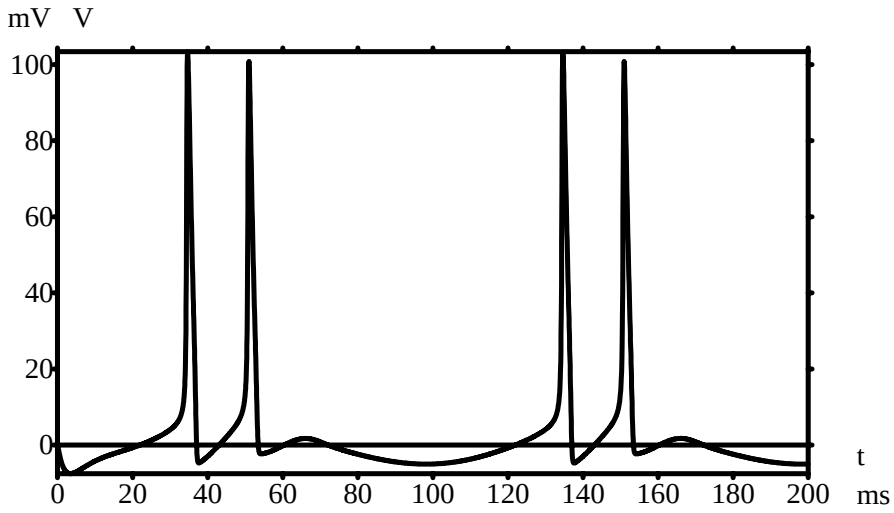

Fig. 5. Dependence of the axon membrane voltage from time at flowing of the external current with frequency 10 Hz and amplitude 60 mA/m^2.

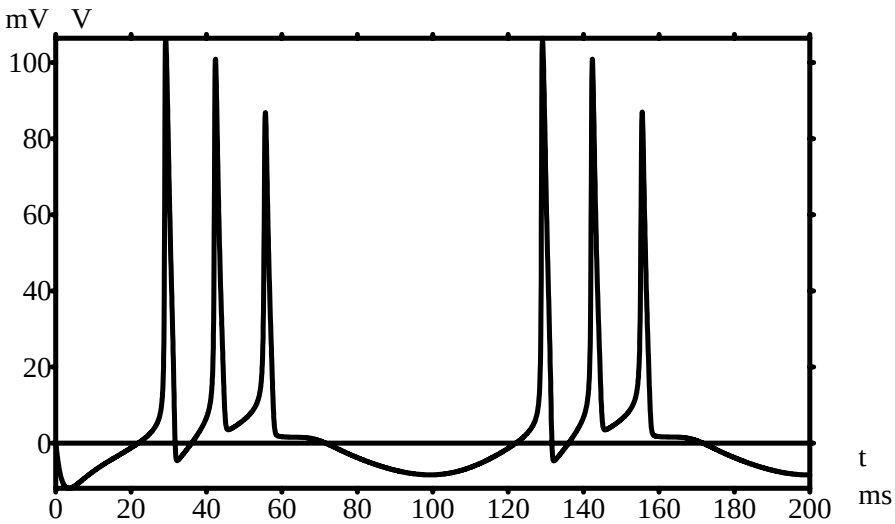

Fig. 6. Dependence of the axon membrane voltage from time at flowing of the external current with frequency 10 Hz and amplitude 100 mA/m^2.

As carried calculations have shown, at simultaneous passage through an axon of an external current J^{ext}, as well as axon excitation current J^{ax}, starting from the defined level of an external current, depending on its frequency, suppression of the excitation pulses occurs if they pass through the axon membrane during negative half-waves of external current (see fig. 7 moment t_1). The same external current does not affect excitation pulses if they appear during positive half-waves (see fig. 7 moment t_2). The carried calculations have shown that current caused by the presence of external field ceases to suppress brain own excitation pulses only when $J^{ext} < J^{ext}_{lim0}$ (where J^{ext}_{lim0} - limit level of current density). For the industrial frequency of 50 Hz this limit level is equl to: J^{ext}_{lim0} =1.5 mA/m^2, for other frequensies it should be calculated.

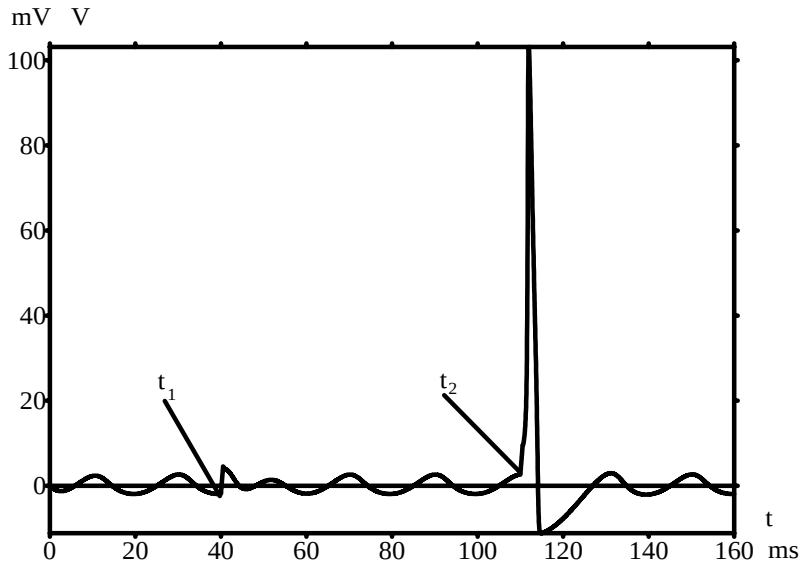

Fig. 7. Dependence of the axon membrane voltage from time at flowing of the external current with frequency 50 Hz and amplitude 10 mA/m^2 and simultaneous flowing of excitation pulses of amplitude J^{ext}=14 μA/cm^2 in the moments t_1, t_2.

It was obtained from the calculations also that to prevent suppression of brain own excitation pulses by the external current of permitted density J^{ext} = 10 mA/m^2, their levels should be increased up to J^{ax} = 18 μA/cm^2 - approximately on 30 % relatively the minimum limiting level of J^{ax}_{min} = 14 μA/cm^2 at which excitation pulses of duration τ^{ax} = 0.5 ms still pass (see fig.8).

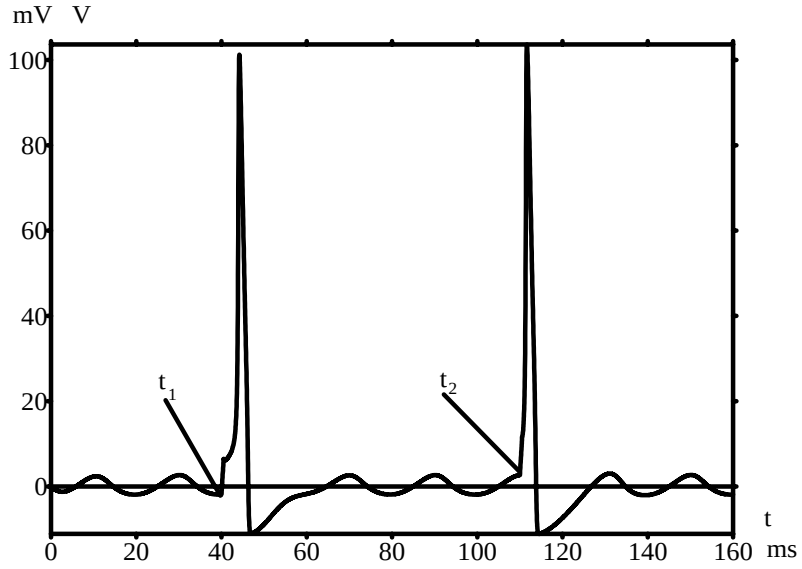

Fig. 8. Dependence of the axon membrane voltage from time at flowing of the external current with frequency 50 Hz and amplitude 10 mA/m^2 and simultaneous flowing of excitation pulses of amplitude J^{ext} = 18 μA/cm^2 in the moments t_1, t_2.

From certain level of external current density, full suppression of the own brain electrical activity has been observed in the calculations. It may be a cause of the analgesic effect during application of the external low frequency EMF due to blocking of action potential propagation.

Thus, from an example of simple calculations, it may be seen that at certain conditions of irradiation, flowing through the membrane of axon of the low frequency external ac can cause suppression of the own excitation signals passing through the membrane. It can cause also generation of the induced excitation signals, as well as increase of the levels of brain own excitation potentials so that they would not be suppressed by the presence of external current, i.e. all phenomena observed in experiment (see [1-5]).

Conclusions.

1. As calculations with the help of Hodgkin-Huxley model have shown, flowing through nervous cells of current with density 10 mA/m^2 and frequency f < 100 Hz in absence of own brain excitation pulses does not cause appearance of the induced excitation potentials. However, simultaneous flowing through an axon of the external very low frequency current $J^{ext}_{lim0} < J^{ext} \leq 10$ mA/m^2 and excitation pulses can cause suppression of the excitation pulses, moreover minimum low frequency current at which this phenomenon still exists, corresponds approximately to 50 Hz, i.e. the most wide-spread industrial frequency.

2. It is possible that at presence of the external very low frequency current, which density level lays in the limits: $J^{ext}_{lim0} < J^{ext} < J^{ext}_{lim1}$ including smaller or equal to the permitted level, brain "adjusts" its work so that suppression of its own excitation signals does not occur, enlarging amplitude of these signals: $J^{ax} > J^{ax}_{min}$. It is possible also that this "tuning" acts some time after removal of the external EMF while brain will not adapt again to the EMF absence, as it was observed in experiment when EEG levels were greater some time after lifting of the low frequency EMF irradiation [2]. It may be also a cause of pain and sensitivity thresholds decrease some time after removal of the low frequency magnetic field exposure (see [12]) as at greater levels of action potentials brain may be more sensitive to lower levels of external pain effects.

References

[1] Bell G., Marino A., Chesson A., Struve F., *"Electrical states in the rabbit brain can be altered by light and electromagnetic fields"*, Brain Research, v. 570, p. 307-315, 1992.
[2] Cook C.M., Thomas A.W., Prato F.S., *"Resting EEG is affected by exposure to a pulsed ELF magnetic field"*, Bioelectromagnetics, v. 25, p. 196-203, 2004.
[3] Marino A.A., Nilsen E., Chesson Jr A.L., Frilot C., *"Effect of low-frequency magnetic fields on brain electrical activity in human subjects"*, Clinical Neurophysiology, v. 115, p. 1195-1201, 2004.
[4] Bell G., Marino A., Chesson A., *"Frequency-specific blocking in the human brain caused by electromagnetic fields"*, NeuroReport, v. 5, No 4, p. 510—512, 1994.
[5] Marino A.A., Nilsen E., Frilot C., *"Nonlinear changes in brain electrical activity due to cell phone radiation"*, Bioelectromagnetics, v. 24, p. 339-346, 2003.
[6] Bédard C., Kröger H., Destexhe A., *"Modeling extracellular field potentials and the frequency-filtering properties of extracellular space"*, Biophysical Journal, v. 86, p. 1829-1842, 2004.
[7] Hodgkin A.I., Huxely A.F., *"A quantitative description of membrane current and its application to conduction and excitation in nerve"*, J. Physiol, v. 117, p. 500-544, 1952.
[8] Adair R.K., *"Biophysical limits on athermal effects of RF and microwave radiation"*, Bioelectromagnetics, v. 24, p. 39-48, 2003.
[9] *"Board statement on restrictions on human exposure to static and time varying electromagnetic fields and radiation"*, Documents of the NRPB, Chilton. Didcot. Oxon, v. 4, No 5, 69 p., 1993.
[10] Gabriel S., Lau R.W., Gabriel C., *"The dielectric properties of biological tissues: II. Measurements in the frequency range 10 Hz to 20 GHz"*, Phys. Med. Biol., v. 41, p. 2251-2269, 1996.
[11] Peasgood W., Dissado L.A., Lam C.K., Armstrong A., Wood W., *"A novel electrical model of nerve and muscle using Pspice"*, J. Phys. D: Appl. Phys., v. 36, p. 311-329, 2003.
[12] Ghione S., Seppia C., Mezzasalma L., Emdin M., Luschi P. *"Human head exposure to a 37 Hz electromagnetic field: effects on blood pressure, somatosensory perception and blood parameters"* Bioelectromagnetics, v. 25, p. 167-175, 2004.

EFFECT OF A SPECIALLY PULSED MAGNETIC FIELD ON WOUND HEALING IN RAT SKIN

*OZLEM ULUKUT

*SELCUK COMLEKCI

**SULEYMAN DEMIREL UNIVERSITY, FACULTY OF ENGINEERING, DEPARTMENT OF ELECTRICAL & COMMUNICATIONS ENGINEERING, 32260, CUNUR, ISPARTA, TURKEY*

e-mail:oulukut@mmf.sdu.edu.tr *e-mail:scom@mmf.sdu.edu.tr*

Abstract

The exact mechanism by which electromagnetic fields affect bone and other tissues has yet to be cleared. Several mechanisms have been proposed, among them changes in cellular ionic calcium, modified receptor and messenger behavior, increased synthesis or degradation of substances, and even direct interaction with genes. Several in vivo studies were conducted to evaluate the effect of pulsed electromagnetic field (PMF) on the healing of skin wounds in rats. Variable results were reported. In some of these studies, exposure of wounds to PMF resulted in a higher rate of wound contraction (WC), enhanced cellular organization, and earlier collagen formation and maturation. However, several other reports failed to show any beneficial effect of PMF on the healing of skin wounds in rats. The aim of this study was to investigate the possible effects of a specially pulsed magnetic field (PMF) on skin wound healing in rats. Thirty male Sprague-Dawley male rats were used in this study. After anaesthetizing and shaving a paired full thickness incision wound (30 mm in length) was made on each side of the dorsal midline of the rats. The rats were randomly divided into three groups each containing 10 rats. Control and two treatment groups which were exposed to 0.45 ms pulse rates of 2.2 kHz. Treatment group1 were exposed PMF (5 mT) for 30 min a day for seven days and treatment group 2 were exposed PMF (2.5 mT) 1 hour a day for seven days after surgery. Control group were subjected to the same procedure, but with the PMF device not activated.

Key words: PMF, wound healing

Introduction

The process of regeneration and repair following injury represents one of the most fundamental defense mechanisms of an organism against environmental damage. Biological processes such as inflammation, proliferation, wound contraction and remodeling lead to the scar formation. Certain systemic diseases, such as injuries to the nervous system, metabolism and aging, have negative influence on the healing process, and lead to chronic wound formation. The use of pulsed magnetic field (PMF) for selective control of cellular function has given biology and medicine a new dimension. PMF stimulators with different characteristics were designed to induce voltages similar to those produced normally, during mechanical deformation of connective tissue. Researchers have used PMF stimulators to promote healing, but the results differ significantly from one another and there are discrepancies between the uses of PMF parameters. Further studies are needed to determine the optimal PMF parameters for the acceleration of wound healing. This study was designed to compare the different PMF pulse rates on skin wound healing in rats.

Milgram et al., (2004), objected to examine the effect of high intensity, short duration PMF on the healing of full thickness skin wounds in rats. Certain type of PMF did not have a significantly beneficial effect on wound healing. Wound healing is characterized by the restoration of the epithelial surface. The process of second intention wound healing consists of contraction and epithelialization.

Basset et al., (1974) including peripheral nerves for regeneration. The influence of PMF on nerve regeneration in vivo has been reported to be acceleration of the recovery of function following peripheral nerve crush or transection and exposure of the proximal nerve segment.

De Haas W.G., Lazarovici M.A., and Morrison D.M. (1979) the object of this experimental work was to evaluate the effect of a noninvasive method of electrical stimulation on the healing of freshly- created osteotomies of the rabbit radius. The apparatus consisted of a solid core electromagnet energized by a square wave unidirectional current. The magnetic field was pulsed transversely across the osteotomy site of the radius while the animal was confined to a restraining device 6 hours daily for 5 days per week. In one group of animals the influence of different pulse frequencies, using 0.1 Hz, 1 Hz, and 4 Hz, was evaluated, while the period of stimulation was kept constant at 2 weeks. In another group of animals, exposure was continued for 3 and 4 weeks while the pulse frequency was kept constant at 1 Hz. Histologic and radiologic comparison with control animals revealed that the initiation of the healing process can be accelerated in magnetic fields pulsed at 1 Hz, but that this effect is not maintained, and that the total period of time required for union is not significantly shortened. In view of these findings, this form of treatment is not recommended for clinical use in the treatment of recent fractures of long bones.

Ieran et al., (1990) PMF have been used clinically for the treatment of chronic skin ulcers of venous origin in humans. In a double blind study PMF have been used clinically for the treatment of chronic skin ulcers of venous origin in humans. In a double blind study the PMF treated group showed no worsening of any the ulcers, whereas four ulcers worsened in the control group.

Stiller et al., (1992), Ieran et al., (1990) by the end of the study, the treated group showed an increased number of healed wounds and a decrease in the rate of recurrence of venous ulcers, compared to the control group. In a multi centre study, a portable PMF device for home use was tested. Fifty percent of the ulcers in the treatment group healed or markedly improved, while none of the ulcers in the placebo group had healed. In the treatment group, no worsening was seen in any of the ulcers, while 54% of the ulcers in the control group exhibited worsening of the ulcers.

PMF Signal Generation and Exposure

The system was fed by a function generator (custom made in the department), producing a 2.2 kHz sine wave with 0.45 ms repetition time. The output of the function generator was connected to the Helmholtz coils: two identical coils (each of 300 turns of enameled copper wire with 0.4 mm radius) were mounted coaxially at a distance of one coil radius (13 cm) from each other to produce a highly uniform horizontal field between them. The coils were connected to the PMF generator.

The pulse duty was defined as the percentage of the time during which the voltage is switched on in one cycle. Helmholtz coil, producing 2.5 mT and 5 mT field effective intensity on the surface of rat skin. During the experiments, field intensity was measured by Philip Harris Probe (Shenstone/England) and Chauvin Arnoux Max3000 TRMS Multimeter (Paris/France). Unilab, Digital Gauss/Tesla Meter (Blackburn/England) was used for purity of the field. Maximum variation was less than 1%. Validation of the intensity measurement, axial magnetic field between the coils was also calculated.

Fig 1. PMF generator and application coil set

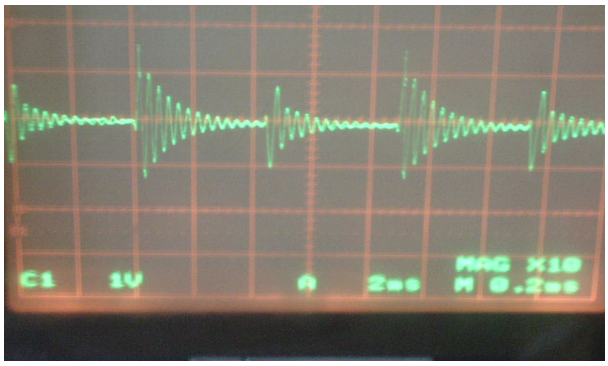

Fig 2. PMF source wave shape

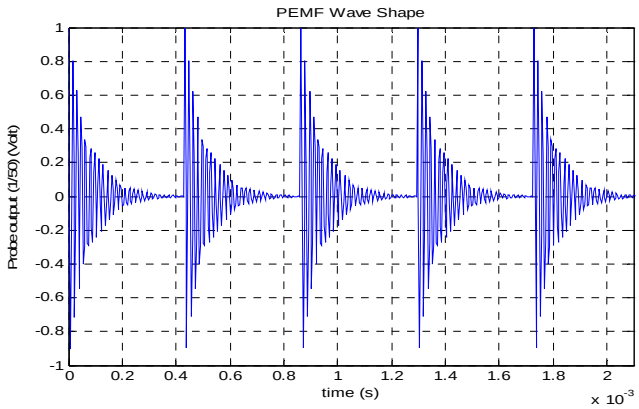

Fig 3. PMF wave shape (MATLAB)

Material and Methods

Thirty Sprague-Dawley male rats, 8-10 weeks old, weighing 200-250 g were used. They were kept in standard cages, food and water were available to them without any restriction. The temperature in the room was 20 ± 2^{o} C, the light cycle was 12/ 12-h light/dark schedule. Anesthesia was performed by the intra-peritoneal injection of ketamine HCL, 100 mg/kg and pompun, 10 mg/kg, 10 minutes before surgery. After shaving and cleaning, a pair of full thickness incisions (30 mm in length) was made parallel to and at a distance of 1.5 cm on each side of the dorsal midline. Then the animals were divided into three groups**.** Treatment group1 were exposed PMF (5 mT) for 30 min a day for seven days and treatment group2 were exposed PMF (2.5 mT) 1 hour a day for seven days after surgery. Control group were subjected to the same procedure, but with the PMF device not activated..

Discussion

Published reports indicated that the PMF stimulators may promote wound healing, but this depends on parameters such as frequency, intensity, exposure time and orientation of PMF. It was suggested that the suitable dosage and optimum PMF parameters involved in wound healing be found. The purpose of this study was to investigate the effects of pulse rates of PMF on skin wound healing in rats.

The animals in the sham group were kept in the restrainer inside the unenergized coil. These conditions may increase stress or temperature of animals, they did not affect wound healing time significantly and it was seen that the animals adapted to these conditions very soon.

Goldman et al.,(1998) have shown enhancement of fibroblast proliferation in response to certain conditions of the electric field (41 mv/m, 10 Hz) and Katsir et al. showed that chick embryo fibroblast proliferation was modified by EMF (60 Hz, 0.7 mT).

Berg et al., (1997) showed that the proliferatory response of yeast to electromagnetic field is frequency dependent and there is a window so that a high proliferation is detected at 15 Hz and a minimum proliferation at 40 Hz. These reports confirm our results in that there is a window between 10 to 80 Hz pulse rates (which is around 20 Hz). The significance in the absolute values and the normalized wound maximal lengths for the 20 Hz group compared to the sham group, verifies that the PMF with 20 Hz pulse rate accelerates wound healing. Our results on the wound surface area indicate that PMF stimulation does not affect wound contraction in rats which is in keeping with Scardino et al. that showed PMF had a positive effect on epithelilization only.

Based on the results obtained in this study it could be concluded that PMF stimulators (which could later become a practical tool for clinical use) are effective devices for the acceleration of wound healing but further studies are required to determine the optimal frequency, direction and intensity of the PMF to be used in soft tissue healing and two clarify the exact mechanisms in involved in this phenomenon.

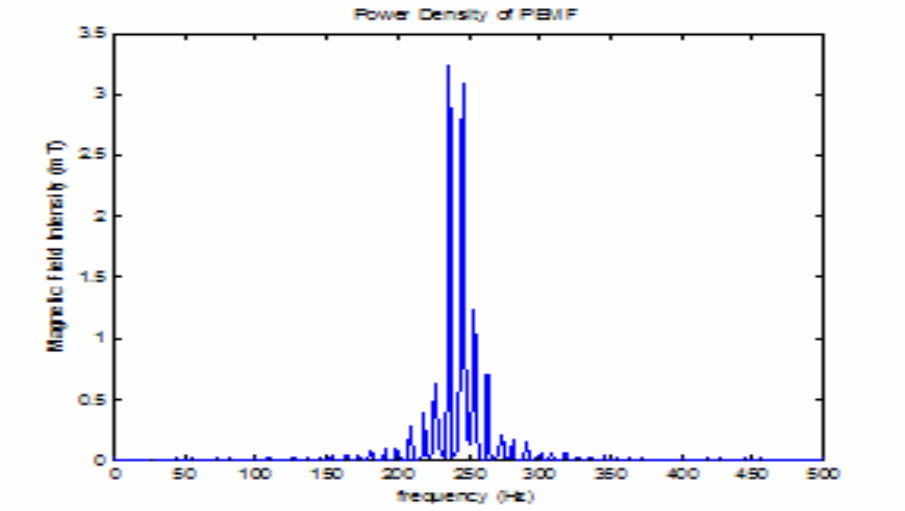

Fig 4. PMF power density

Power spectrum investigation has been conducted by using MATLAB software. Obtained spectrum density of pulsed magnetic field has been shown in Figure 4. As shown in Figure 4 fundamental component of RF energy must be in frequency about 250 Hz. So the main effective portion might be affected calcium permeability of cell membrane .It is known that permeability of cell membrane provides calcium efflux. Consequently target tissues related to wound healing affected by our used waveform.

Fig.5 and Fig. 6 shows the effect of various pulse rates on wound healing.

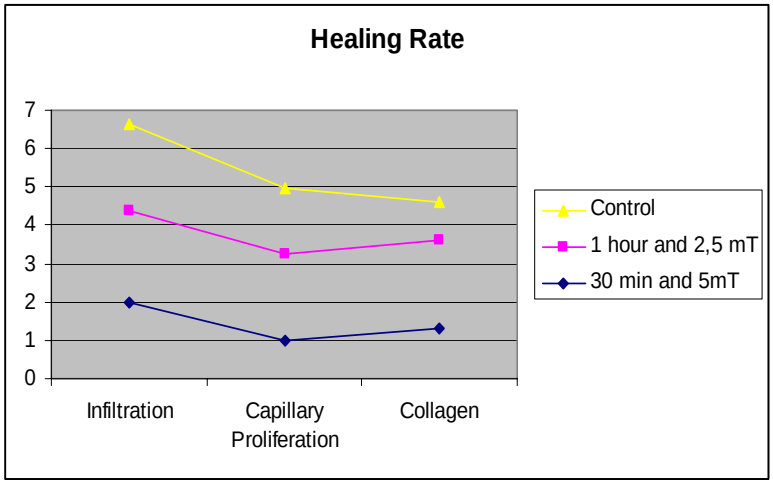

Fig 5. 3rd day's healing results

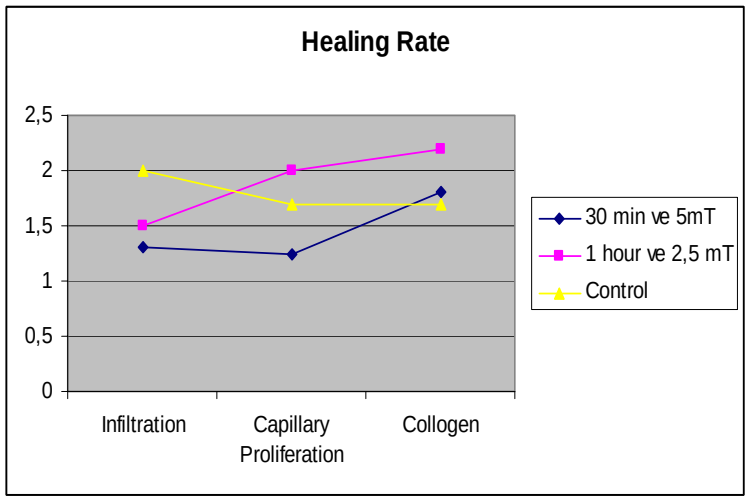

Fig 6. 7rd day's healing results

Conclusions

Changing rate of collagen fibrous and inflammation infiltration are shown in Fig 5. and Fig 6. At the end of the one-week process, decreasing in inflammation infiltration and increasing in collagen fibrous was observed. At incision on dorsal midline, 5 mT a day exposure can decrease healing rate half amount compare to control group. Exposure of 2.5 mT a day can increase the healing rate double amount to control group. The result of beneficial effect about wound healing was found in case of giving exposure with proper PMF. In the study similar results were found as in the scientific literature. Wave shape is as known the waveform which is used by Basset. Using proper exposure type can augment healing rate. The lower the exposure duration, the faster the healing occurs. It is agreeable that in the future, accelerated studies focused on waveform, frequency, power density, and different cell type will give reasonable interesting results.

References

[1] Basset CAL, Pawluk RJ, Pilla AA. 1974. Augmentation of bone repair by inductively-coupled electromagnetic fields. Science 184:575±577.

[2] Berg H, Mehedintu M .Proliferation response of yeast saccharomyces cerevisiae on electromagnetic field parameters. Bioelectrochem.Bioenerg 1997; 43: 67-70.

[3] De Haas W.G., Lazarovici M.A., and Morrison D.M. (1979) The effect of low frequency magnetic fields on the healing of the osteotomized rabbit radius. Clin. Orthop. 245-251.

[4] Goldman RJ, Cheng K. Electric fields and proliferation in a dermal wound model. Bioelectromagnetics 1998*;* 19:68-74.

[5] Ieran M, Zaffuto S, Bangnacani M. Effect of low frequency pulsing electromagnetic fields on skin ulcers of venous origin in humans. J Orthop Res 1990; 8: 276-82.

[6] Milgram, J., Shahar, R., Harrus, T., Kass, P., 2004. The Effect of Short, High Intensity Magnetic Field Pulses on the Healing of Skin Wounds in Rats. Bioelectromagnetics, 25:271 277.

[7] Stiller MJ, Pak GH, Shupack JL, Thaler S, Kenny C, Jondreau L. 1992.Aportable pulsed electromagnetic field (PMF) device to enhance healing of recalcitrant venous ulcers: A doubleblind, placebo-controlled clinical trial. Br J Dermatol 127:
147–154.

[8] Trostel, C. T., Mc Laughlin, R.,M., Lambert, J. G., Cooper, R.C., Elder, S. H., Pool, R. R., Cromiak, J. A., Boyle, C. R., 2003. Effects of Pico-Tesla Electromagnetic Field Treatment on Wound Healing in Rats, Am. J Vet Res, 64: 845-54.

CALCIUM HOMEOSTASIS IN CULTURED EXCITABLE CELLS EXPOSED TO ELF

MARIA A. MARIGGIÒ*•, CATERINA MORABITO*•, GUGLIELMO DI TANO*•, SILVIA BELIA*•, FRANCO CUCCURULLO* AND GIORGIO FANÒ*•

Laboratorio di Fisiologia, *Centro di Studi dell'Invecchiamento – Università "G.d'Annunzio", via Colle dell'Ara, 66013 Chieti – •Istituto Interuniversitario di Miologia (IIM)

Corresponding Author: Prof. Maria A. Mariggiò Lab Fisiologia, Centro di Studi dell'Invecchiamento – Università "G.d'Annunzio"-Chieti-Pescara
via Colle dell'Ara
Chieti 66013, Italy
Tel +39 0871 3554048 Fax +39 0871 3554043
e-mail: mariggio@unich.it

Abstract
It was abundantly but also roughly reported that extremely low-frequency magnetic fields interact with biological systems and in particular with excitable cells, but it remains obscure the mechanism(s) by which ELF are transduced into biological signals. To test if the presence of 50Hz ELF modulates in vitro the activity of excitable cell models, we analysed some features concerning the intracellular calcium homeostasis. In fact, the spatially and temporally defined intracellular calcium variations are the transductive events of numerous extracellular stimuli and this ion can modulate cellular excitability.
Using a single cell approach and a confocal microscope supplemented with a specially designed Helmholtz coils, we recorded intracellular calcium variations during ELF exposure of PC12, GL15 and C2C12 cell lines resembling neuron-like, glial and muscle model respectively. The acute cellular response to ELF was different in each cell line. We observed a differently modulated spontaneous calcium oscillations related to the ELF presence in differentiated C2C12 cells or in undifferentiated GL15 ones; in the other cell models there were not any significant effect in the same experimental conditions. These effects, probably, differently influenced the chronic response on calcium channels, as was revealed by experiments on cell-free samples from 10 days exposed cells.

Introduction
The biological effects of extremely low frequency electromagnetic fields (ELF-EMF) have fascinated scientists for a long time. But it is only during the past decade that the study of EMF interactions with whole organisms or isolated cells has become an increasingly recognized area of research within the biological sciences thank to an increasing number of experimental findings confirming that, under certain conditions, the non-ionizing electromagnetic energy can influence physiological processes in organisms (Gartzke and Lange, 2002; Vaughan et al, 2005). Even if numerous hypotheses have been suggested, none are convincingly supported by experimental findings. Various cellular processes, and systems can be affected by ELF-EMF exposure: i.e. cell membranes, general and/or specific gene expression, cell proliferation and differentiation, metabolic pathways and many other physiological mechanisms correlated directly or indirectly with cell viability (Repacholi and Greenebaum, 1999; Sieron at al, 2004; Ivancsits et al, 2005).
More recently, Simko and Mattsson (2004) suggested that ELF-EMF exposure is capable of increasing intracellular production of free radicals. These are intermediates in natural processes and could be the initial stimulus inducing a first response which then enhances (depending on cell type and status) the release of free radicals (Wolf et al, 2005) in turn leading to different biological events (Droge W, 2002). Mitochondria are the main sites of reactive oxygen species (ROS) formed as a side-product of oxidative phosphorylation, since electrons flowing from reduced substrates are occasionally transferred to oxygen to form superoxide anion and derived products (Chen et al, 2003).
If ROS generation and accumulation can be considered the first cellular event of an ELF-EMF exposure, the modification of Ca^{2+} homeostasis is surely one of the most important mechanisms by which ROS explicate their multiple actions into the cell (Camello-Almaraz et al, 2006). In the past years, many data obtained in various laboratories, showed that the ELF-EMF exposure was able to induce modifications of cytoplasmic Ca^{2+} levels which can be related to different physiological mechanisms: i.e. differentiation of chromaffin cells into neuronal-like cells (Morgado-Valle et al, 1998); cell death by apoptosis induced by several agents in different human cell systems (Fanelli et al, 1999); functional modifications of cells of the immune system (Walleczek J, 1992); etc. All these effects, and more others, can be attributed to modifications of Ca^{2+} homeostasis by ELF-EMF exposure throughout different mechanisms such as the involvement of P2Y membrane receptors (Takahashi et al, 2005); the activation of mechanically operated stretch-activated Ca^{2+} channels (Sun and Cho, 2004); the enhancing of the expression of voltage-gated Ca^{2+} channels (Grassi et al, 2004). All these pathways are constituted at least in part of ionic transmembrane channels that, above all in excitable cells, represent the main way for cell communication. The goal of this paper is to analyse some features involved in the homeostasis of intracellular calcium in excitable cells exposed to ELF-EMF at different intensities (0.1-1.0 mT). In particular we checked if

1. intracellular Ca^{2+} levels are changed
2. alterations of active or passive Ca^{2+} transport through cell membranes can be postulated
3. levels of some proteic factors, directly linked to Ca^{2+} activation, were modified

Results. The experimental plane regards the study of the possible influences of ELF-EMF on calcium homeostasis of excitable cells. For this reason, we used PC12, GL15 and C2C12 cell lines resembling neuron-like, glial and muscle model respectively. The presence of ELF-EMF influences the oxidative system of some excitable cells (Mariggiò et al., 2006) and also in this study some tested cell lines showed ROS production and/or mitochondrial membrane potential variations. Using a confocal microscope equipped with Helmholtz coils, we monitored the cells producing ROS (DCF labelled cells) or their mitochondrial membrane potential (JC-1-labelled cells) during a short exposure time (30 min) to 1.0 mT ELF-EMF. In these conditions, PC12 and GL15 populations showed an increased percentage of cells revealing increased ROS production (3 fold or 10

fold increase compared to PC12 or GL15 controls respectively), while in C2C12 cells no differences compared to control cells were detectable. In addition mitochondrial membrane potential variations were undetectable in PC12 cells, while GL15 and C2C12 cells showed a decreased potential compared to control cells.
The tested cell lines have a peculiar feature common to other excitable cells, which is to show spontaneous intracellular calcium ($[Ca^{2+}]i$) variations. Using the above described experimental single cell approach and a calcium specific fluorescent dye (FLUO4/AM), we assayed spontaneous $[Ca^{2+}]i$ variations during 30 min exposure to 0.1 or 1.0 mT ELF-EMF. Figure 1 shows selected representative frames (0, 15 and 30 min) depicting Fluo4-loaded cells (A) and temporal analysis of single cells (B). Data derived from these experiments showed that the spontaneous $[Ca^{2+}]i$ variations were increased in differentiated cells, above all in NGF-differentiated PC12 cells and in C2C12 myotubes in all experimental conditions (Fig. 1, C). In addition, while no PC12 phenotype was sensible to the presence of ELF-EMF (0.1-1.0 mT), both undifferentiated and differentiated GL15 cells and C2C12 myotubes showed increased spontaneous $[Ca^{2+}]i$ variations during short ELF-EMF exposure time (30 min) (Fig. 1, C).

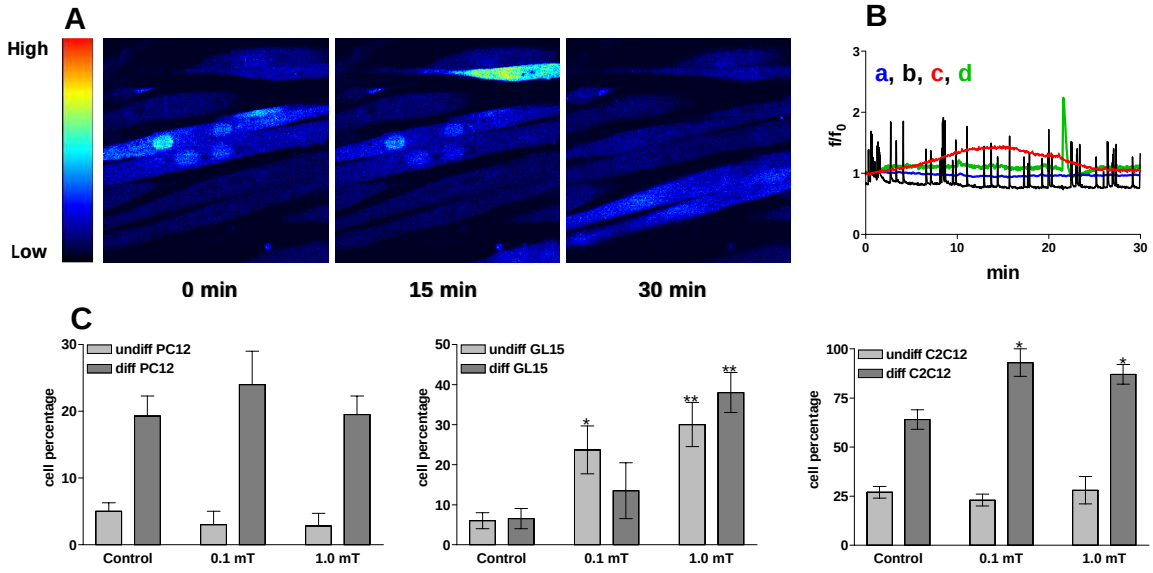

Figure 1: Temporal $[Ca^{2+}]i$ analysis. A: Confocal representative images, acquired at 0, 15 and 30 min, show a pseudo-color representation of Fluo4-loaded cells during a temporal analysis; the pseudo-color bar located to the left of the confocal images indicates a color scale from blue to red related to low (blue) and high (red) Ca^{2+} levels. B: Traces represent the possible $[Ca^{2+}]i$ variations in cells observed in presence or absence of ELF-EMF: a represents no calcium variations, b high frequency calcium variations, c a slow calcium increase and d a single increased pulse of calcium; the traces are the ratio of the single Fluo4-loaded cell fluorescence at time range from 2 to 30 min (*f*) to the mean value of fluorescence intensities after 2 min when, in exposed cells, ELF-EMF were produced (*f*0), as a function of time. C: Graphs represent the cell percentage of spontaneous variations (shown in B) in undifferentiated (undiff) or differentiated (diff) PC12, GL15 and C2C12 cells; bars are mean±SEM, n=5, *p<0.05 and **p<0.01.

Longer cell exposure (3 and 10 days) to ELF-EMF modified basal $[Ca^{2+}]i$ (Fig. 2, A and B). In particular after 3 days exposure at 0.1-1.0 mT ELF-EMF, GL15 cells showed significantly higher basal $[Ca^{2+}]i$ compared to controls; PC12 cells revealed the same increased when exposed to 1.0 mT ELF-EMF after 3 or 10 days exposure, no significant difference was observed after 0.1 mT ELF-EMF exposure. C2C12 cells didn't show any differences at 3 days ELF-EMF exposures, while these cells showed increased basal $[Ca^{2+}]i$ in respect to controls after 10 days exposure to 0.1 or 1.0 mT (Fig. 2, A and B).

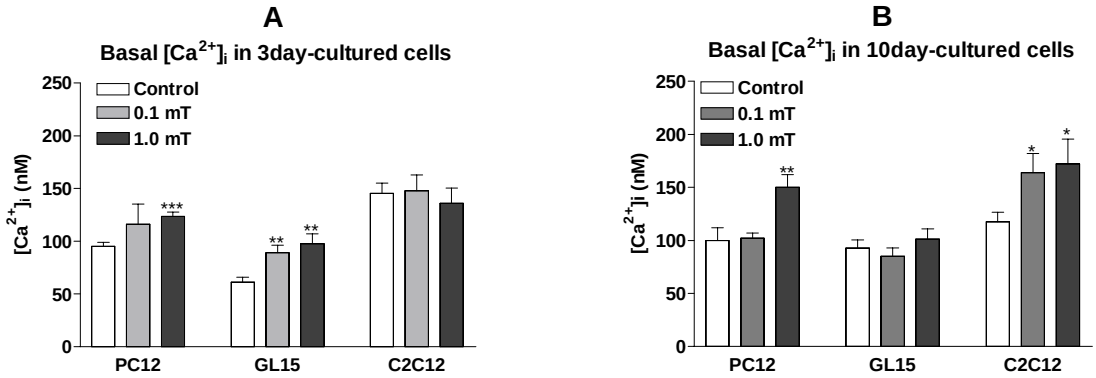

Figure 2: Basal $[Ca^{2+}]$i recorded in cell suspensions after 3 (A) or 10 (B) days (3day- or 10day-cultured) exposure to 0 (Control), 0.1 or 1.0 mT ELF-EMF. Bars are mean±SEM, n=5, *p<0.05, **p<0.01 and ***p<0.001.

The changes in basal $[Ca^{2+}]$i after ELF-EMF exposure could be determined by modifications in the calcium homeostatic system. For this reason we checked some elements involved in calcium homeostasis on long time exposed cells (3 or 10 days to 0.1 or 1.0 mT ELF-EMF). They were: two calcium regulated proteins (calmodulin and calcineurin); the functionality of calcium channels characteristic of excitable cells, voltage-gated dihydropyridine-sensible calcium channel (DHPR) and store ryanodine-sensible channel (RYR); Ca^{2+}/Mg^{2+} ATPase pump activity.

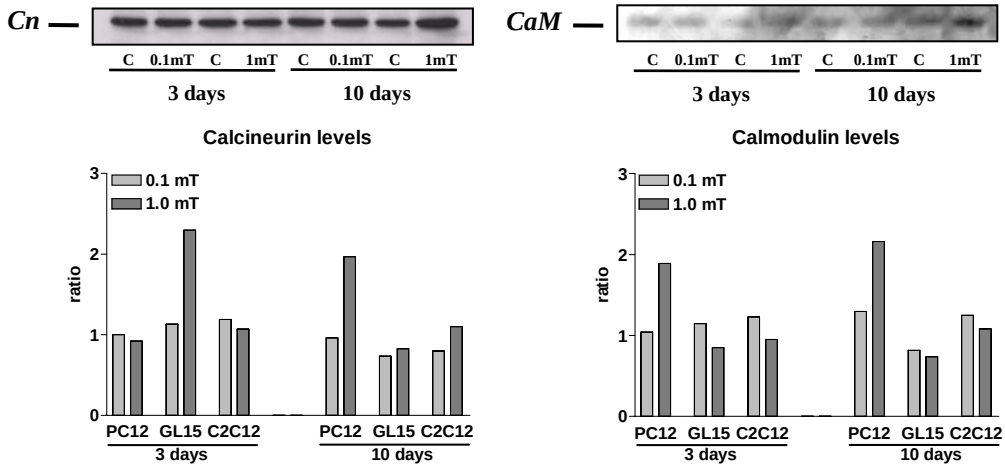

Figure 3: Representative Western blots of calcineurin (Cn) and calmodulin (CaM) in PC12 cells grown in absence (C) or in presence (0.1 or 1.0 mT) of ELF-EMF for 3 or 10 days. The graphs show the summarized densitometric analysis of Western blots of calcineurin and calmodulin in the tested cells. Bars are ratios between ODxmm^2 of each band related to control (C) proteins and ODxmm^2 of the band related to 0.1 or 1.0 mT exposed cells proteins.

Calcineurin levels revealed by Western blot analysis appeared increased in extracts from GL15 cells exposed for 3 days at 1.0 mT ELF-EMF or in those from PC12 cells exposed for 10 days to 1.0 mT ELF-EMF; in the other tested cells no modification was observed in any experimental conditions (Fig. 3). The calmodulin levels appeared increased only in PC12 cells exposed to 1.0 mT for 3 or 10 days (Fig. 3).
Figure 4 shows the data collected from experiments on cell extracts assayed for the functionality of DHPR and RYR channels and ATPase activity.

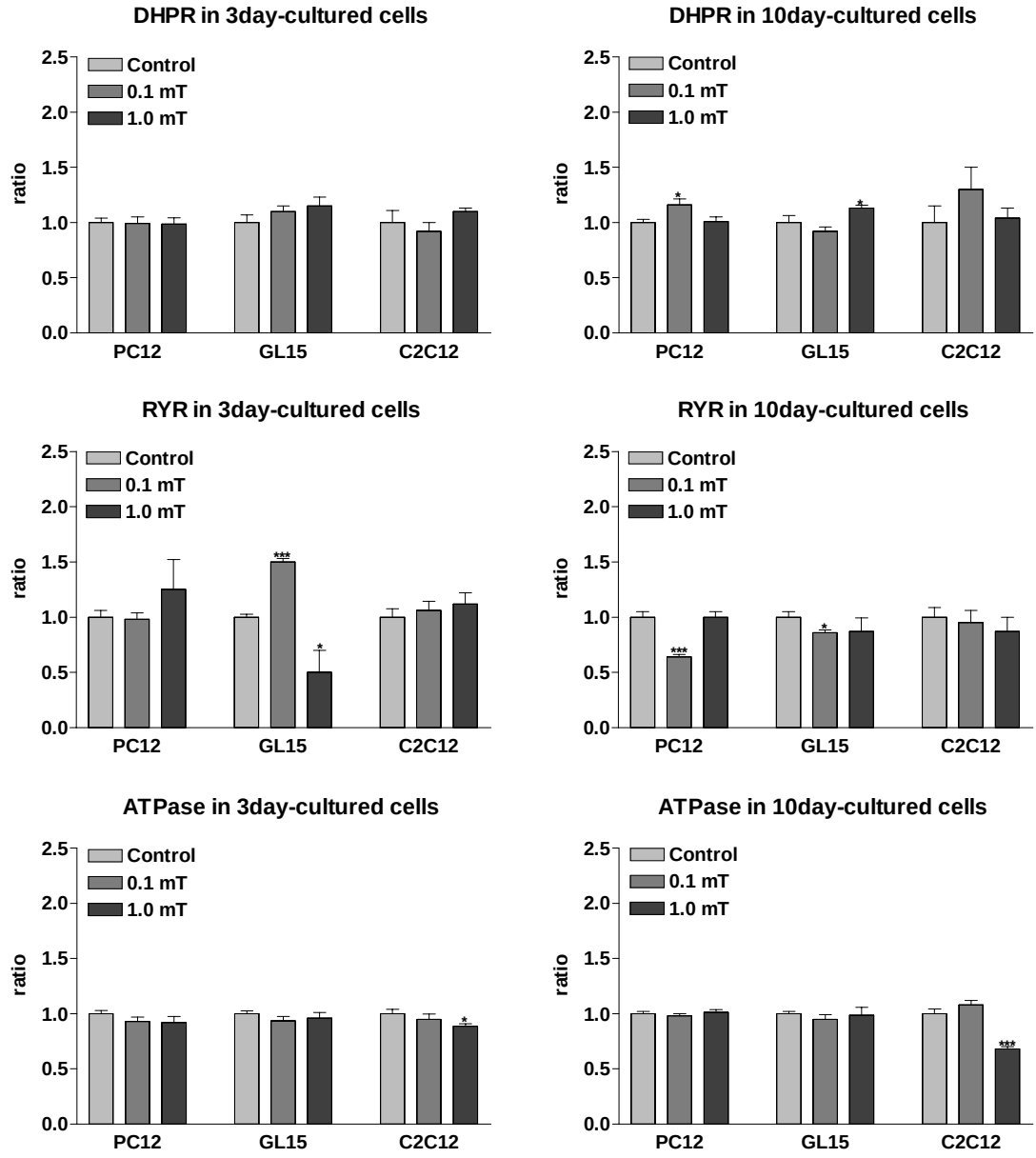

Figure 4: Functional assays on PC12, GL15 and C2C12 cells extracts. After 3 or 10 days (3day- or 10day-cultured cells respectively) exposure to 0 (Control), 0.1 mT or 1.0 mT ELF-EMF, cells were collected, homogenized and assayed for DHPR or RYR binding (calculated as pmol/mg protein and reported as ratio between treated and control cells) and ATPase activity (calculated as specific activity and reported as ratio between treated and control cells). Bars are mean±SEM, n=5, *p<0.05, **p<0.01 and ***p<0.001.

The DHPR and RYR binding assays permitted to monitor the presence of these channels on tested cells, in addition RYR binding experimental protocol revealed the functionally opened RYR channels. The number of DHPR appeared significantly increased on 10 days exposed PC12 and GL15 cells treated with 0.1 and 1.0 mT respectively. Fewer opened RYR channels appeared on 10 days and 0.1 mT exposed PC12 and GL15 cells, in the latter cells this result was evident also at 3 days and 1 mT exposure, while the opened RYR channels increased on 3 days and 0.1 mT exposed GL15 cells. The ATPase assay revealed a decreased ATPase activity on 3 or 10 days and 1 mT exposed C2C12 cells.

In conclusion each cell line showed a peculiar pattern of functional activities probably depending on their biological features.

Discussion. In the excitable cells, the Ca^{2+} ion has shown to play an important role in a wide variety of cellular

functions, such as that related to cell differentiation which involves nerve or muscle growth factors. For this reason, all changes to its cytoplasmic levels and/or transport can be the beginning of modifications able to modify, sometimes also radically, the functional capacity of the cell.
Cells exhibit several Ca^{2+}-mobilizing messengers, which transduce a large variety of extracellular stimuli regulating various intracellular Ca^{2+}-sensitive targets. Recent studies suggest that agonists differentially select their characteristic Ca^{2+} signals but it is still unclear whether different messengers mediate different functions or whether they act in a redundant fashion (Berridge et al, 2000). It is also possible that Ca^{2+} variations, induced by a specific source, are able to activate a sort of negative feed-back mechanism by which the cause of these variations can be suppressed. If this does not happen, then a measurable effect on some specific functional aspects of cell life must take place.
Under our conditions the first cause of Ca^{2+} overload can be found in the ROS generation triggered by ELF-EMF exposure. In fact, in at least two of three tested cell lines (PC12 and GL15), a significant increase of ROS, probably generated from the uncoupling of mitochondrial activity, was evident. As reported by several authors, a close relation between cytoplasmic Ca^{2+} variations and increase of ROS production exists under different experimental conditions. For example: (i) in cardiac tissue, a cytosolic, and subsequently mitochondrial, Ca^{2+} overload impaired mitochondrial bioenergetics (Solaini and Harris, 2005); (ii) in neurons, transient deprivation of oxygen and glucose during temporary ischemia coupled with elevation in cytosolic Ca^{2+} concentration triggers ROS generation and mitochondrial permeabilization, resulting in neural cell death (Brailoiu et al, 2006). Also under our experimental conditions, a significant modification of $[Ca^{2+}]i$ probably dependent on ELF-EMF intensity and/or exposure time, can be observed. Thereafter also some aspects of basal Ca-dependent activity as well as the spontaneous spikes generations, seemed to be influenced from the presence of electromagnetic fields. In fact, we observed differently modulated spontaneous calcium oscillations related to the ELF-EMF presence in differentiated C2C12 cells or in undifferentiated GL15 ones. In this case, it is important to note that modulations of calcium activity was observed during ELF-EMF exposure of single living cells, and the unique experimental procedure used, permitted to strictly correlate, for the first time, the Ca^{2+} variations and the presence of the electromagnetic field. On the other hand, the results from experiments carried out to detect some modifications of Ca^{2+} transport system remain without a clear and complete explanation. This fact could be due to physiological adaptive mechanisms present in the cells. Moreover, it is worth noting that these experiments were performed on cell-free substrate after several days exposure to ELF-EMF, so that the slight, but significant effects observed could be considered other proof of the existence of an interference mechanism induced by ELF-EMF on Ca^{2+} homeostasis

Summary
Cells possess several Ca^{2+}-mobilizing messengers, which couple stimulation at the cell surface, by a multitude of extracellular factors, to the regulation of intracellular Ca^{2+}-sensitive targets. As reported by several authors, a tight relation between cytoplasmic Ca^{2+} variations and an increase of ROS production under different experimental conditions, exists. In particular, the presence of ELF-EMF, with an intensity ranging from 0.1 to 1.0 mT, was able to induce qualitative and quantitative modifications of Ca^{2+} homeostasis (with different features in different cell lines) probably dependent on ELF-EMF intensity and/or time exposure.

Acknowledgments
We wish to thank Dr Cristina Puglielli for her technical assistance in basal $[Ca^{2+}]i$ measurements. This study was supported by grants from MATT (5376/2002/SIAR; DSA/2004/0026772)

References

1. Berridge MJ, Lipp P, Bootman MD. The versatility and universality of calcium signalling. Nat Rev Mol Cell Biol. 2000; 1:11-21.
2. Brailoiu E, Churamani D, Pandey V, Brailoiu GC, Tuluc F, Patel S, Dun NJ. Messenger-specific role for nicotinic acid adenine dinucleotide phosphate in neuronal differentiation J Biol Chem. 2006 Jun 9;281(23):15923-8. Epub 2006 Apr 4.
3. Camello-Almaraz C, Gomez-Pinilla PJ, Pozo MJ, Camello PJ. Mitochondrial reactive oxygen species and Ca^{2+} signalling Am J Physiol Cell Physiol (June 7, 2006). doi:10.1152/ajpcell.00217.2006.
4. Chen Q, Vazquez EJ, Moghaddas S, Hoppel CL, Lesnefsky EJ. Production of reactive oxygen species by mitochondria: central role of complex III. J Biol Chem. 2003; 278:36027-36031.
5. Droge W. Free radicals in the physiological control of cell function. Physiol Rev. 2002; 82:47-95.
6. Fanelli C, Coppola S, Barone R, Colussi C, Gualandi G, Volpe P, Ghibelli L. Magnetic fields increase cell survival by inhibiting apoptosis via modulation of Ca^{2+} influx. FASEB J. 1999; 13:95-102.

7. Gartzke J, Lange K. Cellular target of weak magnetic fields: ionic conduction along actin filaments of microvilli. Am J Physiol Cell Physiol. 2002; 283:C1333-C1346.
8. Grassi C, D'Ascenzo M, Torsello A, Martinotti G, Wolf F, Cittadini A, Azzena GB. Effects of 50 Hz electromagnetic fields on voltage-gated Ca^{2+} channels and their role in modulation of neuroendocrine cell proliferation and death. Cell Calcium. 2004; 35:307-315.
9. Ivancsits S, Pilger A, Diem E, Jahn O, Rudiger HW. Cell type-specific genotoxic effects of intermittent extremely low-frequency electromagnetic fields. Mutat Res. 2005; 583:184-188.
10. Mariggiò MA, Amicarelli F, Grossi MR, Falone S, Morabito C, Fanò G, Cuccurullo F, Di Ilio C. Extremely low frequency electromagnetic fields and oxidative stress in excitable cell lines. Proceedings of 4th International Workshop on Biological Effects of Electromagnetic Fields. 16-20 October 2006, Crete, Greece.
11. Morgado-Valle C, Verdugo-Diaz L, Garcia DE, Morales-Orozco C, Drucker-Colin R. The role of voltage-gated Ca^{2+} channels in neurite growth of cultured chromaffin cells induced by extremely low frequency (ELF) magnetic field stimulation. Cell Tissue Res. 1998; 291:217-230.
12. Repacholi MH, Greenebaum B. Interaction of static and extremely low frequency electric and magnetic fields with living systems: health effects and research needs. Bioelectromagnetics 1999; 20:133-160.
13. Sieron A, Labus L, Nowak P, Cieslar G, Brus H, Durczok A, Zagzil T, Kostrzewa RM, Brus R. Alternating extremely low frequency magnetic field increases turnover of dopamine and serotonin in rat frontal cortex. Bioelectromagnetics 2004; 25:426-430.
14. Simko M, Mattsson MO. Extremely low frequency electromagnetic fields as effectors of cellular responses in vitro: possible immune cell activation. J Cell Biochem. 2004; 93:83-92.
15. Solaini G and Harris DA. Biochemical dysfunction in heart mitochondria exposed to ischaemia and reperfusion. Biochem J. 2005; 390:377-394.
16. Sun S, Cho M. Human fibroblast migration in three-dimensional collagen gel in response to noninvasive electrical stimulus. II. Identification of electro coupling molecular mechanisms. Tissue Eng. 2004; 10:1558-1565.
17. Takahashi K, Doge F, Yoshioka M. Prolonged Ca2+ transients in ATP-stimulated endothelial cells exposed to 50 Hz electric fields. Cell Biol Int. 2005; 29:237-243.
18. Vaughan TE, Weaver JC. Molecular change signal-to-noise criteria for interpreting experiments involving exposure of biological systems to weakly interacting electromagnetic fields. Bioelectromagnetics. 2005; 26:305-322. l
19. Walleczek J. Electromagnetic field effects on cells of the immune system: the role of calcium signaling FASEB J. 1992; 6:3177-3185.
20. Wolf FI, Torsello A, Tedesco B, Fasanella S, Boninsegna A, D'Ascenzo M, Grassi C, Azzena GB, Cittadini A. 50-Hz extremely low frequency electromagnetic fields enhance cell proliferation and DNA damage: possible involvement of a redox mechanism. Biochim Biophys Acta. 2005; 1743:120-129.

Appendix

Instrumentation. The 50Hz electromagnetic fields were generated by two different devices: a solenoid and a pair of Helmholtz coils. These devices were planned and built to deliver variable, homogeneous, sine-wave alternate current magnetic fields with 50 Hz frequency and intensities ranging between 0.1-1.0 mT±2%. The horizontal cylindrical solenoid (length=340mm, diameter=113mm), on a supporting base, was supplied by a power supply Elgar Electronics (mod. CW-801P). The solenoid was used in an incubator (5% CO_2 and 37°C) for long time continuous cell exposures (1-10 days) during which the solenoid's eventual added temperature was negligible (photo A). The pair of Helmholtz coils (r=445mm, distance between coils=400mm), producing homogeneous magnetic field over the specified volume-under-test corresponding to the cell chamber, were located in the working zone of a confocal microscope and connected to a power supply Elgar Electronics (mod. CW-1251P) (photo B). The coils were used to generate 0.1-1.0mT ELF-EMF for short time cell exposure (30 min) during in vivo cell analysis (ROS production, mitochondrial membrane potential variation, $[Ca^{2+}]i$ variation).

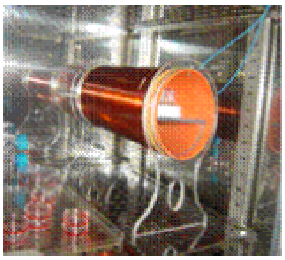

A: Solenoid in a CO_2 incubator

B: Confocal microscope equipped with Helmholtz coils

Cell culture. C2C12 and PC12 (American Culture Collection) and GL15 (functionally characterized in our lab, Mariggiò et al BMC Physiology 1:4, 2001) were cultured as exponentially growing cells in growth medium (GM). The GM for C2C12 and GL15 contains Dulbecco's modified Eagle's medium (DMEM), 10-20% foetal calf serum (FCS), 2-4 mM L-glutamine and 100 UI mL^{-1}-100 μg mL^{-1} Penicillin-Streptomycin. The differentiative phenotype was induced in C2C12 and GL15 cells in GM supplemented only by 2% FCS for 7-10 days. The GM for PC12 cells contains RPMI 1640 with 5% FCS and 10% horse serum, glutamine and antibiotics as mentioned previously. Reagents for cellular cultures were purchased from Gibco (Paisley, Scotland, UK). In PC12 cells, the differentiative phenotype was induced in GM containing 50ng/ml nerve growth factor for 7 days. The cells were seeded on Petri dishes in GM and routinely sub-cultured every three days C2C12 and GL15 and weekly PC12 (Mariggiò et al, BMC Physiology 1:4, 2001; Guarnieri et al, Neuroscience 128:697–712, 2004; Pietrangelo et al., J Physiol.572.3:721-733, 2006). The PC12 cells were cultured on Falcon flask and plated for experiments on collagen-treated wells.

$[Ca^{2+}]i$ and ROS measurements. We plated the cells on glass coverslips that were incubated for 30 min at 37°C in normal external solution (NES) supplemented with 10 mg mL^{-1} BSA and 5 μM FLUO4 AM or H_2DCF-DA (Molecular Probes, Eugene, OR, USA) for $[Ca^{2+}]i$ or ROS determination respectively. The NES solution consisted of 10 mM glucose, 140 mM NaCl, 2.8 mM KCl, 2 mM $CaCl_2$, 2 mM $MgCl_2$, and 10 mM HEPES, pH 7.4. After Fluo4-AM incubation, cells were rinsed with NES and observed. The images were collected using a Bio-Rad MRC-1024 ES confocal system (Bio-Rad Microscience Ltd, Hemel Hempstead, UK) connected to an inverted microscope Zeiss Axiovert 100 equipped with 63x/1.25 PLAN NEOFLUAR oil immersion objective and Helmholtz coils described above. For Fluo4 fluorescence, as well as that of DCF, excitation was fixed at 488 nm and emission was set at 522 nm using a bandpass filter (bandwidth±32 nm). The laser potency, photomultiply and pinhole size were kept constant for the whole experiments. Images were acquired, stored and off line analyzed. Traces deriving from total cell area were calculated as $f/f0$ where f is the fluorescence emission of a single FLUO4 (or H_2DCF-DA) loaded cells at times ranging from two to x seconds and $f0$ is the mean value of fluorescence intensities of the same cell calculated among all the images before turning on the coils. Graphs were plotted using Prism 2.0 (GraphPad Software, San Diego, CA, USA).

Spectrofluorimetric determination of basal $[Ca^{2+}]i$. For basal $[Ca^{2+}]i$ determination on cell suspensions, after 3 or 10 days ELF-EMF exposure, the cells (PC12, C2C12 and GL15) were detached and washed by gentle centrifugation. The cells, resuspended in NES, were loaded with 5 μM Fura 2-AM for 30 min at 37°C and treated for 5 min with 250 μM sulphynpirazone then collected in the quartz cuvette and analysed using LS-5B Perkin-Elmer spectrofluorimeter. The $[Ca^{2+}]i$ was calculated using the formula: $[Ca^{2+}]i = Kd\ (F-F_{min})/(F_{max}-F)$, where F_{max} and F_{min} were the fluorescences recorded at the end of each experiment, after the addition of 1 μM Ionomicin and 5 mM EGTA respectively; Kd (224 nM) is the dissociation constant of Fura2 for calcium (Grynkiewicz et al, J Biol Chem. 260:3440-3450, 1985).

Mitochondrial membrane potential measurements. These were determined using a carbocyanine dye JC-1 (Molecular Probes, Eugene, Oregon, USA) which is taken up by the mitochondria. When the transmembrane potential is high, like in normal cells, JC-1 forms red fluorescence dimers (J-aggregate), while when it is low the red fluorescence disappears and green fluorescence emission appears (monomer). Briefly, the cells on coverslips were incubated in growth medium containing 5 mM of JC-1 for 10 min. After being rinsed three times with PBS, each coverslip was observed and images were recorded with or without the ELF-EMF generated by Helmholtz coils applied to a confocal microscope (excitation was fixed at 488 nm and emission was set to either 522 nm, for green monomer, or 605 nm, for red J-aggregate, using a bandpass filter). To estimate the modification of fluorescence in mitochondria, the change in green and red areas was calculated for the whole image using Scion Image ver. beta 3b (Scion Corporation, Frederick, Maryland, USA). The red/green area ratio, resulting from each single image of the experiment was plotted against time (Castellano et al., Arch. Pharm. Pharm. Med. Chem. 333:373–380; 2000).

Western blots. PC12, C2C12 and GL15 cells were exposed to 0.1 or 1.0 mT ELF-EMF for 3 or 10 days. At the

end of the exposure the cells were collected, rapidly washed on ice with pre-cooled PBS and lysed in buffer containing (mM): 50 Tris-HCl, 100 NaCl, 50 NaF, 40 β-glycerolphosphate, 5 EDTA, 1% Triton X-100, 200 μM NaOrthovanadate, 100 μg/ml phenylmethylsulfonyl fluoride, 10 μg/ml leupeptin, 5 μg/ml pepstatin A, 10 μg/ml benzamidine, pH 7,4. After vortexing for 5 min, the sample were centrifuged at 12,000 rpm for 10 min at 4°C. The protein content of the supernatant was quantified by a colorimetric assay (Bio-Rad Laboratories Srl, Milano, Italy). Samples containing 40 μg of proteins were suspended in Laemmli buffer (8% SDS, 10% glycerol, 5% β-mercaptoethanol, 25 mM Tris-HCl and 0.003% Bromophenol Blue, pH 6,5), boiled for 5-10 min and electrophoresed on 10% SDS polyacrylamide homogenous slab gel (SDS-PAGE). Proteins were electroblotted onto a hydrophobic polyvinylidene difluoride membrane (Hybond-P Amersham-Pharmacia Biotech). The calmodulin and calcineurin proteins levels were detected with specific antibodies (monoclonal mouse anti-Calmodulin and polyclonal rabbit anti-Calcineurin, CALBIOCHEM, Germany). The antibodies were detected by chemiluminescence (ECL Amersham-Pharmacia Biotech).

Binding experiments and ATPase activity measurements**.** For [^{3}H]PN200-110 and RyR binding, and Ca^{2+}-ATPase activity the cells cultured in growth medium were exposed for 3 or 10 days to ELF-EMF electromagnetic fields at 0.1 and 1.0 mT intensity. At the end of the exposure times, the cells were sonicated (1 pulse 2 s^{-1}, 20-40 pulses) in a buffer solution containing 10 mM Hepes and 150 mM KCl. The dihydropyridine receptor (DHPR) concentration was determined according to the procedure of Renganathan et al. (J Membr Biol 157(3):247-253, 1997) using the radioligand [^{3}H]PN200-110. Sonicated cell proteins (40 μg) were incubated in a final volume of 250 μl binding buffer in the presence of 1nM [^{3}H]PN200-110 per 1 h at room temperature, then the samples were filtered with Whatman GF/C filters and washed with 6 volumes of ice-cold washing buffer. Radioactivity was determined by liquid scintillation counting. Non-specific [^{3}H]PN200-110 binding was assessed in the presence of 10 μM unlabeled nifedipine.

The sonicated cell proteins (25 μg), in a final volume of 250 μl, were incubated in a binding buffer (200 mM KCl, 10 mM HEPES pH 7.4, 100 μM $CaCl_2$, 1μg/ml pepstatin, 1μg/ml leupeptin) in agitation with 5 nM [^{3}H]ryanodine for 120 min at 37°C, then filtered with Whatman GF/C filters and washed with 6 volumes of ice-cold 200 mM KCl, 10 mM HEPES, pH 7.4 as described by Fanò et al. (J Muscle Res Cell Motil 22:345-351, 2001). The amount of bound [^{3}H]ryanodine was determined by liquid scintillation counting (Treves et al., Biochemistry 36:11496-11503, 1997).

Ca^{2+}-ATPase enzymatic activity was measured on total sonicated cell proteins according to the procedure of Fanò et al. (J Muscle Res Cell Motil 22:345-351, 2001). The assay was carried out in 1 ml incubation medium (in mM: 5 ATP, 1 $CaCl_2$, 50 Tris-HCl buffer, pH 7.4) containing 25 μg of proteins/sample. After 15 min at 37 °C, the reaction was stopped by the addition of 1 ml of 5% TCA and the precipitate removed by centrifugation at 5000g for 10 min. The released orthophosphate was estimated on 1 ml of clear supernatant, according to Saini and Van Etten (Arch. Biochem. Biophys 191:613-624, 1978). Enzyme specific activity was expressed as μmol of Pi released per min per mg of proteins (A.S.).

Statistical analysis of data was performed using Student's paired t-test, and automatically derived with Prism 2.0 software (GraphPad Software, Inc., San Diego, CA, USA).

THE EFFECTS OF DIFFERENT MAGNETIC FIELD INTENSITY TREATMENTS ON RAT ELECTROPHYSIOLOGICAL PARAMETERS

SEVGI GUNES, BELGIN BUYUKAKILLI

MERSIN UNIVERSITY, MEDICAL FACULTY, DEPARTMENT OF BIOPHYSICS, TURKEY

gunessevgi@yahoo.com, bbuyukakilli@mersin.edu.tr

Abstract

In this study, we investigated the effects of different densities at daily life exposure of sinusoidal magnetic fields on the mass of rats and peripheral nerve regeneration. Magnetic field was applied to 40 rats for 4 hours per day for a week. One of the rat groups were separated as a control the others were separated for 10, 20, and 30 Gauss (G) magnetic field treatment. All of the rats were exposed to crush injury just before the treatment.

In the study, after crush injury of sciatic nerve in the period of first 3 days treatments of magnetic field showed no mass differences compared to control. But 7 days treatment of 30 G magnetic field decreased mass of the rats when compared to control while the other groups did not.

When the electrophysiological results were estimated, in terms of nerve regeneration, it could be suggested that both after 3 days exposition to injury and 7 days treatments of different magnetic field densities have no statistically important effect on the CMAP (Compound Muscle Action Potential) amplitude, area and the rate of conduction.

As a result, it is observed that the density and frequency of magnetic fields used in this study had no effect on transmission and stimulation of nerves consequently so was not effecting the nerve regeneration.

Key words: Electromagnetic field, nerve regeneration, rat mass.

Introduction

All members of modern societies constantly live in electromagnetic fields and waves which intensities are much higher than those found in the nature. The potential negative effects of those on human health continue to be the subject of controversy (1). Most public exposure to ELF fields comes from electrical appliances, household wiring, and AC transmission and distribution lines (2).

In this study we tested whether magnetic fields created with 50 Hz alternating current (AC) affects regeneration of the sciatic nerve or not.

Exposure to PEMF as a pretreatment prior to crush injury also resulted in acceleration of axonal regrowth (3;4). Research in cats and rats suggests that pulsed electromagnetic fields may accelerate the rate of peripheral nerve regeneration (5,6). Stimulation with a 50–Hz alternating magnetic field stimulated regeneration of sensory nerve fibers in the rat sciatic nerve (7). A high-intensity static magnetic field of 1 Tesla has no effect on peripheral nerve regeneration as determined by myelinated axon counts and electrophysiologic studies in our rat sciatic nerve model. Specific orientation of the sciatic nerve with respect to the magnetic field also has no effect on the rate of nerve growth. Periods of restraint of 12 hours per day for 4 weeks inhibit weight gain by rats but have no effect on nerve regeneration in this experimental system (8).

Kolosova at al. [1996] reported that the stimulation observed in the study may not be a direct effect of MWR on regenerating nerve fibers. In their study data show a stimulating effect of low-intensity MWR on regeneration of the rat sciatic nerve. MWR treatment of the femoral skin in the area of suture accelerates the growth rate of the regenerating nerve fibers and their functional maturation (9).

The biological mechanism of action of magnetic fields is poorly understood. Reports of changes in cell membrane permeability suggest that the physiological effect is connected with electrolyte ion exchange (10).

Mean body weights of exposed groups of male and female mice were similar to those of the control groups throughout the study (11). In the another study the data indicated that over 21 days, the PEMF field inhibited young rats ability to recover from the mass loss normally associated with stress from the start of the experiment. In contrast all older rats recovered more slowly than the control young rats in the same study (12).

Materials and Methods

Animals

In present study 40 female Wistar Albino rats (150–200 g) were used. 30 of them were experiment group and the others were the control group. The rats were 12 weeks of age. They lived at 12h light-dark cycle with diet and water available *ad libitum*, without any additional medication. Before the experiment, they are adapted these conditions in a week. The experiment group was divided into three groups. They were given 10, 20 and 30 G respectively. The magnetic field generation coils were not energized, and the control rats were exposed only to the ambient magnetic field in laboratory (0.4-0. 5 G).

Surgical Procedure

All rats were operated on under intramuscular (i.m.) 50 mg/kg Ketamine Hydrochloride anesthesia. The sciatic nerve was exposed to biceps femoris muscle splitting incision unilaterally. Crush lesions were performed using a jeweler's forceps to prevent cutting when applied 15 sec, and the site of the injury was labeled with a 10/0 prolene suture attached to the epineurium. Following recovery from anesthesia, the rats were randomly assigned as a control group or experimental groups.

Magnetic Field Stimulation

A field of 10, 20 and 30 G as calculated from voltages induced in pick up standardized coil probe, placed midfield, was generated in a pair of Helmholtz coils 45 cm in diameter, with 160 turns of 2.2 mm gauge copper wire each. The coils were mounted on a plastic framework, 22.5 cm apart, and connected in series to a generator delivering a sine wave output current of 4.8 A at 50 Hz. Five rats were simultaneously put in a square, nonconductive plastic cage (35x20x45 cm) within the coils and left unrestrained. The coils were placed perpendicular to the table so the magnetic field was horizontal.

The rats were put in square plastic cages (20x20x30 cm) within the coils and exposed to the magnetic field for four hours on every seven days from the day of operation. The action potentials were recorded before experiment and after 3rd, 7th days of exposure to the electromagnetic fields by using a BIOPAC MP 100 Acquisition System Version 3.5.7 (Santa Barbara, USA).

Statistical Analysis

All statistical tests were performed with SPSS software (Statistical Package for the Social Sciences, SPSS, Inc., Chicago, IL, USA). Data obtained from study were compared by one-way ANOVA in term of differences. Bonferroni test was used for determining that the differences between each groups.

Results

The extent of nerve regeneration was studied by CMAPs. The amplitude, duration, area, and latency period of CMAPs were measured, and the conduction velocity of the nerve was calculated.

Table 1

Conduction Velocity (Effect of 50 Hz sinusoidal magnetic field exposure on regeneration of rat sciatic nerve)

Groups	Treatments (h/day)	Magnetic field intensity (G)	Before experiment measurements (m/s)		3rd day measurements (m/s)		7th day measurements (m/s)	
			Average	S D	Average	S D	Average	S D
Control	4	0	103.50	28.55	111.36	0.80	94.44	26.84
Group I	4	10	35.18	18.67	71.15	49.57	87.39	37.03
Group II	4	20	59.74	46.53	101.11	26.75	90.56	41.60
Group III	4	30	101.90	31.36	114.51	23.60	108.33	12.50

S D: Standard Deviation

CMAP rate analysis have showed that 3 days of 10 G treatment elongated duration compared to other three groups and 20 G treatment increased duration more than 30 G treatment. This results show that CMAP period increases while the intensity of magnetic field decreases. When compared to control, 7 days treatment of 20 G decreases total CMAP period more than the other groups. As a result, it is observed that the density and frequency of magnetic fields used in this study had no effect on transmission and stimulation of nerves consequently so was not effecting the nerve regeneration (Table 1).

In the study, after crush injury of sciatic nerve in the period of first 3 days treatments of magnetic field showed no mass differences compared to control. But 7 days treatment of 30 G magnetic field decreased mass of the rats when compared to control while the other groups did not (Table 2).

Table 2

Effect of 50 Hz sinusoidal magnetic field exposure on rats weights

Groups	Measurements	Average weights (g)	Standard deviation
Control (n=10)	1.	152.40	17.57
	2.	159.10	17.02
	3.	161.70	15.83
10 G Group (n=10)	1.	143.70	18.84
	2.	141.30	18.86
	3.	142.70	15.04
20 G Group (n=10)	1.	148.20	19.91
	2.	155.20	20.51
	3.	166.50	19.21
30 G Group (n=10)	1.	169.91	15.27
	2.	172.36	17.77
	3.	175.30	21.32

Conclusions:

We could not prove a neuroprotective effect of electromagnetic field in rat crush injury model using electrophysiological method.

Summary

In this study effects of weak, sinusoidal low frequency magnetic field (MF) stimulation on regeneration of the rat sciatic nerve were investigated. Forty Wistar rats were used: they were underwent unilateral sciatic nerve transaction injury, 30 of them were experiment group and the remaining 10 were control group. The experiment group with sciatic nerve lesion was divided into 3 groups randomly. After the injury all of the experiment groups were exposed to sinusoidal 50 Hz magnetic field of 10, 20 and 30 G respectively. During the experiment the rats were put between a pair of Helmholtz coils for a week for 4 h/day. The other ten rats were used for control.

When the electrophysiological results were estimated on the 3rd and 7th days after the injury, in terms of nerve regeneration, it could be suggested that treatments of different magnetic field densities have no statistically important effect on the CMAP amplitude, area and the rate of conduction.

CMAP rate analysis have shown that 3 days of 10 G treatment elongated duration compared to other three groups and 20 G treatment increased duration more than 30 G treatment. These results show that CMAP period increases while the intensity of magnetic field decreases. 7 days of treatment of 20 G found to decrease total CMAP period more than the control group. As a result, it is observed that the density and frequency of magnetic fields used in this study has no effect on transmission and stimulation of nerves, and also to the peripheral nerve regeneration.

In the study, after crush injury of sciatic nerve in the period of first 3 days treatments of magnetic field showed no mass differences compared to control. But 7 days treatment of 30 G magnetic field decreased mass of the rats when compared to control while the other groups did not.

References

1) Topcu C, Gurbilek M, Akoz M, Acıkgozoglu S. Effect of magnetic fields on the Na^+ K^+- ATPase activity of eritrocyte membrane and the levels of malondialdehyde and glutathione. *T Klin J MED Res*, 2002; 20:119-124.
2) Repacholi MH, Greenebaum B. Interaction of static and extremely low frequency electric and magnetic fields with living systems: health effects and research needs. *Bioelectromagnetics*, 1999; 20:133-160.
3) Sisken BF, Kanje M , Lundborg G, Herbst E, KURTZ W. Stimulation of rat sciatic nerve regeneration with pulsed electromagnetic fields. *Brain Res.* 1989; 24;485(2):309-16.
4) Kanje M, Rusovan A, Sisken B, Lundborg G. Pretreatment of rats with pulsed electromagnetic fields enhances regeneration of the sciatic nerve. *Bioelectromagnetics*, 1993*;* 14:353-359.Michael H. Repacholi B. Greenebaum 1993
5) Raji AM. An experimental study of the effects of pulsed electromagnetic field (diapulse) on nerve repair. *Journal of Hand Surgery.* 1984; 9(2):105-112.
6) Orgel MG, O'Brien WJ, Murray HM. Pulsing electromagnetic field therapy in nerve regeneration: an experimental study in the cat. *Plast Reconstr Surg.* 1984: 73(2):173-83.
7) Rusovan A, Kanje M. Stimulation of regeneration of the rat sciatic nerve by 50 Hz sinusoidal magnetic fields. *Exp Neurol*. 1991; 112(3):312-6.
8) Cordeiro PG, Seckel BR, Miller CD, Gross PT, Wise RE. Effect of a high-intensity static magnetic field on sciatic nerve regeneration in the rat. *Plast Reconstr Surg* 1989; 83(2):301-8
9) Kolosova LI, Akoev GN, Avelev VD, Riabchikova OV, Babu KS. Effect of low-intensity millimeter wave electromagnetic radiation on regeneration of the sciatic nerve in rats. *Bioelectromagnetics*, 1996; 17(1):44-7.
10) Gmitrova A., Ivanco I., Gmitrorov J., Murin M. Biological effect of magnetic field on laboratory animals. Journal of Bioelectricity. 1988 7(1):123-124
11) National Toxicology Program. NTP Toxicology and Carcinogenesis Studies of 60-HZ Magnetic Fields IN F344/N Rats and B6C3F1 Mice (Whole-body Exposure Studies). Natl Toxicol Program Tech Rep Ser. 1999 Apr;488:1-168.
12) Sandrey MA, Vesper DN, Johnson MT, Nindl G, Swez JA, Chamberlain J, Balcavage WX. Effect of short duration electromagnetic field exposures on rat mass. *Bioelectromagnetics.* 2002; 23(1):2-6.

TEMPERATURE AND MICROWAVE FIELD EFFECT ON THE RED FLUORESCENT PROTEIN (DsRed) PHOTOLUMINESCENCE IN SOLUTION

I. BARAK, A.B. COPTY, M. GOLOSOVSKY, AND D. DAVIDOV

The Racah Institue of Physics, The Hebrew University of Jerusalem, 91904 Jerusalem, Israel

Abstract

We compared the effect of microwave irradiation on the red fluorescent protein (DsRed) placed in a cylindrical resonant cavity with that of conventional heating. Our measurements show that the fluorescence intensity in either case decreases by ~ 1% per degree centigrade, indicating that the microwave effect on the sample is mostly a thermal one.

1. Introduction

In this work we studied the influence of microwave field on the DsRed, a red fluorescent protein (RFP) from Discosoma coral[1]. The DsRed has a very stable three dimensional beta-can barrel structure, but its emission spectrum is shifted to longer wavelength , with a maximum intensity at λ=583 nm [2, 3] . The sample, placed in a cylindrical cavity, was excited by the CW excitation at 488 nm by an Argon laser. We performed our experiments on RFP in a buffer solution, and have monitored changes in its photoluminescence under microwave irradiation and compared it to the changes in fluorescence under conventional heating. Previous studies indicate that the microwave field effect on proteins in solution and on living tissues can not be entirely reduced to heating [4, 5, 6,7] , while when the biomolecule is in the crystalline form, the effect of microwave irradiation is indistinguishable from conventional heating[8]. Our group has recently found a specific effect of the microwave field on the Enhanced Green Fluorescent Protein fluorescence in solution [9]. it is surprising since the theoretical analysis of microwave interaction with biological system does not leave many possibilities for non-thermal microwave effect on biological system. Adair [10] showed that the resonance excitation of biological molecules in solution at microwave frequency is highly improbable. Foster[11] demonstrated that thermal gradients on the nanometric scale are exceedingly small. The pupose of our present approach is to study the effect of microwave field on the protein fluorescence in solution in real time.

2. Experimental Setup

We placed a transparent glass pipette filled with buffer solution containing DsRed inside an X-band TE_{011} cylindrical resonant cavity (Fig. 1.). We drilled two small holes in the sidewalls of the cavity to introduce laser beam and to observe fluorescence. The pipette is mounted slightly off-center. The cavity is fed using a HP 83623A synthesized sweeper. We directed a 488 nm Argon laser beam (Omnichrome Series 43) through the pipette and picked up the fluorescence at 90^o using an objective lens coupled to a monochromator (DK480) through an optical fiber (Oriel, Model 77539). The monochromator is connected to a cooled photomultiplier (Product for Research, Model TE177RF) operating in the counting mode (SR400 Two channel Gated photon counter). In some experiments we also used a stereo microscope (Zeiss, Stemi 2000-c) connected to a digital camera.

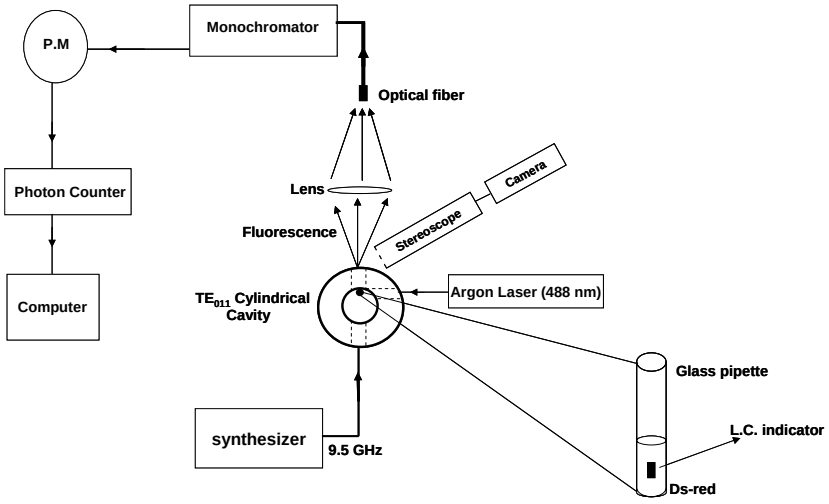

Fig. 1. Experimental setup - Top view. The pipette with a fluorescing solution is mounted in the cylindrical microwave cavity operating at 9.5 GHz. The pipette is slightly off-center of the cavity and it is irradiated by the laser beam through a small hole in the cavity sidewall. The photoluminescence under microwave field is analyzed. The sample is visualized using a stereomicroscope and a digital camera.

3. Mode of operation

Our 63.5 mm diameter cylindrical cavity operates in the TE_{011} mode. Under this mode of operation the currents are annular and there is no electrical current flow in either the radial or longitudinal direction (Fig. 2.). This property enables us to fine tune the frequency by moving the piston-like end plate in and out. A brass screw is used to maximize the coupling between the cavity and the coaxial adaptor.

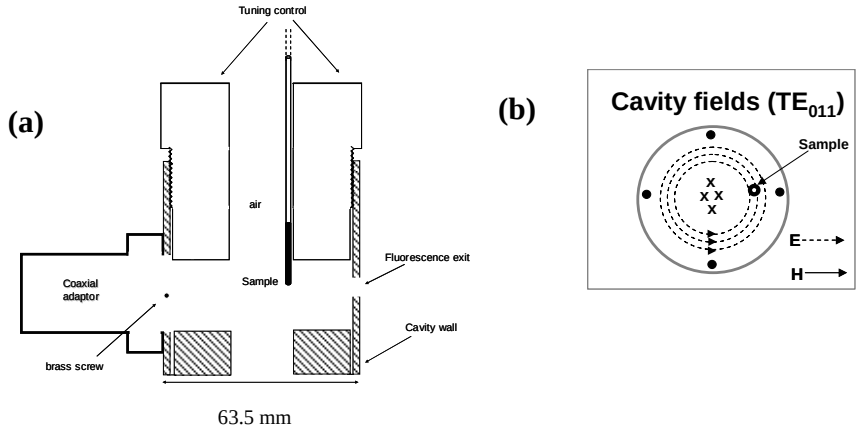

Fig. 2. **(a)** Cavity design – Cross sectional view. The microwave enters the cavity through a coax-to-waveguide adaptor and a coupling hole while the fluorescence exits from the other side of the cavity. **(b)** Cavity fields- Top view.

We measured microwave reflectivity using a vector network analyzer (HP 8510 C). Knowing the field distribution in the cavity, we placed the sample (10 mm long and 1.5 mm wide) slightly off-center where there is some electric field. Note, that the electric field in the center of cavity is zero. Care was taken not to destroy the Q-factor of the cavity (Fig. 3.).

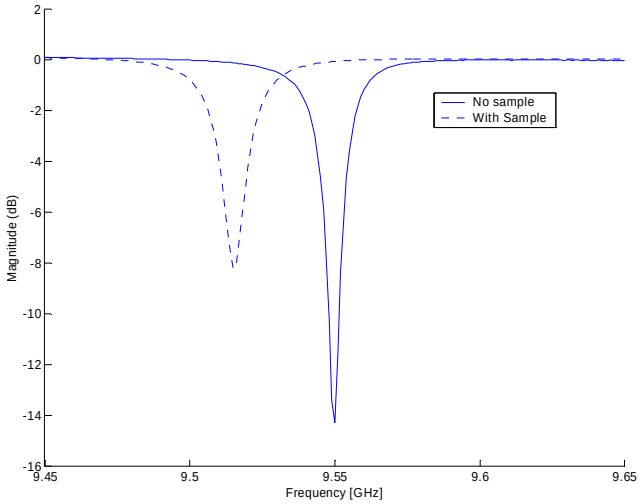

Fig . 3. Microwave reflectivity, S_{11}, with (dashed line) and without (solid line) the sample in a TE_{011} cylindrical cavity. When the sample is placed inside the cavity the resonance curve is slightly perturbed.

Liquid crystal as a temperature indicator

A very important issue in our experiments is independent control of the sample temperature under microwave irradiation. The important requirement here is that the temperature sensor should not perturb microwave field. Therefore, rather than to use a thermocouple, we looked for other methods. We took a thin sheet of commercial film of cholesteric liquid crystal (LC) indicator which changes its color when its temperature is between 35^{o}C- 36^{o}C . Using a stereomicroscope and a digital camera, we first verified that the dry LC indicator alone doesn't change color even under a maximum microwave power of 250 mW. Since our buffer solution consists mainly of water, we filled the same amount of distilled water in a thin glass pipette (just as with the RFP sample), put it inside the cavity together with a small piece of LC (1.3 x 3.3 mm^2) inside and watched for color changes as the incident microwave power is varied. Under maximal incident power the indicator changes its color. When the incident power gets smaller than ≈100mW, the indicator changes. This means that at the incident power of ≈100mW the temperature of the indicator is 35^{o}C- 36^{o}C, i.e. it exceeds ambient temperature (22^{o}C) by 13^{o}C- 14^{o}C. Since the temperature rise is proportional to the incident microwave power, we conclude that each 1 mW of the incident microwave power results in the solution temperature rise of ~ 0.07 ^{0}C.

Fluorescence Spectrum measurement under conventional heating

To observe the temperature dependence of the RFP fluorescence upon conventional heating and in the absence of microwave irradiation, we used a CCD detector (MS 125 ^{TM} 1/8m spectrograph, model 77400 Newport). The glass tube, which is sealed on one side and opened from another allows introduction of a small thermocouple inside the sample (RFP) near the laser-illuminated spot. The pipette with the solution was placed in a heated water bath. The fluorescence was picked up at 90^o to the laser beam by a fiber bundle focusing assemblies (model 77799 Newport), coupled to the CCD detector and to the computer. As we slowly varied the water bath temperature, between 26^o C and 36^o C, we measured the fluorescence spectrum.

4. Experimental Results

The Fig.4 shows the DsRed fluorescence spectrum in the absence and in the presence of the microwave field. First we measured the spectrum without microwave irradiation (dashed line). Then we turned on the microwave for 30 sec., performed the measurement (solid line) and turned it off. Under microwave irradiation the fluorescence intensity is reduced. Having the relation between the microwave power and the temperature we see that there is ~1% fluorescence decrease per one degree centigrade. The process is reversible as can be seen by the spectrum marked by the squares.

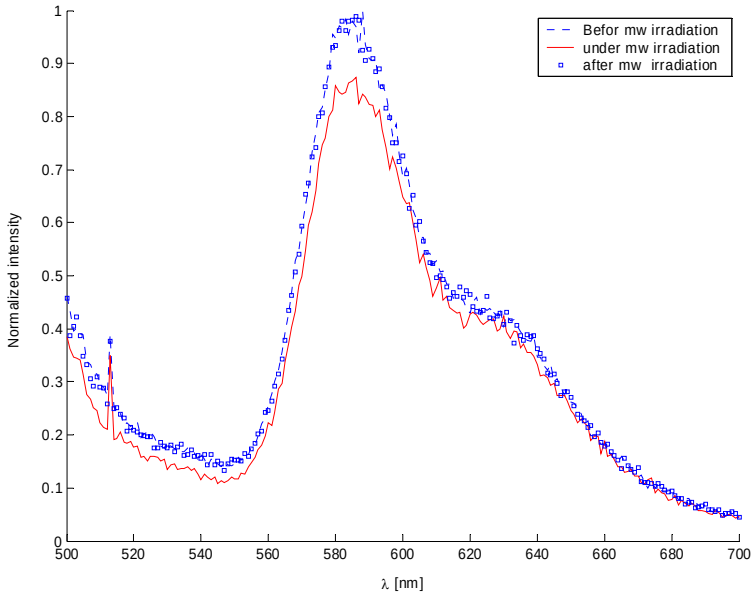

Fig. 4. RFP fluorescence spectrum (normalized with respect to the fluorescence at 583 nm before irradiation) under 488 nm excitation at room temperature before, during and after microwave field. It is seen that under 100 mW microwave irradiation the spectrum is reduced mainly in the peak (λ=583 nm). Note a "valley" at 540 nm.

The next step was to measure the kinetics of microwave effect on the RFP fluorescence (**Fig. 5.**). We picked the wavelength of maximum intensity, turned on the microwave (100mW) and monitored the fluorescence decrease. Then we turned off the microwave and observed how the fluorescence reaches its pre-exposure level. As the power increases the fluorescence "valley" decreases.

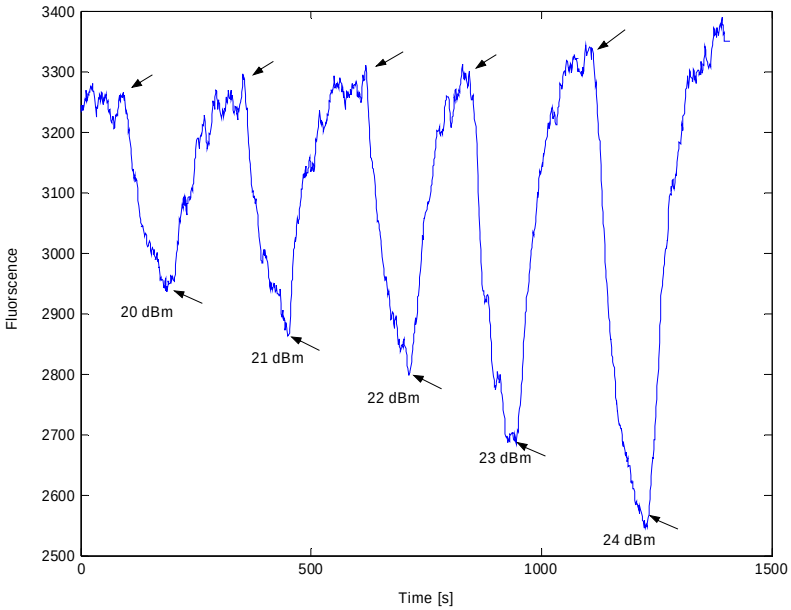

Fig 5. Fluorescence (at λ=583 nm) variation upon switching the microwave field on/off. First arrow on the left upper side indicates the moment when the microwave irradiation is switched on while the arrow at the bottom indicates a moment when the microwave irradiation is switched off.

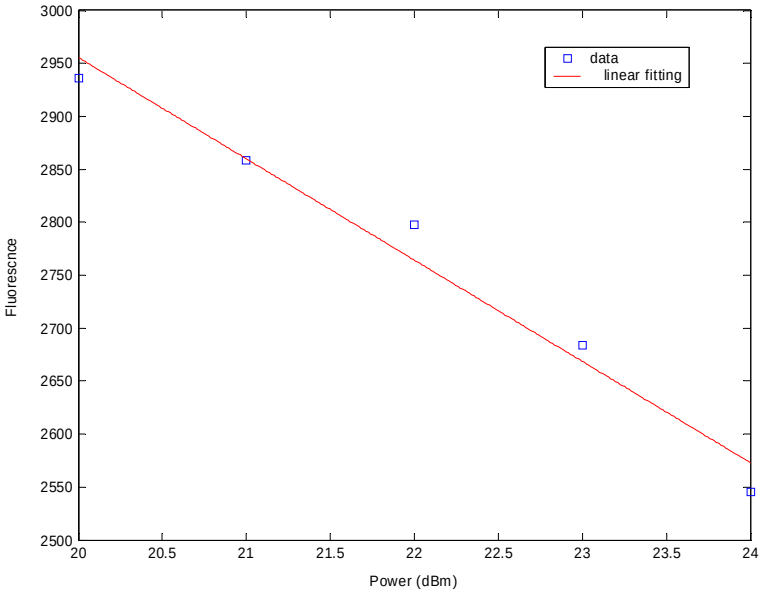

Fig. 6. A decrease in fluorescence (at 583 nm) as a function of the microwave power (dBm).

The effect of microwave on the DsRed should be compared to conventional heating of the protein. Figure 7 below shows the RFP fluorescence spectrum for two different temperatures measured with a CCD detector. Since the glass tube is placed inside a water thermal bath with a thermocouple inside the sample we can measure the fluorescence spectrum for different temperature. When the temperature is slowly increased

from 26°C to 36°C the fluorescence decreases by about 10%. Therefore there is a ~1% decrease per one degree centigrade.

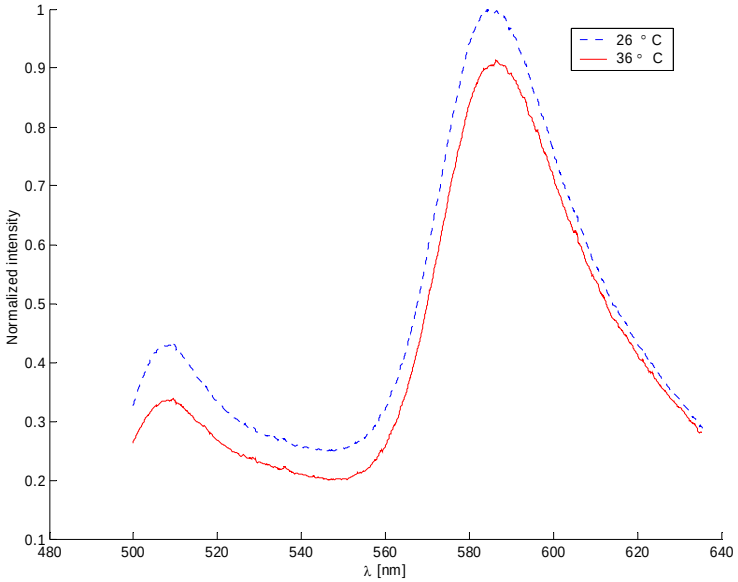

Fig. 7. RFP fluorescence spectrum (normalized) under 488 nm excitation. The glass tube with the protein solution was placed in a heat water bath and the spectrum was measured for two different temperatures using a thermocouple inside the sample. Upon increasing the temperature the fluorescence decreases mainly in the peak (~583 nm).

Since the effect of conventional heating on the fluorescence spectrum of the RFP is wavelength-dependent we present below the temperature dependence of the fluorescence for several wavelengths.

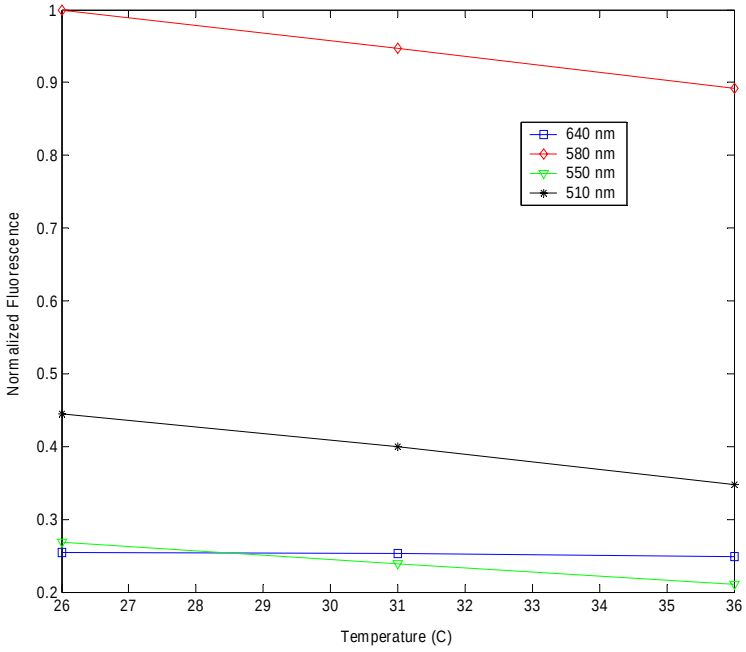

Fig. 8. Normalized fluorescence as a function of the temperature for different wavelengths. Upon increasing temperature the fluorescence does decrease but in different proportion around the spectrum. Watch for example difference of the 580 nm and the 640 nm line.

Summary

Our present experiments indicate that the effect of microwave irradiation on the dsRed fluorescence in solution can be reduced to thermal heating. This is different from our recent experiments with another fluorescent protein [9], EGFP, where we observed that the effect of microwave irradiation was stronger than the heating which accompanies microwave irradiation. Even though the GFP and the DsRed seem to share the same "barrel" form, the latest is known for his greater stability due to his oligomeric structure to elevated temperature and other physical factors [2]. We are now studying the effect of microwave field on the EGFP in our cavity-based set-up as well as the microwave effect on the well-known fluorescence anisotropy of both proteins.

Acknowledgment

We are grateful to F. Sakran for all the technical help and to Dr. Tsafi Danieli and her group for there assistance with RFP handling. We are grateful to O. Popov and V. Lirtsman for the help in optical experiments and for the samples of RFP.

References

[1] Fradkov, A.F. *et al FEBS Lett.* **479**, 127–130 (2000).

[2] V.V. Verkhusha & K.A. Lukyanov, nature Biotechnology **22**,289- 296 (2004).

[3] W. MA, M. Socolich , R. Ranganathan , Nat Struct Biol. 2000 Dec;7(12):1133-8.

[4] H. Bohr and J. Bohr, Phys. Rev. E **61**, 4310, (2000).

[5] D. de Pomerai, C. Daniells, H. David, J. Allan, I. Duce, M. Mutwakil, D. Thomas, P. Sewell, J. Tattersall, D. Jones, and P. Candido, Nature **405**, 417(2000).

[6] M. Porcelli, G. Cacciapuoti, S. Fusco, R. Massa, G. d'Ambrosio, C. Bertoldo, M. DeRosa. and V. Zappia, FEBS Lett**. 402**, 102(1997).

[7] F. Mancinelli, M. Caraglia, A. Abbruzzese, G. d'Ambrosio, R. Massa, and E. Bismuto, J. Cell. Biochem. **93**, 188 (2004).

[8] R. Weissenborn, K. Diederichs, W. Welte, G. Maret, and T. Gisler, Acta Crystallogr. Sect. D (Biol. Cryst.) **61**, 163 (2005).

[9] A.B. Copty, Y. Neve Oz, I. Barak, M. Golosovsky, and D. Davidov Biophys. J. 2006 **91**: 1413-1423.

[10] R.K. Adair Bioelectromagnetics. 24:39-48 (2003).

[11] K.R. Foster , IEEE Trans. Plasma Sci. 28:15-23 (2000).

STUDYING THE EFFECTS OF THE STATIC MAGNETIC FIELD ON THE ENZYMES CATALASE (CAT) AND SUPEROXIDE DISMUTASE (SOD) ACTIVITY IN SUSPENTION CULTURE OF TOBACCO CELLS

PARVIZ ABDOLMALEKI, FAEZEH GHANATI

FACULTY OF SCIENCE, TARBIAT MODARES UNIVERSITY, P.O. BOX 14115/175, TEHRAN, IRAN.

The influence of the magnetic field on the enzyme activity depends on the intensity as well as the period of exposition. In this research the effect of a static magnetic field (SMF) with intensity of 10mT and 30mT on the enzyme activity of superoxide dismutase (SOD) and catalase (CAT) in suspension-cultured of the tobacco cells were investigated. Suspension cultures in the exponential phase of the growth were exposed continuously for 5 days each 5 hours to SMF of 10 and 30 mT. The result showed that the exposure to SMF caused an increase in the activity on the treatment cells (n=24) compared with the controls (n=24). The best obtained average for enzymes activity of SOD on treatment group was 0.88 ± 0.01 (ΔAbs/mg. protein) while the best obtained average for enzymes activity of SOD on control group was 0.55±0.02 (ΔAbs/mg. protein). Similarly, the best obtained average for enzymes activity of CAT on treatment group was 296.61±122.87 (ΔAbs/mg. protein) while the best obtained average for enzymes activity of CAT on control group was 162.72±24.06 (ΔAbs/mg. protein). Our results showed that the exposure of treated cells with a SMF with 10 and 30 mt can cause an increase in the enzyme activity of SOD and CAT.

Introduction

Magnetic fields (MF) are widely distributed in environment and their effects are interesting with the burgeoning development of electrical machines [Ishisaka et al. 2000].There are arguments for both positive and negative effects of EMF on living systems[Yoshikawa et al. 2000]. The exact mechanism of these effects remains unknown and still under investigation. The effects of electromagnetic field exposure on cells can be difficult to interpret because findings are often contradictory. Difficulties may arise because effects are small and because of variations in magnetic field parameters such as strength, duration of exposure and the type of magnetic field (AC or DC). Confounding variables can also arise from differences in the cell type and from the effects of differentiation cues [Mcfarlane et al. 2000]. One of the most important hypotheses is such fields cause an increase the average concentration of free radicals (oxygen free radicals), lengthen their life time, in living organisms which results in the formation of excessive amounts of active oxygen forms [Sobczak et al. 2002, Scaiano et al. 1994, Lee et al. 2004]. They induce change in enzyme activity, gene expression, and release of calcium from intracellular storage sites; affect membrane structure, cell growth, and cell death [Kwee and Rashkmark 1998, Olivares-Barnuelos 2004, [Robison et al. 2002]. Free radicals are very reactive and unstable molecular species that can initiate chain reactions to form new free radicals. Although formed as a result of a wide range of normal biochemical process, they are potentially damaging .Several mechanisms are in place to neutralize and endogenous enzymatic antioxidant defenses that generally hold the production of free radicals and prevent oxidant stress and subsequently tissue damage. The balance between the oxidants and the antioxidants may be disturbed by an increase in free radical production or by a reduction in antioxidants. This imbalance between the oxidants and the antioxidants can lead to oxidative stress which is a series of peculiar and potentially damaging biochemical reactions [Moustafa et al. 2001].

These mechanisms have been initially studied on plants after they used as target model in different stresses. The previous results showed that they produce large amounts of active oxygen species such as superoxide anion (-O2), hydroxyl radical (°OH) and hydrogen peroxide (H2O2) that can result in photoinhibition and photooxidation. We considered the magnetic field as a physical stress and we intended to study the response of the selected cell plant in antioxidant defense systems. We assumed that this response is a protective mechanism that enables cells to survive .It is activated by a wide variety of environment stimuli, such as high temperature,

oxygen starvation, and heavy metals, as well as EMFs. We intended to clarify this point because we know that most organism have enzymatic systems associated with SOD and CAT to scavenge such active oxygen species.
In the present research suspension-cultured tobacco cells (Nicotiana tabacum) were used as a model to evaluate the response of tobacco cells when it exposed to a static magnetic field. Also the intensity of the magnetic field on the rate of enzymes activity was investigated. Tobacco cells were considered as model because there is a potential to extract a homogenate and undifferentiated embryonic batches of cells through carrying out too many subcultures. Thus, the present study was designed to evaluate the effects of exposure to SMF on some parameters indicative of oxidative stress (SOD and CAT) in tobacco cells.
Suspension–cultured tobacco cells (Nicotiana tabacum) were initially grown in Linsmaier & skoog (LS) medium. The calli from which suspensions were established had been maintained in our laboratory for several years. We extract the suspension cultures after 52 subcultures. This provided a homogenate and undifferentiated embryonic batches of cells which could be considered as a good target for our study. Furthermore by doing so, it seems that no longer have they kept their original properties and their physiological response to static magnetic field resembles physiological response of a plant cells regardless of it species. The prepared cells were then incubated at 25°Cin darkness on an orbital shaker at 100 rpm. The suspension of cells were then transferred (1.3gr fresh weight) at 7 day intervals [Kuboi and KAji 1994] into 30ml of fresh medium in a 100ml Erlenmeyer flask. We initially extracted the growth and the differentiation indices of tobacco cell by studying the tobacco growth cells curve. The cells in the exponential phase of the growth curve were then exposed continuously for 5 days (from 3 to 7 sub-cultured) with exposure rate of 5 day to 10 and 30mT in a local designed SMF. The cells were harvested after 5day of treatment and frozen in liquid N2 and kept at – 80 °C until used for biochemical measurements.
The apparatus (Fig.1) which we used to create the static magnetic field had two coils each with 3000 turns of 1mm of enameled copper wire. This provided a highly homogenous field enabling us to put our prepared cells into a large and homogenous field. To intensify the field we used iron surfaces that had been separated by diamagnetic materials to avoid the turbulence currents.
Thirty milliliter cell culture flasks containing tobacco cell cultures were put into the center of cylinder container (length 17cm) that allowed the placement of multiple or single flasks within apparatus simultaneously. The flasks were placed so that laid perpendicular to the direction of the generated magnetic field. The control samples were kept in the same condition regarding the temperature, humidity and light. Using the prepared calibration curve obtained for the apparatus to initialize a magnetic field with the intensity of 10mT and 30mT, a current of 5 ampere and 25 ampere were transferred through the circuit respectively.
Frozen samples (200 mg fresh weight) were homogenized in 3 ml HEPES-KOH buffers (pH 7.8) containing 0.1 mM EDTA. The homogenate was centrifuged at 15000 × g for 15 min. All operation was performed at 4 °C. The supernatant was used for SOD (EC 1.15.1.1) activity [Giannopolitis and Ries 1977]. Reaction mixture (3 ml) consisted of 50 mM HEPES-KOH buffer (pH 7.8), 0.1 mM EDTA, 50 mM Na2CO3 (pH 10.2), 12 mM L-methionine, 75 µM NBT, 300 µL enzyme extract and 1 µM riboflavin. One unit SOD activity was defined as the amount of enzyme required to result in a 50% inhibition of the rate of NBT reduction measured at 560 nm. Activity of CAT (EC 1.11.1.6) was measured in a reaction mixture containing 25 mM Na-phosphate buffer (pH 6.8), 10 mM H2O2 and enzyme extract in a total volume of 1 mL. The decomposition of H2O2 was followed by the decline in absorbance at 240 nm [Cakmak and Horst 1991]. In brief, samples were homogenized in 1 mL of 50 mM Na-phosphate buffer (pH 7.8) containing 5 mM ascorbate, 5 mM DTT, 5 mM EDTA, 100 mM NaCl and 2% (W/V) PVP. The homogenate was centrifuged at 15000 × g for 15 min at 4 °C. The reaction was initiated by adding H2O2 to a final concentration of 44 µM. The reaction rate was monitored by the decrease in absorbance at 290 nm. The rate constant was calculated using the extinction coefficient of 2.8 mM-1 cm-1and corrected for the rate obtained prior to the addition of H2O2. The protein contents were determined by the method of Bradford [1976], using bovine serum albumin (BSA) as standard. All experiments were repeated with at least three independent repetitions and all data were expressed as the mean values ± standard deviation (SD). The Statistical analysis was performed using student's t-test at $p<0.05$ significant level of the difference.
The results showed that the exposure of the magnetic field caused an increase in the antioxidant enzymes activity (SOD & CAT) on the treatment cells (n=24) compared with the controls (n=24). The obtained average for enzymes activity of SOD on treatment group was 0.88 ± 0.01 (nm/mg. protein) while the obtained average for enzymes activity of SOD on control group was 0.55±0.02 (nm/mg. protein) (Fig.2). Similarly, the best obtained average for enzymes activity of CAT on treatment group was 296.61±122.87 (nm/mg. protein) while the best obtained average for enzymes activity of CAT on control group was 162.72±24.06 (nm/mg. protein) (Fig. 3). The average results for the enzymatic antioxidative activity of SOD and CAT for treatment as well as control in two intensities of 10 and 30 mT were presented in table 1. These results showed that the activity of SOD in tobacco cells has been increased for both intensities (10 and 30 mT) in treatment cells. In contrast the activity of CAT showed a significant decreasement in treatment cells compared with control. Our results showed significant difference of enzymes activity in treatment and control cells for SOD (two-tailed $p<0.05$) and CAT (two-tailed $p<0.03$) at 30 mT. Similarly, the enzymes activity in treatment and control cells for SOD

(two-tailed p<0.04) and CAT (two-tailed p<0.01) at 10 mT showed a significant difference. Regardless of enzyme activity obtained for CAT which show a bigger difference at 30 mT compared to 10 mT (fig3), there was not reasonable difference of enzyme activity for SOD as far as the intensity is concern (fig2). These results show that the enzymes activity is not directly dependent to intensity at these two selected intensity of 10 and 30 mT.

Fig.1. Locally designed static magnetic field generator

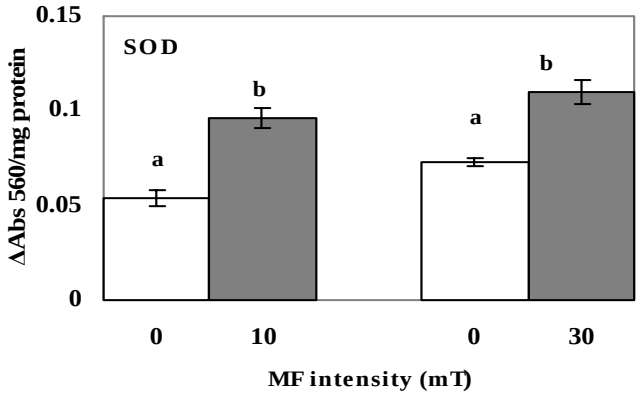

Fig.2. Effect of SMF with different intensities on the activity of SOD in tobacco cells. Data are means of three different experiments in triplicate ± SD. Different letters In each group shows significant difference.

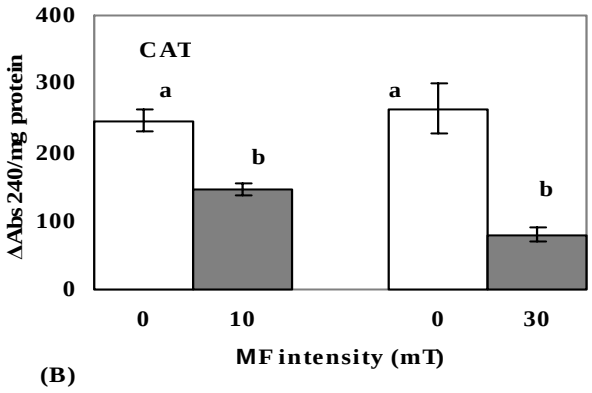

Fig.3. Effect of SMF with different intensities on the activity of CAT in tobacco cells Data are means of three different experiments in triplicate ± SD. Different letters In each group shows significant difference.

Summary

In recent years, the results of experimental studies have revealed that magnetic fields of moderate amplitudes (B=1-100mT) may alter the activity of certain enzyme reactions. An interpretation of the magnetic field activity observed in the enzyme reactions is based on the radical pair mechanisms [Zmyslony et al. 2000]. We actually tried 10 and 30mT in the initial stage of our *in vivo* experiment because these strengths are in the range that humans most often experience in our daily lives [Li and Chow 2001]. Compared to the pervious works which dealing with alternative current (AC) we assume that the effect of static magnetic field using DC current on enzymes activity is more severe. This is justifying because the cycle of 50HZ takes 20ms and the lifetime of a radical pair encounter is no longer than a few microseconds. It is therefore clear that the radical pairs may be affected for a long and continuous time interval by the static magnetic field [Zmyslony et al. 2000]. This may extend the life time of the free radical and its potential damage could be exaggerated.

Plants have several antioxidant enzymes and metabolites located in different plant cell compartments, the main ones being SODs a family metalloenzymes that convert O°2 to H2O2. Because superoxide is the first product of univalent reduction of oxygen, SOD is considered as the “primary defense” against oxygen radicals [Banister et al. 1989]. The product of SOD, hydrogen peroxiode, requires further detoxification. This is achieved by other enzymes and non-enzymatic antioxidants that may differ among the various cellular compartments. H2O2 is reduced to water by ascorbate peroxidase (APX).This enzyme uses a large pool of 10mM ascorbate present in the chloroplast and oxidizes it to monodehydroxyascorbate[Noctor and Foyer 1998]. Also, catalases (CATs) which are tetrameric heme-containing enzymes that similarly catalyze the removal of H2 O2 [Willekens et al. 1995]. Changes in catalase in response to other stress conditions have also previously been reported. Willekens and coworker studied the three isoenzymes of catalases in response to environmental challenges such as UV-B, O3, and SO2 [Willekens et al. 1995]. As a consequence of its sensitivity to environmental conditions, early loss of catalase was suggested as a signal for antioxidant defenses stimulus [Feierabend et al. 1996]. In a similar way, we tried the effect of the exposing to the SMF as another physical stress on catalase inhibition to investigate whether it can mediate defenses in tobacco cells or not.

In our study, a statistically significant CAT activity decrease was observed. Such a condition may indicate abnormal function of the antioxidant system caused by SMF which can lead to a high concentration of H2 O2 in the cells. This incensement in H2 O2 can cause a toxic condition. Spychalla and Desborogh [1990] emphasized that the overproduction of the H2O2–generating SOD must always be combined with increased levels of H2 O2 –metabolizing catalase and/or peroxidase. Such combination can generate a powerful scavenging of toxic oxygen forms. On the contrary, an increase in SOD activity alone might enhance cytotoxicity by active oxygen species likely owing to the accelerated H2 O2 generation and subsequent OH˚ overproduction by the metal catalyzed Haber-Weiss reaction [Piacentini et al. 2001]. Indeed, H2 O2 accumulation may itself lead to higher active oxygen species (AOS) production [Spychalla and Desborogh 1990]. The inconsistent action SOD and CAT enzymes as happened in our study due to the exposing to the static magnetic field contributes to increase the deteriorate effect of H2 O2 and above all the risk of OH˚ formation, the decrease survival and the appearance of signs of senescence. This could be happened through reactivating few oxygen species that cause change vital functions. As a result we can consider that tobacco cells may efficiently metabolize superoxide but may have difficulties in eliminating the hydrogen peroxide when exposing to SMF. Evidence is reviewed here showing that SMF can increase free radicals and alter enzyme reactions which could highlight the activity of oxidant radicals.

Although formed in normal cell metabolism, free radicals are potentially damaging and can initiate chain reactions to form new free radicals. A main protective role against free radicals is attributed to SOD in catalyzing and dismutation of superoxide anions to O2 and H2O2 (Sreenivasulu et al., 2000). The activity of SOD increased from 0.05 ± 0.004 to 0.09 ± 0.005 in 10 mT and from 0.07 ± 0.002 to 0.11 ± 0.006 in 30 mT MF treatments. It means that exposure to MF caused increases by 74% and 87% in unit of SOD activity in 10 and 30 mT-treated tobacco cells, respectively. It implies the first step of the increased production of free radicals by MF in tobacco cells. An increase in SOD activity might enhance cytotoxicity by active oxygen species likely owing to the accelerated H2 O2 generation and subsequent OH• overproduction by the metal catalyzed Haber-Weiss reaction (Piacentini et al. 2001). Likewise, the activity of CAT was also reduced from 247± 15 to 146 ± 8 in 10 mT and from 264 ± 37 to 80 ± 11 in 30 mT MF treatments. Interestingly, the ratio of the reduction of CAT activity in 30 mT-treated cells was remarkably more than those treated with MF of 10 mT (70% versus 41%).

Further experiments involving exposure of cells for a different time and at various magnetic field flux densities make it possible to establish threshold values for this biological effect [Jajte et al. 2001].

References

Banister J.V., Banister W.H., Rotilio G . Aspects of the structure, function, and applications of superoxide dismutase .CRC Crit .Rev.Biochem, 22(1989), 111-180.

Bradford M.B. .A rapid and sensitive method for the quantitation of microgram quantities of protein utilizing the principle of protein-dye binding. Anal. Biochem. 72(1976)248-254.
Cakmak I .. Horst W. J.. Effect of aluminum on lipid peroxidation, superoxide dismutase, catalase and peroxidase activities in root tips of soybean (Glycine max). Plant Physiol. 83(1991)463-468.
Feierabend J ., Streb P ., Schmidt M., Dehne S., Shang W .. Expression of catalase and its relation to light stress and stress tolerance .In: physical Stresses in Plants: Genes and Their Products for Tolerance.In:Physical Stresses in Plants:Genes and Their Products for tolerance, (1996)pp. 223-234. Grillo S.and Leone A.(eds),Springer,Berlin.
Giannopolitis C. N., Ries S. K.. Superoxide dismutase. I. Occurrence in higher plants. Plant Physiol. 59(1977)309-314.
Ishisaka RKanno,T., Inai Y., Nakahara H., Akiyama J.,.Yoshioka T, Utsumi K.,Effects of a magnetic fields on the various functions of subcellular organelles and cells,Pathophysiology 7(2000) 149-152.
Jajte J., Grzegorczyk J., Zmyslony M., Rajkowska E., Kowalska M.S., Kowalski M.L., Influence of a 7mT static magnetic field ,and irons on apotosis and necrosis in rat blood lymphocytes,J Oceup Health 43(2001) 379-381
Kuboi T ., Kaji M.. Establishment of tea cell lines with high growth rate. Tea Res. 80(1994) 1-8 (in Japanese).
Kwee S., Raskmark P. Changes in cell proliferation due to environmental non-ionizing radiation 2.Microwave radiation.Bioelectrochemistry and Bioenergetics 44(1998) 251-255.
Lee B.C.,.Johng H.M,.Lim J.K,.Jeong J.H Effects of extremely low frequency mafnetic field on the antioxidant defense system in mouse brain :a chemiluminescence study.Journal of photochemistry and Photobiology B:Biology 73(2004)43-48.
Li S.H., Chow K.C. Magnetic field induces DNA degradation.Biochemical and Biophysical and Research Communictions 280(2001) 1385- 1388.
Mcfarlane E.H, Dawe G.S., Marks M., Campbell I.C. Changes in neuritis outgrowh but not in cell division induced by low EMF exposure :influence of field strength and culture conditions on responses in rat PC12 pheochromocytoma cells,Bioelectrochemistry 52(2000) 23-28.
Moustafa Y.M., Moustafa R.M., Belacy A., Abou-EI-Ela S.H., Ali, F.M. Effects of acute to the radiofrequency fields of cFellular phones on plasma lipid peroxide and antioxidase activities in human erythrocytes, Journal of pharmaceutical and biomedical analysis 26(2001)605-608.
Noctor G., Foyer C.H. Ascorbate and glutathione: Keeping active oxygen under control .Annu.Rev.Plant Physiol.Plant Mol.Biol. 49(1998)249-279.
Olivares-Barnuelos T., Navarro L., Gonzales A., Drucker-Colin.,R.. Differentiation of chromaffin cells elicited by ELF MF modifies gene expression pattern.Cell Biology International 28(2004) 273-279.
Piacentini M.P., Fraternale D., Piatti E., Ricci D., Vetrano F. Senescence delay and change of antioxidant enzyme levels in Cucumis sativus L.etiolated seedling by ELF magnetic fields. Plant Science 161(2001) 45-53
Robison J.G., Pendleton A.R.,Monson K.O.,.Murray B.K.,.O'Neill K.L. Decreased DNA repair rates and protection from heat induced apoptosis mediated by electromagnetic field exposure.Bioelectromagnetics 23(2002)106-112.
Scaiano Cozens J.CF.L, Mclean J. Model for the rationalization of magnetic field In vivo. Application of the radical-pair mechanism to biological systems .Photochemistry and Photobiology. (1994) Vol.59,pp.585-589.
Sobczak A., Kula. B, Dancii A. Effects of electromagnetic field on free-radical processes in steelworkers.Part II: Magnetic field influence on vitamin A,E and selenium concentrations in plasma .J Occup health 44(2002) 230-233.
Spychalla J.P.,.Desborough S.L. Superoxide dismutase,catalase ,and ;-tocopherol content of stored potato tubers,Plant Physiol.94(1990) 1214-1218.
Sreenivasulu N, Grimm B, Wobus U and Weschke W 2000 Differential response of antioxidant compounds to salinity stress in salt-tolerant and salt-sensitive seedlings of foxtail millet (Setaria italica). Physiol. Plant. 109, 435-442.
Willekens H ., Inze D., Van Montagu M., Van Camp W. Catalases in plants .Mol.Breed. 1(1995)207-228.
Yoshikawa T., Tanigawa M.,.Tanigawa T.Imai,A, Hongo H.,.Kondo, M. Enhancement of nitric oxide generation by low frequency electromagnetic field , Pathophysiology 7(2000) 131-135.
Zmyslony M., Palus J., Jajte J., Dziubaltowska E., Rajkowska E. DNA damage in rat lymphocytes treated in vitro with iron cations and exposed to 7mT magnetic fields (static or 50HZ), Mutat. Res.453 (2000) 89-96.

Analysis of Radiation Hazards to Personnel on Surface Combatants

Avigdor Shechter
Alion Science and Technology
4300 King St.
Alexandria, VA, USA

Moshe Netzer
EMC and Safety Engineering
11 Avigail St.
Haifa, Israel

Abstract: The large number of radio frequency (RF) transmitters employed in combat systems of modern Naval surface combatants requires that they operate in mutual coexistence while posing no danger to operators and equipment despite the limited available physical space. A key to the successful combat system integration is the control of the electromagnetic environment on the combatants' topsides, which might pose radiation hazards (RADHAZ) to personnel (HERP). HERP are caused by transmitter antenna installations that generate intentional EM radiation in excess of the safe levels in zones of personnel activity. Radiation safety to personnel is achieved when the average radiation power density is below the permissible exposure limits (PEL) for HERP at locations of personnel activity and medical equipment operation. This paper describes the analysis tools and techniques for the evaluation of HERP on surface combatants. The same approaches could be employed in the analysis of land site antenna deployment scenarios.

Introduction

Modern surface naval combatants employ a vast array of electronic systems in order to accomplish their warfare missions. Toward this end, electronic systems utilized in combatants comprise powerful transmitters, some of which are broadband such as radar and ECM systems. These systems operate at frequencies from HF to Ka-band in order to perform an assortment of tasks: data and voice communications, radar search and track operations, fire control and weapon guidance activity, electronic warfare, etc.

As the electromagnetic radiation (EMR) sources on combatants' topsides are confined to extremely limited space on the combatants' topsides, they might compromise the EMR safety. Therefore, the EM environment on combatant topsides has to be controlled by either the proper placement of the effectors (hard solutions) or/and by establishing suitable system operational procedures (soft solutions).

RADHAZ are caused by transmitter antenna installations that generate intentional EMR in excess of safe levels in zones of personnel activity, ordnance storage and handling regions, or fueling operations areas. Correspondingly, RADHAZ is categorized according to the following three major groups of hazards of EMR to:

- Personnel (HERP) - harmful effects to humans,
- Ordnance (HERO) – initiation of electro-explosive devices by induced currents,
- Fuel (HERF) – ignition of flammable atmosphere–fuel vapors mixed with air.

In the context of EMR hazard to personnel, HERO and HERF pose indirect hazard; therefore, they will not be discussed.

It follows that during the process of combatant topsides integration, the electromagnetic compatibility (EMC) engineering should address HERP issues by controlling the EM environment, by design. EM Safety is achieved when either all the EMR levels onboard the ship are below the HERP PEL's at topside test point (TP) locations where personnel activity takes place.

From the engineering point of view, the analysis of the EM environment on the combatant topsides should reflect "worst case scenarios". Due to its complexity, combatant topside design is performed by means of computer analysis tools. The methods utilized in the software for topside EM analysis are discussed herein.

Topside EMR and Its Control

The potential for sustained HERP related problems on combatant topsides is due to the high level of EM energy emitted by the onboard intentional topside communications and combat system transmitters. Consequently, the EM environment on the topsides of surface combatants is the aggregate of a variety of RF components of time periodic EMR characterized by either modulated continuous wave (CW) (time harmonic), or repeated pulse (pulse train) modulated EM waves of period T within the range of 1.6 MHz to 36 GHz. Both the CW and pulsed modulated EMR represent finite bandwidth signals having approximate power spectral density (PSD) of similar shape ([1]).

Generally, EMR can be classified into one of the following two categories: ionizing radiation, and non-ionizing radiation. This classification is based on whether the EMR is capable of ionizing atoms and breaking chemical bonds. The EM environments onboard combatants is non-ionizing; thus, its biological effect is to cause dielectric heating. Consequently, the basic interaction of EMR with human tissue is by absorption of the EM energy. Exposure of humans to intense fields produces increased heating whose deposition in the tissue can lead to effects ranging from discomfort, through burns, to protein denaturation. As the human body does not have internal sensors for the sensation of heat, a major source of HERP danger is when the body absorbs

excess radiation, the awareness of the exposed individual. Consequently, as the victim does not feel the need to evacuate the RADHAZ area; thereby, the chance to biological damage increases due to the inability of the victim's body to dissipate the excess heat. Furthermore, strong EMF's induce electric currents in metal objects. The induced currents can cause RF burns or even electric shock to personnel whenever they touch surfaces of high current while standing on the "grounded" deck.

Combatants constitute an environment where personnel are aware of the potential danger of RF exposure associated concurrently with either their routine activity, or incidental transient passage through an area of high EMF. Accordingly, the regulations specifying acceptable limits of EMR exposures in such circumstances are lax as compared to those established for general public environments. Nevertheless, the corresponding RADHAZ permissible exposure limits (PEL's) serve as requirements for certification of combatants. HERP regulations are being regularly updated with the advance of the complex effects of EMR on the human body.

The current industrial specifications for HERP, contained in [1], were used as reference to create the combined HERP regulations for combatants. The resulting frequency dependent PEL's are based on a safety factor of ten over the specific absorption rate (SAR), which might cause bodily harm to humans at each EMR frequency. The graphs in **Figure 1** specify the PEL's for personnel, in terms of the electric field (E-field) strength, for both public and occupational exposure in accordance with [1].

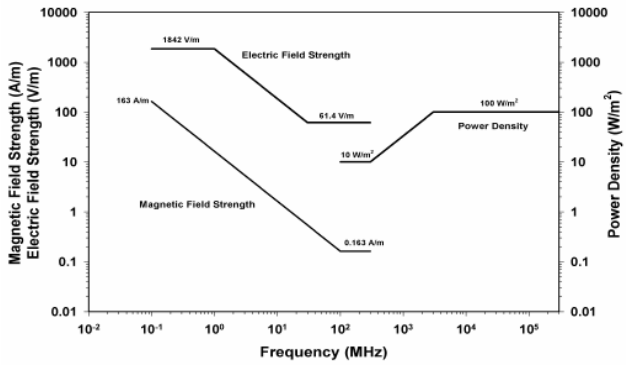

Figure 1 Permissible Exposure Standard for Personnel, IEEE Standard C95.1, 2005

Nevertheless, exceptions to the maximum limits specified in **Figures 1** which allow higher EMR levels do exist ([1]). For example, the power density is allowed to violate the PEL in case of pulsed RF fields, while for cases in which the source is a rotator the power considered for HERP (only!) is reduced according to the following rule:

$$\mathrm{PEL}_{\mathrm{scan}}(f) = \mathrm{PEL}_{\mathrm{fixed}}(f)\frac{2\times \mathrm{Beam\,Width}}{\mathrm{Scan\,Angle}} \qquad (1)$$

where, f is the frequency of the EMR.

Computational EM (CEM) in Topside RADHAZ Analysis

The estimation of HERP from crowded multiple antenna sites can be performed either graphically ([2]), or purely computationally ([3], [4]) based on the following rule ([1], [2]):

$$\left(\frac{E_1}{E_{s1}}\right)^2+\left(\frac{E_1}{E_{s2}}\right)^2+\ldots+\left(\frac{E_N}{E_{sN}}\right)^2<1 \qquad (2)$$

where, $E_1,E_2,...,E_N$, are the E-field strength levels for the frequencies $f_1,f_2,...,f_N$, respectively, and $Es_1,Es_2,...,Es_N$ are the PEL's for the frequencies $f_1, f_2,...,f_N$, respectively. The application of Equation (2) requires the knowledge of the EMF strength or power received at various topside locations from the onboard transmitters. These are obtained via computer-aided predictions based on mathematical models of the topside HERP problem.

Mathematically, the HERP problem is expressed as a radiation/scattering field problem defined over an unbounded domain. However, due to the complexity of the conducting structures, closed form solutions of the topside integration problem are not accessible nor can they be generated using a single method. Thus, topside HERP analyses utilize an array of mathematical methods each suitable to the solution of a different aspect of the topside EMR problem. Due to the complexity of the domain of the topside integration problem, its solution is performed with the aid of numerical analysis tools executed on powerful computers.

The prevalent approach practiced in engineering analysis favors the investigation of the behavior of dynamical systems in the frequency domain (FD) over the time domain (TD). The key to the selection of a suitable FD numerical method is the electrical size of the problem, defined as the ratio of the physical size of the conducting structure to the wavelength, $\lambda \approx 300/f$, of the radiated RF carrier wave where, f is in MHz. At low RF frequencies, the EM wavelengths are of the order of magnitude of the dimensions of the conductor; thus, they interact with it strongly by exciting global resonances; at high RF frequencies, the interactions between the various parts of the conductor are weak; consequently, parts of the structures remote to the RF source location act as scatterers of EMR (i.e., they reflect and diffract the EM waves).

The starting point of all CEM methods are the TD linear Maxwell's curl equations (partial differential equations). The FD CEM methods use the FD version of Maxwell's equations after assuming separation of the time and space dependent variables in conjunction with time-harmonic response postulation. FD CEM methods applied to combatant topside scattering problems are classified according to their FD applicability to the RADHAZ problem as follows:

- Numerical Methods – applied to low frequency analysis,
- Analytically Based Methods – for high frequency analysis.

FD numerical methods belong mostly to the methods known as direct numerical methods. These methods use approximate discrete expressions (interpolations) of the solution functions. The analytically based methods on the other hand, use closed form models (formulae) of wave front propagation (reflection, refraction, and diffraction) in order to calculate EMR fields from EM sources in the presence of scatterers.

In light of the wide range of frequencies of interest in topside RADHAZ analysis in conjunction with the conductor size, the applicability of numerical methods to combatant topside analysis is generally limited to the HF and low VHF (LVHF) ranges (f=2-88 MHz). Consequently, the prediction of topside RADHAZ at UHF and up has to be performed by analytically based methods, as these methods have no applicability limitation in terms of conductor and domain sizes, and the frequency of the source.

Numerical Analysis

Within the framework of the FD modeling of scatterers in unbounded domains, the most popular direct numerical method is known as the method of moments (MoM) ([3]). The method, whose major advantage is the circumvention of the need to model the surrounding non-conducting space, is based on the premise that the total electric field, $\boldsymbol{E}^t$, at any point in space is the sum of the incident and the scattered electric fields. Furthermore, it assumes that the E-field scattered from metallic surfaces is produced by currents induced in the scatterer by the incident field such that the total tangential E-field on its surfaces vanishes (a boundary condition with the unbounded free space); i.e., $\boldsymbol{E}^t = \boldsymbol{E}^s + \boldsymbol{E}^i = 0$. Hence, MoM is a CEM method that uses a specialized analytical solution of Maxwell's equations.

The application of MoM to real conducting structures is accomplished by representing the conducting surfaces of the scatterer as a fine mesh of M thin cylindrical conducting wires of radii a. Consequently, the complete structure can be represented as the sum of the contributions of M wires assuming that their currents are compatible at the nodes of the mesh. Subsequently, the mathematical model, in the sense of MoM, is a system of linear algebraic equations of the general form:

$$[Z]\{I\} = \{E\} \qquad (3)$$

where, $[Z]$ is the global impedance matrix, $\{I\}$ is the unknown global current vector, and $\{E\}$ is the excitation vector.

The impedance matrix in Equation (3) is full rank. It is solved either by means of LU decomposition, or by a more efficient nonlinear programming method such as the conjugate gradient method ([5]). Once the M wire currents are known, the E-field at any TP on the topside can be calculated from the definition of the potential vector $\boldsymbol{A}$:

$$\boldsymbol{E}^s(\boldsymbol{r}) = -j\frac{2\pi}{f}\left[\boldsymbol{A} + j\frac{1}{\mu\varepsilon}\nabla(\nabla\cdot\boldsymbol{A})\right] \quad . \qquad (4)$$

Analytically Based Methods

The solutions obtained via the analytically based methods (also known as semi-analytical methods) are valid for high EMR frequencies in the sense that the EM waves are well formed and locally planar with respect to the conducting structure. It can be inferred that for scatterer sizes larger than two wavelengths, ray-tracing techniques can be utilized in order to calculate the fraction of the EM power reaching topside TP's from topside sources in the presence of scattering obstacles. In order to obtain realistic predictions of the levels of radiation at specified locations, the following source and propagation parameters, among others, should be considered:

- The radiation pattern of each transmitting antenna,
- The near-field (Fresnel Zone) boundaries and intensities,

- Antenna polarization, and cross polarization,
- In-band, out-of-band antenna performance,
- Blockage of line of sight by metallic structural components,
- Presence of radiation absorbing materials (RAM).

The (far-field) pattern of EMR from wanted topside radiation sources is either omni-directional, or directional as depicted in **Figure 2**. Far enough from the source the EMR propagates as a plane wave; nevertheless, often, the topside victims of the excessive radiation are positioned within the near-field regions of the topside sources, which are characterized, irregular field intensities.

Figure 2 – Omni (left), and Directional (right) Radiation Pattern

The calculations of transmission losses of EMR power density due to propagation from topside sources to TP's follows Friis' modeling. Accordingly, the power density, Φ_D, received at a TP located a distance r from a Tx antenna is given by ([4]):

$$\Phi_D = \frac{P_T G_T}{4\pi r^2 L_F} \qquad (5)$$

Where, P_t is the transmitted power, G_T is the (far-field) gain of the Tx antenna, which is a metric characterizing the directivity, $D=4\pi/\Omega_b$ (Ω_b is the 3-dB beam solid angle), and L_F is a path loss factor. Subsequently, the power received at the victim location is just given by $P_R = A_{eff}\Phi_D$ where, A_{eff} is the effective receiving area.

As distances between the EMR sources and victim TP are relatively small for the topside RADHAZ problem, atmospheric propagation losses are negligible. Consequently, the path loss factor is determined by the extent of physical blockage along the line of sight (LoS) between the source and the victim. **Figure 3** (left) shows the possible paths and geometries of EM rays emanating from a generic point source to various observation positions in the presence of a wedge scatterer ([8]). As indicated in **Figure 3** (left), three radiation zones can be identified around the obstacle: direct/reflection/diffraction zone, direct/diffraction zone, and diffraction only zone.

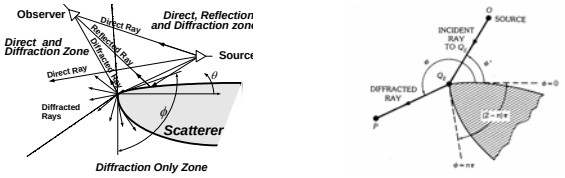

Figure 3 EMR Past a Wedge (left), and Wedge Diffraction (right)

Accordingly, diffraction coefficients are calculated based on the uniform/geometric theory of diffraction (U/GTD). The parameters determining the values of the diffraction coefficients are mainly:

- The incident and diffracted ray angels (found by ray tracing),
- The wave frequency and polarization,
- The wedge angle (where applicable).

A simple analytic GTD expression for wedge diffraction of tip angle $(2\text{-}n)\pi$ (n being some real number) is given by ([8]):

$$D_{\substack{e\\m}} = \frac{\sin\left(\frac{\pi}{n}\right)}{2\pi n\left(\frac{f}{300}\right)^2}\left(\left[\cos\left(\frac{\pi}{n}\right)-\cos\left(\frac{\phi-\phi'}{n}\right)\right]^{-1} \mp \left[\cos\left(\frac{\pi}{n}\right)-\cos\left(\frac{\phi+\phi'}{n}\right)\right]^{-1}\right) \qquad (6)$$

With the incident and diffracted angles indicated in **Figure 3** (right).

Modeling of the Topside RADHAZ Problem

The application of FD methods to the topside EMR problem requires the modeling of EM sources, EMR propagation, and scatterers. The modeling procedure corresponding to the application of both MoM and UTD to RADHAZ analysis is described herein.

Topside transmitting antennas are the sources of the intentional EMR components comprising the topside EM environment. In order to analyze the topside RADHAZ they have to be modeled over the entire RF range. Generally, in MoM analysis the models of sources are constructed to "reproduce" the physics of the real device, whereas in the case of the analytically based methods the models merely reflect the device typical operational characteristics. Once the models of the source of EMR are established, the propagation loss of the radiation from sources to observer (test) points in the presence of scatteres has to be ascertained.

MoM Modeling

Low frequency topside antennas are sources of E-fields. The modeling of E-field sources is implement by inserting a gap of infinitesimal length at the midpoint of a wire located at the position in the wire model corresponding to the real source location and assigning an E-field across it. **Figure 4** depicts the current distribution and the radiation pattern of a 10-wire lineal structure (antenna) radiating in free space in response to a 20 MHz source located at its bottom wire.

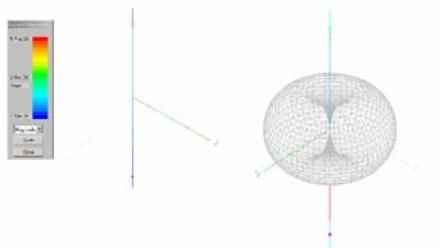

Figure 4 – 10-Wire Model of Monopole Free Space Antenna: Current Distribution (left), Radiation Pattern (right) at 20 MHz

MoM is based on first principles of physics, the correctness of their solutions is indisputable. However, in order to reduce numerical dispersion effects on the approximate solution the use of at least ten sample points within a wavelength is required. Consequently, the maximum length of the longest wire in the model is required to be L=0.1λ, at least. Furthermore, the successful application of the MoM requires that the network of wires representing the conducting structure (including all the topside antennas) follow a specific set of modeling restrictions in order to keep the modeling errors within the engineering acceptable range (a few percent). Furthermore, the ship structure from the waterline up has to be modeled in order to avoid the generation of spurious modes corresponding to any arbitrarily imposed boundaries. An example of a wire mesh model is shown in **Figure 5** for a nominal design of a 50m ship. The model discretizes the ship outer surfaces all the yaw to the waterline using 6,758 wires. The surface of the water is represented as an infinite ground plane having seawater permittivity and conductivity.

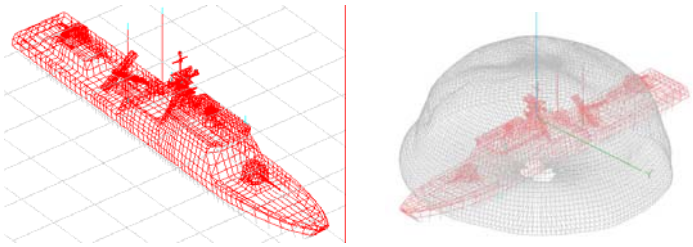

Figure 5. MoM Discretzation of a Nominal Combatant and the Radiation Pattern Of a HF Whip Antenna at 20 MHz

The frequency limitation on the applicability of the MoM is due to its inherent disadvantage that the memory requirement for the discrete model depends quadratically on the size of the conducting structure, while the computational complexity depends on the sixth power of the source frequency. This leads to high computational costs both in terms of computer resources and computation time. Furthermore, as the increase of frequency leads to a numerical model whose spatial resolution exceeds the geometrical confidence level of the design.

Analytically Based Methods Modeling

The limitation of the applicability of the numerical methods to low frequency analyses, requires supplemental methods for handling high frequencies (UHF and up for ships). The idea is to take advantage of the small wavelength relative to the scattering structure in order to generate analytical models that follow geometric arguments.

The general radiation pattern from an EMR source (antenna) is characterized by the presence of a main beam shaped to deliver RF energy along its axis. Nevertheless, due to local diffraction effects, sidelobes and backlobes regions exist as well as depicted

in **Figure 6** (left). Normally the spurious regions show a reduction of 10 dB from mainlobe gain in conjunction with half the beamwidth.

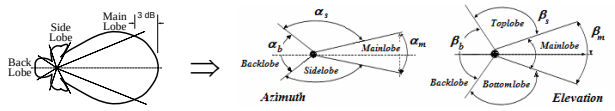

Figure 6 – Simplified Model of Antenna Radiation Patterns

The radiation pattern can be characterized by various analytical approaches. Nonetheless, satisfactory results are also obtained via simplified models based on physical arguments. Accordingly, radiation patterns are classified according to their EM properties via the notion of the antenna gain of the radiation pattern and the effect of its impedance mismatch. Consequently, it is possible to determine the radiation pattern parameters of topside antennas using merely three necessary input parameters: the directional mainlobe gain ($G_0=\eta D$, η radiation efficiency), the azimuth 3dB beamwidth angle (α), and the elevation 3dB beamwidth angle (β) as shown in **Figure 6** (right).

Nevertheless, as often the EMR field at the near-field of the antenna is of interest, the above far field models are corrected to account for near-field EMR. In addition, in order to account for nonlinear effects, empirical harmonic order correction factors for both CW and pulsed transmitter harmonic order attenuations are available.

Due to proximity of the topside transmitters to locations where personnel activity and/or mission critical equipment operate, it is important to consider the location of the near-field border (the point in which a planar wave front is received) corresponding to each topside emitter. The near-field/far-field border location, R_{FF} is determined according to [7] for the two antenna groups:

$$R_{FF}=\begin{cases}5\lambda & \text{for lineal antennas}\\ \frac{2D^2}{\lambda} & \text{for 2D and 3D aperture antennas}\end{cases} \qquad (7)$$

where, D is the maximal lineal dimension of the aperture, and λ is the wavelength. Calculating the "near-field correction", there are different models for three groups of antennas: reflector-aperture antennas, horn-aperture antennas, and lineal antennas.

As the high frequency methods are formulated based on the application of formulae, these methods offer low computational cost both in terms of computing time and machine resources.

Summary

In light of the complexity of topside configurations of modern surface combatants, analysis of topside EM environment is mandatory in order to assure the safety and functionality of the platform. Topside HERP analysis is based on the CEM prediction of EMR levels on the topside. Due to the large physical size of combatants and the wide frequency range employed by their combat systems, topside EMR analysis requires the employment of both low frequency methods, consisting of numerical analysis methods based on MoM, and high frequency methods that are based on ray-tracing algorithms in conjunction with analytically derived formulae. The latter offers high computational efficiency while the former provides accurate physical modeling requiring significant computational resources. HERP safety is achieved as a combination of adequate antenna placement and operating procedures.

References

[1] "IEEE Standard for Safety Levels w.r.t. Human Exposure to RF EM fields, 3 kHz to 300 MHz", IEEE C95.1-2005.

[2] M. Netzer at-al, "A Graphical Method for the Estimation of Radiation Hazards from a Crowded Multiple Antenna Site", Kos Workshop, 2004

[3] R F Harrington, "Field Computation by Moment Methods", IEEE Press, 1992.

[4] J.L.N. Violette et al, "Electromagnetic Compatibility Handbook" Van Nostrad Reinhold Co., NY, 1987.

[5] J.G. Burke, and A.J. Poggio, NEC - Method of Moments Parts I, II and III Technical Document No 116, LLNL, USA 1981.

[6] Balanis, "Antenna Theory – Analysis & Design", Wiley, 2nd Ed., 1997.

[7] "Reference Data for Radio Engineers", 5th ed., ITT, 1973, Howard W. Sams & Co. Inc.

[8] Balanis, "Adv. Engineering. Electromagnetics", Wiley & Sons, 1977.

THEORETICAL ANALYSIS OF VOLTAGE INDUCEMENT ON ORGANELLE MEMBRANES

TADEJ KOTNIK and DAMIJAN MIKLAVČIČ

UNIVERSITY OF LJUBLJANA, FACULTY OF ELECTRICAL ENGINEERING, TRŽAŠKA 25, SI-1000 LJUBLJANA, SLOVENIA

Abstract

Several reports have recently been published on effects of very short and intense electric pulses on cellular organelles; in a number of cases, the cell plasma membrane appeared to be affected less than certain organelle membranes, while with longer and less intense pulses the opposite is the case. The effects are the consequence of the voltages induced on the membranes, and in this paper we investigate the conditions under which the induced voltage on an organelle membrane could exceed its counterpart on the cell membrane. This would provide a possible explanation of the observed effects of very short pulses.

Frequency-domain analysis yields an insight into the dependence of the voltage inducement on the electric and geometric parameters characterizing the cell and its vicinity. The calculations show that at sufficiently high field frequencies, for a range of parameter values the voltage induced on the organelle membrane can indeed exceed the voltage induced on the cell membrane. Particularly, this can occur if the organelle interior is electrically more conductive than the cytosol, or if the organelle membrane has a lower dielectric permittivity than the cell membrane, and we discuss the plausibility of these conditions.

Time-domain analysis is then used to determine the courses of the voltage induced on the membranes by pulses with risetimes and durations in the nanosecond range. The particularly high resting voltage in mitochondria, to which the induced voltage superimposes, could contribute to the explanation why these organelles are the primary target of many observed effects.

1. INTRODUCTION

An exposure of a biological cell to an electric field of sufficient strength can lead to a significant increase in the permeability of the cell plasma membrane (40). If such an exposure is neither too strong nor too long, this phenomenon — referred to as *electroporation* or *electropermeabilization* — is reversible. This allows many otherwise nonpermeant molecules to enter into the cytosol or be inserted into the plasma membrane. Due to its efficiency, electroporation is rapidly becoming an established approach for treatment of solid cutaneous and subcutaneous tumors (22, 47), and it also holds great promise for gene therapy (17).

The mechanism underlying electroporation is the inducement of a voltage on the cell plasma membrane. This voltage is proportional to the field strength and superimposes onto the resting voltage present on the membrane under physiological conditions, typically about –70 mV (37). According to the theory of electroporation, a voltage on the membrane reduces the energy necessary for rearrangements of the membrane lipids that result in formation of aqueous passages (hydrophilic pores) and consequently in increased conductivity and permeability of the membrane. Consequently, as the voltage increases, so does the probability of formation of such passages. The resting voltages normally present on the cell membrane and on the organelle membranes — the largest is in mitochondria, about –140 mV (1) — are insufficient for this, and electroporation is not observed physiologically. However, with exposures to electric fields inducing voltages of several hundreds of millivolts, electroporation of the cell membrane becomes readily achievable and observed in experiments. Both the theory of electroporation (57, 41) and recent computational studies based on molecular dynamics (52, 53, 50) corroborate that as the membrane voltage increases, so does the rate of formation of metastable aqueous passages in the membrane.

The fields used for electroporation are most often delivered as rectangular pulses, with typical amplitudes of several hundred volts per centimeter, durations from tens of microseconds to milliseconds, and risetimes in microseconds. In the first few microseconds after the onset of the pulse, such exposures induce a voltage in the range of several hundred mV on the cell membrane, and this voltage persists until the end of the pulse. Also within microseconds, this leads to the onset of electroporation, detected as a steep increase in electrical conductivity and permeability of the membrane (24, 25).

The exposure of a cell to an electric field also induces voltages on the organelle membranes in the cell interior, but in their steady state, these are several orders of magnitude smaller than the voltage induced on the cell membrane. Thus when the cell membrane is electroporated with typical electroporation pulses with durations of hundreds of microseconds or several milliseconds, the organelle membranes are left unaffected. However, in a number of recent papers it has been reported that with much stronger (typically tens or hundreds of thousands of volts per centimeter) but much shorter (typically tens or hundreds of nanoseconds) pulses, the situation seems to be reversed, with the cell membrane affected less than some internal cell structures (46, 11, 7, 10, 19, 51). In many cases, a mitochondria-dependent apoptosis was observed, which could be due to electroporation of these organelles (6, 8, 58). For brevity, the high-intensity, nanosecond-duration pulses used in these experiments are often referred to as nsPEF (nanosecond-duration pulsed electric fields), and we will also adopt this practice here.

In this paper we explore one possible explanation of the observed effects of nsPEF on intracellular membranes. As discussed above, the steady-state value of the voltage induced on the cell membrane is always much larger than its counterpart on an organelle membrane. But the pulses with durations in the submicrosecond range are too short for the two voltages to approach their steady states, and their time courses become important. These depend on a number of geometric and electric parameters, and here we investigate whether there is a range of plausible parameter values for which the voltage on an organelle membrane can temporarily exceed the voltage on the cell membrane. This explanation has been proposed before, based on considerations of a more qualitative nature (46) and later on finite-elements modeling (29). Here, we derive analytical expressions for the induced voltages and analyze the role of each parameter. In Section 2 we present the expressions for the induced voltages, and in Section 3 we analyze the dependence of these voltages on each of the parameters.

2. DERIVATION OF THE INDUCED VOLTAGES

2.1 The model of a cell with an organelle

For a valid treatment of the membrane voltage induced by alternating fields with frequencies in the MHz and GHz range, or by pulsed fields with risetimes below 1 μs, both the electric conductivities and the dielectric permittivities of the membranes and the surrounding aqueous media have to be taken into account. An analytical treatment of such a system is possible only if the cell is the only object distorting the uniform electric field, and only in geometries where all the boundaries can be expressed as coordinate surfaces. Throughout this work, we will treat a single spherical cell, which meets these requirements. A spherical cell with a uniform interior (i.e. containing no organelles) is widely used in theoretical studies of cells exposed to electric fields, e.g. in derivation of the Schwan equation (38, 31) and its extensions (18, 32, 33, 34). The model with an organelle is then obtained by incorporating into the cell interior another spherical body with a concentric shell. This model (Fig. 1) consists of five regions, each characterized by an electric conductivity (σ, in S/m) and a dielectric permittivity (ε, in As/Vm). From the center outwards, the regions are the organelle interior (subscript 1i), the organelle membrane (1m), the cytosol (2i), the cell plasma membrane (2m), and the cell exterior (e). The radii of the organelle and the cell are denoted by R_1 and R_2, and their membrane thicknesses by d_1 and d_2. Although simplistic, this model is adequate for analyzing the voltages induced on the cell membrane and on organelle membranes (13, 29).

The spatial distribution of the electric potential in and around a spherical cell exposed to a uniform electric field is obtained by solving the Laplace equation in spherical coordinates (39). In each of the five regions of the model shown in Fig. 1, it has the general form

$$\Psi(r,\theta) = \left(A_k r + \frac{B_k}{r^2} \right) \cos\theta \ , \qquad (1)$$

with r the radius measured from the center, θ the angle with respect to the direction of the field, and with constants A_k and B_k specific for each regions. Finiteness of the electric potential at $r = 0$ implies $B_{i1} = 0$, and from uniformity of the field at $r \to \infty$ it follows that $A_e = -E$. The remaining constants A_{1i}, A_{1m}, B_{1m}, A_{2i}, B_{2i}, A_{2m}, B_{2m}, and B_e are determined by the requirement of continuity of the potential, Ψ, and of the normal component of the current density, $\Lambda(\partial\Psi/\partial r)$, at all four boundaries between the regions. In frequency-domain (FD) analysis, Λ is the complex

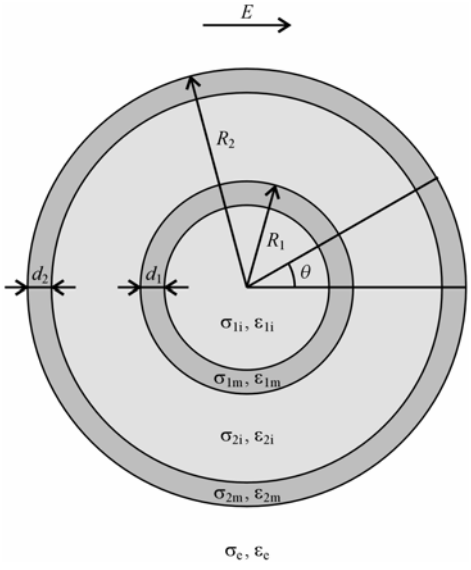

Figure 1

conductivity (admittivity), $\sigma + j\omega\varepsilon$, where ω is the angular frequency of the field, and in time-domain (TD) analysis, it is the admittivity operator, $\sigma + \varepsilon(\partial/\partial t)$, where $\partial/\partial t$ is the operator transforming a function into its time derivative. The continuity requirements for the boundary between the organelle membrane and the cytosol can be written as

$$\begin{aligned} A_{1m} r + \frac{B_{1m}}{r^2} &= A_{2i} r + \frac{B_{2i}}{r^2} \ , \\ \Lambda_{1m}\left(A_{1m} - \frac{2B_{1m}}{r^3} \right) &= \Lambda_{2i}\left(A_{2i} - \frac{2B_{2i}}{r^3} \right) \ , \end{aligned} \tag{2}$$

where in the FD $\Lambda_{1m} = \sigma_{1m} + j\omega\varepsilon_{1m}$, $\Lambda_{2i} = \sigma_{2i} + j\omega\varepsilon_{2i}$, and in the TD $\Lambda_{1m} = \sigma_{1m} + \varepsilon_{1m}(\partial/\partial t)$, $\Lambda_{2i} = \sigma_{2i} + \varepsilon_{2i}(\partial/\partial t)$. Analogous pairs of conditions characterize the other three boundaries. The direct dealing with operators in the TD can be avoided by transferring the treatment into the complex-frequency space, as described in Section 2.3.

The solutions for the eight constants are relatively lengthy expressions, as in general each of them incorporates the geometric and electric parameters of all five regions of the model, but algebraically their determination is elementary, since they form a well-defined system of eight equations with eight unknowns. The derivation and the solutions for the spherical cell with an organelle as shown in Fig. 1 are available at the web address `http://www.biophysj.org/cgi/content/full/biophysj.105.070771/DC1`

Once all the constants are determined, the voltage induced on a membrane is determined as the difference between the potentials $\Psi(r, \theta)$ at the inner and outer surface of this membrane. For the voltage induced on the cell plasma membrane this yields

$$\Delta\Psi_{cell} = \frac{3ER_2 d_2 \left(\begin{array}{l} (R_1 - d_1)^3 (\Lambda_{1i} - \Lambda_{1m}) \left(\begin{array}{l} 2(3R_2^2 - 3R_2 d_2 + d_2^2) \left(\begin{array}{l} (R_2 - d_2)^3 (\Lambda_{1m} - \Lambda_{2i}) \\ + R_1^3 (2\Lambda_{1m} + \Lambda_{2i}) \end{array} \right) \Lambda_{2i} \\ + (3R_2 d_2 - d_2^2) \left(\begin{array}{l} 2(R_2 - d_2)^3 (\Lambda_{1m} - \Lambda_{2i}) \\ - R_1^3 (2\Lambda_{1m} + \Lambda_{2i}) \end{array} \right) \Lambda_{2m} \end{array} \right) \\ + R_1^3 (\Lambda_{1i} + 2\Lambda_{1m}) \left(\begin{array}{l} (3R_2^2 - 3R_2 d_2 + d_2^2) \left(\begin{array}{l} (R_2 - d_2)^3 (\Lambda_{1m} + 2\Lambda_{2i}) \\ + 2R_1^3 (\Lambda_{1m} - \Lambda_{2i}) \end{array} \right) \Lambda_{2i} \\ + (3R_2 d_2 - d_2^2) \left(\begin{array}{l} (R_2 - d_2)^3 (\Lambda_{1m} + 2\Lambda_{2i}) \\ - R_1^3 (\Lambda_{1m} - \Lambda_{2i}) \end{array} \right) \Lambda_{2m} \end{array} \right) \end{array} \right) \Lambda_e}{M} \cos\theta \tag{3}$$

and for the voltage induced on the organelle membrane

$$\Delta\Psi_{org} = \frac{27ER_1 R_2^3 d_1 (R_2 - d_2)^3 \left(3R_1^2 \Lambda_{1i} - d_1 (3R_1 - d_1)(\Lambda_{1i} - \Lambda_{1m}) \right) \Lambda_{2i} \Lambda_{2m} \Lambda_e}{M} \cos\theta \tag{4}$$

where both in (3) and (4)

$$\begin{aligned} M = {} & 2(R_1 - d_1)^3 (\Lambda_{1i} - \Lambda_{1m}) \left(\begin{array}{l} (R_2 - d_2)^3 (\Lambda_{1m} - \Lambda_{2i}) \left(\begin{array}{l} 2(R_2 - d_2)^3 (\Lambda_{2i} - \Lambda_{2m})(\Lambda_{2m} - \Lambda_e) \\ + R_2^3 (\Lambda_{2i} + 2\Lambda_{2m})(\Lambda_{2m} + 2\Lambda_e) \end{array} \right) \\ + R_1^3 (2\Lambda_{1m} + \Lambda_{2i}) \left(\begin{array}{l} (R_2 - d_2)^3 (2\Lambda_{2i} + \Lambda_{2m})(\Lambda_{2m} - \Lambda_e) \\ + R_2^3 (\Lambda_{2i} - \Lambda_{2m})(\Lambda_{2m} + 2\Lambda_e) \end{array} \right) \end{array} \right) \\ & + R_1^3 (\Lambda_{1i} + 2\Lambda_{1m}) \left(\begin{array}{l} (R_2 - d_2)^3 (\Lambda_{1m} + 2\Lambda_{2i}) \left(\begin{array}{l} 2(R_2 - d_2)^3 (\Lambda_{2i} - \Lambda_{2m})(\Lambda_{2m} - \Lambda_e) \\ + R_2^3 (\Lambda_{2i} + 2\Lambda_{2m})(\Lambda_{2m} + 2\Lambda_e) \end{array} \right) \\ + 2R_1^3 (\Lambda_{1m} - \Lambda_{2i}) \left(\begin{array}{l} (R_2 - d_2)^3 (2\Lambda_{2i} + \Lambda_{2m})(\Lambda_{2m} - \Lambda_e) \\ + R_2^3 (\Lambda_{2i} - \Lambda_{2m})(\Lambda_{2m} + 2\Lambda_e) \end{array} \right) \end{array} \right) \end{aligned} \tag{5}$$

The substitution $\Lambda = \sigma + j\omega\varepsilon$ for each of the five regions provides the starting point for analysis of $\Delta\Psi_{cell}$ and $\Delta\Psi_{org}$ in the FD, and the substitution $\Lambda = \sigma + \varepsilon(\partial/\partial t)$ does the same for the TD.

2.2 Analysis in the frequency domain

The frequency domain (FD) is the natural setting for an exposure of a cell to a sinusoidal electric field. Fixing the geometric and electric parameters of the model, inserting for E the amplitude of the field, and writing explicitly $\Lambda = \sigma + j\omega\varepsilon$, the induced voltages $\Delta\Psi_{cell}$ and $\Delta\Psi_{org}$ become functions of a single variable, namely ω, the angular frequency of the field. For a fixed ω, the values of $\Delta\Psi_{cell}$ and $\Delta\Psi_{org}$ are complex numbers, with $|\Delta\Psi_{cell}|$, $|\Delta\Psi_{org}|$ corresponding to the amplitudes of the induced voltages, and $\arg(\Delta\Psi_{cell})$, $\arg(\Delta\Psi_{org})$ to their phase shifts with respect to the external field. It should be emphasized that these values characterize the sinusoidal steady states that are established after the transients occurring at the onset of the field are over.

By considering $\Delta\Psi_{cell}$ and $\Delta\Psi_{org}$ as functions of ω, it is then determined very straightforwardly whether there is a range of parameter values and field frequencies where $\Delta\Psi_{org}$ can — at least temporarily — exceed $\Delta\Psi_{cell}$. The results of such analysis are presented in Section 3.1.

The approach described above can be extended to other periodic time courses of the field representable as uniformly convergent Fourier series. The induced voltages are then given by the series of voltage components induced by individual field components in the Fourier series.

2.3 Analysis in the time domain

The time domain (TD) is the natural setting for exposures of a cell to aperiodic fields, as well as to periodic fields for which the Fourier series is nonuniformly convergent.[*] This class clearly contains a rectangular and a trapezoidal (i.e. having non-zero risetime and falltime) pulse, but it also contains periodic trains of such pulses, as the uniform convergence requirement fails at the pulse edges, which is usually referred to as the Gibbs phenomenon (23). As mentioned in Section 2.1, the most convenient approach here is an interim transfer of the treatment to the complex-frequency space. Denoting the complex frequency by s, the differentiation with respect to time is thereby transformed into multiplication by s, and time courses are replaced by their Laplace transforms. Fixing again the geometric and electric parameters of the model, inserting for E the Laplace transform of the time course of the electric field, $L[E(t)] = E(s)$, and writing explicitly $\Lambda = \sigma + \varepsilon s$, the expressions for $\Delta\Psi_{cell}$ and $\Delta\Psi_{org}$ become functions of s. The time courses of the induced voltages are then obtained as inverse Laplace transforms, $\Delta\Psi_{cell}(t) = L^{-1}[\Delta\Psi_{cell}(s)]$ and $\Delta\Psi_{org}(t) = L^{-1}[\Delta\Psi_{org}(s)]$. This yields the complete time courses, including the transients.

Provided that $E(s)$ is a polynomial in s, $\Delta\Psi_{cell}$ and $\Delta\Psi_{org}$ are rational functions (i.e. fractions of polynomials) of s, and the inverse Laplace transforms are obtained easily. The method is also applicable to all other cases for which the Laplace transform of $E(t)$ and the inverse Laplace transforms of $\Delta\Psi_{cell}$ and $\Delta\Psi_{org}$ can be obtained explicitly. For many of the conceivable time courses of the electric field, the transforms can be found in standard tables (43), while for other sufficiently regular functions they can be derived by means of the Laplace transform integral and the Bromwich integral, respectively (2). For more intricate cases, discretization of time and application of the unilateral Z-transform instead of the Laplace transform would yield approximate solutions.

3. RESULTS AND DISCUSSION

The aim of this paper is to evaluate the voltages induced by nsPEF, which will be approximated as having a trapezoidal shape. As described in the preceding sections, the natural setting for this is the TD, in which this aim will be pursued in Section 3.2. However, there are four geometric and ten electric parameters that have to be investigated with respect to their influence on $\Delta\Psi_{cell}$ and $\Delta\Psi_{org}$, and a trapezoidal pulse is characterized by a risetime, an amplitude, a duration pertaining to this amplitude, and a falltime. For a first insight into the role of the parameters, and for a selection of those to be investigated further, a clearer picture is provided by treating an exposure of a cell to a sinusoidal field, which is characterized only by its amplitude and frequency. Along these lines, Section 3.1 investigates the influence of each of the parameters in the FD, and a much smaller subset of parameters chosen on the basis of this investigation is then used in Section 3.2 in the TD with trapezoidal pulses.

[*] For other periodic fields, the analysis in the frequency domain is simpler, yet the analysis in time domain is nonetheless applicable, due to which it may be viewed as the more general of the two.

3.1 Voltages induced by a sinusoidal field

The purpose of this section is to determine whether in an exposure of a cell to a sinusoidal field, there is a range of parameter values for which $|\Delta\Psi_{org}|$ can exceed $|\Delta\Psi_{cell}|$, or equivalently, for which the ratio $|\Delta\Psi_{org}| / |\Delta\Psi_{cell}|$ can exceed the value of 1. The expressions for $\Delta\Psi_{cell}$ and $\Delta\Psi_{org}$ in Section 2.1 show that this ratio depends on practically all the geometric and electric parameters of the model. The only exceptions are σ_e and ε_e, as the numerators of $\Delta\Psi_{cell}$ and $\Delta\Psi_{org}$ are proportional to $\Lambda_e = \sigma_e + j\omega\varepsilon_e$, while their denominators are identical, so that in the ratio $|\Delta\Psi_{org}| / |\Delta\Psi_{cell}|$ all occurrences of Λ_e cancel out. The simplest method for investigation of the role of the remaining twelve parameters is by means of parametric studies, in which one parameter is varied through a given range while the others are kept at their default values. Restriction to one variable at a time does not completely elucidate the behavior of a function of twelve variables, but the results of such parametric studies are easy to interpret, and will also suffice for the aims of this paper.

Table 1 gives the default values and variation ranges of the parameters. The default values are based on the typical data found in the literature, and the limits of the variation ranges were chosen as physically plausible values. For the reasons discussed above, σ_e and ε_e do not enter the parametric studies, for which the table gives only the default values, which are needed when the two voltages are of interest, and not only their ratio.

Table 1. Default values and variation ranges for parametric studies

Parameter	Default value	Variation range	Parameter	Default value	Variation range
σ_{1i} [S/m]	0.3 [a]	0.1 – 1.0	ε_{1i} [As/Vm]	6.4×10^{-10} [b]	$(3.5 – 7.0) \times 10^{-10}$
σ_{1m} [S/m]	3×10^{-7} [c]	$10^{-8} – 10^{-5}$	ε_{1m} [As/Vm]	4.4×10^{-11} [d]	$(1.8 – 8.8) \times 10^{-11}$
σ_{2i} [S/m]	0.3 [e]	0.1 – 1.0	ε_{2i} [As/Vm]	6.4×10^{-10} [b]	$(3.5 – 7.0) \times 10^{-10}$
σ_{2m} [S/m]	3×10^{-7} [f, g]	$10^{-8} – 10^{-6}$	ε_{2m} [As/Vm]	4.4×10^{-11} [g]	$(1.8 – 8.8) \times 10^{-11}$
σ_e [S/m]	1.2 [h]	—	ε_e [As/Vm]	6.4×10^{-10} [b]	—
R_1 [μm]	3	1 – 8	d_1 [nm]	5	3 – 15
R_2 [μm]	10	5 – 100	d_2 [nm]	5 [k]	3 – 7

[a] set equal to σ_{2i}
[b] physiological saline at 35°C (42, 9)
[c] set equal to σ_{2m}
[d] set equal to ε_{2m}
[e] (21, 26)
[f] from (27), using the conversion given in (3)
[g] (15)
[h] blood serum at 35°C (49)
[k] (1)

Each of the parametric studies was performed for ω spanning the range from 10^5 to 10^{10} s^{-1}, yielding a set of data that can be visualized clearly in a contour plot of the ratio $|\Delta\Psi_{org}| / |\Delta\Psi_{cell}|$ as a function of frequency and the studied parameter. As shown in Figure 2, with the default values assigned to all parameters, this ratio does not exceed the value of 1 for any frequency. A similar result is obtained if the two membranes are assigned realistic dielectric permittivities but zero electric conductivities (13).

However, in eight of the twelve parametric studies, for sufficiently high frequencies the ratio $|\Delta\Psi_{org}| / |\Delta\Psi_{cell}|$ does exceed 1 in a certain range of parameter values. The contour plots showing the results of the parametric studies are given in Figure 3, from which two clear properties emerge. First, in the higher MHz range, either a small increase of σ_{1i} above its default value, or a small decrease of σ_{2i} below its default value suffices for $|\Delta\Psi_{org}|$ to exceed $|\Delta\Psi_{cell}|$. And second, in the higher MHz range and in the GHz range the same is the case for a decrease of ε_{1m} and for an increase of ε_{2m}. A more general

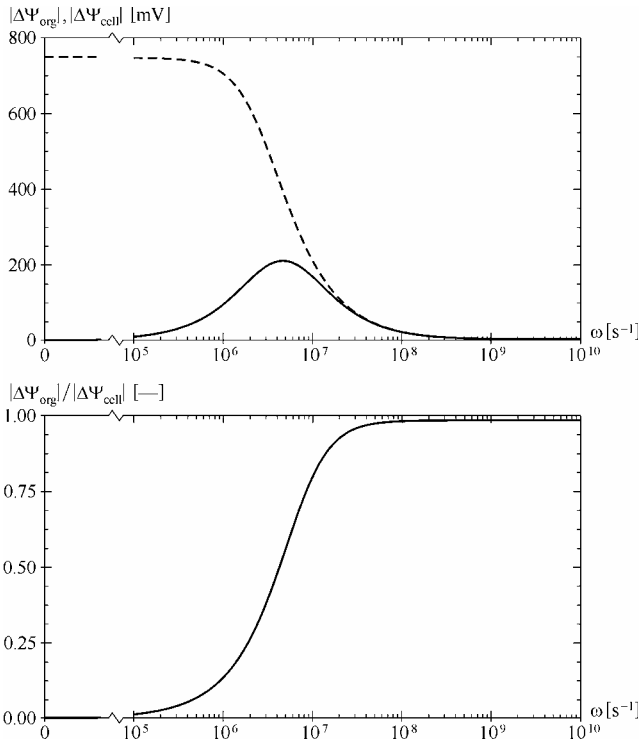

Figure 2

formulation is that the ratio $|\Delta\Psi_{org}|$ / $|\Delta\Psi_{cell}|$ can exceed the value of 1 if the organelle interior has a higher electric conductivity than the cytosol, or if the organelle membrane has a lower dielectric permittivity than the cell membrane. The effect of $\sigma_{1i} > \sigma_{2i}$ is due to the fact that with the increase of frequency, the shielding of the cell interior by the plasma membrane weakens, and the electric current flowing through the cell becomes concentrated in the organelle interior. The effect of $\varepsilon_{1m} < \varepsilon_{2m}$ is also easily explained, as the voltage inducement is faster on the membrane with the lower dielectric permittivity.

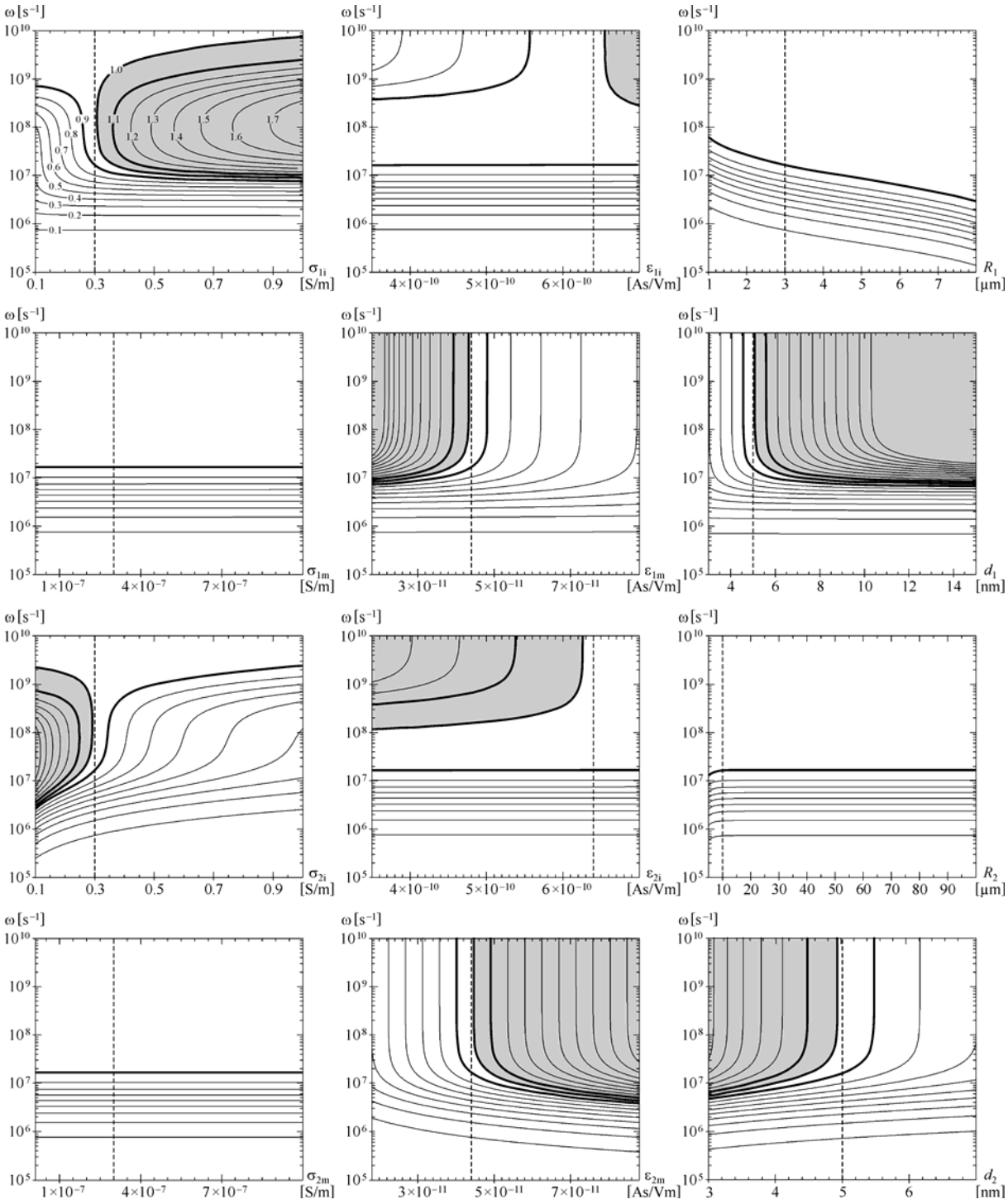

Figure 3

For $\sigma_{1i} > \sigma_{2i}$, the organelle interior would have to contain either a higher total concentration of ions with respect to the cytosol, or a larger fraction of ions with higher mobility (e.g. more potassium and less sodium). In a recent computational analysis, the concentration of potassium ions in the intermembrane space of the mitochondria was

estimated at between 175 and 207 mM (36), which is indeed significantly higher than in the cytosol, where it is typically about 140 mM (37). Among the membranes, the ones with the lowest dielectric permittivity are pure lipid bilayers, and hence for $\varepsilon_{1m} < \varepsilon_{2m}$, the membrane of the organelle under consideration would generally have to contain a smaller fraction of proteins than the cell plasma membrane. This is, however, markedly not the case for the inner mitochondrial membrane, where proteins represent about 76% of the mass — a higher fraction than in any other membrane (37).

The parametric studies also show that $|\Delta\Psi_{org}| / |\Delta\Psi_{cell}|$ can exceed 1 if d_1 is significantly larger than its default value of 5 nm. More generally, a sufficient condition is that the organelle membrane should be thicker than the cell membrane, $d_1 > d_2$. This is realistic for some organelles, such as the nucleus and the mitochondria, as they have a double membrane, and in mitochondria the two membranes are moreover separated by several nanometers of intermembrane space (1). Still, with a thicker membrane, a proportionally larger voltage is required for the same electric field within the membrane. As a consequence, if the electric field in the membrane is the decisive factor in electroporation, with $d_1 > d_2$ the condition $|\Delta\Psi_{org}| / |\Delta\Psi_{cell}| > 1$ is not sufficient for the organelle membrane to be electroporated, but instead roughly $|\Delta\Psi_{org}| / |\Delta\Psi_{cell}| > d_1 / d_2$ would be required.

Finally, a region with $|\Delta\Psi_{org}| > |\Delta\Psi_{cell}|$ is also reached in the parametric studies of ε_{1i} and ε_{2i}, namely at sufficiently high frequencies provided that $\varepsilon_{1i} > \varepsilon_{2i}$. However, as the organelle interior and the cytosol are both aqueous solutions, it is reasonable to assume that ε_{1i} and ε_{2i} are very similar. The choice of variation ranges for these two parameters primarily reflects the dependence of dielectric permittivities on the temperature, but since the cell is too small to contain significant temperature differences, change of the temperature by cooling or heating the cell suspension or a tissue will have nearly the same effect on the two permittivities.

Further analysis reveals that if the cell and organelle membranes are identical in their electric properties and their thickness, and if the cytosol is electrically identical to the organelle interior, then $|\Delta\Psi_{org}| < |\Delta\Psi_{cell}|$ at any field frequency. It should perhaps be stressed here that for such parameter values, the faster charging of the organelle membrane can not cause $\Delta\Psi_{org}$ to exceed $\Delta\Psi_{cell}$, even if the shielding of the organelle by the cell membrane is disregarded. Namely, without shielding, the rate of voltage inducement on a spherical object is inversely proportional to its radius, but the voltage plateau is directly proportional to the radius, so that on a larger object the induced voltage is necessarily larger at all times.[***] As a consequence, the voltage induced on the cell membrane is always larger than its counterpart on the organelle membrane. At low field frequencies the shielding intensifies this effect, as the voltage on the organelle membrane starts decreasing even during the exposure (Fig. 5 illustrates this for an exposure to a direct field).

However, as Figure 3 shows, if some parameters are shifted from their default values, the outcome can change significantly. As an illustration, in Figure 4 we assume that $\sigma_{1i} = 0.5$ S/m, $\varepsilon_{1m} = 3.0 \times 10^{-11}$ As/Vm, and $d_1 = 10$ nm, while keeping the other nine parameters at their default values. This study shows that on a cell characterized by the chosen parameter values, with an exposure to an alternating field with a frequency in the range of tens and hundreds of MHz, the induced voltage on the organelle could exceed its counterpart on the cell membrane by a factor of more than 3. Obviously, this is only relevant provided that σ_{1i} can actually differ that much with respect to σ_{2i}, and similarly for ε_{1m} with respect to ε_{2m}. We discuss the plausibility of this at the end of the paper, whereas we now turn to the voltages induced by a trapezoidal pulse.

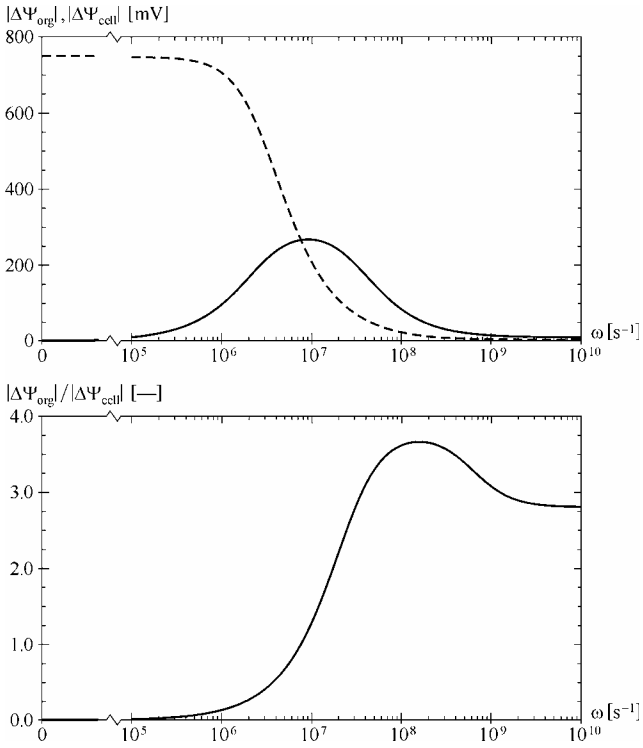

Figure 4

[***] This follows from the fact that for $K > 1$ and $t > 0$, we have $1 - \exp(-t/\tau) < K(1 - \exp(-t/(K\tau)))$. Namely, the two functions are equal at $t = 0$, and for their respective derivatives at $t > 0$ we have $\exp(-t/\tau)/\tau < \exp(-t/(K\tau))/\tau$.

3.2 Voltages induced by a trapezoidal pulse

Before focusing on specific nsPEF, it is instructive to consider the general characteristics of the voltage inducement on a nanosecond time scale. For this, we treat an onset of a direct electric field, and to keep $E(t)$ continuous, we assume that this onset is trapezoidal with a risetime T. Such a time course of the field can be described as a sum of two ramp functions, the first one with a positive slope and starting at the time 0, and the second one with the negative slope of the same size and starting at the time T,

$$E(t) = E_0 \left[\frac{t}{T} u(t) - \frac{t-T}{T} u(t-T) \right] \tag{6}$$

where E_0 is the amplitude of the field that is reached at the end of the risetime. In the complex-frequency space, this becomes

$$E(s) = E_0 \frac{1-e^{-sT}}{s^2 T} \tag{7}$$

In analogy with the FD study shown in Figure 2, we assume that the field amplitude is $E_0 = 5 \times 10^4$ V/m, and treat the situation at $\theta = 0$. In addition, we take $T = 1$ ns, which is on the order of magnitude of the shortest risetimes achievable with nsPEF generators. Proceeding as described in Section 2.3, we insert $E(s)$ into the expressions for $\Delta\Psi_{cell}$ and $\Delta\Psi_{org}$, write all the admittivity operators as $\Lambda = \sigma + \varepsilon s$, assign all the parameters their default values, and apply the inverse Laplace transform to obtain the time courses of the two induced voltages for such an onset of the field. Shown in the top panel of Figure 5, these time courses reveal that the inducement on the cell plasma membrane is a monotonic process, while the inducement on an organelle membrane is transient; with the onset of the field, $\Delta\Psi_{org}$ increases for several hundred nanoseconds, and then recedes back to zero even if the external field persists. This is consistent with the simpler, widely used steady-state consideration of a DC exposure, where the voltage induced on the plasma membrane is given by the static Schwan equation, $\Delta\Psi_{cell} \approx 1.5\ E\ R \cos\theta$, while everywhere in the cell interior the electric potential is practically constant.

The time courses of the two induced voltages also show that with default parameter values, $\Delta\Psi_{org}$ remains below $\Delta\Psi_{cell}$ at all times, as could be expected from the results obtained in the FD (see Fig. 2). However, if in analogy to the second FD study we set $\sigma_{1i} = 0.5$ S/m, $\varepsilon_{1m} = 3.0 \times 10^{-11}$ As/Vm, $d_1 = 10$ nm, and keep the other nine parameters at their default values, the situation changes quite radically. As shown in the bottom panel of Figure 5, $\Delta\Psi_{org}$ now exceeds $\Delta\Psi_{cell}$ considerably during the first tens of nanoseconds. The general properties of the two voltages — a monotonic increase of $\Delta\Psi_{cell}$ and a transient increase of $\Delta\Psi_{org}$ followed by a decrease to zero — are unchanged.

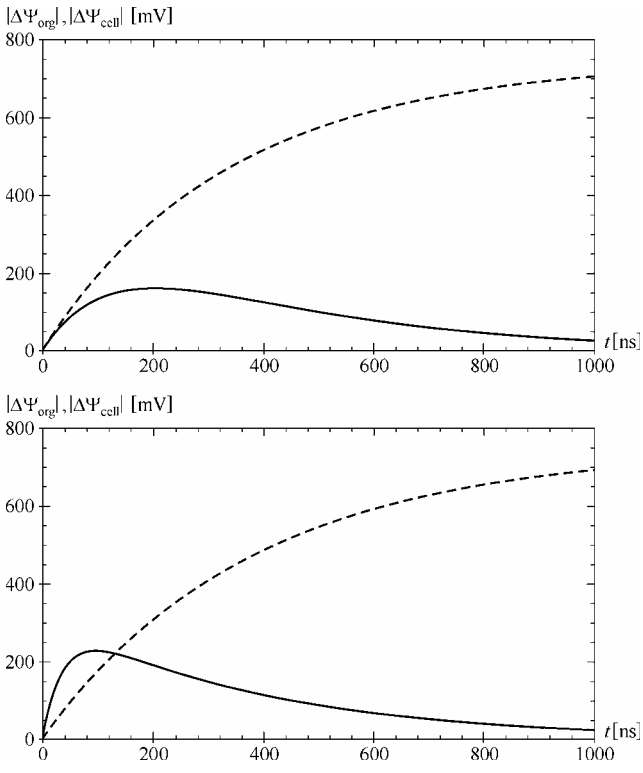

Figure 5

The FD analysis (see Section 3.1) reveals that $\Delta\Psi_{org}$ can only exceed $\Delta\Psi_{cell}$ if either the cell membrane differs from the organelle membrane, or the cytosol differs from the organelle interior. From the results shown in Figure 5 it transpires that moreover, this can only occur during the first hundreds of nanoseconds after the onset of the pulse. Thus only pulse durations shorter than this can allow for selective targeting of intracellular structures, while with longer pulses the cell plasma membrane is always affected to a larger extent.

Further time courses of voltages induced by trapezoidal nsPEFs can be found in (35b).

3.3 Resting voltage on organelle membranes

It was already mentioned in Section 1 that the resting voltage normally present on the mitochondrial membrane is considerably larger than its counterpart on the cell plasma membrane. On each membrane, the voltage induced by an external electric field superimposes to the resting voltage, due to which the total voltage can be higher on a mitochondrial membrane than on the cell plasma membrane even with $\Delta\Psi_{org}$ equal to, or slightly below $\Delta\Psi_{cell}$. As the membrane voltages required for electroporation by nsPEF appear to be in the range of volts (28, 29), it is disputable whether a high resting voltage on an organelle membrane can alone be decisive in making this organelle the primary target of the field. Still, it could be among the reasons why mitochondria are the primary target of many observed effects of the nsPEF. This possibility has been discussed previously by Weaver (56).

3.4 Curvature of organelle membranes

Some theoretical studies suggest that the threshold value of membrane voltage required for electroporation can decrease if the membrane curvature is sufficiently high (54, 41). As the organelles are significantly smaller than the cell, the typical curvatures found in organelle membranes are generally also higher than those in the cell membrane. Due to this, it is conceivable that even with $\Delta\Psi_{org}$ somewhat lower than $\Delta\Psi_{cell}$, electroporation could affect an organelle membrane, but leave the cell membrane intact.

3.5 Voltage-gated channels in organelle membranes

This paper is mainly concerned with the conditions that would allow for electroporation of the organelle membranes, but for completeness it should be noted that some effects caused by nsPEF could also be explained without involving electroporation. Weaver (56) proposed that the membrane voltage induced on the inner mitochondrial membrane could open the mitochondrial permeability transition pore complex (MPTP). As this molecule is voltage sensitive (45, 44) and involved in the induction of apoptosis (20), apoptosis could in this manner be induced also without electroporation of the mitochondrial membranes.

4. CONCLUSIONS

In Sections 3.1 and 3.2, we investigated the circumstances under which the voltage induced by the external field on an organelle membrane can exceed its counterpart on the cell plasma membrane. The results imply that this can not occur if the electric properties of the organelle interior are very similar to those of the cytosol, and if the organelle membrane is very similar to cell membrane. On an organelle membrane considerably thicker than the cell membrane, as in mitochondria, the induced voltage can be higher even under these circumstances, but the electric field in the organelle membrane will remain below the electric field in the cell membrane, making electroporation of the former but not the latter unlikely.

However, if the organelle interior is more electrically conductive than the cytosol, or if the organelle membrane has a detectably lower dielectric permittivity than the cell membrane, the situation changes. For exposures to sinusoidal fields in the MHz range, and for the first tens of nanoseconds of exposures to pulsed fields, the voltage induced on the organelle membrane can easily exceed its counterpart on the cell membrane, as illustrated in Figure 4 and in bottom panels of Figures 5 and 6. These findings are of course only relevant provided that the assumed differences between the organelle interior and the cytosol, or between the cell and organelle membranes are realistic. Higher ionic concentrations in the interior of some organelles could result in higher conductivity of this region with respect to the cytosol, which appears to be a realistic assumption at least in the case of potassium ions in the mitochondria. Experimental estimates obtained by dielectric spectroscopy for the mitochondria (4) and the nucleus (5, 12) also corroborate that the differences between the electric conductivities of the organelle interiors and the cytosol can be considerable, and suggest that organelle membranes can also differ significantly from the cell plasma membrane in their dielectric permittivities.

Finally, as discussed in Sections 3.3, 3.4, and 3.5, there are at least three additional factors that could lead to an organelle membrane being electroporated but the cell membrane left intact: high resting voltage on the organelle membrane, high curvature of the organelle, and voltage sensitivity of certain proteins in the organelle membrane. The first and the third of these factors could also contribute to the explanation why particularly mitochondria often appear to be the primary targets of nsPEF.

References

1. Alberts, B., et al. 1994. *Molecular Biology of the Cell (3rd ed.)*. Garland Publishing, New York.
2. Arfken, G. B., et al. 1995. *Mathematical Methods for Physicists (4th ed.)*. Academic Press, San Diego.
3. Arnold, W. M., et al. 1987. *Biochim. Biophys. Acta.* 905:454–464.
4. Asami, K., and A. Irimajiri. 1984. *Biochim. Biophys. Acta.* 778:570–578.
5. Asami, K., et al. 1989. *Biochim. Biophys. Acta.* 1010:49–55.
6. Beebe, S. J., et al. 2002. *IEEE Trans. Plasma Sci.* 30:286–292.
7. Beebe, S. J., et al. 2003. *DNA Cell Biol.* 22:785–796.
8. Beebe, S. J., et al. 2003. *FASEB J.* 17:1493–1495.
9. Büchner, R., et al. 1999. *J. Phys. Chem. A.* 103:1–9.
10. Chen, N., et al. 2004. *Biochem. Biophys. Res. Commun.* 317:421–427.
11. Deng, J., et al. 2003. *Biophys. J.* 84:2709–2714.
12. Ermolina, I., et al. 2001. *IEEE Trans. Dielect. Elect. Insul.* 8:253–261.
13. Foster, K. R. 2000. *IEEE Trans. Plasma Sci.* 28:15–23.
14. Fröhlich, H. 1958. *Theory of Dielectrics (2nd ed.)*. Oxford University Press, Oxford.
15. Gascoyne, P. R. C., et al. 1993. *Biochim. Biophys. Acta.* 1149:119–126.
16. Gimsa, J., and D. Wachner. 2001. *Biophys. J.* 81:1888–1896.
17. Golzio, M., et al. 2004. *Methods.* 33:126–135.
18. Grosse, C., and H. P. Schwan. 1992. *Biophys. J.* 63:1632–1642.
19. Hall, E. H., et al. 2005. *DNA Cell Biol.* 24:283–291.
20. Halestrap, A. P., et al. 2002. *Biochimie.* 84:153–166.
21. Harris, C. M., and D. B. Kell. 1983. *Bioelectrochem. Bioenerg.* 11:15–28.
22. Heller, R., et al. 1999. *Adv. Drug. Deliv. Rev.* 35:119–129.
23. Hewitt, E., and R. E. Hewitt. 1979. *Arch. Hist. Exact Sci.* 21:129–160.
24. Hibino, M., et al. 1991. *Biophys. J.* 59:209–220.
25. Hibino, M., et al. 1993. *Biophys. J.* 64:1789–1800.
26. Hölzel, R., and I. Lamprecht. 1992. *Biochim. Biophys. Acta.* 1104:195–200.
27. Hu, X., et al. 1990. *Biochim. Biophys. Acta.* 1021:191–200.
28. Joshi, R. P., et al. 2001. *Phys. Rev. E.* 64:011913.
29. Joshi, R. P., et al. 2004. *Phys. Rev. E.* 69:051901.
30. Klösgen, B., et al. 1996. *Biophys. J.* 71:3251–3260.
31. Kotnik, T., et al. 1997. *Bioelectrochem. Bioenerg.* 43:285–291.
32. Kotnik, T., et al. 1998. *Bioelectrochem. Bioenerg.* 45:3–16.
33. Kotnik, T., and D. Miklavčič. 2000. *IEEE Trans. Biomed. Eng.* 47:1074–1081.
34. Kotnik, T., and D. Miklavčič. 2000. *Bioelectromagnetics.* 21:385–394.
35. Kotnik, T., and D. Miklavčič. 2000. *Biophys. J.* 79:670–679.

35b. Kotnik, T., and D. Miklavčič. 2006. *Biophys. J.* 90:480–491.

36. Lemeshko, S. V., and V. V. Lemeshko. 2000. *Biophys. J.* 79:2785-2800.
37. Lodish, H., et al. 1999. *Molecular Cell Biology (4th ed.)*. W. H. Freeman, New York.
38. Marszalek, P., et al. 1990. *Biophys. J.* 58:1053–1058.
39. Morse, P. M., and H. Feshbach. 1953. *Methods of Theoretical Physics*. McGraw-Hill, New York.
40. Neumann, E., et al. 1989. *Electroporation and Electrofusion in Cell Biology*. Plenum Press, New York.
41. Neumann, E., et al. 1999. *Bioelectrochem. Bioenerg.* 48:3–16.
42. Nörtemann, K., et al. 1997. *J. Phys. Chem. A.* 101:6864–6869.
43. Oberhettinger, F., and L. Badii. 1973. *Tables of Laplace transforms*. Springer, Berlin.
44. Palmeira, C. M., and K. B. Wallace. 1997. *Toxicol. Appl. Pharmacol.* 143:338–347.
45. Petronilli, V., et al. 1994. *Biochim. Biophys. Acta.* 1187:255–259.
46. Schoenbach, K. H., et al. 2001. *Bioelectromagnetics.* 22:440–448.
47. Serša, G., et al. 2003. *Cancer. Ther.* 1:133–142.
48. Stratton, J. A. 1941. *Electromagnetic Theory*. McGraw-Hill, New York.
49. Sunderman, F. W. 1945. *Am. J. Clin. Path.* 15:219–222.
50. Tarek, M. 2005. *Biophys. J.* 88:4045-4053.
51. Tekle, E, et al. 2005. *Biophys. J.* 89:274–284.
52. Tieleman, D. P., et al. 2003. *J. Am. Chem. Soc.* 125:6382–6383.
53. Tieleman, D. P. 2004. *BMC Biochemistry* 5:10.
54. Tönsing, K., et al. 1997. *Eur. Biophys J.* 26:307–318.
55. Tsong, T. Y. 1991. *Biophys. J.* 60:297–306.
56. Weaver, J. C. 2003. *IEEE Trans. Diel. El. Insul.* 10:754–768.
57. Weaver, J. C, and Y. A. Chizmadzhev. 1996. *Bioelectrochem. Bioenerg.* 41:135–160.
58. White, J. A., et al. 2004. *J. Biol. Chem.* 279:22964–22972.

TREATMENT PLANNING OF RADIOFREQUENCY ABLATION

T. SAMARAS

ARISTOTLE UNIVERSITY OF THESSALONIKI
RADIOCOMMUNICATIONS LABORATORY, DEPT. OF PHYSICS,
GR-54124 THESSALONIKI, GREECE

ABSTRACT

The treatment of cancer with the use of radiofrequency ablation under imaging guidance has attracted a lot of attention among oncologists in the recent years, as it is a minimally invasive technique of rare complications to the patients. In this work we present the results of treatment planning for the case of liver cancer treated with one electrode operating at 450kHz. We use the finite element method (FEM), implemented in a commercially available software package, to solve the combined electromagnetic and thermal problems. We explore the effect of voltage excitation, as well as of the temperature-dependent conductivity, on the resulting maximum temperature in the tissue. The influence of the blood perfusion term is also taken into consideration in our analysis. The results show that several parameters play a role in the production of a realistic treatment planning and in the investigation of the efficiency of this oncotherapeutic modality, but with the use of the necessary computer resources it is possible to study most of its aspects.

I. INTRODUCTION

The removal of tumor ('tumor ablation') is the destruction of cancerous tissue in an effort to cure the disease. It is clinically applied mainly to non-resectable tumors with the use of either thermal or chemical methods (e.g. ethanol). The thermal methods include the cooling of tissue to temperatures below -40^{o}C (cryoablation) or its heating to temperatures higher than 50^{o}C (thermoablation). The latter is achieved with electromagnetic radiation (RF or microwave), ultrasound and laser. More details on the techniques and the physical principles of tissue ablation can be found in [1].

Apart from liver tumors, where it is considered an established treatment modality, thermoablation is finding an increasing application in other sites like kidney, lung and bone. Most commercially available devices operate with the radiofrequency (RF) current which flows between an electrode (inserted into the tumor under the guidance of medical imaging) and a dispersive electrode (grounding pad), which is placed distally on the body surface of the patient and serves as the return path for the current. The heating of the tissues is larger where the current density is higher, i.e. next to the electrode in the tumor. The temperature can exceed 100^{o}C, although cell death due to coagulative necrosis occurs already above 50^{o}C. However, high tissue temperature may result in tissue carbonization (charring), which is an unwanted situation, not only because it is an irreversible effect, but mainly because it leads to an electrically insulating area which prevents the current from flowing.

There are currently several limitations in tumor thermoablation. Imaging techniques should be improved to allow better guidance of the electrode inside the tumor and evaluation of the thermal lesion. New techniques must be employed (e.g. multiple electrode systems) in order to increase the coagulative zones, instead of inserting a single electrode more than once in the tumor. Finally, the treatment efficiency is compromised next to large blood vessels, which advect a large portion of the heat developed in the target area, leading to lower than expected temperatures [2]. Such shortcomings make the introduction of treatment planning an important factor in securing quality assurance of the treatment and maximizing its outcome.

In this work we will present some of the numerical aspects and problems in the treatment planning of RF ablation with a single electrode inserted inside the liver.

II. METHODOLOGY

Formulation

At first look treatment planning of RF ablation appears like a two-step procedure. In the frequency range of 450–550 kHz, where most probes operate, the wavelength of the electromagnetic field inside the tissue is several orders of magnitude larger than the size of the ablation electrodes, i.e. we deal with a quasi-static problem. At these frequencies conduction current is more important in living tissues (due to electrolyte ions present in them) than displacement current. Therefore, in order to solve the electrical problem it is necessary to use Laplace's equation,

$$\nabla(\sigma \nabla V) = 0 \tag{1}$$

where σ is tissue conductivity (S/m) and V is the electric potential (V). It is assumed that no current sources at the same frequency like the externally imposed current are present inside the human body. Having calculated the electric field, the power per unit mass (W/kg) dissipated in the tissues, i.e. the Specific Absorption Rate (SAR), evaluates to

$$SAR = \frac{\sigma}{\rho}|E|^2 = \frac{1}{\sigma \rho}|J|^2 \tag{2}$$

where ρ is the mass density (kg/m^3) and J the current density (A/m^2). This term can be used as an input to the Bioheat Transfer Equation (BHTE) of Pennes' [3]

$$\rho c \frac{dT}{dt} = \nabla \cdot (k \nabla T) - \rho_b c_b \omega_b (T - T_b) + Q_m + Q_{RF} \tag{3}$$

where k is the thermal conductivity (W/(m K)), c is the specific heat (J/(kg K)), ω_b is the blood perfusion rate (in m^3 of blood per m^3 and per s), Q_m is the metabolic heat generation rate (W/m^3) and Q_{RF} is the volumetric heat generation rate (W/m^3) due to the RF current:

$$Q_{RF} = \rho \, SAR \tag{4}$$

The subscript b denotes 'blood'.
However, equations (1) and (3) are coupled, because electrical conductivity σ changes with temperature, i.e. the problem is non-linear and this can affect the final temperature calculated with numerical techniques [4],[5].

Numerical model
The coupled differential equations were solved numerically with the commercially available software package FEMLAB 3.1i (COMSOL AB, Stockholm, Sweeden), which implements the Finite Element Technique (FEM). The assumed electrode (probe) is shown in Figure 1. The probe had a diameter of 0.3cm and consisted of two parts. The lower tip of 2cm in length was set at a constant voltage V_0, whereas the upper part of 4cm in length was supposed to be insulated electrically. The whole probe was assumed thermally insulated, which is not far from reality for electrodes inserted in catheters.

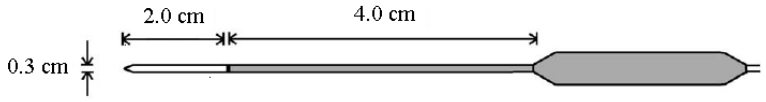

Figure 1. The electrode (probe) assumed in the numerical simulations

The probe was inserted inside a cubical volume of liver tissue with edge dimension of 12cm (Figure 2). The properties of the tissue and blood are given in Table 1. At the sides of the cube Dirichlet boundary conditions were set for both the electric and the thermal problem: The temperature was set at 37^{o}C and the voltage at 0V.

Table 1. Physical properties of model

Property	Value
Electrical conductivity of liver (37^{o}C)	0.143 S/m
Thermal conductivity of liver	0.502 W/(m K)
Specific heat of liver	3600 J/(kg K)
Mass density of liver	1060 kg/m^3
Specific heat of blood	4180 J/(kg K)
Mass density of blood	1000 kg/m^3
Blood perfusion rate	0.0064 1/s
Blood temperature	37^{o}C

The variation of electrical conductivity with temperature was adopted from [4] and can be summarized in

$$\sigma(T) = 0.1151 - [0.00226 \times (25 - T)] + [0.00000925 \times (25 - T)^2] \tag{5}$$

where T is the tissue temperature in ^{o}C. The conductivity and the temperature were sampled every 10 or 30s during the whole simulation of a treatment lasting 15min.

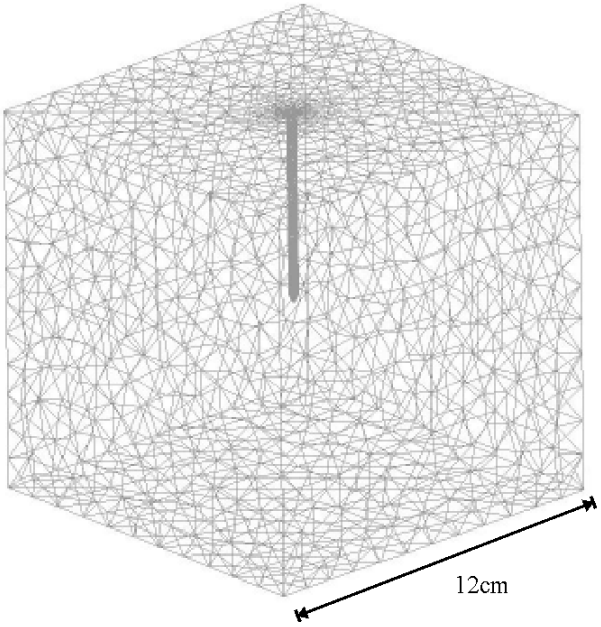

Figure 2. FEM model used for solving the problem

IV. RESULTS

In order to show the differences between the linear and the non-linear problem, the equations were solved both for constant electrical conductivity of liver and for temperature dependent according to equation (5). The shape of the distribution of the electric potential inside the computational domain does not change very much in the two cases (Figure 3), nor does the distribution of the final temperature (Figure 4).
However, the maximum temperature (calculated at the tip of the probe) is different in the two cases for the same voltage V_0 applied. Figure 5 shows that when the conductivity does not vary with temperature the maximum temperature is underestimated; this is especially true for higher probe voltages V_0. It is also clear from Figure 5 that the maximum temperature does not depend linearly on V_0.

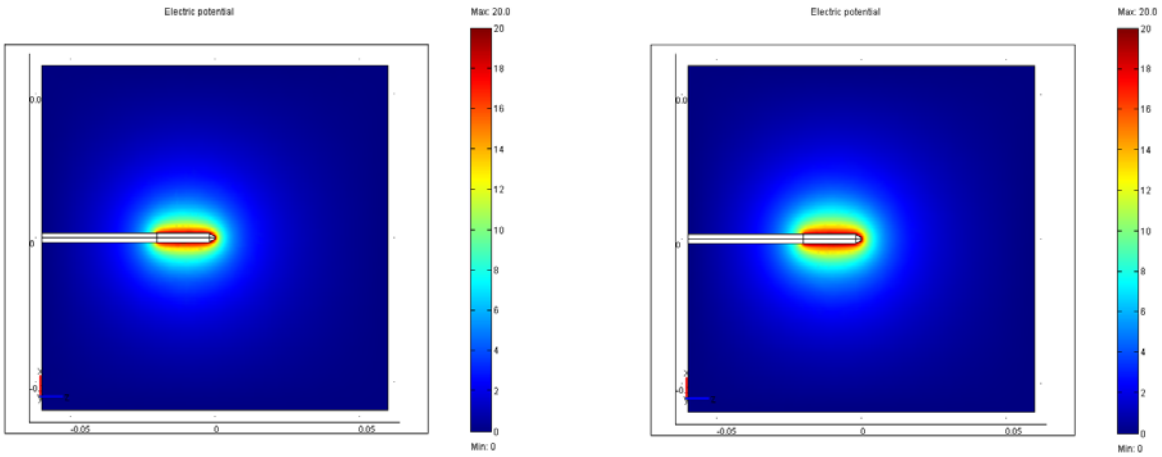

(a) (b)

Figure 3. Distribution of electric potential in the tissue for (a) constant and (b) temperature dependent electrical conductivity

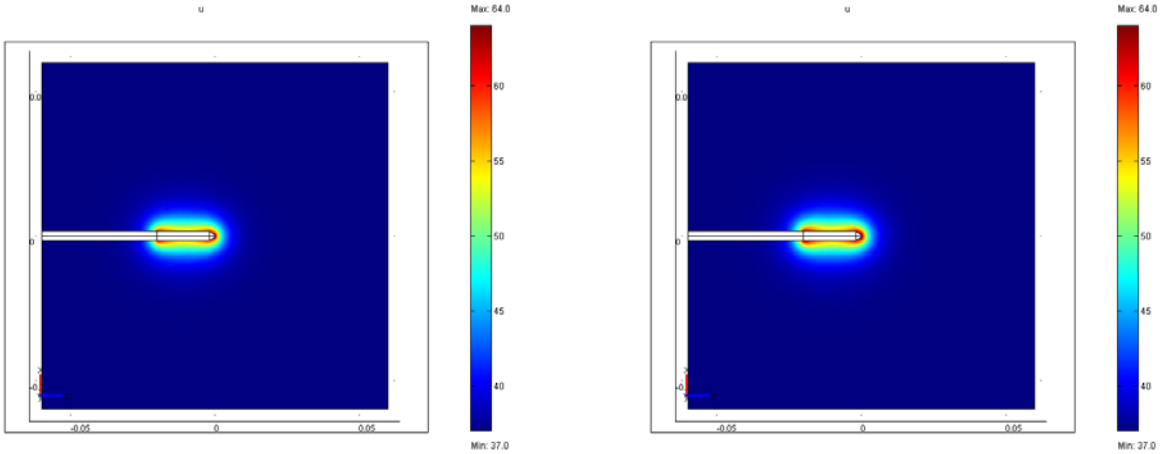

(a) (b)

Figure 4. Final (after 15min) temperature distribution in the tissue for (a) constant and (b) temperature dependent electrical conductivity

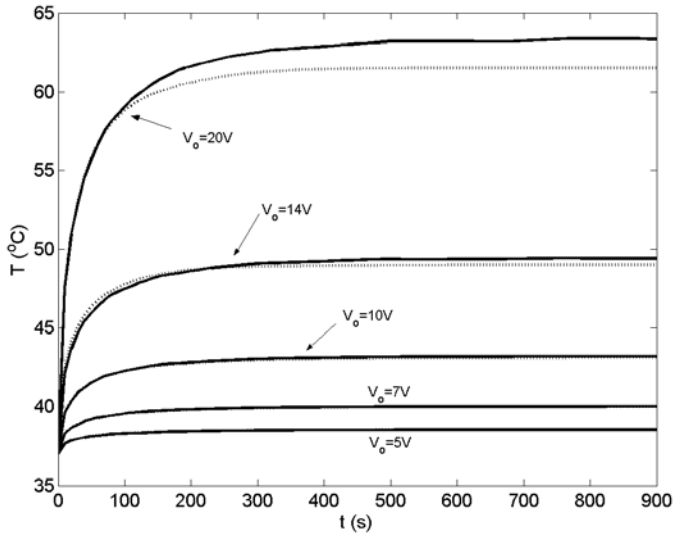

Figure 5. Time course of the temperature at the probe's tip for constant (dashed lines) and temperature dependent (solid lines) electrical conductivity at various source voltages

REFERENCES

[1] D. Haemmerich, "Tissue Ablation", in *Encyclopedia of Medical Devices and Instrumentation*, (John G. Webster, ed.), 2nd Edition, vol. 6, pp. 362-379, John Wiley & Sons, Hoboken, New Jersey, 2006

[2] S. Tungjitkusolmun, S. T. Staelin, D. Haemmerich, Tsai Jang-Zern, Cao Hong, J. G. Webster, F. T. Lee Jr., D. M. Mahvi, V.R. Vorperian, "Three-dimensional finite-element analyses for radio-frequency hepatic tumor ablation", *IEEE Trans. Biomed. Eng.*, vol. 49, no. 1, pp. 3-9, 2002

[3] H. H. Pennes, "Analysis of tissue and arterial blood temperatures in the resting human forearm", *J. Appl. Physiol.*, vol. 1, pp. 93-122, 1948

[4] I. Chang, "Finite Element analysis of hepatic radiofrequency ablation probes using temperature-dependent electrical conductivity", *Biomedical Engineering Online*, vol. 2, 12, 2003

[5] I. A. Chang and U. D. Nguyen, "Thermal modeling of lesion growth with radiofrequency ablation devices", *Biomedical Engineering Online*, vol. 3, 27, 2004

TRANSMIT POWER CONTROL IN MOBILE COMMUNICATIONS AND ITS POTENTIAL FOR A REDUCTION OF EMF EXPOSURE

MICHAEL A. BALDAUF, SANDRA KNÖRZER, THORSTEN KAYSER, AND WERNER WIESBECK

INSTITUT FÜR HÖCHSTFREQUENZTECHNIK UND ELEKTRONIK, UNIVERSITÄT KARLSRUHE (TH), KAISERSTR. 12, 76131 KARLSRUHE, GERMANY

Abstract

The application of transmit power control in mobile communications allows a decrease of the maximum output power to a lower level per link. Technical reasons to utilize transmit power control are the reduction of co-channel interference and an increase in the battery lifetime of the mobile terminal. Considering the well known COST-Hata wave propagation model the steady state transmit powers for base and mobile stations in typical scenarios are calculated. It is shown that for GSM base stations the optional transmit power control has only a small impact onto the human exposure to electromagnetic fields. In contrast to this the transmit power of a GSM mobile phone can be lowered clearly compared to the maximum output power, when applying transmit power control. For UMTS mobile phones there is even a higher potential for an exposure reduction.

Introduction

In mobile radio networks there are basically two sources of electromagnetic fields (EMF). On the one hand there is a fixed base station which transmits a signal with a constant level at all times to allow the mobile station to identify it. The more users there are in a cell the more transmit power is needed to serve the customers with user specific information. On the other hand, there is a mobile station which transmits generally only when the user actively uses the mobile phone e.g. by having a voice connection.

For the far field exposure due to base stations the exposure can be conveniently described by the electric field strength (E) or the power density (S). For the human head held close to a mobile phone there is a strongly varying near field over different tissue types. Therefore, a determination of the specific absorption rate (SAR) is necessary. The exposures which encounter in real life due to base and mobile stations are very different compared to the limit values. Safety distances to base stations based on the ICNIRP Guidelines [1] are typically just a few meters [2]. Thus, the exposures due to base stations are usually well below the limits. However, concerning the exposure to mobile phones some phones are quite close to the SAR limit [3]. In conformance tests the mobile phone transmits with it's maximum transmit power to simulate worst case conditions [4].

The possibility of transmit power control (TPC) allows a reduction of the transmit power. Hence, TPC is a means to reduce interference in mobile cellular networks. Additionally there is a remarkable increase in battery lifetime for mobile terminals. In 3rd generation's UMTS networks TPC at the mobile terminal is a must in order to allow a reception of all users with the wanted signal to noise plus interference ratio (SNIR) at the base station. This paper deals with the potential of the exposure reduction of TPC.

Network layout

In the simulations a simplified hexagonal network layout with three sector antennas in each hexagon is considered. Base stations are placed at the centers of the hexagons (cf. Fig. 1). There are two rings of hexagons surrounding a center hexagon to take the exposure of surrounding cells into account. The technical configuration is the same for all base stations. The exposure is evaluated for the center hexagon. Therefore, this hexagon is overlayed with a regular grid of about 100 000 equidistant points.

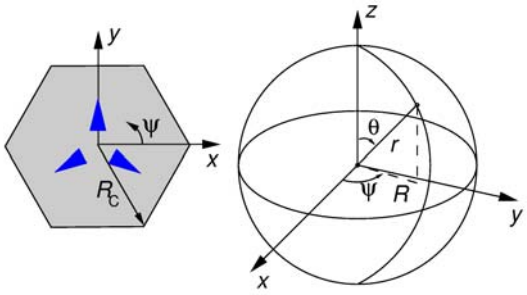

Fig. 1: Left: Hexagonal cell showing the orientation of the sector antennas (arrows). Right: Convention for angles in a spherical coordinate system.

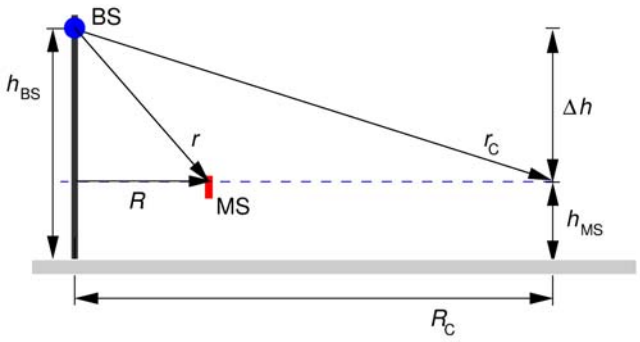

Fig. 2: Exposure scenario.

Exposure Scenario

Fig. 2 shows the considered exposure scenario in a side view. All base stations (BS) are mounted at a height h_{BS}, the mobile stations (MS) are at a height h_{MS} = 1.5 m. The horizontal separation of the MS to the BS is given by the distance R. The variable R_C denotes the cell radius, which is defined in Fig. 1. In the simulations cell radii of R_C = 1 km and R_C = 6.3 km are regarded. Since for smaller cell sizes the antennas are typically mounted at a lower height the antenna heights h_{BS} of the BS are chosen to be dependent on the cell radius R_C. For the smaller cell radius (R_C = 1 km) the antenna height h_{BS} = 12.6 m for the larger cell radius (R_C = 6.3 km) h_{BS} = 41 m.

At the BS there are three Kathrein 742212 antennas [5] mounted with $\psi = \{90°, 210°, 330°\}$ to cover three sectors (cf. Fig. 1). The pattern of the antenna with a gain G_{BS} = 18 dBi is shown in Fig. 3. For the simulation the pattern is smoothed and limited to take an increased field strength due to multipath propagation into account. To concentrate more energy on the ground a declination of the antenna pattern can be done electrically. The considered sector antennas are tilted down slightly. The downtilt angle is chosen in such a manner that the direction where the antenna has its half power beamwidth above the main beam direction is directed at the height of a MS's antenna at the cell radius R_C.

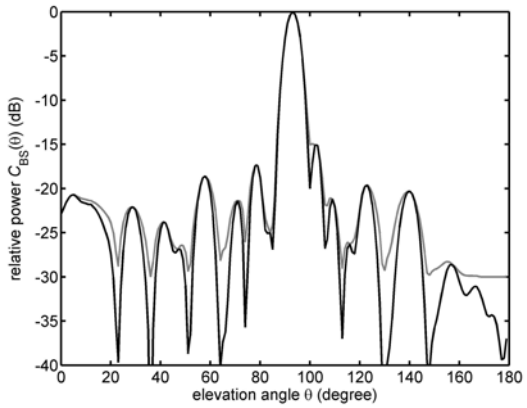

Fig. 3: Elevation pattern of Kathrein's 742212 with 3° electrical downtilt. Shown is the pattern $C_{BS}(\theta)$ for one polarization of the X-polarized antenna. Dark line: unmodified manufacturer data; light line: smoothed and limited pattern data.

Emission versus Exposure

A measure of the biological relevance of electromagnetic fields is the exposure. Transmitters are often classified by their transmit power (emission). In situations where there is no change in the loss between transmitter and the

human body the change in transmit power is directly proportional to the change in exposure. An example is a mobile station held close to the head. As long as the terminal is not moved the exposure is proportional to the transmit power. However, moving e.g. the mobile terminal further away from the head will typically lead to a lower absorption loss of the head. As a result of this, the transmit power can be lowered. Furthermore, the distance to the head is increased. Both facts will lead in sum to an exposure that is lower compared to the situation where the mobile phone is closer to the human head. However, the change in exposure is no longer directly proportional to the change in emission.

Considering two cell radii R_C with different BS antenna heights h_{BS} yields different path losses in the scenarios. Since the exposure is in the far field it can be expressed as power density S. Comparing the power density S allows a direct comparison of the exposure. In contrast to this, for the human exposure due to the mobile phone a constant position of the phone to the head will be assumed. Therefore, the change in exposure is then directly proportional to the change in transmit power.

Path loss model

In order to derive the exposure a knowledge of the path loss L between all sources of EMF and the points that are defined for an evaluation is necessary. The path loss model chosen for the simulations is the well known COST-Hata model [6]. The model takes a correction term for open areas into account [7]. For this reason, the building development can be described by a parameter b. This parameter ranges from $b = 0...1$, $b = 0$ corresponds to an open area whereas $b = 1$ corresponds to an urban area. For more information about the parameter b see [8]. The uplink and downlink frequencies are chosen to be $f = 2$ GHz. A deviation between uplink and downlink frequency is not considered since the frequency difference is usually small in prevalent frequency division duplex (FDD) systems, and therefore has only a negligible influence on the path loss. The isotropic path loss L_i according to the COST-Hata model is given by:

$$\frac{L_i}{\mathrm{dB}} = 158.16 - 13.82 \log\left(\frac{h_{BS}}{\mathrm{m}}\right) + \left(44.9 - 6.55 \log\left(\frac{h_{BS}}{\mathrm{m}}\right)\right) \log\left(\frac{R}{\mathrm{km}}\right) + 32.52\, b \tag{1}$$

where use of the fixed MS antenna height and frequency has been made. Formula (1) gives the path loss for isotropic antennas, therefore the name isotropic path loss L_i. Using directional antennas will change the path loss to:

$$\frac{L}{\mathrm{dB}} = \frac{L_i}{\mathrm{dB}} + \frac{G_{BS} C_{BS}^2(\theta_{BS}, \psi_{BS})}{\mathrm{dB}} + \frac{G_{MS} C_{MS}^2(\theta_{MS}, \psi_{MS})}{\mathrm{dB}} \tag{2}$$

Herein G_{BS} and G_{MS} are the gains of the base and mobile stations, respectively. The gains have to be weighted by the square of the antenna patterns C^2. Since the patterns depend on the viewing angle different indices for the angles θ and ψ are used for the base and mobile station. Depending on the gains G and patterns C the path loss L can be larger or smaller than the isotropic path loss L_i. Typically the base station antennas are directed in order to radiate much energy into directions were the isotropic path loss L_i is large. For the antenna of the mobile station an isotropic radiator is assumed, therefore, the last term in (2) vanishes for the calculation of the path loss L.

For distances close to the base station (1) might yield path losses which are smaller than for a free space propagation (unobstructed line of sight). If this happens the path loss in the model is replaced by the value of the path loss for free space condition.

Path Loss in a Cell

Four cell types were considered for an evaluation of the path loss L in a cell. These are:

- a large urban cell
- a small urban cell
- a large rural cell
- a small rural cell

The term “large” refers to a cell size of $R_C = 6.3$ km, whereas the term “small” refers to a cell size of $R_C = 1$ km. For the urban cell the parameter b in (1) is chosen to be $b = 0.8$ for the rural cell $b = 0.2$. Figs. 4-7 show the distribution of the path losses in the four types of regions for different antenna types. Fig. 4 shows the probability density function (PDF) of the path loss according to (1) with $b = 0.2$. Figs. 5-7 include a log-normal fading with a standard deviation $\sigma = 7$ dB. The left hand sides (LHS) of the figures show the PDF for the larger cell sizes whereas the right hand sides (RHS) show the PDF for the smaller cell sizes. Whereas Figs. 4 and 5 refer to an isotropic antenna at the BS the Figs. 6 and 7 regard the Kathrein 742212 as BS antenna. Comparing

Figs. 4 and 5 shows that considering a log-normal fading shows broader distribution of the PDF. The installation of sector antennas with a high gain will allow a significant reduction of the path loss (compare Figs. 5 and 6). Increasing the building development would yield higher path losses (cf. Fig. 7).

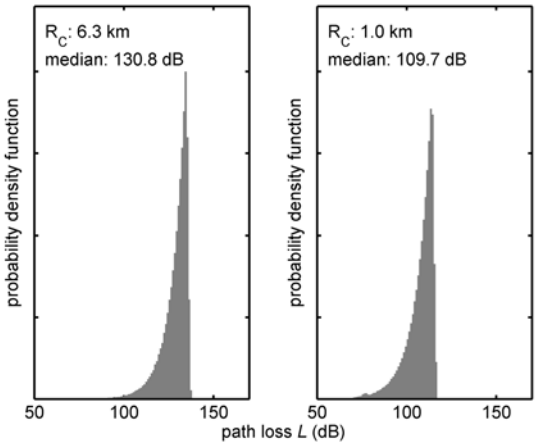

Fig. 4: PDF of the isotropic path loss in a rural region. Parameters: $b = 0.2$. LHS: $R_C = 6.3$ km, RHS: $R_C = 1$ km. No log-normal fading.

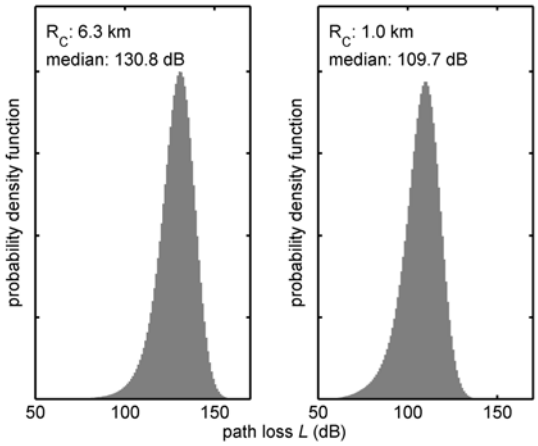

Fig. 5: PDF of the isotropic path loss in a rural region. Parameters: $b = 0.2$. LHS: $R_C = 6.3$ km, RHS: $R_C = 1$ km. Log-normal fading ($\sigma = 7$ dB).

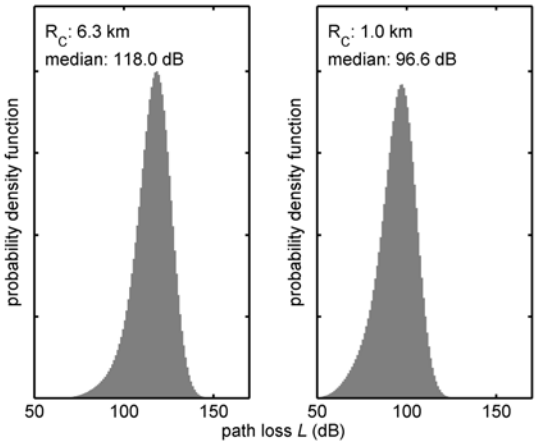

Fig. 6: PDF of the path loss for the considered directional antenna in a rural region. Parameters: $b = 0.2$. LHS: $R_C = 6.3$ km, RHS: $R_C = 1$ km. Log-normal fading ($\sigma = 7$ dB).

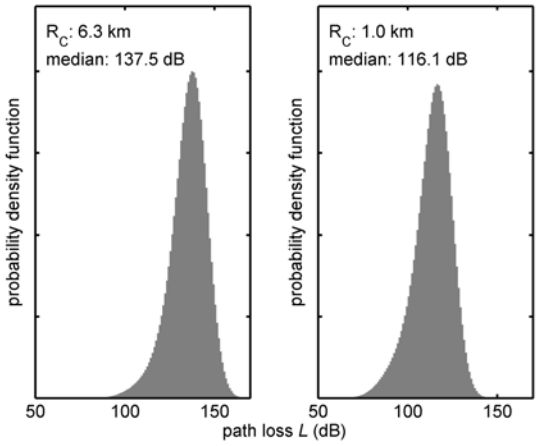

Fig. 7: PDF of the path loss for the considered directional antenna in an urban region. Parameters: $b = 0.8$. LHS: $R_C = 6.3$ km, RHS: $R_C = 1$ km. Log-normal fading ($\sigma = 7$ dB).

Link budget

To decode a signal correctly a minimum required signal quality must be reached. This quality can be given in general as a SNIR (signal-to-noise-plus-interference-ratio). The noise is thermal noise and can't be reduced below a certain value which is dependent on the system temperature and bandwidth. For CDMA systems (e.g. UMTS) where a lot of users share the same frequency at the same time interference has to be taken into account. Interference can be interpreted as noise and vice versa.

GSM systems use frequency division multiple access (FDMA) and time division multiple access (TDMA) to separate users. Assuming sufficient carriers are available the effect of interference needs not to be considered. To determine the required transmit powers at the base and mobile stations it is sufficient to regard the necessary received power P_R per user at the receiving end in combination with the path loss. P_R is independent of the network load and given by the transmit power P_T minus the path loss L between the transmitter and the receiver. Knowing the path loss the minimum required P_T can be determined.

For the determination of the maximum path loss L and therefore also for the mandatory channel no log-normal fading is considered. The transmit power of the base and mobile stations are increased by 20 dB to account for additional propagation losses as the absorption of energy in the human body and effects of small-scale fading. For simplicity fading is not explicitly considered in the determination of the transmit powers. For the mobile stations fading is considered in a later step.

The transmit power of the BS is labeled by $P_{T,BS}$ and the transmit power of the MS by $P_{T,MS}$.

TPC at the BS

If there is no TPC implemented the PDF of the received signal has the same shape as the path loss. Power control can be used only for dedicated channels which don't have to be received at all MS.

The channel configuration of the considered GSM system is shown in Fig. 8. Shown are two carriers which are allocated to different frequencies around $f = 2$ GHz. On the LHS there is the BCCH carrier. Each of the eight bins corresponds to one time slot. Via this carrier information about the cell is transmitted in one slot. The seven other time slots on this carrier are reserved for additional signaling purposes or e.g. SMS services. If the information of these slots is not needed they are filled up with dummy bits and transmitted with full power. This carrier can't be power controlled. Active users having a voice connection are put on another carrier on which power control is available. The transmit power in a power controlled slot is decreased by ΔPC compared to the power of the BCCH carrier. The maximum power reduction which is possible is given by ΔPC_{max}. The simulations were done assuming a varying range of the parameter ΔPC_{max}.

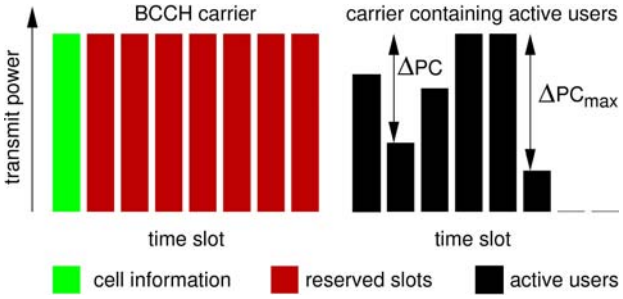

Fig. 8: Channel configuration of the considered GSM system.

In the following three different numbers of carriers N are investigated. The numbers chosen are $N = 1$, 4 and 6. In the case of $N = 1$ only the BCCH carrier is transmitting. $N = 4$ and 6 correspond to typical channel configurations. The required user densities n for these three cases are:

- $n = 0$ ($N = 1$)
- $n = 0.70$ /km^2 ($R_C = 6.3$ km, $N = 4$)
- $n = 1.16$ /km^2 ($R_C = 6.3$ km, $N = 6$)
- $n = 27.71$ /km^2 ($R_C = 1$ km, $N = 4$)
- $n = 46.18$ /km^2 ($R_C = 1$ km, $N = 6$)

Whereas in the large cell ($R_C = 6.3$ km) the considered number of carriers can be filled with small user densities much higher user densities are needed for the smaller cell size ($R_C = 1$ km).

Figs. 9-14 show the transmit power $P_{T,BS}$ per sector and the average power density S_{avg} versus the maximum possible power reduction ΔPC_{max}, respectively, for three cases. There are no results given for the case of the large urban cell. For this case the path loss would be too high for a lot of mobile stations to reach the base stations.

If there is only the mandatory BCCH carrier on air TPC would yield no power reduction since this carrier can't be power controlled ($N = 1$ in the figures). If there are active users in time slots which can be power controlled the total transmit power fed into the sector antenna can be lowered typically by just 3 to 4 dB. A higher value of ΔPC_{max} allows lower transmit powers. Choosing ΔPC_{max} larger than 10 dB shows no further positive effect in terms of transmit power reduction.

The more channels that are in use, the higher is the reduction of the transmit power when using TPC. The increase from 4 carriers to 6 carriers shows no significant effect. A change in transmit power within one configuration is directly proportional to the change in exposure (compare the figures in one row).

Furthermore, the results show that there is no one-to-one equivalence of emission (transmit power) and exposure

(power density). In the case of the rural cell the transmit power of the BS $P_{T,BS}$ in the large cell (cf. Fig. 9) is much higher than in the smaller cell (cf. Fig. 11). However, the exposures in both network configurations are almost the same (compare Figs. 10 and 12). In the small urban cell the transmit power is much higher than in the small rural cell but the exposure is higher by just a small amount. This is due to the fact that in the urban network not only the transmit power is higher but also the path loss is much higher than in the rural case.

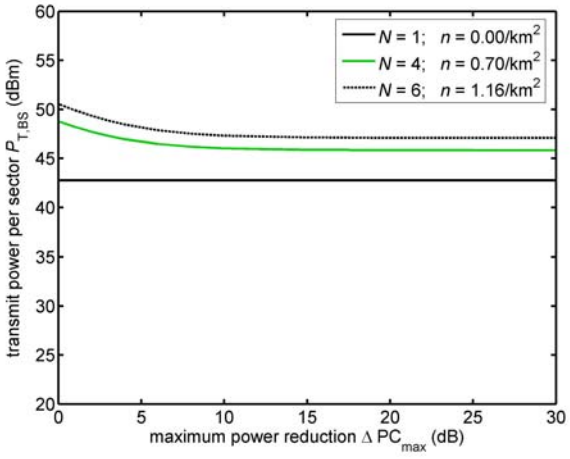

Fig. 9: Transmit power per sector versus the maximum power reduction. Parameters: R_C = 6.3 km, b = 0.2 (rural area).

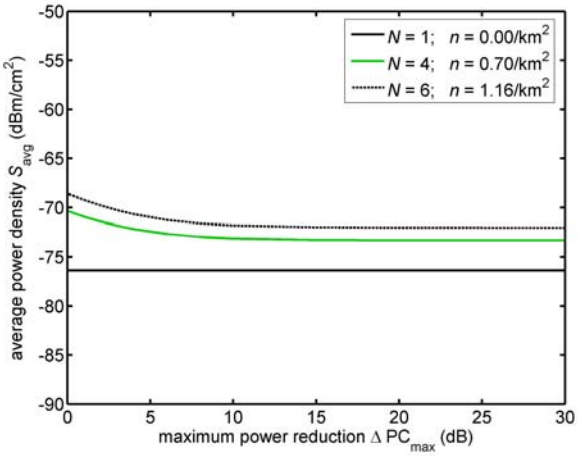

Fig. 10: Average power density versus the maximum power reduction. Parameters: R_C = 6.3 km, b = 0.2 (rural area).

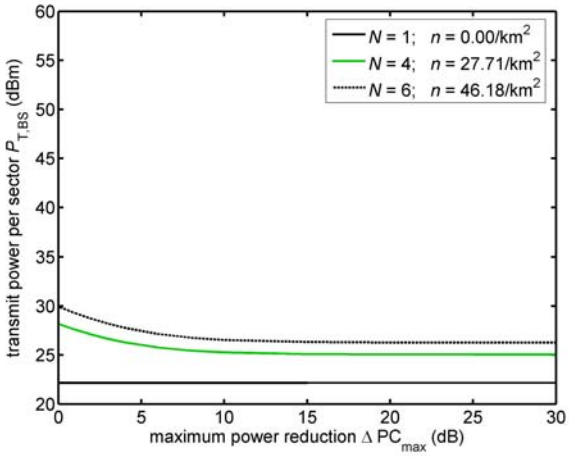

Fig. 11: Transmit power per sector versus the maximum power reduction. Parameters: R_C = 1 km, b = 0.2 (rural area).

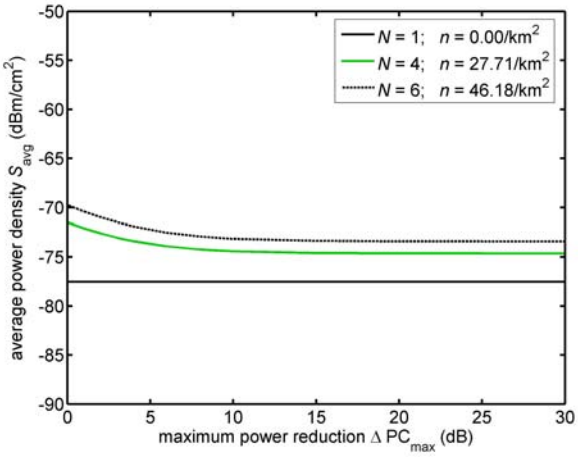

Fig. 12: Average power density versus the maximum power reduction. Parameters: R_C = 1 km, b = 0.2 (rural area).

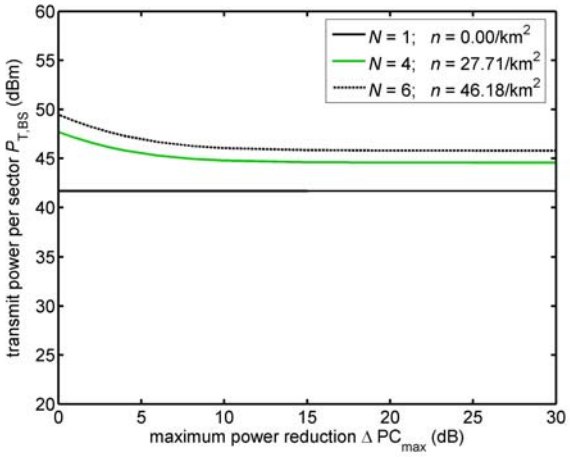

Fig. 13: Transmit power per sector versus the maximum power reduction. Parameters: R_C = 1 km, b = 0.8 (urban area).

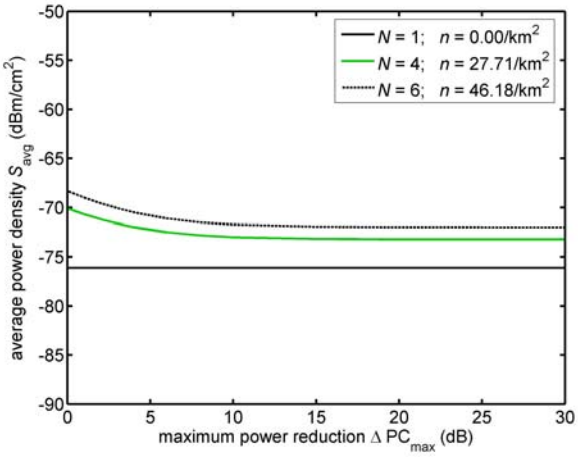

Fig. 14: Average power density versus the maximum power reduction. Parameters: R_C = 1 km, b = 0.8 (urban area).

For UMTS there are also some channels which are transmitted at all times with a constant level. As in GSM, user specific channels can be also power controlled. Simulations have shown that the results for UMTS are very similar to those shown for GSM.

TPC at the MS

The mobile station can adjust it's transmit power in a given range. For GSM 1800 mobile phones the transmit power $P_{T,MS}$ can be adjusted according to the specifications from 0 dBm to 30 dBm [9]. Fig. 15 shows the transmit power of the mobile station when there is no restriction on power control. In the large cell there are some MSs which would transmit with a very high transmit power (LHS of Fig. 15). In practice the maximum TPC is restricted to 30 dBm [9] (LHS of Fig. 16). Since 20 dB are added to the transmit powers as a safety margin there might be a quality decrease for MSs demanding a higher transmit power than possible. MSs that would need more than 50 dBm of transmit power definitely can't be served due to their restriction of the maximum output power of 30 dBm. However, this is only a relatively small part. Comparing large and small cell sizes shows that the transmit power in the smaller cell can be lowered by about 20 dB. Furthermore, comparing the Figs. 15 and 16 it is clear that the implemented lowest transmit power for MSs in GSM networks is not exposure optimized since a lot of MSs would be able to lower their transmit power below $P_{T,MS}$ = 0 dBm in small cells.

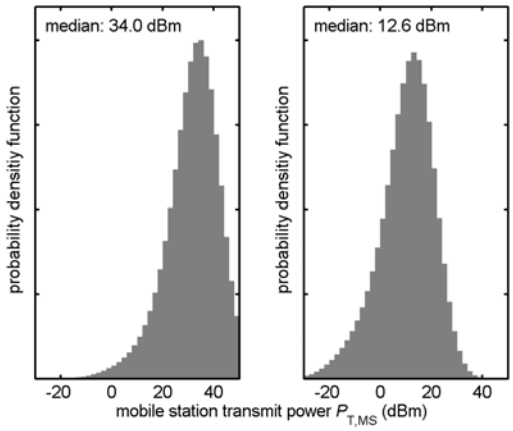

Fig. 15: PDF of the mobile station's transmit power in a rural GSM network. The transmit power can reach arbitrary values. Parameters: b = 0.2; LHS: R_C = 6.3 km, RHS: R_C = 1 km.

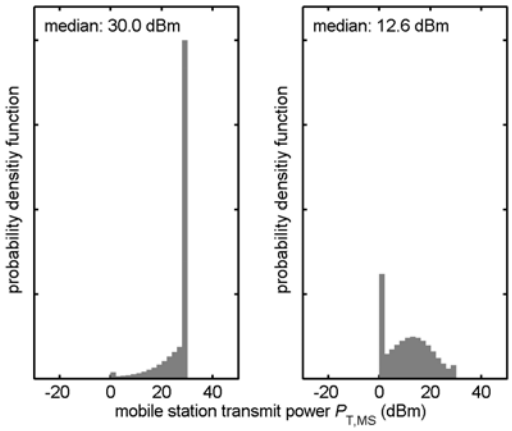

Fig. 16: PDF of the mobile station's transmit power in a rural GSM network. The transmit power can be in the range of the specified TPC. Parameters: b = 0.2; LHS: R_C = 6.3 km, RHS: R_C = 1 km.

For UMTS mobile phones the maximum output power typically used for voice transmissions is $P_{T,MS}$ = +21 dBm. Since every transmitting mobile station produces interference an optimum received power at the base station is a must. The specifications [10] demand a minimum transmit power of $P_{T,MS}$ = -50 dBm or lower. Fig. 17 shows the chosen transmit power of the MS $P_{T,MS}$ if there is no restriction of the TPC. Setting a lower limit of $P_{T,MS}$ = -50 dBm shows that a very small part of the mobile stations in the small cell is then transmitting with a higher power than necessary (cf. Fig.18). Since a transmit power that is too high would cause interference at the BS this situation should be avoided. Therefore, the range of the TPC in UMTS should be extended even further.

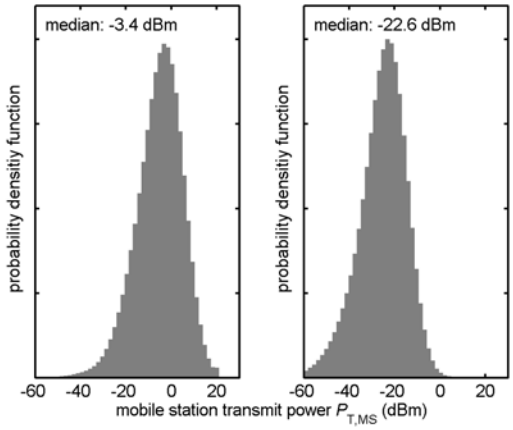

Fig. 17: PDF of the mobile station's transmit power in a rural UMTS network. The transmit power can reach arbitrary values. Parameters: b = 0.2; Channel model: Veh. A, MS speed = 3 km/h. LHS: R_C = 6.3 km, RHS: R_C = 1 km.

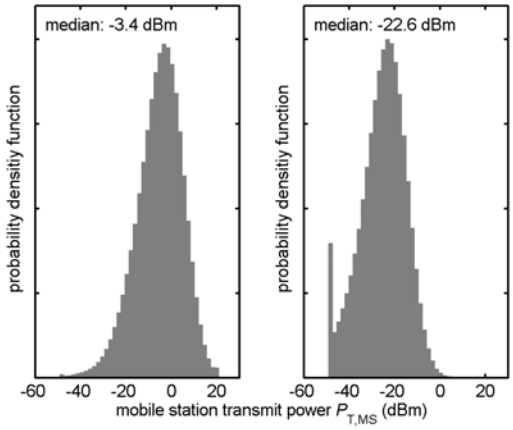

Fig. 18: PDF of the mobile station's transmit power in a rural UMTS network. The transmit power can be lowered only to -50 dBm. Parameters: b = 0.2; Channel model: Veh. A, MS speed = 3 km/h. LHS: R_C = 6.3 km, RHS: R_C = 1 km.

Comparing the results for GSM and UMTS suggests that UMTS MSs need much lower transmit powers than GSM MSs. The reason for this is that typical configurations of the MSs are assumed. Since interference due to the reception of multiple MSs at the same frequency and time is not a dominant problem at GSM BSs, network operators tend to choose transmit powers at the MS which are clearly higher than those needed at a certain instant of time. This is due to fact that the implemented power control can only react very slowly on changing propagation conditions. In contrast to this interference in UMTS networks at the BS is really a problem. Therefore, network operators have to choose the MS's transmit power as low as possible. Fast TPC at the MS helps to adjust the transmit power every 1/1500 seconds. For this reason there is no need for adding a large security factor to account for fading effects as long as the MS is moving with a low speed.

Conclusion

Interference reduction and an increase in battery lifetime are technical reasons to implement transmit power control. The reduction of the human exposure to electromagnetic fields is rather a side effect. It is shown that the decrease in exposure using power control at the base station is rather small since the base station has to transmit site specific information in a broadcast mode at all times. From an exposure point of view a maximum power decrease of 10 dB per power controlled link is sufficient. A larger power reduction will not help to decrease the exposure to electromagnetic fields. Taking advantage of transmit power control at the mobile station the transmit power and, therefore, the exposure due to the mobile phone can be lowered clearly by several orders of magnitude. Whereas the power control range of UMTS mobile phones corresponds in a very good manner to the path loss the power control range of GSM phones is clearly not exposure optimized.

References

[1] ICNIRP, “Guidelines for limiting exposure to time-varying electric, magnetic, and electromagnetic fields (up to 300 GHz)”, *Health Physics*, vol. 74, no. 4, pp. 494-522, 1998

[2] M.A. Baldauf, A. Herschlein, W. Sörgel, W. Wiesbeck, “Safety Distances in Mobile Communications”, *Proceedings of 2nd International Workshop on Biological Effects of Elektromagnetic Fields*, pp. 148-156, Rhodes, Greece, Oct. 2002

[3] http://www.mobile-phones-uk.org.uk/sar.htm

[4] *IEEE Recommended Practice for Determining the Peak Spatial-Average Specific Absorption Rate (SAR) in the Human Head from Wireless Communications Devices: Measurement Techniques*, IEEE Std. 1528-2003, Dec. 2003

[5] KATHREIN Werke KG, Available Online, www.kathrein.de

[6] COST 231, Digital mobile radio towards future generation systems, *European Commission, Directorate General XIII*, EUR 18957, 1999

[7] M. Hata, “Empirical Formula for Propagation Loss in Land Mobile Services”, *IEEE Transactions on Vehicular Technology*, vol. 29, pp. 317-325, 1980

[8] M. A. Baldauf, S. Knörzer, W. Sörgel, and W. Wiesbeck, “Cell Splitting and Exposure in GSM networks”, *13th International Conference on Telecommunications*, published on CD-ROM, Madeira, May 2006

[9] *3rd Generation Partnership Project; Technical Specification Group GSM/EDGE Radio Access Network; Radio transmission and reception (Release 1999)*, Technical Specification, 3GPP TS 05.05, 2003

[10] *3rd Generation Partnership Project; Technical Specification Group Radio Access Networks; User Equipment (UE) radio transmission and reception (FDD) (Release 4)*, 3GPP TS 25.101, 2004

ELECTRIC FIELD ANALYTICAL FORMULAS FOR SINGLE-CIRCUIT POWER LINES WITH TRIANGULAR CONDUCTORS' ARRANGEMENT

A. TZINEVRAKIS **D. TSANAKAS** **E.MIMOS**

Tsanakas@ee.upatras.gr

DEPARTMENT OF ELECTRICAL AND COMPUTER ENGINEERING
UNIVERSITY OF PATRAS
26500, RION, GREECE

Abstract
The electric field produced by electric power lines is usually calculated with the use of numerical methods. However, the analytical calculation of the electric field is preferable, because it leads to a mathematical expression, which shows the field's dependencies from all the line parameters.

Initially, a method to derive the analytical formulas of the intensity of the electric field produced by electric power lines, is presented in this paper. This method is based on the analysis of the intensity of the electric field into the sum of two multipole expansions and in the use of double complex numbers for the simplification of the mathematical expressions. Due to the asymmetry of conductors' charges, they are analyzed in their symmetrical components. Afterwards, accurate analytical formulas of the intensity of the electric field for simple circuit power lines with conductors in triangular arrangement are given, which are valid at any point in the vicinity of lines. Beyond the accurate formulas, simpler approximate formulas are presented, which give the electric field with known precision.

1 Introduction

During the last 25 years the electric and magnetic fields are considered more and more as environmental factors. The International Commission on Non–Ionizing Radiation Protection (ICNIRP) published in 1998 the guidelines [1]. In these guidelines, the limit values are 5kV/m and 100μT for the public exposure and 10kV/m and 500μT for the occupational exposure. The World Health Organization (WHO) and the European Union (E.U.) have adopted the limits of ICNIRP [2,3]. These limits are included in the national legislations of the most countries in the E.U.

In the present paper analytical formulas are developed for the calculation of the intensity of the electric field in the vicinity of single circuit power lines. Corresponding analytical formulas for the calculation of magnetic flux density were published in [4]. The analytical formulas provide the advantage of easy and precise calculation of the field intensities and of a simpler parametrical investigation for evaluating the effect of various parameters, without the use of numerical methods. Therefore, they are appropriate for the assessment of the public exposure, e.g. in the frames of epidemiological studies.

2 Calculation procedure

2.1 Electric field produced by power lines

Figure 1 shows the model of a simple circuit power line and a point of interest P for the calculation of the intensity of the electric field. It is considered that the line route is straight and that its length is very big in comparison with the distances between the conductors and the distances of conductors from the ground. The three conductors in figure 1 bring charges $\underline{Q}_1$, $\underline{Q}_2$ and $\underline{Q}_3$, which are sinusoidal varying in time, while their distances from the point P are R_1, R_2 and R_3 respectively. The intensity of electric field $\underline{\mathbf{E}}_k$ in point P, produced by a conductor k, is given by

$$\underline{\mathbf{E}}_k = \frac{\underline{Q}_k}{2\pi\varepsilon_0}\left(\frac{1}{R_k^{'2}}\mathbf{R}_k^{'} - \frac{1}{R_k^{2}}\mathbf{R}_k\right) \tag{2.1}$$

where $\varepsilon_0 = \frac{1}{36\pi}10^{-9}\frac{A\cdot s}{V\cdot m}$ is the electric permittivity of free space, $\mathbf{R}_k$ the vector distance from the k conductor to the point P, $\mathbf{R}_k^{'}$ the vector distance from the image of the k conductor to point P and R_k, $R_k^{'}$ the modulus of vectors $\mathbf{R}_k$ and $\mathbf{R}_k^{'}$ respectively.

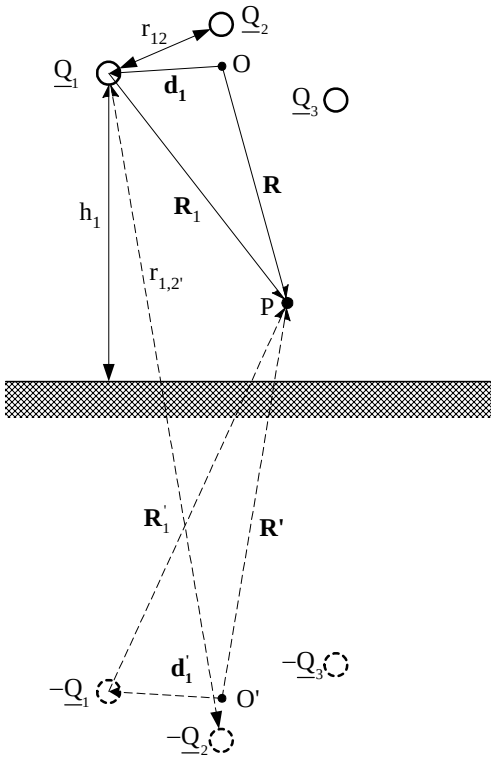

Figure 1. Model of a single circuit power line with the conductors' images

In the general case, a line with n conductors may be considered. Using the superimposition theorem, the intensity of electric field $\underline{\mathbf{E}}$, produced by the line is equal to the sum of the fields produced by each conductor separately,

$$\underline{\mathbf{E}} = \sum_{\kappa=1}^{n}\underline{\mathbf{E}}_k = \frac{1}{2\pi\varepsilon_0}\sum_{\kappa=1}^{n}\underline{Q}_k\left(\frac{1}{R_k^{'2}}\mathbf{R}_k^{'} - \frac{1}{R_k^{2}}\mathbf{R}_k\right) \Rightarrow$$

$$\underline{\mathbf{E}} = \frac{1}{2\pi\varepsilon_0}\sum_{\kappa=1}^{n}\underline{Q}_k\left(\frac{1}{\underline{\mathbf{R}}_k^{'}} - \frac{1}{\underline{\mathbf{R}}_k}\right) \tag{2.2}$$

Relation (2.2) is usually used for the numerical calculation of the intensity of the electric field. However, the summing operation doesn't allow this formula to be readily applied for the calculation of the electric field and makes it unsuitable for reaching general conclusions for the electric field properties and its dependencies on the various parameters of the line.

2.2 Double complex numbers and multipole expansions

The relations for the electric field vector are simplified if complex numbers are used for the representation of vector distances. On the other hand, complex numbers are used for the representation of sinusoidal varying quantities in time (phasors), such as conductors' charges, so finally double complex numbers are required. Book [5] contains the theoritical basis of double complex numbers, in [4] they are used for the calculation of magnetic flux density and in [6] to express the elliptically polarized vector of the electric field of light.

For the representation of space vectors the set of complex numbers C_1 is used, with the imaginary part j, for example $\mathbf{R}_k=x_k+jy_k$, while for the representation of sinusoidal varying quantities in time, the set C_2 with the imaginary part i is used, for example $\underline{Q}_k=Q_k e^{i\varphi_K}$.

Figure 1 shows that each conductor k may characterized by the vector distance $\mathbf{d}_k$ from the reference point O, which is a central point of the real conductors' system. The image of each conductor k may characterized by the vector distance $\mathbf{d}_k^{'}$ from the reference point O΄, which is a central point for the conductors' images' system. The points O and O΄ are close to but not necessarily the centers of the conductors' systems. Their choice is a matter of experience and is made in order to simplify the mathematical expressions.

Replacing $\mathbf{R}_k=\mathbf{R}-\mathbf{d}_k$ and $\mathbf{R}_k^{'}=\mathbf{R}^{'}-\mathbf{d}_k^{'}$ in (2.2), it becomes (2.3).

$$\underline{\mathbf{E}}=\frac{1}{2\pi\varepsilon_0}\sum_{k=1}^{n}\underline{Q}_k\left(\frac{1}{\overline{\mathbf{R}}^{'}-\overline{\mathbf{d}}_k^{'}}-\frac{1}{\overline{\mathbf{R}}-\overline{\mathbf{d}}_k}\right) \tag{2.3}$$

Using the well-known relations (2.4) in (2.3), the intensity of the electric field results as the sum of two multipole expansions, one from the real conductors' system and the other from the conductors' images' system, relation (2.5).

$$\left(\overline{\mathbf{R}}^{'}-\overline{\mathbf{d}}_k^{'}\right)^{-1}=\sum_{\lambda=1}^{\infty}\frac{\overline{\mathbf{d}}_k^{'\,\lambda-1}}{\overline{\mathbf{R}}^{'\,\lambda}} \tag{2.4a}$$

$$\left(\overline{\mathbf{R}}-\overline{\mathbf{d}}_k\right)^{-1}=\sum_{\lambda=1}^{\infty}\frac{\overline{\mathbf{d}}_k^{\,\lambda-1}}{\overline{\mathbf{R}}^{\lambda}} \tag{2.4b}$$

$$\underline{\mathbf{E}}=\frac{1}{2\pi\varepsilon_0}\sum_{k=1}^{n}\underline{Q}_k\left(\sum_{\lambda=1}^{\infty}\frac{\overline{\mathbf{d}}_k^{'\,\lambda-1}}{\overline{\mathbf{R}}^{'\lambda}}-\sum_{\lambda=1}^{\infty}\frac{\overline{\mathbf{d}}_k^{\,\lambda-1}}{\overline{\mathbf{R}}^{\lambda}}\right)\Rightarrow$$

$$\underline{\mathbf{E}}=\sum_{\lambda=1}^{\infty}\underline{\mathbf{E}}_{(\lambda)}^{'}+\sum_{\lambda=1}^{\infty}\underline{\mathbf{E}}_{(\lambda)} \tag{2.5}$$

The terms $\underline{\mathbf{E}}_{\lambda}^{'}$ and $\underline{\mathbf{E}}_{\lambda}$ are called λ order terms and are given by the relations (2.6)

$$\underline{\mathbf{E}}_{(\lambda)}^{'}=\frac{1}{2\pi\varepsilon_0}\cdot\frac{\underline{\mathbf{M}}_{\lambda}^{'}}{\overline{\mathbf{R}}^{'\lambda}} \tag{2.6a}$$

$$\underline{\mathbf{E}}_{(\lambda)}=-\frac{1}{2\pi\varepsilon_0}\cdot\frac{\underline{\mathbf{M}}_{\lambda}}{\overline{\mathbf{R}}^{\lambda}} \tag{2.6b}$$

where the factors $\underline{\mathbf{M}}_{\lambda}^{'}$ and $\underline{\mathbf{M}}_{\lambda}$ are called λ order moments for the conductors' images' system and the real

conductors' system respectively and are given by the relations (2.7).

$$\underline{\mathbf{M}}'_{\lambda} = \sum_{\kappa=1}^{n} \underline{Q}_k \, \bar{\mathbf{d}}_k^{\,\lambda-1} \tag{2.7a}$$

$$\underline{\mathbf{M}}_{\lambda} = \sum_{\kappa=1}^{n} \underline{Q}_k \, \bar{\mathbf{d}}_k^{\,\lambda-1} \tag{2.7b}$$

The multipole expansion, which appears in relation (2.5), is a series of infinite terms, each inversely proportional to an increasing power of the distance and has been used in [4] and [7] for the calculation of magnetic field produced by electric power lines.

2.3 Analysis of charges in symmetrical components

The calculation of the conductors' charges is necessary in order to calculate the intensity of the electric field. In the case of a single circuit power line, figure 1, the conductors' charges $\underline{Q}_1$, $\underline{Q}_2$ and $\underline{Q}_3$ are given by the relations (2.8).

$$\underline{Q}_1 = \frac{\underline{D}_1}{D} \quad , \quad \underline{Q}_2 = \frac{\underline{D}_2}{D} \quad , \quad \underline{Q}_3 = \frac{\underline{D}_3}{D} \tag{2.8}$$

The terms $\underline{D}_1$, $\underline{D}_2$, $\underline{D}_3$ and D are calculated by the relations (2.9)

$$D_1 = \begin{vmatrix} V_1 & S_{12} & S_{13} \\ V_2 & S_{22} & S_{23} \\ V_3 & S_{32} & S_{33} \end{vmatrix} \quad , \quad D_2 = \begin{vmatrix} S_{11} & V_1 & S_{13} \\ S_{21} & V_2 & S_{23} \\ S_{31} & V_3 & S_{33} \end{vmatrix} \quad , \quad D_3 = \begin{vmatrix} S_{11} & S_{12} & V_1 \\ S_{21} & S_{22} & V_2 \\ S_{31} & S_{32} & V_3 \end{vmatrix} \quad , \quad D = \begin{vmatrix} S_{11} & S_{12} & S_{13} \\ S_{21} & S_{22} & S_{23} \\ S_{31} & S_{32} & S_{33} \end{vmatrix} \tag{2.9}$$

where V_1, V_2 and V_3 are the voltages of the conductors 1, 2 and 3 respectively, and

$$S_{ii} = \frac{\ln(2h_i/r_i)}{2\pi\varepsilon_0} \quad , \quad S_{ij} = S_{ji} = \frac{\ln(r_{i,j'}/r_{ij})}{2\pi\varepsilon_0} \quad (i=1,2,3 \text{ and } j=1,2,3) \tag{2.10}$$

The factors h_i, r_i, r_{ij} and $r_{i,j'}$ that appear in relation (2.10) are:
- h_i, distance of the conductor i from the ground
- r_i, radius of the conductor i
- r_{ij}, distance between the conductors i and j
- $r_{i,j'}$, distance between the conductor i and the j conductor's image.

Figure 1 shows, for example, three characteristic distances h_1, r_{12} and $r_{1,2'}$.

The conductors' charges $\underline{Q}_1$, $\underline{Q}_2$ and $\underline{Q}_3$ constitute an asymmetrical system, which impedes the calculation of the intensity of the electric field. The asymmetrical system of charges is analyzed in three symmetrical three phase systems, the positive, the negative and the zero sequence system, according to relation (2.11).

$$\begin{bmatrix} \underline{Q}_{(0)} \\ \underline{Q}_{(1)} \\ \underline{Q}_{(2)} \end{bmatrix} = \frac{1}{3} \cdot \begin{bmatrix} 1 & 1 & 1 \\ 1 & \underline{a} & a^2 \\ 1 & \underline{a}^2 & \underline{a} \end{bmatrix} \cdot \begin{bmatrix} \underline{Q}_1 \\ \underline{Q}_2 \\ \underline{Q}_3 \end{bmatrix} \tag{2.11}$$

where $\underline{Q}_{(0)}$, $\underline{Q}_{(1)}$, $\underline{Q}_{(2)}$ are the zero, the positive and the negative sequence charge respectively and $\underline{a} = e^{i2\pi/3}$.

The intensity of the electric field is calculated for each one of the components of charges separately and the final accurate formulas arise from the superimposition of the results.

3 Electric field of single circuit power lines with conductors in triangular arrangement

3.1 Accurate formula of the electric field

Figure 2 shows a single circuit line with the conductors placed on the corners of an equilateral triangle. The voltages of the three conductors constitute a symmetrical system and are given by relation (3.1).

$$V_a = V\angle 120^0 \quad , \quad V_b = V\angle 0^0 \quad , \quad V_c = V\angle -120^0 \tag{3.1}$$

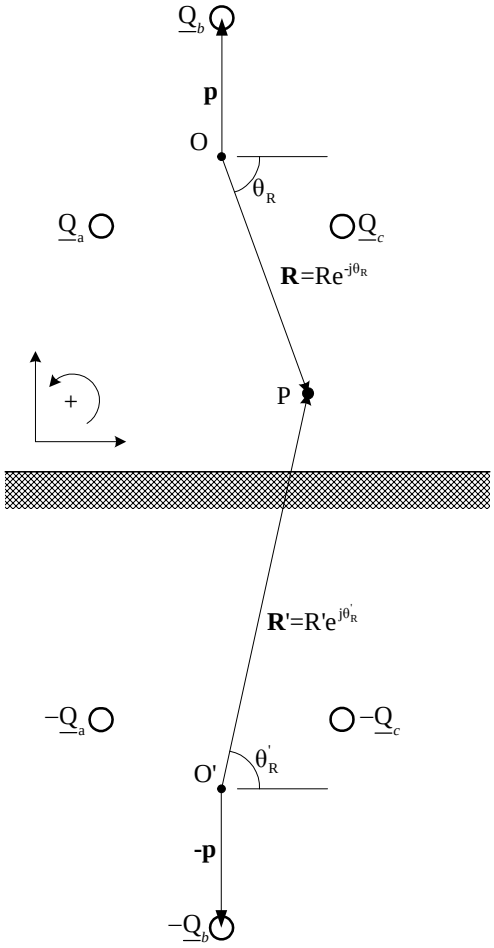

Figure 2. Model of a single circuit power line with the conductors placed on the corners of an equilateral triangle

Choosing the center of the arrangement as the reference point for both the real conductors' system and the conductors' images' system, as shown in figure 2, the distances of the conductors from these points are given in (3.2).

$$\mathbf{d}_a = \mathbf{p}e^{j\frac{2\pi}{3}} \quad , \quad \mathbf{d}_b = \mathbf{p} \quad , \quad \mathbf{d}_c = \mathbf{p}e^{-j\frac{2\pi}{3}} \tag{3.2a}$$

$$\mathbf{d}'_a = \mathbf{p}e^{j\frac{\pi}{3}} \quad , \quad \mathbf{d}'_b = -\mathbf{p} \quad , \quad \mathbf{d}'_c = \mathbf{p}e^{-j\frac{\pi}{3}} \tag{3.2b}$$

where $\mathbf{p}=jp$ is the distance vector between the reference point O and the upper conductor, as shown in figure 2.

Due to $\mathbf{d_k} \neq \mathbf{d}'_k$, the moments $\underline{\mathbf{M}}_\lambda$ and $\underline{\mathbf{M}}'_\lambda$, which are given in relations (2.7), are different,

$$\underline{\mathbf{M}}_\lambda \neq \underline{\mathbf{M}}'_\lambda \tag{3.3}$$

From relation (3.3) results that the real conductors' system is calculated separately from the conductors' images' system.

The conductors' charges are calculated through relations (2.8)-(2.10) and the assymetrical system that results is analyzed in its symmetrical components according to relation (2.11). For all the changes of the distance between the conductors as well as the height h from the ground of the real conductors, it results that the negative sequence charge is practically zero($Q_{(2)}$=0) and that the charges' angles for the positive and zero sequence system, $\theta_{(1)}$ and $\theta_{(0)}$ respectively, remain constant and equal to

$$\theta_{(1)} = \frac{2\pi}{3} \quad , \quad \theta_{(0)} = \pi \tag{3.4}$$

Thus, the intensity of the electric field is calculated only for the positive and zero sequence charges for the two conductors' systems (real conductors and conductors' images) separately.

Considering that the conductors bring only the positive sequence charges, then each conductor's charge is given in relation (3.5)

$$\underline{Q}_a = \underline{Q}_{(1)} \quad , \quad \underline{Q}_b = \underline{a}^2 \underline{Q}_{(1)} \quad , \quad \underline{Q}_c = \underline{a}\underline{Q}_{(1)} \tag{3.5}$$

where according to relation (3.4), results

$$\underline{Q}_{(1)} = Q_{(1)} \cdot e^{i\frac{2\pi}{3}} \tag{3.6}$$

Replacing relations (3.2), (3.5) and (3.6) in relations (2.7), (2.6) and (2.5) and taking into consideration relation (3.3), results the intensity of the electric field that comes from the positive sequence charge and is given in (3.7) for the conductors' images' system and in (3.8) for the real conductors' system.

$$\underline{\mathbf{E}}'_{(1)} = -\frac{3Q_{(1)}\bar{\mathbf{p}}}{4\pi\varepsilon_0\left(\bar{\mathbf{R}}'^{3} + \mathbf{p}^{-3}\right)} \cdot \left[\bar{\mathbf{R}}'(1+ij) - \bar{\mathbf{p}}(1-ij)\right] \tag{3.7}$$

$$\underline{\mathbf{E}}_{(1)} = -\frac{3Q_{(1)}\bar{\mathbf{p}}}{4\pi\varepsilon_0\left(\bar{\mathbf{R}}^{-3} - \mathbf{p}^{-3}\right)} \cdot \left[\bar{\mathbf{R}}(1-ij) + \bar{\mathbf{p}}(1+ij)\right] \tag{3.8}$$

Considering that the conductors bring only the zero sequence charges, then each conductor's charge is given in relation (3.9)

$$\underline{Q}_a = \underline{Q}_{(0)} \quad , \quad \underline{Q}_b = \underline{Q}_{(0)} \quad , \quad \underline{Q}_c = \underline{Q}_{(0)} \tag{3.9}$$

where according to relation (3.4), results

$$\underline{Q}_{(0)} = Q_{(0)} \cdot e^{i\pi} \tag{3.10}$$

Replacing relations (3.2), (3.9) and (3.10) in relations (2.7), (2.6) and (2.5) and taking into consideration relation (3.3), results the intensity of the electric field that comes from the zero sequence charge and is given in (3.11) for the conductors' images' system and in (3.12) for the real conductors' system.

$$\underline{\mathbf{E}}'_{(0)} = -\frac{6Q_{(0)}\bar{\mathbf{R}}'^{2}}{4\pi\varepsilon_0\left(\bar{\mathbf{R}}'^{3} + \mathbf{p}^{-3}\right)} \tag{3.11}$$

$$\underline{\mathbf{E}}_{(0)} = \frac{6Q_{(0)}\bar{\mathbf{R}}^{2}}{4\pi\varepsilon_0\left(\bar{\mathbf{R}}^{3} - \mathbf{p}^{-3}\right)} \tag{3.12}$$

The intensity of the electric field $\underline{\mathbf{E}}$, at any point in the vicinity of the line, arises finally from the

superimposition of all intensities from relations (3.7), (3.8), (3.11) and (3.12), as shown in (3.13).

$$\underline{\mathbf{E}} = \left(\underline{\mathbf{E}}_{(1)} + \underline{\mathbf{E}}_{(0)}\right) + \left(\underline{\mathbf{E}}'_{(1)} + \underline{\mathbf{E}}'_{(0)}\right) \tag{3.13}$$

From (3.13), results the final expression (3.14), which represents the intensity of the electric field as a double complex number.

$$\begin{aligned}\underline{\mathbf{E}} = -\frac{3}{4\pi\varepsilon_0\left(\bar{\mathbf{R}}^{-3} - \bar{\mathbf{p}}^{-3}\right)\left(\bar{\mathbf{R}}'^{-3} + \bar{\mathbf{p}}^{-3}\right)} \cdot [&(Q_{(1)}\bar{\mathbf{p}}\bar{\mathbf{R}}^{-3}\bar{\mathbf{R}}' + Q_{(1)}\bar{\mathbf{p}}\bar{\mathbf{R}}\bar{\mathbf{R}}'^{-3} - Q_{(1)}\bar{\mathbf{p}}^{-2}\bar{\mathbf{R}}^{-3} + Q_{(1)}\bar{\mathbf{p}}^{-2}\bar{\mathbf{R}}'^{-3} + 2Q_{(0)}\bar{\mathbf{R}}^{-3}\bar{\mathbf{R}}'^{-2} \\ &- 2Q_{(0)}\bar{\mathbf{R}}^{-2}\bar{\mathbf{R}}'^{-3} - Q_{(1)}\bar{\mathbf{p}}^{-4}\bar{\mathbf{R}}' + Q_{(1)}\bar{\mathbf{p}}^{-4}\bar{\mathbf{R}} + 2Q_{(1)}\bar{\mathbf{p}}^{-5} - 2Q_{(0)}\bar{\mathbf{p}}^{-3}\bar{\mathbf{R}}'^{-2} - 2Q_{(0)}\bar{\mathbf{p}}^{-3}\bar{\mathbf{R}}^{-2}) + \\ &+ ij(Q_{(1)}\bar{\mathbf{p}}\bar{\mathbf{R}}^{-3}\bar{\mathbf{R}}' + Q_{(1)}\bar{\mathbf{p}}^{-2}\bar{\mathbf{R}}^{-3} - Q_{(1)}\bar{\mathbf{p}}^{-4}\bar{\mathbf{R}}' - Q_{(1)}\bar{\mathbf{p}}\bar{\mathbf{R}}\bar{\mathbf{R}}'^{-3} + Q_{(1)}\bar{\mathbf{p}}^{-2}\bar{\mathbf{R}}'^{-3} - Q_{(1)}\bar{\mathbf{p}}^{-4}\bar{\mathbf{R}})]\end{aligned} \tag{3.14}$$

The rms value of the electric field E is equal to the modulus of the double complex number $\underline{\mathbf{E}}$ and is given in relation (3.15).

$$\begin{aligned}E = \frac{3\sqrt{2}}{4\pi\varepsilon_0} \cdot \left[\frac{1}{\left(R^6 + p^6 - 2R^3p^3\sin 3\theta_R\right)\left(R'^6 + p^6 - 2R'^3p^3\sin 3\theta_{R'}\right)}\right]^{1/2} \cdot \\ [(Q_{(1)}pR^3R'\sin(3\theta_R - \theta_{R'}) - Q_{(1)}p^2R'^3\cos 3\theta_{R'} - Q_{(1)}p^4R'\cos\theta_{R'} + Q_{(0)}R^3R'^2\cos(3\theta_R - 2\theta_{R'}) \\ - Q_{(0)}R^2R'^3\cos(2\theta_R - 3\theta_{R'}) - Q_{(0)}p^3R'^2\sin 2\theta_{R'} + Q_{(0)}p^3R^2\sin 2\theta_R)^2 + \\ + (Q_{(1)}pRR'^3\sin(\theta_R - 3\theta_{R'}) + Q_{(1)}p^2R^3\cos 3\theta_R + Q_{(1)}p^4R\cos\theta_R + Q_{(0)}R^3R'^2\cos(3\theta_R - 2\theta_{R'}) \\ - Q_{(0)}R^2R'^3\cos(2\theta_R - 3\theta_{R'}) - Q_{(0)}p^3R'^2\sin 2\theta_{R'} + Q_{(0)}p^3R^2\sin 2\theta_R)^2 + \\ + (-Q_{(1)}pR^3R'\cos(3\theta_R - \theta_{R'}) + Q_{(1)}p^2R'^3\sin 3\theta_{R'} + Q_{(1)}p^4R'\sin\theta_{R'} - Q_{(1)}p^5 + Q_{(0)}R^3R'^2\sin(3\theta_R - 2\theta_{R'}) \\ - Q_{(0)}R^2R'^3\sin(2\theta_R - 3\theta_{R'}) - Q_{(0)}p^3R'^2\cos 2\theta_{R'} - Q_{(0)}p^3R^2\cos 2\theta_R)^2 + \\ + (-Q_{(1)}pRR'^3\cos(\theta_R - 3\theta_{R'}) + Q_{(1)}p^2R^3\sin 3\theta_R + Q_{(1)}p^4R\sin\theta_R - Q_{(1)}p^5 + Q_{(0)}R^3R'^2\sin(3\theta_R - 2\theta_{R'}) \\ - Q_{(0)}R^2R'^3\sin(2\theta_R - 3\theta_{R'}) - Q_{(0)}p^3R'^2\cos 2\theta_{R'} + Q_{(0)}p^3R^2\cos 2\theta_R)^2]^{1/2}\end{aligned} \tag{3.15}$$

The angles θ_R and $\theta_{R'}$ are shown in figure 2. Relation (3.15) is valid only for the case where the equilateral triangle has the arrangement of figure 2. If the triangle has a different placement in space, then the relative positions of the images would also be different and the calculation of the intensity of the electric field should remade from the beginning.

3.2 Approximate formulas of the electric field

Relation (3.15) is the accurate formula of the intensity of the electric field and depends on the positive and zero sequence charges. This formula is very extensive. A simpler approximate formula may derive taking into account only one of the symmetrical components of the charges.

Figure 3 shows the effect of the positive and zero sequence charge in the intensity of the electric field, for a typical 150kV power line with the conductors in triangular arrangement. From figure 3 results that the positive sequence charge has the bigger effect in the electric field not only close to but also far from the line. However, choosing only the positive sequence charge for the calculation of the electric field, the deviation from the accurate values, mainly close to the line, is considerable.

a)

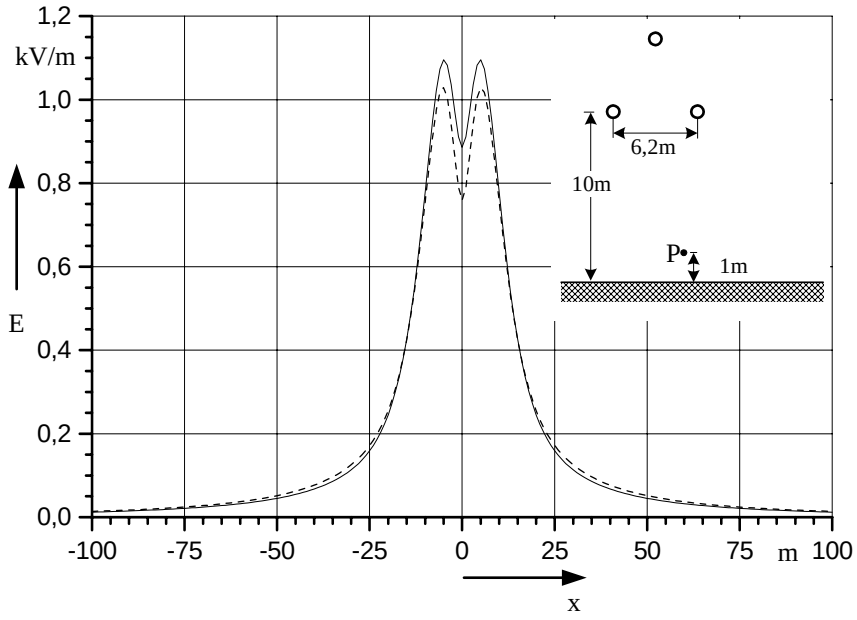

b)

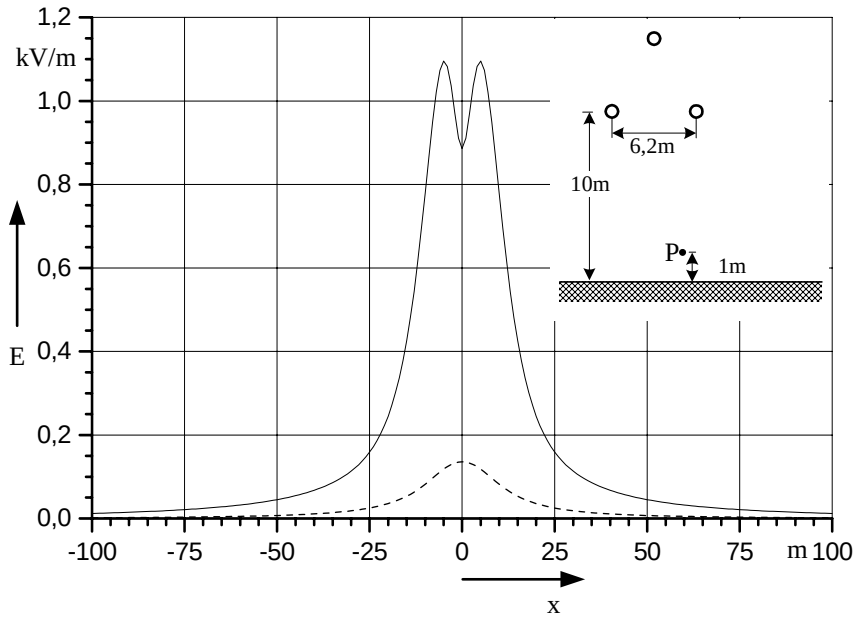

Figure 3. a) Positive and b) zero sequence charge effect in the electric field E that produced by a typical 150kV single circuit line with triangular arrangement of conductors.
——————— Accurate values by formula (3.15) ---------- Symmetrical component's effect

Replacing $Q_{(0)}=0$ in (3.15), the intensity of the electric field by the positive sequence charge is derived in (3.16).

$$E=\frac{3\sqrt{2}Q_{(1)}p}{4\pi\varepsilon_0}\cdot\left[\frac{1}{\left(R^6+p^6-2R^3p^3\sin3\theta_R\right)\left(R'^6+p^6-2R'^3p^3\sin3\theta_{R'}\right)}\right]^{1/2}\cdot$$

$$\left[\left(R^3R'\sin(3\theta_R-\theta_R')-pR'^3\cos3\theta_{R'}-p^3R'\cos\theta_{R'}\right)^2+\left(RR'^3\sin(\theta_R-3\theta_{R'})+pR^3\cos3\theta_R+p^3R\cos\theta_R\right)^2+\right.$$
$$\left.+\left(-R^3R'\cos(3\theta_R-\theta_R')+pR'^3\sin3\theta_{R'}+p^3R'\sin\theta_{R'}-p^4\right)^2+\left(-RR'^3\cos(\theta_R-3\theta_{R'})+pR^3\sin3\theta_R+p^3R\sin\theta_R-p^4\right)^2\right]^{1/2} \quad (3.16)$$

Relation (3.16) is also quite extensive. Taking into account the considerable deviation between the approximate values and the accurate values of the electric field, it results that the approximate formula (3.16) is not efficient.

Another formula may derive considering R=R´ and $\theta_R=\theta_{R'}$. Thus, replacing R=R´ and $\theta_R=\theta_{R'}$ in (3.15), the simpler formula (3.17) arises.

$$E=\frac{3}{2\pi\varepsilon_0}\cdot\frac{1}{\left|R^6+p^6-2R^3p^3\sin3\theta_R\right|}\cdot[Q_{(1)}{}^2p^2\left(R^4\sin2\theta_R-pR^3\cos3\theta_R-p^3R\cos\theta_R\right)^2+$$
$$\left(-Q_{(1)}pR^4\cos2\theta_R+Q_{(1)}p^2R^3\sin3\theta_R+Q_{(1)}p^4R\sin\theta_R-Q_{(1)}p^5+2Q_{(0)}R^5\sin\theta_R-2Q_{(0)}p^3R^2\cos2\theta_R\right)^2]^{1/2} \quad (3.17)$$

Relation (3.17) is the accurate formula of the intensity of the electric field on the surface of ground. This relation can also be a very good approximate formula for the electric field, for low calculation heights (up to 1m), as well as for far distances from the line.

Figure 4 shows the comparison of the electric field E produced by a single circuit line with the conductors in triangular arrangement, as it is calculated by the accurate formula (3.15) and the approximate formula (3.17). In figure 4a the comparison between the two formulas is made for calculation height 1m from the ground, while in figure 4b the comparison is made for calculation height 3m from it.

a)

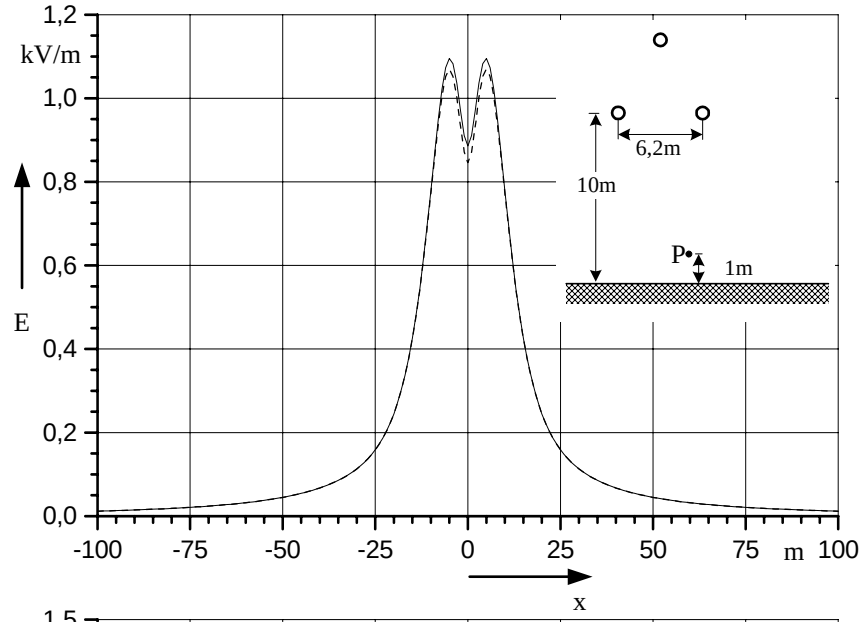

b)

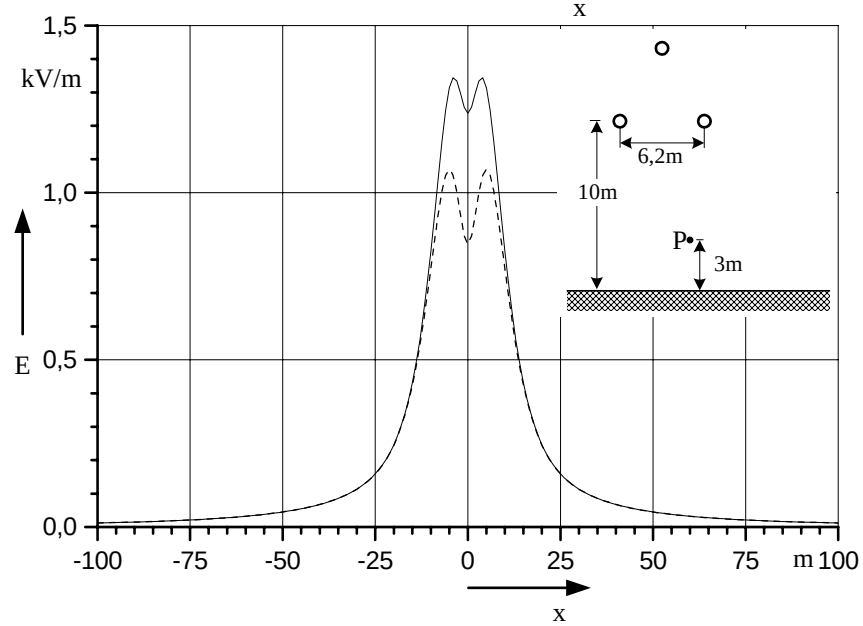

Figure 4. Intensity of the electric field E produced by a typical 150kV single circuit line with triangular arrangement of the conductors, as it is calculated from the accurate formula (3.15) and the approximate formula (3.17) for height a) 1m and b) 3m from the ground.

——————— Accurate formula (3.15) ---------- Approximate formula (3.17)

Figure 4a shows that for low calculation heights (up to 1m), the approximate formula (3.17) gives the intensity of the electric field with exceptional precision, not only far from the line, but also close to it. Figure 4b shows that for bigger calculation heights, the formula (3.17) gives satisfying results only for far distances from the line, while close to it the deviation is significant.

4 Conclusions

The electric field produced by power lines of big length in comparison with the distances between the conductors and the distances between the conductors and the ground, can be expressed with extensive analytical formulas. In the present paper a method to derive the analytical formulas of the electric field has been developed. This method is based on the analysis of the intensity of the electric field into two multipole expansions, one from the real conductors' system and the other from the conductors' images' system. For the simplification of the mathematical expressions double complex numbers are used. Due to the asymmetry of conductors' charges, they are analyzed in their symmetrical components.

Using this method the accurate analytical formula for the intensity of the electric field produced by single circuit lines with the conductors in triangular arrangement is given. This relation may be used for the accurate calculation of the intensity of the electric field, at any point in the vicinity of the lines, close to or far from them. From the accurate formula, a simpler approximate formula with very good precision is derived, which is valid either for low calculation heights (up to 1m) either for bigger heights in far distances from the line.

References

[1] ICNIRP: Guidelines for limiting exposure to time-varying electric, magnetic and electromagnetic fields (up to 300GHz*), Health Physics*, Vol. 74, No 4, pp 494 -522, April 1998.

[2] European Union Council: Recommendation of 12 July 1999 on the limitation of exposure of the general public to electromagnetic fields (0Hz – 300GHz), (1999/519/EC).

[3] European Parliament and Council: Directive 2004/40/EC of 29 April 2004 on the minimum health and safety requirements regarding the exposure of workers to the risks arising from physical agents (electromagnetic fields).

[4] G. Filippopoulos and D. Tsanakas, *Analytical calculation of the magnetic field produced by electric power lines. IEEE Trans. on Power Delivery*, Vol. 20, pp. 1474-1482, 2005.

[5] I. L. Kantor and A.S. Solodovnikov, *Hypercomplex numbers-An Elementary Introduction to Algebras*. Berlin, Germany: Springer –Verlag, 1989

[6] J. Bojanowski, "Vector description of polarized and unpolarized light in double – complex calculus", Optics Lasers Eng., vol. 22, pp. 291-304, 1995.

[7] W. T. Kaune and L. E. Zaffanella, *"Analysis of magnetic fields produced far from electric power lines," IEEE Trans. on Power Del.*, vol. 7, no. 4, pp. 2082-2091, Oct. 1992.

ON THE ANALYSIS OF EMF GENERATED BY POWER LINES

ALESSANDRO MORI

MARIO CALAMIA

DEPARTMENT OF ELECTRONICS AND TELECOMMUNICATIONS,
UNIVERSITY OF FLORENCE,
VIA DI SANTA MARTA, 3
50139 FIRENZE (ITALY)
alessandro.mori@unifi.it
mario.calamia@unifi.it

Abstract

In this paper we discuss the human exposure level for electric and magnetic fields generated by power lines. In particular, we consider the real case of a populated area in Tuscany (Italy) crossed by two high voltage (380 kV) power lines. We carried out a wide measurement campaign and also estimated the electric and magnetic fields generated by the power lines by means of simple and full-wave models (based on the Method of Moments).

The measurement data are used to verify the accuracy of the models. The estimated electric and magnetic fields are then used to evaluate the field exposure in the whole area.

In this paper, we briefly describe the models used in the analysis. We then compare and examine the results obtained from the measurements and the models. Finally, we discuss the model exploitation.

Introduction

The problem of evaluating the power line field exposure is complicated for two reasons. The strong variation of the electric current in a power line reflects on the variation of the generated magnetic field, and the accurate estimation of the electric field generated by a power line can be a very complicated problem due to the complexity of the environment. If the area to be analyzed is large (in our case about 700 m × 250 m) an accurate evaluation of the human exposure level only by measures can be impracticable. Moreover, in case of evaluation of the exposure level for the magnetic field, it is necessary to analyze the field over a large time span (several months – one year). Even for this reason an accurate evaluation of the human exposure level only by measures can be impracticable. On the contrary, the combined utilization of measurements and numerical models allows the characterization of the electric and magnetic fields generated by power lines and the evaluation of the field exposure.

In Italy, the electric and magnetic fields generated by power lines are subjected to the D.P.C.M. (Decree of the Prime Minister) 8th July 2003. It states that the maximum electric field generated by power lines (in accessible areas) has not to exceed the effective value of 5 kV/m. For the effective value of the magnetic flux density (here, for sake of brevity, the magnetic field), the D.P.C.M. establishes three limits. The maximum value has not to exceed 100 μT. In babies playing fields, schools, houses and, in general, in areas where people can stay more than 4 hours/day, the value of 10 μT, evaluated as median over a time span of 24 hours, has not to be exceeded. Finally, in case of a new power line near babies playing fields, schools, houses and, in general, in areas where people can stay more than 4 hours/day, and/or new buildings the median value of 3 μT has not to be exceeded.

The fact to have to evaluate the median value of the magnetic field over 24 hours makes hard to carry out a measurement campaign in a large area. The Italian regulations CEI 211-6 gives suggestions about a measurement campaign and allow the use of a numerical model, recommending measurements where a numerical model estimates a field intensity greater than 50% of the limit value. In our case we have collected a large measurement set (one hundred points / two heights for point / two dates per point), we have used these data in order to evaluate the numerical model accuracy, and we have used the numerical model to estimate the human

exposure level [1], [2].
The Italian regulations CEI 211-4 describes two models (for the magnetic and electric field, respectively) to estimate the fields generated by power lines. These models are two-dimensional, i.e. consider the two-dimensional problem obtained from a perpendicular plane cut of the power line, containing the test point. In order to estimate the magnetic field, the terrain is considered completely transparent, so the Biot-Savart law for a infinite straight wire can be directly used. In order to estimate the electric field, the terrain is assumed as an infinite plane parallel to the power line wires and with an electric potential of 0 V. In order to use these (and the others) numerical models, we have collected all the geometrical and electrical characteristics of the power lines, including the line current and voltage recording (one sample per hour for one year).
We have also used others models, to represent in more detail the real situation. In particular, we have used a three dimensional Biot-Savart model in order to estimate the magnetic field, and a 2D full wave model, based on the Method of Moments [3], in order to estimate the electric field. In this model the profile of the terrain and of buildings on the plane perpendicular to the power line wires and containing the test points are considered at 0 V and are discretized by linear segments with an unknown uniform electric charge distributed on. Also, a three dimensional model is considered, where the AIM (Adaptive Integral Method) [4], [5] approach is used to overcome the computational time and dynamic memory requests of the classical Method of Moments in case of a large number of unknowns.
In the following sections we briefly described the models used, comparing the results with the measurements.

Magnetic field model
We have used two numerical models to estimate the magnetic field generated by power lines. Both models use the Biot-Savart law, in two and three dimensions, respectively. In the following, we describe these models and the results obtained.

Two dimensional model
The two dimensional model follows the Italian regulations CEI 211-4. The fields are considered almost static, the wires of the power lines are assumed as infinite straight wires with uniform current and passing by the intersection between the real wire and the perpendicular plane containing the test point. The terrain and other objects (buildings, etc.) are considered having the same magnetic permeability of the air. So, they are completely transparent to the magnetic field and the classical Biot-Savart law can be employed to evaluate the contribution of a wire to the total magnetic field. This situation is sketched in Fig. 1.
The magnetic field generated by the power line is given by

$$\vec{B}(\vec{r}) = \sum_{i=1}^{M} \vec{B}_i(\vec{r}) = \frac{\mu}{2\pi} \sum_{i=1}^{M} I_i \frac{\hat{u}_i}{d_i} \quad ,$$

where M is the number of wires, I_i is the current phasor flowing on wire i, d_i is the distance between the wire i and the test point on the plane perpendicular to the wire, and

$$\hat{u}_i = \hat{x} \times \hat{d}_i = \hat{x} \times \frac{\vec{d}_i}{d_i} \quad .$$

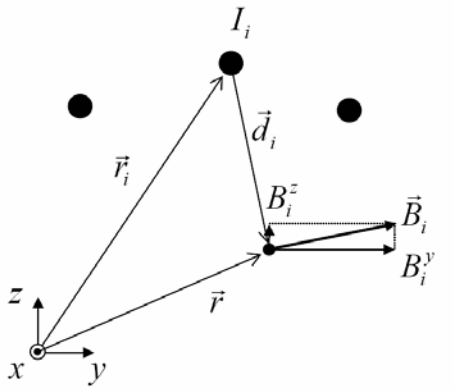

Fig. 1**:** Two dimensional model geometry for the evaluation of the magnetic field.

Respect to the CEI 211-4 specifications, in the two dimensional model the effect of the terrain has been considered through image wires (with current $-I_i$), placed at an height

$$h_i' = h_i + 503\sqrt{2\rho_g / f_0}\ \exp(j\,\pi/4)$$

below the terrain, where h_i is the height of the wire *i* respect to the terrain, f_0 is the frequency and ρ_g is the mean resistivity of the terrain [6]. However, in our case ($\rho_g = 8\,\Omega\,\mathrm{m}$), we have found that the contribution of the images of the real wires is not so significant.

Three dimensional model

In the three dimensional model, with respect to the two dimensional model, the real wires of the power lines are represented as a sequence of linear segments. Moreover, the images of the real wires are not considered. With reference to Fig. 2, the contribution to the magnetic field given by the segment $\overrightarrow{P_1P_2}$ is

$$\vec{B}_{\overline{P_1P_2}}(\vec{r}) = \frac{\mu}{4\pi} I \int_{P_1}^{P_2} \frac{\hat{s}\times\hat{r}}{r^2}\,dl = \frac{\mu}{4\pi} I\hat{u}\int_{P_1}^{P_2} \frac{\sin(\theta)}{r^2}\,dl = \frac{\mu}{4\pi d} I\hat{u}(\cos(\theta_1)-\cos(\theta_2))\,,$$

with $\hat{u} = \hat{s}\times\hat{t}$. The overall magnetic field generated by a power line, with *M* wires subdivided in *N* segments, is

$$\vec{B}(\vec{r}) = \frac{\mu}{4\pi}\sum_{i=1}^{M} I_i\left[\sum_{j=0}^{N+1}\frac{\hat{u}_{i,j}}{d_{i,j}}(\cos(\theta_{i,j})-\cos(\theta_{i,j+1}))\right].$$

Outside the region of interest, the wires are approximated with two semi-infinite segments, so

$$\theta_{i,0} = 0 \quad \theta_{i,N+2} = \pi\,.$$

Results

In Fig. 3 we show a comparison result for the two and the three dimensional model. In every point we have measured the magnetic field 2 m over the floor. Besides the estimated value, an error bar representing the maximum and minimum values relative to an uncertainty of 2 m in the position is showed. The area is near a power line tower, that is the worse situation respect to the straight wire approximation assumed in the two dimensional model. In spite of this, we see that the two dimensional model can be used to verify the Italian regulations compliance of power lines, even if the three dimensional model has higher accuracy and almost the same implementation complexity.

Using a numerical model and the power line current recording we can characterize the magnetic field generated by the power line. Besides contour maps, a product obtainable with a numerical model is shown in Fig. 4.

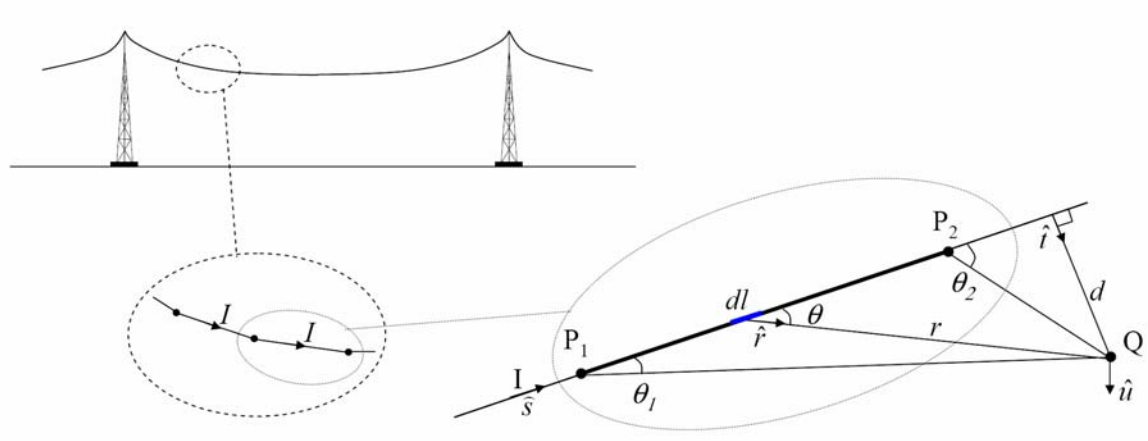

Fig. 2: Three dimensional model geometry for the evaluation of the magnetic field.

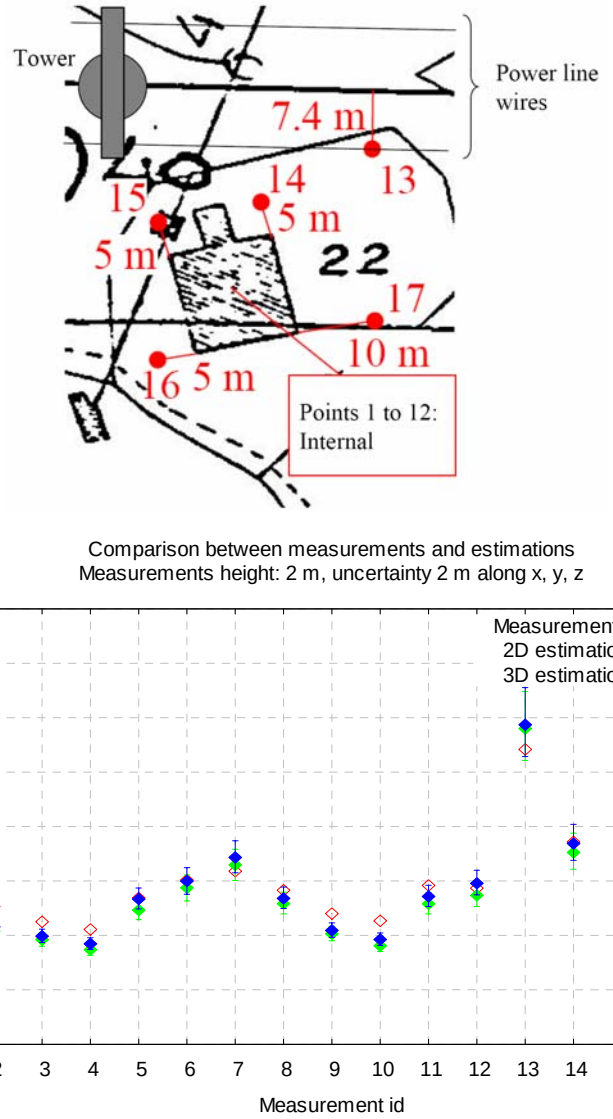

Fig. 3: Comparison between the two and three dimensional model results. Up: position of the measurement points. Down: comparison results. The estimated values are indicated by diamonds. The error bars are relative to assuming a topography and position accuracy of 2 meters.

Electric field model

We have used two 2D models to estimate the electric field generated by power lines. The first one is the model indicated by the Italian regulations CEI 211-4. The second one includes the topography and buildings effects, and is based on the Methods of Moments with pulse basis functions and point matching. We also discuss the 3D extension of the last model, using the AIM formulation in order to reduce the computational complexity of the algorithm. In the following, we describe these models and the results obtained with the 2D models. Results obtained with the 3D AIM model will be shown at the conference.

CEI 211-4 model

As sketched in Fig. 5, the CEI 211-4 numerical model for the electric field generated by power line is the simplest one. The wires of the power line are assumed infinitely straight and parallel, the terrain is assumed perfectly flat and at 0 V potential.

In this case, the electric charge q_i on wire i is obtainable solving the linear system $\underline{V} = \underline{\underline{S}}\,\underline{Q}$, where $\underline{Q}$ and $\underline{V} = [\psi_i - \psi_0 = \psi_i]$ are the vector containing the electric charge and the voltage of the wires, respectively, and the elements of the elastance matrix $\underline{\underline{S}}$ are given by

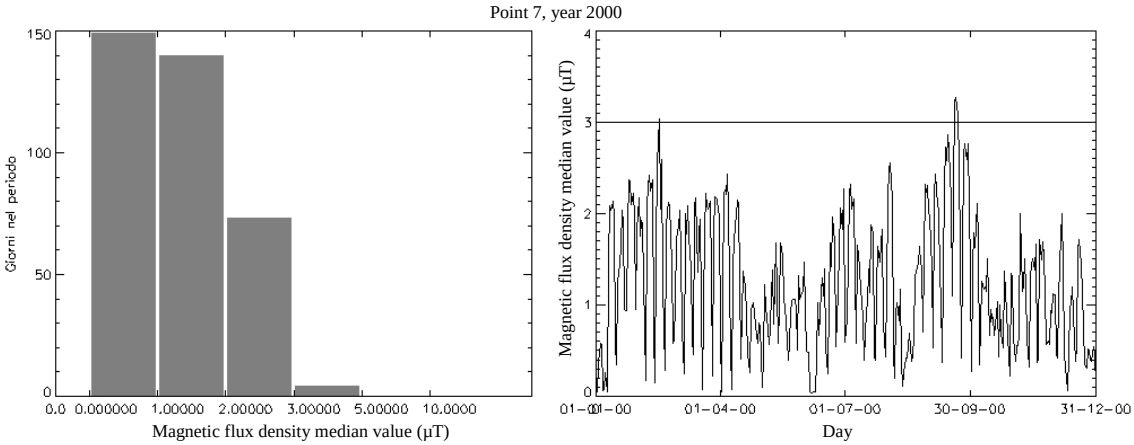

Fig. 4: Median value histogram (left) and graph (right) of the magnetic field as evaluated by the numerical model. The value of 3 μT is the limit indicated by the Italian regulations for a new plant or building.

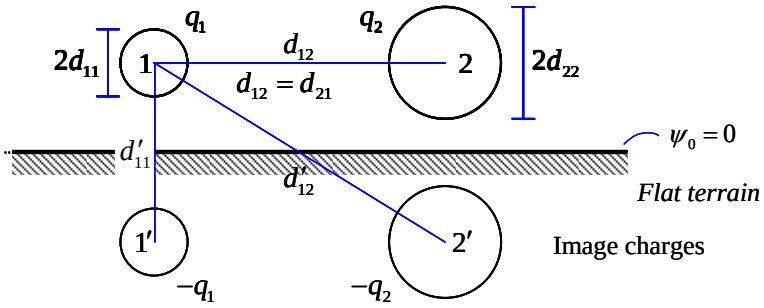

Fig. 5: CEI 211-4 electric field model geometry.

$$s_{ij} = \frac{1}{2\pi\varepsilon}\ln\left(\frac{d'_{ij}}{d_{ij}}\right).$$

When the electric charges are determined, the electric field follows

$$\vec{E}(\vec{\rho}) = \frac{1}{2\pi\varepsilon}\sum_{i=1}^{M} q_i \frac{\vec{\rho}-\vec{\rho}_i}{\left|\vec{\rho}-\vec{\rho}_i\right|^2} - \frac{1}{2\pi\varepsilon}\sum_{i=1}^{M} q_i \frac{\vec{\rho}-\vec{\rho}'_i}{\left|\vec{\rho}-\vec{\rho}'_i\right|^2},$$

where a primed quantity denotes the position of an image and M is the number of wires.

Full 2D model

The full 2D model includes the presence of building and a not flat terrain, as sketched in Fig. 6. It employs a Method of Moments using pulse basis functions to describe the buildings and the terrain, and the point matching technique.

The electric charge on the wires and the amplitude of the linear charge distribution on the segments are again evaluated solving the linear system $\underline{V} = \underline{\underline{S}}\,\underline{Q}$, where the first M elements of the vectors $\underline{Q}$ and $\underline{V}$ are the charge and the voltage of the wires, respectively, and the remaining ones are the amplitude of the linear charge distribution and the voltage (0 V) of the N_S segments representing the buildings and the terrain. The elements of the elastance matrix $\underline{\underline{S}}$ are now given by

$$s_{ij} = \begin{cases} \dfrac{1}{2\pi\varepsilon}\ln\left(\dfrac{d'_{ij}}{d_{ij}}\right) & \text{for } 1 \le j \le M \\ \dfrac{T'_{ij} - T_{ij}}{2\pi\varepsilon} & \text{for } M+1 \le j \le M+N_S \end{cases}$$

where

$$T_{ij} = \frac{1}{L_j} \int_{-L_j/2}^{L_j/2} \ln\left(\left|\vec{\rho}_i - \vec{\rho}_j - \ell\vec{\ell}_j\right|\right) d\ell$$

$$T'_{ij} = \frac{1}{L_j} \int_{-L_j/2}^{L_j/2} \ln\left(\left|\vec{\rho}_i - \vec{\rho}'_j - \ell\vec{\ell}'_j\right|\right) d\ell$$

and L_j is the length of segment *j*, $\hat{\ell}_j$ is its direction, $\vec{\rho}_i$ and $\vec{\rho}_j$ are the position of the wire *i* and of the center of segment *j*, respectively. The electric field is then evaluated as

$$\vec{E}(\vec{\rho}) = \frac{1}{2\pi\varepsilon}\sum_{i=1}^{M} q_i \frac{\vec{\rho}-\vec{\rho}_i}{\left|\vec{\rho}-\vec{\rho}_i\right|^2} - \frac{1}{2\pi\varepsilon}\sum_{i=1}^{M} q_i \frac{\vec{\rho}-\vec{\rho}'_i}{\left|\vec{\rho}-\vec{\rho}'_i\right|^2} +$$

$$+\frac{1}{2\pi\varepsilon}\sum_{i=M+1}^{M+N_s}\frac{q_i}{L_i}\int_{-L_i/2}^{L_i/2}\frac{\vec{\rho}-\vec{\rho}_i-\ell\hat{\ell}_i}{\left|\vec{\rho}-\vec{\rho}_i-\ell\hat{\ell}_i\right|^2}d\ell - \frac{1}{2\pi\varepsilon}\sum_{i=M+1}^{M+N_s}\frac{q_i}{L_i}\int_{-L_i/2}^{L_i/2}\frac{\vec{\rho}-\vec{\rho}'_i-\ell\hat{\ell}'_i}{\left|\vec{\rho}-\vec{\rho}'_i-\ell\hat{\ell}'_i\right|^2}d\ell\,,$$

where the primed entities are relative to the images.

Results

In Fig. 7 we show the comparison between measurements and estimations for two transverse sections respect to the power line in the area under analysis. We consider the presence of the buildings, but do not consider the other obstacles (trees, etc.). This is not enough to obtain a good accuracy. However, the model can give some information about the position of the points were measure the electric field. The power line voltage is almost constant, so we can characterize the electric field generated by the power line by such measurements.

In order to obtain a better accuracy, we can model the power line and the buildings in three dimensions. This brings to increase the number of basis functions, leading the application of the Method of Moments to an unfeasible requests on computational time and/or dynamic memory. An efficient method can be adopted, and in the following we discuss about the use of the AIM formulation in the 3D problem corresponding to the geometry sketched in Fig. 6.

On the use of Adaptive Integral Method

A three dimensional analysis of the area of interest through the Method of Moments to estimate the electric field generated by a power line could be more accurate than a the 2D model, but it leads to unfeasible requests on computational time and/or dynamic memory. In such case the use of a computationally efficient scheme of the Method of Moments gives the opportunity to carry out a 3D analysis. In the following we discuss some implementation notes of the Adaptive Integral Method (AIM). Some results will be presented at the conference.

The Adaptive Integral Method (AIM) [4], [5] has been widely used to solve electromagnetic scattering and radiation problems involving large objects. Its implementation in a Method of Moments (MoM) approach allows, when used with an iterative solver, to accelerate the matrix-vector multiplication and to reduce the number of matrix elements to be stored. In particular, the computational complexity of a matrix-vector multiplication is in the order of $O(N^2)$ using the conventional MoM, where *N* is the number of unknowns, but using the AIM reduces it to $O(N^{1.5}\log N)$ and $O(N\log N)$ for surface and volume scattering, respectively.

The AIM exploits the convolutional property of the free space Green's function. In particular, the interaction between the basis and the testing functions are divided into near and far interactions. The near-interactions matrix elements are evaluated as in the conventional MoM. The other elements (far-interactions matrix elements) are approximated using an auxiliary set of basis function, placed on a uniform cartesian grid. Such auxiliary set of basis function are almost equivalent to the MoM basis function with reference to the elastance matrix elements [5]. By virtue of the auxiliary function are placed on an uniform cartesian grid, and due to the convolutional form of the free space Green's function, the matrix-vector product relative to the far-interactions matrix elements can efficiently evaluated through Fast Fourier Transforms (FFT's).

In case of a half-space limited by a perfectly conductor plane (Fig. 6, extended to three dimensions), the pertinent Green's function doesn't exhibit a convolutional form, so the AIM formulation cannot be applied directly. However, we can exploit the image principle and apply the AIM formulation on the actual object and on its image, increasing the number of points of the uniform cartesian grid to be considered. On the contrary, we can individually consider the real and the image term in the Green's function. In such case, the reflected term exhibits a correlation form on a space variable and its matrix-vector product contribution can be again evaluated by FFT's without increase the number of points of the uniform cartesian grid.

In particular, the needed direct FFT's samples can be obtained from the direct FFT's samples of the auxiliary basis functions of the real objects, obtaining an algorithm with almost the same computational complexity and

dynamic memory requested by the algorithm for the analysis of the object in free space.
In our implementation, the AIM formulation is applied only to the terrain and buildings. The wires of the power line (few unknowns) are considered as in the classical MoM, in order to reduce the number of FFT points along the *z* direction.
Assumed the ground plane at $z = 0$ position, the Green's function has the form

$$g_d\left(|\vec{\rho}-\vec{\rho}'|, z-z'\right)+g_i\left(|\vec{\rho}-\vec{\rho}'|, z+z'\right)=\frac{1}{4\pi\varepsilon\sqrt{|\vec{\rho}-\vec{\rho}'|^2+(z-z')^2}}-\frac{1}{4\pi\varepsilon\sqrt{|\vec{\rho}-\vec{\rho}'|^2+(z+z')^2}},$$

where $|\vec{\rho}-\vec{\rho}'|$ is the distance between source and test position in the *xy* plane. Considering the unknowns images, we have to evaluate

$$\sum_{p'=0}^{N_x-1}\sum_{q'=0}^{N_y-1}\sum_{r'=0}^{N_z-1} g_i\left((p-p')\delta_x,(q-q')\delta_y,2h_z+(r-r')\delta_z\right)\psi(p',q',r')=g_i\left(p\delta_x,q\delta_y,2h_z+r\delta_z\right)\otimes\psi(p,q,-r),$$

where $\otimes$ denotes the three--dimensional convolution, $\delta_{x,y,z}$ denote the cartesian grid spacing along the *x*, *y* and *z*, respectively, h_z is the minimum *z* coordinate of the cartesian grid enclosing the object (0 in our case), and ψ denotes the auxiliary source values.
If $\Psi(i,j,k)$ denotes the FFT samples of $\psi(p,q,r)$, the FFT samples of $\psi(p,q,-r)$ are given by $\Psi(i,j,-k)=\Psi(i,j,\overline{N}_z-k)$, being $\overline{N}_z$ the number of FFT points along the *z* direction.
So, the presence of image sources involves only the multiplication in the transformed domain. The overall computational complexity is dominated by the number of operations required by the direct and inverse FFT and it is almost the same of the free-space case. With similar consideration we can apply the AIM technique also in structure with one or more ground planes, parallel to the coordinate's planes. Such consideration can be useful in evaluation of capacitance for an arbitrary shaped three dimensional structure in the presence of such ground planes.

Conclusions
We have discussed about the use of numerical models of electric and magnetic fields generated by power lines to evaluate the human exposure level. The results obtained from numerical models are been compared to measurements. In case of the magnetic field, a 3D model can be efficiently used, with almost the same complexity of a 2D model. In case of electric field, a 2D numerical model hasn't a good accuracy, even consider the effects of buildings and topography, and measurements are necessary. In such case, a numerical model can be used to choose the measurement's points.
A 3D model can increase the accuracy. We have given some implementation notes about such model (AIM). Results will be shown at the conference.

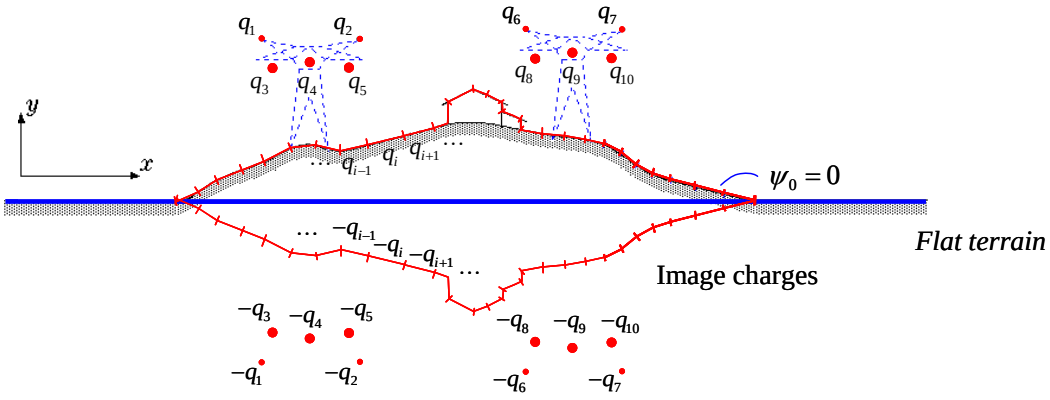

Fig. 6: Full 2D electric field model geometry.

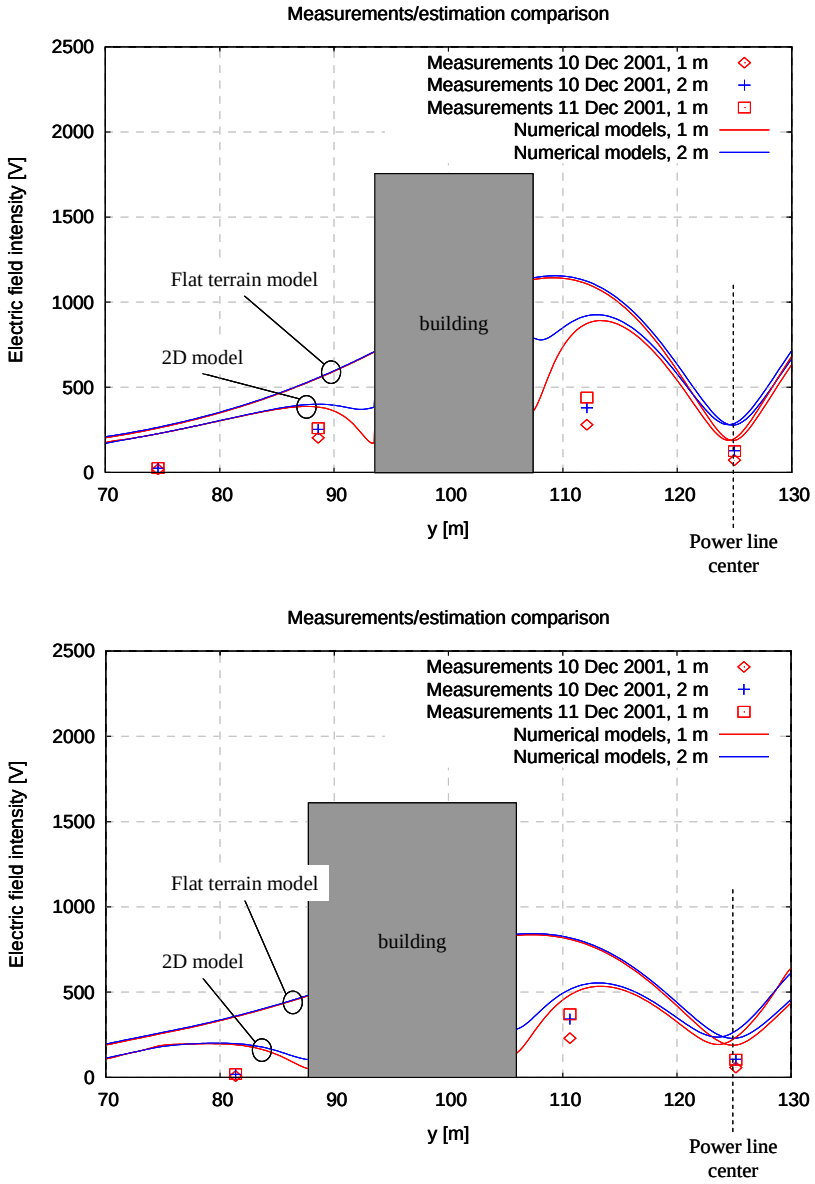

Fig. 7: Comparison between flat terrain and full 2D model results. Two different transverse sections respect to the power line are considered. The number in the legends refers to the quote of the test point.

Bibliography

[1] M. Calamia, "Comune di Montespertoli + 38 contro TERNA S.p.A. – GRTN S.p.A.", *Relazione Tecnica del CTU, 10th April 2002*, filed at Florence Civil Court (Firenze, Italy, in italian).

[2] M. Calamia, "Comune di Montespertoli + 38 contro TERNA S.p.A. – GRTN S.p.A.", *Nota Integrativa alla Relazione Tecnica del 10th April 2002*, 28th August 2004, filed at Florence Civil Court (Firenze, Italy, in italian).

[3] R. F. Harrington, "*Field Computation by Moment Methods*", McMillian Company, New York, 1968.

[4] E. Bleszynski, M. Bleszynski, and T. Jaroszewicz, "AIM: Adaptive integral method for solving large-scale electromagnetic scattering and radiation problems", *Radio Science*, vol. 31, n. 5, Sept.-Oct. 1996, pp. 1225-1251.

[5] C. F. Wang, L. W. Li, P. S. Kooi, and M. S. Leong, "Efficient Capacitance Computation for three-dimensional Structures Based on Adaptive Integral Method", *Progress in Electromagnetics Research PIER*

30, 2001, pp. 33-46.

[6] A Report of the IEEE Magnetic Fields Task Force of the AC Fields Working Group of the Corona and Field Effects Subcommittee of the Transmission and Distribution Committee, "Magnetic Fields From Electric Power Lines Theory And Comparison To Measurements," *IEEE Transactions on Power Delivery*, vol. 3, n. 4, October 1988, pp. 2127–2136.

Overview of IEEE / ISO 11073 RF Wireless: Point-of-care medical device communication – Transport Profiles – Guidelines for the use of RF wireless technology

Joseph J Morrissey

Motorola Labs, 8000 West Sunrise Blvd, Ft. Lauderdale, FL 33322

Abstract: The IEEE / ISO 11073 RF wireless series of standards provides an overview and analysis of the issues related to the use of radio frequency (RF) wireless technology for the transport of data both to and from point-of-care (PoC) medical devices. Currently, several different RF wireless technologies exist that might be applicable, each with different capabilities, stages of maturity in terms of standardization, and active implementation in medical devices and healthcare facilities. It is recognized that RF technologies are rapidly evolving, and new options may become available (or sufficiently established) in the near future offering additional (perhaps superior) solutions for PoC medical device data transport needs. Therefore, the IEEE / ISO 11073 RF wireless series of standards avoids being overly prescriptive but instead aims to assist end users in identifying the necessary requirements and considerations to select an appropriate RF wireless technology solution. Guidance is offered with the objective of allowing medical device manufacturers, wireless equipment manufacturers, healthcare providers, government agencies and any other stakeholders to make reasonable judgments regarding the performance and practical implementation of wireless solutions.

Introduction: Incorporation of wireless technology into point of care (PoC) medical devices has the potential to offer significant benefits to healthcare, specifically home- and mobile- based disease management. An initial IEEE / ISO 11073-30500 Framework and Overview standard outlines use case scenarios to estimate, compare, and contrast the performance of known technologies operating on personal area (wPAN), local area (wLAN), metropolitan area (wMAN), regional area (wRAN), and wide area (wWAN) networks. Major considerations in evaluating performance are 1) the physical requirements of data transport, 2) the quality of service (QoS) requirements associated with the data being transported, and 3) the capabilities of the wireless system. Also considered are related issues such as network architecture, EMI/EMC, co-existence with other data streams, security, cost, power consumption, and technology configurability. Such comparisons are not necessarily intended to endorse an optimal solution, because widely different needs, resources, sizes, and environments associated with healthcare facilities may have a large influence on determining appropriate solutions.

Understanding how these wireless technologies support different quality of service (QoS) requirements (reliability, latency, priority, bandwidth) and how transmit power, link range, battery life and other characteristic features are related to performance is essential [Figure 1]. Optimal performance will largely depend upon the criticality of the medical data and the specific needs and resources of the end user. Related issues include network architecture, EMI/EMC, co-existence with other data streams, security, cost, and technology configurability.

Figure 1. General Overview of Wireless Technology Categories

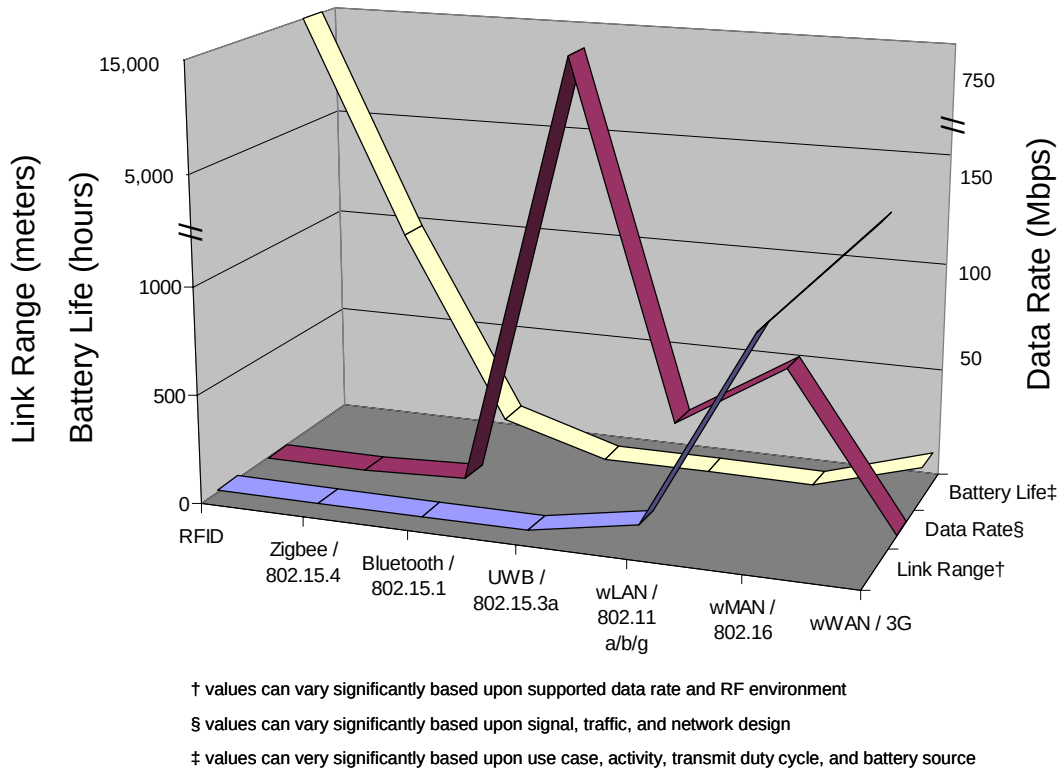

† values can vary significantly based upon supported data rate and RF environment

§ values can vary significantly based upon signal, traffic, and network design

‡ values can very significantly based upon use case, activity, transmit duty cycle, and battery source

Quality of Service (QoS) requirements for medical data [Table 1] are defined in terms of reliability, latency, priority, and bandwidth. The ability of a wireless technology to provide necessary service to medical data in this context would define its QoS support. A variety of different medical devices exist within any given healthcare facility, with medical data streams having different levels of criticality. While some may be good candidates for wireless chip sets, others may perform better on conventional wired systems. This distinction may not be intuitively obvious to medical device and wireless manufacturers or end users without careful consideration of a complex set of variables. Several other considerations, namely increased benefits of mobility of both patients and healthcare staff, must also be considered. It is entirely possible that the added benefits outweigh certain reductions in QoS support.

Table 1. QoS requirements for different categories of medical device data

Data Type	Reliability	Latency	Priority	Bandwidth
Alarms / Alerts (Real-Time)	++++ [AAMI EC-13 - onset of asystole to alarm report]	< 250-500 ms [< 10 sec to central station; AAMI EC-13 - onset of asystole, bradycardia or tachycardia to alarm] < 3 s communication latency	++++	+ (64 bytes/alarm) [intermittent]
Positional alert (Real-Time)	++++	< 3 s communication latency	++++	64 bytes /alert [intermittent] (data is per sensor)
Patient state change (Real-Time)	++++	< 3 s communication latency	++	64 bytes/ state change [intermittent] (data is per sensor)
Sensor watch dog / heartbeat	++++	< 1 min communication latency; ~ 1 time per hour	++	64 bytes/ state change [intermittent]
Reminder (Real-Time)	++++	< 3 s to receive from health care system	++	1632bytes/reminder [intermittent]
Waveforms (Real-Time)	+++	< 300 ms (e.g., during balloon pump in OR / ICU) < 3 s to central station < 7 s for telemetry to in-room monitor	+++	+++ [continuous] EEG: 120-4000+ bit/s (3-12 channels / minimal, monitoring, diagnostic) EEG: 120-250 bit/s (minimal, upper-end, BIS™) Ventilator: 50 - 60 bit/s Sp02: 50 – 120 bit/s
Video/Audio (Real-Time)	+++	< 300 ms	++	4Mbit/s (Bi-directional MPEG2 encoded 320X240 @30fps or 640X480 @30fps audio/video streams) 20Mbit/s (Bi-directional HDTV MPEG-4 video stream; 80kbit/s for VoIP)
Physiologic Parameters (Real-Time) [e.g., episodic bp, hr, SpO_2, $ETCO_2$, temp]	+++	< 10 s to central station < 3 s communication latency from nurse to clinician	+++	+ (20 bytes/param at 1/2 to 1 to 5 Hz) [episodic]
Non-Real-Time Parameters	+++	< 15 s time critical PoCT < 60 s otherwise (CLSI PoCT1-A) < 60 minutes for time-stamped, non time-critical items	++	600 bytes/measurement (CLSI PoCT1-A DML)
Non-Real-Time Events	+++	< 3 s in room < 5 s to central station	++	+ [intermittent]

Control/Settings	+++	< 3 s in room < 5 s to central station	+++	+ [manual]
History / archive retrieval	++	< 5 s pushing < 5 s pulling	+	+++ [manual, bursty]
Web Browsing	++	< 5 s pushing < 5 s pulling	+	+++ [manual, bursty]

In order to address the use of wireless technology in healthcare, realistic use case scenarios have been developed to allow visual navigation of relevant issues involving QoS requirements and support [Figure 2]. These use cases represent a broad range of typical hospital-, home-, and mobile- healthcare scenarios ranging in degree of criticality and complexity.

Figure 2. Use case topological overview

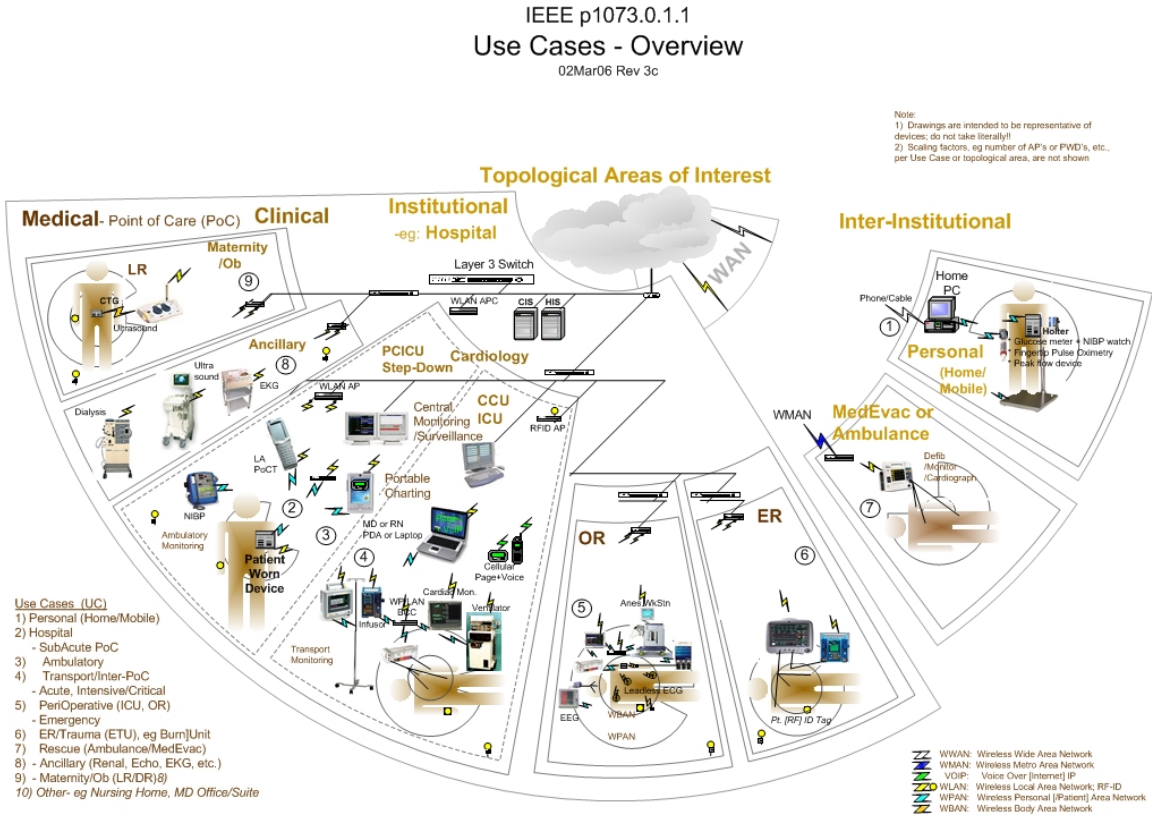

Medical data will often traverse several wireless links en route to the end server / healthcare professional, topological considerations that take different systems into account are necessary [Figure 3]. This example focuses on in-hospital IEEE 802.11 and IEEE 802.15 standards. Other hospital-, home-, or mobile-scenarios were not included to avoid complexity.

Figure 3. Topology Architecture

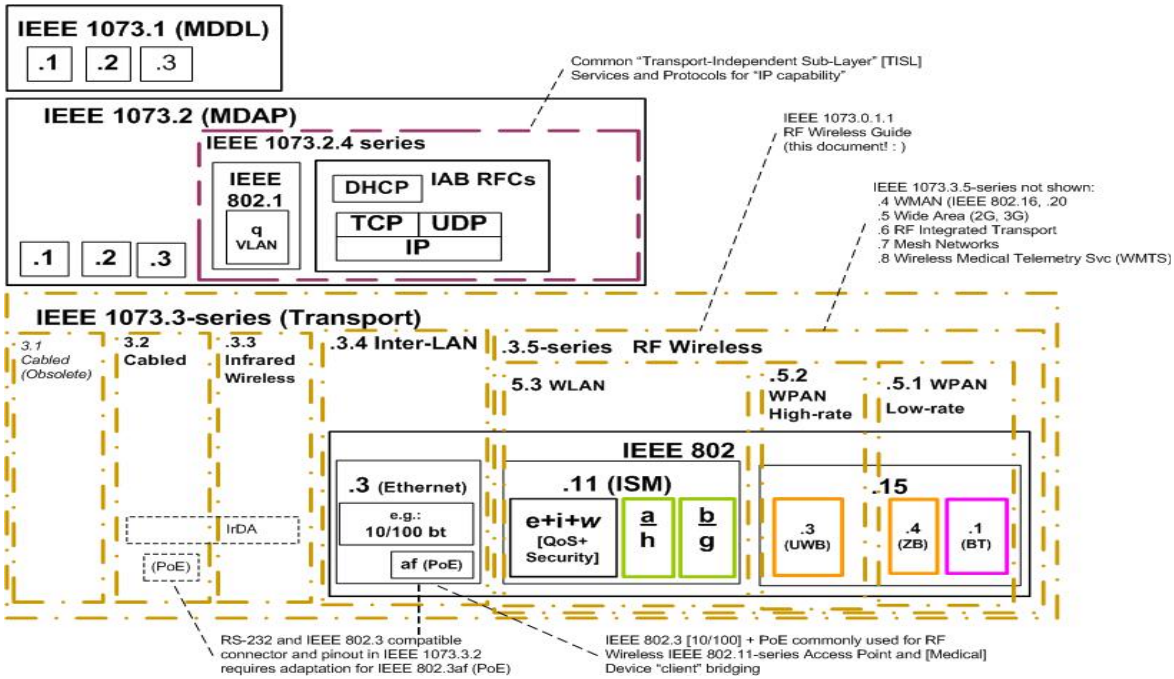

As medical devices become wirelessly enabled, the definition of a "medical device" becomes ambiguous. IEEE / ISO 11073 standards subdivide different stages of medical data transport [Figure 4] to offer some clarification for future assessment and regulation. Traditional definitions of the US-FDA [http://www.fda.gov/cdrh/devadvice/312.html] and UK-MHRA [http://www.mhra.gov.uk/] generally define MDs as products placed on market for patient health / safety that undergo regulatory approval (i.e., CE mark in the EU, FDA approval in the US) and do not address transport of information across wireless links or networks. In the broadest sense, a wireless MD might also include the host (e.g., data collection unit, server, nurse station) and the wireless links (e.g., IEEE 802.11x, IEEE 802.15.x, IEEE 802.16™, telecomm network, IEEE 802.3).

Figure 4. Stages of wireless medical devices

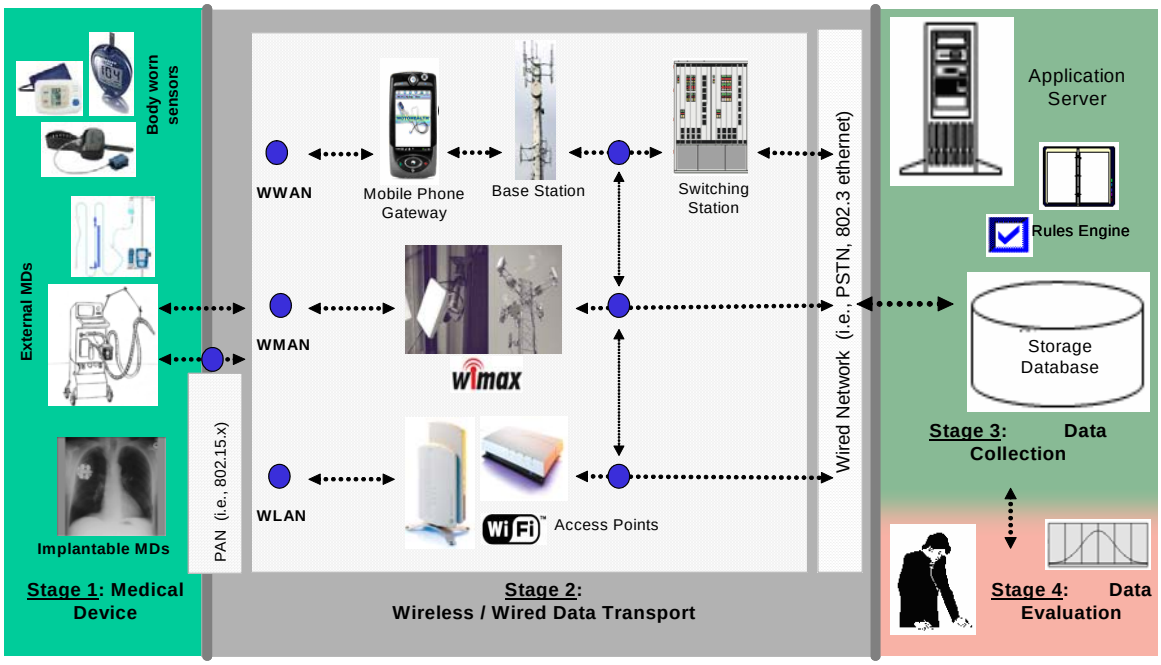

Summary: Proposed, ongoing, and completed IEEE / ISO 11073 RF Wireless Standards [Table 2] will offer guidance to healthcare providers, medical device manufacturers / vendors, wireless equipment manufacturers / vendors, and relevant agency groups for the use wireless technologies for medical data transport. It is a goal of this standards activity to define optimal wireless profiles and promote plug-and-play operability between commercially available medical devices and wireless systems. The effort primarily considers wireless technologies having physical layer protocols defined by industry standards (i.e., IEEE, ISO, ANSI, ITU-R, ITU-T). Compatibility between data exchange formats and upper layer protocols is also an objective to facilitate efficient plug-and-play interfacing and information exchange.

Table 2. IEEE / ISO 11073 RF Wireless family of standards (those in bold are actively in development)

IEEE Project	**Scope**	**Purpose**
IEEE P11073-10101	Nomencature	numeric codes that identify items communicated between systems; partitioned code set that can be use din HL7 messages
IEEE P11073-10201	Domain Information Model (DIM)	Object oriented model: objects, attributes, and methods; all objects specified in ASN.1 notation
IEEE P11073-20000	Application profile – Framework and overview	Scope and purpose for application profile standards - sets and establishes structure for each of the component documents.
IEEE P11073-20400	Application profile – Network service - Framework and overview	Describes the role and types of network services contained within this subset, including their support of transport-specific technologies. This includes key capabilities such as: -Compatibility with IEEE 1073 transport profiles for wPAN, wLAN, wMAN, wWAN -Consistent with QoS outlined in IEEE 802.11e
IEEE P11073-20400	Application profile – Network service - Framework and overview	Describes the role and types of network services contained within this subset, including their support of transport-specific technologies. This includes key capabilities such as: -Consistent with QoS outlined in IEEE 802.11e -Compatibility with IEEE 1073 transport profiles for wPAN, wLAN, wMAN, wWAN
IEEE P11073-20401	Application profile – Network service - Directory	Find and bind services and systems on the network (e.g., a manager for a specific class of devices such as PoCT manager for manufacturer X's devices)
IEEE P11073-20402	Application profile – Network service – Quality of service (QoS) management	Provides a transport-neutral model for application level management of QoS capabilities. This includes detecting the QoS provided by an associated transport profile, as well as setting desired QoS parameters to be negotiated when a connection is established.
IEEE P11073-20403	Application profile – Network services - Location	Patient location, asset tracking, staff location and tracking [throughout supply chain (management) so not counterfeit, correct amount, etc.]
IEEE P11073-20404	Application profile – Network services - Identification	Patient ID, pharmacy ID, supply chain, RFID
IEEE P11073-20500	Application profile – Security – Framework and overview	Overview of issues and strategy for addressing security issues to support plug-and-play medical device communication; incl. security capabilities esp. to support patient demographics data communication[a] consistent / compatible with IEEE 802.11i and HL7 (1073.6.1.1)

IEEE P11073-00101	Technical Report	Guidelines and foundation for RF wireless transport profiles
IEEE P11073-30400	**Transport profile – Internet protocol (IP) [based]**	**Profile the application of IP technologies for use in medical device communication, compatible with IEEE 1073-based Ethernet or wPAN, wLAN, wMAN, wWAN profiles, including vLAN, IP, medical session, QoS, security, UDP, TCP, multicast discovery, addressing characters, wired to wireless infrastructure, etc.**
IEEE P11073-30500	**Transport profile – RF wireless – Framework and Overview**	**Presents the unique concerns and requirements relating to the use of RF wireless technologies for PoC medical device communication. Unique use cases addressed by RF wireless networks; links to guidelines doc 1073.0.0.1**
IEEE P11073-30501	Transport profile – RF wireless – Personal area networks (wPAN), Low-rate	Profile IEEE 802-series standards appropriate for low-rate PoC medical device data transport over short link distances (i.e., personal area networks). [802.15.1[4] Bluetooth, 802.15.4[4] ZigBee]
IEEE P11073-30502	Transport profile – RF wireless – Personal area networks (wPAN), High-rate	Profile IEEE 802-series standards appropriate for high-rate PoC medical device data transport over short link distances (i.e., personal area networks); Ultra wide band (UWB) [802.15.3a[4]]
IEEE P11073-30503	**Transport profile – RF wireless – Local area networks (wLAN)**	**Profile IEEE 802-series standards appropriate for high-rate PoC medical device data transport over in-building networks involving several patient areas (i.e.,802.11a[4], 802.11b[4], 802.11g[4], 802.11n[4] [data prioritization], 802.11i[4] [encrypted transmission to improve security]**
IEEE P11073-30504	Transport profile – RF wireless – Metropolitan area networks (wMAN)	Profile IEEE 802-series standards appropriate for high-rate PoC medical device data transport over large regional areas (i.e., metropolitan area networks) / Broadband / certain UWB technologies
IEEE P11073-30505	**Transport profile – RF wireless – Wide area networks (wWAN)**	**Profile existing licensed telecommunication standards appropriate for PoC medical device data transport over large / regional distances (i.e., wide area networks) / mobile phones (2G [GSM, CDMA, iDEN] and 3G [UMTS, CDMA2000])**
IEEE P11073-30506	RF Integrated Transport[s]	Profile above standards for integrated (e.g., WLAN / WPAN, WPAN / WWAN) data communication
IEEE P11073-30507	Transport profile – RF wireless – Mesh networks	Profile IEEE (802.11s[4], 802.15.5[4]) standards appropriate for low to medium-rate PoC medical device data transport over large / regional distances operating via multiple node relays (i.e., mesh networks)
IEEE P11073-30508	Transport profile – RF wireless – Wireless medical telemetry service (WMTS)	Profile future (IEEE 802-series, other) standards appropriate for PoC medical device data transport developed or modified for operation on WMTS bands

COUPLING TO SPECTACLE FRAMES FROM A 450 MHZ PERSONAL RADIO SOURCE OPERATING ANTERIORLY TO THE HEAD

A. D. BALL, N. E. EVANS, W. G. SCANLON[#], S. J. BURGESS and J. McLAUGHLIN

Centre for Communications Engineering, School of Electrical & Mechanical Engineering, University of Ulster, Shore Road, Newtownabbey, Co. Antrim, N. Ireland, UK, BT37 0QB
 # School of Electrical & Electronic Engineering, Queen's University of Belfast N. Ireland, UK, BT9 5AH.

The RF coupling potential of medium-power UHF personal radios operating in close proximity to wire framed spectacles was quantified in a scenario where the recommended minimum body–radio separation is not respected.

A custom and flexible FDTD simulator written in 'C' (COCA: Code for Coupled Antennas) was used for analysis, with a 2 mm atomically realistic adult head model truncated at the shoulders. The effects of radio orientation and spectacle shape (circular/square) on the polar pattern, induced current profile and SAR distribution was investigated. The undesirable effects of analysing tilted wire elements using the Yee algorithm were overcome by applying Dey-Mittra special update equations. The peak 1 g SAR was situated in the nasal bone region, due to localised parasitic-conductor contact at the bridge of the nose. This parameter was spectacle-shape dependent, as demonstrated by SAR values that were 70 % (rectangular frame) and 174 % (semi-rimless) greater than in the isolated (clean head) case of 3.98 W/kg, for a personal radio input power of 1 W. Partial eye screening occurred when both sets of conducting frames were in place. A maximum coupled current of 16 mA was computed in the semi-rimless frames.

Introduction

Personal radios, transmitting in the lower UHF range (435 MHz), have been identified as primary sources of interference when functioning in close proximity to body worn conductors (e.g. electronic sensing devices [1][2]). Similar effects can also be expected when a PR is operated close to the head, with the user wearing wire framed spectacles [3][4], whereby the minimum body-radio separation of 2.5 cm recommended by a range of manufacturers is not respected, thus placing the transmitting antenna very close to the face and eyes. This is of concern as the eyes are particularly sensitive organs due to their proximity to the surface of the head, their tendency to accumulate damage and cellular debris [5], as well as a limited ability to dissipate heat [6] due to relatively low levels of blood flow compared to other regions of the body.

To date, research into radiation effects in the presence of spectacles has been performed numerically for a cell-phone [7], Personal Digital Assistant applications [8][9], and by measurement [6][10]. The literature shows re-radiation effects [3] along with a rise in peak head SAR [3][8][9], in addition to frequency and spectacle-shape dependence of the average SAR in the eyes [8][9].

The objective of this work was to investigate the effects of a hand held 450 MHz radio fitted with a $\lambda/4$ monopole operated in front of the face (Figure 1a), with a self-developed FDTD program (COCA), by computing the antenna's input impedance, radiation pattern and SAR. These parameters were contrasted to the case when the PR user wore full wire-framed spectacles with rectangular lenses. Dey-Mittra's contour path model was implemented in COCA, enabling the typical practical scenario of a PR tilted by 45° (Figure 1b) to be scrutinised. Finally, COCA was employed to compute the currents induced in a semi-rimless spectacle frame fitted with circular lenses (Figure 1 c & d).

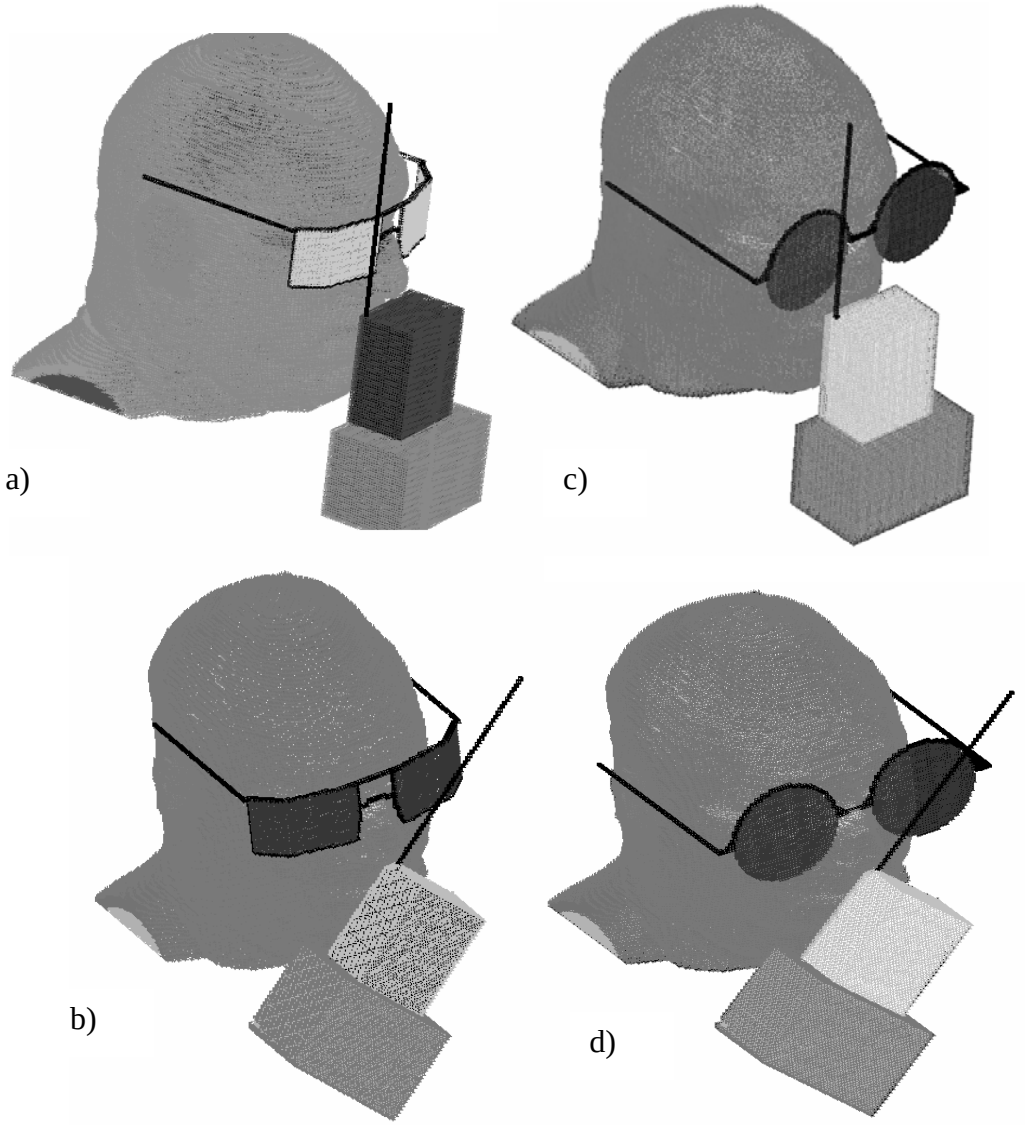

Figure 1: Anterior-head radio / monopole system (vertical & tilted), with wrapped hand. In a) and b) the spectacle frame is 166 mm (0.241 λ) wide, with 122 mm (0.177 λ) legs and lens apertures 68 mm x 40 mm (0.1 λ x 0.06 λ). Cases c) and d) have semi-rimless spectacles, with 152 mm (0.22 λ) legs and a lens diameter of 68 mm.

Methodology

The FDTD computations were performed in a 2 mm grid, using the Brooks anatomically realistic phantom [11] truncated to the head and shoulders. The dielectric properties of the 21 distinct tissue types used (Table 2) were computed at 450 MHz, using a public domain computer program[1] based on published 4-Cole-Cole parameters [12]. The phantom was adapted by removing the normally closed eyelids, so as to leave the eyes exposed as in normal radio use and to investigate the worst-case scenario at the frequency of interest [8][9].

[1] http://niremf.ifac.cnr.it/cgi-bin/tissprop/htmlclie/uniquery

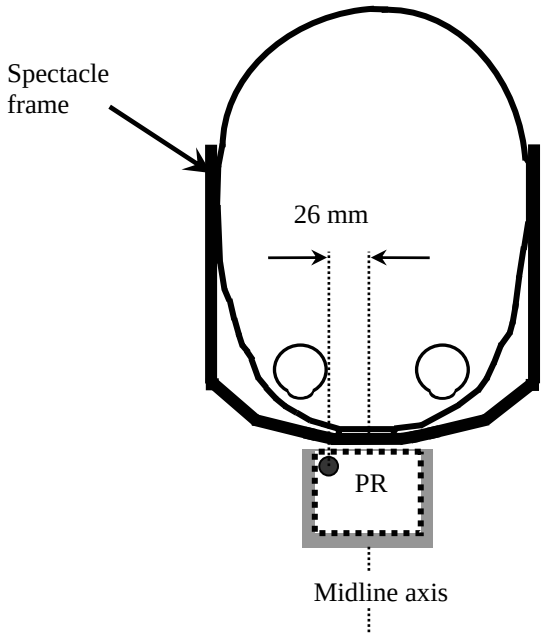

Figure 2: Horizontal section showing relative (rectangular lens) frame, antenna, radio and hand positioning.

The PEC box representing the handset was coated in a loss-less 2 mm insulating layer with $\varepsilon_r = 2$. The $\lambda/4$ monopole, made from 2 mm diameter wire, was corner-located on the top surface of the radio, on the edge nearest the head (4 mm) to mimic worst-case operational conditions (Figure 2). The hand was modelled as a 4 mm core of bone surrounded by a 6 mm layer of muscle and a 2 mm coating of skin, covering all three sides of the handset. The antenna was initially length-adjusted for resonance in isolation, Table 1.

Table 1: Input impedance of a vertical and tilted PR monopole in free space.

	Vertical PR	**Tilted PR**
COCA	74.31+j1.58 Ω	71.69-j1.17 Ω

Table 2: Tissue dielectric properties at 450 MHz.

Material	**Conductivity σ (Sm^{-1})**	**Relative permittivity ε_r**
Blood	1.37	63.7
Blood vessel	0.57	46.6
Bone cancellous	0.24	22.2
Bone cortical	0.09	13
Bone marrow	0.03	5.6
Brain grey matter	0.76	56.5
Brain white matter	0.46	41.5
Cartilage	0.6	45
Cerebellum	1.05	54.7
Cerebro spinal fluid	2.26	70.5
Cornea	1.21	58.5
Eye sclera	1.02	57.2
Fat	0.04	5.5
Lens	0.68	47.8
Ligament	0.57	47
Lymph	0.89	61.23
Mucous membrane	0.69	49.2
Muscle	0.8	56.7
Nerve	0.46	34.9
Skin (dermis)	0.71	45.7
Vitreous humor	1.54	69

The conducting spectacle frame consisted of 2 mm square-section PEC: this was positioned for normal wear, terminating behind the ears. Loss-less optical-glass lenses with ε_r = 7.75 were fitted. The only body surface contact made by the frame was at the top of the nose and near the ears, with a separation of 2 mm (1 Yee cell) representing worst-case conditions.

Polar pattern alteration

At 450 MHz the human body acts primarily as a reflector; the low impedance presented to the wave by the body reduces the electric field nearby, whilst increasing the magnetic field. For antenna-body distances greater than $\lambda/4$ from the transmitter**,** a high impedance is presented to the approaching wavefront, which enhances the electric field at the same time as the magnetic field is reduced. At the far side of the body, away from the antenna, there is a deep null caused by power absorbed in tissue [13]. Because of the dominance of the magnetic field between the monopole and the frames, magnetic coupling occurs. This in turn causes an electric current to flow on the frames, which results in an increased electric field in their vicinity: the wire reradiates and the polar pattern changes.

In all cases studied, the radio is offset from the centre of the face. This results in asymmetric polar patterns as energy is absorbed in the head; see the deep null in Figure 3a). Both backward gains are enhanced by re-radiation from the spectacles: this effectively reduces null depths. The addition of either spectacle frame improves the forward gain and highlights the re-radiation due to induced currents. Tilting the handset has the effect of rotating the radiation pattern: Figure 3 b). Nulls appear both at the front and back of the head, but in the latter case are less pronounced than previously. The frontal null is created due to power absorbed in the nose. The increased forward gain was more noticeable with the square spectacles.

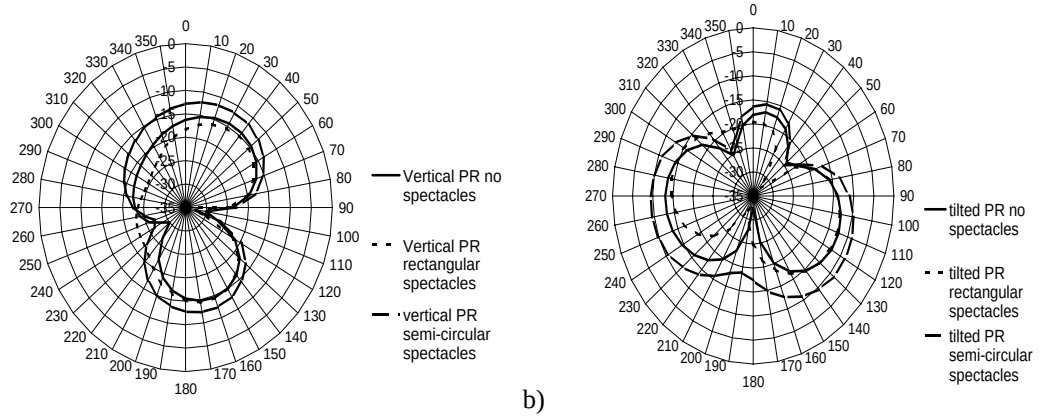

a) b)

Figure 3: E_Φ vertical far field patterns, with and without spectacles, for a) vertical and b) tilted personal radios.

Vertical PR SAR results

Computed SAR values were all scaled for an antenna input power of 1 W, and are summarised in Table 3. When the radio is beside the 'clean' phantom head there is detuning: the input resistance falls to 66.1 Ω and the reactance becomes capacitive, at -j0.72 Ω. With spectacles, the input resistance decreases further to 65.4 Ω, and the reactance becomes inductive.

Table 3: Computed input impedance and peak SAR in the head and eyes in the cases of a vertical and tilted PR proximal to the head. SAR levels were normalised against 1 W transmitter output power.

	Vertical PR			**Tilted PR**		
	Without spectacles	**With rectangular lenses**	**With semi-rimless lenses**	**Without spectacles**	**With rectangular lenses**	**With semi-rimless circular lenses**
Input impedance (Ω)	66.1-j0.72	65.4+j1.4	64.36-j0.7	68.73-j9.41	68.94-j6.4	72.82+j8.83
Peak head SAR (W/kg)						
1-g	3.98	6.77	10.89	3.31	8.53	5.38
10-g	2.65	2.75	2.89	2.14	2.41	2.22
1-g peak eye SAR (W/kg)						
Right	1.16	0.7	0.79	0.23	0.14	0.22
Left	0.35	0.31	0.35	1.01	0.51	1.08

Figure 4 shows the SAR profiles in the relevant vertical head sections, with 0 dB corresponding to maximum power dissipation in each case. For 1 g mass averaged SAR, the displacement of the hotspot in each instance is evident. Without spectacles the maximum SAR in the head was 3.98 W/kg; this occurred in the muscle *(oribicularis oris)* between the oral and nasal cavities, at a tissue depth of 12 mm and in a vertical plane displaced 4 mm towards the antenna from the head's midline axis. With the rectangular-framed spectacles, energy absorption is more spread out over the nose, with a peak 1 g SAR of 6.77 W/kg (a rise of 70 %), in the nasal bone region *(nasalis)* at 4 mm deep in the midline plane, due to localised parasitic-conductor contact at the bridge of the nose. In [8] and [9], it is reported that SAR is dependent on the shape and size of the wearer's spectacles. Similarly here, the SAR with semi-rimless spectacles is concentrated at the upper and lower extremities of the nose, rising to 10.89 W/kg, an increase of 174 % and 61 % compared to the isolated and rectangular-framed cases, respectively. Unsurprisingly, for a higher averaging tissue mass of 10 g, the peak SAR without spectacles was lower at 2.65 W/kg. Increases still occurred in the nasal region (though not as significant), up 3.77 % to 2.75 W/kg with the rectangular frames, and 9.1% to 2.89 W/kg with the semi-circular. The human head is a complex, highly detailed organ; indeed the human eye or pinna/external ear have masses of as little as 10 g [14]. Furthermore, certain cells or neurons in the brain can be misrepresented by 1 g of tissue [14]. An 8 mm^3 Yee grid is employed here, which could explain the relatively high 1 g semi-circular spectacle SAR result. This suggests that the peak 1 g SAR is associated with a single hot-spot rather than a general increase in SAR values within the user's head.

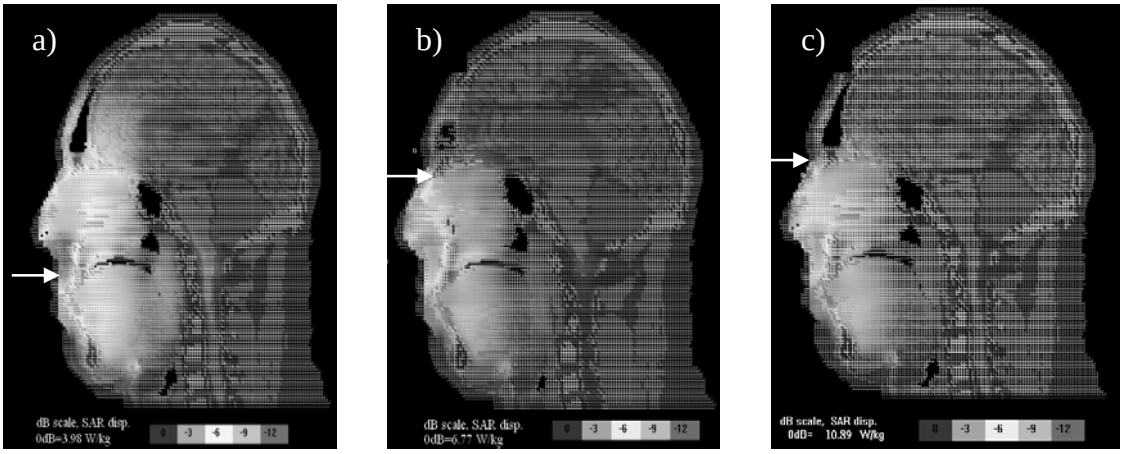

Figure 4: 1 g mass averaged SAR for a vertically-oriented PR beside head a) clean b) with rectangular-framed spectacles and c) with semi-circular frames.

Eye SARs were computed to establish conditions in this particularly sensitive body tissue. With the antenna passing 30 mm from the right eye, and without spectacles, the 1-g peak SAR was 1.16 W/kg. For the left eye, 80 mm from the antenna, the corresponding value was more than 70 % lower (0.35 W/kg). Partial eye screening occurred when both sets of conducting frames were in place; the 1-g SAR fell by 40 % in the right eye and 11.4 % in the left with the rectangular frames in use, as noted in Table 3. A similar phenomenon occurred with the semi-circular frames, with a 32 % SAR reduction in the right eye and an unchanged SAR in the left. All reported SARs were computed for a CW excitation, which implies that they would be further reduced if realistic TDMA duty cycles were taken into account: consequently, they are well within the IEEE guidelines for occupational users. SAR is, however, proportional to the antenna input power, which implies that if transmitter output level rises (a current trend in PR design as hardware improves) then safety limits are likely to be exceeded.

Tilted PR SAR results

Here, the PR was tilted by 45°, as illustrated in Figure 1b. Rotating the radio caused the free space input resistance to decrease by 4.12 %. However, turning the handset had a more noticeable effect on the input reactance, as it became more capacitive - see Table 3.

Placing the spectacles on the phantom caused both the input resistance and reactance to increase positively. Inclination of the radio caused the frame-free 1 and 10 g SARs to be 17 % and 19 % lower than in the vertical PR case, respectively, at 3.31 and 2.14 W/kg. The peak 1g SAR in the eye was situated close to the monopole's feedpoint, in the left eye (1.01 W/kg). Both peak eye SARs without spectacles were less than, or equal to, those with frames and the vertical radio. The 1 g mass averaged SAR profiles with and without spectacles are presented in Figure 5.

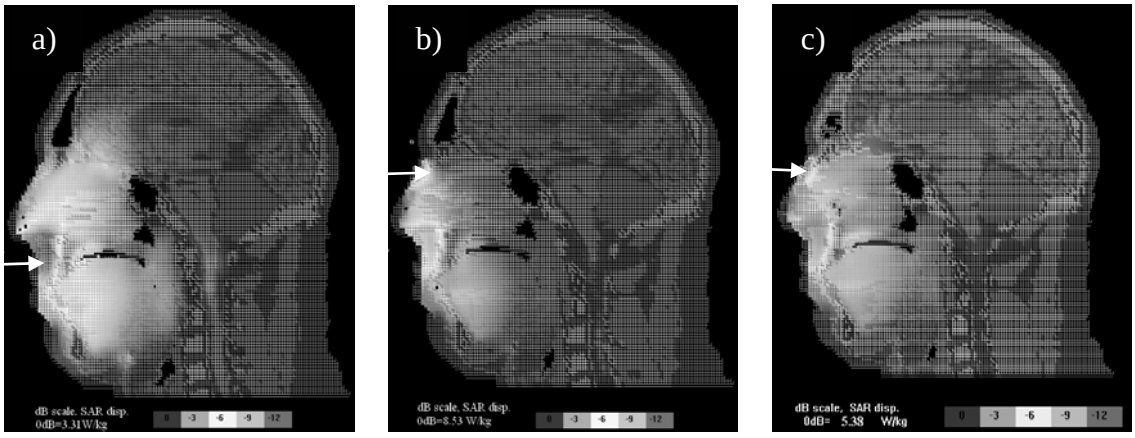

Figure 5: 1 g mass averaged SAR for a tilted PR close to head a) 'clean' b) with a rectangular frame and c) with semi-rimless circular lenses.

As with the vertical PR, the SAR hotspot without spectacles is situated between the oral and nasal cavities. With rectangular-framed spectacles, a second very distinctive concentration is generated at the top of the nasal bone region. There is less SAR 'spread' than in the corresponding vertical PR case (Figure 5b). For semi-circular frames, substantial SAR spreading is again evident.

With the rectangular frames the eyes were partially screened, as substantiated by the 50% reduction of the SAR in the eye nearest the antenna, and 39 % decrease in the other. However, only marginal changes occurred in the case of the semi-circular frames: SAR in the left eye increased by 7 % and decreased in the right by 4 %.

Induced currents

The induced current distribution on spectacle frames has previously been investigated at 1.5 GHz in [7], with a mobile telephone radiating 1 W close to the ear of an anatomically based head model. Two different types of spectacle frames were studied - one with rims and legs both metallic, and the other rimless, with metallic legs only. Current profile discontinuities were present in this model, where the nosepiece intersected each lens' outer contour and at the intersection of the metallic leg and outer rim. The discussion on circular frames has a number of similarities with electrically small loop antennas, which are equivalent to infinitesimal magnetic dipoles; the current distribution in loops of perimeter less than 0.3 λ is taken to be constant around the loop [16].

Computing induced current in a pair of spectacles is challenging in terms of EM simulation, as this creates a number of discontinuities. Because of this, the simulations here were done in two stages. Firstly, a 'flat' spectacle model was assembled (Figure 6a), after which the legs were bent, as depicted in Figure 6b.

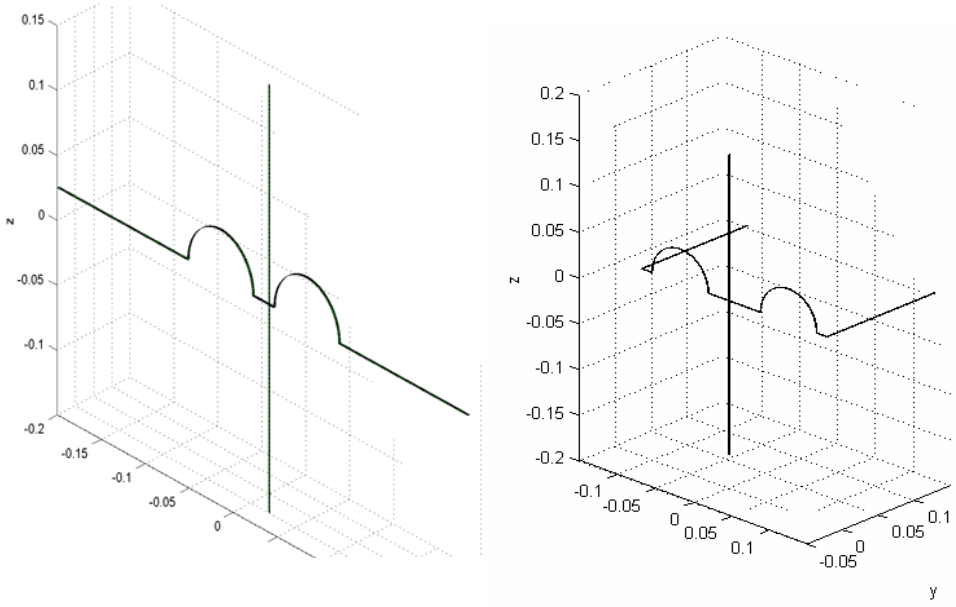

Figure 6: Dipole coupled to a) flat spectacle frame b) a spectacle frame with bent legs; in b) Zin= 64.4–j9.2 Ω.

This done, the induced currents were computed with COCA, as illustrated in Figure 7.

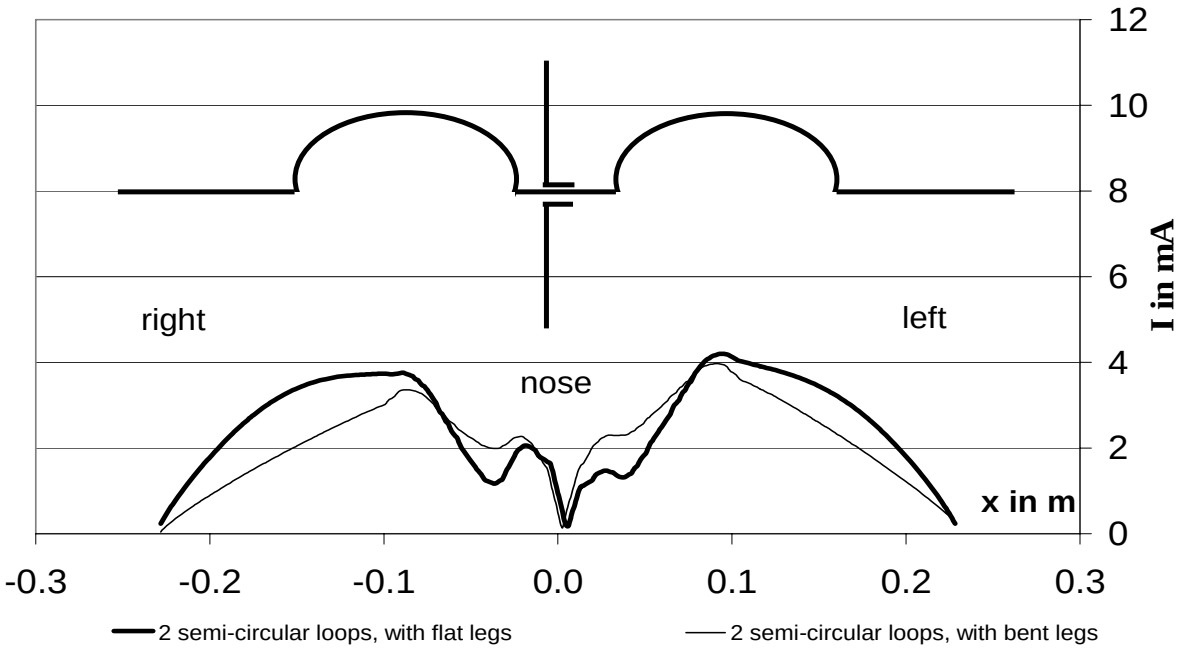

Figure 7: Induced current in the top section of half-rim wire frames adjacent to a 450 MHz dipole (P_{in} = 0.32 W).

The spectacles coupled to the dipole have an overall length of 0.6 λ: two pseudo standing waves are generated that reach minima at the outer extremities of the spectacle legs and at the middle of the nosepiece. Two small reflections at both nosepiece extremities (T junction) emerge, with current maxima of 4 mA at the top of each loop. Bending the legs by 90° causes the induced current to decrease overall. The currents computed are significant, reinforcing the source of the increased forward gains obtained.

Finally, the result of introducing the phantom head was investigated. The PR monopole was corner-located on the handset chassis and held to the right of the user's nose, as illustrated in Figure 2, causing the radiating antenna and case to be strongly coupled to the adjacent semi-circular lens. On this basis, the left lens was shadowed by the nose. This gave a smoother, full standing wave (Figure 8), with current maxima of 16 and 11 mA. The increased current magnitude is because of less detuning in this case, plus the majority of the energy radiated by the monopole is above the PR's 'groundplane'.

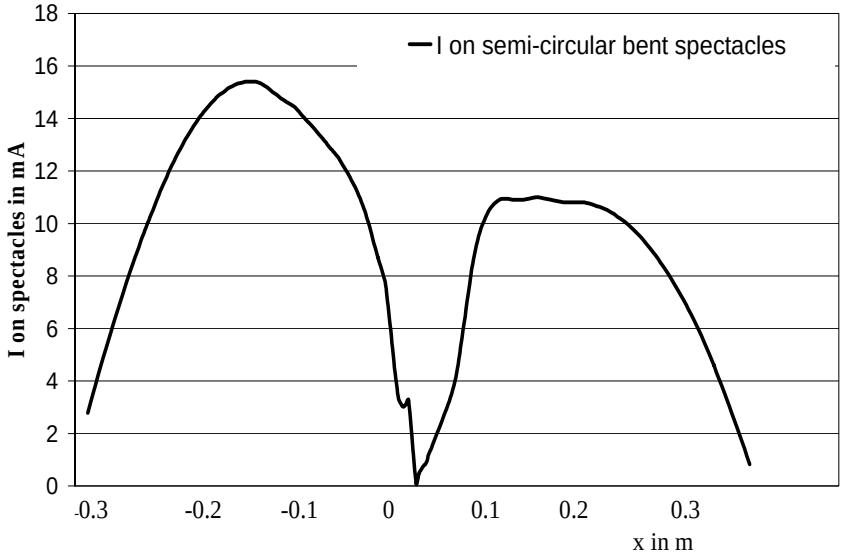

Figure 8: Induced current on semi-circular spectacles with 90° legs, coupled to a vertical 450 MHz monopole / case close to an anatomically realistic head (P_{in}= 0.32 W).

Conclusions

The coupling between a personal radio handset and the human head was investigated at 450 MHz, for two realistic radio orientations, vertical and tilted by 45°. For each orientation, a spectacle-free phantom was contrasted to a model wearing rectangular and semi-circular frames. In each simulation the polar pattern, SAR distribution and induced current profiles were computed.

Absorbed power levels were dependent on the PR's orientation and on the shape of the wire spectacle frames, as evidenced by a 1g SAR ranging between 3.31 and 10.89 W/kg. In the instance of the vertical PR, partial eye screening occurred when both sets of conducting frames were in place. This was only the case with the rectangular frames when the PR was tilted. In general, frame-conductor re-radiation enhances polar pattern forward gain and reduces backward-facing nulls.

Magnetic coupling between the PR and the semi-circular frames caused a cosine-like standing-wave to be developed on the frames, with unequal maxima on the right and left semi-circular loops because of obstructive tissue absorption.

References

[1] Ball A. D., Evans N. E., Troulis S. E., Scanlon W. G. and Burgess S. J., "RF interference (RFI) between uhf personal radios and biomedical monitoring sensors," *Proc. IEE Seminar on Telemetry and Telematics,* London, April 2005, pp. 4/1 - 4/5.

[2] Ball A.D., Evans N. E., Troulis S. E. & Scanlon W. G., "An FDTD study of the interaction between body-worn biomedical-monitor wires and a coupled 435 MHz dipole radiator," *Bioelectromagnetics 2005,* Dublin, June 2005, pp. 92-96.

[3] Troulis S.E., Ball A.D., Evans N.E. and Scanlon W.G., "SAR for adult and child users of 450 MHz Personal-radio handsets operating anteriorly to the head," *3rd International Workshop on Biological Effects of EMF,* Kos, Greece, Oct 2004, pp. 457-464.

[4] Ball A.D., "A Numerical Investigation of the Electromagnetic Coupling Between Body-Worn Conductors and UHF Antennas in Close Proximity," PhD Thesis, University of Ulster, Jordanstown, N. Ireland, 2006.

[5] Dimbylow, P.J. and Mann, S.M., "SAR calculations in an anatomically realistic model of the head for mobile communication transceivers at 900 MHz and 1.8 GHz," *Physics in Medicine and Biology,* Vol. 39, No. 10, Oct. 1994, pp. 1537-53

[6] Anderson, V. and Joyner, K.H., "Specific absorption rate levels measured in a phantom head exposed to radio frequency transmissions from analog hand-held mobile phones," *Bioelectromagnetics,* Vol. 16, No. 1, 1995, pp. 60-69.

[7] Wang J., Joukou T. and Fujiwara O., "Localized specific absorption rate in the human head in metal-framed spectacles for 1.5 GHz hand-held mobile telephones," *Trans. Inst. Electrical Engineers of Japan,* Vol. 118-A (11), 1998, pp. 1234–1240.

[8] Whittow, W.G. and Edwards, R.M.,"A study of changes to specific absorption rates in the human eye close to perfectly conducting spectacles within the radio frequency range 1.5 to 3.0 GHz," *IEEE Transactions on Antennas and Propagation,* Vol. 52, No. 12, Dec. 2004, pp. 3207-12.

[9] Edwards, R.M. and Whittow, W.G., "Applications of a genetic algorithm for identification of maxima in specific absorption rates in the human eye close to perfectly conducting spectacles," *IEE Proceedings-Science, Measurement and Technology,* Vol. 152, No. 3, May 2005, pp. 89-96.

[10] Griffin D.W., "A microwave antenna method of measuring the effect of metal-framed spectacles on microwaves near the eye," *Proc. Antennas and Propagation Society International Symp.,* 1983, Vol 21, pp. 253-256.

[11] Mason, P. A., Ziriax, J. M., Hurt W. D., Walters T. J., Ryan K. L., Nelson D. A., Smith K. I. and D'Andrea J. A., "Recent advancements in dosimetry measurements and modelling," in Radio Frequency Radiation Dosimetry (B. J. Klauenberg and D. Miklavcic, Eds., Kluwer, Norwell, MA, 2000), pp. 141–155.

[12] Gabriel S., Lau R. W. and Gabriel C., "The dielectric properties of biological tissues: III. Parametric models for the dielectric spectrum of tissues," *Phys. Med. Biol.*, Vol. 41, 1996, pp. 2271-2293.

[13] James J.R., Mobile Antenna Systems Handbook, Artech House, 2nd Ed., 2001, ISBN 1580530079.

[14] Lin, J.C., "Specific absorption rates (SARs) induced in head tissues by microwave radiation from cell phones", *IEEE Antennas and Propagation Magazine*, Vol. 42, No. 5, Oct. 2000, pp. 138-1399.

[15] Lin, J.C., "Safety standards for human exposure to radio frequency radiation and their biological rationale," *IEEE Microwave Magazine*, Vol. 4, No. 4, Dec. 2003, pp. 22-26.

[16] Balanis C. A., "Antenna Theory, Analysis and Design," 2nd edition, John Wiley & Sons Inc., 1997.

[17] ANSI, ANSI / IEEE, (1992); *C95.1-1992: IEEE Standard for safety levels with respect to human exposure to radio frequency electromagnetic fields, 3 kHz to 300 GHz,* IEEE, New York.

[18] International Commission on Non-Ionising Radiation Protection, (1999): "ICNIRP statement - health issues related to the use of hand-held radiotelephones and base transmitters," *Health Phys.*, Vol. 70, No. 4, pp. 587- 593.

[19] Troulis S. E., Scanlon W. G., and Evans N. E., "Effect of a hands-free wire on specific absorption rate for a waist-mounted 1.8 GHz cellular telephone handset," *Phys. Med. Biol.*, Vol. 48, 2003, pp. 1675-1684.

EMF DOSIMETRY INSIDE THE EMBRYO EXPOSED BY THE PLANE WAVE IN THE FREQUENCY RANGE OF 10 MHZ TO 3 GHZ

HIROKI KAWAI[1], TOMOAKI NAGAOKA[1], SOICHI WATANABE[1], WOLFGANG KAINZ[2], KAZUYUKI SAITO[3], MASAHARU TAKAHASHI[3], AND KOICHI ITO[4]

[1]NATIONAL INSTITUTE OF INFORMATION AND COMMUNICATIONS TECHNOLOGY, 4-2-1 NUKUI-KITAMACHI, KOGANEI, TOKYO, 184-8795 JAPAN
[2]U.S. FOOD & DRUG ADMINISTRATION, 12725 TWINBROOK PARKWAY, ROCKVILLE, MD, 20852 USA
[3]RESEARCH CENTER FOR FRONTIER MEDICAL ENGINEERING, CHIBA UNIVERSITY, 1-33 YAYOI-CHO, INAGE-KU, CHIBA-SHI, CHIBA, 263-8522, JAPAN
[4] FACULTY OF ENGINEERING, CHIBA UNIVERSITY, 1-33 YAYOI-CHO, INAGE-KU, CHIBA-SHI, CHIBA, 263-8522, JAPAN

Abstract
This paper presents the computational electromagnetic field (EMF) dosimetry inside a woman-torso model, which is exposed to E- and H-polarised waves, in the first gestational month using the finite-difference time-domain (FDTD) method over the frequency range from 10 MHz to 3 GHz. First, parametric models for the dielectric spectrum of fetus and those of amniotic fluid are demonstrated. Second, the whole-body average SAR in the embryo is calculated, when the incident power density of plane waves is ICNIRP or IEEE occupational reference level. As a result, the maximum value is less than 0.4 W/kg (occupational limit) over the frequency range from 10 MHz to 3 GHz. Finally, the internal SAR distributions inside the torso model are also shown at 10 MHz, 100 MHz, and 1 GHz. As a result, the SAR distribution around the embryo is dependent on the frequency and polarized wave in the first gestational month.

1. Introduction

Today many devices emitting EMFs are widely used in the close vicinity of the human body. Consequently, the evaluation of the specific absorption rate (SAR) in various models, such as adults, children, and pregnant women and their fetuses is necessary. Especially the priority on EMF dosimetry in embryos and fetuses is growing [1]. In the early term of pregnancy, it could be possible that the embryos are exposed to EMFs when mothers do not know their pregnancy yet. Therefore, EMF dosimetry in the embryos is important.

Until now, Fleming and Joyner [2] have proposed the EMF dosimetry inside the embryo in 80-100 MHz and fetus across the range 300-1500 MHz, when the pregnant women are exposed to plane wave. In addition, Dimbylow [3] have presented the EMF dosimetry inside a whole-body pregnant woman and her developing fetus in 8-, 13-, 26- and 38-weeks of gestation at 50 MHz. However, the dosimetry inside the embryo over the wide frequency range have not minutely evaluated yet.

Hence, this paper presents the computational EMF dosimetry inside a woman-torso model, which is composed by five types of tissues, in the first gestational month, when the model is exposed to E- and H-polarised waves. Here, the EMF is calculated using the FDTD method [4] over the frequency range from 10 MHz to 3 GHz. Furthermore, the incident power density of plane waves is the international EMF reference revels (ICNIRP [5], IEEE [6], and occupational limit) in each frequency. Moreover, the internal SAR distributions inside the torso model are also calculated at 10 MHz, 100 MHz, and 1 GHz.

2. Models and method

2.1 Dielectric properties of embryo

The dielectric properties of biological tissues are very important parameters for the EMF dosimetry. Gabriel [7] has proposed parametric models for the dielectric spectrum of various types of tissues using the summation of 4-Cole-Cole equation. The dielectric properties at the target frequency are given by the following equation [7].

$$\hat{\varepsilon}(\omega) = \varepsilon_{\infty} + \sum_{n=1}^{4} \frac{\Delta\varepsilon_n}{1+(j\omega\tau_n)^{(1-\alpha_n)}} + \frac{\sigma_i}{j\omega\varepsilon_0} \tag{1}$$

where ε_∞ is the material permittivity at terahertz frequency, ε_0 is the free-space permittivity, σ_i is the ionic conductivity, and $\Delta\varepsilon_n$, τ_n, α_n are material parameters for each dispersion region.However, parametric models of expectant tissues, which are the amniotic fluid, placenta, and fetus (embryo), have not proposed yet in [7].

In fetal tissues, substituted dielectric properties from adult tissues using the variation in the water content [8] are usually used [3]. In addition, the properties of placenta are about the same values of blood, because the composition of the two is about the same. Moreover, Luca *et al* [9] have proposed the parametric model of the conductivity of amniotic fluid over the frequency from 1 MHz to 1 GHz.

Ito *et al* [10] have demonstrated the measured dielectric properties of fetus of rabbit and those of amniotic fluid of human over the frequency range from 100 MHz to 3 GHz. However, their results cannot apply to the other frequency. Therefore, we present the parametric models using the Eq. (1), to expand the wide frequency range. Table 1 describes the parameters of amniotic fluid and those of fetus for the Eq. (1). These parameters are defined using the simplex method based on the differences between the estimated properties by Eq. (1) and measured values as shown in Fig. 1. The parameters can realize the minimization of the difference between the estimated and measured values. In this paper, the dielectric properties based on the parameters in Table 1 are used from 10 MHz to 3 GHz.

Table 1 Parameters of amniotic fluid and those of fetus for the Cole-Cole equation

Tissue	ε_∞	$\Delta\varepsilon_1$	τ_1 [ps]	α_1	$\Delta\varepsilon_2$	τ_2 [ns]	α_2	$\Delta\varepsilon_3$	τ_3 [μs]	α_3	σ_i
A_fluid	4	75	7.23	0.14							1.42
Fetus	4	57	8.38	0.10	6000	133	0.1	1.20E+06	318	0.10	0.12

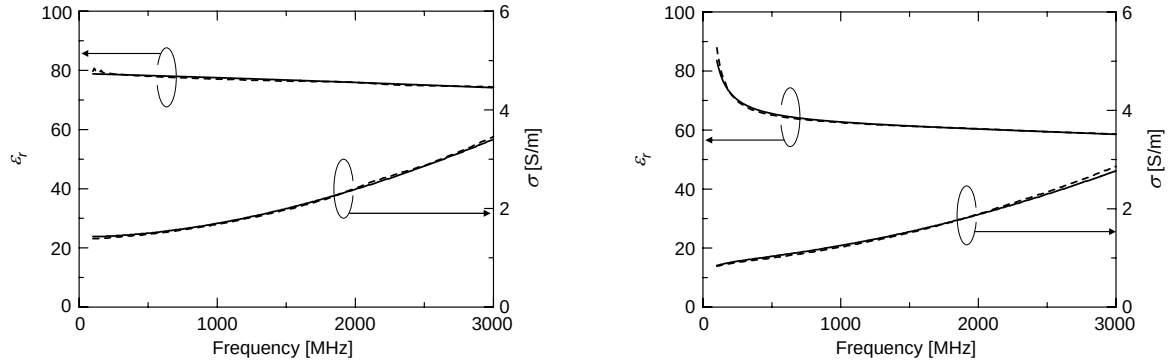

(a) Amniotic fluid (b) Fetus

Fig. 1 Graphic representation of dielectric properties of amniotic fluid and fetus using Eq. (1) and Table 1 (line) together with the measured data (dotted line) [10].

2.2 Numerical model

Figure 2 shows a woman-torso model in the first gestational month. This model was scaled down from a woman-torso model in the 35th gestational week based on the external shape and magnetic resonance (MR) images [11]. The model was segmented seven different types of tissues, which were body, bone, bladder, uterus, embryo, placenta, and amniotic fluid. However, in the first gestational month, the amniotic fluid and placenta have note generated yet. Hence, we substituted the dielectric properties of uterus for the values of the two.

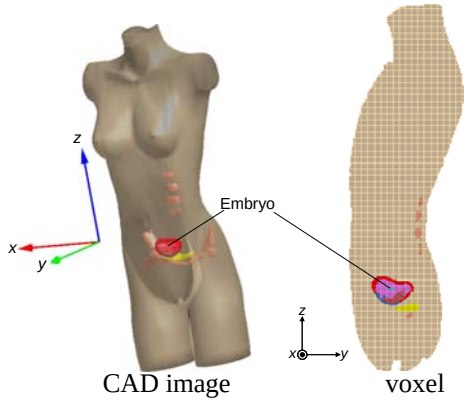

CAD image voxel

Fig. 2 Torso model of woman in the first gestational month.

2.3 Numerical condition

The FDTD software (X-FDTD ver. 6.3.8.3, by Remcom Engineering AG, PA, USA) was used for the EMF calculating inside the torso model. The parameters of FDTD calculation employed in this paper were as follows. The cell size was 2.5 mm. The numerical region was 190 × 150 × 413 cells (475 × 375 × 1032.5 mm^3). In addition, the absorbing boundary condition was the perfectly matched layer (PML) (eight layers).

Dielectric properties of the tissues, which were excluding the fetus, were based on the parametric models in [7]. Here, the properties of body was the 2/3 those of muscle. The incident waves were E- (E_z applied) and H-polarized (E_y applied) waves propagating from the front to the back of the model. The incident power density was from 1 to 5 mW/cm^2 (ICNIRP) or 1 to 10 mW/cm^2 (IEEE), which were the reference levels for occupational exposure to EMFs over the frequency range from 10 MHz to 3 GHz [5], [6].

3. Results

3.1 Whole-body average SAR

Figure 3 (a) and 3 (b) show the calculated results of the whole-body average SAR in the embryo over the frequency range from 10 MHz to 3 GHz, when the incident power density is ICNIRP or IEEE occupational level, which is dependent on the frequency. From Figs. 3 (a) and 3 (b), the SARs by E- and H-polarized waves are less than 0.4 W/kg (occupational limit) from 10 MHz to 3 GHz in both incident levels. In addition, the maximum value by the H-polarized wave is lower than that by the E-polarized wave in the estimated frequency range.

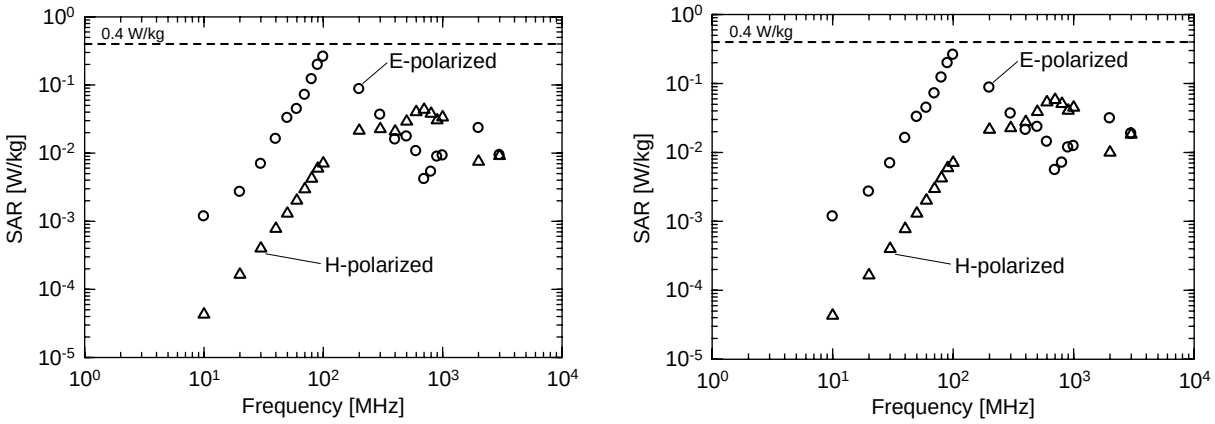

(a) ICNIRP (b) IEEE

Fig. 3 Whole-body average SAR inside the embryo by the plane waves' exposure (circle: E-polarized wave and triangle: H-polarized wave).

3.2 SAR distribution

Figure 4 (a) and 4 (b) illustrate internal SAR distributions on the observational line [see Fig. 4 (lef)] in the median plane of the torso model by the E- or H-polarized wave's exposure at 10 MHz, 100 MHz, and 1 GHz. Here, the incident power density was IEEE occupational reference level in each frequency.

From Fig. 4 (a), the attenuation curve of SAR by the E-polarized wave at 10 MHz is almost equal to that at 100 MHz while the absolute value is significantly different. At these frequencies, in addition, the SAR distribution is almost constant between the uterus and the embryo and higher than the SAR in the frontal body. On the contrary, the attenuation is abruptly varied by the standing wave at 1 GHz.

As shown in Fig. 4 (b), the attenuation curve of SAR by the H-polarized wave in each frequency is about the same. In addition, the peak SAR is arisen on the surface in each frequency. Moreover, the SAR in the embryo and that in the uterus are about the same.

From Fig. 4 (a) and (b), the SAR in the embryo is almost continually varied between the uterus and the embryo in each frequency and incident wave, because the embryo is very small in the first gestational month. These results suggest that the layered structure between the uterus and embryo is not necessary to evaluate the SAR inside the embryo in the first gestational month.

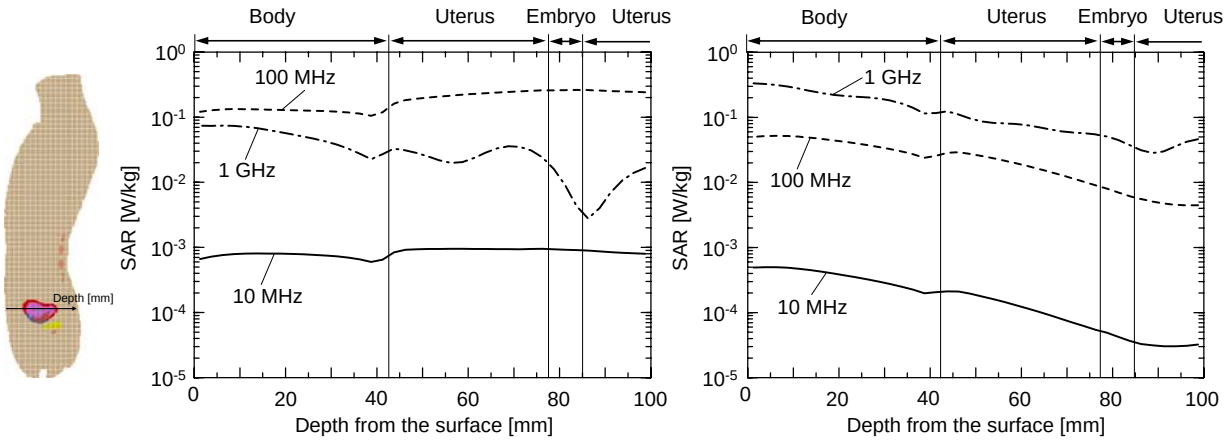

(a) E-polarized wave (b) H-polarized wave

Fig. 4 Internal SAR distributions on the observational line in the median plane of the torso model by the plane wave's exposure at 10 MHz (line), 100 MHz (dotted line), and 1 GHz (dashed-dotted line).

4. Conclusion

This paper presented the computational EMF dosimetry inside the woman-torso model, which was composed by five types of tissues, in the first gestational month using the FDTD method, when the model was exposed to the E- and H-polarized plane waves over the frequency range from 10 MHz to 3 GHz. First, the parametric models for the dielectric spectrum of fetus and those of amniotic fluid were demonstrated. Second, the whole-body average SAR inside the embryo was calculated, when the incident power density of plane waves was ICNIRP or IEEE occupational reference level. As a result, the maximum value in the embryo was less than 0.4 W/kg (occupational limit) by plane waves' exposure over the evaluated frequency range. Finally, the internal SAR distributions inside the torso model were also shown at 10 MHz, 100 MHz, and 1 GHz. As a result, the SAR distribution around the embryo was dependent on the frequency and polarized wave in the first gestational month.

As a further study, the same investigation as above will be done using pregnant and non-pregnant women models, which is segmented much different tissues.

References

[1] WHO, "Children's EMF Research Agenda," The International EMF Project, June 2004.

[2] A.H.J. Fleming and K.H. Joyner, "Estimates of absorption of radiofrequency radiation by the embryo and fetus during pregnancy," *Health phys.*, vol. 74, no. 2, pp. 149-159, Aug. 1998.

[3] P. Dimbylow, "Development of pregnant female, hybrid voxel-mathematical models and their application to the dosimetry of applied magnetic and electric fields at 50 Hz," *Phys. Med. Biol.*, vol. 51, pp. 2383-2394, Apr. 2006.

[4] K.S. Yee, "Numerical solution of initial boundary value problems involving Maxwell's equation in isotropic media," *IEEE Trans. Antennas Propagat.*, vol. 14, no. 3, pp. 302-307, Mar. 1966.

[5] ICNIRP, "Guidelines for limiting exposure to time-varying electric, magnetic, and electromagnetic fields (up to 300 GHz)," *Health Phys.*, vol. 74, no. 4, pp. 494-522, Apr. 1998.

[6] IEEE standard for safety levels with respect to human exposure to radio frequency electromagnetic fields, 3 kHz to 300 GHz, ANSI/IEEE Standard C95.1-2005, Apr. 2006.

[7] C. Gabriel, "Compilation of the dielectric properties of body tissues at RF and microwave frequencies," Brooks Air Force Technical Report, AL/OE-TR-1996-0037, 1996.

[8] J.L. Scheppes and K.R. Foster, "The UHF and microwave dielectric properties of normal and tumour tissues: variation in dielectric properties with tissue water content," *Phys. Med. Biol.*, vol. 25, no. 6, pp. 1149-1159, Nov. 1980.

[9] F.De Luca, C. Cametti, G. Zimatore, B. Maraviglia, and A Pachi, "Use of low-frequency electrical impedance measurements to determine phospholipid content in amniotic fluid," *Phys. Med. Biol.*, vol. 41, no. 9, pp. 1863-1869, Sept. 1996.

[10] K. Ito, H. Kawai, M. Takahashi, K. Saito, T. Ueda, M. Saito, H. Ito, H. Osada, Y. Koyanagi, and K. Ogawa, "Evaluation of the local SAR in a simple abdomen model of pregnant women at 150 MHz," in *Proc. 27th BEMS and EBA meeting*, (CD-ROM), no. 12-2, pp.133-136, Dublin, Ireland, June 2005.

[11] W. Kainz, S. Seidman, R. Qiang, and J. Chen, "The future of anatomical models - anatomical CAD models for numerical dosimetry and implant evaluations," in *Proc. 27th BEMS and EBA meeting*, (CD-ROM), no. P-A-55, pp. 270-272, Dublin, Ireland, June 2005.

ELECTROMAGNETIC POWER ABSORPTION IN CURVED BIOLOGICAL TISSUES

A. SHTROM, D. F. SOLDEA, and P. D. EINZIGER

DEPARTMENT OF ELECTRICAL ENGINEERING,
TECHNION - ISRAEL INSTITUTE OF TECHNOLOGY, HAIFA 32000, ISRAEL

Abstract
Coupled closely to highly absorbing tissues, a source of electromagnetic radiation, such as cellular or hyperthermia antenna, can be greatly affected by the curvature of the absorbing surface. Herein, our previous TE excitation models are extended as to incorporate the TM case, combining an effective and relatively simple procedure for obtaining closed-form corrections for the main power relations involved in the presence of curved-surface absorbing tissues. The derivation is introduced by considering two-dimensional prototype models of surface and line magnetic-type sources radiating in the presence of a half-space and an infinite circular cylinder. The power absorption efficiencies of the cylindrical model are shown to be tightly bounded, both from below and above, by those of the half-space (planar) models.

Introduction
Recently, the study of near-field interactions of electromagnetic sources with highly lossy media, utilizing the Leontovich surface impedance approach [1], [2], has led to analytic readily-interpretable expressions for the main power relations involved in such configurations, namely, source power efficiencies and specific absorption rate [3],[4],[5]. These models, corresponding to a semi-infinite absorbing medium in the vicinity of either finite (current line-source) or infinite (planar current-sheet) sources, lead to an explicit dependence of the power relations on both the geometrical and physical parameters and provided an effective mean for obtaining physical insight into the basic power absorption mechanisms as well as tight bounds and estimates on the power relations. In some realistic configurations, however, such as cellular phone interaction with living tissues [6], [7], electromagnetic hyperthermia-based treatments [8], [9], and highly-sensitive biosensing [10], [11], the absorbing structure's curvature effect should be incorporated into the model in order to render its implementation effective.

Herein, our previous TE excitation models [12] are extended as to incorporate the TM case, utilizing the Leontovich surface impedance approach [1], [2], applied for finite-size two-dimensional (2D) cylindrical absorbing medium. The resultant extension leads to a discrete Parseval's representation for the power relations in terms of the individual cylindrical harmonics' (spectral) power content. These expressions can be interpreted similarly as for the previous (planar) case but with a curvature correction term, continuously depending on the effective surface curvature and the source location. Inclusion of the curvature correction, whenever applicable, enables thereby better understanding and design of prototype systems involving electromagnetic sources closely coupled to highly lossy structures.

Methods
The 2D physical configurations, corresponding to the planar and the cylindrical models, are depicted in Figs. 1(a), 1(b) and Figs. 1(c), 1(d), respectively. Both configurations are characterized by the parameters μ, ε, and σ via: $k_0 = \omega\sqrt{\mu_0\varepsilon_0}$, $Z_0 = \omega\mu_0/k_0 = \sqrt{\mu_0/\varepsilon_0}$, $\sigma_0 = 0$, and $k_1 = \omega\sqrt{\mu_1\tilde{\varepsilon}_1}$, $Z_1 = \omega\mu_1/k_1 = \sqrt{\mu_1/\tilde{\varepsilon}_1}$, $\tilde{\varepsilon}_1 = \varepsilon_1\left(1 - j\sigma_1/\omega\varepsilon_1\right)$ where, assuming a harmonic time-dependence $e^{j\omega t}$, $\Im\{k_1\} \le 0$, and $\Im\{Z_1\} \ge 0$. The analysis and the results for the planar model are well known [2],[3],[4], and thus, summarized herein merely for the sake of comparison, completeness, and clarity. The excitation source locations for both models are given via $y' = d$ (the planar model) and $\rho' = a + d$ (the cylindrical model), where a and d denote the cylinder radius and the sources distance from the lossy tissues, respectively. Additionally, for line sources, $x' = 0$ (the planar model) and $\varphi' = 0$ (the cylindrical model).

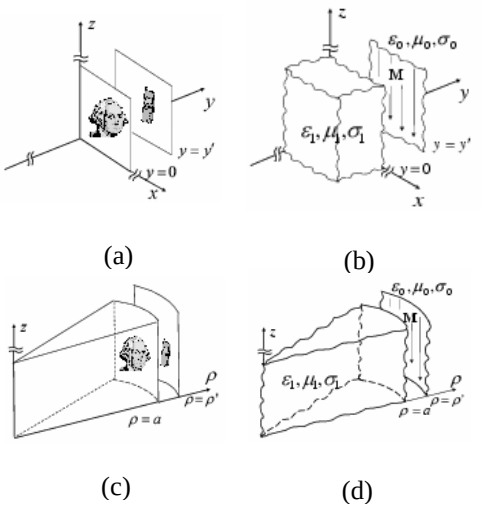

Figure 1: Physical configurations and models for the planar and the cylindrical approaches: (a) Physical configuration, (b) Planar model, (c) Physical configuration incorporating curvature correction, (d) Cylindrical model.

Source representations in terms of surface and line magnetic currents are denoted by $\mathbf{M}^S = -M^S\hat{\mathbf{z}}$ and $\mathbf{M}^L = -M^L\hat{\mathbf{z}}$ respectively, and given in Table 1.

Table 1: Magnetic current sources.

Current source	Planar model	Cylindrical model
M^S	$Ke^{jk_x x}\delta(y-y')$	$I\dfrac{e^{jq\varphi}\delta(\rho-\rho')}{2\pi\rho'}$
M^L	$I\delta(x)\delta(y-y')$	$I\dfrac{\delta(\varphi)\delta(\rho-\rho')}{\rho'}$

The power relations for both models, including radiation power, absorption power, source power, free space source power, power absorption efficiency, and power radiation efficiency, are given via

$$P_{r,\substack{P\\C}} = \mp\frac{1}{2}\Re\left\{\int_{\varphi} E_x H_z^* ds\Big|_{\substack{y'^+\\ \rho'^+}}\right\}, \tag{1}$$

$$P_{a,\substack{P\\C}} = \pm\frac{1}{2}\Re\left\{\int_{\varphi} E_x H_z^* ds\Big|_{\substack{y'^-\\ \rho'^-}}\right\}, \tag{2}$$

$$P_s = P_r + P_a, \tag{3}$$

$$P = P_s\big|_{\varepsilon_1=\varepsilon_0,\sigma_1=0}, \tag{4}$$

$$\eta_a = \frac{P_a}{P_s}, \tag{5}$$

and

$$\eta_r = \frac{P_r}{P_s} = 1-\eta_a, \tag{6}$$

respectively. Note that the distinguishing superscripts S and L (Table 1) and subscripts P and C (Eqs. (1)-(2)), corresponding to the surface and the line currents and to the planar and the cylindrical models, respectively, have been omitted in Eqs. (3)-(6) since these equations apply to both current sources and models. This rule is adapted throughout the entire paper for all the equations that apply to both current sources and models. The fundamental power relations in Eqs. (1)-(4) can be readily expressed in the spectral domain upon expending the transverse components of the electromagnetic field in terms of appropriate modes in conjunction with the Parseval's identity, as summarized in Table 2. The modal fields are represented via plane-waves (continuous spectrum) and cylindrical waves (discrete spectrum) for the planar and the cylindrical models, respectively. The spectral power densities, denoted by P_r, P_a, and P_s in Table 2, are expressed explicitly in Table 3.

Table 2: Spectral representation for the power relations.

Power	Planar-model,		Cylindrical-model,	
relations	current-sheet	line-source	current-sheet	line-source
P_r	$P\frac{\mathcal{P}_r(k_x)}{2}$	$P\int_0^{k_0}\mathcal{P}_r(k_x)\frac{dk_x}{\pi\beta_0}$	$P\mathcal{P}_{r,q}\frac{\left\|H_q^{(2)}(k_0\rho')\right\|^2}{4J_q^2(k_0\rho')}$	$P\sum_{q=-\infty}^{\infty}\mathcal{P}_{r,q}\frac{\left\|H_q^{(2)}(k_0\rho')\right\|^2}{4}$
P_a	$P\frac{\mathcal{P}_a(k_x)}{2}$	$P\int_0^{\infty}\mathcal{P}_a(k_x)\frac{dk_x}{\pi\left\|\beta_0\right\|}$	$P\mathcal{P}_{a,q}\frac{\left\|H_q^{(2)}(k_0\rho')\right\|^2}{4J_q^2(k_0\rho')}$	$P\sum_{q=-\infty}^{\infty}\mathcal{P}_{a,q}\frac{\left\|H_q^{(2)}(k_0\rho')\right\|^2}{4}$
P_s	$P\frac{\mathcal{P}_s(k_x)}{2}$	$P\int_0^{\infty}\mathcal{P}_s(k_x)\frac{dk_x}{\pi\left\|\beta_0\right\|}$	$P\mathcal{P}_{s,q}\frac{\left\|H_q^{(2)}(k_0\rho')\right\|^2}{4J_q^2(k_0\rho')}$	$P\sum_{q=-\infty}^{\infty}\mathcal{P}_{s,q}\frac{\left\|H_q^{(2)}(k_0\rho')\right\|^2}{4}$
P	$\frac{\left\|K\right\|^2}{4\mathcal{Z}_0}$	$\frac{k_0\left\|I\right\|^2}{8Z_0}$	$\frac{k_0\left\|I\right\|^2 J_q^2(k_0\rho')}{8Z_0}$	$\frac{k_0\left\|I\right\|^2}{8Z_0}$

Table 3: Spectral power densities and related functions for the spectral representation.

Planar model		Cylindrical model	
Power Densities And Related functions	Plane-wave Continuous -spectrum	Power Densities And Related functions	Cylindrical-wave Discreet-spectrum
$\mathcal{P}_r(k_x)$	$1+\lvert\Gamma(k_x)\rvert^2+2\Re\left\{\Gamma(k_x)e^{-j2\beta_0 d}\right\}$, $0\le k_x\le k_0$ 0 , $k_0<k_x$	$\mathcal{P}_{r,q}$	$1+\lvert\Gamma_q\rvert^2+2\Re\left\{\Gamma_q\dfrac{H_q^{(1)}(k_0a)H_q^{(2)}(k_0\rho')}{H_q^{(2)}(k_0a)H_q^{(1)}(k_0\rho')}\right\}$
$\mathcal{P}_a(k_x)$	$1-\lvert\Gamma(k_x)\rvert^2$, $0\le k_x\le k_0$ $-2\Im\{\Gamma(k_x)\}e^{-2\lvert\beta_0\rvert d}$, $k_0<k_x$	$\mathcal{P}_{a,q}$	$1-\lvert\Gamma_q\rvert^2$
$\mathcal{P}_s(k_x)$	$2+2\Re\left\{\Gamma(k_x)e^{-j2\beta_0 d}\right\}$, $0\le k_x\le k_0$ $-2\Im\{\Gamma(k_x)\}e^{-2\lvert\beta_0\rvert d}$, $k_0<k_x$	$\mathcal{P}_{s,q}$	$2+2\Re\left\{\Gamma_q\dfrac{H_q^{(1)}(k_0a)H_q^{(2)}(k_0\rho')}{H_q^{(2)}(k_0a)H_q^{(1)}(k_0\rho')}\right\}$
$\Gamma(k_x)$	$\dfrac{1-\mathcal{Z}(k_x)}{1+\mathcal{Z}(k_x)}$	Γ_q	$\dfrac{1-\mathcal{Z}_q w_q}{1+\mathcal{Z}_q w_q^*}\left(\dfrac{w_q^*}{w_q}\right)$
$\mathcal{Z}(k_x)$	$\dfrac{Z_1}{Z_0}\dfrac{\beta_1(k_x)}{k_1}\dfrac{k_0}{\beta_0(k_x)}$	$\mathcal{Z}_q$	$-j\dfrac{Z_1}{Z_0}\dfrac{J_q'(k_1a)}{J_q(k_1a)}$
$\beta_{\substack{0\\1}}(k_x)$	$\sqrt{k_{\substack{0\\1}}^2-k_x^2}$, $\Im\left\{\sqrt{k_{\substack{0\\1}}^2-k_x^2}\right\}\le 0$	w_q	$j\dfrac{H_q^{(1)}(k_1a)}{H_q^{(1)\prime}(k_1a)}$

Results

The limit of high losses, associated with highly lossy tissues, renders $\lvert Z_1/Z_0\rvert\to 0$ (or equivalently $\lvert k_1/k_0\rvert\to 0$) and thus enables the implementation of the well known Leontovich surface impedance approach [1], [2]. This results in a closed-form and relatively simple asymptotic relations for both the planar and the cylindrical models, as summarized in Table 4. These asymptotic relations demonstrate that utilizing the Leontovitch approximation [1], [2] in conjunction with the Debye approximation [13] results in an asymptotic equivalence of the planar and the cylindrical models, when excited by surface currents.

Table 4: The limit of high losses.

Asymptotic limits	Planar model	Cylindrical model
Leontovitch approx. [1],[2] $\left\lvert\dfrac{k_1}{k_0}\right\rvert\to\infty$ or $\left\lvert\dfrac{k_1a}{k_0a}\right\rvert\to\infty$	$\mathcal{Z}(k_x)\sim\dfrac{Z_1}{Z_0}\dfrac{k_0}{\beta_0(k_x)}$ $\Gamma(k_x)\sim 1-2\dfrac{Z_1}{Z_0}\dfrac{k_0}{\beta_0(k_x)}$ $\left.\dfrac{E_x(k_x)}{H_z(k_x)}\right\rvert_{y=0}\sim Z_1$	$\mathcal{Z}_q\sim\dfrac{Z_1}{Z_0}$ $\Gamma_q\sim\left[1-2\dfrac{Z_1}{Z_0}\Re\{w_q\}\right]\dfrac{w_q^*}{w_q}$ $\left.\dfrac{E_{\varphi,q}}{H_{z,q}}\right\rvert_{\rho=a}\sim -Z_1$
Leontovitch approx. [1],[2] & Debye approx. [13] $q=k_0a\sin\theta_q\to\infty$, $\sin\theta_q\ne 1$	$\mathcal{Z}(k_0\sin\theta_q)\sim\mathcal{Z}_q w_q$ $\Gamma(k_0\sin\theta_q)\sim\Gamma_q$	$\dfrac{H_q^{(2)\prime}(k_0a)}{H_q^{(2)}(k_0a)}\sim\pm j\dfrac{\sqrt{(k_0a)^2-q^2}}{k_0a}=\pm j\cos\theta_q$ $w_q\sim 1/\cos\theta_q$

Furthermore, this equivalence establishes an identical asymptotic lower bound on the power absorption efficiency ´s η_a^S in (5) for the planar and cylindrical waves in both models, as demonstrated in Fig. 2, i.e.

$$\eta_a^S \geq \eta_a^S\Big|_{\frac{k_x}{k_0}=0} \text{ or } \frac{q}{k_0 a}=0, \tag{7}$$

in the range, $0 \leq k_0 d < \frac{\pi}{4}$.

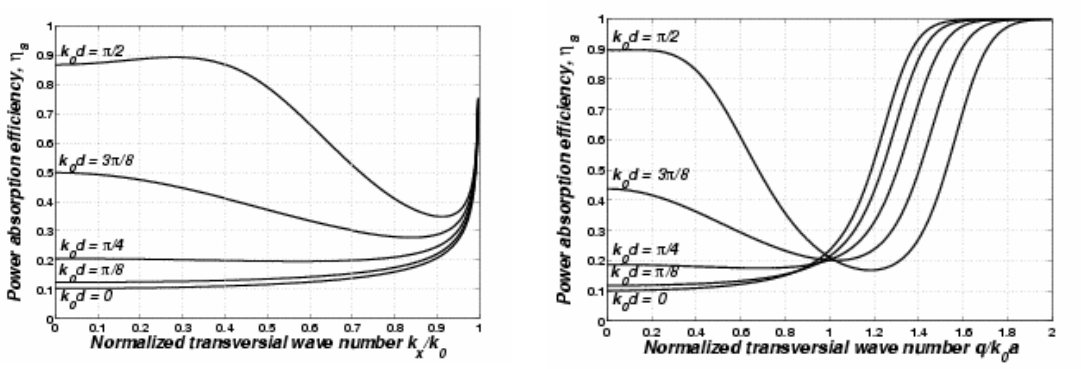

(a) (b)

Figure 2: Power absorption efficiency vs. normalized transversial wave number, $Z_1/Z_0 = 0.1140 + j0.0658$: (a) Plane wave model ($k_0 a \to \infty$) [3], [4], [5], (b) Cylindrical wave model ($k_0 a = 10$).

Noting that Leontovitch and Debye approximations (Table 4) lead to

$$\eta_{a,P}^S\Big|_{\frac{k_x}{k_0}=0} = \eta_a^{TEM} \sim \eta_{a,C}^S\Big|_{\frac{q}{k_0 a}=0}, \tag{8}$$

where η_a^{TEM} is expressed as [4]

$$\eta_a^{TEM} \sim \frac{2\Re\left\{\frac{Z_1}{Z_0}\right\}\left(1-\Re\left\{\frac{Z_1}{Z_0}\right\}\right)}{1-\Re\left\{\frac{Z_1}{Z_0}\right\}-\left(1-2\Re\left\{\frac{Z_1}{Z_0}\right\}\right)\cos^2\left(k_0 d+\Im\left\{\frac{Z_1}{Z_0}\right\}\right)}. \tag{9}$$

This results in an asymptotic common lower bound η_a^{TEM} for both models in (7) and renders a tight asymptotic common lower bound for the line-source power absorption efficiencies $\eta_{a,P}^L$ and $\eta_{a,C}^L$ associated with the planar and the cylindrical models, i.e.,

$$\eta_{a,P}^{L}=\frac{\int_{k_x}\mathcal{P}_a(k_x)\frac{dk_x}{|\beta_0|}}{\int_{k_x}\mathcal{P}_s(k_x)\frac{dk_x}{|\beta_0|}}=\frac{\int_{k_x}\mathcal{P}_s(k_x)\eta_{a,P}^{S}\frac{dk_x}{|\beta_0|}}{\int_{k_x}\mathcal{P}_s(k_x)\frac{dk_x}{|\beta_0|}}\geq\eta_a^{TEM}, \tag{10}$$

and

$$\eta_{a,C}^{L}=\frac{\sum_{q=-\infty}^{\infty}\mathcal{P}_{a,q}\left|H_q^{(2)}(k_0\rho')\right|^2}{\sum_{q=-\infty}^{\infty}\mathcal{P}_{s,q}\left|H_q^{(2)}(k_0\rho')\right|^2}=\frac{\sum_{q=-\infty}^{\infty}\mathcal{P}_{s,q}\eta_{a,C}^{S}\left|H_q^{(2)}(k_0\rho')\right|^2}{\sum_{q=-\infty}^{\infty}\mathcal{P}_{s,q}\left|H_q^{(2)}(k_0\rho')\right|^2}\geq\eta_a^{TEM} \tag{11}$$

respectively.

Finally, in the limit of zero curvature as $k_0a\to 0$, the cylindrical model is asymptotically reduced into the planar model, i.e.,

$$\eta_{a,C}^{L}\sim\eta_{a,P}^{L}, \tag{12}$$

It is readily noted that while the asymptotic result in (8) is valid if Leontovitch and Debye approximations can be applied, for the validity of (12) requires, in addition, that $a/\rho'\to 1$ (or equivalently $d/a\to 0$).

Calculations based on Eq. (5) and Tables 2-3 are now carried out for magnetic line-source excitation (Table 1) utilizing FCC guidelines [14] for evaluation of biological tissues parameters at cellular frequencies (human brain parameters at 900 MHz: $\sigma=0.7[S/m]$, $\varepsilon_1=45\varepsilon_0$). Fig. 3 reveals that the cylindrical model's results correlate well with Eqs. (7)-(12). Furthermore, as expected, the power absorption efficiencies $\eta_{a,C}^{L}$ for the cylindrical model is tightly bounded from above and bellow by the power absorption efficiencies associated with the planar model excited by surface and line magnetic currents (Table 1), respectively, for a broad range of k_0a values, i.e.,

$$\eta_a^{TEM}\leq\eta_{a,C}^{L}\leq\eta_{a,P}^{L},\qquad k_0a>1. \tag{13}$$

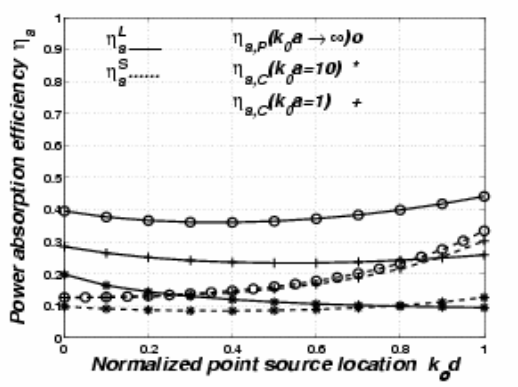

Figure 3: Curvature effect on efficiencies and bounds: FCC parameters at 900MHz [14], $\sigma=0.7[S/m]$, $\varepsilon_1=45\varepsilon_0$.

In conclusion, the power absorption efficiency for the cylindrical model is universally bounded by the planar model efficiencies for both excitations (Table 1), namely, the planar and the line magnetic current sources. Furthermore, as the curvature of the absorbing medium approaches zero, the power relations for the cylindrical model are asymptotically reduced to the results associated with the planar model.

References

[1] T. B. A. Senior, Impedance Boundary Conditions for Imperfectly Conducting Surfaces, *Appl. Sci. Res.*, Sect. B 8, 1959, 418-436.

[2] G. Tyras, *Radiation and Propagation of Electromagnetic Waves*, (New York: Academic, 1969).

[3] D. F. Soldea, D. Razansky, and P. D. Einziger, Plane-Wave Model for Electromagnetic Power Absorption in Biological Tissues, *J. Appl. Phys.*, 94(3), 2003, 2053-2059.

[4] D. Razansky, D. F. Soldea, and P. D. Einziger, Bounds Estimates and Resolution for Power Absorption in 2D Highly-Lossy Configurations - *J. Appl. Phys.*, 95(12), 2004, 8298-8308.

[5] D. Razansky, D. F. Soldea, and P. D. Einziger, Transmission-Line Model for Estimation of Cellular Handset Power Absorption in Biological Tissues- *IEEE Trans. on Electromagn. Compat.*, 47(1), 2005, 61-67.

[6] R.W. P. King, Electric Currents and Field Induced in Cells in the Human Brain by Radiation from Hand-Held Cellular Telephones, *J. Appl. Phys.*, 87(2), 2000, 893-900.

[7] G. Lazzi, O. P. Gandhi, S. Ueno, Guest Editorial, *IEEE Trans. Microwave Theory and Tech.*, 52(8), 2004, 1853 - 1855.

[8] A. J. Fenn, G. L. Wolf, and R. M. Fogle, An adaptive microwave phased array for targeted heating of deep tumours in intact breast: animal study results, *Int. J. Hyperthermia*, 15(1), 1999, 45-61

[9] D. Razansky, P. D. Einziger, and D. R.Adam *Phys. Rev. Lett.*, 93, 2004, 083902.

[10] D. Razansky, P. D. Einziger, and D. R.Adam *Phys. Rev. Lett.*, 95, 2005, 018110.

[11] M. Specht, J. D. Pedarning, W. M. Hechkl, and T. W. Hanisch, *Phys. Rev. Lett.*, 68, 1992, 476.

[12] A. Shtrom, D. F. Soldea, D. Razansky, and P. D. Einziger, Curvature effect for electromanetic power absorption in biological tissues, *Proc. of the 24th IASTED International Multi-Conference on Biomedical Engineering*, Innsbruck, Austria, Feb. 15-17, 2006, 339-343.

[13] M. Abramowitz and I. A. Stegun, *Handbook of Mathematical Functions*, (New York: Dover, 1972).

[14] Federal Communications Commission, Evaluating Compliance with FCC Guidelines for Human Exposure to Radiofrequency Electromagnetic Fields, Supplement C, *OET Bulletin 65*, Ed. 97-01.

RECOGNITION AND ENGULFMENT OF THE APOTOTIC CELLS: INFLUENCE OF THE EXPOSURE TO MODERATE-INTENSITY STATIC MAGNETIC FIELD

LUCIANA DINI, PATRIZIA TARANTINO, BERNADETTE TENUZZO, MAJDI DWIKAT and ALESSANDRA QUARTA

DEPARTMENT OF BIOLOGICAL AND ENVIRONMENTAL SCIENCE AND TECHNOLOGY; UNIVERSITY OF LECCE; LECCE, ITALY

ABSTRACT

Phagocytosis of the apoptotic cells requires distinguishing features on the surface of dead cells, recognition and tethering molecules, as well as the cytoskeletal and other cellular machinery involved in engulfment.

If the details of the interaction between apoptotic cells and phagocytes are still far to be fully understood, even more obscure are the external factors able to modulate the phagocytosis. We have hypothesized that any factors influencing cell surface molecules expression (phagocyte and /or apoptotic cell) can in turn affect recognition of apoptotic cells. This is indeed the case of static magnetic field of moderate intensity that alters the surface of cells after 24 h of continuous exposure.

Therefore, the recognition of apoptotic lymphocytes by liver sinusoidal cells under exposure to 6 mT static magnetic field to define at which extent static magnetic fields are able to modulate this specific type of phagocytosis was studied.

Carbohydrate expression on lymphocyte surfaces was extensively affected by exposure to static magnetic field irrespective of the cell status, i.e. normal or apoptotic. These modifications are responsible of the altered recognition of apoptotic lymphocytes by the sinusoidal liver cells. In particular, the exposure to static MF has been found to be an extremely critical factor for the recognition of not only apoptotic lymphocytes, but especially for control ones.

INTRODUCTION

The interest in the biological effects of non-ionizing electromagnetic fields (EMFs) on the whole organism, as well as on cellular systems, has considerably increased in recent years in consideration of their increased production (from the generation and transmission of electricity, to domestic appliances and industrial equipment, to telecommunications and broadcasting) and of possible health risk for humans. Findings on the effects of (E)MFs exposure on humans are often contradictory and, therefore, difficult to interpret. No direct evidence of tumorigenicity have ever been demonstrated, however, epidemiological studies have associated (E)MFs exposure with increased incidence of cancer. The multiplicity of experimental conditions (i.e., in vitro or in vivo models, intensity and type of field, oscillatory or static, time of exposure, metabolic state of the cells, etc) makes contradictory the data on the biological effects of (E)MFs. Many researches have indicated plasma membrane as the primary site of action of (E)MFs (Santoro et al., 1997). Indeed, the effects on plasma membrane have been described at different levels: on the electrochemical balance of the membrane (Panagopouls et al., 2000), on its surface (Paradisi et al., 1993), on the distribution of membrane proteins (Bersani et al., 1997) and membrane receptors, on the cell-cell and cell-matrix junctions (Somosy, 2000), on lipid peroxidation and generation of reactive oxygen species (ROS) (Ishisaka et al., 2000; Jelenkovic et al., 2006), on DNA damage (Fiorani et al., 1992; Miyakoshi 2005), on the sugar residues on cell membrane (Bordiushkov et al., 2000; Chionna et al. 2003b) and on trans-membrane fluxes of different ions especially calcium (Thompson et al., 2000; Cho et al., 1999 Lyle et al., 1997). As a consequence, cellular processes (physiology and metabolism, i.e. apoptosis, cellular shape, cytoskeleton polymerization) are influenced (Fanelli et al., 1999; Teodori et al., 2002a, b; Chionna et al., 2003a, 2005). In turn, modulation of apoptosis can favor the development of many diseases (Kountouras et al., 2004; Nikitakis et al., 2004).

In particular, apoptosis is an important and widespread process aimed to protect organism by the silent demise of damaged and/or aged cells. Apoptotic cells are usually cleared by phagocytosis *in vivo* with a rapid and efficient process able to remove damaged cells and components by inhibiting inflammation (Savill and Fadok, 2000). The initial event in phagocytosis is the recognition of the target. Successful engulfment requires that apoptotic cells expose at least one "eat-me" signal on their surface (Savill and Fadok, 2000). Apoptosis leads to disruption of the normal phospholipid asymmetry of the plasma membrane, that generates ligands on the cell surface (Williamson and Schleger, 2002), facilitating recognition by specific receptors on the phagocytes. Several *in vitro* study, starting from the pioneering work of Savill et al. (1990), which identified macrophage vitronectin receptor (αvβ3 integrin) as the first receptor to recognize and engulf apoptotic cells, have characterized several recognition systems, mainly by inhibitory studies of the phagocytic process. Table I summarizes the various "eat-me" signals, so far identified, capping the apoptotic cells, that are recognized simultaneously or alternatively by distinct phagocyte receptor molecules.

Table I:*Redundancy in apoptotic cell surface determinants and phagocytes receptors*.

	Present on	
Epitopes and/or receptor	Apoptotic cells surface	Phagocyte surface
phosphatidylserine (PS)	yes	yes
CD31	yes	yes
ATP-binding cassette transporter (ABC1)	yes	yes
phosphatidylserine receptor (PSR)	no	yes
C1q/Mannose Binding Lectin (MBL)	no	yes
calreticulin and CD91	no	yes
CD14	no	yes
αvβ3/αvβ5	no	yes
Scavenger receptors (SRA,CD68,LOX1,CD36)	no	yes
CD11/CD18	no	yes
Lectins	no	yes
Ox-LDL	yes	no
ICAM 3	yes	no
MER	no	yes
αvβ3 integrin	no	yes
β2-GPI receptors	no	yes
bridging molecules:		
Milk Fat Globule Epidermal growth factor 8, (MF-GE8); Growth Arrest Specific gene 6, (Gas6); trombospondin (TSP)		

The same "eat-me" ligand can be recognized by different receptors or bridging molecules, so that recognition possibilities are widely amplified. This redundancy aims to assure maximum clearance efficiency and explains the inability of some individual deletions to efficiently impaired apoptotic cell clearance *in vivo*.

In a wide range of phagocytes, both professional and non-professional, charbohydrate changes on the surface of apoptotic cells are important in triggering recognition (Duvall et al., 1985; Dini et al., 1992; Dini, et al.1993). Initially it has been suggested that healthy hepatocytes ingested apoptotic ones via the asiaologlycoproteins receptor, that is exclusively present on the parenchymal liver cells (Dini et al., 1992). Galactose and mannose- specific recptors of sinusoidal liver cells have been also found play a role in the recognition and engulfment of apoptotic cells, mostly blood circulating (Dini, et al. 1995; Falasca, et al. 1996; Dini and Carlà, 1998), likely in cooperation with other hepatic carbohydrate-specific receptors. Indeed, the mannose receptor of macrophages and liver endothelial cells is the best characterized member of a family of surface lectin receptors that mediates binding and internalization of mannose and fucose (Duvall et al., 1985; Dini et al., 1992; Dini, et al.1993; Dini et al., 1995). CD14, a multifunctional receptor known originally for its role as the lipopolysaccharide (LPS) receptors (Gregory, 2000), could bind the carbohydrate groups that are exposed during the apoptosis.

The overall environmental generation of (E)MFs is due to both natural and artificial sources. Thus, many cell functions can be influenced by the accidental or intentional exposure to (E)MFs. It is likely

that recognition of apoptotic cells could be affected by any environmental factors able to modulate cell surface molecules expression, irrespectively on phagocyte and /or apoptotic cells. Among all the possible factors present in the environment static magnetic field of moderate intensity (static MF 6 mT of intensity) are also included. While it has been reported that static MF can alter surface of cells after 24 h of continuous exposure (Chionna et al. 2003b; 2005), scarce and very contradictory are the data of literature regarding the effects of (E)MFs on phagocytosis (Flipo et al. 1998; Simko et al. 2001).

Aim of the present work has been the study of the *in situ* liver recognition of normal or apoptotic lymphocytes that have been exposed for up to 24 h to 6 mT static MF, to define at which extent static MF are able to modulate this specific type of phagocytosis. In particular, liver is the main site for apoptosis of blood cells, is for lymphocytes either a battlefield or a graveyard (Sun and Shi, 2001; Crispe et al., 2000).

Characterization of cell surface of isolated human lymphocytes: apoptotic versus static MF exposed

Human lymphocytes cells were obtained after Ficoll gradient separation of buffy coats from blood donations of non-smoker healthy males, aged 25–45. They were separated from monocytes by double adherence to plastic. During and after the treatments, they were maintained at a cell density of 1×10^6 cells/ml in complete culture medium at 37 °C supplemented with 10% inactivated fetal calf serum (FCS), 2 mM l-glutamine, 100 IU/ml penicillin and streptomycin in a humidified atmosphere of 5% CO_2; cells were used on the first day of explant. Cell viability was more than 95% at the end of the isolation procedure and it was reduced of about 55 and 70% when cells were induced to apoptosis by using heat shock at 43 °C for 1 h followed by 4 h recovery in fresh medium or cycloheximide (CHX) 10^{-2} M for up to 24 h. The exposure to static MF of 6 mT of intensity, up to 24 h, did not induce any reduction of the cell viability nor modification of cell growth (Fig. 1). Static MF was produced by Neodymium magnetic disks (10 mm in diameter and 5mm in height) of known intensity supplied by Calamit L.td (Milano, Italy) placed under the culture Petri dishes. The intensity of the field generated by the magnet was checked by means of a gaussmeter with a range of operating temperature of 0°C to 50°C and an accuracy (at 20°C) of $\pm$ 1% (Hall-effect gaussmeter, GM04 Hirst Magnetic Instruments Ltd, UK). The laboratory areas between incubators, worktops and tissue culture hood measured 0.08 μT to 0.14 μT (50 Hz) magnetic fields. In the room the background flux density was 10 μT (static) and the local geomagnetic field was approximately 43 μT.

However, when apoptosis was induced under exposure to static MF, the percentage of dead cell was reduced of about 15-20% (Fig. 1). Morphological observation confirmed these results. Indeed, exposure to static MF affected cell shape and surface. Microvilli of control cells became lamellar and cells was more elongated. The surface of lymphocytes induced to apoptosis under exposure was less smooth than not exposed ones (Chionna et al. 2003a).

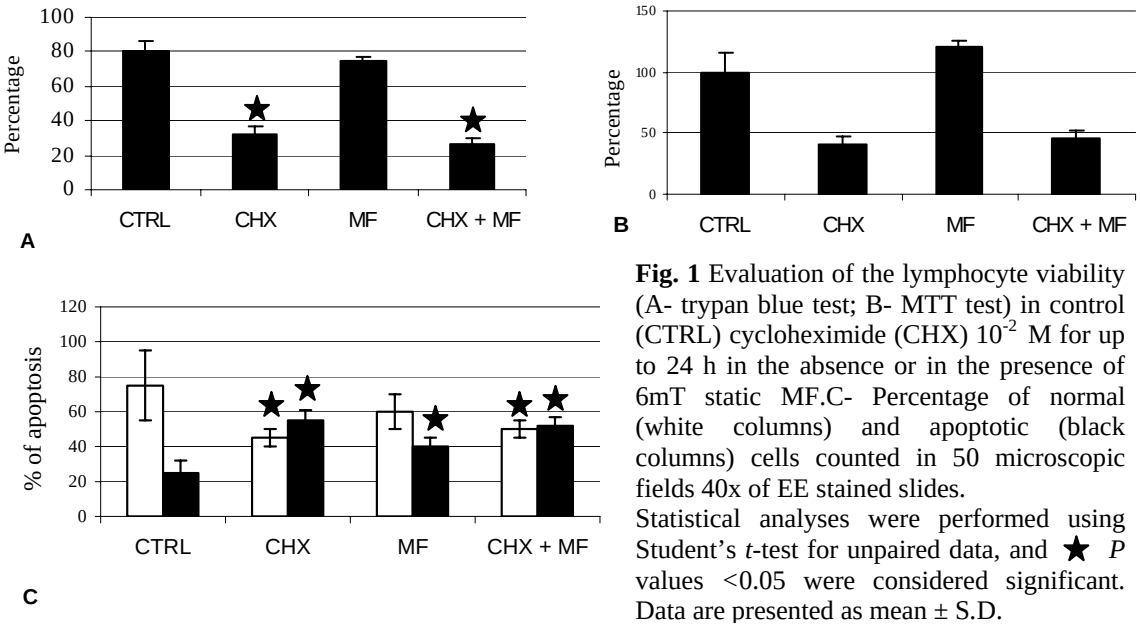

Fig. 1 Evaluation of the lymphocyte viability (A- trypan blue test; B- MTT test) in control (CTRL) cycloheximide (CHX) 10^{-2} M for up to 24 h in the absence or in the presence of 6mT static MF.C- Percentage of normal (white columns) and apoptotic (black columns) cells counted in 50 microscopic fields 40x of EE stained slides.

Statistical analyses were performed using Student's *t*-test for unpaired data, and ★ *P* values <0.05 were considered significant. Data are presented as mean ± S.D.

The liver phagocytosis of apoptotic lymphocytes is mediated by carbohydrate-specific receptors (Dini 2005). In fact, the cell surface of apoptotic lymphocytes express normally hidden sugar moieties like

D-galactose, Mannose, N-acetyl-Dgalactosamine, N-acetyl-Dglucosamine, Fucose. Cells, fixed with 4% formalin in phosphate buffer pH 7.4, 5 min, were labelled with lectin-FITC conjugates, i.e. Concanavalin-A (Con-A) (D-mannose) (40 μg/ml) and Ricinus communis (D-galactose) (2 μg/ml), 30 min in the dark.
Both the apoptotic treatment and the exposure to 6 mT static MF influenced the sugar expression; in addition exposure to static MF modified fluorescence pattern and intensity with respect to the corresponding non exposed cells. In table II are summarized the semiquantitative evaluation of different carbohydrate exposure on cell surfaces of normal, apoptotic and static MF exposed lymphocytes, analyzed with fluorescence microscopy. The carbohydrates whose expression is enhanced after exposure are mannose/D-glucosammine and galactose/D-galactosamine, while the fluorescence pattern resulted modified for all lectins.

Table II Semiquantitiative evaluation of FITC-conjugate lectins for the detection of carbohydrate residues on the cell surfaces of control (CTRL), apoptotic human lymphocytes in the presence or in the absence of static MF

Lectins	CRTL	CTRL+MF	Apoptotic	Apoptotic+MF
Con-A	-	+	++	+
Ricinus Communis	-	++	+++	++

Liver recognition and internalization of lymphocytes
The quantification of adhesion and internalization of the in situ injection of normal, apoptotic and static MF exposed lymphocytes to mouse liver sinusoidal walls is reported in fig. 2. Male Swiss mice, weighting 15-20 g were maintained on a standard laboratory diet and free water access. Before surgery, animals were anaestethized by an i.p. injection with Farmotal (barbiturate anaestethic) (Farmitalia, Italy), 10 mg/100g body weight. All animals received humane care according to the criteria outlined by the national law. For each set of experiments at least three animals were used. Livers were perfused in a non-recirculating system at a flow rate of 1ml/min. $1x10^6$ lymphocytes labelled with Hoechst 33342 were injected into the liver circulation (total volume 10 ml). Lymphocytes used in the different experiments were control, apoptotic, control static MF exposed and induced to apoptosis under static MF. The livers were then extensively washed with culture medium to remove unbound cells. Livers, fixed in 4% paraformaldehyde in phosphate buffer, were processed for routine light microscopy or for cryosectioning. The adhesion of lymphocytes to the sinusoidal wall was evaluated by light and fluorescent microscopy of liver sections. The adhesion specificity was tested in parallel inhibition experiments by adding 80 mM (final concentration) of a sugar cocktail (N-acetyl-D-galactosamine, Mannose, fucose, N-acetilglucosammine) into the perfusion tube before adding apoptotic lymphocytes. To allow internalization warmed solution (37°C) were used. The concentration of lymphocytes used for all experiments was at saturation point, as evaluated by the presence of apoptotic lymphocytes in the medium collected from the liver.
Liver cells were very active in blocking apoptotic lymphocytes, leaving away normal one (less than 6 % of injected cells were bound to sinusoids). Apoptosis was estimated by morphological analysis at the optical level. Light microscopic analysis of apoptosis was done on haematoxylin/eosin stained cells on slides. Haematoxylin-eosin slides were examined for the scoring of cells undergoing apoptosis, by counting in 50 to 100 high-power microscopic fields (x40). Approximately 300 nuclei per slides were counted. The number of apoptotic cells was expressed as number per microscopic field 40x. Slides were also observed for the presence anomalies in the morphologies (normal or altered shape).
Apoptotic lymphocytes were retained by sinusoidal liver cells at high degree, and when internalization was allowed (i.e. perfusion at 37°C), they were found inside the cells. Worth noting, control non exposed lymphocytes were never phagocyted. Surprisingly, when normal lymphocytes were exposed for 24 hr to static MF, they were retained by sinusoidal walls (three times with respect to control) (fig.2) and internalized when allowed.
The percentage of lymphocytes induced to apoptosis under exposure to static MF bound to sinusoidal liver cells was higher than the apoptotic ones. Correspondingly the number of internalized apoptotic lymphocytes was increased. The induction of apoptosis and static MF exposure had a synergic effect. The recognition of apoptotic lymphocytes was, in all cases, specific as indicated by the inhibition experiments. In fact the clearance of apoptotic lymphocytes was mediated by specific receptors, most likely mannose and galactose, able to recognize the surface modifications. Indeed, liver periportal

sinusoidal tracts express higher amount of mannose and galactose-specific receptors than perivenous sinusoidal tracts, thus leading the periportal liver sinusoids to recognize and internalize more apoptotic lymphocytes than the corresponding perivenous cells (Fig.2). Worth noting, the control static MF - exposed cells were recognized at the same extent in the perivenous and periportal tract of the liver sinusoids. The sugar inhibition experiments indicated a synergic recognition between lectin like receptor and not yet known receptor, since the reduction of binding was only partial prevented (Fig. 2).

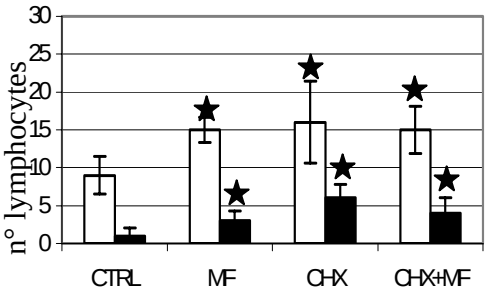

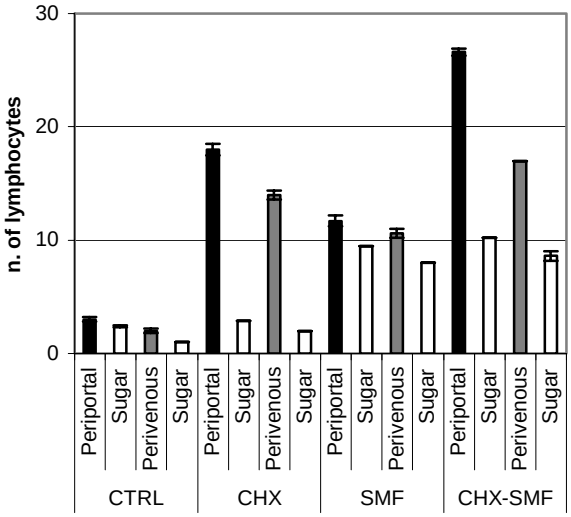

Fig. 2 Number of control or CHX 10^{-2} M for up to 24 h treated lymphocytes in the absence or in the presence of 6 mT static MF for 24 h, adhering (white columns) or internalized (black columns) by liver sinusoidal cells.Statistical analyses were performed using Student's *t*-test for unpaired data, and ★ *P* values <0.05 versus CRTL were considered significant. Data are presented as mean ± S.D.

Analysis of membrane proteins of static MF exposed lymphocytes

The protein pattern of membrane of normal, apoptotic and static MF exposed lymphocytes is reported in fig. 3. Western blot analysis were performed according to Towbin et al. (1979) (Fig.). Specific lectins conjugated to biotin were used: lectin from Concanavalin A specific for α-Mannose and α-glucose residues (at a concentration of 50µg/ml), lectin from *Helix pomatia* specific for N-acetyl-α -D-galactosaminyl residues (at a concentration of 50µg/ml), lectin from *Triticum vulgaris* specific for N-acetyl-β-D-glucosaminyl residues and N-acetyl-β-D-glucosamine oligomere, (at a concentration 50µg/ml), and lectin from *Ulex Europaeus* specific for L-Fucose residues (at a concentration 30µg/ml) (Sigma-Aldrich, Saint Louis, MO, USA). Specific binding of the lectins was detected using streptavidin conjugated to peroxidase (1:1,500 dilution) and visualized using 3-3' diaminobenzidine (DAB) as a substrate in the presence of H_2O_2. Quantification of the glycoprotein bands was performed by using a Biorad Model GS 700 Imaging densitometer.

Differences between exposed and non exposed cells and between control and apoptotic ones have been detected. Apoptosis as well as exposure to static MF induced modifications in the protein profile of cells. In particular, from gel electrophoresis three bands underwent major modifications:130, 95 and 45-43 kDa, while a fourth band was only found in control exposed cells, 60 kDa. The control exposed and the apoptotic non exposed lymphocytes showed an increment of the band of 43KDa. Conversely, the bands of 95 and 130 KDa increased in the presence of static MF while decreased with the CHX treatment. The intensity of the 45KDa band decreased with the treatments respectively with the incubation of CHX, exposure to static MF and CHX incubation in presence of static MF (Fig. 3).

By using different lectins (Concanavalin-A, Ulex europaeus and Triticum vulgaris) the expression of glycidic residues of the proteins was evaluated. The western blots for α-Mannose and α-glucose (Con A) has shown 6 different bands (Fig.5). The 100 KDa α band was modified (+8% versus control) only in the samples incubated with CHX under static MF. The 100 KDa β band was modified at the same extent (- 15%) in both samples exposed to static MF or CHX treated. CHX incubation reduced of about 10% the intensity of the 70 KDa γ band with respect to control. Similar pattern (-8%) was found for 65 KDa δ band,while only the samples exposed to static MF showed a decrement (-9%) of 55KDa ε band. The 30 KDa ζ band was unchanged. The western blots for α-L-Fucose (Ulex europaeus) has shown that the majority of proteins belong to the low molecular weight. Modifications of optical densitometry

with the relative increment or decrement given in percentage with respect to control are reported in fig. 4. The western blots for N−acetyl-D-glucosammine and N−acetyl-neuroaminic (Triticum vulgaris) has shown that the majority of proteins belong to the high molecular weight. Optical densitometry with the relative percentage increments with respect to control are reported in fig.4.

In the present work data have been shown on the strong and reproducible effects that the exposure to static MF exerts on the process of liver phagocytosis of apoptotic lymphocytes.
Liver clearance of apoptotic lymphocytes is a complex mechanism that can be influenced at least at three different levels: phagocyte receptors, apoptotic cell quality and static MF exposure. On the side of the phagocyte receptors, in general, the efficiency of phagocytosis is proportional to the number of expressed receptors. In the liver this aspect is particular evident, since the receptors involved in the recognition of apoptotic cells are modulated in relation to the type of the cells (i.e. Kupffer, endothelial cell, hepatocytes) (Dini and Kolb-Bachofen, 1989), to the physiological or pathological status of the organ and to the cell localization inside the lobule (Dini et al., 2002; Dini, 2000; Dini and Carlà, 1998). With respect to this latter aspect, the efficiency of recognition and internalization is higher in the periportal tracts of the liver lobule, than in the perivenous ones, according to the number of carbohydrate specific receptors.

	treatments			
	ctrl	chx	mf	chx +mf
43kDa	0	0	0.033	0.065
45 kDa	1.23	0.81	0.35	0.76
95 kDa	0.084	0.056	0.11	0.085
130 kDa	0	0	0.064	0.058

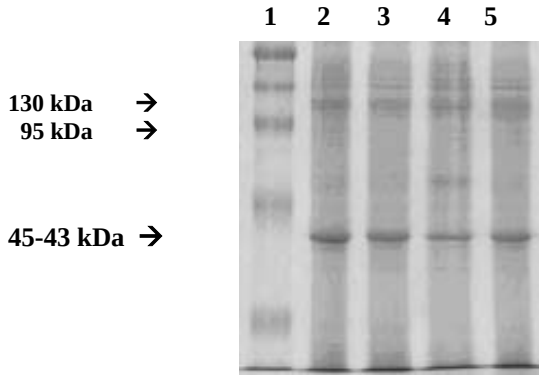

Fig. 3 SDS-PAGE of membrane proteins from control (CRTL), CHX treated lymphocytes in the absence or in the presence of 6 mT static MF for 24 h. Lane 1 Marker; lane 2 control; lane 3 CHX 10^{-2} M for up to 24 h; lane 4 CTRL + static MF for 24 h; lane 5 CHX 10^{-2} M for up to 24 h + static MF for 24 h.

On the side of the edible cells, the quality of apoptotic cells can determine the efficiency of clearance by the liver (Chionna et al., 2003a). It is known that the step in the process of apoptosis (i.e. early, mature or late apoptosis) has influence on the efficiency of removal since the modification of the cell surface changes accordingly with the progression through the apoptotic program (Chionna et al., 2003a). A hierarchy of the expression of specific epitopes on the cell surface of apoptotic lymphocytes has been reported (Chionna et al., 2003a). Therefore, the cell surface of dying cells is progressively changing leading to widely amplified possibilities of a safe recognition and to modulation in the rate of recognition and engulfment. The third level is given by the perturbation exerted by exposure to static MF of moderate intensity. In previous works (Chionna et al., 2003b, 2005; Dini and Abbro 2005;Tenuzzo et al. 2006) we have described the interference of static MF with the process of apoptosis, with cell shape and surfaces, with Calcium ions concentrations, cytoskeleton, differentiation and in the present work, on the liver clearance of normal and apoptotic lymphocytes. Our data confirm those in the literature indicating that cell membranes are the preferential site for the action of the (E)MF (Panagopouls et al., 2000; Paradisi et al., 1993; Bersani et al., 1997; Somosy, 2000).

By using two different experimental approaches, lectin cytochemistry and western blotting of glycoproteins, the modifications of the sugars moieties and/or the glycoproteins of membranes were shown. Apparent discrepancies between lectin cytochemistry and western blots analysis can be due to the labeling of glycolipids of the plasma membranes with cytochemistry methods.
The identification of the (glyco)proteins whose amount has been modified by the exposure to static MF is currently under inestigation. Many of the possible candidate belongs to the transduction pathways and to the adhesion molecules: they are, therefore, molecules that can be involved in the process of

recognition, cell-cell adhesion and the intracellular pathways; processes that are all important for the recognition and engulfment. Indeed, it is not possible to define if the modifications in the cell proteins are due to conformational changes, to transductional or transcriptional modifications or to a synergic effects of all these factors.

	treatments			
	chx e mf	**mf**	**chx**	**ctrl**
Band α	0.334 +8%	0.324 +5%	0.314 +2%	0.307
Band β	0.390 +2%	0.321 -16%	0.326 -15%	0.384
Band γ	0.381 +1%	0.359 -4%	0.339 -10%	0.376
Band δ	0.459 +7%	0.408 -5%	0.393 -8%	0.429
Band ε	0.416 +6%	0.357 -9%	0.374 -5%	0.392
Band ζ	0.448 +6%	0.407 -4%	0.414 -2%	0.424

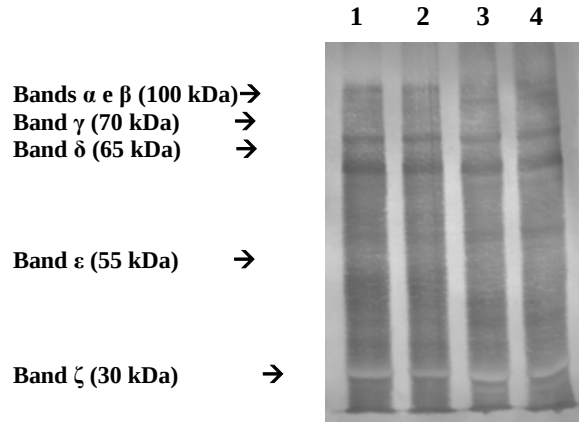

Fig. 4 Western blot assays and O.D. of ConA expression on membrane glycoproteins of isolated human lymphocytes. Lane 1 CHX 10^{-2} M for up to 24 h + static MF for 24 h; lane 2 CTRL + static MF for 24 h; lane 3 CHX 10^{-2} M for up to 24 h; lane 4 control .

Ulex Europeous

	treatments			
	ctrl	chx	mf	chx +mf
Band α	0.398	0.1 -79%	0 -100%	0 -100%
Band β	0.5	0.1 -80%	1.08 +100%	1.12 +100%
Band γ	0.64	0.94 +47%	0.96 +50%	1.35 +100%
Band δ	0	0	0	0

Triticum Vulgaris

	treatments			
	ctrl	chx	mf	chx +mf
Band α	0.643	0.801 +21%	0.819 +27%	0.836 +30%
Band β	0.7	1..0 +42%	1.31 +87%	1.26 +80%
Band γ	0.41	0.23 -43%	0.43 +5%	0.498 +21%
Band δ	0.098	0 -100%	0 -100%	0 -100%

Fig. 5 Optical Density values of one representative western blot of Ulex Europeous and Triticum vulgaris expression in isolated human lymphocytes in control and CHX 10-2M for 24 h treated in the absence or in the presence of 6 mT static MF.

To date, the very few data that have been published on the effects of static MF on gene expression are confusing and, none of them is referring to genes regulating the apoptotic program. Indeed, some studies obtained by using electromagnetic fields at diverse intensities, i.e. ELF and EMF, reported effects on gene expression, particularly at the transcriptional level, after exposure to ELF and EMF of human HL60 (Goodman et al., 1992). Several specific transcripts, i.e. actin, tubulin, H2B histone, c-myc, increased their expression by two to three fold after 20 min of exposure (De Mattei et al., 2005). Conversely, in other reports (Hirose et al., 2003) the exposure to homogeneous static MF at 10 T was unable to affect the expression of c-Jun, c-Fos and c-Myc, while the inhomogeneous static MF at 6T significantly increased c-Jun expression but only at the long-time exposure.

The most intriguing data that has been here shown is the ability of sinusoidal liver cells to retain and to internalize normal exposed lymphocytes. One possible reason of this recognition can be the modifications exerted by static MF on the surface of lymphocytes that share changes with apoptotic cells, thus leading to the removal of control exposed cells via receptors used for the clearance of apoptotic lymphocytes.
It is worth noting to mention that the process of recognition and engulfment of the apoptotic cells has same peculiarity that makes the process of phagocytosis of apoptotic cells different from the phagocytosis of microrganisms or debris (Krysko et al., 2003). In fact, in non-pathological conditions, an efficient clearance is assured by the redundant interaction between apoptotic cell ligands and multiple molecules present on the engulfing cell surface. The apoptotic cell engulfment appears to activate signals able to suppress release of pro-inflammatory cytokines, thus pro-inflammatory responses are not elicited. The phagocytosis of apoptotic cells prevents inflammation (Maderna and Godson, 2003). Therefore, it should be further investigated if the removal of static MF exposed lymphocytes share the characteristic of the phagocytosis of apoptotic cells.

SUMMARY

In summary, evidences of the perturbation exerted by the exposure to 6 mT static MF of human isolated lymphocytes have been reported. In particular, the static MF exposure impaired the apoptotic rate and gave rise to modifications of the cell surface in normal exposed cells similar to the cell surface modifications achieved during the apoptotic program. The cell surface modifications of apoptotic cells are important for their fast and silent removal by professional and amateur phagocytes. Interestingly, the same liver receptorial systems are also used for the recognition of control exposed lymphocytes. The pathological and/or physiological implications are not yet understood and need to be further investigated.
Data showed that the recognition of apoptotic lymphocytes by the sinusoidal liver cells is affected by the exposure to static MFs. Interestingly, exposure to static MFs has been found to be an extreme critical factor not only for the recognition of apoptotic lymphocytes but also for control ones. The imp'lication for human health needs to be deeply investigated.

REFERENCES

Bersani F., Marinelli F., Ognibene A.., Matteucci A.., Checchi S., Santi S., Squarzoni S., Maraldi N.M., 1997**.** Intramembrane protein distribution in cell cultures is affected by 50 Hz pulsed magnetic fields. Bioelectromagnetics 18, 463--469.

Bordiushkov IuN., Goroshinskaia IA.., Frantsiiants EM., Tkacheva GN., Gorlo EI., Neskubina IV.2000. Structural-functional changes in lymphocyte ans erythrocyte membranes after exposure to alternating magnetic field. Vopr Med Khim. 46,72-80. Russian.

Chionna A., Dwikat M., Panzarini E., Tenuzzo B., Carlà EC., Verri T., Pagliara P., Abbro L., Dini L. 2003b. Cell shape and plasma membrane alterations after static magnetic fields exposure European Journal of Histochemistry 47, 299-308.

Chionna A., Panzarini E., Pagliara P., De Luca A., Caforio S., Abbro L., Dini L. 2003a. Hepatic clearance of Apoptotic lymphocytes: simply removal of waste cells? Europ.J.Histochem.47, 97-104

Chionna A., Tenuzzo B., Panzarini E., Dwikat M., Abbro L., Dini L. 2005. Time-dependent modifications of Hep G2 cells during exposure to Static Magnetic Fields. Bioelectromagnetics. 26, 275-286.

Cho MR., Thatte HS., Silvia MT., Golan DE. 1999. Transmembrane calcium influx induced by an electric field. Faseb Journal 13, 677--683.

Crispe IN., Dao T., Klugewitz K., Mehal W.Z., Metz D.P. 2000. The liver as a site of T-cell apoptosis: graveyard, or killing field? Immunol. Rev. 174, 47-62.

De Mattei M., Gagliano N., Moscheni C., Dellavia C., Calastrini C., Pellati A., Gioia M., Caruso A., Stabellini G. 2005. Changes in polyamines, c-myc and c-fos gene expression in osteoblast-like cells exposed to pulsed electromagnetic fields. Bioelectromagnetics 26, 207-214.

Dini L., Kolb-Bachofen V. 1989. Preclustered receptor arrangement is a prerequisite for galactose-specific clearance of large particulate ligands in rat liver. Exp Cell Res.184, 235-40.

Dini L., Abbro L. 2005. Bioeffects of moderate-intensity static magnetic fields. Micron 36,195-217.

Dini L., Autori F., Lentini A., Oliverio S., Piacentini M., 1992. The clearence of apoptotic cells in the liver is mediated by the asialoglycoprotein receptor. Febbs Letters 296, 174--178.

Dini L., Carlà EC., 1998. Hepatic sinusoidal endothelium heterogeneity with respect to the recognition of apoptotic cells. Experimental Cell Research 240, 388--393.

Dini L., Falasca L., Lentini A., Mattioli P., Piacentini M., Piredda L., Autuori F. 1993. Galactose-specific receptor modulation related to the onset of apoptosis in rat liver., Eur. J. Cell Biol. 61, 329-337.

Dini L., Lentini A., Diez Diez G., Rocha M., Falasca L., Serafino L., Vidal-Vanaclocha F. 1995. Phagocytosis of apoptotic bodies by liver endothelial cells., J. Cell Sci 108, 967-973.

Dini L., Pagliara P., Carlà E.C., 2002. Phagocytosis of apoptotic cells by liver: a morphological study. Microscopy Research Techniques 57, 530--540.

Dini, L., 2000. Clearance of apoptotic lymphocytes by human Kupffer cells. Phagocytosis of apoptotic cells in the liver: role of lectin receptors and therapeutic advantages In: Cameron R.G., Feuer G. (Eds), Handbook of experimental pharmacology. Apoptosis and its modulation by drugs. Springer-Verlag Berlin Heidelberg, vol. 142 pp. 319--341.

Duvall E., Wyllie A.H., Morris R.G. 1985. Macrophage recognition of cells undergoing programmed cell death (apoptosis)., Immunology 56, 351-358.

Falasca L., Serafino L., Balabaud C., Dini L. 1996. Human Kupffer cell recognition and phagocytosis of apoptotic peripheral blood lymphocytes., Exp. Cell Res. 224, 152-162.

Fanelli C., Coppola S., Barone R., Colussi C., Gualandi G., Volpe P., Ghibelli L. 1999. Magnetic fields increase cell survival by inhibiting apoptosis via modilation of Ca++ influx Faseb J 13, 95-102.

Fiorani M., Cantoni O., Sestili P., Conti R., Nicolini P., Vetrano F., Dacha M. 1992. Elecrtic and /or magnetic field effects on DNA structure and function in cultured human cells. Mut Res 282, 25-29.

Flipo D., Fournier M., Benquet C., Roux P., Le Boularie C., Pinsky C., La Bella F.S., Krzystyniak K. 1998. Increased apoptosis, changes in intracellular Ca^{2+}, and functional alterations in lymphocytes and macrophages after in vitro exposure to static magnetic field. Journal of Toxicology and Environmental Health 54, 63--76.

Goodman R., Wei L.-X., Bumann J., Henderson AS. 1992. Exposure of human cells to electromagnetic fields: Effect of time and field strength on transcript levels. J. Electro. Magnetobiol, 11. 19–28.

Gregory C.D. 2000. CD14-dependent clearance of apoptotic cells: relevance to the immune system. Curr Opin Immunol.12, 27-34. Review.

Hirose H., Nakahara T., Zhang QM., Yonei S., Miyakoshi J. 2003. Static magnetic field with a strong magnetic field gradient (41.7 T/m) induces c-Jun expression in HL-60 cells. In vitro cell dev boil anim 39, 348-352.

Ishido M., Nitta H., Kabuto M. 2002. The mechanim of biologicalmagnetic field effects on oncostatic actions of melatonin. RIKEN Review No.44, 72-74.

Ishisaka R., Kanno T., Inai Y., Nakahara H., Akiyama J., Yoshioka T., Utsumi K. 2000. Effects of a magnetic fields on the various functions of subcellular organells and cells. Pathophysiol 7, 149-152.

Jelenkovic A.., Janac B., Pesic V., Jovanovic DM., Vasiljevic I., Prolic Z. 2006. Effects of extremely low-frequency magnetic field in the brain of rats. Brain Res Bull. 68, 355-360.

Kountouras J., Zavos C., Chatzopoulos D. 2004. Induction of apoptosis as a proposed pathophysiological link between glaucoma and Helicobacter pylori infection. Medical Hypotheses 62, 378–381.

Krysko DV., Brouckaert G., Kalai M., Vandenabeele P., D'Herde K. 2003. Mechanisms of internalization of apoptotic and necrotic L929 cells by a macrophage cell line studied by electron microscopy. J Morphol 258, 336-345.

Lyle DB., Fuchs TA., Casamento JP., Davis CC., Swicord ML. 1997. Intracellular calcium signaling by Jurkat T-lymphocytes exposed to 60 Hz magnetic field. Bioelectromagnetics 18, 439-445.

Maderna P., Godson C. 2003.Phagocytosis of apoptotic cells and the resolution of inflammation. Biochim Biophys acta 1639, 141-151.

Miyakoshi J. 2005. Effects of static magnetic fields at the cellular level. Prog Biophys Mol Biol. 87, 213-223.

Nikitakis NG., Sauk JJ., Papanicolaou SI. 2004. The role of apoptosis in oral disease: Mechanisms; aberrations in neoplastic, autoimmune, infectious, hematologic, and developmental diseases; and therapeutic opportunities. Oral Surg Oral Med Oral Pathol Oral Radiol Endod. 97, 476-490.

Panagopoulos DJ., Karabarbounis A., Margaritis LH. 2002. Mechanism for action of electromagnetic fields on cells. Biochem Biophys Res Commun. 298, 95-102.

Panagopoulos DJ., Messini N., Karabarbounis A., Philippetis AL., Margaritis LH. 2000. A mechanism for action of oscillating electric fields on cells. Biochemical Biophysical Research Communication 273, 634--640.

Paradisi S., Donelli G., Santini, M.S., Straface E., Malorni W., 1993. A 50 Hz magnetic field induces structural and biophysical changes in membranes. Bioelectronmagnetics 14, 247--255.

Rosen AD. 2003. Mechanism of action of moderate-intensity static magnetic fields. Biochem Biophys Acta 1282: 149-155.

Santoro N., Lisi A., Pozzi D., Pasquali E., Serafino A., Grimaldi S. 1997. Effect of extremely low frequency (ELF) magnetic field exposure on morphological and biophysical properties of human lymphoid cell line (Raji). Biochem. Biophys. Acta 1357:281-290.

Savill J., Dransfield I., Hogg N., Haslett C. 1990. Vitronectin receptor-mediated phagocytosis of cells undergoing apoptosis., Nature, 343, 171-173.

Savill J., Fadok V. 2000. Corpse clearance defines the meaning of cell death., Nature 407, 784-788. Review

Simko M., Droste S., Kriehuber R., Weiss DG. 2001. Stimulation of phagocytosis and free radical production in murine macrophages by 50 Hz electromagnetic fields, European Journal of Cell Biology 80, 562--566.

Somosy Z. 2000. Radiation response of cell organelles. Micron. 31, 165-181.

Sun EW., Shi YS., 2001. Apoptosis: the quiet death silences the immune system., Pharmacol. Therap. 92, 135-145.

Tenuzzo B., Chionna A., Panzarini E., Lanubile R., Tarantino P., Di Jeso B., . Dwikat M, Dini L. 2006. Biological effects of 6mT Static Magnetic Fields on induction of apoptosis: a comparative study in different cell types Bioelectromagnetics in press

Teodori L., Gohde W., Valente MG., Tagliaferri F., Colett D., Perniconi B., Bergamaschi A., Cerella C., Ghibelli L. 2002a. Static magnetic fields affect calcium fluxes and inhibit stress-induced apoptosis in human glioblastoma cells. Cytometry 49, 143-149.

Teodori L., Grabarek J., Smolewski P., Ghibelli L., Bergamaschi A., De Nicola M., Darzynkiewicz Z. 2002b. Exposure of cells to static magnetic fields accelerates loss of integrity of plasma membrane during apoptosis. Cytometry 49, 113-118.

Thompson CJ., Yang YS., Anderson V., Wood AW. 2000. A cooperative model for Ca(++) efflux windowing from cell membranes exposed to electromagnetic radiation, Bioelectromagnetics 21, 455--464.

Towbin H., Staehelin T., Gordon J. 1979. Electrophoretic transfer of proteins from polyacrilamide gels to nitrocellulose sheets: procedure and some applications. Proc Natl Acad Sci USA 76: 4350-4354.

Williamson P., Schleger RA 2002 Transbilayer phospholipid movement and the clearance of apoptotic cells.. Biochim. Biophys. Acta 1585, 53-63.

EFFECTS OF HYDROGEN PEROXIDE AND ADP-RIBOSE ON THE ACTIVATION OF TRPM2 CATION CHANNELS

MUSTAFA NAZIROĞLU

Department of Biophysics,, Faculty of Medicine, Suleyman Demirel University, Isparta, Turkey (mnaziroglu@med.sdu.edu.tr)

***Abstract*:**
It is well known that microwaves from cellular phones or other sources may affect biological systems by increasing free radicals, which may enhance lipid peroxidation levels of the cells, thus leading to oxidative damage. Hydrogen peroxide (H_2O_2) produces during oxidative stress. The Na^+- and Ca^{2+}-permeable melastatin related transient receptor potential channel TRPM2 cation channels can be gated either by adenosine diphosphoribose **(**ADP-ribose) in concert with Ca^{2+} or by H_2O_2, an experimental model for oxidative stress, binding to the channel's enzymatic Nudix domain. Since the mechanisms that lead to TRPM2 gating in response to ADP- ribose and H_2O_2 are not understood, we tested the effects of various antioxidants on ADP-ribose, NAD^+ and H_2O_2-induced TRPM2 currents.

Chinese hamster ovary (CHO) cells were transfected with cDNA coding for TRPM2. Cells were studied with the conventional whole-cell patch clamp technique. The intracellular solution used EDTA (10 mM) as chelator for Ca^{2+} and heavy metal ions. H_2O_2 (10 mM) was added extracellularly although the ADP- ribose (0.3 mM) and NAD^+ (1 mM) were applied intracellularly (i.e. through the pipette).

Non-selective cation currents in whole cell experiments were consistently induced by ADP- ribose, NAD^+ and H_2O_2. The time cause of ADP- ribose and NAD^+ was characterized by a delay of 0.6-3.0 min and a slow current induction to a plateau although the time cause of H_2O_2 was characterized by a delay of 2-5 min and it didn't reach a slow current induction to a plateau

These results demonstrated that all three agonists, H_2O_2, ADP- ribose and NAD+, are capable of activating TRPM2. The three agonists are likely to interact directly with TRPM2 channels, consistent with the idea that they bind to the nudix domain**.**

Introduction

Daily exposures to various types of magnetic fields are increasing in human environment. Extremely low frequency microwaves (MW) from power lines and public transportation systems, high- frequency MW from mobile phones and computers, and strong MW from magnetic resonance imaging in medical diagnosis are the most familiar sources of exposure. Possible biological effects due to exposure various types of MW have become of considerable public interest and concern (McCann et al., 1993; Murphy, 1993).

Reactive oxygen substances (ROS) and lipid peroxides are produced by a free radical chain reaction, which can also be initiated by ROS. The ROS, i.e. singlet oxygen, superoxide anion radical, perhydroxyl radical and hydroxyl radical, contribute to tissue damage (Halliwell and Gutteridge, 1999). ROS also cause injury by reacting with biomolecules such as lipids, proteins and nucleic acids as well as by depleting enzymatic and/or nonenzymatic antioxidants in the brain (Baydaş et al., 2003, Koylu et al., 2006). ROS and/or free radicals may be involved in the action of MW on biological system (Irmak et al., 2002; Ilhan et al., 2004; Koyu et al., 2005; Koylu et al., 2006). Antioxidant treatments in animals and humans could be beneficial in preventing or reducing some complications of low frequency MW (Ilhan et al., 2004; Koyu et al., 2005; Koylu et al., 2006).

Transient receptor potential (TRP) channels were first described in *Drosphila*, where photoreceptor carrying *trp* gene mutations exhibit a transient voltage response to continuous light (Clapham, 2003). These are subdivided into three major subgroups, namely, the vanilloid receptor family, the short TRP channels and melastatin (or long) TRP channels (Kolisek et al., 2005). We have become particularly interested in one member of latter family, known as TRPM2, for a number of reasons a potential role in cell death resulting from oxidative stress (Wehage et al., 2002).

Although TRPM2 is dominantly expressed in brain, it is also detected many other tissues, including bone marrow, spleen, heart, leukocytes, liver, and lung. Native TRPM2 currents have been recorded from U937 monocyte cell line (Perraud et al., 2001), neutrophils (Heiner et al., 2003), and CRI-G1 insulinoma cells (Togashi et al., 2006) where ADP- ribose induces large cation currents that closely match those mediated by

heterologously expressed TRPM2. The Intracellular Ca^{2+} appears to be an important modulator and cofactor of TRPM2, as elevated intracellular Ca^{2+} can significantly increase the sensitivity of TRPM2 toward ADP- ribose (Wehaga et al., 2002; Hara et al., 2002; Kolisek et al., 2005). The channel in human embryonic kidney (HEK)-293 cells can also be gated by H_2O_2, a model substance used as paradigm for oxidative stress (Wehaga et al., 2002; Fonfria et al., 2004; Kolisek et al., 2005). There are conflict reports on the mechanism of H_2O_2- mediated gating of TRPM2. The mechanism has been proposed to be direct or independent ADP-ribose (Wehaga et al., 2002; Hara et al., 2002; Heiner et al., 2003; Kolisek et al., 2005). More recent evidences suggest an indirect mechanism, because H_2O_2- releases ADP- ribose from mitochondria (Fonfria et al., 2004; Kolisek et al., 2005). However, molecular mechanisms of H_2O_2 gates the TRPM2 channels cells are unclear and warrant further studies.

The molecular mechanism by oxidative stress leads to opening of TRPM2 channels need to be elucidated in detail. To study the role of TRPM2 in oxidative stress we used an experimental model, H_2O_2, was applied to TRPM2- transfected cells. Furthermore, the present study was aimed at elucidating the role of the ADP- ribose and NAD+ for gating TRPM2 channels in the chinese hamster ovary (CHO) transfected cells.

Material and methods

Cell culture and transfection

CHO cells were obtained from A.T.C.C. (Rockville, MD, U.S.A.). The cells were cultured in Ham's medium (1 x) (Biochrom, Berlin, Germany), supplemented with 10% (v/v) fetal calf serum (Biochrom), 1 mM sodium-pyruvate (Sigma) and 4 mM L-glutamine (Biochrom, Berlin, Germany). Penicillin (50 U/ml)- streptomycin (50 mg/ml) combination in single- cell experiments was added to the medium. Cells were plated onto Poly-Lysin (0.1 µg/µl, Sigma) coated glass coverslips for 24 h and then transiently transfected with one of the described pcDNA3-EGFP-channel-vector constructs (5 µg) and TransFast Transfection Reagent (7.5 µl; Promega, Mannheim, Germany). As controls, cells were transfected with 2.5 µg „empty" vector-construct and 3.75 µl TransFast Transfection Reagent. Electrophysiological studies were carried out 24-48 h after transfection in cells visibly positive for EGFP.

Electrophysiology

Patch clamp techniques have been described in detail elsewhere (Wehage te al., 2002; Nazıroğlu et al., 2006). Transfected cells were studied with the patch-clamp technique in the whole-cell mode, using a EPC 9 equipped with a personal computer with Pulse and X chart software (HEKA, Lamprecht, Germany). The standard extracellular bath solution contained (in mM) 140 NaCl, 1.2 $MgCl_2$, 1.2 $CaCl_2$, 5 KCl, 10 HEPES, pH adjusted with KOH to 7.4. For Na^+ free solutions, Na^+ was replaced by NMDG (150 mM) and the titration was performed with HCl. For the NMDG solutions with Ca^{2+}, NMDG was partly replaced with $CaCl_2$ (11.2 mM), preserving an osmolarity of about 300 mosmol/l. The noise level in all experiments was minimised by coating the patch electrode tip with agarose (GibcoBRL, paisley, Scotland). The pipettes for whole cell recordings were filled with a solution composed of (in mM) 145 Cs-glutamate, 8 NaCl, 2 $MgCl_2$, 10 EGTA, 10 HEPES, pH 7.2 (adjusted with CsOH). In some experiments, the pipette solution additionally contained ADP-ribose (0.3 mM) or NAD^+ (final concentration 1 mM, added to the pipette solution from a stock of 70 mM in ethanol). Heavy metal concentration of internal buffer affected activation of the channels by H_2O_2. In whole cell experiments, the pipette solution added 10 mM EDTA for EGTA. Cells were held at a potential of –60 mV, and current-voltage (I-V) relations were obtained from voltage ramps from –90 to +60 mV applied over 400 ms. ADP-ribose, NAD^+ and H_2O_2 and all other chemicals were obtained from Sigma.

Data are expressed as mean ± SD. Statistical significance between groups were assessed with Student's t-test. A $p < 0.05$ value was considered significant.

Results

In a previous study (Wehage te al., 2002), authors have characterized TRPM2 currents in TRPM2-transfected HEK-293 cells. The currents were consistently activated by intracellular ADP-Ribose and also by extracellular H_2O_2, but the latter stimulus was effective in only about 25 % of the experiments. A further stimulus of TRPM2 channels, intracellular $NAD^{+,}$ failed in HEK-293 cells. In a further study, we have transfected TRPM2 channels into CHO cells and could stimulate them also with NAD^+; however, no stimulation with H_2O_2 was possible. In the present experiments, we again chose CHO cells but changed the intracellular buffer that used now EDTA rather than EGTA as chelator for Ca^{2+} and probably contaminating

heavy metal ions. Moreover, we chose an intracellular Ca^{2+} concentration calculated to be in the range of 1 µM. Using these conditions, we were able to evoke TRPM2 currents consistently with either of the three stimuli, intracellular ADPR (0.3 mM), intracellular NAD (1 mM), and extracellular H_2O_2 (10 mM) (Figures. 1A and B, 2A and 2B). The currents were non-selective cation currents with a reversal potential close to 0 mV, as previously found to be typical of TRPM2 currents, and were readily blocked in the inside direction when the Na^+ in the bath was replaced by the large impermeant cation $NMDG^+$. No such currents were ever observed when cells were studied that were transfected with a vector only but not with TRPM2; such negative control data were obtained on every experimental day studying TRPM2.

The values for the current densities were 1.87 ± 0.98 pF^{-1} (n=4) and (- 60 mV holding potential) in the absence of NAD^+ and ADP- ribose, 29.16 ± 10.57 pF^{-1} (n=5) and 31.45 ± 23.16 pF^{-1} (n=5) in the presence of NAD^+ and ADP-ribose in the patch- pipette, respectively (Figure 3). The times elapsed before the full response to ADP- ribose and NAD^+ occurred varied between 0.6 -3.0 min. This variability is probably caused by variable diffusion times of ADP- ribose and NAD^+ from pipette bath into cytosol and by metabolism of ADP- ribose and NAD^+ to products that do not active TRPM2 (Perraud et al., 2001; Wehega et al., 2002); metabolism is expected to delay activation of TRPM2 particularly when diffusion is already slow.

The ADP- ribose- and NAD^+ induced inward currents was abolished when extracellular Na^+ was substituted with the large impermeable cation NMDG ((Figures. 1A and B, 2A and 2B). When Ca^{2+} (10 mM) was added to NMDG, a small inward current was restituted (Figures 1B, C and 2B, C). These data indicate that TRPM2 enables non- selective cation currents carried mainly Na^+, but to a small part also by Ca^{2+}, in inward direction and carried by Cs^+ in the autward direction under our experimental conditions. Our results with TRPM2 are essentially identical reports (reviewed in Kuhn et al., 2005).

Figure 1. Stimulator role of intracellular ADP-ribose on the currents of TRPM2 channel. The time where the whole cell period where the normal bath solution (140 nM Na^+) was exchanged to a solution with NMDG as main cation (150 mM, no Ca^{2+} present). The holding potential was –60 mV. **A**. Original recordings from control cell. **B**. Ca^{2+} selectively of TRPM2. A cell expressing TRPM2 currents stimulated with ADP-ribose (0.3 mM) in the pipette. **C**. Current voltage relationships of ADP- ribose currents through TRPM2 in presence of various extracellular cation (same experiments as in panels B).

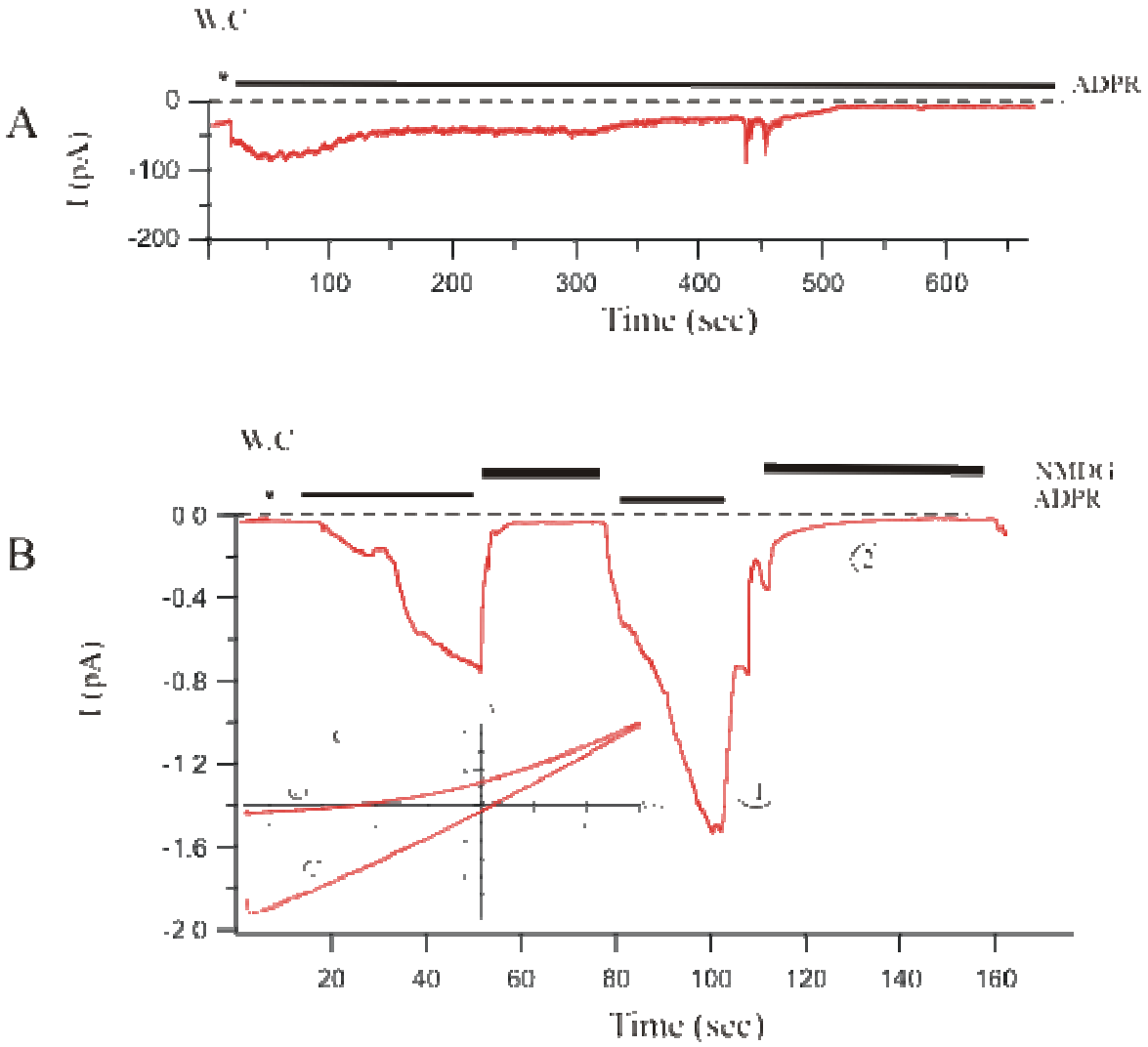

Figure 2. Stimulator role of intracellular β-NAD$^+$ on the currents of TRPM2 channel. The time where the whole cell period where the normal bath solution (140 nM Na^+) was exchanged to a solution with NMDG as main cation (150 mM, no Ca^{2+} present). The holding potential was –60 mV. **A**. Original recordings from control cell. **B**. Ca^{2+} selectively of TRPM2. A cell expressing TRPM2 currents stimulated with β-NAD$^+$ (1 mM) in the pipette. **C**. Current voltage relationships of β-NAD$^+$ currents through TRPM2 in presence of various extracellular cation (same experiments as in panels B).

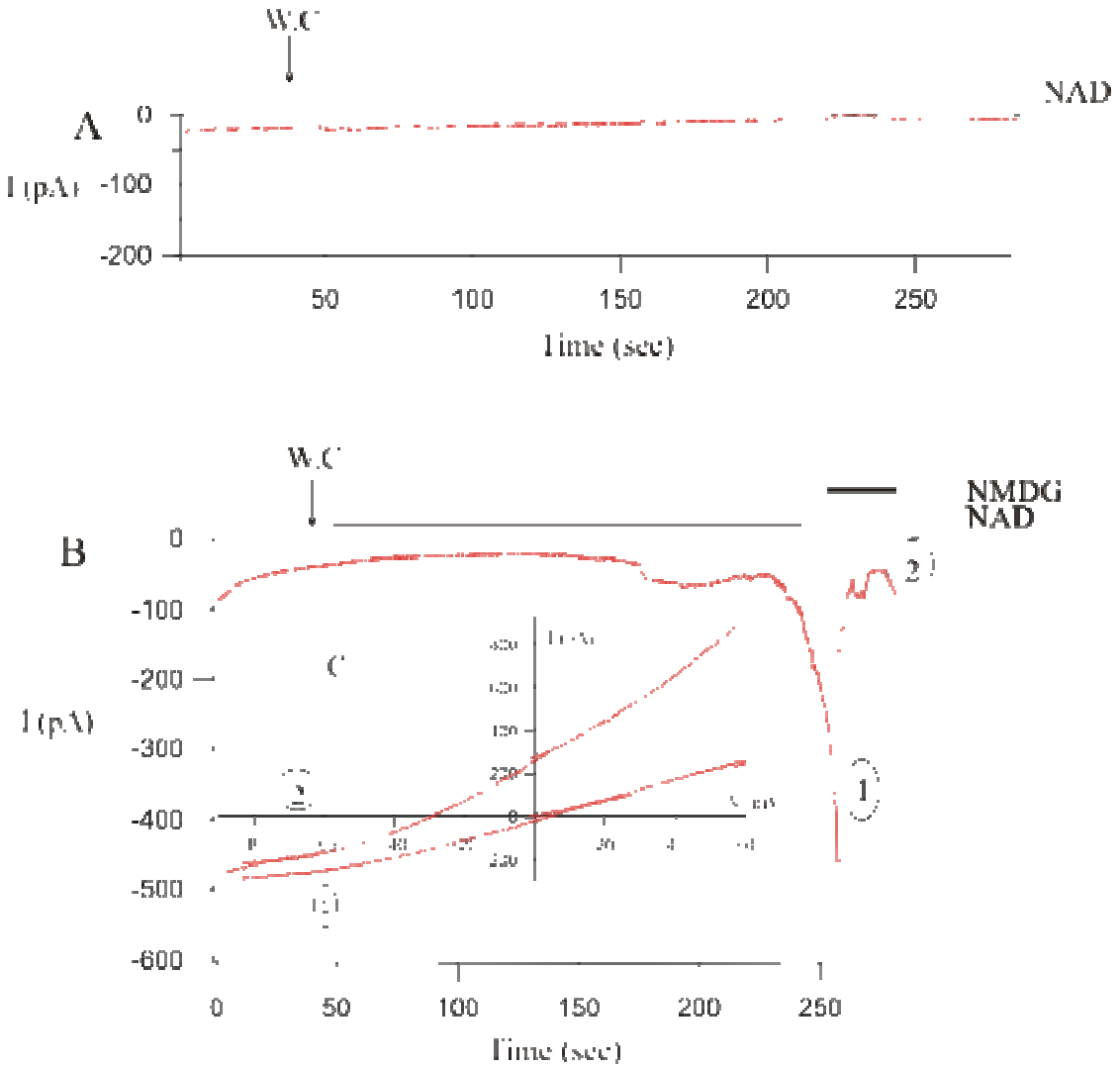

Figure 3. Stimulation of TRPM2 with intracellular β-NAD$^+$ (1 mM) and ADP-Ribose (0.3 mM). For each of the two applicants studied and for pcdfgp (control- transfected cells), the initial current density (current amplitude at –60 mV, divided by the cell capacitance, a measure of cell size as well as maximal current density after dialysis with β-NAD$^+$ and ADP-Ribose was allowed. The numbers of parentheses indicate the number of cells studied; significant stimulation of currents is indicated with *asterisk*. (mean ± SD).

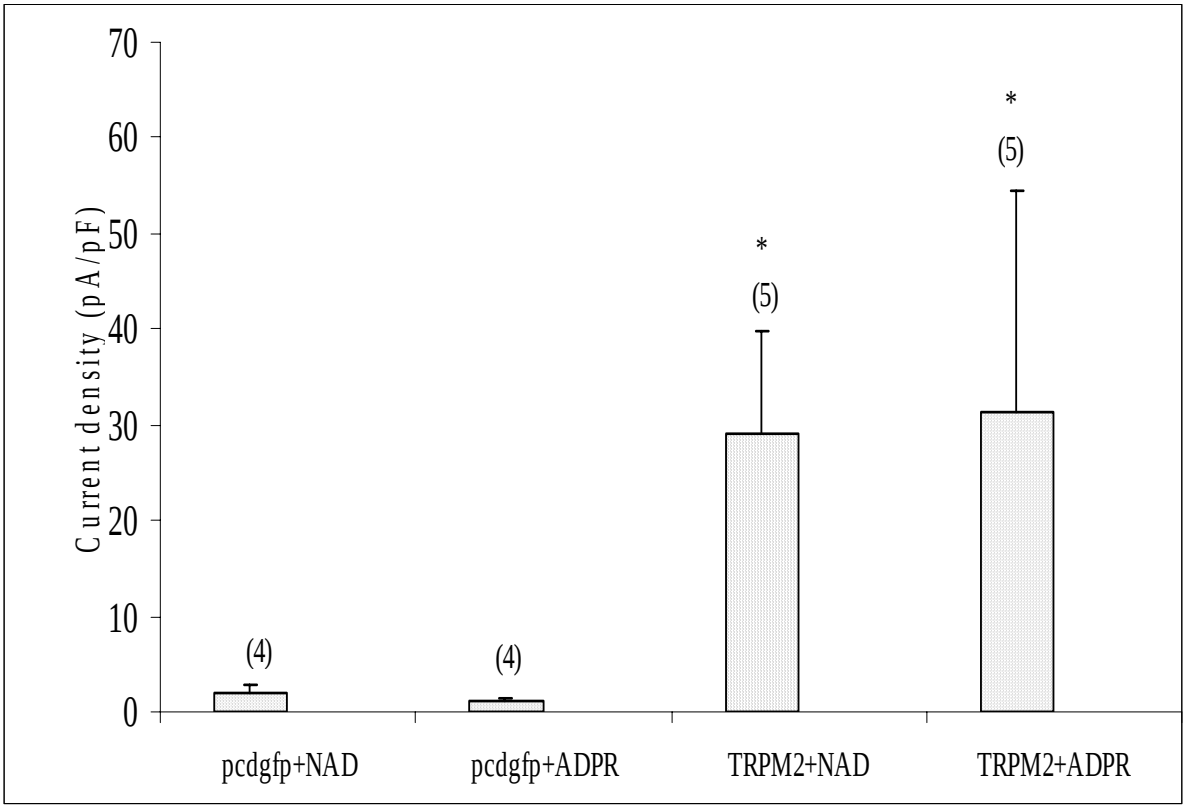

Activation of TRPM2 currents by H_2O_2

It has been well established that mitochondria produce most of the endogenous ROS, including H_2O_2, through oxidative stress. It is therefore rational to propose that the exogenously or endogenously produced ROS via oxidative stress could impair TRPM2 channel function. As a model of oxidative stress, we tested the effects of extracellular H_2O_2 on the TRPM2 channels. H_2O_2 was added to the bath to a final concentration of 10 mM. After a delay of 2-5 min, an inward current developed gradually that was blocked by NMDG and was partly carried by Ca^{2+}. After was-out of H_2O_2, the current initially increased further but then declined almost the base-line levels although a small NMDG- sensitive currents was still present (data were not shown). Re addition of H_2O_2 led to a second current rise. When the cell were exposed to H_2O_2 over more extended times than in Figure 3, the inward currents did not reach a plateau after even 15 min (data were not shown). These data suggest a participation of ROS in the TRPM channel regulation by oxidative stress.

Stimulation currents with H_2O_2 after a characteristic delay was consistently observed more then 16 cells expressing TRPM2. The mean increase in current density was –3.8- to -13.2 (Figures 4). The time elapsed before the full response to H_2O_2 occurred varied between 2-5 min.

Figure 4. Stimulation of TRPM2 with extracellular H_2O_2 (10 mM). For each of the two applicants studied and for pcdfgp (control- transfected cells), the initial current density (current amplitude at –60 mV, divided by the cell capacitance, a measure of cell size as well as maximal current density after dialysis with H_2O_2 was allowed. The numbers of parentheses indicate the number of cells studied; significant stimulation of currents is indicated with *asterisk.* (mean ± SD).

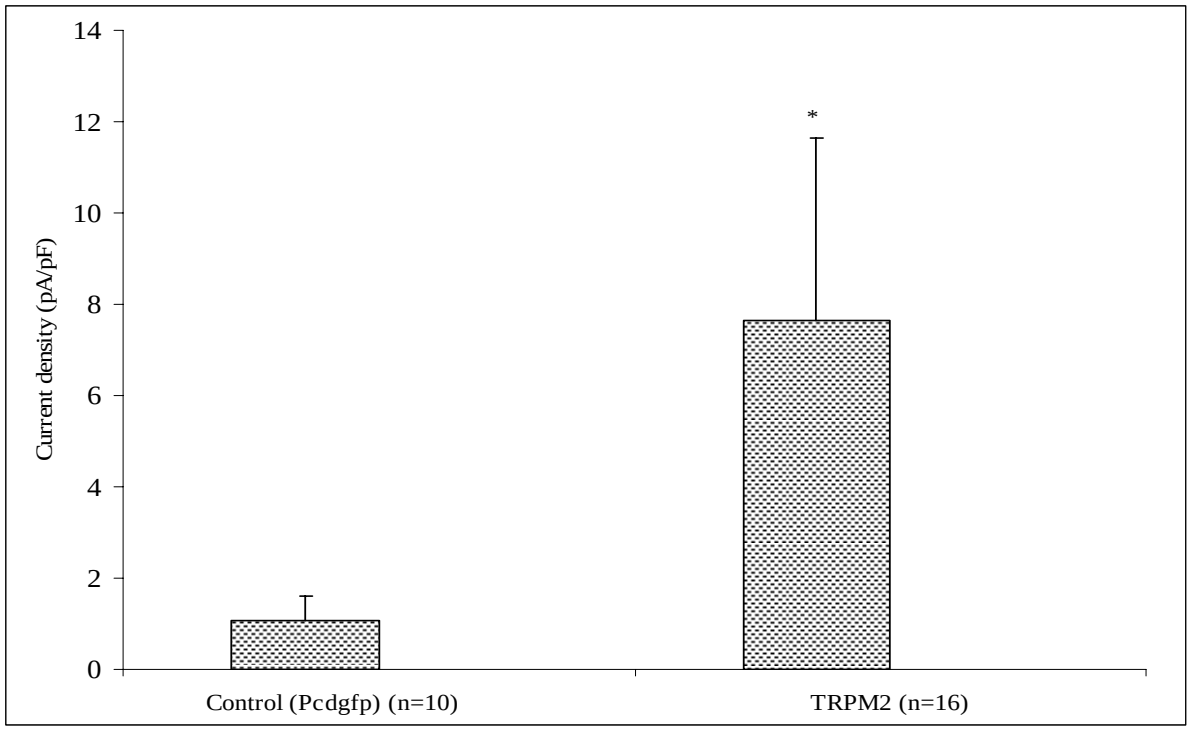

Discussion

The present study was examined effects of H2O2, ADP- ribose and NAD+ on activation of TRPM2 channel. The present study found that the non- selective cation channel currents induced by H_2O_2, ADP- ribose and NAD+.

NAD+ has been reported to stimulate TRPM2 (Sano et al., 2001; Hara et al., 2002). We saw the activation of TRPM2 by NAD+, which support the idea that this substance activates TRPM2 directly. TRPM2 contains as a characteristics structural feature a Nudix domain in its C- terminal cytosolic tail (Perraud et al., 2001). A nudix domain is a consensus region that has been known for a class of pyrophosphatases that degrade nucleoside diphosphates (Heiner et al., 2003). Indeed, the nodix domain of TRPM2 cleaves ADP- ribose, a breakdown product of NAD+ and cyclic ADP- ribose, representing an intacellular second messenger stimulating calcium release mediated by ryanodine receptors. While ADP- ribose is hydrolyzed by TRPM2, it is also activates TRPM2 and induces TRPM2 currents during infusion of ADP- ribose by the patch pipette (Harteneck, 2005). NAD+ has been reported that to stimulate TRPM2 (Hara et al., 2002).

Activation of TRPM2 by H2O2 has been reported from two approaches. One group suggested to gate the channel independently of ADP- ribose (Fonfria et al., 2004; Perraud et al., 2005) and the activation of TRPM2 by H_2O_2 is probably linked to the activity of the poly(ADP- ribose) polymerase (PARP-1), an enzyme transferring multiple ADP- ribose groups to proteins. Evidence for this intracellular pathway resulting in TRPM2 activation has been confirmed by the use of the inhibitors of poly(ADP- ribose) polymerase (PARP-1), which were able to interfer with the hydrogen peroxide induced TRPM2 activation (Reviewed in Harteneck, 2005). However, although evidence has been presented to indicate that PARP- 1 is present in mitochondria, H_2O_2 have also both been suggested to have direct effects on mitochondria (Halliwel and Gutteridge, 1999), such that the interpretation of their capacity to induce DNA damage and active PARP-1 may not be justified. In addition, PARP-1 inhibitors are known to be promiscuous within PARP family because of their structural mimicry of nicotinamide (Ferrais et al., 2003), and the concentrations required to inhibit oxidant mediated TRPM2 gating are well above those required to inhibit PARP-1 *in vitro*, precluding an unambiguous interpretation of the in cell or *in vivo* targets of these compounds. Finally, it is not obvious, at least to these authors, why PARP-1 activation should be connected to activation of a plasma membrane channel (Perraud et al., 2005).

Another group has shown H_2O_2- induced opening of TRPM2 channel directly (Hara et al. (2002; Wehaga et al., 2002; Karft et al., 2003). Indeed, currents through TRPM2 as well as increase in free Ca2+ were consistently observed. In both and TRPM2- transfected HEK-293 cells, authors current responses in whole cell configuration, which also raises the possibility of a direct effect of H_2O_2 on TRPM2 channels. Experiments on COOH- terminal truncated TRPM2 channels, lacking the ADP- ribose pyrophosphatase domain, revealed a loss of ADP- ribose- mediated gating but a retention of H_2O_2- induced activation (Wehaga et al., 2002; Karft et al.,

2003). This observation strongly supports the hypothesis of independent gating mechanisms by H_2O_2 and ADP-ribose.

According to results of current study, the H_2O_2- mediated activation of TRPM2 appears to result from a direct gating mechanism, because TRPM2 activation by H_2O_2 was relatively rapid in whole cell recordings. After adding H_2O_2 to bath, cell in whole cell records was washed by extracellular buffer and then H_2O_2 was given again. The channel was activated again by second administration of H_2O_2. From, this, we can also conclude that H_2O_2- induced, single channel activity observed in excised membrane patches is likely caused by a direct gating mechanism.

Conclusions

These results demonstrated that all three agonists, H_2O_2, ADP- ribose and NAD+, are capable of activating TRPM2. The three agonists are likely to interact directly with TRPM2 channels, consistent with the idea that they bind to the nudix domain (Hara et al. (2002; Wehaga et al., 2002; Karft et al., 2003). However, there remains insufficient evidence to suggest that three agonists are likely to interact directly with TRPM2 channels. Further studies including inside out and cell attached records are necessary to conclude definitively the conclusions.

Acknowledgment

The study was performed in Physiology Institute of RWTH- Aachen (Germany). Prof. Dr. Mustafa NAZIROGLU was supported for the study by an Alexander Humboldt Foundation (AvH) Research Fellowship. We thanks Ilinca Ionescu and Eberhard Jungling for expert technical assistance. Correspondence address is Department of Biophysics Medical (TIP) Faculty, Suleyman Demirel University Posta Kutusu 68 Cunur, TR-32260 Isparta- TURKEY. Tel: +90 246 2113310 Fax: +90 246 2371165 mnaziroglu@med.sdu.edu.tr

References

Baydaş G, Kutlu S, Nazıroğlu M, Canpolat S, Sandal S, Özcan M, Keleştimur H. Inhibitory effects of melatonin on lipid peroxidation induced by intracerebroventricularly administered homocysteine. *J Pineal Res* 2003; **34**: 36-39.

Clapham DE. TRP channels as cellular sensors. *Nature* 2003; **426**: 517-24.

Ferraris D, Ficco RP, Dain D, Ginski M, Lautar S, Lee-Wisdom K, Liang S, Lin Q,Lu MX, Morgan L, Thomas B, Williams LR, Zhang J, Zhou Y, Kalish VJ.Design and synthesis of poly(ADP-ribose) polymerase-1 (PARP-1) inhibitors. Part4: biological evaluation of imidazobenzodiazepines as potent PARP-1 inhibitors for treatment of ischemic injuries. *Bioorg Med Chem* 2003; **11**: 3695-707.

Fonfria E, Marshall, Benham CD, Boyfield I, Brown JD, Hill K, Hughes JP, Skaper SD, McNultym S. TRPM2 channel opening in response to oxidative stress is dependent on activation of poly(ADP-ribose) polymerase. *Br J Pharmacol* 2004; **143**: 186-92.

Halliwell B, Gutteridge JMC. Free radicals, other reactive species and disease. In Free Radicals in Biology and Medicine, 3rd ed.; Halliwell, B., Gutteridge, J.M.C., Eds.; Oxford University Press: New York, 1999, pp 639-645.

Hara Y, Wakamori M, Ishii M, Maeno E, Nishida M, Yoshida T, et al. LTRPC2 Ca^{2+}-permeable channel activated by changes in redox status confers susceptibility to cell death. *Mol Cell* 2002; **9**: 163-73.

Heiner I, Eisfeld J, Luckhoff A. Role and regulation of TRP channels in neutrophil granulocytes. *Cell Calcium* 2003; **33**: 533-40.

Ilhan A, Gurel A, Armutcu F, Kamisli S, Iraz M, Akyol M, Ozen S. Ginkgo biloba prevents mobile phone-induced oxidative stress in rat brain. *Clin Chim Acta* 2004; **340**:153-162.

Irmak MK, Fadillioglu E, Gulec M, Erdogan H, Yagmurca M, Akyol O. Effects of electromagnetic radiation from a cellular telephone on the oxidant and antioxidant levels in rabbits. Cell Biochem Funct 2002; **20**: 279-283.

Kolisek M, Beck A, Fleig A, Penner R. Cyclic ADP-ribose and hydrogen peroxide synergize with ADP-ribose in the activation of TRPM2 channels. *Mol Cell* 2005; **18**: 61-9.

Koliwad SK, Elliott SJ, Kunze DL. Oxidized glutathione mediates cation channel activation in calf vascular endothelial cells during oxidant stress. *J Physiol* 1996; **495**: 37-49.

Köylü H, Mollaoglu H, Ozguner, F., Nazıroğlu, M., Delibaş, N. Melatonin Modulates 900 MHz Microwave-Induced Lipid Peroxidation Changes in Rat Brain. *Toxicol Ind Health* 2006; **22**: 211-16.

Koyu A, Nazıroğlu M, Ozguner F, Yılmaz HR, Uz E, Cesur G. Caffeic acid phenethyl ester modulates 1800 MHz microwave-induced oxidative stress in rat liver. *Electromag Biol Med* 2005; **24**: 135-42.

Kuhn FJ, Heiner I, Luckhoff A. TRPM2: a calcium influx pathway regulated by oxidative stress and the novel second messenger ADP-ribose. *Pflugers Arch* 2005; **451**:212-219.

Kraft R, Grimm C, Grosse K, Hoffmann A, Sauerbruch S, Kettenmann H, Schultz G, Harteneck C. Hydrogen peroxide and ADP-ribose induce TRPM2-mediated calcium influx and cation currents in microglia. *Am J Physiol Cell Physiol* 2004; **286**: C129-37.

McCann J, Dietrich F, Rafferty C, Martin AO. A critical review of the genotoxic potential of electric and magnetic fields. *Mutat Res* 1993; **297**: 61-95.

Mendez F, Penner R. Near-visible ultraviolet light induces a novel ubiquitous calcium- permeable cation current in mammalian cell lines. *J. Physiol* 1998; **507**: 365-377.

Murphy JC, Kaden DA, Warren J, Sivak A. International Commission for Protection Against Environmental Mutagens and Carcinogens. Power frequency electric and magnetic fields: a review of genetic toxicology. *Mutat Res* 1993; **296**: 221-40.

Nazıroğlu M, Lückhoff A, Jungling E. Antagonist effect of flufenamic acid on TRPM2 cation channels activated by hydrogen peroxide. Cell Biochem Funct. 2006 (in press).

Perraud AL, Fleig A, Dunn CA, Bagley LA, Launay P, Schmitz C, Stokes AJ, Zhu Q, Bessman MJ, Penner R, Kinet JP, Scharenberg AM. ADP-ribose gating of the calcium-permeable LTRPC2 channel revealed by Nudix motif homology. *Nature*, 2001; **411**, 595-99.

Sano Y, Inamura K, Miyake A, Mochizuki S, Yokoi H, Matsushime H, Furuichi K.Immunocyte Ca^{2+} influx system mediated by LTRPC2. *Science*. 2001 17; **293 (5533)**: 1327-30.

Togashi K, Hara Y, Tominaga T, Higashi T, Konishi Y, Mori Y, Tominaga M. TRPM2 activation by cyclic ADP-ribose at body temperature is involved in insulin secretion. *EMBO J* 2006; **25** : 1804-15.

Wehage E, Eisfeld J, Heiner I, Jüngling E, Zitt C, Lückhoff A. Activation of the cation channel long transient receptor potential channel 2 (LTRPC2) by hydrogen peroxide. A splice variant reveals a mode of activation independent of ADP- ribose. *J Biol Chem* 2002; **277**: 23150-6.

Appendix: TRMP2 cation channels; Oxidative injury; electromagnetic fields;

3-DIMENSIONAL ITERATIVE FORWARD MODEL FOR MICROWAVE IMAGING

OLEKSIY S. KIM and PETER MEINCKE

ØRSTED•DTU, ELECTROMAGNETIC SYSTEMS
TECHNICAL UNIVERSITY OF DENMARK
ØRSTEDS PLADS, BUILDING 348, DK-2800 KGS. LYNGBY, DENMARK
(osk@oersted.dtu.dk)

Abstract
The efficient solution of a forward scattering problem is the key point in nonlinear inversion schemes associated with microwave imaging. In this paper the solution is presented for the volume integral equation based on the method of moments (MoM) and accelerated with the adaptive integral method (AIM). The proposed technique differs from the usual well-known MoM and AIM in the way the matrices are computed and stored. It is shown that the MoM matrix can be split in parts, which are independent of the material parameters of the scattering object. Then, provided with the actual values of the object parameters, the matrix is promptly restored in each iteration of the nonlinear inversion process. The coefficients of the multipole expansion of the basis functions in AIM are also computed irrespective of the object properties, so that the far-field contribution is computed on-the-fly via FFT in each iteration of the forward solution. Thus, the presented technique allows us to avoid the time-consuming procedure of the MoM matrix filling in each inversion iteration. Furthermore, the forward solution from the previous inversion iteration can be utilized in the next one as an initial guess, thus reducing the solution time for the forward model.

Introduction
Nonlinear inversion schemes applied in microwave imaging involve the solution of a forward scattering problem, which takes the major part of the overall solution time. Therefore, it is of great importance to make the forward model fast and efficient to ensure the rapid convergence of the imaging procedure.

If a single-frequency inversion technique is utilized, it implies a frequency-domain forward scattering model. The volume integral equation (VIE) technique or the finite element method (FEM) can be applied in this case. The VIE solution converges much faster than FEM [1]. However, its memory demand is also significantly higher. The FEM generates a sparse matrix, while the method of moments (MoM) applied to transform the integral equation into a system of linear equations yields a matrix with a very high fill-in. The large memory requirements of MoM for integral equations can be a bottleneck for imaging of dense inhomogeneous dielectric objects. To overcome this difficulty an accelerated MoM solver, such as the multilevel fast multipole method (MLFMM) or the adaptive integral method (AIM), can be applied.

In this paper, we present the solution for the volume integral equation by the method of moments accelerated with the adaptive integral method. The proposed technique differs from the usual well-known MoM and AIM in the way the matrices are computed and stored.

Nonlinear inversion process involves an iteration procedure, in which a forward problem is solved in each iteration with a relatively small variation of the material parameters of the object under investigation. To improve the efficiency of the algorithm the forward solution can take advantage of the solution from the previous iteration. First of all, the time consuming MoM matrix filling process can be almost eliminated if the matrix is split into parts independent of the material parameters of the scattering object. These parts can be computed only once and stored in computer memory or on a hard disk. Then, provided with the actual values of the object parameters, the matrix is promptly restored in each iteration of the nonlinear inversion process. Thus, a significant saving in the computational time can be achieved as compared to the case when the MoM matrix is

computed from scratch in each iteration. Furthermore, the forward solution from the previous inversion iteration can be utilized in the next one as an initial guess, thus reducing the solution time for the forward model.

Method of Moments for Volume Integral Equation

The volume integral equation represents the total electric field $\bar{E}(\bar{r})$ in the volume V as a sum of the incident $\bar{E}^i(\bar{r})$ and the scattered $\bar{E}^s(\bar{r})$ electric fields as

$$\bar{E}(\bar{r}) = \bar{E}^i(\bar{r}) + \bar{E}^s(\bar{r}), \qquad \bar{r} \in V. \tag{1}$$

The scattered electric field $\bar{E}^s(\bar{r})$ can be written in terms of the magnetic vector potential $\bar{A}(\bar{r})$ and scalar potential $\Phi(\bar{r})$ as

$$\bar{E}^s(\bar{r}) = -j\omega\bar{A}(\bar{r}) - \nabla\Phi(\bar{r}), \tag{2a}$$

$$\bar{A}(\bar{r}) = \mu_b \int_V G(\bar{r},\bar{r}')\bar{J}(\bar{r}')dv', \tag{2b}$$

$$\Phi(\bar{r}) = \frac{1}{\varepsilon_b}\int_V G(\bar{r},\bar{r}')\rho(\bar{r}')dv', \tag{2c}$$

where $G(\bar{r},\bar{r}')$ is the free space Green's function and $\bar{J}(\bar{r})$, $\rho(\bar{r})$ are the unknown induced electric volume current and charge densities, respectively. In (2), ε_b is the permittivity and μ_b is the permeability of the background medium. It is noted that the VIE is more conveniently solved with respect to the electric flux density $\bar{D}(\bar{r})$ because its normal component is continuous across the boundary between two different dielectric materials. The substitution in variables is carried out as

$$\bar{J}(\bar{r}) = j\omega K(\bar{r})\bar{D}(\bar{r}) == j\omega\frac{\varepsilon(\bar{r})-\varepsilon_b}{\varepsilon(\bar{r})}\bar{D}(\bar{r}). \tag{3}$$

To discretize the VIE in (1) the scattering object is divided into cells using curvilinear hexahedral elements. Then, the unknown function $\bar{D}(\bar{r})$ is expanded locally in each cell in terms of the higher-order hierarchical Legendre basis functions $\overline{f_n}(\bar{r})$ [2]. Finally, the Galerkin's testing is employed to transform the VIE in (1) into a system of linear equations. Assuming the dielectric permittivity $\varepsilon(\bar{r})$ to be constant within each cell and taking into account that $\rho(\bar{r}) = j\omega^{-1}\nabla\cdot\bar{J}(\bar{r})$, an element z_{mn} of the resulting MoM matrix $[Z]$ can be written as

$$\begin{aligned} z_{mn} &= \frac{\left\langle \overline{f_m}(\bar{r}), \overline{f_n}(\bar{r})\right\rangle}{\varepsilon_l} + K_l\left\{-\omega^2\mu_b\left\langle \overline{f_m}(\bar{r}), \int_{V_l} G(\bar{r},\bar{r}')\overline{f_n}(\bar{r}')dv'\right\rangle\right. \\ &\left. -\frac{1}{\varepsilon_b}\left\langle f_m(\bar{r}), \nabla\left(\int_{V_l} G(\bar{r},\bar{r}')\left[\nabla'\cdot\overline{f_n}(\bar{r}')\right]dv' - \int_{S_l} G(\bar{r},\bar{r}')\left[\overline{f_n}(\bar{r}')\cdot\overline{dS'}\right]\right)\right\rangle\right\} \\ &= \frac{z'_{mn}}{\varepsilon_l} + K_l z''_{mn}, \end{aligned} \tag{4}$$

where $\langle\cdot,\cdot\rangle$ is the inner product, and the subscript l denotes the cell, in which the function $\overline{f_n}(\bar{r})$ is defined. The surface integral in (4) is taken "just inside" the surface of the cell l. It is seen that both z'_{mn} and z''_{mn} are independent on the material parameters of the object. However, the expression (4) is valid only for a subset of the higher-order hierarchical Legendre basis functions $\overline{f_n}(\bar{r})$, namely those that are defined within one cell. For the basis functions that span two neighbor cells (rooftop, for instance), so that $\overline{f_n}(\bar{r}) = \overline{f_n^-}(\bar{r}) + \overline{f_n^+}(\bar{r})$, the expression (4) can be modified as

$$\begin{aligned} z_{mn} &= \frac{\left\langle \overline{f_m}(\bar{r}), \overline{f_n^-}(\bar{r})\right\rangle}{\varepsilon_l^-} + \frac{\left\langle \overline{f_m}(\bar{r}), \overline{f_n^+}(\bar{r})\right\rangle}{\varepsilon_l^+} + K_l^- z''^-_{mn} + K_l^+ z''^+_{mn} \\ &= \frac{z'^-_{mn}}{\varepsilon_l^-} + \frac{z'^+_{mn}}{\varepsilon_l^+} + K_l^- z''^-_{mn} + K_l^+ z''^+_{mn}. \end{aligned} \tag{5}$$

Again, the expressions for $z'^{\pm}_{mn}$ and $z''^{\pm}_{mn}$ do not contain the material parameters of the scattering object. Consequently, the matrices $[Z''^{-}]$ and $[Z''^{+}]$ can be precomputed and stored for the subsequent iterations of the nonlinear inversion process. The first two terms in (5) do not require precomputation. They can be computed "on the fly", since no time-consuming Green's function calculations are involved.

Adaptive Integral Method for Volume Integral Equation

The adaptive integral method accelerates the solution of the VIE by separating elements of the MoM matrix $[Z]$ responsible for near- and far-interactions [3], as

$$[Z] = [Z^{near}] + [Z^{far}]. \tag{6}$$

The near-field elements $[Z^{near}]$ constitute a relatively small part of the full matrix. They are computed explicitly and stored in a sparse matrix format. The far interactions are accounted implicitly in the matrix-vector product $[Z^{far}][X]$, where $[X]$ is the unknown solution vector in each iteration of the iterative solution of the MoM matrix system. The following procedure makes it possible to apply the FFT to speed up the matrix-vector multiplication.

The induced volume current and charge densities are represented by point-like sources located at nodes of a regular rectangular grid enclosing the scattering object. Mathematically, it is equivalent to the expansion of the components of the functions $\overline{f_n}(\bar{r})$ and $\nabla \cdot \overline{f_n}(\bar{r})$ in terms of Dirac delta-functions as

$$f_\alpha(\bar{r}) \cong \sum_{\bar{u} \in C_\alpha} \Lambda_{\alpha\bar{u}} \delta(\bar{r} - \bar{u}), \tag{7}$$

where f_α denotes f_{nx}, f_{ny}, f_{nz}, or $\nabla \cdot \overline{f_n}$, and C_α is a cube of $(M+1)^3$ nodes. The coefficients $\Lambda_{n\bar{u}}$ are chosen so that the expansion (7) reproduces the far field radiated by the current element $\overline{f_n}(\bar{r})$. This can be achieved in different ways, depending on approximation criteria established. Here, we use a multipole expansion described in [3].

To make the expansion (7) consistent with the representation (5) for the rooftop basis function, we can similarly write

$$f_\alpha(\bar{r}) = f_\alpha^-(\bar{r}) + f_\alpha^+(\bar{r}) \cong \sum_{\bar{u} \in C_\alpha^-} \Lambda_{\alpha\bar{u}}^- \delta(\bar{r} - \bar{u}) + \sum_{\bar{u} \in C_\alpha^+} \Lambda_{\alpha\bar{u}}^+ \delta(\bar{r} - \bar{u}). \tag{8}$$

Thus, the elements of the matrix $[Z^{far}]$ can be approximated as

$$z_{\beta\alpha}^{far} \cong K_l^- \sum_{\bar{v} \in C_\beta} \sum_{\bar{u} \in C_\alpha^-} \Lambda_{\beta\bar{v}} G(\bar{v} - \bar{u}) \Lambda_{\alpha\bar{u}}^- + K_l^+ \sum_{\bar{v} \in C_\beta} \sum_{\bar{u} \in C_\alpha^+} \Lambda_{\beta\bar{v}} G(\bar{v} - \bar{u}) \Lambda_{\alpha\bar{u}}^+. \tag{9}$$

In (9), we assume that constants, such as ω, ε_b, μ_b, are included in the corresponding coefficients Λ. Based on the expression (9) it can be observed that the matrix vector-product $[Z^{far}][X]$ can be effectively computed by FFT's.

The coefficients $\Lambda^{\pm}$ are independent of the material parameters of the scattering object, and therefore calculated once they can be reused throughout the nonlinear inversion process.

Forward Solution Procedure in the context of the Nonlinear Inversion Process

The computational procedure for the solution of the forward scattering problem in the context of the nonlinear inversion process is as follows:

1. Set initial values for the material parameters of the object under investigation.
2. Discretize the object.
3. Set the expansion order for the unknown function $\overline{D}(\bar{r})$ in each cell according to its electrical size.
4. Specify a regular rectangular grid enclosing the scattering object and compute the coefficients $\Lambda^{\pm}$.
5. Compute the terms $z''^{\pm}_{mn}$ for the elements of $[Z^{near}]$ and store them in a sparse matrix format.
6. Reconstruct the matrix $[Z^{near}]$ using the precomputed $z''^{\pm}_{mn}$ and actual material parameters of the object (Equation (5)).

7. Solve the MoM matrix system using an iterative solver. The product $[Z^{far}][X]$ is calculated by FFT's in each iteration using the precomputed $\Lambda^{\pm}$.
8. If necessary update the material parameters of the object and return to step 6.

It should be noted that the procedure presented above is valid only for a reasonable variation of the material parameters of the object (within 10-20%). Otherwise, to avoid over- or under-discretization the procedure should be repeated starting from step 3. If our method of moments solution were based on low-order basis functions (pulse, RWG, etc.) the procedure should have been repeated starting from step 2.

Numerical Results

To verify the proposed technique, we consider scattering by a solid dielectric cube with the side length $1.4\lambda_0$. The cube is made of lossless dielectric with the relative permittivity $\varepsilon_r = 4.0$, except its central slice of width $0.28\lambda_0$ (see Fig. 1). The relative permittivity of the slice is varied from $\varepsilon_r = 4.1 - j0.05$ to $\varepsilon_r = 5.1 - j0.55$ in 11 cycles, which represent the iterations of a nonlinear inversion process. An x-polarized plane wave illumination is considered. The object is discretized with 1000 identical cells, and the second expansion order is utilized to expand the unknown electric flux density in each cell. The discretization yields 25200 unknowns, which would require about 4.7 GB of computer memory to store the full MoM matrix. For the modified MoM and AIM techniques presented in this paper the memory requirement is 510 MB.

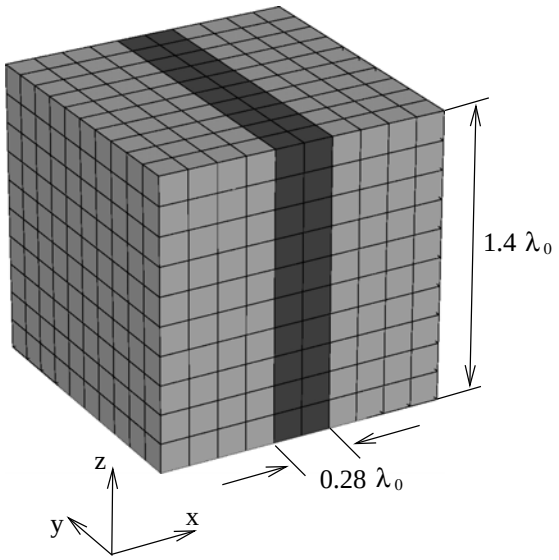

Fig.1. Solid dielectric cube with a central slice made of different dielectric material.

In the numerical experiments the Generalized Minimal Residual (GMRES) iterative solver with restarts after 30 iterations is employed. The time to fill the MoM matrix and the number of iterations to convergence to a relative residual error of 10^{-5} is summarized in Table 1 for all 11 cycles. In the first cycle all necessary calculations to precompute the data for the subsequent cycles are carried out, i.e., steps 1-5 of the solution procedure described in the previous section. Then steps 6-8 follow. In the subsequent cycles only steps 6-8 are involved. It is seen that a significant saving in time in cycles 2-11 is achieved by eliminating the matrix filling process and reusing precomputed result from the first cycle. The matrix reconstruction at the step 6 is extremely fast. Moreover, the number of iterations to converge is also decreased by employing as an initial guess the solution vector from the previous cycle.

Table 1. MoM matrix filling time and the number of iterations to converge.

Cycle	1(setup)	1	2	3	4	5	6	7	8	9	10	11
Permittivity	4.1-*j*0.05	4.1-*j*0.05	4.2-*j*0.10	4.3-*j*0.15	4.4-*j*0.20	4.5-*j*0.25	4.6-*j*0.30	4.7-*j*0.35	4.8-*j*0.40	4.9-*j*0.45	5.0-*j*0.50	5.1-*j*0.55
Filling time, sec	33547	15	15	15	15	15	15	15	15	15	15	15
Iterations	–	1559	1000	965	934	908	885	861	840	822	805	789

The configuration of the cycle 11 is also simulated from scratch using the classical MoM accelerated with the AIM. In Fig. 2, the obtained bistatic radar cross section (RCS) is compared to the result of the cycle 11. As expected, no difference is observed, which illustrates the correctness of the derivation and implementation of the presented technique.

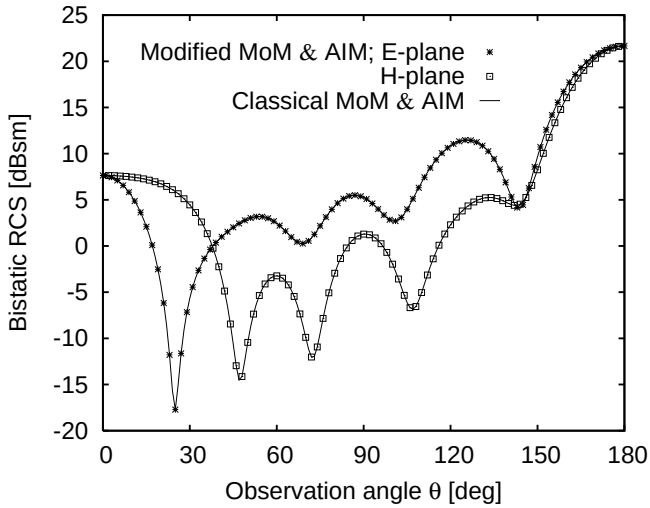

Fig.2. Bistatic RCS of the dielectric cube with a central slice made of dielectric with $\varepsilon_r = 5.1 - j0.55$.

Conclusions

The formulation for the classical method of moments for the volume integral equation, which is employed to solve the forward scattering problem, is modified so that the time consuming matrix filling procedure is moved to the setup phase of a nonlinear iterative inversion process. This is accomplished by splitting the MoM matrix in parts, which are independent of the material parameters of the scattering object. Once computed in the setup phase these parts are stored in the memory or on a hard disk. Then, provided with the actual values of the object material parameters, the matrix is promptly restored in each iteration of the nonlinear inversion process. Similar modifications are made in the adaptive integral method, which is applied to accelerate the MoM solution as well as to reduce its memory demands. The given numerical results show that the present technique allows the forward model to be solved fast and efficiently in each iteration of a nonlinear inversion process.

Acknowledgments

The Danish Technical Research Council is acknowledged for supporting this work.

References

1. Volakis J.L., Sertel K., Jorgensen E., Kindt R.W., “Hybrid finite element and volume integral methods for scattering using parametric geometry”, *Computer Modeling in Engineering & Sciences*, vol. 5., no. 5, pp. 463-476, 2004.

2. Kim O.S, Jørgensen E., Meincke P., Breinbjerg O., “Method of moments solution of volume integral equations using higher-order hierarchical Legendre basis functions”, *Radio Sci.*, 39, RS5003, doi:10.1029/2004RS003041.

3. Bleszynski E., Bleszynski M., Jaroszewicz T., “AIM: adaptive integral method for solving large-scale electromagnetic scattering and radiation problems”, *Radio Sci.*, vol. 31, no. 5, pp. 1225-1251, 1996.

USING COMPUTER PROGRAMS TO EVALUATE EFFICIENCY OF DIFFERENT SHIELDS CONFIGURATION

KUREK KRZYSZTOF[1)], GRYZ KRZYSZTOF[2)], KARPOWICZ JOLANTA[2)], KUREK ALICJA[1)], SMALCERZ ALBERT[1)], ZRADZIŃSKI PATRYK [2)]

[(1)] SILESIAN UNIVERSITY OF TECHNOLOGY, DEPARTMENT OF ELECTROTECHNOLOGY, 8 KRASIŃSKIEGO STR., 40-019 KATOWICE, POLAND
[(2)]CENTRAL INSTITUTE FOR LABOUR PROTECTION-NATIONAL RESEARCH INSTITUTE, 16 CZERNIAKOWSKA STR, 00-701 WARSAW, POLAND

Abstract
The issue of limiting negative influence of effect of electromagnetic fields from induction heating devices using electromagnetic shields has been presented in the paper. The effectiveness of shielding for fields of different frequencies has been examined considering the material, thickness and size of shields as well as multilayer systems. The research was conducted applying computer simulation method using Flux3D and CST EM Studio programs and subsequently experimentally verified at laboratory stand. The satisfactory similarity of simulation and experimental results allows for using the simulation method in designing shields for industrial use.

Introduction
Induction as well as magnetohydrodynamic (MHD) heating devices are commonly used in industry especially in metallurgy and machine building. Conversion of energy into heat or generation of electrodynamic forces moving liquid metal happens through electromagnetic fields of low frequencies of 50 and 60 Hz, medium ones of around 30 kHz and high ones of up to around 400 kHz. Because of it the supplying sources of induction or MHD devices have negative influence on the surrounding environment. One of the technical means most often used for limiting electromagnetic radiation is electromagnetic shielding. Technical surroundings in industrial environment very frequently cause unexpected distribution of field around the devices, which makes proper design and production of effective shielding a very complicated issue. Usually adequate experience is required as well as suitable research methods need to be applied. In the authors' opinion a computer simulation method is very useful to achieve these aims provided that it is properly experimentally verified [1,2].
The multivariant calculations in the paper have been carried out applying programs using the finite elements and boundary integrals method for calculations of magnetic field intensity in front and behind the shield, since in case of induction or MHD devices these are the real risks. Different shield structures: single-layer and double-layer have also been examined taking into consideration the material they have been made from, their size and positioning in relation to the measuring point. The calculations have been performed for the frequency range most often used in induction heating and metallurgical MHD devices.

Simulation results
The simulation calculations have been made in a system (Fig.1) consisting of an inductor loaded with a charge being a field source and a shield placed between the inductor and the points in space in which the field intensity have been calculated. Flux3D computer programs were used for calculation basing on Maxwell's equations solution applying finite elements method and respectively CST EM Studio using boundary integrals method. Physical properties of materials being subject of simulation have been put into Table 1.
Shielding effectiveness has been calculated in accordance with the relation [3]:

$$S_H = 20 lg \frac{H}{H_S}$$

where: H – magnetic field intensity in a system without a shield, H_S - magnetic field intensity in a system with a shield.

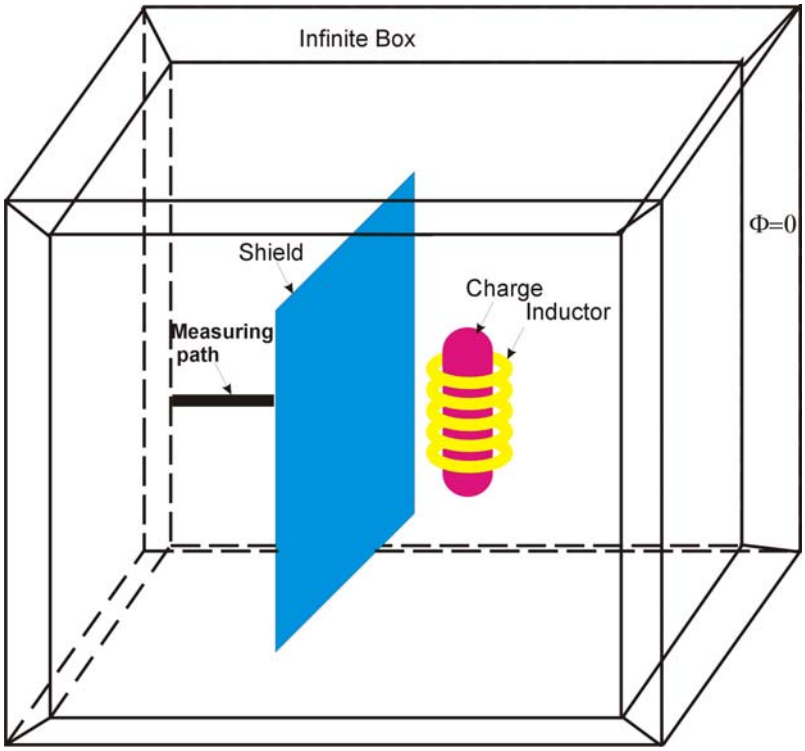

Fig.1. 3D calculation model for simulation of shielding effectiveness of induction devices

The influence of the shield's material, its thickness, structure, existence of one or two layers and the placing between source and a measuring point on shielding effectiveness has been examined with certain supplying parameters. The simulation results are shown in Figures 2-5.

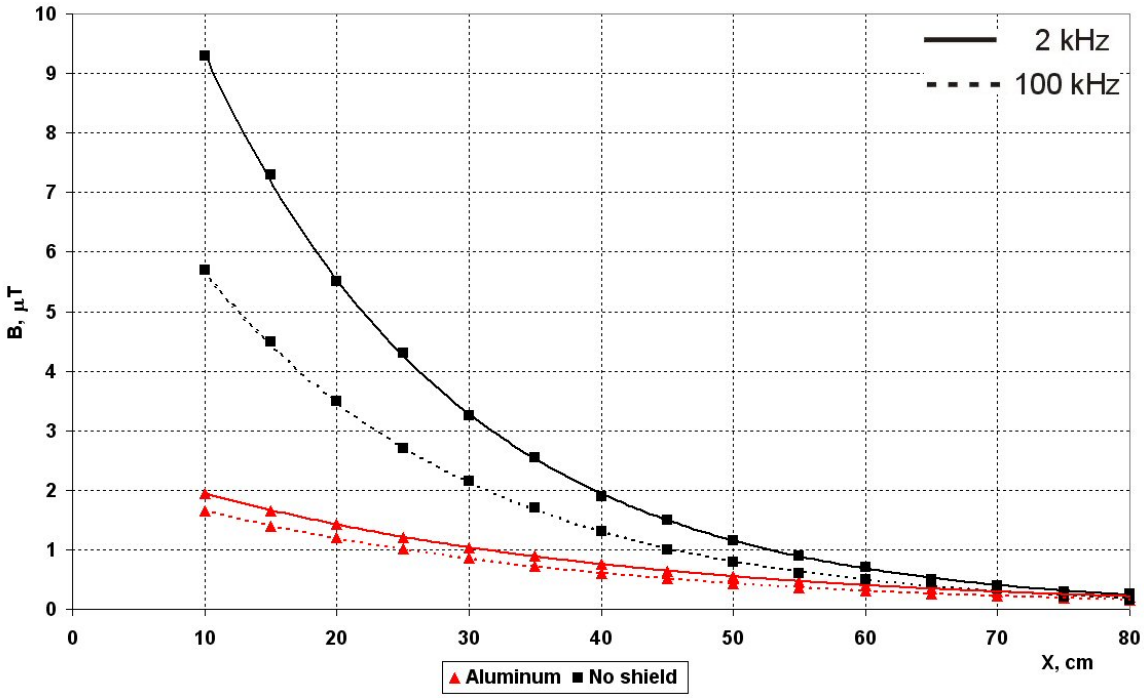

Fig. 2. Effect of using shield on magnetic induction value on measuring path outside shield

Using an electromagnetic shield (Fig.2) leads to a rapid four times decrease of magnetic induction value in places outside the shield especially in its nearest proximity, since with moving away from the source the field weakens in a natural way.

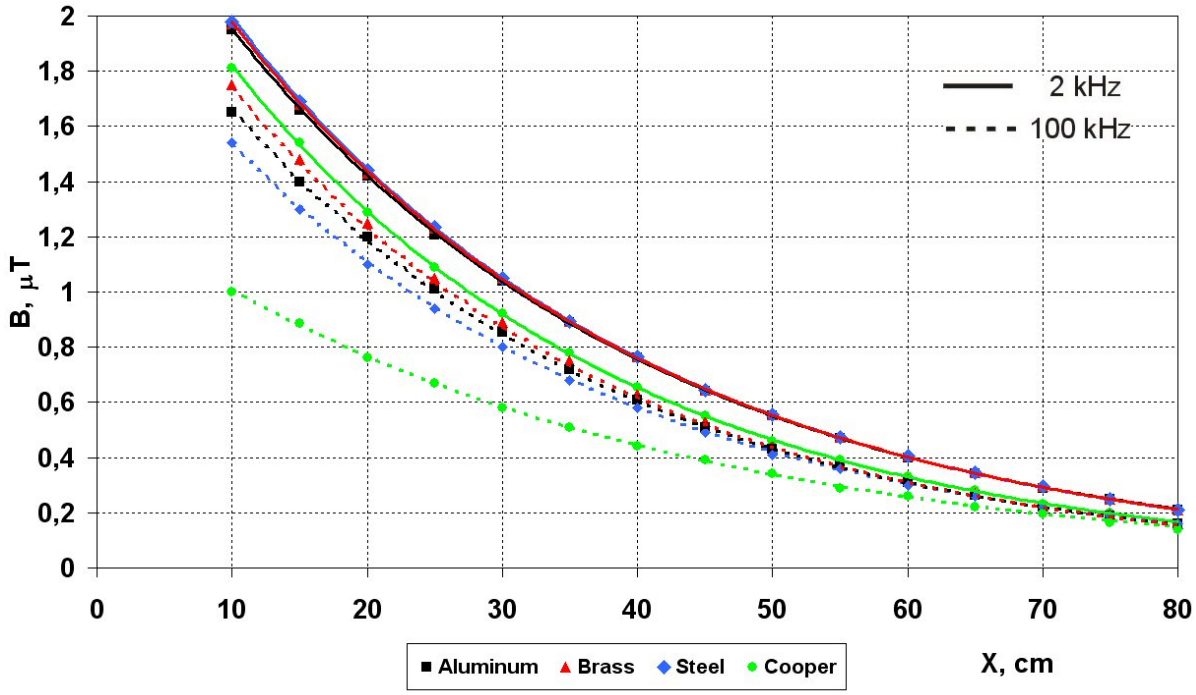

Fig.3. Calculated magnetic induction values for shields made of various materials

The materials of high conductivity and possibly of high magnetic permeability (ferromagnetics) have the best shielding properties (Fig.3) by certain shield thickness. One has to however bear in mind that using ferromagnetics as shields is limited and near the sources with medium and high frequencies even impossible due to their quick heating leading to melting in places. While choosing the material its costs also have to be considered. This makes using of copper very problematic and therefore aluminum and non-magnetic steel are used far more often

Tab. 1. Physical properties of materials

Material	Conductivity, MS/m	Magnetic permeability
Aluminum	33	1
Brass	25	1
Steel	4,3	1000
Copper	55	1

Figure 4 indicates that the shield should not be to thin (0,5 mm) in relation to the depth of electromagnetic field penetration

$\delta = \sqrt{\frac{2}{\mu\gamma\omega}}$, where μ - magnetic permeability of the shield, γ – electrical conductivity of the shield, ω – pulsation of the coil current ($\omega = 2\pi f$). Nevertheless further increase of its thickness to over 2 mm is purposeless since the production costs grow significantly with slight decrease of induction value.

On the other hand the course of curves shown in Figure 5 indicates that application of double-layer structures (two different materials) is reasonable only for a system conductor (Cu or Al) – ferromagnetic. It seems that this has to be subject of further research.

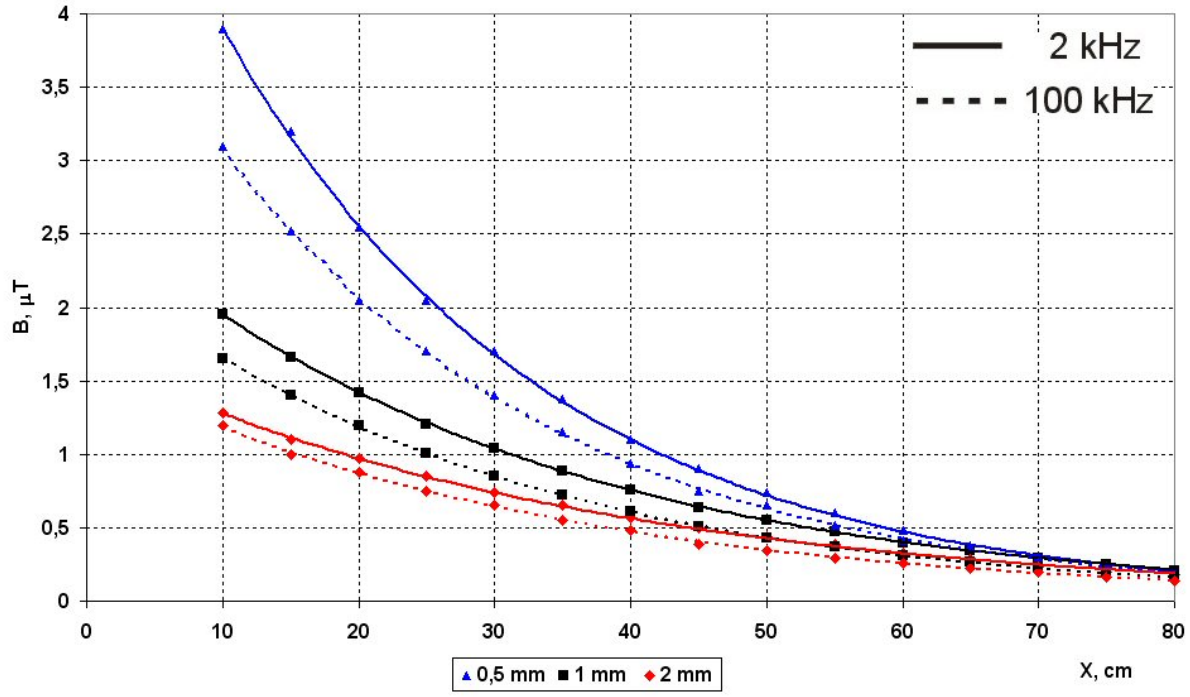

Fig.4. Calculated values of magnetic induction for aluminum shields of various thicknesses

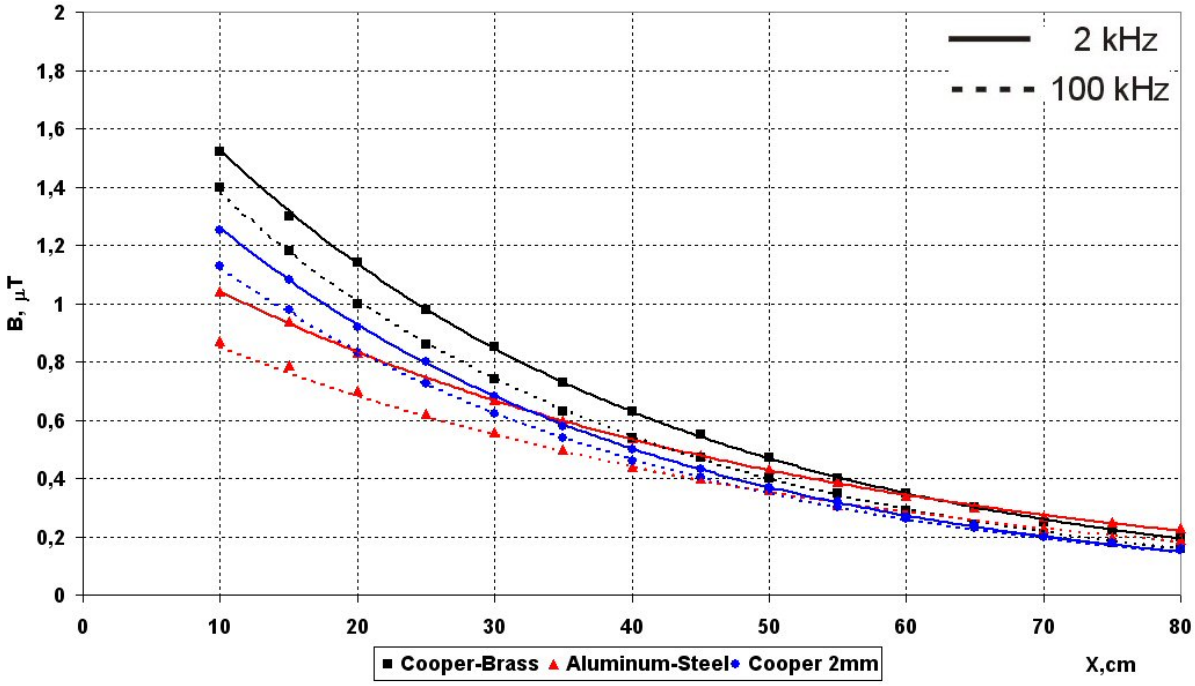

Fig. 5. Calculated values of magnetic induction for double-layer shields in relation to single-layer shield made of copper with same thickness as double-layer shields

Experimental verification

The carried out simulation research was experimentally verified in the laboratory of Electromagnetic Risks Workroom in the Central Institute of Work Protection. The examinations have been performed in the system as in Figure 6 and covered determination of frequency characteristics of shielding effectiveness for metal shielding structures, comprising of various combinations of sheet metal. The frequency characteristics have been determined for electromagnetic fields' frequency of 20 to 100 kHz. The Helmholtz's coils were used as electromagnetic field source during examinations. The supplying system consisted of a HAMEG HM8130 generator, PA-300S power supplier, H/PA-300S adjusting system. The stability of the generated magnetic field

was monitored with excitation check using HP 34401A voltmeter. The shielding effectiveness was determined on the basis of magnetic induction measurements using Narda ELT-400 meter (S/N K-0036) with 1Hz-400kHz probe (S/N K-0042), applied in a RMS 320μT, LowCut 1Hz working mode. Comparison of shielding effectiveness results obtained from simulation and measurements has been shown in Figure 7 and 8.

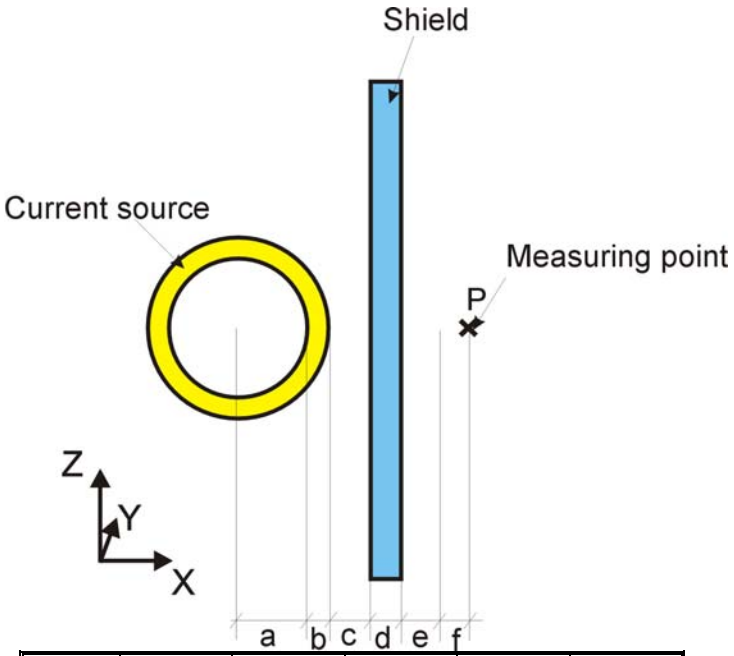

a	b	c	d	e	f
mm	mm	mm	mm	mm	mm
150	20	10	10	50	50

Fig.6. Measuring system for experimental verification of shielding effectiveness

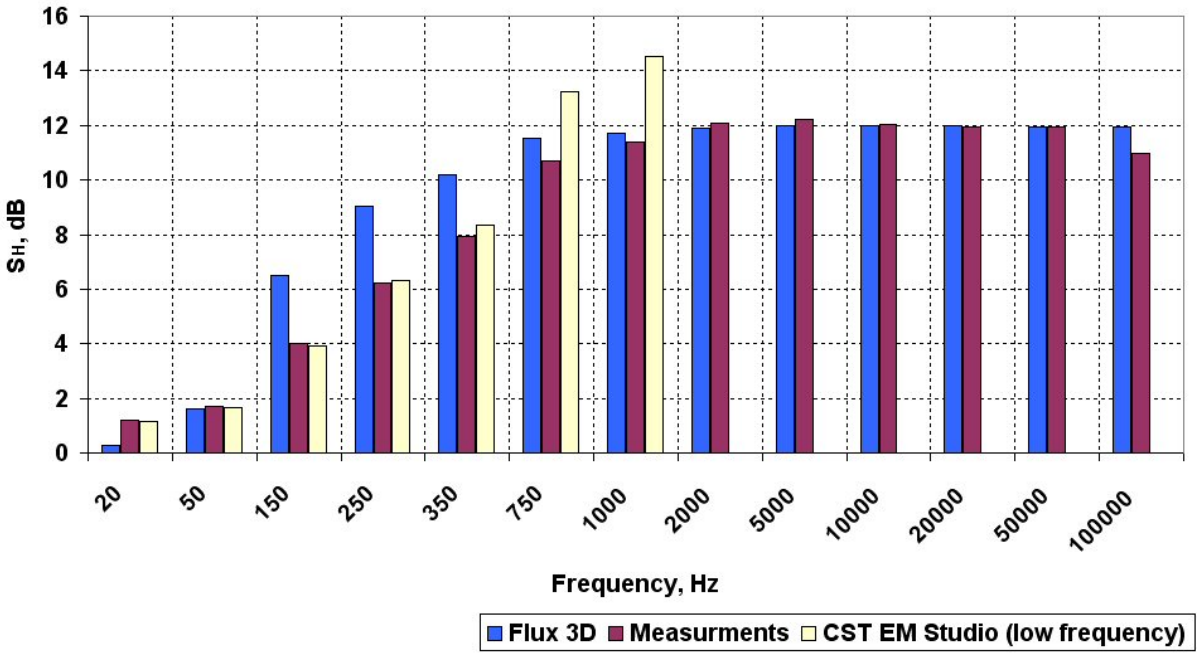

Fig.7. Comparison of shielding effectiveness results obtained from simulation (Flux3D, CST Studio) and measurements for shield made of sheet copper of 1 mm thickness

The presented comparison show that the calculation carried out using Flux3D program for medium and high frequencies > 750 Hz are very similar to experimental results (Fig.7) for single-layer shield and a little less so for

double-layer shield (Fig.8). In both cases good conformity of CST Studio and experimental results has been obtained for low frequencies < 250 Hz.

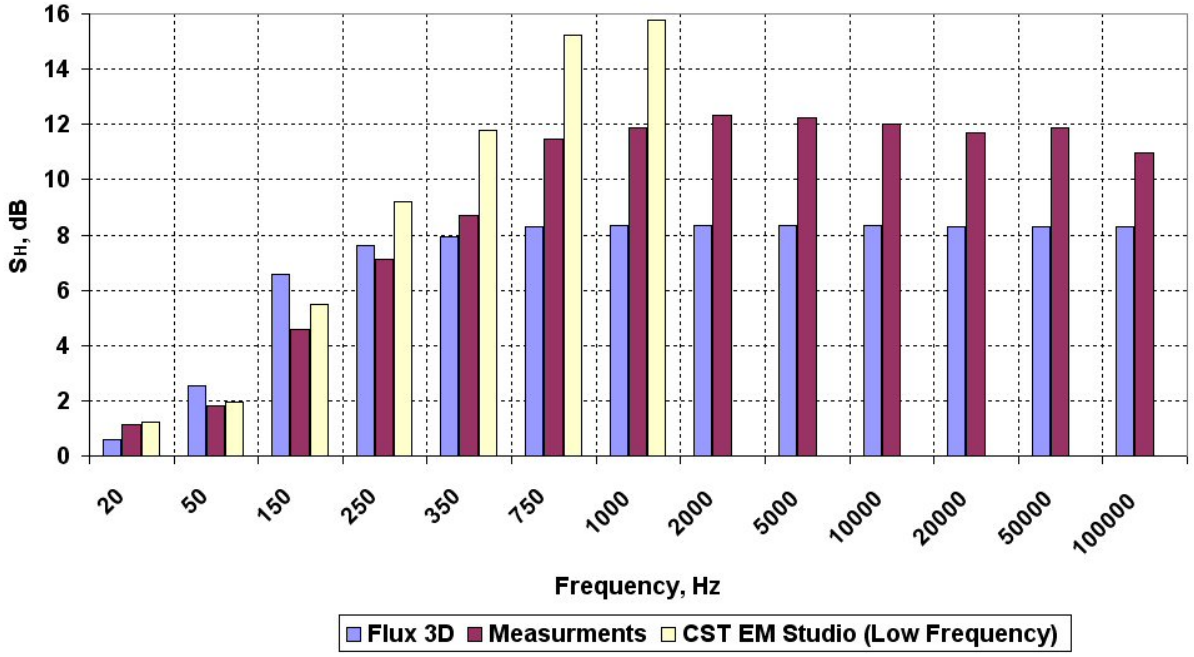

Fig.8. Comparison of shielding effectiveness results obtained from simulation (Flux3D, CST Studio) and measurements for double-layer shield made of sheet copper of 1 mm thickness and made of brass of 1 mm thickness

Summary

Usability of computer simulation method for research on shielding effectiveness and consequently on limitation of electromagnetic radiation levels around induction devices has been presented in the paper. The carried out examinations proved that that for frequency ranges applied in induction heating the best results of shielding effectiveness were obtained for copper shields of thicknesses up to 2 mm. Only slightly worse results were obtained for aluminum, but considering the cost of both materials, the latter will be much more frequently used. Interesting results have been obtained for double-layer systems especially for aluminum-steel, however this requires further research in order to select the optimum sort of sheet steel and thickness of both layers.

Application of computer simulation may be a basic tool in the design process of electromagnetic shields in industry installations.

Acknowledgments

This paper was supported by the State Committee for Scientific Research under research grants number 3 T08B 051 29 and 3 T08B 033 27.

References

1. Kurek K., Smalcerz A.: Methods of reduction of electromagnetic radiation around the induction devices, Workshop Warsaw, 2005, pp. 53-57 s. VI
2. Kurek K., Smalcerz A.: Electromagnetic fields exposure around induction heaters and methods of its limitation, International Conference on Electromagnetic Fields, Health and Environment, EHE'06, Funchal, Madeira, Portugal, April, 2006 pp. 1.93-1.98
3. Korniewicz H.: Ekranowanie źródeł pól elektromagnetycznych 0,1-300 MHz. Prace CIOP 1984, Polish pp.3-26

NEW FEATURES IN THE IEEE C95.1-2005 RF EXPOSURE STANDARD

C-K. CHOU[1], JOHN A. D'ANDREA[2], RICHARD A. TELL[3], J. PATRICK REILLY[4], ELEANOR R. ADAIR[5], MAYS L. SWICORD[6], SAKARI LANG[7], JOHN J. DEFRANK[8], RONALD C. PETERSEN[9]

[1]MOTOROLA LABS, CK.CHOU@MOTOROLA.COM
[2]NAVAL HEALTH RESEARCH CTR., JOHN.DANDREA@NAVY.BROOKS.AF.MIL
[3]RICHARD TELL ASSOCIATES, RTELL@RADHAZ.COM
[4]METATEC ASSOCIATES, JPREILLY@IEEE.ORG
[5]INDEPENDENT CONSULTANT, EADAIR@COMCAST.NET
[6]MOTOROLA LABS, MAYS.SWICORD@MOTOROLA.COM
[7]NOKIA CORPORATION, SAKARI.LANG@NOKIA.COM
[8]USACHPPM, JOHN.DEFRANK@AMEDD.ARMY.MIL
[9]R C PETERSEN ASSOCIATES, R.C.PETERSEN@IEEE.ORG

Abstract
C95.1-2005 "IEEE Standard for Safety Levels with Respect to Human Exposure to Radio Frequency Electromagnetic Fields, 3 kHz to 300 GHz" was approved on October 5, 2005 and published on April 19, 2006. This revision (of C95.1-1991) is based on an evaluation of the scientific literature through 2003. The recommendations are intended to protect people of all ages against established RF adverse health effects. Major changes (compared with the 1991 standard) are: 1) The maximum permissible exposure values of the lower tier are harmonized with other standards between 30 MHz and 100 GHz. 2) The upper frequency for the basic restriction on whole-body averaged SAR has been reduced from 6 to 3 GHz. 3) The BRs on peak spatial-average SAR have been changed from 1.6 W/kg and 8 W/kg for the lower and upper tiers to 2 W/kg and 10 W/kg, respectively, and the corresponding averaging mass from 1 to 10 g of tissue in the shape of a cube. For the extremities (including forearms and lower legs) and pinnae, the permitted peak SAR averaged over 10 g of tissue is now 20 W/kg for the upper tier and 4 W/kg for the lower tier. 4) The averaging times for both the upper and lower tiers have been changed to more realistic values for frequencies above 3 GHz.

Introduction

The purpose of IEEE Std. C95.1-2005 [1] is to provide exposure limits (basic restrictions and derived limits) to protect against established adverse effects to human health associated with exposure to RF electric, magnetic and electromagnetic fields over the frequency range of 3 kHz to 300 GHz. This standard is a revision of IEEE Std C95.1-1991 (1999 edition) [2] and IEEE Std C95.1b-2004 [3]. In revising the standard, findings of studies published between 1950 and December 2003[1] were considered, including those studies that involve low level exposures where increases in temperature could not be measured or were not expected. New insights gained from improved experimental and numerical methods and a better understanding of the effects of acute and chronic RF electromagnetic field exposures of animals and humans are included. A lack of credible scientific and medical reports showing adverse health effects for RF exposures at or below corresponding exposure limits in past standards supports the protective nature of the standards. This standard for the first time includes guidance on the necessity of an RF exposure control program (C95.7-2005) [4].

Below 100 kHz, the effect being minimized is aversive or painful electrostimulation. Above 100 kHz there can be a sensation of heating, which is not considered adverse. The limits in this standard may not prevent such

[1] Although the literature cutoff date was December 2003, several papers published in 2004 and 2005 were included.

thermal sensations; they are designed to protect against adverse health effects resulting from tissue heating, the only established mechanism relating to adverse effects of exposure to RF energy at frequencies above 100 kHz.

The standard consists of two main parts. The normative part includes an overview of the document (scope, purpose, and introduction), references, definitions, and recommendations. The informative part is comprised of 7 Annexes, with the first three explaining the revision process, summary of literature, and rationale of the revision. Examples of practical applications are shown in Annex D. The last three annexes are glossary, literature database (with 1143 references) and bibliography. This paper summarizes the 250 page standard, with emphasis on the new features. For details, especially on the literature summary of about 1300 peer reviewed papers (Annex B) and rationale of all changes (Annex C), please refer to the original standard [1].

Recommendations

The recommendations are expressed in terms of basic restrictions (BRs) and maximum permissible exposure (MPE) values (sometimes called reference levels, or investigation levels). The BRs are limits on internal fields, specific absorption rate (SAR), and current density; the MPEs, which are derived from the BRs, are limits on external fields and induced and contact current. The recommendations, which protect against effects associated with electrostimulation and tissue and whole body heating, are intended to apply to all human exposures except for exposure of patients by, or under the direction of, physicians and medical professionals.

BRs and MPEs for frequencies between 3 kHz and 100 kHz

Table 1 lists basic restrictions for particular areas of the body in terms of the electric field within the biological tissue (*in situ*). Two parameters are listed in the table: the rheobase *in situ* field, E_0, and a strength-frequency parameter, f_e. Limits are determined from Table 1 as:

$$E_i = E_0 \text{ for } f \leq f_e$$

$$E_i = E_0 (f/f_e) \text{ for } f \geq f_e$$

Where E_i is the maximum allowed induced in situ electric field.

Table 1 – BRs applying to various regions of the body

		Action Level[a]	**Persons in Controlled Environments**
Exposed tissue	f_e (Hz)	E_0 (rms) (V/m)	E_0 (rms) (V/m)
Brain	20	5.89×10^{-3}	1.77×10^{-2}
Heart	167	0.943	0.943
Extremities	3350	2.10	2.10
Other tissues	3350	0.701	2.10

[a] Within this frequency range the term "action level" is equivalent to the term "general public".

Table 2 lists the MPEs for the magnetic field (flux density, *B*, and magnetic field strength, *H*) for exposure of the head and torso. The averaging time for an rms measurement is 0.2 second.

Table 2 – MPE for exposure of head and torso: f = 3 kHz to 5 MHz

Frequency range (kHz)	Action Level		Persons in Controlled Environments	
	B_{rms} (mT)	H_{rms} (A/m)	B_{rms} (mT)	H_{rms} (A/m)
3.0 – 3.35	0.687/f	547/f	2.06/f	1640/f
3.35 – 5000	0.205	163	0.615	490
NOTE—f is expressed in kHz.				

The MPEs for the limbs (entire arms and legs) are listed in Table 3.

Table 3 – MPE for the limbs: f = 3 kHz to 5 MHz

Frequency range (kHz)	Action Level		Persons in Controlled Environments	
	B_{rms} (mT)	H_{rms} (A/m)	B_{rms} (Mt)	H_{rms} (A/m)
3.0 – 3.35	3.79/f	3016/f	3.79/f	3016/f
3.35 – 5000	1.13	900	1.13	900
NOTE—f is expressed in kHz.				

Table 4 lists MPEs in terms of the undisturbed (absent a person) external electric field, E.

Table 4 – Electric field MPE – whole body exposure: f = 3 kHz to 100 kHz

	Action Level	Persons in Controlled Environments
Frequency range (kHz)	E (rms) (V/m)	E (rms) (V/m)
3 kHz to 100 kHz	614	1842

The limits in Table 5 protect against adverse electrostimulation effects.

Table 5 – RMS induced and contact current limits for continuous sinusoidal waveforms, f = 3 kHz to 100 kHz

Condition	Action Level (mA)	Persons in Controlled Environments (mA)
Both feet	0.90f	2.00 f
Each foot	0.45f	1.00 f
Contact, grasp[a]	--	1.00 f
Contact, touch	0.167f	0.50 f
NOTE 1— f is expressed in kHz. NOTE 2—Limits apply to current flowing between the body and a grounded object that may be contacted by the person. NOTE 3—The averaging time for determination of compliance is 0.2 s.		

[a] The grasping contact limit pertains to controlled environments where personnel are trained to make grasping contact and to avoid touch contacts with conductive objects that present the possibility of painful contact.

BRs and MPEs for frequencies between 100 kHz and 3 GHz

The whole-body-average BRs shown in Table 6 are based on established adverse health effects associated with heating of the body during whole-body exposure. Consistent with the approach used in the prior standard to derive exposure limits, a traditional safety factor of ten (10) has been applied to the established SAR threshold for such effects, yielding an SAR of 0.4 W/kg averaged over the whole body. In the absence of an RF safety program, the BRs of the lower tier (action level) may also be used for the general public. Applied to members of the general public, the lower tier provides more assurance that continuous, long-term exposure of all individuals in the population, will be without risk of adverse effects. The localized exposure BRs shown in Table 6 are established to protect against excessive temperature rise in any part of the body that might result from localized or non-uniform exposure. When averaging SAR over a 10-g volume of tissue in the extremities and the pinnae, only SAR values for that tissue may be considered. If any cubic volume contains tissue from both the body and the extremities or pinna, each must be considered separately.

Table 6 – BRs for frequencies between 100 kHz and 3 GHz

		Action Level [a] SAR[b] (W/kg)	Persons in Controlled Environments SAR[c] (W/kg)
Whole-body exposure	(Whole-Body Average— WBA)	0.08	0.4
Localized exposure	(Local peak spatial-average)	2[c]	10[c]
Localized exposure	(Extremities[d] and pinnae)	4[c]	20[c]

[a] BR for the general public when an RF safety program is unavailable.

[b] SAR is averaged over the appropriate averaging times as shown in Table 8 and Table 9.

[c] Averaged over any 10 g of tissue (defined as a tissue volume in the shape of a cube)[2].

[d] The extremities are the arms and legs distal from the elbows and knees, respectively.

[2] The volume of the cube is approximately 10 cm^3.

Contact and induced current limits, 100 kHz to 110 MHz

In the transition region of 100 kHz to 5 MHz, two sets of contact and induced current limits apply. The limits in Table 5 protect against effects associated with electrostimulation and the limits in Table 7 protect against effects associated with tissue heating. Contact and induced current shall both be limited as specified in Table 7.

Table 7 – RMS induced and contact current limits for continuous sinusoidal waveforms, *f* = 100 kHz to 110 MHz

Condition	Action Level [a] (mA)	Persons in Controlled Environments (mA)
Both feet	90	200
Each foot	45	100
Contact, grasp[b]	-	100
Contact, touch	16.7	50
NOTE 1—Limits apply to current flowing between the body and a grounded object that may be contacted by the person. NOTE 2—The averaging time for determination of compliance is 6 minutes.		

[a] MPE for the general public in absence of an RF safety program.

[b] Grasping contact limit pertains to controlled environments where personnel are trained to make grasping contact and to avoid touch contacts with conductive objects that present the possibility of painful contact

BRs for frequencies between 3 GHz and 300 GHz

BRs to protect against adverse effects associated with heating are established for incident power density for frequencies between 3 GHz and 300 GHz. Such restrictions are derived with consideration of adverse effects thresholds (based on the literature review and evaluation), their distribution among the population, and safety factors. The BRs for frequencies between 3 GHz and 300 GHz are the same as the corresponding MPEs shown in Table 8 and Table 9, and are considered appropriate for all human exposure.

Table 8 – MPE for the upper tier (people in controlled environments)

Frequency range (MHz)	RMS electric field strength (E)[a] (V/m)	RMS magnetic field strength (H)[a] (A/m)	RMS power density (S) E-field, H-field (W/m^2)	Averaging time $\|E\|^2$, $\|H\|^2$ or S (min)
0.1–1.0	1842	$16.3 / f_M$	$(9000, 100\,000 / f_M^2)$ [b]	6
1.0–30	$1842 / f_M$	$16.3 / f_M$	$(9000 / f_M^2, 100\,000 / f_M^2)$	6
30–100	61.4	$16.3 / f_M$	$(10, 100\,000 / f_M^2)$	6
100–300	61.4	0.163	10	6
300–3000	—	—	$f_M / 30$	6
3000–30 000	—	—	100	$19.63 / f_G^{1.079}$
30 000–300 000	—	—	100	$2.524 / f_G^{0.476}$
NOTE—f_M is the frequency in MHz, f_G is the frequency in GHz.				

[a] For exposures that are uniform over the dimensions of the body, such as certain far-field plane-wave exposures, the exposure field strengths and power densities are compared with the MPEs in the Table. For non-uniform exposures, the mean values of the exposure fields, as obtained by spatially averaging the squares of the field strengths or averaging the power densities over an area equivalent to the vertical cross section of the human body (projected area), are compared with the MPEs in the Table.

[b] These plane-wave equivalent power density values are commonly used as a convenient comparison with MPEs at higher frequencies and are displayed on some instruments in use.

Table 9 – Action level (MPE for the general public when an RF safety program is unavailable)

Frequency range (MHz)	RMS electric field strength (E)[a] (V/m)	RMS magnetic field strength (H)[a] (A/m)	RMS power density (S) E-field, H-field (W/m^2)	Averaging time $\|E\|^2$, $\|H\|^2$ or S [b] (min)	
0.1–1.34	614	$16.3 / f_M$	$(1000, 100\,000 / f_M^2)$ [c]	6	6
1.34–3	$823.8 / f_M$	$16.3 / f_M$	$(1800/ f_M^2, 100\,000 / f_M^2)$	$f_M^2 / 0.3$	6
3–30	$823.8 / f_M$	$16.3 / f_M$	$(1800/ f_M^2, 100\,000 / f_M^2)$	30	6
30–100	27.5	$158.3 / f_M^{1.668}$	$(2, 9\,400\,000 / f_M^{3.336})$	30	$0.0636 f_M^{1.337}$
100–400	27.5	0.0729	2	30	30
400–2000	—	—	$f_M / 200$	30	
2000–5000	—	—	10	30	
5000-30 000	—	—	10	$150 / f_G$	
30 000-100 000	—	—	10	$25.24 / f_G^{0.476}$	
100 000-300 000	—	—	$(90 f_G - 7000)/200$	$5048/[(9 f_G - 700) f_G^{0.476}]$	
NOTE—f_M is the frequency in MHz, f_G is the frequency in GHz.					

[a] For exposures that are uniform over the dimensions of the body, such as certain far-field plane-wave exposures, the exposure field strengths and power densities are compared with the MPEs in the Table. For non-uniform exposures, the mean values of the exposure fields, as obtained by spatially averaging the squares of the field strengths or averaging the power densities over an area equivalent to the vertical cross section of the human body (projected area), are compared with the MPEs in the Table.

[b] The left column is the averaging time for $|E|^2$, the right colum is the averaging time for $|H|^2$. For frequencies greater than 400 MHz, the averaging time is for power density S.

[c] These plane-wave equivalent power density values are commonly used as a convenient comparison with MPEs at higher frequencies and are displayed on some instruments in use.

RF safety programs

Throughout the RF spectrum applicable to this standard, the MPEs apply to exposure of people, i.e., compliance with this standard is determined by whether or not exposures of people to RF fields, currents and voltages exceed the applicable MPEs. Where there may be access to RF fields, currents, and/or voltages that exceed the lower tier (Action Level) of this standard, an RF safety program such as detailed in IEEE Std C95.7-2005 [4] shall be implemented to ensure that exposures do not exceed the MPEs or BRs for persons in a controlled environment.

Similarities and differences between this standard and IEEE Std C95.1-1991

Similarities:

a) All relevant reported biological effects at either low ("non-thermal") or high ("thermal") levels were evaluated. Research on the effects of chronic exposure and speculations on the biological significance of low-level interactions have not changed the scientific basis of the adverse effect level.

b) WBA and peak spatial-average SAR remain the basic restrictions of exposure over much of the RF spectrum. The whole body average SAR values remain the same as in IEEE Std C95.1-1991, i.e., 0.4 and 0.08 W/kg.

c) The MPE for exposures in controlled environments remain the same as in IEEE Std C95.1-1991.

d) The averaging time remains six minutes for frequencies below 3 GHz for effects associated with tissue heating. For electrostimulation effects, the averaging time is 0.2 s for an rms measurement. Peak electrostimulation limits apply to instantaneous values within the applicable bandwidth.

Differences:

a) IEEE Std C95.1-1991 contains two tiers; an upper tier for "exposures in controlled environments" and a lower tier for "exposures in uncontrolled environments." In this standard, two tiers have also been set. As in the 1991 standard, an upper tier has been set for exposure of persons in controlled environments. While the weight of scientific evidence supports the conclusion that no measurable risk is associated with RF exposures less than the upper tier of this standard, it is impossible to scientifically prove absolute safety (the null hypothesis). Thus a lower tier has been set with an extra margin of safety that applies to all other individuals. The lower tier, called an "action level," recognizes public concerns, takes into account uncertainties in laboratory data and in exposure assessment, and supports the process of harmonization with other standards, e.g., the NCRP recommendations [6] and the ICNIRP guidelines [7]. For practical purposes, the lower tier may be used for the general public or as an action level, above which an RF safety program shall be implemented to protect against exposures that exceed the upper tier.

b) The upper frequency boundary over which whole body average SAR is deemed to be the basic restriction has been reduced from 6 GHz to 3 GHz.

c) The long-term MPEs for the lower tier are different from those in IEEE Std C95.1-1991 and are in general more restrictive between 300 MHz and 300 GHz.

d) The peak spatial-average SAR values have been changed from 1.6 W/kg and 8 W/kg for lower and upper tiers to 2 W/kg and 10 W/kg, respectively.

e) The averaging mass for determining the peak spatial-average SAR has been changed from 1 g of tissue in the shape of a cube to 10 g of tissue in the shape of a cube.

f) Although implicit in previous versions of IEEE Std C95.1, the present standard explicitly relies on "basic restrictions".

g) The standard now requires the development and implementation of an RF safety program in controlled environments.

h) The averaging time for both the upper and lower tiers has been changed for frequencies above 3 GHz.

i) The upper frequency at which maximum induced and contact currents are specified is now 110 MHz compared with 100 MHz in the previous standard.

j) The frequency at which the upward ramp begins for the relaxation of the power density limits for localized exposure has been changed from 6 GHz to 3 GHz.

k) In recognition of the differing impact of exposure to particular frequencies, the standard provides sections devoted to three frequency bands: 3 kHz to 5 MHz, 100 kHz to 3 GHz and 3 GHz to 300 GHz. The limits in the first band minimize adverse effects associated with electrostimulation. This overlaps the second band where the limits also protect against effects associated with heating. The limits in the third band protect against effects associated with heating. Differences within each of those bands are provided below.

Features:

a) **3 kHz to 5 MHz** – The standard defines basic restrictions (BR) in terms of the *in situ* (within biological tissue) electric fields for different regions of the body. Magnetic field MPEs are specified for the arms and legs and for the head and torso, but compliance with the standard can be demonstrated for uniform sinusoidal magnetic fields by showing that either the *in situ* electric field BR or the magnetic field MPE is satisfied. If the magnetic field is not constant over the head and torso, it is sufficient to demonstrate that the basic restrictions are satisfied, or that the spatial peak of the magnetic field MPE is not exceeded. Based on current knowledge of adverse effects on humans within this frequency range, the whole body electric field MPE for the controlled environment has been increased. Similarly, the magnetic field MPEs, with separate requirements for body portions as noted above, have been increased for both the general public and controlled environments and have been made frequency dependent. Averaging time for an RMS measurement is 0.2 second. Formulas have been included for determining maximum permitted peak electric fields for both *in situ* and environmental considerations.

b) **100 kHz to 3 GHz** – In this frequency range where SAR is the controlling criterion, the revised standard confirms the presumed threshold whole body average SAR of 4 W/kg for potentially adverse effects. Localized exposure restriction criteria (peak spatial-average SAR) have been changed for both the upper and lower tiers. Peak spatial average SAR for any body tissue including the hands, wrists, forearms, feet, ankles, lower legs and pinnae, is required to be determined over 10 g of tissue in the shape of a cube. Peak spatial average SAR for the 10-g sample is to be no greater than 10 W/kg for the upper tier and 2 W/kg for the lower tier. For the hands, wrists, forearms, feet, ankles, lower legs and pinnae, the permitted peak spatial average remains as specified previously in 10 g of tissue, *i.e.*, 20 W/kg for the upper tier and 4 W/kg for the lower tier. The contact current limits for the frequency range of 100 kHz to 110 MHz have been subdivided into touch and grasping conditions, with the grasping condition confined to the controlled environment. The permissible touch contact current has been reduced for both the controlled environment and the general public. The lower part of this frequency range, i.e., 100 kHz to 5 MHz, is a transition region where the limits protecting against electrostimulation and the limits protecting against effects associated with heating must be met.

c) **3 GHz to 300 GHz** – In this frequency range, the interactions become quasi-optical, and the MPEs are expressed in terms of incident power density and exposure duration. The principal change in the standard has been in the MPE frequency dependence above 300 MHz for the lower tier (general public).

Summary

IEEE C95.1-2005 provides recommendations to protect against established adverse effects in human beings exposed to electromagnetic fields in the frequency range from 3 kHz to 300 GHz. Similarities and differences from the IEEE C95.1-1991 (and its two amendments) are discussed. A notable revision to the new standard is the recommendation of peak spatial average SAR of 2 and 10 W/kg averaged over 10 g tissue for the lower and upper tier limits, respectively. This revision resolves a major harmonization issue with other RF standards and guidelines. Cooperative efforts should be continued to achieve internationally harmonized exposure limits.

References

[1] IEEE C95.1-2005, "IEEE Standard for Safety Levels with Respect to Human Exposure to Radio Frequency Electromagnetic Fields, 3 kHz to 300 GHz".

[2] IEEE C95.1-1991, "IEEE Standard for Safety Levels with Respect to Human Exposure to Radio Frequency Electromagnetic Fields, 3 kHz to 300 GHz", (1999 edition).

[3] IEEE C95.1b-2004, "IEEE Standard for Safety Levels with Respect to Human Exposure to Radio Frequency Electromagnetic Fields, 3 kHz to 300 GHz - Amendment 2: Specific Absorption Rate (SAR) Limits for the Pinna)".

[4] IEEE C95.7-2005, "Recommended Practice for Radio Frequency Safety Programs".

[5] IEEE C95.6-2002, "IEEE Standard for Safety Levels with Respect to Human Exposure to Electromagnetic Fields, 0 to 3 kHz".

[6] NCRP, Biological Effects and Exposure Criteria for Radiofrequency Electromagnetic Fields. Bethesda: NCRP Report no. 86, National Council on Radiation Protection and Measurements, Bethesda, MD, 1986

[7] ICNIRP (International Commission on Non-Ionizing Radiation Protection), "Guidelines for limiting exposure to time-varying electric, magnetic, and electromagnetic fields (up to 300 GHz)," *Health Physics*, vol. 74, pp. 494 - 522, 1998

EXPERIMENTAL DOSIMETRY FOR THE UK MOBILE TELECOMMUNICATIONS AND HEALTH RESEARCH PROGRAMME

BENJAMIN LOADER
NATIONAL PHYSICAL LABORATORY,
HAMPTON ROAD, TEDDINGTON MIDDLESEX, UK, TW11 0LW

Abstract
This paper presents a review of the dosimetry in the UK Mobile Telecommunications and Health Research (MTHR) programme. It describes the exposure systems used in the human volunteer studies, their output characteristics, and the rationale behind their specifications. It also describes how traceability to national standards was established for the *in vitro* studies. Problems encountered during the development of these systems are also presented.

Introduction
The Link Mobile Telecommunications and Health Research Programme (MTHR) resulted from the publication of the report by the Independent Expert Group on Mobile Phones [1]. The MTHR has funded research in the UK to a value of £8.8 million to investigate the impact of mobile telecommunications on health. In determining the research priorities, the programme has sought to take into account public concerns about mobile communications technology as well as other research conducted nationally and internationally. To date, MTHR has funded twenty projects, and another six projects have been funded as an adjunct to the programme by the UK Department for Trade and Industry or the Home Office. Effective and accurate dosimetry is essential if meaningful conclusions are to be drawn from these studies. Under the programme, the National Physical Laboratory (NPL) has provided dosimetry support to the research projects. This support has included advice regarding the specification of exposure systems, independent verification that the systems used meet these specifications, and calibration to provide traceability to National Standards. Staff at NPL have also measured and characterised other aspects of the systems' performance, such as the low frequency magnetic fields that they emit [2].

For dosimetry purposes, the studies fall into the following categories: human volunteer studies on handset exposure, human volunteer studies on base station exposure, *in vitro* studies, in *vivo* studies, and epidemiology. This paper considers the exposure systems used for the human volunteer and *in vitro* studies. It provides a description of the devices used for generating the exposures, the rationale behind the choice of signal characteristics and exposure levels, and problems that were encountered during their development. The paper also examines how traceability to National Standards was established for exposures in the *in vitro* studies, and how the systems were characterised at NPL.

1. Human-volunteer studies
Handset exposure. During typical phone use there is a wide variation in exposure. This is dependent on the phone type, radio reception conditions, pattern of speech or type of data sent, the way the phone is held, and whether it is used in the left or right hand. Along with the RF signals, the phone will generate low frequency magnetic fields caused by the pulsed nature of the battery currents and static magnetic fields caused by the earpiece in the phone. Movement of the phone may modulate such static fields during use. There will be some heating of the skin in the region of the phone because the circuits dissipate heat and the use of the phone may also affect the subject's posture. All of these factors could potentially affect the outcomes of human volunteer studies. It would be impossible to encompass all possible variations in exposure conditions within a single experiment. Practical considerations limit the duration of test sessions for human volunteer studies, and therefore the number of exposure conditions that can be tested. Whilst a system could be designed to generate uniform exposure to cover all possible regions exposed during phone use, such a system would not give realistic patterns of exposure, and in particular, any effects due to the field gradients in the head would not be apparent.

MCL (www.mcluk.org), in collaboration with the Department of Electronics at York University, developed the handsets that were used for all the human volunteer studies on handset exposure within the MTHR programme (Fig. 1). These handsets are designed to give accurate and reproducible exposures representative of those from GSM [3] or TETRA [4] phones, and to facilitate double-blind experiments. The handsets are battery powered, to allow free movement of the subjects during the tests and also to avoid coupling effects that occur if a cable connects the antenna to the signal source. They can operate for approximately one hour before the batteries need

charging and there is an audible low battery warning. They operate as "stand alone" transmitters without the requirement for an operational network.

Three modes of exposure were used for the MTHR studies; pulsed mode (GSM or TETRA), continuous wave (CW) mode, which produces an unmodulated signal with the same frequency and average power as the pulsed mode, and sham mode. CW mode was included to determine whether any observed effects are due to the pulsed nature of mobile phone signals. Selection of the mode of operation is by two 16-position rotary switches, the codes for each mode being assigned randomly for each handset and held by the manufacturer. This facilitates double blind experiments. The characteristics of the output from the handsets in each mode are shown in Table 1.

Figure 1: Picture of the MTHR handsets. Front and rear view. The antenna is angled slightly towards the head to increase specific absorption rate (SAR) level. Visible are two rotary mode switches and RF test connector used to check correct operation prior to test sessions.

Table 1: Comparison of exposure modes.

Output characteristics	**Mode**		
	GSM or TETRA	**CW**	**Sham**
RF exposure level	1.4 Wkg^{-1}	1.4 Wkg^{-1}	0.002 Wkg^{-1}
Pulse modulation of signals	Yes	No	No
Low frequency magnetic fields	Yes	No	No
Static magnetic field	Yes	Yes	Yes
Heat dissipation from circuits in phone	Yes	Yes	Yes

The characteristics of the modulation for the GSM and TETRA modes are given in Table 2. The transmission frequency was chosen to be 888 MHz for the GSM handset and 381 MHz for the TETRA phone. The GSM handset frequency is just outside the normal operating band of the GSM system, and this is to avoid interference with operational networks. Signal modulation gives rise to a low frequency magnetic field, which is the case for a real phone, and these are shown in Fig. 2. In the sham mode, the CW signal is generated and a switch diverts the signal to an internal load so that the antenna does not transmit it. This gives the same battery life and operating temperature as the transmitting modes, which is a requirement for double blinding. The sham mode therefore produces the same static magnetic field as the CW mode. The circuit boards within the handset also radiate electromagnetic fields in the sham mode and this, rather than the performance of the RF switch used, limits the degree of isolation that can be achieved. In the "sham" mode the exposure level is reduced by at least 20 dB compared to the exposed modes. The field level in air at 10 cm from the handset is between 0.5 Vm^{-1} and 1 Vm^{-1} for the sham mode, compared to 13 V/m for the CW exposed mode.

Table 2: Main characteristics of GSM & TETRA signals.

GSM			TETRA	
Handset characteristics	Included in MTHR handset		Handset characteristics	Included in MTHR handset
GSM 900	Yes		Voice plus data mode (V + D)	Yes [2]
GSM 1800	No		Direct mode (DMO)	No
GSMK mask for pulse shape (GSM)	Yes		Packet data optimised mode (PDO)	No
PSK modulation (GSM)	Yes		DQPSK modulation [3]	Yes
Super- and Hyper-frame structures.	Yes		Hyper and Multi-frame structure	Yes
Variation in slot transmit power (adaptive power control)	No		Variation in slot transmit power (adaptive power control)	No
GSM DTX mode[1]	No[1]		Correct pulse shape	Yes
Frequency hopping	No		Frequency hopping	No
Multi-slot operation	No		Multi-slot operation	No

Notes:

1. The handsets have this capability, but it was not used for the MTHR trials. Discontinuous Transmission (DXT) mode will alter the low frequency magnetic fields produced by the handset.
2. V + D is the most common mode of operation for TETRA. Only voice communication is included.
3. DQPSK = Π/4 Differential Quaternary Phase Shift Keying.

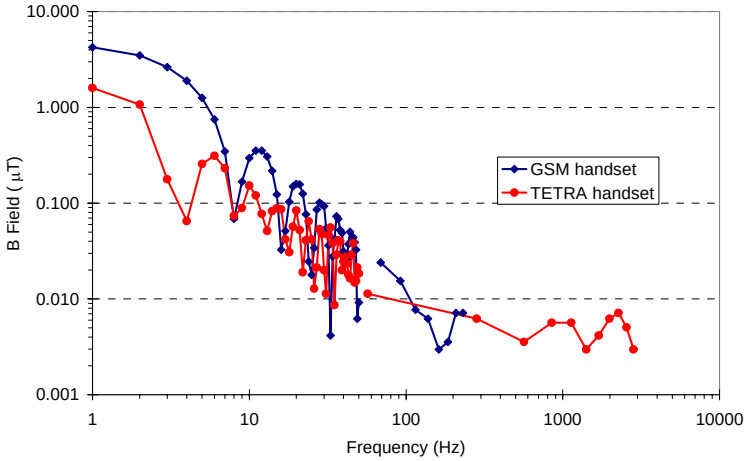

Figure 2. Magnetic field from MTHR handsets in GSM and TETRA "exposed" mode [2].

SAR is the specific absorption rate of RF energy in tissues in watts per kilogram (Wkg^{-1}). The target level for the GSM, CW and TETRA exposures was chosen as 1.4 Wkg^{-1} averaged over a 10 g mass. This is the highest level that ensures volunteers will not be exposed above the ICNIRP limit of 2 Wkg^{-1} for public exposure, allowing for the uncertainty of the dosimetry. Most available GSM handsets are designed to comply with IEEE limit [5] of 1.6 Wkg^{-1} averaged over a 10 g mass, so this level is representative of GSM phones. TETRA handsets with 1 W peak power produce similar SAR levels to GSM phones when used in voice communication mode [6, 7]. However, TETRA handsets having 3 W peak power can produce higher SAR levels [7]. The SAR from each handset was measured to an accuracy of ± 30 % by an accredited test laboratory and was checked and adjusted periodically during the studies. The handsets incorporate a test mode that allows the modulated or CW signal to be measured with a power meter prior to each test session, to confirm that the handset is operating correctly. Fig. 3 shows the measured SAR distribution from the GSM handset. The 10 g averaged SAR from the antenna is 1.4 Wkg^{-1}. The 10 g averaged SAR in the region of the body of the handset is 0.4 Wkg^{-1}.

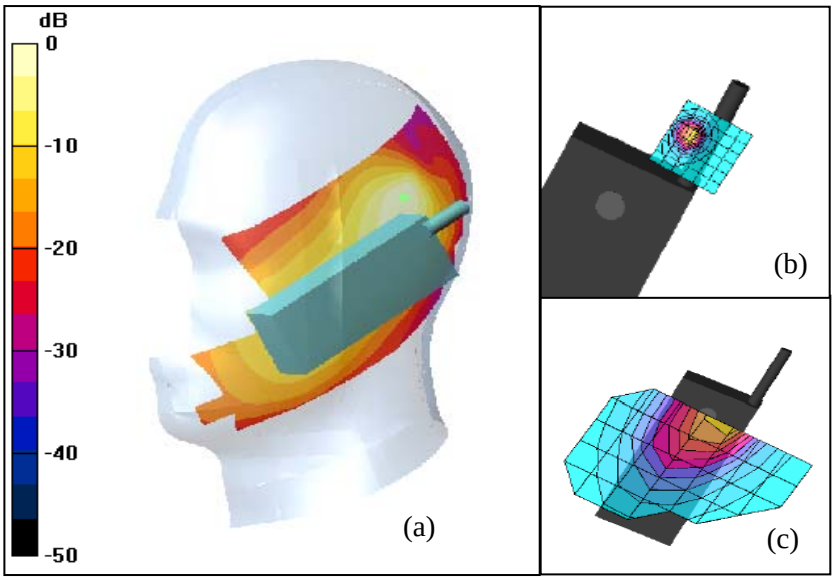

Figure 3. SAR distributions from the MTHR GSM handset (reproduced courtesy MCL Ltd). (a) Position of the handset for left hand exposures. (b) SAR distribution from antenna. (c) SAR distribution from circuits in the handset.

Both left hand and right hand use of the phone were considered in the studies. The phone was positioned in the "cheek position" defined in [8] when used on the left-hand side of the head. When used on the right-hand side of the head, it was shifted upwards from this position by 4 cm. This ensures that the position of the maximum SAR relative to the ear remains the same for both sides of the head, even though the antenna is not located symmetrically on the handset. The region of brain exposed may affect whether a particular effect is detected.

From switch on to the point the low battery audible warning activates, there is a gradual reduction in the power radiated by the handset, as shown in Fig. 4. Note that during all sessions, the handsets are switched on three minutes prior to beginning the tests.

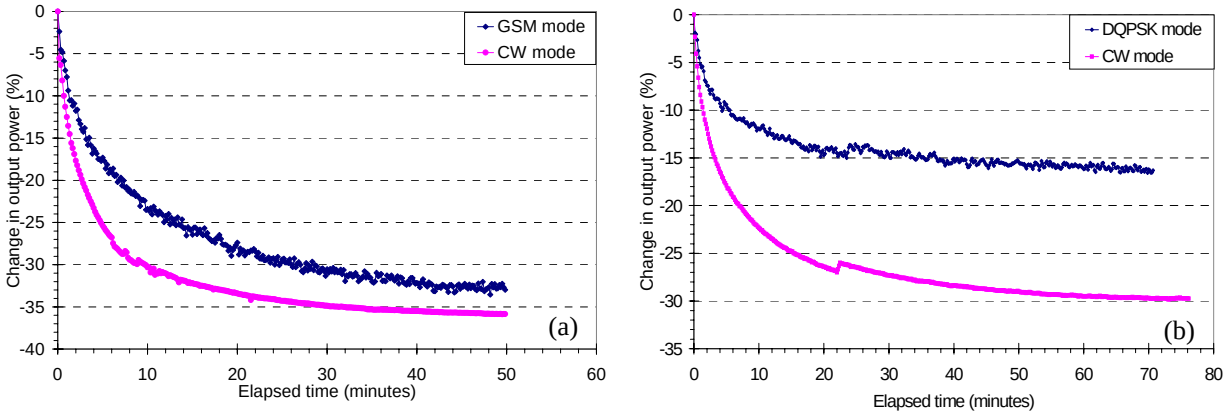

Figure 4. Change in radiated power versus time from switch on. (a) GSM handset, (b) TETRA handset

Achieving double blinding for the handsets was quite challenging. Each mode of operation must discharge the battery at the same rate, must result in the same degree of heating of the handset, and produce no audible or visual indications. Initial trials of the handsets showed that they got hotter in CW mode than modulated mode, and subjects were able to detect this difference. Adding an additional resistor to generate heat in the pulsed mode rectified this, but meant the handsets may get slightly hotter than is the case for a normal phone. In very quiet environments, some subjects were able to hear a clicking noise from the battery when the handset was in pulsed modes. Some low-level background noise was necessary to mask this sound during the experiments.

Studies look for differences in a measurable response resulting from the different exposure modes. Given the nature of the three exposure conditions from the MTHR handsets, studies using the handsets would show: *1. Effects that are due to GSM or TETRA signals from the handset in the presence of static magnetic fields, low frequency magnetic fields and contact heating that is typical of a real phone. 2. Effects arising from a CW signal whose severity increase with exposure level*. However, the following are not tested, since these are present in both the exposed and sham conditions: *1. Effects due to CW signals with a threshold that is below the sham level and whose severity does not increase with exposure level. 2. An effect arising solely from the static magnetic field of the handset. 3. Effects caused solely by the very slight heating of the head that occurs through contact with the warm phone.*

Base Station exposure. Base stations may have multiple traffic and control channels. The control channels always have full slot occupancy and maximum power level. The traffic channels have variable slot occupancy, and some designs have variable power level for the bursts (down-link power control). The inter-slot guard period that separates bursts are synchronised between channels. In real-life situations, the signal is reflected and attenuated by buildings and structures. As a person moves through the field, the amplitude of the signal may increase and decrease (fading multi-path). They will be exposed to many different radio signals simultaneously. The height of the antenna and the elevation pattern mean exposure may not decrease with distance from the antenna. Base stations may generate electromagnetic fields other than the transmitted signals, but these emissions are limited by the GSM specifications [3].

The base station exposure system used by MTHR was developed by Red-M Ltd [9], and installed at the University of Essex in an absorber-lined screened room supplied by NPL. The system provides three exposure modes; GSM mode, UMTS mode and sham mode. The sequence of exposure for each test session is determined by a test code that is assigned to each volunteer in the study, and these are randomised. This facilitates double blinding of the studies. In addition there is an open provocation mode. Fading multi-path effects were not simulated in the exposure system. Whilst fading multi-path simulators to represent different environments are available, this would have added considerably to the cost of the exposure system, and the choice of which environment to simulate would be difficult. The system uses a Rhode and Schwarz SMU 200A digital signal generator. For GSM mode, the amplitude-quadrature (I/Q) data of the traffic and control channels is generated externally and sent to the modulation inputs of the signal generator. An external circuit then adds the inter-slot guard period to give the correct pulse shape. As a result the data sent is not synchronised to the bursts. For UMTS, the signal generator generates the signal internally. In the sham mode the modulation and RF output

from the signal generator are turned off. The signals are amplified before being transmitted by a vertically polarised log periodic dipole array (LPDA) located inside the screened room. The antenna is at a distance of 5 m from the subject and is concealed behind a curtain. Forward and reverse power to the antenna are monitored prior to test sessions to confirm correct operation of the system. To reduce the field level that is present in the sham mode, the signal generator and amplifier are located outside the screened room used for the exposures. The system is calibrated every six months during the study to ensure that its output remains stable.

The total power density in the GSM mode and also the UMTS signal is 10 mWm^{-2} ± 30%. The choice of this exposure level was based on a detailed survey of seventeen macro-cellular base station sites in the UK, which found a maximum power density of 8.3 mWm^{-2} [10]. Exposure to members of the public from Microcell and Picocell base stations may exceed 100 mWm^{-2} [11], so this does not represent a maximum exposure for all types of base station. The variation in power density over the region occupied by the seated volunteer (a 1 m by 0.9 m plane orthogonal to the antenna boresight) is no more than ± 3.2 dB. The power density in the sham mode is 54 dB lower than for the transmit mode, and is a CW signal.

The GSM signal is representative of a GSM macro-cell base station without downlink power control on the traffic channels. The main characteristics of the GSM signal are given in Table 3. The pulse shape and inter-slot guard interval, Fig. 5(a), conform to the GSM specifications [3]. There are two traffic channels, one at 886.8 MHz and one at 1877 MHz, and two broadcast channels, one at 888.8 MHz and 1879 MHz and these signals are transmitted simultaneously. The broadcast channels have all eight slots in the frame continuously transmitted at a constant power level. The traffic channels have constant pulse amplitude but variable slot occupancy, the slot occupancy being generated stochastically, Fig. 5(b). The peak amplitude of the signal at the four frequencies are approximately equal.

Table 3: Main characteristics of GSM signals from the base station exposure system.

GSM base station	Included in MTHR exposure system
GSM 900 band	Yes
GSM 1800 band	Yes
Traffic channel	Yes
Control channel	Yes
Variations in slot transmit power on traffic channels (downlink power control).	No
PSK modulation	Yes
GSMK mask for pulse shape	Yes
Variable slot occupancy for traffic channel	Yes -this is generated stochastically
EMC emissions from base station	No
Fading multi-path effects	No

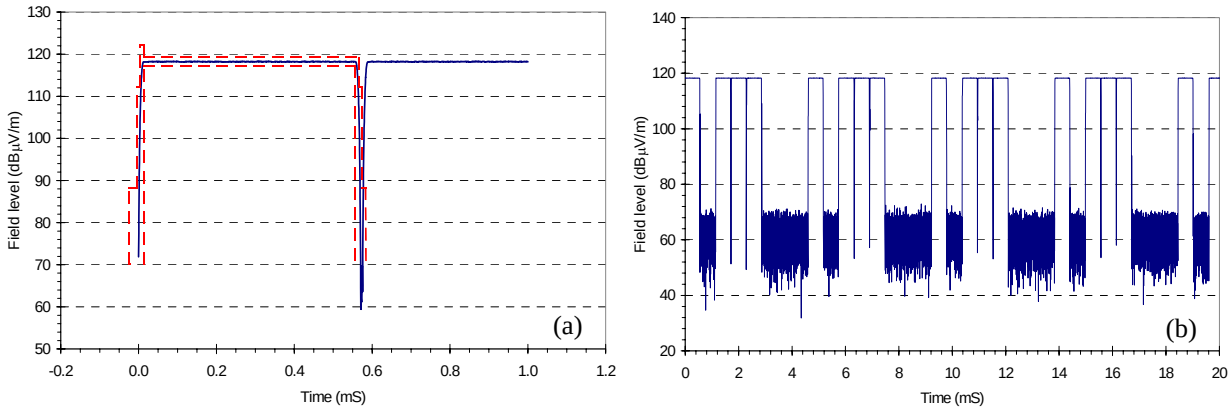

Figure 5. GSM 900 Traffic Channel: (a) Single pulse, dashed-line shows pulse limits from GSM specifications [3], (b) Multiple pulses, showing slot occupancy within the GSM fames.

The UMTS mode is based on test mode 1 specified in the 3GPP standard [12] and is representative of a realistic traffic scenario with high peak to average ratio. It is a single channel with 5 MHz bandwidth, as shown in Fig. 6. The signal was decoded using an Agilent PSA spectrum analyser, and the results are shown in Table 4

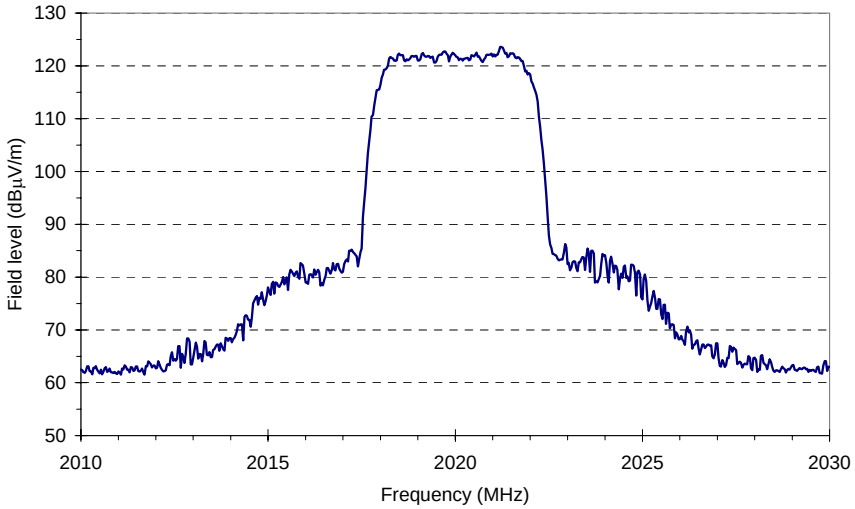

Figure 6. Peak amplitude versus frequency for UMTS signal.

Table 4. Composition of UMTS signal

Signal component	Level [1]
Common Pilot Channel (CPICH)	-24.009 dBc
Primary Synchronisation Channel (PSCH)	-43.09 dBc
Secondary Synchronisation Channel (SSCH)	-43.82 dBc
Number of active channels	none
Maximum power for inactive channel	-21.762 dBc
Average power for inactive channel	-27.093 dBc

Note.
1. $$dBc = 10\log_{10}\left(\frac{channel\ \ power(W)}{Power\ at\ centre\ carrier\ \ frequency\ (W)}\right)$$

2. Exposure systems for in vitro studies.

Great care must be taken when designing and calibrating experimental exposure systems, and the scale of this task should not be underestimated when planning a study. As well as establishing known and accurate exposure levels with suitable signal characteristics, all other environmental factors must be considered and relevant parameters monitored during the experiments. A high efficiency at inducing SAR is desirable, since any power losses within the exposure device are likely to cause heating in the samples in addition to the heating due to their dielectric losses. Transverse Electromagnetic (TEM) cells [13], which are widely used for generating exposures, generally have a low efficiency for inducing SAR in small samples. Sample containers should not be placed directly on the conductors of the TEM line, as this allows thermal conduction to occur. For matched systems, heat may be transferred from the termination, and this should be remote from the exposure set up. For exposure systems used in incubators, there should be sufficient airflow to ensure the samples are at the same temperature as the incubator. In this respect open-sided transmission lines are better than closed TEM cells. It is essential to measure the heating of the biological samples that occurs during the exposure, and assess the effect that this will have. Where such heating occurs, rate of temperature rise measurements will over-estimate the SAR arising from absorption of RF energy. Systems with high VSWR may give higher efficiencies, but uncertainty in the position of the standing wave will lead to large uncertainties in the exposure. The position of the standing wave is dependent on the complex impedance of the source and termination. Determining the level at which samples should be exposed for a particular experiment is difficult. Whilst SAR measurements in homogeneous phantoms can be used to determine conservative estimates for the maximum 1 g or 10 g averaged SAR from a device, they cannot predict the SAR level in a particular biological tissue within a person or animal exposed to electromagnetic fields, and this can usually only be determined by computer simulations.

Calibrating *in vitro* exposure systems is difficult, and dosimetry may rely heavily on computer simulations. Systems that operate at 37°C, should be characterised at this temperature, as the conductivity of the samples, and therefore the energy absorption, will change with temperature. For multi-well plates the exposure will not be the same for all the wells. This should be taken into account when designing the experimental protocol. Uniformity of exposure may be enhanced by filling the regions between the wells with dielectric material having similar permittivity to the samples. Non-uniformity of samples and meniscus effects add to exposure uncertainty [14]. Whilst it is possible to measure the SAR in the media containing cells or organisms, the measurement techniques generally have insufficient resolution to determine the SAR within the biological material of interest. There is a clear need to develop techniques of dosimetry with much higher spatial resolution for this purpose (micro-dosimetry).

Two types of system were used to generate exposures for the in-*vitro* studies in the MTHR programme; a TEM cell for use in incubators (University of Nottingham) and open-sided transmission lines for use in microscope systems (Babraham Institute, Cambridge). The systems were calibrated at NPL to provide exposures that were traceable to National Standards. The method of calibration is to use a 1.4 mm diameter electric field probe to compare the electric field within the exposed samples with a known electric field in the same material generated within a matched waveguide system [15]. This may require several litres of sample at 900 MHz for the measurement in the matched waveguide. The measurement in the exposure system must be performed using a higher input power than is used for the experiments, and the results scaled to the correct power level. This is because the small size of the E-field probe yields poor sensitivity. A sample depth of at least 5 mm is necessary to avoid errors. For these systems, the field strength in the air above the sample is much higher than the field in the sample itself, and the probe will over-read if the sensors are not immersed sufficiently in the sample. Accuracy is improved by using the same power sensor to determine the input power to the waveguide and the exposure system. The material density must be measured to determine the SAR level, but the conductivity of the material is not used in the calculation using this method. The temperature rise in the samples was measured using a SPEAG TV1V3 temperature probe for different power levels.

The system used by the University of Nottingham for previous studies into effects of RF exposures on nematodes [16, 17, 18] has a twenty-four well *petri* dish located within the TEM cell. The exposure system is placed inside an incubator. As part of the MTHR programme, the performance of this system was assessed at NPL. Fig. 7(a) shows the measured SAR value at the centre of a 1 ml sample of K-medium (permittivity 78.30 – 22.96 j at 900 MHz and 22.5ºC) for each of the wells in the *petri* dish. There is considerable variation in the SAR level between wells in the *petri* dish. The SAR level averaged across all the wells was 0.0141 Wkg^{-1} for 1 W at input power, so the system has relatively low efficiency at inducing power absorption in the samples. It is important to note that the SAR was measured in the K-media used to support the nematodes, and not within the nematodes. The variation in SAR with sample volume and probe height is shown in Fig. 7(b). Note that the probe is over-reading as it comes into proximity of the surface of the sample because the field in air above the sample is much higher than the field within the sample.

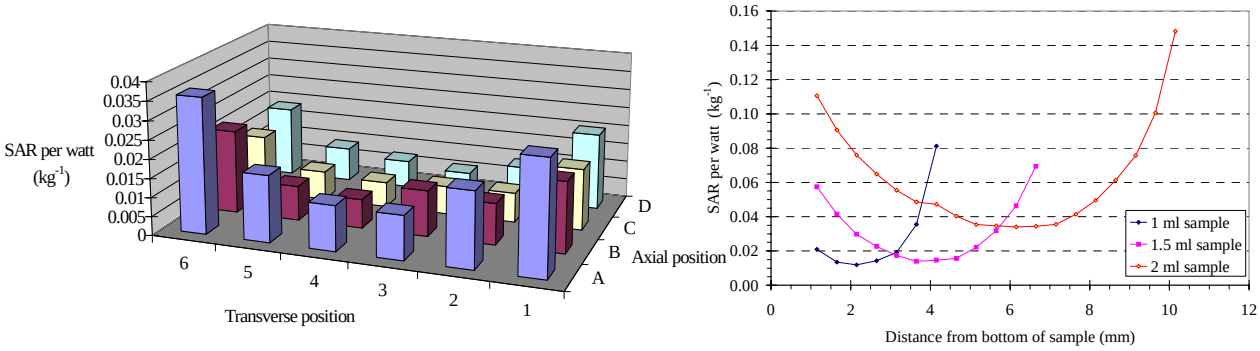

(a) (b)

Figure 7. (a) Variation in SAR level for different wells in a multi-well petri-dish, (b) Variation in SAR with probe height for different sample volumes.

The temperature rises at the centre of the samples were measured at NPL in a temperature controlled laboratory. Cycling the power on and off allowed heating due to the RF power to be distinguished from any changes in the ambient temperature. It became apparent that the power loss in the TEM cell was giving rise to additional heating of the samples, and this was not predicted from SAR calculations. To reduce this loss, the following modifications were made to the system; the foam filler that originally filled the lower chamber of the TEM cell was removed; the BNC connectors used at either end of the TEM cell were replaced with APC3.5 connectors (BNC connectors are for frequencies up to 500 MHz); the TEM cell was silver-plated. The results of the sample temperature measurements before and after modification are shown in Fig. 8 and in Table 5. The temperature measurements were repeated with the system in the incubator used for the experiments and the results confirmed. Previously reported effects from the studies could not be replicated once the unwanted sample heating caused by the exposure system was reduced in this way [19]. It is probable that the nematodes used for the studies were sensitive to the temperature changes that were occurring in the original exposure system.

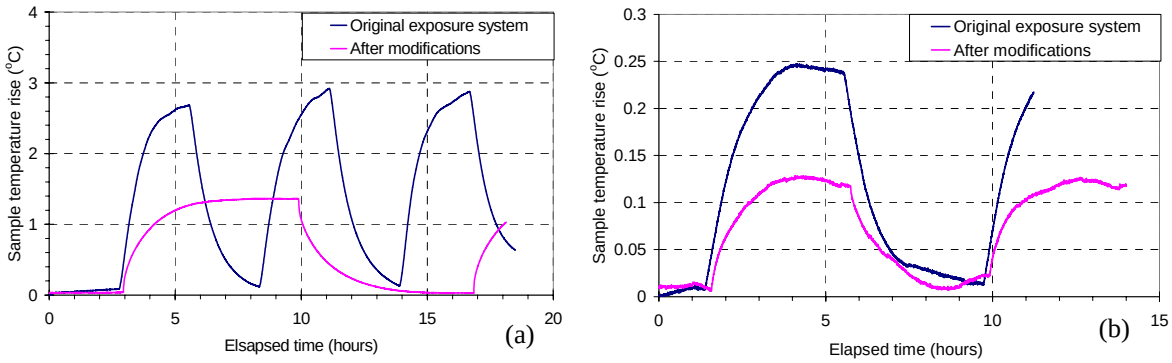

Figure 8. Temperature rises in samples for; (a) an input power of 10 W, (SAR level 0.14 Wkg^{-1}) and (b) an input power of 1 W (SAR level 0.014Wkg^{-1}) before and after modification of the exposure system.

Table 5: Performance of exposure system before and after modification.

Parameter	Original exposure system	After modification
Power loss at 900 MHz	8.47%	1.09%
Sample Temperature rise for 1 W input power	0.25ºC	0.12ºC
Sample temperature rise for 10 W input power	3.6ºC	1.4ºC
Average SAR level in samples for 1 watt input power.	0.014 Wkg^{-1}	(0.014 Wkg^{-1})

The system used by Babraham Institute [20, 21] is shown in Fig. 9. An inner conducting plate, and two outer conducting plates form an open-sided TEM transmission line. The sample is placed on the lower conductor directly above an aperture, and this allows it to be viewed with a microscope during exposure. Table 6 gives the measured SAR levels for 1 watt input power at five positions (Fig. 10) in HEPES and DMEM. The measurements were made at 22.2°C. This is because the National Standard for SAR is controlled at this temperature. However, the exposure system is normally used in an incubator at 37°C. The dielectric properties for these materials at 22.2°C and 37°C are given in Table 7. The SAR levels in the sample will be proportional to the conductivity, so the measured SAR values must be adjusted to account for temperature. The efficiency at inducing SAR in the samples is twenty times that of the Nottingham system, due to the smaller separation of the conductors, and no significant sample heating occurs.

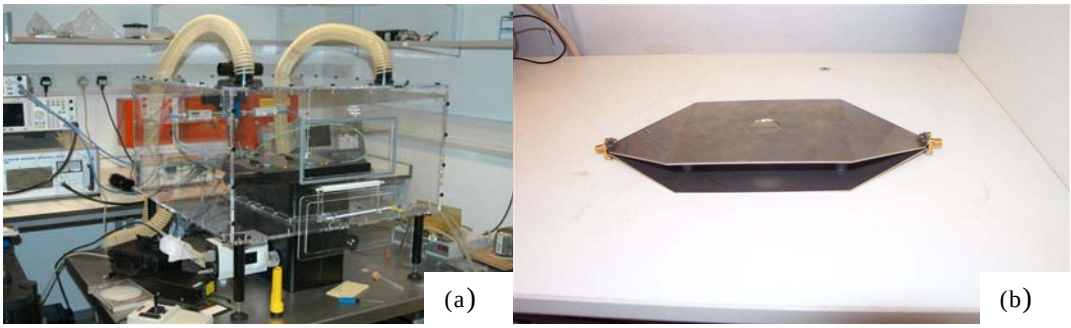

Figure. 9: Exposure system used at Babraham Institute (Courtesy Rod O'Connor, Babraham Inst.). (a) Enclosure for environmental control. (b) TEM-line used to generate RF exposures to samples.

Table 6: SAR levels per watt measured in different growth media at 22.2°C

	SAR (Wkg^{-1}) per watt	
Position	HEPES	**DMEM**
Centre	0.49	0.57
Left	0.56	0.71
Right	0.52	0.69
Front	0.51	0.68
Back	0.57	0.64
Average	**0.53**	**0.66**

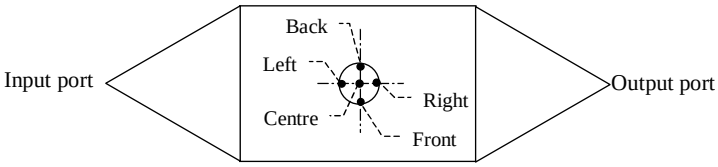

Figure 10. SAR measurement positions

Table 7: Dielectric properties of HEPES and DMEM at 22.2°C and 37°C.

Liquid	Temperature °C	ε′	ε″	σ (Sm^{-1})
HEPES[1]	22.2	76.7	32.2	1.61
	37.0	60.1	21.8	1.10
DMEM[2]	22.4	76.8	34.1	1.71
	37.0	68.7	40.3	2.02

[1] N-2-Hydroxyethylpiperazine-N-2-Ethanesulfonic Acid, [2] Dulbeco's Modified Eagle's Medium.

Conclusions

The MTHR programme has adopted sound metrological principles to ensure the studies funded within the programme produce meaningful, and reproducible results. The National Physical Laboratory has provided consultancy to the researchers within the programme and has characterised and calibrated some of the exposure systems used. Human volunteer studies into handset exposure have used standard exposure handsets that generate the main characteristics of both the RF and magnetic fields produced by real GSM and TETRA handsets. The exposure level of 1.4 Wkg^{-1} 10 g averaged SAR ensures volunteers are not exposed above ICNIRP guideline levels. The base station exposure system produces exposures representative of a GSM macrocell base station at 10 mWm^{-2}. The system also generates representative UMTS signals. Both systems facilitate double blind experimental protocols. For the *in vitro* studies within the programme, the system used to generate exposures have been traceably calibrated to National Standards at NPL. Unwanted heating effects in one system were rectified, and previously reported effects of RF exposure could not then be replicated.

Acknowledgements:

The author would like to acknowledge the help and support of: Phil Chadwick (MCL); Myles Capstick (University of York); Bachir Belloul (Red-M Limited); David de Pomerai, Adam Dawe and Steve Greedy (University of Nottingham); Elaine Fox, Stacy Eltiti and Denise Wallace (University of Essex); Rod O'Connor (Babraham Institute); Andrew Gregory and Michael Hall (NPL) and members of the Dosimetry Working Group, UK Mobile Telecommunications and Health Research Program.

References

[1]"Mobile Phones and Health", Report of the Independent Expert Group on Mobile Phones (the Stewart Report), May 2000, ISBN 0-85951-450-1, (www.iegmp.org.uk/report/text.htm)

[2] Hall, M, "Measurement of electromagnetic flux density from mobile handsets", NPL Report DEM-ES(RES) 004, April 2006.

[3] ETSI Standard TS145 005 V6.11.0 (2005-09), "Digital Cellular Telecommunications System (Phase 2+); Radio Transmission and Reception" (www.etsi.org)

[4] ETSI Standard EN 300 392-2 V2.1.1 (2000-12). "Terrestrial Trunked Radio (TETRA) Voice plus Data (V+D), Part 2: Air Interface (AI)". (www.etsi.org)

[5] IEEE C95-1, "IEEE Standard for Safety Levels with respect to Human Exposure to Radio Frequency Electromagnetic Fields, 3 kHz to 300 GHz", IEEE 1999.

[6] Chadwick, P, "Assessment of Specific Absorption Rates from Second Generation Airwave Equipment: TETRA radios and accessories, MCL report, January 2003, (www.mcluk.org).

[7] Dimbylow P, Khalid M, and Mann S, (2003), “Assessment of specific energy absorption rate (SAR) in the head from a TETRA handset”, Phys Med Biol, 48, 3911-3926.

[8] British Standard BS EN 503361:2001. “Basic standard for the measurement of specific absorption rate related to human exposure to electromagnetic fields from mobile phones (300 MHz – 3 GHz)”.

[9] Belloul, B, “EM Exposure System: Technical Reference Manual”, Version 1.4, Dec 2005, CDS Doc: GCD-RTG 1291/2004. (www.red-m.com)

[10] S M Mann, T G Cooper, S G Allen, R P Blackwell and A J Lowe, “Exposure to Radio Waves near Mobile Phone Base Stations”, NRPB-R321, 2000, ISBN 0 85951 455 2

[11] Cooper TG, Mann, SM, Khalid, M, and Blackwell, RP. “Public exposure to radio waves near GSM microcell and picocell base stations”, J Radiat Prot, 26, 2006, 199-211.

[12] 3GPP TS 25.141 V6.3.0 (2003-09) “Technical Specification Group Radio Access Network; Base Station (BS) conformance testing (FDD) (Release 6)”, (www.3gpp.org/ftp/Specs/html-info/25141.htm)

[13] Crawford, ML, “Generation of standard fields using TEM transmission cells”, IEEE Trans. on EMC, 1974, 16 (4), pp. 189 - 195.

[14] Schuderer J, Kuster N, “Effect of the meniscus at the solid/liquid interface on the SAR distribution in Petri-dishes and flasks”, Bioelectromagnetics 2003, Feb; 24(2), 103-8.

[15] Pokovic, KT, T.Schmid and N.Kuster, “Robust set-up for Precise Calibration of E-field probes in Tissue Simulating Liquids at Mobile Phone Frequencies”, Proceedings ICECOM 1997, pp 120 – 124, Dubrovnik, Croatia Oct 12-17.

[16] Daniells C, Duce I, Thomas D, Sewell P, Tattersall J, de Pomerai D.. “Transgenic nematodes as biomonitors of microwave-induced stress”, Mutat Res, 1998, 399:55–64.

[17] de Pomerai D, Daniells C, David H, Allan J, Duce I, Mutwakil M,Thomas D, Sewell P, Tattersall J, Jones D, Candido P, “Non-thermal heat-shock response to microwaves”. Nature, 2000, 405:417–418.

[18] de Pomerai D, Daniells C, David H, Allan J, Duce I,MutwakilM, Thomas D, Sewell P, Tattersall J, Jones D, Candido P, “Microwave radiation induces a heat-shock response and enhances growth in the nematode Caenorhabditis elegans”, IEEE Transact Micr Theor Tech, 2000, 48:2076–2081.

[19] Dawe A S, Smith B, Thomas D W P, Greedy S, Vasic N, Gregory A, Loader B, and de Pomerai D, “A small temperature rise may contribute towards the apparent induction by microwaves of heat-shock gene expression in the nematode, Caenorhabditis elegans”, Bioelectromagnetics, 2006, 27(2), 88-97.

[20] Collin A., Cueille M., O'Connor R, Leveque P. (2005) Dosimetry and Microdosimetry including Electromagnetic, Thermal and Convection for in vitro Microwave exposure System. XXVIIIth General Assembly of the International Union of Radio Science (URSI), paper KP.4(0140), New Delhi, India.

[21] Cueille M., Collin A., O'Connor R., Leveque P. (2005) Dosimetry based on Electromagnetic, Thermal and Convection simulations for in vitro Microwave Exposure System. Proceedings BioEM 2005, Dublin, pp. 462-463.

TOWARDS A STANDARDIZATION OF SAR NUMERICAL EVALUATION

L. CATARINUCCI, A. COLUCCIA, L. TARRICONE

D.I.I. UNIVERSITY OF LECCE, LECCE – ITALY
mail: luca.catarinucci@unile.it; luciano.tarricone@unile.it

Abstract
The numeric evaluation of the specific absorption rate (SAR) referred to a certain quantity of biological tissue, plays a main role when radioprotection aspects connected to the interaction between humans and electromagnetic (EM) fields are investigated, as highlighted in the related guidelines both in European Community (ICNIRP) and in USA (IEEE C95.1).
Nevertheless, it is important to observe how SAR values are strongly influenced by many factors as, for instance, the shape of the volume containing the reference mass; such a shape is imposed as cubical in IEEE guidelines, whilst this is not clearly stated in ICNIRP ones. Moreover, several other aspects, such as the optimum discretization step or the treatment of internal air (just to mention some of them), cause discrepancies among results obtained by different research groups.
In this work an overview on some SAR algorithms is firstly presented, and a discussion on their potential differences reported. Then, such algorithms and new ones proposed by the authors, are used to evaluate the SAR in some practical human-antenna interaction cases. The remarkable differences highlighted from the comparison, enforce the necessity to individuate an algorithm to be elected as "canonical", as discussed in conclusion of the work.

Introduction
The frequent exposure to the field emitted by electromagnetic (EM) sources is nowadays a matter of fact; consequently, in recent years, there has been an increasing public concern about the possible risks for human health due to the interactions with antennas. For this reason, the major public organizations in the world have established safety guidelines for radiofrequency (RF) exposure, as for instance the recently revised IEEE RF Safety Standard C.95.1-2006 [1], adopted in United States, and the International Commission on Non-Ionizing Radiation Protection (ICNIRP) Safety Standard [2], adopted in European Community. Such guidelines are based on the specific absorption rate (SAR) averaged over a certain reference tissue mass, usually 1 g, 10 g or the whole body mass; safety limits are accurately fixed distinguishing among different categories of workers and different body parts, and they are also frequently updated as a consequence of the results produced by the scientific community. The last confirmation of that is given by the introduction for the first time in a guideline [1] of new safety limits specific for the pinna, after the publication of some works, aiming at demonstrating the necessity of paying due attention to the anatomic details of the ear and to their effects in the exposure to cellular phones [3]-[5]; such diversification had not been considered neither in the previous IEEE standards [6], [7] nor in ICNIRP ones.
Nevertheless, in contraposition to the constant attention dedicated to the refinement of the safety limits, diversifying them in terms of kinds of workers, exposure time and exposed body portions, it is quite evident a lack of indications about how the SAR should be evaluated; indeed, despite the apparent easiness of the formulae for the SAR evaluation, such relations actually open themselves to different interpretations which could cause discrepancies in the estimation of the absorbed energy. As well known, in fact, the SAR is defined as the "time derivation of the incremental energy absorbed by, or dissipated in, an incremental mass contained in a volume element of a given density, normalized to that mass", which can be synthesized as:

$$SAR = \frac{\partial}{\partial t}\left(\frac{\partial W}{\partial m}\right). \tag{1}$$

In the context of RF and/or microwave (MW) exposure, where the energy absorption by tissues is only due to the Joule effect, two more convenient forms are often used, allowing the SAR evaluation from either electric field or temperature measurement through the following formulae:

$$SAR = \frac{\sigma |E^2|}{2\rho} = c\frac{\Delta T}{\Delta t}, \quad (2)$$

Where σ [S/m] is the tissue conductivity, E[V/m] the electric field, ρ [kg/m^3] the tissue density, c the tissue specific heat capacity and ΔT [°C] the temperature change caused by the exposure for a time Δt [s].
Consequently, considering the first of the (2), the SAR averaged over a certain reference mass, can be written as:

$$SAR_{rm} = \frac{\int_{V(rm)} \sigma |E|^2 / 2 \; dv}{\int_{V(rm)} \rho \; dv}, \quad (3)$$

Where rm is the reference mass (usually 1g, 10g or the whole body mass) and $V(rm)$ is the volume containing rm.
It can be noted that, although the shape of the volume containing the reference mass does not affect the divisor in (3), which is anyhow equal to rm, its impact on the dividend could be relevant; the distribution of the electric field, in fact, varies greatly from point to point inside the tissues, so that the use of different volumes could generate strong discrepancies.
It is reasonable wondering, hence, how the shape of the volume containing the reference mass can impact the SAR value itself and if, consequently, such a shape must conveniently be standardized. Can, for instance, the SAR averaged over 10 g of tissue assume a different value if the volume shape is changed? If so, which is the most appropriate shape to be considered?
The just opened problem is almost completely neglected in international guidelines. Despite the common sense would suggest that a spherical volume should be the most logical choice, because it does naturally select the set of points which are as close as possible to the evaluation point, IEEE guideline bases its safety limits on cubical volumes. Even more debatable is the position assumed on ICNIRP standards, where the absolute lake of indications in matter, leave the scientist the faculty of the choice.
Moreover, it is commonly accepted from the scientific community, that the use of numerical dosimetry for the energy absorption estimation is the most appropriate approach; experimental dosimetry, in fact, evidences strong difficulties both in using real subjects and in carrying out adequately accurate phantoms, capable therefore to correctly reproduce the human characteristics. Vice versa, the use of EM full-wave methods, such as the Finite Difference Time Domain (FDTD) algorithm or the Finite Element Method (FEM), jointly with the availability in literature of some accurate numerical phantoms, as for instance the one proposed in [8] or the one proposed in [9], allows the rigorous evaluation of the SAR also in complex realistic human-antenna exposure problems. However, when numerical methods are used, a spatial discretization must be implemented, thus accentuating even more the problems connected to the SAR evaluation. In such a case, in fact, the averaged SAR can be computed through the following formula:

$$SAR_{rm} = \frac{\sum_{i \in \bar{V}(rm)} \sigma_i |E_i|^2 / 2}{\sum_{i \in \bar{V}(rm)} \rho_i}, \quad (4)$$

where the index i indicates the generic elementary cell of the discretized space and $\bar{V}(rm)$ the discretized volume containing the reference mass rm. The use of a volume $\bar{V}(rm)$ consisting of several cells, is itself a degree of freedom and consequently a source of non-uniqueness of the results, the SAR value being dependent on which cells are chosen, among the several possible, to better represent the desired volume shape. Moreover, also the spatial discretization step could play a major role: a space step as large as a significant portion of the reference mass, for instance, besides emphasizing the just mentioned problem, causes strong discrepancies between rm and the actual considered averaging mass.
To the topics now pointed out, some others can be added, each one increasing the uncertainty to the estimated SAR values. The peak SAR values, for instance, are often founded in points close to the human surface, where

the chosen volume shape must be modified in order to consider only tissue and not air. Which is the best algorithm in that sense?
Moreover, as well known, if the FDTD method is used, the obtained electric field components are not centered in the elementary cells [10]. Recently, some algorithms have been proposed to refine SAR calculation [11], and they are herein discussed.
Furthermore, another key-point is the one of how to treat the presence of internal air, which is also here specifically addressed.
More specifically, in the following sections some commonly used SAR algorithms will be described and compared, and some new ones proposed by the authors presented. Such algorithms are then applied to a difficult case of interaction between humans and radio base station antennas (RBA) using both cubical and spherical reference volumes, and results showed and discussed.

Common SAR numerical algorithms

In this section, a brief overview of the most commonly adopted algorithms for the numerical evaluation of the SAR, is presented. Despite the appreciable differences among the algorithm structures, it is important to highlight here that the main goal of this treatment is neither the individuation of an algorithm to be elected as a reference, nor the eventual discredit of some of them; on the contrary, in fact, what is sustained in this work is that, although different numerical strategies give out different SAR values, none of them contravene any of the indications reported in the safety guidelines.
One of the usually adopted approaches, for instance, computes the SAR_{rm} on a certain point by considering the contributes coming from the cells which belong to a cubical volume centered in that point. In [12] and [13] such a volume is prefixed, i.e. is the same for each computation point, and it is dimensioned in order to roughly contain the reference mass. The non modifiability of the volume shape causes the evaluation of the SAR in presence of air together with tissues and consequently an averaged value obtained integrating over a mass different from rm. In order to avoid the evaluation of the SAR in cases where a too large portion of the volume does not contain tissues, a maximum tolerable percentage of air is imposed: if the percentage of air is superior to the fixed limit, SAR remains undetermined.
It is important to observe that such an approach does not allow the evaluation of the absorbed energy in the most external points of the exposed target where, though, high SAR values or even the peak SAR itself, are located.
Furthermore, also where the volume does not contain air, it is often impossible to reach exactly rm using a cube, the number of needed cells being strongly dependent on the discretization step.
In order to avoid some of the listed problems, parallelepipeds instead of cubes are used in [14], but also this solution is not devoid of lacks; such a choice, in fact, forces the use of a volume which is unbalanced respect to the evaluation point and, consequently, causes the use of too far contributes.
A first improvement of the previous techniques can be obtained through the use of a cubic volume which dynamically adjusts itself in order to consider exactly the rm and tolerates up to a certain percentage of air, as proposed in [11]. The algorithm builds a sequence of cubes of dimension progressively increasing till a mass superior to rm is reached. At each step the percentage of air is evaluated and if it is greater than the prefixed limit, the SAR in that point remains undetermined. Vice versa, the last cube of the sequence with mass inferior than rm is used as the core for the SAR evaluation and only an accurately evaluated portion of the adjacent cells is added in order to exactly reach rm. Anyhow, a big limit of this algorithm remains: the incapability to determine the SAR in points closed to the surface of the exposed target; in [15] a further improvement in that sense is proposed. The concept of a volume perfectly cubical is not considered indispensable anymore; the cells are assembled around the reference one by following established criteria and excluding the air. The algorithm, here named Adaptive Cube (AC), stops the insertion of new cells when the total mass is equal to rm for each computed value, but the shape of the volume is given by the set of cells which better approximate a cube intersected with non-tissue points. In such a way, in each point, included those belonging to the most external regions, the SAR can be evaluated.
The comparison among the presented numerical techniques shows that even radically different algorithms for the evaluation of the SAR can comply with the few indications reported in RF safety guidelines, despite it is easily

predictable that they could generate discrepant results. Consequently, an integration of the guidelines with detailed indications on a SAR numerical algorithm to be elected as a reference, appears to be at least expected.

New kinds of SAR algorithms

The conceptual differences among the commonly used algorithms for the SAR numerical evaluation and the consequent observations reported at the end of the previous section, pave the way to a more deep theoretical discussion about how the algorithms should be conceived. Even if at a first glance it could seem a mere implementation problem, it addresses instead to a more general consideration: which is the most suitable volume shape for the SAR evaluation? If it is true that when numerical methods and orthogonal meshes are used, it is quite easy and natural to choose cubical volumes which contain 1g or 10g (the rm) of tissue, it is as much true that the acceptance of such an assumption signifies to be aware of the limits which derive from that, and that the obtained results could be at least debatable.

Anyhow, even if, for instance, the AC algorithm is basically oriented towards cubical shapes, the eventual presence of air could cause a strong deformation of the volume, such as in the case of the SAR evaluated in the fingers, where the cube becomes more likely similar to a thin parallelepiped. This is not surprising, the choice of the cube being justified only by its implementation easiness; nevertheless, it is reasonable wondering which should be the most appropriate volume, regardless to eventual implementation problems.

To the opinion of the authors, there is no doubt that a spherical volume is the best one. Spheres, in fact, select the most close cells to a reference point, thus allowing the most natural evaluation of the SAR; any other volume, in fact, would take into account too far contributes, as for the cube case, where the vertexes are considered instead of more close points.

Nevertheless, to adequately take into account a spherical volume when discretized spaces are considered, some observations are necessary. In a continuous space, in fact, it is possible to determine an ideal sphere (ideal circle in 2D) which contain exactly a quantity of tissue equal to rm, but in a discretized space this is quite complicated. For the 2D case, an hypothetical ideal circle is reported in Figure 1; the yellow cell in the center is the one where the SAR must be evaluated. Some of the cells are entirely contained in the ideal circle, whilst some others (the violet ones in Figure 1) are intersected by that circle; such cells are called here “peripheral cells” and will play a major role in the formulation of new algorithms. The SAR, in fact, should ideally be calculated by adding the contribute of the internal cells to the contribute of the partial volumes of the peripheral cells, so that the approximation of such partial volumes becomes the real difficulty of spherical algorithms.

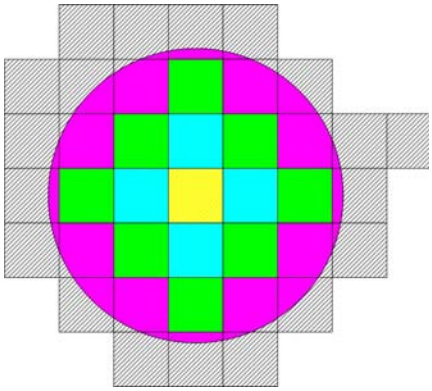

Figure 1. Representation of the ideal circle which includes the rm.

In the following four new algorithms will be presented, all based on spherical volumes, even though the same strategies can be easily applied to cubical volumes.

A: Onion Skin Algorithm

The first algorithm which is here proposed considers a sphere as the reference volume and, when necessary, modifies the shape in order to include only tissues and not air. The strategy that regulates the addition of a new cell to the partial volume, gives the name to the proposed algorithm: “Onion Skin” (OS); if the mass contained in a sphere of radius r (onion) is inferior to rm, in fact, new cells are added selecting them out among those belonging to the layer which radius is $r+1$ (skin). Such an algorithm is similar to the AP one proposed in [15] apart from the shape of the volume.

The main steps of the algorithm for the evaluation of the SAR_{rm} in a cell of coordinates $< x, y, z >$ can be synthesized as follows:

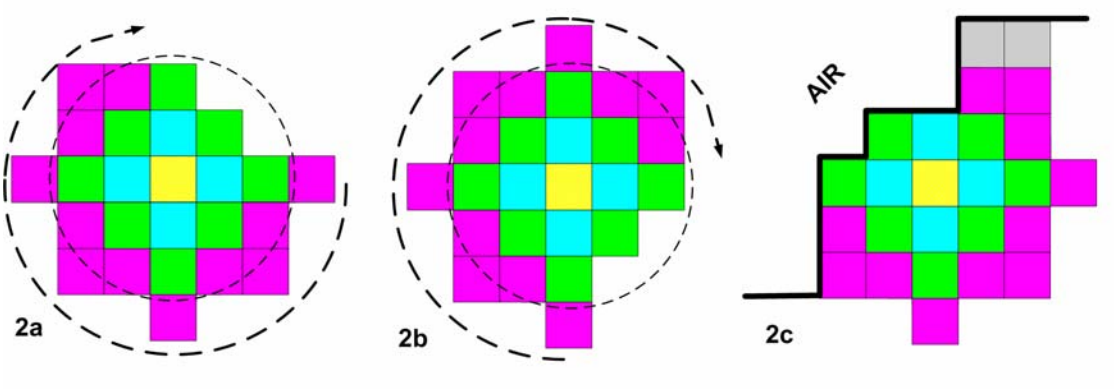

Figure 2. Onion Skin algorithm applications examples.

1. initialize the radius $r = 1$ and set the center in $< x, y, z >$;
2. select the set of possible candidate cells as those belonging to the layer of radius r centered in $< x, y, z >$ and representative of tissues (air is excluded);
3. add one of the individuated cell to the partial volume and compute the new partial mass pm.
4. repeat step 3 until all the cells individuated in 2 have been added or the condition $pm \geq rm$ is verified;
5. if $pm \geq rm$ has not been verified yet, impose $r = r + 1$ and come back to 2. Else (the volume is founded) go to 6;
6. Evaluate the SAR_{rm} by using the individuated volume.

The method guarantees that the desired 1g or 10g of rm are obtained with a tolerance on the order of a fraction of the last added cell mass. It is quite evident that the algorithm is based on the iterated addiction of layers to the central cell until rm is reached; it is highly probable, though, that the last layer will not be completed, thus causing an unbalancing of the volume respect to the cell in $< x, y, z >$. In Figure 2, a bi-dimensional schematization of the volume individuated by the OS algorithm is reported for a simple case of absence of air and supposing that 25 cells guarantee a mass of almost rm. The different colors of the cells individuate different layers. More specifically, in Figure 2a the reference cell (the yellow one) is supposed to be far enough from every air region so that for each successive layer all the cells can be considered potential candidates to be part of the averaging volume; as apparent, three complete layers and a partial one are needed. The cells of the last layer, however, could be chosen in different ways as evidenced in Figure 2b, and consequently the obtained SAR could assume different values. This represents the most substantial lake of the OS algorithm. Finally, Figure 2c shows what happens when the evaluation cell is quite close to air regions, with the consequent modification of the volume shape in order to guarantee anyhow an averaging mass equal to rm as well as the use of only tissue cells.

B: Graded Peripheral Cells Algorithm

As previously observed, the best way for considering spherical volumes in orthogonal meshes, would be that of taking into account the whole contribute coming from all the cells entirely contained in the ideal sphere, and the partial contribute given by the peripheral cells. The problem, actually not trivial, consists on the accurate evaluation of the partial volume to be considered for each of the peripheral cells; this problem is quite difficult to solve analytically because of the high number of possible intersections between spheres and cubes: approximations are, hence, strongly necessary.

The herein proposed approach, called Graded Peripheral Cells (GPC), considers an equal fraction of all the peripheral cells, regardless to the effective volume individuated by the ideal sphere (or ideal circle in 2D). The algorithm analyzes all the non-air cells around the evaluation point, and marks them as internal, external or peripheral, respect to the ideal sphere; in order to perform such an operation, the number of vertexes internal to the sphere is computed.

Once such a preprocessing analysis has been performed, the mass of the internal cells is known, as well as the remaining quantity necessary for reaching rm. Such a quantity is considered as equally distributed among all the peripheral cells which proportionally contribute to the final SAR value.
In Figure 3 the individuated resultant volume is reported for the same case of Figure 2a. The small internal squares sketched inside the peripheral cells, represent the considered portion of mass. By comparing such a volume with the one obtained with the OS algorithm, it can be noticed how the problem of the unbalancing respect to the central cell is substantially bypassed. Nevertheless, the assumption that all the peripheral cells contribute with the same mass, seems to be too approximate, because some of the cells are only slightly intersected from the ideal sphere whilst some others are almost completely internal. The next proposed algorithms can be considered as a refinement of the GPC one, aimed at better approximate the ideal situation described in Figure 1.

C: Graded Peripheral Vertex Algorithm

The Graded Peripheral Vertex (GPV) algorithm represents a more refined version of the GPC algorithm. As previously shown, in fact, in GPC the same portion of mass is considered for each one of the peripheral cells; if a method is found for discriminate how much of a cell is internal to the ideal sphere, a non-uniform weighting can be effectively applied. Actually, the same strategy used for discriminating if a cell is or not peripheral, can be extended in that direction; a cell is peripheral, in fact, if at least one vertex is internal to the ideal sphere and contemporaneously at least one vertex is external. The number of internal vertexes, hence, could be a good parameter to be used. Despite it is still an approximation, it is evident that a cell with only one internal vertex contributes with a portion of its volume larger than that of a cell with more internal vertexes.
The GPV algorithm, hence, calculates the portion of a peripheral cell to be considered, proportionally to the number of internal vertexes; more specifically, if $1 \le n \le 8$ ($1 \le n \le 4$ in 2D cases) is the number of internal vertexes of one of the examined cells, then $n/8$ of its mass is considered. Figure 4 shows, reporting also the number of internal vertexes for each peripheral cell, how the application of the GPV algorithm allows a better distribution of the mass respect to the GPC and the OS ones, increasing the accuracy of the approximation respect to the ideal case of Figure 1 and thus improving the quality of the result.

D: Graded Peripheral Vertex-3 Algorithm

The Graded Peripheral Vertex-3 (GPV3) algorithm is a modification of the GPV algorithm, where the contribute of each peripheral cell is not proportional to the number of internal vertexes n, but to its cube (its square in 2D), i.e. to n^3. This criterion is based on the observation that the dependence of the internal volume on the number of internal vertexes is, in most cases but not always, almost cubical. In such an algorithm, hence, the mass of a cell is divided into 64 parts (16 in 2D) and $n^3/64$ is the fraction of mass (and volume) considered for a peripheral cell with n internal vertexes.
Even if none among GPV and GPV3 is definitively better than the other, above all in 3D cases the GPV3 seems to guarantee better approximations.

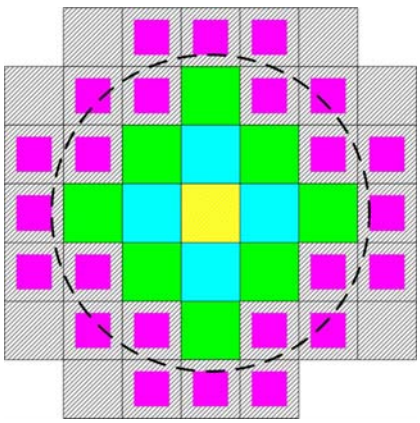

Figure 3. Graded Peripheral Cell algorithm application

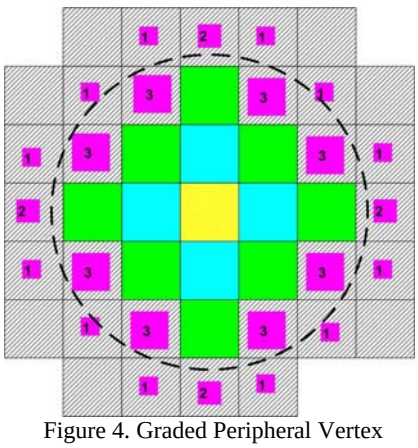

Figure 4. Graded Peripheral Vertex algorithm application

Results

In this section some of the presented algorithms are tested on a practical case and results compared and discussed. More specifically the difficult problem of the interaction of a human with the field emitted by a radiobase station

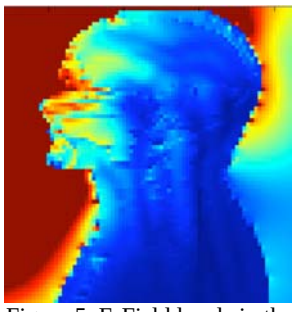

Figure 5. E-Field levels in the studied case

Peak SAR comparison		
SAR Algorithm	**Peak SAR (1g)**	**Peak SAR (10g)**
Adaptive Cube (AC)	**27.93**	**14.39**
Onion Skin (OS)	**27.00**	**14.32**
Graded Peripheral Cell (GPC)	**27.65**	**14.73**
Graded Peripheral Vertex (GPV)	**27.89**	**14.78**
Graded Peripheral Vertex-3 (GPV3)	**28.03**	**14.85**

Table I. Peak SAR values using different algorithms.

antenna has been solved by using the FDTD method [16], and the SAR averaged over 1g and over 10g of tissue has been evaluated in each point of the exposed subject (which is the numerical phantom proposed in [8]). In Figure 5 the electric field distribution in a section of the head is reported. Five different algorithms have been used: the AC one, representative of the cubical shape algorithms, the Onion Skin one, which applies the same strategies of the AC but to spherical volumes, and the three successive refinements, respectively GPC, GPV and GPV3. The other presented algorithms, instead, have not been tested, because their inability to evaluate the SAR in superficial points makes the comparison with most sophisticated strategies impossible.

In Table I the peak SAR values are reported both for $rm = 1g$ and for $rm = 10g$. It can be observed that all the tested algorithms give comparable results. This is not surprisingly: even if the algorithms are quite different, in fact, the peak SAR is found in the proximity of the phantom surface where the electric field assumes the highest values all around a region as large as many rm. In such points, the volumes are also strongly deformed by the phantom shape, so that the refinement strategies becomes unappreciable. Anyhow, it is important to recall again that, among the possible, only algorithms which can evaluate the SAR everywhere in the phantom have been tested; the others algorithms, such as the one proposed in [12] and [13] or the one proposed in [14], would have been unable to determine the SAR in such points. This observation is itself enough to justify the requirement of a standardization of the SAR numerical evaluation techniques.

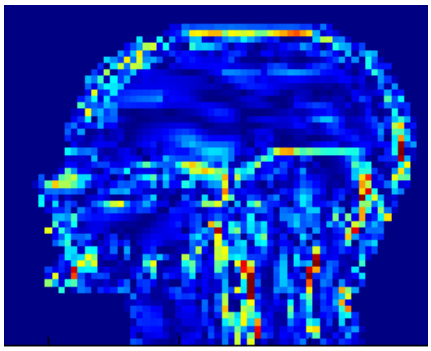

Figure 6. AC versus OS: percentage difference in each phantom point.

In order to appreciate, though, the differences among the various algorithms, all the SAR values, and not only the peak one, should be compared.

In Figure 6, for instance, the percentage difference among AC and OS is graphically reported. The chromatic scale, from blue to red, represents increasing differences from 0 up to 45%. It is quite apparent the strong diversity in some investigated phantom points, even though only the shape, and not the strategy, differentiates the algorithms.

In Table II, instead, the GPV3 algorithm is used as the reference one, and the percentage difference with the others is reported. More specifically two parameters are computed: the average percentage difference and the maximum percentage difference.

Percentage Difference				
SAR Algorithm	**SAR (1g)**		**SAR (10g)**	
	Average %	**Maximum %**	**Average %**	**Maximum %**
AC versus GPV3	**8.43**	**99.08**	**5.12**	**69.95**
OS versus GPV3	**6.90**	**95.39**	**3.31**	**53.71**
GPC versus GPV3	**4.93**	**90.14**	**0.14**	**3.04**
Graded Peripheral Vertex (GPV)	**2.66**	**42.89**	**0.08**	**2.33**
Graded Peripheral Vertex-3 (GPV3)	**---**	**---**	**---**	**---**

Table II. Average and Maximum percentage difference respect to GPV3 algorithm.

Through the analysis of the data reported in the table, some conclusions can be drawn. First of all, by improving the accuracy of the algorithms, all the percentages decrease. As expected, hence, by using more refined spherical algorithms a better discrimination of the absorbed power in the various points can be performed, so that the SAR values can be better estimated. Also, it can be observed that differences referred to the SAR_{10g} are always inferior to those referred to the SAR_{1g} and this for two different reasons: first of all, by increasing the rm, the consequent smoothing effect due to the integration over a bigger volume causes the attenuation of the differences among the methods. Secondly, the number of peripheral cells increases with the volume and the contribute of each of them becomes less relevant.

Even more interesting are the deductions coming from the analysis of the maximum percentage error; two sophisticated algorithms, such as OS and GPV3, give in some points difference up to 90% for the SAR_{1g} and up to 50% for the SAR_{10g}. Even two quite similar algorithms, GPV and GPV3, show strong differences in the 1g case. In order to better appreciate the impressive differences among the algorithms in every points of the phantom head, finally, the percentage difference of GPV3 respect to OS and respect to GPC for the SAR_{1g} are reported in Figure 7.

Conclusions

In this work some commonly adopted algorithms for the numerical evaluation of the Specific Absorption Rate (SAR) averaged over a certain mass have been reported and some new ones have been presented and compared. Among the most important conclusions which can be drawn, the main aspect seems to be that of the necessity of a standardization of the techniques for the SAR calculation. The discrepancies among results obtained through different algorithms are impressive, even though all of the tested techniques do not contravene any of the indications, probably inadequate, reported in the most important radiofrequency safety standards. This enforces, also, a more detailed discussion about the consideration of local SAR values.

The work itself gives some indications in that sense, discussing the role plaid by the shape of the integration volume along with other important issues. The use of a spherical volume rather than a cubical one, represents for the authors the main necessary modification, and the four proposed algorithms could be used as the starting point which paves the way to a more deep discussion.

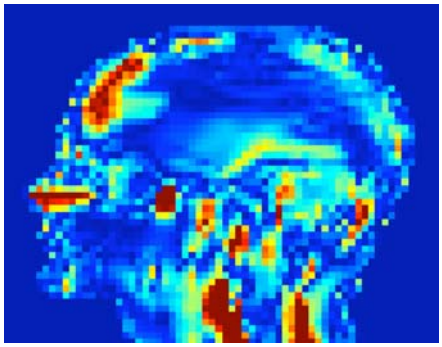

a)

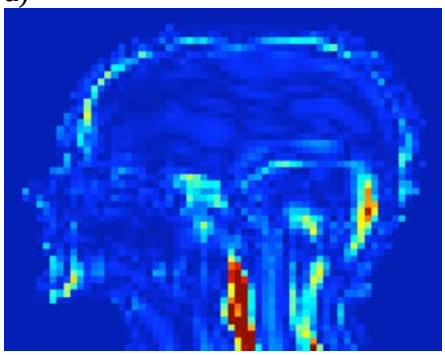

b)

Figure 7. GPV3 versus OS (a) and GPV3 versus GPC (b) percentage difference in each phantom point.

References

[1] IEEE C95.1 – 2006, “Standard for Safety Levels with Respect to Human Exposure to Radiofrequency Electromagnetic Fields, 3 kHz to 300 GHz”, IEEE Standards C95.1, Coordinating Committee 28.4, 2006.

[2] ICNIRP, “Guidelines for limiting exposure to time-varying electric, magnetic and electromagnetic fields (up to 300 GHz),” Health Phys.: International Commission on Non-Ionizing Radiation Protection (ICNIRP), vol. 74, pp. 494-522, 1998.

[3] O.P. Gandhi, Gang Kang, “Inaccuracies of a plastic "pinna" SAM for SAR testing of cellular telephones against IEEE and ICNIRP safety guidelines”, MTT IEEE Trans. on MTT, Volume 52, Issue 8, Part 2, Aug. 2004 Page(s):2004 – 2012

[4] Beard et al, “Comparisons of computed mobile phone induced SAR in the SAM phantom to that in anatomically correct models of the human head”, IEEE Transaction on EMC, Volume 48, Issue 2, May 2006 Page(s):397 – 407

[5] M. Burkhardt, N. Kuster, “Appropriate modeling of the ear for compliance testing of handheld MTE with SAR safety limits at 900/1800 MHz”, IEEE Trans. on MTT, Volume 48, Issue 11, Part 1, Nov. 2000 Page(s):1927 – 1934

[6] ANSI C95.1-1982, “American National Standard Safety Levels With Respect to Human Exposure to Radiofrequency Electromagnetic Fields, 300 kHz to 100 GHz”, The Institute of Electrical and Electronics Engineers, Inc., New York, NY.

[7] IEEE C95.1 – 1999, “IEEE Standard for Safety Levels With Respect to Human Exposure to Radiofrequency Electromagnetic Fields,

3 kHz to 300 GHz" IEEE Standard C95.1, 1999.
[8] I. C. Zubal, C. R. Harrell, E. O. Smith, Z. Rattner, G. Gindi, P. B. Hoffer, "Computerized 3D Segmented Human Anatomy", Medical Physics, 21, 2, pp. 299-304, 1994.
[9] P. A. Mason, J. M. Ziriax, W. D. Hurt, T. J. Walters, K. L. Ryan, D. A. Nelson, K. I. Smith, and J. A. D'Andrea, "Recent advancements in dosimetry measurements and modeling," in Radio Frequency Radiation Dosimetry, B. J. Klauenberg and D. Miklavcic, Eds. Norwell, MA: Kluwer, 2000, pp. 141–155.
[10] A. Taflove, 'Computational Electrodynamics: The Finite-Difference Time-Domain Method', Norwood, MA, Artech House, 1995
[11] K. Caputa, M. Okoniewski, M. A. Stuchly, "An algorithm for computations of the power deposition in human tissue, IEEE Antennas Propagat. Mag., vol. 41, pp. 102-107, Aug. 1999.
[12] K. S. Nikita et al, "A Study of Uncertainties in Modeling Antenna Performance and Power Absorption in the Head of a Cellular Phone User", IEEE Transactions on MTT, vol. 48, n.12, Dec. 2000.
[13] Jianqing Wang, Osamu Fujiwara, Soichi Watanabe, Yukio Yamanaka, "Computation With a Parallel FDTD System of Human-Body Effect on Electromagnetic Absorption for Portable Telephones", IEEE Transactions on MTT, vol. 52, n. 1, January 2004.
[14] O.P. Gandhi, G. Lazzi, C.M. Furse, "Electromagnetic Absorption in the Human Head and Neck for Mobile Telephones at 835 and 1900 MHz", IEEE Transactions on MTT, vol. 44, n.10, October 1996.
[15] A. Lee, J. Pack, "Study of the Tissue Volume for Spatial-Peak Mass-Averaged SAR Evaluation", IEEE Transactions on EMC, vol. 44, n. 2, May 2002.
[16] L. Catarinucci, P. Palazzari, L. Tarricone, "Human Exposure to the Near-Field of Radiobase Antennas: a Full-wave Solution using Parallel FDTD", IEEE Trans. on MTT, March 2003.

ON THE USE OF A GRID REFINEMENT ALGORITHM IN FDTD FOR EVALUATING THE SAR IN VARIOUS EXPOSURE CONDITIONS

R. PONTALTI, A. VACCARI, C. MALACARNE, L. CRISTOFORETTI

ITC-IRST - CENTRO PER LA RICERCA SCIENTIFICA E TECNOLOGICA

VIA SOMMARIVE, 18 - 38050 POVO, TRENTO – ITALY

Abstract

Whole-body averaged and local SAR depends on many factors including stature, gender and posture of the exposed subject. In RF dosimetry, various numerical phantoms of women and men are gradually becoming available as well as numerical techniques able to virtually rotate the main joints in order to change their posture. Other variables which deserve investigation are field polarization and impinging direction of the incident wave. To assess the SAR distributions in these structures a high spatial resolution of the human numerical models is mandatory. At the same time, it is usually requested to model a large embedding domain which may accommodate a near field source. This imposes the use of subgridding techniques. Practical examples of the FDTD implementation with a domain refinement algorithm, in the range 100 MHz – 4 GHz, are reported

Introduction

Numerical phantoms involving sophisticated complex permittivity representations of the human body are a useful tool for investigating the connection between external fields and induced internal SAR. These phantoms are obtained either by image segmentation and assignment of the proper permittivity values to each tissue or by semi-automatic methods which take into account the complex permittivity variations into every tissue. Both methods use sets of anatomical images obtained by CT (Computerized Tomography) or by Magnetic Resonance Imaging (MRI).

The human exposure was first studied by using models of a man in standing position frontally impinged by a plane wave with vertical polarization, having these states been recognized as generally maximizing the absorption. Nevertheless, these conditions (male model, standing position and plane wave) are too generic to accurately evaluate the exposure in a realistic environment. Different postures, body shape and composition can determine SAR differences. A number of postures have already been studied [1][2] and, in the last years some works focussed on the gender differences [3].

After having developed their own male [4] and female phantoms [5], the authors used them in some works dedicated to the understanding of the differences found in the whole body averaged SAR between male and female [3][6].

Recently they developed a technique for numerically rotating the main joints of the body preserving, at the same time, a reasonably realistic anatomic aspect. Since a posture in which a subject spends a considerable part of its living time is sitting, arms and legs of the male phantom were rotated in a way to simulate that condition.

A paper published very recently [2] demonstrates that different parts of the body (trunk, limbs or forelimbs) may show their own resonance when stimulated with the proper frequency and polarization. It causes a large variety of conditions determined by the posture and by the parameters of illumination, depending on the relative orientation of the field with specific portions of the body which – in case of a more complex posture than standing with aligned arms – cannot be anymore considered as a simple linear antenna.

The attention is focused on the range of the RF spectrum located above the body resonance (here meant standing, i.e. about 40 or 80 MHz depending on grounded or isolated condition), in which the largest part of artificial sources for broadcasting and mobile communication is allocated: 0.1–4 GHz.

For calculating SAR distribution the Finite-difference time-domain (FDTD) solution method of Maxwell's equations, a widely used numerical technique in computational electromagnetics, has been used. It is commonly retained that only analyses at frequencies corresponding to wavelengths no shorter than 10 times the space sampling size are fairly accurate. But when, at a given frequency, the structures' electrical density augments, such as in biological tissues, wavelengths are unavoidably shortened. Many efforts have then been made to develop local mesh refinement algorithms for the FDTD method. A reported problem of the various attempts is their tendency to become unstable.
In this work, a robust and economic subgridding algorithm has been used [7] to achieve higher spatial resolution in the region of interest. This method, called filtering-based (FB) subgridding, is applied to allow a refined calculation of SAR, while maintaining a rather large cushion of free space all around the bodies.
It is as economic as possible, both in terms of memory request and in the number of floating point operations. To this end we devised a coupling scheme between two FDTD meshes, one of them having an higher resolution by a factor of 3, 5 or 7 than the other. The subgridding algorithm at the fine-coarse interface is based on a spatial-differentiation low-pass filter which is analytically justified. It requires only a certain number of extra floating point operations, but no extra memory allocation.
Firstly this work considers the DAM phantom developed in our laboratories and the numerical algorithm used to rotate the principal joints (arms, legs and hips). A brief description of the used subgridding technique will follow. Finally, some examples about the use of the subgridding technique applied to a real dosimetric problem are shown. In particular it will be studied the comparison of whole body averaged SAR in seated and standing male models undergone to various exposure conditions in terms of H or V polarization and frontal or lateral incidence.

Numerical human body model

A semi-automatic procedure to develop numerical human Dielectric Anatomical Models (DAM) was developed in the last years at the ITC-irst laboratory. The procedure is based on MRI image acquisition and by relating grey levels of each voxel to the proper complex permittivity value. The rationale is briefly described as follow. Detailed description of the technique is reported in [4], [5].
Whole body MRI scanning of a male (height: 1.73 m, weight: 63.8 kg) and female (height: 1.62 m, weight: 48.7 kg) volunteers (to obtain mDAM and fDAM respectively) were carried out. The acquisition of the images was performed by a 1 Tesla whole-body imager (1T, 42.5 MHz); body and head coils were used. Data sets were processed to improve the erected posture of the body. Ankle angle was also modified to ameliorate the contact of the feet with the ground. Afterwards, the images were interpolated, obtaining models of 5,999,472 voxels (fDAM) and of 7,795,509 voxels (mDAM), 2×2×2 mm^3 each. After the processing needed to correct the MR image non-uniformities, an automatic technique has been applied to obtain the dielectric models (Figure 1).

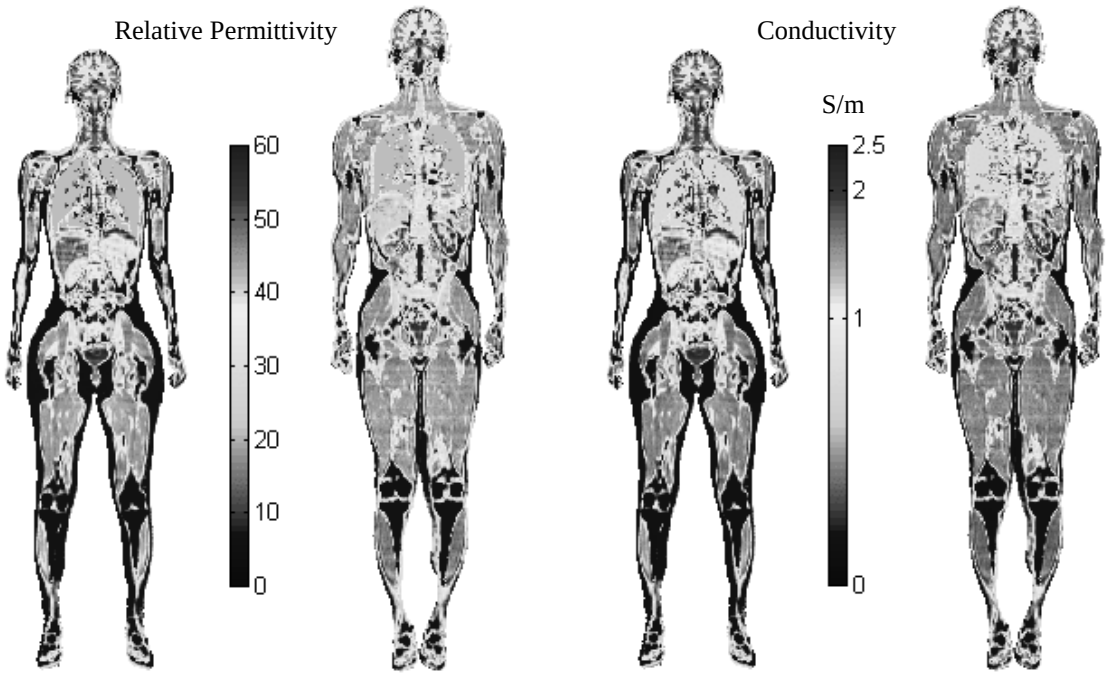

Figure 1. Relative permittivity and conductivity at 2 GHz for the female (left) and the male (right) models

To correlate the image grey levels to the complex permittivity values, transfer functions based on mixture theory were implemented for both high water content and low water content tissues. Since the equations of mixture theory were obtained from data over the frequency range 0.1 ÷ 18 GHz, the validity of the transfer functions lies in this same range.

Rotation of joints

In recent dosimetric studies, the attention has been increasingly devoted to the realistic representation of the human body; this means that, while initially only an average male man in standing position was considered, nowadays many phantoms of different heights, weights, genders, ages and positioned in different postures have been represented [1][2]. Among these aspects, the present work focuses its attention to the development of a modified phantom repostured in order to represent a seated man, being this latter a very frequent condition, both for workers and general public. However, aim of this study was not only to reach such kind of result, but more generally to develop a numerical algorithm able to manipulate the original numerical phantom, in order to model as many postures as possible.

The problem of the realistic geometric modelling of humans has been faced in many fields, from dosimetry to mechanobiology or computer graphics [8][9]. In these latter fields a very high level of anatomical modelling have been reached, with accurate representations of the organs both from a geometrical, anatomical and even dynamic point of view. The starting point in these cases is the detailed knowledge of the internal structures, which are segmented [10]. In this way each single structure is not only geometrically well-confined, but also dynamically characterised, and therefore able to discriminate that, for example, only the muscle is able to undergo active contraction or that the rigidity of the bone actually prevent its deformation.

Conversely, the original phantom used in this study is not segmented. While this condition enables on the one side the highest accuracy in the dielectric properties dispersion modelling, on the other side it partially hinders the accuracy in performing joint movements.

Nevertheless, some general criteria are anyway applicable, such as: to deform as little as possible the rigid structures like the bones, to preserve the total length of each deformed part (alongside its central axis), and finally to properly modify some regions (muscle) in order to maintain the total mass amount constant guaranteeing at the same time a good anatomical resemblance. It is evident that, in this case, the criteria are no longer applicable to well-defined districts, but rather to regions principally containing one tissue or the other.

The procedure followed to obtain the seated phantom is summarisable as follows:

- first of all the sub-volumes to rotate were identified and isolated, one at a time, from the remaining part of the body. In this specific case four sub-volumes were obtained: one for the legs, one for the pelvis and the two latter for the arms;
- for each sub-volume some ‘fiducial point’ couples (one point in the subvolume, the other one in the remaining part) were located. These were chosen in correspondence of the interface–the region that will be deformed the least– in order to facilitate the successive re-assembling of the two parts;
- the rotation plane and axis were defined with respect to the sub-volume and this latter was considered as a succession of slices parallel to the rotation plane and one voxel thick;
- each slice was further subdivided longitudinally in order to obtain several geometrical structures (called *fibres* hereafter in the text), parallel one to the other and roughly following the direction of the part to bend. The aim of this operation is to guarantee the necessary continuity alongside the structure (for example the wrapping around the elbows, knees, etc.);
- in correspondence of each slice there was one only *fibre* which passed through the rotation axis. This *fibre* underwent the only rotation operation, whilst, as the *fibres* were away from the central one, they underwent also a deformation. It is worth noting that, considering the slices where the bone was present, the central *fibre* coincided just with the bone and was therefore suitable to represent its rigid behaviour.
- Besides the rotation, other two types of deformations were applied: i) in correspondence of the rotation axis surroundings, in order to guarantee the necessary continuity of the tissue in this region, and ii) the height augmentation of the most external *fibres* containing tissues, applied in correspondence of the middle part of the segment(s) upper (and lower) with respect to the rotation axis. All these operations were applied at *fibre* level.

  The first operation consisted in the assignment of a new value–obtained by interpolation of the nearest voxel values– to both the new empty voxels and those superimposed as a consequence of the rotation. The second deformation had instead the aim to reproduce the muscle augmentation as a consequence of its contraction (active in the case of the upper-limb, and passive for the lower-limb). This latter kind of deformation was customizable, by initially setting two parameters which had effect, the first, on the amplitude of the deformation, and the second on the extent of the region to deform. These operations were performed in an automated way through an algorithm implemented by the authors.

The figure 2 shows, as an example, the different effects obtained by applying some kinds of deformations to the DAM's original left arm (a), and thus obtaining a simply rotated arm (b) or a rotated arm with augmented muscle in correspondence of the upper-limb (active contraction, (c)), or both the upper- and lower-limb (active and passive contraction, (d)).
A direct consequence of these kinds of deformations was a little mass variation. In particular, even the rotation without muscle augmentation led to a mass increasing as long as the structure to bend was rather thin (arm, legs), but the mass was found to be reduced while bending larger structures such as the pelvis. Therefore, particular attention had to be paid in assigning the suitable deformation parameters, in order to guarantee the total mass conservation.
A picture of the final result, that is the seated DAM phantom, is shown in Figure 3, laterally on the right.

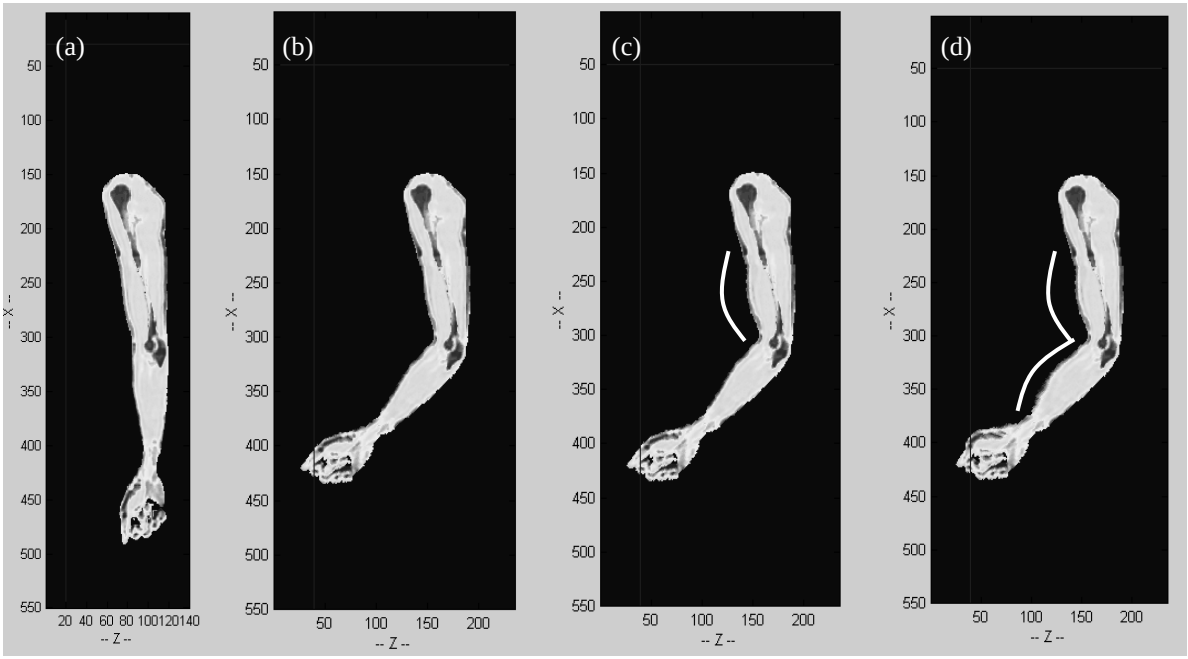

Figure 2: The pictures show four slices corresponding to the same depth of the DAM arm: in the original position (a), bended with a rotation of 45 degrees (b), as well as deformed to reproduce the muscle contraction, only in correspondence of the upper-arm (c), or both in the upper- and fore-arm. The white curves roughly indicate the regions where the deformations were applied.

FDTD calculation

Following a well known procedure, in classic FDTD [11] one writes centred finite difference analogues of the six partial differential scalar equations corresponding to the two Maxwell's curl time domain ones. Due to the particular choice of the lattice fields' sampling points, such finite equations are second-order accurate, both in space and time. As an initial value problem (IVP) fully explicitly formulated, the classic FDTD method is subjected to a stability condition, the so-called Courant–Friedrichs–Lewy (CFL) condition.
Moreover, the FDTD method needs to be supplemented by a suitable boundary condition (BC) on the outer surface of the computational domain to truncate the lattice and thus overcoming finite memory allocation capabilities. To this end many authors developed special BCs which are known, in the FDTD community, as absorbing boundary conditions (ABCs) or radiation boundary conditions (RBCs). They permit a mesh truncation with a minimum amount of back-reflection into the computational domain.
In our work we implement the anisotropic PML condition [12], which makes use of a uniaxial anisotropic lossy Maxwellian (i.e., unsplit) material. Our absorbing layer depth is standardized to 20 extra cells. Special care has to be given to the 8 corner, the 12 edges and the 6 faces of such an additional outer absorbing lattice. The coefficients for the various sub-regions and other relevant parameters are pre-calculated before the FDTD iterations start. Cubic smooth onsets of the conductivities are also used. A very low residual reflectivity is accomplished.
We also adopt the so-called "pulsed" FDTD method, which makes use of compact excitation pulses and an in-line discrete Fourier transform (DFT) of the system response. The DFT is updated every space sampling point at each time iteration. A plane wave excitation is launched on the six faces of a so-called Huygens' box, by means

of the addiction of electric and magnetic surface equivalent currents, which permit the total field, here meant incident+scattered, is present within the box but only the scattered one travels outside his volume. This allows an optimal functioning of the RBCs since they work on fields having lower amplitude than that of the total field and with incidence near to the normal to the boundary. The conditions on this box are parameterized in order to launch the desired excitation (i.e., progressive or regressive plane waves with different polarizations) without changing and/or recompiling the code. The model of the body target is contained in a sub-domain separately dealt with by the subgridding FDTD routine, which works coupled with the exterior one.
In [7] it is demonstrated that refining techniques are prone to instabilities because the interface between fine and coarse grids can trigger the onset and/or the amplification of high frequency components. This is due to the different numerical dispersion properties of the two grids. In particular, components which may freely propagate in one grid may have frequency greater than the Nyquist limit of the other one. Usually these frequencies are over the maximum frequency of interest and then may be treated as spurious components. The countermeasure proposed in [7], and here implemented, is to filter out such frequencies directly at the fine-coarse interface. That is why we call the technique FB-algorithm (Filtering Based).
It is not straightforward to deal with filters in time domain calculations such the FDTD method. In principle, simple low pass filters are applicable by using recursive techniques. The problem is that they would introduce phase delays which generate unphysical propagation and ultimately lead to instabilities. On the other hand, implementing a zero-delay filter would imply having at hand the whole time history of the quantity to be filtered, a thing which is impossible because of the evolutive nature of the FDTD method itself.
The problem has been solved [7] by transforming the temporal double derivative and his higher orders (used to implement the filter) into a set of spatial ones by means of the wave equation. Without entering in details here, the filtering action is obtained by a sort of spatial averaging with given weight coefficients. Acting at the space level permits the in-line updating during the time iterations. This allows a drastic mitigation of the instabilities, giving us the chance of using straight refinement factors of up to 7 or more, without resorting to the recursive nesting of grids (as instead it was usually done in case of use of such high refinements) which is severely computationally onerous.

Results and conclusions

In order to complement the findings of [2] who found that posture may give rise to secondary resonance peaks, a number of frequencies in the range 0.1–4 GHz have been evaluated. For each of them, the male phantom was accommodated in two postures (sitting and standing) and exposed in H or V polarization with the wave impinging the body frontally and laterally. The results are summarized in Figures 3 and 4. Since our method for obtaining the phantom does not allow going down below 100 MHz, we could not evaluate the resonant region of the spectrum. Nevertheless, results in the analyzed range are very important for radioprotection studies since the large part of broadcasting and mobile communication sources are located within it.
By using the data published in [13] it has been observed that, for Visible Human phantom, an empirical relationship holds for a 0.9 GHz plane wave exposure. It states that the whole body averaged SAR may be approximately calculated as 0.6 times the flux of the Poynting vector, times the minimal rectangular area circumscribing the largest coronal section of the body (it was illuminated frontally) and divided by the weight of the body.
By analyzing our phantoms, we found that the factor 0.6 is equivalent to the ratio between the area of the largest coronal section of the body and the minimal rectangular area circumscribing it. Then the above mentioned empirical relationship may be rewritten as:

$$SAR_{wb} \approx S\frac{A}{M} \qquad \{1\}$$

where S is the power density in W/m^2, A is the body area meant as the maximum cross section perpendicular to the wave number vector, and M is the mass of the body. This is not surprising, because it establishes that the power absorbed by the body is the Poynting flux by the section area; then this power distributes in the body and the averaged SAR is calculated dividing it by the body weight.
It is expected that this holds just at high frequencies where the absorption is eminently superficial. For this reason we report this approximated value only above 3 GHz in the graphs.
Since the computational burden involved in the calculation is rather high we could not provide results on a dense set of frequencies; thus, in case a fine structure were present in the spectrum, it would not be discriminated. However, it is probably unrealistic that a highly irregular behaviour in the SAR_{wb} would occur between a data point and the other one, even though they are rather sparse.
In [2] sub-resonances were seen slightly above 100 MHz for the sitting posture. Although we cannot confirm those results until a very dense set of frequency points will be available, we may draw some conclusions from the data here reported.

In the grounded state (as are the phantoms in the present study) main body resonance for the standing posture, occurs around 40 MHz. At 100 MHz, first point of our set, the tail of the resonance peak is still evident when the polarization is vertical in both orientations. It is more pronounced in the standing posture despite the sitting one has a shorter equivalent height and, consequently, a resonant frequency nearer to 100 MHz. Probably, since the shape of the body does not resemble anymore a linear antenna, the absorption is smeared on a larger, but less intense, resonance peak. It is also evident from the graphs that the peak is polarization-dependent: the SAR_{wb} is minimal at 100 MHz with horizontal polarization, which seems instead to show its maxima around 500 MHz or above.

Probably the most remarkable conclusion which can be drawn by the graphs is how good the very simple formula {1}, is able to provide an order-of-magnitude SAR_{wb} estimation above 500 MHz for both body orientations (frontal and lateral). The larger difference between the two body orientations is found for the standing posture, where the cross sectional area exposed to the wave almost doubles in passing from lateral to frontal orientation. Minor differences are instead visible for the seated case where the frontal cross section is diminished by the femurs' region with respect to the standing one.

These preliminary results suggest that, despite the roughness of formula {1}–which takes into account neither the dielectric properties of the body, nor its shape along the propagation direction–it gives reasonably good approximation of the SAR averaged over the whole body, at least above 500 MHz.

A conclusive statement about fulfilling of ICNIRP [14] limit can also be formulated: thresholds for whole body averaged SAR is 0.4 and 0.08 W/kg for occupational and general public, respectively. From that, the reference levels, under conservative assumptions, were calculated as: 10 and 2 W/m^2, till 400MHz, a linear connection follows up to 50 and 10 W/m^2 at 2 GHz and above this frequency values remain unchanged till 300 GHz. Scaling the SAR_{wb} to these limits allows the threshold of Figures 3 and 4 to be calculated. As it is shown in the graphs, the standing posture with frontal exposure and vertical polarization remain the conditions for which the absorption goes nearer to threshold although never reaching them.

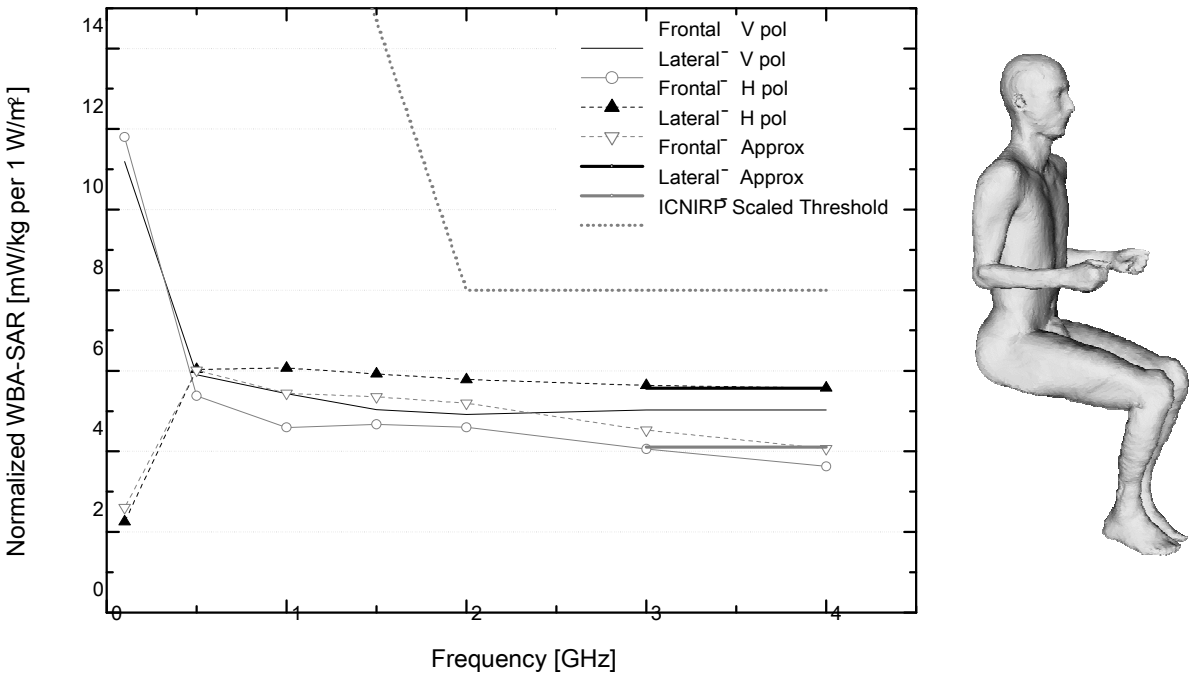

Figure 3: Whole body averaged SAR (Poynting flux of 1 W/m^2) for the sitting male phantom. In black and gray the frontal and lateral exposition, respectively. The polarization is vertical (solid lines) or horizontal (dashed lines). Approximated values are obtained by formula {1}. Dotted line is the scaled ICNIRP threshold which is applicable for both occupational and general public.

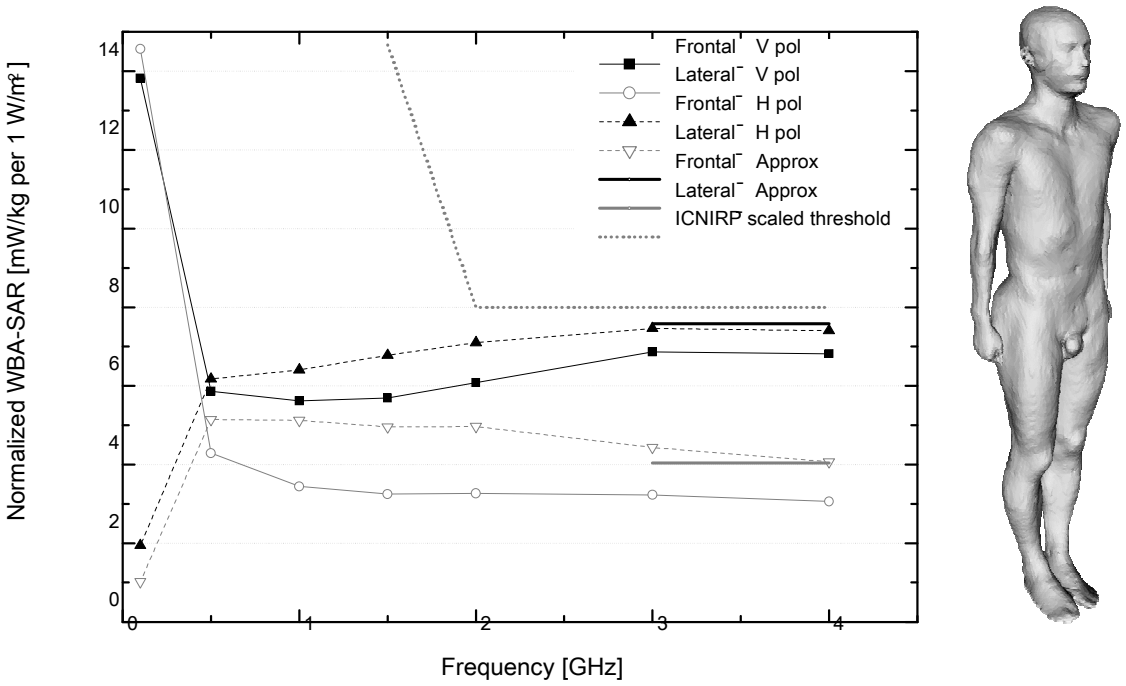

Figure 4: Whole body averaged SAR (Poynting flux of 1 W/m^2) for the standing male phantom. In black and gray the frontal and lateral exposition, respectively. The polarization is vertical (solid lines) or horizontal (dashed lines). Approximated values are obtained by formula {1}. Dotted line is the scaled ICNIRP threshold which is applicable for both occupational and general public.

References

[1] R. P. Findlay and P. J. Dimbylow, Effects of posture on FDTD calculations of specific absorption rate in a voxel model of the human body, *Physics in Medicine and Biology*, 50, 3825–3835, 2005

[2] R. P. Findlay and P. J. Dimbylow, FDTD calculations of specific energy absorption rate in a seated voxel model of the human body from 10 MHz to 3 GHz, *Physics in Medicine and Biology*, 51, 2339–2352, 2006

[3] L. Sandrini, A. Vaccari, C. Malacarne, L. Cristoforetti and R. Pontalti, RF dosimetry: a comparison between power absorption of female and male numerical models from 0.1 to 4 GHz, *Physics in Medicine and Biology*, 49, 2, 5185-5201, 2004

[4] M. Mazzurana, L. Sandrini, A. Vaccari, C. Malacarne, L. Cristoforetti and R. Pontalti, A semi-automatic method for developing an anthropomorphic numerical model of dielectric anatomy by MRI, *Physics in Medicine and Biology*, Vol. 48, No. 19, 3157-3170, 2003

[5] M. Mazzurana, L. Sandrini, A. Vaccari, C. Malacarne, L. Cristoforetti and R. Pontalti, Development of numerical phantoms by MRI for RF electromagnetic dosimetry: a female model, *Radiation Protection Dosimetry*, 111, 4, 445-451 2004

[6] R. Pontalti, L. Sandrini, A. Vaccari, C. Malacarne and L. Cristoforetti, Body-District Averaged-SAR in Female and Male Subjects Exposed to RF Plane Wave. *Proceedings of the 3rd International Workshop on Biological Effects of Electromagnetic Fields* - Volume I, Kos, Greece, 4-8 October 2004, P. Kostarakis Ed., pp. 447-456

[7] A. Vaccari, R. Pontalti, C. Malacarne, L. Cristoforetti, A Robust and Efficient Subgridding Algorithm for the Finite-Difference Time-Domain Simulation of Maxwell's Equations, *Journal of Computational Physics*, 194, 117-139, 2004

[8] J. W. Fernandez, P. Mithraratne, S. F. Thrupp, M. H. Tawhai, P. J. Hunter, "Anatomically based geometric modelling of the musculo-skeletal system and other organs",Biomechan Model Mechanobiol Vol. 2, pp 139–155, 2004

[9] J. Teran, E. Sifakis, S. S. Blemker, V. Ng-Thow-Hing, C. Lau, and R. Fedkiw, "Creating and Simulating Skeletal Muscle from the Visible Human Data Set", IEEE Transactions On Visualization And Computer Graphics, Vol. 11, No. 3, pp 317–328, May/June 2005

[10] F. Dong, G. J. Clapworthy, M. A. Krokos, and J. Yao, "An Anatomically-Based Approach to Human Muscle Modeling and Deformation", Ieee Transactions On Visualization And Computer Graphics, Vol. 8, No. 2, pp 154–170, April/June 2002

[11] K.S. Yee, Numerical solution of initial boundary value problems involving Maxwell's equations in isotropic media, *IEEE Trans. Antenna Propagat*. 14, 302–307, 1966

[12] S. D. Gedney, "An anisotropic perfectly matched layer-absorbing medium for the truncation of FDTD lattices," *IEEE Trans. Antennas Propagat.*, vol. 44, pp. 1630–1639, Dec. 1996

[13] P. Bernardi, M. Cavagnaro, S. Pisa, and E. Piuzzi, "Specific absorption rate and temperature elevation in a subject exposed in the far-field of radio-frequency sources operating in the 10-900-MHz range", *IEEE Trans. on Biomed. Eng.*, vol. 50, no. 3, pp. 295 -304, Mar 2003

[14] ICNIRP, "Guidelines for limiting exposure to time-varying electric, magnetic, and electromagnetic fields (up to 300 GHz)", *Health Physics*, vol. 74, pp. 494–522, 1998

INFLUENCE OF MICROWAVE RADIATION ON CELL MEMBRANE STIFFENING

GEORGE SAJIN[(*)], TUDOR SAVOPOL[(**)], MARIA SAJIN[(**)] EUGENIA KOVACS[(**)], IRINA MIRON[(**)]

[(*)]NATIONAL RESEARCH INSTITUTE FOR MICROTECHNOLOGIES, STR. EROU IANCU NICOLAE 32B, 077190, BUCHAREST, ROMANIA
[(**)]"CAROL DAVILA" MEDICAL UNIVERSITY, BIOPHYSICAL RESEARCH DEPARTMENT, STR. DIONISIE LUPU 37, BUCHAREST, ROMANIA

Abstract
The purpose of our experiments was to measure the effects of 1800 MHz microwave radiation on membrane anisotropy of a human blood monocitar and trombocitar cell population. Power level of the applied CW microwave radiation was low enough to consider it to be athermal. Experience demonstrates that the natural tendency to decrease of cell membrane anisotropy is favourised by microwave irradiation. This tendency maintains after the ceasing of microwave irradiation.

Introduction
Due to the extensive use of electromagnetic fields in everyday life, more information is required to detect the mechanisms of interaction and the possible side effects of microwave radiation on the structure and function of the organism. The target of these experiments was to find the effects of 1800 MHz microwave radiation on human cells. This frequency was chosen because it is used for the extension of mobile telephony systems. The biologic parameter followed in experiments was the membrane anisotropy of human blood monocytes and trombocytes.

Experimental method

Principle of the method
The membrane fluidity of irradiated and nonirradiated human blood cells was monitored by fluorescence anisotropy measurements of TMA – DPH labeled cells. Fluorescence anisotropy was measured before, during and after microwave irradiation of human blood monocytes and trombocytes.

The principle of the method consists in labeling the cellular membrane with a specific fluorescent dye. TMA – DPH with the formula shown in Fig.1 binds on the hydrophilic external surface of the cell membrane.

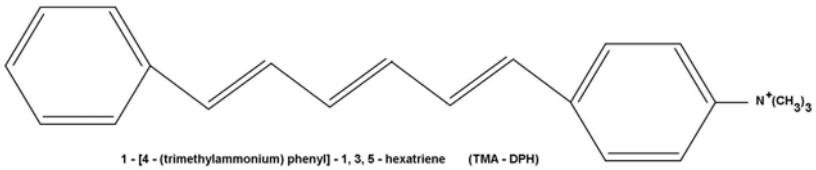

Fig.1. Formula of 1 – [4 – (trimethilammonium) phenyl] – 1, 3, 5 – hexatriene (TMA – DPH)

The biological sample is then illuminated with vertically polarized light.

Upon excitation of a molecule with vertically polarized light, the molecule will emit a fluorescent radiation more or less polarized, depending on the degrees of freedom of the molecule during the lifetime of the excited state. Depolarization degree of fluorescent light is a measure of the fluorophore freedom and therefore it is a measure of fluidity of the surrounding medium. Both the absorption and the emission of polarized light by a molecule are due to electronic transitions. A molecule can absorb a photon only if the molecular transition moment lies in the polarization plane of the exciting incident light. Reciprocal, when it comes back in the initial

status, the excited molecule emits light polarized in the plane of molecular transition moment. It follows that from a populations of molecules randomly oriented, illuminated with polarized light, only a sub-population will be excited (those with the molecular transition moment properly oriented).

An excited molecule will remain in this status only a small (some nanoseconds) time – naturally lifetime of excited status. After this time it will relax emitting polarized light in the manner described above. If during naturally lifetime of excited status the molecule changes its position (due to the thermal agitation) the emitted light will be in other direction that the absorbed exciting light. It follows that, naturally, the emitted light from this molecular population will have a polarizing index smaller than the incident light. The depolarizing degree is a measure of the freedom of movement of the molecules in the fluid, therefore a measure of the fluidity.

Usually, the incident light is vertically polarized and the measurement of the polarization of the emitted light are made in vertical (I_{VV}) and in the horizontal plane (I_{VH}) where the indexes v and h refers to the vertical, respectively horizontal polarizing plane.

The monitored parameter is the fluorescence anisotropy index **r** of the emitted light defined as:

$$r = \frac{I_{VV} - GI_{VH}}{I_{VV} + 2GI_{VH}} \quad (1)$$

where:

I_{VV} = recorded intensity of vertically polarized fluorescence light when excitation light is vertically polarized;

I_{VH} = recorded intensity of horizontally polarized fluorescence light when excitation light is vertically polarized;

G = correction factor depending on the fluorimeter used in measurements; it is due to the imperfection of the detection system and of monochromators.

$$G = \frac{I_{HV}}{I_{HH}} \cong 1 \quad (2)$$

where:

I_{HV} = recorded intensity of vertically polarized fluorescence light when excitation light is horizontally polarized;

I_{HH} = recorded intensity of horizontally polarized fluorescence light when excitation light is horizontally polarized;

The wavelength of excitation and emission light were $\lambda_{excitation}$ = 356 nm and $\lambda_{emission}$ = 429 nm, respectively.
By measuring the depolarizing of the light emitted by this fluorescent material it is possible to evaluate the membrane fluidity. A high value of anisotropy means the stiffening of the membrane and inverse, a low value corresponds to a more fluid membrane.

The purpose of our experiments was, using the above exposed method, to measure the membrane anisotropy of a monocitar human blood cell population irradiated with 1800 MHz microwave radiation and to compare it with the membrane anisotropy of non-irradiated cells.
Biological material (blood platelets) used in experiments was taken over from two healthy human donors and separated by centrifugation. Labeling of the blood cell (monocytes and trombocytes) membranes was done in 5 μl of TMA – DPH stock solution (0.5 mM TMA – DPH in dimetylformamide – DMF) and 1 ml of cell suspension were added to 1 ml Ringier solution in a fluorimeter cuvette with dimensions 1×1×5 cm^3.

Microwave experimental setup

The experimental arrangement allows simultaneous application of the polarized light and of the microwave radiation. The microwave experimental setup, it is presented in Fig.2. It consists in a microwave generator followed by a variable attenuator and an isolator with the role to prevent the reflected waves to reach the emitting device. The microwave chain contains two 20 dB directional couplers mounted as in Fig.2 in order to measure the direct and reflected power traveling in setup. Via two identical detectors, two voltages proportional

with the direct and reflected microwave powers are displayed on the voltmeters (1) and (2). Prior the beginning of the experiments a calibration step is performed.

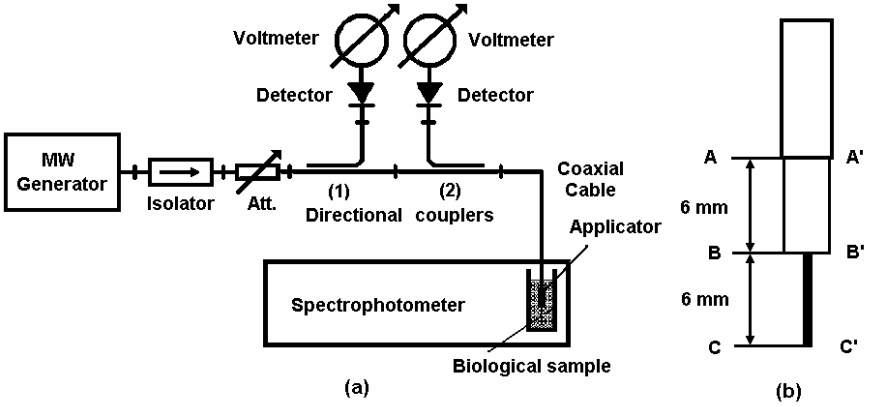

Fig.2. The microwave setup (a) and the applicator (b)

The radiating element is a λ/2 antenna (applicator) made using a semi-rigid cable. The external metallic shield of the cable was removed on a length of 12 mm (section AA') and the cable dielectric was removed on a length of 6 mm (section (BB') exposing 6 mm of central conductor. The antenna is introduced in the container in such a manner that the exposed dielectric and the central conductor are totally submersed in the biological fluid (up to the section AA').
The microwave power level effectively injected in the biological sample is the difference between direct power level and reflected power level and minus the losses in cables and transitions.

Experiments and results

Experiments on human monocytes membrane anisotropy
From the power balance previously presented results a microwave power of approx. 70 mW CW effectively injected in the biological sample. Because the content of the mini-container is approx. 4 g of biological sample it results a SAR = 18 mW/g.

Anisotropy of monocyte membrane was measured for 90 min at time intervals of 5 min. In the first 30 min the microwave radiation was not applied so that the anisotropy variation in this time interval vas considered as a measure for natural anisotropy decrease. In the next 30 min the biological samples were irradiated in the conditions presented above. Finally, for the last 30 min the microwave radiation was interrupted but the measurements continued at the same time interval of 5 min each in order to see the evolution of anisotropy following the irradiation.

The obtaining results are displayed in Tab.1 prior to, during and after the microwave irradiation. The normalization was made to the values of anisotropy at the beginning of the experiments. One can see that the natural tendency of anisotropy is to decrease (in the first 30 min) and this tendency is maintained during the irradiating session and also after the interruption of microwave application.

In order to have a better understanding of the microwave effects, a number of samples pairs were chosen following the criterion of closest values of the rate of the anisotropy decrease in the first 30 min (without microwave irradiation). One of the components of each pair was then irradiated with microwaves and the other was kept as reference. The rate of anisotropy decrease was measured during the microwave application and in the post-irradiation time.

The results for four pairs of biological probes are presented in Table 2. There is shown the difference between rates of the anisotropy decrease in the two biological samples in each pair. One may see an increasing rate of this parameter during the irradiation time, tendency maintained also in post-irradiation time.

TABLE 1
DECREASING OF THE ANISOTROPY (NORMALIZED VALUES)

Pre-irradiation		Irradiation		Post-irradiation	
Time (min)	Value	Time (min)	Value	Time (min)	Value
5	0,974	35	0,884	65	0,846
10	0,953	40	0,886	70	0,848
15	0,921	45	0,878	75	0,808
20	0,910	50	0,867	80	0,841
25	0,904	55	0,835	85	0,850
30	0,900	60	0,847	90	0,811

TABLE 2
DIFFERENCE BETWEEN ANISOTROPY DECREASE RATES OF THE MONOCYTIC CELLS IN EACH SAMPLE PAIR.

Time (min)	Differences in rates of anisotropy decrease (absolute values)			
	1st pair	2nd pair	3rd pair	4th pair
0	0.000	0.000	0.000	0.000
5	0.010	0.010	0.018	0.000
10	0.009	0.016	0.005	0.004
15	0.011	0.014	0.014	0.006
20	0.010	0.026	0.006	0.003
25	0.012	0.006	0.004	0.005
30	0.011	0.018	0.018	0.005
35	0.013	0.023	0.060	0.006
40	0.014	0.010	0.026	0.008
45	0.026	0.013	0.036	0.019
50	0.027	0.022	0.024	0.017
55	0.025	0.017	0.044	0.015
60	0.035	0.063	0.048	0.014
65	0.040	0.066	0.033	0.022
70	0.034	0.050	0.028	0.021
75	0.032	0.064	0.029	0.027
80	0.041	0.046	0.042	0.028
85	0.032	0.055	0.041	0.033
90	0.039	0.083	0.004	0.034

The results showing the anisotropy increasing rate were drawn for the first and the second biological sample pairs in Fig.3 … 6.

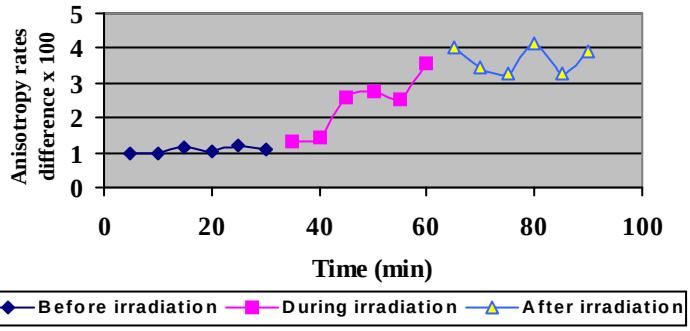

Fig.3. Anisotropy decreasing rate for the first biological monocytic sample pair (see Table II)

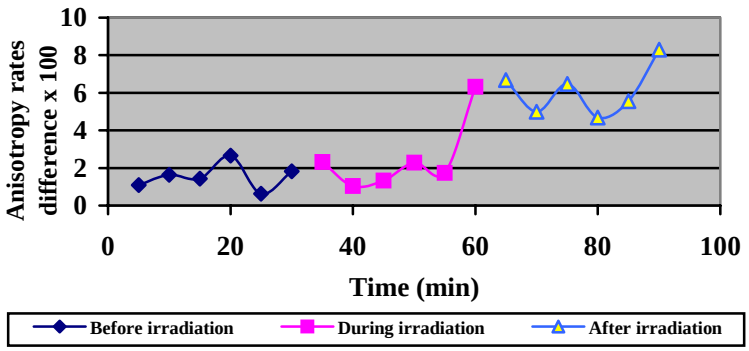

Fig.4. Anisotropy decreasing rate for the second biological monocytic sample pair (see Table II)

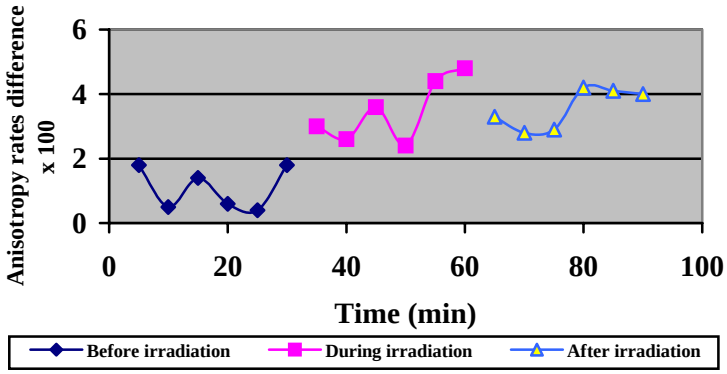

Fig.5. Anisotropy decreasing rate for the third biological monocytic sample pair (see Table II)

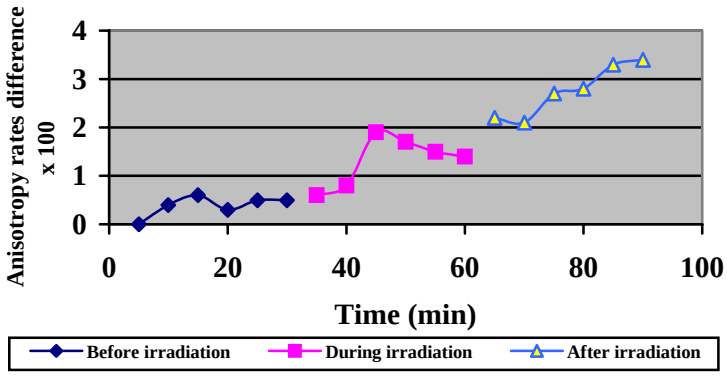

Fig.6. Anisotropy decreasing rate for the fourth biological monocytic sample pair (see Table II)

Experiments on human trombocytes membrane anisotropy

Experiments made using a trombocitar population obtained from human blood are similar with those concerning monocitar population. The same microwave irradiation setup was used. There are, nevertheless, some differences.

a) The experiments were made using two microwave power levels: 7 mW and 60 mW, meaning SAR values of 1.75 mW/g and respectively 15 mW/g.

b) The total experimental time was 3 h, each measurement being made at 5 min time interval. The microwave irradiation was applied in the second hour of the experiment (between minutes 60 and 120).

c) In each day was made an experiment using the same trombocitar concentrate. There were four experiments in four days but, for the sake of space saving, only the results of first two experiments are presented. The other results are very similar.

The power levels are done at the point (a).

The values of anisotropy obtained in these experiments are presented in Table 3 and the graphs representing these values are presented in Figs. 7 – 10.

TABLE 3

NORMALIZED VALUES OF TROMBICYTIC MEMBRANE ANISOTROPIES OBTAINED BY MICROWAVE IRRADIATION

Time (min)	First day experiments		Second day experiments	
	7 mW	60 mW	7 mW	60 mW
0	1.000	1.000	1.000	1.000
10	0.972	0.993	1.030	0.980
20	0.974	1.003	0,980	1.024
30	1.001	0.995	0.962	1.000
40	0.961	0.970	0.97	0.975
50	1.000	0.952	0.93	0.950
60	0.960	0.982	0.95	0.951
70	0.968	0.980	0.922	0.962
80	0.961	0.969	0.913	0.957
90	0.921	0.971	0.918	0.971
100	0.950	0.961	0.892	0.950
110	0.926	0.954	0.887	0.938
120	0.940	0.960	0.861	0.930
130	0.962	0.950	0.862	0.900
140	0.93	0.948	0.864	0.870
150	0.932	0.945	0.888	0.870
160	0.92	0.915	0.880	0.800
170	0.908	0.900	0.847	0.770
180	0.912	0.874	0.830	0.720

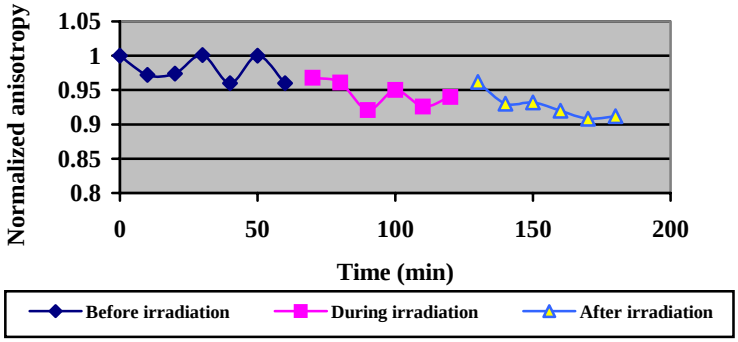

Fig.7. Evolution of the trombocytes membrane anisotropy in the first day of experiments. Applied microwave power: 7 mW

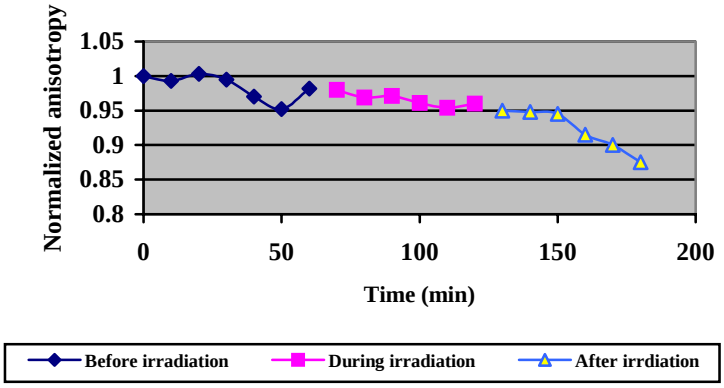

Fig.8. Evolution of the trombocytes membrane anisotropy in the first day of experiments. Applied microwave power: 60 mW

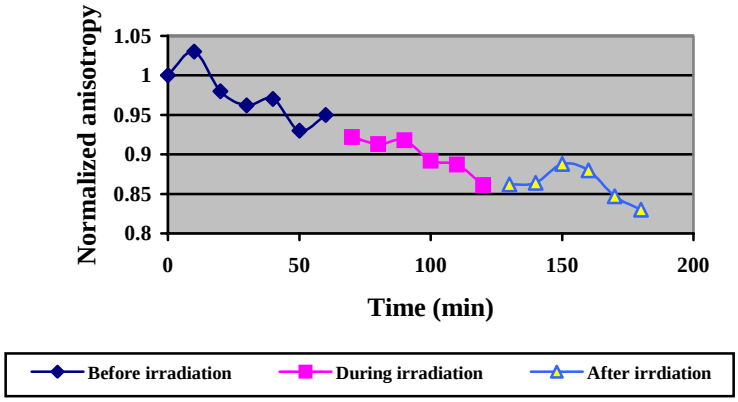

Fig.9. Evolution of the trombocytes membrane anisotropy in the second day of experiments. Applied microwave power: 7 mW

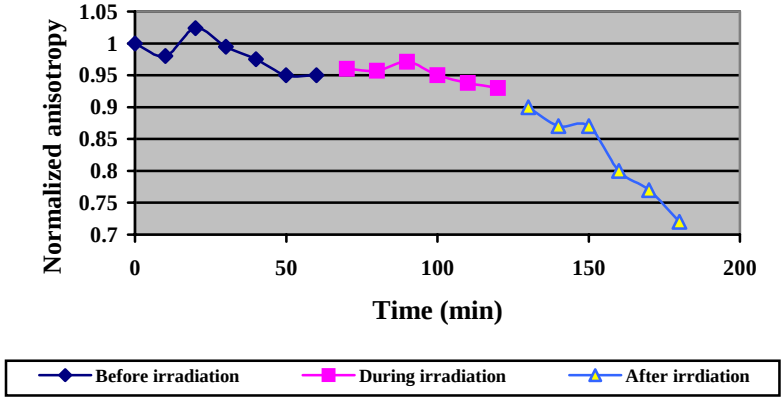

Fig.10. Evolution of the trombocytes membrane anisotropy in the second day of experiments. Applied microwave power: 60 mW

Conclusions

In the above presented experiments power level of the applied microwave radiation was low enough to consider it to be athermal. From the numerical data and the drawings presented in this paper one may conclude the following:

a) During the experience (with or without microwave irradiation) the tendency of anisotropy of human blood monocytes membrane anisotropy is to decrease;

b) This decrease is greater when 1800 MHz microwave radiation is applied. This tendency is maintained after the ceasing of microwave irradiation.

c) For a better emphasizing of this result, for monocytes cellular population, samples pairs of blood samples were chosen following the criterion of closest values of the speed of the anisotropy decrease in the first 30 min. The speed of the anisotropy decrease was evaluated in the time and after the microwave irradiation. The result is presented in Table 2 and in Figs 1 and 2, showing the same effect on the speed of anisotropy decrease.

d) For a population of trombocytic cells, the anisotropy of the cellular membrane, also, decrease both during and after ceasing of the microwave radiation..

e) The slope of the decreasing curve is greater after irradiation with 60 mW microwave radiation. It seems like RF radiation favours the decrease rate of membrane anisotropy.

Acknowledgements

This paper is the result of studies made in National Research Institute for Microtechnologies, Bucharest, Romania, on the basis of the Project 31CEEX 103/2005.

CARDIOVASCULAR RISK IN PHYSIOTHERAPISTS UNDER ELECTROMAGNETIC RADIATION

KATIA VANGELOVA, MICHEL ISRAEL, CHRISTO DEYANOV, MICHAELA IVANOVA

NATIONAL CENTER OF PUBLIC HEALTH PROTECTION,
15 ACAD. IVAN GESHOV BLVD, 1431 SOFIA, BULGARIA

Abstract

The aim of the study was to assess the long-term effects of electromagnetic radiation (EMR) on cardiovascular system of medical staff in physiotherapies. 52 exposed subjects (4 male and 48 female; aged 47.3 ± 8.7 yrs.) and a control group of 52 subjects, matched by sex and age, with similar job characteristics except for EMR were studied. The EMR exposure from appliances emitting at 50 Hz, 150 kHz, 27.12 MHz, 2.45 GHz was assessed. The workload and psychosocial factors were followed, too. The cardiovascular risk factors arterial pressure, lipid profile, body mass index, waist/hip ratio, smoking, alcohol consumption, nutrition, family history of cardiovascular disease were studied. The incidence of hypertension was moderate with the studied physiotherapists (26.9 % v.s. 23.8 % with the control group). The total cholesterol (TC) and low-density lipoprotein cholesterol (LDL-C) were significantly higher in the exposed group. The odds ratios indicate higher chance of becoming dyslipidemic with the exposed to EMR subjects [for TC OR (95 % CI) = 1.570 (1.048 – 2.351) and for LDL-C OR (95 % CI) = 1.840 (1.158 – 2.924)]. In conclusion, our data show that the EMR exposure of the medical staff in physiotherapies is associated with the adverse effects on cardiovascular system.

Key words: Arterial hypertension, dyslipidemia, EMR exposure, long-term effects, health risk

Introduction

Physiotherapetists are exposed to many risks in their work environment, some common for the health care workers, and some specific for the profession, such as the exposure to electromagnetic radiation (EMR), emitted from pulsed magnets, d'Arsonvale devices, equipment for microwave and high frequency diathermy, optical sources (UV, IR and visible), lasers. Some of the devices emit electromagnetic radiation above the exposure limits, rising health concerns.

The general health status of physiotherapiscs is largely unknown (Cromie et al. 2002), but some studies suggest possible adverse health effects of the EMR exposure, including increased risk of cardiovascular diseases. Hamburger et al. (1983) found positive relation between the EMR exposure and heart disease in physiotherapists, but in the study the exposure was categorized as either high or low on the base of mean number of employed years and mean number of treatments delivered by week. More attention has been paid to the health risks of radiofrequency EMR exposures in communications, but there still exist controversies concerning the effects of long-term exposures to low-level EMR (recent reviews Repacholi, 1998, Krewski et al. 2001, Vangelova and Deyanov 2003. Jauchem (1997) reviewed the epidemiological studies with a general conclusion that they had not yielded any obvious cardiovascular related hazards on long-term low-level exposures, in spite of the presence of various physiological effects. Our earlier data showed high rate of hypertension in broadcasting and TV station operators (Israel and Tomov, 2000). A second study was carried by our group in 49 broadcasting and 61 TV station operators (Vangelova et al. 2006) in order to confirm the previous findings, enlarged with serum lipids, and showed significantly higher chance of becoming hypertensive and dyslipidemic in broadcasting and TV station operators exposed to radiofrequency EMR. Slight, subclinical ECG abnormalities, accompanied by symptoms of sympathicotony in heart variability, shifts in the diurnal rhythms of blood pressure and heart rate in 77 AM broadcasting station operators (0.7-1.5MHz) were reported (Bortkiewicz, 1995; Szmigielski, 1998). Szmigielski (2000) confirmed the above data in a study on 38 workers in radio transmitting centers, exposed to 10-30 MHz EMF.

The aim of the study was to assess the long-term effects of EMR on the cardiovascular system of medical staff in physiotherapies.

Material and methods

The cardiovascular risk was assessed in 52 physiotherapists (4 males and 48 females) working with EMR emitting devices of age 47.3 ± 8.7 years and length of service 23.0 ± 9.5 years. A control group of 52 subjects from the same hospitals were examined, matched by sex, age and shift work schedules, with similar job characteristics except for the EMR. Their age was 47.8 ± 8.5 and length of service of 21.6 ± 4.6 years. The investigated subjects signed an informed consent.

EMR exposure assessment

There are a variety of sources of EMR in physiotherapies, emitting in the frequency range from constant fields (F = 0 Hz) to optic radiation. This puts substantial difficulties to the elaboration of a precise workplace exposure assessment, complicated by variety of situations in different cabinets, number of patients, etc. The scope of the devices in the studied units is the following:

- Devices for local thermotherapy ("Chinese vacuum cleaner" – Qi Gong);
- Equipment for galvanotherapy, ion - galvanotherapy and electrostimulation, "bipulsator" (for therapy with electric pulses), diadynamic;
- Devices for local franklinization – "ion shower";
- Equipment for low frequency diathermy, diathermal ion galvanization and diathermal electrostimulation;
- D'Arsonvale devices;
- Equipment for treatment with magnetic/electric field within the radiofrequency (RF) range (27.12 MHz), and with microwaves (2,45 GHz) for inductive-thermal therapy;
- Microwave electropyrexia;
- Devices for photo-therapy:
  - Solariums;
  - UV lamps for individual UV therapy;
  - UV sources application of the PUVA method of therapy;
  - Lamps of types "SOLUX" and "INFRAROUGE";
  - Laser diodes, gas lasers and other sources of coherent light.

We used the approach of individual assessment of EMR in physiotherapies, described earlier (Israel and Tschobanoff, 2006). In order to establish unified conditions for exposure assessment for different frequencies (over the overall frequency range) we applied a general unified indicator associated with the energetic irradiation dose, according to the ICNIRP Guidelines (1), ACGIH TLVs (2), and the Bulgarian National Standards (3, 4).

The energy load of the human organism is defined for three cases as a derived quantity of energy falling at external irradiation: $\boldsymbol{W_E}$, $\boldsymbol{W_H}$ and $\boldsymbol{W_S}$, based on dispersed energy per time unit on human body during the official working shift. Measurable quantities are used – intensities and power density according to the distance from the generator to the measuring device and the respective frequency range of the single photon.

SAR is the specific value of power absorbed by the recipient; ***SA*** is the specific value of the respective absorbed energy according to the calculated ***SAR***.

As ***SAR*** is introduced by the dimension of base metabolism of an adult man (175 cm/70 kg) the dimension of ***SA*** is the dimension of ***SAR*** by the time, that is

$$SA = SAR.t \quad [J/kg]$$

The two types of quantities - $\boldsymbol{W_E}$, $\boldsymbol{W_H}$ and $\boldsymbol{W_S}$ on the one side, and ***SAR, SA*** on the other do not differ substantially in conditions of air equivalent environment and a human body situated in it.

SAR is introduced through Human Equivalent Antenna. If the respective effective area is $\boldsymbol{A_e}$, then through relationships between the dimensions of the quantities ***W*** and ***SA*** following by the definition for power and from the way of determining human body exposure, the quantity ***W*** corresponds to whole body value of ***SA*** at constant body weight and unchanging mean conductivity of the tissue, standardized to the effective exposure area $\boldsymbol{A_e}$. The magnitude of the latter on its part depends on the mutual orientation of a standing person and the intensity of the falling electric field ***E***.

The measurable quantity in all cases is the same – ***E [V/m].*** Consequently $\boldsymbol{W_E}$ will incorporate the definition of ***SA*** and vice versa.

The exposure duration: real exposure time at work with a device $\boldsymbol{T_{app}}$ ***[h]***, followed by chronometer measurements, and a total duration of the working shift ***T [h***.were registered. The duration time is introduced by the number of devices and the number of patients serviced by the individual.

The method was unified for the equipment, the distances to the particular device and the mandatory restrictions to the behavior of the physicist/engineer, performing the measurement. The major characteristics of the method are the 6 mandatory distances to the different types of generators determined depending on the frequency range of the radiation. They conform to the requirements for measurement in the far and near field zones and the requirements for determination of ***SAR*** in different cases of electromagnetic energy falling on a standing human.

The dose as a function of the squared mean measured intensity was presented by the ***SAR*** quantity. Our calculation formulation were based on the vision of the averaged dose: the dose (calculated with the actual measured values of the field and exposure time) multiplied by the mean geometric value of the partial doses on the distance from the physician/nurse to the patient $\boldsymbol{r_1}$ and the dose of the same to another characteristic distance (one of the cited – $\boldsymbol{r_i}$, i ≠ 1). Thus a characterizing quantity was obtained which is a non-dimensional growing sum $\overline{D}$:

$$\overline{D} \approx \sum \frac{1}{q} \sqrt{D(r_1)} \sqrt{D(r_{i\neq 1})}$$

Here ***1/q*** was a non-dimensional quantity – ratio.

The squared field strength ($\boldsymbol{E^2}$) used for the dose assessment was equal to the product of the measured intensity of the field at distance $\boldsymbol{r_1}$ and the sum of weighed intensities of the other 5 distances. The method allows, at unified measurements, the elaboration of individual exposure assessment for each person in physiotherapy through calculations depending on the number of devices, number of patients and the actual configuration of the ward.

Physiotherapy devices and calculated values of the exposure for every device/for one person of the personnel were as follows:

1. Device “Megatherm”:
SAR ≤ 3.71 W/kg
f = 27.12 MHz; basic restrictions (br) for whole body SAR: SAR_{br} = 0.4 W/kg

2. UHF acoustic generator for ultrasound therapy: f ≤ 2.5 MHz:
(measurements in the frequency range f ≤ 2 kHz)

$$j \approx 3.8\ mA/m^2$$

f ≤ 2 kHz; basic restrictions for the induced current: $j_{br} \leq 2\ mA/m^2$

3. UHF 66 (Russia):
SAR ≤ 9.8 W/kg
f ≤ 2 kHz; basic restrictions for the induced current: $j_{br} \leq 2\ mA/m^2$

4. Magnet N 80 (Bulgaria):

$$j \approx 0.31\ A/m^2$$

5. Magnet NM (Bulgaria):

$$j \approx 0.28\ A/m^2$$

Light sources (polychromatic):
restrictions according to ACGIH (2004):
IR: $S \leq 1.8.t^{-3/4}\ W/cm^2$ (for cornea and lens)
IR: $S \leq 0.6/\alpha\ W/cm^2.sr$ (for retina protection)
IR (with blue light filter – B1): 1 $\mu W/cm^2$, and : $t_{max} \leq 10\ mJ/cm^2/S$
UV and visible light: $t_{max} \leq 0.003\ J/cm^2/S$

6. Quartz (UVB-1, UVB, UVA, Visible:

$$S \approx 17.6\ mW/cm^2$$

7. Solux Infrarouge, without filters:

$$S \approx 286.1\ mW/cm^2$$

8. Solux Infrarouge, with filter B1:

$$S \approx 4.9\ mW/cm^2$$

9. Interferenz - Endovak:

$$j \approx 0.69\ A/m^2$$

$f \leq 100$ kHz; basic restrictions for the induced current: $j_{br} \leq 1\ A/m^2$

10. Diadynamik (Bulgaria):

$$j \approx 0.15\ mA/m^2$$

11. Galvanostat (Bulgaria):

$$j \approx 0.15\ mA/m^2$$

$f = 150 \div 300$ kHz; basic restrictions (br) for whole body SAR: $SAR_{br} = 0.4$ W/kg

12. D'Arsonval:
SAR ≤ 0.4 W/kg
$f = 27.12$ MHz; basic restrictions (br) for whole body SAR: $SAR_{br} = 0.4$ W/kg

13. UHF 66 (Russia):
SAR ≤ 9.8 W/kg
$f = 2450$ MHz; basic restrictions (br) for whole body SAR: $SAR_{br} = 0.4$ W/kg;
for limbs $SAR_{loc} = 20$ W/kg
for head $SAR_{loc} = 10$ W/kg

14. Radarmed (2 devices):
with symmetric applicators
SAR ≤ 0.31 W/kg
with conical applicator
SAR ≤ 5.3 W/kg
Light sources (polychromatic):
restrictions according to ACGIH (2004):
IR: $S \leq 1.8.t^{-3/4}$ W/cm^2 (for cornea and lens)
IR: $S \leq 0.6/\alpha$ W/cm^2.sr (for retina protection)
IR (with blue light filter – B1): 1 μW/cm^2, and : $t_{max} \leq 10$ mJ/cm^2/S
UV and visible light: $t_{max} \leq 0.003$ J/cm^2/S

The relative values for the whole frequency range in each physiotherapy were calculated and the obtained quota was much larger than 1.

Confounding factors as noise, microclimate and psychosocial factors were followed and showed no differences between the groups.

The cardiovascular risk was assessed on the base of arterial pressure, lipid profile, body mass index (BMI), waist circumference, smoking habits, family history for cardiovascular disease, etc. The arterial pressure was measured with Hg sphygmomanometers two times in a period of three months. The hypertension was defined using the JNC VI (1997), as well as preliminary physicians diagnosis. Weight, height and circumferences at the narrowest part of the waist were recorded, and the BMI was calculated.

Blood for analysis was obtained after an overnight fast. The lipid profile included the following indices: total cholesterol (TC), high density lipoprotein cholesterol (HDL-C), low density lipoprotein cholesterol (LDL-C), triglycerides and TC/HDL-C ratio. The assessment of the lipid indices was performed with enzymatic tests. The HDL was separated by precipitation of LDL and VLDL and the cholesterol was assayed in the HDL fraction. The LDL-C was calculated using the formula of Friedewald for triglycerides < 4.3 mmol/l. The ratio TC/HDL-C was calculated, too.

The data were analyzed using SPSS software. Analysis of variance (one-way ANOVA), correlation analysis, $\chi 2$ and odds ratio were applied.

Results

The incidence of hypertension was moderate in the medical staff and did not differ significantly between the studied groups (26.9 % with the staff exposed to radiofrequency EMR v.s. 23.8 % with the control group). No significant differences both in systolic and diastolic blood pressure (SBP and DBP) were found between the exposed group in comparison to the control one (Table 1). The BMI did not significantly differ between the studied groups, but the waist was slightly higher with the exposed group. The TC, HDL-C and LDL-C were significantly higher in the radiofrequency EMR exposed group with comparison with the control group.

Table 1.
The blood pressure, anthropometric and metabolic variables of medical staff from physioterapies, exposed to EMR and control group

Indices/Groups	Medical staff from physioterapies	Control group
SBP (mmHg)	124.8 ± 19.7	122.4 ± 16.2
DBP (mmHg)	80.2 ± 12.6	78.2 ± 8.5
BMI (kg/m^2)	24.5 ± 3.8	23.3 ± 3.6
Waist (cm)	83 ± 11.9	81.5 ± 11.1
TC (mmol/l)	5.44 ±1.06**	4.97 ± 0.69
HDL-C (mmol/l)	1.53 ± 0.28*	1.39 ± 0.34
LDL-C (mmol/l)	3.42 ± 0.91**	3.07 ± 0.70
Triglycerides (mmol/l)	1.23 ± 0.71	1.19 ± 0.57
TC/HDL-C ratio	3.64 ± 1.02	3.57 ± 0.87

* $p < 0.05$; ** $p < 0.01$

The rate of distribution of some of the main cardiovascular risk factors is presented in Table 2. Significantly higher rate TC > 5.2 mmol/l and LDL-C > 3.4 mmol/l was found with the exposed to EMR medical staff, with higher significance for LDL-C. The odds ratios indicate higher chance of becoming dyslipidemic with the exposed to EMR subjects [for TC OR (95 % CI) = 1.570 (1.048 – 2.351) and for LDL-C OR (95 % CI) = 1.840 (1.158 – 2.924].

Table 2.
The frequency of distribution of the main cardiovascular risk factors in medical staff from physioterapies, exposed to EMR and a control group.

Indices	Medical staff from physioterapies	Control group	χ^2	Corrected χ^2	P
TC > 5.2 mmol/l	59.6 %	36.5 %	5.254	5.200	.018
HDL-C < 1 mmol/l	14.9 %	28.8 %	2.781	2.752	NS
LDL-C > 3.4 mmol/l	55.3 %	26.9 %	8.267	8.183	.004

The rate of smoking was high in both studied groups, slightly higher in the control one (44.2 % v.s. 40.4 % in the medical staff from physioterapies). There were no considerable differences in the self reported degree of smoking (33.3 % of the medical staff from physioterapies smoked 5-10 cigarettes/day, 57.1 % smoked 10-20 cigarettes/day and 9.5 % more than 20 cigarettes/day while in the control group 39.1 % smoked 5-10 cigarettes/day, 47.8 % smoked 10-20 cigarettes/day and 13 % more than 20 cigarettes/day). 47.6 % of the medical staff from physioterapies smoked for more than 20 years v.s. 43.5 % of the control group. There was no difference in the proportion of self reported drinkers between the investigated groups, nor in the number of beverages per week among the alcohol users. The self reported nutrition habits and physical activity during the free time did not differ between the groups, too.

Discussion

Our data show higher rate of dyslipidemia with the exposed to EMR physiotherapists, thus supporting the findings of Hamburger et al. (1983) for positive relation between the EMR exposure and heart disease in physiotherapists and confirming the data for higher rate of dyslipidemia under EMR exposure in other occupational groups as broadcasting and TV transmitting operators (Vangelova et al. 2006). The greater chance of becoming dyslipidemic of the physioterapetists exposed to EMR was confirmed by the calculated odds ratio. We suppose that the variations of TC and LDL-C were mediated to some extent by the stress system. Our data show significant EMR exposure-effect on the excretion rates of stress hormones in physiotherapists (Israel et al. 2006) and in other occupational groups (Vangelova et al., 2005). The elevation of stress hormones under

occupational stressors has been shown to interact with cardiovascular risk factors (Rosmond 1998, Fraser et al. 1999, Vrijkotte et al. 1999, Chrousos, 2000).

The higher rate of dyslipidemia in the medical staff from physioterapies can be associated mainly with the EMR exposure as the confounding factors as noise, microclimate, work organization, work control, work content, etc. were controlled (unpublished data), and the studied subjects had the same social class, found to be an important confounder (Boggild et al., 1999b). Although our study was controlled we do not exclude some synergistic effects of EMR with other occupational stressors, as emotional load of dealing with patients, work tasks requiring intense concentration, a feeling for risk of infections, strain, etc.

The rate of hypertension was similar in the exposed to EMR and control group medical staff for difference of earlier findings for higher rate of hypertension in broadcasting and TV transmitting operators working under radiofrequency EMR (Bortkiewicz 1997, Israel and Tomov, 2000, Vangelova et al. 2006). There are several differences between the cited previous studies and the present one. First, the EMR exposure was different. The physioterapetists were exposed for very short periods of time to high intensities, while the studied broadcasting and TV transmitting operators were exposed during all the working time, but with lower intensities. Second, the job task was quite different. The broadcasting and TV transmitting operators work was monotonous, while the job task of physiotherapetists was mobile, associated with emotional load of dealing with patients. Third at the last, but not at the least of importance, the broadcasting and TV transmitting operators groups consisted mainly of males, while the medical staff from physioterapies were mainly females. So the gender differences might contribute to inconsistency of the results concerning hypertention. There are data that the impact of stress is greater on arterial pressure in men and on indices associated with insulin resistance, as lipid profile indices, in females (Chrousos, 2000).

The body mass index did not differ between the groups, but the medical staff from physioterapies had more centrally disposed adipose tissue, well known risk factor for cardiovascular disease (CVD). The rate of smoking was high in the two studied groups, slightly higher in the control one. The differences in the self reported degree of smoking and the duration of smoking between the studied groups were negligible. No differences of self-reported alcohol consumption, nutrition habits, physical activity were found.

Summing up, our data suggest that the medical staff exposed to EMR was at greater risk of becoming dyslipidemic. Further studies are needed to investigate the effect of EMR on cardiovascular risk factors in the medical staff in physiotherapies, using an approach of studying the personal long-term EMR exposure in order to reach better understanding of the possible adverse effects of EMR on cardiovascular system.

References

1. Bulgarian National Standard 14425 –90. Labour protection. Electromagnetic fields – radiofrequency range. Admissible values and requirements for control (in Bulgarian).
2. Bulgarian National Standard 17137-90. Labour protection. Electromagnetic fields – microwave range. Admissible values and requirements for control (in Bulgarian).
3. Boggild, H., Suadicani, P., Hein, H.O., Gyntelberg F. Shiftwork, social class, and ischaemic heart disease in middle aged and elderly men; a 22 year follow up in the Copenhagen male study. Occup. Environ. Med. 1999 (b): 56(9): 640-645.
4. Bortkiewicz, A., Zmyslony, M., Gadzicka, E. Ambulatory ECG monitoring in workers exposed to electromagnetic fields. J. Med. Eng. Technol. 1997; 21(2): 41-46.
5. Chrousos, G.P. The role of stress and the hypothalamic-pituitary-adrenal axis in the pathogenesis of metabolic syndrome: neuroendocrine and target tissue-related causes. Intern. J. Obesity 2000; 24 (Suppl. 2): S50-5.
6. Cromie J.E., Robertson V.J., Best M.O. Occupational health in physiotherapy: General health and reproductive outcomes. Austr. J. Physiotherapy 2002; 48: 287-294.
7. Fraser, R., Ingram, M.C., Anderson, N., Morrison, C., Davies, E., Connell, J.M.C. Cortisol effects on body mass, blood pressure, and cholesterol in general population. Hypertension 1999; 3: 1374-8.
8. Hamburger S., Logue L.G., Silvermen P.M. Occupational exposure to non-ionizing radiation and an association with heart disease: An exploratory study. J.Chronic Diseases 1983; 36:791-802.
9. ICNIRP. Guidelines for limiting exposure to time-varying electric, magnetic and electromagnetic fields (up to 300 GHz). Health Physics 1998; 74(4): 494–522.
10. Israel, M., Tomov, P. Epidemiological study of the effect radiofrequency radiation on operators in radio, TV and relay stations. Proceedings of Eastern European Regional EMF Meeting and Workshop (M. Israel, M. Repacholi, eds.), 2000; VM-OFSET Sofia: pp. 145-154.
11. Israel, M., Tschobanoff, P. Exposure to non-ionizing radiation of personnel in physiotherapies. In: Bioelectromagnetics. S. N. Ayropetyan and M. S. Markov (eds.), Springer Press, 2006:
12. Israel, M., Vangelova K., Velkova D., Ivanova M. Stress hormone reactivity in medical staff exposed to electromagnetic radiation. Proceedings of the 4th International Workshop on Biological Effects of

Electromagnetics, 2006, Crete, Greece (in print).
13. Jauchem, J. Exposure to extremely–low–frequency and radiofrequency radiation: cardiovascular effect in humans. Int. Arch. Occup. Environ. Health 70, 9-21 (1997).
14. JNC VI. Classification of blood pressure of adults of age 18 years and older. Arch. Intern. Med. 1997; 157: 2413-2446.
15. Krewski, D., McBride, M., Salem, T. Potential health risks of radiofrequency fields from wireless telecommunication devices. J. Toxicol. Environm. Health 2001; 4 (B): 1-143.
16. Repacholi, M.H. Health effects of exposure to non-thermal levels of radiofrequency fields. Bioelectromagn. 1998; 19: 155-168.
17. Rosmond, R., Dallman, M.F., Bjorntorp, P. Stress related cortisol secretion in men: Relationships with abdominal obesity and endocrine, metabolic and hemodinamic abnormalities. J. Clin Endocrinol. Metab. 1998; 83: 1853-1859.
18. Szmigielski, S., Bortkiewicz, A., Gadzicka, E. Alterations of diurnal rhythms of blood pressure and heart rate of workers exposed to radiofrequency electromagnetic fields. Blood Press. Monit. 1998; 3(3): 323-330.
19. Szmigielski, S., Sobiczewska, A., Kubacki, R. Dysregulation of autonomic control of cardiac function and shift of diurnal rhythms of blood pressure in workers exposed to RF electromagnetic fields. In: Mobile Telephones and Health – and Update of the Latest Research (Bolton S. and Gemmel C., eds), 1999; Rad City and Financial Document Department Print Consultancy, Surrey, UK: pp. 117-136.
20. Threshold Limit Values for Chemical Substances and Physical Agents & Biol. Exp. Indices, ACGIH, Signature Publications, 2004.
21. Vangelova K., Israel M., Mihailov S. The effects of low level radiofrequency electomagnetic radiation on the excretion rates of stress hormones in operators during 24 hour shifts. Centr. Eur. J. Public Health 2002; 10, 23-27.
22. Vangelova K., Deyanov C. The effect of electromagnetic fields on the synthesis and secretion of melatonin, stress hormones and cardiovascular system. Review. Problems in Hygiene 2003; XIV (2): 41-47 (in Bulgarian).
23. Vangelova K., Israel M. Variations of melatonin and stress hormones under extended shifts and radiofrequency electromagnetic radiation. Rev. Environ. Health 2005, 20 (2): 151-161.
24. Vangelova K., Deyanov C., Israel M. Cardiovascular risk under radiofrequency electromagnetic radiation. Int. J. Hyg. Environ. Health 2006; 209: 133-138.
25. Vrijkotte, T.G.M, van Doornen, L.J.P, de Gues, E.J.C. Work stress and metabolic and hemostatic risk factors. Psychosom Med 1999; 61: 796-805.

RF-ABSORPTION AND TEMPERATURE ELEVATIONS IN THE INNER EAR AND THE EYE DUE TO EXPOSURE FROM HANDHELD DEVICES IN THE 400 MHZ TO 1850 MHZ RANGE

G. SCHMID[1], R. ÜBERBACHER[1], T. SAMARAS[2]

[1]ARC SEIBERSDORF RESEARCH GMBH, A-2444 SEIBERSDORF, AUSTRIA
[2]RADIOCOMMUNICATIONS LABORATORY, DEPARTMENT OF PHYSICS, ARISTOTLE UNIVERSITY OF THESSALONIKI; GR-54124 THESSALONIKI, GREECE

ABSTRACT

In order to allow detailed numerical RF dosimetry and computation of RF-induced temperature elevations in small anatomical structures, numerical models of the human eye and the inner ear organs (cochlea, labyrinth, auditory nerve, hearing bones) were developed based on frozen section techniques at a spatial resolution of 0.1 mm. After inserting these high resolution models into a commercially available head model, FDTD computations of SAR distribution and temperature elevations due to RF absorption were carried out using the SEMCAD X simulation platform. Generic models of handsets at 400 MHz, 900 MHz and 1850 MHz, operated in close proximity to the head, were considered as radiation sources.

Due to the heterogeneity in the area of the cochlea and the labyrinth (actually comprising highly conductive liquids surrounded by compact bone), the results showed a highly heterogeneous SAR distribution and SAR-peaks inside the cochlea and the labyrinth. However, temperature computations showed, that temperature elevations inside these organs are well below 0.1°C, when considering typical output power values of handheld devices (maximum for 400 MHz exposure).

In case of frontal exposure maximum temperature elevations in the eye of approximately 0.6°C were found for typical device output powers.

I. INTRODUCTION

The analysis of RF-power absorption and RF-induced temperature elevations in the human head, caused by handheld mobile communication devices, has been investigated in numerous scientific publications in recent years (e.g. [1]-[18]). In most cases computational techniques based on the Finite Difference Time Domain (FDTD) method were used for solving both the electromagnetic and the thermodynamic problem; the latter was mostly described by the Pennes' *Bioheat Transfer Equation* (BHTE) [19]. However, a detailed quantitative comparison of the results reported by these studies is difficult because of the variety of considered exposure situations and RF-source power levels, as well as the different head models used, which significantly affect the correlation between mass averaged Specific Absorption Rate (SAR) in the head and the temperature increase in specific tissues, as reported by [10]. When relating the temperature increase to the maximum10g averaged SAR in the head, the reported maximum temperature elevations in brain tissue are ranging between approximately 0.05°C/(W/kg) and 0.16°C/(W/kg). Concerning eye exposure, plane wave irradiation was considered in most cases in the past, mainly at frequencies beyond 1 GHz. Relating the maximum temperature increases in the eye found by these studies to the incident power density, the reported values are ranging between 0.003 °C/(W/m^2) and 0.006°C/(W/m^2).

The original spatial resolution of the numerical head models used in the above mentioned studies was usually not better than approximately 0.5 mm in horizontal direction and 1-2 mm in vertical direction (except [18], which were using 0.25 mm resolution for the eye). Due to this fact, anatomically small structures like the inner ear organs are, if at all, not accurately represented in these head models. Consequently, no detailed analysis of RF absorption in these organs and structures was possible so far.

In order to enable detailed RF dosimetry in the inner ear organs and in a detailed model of the eye, numerical models of the inner ear and the eye at a spatial resolution of 0.1mm x 0.1mm x 0.1mm were developed in this study and first results regarding RF-absorption and temperature elevations caused by generic phone models in the frequency range 400 MHz – 1850 MHz are presented.

II. MATERIAL AND METHODS

II.1. High resolution anatomical models of the inner ear and the eye

For developing the numerical model of the inner ear, vertical slices at a separation distance of 0.1 mm of a section of the left hemisphere of a real male human head (provided by the Center for Anatomy and Cell Biology, Medical University of Vienna) were obtained by frozen section technique (figure 1).
Each slice was scanned at a resolution of 1200 dpi using a commercially available document scanner (HP ScanJet 3970). Based on these digital images the segmentation (0.1 mm x 0.1 mm) of the *cochlea*, the *vestibulum*, the *canales semicirculares*, the *auditory ossicles* and the *tympanic membrane* as well as the conversion into a SAT-File format was carried out by IT'IS Foundation, Zurich, Switzerland. Exactly the same procedure was used for the development of the eye model, where *cornea*, *sclera*, *lens* and the optic nerve were distinguished during segmentation.

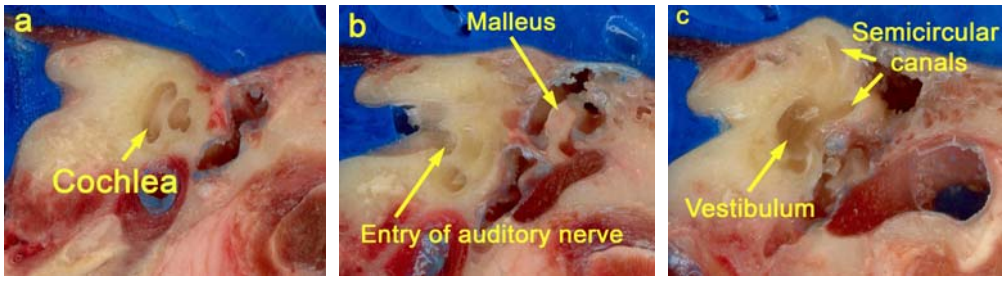

Figure 1: Examples of vertical cross sections through the human inner ear

Using the FDTD-based simulation platform SEMCAD X, the developed high resolution models of the inner ear organs and the eye were then inserted into a commercially available male head model based on the visual human data set (0.5 mm x 0.5 mm horizontal, 2 mm vertical resolution, 47 different tissue regions). In case of the inner ear model, the tympanic cavity, the external auditory canal as well as the auditory nerve were added by manual modeling and adjusted correspondingly in order to have an anatomically correct representation (figure 2). The yellow colored structure in the close-up view in figure 2 corresponds to the inner space of the labyrinth (cochlea, vestibulum, semicircular canals), which is filled with approximately 200 µl of perilymph- and endolymph-liquid. This structure is embedded in the highly compact petrous bone. In case of the eye model the lens' nucleus was added manually (figure 3).

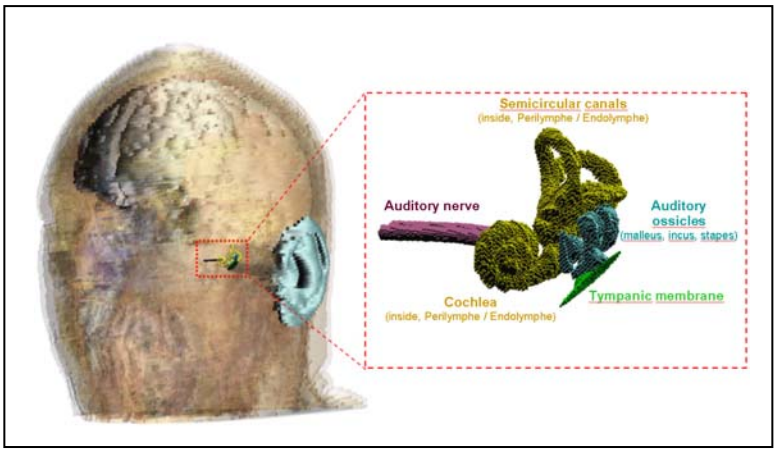

Figure 2: Anatomically correctly positioned high resolution inner ear organs inside a commercially available numerical head model

Figure 3: High resolution eye model in 3D view (top) and in a horizontal cross section (bottom)

II.2. Considered exposure conditions

Three different generic models of handsets, one per frequency, were considered as radiation sources. At 400 MHz a resonant helix antenna (axial length 61 mm, helix diameter 8.6 mm, wire diameter 1 mm, 14 turns) on top of metallic box (130 mm x 50 mm x 30 mm) was considered as a representative model for a hand held radio set such as used for example in a TETRA system. For 900 MHz and 1850 MHz quarter wave

monopoles (diameter 2 mm) on top of a metallic box (100 mm x 40 mm x 20 mm) were chosen as representatives for mobile phones of the GSM900 and the DCS1800 and UMTS systems, respectively. For each radiation source lateral exposure in "Tilt" position as well as frontal exposure with a distance between the antenna's feedpoint and the left eye of approximately 2.5 cm were considered. Figure 4 shows the 6 different exposure conditions.

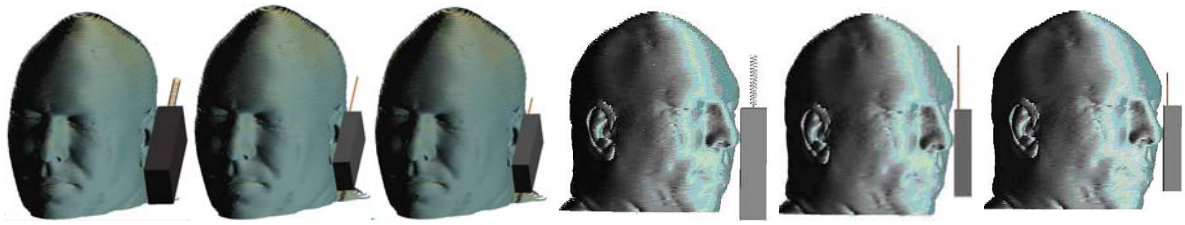

Figure 4: Considered exposure conditions. left: lateral exposure in "tilt" position at 400 MHz, 900 MHz and 1850 MHz, right: frontal exposure at 400 MHz, 900 MHz and 1850 MHz

II.3. Computational techniques used

The FDTD based SEMCAD X simulation platform was used for both the electromagnetic as well as the thermodynamic computations. The used thermodynamic solver was based on Pennes' BHTE and both the electromagnetic as well as the thermodynamic computations were carried out on the same FDTD grid, using a graded mesh with mesh size between 0.25 and 5 mm. However, in the irradiated hemisphere the maximum grid step was kept below 1.5 mm and constant at 0.25 mm in the region of the high resolution models of the inner ear region and the eye. This resulted in a total of approximately 20-25 million FDTD cells, depending on the considered source model.

II.4. Tissue parameters and boundary conditions

For the dielectric properties of the tissues values according to [20] were taken. With respect to the thermal properties 19 different materials were allocated to the more than 50 different tissue regions in the head model (including the high resolution inner ear and eye). Table 1 lists the used thermal properties, which were derived from several sources in the literature (e.g. [1],[13],[21]).

Table 1: Thermal tissue properties used

material	density [kg/m³]	specific heat [J/kg.K]	thermal conductivity [W/m.K]	perfusion [ml/min.kg]	metabolic heat [W/kg]
blood	1060	3780	0.51	10000	0
bone	1850	1300	0.39	11.5	0.15
brain average	1040	3650	0.55	608.5	9.70
cartilage	1100	3521	0.46	50	0.18
cerebellum	1040	3670	0.55	510	9.70
cerebrospin. fluid	1005	4116	0.59	0	0
cornea	1076	3793	0.52	38	0.32
fat (not infiltrated)	920	2493	0.24	25.3	0.15
gland tissue	1040	3600	0.53	3059	9.79
grey matter	1040	3684	0.57	608.5	9.70
lens	1080	3133	0.43	0	0
marrow	1020	3120	0.32	219	5.50
muscle	1045	3580	0.5	26.6	0.67
nerve tissue	1040	3582	0.46	37.7	9.61
skin dry	1140	3600	0.37	86.6	0.18
skin wet	1140	3600	0.37	86.6	0.18
tongue	1045	3580	0.5	26.6	0.67
vitreous humor	1003	3997	0.59	0	0.34
white matter	1040	3611	0.5	262.5	9.70

At the thermal boundary between the head model and the ambient a heat transfer of 8 W/(m^{2}K) at a nominal ambient temperature of 25°C was assumed. Thermal boundaries between air filled cavities inside the head model and their bounding tissues were assumed to be 4 W/(m^{2}K) at 37°C, except for the nasal cavity and the ear channel, where 30 W/(m^{2}K) at 35°C and 6.3 W/(m^{2}K) at 35°C were chosen, respectively.

III. RESULTS

Lateral exposure

Figure 5 depicts the distribution of SAR (not averaged, normalized to 1W radiated power) in a cross section of the head through the cochlea for all three frequencies considered. With respect to the inner ear, relatively high local SAR values appear inside the peri-/endolymph-filled labyrinth compared to the surrounding bone, especially at 400 MHz. This is due to the relatively high conductivity of peri-/endolymph, which is very similar to cerebrospinal fluid. In the last row of figure 5 the SAR distribution on the surface of middle- and inner ear organs (labyrinth, auditory nerve, tympanic membrane, auditory ossicles, compare figure 2) is shown.

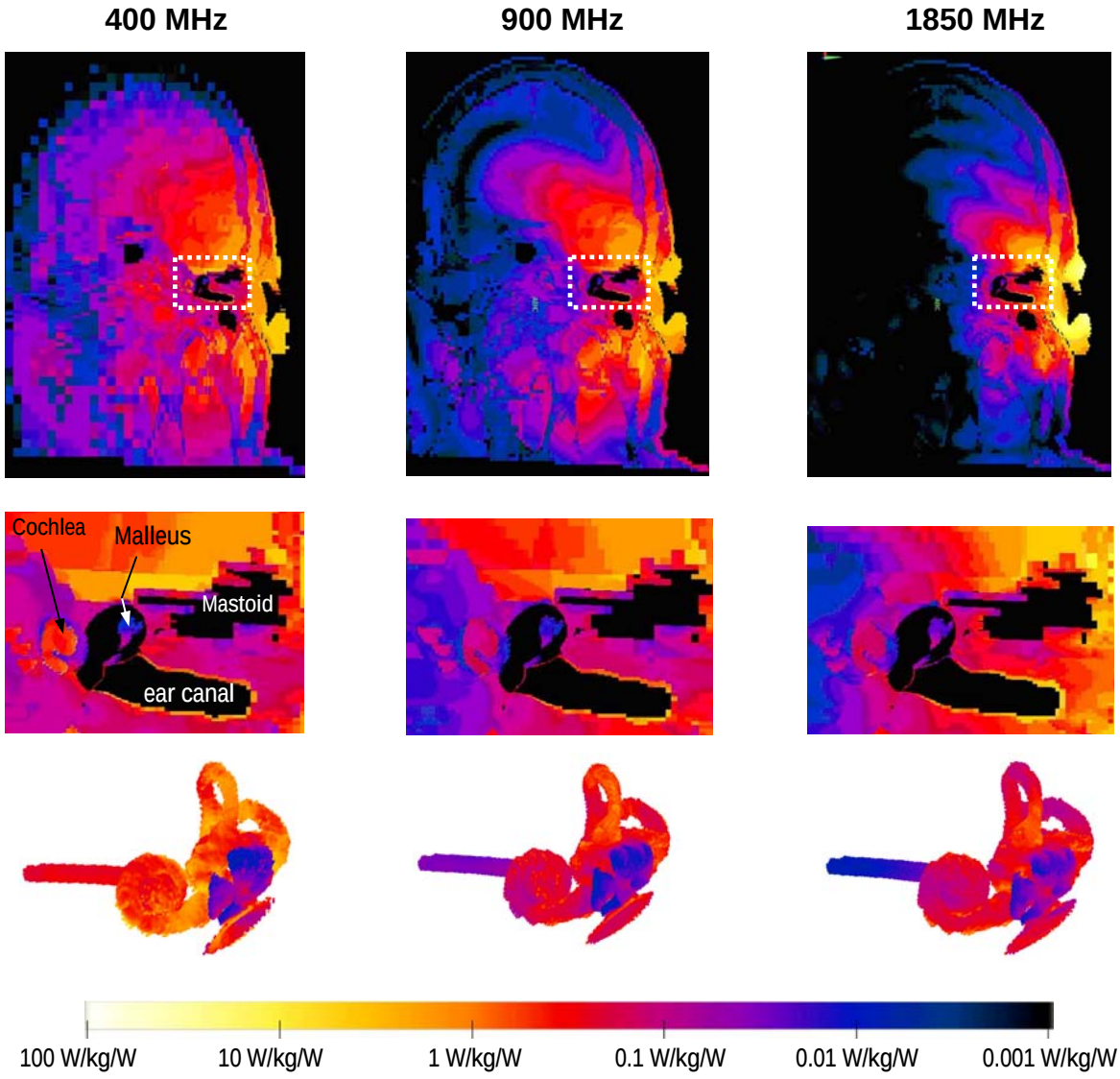

Figure 5: SAR distributions (not averaged, normalized to 1W source power) in a cross section of the head through the cochlea for 400 MHz (left column), 900 MHz (center column) and 1850 MHz (right column). At the bottom the SAR distribution on the surface of the middle- and inner ear organs is shown.

Despite of the inhomogeneous distribution of SAR inside the head, the thermodynamic computations show only very low temperature increases in it. Figure 6 illustrates the maximum temperature elevation in specific tissues, within the time period from switching on the radiation until thermal equilibrium is reached (after approx. 20 minutes). Note that the values in figure 6 are normalized to the case of a 10g averaged SAR of 2 W/kg in the head, i.e., the limit for localized exposure according to [22] and [23].

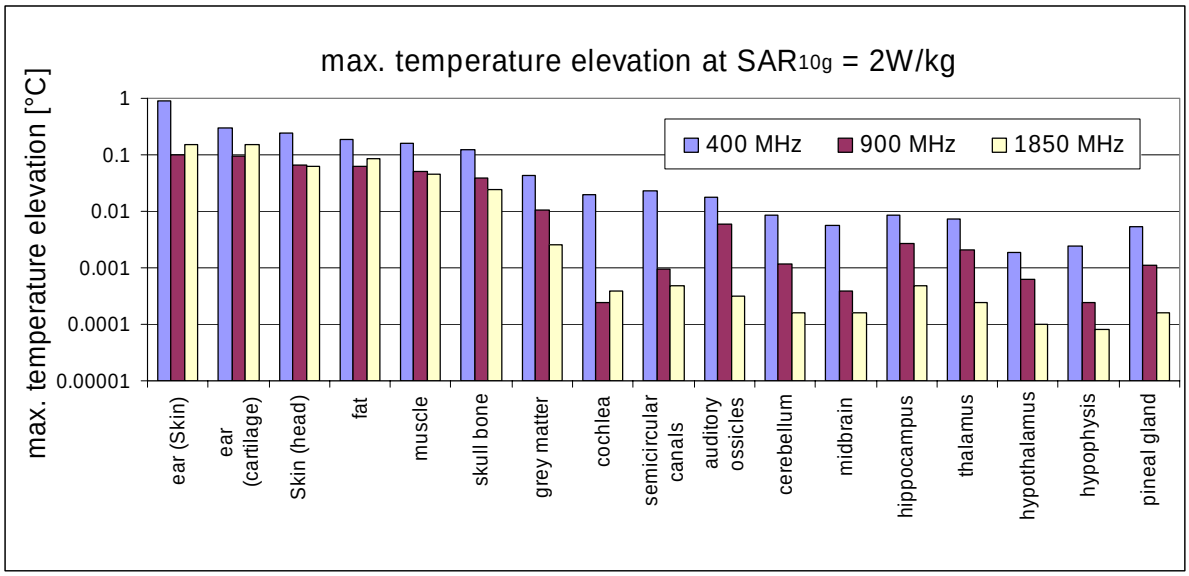

Figure 6: Maximum temperature elevation in specific tissues and organs due to a lateral exposure according to the current limit for localized exposure according to [22] and [23].

As it can be seen from the figure maximum temperature elevations are highest for 400 MHz due to the high penetration depth and the more homogeneous heating of the head, which causes lower temperature gradients and therefore less effective heat conduction inside the head. However, the absolute values of the obtained temperature elevations are rather small. They are below 0.05°C for grey matter, below 0.025°C in the inner ear organs and below 0.01°C in deep brain tissues. More superficial tissues as bone, muscles, fat and the skin on the head showed an increase in temperature between 0.1°C and 0.25°C. The absolute maximum temperature increase was obtained in the skin of the pinna and was approximately 0.9°C.

Front exposure

The distribution of SAR in case of having the radiation source in front of the left eye is shown in figure 7. Non averaged SAR values, normalized to 1 W radiated power are shown in a horizontal cross section of the head through the eye.

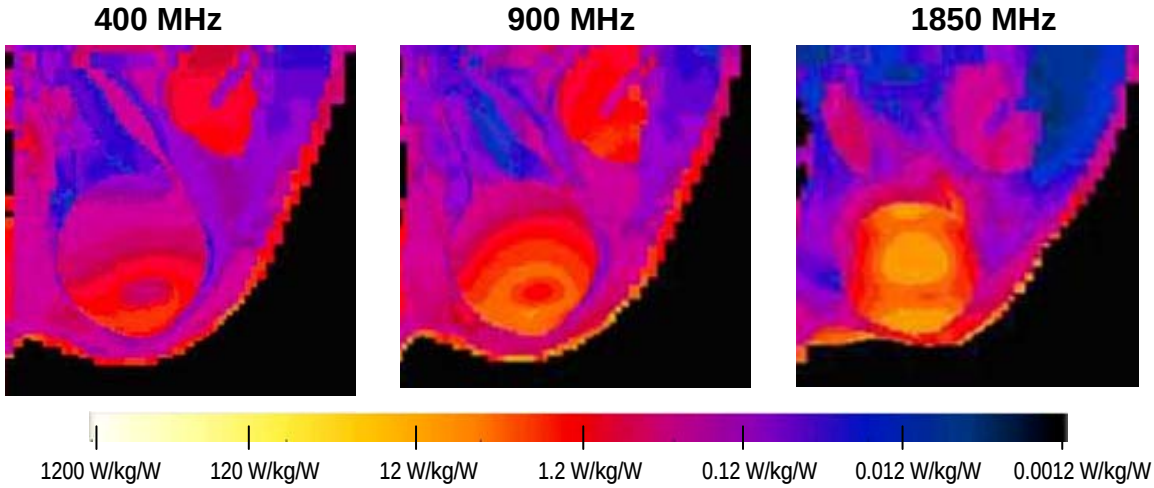

Figure 7: SAR distributions (not averaged, normalized to 1W source power) in a cross section of the head through the eye for 400 MHz (left column), 900 MHz (center column) and 1850 MHz (right column).

RF absorption in the eye increases with frequency and at 1850 MHz a “standing wave pattern” with a SAR maximum approximately in the center of the eye can be observed. This is due to the fact that at 1850 MHz the eye diameter is approximately one wavelength (in tissue) of the radiation frequency.
The maximum temperature elevations in specific tissues, within the time period from switching on the radiation until thermal equilibrium is reached (after approx. 20 minutes) are depicted in figure 8. Again the given values are normalized to the case of a 10g averaged SAR of 2 W/kg in the head.

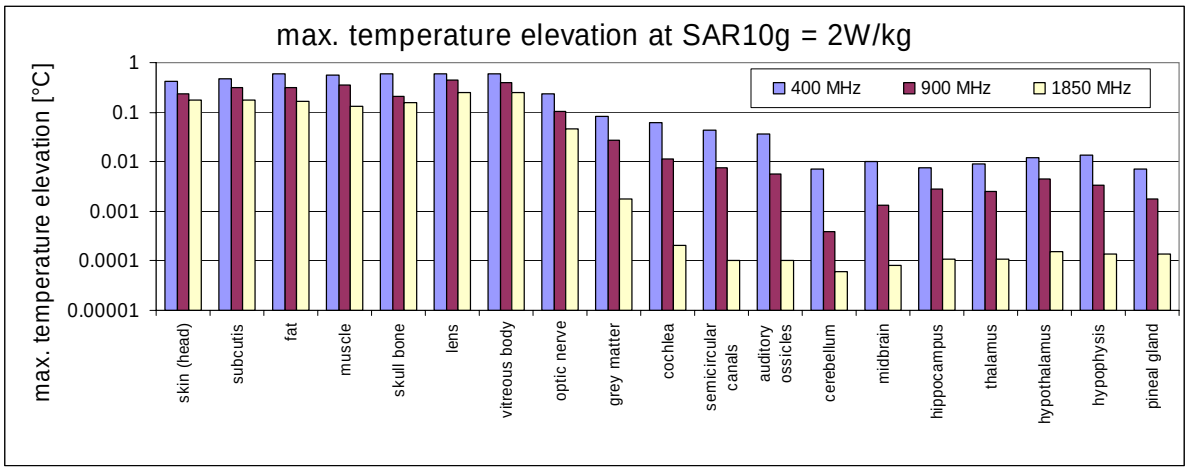

Figure 8: Maximum temperature elevation in specific tissues and organs due to a frontal exposure according to the current limit for localized exposure according to [22] and [23].

Although the highest peak SAR values in the eye were obtained for the high (1850 MHz) frequency, the maximum temperature elevations appear again for a 400 MHz irradiation. The absolute maximum temperature elevation was observed in the lens and was approximately 0.6°C. Maximum temperature elevations in other (superficial) tissues are approximately in the same order of magnitude, ranging from 0.2°C to 0.6°C. In the optic nerve and in grey matter tissue temperature elevations up to approximately 0.25°C and 0.09°C were found, respectively. Interestingly, the temperature elevations in the middle and inner ear regions appear somewhat higher during frontal exposure compared to the case of lateral exposure. This effect, however needs to be investigated further, because it might be affected by the different spatial discretizations of the computation domain used for frontal and lateral exposure.

Influence of perfusion and ambient temperature

In order to estimate the impact of variations in the ambient temperature and in blood perfusion, computations (at 400 MHz) were carried out with tissue perfusion (all tissues) reduced to 50% of the nominal values listed in table 1, and an ambient temperature of 35°C (instead of a nominal value of 25°C). All other parameters remained unchanged. The results clearly show that for tissue regions deep inside the head a change in ambient temperature does not play an important role, whereas a reduction of perfusion by 50% increases the observed maximum temperature elevations by up to a factor of 2.5 in these tissues. For more superficially located tissues (skin, cartilage, fat, subcutis, bone) both perfusion as well as ambient temperature play a role with respect to the maximum temperature elevation.

Pulsed radiation

Current safety standards, e.g. [22], define the basic restriction for localized exposure in terms of a 6 minute average SAR. This means that for shorter times higher temporal peak SAR values are allowed. Therefore we investigated (at 400 MHz) the effect of pulsed radiation by applying short exposure peaks (in terms of 10g averaged SAR) of 4 W/kg, 12 W/kg and 72 W/kg for 180 s, 60 s and 10 s within a continuously repeated 6 minute interval, respectively. All of these cases lead to a 6 minute average SAR of 2 W/kg. The comparison of the pulsed exposure with a continuous wave exposure at 2 W/kg showed increased maximum temperature elevations for the mentioned kind of pulsed exposure. Tissues deep inside the head were significantly more affected by this effect than superficial tissues. The worst of the considered cases was the repeated 10 s / 72 W/kg lateral exposure, which, for example, leads to a relative increase of the maximum temperature elevation in the skin by a factor of 2 compared to a factor of 11 in the hypothalamus.

IV. CONCLUSION

In general, the obtained results showed that for exposure situations typical for usage of modern digital mobile phones the RF-induced temperature elevations inside the head are rather small. Although a very heterogeneous pattern of RF power dissipation could be observed due to the significantly different dielectric properties of the different tissues, no temperature "hot spots" are to be expected due the efficient heat transfer mechanisms taking place in the tissues (heat conduction and heat transfer by perfusion). As far as comparable, when relating the maximum temperature elevations to the 10g averaged SAR in the head, our results are in line with results reported by other authors ([1]-[18]), even though our results appear to be at the lower end of the range of RF-induced temperature elevation stated in [1]-[18]. This might be caused by the specific properties of the used head model (based on the visual human data set) with respect to its tissue composition [10].
The observation that, with respect to the maximum RF-induced temperature elevations, inner tissues are significantly more affected by pulsed radiation at constant 6 minute averaged SAR than superficial tissues might be of biological interest, because heat perception mainly takes place inside the superficially located skin. However, it has to be noted that the time course of the exposure and the required peak RF power leading to such effects (a single high peak in repeated 6 minute intervals) are not typical for mobile communication devices.

ACKNOWLEDGEMENTS

This work was sponsored by the Federal Office for Radiation Protection, Germany, in the frame of the German Mobile Telecommunication Research Program. Furthermore the authors gratefully acknowledge the support by Prof. Manfred Tschabitscher, Center for Anatomy and Cell Biology, Medical University of Vienna, and Anja Klingenböck, IT'IS, Zurich, Switzerland.

REFERENCES

[1] G. M. J. van Leeuwen, J. J. W. Lagendijk, B. J. A. M. van Leersum, A. P. M. Zwamborn, S. N. Hornsleth and A. N. T. J. Kotte, "Calculation of change in brain temperatures due to exposure to a mobile phone", Phys Med Biol, vol. 44, pp. 2367-2379, 1999.

[2] O. P. Gandhi, Q.-X. Li and G. Kang, "Temperature rise for the human head for cellular telephones and for peak SARs prescribed in safety guidelines", IEEE Trans Microwave Theory Techn, vol. 49, pp. 1607-1613, 2001.

[3] J. Wang and O. Fujiwara, "FDTD computation of temperature rise in the human head for portable telephones", *IEEE Trans Microwave Theory Techn*, vol. 47, pp. 1528-1534, 1999.

[4] International Commission on Non-Ionizing Radiation Protection, "Guidelines for limiting exposure to time-varying electric, magnetic, and electromagnetic fields (up to 300 GHz)", *Health Physics*, vol. 74, pp. 494-522, 1998.

[5] P. Bernardi, M. Cavagnaro, S. Pisa and E. Piuzzi, "Specific absorption rate and temperature increases in the head of a cellular-phone user", *IEEE Trans Microwave Theory Techn*, vol. 48, pp. 1118-1126, 2000.

[6] P. Bernardi, M. Cavagnaro, S. Pisa and E. Piuzzi, "Power absorption and temperature elevations induced in the human head by a dual-band monopole-helix antenna phone", *IEEE Trans Microwave Theory Techn*, vol. 49, pp. 1118-1126, 2001.

[7] P. Wainwright, "Thermal effects of radiation from cellular telephones", *Phys Med Biol*, vol. 45, pp. 2363-2372, 2000.

[8] T. V. Yioultsis, T. I. Kosmanis, E. P. Kosmidou, T. T. Zygiridis, N. V. Kantartzis, T. D. Xenos and T. D. Tsiboukis, "A comparative study of the biological effects of various mobile phone and wireless LAN antennas", *IEEE Trans Magn*, vol. 38, pp. 777-780, 2002.

[9] A. Hirata, M. Morita and T. Shiozawa, "Temperature increase in the human head due to a dipole antenna at microwave frequencies", *IEEE Trans Electromagn Compat*, vol. 45, pp. 109-116, 2003.

[10] A. Hirata and T. Shiozawa, "Correlation of maximum temperature increase and peak SAR in the human head due to handset antennas", *IEEE Trans Microwave Theory Techn*, vol. 51, pp. 1834-1841, 2003.

[11] J. A. Scott, "A finite element model of heat transport in the human eye", *Phys Med Biol*, vol. 33, pp. 227-242, 1988.

[12] A. Taflove and M. E. Brodwin, "Computation of the electromagnetic fields and induced temperatures within a model of the microwave-irradiated human eye", *IEEE Trans Microwave Theory Techn*, vol. 23, pp. 888-896, 1975.

[13] P. Bernardi, M. Cavagnaro, S. Pisa and E. Piuzzi, “SAR distribution and temperature increase in an anatomical model of the human eye exposed to the field radiated by a user antenna in a wireless LAN”, *IEEE Trans Microwave Theory Techn*, vol. 46, pp. 2074-2082, 1998.
[14] A. Hirata, G. Ushio and T. Shiozawa, “Calculation of temperature rises in the human eye exposed to EM waves in the ISM frequency bands”, *IEICE Trans Comm*, vol. E83-B, pp. 541-548, 2000.
[15] A. Hirata, S. Matsuyama and T. Shiozawa, “Temperature rises in the human eye exposed to EM waves in the frequency range 0.6-6GHz”, *IEEE Trans Electromagn Compat*, vol. 42, pp. 386-393, 2000.
[16] A. Hirata, H. Watanabe and T. Shiozawa, “SAR and temperature increase in the human eye induced by obliquely incident plane waves”, *IEEE Trans Electromagn Compat*, vol. 44, pp. 592-594, 2000.
[17] A. Hirata, “Temperature increase in human eyes due to near field and far field exposures at 900 MHz, 1.5 GHz and 1.9 GHz”, IEEE Trans Electromagn Compat, vol. 47, (1), pp.68-76, 2005
[18] V.V.M. Flyckt, B.W. Raaymakers, H.Kroeze, J.J.W. Lagendijk,"Temperature rise in the human eye and orbit due to RF exposure calculated with a realistic vascularized model: temperature distributions and the enormous impact of cooling by perfusion", 17th International Zurich Symposium on Electromagnetic Compatibility, Singapore, 2006
[19] H. H. Pennes, “Analysis of tissue and arterial blood temperatures in the resting human forearm”, J Appl Physiol, vol. 1, pp. 93-122, 1948.
[20] Gabriel S, Lau RW, Gabriel C (1996c). ”The dielectric properties of biological tissues: III. Parametric models for the dielectric spectrum of tissues”, Phys. Med. Biol. 41:2271-2293.
[21] F.A. Duck, ”Physical Properties of Tissue, A comprehensive reference book”, Academic Press Ltd., London, 1990, ISBN 0-12-222800-6
[22] ICNIRP International Commission on Non-Ionizing Radiation Protection, “Guidelines for limiting exposure in time-varying electric, magnetic and electromagnetic fields (up to 300 GHz)”, Health Physics 74, 494-522, 1998.
[23] IEEE Std C95.1-2005, “Standard for Safety Levels with Respect to Human Exposure to Radio Frequency Electromagnetic Fields, 3 kHz to 300 GHz”, IEEE, New York, USA, 19.04.2006

MODEL FOR NECK WHEN ESTIMATING EXPOSURE TO ELECTRIC FIELDS AT 400 KV SUBSTATIONS

TONI LÅNGSJÖ[1], JARI LATVA-TEIKARI[1], JARMO ELOVAARA[2], LEENA KORPINEN[1,3]

[1] LAB.OF ELECTRICAL ENGINEERING AND HEALTH, TAMPERE UNIV, OF TECH., P.O. BOX 692, 33101 TAMPERE, FINLAND
[2] FINGRID OYJ, P.O. BOX 530, 00101 HELSINKI, FINLAND
[3] FACULTY OF TECH., THE DEPARTMENT OF ELECTRICAL ENGINEERING AND AUTOMATION, UNIV. OF VAASA, P.O. BOX 700, 65101 VAASA, FINLAND

Abstract

Directive 2004/40/EC sets action and exposure limit values for people working in electric and magnetic fields. Electric field action values for 50 Hz frequency might be exceeded in existing 400 kV air-insulated substations. Therefore measurements in Finnish 400 kV substations were conducted to find out whether the limit value of induced current density (10 mA/m^2) is exceeded in the human central nervous system. One of the most critical areas is the neck. Measurements were made with a specific system connected to the test person, who simulated practical work in actual and practical working conditions. The developed system measures the current induced in the head as well as the total current induced in the body of the test person.

The maximum average current density in the cross-sectional area of 40 cm collar-size neck was 6.81 mA/m^2, even if the action value for the electric field strength was clearly exceeded. The margin to the limit value 10 mA/m^2 is obvious, but further analysis was necessary due to individual variations etc. Consequently, a model for analyzing current densities in the cross-sectional area of the neck, especially in central nervous system, was developed.

The model described 9 different tissues in the neck area. Currents and current densities in the tissues were calculated when the average current density had a given value. The result was that only 0.13 % of the total current in the neck area flows through the spinal cord causing in it a current density 0.72 mA/m^2 when the average current density in the neck area is 6.81 mA/m^2 (collar size 40 cm assumed). Thus, it seems that the substation workers are not exposed to current densities in practical work situations within the body, which would exceed the directive's limit value.

Keywords: *occupational exposure, induced current density, central nervous system*

1. Introduction

Power frequency electric and magnetic fields occur in electricity generation, transmission, distribution and consumption. Occupational exposure to electric fields is common especially in electricity transmission and distribution. Accordingly, exposure in certain places is larger than in other places. In 400 kV air-insulated outdoor substations the exposure of the workers to the electric fields is one of the largest areas. We will concentrate on electric fields instead of magnetic fields, because in 400 kV outdoor substations electric fields in practice cause more remarkable current density in the human body than magnetic fields.

The European Union (EU) sets action and limit values for occupational exposure to electric fields in directive 2004/40/EC. The action value for 50 Hz electric field is set as electric field strength and it is 10 kV/m. In case action value is exceeded the employer has to make sure the limit value will not be exceeded. Limit value is set as induced current density in the central nervous system in the head or trunk and it must not exceed 10 mA/m^2. Limit value is set to protect tissues in the central nervous system for acute effects of exposure. [1]

When estimating exposure to electric fields, the neck is a critical area, because current induced in the head flows through the neck into the trunk and the cross-section area in the neck is small compared with the trunk. Furthermore, the spinal cord as a part of the human central nervous system makes the neck an interesting area.

The Laboratory of Electrical Engineering and Health (LEEH) at Tampere University of Technology (TUT) has made several electric field measurements at Finnish 400 kV substations. At 75 % of the measured substations the action value 10 kV/m was exceeded already at the ground level. Higher values can be expected in maintenance situations, although live-line work tasks are not carried out in 400 kV level. Therefore further study of induced current densities was seen as necessary.

A study of induced current densities was done by using special measuring equipment which consists of a helmet coated with copper and having a transparent but conductive face shield, two commercial current recording ammeters, a commercial medical electrode and leads. The current induced in the helmet and shield was conducted away with a lead connected to the helmet. An ammeter was connected to the lead and the other end of the lead was connected to a medical electrode in test person's wrist. The test person wore insulated shoes and gloves and the medical electrode in the wrist was earthed with another insulated lead going along the body of the test person. Also the grounding lead had a recording ammeter. Hence, both the induced current in the helmet with face shield and in the whole body current could be measured. A schematic picture of the measuring arrangement is shown in Fig. 1.

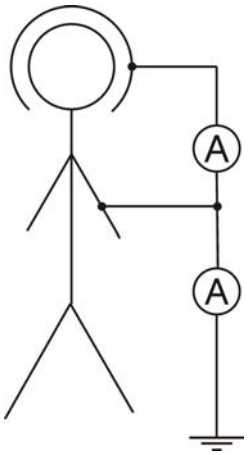

Fig. 1 Schematic picture of the measuring arrangement [2]

The current induced in the helmet and shield is called helmet current I_{helmet}. Because the helmet is slightly larger than head, current induced in the helmet is larger than the induced current in the head in normal conditions. This error was compensated for by multiplying the helmet current by empirically defined correction coefficient *k*, which is 0.819.

LEEH made induced current measurements at 7 different 400 kV air-insulated substations. Altogether 125 measurements were made in 12 different work tasks. The tasks consisted of normal walking in the substation, climbing in the maintenance and inspection platforms as well as maintenance work from ladders or from persons being lifted. The largest value for induced helmet current was 105.8 µA. This current causes current density 6.81 mA/m^2 in the neck area when the neck cross-sectional area is assumed to be a circle with circumference 40 cm (typical collar size for men is 40 cm).

Current density 6.81 mA/m^2 gives an obvious margin to the limit value 10 mA/m^2. However, individual variations in collar size may be rather considerable. Consequently, in order to get further analysis about 50 Hz currents and current densities in different tissues in the neck and especially in the central nervous system LEEH developed a model based on the cross-section of the neck.

2. Objectives and methods

2.1 Aim of the Study

The main aim of this study was to estimate with a developed model current densities in different tissues, especially in the spinal cord in the neck cross-sectional area. The purpose was to find current densities at 35 cm, 40 cm and 50 cm neck circumferences. Another aim of the study was to find out current percentages of induced head current in different tissues.

2.2 Description of the Model

The model is based on the anatomical picture of the cross-sectional area of neck. The anatomical picture was taken from source [3]. Each tissue in the anatomical picture was modeled by using circles, rings and half-rings as modeling shapes so that the shape fitted the anatomical picture of tissue as well as possible. The neck was also assumed to be a circular shape. A cross-sectional picture of the model is presented in Fig.2.

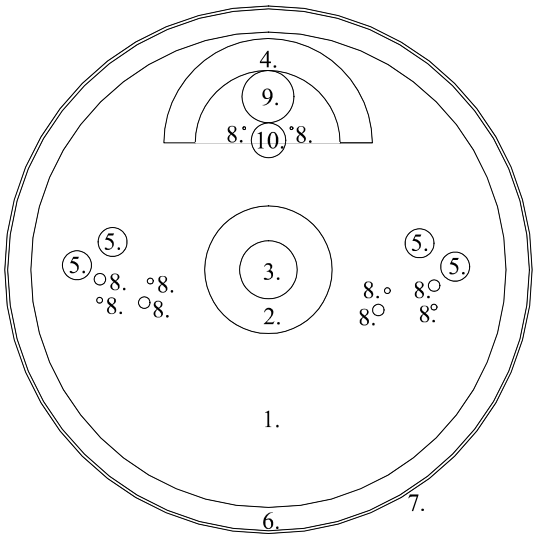

Fig. 2 Cross-sectional picture of the model

Tissue 5 includes arteries and veins, which are located on both sides of the model. Tissue 8 consists of five different nerves: spinal nerve, vagus nerve, phrenic nerve, sympathetic trunk and recurrent laryngeal nerve.

Windpipe (number 10) is assumed air with conductivity of 0 S/m. Muscle (number 1.) is a circle area, where tissues 2, 3, 4, 5, 8, 9, 10 create holes in.

Dimensions of the model are scaled when circumference of neck (collar size i.e. circumference of circle 7.) is changed. Dimensions of the tissues are presented in Table 1, when the diameter of the model is assumed *d*.

Table 1 Dimensions of the model, when the largest diameter is assumed as *d*.

Tissue	Dimensions	
1. Muscle	0.901*d*	
2. Bone trabecular	0.242*d*	
3. Spinal cord	0.110*d*	
4. Thyroid gland	0.396*d*	0.275*d*
5. Blood	0.055*d*	
6. Fat layer	0.989*d*	
7. Skin	*d*	
8. Nerves	constants	
9. Gullet	0.066*d*	
10. Windpipe	0.099*d*	

Nerves are the only tissue in model, which have constant dimensions at all collar sizes. Diameters are for spinal and vagus nerves 0.20 cm, phrenic nerve and sympathetic trunk 0.10 cm and recurrent laryngeal nerve 0.05 cm.

Each tissue has its own conductivity value. Tissues with conductivity values are presented in Table 2.

Table 2. Tissues used in the model and their conductivities at 50 Hz. [4], [5]

Tissue	Conductivity (S/m)
1. Muscle	0.3500
2. Bone trabecular	0.0700
3. Spinal cord	0.0300
4. Thyroid gland	0.5200
5. Blood	0.7000
6. Fat layer	0.0400
7. Skin	0.1000
8. Nerves	0.0274
9. Gullet	0.5200
10. Windpipe (air)	0

2.3 Induced Currents and Current Densities

All the tissues in the model are connected in parallel. In a resistive model the conductance value G_i for the tissue i can be calculated by using equation (1), when conductivity value σ_i and total area A_i of the tissue i are known. Length of the neck is l (constant).

$$G_i = \sigma_i \frac{A_i}{l}, \text{ where } i = 1\ldots9 \tag{1}$$

By using current distribution law in parallel connected circuit, currents I_i in tissues can be calculated by using equation (2).

$$I_i = k \cdot I_{helmet} \frac{G_i}{\sum_{i=1}^{9} G_i}, \text{ where } i = 1...9 \tag{2}$$

Current percentages of head current p_i in tissue i can be calculated by using equations (1) and (2). Hence, we get final equation (3) for current percentages of head current.

$$p_i = \frac{\sigma_i A_i}{\sum_{i=1}^{9} \sigma_i A_i} \cdot 100\%, \text{ where } i = 1\ldots9 \quad (3)$$

Current densities J_i in tissue i can be calculated by using equation (4).

$$J_i = \frac{I_i}{A_i} = k \cdot I_{helmet} \frac{\sigma_i}{\sum_{i=1}^{9} \sigma_i A_i} \quad (4)$$

3. Results

The model gives the current densities in various tissues in the neck area. Results were calculated with 35 cm, 40 cm and 50 cm collar sizes and maximum measured helmet current 105.8 µA by using equation (4). This helmet current corresponds to working in conditions where the local electrical field strength is highly non-uniform and clearly exceeds the action value limit. Induced current densities in each tissue are presented in Table 3. Average current densities in cross-sectional area of the neck are also presented.

The largest current densities in the neck area occur in blood (arteries and veins), thyroid gland, gullet and muscle. Current densities in bone, spinal cord, fat layer, skin and nerves stay below or near to 3 mA/m^2 even at 35 cm collar size.

Spinal cord is critical part in exposure because it is a part of the human central nervous system. According to the results current densities in central nervous system seem to stay below 1 mA/m^2 even at 35 cm collar size.

Table 3. Calculated current densities (mA/m^2) in different tissues at collar size 35 cm, 40 cm and 50 cm.

Tissue	**Collar size**		
	35 cm	**40 cm**	**50 cm**
1. Muscle	10.95	8.38	5.36
2. Bone trabecular	2.19	1.68	1.07
3. Spinal cord	0.94	0.72	0.46
4. Thyroid gland	16.27	12.45	7.97
5. Blood	21.90	16.76	10.72
6. Fat layer	1.25	0.96	0.61
7. Skin	3.13	2.39	1.53
8. Nerves	0.86	0.66	0.42
9. Gullet	16.27	12.45	7.97
Average current density in neck area	8.89	6.81	4.36

Current percentages in tissues were calculated by using equation (3). Results are presented in Table 4 at 40 cm collar size. Current distribution in tissues varies a bit depending on collar size. This results from nerves, which are not scaled as other tissues. However, the maximum variation is 0.1 % when varying collar size between 35 cm...50 cm.

Table 4. Current percentages in different tissues at collar size 40 cm.

Tissue	Percent of head current (p_i)
1. Muscle	84.43
2. Bone trabecular	1.14
3. Spinal cord	0.13
4. Thyroid gland	7.41
5. Blood	2.97
6. Fat layer	2.34
7. Skin	0.77
8. Nerves	0.01
9. Gullet	0.80

According to results most of induced current flows through muscle. This is due to its conductivity and a large area in cross-sectional area.

4. Discussion

The model gives a more specific estimation about current distribution in the neck area. According to results current densities in the central nervous system stay clearly under limit value 10 mA/m^2 even if the collar size is small (35 cm). Hence, it seems that substation workers in practical outdoor work situations in 400 kV substations are not exposed to current densities that exceed the limit value of the directive 2004/40/EC.

According to the model the collar size for neck should be 16.5 cm in order to exceed the limit value. Such a narrow neck circumference is extremely rare, if not undiscovered in the working age population.

There are some simplifications in the model that cause errors in calculations. Modeling shapes differ from real tissue shapes and so they do not fit into tissues perfectly. This difference relates also to the circumference of the neck cross-sectional area, which is not exactly circular in the anatomical picture. Another principal difference from reality in the model is that cross-sectional area of neck is assumed the same in every position of neck length *l*. In reality the proportions of tissues varies depending on the position of cross-sectional area on neck.

One limitation of the model is that it is purely resistive and it does not take account mutual inductances, which occur between different parallel-connected tissues. However, impedances of biological material are mostly resistive below 100 Hz and contribution on capacitive component is of the order of 10 % in most cases [5]. Hence, the error caused by this limitation does not seem to be large.

When comparing current densities to a study by Dimbylow, P. [4], we can notice that current densities in the spinal cord are larger than in our study. Our neck model is suited to a ballpark estimation. A three-dimensional model based on for example MRI scan gives us a more accurate estimation.

For further analysis of induced current densities it may be necessary to develop cross-sectional practical models also for other areas in the human body. Such areas could for example be the chest or stomach, because the spinal cord as a part of central nervous system is part of both cross-sectional areas.

References

[1] 2004/40/EC, 2004. Directive on the minimum health and safety requirements regarding the exposure of workers to the risk arising from physical agents (electromagnetic fields). The European parliament and the council. Official journal of the European Union, 159. 26 p.

[2] Långsjö, T., Latva-Teikari, J., et al. Occupational exposure to 50 Hz electric fields at substation. 16th World Congress on Ergonomics. Maastricht, Netherlands. 10. – 14.6.2006.

[3] Frank H. Netter, M.D. Atlas of Human Anatomy. Second Edition. East Hanover (N.J.): Novartis, 1997

[4] Dimbylow, P. Development of the female voxel phantom, NAOMI, and its application to calculations of induced current densities and electric fields from applied low frequency magnetic and electric fields. Physics in Medicine and Biology. 23 February 2005.

[5] Italian National Research Council, Institute for Applied Physics. Calculation of the Dielectric Properties of Body Tissues in the frequency range 10 Hz - 100 GHz. Available from: http://niremf.ifac.cnr.it/tissprop/ Referred 14.06.2006.

THERMODYNAMIC LAW AND THE PROBLEM OF STANDARDIZATION OF RADIOFREQUENCY ELECTROMAGNETIC RADIATION

YULIA CHUKOVA

Russian People's Academy of Science, Krasnopresnenskiy Ecological Fund. Moscow

Malaya Gruzinskaya St. 6 – 42, 123242, Moscow, Russian Federation

e-mail: y.Chukova@mtu-net.ru

Abstract

The problem of radiofrequency radiation standardization is the most important problem of up-to-date-ness because all frequencies of radiofrequency radiation are used in different technical and domestic devices. The sharpness of this problem was elucidated half a century ago, when the USSR standard for microwave radiation was 1000-fold lower than the USA standard. In the USA and in many other countries, a power density of 10 mW/cm^2 has been adopted as a standard safety level, but in the USSR a value of 10 $\mu W/cm^2$ was adopted.

This problem exists both for microwave radiation and other radiofrequencies at the present time.

The thermodynamic theory of systems under electromagnetic radiation gives the general law of electromagnetic energy conversion into energy of chemical bonds (the Helmholtz free energy). This law gives the dependence of bioeffects on absorbed power. The thermodynamic law shows that there are two regions of bioeffects of radiofrequency radiation: thermal effects and isothermal ones (endergonic + exergonic effects). The USA standard is good only for thermal effects, but the USSR standard is valid for thermal and isothermal effects.

It is discussed a role of a good social decision for conservation of public health.

Introduction. The general principle of hygienic standardization

The general principle of hygienic standardization is simple. Hygienic research begins with the most great influences. In these conditions, there is a hundred-per-cent adverse effect (death, illness etc). Then the influence decreases and the adverse effect decreases too. At last a hygienist does not see an adverse effect. This point is called the no-observed-adverse-effect level (NOAEL) or no-observed-effect dose. This point is the final one of natural research. The following decision (standard) is the social act because all levels and doses below the NOAEL or no-observed-effect dose are determined as safe levels or doses (Fig.1). This statement was the general paradigm of safety in 20th century. This paradigm prevails today.

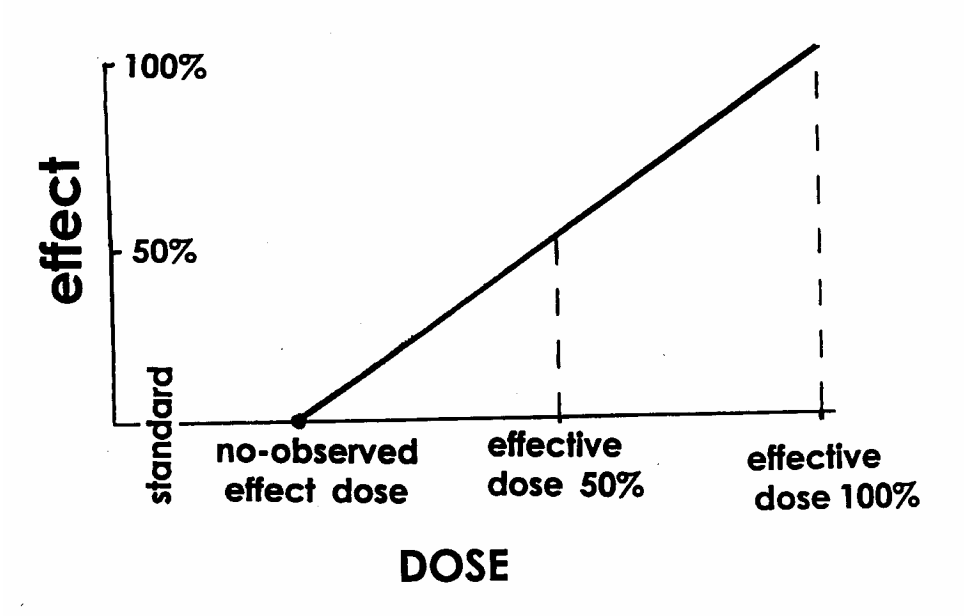

Fig.1

The principle of radiofrequency radiation standardisation in the 20th century

During the second part of the 20th century, there was considerable development and increase in the number of devices that emit nonionizing radiofrequency radiation. For example, microwaves (MW) were used in all sectors of our society for military, industrial, telecommunications, medical and consumer applications. This is the frequency range receiving the most attention in terms of biological interaction. This is due to the widespread use of high MW energy densities in highly populated areas. High energy densities of MW radiation cause heating of the human body. This is a dangerous effect and the principle of 20th century standardization for radiofrequency radiation was simple and common [1]. It has needed to determine the no-observed- heating-effect level. Safe conditions must be lower than the no-observed-heating-effect level. This statement was the general paradigm of safety in the 20th century for radiofrequency radiation and prevails today. In the USA, a power density of 10 mW/cm^2 has been adopted as the standard safety level [2]. Standards in different countries are different because shifts from the no-observed-heating-effect level are not equal.

For a long time there was only one exception to this rule: it was the Soviet standard on adverse microwave radiation effects. This standard was 1000-fold lower than the USA standard. Such a huge difference in the representation of an adverse effect was a result of the great experimental programme in the USSR in the middle of the 20th century.

In the USSR, standardization for microwave radiation was begun in 1956. Soviet hygienists studied at first the thermal effects of high-intensity radiation and then they took an interest in low-intensity radiofrequency radiation. They revealed that changes resulting from chronic or repeated exposure to low intensities of radiation are specific, initially reversible and affect the nervous system, myocardium, kidneys etc. About 70 photos of those changes are in an English book [3]. The reversible changes disappear after some time, if the exposure is ended. In other cases, the changes are permanent. The results of these researches were published both in Russian and in English [3, 4].

In the end, the Doctor-hygienist Z.V. Gordon (head of the laboratory of radiofrequency electromagnetic waves of the Institute of Labour Hygiene and Occupational Diseases of the Academy of Medical Science of the USSR) proposed for the Soviet microwave hygienic standard a power density of 10 $\mu W/cm^2$. Her suggestion

was supported by Admiral A.I.Berg , Deputy Defence Minister for the USSR . So, in the USSR the value of 10 $\mu W/cm^2$ was adopted as the safety standard for microwave radiation. This led to the well-known difference of a factor of 1000 between the safety standards in the USSR and the USA. Thus, the Soviet standard was the most stringent standard in the world.

The Soviet standard has taken into account adverse non-thermal effects. It means that in the second part of the 20^{th} century in Russia, the other independent paradigm of hygienic standardization of radiofrequency radiation has been adopted. This confusing picture was indeed the beginning of a hygienic discussion which has been long and unsuccessful. The situation can be changed by the thermodynamic theory of systems under electromagnetic radiation.

Thermodynamics is free from the terms “adverse effect”, “hazard” etc. These terms are known in medicine and biology. Thermodynamics deals with thermal and isothermal processes, the endergonic and exergonic ones, but every process can be useful or adverse from a view of life and from a human standpoint. The method of thermodynamics of irreversible processes in systems under electromagnetic radiation yielded interesting results for up-to-date hygiene and physiology. One result is related to the radiofrequency safety problem.

Resume of advances in the nonequilibrium thermodynamics of isothermal processes in systems under electromagnetic radiation

Thermodynamics deals with the energy of processes and the efficiency of energy conversion. It began with a study of technical systems under electromagnetic radiation (luminescent lamps and solar cells). The considered system is given in Fig.2, with the definitions. In this system, there are three kinds of energy conversion: radiation into radiation, radiation into Helmholtz free energy and radiation into heat.

The basic theoretical work was done by L. Landau in 1946 [5]. At that time, he was not yet a Nobel prize winner. Landau has estimated the first way – luminescence. The result for luminescence, which has been obtained by L. Landau, has struck scientists very much. Only some scientists can believe that optical cooling is possible. Optical heating is habituated for us. But during the 1970s the thermodynamically predicted result was obtained in many systems under laser light; and in 1997 the Royal Swedish Academy of Sciences decided to award the Nobel Prize in Physics jointly to Steven Chu (USA), Claude Cohen-Tannoudji (France) and William D. Phillips (USA) for the development of methods of cooling atoms with laser light.

It is foreseeable that in the future a device will be designed which combines the characteristics of a radiation-source and a refrigerator. Thermodynamics does not forbid a such device.

The second way is interesting for solar sells and bioeffects of electromagnetic radiation. For the second way of energy conversion, thermodynamics did not give any wonderful result [6], but the solar cell presented a possibility of direct numerical verification of the thermodynamic theory through a correlation with experimental data. This comparison became possible because theoretical physicists have gone from the thermodynamic limit efficiency estimation to the real efficiency calculation for processes with losses. The numerical correlation of experimental data with the theory was not only satisfactory, but the fit of theory and experiment was also quite good. Furthermore, the thermodynamic method may work even for living systems. It allowed understanding and explanation of many experimental results in living systems, which had not previously been exhaustively explained [7,8].

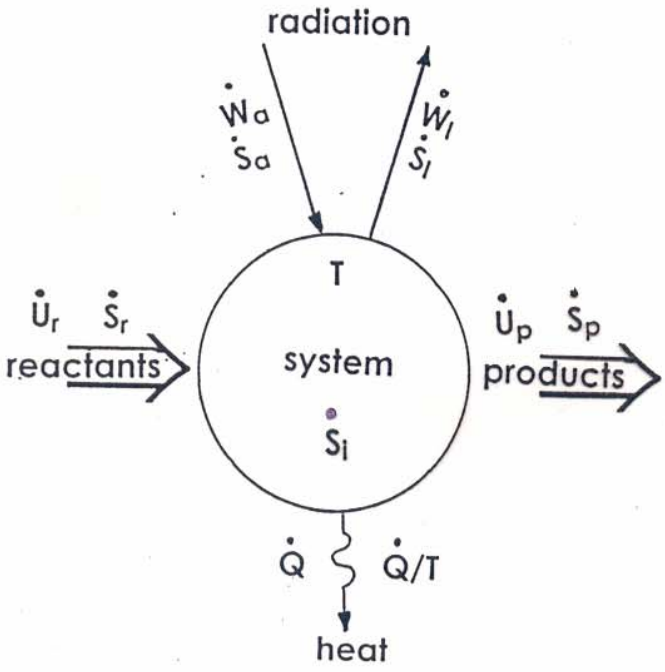

Simbols and Notations:

T - temperature

• time derivative sign

Energy	Corresponding entropy flux
U_r - internal energy of reactants	$\dot{S}_r$
U_p - internal energy of products	$\dot{S}_p$
$\dot{W}_a$ - absobed power	$\dot{S}_a$
$\dot{W}_l$ - power of luminescence	$\dot{S}_l$
$\dot{Q}$ - thermal flux	$\dot{Q}/T$

$\dot{S}_i$ - entropy generation rate in system

F - Helmholtz free energy $F = U - TS$ (1)

η - real efficiency $\eta = (F_p - F_r)/W_a = \Delta F/W_a$ (2)

$\Delta F > 0$ endoergonic process
$\Delta F < 0$ exoergonic process

For bioeffects of electromagnetic radiation, there is a need to examine conversion of energy of electromagnetic radiation into energy of chemical bonds, i.e. into Helmholtz free energy. The efficiency of this conversion is given by formula (2). On the basis of the first and second equations of thermodynamics, for the steady state of a system, the efficiency η of MM radiation conversion at constant temperature is given by:

$$\eta = 1 - T\,(\dot{S}_a + \dot{S}_i)/\dot{W}_a \qquad (3)$$

From formula (3) it is obvious that the efficiency η is determined by two entropy terms. The first entropy term $\dot{S}_a$ (entropy flux of absorbed power) is dictated by the absorbed power characteristics and is defined by formula (4):

$$\dot{S}_a = 2\pi k c^{-2} \int \nu^2 (1 + \ln\rho)\, d\nu \qquad (4)$$

where c is the velocity of light, k is the Boltzmann constant, ν is a frequency and

$$\rho = c^2 E_\nu / 2\pi h \nu^3 \qquad (5)$$

E_ν is the spectral density of absorbed power $\dot{W}_a$

$$\dot{W}_a = \int E_\nu \, d\nu \qquad (6)$$

The second entropy term $\dot{S}_i$ (entropy generation rate) is determined as

$$\dot{S}_i = \alpha \dot{W}_a + \beta \dot{W}_a^{\,n} \qquad (7)$$

where α, β and $n \neq 1$ are constants connected with the system characteristics.

According to formulas (3 – 7), the dependence of efficiency on absorbed power $\dot{W}_a$ (or spectral density of absorbed power E_ν) is given by the left-hand curve of Fig.3

Fig.3 demonstrates two simple and important results:

1) A system at constant temperature can show three types of behaviour in response to energy absorption. In order increasing absorbed power, they are:

– exergonic isothermal processes
– endergonic isothermal processes
– endergonic nonthermal processes

2) Endergonic processes have a beginning and an end.

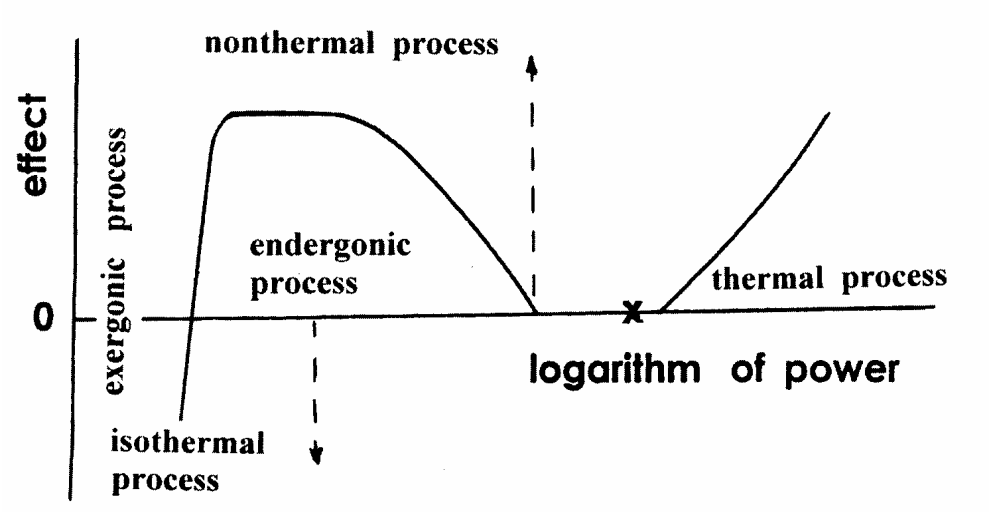

Fig.3

The rapid rise and the plateau of the left-hand curve of Fig.3 are determined by the entropy of absorbed power according to (4), but the position of the curve on the logarithm of absorbed power axis (the point of its intersection with the absorbed power axis, where the real endergonic processes are balanced out by exergonic processes) is dictated by the linear term of the entropy generation rate according to (7). The falling region of the left-hand curve is defined by the nonlinear term in the entropy generation rate. This is the second term in formula (7) for the condition $n > 1$.

A qualitative agreement between the thermodynamic theory of endergonic processes and experimental data was demonstrated in a series papers [9 –12] and in two books [7, 8]. That is why this aspect of the problem will be omitted in the present paper.

So, endergonic processes have a beginning and an end at some level of absorbed power, but an experimentalist can study the system not only at constant temperature, but also at increasing temperature for high absorbed power. According to thermodynamic theory in this case, we have two results: a system with no biological effects; and thermal processes in a system (right-hand curve in Fig.3).

Thermal effects of radiofrequency radiation have been studied for almost one hundred years and for thermal processes there is sufficient scientific clarity. That is why this aspect of the problem is omitted in the present paper. The interval without biological effects is poorly understood and it is therefore useful to recall a paper by scientists at the University of Utah (Salt Lake City, USA), who studied this interval [13]. They exposed monolayer cell cultures (for example BHK-21/C13 cells) to high levels of microwave radiation without significant microwave-induced heating ($\leq 0.1°$ C). They showed that for the frequency interval 38-48 GHz at a power density of 292 mW/cm^2 and for 65-75 GHz at a power density of 177 mW/cm^2 bioeffects of microwaves were absent [13].

Thermodynamic conclusions for hygienic standardization

The curves of Fig.3 are very important for the hygienic standardization of radiofrequency radiation. They show that the 20^{th} paradigm of hygienic standardization takes into account only thermal processes in living systems under electromagnetic radiation. In the light of thermodynamic theory, it is clear that the experimentalists finished their research when they reached the interval between thermal and nonthermal effects. All current hygienic standards, except the Russian standards, lie in this interval (cross).

The standards of different countries are different because they are not equally close to the no-observed-heating level (the starting point for thermal processes). But they are all interposed between thermal effects and nonthermal endergonic ones.

From thermodynamics it is obvious that current international standards relate to thermal processes only.

The Soviet hygienic standard for radiofrequencies holds both for thermal and for isothermal processes. That is why it is 1000-fold more severe than the USA standard and all other standards.

It is obvious that in the future national and international standards will be changed. They will become more severe and, in the long run, isothermal effects will taken into account. Then the science of hygiene will have a theoretical basis as a third point of support, in parallel with the experimental and social ones. This is demonstrated schematically in Fig.4. But hygienists do not at present know the theoretical basis and the situation is therefore not simple.

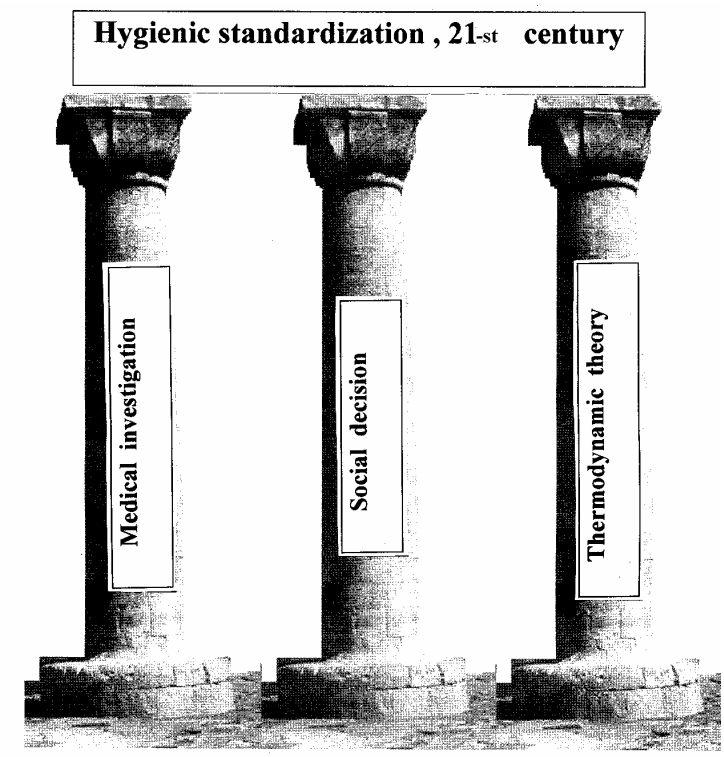

Fig.4

Radiofrequency hygiene of the transitional period

The main current international documents, "Directive 2004/40/EC of the European Parliament and the Council of 29 April 2004 on the minimum health and safety requirements regarding the exposure of workers to the risk arising from physical agents" and "ICNIRP Guidelines for limiting exposure to time-varying electric, magnetic, and electromagnetic fields (up to 300 GHz)", take into account only thermal processes under radiofrequency radiation. How should hygienists deal with real situations today? There are two ways. One way is very simple: it is to wait for laboratory isothermal experiments to show scientifically what the standard of absorbed power must be. In this case, hygienists will leave the people without protection for a long time. But there is another way: a social resolution of the problem, i.e. a precautionary approach. Social decisions may vary, which means that national standardizations will be original, as is now indeed the case. Some examples are given below.

Poland

Polish hygienists understand that limits based on ICNIRP are not too liberal in the case of chronic occupational exposure, and the regulations established in Poland contain limits on permissible exposure which are more restrictive than the EC Directive and the ICNIRP Guidelines. The Polish standardization system allows harmonisation with the EC Directive/ICNIRP basic restrictions and, at the same time, the practical application of a precautionary approch in the occupational environment.

In Poland, there are three levels of exposure [14]:

- high-level and dangerous zone,
- medium-level and safety zone,
- low-level for outside the safety zone.

For pregnant women and young workers (below 18 years), the levels of restricted occupational exposure in Polish Standards (2002) are 2-3 times lower than international regulations. For thresholds of permissible environmental exposure, they are 10 times lower.

Sweden

It has long known that the Swedish occupational standards for personal computers are more severe than international ones.

Austria

The strictest precautionary approach has been established in Austria. It is the so-called "Salzburg Model" [15,16]. The "Salzburg Model" was created in the city of Salzburg in 1997- 1998, when the Department of Public Health of the Federal State of Salzburg was requested by the Salzburg Provincial Parliament, the director of the Department of Health and several mayors to provide a medical evaluation of the GSM fields emitted from mobile telecommunications base stations. The aim of the Salzburg Model is the implementation of a precautionary strategy for the protection of public health against electromagnetic fields.

The so-called "Salzburg precautionary value" is equal to $1 mW/m^2$ (or $0.1\ \mu W/cm^2$) for the bands of 900 MHz – 1800 MHz. This frequency band is used by GSM base stations. It is useful to compare the "Salzburg precautionary value" with the ICNIRP (1998) standard of $4 – 10\ W/m^2$, which is based on thermal effects in the same frequency range. The difference is 4 orders of magnitude. This difference accords well with theoretical estimates of the difference between the thresholds for thermal and isothermal processes.

Austrian hygienists understand that the Salzburg precautionary value is based on biological effects of low-intensity exposure (isothermal effects).

The decision of the Salzburg authority is a wise decision, and is in accordance with the WHO policy [23]. One can compare this decision with Napoleon's decision. As is known, Napoleon Bonaparte created a domestic code. According to Napoleon's code, the father of a child born in wedlock is the husband. In real situations, if the father is unknown, the husband is considered as the father. This decision is dictated by expediency, rather than truth. Napoleon's decision has been a wise decision, because it has saved the law-courts and the population from unnecessary trouble. Napoleon's decision has became a principle of legislation in many European countries for two centuries. Today, this problem is solved by scientific methods because science can establish paternity with high accuracy.

The "Salzburg Model" offers some advantages over Napoleon's decision, because the "Salzburg Model" corresponds to thermodynamic predictions. Thermodynamic law supports the Salzburg precautionary level.

It is now apparent that this work will be the subject of experimental investigation, as attested by the Austrian-Spanish paper [17].

Summary

Thermodynamic theory shows that there are two independent regions of biological effects of radiofrequency radiation: thermal and isothermal ones. Thermal effects are very simple, well studied and standardized. Isothermal effects are complicated to study and their standardisation is for the future.

The precedents of the Salzburg model and the Soviet (Russian) standard are the first steps in a new hygienic science and a new system of standardisation, which will be able to protect public health against adverse effects of radiation. These are real attempts to execute the WHO plans and intentions.

Acknowledgement

I wish to thank Prof. O.P. Gandhi (University of Utah, Salt Lake City, USA), who made available a complete set of his papers on this subject.
I thank the research workers of the University of Utah for a very difficult experiment, which is very important for thermodynamics and hygiene.

References

1. M.H. Repacholi Development of standards – Assessment of health hazards and other factors. Biological effects and dosimetry of nonionizing radiation. Ed. M. Grandolfo, S.M. Michaelson, A.Rindi v.49, 1983, Plenum Press, N.Y., London.

2. Johnson C.C., Guy W. - Nonionizing electromagnetic wave effects in biological materials and systems - Proceedings of the IEE, 1972, v.60, No 6 , pp.692-71

3. Tolgskaya M.S., Gordon Z.V. *Pathological effects of radio waves.* Consultants Bureau, N.Y., London, 1973

4. Biologic effects and health hazards of microwave radiation. Proceeding International Symposium, Warsaw. 1973. Polish Medical Publishers, 1974, pp.22-35, 289 -293

5. L. D. Landau,- On the thermodynamics of photoluminescence. J. Phys. USSR, 1946 ,v.10, p.503 -506

6. P.T. Landsberg , G.Tonge - Thermodynamic energy conversion efficiencies.- J. Appl. Phys. 1980, v.51, N7, p.R1 - R20

7. Yu.P. Chukova. Advances in nonequilibrium thermodynamics of the systems under electromagnetic radiation, 2001, Moscow, Khrizostom, ISBN 5-7508-0285-X

8. Yu.P. Chukova , Low-level influence effects. Thermodynamic, experimental (medical and biological), social, legislative, international and philosophical aspects of problem. Moscow, 2002, ISBN 5-89047-013-2.

9. Chukova Yu.P. Biological response to radiofrequency electromagnetic radiation.- Dokl. Biological Sciences.Proceedings of the Academy of Sciences of the USSR,1990, v.311,p.237-239

10. Yu.P. Chukova, Reasons of poor replicability of nonthermal bioeffects by millimetre waves, Bioelectrochemistry and bioenergetics, Vol. 48, 1999, pp. 349 – 353.

11. Yu.P. Chukova, Thermodynamics of isothermal processes of electromagnetic radiation and practical conclusions. Proceeding of the Millennium Workshop on Biological effects of electromagnetic fields. Crete, Greece, 2000, p. 338 - 341

12. Yu.P. Chukova, Bioeffects under electromagnetic radiation. Theory and experiment, Biological effects of EMFs. 2nd International workshop. Proceedings. Kos, Greece, 2004, Vol. 2, pp. 775 – 783

13. L.G. Bush, D.W. Hill, A Riazi, L.J. Stensaas, L.M. Partlow and O.P. Gandhi. Effects of millimeter-wave radiation on monolayer cell cultures.III. A search for frequency-specific athermal biological effects on protein synthesis. Bioelectromagnetics 1981,v. 2, pp.151-159.

14. Karpowicz J., Gryz K. – EMF exposure's occupational risk assessment – Approach implemented by EC directive 2004|40 and national regulations in Poland. Kos, 2004, v.2, p.1190 – 1195

15. G. Oberfeld, C. Konig , The Saltzburg Model: a precautionary strategy for sitting of base station. Biological effects of EMFs. 2nd International workshop. Proceedings. Rhodes, Greece, 2002, Vol..2, p.621-625

16. E. Marsalek. A possible regulatory framework for the erection of mobile phone base station within the European community, The "Round-table-consensus-Model" (So called "Saltzburg model"), Biological effects of EMFs. 2nd International workshop. Proceedings. Rhodes, Greece, 2002, Vol .2, pp. 611-620

17. Oberfeld G., Navarro A.E., Portoles M., Maestu C., Gomez-Perretta C. The microwave syndrome – further aspects of a Spanish study. Biological effects of EMFs. 3rd International workshop. Proceedings. Kos, Greece, 2004, v.2, p.728 – 735.

EFFECTS OF MOBILE PHONE EXPOSURE ON HUMAN COGNITIVE FUNCTION

ANDREW WOOD

CON STOUGH

RODNEY CROFT

VANESSA KEETLEY

DENISE HAMBLIN

SARAH LOUGHRAN

BRAIN SCIENCES INSTITUTE, SWINBURNE UNIVERSITY OF TECHNOLOGY, HAWTHORN, VICTORIA 3122, AUSTRALIA

Abstract

This presentation will summarize the results of several human volunteer studies carried out at Swinburne University over the last 7 years. The outcomes (significant unless otherwise stated) were:

- Tests of cognition (n = 120 subjects; battery of 8 tests): When adjusted for co-variables, worse performance in simple reaction time and choice reaction time; worse performance in some measures of information retrieval, but improved speed of processing of information held in memory.
- Event Related Potential pilot study (n = 12 subjects; auditory stimuli): Reduced N1 amplitude and latency to non-target and increased P3 latency to oddball target stimuli; worse reaction time performance.
- Event Related Potential main study (n = 120 subjects; auditory, visual and cognitive task stimuli): no significant changes in ERP-related parameters.
- Sleep study (n = 50; polysomnography): REM latency reduced by 16%. EEG alpha power enhanced by 8% during 1st non-REM period.
- Overnight melatonin (metabolite) output (n = 55): Overall no change, but 27% reduction in normalized output pre-bedtime.

These results will be compared for overall internal consistency and with studies from other laboratories. Part of the program of the Australian Centre for Radiofrequency Bioeffects Research is to extend some of the studies.

Introduction

The basic question our research program has sought to answer is: do the emissions from mobile phone handsets lead to an immediate change in a person's neuropsychological performance, such as ability to react to stimuli, recall information, perform tasks accurately, get a good night's sleep and so on? The specific hypotheses we formulated were on the basis of research available to us in the planning phase. An extensive literature review was taken at this time (Hamblin & Wood 2002). This identified EEG alpha power increase in response to radiofrequency (RF) exposure as being the most consistent observation

Methods

Exposure to RF was accomplished by the use of a popular handset, programmed into GSM pulsed mode (0.25 W average) using the manufacturer's software, giving a constant output over the time of the experiment, typically 1 – 2 hours. The output was checked in three ways: i) with dipole antenna; ii) direct connection to RF power meter and iii) by measurements in SAR phantom. The maximum 10g-averaged SAR value obtained was 0.11 W/kg (Hamblin et al 2006), with the phone attached to a cradle placing the handset in a normal position next to cheek. A number of checks were made: firstly, that the participants could not detect audible cues from the handset circuitry; secondly that ELF pickup in EEG electrode leads was not significant (Wood et al 2003) and thirdly that the SAR value was not affected by the presence of EEG lead wiring. In the case of auditory stimuli, an additional test ensured that the test tones (which were delivered by air-tube ear inserts) were uncontaminated by EMI from the phone handset.

A number of biological endpoints were assessed as follows: a) speed & accuracy in performing (mainly paper & pencil) cognitive tasks; b) Event-related potentials (ERPs): specific changes in EEG evoked by visual, auditory & cognitive stimuli; c) sleep architecture: quality and type of sleep following 30 min of phone exposure just prior to going to bed and d) the output of urinary melatonin metabolite: before and after sleep in both exposure conditions.

The basic procedure followed was of two types: for the cognition & ERP experiments, there were two testing sessions 1 week apart each with one of two exposure conditions: a random number generator determined which of exposure condition A (sham) or B (actual exposure) occurred first. To minimise practice effects alternate forms of the cognitive tests were given: the tests in each battery were given in random order (but in the same order between the two exposure conditions). The test were given twice at each session (4 times altogether), one before and once during the (real or sham) exposure. The outcomes were scored as a difference between performance before and performance during exposure, then score for weeks A & B were compared.

For the sleep study the procedure was somewhat different: participants stayed overnight for the Saturday and Sunday nights of two successive weekends. The Saturday nights were for adaptation to sleeping in the laboratory and on the Sunday nights the A or B type exposure was given for a period of 30 minutes prior to getting into bed. The monitoring electrodes were not attached until the exposure had finished. Polysomnography was carried out until 6 am the next morning. Urine was collected before getting into bed and at 6 am: urine volumes, creatinine and 6-hydroxy-melatonin sulphate (aMT6s) concentrations were measured.

In statistical analysis of results the potential confounding of multiple comparisons was recognised. Where possible we used prior hypotheses based on literature expectations: in these confirmatory hypotheses $p < 0.05$ was taken as the critical value for changes being regarded as significant. In hypothesis-generating comparisons, the critical p value was taken as 0.05 divided by an effective number of independent comparisons. For example, where the EEG was typically measured from 62 scalp sites: data from several sites were grouped and trends across the scalp studied (giving just 2 levels of laterality and 3 levels in the front/back direction).

Outcomes

1. Effects on Cognition (Keetley et al 2006)

In this study of 120 volunteers, a battery of 8 tasks were given, but task scores yield 18 measures of cognitive performance. The results were adjusted for co-variables: sex, age & educational level where there was literature evidence for this. It was found that participants scored worse in reaction time & information retrieval tests, but showed improvement in speed of processing of information held in memory. We concluded that basic memory tasks were impaired, but higher cortical functions improved

2(a). ERP pilot study (Hamblin et al 2004)

This was a small hypothesis-generating study of 12 volunteers. An auditory 'oddball' task was studied: responses to the 'oddball target' stimulus (t) and 'non-target' stimuli (nt) were considered separately. For the 'nt' responses, N1 amplitude was reduced (50%) and latency was 8.7% less with exposure. For 't' responses, P3 latency was 8% longer. Reaction Time (RT) was 10% worse.

2(b). ERP main study (Hamblin et al 2006)

This followed on from the above and was a study of 120 volunteers. For the auditory and visual 'oddball' tasks: 't' and 'nt' responses were considered separately. ERP amplitudes and latencies at specific sites were analysed, along with RT to 't' responses in both the auditory and visual tasks. No significant changes were found in relation to these parameters. Future analysis will concentrate on ERP changes from various scalp regions derived from factor analyses together with Event Related-Desynchronisation/Synchronisation (ERD/ERS) and Choice

Reaction Time (CRT) recorded during a cognitive task, which was a card-sorting task which was also conducted as part of the test battery. Psychological activation, as well as investigation into all above parameters by age, gender, previous mobile phone use, hemisphere exposed and laterality is also currently being undertaken.

3. Sleep study stages (Loughran et al 2005)
This was of a group of 55 volunteers (5 who had to be excluded because a sleep disorder was revealed during the subsequent sleep analysis). Ten standard sleep parameters were compared for RF effect: all were non-significant, except for rapid eye-movement (REM) sleep latency, which was reduced 16% by exposure (and which was a serendipitous finding). The EEG Alpha band power (range 11.5 – 12.25 Hz) was shown to be significantly enhanced (by 8%) in the 1st non-REM period (and this supported a prior hypothesis).

4. Sleep study melatonin (Wood et al 2006)
The urine melatonin metabolite (aMT6s) was measured in pre-and post bed-time samples in the same 55 volunteers involved in study 3. Overall, there was no change in total output (pre- + post-bedtime: 14.1 vs 14.6 µg). When values were normalised to urine creatinine concentration (which is considered to give a more precise estimate of aMT6s output), there was a significant reduction (by 27%) in pre-bedtime samples (Sham: 7.7; Exposed 5.6; units: ng aMT6s/mg creatinine). However, the distribution showed that 4 of the subjects were outlying the normal distribution (all in the same direction). If these were eliminated from the analysis the difference was not significant.

Summary
The results of these separate studies are currently being evaluated for internal consistency and for consistency with results from other laboratories. Under the program of the Australian Centre for Radiofrequency Bio-effects Research some of these studies are being replicated using some of the same cohort of subjects and using 3-G type exposures.

Grant Support
This research was supported by grants 78/3718 (Stough & Wood) and 154905 (Wood & Stough) from the National Health and Medical Research Council of Australia.

References

Hamblin DL, Croft RJ, Wood AW, Stough C, Spong J. 2006. The sensitivity of human event-related potentials and reaction time to mobile phone emitted electromagnetic fields. *Bioelectromagnetics* 27:265-73

Hamblin DL, Wood AW. 2002. Effects of mobile phone emissions on human brain activity and sleep variables. *Int J Radiat Biol* 78:659-69

Hamblin DL, Wood AW, Croft RJ, Stough C. 2004. Examining the effects of electromagnetic fields emitted by GSM mobile phones on human event-related potentials and performance during an auditory task. *Clin Neurophysiol* 115:171-8

Keetley V, Wood AW, Spong J, Stough C. 2006. Neuropsychological sequelae of digital mobile phone exposure in humans. *Neuropsychologia* 44:1843-8

Loughran SP, Wood AW, Barton JM, Croft RJ, Thompson B, Stough C. 2005. The effect of electromagnetic fields emitted by mobile phones on human sleep. *Neuroreport* 16:1973-6

Wood AW, Hamblin DL, Croft RJ. 2003. The use of a 'phantom scalp' to assess the possible direct pickup of mobile phone handset emissions by electroencephalogram electrode leads. *Med Biol Eng Comput* 41:470-2

Wood AW, Loughran SP, Stough C. 2006. Does evening exposure to mobile phone radiation affect subsequent melatonin production? *Int J Radiat Biol* 82:69-76

THE EFFECT OF A SPECIFIC PULSED MAGNETIC FIELD ON MICROCIRCULATION

MCKAY JC [1,2], TYML K [2], PRATO FS [1,2,3], THOMAS AW [1,2,3]

[1]BIOELECTROMAGNETICS, IMAGING PROGRAM, LAWSON HEALTH RESEARCH INSTITUTE, LONDON, ONTARIO, CANADA, N6A 4V2
[2]DEPARTMENT OF MEDICAL BIOPHYSICS, SCHULICH SCHOOL OF MEDICINE AND DENTISTRY, UNIVERSITY OF WESTERN ONTARIO, LONDON, ONTARIO, CANADA, N6A 5B8
[3]DEPARTMENT OF IMAGING AND NUCLEAR MEDICINE, ST. JOSEPH'S HOSPITAL, LONDON, ONTARIO, CANADA, N6A 4V2

ABSTRACT

The effect of magnetic field (MF) exposure on microvascular blood flow is controversial with no clear evidence of any one effect. In this study, we investigated the effect of a complex, low frequency, electromagnetic pulse (CNP) on microvascular blood flow when stimulated with acetylcholine (vasodilator). The effect of CNP exposure on blood flow (after 30 and 60 min) when stimulated by 3 concentrations of acetylcholine (Ach) was tested in the peripheral muscle microvasculature of a rat and measured using laser Doppler flowimetry. A mixed design ANOVA indicated that there was a main effect of time, and a main effect of Ach concentration (positive control). There was no significant interaction between time and exposure type due to the large variance created by the Ach concentration; however, a power analysis projection of the data suggests that with additional rats a significant effect would be present at the 0.1 mM Ach concentration. This data will further be analyzed using spectrographs to identify possible imprints of the CNP in the blood flow recordings, as well as any other frequency differences that are present between the sham- and CNP-exposed animals. In light of the present results, it would appear that the CNP modestly increases microvascular blood perfusion after 60 min of exposure in the rats that received 0.1 mM Ach compared to sham-exposed animals. These findings are important in that one potential 'side-effect' of MF exposure to this particular MF sequence has been investigated.

MICROCIRCULATION AND CNP

INTRODUCTION

The effect of magnetic field (MF) exposure on microvascular blood flow is controversial with no clear evidence of any one effect. Published literature is mixed, however, it could be suggested that results are mostly divided into 2 categories[1]: those studies that suggest that MFs lead to an increase in perfusion, and those studies that support a biphasic effect of MFs. The former group of studies indicates that when blood vessels are resting at a normal tone, MF exposure leads to an increase in perfusion (both during and after exposure) [2,3]; while the latter studies indicate that when vessel tone is either low or high, MF exposure alters vasomotion so that normal vessel tone is re-established[4]. The observed variation in published studies is likely attributed to the variation in tested parameters (duration of exposure, time-varying vs. static MF, localization of exposure, MF strength) and species (mice, rats, humans).

In this study, we investigated the effect of a specific pulsed MF sequence, a complex neuroelectromagnetic pulse (CNP), on microvascular blood flow when stimulated with a vasodilator (acetylcholine). The CNP has been shown by our lab to be effective in providing analgesia[5] for snails, mice, and humans, therefore we were interested in its potential effects on other biological systems, such as the microcirculatory system.

Numerous applications and benefits could be derived from locally manipulating microcirculatory blood flow. For instance, the ability to locally modify blood flow may be of benefit to wound healing, site-specific absorption of drugs, and re-perfusion of ischemic tissue. Conversely, if an individual was receiving MF therapy for a particular condition unrelated to blood flow, understanding other effects of that MF (e.g. microcirculatory effects) would be of importance.

According to previous research, results from this study should be explained by 1 of 2 theories: A.) The CNP will provide a homeostatic effect. That is, when acetylcholine (Ach) is administered, blood flow should increase, however, the CNP will cause resistance against this blood flow increase and no effect or a reduced effect on perfusion should be observed. B.) In agreement with our preliminary data[6] and other research showing that MFs increase perfusion, the CNP will in some way enhance the effects of Ach on blood flow leading to an increase in perfusion. It is proposed that nitric oxide may be involved in the potential interaction of Ach with the CNP.

OBJECTIVE

The objective of this experiment was to determine the effect of CNP exposure (after 30 and 60 min) on blood flow when stimulated by Ach in the peripheral muscle microvasculature of a rat.

METHOD

100 male Sprague-Dawley rats (210-290 g) were housed on a 12hr/12hr light/dark cycle and were provided with food and water *ad libitum*. All procedures were performed in accordance with the *Ethics Review Board* at the *University of Western Ontario*.

Rats were anesthetized using pentobarbital sodium (65mg/kg of mass) and surgery was performed on the left hind limb. The extensor digitorum longus (EDL) muscle was carefully exposed and allowed to stabilize for half an hour prior to the MF exposure. Individual rats were then placed within the set of Helmholtz-like coils and a laser Doppler flow meter probe was lowered directly on top of the EDL. Specifics of the coils and MF are as follows: 1.2 m diameter for the coil that generates the vertical low frequency (< 1000 Hz) MF with a 200 μT peak (400 mT/s). The sequence consists of 5 pulse segments (each 853 ms) with an average frequency of 72 Hz separated by an increasingly long refractory period (110-1200 ms).

A Time 0 (prior to MF exposure) measurement was taken for 8 min using PeriMed for Windows software. The MF (CNP) was then turned on. After 30 min had elapsed from the end of the Time 0 recording, a second measurement was taken (Time 30) for 8 min. After 60 min had elapsed from the end of

the Time 0 recording, a final (Time 60) measurement was made again for 8 min. For each recording, the same procedure was followed: 20 sec of un-stimulated blood flow was recorded to obtain a baseline and then Ach was dropped directly on top of the EDL. Three different concentrations of Ach were used: 0.1, 1, and 10 mM. Prior to each Ach injection, phosphate-buffered saline was injected on the EDL as a control measure.

At the end of the experiment, rats were euthanized via an intra-cardiac injection of pentobarbital. The Time 30 and Time 60 peak blood flow values were normalized to the Time 0 peak values and the results were analyzed using SPSS 12.0.

RESULTS

A mixed design analysis of variance was performed to test the effects of CNP exposure on blood flow, using time as a repeated measure. There was a significant difference in peak blood flow response across the 3 tested time points ($F(2, 179) = 18.15$, $p < 0.001$). The Time 60 values were lower that the Time 30 values. Also, as expected, there was a significant interaction between injection type (0.1, 1, or 10 mM Ach), our positive control, and time of exposure ($F(4, 184) = 3.92$, $p < 0.05$). There was no significant interaction between time and exposure type due to the large variance created by the Ach concentration; however, a power analysis projection of the data suggests that with additional rats a significant effect would be present at the 0.1 mM Ach concentration. Please refer to Figure 1 for the normalized peak blood flow response to Ach over time. Note that the greatest effect of the CNP appears to be occurring at the lowest concentration of Ach (0.1 mM). This is illustrated in Figure 2.

CONCLUSION

In light of the present results, it would appear that theory B – 'CNP increases microvascular blood perfusion' could possibly explain the obtained data. After 60 min of CNP exposure, the rats that received 0.1 mM Ach showed a modest increase (12 %) in peak blood flow response compared to sham-exposed animals. Analysis of a greater sample size is required to confirm this finding; however, these results are in support of preliminary data collected from our lab[6].

These findings are important in that one potential 'side-effect' of MF exposure to this particular MF sequence has been investigated. It would appear that MF exposure of this type modestly increases blood flow in the microvasculature after 60 min of exposure.

SUMMARY

The objective of this experiment was to determine the effect of 30 and 60 min exposure to a specific pulsed electromagnetic field (CNP) in the peripheral muscle microvasculature of a rat. Changes in blood flow, when stimulated by 3 different concentrations of acetylcholine (a vasodilator), were recorded using laser Doppler flowimetry. After 60 min of CNP exposure, the rats that received 0.1 mM acetylcholine (the lowest concentration) showed a modest increase (12 %) in peak blood flow response compared to sham-exposed animals. Analysis of a greater sample size is required to confirm this finding. These findings are important in that one potential 'side-effect' of MF exposure to this particular MF sequence has been investigated.

ACKNOWLEDGEMENTS

St. Joseph's Health Care (London) Foundation, The Lawson Health Research Institute Internal Research Fund, Natural Sciences and Engineering Research Council of Canada (NSERC), Canadian Institutes of Health Research (CIHR), the Ontario Research and Development Challenge Fund (ORDCF), Canada Foundation for Innovation (CFI), and the Ontario Innovation Trust (OIT).

REFERENCES

[1]McKay JC, Prato FS, Thomas AW. Bioelectromagnetics (accepted July 2006).
[2]Gmitrov J, Ohkubo C, Okano H. Bioelectromagnetics 23: 224-9, 2002.
[3]Xu S, Okano H, Ohkubo C. Bioelectrochemistry 53: 127-35. 2000
[4]Okano H, Ohkubo C. Bioelectromagnetics 22: 408-18, 2001.
[5]Thomas AW, Kavaliers M, Prato FS, Ossenkopp KP. Neurosci Lett 222: 107-10, 1997.
[6]Hensel JM, Bohnert R, Tyml K, Prato FS, Thomas AW. Bioelectromagnetics Soc Abstracts 25, 2003.

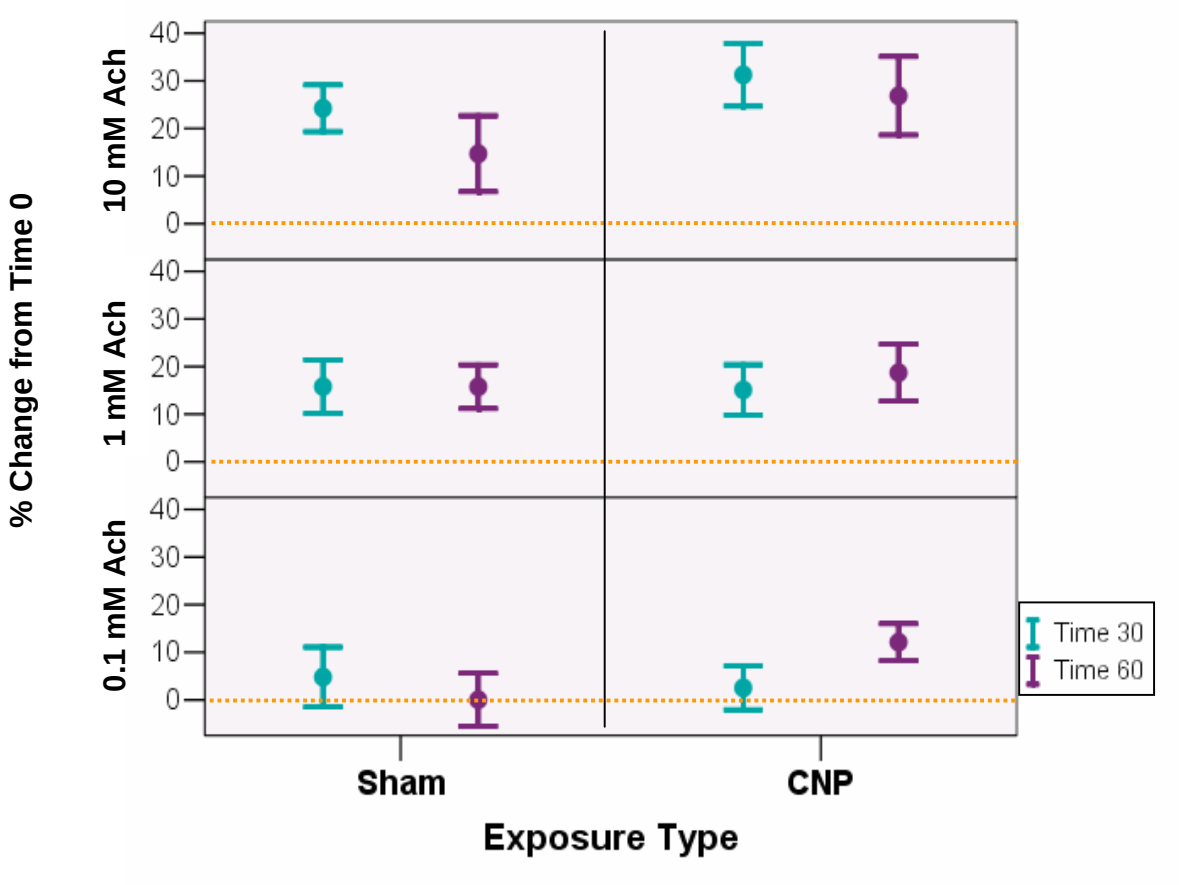

FIGURE 1. Change in microvascular blood flow after 30 and 60 min of exposure to the CNP relative to pre-exposure blood flow baseline. The line of reference at point 0 indicates 'no change' from the Time 0 blood flow values. The most noted difference in peak blood flow response between the sham- and CNP-exposed animals occurs at the lowest concentration of Ach (0.1 mM) after 60 min of exposure. Within each of the sham and CNP cells, the left hand points and error bars refer to the Time 30 measurements and the right hand points and error bars refer to the Time 60 measurements.

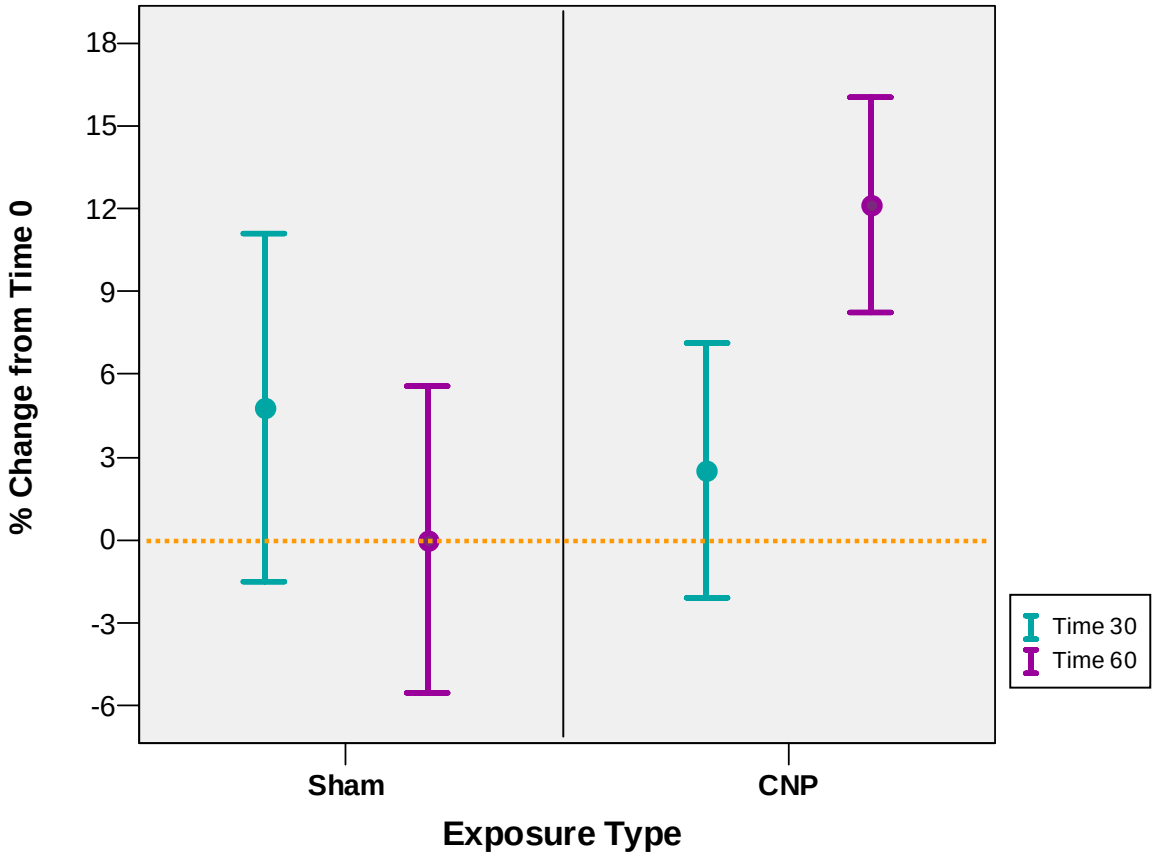

FIGURE 2. Percent change (from Time 0) in peak blood flow response to 0.1 mM Ach after 30 and 60 min of sham and CNP exposure. The line of reference at point 0 indicates 'no change' from the Time 0 blood flow values. Within each of the sham and CNP cells, the left hand points and error bars refer to the Time 30 measurements and the right hand points and error bars refer to the Time 60 measurements.

ABSENCE OF LINEAR CORRELATION BETWEEN BIOLOGICAL EFFECTS AND POWER DENSITY IN THE NON-THERMAL RF RADIATION RANGE

SIANETTE KWEE
DEPARTMENT OF MEDICAL BIOCHEMISTRY, UNIVERSITY OF AARHUS, BUILDING 170,
DK-8000 AARHUS C, DENMARK.

Abstract

During the past years many studies, including our own, have shown significant changes in various cellular processes caused by rates of adsorption at very low level of RF irradiated tissue.
In our investigations we found that MW-EMF exposure of cells down to SAR 0.0002 - 0.002 W/kg caused changes in the cell cycle, which could explain the resulting changes in cell proliferation. Therefore it can be assumed that the observed changes were due to non-thermal RF effects. This could also be concluded from our experiments at various temperatures, which showed that changes in cell proliferation were significantly higher in RF exposed cells than in non-exposed cells at the same temperature.
Nevertheless present safety levels are still based on thermal effects only.
Another argument in favour of non-thermal effects are the socalled "window" effects, i.e. only at specific power densities and/or frequencies, significant effects are seen. These "window" effects have only been observed in the non-thermal range. The same applies to the phenomenon of adaptation.
In this study it will be shown that, though changes in cell proliferation following RF exposure varied with the different SAR levels, they were not linearly proportional with increasing SAR levels, but exhibiting so- called "window" effects.
Effects also varied with the length of exposure time and after 24 h of exposure no changes in cell growth were detected any more. Moreover repeated exposure did no show any difference from results found at a single exposure. This can only be explained by adaptation of cell growth to RF exposure.
So a maximum increase in cell proliferation was only found at certain power densities and exposure times. This can be considered to be characteristic for non-thermal effects.

S.KWEE

Introduction

This study is part of our on-going work to find a mechanism for the biological effects of electromagnetic fields (EMF), in particular non-thermal effects.
From laboratory, clinical and epidemiological studies various effects have been reporterd after exposure to microwave electromagnetic fields. In course of time many theories have been proposed for these effects. On the other hand, very few experimental studies have appeared that offer an explanation for the reported effects.
At first it was assumed that biological effects of radiofrequency (RF) or microwave (MW) fields are solely the result of heat generation. Unfortunately the misconception still persists that all effects of MW-EMF are thermal. Even though we have started to talk about non-thermal effects of MW fields, they are being discussed in terms traditionally applied to heat effects. This is also reflected in the official standardlevels for safe exposure that are only based on heating and are based on average, whole-body irradiation of laboratory animals. However, a lot of tissue damage has been done long before a laboratory animal shows behaviour changes or dies from thermal effects.
At present we have enough experimental evidence to question the validity of standards based only on thermal effects. In particular fundamental research on cell tissue cultures has presented the strongest evidence. During the past years many studies, including our own, have shown significant changes in various cellular processes caused by rates of adsorption at very low level of RF irradiated tissue. At these levels it was also observed that the biological effects were not always linearly proportional with higher power densities or exposure times, but there were so-called "window effects". It also appeared that these window effects are characteristic for non-thermal effects.
We have chosen cell proliferation as the parameter to follow the changes in mammalian cell tissue cultures after exposure to EMF. Our experiments were all done at very low field strength, so the observed changes could be considered as non-thermal effects of EMF.

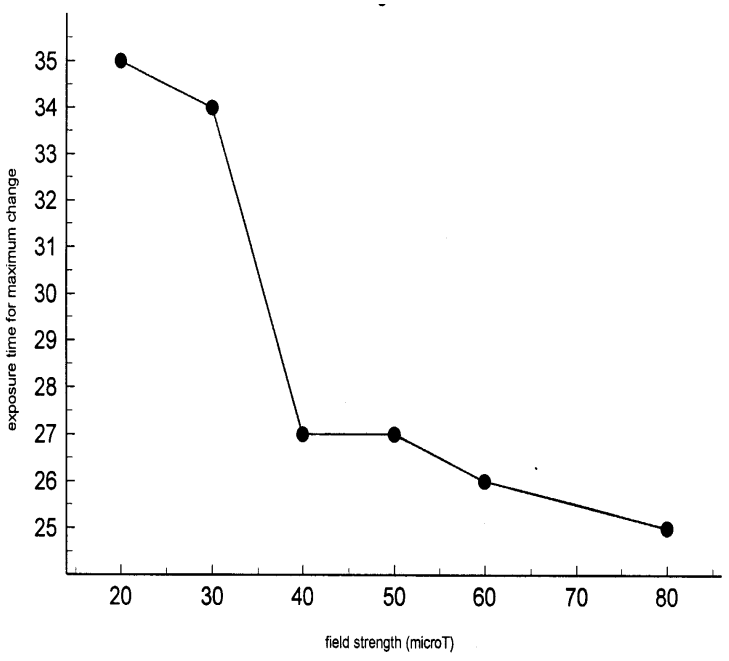

Figure 1:ELF electromagnetic fields: Dependance of maximum change in proliferation rate on exposure time and field strength.

Methods

Materials, cell cultures, EMF - MW exposure, experimental protocol and calculations have been described before [1-4].

Results and discussion

ELF magnetic fields

In previous work [3] we showed that in case of ELF-EMF exposure there was a linear correlation between field strength and the exposure time to obtain a maximum effect as shown in Fig. 1. However it can be seen that this proportionality is not present within a certain power range. As shown in Table 1 there is a plateau at 40-50 µT or a socalled " window".

TABLE 1

Dependance of maximum changes in proliferation rate on exposure time and ELF magnetic field strength in AMA cell cultures .

Field strength µT	Exposure time for maximum change in proliferation rate min
20	35
30	34
40	27
50	27
60	26
80	25

MW magnetic fields

The cell cultures were exposed to 960 MHz microwave fields at various power levels and exposure times. As shown in Table 2 and 3 this resulted in a significant change in cell growth, dependent on energy level and exposure time. Repeated periods of exposure did not seem to change the effects.

It is notable that increased energy levels are not proportional to an increased change in cell growth. At certain levels there is a negative change, while others show a positive change. Also linearity between exposure time and change in cell growth is different and dependent on energy levels. At varying energy levels the maximum change is seen at 20 or 30 or 40 min (Table 4).

At specific levels there is an increase and at others a decrease in growth change at longer exposure times. The latter could indicate adaptation. So adaptation is apparently also dependent on energy level, since at certain levels adaptation takes place already at shorter exposure times than at other levels.

TABLE 2

Percent change in proliferation rate in AMA cells after exposure to MW-EMF of varying energy levels and different exposure times.

Field strength SAR mW.kg^{-1}	Exposure time min	Change in proliferation rate		
		mean	95% confidence limit	
21	20	- 3.5*	-43	87
21	30	-75	-55	199
21	40	-120	14	219
52	10	70	-5	200
52	20	80	-17	204
52	30	645	-4	191
21	20	- 1.75*	-76	111
21	30	-90	-4	191
21	40	- 4.8*	-194	289
11	10	50	-5	223
11	20	230	-9	312
11	30	40	-99	126
21	20	1.3*	-99	126
21	30	-55	17	108
21	40	-103	58	148

* not significant. P value > 0.5 (paired t-test)

TABLE 3

Percent change in proliferation rate in AMA cells after **30 min** exposure to pulsed microwave fields of varying power levels.

Field strength SAR mW.kg^{-1}	**% change in proliferation rate**		
	mean	95% confidence limit	
6	665	-43	87
7	376	-55	199
12	-40	14	219
16	246	-3	160
21	-750	-55	190
23	-48	-220	105
4	924	-76	111
5	645	-4	191
8	832	-194	289
9	-752	-55	190
16	- 0.62*	-46	105
21	-90	-4	191
26	4.0*	-99	126
33	398	17	108
56	472	58	148
107	-38	-43	87
21	-55	17	108

* not significant. P value > 0.5 (paired t-test)

TABLE 4

Dependance of maximum changes in proliferation rate on exposure time and RF field strength.

Field strength SAR mW.kg^{-1}	**Exposure time for maximum change in proliferation rate min**
21	40
52	20
21	30
11	20
21	30

In conclusion it can be said that the same lineair correlation between power level, exposure time and growth change was not as clear in the case of RF exposure as it is for ELF exposure. As observed also by others the effects registered are not linear over the whole radiofrequency field density spectrum. This can be related to the oscillatory nature of cell growth. Apparently the interaction of microwave radiation with cellular oscillators contributes more to these effects than in case of ELF electromagnetic fields.

Summary

We have studied the effects of ELF and RF exposure on cell growth in cell tissue cultures. Our experiments were done at very low field strength and in case of RF fields corresponding to a SAR not exceeding 2.1 $mW.kg^{-1}$. So the changes observed can be considered as non-thermal effects.
In case of exposure to ELF we can see one specific window at a field strength of 40-50 μT.
In case of RF exposure the picture is more complicated: there are several windows or rather maxima and minima dependant not only on fieldstrength, but also on exposure times. This is certainly due to the different nature of RF radiation and also the modulating frequencies. It has been shown that at constant frequencies the biological effects are much less or even absent.
Longer exposure times and recording periods will result in adaptation and this might be the reason why under different experimental conditions no changes were observed. Due to the process of adaptation it may often no longer be possible to measure changes in cell proliferation when repeated exposures or and much longer exposure times are applied. It is known that under these conditions increasing Hsp concentrations are required to produce the effects as described above. So the Hsp mechanism is certainly also responsible for the resulting adaptation.
It is clear that these window and adaptation effects are crucial for long-term health effects of RF radiation [5] at non-thermal level.
In the thermal range these effects cannot be observed [6]. This is another reason to reconsider the present safety standard, which only applies to thermal effects of RF radiation.

Acknowledgements

The complete exposure system, including the SAR calculations, were designed and assembled by the late prof. Povl Raskmark.

References

[1] S. Kwee, P. Raskmark, Changes in cell proliferation due to environmental non-ionizing radiation. 1. ELF electromagnetic fields, Bioelectrochem. Bioenerg. 36: 109-114, 1995.
[2] S. Kwee, P. Raskmark, Changes in cell proliferation due to environmental non-ionizing radiation. 2. Microwave radiation, Bioelectrochem.Bioenerg. 44: 251-255, 1998.
[3] S. Kwee, P. Raskmark, Radiofrequency electromagnetic fields and cell proliferation, in Electricity and Magnetism in Biology and Medicine, F.Bersani, ed., Kluwer Academic/Plenum Publishers, New York, 187-190, 1999.
[4] S. Kwee, P. Raskmark, S. Velizarov, Changes in cellular proteins due to environmental non-ionizing radiation. 1. Heat-shock proteins, Electromagnetobiology 20(2):141-152, 2001.
[5] S. Kwee, Effects of concentration chances in certain cellular proteins due to microwave radiation, 3rd International Workshop on Biological effects of EMFs, Kos, Greece 2004.
[6] S. Velizarov, P. Raskmark, S. Kwee, The effects of radiofrequency fields on cell proliferation are non-thermal, Bioelectrochem. Bioenerg. 48:177-180, 1999.

MAGNETIC FIELD EXPOSURE METERING

TOMMI KEIKKO
TAMPERE UNIVERSITY OF TECHNOLOGY, P.O. BOX 692, FIN-33101 TAMPERE, FINLAND

REINO SEESVUORI
TAMPERE POWER DISTRIBUTION, P.O. BOX 175, FIN-33101 TAMPERE, FINLAND

SEPPO VALKEALAHTI
TAMPERE UNIVERSITY OF TECHNOLOGY, P.O. BOX 692, FIN-33101 TAMPERE, FINLAND

Abstract
A magnetic field exposure metering system has been developed to be utilized in indoor MV/LV substation measurements. The metering system follows the guidelines published by the International Commission on Non-Ionizing Radiation Protection (ICNIRP) and the EU directive of 2004 for public and occupational exposure. It can be used to measure magnetic field values, total harmonic distortion of the magnetic field, magnetic field exposure ratios for public and workers, load current values and total harmonic distortion of the load current. This paper presents the developed magnetic field exposure metering system, quantities to be measured by the system and exemplary measurements.

1. Introduction
Measurements of electric and magnetic fields in living and working environment have increased because the public concern on the fields has increased. Due to their possible health effects, the International Commission on Non-Ionizing Radiation Protection (ICNIRP) has published guidelines, in which upper limits for public and occupational exposures have been presented /1/. Based on these guidelines, European Parliament and Council have adapted a Directive on minimum health and safety requirements regarding the exposure of workers to electromagnetic fields in 2004 /2/. The European Parliament and Council Directive has to be nationally implemented in 2008. In Finland and in several other EU countries the legislation for occupational exposure to low frequency electric and magnetic fields is still missing. In addition to that common practices and standards have to be created for everyday measurements and estimation of magnetic field exposures.

Table 1 presents occupational exposure reference levels of the ICNIRP guidelines and the Directive. The limit for allowed public exposure to 50 Hz magnetic fields is 100 μT and for occupational exposure 500 μT.

Table 1. Public /1/ and occupational /1, 2/ magnetic field exposure reference values.

Frequency, f (Hz)	**Public allowed magnetic flux density, B (μT)**	**Occupational allowed magnetic flux density, B (μT)**
Up to 1	4×10^4	2×10^5
1-8	$4 f^{-2} \times 10^4$	$2 f^{-2} \times 10^5$
8-800	$5 f^{-1} \times 10^3$	$25 f^{-1} \times 10^3$
800-820	6.25	$25 f^{-1} \times 10^3$
$(0.82\text{-}65) \times 10^3$	6.25	30.7
$(0.065\text{-}0.15) \times 10^6$	6.25	$2 f^{-1} \times 10^6$
$(0.15\text{-}10) \times 10^6$	$0.92 f^{-1} \times 10^6$	$2 f^{-1} \times 10^6$
$(10\text{-}400) \times 10^6$	0.092	0.2
$(0.4\text{-}2) \times 10^9$	$4.6 f^{0.5} \times 10^{-6}$	$10 f^{0.5} \times 10^{-6}$
$(2\text{-}300) \times 10^9$	0.2	0.45

In 2003 ICNIRP expanded their guidelines by taking into account the harmonic components of the magnetic field with phase angles /3/. This statement provides accurate guidelines, in practice, to estimate the magnetic

field exposure due to harmonic components, but it has not been referenced widely. In the case of electricity transmission and distribution only frequencies from 50 Hz to 65 kHz contribute to magnetic field exposure. So far, there is only one commercial magnetic field exposure meter, which is able to consider this frequency range including the phases of the magnetic field components. Measurement method utilized in that meter seems to stands up to a close examination. However, the output of the results in this commercial meter is inadequate for advanced measurements.

Electromagnetic fields have been studied at the Tampere University of Technology (TUT) since the 1980's. In recent years, the research has concentrated on evaluating exposure to magnetic fields. Previously, measurement system at TUT was based on commercial magnetic field meters and power quality analyzers /4/. In that system, the exposure was calculated afterwards enabling advanced magnetic field exposure measurements considering the phases of the harmonic components. However, load current of the indoor MV/LV substation and magnetic field were measured with different equipments, thus not exactly simultaneous. There was a clear need for an improved measurement system providing directly simultaneous measurements of all physical quantities of interest. In this paper we will describe a magnetic field exposure metering system utilized in indoor MV/LV substation measurements meeting these requirements.

2. Measurement methods

In addition to magnetic field exposure measurements, the system measures synchronously load currents. The measurement system saves magnetic field values, total harmonic distortion of the magnetic field, magnetic field exposure ratios for public and workers, load current values and total harmonic distortion of the load current.

A conservative estimate of the cumulative magnetic field *K'* normalized to the measured 50 Hz magnetic field value B_1 is calculated according to the ICNIRP guidelines /1/ by

$$K' = 1 + \sum_{k=2}^{16} k \frac{B_k}{B_1} + \sum_{k=17}^{1300} 16 \frac{B_k}{B_1}, \tag{1}$$

where k is the index of harmonic frequency and B_k is the measured magnetic field of the harmonic component k /5/. According to the ICNIRP guidelines the magnetic field exposure ratio *R'* is

$$R' = \frac{B_1}{B_{L,1}} K', \tag{2}$$

where $B_{L,1}$ is the 50 Hz magnetic field reference level. The allowed upper limit for the magnetic field exposure ratio *R'* is 1. The method presented in equations 1 and 2 has been shown to overestimate the exposure ratio close to 50% in indoor distribution substation by /4/.

According to the ICNIRP statement /1/ and the anticipated implementation of the EU Directive /2/ the maximum cumulative magnetic field K normalized to the 50 Hz magnetic field component B_1 can be obtained as the maximum value of the sum of harmonic components inside a cycle time of 20 ms as follows

$$K = \left\{ 1 + \sum_{k=2}^{16} k \frac{B_k}{B_1} \cos(k\omega_1 \tau + \varphi_k + \phi_k) + \sum_{k=17}^{1300} 16 \frac{B_k}{B_1} \cos(k\omega_1 \tau + \varphi_k + \phi_k) \right\}_{\max}, \tag{3}$$

where ω_1 is $2\pi f_1$, φ_k is the phase angle of B_k, ϕ_k is the biological correction angle at frequency $k \times f_1$, f_1 is fundamental frequency of 50 Hz. Further, the magnetic field exposure ratio R is

$$R = \frac{B_1}{B_{L,1}} K. \tag{4}$$

The calculation procedure of equations 3 and 4 was presented by /6/ and also by /3/ and /7/. The calculation procedure of the magnetic field exposure ratio based on equations 3 and 4 was earlier used to study the validity of the method based on equations 1 and 2 in indoor distribution substation environment by /4/.

The maximum cumulative magnetic field K of equation 3 can be presented in a more general form as a function of time t for long term measurements as follows

$$K(t) = \left\{ \sum_{f=8Hz}^{800Hz} \frac{f}{f_1} \frac{B_f(t)}{B_1(t)} \cos\left[\omega\tau + \varphi_f(t) + \phi_f\right] + \sum_{f>800Hz}^{150kHz} 16 \frac{B_f(t)}{B_1(t)} \cos\left[\omega\tau + \varphi_f(t) + \phi_f\right] \right\}_{\max}. \tag{5}$$

This approach, in principle, is a continuous integration of the magnetic field spectrum corresponding closely to the weighted peak approach /3, 6/. In the weighted peak approach the waveform is weighted with a simple high-pass filter with a 3 dB cut-off frequency at 800 Hz. This approach has been used in the measurements of this paper. However, one must note that a discrete summation of equation 3 is quite adequate for power engineering applications and takes into account all essential frequencies.

3. Meters

In the measurements a 3-axial EnviroMentor BMM-3000 magnetic field meter (accuracy ±5%, RMS) was used. Measured signal was further processed and stored with data acquisition system NI-DAQPad-6015 by National Instruments. Measurement program is named as Keikko6 and created with LabView 7.1. Fig. 1 presents an exemplary screen from a magnetic field measurement.

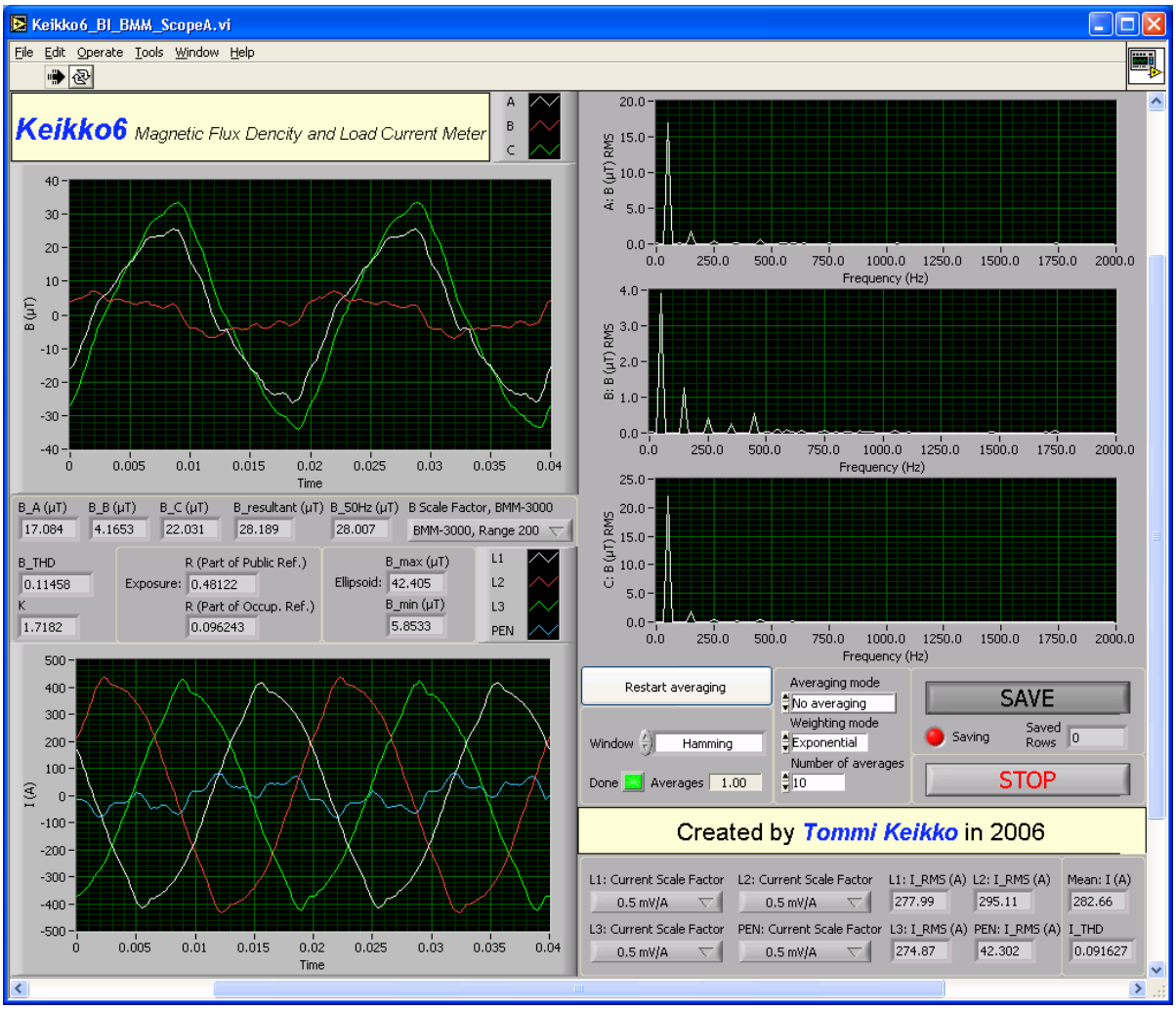

Figure 1. Output screen of the magnetic flux density and load current meter with exemplary measurement results.

The developed metering system saves magnetic field values, total harmonic distortion (THD) of the magnetic field, magnetic field exposure ratios for public and workers, load current values and total harmonic distortion of the load current. Magnetic field values *B_A*, *B_B*, and *B_C* in Fig. 1 are RMS components of the orthogonal magnetic flux density values B_x, B_y, and B_z. Also their resultant value and the resultant 50 Hz value are shown. Total harmonic distortion of the magnetic field B_{THD} is calculated, as follows

$$B_{THD} = \sqrt{\frac{\sum_{k=2}^{1300} \sum_{D=x,y,z} B_{k,D}^2}{\sum_{D=x,y,z} B_{1,D}^2}}, \tag{6}$$

where D is the index of the orthogonal magnetic field component. Further, the cumulative magnetic field K normalized to 50 Hz, and public and occupational magnetic field exposures are saved as well.

In addition, elliptic polarization of the magnetic flux density is measured. Ellipsoid based on maximum and minimum magnetic field values during five 50 Hz cycles presents the polarization grade of the vibration.

Load current values *I_RMS* are RMS values for the three phase currents I_{L1}, I_{L2} and I_{L3} and the combined protective earth and neutral conductor current I_{PEN}. Mean current is the average value of the three phase currents.

Mean total harmonic distortion of the load current $I_{THD,Mean}$ (*I_THD* in Fig. 1) is determined and calculated from the load currents of the phases, as follows

$$I_{THD,Mean} = \sqrt{\frac{1}{3}\sum_{L=L1,L2,L3}\frac{\sum_{k=2}^{n} I_{k,L}^2}{I_{1,L}^2}}, \quad (7)$$

where L is the index of phases.

4. Measurement set-up

Magnetic field and load current measurements were performed inside 12 indoor MV/LV substations. Fig. 2 presents a photo of an indoor distribution substation, its surroundings and the measurement set-up in one typical substation structure having the LV connection near the ceiling. The magnetic field measurement point nearby the LV connections was determined by considering public exposure in the residence above an indoor distribution substation. The structure of the substation and the building was examined before each measurement.

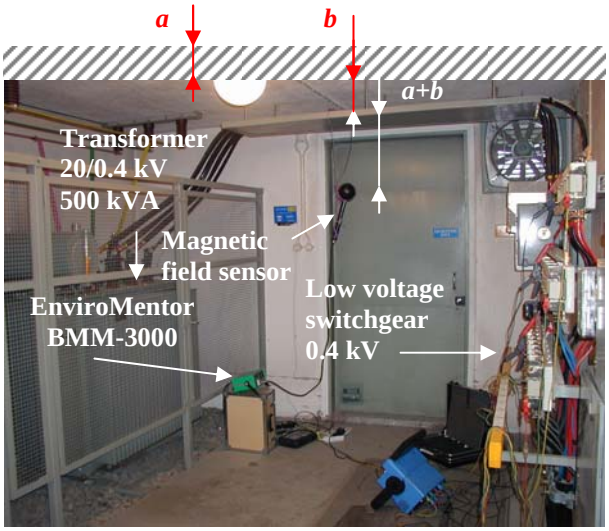

Figure 2. Measurement set-up in a typical indoor distribution substation having the LV connection near the ceiling. Dimension *a* is the thickness of the ceiling and dimension *b* is the distance between the LV connection and the ceiling. /4/

In cases, where the LV connection was not close to the ceiling, the magnetic field sensor was located in the ceiling of the substation above the LV connection or above the expected highest magnetic field source, if possible. Fig. 3 presents a typical measurement set-up, where the LV connection goes on the floor level. Low voltage switchgear can be seen in left-hand photo.

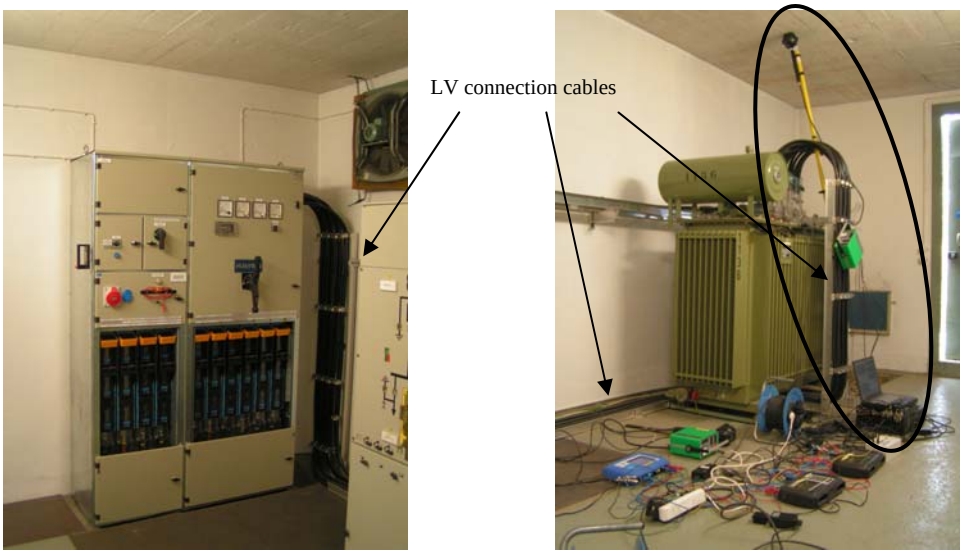

Figure 3. Photos of a measurement set-up in an indoor MV/LV distribution substation, where LV connection is located on the floor level.

Right-hand photo presents the MV/LV transformer. Meters and other measurement equipment are on the floor of the substation. What comes to the public exposure on magnetic fields in the residence above the substation, the space above the transformer is the interesting area to be measured. This area is rounded in the right-hand photo in Fig. 3 and is considered in this paper.

5. Measured magnetic field waveform exposures

Different types of indoor distribution substation structures were selected for measurements to obtain an overall picture on the public magnetic field exposure. Measurements were carried out during the spring 2006. Loads were apartment houses, office buildings or school buildings. The loads of the distribution substations were mostly heat loads, fluorescent and tungsten lamps, computers, and other electronic devices. These loads cause harmonics in the load current that increase the total magnetic field in the substation and decrease the allowed reference value of the 50 Hz magnetic field component. Measured locations and periods are presented in Table 2, where I_{max} is the highest 15 minutes average load current during the previous year and I_{Rated} is the rated load current.

Table 2. Measured indoor distribution substations in spring 2006.

Substation	Transformer		LV connection structure	Measurement period (h:min)
	I_{max} (A)	I_{Rated} (A)		
A	1000	1155	Cables near ceiling	21:35
B	1100	1155	Cables in floor	18:28
C	350	722	Cables near ceiling‡	Period 1: 69:57 Period 2: 28:55§
D	650	1443	Bus bars near ceiling	22:19
E	560	722	Cables near ceiling	18:08
F	730	722	Cables near ceiling	117:11
G	500	722	Cables in floor	21:55
H	T1: 500 T2: 300	T1: 722 T2: 433	Cables near ceiling	44:56
I	T1: 440 T2: 290	T1: 722 T2: 433	Cables near ceiling	73:18
J	450	722	Cables in floor	18:39
K	T1: 350 T2: 750	T1: 1155 T2: 722	Cables near ceiling	21:29
L	560	722	Bus bars near ceiling	66:34

‡ special structure: two × tree phase cables

§ measured in two periods and two locations, period 1 near LV switchgear and period 2 near transformer

Magnetic fields were measured during 1 to 5 day periods. Transformers in substations B, F and K were near their capacity limits. The other substations were clearly within the capacity of their transformers. More detailed results are presented for substation A to describe the advantages of our metering system. Long periods can be measured to consider varying load situations when metering exposure to magnetic field. Due to data handling purposes long measurements can be saved automatically to several files. We used a measurement interval of 1 s and saved 30 000 measurements in one output file i.e. a measurement of 8 hours and 20 minutes. In the following we present a set of measurements done during the first metering lot for substation A to demonstrate our metering systems. This substation has the same type of structure as in Fig. 2.

Fig. 4 presents 50 Hz magnetic field component and public exposure ratio during the first metering lot for substation A. The public exposure ratio correlates, on the average, well with the fundamental magnetic field component, which is in accordance with small variations of $K(t)$ as a function of time being close to 2 (Fig. 5). Thus, according to equation 4, the public exposure ratio has to be multiplied by a factor of 50 μT to obtain the 50 Hz magnetic field component in Fig. 4. This simply means, that the total magnetic field exposure including the harmonic components is, in practice, two times the exposure due to the fundament frequency.

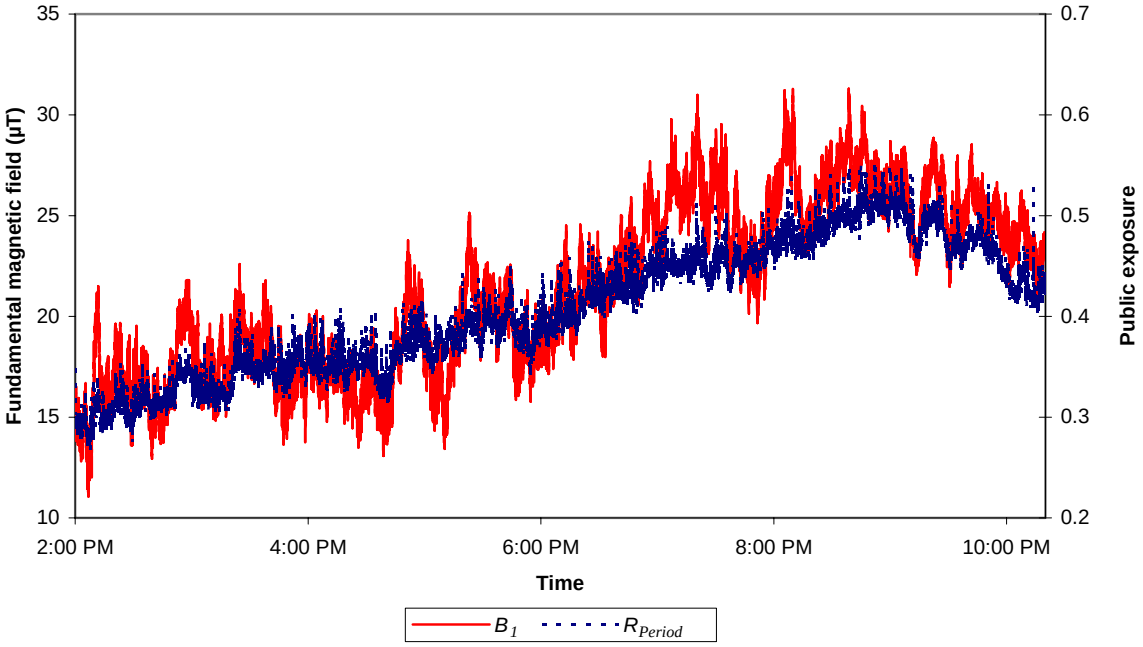

Figure 4. Measured 50 Hz magnetic field component and the public exposure ratio in substation A.

Candidates to explain varying *K(t)* are the total harmonic value for the magnetic field and the relative load current defined as load current divided by the rated current of the transformer (1155 A for substation A), which are presented in Fig. 5. There seems to be a slight negative correlation between the cumulative magnetic field normalized to 50 Hz and the relative load current in agreement with earlier observations /4/. The same negative correlation exists also between B_{THD} and the relative load current. A strong positive correlation is seen between *K(t)* and B_{THD}, as expected.

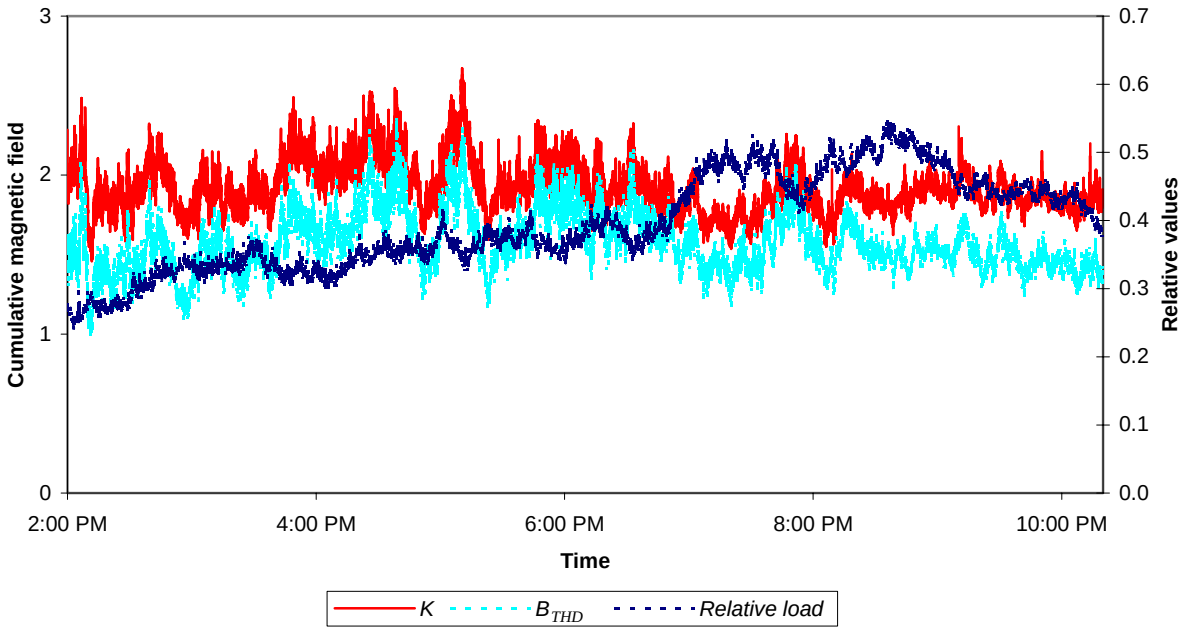

Figure 5. Measured *K(t)*, B_{THD} and relative load current as a function of time for substation A.

Based on Fig. 5 the correlation between *K(t)* and B_{THD} is clear. The shapes of the curves seem to be almost similar having only minor differences. Further, based on /4/ load current and magnetic field harmonics had correlation. The same was tested for substation A in Fig. 6. Correlation between the load current and the magnetic field total harmonic distortions is clear also in these measurements.

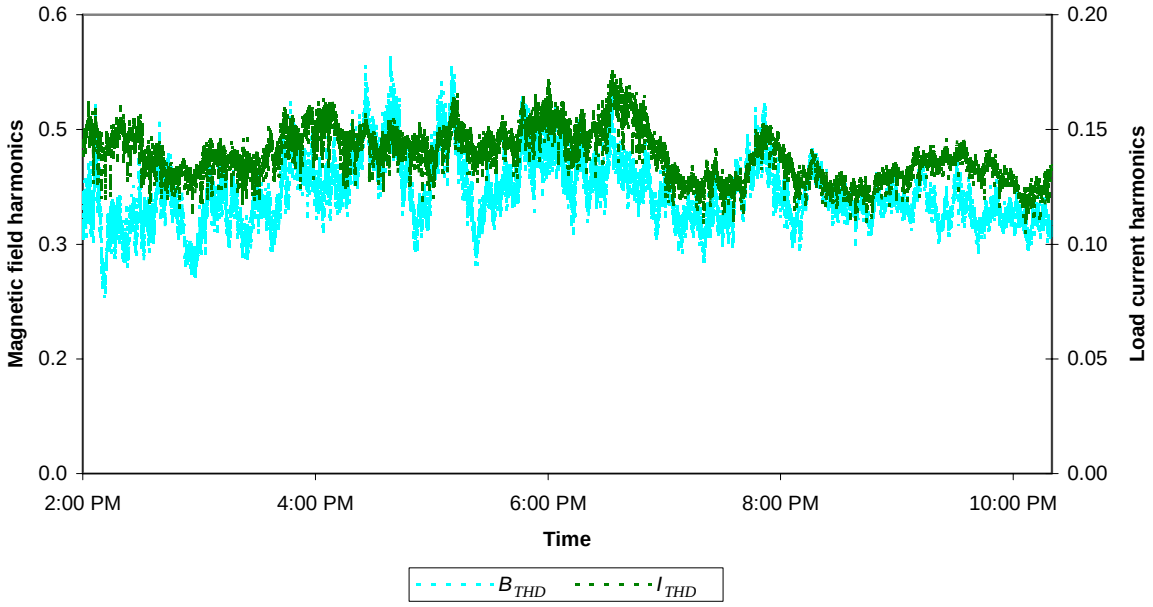

Figure 6. Load current and magnetic field harmonics for substation A.

The coefficient between I_{THD} and B_{THD} is close to 3 in this measurement. This coefficient is the same than in /4/, although the determination of the total harmonic distortion values differs. Previously the values were determined based on the highest load current and highest magnetic field component. The more advanced determinations in this paper were presented in equations 6 and 7.

Summary of the results for all measurement periods is presented in Table 3, where I_{load} is the highest load current, B_{period} is the highest magnetic field and R_{period} is the highest magnetic field public exposure ratio during the measurement period. Significance of the measurement result is determined based on congruence between the measured location and the possible public exposure so that ** means a significant result and * means a indicative result. R_{max} is the highest magnetic field public exposure ratio during the measurement period scaled to the rated load current.

Table 3. Key results for the measurement periods.

Substation	Significance	I_{load} (A)	B_{period} (µT)	R_{period} (%)	R_{max} (%)
A	**	633	32.7	0.73	1.33
B	*	851	120.8	1.57	2.13
C	**	Period 1: 326	Period 1: 7.90	Period 1: 0.17	Period 1: 0.37
	*	Period 2: 279	Period 2: 41.6	Period 2: 0.90	Period 2: 2.32
D	**	688	44.3	0.71	1.49
E	**	349	26.7	1.37	2.83
F	**	478	51.4	0.82	1.24
G	*	378	7.40	0.27	0.51
H	**	454	75.4	1.37	2.18
I	**	352	13.1	0.20	0.42
J	*	343	27.5	0.41	0.86
K	**	567	12.1	0.33	0.67
L	**	445	75.6	1.73	2.81

Significance is valuated based on the structure of the indoor MV/LV substation. For bus bars or cables near the ceiling the location of the magnetic field sensor corresponds to the floor of the space above the substation. If the sensor is located in the ceiling of the substation, the results of the measurement periods are indicative. In the Table 3 the public exposure ratio during the measurement period exceeded value one in 3 out of 9 significant measurement periods. When the exposure ratio is scaled with the rated load current the value one is exceeded in 6 out of 9 significant measurement periods. The exposure ratios exceeded one in 1 and 2 out of 4 indicative measurement periods, respectively.

6. Summary

Magnetic field exposures are presented considering harmonics for the case of 12 indoor MV/LV distribution substations. Based on the measurements, the public exposure often exceeded the reference value in rooms above indoor distribution substations. Further, this means that indoor distribution substations can cause public exposure. Another relevant question is do the structures of the present indoor MV/LV distribution substations produce too high magnetic fields considering the EU Directive /2/, which will be nationally implemented within the EU by 2008.

In this paper, magnetic fields were measured with a new and advance metering system. All important magnetic field and load current values were measured with a simultaneous measurement. This new metering system gave relevant results and made further analyses possible. Previous measurements and references supported results and analysis made with the new metering system. Furthermore, magnetic fields can cause disturbances in measurement or control systems and in electrical devices, and that is another possible use of this new metering system.

Based on the measurements of substation A, the load current is the primary cause for the magnetic field level. Fig. 7 presents the measured magnetic field generation defined as magnetic field divided by the load current for substation A.

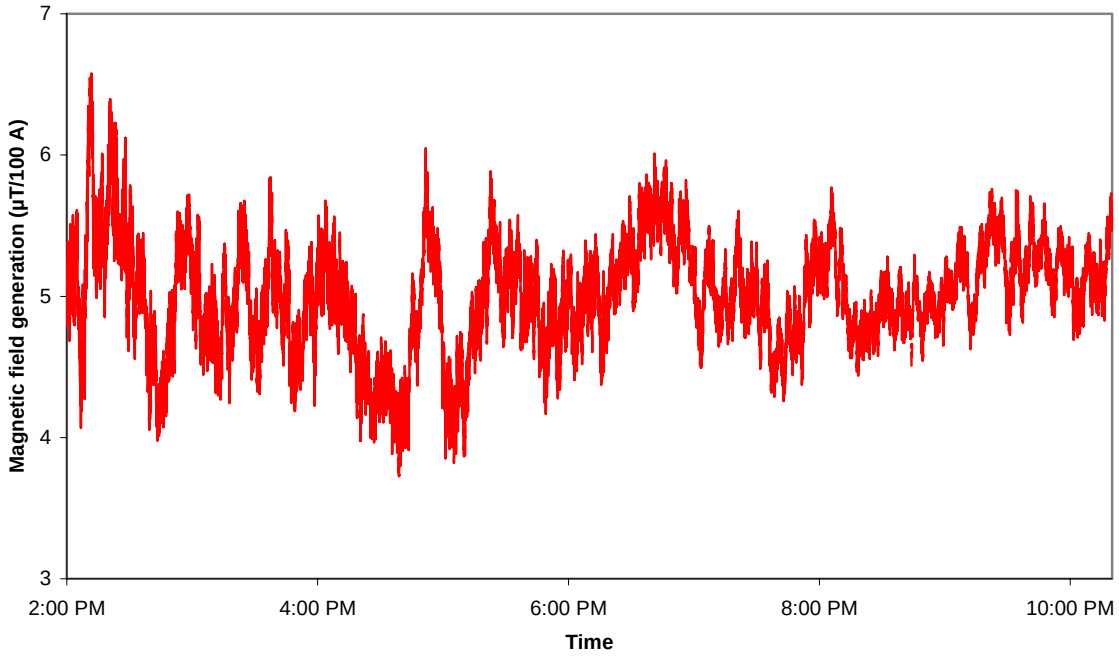

Figure 7. Measured magnetic field generation in substation A.

A generally accepted basic approximation is that the magnetic field is considered to be directly proportional to the load current. This seems to be roughly true for substation A. The average value for the magnetic field generation in Fig. 7 is around 5 µT/100 A. However, it varies most of the time between 4 and 6 µT/100 A. Because the curve in Fig. 7 is not linear, the phase angle differences of the currents have important role when estimating magnetic fields.

The structural differences between indoor distribution substations will have a significant impact on magnetic fields. Therefore, to create general magnetic field exposure estimates, a wider range of grouped structures of the indoor MV/LV distribution substations and with grouped load parameters should be analyzed.

References

1. ICNIRP. Guidelines for limiting exposure to time-varying electric, magnetic, and electromagnetic fields (up to 300 GHz). Health Phys 74:494-522; 1998.

2. Directive 2004/40/EC of the European Parliament and of the Council on the minimum health and safety requirements regarding the exposure of workers to the risks arising from physical agents (electromagnetic fields). Brussels; 2004.

3. ICNIRP. Guidance on determining compliance of exposure to pulsed and complex non-sinusoidal waveforms below 100 kHz with ICNIRP guidelines. Health Phys 84:383-387; 2003.

4. Keikko T, Seesvuori R, Valkealahti S. Exposure to magnetic field harmonics in the vicinity of indoor distribution substations. Health Phys 2006. (In press.)

5. Keikko T, Isokorpi J, Korpinen L, Elovaara J, Vanhala P. Considering electric and magnetic fields in electric power system design in Finland. In: Proceedings of a CIGRE, International Conference on Large High Voltage Electric Systems. Paris: CIGRE; ID 36-102; 2000.

6. Jokela K. Restricting exposure to pulsed and broadband magnetic fields, Health Phys 79: 373-388; 2000.

7. Keikko T. Technical management of the electric and magnetic fields in electric power system. Dr.Tech. dissertation, Dept. El. Eng. Tampere: Tampere University of Technology; 2003.

ALGORITHM FOR NOISE-DATA REDUCTION FOR LONG-TERM EMF MONITORING SYSTEMS

H. HAIDER[1], A. NÖHRER[1], G. NEUBAUER[1]

[1]*ARC SEIBERSDORF RESEARCH GmbH, A-2444 SEIBERSDORF, AUSTRIA*
HARALD.HAIDER@ARCS.AC.A T

Abstract
In addition to present popular 'in situ' EMF-measurements performed at critical locations like schools, hospitals or in front of base stations for one-time, long-term evaluations of RF-fields become more and more essential. This is especially because of the continuously increasing number of new applied technologies and even more emitting base stations. To perform such long-term investigation, fully automatic, stand alone EMF-monitoring stations are suited very well. Typically, several of such stations are connected to one environmental network, fully remote controlled by one server. To yield maximum of information, each station is continuously in operation, performing frequency selective measurements and generating an enormous amount of measurement data. The data communication often represents the bottleneck of such systems and therefore the reduction of these data becomes very essential. By implementing an intelligent algorithm for data reduction directly on the measurement station this problem could be reduced. Therefore we will provide in this paper a methodology suited for a considerable reduction of noise points without loosing any relevant signal information. The specific nature of this algorithm and his efficiency in data reduction will be discussed and explained, including how it works and what parameters are needed. The results which can be achieved with this technique are demonstrated with the existing monitoring system 'Field Nose' from ARC Seibersdorf research.

I. **Introduction**

Today more than 1 billion people are using mobile telephones world-wide, about 360 million people of them in Europe. Such wide use of this technology led to an increase in the environmental exposures to RF-fields and the introduction of new, additional technologies has intensified this process.

In the meantime most countries have national laws, regulations, guidelines or standards and more or less accurate defined measurement procedures and protocols how to handle RF-exposure. The ICNIRP guidelines [1] are used as reference in most European countries. However, many countries apply more restrictive limits, e.g. Switzerland and Italy [2]. Independent of the absolute values of limits, different measurement procedures are used in different countries. In general, the limit are frequency dependent and given over a wide frequency range. There are different concepts regarding the kind of exposed people and the considered areas, i.e. general public versus workers or controlled versus uncontrolled areas. For EMF-exposure evaluation, the contributions of all relevant RF-emitters for the whole body have to be investigated, considering individual signal form, frequency range, bandwidth, polarisation, direction and deviation over time. This leads to a lot of essential requirements for EMF measurement systems and especially also for the data evaluation procedures of such equipment. Another need for adequate measurement and evaluation techniques is the demand for epidemiological studies on the potential health effects caused by the numerous RF-emitters. In the frame of an international project the feasibility of epidemiological studies on potential health effects arising due to the exposure from mobile telephone base stations was jointly assessed by a team of RF experts and epidemiologists. A major outcome of this study was the need for reliable exposure assessment procedures [3]. Frequency selective, monitoring exposure assessment equipment is one of the best suited approaches to assess exposure in a reliable way. Also one COST 281 program activities are focusing at that topic.

II. EMF Measurement Systems

One of the most important requirements for EMF-measurement systems for exposure evaluation is an isotropic (receiving) radiation characteristic over the whole frequency range to add all contributes of different RF-emitters (technologies) in the same way, independent of their distance and direction in relation to the measurement point

and their polarisation. Further the sensitivity of the measurement systems have to be high enough to measure very small signals of modern communication technologies of a few mV/m as well as the dynamic range has to be large enough to consider signals close to the limit level, which is typical at 4 V/m to 60 V/m. Of course measurements have to consider the effective field strength or power flux density independent on the kind of signal or technology (e.g. modulation, pulsing or frequency hopping) and they should be fast, easy to handle, accurate and reliable. The instruments should be small, low cost, easily to operate and the requirement to enable long-term evaluation is essential for RF-dosimetry. Currently three different technical solutions are on the market to perform EMF measurements and each one has its individual assets and drawbacks in relation to the requirements mentioned above.

First there are the well known wideband field probes. They are low priced, easy to handle, have a wide frequency range typically from 100 kHz to 3 GHz, good isotropic characteristic and they are popular also for other kind of measurements e.g. for classical EMC. Some types also enable to select some frequency dependent limits and return the result in percentage of that limit. Unfortunately this is a global result without any information of the relative contribution of the considered transmitters. Also the sensitivity is limited at about 0.1 V/m. Therefore field probes are popular and well suited for preliminary measurements, e.g. to decide if and at what position frequency selective measurements should be performed.

A second group is represented by so called transmitter-selective or narrowband instruments. With these instruments, which are relatively new on the market, fixed or user definable frequency bands corresponding with the bands of transmitter-technologies are measured. Each narrowband is evaluated separately but of course there is, similar to field probes, no possibility to get any information about signal intensity within a band e.g. any differences in channels or for competitive providers. Depending on the system, data acquisition in the time domain is very flexible, from milliseconds to minutes for long-term evaluations. Typically 7 to 15 narrow-bands are measured together at each time cycle and therefore the resulting data amount is relatively easy to handle. Some systems are small enough to carry them on the body or in a rucksack and use these instruments for ‘live time’ RF-dosimetry during the whole day or to evaluate typical exposure at a working place. Typical limitations of those systems are given if signals occur out of the predefined narrow-bands because they were totally ignored. Another problem is caused by crosstalk of bands close together which is often used for up- and downlink of one technology, but could also affect different technologies, if their frequency bands are proximate to each other. Increasing the number of RF-technologies or even the number of bands which should be evaluated will increase that crosstalk problematic. The sensitivity of the systems is typically given at the data-sheets with 10 to 50 mV/m, which is suitable for most applications. Unfortunately the isotropic behaviour and measurement uncertainty are often not clearly specified especially if these data are needed for the individual bands.

The third group of systems is a more or less traditional method using a wideband antenna or field sensor in combination with a frequency selective measurement instrument like a spectrum analyser. Due to the fact that no antenna has an isotropic radiation characteristic by itself, one solution consists in the addition of the contributions of three measurements of an antenna with a dipole like radiation pattern to yield an isotropic receiving characteristics for the system. ARC Seibersdorf research developed small RF-antennas with a dipole like radiation pattern and established the so-called ‘Add3D Method’ [2] in 2002. An automatic positioner can be used to realize the three orthogonal antenna orientations. Figure 2 is showing a schematic drawing of the ARC Seibersdorf research system ‘Field Nose Complete’ and a picture of the real system (see also at http://www.seibersdorf-rf.com). This EMF-measuring and monitoring system is fully remote controlled by the software ‘Nose’, and enables the user to perform automatic measurements as well as many data evaluation procedures. The following examples and evaluations of that publication are based on this system.

Other manufacturers offer systems based on three small sensors with dipole characteristic and switch between them or combine them by an electrical network. In those cases there is the challenge to get an acceptable isotropic radiation pattern of the system because the three sensors interfere with each other. On the other hand such systems are faster, because they need no time to rotate the receiving antenna.

All these systems based on frequency selective spectrum analyser measurements enable individual RBW-settings, rms-, peek- or average signal detection, max-hold trace functionality, very high dynamic range and best sensitivity (low noise level) caused by the performance of state of the art spectrum analysers. The measurement time for a frequency scan is different and mainly depending on the trace speed, the analyser settings, the number

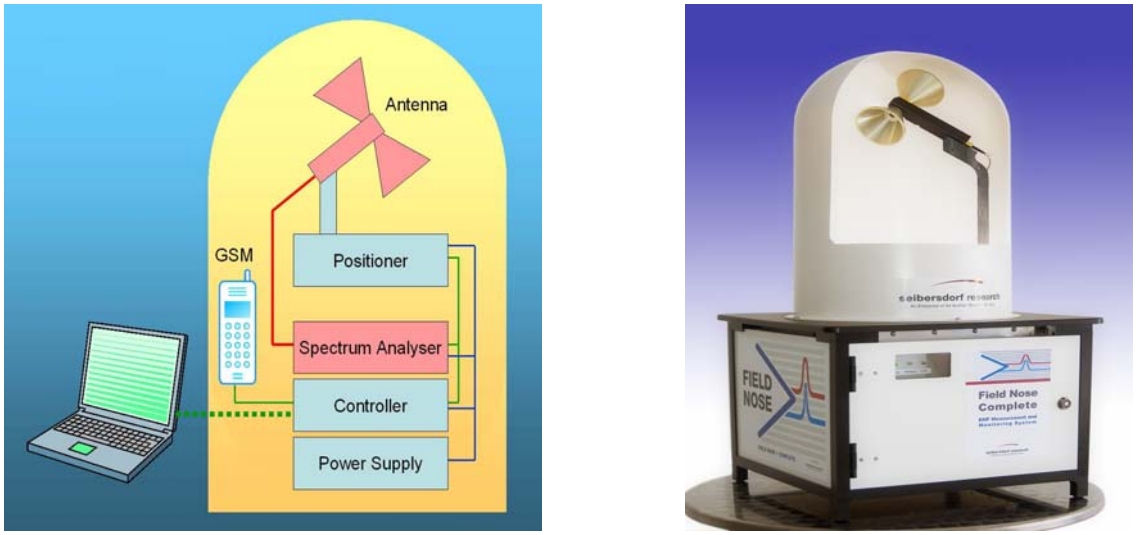

Figure 2: EMF-monitoring system Field Nose Complete (schema and picture)

of repetitions and the sensor type. Measurement cycles of a scan from e.g. 80 MHz to 2.5 GHz can be done within a minute or less. With these frequency selective measurements most information is generated and available for evaluation on the one hand. On the other hand especially that large amount of data can make problems. One possible way of the challenging task to reduce the amount of data without any loss of relevant information is presented in the next chapters.

III. Evaluation problematic of frequency selective systems

Figure 3 is showing a measurement trace and the corresponding data evaluation of a frequency selective, wideband EMF-measurement performed in the centre Vienna. Radio and TV signals as well as the typical downlink signals of mobile phone technologies (GSM 900, DCS 1800 and UMTS) can be seen. The frequency bands of those technologies are marked by coloured, vertical areas corresponding to technology bands as common for band-selective data evaluation. The measurement was done from 80 MHz up to 2.5 GHz using a Field Nose system with a PCD8250 antenna, a 5 m long RF-cable and an Anritsu MS 2711D spectrum analyser.

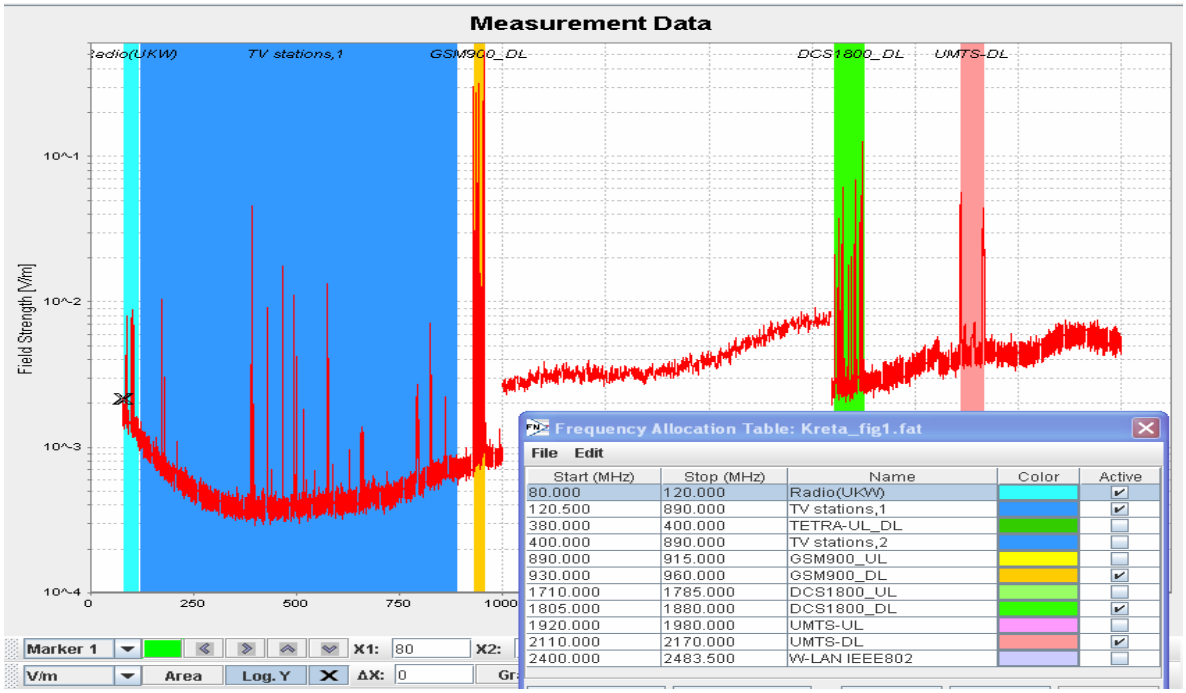

Figure 3: Frequency selective EMF-wideband measurement trace (overview measurement) from Vienna

The characteristic ‘bathtub’ noise floor for this frequency selective, wideband measurement trace can be seen very clearly because of the logarithmic scaling of the field strength axis. It is caused by the noise floor of the spectrum analyser itself (primary depending on its RBW setting, internal attenuator setting or an activated preamplifier), the cable- and connector losses and the antenna factor of the used PCD-antenna. Also caused by the logarithmic scaling and the high sensitivity of the system, the small signals from radio and TV-stations and less strong mobile technology signals with a few mV/m can be detected well. For the measurements from 80 MHz to 1 GHz and from 1.8 GHz to 2.5 GHz a RBW-setting of 100 kHz was used to get a good frequency resolution of the measured technologies. Between those bands we do not expect any signals. Therefore the RBW at that frequency range was set to 1 MHz to save time for the frequency scans and to reduce the number of measurement points too. The higher noise floor does not disturb in that case because of the lack of public communication technologies in that range.

Caused by the selected RBW-settings with 100 kHz respectively 1 MHz and the wide frequency range, 17.000 measurement points are needed for the one single scan according to Figure 3. For example if one scan should be performed each 5 minutes during one day, 288 scans respectively nearby 5 million measurement points are needed. To save that data including measurement information like settings, used antenna and cable factors, time and date, the Field Nose system needs approximately 15 MByte of memory, if the data was stored in a binary format. Even up-to-date computers need considerable time (from a few seconds to minutes) to process such big amount of data, e.g. to print them on screen, perform any data calculations, load and save them or to send them to a host system computer in case of a monitoring system consisting of several measurement stations. In practice measurement may differ to that example, but still a huge amount of data could be produced and the resulting time delay for data processing will not be accepted by the user. This would limit the application of frequency selective systems for long-term evaluation in a considerable way.

IV. Algorithm for noise-data reduction

Having a look to Figure 3, it can be seen that most of the measurement points are representing noise. The only important information of this noise floor is that all signals below that level could not be detected by the measurement system and not considered for any evaluation. On the other hand if the level of noise is deep enough, the signals below that do not affect the evaluation results in a significant way. This fact is the starting point to overcome the problem of extremely large amount of data for frequency selective measurements. Based on an effective signal detection method it should be possible to divide the signals from noise sequences and reduce or eliminate the noise data. Of course the efficiency of that process depends on the relation of signal and noise parts in a measurement scan but especially for wideband measurements it should reduce the number of data points in a considerable way and help to speed up the systems.

The simplest solution segmenting noise and signals is a user defined threshold line near above the noise. All values above that threshold will be accepted as signals. Unfortunately this works only for small frequency ranges because for wideband measurements the noise floor usually is frequency dependent and there is the question where to set the threshold limit. Another method is to select the largest signals by a peak detection algorithm. There of course is always the question of a proper predefinition of the number of relevant peaks as well as the problem that the highest signals not necessary are the one with most of energy because of different bandwidths. Approaches like they are typical in the noise reduction of sound signals were not applicable because of the fact that EMF signals sometimes look like noise to them. Other approaches which are used in image processing are not really applicable too.

Therefore we developed a specific algorithm for signal detection considering the unique requirements in the area of EMF signal processing. The processing of the data can be applied to measured data that is already available, but the main intention was to perform the reduction during measurements on the embedded system of the Field Nose Complete system. Therefore the reduction algorithm works completely automatically but it is also possible to set some parameters manually to improve the results for certain measurements. The noise data can be reduced so that the noise floor is still present or it is possible to remove the noise data completely. Signals are not affected by the algorithm in any way.

The noise data reduction algorithm itself works in the way that first the noise floor is detected and segmented from the signals. The next step is to calculate the new reduced noise floor with less data points and finally this new noise floor is merged with the original signal data. The most difficult part was to find a way how to distinguish very efficient between the noise floor and the signals because sometimes signals share many characteristics with the noise. For that purpose an upper and a lower envelope of the noise are calculated by

using a 'Noise Height' factor in dB. Based on this predefined noise-amplitude factor the decision is derived if the measured points are noise or not. If a Gaussian distribution function is assumed for the noise, this factor should be 2 sigma of the noise amplitude to catch approximately 99 % of noise by the envelope curves. For that process it is essential to consider not only the difference between adjacent measurement points, but also the amplitude differences of proximate points have to be considered.

Between the envelope curves of the noise a new noise curve is calculated with much less points in correlation to the original measured curve. The reduction of noise points for the calculated noise curve is predefined in the software or can be selected manually by a percentage value, which is typically around 90 % (this is an input value for the software and not correlating with exact 90 % of noise point reduction; see also Table 1). The resulting, data reduced measurement curve consists of the original signals matched with the sequences of reduced noise points. In Figure 4 an example of the signals is displayed. The thick (red) curve is the new calculated curve with reduced number of points in the noise sequences and unchanged points for all signals.

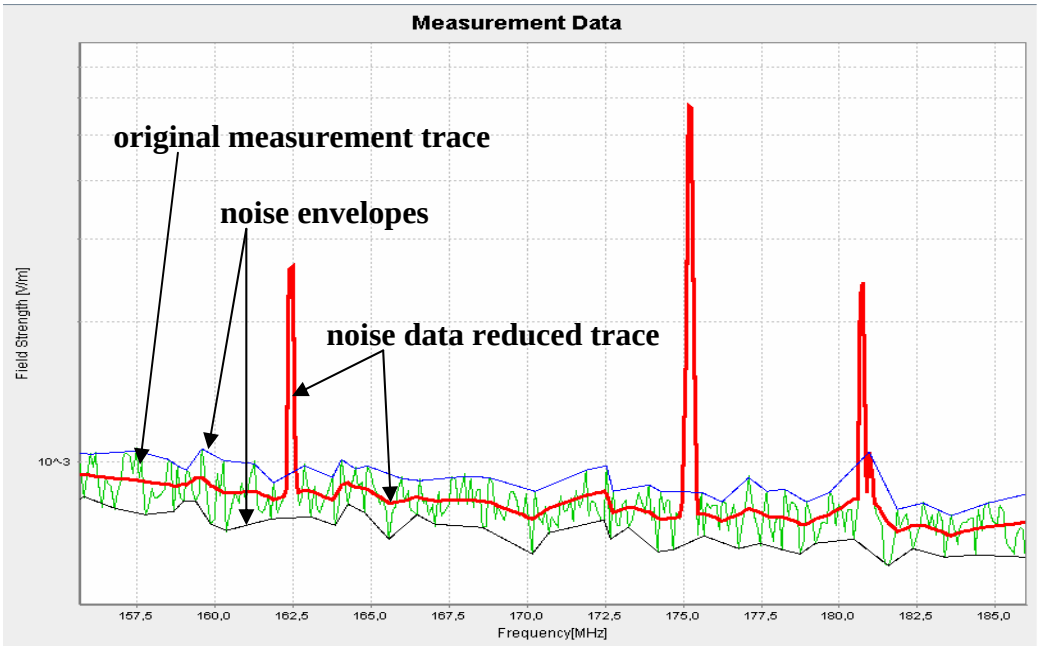

Figure 4: Noise points reduced measurement trace with noise envelopes

However there are still some kinds of signals making problems like typical UMTS signals. Because of their 5 MHZ bandwidth and the RBW-setting of 100 kHz these signals look like noise to the algorithm. This can be solved in a second signal check, where it is assumed that the noise floor is continuous. Jumps in the noise floor because of different analyser settings are handled by the evaluation of each measurement trace separately.

The next step to reduce the amount of data is to eliminate the noise sequences totally. Therefore simply all noise points are neglected and only the signals are still part of the data reduced, noise points excluding trace. In the graphic chart the flanks of signals are connected by a line. In Figure 5 the UMTS-DL band of the overview measurement from Vienna (Figure 3) is shown magnified. For the original measurement trace the noise data reduced trace and the trace with eliminated noise points were calculated and displayed together. The difference in the number of needed data points for these three signals is obvious.

Another powerful effect of the presented algorithm besides the data reduction is the possibility to evaluate the effective signal power without any incorrect additional integration of noise to the signals. To demonstrate that we have again a look at the UMTS band of Figure 5 respectively Figure 6 at left side. This time the vertical bands in Figure 6 are representing the DL-channels of the Austrian UMTS providers, which are used for data evaluation of the three UMTS-traces. On the right side of this figure the evaluation results are given. In all 3 diagrams the results for the active channels are identical because the algorithm does not affect the signal parts.

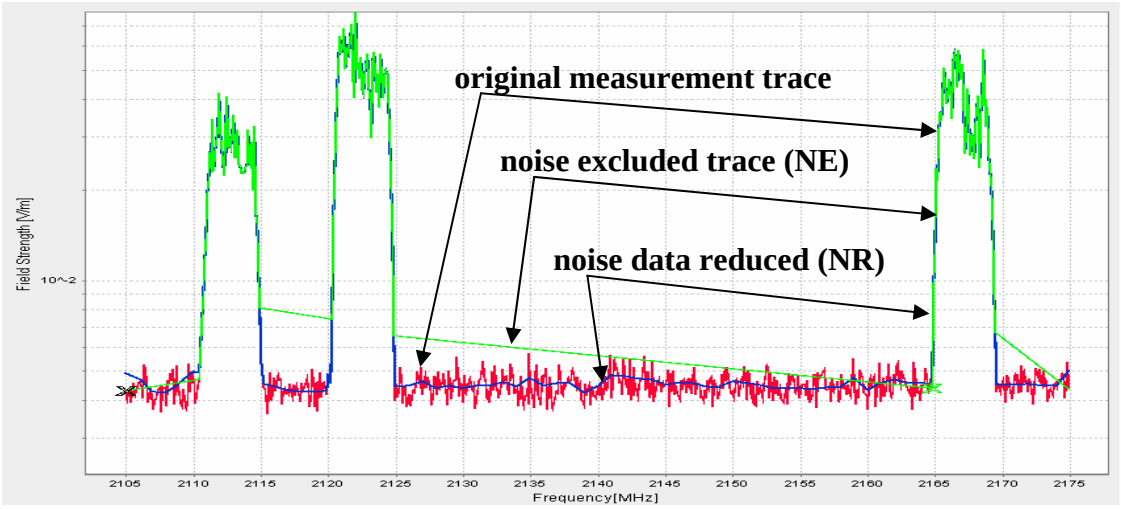

Figure 5: UMTS-DL traces after noise data reduction

Also the results of the other channels, representing the noise power, are very similar for the original trace and the noise data reduced trace. However for the trace without any noise points the evaluation result for inactive bands is zero. Therefore the presented algorithm enables the user to add only the power of measured signals to yield in fact EMF-field strength evaluation results without any disturbing noise contributes.

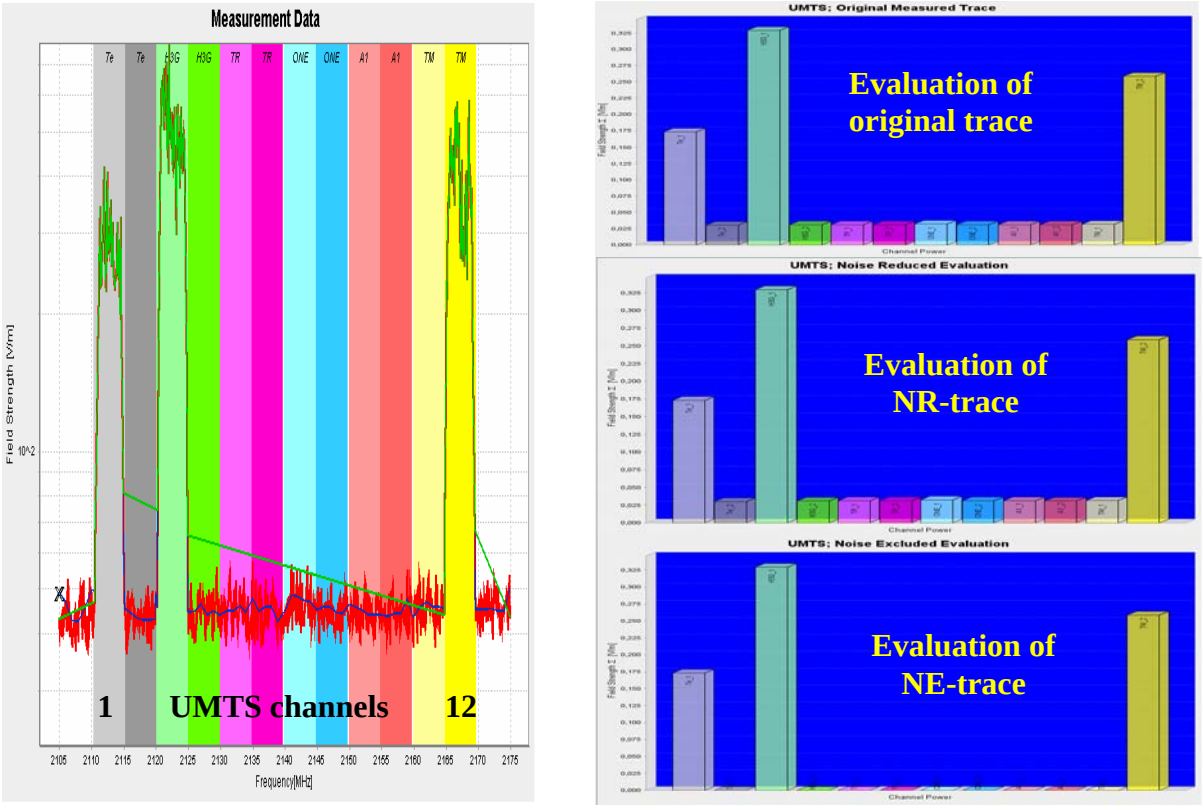

Figure 6: UMTS-DL traces and corresponding channel selective evaluation results

V. Results

Figure 7 is showing 4 original measurement traces and the noise excluded traces after implementation of the algorithm to the original measurement traces. At the top there are typical GSM900-DL measurements performed from 930 MHz to 960 MHz. The left one was made in the rural environment at Seibersdorf and the right during an EMC-exhibition at Stuttgart in 2005. Below them there are 2 of the overview measurements corresponding to

the measurements described in Figure 3. The left one is again from Seibersdorf and the other one from the centre of Vienna. These 4 pictures are showing typical traces which are used to investigate the efficiency in data reduction of the presented algorithm. The results are given in Table 1 for one, ten and fifty similar measurement traces (repetitions) for each of the 4 signal groups.

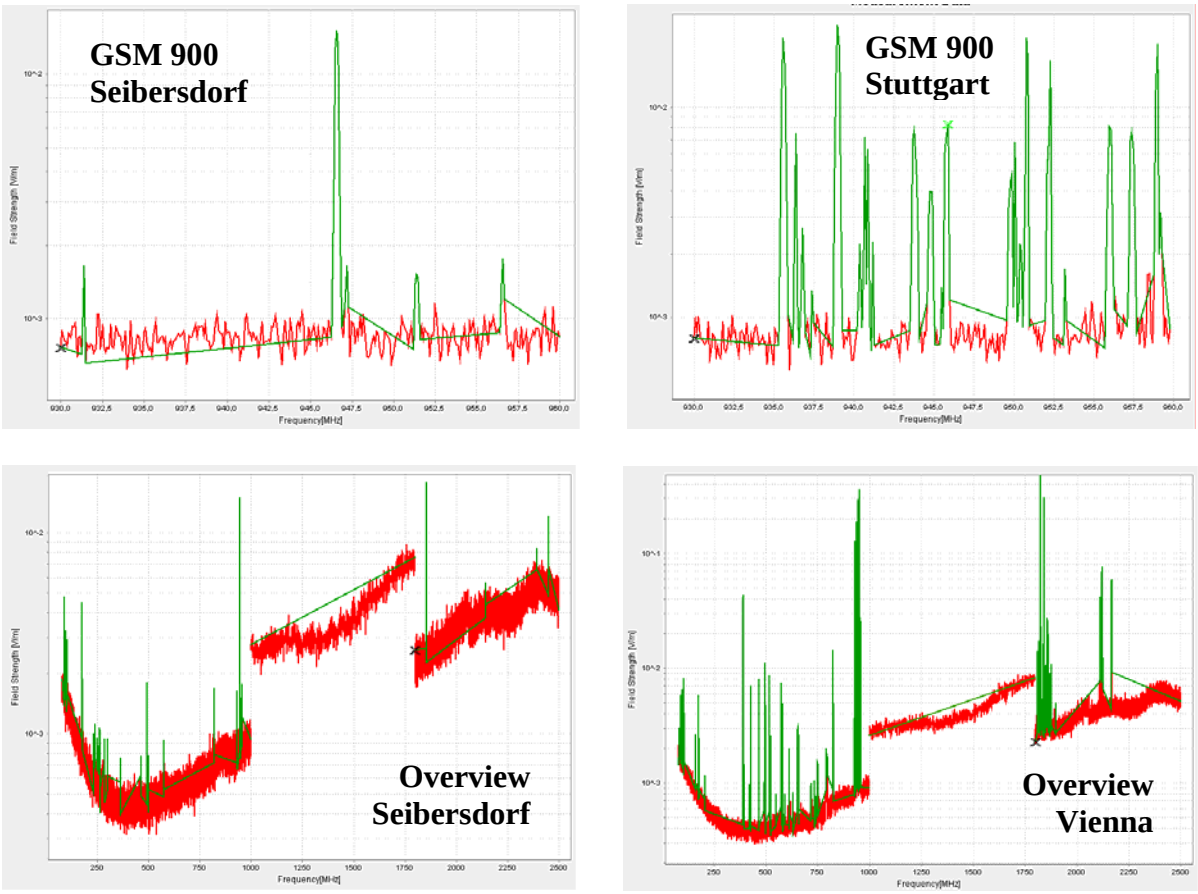

Figure 7: Example traces for the evaluation of Table 1

The values given in percentage are relating to the original measurement traces and give the amount of needed disk space after data reduction. That means a number of 30 % corresponds with a data reduction of 70 %. For the original measured traces the necessary disc space to save the measurement including all settings, factors and other useful information is given in kByte.

	Signal Group	GSM 900; Seibersdorf	GSM 900; Stuttgart	Overview; Vienna	Overview; Seibersdorf
1 Trace	Original Sig. [kB]	9	9	178	178
	NR [% of the original sig.]	77,8	77,8	19,7	14,6
	NE [% of the original sig.]	66,7	77,8	8,4	3,9
10 Traces	Original Sig. [kB]	34	34	1721	1721
	NR [% of the original sig.]	52,9	61,8	12,9	12,3
	NE [% of the original sig.]	32,4	44,1	1,8	1,6
50 Traces	Original Sig. [kB]	140	140	8515	8515
	NR [% of the original sig.]	54,3	59,3	12,3	12,1
	NE [% of the original sig.]	32,9	37,9	1,6	1,5

Table 1: Efficiency of the data reduction algorithm (Noise Height factor = 5dB and 90 % Reduction Value)

As expected the best results are given for overview measurements in a rural environment like Seibersdorf. There are only a few signals present and the noise reduction is very efficient with up to 87,9 % data reduction for the noise data reduced traces and up to 98,5 % for the noise excluded traces at 50 repetitions. That means that the needed disc space is reduced from about 8.5 MByte to less than 130 kByte. This is a data amount which can be processed easily within short time by computers. Also for the noise excluded wideband trace performed in the city of Vienna the reduction is quite similar with 1.6 % of remaining data instead of 1.5 % like Seibersdorf. For the scenario of 288 wideband traces during one day as assumed in chapter III including the evaluation problematic for frequency selective measurements, a total disc space of about 620 kByte would be generated if the presented algorithm is used. This data amount is still not a large problem to process at modern PCs and therefore in fact this algorithm supports frequency selective EMF-measurement systems to overcome the problematic of time delay caused by too much data generation. For a single overview trace the efficiency of the data reduction is a little bit less because of the data overhead necessary for each measurement job independent of its number of repetitions but with about 80 % to 95 % still excellent. For the GSM900 evaluations the reduction of data is from about 22 % for noise reduced signals for one single trace up to 77 % at the 50 noise excluded traces for the GSM900 band at Seibersdorf, but the absolute amount of data is much less than for the overview measurements and therefore not a problem in processing. In addition to that it is a big advantage of the algorithm too, that it is working automatically as a selector to differ between the existing signals and noise, which is not of interest. Only pure signal information is kept in opposite to other methods like band-selective methods or by wideband measurements using field probes where signal and noise is mixed without any possibility for differentiation.

VI. Conclusion

Recapitulating it was found that especially for wideband measurements with a lot of repetitions the presented algorithm has its best efficiency with typically more than 98 % of data reduction for the investigated traces and measurement settings. This enables frequency-selective measurements for sophisticated single investigations on site as well as for long-therm monitoring e.g. for dosimetry studies. Caused by the fact that the data reduction algorithm can automatically be applied in real-time to the measured data and it is not specific for any spectrum analyser, it could be used generally for data reduction purposes. Another big advantage of that data reduction process is the differentiation between signal and noise. This enables the user to define the pure signal power for EMF-evaluation instead of a mixture of signal and noise contributes. Furthermore the frequency selective measurement method is still the most sensitive procedure which allows best isotropic behaviour, sharp frequency differentiation and accurate uncertainty estimation. Drawbacks of those systems are the relatively high cost, large mechanical dimension of the some equipment and typically the engineer needs measurement expertise and experience to perform well suited settings that the advantages of frequency selective systems could be utilized.

References

[1] ICNIRP: "Guidelines for limiting exposure to time-varying electric, magnetic, and electromagnetic fields.", Health Physics 74 (4), pp 494 – 522, 1998.

[2] W. Müllner, G. Neubauer, H. Haider: "Add3D, a new technique for precise power flux density measurements at mobile communications base stations", 10. Internationale Fachmesse und Kongress für EMV, Düsseldorf, pp 305–312, 2002

[3] Neubauer, G.; Röösli, M.; Feychting, M.; Hamnerius, Y.; Kheifets, L.; Kuster, N.; Ruiz, I.; Schüz, J.; Wiart: „Feasibility of future epidemiological studies on possible health effects of mobile phone base stations", Platform Presentation at the BioEM 2005 (joint meeting of the Bioelectromagnetics Society and the European BioElectromagnetics Association), June 20.-24., 2005, Dublin, Ireland, Abstract Book pp. 102-103.

Long term effects of microwaves from GSM mobile phones on the rat brain

Jacob L. Eberhardt[1], Bertil R.R. Persson[1], Arne Brun[2], Lars Malmgren[4], Gustav Grafstrom[1], and Leif G. Salford[3]

Department of Radiation Physics[1], Neuropathology[2], Neurosurgery[3] and The MAX-lab national facility[4], University of Lund, Lund, Sweden.

1. INTRODUCTION

Our group has since 1988 studied the effects of different intensities and modulations of 915 MHz RF in a rat model. In series of more than 1600 animals, we have proven that subthermal energies from both pulse-modulated and continuous RF fields including those from real GSM mobile phones - have the potency to significantly open the BBB
for the animals own albumin (but not fibrinogen) to pass out into the brain and to accumulate in the neurons and glial cells surrounding the capillaries. These results are duplicated recently in another laboratory [1]. Similar results are found by others [2]. In a recent study, we found signs of neuronal damage in the rat 28 and 50 days after a 2 hours exposure for GSM microwaves at 900 MHz with SAR < 0.2 W/kg [3,4].

2. OBJECTIVE

To investigate in the rat the occurrence behavioral changes, leakage of the blood-brain barrier and of neuronal damage after a one year period of weekly 2 hour exposures to radiation from a GSM mobile phone at different intensities.

3. METHODS

48 male and female Fischer 344 rats were exposed or sham exposed for two hours once a week for 55 weeks in TEM-cells to radiation from a software programmable GSM-900 mobile telephone. The animals were awake during the exposure and could move and turn within the exposure chamber. The peak output power fed into the TEM cells were 5 or 500 mW, resulting into average whole body specific absorption rates of 1 or 100 mW/kg. A further 8 animals served as cage controls: The latter stayed ndisturbed in the animal facility during the whole period of the investigation. 3 weeks after the last exposure, all animals were subjected to two different behavioral test: (i) the Open Field
test for testing exploratory and motor behavior as well as anxiety, and (ii) the Episodic-like memory task for testing episodic memory and novelty preference [6]. After the behavioral testing period, the animals were anaesthetized and sacrificed by perfusion-fixation with 4% formaldehyde. Brain slices were stained for RNA/DNA with cresyl violet and HSP70 for heat shock protein. Applying albumin antibodies (Dakopatts), albumin in the brain tissue and albumin uptake into neurons is revealed.

4. ANALYSIS and RESULTS

The occurrence of blood-brain barrier leakage and damaged (dark) neurons in different parts of the brain were judged semi-quantitatively by the neuropathologist. No increased number of albumin foci or dark neurons were found in exposed animals as compared to sham-exposed. The Open Field test revealed no effect of exposure on exploratory and motor behavior. The episodic memory test revealed worse short-term memory for exposed animals as compared to sham exposed animals.

A grant from the Swedish Council for Working Life and Social Research is gratefully aknowledged.

1. F Tore, P-E Dulou, E Haro, B Veyret, P Aubineau. Two-hour exposure to 2 W/kg, 900 MHz GSM microwaves induces plasma protein extravasation in rat brain. In: Proceedings from the 5th International Congress of the European Bioelectromagnetics Association. (M Hietanen, K Jokela, J Juutilainen, eds) 2001, pp 43-45.

2. K Fritze, C Sommer, B Schmitz, G Mies, K Hossman, M Kiessling, et al. Effect of global system for mobile communication (GSM) microwave exposure on blood-brain barrier permeability in rat. Acta Neuropathology (Berlin) 1997, 94, pp 465-470.

3. LG Salford, AE Brun, JL Eberhardt, L Malmgren, BRR Persson. Nerve cell damage in mammalian brain after exposure to microwaves from GSM mobile phones. Environmental Health Perspectives, 2003, 11(7), pp 881-883.

4. JL Eberhardt, BRR Persson, LOG Malmgren, AE Brun and LG Salford. Blood-brain barrier permeability and nerve cell damage in the rat brain 14 and 28 days after exposure to microwaves from GSM mobile phones. Manuscript 2006.

5. FA Malek, K-U Moritz, J Fanghanel. Formaldehyd inhalation and open field behavior in rats. Indian Journal of Medical research 2003, 118, pp 90-96.

6. E Dere, JP Huston, MA De Souza Silva. Integrated memory for objects, places, and temporal order: Evidence for episodic-like memory in mice. Neurobiology of Learning and Memory 2005, 84, pp 214-221.

THE TREATMENT OF PERIPHERAL NERVE TRANSECTION INJURY UNDER 50 HZ ELECTRIC FIELD EXPOSURE

*OZLEM ULUKUT

*SELCUK COMLEKCI

**SÜLEYMAN DEMİREL UNIVERSITY, FACULTY OF ENGINEERING, DEPARTMENT OF ELECTRICAL & COMMUNICATIONS ENGINEERING, 32260, ÇÜNÜR, ISPARTA, TURKEY*

e-mail:oulukut@mmf.sdu.edu.tr *e-mail:scom@mmf.sdu.edu.tr*

Abstract

Merely electric field exposure is often occurred by electric transmission lines, electric appliances without current flow. The aim of this study was to investigate the effects of a 50 Hz electric field on peripheral nerve regeneration in rats. The exposure system was based on parallel-plate-capacitor system. Electric field exposure set-up was established for studies on forty male Sprague-Dawley rats. The rats were randomly divided into four groups each containing 10 rats. Four groups examined variables associated with the method and timing of surgical repair, the arrest of Wallerian degeneration, and the role of electric field in functional recovery. Treatment group1, treatment group 2 and treatment group 3 were subjected to electric fields of 10 kV/m strengths. Control group were subjected to the same procedure, but with the device not activated. The ambient temperature and relative humidity percent of the room housing this facility were maintained at 24 ± 2 °C and 55 ± 5 respectively. Standard poly-carbonate animal cages with PVC lids were kept between the parallel plates producing vertical component of electric field for exposing the animals. The duration of exposure of rat was 1 months. Treatment group1, treatment group 2 and treatment group 3 showed that a vein-graft conduit did not improve functional recovery compared with standard epineurial repair. Also, delayed repair compared favorably with immediate repair.

Key words: Electric field, parallel plate, peripheral nerve regeneration

Introduction

Extremely low frequency (ELF) electric field (EF) and electromagnetic field (EMF) were demonstrated to affect biological systems in vitro and in vivo [World Health Organization, 1984]. Unlike the ionizing radiation and radiofrequency waves, the energy transferred to the biological tissues by the ELF fields is no significant. Some biological processes may be more sensitive than others to ELF EMFs resulting in measurable outcomes.

Weak DC EF was applied to accelerate nerve regeneration following different peripheral nerve injury models [Politis et al., 1988; Kerns et al., 1991; Kerns and Lucchinetti, 1992]. Pulsed electromagnetic field (PEMF), as a non-invasive modality was also effective in enhancing nerve regeneration [Ito and Bassett, 1983; Orgel et al., 1984; Sisken et al., 1989; Walker et al., 1994].

The sinusoidal AC magnetic field was found to accelerate nerve regeneration following a crush injury [Rusovan and Kanje, 1991]. To our knowledge, how ELF EF affects nerve regeneration has not been studied before. Animal studies focused on the magnetic field components, whether they investigate hazards or benefits associated with ELF EMFs. The theoretical background is that the magnetic field is almost unperturbed by tissues as opposed to EFs. Magnetic field is created when electric current flows. EF represents the force that a charge exerts on other charges and a potential difference is sufficient for its presence even when a current does not flow. Pure EFs may have biological effects [Repacholi and Greenebaum, 1999].

Materials and Methods

In this study the experiment was performed on forty young adult, male Sprague–Dawley rats weighing 180–240 g. The study was approved by the Institutional Review for Animal Research Board of SDU and conducted in accordance with the institutional guidelines. The rats were randomly divided into four groups each containing 10 rats. Four groups examined variables associated with the method and timing of surgical repair, the arrest of wallerian degeneration, and the role of electric field in functional recovery. Treatment group1, treatment group 2 and treatment group 3 were subjected to electric fields of 10 kV/m strengths. Control group were subjected to the same procedure, but with the device not activated. The ambient temperature and relative humidity percent of the room housing this facility were maintained at 24 ± 2 °C and 55 ± 5 respectively. Standard poly-carbonate animal cages with PVC lids were kept between the parallel plates producing vertical component of electric field for exposing the animals. The duration of exposure of rat was 1 months.

Surgical Procedure

The animals were anesthetized by intraperitonel injection of ketamine (90 mg/kg) and xylazine (6mg/kg). By using a surgical microscope common peroneal nerve was isolated through a short lateral thigh incision on the left side. Two centimeters proximal to its entrance into the lateral crural compartment, peroneal nerve was crushed twice with a no. 3 jeweler's forceps for 30 s, so that only a transparency of the neural sheath was seen at the injury site.

Electric Field Application Set Up

The theory of EF between the plates of parallel plate capacitors was utilized for EF exposure settings [Lorrain and Corson, 1970]. The setup was schematically illustrated in Figure 1. The EF strength was calculated according to the equation E=V/d where V is electric potential between the plates, d is the distance, and E is the EF intensity in volt/meter. Plates were made of a perfect conductor for free charges to disperse homogenously in order to produce uniform EFs. Zinc plated tin sheets of 2 mm thickness were selected for this purpose. Plates of 50X100 cm in dimension were cut out of them and perfectly flattened. The corners were rounded to get rid of corruptions due to end effect. They were placed upright on wooden stands and positioned parallel to each other. In order not to disturb the field, leads were connected to the center of the plates on their outer sides.

The plates were spaced at 50 cm in distance. Three ungrounded plastic cages were placed inside as seen in Figure 1. Three or four rats were housed in each cage. Cages were in adequate size to ensure free movement of rats and hence homogenous shielding of each other. In addition to weekly cleanups of the plates and cages, the setups were frequently scrutinized for gross soil and wetness that would disturb the homogeneity of EF. The attenuation due to routine soiling could be estimated to cause very small variation in EF. From the equation above, average EF densities between the plates were calculated to be 5000 V/0.5 m=10000 V/m (10 kV/m) in 50 Hz groups. Max 3000 TRMS Multimeter (Chauvin Arnoux, Paris, France) was used for voltage measurements.

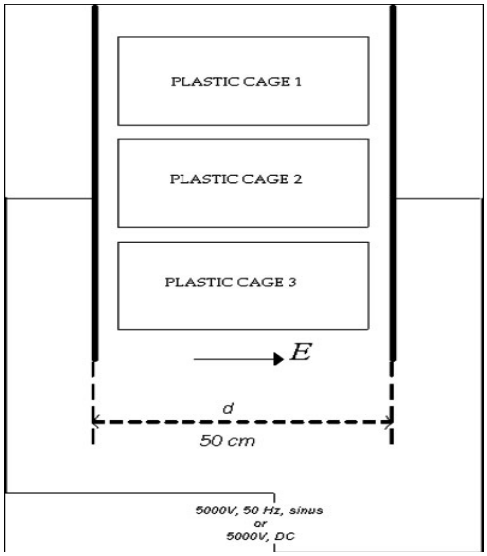

Figure 1. The electric field application set up.

Discussion and Conclusion

International standard commissions (ICNIRP, IEEE) are generally warn about magnetic radiation to public. General consensus that is below 10 kV/m will be harmless. In this study we tried to show that pure electric field was able to affect on a living tissue.

We designed the study to determine whether any changes occur in the rate of nerve regeneration when rats are continuously exposed to strong EFs for 4 weeks following a crush injury. Treatment group1, treatment group 2 and treatment group 3 showed that a vein-graft conduit did not improve functional recovery compared with standard epineurial repair. Also, delayed repair compared favorably with immediate repair. All differences found between the exposure groups of this study were in accordance with lower rates of Wallerian degeneration and nerve regeneration in 50 Hz EF group.

However, their concordance in direction of effect with each other suggests that continuous 50 Hz EF exposure has a weak effect that is detrimental mostly to the rate of early nerve regeneration in a crush injury model. Although the internal EFs induced by 50 Hz EF in this study are estimated to be within the lower limits of endogenous noise. This suggests that electric induction may be required for pure EF effects even though the density of induced fields is not above the endogenous background level.

References

[1] Mustafa Asim Aydin, Selcuk Comlekci, Meltem Ozguner, Gokhan Cesur, Serdar Nasir, Zeynep Dilek Aydin, The influence of continuous exposure to 50 Hz electric field on nerve regeneration in a rat peroneal nerve crush injury model, Bioelectromagnetics, 27:401-413 (2006).

[2] Bassett CA. 1983. Effect of weak, pulsing electromagnetic fields on neural regeneration in the rat. Clin Orthop 181:283–290

[3] Kerns JM, Lucchinetti C. 1992. Electrical field effects on crushed nerve regeneration. Exp Neurol 117:71–80.

[4] Kerns JM, Fakhouri AJ, Weinrib HP, Freeman JA. 1991. Electrical stimulation of nerve regeneration in the rat: The early effects evaluated by a vibrating probe and electron microscopy. Neuroscience 40:93–107.

[5] Lorrain P, Corson D. 1970. Chapter 2: Electrostatic fields. In: Lorrain P, Carson D, editors. Electromagnetic fields and waves. San Fransisco: WH Freeman and Co. pp 40–84.

[6] Politis MJ, ZanakisMF, Albala BJ. 1988. Facilitated regeneration in the rat peripheral nervous system using applied electric fields. J Trauma 28:1375–1381.

[7] Repacholi MH, Greenebaum B. 1999. Interaction of static and extremely low frequency electric and magnetic fields with living systems: Health effects and research needs. Bioelectromagnetics 20:133–160.

[8] Rusovan A, Kanje M. 1991. Stimulation of regeneration of the rat sciatic nerve by 50 Hz sinusoidal magnetic fields. Exp Neurol 112:312–316.

[9] Orgel MG, O'Brien WJ, Murray HM. 1984. Pulsing electromagnetic field therapy in nerve regeneration: An experimental study in the cat. Plast Reconstr Surg 73:173– 183.

[10] Sisken BF, Kanje M, Lundborg G, Herbst E, Kurtz W. 1989. Stimulation of rat sciatic nerve regeneration with pulsed electromagnetic fields. Brain Res 485:309–316.

[11] Walker JL, Evans JM, Resig P, Guarnieri S, Meade P, Sisken BS. 1994. Enhancement of functional recovery following a crush lesion to the rat sciatic nerve by exposure to pulsed electromagnetic fields. Exp Neurol 125:302– 305.

[12] World Health Organization. 1984. Environmental heath criteria 35: Extremely low frequency (ELF) fields. Geneva.

The influence of Pulsed Magnetic Fields (PMF) on the synaptic transmission and on the action potential in the mouse nervous system.

Zaghloul Ahmed[2] and Andrzej Wieraszko [1,2],

[1]Department of Biology/CSI/IBR Center for Developmental Neuroscience, The College of Staten Island, City University of New York, [2] Ph.D. Program in Biology, The Graduate School and University Center of NY, New York.

Abstract

We demonstrated previously that exposure of brain tissue to pulsed magnetic fields (PMF) significantly amplified the magnitude of the evoked potentials. Either increase in the amplitude of the action potential, or amplification of the synaptic efficiency could explain observed results. Further investigation revealed, that Paired Pulse Facilitation (PPF), a form of synaptic plasticity observed in the central nervous system was significantly modified by the exposure to PMFs. Although these results pointed at the synapse, as the site of PMF action, the enhancement of an antidromically evoked potentials, recorded from hippocampal slices implied, that PMF can influence nonsynaptic mechanisms as well. This assumption was supported by PMF-induced amplification of the action potential recorded from isolated, peripheral mouse nerve in vitro. It has been determined, that PMF reduced the axonal threshold, making nerves more excitable. Additional studies demonstrated, that the action of PMF is exerted by modifying the action of ion channels, responsible for synaptic transmission and generation of an action potential. The action of PMF was very specific and related to their frequency.

Introduction.

Our previous investigation revealed that Pulsed Magnetic Fields (PMFs) increased neuronal activity recorded from mouse hippocampal slices (Wieraszko et al., 2005). The enhancement in the activity of the nerve cells was expressed as an increase in the amplitude of electrophysiologically recorded evoked potentials (Wieraszko, 2004), which was correlated with an enhancement of the release of neurotransmitter (glutamate) (Wieraszko et al., 200), and an elevation in the concentration of the second messenger, cAMP (Hogan and Wieraszko, 2004).

The intensity of neuronal activity was measured as the amplitude of the population spike (PS), which represents synchronized firing of the pyramidal neurons **(**Andersen et al., 1971). While the population spike illustrates synaptic activation of neurons, it has to be preceded by the action potential generated non-synaptically. The diagram in Fig 1 shows the sequence of these events. Presynaptic action potential, induced by stimulating electrodes (S), propagates towards the end of the axon and initiates the release of the neurotransmitter (glutamate in our preparation) at the presynaptic terminal (Pre). The neurotransmitter released from the presynaptic part stimulates the postsynaptic part (Post), generating population spike (potential # 3). The same stimulation can also generate the action potential, which will propagate toward the cell body of neuron A initiating antidromically evoked potential # 1. No synaptic transmission is involved in generation of this potential. Therefore, the influence of PMF on both: 1) the presynaptic mechanism of generation of an action potential and, 2) synaptically mediated mechanism of generation of the population spike may contribute to the PMF-induced modifications of the amplitude of the population spike. The purpose of the current research was to evaluate the contribution of the presynaptic and postsynaptic mechanisms in modulation of the population spike by PMF.

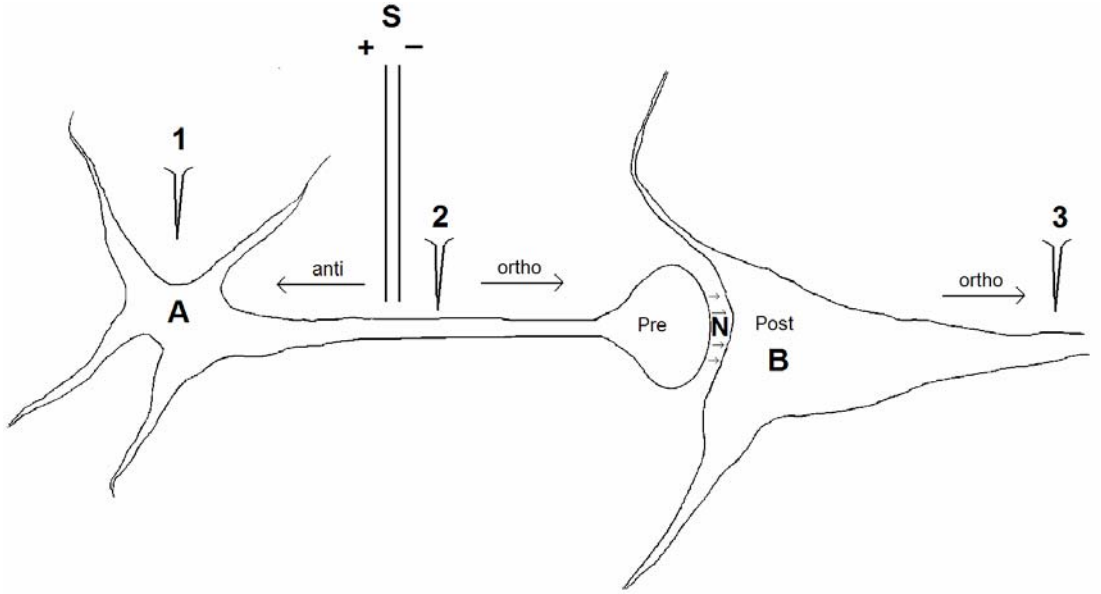

Fig1. The diagram of neuronal activities recorded in the experiments on hippocampal slices. Stimulating electrode (S) initiates the generation and orthodromic propagation of an action potential # 2. This potential reaches the nerve terminal (Pre) stimulating the release of neurotransmitter (N), which activates postsynaptic part initiating generation of the population spike (potential # 3) in neuron B. Thus, the population spike (potential # 3) is generated, as a result of presynaptic and postsynaptic activities. The action potential initiated by stimulating electrode (S) can also propagate towards the cell body of neuron A (antidromic stimulation) generating an action potential # 1. This potential is generated without the involvement of synaptic transmission.

While the mouse hippocampal slices were used to evaluate the involvement of presynaptic and postsynaptic mechanisms, the segments of the mouse sciatic nerve were used to verify the results related to presynaptic component.

Methods

The biological preparation (hippocampal slices, or segments of sciatic nerve) have been incubated in a chamber shown in Fig 2, and exposed to pulsed magnetic fields for 30 minutes. The evoked, neuronal activity of the preparation was followed before, during and after exposure to PMF.

PMF exposure

The pulsed magnetic field (PMF) was generated by DC-powered coils (Trabulsi et al., 1996; Wieraszko, 2004), wound around an acrylic frame, which surrounded the interface-recording chamber. The activation and deactivation of the coils was operated by a programmable timer, which was set at different frequencies to meet the goal of the specific experiment. A plastic tube connected to the building air supply secured the flow of the air indicated by arrows E. The flow of air prevents the water chamber from overheating during electromagnetic field activation (Trabulsi et al., 1996; Wieraszko, 2004) (Fig 2). Regardless of the frequency of the pulsed magnetic field, each pulse has four phases: rising phase (period of coils charging), static magnetic field phase (period of no change; the power supply on), falling phase (period of coils discharging), and then an “off” phase (power supply off), (Fig 3 and 4). The duration of the rising and falling phases (measured as shown in Fig 4) was equal for all frequencies generated by our magnetic field setup; however, the number of these phases is substantially different for different frequencies. Unless specified otherwise, the frequency that was used was 0.16 Hz. The same field was used for hippocampal slices and for sciatic nerve preparation. The one "on" and "off" period was considered as one cycle and the frequency of magnetic field stimulation was expressed as number of these cycles per second (Fig 3). The graph in Fig 3 shows magnetic field pulse recorded on-line for the

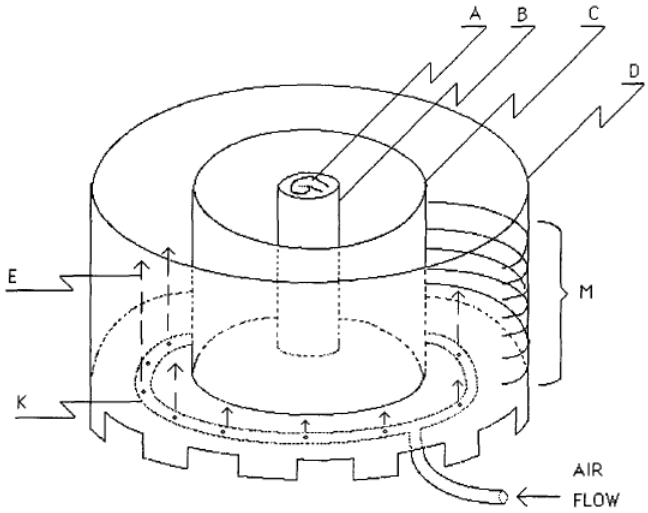

Fig. 2. A diagram of the experimental system. The slice (A) is placed in the chamber (B) that is filled with Ringer's solution and oxygenated with 95%/5% O2/CO2. The water chamber (C) contains the temperature sensor (H) and the oxygenating airflow. The magnetic coil (M) encircled the acrylic frame (D). During the magnetic field application, airflow circulating through a holed tube (K) is turned on, creating an air flow (E) to dissipate any accumulated heat. (According to Wieraszko, 2004).

period of thirty minutes. Neither change in the PMF strength nor shape was observed. A, B and C show on-line PMF recording for 4 minutes in the beginning, middle, and at the end of thirty minute period.

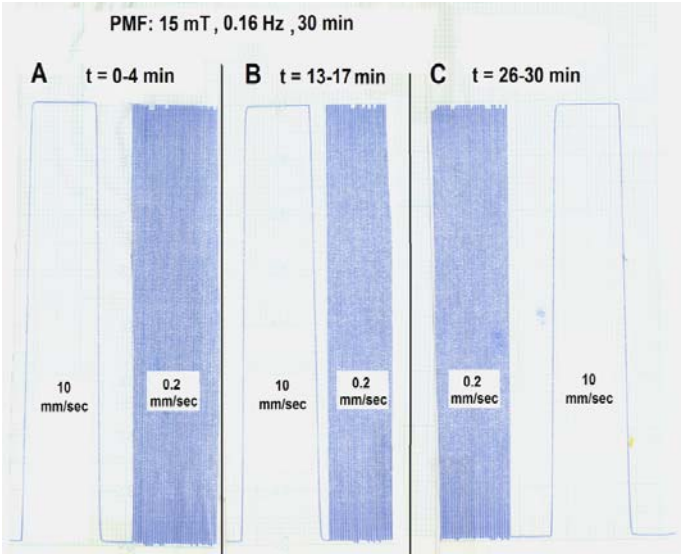

Fig. 3. Thirty minutes of PMF recording. This graph shows - on line - magnetic field pulse recording for the period of 30 minutes that illustrates neither change in the PMF strength nor shape. A, B and C show on-line PMF recording for 4 minutes in the beginning, middle, and at the end of 30 minutes.

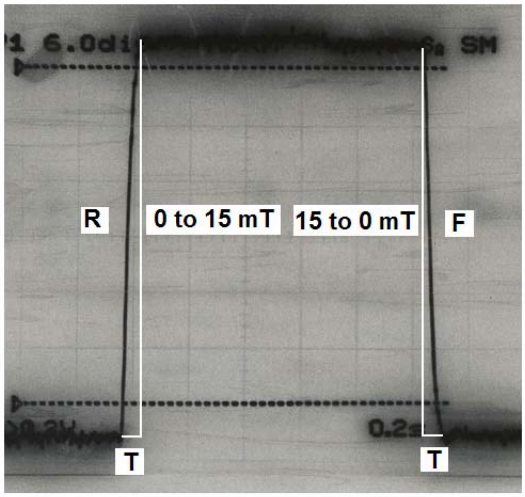

Fig. 4. A photograph of the PMF pulse taken from oscilloscope screen. It shows the rising (R), and falling phases (F). The white vertical lines and horizontal lines (T) were drawn to calculate the slope of the rising and falling phases of magnetic pulse (black trace). The duration of the "on" phase, and the intensity of the field shown on this photograph is 3 sec. and 15 mT, respectively.

Results

A. The influence of PMF on synaptic and nonsynaptic component of neuronal activity tested on hippocampal slices.

The hippocampal slices were prepared from CD-1 strain of mice, as described previously (Wieraszko,

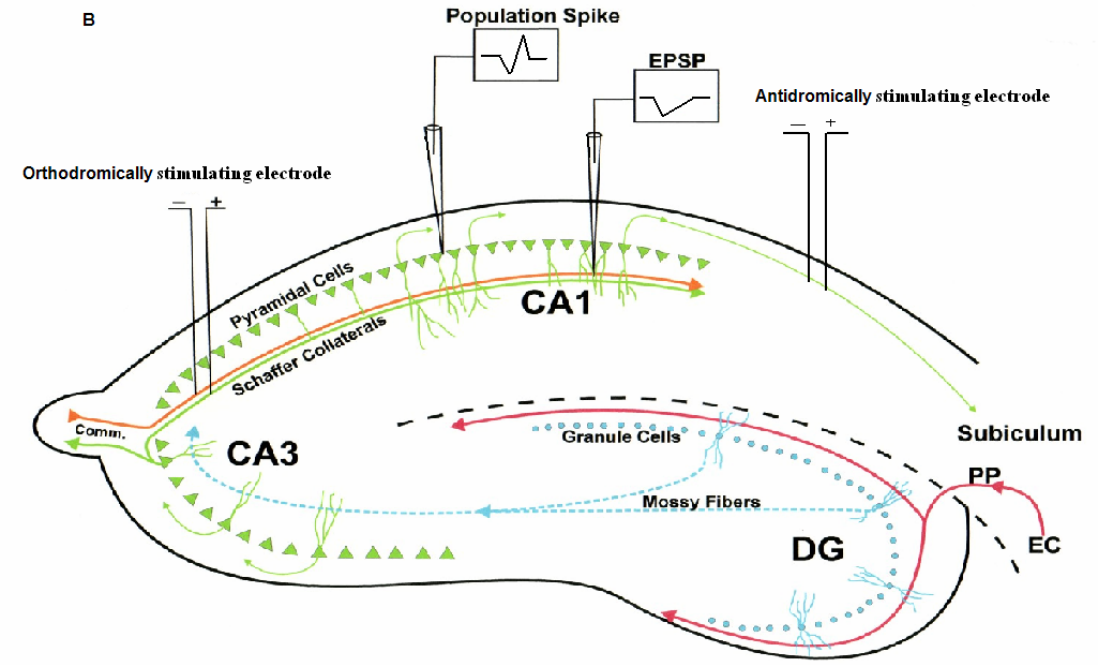

Fig. 5. Hippocampal pathways and recording of their activities. The diagram shows the hippocampal pathways and the location of stimulating and recording electrodes. The electrode stimulating orthodromically is located in CA3 hippocampal subfield. When activated, it evokes the action potential, which propagates towards CA1. This action potential, in turn, synoptically activates CA1 pyramidal neurons, which generate population spike. Pyramidal neurons can be also stimulated nonsynaptically with antidromically stimulating electrode.

1983). The diagram of the cross-section of the hippocampus is depicted in Fig 5. The population spike can be evoked by either orthodromic stimulation of the Schaffer collateral and then recording from the CA1 pyramidal cell layer (this involves synaptic transmission), or by the antidromic stimulation, which is defined as the stimulation of the axonal area of the CA1 and recording from CA1 pyramidal cell layer (it does not involve synaptic transmission). See also Fig 1 for further explanation.

A.1. Effects of PMF on paired pulse facilitation (PPF)

Our previous experiments (Wieraszko, 2004) demonstrated a PMF induced increase in the magnitude of the population spike evoked by single-pulse electrical stimulation applied at the frequency of 0.16 Hz. To analyze this phenomenon further we applied paired-pulse stimulation paradigm, which is considered a good indicator of the changes in the mechanism of orthodromically induced synaptic processes of the neurotransmitter release. Two pulses, separated by the interstimulus interval of 15-55 ms were applied with the frequency of 0.16 Hz to evoke two population spikes. Paired-Pulse Facilitation (PPF) was expressed as an increase in the magnitude of the second population spike as compared to the first one. PPF was calculated as the difference in amplitude between the first population spike (PS1) and the second population spike (PS2). An increase in the second population spike relative to the first will produce higher PPF. The expression of PPF as the difference rather than the ratio has been chosen, since PMF increased both PS1 and PS2 (Fig 6). The experiment was initiated by recording of the PS for 20 minutes prior the exposure to PMF (baseline). The average of the PPF measurements that were calculated from the baseline period was compared to the averages taken from the recordings after the exposure to PMF. The result of ten experiments showed significant increase in PPF after the PMF exposure (n=10, 150 %, p=0.000317, paired sample t test was used). Note, that although the magnitude of both population spikes increased following PMF exposure, the facilitation of the second one exceeded the facilitation of the first (Fig 6).

Statistical analysis revealed, that there was no correlation between initial PPF and the change in the amplification of PPF. Therefore we assumed, that the amplification of PPF was not due to PMF-

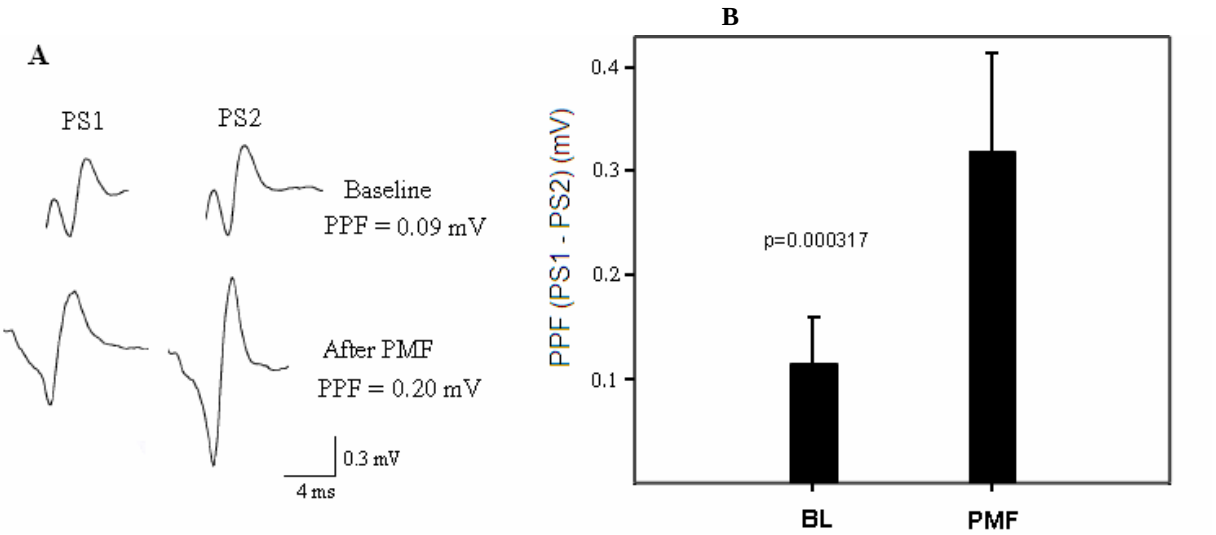

Fig. 6.The influence of PMF on paired pulsed facilitation. A - Potentials marked PS1 and PS2 correspond to the first and second evoked potentials, respectively and were initiated by two consecutive pulses applied with a frequency of 0.16 Hz; inter pulse intervals (IPI) was adjusted accordingly to get the largest PPF (25 – 55 ms). The PPF was calculated as PS2 minus PS1. The upper and lower potentials represent potentials that were recorded during the baseline and after the PMF exposure, respectively. PPF was increased by about 120% after the exposure to PMF. Note, that both PS1 and PS2 increased after exposure. B - the average changes in PPF after the exposure to PMF applied at the frequency of 0.16 Hz (n = 11). The baseline bar (BL) represents the average of PPF from the first 10 - 15 minutes before the application of PMF. The PMF bar represents the average of PPF during maximal effect of PMF amplification. The result of the paired t test is shown in the graph.

induced increase in the number of firing neurons, but due to an increase in the excitability of the same population of neurons, which were active before PMF exposure.

A.2. The effect of PMF on antidromically evoked population spike in the hippocampal slices

To inquire into the mechanisms of PMF, we considered an experimental paradigm that would express the action potential without concomitant involvement from synaptic transmission. Stimulating the hippocampal pyramidal cell layer CA1 with antidromic stimulus (stimulating electrode on the subiculum,

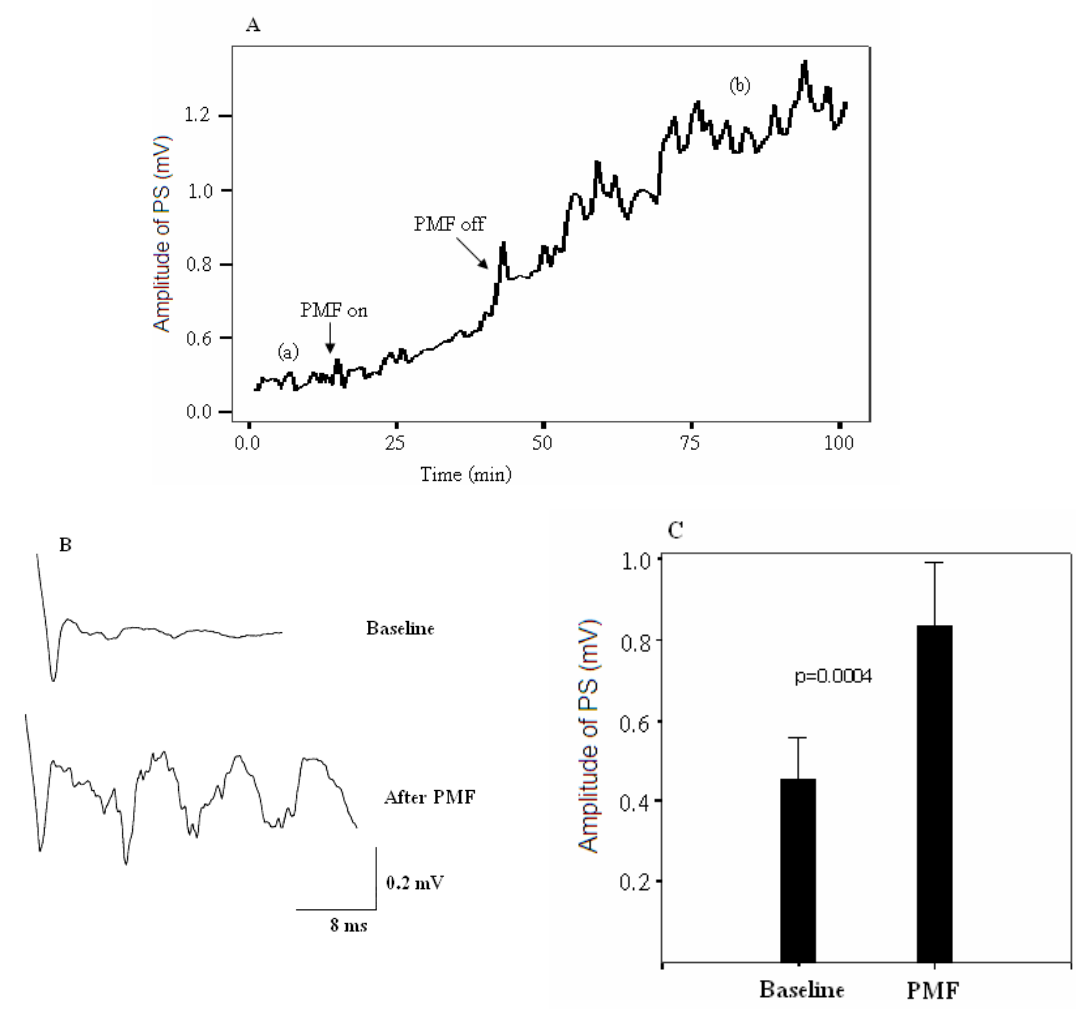

Fig.7. The effect of PMF on the antidromically evoked population spike. The slices were incubated in a calcium free medium and with 2mM kynurenic acid. A – a representative experiment showing the amplitude of the population spikes before (a) and after (b) the application of PMF. B – A waveform that shows the potential amplitude before and after PMF exposure; note the generation of multiple potentials . C – Average results of baseline and at maximal PMF effect (n = 15, p = 0.0004). Paired t test was used.

recording electrode on the pyramidal cell layer CA1) (Fig. 1 and 2) would induce pre-synaptic action potentials only. The addition of kynurenic acid (a blocker of glutamergic receptors) to the slice containing chamber and the omission of calcium would eliminate any contribution of glutamergic synaptic transmission to either the initiation or size of recorded potentials. Fifteen experiments on 15 different slices taken from 5 animals were performed. The potentials were recorded for 20 minutes to create a stable baseline, and then a PMF of 0.16 Hz was turned on for 30 minutes. Averages from the baseline and at the maximal effect of PMF (20 potentials) were compared. The PMF has not only

increased significantly the size of population spikes (n=15, 183.3%, p=0.0004, Fig 7A, B) but also induced multiple firings and seizure like activity (Fig 7 B). There was no correlation between the amplitude of the baseline and the amplitude of the change (the PS amplitude after PMF exposure minus the PS amplitude of baseline) after the exposure to PMF. That means that the effect of PMF was independent of the amplitude of the initial population spike.

B. The influence of PMF on the action potential recorded from the sciatic nerve.

CD-1 strain of mice was used to prepare segments of sciatic nerve. Following decapitation both hind limbs were skinned. The upper thigh muscles were then cut and either the femoral bone was broken or the hip joint was dislocated. The broken limb was pulled away and muscle tissue of the thigh were cut to expose the sciatic nerve from its origin in the vertebral column. The two ends of the sciatic nerve were cut and the nerve was pulled out and placed in the ice-cold Ringer's solution. The nerve was then cut into 4 to 6 mm segments, which were placed in an incubation chamber maintained at 33^{o}C, and constantly oxygenated with a 5%/95% CO_2/ O_2. The individual segment was transferred in turn into a recording chamber. The epineurium (the outermost layer of connective tissue surrounding the entire peripheral nerve) remained intact. The recording electrode was placed inside the epineurium at the end of the cut and the stimulating electrode was placed out side the epineurium at a distance that was varied to obtain the robust compound action potential (CAP) (Fig 8).

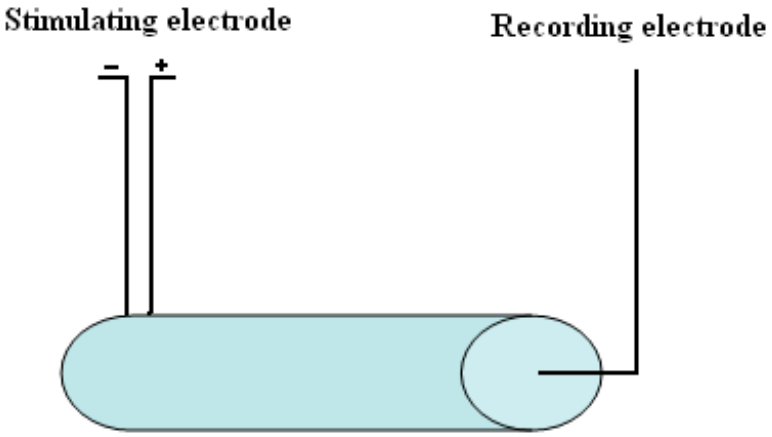

Fig. 8. The placement of the electrodes on a sciatic nerve segment.

B.1. Effects of PMF on compound action potential (CAP)

It can be surmised from the preceding experiments that the PMF effect probably influences the mechanism of action potential through changes in its initiation and propagation. Therefore, we decided to investigate the effect of PMF exposure on the sciatic nerve, which represents simpler preparations without any synaptic connections. The interpretation of the PMF-induced effect could then be circumscribed to the processes responsible for generating, modulating and propagating action potentials.
To investigate the effect of PMF on the compound action potential recorded from the sciatic nerve, 10 experiments were performed. A typical experiment is depicted in Fig 9. The averages of the CAP amplitude recorded in the first 20 minutes (baseline), were compared to the averages of the CAP amplitude recorded 30 minutes after the exposure to PMF. The PMF increased the mean amplitude of the CAP significantly (n=10, 187.1%, p = 0.005, Fig 10). Control experiments revealed, that the amplitude of CAP remained constant for at least 2 hrs, when PMF was not applied. The PMF-induced amplification of the amplitude of the compound action potential occurred independently on electrical stimulation used to induce neuronal activity. When the electrical stimulation was discontinued during PMF exposure, there was still an increase in CAP amplitude (Fig 11).

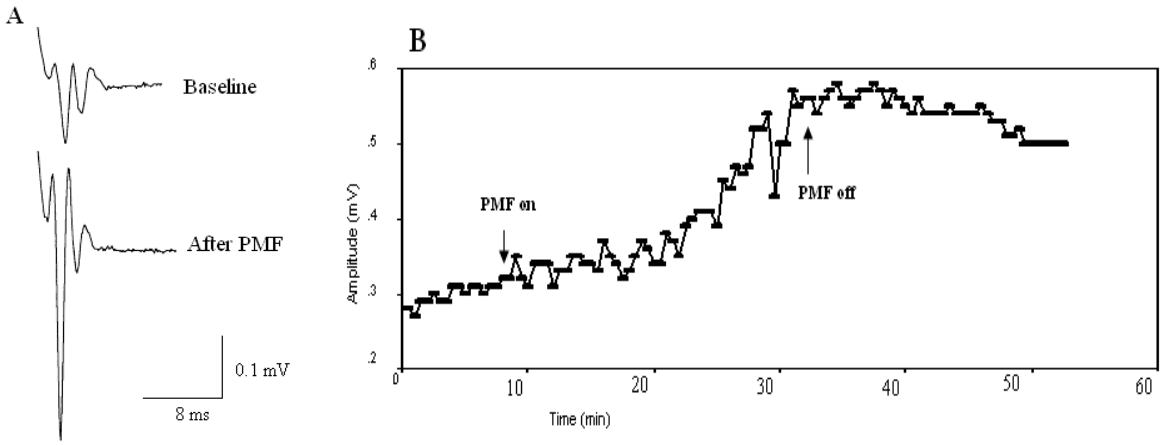

Fig. 9. A representative experiment demonstrating the influence of PMF on CAP. A – The upper and lower potentials represent the CAP before and after PMF exposure, respectively. B – the change in the amplitude of CAP during entire experiment; "PMF on/PMF off" indicates initiation and termination of the magnetic field exposure, respectively.

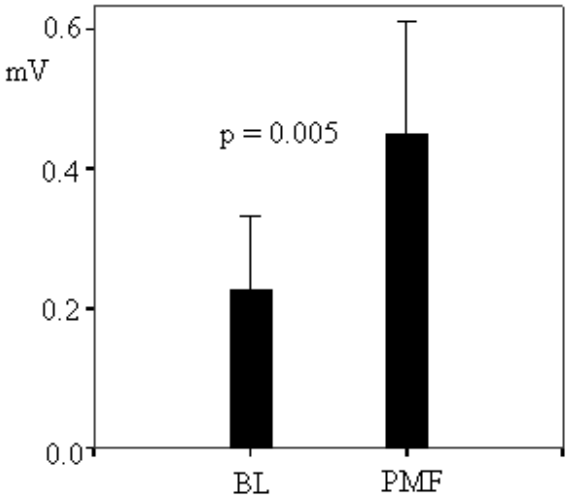

Fig. 10. The influence of PMF on CAP recorded from the sciatic nerve. The bars show the averages of 10 experiments, performed on ten different segments of the sciatic nerve prepared from eight mice. BL refers to the baseline-recording period. The PMF bar represents the recordings at the maximal effect of the PMF. PMF significantly increased the compound action potential (n=10, 187.1%, p = 0.005). Wilcoxon signed ranks test, for 2 related samples was used.

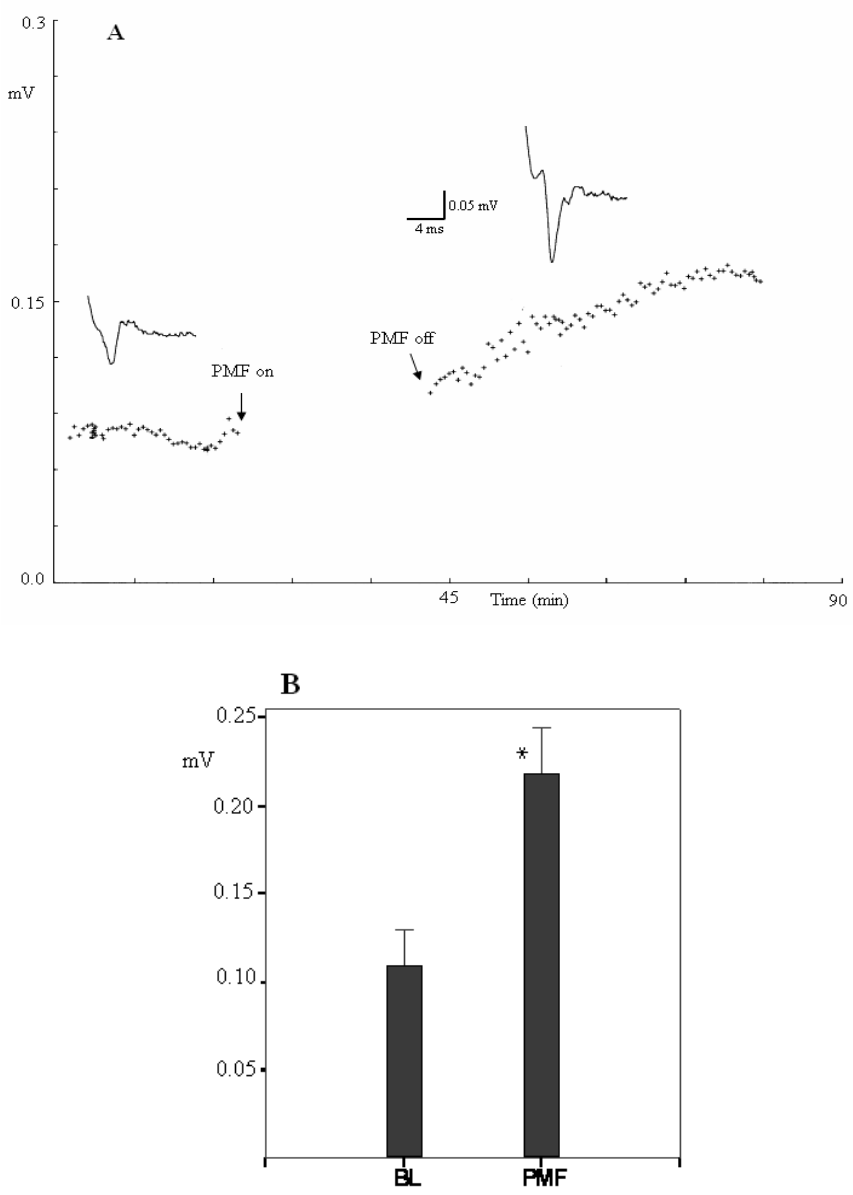

Fig. 11. PMF effect was independent of the concurrent electrical stimulation used to evoke CAP. The recording was followed for 20 minutes and then the electrical stimulation was stopped during the 30 minutes exposure to PMF. After the PMF was turned off, electrical stimulation was resumed and potentials were followed for another 30 minutes. A – An example of a typical experiment: the upper part of the graph represent potentials recorded before and after PMF exposure and the lower part of the graph shows the potential amplitude that was followed throughout the experiment except the period of PMF exposure. Note that during PMF exposure no electrical stimulation was applied and no records of CAP were taken. B – Bars represent the averages that were taken from the baseline period (BL) and at the maximal effect after the PMF exposure (PMF). PMF induced significant increase of the CAP amplitude (n=11, p=0.002, 185.7%, Wilcoxon signed ranks test).

We have also investigated the influence of PMF on the axonal threshold. In most of the experiments, 0.1 V was the lowest strength used to evoke the lowest compound action potential, and for maximal strength one Volt was used. Any stimulus strengths above one Volt were considered supra maximal. During the baseline period of each experiment, one recording was taken at the strength of each stimulus and repeated after the PMF exposure. Note that the same electrical stimulus strength evoked higher CAP amplitude after the PMF exposure. Figure 12 shows that the PMF reduced the threshold

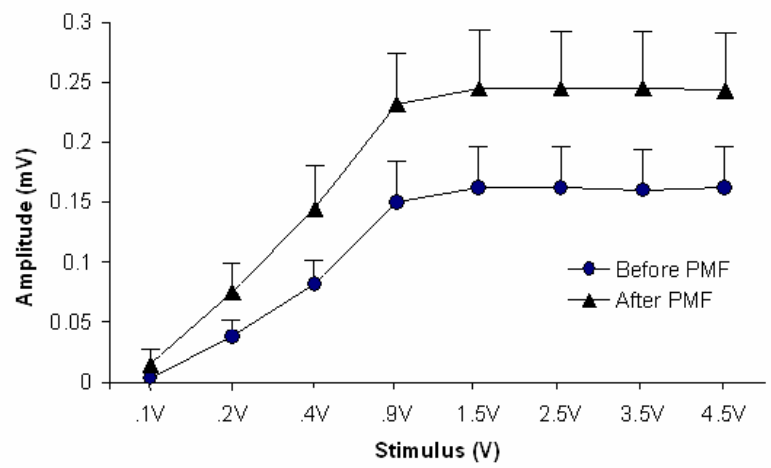

Fig. 12. Effects of PMF on the sciatic nerve threshold. The stimulus strength ranging from 0.1 V to 4.5 V was applied to the sciatic nerve preparation before (● ●) and after (▲ ▲) the exposure to PMF. Eight measurements (one measurement at each value of stimulus strength) were taken from each experiment before PMF exposure (solid circles) and another eight measurements were taken after the PMF exposure (solid triangles). The PMF shifted the threshold curve to the left, which suggests reduction in the axons threshold. That left shift was statistically significant in all stimulus strength values ($p<0.05$, $n=8$) except at 0.1V ($p>0.05$, $n=8$, paired Samples t test). Each point on the graph represents the average of eight experiments.

significantly ($n = 9$, $p<0.05$) in all stimulus strengths except at 0.1 V, where the reduction of the threshold was small and statistically insignificant ($p>0.05$).

B. 2. The effect of PMF on sodium channels

The experiments previously described, suggest that Na^+ and K^+ channels are involved in the mediation of the PMF-induced effect. Therefore the effects of PMF on CAP was studied in the presence of 10nM TTX (a potent sodium channel blocker).

After stable baseline recordings were established, TTX (10nM) was added to the recording chamber. TTX significantly reduced the CAP amplitude ($p = 0.009$, 68.2%, $n = 6$). Fig 13 A and B show a typical experiment and the average of all data, respectively. When the amplitude of the potential stabilized at its minimum value after the addition of TTX (15 - 20 minutes), the PMF was applied for 30 minutes. The depressive effect of TTX was not only eliminated within first 10 minutes of the PMF application, but was reversed to amplification in the later stages of the PMF exposure ($p=0.027$, 80% ± 55%, $n=6$). Figure 13A shows a representative experiment showing the CAP potentials and the change in their amplitudes depicted as the upper and lower parts of the graph, respectively. The bars in figure 13B represent the averages of potentials recorded during three periods of the experiment: 1) baseline (before the addition of TTX and the PMF exposure) marked as (BL); 2) at the maximal of the depressive effect of TTX (TTX) and 3) at the maximal amplification after the PMF exposure (PMF). We have also investigated the effect of the PMF on CAP in the presence of lidocaine, a strong local anesthetic whose action is mediated by the blocking of sodium channel. After stabilization of the potential, lidocaine (150 µM) was added to the recording chamber. It significantly reduced the amplitude of the compound action potential ($p = 0.0005$, $n = 8$). When the amplitude of the potentials stabilized at its minimum value after the addition of lidocaine (15 -20 minutes), the PMF was turned on for thirty minutes. Surprisingly, the

PMF reversed the depressive effect of lidocaine within 7-10 minutes (Fig 14A). The reversal effect of the PMF was significant (p = 0.0005, n = 8, Fig 14B). Washing away the lidocaine amplified the potential even further (p = 0.003, n = 8). Figure 14A depicts a typical experiment that shows the potential shape

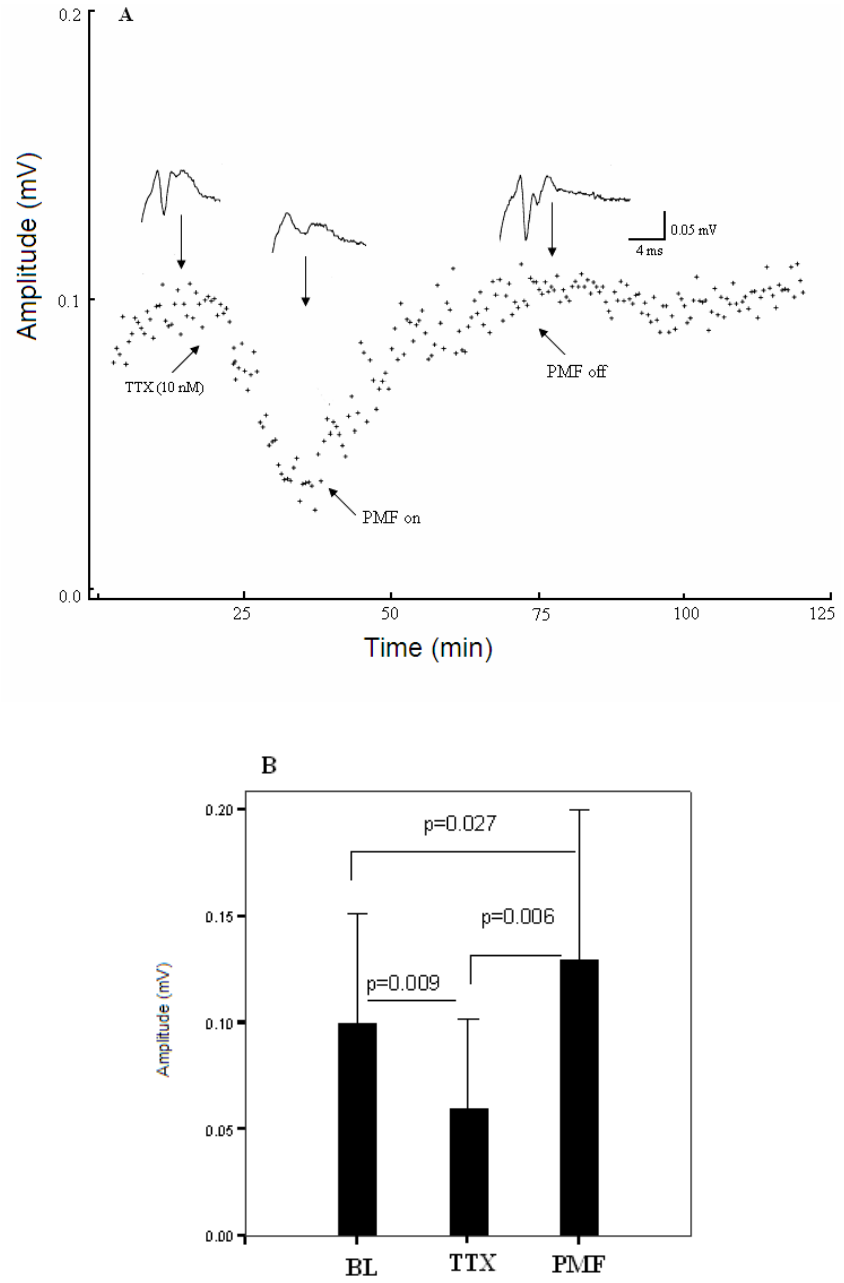

Fig.13. The influence of PMF on TTX-induced depression of CAP. A – A representative experiment. Following 15 minutes of baseline, TTX was added to the recording chamber. TTX reduced the CAP significantly (p=0.009, 68.2%). After the recording in the presence of TTX showed stability, PMF was turned on for 30 minutes. It reversed the TTX-induced depression and in later stage it significantly amplified the potential over the baseline. B - the averages of the potentials recorded during different stages of the experiment: the baseline (BL), after TTX addition (TTX) and after PMF exposure (PMF). PMF significantly reversed the effect of TTX and increased the CAP significantly (p=0.006, 80%, n=6, paired samples t-test).

and amplitude at different periods of the experiment. Bars in Figure 14B represent the average potential for different periods of the experiments.

In control experiments (no PMF) the potential depressed by lidocaine was followed for over an

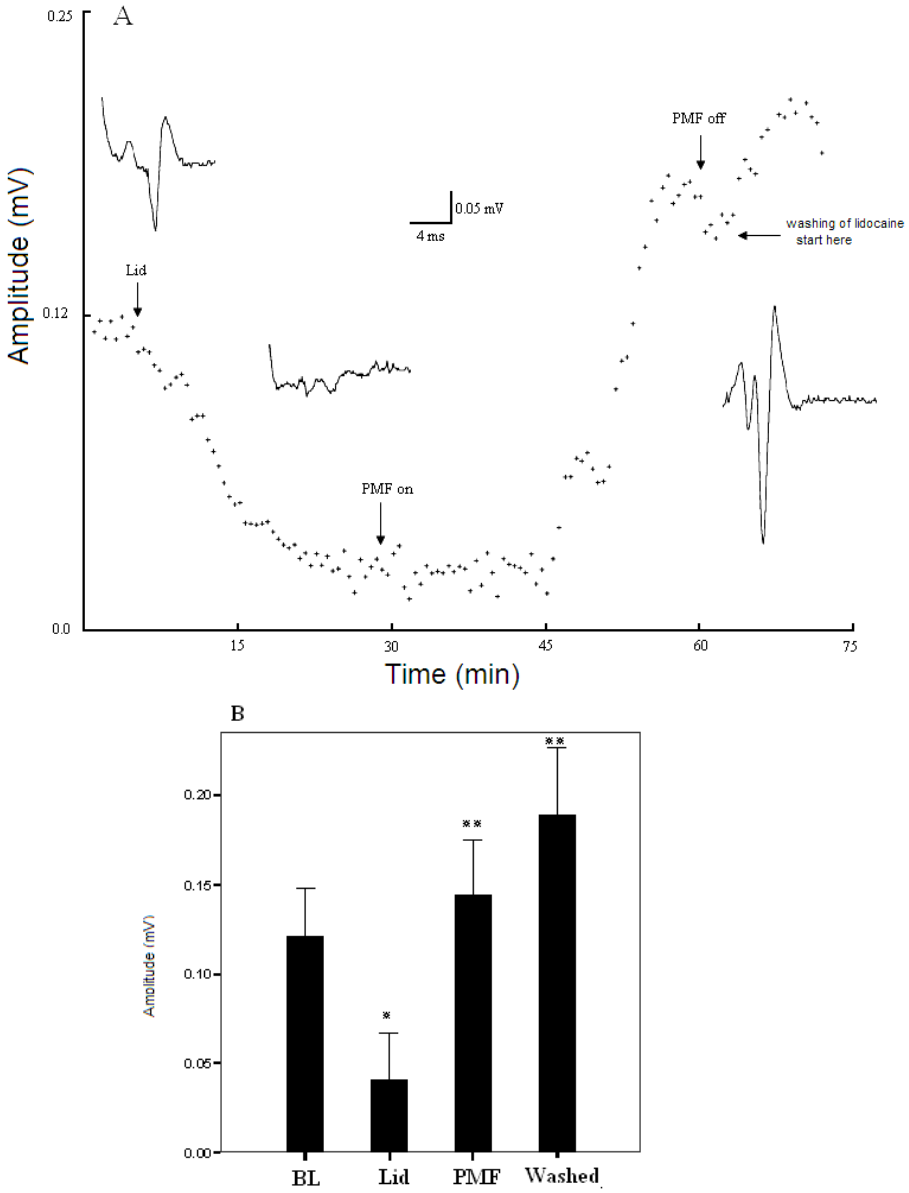

*Fig.14. The influence of PMF on lidocaine-induced depression of CAP. A – A representative experiment demonstrating the depression of CAP by lidocaine (150μM) and the reversal of lidocaine's action by PMF exposure. B – The magnitude of CAP in baseline (BL), after the addition of lidocaine (Lid), after PMF exposure (PMF), and after lidocaine was washed away (Washed). Lidocaine-induced attenuation of CAP (p=0.0005, n=8), was reversed by PMF exposure (p = 0.0005, n = 8, paired t-test). The increase that was induced by PMF exposure was significantly higher than the mean of the CAP of the baseline (p=0.04). Washing of lidocaine away induced additional increase in CAP amplitude, which exceeded the value of the potentials recorded after PMF exposure (p=0.003). *denotes a statistically significant difference (p<0.05) between the baseline and after the addition of lidocaine. **denotes a statistically significant difference (p<0.05) between after PMF and after washing and both baseline and lidocaine.*

hour and no spontaneous recovery was observed, unless the lidocaine was washed away with fresh Ringer's solution (Fig 14B).

The results of experiments with lidocaine and TTX inspired us to investigate the idea, that PMF amplifies the action potential by modifying the gating process of the sodium channel. To verify our assumption we used veratridine, which modifies inactivation gate and induces a persistent activation of the sodium channel (Hille, 2001). In the sciatic nerve preparation veratridine did not change the size of CAP (n = 10, p = 0.619) but reversed the action of the PMF from facilitation to depression (p = 0.002). These results indicate that the PMF potentiated the effect of veratridine probably by facilitating its binding ability.

B.3. The pulsed magnetic field frequency and its effect on CAP.

We have also investigated the influence of magnetic field frequency on the changes in the CAP amplitude. Five frequencies have been selected: 0.5 Hz, 0.16 Hz, 0.07 Hz, 0.03 Hz, 0 Hz (static). The static magnetic field was used to compare the results obtained on sciatic nerve with our previous data on hippocampal slices (Wieraszko, 2000). Interestingly, although the static magnetic field initially reduced the CAP, (n = 16, p =0.0009), it induced recovery/amplification of the potential in the later stage of its application (p = 0.481, Fig. 15 and 16).Figure 15 shows an example of a typical experiment that represents the amplitude of the potential, and Fig 16 depicts the potential shape at different stages of the experiment**.**

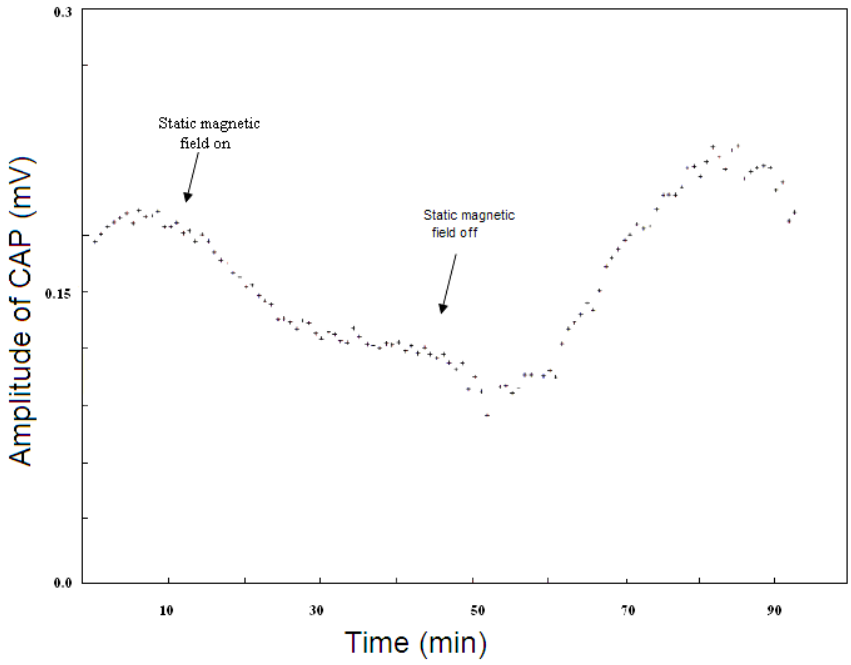

Fig. 15. A representative experiment showing the influence of static magnetic field on CAP recorded from the sciatic nerve. Static magnetic field induced biphasic effect: depression phase during the application of field and recovery/amplification phase after the termination of the field.

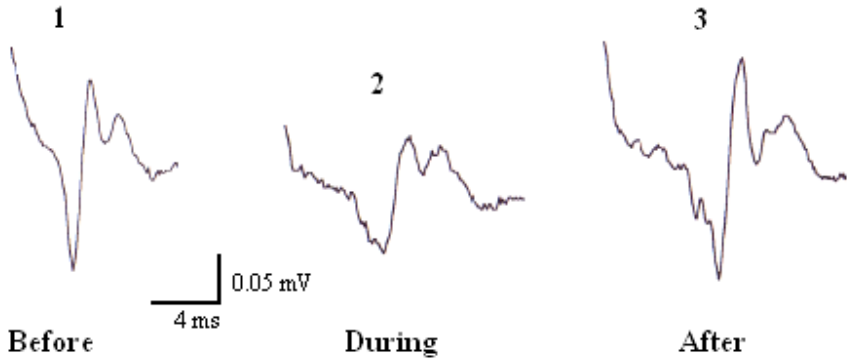

Fig. 16. Three waveforms show the shape and the amplitude of CAP: before (1), during (2), and after (3) exposure to the static magnetic field..

The influence of different frequencies of PMF on the magnitude of CAP is shown in Fig 17.

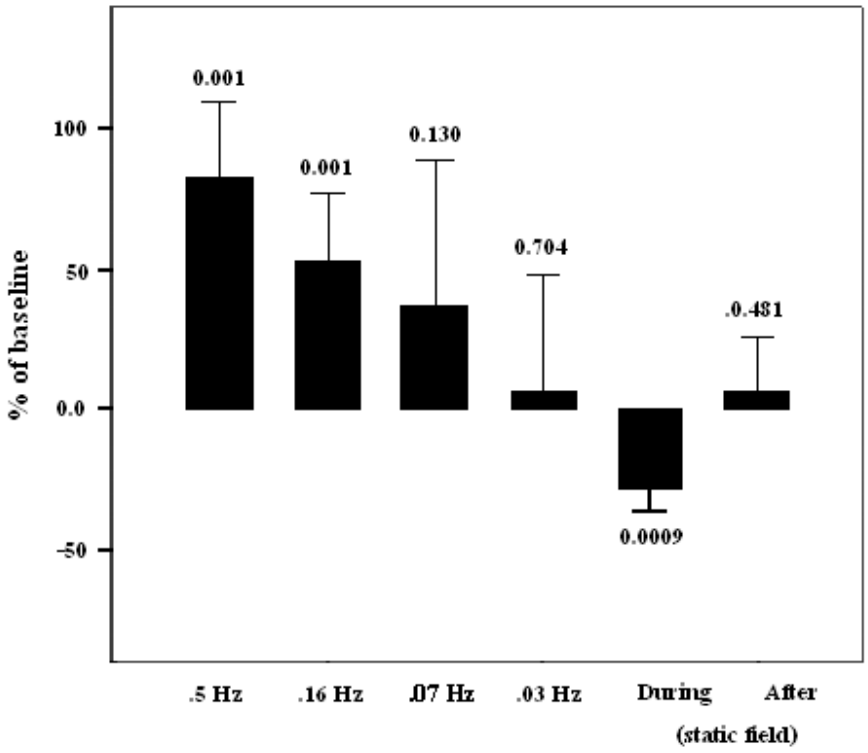

Fig.17. The influence of different frequencies of PMF on CAP recorded from the sciatic nerve. The bars represent the percentage of control calculated as the difference between the average before and after the PMF exposure divided by the average before PMF exposure. The numbers above the bars represent the p value, which was calculated using one sample t test. The difference between groups was statistically significant One way ANOVA was used (F = 7.566, p = 0.0002).

C. Discussion.

Our findings support our previous reports on the effect of PMF on the nervous system (Trabulsi et al., 1996; Wieraszko, 2000; Wieraszko, 2004; Wieraszko, et al., 2004). The effect was frequency-dependent and mediated by synaptic and non-synaptic mechanisms. The enhancement of the paired-pulse facilitation (PPF) implies PMF-induced modulation of presynaptic mechanism, most likely the processes regulating neurotransmitter release. This supports our previous results demonstrating PMF-induced reduction in glutamate uptake (Wieraszko et al., 2005). One can hypothesize, that PMF-induced decrease in Ca^{2+} buffering, amplification of Ca^{2+} release from the internal stores, and/or increase of the influx of Ca^{2+} through calcium channels at the pre-synaptic terminal may be involved in observed effects.

The result from the experiments with antidromic stimulation of the hippocampal slices provided the first clue toward the axonal involvement in the PMF-induced increase in excitability. When synaptic transmission was blocked, the PMF was effectively inducing an increase in the antidromically recorded population spike. Further analysis of the result of these experiments indicated that the population spike amplification was not due to an increase in the number of firing neurons but resulted from an increase in excitability of the same population of neurons. This assumption was further supported by the experiments performed on sciatic nerve. The compound action potential (CAP), recorded from this preparation was permanently amplified following PMF exposure. This amplification was correlated with PMF-induced reduction in the axonal threshold. The plateau of curve illustrating the relationship between CAP amplitude and the strength of the stimulus was similar in the exposed and unexposed preparations. This supports the conclusion that the PMF-induced increase in the CAP amplitude was due to an increase in excitability of the same population of axons and not by the recruitment of new axons.

PMF has been shown not only to reverse the depressive action of TTX and lidocaine, but to amplify the CAP at a later time in the experiment. Apparently, PMF exposure changed the properties of sodium channel reducing its affinity for both ligands. Local anesthesia drugs such as lidocaine can shed more light on how PMF induced hyperexcitability. In the presence of lidocaine sodium channel inactivation is greatly amplified. Hyperpolarization of the cell membrane is needed to relieve this inactivation of the channel (Hille, 2001). Theoretically, lidocaine binds to a site inside the channel pore and its binding is voltage dependent. Since depolarization is needed for the drug to block the channel, it is assumed that lidocaine binds more tightly to an inactivated sodium channel (Hille 2001). These phenomena can explain why the PMF eliminated the lidocaine effect on sodium channels. Hyperpolarization of the cell membrane by PMF initiates following, sequentially occurring events: 1) it opens the inactivated gate more readily; 2) it loosens drug binding; 3) it makes the drug more prone to site dissociation. However, hyperpolarization cannot alone explain all the PMF induced effects mentioned above, and experiments with TTX suggest that PMF exposure induces also changes in the channel protein confirmation. TTX binds to the extracellular site of the sodium channel in a voltage-independent way, blocking stimulated and non-stimulated axons. Since TTX does not react with the channel gating system hyperpolarizing of the cell membrane would not affect the action of TTX. Therefore, the changes in the channel protein conformation, not change in the membrane potential could explain the effect of PMF on TTX-sodium channel interaction.

PMF induced effect was blocked by veratridine. Veratridine reduces the conduction of sodium channel and prevents its inactivation (Hille 2002). The action of veratridine is activity-dependent and it does not affect the activation gate of sodium channels. Veratridine modifies the inactivation gate of sodium channels and the lifetime of that modification is in milliseconds. The reaction of the drug (binding and unbinding) develops from the open state of sodium channel (Hille, 1968; Sutro 1968; Leibowitz et al. 1986; Wang et al. 1990). The dependence of veratridine action on the open state of sodium channel explains the cooperative effect between the PMF and veratridine actions. The PMF increased the rate of activation of sodium channels and that in turn intensified the action of veratridine. Thus, veratridine together with PMF reduced the amplitude of CAP2. Being that PMF did not reverse the action of veratridine, it means that the PMF effect on the shape of the channel protein is specific. If the change in the channel complex is general, it would have affected its affinity to all three antagonists. Instead, the PMF changed the affinity of lidocaine and TTX and reversed their actions, but it did not diminish the affinity for veratridine. Just to the opposite, it intensified its action. This observation points to the probability of the presence of particular sites in the channel complex with different sensitivities to magnetic field exposure.

Although the PMF used in this study is a very specific form of magnetic field spectrum, the findings and their analysis can be applied as a basis for other magnetic field forms biological effects. Magnetic field in general is approved to be beneficial as an adjunct therapy in medicine (see review by Shupak, 2003). The lack of mechanisms of magnetic field action hindered its research toward therapeutics (Rubik, 1997). Here we introduced a mechanistic basis for their effect, which would help and guide clinicians and researchers to the best possible utilization of magnetic field in the treatment of the pathology. A clinical based research could test the effect of PMF on the peripheral nervous system on humans.

Acknowledgements
This research was supported by NIH grant # 1RO1ES110022, PSCCUNY grants # 662850035 and 670890036, and by OMRD Fellowship to CSI/IBR Center for Developmental Neuroscience.

References

Andersen P., Bliss TVP., Skrede KK., (1971). Unit analysis of hippocampal population spike. Exp. Brain Res., 13: 208-221.

Hille, B. (1968). Pharmacological modification of the sodium channel of the frog nerve. J. Gen. Physiol. 51: 199 – 219.

Hille, B. (1968). Charges and potentials at the nerve surface: Divalent ions and PH. J. Gen. Physiol. 51:221 – 236.

Hille, B. (2001). Ion channels of excitable membrane. Third edition, Sinaur Associates, Inc. publishers Sunderland, Massachusetts U.S.A.

Hogan MV, Wieraszko A (2004).An increase in cAMP concentration in mouse hippocampal slices exposed to low-frequency and pulsed magnetic fields. Neurosci. Lett. 366:43-47.

Keynes, R. D., (2002). Studies of multimodal gating of the sodium channel. Sodium channels and neuronal hyper-excitability, published by John Wiley and sons Ltd, pp5-14.

Leibowitz, M. D., J. B.Sutro and B. Hille, (1986). Voltage-dependent gating of veratridine-modified Na channels. J. Gen. Physiol. 87: 25-46.

Rubik, B., (1997). Bioelectromagnetic and the future of medicine. Administrative radiology Journal. 16: 38 – 46.

Semm P, Schneider T, Vollrath L (1980). Effects of an earth-strength magnetic field on electrical activity of pineal cells. Nature, 11: 288(5791):607-8.

Shupak, M. Naomi (2003). Therapeutic uses of pulsed magnetic-field. Radio Science Bulletin, No 307, 9 – 32.

Sutro, J. B. (1986). Kinetics of veratridine action on Na channels of skeletal muscle. J. Gen. Physiol. 87: 1-24.

Trabulsi R, Pawlowski B, Wieraszko A (1996).The influence of steady magnetic fields on the mouse hippocampal evoked potentials in vitro. Brain Res. 728:135-139.

Wang H, Wang X, Scheich H (1996). LTD and LTP induced by transcranial magnetic stimulation in auditory cortex. Neuroreport, 7:521-5.

Wang, G. K., M. Dugas, B. I., Armah and P. Hornerjager, (1990). Sodium chanel comodification with full activator reveals veratridine reaction dynamics. Mol. Pharmacol. 37: 144-148.

Wieraszko A (2000). Dantrolene modulates the influence of steady magnetic fields on hippocampal evoked potentials in vitro. Bioelectromagnetics. 21:175-82.

Wieraszko, A. (2004). Amplification of evoked potentials recorded from mouse hippocampal slices by very low repetition rate pulsed magnetic fields. Bioelectromagnetics 25:537-544.

Wieraszko A., J. Armani, A. Hanna, N. Maqsood, H. Raja, M.V. Hogan (2004) . Changes in neurotransmitter turnover and second messenger levels in brain tissue exposed to magnetic fields. Proc., 3rd Int. Workshop: Biological effects of EMFs, Kos, Greece, pp. 614-632.

Wieraszko, A., Armani, J., Maqsood, N., Raja, H., Philip, S., (2005). Modification of the synaptic glutamate turnover in the hippocampal tissue exposed to low-frequency, pulsed magnetic fields. Brain Res., 1052: 232-235.

Wieraszko A (1983). Uptake of D-[3H] aspartic acid by hippocampal slices: the influence of low and high frequency activation of nerve endings. Brain Res. 259:324-326.

INDIVIDUAL CHANGES IN HUMAN EEG CAUSED BY MODULATED 450 MHz MICROWAVE

RUTH TOMSON[1], MAIE BACHMANN[1], JAAN KALDA[2], MAKSIM SÄKKI[2], JAANUS LASS[1], VIIU TUULIK[1], AND HIIE HINRIKUS[1]

[1]Biomedical Engineering Centre, Tallinn University of Technology

Address: 5 Ehitajate Rd, EE19086 Tallinn, Estonia

[2]Institute of Cybernetics at Tallinn University of Technology

Address: 21 Academy Rd, EE12618 Tallinn, Estonia

Abstract

During resent years our studies have been focused on the effect of modulated low-level microwaves on human EEG rhythms. In this study the experiments with 450 MHz microwave modulated at 40 Hz and 70 Hz frequencies were carried out on a group of 15 volunteers. The field power density at the scalp was 0.16 mW/cm^2. Ten cycles of the exposure (1 min on and 1 min off) with each modulation frequency were applied. The energies of 8 EEG channels FP1, FP2, T3, T4, P3, P4, O1 and O2 were analysed for individuals by two different methods: nonlinear method of scaling analysis for length distribution of low variability periods (LDLVP) and relative changes in EEG energy between segments with and without exposure (*S*-parameter). Statistical analysis of the calculated measures with post-hoc Bonferroni correction by approach with a 0.05 confidence level was applied.

The exposure caused increase of the EEG energy; changes were stronger in temporal and parietal regions and EEG beta rhythms. Statistically significant changes in EEG were detected for 4 subjects (26.7%) with 40 Hz modulation frequency. The rate of multiple chemical sensitivity (between 2 and 10 %) is even lower than sensitivity to microwave.

Keywords: EMF effects, nonionising radiation, microwave radiation, time variability, scaling analysis, spectral analysis, EEG rhythms.

Introduction

The nervous system has been thought to be most sensitive to external electromagnetic field (EMF) since there is a tremendous electrical activity in neural processes. Information processing and transmission in nervous system is based on bioelectromagnetic phenomena. Therefore, can be expected that EMF effects at system level appear most likely in nervous system.

Modulated microwave radiation at non - thermal level of field power density can affect human central nervous system in a sensible way. Except in unhealthy artificial conditions the effect is weak and difficult-to-detect. Reports of possible non-thermal EMF effects are often contradictory and the difficulties in independent repeating of the experimental results cause doubts. Mechanisms behind the effects are still unclear. Several investigators have reported that low-level exposure produces alterations in the EEG signal and brain behavior [1 - 7], while others conclude that exposure to electromagnetic field does not alter resting EEG [8, 9].

In our previous studies the relative changes in the EEG rhythms energy caused by microwave radiation modulated inside the EEG physiological spectrum at frequencies 7 Hz, 14 Hz and 21 Hz were investigated [10]. The conclusion was that the effect produced by microwave radiation has a clear frequency dependence and increases with modulation frequency. The influence of microwave with modulation frequency 217 Hz – technical frequency much higher than the EEG rhythms – has been also reported to produce statistically significant changes in time variability and intensity of the EEG signal for 10-20% of healthy subjects [11].

This study is aimed to evaluate the effect of microwave modulated with intermediate frequencies 40 Hz and 70 Hz. The same exposure conditions utilized in our previous studies were applied. Two methods were selected for EEG analysis: scaling analysis of length distribution of low variability periods (LDLVP) as sensitive to signal time variability [12] and relative change in the EEG energy of segments of the signal with and without exposure as sensitive to the changes in signal level [6].

Method and equipment

Subjects

An experimental study was carried out on a group of volunteers. The group consisted of 15 young persons (aged 21-24): 8 male and 7 female. Their physical and mental condition (tiredness, sleepiness) before the experiment was evaluated by a questionnaire and a clinical interview. All the subjects selected were healthy, without any medical or psychiatric disorders; tired or sleepy people were excluded. After the recordings, they described how they felt during the experiment. The subjects reported neither alertness nor any strain experienced during the recordings.

The experiments were conducted with the understanding and written consent of each subject. The study was conducted in accordance with the Declaration of Helsinki and has been formally approved by the local Medical Research Ethics Committee.

The measurements were performed in a dark laboratory, but no other special conditions were provided. The subjects lay in a relaxed position, with eyes closed and ears blocked during the experiments.

All the subjects were exposed and sham exposed. Only one experimental EEG recording was performed for a subject during a day. The measurements were double blinded. During each test session, the exposed and sham-exposed subjects were randomly assigned. The subjects were not informed of their exposure; however, they were aware of the possibility of being exposed. Subjective factors were also excluded from the computer-performed data analysis: the same algorithms were applied for all the recordings (both for exposed and sham-exposed subjects).

Microwave Exposure

The modulated microwave radiation at non-thermal level of field power density, identical to our previous studies [5, 6, 10, 11, 12], was used. Microwave exposure conditions were the same for all subjects.

The 450 MHz microwave radiation was generated by the Rhode & Swartz (Germany) signal generator model SML02. The RF signal was 100% amplitude modulated by the pulse modulator SML-B3 at 40 or 70Hz frequency (duty cycle 50%). The generator signal was amplified by the Dage Corporation (USA) power amplifier model MSD-2597601. Located in the laboratory, the generator and amplifier were carefully shielded. The 1W EMF output power was guided by a coaxial lead to the 13cm rod antenna NMT450 RA3206 by Allgon Mobile Communication AB, Sweden, located 10 cm from the subject's skin on the left side of the head.

The calculation of the specific absorption rate (SAR) inside the brain was based on the known field power density on skin. The Central Physical Laboratory of the Estonian Health Protection Inspection measured the spatial distribution of the microwave power density by the Fieldmeter C.A 43 Chauvin Arnoux (France) field strength meter. The calibration curves of the field power density dependence on the distance from the radiating antenna were obtained from these measurements taken in the actual conditions of the experiment. During the experiments, the stability of the microwave level was monitored by the IC Engineering (USA) Digi Field C field strength meter.

Estimated from the measured calibration curves, the field power density at the skin was 0.16 mW/cm2. The level of power density was so low that thermal effects were extremely unlikely.

Recording protocols and equipment

The study consisted of three experimental protocols, identical for all subjects. The first protocol was recorded as described below.

First, the reference EEG was recorded over 60 s.

Secondly, modulated microwave radiation was applied. The duration of the exposure was 60 s, and the compensatory pause after the exposure was 60 s. Continuous EEG recordings were made during and 60 s after exposure. The procedure of the cycle was repeated ten times. The microwave exposure was switched on every first 60 s of the cycle. During ten cycles of microwave exposure, the modulation frequency always remained at 40 Hz.

The recording protocol for one subject lasted for 21 min, during which the EEG was continuously recorded.

The second protocol included the same steps, except that the modulation frequency was 70 Hz and the third protocol for the sham-exposure included also the same steps, except that the microwave generator was switched off.

The Cadwell Easy II EEG measurement equipment was used for the EEG recordings. The EEG was recorded by means of 19 electrodes, placed on the subject's head according to the international 10-20-electrode position classification system, with Cz as reference. The EEG recordings were stored on a computer at a sampling frequency of 400 Hz. The recorded EEG signals were examined by an experienced neurologist. Artifacts were detected by visual inspection. The recordings containing multiple artifacts were removed, and the whole recording was repeated.

The pre-processing of the signals was performed in the LabVIEW programming and signal-processing environment. The EEG spectrum 0.5 - 39 Hz was selected for the analysis. The results of the preceding validation of the set-up confirmed the absence of modulation components, caused by parasitic interference between EEG and radio frequency equipment.

Analysis of the EEG based on the LDLVP method

Initially, all the EEG recordings were divided into two sub-signals. The recordings performed with the first and second recording protocol were divided as follows:

- the first subsignal contained all 1 min periods without microwave exposure (all the odd minutes from the initial EEG recording),
- the second subsignal contained all minutes with microwave exposure (all even minutes of the initial EEG recording).

The recordings performed with the sham recording protocol were divided similarly:

- the first sham subsignal contained all the odd minutes,

· the second sham subsignal contained all the even minutes of the initial recording.

The scaling analysis utilizing LDLVP method was applied for two sub-signals.

The LDLVP method has been used and described in details in our previous studies [12 – 14]. Here we provide a brief summary of this method.

First, we define the local variability as the deviation of the current value of the signal from the local average

$$\delta V(t) = V(t) - T^{-1} \int_{-T/2}^{T/2} V(t+\tau) d\tau , \quad (1)$$

where V(t) is the recorded voltage, and the time-window width T is a free (adjustable) parameter. For EEG signals, a reasonable value is provided by T = 60 ms [14].

Secondly, low-variability periods are defined as continuous intervals with

$$\delta V(t) < \delta_0 . \quad (2)$$

Finally, the number of low-variability periods N exceeding length T_0 is plotted against length T_0, see Figure 1.

The value of δ_0 was adjusted for each recording individually, reaching a minimum value so that, for both subsignals, the length of the longest low-variability period was at least 3750 ms.

The hypothesis of this work was that microwave exposure increases EEG variability. Owing to higher variability, there are fewer long low-variability periods. Therefore it is expected that microwave exposure decreases the area of the $T_0(N)$ -curve (see Fig 1), due to faster cut-off at large values of T_0. According to this assumption, the weighted area

$$S_W = \sum_{N=1}^{128} \ln\left(\frac{N}{\max(N-1,1/4)} \right) \ln(T_0) N^{1/2} \quad (3)$$

of the function $T_0 = T_0(N)$ was selected as the non-linear quantitative measure.

Analysis of the EEG based on the *S*-parameter method

Relative changes in the EEG energy between segments with and without exposure *S*-parameter was selected as a measure for detection of the effect on signal intensity.

The analysis method was applied in our previous study [10], except for different comparison intervals. The energies of the different EEG rhythms were analyzed separately. Average energies for segments with and without stimulation were compared. The first 30 s of a 60 s recording segments with and without stimulation were selected as intervals for comparison. The average energy of an arbitrary comparison interval was calculated for the recording segment as follows:

$$s_i = \frac{1}{N} \sum_{r=1}^{N} \left[x(r) \right]^2 \quad (4)$$

where x is the amplitude of the recorded signal and N is the number of samples, during 30 seconds N = 12000. The relative change in the energy of the recording segments with and without stimulation was selected for further analysis. Finally, parameter S was calculated as follows:

$$S = \left(\frac{s_2}{s_1} - 1 \right) \times 100\% \quad (5)$$

where s_1 and s_2 were the average energies inside the comparison intervals without and with stimulation respectively. For sham recordings the same parameter was calculated for comparison intervals as even and odd minutes of the recordings.

At first, the energies of the four basic EEG rhythm frequencies, theta (4 – 7 Hz), alpha (8 – 13 Hz), beta1 (15 – 20 Hz) and beta2 (22 – 38 Hz), were extracted from the total EEG signal (0.5 – 48 Hz) by filtering. The parameter S was calculated separately for the EEG energies of the theta, alpha, beta1 and beta2 rhythms.

Signal processing and calculation of parameters were performed in the LabVIEW programming and signal processing environment.

Statistical analysis

For sham recordings, sub-signals were completely equivalent. The mathematical expectation of the difference in their spectral powers is zero, $\left\langle \tilde{W}_0 - \tilde{W}_1 \right\rangle = 0$. Next, an estimate of the variance could be obtained as the mean of squared differences:

$$\sigma_f{}^2 = \frac{1}{15}\sum_{n=1}^{15}\left(\tilde{W}_{0nf} - \tilde{W}_{1nf}\right)^2 \qquad (6)$$

According to the "zero hypothesis", the EEG recordings of subjects under microwave exposure cannot be distinguished from sham signals. Thus, the "zero hypothesis" implies that $\left\langle W_0 - W_1 \right\rangle = 0$ and $\left\langle \left(W_0 - W_1\right)^2 \right\rangle = \left\langle \left(\tilde{W}_0 - \tilde{W}_1\right)^2 \right\rangle$. Consequently, if the zero hypothesis is true, the quantity $x_f = \left(W_{0nf} - W_{1nf}\right)^2 \sigma_f{}^{-2}$ is an *f*-distributed random quantity, the cumulative distribution of which is routinely designated as $F_{1,15}(x_f)$; the indices 1 and 15 stand for the numbers of the degrees of freedom.
Accordingly, the ratio of the computed power difference to the standard deviation of the differences can be used as a quantitative measure, showing how well the zero hypothesis is satisfied; respective *p*-values are obtained by means of the cumulative *f*-distribution:

$$p_f = F_{1,15}\left[\left(W_{0nf} - W_{1nf}\right)^2 \sigma_f{}^{-2}\right] \qquad (7)$$

The same technique has been applied to the non-linear quantitative measure (derived from LDLVP), resulting in another two series of *p*-values for recordings at modulation frequency 40 Hz and 70 Hz.

For post hoc analysis the modified Bonferroni correction was applied according to which the smallest p-value is to be multiplied by the number of data points 15, the second smallest is to be multiplied by 15/2=7.5 etc.

Results

The results of LDLVP analysis for a subject are presented in Figure 1. The number of low-variability periods N exceeding the length T_0 is plotted versus the length T_0 for the first and second sub-signal for exposed recording. As can be seen, microwave exposure lowers the curve at the right-hand part of the graph (large values of T_0). Such a change in curve indicates that microwave exposure increases variability of the EEG signal: owing to higher variability there are fewer long low variability periods.

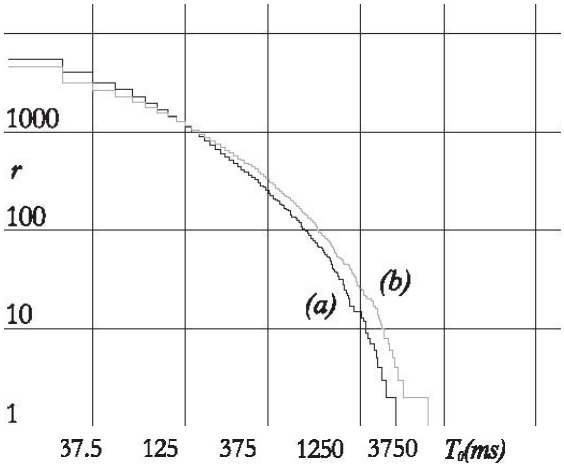

Figure 1. The number of low-variability periods *N* exceeding the length T_0 for a significant subject: black line (a) – second sub-signal of exposed recording (intervals with microwave); grey line (b) – first sub-signal of exposed recording (intervals without microwave).

The results of statistical analysis of the LDLVP quantitative measures for sham and microwave-exposed at modulation frequency 40 and 70 Hz recordings, calculated for each subject, are presented in Table 1. For sham recordings there were no significant results. The ratio of the computed power difference to the standard deviation of differences $\sqrt{x}$ of more than three were considered as significant deviations from the zero hypothesis and are marked in bold. After Bonferroni correction *p*-values not larger than 0.05 were considered as significant deviations from the zero hypothesis and are marked in bold. As can be seen, the analysis resulted in *p*-values lower than 0.05 for 4 cases in the case of microwave exposure at modulation frequency 40 Hz and none for 70 Hz frequency.

Table 1. Calculated using LDLVP method $\sqrt{x}$ and *p*-values as a result of Bonferroni correction for different microwave exposure conditions in P-channels

Frequency band	0.5 – 39 Hz					
	sqrt(x)			*p* - value		
Subject	sham	40 Hz	70 Hz	sham	40 Hz	70 Hz
1	0.07	0.95	1.93	1.000	0.591	0.339
2	-0.11	**-3.02**	-0.77	0.582	**0.025**	0.842
3	1.02	1.30	-0.60	1.000	0.392	0.836
4	0.81	-0.21	-0.60	0.876	0.835	0.760
5	0.67	-0.39	1.68	0.963	0.812	0.403
6	0.81	-0.28	-0.04	0.844	0.838	0.972
7	0.98	-0.63	-0.98	0.837	0.802	0.723
8	-1.23	-1.51	-0.11	0.804	0.315	0.983
9	1.86	**3.69**	0.35	0.715	**0.022**	0.912
10	-0.28	2.49	-0.21	0.769	0.065	0.964
11	0.88	0.46	2.14	1.000	0.816	0.336
12	0.00	**3.09**	-2.74	1.000	**0.029**	0.190
13	-0.04	1.93	1.16	1.000	0.170	0.781
14	-1.30	**-3.69**	0.77	1.000	**0.011**	0.748
15	1.93	0.49	-1.05	1.000	0.857	0.762

The results of the *S* - parameter analysis for the whole group are presented in Figure 2. The graph illustrates the effect of microwave exposure – changes between exposed and not exposed segments of the recordings on different EEG rhythms and for sham, 40 Hz and 70 Hz modulation frequency. As can be seen, microwave exposure causes increase in energy of the EEG beta1 and beta2 rhythms.

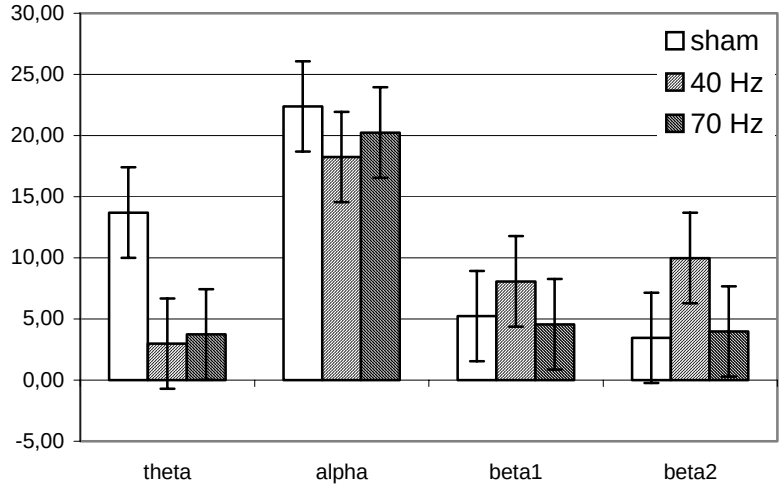

Figure 2. The relative average changes in % (*S* – parameter) of the EEG rhythms total energy of the recording segments with and without microwave exposure in P – channels for the whole group.

The results of statistical analysis of the *S* - parameter are presented in Table 2. For sham recordings there were no significant results. Microwave exposed recordings at modulation frequency 40 Hz have 2 significant values in beta2 region.

Table 2. Calculated *p*-values for different EEG rhythms in P-channels as a result of analysis by post – hoc Bonferroni correction for different microwave exposure conditions

Frequency band	*p*-value											
	Theta			Alpha			Beta1			Beta2		
Subject	sham	40 Hz	70 Hz	sham	40 Hz	70 Hz	sham	40 Hz	70 Hz	sham	40 Hz	70 Hz
1	1.000	1.000	1.000	1.000	1.000	1.000	1.000	0.433	1.000	0.935	1.000	1.000
2	1.000	1.000	1.000	0.612	1.000	1.000	0.902	0.664	1.000	0.780	**0.000**	0.053
3	0.342	1.000	1.000	1.000	1.000	1.000	0.876	1.000	1.000	0.903	0.880	0.671
4	1.000	1.000	1.000	1.000	1.000	1.000	0.983	1.000	1.000	0.875	1.000	0.825
5	1.000	1.000	1.000	1.000	1.000	1.000	0.819	1.000	1.000	0.780	1.000	0.670
6	1.000	1.000	1.000	1.000	1.000	1.000	0.859	1.000	1.000	0.905	1.000	0.543
7	1.000	1.000	1.000	1.000	1.000	1.000	0.780	1.000	1.000	0.781	1.000	0.575
8	1.000	1.000	1.000	1.000	1.000	1.000	0.767	1.000	1.000	1.000	1.000	0.624
9	1.000	1.000	1.000	1.000	1.000	1.000	0.680	1.000	1.000	0.836	0.988	0.573
10	1.000	1.000	0.358	1.000	1.000	1.000	0.837	0.609	1.000	0.800	0.595	0.715
11	0.151	1.000	1.000	1.000	1.000	1.000	1.000	1.000	1.000	1.762	1.000	0.840
12	1.000	1.000	1.000	1.000	1.000	0.066	0.705	1.000	1.000	0.837	1.000	0.818
13	0.548	1.000	1.000	0.077	1.000	1.000	0.794	1.000	1.000	0.757	1.000	0.994
14	1.000	1.000	1.000	1.000	1.000	1.000	1.000	0.383	0.423	0.935	**0.003**	0.690
15	1.000	1.000	1.000	1.000	1.000	1.000	1.000	1.000	0.268	1.000	1.000	0.874

The graphs of changes of the EEG rhythms energy for a significant subject are presented in Fig. 3. In this case increase in the EEG beta2 rhythm energy is more clearly indicated than in Fig. 2 for average changes in the whole group. Effect of 40 Hz modulated microwave is more evident than 70 Hz modulated microwave.

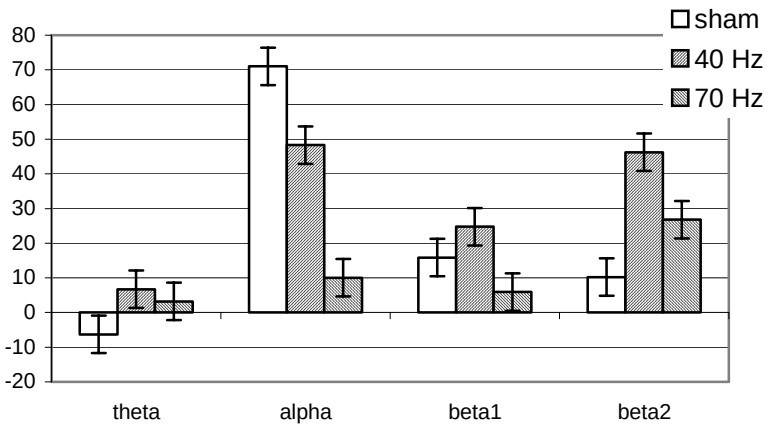

Figure 3. The relative changes (S – parameter in %) of the EEG rhythms total energy in P – channels for a significant subject.

Discussion

As table 1 illustrates, the LDLVP presents the best outcome at modulation frequency 40 Hz, resulting in significant results for 4 subjects. Accordingly, significant effect of exposure to the EEG signal was detected for 26.7 % of subjects. Modulation at frequency 70 Hz was not as effective as 40 Hz; however, it was distinguishable from sham signals, which did not result in any significant deviation.

Considering the direction of influence at modulation frequency 40 Hz, for two subjects under the exposure the computed LDLVP weighted area increased, and for two it decreased. For all subjects, the departure from the sham behavior is statistically reliable. This is somewhat different from what has been observed for the modulation frequency 7 Hz, when the sign of the departure was always negative (corresponding to increased variability) [12]. However, a study at modulation frequency 217 Hz resulted with the outcome, in which for half of the subjects the computed LDLVP weighted area decreased and for another half it decreased [15]. This observation gives us a hint that the physiological effect of the microwave stimulation depends on the modulation frequency (at least there is a difference between the 40, 217 Hz, and the 7 Hz frequencies).

The *S*-parameter measures exceeded the limit of significant deviation from zero hypothesis also at modulation frequency 40 Hz in beta2 frequency band (Table 2), providing 2 significant cases out of 15, that is 13.3 %. There were no significant results at modulation frequency 70 Hz. In an earlier study [10] it was suggested that microwave exposure causes a significant effect when the modulation frequency is higher or comparable with EEG rhythm frequency.

As with both methods, modulation at frequency 70 Hz is not as effective as at 40 Hz. Here we can see that achieved effect is probably concentrated to the lower frequencies. In our previous study with modulation inside the EEG physiological frequencies band the effect has been reported to be more evident at higher modulation frequencies [16]. Possible reason is that 40 Hz is quite close to the EEG physiological frequencies and the switching with brain oscillations more effective.

From those results it is difficult to conclude which measure, LDLVP or *S*-parameter, is more effective and whether the effect of modulation frequencies 40 and 70 Hz appear rather in intensity (*S*-parameter) or time variability (LDLVP) of the EEG signals. The results reported in our previous study with 7 Hz modulated microwave lead to the conclusion that the effect appears in time variability [12], while the next study concerning modulation frequency 217 Hz concluded that the effect is rather in intensity [15].

From Tables 1 and 2, it can be seen that the subjects having significant results overlap. On the other hand, with the LDLVP method, there are 4 significant results compared to 2 with the *S*-parameter. This indicates that microwave stimulation causes different effects for different subjects and there is a need for various methods to detect those effects.

The analysis by the LDLVP method detected the effect of exposure at modulation frequency 40 Hz for 26.7 % of subjects. For instance, the rate of multiple chemical sensitivity (MCS) occurrence is estimated to be between 2 and 10 % in the general population [17]. MCS is characterized by recurrent symptoms involving multiple organ systems and occurring in response to demonstrable exposures to multiple chemically unrelated compounds at doses far below those established to cause harmful effects. Taking this into consideration, LDLVP and *S*-parameter methods demonstrated good sensitivity detecting the effects of microwave stimulation at modulation frequency 40 Hz.

Main trend of changes caused by microwave exposure modulation frequencies was increase of the EEG energy in beta rhythm. Increased beta absolute power was also observed in alcohol-dependent subjects [18].

Conclusion

1. The modulated with 40 Hz 450 MHz microwave exposure caused statistically significant changes in the EEG time variability (26.7% of subjects) and energy variations (13.3% of subjects).

2. Main trend of changes was increase in the EEG beta rhythm energy.

3. The effect is more evident with the modulation frequency closer to the physiological EEG rhythms band.

References

[1] Mann, K., Roschke, J. “Effects of pulsed high-frequency electromagnetic fields on human sleep,” *Neuropsychobiology* 1996, **33**: pp. 41-47

[2] Borbely, A.A., Huber, R., Graf, T., Fuchs, B., Gallmann, E., Acherman, P., “Pulsed high – frequency electromagnetic field affects human sleep and sleep electroencephalogram” *Neurosci. Lett.* 1999, **275**: pp. 207 - 210

[3] Huber, R., Graf, T., Cote, K.A., Wittmann, L., Gallmann, E., Matter, D., Schuderer, J., Kuster, N., Borbely, A.A., Achermann, P. “Exposure to pulsed high-frequency electromagnetic field during waking affects human sleep EEG,” *Neuroreport* 2000; **11**: pp. 3321-3325

[4] Krause, C.M., Sillanmäki, L., Koivisto, M., Häggqvist, A., Saarela, C., Revonsuo, A., Laine, M., Hämäläinen, H. “Effects of electromagnetic field emitted by cellular phones on the EEG during a memory task,” *Neuroreport* 2000; **11**: pp. 761-764.

[5] Lass, J., Tuulik, V., Ferenets, R., Riisalo, R., Hinrikus, H. "Effects of 7Hz-modulated 450 MHz electromagnetic radiation on human performance in visual memory tasks," *Int. J. Radiat. Biol.* 2002; **78**: pp. 937-944
[6] Hinrikus, H., Parts, M., Lass, J. and Tuulik, V.: 2004, Changes in Human EEG Caused by Low – Level Modulated Microwave Stimulation, *Bioelectromagnetics*, **25**: pp. 431 – 440
[7] Curcio, G., Ferrara, M., Moroni, F., D'Inzeo, G., Bertini, M., De Gennaro, L. "Is the brain influenced by a phone call? An EEG study of resting wakefulness" *Neurosci. Res.* 2005, **53**: pp. 265 - 270
[8] Hietanen, M., Kovala, T. , Hamalainen, A.M. "Human brain activity during exposure to radiofrequency fields emitted by cellular phones," *Scand J Work Environ Health* 2000, **26**: pp. 87-92
[9] Krause, C.M., Sillanmäki, L., Koivisto, M., Häggqvist, A., Saarela, C., Revonsuo, A., Laine, M., Hämäläinen, H. "Effects of electromagnetic fields emitted by cellular phones on the electroencephalogram during a visual working memory task," *Int J Radiat Biol* 2000, **76**: pp.1659-1667
[10] Hinrikus, H., Bachmann, M., Tomson, R., Lass, J. "Non-thermal effect of microwave radiation on human brain" *The Environmentalist* 2005, **25**: pp. 187 – 194
[11] Bachmann, M., Kalda, J., Lass, J., Tuulik, V., Hinrikus, H. "Power spectrum distinguishes the effect of microwave stimulation on human EEG at rest" Biological Effects of EMFs 3rd International Workshop, Kos, Greece, 4 – 8 October 2004, pp. 75 – 81
[12] Bachmann, M., Kalda, J., Lass, J., Tuulik, V., Säkki, M., Hinrikus, H. "Non-linear analysis of the electroencephalogram for detecting effects of low-level electromagnetic fields," *Med Biol Eng Comput* 2005; **43**: pp. 142-149
[13] Kalda, J., Säkki, M., Vainu, M., and Laan, M. (2001): 'Zipf's law in human heartbeat dynamics', available: http://arxiv.org/abs/physics/0110075
[14] M. Säkki, J. Kalda, M. Vainu, M. Laan, "The distribution of low-variability periods in human heartbeat dynamics," *Physica A* 2004; **338**: pp. 255-260.
[15] Bachmann, M., Säkki, M., Kalda, J., Lass, J., Tuulik, V., Hinrikus, H. "Effect of 450 MHz microwave modulated with 217 Hz on human EEG in rest" *The Environmentalist* 2005, **25**: pp. 165 – 171
[16] Lass, J., Hinrikus, H., Bachmann, M., Tuulik, V. Microwave radiation has modulation frequency dependent stimulating effect on human EEG rhythms. *Proceedings of the 26th Annual International Conference of the IEEE EMBS* San Francisco, USA, September 1-5, 2004, pp. 4225-4228
[17] Cullen, M.R. "Workers with multiple chemical sensitivities," Occupational medicine: state of the art reviews. Philadelphia: Hanley & Belfus, Inc. 1987; 2: pp. 655-661.
[18] Rangaswamy M, Porjesz B, Chorlian DB, Wang K, Jones KA, Bauer LO, Rohrbaugh J, O'Connor SJ, KuperKuperman S, Reich T, Begleiter H. Beta power in the EEG of alcoholics. *Biol Psychiatry*. 2002 15; 52(8):831-842.

ELECTRIC-FIELD METERS FOR ASSESSING THE EXPOSURE RATIO FROM MULTIPLE RADIO SOURCES AND IMT-2000 CELLULAR BASE STATIONS EMPLOYING THE ISOTROPIC SLEEVE DIPOLE SENSOR AND CODE SELECTIVE RECEIVERS

JUNJI HIGASHIYAMA, KOHJIROH OHSHITA, HIROAKI KOYAMA, YOSHIAKI TARUSAWA, AND SHINJI UEBAYASHI

WIRELESS LABORATORIES, NTT DOCOMO, INC.
3-5 HIKARI-NO-OKA, YOKOSUKA-SHI, KANAGAWA*, 239-8536, *JAPAN

Abstract

This paper proposes novel electric-field (E-field) meters that comprise an isotropic sleeve dipole sensor for a wideband frequency range, code selective receivers, and a GPS receiver.

The sensor achieves isotropy and a wideband frequency range with a high sensitivity level to measure the total exposure ratio from radio sources in the in-situ environment including a scattering domain and where multiple radio sources have different frequencies.

The strength of the E-field from a cellular base station varies dynamically because the transmission power varies depending on the amount of communications traffic. Therefore, for cellular operators, it is important to estimate conservatively the exposure ratio from their base stations at the designed maximum transmission power. A code selective receiver is adopted for conservative estimation of the exposure ratio from the IMT-2000 cellular base stations, which are becoming commonplace worldwide.

The proposed E-field meters can accurately assess the total exposure ratio from 30 MHz to 3 GHz and the profile of the human exposure ratio from IMT-2000 cellular base stations based on in-situ measurement. In addition, we show that the exposure ratio from a typical IMT-2000 cellular base station is less than 1/10000 of the E-field strength reference level given in the ICNIRP guidelines.

Keywords: IMT-2000 cellular system; the ICNIRP guidelines; radio receivers

1. Introduction

When starting the service of a new cellular base station, the E-field strength from the base station must be below the E-field reference level given for the country in which the base station is established. Furthermore, if there are other radio stations around the base station, the electromagnetic environment including the radio waves from the surrounding stations must be evaluated comprehensively. The reference levels for the E-field strength are different for each radio law. However, many radio laws adopt the reference levels given in the ICNIRP guidelines (the ICNIRP reference levels) [1]. The ICNIRP reference levels are different for each radio wave frequency. Therefore, if the E-field strength levels are evaluated in an environment where the radio waves from multiple radio stations have different frequencies, it is important to asses the total exposure ratio considering the difference between the E-field strength levels at each frequency.

For cellular operators, it is important not only to comply with the ICNIRP reference levels, but also to communicate to the general public to enhance public confidence and acceptability for radio frequency (RF) exposure as indicated in the fact sheet issued by the World Health Organization [2]. Therefore, an E-field meter that accurately assesses the total exposure ratio, which is the summation of the squared ratios of the E-field strengths to the ICNIRP reference levels, in the in-situ environment is required.

In order to enhance public confidence and acceptability for RF exposure, it is important to estimate not only the total exposure ratio, but also the profile of the exposure ratio from a cellular base station. The radio waves from cellular base stations include many kinds of digital modulated waves with different frequencies. In addition, the E-field strength from a cellular base station varies dynamically because the transmission power varies depending on the amount of communications traffic. In order to assess the maximum exposure radio from a cellular base station, an assessment of the E-field strength from the base station at the maximum designed transmission power is required. Therefore, the E-field meter that accurately assesses the profile of the exposure

ratio from a cellular base station in the in-situ environment is required to be optimized to the digital modulated waves.

The objective of this paper is to specify, for such an E-field meter and when it is put into service in its operational environment, the methods to assess the value of the total exposure ratio in relevant public-access areas in order to communicate the risk to the general public.

This paper proposes the following two E-field meters.

a) An E-field meter for assessing the total exposure ratio.

b) An E-field meter for assessing the profile of exposure ratio from a cellular base station.

In particular concerning b), the E-field meter for the IMT-2000 cellular system, which is the 3rd generation cellular system and is becoming commonplace worldwide, is proposed.

2. Basic Configuration

a) E-field meter for assessing the total exposure ratio

In order to conform to the ICNIRP reference levels, the total exposure ratio should be less than or equal to one. The total exposure ratio is estimated using (1),

$$e_t^{\,2} = \sum_{i=100\,\mathrm{kHz}}^{1\,\mathrm{MHz}} \left(\frac{E_i}{c} \right)^2 + \sum_{i>1\,\mathrm{MHz}}^{300\,\mathrm{GHz}} \left(\frac{E_i}{E_{L,i}} \right)^2 , \tag{1}$$

where e_t^2 is the total exposure ratio, E_i V/m is the E-field strength at frequency i, and c and $E_{L,i}$ V/m are the ICNIRP reference levels at frequency i.

An E-field meter that measures the strength of the E-fields including those from cellular base stations, FM radio stations, and TV stations, must have a high level of sensitivity throughout a wideband frequency range. In the construction of a wideband E-field sensor, a shorted-dipole element that is shorter than the wavelength is often combined with a diode detector. The detection sensitivity limit of this sensor is approximately 0.1 V/m (100 dBμV/m). However, in order to measure the strength of the E-fields around a cellular base station in the in-situ environment for practical purposes, the detection sensitivity of the E-field sensor must be 1 mV/m (60 dBμV/m).

In addition, in order to measure the E-field strength accurately, the sensor polarization must be set to conform to the target electromagnetic wave polarization. However, in the in-situ environment in which the equipment is surrounded by many reflectors, which is representative of many urban areas, accurate measurement is difficult due to the presence of the scattering domain in the case of measurement using the E-field sensor comprising a shorted dipole. On the other hand, the isotropic E-field sensor enables measurement of the E-field strength without depending on the polarization of the target wave. Therefore, in an in-situ measurement the isotropic E-field sensor must be used.

The target measuring frequency range of the proposed E-field meter is assumed to be from 30 MHz to 3 GHz, which includes the frequencies used by cellular services and many other wireless services. When measuring the strength of the E-field from a cellular base station, as mentioned above, it is practical to have the detection level of 60 dBμV/m. In order to satisfy this requirement, the construction of the proposed E-field sensor is based on a frequency tuning measurement instrument for detection. The relationship between the required sensitivity and antenna factor (AF) for the E-field sensor is given as (2),

$$E_{REQ} = n + SNR + AF_{REQ} + 107 , \tag{2}$$

where E_{REQ} dBμV/m is the required sensitivity level, AF_{REQ} dB/m is the required AF, n dBm is the noise floor of the instrument, and SNR dB is the signal-to-noise ratio (SNR).

If a general spectrum analyzer with the noise floor of -90 dBm for the resolution bandwidth of 100 kHz is adopted as the frequency tuning measurement instrument, in order to achieve the sensitivity of 60 dBμV/m, the AF of 40 dB/m is required for the E-field sensor. In this regard, it is assumed that the E-field sensor can detect the E-field strength, if the SNR is greater than 3 dB.

In order to achieve sensor elements and baluns that exhibit a high sensitivity level across a wideband frequency range, the sensor element design is based on a sleeve dipole and divided sub-elements that correspond to each frequency range. The proposed sensor element comprises a radiator, a sleeve, and a coaxial feeder as shown in Fig. 1.

The radiator comprises multiple cylindrical conductors connected by inductors. The lengths of each conductor are based on a log periodic rule. The inductors function to change the effective length of the radiant region for each frequency because the impedance of the inductors increases with an increase in the frequency. The sleeve is also basically constructed in the same manner as the radiator. However, in the sleeve region, the

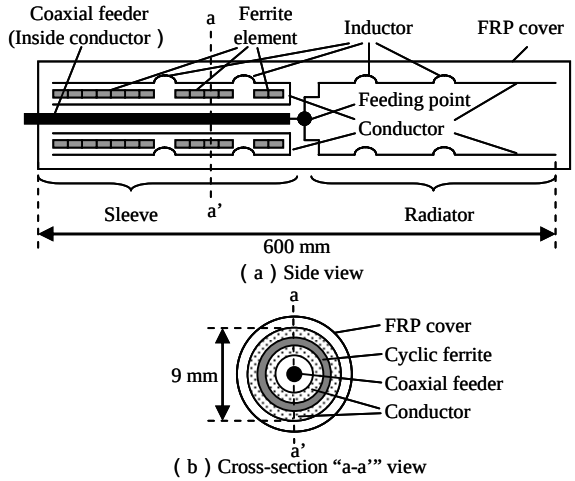

Fig. 1. Construction of proposed sensor element for assessing the total exposure ratio

coaxial feeder is at the center of the conductors, and ferrite elements are inserted between the feeder and the conductors. These ferrite elements provide a sufficient degree of isolation between the feeder and the conductors of the sleeve.

The length of the proposed sensor element including the radiator and sleeve regions is 600 mm, the diameter of the outside conductors is 9 mm, and the entire sensor element is covered with fiber-reinforced plastic (FRP).

Isotropic sensitivity is required for the E-field sensor in the in-situ measurement as mentioned above. Therefore, the proposed E-field senor comprises three sensor elements that cross orthogonally in a three-dimensional Cartesian coordinate system for the isotropic sensitivity.

The proposed E-field meter integrates the proposed wideband 3-axis isotropic E-field sensor above, a switch box for RF signals, a spectrum analyzer, and a notebook PC to control the switch box and spectrum analyzer. A schematic and a photo of the equipment are given in Figs. 2 and 3, respectively.

The spectrum analyzer detects the signal induced at an axis of the proposed E-field sensor. The E-field strength detected by the axis of the proposed sensor is calculated using (3),

$$E_x = P_x + AF_x + L_x + 107\,, \tag{3}$$

where E_x dBμV/m is the E-field strength detected at the x axis, P_x dBm is the received power for the x axis detected by the spectrum analyzer, AF_x dB/m is the AF of the x axis, and L_x dB is the cable loss between the x axis of the sensor and the spectrum analyzer. E_y and E_z are the same as E_x.

The E-field strength of a point of interest is calculated using (4),

$$E = \sqrt{E_x^2 + E_y^2 + E_z^2}\,, \tag{4}$$

where E μV/m is the root mean square of E-field strength of E_x, E_y, and E_z.

The switch box selects the connection to an axis element of the proposed sensor and the spectrum analyzer. The notebook PC controls the switch box and spectrum analyzer, calculates the total exposure ratio using (3), (4), and (1), and shows the frequency spectrum with the ICNIRP reference level and the total exposure ratio.

b) E-field meter for assessing the exposure ratio profile from a IMT-2000 system base station

In order to assess the strength of the E-field from a cellular base station at the maximum designed transmission power, it is effective to utilize characteristics of the transmission power allocated to the control channel. These characteristics are that the transmission power is constant at each cellular base station and that the power is independent of the amount of communications traffic.

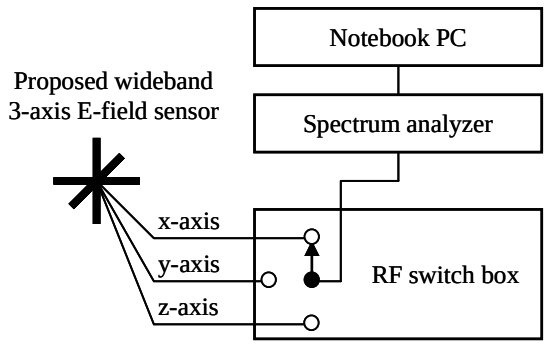

Fig. 2. Construction of proposed E-field meter for assessing the total exposure ratio

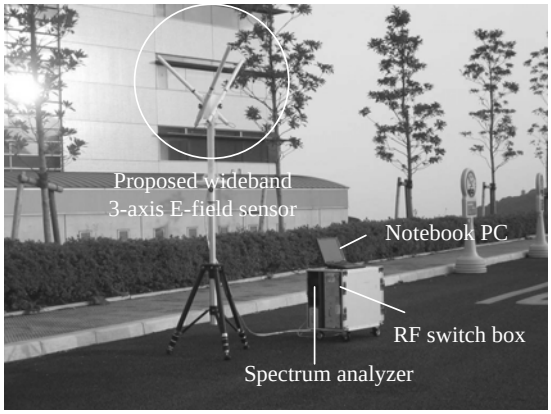

Fig. 3. Proposed E-field meter for assessing the total exposure ratio

The relationship between the total exposure ratio and the exposure ratio from a cellular base station at the designed maximum transmission power is given as (5),

$$e_t^2 = e_{EUT}^2 + e_x^2, \tag{5}$$

where e_t^2 is the total exposure ratio, e_{EUT}^2 is the exposure ratio from a cellular base station at the designed maximum transmission power, and e_x^2 is the exposure ratio from other radio sources.

In the 2nd generation cellular systems, since the access system is based on the frequency division multiple access (FDMA) system, the strength of the control channel E-field can be adequately measured at the frequency range assigned to the control channel by frequency tuning using a spectrum analyzer. On the other hand, the 3rd generation cellular systems are based on the code division multiple access (CDMA) system. In this system, the frequency spectra of the communication channels overlap. Therefore, in order to measure the E-field strength of the control channel in the wideband code division multiple access (W-CDMA) system, code selective receivers are required. The control channel is called the primary common pilot channel (P-CPICH) in the 3GPP specification [3].

The exposure ratio from W-CDMA system base stations is given as (6) and (7),

$$e_{EUT}^2 = \sum_{i=1}^{N_{EUT}} \left(\frac{E_{rec,i}}{E_{L,i}} \right)^2, \tag{6}$$

$$E_{rec,i}^2 = N_{code} \times E_{P-CPICH}^2, \tag{7}$$

where e_{EUT}^2 is the exposure ratio from a cellular base station at the designed maximum transmission power, N_{EUT} is the number of radio sources at the W-CDMA system base station, $E_{rec,\,i}$ is the received E-field strength due to *i*-th radio source at W-CDMA system base station, $E_{L,\,i}$ is the ICNIRP reference level at the *i*-th radio frequency, N_{code} is the number of traffic codes, and $E_{P\text{-}CPICH}$ is the E-field strength of the P-CPICH code.

The proposed E-field meter integrates an isotropic E-field sensor comprising the 3-axis dipole elements used in the in-situ measurement, three code selective receivers to detect the W-CDMA system signals, a GPS receiver to detect the geometrical position, and a notebook PC to control the receivers. A schematic and a photo of the equipment are given in Figs. 4 and 5, respectively.

The E-field sensor comprises the 3-axis mutually-perpendicular dipole elements because isotropic sensitivity is required for the E-field sensor in the in-situ measurement as described above. The three code selective receivers correspond to each axis of the isotropic sensor, and detect only the P-CPICH intensity.

The notebook PC controls the code selective receivers and calculates the exposure ratio from the target base station at the designed maximum transmission power. The P-CPICH E-field strength of an interesting point is calculated using (3), (4), and (7). The exposure ratio from a base station at the designed maximum power is calculated using (6). Furthermore, this equation obtains the geometrical position information from the GPS receiver and shows the geometrical profile of the exposure ratio from the target base station.

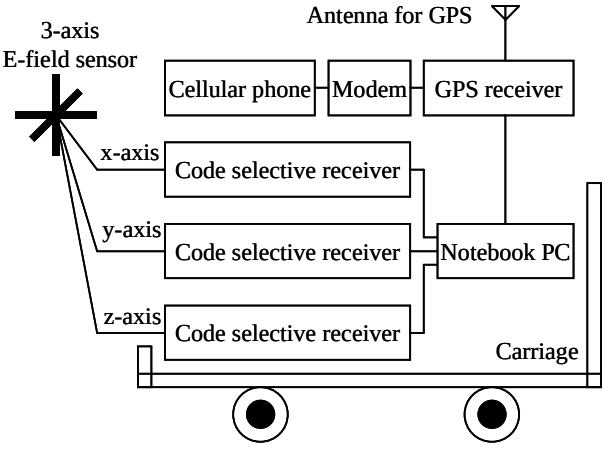

Fig. 4. Construction of proposed E-field meter for assessing the exposure ratio from IMT-2000 system base station

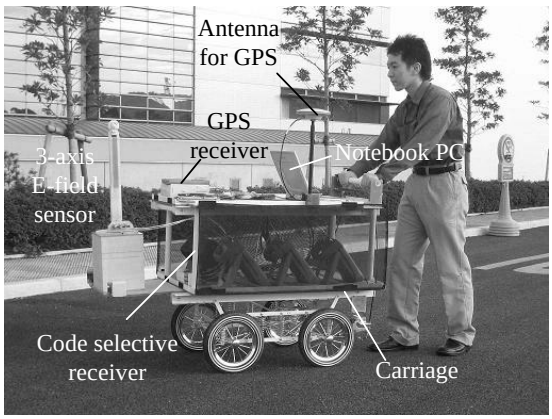

Fig. 5. Proposed E-field meter for assessing the exposure ratio from IMT-2000 system base station

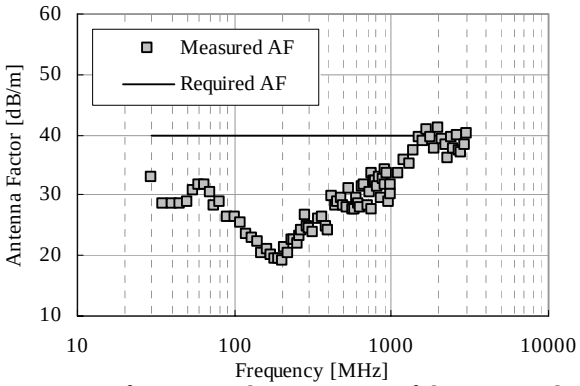

Fig. 6. AF frequency characteristics of the proposed E-field sensor for assessing the total exposure ratio system base station

Table 1. Code Selective Receiver Characteristics for Exposure Ratio from IMT-2000 System Base Station

Item	Value
Frequency Range	2110~2200 MHz
Dynamic Range	-117~-33 dBm
Resolution	0.1 dB
Accuracy	±2 dB
SIR Accuracy	±3 dB
Sampling Interval	10 ms

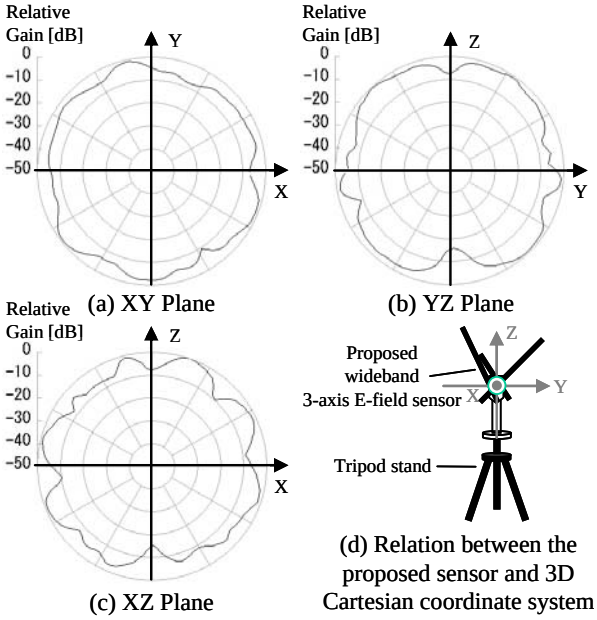

Fig. 7. Isotropic responses of the proposed E-field sensor for assessing the total exposure ratio

3. Characteristics

a) E-field meter for assessing the total exposure ratio

The AF frequency characteristics of the proposed E-field sensor are shown in Fig. 6. The AF is calibrated by using a standard antenna.

The E-field sensor achieves an AF value of 40 dB/m from 30 MHz to 1.7 GHz, and 41 dB/m from 1.7 GHz to 3 GHz.

The isotropic response of the proposed sensor is measured using an SG system (Satimo S. A.). The measurement values at 2 GHz, which is used by W-CDMA systems, are shown in Fig. 7.

Figure 7 shows that the isotropic response of the proposed sensor is within ±5 dB except for below the proposed sensor where there is a tripod stand.

b) E-field meter for assessing the exposure ratio profile from a IMT-2000 system base station

The characteristics of the code selective meter are given in Table 1. For example, at 2 GHz, the AF value of the isotropic sensor in the proposed E-field meter is 45.2 dB/m. Therefore, the proposed E-field meter is estimated to achieve the sensitivity of 0.06 mV/m using (2).

4. Measurement example

a) E-field meter for assessing the total exposure ratio

The total exposure is measured using the proposed E-field meter in an urban area and is shown in Fig. 8.

Figure 8 shows that the proposed E-field meter can assess the exposure ratios from not only cellular base stations, but also other stations such as TV stations. In addition, it shows that the total exposure ratio is approximately 1/5000 (2.08e-2%), and is sufficiently lower than the ICNIRP reference level.

b) E-field meter for assessing the exposure ratio profile from a IMT-2000 system base station

The exposure ratio from a W-CDMA system base station is assessed using the proposed E-field meter. The base station antenna is located in a rural area. The total exposure ratio is assessed approximately every 50 cm from under the antenna to approximately 1.6 km away. The height of the upper end of the antenna attached to a mast is 39.7 m. The total transmission power is 48 W per radio sector. The ICNIRP reference level for the 2-GHz band indicated in the ICNIPR guidelines is 61.4 V/m [1]. The assessed profile for the total exposure ratio is shown in Fig. 9. The figure shows that the maximum value of the total exposure ratio from this base station is approximately 1/10000 of the ICNIRP reference level.

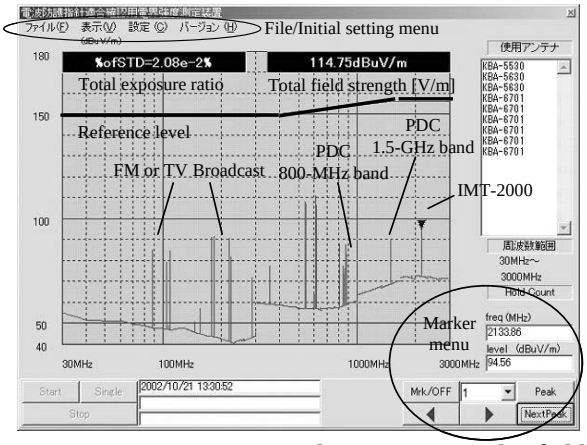

Fig. 8. Measurement example using proposed E-field meter for assessing the total exposure ratio

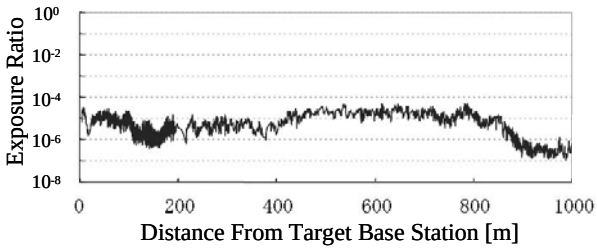

Fig. 9. Measurement example using proposed E-field meter for assessing the exposure ratio from IMT-2000 system base station

5. Summary

The proposed E-field meters achieved the following points.

1) The sensitivity of 1 mV/m was achieved using only one E-field sensor in the frequency range from 30 MHz to 3 GHz, and the total exposure ratio from multiple radio stations was assessed in the frequency range.

2) The E-field meter for assessing the exposure ratio profile from an IMT-2000 system base station comprises code selective receivers was presented, and the exposure ratio profile was assessed.

3) The total exposure ratio is less than 1/5000 of the ICNIRP reference level in an urban area.

4) The maximum value of the exposure ratio profile from a W-CDMA base station is less than 1/10000 of the ICNIRP reference level in a rural area.

References

[1] International Commission on Non-Ionizing Radiation Protection, "Guidelines for limiting exposure to time-varying electric, magnetic, and electromagnetic fields (up to 300 GHz)," April 1998.

[2] World Health Organization, "Electromagnetic fields and public health –Base stations and wireless technologies," Fact sheet N° 304, May 2006.

[3] 3GPP Organization Partners, "3rd Generation Partnership project; Technical Specification Group Radio Access Network; Base Station conformance testing (FDD) (Release 5)," pp. 40-41, 3GPP Organization Partners, June 2005.

THE EFFECT OF HUMAN OPERATOR ON THE MEASUREMENT OF THE ELECTROMAGNETIC FIELD WITH A BROADBAND PROBE

T. SAMARAS, G. TSANIDIS, J. N. SAHALOS

ARISTOTLE UNIVERSITY OF THESSALONIKI
RADIOCOMMUNICATIONS LABORATORY, DEPT. OF PHYSICS,
GR-54124 THESSALONIKI, GREECE

ABSTRACT

In this work we investigated the effect of the human operator body on the measurement of an electric field with a broadband probe. The finite-difference in time-domain technique was used to evaluate the influence. A numerical model of a commercially available probe was created and examined for its operation both within and outside its intended frequency use. Two homogeneous models of the human operator made of dispersive muscle-like material were considered. The first one was with the arm raised above the head at an angle of 45^o with the horizon and the second one was with the arm extended in front of the thorax. Several angles of incidence of the plane wave were simulated and it was shown that the former configuration (arm raised) resulted in more accurate measurements than the latter one. Furthermore, it was established that not only the presence of the human was responsible for the discrepancy of the measured values, but also the input impedance of the probe's dipoles which changed, due to coupling with the human body, thus altering the antenna factor that had been calculated during calibration.

I. INTRODUCTION

In the recent years, the concern, which arose about the possible health hazards of non-ionizing electromagnetic radiation, has led to the introduction of standards or safety guidelines on exposure. In order to compare with the limiting values set in such documents, it is necessary to have a probe that can accurately measure the electric field. There are a lot of factors, which reduce measurement accuracy. The most typical and frequent factors result mainly from the type of antenna used inside the probe, its size, and the mutual coupling between the antenna and the radiation source. Apart from the above, other factors include the detector's dynamic characteristics, the termination of the measurement probe and the deformation of the measured field, which is caused, e.g. by the person performing the measurement.
In the present study, we examine the influence of the human operator on the calibrated characteristics of a field probe and, consequently, on the measurement accuracy. In particular, we investigate what is the effect of the proximity of the human body on the probe's frequency response, its isotropicity and the calculated antenna factor (AF).

II. MATERIALS AND METHODS

Principle of operation of a broadband probe

A broadband probe of the electric field usually consists of a dipole antenna, a non-linear detector, lumped elements, which are used for filtering and shaping, a transmission line and some monitoring instrumentation. The principle of operation of the probe is based on the production of a voltage across the detector at the antenna terminals, when a continuous wave field is applied. This radiofrequency voltage has a dc component proportional to the square of the incident field, due to the non-linear characteristics of the detector. This component is filtered and is conveyed over the transmission line to the monitoring instrumentation. In order to obtain an omnidirectional pattern of the measurement probe, it is necessary to use three mutually perpendicular antennas and to sum their output voltages, so as to result to the output voltage [1].

Numerical model of the broadband probe

The numerical modeling was performed with the use of the finite-difference in time-domain (FDTD) technique. The model of the probe was based on a real product (Narda Model 8760), which operates in the frequency range from 300kHz to 1GHz. The isotropicity of the probe was achieved with three dipoles, which were placed on planar substrates combined to form a beam with the cross section of an equilateral triangle. Each of the orthogonal dipoles formed an angle of 54.74^o with the axis of the beam (Figure 1). These dipoles consisted of a

layer of a perfect electrical conductor with 9cm length, 4cm width and 0.2 mm thickness, printed on a dielectric substrate 1.4mm thick, of which the dielectric constant was assumed to be 3. Across the gap between the two parts of the dipole antenna a lumped element was mounted with resistance 1MΩ, where the induced voltage was measured due to the incident electric field (linear detector). The effective voltage of the measurement probe resulted from the summation of the induced voltages of the three dipoles, after squaring them. This structure was placed inside an empty cup, whose shape was conical. The shaft of the probe was assumed made of dielectric material, with the same dielectric constant 3, and had a radius of 2cm.

(a) (b)

Figure 1: (a) Cross section of the probe (b) Side view of the probe with the dipoles

During the process of calibration, the probe was excited by a plane wave with vertical polarization and field strength of 1V/m. Figure 2 presents the frequency response of the probe in the frequency range from 300kHz to 2.4GHz. The response in the operation range of the probe was almost frequency independent and its flatness was within ±0.75dB. When the frequency was increased beyond the point where the dipole antenna is electrically short ($\beta_o h<0.3$), the response was seen to peak in the vicinity of the frequency for the first resonance of the dipole antenna ($\beta_o h=\pi/2$), which is approximately at 1.6GHz. The curves of Figure 3 indicate that the probe's linearity is very weakly dependent on the frequency in its operation range. The radiation pattern of the probe (not shown here) confirms that isotropy is achieved by the mutually orthogonal configuration of the three dipoles.

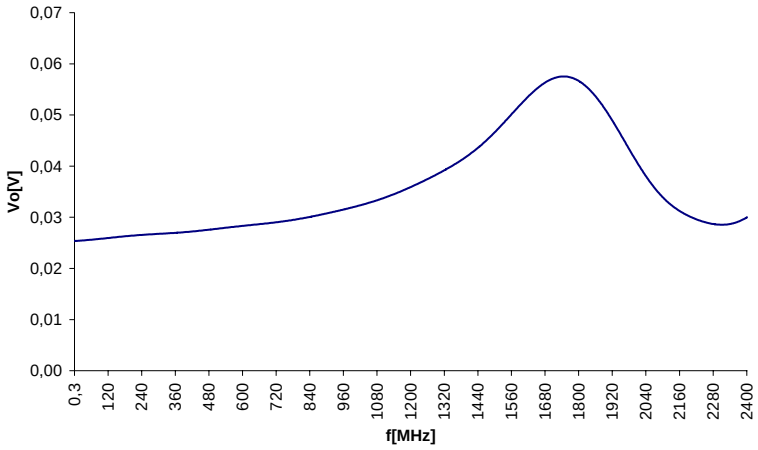

Figure 2. Frequency response of the numerical model of the probe to a plane wave of vertical polarization and electric field strength of 1V/m

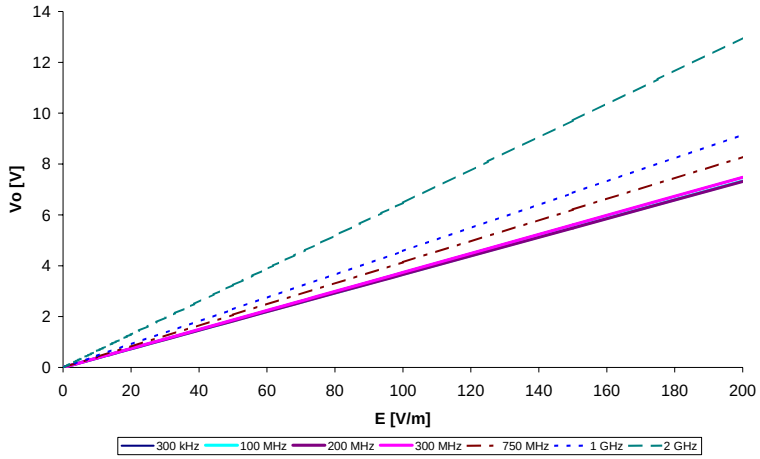

Figure 3. Response of the numerical model of the probe to a plane wave of vertical polarization and varying electric field strength for several frequencies

Through the process of calibration the antenna factor (AF) in dB(1/m) can be determined:

$$AF = 20\log_{10}(\frac{E}{V}) \quad (1)$$

where E is the electric field incident on the antenna and V is the voltage developed across the output of the antenna. Accordingly, an unknown electric field can be determined by the calibrated probe in terms of the measured voltage. Figure 4 shows the calculated AF, which seems to be approximately flat in the operation range, while the range of the first resonance of the dipoles is obvious.

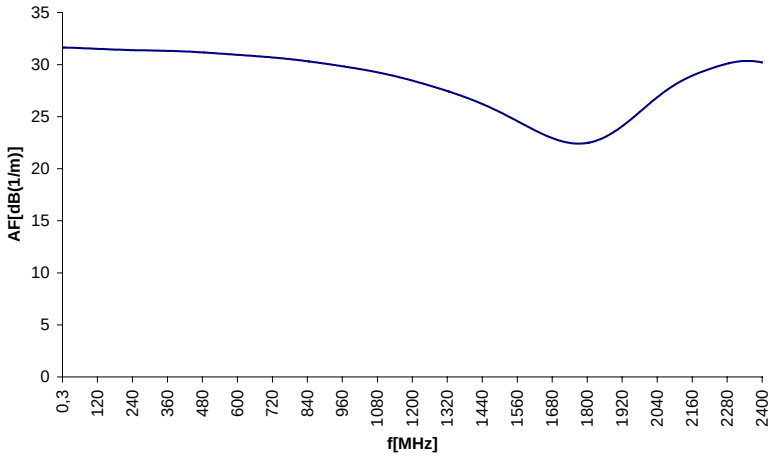

Figure 4. The antenna factor (AF) of a probe calibrated with a plane wave of vertical polarization

Numerical model of the human operator

Our computations assumed a human model of 1.70m height, 0.4625 width and 0.47m depth, which was available on the internet (www.3dcafe.com). The hand of the model was moved with program CtrlView® (www.ctrlview.com) to create two different human models. Figure 5a shows the human model for which the direction of the hand forms a 45^{o} angle with the horizon. For the second model the direction of the hand coincided with the direction of the horizon (Figure 5b). Both models were homogenous and consisted of material corresponding to human muscle. The dielectric properties of the muscle-simulating material were described by a 2nd order Debye model, in order to take into account the frequency dependency of them in the range of 300kHz to 2.4GHz. The constants assumed were ε_{∞}=40, ε_{s1}=3948, ε_{s2}=59.09, τ_1=4.62×10^{-8}s, and τ_2=9.11×10^{-10}s.

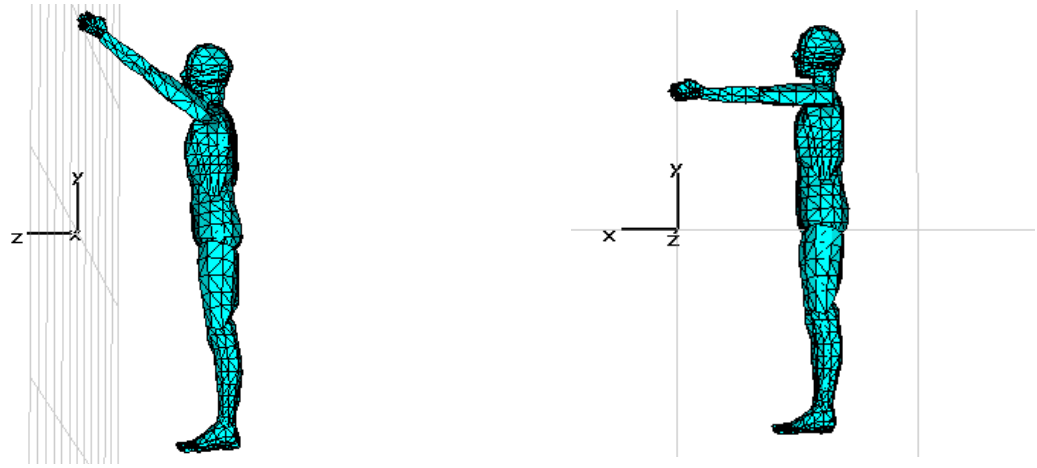

(a) (b)

Figure 5: (a) Human model with raised arm (b) Human model with extended arm

III. RESULTS

In the following we discuss the influence of the human body on the frequency response and the isotropicity of the calibrated probe. Figure 6 presents the frequency response of the probe, when the latter was used by the first and second human model respectively and was illuminated by a plane wave similar to that used in the calibration procedure. In both cases the variation with frequency was more intense than when the probe was in free space, a fact which confirms that the presence of the human affects the electromagnetic environment. In the case of the second model (Figure 6b), the influence of the human was more evident, because the measurement was performed in front of the body, which results in the probe being influenced by all the changes of the field caused by the human. In both models alterations were also observed in the isotropicity of the measurement probe, especially in the vertical plane. The second model seems to have affected more the isotropicity of the probe than the first one and especially in the higher frequencies, where the wavelengths became smaller than the model's dimensions.

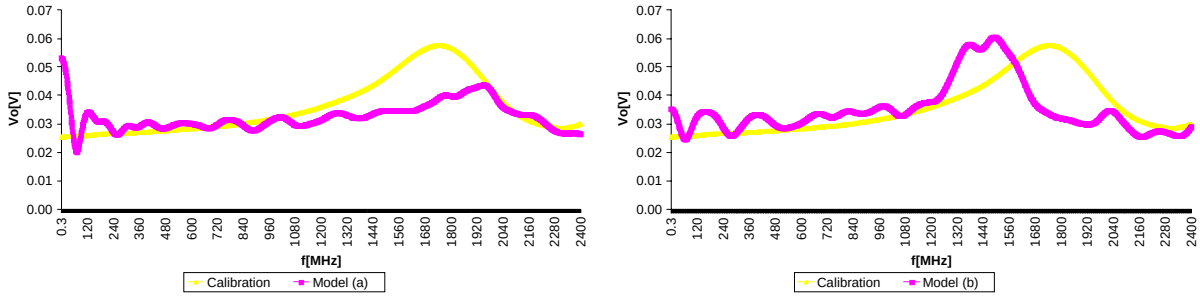

(a) (b)

Figure 6: Calibration response of the probe in the presence of the human model (a) and (b) of Figure 5.

In the present study we also investigated a series of measurement configurations, in which the probe was held by the human model and was excited by plane waves with different polarizations and from different directions. Initially we simulated the first human model (raised arm) with the probe for a vertically polarized incident plane wave coming from the front of the model. With regard to the accuracy of the measurement, we always compute the percent relative divergence of the measured and the actual field based on:

$$J[\%] = \frac{E_{TRUE} - E_{MEASURED}}{E_{TRUE}} \times 100 \quad (2)$$

Figure 7 demonstrates the deviation as a function of the frequency of the incident wave. It seems that the measured field followed to a satisfactory degree the variations of the actual field in the probe's operation range (300kHz - 1GHz), where the deviation was less than 1.6dB. This divergence of field was caused by the changes of the dipole's input impedance, because of the coupling, which takes place between the human model and the measurement probe. This variation of impedance of the three dipoles is shown in Figure 8, where it can be noticed that there fluctuations in the lower frequencies and a stabilization in the range above 200MHz.

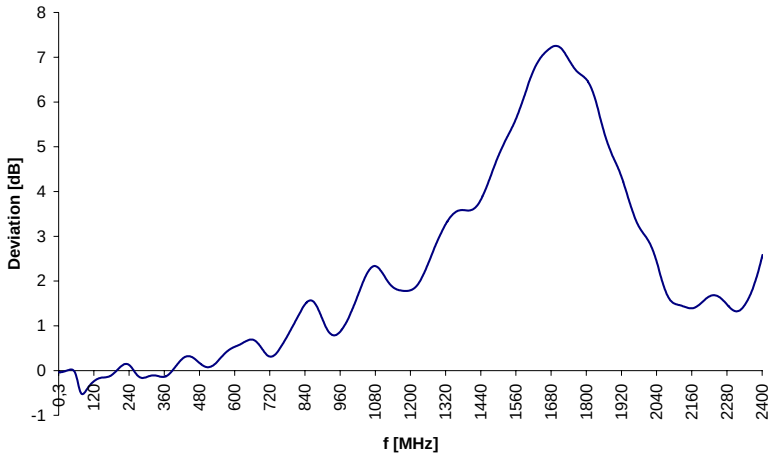

Figure 7. Deviation of the measured electric field from the true electric field for the human model with the raised arm

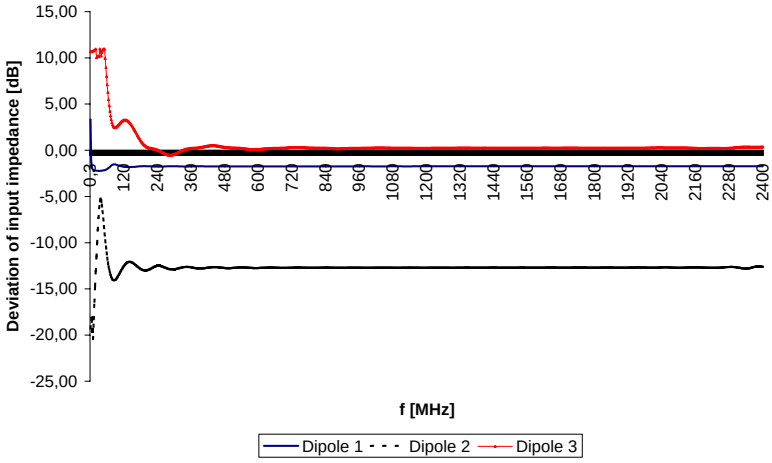

Figure 8. Deviation of the input impedance of the probe's dipoles due to coupling with the human body

In the higher frequency range (above 1 GHz) the difference between the measured and the actual field was greater than in the operation range, not only due to the change of the impedance of the dipoles, but also because of the reduction in the calculated AF, since this is the range of dipole resonance. As a result there was an underestimation of the electric field up to 55%. This means that when the probe is used in an environment of multiple sources, there must be adequate filtering, so that the measurement is not contaminated by fields in the frequency range, where the probe fails to operate correctly.

As a further step, we examined the incidence of the plane wave from various other angles and not only from the front of the model. The different deviation between measured and actual field established that the coupling between human and probe was dependent on the direction of the incident field. Moreover, we simulated a horizontally polarized plane wave irradiating the human operator from the front, showing that coupling also depended on field polarization.

We repeated the above procedure for the second human model (extended arm). Figure 9 shows that this model affected more the accuracy of measurement than the first one, when it was illuminated from the front, because of the fields scattered by the human body. In this case, the deviation of the measured value from the true one reached 4dB. However, for the higher frequencies (> 100MHz), this deviation became less than 2dB, when the field was incident from the back of the human operator.

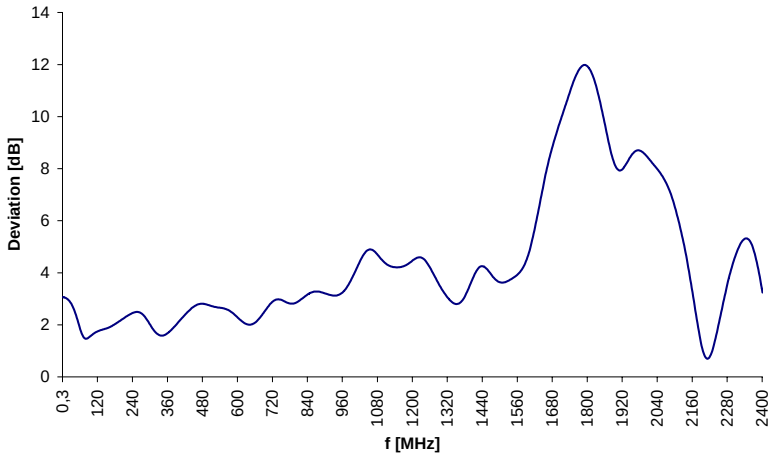

Figure 9. Deviation of the measured electric field from the true electric field for the human model with the extended arm

IV. DISCUSSION - CONCLUSIONS

The use of a probe consisting of three mutually vertical dipoles can be used for the measurement of electric fields only in its operation range. The frequency response of the probe is limited by the dipoles dimensions. The cup or the shaft of the probe do not seem to affect the measurement, as long as they are present in its calibration. However, the presence of the human operator changes the incident electromagnetic field. As a result the probe does not measure the real incident field, but the one developed around the human operator. The deviation is larger when the operator holds the probe with an extended arm in front of him/her and becomes smaller when he/she holds it with an arm raised above his/her head at an angle of 45^{o} with the horizon. This is actually the way of use proposed by the manufacturer and has been confirmed by the simulations conducted in this study. For this configuration, it was found also (not presented here) that the effect of the ground is minimized, since the probe is high above it.

Another source of inaccuracy in the measurement is the change of input impedance of the dipoles, since they couple with the dielectric body of the human operator. This change in impedance leads to a different AF from the one evaluated during the calibration. Therefore, even if the incident field remained unchanged, the probe would still give a wrong field value. The coupling of the probe with the human body depends on the angle of arrival, the frequency and the polarization of the incident field, making the introduction of a correction factor impossible.

REFERENCES

[1] H. I. Bassen and G. S. Smith, “Electric Field Probes – A Review”, *IEEE Trans Antennas Propagat*, vol. 31, no. 5, pp. 710-718, 1983

VARIATION OF RFR VIA APPLIED HUMAN VOICE AND PURE TONE IN DIFFERENT STRENGTHS & FREQUENCIES TO MOBILE PHONE

ELCIN OZGUR, GOKNUR GULER

BIOPHYSICS DEPARTMENT, GAZI UNIVERSITY MEDICAL FACULTY
GAZI UNIVERSITESI TIP FAKULTESI BIYOFIZIK ANABILIM DALI
06510 BESEVLER ANKARA TURKEY
elcinozgur@gazi.edu.tr, gozturk@gazi.edu.tr

Abstract
GSM DCS 1800 mobile phone radiation emitted by Nokia 3210 (0.81 W/kg digital SAR) was measured by electromagnetic radiation meter while speaking into phone by different frequency-strength pure tone and human voices generated sound production device, also in quiet condition in the sound-proof room. The measurements are taken in 2-second-periods as instantaneously during 6 minutes and saved in high configuration computer. Average values of these measurement data were calculated after whole experiment concluded.
In quiet condition, 7.7 V/m external E fields were averaged. Applied pure tone, man and woman voices, between 0-120 dB strength and 125-8000 Hz frequency range made E field values increase approximately as 24 V/m.
It was detected that all types of sound in 60 dB strength and having 3-4 kHz frequencies, daily life speech range are the threshold for mobile phone radiation increment. Statistically insignificant change was observed between quiet condition and below 60 dB range. 60 dB and loader voices in the range of 1-4 kHz frequencies generated nearly the same E field values as 24 V/m.

Introduction
Number of mobile phone users already above 2 billion and it is anticipated that this number will reach to 5 billion next 5 years. Not only basic qualifications such as voice, data and image transfer, but also mobile phones becoming multi terminal devices make the body of consumer grow. Innovations on mobile phone technology are actualized everyday such as models taking picture, recording video, for babies and having options of “push and talk” which teenagers like and use very often. The wide and growing use of cellular phones has also raised questions about the possible health risks associated with Radio Frequency (RF) electromagnetic fields. In order to estimate health risks, cellular phone users have to obtain the relative exposure levels. However, the RF exposure level is very difficult to measure accurately and quantify for all individuals as SAR (Specific Absorption Rate) because exact measurements of SAR in vivo, which has a direct effect on user in relation to the output level of cellular phone, are almost impossible[1]. ICNIRP (International Commission for Non-Ionizing Radiation Protection) prepared guidelines for limiting EMF exposure directly related to adverse health effects caused by EMF radiation by means of coupling with body directly or indirectly. Two classes of guidance are presented as Basic restrictions and Reference levels. Basic restrictions are the restrictions on exposure to time-varying electric, magnetic, and electromagnetic fields that are based directly on established health effects. Depending upon the frequency of the field, the physical quantities used to specify these restrictions are current density (**J**), specific energy absorption rate (SAR), and power density (**S**). Reference levels are provided for practical exposure assessment purposes to determine whether the basic restrictions are likely to be exceeded. Some reference levels are derived from relevant basic restrictions using measurement and/or computational techniques, and some address perception and adverse indirect effects of exposure to EMF. The derived quantities are electric field strength (**E**), magnetic field strength (**H**), magnetic flux density (**B**), power density (**S**), and currents flowing through the limbs (*IL*)[2,3]. In other words, determining of the reference levels gives information about if the basic restrictions are exceeded.
In this study, we measure the cellular phone radiation operating in GSM DCS 1800 MHz by using electromagnetic radiation meter in order to determine the individuals’ exposure levels to inform the quantity of exposure and estimate health risks. Mobile phone, Nokia 3210 with 0,81 W/kg digital SAR value was used.

Measurements were executed while pure silence, and also applying pure tone, man and woman voices, between 0-120 dB strength and 125-8000 Hz frequency range spoken into the mobile phone in a pure silent room.

Materials and Methods

Two identical Nokia 3210 (0.81 W/kg) were chosen as mobile phones for which we obtain the exposure level while speaking into the phone with the human voices in different frequencies and intensities. Also we measured the exposure value when pure tone applied. Pure tone, artificial sound not exist in nature, was generated by audiometer (Interacoustics Clinical Audiometer AC 40) applied to mobile phone microphone as receiver using headphone (SONY). Audiometer operates pure tone in 0-120 dB strength and 125-8000 Hz frequency range. Also, it can modulate average tone of man and woman voices into different frequencies and strengths in the same range. A woman and a man volunteers whose voices are in the average range of frequencies. NARDA EMR 300 and type 8.3 probe were used as radiation measurement device. Measurements were taken for duration of 10 minutes per 2 seconds and the data saved to the computer connected to device via fiber optic cable. The whole data were averaged before statistical analysis.

4 cases as “pure silence”, “pure tone”, “woman voice”, “man voice” are analyzed if measured external E field levels change with respect to type, frequency and intensity of voice.

Result

For Nokia 3210, there is an increase for certain frequencies and strengths in tree of these four cases of which “pure tone”, “woman voice”, “man voice” with respect to “pure silence”($p<0.05$). However, this increase is independent of voice type, namely external E field levels are the same for “pure tone”, “woman voice”, “man voice”.

For 125 Hz, E field is 7,68 V/m same as in pure silence mode in all intensities starting from 0 dB up to 120 dB. For 250 Hz, with the voice of 90 dB, 100 dB and 110 dB intensities speaking into mobile phone changing the external E field level as 23,89 V/m ; 24,26 V/m ; 24,19 V/m respectively. For 500 Hz; changes in E field beginning between of 90 dB and 120 dB the intensities as 24,13 V/m by 90 dB; 24,26 V/m by 100 dB; 24,17 V/m by 110 dB and 24,17 V/m by 120 dB. For 750 Hz; voices between 80 dB-120 dB intensities makes field values as 24,1 V/m; 23,83 V/m; 24,25 V/m; 24,16 V/m and 24,15 V/m respectively. Also, the E field level changed by applying the voice intensity of the same range for 1 kHz as 24,15 V/m; 23,87 V/m; 24,23 V/m; 24,18 V/m and 24,15 V/m . The threshold intensity that change the E field level generated by mobile phone for 1.5 kHz sound is 70 dB. The E field levels for intensities between 70 dB and 120 dB are 24,13 V/m; 24, 13 V/m; 23,9 V/m; 24,18 V/m; 24,15 V/m respectively. Again for voice having 2 kHz frequency and intensities changing from 70 dB to 120 dB, the field values are 24,13 V/m; 24,13 V/m; 24,07 V/m; 24,23 V/m; 24,16 V/m and 24,16 V/m.

Voice in frequency of 3 kHz makes the E field value change if these voices are 60 dB and more strength. For 2 kHz and 60 dB voice makes E field level as 23,81 V/m. and for the other intensity of voices in this frequency which increase the level of mobile phone’s radiation are 24,12 V/m; 24,29 V/m; 24,28 V/m; 24,25 V/m and 24,22 V/m respectively. For 4 kHz also there are the same range of intensity as 60 dB – 120 dB having E field value as 23,95 V/m; 24,13 V/m; 24,13 V/m; 24,43 V/m; 24,41 V/m and 23,73 V/m and 23,55 V/m respectively. In 6 kHz, only 110 dB and 120 dB voices increase the radiation as 24,22 V/m and 24,20 V/m. For 8 kHz voices in all strengths, E field value measured as 7,89 V/m nearly the same as in pure silence mode. Table 1 contains all these data in detail. For this reason, whole data averaged for three types of voices (Table 1, Figure 1-4)

Discussion

The use of mobile phone by adult, young people, children and the elderly has grown rapidly which causes increased concern of public, scientists and experts about the health effects of these phones in the last years. Therefore, the intensive research continues to be carried out in order to find if they cause any possible health risk for humans.

GSM-1800 signals SAR levels ranging from 0.1 to 2 W/kg. Modulations named as GSM-217, GSM-Basic, GSM-DTX or GSM-Talk have SAR values between this range.

GSM-217Hz is GSM signals are amplitude modulated by rectangular pulses with a repetition frequency of 217 Hz and a duty cycle of 1:8 (pulse width 0.576 ms), corresponding to the dominant modulation component of GSM. The ratio between slot average SAR and time average SAR is 8. GSM- Basic is in addition to this basic GSM-217Hz TDMA frame, every 26th frame is idle, which adds an 8 Hz modulation component to the signal . The ratio between slot average SAR and time average SAR is 8.3. The discontinuous transmission mode (DTX) is active during periods without speaking into the phone. To save battery power, the transmission is reduced to 12 frames per intermediate multiframe of 104 frames (compared to 100 frames for GSM Basic). The frame structure of the DTX signal results in 2, 8 and 217 Hz components. The ratio between slot average SAR and time average SAR is 69.3.

GSM-Talk generates temporal changes between GSM-Basic and GSM-DTX and simulates a conversation with an average duration of 97s and 50s for Basic and DTX, respectively. The ratio between slot average SAR and time average SAR is 11.9. Furthermore, arbitrary field on/off intermittence in the range from seconds to hours can be applied [4,5,6].

In this study, Mobile phone Nokia 3210, spoken into the phone, mostly in GSM Basic mode measured externally in order to obtain an opinion about how much user exposure. All in all, we found that the external E field which mobile phone generates while user speaks into phone without cease is triple of the measured value while nobody speaks into phone when conversation is ended for both user.

In Lonn at al. study, the output power for all mobile phone callas managed by GSM operator Telia Mobile was recorded during one week in four defined areas (rural, small urban, suburban and city area) in Sweden [7]. The recording included output power for 900 MHz and the 1800 MHz frequency band. Conclusion of this report is that in rural areas where base stations are sparse, the output power level used by mobile phones are on average considerably higher than in more densely populated areas. So, our experiment was done in pure silent room in the city center where the base stations near and actively operated and in the time period of before primetime (09.00-11.30 AM), prime time(12.00- 13.30 AM) and after prime (14.00-17.00 AM) time of weekdays.

As a result, we found that mobile phone user expose more RF radiation when he / she is talking in the periods out of prime time. In the period called as prime time the external E field value is constant both for silence and speaking into mobile phone.

There is no difference if the voice belonging to woman, man or child on the level of external E field that mobile phone generates. There is threshold level of sound intensity changing mobile phones technology. 50 decibels (dB) the range of whispering is the threshold strength in order to recognize the voice which is speaking into mobile phone Nokia 2100 although 60 dB can be solely threshold for Nokia 3210.

A quantitative assessment of individual exposure to radiofrequency fields epidemiological studies of possible health effects for many reasons.

Table 1: External electric field values (V/m) generated by Nokia 3210 in GSM-Talk modulation with pure tone, woman and man's voices in a sound proof room.

Intensity/ Frequency	**Nokia 3210**			
(dB/Hz)	**Pure Silence**	**Pure Tone**	**Man's Voice**	**Woman's voice**
0 /125	7.68	7.68	7.7	7.68
10 /125	7.68	7.68	7.7	7.68
20 /125	7.68	7.68	7.7	7.68
30 /125	7.68	7.68	7.7	7.68
40 /125	7.68	7.68	7.7	7.68
50 /125	7.68	7.68	7.7	7.68
60 /125	7.68	7.68	7.7	7.68
70 /125	7.68	7.68	7.7	7.68
80/125	7.68	7.68	7.7	7.68
90 /125	7.68	7.68	7.7	7.68
0 /250	7.68	7.69	7.69	7.69
10 /250	7.68	7.69	7.69	7.69
20 /250	7.68	7.69	7.69	7.69
30 /250	7.68	7.69	7.69	7.69
40 /250	7.68	7.69	7.69	7.69
50 /250	7.68	7.69	7.69	7.69
60 /250	7.68	7.69	7.69	7.69
70 /250	7.68	7.69	7.69	7.69
80/250	7.68	7.69	7.69	7.69
90 /250	7.68	23.87	23.9	23.89
100 /250	7.68	24.26	24.27	24.26
110 /250	7.68	24.19	24.2	24.19
0 /500	7.68	7.9	7.9	7.9

10 /500	7.68	7.9	7.9	7.9
20 /500	7.68	7.9	7.9	7.9
30 /500	7.68	7.9	7.9	7.9
40 /500	7.68	7.9	7.9	7.9
50 /500	7.68	7.9	7.9	7.9
60 /500	7.68	7.9	7.9	7.9
70 /500	7.68	7.9	7.9	7.9
80/500	7.68	7.9	7.9	7.9
90 /500	7.68	24.1	24.15	24.13
100 /500	7.68	24.26	24.27	24.26
110 /500	7.68	24.17	24.17	24.17
120 /500	7.68	24.17	24.18	24.17
0 /750	7.68	7.62	7.62	7.62
10 /750	7.68	7.62	7.62	7.62
20 /750	7.68	7.62	7.62	7.62
30 /750	7.68	7.62	7.62	7.62
40 /750	7.68	7.62	7.62	7.62
50 /750	7.68	7.62	7.62	7.62
60 /750	7.68	7.62	7.62	7.62
70 /750	7.68	7.62	7.62	7.62
80/750	7.68	24.1	24.1	24.11
90 /750	7.68	23.85	23.8	23.84
100 /750	7.68	24.25	24.26	24.25
110 /750	7.68	24.15	24.17	24.15
120 /750	7.68	24.15	24.15	24.15
0 /1000	7.68	7.9	7.9	7.9
10 /1000	7.68	7.9	7.9	7.9
20 /1000	7.68	7.9	7.9	7.9
30 /1000	7.68	7.9	7.9	7.9
40 /1000	7.68	7.9	7.9	7.9
50 /1000	7.68	7.9	7.9	7.9
60 /1000	7.68	7.9	7.9	7.9
70 /1000	7.68	7.9	7.9	7.9
80/1000	7.68	24.15	24.13	24.18
90 /1000	7.68	23.85	23.87	23.88
100 /1000	7.68	24.2	24.26	24.24
110 /1000	7.68	24.16	24.2	24.17
120 /1000	7.68	24.16	24.17	24.15
0 /1500	7.68	7.9	7.9	7.9
10 /1500	7.68	7.9	7.9	7.9
20 /1500	7.68	7.9	7.9	7.9
30 /1500	7.68	7.9	7.9	7.9
40 /1500	7.68	7.9	7.9	7.9
50 /1500	7.68	7.9	7.9	7.9
60 /1500	7.68	7.9	7.9	7.9
70 /1500	7.68	24.13	24.1	24.2
80/1500	7.68	24.14	24.1	24.14
90 /1500	7.68	23.85	24	23.85

100 /1500	7.68	24.25	24.2	24.25
110 /1500	7.68	24.15	24.17	24.15
120 /1500	7.68	24.14	24	24.13
0 /2000	7.68	7.96	7.96	7.96
10 / 2000	7.68	7.9	7.9	7.9
20 /2000	7.68	7.96	7.96	7.96
30 /2000	7.68	7.9	7.9	7.9
40 /2000	7.68	7.96	7.96	7.96
50 /2000	7.68	7.9	7.9	7.9
60 /2000	7.68	7.9	7.9	7.9
70 /2000	7.68	24.13	24.14	24.13
80/2000	7.68	24.14	24.12	24.14
90 /2000	7.68	24	24.11	24.1
100 /2000	7.68	24.24	24.2	24.26
110 /2000	7.68	24.17	24.13	24.18
120 /2000	7.68	24.14	24.16	24.19
0 /3000	7.68	7.89	7.89	7.89
10 / 3000	7.68	7.89	7.89	7.89
20 / 3000	7.68	7.89	7.89	7.89
30 / 3000	7.68	7.89	7.89	7.89
40 / 3000	7.68	7.89	7.89	7.89
50 / 3000	7.68	7.89	7.89	7.89
60 / 3000	7.68	23.83	23.8	23.81
70 / 3000	7.68	24.11	24.13	24.1
80/ 3000	7.68	24.11	24.13	24.1
90 / 3000	7.68	24.23	24.33	24.3
100 / 3000	7.68	24.3	24.2	24.33
110 / 3000	7.68	24.2	24.2	24.34
120 / 3000	7.68	24.17	24.17	24.31
0 / 4000	7.68	7.89	7.89	7.89
10/ 4000	7.68	7.89	7.89	7.89
20 /4000	7.68	7.89	7.89	7.89
30 /4000	7.68	7.89	7.89	7.89
40 /4000	7.68	7.89	7.89	7.89
50 /4000	7.68	7.89	7.89	7.89
60 /4000	7.68	24.01	23.91	23.92
70 / 4000	7.68	24.13	24.13	24.13
80/ 4000	7.68	24.13	24.13	24.13
90 / 4000	7.68	24.43	24.43	24.43
100 / 4000	7.68	23.41	23.41	24.41
110 / 4000	7.68	23.59	23.69	23.9
120 / 4000	7.68	23.58	23.59	23.48
0 / 6000	7.68	7.94	7.94	7.94
10/ 6000	7.68	7.94	7.94	7.94
20 / 6000	7.68	7.94	7.94	7.94
30 / 6000	7.68	7.94	7.94	7.94
40 / 6000	7.68	7.94	7.94	7.94
50 / 6000	7.68	7.94	7.94	7.94

60 / 6000	7.68	7.94	7.94	7.94
70 / 6000	7.68	7.94	7.94	7.94
80/ 6000	7.68	7.94	7.94	7.94
90 / 6000	7.68	7.94	7.94	7.94
100 / 6000	7.68	7.94	7.94	7.94
110 / 6000	7.68	24.17	24.26	24.17
120 / 6000	7.68	24.21	24.24	24.16
0 / 8000	7.68	7.89	7.89	7.89
10/ 8000	7.68	7.89	7.89	7.89
20 / 8000	7.68	7.89	7.89	7.89
30 / 8000	7.68	7.89	7.89	7.89
40 / 8000	7.68	7.89	7.89	7.89
50 / 8000	7.68	7.89	7.89	7.89
60 / 8000	7.68	7.89	7.89	7.89
70 / 8000	7.68	7.89	7.89	7.89
80/ 8000	7.68	7.89	7.89	7.89
90 / 8000	7.68	7.89	7.89	7.89
100 / 8000	7.68	7.89	7.89	7.89
110 / 8000	7.68	7.89	7.89	7.89

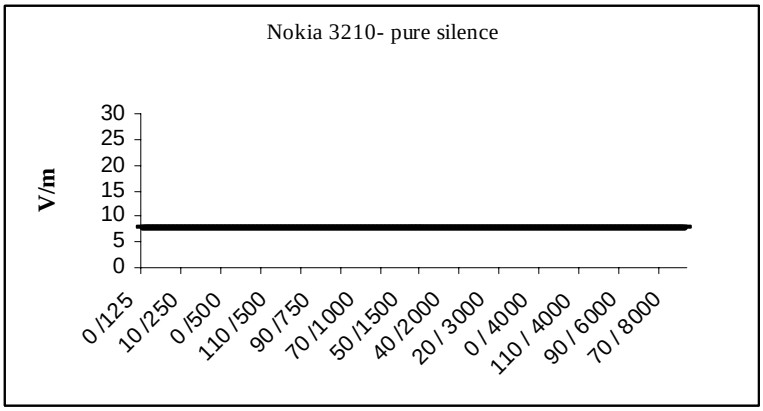

Figure 1: External electric field values (V/m) generated by Nokia 3210 in GSM-Talk modulation in pure silence in a sound proof room

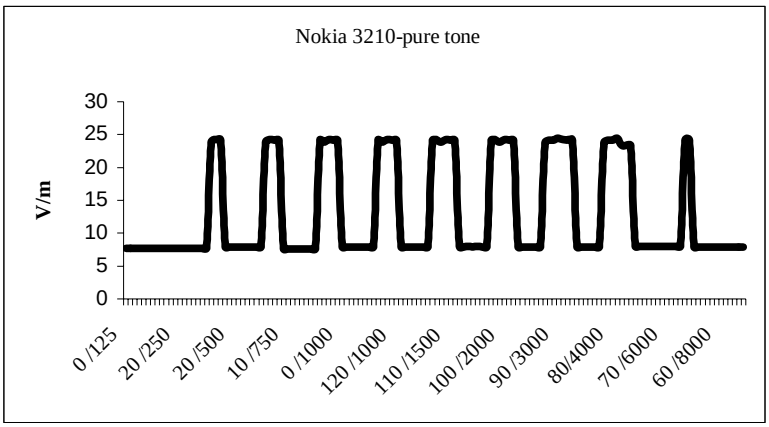

Figure 2: External electric field values (V/m) generated by Nokia 3210 in GSM-Talk modulation with pure tone in a sound proof room.

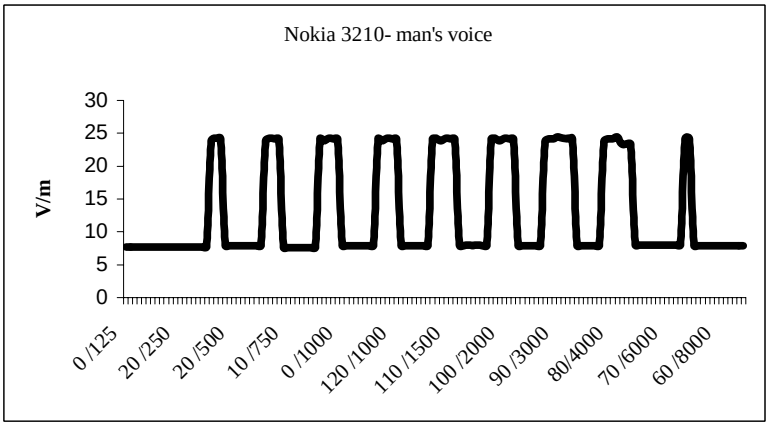

Figure 3: External electric field values (V/m) generated by Nokia 3210 in GSM-Talk modulation with man's voices in a sound proof room.

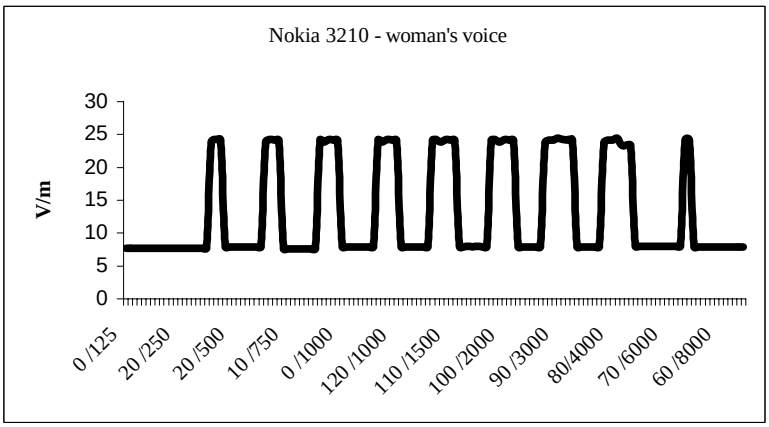

Figure 4: External electric field values (V/m) generated by Nokia 3210 in GSM-Talk modulation with woman's voices in a sound proof room.

References

1) Kim, S.C., Nam, K.C., Kim, D.W. (2005). Estimation of relative exposure levels for cellular phone users using a neural network, Bioelectromagnetics online,DOI 10.1002/bem.20203,www..interscience.wiley.com
2) ICNIRP 1998 Standards: Guidelines for Limiting Exposure to Time Varying Electric and Magnetic Fields (Up to 300 GHz), International Commission on Non-Ionizing Radiation Protection, Health Physics, 74, 494-522, (1998).
3) ICNIRP Health Issues Related to the Use of Hand-Held Radiotelephones and Base Transmitters. Health Physics, 70 , 587 (1996).
4) Capri, M., Scarcella E. ,Bianchi, E., Fumelli, C., Mesirca, P., Agostini, C., Remondini, D., Schuderer, J., Kuster, N., Franceschi, C., Bersani, F. (2004). 1800 MHz radiofrequency (mobile phones, different Global System for Mobile communication modulations) does not affect apoptosis and heat shock protein 70 level in peripheral blood mononuclear cells from young and old donors. *International Journal of Radiation Biology* 80: 389 – 397
5) Wiart, J. Dale, C. Bosisio, A.V. Le Cornec, A. (2000). Analysis of the influence of the power control and discontinuoustransmission on RF exposure with GSM mobile phones, *Electromagnetic Compatibility, IEEE Transactions*, 42, 376-385
6) REFLEX,(2004). Risk Evalution of Potential Environment Hazards From Low Frequency Electromagnetic Field Exposure Using Sensitive in vitro Methods, Final Report, EU Quality of Life and Management of Living Resources, QLK4-CT-1999-01574.
7) Lönn1, S., Forssén1,U., Vecchia,P., Ahlbom1,A. and Feychting, M.(2004). Output power levels from mobile phones in different geographical areas; implications for exposure assessment. *Occupational and Environmental Medicine* 61:769-772

MAGNETIC FIELDS FOR RELIEF OF MYOFASCIAL AND/OR LOW BACK PAIN THROUGH TRIGGER POINTS

Carlton F. Hazlewood, Marko S. Markov

Research Consultants International, Houston, USA, e-mail: carltonh@swbell.net;
Research International, Buffalo USA email: msmarkov@aol.com

Abstract

It is known that a significant fraction of both acute and chronic pain experience is myofacial in nature. This paper address the potential for pain relief to be induced by placing magnets over the trigger points associated with that referred pain. This is even more important in patients with various disabilities and experiencing chronic sacro-iliac and/or low back pain.

It is well recognized that a trigger point is a functional, rather than an anatomical, entity. From the point of view of magnetotherapy it appears to us that the trigger points represent a plausible physiological/tissue "window" and/or pathways which allows magnetic fields to penetrate through physiological barriers and thus returning injured tissues to the homeostatic state. It should be noted that these "tissue windows" represent physiological "entrance points" for eventual exogeneous stimulations, mainly physical by nature, to enter the body.

There is evidence that the application of magnetic field (via permanent magnets) on trigger points is more effective for pain relief as compared to other parts of the body surface. The systemic effects should also be considered when magnetic field effects are discussed. (We first presented this idea at the 2004 meeting in Kos.)

We discuss the mechanisms of action related to ion transport as central to the integrity and proper functioning of nerve excitability and muscle contraction. Any disruption of their normal function would directly and markedly affect human neurosensory and neuromotor performance. Biophysical phenomena associated with modification of ion transport are in the millivolt and picoampere range. Therefore, electrophysiological changes in ion channel functions are among the most sensitive indicators, if not the most sensitive indicator, to detect and quantify physiological effects of electromagnetic fields.

We postulate that in addition to the known effect of magnetic fields on water structure there could be a change in the tensile properties of cartilage, ligaments, and other soft tissue structures which secondarily may relieve tension on arthritic joints or on chronically "inflamed" areas.

Introduction

Increasing interest in alternative and complimentary medicine has attracted the attention of scientists and clinicians to the potential benefit of using various static magnetic fields and EMFs for therapeutic purposes. It is now clear that magnetic fields interact with biological tissues in a way that specific physiological changes occur. Both static and time varying magnetic fields were successfully applied to treat therapeutically resistant problems in the musculoskeletal system (Bassett, 1989 and 1994; Pilla and Markov 1994; Markov 1995; Itoh, et al., 1991; Markov and Pilla 1995; Shupak, 2003; Rosch and Markov, 2004). It is accepted that EMFs provide a practical, exogenous method for inducing cell and tissue modifications that can correct selected pathological sites. The most effective clinical applications of these physical factors are related to bone unification as well as reduction of pain and edema in soft tissues (Bassett 1989; Markov and Pilla 1995). For musculoskeletal injuries and post-surgical, post-traumatic and chronic wounds, magnetic fields are recognized as a modality that contributes to reduction of edema. It is well known that edema reduction can be a major therapeutic instrument in the acceleration of pain and stress relief. Surprisingly, edema reduction has been reported with low amplitude (in the range of 1-50 mT), low frequency (in the range of 1-100 Hz), and pulsed radiofrequency (27.12 MHz) signals applied to the site of injury/pain (Markov and Pilla 1995; Rosch and Markov, 2004).

Static and time-variable electromagnetic fields have been applied with apparent success in the management of pain in a variety of orthopedic conditions, most commonly traumatic bone fractures or surgical osteotomies (Becker and Selden, 1985; Becker, 1990; Miner and Markoll, 1993, Trock *et al.*, 1994; Bassett,1994). Carpenter and Ayrapetyan (1994) and Rosch and Markov (2004) edited books that provide excellent overviews of the biological effects of electric and magnetic fields. It is clear that this is an emerging field in biology and medicine. Attempts are being made to scientifically document the impact of electric and magnetic fields on biological systems.

The remarkable observations that there are no known adverse effects with using permanent magnets or low frequency EMF stimulation, lends support for the therapeutic use of magnetic fields is (Rosch and Markov, 2004). In addition, the large body of scientific publications supports the notion that magnetic therapy may have utility in the treatment of pain (Foley-Nolan et al. 1990 and 1992; Ellis 1993; Trock et al. 1993a, 1993b, and 1994; Markov and Pilla 1995; Vallbona et al. 1997; Sartucci et al. 1997; Sherman et al. 1998). However, it should be noted that despite a number of clinical studies performed world-wide indicating successful use of magnetic fields for treatment of various diseases and pathologies, little is known regarding the effectiveness of magnetic fields in relieving low back pain (LBP).

One of us (CFH) has placed magnets on his body in order to test for pain relief. Placing the magnet on the site of the pain experience led to some relief, but never considered satisfactory, except on rare occasions. Upon seeing a figure from Travell and Simons (1983), in a pain clinic, which schematically showed a trigger point at the mid-thigh area near the groin referring pain to the right knee cap, the idea surfaced, that one could possibly "inter the body magnetically" at the site of the trigger point. If that were the case, would pain relief be experienced? The procedure was completed within one and one half hours—the patellar pain (chronic for CFH) completely dissipated. This experience was shared with another physician-scientist, more elaborate experimental designs were considered and executed. Also, by applying the magnets to trigger points of referred pain, volunteer subjects have been relieved of their pain within twenty to forty minutes (Vallbona *et* al., 1997).

Herein, we discuss the use of static magnetic fields to provide pain relief in specific, and therapy for myofascial problems in general.

Chronic Pain Symptoms

Chronic pain can be defined as pain that persists past the normal time of healing and lasts at least six months. Chronic pain is not only a burden to the individual who must cope with the experience of persistent pain symptoms, but also to the health care system that is often unable to permanently alleviate the suffering experienced by the individual. The experience of chronic pain is a complex mixture of factors that include pathological tissue changes eliciting nociception as well as psychosocial and psychophysiological behaviors elicited by pain. By definition, pain is a subjective phenomenon. Therefore it is well understood that, in order to obtain an accurate assessment of the pain experienced by an individual, a self-report of the pain intensity and symptoms must be considered along with other appropriate medical assessments (Goodman and McGrath 1991).

Even with the rapid, and often successful advances in surgical techniques and non-invasive therapies for the treatment of painful conditions such as low back pain, many individuals suffering from these conditions continue to experience pain after medical interventions have been performed (Mayer and Gatchel 1988). The risk of anesthesia, the length and tolerance of postoperative immobility, and the effects of the biomechanics of the spine have to be considered with respect to possible surgical interventions. Bed rest, anti-inflammatory medications, steroidal injections, and physical therapy programs are often prescribed. In many of these individuals, the incidence of overuse or misuse of medication (Kouyanou et al. 1997) and excessive activity limitation (Haythornthwaite et al. 1991; Vendrig and Lousberg 1997) are not uncommon pain behaviors.

Myofascial pain: chronic pain in a different perspective .

What is myofascial pain? Let us first say some words about "myofascial problem". Physiologist have known for relatively long time that each and everyone of the some 400 skeletal muscles in the human

body are surrounded by connective tissue called fascia. For various reasons myofascial problems could occur at the surface of interaction between muscle and fascia, in many cases caused by an inflammation. The demonstration of the problem that occurs might be the appearance of a localized sensation of pain at a given spot of the body which is manifested also at the body surface as a myofascial trigger point. In many cases the trigger point might be distant from the place at which myofascial problem originated. Such trigger points might be found at different areas over the body and when touched the pain might be aggravated. Further, a myofascial trigger point is defined as a hyperirritable spot, usually within a taut band of skeletal muscle or in the muscle's fascia, that elicits a painful experience upon touch (Travell and Simons, 1983, Vol. 1, p. 3). Myofascial pain syndrome is discussed, in detail, through out the two volume set by Travell and Simons (1983, Volumes 1 and 2) entitled: MYOFASCIAL PAIN AND DYSFUNCTION. As pointed out by Travell and Simons, the word "myofascial" was used, as early as 1940, "…to describe the identification and treatment of trigger areas in muscles of the low back and by 1948, in pectoral muscles" (Vol. 1, p. 10). Janet Travell, in 1952, adopted the term *myofascial*. She observed that during an infraspinatus muscle biopsy, stroking or pinching either the superficial fascia or the contractile tissue of the muscle evoked the referred pain pattern from the muscle" (Travell and Simons, 1983, Vol. 1, p.10). In addition, Travell and Simons record that "*The expressions, 'myofascial pain' and 'myofascial syndrome,' have the advantage that they clearly situate the illness in the muscle or its fascia, and that they have been used consistently to identify TP [trigger point] phenomena…*"

Trigger points.

Trigger points may be latent or active and Travell and Simons (1983) define them as "a focus of hyperirritability in a tissue that, when compressed, is locally tender and, if sufficiently hypersensitive, gives rise to referred pain and tenderness..." Thus, a trigger point is a functional, rather than an anatomical, entity. Nevertheless, the identification of trigger points with its referred pain experience, is relatively easy to identify with the Trigger Point Manual of Travell and Simons. When a trigger point is inactive, it is difficult to identify, yet when the process of activation begins the sensitivity of the trigger point becomes greater and greater to touch—hence, easier to identify. This onset of sensitivity may be referred to as a latent trigger point. Note: an active myofascial trigger point is always associated with pain, while a latent trigger point, is not usually associated pain. The latent trigger point, however, may cause restriction of motion and weakness of the affected muscle. The latent trigger point may persist for years after partial recovery from injury has begun. Acute attacks of pain may exist, since minor overstretching, overuse, or cooling of the muscle may serve to reactivate it (Travell and Simons, 1983). In summary, both latent and active trigger points cause dysfunction, and active trigger points cause pain. Finally, it should be recognized that myofascial trigger points are to be distinguished from those of other tissues such as skin, ligaments and periosteum (Travell and Simons, 1983).

Normal muscles do not contain detectable trigger points. Normal muscles have no taut bands of muscle fibers, are not tender to firm palpation, exhibit no local twitch responses, and do not refer pain in response to applied pressure. Males or females of any age can develop trigger points--particularly sedentary, middle-aged women. Except in later years, women seem somewhat more likely than men to develop myofascial pain syndromes. It appears that women are more likely (rather than men) to seek medical aid for pain of myofascial origin (Travell and Simons, 1983).

Active trigger points are more likely to reside in postural muscles of the neck, shoulder, pelvic girdles, and the muscles of mastication. Again, the upper trapezius, scalenes, sternocleidomastoids, levator scapulae and quadratus lumborum muscles are commonly involved. *Myofascial pain is referred from trigger* points in *specific patterns characteristic of each muscle* (Travell and Simons, 1983). The trigger points, for spontaneous pain, are rarely located in the spatial area of the pain experience. That is, trigger points and the area of the pain experience are spatially displaced. Referred pain of myofascial trigger points usually is described as dull and aching, often deep, with intensity varying from low-grade discomfort to severe and incapacitating. It may occur at rest, or only on motion.

Digital pressure on a given trigger point (or penetrating the trigger point with a needle) elicits referred pain or causes an increase in intensity of that pain. The more hypersensitive the trigger point, the more intense and consistent is the referred pain, and the more extensive and sustained is its distribution. In various myofascial trigger point syndromes, pain is rarely completely symmetrical across the body. At examination, the patient usually complains of pain from the most recently activated trigger point. When this trigger point is eliminated, the pain pattern may shift to that of an earlier trigger point that also must be inactivated. If the initial (or dominant) trigger point is inactivated first, the patient may recover without further treatment. Travell and Simons (1983) point out that Pain referred from myofascial trigger points do not

follow simple segmental patterns, familiar neurological patterns, nor the known patterns for referred pain of visceral origin.

The severity and extent of the referred pain pattern depends on the degree of irritation, and/or inflammation of the trigger point, not on the size of the muscle. Trigger points are activated directly by acute overload, overwork fatigue, direct trauma, and by chilling. Primary myofascial trigger points also develop in muscles subject to excessive repetitive or sustained contractions (overload fatigue). Secondary trigger points are likely to develop in adjacent muscles that are chronically overloaded by spasms. It is well known that active myofascial trigger points vary in irritability from hour-to-hour and from day to day. The amount of stress required to produce myofascial pain is highly variable, compared with other muscular pains, including angina and intermittent claudication, that are due to arterial insufficiency. Trigger-point irritability may be increased *from a latent to an active level by* many factors. The amount of stress needed to activate a latent trigger point and thus cause a clinical pain syndrome depends on the degree of conditioning of the muscle; the greater the exercise tolerance of the muscle, the lower the susceptibility of its trigger points to activation.

Once, knowledge of the referred pain by trigger points was clear, an assumption was made that magnetic fields, applied to trigger points, would reduce or abolish the pain referred by the specific trigger point. The first test of this hypothesis was initiated in pilot study of a small population of subjects with a chronic pain condition known as the Post Polio syndrome. In this clinical setting, the trigger points and their sites of referred pain were well delineated.

Post-polio syndrome.

Overuse of body parts is perhaps the largest cause of myofascial type pain. The magnitude of the population involved with the malady is unknown; however, one well-known group within the broad group of disabilities is the survivors of polio. Within this group is found a sizable number people suffering from both chronic and acute pain: the Post-polio syndrome (PPS). Halstead *et al.* (1985) compiled responses to questionnaires sent in 1985 to polio survivors identified through informal networks. The pain was classified as myofascitis secondary to progressive denervation; and this continues to be reasonable. For example, Trojan and Cashman (2005) point out that "The cause of PPS remains unclear, but is likely due to distal degeneration of enlarged post-poliomyelitis motor units.". Subsequent observations, revealed psychological and social effects that cause changes in both quality of life and in lifestyle (Hollingsworth, *et al*, 2005). In regard to numbers: one of the latest estimates of the size of the population of polio survivors is set at one million. Within that group, the population of people with post-polio syndrome is stated to be on the order of 80% (Elrod et al., 2005) In this project, 75.5% of the patients had muscle pain and 75.4% had joint pain. The types of pain experiences in this group are multiple, including a lot of diffuse muscle and joint pain (Smith and Mabry, 1995). Recovery from the diffuse muscle pain can take many months and requires considerable compliance (Peach and Olejnik, 1991). The joint pain is thought to be due to degenerative arthritis caused by age. Subacute or chronic sacroilitis occurs very often, but many times it is not recognized because other forms of low back pain mask it.

Clinical study of Postpolio Patients. A double blind, randomized clinical trial was conducted in postpolio patients to determine if pain was relieved by application of static magnetic fields applied directly over an identified pain trigger point (Vallbona et al. 1997). The devices used in this study were Bioflex magnets (Magnalex, Inc., Corpus Christi, TX) which have a pattern of concentrically arranged circles of alternating magnet polarity. Depending on the area involved, the device was a disc (40 or 90 mm in size), a credit card-sized pad, or a strip. The magnetic field intensity of the device was rated at 500 Gauss at the device surface for the 40-mm disc and the strips. The 90-mm discs and credit-card pads were rated at 300 Gauss at the surface. Placebo devices were of identical sizes and shapes.

Fifty postpolio patients with muscular or arthritic pain participated in this study. Twenty-nine patients (5 males, 24 females; mean age=51.5 years) were randomly selected to receive treatment with the active magnetized device; 21 patients (6 males, 15 females; mean age=55.9) received treatment with the inactive device. Patients were asked to complete a McGill Pain Questionnaire to provide a subjective evaluation of his or her general pain experience (a validated method for analyzing pain). Only one area of pain was evaluated, even thought multiple sites may have been present. A trigger point associated with the site of pain was grossly elicited first by finger palpation and then by firm application of a blunt object, which in non-painful areas produced a sensation of pressure but no pain. The patient was asked to subjectively grade the pain at the trigger point on a scale from 1 to 10 (with 1 being the least and 10 being

the maximum). The appropriately sized magnetic or placebo device was placed on the area of pain with adhesive tape for 45 minutes. After removal of the device, the patient was asked to assess the intensity of pain again using the McGill Pain Questionnaire. The proportion of patients in the active-device group who reported a pain score decrease greater than the average placebo effect was 76%, compared with 19% in the placebo-device group ($p < .0001$) (Vallbona, *et al.*, 1997).

Chronic Low Back Pain

Low back pain (LBP) represents an important health problem in which medical costs and lost work capacity are major issues. Disorders of the low back are a major cause of disability of people under the age of 45 (Mayer and Gatchel 1988). In fact, work incapacity resulting from LBP has been estimated to vary between 2% and 8% in Western Europe and North America (Nachemson 1992). The medical costs associated with the treatment of low back disorders have been estimated to fluctuate between $4.6 and $60 billion annually in the U.S. (Lee 1994; Miedema et al. 1998).

Static and time-varying EMFs have been applied with apparent success in the management of pain in a variety of orthopedic conditions, most commonly traumatic bone fractures or surgical osteotomies (Bassett 1989). Furthermore, in the domain of osteoarthritis several double blind, placebo-controlled studies demonstrated the efficacy of pulsed EMFs for the relief of pain (Trock et al. 1993a, 1993b, and 1994).

A large body of scientific literature suggests that magnetic therapy my have utility in the treatment of pain (Foley-Nolan et al. 1990 and 1992; Ellis 1993; Trock et al. 1993a, 1993b, and 1994; Markov and Pilla 1995; Vallbona et al. 1997; Sartucci et al. 1997; Sherman et al. 1998). However, it should be noted that despite a number of clinical studies performed world-wide indicating successful use of magnetic fields for treatment of various diseases and pathologies, little is known regarding the effectiveness of magnetic fields in relieving LBP.

In the experimental design, trigger points were identified for the subject's pain experience. Magnets of a specific design were placed over the trigger points responsible for the pain experience. These magnets had been charged to surface field strengths between 300 to 500 Gauss and were disc-shaped. The disc magnets can be kept in place by means of adhesive tape and/or specially made double sided adhesive, which is attached directly to the disc surface. It is clear from initial studies that the application of the magnets to a trigger point can reduce or eliminate (by subjective measure) the pain referred from that trigger point. The mechanisms of the effect of magnetic fields on soft tissues have not been elucidated.

The hypothesis

One of us (MSM) have been studied the biological and clinical effects of magnetic fields for several decades. The hypothesis for "biological windows" have been proposed in 1976 and further developed. This term refers to existing preferred values of magnetic fields that cause significant biological response. It appears that Mother Nature, during evolution, created mechanisms for response at which selected magnetic fields are detected, while living creatures neglected other signals, which could be even stronger (Markov, 1994). The existence of such windows have been proven in studies with various living systems as well as with different systems in human body. Probably we should speak about "biophysical windows" instead of "biological windows". The difference should be that this idea is more related to the physical parameters of the applied endogenous signal rather than to biological characteristics. From a biological point of view, one plausible mechanism could be linked to the idea proposed by Blank (2004), who reported existence of a domain in the heat shock protein HS70 that is responsible for detecting the MF signal.

We are proposing a hypothesis that trigger points represent a real biological "window" or "door" for delivering the magnetic field to the muscles or other body parts that experience pain. Let us make a following model: The part of the body that represents an activated trigger point virtually could open the door for any physical influence. When appropriate magnetic field is applied, like a key for the locker, the door "opens" and allows the magnetic field, virtually to enter the body. Next, via the systemic effect (presented by us at Kos meeting 2003), the signal is delivered to the source of the problem – where irritation, inflammation, or some other pathophysiological disturbances took place. In that part of the body, inflammation may invoke T-lymphocytes for fighting the inflammation. As it was shown, by one of us, at the Rhodes meeting (Nindl et al, 2002) and in our recent publication (Markov et al., 2006), magnetic fields more significantly influence the lymphocytes activated by the disturbances.

This hypothesis might be summarized as follows:

- A trigger point becomes activated due to inflammation at the interface between muscles, and fascia
- If an appropriate magnetic field is applied, the trigger point secures the pathway for the magnetic field
- Via systemic effect, the signal is delivered to the source of inflammation (i.e., the interface between muscle and fascia
- Magnetic fields stimulate those T-lymphocytes that have been activated by inflammation, thus reducing the inflammation and, in turn, bring about pain relief.

We also postulate that, there could be a change in the tensile properties of cartilage, ligaments, and other soft tissue structures, which secondarily may relieve tension on arthritic joints or on chronically "inflamed" areas. Such ideas seem very possible in light of the work of Becker and Selden (1985) and Vallbona, *et* al. (1983). That the magnetic fields interact with the biological “transmission lines” contained within the trigger point area; and, that the “transmission lines” possibly communicate with the inflamed area of the pain experience. Such speculation is consistent with the concept of the systemic effect (Ericsson, *et al.*, 2005) (Markov, *et al.*, 2006).

Continuing with this line of thought, we remind the reader that connective (i.e., the extracellular matrix) has been suggested to be involved in myofascial pain as well as in pain relief. As discussed above, a network of connective tissue surrounds each muscle fiber of a given muscle, all muscle groups (arms, legs, trunk, head, and neck), all nerve fibers, neuromuscular junctions, etc. (Fawcett, 1994, Chapters 5, 10, and 11; Barker, 1974). It has been hypothesized that contraction-relaxation units exist throughout the extracellular matrix of the body (Hazlewood, 2003). It is proposed that shortening of these "units” do induce pain, and relaxation of these "units" do induce pain relief. For myofascial type pain the possibility of the involvement of the connective tissues as a player in various pain syndromes is reasonable.

In conclusion: We realize that the speculations put forth in this presentation may be a little overwhelming. Nevertheless, we ask for your indulgence--please remember, these speculations are intended to provoke both thought and experimentation. Note: We are searching for an explanation of the observation that the probability of pain relief is enhanced when a magnet is placed over a trigger point as opposed to direct placement on the painful area; and, therefore ask the question: Could trigger points serve as a sensitive “tissue window” providing pathways of stimulation to the needed area?

References

Barker, D. 1974 The morphology of muscle receptors. In: Muscle Receptors. By Barker, D., Hunt, C.C., and McIntyre, A.K. Ed. By Hunt, C.C. Springer-Verlag Berlin. 310 pp.

Bassett, C.A.L. 1989. Fundamental and practical aspects of therapeutic uses of pulsed electromagnetic fields (PEMFs). Critical Reviews in Biomedical Engineering. 17:451-529.

Bassett, A. 1994. Therapeutic Uses of Electric and Magnetic Fields in Orthopedics. In: Carpenter, D.O., and Ayrapetyan, S. Biological Effects of Electric and Magnetic Fields--*Beneficial and Harmful effects*. Vol. 2. Academic Press, Inc. pp.13-48.

Becker, R.O**.** 1990. Cross Currents. The perils of electromedicine, the promise of electromedicine. The Putnam Publishing Group, New York, NY

Becker, R.O**.**, and Selden, G. 1985. The Body Electric: Electromagnetism and the Foundation of Life:William Morrow & Company, Inc., New York, p 364.

Blank, M. and Goodman R. 2004. A biological guide for electromagnetic safety: The stress response. Bioelectromagnetics. 25: 642-646

Carpenter, D.O. and Ayrapetyan, S. (Eds.) 1994. Biological Effects of Electric and Magnetic Fields. Vol. 1, *Sources and Mechanisms* and Vol. 2, *Beneficial and Harmful Effects*. Academic Press.

Ellis, W.V. 1993. Pain control using high-intensity pulsed magnetic stimulation. Bioelectromagnetics. 14:553-556.

Elrod, L.M., Jabben, M., Oswald, G., Szirony, G.M. 2005. Vocational Implications of Post-polio syndrome. *Work.*25(2): 155-161.

Environmental Health Criteria 69: Magnetic Fields World Health Organization, Geneva 1987, p 197.

Fawcett, D.W. 1994. Bloom and Fawcett: A Textbook of Histology. Twelfth edition. Chapman & Hall, New York. 964 pp.

Foley-Nolan, D., Barry, C., Coughlan, R.J., O'Connor, P., and Roden, D. 1990. Pulsed high frequency (27MHz) electromagnetic therapy for persistent neck pain. A double blind, placebo-controlled study of 20 patients. *Orthopedics* **13**:445-451

Foley-Nolan, D., Moore, K., Codd, M., Barry, C., O'Connor, P., and Coughlan, R.J. 1992. Low energy high frequency pulsed electromagnetic therapy for acute whiplash injuries. A double blind randomized controlled study. *Scand. J. Rehab. Med.* **24**:51-59.

Glassman, L.S., McGrath, M.H. and Bassett C.A.L. 1986. Effect of external pulsing electromagnetic fields on the healing of soft tissue. Ann. Plast. Surg. 16:287-295.

Grande, D.A., Magee F.P., Weinstein, A.M., and McLeod, B.R. 1990. The effects of low-energy combined AC and DC magnetic fields on articular cartilage metabolism. Annals N.Y. Acad. Sci. 404-407.

Halstead, L.S., Wiechers, D.O., Rossi, C.R. 1985. Late effects of poliomyelitis: A national survey. In: Halstead LS, Wiechers DO (eds): *Late Effects of Poliomyelitis.* Miami, Florida: Symposia Foundation.

Hazlewood, C. F. 2003. Treatment of Post-Polio Pain with a Static Magnetic Field and Some Notions on Mechanism. In: "Magnetotherapy: Potential Therapeutic Benefits and Adverse Effects". Ed. By Michael J. McLean, Stefan Engstrőm and Robert R. Holcomb Floating Gallery Press. pp. 191-207.

Haythornthwaite, J.A., W.J. Sieber, and R.D. Kerns. 1991. Depression and the chronic pain experience. Pain. 46:177-184.

Health and Safety Guide No. 27: Magnetic Fields Health and Safety Guide. World Health Organization. 1989, p 24.

Herman, E., R. Williams, P. Stratford, A. Fargas-Babjak, and M. Trott. 1994. A randomized controlled trial of transcutaneous electrical nerve stimulation (CODETRON) to determine its benefits in a rehabilitation program for acute occupational low back pain. Spine. 19:561-568.

Hollingsworth, L., Diderot, M.J., and Levington, C. 2005 Post-polio Syndrome: Psychological Adjustment to Disability. *Issues Ment. Health Nurs* 23(2): 135-156.

Itoh, M., Montemayor, J.S., Matsumoto, E., Eason, A., Lee, M.H., and Folk, F.S. 1991. Accellerated wound healing of pressure ulcers by pulsed high peak power electromagnetic energy (Diapulse). *Decubitus* **4**:29-34,

Loeser, J.D. 1980. Perspectives on pain. In: Clinical Pharmacology and Therapeutics. P. Turner, ed. University Park Press:Baltimore. pp. 313-316.

Markov, M.S. 1995. Electric current and electromagnetic field effects on soft tissue: Implications for wound healing. Wounds. 7:94-110.

Markov, M.S. and Pilla, A.A. 1995. Electromagnetic field stimulation of soft tissues: pulsed radio frequency treatment of post-operative pain and edema. Wounds. 7:143-151.

Markov, M.S., Hazlewood, C.F., Ericsson, A.D. 2004. Systemic effect – a plausible explanation of the benefit of magnetic field therapy: A hypothesis - 3rd International Workshop on Biological Effects of EMF – Kos, Greece, October 4-8, 2004, 673-682, ISBN 960-233-151-8.

Mayer, T.G. and R.J. Gatchel. 1988. Introduction and overview of the problem. In: Functional Restoration for Spinal Disorders: The Sports Medicine Approach. T.G. Mayer and R.J. Gatchel, eds. Lea & Febiger:Philadelphia, PA. pp. 3-15.

McCray, R.E. and N.J. Patton. 1984. Pain relief at trigger points: a comparison of moist heat and shortwave diathermy. JOSPT. 5:175-178.

Miner, W.K., and Markoll, R. 1993. A Double-Blind Trial of the Clinical Effects of Pulsed Electromagnetic fields in Osteoarthritis. *J. Rheumatol.* 20: 456-460.

Nachemson, A.L. 1992. Newest knowledge of low back pain: a critical look. In: Clinical Orthopaedics and Related Research. M.R. Urist, ed. J.P. Lippincott Co.:Philadelphia. pp. 8-20.

National Research Council (NRC). 1996. Possible Health Effects of Exposure to Residential Electric and Magnetic Fields. Executive Summary. Committee on the Possible Effects of Electromagnetic Fields on Biological Systems, Board on Radiation Effects Research, Commission on Life Sciences, and National Research Council. National Academy Press:Washington, D.C. pp. 1-7.

Nindl, G., Johnson, M.T., Hughes, E.F., Markov, M.S. 2002. Therapeutic electromagnetic field effects on normal and activated Jurkat cells - International Workshop of Biological effects of Electromagnetic fields, Rhodes, Greece, 7-11 October 2002, p.167-173. ISBN # 960-86733-3-X.

Pfingsten, M., J. Hildebrandt, E. Leibing, C. Franz, and P. Saur. 1997. Effectiveness of a multimodal treatment program for chronic low-back pain. Pain. 73:77-85.

Peach, P. and Olejnik, S. 1991. Effect of Treatment and Non-Compliance on Post-Polio Sequelae. *Orthopedics* **14**: 1199-1203.

Pilla, A.A. and Markov, M.S. 1994. Bioeffects of weak electromagnetic fields. Reviews on Environmental Health. 10:155-169.

Rosch P.J. and Markov M.S.(eds.) 2004. Bioelectromagnetic Medicine, Marcel Dekker NY, 850 pp.

Sartucci, F., Bonfiglio, L., Del Seppia, c., Luschi, P., Ghione, S., Murri, L., and Papi, F. 1997. Changes in pain perception and pain-related somatosensory evoked potentials in humans produced by exposure to oscillating magnetic fields. Brain Research. 769:362-366.

Sherman, R.A., Robson, L., and Marden, L.A. 1998. Initial exploration of pulsing electromagnetic fields for treatment of migraine. Headache. 38:208-213.

Shupak N.2003. Therapeutic uses of pulsed magnetic-field exposure: A review. Radio Science Bulletin # 307; 9-32

Travell, J.G. and Simons, D.G. Myofascial Pain and Dysfunction The Trigger Point Manual: Volume 1, The Upper Extremities, published in 1983 and Volume 2, The Lower Extremities, published in 1992. Williams and Wilkins.

Trock, D.H., A.J. Bollet, R.H. Dyer, Jr., L.P. Fielding, W.K. Miner, and R. Markoll. 1993a. A double-blind trial of the clinical effects of pulsed electromagnetic fields in osteoarthritis. J. Rheumatol. 20:456-460.

Trock, D.H., A.J. Bollet, and R. Markoll. 1993b. Treatment of osteoarthritis with pulsed electromagnetic fields. Arthritis and Rheumatism. 36:130-131.

Trock, D.H., Bollet, A.J., and Markoll, R. 1994. The Effect of Pulsed Electromagnetic Fields in the Treatment of Osteoarthritis of the Knee and Cervical Spine. Report of Randomised, Double Blind, Placebo Controlled Trials. *J. Rheumatol.* **21**:1903-1911.

Trojan, D.A., and Cashman, N.R. 2005 Post-poliomyelitis Syndrome. *Muscle Nerve.*31(1): 6-19

Vallbona, C., Hazlewood, C.F. and Jurida G.. 1997. Response of pain to static magnetic fields in postpolio patients: a double-blind pilot study. Arch. Phys. Med. Rehabil. 78:1200-1203.

Varcaccio-Garofalo, G., Carriero, C., Loizzo, M.R., Amoruso, S., and Loizzi, P.. 1995. Analgesic properties of electromagnetic field therapy in patients with chronic pelvic pain. Clin. Exp. Obst. Gyn. 22:350-354.

Vendrig, A.A. and Lousberg, R. 1997. Within-person relationships among pain intensity, mood and physical activity in chronic pain: a naturalistic approach. Pain. 73:71-76.

Wagstaff, P., Wagstaff, S., and Downey, M. 1986. A pilot study to compare the efficacy of continuous and pulsed magnetic energy | short-wave diathermy | on the relief of low back pain. Physiotherapy: 72:563-566.

World Health Organization (WHO). 1987a. Magnetic Fields. United Nations Environment Programme, World Health Organization, and The International Radiation Protection Association. Environmental Health Criteria 69. pp. 25-33, 119-127.

World Health Organization (WHO). 1987b. Magnetic Fields Health and Safety Guide. United Nations Environment Programme, World Health Organization, and The International Radiation Protection Association. Health and Safety Guide No. 27. pp. 7-24.

FLUIDIC MICROSYSTEMS FOR BIOlOGICAL CELL SAMPLE HANDLING AND ANALYSIS

KARAN KALER, YOULAN LI, THIRUKUMARAN T. K.,

COLIN DALTON AND RANJIT PRAKASH

DEPARTMENT OF ELECTRICAL AND COMPUTER ENGINEERING
SCHULICH SCHOOL OF ENGINEERING,
UNIVERSITY OF CALGARY,
2500 UNIVERSITY DRIVE N.W.,
CALGARY, CANADA (T2N-1N4)

Abstract

The ability to manipulate volumes of liquid and their constituent components, such as cells, organelles and their nucleic acids, utilizing very small (microliter) sample volumes provides new and novel opportunities and capabilities in microchip based bio-analysis and detection or lab-on-a-chip based diagnostics. The low sample volume requirements and rapid real-time processing capability enables parallel and multi processing capability without adverse impact on sample degradation.

Our research effort has focused on the development and application of non-invasive cell manipulations and separation techniques to facilitate fraction of diseased and healthy cells on a microchip in a rapid fashion with minimal amount of sample preparation. The cell sample processing capability is provide by electrokinetic based manipulation on-chip by leveraging the phenomena of dielectrophoresis (DEP). We explore the integration of electrokinetic methods for both particle and liquid manipulations utilizing conventional "closed channel" microfluidic structures as well as surface fluidic or "open channel" schemes.

Utilizing closed channel microfluidic structures, we have demonstrated DEP cell separation capability on batch and continuous flow through samples. We have furthermore explored the combined use of liquid and particle DEP to provide alternate means of processing/manipulating micro litre sized liquid droplets containing cells. This cell sample preparation capabilities provided by the integrated DEP and microfluidic, when integrated with other down stream processing components, such as cell lyses, genetic amplification and nucleic acid detection capability, has the potential of providing a complete bio-analysis on a chip. The proposed platform technology is not limited to applications targeted to disease detection; it is equally suitable for the detection of environmental agents and pathogens that have adverse impact on human health, Furthermore, the technology makes available useful small sample handling and analysis capabilities, which can be leveraged to benefit investigations concerning interaction of E.M. fields with biological cells.

1. Introduction

In recent years, as a result of advances in microfabrication methods, materials and process technology and coupled with it's availability to the research community has resulted in many new and novel application of the technology in many diverse areas in addition to the traditional semiconductors and microchip industry [1, 2]. For example the ability to lithographically pattern and etch microscopic scale micro-channels in glass provided a compact footprint for the development of capillary electrophoresis, with improved sample handling, detection and throughput [3]. Furthermore the miniaturization of such devices has made it possible for their infield deployment and handheld operation. Despite the success of such development in fluidic microsystems, a number of issues and obstacles need to be addressed before the technology can be considered reliable and mature enough to be applied successfully in the more critical and demanding arena pf biomedical diagnostics, on a routine basis. Of major concern and a significant challenge in this regard is the availability of suitable on-chip low volume sample preparation and handling methods [4, 5] in additional to suitable sample isolation (valving), pumping, mixing components.

Recent advances in the development and application of A.C. electrokinetics has shown that simultaneous handling and manipulation of very small quantity of fluids and particles, such as cells can be achieved utilizing the traditional closed channel microfluidic and more recently open channel surface microfluidic devices [6]. In the past, A.C. electrokinetic systems leveraging the phenomena of Dielectrophoresis (DEP) have been developed

primarily employing closed fluidic chambers or microfluidic channels and intersections that are interfaced to external fluid pumping and sample injection hardware [7-9]. Such systems, particularly those employing microfluidic channels for cell collection and separation usually require sample preprocessing and are frequently plagued by micro-channel blockage. Such problems need to be overcome in order to successfully commercialize microfluidic cell analysis/sorting devices. The closed channel microfluidic systems are furthermore less amiable to creating complex cell processing structures, due to pressure and flow related problems and the need for extensive valving and flow control devices on-chip and capable of withstanding high operating pressures . In the paper we discuss the utility, application and merits of example "open channel" or surface microfluidics and "closed channel" microfluidic systems for biological cell sample handling and analysis utilizing A.C. electrokinetic approaches.

2. AC electroactuation and manipulation of cells and microfluids by dielectrophoresis (DEP)

Electrical field effect phenomena have been extensively investigated and demonstrated to provide novel ways of manipulating and interrogating individual microscopic sized particles and intact biological cells, immersed in fluid media [10-12]. In this paper we focus on the capabilities and utility of non uniform A.C. (alternating current) electric field effect, referred to as dielectrophoresis (DEP), in providing particle, liquid, droplet actuation at microscopic scales to facilitate the deployment of fluidic microsystems or LOC for the handling and manipulation of cells and subsequently the genetic material of the individually selected or fractionated cell population.

(a) Particle DEP actuation

To illustrate the salient features and basis for particle DEP actuation, consider a microscopic sized spherical shaped particle or object that is immersed or surrounded by another medium and subjected to an externally imposed non uniform electric field. We further assume that the particle and the surrounding medium are characteristically different in terms of the electrical permittivity and conductivity. The time averaged DEP force $\langle \vec{F}_{DEP} \rangle$ acting on a spherical body of radius a, due to a spatially non uniform ac electric field, is summarized as follows [13]:

$$\left\langle \vec{F}_{DEP} \right\rangle = 2\pi\varepsilon_m a^3 \,\mathrm{Re}\left[K_e\right] \nabla E_{rms}^2 \qquad (1)$$

where, $K_e = \dfrac{\varepsilon_p^* - \varepsilon_m^*}{\varepsilon_p^* + 2\varepsilon_m^*}$

In the DEP force expression (Eqn. 1), the quantity $\mathrm{Re}\left[K_e\right]$ refers to the real part of excess polarizability or frequently referred to as the Claussius-Mosotti factor (CMF). The quantities $\varepsilon_p^* = \varepsilon_p - j\frac{\sigma_p}{\omega}$ and $\varepsilon_m^* = \varepsilon_m - j\frac{\sigma_m}{\omega}$ are the complex permittivity of the particle and medium respectively. ε_m , ε_p represent the real dielectric permittivity of the medium and particle σ_m , σ_p refer to the conductivity of the particle; and the medium and $\omega = 2\pi f$ is the radian frequency, where f (Hz).is the applied A.C. electric field frequency. The CMF reflects the polarizability difference the particle and media, and is usually a sensitive function of the applied field frequency. The term ∇E_{rms}^2 is the gradient of the electric field squared.

It is apparent, from Eqn. (1), that the DEP force depends on the particle size (volume), the gradient of electric field squared and the Claussius–Mosotti factor which is frequency dependent. Furthermore, when Re [K_e] > 0, at a particular frequency, the DEP force is positive (+ve DEP) and directed towards the region of increasing field intensity [12]. In contrast, when Re [K_e] < 0, the DEP force is negative (-Ve DEP) and impels the particles to regions of field intensity minimum [14]. The impact of +Ve and –Ve DEP forces acting on particle subjected to nonuniform field, as synthesized by a set of coplanar electrodes, is shown schematically in Figure 1. The +Ve and –Ve DEP effect has the beneficial effect of physically separating or concentrating the particles in regions of field intensity maxima (at the electrode surfaces) and minima (located away from the electrode surfaces).

Most microscopic particles of practical interest, including biological cells, due their structural heterogeneity and differences in the electrical properties of the various ultra structures compared to that of the suspending media may exhibit both +Ve and –Ve DEP behavior in different region of the applied field frequency spectrum [15]. It is due to such characteristic differences in the frequency dependent polarization and the resulting DEP response which enables selective and differential manipulation and physical separation of one or more types of particles or cells in a mixed population suspension.

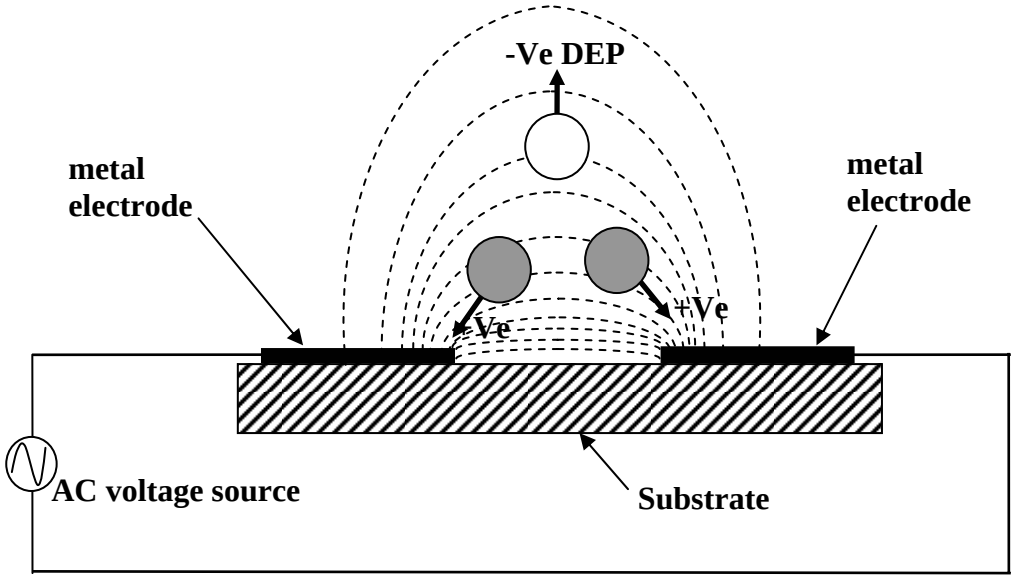

Figure 1. A cross-sectional view of a co-planar electrode geometry, showing the differing +Ve and –Ve DEP forces exerted on particles, induced by a nonuniform AC field, as depicted by the dashed lines the diagram. The shaded particle, experiencing +Ve DEP, are impelled towards and collected at the electrodes, while particle experiencing –Ve DEP body force is impelled upwards into a region of local field intensity minima.

(b) Liquid DEP actuation and droplet dispensing

The utility of the DEP effect is not limited to particulate matter, but maybe made to manifest and exert body forces on aqueous polarizable media [14-16]. The practical and useful utility of the phenomena, especially at the micro scale, enables novels means of handling and manipulating aqueous biological fluid samples, without the need for valving and/or pumping required for isolation, steering and fluid transport in conventional microfluidic systems. Thus, the DEP effect, in addition to serving to electro-actuate microscopic particles and thereby facilitate their manipulation may furthermore be leveraged to enable noninvasive handling and manipulation of microliter volume droplets of aqueous dielectric media on open surfaces. Such open surface manipulation of biological samples circumvents a variety of issues that plague closed channel systems.

The first demonstration of macro scale liquid actuation by DEP was reported by Pillet [16]. By partially immersing two parallel plates in a bath of aqueous dielectric media (oil) and applying an A.C. potential to the plates, he observed that a column of liquid was raised between the plates to a new equilibrium.

More recently, the work of Jones et al [17, 18], Ahmed et al [19] and Kanagasabapathi et al [20] have shown that similar type of controlled actuation of a small quantities of dielectric liquids (oils and low conductivity water), on top of planar surfaces can be achieved by employing a pair of thin coplanar metal electrodes, coated with a thin film dielectric material, of a suitable contact angle ($< 70^0$), as shown in Figure 2.

For satisfactory operation, liquid that is to be actuated and dispensed is usually introduced as a parent drop at one end on the electrode structure. On application of an AC voltage, typically ~ $230V_{RMS}$ @ 100 kHz, a jet of liquid in the form of finger, confined to the width of the electrodes, protrude from the parent droplet and very rapidly extend to the end of the electrode structure.

The characteristics of this liquid finger formation has been analysed by Jones et al [21]. A reduced-order lumped parameter model was proposed that takes into account liquid surface tension viscous drag, and the DEP force. The resulting expression, describing the DEP force induced on the liquid finger, is as follows [19]:

$$F_{liquid\ DEP} = \frac{(\varepsilon_{liq} - 1)C_d^2 C_{air} V^2}{2(C_d + 2\varepsilon_{liq} C_{air})(C_d + 2C_{air}))} \qquad (2)$$

The liquid DEP force imparted, varies as the square of the applied voltage (V), the permittivity of the liquid (ε_{liq}) and the characteristics of the field in the liquid media, controlled by the electrode structure, dielectric coating and geometry. Upon removal of the voltage, the liquid finger breaks up into one or more smaller sized daughter droplets that are spaced almost uniformly on top of the electrodes. Further refinements in the basic coplanar structure, such a three electrode system, the judicious location of semicircular metal bump areas and their spacing to satisfy the Raleigh jet break criterion have enabled the controlled dispensing of aqueous media (deionized water) in the form multiple identical sub-microliter droplets [19]. These are included in the structure shown Figure 3(a), while figure 3(b) shows the daughter droplets populating the metal bump regions spaced at regular intervals along the coplanar electrode structure.

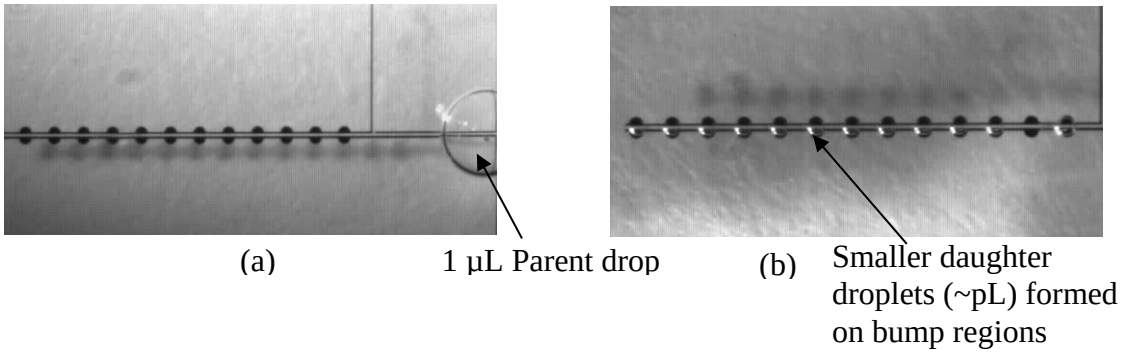

Figure 3. (a) Photographs showing the 3-electrode structure with metal bumps, for improved droplet formation. (b) Successful population of the bump regions with smaller daughter droplets after the applied voltage is removed.

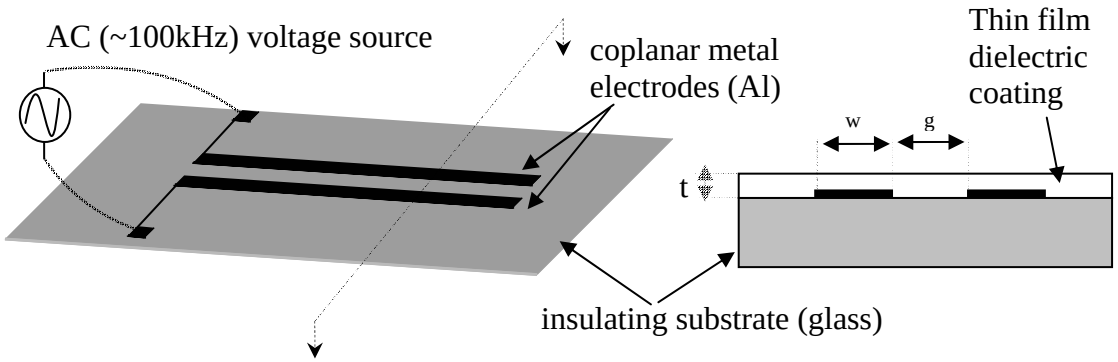

Figure 2. A schematic (a) plan and (b) cross-sectional views of the co-planar electrode geometry, coated with a thin dielectric film, employed for DEP actuating liquid. Nominal dimension of the structure are as follows: t ~ 0.5 µm; w = 30 µm; g = 30 µm.

Thus, successful development and implementation of liquid actuation, droplet formation and transport on open surfaces utilizing liquid DEP, open up a variety of new application in the microfluidics domain concerning the manipulation of minute quantities of fluid sample and it's components. Some such example surface fluidic manipulations are discussed in a later section in this article.

3. Integration of on-chip DEP with microfluidics

Having provided a basis for DEP manipulation of particles and liquid samples, we now turn to its application and utility for lab-on-a chip applications. .In this article we specifically focus on microfluidic devices that integrate DEP for particle/cell handling or processing. The level and extent of the integration effort demanded is very much governed by the application (i.e. application specific). For example, a fully integrated microfluidic device for chip based genetic analysis requires a number of different microfluidic component blocks to facilitate cell manipulation, nucleic acid processing (genetic amplification and separation) and a suitable electro-optical detection system. More specifically a fully integrated platform would include cell sorting and fractionation and /or concentration, cell lysis step to extract the genetic material (DNA, RNA), genetic amplification procedure, such as on-chip PCR and subsequent DNA separation and detection utilizing on-chip capillary electrophoresis.

Thus on-chip sample preparation, including cell separation, is a key and much needed capability that can have a dramatic impact of the overall performance and capabilities of integrated microfluidic chips for bio-analysis and detection. In the past a variety of different techniques methods have been proposed to handle the sample preparation needs, however, many of the proposed approaches, unlike DEP are not readily incorporated on-chip. Here we examine two different approaches, a batch sorting scheme and a continuous DEP based cell fractionation in affecting cell separation in microfluidic channels. A fundamental requirement of all devices that leverage DEP is appropriate synthesis of a nonuniform electric field, which is achieved quite readily using metal electrodes of appropriate dimension, spacing/geometry. However, in order to integrate DEP electrode structures in microfluidic channels, we are limited to the use of planar electrode structures which can be photo lithographically patterned. Furthermore, to facilitate microfabrication, the planar electrodes are limited to locations on the top or bottom sides of the microchannels. The choice of material for the metal electrode material has to be given due consideration. If the channels contents are to be visually inspected or the contents monitored, then it is appropriate to transparent electrodes material such as indium tin oxide (ITO), otherwise either titanium-platinum of chrome-gold electrodes have been shown to suitable and readily deposited and patterned lithographically.
An example of a DEP based microfluidic chip fabricated to make available binary DEP fraction of cells in a continuous fashion [22], is shown in Figure 4.

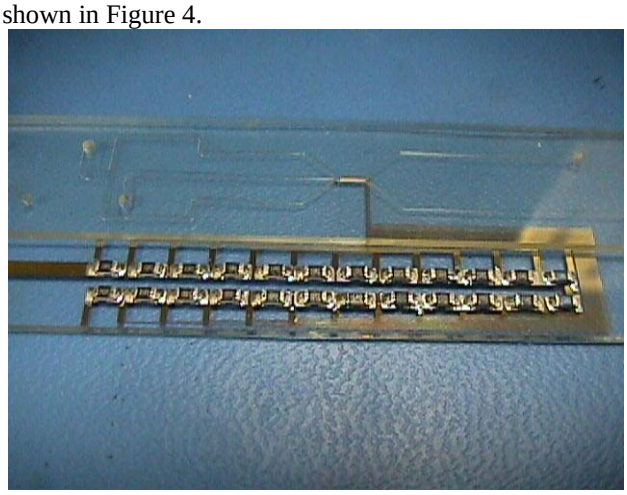

Figure 4 A closed channel microfluidic DEP fractionation chip, showing the microfluidic channels with in-channel microelectrodes for DEP cell sorting

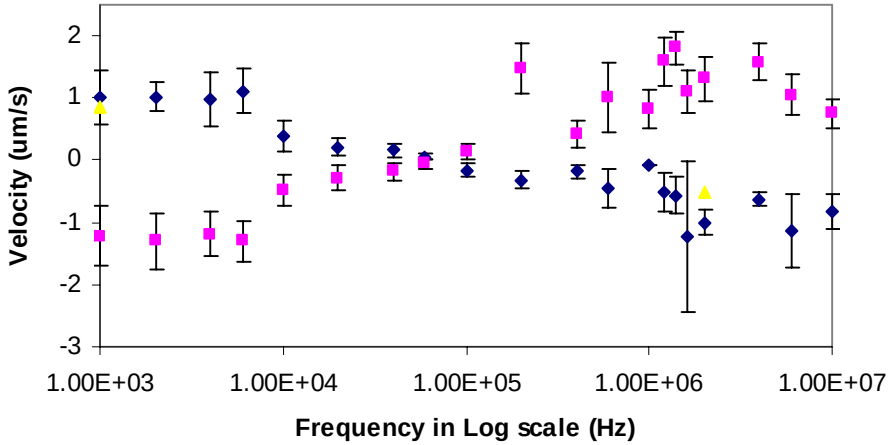

Figure 5. Plot of the DEP velocity spectrum of viable and nonviable yeast cells versus frequency. showing +Ve DEP and –Ve DEP responses [21].

The device is comprised of a cell and sheath injection ports that facilitates the injection of a cell sample into the chamber using off-chip pumping. The dimensions of the sheath flow and cell sample channels are designed to enable hydrodynamic focus of the cell stream under laminar flow. The focused injected cell stream is subjected to a nonuniform isomotive electric field, synthesized by an array of individual biased electrodes. In this isomotive field region cells, depending on their frequency dependent polarizability, may experience positive or negative DEP depending on the frequency of the applied field, and hence are deflected in opposite directions and

normal to the fluid flow. Thus cells experiencing +Ve and –Ve DEP are physically separated and subsequently collected as purer subpopulations downstream. Example DEP spectral of viable and non-viable yeast cell, obtained using the device is shown in Figure 5. The plot reveals that binary fractionation of viable from nonviable yeast cells, suspended in deionized water, and is most efficiently attained over specific regions (10 kHz to 80 kHz and 1 MHz to 5 MHz) of the frequency spectrum. Further integration of the chip, incorporating near-field hybrid attached to the glass substrate facilitates real-time monitoring of cell separation at the outlet ports of the device [23].

An alternative approach to the continuos fraction of cells utilizing DEP is to adopt a batch sorting /separation which is perhaps more suitable in cases where a dilution of the cell sample concentration by the sheath flow as in the continuous separation is not desirable. An example of this batch cell separation device is shown in Figure 6. Unlike the continuous cell sorting device, requiring metallized electrodes on the to and bottom faces of the microfluidic channels, the batch scheme can be readily implemented with an array of electrodes house on a glass substrate while the microchannels enclosing the electrodes are cast in Poly(dimethyl siloxane) (PDMA) and affixed on top of the glass substrate[24]. The use of PDMS polymer for microfluidics, is advantageous as it reduces the time, complexity and cost of prototyping and manufacturing. PDMS is hydrophobic and can easily nucleate air bubbles, however, by exposing the cured PDMS layer to oxygen plasma at a pressure of 0.15 torr renders the surface hydrophilic and makes it compatible for microfluidic handling. The assembled microfluidic DEP device can withstand moderate chamber pressures, typically ~ 30-50 psi.

In such a batch DEP device, a dilute cell suspension is introduced in to the chamber employing pressure driven flow and an AC voltage is applied to the electrode array. Cells experiencing +Ve DEP are collected in the high field regions, while cells experiencing negative DEP are repelled from the electrode surfaces and levitated or trapped in local filed intensity minima (see Figure 7). Since the +Ve DEP cells are strongly held on to the electrode surface and the -Ve DEP cells can be flushed while retaining the cells collected at the electrodes in the chamber. Such batch DEP devices, although simple in design compared to the continuous cell sorting system, finding utility in applications that require concentration of cell sample into a smaller volume.

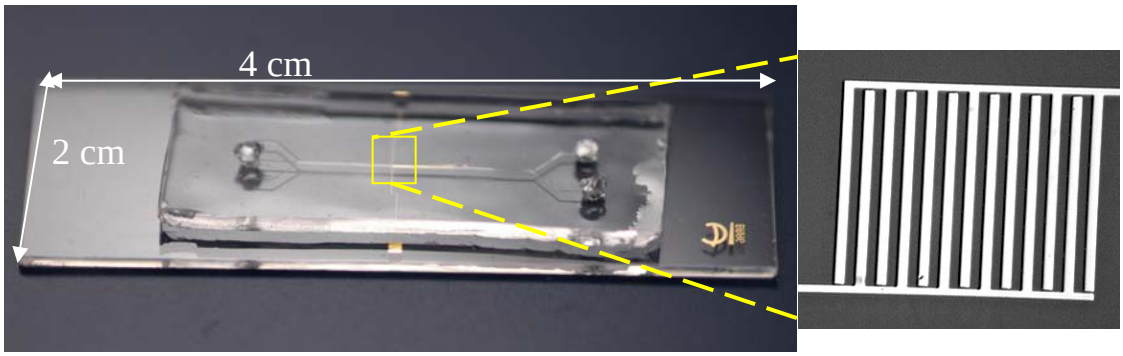

Figure 6. A glass-PDMS microfluidic device for batch DEP cell separation with in-channel planar interdigitated microelectrodes electrodes (electrode width = 20 µm; electrode spacing= 20 µm

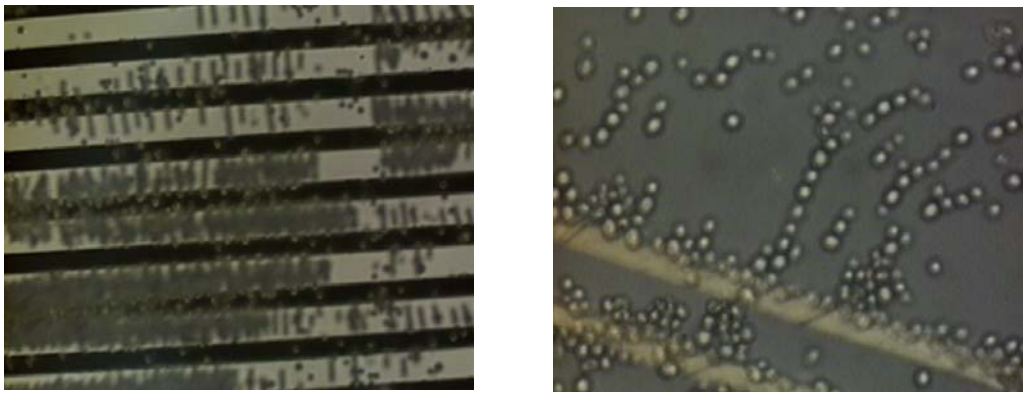

(a) (b)

Figure 7 Photographs showing(a) microscopic sized latex beads (10 µm in diameter) suspended in low conductivity media (water) exhibiting –Ve DEP and levitation above the electrode plane and (b) +Ve DEP collection of yeast cells at electrode edges [23].

4. Surface Fluidic Structures for Integrating Liquid and Particle DEP

Conventional microfluidic devices or systems to a large extent are comprised of microfluidic channels, which traditionally are etched in glass or more recently patterned in PDMS or other suitable polymeric substrates. The substrate with the etched channels are then suitably bonded or sealed to another or identical substrate material to form closed microchannel structures. As discussed earlier there are a number of issues concerning the utility and applicability of such devices in the domain of microfluidic when handling or processing of aqueous biological sample containing cells or macromolecules in suspension. Recently, the emergence of Liquid DEP as alternate means of manipulating and processing small quantities, has suggested new and novel schemes of manipulating liquids samples comprised of cell (cell suspensions), macromolecules and/or reagents.

An example surface fluidic structure illustrating the combined manipulation of both liquids and particles (cells) utilizing Liquid and particle DEP phenomena [19] is illustrated in Figure. 8. The microelectrode structure basically combines the liquid actuation and droplet formation station with the particle DEP microelectrode array. The key capabilities of this integrated structure are (1) it's ability to dispense and form droplets of a cell suspension at locations as specified and implemented by the Liquid DEP structure (2) the ability to subject cells suspended in the daughter droplets, formed by liquid actuation, to one or more DEP field frequencies and subsequently convey the sample to another location in the structure. The structure illustrated in Figure 9 was microfabricated integrating different electrode arrangements at the bump regions.

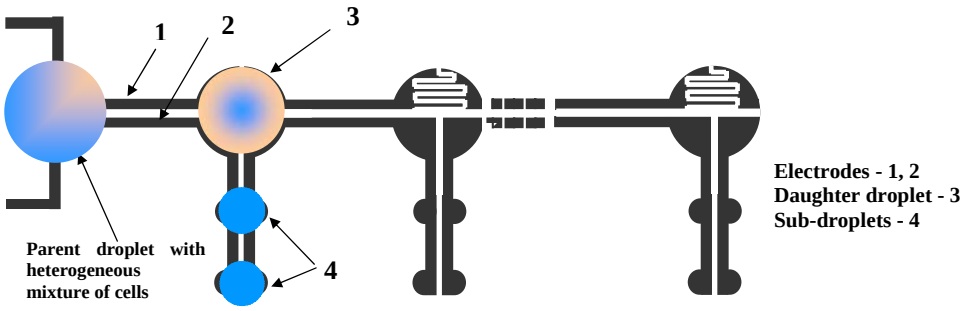

Figure 8. A schematic diagram of surface fluidic structure integrating liquid and particle DEP [20].

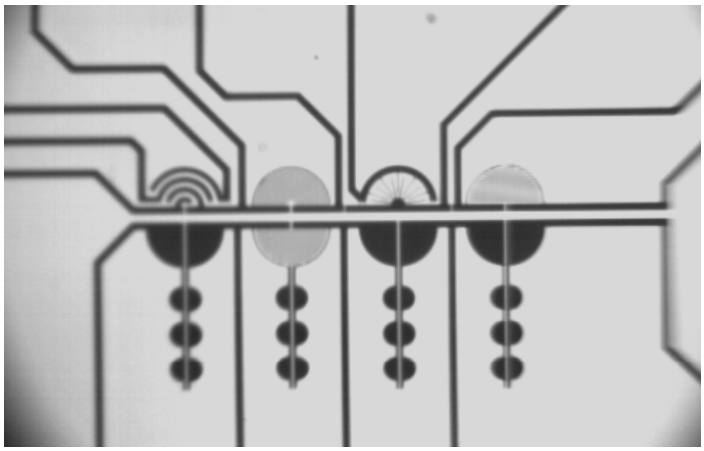

Figure 9. Photograph of the fabricated surface fluidic structure for the combined DEP manipulation of liquid parent droplet and particle within the daughter droplets. Four different electrode arrangements are incorporated in the structure for DEP manipulation of particles.

To verify the particulate DEP effects on open droplets, sample media containing yeast cells (Saccharomyces Cerevisiae) placed directly on the bump region. An AC voltage of 2.47 V_{RMS} was applied at 600 kHz, yeast cells were observed to be pulled towards the electrodes and furthermore forms pearl chain along the periphery of the bump region due to +Ve DEP effect (Fig. 10a). However, at frequencies above 10 MHz, the same cells were repelled from the electrode periphery (-Ve DEP) as in Fig. 10b. Under –Ve DEP conditions, some cells are trapped within the interdigitated electrodes, this phenomenon though not quantified can be attributed to the smaller electrode gaps resulting in very high particle-particle interaction and thereby forming cell-traps. Cells repelled under –Ve DEP conditions were actuated along the electrodes below the bumps, forming picolitre droplets on the lower bumps.

Since liquid actuation, droplet formation and subsequent particle DEP are achieved in rapid fashion, we are

presently engaged in the integration of near-filed optical sensors to detect the presence of a liquid finger, droplets and particle (cell) at suitable locations in the structure.
The combined liquid actuation with droplet formation and muti-frequency DEP examination of cell suspension sample, as well as providing novel opportunities of providing sample preparation, including sorting, analysing and/or separation of cells.

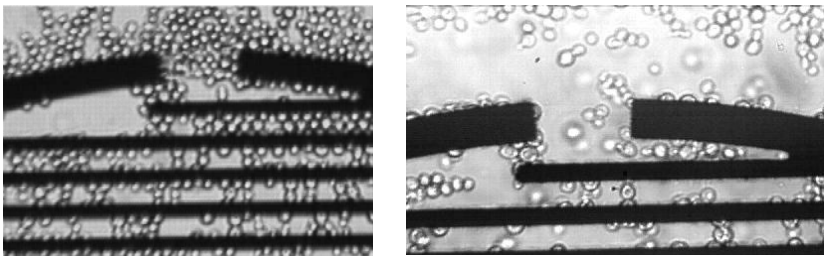

(a) (b)

Figure 10. (a) The +Ve DEP of yeast cells at an applied voltage of 2.47 V_{RMS} and frequency 500 kHz; (b) -Ve DEP of yeast cells at 10 MHz [20].

5. Integration of Liquid/particle DEP with genetic amplification (PCR) and detection

Having demonstrated the particle and liquid handling, we now focus on the integration of other additional liquid handling or processing capabilities necessary to implement genetic amplification utilizing PCR and detection. A fundamental requirement, in addition to thermal cycling, is the mixing of the sample with reagents and buffers. To demonstrated such mixing capabilities we employed DEP liquid actuation to project a finger from the parent droplet housed on top of the coplanar electrodes (see Figure 11) [25]. The electrodes were designed such that they terminated on the edge of a sample well containing PCR mix. The PCR well was coated with Teflon to minimize DNA adsorption and further aided in preventing the liquid in the PCR from forming a finger. Thus once an AC voltage (230V, 100 kHz) was applied to the coplanar electrodes a liquid finger was actuated from the parent drop containing known template DNA and contacted the PCR mix in the well, approximately 10% of the sample DNA was transferred to the PCR well. The chip was then thermal cycled 20 times to amplify the template DNA, transferred by finger actuation into the PCR well. The PCR amplified product was analysed by on-chip capillary electrophoresis to verify the presence of template DNA in the mixed and amplified sample. This is the first demonstration of a microfluidic chip that integrates DEP actuated surface fluidic sample mixing, with conventional closed channel well PCR and CE detection. These finding suggest novel ways of combing the sample preparation afforded by DEP on surfaces with the closed channel amplification and detection on a common substrate.

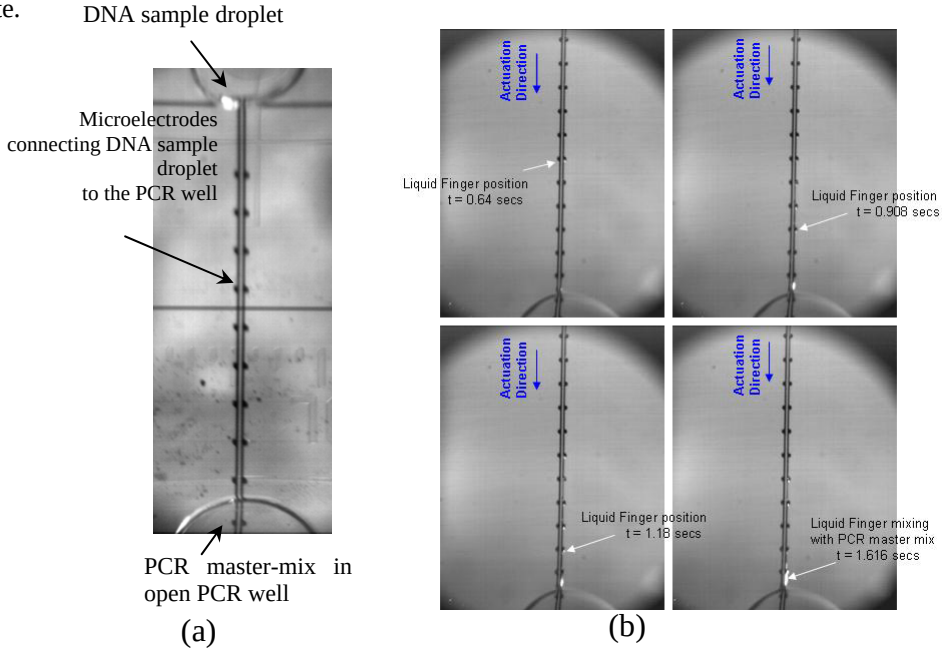

(a) (b)

Figure 11. (a) Liquid mixing structure, showing sample and PCR drops located at the end of the Liquid DEP actuation structure. (b) Time sequence of liquid finger drawn from the sample drop and mixed with PCR drop in an open PCR well [25].

An alternative approach to the liquid DEP actuated mixing, as illustrated earlier, is to utilize a whole droplet actuation scheme. The actuation of small droplets confined on top of coplanar electrodes is readily achieved by coating the surface of the electrodes with a hydrophobic coating, such as Teflon. The dimensions of the electrodes are based on the droplet volume to be actuated. Unlike the liquid DEP assisted mixing, achieved by employing high frequency fields, whole droplet actuation and transport is achieved at much lower field frequencies [26]. To illustrate whole droplet mixing approach, two drops, one larger (5 µL) than the other (1.5 µL) were placed onto at the ends of a coplanar electrode structure, coated with SU-8 + Teflon film (`thickness ~ 1.6 µm). The contact angle of the water droplets on the Teflon coated surface was 110^0. When an AC voltage (93 V_{RMS} @ 90 Hz) is applied, the smaller (1.5 µL) droplet was conveyed (35.62 mm/sec) towards the larger droplet, located at the opposite other end of the electrode structure. As the droplet is transported along the electrode track, it exhibits small lateral oscillations. A time sequence showing such actuation of the whole droplet is shown in Figure 12. The ability to actuate whole microliter sized droplets and successfully mix them is particularly important when dealing with protein and enzyme samples, which tend to rapidly collapse, due to adsorption when placed on hydrophilic surfaces.

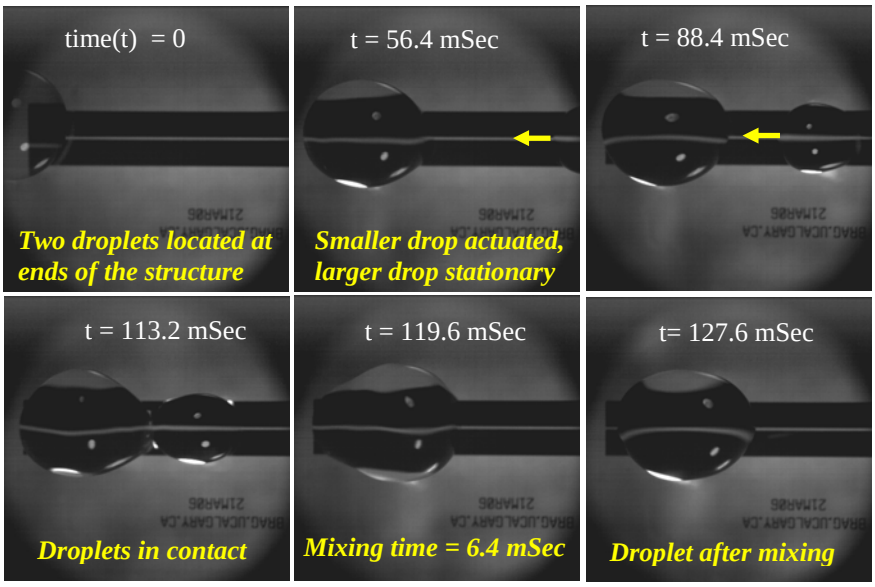

Figure 12. A sequence of photographs, showing the electro-actuation of a µL drop of water. The larger stationary parent drop is mixed with an actuated smaller daughter drop. The details of electrode structure and surface treatment are as follows: Electrode width = 500 µm, Gap = 50µm and Length = 7700 µm; Surface dielectric coating: SU 8-2000.5 + Teflon (~1.6 µm)

6. Conclusion

In this paper we have illustrated both the phenomena of DEP and its practical utility in potential lab-on-chip devices for clinical diagnostic and laboratory applications in the life sciences. These DEP-microfluidic devices provide the on-chip capability of selective and non-invasive manipulation of cells (trapping, levitating, sorting, concentration, purification) in suspension in closed channel microfluidic devices. We have furthermore reviewed new approaches in liquid and particle processing employing DEP forces, generated by co-planar microelectrodes, for combined particle and liquid actuation on top of open surfaces (surface fluidics). This combined liquid/particle processing capability provides unique handling and processing of biological samples in a rapid fashion. We have specifically illustrated this capability in parallel multi-frequency DEP cell fractionation device, which can serve as the front end sample preparation stage of a more complex lab-on-a-chip devices, target for example genetic finger printing and analysis.

7. Acknowledgements

The authors gratefully acknowledge the financial support provide by NSERC, Western Economic Diversification (WED), Canadian Institute for Heath Research (CIHR). We furthermore acknowledge the fabrication support provided by Micralyne Inc and CMC Microsystems, in support of the work presented in this article and the valuable assistance provided by the staff of the U of Alberta Nanofab and the U of Calgary CCIT clean room facility.

References

[1] Kamholz, A.E. (2004) *"Proliferation of microfluidics in literature and intellectual property"*, Lab on a

Chip, **4**(2): pp. 16N-20N.
[2] Kopp, M.U., H.J. Crabtree, and A. Manz (1997) *"Developments in technology and applications of microsystems"*, Current Opinion In Chemical Biology", **1**(3): pp. 410-419.
[3] Manz A., Fettinger J.C., Verpoorte E., Ludi H., Widmer H.M., Harrison D.J. (1991) *"Micomachining of Monocrystalline Silicon and Glass For Chemical-Analysis Systems - A Look Into Next Century Technology Or Just A Fashionable Craze"*, Trac-Trends In Analytical Chemistry **10** (5): pp 144-149.
[4] Koo, J.M. and C. Kleinstreuer (2003) *"Liquid flow in microchannels: experimental observations and computational analyses of microfluidics effects"*, Journal of Micromechanics and Microengineering, 2003. **13**(5): pp. 568-579.
[5] Xuan, X.C. and D.Q. Li (2004) *"Analysis of electrokinetic flow in microfluidic networks"*, Journal of Micromechanics and Microengineering, **14**(2): pp. 290-298.
[6] Hughes, M.P (2002) *"Strategies for dielectrophoretic separation in laboratory-on-a-chip systems.* Electrophoresis, **23**(16): pp. 2569-2582.
[7] Talary, M.S. Burt, J.P.H., Tame, J.A. and Pethig, R.(1996) *"Electromanipulation and separation of cells using travelling electric fields"*, Journal of Physics D-Applied Physics, **29**(8): pp. 2198-2203.
[8] Pethig, R. (1996) *"Dielectrophoresis: Using inhomogeneous AC electrical fields to separate and manipulate cells"*, Critical Reviews in Biotechnology, **16**(4): pp. 331-348.
[9] Li, Y.L. and K. Kaler (2004) *"Dielectrophoretic fluidic cell fractionation system"*, Analytica Chimica Acta, **507**(1): pp. 151-161.
[10] Kaler, K., T.B. Jones, and R. Paul (1995) *"Low-Frequency Micromotions of Dep-Levitated Plant-Protoplasts.1",*. Journal of Colloid and Interface Science, **175**(1): p. 108-117.
[11] Wang, X.B., Yang, J.; H., Y.; Vykoukal, J.; B., F. F.; Gascoyne, P. (2000) *"Cell separation by dielectrophoretic field-flow-fractionation"*. Analytical Chemistry, **72**(4): pp. 832-839.
[12] Rousselet, J., G.H. Markx, and R. Pethig (1998) *"Separation of erythrocytes and latex beads by dielectrophoretic levitation and hyperlayer field-flow fractionation"*, Colloids and Surfaces A-Physicochemical and Engineering Aspects, **140**(1-3): pp. 209-216.
[13] Jones, T. B., 1995 *Electromechanics of particles*, Cambridge University Press.
[14] Pohl, H. A., 1978, *Dielectrophoresis: The behaviour of neutral matter in non-uniform electric fields*, Cambridge University Press.
[15] Kaler K.V.I.S., Xie, J. Jones, T. B. and Paul, R., (1992) *"Dual-frequency dielectrophoretic levitation of canola protoplast"*, J. Biophys. 63 (1), pp. 58-69.
[16] Pellat, H. (1895) *Mesure de la force agissant sur les dielectriques liquides non electrises places dans un champ elitrique"*. C. R. Acad. Sci. Paris, (119): pp. 691-694.
[17] Jones, T.B.(2001) *"Liquid dielectrophoresis on the microscale"*, Journal of Electrostatics, **51**: pp. 290-299.
[18] T. B. Jones M. Gunji, and M. Washizu,, (2001) *"Dielectrophoretic Liquid Actuation and Nanodroplet Formation,"* Journal of Applied Physics, vol. **89**, pp. 1441-1448.
[19] Ahmed, R., Hsu, D., Bailey, C. and Jones, T.B. (2004) *"Dispensing picoliter droplets using dielectrophoretic (DEP) microactuation"*, Microscale Thermophysical Engineering, **8**(3): pp. 271-283.
[20] Thirukumaran T.K., T.B. Jones and KV.I.S. Kaler, *"Droplet-based DEP Microfluidics - High Speed Liquid Actuation on Planar Substrates and Factors Influencing Picolitre Droplet Formation,"* Proceedings of nano2005, vol. 2, pp. 615-622, Sivakasi, India, July 13-15, 2005.
[21] Jones, T.B., *"Dynamics of Dielectrophoretic Liquid Microactuation"*. Proceedings of 4th Int'l Conference on Applied Electrostatics, Dalian, China, 2001.
[22] Youlan Li, Colin Dalton, John Crabtree, Gregory Nilsson and Karan V.I.S. Kaler*, *"Continuous Dielectrophoretic Cell Separation Microfluidic Device"* (manuscript in press).
[23]`Lee Hartley, Karan V.I.S. Kaler, Orly Yadid-Pecht, "Hybrid Integration of an Active Pixel Sensor and Microfluidics for Cytometry on a Chip" TCAS-I Special Issue Smart Sensors (In press).
[24] Thirukumaran T. Kanagasabapathi, Christopher J. Backhouse and Karan V.I.S. Kaler, *"Dielectrophoresis (DEP) of Cells and Microparticle in PDMS Microfluidic Channels"*, Nanotech 2004, Vo1. 1, pp.81-84.
[25] Thirukumaran Kanagasabathi, A. Ranjit Prakash, Karan V.I. S. Kaler, *"Integration of surface microfluidics to closed-channel fluidics for a valveless multi-layer genetic analysis chip"* µTAS 2006, Nov, 2006, Tokyo Japan.(paper accepted).
[26] M. Gunji and M. Washizu,(2005) "Self-propulsion of a water droplet in an electric field," Journal of Physics D-Applied Physics, Vol. 38, pp. 2417-2423.

IN VITRO EXPERIMENTS TO ASSESS ELECTROMAGNETIC FIELDS EXPOSURE EFFECTS FROM RFID READER/WRITER FOR PACEMAKER PATIENTS

S. FUTATSUMORI[1], T. HIKAGE[1], T. NOJIMA[1], B. KOIKE[2], H. FUJIMOTO[3], T. TOYOSHIMA[3]

[1]GRADUATE SCHOOL OF INFORMATION SCIENCE AND TECHNOLOGY, HOKKAIDO UNIVERSITY
KITA 14, NISHI 9, KITA-KU, SAPPORO, HOKKAIDO, 060-0814 JAPAN

[2]JAPAN AUTOMATIC IDENTIFICATION SYSTEMS ASSOCIATION
1-9-5 IWAMOTO-CHO, CHIYODA-KU, TOKYO, 101-0032 JAPAN

[3]MEDTRONIC JAPAN CO., LTD.
SOLID SQUARE WEST TOWER, 580 HORIKAWA-CHO, SAIWAI-KU, KAWASAKI, KANAGAWA, 210-0913 JAPAN

Abstract
Today, the use of implantable cardiac pacemakers has become more widespread and more than 50,000 devices are implanted in Japan per year as of 2005. Implantable cardiac pacemaker patients are excluded from the recommended electromagnetic fields (EMF) level of guidelines such as ICNIRP reference levels. Recently, many communication devices including Radio Frequency Identification (RFID), Electronic Article Surveillance (EAS), and contactless IC cards have been introduced to our daily lives. They are expected to achieve more widespread applications. Accordingly, the assessment of EMF exposure limits for pacemaker patients should be required to complement the EMF safety guidance.
In this paper, electromagnetic interference (EMI) from commercially available RFID reader/writers on implantable cardiac pacemakers and cardioverter-defibrillator (ICD) were investigated. The newly constructed in-vitro experimental test system based upon an Irnich's flat torso phantom was applied. EMI test experiments on 10 types of RFID reader/writers and 13 types of implantable pacemakers and ICDs were conducted. Frequency bands were 125 kHz and HF (13.56 MHz), as well as UHF (950 MHz) and 2.45 GHz. In addition, electromagnetic field distributions of RFID reader/writer antennas were measured in detail. Finally, results of in-vitro EMI test experiments were introduced and characteristics of interferences were discussed.

Introduction
ICNRP guidelines for limiting human exposure were published in 1998 for the purpose of protecting electromagnetic fields (EMF) effects for health [1]. These guidelines include reference levels for occupational and general public exposures. However, these guidelines do not apply to people who wear implantable medial devices. To prevent electromagnetic interference (EMI) on the functions of these devices, it is necessary to find out the conditions which cause malfunctions. A lot of research is being carried out with an increasing in the use of wireless communication devices. In particular, EMI due to mobile phone systems are investigated precisely [2]-[8]. In Japan, guidelines to prevent the EMI is provided and operated under technical report [7].

Radio frequency identification (RFID) technologies are assumed to have widespread application as an automatic recognition method in ubiquitous networks. Scope of the technology includes product management and identification instead of the conventional barcode technology. RFID systems are essential devices to achieve future ICT society.

Several frequency bands, some modulation methods and many types of antenna are employed for RFID systems. For the various types of systems, the effect on implantable cardiac pacemakers and implantable cardiac-defibrillators (ICD) patients should be precisely taken into account. Table. 1 indicates ICNRP reference levels at operating frequency bands of RFID systems. In order to assess the EMI from RFID systems, EMF strengths which cause effects for operations of these devices are required to be examined from experimental and measured results. Then, these threshold field strengths can be compared with the reference levels.

Table 1
ICNRP reference levels for general public exposure to time-varying electric and magnetic fields.
Field strength at RFID operating frequency bands.

Frequency bands	E-field strength (V/m)	H-field strength (A/m)	B-field (μT)
125 kHz	87	5	6.25
HF (13.56 MHz)	28	0.073	0.092
UHF (950 MHz)	42	0.11	0.14
2.45 GHz	61	0.16	0.20

In this paper, in-vitro experiments to assess the electromagnetic field effects due to RFID reader/writers on both pacemakers and ICDs patients are discussed. First, test experiments to obtain EMI characteristics of pacemakers and ICDs are investigated. Combinations of 13 types of implantable devices and 10 types of commercially produced RFID reader/writers are tested using a newly developed test system. Secondly, to obtain the field strength for the estimation of EMI, radio waves from RFID reader/writer antennas are measured precisely. Finally, experimental results are introduced and characteristics of the EMI are discussed.

In vitro electromagnetic interference test experiments

To obtain EMI data and characteristics of RFID reader/writer antennas, test experiments on 10 types of commercially available antennas and 13 types of pacemakers and ICDs are carried out. Tested pacemakers and antennas are shown in Table 2 and Table 3. Pacemakers and ICDs have many operating modes and functions - pacing/sensing polarity, single/dual chamber mode, and antitachycardia functions. The total test mode is 768 modes at different function modes, frequency bands and RFID reader/writer antennas.

The test system is based upon the previously proposed one for the estimation of EMI due to mobile phones described in [2], [3], [5] and [10]. The system is also employed in EMI test experiments reported by Ministry of Internal Affairs and Communications (MIC) of Japan [8] and [9]. The test system consists of a flat human torso phantom, an electrocardiogram (ECG) signal generator/detector, a chart recorder, an oscilloscope, a measurement platform and a RFID reader/writer antenna as shown in Fig. 1, Fig. 2 and Fig. 3.

The torso phantom used in this experiment is some modifications of Irnich's model in the reference described above. Both atrial and ventricular electrode are improved which enables us to separate each chambers' ECG signal levels of more than 20dB. It is therefore taking advantage to examine EMI with low interference by another chambers' signal. In addition, the size of the phantom is slightly different. The tank of the phantom is made of acrylic material and filled with a saline solution (NaCl 1.8g/L). At low frequency, the saline solution provides same electric conductivity 0.2 S/m as human bodies. This means ECG signals between lead wire of a pacemaker and electrodes go through without direct connection. In addition, it is known this concentration of saline solution gives less attenuation constant than actual human body at radio frequency [5]. The torso phantom is suitable for the EMI test experiment, because it allows more conservative results for EMI estimations.

RFID systems are typically operated at the frequency bands - 125 kHz, HF (13.56 MHz), UHF (950 MHz) and 2.45 GHz, as shown in Table 3. Furthermore, these antennas usually have different shapes, locations and radiating fields depending on their purpose, operating frequency bands and their manufacturers. Moreover, positions between a human torso phantom and RFID reader/writer antennas must be determined precisely and be variable. It is required to measure the EMI due to various antennas with accuracy and repeatability. The two-axis sliding measurement platform shown in Fig. 2 enables us to measure RFID antennas moving parallel to the torso phantom (*y*-axis direction), while maintaining the same distance between the phantom and antennas (*x*-axis direction). All parts of this platform are made of dry wood. This system has advantages of high efficiency and data obtained can be reliability assessed.

The number of each RFID system is shown in Table 3. 125 kHz and HF band RFID systems employ amplitude-shift keying (ASK) as modulation method. HF band systems are also compliant with ISO/IEC15693 international standard [11]. In addition, modulation method of UHF band and 2.45 GHz RFID systems are double sideband (DSB) ASK or single sideband (SSB) ASK and frequency hopping spread spectrum (FHSS) or ASK, respectively. EPC Class 1 Generation 2 [12] for UHF band, ARIB STD-T81 [13] or RCR STD-1 [14] for 2.45 GHz are applied as specifications, respectively. In lower frequency bands such as 125 kHz and HF band, an inductive coupling between reader/writer antennas and tags realize their communications. On the other hand, the UHF band and 2.45 GHz systems use electromagnetic waves to communicate with each other. Owing to this dissimilarity, the test procedure introduced in the next section is different.

Table 2
Pacemakers and implantable cardioverter-defibrillators.

Tested devices	Type of chambers	Number of devices
Pacemaker	Single chamber	5
	Dual chamber	5
Implantable Cardioverter-Defibrillator	Single chamber	1
	Dual chamber	2
Total		13

Table 3
RFID reader/writer antennas.

Frequency bands	Modulation methods	Number of antennas
125 kHz	ASK	4
HF (13.56 MHz)	ASK	2
UHF (950 MHz)	DSB-ASK or SSB-ASK	2
2.45 GHz	FHSS or ASK	2
Total		10

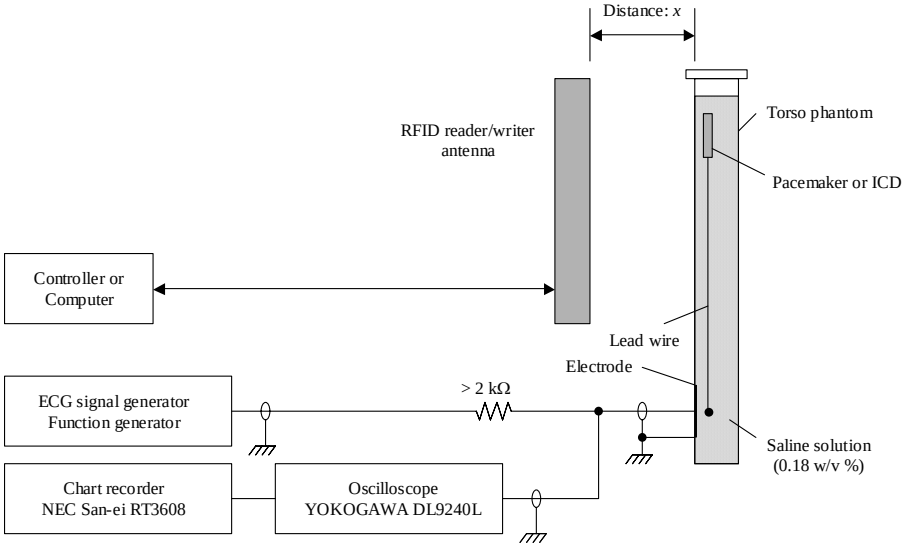

Fig. 1. Configuration of the test system.

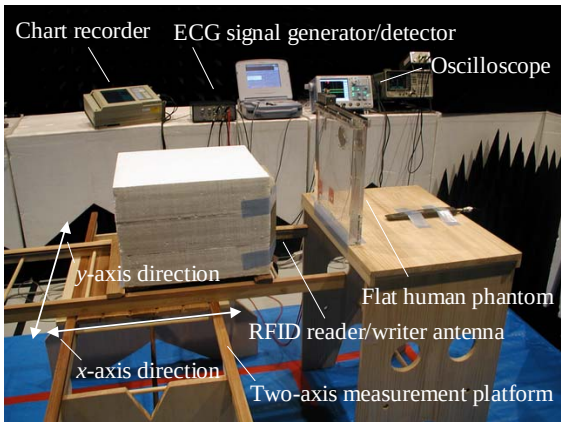

Fig. 2. Overall view of the in-vitro experimental system.

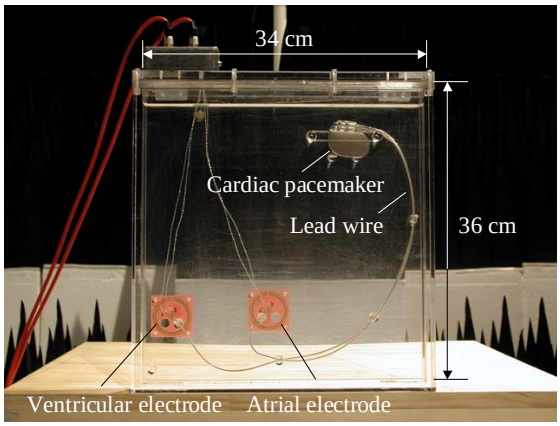

Fig. 3. The human torso phantom.

The in-vitro EMI test experiments procedure is explained as shown in Fig. 4. First of all, in order to obtain most conservative results, both sensitivity and refractory period of pacemakers and ICDs are programmed to maximum sensitivity and minimum time, respectively. Second, configurations of RFID reader/writers are prepared to actual operating mode. The next step depends on frequency bands of RFID reader/writer. EMI of 125 kHz and HF band are assumed to be caused by induced voltage, which follows Faraday's law of induction [4]. Malfunctions may happen when ”an inductor coil” composed of lead wire of pacemakers and ICDs receive changing magnetic field radiated from RFID reader/writer antennas. Because of this mechanism, interferences are examined while the phantom is exposed to changing magnetic field. Antennas are moving in *y*-axis direction (as shown in Fig. 2) and closely attached to the torso phantom. EMI of UHF band and 2.45 GHz band occurs due to direct coupling between antennas and terminals of pacemakers and ICDs [4]. Interference is investigated while the antenna is located at a fixed position and closely attached to the torso phantom.

Then, the ECG signal for each mode is recorded on the paper for 100 seconds. In addition, the distance between antennas and the torso phantom (*x*-axis direction in Fig. 3) is increased when interference occurs. In this case, the maximum interference distance (distance where EMI disappears) is found out and recorded in centimetres. As long as interference exists, sensitivity of pacemakers and ICDs are stepped down to five levels (maximum, 1.0 mV, 2.4 mV, 5.6 mV, minimum) and the maximum interference distance is also recorded. Breakdowns of the EMI test modes and settings are shown in Table 4.

Operating modes of pacemakers and ICDs are VVI mode (the Ventricle chamber is paced, the Ventricle chamber is sensed, and the response to sensing is Inhibited) and AAI mode (the Atrium chamber is paced, the Atrium chamber is sensed, and the response to sensing is Inhibited). In addition, unipolar and bipolar modes are chosen to their sensing/pacing polarity. For each of the operating modes, there are two types of EMI test modes are conducted - one with an injected ECG signal (typical inhibition), and one with no injected ECG signal (typical asynchronous pacing). With ICDs, there are two additional test modes. False Positive mode (one with no injected ECG signal and false detection of fibrillation), and False Negative mode (one with injected ECG signal and false non-detection of fibrillation) are investigated. The EMI test experiments are conducted in a closed, electromagnetic shielded anechoic chamber in Hokkaido University.

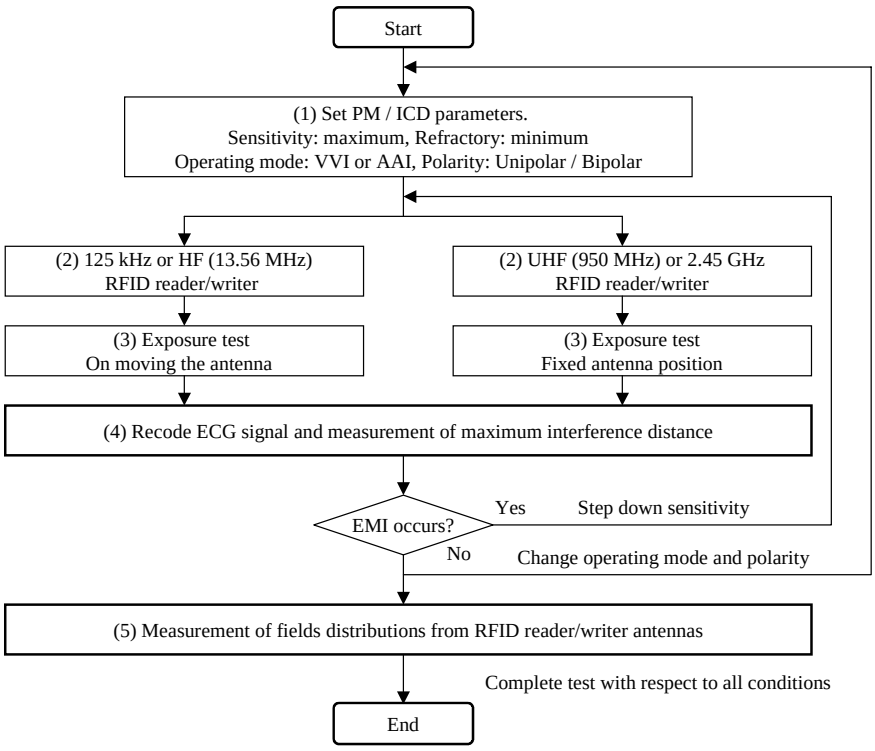

Fig. 4. In-vitro EMI test experiments procedure.

Table 4 EMI test modes and settings.

EMI test modes		Inhibit		Asynchronous		Inhibit		Asynchronous		False Positive	False Negative	Total Modes
PM/ICD Operating modes		VVI		VVI		AAI		AAI		AAI	AAI	
PM/ICD Sensing/Pacing Polarity		UNI	BI	UNI	BI	UNI	BI	UNI	BI	BI	BI	
RFID Reader/writer Frequency Bands	125 kHz	28	40	28	40	32	40	32	40	20	20	320
	HF (13.56 MHz)	14	20	14	20	16	20	16	20	10	10	160
	UHF (950 MHz)	16	20	16	20	12	12	12	12	4	4	128
	2.45 GHz	14	20	14	20	16	20	16	20	10	10	160
Total modes		72	100	72	100	76	92	76	92	44	44	768

PM: Pacemaker, ICD: Implantable cardioverter-defibrillator

UNI: Unipolar, BI: Bipolar

Finally, measurements of field distributions described in the next section are carried out. The measurement area is determined based on the experimental results. In order to find out the correlation between obtained EMI data and field strength, precise measurement is required.

Field distribution measurements of RFID reader/writer

To obtain detailed data to clear up correlations between EMI and EMF strength, field distributions of RFID reader/writers antennas are measured. Both electric and magnetic fields are determined for all RFID reader/writers antennas shown in Table 3. The reason for this is a near field of the antennas is not proportioned to each other. For 125 kHz and HF band, measurement of 729 sample points which include 70 cm × 70 cm × 70 cm (width × height × depth) at 10 cm separation are carried out. In addition to this wide area measurement, we examined more fine separation for the depth direction (*x*-axis direction in Fig. 2). We measure 1029 sample points which include 70 cm × 70 cm × 20 cm (width × height × depth) at 1 cm separation for the depth direction. Figure 6 shows the probe positioners for low frequency bands, which is made of styrene foam. This positioner enables reliable measurement taking the advantages of low reflection or absorption of EMF. Electric field probe EMR-300 (Wandel & Goltermann GmbH, Germany) and magnetic field probe 11941A (Agilent technologies Inc., Palo Alto, CA, USA) are used. For the UHF band and 2.45 GHz, measurements of 3459 sample points are also performed. These measurements include the area of 36 cm × 36 cm × 20 cm (width × height × depth) at 3 cm separation for the width and height direction and at 1cm separation for the depth direction. Electric field probe IXP-050 (IndexSAR Ltd., Newdigate, England) and magnetic field probe 7405-903 (ETS-Lindgren, Cedar Park, TX, USA) are employed.

Figure 6 is a typical 3-dimensional magnetic field radiated from a HF band antenna. In addition, differences of field strength radiated from 4 types of 125 KHz antennas are shown in Fig. 7. This figure indicates 1-dimensitonal magnetic field strengths at the central axis of the antennas. Values of *y*-axis are normalized to the maximum field strength out of 4 types of antennas.

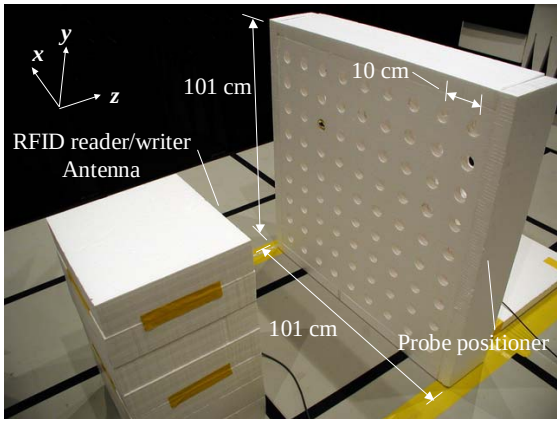

Fig. 5. The probe positioner for low frequency bands. 125 KHz and HF band.

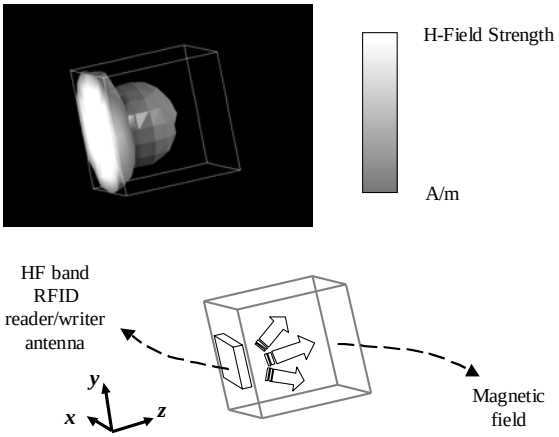

Fig. 6. Typical 3-dimensional magnetic field distribution from a HF band antenna.

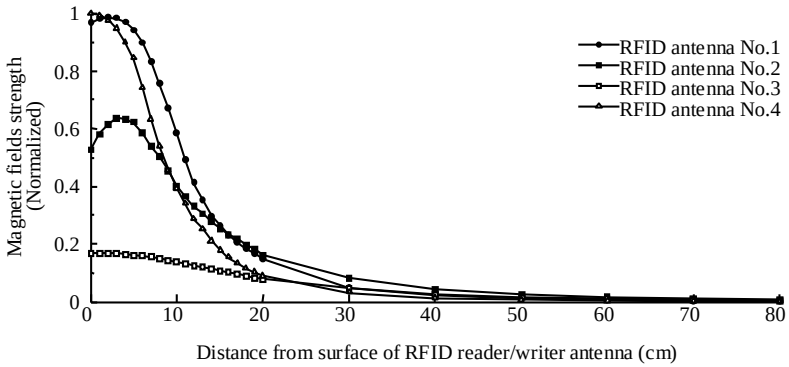

Fig. 7. 1-dimensional magnetic field distributions of 125 KHz RFID reader/writer antennas. Magnetic field strength on the central axis of antennas.

Results & Discussions

First, results of the EMI test experiments are discussed. A total of 768 test modes are used in the experiments. As shown in Fig. 8, 107 modes are affected when pacemakers and ICDs are programmed to maximum sensitivity. Therefore the affected rate is about 14 %. Under these conditions, the maximum interference distance is 15cm. In addition, when the sensitivity is stepped down to minimum sensitivity, the affected mode and rate are 26 modes and about 3 %, respectively. The maximum interference distance of this sensitivity is 11 cm. From this EMI test experiment, when the radio wave from antennas are continuous wave or do not have time-varying envelope curve, no malfunctions happen on pacemakers and ICDs. On the other hand, if they are exposed to changing fields such as pulse modulated wave or changing magnetic field due to movement of antennas, probability of the EMI occurrence is much higher than another condition.

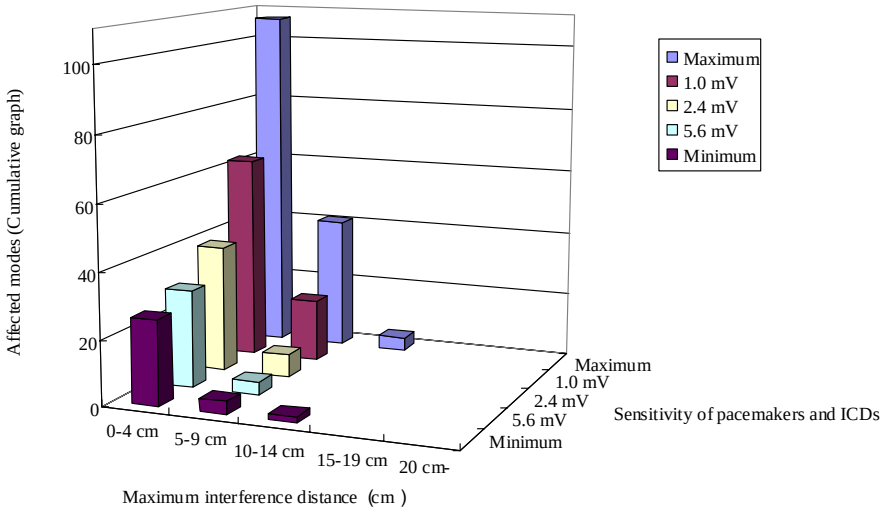

Fig. 8. The results of in-vitro EMI experiments.
Affected modes (Cumulative) and maximum interference distance
depending on sensitivity of pacemakers and ICDs.

Summary

In this paper, to assess the EMF fields' exposure effect from RFID reader/writer antennas, field strengths which cause effects for these implantable devices operations were examined from experimental and measured results. First, EMI due to commercially available RFID reader/writers on pacemakers and ICDs were investigated using newly constructed in-vitro experimental test system. This system was based upon an Irnich's flat torso phantom. In vitro EMI test experiments on 10 types of RFID reader/writers and 13 types of implantable pacemakers and defibrillators were conducted. The frequency bands were 125 kHz, HF (13.56 MHz), UHF (950 MHz) and 2.45 GHz. Secondly, EMF distributions of RFID reader/writer antennas were measured in detail. Finally, results of EMI test experiments were introduced and characteristics of interferences were discussed.

The correlation between the EMI test experiments results and field strength radiated from RFID reader/writers are now being investigated in detail. Further results and discussions are shown in later.

Acknowledgement

The authors would like to thank the members of the Pacemaker Committee of Japan and Japan Automatic Identification Systems Association for their cooperation and support.

References

[1] International Commission on Non-Ionizing Radiation Protection (ICNIRP), "Guidelines for limiting exposure to time-varying electric, magnetic and electromagnetic fields (up to 300 GHz)," Health Phys., vol.74, pp.494-522, 1998.

[2] W. Irnich, L. Batz, R. Muller, and R. Tobisch, "Electromagnetic interference of pacemaker by mobile phones," PACE, vol. 19, pp.1431-1446, Oct. 1996.

[3] V. Barbaro, P. Bartolini, A. Donato, and C. Militello, "Electromagnetic interference of analog cellular telephone with pacemakers," PACE, vol. 19, pp. 1410-1418, Oct. 1996.

[4] T. Toyoshima, M. Tsumura, T. Nojima, and Y. Tarusawa, "Electromagnetic interference of implantable cardiac pacemakers by portable telephones," Japanese journal of cardiac pacing and electrophysiology, vol. 12, no.5, pp. 488-497, 1996.

[5] Y. Tarusawa, K. Ohshita, Y. Suzuki, T. Nojima, and T. Toyoshima, "Experimental estimation of EMI from

cellular base-station antennas on implantable cardiac pacemakers," IEEE Trans. Electromagn. Compat., vol. 47, no. 4, pp.938-950, Nov. 2005.
[6] T. Nojima, and Y. Tarusawa, "A new EMI test method for electronic medical devices exposed to mobile radio wave," IEICE trans. Commun., vol.E88-B, no.1, pp. 11-18, Jan. 2001.
[7] Guidelines on the use of radio communication equipment such as cellular telephones - Safeguards for electric medical equipment, presented at the EMC Conf. Japan, Electromagnetic Medical Equipment Study Group, 1997.
[8] Investigation and research report of electromagnetic interference on medical devices (in Japanese), Ministry of Internal Affairs and Communications (MIC) of Japan, Mar. 2005.
[9] Investigation and research report of electromagnetic interference on medical devices (in Japanese), Ministry of Internal Affairs and Communications (MIC) of Japan, Mar. 2004.
[10] Active Implantable Medical Device - Electromagnetic Compatibility - EMC Test Protocols for Implantable Cardiac Pacemakers and Implantable Defibrillators, AAMI Standard PC69, 1999.
[11] ISO/IEC15693: Identification cards - Contactless integrated circuit(s) cards - Vicinity cards - Part1 : Physical characteristics, International Organization for Standardization, 2000.
[12] EPC Radio-Frequency Identity Protocols Class-1 Generation-2 UHF RFID Protocol for Communications at 860 MHz-960 MHz, Version 1.0.9., EPCglobal, Inc., 2005.
[13] Standard ARIB STD-T81: 2.4GHz-Band RFID Equipment Using Frequency Hopping System for Specified Low Power Radio Station, Association of Radio Industries and Businesses, Japan, 2006.
[14] Standard RCR STD-1: 2.4GHz-Band RFID Equipment for Premises Radio Station, Association of Radio Industries and Businesses, Japan, 2006.

7 HZ ELECTROTHERAPY FOR THE TREATMENT OF SKIN UNDIFFERENTIATED DESEASES

ALBERTO FOLETTI M.D.[1] MARIO LEDDA[2] , EMANUELA ROSOLA[2] , ANTONELLA LISI[2], ENRICO D' EMILIA[4] , SETTIMIO GRIMALDI [2],

[1]Quantech – Milan, Italy
[2]Istituto di Neurobiologia e Medicina Molecolare CNR –Rome, Italy
[4]ISPESL DIPIA Rome Italy

Corresponding Author:
Settimio Grimaldi
Istituto di Neurobiologia e Medicina Molecolare–Consiglio Nazionale delle Ricerche
Via Fosso del Cavaliere 100, 00133 Rome, Italy
Phone 39 06 49934230; Fax 39 0649934231
E-Mail settimio.grimaldi@artov.inmm.cnr.it

Running Title: Effect of electric field on keratinocytes
Key words: NIR, growth differentiation, keratinocytes.

Abstract

Electrotherapy is a treatment method in which an electric stimulus is used to achieve physiological changes in the body.
The specific aim of the present work concerns the effectiveness of low frequency electric fields treatment to modify biochemical properties of human keratinocytes (HaCaT).
Cells exposed to a 7 Hz electric field for one hour (twice daily), showed by Scanning Microscopy modification in shape and morphology; these modifications were also associated to different actin distribution revealed by phalloidin fluorescence analysis.
Indirect immunofluorescence with fluorescent antibodies against involucrin and β catenin, both differentiation and adhesion markers, revealed an increase in involucrin and β catenin expression, supporting that exposure to electric field carries keratinocytes to an upper differentiation level.
Such study confirmed our previous observation and support the hypothesis that 7 Hz electric field, may modify cell biochemistry and interfere in differentiation and cellular adhesion of normal keratinocytes.

INTRODUCTION

In the last twenty years there has been an increasing interest to investigate the possible effect of extremely low frequency (ELF) electric and magnetic fields (Chiabreara 1985, Zhadin 2001) on human health. The experimental approach to the electromagnetic field (EMF) effects on living systems is complicated by various reported non linearities (intensity, frequency and time windows of the fields) and peculiarities (cell type, age, treatment) so that extrapolation or replications among laboratories can hardly be made. The possible mechanisms of the induced effects are still not known, although a number of theoretical models have been proposed (Glaser 1992, Liburdy 1992, Barnes 1996,). This may be partially due to the difficulties in demonstrating reproducible results.
The aim of the present work is to clarify the action's mechanism at cellular level of an electrotherapy procedure performed by an electro-medical device still in clinical use and so easily reproducible in each bio-physical setting like frequency, intensity and exposure's time.
Moreover a second aim of this work is to validate the effectiveness of the current clinical application protocols.
This work concerns the effect of 7 Hz electric field exposure on morphological and biochemical properties of normal human keratinocytes.

Human skin and mucosa, majorly constituted of keratinocytes, are the most exposed cells to the impact with electromagnetic radiation.
Keratinocytes are so an ideal model to analyse the biological effects of non ionising electromagnetic field, because they are the first cells to which the energy associated to the radiation, will directly be transferred.
HaCaT are epithelial cell line, ideal to understand if a physical agent such as electric field exposure (7 Hz) can interfere with cell morphology, biochemistry and modulate keratinocytes differentiation.
Our results indicate that two ours exposure daily to 7 Hz electric field could be responsible to a different morphological and cytoskeletal assept on HaCaT, together with the increase in involucrin expression, suggesting that EMF takes such cells at an upper differentiation level.
This data strongly support the efficacy of 7 Hz therapy for the treatment of skin deseases as well as a co adjuvant in the therapy of undifferentiated deseasaes.

MATERIALS AND METHODS

Cell Cultures

Cells were grown in Serum Free Medium (GIBCO Laboratories, Scotland) supplemented with antibiotics (110 IU /ml of penicillin and 100 μg/ml of streptomycin) at 37 ± 0.3 °C, 5% CO_2, and sub-cultivated once a week at a 1:3 ratio.

Exposure System.

The flask containing cells were placed between two electrode and exposed twice daily for 1 hours to a 7 Hz electric field at 100mV in a cells incubator under controlled condition (37 °C and 5% CO_2).
As a control experiment other sample of the same cells was placed in the cell incubator with no field, in the same conditions of the exposed one.
No differences were detected between control and sham cells.

Immunofluorescence Assay

HaCaT cells were cultured in SFM medium, starting at a concentration of 6 X 10^5/ml. Exposed cells were cultivated in the same conditions in the exposure system at 7 Hz electric field for 72 hours. Cells were washed, air dried, fixed in paraformaldeide 4% in PBS for 15 minutes and tested by indirect immunofluorescence for the presence of involucrin, β catenin. Antibody against involucrin (Sigma) was used at 1:100 dilution, anti β catenin (Calbiochem) at a 1:500 dilution. After 45 minutes incubation in primary antibody, the slides were washed three times with PBS, dried and stained with fluorescein –isothiocyanate-conjugated goat antiserum to human immunoglobulin G (Amersham) at a dilution of 1:200. After further incubation for 45 minutes the slides were washed and examined by fluorescence microscopy. Four different sets of experiments were performed.

Electrophoresis

SDS-polyacrylamide gel electrophoresis (SDS-Page) was carried out according to Laemmli, 1970 . After 72 hours exposure to electromagnetic fields, equal amount of cell proteins from control and exposed cells , measured by Lowry test, were loaded for each line, after lysis in sample buffer. The samples were boiled for 5 minutes . Electrophoresis was carried on 7.5% SDS polyacrilamide gel at 30 mA for about 2 hours. Gel was subsequently transferred on nitrocellulose membrane (Biorad) at 200 mA for 3 hours, and membrane, after blocking in 3% not dried fat milk for 1 hours at room temperature, was incubated with EGF receptor antibody (Sigma) at a dilution of 1:100 as suggested by manufacturer and revealed by ECL (Amersham).
Three different sets of experiments were performed.

RESULTS

Indirect Immunofluorescence microscopy of modulation of Involucrin, and β-Catenin expression after exposure at 7 Hz electric field

The effect of EMF exposure on HaCaT cell expression of differentiation (Involucrin) and adhesion (βCatenin) markers is respectively reported in Tab and Fig. 1.
Exposed HaCaT cells showed an apparent increase in cells becoming positive to involucrin expression after field exposure compared to control cells. The increase in Involucrin positivity can suggests that 7 Hz HaCaT exposed cells were driven to an upper differentiation level.
As reported for the involucrin experiment also βCatenin seems to be more evident in cells after fiels exposure. The amount of cells positive to β Catenin and involucrine by indirect immunofluorescence is reported in Tab.1

The increase in β Catenin positivity in 7 Hz electric field exposed HaCaT cells, indicates a major cellular adhesion capacity compared to control cells.
Western blot analysis of both involucrin and β Catenin after 7 Hz exposure is reported in Fig. 1. The amount in both proteins seems to be affected by the treatment with the electric field.

DISCUSSION

In the last two decades, reports of biological effects of low-energy EMF have been increasing (Adey 1993, Pilla 1992, Hinsenkamp 1997). Particularly debated is the question of the epidemiological evidence (14) of adverse effects of an extremely low frequency magnetic field (ELF) generated by 50-60 Hz high voltage power transmission lines, video display terminals, electric blankets and other home appliances, which raise the possibility of deleterious health effects (Adey 1981) from exposure to radio frequency (Tenforde 1995) or low frequency fields (Savitz 1987). A valid objection is that field intensity is many orders of magnitude below the noise threshold so that selective, cooperative, or amplifying mechanisms must be postulated. There also problems of reproducibility of reported effects. The therapeutic potential of ELF can be seen in the proven efficacy of low-energy, pulsed magnetic fields in non-union bone fracture healing (Weaver 1990), confirming that under certain conditions non-ionising electromagnetic energy can influence physiological processes in organisms (Kaiser 1988). Physiological paradigms for ELF effects are required. Clues may be found in the mechanisms by which ELF interacts with cultured cells under controlled laboratory conditions and by correlating in vivo evidence with in vitro data (Glaser 1992). Low frequency magnetic fields at 50 or 60 Hz are also reported to stimulate nerve regeneration (Phillips 1992) or alter gene transcription. They may also play a synergic role in cellular processes that are already activated, such as cell proliferation (Walleczeck 1992). The role of Ca^{2+} in the transduction of these effects has been suggested, and indirect evidence of its involvement has been shown (Karabachtsian 1994).
In our work we analysed the effect of 7Hz ELF therapy on human epithelial cell line (HaCaT). Epithelial cells are an interesting model to study the biological effect of the interaction with non-ionising radiations, are not shielded by any other stratum of cells in the impact with electromagnetic radiation, and so they are totally available to the field.
Human keratinocytes cells are also a very good model to investigate the epithelial switch between proliferation and differentiation (Medema 1994).
The effect of 7 Hz exposure on HaCaT cells by ultra microscopy (data not shown), at cells confluency showed a modified morphological aspect: they are bigger and more elongated than controls. Exposed cells lost filopodia, and show a higher number of lamellipodia, specialized structures for cell-cell contact. The augment of cell-cell contact junctions , is also supported by the different distribution in β-Catenin as reported in and Tab.1.
β-Catenin is a protein implicated in cell-cell-adhesion, binding cytoplasmic domain of cadherin, and in signal transduction (Szabo 2001, Vasioukin 2001).
Cell adhesion molecules and their association with actin cytoskeleton play an important role not only in the maintenance of tissue integrity, but also in proliferation and differentiation .
Exposure to the field also causes rearranging of actin filaments (data not shown), leading to an increase in actin expression and in formation of stress fibres that cross parallel to the elongated cells.
Since modification of cellular growth rate and gap junction number with the consequent cytoskeleton rearrangement are implicated in cells transformation (Hsu 2000) we analysed the expression of involucrin as a differentiation marker of keratinocytes (Batta 2000). In human epidermis, involucrin is first observed in the cytoplasm of spinous and granular layer cells. In transition cells, it is equally distributed between the cytoplasm and the nascent corneified envelope, while in the corneocytes it is largely corneified envelope associated. In our experiments involucrin and epecially β catenin expression in the exposed cells, is increased compared to control. (Fig .1). Since involucrin is a keratinization-associated molecules our observation may suggest that the exposed cells are at an upper differentiation level than controls..
This is a very important point suggesting a possible application of electrotherapy in the therapy of skin proliferative diseases. It would be very interesting, for example, to analyse the possibility of using electrotherapy as non invasive chemoterapic agent. Other authors have just reported therapeutical effects of electromagnetic radiation for clinical aims (Basset 1993, Leszczynski 2001, Pletnev 2000).
In summary, 7Hz electric field induces an alteration of growth and differentiation pattern on HaCaT cells. The modification of morphology, cytoskeletal assept, and expression of adhesion and differentiation markers confirm our previous data that exposed cells are at an upper differentiation level.
Our results strongly suggests the possibility to use physical agents such as electric or electromagnetic field, in support to chemiotherapy to fight epithelial proliferation diseases, as well as all the deseases in which cells are characterized to a lower differentiation state

LEGENDS

Tab.1 7 Hz Electric Field modulation of Involucrin and β Catenin by Indirect Immunofluorescence Microscopy.

Tab 1 shows modulation of involucrin and β Catenin expression in control and exposed cells.

Experiment is representative of cells at 72 hours growth and exposure.

Figure 1. Western Blotting of β Catenin and Involucrin

In the first (left) lane: proteins extracted by control cells, in the second (right) lane: proteins extracted by 7 Hz, exposed cells. The amount of proteins inoculated is the same for control and exposed samples, quantitated by Lowry test.

REFERENCES

Adey W.R: Tissue interaction with non-ionizing electromagnetic field. Physiological Review, 61: 435-514, 1981.

Adey W.R: Biological effects of electromagnetic fields. J Cell Biochem 51(4): 410-6, 1993.

Barnes P.S.: Effect of electromagnetic field on the rate of chemical reactions. Biophysics, 41: 801-808, 1996.

Basset C.A.L: Beneficial effects of electromagnetic fields. Journal of Cellular Biochemistry, 51: 387-393, 1993.

Batta K., Rugg E.L., Wilson N.J., West N., Goodyear H., Lane E.B., Gratian M., Dopping-Hepenstal P., Moss C., Eady R.A. A keratin 14 'knockout' mutation in recessive epidermolysis bullosa simplex resulting in less severe disease. Br J Dermatol, 143(3): 621-7, 2000.

Chiabrera A., Nicolini C., Schwan H.P.: Interactions between electromagnetic fields and cells. In Chiabrera eds, Plenum, New York, 1985.

Dominey A.M., Wang X.J., King L. jr, Nanney L.B., Gagne T.A., Sellheyer H., Bundman D.S., Longley M.A., Rothnangel J.A., Greenhalg D.A., et al. Targeted over expression of transforming growth factor alpha in the epidermis of transgenic mice elicits hyperplasia, hyperkeratosis, and spontaneous, squamous papillomas. Cell Growth Differ., 4: 1071-1082, 1993.

Fukunaga M., Oka M., Ichihashi M., Yamamoto T., Matsuzaki H., Kikkawa U. UV-Induced Tyrosine Phosphorylation of PKC delta and Promotion of Apoptosis in the HaCaT Cell Line. Biochem, Biophys, Res, Commun., 30; 289(2):573-9, 2001.

Glaser R.: Current concepts of the interaction of of weak electromagnetic fields with cells. Bioelectrochem. Bioener., 27: 255-268, 1992.

Hinsenkamp M., Jercinovic A., De Graef Ch., Wilaert F., Heenen M. Effects of low frequency pulsed electrical current on keratinocytes in vitro. Bioelectromagnetics, 18 : 250-254, 1997.

Hsu M., Andl T., Li G., Meinkoth J.L., Herlyn M. Cadherin repertoire determines partner-specific gap junctional communication during melanoma progression. J Cell Sci, 113 (pt9): 1535-42, 2000.

Kaiser F. Theory of non-linear excitation. In : Frolich H. et al. (eds). Biological coherence and response to external stimuli. Springer Heidelberg Germany, 25-48, 1988.

Karabakhtsian R., Bronde N., Shalts N., Kochlatyi S., Goodman R., Henderson A.S. : Calcium is necessary in the cell response to EM fields. FEBS Lett., 301: 53-59, 1994.

John C.F., Morris K., Jordan B.R., Thomas B., A-H-Mackerness S:
Ultraviolet-B exposure leads to up-regulation of senescence-associated genes in Arabidopsis thaliana. J. Exp. Bot., 52(359):1367-73, 2001.

Jost M., Kari C., Rodeck U. The EGF receptor-an essential regulator of multiple epidermal functions: Eur J Dematol., 10: 505-510, 2000.

Laemmli U.K.: Cleavage of structural proteins during the assembly of the head bacteriophage T4. Nature, 227: 680-685, 1970.

Alberto Foletti M.D. Mario Ledda , Emanuela Rosola , Antonella Lisi, Enrico D' Emilia , Settimio Grimaldi

Liburdy R.P.: Calcium signalling in lymphocytes and ELF fields: evidence for an electric field metric and a site of interaction involving calcium ion channels. FEBS Lett., 301(1): 53-59, 1992.
Leszczynski D., Pitsillides C.M., Pastila R.K., Rox Anderson R., Lin C.P: Laser-beam-triggered microcavitation: a novel method for selective cell
destruction. Radiat. Res., 156(4):399-407, 2001.

Medema J.P., Sark M.W., Backendorf C., Bos J.L. Calcium inhibits epidermal growth factor-induced activation of p21ras in human primary keratinocytes. Mol Cell Biol, 14(11): 7078-85, 1994.
Pilla A.A., Markov M.S: Bioeffects of weak electromagnetic fields. Rev Environ Health, 10(3-4): 155-69, 1992.
Phillips J.L., Haggren W., Thomas W.J., Jones T.I., Adey W: Magnetic field-induced changes in specific gene transcription. Biochimica Biophysica Acta, 1132: 140-144, 1992.
Peus D., Hamacher L., Pittelkow M.R. EGF-receptor tyrosine kinase inhibition induces keratinocytes growth arrest and terminal differentiation. J.Invest. Derm., 109: 751-756, 1997.

Pletnev S.D.: The use of millimeter band electromagnetic waves in clinical oncology. Crit. Rev. Biomed. Eng., 28(3-4): 573-87, 2000.
Rusovan A. and Kanje M. Magnetic fields stimulate peripheral nerve regeneration hypophyctiomia rats. Neuroreport 3 (12) : 1039-1041, 1992.
Savitz D.A., Pearce N., Poole C. Update on methodological issues in the epidemiology of electromagnetic fields and cancer. Epidemiological Rewievs,. 15: 558-566, 1987.

Szabo I., Rojavin M.A., Rogers T.J., Ziskin M.C. Reactions of keratinocytes to in vitro millimeter wave exposure. Bioelectromagnetics, 22: 358-364, 2001.
Tenforde T.S: Interaction of extremely low frequency electric and magnetic fields with humans. In C. Polk, E. Postow Eds: "Handbook of biological effects of electromagnetic fields". 2nd Ed., CRC Press, Boca Raton, 185-230, 1995.
Vasioukhin V., Bauer C., Degenstein L., Wise B., Fuchs E. Hyperproliferation and defects in epithelial polarity upon conditional ablation of alpha-catenin in skin. Cell, 23: 104 (4): 605-617, 2001.
Weaver J.C., Astumian R.D. The response of living cells on very weak electric fiels: the thermal noise limit. Science, 247:459-462, 1990.
Walleczeck J: Electromagnetic field effect on cells of the immune system: the role of calcium signalling. Faseb Journal, 6 : 3177-3185, 1992.
Zhadin M.N.: Review of russian literature on biological action of DC and low-frequency AC magnetic fields. Bioelectromagnetics, 22(1): 27-45, 2001.

Aknowledgements
Specially thanks for the realisation of this work is due to Italian Medical Society for Bio-Physical Information Therapy.

Fig.1

Involucrin

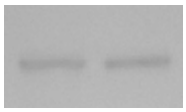

β catenin

Table 1. % HaCaT cells increasing Involucrin and β Catenin Immunofluorescence positivity after 7 Hz electric treatment

	% Positive Cells
Involucrin	**8 ± 1**
β Catenin	**10 ± 1**

– **±S.D**

STATIC MAGNETS AND PC6 CELLS: DIFFERENTIATION AND PROLIFERATION

Amanda B. Spence and Betty F. Sisken

Dept. of Biological Sciences and Center for Biomedical Engineering, University of Kentucky, Lexington, KY 40506

The objective of this study was to assess the effects of static magnetic fields on proliferation and differentiation of PC6 cells. Proliferation was measured by counting the number of cells in four different quadrants of each well in a 6-well plate after 2 days of incubation. Differentiation was assessed in the same wells by measuring the percentage of cells with neurites (cell extensions) growing from the cell bodies.

We used two Tectonic ceramic magnets (800 Gauss surface field strength, 4 cm in diameter) one under a well at each end of the plate and exposed the cells for three hours /day for each of 2 days . Culture plates were placed directly on the surface of the two magnets. Nerve growth factor (NGF) in phosphate buffered saline (PBS) or PBS alone was added to the cultures; the final concentration of NGF tested was 10 and 20 ng/ml.

A significant effect on differentiation ($p=0.0215$) was found when comparing cultures treated with either concentration of NGF and cultures treated with PBS. The presence of a static magnetic field had no additive effect with the NGF nor did it have any effect alone. Growth, in terms of number of cells, was not affected by the magnetic field + PBS, NGF alone, or NGF + magnetic field.

We also asked the question whether the magnetic fields had any direct effect on the culture media alone or with the addition of PBS or NGF. Therefore, the culture media (+PBS or +NGF) was exposed to the magnetic fields for 3 hours and then the PC 6 cells were added. After 2 days of incubation the results demonstrated that the fields did not affect NGF action since cell differentiation was still increased to the same extent over PBS controls, and no differences were found in growth (proliferation) assessments.

These results are can be compared and contrasted to those found when we tested
2 Hz pulsed electromagnetic fields (PEMF) on PC6 cells, where neurite outgrowth was inhibited (Shah et al, 2001) and with 15 Hz PEMF where differentiation of dissociated sensory neurons was inhibited (Webb et al, 1994). In contrast, we described a stimulation of neurite outgrowth from explants of chick sensory ganglia (Sisken et al, 2000) using the same 800 gauss static magnetic field + NGF. The mechanisms underlying these effects are not known, but may involve magnetic field regulation of NGF activity. Since this dose of magnetic fields may be outside the biological window for single cells, future studie will be run in which the magnetic fields are reduced in strength.

EFFECTS OF GSM-900 JAMMER'S ELECTROMAGNETIC FIELD ON HUMAN ELECTROENCEPHALOGRAM

R. MASKANI

DEPARTMENT OF MEDICAL PHYSICS, TARBIAT MODARES UNIVERSITY, TEHRAN, IRAN

maskany@modares.ac.ir

S.M.P. FIROOZABADI

DEPARTMENT OF MEDICAL PHYSICS, TARBIAT MODARES UNIVERSITY, TEHRAN, IRAN

pourmir@modares.ac.ir

B. JALALIAN

SHAHRUD CAMPUS OF ISLAMIC AZAD UNIVERSITY, SHAHRUD, IRAN

jalalianbabak@hotmail.com

Abstract

Widespread use of mobile phones and the necessity for restriction of it in some places have increased the growth of mobile phone jammer (MPJ). The MPJ produces an electromagnetic field (EMF) that blocks the mobile phone communications. It generates noisy signals at a frequency in order of the mobile phone. People, who exposed to the MPJ field, usually are unaware about its effects on their health. So, at this study the influences of mobile phone jammer's exposures on human electroencephalogram (EEG) are evaluated experimentally.

Thirty healthy participants attended two sessions, one week apart. In experimental and sham session, before exposure, 19 Channels EEG signal was recorded with closed eyes. In experimental session, they exposed to the MPJ's EMF for twenty minutes. In sham session, MPJ was turned off. Then, in two sessions, EEG signal was recorded twenty minutes after beginning of each session. The follow-up EEG signal was recorded at fortieth minutes. Then, power spectrum of EEG signals was calculated using Matlab toolbox.

The analysis of results showed that area under power spectrum curve off EEG signals in some channels has changed between sham and exposure session. The frequency parameters of EEG signals have been changed due to the MPJ exposures, especially in the alpha and theta band of frequency domain. We concluded that this radiofrequency exposure could affect the participant's awareness

Keywords*:* Electromagnetic Field, Mobile Phone Jammer, GSM 900MHz, EEG

Introduction

Widespread use of mobile phones and the necessity for restriction of it in some places have increased the growth of mobile phone jammer (MPJ). The MPJ produces an electromagnetic field (EMF) that blocks the mobile phone communications. GSM use 900MHz EMF as a carrier for communications. But MPJs generate noisy signals at a frequency in order of the mobile phone. Therefore in study of MPJ's effects we can refer to researches of mobile phone effects. Should be noted that MPJs just used for produce noise and may be have other deferent frequencies that defer between company's products and their noise production methods.

The first cell phone jammer was marketed in 1998 after Goldshtein. MPJs are used in some places that mobile phone usage is forbidden such as exams or in places that quite is necessary, for example banks, mosques, churches, theaters and meetings. Furthermore People may be resident long time near MPJ, for example in offices or prisons. Operation of these devices is illegal or very limited in some countries and discussions about its usage continue [1]. These discussions are on two subjects; MPJs usage limits mobile benefits essentially in emergency situations, and probable health hazard of MPJ's EMF [2].

On the other hand, some people that think mobile phone ring and their families and friend's irregular call is ruining their rest and Security and has contrast with their relationship with another people, interest to use low power MPJs and try to make this a manner [3].

People, who exposed to the MPJ field, usually are unaware about its effects on their health. So it's necessary to validate the effect of MPJ on human health.

Generally EMF effects can be divided in to thermal and non-thermal effects. More Standards are based on released heat from EMF that SAR (specific energy absorption rate) is famous standard. But in order weak Electric field that emitted from mobile phone and MPJs non-thermal effects is more probable [4].

Non-thermal effects of EMF that often has been considered are effect on carcinogenic processes, tumor growth, etc. until now Scientific can't find any exact relationship between Mobile phone or MPJ usage and human physiology and pathology. Among researches effect on brain and nervous system has been considered, specially.

Some of probable effects of EMF on nervous system are effect on function of neural membrane, calcium efflux, neuronal excitability, neurotransmitter systems, thermoregulatory behavior, Motor activity, auditory responses, learning and memory, blood–brain barrier and finally effect on brain activity such as EEG and ERP [5].

EEG is an immediate reflection of change in function of nervous system that make it considerable. The effect of EMF on brain activity has been studied later in number of experiments. Studies often report EMF exposure of mobile phone increase spectral power of resting EEG, especially in alpha band [6,7,8,9,10,11,12] but in another research didn't observe such changes [13,14,15].

In some experiment spectral power of Sleep EEG increased due to EMF exposure of mobile phone [10,16,17,18,19,20,21,22] and in another studies didn't result these effects [23,24,25,26].

About effects of mobile phone exposure on EPs some researches have been done. Some of this research report changes in measured parameters [7,9,26,27,28,29,30,31,32] and in another studies can't observed any changes [33,34,35,36].

At this study the influences of mobile phone jammer’s exposures on human resting electroencephalogram (EEG) are evaluated experimentally.

Materials and methods

Subjects

Thirty healthy males aged between 18 and 27 years participate in the study. Participants often had university degrees and easily have been described about purpose and procedures of the study. Before participate in experiment any participant was introduced with experimental tools and situation.

Participant were asked about any nerves illness and difficulties such as long term headache, sleep disorder etc. also in first session of experiment an EEG with clinical order has been recorded and a neural specialist reviewed this record and finally sample with neural difficulty has been forgave from experiment and invited for more clinical exam. During the experiment two peoples were invited for clinical difficulty investigating exams.

Before first session participants have been noted that had sufficient sleep and didn't use sleepy and neural drugs. Before experiment any participant wrote an informed consent that contained detail of study.

Procedure

Participants attended two sessions, one week apart, for experimental and sham session. In each session participant seat on a comfortable armchair and an expert technician placed the electrodes on his head. Before exposure, 19 Channels EEG signal was recorded with closed eyes. In experimental session, they exposed to the MPJ EMF for twenty minutes from right side. In sham session, MPJ was turned off and participants were unaware that MPJs was on or off. In two sessions, EEG signal was recorded twenty minutes after beginning of each session. The follow-up EEG signal was recorded at fortieth minutes. The experimental protocol is shown in table 1.

Table 1: experimental protocol

Session	30 s EEG Recording	20 min being near the MPJ	30 s EEG Recording	20 min after Second record	30 s EEG Recording
First	Background	ON Exposure / OFF	After	Follow-up time	Follow-up
Second		OFF Exposure / ON			

EMF exposure

GSM 900 use 890-960 MHz EMF as a carrier for communications. This wide band divided to two bands, uplink band 890-915 MHz, and downlink band 935-960 MHz. downlink is the transmission path from a Base Station to the Cell Phone. Uplink is the transmission path from a mobile station to the base station [37].

MPJs emit EMF similar to downlink (935-960 MHz) but with ramp modulation, which block mobile communications around itself. MPJs emit EMF similar to carrier of GSM, but in a stable frequency band and with constant power for a long time. These make MPJ a suitable EMF generator for our study.

EMF emitter that has been used in our study was MPJ 101 (Moje Nasr Gostar co.) that emits noisy 935-960 MHz EMF with power of 1 W and can block GSM900 communications in a 15 meters circle. Fig 1

Frequency of EMF that emitted form MPJ 101 was tested with a Spectrum Analyzer (TR4131) that has correct frequency band

Fig 1: MPJ 101

MPJ 101 has an 8 cm, quarter wavelength antenna. Participants sat approximately 50 cm apart the MPJ. It can be assumed that participants placed in far field of antenna. Therefore power density on volunteer head can be estimated:

$$\frac{I}{S}=\frac{I}{4\pi r^2}=\frac{1}{4\pi(0.5)^2}\left(\frac{W}{m^2}\right)=0.32\ Wm^{-2}$$

Public standard level for power spectrum that ICNIRP determined in 935 MHz is 4.68 Wm^{-2}. It can be seen that power spectrum is smaller than standard level.

Data acquisition

EEG was recorded using a 19 Channels EEG recording system (sholeh danesh co.). It has an 8-bit A/D card and its sampling rate is 250 Hz. 19 Ag-AgCl Saline Pad Electrodes placed on participant's head using 10-20 system and fixed with a head cap strap. Two earlobe electrodes were hanged to ears with ear clip as reference and recording was performed with monopole montage.

Data acquisition, Preview and primary analysis performed using SD-C24 EEG software that install on recording PC. Default mode of recording system that performed for clinical application has a 35 Hz low pass

and a 1 Hz high pass filter. We were using this mode for clinical exam of participants that has been said before. For experimental record a 70 Hz low pass and a 0.3 Hz high pass filter were used.

More than 30 s EEG with closed eye was recorded in any record (background, after and follow-up) that has been said before.

Data analyzes

Recording data was saved in special file format. This primary format has been converted to a data array with Matlab software format (MathWorks, Inc. version 7) that can be analyzed in Matlab toolboxes. The MAT file after convert has been reviewed with eeglab4.515 toolbox [38] and compared with printed records to validate conversion program.

Recorded EEG was reviewed with eeglab4.515 toolbox and in any record (background, after and follow-up), 10 without movement artifact 1 s windows have been selected.

Frequency analysis has been done in the Matlab. FFT (Fast Fourier Transform) was performed on each 1 s data to calculate power spectrum. Because frequency contents of normal adult lie between 0.1-40Hz [39] in power spectrum calculation we abandoned upper than 45 Hz contents. We also abandoned frequency content lower than 1Hz because our frequency resolution in power spectrum calculation. Then Relative Power Spectrum (RPS) has been calculated as below.

RPS= Area under Power Spectrum curve of any rhythm / Total area under Power Spectrum curve

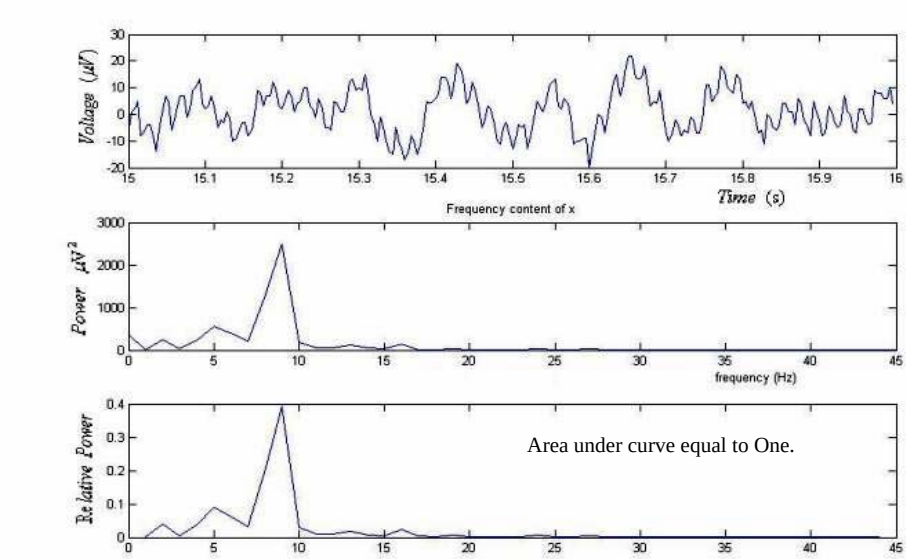

Fig 2: Original EEG wave ,Voltage as a function of time (first), Power Spectrum (second) and RPS (third)

Then power spectrum has been averaged in 10 second. For evaluation of changes in EEG rhythms, RPS has been summed in each rhythm. EEG rhythms have been determined as shown below

Delta	δ	1-3 Hz
Theta	θ	4-7 Hz
Alpha	α	8-13 Hz

Beta	β	14-35 Hz
Gamma	γ	36-45 Hz

Essentially EEG RPS may change as a function of time during each session. For finding any effect of EMF exposure, recording data during the real exposure with that recorded in sham session should be compared. In each session, Growth Ratio (GR) from background to after, from after to follow-up and from background to follow-up records were calculated as below.

GR=(after RPS-background RPS)/background RPS …

Therefore we could compare between two sessions with three GRs.

Statistical analyses

Statistical analyses were performed with SPSS (SPSS Inc. version 11.5.) software Paired T-test was performed for GR of RPS between two sessions. Differences were considered statistically significant at $P< 0.05$. Paired T-test was performed for each 19 electrodes in all rhythms separately.

For Paired T-test the data should be normal. Therefore normality of data was checked in One-Sample Kolmogorov-Smirnov Test. If normality test failed nonparametric test (Wilcoxon signed rank test) would use.

Additionally for evaluation the inherent changes of EEG rhythms due to time, Repeated measures have been performed on background, after and follow-up records in each session separately. Mauchly's Test of Sphericity Were performed before Repeated measures tests. If Mauchly's Test of Sphericity failed, other methods (Greenhouse-Geisser, Huynh-Feldt and Lower-bound) would perform.

Result

Repeated measures of data showed changes in EEG rhythm due to time especially in Theta and Alpha rhythms. Analyze of differences showed significant changes in GR from background RPS to after, between two sessions in some electrode and in some rhythms. As be shown in Table 2. Positive sign in the table shows increase in RPS change in those rhythm and negative sign show decrease in it. It seems that immediately after exposure the natural changes of EEG rhythms were modified. Slow brain potentials increased due to exposure. Analyze of GR from follow-up to after record also showed more differences between sham and experimental sessions as shown in Table 3. Comparing sham and experimental records showed decrease in GR in Theta rhythms. Result of comparing GR from follow-up to background record showed less change in two sessions(Table 4).

Discussion

Our result showed RPS of slow brain potential increased immediately after exposure in some electrode, it is inconsistent with result of more experiment that have reported increase in alpha rhythm due to exposure. It may be result of large widespread data in upper rhythms that unable us to see significant differences.

Comparing GR from follow-up to after record in sham and experimental records showed decrease in natural changes in Theta rhythms.

Results showed increase in GR from background to after record and decrease from after to follow-up record in Theta rhythm due to EMF exposure that is reasonable.

Analogizing GR from background to follow-up record in two sessions showed partially increase in beta rhythm that perhaps it happens accidentally.

In our study the frequency parameters of EEG signals have been changed due to the MPJ exposures, especially in the alpha and theta band of frequency domain. We concluded that this radiofrequency exposure could affect the frequency content of EEG and participant's awareness.

Table 2- changes in RPS from background to after records due to EMF exposure

Location	Delta 1-3 Hz	Theta 4-7 Hz	Alpha 8-13 Hz
C3			-
Cz		+	
F7	+		-
Fp2		+	
Fz		+	
P3	+		
T3	+		-
T5	+		

.

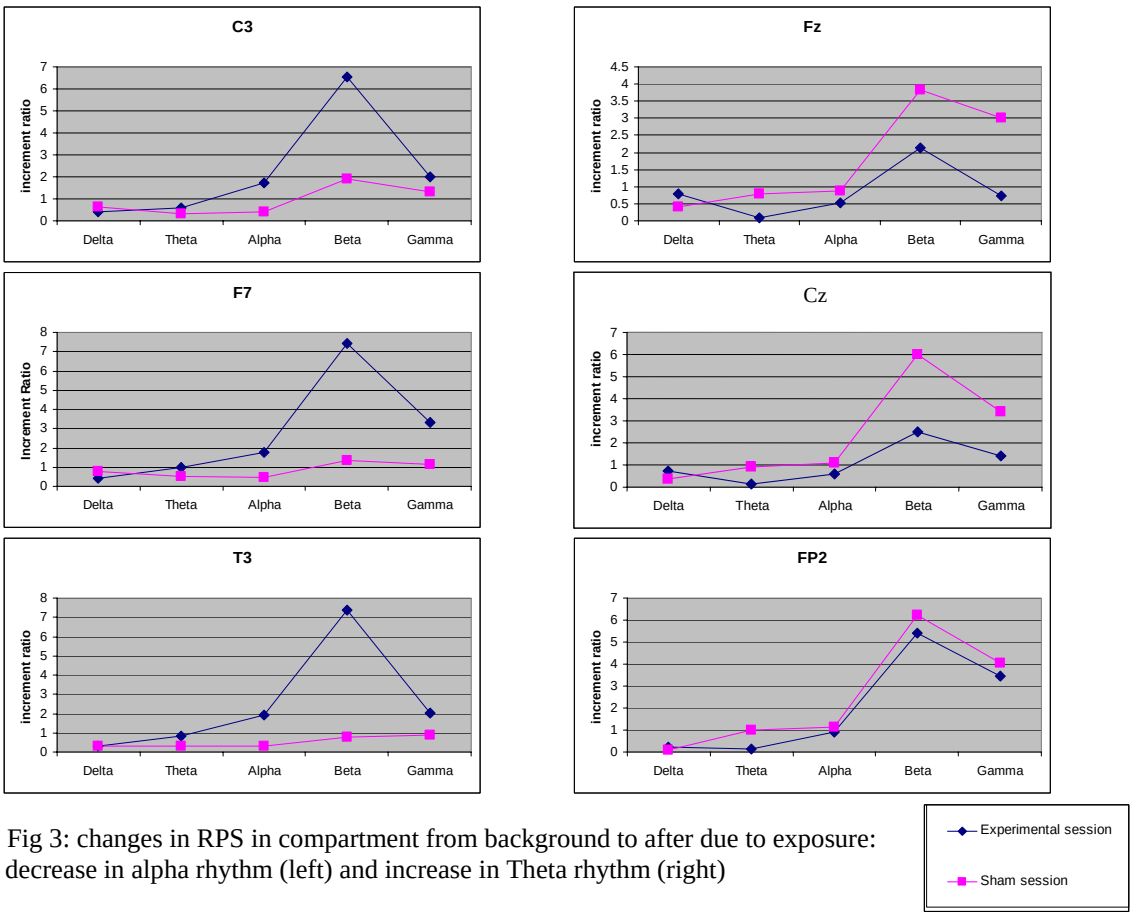

Fig 3: changes in RPS in compartment from background to after due to exposure: decrease in alpha rhythm (left) and increase in Theta rhythm (right)

Table 3- Changes in RPS from after to follow-up records due to EMF exposure.

Location	Delta 1-3 Hz	Theta 4-7 Hz	Alpha 8-13 Hz
C3		-	
CZ		-	
Fp1			+
Fp2		-	
Fz		-	
O1		-	
O2		-	
Pz		-	
T3			+

Table 4- Changes in RPS between from background to follow-up records due to EMF exposure.

Location	Delta 1-3 Hz	Theta 4-7 Hz	Alpha 8-13 Hz
C3	+	-	
F8	+		
O1	+		
P3	+	-	

References

[1] James Careless, Canada phones face legalized jammers, Wireless Week; Mar 26, 2001; 7, 13; ProQuest Telecommunications, pg. 71
[2] Australian Communications Authority (ACA) Report, mobile phone jammers, July 2003
[3] Limor Fried, Social Defense Mechanisms: Tools for Reclaiming Our Personal Space, thesis, Department of Electrical Engineering and Computer Science, Massachusetts Institute of Technology, January 2005
[4] IEGMP Independent Expert Group on Mobile Phones. Mobile phones and health. 2000, ISBN 0-8591-450-1, http://www.iegmp.org.uk.
[5] EMF international project, http://www10.who.int/peh-emf/emfstudies/database.cfm
[6] Reiser H-P, Dimpfel W, Schober F. The influence of electromagnetic fields on human brain activity. Eur J Med Res 1995;1:27–32.
[7] Thuroczy G, Kellenyi L., Faludy B., Lenard L, effects of mobile gsm radiotelephone exposure on the auditory brainstem response (ABR), Neurobiology, Vol. 7, Pg. 79 - 81, 1999
[8] Lebedeva N. N., cellular phone electromagnetic field effects on bioelectric activity of human brain, Crit Rev Biomed Eng, Vol. 28, Pg. 323 - 337, 2000
[9] Croft R. J., Chandler J. S., Burgess A. P., Barry R. J., Williams J. D., Clarke A. R., Acute mobile phone operation affects neural function in humans, J Altern Complement Med., Vol. 8, Pg. 427 - 435, 2002.
[10] Hamblin D. L., Wood A. W. Effects of mobile phone emissions on human brain activity and sleep variables, Int. J. Radiat. Biol., Vol. 78, Pg. 659 - 669, 2002.
[11] D'Costa H., Trueman G., Tang L., Abdel-rahman U., Abdel-rahman W., Cosic I., Human brain wave activity during exposure to radiofrequency field emissions from mobile phones, Australian Physical and Engineering Sciences in Medicine, Vol. 26, Pg. 162 - 167, 2003.
[12] G. Curcio, M. Ferrara, F. Moroni, G. D'Inzeo, M. Bertini, L. De Gennaro, Is the brain influenced by a phone call? An EEG study of resting wakefulness, Neuroscience Research 53 (2005) 265–270
[13] Roschke J, Mann K. No short term effects of digital mobile radio telephone on the awake human electroencephalogram. Bioelectromagnetics 1997;18:172–176.
[14] Kim Y. S, Characteristics of eeg and aep in human volunteers exposed to RF, Korean Journal of Environmental Health Society, Vol. 24, Pg. 58 - 65, 1998.
[15] Hietanen M, Kovala T, Hamalainen AM. Human brain activity during exposure to radiofrequency fields emitted by cellular phones. Scand J Work Environ Health 2000;26(2):87–92.
[16] Mann K, Ro¨schke J. Effects of pulsed high-frequency electromagnetic fields on human sleep. Neuropsychobiology 1996;33:41–7.
[17] Borbely A, Huber R, Graf T, Fuchs B, Gallman E, Achermann P. Pulsed high-frequency electromagnetic fields affects human sleep and sleep electroencephalogram. Neurosci Lett 1999;275:207–10.
[18] Huber R., Graf T., Cote K. A., Wittmann L., Gallmann E., et al, Exposure to pulsed high-frequency electromagnetic field during waking affects human sleep EEG NeuroReport, Vol. 11, Pg. 3321 - 3325, 2000
[19] Lebedeva, N.N.; Sulimov, A.V.; Sulimova, O.P.; Korotkovskaya, T.I.; Gailus, T. Investigation of brain potentials in sleeping humans exposed to the electromagnetic field of mobile phones. Biomedical Engineering 2001; 29(1):125-133
[20] Huber R., Treyer V., Borbely A. A., Schuderer J., Gottselig J. M., et al ., Electromagnetic fields, such as those from mobile phones, alter regional cerebral blood flow and sleep and waking, J. Sleep Res., Vol. 11, Pg. 289 - 295, 2002
[21] Huber R., Schuderer J., Graf T., Borbely A. A., Kuster N., Achermann P., Radio frequency electromagnetic field exposure in humans: estimation of sar distribution in the brain, effects on sleep and heart rate, Bioelectromagnetics, Vol. 24, Pg. 262 - 276, 2003.
[22] Mann K., Roschke J., Sleep under exposure to high-frequency electromagnetic fields, Sleep Medicine Reviews, Vol. 8, Pg. 95 - 107, 2004.
[23] Wagner P, Roschke J, Mann K, Hiller W, Frank C. Human sleep EEG under the influence of pulsed radiofrequency electromagnetic fields: a polysomnographic study using standardised conditions. Bioelectromagnetics 1998;19:199–202.
[24] de Seze R., Effects of radio cellular telephones on human sleep, J. Sleep Research, Vol. 9(Suppl 1), Pg. 18 - , 2000.
[25] Wagner P, Roschke J, Mann K, Fell J, Hiller W, Frank C, Grozinger M. Human sleep EEG under the influence of pulsed radio frequency electromagnetic fields. Neuropsychobiology 2000;42:207–212.
[26] Jech R, Sonka K, Ruzicka E, Nebuzelsky A, Bohm J, Juklyckova M, Nevsymalova S. Electromagnetic field of mobile phones affects visual event related potential in patients with narcolepsy. Bioelectromagnetics, 2001;22:519–28.
[27] Freude G, Ullsperger P, Eggert S, Ruppe I. Effects of microwaves emitted by cellular telephones on human slow brain potentials. Bioelectromagnetics 1998;19:384–7.

[28] Krause C. M., Sillanmäki L., Koivisto M., Häggqvist A., Saarela C., et al., Effects of electromagnetic field emitted by cellular phones on the eeg during a memory task, NeuroReport, Vol. 11, Pg. 761 - 764, 2000.
[29] Krause C. M., Sillanmaki L., Koivisto M., Haggqvist A., Saarela C., Revonsuo A., effects of electromagnetic fields emitted by cellular phones on the electroencephalogram during a visual working memory task, Int. J. Radiat. Biol., Vol. 76, Pg. 1650 - 1667, 2000.
[30] Freude G, Ullsperger P, Eggert S, Ruppe I. Microwaves emitted by cellular telephones affect human slow brain potentials. Eur J App Physiol 2000; 81:18–27.
[31] Hamblin D. L., Wood A. W., Croft R. J., Stough C., Examining the effects of electromagnetic fields emitted by gsm mobile phones on human event-related potentials and performance during an auditory task, Clinical Neurophysiology, Vol. 115, Pg. 171 - 178, 2004.
[32] Maby E., Jeannes R. L., Faucon G., Liegeois-Chauvel C., de Seze R., Effects of gsm signals on auditory evoked responses Bioelectromagnetics, , Pg. - , 2005
[33] Urban P, Lukas E, Roth Z Does acute exposure to the electromagnetic field emitted by a mobile hone influence visual evoked potentials? a pilot study. Cent Eur J Pub Health 1998;6:288–90.
[34] Krause C. M., Haarala C., Sillanmaki L., Koivisto M., Hamalainen H., et al. , Effects of electromagnetic field emitted by cellular phones on the eeg during an auditory memory task - a double blind replication study, Bioelectromagnetics, , Vol. 25, 2004, Pages: 33-40
[35] Arai N., Enomoto H., Okabe S., Yuasa K., Kamimura Y., Ugawa G., Thirty minutes mobile phone use has no short-term adverse effects on central auditory pathways, Clinical Neurophysiol., Vol. 114, Pg. 1390 - 1394, 2003.
[36] Oysu C, Topak M, Celik O, Yilmaz HB, Sahin AA., Effects of the acute exposure to the electromagnetic field of mobile phones on human auditory brainstem responses, Eur Arch Oto-Rhino-Laryngology, , 262(10):839-43,2005.
[37] Wikipedia, http://en.wikipedia.org/wiki/Main_Page
[38] http://sccn.ucsd.edu/eeglab, Swartz Center for computational Neuroscience, University of California, San Diego.
[39] Ernest Niedermeyer, The Normal EEG of Waking Adult, Electroencephalography Basic Principle, Clinical Applications and Related Fields. Second edition, P 97-117, 1987

WAVELET ANALYSIS OF THE EFFECT OF A 900MHZ ELECTROMAGNETIC FIELD ON EVENT RELATED POTENTIALS OF EEG SIGNALS.

NANOU ELENA[1], PAPAGEORGIOU CHARALAMBOS[2, 3], HOUNTALA CHRISSANTHI[1], MAGANIOTI ARGIRO[1], TSIAFAKIS VASILEIOS[1], KAPARELIOTIS EVANGELOS[1], SOLDATOS KONSTANTINOS[2], RABAVILAS ANDREAS[3] CAPSALIS CHRISTOS[1]

[1] NATIONAL TECHNICAL UNIVERSITY OF ATHENS, DEPARTMENT OF ELECTRICAL ENGINEERING, DIVISION OF INFORMATION TRANSMISSION SYSTEMS AND MATERIAL TECHNOLOGY, GREECE

9 IROON POLYTECNEIOY STR., ATHENS, GREECE, 15773, Tel: ++30210-7722574, Fax: ++30210-7723520, email:enanou@mail.ntua.gr

[2] DEPARTMENT OF PSYCHIATRY, EGINITION HOSPITAL, UNIVERSITY OF ATHENS, GREECE
email: cpapage@eginitio.uoa.gr

[3] UNIVERSITY MENTAL HEALTH RESEARCH INSTITUTE, ATHENS, GREECE.

Abstract

Wavelet analysis has proven a useful tool for time-frequency analysis of EEG and Event Related Potential (ERP) signals. Moreover the effect of electromagnetic fields (EMFs) on brain activity is an important issue that requires further investigation.

The present study focused on the temporal analysis of the early components of ERPs stimulated by sounds of different frequencies (low=500 Hz and high=3000Hz), using wavelets. The ERPs were recorded at 16 scalp electrodes during a working memory test with and without electromagnetic radiation (900 MHz). The sample included 10 women and 9 men. Temporal comparisons were made between the energies, averaged at the time intervals before and after the P50 amplitude peak (30-80 msec after warning stimulus onset).

Results showed that the maximum energy variability was observed for the α-band at the C4 electrode. In the absence of radiation men exhibited a significant increase after the P50 peak of the energy for the low frequency stimulus, while women exhibited this significant increase for the high frequency stimulus. Conversely the presence of radiation seemed to suppress this energy increase for both sexes with the exception of women for the low tone.

Introduction

Since the advent of GSM-based cellular phone networks general concerns have been raised regarding potential health effects of high frequency electromagnetic fields (EMF). The close proximity of a mobile phone to the user's head leads to the absorption of part of the EMF energy in the head and the brain [1]. This is especially important in view of the observation that the shape of the head is oval, with a short axis of 15 – 17 cm in length, which is half the wavelength of the 900MHz transmission signals of the cellular phones. Consequently, the head may serve as a lossy resonator absorbing much of the energy emitted by cellular phones [2]. The above considerations necessitate the study of the possible effects of EMF on brain and behavior [3].

Analysis of EEG signals proved a useful and appropriate approach in measuring the level and spatial distribution of cortical activation during cognitive task performance. Several reports provide evidence that the exposure to EMFs increases the cortical activity as it is reflected in the increase of spectral power in the alpha band of the EEG signal. [4, 5, 6, 7]. However, there are reports which do not confirm these results [8].

The event-related brain potentials (ERPs) consist of a series of positive and negative peaks of the brain signals occurring at a fixed time relative to an event. These component peaks are studied with the assumption that they index meaningful aspects of cognitive processing [9]. Specifically the earlier components of the ERPs (0 – 100 msec after stimulus) are thought to represent the activity of the sensory pathways that transmit the signal generated at peripheral receptors to central processing systems.

There have been several studies of mobile phone emissions on the brain activity using the sensory components of ERPs methodology with various results [10, 11, 12, 13, 14 and 15]. It should be noted that the early components are 'modality specific', that is they are influenced primarily by the stimulus parameters such as intensity and frequency [16].Our team recently found that the MP-EMF affect the patterns of the auditory P50 component of ERPs (generally 30-80 msec post-stimulus)[17]. In particular the amplitude of P50 evoked by low frequency stimuli at Fp1 and O1 electrode is statistically significant increased in the presence of MP-EMFs. In contrast the exposure to MP-EMFs revealed statistically significant decrease of the amplitude of P50 evoked by high frequency stimuli, at Fp1 electrode as compared to themselves without MP-EMF exposure. These findings have been conceived as evidence that the MP-EMF emitted by mobile phone affect pre-attentive information processing reflected by the synchronized responses of the thalamocortical system of the P50 component of ERPs. [18, 19]

Moreover, having in mind that EEG and ERP data sets are nonstationary a useful tool to analyze these signals in both time and frequency domain is the Wavelet Analysis. Many studies have used wavelets in order to explore EEG and ERP waveform structure. Rosso and Figliola [20] used the wavelet transformation at generalized epileptic tonic/clonic EEG signals and showed that the Relative Wavelet Energy describes accurately the epileptic recruitment rhythm. Samar et al. applied wavelets at data collected from a sample consisted of controls and alcoholics in order to compare ERP values at different frequency levels [21]. They found significant group differences at the theta band at the span of P300 and also at the alpha band for the P100-N100-P200-N200. However, up to our knowledge, there are no studies specifically examining the effect of EMFs on ERPs using wavelets.

On the other hand the gender-dependent brain function is a subject under research. In a study about sex differences in resting EEG activity it was reported that EEG power for females was greater than the EEG power for males, with significant differences observed for delta, theta and beta bands, but not for the alpha band [22]. These findings concur with the results of a study of Briere et al. where women were found to have higher EEG power values at the central, parietal and left temporal electrodes [23]. Only one study has so far investigated EEG gender-related differences under exposure to mobile phone EMFs [24]. The subjects' EEG was recorded during the anticipatory period of performance on an auditory Wechsler test for 500 ms, either under real (900 MHz CW with a mean power at 0.64 W) or sham exposure. The amount of baseline EEG spectral energy of males was greater than that of females, while EMF exposure decreased the EEG energy of males and increased that of females. The above findings indicate that it is necessary to examine the possible impact of EMFs on brain activity separately for males and females in order to avoid the confounding effects of gender.

In summing up, cortical activation during the early components of the ERP signal is thought to be gender, modality and frequency specific. In view of the above considerations, the wavelet analysis of energy changes at the time intervals before and after the P50 could be of value in identifying possible pathophysiological alterations evoked by EMFs. Thus, the present study was designed to determine the time dependence of the effect of EMF exposure on the energy of early components of ERP during a working memory test.

Methods

Participants

Nineteen healthy individuals (9 men and 10 women, mean age = 23.3 ± 2.23 years, mean education = 16.9 ± 1.82 years) participated in the experiment. The male and female subgroups were homogeneous with regards to age and educational level. All participants were right-handed and had no history of any hearing problem. Informed consent was obtained from all subjects.

Experimental setup and Measurement Procedure

The subjects were evaluated with the digit span Wechsler Auditory test [25]. A warning stimulus of either high "(3000 Hz)" or low frequency "(500 Hz)" was presented through earphones to the subjects, who were asked to memorize the numbers that followed. The warning stimulus lasted 100msec. A one second interval followed the onset of the warning stimulus and then the numbers to be memorized were presented by a male voice. At the end of the number sequence presentation, the same signal tone was repeated. If the frequency of the signal tone was low the subjects had to recall the numbers in the same order as that presented, else, if the frequency was high, the subjects had to recall the numbers in the opposite order. Before any ERPs' recording, practice trials were administered until the subjects could clearly discriminate the warning stimuli (tones). After completion of the above-mentioned process, i.e. the practice trials, a rest period of five minutes followed, before the recording of the ERPs.

The experimental setup included a Faraday room, which screened any electromagnetic interference that could affect the measurements. The subjects sat in an anatomical chair and a certified dipole antenna was fixed near their right ear. The dipole's model was ELECTRO-METRICS EM6924 and the antenna factor was 27.4dB/m at 900MHz. Care was taken so that the distance between telephone and ear (about 20 cm) was constant during the whole session. The antenna was driven by a signal generator, which could be switched on or off. In the on mode the antenna emitted a 900 MHz electromagnetic field with mean power at 64 mWatt. [24] The signal was not modulated. The field strength was 3V/m at the point where the subjects' head was standing.

ERPs were recorded during 1.1 sec between the onset of the warning stimulus and the onset of the first administered number. The electrophysiological signals were recorded with Ag/AgCl electrodes. Electrode resistance was kept constantly below 5 kΩ. EEG activity was recorded from 15 scalp electrodes based on the International 10-20 system of Electroencephalography [26], referred to both earlobes. An electrode placed on the subject's forehead served as ground. The bandwidth of the amplifiers was set at 0.05 Hz to 35Hz. During the administration of stimuli, the subjects had their eyes closed in order to minimize eye movements and blinks. Eye movements were recorded through electro-oculogram (EOG) and recordings with EEG higher than 75mV were rejected. Warning stimuli, as well as learning material, i.e. the numbers to recall, were presented binaurally via earphones at an intensity of 65dB sound pressure level. The earphones did not have metal components in order to avoid EMF concentration.The evoked biopotential signal was submitted to an analogue-to-digital conversion, at a sampling rate of 1 KHz. Each recording session consisted of 52 repetitions of the trial.

The subjects performed the task twice, with (on mode) and without (off mode) radiation, with an interval of two weeks between the measurements. The order in which the subject was exposed at the EMF (exposure at the first or second visit) was random.

Because the P50 component is included in the array of early-endogenous ERPs components, which normally are modality specific, the ERPs induced by the two modal stimuli were averaged separately [16]. In particular, two varieties of P50 waveforms were obtained, one (low P50) evoked by the low frequency modality (26 trials) for each lead in all subjects and another (high P50) evoked by the high frequency modality (26 trials) for each lead in all subjects .

Wavelet Analysis

The Discrete Waveform Transform (DWT) was applied at the collected ERP data. The DWT analyzes the signal at different frequency bands with different resolutions by decomposing the signal into a coarse approximation and detail information. DWT employs two sets of functions, called scaling functions and wavelet functions, which are associated with low pass and high pass filters, respectively. The decomposition of the signal into different frequency bands is simply obtained by successive high pass and low pass filtering of the time domain signal. The original signal is first passed through a half band high pass filter and a low pass filter. After the filtering, half of the samples can be eliminated according to the Nyquist's rule, since now the highest frequency of the signal is half of this before filtering. The signal can therefore be subsampled by 2, simply by

discarding every other sample. This constitutes one level of decomposition. The "mother" wavelet function that was used to our analysis was Daubechies 1 (db1) and the levels of decomposition were seven.

This decomposition halves the time resolution since only half the number of samples now characterizes the entire signal. However, this operation doubles the frequency resolution, since the frequency band of the signal now spans only half the previous frequency band, effectively reducing the uncertainty in the frequency by half. At every level, the filtering and subsampling will result in half the number of samples (and hence half the time resolution) and half the frequency band spanned (and hence doubles the frequency resolution). The ERP data of the experiment consisted of 1000 values for each channel for each person after the averaging. In order to obtain high frequency resolution in δ band, the 1000 value sample was artificially subsampled. That is, the average of each 8 successive measurements of the signal was calculated the and consequently, 125 values were formed to which the Wavelet transform (WT) was applied.

The second step of the analysis was the reconstruction of the signal (or in our case the reconstruction of the details of the signal), that is how its components can be assembled back into the original signal without loss of information. The details of the signal at each level j are given by the function

$$D_j(t) = \sum_{k \in Z} C_{j,k} \psi_{j,k}(t)$$

where $\psi_{j,k}$ is the mother wavelet and $C_{j,k}$ are the wavelet coefficients which were calculated at the previous step. The wavelet coefficients $C_{j,k}$ can be interpreted as the local residual error between successive signal approximations at scales j-1 and j. $D_j(t)$ is the residual signal at scale j. It contains the information of the signal at frequencies $2^{j-1}f_s \leq |f| \leq 2^j f_s$.

Then the energy at each resolution level j=1,…,7 and at each instant, was calculated. This is the energy of the reconstructed detail signal:

$$E_j(t) = | D_j(t) |^2$$

The energies of the last three levels ($E_5(t)$,$E_6(t)$, $E_7(t)$) were summed up so that the sum stands for the energy at the time domain of the delta band (frequency 1-4 Hz). Each one of the remaining four levels with descending order represents the energy of the basic EEG rhythms theta, alpha, beta and gamma respectively.

The total energy at each time was calculated as follows:

$$E_{tot}(t) = \sum_{j=1}^{N} E_j(t)$$

The accuracy of the results was confirmed by comparing them with those derived from previous analysis with the FFT [24].

Finally the energy at each band was evaluated on a temporal basis. This means that the energies, were averaged at the time intervals before and after the P50 amplitude peak (30-80 msec after warning stimulus onset) and comparisons were made between these energies (before – after P50).

Statistical analysis

The parameter under consideration is the energy calculated with the Wavelet Transform. Preliminary statistical analysis was carried out independently for each modality (high, low) and for each frequency band (delta, theta, alpha, beta and gamma). The energies at the 15 leads were subjected to three way MANOVA with radiation (on – off), gender (male – female) and time interval (before – after the P50 peak) as the three independent factors. When the MANOVA procedure revealed statistical significance, the energies before and after the P50 peak were subjected to multiple pairwise comparisons for each lead, gender and radiation condition independently. Statistical significance was set at the 0.05 level.

Results

The MANOVA procedure revealed that significant energy differences were found only at the alpha frequency band. Figure 1 displays the energies before and after the P50 component and Table 1 displays the energy differences after – before the P50 component for tones, genders and EMF conditions. . In Figure 1 asterisks indicate the electrodes for which the energy differences are statistically significant. It seems that these temporal energy differences are mostly positive and highly dependent on the interaction among modality, gender and EMF. In the absence of radiation men witnessed a significant increase of the energy of the alpha frequency band

for the low stimulus at electrodes F3,C5,C6,P3,Pz and Fz, while women evidenced the same increase for the high stimulus at electrodes F3,Fp2,F4,C6 and C4. The presence of radiation seems to suppress this temporal energy increase with the exception of women for the low tone at electrodes C6 and P4.

Electrodes	Energy (Joule) Differences after – before P50 for *low* stimulus				Energy (Joule) Differences after – before P50 for *high* stimulus			
	Male		Female		Male		Female	
	EMF Off	EMF On	EMF Off	EMF On	EMF Off	EMF On	EMF Off	EMF On
Fp1	5.56	5.32	0.43	2.55	-3.35	2.45	0.83	2.33
F3	**5.49**	6.07	-0.18	7.98	-6.22	6.78	**5.57**	-5.88
C5	**5.12**	4.37	-0.26	4.17	0.88	3.23	3.28	-4.3
C3	4.8	4.28	-1.43	7.21	-1.05	2.64	3.69	-4.01
Fp2	4.23	3.46	2.7	6.48	-4.05	2.16	**4.09**	-1.92
F4	5.46	5.06	2.49	7.58	-0.94	4.65	**7.37**	-3.43
C6	**6.63**	2.16	2.91	**7.18**	-1.02	3.29	**6.14**	-0.7
C4	6.17	1.79	2.22	7.68	-3.2	5.79	**6.58**	-1.42
O1	1.55	-0.11	-0.29	1.82	-4.98	-1.55	1.05	2.88
O2	1	-4.66	-1.37	-0.66	-4.53	-1.05	1.43	-1.31
P4	**5.6**	-2.3	1.09	**5.71**	-2.96	0.81	4.41	5.52
P3	2.79	2.39	-0.71	2.42	-4.56	1.68	3.03	-2.69
Pz	**3.83**	-5.84	-1.52	4.94	-7.2	3.07	6.15	-4.67
Cz	6.39	4.38	-1.97	10.93	-3.98	7.66	4.22	-6.59
Fz	**5.54**	5.33	0.05	7.08	-3.54	4.28	3.95	0.85

Table 1. Energy differences after – before the P50 component for tones, genders and EMF conditions.

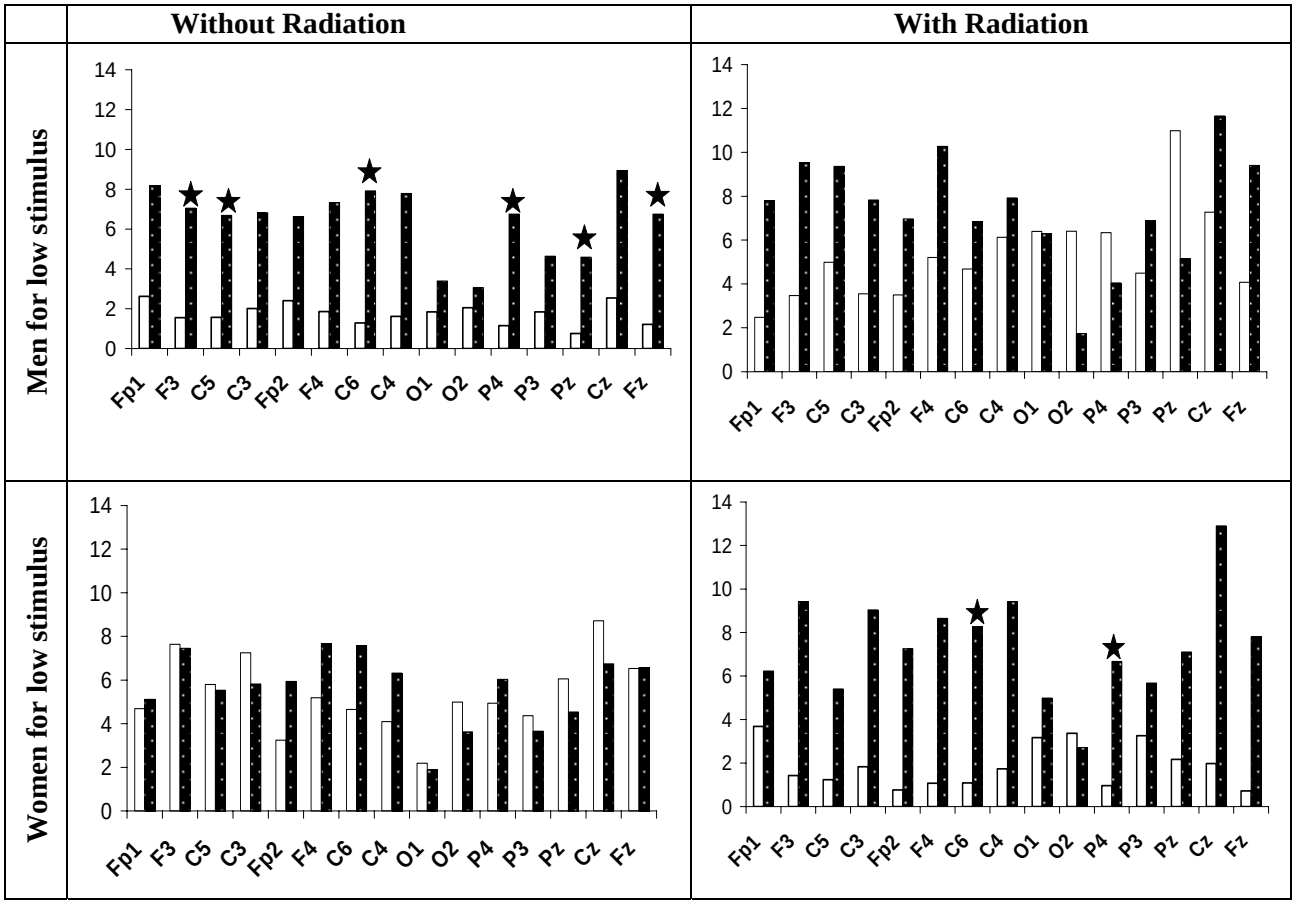

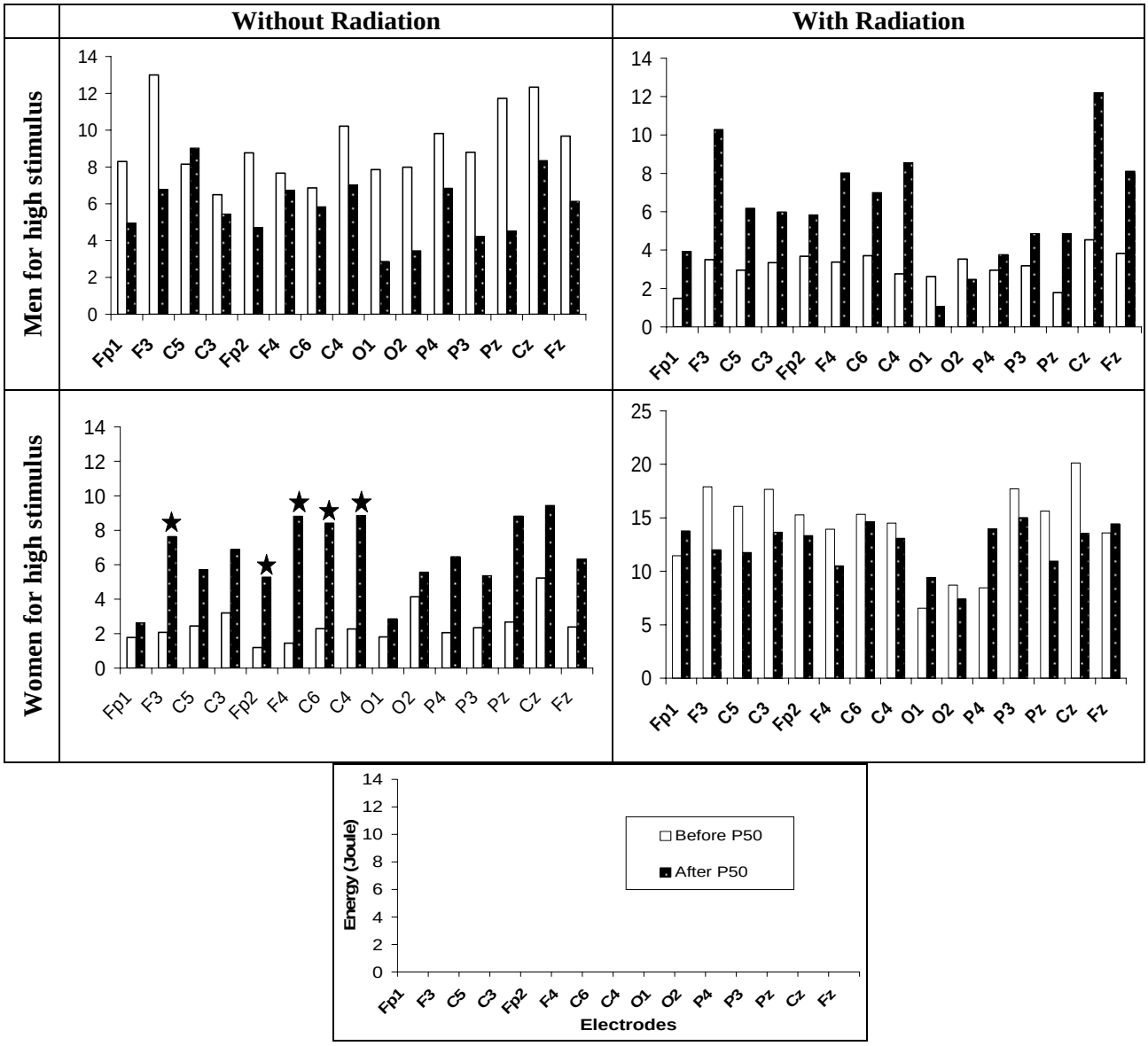

Figure 1. Energies before and after the P50 component for tones, genders and EMF conditions.

Discussion

The main objective of this study was the investigation of the influence of EMF on the sensory components of ERPs (within, 100msec after warning stimulus onset) elicited during a WM task. In order to retain both time and frequency domain information of ERPs we used the Wavelet analysis. Utilizing the two key aspects of Wavelet analysis-its multiresolution nature and its adaptivity to nonstationarity in ERP data elicited during a WM task- temporal comparisons between the energies, averaged at the time intervals before and after the P50 amplitude peak (30-80 msec after warning stimulus onset) were made.

The most robust findings were observed in alpha-frequency band activities. In particular in the absence of radiation, comparing the energies of the alpha frequency band before and after the P50 component, men exhibited a significant increase for the low stimulus at electrodes F3,C5,C6,P3,Pz and Fz, while women evidenced the same increase for the high stimulus at electrodes F3,Fp2,F4,C6 and C4. The importance of the obtained results may be explained, considering the activation of 'alpha system', using the so called conventional ways of EEG variables (power-, amplitudes-, network connection measures and phase delays). When a subject is stimulated (e.g. auditory stimulus) the flow of information is accompanied by alpha enhancement involving structures in the auditory pathways (e.g. reticular formation, medial geniculate nucleus, thalamus, hippocampus and the auditory cortex). [27]

Neurophysiological studies underscore that the alpha-band of evoked potentials is strongly correlated

with sensory function (e.g. thalamo-cortical circuits associated with working memory and probably with long – term memory engrams) [28]. It was also suggested that the alpha-band activity reflects a cortical –deactivation (the augmentation of attention-demanding mental activity is associated with decrease of alpha rhythm) [29]. In the light of these theories, the stimulus-related increase of the energy (before and after the P50), mostly for the alpha activity, which was found here, could though speculative, point to the possibility that the underlying neural networks of pre-attentive operation needs to be deactivated (relaxed) when the process of attention is ongoing. Conventionally the waveform of P50 which (as noted earlier) reflects pre-attentive operations is followed by the N100 waveform which represents the process of attention [16].

A second striking finding was the effect of gender on the patterns of energy changes within the time-window of the sensory components of ERPs for the alpha frequency. Gender has been shown to influence a variety of electrophysiological measures. However, the factors that mediate gender-related electrophysiological differences are not well understood. One possible mechanism which has been postulated is that steroid hormones estrogens and testosterone might be related to the neural oscillations associated with thalamocorical circuits which underlie alpha band activity [30]. Within this context, in order to understand better the observed gender-related differences concerning the two warning stimuli (high- vs low-warning tone) which evoked the measured ERPs, it seems reasonable to keep in mind that the auditory pathways from cochlear nucleus to the auditory cortex exhibit tonotopic organization during the ontogenesis.[31] In the light of these theoretical assumptions , it could be speculated that males and females have different neural networks activities involved in the transfer of information in thalamo-cortical circuits. This is in line with neurophysiological studies indicating that during the adolence in males the volume of white matter increases faster than in females. [32]

Moreover, the observed increase of the energy, before - after the P50 amplitude peak, points to an increased cortical activation as a direct consequence of EMF exposure. Such an effect may be due either to the psychophysic effect of the EMF exposure on brain tissue and/ or to its neurophysiological consequences (e.g. influence on blood brain barrier and/or thermal alterations). In relation to the neurophysiological point of view recent studies provide evidence, indicating the involvement of blood brain barrier (BBB) permeability, in the effect of mobile phones on the brain [33]. For instance it has been shown that EMF radiation has the potency to significantly open the BBB in a way that not only small but also large molecules, including toxic ones, can pass the BBB producing neuronal damage in the cortex, hippocampus and basal ganglia of rats exposed to EMF radiation for two (2) hours [34, 35]. On the other hand the EMF radiation is associated with enhancement of the temperature of the underlying tissues of the brain. It has been reported local heating (estimated to $0.11^{O}C$ rise in brain) due to radiation of EMF [36]. Interestingly, psychophysiological and neurophysiological studies have provided a direct relationship between alpha EEG activity regarding both thermal stimulations of the brain and changes of BBB. For example EEG coherence in alpha band significantly decreased in human subjects during tonic thermal stimulation [37]. Within this context, a brain imaging study by Korn et al., 2005 [38] using single photon emission computed tomography (SPECT) and addressing to both cortical- and BBB function in patients with postconcussion syndrome found significantly lower power in the alpha band compared with matched controls in conjunction with BBB disruption. Therefore, the changes described regarding the alpha EEG activity would seem to indicate adverse effects of EMF upon brain operation, which possibly may be mediated through the thermal and BBB alterations induced by EMF radiation.

In summary, the present study is an attempt to find sensory ERPs correlates associated with possible effects on human brain after exposure to EMFs. In order to retain both time and frequency domain information of ERPs we used the Wavelet analysis. Temporal comparisons between the energies, averaged at the time intervals before and after the P50 amplitude peak (30-80 msec after warning stimulus onset) were made. It was found that only for the alpha band the energy was mostly increased and this change is highly dependent on the interaction among modality, gender and EMF exposure.

Acknowledgements

The authors would like to thank Mr. M.Kyprianou, Scientific Investigator, Athens, Greece, for his professional support on the statistical analysis of the experimental results.

References

[1] F. Schönborn, M. Burkhardt, N. Kuster, Differences in energy absorption between heads of adults and children in the near field of sources. Health Phys. 74 (1998) 160-168.

[2] Z. Weinberger, E. D. Richter, Cellular telephones and effects on the brain: The head as an antenna and brain tissue as a radio receiver, Med. Hypotheses 59(2002) 703-705.

[3] R. Westerman, B. Hocking, Diseases of modern living: neurological changes associated with mobile phones and radiofrequency radiation in humans, Neurosci. Lett. 361 (2004) 13-16.

[4] H. Reiser, W Dimpfel, F Schober, The influence of electromagnetic fields on human brain activity, Eur J Med Res. 1995 Oct 16;1(1):27-32.

[5] R Huber, V Treyer, AA Borbely, J Schuderer, JM Gottselig, HP Landolt, E Werth, T Berthold, N Kuster, A Buck, P Achermann, Electromagnetic fields, such as those from mobile phones, alter regional cerebral blood flow and sleep and waking EEG. J Sleep Res. 2002 Dec;11(4):289-95.

[6] RJ Croft, JS Chandler, AP Burgess, RJ Barry, JD Williams, AR Clarke, Acute mobile phone operation affects neural function in humans. Clin Neurophysiol. 2002 Oct;113(10):1623-32.

[7] Curcio G, Ferrara M, Moroni F, D'Inzeo G, Bertini M, De Gennaro L. Is the brain influenced by a phone call? An EEG study of resting wakefulness. Neurosci Res. 2005 Nov;53(3):265-70. Epub 2005 Aug 15.

[8] J Roschke and K Mann, No short-term effects of digital mobile radiotelephone on the awake human electroencephalogram. Bioelectromagnetics 1997; 18:172–176.

[9] N Yeung, R Bogacz, B Clay Holroyd,, JD Cohen, eds. Psychophysiology, Blackwell Publishing Inc. Printed in the USA. 41 (2004), 822–832.

[10] C. Eulitz, P. Ullsperger, G. Freude, T. Elbert, Mobile phones modulate response brain activity, Neuroreport 9 (1998) 3229-3232.

[11] G. Freude, P. Ullsperger, S. Eggert, I. Ruppe, Effects of microwaves emitted by cellular phones on human slow brain potentials, Bioelectromagnetics, 19 (1998)384-387.

[12] W. A. Preece, G.Iwi, A. Davies-Smith, K. Wesnes, S. Butler, E. Lim, A. Varey, Effect of a 915-MHz simulated mobile phone signal on cognitive function in man. Int J Radiat Biol. 75 (1999) 447-456.

[13] M. Koivisto, A. Revonsuo, C. Krause, C. Haarala, L. Sillanmaki, M. Laine, H. Hamalainen, Effects of 902 MHz electromagnetic field emitted by cellular telephones on response times in humans. Neuroreport 11 (2000) 413-415.

[14] M. Koivisto, M.C. Krause, A.Revonsuo, M. Laine, H. Hamalainen, The effects of electromagnetic field emitted by GSM phones on working memory. Neuroreport 11 (2000) 1641-1643.

[15] M.C. Krause, L. Sillanmaki, M. Koivisto, A. Haggqvist, C. Saarela et al. Effects of electromagnetic fields emitted by cellular phones on the electroencephalogram during a visual working memory task. Int J Radiat Biol. 76 (2000) 1659-1667.

[16] M.Fabiani, G. Gratton, M. Coles, Event-related potentials: methods, theory, and applications. In: Cacioppo J, Tassinary L, Bernston G, eds. Handbook of psychophysiology. Cambridge University Press, New York, 2000, pp53–84.

[17] Papageorgiou C., Nanou D., Tsiafakis V., Kapareliotis E., Kontoangelos K., Capsalis C, Rabavilas A., Soldatos C.Acute mobile phone effects on pre-attentive operation, Neuroscience Letters 2006 (Paper in press).

[18] A.B.Clementz, D.L. Blumenfeld, S. Cobb, The gamma band response may account for poor P50 suppression in schizophrenia. Neuroreport. 8(18) (1997)3889-3893.

[19] G. Zouridakis, N.N. Boutros, H.B. Jansen, A fuzzy clustering approach to study the auditory P50 component in schizophrenia. Psychiat. Res. 69 (1997) 169-181.

[20] Rosso O.A., Figliola A. Order/disorder in brain electrical activity, Revista Mexicana de Fisica 50(2) (2004) 149-155.

[21] Samar V.J., Begleiter H., Chapa J.O., Raghuveer M.R., Orlando M., Chorlian D., Matched Meyer neural wavelets for clinical and experimental analysis of auditory and visual evoked potentials, 1996,In G. Ramponi, G.I. Sicuranza, S. Carrato and S.Marsi(Eds.), Signal processing: VII. Theories and applications, Proceedings of EUSIPCO-96(pp. 387-390). Trieste: Edizioni LINT.

[22] Horita M, Takizawa Y, Wada Y, Futamata H, Hashimoto T. Sex differences in EEG background activity: a study with quantitative analysis in normal adults. Rinsho Byori 43(2): 177-80, 1995Feb.

[23] Briere ME, Forest G, Chouinard S, Godbout R. *Evening and morning EEG differences between young men and women adults*. Brain Cogn 53(2): 145-8, 2003 Nov.

[24] C. Papageorgiou, E. Nanou, V. G. Tsiafakis, C. Capsalis, A. D. Rabavilas, Gender related differences on the EEG during a simulated mobile phone signal, Neuroreport, 15 (2004) 2557-2560.

[25] D. Wechsler, Manual for the Wechsler adult intelligence scale. New York: Psychological Corporation, 1955.

[26] H. Jasper, The ten-twenty electrode system of the international federation. Electroencephalogr Clin Neurophysiol. 10 (1958) 371–375.

[27] Basar E.Memory as the "whole brain work": a large-scale model based on "oscillations in super-synergy".Int J Psychophysiol. 2005;58(2-3):199-226.

[28] Basar E, Basar-Eroglu C, Karakas S, Schurmann M.Gamma, alpha, delta, and theta oscillations govern cognitive processes.Int J Psychophysiol. 2001;39(2-3):241-8.

[29] Laufs H, Kleinschmidt A, Beyerle A, Eger E, Salek-Haddadi A, Preibisch C, Krakow K. 2003. EEG-correlated fMRI of human alpha activity. Neuroimage 19:1463-1476.

[30] Carozzo S, Fornaro S, Garbarino S, Saturno M, Sannita WG.From neuroscience to application in neuropharmacology: A generation of progress in electrophysiology.Clin EEG Neurosci. 2006 Apr;37(2):121-34. Review.

[31] Romand R. Modification of tonotopic representation in the auditory system during development. Prog Neurobiol. 1997 ;51(1):1-17.

[32] De Bellis MD, Keshavan MS, Beers SR, Hall J, Frustaci K, Masalehdan A, Noll J, Boring AM.Sex differences in brain maturation during childhood and adolescence.Cereb Cortex. 2001 Jun;11(6):552-7.

[33] Hossmann KA and Hermann DM. Effects of electromagnetic radiation of mobile phones on the central nervous system. Bioelectromagnetics 2003;24:49–62.

[34] Persson BR, Salford LG, Brun A, Eberhardt JL, Malmgren L. Increased permeability of the blood-brain barrier induced by magnetic and electromagnetic fields. Ann N Y Acad Sci. 1992 Mar 31;649:356-8. No abstract available.

[35] Salford LG, Brun AE, Eberhardt JL, Malmgren L, Persson BR. Nerve cell damage in mammalian brain after exposure to microwaves from GSM mobile phones. Environ Health Perspect. 2003 Jun;111(7):881-3;

[36]Van Leeuwen GM, Lagendijk JJ, Van Leersum BJ, Zwamborn AP, Hornsleth SN, Kotte AN. Calculation of change in brain temperatures due to exposure to a mobile phone. Phys Med Biol. 1999 Oct;44(10):2367-79.

[37] Huber MT, Bartling J, Pachur D, Woikowsky-Biedau SV, Lautenbacher S.EEG responses to tonic heat pain.Exp Brain Res. 2006;173(1):14-24.

[38] Korn A, Golan H, Melamed I, Pascual-Marqui R, Friedman A. Focal cortical dysfunction and blood-brain barrier disruption in patients with Postconcussion syndrome. J Clin Neurophysiol. 2005 Jan-Feb; 22(1):1-9.

MODULATED MICROWAVE EFFECT ON DEPRESSION

MAIE BACHMANN[1], HIIE HINRIKUS[1], KAIRE AADAMSOO[2], ÜLLE VÕHMA[2], JEKATERINA RUBLJOVA[1], ANNA SUHHOVA[1], JAANUS LASS[1], JEVGENI RIIPULK[1]

[1]Biomedical Engineering Centre, Tallinn University of Technology

Address: 5 Ehitajate Rd, EE19086 Tallinn, Estonia

[2]Clinic of Psychiatry, North Estonia Regional Hospital,

Address: 19 J.Sütiste Rd, EE13419 Tallinn , Estonia

Abstract

The preliminary experiments were carried out on the group of depression patients (women, 18 subjects) and comparison group of healthy volunteers exposed during 30 min to 450 MHz microwave radiation modulated with 1000 Hz frequency. The field power density at the scalp was 0.9 mW/cm^2. As a subjective criteria of depression mood, the Brief Affect Scale (BAS) and Visual Analogue Scale (VAS) before and after each exposure procedure was used. Parallel a ratio of the EEG power in symmetric EEG channels of the different brain hemispheres FP1/ FP2, T3/T4, P3/P4 and O1/O2 was evaluated. Statistical analysis of these parameters for individuals with post-hoc Bonferroni correction was applied.

The BAS revealed mood improvement after exposure for majority of depressive subjects (11) and no changes for others (7). The VAS detected significant improvement in subjective mood score after exposure. The EEG analysis showed the biggest difference in symmetry between hemispheres in temporal area. Average values are higher in higher EEG rhythms. The difference was significant in 3 cases of exposed and in 5 cases of sham recordings. Significant results in sham condition indicate that the parameter selected as a measure is not very steady among depressive patients. This makes difficult to detect the effect caused by the EMF exposure.

Keywords: EMF effect, depression, Brief Affect Scale, EEG analysis, symmetry of brain hemispheres.

.

Introduction

Clinical treatment approaches for depression disorder utilize primarily pharmacologic agents, antipsychotic and antidepressant drugs, that sometimes are of limited efficacy and may have objectionable side effects. ECT is usually effective as a treatment for depressive disorder, but it involves general anesthesia and some degree of memory loss, and its effects can be transient. Repetitive transcranial magnetic stimulation (rTMS), initially developed to test gross central nervous system function, more recently has been applied with some success in the treatment of depression [1–3]. The success of rTMS in the treatment of depression has been varied and has been described in a recent review as "often statistically significant (but) below the threshold of clinical usefulness" [1]. rTMS treatment can be unpleasant, with some patients declining participation due to scalp pain induced by the apparatus [4]. There is also a small risk of seizure [5].

Recent report has suggested mood improvement in patients with bipolar disorder immediately after they underwent an echo-planar magnetic resonance spectroscopic imaging (EPMRSI) procedure that can be performed within clinical MR system limits [6]. The mood states of subjects in an ongoing EP-MRSI study of bipolar disorder were assessed by using the Brief Affect Scale, a structured mood rating scale, immediately before and after an EP-MRSI session. The characteristics of the electric fields generated by the EP-MRSI scan were analyzed. Mood improvement was reported by 23 of 30 bipolar disorder subjects who received the actual EP-MRSI examination, by three of 10 bipolar disorder subjects who received sham EP-MRSI, and by four of 14 healthy comparison subjects who received actual EP-MRSI. Significant differences in mood improvement were found between the bipolar disorder subjects who received actual EP-MRSI and those who received sham EP-MRSI. The electric fields generated by the EP-MRSI scan were smaller (0.7 V/m) than fields used in repetitive transcranial magnetic stimulation (rTMS) treatment of depression (1–500 V/m) and also extended uniformly throughout the head, unlike the highly nonuniform fields used in rTMS. The EP-MRSI waveform, a 1-kHz train of monophasic trapezoidal gradient pulses, differed from that used in rTMS. These preliminary data suggest that the EP-MRSI scan induces electric fields that are associated with reported mood improvement in subjects with bipolar disorder. The findings are similar to those for rTMS depression treatments, although the waveform used in EP-MRSI differs from that used in rTMS.

The findings reported above allowed expecting EMF effect on depression at the field power density much lower than used in TMS. In our previous studies the effect of the modulated 450 MHz microwave radiation on human EEG has been detected at the EMF level 0.16 mW/cm^2, lower than the recommended health protection limit [7-10]. In majority of modulation frequencies and EEG rhythms the exposure increases the EEG energy level and variability. Has such stimulation any effect on depression?

The aim of this study is to investigate the effect of modulated microwave exposure to the state of depression. In the study we tested the hypothesis that the modulated with 1000 Hz frequency 450 MHz EMF has an effect on subjects with depressive disorder. Distinction of reactions to microwave exposure will be performed by 1) clinical rating utilising psychiatric tests 2) EEG analysis.

Method and equipment

Subjects

The experiments were carried out on two groups of volunteers: a group of patients with major depressive disorder and a group of healthy comparison subjects. The group of subjects consisted of 18 persons, mean age 39 years, standard deviation 10 years.

The study was conducted in accordance with the Declaration of Helsinki and has formally approved by the local Medical Research Ethics Committee. All risks, benefits and possible adverse events associated with EMF study participation were explained to subjects, who provided written informed consent before entering the study.

Subjects with major depressive disorder were selected from hospital inpatient unit. Subjects with non-psychotic major depressive disorder as defined by ICD-10 criteria and determined by 17-item Hamilton Depression Rating Scale (HAM-D) score more than 14 were eligible. The average HAMD score for the group was 21 (SD 3.3). Subjects were without antidepressant treatment, only regular (same dosage for more than 3 weeks) benzodiazepine use was allowed. Concomitant treatments for current general medical conditions were permitted on the basis of clinical judgment (patients receiving medication with known CNS side effects were not eligible).

All the subjects passed two experimental procedures - with exposure and sham. During each test session, the succession of exposure-sham was randomly assigned. Only one experimental EEG recording was performed for a subject during a day between time interval 9 a.m. to noon. The subjects were not informed of their exposure, however, they were aware of the possibility of being exposed.

Subjects were asked to evaluate Becks Depression Inventory (BDI) and Visual Analogue Scale (VAS) before and after each EMF procedure (both exposure and sham). Subjects were also asked to evaluate Brief Affect Scale (BAS) after each EMF procedure.

Microwave exposure

The 450 MHz microwave radiation was generated by the Rhode & Swartz (Germany) signal generator model SML02. The RF signal was 100% amplitude modulated by the pulse modulator SML-B3 at 1000 Hz requency (duty cycle 50%). The generator signal was amplified with the Dage Corporation (USA) power amplifier model MSD-2597601 and additional laboratory amplifier (Miteq-Eesti, Estonia). The generator and amplifier were carefully shielded and located in the laboratory room. The 10W EMF output power was guided by a coaxial to the quarter-wave antenna NMT450 RA3206 by Allgon Mobile Communication AB, Sweden, located at 10 cm from skin from the left side of the head.

The spatial distribution of the microwave power density was measured by the Fieldmeter C.A 43 Chauvin Arnoux (France) field strength meter. The calibration curves of the field power density dependence on the distance from the radiating antenna were obtained from these measurements performed in the real condition of the experiment. During the experiments, the stability of the microwave level was monitored by the IC Engineering (USA) Digi Field C field strength meter. Estimated by the measured calibration curves, the field power density at the skin from the left side of the head was 0.9 mW/cm^2. The spatial distribution of the field density around the head and upper torso was not uniform: Digi Field C field strength meter indicated maximum level of 0.9±0.1 mW/cm^2 at the left side of the head, minimum level of 0.14±0.05 mW/cm^2 at the right side of the head and 0.45±0.05 mW/cm^2 above the head. Measured field power density was 0.8±0.15 mW/cm^2 at 10 cm distant from the left ear, near and the left shoulder and 0.17±0.05 mW/cm^2 near the right shoulder. The SAR value, calculated based on the maximum field power density, is 2 W/kg.

Experimental procedure and EEG recording equipment

The study consisted of two experimental procedures identical for all subjects. The first protocol included continuous EEG recording during 30 minutes. The 450 MHz 1000 Hz modulated microwave exposure is switched on during all recording. The second protocol is the same except that the microwave exposure is switched off.

The experimenter and the subjects were in the same laboratory room during the experiments. The room was dark but no other special conditions were provided. The subjects were lying in a relaxed position, eyes closed and ears blocked during the experiments.

The Cadwell Easy II EEG measurement equipment was used for the EEG recordings The EEG was recorded using 32 electrodes, which were placed on the subject's head according to the international 10-20-electrode position classification system. The channels for analysis were chosen to cover the entire head: frontal - FP1, FP2; parietal P5, P4, temporal - T3, T4; occipital O1, O2 and the reference electrode Cz). The EEG recordings were stored on a computer with a 400 Hz sampling frequency. The recorded EEG signals were observed by an experienced neurologist. The artifacts were detected by visual inspection. The recordings containing multiple artifacts were removed and the recording was repeated.

Afterwards, off-line data processing was executed. The energies of the five basic EEG rhythm frequencies (delta, theta, alpha, beta and beta2) were extracted from the total EEG signal (0.5 - 48 Hz) by filtering.

Clinical evaluations

Each subject completed the Visual Analogue Scale (VAS) and the Brief Affect Scale (BAS) based on their subjective feeling and symptoms before and/or after every experimental procedure.

Visual Analogue Scale (VAS) was introduced for subject self-evaluation of mood. VAS is 100-millimeter line with one end matching mood “very bad” and second end matching as “very good”. Subject has to determine visually her mood on the day of evaluation marking this on the line. In our study subjects evaluated VAS on the day before and the day after EMS procedure (both exposure and sham). This allows to determine immediate effect as scale can be to be applied every day. The lengths of the lines from beginning up to the marker were manually measured afterwards (results from 0 to 100 are possible). The lower numeric results in VAS show more depressive mood. VAS was introduced to determine immediate effect of EMS, as HAMD and BDI are designed for longer period (minimum 1 week).

The Brief Affect Scale was applied to the study after the experimental protocols. The subjects were asked to fill out the form and answer how much, if any, their feeling had improved or worsened since the time before experimental protocol. The subjects provided their responses on a 7-point scale, as follows: 3, very much improved; 2, much improved; 1, minimally improved; 0, no change; –1, minimally worse; –2, much worse; and –3, very much worse. These numerically ranked responses were grouped into the categories of improved (3 to 1), same (0), and worse (–1 to –3) for statistical treatment. This grouping is referred to as the Brief Affect Scale ratings.

The two-tailed paired Student t-test was used to estimate differences between exposed and sham exposed results for depressive and healthy subjects. All *p* values lower than 0.05 were considered as significant.

EEG analysis

The dynamics of the EEG energy of the theta (4-8 Hz), alpha (8-13 Hz), beta1 (13-20 Hz) and beta2 (20-40 Hz) rhythms frequencies was analyzed.

Assymmetry between left and right brain hemisphare EEG channels was selected as a measure for estimation of the effect. The ratio of the power spectral density of the signals for the symmetric channels FP2/FP1, T4/T3, P4/P3, O2/O1 from right and left hemispheres was calculated and analysed.

The power spectral density (PSD) was estimated by means of Welch's averaged periodogram method. The signal was divided into overlapping sections (50%), with the length of 2048 points and windowed by the Hanning window. Afterwards, the power on the theta, alpha, or beta band W_{mn} was computed for each subject (indexed by $n \in [1,18]$) and hemisphere (indexed by $m=1,2$) as the area under the spectrum for the corresponding frequency band (integral of the band).

The relative misbalances of the PSD in symmetric channels were selected for further analysis. Finally, parameter *A* for a subject was calculated as follows:

$$A=(W_{1n} / W_{2n} -1)*100\ \%,$$

where W_{1n} and W_{2n} were the power spectral densities of the right and left symmetric channel respectively.

The average values and standard deviations of parameter *A* for different EEG channels pairs for the individual subjects and for the whole group were calculated.

Statistical analysis was performed for the differences between exposed and sham exposed recordings. For sham recordings, normal physiological processes determine the asymmetry between hemispheres and the standard deviation σ for the parameter *A* was calculated.

According to the “zero hypothesis”, the EEG recordings of subjects under microwave exposure cannot be distinguished from sham signals. Thus, the “zero hypothesis” implies that and $\left\langle \left(W_1 - W_2\right)^2 \right\rangle = \left\langle \left(\tilde{W}_1 - \tilde{W}_2\right)^2 \right\rangle$. Consequently, if the “zero hypothesis” is true, the quantity $x = \left(W_{1n} - W_{2n}\right)^2 \sigma^{-2}$ is a *f*-distributed random quantity, the cumulative distribution of which is routinely designated as $F_{1,15}(x)$; the indices 1 and 18 stand for the numbers of the degrees of freedom.

Accordingly, the ratio of the computed power difference to the standard deviation (calculated on the basis of sham signals) of the differences can be used as a quantitative measure, showing how well the “zero hypothesis” is satisfied, respective *p*-values are obtained by means of the cumulative *f*-distribution:

$$p = F_{1,15}\left[(W_{1n} - W_{2n})^2 \sigma^{-2}\right].$$

Post-hoc mean comparisons were tested by Bonferroni approach with a 0.05 confidence level.

Signal processing and calculation of parameters were performed in the LabVIEW and MatLab programming and signal processing environment.

Results

The results of psychiatric tests are presented in Table 1. Most of the depressive subjects reported improvement of her mood after exposure (11). This number is less for sham procedure (7). Numbers of the subjects with no changes of mood is less for exposed subjects (7) and higher for sham subjects (10). Only one subject reported worsening of her mood during sham procedure.

The changes in mood during procedure are quite well reflected in score of the BAS test: average score for exposed procedure is 0.81 and sham procedure 0.62.

VAS test revealed significant change between scores before (average 33.3) and after (average 40.2) for exposed subjects and no significant change for sham exposed subjects.

These results are in good agreement with the study [6], where mainly the Brief Affect Scale was used for evaluation of the mood improvement in bipolar depression. Anyway, such results may be caused by the factors different from EMF as inconveniences related to MRI equipment or EEG cap.

Table 1. Data of the Brief Affect Scale (BAS) and Visual Analogue Scale (VAS) tests for depressive subjects

	Total number of subjects	Sub. Reporting improvement	Sub. Reporting worsening	Sub. Reporting no change	BAS		VAS			
							Before		After	
					Mean for group	SD	Mean for group	SD	Mean for group	SD
Depression subjects exposed	18	11	0	7	0.81	0.75	33.34	17.97	40.21	25.18
							p=0.04			
Depression subjects sham exposed	18	7	1	10	0.62	1.20	35.68	19.46	40.29	21.21
							p=0.25			

Data of the EEG analysis are presented in Figures 1 and 2. Figure 1 presents the average values of *A* for different frequency bands, for control group in sham (1a) and EMF condition (1b). As can be seen, those values behave quite similarly. The biggest difference seems to be in frontal region. However, trends in different channels are the same in sham and EMF condition.

As expected, for control group, there were no significant results in the ratio of the computed power difference to the standard deviation of differences (calculated on the basis of sham signals) in the case of sham recordings nor recordings under the influence of EMF.

Figure 2 presents the average values of A for different frequency bands, for depressive group in sham (2a) and EMF condition (2b). The results are not as similar between two EMF conditions as they were in control group. The biggest difference occurs in temporal area. Average values are higher in higher EEG rhythms, however having opposite signs. Beta rhythms are more influenced also in frontal area. Trends in other brain regions are mostly the same in sham and EMF conditions.

In the case of EMF recordings of depressed patients, the ratio of the computed power difference to the standard deviation of differences (calculated on the basis of sham signals) was significant in 3 cases, and in the case of sham recordings in 5 cases. Significant results in sham condition indicate that parameter *A* is not very steady among depressive patients. This makes difficult to detect which deviation of the parameter is caused by EMF.

1a)

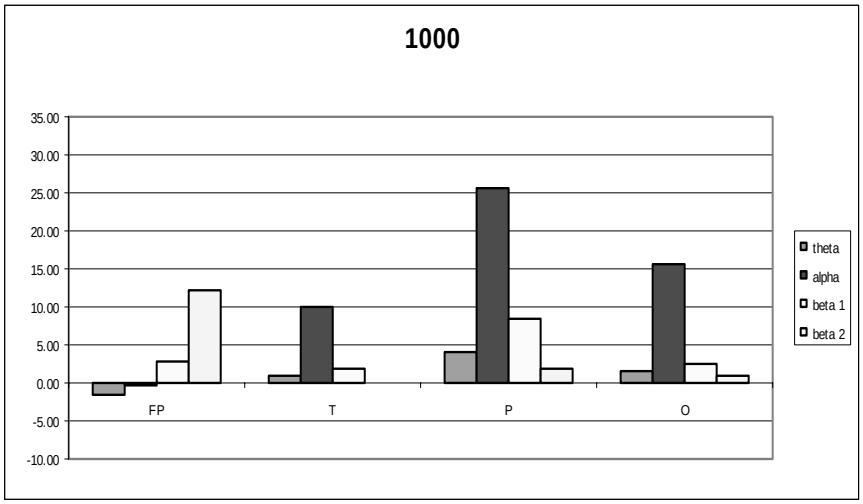

1b)

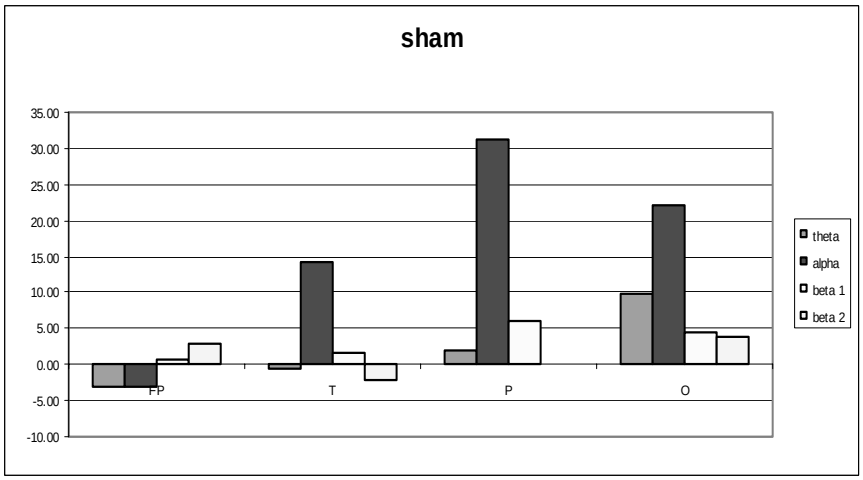

Figure 1. The average asymmetry of hemispheres (average values of *A*) for different EEG rhythms for control group in EMF (1a) and sham (1b) condition.

To investigate the behaviour of parameter *A* with depression, the depressive patients' sham recordings were compared with the sham recordings of the control group.

Now, the ratio of the computed power difference to the standard deviation of differences (calculated on the basis of sham signals) for control group sham recordings was zero and depressive group sham recordings had 7 significant results. The influence was highest in frontal theta rhythm 16.7% and the depression slightly influenced also the beta1 and beta2 rhythms in frontal and temporal region (5.6%).

2a)

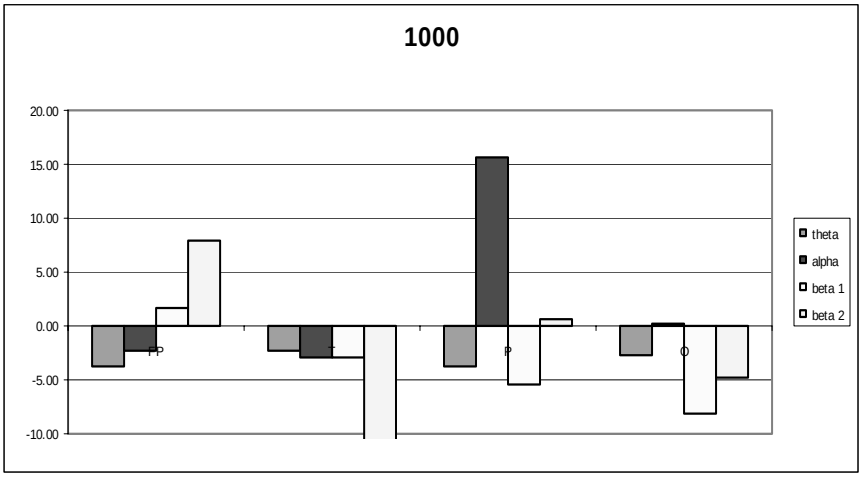

2b)

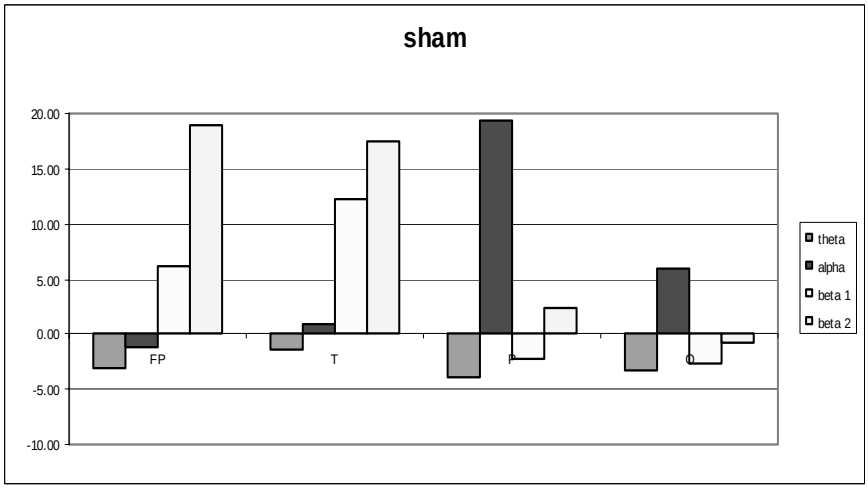

Figure 2. The average asymmetry of hemispheres (average values of *A*) for different EEG rhythms for the group of patients with major depressive disorder in EMF (2a) and sham (2b) condition.

Summary

The BAS revealed mood improvement after microwave exposure for majority of depressive subjects (11) and no changes for others (7). The VAS detected significant improvement in subjective mood score after exposure. These results support the recent promising research where mood improvement in bipolar depression by low-frequency magnetic field has been reported [6].

The EEG analysis based on evaluation of symmetry between brain hemispheres detected the biggest difference related to EMF exposure in temporal area. Average values are higher in higher EEG rhythms. But the difference related to EMF was significant in 3 cases, and in the case of sham recordings in 5 cases. Significant results in sham condition indicate that the parameter selected as measure is not very steady among depressive patients and makes difficult to detect which deviation of the parameter is caused by EMF exposure.

The preliminary results are promising and the further investigation should be aimed to finding a better measure for EEG analysis and performing experiments on larger number of subjects.

Acknowledgement

This study has been supported by the Estonian Science Foundation grant No 6632.

References

1. Wassermann EM, Lisanby SH: Therapeutic application of repetitive transcranial magnetic stimulation: a review. Clin Neurophysiol 2001, **112**:1367–1377.
2. McNamara B, Ray JL, Arthurs OJ, Boniface S: Transcranial magnetic stimulation for depression and other psychiatric disorders. Psychol Med 2001, **31**:1141–1146.
3. Lisanby SH: Focal brain stimulation with repetitive transcranial magnetic stimulation (rTMS): implications for the neural circuitry of depression. Psychol Med 2003; **33**:7–13.
4. George MS, Nahas Z, Molloy M, Speer AM, Oliver NC, Li XB, Arana GW, Risch SC, Ballenger JC: A controlled trial of daily left prefrontal cortex TMS for treating depression. Biol Psychiatry, 2000; **48**:962–970.
5. Wassermann EM: Risk and safety of repetitive transcranial magnetic stimulation: report and suggested guidelines from the International Workshop on the Safety of Repetitive Transcranial Magnetic Stimulation, June 5–7, 1996. Electroencephalogr Clin Neurophysiol 1998; *108*:1–16.
6. Rohan M, Parow A, Stoll AL, Demopolus C, Friedman S, Dager S, Hennen J, Cohen BM, Renshaw PF, 2004. Low-field magnetic stimulation in bipolar depression using an MRI-based stimulator. Am J Psychiatry; **161**: 93-98.
7. Hinrikus, H., Parts, M., Lass, J., Tuulik, V. Changes in Human EEG Caused by Low Level Modulated Microwave Stimulation. Bioelectromagnetics . 2004, **25**: 431-440.
8. Bachmann, M., Kalda, J., Lass, J., Tuulik, V., Sakki, M., Hinrikus, H. Non-linear analysis of the electroencephalogram for detecting effects of low-level electromagnetic fields. Medical & Biological Engineering & Computing, 2005, **43**:142-149.
9. Lass, J., Hinrikus, H., Bachmann, M., Tuulik, V. Microwave radiation has modulation frequency dependent stimulating effect on human EEG rhythms. Proceedings of the 26th Annual International Conference of the IEEE EMBS San Francisco, USA, 2004, 4225-4228.
10. Bachmann, M., Säkki, M., Kalda, J., Lass, J., Tuulik, V., Hinrikus, H. (2005): Effect of 450 MHz microwave modulated with 217 Hz on human EEG in rest. The Environmentalist, 2005, **25**: 65-171.

EFFECTS OF THE STATIC MAGNETIC FIELD GENERATED BY 0.5 T MRI UNIT ON TNF-α RELEASE OF HUMAN PBMC FROM PATIENTS WITH RHEUMATOID ARTHRITIS.

ANTONIO LO CASTO[1], CARMELA LA MENDOLA[2], SERGIO SALERNO[1], GIUSEPPE MAMONE[1], NADIA CACCAMO[2], ROBERTO LAGALLA[1]

[1] Sezione di Scienze radiologiche - Dipartimento di Biotecnologie mediche e Medicina legale - Università degli Studi di Palermo
[2]Dipartimento di Biopatologia - Università degli Studi di Palermo

Abstract
The aim of this study was to investigate the effects of a 0.5 T static magnetic field (SMF) of a MRI clinical unit on TNF-α release from peripheral blood mononuclear cells (PBMC) obtained from patients with rheumatoid arthritis (RA). These patients didn't take biological drugs, as receptor TNF-α or anti-TNF-α monoclonal antibodies, at the time of collecting samples. PBMC were isolated and cultured in complete medium and split into 2 groups of samples, one to be exposed and the other one as control. After 2 hrs of exposure to the SMF at 37°C, cells were stimulated or non stimulated with a mitogen, and incubated for 48 hrs. After the incubation the supernatants were collected and assayed by ELISA technique for TNF-α production. The results demonstrated a significant decrease of TNF-α release in PBMC of patients with RA exposed to 0.5 T SMF. RA is a multisystem disorder. It predominantly causes inflammation in synovial joints and tendon sheaths and results in suppressed erythropoiesis, but can also lead to serositis, alveolitis, ocular scleritis, subcutaneous nodules and hepatosplenomegaly. The positive clinical response to drug therapy with TNF-α-neutralizing agents shows that the inflammation is largely TNF-α dependent, at least in the synovium.

Introduction
Static magnetic field (SMF) produces different bioeffects on cells of the human immune system. A strong SMF is commonly employed by magnetic resonance devices in clinical practice to obtain tomographic images of the whole body (MRI, magnetic resonance imaging). Immune system cells represent a well known and sensitive model for the study of magnetic field bioeffects [1-3]. We have previously demonstrated that the SMF generated by a 0.5 T superconducting MRI clinical unit causes *in vitro* alteration on cytokine release in human peripheral blood mononuclear cells (PBMC) from healthy volunteers [1, 3]. Among these cytokines, it was observed a decreased release of TNF-α in exposed cells [4, 5]. TNF-α is a regulator of the immune response, playing an important role in several inflammatory conditions, such as rheumatoid arthritis (RA) [6, 7]. Some papers have dealt the effects of electromagnetic fields (emf) as a potential therapy in the treatment of arthritis [8, 9]. The aim of this study was to investigate the effects of a 0.5 T SMF of a MRI clinical unit on TNF-α release from PBMC obtained from patients with rheumatoid arthritis (RA).

Materials and methods
PBMC of 4 patients affected by RA and that didn't take biological drugs, as receptor TNF-α or anti-TNF-α monoclonal antibodies, at the time of collecting samples, were used for the experiment. PBMC were isolated from heparinized blood by centrifugation on Ficoll-Hypaque (Pharmacia, Uppsala, Sweden). Cells were maintained in RPMI-1640 (Gibco, Grand Island, NY) supplemented with 10% heat-inactivated pooled human AB^+ serum, 2 mM L-glutamine, 20 mM HEPES, 100 U/ml penicillin, 100 μg/ml streptomycin, 5 x 10^{-5} M 2-mercaptoethanol and 150 IU/ ml rIL-2. PBMC were split into two groups of samples, one to be exposed and the other one as control to be kept under isothermal conditions for the whole time of the experiment. After 2 hrs of exposure to the SMF, cells were stimulated with a mitogen, lypopolisaccaride (LPS), employed at a 0.5 μg/ml suboptimal concentration. After 48 hrs of culture supernatants were collected and stored at –70° C until tested. TNF-α content was assessed using immunoenzymatic methods. The commercial enzyme-linked immunosorbent assay (ELISA) was reagent set human TNF-α (EUROCLONE, Devon, UK). A superconducting MRI unit (Vectra; GE Medical Systems, Milwaukee, WI, USA) commonly employed for clinical examinations was the source of the 0.5 T SMF. A specific device for keeping the cell samples at 37° C was used; it was constituted

by a thermostated water bath in which a plexiglass tube holder, with the tubes containing cell samples, was placed before its introduction within the gantry of the MRI unit.

Results

After 48 hrs of *in vitro* culture, a significant decrease of TNF-α release was observed in PBMC of 4 patients affected by RA exposed for 2 hrs to a 0.5 T SMF, stimulated or not stimulated with LPS, in comparison with sham-exposed cells (Fig. 1).

Discussion

It has been previously observed that exposure of human PBMC from healthy volunteers for 2 hrs at 37 °C to the 0.5 T SMF of a MRI clinical unit caused a decreased release of cytokines in exposed cell [1, 3]. It was also demonstrated a decreased release of TNF-α in human macrophages under the same condition of exposure [4]. A related decrease of intracellular free calcium -whose compartimentalization through cell membrane is a part of the cell response mechanism to magnetic fields and inhibits activation of immune system cells- was also found in the exposed macrophages [5]. In this study the effects of a 0.5 T SMF of a MRI clinical unit on TNF-α release from PBMC obtained from patients with RA was evaluated. RA is a chronic inflammatory disease affecting 1% of the population [6]. TNF–α is a cytokine that promotes the inflammation and its associated with fever and signs (pain, tenderness, and swelling) in several inflammatory conditions, including RA [6, 7]. Some drugs have been introduced that, blocking the action of TNF-α, reduce the signs and symptoms of inflammation and stops the progression of joint damage [10]. Moreover, TNF–α is now recognized as a critical cytokine orchestrating differentiation and proliferation, as well as the ability to induce cell death [6]. TNF–α has been implicated as the causative agent in a number of pathologies, including cachexia, septic shock, rheumatoid arthritis, autoimmunity, and induction of HIV expression. Activated T cells, macrophages, and other non-lymphoid cells produce TNF–α. In RA, the antibodies (IgM) produced react with connective tissue components such as collagen and proteoglycans as well as with determinants in the Fc region of IgG and form IgG–IgM complexes, which get deposited in the joints and activate complement cascade [11]. This mechanism leads to erosion of cartilage and bone. The existing treatments available for RA cannot be considered as curative or definitive therapy. Hence, alternative and safe therapy regulating signaling pathways is absolutely essential. There is an increasing interest in the therapeutic use of emfs in arthritis, stimulated in large part by recent advances in alternative and complementary medicine [8, 9]. In this paper, after 48 hrs of *in vitro* culture, a significant decrease of TNF-α release was observed in PBMC of patients affected by RA exposed for 2 hrs to the 0.5 T SMF of a MRI clinical unit. Although these preliminary results, obtained from PBMC of only 4 patients affected by RA, need to be confirmed on wider population, this work may supply a key to the comprehension of mechanisms responsible of the therapeutic effects of emfs in arthritis. Interesting perspectives in the use of emfs as an adjuvant or alternative form of therapy in arthritis may furthermore develop.

References

1. Salerno S, Lo Casto A, Caccamo N, D'Anna C, De Maria M, Lagalla R, Scola L, Cardinale AE. Static magnetic fields generated by a 0.5 T MRI unit affects in vitro expression of activation markers and interleukin release in human peripheral blood mononuclear cells (PBMC). Int J Radiat Biol 1999; 75:457-63.
2. Aldinucci C, Garcia Blanco J, Palmi M, Sgaragli G, Benocci A., Meini A, Pessina F, Rossi C, Bonechi C, Pessina GP. The effect of strong static magnetic fields on lymphocytes. Bioelectromagnetics 2003; 24:109-117.
3. Salerno S, La Mendola C, Lo Casto A, Mamone G, Caccamo N, Cardinale AE, Salerno A. Reversible effect of MR and ELF magnetic fields (0.5 T and 0.5 mT) on human lymphocyte activation patterns. Int J Radiat Biol 2006; 82:77-85.
4. Lo Casto A, La Mendola C, Salerno S, Mamone G, Caccamo N, De Maria M. Effects of the static magnetic field generated by 0.5 T MRI unit on the release of TNF-α from human monocytes. Proceedings Biological effects of EMFs, 7-11 October, Rhodes, Greece, 2002: 363-366.
5. Lo Casto A, La Mendola C, Salerno S, Mamone M, Caccamo N, Lagalla R. Effects of the static magnetic field generated by 0.5 T MRI unit on intracellular calcium concentration and TNF-α release of human macrophages. Proceedings Biological effects of EMFs – 3rd International Workshop, 4-8 October, Kos, Greece, 2004: 70-73.
6. Beutler B. TNF in pathophysiology: biosynthetic regulation. J Invest Dermatol 1990; 95:81S–84S.
7. Kunkel SL, Spengler M, Kwon G, May MA, Remick DG. Production and regulation of tumor necrosis factor alpha. A cellular and molecular analisys. Methods Achiev Exp Pathol 1988; 13: 240-249.
8. Kumar VS, Kumar DA, Kalaivani K, Gangadharan AC, Raju KV, Thejomoorthy P, Manohar BM, Puvanakrishnan R. Optimization of pulsed electromagnetic field therapy for management of arthritis in rats. Bioelectromagnetics 2005; 26:431-9.
9. Fischer G, Pelka RB, Barovic J. Adjuvant treatment of knee osteoarthritis with weak pulsing magnetic fields. Results of a placebo-controlled trial prospective clinical trial. Z Orthop Ihre Grenzgeb. 2005; 143:544-50.

10. Iannone F, Trotta F, Montecucco C, Giacomelli R, Galeazzi M, Matucci-Cerinic M, Ferri C, Cutolo M, Bambara LM, Triolo G, Ferraccioli G, Valentini G, Lapadula G. Etanercept maintains the clinical benefit achieved by infliximab in patients with rheumatoid arthritis who discontinued infliximab due to side effects. Ann Rheum Dis. 2006 Jul 12; [Epub ahead of print].
11. Kohl J, Gessner JE. On the role of complement and Fc gammareceptors in the arthus reaction. Mol Immunol 1999; 36:893-903.

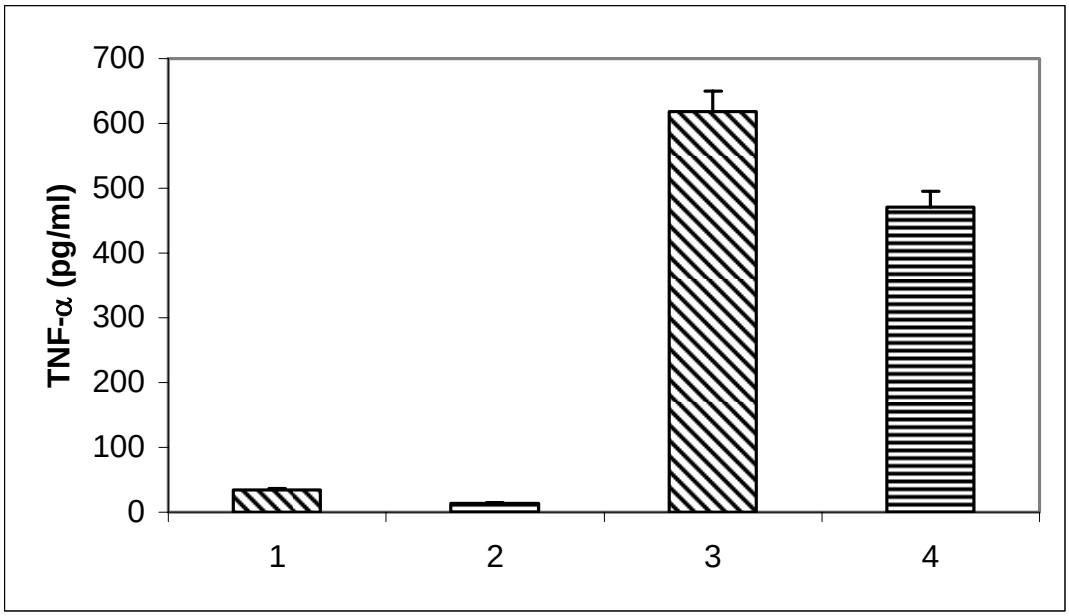

Fig.1. Release of TNF-α by human PBMC exposed to a 0.5 T SMF
Legends:

1. Sham exposed PBMC after 48 h of culture in complete medium.
2. SMF exposed PBMC after 48 h of culture in complete medium.
3. Sham exposed PBMC stimulated with mitogen (LPS) after 48 h of culture in complete medium.
4. SMF exposed PBMC stimulated with mitogen (LPS) after 48 h of culture in complete medium.

Overview of ISO TC215 Technical Report #21730: "Health informatics - Use of mobile wireless communication and computing technology in healthcare facilities - Recommendations for electromagnetic compatibility with medical devices

Joseph J Morrissey

Motorola Labs, 8000 West Sunrise Blvd, Ft. Lauderdale, FL 33322

Abstract: Worldwide, healthcare facilities are recognizing the need to incorporate new technology and provide better point-of-care information to improve healthcare delivery, while reducing medical errors. Computing technologies, electronic medical record systems, and seamless access to information using wireless communication can offer significant advancements to healthcare communication and health informatics exchange. Such wireless technologies include the use of mobile phones, handheld computers / PDAs, WiFi / 802.11.x local area networks, personal area networks including 802.15.1 (Bluetooth) / 802.15.4 (Zigbee) / WiMedia / UWB Alliance (UWB), two-way pagers, radios, etc. In addition, visitors and patients are also finding use of personal mobile phones and other wireless devices increasingly valuable, especially in times of crisis. Previously, no uniform international guideline existed for the appropriate deployment, use, and management of mobile wireless communication and computing technology within healthcare facilities to mitigate potential electromagnetic interference (EMI) with medical devices. At one extreme, overly-restrictive policies in some healthcare facilities may inadvertently act as obstacles to the deployment of beneficial technology. At the other extreme, unmanaged use of mobile wireless handsets in healthcare facilities can place patients at risk. An equally important factor in this issue is that healthcare organizations throughout the world have a variety of different resources, needs, concerns, and RF environments that may not all be addressed by implementation of a single prescriptive management strategy. The current Technical Report offers balanced guidance to allow diverse healthcare organizations realize the benefits of mobile wireless technology while also providing necessary and sufficient safeguards against undesired and unintended risks of EMI.

Introduction: The non-controlled/unmanaged use of mobile wireless equipment by individuals visiting or working in healthcare facilities has steadily increased, regardless of existing healthcare policy. However, published reports suggest that the level of risk for accidental EMI events from government and other non-profit health agency sources appears to be relatively small, although underreporting of such events may be substantial. Anecdotal observations of suspected EMI events or incidents with ECG and EEG machines, apnoea monitors, ventilators and radiant warmers, infusion pumps, wheelchairs, and other devices have been reported or referred to in a number of publications [1]-[15]. Ad hoc test studies [16]-[28] have confirmed that EM interference effects can be caused by certain wireless transmitters in susceptible medical devices, although this generally requires specific conditions (transmission at higher power levels, close proximity, for extended periods of time) that may not be common during normal use.

Although the recently approved second edition of the IEC International Standard 60601-1-2 specifies general immunity levels of 3 V/m for medical equipment and systems that are not life-supporting and 10 V/m for life-supporting medical equipment and systems, manufacturers in the US and many other countries are allowed to justify lower levels and there is no consistent international regulation enforcing this standard. Many mobile wireless handsets exceed the 3 and 10 V/m limits when operating at maximum power and in close proximity. Further, older medical devices still in use may not have been constructed or tested to the same EM immunity level. Despite the potentially serious level of risk due to unmanaged mobile wireless handset use, most mobile wireless equipment might be allowed to operate, even where potentially susceptible medical devices are used, if comprehensive management procedures are implemented.

Recommendations: The following recommendations are intended to help the healthcare facility achieve a reasonable assurance of EMC with their medical devices while allowing for the deployment of wireless RF technology. These recommendations are built on the foundations from the AAMI TIR 18-1997, recommendations from the AMA Council on Scientific Affairs, the American Society for Healthcare Engineers,

and several other publications and reports. In general, the healthcare facility should create a management, testing, procurement, and education program and policies addressing electromagnetic compatibility with active medical devices and the deployment of wireless technology. Because of the wide range of wireless technology involved, there are specific recommendations dealing with both the wireless emitters that are controlled or managed by the healthcare facility and wireless emitters that are not easily controlled by the facility (e.g., patient or visitor PDAs, computers, or cellular telephones). The following flow chart illustrates basic steps outlined in the specific recommendations to develop a facility strategy allowing wireless equipment to operate without unnecessary restrictions while at the same time sufficiently managing and mitigating potential EMI issues.

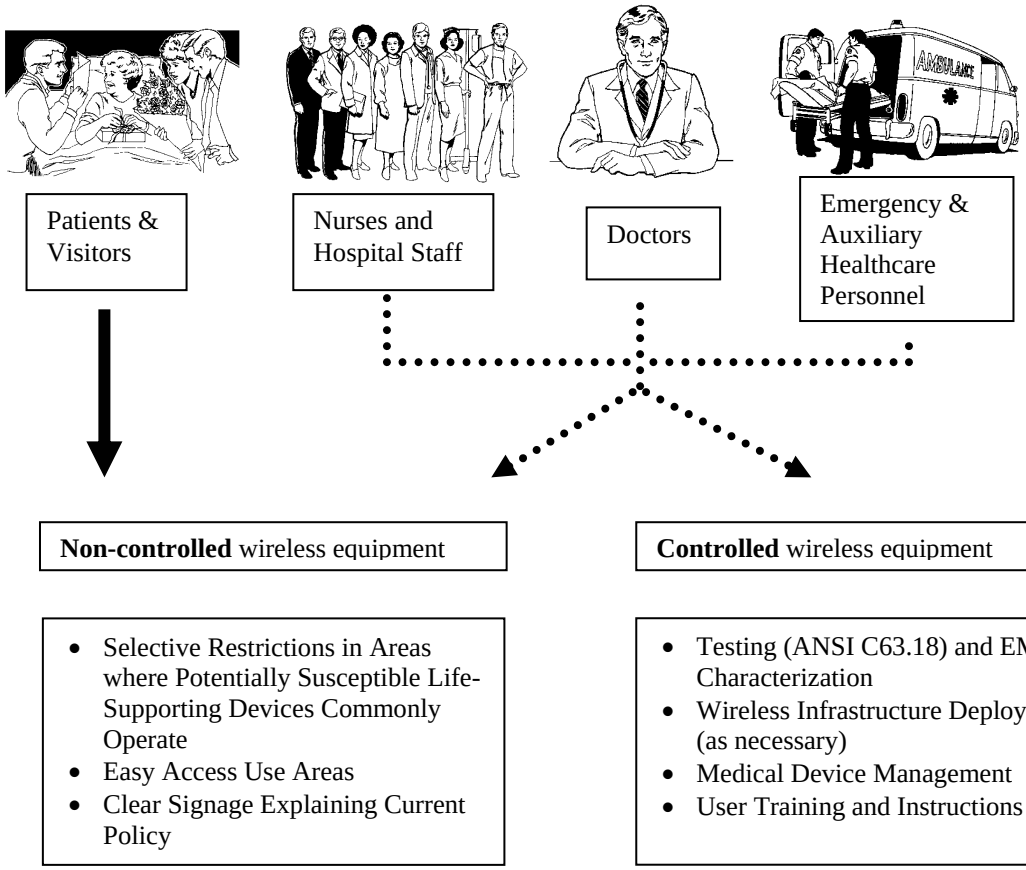

Important recommendations are made equally to Medical Device Manufacturers, Healthcare facilities, and Wireless Equipment Manufacturers.

Risk management of medical devices is covered in ISO 14971. All medical devices (including systems of medical devices such as would be formed with wired or wireless communication devices) should meet that standard and be managed to take into account compliance with ISO 14971 over the life cycle of the device.
For Medical Device Manufacturers, they should continue to meet and exceed current IEC 60601-1-2 [33] listed electromagnetic immunity levels in the design of new medical equipment. Medical devices that are not directly covered by this technical report should also be designed, manufactured, and deployed using the appropriate consensus standards with respect to EMC. (e.g., active implanted devices [55], in vitro diagnostics [56]). It is expected that medical devices will increasingly operate in environments where emissions from mobile RF/wireless transmitters are increasingly common.

For Healthcare facilities, they should manage wireless equipment within their facility in accordance with the following guidelines, and neither unduly limit the use of otherwise beneficial technology or ignore the potential for EMI issues. Similar recommendations electromagnetic compatibility with medical devices should also be directly incorporated into corporate policies, strategic plans, and / or governance models.
For Wireless Equipment Manufacturers, they should have full understanding of the potential EMI issues that can arise in worse case scenarios with medical devices as well as other wireless equipment, and deploy their equipment and systems appropriately in accordance with the following recommendations.

Responsibility within healthcare facilities
Within the healthcare facility, clinical/biomedical engineers or other appropriate technical personnel (e.g., spectrum management, IT, telecom, and building services) should be the focal point for EMC, EMI mitigation, and EMC/EMI education and training. Qualifications are not specified in this document, although consideration should be given to appropriate education, expertise, and experience of the responsible individuals

Inventory within healthcare facilities
The medical device inventory within a healthcare facility should be managed to the extent possible and practical to ensure compatibility with the ever-increasing RF environment.
a) In the purchase of new medical devices by healthcare facilities, every effort should be made to ensure the equipment meets (and exceeds if possible) minimum EMC immunity requirements set out by IEC 60601-1-2:2001 or other appropriate medical device EMC standard. Older equipment found to be particularly susceptible to EMI caused by mobile wireless transmitters should be phased out as is possible and practical within the healthcare facility budget.

b) While significant modifications to medical devices should not be made by healthcare facilities, certain simple precautions can be taken to reduce the risk of EMI caused by mobile wireless transmitters. EMI susceptibility in all medical devices can be reduced by positioning cables, sensors, and electrical accessories in such a way as to increase the distance between these components and RF transmitters operating in the area. Life-supporting medical devices or those known or suspected of being susceptible to EMI can be positioned away from high traffic areas or adjoining rooms where mobile wireless equipment may be in routine operation.

Testing within healthcare facilities
The **IEEE / ANSI C63.18** protocol is recommended for comprehensive ad hoc, on site testing of all mobile wireless equipment that might be used in the healthcare facility by doctors, staff, visitors, or patients. However, it is fully understood that exhaustive testing is rarely feasible, and different needs, resources, and personnel constraints of the healthcare facility may dictate widely different approaches. General recommendations regarding EMC testing are as follows:

a) Testing should be performed, whenever possible and practical, on selected medical devices in the equipment inventory that are considered to have life supporting functions (i.e., according to the prioritization recommendations of ANSI C63.18) using one of the mobile handsets as a test transmitter (see ANSI C63.18 for details on the test protocol).

b) Testing should take special consideration of older medical devices, life-supporting medical devices, and any device where EMI is suspected. Testing can be extended to other medical devices where feasible and practical (see ANSI C63.18 for details on a recommended prioritization).

c) Periodic testing should be performed on a regular schedule (e.g., once per year), and especially after changes such as the introduction of new communication devices, new medical equipment, or significant repositioning on a regular basis

d) If comprehensive testing of mobile wireless equipment is not possible, focused testing on mobile wireless equipment routinely operating within the healthcare facility that can transmit at higher power (e.g., two-way radios, mobile / cellular phones) may be most appropriate (see section 3, Table 1, and Annex A sections 4 and 5 for more detailed information about the frequency and RF output power for several types of wireless equipment). If testing of mobile wireless equipment is not possible at all, some information may be obtained by communicating with larger healthcare facilities that have performed prior testing or from ad hoc EMI testing databases found on the internet (one such ad hoc EMI testing database is currently being developed in cooperation with ASHE, although as of this revision it is not yet operational).

e) Assistance with obtaining transmitter equipment, setting the equipment in test mode for constant output at maximum power, and performing ad hoc testing can often be requested from mobile wireless equipment manufacturers and/or network providers.

f) Consideration may be given to have testing performed by an independent third party, in conjunction with the healthcare organization's clinical engineering group. The involvement of a third party may facilitate a consistent

and impartial evaluation of EMI issues and proposed management strategies, and more importantly may offer an independent analysis in cases where a further level of indemnity for the healthcare facility, equipment manufacturer, and/or network service provider is desired.

g) Medical devices found in ad hoc testing to be susceptible to EMI should be replaced whenever feasible and practical with more electromagnetically compatible devices, e.g. those compliant with new IEC 60601-1-2:2001 and other relevant immunity requirements. However, it should be noted that medical devices meeting 60601-1-2 can still be susceptible to emissions from mobile wireless equipment such as mobile / cellular phones at close range where the electromagnetic fields exceed the immunity testing levels specified in this standard.

h) Results from ad-hoc testing tend to be variable, due to variability in RF source power, medical-device differences, and test-site differences. It is important to understand that the primary function of ad-hoc testing is to identify unreasonably-susceptible medical devices so that they can be managed appropriately, not act as a quantitative assessment of their susceptibility.

Controlled use within healthcare facilities
For controlled mobile wireless equipment to be used by doctors and healthcare organization staff under managed conditions, it is recommended that necessary and sufficient procedures be implemented to identify, characterize, and mitigate potential EMI problems.

a) The **IEEE / ANSI C63.18** recommended practice (as outlined above) is the suggested test protocol for rapid ad hoc, on-site RF EMI testing for EMI identification and characterization.

1) Testing should be performed using the mobile wireless handsets to be used in the controlled system as a test transmitter. If multiple in-house systems are to be deployed, testing should be performed with each different RF signal. If new in-house systems are deployed, each different RF signal should be tested. Different EMI effects can be caused by different RF signals.

2) Ad hoc testing should be an ongoing effort, with a record of EMI test results kept including characterization of new medical device acquisitions and investigation / verification of reported EMI incidents, making any necessary adjustments to policy.

3) Periodic testing should be performed on a regular schedule (e.g., once per year), and especially after changes such as the introduction of new communication devices, new medical equipment, or significant repositioning on a regular basis.

4) Given the qualitative nature of the ANSI C63.18 ad hoc testing, even if no significant EMI issues are identified, nominal management policies including recommended minimum separation distances may still be prudent.

b) For mobile handsets that transmit at a constant output power, having no dynamic power control (e.g., standard two-way radios, family radios, two-way pagers, 802.11 systems), EMC management should involve ensuring adequate separation from identified susceptible medical devices. In the case of radio transmitters with relatively high constant power output (1 W or more), this may require significant separation distances and possibly necessitate their restriction from certain areas of the healthcare facility. In the case of pagers with extremely short burst transmissions or IEEE 802.11 a/b/g / Local Area Network or IEEE 802.15 / Bluetooth / Zigbee / IEEE 802.15.3a PAN equipment (see table 1 for more information about these) with relatively low constant power output (~10 milliwatts), the risk of EMI may be significantly less than for equipment such as two-way radios. Testing is still recommended whenever possible, although it is understood that it may reveal little susceptibility and the feasibility and practicality of all testing must be considered and prioritized.

c) If mobile wireless transmitters are dynamically power controlled (e.g., mobile / cellular phones, PDAs operating on wide area networks), EMC management should involve network characterization, design, and in-building engineering to supplement the wide area network as necessary to insure handsets are directed to transmit at RF power levels sufficient to minimize EMI issues. The existence of numerous shielding and reflecting objects in a healthcare facility may create areas with variations in downlink signal coverage, some of which could lead to significant intermittent changes in transmit power of the handsets causing them to deviate from their normal output power. Such areas should be characterized (by measuring existing signal strength with the mobile wireless handset set to a "trace" mode – this can often be done by the network service provider) and managed appropriately.

d) Medical device management procedures may include identification through labelling, repositioning or other means to reduce exposure to the wireless emissions, or replacing particularly susceptible devices with newer model units. Because of medical device regulations, modifications to a medical device should only be made by the device manufacturer.

e) User guidelines can be provided as an additional layer of management directing healthcare staff to maintain a predetermined and practical separation distance between their mobile wireless handsets and potentially susceptible medical devices (between 25 cm and 2 meters).

f) The AAMI TIR 18 is recommended for additional details on medical device management and EMC/EMI guidelines.

g) Testing of specific fixed-infrastructure components such as local electrical circuits and circuit breakers can be considered for testing if failure could represent a significant hazard, and if testing can be performed without placing the facility at risk.

h) Healthcare facilities should actively manage spectrum usage (e.g, maintain a list of all controlled-use RF sources indicating where they are authorized to operate, as well as the maximal number of such units permitted within each area or zone).

i) Wireless security issues (which are outside of the scope of this document) must be properly considered, otherwise patient safety may be threatened if the informatics system becomes compromised or incapacitated

Non-Controlled use within healthcare facilities
For non-controlled mobile wireless equipment that may be brought randomly into the healthcare facility by visitors, patients, or staff and transmit a variety of different signals at different output power levels:
a) Separate EMC/EMI management policies than those listed for controlled mobile wireless handsets should be applied. While ad hoc testing and management solutions are always encouraged whenever possible, this may not be practical for every wireless system.

1) While certain mobile handsets may be able to operate compatibly throughout a healthcare facility environment, other mobile handsets may have greater potential to cause EMI events due to local differences in output power or signal type. As the number of handsets continues to increase and new models reduce size, internalize antennas, and combine technologies (i.e.; mobile phone / pager / PDA device / local area IEEE 802.11a/b/g / personal area IEEE 802.15.1 / UWB / IEEE 802.15.4, etc), it is becoming increasingly difficult to differentiate between RF transmitter types based upon visual appearance alone. Further confounders include the growing number of wireless headsets and accessories that relocate the actual RF transmitter to a pocket or purse, keeping them from obvious view even when in use. An increasing number of mobile wireless handsets can transmit multiple signal types, including data transmission that may use different bursting technologies (i.e., GPRS, WAP). Wireless laptop cards and PDAs may operate on either wide area (mobile phone-type) or local (IEEE 802.11.x - type) networks with different carrier frequencies, signal types, and power output. Ultimately, it may be impossible to enforce any policy that differentiates between different non-controlled mobile wireless handset types with regard to their use in the healthcare facility based upon visual appearance. For this reason, all non-controlled mobile wireless handsets should be treated with the same management / restrictions regardless of whether or not they appear to be the same as controlled handsets.

2) Restrictive policies might involve requesting that individuals not use their personal mobile wireless handsets in areas of the facility where potentially susceptible medical devices are used. This should involve requesting by appropriate signage or some other reliable mechanism that non-controlled mobile wireless equipment is turned off before entering areas where potentially susceptible life-supporting medical devices are commonly operating, as even well-intentioned individuals may feel compelled to receive and respond to incoming calls or messages.

3) Implementation and enforcement of restrictive policies should be facilitated by signs, especially in areas where potentially susceptible medical devices are commonly located, to make patients and visitors aware of the existing healthcare facility policy. Compliance with existing policy can be facilitated by defining numerous areas with easy access where the use of wireless handsets by patients, visitors, and staff is unlikely to interfere with medical devices.

4) Any restrictive policy should be balanced between an informed assessment of EMI risk and the increasing need among patients, visitors, and healthcare facility staff for mobile wireless communication and computing. In the extreme, healthcare facilities could ban the use of all non-controlled mobile wireless handsets altogether, although such measures are likely to be excessive from an EMI management perspective (58) and not responsive to the growing needs of individuals for direct access to mobile wireless communication, especially in times of emergency and crisis.

b) While instructing patients and visitors to maintain a minimum separation distance between their personal mobile wireless handsets and medical devices might theoretically act as a safeguard against EMI events, such a recommendation may be impractical in many facility areas, and further be exceedingly difficult to monitor and enforce. Such minimum separation requirements are not recommended as a primary management strategy. However, the minimum separation distances determined from ad hoc testing can be used as an added layer of management in areas where potentially susceptible life-supporting medical devices are commonly operating.

RF emissions from network sources

a) RF emissions from in-building system network antennas (WAN microcells or repeaters, LAN access points) are most appropriately managed by locating them in a place where separation distance mitigates medical device EMI effects, such as the roof of corridors and rooms.

b) RF emissions from base station sites physically located on healthcare facility roof-top or building structures should conform to existing national radio regulations to limit emissions directly into the supporting building structure.

Medical devices within healthcare facilities

a) Although outside the current scope of this recommendation, the placement and operation of RF-emitting medical devices within the healthcare environment is an area that should be carefully considered. There are many types of medical devices that generate and use electromagnetic energy for their medical function. For example, Electric scalpels (e.g. high frequency electrosurgical equipment) often generate RF and microwave fields for cauterization purposes, physio-diathermy units may emit 915, 433, 2450 MHz or other frequencies for deep tissue heating (36), and ultrasound machines may radiate up to their operating frequency of ~ 3 - 20 MHz. The healthcare facility should exercise caution in where and how these types of emitters are used in the vicinity of other potentially susceptible medical devices.

b) Electromagnetic type security and inventory systems such as metal detectors, anti-systems, and RFID emit signals that may disrupt potentially susceptible medical devices. The policies and practices of the healthcare facility should address this equipment. For example, RFID tags used in the healthcare environment may be passive emitters, activated by inductive processes when brought into proximity of RFID readers. However, the readers may emit high field strength magnetic fields and should be included as a transmitter in ad hoc testing and in EMC/EMI management policies. The recently published ASTM F 2401-04 “Standard Procedures for Security Checkpoint Metal Detector Screening of Persons with Medical Devices” provides useful information [57]

c) For medical devices used outside the healthcare facility in a domiciliary setting, such as dialysis equipment, blood glucose analyser, infusion pumps, etc, instruction should be provided to patients advising them to maintain at least 1 meter of separation distance between the medical device and mobile wireless equipment while it is in operation.

References:

1) Segal B et al (2001) Risk of Patient Injury due to Electromagnetic Interference Malfunctions: Estimation and Minimization. Proc 2001 IEEE International Symposium on Electromagnetic Compatibility, p. p. 1308-1312.

2) ECRI "Cellular Telephones and Radio Transmitters—Interference with Clinical Equipment". Health Devices 1993 Aug-Sep;22[8-9]:416-8

3) ECRI "Electromagnetic Interference and Medical Devices: An Update on the Use of Cellular Telephones and Radio Transmitters in Healthcare Facilities". Health Devices Feb-Mar 1996;25(7):263

4) Segal B et al (1994) The Health Canada Medical Devices Bureau Roundtable Discussion on Electromagnetic Compatibility in Healthcare. Biomedical Instrumentation Technol 29:350-354

5) Bassen H.I., Ruggera, P.S., O'Bryan, E.R., Casamento, J.P., Silberberg, J.L. (1992) Medical Device RF Susceptibility - Research and Proposed Standards for Infant Apnea Monitors. EMC Technology Magazine Expo '92 International Conference on Electromagnetic Compatibility Technical Record, pp. 256-260

6) Sykes, S., ed. Forum on Electromagnetic Compatibility. FDA/AAMI Conference Report (proceedings available from the Association for the Advancement of Medical Instrumentation, Arlington, Virginia), May 1995 (ISBN 1-57020-054-8).

7) Silberberg JL (1993) Performance Degradation of Electronic Medical Devices Due To Electromagnetic Interference. Compliance Engineering 10:25-39

8) ECRI (2001) Wireless communication devices and electromagnetic interference. ECRI's updated recommendations. Health Devices (2001) Nov;30(11):403-9

9) Silbert PL (1994) J. Polysomnographic Technology 10:20-22

10) AAMI TIR 18 (1997) Guidance on Electromagnetic Compatibility of Medical Devices for Clinical/Biomedical Engineers. Part 1: Radiated Radio Frequency Electromagnetic Energy

11) Paperman WD et al (August 1994) Electromagnetic Interference: Causes and Concerns in the Health Care Environment, Healthcare Facilities Management Series, Number 055110, AHA/ASHE.

12) David Y et al (June 1997) EMC: How to Manage the Challenge, Healthcare Facilities Management Series, Number 055144, AHA/ASHE.

13) MDA Bulletin (MDA DB 9702, MDA SN2001 (06): http://www.medical-devices.gov.uk/sn2001(06).htm March 1997

14) MDA update (MDA SN 2001(06): http://www.medical-devices.gov.uk/mda/mdawebsitev2.nsf/webvwSearchResults/37CE5B0D2F6E45C900256A99005B8734?OPEN

15) Silberberg JL (2001) Achieving Medical Device EMC: The Role Of Regulations, Standards, Guidelines, and Publications. Proc 2001 IEEE International Symposium on Electromagnetic Compatibility, p. p. 1298-1307.

16) Irnich et al (1999) Mobile Phones In Hospitals. Biomed Instrum Technol 33:28-34

17) Morrissey et al, Characterization of Electromagnetic Interference of Medical Devices in the Hospital Due To Cell Phones. Health Physics (2002) 82:45-51

18) Barbaro Electromagnetic Interference by GSM Cellular Phones and UHF Radios with Intensive Care and Operating Room Ventilators. Biomedical Instrumentation & Tech (2000) 34:361-369

19) Handa Electromagnetic Interference on Medical Equipment by Low Power Mobile Telecommunication Systems. IEEE Trans Electromagnetic Compatibility (2000) 42:470-475

20) Sibakov and Hietanen Safe Use of Mobile Phones in Hospitals. Health Physics (2000) 79(suppl):S77-S84

21) Bassen HI, Moore HJ, Ruggera PS. Cellular Phone Interference Testing of Implantable Cardiac Defibrillators In Vitro. Pacing Clin Electrophysiol. 1998 Sep;21(9):1709-15.

22) Davis D, Segal B, Pavlasek T. Can Minimum Separation Criteria Ensure Electromagnetic Compatibility in Hospitals? An Experimental Study. Biomed Instrum Technol. 1999 Sep-Oct;33(5):411-6.

23) Sibakov and Hietanen VTT Technical Bulletin (ESPOO 1998)

24) Rice (2000) 2.4 GHz RF LAN EMI in Medical Devices. J. Clin Engineering (Sep/Oct 2000) 260-264

25) Turcott & Witters Biomed Instrum Technol (1998) A Practical Technique for Assessing EMI in the Clinical Setting: Ad Hoc Testing. May-Jun;32(3):241-52

26) Tri et al, Cellular Phone Interference with External Cardiopulmonary Monitoring Devices. Mayo Clinic Procedings (2001) 76:11-15

27) Aki W et al (2002) Influence of Electromagnetic Waves on Portable Electronic Instruments in Medicine [Japanese]. Nippon Hoshasen Gimutsu Gakkai Zasshi [Japanese] 58:948-956

28) Medicine and Health Products Regulatory Agency: http://www.medical-devices.gov.uk/mda/mdawebsitev2.nsf?Open

ELECTROMAGNETIC COMPATIBILITY BETWEEN WiFi ACCESS POINT AND EEG SIGNALS.

KAPARELIOTIS EVANGELOS[1], NANOU ELENA[1], TSIAFAKIS VASILEIOS[1], SOTIRIOU APOSTOLOS[1], PRAGIATIS LAZAROS[1], CAPSALIS CHRISTOS[1]

[1] NATIONAL TECHNICAL UNIVERSITY OF ATHENS, DEPARTMENT OF ELECTRICAL ENGINEERING, DIVISION OF INFORMATION TRANSMISSION SYSTEMS AND MATERIAL TECHNOLOGY, GREECE

9 IROON POLYTECNEIOY STR., ATHENS ,GREECE, 15773, Tel: ++30210-7722574, Fax: ++30210-7723520, email:enanou@mail.ntua.gr

Abstract

In the current work, we study the EMC problem that involves the usage of an electroencefalographer in an environment with electromagnetic radiation produced by a WiFi access point.

The experimental setup was situated in an anechoic chamber so that no electromagnetic interference would affect the measurements. The amplifier room, outside the anechoic room, situated the other part of the experimental apparatus. 32 electrodes entered a low-pass filter placed at the boundary wall of the Faraday screen room. The signal was amplified, before entering a 32-bit analog to digital converter. The recording frequency was at 1 kHz.

The wireless access point operated at the typical frequency band of 2.4 – 2.4835 GHz and the maximum EIRP allowed in Europe that is 100mW. The distance of the access point to the electroencephalographer was 10cm. Two sets of measurements were performed. One with measuring the noise of the system and the other with the WiFi transmitter switched on.

The results showed that there was no interference of the WiFi Access point to the measured signals. This is of great importance because of the great expansion of wireless technology.

Introduction

Since the early 1990s, reports of medical device failure from electromagnetic interference have increased [1, 2]. This is due to several factors. The number of electronically controlled medical devices has burgeoned in hospitals and other medical facilities. The modern instruments are often more sensitive to electromagnetic interference (EMI) because they incorporate low power integrated electronic circuitry that can be much more sensitive to electromagnetic fields than their electrical and electromechanical predecessors. Digital wireless communications systems often utilize pulsed amplitude modulation, a type of modulation that can enhance the potential for EMI.

The European Union has gotten much of attention with regard to the regulation of electromagnetic compatibility (EMC) and medical electronics. Today, most medical EMC regulations originate within the International Electro technical Commission (IEC). The standard EN60601-1-2 [5] defines limits for emissions and levels of immunity and was updated to encompass the frequencies used by mobile phones and other communication technologies such as wireless local area networks (WLAN). The IEC standard states that electronic medical equipment must operate normally in electric field intensity of 3 V/m and at a 10 V/m threshold for life – sustaining equipment.

The Electroencephalograph (EEG) is a recording equipment of brain signals with typical voltage of 100 μV and frequency range (EEG bands) 0.5 Hz up to several hundreds Hz. The EEG is connected directly to the patient in order to detect these small physiological signals which are then amplified. The EEG is known to be very sensitive to EMI due to the fact that the pulsed RF signals maybe demodulated by non-linear elements in amplifier circuits. [Robinson 2003]. Morrisey et al. reported distortion of EEG bands throughout the 0-70 Hz range during full power exposure to CDMA and GSM signals for both frequencies of 1.800 and 1900 MHz at distances of between 0.25 to 0.5 m.[Morrisey 2002].

Wireless Local Area Networks (WLANs) in a hospital typically consist of multiple antenna sites (known as base stations) interspersed throughout the hospital building that connect to a central “hub” or “router” unit. This latter unit connects the WLAN with the wired hospital network. WLANs transmit and receive signals with various handheld devices (or laptop computers, etc) as these devices roam throughout the coverage net work in the building. WLANs typically use the 802.11 standards that operate on frequencies around 2.45 GHz and 5.8 GHz. The handheld devices are not power controlled, but transmit at a very low constant power (on the order of 1-10 milliwatts) as they are designed to never be very far away from the nearest network node. As a consequence, the likelihood of electromagnetic interference of W LANs with critical and life support medical equipment is very small, since they transmit at power levels t hat are well below the IEC recommended levels. The WLAN base stations transmit at a higher power level (typically around 500 mW), which increases the chances for electromagnetic interference. Research by [13] revealed that peak values of such base stations often exceed the critical 10V/m field strength value.

Taking into account the above considerations, in our current work, we study the EMC status that involves the usage of an electroencefalograph in an environment infested with electromagnetic radiation produced by a WiFi Access Point. The purpose is to observe the effects of the WiFi signal on the EEG signal.

Materials and Methods

The experimental setup (Fig 1) was situated in a Faraday chamber so that no electromagnetic interference would affect the measurements. A head phantom was placed in the chamber and the signals were recorded from thirty two electrodes (Fp1, Fp2, Fpz, AFz, F2, F3, F4, F7, F8, FC1, FC2, FC5, FC6, C2, C3, C4, A1, A2, CP1, CP2, CP5, CP6, P3, P4, Pz, T3, T4, T5, T6, O1, O2,Oz) with a surface of Ag/ AgCl, which were placed on the scalp of the model-head. The electrodes were positioned according to the International 10-20 system of electroencephalography [8]. The measured magnitude was the voltage at the edges of a 2 kΩ resistance placed between each electrode and a common ground. The total electrode impedances were below 5 kΩ. The amplifier room, outside the Faraday room, situated the other part of the experimental apparatus. The electrodes entered a low-pass filter placed at the boundary wall of the Faraday screen room. The filter cut frequencies over 35 Hz so that the signal of the power supply network which is at 50 Hz would not interfere with the signal. The signal was amplified by a Braintronics DIFF/ISO-1032 amplifier, before entering a 32- bit analogue to digital converter (NI SCB-68) which has a GPIB output. The digitized signal comprises an input for a Data Acquisition Card (32 bit NI 6035E DAQ Card). The PC with the DAQ Card ran a LabView program for the recording of the signals, which can be monitored by an on-screen graphical representation. The recording frequency was at 1

kHz. Another PC, connected with the one described above, ran a program which triggered the other PC to save the brain signals whenever the user wanted .The recording time was 1.5 sec so the saved signal consisted of 1500 values. The total task consisted of 55 repetitions.

The WiFi Access Point was placed in the Faraday room and made a link with a laptop that was inside the room. The WiFi signal was radiated by a dual dipole antenna,, with 20dBm power and QPSK modulation. The Access Point was placed at a distance of 1m from the head.

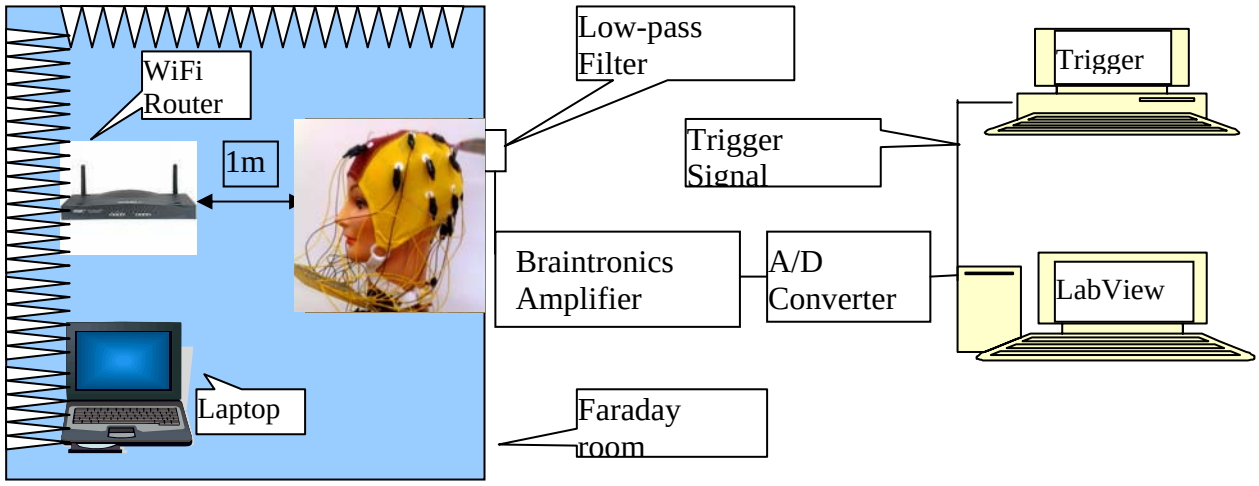

Figure1. Experimental Setup

The experimental procedure was done twice. The first time the WiFi Access Point was off and practically the noise of the device was measured and the second time the WiFi was functioning.

Regarding the collected data analysis, in order to optimize the signal to noise ratio (SNR) the grand average across the 55 repetitions for each channel was calculated according to the following equation:

$$\bar{V}_t = \frac{1}{55} * \sum_{j=1}^{55} V_{jt}$$

Where Vjt is the value that results after the subtraction of the amplification and the average referencing and corresponds at the time t of the trial j. This SNR optimization procedure is considered a standard practice when it comes to brain signal measurements, which are generally considered to be quite noisy. (Roth et al., 1995, pp.805-910)

The final data for analysis for each EMF condition consisted of 1500 amplitude values for each electrode, expressed in μVolts corresponding to the 1500 msec of the time period as described above.

For each electrode, the following magnitudes were also calculated:

- the energy E of the recorded signals ($E=V_t^2$)
- the amplitude in the frequency domain by using the Fourier Transform (FFT).

Data analysis

The differences between the values of the energy at the two EMF conditions were calculated for each of the thirty two leads. The data were also compared to real EEG recordings at certain representative electrodes. The mean values and the standard deviations of the final data were calculated for each group (WiFi Off, WiFi On, EEG) at these electrodes.

Results

The data analysis revealed that the maximum difference between the values of the signal energies for each EMF was 0.7 Joules with the exception of T5 electrode, which is a small value if compared with the energy values. Figure 1 is quite helpful in explaining this fact. The white bars denote the calculated energy in the absence of the WiFi signal while the black bars denote the signal energy in the presence of the WiFi signal.

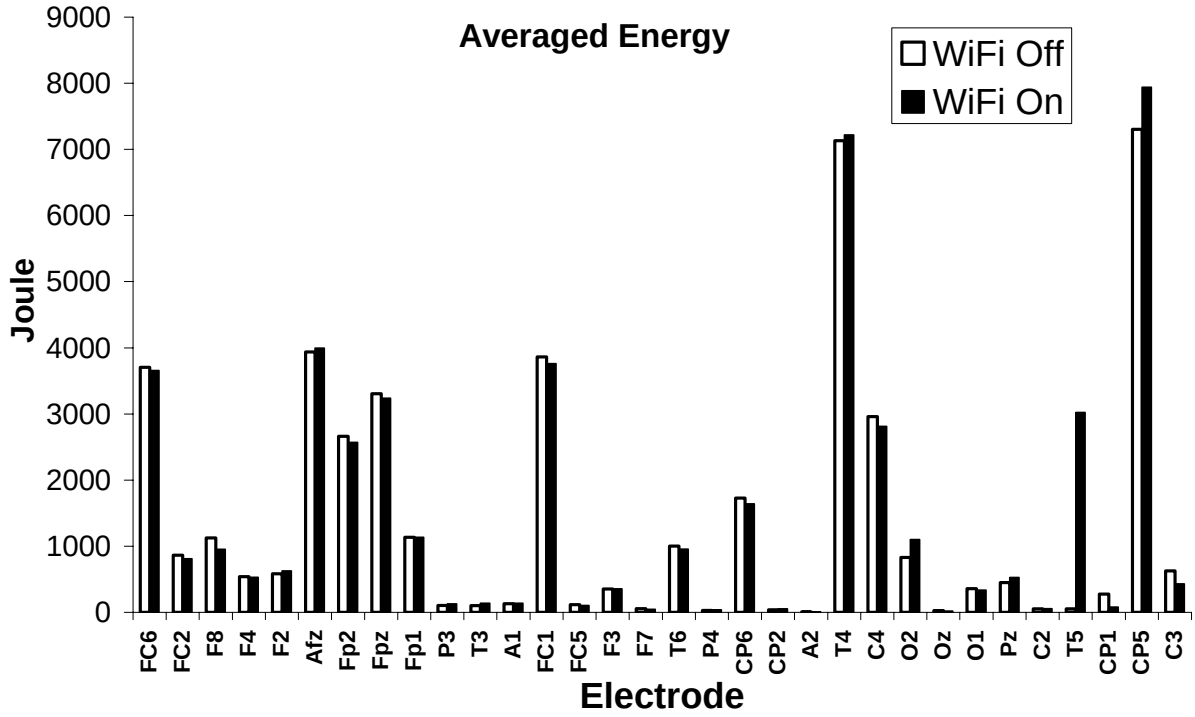

Figure 2. Averaged Energy at each electrode and each radiation condition. . The white bars denote the calculated energy in the absence of the WiFi signal while the black bars denote the signal energy in the presence of the WiFi signal.

Table 1 shows the mean values and the standard deviations at some representative electrodes, of the three groups of data at different conditions: absence of WiFi Signal, presence of the WiFi signal and EEG recordings. It is notable that the mean values and the standard deviations for the first two cases (WiFi Off, WiFi On) are very similar. The comparison of these values to the respective values of the data that come from human measurements reveals great variation.

	Mean Values			SD		
Electrode	**WiFi Off (Noise)**	**WIFi On**	**Human**	**WiFi Off (Noise)**	**WiFi**	**Human**
F4	-0.59	-0.59	-0.27	0.08	0.10	2.58
Fz	-0.62	-0.64	-1.37	0.09	0.11	2.91
Fp2	1.33	1.30	-1.61	0.11	0.11	3.14
Fp1	-0.86	-0.86	-1.37	0.09	0.12	3.45
P3	0.25	0.28	2.65	0.08	0.10	3.01
F3	0.48	0.48	-0.52	0.09	0.09	2.74
P4	-0.06	-0.12	2.33	0.12	0.11	2.89
C4	-1.40	-1.36	0.95	0.14	0.12	3.00
O2	-0.74	-0.73	2.97	0.09	0.45	2.89
O1	-0.48	-0.46	1.52	0.09	0.11	2.05
Pz	0.54	0.58	2.87	0.12	0.12	3.54
C3	-0.63	-0.52	2.02	0.14	0.14	3.35

Table1. Mean values and standard deviations for three conditions (WiFi Off, WiFi On, EEG) at a number of electrodes

Figure 3 is a representative diagram of the grand averaged amplitudes during a recording period for the three experimental conditions at the electrode O1. The diagram helps in realising the considerable variation of the EEG data .

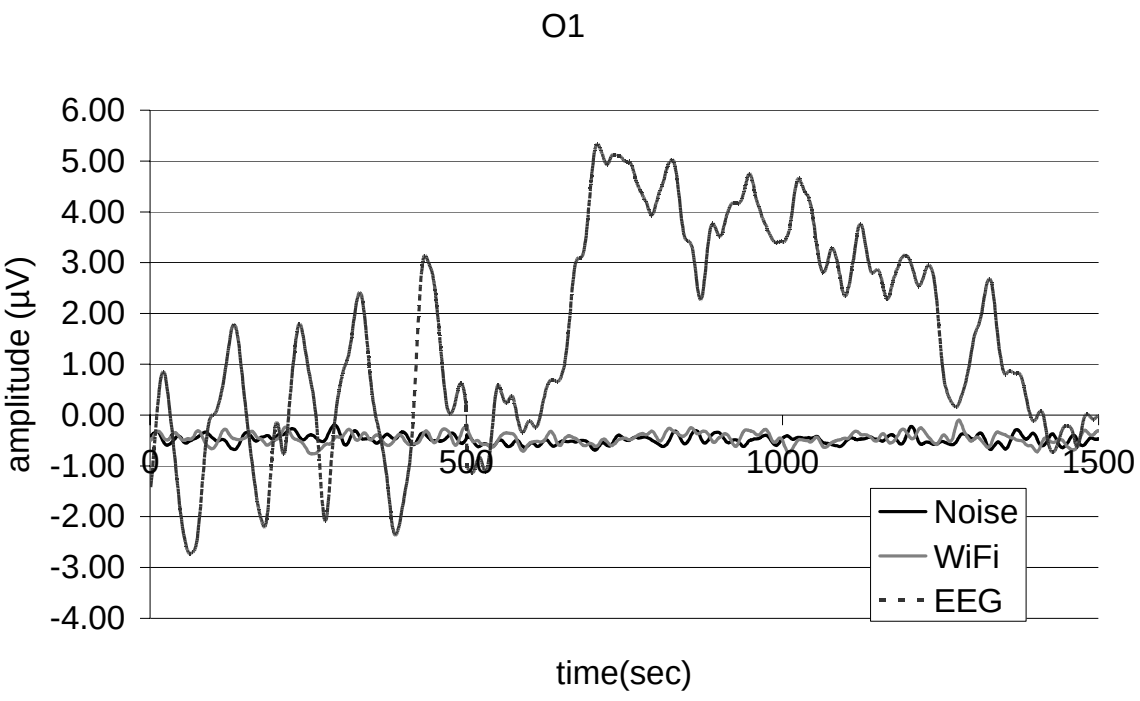

Figure 3. Grand averaged amplitudes for the three experimental conditions at the electrode O1

Discussion

From the data analysis and the results which aroused, there is no evidence that a WiFi signal at a distance of 1m from EEG electrodes causes interference at the EEG recordings. WiFi is a low power protocol that has flexible power settings and can be deployed in various conditions in order to ensure that all radiation is well within the limits set even by the most strict hospital authority. Other tests [14] indicate that not only WiFi shows no interference to medical equipment but has the edge when compared to other wireless technologies. Wireless communication is a promising opportunity for future medical systems in the hospital. Today's wireless standards with moderate output power represents no real danger for the operation of medical equipment [14] and seems to be suitable for medical environment even with several wireless devices used simultaneously. The various applications that hospitals can create through the use of WiFi in a quick and cost effective fashion have been the subject of many a discussions, wireless patient monitoring in steady state [15] or in IC units or in OR units [14,16] is an application of great importance that will greatly improve the working conditions of the staff but moreover it will make the care of patients more efficient. Even though the results indicate that there is more tests are no interference between EEG and WiFi we need to investigate further in order to verify the suitability and assure the reliability of WiFi communication in medical equipment of any sort.

References

1. Silberberg JL: Performance degradation of electronic medical devices due to electromagnetic interference. Compliance Eng 10(5):25-39, 1993.

2. Joyner K, Anderson V, Wood M: Interference and energy deposition rates from digital mobile phones. In: Abstracts Annual Meeting of the Bioelectromagnetics Society 16:67-68, 1994

3. Silberberg JL: Medical device electromagnetic interference issues, problem reports, standards, and recommendations. In: Proc Health Canada Medical Devices Bureau Round-Table Discussion on Electromagnetic Compatibility in Health Care, Ottawa, Canada, pp. 11-20, 1994.

4. Segal B, Skulic B, Liu-Hinz C, Retfalvi S, Lorange M, Pavlasek T: Preliminary study of critical-care medical device susceptibility to portable radiofrequency sources. In: Proc Annual Meeting and Exposition of the Association for the Advancement of Medical Instrumentation 13:83, 1995.

5. International Electrotechnical Commission, "IEC 60601-1-2, Medical Electrical Equipment Part 1: General Requirements for Safety, Amendment No. 2. Collateral Standard: Electromagnetic Compatibility—Requirements and Tests," 1st ed., Geneva, 1993.

6. Barbaro V, Bartolini P, Militello C, Altamura G, Ammirati F, Santini M: Do European GSM mobile phones pose a potential risk to pacemaker patients: Invitro observations. PACE 18(6):1218- 1224, 1995.

7. Joyner, K., Wood, M., Burwood, E., Allison, D., Strange, R: Interference to Hearing Aids by the New Digital Mobile Telephone System, Global System for Mobile (GSM) Communications Standard. National Acoustic Laboratories, Australian Hearing Services, Sydney Australia, 1993.

8. Jasper H. The ten-twenty electrode system of the international federation. Electroencephalogr Clin Neurophysiol, 1958

9. S Kirk, "Designing Medical Equipment for Electromagnetic Compatibility," Medical Device Technology 3, no. 4 (1992): 42-49.

10. D Davis, B Segal, and T Pavlasek, "Can Minimum Separation Ensure Electromagnetic Compatibility in Hospitals? An Experimental Study," Biomedical Instrumentation and Technology/Association for the Advancement of Medical Instrumentation 33, no. 5 (1999): 411- 416.

11. S Kirk, "Solving Electromagnetic Problems in Medical Equipment," Medical Device Technology 3, no. 1 (1992): 27-30

12. Roth, W.T., Ford, J.M., Pfefferbaum, A. and Elbert, T.R. Methodological issues in event-related potential and magnetic field studies. Chapter 78 in Psychopharmacology: The Fourth Generation of

Progress, F.E. Bloom and D.J. Kupfer (Eds.), pp. 895-910. New York, NY: Raven Press, 1995

13. Rice, WP 2.4 GHz RF WLAN EMI in medical devices. J. Clin. Engineering(Sept/Oct) 2000: 260-264

14. Jan Olav Høgetveit, Ilangko Balasingham, Karl Øyri, Øystein Jensen The 3rd European Medical and Biological Engineering Conference: Introducing Multiple Wireless Connections To The Operating Room, Interference Or Not?

15. WLAN-based, indoor medical residents positioning system Ke Yu; Chen, J.; Refai, H.H.;Wireless and Optical Communications Networks, 2005. WOCN 2005. Second IFIP International Conference on 6-8 March 2005 Page(s):556 - 560 Digital Object Identifier 10.1109/WOCN.2005.1436088

16. Patient's data browsing in wireless LAN in TELEMEDIK Kundu, S.; Mukherjee, J.; Majumdar, A.K.; Personal Wireless Communications, 2005. ICPWC 2005. 2005 IEEE International Conference on 23-25 Jan. 2005 Page(s):272 - 275 Digital Object Identifier 10.1109/ICPWC.2005.1431347

LACK OF PROMOTING EFFECTS OF CHRONIC EXPOSURE TO 1.95-GHZ W-CDMA SIGNALS FOR MIT-2000 CELLULAR SYSTEM ON DEVELOPMENT OF N-ETHYLNITROSOUREA-INDUCED CENTRAL NERVOUS SYSTEM TUMORS IN F344 RATS

TOMOYUKI SHIRAI[1*], TOSHIO ICHIHARA[2], KANAKO WAKE[3], SO-ICHI WATANABE[3], YUKIO YAMANAKA[3], MAYUMI KAWABE[2], MASAO TAKI[4], OSAMU FUJIWARA[5], JIANQING WANG[6], SATORU TAKAHASHI[1]AND SEIKO TAMANO[2]

[1]DEPARTMENT OF EXPERIMENTAL PATHOLOGY AND TUMOR BIOLOGY, NAGOYA CITY UNIVERSITY GRADUATE SCHOOL OF MEDICAL SCIENCES, NAGOYA 467-8601, JAPAN.E-mail: tshirai@med.nagoya-cu.ac.jp
[2]DIMS INSTITUTE OF MEDICAL SCIENCE, INC, ICHINOMIYA, AICHI, JAPAN
[3]COMMUNICATIONS RESEARCH LABORATORY, TOKYO, JAPAN
[4]DEPARTMENT OF ELECTRICAL AND ELECTRONIC ENGINEERING, TOKYO METROPOLITAN UNIVERSITY, TOKYO, JAPAN
[5]DEPARTMENT OF ELECTRICAL AND COMPUTER ENGINEERING, NAGOYA INSTITUTE OF TECHNOLOGY, NAGOYA, JAPAN
[6]DEPARTMENT OF COMPUTER SCIENCE AND ENGINEERING, NAGOYA INSTITUTE OF TECHNOLOGY, NAGOYA, JAPAN

ABSTRACT

The present study was performed to evaluate effects of a 2-year exposure to an electromagnetic near-field (EMF) equivalent to that generated by cellular phones on tumor development in the central nervous system (CNS) of rats which were born from ENU-treated F344 mother rats. A total of 500 pups were divided into 5 groups, each composed of 50 males and 50 females. A 1.95 GHz W-CDMA signal for IMT-2000, was used for the exposure of the rat head starting from 5 weeks of age, 90 min a day, 5 days a week, for 104 weeks. Brain average specific absorption rate (SAR) was designed to be 0.67 and 2.0 W/kg for low and high exposures, respectively. Whole-body average SAR was less than 0.4 W/kg. The incidence and number of brain tumors in female rats exposed to 1.95 GHz EMF had a tendency to be increased but there was no statistical significance. Overall, no increase in their incidences or numbers per group, either in the males or females, was detected in the EMF-exposed groups. Thus, under the present experimental conditions, 1.95 GHz W-CDMA signal for IMT-2000 exposure to the heads of rats for a 2-year period did not accelerate or affect ENU-initiated brain tumorigenesis.

INTRODUCTION

Since there is serious concern that exposure to an electromagnetic field (EMF) due to cellular phones is associated with an increase risk of disease such as brain dysfunction and/or brain tumor development, many epidemiological and experimental research studies to explore this possibility. However, none of epidemiological studies revealed a clear association between exposure to EMF and development of brain tumors. Furthermore, none-of 5 long-term (2-year period) animal experiments which had been performed demonstrated the presence of association of exposure to time-division multiple access (TDMA) or frequency-modulated signals with tumor development in the central nervous system of rats. Recently we also conducted a 2-year EMF exposure experiment in an ENU-exposed rat model with a 1.439-GHz TDMA signal for the Personal Digital Cellular (PDC), Japanese standard cellular system at brain average specific absorption rates (SARs) of 0.67 and 2.0 W/kg for low and high exposures. The results disclosed no inter-group differences in body weights, food

consumption, or survival rates and no increase in the brain and spinal tumor incidences or numbers per group, either in males or females of the EMF-exposed groups [Shirai, et al. 2005].

Recently the International Telecommunication Union (ITU) has introduced the new mobile telecommunication system, i.e., International Mobile Telecommunication 2000 (IMT-2000) which has also been named the 3rd generation (3G). The wide-band code division multiple access (W-CDMA) is also termed the Universal Mobile Telecommunication System (UMTS) in the EU. The first IMT-2000 service was started in Japan in 2001. This service, the freedom of mobile multimedia access (FOMA) by NTT DoCoMo, uses W-CDMA signals and the 1.95 GHz region for up-links and the 2.14 GHz region for down links. The number of subscribers to the W-CDMA system in Japan was about 28 million in April 2006 while that to the TDMA systems was about 41 million. Because the number of W-CDMA users is rapidly increasing, this type of signal will probably become the most major digital signal for the Japanese general public in near future.

Therefore, the present study was designed as a first long-term investigation of effects of chronic exposure to 1.95-GHz W-CDMA signals for MIT-2000 cellular system on development of ENU-induced CNS tumors in F344 rats. It was conducted in compliance with the Good Laboratory Practice (GLP) Standards of the Japanese Ministry of Health and Welfare Ordinance No, 21. This is the first experimental result on a long-term effects of MIT-2000 cellular system on development of central nervous system tumors.

MATERIALS AND METHODS

A total of 100 pregnant F344 rats were purchased from Charles River Japan (Atsugi, Kanagawa Japan) and given a single intravenous administration of ENU on gestational day 18. ENU (Nacalai Tesque Tokyo, Japan) was dissolved in physiological saline for this purpose and injected into the tail vein at a dose of 4 mg/ml/kg body weight. ENU-exposed pups of both sexes were allocated to 4 groups, each composed of 50 females and 50 males. Pups (50 males and 50 females) from mothers that received the vehicle instead of ENU served as complete controls. Dummy animals were used to cover any vacancy in EMF exposure boxes due to interim death to maintain the exposure conditions unchanged. All animals were allowed free access to pelleted diet and drinking water.

The rats in Groups 1 to 5 were exposed to EMF; Group 1 was a complete control without any treatment. Group 2 received ENU alone and was kept in cages throughout the experiment. Group 3 was given ENU set in exposure boxes in the same manner as in Groups 4 and 5 but with no actual exposure to EMF (sham exposure group). Groups 4 and 5, given ENU, then were exposed to EMF at low (SAR: 0.67 W/kg) and high (SAR: 2.0 W/kg) levels, respectively.

The exposure box was 90 x 90 x 60 cm. Ten rats fixed individually in plastic tubes were set on disk-shaped plates like a carousel with the nose pointing to the center. Each plate was 65 cm in diameter, with adjustable height supported by a center hollow cylinder pole. A resonant monopole antenna for 1.95 GHz was set from the ceiling of the exposure box in order to fit in the center of the disk-shaped plate. The distance between the antenna and each rat nose was set at 30 mm.

A 1.95-GHz W-CDMA signal from Cellular Phones for MIT-2000 Cellular system was applied. Long-term intermittent exposure to the heads of the rats (90 min a day, 5 days a week, Monday through Friday) was started at 5 weeks of age and continued for 104 weeks. All exposures including sham exposure were controlled with the assistance of a computer system. If the number of rats became less than 10 in an exposure box due to loss through mortality, dummy rats were used to maintain the symmetrical arrangement of animals and the scheduled specific absorption rate (SAR) of EMF exposure.

SAR distributions in rats were evaluated by numerical dosimetry with the Finite Difference Time Domain method (FDTD). Brain average SAR was set at levels, 0.67 and 2.0 W/kg, respectively. Whole-body average SAR averaged over the 2-year experimental period was limited within lower level which cannot cause any thermal effects; the highest whole-body averaged SAR was 0.464 W/kg which is much lower than 4 W/kg, the threshold for thermal effects.

All surviving animals after the 104 week-exposure to EMF were killed under light anesthesia with ethyl ether and aorta blood was collected from all rats for hematology analysis, before a complete autopsy was performed. Organ weights were measured for the brain, heart, liver, kidney, spleen, pituitary gland, adrenal glands, testes and ovaries. All organs including the CNS and macroscopically observable lesions were fixed in 10% buffered formalin routinely processed for embedding in paraffin and sections (4 m thickness) were stained with H & E for histological examination. Rats that died or became moribund during the experiment were also autopsied.

RESULTS

There were no significant differences in growth rates between rats receiving maternal ENU and untreated controls (Group 1) in either males or females. Restraint of rats in the plastic holders in the exposure

boxes itself suppressed growth, particularly in the males, but this suppression was not exacerbated by actual EMF exposure. No significant inter-group differences in survival rates were observed in either sex. No clear increase in death rates with EMF exposure was observed in males or females. There were no significant differences in food consumption among groups throughout the experiment in either the females or the males. There were no inter-group differences in the relative organ weights of the brain, heart, liver, kidney, spleen pituitary gland, adrenal glands and testes or ovaries.

In this study, one CNS tumor was also observed in a female not receiving ENU. The lesions were astrocytomas, oligodendrogliomas, mixed gliomas, ependymomas, meningiomas, granular cell tumors and malignant reticulosis. The major type was the astrocytoma. The incidences of brain tumors in the females ranged from 2 to 22% and the numbers of rats ranged from 1 to 11. The incidences and numbers of brain tumors were very similar in males and females. While values in female rats exposed to 1.95-GHz W-CDMA signals for IMT-2000 had a tendency to be increased, this was no statistical significant. Spinal cord tumors were sporadically found in the males but not the females. There were no statistically significant differences in CNS tumors in males among the groups given ENU. Thus, the data for both sexes indicate that EMF does not accelerate ENU-initiated CNS tumor development.

Besides CNS tumors, sporadic tumors were noted in other organs/tissues. Among these tumors, skin fibromas and large granular lymphocytic leukemia were less frequent in the EMF exposed males and there was a statistical significance between sham exposed and the high dose EMF group at $p<0.05$.

DISCUSSION

In the literature, there are conflicting epidemiological data regarding the risk of EMF exposure for brain tumor development; some demonstrating very small association between workers in electrical industry and in the US Air Force population and brain tumors. However, there are five recent epidemiological studies that did not demonstrate any association between cellular telephone use and brain tumor risk.

With such conflicting epidemiological data, long-term animal experiments are essential for scientific evaluation of the risk of EMF with reference to brain tumor development. Four animal studies specifically targeting this question had already been performed prior to the present work. Neither 2-year animal bioassays with digital nor frequency-modulated signals found any detrimental effects of EMF exposure after intrauterine administration of ENU. A similar experiment with Sprague-Dawley rats carried out by others resulted in no initiation or promotion of brain tumors by any of the RF fields tested. Our group also previously conducted a long-term exposure animal experiment with intrauterine treatment with ENU for brain tumor initiation and we concluded that exposure to 1.439-GHz TDMA signal for 1.5 h/day, 5 days for 2-year period, did not accelerate ENU-initiated CNS tumor development in rats.

The present experimental design with 1.95GHz W-CDMA signals for IMT-2000 cellular system was also planned by the Committee of the Study on Human Exposure to EMF in Japan established in 1997 with the aim of scientifically clarifying any effects of radio waves from mobile telephone terminals on the human body. The whole body average SAR was limited as far as possible in order to avoid significant thermal stress and was less than 0.464 W/Kg. In the present experiment, there were no statistically significant inter-group differences in the incidences of CNS tumors in either males or females initiated with ENU although there was a tendency of slight increase in brain tumor development in the females exposed to EMF. No increase in spinal tumor development by EMF exposure was observed in either sex. Furthermore, development of tumors in organs other than CNS was not enhanced. Thus, it can be stated that the present data demonstrate that 1.95-GHz W-CDMA signals for IMT-2000 Japanese cellular system at a brain average SAR of 0.67 or 2.0W/kg for 2 years do not possess promotion potential for ENU-initiated CNS tumor development in either sex of F344 rats. In our previous study with 1.439 GHz TDMA signal, the incidences of pituitary tumor in both sexes received ENU showed a tendency for increase, but were clearly suppressed by 2.0 W/kg EMF, with statistical significance in males. However, such increase by ENU and suppression by EMF were not evident in the present study. Since the increase of pituitary tumor development in EMU-treated animals was concluded to be within the wide range of background data, the present data for pituitary tumor incidence seem reasonable.

In conclusion, the present large scale 2-year exposure experiment to 1.95GHz W-CDMA signals for IMT-2000 cellular system demonstrated that EMF at brain average SAR of 0.67 or 2.0W/kg does not promote ENU-induced rat brain carcinogenesis, providing additional evidence in support of no association between EMF and brain tumor risk in man.

Acknowledgement

This work was supported by a Grant from the Ministry of Internal Affairs and Communications, Japan

ORDER CHANGES IN CELL MEMBRANE INDUCED BY APPLIED ELECTROMAGNETIC FIELD

E. KOVACS[1], T. SAVOPOL[1], D. MARTIN[2], N. IACOB[2], M. MOISESCU [1]

[1]Biophysics and Cell Biotechnology Dept., « Carol Davila » Medical University, P.O. Box 35-43, 050461 Bucharest, Romania,
[2]National Institute for Lasers, Plasma and Radiation Physics

Abstract

Changes in membrane order are known to alter the function of integral proteins. Consequently, microwave induced changes of membrane lipid order may have physiological implications. The detailed biophysical mechanisms for these effects are not currently available and experiments on in vitro models are expected to offer the keys to understanding the nature of microwaves non-thermal and windowed effects.
We studied the changes in membrane fluidity (fluorescence depolarization) and generalized polarization of human platelets extracted from freshly donated blood, induced by irradiation with 2.45 GHz microwaves, CW at 24 mW incident power, SAR 10 W/kg. The experimental arrangement consisted mainly in a 2.45 GHz generator of adjustable output power in the range of 0 – 30 mW and a modified conventional coaxial probe used for two functions: as impedance matching device and as microwave (MW) irradiating antenna. Irradiation of samples during fluorescence anisotropy and generalized polarization records was made by introducing the antenna into the fluorometric cuvette. Changes of the same membrane parameters of a liposome suspension irradiated by microwaves was performed in order to have as reference a simple lipid bilayer, consisting of a single type of lipids.
Studies of membrane phase-transition temperature and other physical and chemical parameters lead to the conclusion that the liposome and platelet membranes, whose isothermal electric susceptibility is dramatically increased around phase-transition temperature, undergo order changes by interacting with oscillating electromagnetic field; these are reflected in the observed shift of the phase transition temperature of the microwave exposed liposomes comparatively to the sham exposed samples as well as in the higher values of generalized polarization (GP) of the cell/liposome membrane.
Membrane dipolar components such as polar amino acid side chains and cell membrane associated bound water which undergo orientation resulting in rotational motions with an associated time constant similar to the wave number of the impressed oscillating electromagnetic field, are the most probable targets which trigger the observed membrane order changes.

Introduction

Decades of experimental and theoretical research stay behind the attempts to reveal and account for the observed biological effects of RF and microwaves. Despite the investment of creativity, funds and hard work, few sound statements and facts concerning the specific interaction of microwaves with living structures/cells are available.
In our work, we choose simple phenomena and biological models in the attempt to dissociate the specific microwave interaction with the substrate from the non-specific thermal effect; the assumption is that while a great part of incident microwaves energy is dissipated as heat, the other part is absorbed resonantly by specific structures accounting for non-thermal "biological effects".
Two phenomena were chosen to analyse the specific interaction mechanisms.
1/The changes of *lipid packing* in *membrane bilayer* potentially induced by microwaves and formally reflected in a fluorescent marker mobility and in critical events accompanying the phase transition of the lipid bilayer. These changes would shift the temperature dependence curves and phase transition temperature in irradiated versus control samples as shown by fluorescence depolarization recordings.
2/ The change in *generalized membrane polarizability* induced by microwave application which must be reflected in fluorescent emission of Laurdan – a fluorescent dye, sensitive to polarization of hydrophilic environment within the lipid bilayer.

Method and results

Fluorescence depolarization

Fluorescence depolarization measurements of a membrane fluorescent marker (TMA-DPH in our case) provide information about the rigidity of lipid tails packing around the site of marker insertion. As higher is fluorescence anisotropy (r) as less fluid may be considered the membrane in the region of marker insertion (in case of TMA-DPH, below the polar heads in the outer lipid layer). A lipid bilayer is characterized by a specific phase – transition temperature, when it switches from a gel-like organization (lipid packing) to a liquid-crystalline organization, when lipid packing is looser (more fluid). The degree of looseness of lipid packing is critical for many membrane functions which rely on protein conformational changes within or across the membrane. It is considered that subtle conformational changes of proteins which occur along the signal transduction pathways may be hindered under low level microwave irradiation although no plausible physical mechanism for explaining this effect is yet available.

Here we use a simple model of lipid bilayer, *the liposome membrane*, to check if lipid packing is influenced by microwave irradiation. The fluorescence marker used is a TMA-DPH molecule.

1-[4-(trimethylammonium)phenyl]-1,3,5-hexatriene (TMA-DPH)

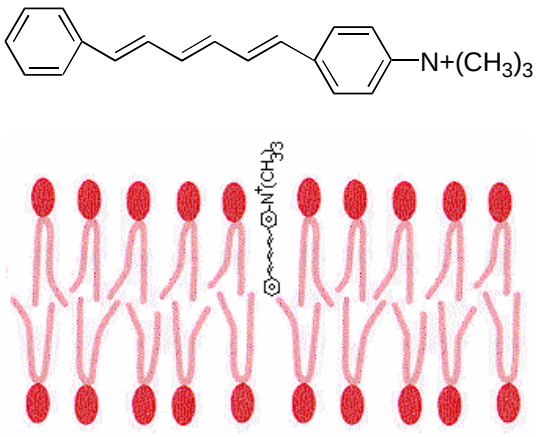

Fig. 1 The insertion of the fluorescent probe (TMA- DPH) in the lipid bilayer

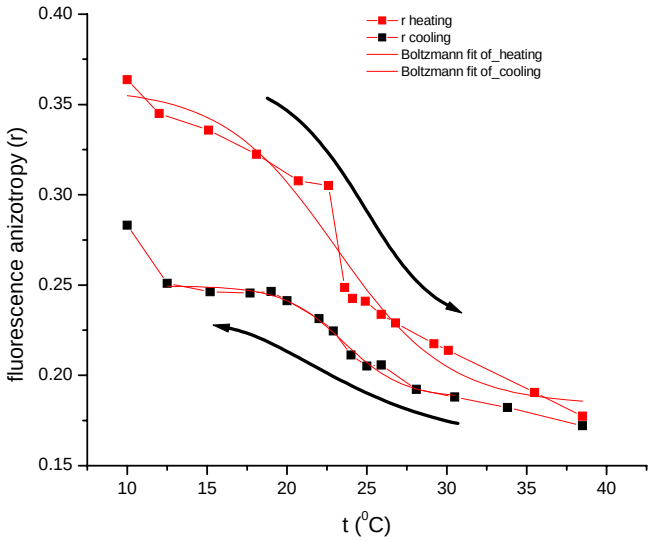

Fig.2 Fluorescence anisotropy of 1,2-dimyristoyl-sn-glycero-3-phosphocholine (DMPC) liposomes recorded versus temperature increase (red squares) and temperature decrease (black squares). The sigmoid fit of the experimental curves indicate a phase transition around 23 ^{o}C.

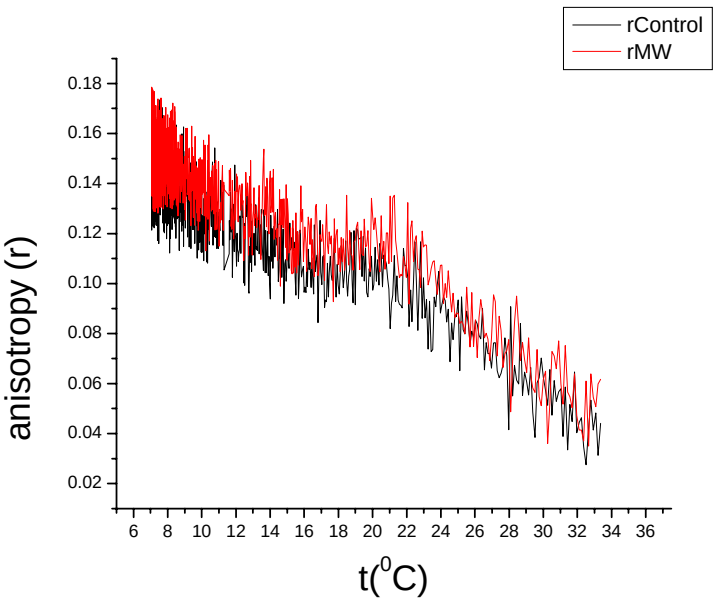

Fig.3 Fluorescence anisotropy of 1,2-dimyristoyl-sn-glycero-3-phosphocholine (DMPC) liposomes recorded versus temperature increase induced by thermostate (black) and microwave heating (red).

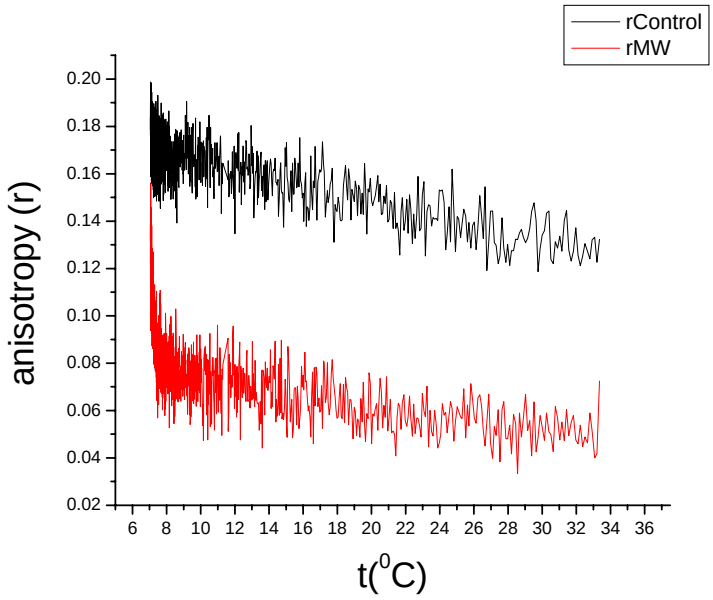

Fig.4 Fluorescence anisotropy of human platelet membranes vs. temperature increase at thermostate (black) and microwave (red) heating

Generalized polarization (GP)

Laurdan (6-dodecanoyl-2-(dimethylamino)-naphthalene) is a fluorescent dye which spontaneously incorporates into phospholipid membranes due to its long hydrophobic tail, as shown in the scheme below:

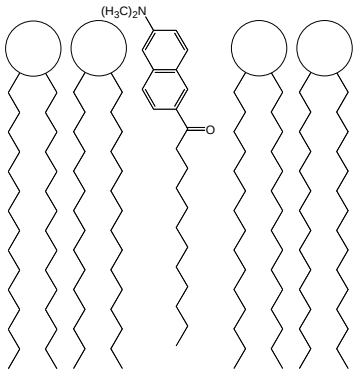

The molecule in the ground state has a very low dipole moment, while excited it has a high dipole (due to the existence of donor and acceptor functional groups).

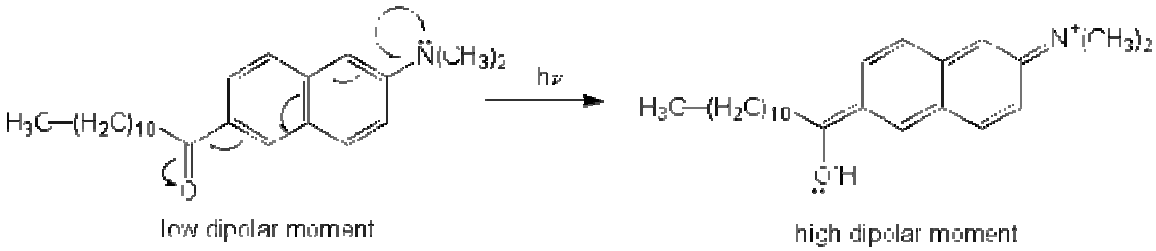

When the membrane contains dipolar molecules (e.g. water), these molecules will strongly interact with the excited form of Laurdan, shifting its emission spectrum toward lower energies (higher wavelengths), because part of the excitation energy is dissipated in the reorientation process. This phenomenon is illustrated in the diagram bellow:

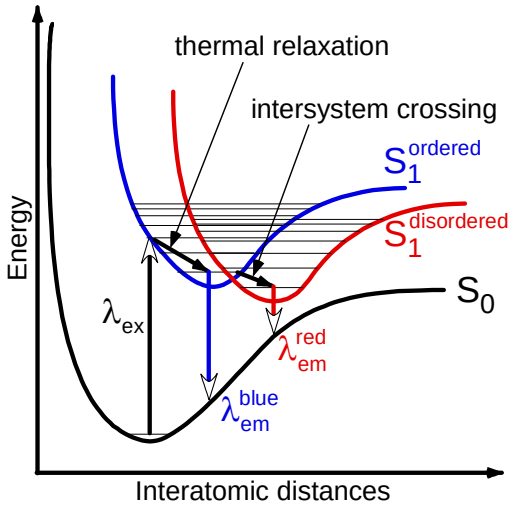

In MW fields, the permanent dipoles of water are supposed to align along the electric field lines. This "ordering" phenomenon of the molecules inside the membrane will hinder the energy transfer process between the excited molecules of Laurdan and the surrounding water molecules, compared with the same process in a non-irradiated sample. Thus, when heating a sample, the profiles of the plots representing the emission maxima position vs. temperature, will depend on the heating procedure ("thermal" or by MW irradiation).

In the case of simple membranes, containing one single component, like liposomes, the plot of λ_{max} vs. temperature has an S-shaped aspect, showing a quite sharp inflexion point corresponding to the phase transition temperature of the phospholipid used for liposomes preparation.

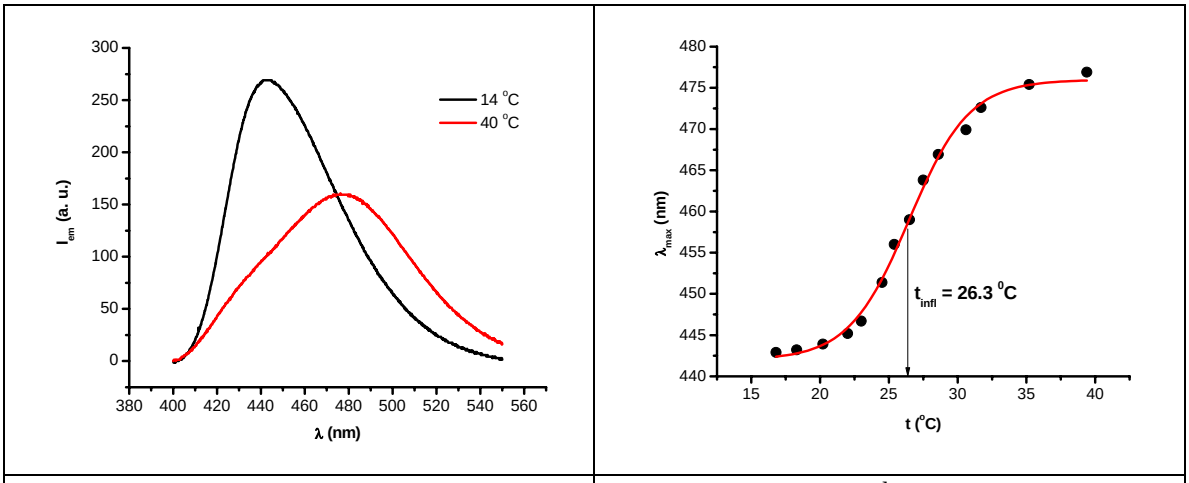

a b

Fig.5 Modification of emission spectra of Laurdan in 1,2-dimyristoyl-sn-glycero-3-phosphocholine (DMPC) liposomes, induced by "thermal" heating. a) Aspect of emission spectra at two extreme temperatures (14 and 40 °C); b) Shift of the emission maxima as a function of temperature.

As concerns the generalized polarization, it depends on the temperature in the same S-shaped way as the emission maxima, but in a less well defined manner, presenting the inflexion point at approximately the same temperature:

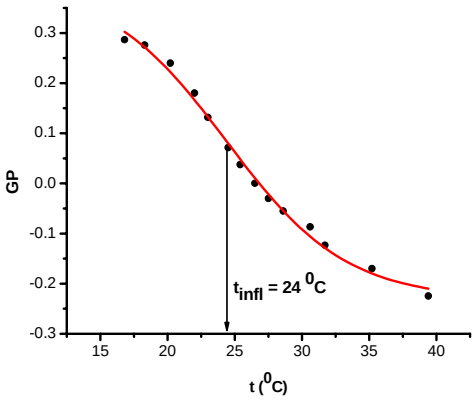

Fig.6 The temperature dependence of generalized polarization. The difference between the values of the inflexion point as determined by GP and λ_{max} lays within the standard error of the two computation methods

When the same heating is performed by applying MW, the corresponding plot looks like:

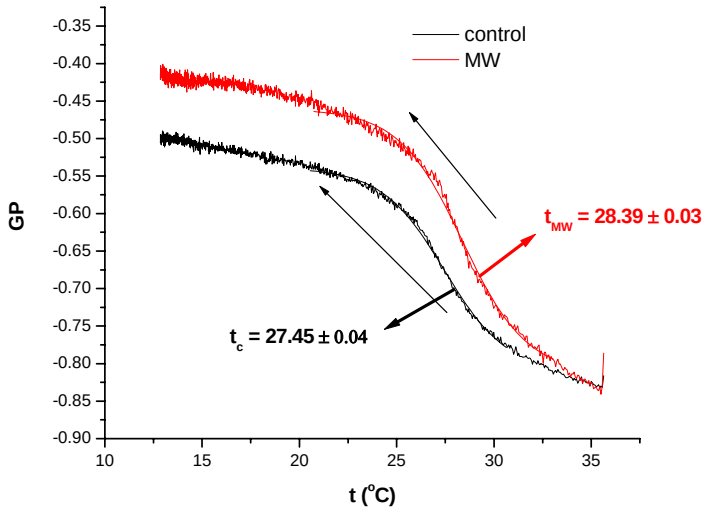

Fig.7 General polarization of DMPC liposome suspension cooled in the presence (red curve) and the absence (black curve) microwave irradiation (SAR 10mW/g).

Containing cholesterol and many other lipidic or non-lipidic components, many cell membranes do not elicit a clear critical temperature of phase transition, the different phases coexisting in various proportions. In the figure below, the record of GP at warming and cooling of platelets suspension in the absence of MW irradiation is shown.

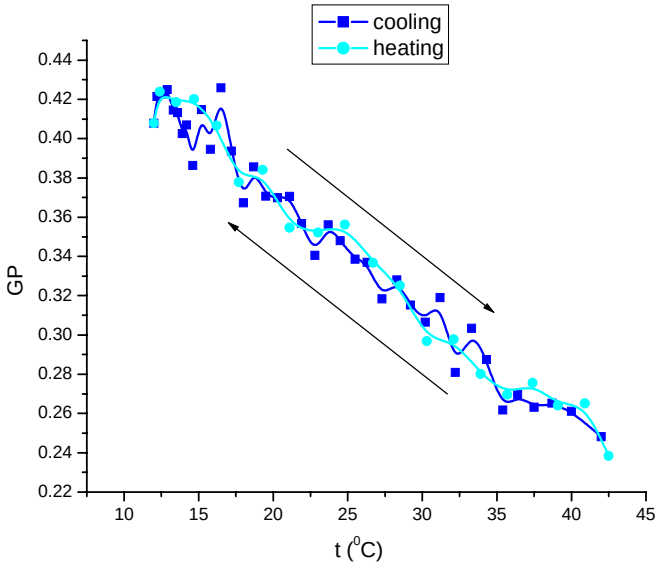

Fig.8 General polarization of human platelets suspension in HBBS buffer as evaluated by Laurdan fluorescence. No obvious inflection point (phase transition temperature) can be noticed.

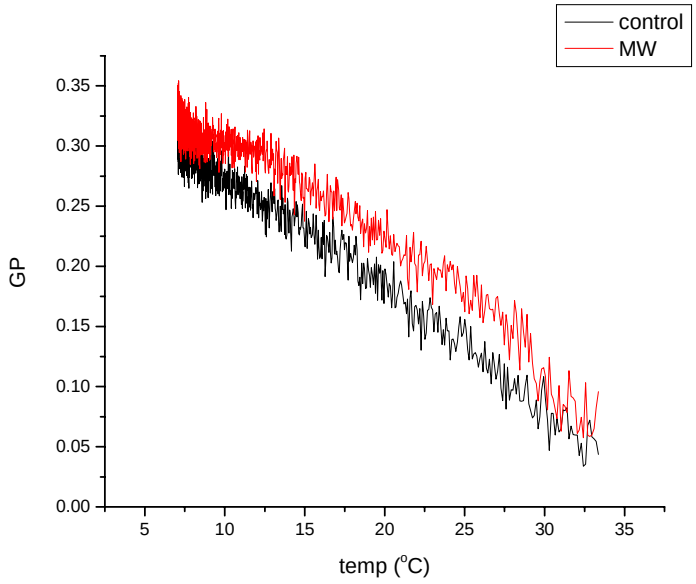

Fig.9 Generalized polarization of human platelets suspension in HBBS buffer as evaluated by Laurdan fluorescence. Higher GP of irradiated sample (red) show a predominance of non-relaxed Laurdan population

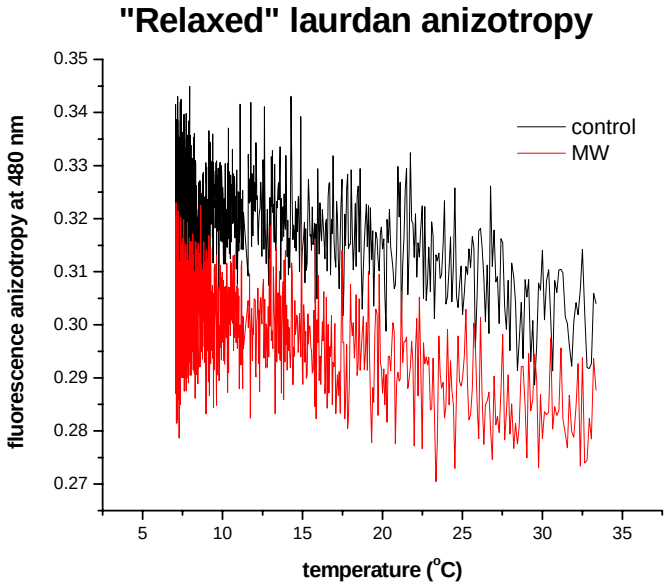

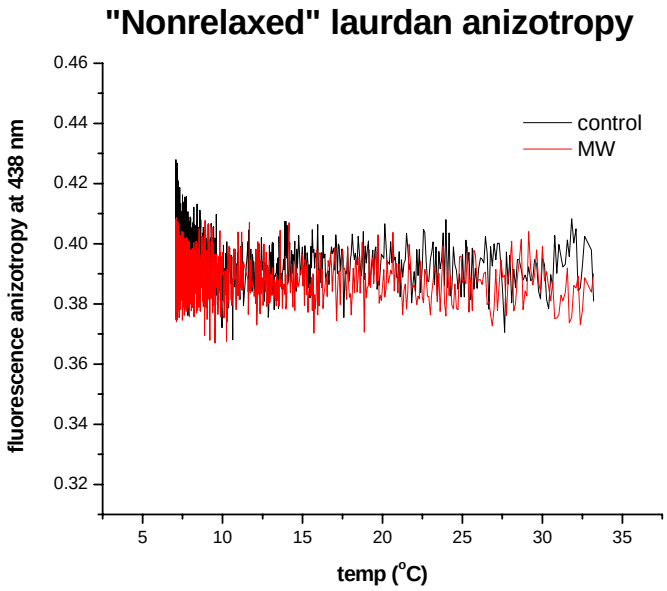

Fig.10 Fluorescence depolarization platelets membranes labelled by Laurdan, recorded at a/ λ_{em48o} and b/λ_{em438} nm

Discussion

The higher values of generalized polarization in irradiated lipid vesicles as well as in platelets reflect formally an increase in population of non-relaxed Laurdan molecules which cannot orient locally the polar, hydrophilic molecules (water). We could expect this, since water molecules are already oriented by microwave field, contributing to a more rigid, gel-like lattice at low temperatures (see figure 7). This is also why the phase – transition temperature is higher in irradiated liposome sample. As system pass to a liquid-crystal phase (above T_c), the difference between the two samples vanishes since thermal motion oppose the dipole orienting effect of the field.

The same effect can be observed in recording the fluorescence anisotropy based on emission of relaxed and nonrelaxed laurdan molecules. Under microwave irradiation the anisotropy of relaxed Laurdan emission is lower comparatively to that of the non-relaxed Laurdan due to the greater mobility of the fluorescent marker in the lipid environment when it cannot strongly orient the neighboring dipoles (water, aminoacids) already oriented in the direction of the applied field.

In case of TMA-DPH fluorescence measurements the local mobility of lipid tails packed within the membrane bilayer is followed up. While in case of model liposome membrane no dramatic effect of irradiation was observed (fig.3), in case of platelet membrane a pronounced loosening (decrease of fluorescence anisotropy) of lipid packing is noticed (fig.4) similar to that recorded when using Laurdan (fig.10).

Conclusion

Based on evidence of the effects of radiofrequency fields in different biological endpoints, it has been suggested (Adey 1993), that co-operative interactions on the surface of cell membranes may allow weak fields to influence cellular processes through signal amplification and transduction processes.

At frequency used in our measurements (2.45 GHz), the basic interaction mechanism is the rotation of molecules in which positive and negative charges are separated in space (polar molecules). The most common such molecule in biological matter is water. Polar molecules tend to align themselves with the electric field and, as this oscillates, they tend to follow these oscillations. In this process energy is dissipated in the form of heat.

To discuss on *long lasting* effects of microwave application on a living system is only meaningful in terms of interference with signal pathways and this is, most probable, the specific “nonthermal” effect of microwaves although, as mentioned above, it may be accompanied by system heating.

An example of (interfacial) membrane polarity modulating the binding of signal molecules is the case of protein kinase C (PKC). This enzyme plays an important role in signal transduction. It is an amphitropic enzyme, existing in both aqueous and membrane phases. Binding of PKC to membranes increases its activity against most substrates. Membrane interfacial properties affect both the binding of the enzyme to a membrane as well as the activity of the enzyme in the membrane-bound state (Giorgione et al., 1998).

Our experiments provide the evidence that in simple bilayer systems (liposomes) as well as in a living cell membrane there is a change in local order of lipid packing (membrane fluidity) and polar molecules orientation induced by microwave irradiation. These changes are consistent with many reported cellular effects of microwaves and provide a meaningful biophysical mechanism for them.

References

Adang D., Remacle C., Vander Vorst A., *Long-term and low-thermal biological effects of microwaves, WIT Transactions on Biomedicine and Health, Vol 9, © 2005 WIT Press, www.witpress.com, ISSN 1743-3525 (on-line)*

Adey, W.R. *Biological effects of electromagnetic fields.* J. Cellular Biochem. 51. (1993) 410-416.

Adey, W.R. *Electromagnetics in biology and medicine In: H. Matsumoto ed. Modern Science* (1993) Oxford Univ. Press 227-245.

Ambrosini A., Zolese G., Balercia G., Bertoli E., Arnaldi G., Mantero F., *Laurdan* fluorescence: a simple method to evaluate sperm plasma membrane alterations,* Fertility and Sterility, 76, (2001) 501-505

CSIRO - *BIOLOGICAL EFFECTS AND SAFETY OF EMR* , June 1994

De Vequi-Suplicy C., Benatti C., Lamy T., *Laurdan in Fluid Bilayers- Position and Structural Sensitivity,* Journal of Fluorescence, 16(2006), 431-439

Epand R., Kraayenhof R., *Fluorescent probes used to monitor membrane interfacial polarity*, Chemistry and Physics of Lipids, 101 (1999) 57–64

Giorgione J., Kraayenhof R., Epand R.,*Interfacial membrane properties modulate protein kinase C activation: role of the position of acyl chain unsaturation*, Biochemistry 37 (1998) 10956-10960

Lee-Gou Chong P., Sugar I., *Fluorescence studies of lipid regular distribution in Membranes,* Chemistry and Physics of Lipids, 116 (2002) 153–175

Liburdy R, Vanek PJr., *Microwaves and the cell membrane. II. Temperature, plasma, and oxygen mediate microwave-induced membrane permeability in the erythrocyte,* Radiat Res.102 (1985) 190-205

Parasassi T., KrasnowskaE., Bagatolli L., Gratton E., *Laurdan and Prodan as Polarity – Sensitive Fluorescent Membrane Probes*, Jornalof Fluorescence, 8 (1998) 365-373

Zubiri D., Domecq A., Bernik D., *Phase behavior of phosphatidylglycerol bilayers as a function of buffer composition: fluorescence studies using Laurdan probe,* Colloids and Surfaces B: Biointerfaces 13 (1999) 13–28

The Use of Electromagnetic Noise as a Universal Inhibition Factor for the Mitigation of Biological Effects from Exposure to Electromagnetic Fields

Miguel Penafiel

Vitreous State Laboratory
The Catholic University of America
Washington, DC
USA

Running Title: Inhibition of bio-effects with ELF noise

Please send correspondence to:

Miguel Penafiel
Vitreous State Laboratory
Catholic University
Hannan Hall, Room 410
Washington, DC 20064
USA

Telephone: 202-319-5335
FAX: 202-319-4469
Email: Penafiel@vsl.cua.edu

Abstract

Numerous studies have reported biological effects from exposure to electromagnetic fields both in the ELF and RF ranges, but there is a lack of consensus about the validity of observed effects. In part this is due to replication difficulties. At the core of this issue is the fact that observed effects, while significant, can be of a subtle nature and can be easily masked by equally subtle changes in experimental conditions. The result is that effects that are observed in one experimental setting may not be observed in another seemingly equivalent setting. An alternate approach to verify the validity of observed effects that overcomes the difficulties associated with attempting to duplicate experimental conditions is to intentionally use an inhibition factor to demonstrate that observed effects can be elicited or negated at will. Our own research and that of others supports the notion that a universal inhibition factor is ELF electromagnetic noise. The superposition of ELF noise to inhibit biological effects elicited by exposure to electromagnetic fields has been found to be effective in all instances tested. Inhibited effects include: changes in enzymatic activity, changes in hormone levels, changes in oncogene transcript levels, alterations in gap junction intercellular communication, increases in DNA breaks, activation of stress proteins, increases in cell proliferation, teratogenic effects, and memory effects. The superposition of ELF noise has been shown to be equally effective in blocking ELF and RF induced effects. A physical understanding of how EM noise acts to block EMF induced effects can be formulated in terms of a detection process of the EM stimulus

analogous to the detection of chemical gradients in bacterial chemotaxis. This theory hypothesizes a temporal sensing mechanism involving two characteristic time constants: τ_a, the "averaging" time (~0.05s), and τ_m, the "memory" time (~5s). To elicit a full response a stimulus of constant intensity over τ_a must be applied for a time period greater than τ_m. The superposition of EM noise effectively inhibits the response by destroying amplitude uniformity of the EM stimulus over the required time scale.

Key words: ELF noise, temporal sensing, inhibition factor

Introduction

As far back as the 1980's reports about so-called nonthermal biological effects of exposure to weak electromagnetic fields (EMFs) were being widely circulated (Luben et al. 1982). These reports created a great deal of controversy as they went against the then commonly held belief that electromagnetic exposure could be of biological consequence only when the energy transfer was sufficient to produce measurable increases in temperature. Today, more than 25 years later and after hundreds of studies the controversy still remains. But the source of the controversy is not that biological effects from exposure to nonthermal fields have not been observed, but rather that biological mechanisms that explain the observed phenomena are still not well understood and cannot be easily explained, leading some to believe that effects are not plausible in spite of the evidence (Adair 1991, 2003).

All life on earth has evolved in the presence of environmental factors that include a broad spectrum of electromagnetic radiation. Much of this radiation is from natural sources that have been an essentially constant part of the environment in recorded time. But the technological leap that has taken place over the last 75 years or so has substantially increased the background radiation. This increase is particularly evident in the Extremely Low Frequency (ELF) range due to the ever-expanding electric power distribution grid, and in the Radio Frequency (RF) range due to the exponential growth of telecommunication networks. The increased exposure to man-made fields has fuelled the interest in understanding biological interactions, not only as a means to gain scientific knowledge, but also to assist in the setting of regulatory guidelines for exposure to such fields.

The issue of regulatory guidelines is most relevant in connection with the use of the ubiquitous cellular phone. Present guidelines, which coincide with practical limitations for the deployment of these devices, are based on the assumption that only effects accompanied by strong thermal interactions are likely. Yet there are hundreds of studies that show effects from nonthermal exposure (Adair 2003). Most of the observed effects are of a subtle nature and are therefore susceptible to numerous factors that make replication difficult. In part due to replication difficulties, some have suggested that all of the studies that show effects are somehow flawed (Adair 2003). The alternative is that there are as yet not clearly defined biological mechanisms that have escaped scientific understanding. Of course, the lack of a full understanding does not make observed effects invalid. Such is the case, for instance, with EMF-mediated bone fracture repair, which is clinically effective but still not well understood (Aaron et al. 2004).

Published studies that have reported biological effects from exposure to weak ELF and RF fields are too many to mention individually. Effects in the ELF range include changes in enzymatic activity (Litovitz et al.1997), teratogenic effects (Farrell et al. 1997), changes in gene expression (Lin et al. 1994), stress response effects (Lin et al.1997, DiCarlo et al. 2002), and DNA damage effects (Lai and Singh 1997). RF effects include changes in enzymatic activity (Penafiel et al. 1997), memory effects (Lai et al. 1994, Wang and Lai 2000), and DNA damage effects (Lai and Singh 1996). There are also a number of experiments that show similar effects for both ELF and RF exposure indicating that common biochemical pathways may be involved in the response. These effects include changes in enzymatic activity (Penafiel et al. 1997), memory effects on rats (Lai et al. 1994, 1998) and effects on chromatin conformation (Belyaev et al. 2005).

While the evidence for biological effects from exposure to weak EMFs is extensive, it is important to point that a number of experiments have also reported null effects. Many of these are experiments that have attempted to replicate previously reported results (Desta el al. 1999, Cosquer et al. 2005). Such null effects bring into question either the validity of reported effects or the accuracy of replication conditions (Krause et al. 2004). The issue of replication was also evident in our own laboratory while studying teratogenic effects from ELF EMF exposure of chick embryos. Statistically significant effects were observed in some experimental campaigns but not in others even though experimental conditions appeared to be the same. The discrepancy in the results was eventually tracked down to a change in the chick progenitor flock. The unknown factor causing the variability in results was apparently a genetic factor (DiCarlo and Litovitz 1999).

The ability to examine experimental data to look for unknown factors usually requires that a large number of experiments be performed. More often than not this is not possible. The issue of experimental validity when exact replication is difficult to achieve can be best addressed using a suitable inhibition factor, if such a factor can be found. We have previously demonstrated in a number of instances, that in the case of exposure to weak ELF and RF EMFs, the inhibition factor is ELF electromagnetic noise (e.g.,Litovitz et al. 1993, 1994, 1997b). The purpose of this paper is to show that the inhibiting ability of ELF noise covers a wide range of biological effects thereby suggesting that it might be a universal inhibition factor for EM induced biological effects.

Temporal characteristics of a bio-effecting stimulus

One of the issues concerning the general acceptance of experimental results that show effects from exposure to weak electromagnetic field is one of plausibility based on accepted demonstrable mechanisms. By one argument, weak EMFs do not carry sufficient energy to cause biologically significant interactions in the presence of local thermally driven electromagnetic noise. Calculations based on general physical properties of biological matter, which do not account for biological complexity, do indeed appear to demonstrate that local noise considerations make such interactions unlikely (Adair 1991, 2003). For interactions within the cellular membrane the magnitude of the local electromagnetic noise, thus calculated, is of the order of 500 V/m, which is many orders of magnitude larger than induced fields within humans from background ELF EMFs (< 0.001 V/m). Yet undisputable effects associated with research on bone fracture repair, which appears to be rooted in membrane bound interactions, have been observed with induced electric fields of 0.1V/m or even less (Luben et al. 1982). This evidence suggests that thermal noise considerations are not sufficient to render certain effects implausible.

If we accept that certain bio-effecting interactions are possible, notwithstanding thermal noise considerations, then it is of interest to find alternate approaches to determine the viability of such interactions. Clearly, EMFs affect biological material at an elemental level, but beyond the obvious primary interaction the biological response is determined by the signal processing characteristics of the living biological entity. These characteristics are an inherent property of the living system defined by a complex transfer function, which if known, would predict what signals are filtered out and what signals are passed through. An important consideration in this simple model is how stimulating signal varies as a function of time.

The biological response to an environmental stimulus is a multi-step process involving a series of chained biochemical reactions characterized by varying rate constants, which form what is referred to as a signalling cascade. The net response results from the interplay of the biochemical events in the signalling cascade. This process, which incorporates the functions of signal detection and discrimination and control of the endogenous cellular reply, is referred to as signal transduction. A model system for the study of signal transduction is that of bacterial chemotaxis. This model involves two time-dependent processes that together constitute a rudimentary memory system. One is a fast process, occurring on a time scale of the order of 0.04s, which performs the function of measuring the concentration of chemotactant molecules through binding of these molecules to surface receptors. The other is a slower process, taking place on a time scale of the order of 5s, which performs a comparison function by modification of the receptors when no changes in chemotactant concentration are detected. This is a process of temporal sensing through which the bacterium makes continuous measurements of chemotactant concentration, compares successive measurements, and responds to the difference between them.

A model analogous to that of bacterial chemotaxis can describe the biological response to weak EMF exposure (Litovitz et al 1997a). The parameters of this model were determined in studies of the effect of EMF stimulation on ODC activity. A constantly applied 60 Hz EMF stimulus yielded a consistent doubling of the ODC activity. Changes in the ODC response were first examined by introducing zero-field gaps of varying duration in the exposure signal. It was determined that the magnitude of the response decreased as the frequency of the gaps increased. The full response was elicited when a field of constant intensity was applied, without interruption, for a minimum of 10s. The characteristic time associated with the response to this gapped stimulus was found to be 5s and was termed the memory time, $\tau_{m.}$. Knowing the requirements to elicit a full response, zero-field gaps were introduced periodically at 1s intervals for much shorter intervals that were increased until the response was negated. The magnitude of the response was found to decrease with increasing gap duration. No response was obtained when the gap duration was 100ms. The characteristic time constant associated with the response to this second gapped stimulus was found to be 0.05s and was termed the averaging time, τ_a. In essence these results showed that the ODC response to EMF stimulation involved two processes with rudimentary memory. Continuous measurements averaged over a time τ_a are compared successively. The response is elicited when a constant measurement persists over a time greater than $\tau_{m.}$

The use of ELF noise to negate electromagnetic effects

The similarities of the temporal characteristics of the response to EMF exposure, as determined for the ODC model, with those of bacterial chemotaxis suggests that this may be a more general model applicable to the response to weak environmental stimuli. Furthermore, the requirement that certain temporal characteristics must be met to elicit a response suggests that strategies to alter the temporal characteristics of a stimulus could be devices for the purpose of negating the response. Such a scheme might be useful, for instance, for the mitigation of unwanted effects from EMF exposure.

The simplest strategy to alter the temporal parameters of an EMF stimulus is by the superposition of another EMF stimulus whose temporal characteristics do not meet the requirements to elicit a response. One such signal is ELF magnetic noise. Using the temporal sensing model with $\tau_a = 0.05$s and $\tau_m = 5$s, it can be shown a noise signal with bandwidth in the biologically active frequency range below 100 Hz will not elicit a response. The superposition of a noise EMF stimulus over an existing stimulus results in a new stimulus which is noisy itself and is the sum of the local stimulus s(t) and the superimposed noise n(t). In order to fully negate the response n(t)/s(t) must be greater than or equal to 1.

Measurements with the ODC model confirmed that the superposition of ELF noise could indeed negate the response (Litovitz 1994, 1997b). Other studies in our laboratory demonstrated that noise could also be used to inhibit teratogenic effects and effects on the stress response in chick embryos (Litovitz 1993, DiCarlo 1998, 1999b, 2000, 2002, Shallom 2002). Furthermore, it was also found that ELF noise could inhibit biological effects induced by mild mechanical vibration (DiCarlo 2002). Considered together this evidence makes a strong case for the argument that the inhibiting effect of ELF noise may be universal to weak stimuli.

Experiments carried out in other laboratories have also demonstrated the efficacy of ELF noise to inhibit both ELF and RF effects. Table 1 shows a list of published results that show the range of effects negated by the superposition of ELF noise. In the ELF domain effects elicited with field intensities between 1uT and 400 uT have been blocked. In the RF domain effects from exposure to fields of the order of 1 to 3 W/kg have been negated. The lower intensity cases represent situations in which the viability of effects might be called into question based on thermal noise consideration. The thermal noise issue can still be a possible argument against viability in the higher intensity cases, but it is a less convincing argument particularly since equivalent field intensities have been demonstrated to be bio-effecting in bone growth stimulation studies (Luben et al 1982). The results of Table 1 show that the outcome of the observed response can be manipulated through the use of another stimulating agent of the same type as the bio-effecting agent, thereby lending credibility to the existence of such effects.

Table 1: Biological effects inhibited by the superposition of ELF noise			
Model	*Exposure field*	*Effect inhibited*	*Reference*
Chick embryos	4 uT, 60 Hz sine	Two-fold increase/shift in ODC activity	Farrell et al. 1993
Chick embryos	1 uT peak, 100 Hz pulsed	Two-fold increase in developmental abnormalities	Litovitz et al. 1993
L929 cells	10 uT, 60 Hz sine	Two-fold increase in ODC activity	Mullins et al. 1993
L929 cells	10 uT, 60 Hz	Two-fold increase in ODC activity	Litovitz et al 1994
HL60 cells	6.7 uT, 60 Hz sine	40 % increase in c-myc transcript	Lin et al. 1995
Chick embryos	4 uT, 60 Hz sine	40 % reduction in the activity of 5'-nucleotidase	Martin et al. 1995
AMA cells	5uT, 50Hz sine	15% increase in cell proliferation	Rasmark et al. 1996
PC12 cells	8 uT, 60 Hz sine	15% decrease in intracellular dopamine	Opler et al 1997
L929 cells	835 MHz amplitude modulated, 2.5 W/Kg	40-100% increase in ODC activity	Litovitz et al. 1997
Chick embryos	4 uT to 10 uT, 60 Hz sine	Two-fold enhancement of survival of chick embryos in anoxic conditions by EM pre-conditioning	DiCarlo et al. 1999
Chick embryo	8 uT, 60 Hz sine 915 MHz CW, 1.7 W/kg repeated	27% decrease in HSP70 levels consistent with decreased cyto-protection	DiCarlo et al. 2002
Chick embryo	915 MHz CW, 1.75 or 2.5 W/Kg	Increase in HSP70 by preconditioning consistent with increased survival after hypoxia	Shallom et al. 2002
NIH3T3 cells	0.4 mT 50Hz	40% suppression in gap junction intercellular communication	Zeng et al 2002
Rats	2.45 GHz CW, 1.2 W/Kg	35% learning deficit	Lai 2004
NIH3T3 cells	0.2 mT 50Hz	50% co-suppression in gap junction intercellular communication with phorbol ester	Gao et al 2004
NIH3T3 cells	0.4 mT, 0.2 mT, 50Hz	30% suppression in gap junction intercellular communication	Zeng et al 2006

Discussion

In spite of hundreds of published results that claim the existence of biological effects from exposure to weak ELF and RF EMFs using a broad range of end points, there is still a great deal of uncertainty about whether these effects are real. Part of the problem is that effects have often been difficult to replicate and proposed biological mechanisms have not been substantiated and thus often remain speculative. But even when effects are generally accepted, a full understanding of the underlying biological mechanisms can still be lacking. Such is the case, for instance, in the case of EMF induced bone growth stimulation (Aaron et al. 2004).

Stimulation of living biological entities by weak exogenous stimuli involve signal transduction processes which often include signal integration and amplification. A model proposed in bacterial chemotaxis, which may apply to many other weak signal detection situations, assumes the existence of long-range cooperative interactions between receptors as a means to achieve signal amplification (Sourjik and Berg 2004). Other processes that could result in further signal amplification and discrimination are communication interactions between cells through gap junction channels. Direct cell to cell communication, evident in organized tissues and even in cell cultures as demonstrated by contact growth inhibition, is critical to bone-forming cells (Lecanda et al 1998). Biological effects could result from the disruption of any of the signalling pathways of the signal transduction process.

The biochemical basis for the interaction of EMFs with living entities is not clear. It is possible that the primary site of interaction is at the cellular membrane via modulation of receptor binding. If this were the case, a myriad

of downstream signalling pathways could be affected leading to observable effects. But the ability of noise to inhibit many of these effects provides a common link that sheds some light about the nature of the response. It is generally accepted that at a fundamental level the extent of the electromagnetic interaction is proportional to the intensity of the stimulus. As the intensity level increases direct heat dissipation resulting in measureable increases in temperature could be a consequence of the exposure. At such levels the superposition of a signal of equivalent intensity would only result in further heating. But at exposure levels for which heating is not an issue, such as the experiments listed in Table 1, the inhibiting ability of superimposed ELF noise indicates that these interactions are a signalling events with common temporal sensing characteristics. This also suggests that while the effects of EMF exposure may be evident in a multitude of observable parameters, it is possible that such responses might share a few key common biochemical pathways. The shared common pathways would be those that establish the signal averaging time, τ_a, and the memory time, τ_m of the temporal sensing process.

The evidence shown in Table 1 is suggestive of a general effect that may be universally applicable. This inductive conclusion would be difficult to prove for all cases. However, the fact that ELF noise inhibition has been effective in all instances in which it has been examined adds to the weight of the evidence supporting this argument.

Conclusions

A review of experimental results on the use of the superposition of ELF noise for the inhibition of effects induced by exposure to weak EMFs shows the efficacy of this technique to negate observed effects. These results apply to a broad range of end points and over a wide range of signal intensities suggesting that a common factor is at play. This common factor is likely to be a temporal sensing process characterized by two common rate constants. The broad scope of inhibited effects also suggests the applicability of the temporal sensing hypothesis as a general signal transduction mechanism for the interaction of EMFs with living systems.

Two general conclusions can be drawn from the foregoing review which shows that the superposition of ELF noise is an effective inhibiting factor in bioelectromagnetic effects: 1) the use of ELF noise in a pseudo-sham exposure condition would be beneficial in determining whether observed effects are attributable to EMF exposure, and 2) the superposition of ELF noise would be effective as a prophylactic means to inhibit unwanted biological effects in situations where exposure is unavoidable.

References

Aaron RK, Boyan BD, Ciombor DM, Schuartz Z, Simon BJ. 2004. Stimulation of growth factor synthesis by electric and electromagnetic fields. Clin. Orthop. Relat. Res. 419:30-37.

Adair RK. 1991. Constraints on biological effects of weak extremely low frequency electromagnetic fields. Phys. Rev. A 43:1049-1048.

Adair RK. 2003. Biophysical limits on athermal effects of RF and microwave radiation, Bioelectromagnetics 24(1):39-48.

Belyaev IY, Hillert L, Protopopova M, Tamm C, Malmgrem LO, Person BR, Selivanova G, Harms-Ringdahl M. 2005. 915 MHz Microwaves and 50 Hz Magnetic field affect chromatic conformation and 53BP1 foci in human lymphocytes from hypersensitive and healthy persons. Bioelectromagnetics 26:173-184.

Cosquer B, Kuster N, Cassel JC. 2005. Whole-body exposure to 2.45 GHz electromagnetic fields does not alter 12-arm radial-maze with reduced access to spatial cues in rats. Behav Brain Res. 161:331-334.

Desta AB, Owen RD, Cress LW. 1999. Ornithine decarboxylase activity in developing chick embryos after exposure to 60-hertz magnetic fields. Biochem Biophys Res. Comm. 265:211-213.

DiCarlo AL, Farrell JM, Litovitz TA. 1998. A simple experiment to study electromagnetic field effects: Protection induced by short-term exposures to 60 Hz magnetic fields. Bioelectromagnetics 19:498-500.

DiCarlo AL, Litovitz TA. 1999a. Is genetics the unrecognized confounding factor in bioelectromagnetics? Flock-dependence of field-induced anoxia protection in chick embryos. Bioelectrochem Bioenerg. 48:209-215.

DiCarlo AL, Farrell JM, Litovitz TA. 1999b. Myocardial protection conferred by electromagnetic fields. Circulation. 99:813-816.

DiCarlo AL, Mullins JM, Litovitz TA. 2000. Electromagnetic field-induced protection of chick embryos against hypoxia exhibits characteristics of temporal sensing. Bioelectrochemistry 52:17-21.

DiCarlo A, White N, Guo F, Garrett P, Litovitz T. 2002. Chronic electromagnetic field exposure decreases HSP70 levels and lowers cytoprotection. J. Cell. Biochem. 84:447-454.

Farrell JM, Barber M, Doinov P, Krause D, Litovitz TA. 1993. Superposition of a temporally incoherent magnetic field suppresses the change in ornithine decarboxylase activity in developing chick embryos

induced by a 60 Hz sinusoidal field. In: Blank M, ed. Electricity and Magnetism in Biology and Medicine. San Francisco, USA: San Francisco Press.
Farrell JM, Litovitz TL, Penafiel LM, Montrose CJ, Doinov P, Barber M, Brown KM, Litovitz TA. 1997. The Effect of Pulsed and Sinusoidal Magnetic Fields on the Morphology of Developing Chick Embryos, Bioelectromagnetics 18:431-438.
Gao XW, Xu ZP, Huo YN, Jiang H, Fu YT, Lu DQ, Zeng QL. 2004. [Noise magnetic fields block co-supression effect induced by power frequency magnetic field and phorbol ester]. Zhonghua Yu Fang Yi Xue Za Zhi 38:11-13.
Krause CM, Haarala C, Sillanmaki L, Koivisto M, Alanko K, Revonsuo A, Laine M, Hamalainen H. 2004. Effects of electromagnetic field emitted by cellular phones on the EEG during an auditory memory task: a double blind replication study. Bioelectromagnetics 25:33-40.
Lai H, Horita A, Guy AW. 1994. Microwave irradiation affects radial-arm maze performance in the rat. Bioelectromagnetics 15:95-104.
Lai H, Singh HP. 1996. Single- and double-strand DNA breaks in rat brain cells after acute exposure to radiofrequency electromagnetic radiation, Int J Radiat Biol. 69:513-21.
Lai H, Singh HP. 1997. Acute exposure to a 60 Hz magnetic field increases DNA strand breaks in rat brain cells, Bioelectromagnetics 18:156-65.
Lai H, Carino MA, Ushijima I. 1998. Acute exposure to a 60 Hz magnetic field affects rats' water-maze performance. Bioelectromagnetics 19:117-122.
Lai H. 2004. Interaction of microwaves and a temporally incoherent magnetic field on spatial learning in the rat. Physiology and Behavior 82:785-789.
Lecanda F, Towler DA, Ziambaras K, Cheng SL, Koval M, Steinberg TH, Civitelli R. 1998. Gap junctional communikcation modulates gene expression in osteoblastic cells. Mol. Biol. Cell. 9:2249-2258.
Lin H, Goodman R, Shirley-Henderson A. 1994. Specific region of the c-myc promoter is responsive to electric and magnetic fields, J Cell Biochem 54:281-8.
Lin H, Goodman R. 1995. Electric and magnetic noise blocks the 60 Hz magnetic field enhancement of steady state c-myc transcript levels in human leukemia cells. Bioelectrochem. Bioenerg. 36:33-37.
Lin H, Opler M, Head M, Blank M, Goodman R. 1997. Electromagnetic field exposure induces rapid, transitory heat shock factor activation in human cells, J Cell Biochem 66:482-488.
Litovitz TA, Montrose CJ, Doinov P, Brown KM, Barber M.1993. Superimposing spatially coherent electromagnetic noise inhibits field-induced abnormalities in developing chick embryos. Bioelectromagnetics.15:105-113.
Litovitz TA, Krause D, Penafiel M, Elson EC, Mullins JM. 1993. The Role of Coherence Time in the Effect of Microwaves on Ornithine Decarboxylase Activity, Bioelectromagnetics 14:395-403.
Litovitz TA, Krause D, Montrose CJ, Mullins JM. 1994. Temporally incoherent magnetic fields mitigate the response of biological systems to temporally coherent magnetic fields. Bioelectromagnetics 15:399-409.
Litovitz TA, Penafiel M, Krause D, Zhang D, Mullins JM. 1997a. The role of temporal sensing in bioelectromagnetic effects. Bioelectromagnetics 18:388-395.
Litovitz TA, Penafiel LM, Farrel JM, Krause D, Meister R, Mullins JM. 1997b. Bioeffects induced by exposure to microwaves are mitigated by superposition of ELF noise. Bioelectromagnetics 18:422-430.
Luben RA, Cain CD, Chen MC, Rosen DM, Adey WR. 1982. Effects of electromagnetic stimuli on bone and bone cells in vitro: Inhibition of responses to parathyroid hormone by low-energy low-frequency fields, Proc. Natl. Acad. Sci. USA 79:4180-4184.
Martin AH, Moses GC. 1995. Effectiveness of noise in blocking electromagnetic effects on enzyme activity in the chick embryo. Biochem. Mol. Biol. Int. 36:87-94.
Mullins JM, Krause D, Litovitz TA. 1993. Simultaneous application of a spatially coherent noise field blocks response of cell cultures to a 60 Hz electromagnetic field. In: Blank M, ed. Electricity and Magnetism in Biology and Medicine. San Francisco, USA: San Francisco Press.
Opler M, Rukenstein A, Cote L, Goodman R. 1997. Reduced dopamine levels in PC12 cells exposed to low frequency electromagnetic fields. Bioelectrochem. Bioenerg. 42:235-239.
Penafiel LM, Litovitz TA, Krause D, Mullins JM. 1997. Role of Modulation on the Effect of Microwaves on Ornithine Decarboxylase Activity in L929 Cells. Bioelectromagnetics 18:132-141.
Raskmark P, Kwee S. 1996.The minimizing effect of electromagnetic noise on the changes in cell proliferation caused by ELF magnetic fields. Bioelectrochem. Bioenerg. 40:193-196.
Shallom JM, DiCarlo AL, Ko D, Penafiel LM, Nakai A, Litovitz TA. 2002. Microwave exposure induces Hsp70 and confers protection against hypoxia in chick embryos. J. Cell. Biochem. 86:490-496.
Skyberg K, Hansteen IL, Vistnes AI. 2001. Chromosomal aberrations in lymphocytes of employees in transformer and generator production exposed to electromagnetic fields and mineral oil. Bioelectromagnetics 22:150-160.

Sourjik V and Berg HC. 2004. Functional interactions between receptors in bacterial chemotaxis. Nature 428:437-441.

Wang B, Lai H. 2000. Acute exposure to pulsed 2450-MHz Microwaves Affects water-maze performance of rats. Bioelectromagnetics 21:52-56.

Zeng QL, Chiang H, Fu YT, Lu DQ, Xu ZP. 2002. [Electromagnetic noise blocks the gap-junctional suppression induced by 50 Hz magnetic field], Zhonghua Lao Dong Wei Sheng Zhi Ye Bing Za Zhi 20:243-245.

Zeng QL, Ke XQ, Gao XW, Fu YT, Lu DQ, Chiang H, Xu ZP. 2006. Noise magnetic fields abolish the gap junction intercellular communication suppression induced by 50 Hz magnetic fields, Bioelectromagnetics 27:1-6.

ELF and RF/MW Electric fields as bioeffectors: a much needed new direction in bioelectromagnetics?

ROGER COGHILL

For several decades now Western research attention in bioelectromagnetics has largely centred on the magnetic component of the electromagnetic wave. In their original 1979 paper, which some argue heralded much of the subsequent scientific interest, Wertheimer and Leeper concluded that the elevated incidence of childhood cancer near pole-mounted transformers in Denver was probably due to the magnetic field. Their conclusion was based on preceding research, which had reported magnetic field sensitivities of some animals and fishes. Savitz et al. later attempted to include electric field measurements in their replication of the Denver study, but abandoned their effort through an inability to address the topic of chronic exposure. It may have escaped the notice of both authors that pole mounted transfoirmers inevitably generate large electric fields in converting the primary to the secondary induced voltage. Moreover, electric fields (unlike magnetic) are present wherever there is connection to the main supply, so the electric component was actually an equal candidate for Wertheimer and Leeper's speculations.
The world's power utilities have also favoured magnetic field research, comforted by the recognition that few homes will experience the 0.4uT commonly used as a cut point in epidemiological studies to define relative risk. The popular EmDEX probes (designed for EPRI) indeed do not even permit the user to collect electric field data without elaborate engineering modification.

Eastern bloc countries do not share this view, arguing that mankind has always had evolutionary experience of magnetic fields, in that we all live on the large magnet of the Earth.: and if anything new has occurred on the planet since the advent of electricity then it is the alternating electric field, for which there is no evolutionary counterpart (Shandala et al, 1988). The search for a mechanism of interaction incorporating the magnetic field only has proven inconclusive to date despite the evidence of many non thermal effects. It might therefore be more fruitful to reappraise the role of the electric component.

Out of eight published domestic epidemiological studies of the electric field only three took proper measurements, and these together offer strong support for the electric field at the nocturnal bedplace as the active parameter (see Table 1). The remaining five used spot or portable probes, or room centre measurements which do not adequately characterise bedplace exposure (see Table 2). The three pertinent studies show a consistent dose response pattern indicating that chronic exposure to ELF electric fields above 20V/m are hazardous to child health.

Table 1: Bedplace ELF electric field exposure in childhood cancer homes

Study	Exposure measures	**Odds ratio (OR) or relative risk (RR)**	95CI%
Coghill, Steward et al, 1996	12 hours TWA, bedplace only	**4.69**	1.17-27.0
Dockerty, Elwood et al, 1997	24 hours TWA, bedroom and one other room	**2.3**	0.4 – 12.7
Skinner Mee et al., 2002	Spot, 48 hours apart, bedplace and one other room	**1.42**	0.88-2.27

Table 2: Residential ELF electric field studies with poor characterisation

Study	Year	Deficiency
Savitz, Wachtel et al, *	1988	room centres only
Green et al,	1999	daytime personal monitor
McBride, Gallagher et al.,	1999	48hrs personal monitor
Tynes and Haldorse	1997	room corner nearest HT line
London, Thomas et al,	1991	spot measurements only

- abandoned a third way through the collection

Our laboratory has recently reported that ELF electric fields at levels commonly seen near powerlines and domestic electric appliances can create nitrites in aerated distilled water to a concentration reported by other studies to cause ill health. The effect is robust over many experiments. This simple physico-chemical effect (paralleling the effect in respiring organisms largely composed of aqueous solutions) may explain the thirty year old mystery of how such weak fields can cause ill health in the absence of heating.

Other studies show that many of the disorders associated with chronic ELF EM field exposure are also associated with excess nitrites found in the patients biological fluids. In childhood leukaemia for example the nitrite level is four times normal in serum and two orders of magnitude higher than normal in the CSF.

An appraisal of the literature as presented in this paper offers the conclusion that more research attention should be paid to electric fields and this in turn may lead to new standard setting which recognises at last the importance of non-thermal effects.

EFFECT OF LOW POWER MILLIMETER WAVES IRRADIATION ON $C_{12}EO_5/^2H_2O$ MEMBRANE MODEL: A ^{2}H-NMR SPECTROSCOPY INVESTIGATION.

LUIGI FILIPPELLI, AMERIGO BENEDUCI, GIUSEPPE CHIDICHIMO.

CHEMISTRY DEPARTMENT, UNIVERSITY OF CALABRIA, 87036 ARCAVACATA DI RENDE (CS), ITALY

CORRESPONDING AUTHORS: - l.filippelli@unical.it , beneduci@unical.it

Abstract

The influence of low power millimeter wave (MMW) irradiation in the 53.57-78.33 GHz frequency range, on water molecules of a model membrane has been investigated by Deuterium Nuclear Magnetic Resonance (^{2}H-NMR) Spectroscopy. The quadrupole splitting (Δ) of deuterated water within the lamellar mesophase of the $C_{12}EO_5/^2H_2O$ binary system has been measured, at 25°C constant temperature. It has been found that continuos wave (wide band 53.57-78.33 GHz) irradiation of the above membrane model system produces, a significant increase of the quadrupole splitting of deuterated water molecules. The observed variation of the Δ for heavy water is opposite with respect to a temperature increase and it depends on the level of hydration of the lamellar sample: in samples with an higher water content, MMW irradiation produced a larger Δ increase. The observed effect was totally reversible. In few hours the splitting came back to the initial value. We propose an explanation in terms of variation of the free/bound water population ratio and calculate the change in the Gibbs free energy of the system after the irradiation treatment. The interaction model membrane-MMW, might involve the structures that liquid water can adopt by using hydrogen bonds.

Short running title: millimeter wave effect on membrane hydration
Key words: membrane hydration; low power millimeter waves; ^{2}H-NMR spectroscopy

Introduction

The interaction between low power millimeter waves (power density below 1 mW/cm^2) and biological systems, concern either the effects induced by this radiation on the systems, or the basic mechanisms of interaction.

In 1968 Webb and Dodds observed the inhibitory effect of MMW on the growth of the *E. Coli* bacterium [Webb, 1968]. Afterwards H.D. Devyatkov [Devyatkov, 1974, 1981, 1983] and other Russian scientists [Sevastyanova, 1974, 1981] observed the influence of such radiation on various biological systems. Interesting studies on the growth of Saccaromices cerevisiae were performed by Grundler and Keilmann [Grundler, 1977, 1978, 1983]. A review of the most important results, in which some physical-chemical aspects of the MMW-biological systems interaction are also reported, is due to Pachomov et al. [Pachomov, 1998]. The effects observed on MMW irradiated cell systems go from cell growth variations, to changes in DNA morphology [Brill, 1993]. Ionic membrane transport alterations were also reported [Brovkovich, 1991, Geletyuk, 1995, Kataew AA, 1993].Since 2002, we have shown that low power (<10 mW/cm^2) electromagnetic radiation, in the millimeter wavelength range (3.84-5.78 mm), could be used as a physical mean in order to influence the proliferative behavior of several cultured cells [Chidichimo, 2002]. It should be highlighted that the proliferation rate of the investigated tumoral systems was inhibited by MMW in certain exposure conditions, whereas that of the healthy cell systems was not. Moreover, we have also shown that the frequency of the radiation and the irradiation time [Beneduci, 2005a] influence the observed effects. Besides the effect on cell proliferation, significant morphological alterations were observed on human melanoma, breast carcinoma and erythromyeloid leukemia cells [Beneduci, 2005a,b, Beneduci, 2006].

Until now however, there is not a generally accepted point of view on the biophysical mechanism of interaction between millimeter radiation and biological systems. Besides thermal effects that occur at high powers (>10 mW/cm^2), it was hypothized that the MMW-biosystems interaction could involve resonant nonthermal mechanisms at very low powers [Fröhlich, 1968, 1977, 1980, 1983, 1986a, b, Kaiser, 1988, Sinizin, 1998;]. Data on the dielectric properties of water [Ellison, 1996] and of biological systems [Schwan, 1983, Grant, 1984] agree on the fact that water is the only molecular system, able to directly interact with electromagnetic waves in the millimeter range above 1 GHz [Beneduci, 2006].

However, besides the direct field effect on water dipoles, any biological effects could be explained only if the electromagnetic field affects the reaction sensitivity of some cellular processes, that is crucially determined by the reaction moments [Neumann,2000].

The absorption of microwave radiation by water molecules may induce changes in the equilibrium free water/bound water involved in several cellular processes in which a chemical control is exerted [Neumann,2000]. Water plays also crucial roles in proton transfer reactions and in transport processes through narrow channels or pores in which water molecules assume particular interfacial orientations [Neumann,2000]. The millimeter radiation could affects the orientational dynamics of water molecules in such systems, causing several bio-effects.

The above considerations and the morpho-functional alterations of the membrane observed on some *in vitro* cultured tumoral cells after MMW irradiation [Chidichimo 2002, Beneduci 2005b, Beneduci, 2006, Szabo 2006, Chen 2004], brought us to begin the study of the MMW-membrane interaction.

The present work therefore, deals with some aspects of the physico-chemical mechanisms that occur when a model membrane system interacts with the millmeter waves.

All the biological membranes exist because of the intermolecular forces occurring between the components of the system (hydrophobic interactions, dipole-dipole, ion-dipole, hydrogen bonds network) . The water molecules interacting with the polar head groups of the anfiphilic molecules by non-bonding forces are in chemical equilibrium with those ones that constitute the bulk water and are the so called “free water” molecules. A general reaction step that summarizes such type of chemical process occurring at the polar interface of a double layer is the following:

$$S(H_2O)_r + nH_2O \xleftrightarrow{K_{eq}} S(H_2O)_{r+1} + (n-1)H_2O \qquad (1)$$

where $S(H_2O)_r$ is the amphiphilic molecule that binds r water molecules and being in thermodynamic equilibrium with the species $S(H_2O)_{r+1}$ that bind r+1 water molecules, $(n-1)H_2O$ being the free water molecules. The model membrane system investigated in the present work was the penta(oxyethylene)n-dodecylether/water lamellar lyotropic-liquid crystal system, which has been extensively studied in the past [Mitchell, 1983, Dimitrova et al., 1996,]. Such binary system was conveniently adopted by us because it easily forms double layer of lamellar structures (like biomembranes), at room temperature in a relatively wide range of compositions.

If a model membrane is made by using heavy water (^2H_2O) instead of ordinary water (H_2O), one can record a deuterium NMR spectrum which will be the result of a superposition of spectral doublets whose peak separation (in Hz) depends on the orientation of the double layer (lamella) with respect to the NMR static magnetic field [Pake 1948]. When the plane of the lamella is oriented parallel to the static magnetic field, the peak separation is called quadrupole splitting, Δ.

In the case under study, the $C_{12}EO_5/^2H_2O$ system, Δ is proportional to the total fraction of water molecules bound to the polar head group of the surfactant, p_b, and to an average order parameter S_b that brings information about the local motion of the O-D bonds in heavy water:

$$\Delta = \frac{3}{4}\nu_q p_b S_b \qquad (2)$$

where, ν_q is the quadrupole coupling constant. The equilibrium reaction that concern the hydration process of the surfactant molecules in the lamellar structures, could be written in the general form (3) [Mitchell et al., 1983], where S_f are the free surfactant molecules, W_f the free water molecules, $S_b(W_b)_r$ are the complexes formed by a surfactant molecule and r water molecules and K_b is the thermodynamic equilibrium constant.

$$S_f + rW_f \xleftrightarrow{K_b} S_b(W_b)_r \qquad (3)$$

It is clear that any cause affecting the free/bound water equilibrium must reflects a change in the value of the quadrupole splitting that can be conveniently measured by the ^{2}H-NMR technique [Mitchell et al., 1983].

Materials and methods

Deuterium NMR spectra were recorded on a 300 MSL Bruker spectrophotometer operating at 46.053 MHz deuterium resonance frequency, using a 10 mm tunable probe. To record the spectra, samples were introduced in a 10 mm NMR tube. Each spectrum is the Fourier transform of a FID obtained integrating 400 scans, with a 1 sec repetition time. Each scan is a quadrupolar echo pulse sequence, with a 9 µs 90° pulse and a 88 µs delay time. Sample temperature was constantly maintained at 25°C by the spectrophotometer variable temperature controller VT 1000.

Chemicals

Normaldodecylpentaoxyhetylene ether ($C_{12}EO_5$) was purchased from Sigma-Aldrich (99% purity) and deuterated water from Cambridge Isotope Laboratories, Inc. (99.9% purity). Both chemicals were used without

further purification. Lamellar lyotropic liquid crystal samples, $C_{12}EO_5/^2H_2O$, were prepared by weight adding the right amount of heavy water to the surfactant placed in a 5 mm NMR tube. The mixtures were then warmed up and vortex stirred to achieve homogeneity . Three samples were prepared containing 30% (sample A),25% (sample B) and 20% (sample C) by weight D_2O. A 4 mm glass bar was introduced inside a 5 mm NMR tube to obtain a thin layer (0.5 mm) of lamellar phase (fig.1). Samples were then sealed and stored at 25°C for about three days.

Experimental MMW facilities and sample irradiation

The MMW radiating apparatus AMFIT 32 (made in Russia by the UWOM company of Nizhnj Novgorod), was used as radiation source. It is a microwave noise generator diode, able to supply a 53.57-78.33 GHz frequency band at a global mean power density < 1μWatt. Samples were placed at the end of the conical antenna of the instrument and were irradiated for 7 hours. Temperature was strictly controlled and maintained at 25 °C along the experiment. Samples were weighted after the irradiation treatments to check for evaporation of water but weights remained constant.

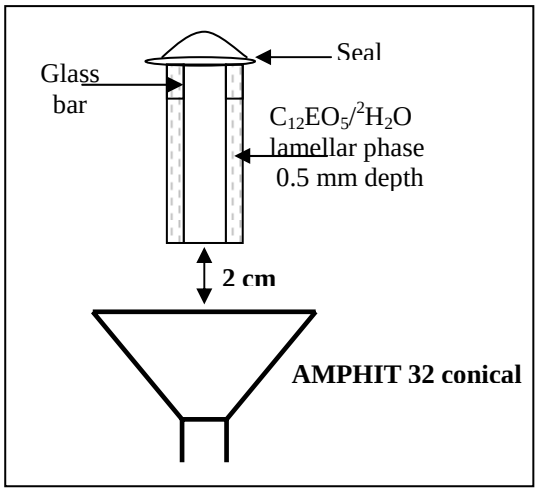

Fig. 1. Schematic representation of the lamellar sample and of the irradiation geometry (not in scale).

Results

Stability of the system under constant temperature condition

Prior to perform any irradiation experiment, the stability of the lamellar samples was tested under 25°C constant temperature condition. In fig. 2, the variation (%) of the quadrupole splitting is showed for a time course of 4 days, in the case of the sample A. It could be noted that Δ resulted very stable showing only restricted oscillations of the order of ± 0.25% (N=96), around the equilibrium Δ value. These random variations could be attributed to small fluctuations of the temperature of the thermostated chamber (probe). Analogous behaviour was observed for the other samples B and C (data not shown).

Quadrupole splitting behavior of heavy water under MMW irradiation

Typical ^{2}H-NMR spectra recorded before and after three irradiation treatments, were reported in fig.3 **A**, **B** for sample **A** and **B**. Significant increases of 5.3±1.0% (N=3) and 2.6±0.5% (N=3) of the quadrupole splitting of heavy water, were observed in the irradiated samples **A** and **B** respectively. A negligible perturbation of the Δ, was also observed in the irradiated sample **C** (data not shown).

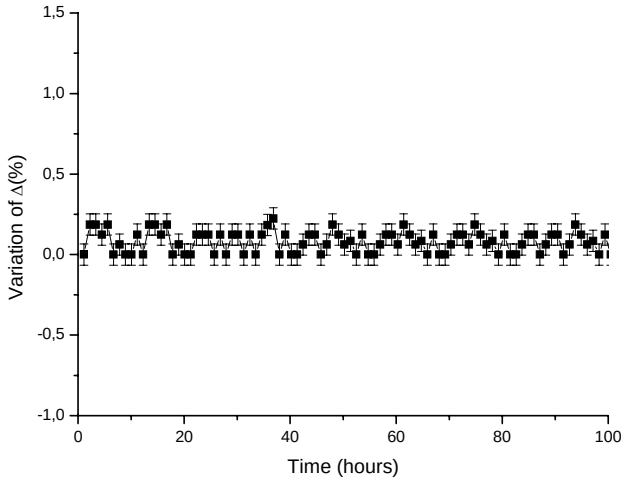

Fig. 2. Sample A before irradiation. Quadrupole splitting variation of ^2H_2O as a function of time (T=25°C). Spectra were recorded along 4 days with 1 hour steps. The sample is very stable.

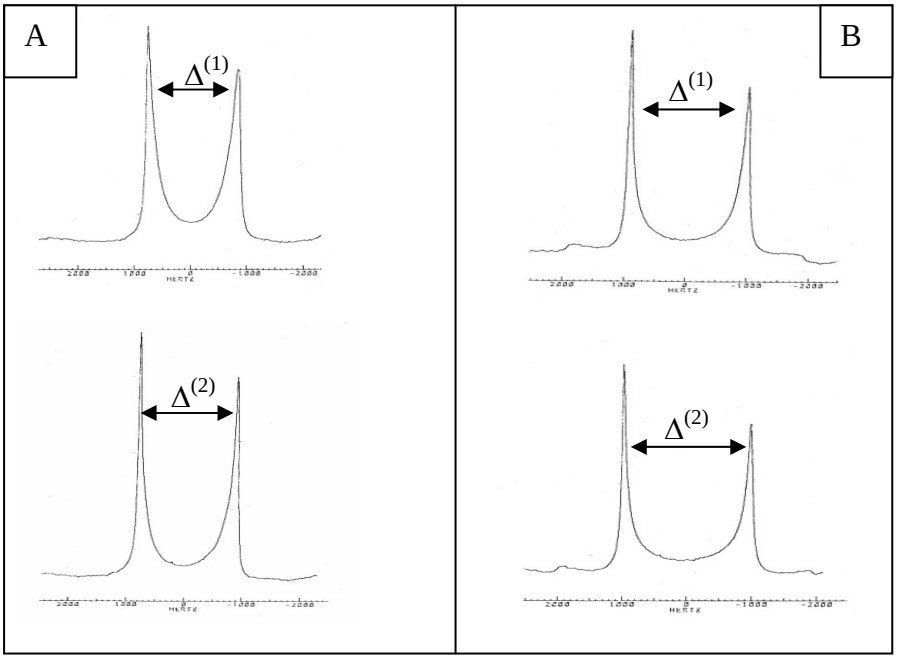

Fig 3. ^2H_2O-NMR spectra of the investigated samples. The Δ of heavy water in sample A ($\Delta^{(1)}$=1608 Hz) gained 80 Hz after the irradiation ($\Delta^{(2)}$=1688 Hz). The increase of the Δ for the sample B was 45 Hz ($\Delta^{(2)}$=1918 Hz; $\Delta^{(2)}$=1963 Hz).

The observed variations are very far from those which could be induced by thermal fluctuations. Actually, from control sample data, we have seen that thermal fluctuations (of less than 1 degree) caused statistical random variations of the quadrupole splitting about the equilibrium value at 25°C, which were not larger than 4 Hz (0.25%).

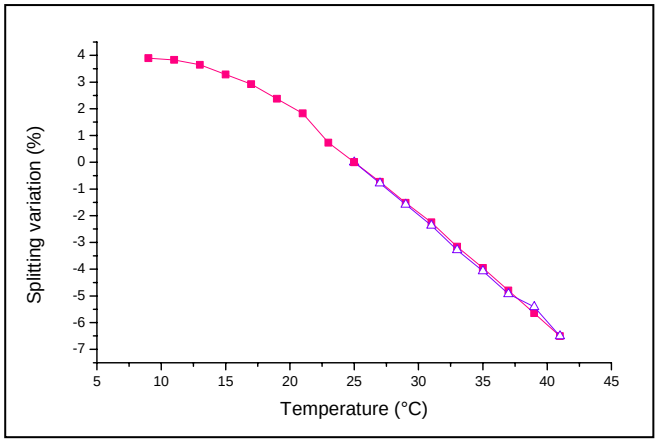

Fig. 4. Sample A.Variation of the splitting value in percentage as a function of temperature. The point zero on the ordinates corresponds to 25 °C.

^2H_2O quadrupole splitting temperature dependance

In fig.4 the variation of the quadrupole splitting of heavy water relative to sample **A** was shown as a function of temperature, in the range 9°C – 41°C. The thermal process, from 9°C to 41°C, is reversible (see upfacing triangle in fig. 4). At this point, two fundamental findings have to be underlined: 1) to produce a 6% increase in Δ in such a system (sample **A**), equal to that observed under MMW irradiation, it was necessary to reduce the temperature of the system of about 15°C. 2) MMW irradiation produced an increase of Δ while a temperature increase produced a Δ decrease. This temperature dependence was similar for the other two samples (**B** and **C**), as previously reported [Rendall K, 1984].

MMW irradiation increases membrane hydration

In view of equation (2), the quadrupole splitting (Δ) can change only if p_b and/or S_b changes. Summarizing the results, the variation of the quadrupole splitting of D_2O contained in the irradiated model membranes, increases as the percentage of heavy water within the samples increases. Going from the less hydrated (C) to the more hydrated system (A) the free water dispersed between the surfactant lamellae gradually increase. Hence a crucial parameter influencing the variation of Δ after MMW irradiation, must be the amount of free water present in the system. More precisely, we observed that the effects produced on the quadrupole splitting of heavy water by the MMW irradiation increases as the free water/ bound water (p_b) ratio increases. A variation of only the order parameter S_b cannot explain the observed trend. Indeed, such a parameter reflects the local orientational order of the bound water. Thus the value of S_b depends on the mobility of water molecules linked to the surfactant polar heads. If the MMW irradiation had acted on this physical property of the system, the variation of Δ should not depend on the sample composition. Thus, we interpreted our experimental findings, identifying a primary interaction occurring between the millimeter radiation and the free water of the membrane system that strongly absorbs the MMW. As first order effect, consequence of such direct interaction, is the shift of the thermodynamic equilibrium (3) towards right. Hence, the membrane resulted more hydrated (greater *pb* values) after the MMW irradiation treatment, than the equilibrium initial condition. Such fundamental perturbation was observed as a quadrupole splitting increase. In thermodynamic terms, this means that the Gibbs free energy variation relative to the process (3), expressed by equation (4) is shifted towards more negative values (more favoured thermodynamic process) by millimeter wave irradiation.

$$\Delta G = G_{W_b} - G_{W_f} \tag{4}$$

The first term (G_{Wb}) of eq.4 is the Gibbs free energy of a mole of bound water molecules. Its value depends on local thermodynamic properties of water molecules bound to the polar heads of the surfactant, that are not susceptible to change under irradiation. Then, $G_{Wb,}$ does not change. Hence we can write equation (5)

$$G_{W_b}^{(1)} = G_{W_b}^{(2)} \tag{5}$$

where the superscript (1) and (2) refer to the state of the system before and after MMW irradiation, respectively.

Variation of the Gibbs free energy of the system under MMW Irradiation

We derived the change in the Gibbs free energy variation of the system produced by MMW (ΔG_{MW}). Using equation (4), the equality (5), and defining the states of the system before and after irradiation by the superscript (1) and (2) respectively, we can write the following equations:

$$\Delta G^{(1)} = G_{W_b}^{(1)} - G_{Wf}^{(1)} = -RT \ln K_b^{(1)} \quad (6)$$

$$\Delta G^{(2)} = G_{W_b}^{(2)} - G_{Wf}^{(2)} = -RT \ln K_b^{(2)} \quad (7)$$

We can express thus, the quantity ΔG_{MW} as the difference between the Gibbs free energy variation relative to equilibrium (3) before and after irradiation:

$$\Delta G_{MW} = \Delta G^{(2)} - \Delta G^{(1)} = -[G_{W_f}^{(2)} - G_{W_f}^{(1)}] \quad (8)$$

Equation (8) tells us that energetic changes of the state of the system, produced by MMW irradiation, are due to changes, opposite in sign, in the energetic state of free water present in the system.
We can correlate the quantity ΔG_{MW} with the thermodynamic equilibrium constant K_b relative to process (3) before and after MMW irradiation:

$$\Delta G_{MW} = -RT \ln \frac{K_b^{(2)}}{K_b^{(1)}} \quad (9)$$

In table 1, quadrupole splitting experimental values and calculated thermodynamic data relative to systems **A**, **B**, and **C** were collected.
The p_b values were determined by means of equation (2) and using the S_b value as reported by Mitchell et.al . The increase of the Gibbs free energy of free water, produced on the systems after irradiation, is greatest for sample **A** (+2882 J/mol). Consequently, equilibrium (3) is shifted towards the water-surfactant complex ($K_b^{(2)}$ 3.2 fold greater than $K_b^{(1)}$ after irradiation). This effect is less pronounced in system **B** (+834 J/mol; $K_b^{(2)}$ 1.4 fold greater than $K_b^{(1)}$ after irradiation). No net increase was observed in system **C**.

Table 1

State of the System	Δ (KHz)	p_b	S_b	$K_b^{(2)} / K_b^{(1)}$	ΔG_{MW} (J)	$C_{12}EO_5/^2H_2O$ %(w/w)
1	1.608	0.51	0.0146	3.2	-2882	70
2	1.688	0.54				
1	1.918	0.61		1.4	-834	75
2	1.963	0.63				
1	1.946	0.62		≈1	0	80
2	1.956	0.63				

Table 1. Experimental and calculated data of the parameters characterizing the lamellar system. Low power MMW irradiation induces an increase of the fraction of water molecules bound to the surfactant. See text above for details.

Summary
The quadrupole splitting of deuterated water of a $C_{12}EO_5/^2H_2O$ membrane model was measured by ^{2}H-NMR spectroscopy. By irradiating the model membranes utilizing low power millimeter waves (wide band 53.57-78.33 GHz, continous wave), we modified (increase) the splitting value of the heavy water. This cannot be explained in terms of solely provided heat. In fact, raising temperature produces an opposite behaviour of the monitored parameter (splitting decrease). Weighting the samples after millimeter waves exposure, allowed us to be sure that water did not evaporate. We also found that the effect is completely reversible after few hours. Furthermore, the most hydrated samples were more sensitive to the irradiation treatment. Making some assumptions we propose that the MMW interact primarly with the free water trapped between the layers of the system, inducing the water molecules to bound the surfactant. Literature data and studies we are carrying out on the dielectric constant of both normal and deuterated water (data to be published), strongly indicate that water is the primary absober of the millimeter wavelengths and the obtained dielectric data are different for the two kind of water at the same frequencies. Works in progress are clearly indicating that very likely the structures that water can adopt by means of hydrogen bond network play a central role in the observed effects; phospholipid model and in vitro cultured cells, respond to some specific frequencies rather than others.

Acknowledgements
This work was supported by Fondazione CARICAL, Lega Italiana per la Lotta Contro i Tumori Sezione Cosenza and Regione Calabria (POR 2000/2006, misura 3.16, progetto PROSICA)

References

Beneduci A et al. 2005a. Frequency and irradiation time-dependant antiproliferative effect of low-power millimeter waves on RPMI 7932 human melanoma cell line, Anticancer Research 25:1023-1028.

Beneduci A et al. 2005b. Transmission electron microscopy study of the effects produced by wide-band low-power millimeter waves on MCF-7 human breast cancer cells in culture, Anticancer Research 25:1009-1014.

Beneduci A et al. 2006. Antiproliferative effect of millimeter radiation on human erythromyeloid leukemia cell line K562 in culture: ultrastructural-and metabolic-induced changes, *Bioelectrochemistry* (2006), doi:10.1016/j.bioelechem.2006.07.008.

Brill G et al. 1993. Effect of low level extremely high frequency radiation on the genetic activity of polytene chromosomes of Chironomus plumosus. Fizicheskaia Meditzina 3:69.

Brovkovich VM et al. 1991. Action of millimeter-range electromagnetic radiation on the Ca^{++} pump of sarcoplasmic reticulum. Radiobiologia 31: 268.

Chen Q et. al. 2004. Millimeter wave exposure reverses TPA suppression of gap junction intercellular communication in HaCaT human keratinicytes. Bioelectromagnetics 25:1-4.

Chidichimo G et al. 2002. Selective inhibition of tumoral cells growth by low power millimeter waves. Anticancer Research 22:1681-1688.

Devyatkov ND et al. 1974. Sov. Phis-Usp. 16, 4: 568-579.

Devyatkov ND. 1981. Non thermal effects of millilmeter wave irradiation. In: Devyatkov ND, editor. Use of Low Intensity Millimeter Radiation in Biology and Medicine. Moscow: Inst Radiotech Electrotech Moscow. Acad. Sci USSR (in Russian).

Devyatkov ND. 1983. Non thermal effects of millilmeter wave irradiation. In: Devyatkov ND, editor. Use of Low Intensity Millimeter Radiation in Biology and Medicine. Moscow: Inst Radiotech Electrotech Moscow. Acad. Sci USSR (in Russian).

Dimitrova GT. 1996. Investigation into phase behavior of nonionic ethoxylated surfactanst using ^{2}H NMR spectroscopy. Langmuir 12:315-318.

Ellison WJ. 1996. Water : A dielectric reference. Journal of Molecular Liquids 68:171-279.

Fröhlich H. 1968. Long range coherence and energy stored in biological systems. Int J Quantum Chemistry 2:641-649.

Fröhlich H. 1970. Long range coherence and the action of enzymes. Nature 228:1093.

Fröhlich H. 1980. The biological effects of microwaves and related questions In: Marton L ed. Advances in electronics and electron physics. Academic Press, New York, pp. 53:85-152.

Fröhlich H. 1983. Evidence for coherent excitation in biological system Int. J. Quantum Chem 23:1589-1595.

Fröhlich H. 1986. Coherent action of enzymes. In: R. Welch ed. The fluctuating enzymes. John Wiley, New York, pp. 421-449.

Fröhlich H. 1986. Coherent excitation in biological systems. In: F. Gutmann, H. Keyser, eds. Modern bioelectrochemistry Plenum, New York, pp 241-261.

Geletyuk VI et al. 1995. Dual effects of microwaves on single Ca^{++} activated K^{+} channels in cultured Kidney cells *Vero*. FEBS Lett 359:85-88.

Grant EH. 1983. Molecular interpretation of the dielectric behavior of biological materials. In: Grandolfo M, Michaelson SM and Rindi A eds. Biological Effects and Dosimetry of Nonionizing Radiation, NATO Advanced Study Institutes Series. Series A, Life Sciences; v. 49, Plenum Press New York and London pp 179-194.

Grundler W, Keilmann F. 1977. Resonant growth rate response of yeast cells irradiated by weak microwaves. Phys Lett 62A:463-466.

Grundler W, Keilmann F. 1978. Nonthermal effects of millimiter microwaves on yeast growth. Z Naturforsch 33c:15-22.

Grundler W, Keilmann F. 1983. Sharp resonances in yeast growth prove non-thermal sensitivity to microwaves. Phys. Rew. Lett 51:1214-1216.

Kaiser F. 1988. Theory of Non-Linear Excitations In: H. Fröhlich ed. Biological Coherence and Response to External Stimuli, Springer-Verlag pp 25-48.

Kataew AA et al. 1993. Frequency-dependent effects of the electromagnetic millimeter waves on the ion current in the cell membrane of Nitellopsis obtusa: non thermal action. Biofizika 38:446-462.

Mitchell DJ et al. 1983. Phase behavior of polyixyethylene surfactants with water J. Chem. Soc., Faraday Trans 19:975-1000.

Neumann E 2000. Digression on chemical electromagnetic field effects in membrane signal transduction–cooperativity paradigm of the acetylcholine receptor, Bioelectrochemistry 52: 43-49.
Pake GE. 1948. J Chem Phys 16:327.
Pakhomov G. 1998. Current state and implication of research on biological effects of millimeter waves: a review of the literature. Bioelectromagnetics 19:393-413.
Rendall K and Tiddy GJT. 1984. Interaction of water and oxyethylene group in lyotropic liquid crystalline phases of poly(oxyethylene)n-dodecyl ether surfactants studied by ^{2}H Nuclear Magnetic Resonance spectroscopy. J Chem Soc Faraday Trans 80:3339-3357.
Schwan HP. 1983. Dielectric properties of biological tissue and cells at RF-and MW-frequencies. In: Grandolfo M, Michaelson SM and Rindi A eds. Biological Effects and Dosimetry of Nonionizing Radiation, NATO Advanced Study Institutes Series. Series A, Life Sciences; v. 49, Plenum Press New York and London pp 179-194.
Sevastyanova LA, Vilenskaya RL. 1974. A study of the effect of millimeter-band microwaves on the bone marrow of mice. Sov. Phis-Usp (Engl Transl) 16:570.
Sevastyanova LA, Vilenskaya RL. 1981. Specific influence of millimeter waves on biological objects. In: Devyatkov ND, editor. Non thermal effects of millilmeter wave irradiation. Moscow: Inst Radiotech Electrotech Moscow. Acad. Sci USSR (in Russian) pp 86-113.
Sinizin NI. 1998. The special role of the Millimeter waves-aqueous medium interaction in nature. Biomedicina Radiotecnika 5:5-23 (in Russian).
Szabo I et. al. 2006. Millimeter wave induced reversibile externalization of phosphatidylserine molecules in cells exposed in vitro. Bioelectromagnetics 27:233-244.
Tanaka H. 1998. Simple physical explanation of the unusual thermodynamic behavior of liquid water Phys Rev Lett 80:5750-5753.
Tanaka H. 2000. The two state model of water. J Chem Phys 112:799-809.
Tanaka H. 2000. Thermodynamic anomaly and polyamorphism of water. Europhys Lett 50(3):340-346.
Webbs SJ, Dodds D. 1968. Inhibition of bacterial cell growth by 136gc microwaves. Nature 218: 374-375.

BIOLOGICAL COMPLEXITY AND MAGNETIC-FIELD SENSITIVITY

PIETRO VOLPE AND TAMILLA EREMENKO

AREA OF BIOPHYSICS OF THE DEPARTMENT OF BIOLOGY, UNIVERSITY OF ROME "TOR VERGATA", ROME, ITALY (volpe@bio.uniroma2.it)

Abstract. This contribution points to the mechanisms of zero-frequency (DC) and oscillating (AC) magnetic field (MF) bioeffects. The survey pays particular attention to the action of artificial MFs not only at the ionic, molecular or macromolecular levels, but also at the levels of *in vitro* cycling cells, *in situ* functioning tissues or organs and total bodies. The significance of crucial findings concerning the MF-dependence of cell proliferation *vs*. cell death, extent of necrosis *vs*. apoptosis and cell membrane fluidity is judged by comparing the results obtained in a solenoid (SLD), where an MF can be added to the geomagnetic field (GMF), with those obtained in a magnetically shielded room (MSR), where the MFs can be partially attenuated or null. This comparative criterion is required because the differences detected in the experimental samples against the controls are often rather small *per se*, as observed in estimating the MF-dependence of expression of single genes or of the rates of total DNA replication, RNA transcription and protein translation. The analysis also considers the MF-dependence of the interactions between host eukaryotic cells and infecting bacteria. In the framework of studies on the origin and adaptation of life on Earth, theoretical insights paving the way to elucidate the mechanism(s) of MF-interaction with biostructures and biosystems of different orders of organization are considered.

Introduction

Since life on Earth originated in natural MFs, while a large part of the living matter became subjected to artificial MFs only in the XXth Century, a question concerning the adaptation of organisms to these new unexpected fields emerged. For instance, would an animal maintain the normal ontogenesis in an artificial MF characterized by an amplitude much greater than that in which it evolved?

In recent years, the number of reports posing this question has increased. In particular, the epidemiological aspect was debated with emphasis since the negative effects of extremely low frequency (ELF) MFs generated by 50 Hz high voltage power transmission lines, video screens, electric blankets or other home appliances, was forcibly denounced as time went by [1]. The belief that the field intensity was rationally fixed below a risk threshold functioned as objection to the alarm. However, the available data were contradictory [2]. On the one hand, a benefit from the low-energy pulsed MFs in non-union bone fracture healing and in cell regeneration was reported [3]. On the other, the influence of MFs at 50-60 Hz exerted on the nervous system [1] induced preoccupation.

In any case, the MFs showed a distinct influence on cell proliferation (Figs. 1 and 2) [4] and on the role of the calcium ions in the transduction of this influence [5-10]. In particular, it was reported that a 22 μT MF at 60 Hz modulated the calcium influx [8]. The MF-dependence of the state of the cell membrane was studied through microscopy [11] and cytofluorimetry [12]. The influence of 1-10 μT MFs at 50 Hz on the membrane conductivity and permeability was taken into account [11]. A study was performed on the effects of very weak MFs (10^{-6} to 10^{-5} T) on chicken embryogenesis [13]. The results of this investigation were confirmed in some laboratory conditions [14] and contradicted in others [15,16].

The divergences encountered in the literature with respect to the MF-dependence of certain biological structures and functions are not due only to the differences of equipment facilities or experimental accuracy, but rather to the adequacy of proposed methodological approaches. In addition, there is still a largely recognized lack of theoretical analysis to explain the mechanisms which underlie the interactions between the MFs and the various cellular targets. Thus, the main aim of this report is to draw the attention on the efforts that have been made to define the basic physical laws describing MF-biosensitivity.

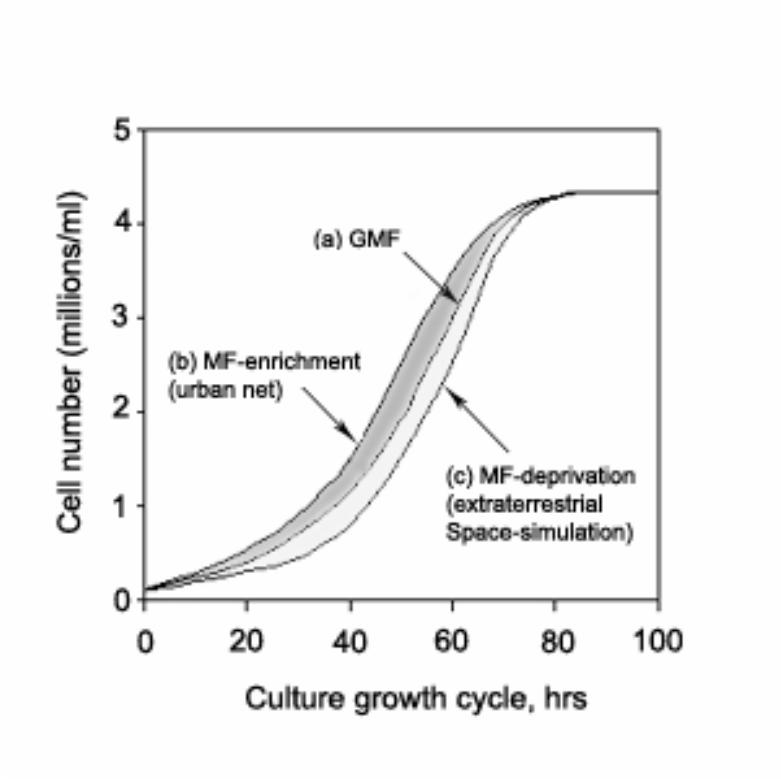

Fig. 1. *Acceleration and deceleration of cell proliferation after addition or subtraction of MFs* [4]. Cultures of *Friend erythroleukemia* cells were left to grow in parallel for about 100 hrs: (a) under the control 45 μT DC of the Earth's MF, (b) in an LSD where 70 μT at 50 Hz were added to the 45 μT DC of the Earth's MF and (c) in a MSR where the highly attenuated field essentially reflected the residual 20 nT DC of the Earth's MF and the 2.5 pT AC of the power line MF (in the MSR the 45 μT DC of the Earth's MF was attenuated 2500 times at 0.0 Hz because the AC shielding factor was estimated to be about 2500 for frequencies between 0.001 and 10000 Hz, while the applied AC MF was 30000-40000 times smaller at 50 Hz). The results represent the mean of five experiments for (b) *vs*. (a) and three experiments for (c) *vs*. (a). The Student's paired *t* test showed *P* values of 0.02 for both (b) *vs*. (a) and (c) *vs*. (a).

Is the question of the mechanisms of magnetic-field bioeffects still open?

Following the well known contributions of several laboratories which attracted the attention of the scientific community on the possible involvement in MF bioeffects of resonance at the cyclotron frequency under the combined influence of DC and AC MFs [17-20], Blanchard and Blackman [21] tried to enrich the Magnetobiology with a theory based on an ion parametric resonance model.

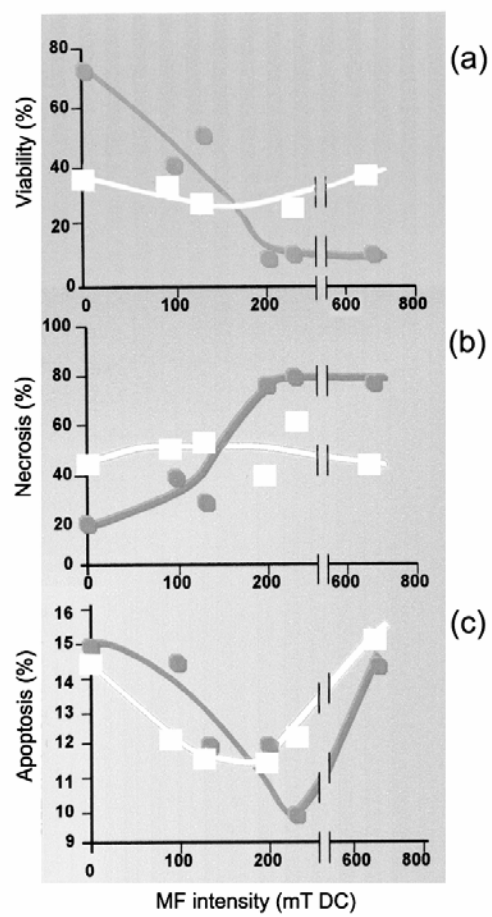

Fig. 2. *Dependence of the human macrophage viability, necrosis and apoptosis, in the absence and in the presence of mycobacterial infection, upon static MFs* [39,40]. Macrophages (MDMs), separated from PMB cells attached for 1 hr to the bottom of a flask, were subdivided, using dishes, into a number of equal samples each consisting of $1 \cdot 10^6$ MDMs in 1.5 ml of RPMI-1640 medium. Five samples were maintained for 5 days under DC MFs of various intensity, while a control sample was kept in the absence of any MF. At the end of the fifth day of exposure, each sample was washed twice with PBS, while the MDMs were detached from their dish, treated with PI and analyzed cytofluorimetrically. A parallel set of samples (each also consisting of $1 \cdot 10^6$ MDMs in 1.5 ml of RPMI-1640 medium), after a 5-day permanence in culture without MF, was infected with *Mycobacterium tuberculosis* (MTB) and maintained for another 2 days under the same MFs of various intensity (a control MTB-infected MDM sample was kept for 2 days in the absence of any MF). At the end of the second day of exposure, each MTB-infected MDM sample was washed twice with PBS, detached from the dish bottom, treated with PI and analyzed cytofluorimetrically. (**a**) Viability of the uninfected MDMs *vs*. that of the MTB-infected MDMs; (**b**) necrosis of the uninfected MDMs *vs*. that of the MTB-infected MDMs; (**c**) apoptosis of the uninfected MDMs *vs*. that of the MTB-infected MDMs. (λ-λ) Uninfected MDMs; (ρ–ρ) MTB-infected MDMs. The values represent the mean of three experiments, each performed in triplicate. The Student's paired *t* test showed *P* values of 0.04 for (a), 0.01 for (b) and 0.05 for (c).

Anyway, from a unifying physico-chemical point of view and despite the list of MF bioeffects reported earlier, the research is still unable to provide a proper explanation. For this reason, it is convenient to re-

consider, in detail, other contributions which could make the efforts more circumstantiated and allow a comprehensive theory of the MF bioeffects.

Long ago, it was suggested that the rise of a ponderomotive force caused in a biostructure by non-uniform static MFs could lie on the basis of the magnetotropism of plants, where the "paramagnetic cells" representing a minor biomass, would be forced towards a point of maximal field while the "diamagnetic cells" representing a major biomass would be forced towards the opposite direction. Studying the interaction of the neuromembrane ionic channels with the spreading action potential, Volobuev and Coworkers [22] proposed that "external" MFs interact with hypothetical "internal" MFs created by the ionic channels and nodes of Ranvier. This could explain the decrease observed in the speed of propagation of the action potentials in static MFs. Another study by Agulova and her Colleagues [23], concerning the behaviour of non-equilibrium systems in low-frequency/low-intensity MFs, distinguished the direct perception of the MF by biomolecular structures from the signalling role of the MF through the central nervous system.

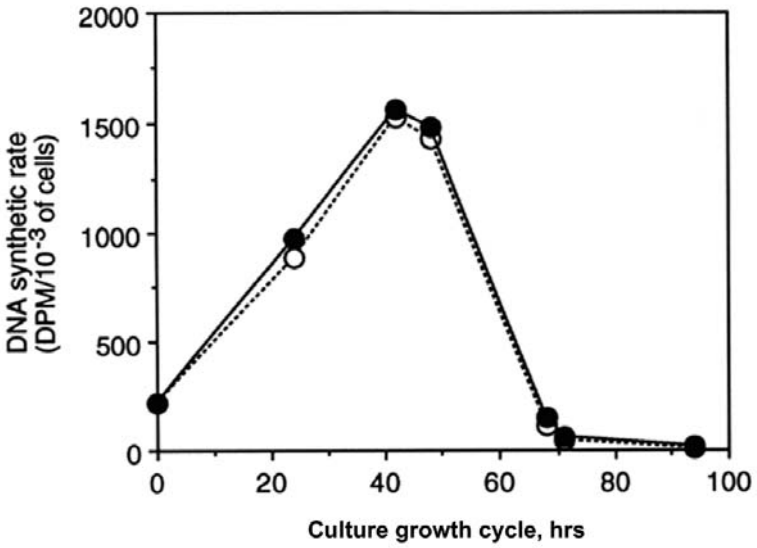

Fig. 3. *Stability of the rates of DNA replication in Friend erythroleukemia cells after their long exposure to an AC MF* [42]. The cells were pre-exposed to 70 μT at 50 Hz plus 45 μT DC of the Earth's MF for 318 days, during which they were necessarily reinoculated into a fresh medium twice per week (during each reinoculum, the cells remained in the absence of irradiation for 20 min). Then, two samples were inoculated at a density of $0.3 \cdot 10^6$ cells/ml and followed during their culture growth cycle. At intervals of 24 hrs, $2 \cdot 10^6$ cells were incubated in 2 ml of the same medium in which they grew (containing ten per cent foetal calf serum) with 2 μCi of [^{3}H]thymidine (86.1 Ci/mmol). The incubation lasted 50 min at 37 ^{o}C under shaking, in the absence of 5% CO_2 in air. The labelled cells were washed three times with PBS (without Ca^{2+} and Mg^{2+}), harvested and treated with 1 ml of 10% TCA at 4 ^{o}C for 1 hr. The TCA-precipitable material was loaded through a 0.45 μm Millipore filter and washed twice: first, with 15 ml of cold 5% TCA and, second, with 5 ml of 70% ethanol. The yielded sediment was dried at 20 ^{o}C and introduced into 10 ml of Ultima Gold scintillation liquid to measure its radioactivity. (μ-μ) Cell proliferation outside the SLD under the sole 45 μT DC of the Earth's MF; (λ-λ) cell proliferation inside the SLD under 70 μT at 50 Hz plus 45 μT DC of the Earth's MF. The experiments were repeated three times. The Student's paired *t* test showed *P* values of 0.06.

They noted an influence of the GMF variations on the precipitation and agglutination reactions in aqueous solutions and on the Piccardi test [24]. Kislovsky [25], in an attempt to explain the biovariations caused by GMF perturbations, suggested the occurrence of dissipative clathrate structures in the aqueous medium and on its borders in non-equilibrium conditions. The length of conservation of these structures was taken as an example

of near-critical phenomena that are close to the temperature of phase transitions of the second kind: liquid-liquid. In such a case, the phase transitions would be at the lower critical temperatures of stratification of the aqueous solutions, when the elements of short-range order inherent in clathrate structures are abolished.

Zhvirblis [26], being interested in the influence of solar activity on the biosphere, paid attention to the correlation of some medico-biological tests with the index of GMF perturbation, in which sector boundaries of the interplanetary MF, associated with the solar wind, were taken as zero. This study revealed that the direction along the phase trajectory contour changed when the Earth crossed the sector boundary. Vladimirsky and Temurjants [27,28], on the basis of the fact that the Piccardi test was sensitive to the polarity of a radial component of the interplanetary MF, supposed that this sensitivity could be due to the geomagnetic micropulsations in the range from 0.007 to 0.1 Hz. Therefore, they presented a list of principles concerning the influence of weak ("non-thermal") and ultraweak ("natural") AC MFs on inorganic and biological systems.

In contrast with the opinion of Binhi [29] who considered the nuclear magnetic resonance as impossible in biological magnetoreception, this list re-encouraged the idea of a possible role of nuclear magnetic resonance in the GMF variations. Hence, Lednev and Coworkers [30] suggested that the calcium-binding proteins constitute the place of primary action of combined MFs. In their opinion, these proteins cause a splitting of energetic levels of the calcium ion oscillation in the protein (*Zeman effect*) while the width of the splitting is equivalent to the cyclotron frequency of calcium and the applied DC MF. On this basis, the parametric resonance was thought as a mechanism for increasing ionic energy. Moreover, the same Authors proposed that DC, AC and combined DC+AC MFs can change the polarization degree, while the biological effects of the MFs can be induced by the same polarization degree of the calcium ion oscillation.

Binhi and Coworkers [31-33] studied the mechanism of the magnetosensitive ion binding by proteins, under the influence of external AC MFs, in the framework of an idealized quantum model. It turned out that the dissociation probability of an ion-protein complex depends on frequency and amplitude. This was shown to be a consequence of the interference of angular modes of the ion wave function.

Moreover, attention was drawn on the problem of the dielectric response of some biological tissues [34] (in relation with the orientation, in a DC MF [35], of ions, molecules and cells), while Zhadin [36] investigated the thermal oscillations of the calcium ion in a calcium-binding protein, under the influence of combined DC+AC MFs. From the study it emerged that the DC MF causes the Larmor procession of ion oscillations. Since the cyclotron frequency is twice the Larmor frequency, this led to the suggestion that the phenomenon could serve as a basis for increasing the kinetic energy of the calcium ion due to parametric resonance. In harmony with this suggestion, an AC electric field perpendicular to a DC MF (or an AC MF parallel to a DC MF) was expected to increase the ionic energy while a maximal effect was expected at the cyclotron frequency of an AC MF.

Zhadin [36] tried to solve equations of motion of the ion in a macromolecule under the influence of the MFs, considering the damping effects and the influence of particles surrounding this ion. In contrast with Lednev and Coworkers [30] and Blanchard and Blackman [21], he showed that the possibility of parametric resonance is not credible for the AC MF frequencies, being many orders of magnitude lower than the natural frequency of an ion in a macromolecule. Indeed, resonance-like phenomena were found to be induced by the influence of a DC MF alone and by a combined DC and AC MFs without any parametric resonance. Zhadin [36] estimated that the MFs may cause changes in energy of the ionic thermal motion which, in turn, would be sufficient to trigger variations in the conformational state of a macromolecule.

Does the MF-effect depend upon the complexity of given biostructures or biosystems?

The debate was focused on the theoretical basis of the MF-action on macromolecules (Fig. 3): on the one hand, it was suggested that weak extremely low-frequency MFs affect intracellular DNA directly, since the MFs must exert a force of the order of $I_{DNA} = 1.6 \cdot 10^{-13}$ A on the currents that flow in the DNA [37]; on the other, it was claimed that this conclusion is not in agreement with physical principles, since the force on the current carrying strands generated for example by a MF, B = 5 μT, would be extremely weak, i. e. equal to $F = BI_{DNA} = 8 \cdot 10^{-19}$ N/m [38]. In other words, a motion of a 1 mm long strand through a distance equal to that of the strand diameter of 2 nm represents an energy of $1.6 \cdot 10^{-33}$ J or $3.7 \cdot 10^{-13}$ kT (hence, the energy transfer from the action of the MF on the strand would be negligible compared to the energy of thermal agitation).

Whatever the conclusion of the debate will be, several years ago we suggested that, at variance with the influence of a weak AC MF on cell-cycle kinetics [4] and cell membrane fluidity [12], this field is insufficient to exert an appreciable influence on macromolecular biosynthesis [41]. This was also in harmony with recent studies concerning, on the one side, the genome stability *vs*. deprivation or enrichment of the GMF [42] and, on the other, the gene expression in a Space-simulating magnetically shielded environment [43].

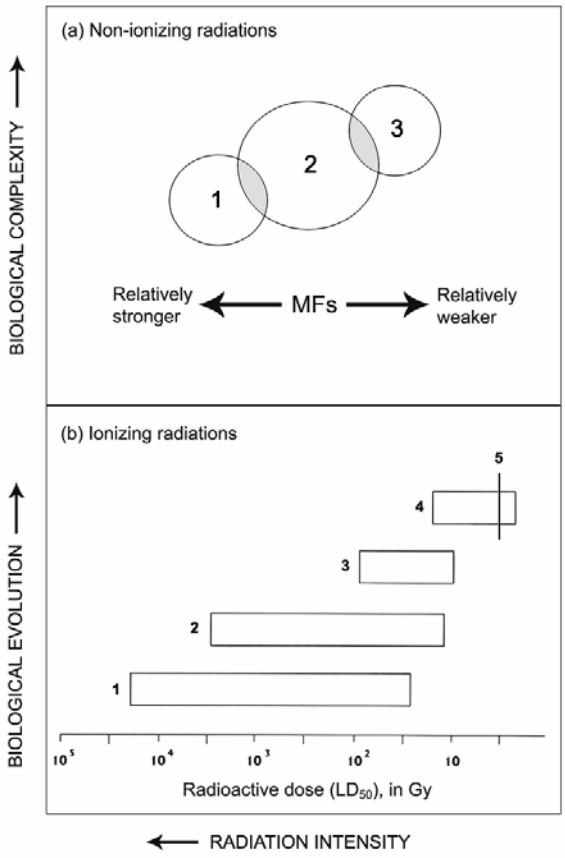

Fig. 4. *MF-sensitivity as a function of complexity of the irradiated biological target*. (**a**) Orders of organization of biostructures or biosystems invested by non-ionizing radiations: 1. molecules and macromolecules; 2. biostructures; 3. biosystems. The size of the areas reflects the results of 100 experiments, estimated from the literature, performed by using DC MFs for about 30% and AC MFs for about 70%. (**b**) Evolution of biosensitivity to ionizing radiations [85]: 1. bacterial cells; 2. plants; 3. animals with cold blood; 4. animals with warm blood; 5. Man.

Therefore, the state of the art suggests that the mechanism or the mechanisms which underlie the interactions of the MFs with the biostructures and biosystems (Fig. 4) are still an open question [44]. In this respect, it was suggested that the approach towards the non-equilibrium thermodynamics of the systems under electromagnetic (EM) waves was of primary importance [45].

It still remains to be explained why pulsed EM fields can be more active biologically than continuous ones [46]. This acquires interest in connection with the fact that an alternative basic mechanism of MF bioeffects could be the forced-vibration of all the free ions in proximity of a cell plasma membrane caused by an external AC field. The model proposed by Del Moral and Coworkers [47] explaining the bioelectric activity of single

unit neurons under DC and ELF MFs, based on the strong anisotropy of diamagnetic susceptibility of membrane phospholipids acting cooperatively (superdiamagnetism), would also seem to deserve special attention.

Remarks on the order of organization of a biological target

The observations concerning the MF-dependence of the volume of a whole cell or its nucleus [4,48] were supported by those regarding the MF-dependence of the electrokinetic properties of nuclei in human buccal epithelial cells [49]. Other studies were devoted to the analysis of the so-called "electromagnetic man" *vs*. the magnetic resonance tomography [50] and of the effect of MFs on synchronization of mammalian cell permeabilization *vs*. the MF-dependence of gene delivery [51].

From a methodological point of view, attempts were made to employ the programmed chrono-potentiometry as a tool to study electroporation and resealing of pores in bilayer lipid membranes [52] while an eu-wide initiative, to characterize the biological effects of an electromagnetic field (EMF) on human and mouse cell lines by gene expression, was taken [53].

There is a consensus about the effect of MFs on cell-cycle kinetics. In fact, the changes of FL cell-cycle kinetics, following the addition or deprivation of MFs (Figs. 1 and 2a,b) [4], were consistent with the alteration of the onset of S-phase observed after a 50 Hz MF exposure of normal human fibroblasts [54] and with variation of cell-cycle kinetics and colony forming ability after exposure of budding yeast to 50 Hz magnetic radiation [55]. This was shown to influence, in turn, the change in growth and differentiation of PC6 cells exposed to pulsed EMFs [56].

Although the question about the influence of MFs on the development of programmed cell death remains in many respects open (Fig. 2c), especially in terms of the correlation of ion homeostasis and apoptosis [57], investigations strikingly suggested that the MF causes an inhibition of apoptosis [58]. In fact, Annexin V was shown to counteract apoptosis by inducing calcium influx in human lymphocytic T cells [59] while it was demonstrated that by using the patch clamp technique there is an effect of MF exposure on the calcium channel currents [60]. It was also suggested that membrane dielectric changes may indicate induced apoptosis in HL-60 cells [61]. In any case, there was no question about the influence of the MFs on apoptosis: a transient suppression of X-ray-induced apoptosis by exposure to power frequency MFs in MCF-7 cells was evidenced [62], a change in the rate of DNA repair due to apoptosis mediated by MF exposure was detected [63], an exposure of a neuroblastoma cell line to 50 Hz MFs definitely caused changes in the apoptotic rate [64].

Here follows a list of the harmful AC bioeffects investigated at various levels.

At the morphological level, developmental changes in *Drosophila melanogaster* following exposure to alternating EMFs were observed [65] while effects of permanent MF on wing size parameters of the same insect were found [66].

At the cellular level, there were some effects of extremely low frequency EMFs on mammalian follicle development [67]. ELF EMFs as well as heat shock proved to increase microvescicle motility in astrocytes [68]. In addition, it was observed that both sedimentation and aggregation of erythrocytes were MF-dependent [69].

At the macromolecular level, while stability of the DNA replication reaction to MFs was observed (Fig. 3), electric relaxation processes were shown in lipid-bilayers after exposure to weak magnetic pulses [70]. In the framework of the studies on genotoxicity of radiofrequency signals, the occurrence of DNA damage in cultured human blood cells was seen [71] while there were clear cytogenetic effects of 900 MHz microwaves on human lymphocytes [72]. Also, there were an increase in X-ray-induced gene mutations by exposure to AC MFs in NF-kappa B-inhibited cells and an increase in hypoxanthine-guanine phosphoribosyl transferase gene mutations by exposure to electric fields [73]. ELF-pulsed MFs modulated gene expression in myocardial cells [74] while an effect of UV B radiation and 100 Hz EMFs on DNA synthesis of Jurkat cells was detected [75]. As for protein macromolecules, there was an influence of the high ELF MFs on DNA and RNA polymerases *in vitro* and on a cell-free mismatch repair [76].

At the molecular level, effects of exposure to weak radiofrequency fields on acethylcholine release in hippocampus of freely moving rats were revealed [77]. Effects of 60 Hz MF on the immune system in wistar rats was denounced [78]. Also, at the level of ionic events, factors distorting cytosolic calcium measurements in Jurkat cells during exposure to ELF MFs were revealed [79] while there was a calcium spiking in ROS 17/2.8 cells exposed to ELF EMF [80].

The hypothesis suggesting that the rescue of damaged cells may be the mechanism explaining why MFs, which are not mutagenic *per se*, are often able to increase mutation and tumor frequencies [58], is being considered in a number of laboratories. As a matter of fact, there seems to be a general consensus on MFs which may be indeed correlated with cancer [81]. Effects of a 50 Hz MF exposure were also observed on tumor experimental models [82]. The correlation of the MF action with cancer must also be added to the general concern about the harmful effect of MFs on human health.

Summary

Both old [1-16] and new [83] contributions continue to recognize, on the one hand, that the mechanisms of the MF-bioeffects are not yet understood [84] and, on the other, pave the way towards the assumption of an inverse correlation between the degree of MF-sensitivity and the order of complexity of the biological target (Fig. 4a). Such a hypothesis, by analogy, could be judged in the framework of the known inverse correlation existing between the intensity of the ionizing radiation and the evolutionary state of the species (Fig. 4b) [85]. In other words, although both AC and DC MFs do not cause electron movements inside the atom, their final action might depend on peculiar ontological and phylogenetic features of biodiversity. This idea emerged particularly from the comparison of the interactions between the MFs and the living matter at the molecular, tissue and total-body levels [84]. In fact, at variance with cell-cycle kinetics and cell membrane molecular dynamics, which unequivocally depend upon low-frequency/low-intensity MFs [4,12], the single molecular reactions, as some of those occurring in gene expression, react to these fields to a lesser extent [41-43]. An interest of the differential response to MFs, evolving as a function of the biological complexity, would also appear if one correlated Markov's "biological windows" [86] with the heterogeneous MF-sensitivity established for the various cell-cycle stages [4,54] and, thus, for the whole cell proliferation process.

Acknowledgements

This study was supported by the University of Rome "Tor vergata" and a MIUR-CNR-ENEA Project.

References

[1] A. F. Lawrence and W. R. Adey. Non linear wave mechanisms in interactions between excitable tissue and electromagnetic fields. *Neurol. Res.* 4, 115-53 (1982).

[2] A. Lacy-Hulbert, J. C. Metcalfe and R. Hesket. Biological responses to electromagnetic fields. *FASEB J.* 12, 395-420 (1998).

[3] C. A. Basset. Beneficial effects of electromagnetic fields. *J. Cell. Biochem.* 51, 387-393 (1993).

[4] T. Eremenko, C. Esposito, A. Pasquarelli, E. Pasquali and P. Volpe. Cell-cycle kinetics of *Friend erythroleukemia* cells in a magnetically shielded room and in a low-frequency/low-intensity magnetic field. *Bioelectromagnetics* 18, 58-66 (1997).

[5] M. Blank. The surface compartment model: a theory of ion transport focused on ionic processes in the electric double layers at membrane protein surface. *Biochim. Biophys. Acta* 906, 277-294 (1987).

[6] J. Walleczeck. Electromagnetic field effect on cells of the immune system: the role of calcium signaling. *FASEB J.* 6, 3177-3185 (1992).

[7] R. Glaser. Current concepts of the interaction of weak electromagnetic fields with cells. *Bioelectrochem. Bioenerg.* 27, 255-268 (1992).

[8] R. P. Liburdy. Calcium signaling in lymphocytes and ELF fields. Evidence for an electric field metric and a site of interaction involving the calcium ion channel. *FEBS Lett.* 301, 53-59 (1992).

[9] R. Karabakhtsian, N. Broude, N. Shalts, S. Kochlatyi, R. Goodman and A. Henderson. Ca^{2+} is necessary in the cell response to EM fields. *FEBS Lett.* 349, 1-6 (1994).

[10] F. S. Barnes. Effect of electromagnetic fields on the rate of chemical reactions. *Biophysics* 41, 801-808 (1996).

[11] S. Paradisi, G. Donelli, M. T. Santini, E. Straface and W. Marloni. A 50 Hz magnetic field induces structural and biophysical changes in membranes. *Bioelectromagnetics* 14**,** 247-255 (1993).

[12] P. Volpe, T. Parasassi, C. Esposito, G. Ravagnan, A. M. Giusti, A. Pasquarelli and T. Eremenko. Cell membrane lipid molecular dynamics in a solenoid *vs*. a magnetically shielded room. *Bioelectromagnetics* 19, 107-111 (1998).

[13] J. M. Delgado, J. Leal, L. Moneagudo and G. Gracia. Embryological changes induced by weak ELF EMF. *J. Anat.* 134, 533-551 (1982).

[14] A. H. Martin. Development of chicken embryos following exposure to 60 Hz MF with differing waveforms. *Bioelectromagnetics* 13, 223-230 (1992).

[15] S. Maffeo, M. Miller and E. Carstensen. Lack of effect of weak low-frequency EMF on chick embryogenesis. *J. Anat.* 139, 613-618 (1984).

[16] B. F. Sisken, I. Fowler, C. Mayaud, J. Ryaby and A. Pilla. Pulsed EMF and normal chick development. *J. Bioelectr*. 5, 25-34 (1986).

[17] A. R. Liboff. Geomagnetic cyclotron resonance in living cells. *J. Biol. Phys.* 9, 99-100 (1985).

[18] B. R. McLeod and A. R. Liboff. Cyclotron resonance in cell membranes: the theory of the mechanism. In "*Mechanistic Approaches to Interactions of Electric and Electromagnetic Fields with Living Systems"* (M. Blank and E. Findl, eds.), Plenum Press, New York, pp. 97-108 (1987).

[19] A. Chiabrera, B. Bianco, J. J. Kaufman and A. A. Pilla. Quantum dynamics of ions in molecular crevices under electromagnetic exposure. In "*Electromagnetics in Biology and Medicine*" (C. T. Brighton and S. R. Pollak, eds.), San Francisco Press, San Francisco, pp. 21-26 (1991).

[20] D. T. Edmunds. Larmor procession as a mechanism for the detection of static and alternating magnetic fields. *Bioelectrochem. Bioenerg* 30, 3-12 (1993).

[21] J. P. Blanchard and C. F. Blackman. Clarification and application of an ion parametric resonance model for magnetic field interactions with biological systems. *Bioelectromagnetics* 15, 217-238 (1994).

[22] A. N. Volobuev, B. N. Zhukov, A. U. Bakhito, E. L. Ovcinnikov and I. A. Trufanov. Influence of constant magnetic field and laser emission on neurophysiological processes. *Biofizika* 38, 372-377 (1993).

[23] L. P. Agulova, A. M. Opalinskaja and V. C. Kirjanov. Specific features of reactions of different objects sensitive to change in cosmophysical factors and action of weak electromagnetic fields. In "*Problems of Cosmic Biology*" (M. N. Gnevishev, ed.), Nauka, Leningrad, Vol. 65, pp. 160-181 (1989).

[24] G. Piccardi. The Chemical Basis of Medical Climatology, Springer, New York (1962).

[25] L. D. Kislovsky. Reaction of biological system to weak low-frequency electromagnetic fields adequate for it. In *"Problems of Cosmic Biology*" (A. M. Ugolev, ed.), Nauka, Moscow, Vol. 43, pp. 148-166 (1982).

[26] V. E. Zhvirblis. On reproducibility of heliobiological experiments. In "*Problems of Cosmic Biology*" (M. N. Gnevishev, ed.), Nauka, Leningrad, Vol. 65, pp. 145-160 (1989).

[27] B. M. Vladimirsky. Biological rhythms and the solar activity. In "*Problems of Cosmic Biology*" (V. N. Chernigovsky, ed.), Nauka, Moscow, Vol. 41, pp. 289-315 (1980).

[28] B. M. Vladimirsky and N. A. Temurjants. Nuclear magnetic resonance of weak electromagnetic field action on biological, physical and chemical systems. *Biofizika* 38, 372-377 (1996).

[29] V. N. Binhi. Nuclear spins in primary mechanisms of biomagnetic effects. *Biofizika* 40, 671-685 (1995).

[30] V. V. Lednev, N. A. Belova, I. K. Srebnitskaja, E. N. Iljasova, Z. N. Rozhdesvenskaja, A. A. Klimov, N. A. Belova and K. P. Tiras. Magnetic parametric resonance in biosystems: experimental verification of the theoretical predictions with the use of regenerating planarians *Dugestia tigrina* as a test system. *Biofizika* 41, 815-825 (1996).

[31] V. N. Binhi, Y. D. Alipov and I. Y. Belyaev. Effect of static magnetic field on *E. coli* cells and individual rotations of ion-protein complexes. *Bioelectromagnetics* 2001, 22, 79-86.

[32] V. N. Binhi. On the model ion channel-electrical solenoid. *Biofizika* 40, 549-550 (1995).

[33] V. N. Binhi. Mechanism of magnetosensitive ion binding by some proteins. *Biofizika* 42, 338-342 (1997).

[34] A. El-Lakkani. Dielectric response of some biological tissues. *Bioelectromagnetics* 22, 272-279 (2001).

[35] R. Emura, N. Ashida, T. Higashi and T. Takeuchi. Orientation of bull sperms in static magnetic fields. *Bioelectromagnetics* 22, 60-65 (2001).

[36] M. N. Zhadin. Action of magnetic fields on the ion motion in a macromolecule: theoretical analysis. *Biophyzika* 41, 832-850 (1996).

[37] M. Blank and R. Goodman. Do electromagnetic fields interact directly with DNA? *Bioelectromagnetics* 18, 111-115 (1997).

[38] R. K. Adair. Extremely low frequency electromagnetic fields do not interact directly with DNA. *Bioelectromagnetics* 19, 136-137 (1998).

[39] F. Mariani, G. Cappelli, T. Eremenko and P. Volpe. Influence of static magnetic fields on cell viability, necrosis and apoptosis. *J. Biol. Res*. 77, 71-84 (2001).

[40] P. Volpe, G. Cappelli, F. Mariani, A. Serafino and T. Eremenko. Macrophage sensitivity to static magnetic fields. In "*Biological Effects of EMFs*" (P. Kostarakis, ed.), University of Ioannina and NCSR Demokritos Publishers, Rhodes, Vol. 1, pp. 374-381 (2002).

[41] T. Eremenko, C. Esposito, P. Iacovacci, E. Tartaglini and P. Volpe. Regulation of macromolecular biosynthesis in growing erythroleukemia cells exposed to a magnetic field. In "*Annual Review of Research on Biological Effects of Electric and Magnetic fields*" (D. Wisecup, ed.), San Diego, A15, pp. 1-2 (1992).

[42] P. Volpe and T. Eremenko. Genome stability *vs*. deprivation or enrichment of the geomagnetic field. *The Environmentalist* 25, 72-82 (2005).

[43] P. Volpe and T. Eremenko. Gene expression in a Space-simulating magnetically shielded environment. *The Environmentalist* 25, 83-92 (2005).

[44] C. M. Cook, A. W. Thomas and F. S. Prato. Human electrophysiological and cognitive effects of exposure to ELF magnetic and ELF modulated RF and microwave fields: a review of recent studies. *Bioelectromagnetics* 23, 144-157 (2002).

[45] Y. P. Chukova. The general laws of biological effects of optical electromagnetic fields. In "*Biological Effects of EMFs*" (P. Kostarakis, ed.), University of Ioannina and NCSR Demokritos Publishers, Rhodes, Vol. I, pp. 318--326 (2002).

[46] D. J. Panagopoulos, N. Messini, A. Karabarbounis, A. L. Filippetis and I. H. Margaritis. A mechanism for action of oscillating electric fields on cells. *Biochem. Biophys. Res. Commun.* 272, 634-640 (2000).

[47] A. Del Moral, M. J. Azanza, A. C. Calvo and R. N. Perez-Bruzon. Cooperative diamagnetism and Ca^{2+} liberation of plasma membrane molecules explains the neuron responses to applied static and extremely low frequency magnetic fields. In "*Biological Effects of EMFs*" (P. Kostarakis, ed.), University of Ioannina and NCSR Demokritos Publishers, Rhodes, Vol. 1, pp. 298-308 (2002).

[48] S. Grimaldi, D. Pozzi, M. Santoro, A. Lisi, E. Pasquali, A. Serafino, L Giuliani, M. Vignati, T. Eremenko and P. Volpe. Magnetic field is affecting biophysical and morphological properties of mammalian cells. In "*2nd Workshop on Biostructures and Biosystems*" (Italian Society of Biophysics, ed.), SIB Publishers, Portonovo, Abstr., C, 25 (1997).

[49] Y. G. Shokorbatov, V. G. Shakhbazov and A. O. Rudenko. Modification of electrokinetic properties of nuclei in human buccal epithelial cells by electric fields. *Bioelectromagnetics* 22, 106-111 (2001).

[50] F. Bistolfi. Electromagnetic man and magnetic resonance tomography: Update on the biological effects and new paths of research. *Riv. Neuroradiol*. 14, 63-82 (2001).

[51] M. Golzo, J. Teissie and M. P. Rols. Cell synchronization effect on mammalian cell permeabilization and gene delivery by electric field. *Biochem. Biophys. Acta* 1563, 23-28 (2002).

[52] S. Koronkievicz, S. Kalinowsky and K. Bryl. Programmable chronopotentiometry as a tool for the study of electroporation and resealing of pores in bilayer lipid membranes. *Biochem. Biophys. Acta* 1561, 222-229 (2002).

[53] C. Maercker, J. Czyf, A. M. Wobus, W. Huber, A. Poustka, S. Ivancsits, H. W. Ruediger, O. Jhan, E. Diem, J. Schuderer, N. Kuster, D. Fornasari, F. Clementi, K. Schlatterer, R. Tauber, R. Fitzner, J. Reivenen, F. Aldokofer and D. Leszczynski. An eu-wide initiative to characterize the biological effects of EMF on human and mouse cell lines by gene expression profiling. In "*Biological Effects of EMFs*" (P. Kostarakis, ed.), University of Ioannina and NCSR Demokritos Publishers, Rhodes, Vol. II, pp. 588-594 (2002).

[54] N. A. Cridland, R. G. E. Haylock and R. D. Saunders. 50 Hz magnetic field exposure alters onset of S-phase in normal human fibroblasts. *Bioelectromagnetics* 20, 446-452 (1999).

[55] A. Markkanen, J. Juutilainen, S. Lang, J. Pelkonen, T. Rytomaa and J. Naarala. Effects of 50 Hz magnetic field on cell-cycle kinetics and the colony forming ability of budding yeast exposed to ultraviolet radiation. *Bioelectromagnetics* 22, 345-350 (2001).

[56] J. P. Shah, P. Midkiff, P. C. Brandt and B. F. Sisken. Growth and differentiation of PC6 cells: the effects of pulsed electromagnetic fields (PEMF). *Bioelectromagnetics* 22, 267-271 (2001).

[57] S. P. Yu, L. M. T. Canzoniero and D. W. Choi. Ion homeostasis and apoptosis. *Curr. Opin. Cell Biol.* 13,405-411(2001

[58] C. Fanelli, S. Coppola, R. Barone, C. Colussi, G. Gualardi, P. Volpe and L. Ghibelli. Magnetic fields increase cell survival by inhibiting apoptosis via modulation of Ca^{2+} influx. *FASEB J.* 13, 95-102 (1999).

[59] C. Gidon-Jeangirard, E. Solito, A. Hofman, F. Russo-Marie, J. M. Freyssinet and M. C. Martinez. Annexin counteracts apoptosis while inducing Ca^{2+} influx in human lymphocytic T cells. *Biochem. Biophys. Res. Commun.* 265, 265-215 (1999).

[60] M. Obo, S. Konishi, Y. Otaka and S. Kitamura. Effect of magnetic field exposure on calcium channel currents using patch clamp technique. *Bioelectromagnetics* 23, 306-314 (2002).

[61] X. Wang, F. F. Becker and P. R. C. Gascoyne. Membrane dielectric changes indicate induced apoptosis in HL-60 cells more sensitively than surface phosphatidylserine expression or DNA fragmentation. *Biochem. Biophys. Acta* 1564, 412-420 (2002).

[62] G. R. Ding, T. Nakahara, R. R. Tian, Y. Guo and J. Miyakoshi. Transient suppression of X-ray-induced apoptosis by exposure to power frequency magnetic fields in MCF-7 cells. *Biochem. Biophys. Res. Commun.* 286, 953-957 (2001).

[63] J. G. Robinson, A. R. Pendieton, K. O. Manson, B. K. Murray and K. L. O'neill. Decreased DNA repair rates and protein from heat induced apoptosis mediated by electromagnetic field exposure. *Bioelectromagnetics* 23, 106-112 (2002).

[64] A. Negroni, M. C. Pirozzoli, G. A. Lovisolo, L. Mosiello, C. Laconi and C. Marino. Exposure to 50 Hz magnetic fields of a neuroblastoma cell line: effects on apoptosis. In "*Biological Effects of EMFs*" (P. Kostarakis, ed.), University of Ioannina and NCSR Demokritos Publishers, Rhodes, Vol. II, pp. 865--868 (2002).

[65] G. Mirabolghasemi and M. Azarnia. Developmental changes in *Drosophila melanogaster* following exposure to alternating electromagnetic fields. *Bioelectromagnetics* 23, 416-420 (2002).

[66] M. Stamenkovich-Radak, I. Kitanovic, Z. Prolic, I. Tomisic, B. Stoijkovic and M. Andjelkovic. Effects of permanent magnetic field on wing size parameters in *Drosophila melanogaster*. *Bioelectromagnetics* 22, 365-369 (2001).

[67] S. Cecconi, G. Gualtieri, A. Di Bartolomeo, G. Troiani, M. G. Cifone and R. Canipari. Evaluation of the effects of extremely low frequency electromagnetic fields on mammalian follicle development. *Hum. Reprod.* 15, 2319-2325 (2000).

[68] F. Golfert, A.Hoter, M. Thrummler, H. Bauer and R. H. W. Funk. Extremely low frequency electromagnetic fields and heat shock can increase microvesicle motility in astrocytes. *Bioelectromagnetics* 22, 71-78 (2001).

[69] M. Lino and Y. Okuda. Osmolality dependence of erhythrocyte sedimentation and aggregation in strong magnetic field. *Bioelectromagnetics* 22, 46-52 (2001).

[70] A. Pazur. Electric relaxation processes in lipid-bilayers after exposure to weak magnetic pulses. *Zeitschr. Natur. J. Biosci.* 56, 831-837 (2001).

[71] R. R. Tice, G. G. Hook, M. Donner, D. I. McRee and A. W. Guy. Genotoxicity of radiofrequency signals: I. investigation of DNA damage and micronuclei induction in cultured human blood cells. *Bioelectromagnetics* 23, 113-126 (2002).

[72] A. Maes, M. Collier and L. Vershaeve. Cytogenetic effects of 900 MHz (GSM) microwaves on human lymphocytes. *Bioelectromagnetics* 22, 91-96 (2001).

[73] G. R. Ding, K. Wake, M. Taki and J. Miyakoshi. Increase in hypoxanthine-guanine phosphoribosyl transferase gene mutations by exposure to electric field. *Life Sci.* 68, 1041-1046 (2001).

[74] C. Ventura, M. Maioli, G. Pintus, G. Gottardi and F. Bersani. Elf-pulsed magnetic fields modulate opioid peptide gene expression in myocardial cells. *Cardiov. Res*. 45, 1054-1064 (2000).

[75] G. Nindi, E. F. Hughes, M. T. Johnson, D. N. Vesper and W. X. Balcavage. Effect of ultraviolet B radiation and 100 Hz electromagnetic fields on proliferation and DNA synthesis of Jurkat cells. *Bioelectromagnetics* 23, 455-463 (2002).

[76] S. Herada, S. Yamada, O. Kuramela, Y. Gunji, M. Kawasaki, T. Miyakawa, H. Yonekura, S. Sakurai; K. Bessho, R. Hosono and H. Yamamoto. Effects of high ELF magnetic fields on enzyme-catalyzed DNA and RNA synthesis *in vitro* and on a cell-free mismatch repair. *Bioelectromagnetics* 22, 260-268 (2001).

[77] G. Testylier, L. Tonduli, R. Malablau and J. C. Debouzy. Effects of exposure to low level radiofrequency fields on acethylcholine release in hippocampus of freely moving rats. *Bioelectromagnetics* 23, 249-255 (2002).

[78] A. C. T. De Lucia, C. W. S. F. Anselmo, I. M. Oliveira, M. B. Filho and M. T. J. De Almeida Catanho. Effects of 60 Hz electric and magnetic field on the immune system in the wistar rats. In "*Biological Effects of EMFs*" (P. Kostarakis, ed.), University of Ioannina and NCSR Demokritos Publishers, Rhodes, Vol. II, pp. 837--845 (2002).

[79] C. R. McCreary, A. W. Thomas and F. S. Prato. Factors confounding cytosolic calcium measurements in Jurkat E6.1 cells during exposure to ELF magnetic fields. *Bioelectromagnetics* 23, 315-328 (2002).

[80] R. Shahidain, R. D. Mullins and J. E. Sisken. Calcium spiking and baseline calcium levels in ROS 17/2.8 cells exposed to extremely low frequency electromagnetic fields (ELF EMF). *Internat. J. Rad. Biol.* 77, 241-248 (2001).

[81] C. E. Minder and D. H. Pfluger. Minder and Pfluger respond to "Electromagnetic fields and cancer in railway workers" by Savitz. *Amer. J. Epidemiol*. 153, 839-840 (2001).

[82] P. Galloni and C. Marino. Effects of 50 Hz magnetic field exposure on tumor experimental models. *Bioelectromagnetics* 21, 608-614 (2000).

[83] A. Morelli, S. Ravera, I. Panfoli and I. M. Pepe. Effects of extremely low frequency electromagnetic fields on membrane-associated enzymes. *Arch. Biochem. Biophys*. 441, 191-198 (2005).

[84] P. Volpe. Interactions of zero-frequency and oscillating magnetic fields with biostructures and biosystems. *Photochem. Photobiol. Sci.* 2, 637-648 (2003).

[85] P. Volpe. Introduzione alla Biofisica delle Radiazioni. Unesco Office Publishers, Venice, pp. 1-256 (1999).

[86] M. S. Markov. Myosin phosphorylation - a plausible toole for studying "biological windows". In "*Biological Effects of EMFs*" (P. Kostarakis, ed.), University of Ioannina and NCSR Demokritos Publishers, Kos, Vol. I, pp. 1-9 (2004).

MODELS OF NEURONE DYNAMICS: SPONTANEOUS AND UNDER ELF ALTERNATING MAGNETIC FIELD

A. DEL MORAL(*), MARÍA J. AZANZA(+) AND R. N. PÉREZ-BRUZÓN(+)

(*) LABORATORIO DE MAGNETISMO DE SÓLIDOS, DEPARTAMENTO DE FÍSICA DE MATERIA CONDENSADA AND ICMA, UNIVERSIDAD DE ZARAGOZA AND CSIC, 50009 ZARAGOZA, SPAIN.
(+) LABORATORIO DE MAGNETOBIOLOGÍA, DEPARTAMENTO DE ANATOMÍA E HISTOLOGÍA HUMANAS, FACULTAD DE MEDICINA, UNIVERSIDAD DE ZARAGOZA, 50009 ZARAGOZA, SPAIN.

Abstract

We report about a developed model of single neurone dynamics from where we calculate the effects of low frequency (ELF) magnetic field (MF) upon single neurones and simple neurone networks. Calculations are based on the membrane phospholipids (PP) superdiamagnetism and Ca^{2+} coulomb explosion model and on an extension of the Hodgkin & Huxley (HH) equation under MF. *Integration* of HH equation, under AC MF application, by assuming the membrane as a Kirchoff electrical knot, and within the relaxation-time, τ approximation for the HH n(t), m(t) and h(t) characteristic conductance functions have been performed, obtaining the theoretical time dependence of membrane voltage for hyperpolarization (H) and depolarization (D) processes, so allowing a determination of K^+, τ_K, and Na^+, τ_{Na} relaxation times. Calculated frequency spectra of single bioelectric impulse H and D voltages are *lorentzians*, as experimentally observed in single unit neurones of mollusc *Helix aspersa*. On the other hand a model which explains the *frequency window effect* (FWE) in neural tissue is developed, explaining Bawin & Adey's first FWE observation in chicken brain and also our observations of FWE in mollusc *Helix aspersa*, both respectively showing *lorentzian* dependencies for Ca^{2+} efflux, $\phi(f_M)$ and bioelectric frequency $f(f_M)$ with AC MF frequency, f_M i.e a resonance when spontaneous $f_0 = f_M$.

1.- Introduction.-

In the bioelectric activity of neural tissue, either spontaneous or under applied magnetic field (MF) there appear two issues: the generation and structure of the bioelectric impulse and the frequency of it, to which we should add the sinusoidal or alternating (AC) MF induced firing correlation observed between neurones or *AC-MF-synchronization effect* (1). The generation of the impulse, after the refractory time, is one of the main problems of neurone physiology, during which the ATP-Na/K pumps operate. The process by which the impulse starts it is thought to be the result of small sub-threshold voltages sum up to a threshold voltage, V_S where the depolarization (D) process starts, with the entrance of Na^+ ions to the cell, through voltage activated Na^+-channels. We are not going to treat here this problem, but about the time shape of the impulse once it is formed, dividing it in D and hyperpolarization (H, due the sorting out of K^+ ions through delayed rectifier voltage-operated K^+-channels). The MF effect on electrogenic pumps, which promote the entrance of $3\,K^+$ ions against the sorting out of $2\ Na^+$ ions, making the membrane going to the resting potential, was already considered elsewhere (2), so completing the full scenario. The MF effect on the refractory process is the decrease of impulse D amplitude. All those impulse parts we will see are explained by the *integration* of the Huxley & Hodgkin (HH) equation (3), supplemented by the MF produced Ca^{2+} current, that has been done by assuming the membrane as a Kirchoff *electric knot*, instead of as a parallel conductances network as done so far (4). Regarding to the second issue, the neuron impulse frequency, *f* strongly changes with the MF intensity, B and in the case of AC MF with the RMS field intensity, $B_{eff} = B_0/\sqrt{2}$ (B_0 is the AC MF amplitude) and also with the AC MF frequency, f_M. With all those models we have conformed a full picture of the single unit neurone bioelectric behaviour, either for spontaneous regime or under AC MF, this of extremely low frequencies (ELF).

2.- Superdiamagnetism (SD) and Ca^{2+} coulomb explosion (CE) model under AC magnetic fields.-

The explanation of above effects will be based on the membrane phospholipid (PP) *superdiamagnetism* (SD) and Ca^{2+} *coulomb explosion* (CE) model (5, 6). This model has been widely tested in single neurones and simple neurone networks under static and ELF MF respectively, where in the latter the MF also induces a *synchronized* bioelectric activity within those networks (1, 7). The model contemplates three ingredients: i) the anisotropy of the diamagnetic susceptibility tensor components, $\tilde{\chi}$ (< 0) of the long PP "rods", or difference $\Delta\chi = \chi_{\parallel} - \chi_{\perp}$, between the directions parallel ($\parallel$) and perpendicular ($\perp$) to the PP axis; ii) the well proved cluster formation in the membrane liquid crystal of *correlated* PP long axes through their electric quadrupolar moments, $\tilde{Q}_i$ interaction, of pair (i, j) correlation function $C_Q = \langle \tilde{Q}_i \tilde{Q}_j \rangle - \langle \tilde{Q}_i \rangle \langle \tilde{Q}_j \rangle$, by which the PPs cooperatively rotate out from the MF **B** axis (SD; PP electric dipolar moment is very weak). $\langle ... \rangle$ is the ensemble thermal average. The correlation length, ξ usually exceeds a single neurone, *via* the PPs of the interposed glia membranes between neurones, and through the gap junctions (8); iii) when the Ca^{2+} ions attached to their PP bilayer inner and outer binding sites (polar heads) happen to be nearest-neighbours (NN, in number N_{nn} per cluster face, with estimated $N_{nn} \cong 0.007\, N_c$, N_c being the PP number per cluster), and the NN PPs suffer opposite (with clearly 1/2 probability) magnetic torques $\boldsymbol{\tau}_m = \pm \mathbf{m} \times \mathbf{B}$, the weak ionic bindings are broken by their mutual coulomb repulsion, of energy ε_{coul}. This produces a *simultaneous* detaching (coulomb explosion, *CE*) of Ca^{2+} pairs (see Fig.1 for a view of the mechanisms involved). Note that the Ca^{2+} water solvating and dielectric mem-

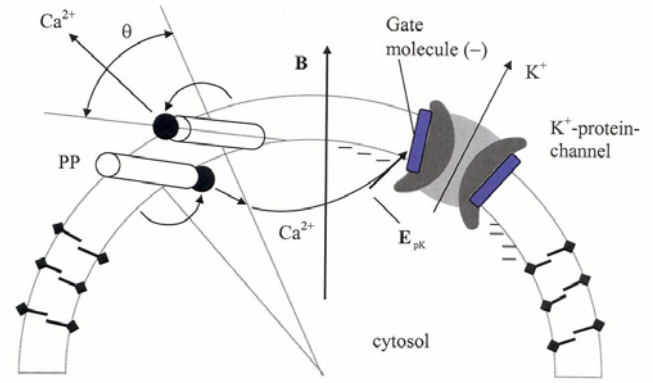

Fig.1.- Schematic view of the mechanisms involved in the SD-CE model. The circular shell represents the membrane neurone phospholipid (PP) bilayer. Two nearest-neighbour Ca^{2+}-charged phospholipids (rods) rotate under their assumed opposite magnetic torques, approaching the Ca^{2+} ions (black circles), attached to the PP negatively charged heads (lozenges). The ions become simultaneously detached from the membrane surfaces when their weak ionic bonds to the heads are broken due to Ca^{2+}-Ca^{2+} coulomb repulsion. Within the cytosol the Ca^{2+} ions diffuse towards the K^+-protein channels, which are opened when Ca^{2+} is captured by the "gate" molecule (calmodulin), giving rise to the K^+ outwards current (hyperpolarization).

brane negative electric images formation reduce the Ca^{2+} effective charge to only $q_{ef} \cong 0.025\ q_{Ca^{2+}}$, making the ionic bond energy, ε_{bind} rather weak. But since ε_{bind} is supplemented by the water-PP surface tension energy the bond becomes stable against *normal* to the surface thermal fluctuations (of energy $(1/2)k_B T \cong 8$ meV at r.t.) (5)**.** $\mathbf{m} = \tilde{\chi}\mathbf{H}$ is the field induced diamagnetic PP magnetic moment and it rotates out from **B** axis because $|\chi_{\parallel}| > |\chi_{\perp}|$, therefore alternatively approaching the NN Ca^{2+} charged PP heads (Fig.1). The PP magnetic energy is given by $\varepsilon_m = -(1/2\mu_0)B^2(\chi_{\perp} + \Delta\chi \cos^2\theta)V$, where θ is the angle formed by the PP axis with **B** and $\boldsymbol{\tau}_m = -(\partial\varepsilon_m/\partial\theta)\hat{\boldsymbol{\theta}}$, which acts against the opposite coulomb repulsion torque, $\boldsymbol{\tau}_r = -(\partial\varepsilon_{coul}(\theta)/\partial\theta)\hat{\boldsymbol{\theta}}$ (V is the PP volume). Under AC MF the scenario is the detaching from the cluster of gaussian bursts of Ca^{2+} ions for about half a MF cycle, since the magnetic torque is oscillatory, i.e. $\tau_m = (1/2\mu_0)B_0^2 \Delta\chi \sin 2\theta(t) \sin^2\omega_M t$. The Ca^{2+} detaching occurs when $N_{nn}(\varepsilon_{coul}(\theta) - \varepsilon_{bind}) + N_c\varepsilon_m(\theta) \cong 0$, a condition that allows to weak MF to detach about 7 Ca^{2+} per 10^3 PP for large enough N_c (5, 6). Note that the small q_{eff}, the interposed membrane dielectric constant ($\in_r \cong 2.6$) and the final Ca^{2+}-Ca^{2+} approaching distance $d_f \cong 5.3$nm yield a small energy $\varepsilon_{coul}(\theta_f) = (1/4\pi \in_r \in_0)(q_{eff}^2/d_f^2)$ at the coulomb explosion angle θ_f. The MF detaching process, which occurs within a spherical apex of 120º around **B**, produces a cytosol Ca^{2+} concentration about ten times the normal one and similar to the produced one in the D process (see (6) for greater detail).

The main result from the SD-CE model (5, 6) is the *field intensity dependence* of the neurone bioelectric frequency, $f(B_{eff},T)$. This frequency is controlled by chemistry mass action law between Ca^{2+} and membrane binder radical, R^- (sialic acid outside and phosphatidylserine inside), i.e. $[Ca^{2+}][R^-]=k(T,B_{eff})[CaR]$, where k is the kinetics constant. Thus $f \propto [R^-]$ becomes inversely proportional to the number of Ca^{2+} ions detached per cluster, $N^c_{Ca^{2+}} = N_{nn}\exp(-\Delta E_c/k_BT)$, where $\Delta E_c(\theta)=-(N_c\varepsilon_m+N_{nn}\varepsilon_{coul})$ is the *dynamic* Peierls's energy barrier to be overcome by the Ca^{2+} ion in order for the PP to steadily rotate. Moreover under AC MF the H process (where the cytosol becomes more negative due the K^+ ions sorting out) is modified by the Ca^{2+} ions (in number of four) binding to the K^+ protein-channel (more specifically to the calmodulin "gate" molecule) and opening it due to the calmodulin electrical unfolding (9). Therefore it should be $f \propto 1/N_{Ca^{2+}}$, to first order. Summing now $N^c_{Ca^{2+}}$ from all the PP clusters in membrane (s), the final result is that the neurone bioelectric frequency varies with RMS MF as (5, 6)

$$f(B_{eff},T)=f(0,T)\exp(-\alpha B^2_{eff}), \qquad [1]$$

where $f(0,T)\equiv f_0$ is the *spontaneous* frequency and the parameter $\alpha = N_c|\chi_\perp|V/2\mu_0 k_B T$, that encompasses the PP cluster physical properties and membrane temperature, T. As mentioned before for ELF AC MF (quasistatic) we have introduced in [1] the RMS B_{eff}, since magnetic energy density stored in the membrane is $B(t)^2/2\mu_0$, of time average $B^2_{eff}/2\mu_0$. Eq.[1] has been widely and firmly tested in single neurones of *Helix aspersa* for static (5) and ELF weak MF (1,11) and for T modification, by using standard microelectrode transmembrane voltage real time recording technique. In fact for weak ELF MF the observed *f* in *Helix* neurones follows a dependence $f(B_{eff})\cong f(0)(1-\alpha B^2_{eff})$, which precisely is the obtained one by performing a series expansion of [1] for $\alpha B^2_{eff} << 1$ (1). Regarding to *f* (T) dependence, preliminary observations in mapped *Helix* neurones F47 and F2 show that *f* first decreases with increasing T at fixed B_{eff}, in disagreement with eq.[1] (see Fig.2). The reason is that those neurones belong to the $\approx$ 26% of studied ones where *f increases* with increasing B_{eff} (6). The responsible mechanism is that the by MF detached Ca^{2+} ions depolarize the membrane, cytosol becoming more positive, so opening Na^+ and/or Ca^{2+} channels operated by voltage. Also D amplitude V_d *decreases*, the calculated variation in V_d being $\Delta V_d(B_{eff})=-(4\pi/N_c)E_p\exp(+\alpha B^2_{eff})$, where E_p is the pump e.m.f. , due to opposite to PP protein pump rotation (since $|\chi_\parallel|<|\chi_\perp|$), where PP partially cover the protein pump (2). Also observed are two transitions in the form of increasing *f* within a ΔT small interval, at $T_{f1}\approx 30^oC$ and $T_{f2}\approx 37^oC$, corresponding to phase transitions within the membrane liquid crystal. After second transition *f* decreases with T increase, now in agreement with [1], although temperature behaviour requires deeper investigation, and PP liquid crystal viscosity energy dissipation, $\varepsilon_v=-\eta_r(T)\theta(t)$ introduction in SD - CE model (η_r is the viscosity coefficient).

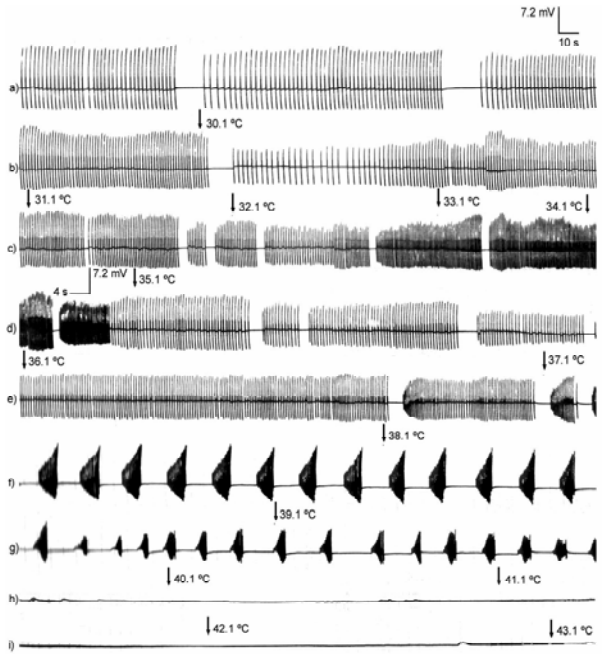

Fig.2.- Temperature effect for neurone F47 bioelectric activity. Transitions at 30ºC and 37ºC are observed.

3.- Biolectric impulse shape and frequency spectrum.-

The D and H main trams of bioelectric impulse (Fig.3) in neurones are controlled by the well known Hodgkin & Huxley equation (3). This equation has been usually referred to an equivalent electric circuit of in

parallel conductances, membrane capacitance, C_m and DC generators, the latter being the equilibrium Nersnt $Na^+$and K^+e.m.f., E_{Na} and E_K, due to the ions electrochemical gradients. Consideration of this network by meshes does not allow its solution, and we will consider the membrane as a knot where the currents concur

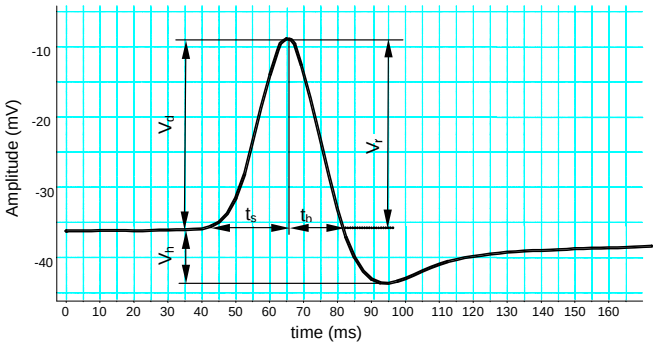

Fig.3.- Neurone V-14 impulse of *Helix* , with D, R and H trams.

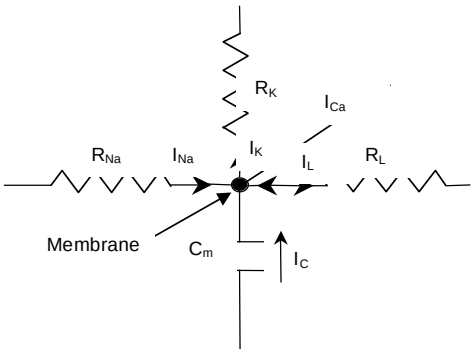

Fig.4.- Membrane equivalent Kirchoff electric knot.

(Fig.4). Therefore HH equation takes the knot law of charge conservation (no charge accumulation in membrane),

$$C_m(dV/dt)+g_{Na}m(t)^3h(t)(V-E_{Na})+g_K n(t)^4(V-E_K)+g_L(V-V_L)-I_{Ca}(B_{eff},t)=0 \quad , \qquad [2]$$

where V is the transmembrane voltage, g_i (i =Na, K, L) the channels conductances. m and n are the HH channel excitatory and h inhibitory functions, of microscopic origin not yet well known, although the phenomenologically needed powers four, point out to four independent processes, acting for the opening (m, n) and closing (h) of corresponding channels. Leakage (L) channels and ligand operated ones are probably responsible for the setting of the threshold voltage, V_s but current through them is weak and here neglected. Finally, HH currents have been supplemented by the Ca^{2+} current produced by MF (*HH magnetic* (HHM) equation). We will solve eq.[2] in the *relaxation time, τ, approximation* for the HH functions, where e.g.

$$dn/dt=-n(t)/\tau_K \qquad [3]$$

where n(t) is assumed to be proportional to the number of K^+-channels which remain closed at time t. Integration of [3] taking t = 0 at the beginning of repolarization (R) plus H process, yields $n(t)=n_0\exp(-t/\tau_K)$. Similarly taking t = 0 at the beginning of D process we obtain that function $m(t)=m_0\exp(-t/\tau_{Na})$. Otherwise the inhibition function at D process follows the equation $dh/dt=+h(t)/\tau_{inh}$, of integral $h(t)=h_0\exp(+t/\tau_{inh})$. We will now obtain the membrane voltage V(t) dependence, partitioning the impulse in the mentioned regimes.

Repolarization and hyperpolarization: these two processes follow one after other and it is well known that in the R+H process only K^+-channels are open and therefore [2] becomes, $C_m(dV/dt)+g_K n(t)^4(V-E_K)-I_{Ca}(B_{eff},t)=0$, which integration after substitution of n(t) yields

$$V_K(t)=E_K+(E_{Na}-E_K)\exp\left[-(g_K n_0^4\tau_K/4C_m)(1-e^{-4t/\tau_K})+\int_0^t dt'\,I_{Ca}(B_{eff},t')/(V_K(t')-E_K)\right], \qquad [4]$$

which is an integral equation with kernel $I_{Ca}(B_{eff},t)$. We will show below (from [1] and [9]) that $I_{Ca}(B_{eff},t)=-(N(0)f(B_{eff}=0)q_{Ca}/\tau_{Ca})\exp(-\alpha B_{eff}^2)\exp(-t/\tau_{Ca})$, where N(0) is the initial Ca^{2+} ion number in a burst and τ_{Ca} the Ca^{2+} relaxation time (diffusion time in the cytoplasm) (t origin in [4] is taken at $V(t)=E_{Na}$, origin of R). For comparison with experimental results in single neurones, it is useful to work in frequency domain, ω, so that we will obtain the *frequency spectrum* of spontaneous impulse $V_K(t)$. Fourier transform of [4] exp[…] function is unknown, but for $t<\tau_K$ first exponential can be series expanded, so obtaining

$$V_K(t)\approx E_K+(E_{Na}-E_K)\left[1-(g_K n_0^4\tau_K/4C_m)(1-e^{-4t/\tau_K})+\int_0^t dt'\,I_{Ca}(B_{eff},t')/(V_K(t')-E_K)\right]. \qquad [5]$$

The ω spectrum of [5] *spontaneous* $V_K(t)$ ($I_{Ca} = 0$) is obtained by Fourier transforming $V_K(t)$ around a central frequency ω_0^*, characteristic of the impulse, yielding (except for a Dirac $\delta(\omega - \omega_0^*)$ artefact introduced by the exponential series cut-off)

$$V_{Na}(\omega) = A^* \Big/ \left[(\omega - \omega_0^*)^2 + (\Delta\omega/2)^2 \right] , \qquad [6]$$

where $A^* \equiv g_K n_0^4 \tau_K / 4C_m$ and $\Delta\omega/2 = 2\pi/\tau_K$ the HMHW, which provides τ_K. Therefore the impulse spectrum is the familiar *lorentzian* function, taking its maximum value at $\omega = \omega_0^*$. Eqs. [5] and [6] can be easily extended to the real situation of having different types of K^+-channels (up to seven in *Helix aspersa* (13)), but this extension is not suitable for comparison with the impulse because of the too large number of parameters involved.

Depolarization: this process follows after the refractory time and threshold voltage establishment, and since involved Na^+ channels are operated by voltage, inclusion of Ca^{2+} current sums only a term to $V_{Na}(t)$. But also retarded in time K^+ channels are opened, although being in small number during D tram their current can be neglected. The HHM relevant equation is then $C_m(dV/dt) + g_{Na} m(t)^3 h(t)(V - E_{Na}) - I_{Ca}(B_{eff}, t) = 0$, which in presence of MF yields another integral equation. Integration followed by the first exponential expansion as before yields

$$V_{Na}(t) \approx E_{Na} \left[1 - (g_{Na} m_0^3 h_0 \tau_{eff} / 3C_m) \exp(-t/\tau_{eff}) + \int_0^t dt' \, I_{Ca}(B_{eff}, t') \Big/ (V_{Na}(t') - E_{Na}) \right], \qquad [7]$$

where the relaxation time is given by $\tau_{eff}^{-1} = \tau_{Na}^{-1} - \tau_{inh}^{-1}/3$, since the inhibition and activation are independent processes. As before the ω-spectrum of spontaneous $V_{Na}(t)$ is lorentzian of $\Delta\omega/2 = 2\pi/\tau_{eff}$, and $A^* \equiv g_{Na} m_0^3 h_0 \tau_{eff} / 3C_m$. Extension to different kinds of Na^+-channels is not worthwhile because of above mentioned reason.

Comparison with experiments in single neurones: we will compare our HHM model with electrophysiological experiments performed on *Helix aspersa* single unit neurones, a good bench for present studies. Thus in Fig.5 we present the spontaneous ($B_{eff} = 0$) R+H potential time variation for two mapped neurones (14), fitted by the approximate solution [5], the agreement being reasonable, but where we do not reproduced the sigmoidal variation at the ends, due to the series cut-off in [4]. The more "accurate" used "sigmoidal" fit by $(1 - e^{-t/\tau_K})^4$ is also shown, but its basis is purely phenomenological. We took $E_K = -75\,mV$, $E_{Na} = +50\,mV$ (this e.m.f. rectified by the delayed K^+ channels), $g_K = 1.6 \times 10^{-7} m^{-2} \Omega^{-2}$ and $C_m = 4 \times 10^{-2} Fm^{-2}$, and from the fits we obtained the n_0 and τ_K values quoted in Table 1. Clearly we can not identify n_0 with the number of K-protein channels (KP), with a density of ≈ 7 KP/μm^2, which for a neurone of 100 μm diameter yields $\approx 2x10^4$ KP. In Fig.6 we show the frequency spectrum of a bioelectric impulse of neurone V19, together with the fitted theoretical one by eq. [6] , using the parameter values of Table 1 the agreement being excellent, the same happening for other neurones (not shown). Under applied AC MF we have observed that shape of the impulse becomes *unmodified*, which means that the solution of full integral eq.[4] is not needed. Integral eqs. [4] and [7] can be easily transformed into second order linear differential equations of well known solutions, not given here.

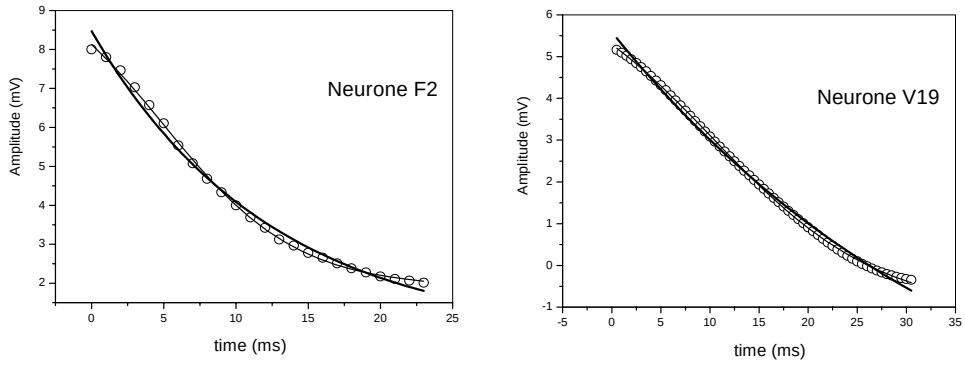

Fig.5.- Experimental (o) and model (thick line) R+H time variations for neurones F2 and V19; sigmoid (thin line).

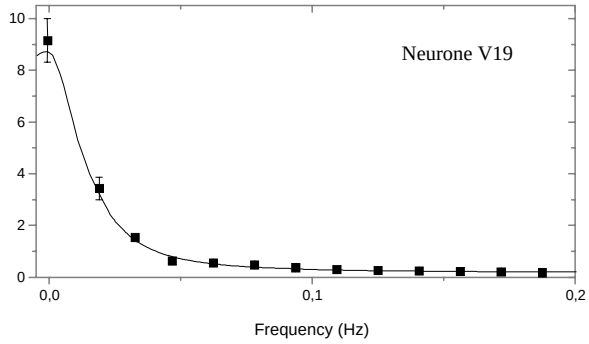

Fig.6.- Frequency spectrum of R+H tram impulse. Experiment (v) and model fit (full line).

Similarly in Figs. 7 we show the D voltages for the same neurones impulses, fitted by [7], using the above parameter values and $g_{Na} = 1.9 \times 10^{-7}\, m^{-2}\, \Omega^{-2}$, from the fits obtaining the values of $\left(m_0^3 h_0\right)^{1/4}$ and τ_{eff} quoted in Table 1. Values of $\left(m_0^3 h_0\right)^{1/4}$ are larger than n_0 ones, and same above consideration apply to them. Also sodium τ_{eff} are larger than τ_K, although in the impulse times $t_S < t_b$ because $V_{Na}(t)$ is interrupted at the smaller (abs.value) E_{Na} than E_K for $V_K(t)$. In Fig.8 is shown the frequency spectrum of $V_{Na}(t)$ for neurone V-19, and the fit by the corresponding lorentzian. D voltage is unmodified by applied AC MF and again solving of R+D equation under MF with I_{Ca} term is not needed.

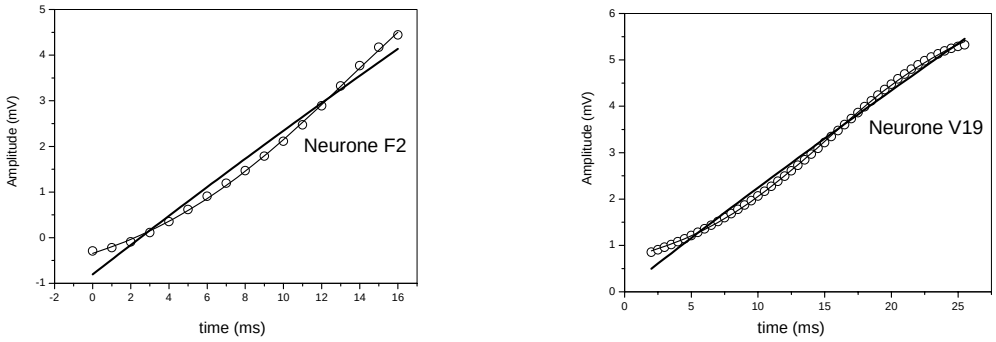

Fig. 7.- Ibidem Fig.5 for the depolarisation (D) process; lines: thick, model fit; thin, sigmoid.

Overall our HHM model explains well the spontaneous time dependence of the bioelectric impulse and its frequency spectrum. Demonstration that AC MF produced voltage, V_{Ca} is negligible is a mathematical problem of HHM differential equation resolution as mentioned before. As we will see in Section 3, the main effect of $I_{Ca}(B_{eff}, t)$ is upon the neurone bioelectric *frequency*.

Table 1.- Initial values of n, m, and h HH functions and K^+ and Na^+ relaxation times.

Neurone	n_0	τ_K (ms)	$\left(m_0^3 h_0\right)^{1/4}$	τ_{eff} (ms)
F1	200	33.0	51	92.7
F2	188	49.4	45	149.9
V3	202	45.0	49	109.6
V14	272	12.4	58	57.0
V19	155	156.7	41	222.8

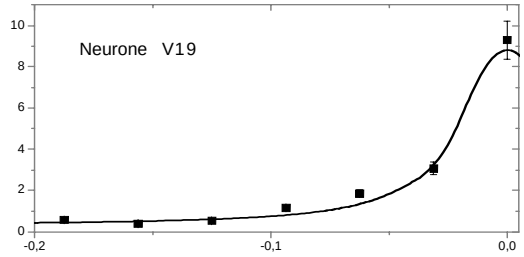

Fig.8.- Frequency spectrum (v) for impulse depolarization of neurone V-19. Line is the lorentzian fit, $L(f)$.

4.- Magnetic field frequency dependence of biolectric activity: frequency window effect.-

The experiments initiated in 1975 by Adey and co. (15) about the effects of ELF MF upon neural tissue are a breakthrough in the understanding of how AC ELF MF interacts with this tissue, apart from its *negligible* Joule heating. They prepared newborn chicken brain slices and embedded them in a physiological HCO_3^- water solution doped with radioactive $^{45}Ca^{2+}$ as marker. The tissue was then irradiated with a radiofrequency (RF) field of 147 MHz, *amplitude modulated* by an ELF MF (of amplitude 25 - 30 nT) in the interval 0.5 - 35 Hz, observing an increase of $^{45}Ca^{2+}$ efflux from the tissue. The experiments demonstrated two things: i) the RF (147 MHz) electromagnetic field (EMF) does *not* produce a measurable efflux increase; ii) a calcium efflux increase was observed for the tissue irradiated with the modulated wave, but only within an interval of about 5-25 Hz, so called *frequency window* effect (FWE) (see Fig.9). Recently we have found a FWE in *Helix aspersa* brain, irradiated with microwaves of 9.6 GHz amplitude modulated between 2-25 Hz. Since Ca^{2+} electrochemical gradient, E_{Ca} displaces these ions to the cell interior, the observed efflux was interpreted as Ca^{2+} liberation from the external membrane surface. FWE was afterwards found in many other kinds of cells and experimental conditions (see (6) for a review), in particular for the bioelectric *frequency, f* dependence with the applied ELF MF frequency, f_M in *Helix aspersa* single neurones (16). Our new observation is that the calcium efflux closely follows a *lorentzian* curve, written now in the normalized form,

$$\phi(\omega_M) = \phi(\omega_0)(\Delta\omega/2)^2 \Big/ \left[(\omega_M - \omega_0)^2 + (\Delta\omega/2)^2\right] \quad , \qquad [8]$$

where ω_0 is the frequency at the maximum efflux $\phi(\omega_0)$. Effectively, in Fig.9 the continuous line is the fit by [8] to the experimental calcium efflux (v points), and where $f_0 = \omega_0/2\pi \cong 14$ Hz and $\Delta f = \Delta\omega/2\pi = 14.8$ Hz.

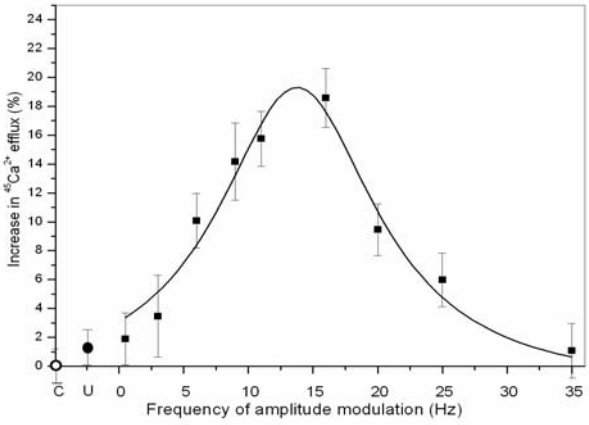

Fig.9.- The points (v) are the experimental $^{45}Ca^{2+}$ efflux increase from chicken brain under application of 147 MHz EMF carrier (intensity $0.8\,mW/cm^2$), *amplitude modulated* by a MF of frequency, f_M between 0.5-35 Hz and $B_0 \cong 30$ nT (15). The curve is the theoretical lorentzian, fitted according to the model eq.[8] (symbols C (o) and U (λ) respectively correspond to control and unmodulated EM wave experiments).

The quantitative explanation of such a FWE, although profusely mentioned and discussed since then (6), has remained unknown. Although those workers considered that the electric field of the ELF EMF was the responsible for the effect, it seems now clear that it is the MF the responsible one (16). This conclusion also stems from our experiments performed upon single neurones of *Helix aspersa*, submitted to an AC MF, of amplitude $B_0 = 0.1\mu$T-1 mT in the range of 0.1 - 80 Hz. We observed for $\approx$ 56% of the neurones studied a *decrease* in their bioelectric frequency, *f* with the increase of MF frequency, f_M ($\omega_M = 2\pi f_M$), and that the frequency dependence $\omega(\omega_M)$ follows a *lorentzian* function as well, i.e. there appears a FWE too. Moreover in other experiments at the fixed frequency of 50 Hz and with variable amplitude AC MF, we found a *decrease* of the bioelectric frequency with field, of the form [1] for also about 56% of the neurones studied (1, 11**).**

The *lorentzian* frequency, f_M dependence either of the calcium efflux to the extra-cellular fluid from chicken neurones, $\phi(\omega_M)$ or the bioelectric frequency dependence $f(f_M)$ in *Helix aspersa* neurones suggest a common origin for the time dependence of the mechanism involved in the Ca^{2+} ions detaching from their binding sites and their final sequestration or capture. This dependence merely is that the amount of Ca^{2+} ions

either freed to the external or to the cytosol sides from the membrane *must* vary in the form

$$N(t) = N(0)\exp(-t/\tau_{Ca}) \,, \qquad [9]$$

for an applied ELF MF starting at t = 0. This is so *because the Fourier transform of a lorentzian function is an exponentially time decaying function* (i.e. a relaxation mechanism), with relaxation time $\tau_{Ca} = 2/\Delta f$, as we have shown in Section 2. This is our main point in favour of a *resonance* effect for the FWE. The time τ_{Ca} is the one required for performing the process of Ca^{2+} liberation from membrane binders, mainly Ca^{2+} diffusion within the external or cytosol fluids and final Ca^{2+} sequestration either by a protein channel (or by other cytosol structures) or incoming to the radioactivity counter for the externally freed $^{45}Ca^{2+}$ ions. In their diffusion the Ca^{2+} ions traverse a RMS distance $\sqrt{\langle \ell^2 \rangle} \cong \sqrt{D\tau_{Ca}}$, the one for a random walk, where *D* is the diffusion coefficient of the ion in the fluid (17). Therefore we come up with $N(t)$ obeying a dynamic equation of relaxation $dN/dt = -N/\tau_{Ca}$, as we would expect for a two states system (freed Ca^{2+} and bonded Ca^{2+} to its sites) in thermodynamic equilibrium, with Ca^{2+} decay between the two states. For the Ca^{2+} ions freed to the extra-cellular fluid they will end up fully thermalized and dissolved in it, increasing its concentration ($^{45}Ca^{2+}$ efflux in Adey & Bawin's experiment). For the Ca^{2+} ions liberated to cytosol, they will diffuse and finally will have a certain probability of being captured by a K^+-protein channel through the calmodulin attractive electric field, $\mathbf{E}_{pK}$ (see Fig.1).

We can quantitatively express the above considerations by Fourier transforming the observed lorentzian function $L(\omega_M)$, which represents either the efflux $\phi(\omega_M)$ or the bioelectric frequency $\omega(\omega_M)$ dependencies, around the neurone spontaneous frequency, ω_0, i.e.

$$N(t) = \int_{-\infty}^{+\infty} L(\omega_M)\,\omega(B_{eff}=0)\exp(-\alpha B_{ef}^2)\exp(-i(\omega_M-\omega_0)t)\,d\omega_M = \qquad [10]$$

$$\omega(B_{eff}=0)\exp(-\alpha B_{eff}^2)\int_{-\infty}^{+\infty} \frac{2(\Delta\omega/2)}{(\omega_M-\omega_0)^2+(\Delta\omega/2)^2}\exp(-i(\omega_M-\omega_0)t)\,d\omega_M = \omega(B_{eff}=0)\exp(-\alpha B_{eff}^2)\exp(-t/\tau_{Ca}).$$

If we now call $N(0) = \omega(B_{eff}=0)\exp(-\alpha B_{eff}^2)$ to the initially (at t = 0) detached Ca^{2+} ion number within a burst, we end up with the Ca^{2+} relaxation [9] (note, in [10] $\omega(B_{eff}=0)$ is dimensionless). Since τ_{Ca} is related to $\Delta\omega/2$, which is experimentally accessible from the spectra $L(\omega_M)$, we can determine that time from experiment.

The central frequency ω_0 in [10] is assumed to be the spontaneous average bioelectric frequency, so that we obtain a *resonance* or maximum of calcium efflux when $\omega_M = \omega_0$. This resonance mechanism should not be confused with the unspecific stochastic resonance model one. This model is based also on a two-states system, but assuming a critical noise which is modulated by the AC driving agent and reaches a threshold value (18). A difficulty with this model is that the *physical* mechanism involved in the weak AC agent interaction with the system is neither specified nor quantified. Therefore it becomes of questionable application to the distribution of spontaneous bioelectric frequencies, $D(\omega_0)$ (density of frequencies) for the biological system (membrane), also *lorentzian* (setting $\omega_M = 0$ in [8] and [10]). In fact such a distribution has been clearly inferred from our experiments with *Helix* brain neurones, in the form of repetitive narrow bursts of higher frequency (Fig.10), localized in time when f_M is increased, and superposed to the main $f(f_M)$ lorentzian decrease below ω_0 (12).

f_M = 0 Hz f_M = 0.5 Hz f_M = 1 Hz

Fig.10.- Neuron D-5 spontaneous bursts of variable f.

In Fig.9 we show the excellent fit by [8] of the calcium efflux increase vs. f_M, and which means that our SD-CE and Ca^{2+} kinetics model gives a physical and quantitative explanation to the Adey & Bawin's FWE observation (15). According to our assumption chicken cerebral neurones average bioelectric frequency should be $f_0 \cong 14$ impulses/s, to some extent comparable with the mollusc neurones with $f_0 \approx 0.1-5$ impulses/s.

Similarly in Fig.11 we present, the bioelectric frequency *f* vs. f_M variation for *Helix aspersa* brain mapped neurones F1 and V14, under AC MF of B_0=1 mT. The fit of $f(f_M)$ by $L(\omega_M)$ is also rather good. Now, as above mentioned, the bioelectric activity is commanded by the AC MF Ca^{2+} ions internally detached towards the cytosol, which join the K^+-protein channels and open them, giving rise to the bioelectric impulse of K^+ ions sorting out. Therefore this mechanism should be also operative in the chicken brain bioelectric activity, and therefore both experiments reveal the Ca^{2+} simultaneous detaching from both surfaces of the membrane. Besides the determined Ca^{2+} relaxation times, τ_{Ca} are 135 ms (chicken brain) and between 93-365 ms for the studied neurones of *Helix aspersa*. An *ab-initio* calculation of the Ca^{2+} relaxation time, τ_{Ca} is difficult, if we consider the mentioned above kinetics involved. In fact a first principles calculation of the K^+ and Na^+ relaxation times in HH equations is still an open problem, relaxation times left as adjustable parameters as we did in section 2. However for τ_{Ca} if we estimate the mean diffusion length of Ca^{2+} in water, taking $D \approx 10^{-9}\ m^2 s^{-1}$, the typical diffusion coefficient for small molecules in water (18**)**, we obtain $\sqrt{\langle \ell^2 \rangle} \approx 30-60\ \mu m$, reasonable values for the studied neurones of average diameter $d \approx 100\ \mu m$ (1, 14).

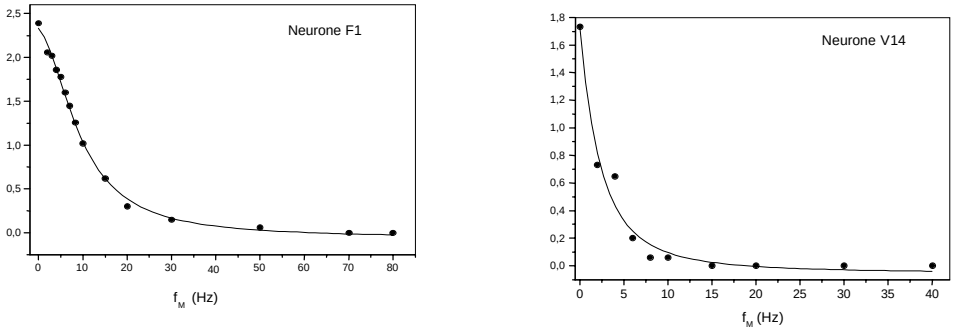

Fig.11.- Variation of bioelectric frequency, *f* with MF frequency, f_M. Experiment (λ); lines are lorentzian fits $L(f_M)$, with f_0=2.5, 2.0 Hz and $\Delta f/2$ = 9.9, 2.7 Hz for neurones F1 and V14 respectively.

A final check of the SD-CE model suitability is the obtaining of the clusters PP numbers, N_c in *Helix aspersa* neurones. This can be done by determining the parameter α from the slopes of the above $f(B_0)$ mentioned plots from time synchronized neurone pairs under f_M = 50 Hz MF field. (1,7). In Fig.12 are shown such a plots for the pair V13-V23 of the visceral ganglion. Taking $\chi_\perp \cong -0.56\times10^{-7}$, determined in erythrocyte membranes by combined SQUID magnetometry ($\Delta\chi$) and electrophysiological experiments (5,19**)**, $V \approx 5\times10^{-28}\ m^3$**,** T≅293K and α values, obtained from the slopes, we respectively obtain $N_c \approx 4$ and 1 x10^{12} PP in a cluster. Considering that the numbers of PP in such a membranes, of average diameters 120 and 103 μm respectively, are $N_{pp} \approx$ 2 and 1.5 x10^{11} (1, 7**),** that numbers throw about $c = N_c/N_{pp} \approx 42$ and 16 correlated neurones respectively, firing in *synchronized* way with the probe ones, i.e. forming "giant" PP clusters of linear extension ≈ 300 μm (the visceral ganglion has a diameter of about 600 μm and *Helix* brain has $\approx 2\times10^4$ neurones) (14). Therefore neurones form correlated small networks under ELF weak MF. In the case of the chicken brain we do not dispose of data about the calcium efflux dependence with the modulating MF amplitude B_0 and that calculation is not possible.

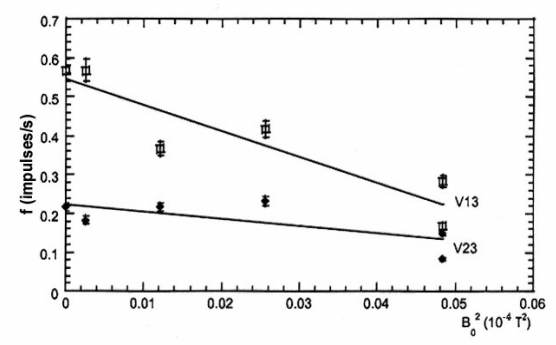

Fig.12.- Plots of the bioelectric frequency, *f* vs. B_{eff}^2 (f_M = 50 Hz) for *Helix aspersa* neurone pair V23-V13 (14), showing *synchronization* under MF. From line slopes is determined the α parameter.

5.- Conclusions.-

We have integrated, by the first time to our knowledge, the Hodgkin & Huxley (HH) equation for the biolectric impulse, by considering the membrane as a Kirchoff *electric knot*. Integration has been performed

under applied AC MF, by partitioning the bioelectric impulse in its depolarization (D) and repolarization (R) plus hyperpolarization (H) regimes. For the spontaneous regimes we have obtained the time variations of the D and R+H voltages, in reasonable agreement with our experiments on single unit neurones of mollusc *Helix aspersa*. The HH characteristic functions n(t) and m(t) (excitatory) and h(t) (inhibitory) have been treated within the relaxation time,τ approximation, from the comparison with the bioelectric impulse obtaining τ_{Na} and τ_K, as well as the initial values of those functions. The calculated frequency spectrum of the impulse is *lorentzian*, in good agreement with experimental one, from the HMHW also determining τ_{Na} and τ_K. The cytosol Ca^{2+} ion current, produced by the SD and CE under AC MF has been calculated, although experimentally the *single* impulse is *not* modified by weak applied MF to *Helix aspersa* neurones. This means that MF produced extra-voltage, $V_{Ca}(t)$ is negligible, its numerical calculation value being deferred for further work.

On the other hand, we have shown that the hallmark Adey & Bawin's *frequency window effect* is a consequence of the phospholipids superdiamagnetism and Ca^{2+} coulomb explosion in the outer surface of the neurones, and that the effect is a *resonance* of *lorentzian* shape, when the MF frequency matches the neurone spontaneous frequency. In *Helix aspersa* single neurones, same mechanism is operating but now due to the Ca^{2+} liberation from the inner membrane surface towards the cytosol, so operating the K^+ channels. In both situations the *lorentzian* spectrum is a consequence of the exponentially decaying relaxation followed by the Ca^{2+} current, freed by the MF to the extra-cellular or cytosol fluids, ions suffering *diffusion* before capture. This diffusion mainly determines the lorentzian spectrum vs. applied MF frequency f_M.

Acknowledgements.

We acknowledge financial support of Fundación Humanismo y Ciencia (Madrid) and of Diputación General de Aragón (Zaragoza) under project B-43.

References

(1) Azanza M.J., Calvo A.C. and del Moral A. Evidence of synchronization of neurones activity of molluscan brain ganglia induced by alternating 50 Hz applied magnetic field. Electro-Magnetobiology. 21: 221-232, 2002.
(2) Azanza M.J., and del Moral A. Isolated neuron amplitude spike decrease under static magnetic fields. J. Magn. Magn. Mat. 157-158: 593-594, 1996.
(3) Hodgkin A. I. and Huxley A.F. A quantitative description of membrane current and its application to conduction and excitation in nerve. J.Physiol. 117: 500-544, 1952.
(4) Kandel E.R., Schwartz J.H. and Jessell T.M. *Principles of neural science*. McGraw Hill, New York, 2000.
(5) del Moral A., and Azanza M.J. Model for the effect of static magnetic field on neurons. J. Magn. Magn. Mat.114: 240-242, 1992.
(6) Azanza M.J., and del Moral A. Cell membrane biochemistry and neurobiological approach to biomagnetism. Prog. Neurobiol. 44: 517-601, 1994.
(7) Azanza M.J., Pérez-Bruzón R.N., Calvo A.C. and del Moral A. Elemental neuron network dynamics under applied sinusoidal magnetic fields. Bioelectromagnetics. 2005 Congress, pp. 312-314, Dublín, 2005.
(8) Azanza M.J., Pes N., Raso M., Pérez-Bruzón R.N., Junquera C., Pérez-Castejón C., Maestú C., Aisa J., Lahoz M., Martinez-Ciriano C., Vera-Gil A. and del Moral A. Characterization of connexins in *Helix aspersa* suboesophageal brain ganglia neurons and glia cells by immunocitochemistry, Histol. Histopathol., 2006, (in press).
(9) Babu Y.S., Sack J.S., Greenough T.J., Bugg C.E., Means A.R. and Cook W.J. Three-dimensional structure of calmodulin. Nature. 315: 37-40, 1985.
(10) Azanza M.J., and del Moral A. ELF-magnetic field induced effects on the bioelectric activity of single neurone cells. J. Magn. Magn. Mat. 177-181: 1451-1452, 1998.
(11) Azanza M.J. and del Moral, A. ELF-magnetic field induced effects on the bioelectric activity of single neuron cells. J. Magn. Magn. Mat. 177-181: 1451-1452, 1998.
(12) del Moral A., Pérez-Bruzón R.N. and Azanza M.J., to be published.
(13) Pérez-Castejón C., Junquera C., Pueyo A., Pérez-Bruzón R.N., Azanza M.J., Raso M., Pes N., Maestu C., Aisa J., Lahoz M., Martínez-Ciriano C., Vera-Gil A., and del Moral A. Charaterization of neuron membrane ionic protein channels involved in the responses to applied ELF-Magnetic fields observed in *Helix aspersa* brain ganglia neurons. Histol. Histopathol. Suppl.1: S134, 2005.
(14) Kerkut G.A., Lambert J.D.C., Gayton R., Loker J.E. and Walker R.J. Mapping of nerve cells in the ganglia of *Helix aspersa* neurons. Comp. Biochem. Physiol. 50A: 1-25, 1975.
(15) Bawin S.M., Sheppard A. and Adey W.R., Bioeletrochem. Bioenergetics. 5: 67, 1978.
(16) Pérez-Bruzón R.N., Azanza M.J and del Moral A. J. Magn. Magn. Mat. 272-276: 2424, 2004.
(17) See e.g. Nelson P., *Biological Physics, Energy, Information, Life*, Freeman, New York, 2004.
(18) See e.g. Wellens T., Shatokhin V. and Buchleitner A. Stochastic resonance. Rep. Prog. Phys. 67: 45, 2004.
(19) Azanza M.J., Blott B.H., del Moral A. and Peg M.T., Bioelectrochem. Bioenergetics. 30: 45,1993.

EFFECTS OF EXTREMELY LOW FREQUENCY ELECTROMAGNETIC FIELDS ON MEMBRANE-BOUND ENZYMES. AN OVERVIEW.

I.M.PEPE, S. RAVERA, D. CALZIA, I. PANFOLI, C. CUGNOLI and A. MORELLI

DEPARTMENT OF BIOLOGY, UNIVERSITY OF GENOA, VIALE BENEDETTO XV, 3 GENOVA, 16131 ITALY, e-mail: mario.pepe@unige.it.

Abstract

In order to give an interpretation at molecular level of the macroscopic effects produced by ELF-EMFs on biological systems, the activities of different enzymes were studied under exposure to electromagnetic fields of 75 Hz. The activities of cytosolic enzymes as well as those of integral or periferal membrane enzymes were not affected by the field exposure. Only the activities of some lipid-linked enzymes decreased approximately of about 54 % to 61 % with field amplitudes above different thresholds (from 0.66 to 1.35 mTesla). The decrease in enzymatic activity of the field-sensitive enzymes was independent of the time of permanence in the field and was completely reversible. When these enzymes were solubilized with Triton, no effect of the field was obtained on the enzymatic activity, suggesting the crucial role of the membrane, as well as the linkage to it, in determining the conditions for enzyme inactivation.

INTRODUCTION

The interactions between electromagnetic fields of extremely low frequency (ELF-EMFs) and biological systems have been widely investigated [Walleczek, 1995; Kaiser, 1996; Eremenko et al., 1997; Berg, 1999; Ivancsits et al., 2002;Volpe, 2003]. The problem concerning the mechanisms which can determine biological effects is not yet solved [Lawrence and Adey, 1982; Glaser, 1992; Basset, 1993; Barnes, 1996; Lacy -Hulbert et al., 1998; McCann et al.,1998; Weaver, 2002]. The related phenomena are still not clear, but their existence is certain at least in many specific cases. However, a generally accepted interaction model able to explain these phenomena is lacking. A contribution in this direction could be that of an interpretation at molecular level of the macroscopic effects produced by ELF- EMFs. Therefore, our attention was focused on the enzymatic activity which are known to be underlying many biological processes. The hypothesis that ELF EMFs could affect enzymes activities was tested on a number of soluble enzymes as well as on membrane-associated enzymes. Among cytosolic enzymes hexokinase, pyruvate kinase**,** glucose 6 phosphate dehydrogenase and adenylate kinase were chosen. The membrane-associated enzymes were: integral membrane proteins such as CaATPase, Na/K,ATPase, succinic dehydrogenase; periferal membrane proteins such as photoreceptor phosphodiesterase 6 (PDE); lipid-linked proteins such as alkaline phosphatase and acetylcholinesterase. Membrane-bound phosphoglycerate kinase was also assayed.

When exposed to ELF-EMFs of 75 Hz , the activities of soluble enzymes were not affected by the field, whilst those of four enzymes out of eight bound to membrane were lowered dramatically of about 54% to 61%. Moreover, the effects of the applied field on these enzymes vanished when they were mildly solubilized by Triton, suggesting that the membranes could have an important role for mediating the effect of the field on the enzymatic activity. In fact, interesting results involving biological membranes exposed to ELF electromagnetic fields has been already reported [Miller, 1991; Paradisi et al., 1993; Astumian et al., 1995; Baureus-Koch et al., 2003;]. In particular, measurements by fluorescent probes showed changes in lipid molecular dynamics of the cell membrane [Volpe et al., 1998], while electron microscope images of freeze-fractured membranes exposed to the field indicated a significant clustering of the distribution of the intramembrane proteins [Bersani et al., 1997]. The applied field could modify the membrane organization and structure by acting directly on the strong anisotropy of diamagnetic susceptibility of membrane phospholipids [Del Moral et al., 2002]. An interesting result on the effects of ELF EMFs on carbonic anhydrase entrapped in liposomes seems to exclude the role of the enzyme molecule in favour of the direct action of the field on charged lipids of the membrane [Ramundo-Orlando et al., 2000].

METHODS

Electromagnetic field production. EMFs were produced by an equipment (Biostim Igea, Modena, Italy) mainly used for clinical application and already described [De Mattei et al., 2003; Ravera et al., 2004]. The generator system supplies a square wave with a maximal applied tension of 180 V, a period of 13.3 ms (75 Hz of frequency), a duty cycle of 10%, to a couple of identical coils aligned on a central axis. Each coil, made up of 1000 turns of copper wire of 0.2 mm of diameter, had internal and external diameter of 72.5 mm and 82.5 mm respectively. As the current supplied by the equipment to the coils was not adjustable, different amplitudes of magnetic field were obtained by separating the two coils with different distances. Measurements of the magnetic field B maximal intensity with a gaussmeter showed that it was fairly constant midway between the coils, giving values of about 2.20 ± 0.08 mT when the distance between the coils was 12 cm and about 0.45 ± 0.02 mT at 29.6 cm distance. An error of 0.5 cm in determining the distance between the coils gave an error of 4% in the field measurements. The values of the field near the threshold (see Fig 1) were determined more accurately (sd of 1 % , n=10). Time course of the magnetic field as well as that of the induced electric field were measured as already described [De Mattei et al., 2003; Ravera et al., 2004], at the center of the distance between the two coils where the samples were always placed. Temperature variations of the order of magnitude of experimental error (± 0.1 ° C) were measured with a termocouple inside the sample in the presence of the applied field.

Enzymatic activities measurements.

Hexokinase activity assay. Hexokinase activity was measured in the presence or in the absence of the field for 1 min after glucose addition (200 mM final concentration) to the reaction mixture containing the purified enzyme. The reaction mixture contained 100 mM Tris–HCl pH 8, 8 mM $MgCl_2$, 1 mM ATP and 2 µl of Hexokinase (Cat n° 11 426 362 001, Roche), in final volume of 1 ml. Before and after 1 min of incubation 100 µl of the reaction mixture were withdrawn and added to 50 µl of 25% PCA. Each sample was centrifuged shortly at 14,000 rpm and then 100 µl of supernatant was withdrawn and neutralized with 50 µl K_2CO_3. The centrifugation was repeated to remove potassium perchlorate. Aliquots of 100 µl of each neutralized extract were used to assay Glucose-6-phosphate, monitoring NADPH formation by spectrophotometer (340 nm), according to Bergmeyer et al.[1983].

Pyruvate Kinase activity assa.y Pyruvate Kinase activity was measured in the presence or in the absence of the field for 1 min after phosphoenol-pyruvate (PEP) addition (0.6 mM final concentration) to the reaction mixture containing the purified enzyme. The reaction mixture contained 100 mM Tris–HCl pH 8, 8 mM $MgCl_2$, 5 mM ADP and 0.5 µl of Pyruvate Kinase (Cat n° P-1506, Sigma), in final volume of 1 ml. Before and after 1 min of incubation 100 µl of the reaction mixture were withdrawn and added to 50µl of 25% PCA. Each sample was centrifuged shortly at 14,000 rpm and then 100 µl of supernatant was withdrawn and neutralized with 50 µl K_2CO_3. The centrifugation was repeated to remove potassium perchlorate. Aliquots of 100 µl of each neutralized extract were used to assay Pyruvate, monitoring NAD^+ formation as already described [Bergmeyer et al., 1983].

Glucose 6 phosphate dehydrogenase (G6PD) activity assay. Glucose 6 phosphate dehydrogenase activity was measured in the presence or in the absence of the field for 1 min after glucose-6-phosphate addition (10 mM final concentration) to the reaction mixture containing the purified enzyme. The reaction mixture contained 100 mM Tris–HCl pH 8, 8 mM $MgCl_2$, 0.5 mM NADP and 0.25 µl of Glucose-6- phosphate dehydrogenase (Cat n° G-5760, Sigma), in final volume of 1 ml. Before and after 1 min of incubation 100 µl of the reaction mixture were withdrawn and added to 50 µl of pure Aceton. Each sample was centrifuged shortly at 14,000 rpm and then 100 µl of supernatant was withdrawn, added to 900 µl of water and immediately assayed to spectrophotometer (340 nm), to observe the NADPH formation.

All the other enzymatic activities presented in Table 1 were measured following the methods described in the Appendix

Protein concentration

Protein concentrations were determined using the Bradford method [1976].

RESULTS AND DISCUSSION

In order to measure the direct effects of ELF - EMFs on enzymatic activities, the enzymes were studied in purified state when available or in rough extracts from cell-free homogenates. Different length of exposure to the fields lasted from 1 min to 60 min. The effects on enzymatic activities were detectable only during the field exposure. No effects were measured immediately after the withdrawal of the field, suggesting a perfect

reversibility of the mechanism. Table 1 shows the activities of different enzymes exposed to ELF - EMFs of 75 Hz frequency and 3.0 mT magnetic field amplitude for 20 min. The activities of the cytosolic enzymes, that is: hexokinase, pyruvate kinase**,** glucose 6 phosphate dehydrogenase and adenylate kinase were not affected by the field exposure with a statistical significance of $P < 0.001$. Among membrane-associated enzymes instead: alkaline phosphatase, acetylcholinesterase from ghosts or from synaptosomes, phosphoglycerate kinase and membranous adenylate kinase, decreased their activities of about 54%, 60%, 58% 61% and 54% respectively, while either integral membrane enzymes such as CaATPase, Na/K,ATPase and succinic dehydrogenase, or periferal membrane enzymes such as photoreceptor PDE were insensitive to the applied field.

Table 1. Activities of different enzymes upon 20 min exposure to a field of 75 Hz and 3.0 mT.

Enzyme	Control sample	Sample + field
Hexokinase	47 ± 2 U/mg	47 ± 2 U/mg
Pyruvate Kinase	175 ± 10 U/mg	177 ± 10 U/mg
Glucose 6 phosphate dehydrogenase	75 ± 7 U/mg	73 ± 6 U/mg
Cytosolic adenylate kinase	385 ± 33 U/mg	390 ± 30 U/mg
Alkaline phosphatase	61 ± 2 U/mg	28 ± 1 U/mg
Acetylcholinesterase from ghosts	3.5 ± 0.1 U/mg	1.4 ± 0.1 U/mg
Acetylcholinesterase from synaptosomes	13.7 ± 0.2 U/mg	5.8 ± 0.1 U/mg
Phosphoglycerate kinase	0.465 ± 0.005 U/mg	0.18 ± 0.01 U/mg
membrane Adenylate kinase	177 ± 10 U/mg	81 ± 5 U/mg
CaATPase	21 ± 1 U/mg	20 ± 1 U/mg
Na/K,ATPase	78 ± 5 U/mg	80 ± 5 U/mg
Succinic dehydrogenase	100 ± 5 U/mg	101 ± 5 U/mg
rod outer segment PDE	50 ± 5 U/nmol of Rhodopsin	48 ± 5 U/nmol of Rhodopsin
Alkaline phosphatase in 0.1% Triton	58 ± 2 U/mg	56 ± 2 U/mg
Acetylcholinesterase from ghosts in 0.1% Triton	3.3 ± 0.2 U/mg	3.0 ± 0.2 U/mg
Acetylcholinesterase from synaptosomes in 0.1% Triton	15.1 ± 0.2 U/mg	14.5 ± 0.2 U/mg
Phosphoglycerate kinase in 0.1% Triton	0.43 ± 0.01 U/mg	0.43 ± 0.01 U/mg
membrane Adenylate kinase in 0.1% Triton	175 ± 10 U/mg	180 ± 10 U/mg

Each value represents the mean ± SD of five measurements. The enzymatic activity is expressed as Units/mg (nmoles of substrate transformed /min/ mg protein). The activity of each enzyme was measured for 1 min before the withdrawal of the field. The solubilization with Triton in itself did not affect the activity of alkaline phosphatase or acetylcholinesterase from blood cells but decreased of about 7.5 % the activity of phosphoglycerate kinase while enhanced of about 10% the activity of acetylcholinesterase from synaptosomes. Such activity differences are usually observed when membrane bound enzymes are solubilized in low concentration of a mild detergent [Helenius and Simons, 1975].

The activities of the field-sensitive enzymes were measured in function of the concentration of their substrates and the resulting Michaelis-Menten kinetics showed a behaviour of a pure noncompetitive inhibition where only V_{max} was affected by a field exposure. The Lineweaver-Burk plot of the data obtained for acetylcholinesterase from blood cell ghosts showed that K_M remained constant whereas V_{max} dropped of about 60% when exposed to the field.

The decrease of the enzymatic activities shown in Table 1 of the four enzymes was independent of the time of permanence in the field and appeared constant within the experimental errors under exposure lengths of 1 min to 60 min. In other words, the same decrease in the enzymatic activity was measured independently of the

exposure time, indicating that the effect of the field starts within the first min exposure and remains constant during all the the field permanence. The action of the field seems that to switch the enzyme to a state of a reduced activity which is immediately restored when the enzyme is removed from the field.

The decrease of the enzymatic activities was studied at different amplitudes of the applied field. Fig 1 shows that field amplitude of about 1.35 ± 0.05 mT or 0.80 ± 0.03 mT were the lowest value which produced a supra-threshold response respectively for alkaline phosphatase and acetylcholinesterase from blood cells. At field amplitudes under the thresholds the enzymatic activities were statistically indistinguishable from those of the controls. Similar data were found for the other two field-sensitive enzymes and the corresponding suprathreshold field values were 0.66 ± 0.02 mT or 0.85 ± 0.03 mT for phosphoglycerate kinase or acetylcholinesterase from synaptosomes respectively. The effect of the field on enzymatic activities seems independent of its amplitude above the threshold up to 2.2 mT as well as for the amplitude of 3.0 mT reported in Table 1.

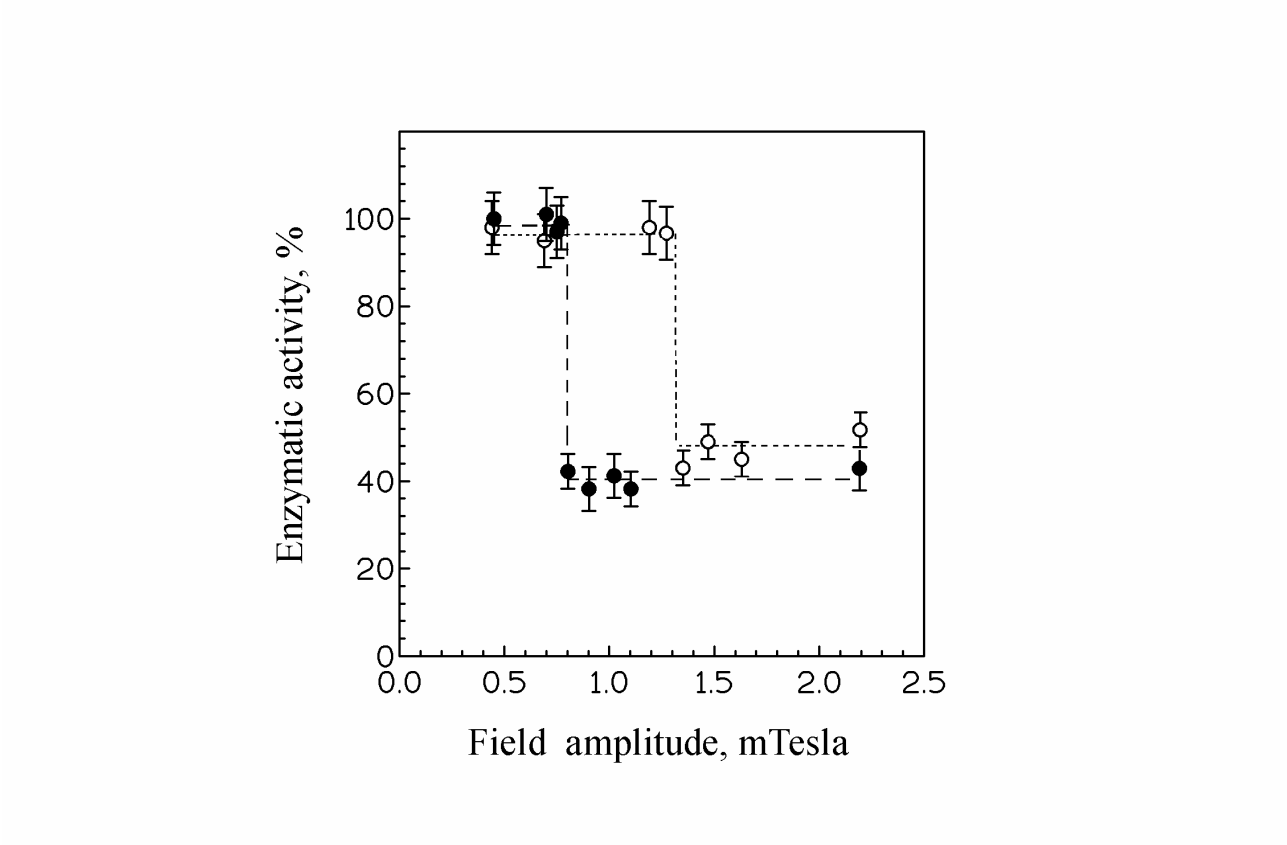

Fig 1. Enzymatic activity of alkaline phosphatase (○) or acetylcholinesterase from ghosts (●) measured during 10 min exposure to 75 Hz magnetic field of different amplitudes. Each value represents the mean ± SD of five measurements.

When the same experiments were run on the field-sensitive enzymes solubilized by 0.1 % Triton, the results showed that the activities of the solubilized enzymes were not affected by the field (see the last five lines of Table 1) with a statistical significance of $P < 0.001$.

Changing of enzymatic activities due to exposure to ELF-EMFs have already been reported by different workers. However, the differences in the observed effects could be due to the wide variety of the experimental conditions used by the various authors. The choice of field frequency is crucial as the quantistic interaction of the electromagnetic wave with molecules can only operate through frequency windows. However, fields of 60 Hz frequency, close to 75 Hz used in our experiments, caused opposite and small effects on soluble enzymes [Zhang and Berg, 1992; Litovitz et al., 1991; Thumm et al., 1999; Harada et al., 2001]. Many reported changes of enzymatic activities in whole cells and tissues suggest that ELF-EMFs may stimulate a general response to electromagnetic stress. In the case of ornithine decarboxylase for instance, the enzymatic activity was enhanced approximately 1.5 to 4-fold when exposed to ELF- EMFs [Mullins et al., 1999]. However, in this case the experiments were run on entire fibroblasts cells and the exposure to 60 Hz field for 4 hours presumably did not affect the enzyme activity directely. The activity of another soluble enzyme such as enolase was found

decreased by 28% in *Escherichia coli* colture exposed for 30 min to a field of 60 Hz [Dutta et al., 1994]., In this case however, the enzymatic activity was assayed in cell extracts, after the withdrawl of the field, and its decrease maybe be due to stress effects induced by the field and not to a direct interaction of the field with the enzyme molecule.

Among integral membrane protein, Na/K,ATPase and cytochrome oxidase were found to increase its enzymatic activity by approximately 30 % and 40% respectively in experimental conditions similar to those described in this paper, under exposure to a pulsed magnetic field of 60 Hz with an amplitude of only 10 μT [Blank and Soo, 2001]. The frequency window for Na/K,ATPase was very sharp with a maximal change at 60 Hz while at 100 Hz the change in enzymatic activity was only 10%.

The results shown in Table 1 strongly suggest that the field action is mediated by the membrane organization and structure which is crucial in determining the conditions of the enzyme inactivation. However, the effect of the field on the membrane is not sufficient alone to explain the decrease in enzymatic activity: in the case of acetylcholinesterase, it was independent of the source of the membrane, as the activity decrease for the enzyme coming from blood cells (60 % ± 4%) was not statistically different from that prepared from synaptosomes (58 % ± 5 %).On the other hand, integral membrane enzymes such as Ca,ATPase and Na/K,ATPase or periferal membrane enzymes such as PDE were not affected by the field suggesting the importance of the linkage to the membrane. Alkaline phosphatase, acetylcholinesterase from blood cell or from synaptosomes and adenylate kinase from rod disk membranes are lipid-linked membrane enzymes: alkaline phosphatase as well as acetylcholinesterase are known to be anchored to the membrane through a glycosylphosphatidylinositol while adenylate kinase is presumably bound to rod disk membranes through a myristic fatty acid [Notari et al., 2003]. Instead, the kind of attachment to red blood cell membranes of the field-sensitive enzyme phosphoglycerate kinase is not yet known, although a covalent linkage to hydrophobic group such as myristylate has been suggested [Concepcion et al., 2001]. In a recent report [Caseli et al., 2005], the enzymatic activity of alkaline phosphatase incorporated into artificial phospholipid monolayers dropped of about 40 % following a lipid phase transition from liquid expanded to liquid condensed state, when surface pressure increased above 18 mN/m. Fluorescence microscopy revealed that above this pressure, proteins aggregated and formed clusters which would affect the substrate accessibility to the catalytic site and therefore decrease the enzymatic activity. It has also been reported that a pulsed field of 50 Hz is able to induce a decrease in lipid molecular dynamics of cell membranes [Volpe et al., 1998] and significant clustering of the distribution of the membrane proteins [Bersani et al., 1997]. Therefore, we can speculate that the field of 75 Hz would be able to induce a transition of the lipid bilayer to a more liquid ordered phase, as suggested by the sharp threshold behaviour shown in Fig 1, followed by the partition of the lipid-anchored enzymes in clusters with a subsequent activity decrease.

However, the results presented in this paper are important for the interpretation at molecular level of macroscopic effects produced by ELF- EMFs on biological systems. An example could be that of the clinical application of weak EMFs of 75 Hz frequency currently used to accelerate the healing of bone fractures. The molecular mechanisms underlying these empirical observations could originate from alkaline phosphatase inhibition by the pulsed field. As a matter of fact, alkaline phosphatase is commonly used as an osteoblast differentiation marker, although its role in bone formation is still controversial as it could be involved in the process of bone mineralization or in the organic matrix synthesis as well. However, a decrease in its activity was found in concomitance with an increase of the number of human bone cells in culture following dynamic strain [Kaspar et al., 2000].

Another example of field effect which needs a molecular interpretation comes from several studies that indicate that ELF-EMFs affect cell division timing and embryos development of many organisms [Delgado et al., 1982; Dixey and Rein, 1982; Koch et al., 1993]. In particular, the effects of low-intensity electromagnetic fields on the early development of the sea urchin *Paracentrotus lividus.* [Falugi et al., 1987] could be interpreted as due to acetylcholinesterase inhibition. A recent report on exposure of fertilized eggs of the sea urchin *Paracentrotus lividus* to an electromagnetic field of 75 Hz frequency, shows a dramatic loss of synchronization of the first cell cycle, with formation of anomalous embryos linked to irregular separation of chromatides during the mitotic events [Ravera et al., 2006.]. As acetylcholinesterase is thought to regulate the embryonic first developmental events of the sea urchin [Shmukler et al., 1998], its enzymatic activity was assayed in embryo homogenates and found it decreased by 48% when exposed to the same pulsed field. This enzymatic inactivation had a threshold of about 0.75 mTesla, the same field threshold found for the effect on the formation of anomalous embryos. The conclusion is that one of the main causes of the dramatic effects on the early development of the sea urchin by field exposure could be the accumulation of acetylcholine due to acetylcholinesterase inactivation. Moreover, the effects of accumulation of acetylcholine last presumably even after the removal of the field and the consequent reversible restoration of acetylcholinesterase activity. In other words, even though the effects of ELF-EMFs are likely transient, the consequences of the exposure may not be overlooked as they can be irreversible.

On the other hand, some field bioeffect could be positive. It was reported that cholinesterase inhibitors, such as methanesulfonyl fluoride, improve cognitive performance in patients with senile dementia of the Alzheimer type [Moss et al.,1999]. In this case, ELF-EMFs may be of some help for treatment of the desease as a mild tool without farmacological side effects.

Summary

The hypothesis that ELF EMFs could affect directly enzymes activities was tested on a number of soluble enzymes as well as on membrane-associated enzymes. Among cytosolic enzymes, hexokinase, pyruvate kinase**,** glucose 6 phosphate dehydrogenase and adenylate kinase were chosen; among integral membrane protein: CaATPase, Na/K,ATPase, succinic dehydrogenase; among periferal membrane proteins: photoreceptor phosphodiesterase 6 (PDE); among lipid-linked proteins: alkaline phosphatase, acetylcholinesterase and membranous adenylate kinase. Membrane-bound phosphoglycerate kinase was also assayed. When exposed to ELF-EMFs of 75 Hz , the activities of soluble enzymes as well as those of integral or periferal membrane enzymes were not affected by the field, whilst those of lipid-linked enzymes were lowered dramatically of about 54% to 61%. Moreover, the effects of the applied field on these enzymes vanished when they were mildly solubilized by Triton, suggesting that the membranes, as well as the protein linkage to them, could have an important role in mediating the effect of the field on the enzymatic activity.

REFERENCES

Astumian, R.D. Weaver, J.C. Adair,R.K. 1995 Rectification and signal averaging of weak electric fields by biological cells. *Proc.Natl.Acad.Sci.U.S.A.* 92(9): 3740-3743.

Barnes, F. S. 1996. Effect of electromagnetic fields on the rate of chemical reactions. *Biophysics*. 41: 801-808.

Basset, C. A. 1993. Beneficial effects of electromagnetic fields. *J. Cell. Biochem.* 51: 387-393.

Baureus-Koch,C.L. Sommarin,M. Persson,B.R. Salford,L.G. and Eberhardt,J.L. 2003 Interaction between weak low frequency magnetic fields and cell membranes. *Bioelectromagnetics.* 24(6): 395-402.

Berg, H. 1999. Problems of weak electromagnetic field effects in cell biology. *Bioelectrochem. Bioenerg*. 48: 355-360.

Bergmeyer H.U. Grassl M. Walter H-E, 1983, Enzymes, in: H.U. Bergmeyer (Ed.), Methods of enzymatic analysis vol 2, Verlag Chemie, Weinheim, pp. 126-281.

Bersani, F., Marinelli ,F., Ognibene, A., Matteucci, A., Cecchi,S., Squarzoni, F., and Maraldi, N.M. 1997. Intramembrane protein distribution in cell cultures is affected by 50 hz pulsed magnetic fields. *Bioelectromagnetics* 18: 463-469.

Blank, M. Soo, L. 2001. Optimal frequencies for magnetic acceleration of cytochrome oxidase and Na,K-ATPase reactions. *Bioelectrochemistry* 53: 171-174.

Bonner W. 1955. Succinic dehydrogenase, assay method. *Meth. Enzymol*. 1: 722-729.

Bradford M. 1976. A quantitative, semiquantitative and qualitative assay of protein, *Anal. Biochem.* 72: 248-256.

Caseli, L., Oliveira R. G., Masui D. C., M.Furriel R. P., Leone F. A., Maggio B., and Zaniquelli M.E.D. 2005, Effect of Molecular Surface Packing on the Enzymatic Activity Modulation of an Anchored Protein on Phospholipid Langmuir Monolayers. *Langmuir* 21:4090-4095.

Concepcion J. L., Adje´ C. A. Quinones W., Chevalier N., Dubourdieu M. and Michels P.A.M. 2001. The expression and intracellular distribution of phosphoglycerate kinase isoenzymes in *Trypanosoma cruzi. Molecular & Biochemical Parasitology* 118: 111–121.

Delgado, J. M. R., Leal, J., Monteagudo, J.L., Gracia, M.G.J. 1982, Embriological changes induced by weak extremely low frequency electromagnetic field. *J. Anat.* 134: 533-551.

Del Moral, A., Azanza, M. J., Calvo A. C., and Perez-Bruzon, R. N. 2002. Responses to applied static and extremely low frequency magnetic fields. *In* Biological Effects of EMFs. P. Kostarakis, editor. Demokritos Publishers, Rhodes. vol. 1, 298-308.

Dixey, R. and Rein, G. H. 1982, Noradrenaline Release Potentiated in a Clonal Nerve Cell Line by Low-Intensisty Pulsed Magnetic Fields. *Nature* 296: 253-255.

De Mattei M, Pasello M, Pellati A, Stabellini G, Massari L, Gemmati D and Caruso A. 2003. Effects of electromagnetic fields on proteoglycan metabolism of bovine articular cartilage explants. *Connective Tissue Research*. 44(3-4):154-159.

Dutta; S.K., Verma, M.; Blackman, C.F. 1994. Frequency-dependent alterations in enolase activity in Escherichia coli caused by exposure to electric and magnetic fields. *Bioelectromagnetics.* 15: 377-83.

Eremenko T., C. Esposito, A. Pasquarelli, E. Pasquali and P. Volpe. 1997. Cell-cycle kinetics of Friend erythroleukemia cells in a magnetically shielded room and in a low-frequency/low-intensity magnetic field. *Bioelectromagnetics.* 18: 58-66.

Falugi, C., Grattarola, M., Prestipino, G. 1987 Effects of low-intensity pulsed electromagnetic fields on the early development of *Paracentrotus lividus*. *Biophys. J.* 51: 999-1003.

Glaser, R. 1992. Current concepts of the interaction of weak electromagnetic fields with cells. *Bioelectrochem. Bioenerg.* 27: 255-268.

Harada S., Yamada S., Kuramata O., Gunji Y. Kawasaki M., Miyakawa T., Yonekura H., Sakurai S., Bessho K., Hosono R., Yamamoto H. 2001. Effects of high ELF magnetic fields on enzyme-catalyzed DNA and RNA synthesis in vitro and on a cell-free DNA mismatch repair. *Bioelectromagnetics* 22(4): 260-266.

Helenius, A., Simons K. 1975. Solubilization of membranes by detergents, *Biochim. Biophys. Acta* 415: 29-79.).

Ivancsits, S., Diem, E., Pilger, A., Rudiger, H., and Jahan, O. 2002. Induction of DNA strand breaks by intermittent exposure to extremely-low-frequency electromagnetic fields in human diploid fibroblasts. *Mutation Res*. 519: 1-13.

Kaiser, F. 1996. External signals and oscillation dynamics: biophysical aspects and modelling approaches for interactions of weak electromagnetic fields at the cellular level. *Bioelectrochem. Bioenerg*. 41: 3-18.

Kaspar D, Seidl W, Neidlinger-Wilke C and Claes L. 2000. In vitro effects of dynamic strain on the proliferative and metabolic activity of human osteoblasts. *J. Musculoskelet. Neuronal. Interact*. 1: 161-164.

Koch, W.E.,Koch, B.A., Martin, A.H. and Moses, G.C. 1993, Examination of development of cicken embryos following exposure to magnetic fields. *Comp. Biochem. Physiol., Comp. Physiol.* 105: 617-624.

Lacy-Hulbert, A., Metcalfe, J. C., and Hesket, R. 1998. Biological responses to electromagnetic fields. *FASEB J.* 12: 395-420

Lawrence, A. F., and Adey, W. R. 1982. Non linear wave mechanisms in interactions between excitable tissue and electromagnetic fields. *Neurol. Res.* 4: 115-53.

Litovitz, T.A., Krause, D.J., and Mullins, J.M. 1991. Effect of coherence time of the applied magnetic field on the enhancement of ornithine decarboxylase activity. *Biochem. Biophys. Res. Commun.* 178: 862–865)

Martin J.B. and Doty D.M. 1949, Determination of inorganic phosphate; modification of isobutyl alcohol procedure, *Anal. Chem.* 21: 965–967.

McCann, J., Dietrich, F., and Rafferty, C. 1998. The genotoxic potential of electric and magnetic fields: an update. *Mutation Res*. 411: 45-86.

Miller, D. L. 1991, Electric fields induced in chicken eggs by 60-Hz magnetic fields and the dosimetric importance of biological membranes. *Bioelectromagnetics.* 12(6): 349-360.

Moss D.E., Berlanga P.,. Hagan M.M, Sandoval H. and Ishida C. 1999, Methanesulfonyl fluoride: a double-blind, placebo-controlled study of safety and efficacy in the treatment of senile dementia of the Alzheimer type, *Alzheimer Dis. Assoc. Disord.* 1**3**: 20–25.

Mullins, J.M. Penafiel, L.M. Juutilainen, J. Litovitz, T.A. 1999 Dose-response of electromagnetic field-enhanced ornithine decarboxylase activity. *Biochemistry and Bioenergetics* 48(1): 193-199.

Notari L., Morelli A. and Pepe I.M. 2003. Studies on adenylate kinase isoform bound to disk membranes of rod outer segment of bovine retina. *Photochem. Photobiol. Sci*.2: 1299-1302.

Paradisi, S., Donelli, G., Santini, M. T., Straface E., and Marloni, W. 1993. A 50 Hz magnetic field induces structural and biophysical changes in membranes. *Bioelectromagnetics.* 14: 247-255.

Pontremoli S., Salamino F., Sparatore B., Melloni E., Morelli A., Benatti U., De Flora A. 1979, Isolation and partial characterization of three acidic proteinases in erythrocyte membranes, *Biochem. J.* 181: 559-568.

Ramundo-Orlando, A., Morbiducci, U., Mossa, G., D'Inzeo, G. 2000, Effects of low frequency, low amplitude magnetic fields on the permeability of cationic liposomes entrapping carbonic anhydrase *Bioelectromagnetics*, 21: 491-498.

Ravera S. Repaci E. Morelli A. Pepe I.M. Botter R. and Beruto D. 2004. Effects of extremely low frequency electromagnetic fields on the adenylate kinase activity of rod outer segment of bovine retina. *Bioelectromagnetics*. 25: 545-551.

Ravera, S. Falugi, C. Calzia, D. Pepe, I.M. Panfoli, I. Morelli, A. 2006 First cell cycles of sea urchin *Paracentrotus lividus* are dramatically impaired by exposure to extremely low frequency electromagnetic field. *Biology of Reproduction* (in press)

Rawls S.M., McGinty J.F., Terrian D.M. 1999, Presynaptic K-opioid and muscarinic receptors inhibit the calcium-dependent component of evoked glutamate release from striatal synaptosomes, *J. Neurochem.* 73: 1058-1065

Schnetkamp P.P. and F.J. Daemen. 1982 Isolation and characterization of osmotically sealed bovine rod outer segments. *Methods Enzymol*. 81: 110-116.

Shmukler, Y.B. and Buznikov, G.A. 1998, Functional Coupling of Neurotransitters with second messengers During Cleavage Divisions. Facts and Hypotheses. *Perspect. Developmental Neurobiol.* **5**, 469-480.

Smith, H.G., Stubbs G.W., and Litman, B.J. 1985. The isolation and purification of osmotically intact discs from retinal rod outer segments. *Exp.Eye Res*. 20: 211-217.

Thumm, S., Loschinger, M., Glock, S., Hammerle, H., and Rodemann, H.P.1999. Induction of cAMP-dependent protein kinase A activity in human skin fibroblasts and rat osteoblasts by extremely low-frequency electromagnetic fields. *Radiat. Environ. Biophys*.38: 195-199.

Volpe, P., Parasassi, T., Esposito, C., Ravagnan, G., Giusti, A. M., Pasquarelli, A., and Eremenko, T. 1998. Cell membrane lipid molecular dynamics in a solenoid *vs*. a magnetically shielded room. *Bioelectromagnetics.* 19: 107-111.

Volpe, P. 2003. Interactions of zero-frequency and oscillating magnetic fields with biostructures and biosystems. *Photochem. Photobiol. Sciences* 2: 637-648.

Walleczek, J. 1995. Electromagnetic fields: Biological interactions and mechanisms. *In* Advances in Chemistry Series vol. 250. Blank, M. editor., ACS, Washington, pp 396-404.

Weaver, J.C. 2002. Understanding conditions for which biological effects of nonionizing electromagnetic fields can be expected. *Bioelectrochem*. 56: 207-209

Zhang, L, and Berg, H. 1992. Electrostimulation of the dehydrogenase system of yeast by alternate current. *Bioelectrochem. Bioenerg*. 28: 341-353.

Appendix

Erythrocyte membranes (ghost) preparation Erythrocytes, completely free of leucocytes and platelets, were obtained following a method already reported [Pontremoli et al., 1979] with minor modifications, starting from 25 mls human blood treated with 1mg/ml EDTA to avoid coagulation. The sample was centrifuged at 3,500 rpm for 15 min at 4 °C and the pellet containing erythrocytes was collected and resuspended in 130 mM KCl and 20 mM Tris-HCl pH 7.4 (1:1 v/v) and centrifuged thrice at 3,500 rpm for 15 min. In order to obtain the erythrocytes membranes the last pellet was resuspended in hemolysis buffer (1:5 v/v) containing 1 mM EDTA-Na and 10 mM Tris-HCl pH 7.4 and centrifuged at 17,000 rpm for 40 min. The pellet containing erythrocyte membranes was resuspended in few mls of distilled water. Samples were stored at –80°C.

Synaptosomal preparation For synaptosomal preparation, the method published by Rawls [1999] was followed with minor modifications. For each preparation, six dorsal striata were removed from decapitated *Mus musculus* mouse and pooled in ice-cold 100 mM Tris buffer pH 7.4. The striata were transferred to 0.32 M unbuffered sucrose and manually disrupted in a glass homogenizer with a Teflon pestle. The homogenate was centrifuged at 3,000 *g* for 2 min. The supernatant was centrifuged at 14,000 *g* for 12 min. The soft pellet was resuspended in 0.32 M sucrose containing 10 mM N-tris(hydroxymethyl)-methyl-2-aminoethanesulfonic acid (TES, pH 7.4), and 4-ml aliquots were loaded onto discontinuous gradients consisting of three layers of Ficoll (Sigma) in sucrose (wt/vol ; 12%, 4 ml ; 9%, 1 ml ; 6%, 4 ml). The gradients were centrifuged at 62,483 *g* for 35 min. Synaptosomes were harvested from the 9% layer, diluted with 3 volumes of 10 m*M* TES buffer containing 140 m*M* NaCl, 5 m*M* KCl, 5 m*M* $NaHCO_3$, 1.2 mM Na_2HPO_4, 1 mM $MgCl_2$, and 10 mM glucose (pH 7.4), and centrifuged at 14,000 *g* for 12 min. Synaptosomes were resuspended in 0.5 ml of 10 mM TES buffer (pH 7.4). The preparation was divided into aliquots containing 0.8 mg of protein and centrifuged at 10,000 *g* for 2 min. Synaptosomes were overlaid with 200 µl of 0.25 M sucrose containing 5 mM TES (pH 7.4) and stored as pellets at –80°C.

Acetylcholinesterase activity Acetylcholinesterase activity was measured by using acetylthiocholine chloride (Sigma) as substrate and monitoring the thiocoline production as already described [Bergmeyer et al., 1983]. Synaptosomal (100 µg of protein) or erythrocyte membranes preparations (200 µg of protein) were added to a reaction mixture containing 0.4 mM acetylthiocholine in 50 mM phosphate buffer pH 7.2. The final volume of 1 ml was kept in the electromagnetic field 75 Hz, 2.5 mT. At different time intervals, aliquots of 100 µl were withdrawn and added to 50 µl of 25% PCA. Control samples were run in the same experimental conditions as above but in the absence of field. Each sample was centrifuged for 3min at 14,000 rpm and then 100 µl of supernatant was withdrawn and neutralized with 50 µl 2 M K_2CO_3. Centrifugation was repeated to remove potassium perchlorate. Aliquots of 100 µl of each neutralized extract were used for thiocoline assay by addind 0.5 mM DTNB in phosphate buffer pH 7.2 (1 ml final volume). Thiocoline reaction with DTNB gave thionitrobenzoate formation (ε_{405} = 1.33 mM^{-1} cm^{-1}) which was monitored spectrophotometrically by following the rise in absorbance.

Phosphoglycerate kinase activity Phosphoglycerate kinase activity was measured in red blood cell ghosts by following a method already described [Bergmeyer et al., 1983] with minor modifications. Ghosts (100 µg) were added to a solution containing 6.5mM glycerate-3-phosphate and 1.2mM ATP in 40 mM Tris HCl pH 8, 120 mM KCl, 10 mM $MgCl_2$. The final volume of 1 ml was kept in the electromagnetic field of 75 Hz and 2.5 mT.

At different time intervals, aliquots of 100 µls were withdrawn and added to 50 µl of 25% PCA. Control samples were run in the same experimental conditions as above but in the absence of the field.

Each sample was centrifuged for 3min at 14,000 rpm and then 100 µl of supernatant was withdrawn and neutralized with 50 µl 2 M K_2CO_3. Centrifugation was repeated to remove potassium perchlorate. Aliquots of 100 µl of each neutralized extract were used for the enzymatic assay by addind 2µl of glycerate–3-phosphate dehydrogenase, 0.2 mM NADH, 10 mM $MgCl_2$, 50mM Tris HCl buffer pH 8 (1 ml final volume). The corresponding NADH oxidation was monitored spectrophotometrically by following the decrease in absorbance at 340 nm (ε_{340} = 6.22 mM^{-1} cm^{-1}).

(Na, K)ATPase activity Plasma membrane Ca-ATPase activity was measured in erythrocyte membranes preparation through inorganic phosphate release. The standard reaction mixture contained 30 mM HEPES, pH 7.6, 140 mM KCl, 0.2 mM ouabain, 2 µg/ml CaATPase activity calmodulin, 2 mM ATP and 0.005 mM free Ca^{2+} (obtained with a Ca^{2+}-EGTA buffer; EGTA was 2mM). 2mM EGTA) in a final volume of 1 ml. Aliquots of erythrocyte membranes preparation (about 70 µg proteins) were added to the reaction mixture and incubated at room temperature for 20 min in the presence or in the absence of the field of 75 Hz and 2.5 mT. The final volume of 1 ml was kept in the electromagnetic field. At different time intervals, aliquots of 100 µls were withdrawn and added to 50 µl of 25% PCA. Each sample was centrifuged for 3min at 14,000 rpm and then 100 µl of supernatant was withdrawn and neutralized with 50 µl 2 M K_2CO_3. Centrifugation was repeated to remove potassium perchlorate. Control samples were run in the same experimental conditions as above but in the absence of field. The released inorganic phosphate was determined colorimetrically as described by Martin and Doty (1949). Blank subtraction was obtained by considering the amount of inorganic phosphate released by parallel samples incubated in the absence of Ca^{2+} and in the presence of 2 mM EGTA.

ATPase activity of erythrocyte membranes was assayed by the pyruvate kinase, lactate dehydrogenase system in which hydrolysis of ATP is coupled to the oxidation of NADH. ATP hydrolisis was measured in the presence or in the absence of the field for 20 min. An aliquot of 0.145 mg/ml erythrocyte membranes preparation was added to the reaction mixture containing 100 mM Tris–HCl pH 8, 2 mM $MgCl_2$, 150 mM NaCl, 50 mM KCl, 1 mM ATP. Aliquots of 100 µl of the reaction mixture were withdrawn and added to 50 µl of 25% PCA. Each sample was centrifuged shortly at 14,000 rpm and then 100 µl of supernatant was withdrawn and neutralized with 50 µl of 2M K_2CO_3. The centrifugation was repeated to remove potassium perchlorate. In order to measure the amount of ATP hydrolized, 100 µl aliquots of each neutralized extract were added to 1 ml final vol of reaction mixture containing 0.16 mM NADH, 1.5 mM phosphoenolpyruvate, 8 µg/ml pyruvate kinase, 8 µg/ml lactate dehydrogenase, 100 mM Tris–HCl pH 8.0; 5 mM $MgCl_2$. ATP hydrolysis coupled to oxidation of NADH was followed at 340 nm (ε_{340} for NADH=$6.22\times10^3 M^{-1}cm^{-1}$) in spectrophotometers. Ouabain-sensitive (Na^+,K^+)ATPase was determined as the difference between the enzyme activities in the presence and in the absence of 0.1 mM ouabain.

Microsome preparation Bovine liver was chopped and homogenized in 20 mM Tris-HCl pH 7.5 containing 0.25 M sucrose in a Potter apparatus. The homogenate was centrifuged for 10 min at 900 g. The supernatant was collected and centrifuged for 20 min at 20,000 g. The resulting supernatant containing cytosol and microsomes was collected and centrifuged at 100,000 g for 1 hr. The pellet containing microsomes was stored at –80°C.

Alkaline phosphatase activity Alkaline phosphatase activity was measured by using 4-nitrophenylphosphate (Sigma) as substrate and monitoring 4-nitrophenol formation as already described [Bergmeyer et al., 1983]. Microsomes from liver (100 µg of protein/ml) were added to a reaction mixture containing 4-nitrophenylphosphate (12 mM) 0.1 M glycine, 0.1 mM $ZnCl_2$, 1mM $MgCl_2$ (glycine buffer pH 10.5). The final volume of 1 ml was kept in the electromagnetic field for 20 min. At different time intervals, aliquots of 100 µls were withdrawn and added to 50 µl of 25% PCA. Control samples were run in the same experimental conditions as above but in the absence of field. Each sample was centrifuged 3 min at 14,000 rpm and then 100 µl of supernatant was withdrawn and neutralized with 50 µl 2 M K_2CO_3. Centrifugation was repeated to remove potassium perchlorate formed by the reaction between PCA and K_2CO_3. Aliquots of 100 µl of each neutralized extract were used for 4-nitrophenol assay by adding 0.1 M glycine buffer pH 10.5 (1 ml final volume) and measuring spectrophotometrically the increase in absorbance at 405 nm (ε = 1.85 $mmol^{-1}$ x cm^{-1}) which is proportional to the nitrophenol produced.

Mitochondria preparation Pieces of rat liver (3 g) were homogenated at ice temperature by Potter-Elvehjem system in 20 ml Buffer containing 0.25M Sucrose, 5 mM HEPES pH 7.2, 1mM EDTA. The liver homogenate was centrifuged for 10 min at 500g, at 4°C. After centrifugation, precipitate was discarded and supernatant was centrifuged again for 20 min at 20,000g. Then the pellet was collected and dissolved in 2 ml of homogenizing Buffer.

Succinic dehydrogenase activity Succinic dehydrogenase activity was assayed by the oxidation of succinic acid to fumaric acid coupled with $K_3Fe(CN)_6$ reduction, following the method of Bonner [1955] with minor modifications. The enzymatic activity was measured in the presence or in the absence of the field of 75 Hz and 2.5 mT for 20 min after addition of mitochondria preparation (0.1 mg of proteins) to 1 ml final volume of the

reaction mixture containing 100 mM Phosphate buffer pH 7.6, 70 mM Na succinate, 2 mM $K_3Fe(CN)_6$. At different time intervals, aliquots of 100 µls were withdrawn and the reaction was stopped with 0.25 ml Aceton. Then the samples were centrifuged for 3 min at 14,000 rpm, and supernatant was used for the succinic acid oxidation coupled to reduction of $K_3Fe(CN)_6$, which was followed spectrophotometrically at 400 nm (ε_{400} for $K_3Fe(CN)_6$ = 920 $M^{-1}cm^{-1}$).

Rod outer segments and disk membranes preparations In a typical experiment, rod outer segments (ROS) were isolated from 30 bovine retina in dim red light by following the method of Schnetkamp and Daemen [1982] by sucrose gradient centrifugation. Intact ROS were first washed in an isotonic medium containing 40 mM Tris-Maleate pH 7, 120 mM KCl and then centrifuged for 10 min at 1,500 g. Osmotically intact disks were obtained after bursting intact ROS for 3 h in 30 ml of 5% Ficoll (Sigma) in distilled water containing 5 mM DTT and 70 mg/ml leupeptin and then by collecting them in dim red light at the 5% Ficoll surface after centrifuging for 2 h at 25,000 rpm in a Beckman FW-27 rotor [Smith et al., 1985]. The disk membranes were washed in distilled water and centrifuged for 10 min at 1,500 g. The pellet (purified disk membrane preparation) was resuspended in the initial volume of distilled water and stored in the dark at - 80° C.

Rod disk phosphodiesterase activity cGMP Phosphodiesterase was assayed as follows. The reaction mixture contained 100 mM MOPS (pH 7.1), 140 mM KCl, 20 mM NaCl, 5 mM $MgCl_2$, 2mM GTP and 5 mM cGMP. The reaction was started by adding 50 µl of reaction mixture containing 4 µCi [8-^{3}H] cGMP (specific activity: 12.7 Ci/mmol) to 50 µl of purified disk membrane preparation previously bleached in the room light (final concentration: 1 – 2 mg/ml protein). The reaction was run in the presence or absence of ELF-EMF of 75 Hz and 2.5 mT, at room temperature and stopped after 1, 3, 5, 10 and 20 min by adding 5 µl of 100 mM EDTA to each 20 µl withdrawn sample and boiling for 2 min. After centrifuging, 10 µl of the supernatants were analysed by TLC on polyethyleneimine-cellulose developed in one dimension with 1M LiCl. 5'-GMP was added as internal standard. The separed spots corresponding to cGMP and 5'-GMP, visualized under UV light, were cut into scintillation vials, eluted in 0.5 ml of 0.7M MgCl2/1M TrisHCl pH 7.4 (10/2 v/v) , added to 3 ml of Instagel, left overnight and then counted in a LKB liquid scintillation counter.

LIPOSOME: A MODEL FOR PROBING THE INTERACTION OF ELECTROMAGNETIC FIELDS AND BIOSYSTEMS

ALFONSINA RAMUNDO-ORLANDO[a], GUGLIELMO D'INZEO[b], GIAN PIERO GALLERANO[c]

[a]INSTITUTE OF NEUROBIOLOGY AND MOLECULAR MEDICINE OF ITALIAN RESEARCH COUNCIL, VIA DEL FOSSO DEL CAVALIERE, 00133 ROME, ITALY; [b]DEPARTMENT OF ELECTRONIC ENGINEERING, UNIVERSITY 'LA SAPIENZA', VIA EUDOSSIANA, 18-00184 ROMA, ITALY; [c]UTS TECNOLOGIE FISICHE AVANZATE, ENEA-FRASCATI, VIA ENRICO FERMI 4, P.O. BOX 65, 00044 FRASCATI –ITALY.

Abstract

Liposomes are very useful model membrane systems: Although they are unable to mimic all the complexity of a cell membrane, they have a well-defined chemical composition, the capacity to arrange themselves in bilayers, selectivity to ionic species and molecules, and many other useful features. Interactions can take place between this model system and electromagnetic fields (EMFs) at different frequencies, from extremely low frequency up to microwave and THz range, so that, a comparative evaluation of the observed effects with different EMF components is allowed. In this context we used cationic Carbonic Anhydrase (CA)-loaded liposomes. The CA was entrapped into these liposomes and the hydrolysis rate of substrate p-nitrophenyl acetate (p-NPA) added in the bulk aqueous phase was adopted as the index of membrane permeability changes. In fact previous kinetic experiments showed a very self-diffusion rate of p-NPA across intact liposome bilayer. Observations reported by our group evidenced that combined 7 Hz sinusoidal (B_{acpeak} = 50μT) and parallel static (B_{dc} = 50μT) magnetic fields can induce permeability changes in these liposomes. Further, we reported on the effects of 2.45 GHz microwave exposure (6 mW/g) on the permeability of these cationic liposomes. Finally, we report on the effects of 130 GHz radiation modulated at low frequency of 5, 7 and 10 Hz on the permeability of these cationic liposomes. The enzyme activity, as function of increased diffusion of p-NPA, rises from 23% to 61% over 3 min of 130 GHz radiation modulated at 7 Hz, at incident intensity of 10.5 mW/cm^2, and a peak electric field of 2.6 kV/cm. The increase of the incident intensity up to 17 mW/cm^2 did not further increase the enzyme activity. This biological model demonstrates an extraordinary sensibility in revealing the influence of EMFs on the lipid bilayer permeability and allowed an interaction mechanism with an ELF magnetic field to be derived.

Introduction

When considering the action of electromagnetic fields (EMFs) on a biological system, the cell membrane is indicated by the most part of studies as the primary site of interaction [1]. Living organisms are made of cells bound by their membranes. They are self-assembly entities; each is organizing a particular combination of phospholipids in the form of a bilayer with other constituents (e.g. proteins) embedded in it. This lipid bilayer existing in all biomembranes is most unique; it serves not merely as a physical barrier but functions as a two-dimensional matrix for reactions. Also the lipid bilayer acts as a conduit for ion transport, as a framework for antigen-antibody binding, as bipolar electrode for redox reactions, and as a reactor for energy conversion (e.g. light to electric to chemical). Further, a modified lipid bilayer performs as a transducer for signal transduction (i.e., sensing), and numerous other functions as well. All these myriad activities require the ultra thin lipid bilayer. In particular, molecular systems that have been suggested to be candidates for direct modulation by

EMFs are the binding of extracellular ligands to the cell-surface receptor sites, and translocation of charged ionic species across the lipid bilayer. Both events lead to the activation of diverse biochemical pathways that transduce signals to internal sites within the cell [2].

In spite of the huge number of papers that have studied the biological effects of EMFs exposure on cell membrane, from an experimental and theoretical point of view [see reviews 3-6], we reckon to have a nearly complete knowledge by now only in the case of thermal effects. These are due to a sharp increase of temperature that can be systemic or localized. Such effects typically correspond to high power radiation. On the other hand, the complexity of the cell membrane we want to study the interaction with leads to hypothesize the possibility of more subtle specific or non-thermal effects. These are due to phenomena that have no dependence on the thermal energy deposited, or for which temperature is merely one of many significant parameters, and can occur even if the external EMF is weak. Research on these specific effects requires an experimental approach enabling to reduce the complexity of the systems involved.

The cell membrane acts as a gateway to the cell, 30% of all proteins within the body are membrane proteins and 60% of drug targets are membrane proteins. Despite its immense complexity, however, the functionality of the membrane is ultimately determined by its mechanical and electrical properties.

In order to reduce the complexity of this biological system, we suggest the use of membrane model so that physical, biochemical, and physiological processes may be isolated and analysed in molecular terms. Amongst these model systems, liposomes are very useful, although they are unable to mimic all the complexity of a cell membrane; they have a well-defined chemical composition, the capacity to arrange themselves in bilayers, selectivity to ionic species and molecules, and many other useful features [7-8]. Liposomes occur naturally and can be prepared artificially from natural or synthetic lipid molecules [9]. They can encapsulate or bind a variety of molecules, such as drug molecules, proteins, nucleotides and even plasmids, into or onto the membrane [10].

For more than 15 years our laboratory has been studying the possibility of the use of liposomes in an effort to clarify the mechanism of how EMFs exposure induce alterations of membrane permeability, focusing the attention mainly on the membrane phospholipidic components [11-14].

In this context cationic CA-loaded liposomes (Fig.1) revealed an extraordinary sensibility toward the EMFs induced-effects.

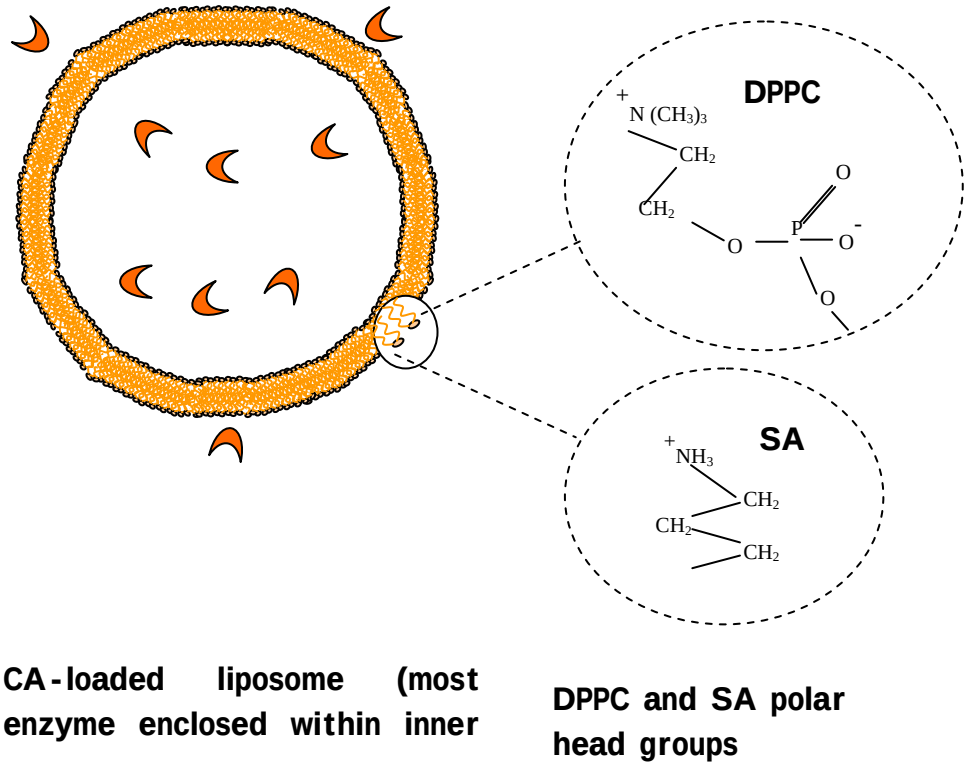

Fig. 1. Schematic representation of CA-loaded liposomes where the dipolar (e.g. DPPC) and unipolar (e.g. SA) chemical structures in the lipid bilayer are depicted.

They are formed by controlled dialysis of detergent (DIAL) and containing dipalmitoylphosphatidylcholine (DPPC), cholesterol (CHO), and the charged lipid stearylamine (SA). Because entrapping Carbonic Anhydrase (CA) these liposomes could be considered as a bioreactor. To follow any alteration due to EMFs exposure on the permeability of lipid membrane we add in the bulk aqueous phase the substrate p-nitrophenyl acetate (p-NPA) in great excess to have a steady-state condition limited only by the enzyme activity. Because the p-NPA cannot pass freely across the lipid bilayer, or with a very low self-diffusion, any enhancement of its hydrolysis rate can be assumed due to permeability change enabling the p-NPA to reach the enzyme into the inside of liposomes. We carry out kinetic measurements by monitoring the appearance of the product of p-NPA hydrolysis at its peak of absorbance at 400 nm in a Cary50 spectrophotomer. Typical recorded curves of change of absorbance at 400 nm against time (min) in the sham and exposed samples are shown in Fig. 2. The difference between the p-NPA hydrolysis rate in the exposed sample and the sham one is taken as an index of permeability changes due to the exposure. The temperature is always recorded during the entire exposure time.

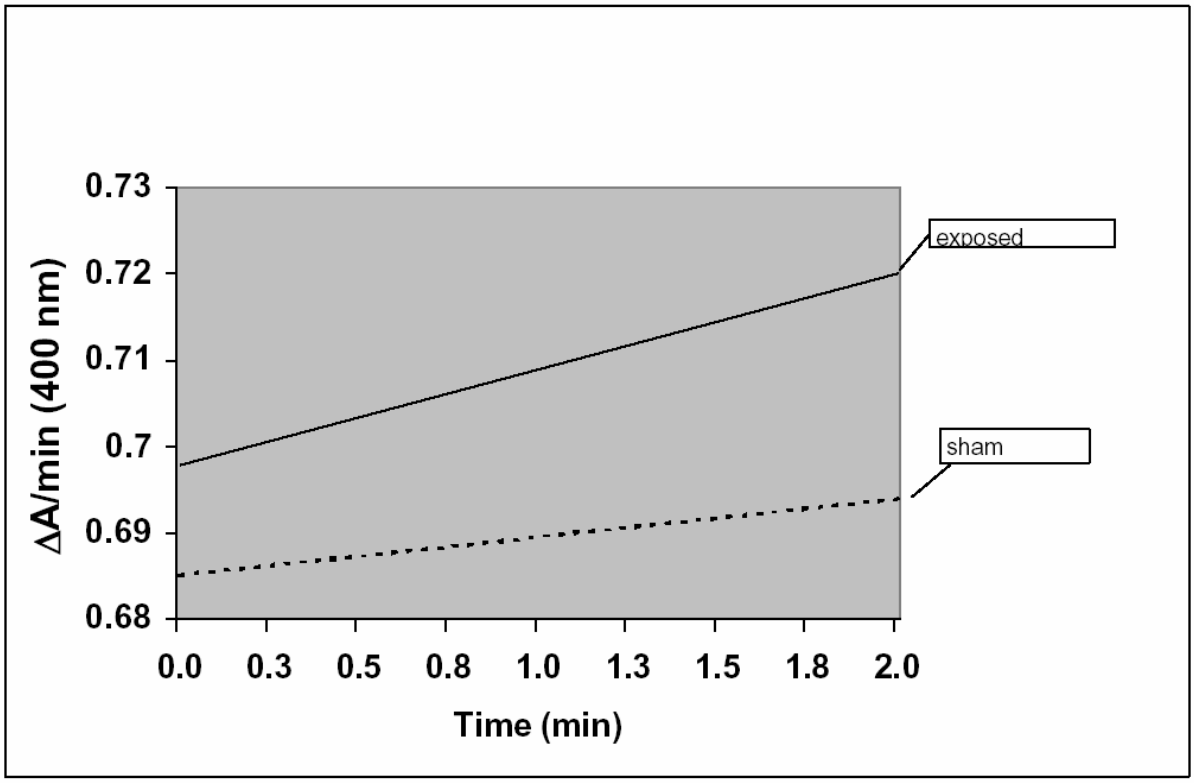

Fig. 2. Typical recorded curves of the p-NPA hydrolysis rate of CA-loaded liposomes during EMFs exposure are shown.

Typically, in these cationic liposomes, a non-zero p-NPA hydrolysis rate resulted in the sham samples (Fig. 2). Indeed, due to electrostatic interactions between the enzyme and the positive charge on the lipid membrane, a small fraction of enzyme is located on the surface of liposomes.

In order to normalize the kinetic data obtained with several liposome preparations used throughout our studies, we determine the total activity of CA (100%) released from each liposome preparations after their disruption with detergent (n-octyl-β-glucopiranoside). Then, the relative *p*-NPA hydrolysis rates in intact liposomes are expressed as percentage values (%), and calculate for every exposed and sham sample toward 100% of CA.

We speculated that the above experimental system, in contrast to living cells, was well defined and had

only a limited number of parameter, thus allowed to evaluate in a comparative way the biological effects induced by EMFs with different components. This idea was supported by the following findings.

We found that 2.45 GHz microwave radiation (6 mW/g) induced an increase of p-NPA hydrolysis rate from 41% ± 7 to 80% ± 11 in eight different CA-loaded liposome preparations [15]. An S-band exposure chamber, with a coax-waveguide transition bandwidth input 1.7-2.6 GHz, was used. The SAR of the samples was calculated by the experimental curve of the temperature increase inside a water-filled cuvette in absence of thermostatic control. We speculated that the net surface charge in the vesicles might be involved in the response of liposomes to MW field exposure, since the permeability effect could be dependent on electrostatic charge. This idea was supported by the finding that liposomes with higher net surface charge (i.e., DPPC:CHO:SA at 5:3:2 lipid ratio) showed an higher effect than ones with 6:3:1 ratio. We also found that the MW induced-effect on substrate permeation occurred well below (20°C) the phase-transition temperature of liposomes (≈ 40°C), in agreement with literature data [16-17]. It should be noted that liposomes exhibit phase transitions which can be triggered by (inter alias) changes in the total or average area of polar heads on the outer monolayer, these transitions has been proposed to induce changes in the membrane permeability which are analogous to microwave-induced permeability changes [18].

We used the same experimental approach in an effort to clarify the mechanism for how extremely low frequency (ELF) electromagnetic fields exposure influences the trans-membrane movement of free ions in cell membranes [19-21]. Such experimental evidences demonstrate a change in free calcium concentration between the extra- and the intracellular medium under the presence of an ELF magnetic field combined with a static magnetic field.

In this context, we investigated whether combined sinusoidal (AC) and static (DC) magnetic fields could affect the permeability of our cationic CA-loaded liposomes under well-controlled field exposure conditions. The magnetic field was generated by a series of perpendicular nested coils. Each set of coils controls the component direct along its axis. In the center of the apparatus a large isofield region (8 cm^3) with a field uniformity of 1% was obtained. The values of the three components of the magnetic field were generated and maintained by the feedback system [22]. We found that 7 Hz sinusoidal (Bacpeak = 50μT) and parallel static (Bdc = 50μT) magnetic fields exposure induced an increase in the hydrolysis rate of p-NPA in these liposomes [22]. We speculated that the positive charges of SA on the liposome surface might be responsible for the effect. This idea was supported by the findings that the effect was linear with the increase of SA concentration in the lipid mixture and nullified by neutralizing the positive charge of SA, upon going from pH 7.55 to 8.95 in the reaction medium. Moreover, the presence of CA partially located on the external surface of these liposomes would be expected to be a confounding factor in determining the primary target on the membrane for the interaction of the ELF magnetic field. Therefore we studied the influence of ELF magnetic field on the catalytic parameters of the CA. No structural change of the enzyme, as revealed by the K_m values, was found when CA was either free in solution or loaded in liposomes. Further a specific treatment of the liposomes with a protease able to remove the CA partially located on their surface did not indicate any role for the enzyme itself in the effect [23].

Based on these results an interaction model between the magnetic field and the polar structures embedded in the liposomes has been proposed [23]. The proposed model shows the possibility of inducing a precessional motion by applying suitable dynamic magnetic field. As a result, the charged structures (e.g. - $CH_2CH_2NH_3^+$ in SA) on the lipid membrane could move in a way such as to facilitate the passage of external substances right through the membrane [23-24].

The increasing interest in the THz (Tera-Hertz) region of the electromagnetic spectrum, extending from 100 GHz to 10 THz, in biomedical science [25-26], and the scarce knowledge about the biological effects of this THz region on living systems, suggested us to use our experimental approach in the context of the European Project THz-BRIDGE dealing specifically to investigations on diagnostic and potential genotoxic effects induced by THz radiation.

A series of experiments examining the effects of 130 GHz radiations, modulated at low frequency (5, 7 and 10 Hz) on membrane permeability were carried out. The THz radiation were conducted by using a Compact THz Free Electron Laser (FEL) providing coherent radiation at 130 GHz with a 10% relative bandwidth in the form of a "train" of micro pulses of about 50 ps duration each, with 330 ps spacing between adjacent pulses [27]. The overall duration of the train (macro pulse) is 4 μs. Macro pulses can be produced up to a maximum repetition frequency of 10 Hz.

We found that the THz exposure induces an increase of the p-NPA hydrolysis rate on CA-loaded liposomes in a dose-dependent manner. Indeed, by applying an incident power lower than 8 mW/cm^2 the effect was found only for modulation at 7 Hz. By increasing the field power the effect was also found at modulation of 5 and 10 Hz, though always much more less significant than at 7 Hz. We speculated that probably a temperature rise in the exposed sample rather than a modulation at a specific frequency might be responsible for the effect. Therefore, we studied exposure induced membrane changes on liposome at a different phase transition state by exchanging the DPPC with POPC in the lipid mixture. Further, we prepared the latter

liposome in a different manner avoiding the detergent dialysis, thus producing VET liposome populations with a higher diameter *vs.* DIAL ones. POPC liposomes, which are in fluid phase, showed that THz exposure does not induce any increase in liposome permeability, and that the temperature variations recorded in the samples during the exposure were negligible. Based on these results we excluded a thermal-based explanation for the effect.

Electrical double layers form at each side of the cell membrane, in equilibrium, this potential is of the order 100 mV ($E_{bilayer} \sim 10^7$ Vm^{-1}) when the net ion flux (mainly K^+, Na^+, Cl^-, Ca^{2+}) through the membrane is zero, and any disturbance of the membrane (e.g. by absorption of electromagnetic radiation in the membrane) can result in a change in the potential difference across the system. In the 130GHz experiments noted above, the peak electric field (E_{130GHz}) was two orders of magnitude lower than naturally developed across bilayers. Despite this comment, the influence of the electric field cannot be excluded for the effect of permeability change on lipid membrane, as the effects appear be pronounced only within a certain field range (Fig. 3). As living organisms are not adapted to this spectral range of radiation, and the possible resonance characteristics of its action, it may be possible that a relatively small influence causes a pronounced effect.

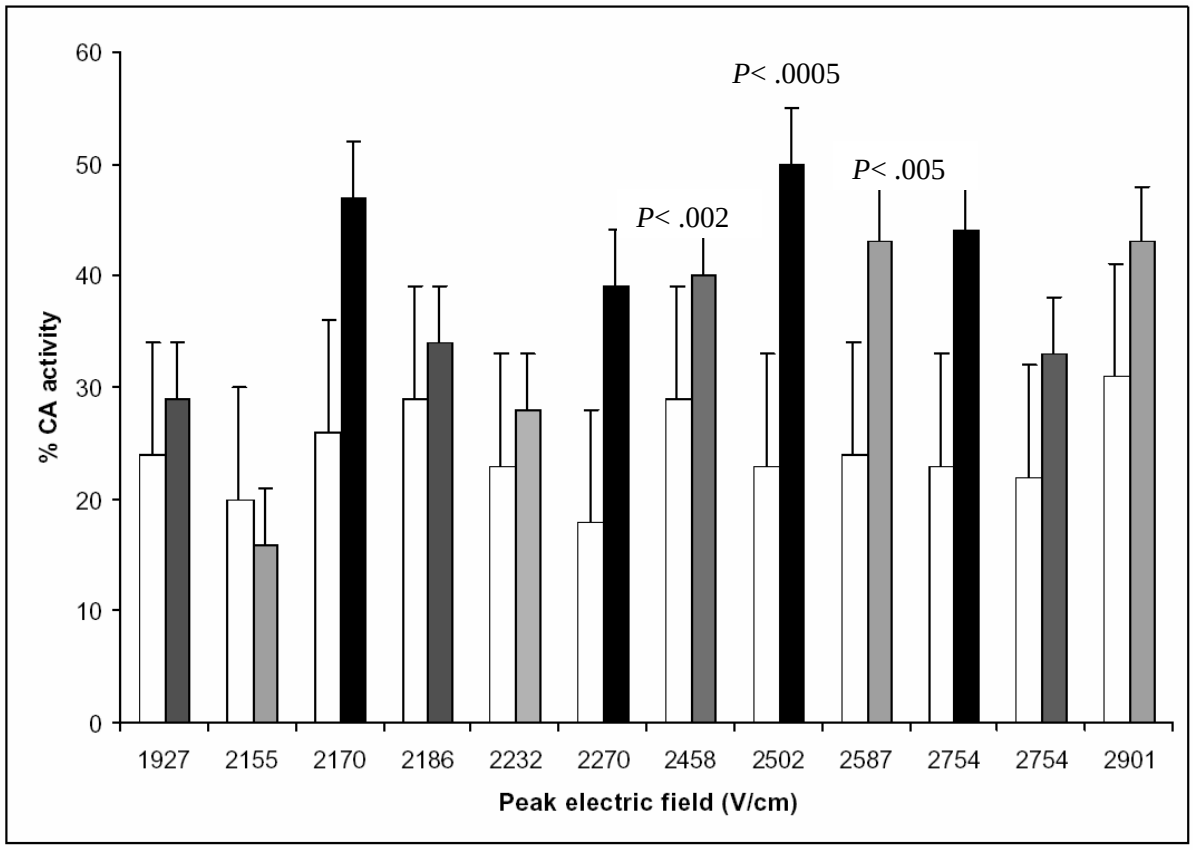

FIG. 3. Effect of 130 GHz radiation on CA reaction rate of DIAL liposomes. % CA reaction rates as a function of the peak electric field are shown for three different pulse repetition rates: 10 Hz (dark grey), 7 Hz (black) and 5 Hz (light grey), sham (white). Statistical significances are presented as P of unpaired two-tailed t-test at 95% confidence intervals.

Summary

The use of cationic liposomes entrapping an enzyme for the evaluation of permeability changes induced by EMFs on cell membrane has been proposed. This system allows comparative evaluation of the induced effects by exposure at different EMF components. Specifically, membrane components, with typical dipolar (e.g. phospholipids), or unipolar (e.g. cationic amines) structures, may be focused to study and find interpretation keys on the biointeraction phenomenon, under EMFs exposure conditions.

References

1. C. Polk, E. Postow. Biological Effects of Electromagnetic Fields. CRC Press, Boca Raton, 2nd Edition, 1996.

2. Rodbell, E. Signal transduction: evolution of an idea. *Biosci. Rep.* 15 :117-133, 1995.

3. Zhadin, M. N. Review of Russian literature on biological action of DC and low-frequency AC magnetic fields. *Bioelectromagnetics* 22:27-45, 2001.

4. Repacholi, M.H. Health risks from the use of mobile phones. *Toxicology Letters* 120:323-331, 2001.

5. Litvak, E. Foster, K.R., Repacholi, M.H. Health and safety implications of exposure to electromagnetic fields in the frequency range 300 Hz to 10 MHz. *Bioelectromagnetics* 23:68-82, 2002.

6. Fedorov, V.I., Popova, S.S., Pisarchik, A.N. Dynamic effects of submillimeter wave radiation on biological objects of various levels of organization. *Int. J. Infrared Millimetr Wave* 24:1235-1253, 2003.

7. Gregoriadis G. (Editor) Liposome Technology 2nd Edition Boca Raton CRC, 1993.

8. Walde P. Preparation of vesicles. Encyclopedia of Nanonoscience and Nanotechnology in: H.S. Nalwa (Ed.) American Scient. Publishers, vol. X, pp. 1-37, 2003.

9. Lasic, D. D. Liposomes: from physics to applications. *Trends in Biotechnology* 16:307-321, 1998.

10. Ramundo-Orlando, A., Serafino, A., Villalobo, A. Gap junction channels reconstituted in two closely apposed lipid bilayer. *Archives of Biochemistry and Biophysics* 436:128-135, 2005.

11. Ramundo-Orlando, A., Arcovito, C., Palombo, A., Serafino. A.L., and Mossa, G. Enzymatic kinetic change of Ascorbate Oxidase loaded into liposomes induced by microwave fields exposure. *Journal of Liposomes Research* 3(3): 717-724, 1993.

12. Ramundo-Orlando, A., Gensabella, R., and d'Inzeo, G. The enhancement of lipid peroxidation kinetics in phosphatidylcholine liposomes by microwave radiation. *Res. Commun. Biochem. Cell & Mol. Biology* 3, 233-250, 1999.

13. Ramundo-Orlando, A., Liberti, M., Mossa, G., and d'Inzeo, G: Effect of 2.45 GHz microwave fields on liposomes entrapping glycoenzyme ascorbate oxidase. Evidence for oligosaccharide side chains involvement. *Bioelectromagnetics* 25: 338-345, 2004.

14. Ramundo-Orlando, A., Serafino, A., Schiavo, R., Liberti, M., d'Inzeo, G. Permeability changes of connexin32 hemichannel reconstituted in liposomes induced by extremely low frequency, low amplitude magnetic fields. *BBA-Biomembranes* 1668(1): 33-40, 2005.

15. Ramundo-Orlando, A., Mossa, G., and d'Inzeo, G. Effect of microwave radiation on permeability of Carbonic Anhydrase loaded unilamellar liposomes. *Bioelectromagnetics* 15(4): 303-313, 1994

16. Liburdy R.P. Fingado, B. "Effects of MW fields on liposome permeability: Non-phase transition liposome vesicles" 12th Annual BEMS Meeting, San Antonio, Texas, 10-14 June, 1990

17. Saalman, E. Norden, B., Arvdsson, L., Hamnerius, Y., Hojevik, P. Connell, K.E., Kurucsev, T. Effect of 2.45 GHz microwave radiation on permeability of unilamellar liposomes to 5(6)-carboxyfluorescein. Evidence of non-thermal leakage. *Biochem. Biophys Acta* 1064:124-130, 1991.

18. Liburdy, R.P. Magin, R.L. Microwave stimulated drug release from liposomes. *Radiat. Res.* 103:266-275, 1985

19. Liboff, A.R. Cyclotron resonance in membrane transport. In Interaction between EMFs and cells". Chiabrera A.,Nicolini, C. and H.P. Schwan (eds), London, Plenum Press, pp. 281-296, 1985.

20. Liboff, A.R. Smith, S.D. and McLeod B.R. Experimental evidence forion cyclotron resonance mediation of membrane transport. In Mechanistic Approach to Interaction of Electric and EMFs with living systems, M. Blank and E. Findl (eds), New York, Plenum Press, pp.109-132, 1987.

21. Blackman C. F., Benabe, S.G., House, D.E. and Joines W.T. Effects of ELF(1-120 Hz) and modulated (50 Hz) RF fields on the efflux of calcium ions from brain tissue in vitro. *Bioelectromagnetics*, 6:1-11, 1985.

22. Ramundo-Orlando, A., Morbiducci, U., Mossa, G., and d'Inzeo, G. Effect of low-frequency, low-amplitude magntic fields on the permeability of cationic liposomes entrapping carbonic anhydrase.I. Evidence for charged lipid involvement. *Bioelectromagnetics* 21:491-498, 2000.

23. Ramundo-Orlando, A., Mattia, F., Palombo, A., and d'Inzeo, G. Effect of low-frequency, low-amplitude magntic fields on the permeability of cationic liposomes entrapping carbonic anhydrase.II. No evidence for surface enzyme involvement. *Bioelectromagnetics* 21: 499-507, 2000.

24. Cappelli, M. d'Inzeo, G. Apollonio, F. and Liberti, M. A possible mechanism explaining variation in membrane permeability under exposure to weak magnetic fields. Proceedings of 26th IEEE-EMBS Congress, 1-5 Sept. 2004.

25. Woodward R. 2004. Terahertz Technology in the Medical and Pharmaceutical Industry. *Preclinica* 2:328-335.

26. Woolard DL, Brown ER, Pepper M, Kemp M. 2005. Terahertz frequency sensing and imaging: a Time of reckoning future applications? Proceedings IEEE 93:1722-1743.

27. Gallerano GP, Doria A, Giovenale E, Renieri A. Compact free electron lasers: from Cerenkov to waveguide FELs. *Infr. Phys. Tech.* 40:16-20, 1999.

ELF MAGNETIC FIELDS AFFECT STEM CELL DIFFERENTIATION: RESULTS AND PERSPECTIVES

F. BERSANI*, C.VENTURA§, P.MESIRCA*, M. MAIOLI‡
*DEPARTMENT OF PHYSICS, UNIVERSITY OF BOLOGNA, ITALY
§INSTITUTE OF CARDIOLOGY, UNIVERSITY OF BOLOGNA, ITALY
‡DEPARTMENT OF BIOMEDICAL SCIENCES, UNIVERSITY OF SASSARI, ITALY

Abstract

The exposure of mouse embryonic stem (ES) cells to extremely low frequency magnetic fields (ELF-MFs) triggered the expression of GATA-4 and Nkx-2.5, acting as cardiac lineage-promoting genes in different animal species, including humans. ELF-MFs also enhanced prodynorphin gene expression, and the synthesis and secretion of dynorphin B, an endorphin playing a major role in cardiogenesis. These effects occurred at the transcriptional level and ultimately ensued into a remarkable increase in the yield of ES-derived cardiomyocytes. These results demonstrate the ability of ELF-MFs to modify the gene program of cardiac differentiation in ES cells without the aid of gene transfer technologies.

INTRODUCTION

Extremely low frequency Magnetic fields (ELF-MFs) have been shown to elicit behavioural changes in intact organisms (1) and affect proliferation and growth factor expression in cultured cells (2,3).
Nevertheless, only a few reports suggest that ELF-MFs may affect cell differentiation (4-6).

In the present study, we used murine embryonic stem (ES) cells as an in vitro model of cardiac differentiation and assessed whether ELF-MF (Fig. 1) may be involved in the activation of a gene program of cardiac lineage commitment

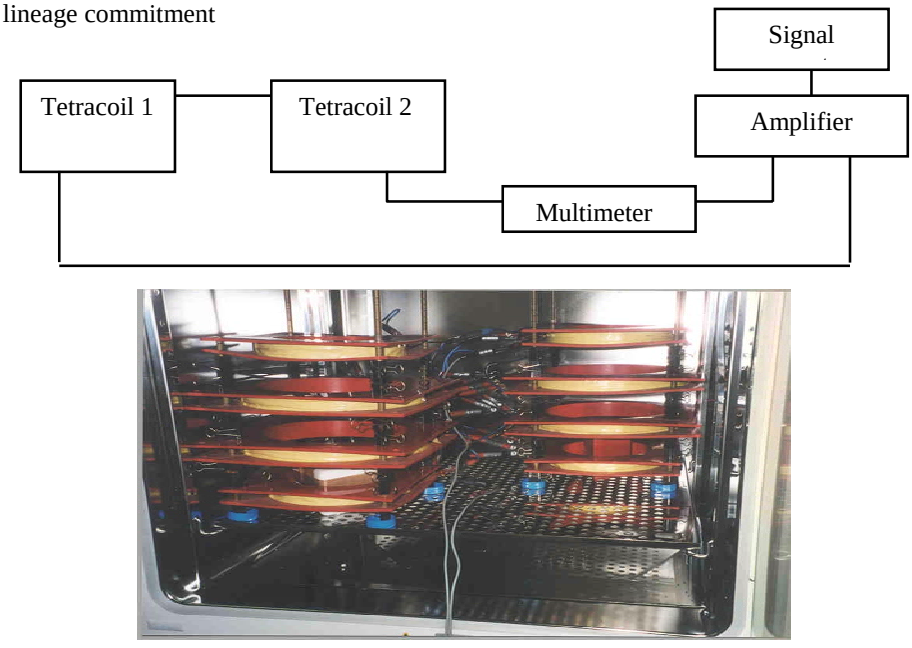

Figure 1

Exposure system and signal characteristics:

- signal generator: Beckman FG3A
- c.c. current amplifier (home made) for low resistive load
- multimeter: Fluke 85III

- two tetracoils, each composed of four coaxial coils, 40 (20+20) turns each, which were double-wrapped to obtain wound (active) or counter-wound (sham) configuration. The inner coils have radii of 10 cm, and the outer of 7 cm. With this configuration a very large region of magnetic field uniformity can be obtained.
- Signal: 50 Hz, sinusoidal, intensity 0.8 mT_{rms}
- The two tetracoils were placed inside the same incubator as shown in the picture.

ELF-MFs were applied to GTR1 ES cells, a derivative of R1 ES cells bearing the puromycin resistance gene driven by the cardiac specific MHC promoter (GTR1 cells were kindly provided by Dr. William L. Stanford, University of Toronto and Centre for Modeling Human Disease, Canada). ES cells were maintained in the undifferentiated state by culturing in KNOCKOUT D-MEM containing 15% FBS, supplemented with 1000 U/ml LIF (Leukemia Inhibitory Factor). To induce cardiac differentiation, cells were plated onto special plates (Costar ultra low attachment clusters), containing KNOCKOUT D-MEM, lacking supplemental LIF. After 2 days, the resulting embryoid bodies (EBs) were plated onto tissue culture dishes. When spontaneous contractile activity was noticed, puromycin (2µg/ml) was added to eliminate non-myocardial cells. After 2 days, puromycin selected cells were transferred to new tissue culture dishes. EBs, collected at several stages after plating, as well as puromycin-selected cells were processed for gene expression analyses. Following LIF removal and throughout puromycin selection, GTR1 cells were also exposed to a sinusoidal ELF-MF (50 Hz, 0.8 mT_{rms}). The analysis of mRNA expression was performed by RT-PCR technique.

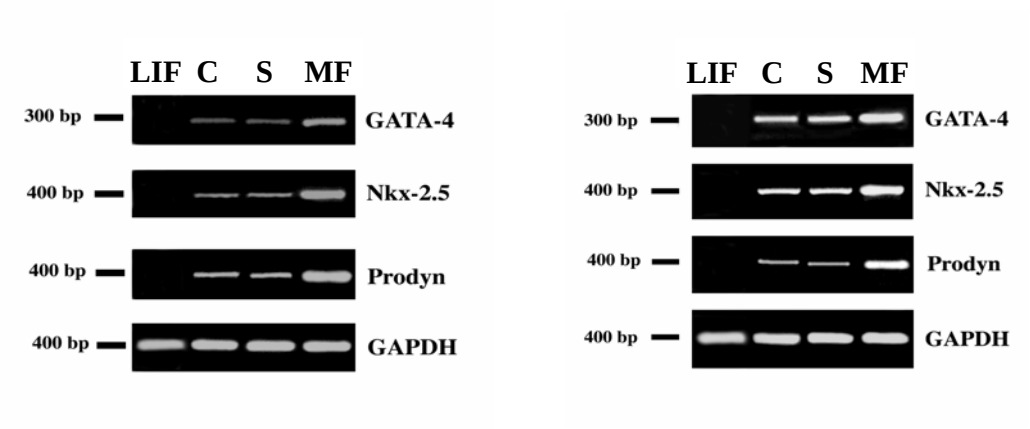

Figure 2

Effect of ELF-MFs on a cardiogenic transcriptional profile in embryoid bodies (left panel) and puromycin-selected cardiomyocytes (right panel). LIF, leukemia inhibitory factor; C, control; S, sham; MF, magnetic field; Prodyn, prodynorphin. GAPDH, (Glyceraldehide-3-phosphate dehydrogenase) was used as reference.

Exposure to ELF-MFs triggered the expression of GATA-4 and Nkx-2.5 mRNA in both EBs and puromycin-selected cardiomyocytes. Notably, these transcripts encode for a zinc finger-containing transcription factor and a homeodomain, that are both essential for cardiac lineage commitment in different animal species, including humans (7-9). Moreover, ELF-MF increased the expression of the prodynorphin gene, which encodes for the dynorphin family of endorphin peptides, previously shown to act as orchestrators of the transcription of both cardiogenic and cardiospecific genes in mouse ES cells (10,11). Consonant with our previous findings (12), the increase in prodynorphin mRNA was associated with an increase in the expression of dynorphin B, a bioactive end-product of the gene (not shown).

The attainment of a cardiac fate was inferred by the observation that ELF-MFs also elicited the expression of cardiac specific genes, including myosin light chain 2-V and alpha-myosin heavy chain, as shown in Fig. 3.
On the whole, the over-expression of both cardiogenic and cardiac-specific genes induced by ELF-MFs ensued in a remarkable increase in the yield of ES-derived spontaneously beating cardiomyocytes.

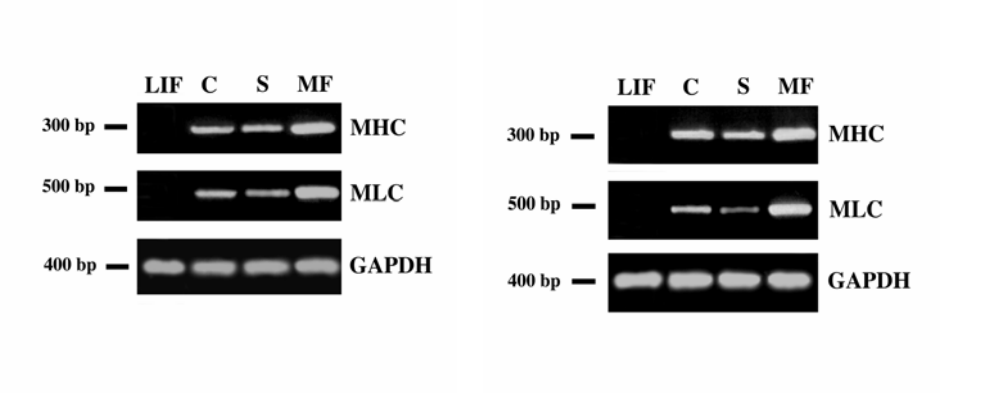

Figure 3
Effect of MF on the Expression of Cardiac Specific Genes.

Left panel, ELF-MF was applied from the time of LIF removal and EBs were collected after 3 days.
Right panel, ELF-MF was applied from the time of LIF removal throughout puromycin selection. Four days after puromycin addition, ES-derived cardiomyocytes were processed for gene expression analyses.
MHC, alpha-myosin heavy chain; MLC, myosin light chain-2V; C, control cells; S, Sham; MF, magnetic field.

To assess whether commitment to other cell lineages were recruited by ELF-MF, we investigated the expression of neurogenin-1, a gene involved in neuronal specification, and myoD, a transcript associated with skeletal myogenesis. While myoD was not affected by cell exposure, neurogenin-1 mRNA was only slightly increased in EBs (Fig. 4).

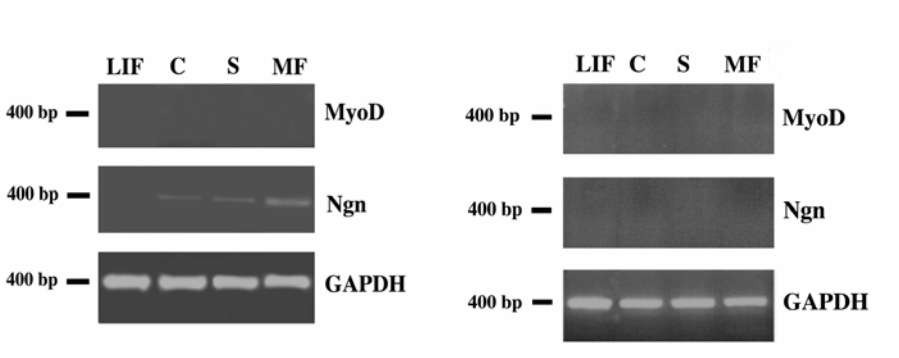

Figure 4
Effect of ELF-MF on the expression of genes promoting non-myocardial lineages.
Left Panel, ELF-MF was applied from the time of LIF removal and EBs were collected after 3 days.

Right panel, ELF-MF was applied from the time of LIF removal throughout puromycin selection. Four days after puromycin addition, ES-derived cardiomyocytes were processed for gene expression analyses. Ngn, neurogenin1, determination gene; C, control; S, Sham; MF, magnetic field.

Summary

The development of a model of *in vitro* cardiogenesis based on "gene trapping" selection of cardiomyocytes from pluripotent GTR1 cells provided a homogeneous and reproducible approach to assess the effect of MF on developmental decisions in ES cells.

In this model of cardiogenesis, MF elicited the expression of a gene program of cardiogenesis, along with the induction of cardiac-specific transcripts.

MF failed to activate skeletal myogenesis but slightly enhanced the expression of a vertebrate neural determination gene.

These results demonstrating the potential use of magnetic fields for modifying the gene program of cardiac differentiation in ES cells without the aid of gene transfer technologies may pave the way for novel approaches in tissue engineering and cell therapy. Within this context we are now planning to investigate whether ELF-MF with different physical characteristics (frequency, amplitude and wave shape) may influence cell lineage commitment even in human mesenchymal stem cells.

Acknowledgments

This work was supported by the European Project "Risk evaluation of potential environmental hazards from low-energy electromagnetic field exposure using sensitive in vitro methods" (REFLEX), by Ministero dell'Istruzione, dell'Università e della Ricerca (MIUR) 5% "Salvaguardia dell'uomo e dell'ambiente dalle emissioni elettromagnetiche," by MIUR Fondo Integrativo Speciale per la Ricerca – 2001, and by Ministero della Sanità (Attività di Ricerca Finalizzata – 2002).

References

1. Lai H, Carino MA, Horita A, Guy AW. Effects of a 60 Hz magnetic field on central cholinergic systems of the rat. *Bioelectromagnetics.* 1993;14:5–15.
2. Cossarizza A, Monti D, Bersani F, Cantini M, Cadossi R, Sacchi A, Franceschi C. Extremely low frequency pulsed electromagnetic fields increase cell proliferation in lymphocytes from young and aged subjects. *Biochem Biophys Res Commun.* 1989;160:692-8.
3. Cossarizza A, Angioni S, Petraglia F, Genazzani AR, Monti D, Capri M, Bersani F, Cadossi R, Franceschi C. Exposure to low-frequency pulsed electromagnetic fields increases interleukin-1 and interleukin-6 production by human peripheral blood mononuclear cells. *Exp Cell Res.* 1993; 204:385–7.
4. Diniz P, Shomura K, Soejima K, Ito G. Effects of pulsed electromagnetic field (PEMF) stimulation on bone tissue like formation are dependent on the maturation stages of the osteoblasts. *Bioelectromagnetics.* 2002;23:398-405.
5. Manni V, Lisi A, Rieti S, Serafino A, Ledda M, Giuliani L, Sacco D, D'Emilia E, Grimaldi S. Low electromagnetic field (50 Hz) induces differentiation on primary human oral keratinocytes (HOK). *Bioelectromagnetics.* 2004;25:118-26.
6. Lisi A, Ciotti MT, Ledda M, Pieri M, Zona C, Mercanti D, Rieti S, Giuliani L, Grimaldi S. Exposure to 50 Hz electromagnetic radiation promote early maturation and differentiation in newborn rat cerebellar granule neurons. *J Cell Physiol.* 2005;204:532-8.
7. Biben C, Harvey RP. Homeodomain factor Nkx-2.5 controls left/right asymmetric expression of bHLH gene eHand during heart development. *Genes Dev.* 1997;11:1357–69.
8. Lints TJ, Parsons LM, Hartley L, Lyons I, Harvey RP. Nkx-2.5: a novel murine homeobox gene expressed in early heart progenitor cells and their myogenic descendants. *Development.* 1993;119:419–31.
9. Benson DW, Silberbach GM, Kavanaugh-McHugh A, Cottrill C, Zhang Y, Riggs S, Smalls O, Johnson MC, Watson MS, Seidman JG, et al. Mutations in the cardiac transcription factor Nkx-2.5 affect diverse cardiac developmental pathways. *J Clin Invest.* 1999;104:1567–73.

10. Ventura C, Zinellu E, Maninchedda E, Fadda M, Maioli M. Protein kinase C signaling transduces endorphin-primed cardiogenesis in GTR1 embryonic stem cells. *Circ Res.* 2003;92:617–22.
11. Ventura, C., Zinellu, E., Maninchedda, E., and Maioli, M. Dynorphin B is an agonist of nuclear opioid receptors coupling nuclear protein kinase c activation to the transcription of cardiogenic genes in GTR1 embryonic stem cells. *Circ Res.* 2003;92:623–29.
12. Ventura C, Maioli M, Asara Y, Santoni D, Mesirca P, Remondini D, Bersani F. Turning on stem cell cardiogenesis with extremely low frequency magnetic fields. *FASEB J.* 2005;19:155-7.

EFFECTS OF GSM BASE STATION ELECTROMAGNETIC RADIATION ON OXIDATIVE STRESS IN RATS

ALI IHSAN YUREKLI, MSC
TUBITAK – UEKAE, P.K.74 GEBZE 41470 KOCAELI, TURKEY

MEHMED OZKAN, PROF.DR.
BOGAZICI UNIVERSITY, INSTITUTE OF BIOMEDICAL ENGINEERING
34342 BEBEK-ISTANBUL, TURKEY

TUNAYA KALKAN, PROF.DR.
ISTANBUL UNIVERSITY, CERRAHPASA MEDICAL FACULTY,
BIOPHYSICS DEPARTMENT, ISTANBUL, TURKEY

HALE SAYBASILI, ASSOC.PROF.DR.
BOGAZICI UNIVERSITY, INSTITUTE OF BIOMEDICAL ENGINEERING
34342 BEBEK-ISTANBUL, TURKEY

HANDAN TUNCEL, PHD
ISTANBUL UNIVERSITY, CERRAHPASA MEDICAL SCHOOL,
BIOPHYSICS DEPARTMENT, ISTANBUL, TURKEY

PINAR ATUKEREN, PHD
ISTANBUL UNIVERSITY, CERRAHPASA MEDICAL SCHOOL,
BIOCHEMISTRY DEPARTMENT, ISTANBUL, TURKEY

KORAY GUMUSTAS, PROF.DR.
ISTANBUL UNIVERSITY, CERRAHPASA MEDICAL SCHOOL,
BIOCHEMISTRY DEPARTMENT, ISTANBUL, TURKEY

SELIM SEKER, PROF.DR.
BOGAZICI UNV., FACULTY OF ENG., ELECTRICAL-ELECTRONICS ENG.
DEPARTMENT, 34342 BEBEK-İSTANBUL, TURKEY

Abstract:

The ever-increasing use of cellular phones and increasing number of associated base stations are becoming a widespread source of non-ionizing electromagnetic radiation.
In this study, we submit an animal study in a confined, well-controlled environment, with an intention to investigate effects of GSM Base Transceiver Station (BTS) EM radiation on oxidative stress and generation of free radical. During this study a group of young adult male Wistar albino rats was exposed to EM fields inside a test chamber, while another group was sham-exposed under the same conditions. Malondialdehyde (MDA) levels were assessed as a marker of lipid peroxidation and the activities of GSH and SOD were determined in order to evaluate antioxidant status in the blood samples of exposed rats.

MDA level was increased significantly ($p<0.0001$) for the experiment group when compared to the sham-exposed group. SOD activity was also increased for the experiment group, although less significantly ($p=0.019$), when compared to the sham-exposed group. GSH concentration decreased significantly ($p<0.0001$) for the experiment group when compared to the sham exposed group.
Our results indicate that exposure to EM fields at BTS frequencies may modulate the oxidative stress of free radicals by enhancing lipid peroxidation and reducing the concentration of GSH.
Keywords: Electromagnetic field, base transceiver station, antioxidants, oxidative stress, GTEM.

1. INTRODUCTION

The fast growing second generation mobile phone system, Global System for Mobile Communications (GSM), has become the world's largest mobile telecommunications system, with its one billion subscribers in over 200 countries [1]. Electromagnetic (EM) radiation produced by mobile phone and their base station antennas are in the 890 – 960 MHz frequency range for the GSM900 system. While mobile phones emit low power (2 Watts or less) EM fields in the 890 – 915 MHz range, the base station emissions are much higher in power and in the 935 – 960 MHz range. Since mobile phones are kept and used near the body, in particular near the head, emissions should be analyzed in the near field. On the other hand, base station radiation must be modeled with far field considerations. Another concern on base stations is the continuous emission of EM radiation. Therefore, residents who live close to base stations may have a bigger health concern than the casual users of the mobile phones.

There are a number of governmental and independent organizations working on the regulation of the EM radiation from mobile phones and their base stations. As a result useful guidelines and directives have been placed in act [2, 3]. These guidelines, however, focus on the SAR values, which addresses the energy deposition in the body in terms of heat. In May 2000, in IEGMP *Mobile Phones and Health* report [4], concerns were reaffirmed in the following statement, as: "…There is now scientific evidence, however, which suggests that there may be biological effects occurring at exposures below these guidelines…"

A relatively recent comprehensive survey on mobile phone health effects, published by NRPB (UK) [5], summarizes 26 reports from several countries. The survey concludes that although the possibility of low level EM field exposure causing adverse health effects remain "unproven", additional well targeted, high quality research will be valuable to explore the remaining uncertainties further.

One of the areas of interest by scientists in recent years is the EM radiation induced oxidative stress in biological systems. The issue was first studied for the extremely low frequency (ELF) range, particularly for the power-line frequency the magnetic fields [6, 7]. Some recent studies also address effects in radio frequency (RF) range, especially for the mobile telecommunications emissions [8, 9, 10, 11].

Free radical is a molecule or ion that has an unpaired electron in its outer orbit. Radical particles are unstable and are very reactive. Most common free radicals are produced from oxygen metabolism and are, thus, called as reactive oxygen species (ROS). Free radicals start chain reactions as the unpaired electron is transferred from one molecule to another. One known consequence of this kind of a chain reaction is the lipid peroxidation, where reactive radicals, such as NO_2^-, OH^- or $CCl_3O_2^-$, abstract an atom of hydrogen from poly-unsaturated fatty acid (PUFA) side chains in membranes or lipoproteins. This leaves an unpaired electron on carbon. The carbon radical reacts with oxygen and the resulting peroxyl radical attacks adjacent fatty acid side chains to generate new carbon radicals and so the chain reaction continues. The attack of one reactive free radical can oxidize multiple fatty acid side chains to lipid peroxides, damaging membrane proteins. This makes the membrane leaky and eventually causes complete membrane breakdown [12]. MDA is one of the end products of lipid peroxidation which is mostly used as an oxidative stress marker.

There are experimental evidences that oxidative stress and consequent free radical production are important causative factors in the pathology of several degenerative disorders; such as neurodegenerative diseases, carcinogenesis, atherosclerosis, hypertension and diabetic mellitus [13,14,15,16]. Oxidative stress refers to the cytotoxic consequences of oxygen radicals, such as superoxide anion ($O_2^{\cdot -}$), hydroxyl radical ($OH\cdot$) and hydrogen peroxide (H_2O_2), which are generated as byproducts of cellular aerobic metabolism. Oxygen radicals can attack DNA, proteins and lipid membranes, thus disturbing their physical function.

Fortunately, there are enzymatic systems to counterbalance the production of ROS. Superoxide dismutase (SOD), catalase (CAT) and glutathione peroxidase (GSH-Px) are enzymes responsible for

degradation of $O_2^{\cdot -}$. While SOD converts $O_2^{\cdot -}$ to H_2O_2, GSH-Px converts H_2O_2 to water and oxygen. GSH-Px uses H_2O_2 to oxidize reduced glutathione (GSH). Decreased activity of GSH-Px leads to accumulation of H_2O_2, which in the presence of iron and copper promotes the Fenton reaction to yield $OH^{\cdot}$. Hydroxyl radical is the most reactive form of oxygen radicals that can initiate a chain reaction to generate numerous toxic reactants. GSH-Px also participates in detoxification of lipid peroxyl radicals [17, 18].

In this article, we submit an animal study in a confined, well-controlled environment, with an intention to investigate effects of GSM Base Transceiver Station (BTS) EM radiation on oxidative stress and generation of free radical. During this study a group of young adult male Wistar albino rats was exposed to EM fields inside a test chamber, called Gigahertz Transverse Electromagnetic (GTEM) Cell, while another group was sham-exposed under the same conditions. Malondialdehyde (MDA) levels were assessed as a marker of lipid peroxidation and the activities of GSH and SOD were determined in order to evaluate antioxidant status in the blood samples of exposed rats.

2. METHODS

2.1 Exposure Environment

The test setup is a general purpose EM shielded chamber that is suitable to house laboratory animals. In this exposure environment electromagnetic radiation of specific energy, frequency and waveform can be applied. The main element of the setup (Figure 1) is a GTEM Cell [GTEM 1750, MEB, Germany], installed in Electromagnetic Compatibility (EMC) Laboratory of TUBITAK-UEKAE.

GTEM Cell is a radiated field generation and measurement device that has a single input/output port for EM immunity and emission test purposes. GTEM Cell, in essence, is a transmission line terminated with 50 Ω load. The asymmetrical inner conductor (called “septum”) is designed to match the impedance of a tapered, rectangular wave guide cross section. The outer surface of the GTEM Cell is made of metal sheets with an attenuation of around 60 dB at high frequency EM fields. Note that honeycomb waveguides are installed at the bottom of the GTEM Cell for ventilation purposes. Electric field level is directly proportional to the amplitude of the voltage applied to the input port and inversely proportional with the septum height. In order to obtain increased field level with constant input power, cages that contain the test subjects are designed and placed closer to the input port of the GTEM Cell for the purpose of biological effect studies as illustrated in Figure 2

Signal generators, are used to feed the input port of the GTEM cell in order to imitate the electromagnetic fields emitted from base transceiver stations. A properly selected signal generator [SMY01, Rohde&Schwarz, Germany] generates the 945 MHz carrier wave which is then pulse modulated at 217 Hz [using Stanford Research Systems DG535 Digital Delay/Pulse Generator, USA] in accordance with GSM specifications. Output of the signal generator is then connected to a 100W power amplifier [757LCB-CE, Kalmus, USA]. Power feed to the GTEM cell input is provided through a directional coupler. One port of the directional coupler is connected to a power meter [Rohde&Schwarz NRVS with thermal probe NRV-Z51] through which applied power level is monitored (Figure 1).

The rats are enclosed inside two “*metabolic cages*” which are placed adjacent to each other. These cages are designed so as to feed and water the rats and collect urine samples through its structure. The cages are composed of transparent Plexiglas material. It is thus assumed that the cages have minimal effect on the applied electric field. The rats are free to move inside a volume of 24 cm (W) x 34 cm (L) x 12.5 cm (H). The applied electric field is perpendicular to the plane on which the rats move; therefore each animal is exposed to the field without any obstruction caused by its “neighbors”.

2.2 SAR Calculation

It is necessary to make the dosimetric evaluation of an electromagnetic field exposure experiment in order to deduce meaningful results and compare various biological effects produced with different test setups. Dosimetric evaluation is performed, in general, in terms of Specific Absorption Rate, known as “SAR” in short. Since exposure from Base Transceiver Stations (BTS) is generally in the far field, whole-body average SAR is taken into consideration in this experiment. Whole-body average SAR is defined as the total energy, transferred to the body per unit time, divided by the total mass.

.

The Finite-Difference Time-Domain (FDTD) method implemented in a MATLAB program was used to compute the expected SAR values on the subjects in a simulation environment.

In order to validate the numerical model and MATLAB implementation of the FDTD technique, electric field levels were measured at 10 selected positions on an XY plane located at the middle of the Z axis and compared with those that were obtained by the FDTD technique. These points were selected such that they represent the position of the rats in metabolic cages during actual EM exposure. The simulation software was executed for three times for different input power levels. Electric field levels were also measured by an electric field meter [Acterna EMR-300 with Type 8 E-field probe, Germany], again at those specified input power levels. We found out that FDTD model closely simulates the actual exposure environment (less than 7% difference in the average electric field levels). Thus, the model is a good approximation of the real life measurements. Electric field measurement results also indicated that a fairly uniform electric field was applied to the test subjects in the exposure environment.

The test subject was, on the other hand, modeled roughly with an effort to maintain some details of its geometry. The rat, as a whole, was modeled using electrical properties at 945 MHz, calculated for average muscle tissue, corresponding to: ε =55.853462 and σ=0.985515. Rat muscle tissue density was taken as, ρ=1040 mg/cm^3. For the sake of simplicity, rat cages were not included in the model since they are transparent to electromagnetic radiation. Normalized SAR value for this exposure environment was found to be 0.90 mW/kg per input W. Thus, when this exposure setup is used for assessment of biological effects, we can compute the SAR values through the FDTD model easily once the GTEM input power level is given.

2.3 Electromagnetic Exposure

Calculations above show that in this test environment SAR values we can induce are well below the safety standards [3]. A set of exposure experiments was performed in two phases to investigate the biological effects of the electromagnetic fields at GSM BTS frequency. The first phase was the EM field exposure experiment and the second was the sham exposure (see Table 1). In each phase, the following procedure was applied:

The animals were obtained from the Experiment Animals Center of Istanbul University Cerrahpasa Medical School. For each of the two phases a set of 9 healthy, young adult male Wistar albino rats were used. The rats were cared for in accordance with the Guide for the Care and Use of Laboratory Animals [20]. The rats have been fed with standard pellet food and watered by tap water ad libitum. The rats have been weighted before, after and at each day of the experiment. Average weights of both groups before and after the experiment and their average food and water consumption are given in Table 2.

The subjects were placed inside two metabolic cages, 5 rats in one cage and 4 rats in the other. The cages were placed in the test volume inside the GTEM cell as shown in Figure 2. Radiofrequency EM field (3.67 W/m^2 power density) was applied onto the exposure group for the first phase, while there was no EM field exposure onto the sham group, in the second phase. We could only apply a low power level, which corresponds to a SAR value of 11.3 mW/kg, because of the time averaging of the applied peak power level in accordance with the GSM modulation of the carrier wave. The cages containing the rats were kept inside the GTEM Cell for 7 hours for a period of 8 days for each group.

2.4. Metabolite Gathering and Analysis

At the end of each phase, the animals were anesthetized. After exploration of the thorax, intracardiac blood was quickly obtained. The tubes containing the processed blood samples were stored at -24 ^{o}C until they were analyzed at the Cerrahpasa Medical School Biochemistry Laboratory. These samples were processed for measuring MDA, GSH and SOD levels. The materials collected were analyzed using a spectrophotometer [JASCO V-530 UV/VIS] according to standard laboratory procedures [21,22].

MDA level was determined in plasma using the principle of spectrophotometric determination of absorbance at 535 nm of colored complex which is formed by condensation of two molecules of thiobarbituric acid and one molecule of the material that it reacts with. For this purpose, 1 ml of a stock solution, which was prepared from trichloroacetic acid, thiobarbituric acid and hydrochloric acid, was added to 0.5 ml of plasma. After pippeting, tubes were closed and put inside a boiling water bath for 20 minutes. After cooling down, they were centrifuged at 2000 cycles/min for 10 minutes. Absorbance of the supernatant solution was read against the blind solution. MDA level is given in millimoles per liter (mM/L).

GSH concentration was determined in total blood by color reading at 412 nm of the solution that is formed by the reaction of free sulfhydryl compounds in the whole blood with 5,5'-Dithiobis (2-nitrobenzoic acid) (DTNB). Note that DTNB is a disulfide chromogen that is readily reduced by sulfhydryl compounds to an intensely yellow compound and the absorbance of the reduced compound is directly proportional to the GSH concentration. Cuverts were prepared for GSH calibrator, erythrocyte and precipitating agent. After incubating at room temperature for 5 minutes, the solutions were centrifuged at 3000 cycles/min for 10 minutes. Upper phase was extracted and phophate buffer, DTNB and distilled water were added. The color reading was performed at 412 nm against the blind solution in 4 minutes. Using glutathione standard curve did the calculation. GSH concentration was expressed in milligrams per gram hemoglobin (mg / g Hb).

The method of determination of SOD activity was based on the reduction of nitroblue tetrazolium by superoxide anions that were formed by xanthine/xanthine-oxidase system and then inhibition of superoxide anions by SOD. Reaction mixture used to determine the SOD activity in erithrocytes was prepared using xanthine, EDTA, nitroblue tetrazolium, Na_2CO_3 and bovin serum albumin at specified concentrations inside a 200 ml flask. Reaction mixture was set to a pH level of 10.2. Supernatant solution was prepared using chloroform letanal, erythrocyte and distilled water. This solution was centrifuged at 15000 cycles/min for 10 minutes. Test and blind solutions of 1.07 ml were incubated at 25 ^oC for 20 minutes.After adding 0.05 ml of $CuCl_2$ (8 mM/l) reaction was stopped. Note that the 50 % inhibition with respect to the blind inside the reaction tube corresponds to 1 unit of SOD activity. The units of SOD activity was determined by simple linear ratio. But it had to be further determined with respect to the hemoglobin concentration inside the solution, so the resultant SOD activity was formulated in terms of units per gram hemoglobin (or U / g Hb).

Hemoglobin concentration for GSH and SOD analysis was determined using Drabkin's reagent. 3 mL reagent was mixed with 1:20 hemolysate and kept in dark for 10 minutes. Absorbance at 540 nm was read against a blank of Drabkin's solution and hemolysate hemoglobin concentration was determined from a calibration curve.

Data was presented as means standard deviation. SPSS software package (SPSS for Windows release 11.50) was used for statistical analysis. The analysis results were evaluated based on Mann-Whitney U test statistics and a $p<0.05$ was considered significant.

3. RESULTS

Lipid peroxidation (MDA – malondialdehyde), GSH (reduced glutathione) and SOD (superoxide dismutase) analysis results are given in Figure 3, Figure 4 and Figure 5, respectively. Levels of all the three parameters of interest have been changed significantly under EM radiation effect. MDA level was increased significantly ($p<0.0001$) for the experiment group (10.20 ± 0.78 mM/L) when compared to the sham-exposed group (6.77 ± 0.60 mM/L). SOD activity was also increased for the experiment group (2.53 ± 0.87 Units / mg Hb), although less significantly ($p=0.019$), when compared to the sham-exposed group (1.79 ± 0.72 Units / mg Hb). GSH concentration, on the other hand, decreased significantly ($p<0.0001$) for the experiment group (7.84 ± 1.15 mg / g Hb) when compared to the sham exposed group (19.19 ± 1.64 mg / g Hb).

4. DISCUSSION AND CONCLUSION

A two-phase experiment was designed in order to investigate the effects of EM fields at GSM BTS transmitter frequencies. In the first phase, EM field at 945 MHz of 3.67 W/m^2 power density, which is calculated to produce a SAR value of 11.3 mW/kg, was applied on a group of 9 rats inside a GTEM Cell. In the second phase, the same number of rats was sham exposed under the same conditions. The duration was 7 hours/day for a period of 8 days, in each phase.

Biochemical analysis of blood samples indicate that the GSM BTS EM radiation exposed rats have higher concentration levels of MDA (malondialdehyde) and lower GSH (glutathione) concentrations when compared to the sham exposed group. This outcome is in agreement with the results of some previous studies. Dasdag et al. [9] studied the effects of mobile phone EM radiation on rat brain tissues, where rats are exposed to EM fields for 20 min/day for 30 days (SAR=0.52 W/kg). The MDA levels in rat brain tissues increased significantly after exposure. In another study by Ozguner et al. [11], renal impairment in rats was investigated under mobile phone radiation (SAR=0.016 W/kg). Rats were exposed 30 min/days for 90 days and the result was increase of renal tissue MDA, NO (nitric oxide) and urinary NAG (N-acetyl-β-D-glucosaminidase) levels

and significant decrease of tissue SOD, CAT (catalase) and GSH-Px (glutathione peroxidase) levels. Ilhan et al. [10] studied mobile phone induced oxidative stress in rat brain. Rats were exposed to mobile phone emissions (SAR=0.25 W/kg) for 1 hour/day for 7 days. MDA and NO levels were increased whereas GSH-Px and SOD activities were decreased significantly in rat brain tissue. Additionally, XO and ADA levels were also increased. Moreover, Moustapha et al. [24] have studied acute mobile phone exposure effects on human volunteers and found out that MDA level in plasma was increased and GSH-Px and SOD activities were decreased in human erythrocytes after 1h, 2h and 4h of exposure. No significant change was observed for CAT activity in this study.

However, some other studies in literature have concluded in no relation between EM field exposure and free radical activity. Irmak et al. [24] have shown that EM radiation from mobile phones applied 30 min/days for 7 days on rabbits had no significant effect on rabbit brain, suggesting that oxygen free radicals were not generated. But, they have observed a significant increase in serum SOD activity in the exposed group. In addition, Zmyslony et al. [8] have exposed rat lymphocytes in vitro to 930 MHz continuous wave (CW) radiation inside a GTEM Cell (SAR=1.5 W/kg). Five min and 15 min acute exposure resulted in no change in reactive oxygen species production in living cells. However, change was observed when lymphocytes were treated with $FeCl_2$ as a stimulating agent.

Some research studies relates oxidative stress to certain diseases. In a Parkinson's disease model SOD, CAT and GSH-Px activities were increased in striatum and ventral midbrain of mice [25]. In another Parkinson's disease model Thiffault et al. [26] showed an increase in SOD activity with no increase in GSH-Px activity in mice brain. Neuronal GSH deficiency and age dependent neurodegeneration were found to be related with the down regulation of excitatory amino acid transporters in mice [27].

According to our results, MDA level and SOD activity were increased, whereas GSH concentration was decreased in EM radiation exposed rats when compared to sham-exposed group. We think that decreased GSH concentration may be due to the higher consumption of GSH for scavenging the higher production of free radicals. The lower GSH concentration may have some relation to the increased SOD activity. Note that the endogenous GSH has a protective function in scavenging radicals and in molecular repair. However, such scavenging can set up a superoxide-dependent chain production of H_2O_2 and oxidized glutathione, which would oxidatively stress the cell. Therefore, the increased SOD activity may be a response to suppress the higher chain oxidation of GSH, or a response to balance the decreased GSH concentration.

Thus, the up regulated SOD activity converts $O_2^{\cdot}$ to H_2O_2 and down regulated GSH concentration leads to the insufficient detoxification and accumulation of H_2O_2 in the system. H_2O_2 is known to be converted to hydroxyl radical in the presence of iron rapidly, which is the most damaging form of ROS. Note that the balance between GSH-Px and SOD appears to be important for the cellular resistance to oxidative stress [28].

In conclusion, our results indicate that exposure to EM fields at BTS frequencies may modulate the oxidative stress of free radicals by enhancing lipid peroxidation and reducing the concentration of GSH. It is highly probable that detoxification of lipid peroxyl radicals can not be accomplished in our system. We note that reactive oxygen species may have a probable role on adverse effects of EM fields at mobile telecommunication frequencies. The outcome of this study needs confirmation by repetitive laboratory studies, including higher dose and longer duration exposure, and theoretical mechanisms underlying this effect should also be addressed in future.

Acknowledgements:

The authors thank Mehmet YAZICI for his help on SAR calculation using FDTD method and Dr. Huseyin AKSU for his help on statistical evaluation.

The present work was supported by the Research Fund of Istanbul University. Project No: 859/16082006.

This research is sponsored by Bogazici University Research Fund, project number: 01HX102D.

References:

1. NRPB. Mobile Phones and Health 2004. National Radiation Protection Board Report. **2004** 15:5. UK. Available from: http://www.hpa.org.uk/radiation/publications/documents_of_nrpb/abstracts/absd15-5.htm

2. ICNIRP. Guidelines for limiting exposure to time-varying electric, magnetic and electromagnetic fields (up to 300 GHz). Health Physics **1998**, 74, 494-522.
3. CENELEC. EN 50360. Product standard to demonstrate the compliance of mobile phones with the basic restrictions related to human exposure to electromagnetic fields (300 MHz - 3 GHz). European Standards Organization. Directive 199/5/EC on Radio Equipment and Telecommunications Terminal Equipment and the mutual recognition of their conformity. **2001**.
4. IEGMP. Mobile Phones and Health. Report of Independent expert Group on Mobile Phones. National Radiation Protection Board Report. Oxon, UK. **2000**. Available from: http://www.iegmp.org.uk/report/text.htm.
5. Sienkiewicz ZJ, Kowalczyk CI.. A Summary of Recent Reports on Mobile Phones and Health (2000–2004). National Radiation Protection Board Publication. W65. UK. **2005**. Available from: http://www.hpa.org.uk/radiation/publications/w_series_reports/2005/nrpb_w65.htm
6. Brocklehurst B, McLauchlan KA.. Free radical mechanism for the effects of environmental electromagnetic fields on biological systems. Int J Radiat Bio **1996**, 69, 3-24.
7. Lacy-Hubert A, Metcalfe JC, Hesketh R. Biological responses to electromagnetic fields. FASEB Journal **1998**, 12, 395-420.
8. Zmyslony M, Politanski P, Rajkowska E, Szymczak W, Jajte J. Acute exposure to 930 MHz CW electromagnetic radiation in vitro affects reactive oxygen species level in rat lymphocytes treated by iron ions. Bioelectromagnetics **2004**, 25, 324-328.
9. Dasdag S, Akdag MZ, Aksen F, Bashan M, Buyukbayram H. Does 900 MHz GSM Mobile Phone Exposure Affect Rat Brain? Electromagnetic Biology and Medicine **2004**, 23, 201-214.
10. Ilhan A, Gurel A, Armutcu F, Kamisli S, Iraz M, Akyol O, Ozen S. Gingko biloba prevents mobile phone-induced oxidative stress in rat brain. Clinica Chemica Acta **2004**, 340, 153-162.
11. Ozguner F, Oktem F, Ayata A, Koyu A, Yilmaz HR. A novel antioxidant agent caffeic acid phenetyl ester prevents long-term mobile phone exposure-induced renal impairment in rat. Molecular and Cellular Biochemistry **2005**, 277, 73-80.
12. Anderson D. Antioxidant defences against reactive oxygen species causing genetic and other damage. Mutation Research **1995,** 350, 103-108.
13. Simonian NA, Coyle JT. Oxidative Stress in Neurodegenerative Diseases. Annu Rev Pharmacol Toxicol **1996**, 36, 83-106.
14. Turner RN. Free radicals and disease: the toxaemia hypothesis, Complementary Therapies in Medicine **1996**, 4, 43-47.
15. Mahboob M, Shireen KF, Atkinson A. Lipid peroxidation and antioxidant enzyme activity in different organs of mice exposed to low level of mercury. J Environ Sci Health B. **2001**, 36, 687-697.
16. Maritim AC, Sanders RA, Watkins JB 3rd. Diabetes, oxidative stress, and antioxidants: a review. J Biochem Mol Toxicol **2003**,17, 24-38.
17. Stadtman ER. The Role of Free Radical Mediation of Protein Oxidation in Aging and Disease. In Özben T (eds.): Free Radicals, Oxidative Stress, and Antioxidants). New York: Plenum Press, **1998**, 131-143.
18. Coyle JT, Puttfarcken P. Oxidative Stress, Glutamate and Neurodegenerative Disorders. Science **1993**, 262, 689-694.
19. Chou CK, Bassen H, Osepchuk J, Balzano Q, Petersen R, Meltz M, Cleveland R, Lin JC, Heynick L. Radiofrequency Electromagnetic Exposure: Tutorial Review on Experimental Dosimetry. Biolectromagnetics **1996**, 17, 195-208.
20. National Research Council. Guide for the Care and Use of Laboratory Animals, National Academy Press Washington, D.C. **1996**.
21. Burtis CA, Ashwood ER, Tietz NW. Tietz Textbook of Clinical Chemistry. W.B. Saunders Company. 3rd Ed. **1999**.
22. Yi Sun, Oberley LW, Ying Li,. A simple method for clinical assay of superoxide dismutase. Clinical Chemistry **1988** , 34, 497-500.
23. Moustapha YM, Moustapha RM, Belacy A, Abou-El-Ela SH, Ali FM. Effects of acute exposure to radiofrequency fields of cellular phoneson plasma lipid peroxide and antioxidase activities in human erythrocytes, Journal of Pharmaceutical and Biomedical Analysis **2001**, 26, 605-608.
24. Irmak K, Fadillioglu E, Gulec M, Erdogan H, Yagmurca M, Akyol O.Effects of electromagnetic radiation from a cellular telephone on the oxidant and antioxidant levels in rabbits. Cell Biochemistry and Function **2002**, 20, 279-283.
25. Cassarino DS, Fall CP, Swerdlow RH, Smith TS, Halvorsen EM, Miller SW, Parks JP, Parker WD, Bennett JP. Elevated Reactive Oxygen Species and Antioxidant Enzyme Activities in Animal and Cellular Models of Parkinson's Disease. Biochimica et Biophysica Acta **1997**, 1362, 77-86.
26. Thiffault C, Aumont N, Quirion R, Poirier J.Effect of MPTP and L-Deprenyl on Antioxidant Enzymes and Lipid Peroxidation Levels in Mouse Brain. J Neurochem **1995**, 65, 2725-2733.
27. Aoyama K, Suh SW, Hamby AM, Liu J, Chan WY, Chen Y, Swanson RA. Neuronal glutahione deficiency and age dependent neurodegeneration in the EAAC1 deficient mice. Nature Neurosci , **2005**, 9, 110-126.
28. Amstad P, Moret R, Cerutti P. Glutathione Peroxidase Compensates for the Hypersensitivity of Cu, Zn-Superoxide Dismutase Overproducers to Oxidant Stress. J Biol Chem **1994**, 269, 1606-1609.

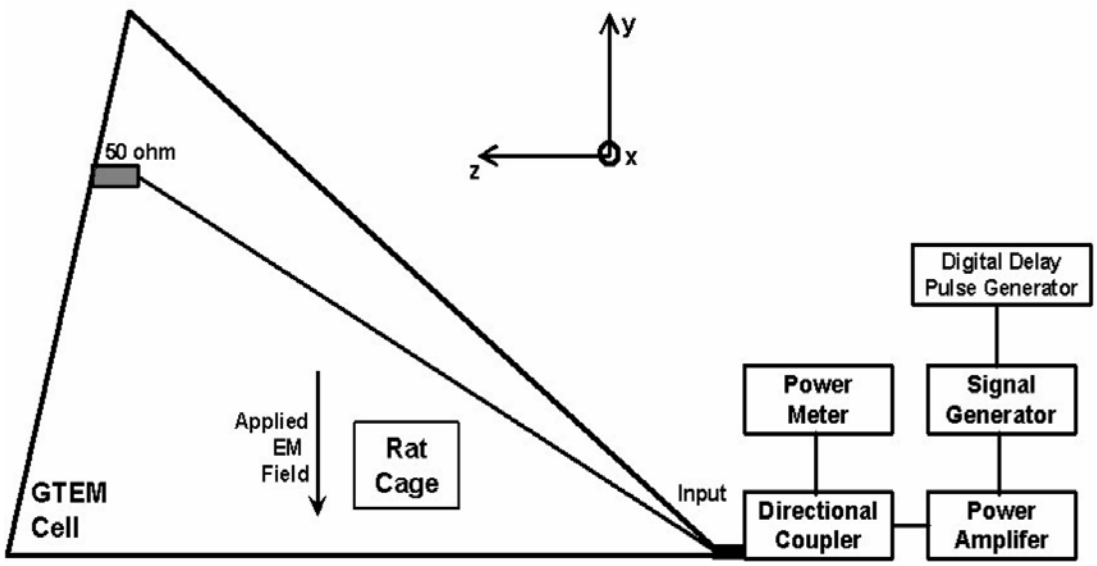

Figure 1. Electromagnetic field exposure setup.

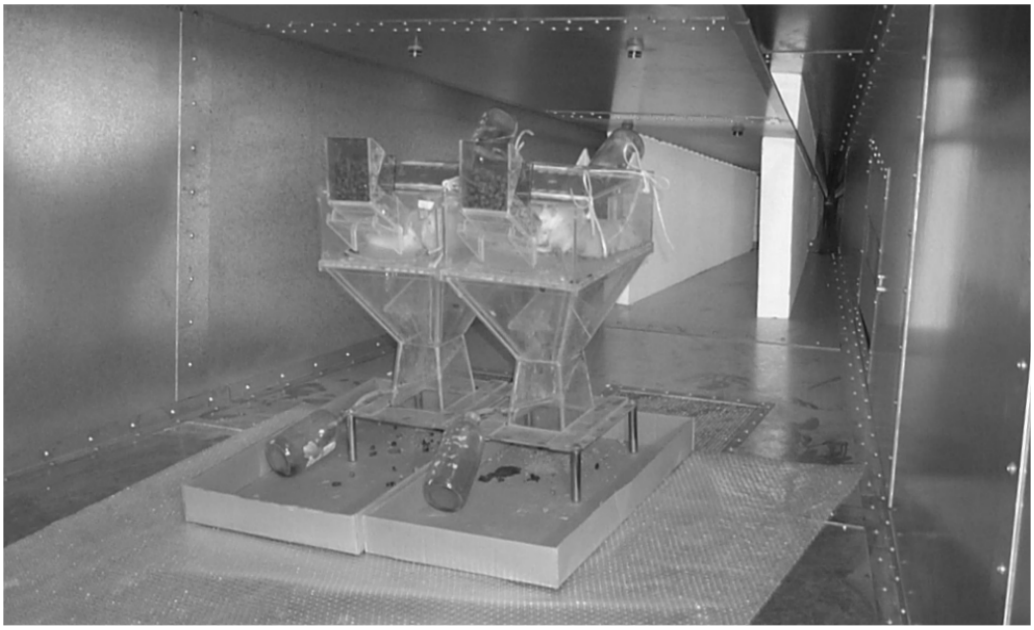

Figure 2. A group of rats contained in two metabolic cages inside GTEM Cell.

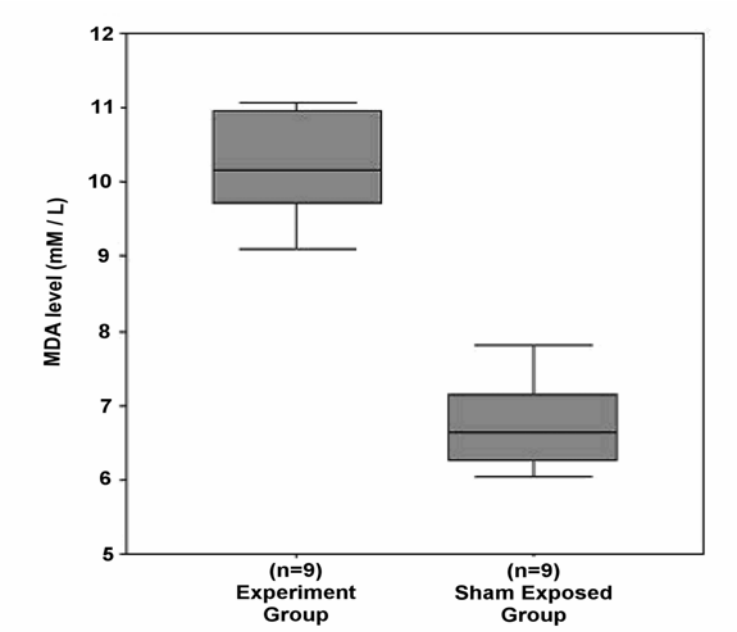

Figure 3. Effects of 945 MHz electromagnetic radiation on lipid peroxidation levels in rat blood samples (mean ± SD). $p<0.0001$ vs. sham according to Mann-Whitney U test.

Table 1. Exposure parameters.

Phase	# Rat	GTEM Input Power (W)	Applied E Field Level (V/m)	Power Density (W/m^2)	SAR (mW/kg)	Exposure Duration (days)	Effective Exposure Time (hours/day)	Time Spent in GTEM Cell (hours/day)
Experiment	9	12.5	37.2	3.67	11.3	8	7	7
Sham Exposure	9	-	-	-	-	8	-	7

.

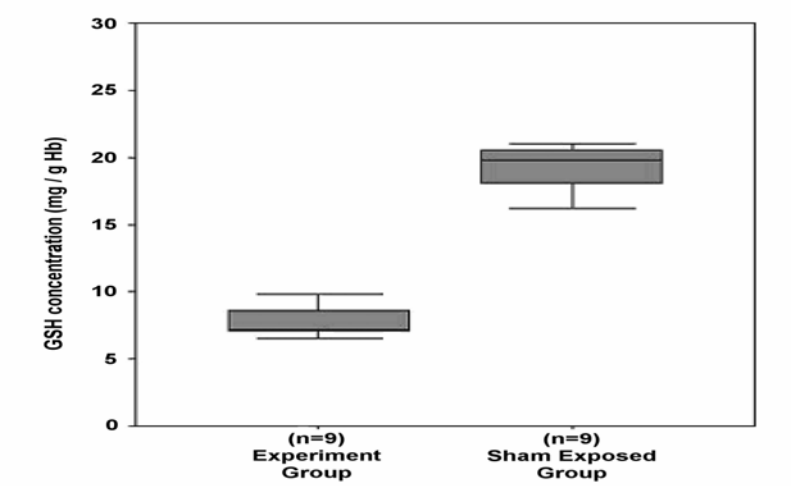

Figure 4. Effects of 945 MHz electromagnetic radiation on GSH concentration in rat blood samples (mean ± SD). $p<0.0001$ vs. sham according to Mann-Whitney U test.

Table 2. Average weights of the rats before and after the experiment and their average food and water consumption.

GROUPS	Initial Weights (g)	Weights After Exposure (g)	Average consumed food per day by single rat (g)	Average consumed water per day by single rat (ml)
Experiment	190 ± 40	220 ± 38	22	21
Sham Exposure	162 ± 43	191 ± 44	30	18

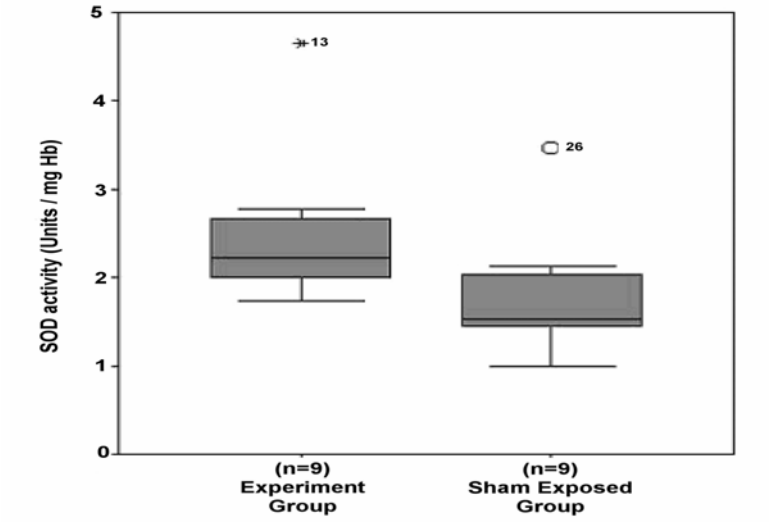

Figure 5. Effects of 945 MHz electromagnetic radiation on SOD activity in rat blood samples (mean ± SD). $p=0.019<0.05$ vs. sham according to Mann-Whitney U test.

THE PHYSIOLOGICAL BASIS FOR BASIC RESTRICTIONS IN EXTREMELY LOW FREQUENCY STANDARDS AND GUIDELINES

ANDREW W WOOD

BRAIN SCIENCES INSTITUTE, SWINBURNE UNIVERSITY OF TECHNOLOGY, HAWTHORN, VICTORIA 3122, AUSTRALIA

Abstract

In the range 0.1 – 3,000 Hz, there are significant disparities between basic restrictions in the ICNIRP guidelines and the IEEE (ICES) standard, even though in both these are derived from consideration of abnormal retinal responses (phosphenes) and peripheral nervous system stimulation. Considerable uncertainties exist in i) interpreting the available data ii) in determining the point at which bioeffects become health effects and iii) deciding on an appropriate margin for safety for occupational and general public exposure. The available data tend to be rather sparse outside the range 20 – 60 Hz.

Recent data from large-scale voxel models and from human volunteer and modeling studies of the effects of MRI switching field gradients permit some comparisons between external fields known to cause certain bio-effects and external fields estimated from basic restriction values. Some interpolation and extrapolation across the frequency range is possible. In particular, electric field limits, which were previously thought to be entirely determined by indirect effects (contact currents and micro-shock) should now, because of results from recent voxel-based modeling, be determined more by direct effects derived from basic restrictions.

The presentation will review the approach taken by a Working Group for the development of the Australian ELF Standard

Introduction

The Australian ELF Standard Working Group, from their first meeting, faced the dilemma of whether to follow the approach of ICNIRP (ICNIRP 1998) or of IEEE (IEEE 2002) in recommending basic restrictions for protection. For example, at power frequencies and for the general public, the former approach limits induced current density (J) to 2 $mA.m^{-2}$ (averaged over 1 cm^2 of tissue, perpendicular to current direction) and the latter limits induced electric field (E_{int}) to different limits in different parts of the body (averaged over a 0.5 cm line segment in the body). In the most sensitive value, the brain, the 50 Hz value is 14.7 V/m. Since the two quantities can be related via $J = \sigma E_{int}$, the two approaches can be made equivalent by taking $\sigma = 0.136$ S/m, which is not too different from the average value of 0.2 S/m often used as an average value for tissue conductivity. However, because of the different assumed frequency variation, the disparities become very large at non-power frequencies. For example, the difference at 750 Hz (assuming $\sigma = 0.136$ S/m) is 15-fold (with IEEE less conservative) and at 1 Hz, 10-fold (with IEEE more conservative at these lower frequencies). This forced the Working Group to re-examine the experimental data upon which these limits (and the associated reference levels) were derived. A number of important issues emerged, as follows:

Synaptic effects in the retina

A number of experimental reports are relevant to making estimates of the threshold tissue E_{int} for a measurable physiological response to occur. Most identify 20 Hz as the frequency for the lowest threshold. Eight studies involve the application of current to the retina (electro-phosphenes) and three the application of alternating magnetic fields (magneto-phosphenes). Considerable assumptions need to be made in each case to estimate tissue threshold, which range from 1 to over 600 mV/m. Although there is a large overlap, the electro-phosphene thresholds tend to be higher than the magneto-phosphene. The pooled value (assuming the two phenomena to be equivalent) is 56 mV/m (95% CI 2.3 – 1330 mV/m). This is very close to the RMS value used as the basis of the IEEE standard.

Peripheral neural stimulation

Some recent work on human perception and of associated mathematical modelling of neural stimulation allows limits to be estimated for this phenomenon. Most of this refers to work on the fields associated with the switching of gradient fields in Magnetic Resonance Imaging, which induce currents in the body and have characteristic frequencies typically in the range 500 – 1,000 Hz. A threshold for perception of just over 2 V/m was identified by Nyenhuis (Nyenhuis et al 2001) but further analysis using more sophisticated models gives a rather higher value of around 4 V/m (So et al 2004). Other work (Liu & Crozier 2004; Liu et al 2003), tends to confirm that the threshold value for sensation is lower than the 6.15 V/m value which form the basis for peripheral nerve stimulation in the IEEE standard (and which was derived using a mathematical model of a long, 20 μm diameter myelinated nerve).

Safety margins

There is considerable debate on the margin that should exist between the thresholds just discussed and basic restrictions for a) occupational or 'controlled environment' and b) general public categories of exposure. ICNIRP uses margins of 10, 5 or 2 depending on the context, whereas IEEE uses margins of either 1 or 3. The justifications for the actual values uses are often not fully substantiated. Another area of debate is on whether the basic restriction should be related to a threshold for sensation or for harm/pain, and what the relationship between these two levels is. There is some useful information emerging on the distribution of thresholds within the general population.

Reference or Maximum Permissible Exposure Levels: relationship with Basic Restrictions

Both the IEEE and ICNIRP standards use simple homogeneous geometrical models of the human torso/head in order to derive equivalent external field limits. In recent years highly sophisticated, voxel-based, models of both the adult male and female have become available (Caputa et al 2002) (Dimbylow 2000; Dimbylow 2005; Dimbylow 1998). In addition, models of the child (Hirata et al 2001) and the pregnant female Dimbylow (Dimbylow 2006) have also been studied. Given tissue-specific Basic Restriction values, the corresponding external fields required to produce these can be found. Although most of this work is at power frequencies, other frequencies in the ELF range have also been studied (Dimbylow 2005; Dimbylow 1998). This allows reference levels to be calculated for both the avoidance of retinal and peripheral nerve stimulation effects, the latter becoming more of a concern above a few hundred Hz. For magnetic (*B*) fields reference levels can be derived fairly straightforwardly, but levels for electric (*E*) fields are a little more complicated.

Electric field limits: direct and indirect effects

Previous standards have assumed that E_{int} induced by external electric (rather than magnetic) fields are of the order of fractions of mV/m per kV/m external. Electric (*E*) field reference levels have been set to avoid indirect effects such as contact current and micro-shock. The former effectively limits *E* fields via the Deno formula (Deno 1975) since the magnitude of contact current is directly proportional to *E*. Contact current is in turn limited by considerations of annoyance thresholds for the general population. However, the voxel-based modelling studies just described predict much larger E_{int} values than previously supposed (up to 50 mV/m per kV/m in bone, for example). Consideration of E_{int} in excitable tissue gives more conservative values for external *E* than are given by the Deno formula. However, data on micro-shock still determine *E*-field reference levels for the range of frequencies less than 100 Hz (and including DC).

Giving protection below 0.1 Hz

Here, external *E*- and *B*-fields need to be considered separately: for E-fields the need to avoid the production of micro-shocks in DC fields gives similar reference levels to those at power frequencies. On the other hand, data on *B*-fields is much more sparse, but it would appear that the reference level at DC should be at least two orders of magnitude higher than at power frequencies.

Progress within the Australian Working Party for an ELF Standard

The Working Party has developed a draft, incorporating the considerations just outlined, which it hopes will be available for public comment before the end of the year. At power frequencies, analysis along the lines just described tend to the view that the ICNIRP *B*-field reference levels are too conservative and the *E*-field levels too lax. Other considerations include: whether in controlled circumstances or activities reference levels can be relaxed for both occupational and general public exposures; what precise tissues (and what volume) do the basic restrictions refer to; what the safety margins should be? A Regulatory Impact Statement, which will include cost-benefit analyses of a) regulatory adoption or b) voluntary compliance (with the standard as an educative document), is being prepared.

The author chairs the ELF Standard Working Group set up by the Radiation Health Committee of the Australian Radiation Protection and Nuclear Safety Agency (ARPANSA). The views presented are personal to the author and should not be taken as representing those of ARPANSA or of the Australian Government.

References

Caputa K, Dimbylow P, Dawson T, Stuchly M. 2002. Modelling fields induced in humans by 50/60 Hz magnetic fields: reliability of the results and effects of model variations. *Phys Med Biol*. 47:1391-8

Deno DW. 1975. Currents induced in the body by high voltage transmission line electric field - measurement and calculation of distribution and dose. *IEEE Trans Power App Syst* 96:1517-25

Dimbylow P. 2000. Current densities in a 2 mm resolution anatomically realistic model of the body induced by low frequency electric fields. *Phys Med Biol.* 45:1013-22

Dimbylow P. 2005. Development of the female voxel phantom, NAOMI, and its application to calculations of induced current densities and electric fields from applied low frequency magnetic and electric fields. *Phys Med Biol* 50:1047-70

Dimbylow P. 2006. Development of pregnant female, hybrid voxel-mathematical models and their application to the dosimetry of applied magnetic and electric fields at 50 Hz. *Phys Med Biol* 51:2383-94

Dimbylow PJ. 1998. Induced current densities from low-frequency magnetic fields in a 2 mm resolution, anatomically realistic model of the body. *Phys Med Biol* 43:221-30

Hirata A, Caputa K, Dawson TW, Stuchly MA. 2001. Dosimetry in models of child and adult for low-frequency electric field. *IEEE Trans Biomed Eng* 48:1007-12

ICNIRP. 1998. Guidelines on limits of exposure to time-varying electric, magnetic and electromagnetic fields (1 Hz - 300 GHz). *Health Phys* 74:494-522

IEEE. 2002. IEEE standard for safety levels with respect to human exposure to electromagnetic fields, 0-3 kHz. *Rep. IEEE Std C95.6*, IEEE, New York

Liu F, Crozier S. 2004. A distributed equivalent magnetic current based FDTD method for the calculation of E-fields induced by gradient coils. *J Magn Reson* 169:323-7

Liu F, Zhao H, Crozier S. 2003. On the induced electric field gradients in the human body for magnetic stimulation by gradient coils in MRI. *IEEE Trans Biomed Eng* 50:804-15

Nyenhuis J, Bourland J, Kildishev A, Schaefer D. 2001. Health effects and safety of intense gradient fields. In *Magnetic resonance procedures: health effects and safety*, ed. F Shellock, pp. 31-53. Boca Raton, FL: CRC Press

So PP, Stuchly MA, Nyenhuis JA. 2004. Peripheral nerve stimulation by gradient switching fields in magnetic resonance imaging. *IEEE Trans Biomed Eng* 51:1907-14

METHODOLOGICAL PROBLEMS IN THE ASSESSMENT OF THE CARDIOVASCULAR FUNCTION IN WORKERS EXPOSED TO ELECTROMAGNETIC FIELDS

BORTKIEWICZ A., GADZICKA E., ZMYSLONY M.,SZYMCZAK W.

NOFER INSTITUTE OF OCCUPATIONAL MEDICINE,
91-348 LODZ, 8 TERESY ST., POLAND, e-mail: alab@bg.p.lodz.pl

Abstract
The aim of the study was evaluation the effect of occupational exposure to electromagnetic fields (EMF) on the cardiovascular system.
The examinations covered all technical personnel employed at selected AM Broadcast Stations (738 -1503 kHz) - (I), radio services (150 - 170 MHz - (II), power substations (50 Hz) - (III), radio and TV broadcasting stations (VHF 30-300 MHz and UHF 0.3-3 GHz) - (IV), and Radio Link Stations (no EMF exposure) - (0). Maximum electric field strength (E_{max}) and magnetic flux density (B_{max}) were assessed and doses per work shift – E_{dose} and B_{dose} were calculated. 287 male workers aged 21-69, with employment duration 1- 42 years, underwent medical examination, resting and 24-h ECG, ambulatory blood pressure monitoring (ABPM). Risk of abnormalities (mostly ventricular arrhythmia) in resting and/or 24-h ECG was significantly higher for group I than for controls (OR= 6.6). In the group III, ABPM revealed a significantly higher risk of increased BP values, referred mainly to systolic BP at night-time (OR=12.5). Also in group IV, BP disturbances were significantly more frequent than in controls (OR=8.6). Cardiovascular abnormalities correlated with EMF maximum value as well as its dose. In all cases, the exposure levels were below Polish OEL values. Nevertheless, significant cardiac abnormalities, related to EMF frequency and intensity, were observed.

Introduction
The electromagnetic fields are commonly present both in the communal and work environments. The potential hazard they may pose to human health is a matter of dispute among scientists. The external electric and magnetic fields have a theoretical potential to affect the functions of different body systems through generating electric impulses within them. Most sensitive to EMF influence are the cardiovascular and nervous systems, particularly the autonomic nervous system responsible, among others, for neurovegetative regulation of the cardiovascular function. The experimental studies conducted thus far indicate that EMF within radio-, microwave and power frequencies can produce measurable biological effects. However, there is no simple relation between the biological and health effects. The biological effects detected at the cell or tissue level may not, and most often do not, translate into overt health effects, owing to the adaptation and repair mechanisms of the living organisms. Moreover, the findings of experimental animal studies can hardly be extrapolated to humans in view of the anatomic and functional differences between species.

Therefore, for evaluating health effects of EMF exposure, the most significant are experimental, clinical or epidemiological studies on humans. The experimental studies make it possible to assess immediate response but not the delayed effects. Consequently, they are of little use for the assessment of effects of occupational exposure that may last several years. Much more valuable are the clinical studies. However, these have been rather scarce so far. Although there are quite a few reports on such studies conducted in the former Soviet Union, they have been commonly criticized for several methodological drawbacks and deficiencies, including ad hoc selection of the study population, lack of control group, lack of accurate assessment of electromagnetic environment, and lack of adjustment for the confounding factors [1]. Further, the methods applied may not have been relevant to the study objectives. To assess the cardiovascular function, the authors most frequently used resting ECG and office BP measurements which are inadequate for detecting functional impairments or early subclinical signs of cardiac dysfunction.

Epidemiological studies can provide the best evidence on the possible health effects of EMF exposure. The studies performed thus far were intended mostly for the assessment of cancer risk from EMF exposure. The results of the first epidemiological study concerning the cardiovascular system were published in 1999. Savitz et al. [2] examined the mortality from cardiovascular diseases in relation to occupational exposure to 50 Hz EMF in a cohort of 138 903 male electric utility workers from five US companies over the period of 1950-88. Age-, race-, and social class-adjusted long-lasting exposure to high level EMF was associated with an increased risk of

death from arrhythmia-related conditions: (n=212) SMR=1.11-2.04 and acute myocardial infarction: (n=4238) SMR=1.07-1.66. These data suggest a possible association between occupational EMF exposure and arrhythmia-related heart disease.

Few epidemiological studies on non-carcinogenic effects of radio frequency and microwave EMF exposures have been published. It was only the questionnaire studies on subjective complaints among mobile phone users and physiotherapists [3-5].

Since 1993, in Nofer Institute of Occupational Medicine, has been conducting comprehensive studies on the neurovegetative regulation of the cardiovascular function in workers exposed to different frequency EMFs [6-9]. The aim of these studies is to investigate the influence of EMF exposure on the cardiac function and find out whether and to what extent the EMF frequency and exposure level can determine the type of cardiovascular abnormalities and neurovegetative function affected.

Methods

For the study, the non-invasive methods of 24-h ECG (Holter) and blood pressure monitoring (ABPM) have been applied which are useful for the examinations of healthy individuals during their normal professional and daily activities. These methods are helpful in detecting not only the clinical manifestations of the disease, but also in early diagnostics of a dysfunction of the cardiovascular system. The examinations were carried out in compliance with the standards of the International Society for Holter and Noninvasive Electrocardiology [10]. The protocol was approved by the Regional Biomedical Ethics Committee.

In all workers the following examination were performed:

- *anamnesis*, with an interview on the risk factors of cardiovascular diseases: family history of metabolic and cardiovascular diseases, lifestyle, nutritional habits and physical activity,
- *routine physical examination*, with office blood pressure measurement (according to WHO guidelines),
- *routine ECG* during rest in the supine position, using Medea system (Gliwice, Poland) from 12 typical leads. The results obtained were evaluated based on generally adopted standards,
- *24 h ECG monitoring* on normal workday, using Medilog Suprima (Oxford, England) set from three bipolar leads. This method is thought to ensure the most accurate diagnostics of cardiac rhythm disturbances, conduction impairments and ischemia, especially silent ischemia. Final results, including heart rate, symptoms of ischemia, arrhythmia and conduction disturbances were related to the international standards for Holter ECG [10],
- *Blood pressure monitoring (ABPM)* - 24-h ambulatory blood pressure monitoring was performed during everyday professional and other activities using DX-Medilog Systems. The measurements were carried out automatically, every half hour during daily activities and every hour during sleep. Mean, systolic (BPS) and diastolic (BPD) blood pressure and heart rate (HR) for 24 hours (O), day-time activity (D) and night-time rest (N) were calculated and related to the Staessen's standards of arterial blood pressure as the reference values [11]. The day-night ratios were determined for systolic and diastolic blood pressure (BPSD/BPSN, BPDD/BPDN). Subjects with BP ratio lower than 1.1 are called the ‘non-deepers’ (subjects without a physiological nocturnal decrease in systolic and/or diastolic blood pressure).
- *Exposure evaluation:* To assess the worker’s individual exposure to EMF, the following parameters were measured:
  I. in workers at AM broadcasting stations: maximum value of electric field strength (E_{max}) and dose per workshift (E_{Dose}),
  II. in workers of radioservices, who were periodically exposed to EMF emitted by the repaired equipment only (E_{max}) were measured, because it was impossible to calculate (E_{Dose}),
  III. in workers at substations: maximum value of electric field strength (E_{max}), maximum value of magnetic flux density (B_{max}) and doses per workshift - E_{Dose} and B_{Dose},
  IV. in workers at broadcasting stations: maximum value electric field strength (E_{max}), mean value of E (E_{mean}) and lifetime dose of E (E_{dose}) separately for VHF, UHF and VHF+UHF. Our assessment of exposure was based on the spectrum analysis of a typical station broadcasting in UHF and VHF bands and on the specifications of the apparatus installed there.

The EMF dose was determined using quasi-dosimetric method. The following procedures had to be completed prior to final exposure assessment:

1. Assessment of the average time the workers spent in particular functional units of the object within a workshift. This was based on an interview and work timing of each worker.
2. Calculation of the mean intensity of electric and magnetic field (if it was measureable) This was done by carrying measurements in several-several dozen locations all over each unit where the workers were

staying. The results of these partial measurements were then averaged for the whole area of the unit. In each of such areas, the maximum values were recorded of electric and magnetic field intensities that the workers had been exposed to.

3. For exposure assessment, the highest of the maximum value of EMF and the total E and H doses per workshift were considered. Lifetime dose was calculated for each worker from the history of employment and job timetable.

For electric field intensity measurement, the HOLADAY Ind. (USA) measuring set and broad-band MEH-1a meter (Technical University, Wroclaw, Poland) were applied
For measurements of magnetic field intensity, the MNP89 meter (Technical University of Wroclaw, Poland) was applied.

Subjects
The groups under study consisted of technical personnel and security service workers who were qualified by the occupational health practitioners as capable for work at permissible EMF levels. The subjects were randomly selected from the total number of such stations in Poland. All workers at each appointed station were examined. All subjects from the exposed and control groups gave their formal consent prior to inclusion in the study. Before the onset of the examinations, all the procedures were explained in detail to each participant.
The examinations were carried out in:

- AM broadcasting stations - exposed group I. The AM stations selected for the study operate at frequencies ranging from 738 kHz to 1503 kHz. These objects can be characterized by permanent exposure of their workers to electromagnetic fields (mostly electric). The main source of EM fields in the AM stations are the transmitting antennas (half-wave dipole), radio transmitters and feeders (which conduct radio signals from the transmitter to the antenna),
- Radio-services - exposed group II. Mobile radio-communication network requires permanent technical supervision by radio-service units. During the service operations, undesirable EM fields are generated by unscreened transmitters, improper tuning instruments and transmitting-receiving antennas installed in the service-rooms. The radio-service workers under study were exposed to EM fields with frequency varying from 150 to 170 MHz,
- Substations - exposed group III. Substations are the element of a power system, in which electric power is distributed and/or transformed. The substations under study work at high and extra high voltage (110 kV-400 kV). The substation equipment is a source of 50 Hz electric and magnetic field,Broadcasting stations that operate at frequencies ranging from 66 MHz to 727 MHz – exposed group IV,The operators of radio- and TV stations are exposed to different EMF levels, depending on various factors such as transmitter technological characteristics, feeder quality, distance from the antenna, etc. These factors differ considerably between the individual broadcast stations.Radio Link Stations - the control group (0). Radio Link Stations are the elements of a telecommunication system in which signals are transmitted using EM waves focused into very row beams by directional (mostly parabolic) antennas. As the antennas are installed in highly inaccessible locations and the radiation beams run high above the ground, the workers of the Radio Link Stations are free from being exposed.

Table 1. Characteristics of the study population

	Exposed groups				**Control group**
	AM Broadcasting Stations (I)	Radioservices (II)	Substations (III)	Broadcasting stations (IV)	Radio Link Stations (0)
Number of subjects	71	40	63	71	42
Age (years)	46.9±13.1*	36.9±11.5	39.0±10.0	45.3±9.4	40.7±2.2
Employment (years)	18.6±12.1	12.5±9.5	15.0±10.0	19.1±8.8	17±13
Diseases diagnosed: hypertension diabetes, type II Subjective symptoms	 12 (17%) 1 31 (44%)	 6 (15%) 0 26 (65%)	 11 (17%) 0 30 (46%)	 11 (15%) 1 36 (51%)	 8 (19%) 1 15 (29%)
BMI	26.0±3.0	25.0±3.0	26.0±4.0	26.9±3.8	25.4±4.0
No. of smokers (more than 10 cigarettes/day)	33 (47%)*	15 (37.5%)	21 (33%)	17 (24%)	17 (40%)

BMI (body mass index) = body mass/height^2 (kg/m^2)

* statistically significant difference ($p \leq 0.05$)

The exposed groups were similar with respect to the level of leisure time physical activity, and dietary and smoking habits. They differed only with regard to the age. The possible influence of this difference on the study results was eliminated using statistical methods.

Results

In all the exposed groups, the assessment of EMF exposure revealed levels not higher than those attributed to the hazard area according to Polish OEL values.

Table 2. EMF exposure in the study groups

Groups	**Exposed** AM Broadcast Stations (I)	Radio-services (II)	Substations (III)	Broadcasting stations (IV)	**Non-exposed** Radio Link Stations (0)
EMF frequency	738-1503 kHz	150-170 MHz	50 Hz	66-727 MHz	0
E_{max}	50-550 [V/m]	2-55 [V/m]	4.3-6.7 [kV/m]	7.9-16.7 [V/m]	0
B_{max}	negligible	negligible	26.1-37.3 [mT]	negligible	0
E_{dose}	50-260 [(V/m)h]	irregular exposure	0.2-15.2 [(kV/m)h]	50-260 [(V/m)h]	0
B_{dose}	negligible	negligible	1.4-38.9 [mTh]	negligible	0

Our studies did not reveal any significant differences between the exposed and non-exposed groups with respect to the frequency of abnormalities in resting ECG. Significant differences between group (I) and other groups, were found in Holter 24-h ECG and when the resting and Holter ECGs were regarded as complementary (table 3) In group (II-IV) the abnormalities in 24-h and/or resting ECG were more frequent than in non-exposed group, but the differences were insignificant. In group (I) among the abnormalities in Holter ECG records dominated the ventricular heart rhythm disturbances, in others repolarization impairments. In switch-yard substation workers (group III) exposed to high and extremely high voltages ranging from 110 kV to 400 kV blood pressure changes prevailed among the recorded cardiovascular impairments and were significantly more frequent in the exposed group than in controls (table 3). The ambulatory blood pressure monitoring revealed an increased frequency of subjects with elevated BP in substation workers (38%), and Broadcasting Stations workers (32%) as compared with the non-exposed subjects (23%).

Table 3. Percentage of subjects with ECG and blood pressure abnormalities

Groups	A: resting ECG	B: Holter monitoring	A and/or B	ABPM	Office BP
AM broadcasting stations (I)	34	56	83	6	20
Radioservices (II)	30	32.5	55	20	22.5
Substations (III)	29	40	48	38	19
Broadcasting stations (IV)	34	44	59	70	34
Radio Link Stations (0)	26	31	40	23	19
p	ns	I vs. 0 (p=0.02)	I vs. 0 (p=0.001)	III vs. 0, IV vs. 0 (p=0.04)	ns

In group (III) and (IV) the mean systolic blood pressure for 24 hours, day-time activity and night-time rest were significantly higher than in the controls. Mean values of diastolic blood pressure for 24 hours (24-h) and night-time rest were significantly higher in the group IV (Fig. 1). In groups I and II in comparison with control group it has been found that mean blood pressure, both 24-h and that recorded during daytime and at night, did not show statistically significant differences. Only the diastolic blood pressure recorded during the night hours was higher in group I, II and IV than in the control, but the difference was on the border of the statistical significance ($p = 0.0512$).

Number of non-dippers was significantly higher in group I (37%) and III (48%) and IV (61%) in comparison with control group (23%) and group II (28%). HRD was found to be significantly lower in the groups I and III than in the

control group, despite the fact that physical and mental load during work and leisure time were similar. HRD/HRN was significantly lower in the groups I, II and III than in the control group. The decreased value of this parameter may indicate a dysfunction of the neurovegetative regulation.

In the group IV it was a significantly higher percentage of subjects with impaired BP regulation, expressed as the absence of physiological nocturnal systolic and diastolic BP drop.

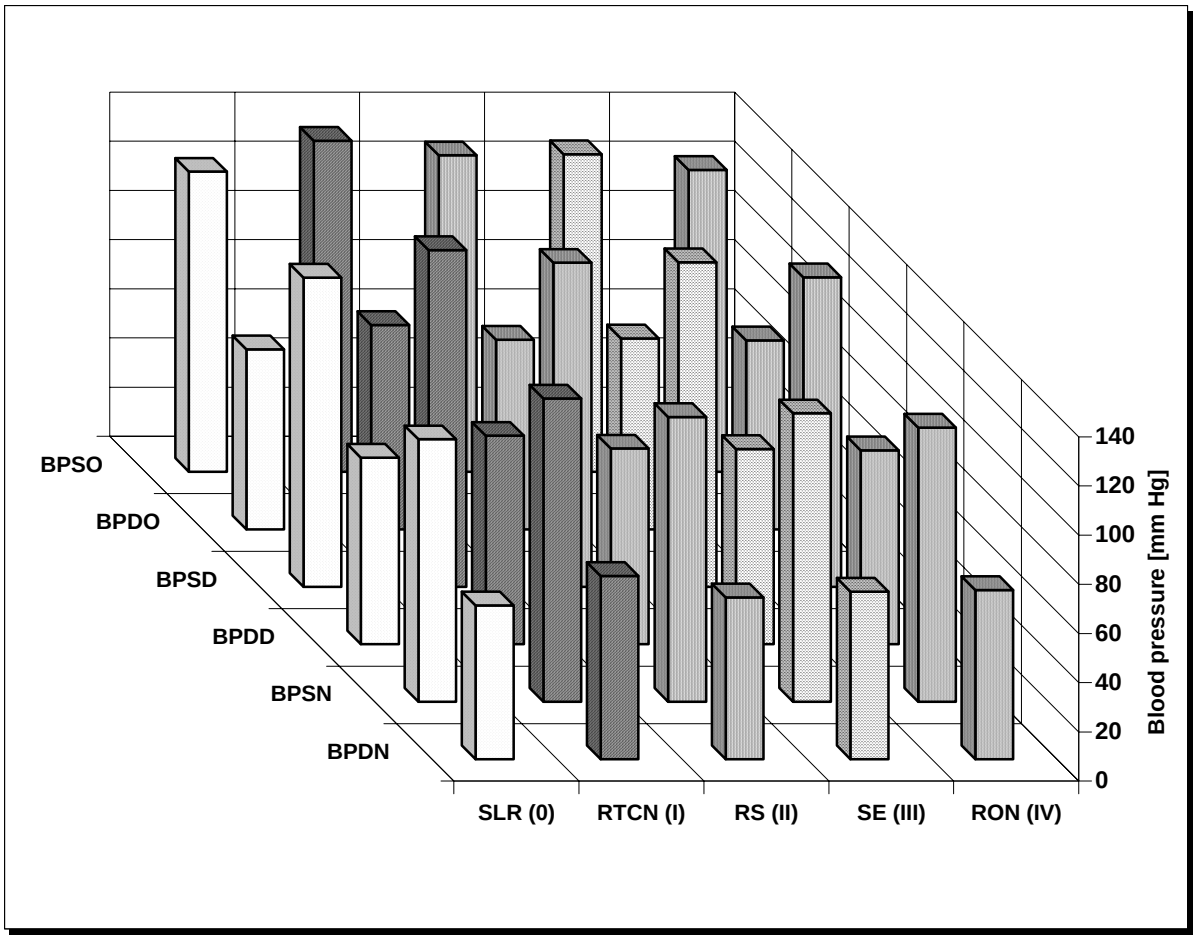

Fig. 1. Blood pressure in the study groups (ABPM results)

The risk analysis revealed that the probability (odds ratio) of abnormalities in resting and/or 24h ECG was 6.6 for group I, 2.0 for group II, 1.4 for group III and 4.5 for group IV, as compared with the control group. On the other hand, the ABPM monitoring revealed that when compared to the values found for controls, the risk of elevated blood pressure was lower in group I, comparable in group II, and significantly higher in group III and IV. The increased BP values referred mainly to systolic pressure at night (odds ratio=12.5). In group IV, the risk of elevated arterial blood pressure was 8.6.

Relationship between cardiovascular disturbances and parameters characterizing the level of exposure.

The disturbances in ECG and blood pressure regulation were dependent on EMF exposure level. In group I, a significant relationship was found between mean BPSN and E_{dose} ($p=0.004$) as well as between BPSN and E_{max} ($p = 0.03$). In group II, the relationship between BP level and exposure parameters was not analysed. Such an analysis could not be performed due to the specific job characteristics in this group - the workers were periodically exposed to EMF emitted by the repaired equipment and it was impossible to determine the level of their exposure. In group III, BP disturbances significantly correlated with exposure parameters. BPDO, BPDD, and BPDN were found to depend on the period of employment ($p=0.023$, $p=0,05$, $p=0.001$ respectively). A significant correlation was found between BPSN and BPDN and the maximum values of electric and magnetic fields ($p=0.043$ and $p=0.026$). In group IV, the disturbances in blood pressure regulation were dependent on EMF

exposure parameters. The risk of BP changes increased with higher lifetime dose in the UHF-VHF bands (OR=2.3) as well as higher E_{mean} in the UHF and VHF bands (OR=2.3, OR=2.5, respectively). The risk of impaired BP regulation (no nocturnal blood pressure drop) significantly increased with lifetime dose in the UHF range (OR=2.6) and with a growing E_{mean} in the VHF range (OR=2.1).

Summary

Although the occupational exposure limits, as laid down in respective Polish regulations, were not exceeded, the different impairments in circulatory system were observed in exposed workers. In workers at AM broadcasting stations, heart rhythm disturbances, detected by 24-h ECG monitoring, were more frequent than in the non-exposed workers as well as workers exposed to 50 Hz EMF. On the other hand, in workers at substations and broadcasting stations, an increased frequency of elevated BP (detected with ABPM) was found, compared with other groups. Our results suggest that the frequency of EMF determines the type of the observed cardiovascular disturbances.

Significant BP disturbances occurred mainly at night; therefore, the office BP measurement is inadequate to detect them. It is also worth noting that in EMF-exposed workers, increased BP levels in ABPM could be found both in the persons showing normal and increased BP values in a single office measurement. Therefore, the present scope of prophylactic examinations seems to be inadequate for workers occupationally exposed to EMF and it should be extended with 24h monitoring of the ECG and blood pressure.

References

[1] M.H. Repacholi, "Low level exposure to radiofrequency electromagnetic fields. Health effects and research needs," *Bioelectromagnetics*, vol. 19, pp. 1-19, January 1998.

[2] D.A. Savitz, L. Duanping, A. Sastre, R.C. Kieckner, and R. Knave, "Magnetic field exposure and cardiovascular disease mortality among electric utility workers," *Am J Epidemiol*, vol. 149, pp. 135-142, January 1999.

[3] B. Hocking, "Preliminary report: Symptoms associated with mobile phone use," Occup. Med., vol. 48, pp. 357-360, October 1998.

[4] G. Oftedal, J. Wilen, M. Sandstrom, and K.H. Mild, "Symptoms experienced in connection with mobile phone," *Occup. Med.*, vol. 50, pp. 237-245, May 2000.

[5] Hamburger S., Logue J.N., and Silverman P.M., "Occupational exposure to non-ionizing radiation and an association with heart disease: An exploratory study," *J.Chron.Dis*., vol. 36, pp. 791-802, November 1983.

[6] A. Bortkiewicz, M. Zmyslony, C. Palczynski, E. Gadzicka, and St. Szmigielski, "Dysregulation of Autonomic Control of Cardiac Function in Workers at AM Broadcast Stations (0.738-1.503 MHz)," *Electro-and Magnetobiology*, vol.14, pp. 177-191, November 1995.

[7] A. Bortkiewicz, E. Gadzicka, and M. Zmyslony, "Heart rate variability in workers exposed to medium-frequency electromagnetic fields," *J Auton Nerv Syst*., vol. 59, pp. 90-97, July 1996.

[8] St. Szmigielski, A. Bortkiewicz, E. Gadzicka, M. Zmyslony, and R. Kubacki, "Alteration of diurnal rhythms of blood pressure and heart rate in workers exposed to radiofrequency electromagnetic fields," *Blood Press Monit*, vol. 3, pp. 323-330, June 1998.

[9] A. Bortkiewicz, E. Gadzicka, M. Zmyslony, and W. Szymczak, "Neurovegetative disturbances in workers exposed to elektromagnetic fields, " in *Proceedings of the International Federation for Medical & Biological Engineering IX Mediterranean Conference on Medical and Biological Engineering and Computing Medicon 2001*, ed.: R. Magjarević, S. Tonković, V. Bilas, and I. Lacković., Pula, Croatia 2001, pp. 769-772., June 2001.

[10] ACC/AHA Clinical Competence Statement on Electrocardiography and Ambulatory Electrocardiography. *Circulation*, 104, pp. 3169-3178, December 2001

[11] J. Staessen, R. Fagard, P. Lijnen, L. Thijs, R. Van Hoof, and A. Amery, "Reference values for ambulatory blood pressure: a meta- analysis," *J. Hypertension*, vol. 8 (suppl 6), pp. S57-S64, December 1990.

EXTERNAL ELECTRIC & MAGNETIC FIELD ASSESSMENT ON THE GENERAL PUBLIC NEAR A 132 KV TRANSMISSION LINE RIGHT OF WAY

M. M. Dawoud, *Fellow IEE*, *Senior Member*, *IEEE*, C. A. Belhadj, *Member*, *IEEE*, I.O. Habiballah, *Member*, *IEEE*, T. K. Abdel-Galil, *Member*, *IEEE*, and M. Arif Abdul-Majeed.

King Fahd University of Petroleum and Minerals, Dhahran 31261, Saudi-Arabia.
(e-mail: mmdawoud@kfupm.edu.sa)

Abstract

The external electric and magnetic fields have been evaluated near a 132 kV transmission line, where members of the general public are likely to be exposed. A double circuit existing transmission line is used for the assessment. The fields have been generated using EPRI's EMF workstation software. The field calculations are based on the charge simulation method for the electric field, and Biot-Savart law for the magnetic field. The predicted electric field at the right of way was found to be 0.165 kV/m and the magnetic field was 21.4 mGauss. The results are presented in the form of field profiles at ground level around one span for both sides of the transmission line, and up to 250 ft. from the centre of the transmission line. The results for both the electric and magnetic fields have been compared with the international standards for the maximum allowable level. The comparison shows that members of the general public are exposed to field levels below those set by the standards.

Introduction

Exposure of the general public to electric and magnetic fields resulting from high voltage power transmission lines has been of prime concern for many years among electric power establishments as well as the general public. Field assessment and epidemiological studies drew a lot of attention to this during the past few decades. The aim of these studies has been to establish the safe exposure levels to power frequency electric and magnetic fields for the general public as well as line workers. Limited knowledge and information available regarding the general public exposure to these fields tends to magnify intensively the risk of exposure to extremely low frequency fields. The SEC transmission networks above 110 kV spans a total length of 33,685 circuit-km (ckm). This consists of 7,490 ckm for 110 – 115 kV, 14,451 ckm for 132 kV, 3,850 ckm for 230 kV and 7,894 ckm for 380 kV of transmission networks [1]. These figures indicate the proximity of high voltage transmission lines and locations of residential areas occupied by the general public. They also justify the need for the assessment of the electric and magnetic fields at and beyond the right of way (ROW) of the high voltage transmission lines.

There has been rising interest over the years in determining the safe exposure levels of people, mainly workers, and the general public, to power frequency electric and magnetic fields [2]-[8]. Several organizations have developed standards and guidelines for such permissible exposure levels. By far, the most important organizations that have contributed to the establishment of these standards and guidelines are the Institute of Electronic and Electrical Engineers (IEEE) [2], and the International Commission on Non-Ionizing Radiation Protection (ICNIRP) [3]. There are other organizations such as the American Conference of Governmental Industrial Hygienists (ACGIH) [4], and the National Radiological Protection Board (NRPB) that have made a major contribution [5],[6]. There are many government agencies and organizations that have published articled on this subject [7],[8].

The permissible levels quoted in many countries refer to the permissible levels set by the IEEE standard, and the ICNIRP guideline. Table 1 lists a summary of the external exposure limits for 60 Hz for the IEEE, ICNIRP, NRPB, and ACGIH for the general public.

TABLE 1
SUMMARY OF EXTERNAL EXPOSURE LIMITS FOR THE GENERAL PUBLIC.

Organization	E (kV/m)	$Bx10^4$ (mG)
IEEE	5	0.833
ICNIRP	4.2	0.1
NRPB	12	1.3
ACGIH	No specific standard for general public.	

This paper presents an exposure assessment study for the general public exposed to a practical double circuit HV transmission line. The selected line spans from substation 8114 (Qortoba Area) to substation 8079 (Alhamra Area-Khorais) in the Riyadh region of Saudi Arabia. Its nominal voltage and power ratings are 132 kV and 293 MVA respectively. This paper introduces detailed system data after this introduction. A description of the charge simulation method and Biot-Savart law used in the evaluation of the electric and magnetic fields follow the data section. The results of the external fields, with emphasis on the right of way and beyond are then presented. The following section introduces a comparison between the evaluated fields and the standards set by the IEEE, ICNIRP, ACGIH, and the limits recognized and used by several countries all over the world. The paper terminates with a conclusion, acknowledgment, and references.

System Data

A real double circuit transmission line is selected by SEC for the study of the exposure to electric and magnetic fields. The selected line spans from substation 8114 (Qortoba Area) to substation 8079 (Alhamra Area-Khorais) in Riyadh region. The nominal voltage and power ratings are 132 kV and 293 MVA respectively. Detailed line data and tower dimension are presented in Fig.1. and line details is delineated in Table 2.

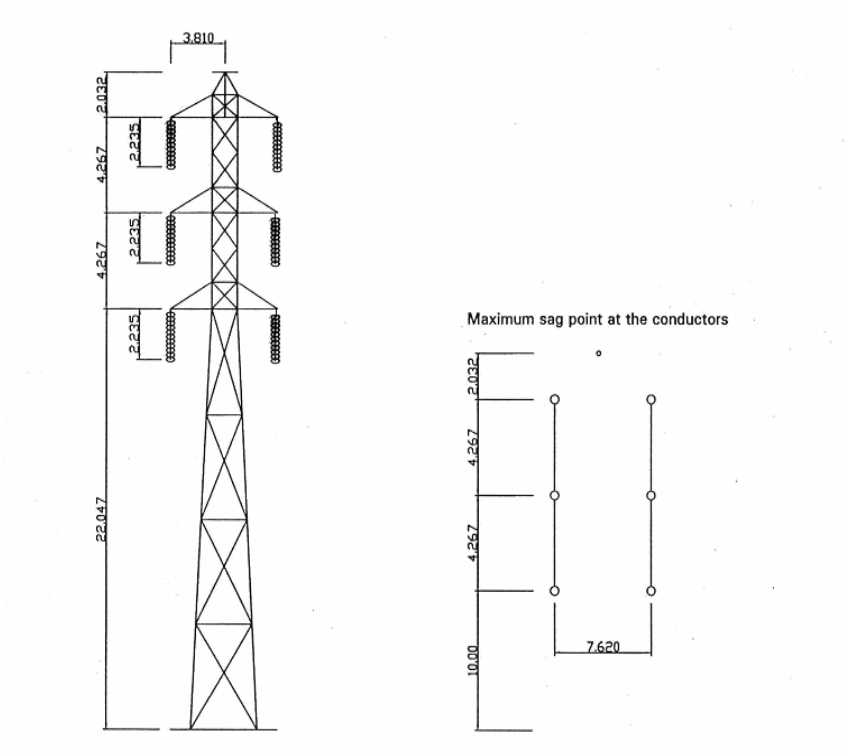

Fig. 1. Tower dimension for the 132 kV transmission line.

TABLE 2
TRANSMISSION LINE DATA FOR THE 132 KV LINE.

Line Ratings		
Rating (MVA)	293 MVA	
Nominal Line Voltage (kVL-L)	132 kV	
Actual Line Voltage (kVL-L)	132 kV	
Nominal Line Current (kA)	1.284 kA	
Peak Load Current (kA), for Both Circuits	Circuit 1	Circuit 2
	603 A	603 A
Line Conductor And Overhead Ground Wire Parameters		
Conductor/Ground Wire	Conductor	Ground Wire
Diameter (cm)	2.773 cm	1.03 cm
Number of Sub-conductors	SINGLE	
Phase Relation of Conductors	VERTICAL (R-Y-B)	
Right of Way	40 m	
Full span (m)	305 m	
Mid Span height (m) or Sag (m) (lowest point)	10 m	

The external field evaluation has been carried out at ground level and for distances up to ± 250 ft from the centre of the transmission line. This range encompasses the right of way of the transmission line and beyond and gives a good indication of the level of exposure of the general public to the electric and magnetic fields resulting from the near by transmission line. Similar results concerning line workers have been reported in [15].

External Electric and Magnetic Field Calculations

The basic physics of quasi-static fields allow separate discussion of power frequency electric and magnetic fields [9]. The solution methodology for both the electric and magnetic fields are highlighted in this section.

A. Charge Simulation Method

The solution methodology for electric field is based on the two-dimensional charge simulation method. This commonly used approach consists essentially of two stages: (l) calculation of the equivalent charges per unit length of conductor and (2) calculation of the electric field produced by these charges. A detailed treatment of the calculations is given in [10]-[13] and summarized here. The general relationship used to calculate the charges on a multi conductor system is presented in matrix form in (l).

$$[Q] = [P]^{-1} [V] \quad (1)$$

Where: [Q] is a column vector of the linear charge on each conductor; [V] is a column vector of the potentials of the conductors; $[P]^{-1}$ is the inverted matrix of the Maxwell potential coefficients of the conductors. A set of image conductors is used with charges opposite to those of the transmission line. The actual conductors and their images are characterized by real and imaginary voltages and diameters. Overhead shield wires are also included in this method (and assumed to be at zero potential). For bundled conductors, a single conductor with an equivalent diameter is used, on the basis of the following formula:

$$d_{eq} = D \sqrt[n]{\frac{n\,d}{D}} \quad (2)$$

where

d_{eq} is equivalent single conductor diameter; n is number of sub conductors; d is diameter of individual sub conductor ; D is geometric diameter of the bundle. The self and mutual Maxwell potential coefficients are calculated for the conductor system on the basis of line geometry and conductor diameter using the following equations.

Self:

$$P_{ii} = \frac{1}{2\pi\varepsilon} \ln\left(\frac{2y_i}{d_i}\right) \quad (3)$$

Mutual:

$$P_{ij} = \frac{1}{2\pi\varepsilon} \ln\left(\frac{(x_i - x_j)^2 + (y_i + y_j)^2}{(x_i - x_j)^2 + (y_i - y_j)^2}\right)^{1/2} \quad (4)$$

where

$\varepsilon = 8.85 * 10^{-12}$ F/m (Dielectric constant of air); di is conductor diameter or equivalent bundle diameter of conductor i ; yi, yj = heights of conductors i and j above ground; xi, xj = horizontal coordinates of conductors i and j with respect to a reference. The inverted potential coefficient matrix $[P]^{-1}$ is multiplied by the column matrix of line-ground conductor voltages to yield the charges per unit length of the conductor, as shown in (l). These charges are then used to calculate the real and imaginary parts of the horizontal and vertical components of the electric field [13].

B. BIOT-SAVART Law

The basic equation for calculating the magnetic field of a long, straight wire is derived from Ampere's Law [11,14] and given in (5):

$$H = \frac{i}{2\pi r} \quad (5)$$

Where: H is the magnetic field intensity (A/m); i is the electric current in the wire (Amperes); r is the distance between the wire and the point of interest (meters)

The fundamental unit for the magnetic field intensity, *H*, is the Ampere per meter (A/m). However, magnetic field exposure technology often uses the magnetic flux density, *B*. The relationship between H and B is given by

$$B = \mu H \quad (6)$$

where:; B is the magnetic flux density (Gauss); μ = Permeability constant used for both air and ground ($4\pi * 10^{-7}$ Henry/m)

The magnetic field is a vector field with both vertical and horizontal components. The field, as computed in Eq. 6, is separated into vertical and horizontal components by multiplying by $\sin(\theta)$ and $\cos(\theta)$. In general, both components must be retained. For three-phase ac fields, the vertical and horizontal components must be combined individually as phasors, regarding the angles of the different currents. The total magnetic field is the sum of all the contributions from the line currents as given in (7).

$$B_{i,j} = \sum\left[\frac{\mu I_i}{(2\pi r_{i,j})}\right] \varphi_{i,j} * 10^4 \quad (7)$$

Where: $r_{i,j}$ is the distance between point and conductors and $\varphi_{i,j}$ is the unit vector in the vector cross-product direction of the current vector and the vector segment $r_{i,j}$. For a three phase ac transmission line, the field at any point can be described by the field ellipse (similar to the electric field).

Evaluation of the External Electric & Magnetic Fields

In this study the electric and magnetic fields produced by the transmission line at ground level, have been modelled using the subroutine EXPOCALC of the EPRI's software EMF Workstation, Version 2.51 [14]. The software package used, starts by setting the general required parameters such as the designated area of concern parameters, the structure position, boundary area, as well as the field calculation height. The line design parameters are entered in a detailed manner and that includes phase structure of the line, conductor size, applied voltage and the operating current. The span specifications are then taken into consideration.

EMFW software provides the calculated field values in a 3-D volume around the transmission line space. Fig. 2 shows the 3-D calculated electric field around the transmission line between the mid-span point and the tower location.

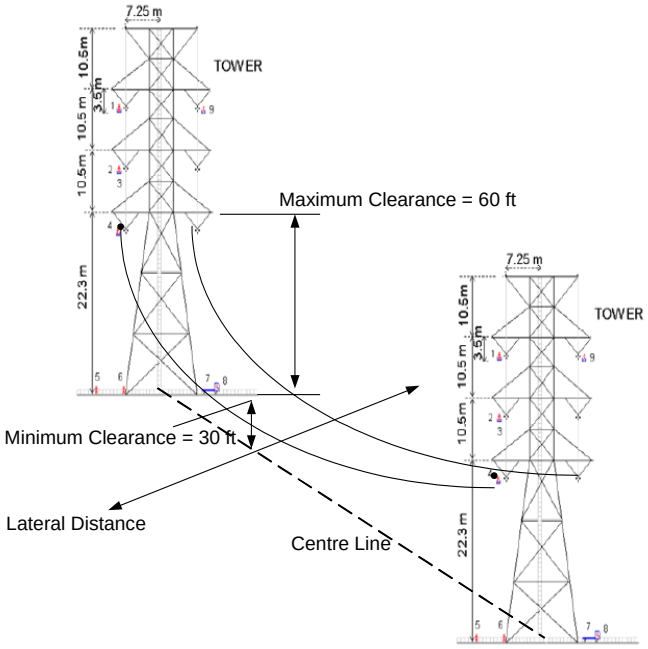

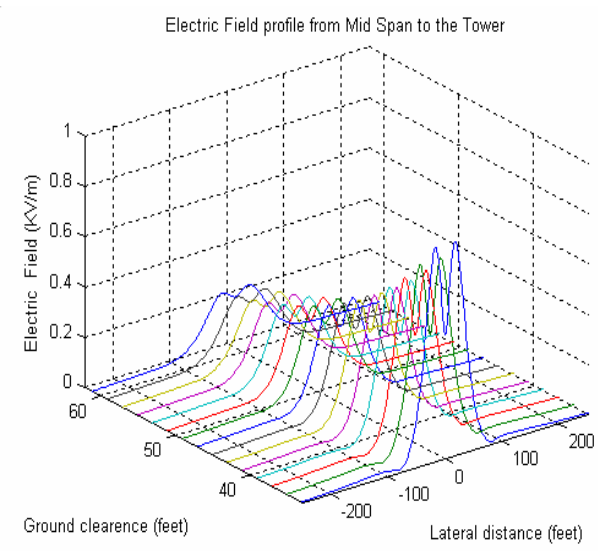

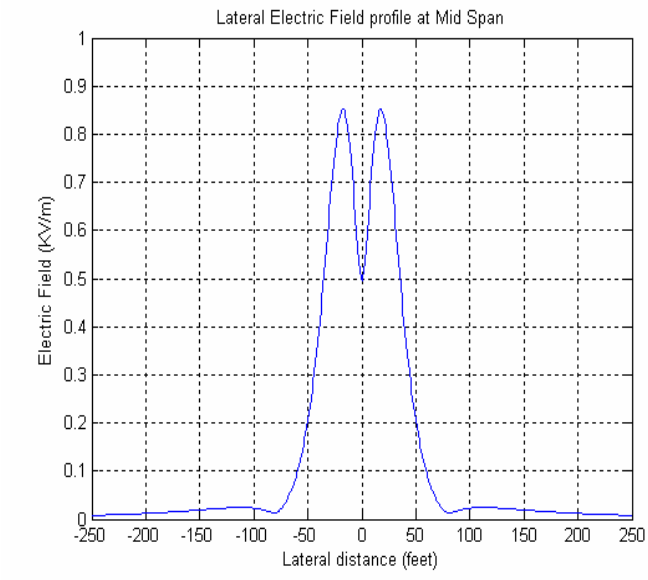

Fig. 2 Calculated External Electric Field Around the Transmission Line between Mid-Span and the Tower Location.

(a) Tower-to-tower geometry, showing mid-span between two towers.
(b) 3-D Electric field profile from mid-span to the tower for a lateral distance ranging between ± 250 ft. from the centre line.
(c) 2-D Electric field profile at mid-span.

The 2-D electric field profile shows that the calculated E field at the right of way is 0.165 kV/m. The E field decreases with increased distance from the centre line of the transmission line.

Similar behaviour is observed for the calculated magnetic field. This is shown in Fig. 3 (a and b).

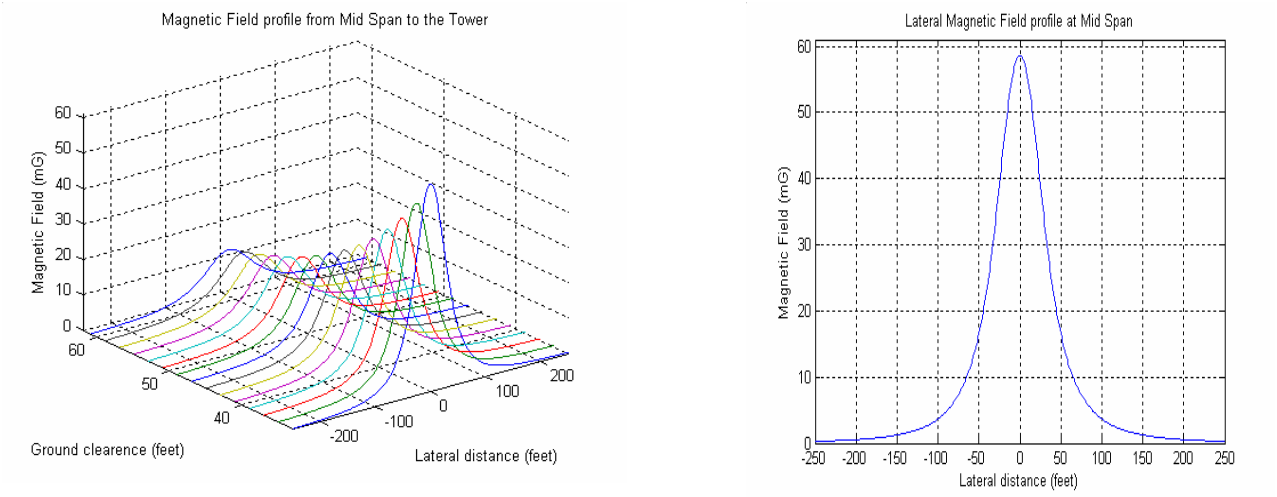

(a) (b)

Fig. 3 (a) 3-D Magnetic field profile from mid-span to the tower for a lateral distance between ± 250 ft.
(b) 2-D Magnetic field profile at mid-span.

The results shown in the 2-D profile indicate that the magnetic field value at the right of way is 10 mG, which is far below the standards set by the IEEE, ICNIRP and NRPB. The maximum calculated magnetic field at the right of way is 21.4 mG, which is still far lower than all the standards set for the general public exposure.

Comparison to the International Standards

The calculated electric and magnetic field exposure levels are compared to the universal standards such as IEEE Standard C95.6 [2], ICNIRP guidelines [3], and NRPB [4]. The comparison is given in table 3. The IEEE Standard C95.6 recommends limits on exposures to electric and magnetic fields in the frequency range of 0 to 3000 hertz (Hz).

TABLE 3
COMPARISON OF THE CALCULATED FIELDS AT THE RIGHT OF WAY TO THE INTERNATIONAL STANDARDS

Organization	E (kV/m)	$Bx10^4$ (mG)
IEEE	5	0.833
ICNIRP	4.2	0.1
NRPB	12	1.3
ACGIH	No specific standard for general public.	
At ground level(ROW)	0.165	0.00214

The highest electric field exposure level computed at the right of way (ROW) is 0.165 kV/m. However, the Maximum Permissible Exposure (MPE) for the power frequency electric field as per the IEEE Standard C95.6 is 5 kV/m for a controlled (occupational) environment. The maximum permissible level according to the ICNIRP guidelines for occupational exposure is 4.2 kV/m. The limit according to the NRPB Guidelines for Exposure to 60 Hz EMF is 12 kV/m.

The maximum magnetic field computed at the right of way is 21.4 mG. However, the Maximum Permissible Exposure for the power frequency magnetic field by the general public as per the IEEE Standard is 0.833×10^4 mG. The maximum permissible level according to the conservative standard ICNIRP guidelines is 0.1×10^4 mG. The limit according to the NRPB for Exposure to 60 Hz EMF is 1.3×10^4 mG. There are no limits set by the ACGIH for the general public.

The highest electric and magnetic fields exposure level for the SEC 132 kV transmission line, therefore, is well below the limits set by the different standards for general public exposure.

Conclusion

The exposure of the general public to the electric and magnetic fields associated with a 132 kV HV transmission line has been evaluated. The EPRI's EMF Workstation software has been used to calculate the external electric and magnetic fields due to the 132 kV high voltage transmission line at ground level and for distances starting from the right of way of the transmission line. Comparison of the values of external electric and magnetic fields, with the allowable limits set by international standards reveals that the level of exposure of the general public to extremely low frequency electric and magnetic fields are well below the limits recommended by these international standards.

Acknowledgment

The authors acknowledge the support of King Fahd University of Petroleum & Minerals in conducting this research.

References

[1] Saudi Electricity Company, "Annual Report", Saudi Arabia, 2004.

[2] IEEE Std C95.6., "IEEE Standard for Safety Levels with Respect to Human Exposure to Electromagnetic Fields, 0–3 kHz", 2002.

[3] International Commission on Non-Ionizing Radiation Protection:, "Guidelines limiting exposure to time-varying electric, magnetic, and electromagnetic fields (up to 300 GHz)", Health Physics, Vol. 74, No. 3, pp. 494-522, 1998.

[4] American Conference of Governmental Industrial Hygienists, TLVs and BEIs, Cincinnati: ACGIH, 2001

[5] Advisory Group on Non-Ionizing Radiation (AGNIR) of the UK National Radiological Protection Board (NRPB), "Limiting Exposure to Electromagnetic Fields (0 300 GHz)", Doc. NRPB, Vol. 15, No. 2, 2004.

[6] National Radiological Protection Board, "Restrictions on human exposure to static and time varying electromagnetic fields and radiation: scientific basis and recommendation for implementation of the Board's statement", Doc. NRPB, Vol. 4, pp. 8–69, 1993.

[7] Olden, K. O., "Health Effects from Exposure to Power-Line Frequency Electric and Magnetic Fields", National Institute of Environmental Health Sciences, NIH Publication 99-4493, 1999.

[8] International Agency for Research on Cancer (IARC), Non-Ionizing Radiation, Part 1: "Static and Extremely Low Frequency Electric and Magnetic Fields", Publication 80, 2002.

[9] Electric Power Research Institute, "Transmission Line Reference Book 345 kV and Above", Fred Weidner and Sons, New York. NY., 1975.

[10] Singer, H., H. Steinbigler, and P. Weiss, "A charge simulation method for the calculation of high voltage fields", IEEE Trans. PAS, v. 93, pp. 1660-1668, 1974.

[11] Shen, L., and J. Kong, "Applied Electromagnetics", Brooks/Cole. Engineering Division, 1983.

[12] Foe, P. Y., and S. Y. King, "Bundle Conductors Electric Field by Integral Equations Method", Proc. IEE, Vol. 123, No. 7, pp. 702-706, 1976.

[13] Singer, H., H. Steinbigler, and P. Weiss, "A charge simulation method for the calculation of high voltage fields", IEEE Trans. PAS, Vol. 93, pp. 1660-1668, 1974.

[14] Electric Power Research Institute (EPRI), "Electric and Magnetic Fields Workstation (EMF WORKSTATION)", Users Manual Version 2.51.

[15] I.O. Habiballah, T. K. Abdel-Galil, M. M. Dawoud, C. A. Belhadj, M. Arif Abdul-Majeed, and T.A. Al-Betairi, "ELF Electric and Magnetic Fields Exposure Assessment of Live-Line Workers for 132 kV Transmission Line of SEC", 2006 IEEE PES Transmission and Distribution Conference and Exposition: Latin America, August 15-18, 2006, Caracas, Venezuela, Accepted.

TINNITUS AND MOBILE PHONE USE: IS THERE A CONNECTION?

HANS-PETER HUTTER[1], HANNS MOSHAMMER[1], PETER WALLNER[2], MONIKA CARTELLIERI[3], DORIS-MARIA DENK-LINNERT[4], MICHAELA KATZINGER[4], KLAUS EHRENBERGER[4], MICHAEL KUNDI[1]

[1]INSTITUTE OF ENVIRONMENTAL HEALTH, MEDICAL UNIVERSITY OF VIENNA, AUSTRIA
[2]MEDICINE AND ENVIRONMENTAL PROTECTION [MUS], VIENNA, AUSTRIA
[3]EAR NOSE AND THROAT DEPARTMENT, KAISER-FRANZ-JOSEF-SPITAL, VIENNA, AUSTRIA
[4]EAR NOSE AND THROAT DEPARTMENT, MEDICAL UNIVERSITY OF VIENNA, AUSTRIA

Abstract

Background: Recent studies suggest that about 10-15% of the adult population experiences tinnitus. As there are indications that mobile phone use could be a risk factor for the occurrence of tinnitus, we performed a case-control study on this issue.

Methods: One hundred patients presenting with tinnitus at the Ear-Nose-Throat (ENT) Department of the Medical University of Vienna were enrolled into the study. For each case a control subject was randomly selected matched for sex and age with various diagnoses not related to tinnitus. A standardized questionnaire (based on the protocol of the Interphone study) was answered by study participants. Patients' history was obtained and clinical examinations were conducted to exclude known underlying causes of tinnitus. Only patients were included that were negative in this respect and therefore suffered from “idiopathic” tinnitus. Odds ratios were computed based on conditional logistic regression with age, sex, years of education, and living in an urban area as covariates.

Results: Mobile phone use was highly prevalent in cases as well as controls (>90%). Concerning mobile phone use up to the index date (onset of tinnitus) neither regular use nor intensity or cumulative hours of use had a significant effect. However, prolonged use (four years or more) of a mobile phone was associated with a significant odds ratio of 1.95 (CI 1.003-3.80).

Conclusions: There could be an association between mobile phone use and the occurrence of tinnitus with a latency of several years.

Introduction

Subjective tinnitus (tinnitus aurium) is defined as a sound sensation that cannot be attributed to an external sound source. It is a symptom of different underlying diseases, not a disease itself. The numerous mechanisms that produce tinnitus are not fully known and associated with nearly all diseases and disorders of the ear (middle ear, inner ear) and retrocochlear disease also causing hearing loss. Different hypotheses explain the various pathophysiological aspects of tinnitus [1]. Tinnitus seems to be generated predominantly in the primary afferent synapses of the cochlea [2,3], but leads to a cortical reorganisation [3]. Tinnitus is experienced by the patients either uni- or bilateral as a sound in the ear/head of varying quality (e.g. roaring, hissing, ringing); it may occur of non-pulsatile or pulsatile character, the latter may be due to vascular pathology.

Most often tinnitus sensation is intermittent and sometimes associated with specific conditions - such as listening to loud music, fever, use of aspirin or quinine, or transient perturbations of the middle ear - and subsides over a period of time ranging from a few seconds to a few days. Studies indicate that the prevalence of tinnitus in adults falls in the range of 10-15% [4-6].

At least in 1-3% of the general population tinnitus affects the quality of life, involving sleep disturbance, work impairment and psychic distress [7].

Tinnitus is more common in the elderly but may also occur in children. It could become more common in the future as a direct consequence of the rise in recreational-noise-induced hearing loss (i.e. from overly loud music) combined with an increased life span. Due to the various pathophysiological mechanisms of tinnitus, therapy is problematic, and evidence-based therapeutic interventions are rare. There currently are very few interventions available that reduce tinnitus loudness and annoyance effectively [8]. Therefore it is important to focus research on possible (environmental) risk factors.

During the last years the habit to extensively use mobile telephones has emerged, such that the majority of the population of Western and Middle-European countries are regularly using these phones. There are concerns that mobile telecommunication could be a possible risk factor for the occurrence of tinnitus (complaints of patients to environmental out-patient departments, neighbours of basestations [e.g.9]). However, up to now there have been no systematic investigations of this problem.

Our study should provide first answers to the question whether or not intensive use of mobile phones increases the risk of tinnitus occurrence.

Methods

Study design and participants

The study was carried out as a hospital-based case-control study at the Ear-Nose-Throat (ENT) Department Medical University of Vienna, Austria. Cases were enrolled consecutively as they presented at the out-patient unit. For each case a control was selected from the same department, of the same age group (±2,5 years < 55 years; ±5 years > 55 years), the same sex and ethnic group. Exclusion criteria were diseases of the middle ear, status post middle ear surgery, retrocochlear disease, severe psychiatric and systemic diseases and medication with drugs that can influence tinnitus (ototoxic or psychopharmacological drugs). Patients with acute and chronic tinnitus who attended the ENT department (age 16 to 80 years) were included.

Controls were patients without any concomitant condition that is related to tinnitus (except for unspecific causes such as hypertension).

Diagnostics/investigation procedure

For the selection of patients, the diagnostic test battery contained the following procedures

- careful history with special regard to tinnitus and its risk factors
- clinical ENT examination with otomicroscopy
- pure-tone and speech audiogram
- tympanogram and testing of the stapedius reflex
- subjective rating of the tinnitus
- tinnitus matching
- MRI (if indicated, to exclude retrocochlear pathology)

Each case that was enrolled received a standardized questionnaire (Structured Tinnitus Interview, STI [8]). Items refer to central characteristics of tinnitus history, etiological factors and tinnitus-related psychological complaints. In addition, a medical interview was conducted. Patients' history and clinical examination concerning possible underlying causes of tinnitus were obtained by usual clinical procedures. For each patient a CRF (Case Report Form) was compiled that was maintained according to GCP (Good Clinical Practice) guidelines.

Pure-tone and speech audiometry (Clinical Audiometer AC 40, Interacoustics©) were applied in order to exclude tinnitus related to sudden deafness and Morbus Menière. Tympanometry and stapedius reflex measurements (Impedanz Audiometer AZ 26, Interacoustics©) were carried out in order to exclude tinnitus related to conductive hearing loss. If retrocochlear hearing loss was suspected, cranial MRI was applied.

For the evaluation of tinnitus, both a subjective rating of the tinnitus on a five-point scale (0 = no tinnitus; 1 = slight; 2 = moderate; 3 = severe; 4 = tormenting tinnitus) and a tinnitus matching as a psychoacoustic measurement of tinnitus were carried out.

The audiometric tinnitus simulation test (= tinnitus matching) (Clinical Audiometer AC 40, Interacoustics©) determined character (pure-tone, narrow and wide band), frequency and intensity of the tinnitus. Tinnitus matching was performed contralaterally.

With the help of this procedure tinnitus subtypes (esp. temporo-mandibular joint dysfunction related tinnitus, cervical tinnitus, acute tinnitus/sudden deafness/noise trauma, suspected cochlear-synaptic tinnitus) could be identified. This information was used to exclude patients with known underlying pathophysiology.

For the exploration of the mobile phone habits we used a standardized questionnaire (based on the protocol of the Interphone Study of the WHO). In short, for each mobile phone the subject used or has used, the type of phone, duration and intensity of use, side of the head the phone was predominantly held, use of head sets, use in urban/rural areas and in cars was assessed. In addition, to assess individual microwave exposure for future investigations we took two photos of the participants while using a mobile phone in typical position. Furthermore, somatometry of the head was performed on specific anthropogenic diameters (e.g. tragus - tragus, biauricular diameter) with a calliper.

Statistical Methods

Data on mobile phone use were censored at the date of first occurrence of tinnitus. Index date of controls was the occurrence of tinnitus in the matched case. Intensity of use, cumulative number and duration of calls were categorized based on the distribution of these variables in controls: The median (excluding never users) was chosen as cut-off. Reference category was never use of a mobile phone (prior to index date). In all cases data on mobile phone use were adjusted for the use of hands-free devices. Further adjustments were applied for the side of the head of predominant use. Mobile phone use was only counted if it occurred on the same side of the head as the tinnitus (controls were assigned the side of the matched case). Duration of mobile phone use was categorized into three groups: never use or use for less than one year (reference), 1 to 4 years, and longer than 4 years.

Conditional logistic regression analyses for individually-matched data were used to estimate odds ratios and 95% confidence intervals. All analyses were adjusted for gender, age, years of education (less than and 12 years or more) and living in an urban area.

Results

Subjects' characteristics were comparable in cases and controls (table 1). Due to matching for gender and age these variables were in agreement, but also other personal characteristics did not differ significantly between cases and controls. There was a slight tendency for a somewhat higher socio-economic status (SES) implied by the higher education, higher rate of white collar workers and urban residents in controls.

Table 1. Demographic characteristics of cases and controls[+)]. p-value for comparison of non-matching variables.

	Cases	Controls	p-value
Gender			
male	54	54	
female	46	46	
Age (mean±SD)	42.5±14.4	42.5±14.5	
Partner			
with	66	69	0.742
without	28	28	
Education			
<12 years	36	29	0.371
≥12 years	63	69	
Occupation			
unemployed	6	6	0.624
retired	16	16	
in education	15	10	
blue collar	9	10	
white collar	48	53	
City resident			
yes	70	76	0.361
no	23	18	

[+)] Percentages not summing up to 100 due to missing values

Almost all subjects at time of inquiry used a mobile phone (92% and 93% for cases and controls, respectively), however, at the time of first occurrence of tinnitus (and the respective index date in controls) only 73% of cases and 67% of controls were using a mobile. Another 7% of cases and 8% of controls used the mobile at that time for less than one year. For ever users prior to occurrence of tinnitus there was a slightly but not significantly increased odds-ratio of 1.37 (95% CI: 0.73-2.57). Moderate increases of odds-ratios were noted for all variables of intensity of use: average daily duration of use for 10 minutes or more was associated with an odds-ratio of 1.71 (95% CI: 0.85-3.45), cumulative hours of use of 160 or more gave an odds ratio of 1.57 (95% CI: 0.78-3.19), cumulative number of calls in excess of 4000 an odds-ratio of 1.28 that was less than for lower number of calls (odds-ratio 1.46) possibly indicating greater importance of duration as compared to number of calls. A borderline significant result was obtained for duration of use of 4 or more years: odds-ratio 1.95 (95% CI: 1.003-3.80). Test of trend for duration of use was also significant (p=0.046).

Table 2. Mobile phone use and risk of tinnitus.

	No. of cases	No. of controls	OR	95% CI
Mobile phone use				
never	27	33	1.00	
ever	73	67	1.37	0.73-2.57
Average duration				
never	27	33	1.00	
<10 min/day	39	34	1.02	0.48-2.16
≥10 min/day	43	33	1.71	0.85-3.45
Cumulative hours of use				
never	27	33	1.00	
<160 h	31	34	1.17	0.56-2.42
≥160 h	42	33	1.57	0.78-3.19
Cumulative number of calls				
never	27	33	1.00	
<4000 calls	37	33	1.46	0.71-3.00
≥4000 calls	36	34	1.28	0.62-2.63
Years of mobile phone use				
never, <1	34	41	1.00	
1-3	33	36	1.23	0.61-2.47
≥4	33	23	1.95	1.003-3.80

Discussion

The prevalence of tinnitus has increased over the past decade and is currently 10-15% in industrialized countries [7]. Increase in incidence may be due to better diagnostic tools and increased awareness of the disease; however, a number of environmental factors have been implicated to increase the risk of tinnitus. The suspected factors include electromagnetic fields emitted by hand-held cellular telephones.

Since the majority of the population is using mobile phones more or less intensively people were concerned about effects on wellbeing [11,12]. Practitioners are confronted with reports of sensation of tinnitus related to mobile phone use by their patients [13].

In our study slight increases in risk were noted for all variables of intensity of use. The study was designed to detect a twofold increase of risk with 80 percent power. Further investigations esp. multicenter designs will be more efficient to detect these moderately increased risks. Because of the high prevalence of tinnitus and the widespread use of mobile phones even a small enhancement of the risk could be of public health importance.

From a theoretical point of view this possible association of mobile phone use and occurrence of tinnitus has some plausibility, because the cochlea is located in an anatomic region where a considerable amount of the power emitted by cell phones is absorbed [14]. One etiologic factor for tinnitus is calcium imbalance in the neural acoustic pathway. It is well known that exposure to modulated high-frequency electromagnetic fields (HF-EMF) has the potential to affect calcium homeostasis especially in neural tissue [15].

Because some mobile telephones (especially newer types) cause rather high exposure of the cochlea [14] and along the acoustic pathway it is possible that tinnitus could be caused by calcium efflux. Effects of exposure on calcium homeostasis was also implied as one factors in the development of acoustic neuroma. Ten studies [16-25] investigating the association between mobile phone use and acoustic neuroma have been published so far.

Half of theses studies found indications of an association [21-25], the other 5 were those with shorter duration of mobile phone use and/or smaller number of long-term users of a mobile [16-20].

Tinnitus strongly interferes with the daily lives of people. In industrialized countries, 10-15% of the adult population currently experience tinnitus. There are very few interventions available that effectively reduce tinnitus loudness and annoyance. Therefore, all measures should be taken to avoid further increase of tinnitus prevalence.

Results indicate that high intensity and long duration of mobile phone use might be associated with occurrence of tinnitus. As more persons start using mobile phones at younger age, this indeed may become a public health problem.

Acknowledgements

We thank Elisabeth Cardis, International Agency for Research on Cancer, Lyon, for permitting use of the Interphone Questionnaire. Furthermore the assistance of Brigitte Piegler is gratefully acknowledged.

References

[1] Eggermont J (2005): Tinnitus: neurobiological substrates. Drug Discovery Today 10:1283-1290.
[2] Ehrenberger K, Brix R (1983): Glutamic acid and glutamic acid diethyl ester in tinnitus treatment. Acta Otolaryngol (Stockholm) 95:599-605.
[3] Eggermont J (1990): On the pathophysiology of tinnitus; a review and a peripheral model. Hear Res 48:111-23.
[4] Heller AJ (2003): Classification and epidemiology of tinnitus. Otolaryngol Clin North Am 36:239-248.
[5] Marsot-Dupuch K (2001). Pulsatile and nonpulsatile tinnitus: a systemic approach. Semin-Ultrasound-CT-MR 22:250-270.
[6] Henry JA, Dennis KC, Schechter MA (2005): General Review of Tinnitus: Prevalence, Mechanisms, Effects, and Management. Journal of Speech, Language, and Hearing Research 48:1204-1235.
[7] Dobie RA (2003): Depression and tinnitus. Otolaryngol Clin North Am 36, 383-388.
[8] Denk D-M, Heinzl H, Franz P, Ehrenberger K (1997): Caroverine in tinnitus treatment: a placebo-controlled blind study. Acta Otolaryngol (Stockholm) 117:825-830.
[9] Navarro EA, Segura J, Portosolés M, Gómez-Perretta de Mateo C (2003): The microwave syndrome: a preliminary study in spain. Electromagnetic Biology and Medicine 22:161-169.
[10] Hiller W, Goebel G, Schindelmann U (2000): Systematische Fremdbeurteilung von Patienten mit chronischem Tinnitus (Strukturiertes Tinnitus-Interview). Diagnostica 46:93-102.
[11] Hutter HP, Moshammer H, Wallner P, Kundi M (2004): Public perception of risk concerning celltowers and mobile phones. Sozial- und Präventivmedizin 49:62-66.
[12] Siegrist M, Earle TC, Gutscher H, Keller C (2005): Perception of Mobile Phone and Base Station Risks. Risk Analysis 25:1253-1264.
[13] Huss A, Röösli M (2005): Befragung von Ärztinnen und Ärzten zum Thema elektromagnetischer Felder in der hausärztlichen Praxis. Studie im Auftrag des Bundesamtes für Gesundheit (BAG). Institut für Sozial- und Präventivmedizin, Universität Bern, September 2005.
[14] Überbacher R, Schmid G, Tschabitscher M (2006): New high resolution numerical model of inner ear organs for RF-dosimetriy – preliminary results in the 900 MHz – 10 GHz range. The Bioelectromagnetics Society`s 28th Annual Meeting (June 11-15, 2006; Cancun, Mexico).
[15] Blackman CF (1992): Calcium release from neural tissue: experimental results and possible mechanisms. In Norden B, Ramel C (eds): "Interaction Mechanisms of Low-Level Electromagnetic Fields in Living Systems." Oxford: Oxford University Press, pp. 107-129.
[16] Hardell L, Nasman A, Pahlson A, Hallquist A, Hansson Mild K (1999): Use of cellular telephones and the risk for brain tumours: A case- control study. International Journal of Oncology 15:113-116.
[17] Johansen C, Boice J, Jr., McLaughlin J, Olsen J (2001): Cellular telephones and cancer—a nationwide cohort study in Denmark. J Natl Cancer Inst 93:203-720.
[18] Inskip PD, Tarone RE, Hatch EE, Wilcosky TC, Shapiro WR, Selker RG, Fine HA, Black PM, Loeffler JS, Linet MS (2001): Cellular-telephone use and brain tumors. N Engl J Med 344:79-86.
[19] Muscat JE, Malkin MG, Shore RE, Thompson S, Neugut AI, Stellman SD, Bruce J (2002): Handheld cellular telephones and risk of acoustic neuroma. Neurology 58:1304-1306.
[20] Warren HG, Prevatt AA, Daly KA, Antonelli PJ (2003): Cellular telephone use and risk of intratemporal facial nerve tumor. Laryngoscope 113:663-667.

[21] Hardell L, Hansson Mild K, Carlberg M (2003): Further aspects on cellular and cordless telephones and brain tumours. International Journal of Oncology 22:399-407.
[22] Christensen HC, Schuez J, Kosteljanetz M, Poulsen HS, Thomsen J, Johansen C (2004): Cellular telephone use and risk of acoustic neuroma. American Journal of Epidemiology 159:277-283.
[23] Loenn S, Ahlbom A, Hall P, Feychting M (2004): Mobile Phone Use and the Risk of Acoustic Neuroma. Epidemiology 15:653-659.
[24] Hardell L, Carlberg M, Hansson Mild K (2005): Case-Control Study on Cellular and Cordless Telephones and the Risk for Acoustic Neuroma or Meningioma in Patients Diagnosed 2000-2003. Neuroepidemiology 25:120-128.
[25] Schoemaker MJ, Swerdlow AJ, Ahlbom A, Auvinen A, Blaasaas KG, Cardis E, Christensen HC, Feychting M, Hepworth SJ, Johansen C, Klaeboe L, Loenn S et al. (2005): Mobile phone use and risk of acoustic neuroma: results of the Interphone casecontrol study in five North European countries. British Journal of Cancer 93:842-848.

EFFECTS OF 2.45 GHz ELECTROMAGNETIC FIELDS WITH A WIDE RANGE OF SAR ON CELLULAR GENOTOXICITY IN CULTURED CELLS

JUNJI MIYAKOSHI, SHIN KOYAMA, YOSHIKI KOMATSUBARA, JIN WANG, TOMONORI SAKURAI

GRADUATE SCHOOL OF HEALTH SCIENCES, FACULTY OF MEDICINE, HIROSAKI UNIVERSITY, HIROSAKI, AOMORI, 036-8564, JAPAN

Abstract

High-frequency electromagnetic fields (HFEMF) used for mobile phones may be of great concern for human health. In order to investigate the properties of HFEMF, we have examined the genotoxic effects of 2.45 GHz EMF on micronucleus (MN) formation, DNA strand breaks, and chromosomal aberrations in cultured cells. Chinese hamster ovary (CHO)-K1, human glioma MO54, and mouse m5S cells, respectively, were used in these experiments for MN formation, DNA strand breaks, and chromosomal aberration. The DNA strand breaks were detected using an alkaline comet assay. Cells were exposed to HFEMF for 2 h at average specific absorption rates (SARs) from 5 to 200 W/kg, and the effects on these cells were compared with those in sham-exposed cells. Heat treatment as a heat control was performed at temperatures of 37 to 44°C. MN frequency at SAR of lower than 50 W/kg did not differ from the sham-exposed controls, while MN frequency at SARs of 100 and 200 W/kg was significantly higher. No significant differences in the DNA strand breaks and the chromosomal aberrations were observed following exposure to HFEMF from 5 to 200 W/kg, compared with sham-exposed control. In summary, HFEMF exposure at 2.45 GHz for 2 h up to SAR of 50 W/kg does not induce MN formation, DNA strand breaks and chromosomal aberrations.

Introduction

In recent years there has been a rapid increase in the use of devices and systems employing high-frequency electromagnetic fields (HFEMF) in our lives, including radio and TV transmitters, microwave ovens, telecommunication links, and satellite communications, as well as mobile phones and their supporting transmitters (base stations). Thus exposure to HFEMF in the environment is greater than any of the former ages of human. A consequent result of this has been increased concern about the association between environmental exposure to HFEMF and cancer. Although several theoretical models have been proposed [1-3], the association between HFEMF and cancer remains unclear.

General concerns regarding the potential hazards of exposure to HFEMF have led to many epidemiological investigations [4-6]. Several studies have suggested that exposure to HFEMF can interact with behavior [7, 8]. *In vitro* studies have reported the effects of HFEMF on several end-points, including effects on DNA damage [9], chromosome aberrations [10], mutation [11], cell transformation [12] and gene expression [13]. In these studies, cells were typically subjected to exposures as low as specific absorption rates (SARs) of 10 W/kg to estimate the

---

Effects of 2.45 GHz Electromagnetic Fields with a Wide Range of SAR on Cellular Genotoxicity in Cultured Cells
Junji Miyakoshi, Shin Koyama, Yoshiki Komatsubara, Jin Wang, Tomonori Sakurai
Graduate School of Health Sciences, Faculty of Medicine, Hirosaki University, Hirosaki, Aomori, 036-8564, Japan

risk of weak HFEMF that we are actually exposed to daily, since this is the final goal of these studies. However, exposures to a higher intensity are also necessary to explore the effects of HFEMF for safety evaluation. We have previously reported that exposure to 2.45 GHz electromagnetic fields for 2-16 h induced Hsp70 in human glioma MO54 cells [14], and exposure to HFEMF at 100 W/kg did not cause any DNA damage according to the comet assay system [15]. HFEMF at high SAR mainly results in heating of the cells. Heat is known to cause many biological changes and the heating effect of HFEMF is well established [16]. However, there have been claims that HFEMF could exert non-thermal effects on biological systems. Hence, with exposure conditions used in these experiments it becomes very important to establish the differences between thermal and non-thermal effects.

Considering these previous data, we have examined the frequency of micronucleus (MN) formation in Chinese hamster ovary (CHO)-K1 cells following HFEMF exposure. MN formation is derived from clastogenic activity arising from chromosomal fragments that are not incorporated into daughter nuclei at mitosis. This occurs because of the lack of a kinetochore. MN formation is also derived from an aneugenic process when the whole chromosome is not correctly integrated into the two daughter nuclei at the time of cell division [17-20]. In the present study, we also examined the presence or absence of single-strand DNA breaks and chromosomal aberrations in mammalian cells exposed to 2.45 GHz HFEMFs with a wide range of SAR (5 W/kg to 200 W/kg) in human glioma MO54 and mouse m5S cells, respectively.

Materials and methods

1. Exposure system

The exposure system of HFEMF was described elsewhere [21-23]. In brief, the applicator is based on a rectangular waveguide, with its size determined to be 110 mm (wide) × 55 mm (high) × 310 mm (deep). The electromagnetic waves are propagated along the waveguide in TE_{10} mode. One end of the applicator is terminated with a short-circuiting plate to generate standing waves in the waveguide.

A rectangular culture dish is placed on two slits, which were bored into the wider wall of the waveguide. The cells in the dish are exposed to the HFEMF through these slits. The two slits are pinch shaped, which enhances the coupling of the electromagnetic field to increase the effective exposure area. The culture dish is divided into four compartments. The distribution of the electric field in the medium depends on the thickness of the medium. Therefore, it is preferable to choose a thickness that maximizes the SAR at the bottom of the well, where the cells are present. Numerical analysis indicates that the appropriate thickness is 8 mm, which corresponds to a half wavelength in the medium.

The SAR distribution in the exposure apparatus was calculated using the Finite Difference Time Domain (FDTD) method. An each compartment has a different value of SAR. The maximum SAR appears in compartment 3. The maximum SAR values in compartment 2 and 4 are 80% and 85% of the maximum SAR value in compartment 3. The minimum SAR in compartment 1 is 1% of the maximum value.

2. Cells and culture conditions

CHO-K1 cells were obtained from the Japanese Cancer Research Bank, Tokyo. Cells were maintained in Ham's F-12 medium (Nikken Bio Medical Laboratory, Kyoto, Japan) supplemented with 10% fetal bovine serum (Gibco, BRL) at 37°C in 95% air and 5% CO_2 [21].

MO54 cells, derived from a human malignant glioma, were used in this study. Cells were cultured in Dulbecco's modified Eagle's medium (Nikkenn Bio Medical Laboratory) supplemented with 10% fetal bovine serum (GIBCO, BRL) at 37°C in an atmosphere of 95% air and 5% CO_2 [22].

Mouse m5S cells are a near-diploid cell line established from embryonic skin; they are immortalized but non-tumorigenic [24]. The cells were grown as monolayers in Dulbecco's modified Eagle's medium supplemented with 10% fetal bovine serum (BioWest, Rue de la Caille 49340 Nuaill, br, France) at 37°C in an atmosphere of 95% air and 5% CO_2 [23].

3. MN analysis

After a 2 h exposure to HEFMF, the cells were trypsinized and seeded in 10 cm culture dishes in medium containing cytochalasin B at a final concentration of 3 μg/ml for 18 h, in order to prevent cell division. A sham-exposure experiment was performed as a negative control. Cells were treated in the same way to those that underwent HFEMF exposure, except that HFEMF exposure itself was omitted. Instead, the cells were incubated for 2 h in a conventional incubator. In addition, the cells were treated with bleomycin alone as a positive control, using the same conditions as those used for sham exposure.

The cells were collected at a concentration of 2.7×10^4 cells/ml, and samples of 0.2 ml were centrifuged onto slides, using a Cytospin centrifuge (Shandon Southern Ltd.) at 100 × g for 5 min. The cells were then fixed with 80% cold ethanol for 30 min. The slides were washed gently with PBS and soaked in new PBS for 5 min to

completely remove the ethanol.

The cells on the slides were stained with 20 µl of propidium iodide (PI) diluted in glycerol (to a concentration of 0.2 µg/ml), and kept in the dark until counting was performed. A total of 1000 binucleated cells were scored for evaluation of the frequency of induction of MN, using fluorescence microscopy (Olympus). Cells were counted as having MN formation when they contained at least one micronucleus. The procedure was performed in a double-blind manner, and followed the method described by Countryman and Heddle [20]. Statistical analysis of the data in the control and experimental groups was conducted using ANOVA (analysis of variance) followed by Fisher's Protected Least Significant Difference (PLSD) test.

4. Comet assay

To detect DNA damage at the single-cell level, an alkaline comet assay was performed. The method of the comet assay has been described previously [25]. In brief, we used a Trevigen Comet Assay system (Trevigen, Inc., Gaithersburg, MD). After the treatments, the cells were rinsed with phosphate-buffered saline (Ca^{++} and Mg^{++} free; PBS) and treated with trypsin. Cell suspension in 1×PBS on ice was mixed with low melting agarose at 37 °C (cell suspension : agarose = 1 : 8). The mixture of cell suspension and agarose was kept on a slide in the dark at 4 °C, underwent 5 minutes of fixation, and was then immersed in a lysis solution at 4°C for 40 min. The slide was placed in the alkali buffer for 15 minutes. Electrophoresis was performed as reported previously [26]. After the electrophoresis, the samples were fixed in ethanol for 5min and then dried. DNA in agarose was stained with SYBR Green according to the manufacturer's recommended procedure.

DNA Strand breaks were analyzed by using IDL Comet 6.0 (Adamnet, Tokyo, Japan). Tail length is the destance from the first non-zero element to the last non-zero elements in tail content. Tail content was calculated as the integrated value of the fluorescent brightness of the total comet minus the integrated value of the fluorescant brightness of the comet head. The unit of the parameter is given as "pixels". The tail length is the distance between the first and last non-zero elements in the tail content. The tail moment was calculated according to the following equation:

Tail moment = Differential between means ×% in tail.

For a statistical evaluation of the tail moment, tail length, and tail percent, An analysis of variance (ANOVA) test was used to determine any inte-group differences. When a significant *F* value was found ($p<0.05$), the Bonferroni/Dunn test was used for a multiple comparison. *P*-value that were less than 0.05 were considered statistically significant.

5. Chromosomal aberrations

After exposure, the cells were removed and cultured in a conventional incubator for 24 h. Colcemid (0.1µg/mL, Sigma) was added during the last 4 h. Unexposed control cells were incubated for the same period in a conventional incubator. Chromosome preparations were made according to the standard air-drying method and stained with 3% Giemsa solution (pH 6.4). For each culture, a minimum of 200 cells was assesed for the types and frequencies of chromosomal aberrations; all structural chromatid-type and chromosome-type changes, including gaps, were recorded. The scoring was conducted in a double-blind manner.

The experimental data are presented as the mean ± S.E.M. *Chi* square tests were performed to determine whether there was a significant difference in the proportion of cells with aberrations between the cells exposed to HFEMF and unexposed cells. The statistics were calculated either including or excluding gaps.

Results

1. MN formation

There was no increase in MN formation in cells exposed to HFEMF at SAR from 5 to 50 W/kg. However, the frequency of MN formation in cells exposed to HFEMF at SAR of 100 and 200 W/kg was statistically significantly different to that observed following sham-exposure (Fig. 1). The frequency of MN formation following treatment with bleomycin alone was statistically higher, compared with the sham-exposed control (Fig. 1). Although there was no increase in MN formation in cells treated with a combination of bleomycin and HFEMF exposure at SAR from 5 to 100 W/kg, there was a statistically significant difference in MN formation between treatment with bleomycin alone and combined treatment with bleomycin and HFEMF exposure at a SAR of 200 W/kg.

The frequency of MN formation with heat treatment increased in a temperature-dependent manner. However, there was no difference between bleomycin-treated cells and cells treated with a combination of heat and bleomycin for temperatures from 38 to 41°C (data not shown).

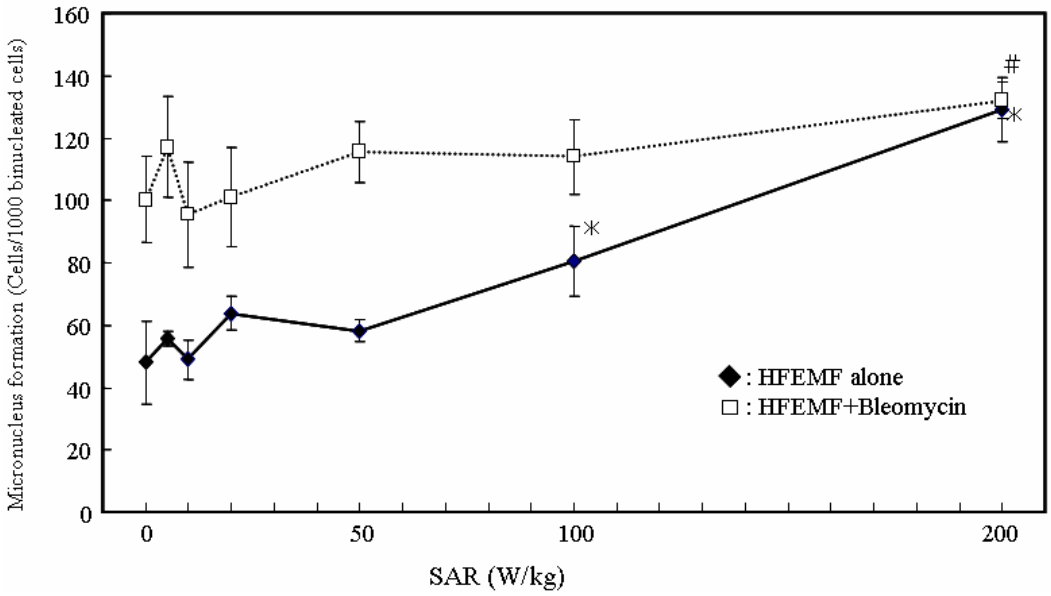

Figure 1. The frequency of MN formation in CHO-K1 cells exposed to HFEMF with or without bleomycin, compared to that following sham-exposure. The bars show standard deviations, based on three experiments. An asterisk indicates a statistically significant difference between sham- exposure and HFEMF exposure (p<0.01). A sharp indicates a statistically significant difference between treatment with bleomycin alone and combined treatment with HFEMF exposure and bleomycin (p<0.01).

2. DNA strand breaks

No significant difference in tail moment was seen for each exposure condition at SAR levels from 5 W/kg to 200 W/kg (Table 1).

Table 1 Comparison of Comet Parameters in MO54 Cells Exposed to 2.45GHz Continuous-Wave HFEMF, Sham and 100μg/mL bleomycin

Exposure Condition	Sham	5 W/kg	10 W/kg	20 W/kg	50 W/kg	100 W/kg	200 W/kg	Bleomycin
Tail Moment	406.6 ± 113.2	365.1 ± 13.9	425.1 ± 30.5	353.2 ± 44.0	372.3 ± 83.7	335.6 ± 53.9	432.6 ± 70.4	2071.9 ± 419.8*
Tail Length	54.7 ± 23.6	76.0 ± 8.5	80.3 ± 13.8	68.6 ± 25.4	61.2 ± 18.5	48.5 ± 3.9	53.9 ± 3.6	118.9 ± 41.1*
Tail Percent	24.5 ± 5.1	24.6 ± 1.1	25.2 ± 5.2	24.8 ± 0.8	24.3 ± 2.6	22.7 ± 3.2	25.0 ± 3.2	40.1 ± 9.7*

Data are presented as the mean ± standard deviation, based on three experiment.
The units of each parameter are Tail moment = arbitrary unit, Tail length – pixel, and Tail percent - %.
*Significantly different (at p<0.01) from Sham, HFEMF exposure and heat treatment groups.

No significant differences were observed in tail moment for each of the treatment conditions with sham and heating at 39 - 44°C. No cell killing was observed after the HFEMF exposure at the SARs of 5, 10, 20, 50 and 100 W/kg, while cell viability was slightly decreased at 200 W/kg (83.4 ± 4.9% (data not shown), No significant difference vs Control). No cell killing was also observed immediately after heat treatment at 39 and 41°C and the treatment with bleomycin. The cell viability at 44℃ was decreased (77.1 ± 2.5%, $p < 0.01$, Significantly different vs Control).

3. Chromosomal aberrations

A summary of chromosomal aberration data is showed in Table 2.

Table 2 Chromosomal aberration in m5S cells after treatment with HFEMF, MMC, or X-rays

Treatment	No. of cells analysed	Chromatid-type				Chromosome type				Aberrations/100 cells		%Aberrant Cells	
		ctg	csg	ctb	cte	Frag	Min	Dic	Ring	Total	Excl	Total	Excl
Sham	200	3	0	0	0	1	1	0	0	2.5	1	2.5	1
5 W/kg	200	2	0	2	0	0	0	0	0	2	1	2	1
10 W/kg	200	0	0	0	0	0	0	1	0	0.5	0.5	0.5	0.5
20 W/kg	200	1	0	0	0	0	0	0	0	0.5	0	0.5	0
50 W/kg	200	1	1	0	2	0	0	0	0	2	0.5	2	1
100 W/kg	200	1	0	1	1	0	2	0	0	2.5	1	2.5	2
MMC (0.1 μg/mL)	200	4	0	11	78	2	3	1	1	50	43.5	44.5	43.5
X-rays (3 Gy)	200	4	1	5	14	4	18	4	0	25	19	21.5	19

ctb= chromatid breaks, csg= isochromatid gaps, cte= chromatid exchanges.
Isochromatid breaks (csb) were included in acentric fragments (Frag).
Min=minute chromosomes, Dic dicentrics. Excl=excluding gaps.

The rate of incidence of chromosomal aberrations was less than 0.02. No differences were observed between control and HFEMF exposure. The frequency of chromosomal aberration appearance is less than 2.5% between 5 W/kg to 100 W/kg HFEMF exposures. In contrast, X-rays and MMC treatment resulted in chromosomal aberrations in 45% and 20% of the cells, respectively. Results obtained by chromatid and chromosome aberration analysis did not exhibit any statistically significant differences between sham control and HFEMF exposure conditions from 5 W/kg to 100 W/kg. As expected, MMC and X-ray treatment significantly increased ($p < 0.001$) the frequency of chromosomal aberration, chromatid aberration and total chromosomal aberration compared with sham controls.

Conclusions

In conclusion, HFEMF exposure at 2.45 GHz for 2 h up to SAR of 50 W/kg does not induce MN formation. We did not detect the increase in DNA strand breaks and chromosomal aberrations, even at 100 W/kg. For the MN formation, there were statistically significant increases at SARs of 100 and 200 W/kg, compared with the sham-exposed control. However, we also observed that the temperature elevation induced the increased MN formation. Although more research is required, the present study has shown that MN formation at SAR from 5-200 W/kg is connected to temperature raise caused by HFEMF.

In addition, we have reported the effect of HFEMF on cell growth rate, cell cycle distribution, Transformation, and heat-shock protein (hsp) expression. Cell growth rate and cell cycle distribution were not affected by exposure to HFEMF at SAR of lower than 100 W/kg for 2 h [27], No significant differences were observed in the malignant transformation (Type II + Type III) frequency between the sham-control and the HFEMF at SARs of 5 to 200 W/kg for 2 h [28]. The expression of hsp70 increased in a time and dose-dependent manner at SAR of over 50 W/kg for 1-3 h [29]. However, a similar effect was also observed in corresponding heat controls.

From these results, we considered that HFEMF exposure at 2.45 GHz for 2 h did not affect cell growth, cellular genotoxicity, cell transformation, and hsp70 expression, even at exposure level of 5 to 50 W/kg. Therefore, we can conclude that our investigations have indicate the absence of any relationship between

exposure to the HFEMF at an environmental level and adverse health effect. However, experiments should still be performed to evaluate the safety of the HFEMF exposures.

Acknowledgments

We thank Drs. M. Taki and Y. Suzuki (Tokyo Metropolitan University, Japan) for the supply of HFEMF exposure system. This work was supported in part by the committee to Promote Research on the Possible Biological Effects of Electromagnetic Fields, Ministry of Public Management, Ministry of Internal Affairs and Communications, Japan.

References

1. R Glaser (1992) Current concepts of the interaction of weak electromagnetiv fields with cells. Bioelectrochemistry and Bioenergetics, 27: 255-268.
2. PS Liburdy (1992) Calcium signaling in lymphocytes and ELF fields: evidence for an electric field metric and a site of interaction involving calcium ion channels. FEBS Lett., 301: 53-59.
3. PS Barnes (1996) Effect of electromagnetic field on the rate of chemical reactions. Biophysics., 41: 801-807.
4. L Hardell, A Nasman, A Pahlson, A Hallquist and K Hansson Mild (1999) Use of cellular telephones and the risk for brain tumours: a case-control study. Int J Oncol., 15: 113-116.
5. A Ahlbom, A Green, L Kheifets, D Savitz and A Swerdlow (2004) International Committee for Non-Ionizing Radiation Protection (ICNIRP) Standing Committee on Epidemiology. Epidemiology of health effects of raiofrequency exposure. Environ Health Perspect, 112: 1741-1754 .
6. A Lahkola K Tokola and A Auvinen (2006) Meta-analysis of mobile phone use and intracranial tumors. Scand J Woork Environ Health, 32: 171-177.
7. JA D'Andrea, ER Adair and JO de Lorge (2003) Behavioral and cognitive effects of microwave exposure. Bioelectromagnetics, 6: S39-S62.
8. LN Heynick, SA Johnston and PA Mason (2003) Radio frequency electromagnetic fields. Cancer, mutagenesis, and genotoxicity. Bioelectromagnetics, 6: S74-S100.
9. H Lai and NP Singh (1995) Acute low-intensity microwave exposure increases DNA single-strand breaks in rat brain cells. Bioelectromagneitcs, 16: 207-210.
10. Vijayalaxmi, KS Bisht, WF Pickard, ML Meltz, JL Roti Roti and EG Moros (2001) Links chromosome damage and micronucleus formation in human blood lymphocytes exposed in vitro to radiofrequency radiation at a cellular telephone frequency (847.74 MHz, CDMA). Radiat Res., 156: 430-432.
11. P Gos, B Eicher, J Kohli and WE Heyer (2000) No mutagenic or recombinogenic effects of mobile phone fields at 900 MHz detected in the yeast Saccharomyces cerevisiae. Bioelectromagnetics, 21: 515-523.
12. JL Riti Roti, RS Malyapa, KS Bisht, EW Ahern, EG Moros, WF Pickard and WL Straube (2001) Neoplastic transformation in C3H 10T(1/2) cells after exposure to 835.62 MHz FDMA and 847.74 MHz CDMA radiations. Radiat Res., 155: 239-247.
13. D Leszczynski, S Joenvaara, Reivinen and R Kuokka (2002) Non-thermal activation of the hsp27/p38MAPK stress pathway by mobile phone radiation in human endothelial cells: molecular mechanisim for cancer- and blood-brain barrier-related effects. Dfferentiation, 70: 120-129.
14. F Tian, T Nakahara, K Wake, M Taki and J Miyakoshi (2002) Exposure to 2.45 GHz electromagnetic fields induces hsp70 at a high SAR of more than 20 W/kg but not at 5W/kg in human glioma MO54 cells. Int J Radiat Biol., 78: 433-40.
15. J Miyakoshi, M Yoshida, Y Tarusawa, T Nojima, K Wake and M Taki (2002) Effects of High-Frequency Electromagnetic fields on DNA strand breaks using comet assay method. Elecrical Engineering in Japan, 141: 9-15.
16. GM Van Leeuwen, AN Kotte, BW Raaymakers and JJ Lagendijk (2000) Temperature simulations in tissue with a realistic computer generated vessel network. Phys. Med. Biol., 45: 1035-1049.
17. R Gudi, SS Sandhu, and RS Athwal, (1990) Kinetochore identification in micronuclei in mouse bone-marrow erythrocytes: an assay for the detection of aneuplodity-inducing agents. Mutat. Res., 234: 263-268.
18. GM Krishna, R Fiedler and JC Theiss (1992) Simultaneous evaluation of clastogenicity, aneugenicity and toxicity in the mouse micronucleus assay using immunofluorescence. Mutat. Res., 282: 159-167.
19. M Fenech and AA Morley (1989) Kinetochore detection in micronuclei: an alternative method for measuring chromosome loss. Mutagenesis, 4: 98-104.
20. PI Coutryman and JA Heddle (1976) The production of micronuclei from chromosome aberrations in irradiated cultures of human lymphocytes. Mutat. Res., 41: 321-332.

21. S Koyama, Y Isozumi, Y Suzuki, M Taki and J Miyakoshi (2004) Effects of 2.45 GHz electromagnetic fields with a wide range of SARs on micronucleus formation in CHO-K1 cells, Scientific World Journal, 4: 29-40.
22. Y Komatsubara, H Hirose, T Sakurai, S Koyama, Y Suzuki, M Taki and J Miyakoshi (2005) Effect of 2.45GHz electromagnetic fields with a wide range of SARs on DNA damage in MO54 cells. European Biology and Bioelectromagnetics, 1: 148-170
23. Y Komatsubara, H Hirose, T Sakurai, S Koyama, Y Suzuki, M Taki and J Miyakoshi (2005) Effect of high-frequency electromagnetic fields with a wide range of SARs on chromosomal aberrations in murine m5S cells. Mutat. Res., 587: 114-119
24. MS Sasaki and S Kodama (1987) Establishment and some mutational characteristics of 3T3-like near-diplold mouse cell line, J. Cell Phys., 131: 114-122.
25. J Miyakoshi, M Yoshida, K Shibuya and M Hiraoka (2000) Exposure to strong magnetic fields at power frequency potentiates X-ray-induced DNA strand breaks. J. Radiat. Res., 41: 293-302.
26. PL Olive, D Wlodek, RE Durand and JP Banath (1992) Factors influencing DNA migration from individual cells subjected to gel electrophoresis. Exp vell Res., 198: 259-267.
27. Y Takashima, H Hirose, S Koyama, Y Suzuki, M Taki and J Miyakoshi (2006) Effects of continuous and intermittent exposure to RF-fields with a wide range of SARs on cell growth, survival and cell cycle distribution. Bioelectromagnetics, 27: 392-400.
28. J Wang, T Sakurai, S Koyama, Y Komatubara, Y Suzuki, M Taki and J Miyakoshi (2005) Effects of 2450 MHz Electromagnetic fields with a Wide Range of SARs on Methylcholanthrene-induced Transformation in C3H10T1/2 Cells. J. Radiat. Res., 46: 351-361
29. J Wang, S Koyama, Y Komatubara, Y Suzuki, M Taki and J Miyakoshi (2006) Effect of a 2450 MHz high-frequency electromagnetic field with a wide range of SARs on the induction of heat-shock proteins in A172 cells. Bioelectromagnetics, *(in press)*.

ELECTROMAGNETIC RADIATION EFFECTS ON ELECTRONIC PARTICLES TRANSFER IN DNA – APPLICATIONS TO MILLIMETER AND OPTICAL RANGES

Gérard DUBOST
Institut d'Electronique et de Télécommunications de Rennes
UMR CNRS 6164, Université de Rennes 1,
Avenue du Général Leclerc, Campus de Beaulieu, 35042 – Rennes Cedex – France

André BELLOSSI
Villa Gabrielle, Chemin du Goh Vras, 56730 – Saint Gildas de Rhuys – France

ABSTRACT

We justify the validity of the biexponential Debye relaxation model of the pure water extrapolated until the optical range by means of experiments results obtained on the human skin. The pure water attenuation per wavelength is maximum in the millimeter-wave range. We confirm the measurements which have shown appreciable AC conductivity of DNA due to relaxation losses of their surrounding water dipoles. We extend this property to the UV range showing the action of photons upon free electrons. Excited ions, by means of our external plasma device generator of solitary-waves is the object of photon emissions in the optical range. In particular in UV range the free electron alone is liable to be propeled by a photon with a kinetic energy with a some idea of the size to 10^{-23} Joules. In a large range until millimeter waves, the excited ions can attract electrons showing a kinetic energy of 10^{-21} Joules. They can be used to activate control and explain the division of fibroblasts and the cancer mechanisms of human skin, the main modification of DNA molecules by UV radiation being the formation of pyrimidine dimers. Finally we can conclude that the molecule of DNA has a conducting which is always increasing with the frequency, but can be considered as a real conductor only in the millimeter-wave range with an important absorption per wavelength. The "conduction quality" is the ratio of the conduction to the displacement currents.

INTRODUCTION

PRELIMINARY CLARIFICATION

The electronic conduction in DNA is a polemic subject always going on nowadays. Is DNA conductive or not ? DNA has been reported to be a metal, a semiconductor, an insulator and even a proximity effect induced superconductor. Above all it was advisable to go back to some reminders. In a recent paper [1] it as been shown that appreciable AC conductivity of DNA, measured in the millimeter wave range, is largely ascribed to relaxational losses of the surrounding water dipoles. So it was necessary from the theoretical complex dielectric constant $\tilde{\varepsilon}_r = \varepsilon_r - j\sigma/\omega\varepsilon_o$ of bulk pure water, described by a biexponential Debye relaxation model [2], to calculate its conductivity σ, and the coefficient of absorption A given by the classical expression :

$$A\ (\text{Neper}/\lambda_o) = 2\pi\left[-\frac{\varepsilon_r}{2}+\frac{1}{2}\sqrt{\varepsilon_r^2+(\sigma/\omega\varepsilon_o)^2}\right]^{1/2} = \frac{\lambda_o}{\delta} \quad (1)$$

δ is the thickness penetration and λ_o the free space wavelength.

We introduced the "conduction quality" C_p which is the ratio of the conduction to the displacement currents equal to : $C_p = \sigma / 2\pi f\, \varepsilon_o\, \varepsilon_r$ (2)

The **Table I** shows the various parameters in terms of the frequency for the pure water at 20 °C. We can conclude :

a) The conductivity σ is increasing with the frequency.
b) The absorption coefficient $A(N/\lambda_o)$ has a maximum in the millimeter range (N means Nepers : 1N = 8.69 dB).
c) The absorption per unit of length (dB/mm) is increasing with the frequency.
d) In the millimeter wave range the water can be considered as a "conductive medium" (C_p >1), and as an insulator medium (C_p <1) when f < 2.10^{10} Hz or f > 2.10^{11} Hz. Nevertheless its conductivity σ is always increasing with the frequency.
e) We can justify the values of the conductivity and the absorption in the UV range deduced from the experiments realized on the epidermis. The epidermis is composed, from the skin surface to the depth, by the stratum corneum, the stratum granulosum, the stratum spinosum and the stratum basale. Due to the water content of the cells we can put together the three later layers ; we call them mucus body.

The **Table II** shows the values extracted from measurements upon the human skin which must be compared with these given in **Table I**.
The range UV is separated into two ranges : UVA and UVB. For each of them, and from the measured transmission coefficient [18], we deduced the conductivity σ and the absorption related to the stratum corneum and the mucus body. We note that the bulk water theoretical conductivity is comprised between those of the stratum corneum and mucus body.

f(Hz)	λ_o	(2) C_p	$\sigma(S/m)$	(1) δ	v_p/c	ε_r	(1) $A(N/\lambda_o)$	A(dB/mm)
10^9	300 mm	0.05	0.22	0.21 m	0.11	80.0	1.4	0.04
5.10^9	60 mm	0.25	5.2	9 mm	0.11	75.2	6.7	0.97
10^{10}	30 mm	0.49	17.3	2.5 mm	0.12	63.6	12.0	3.5
2.10^{10}	15 mm	0.93	41.6	0.9 mm	0.145	40.2	17.1	9.9
5.10^{10}	6 mm	1.72	68.7	360 µm	0.22	14.4	16.7	24
7.10^{10}	4.3 mm	1.85	73.3	290 µm	0.25	10.2	14.9	30
10^{11}	3.0 mm	1.79	76.5	250 µm	0.29	7.7	12.0	35
5.10^{11}	600 µm	0.74	99.7	125 µm	0.43	4.9	4.8	70
10^{12}	300 µm	0.54	131	86 µm	0.47	4.2	3.5	100
5.10^{12}	60 µm	0.18	172	57 µm	0.54	3.4	1.06	150
10^{13}	30 µm	0.10	176	38 µm	0.55	3.3	0.80	230
10^{14}	3 µm	10^{-2}	177	38 µm	0.55	3.3	0.08	230
10^{15}	0.3 µm	10^{-3}	177	38 µm	0.55	3.3	0.008	230

Table I : Electrical parameters of pure bulk water at 20 °C in terms of frequency

Range (μm)	λ_m (μm) (mean)	Mean Transmission T [18]	T_{SC} (dB)	T_{MB} (dB)	A(dB/mm)	σ(S/m)	
UVA (0.315 – 0.390)	0.352	4.6 % - 13.4 dB	-9	-4.4	529 67	588 74	SC MB
UVB (0.280 – 0.315)	0.298	0.9 % - 20 dB	-14	-6	823 92	914 102	SC MB
UV (0.280 – 0.390)	0.335	3.5 % - 14.6 dB	-10	-4.6	588 70	653 78	SC MB

Table II (valid for $\varepsilon_r = 3.3$ and $\sigma/\omega\varepsilon_o << \varepsilon_r$)

SC : Stratum corneum : thickness : 17 μm Transmission : T_{SC}

MB : Mucus body thickness : 65 μm Transmission : T_{MB}

$$\text{With : } T = T_{SC} + T_{MB} \quad \text{and} \quad \sigma(S/m) = \frac{A(dB/mm)}{0.9}$$

CHARGE TRANSPORT IN SYNTHETIC DNA

The denaturation of the DNA is due to the breaking of the hydrogen bonds, which keep in position the two strands (fig. 1).
In the course of the DNA duplication, two complementary strands give birth to two new DNA molecules. The DNA macromolecule structure was introduced in 1953 by Watson and Crick.

Electronic transport along DNA is crucial for the repair mechanism after radiation damage and biosynthesis [3]. In 1989 Peyrard-Bishop study the structure by means of global energies expressed with a Lagrangian.

The various parameters used are :

- the relative displacements of the nucleotidic bases at different sites of each DNA strand,
- the equivalent mass m of a nucleotide pair equal to 300 amu ($m = 5.10^{-25}$ Kg),
- the Morse potential which is the energy of a hydrogen bond between a pair of nucleotides,
- the average of the energy values for the guanine-cytosine basis (G-C) and for the thymine-adenine basis (A-T), which is called the well depth or Morse depth. It corresponds to the dissociation energy of a base pair and is equal do D = 0.04 eV let us be $0.64\ 10^{-20}$ J,
- the width of the well equal to : w = 0.224 Å,
- the stacking energy between neighboring bonds,
- the energy of the dipole-dipole interaction,
- the dipole parameter expressed in terms of electric charge transfer and of the distance between neighboring base pairs,
- the potential energy between two consecutives bases along a strand V_o = 0.1eV in an equilibrum state,
- the linear frequency of the isolated oscillator which is equal to :

$$f_o = (1/2\pi)\left(2D/mw^2\right)^{1/2} = 1.14\,10^{12} \text{ Hertz} \qquad (3)$$

One considers the radial displacement of the base unit and the angular rotation between two adjacent base pairs from their equilibrium state. The lattice oscillations are designed by pulsation Ω_r for the radial displacement and Ω_p for the twist one.

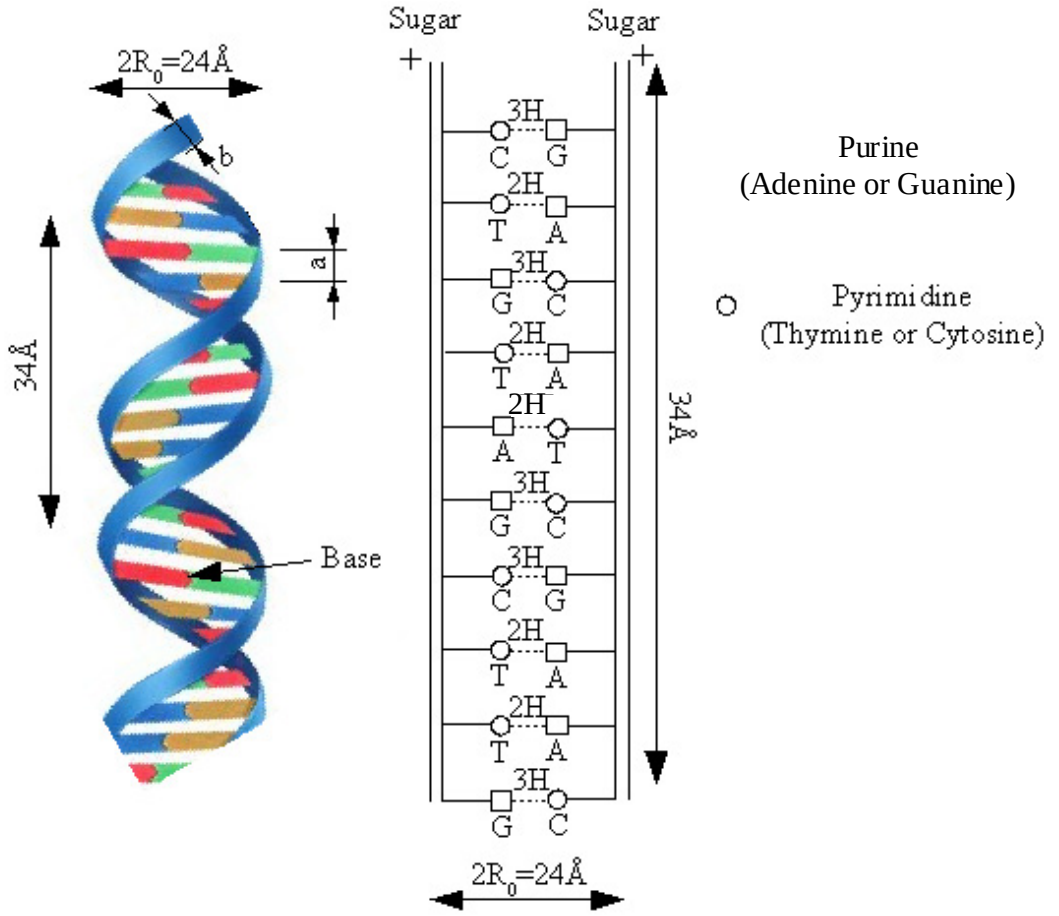

Fig. 1.

The adiabaticity parameter $(h/2\pi)(\Omega_r / V_o)$ (4) equal to : 0.041 proves the adiabatic right hypothesis during a quasi instantaneous displacements. From the fixed parameters at an equilibrium state : a = 3.4 Å, $\theta_o = 36°$, $R_o = 12$ Å, we deduced the distance ℓ_o between two consecutive bases along a strand :

$$\ell_o = \sqrt{a^2 + 4R_o^2 \sin^2(\theta_o/2)} = 8.16 \text{ Å}$$

The potential energy V_o is equal to :

$$V_o = p_o.q/4\pi\varepsilon_o \ell_o^2 \qquad (5)$$

where p_o is the moment of the charge. With $V_o = 0.1\text{eV}$ we deduced : $q.p_o = 1.18\,10^{-48}$. Taking $p_o = q.1$ Å, gives : $q = 1.08\,10^{-19}\text{C}$ which is approximately the electron charge. The mobility of the charge is possible in the presence of random parametrical and structural disorders inherent to DNA molecules [3].

Recently some authors [4] have considered the charge q when hydrogen bonds stretch using quantum chemical methods taking into account the nucleoside pairs (sugar linked to base). The value of the dipole parameter $J = q^2/4\pi\varepsilon_o a^3$ (6) is equal to : $3.3\,10^{-3}\text{eV/Å}^2$ let us be $0.053\,\text{J/m}^2$ with q = - 0.095 e, which is the charge transfer intermediate between the A-T and G-C base pairs [1].

The stacking parameter is given by some authors [5] equal to 0.96 J/m^2 (let us be 0.06 eV/ Å^2), and by others [6] comprised between 0.01 and 10 eV/ Å^2. It has been then considered as adjustable parameter [4]. In short we can report according [4] that solitons or "discrete breathers" can be also generated from or exist among random thermal fluctuations. Moving breathers with speed comprised between 4 and 24 m/s, behave as quasiparticles, having an effective mass between 30 and 46 amu and a kinetic energy comprised between $6.5\,10^{-25}$ J and

2.10^{-23}J, which is able to pass over a bending point in function of the strand curvature. For T = 310° K the thermal energy is $KT = 4.310^{-21}$J or 2.710^{-2}eV. The conduction mechanism in DNA was recently studied [7], showing the impact of disorder. Evidently the charge motion is influenced by the vibrational modes of the double helix. Results concerning the electron transport in synthetic DNA polymers had been recently published [8]. For many organs we know that beyond a frequency of 2.10^{10} Hertz, the conductivity trends upward very quickly [Gabriel King's College, London, June 1996]. To establish the theory of the cell division Popp [8] supposed a high conductivity for the cell membrane without indication of its value. Albrecht-Buehler [9] thinks that centriolar "blades" have a high conductivity. Centrosome is an intracellular organelle composed of 2 centrioles and pericentriolar material. The centrioles are a pair of cylinder-like structures. (0.8 × 0.15 µm) often disposed in an orthogonal way to each other. Each centriole is composed of 9 separate protofilaments (0.8 µm × 40 nm). Electrons of very low energies can induce substantial yields of single and double strand breaks of DNA in near infrared spectrum [10] and [11]. To be in a good agreement with numerous experimental results in near infrared, visible and near ultraviolet spectra we must choose a conductivity of 10^5S/m for the membrane medium [12].

The figure 2 gives the theoretical velocity v of the moving electron along the DNA chain, as a function of the amplitude E_o of the periodic field parallel to the double helix axis, for different frequencies in the millimeter wave ranges. It is taken out from [3] but expressed now with more convenient parameters. The normalized frequency given in [4] is related to the frequency f_o (3), with D = 0.04 eV, w= 0.224Å and $m = 5.10^{-25}$Kg. Coherent electron transfer can be stimulated when the frequency of the applied field is such that : $10^{11} < f < 3.10^{12}$ Hz .To be efficient the applied external electric energy $eE_o\ell_o$ has to be higher than V_o let us be : $E_o\ell_o > 0.1V$ with $\ell_o = 8.16$ Å that is $E_o > 10^8$ V/m.

Moreover the electron kinetic energy comprised between 4.10^{-26} and , 610^{-26}J, is very weak compared with the thermal fluctuation kT.

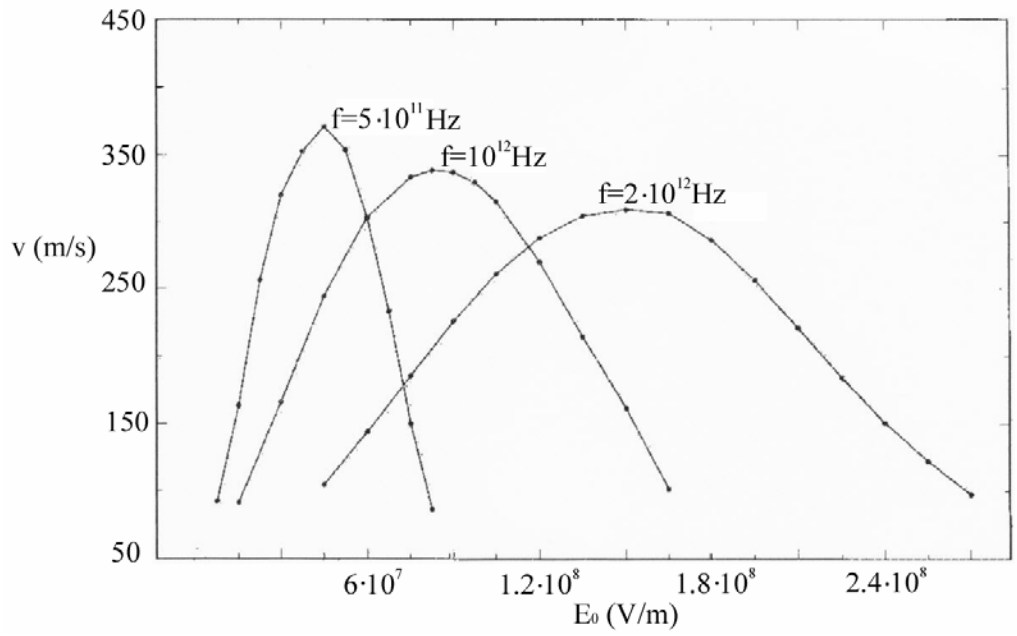

Fig. 2

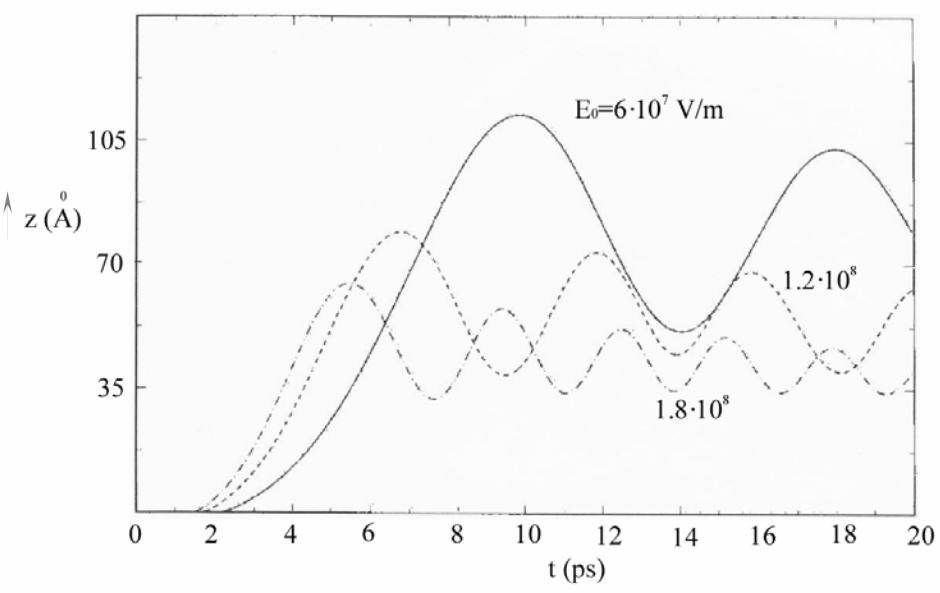

Fig. 3 : Temporal electronic occupation probability

The figure 3 shows the temporal behavior of the electronic occupation probability of the electron along the DNA axis in the presence of the external field at $f = 10^{11}$ Hz for different amplitudes E_o and a disorder of 0.02 eV. The position $z(\text{Å})$ corresponds to the electronic occupation probability after a propagation from a starting one for t = 0. When the field amplitude is enlarged the dynamic of the electron and the amplitude of the oscillations become weaker. The oscillation frequencies f_{osc} are higher than the electronic one equal to 10^{11} Hz as indicated in Table III.

$E_o\,(V/m)$	6.10^7	$1.2\,10^8$	$1.8\,10^8$
f_{osc} (Hertz)	$1.25\,10^{11}$	2.10^{11}	$2.8\,10^{11}$

Table III (valid for $f = 10^{11}$ Hz)

Whatever E_o, the maximum velocity v_M at $f = 10^{11}$ Hz is equal to $2.3\,10^3\,m/s$. All these results, valid for a relative strong disorder ΔE on site electronic energy equal to 0.02 eV, are due to the nonlinear physics applied to DNA.

COMPARISON BETWEEN THEORY AND EXPERIMENTS IN MILLIMETER RANGE

AC conducting DNA in the millimeter range has been measured. Several authors have shown an appreciable conducting which approaches that of a well-doped semiconductor. Nevertheless it has been found that the high AC conductivity of DNA can be attributed largely to relaxational losses of the dipoles of the water molecules in surrounding hydratation layers [1]. The total number of water molecules per nucleotide has to be correlated with the relative humidity [13]. For instance the adsorption of water molecules per nucleotide is equal to 13 for a rate of humidity (R.H) equal to 84 % and 4 for a R.H of 60 %. For an R.H of 0 %, there are 2.5-3 water molecules

per nucleotide which cannot be removed from the helix. The table IV shows the AC conductivity of calf thymus DNA measured in terms of the frequency [1].

f(Hz)		10^{11}	$2\,10^{11}$	$5\,10^{11}$	10^{12}
RH : 0 % σ (S/m) [1]		1	12	35	100
RH : 84%	σ(S/m) [1]	25	50	70	110
	A(N/λ_o) (1)	4.9	5.4	3.5	3.0
	C_p (2)	0.60	0.75	0.40	0.50

Table IV : conductivity σ measurements of calf thymus DNA

The conductivity σ, which is increasing with the frequency and the rate of humidity, can be attributed largely to the water layer surrounding the DNA blackbone. In effect, for a R.H equal to 84 % the absorption A(N/λ_o) and C_p were calculated with the relations (1) and (2) using the experimental conducting σ [1] and ε_r given in **Table I**. The experimental values σ [1] and the deduced absorption A(N/λ_o) shown in **Table IV** are normally as should be weaker than these shown in **Table I** valid for the bulk pure water. The measured conductivities of the single and double strands have been found identical [1]. Considering the weak values of C_p we can say that the DNA can be reported to a dielectric medium in spite of its important conductivity. Previously reported conductivity value of 240 S/m was evaluated from the measured loss of highly sensitive resonant cavities operating at 12 and 100 GHz [14].

SOLITARY-WAVE EMISSIONS

The emission are due to solitary-waves or solitons issued from an external confined plasma device [15]. The induced emission lifetime of the ion in vivo medium is given [17] :

$$\tau_B = \frac{78}{\pi^2}.\left(\frac{c}{f_r}\right)^3.\frac{h^2}{Z^2}.\sqrt{\frac{\varepsilon_o}{\mu_o}}.\frac{\varepsilon_o}{P_t^2}\left[2\pi e(\Delta n_i)V_p\frac{L}{r}\right]^{-2}.|\tilde{n}|^2 \qquad (7)$$

$\tilde{n}$ is the mean complex, index of refraction at f_r in the vivo medium.
The parameters inserted between brackets are related to the plasma device.
P_t is the electric moment of the dipolar transition. Z is the atomic number of the ion. f_r is the square signal modulation frequency of a high RF frequency used to light the discharge inside the plasma tube. The density of the ions at the fundamental state in a strong electrolyte, equivalent to the interstitial liquid, which has been carried is equal to : $N_1 = 1.85\,10^{26}/m^3$: [16].
From [17] we deduced in the vivo medium :

$$N_2 = N_1\,3.7\,10^{16}\left(\frac{f_r}{\nu}\right)^3.\frac{1}{|\tilde{n}|^2} \qquad (8) \qquad\qquad \tau_B = 4.10^{20}\,f_r^{-3}.|\tilde{n}|^2 \qquad (9)$$

N_2 is the density of excited ions per unit of volume and ν the frequency of their photonic emission. From N_2 we deduced the mean distance between sollicitaded ions by the expression : $d = (N_2)^{-1/3}$ (10)

We showed that a low frequency f_r acting upon ion produce an ionizing radiation in the optical range [17]. The **Table V** shows the calculated values related to the ion induced emissions in terms of the free wavelengths for a higher modulation frequency f_r and a weak lifetime.

λ_o	0.25 µm	1µm	10 µm	100 µm	1 mm	1.78 mm
d	16 µm	4 µm	0.4 µm	400 Å	40 Å	22 Å
$n = N_2 / N_1$	$1.3\,10^{-12}$	$8.8\,10^{-11}$	$8.8\,10^{-8}$	$8.8\,10^{-5}$	$8.8\,10^{-2}$	0.5
N_2 / m^3	$2.4\,10^{14}$	$1.6\,10^{16}$	$1.6\,10^{19}$	$1.6\,10^{22}$	$1.6\,10^{25}$	$9.2\,10^{25}$
ν(Hz)	$1.2\,10^{15}$	3.10^{14}	3.10^{13}	3.10^{12}	3.10^{11}	$1.69\,10^{11}$
$W = h\nu$ (J)	8.10^{-19}	2.10^{-19}	2.10^{-20}	210^{-21}	2.10^{-22}	$1.1\,10^{-22}$
d / λ_o	64	4	0.04	4.10^{-4}	4.10^{-6}	$1.2\,10^{-6}$

Table V : Ion induced emission

valid for $f_r = 4.10^6$ Hz, $\tau_B = 6.10^3$ s (9), $N_1 = 1.85\,10^{26} / m^3$, $|\tilde{n}|^2 = 10^3$,

When the wavelength is enlarged the mean distance d between the sollicited ions and the energy of the quantic oscillator W are decreasing, while their density N_2 increases. We have shown in [17] that when $d / \lambda_o < 1/\pi$ two adjacent dipoles have a strong mutual coupling such that the radiation of the array due to the whole excited ions was suppressed. Nevertheless the electric field amplitude E_o due to one ion is given by :

$$E_o = P_t / 4\pi\varepsilon_o r^3 \qquad (11)$$

P_t is the electric moment of the dipolar transition approximately equal to :

$$P_t = e.1\,Å = 1.6\ 10^{-29}\ (C.m)$$

For r = 10Å, we obtain from (11) : $E_o = 1.4\,10^8$ V / m . Let us consider the electrostatic attraction of an electron by the ion when the viscosity strength is taken into account. We calculate for r = 10 Å a speed of $5.510^4 m/s$, that is a kinetic energy equal to 10^{-2} eV. Let be a free electron motionless knocked by a photon of $W = h\nu$ energy. We suppose a perfectly elastic shock. Before and after the shock the whole impulse is unchanged. If we neglect the Compton effect, that is the frequency variation of the photon, we can write :

$$\frac{2h\nu}{c} = m_e v_e \qquad (12),$$

With : $h\nu = 5.1\,eV$, $m_e = 0.91\,10^{-30}$ Kg, we deduced from (12) the electron speed : $v_e = 6.10^3 m/s$. So the electron kinetic energy is equal to : 1.610^{-23} J, that is 10^{-4} eV. The photon which is associated with an electromagnetic wave is moving along the DNA with a speed equal to : $v_p = 1.65\,10^8$ m / s (see Table I). The photon can be also absorbed by the particle. Then the photo-ionization principle may give birth to an electron, with an energy higher than 10^{-4} e V .

SUMMARY

a) We introduced the ratio of the conduction to the displacement currents to express the conduction quality C_p (2) of a medium. Thus the pure water has a conduction σ which is always increasing all along the frequency range, while the conduction quality C_p is the highest in the millimeter wave range (**Table I**).

b) We justify the validity of the biexponential Debye relaxation model of the pure water extrapolated until the U.V range, by means of experimental results obtained on the human skin.

c) **Table I** shows the attenuation per wavelength which is maximum in the millimeter-wave range. Recent measurements in that range have shown appreciable AC conductivity of DNA which is largely ascribed to relaxational losses of the surrounding water dipoles [1]. We have extended this property to the UV range **(Table II),** showing further the action of photons upon free electrons.

d) Excited ions, by means of our external plasma device generator of solitary waves, is the object of photon emissions where an example is given in the Table V. An electron can be shocked by a photon in UV, showing a kinetic energy equal to 10^{-4} eV. What's more by means of the electrostatic attraction of one ion, an electron can show a kinetic energy equal to 10^{-2} eV. They can be used to activate, control and explain the division of fibroblasts and the cancer mechanisms of human skin, the main modification of DNA molecules by U.V radiation being the formation of pyrimidine dimers [11].

REFERENCES

[1] **M. BRIMAN, N.P. ARMITAGE et all**, *Dipole relaxation losses in DNA*. Depart. of Physics and Astronomy, University of California, Los Angeles, CA 90095, 8 Nov. 2005.

[2] **C. RONNE et al**, J. Chem. Phys. 107, 5319 (1997).

[3] **D. HENNING, J.F.R. ARCHILLA** , *Polaronic charge transport mecanism in DNA.* Elsevier Preprint, May 18, 2005.

[4] **J. CUEVAS, E.B. STARICOV et all**, *Moving breathers in bent DNA with realistic parameters* ar Xiv : nlin.PS/0404029V3,4, Nov. 2004.

[5] **T. DAUXOIS, M. PEYRARD, A.R. BISHOP**, Phys. Rev. E 47, 684 (1993).

[6] **J. CUEVAS, J.F.R. ARCHILLA et all,** *Moving breathers in a DNA with competing short and long-range dispersive interactions*, Physica D 163 : 106, 2002.

[7] **P. CARPENA, P. BERNAOLA-GALVAN et all**, Nature 418, 955 (2002).

[8] **F.A. POPP,** *Basic theory of cancer development and defense*, Intern. Conf. Biological Cancer Defense in Heidelberg, May 3-5, 2002.

[9] **G. ALBERCHT BUEHLER,** *Altered drug resistance of microtubules in cells exposed to infrared light pulses*. Cell mobility and cytoskeleton, 1998, vol. 40, pp. 183-192.

[10] **A. BOUDAFFA, P. CLOUTIER et all**, *Resonant formation of DNA strands breaks by low energy electrons*, Science 3 March, 2000, vol. 287.

[11] **J. HUGO, NIGGLI**, *Ultra weak photon emission in differentiated fibroblasts.* Conference on biophotons, 1999.

[12] **G. DUBOST, A. BELLOSSI**, *Cell membrane physical model in near infrared, visible, and near ultraviolet spectra*. Biological Effects of EMFS, 3rd Intern. Workshop Kos, Greece, 4-8 October, 2004, p. 492 to 500.

[13] **S. BRAUNAUER, P. EMMETT et all**, J. Am. Chem. Soc., 80, 309 (1938).

[14] **K.H. YOO, D.H. HA et all**, Phys. Rev. Lett. 87, 198102 (2001).

[15] **G. DUBOST, A. BELLOSSI, J. BARE**, *Efficiency of solitary-waves radiated by the discharge in a confined plasma column*. Biological Effects of EMFS, 3rd Intern. Workshop Kos, Greece, 2004, p.473 to 481.

[16] **G. DUBOST, A. BELLOSSI**, *Electromagnetic field diffracted by a nervous fiber excited by an external electric field.* Biological Effects of EMFS, 3rd Intern. Workshop Kos, Greece, 2004, p. 482 to 491.

[17] **G. DUBOST, A. BELLOSSI, J. BARE**, *Solitary waves effects on Ions Emissions in the living matter.* MMS Proceedings : MSA6, pp. 210-215, sept. 6-8, 2005, Athens, Greece.

[18] **K. HOFFMANN, K. KASPAR, P. ALTMEYER, T. GAMBICHLER**, *UV Transmission Measurements of Small Skin Specimens with Special Quartz Cuvettes*. Dermatology 2000; 201; 307-311, Ruhr University, Bochum, Germany.

PARAMETERIZATION OF ALTERED HUMAN ERYTHROCYTE SHAPES. APPLICATION TO THE CALCULATION OF THE INDUCED TMP AND STRESS FORCES

J.L. SEBASTIÁN

S. MUÑOZ

M. SANCHO

J.M. MIRANDA

DPT. DE FÍSICA APLICADA III, FACULTAD DE CIENCIAS FÍSICAS
UNIVERSIDAD COMPLUTENSE, 28040 MADRID, SPAIN

Abstract
Simple parametric equations are presented in terms of Jacobi elliptic functions that provide a realistic model of abnormal variations in size which maintain the biconcave shape of a normal erythrocyte (anisocytosis), and abnormal variations in shape which maintain the original volume of the erythrocyte (poikilocytosis), as well as continuous deformations from the normal to the altered shapes. We illustrate our results with parameterizations of spherocytes, ellipsoids, microcytes, macrocytes and stomatocytes, and apply these parameterizations to the numerical calculation of the induced transmembrane potential in stomatocytes and the induced electric stress on the membrane of erythrocytes when both cells are exposed to an external electromagnetic field of 1800 MHz.

Introduction
Erythrocytes are the most numerous cells in the blood and their complete characterization has attracted much effort. In particular it has been known experimentally for more than fifty years that a variety of agents can modify systematically and reversibly the normal erythrocyte shape and size [Ponder 1948]. From a biophysical point of view changes in shape have been related to different mechanisms, such as variations of the membrane potential and temperature [Glaser 1979], to anion-exchange protein band 3 [Wong 1994, Gimsa 1998] or to the influence of the cytoplasmatic pH [Gedde et al. 1995]. From a complementary point of view, the increasing use of numerical techniques in the calculation of multiple-cell phenomena has prompted the development of realistic mathematical models for the shape of normal erythrocytes [Gray 1998, Bloor and Wilson 2000, Oroz 2004]. In fact, we have shown in previous work the crucial role played by an accurate geometry of the cell in the study of the response of normal erythrocytes to electromagnetic fields [Sebastian et al. 2001, 2004, Muñoz et al. 2003]. However, we are not aware of any simple geometrical model for altered erythrocyte shapes.

In this paper we address the modeling of abnormal variations in size which maintain the basic biconcave shape of the normal erythrocyte (anisocytosis), and abnormal variations in shape which maintain the original volume of the erythrocyte (poikilocytosis).

Anisocytosis is the generic term used to describe an abnormally wide distribution of the sizes of the erythrocytes in the blood, be it due to the presence of young red blood cells such as macrocytes which are larger than mature normal red blood cells, or to the presence of smaller red blood cells such as microcytes. Although anisocytosis by itself is not diagnostic, an improved anemia classification might be available by combining measures of red blood cell size variability with mean corpuscular volume [Simel et al. 1988]. Microcytic cells occur in immune-

mediated hemolytic anemia, microvascular constriction, early Heinz-body anemia and iron-deficiency anemia. Macrocytic cells occur with regenerative anemia and rarely with erythrocytic leukemia.

The rather non-specific term poikilocytosis is used to describe an unusually high (greater than 10%) population of abnormally shaped erythrocytes in peripheral blood [Harvey 2001]. These morphologically abnormal erythrocytes (poikilocytes) may be caused by a variety of conditions, including fragmentation of erythrocytes, oxidative injury, immune-mediated damage, and congenital abnormalities [Cowell et al.1999]. Among these morphologically abnormal cells are the spherocytes and stomatocytes. Spherocytes are red blood cells that are almost spherical in shape. They have no area of central pallor like a normal red blood cell. Large spherocytes (macrospherocytes) are seen in hemolytic anemia, whereas small spherocytes (microspherocytes) are sometimes seen in severe burn cases. Stomatocytes are characterized by a slit-like zone of central pallor. Stomatocytes are usually the result of a water content increase, an alteration of cation content and flux or and amphipathic drug use [Lim et al. 2002, Fujii et al. 1979, Elgsaeter and Mikkelsen 1991, Isomaa et al. 1987]. This altered erythrocyte shape is particularly interesting because of its abnormal increase in osmotic fragility which could lead to mechanical damage in turbulent blood flow circulation.

Considering the essential role played by the shape and size of the red blood cells in all the processes mentioned above, realistic cell models for spherocytes, macrocytes, microcytes and stomatocytes (as typical representatives of poikilocytes) must be used in any morphological cell analysis. In particular, the variation of the transmembrane potential when the cell is exposed to an electromagnetic (EM) field is a good probe of the interaction mechanism between biological cells and external radiation.

The layout of this paper is as follows: in the next section we briefly review existing mathematical models for the normal erythrocyte shape, and then present a new set of simple parametric equations that by means of free parameters model accurately continuous deformations from a simple sphere to the final erythrocyte altered shapes; then, as applications of these equations, we determine the transmembrane potential and the electric stress forces induced in the membrane of different cell shapes when they are exposed to an external EM field; the paper ends with a brief summary.

Parameterizations of erythrocyte shape abnormalities

Among the methods frequently used to model the erythrocyte normal shape [Sebastian et al. 2004, Moon and Spencer 1998] we mention the surface of revolution generated by a Cassini curve [Gray 1998]. Its main advantage is that Cassini curves have simple parametric representations in terms of trigonometric functions; its main limitations are that Cassini curves are determined by only two parameters (which can be used to fix only the length and the height of a real erythrocyte), and that the implementation of anisotropic deformations is not straightforward (in particular poikilocytosis and the changes in the shape of membranes which occur spontaneously when the cells are immersed in an aqueous environment under appropriate conditions [Jie et al. 1998]).

At the other end in complexity is the approach proposed by [Bloor and Wilson 2000], who use an elliptic partial differential equation in combination with an expression for the membrane surface energy to give a most realistic representation of the shape of the membrane surface. This approach, however, lacks the advantages of a simple parametric representation.

To find a reasonably simple parametric representation that allows for the modeling of the deformations we finally recall the parametric representation of the normal biconcave erythrocyte in terms of the $\mathrm{sn}(u|m)$, $\mathrm{cn}(u|m)$ and $\mathrm{dn}(u|m)$ Jacobi elliptic functions with three free parameters [Kuchel and Fackerell 1999], which we prefer to write directly in terms of as many physically measurable parameters as possible:

$$\mathbf{r}(u,\phi)=\left(\frac{\ell}{2}\mathrm{cn}(u|m)\cos\phi,\frac{\ell}{2}\mathrm{cn}(u|m)\sin\phi,\pm h_0\,\mathrm{sn}(u|m)\frac{\mathrm{dn}(u|m)}{\mathrm{dn}(U|m)}\right), \tag{1}$$

where ℓ is the diameter of the erythrocyte, $2h_0$ is the height of the erythrocyte at its center, $U=K(m)$ is the corresponding complete elliptic integral of the first kind (which satisfies $\mathrm{cn}(U|m)=0$, $\mathrm{sn}(U|m)=1$ and

$\mathrm{dn}(U|m)=\sqrt{1-m}$, although for clarity we keep the functional form of this last expression in the parametric equations), $u\in[0,U]$, $\phi\in[0,2\pi]$, and the plus and minus signs correspond to the upper and lower half of the cell respectively. The only remaining parameter is $m\in[0,1)$, which can be used to fix for example $2h_{\max}$, the maximum height of the erythrocyte. Equation (1) is obviously suitable to model not only normal erythrocytes but also macrocytes and microcytes, because they essentially keep the normal erythrocyte shape and only differ in that they have different values for the diameter and height of the cell (and therefore different volumes).

To discuss the parameterization of altered shapes we first proceed by example: our model of the stomatocyte is generated by the equations

$$\mathbf{r}_{+}(u,\phi)=\left(\frac{\ell}{2}\mathrm{cn}(u|m_{+})\cos\phi,\frac{\ell}{2}\mathrm{cn}(u|m_{+})\sin\phi,h_{+}\,\mathrm{sn}(u|m_{+})\left(\frac{\mathrm{dn}(u|m_{+})}{\mathrm{dn}(U_{+}|m_{+})}\right)^{3}\right), \tag{2a}$$

$$\mathbf{r}_{-}(u,\phi)=\left(\frac{\ell}{2}\mathrm{cn}(u|m_{-})\cos\phi,\frac{\ell}{2}\mathrm{cn}(u|m_{-})\sin\phi,-h_{-}\,\mathrm{sn}(u|m_{-})\left(\frac{\mathrm{dn}(u|m_{-})}{\mathrm{dn}(U_{-}|m_{-})}\right)^{2}\right), \tag{2b}$$

for the upper and lower parts of the cell respectively. Note that in addition to the different powers (cube and square respectively) of the Jacobi $\mathrm{dn}(u|m)$ function in the third component of $\mathbf{r}_{\pm}(u,\phi)$, we also use independent values of the parameters $h_{\pm}$ and $m_{\pm}$ (and the ensuing $U_{\pm}=K(m_{\pm})$) for the upper and lower part of the cell.

Figure 1 shows the parameters and 2D generating curves for the sphere, ellipsoid, basic discocyte and a stomatocyte of the same volume obtained from Eqs. 1 and 2 respectively. Similarly, Figure 2 shows the 3D

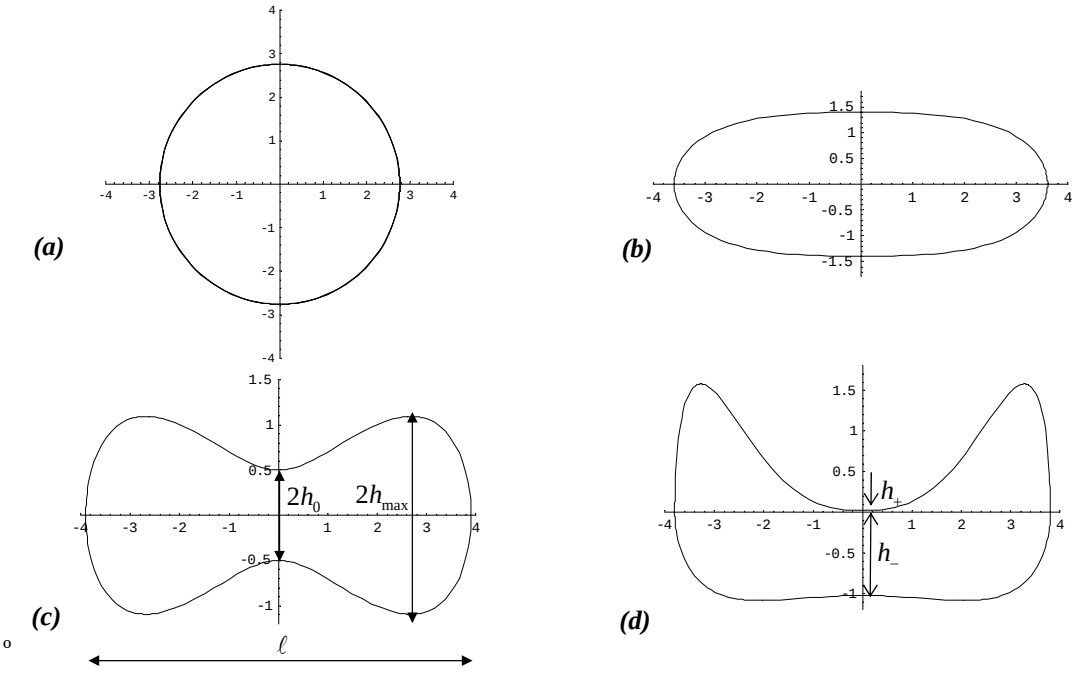

Fig. 1 2D generating curves obtained from equations 1 and 2 for a) spherocyte b) ellipsoid c) normal biconcave erythrocyte and d) Stomatocyte. The different modeling parameters used in the equations are shown in Table 1.

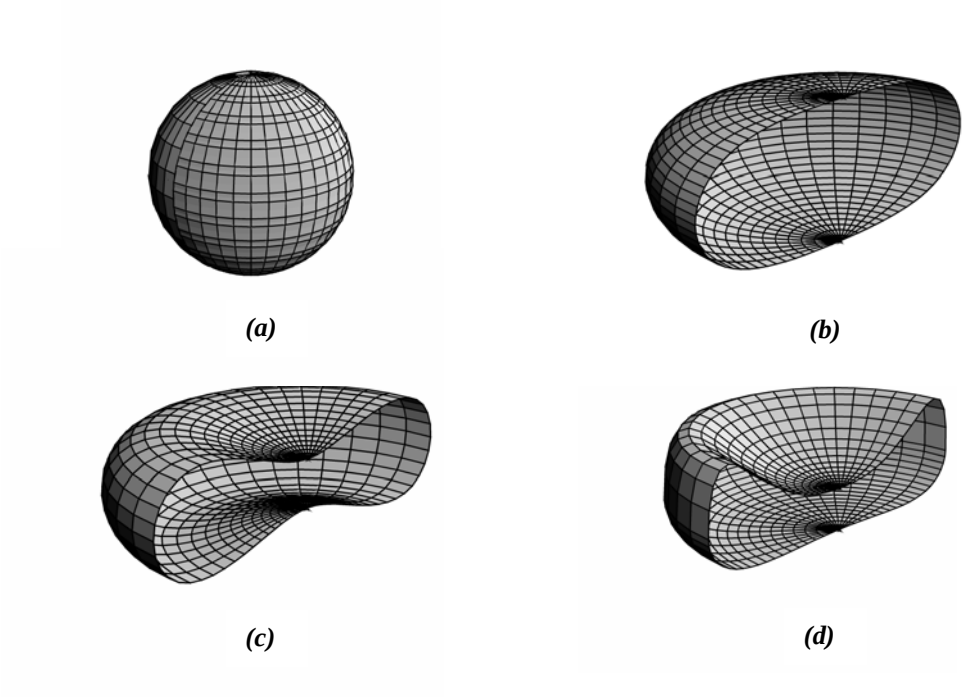

Fig. 2 3D view of the spherocyte, ellipsoid, erythrocyte and stomatocyte models generated using *Mathematica*.

cell geometries generated in *Mathematica* [Wolfram 2003] by rotation of these curves around the vertical axis. As it can be easily seen in both the 2D and the 3D figures, our stomatocyte model has a deep dimple. This degree of severity of the invagination determines that it belongs to subclass II [Bessis 1977] and is perfectly modeled by the modified Eq. 2. In Table 1 we present the numerical values of the parameters of these cells as well as of the parameters of the macrocyte and microcyte. Note that the maximum height of the stomatocyte has to be determined by using the inverse functions $u_{\pm} = \mathrm{sn}^{-1}(x, m_{\pm})$, and that the volumes of the upper and lower parts of the cells can be readily calculated thanks again to the parametric equations:

$$V_{\pm} = -2\pi \int_0^{U_{\pm}} x'(u, m_{\pm}) x(u, m_{\pm}) z(u, m_{\pm}) du \,, \tag{3}$$

where the prime denotes derivation with respect to *u*.

Cell	$\ell\,(\mu\mathrm{m})$	$h\,(\mu\mathrm{m})$	m	$V\,(\mu\mathrm{m}^3)$	$2h_{\max}\,(\mu\mathrm{m})$	$\delta\,(\mathrm{nm})$
Spherocyte	5.46	2.73	0	85.29	5.46	8
Ellipsoid	7.2	1.4	0.3954	85.17	2.8	8
Normal erythrocyte	7.8	0.5	0.9447	85.1	2.19	8
Microcyte	5	0.4	0.9520	29.8	1.87	8
Macrocyte	10	0.65	0.8446	118.1	1.79	8
Stomatocyte II $(+,-)$	7.6	(0.1242,1.4037)	(0.9741,0.4720)	85.02	2.19	8

Table 1. Parameters used in Eqs. 1 and 2 to model the different cell shapes: ℓ is the diameter of the cell, $2h$ ($h_+ + h_-$ for the stomatocyte) is the height at the centre, m (m_+ and m_- for the stomatocyte) is the parameter in the Jacobi elliptic functions, V is the volume, $2h_{\max}$ the maximum height and δ the thickness of the membrane.

We now proceed to discuss the rationale behind and the generalization of the parameterization given by Eq. 2. Note that the common structure of Eqs. 2a and 2b is

$$\mathbf{r}(u,\phi)=\left(\frac{\ell}{2}\mathrm{cn}(u|m)\cos\phi,\frac{\ell}{2}\mathrm{cn}(u|m)\sin\phi,h\,\mathrm{sn}(u|m)\left(\frac{\mathrm{dn}(u|m)}{\mathrm{dn}(U|m)}\right)^{p}\right) \tag{4}$$

where the exponent *p* (here equal to 3 and 2 respectively) is a new parameter which in effect controls the gross features of the shape. Note also that the original parameterization of the normal erythrocyte shape of Kuchel and Fackerell is the particular case $p=1$ of our Eq. 4. In fact, taking into account that the Jacobi elliptic functions can be considered as deformations of the familiar trigonometric functions to which they reduce for $m=0$ ($\mathrm{sn}(u|0)=\sin u$, $\mathrm{cn}(u|0)=\cos u$ and $\mathrm{dn}(u|0)=1$, in which case the parametric Eq. 4 represents a revolution ellipsoid) and taking into account also the elementary properties of these Jacobi functions [Abramowitz and Stegun 1972], it can be seen that the essential features of the parameterization (4) are maintained for positive (not necessarily integer) values of *p*. This new, continuous parameter can be used to advantage in the modeling not only of altered shapes, but of continuous deformations of the normal erythrocyte into these deformed shapes.

Finally, we have insisted on the advantages of an explicit parametric representation: in particular we can easily generate the uniform shell representing the membrane by shifting any parametric surface given by Eq. 4 by a constant distance δ along the outer normal at each point, i.e., the outer layer of the membrane is given by

$$\mathbf{r}_{\delta}(u,\phi)=\mathbf{r}(u,\phi)+\delta\,\mathbf{n}(u,\phi) \tag{5}$$

where

$$\mathbf{n}(u,\phi)=\frac{(\partial\mathbf{r}/\partial\phi)\times(\partial\mathbf{r}/\partial u)}{\left\|(\partial\mathbf{r}/\partial\phi)\times(\partial\mathbf{r}/\partial u)\right\|}\,. \tag{6}$$

Eqs. 4, 5 and 6 summarize our rather general model of normal or altered erythrocytes.

Applications

To illustrate the practical use of these parameterizations, we present (1) the numerical calculation of the induced transmembrane potential in stomatocytes and (2) the induced electric force (electrical stress tensor) on the interface between the realistic curved membrane and the external medium in normal erythrocytes. Both cells are exposed to an 1800 MHz plane wave, a typical carrier frequency in cellular phones and in wireless surveillance systems.

The resting transmembrane potential is a basic magnitude to the physiological state of the cell [Gedde and Huestis 1997, Glaser 1998, Bifano et al.1984], and therefore the determination of induced field strengths and transmembrane potentials can provide a good insight on the relation between the exposition to radiofrequency fields and subsequent cell changes. The relevance of the induced transmembrane potential can be inferred from the numerous papers previously published by different authors [Grosse and Schwan 1992, Kotnik and Miklavcic 2000a, 2000b and therein]. However, these former studies have generally used simplified spherical or spheroidal cell geometries (also a particular case of Eq. 4), or at most the more realistic parameterization of the normal erythrocyte by a Cassini curve. Given the numerical precision that can be attained in these calculations we do not expect a significant difference between the results for a normal erythrocyte parameterized by a Cassini curve and a normal erythrocyte parameterized by Eq. 1. However, Eqs. 4-6 permit us to perform the corresponding calculations for abnormal erythrocytes, which to our knowledge has not been carried out before.

Our model of cell (stomatocyte and erythrocyte) is formed by two media: the membrane and the cytoplasm. The cytoplasm is a physiological saline solution with a protein volume fraction of 0.26. The membrane will be represented by a shell of constant thickness $\delta=8\mathrm{nm}$ that has a very low conductivity and a frequency-independent relative permittivity [Gimsa et al. 2001]. The cell is immersed in an external continuous medium - the radiation region - formed by an electrolyte with the dielectric properties of physiological saline. Table 2 shows the electrical parameters for the membrane, cytoplasm and external medium. These values are typical for the erythrocyte structure and have been extensively used in the literature [Simeonova et al. 2002].

As the cell dimensions (≈ 8 μm) are much smaller than the wavelength at the working frequency (≈ 2 cm), we can assume that the cell is exposed to a uniform field. Therefore a quasistatic approximation holds and we can calculate the field distribution by solving directly the full Maxwell equations using a discretization of the cell model geometry into tetrahedral elements with an adaptive mesh.

Cell	$\varepsilon/\varepsilon_0$	$\sigma\ (S/m)$	Loss tangent
Cytoplasm	50	0.53	0.10590
Membrane	9.04	$1x10^{-6}$	$1.1052x10^{-6}$
External medium	80	0.12	0.014986

Table 2. Relative permittivity $\varepsilon/\varepsilon_0$, conductivity $\sigma\ (S/m)$, and loss tangent for the cytoplasm, membrane and external continuous medium at 1.8 GHz.

In this paper we use a finite element (FE) technique [Jin 1993, Douglas et al. 2000] with a variable density mesh to determine the electric field intensity within the different layers of the cell. The cells are exposed to a linearly polarized EM plane wave of frequency 1.8 GHz propagating along the *y* axis, with the **E** and **H** field vectors parallel to the *z* and *x* axes. The radiation region is taken to be a cube in which the cells are immersed. This region is filled with the external medium and surrounded by perfectly matched layers (PML). This setup provides a reflectionless interface between the region of interest and the PML layers at all incident angles [Becache and Joly 2001]. We achieve a good compromise between accuracy and computing resources by extending the dimensions of the radiation region to the order of four wavelengths in the external medium. This FE numerical technique has already been validated by the authors in previous works with simpler [Sebastian et al. 2001, Muñoz et al. 2003] and more complex geometries [Muñoz et al. 2004, Sebastian et al. 2005]. For normalizing purposes the electric field intensity is set to 1 V/m.

a) Determination of the induced transmembrane voltage in stomatocytes

In contrast to the symmetrical erythrocyte shapes, the asymmetry of the stomatocyte around the major axis leads to different values of the induced transmembrane potential in the upper and in the lower parts of the cell. Figure 3 shows this induced transmembrane potential both in the upper and in the lower parts of a stomatocyte as a

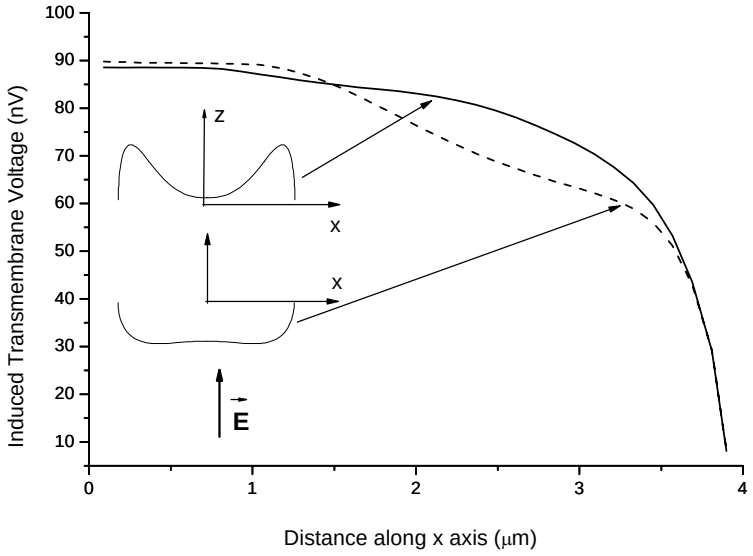

Fig. 3 Induced transmembrane potential in the upper and lower parts of a stomatocyte as a function of the distance *x* along the major axis of the cell. The cells are exposed to an RF field of frequency 1800 MHz. The electric field has an intensity of 1 V/m and is linearly polarized parallel to the vertical axis.

function of the distance *x* along the major axis. Again, the incident external electric field is parallel to the vertical axis. Note that in the flattest regions of the lower and upper parts of the stomatocyte the applied external field is perpendicular to the membrane surface. As the values of the conductivities of both the external medium and the

membrane are very low, the induced transmembrane voltage in these regions is, as expected, mainly governed by the ratio of the respective permittivities.

b) Determination of the induced electric stress forces on the membrane of erythrocytes

An obvious assumption concerning the field **E** in the membrane is that it generates a Maxwell stress which will compress the membrane. This electrical stress plays a fundamental role in electroporation processes. In the quasistatic case, the forces exerted on a finite volume of material by the electric field can then be expressed as a result of forces acting on the surface limiting this volume by (Giner *et al* 1995)

$$f_i = \int_S T_{ij} dS_j \tag{7}$$

with the stress tensor for the electric field in a material medium defined by

$$T_{ij} = \varepsilon E_i E_j - \frac{1}{2}\delta_{ij} E^2 (\varepsilon - \eta \frac{d\varepsilon}{d\eta}) \tag{8}$$

In this work, we have not considered any variations of the electric permittivity of both media with their respective mass densities, i.e. $d\varepsilon_i / d\eta_i = 0$, and therefore Eq. 8 is greatly simplified.

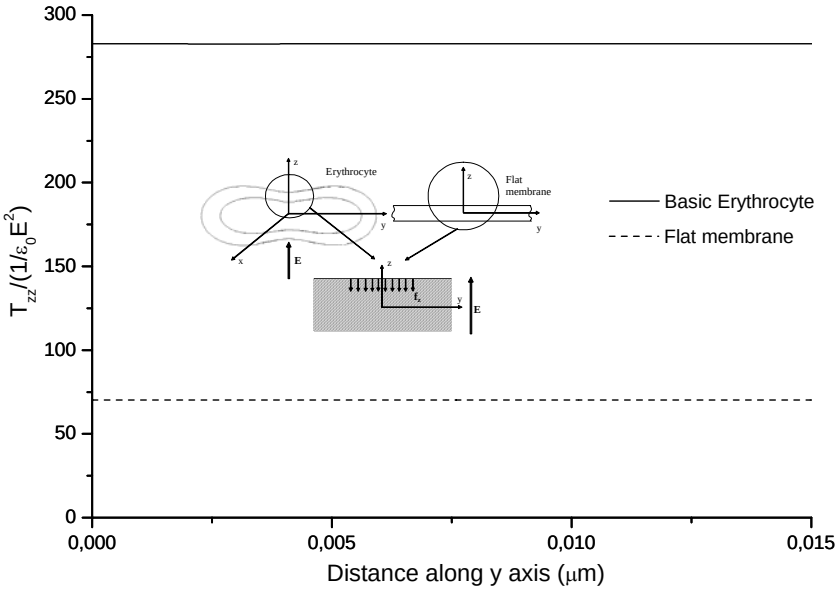

Figure 4 Stress force density (T_{zz}) exerted on the centre of the curved erythrocyte membrane (solid line) and on a flat membrane (dashed line). The force density is directed inward the membrane (along the negative *z* axis as shown in the inset) and is normalized with respect to the external field ($\varepsilon_0 E^2$).

Although our analysis has only been limited to electrical stress and to a very short radius around the *z* axis of the erythrocyte (as it would be the case of a pore), the results clearly show that the electrical forces favour deforming of the membrane. The shape and size evolution of the cell will eventually be determined by a combination of electrical and mechanical forces. A comparison of the force densities obtained for an unstretched flat membrane and for the realistic erythrocyte model shows that the curvature of the membrane cannot be neglected.

Summary

We have given a simple parameterization of erythrocyte shapes which includes as a special case the normal biconcave erythrocyte of Kuchel and Facherell (and consequently spherical or ellipsoidal models), but allows for continuous deformations from this normal shape to rather general altered shapes (like stomatocytes). As an

added advantage of having a simple, explicit parameterization, we can generate a realistic three dimensional model of these erythrocytes by shifting the inner surface a constant distance along the outer normal.

As an application of this parameterization we have performed numerical calculations of the transmembrane potential induced by an electromagnetic field of 1800 MHz and 1 V/m in stomatocytes and normal erythrocytes. The results for the unsymmetrical stomatocyte depend essentially on the new parameterization, and have to be given separately for the upper and the lower parts of the cell.

Our calculations give insight into electrical stresses on realistic curve membranes of cells immersed in an electric field. This work can be applied to different cell shapes and the refinements thereof may be of potential value in understanding the kinetics of the rupture of membranes and related phenomena such as electrorotation and dielectrophoresis.

Finally, we point out that this analysis is purely theoretical and has been performed for a particular orientation of the external RF field, and as such necessarily calls for further investigations.

Acknowledgements
This work was supported by the Comunidad de Madrid under Grant number: PR45/ 05 - 4166

References

Abramowitz M., and Stegun I.A. Eds., Handbook of Mathematical Functions (Dover, New York, 1972).

Becache E. and Joly P., Tech. Rep. 4164, INRIA, 2001.

Bessis M., Blood Smears Reinterpreted (translated by George Brecher) (Springer-Verlag, Berlin, 1977) pp. 68-70.

Bifano T., Novak S. and Friedman J.C., Relationship between the Shape and the Membrane Potential of Human Red Blood Cells, J. Membr. Biol. 82 (1984): 1-13.

Bloor M.I.G and Wilson M.J., Method for Efficient Shape parametrization of Fluid Membranes and Vesicles, Phys. Rev. E, 61(4) (2000): 4218-4229.

Cowell R.L, Tyler R.D. and Meinkoth J.H., Diagnostic Cytology and Hematology of the Dog and Cat, 2nd ed. (Mosby, St. Louis, 1999).

Douglas J. Jr., Santos, J. E. and Sheen D., A Nonconforming Mixed Finite Element Method for Maxwell's Equations, Math. Models Meth. in Appl. Sci. (M3AS),10 (2000): 593-613.

Elgsaeter A. and Mikkelsen A., Shape and Cell Changes in Vitro in Normal Red Blood Cells, Biochimica et Biophysica Acta 1071 (1991): 273-290.

Fujii T., Sato T., Tamura A., Wakatsuki M. and Kanaho Y., Shape Changes of Human Erythrocyte Induced by Various Amphipathic Drugs Acting on the Membrane of the Intact Cell, Biochem. Farma. 28 (1979): 613-620.

Gedde M., Yang E. and Huestis W.H., Shape Response of Human Erythrocytes to Altered Cell pH, Blood 86 (1995): 1595-1599.

Gedde M. and Huestis W.H., Membrane Potential and Human Erythrocyte Shape, Biophys. J. 72 (1997): 1220-1233.

Gimsa J., A Possible Molecular Mechanism Governing Human Erythrocyte Shape, Biophys J. 75 (1998): 568-570.

Gimsa J.and Wachner D., Analytical description of the transmembrane voltage induced on arbitrarily oriented ellipsoidal and cylindrical cells *Biophys J.* 81 (2001): 1888-96.

Giner V, Sancho M and Martinez G Electromagnetic forces in dissipative dielectric media *Am. J. Phys*. 63 (8) (1995): 749-53.

Glaser R., The Shape of Red Blood Cells as a Function of Membrane Potential and Temperature, J. Membrane Biol. 51 (1979): 217-228.

Glaser R., Does the Transmembrane Potential or the Intracellular pH Control the Shape of Human Erythrocyte? Biophys. J. 75 (1998): 569-570.

Gray A., Modern Differential Geometry of Curves and Surfaces with Mathematica, 2nd Ed. (CRC Press, Boca Raton, 1998).

Grosse C. and Schwan H.P., Cellular Membrane Potentials Induced by Alternating Fields, Biophys. J. 63 (1992): 1632-1642.

Harvey J.W., Atlas of Veterinary Hematology: Blood and Bone Marrow of Domestic Animals, (WB Saunders, Philadelphia, 2001).
Isomaa D., Hagerstrand H. and Paatero G., Shape Transformations Induced by Amphiphiles in Erythrocytes, Biochimica et Biophysica Acta 899 (1987): 93-103.
Jie Y., Quanhui L., Jixing L, and Ou-Yang Zhong-Can, Numerical Observation of Nonaxisymmetric Vesicles in Fluid Membranes, Phys. Rev. E 58 (1998): 4730-4736.
Jin J., The Finite Element Method in Electromagnetics (Wiley, New York, 1993).

Kotnik T. and Miklavcic D., Second Order Model of Membrane Electric Field Induced by Alternating External Electric Fields, IEEE Trans on Biomed. Eng. 47 (2000)a: 1074-1081.
Kotnik T. and Miklavcic D., Analytical Description of Transmembrane Voltage Induced by Electric Fields on Spheroidal Cells, Biophys. J. 79 (2000)b: 670-679.
Kotnik T. and Miklavcic D., Theoretical Evaluation of the Distributed Power Dissipation in Biological Cells Exposed to Electric Fields, Bioelectromagnetics 21 (2000)c: 385-394.
Kuchel P. and Fackerell E., Parametric Equation Representative of Biconcave Erythrocytes, Bulletin of Mathematical Biology 61 (1999): 209-220.
Lim H.W.G., Wortis M. and Mukhopadhyay R., Stomatocyte-discocyte-echinocyte Sequence of the Human Red Blood: Evidence for the Bilayer Couple Hypothesis from Membrane Mechanics., Pnas 99 (26) (2002): 16766-16769.
Moon P. and Spencer D.E., Field Theory Handbook: Including Coordinate Systems, Differential Equations and Their Solutions (Springer, Berlin, 1998).
Muñoz S., Sebastián J.L, Sancho M. and Miranda J.M., A Study of the Electric Field Distribution in Erythrocyte and Rod Shape Cells from Direct RF Exposure, Phys. Med. Biol. 48 (2003): 1649-1659.
Muñoz S., Sebastian J.L., Sancho M., and Miranda J.M., Transmembrane Voltage Induced on Altered Erythrocyte Shapes Exposed to RF Fields, Bioelectromagnetics 25 (2004): 631-634.
Oroz L.M.A., Morphologie Mathematique en Coordonnees Logarithmique-polaires et Methodes Geometriques de Classification. Application a L´etude des Erythocytes, (Master Thesis, Ecole des Mines de Paris, 2004).
Ponder E., Hemolysis and Related Phenomena (Grune & Stratton, New York, 1948).

Sebastian J.L., Muñoz S, Sancho M. and Miranda J.M., Analysis of the Influence of the Cell Geometry, Orientation and Cell Proximity on the Electric Field Distribution from Direct RF Exposure, Phys. Med. Biol. 46 (2001): 213-225.
Sebastian J.L., Muñoz S, Sancho M. and Miranda J.M., Modeling the Internal Field Distribution in Human Erythrocytes Exposed to MW Radiation, Bioelectrochemistry 64 (2004): 39-45.
Sebastian J.L., Muñoz S., Sancho M., Miranda J.M. and Álvarez G., Erythrocyte Rouleau Formation under Polarized Electromagnetic Fields, Phys. Rev. E 72 (2005): 31913(9).
Simel D.L., DeLong E. R., Feussner J.R., Weinberg J.B. and Crawford J., Erythrocyte Anisocytosis. Visual Inspection of Blood Films vs Automated Analysis of Red Blood Cell Distribution Width, Arch Intern Med. 148(4) (1998): 822-824.
Simeonova M., Wachner D. and Gimsa J., Cellular Absorption of Electric Field Energy: Influence of Molecular Properties of the Cytoplasm, Bioelectrochemistry 56 (2002): 215-218.
Wolfram S., The Mathematica Book (Wolfram Media, Champaing 2003).

THE DEPENDENCE OF BIOLOGICAL EFFECTS ON THE AMPLITUDE OF EXTREMELY WEAK POWER - FREQUENCY MAGNETIC FIELD

N.A. BELOVA, O.N. ERMAKOVA, A.M. ERMAKOV[1], V.V. LEDNEV

INSTITUE OF THEORETICAL AND EXPERIMENTAL BIOPHYSICS RAS

[1]PUSHCHINO STATE UNIVERSITY

E-MAIL: belova@iteb.ru

Abstract.

We report the results of a study on the influence of extremely-weak power frequency (60 Hz) magnetic field on the rate of regeneration in planarians Girardia tigrina and on the rate of gravitropic curvature development in the segments of the line stems. The data presented here demonstrate that the dependence of biological effects on the field's amplitude in the range from 0.5 to 8 μT is polyextremal. In particular, the maxima of effects (activation of regeneration) is observed at B_{AC} = 1.3 and 3.9 μT, while at B_{AC} = 2.5 and 5.4 μT the value of bioeffects are close to zero. The experimentally observed dependence of bioeffects on the field's amplitude can be reasonably well approximated by the theoretical expression, which we obtained earlier. At the values of B_{AC} >8-10 μT the bioeffect changes its sign – activation of planarian's regeneration starts to be replaced by its inhibition. The inhibition takes place for the range of the amplitudes from 10 to 140 μT. Simple theoretical estimates indicate, that the observed change in the sign of the effect may result due to the prevalence of the effects caused by the induction of the alternating currents in the test-system at relatively high B_{AC} – amplitudes. These results provide additional evidences for the model, explaining the interaction of weak and extremely weak alternating magnetic fields with biosystems, suggested earlier and provide the basis for planning of the epidemiological studies and interpretation of the corresponding results.

1. Introduction.

At present time it is generally accepted, that low-frequency alternating magnetic fields (AMF) with amplitudes (magnetic induction values, B_{AC}) equal or exceeding 10 μT are capable to induce the biological effects in a number of biosystems. This kind of magnetic fields are widely used in medicine, in particular, to stimulate regeneration of bones and soft tissues. However, humans in living and working places are exposed to the influence of rather weak or exteremely weak alternating magnetic fields (EW AMF), originating from technogenic and natural sourses. The amplitudes of the power-frequency magnetic fields in most of the living places range from 0.01 to 1-2 μT, while at some working places it may reach 5-6 μT [1]. Some experimental studies indicate that EW AMF may substantially influence some biological systems [1-16]. It should be noted, that in most cases the experiments with AMF are usually performed on the background of the static Earth's magnetic field, B_{DC}, with the value of magnetic induction of about 50 μT. Correspondingly, in a general case the term EW AMF means, that one is using the combined magnetic field, which contains both static and exteremely weak alternating components. This circumstance is important for understanding of the physical mechanism the of influence of EW AMF on biological systems. Nevertheless, the term " bioeffects of EW AMF " is often used for brevity and also to emphasize the specificity of the mechanism of action of such fields.

It is necessary to note, that reports on the bioeffects of AMF with the amplitudes higher than 10 μT, as a rule, do not cause any doubts. At the same time some authors deny even a mere possibility of bioeffects of AMF with the amplitudes less than 10 μT. Contrary to the claims denying the possible existence of biological effects of low-frequency magnetic fields with the amplitudes ≤ 2 μT in the frame of traditional physics and biology [8, 17], there is a considerable number of experimental evidence confirming this kind of effects. It is remarkable, that the

important data demonstrating the inhibiting influence of sinusoidal magnetic field (B_{AC} =1.7 μT, f_{AC} = 60 Hz) on the oncostatic action of melatonin in a culture of human breast cancer cells have been obtained independently by several laboratories [5, 6, 7, 14, 15].

Despite of a certain, although quite slow, progress in the experimental proof of biological efficiency of some types of EW AMF, there is still no clear understanding of the corresponding mechanisms. In order to develope the possible theoretical models for the interaction of EW AMF with biosystems it is necessary to have the thorough experimental data on the dependence of bioeffect's value on the parameters of the magnetic field.

We have shown recently, that EW AMF with the values of amplitudes in the microtesla, nanotesla and even picotesla range substantially influence the properties of biological test-systems prepared from animal and plant sourses [18, 19]. In particular, such fields were found to affect the rate of regeneration in planarians (*Girardia tigrina*) and also the rate of gravitropic response in the stem segments of flax (*Linum bienne*). We have found that the maximal and minimal values of the bioeffects were observed at certain (identical for the different test-systems) values of the amplitude/frequency - ratio of the AMF; the values of the bioeffects did not change with a simultaneous proportional change of the amplitude and the frequency of AMF.

The theoretical analysis of the obtained experimental data has shown, that in the range of frequencies and amplitudes used in our experiments, the value of bioeffects of EW AMF strongly depends on the parameter $\gamma B_{AC} / f$, where γ - gyromagnetic ratio for the particular type of magnetic moment, and B_{AC} - and f_{AC} – correspond to magnetic induction and frequency of the alternating magnetic component [19]. We have shown, that experimental dependence of the value of bioeffects on the frequency of alternating component (in a range from 10 to 320 Hz) at constant amplitude (B_{AC} = 1.6 μT) may be approximated by a theoretical curve with γ = 42.578 Hz/μT, corresponding to the gyromagnetic ratio of the nuclear spins of hydrogen atoms. The dependence of bioeffect's value on $\gamma B_{AC} / f$ - parameter is polyextremal: well expressed maxima are observed at $\gamma B_{AC} / f$ = 0.9; 2.75 and minor maxima – at $\gamma B_{AC} / f$ = 4.5; 6.1. The bioeffects are absent at $\gamma B_{AC} / f$ = 1.8; 3.8; 5.3; 6.7 [19].

In order to estimate the biotropic action of the particular exteremely weak power-frequency magnetic field (on the background of the geomagnetic field), it is nessesary to obtain the dependence of the bioeffect's value on the amlitude of the field at fixed frequency. Here we present the corresponding experimental data, indicating that at rather small amplitudes (0< B_{AC} <10 μT) of 60 Hz magnetic field the maxima and minima of the corresponding bioeffects are observed at exactly the same values of the $\gamma B_{AC} / f$ - parameter, which were found earlier [19] in the frequency- dependence studies (as it was expected).

2. Experimental section.

2.1. Magnetic fields.

The exposure of the test-systems to the power – frequency magnetic field (60 Hz) with the value of magnetic induction, B_{AC}, was carried out on a background of an ambient static magnetic field, $B_{DC} \cong 42.0$ μT. The alternating (sinusoidal) magnetic field, generated with the use of Helmholtz coils (39 cm in diameter) was oriented co-linear with a vector of the Earth's magnetic field. The Helmholtz coils have been fed by standard signal generators G4-153 or G6-28. The control test-systems were exposed to the static Earth's magnetic field. The necessary values of alternating magnetic field were established taking into account the transmission coefficient for a Helmholtz coil, equal to 10 μT/1V.

The experiments were performed using EW AMF with the following parameters:

f_{AC} = 60 Hz; 0.1 μT < B_{AC} < 140 μT; B_{DC} = 42.0 μT.

The value of magnetic induction of the background alternating (50 Hz) magnetic field at the position of experimental test-systems inside of the Helmholtz coils was 15 nT. Experiments were conducted at room temperatures of about 20-22 ^{0}C.

2.2. Test-systems.

2.2.1. Regnerating planarians. Preparation, computer morphometry, data analysis.

The flat worms (planarians *Girardia tigrina*), asexual laboratory race were reared in pond water at room temperature and were fed once a week with the Diptera larvae. For the experiments the animals of about 7-8 mm in length were selected. The feeding of the selected planarians was stopped one week prior to the start of the experiment. The head portions of planarians were amputated with an eye scalpel under a binocular microscope: approximately 1/5 part of a body containing head ganglion was dessected. Then regenerants were placed in two glass vessels filled with 50 ml of pond water (30 regenerating planarians per vessel).

The rate of regeneration in experimental and control animals was estimated with the use of computer morthometry method, based on of photocontrast between old (pigmented) and new (transparent) parts of a planarian's body.Each planarian has been photographed with the use of binocular microscope and videocamera in 3 days after amputation. It takes about 30 minutes to get photo pictures of a groop of 30 animals. The video images of rgenerating planarian were introduced into computer. Using the special program for image analysis, we determined the area, S, of whole planarian and the area, s, of the newly formed (transparent) blastema (Fig.1). The results of these measurements were used in calculations of the regeneration index, $R = s / S$, averaged over 30 planarians in control and experimental animals. The values of the EW AMF bioeffect was determined according to the expression:

$\Delta R\ (\%) = \dfrac{(R_{\exp} - R_{con}) \pm (\delta_{\exp} + \delta_{con})}{R_{con}} \times 100\%$, where $\delta_{\exp}$ and δ_{con} - standard errors of the average values, obtained for the experimental and control animals.

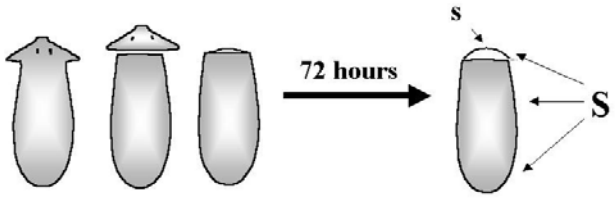

Figure 1. The scheme of measurements of the planarian's regeneration index; *s* - the area of newly formed tissue (blastema), *S* – the area of the whole body of planarian; *s/S* – regeneration index

2.2.2. Segments of flax stems. Preparation, stimulation of gravitropic bending, data analysis.

Seedlings of flax (*Linum bienne*) were grown from the seeds at thermostat at 26 ^{0}C in complete darkness during 4 days. In 4 days the stems seedlings were about 3-4 cm long. The apical parts (2.5 cm in length of stems) were excised and the leaves were removed from the obtained segments. The segments were placed horizontally in the Petri dishes (90mm in diameter) on the filter paper moistened with 2 ml of distilled water. The basal ends of the segments were fixed by the rings cut off from the silicon tube. Two dishes (with 20 segments per dish) were exposed to magnetic field and two dishes were used as a control. The gravitropic upward bending in segments begins in about 30 min after placing them in horizontal position and in about 3 hours the apical ends of segments attain the vertical positions with the tips directed against the gravity force vector. The value of the gravitropic bending in segments was defined as an averaged (over the number of 40 segments) angle formed between the apical end of a segment and the horizontal plane, $\alpha \pm \delta$, where δ -standard deviation of the mean (Fig. 2).

The measurements were performed with a protractor in 2 hours after beginning of the experiment. The collection of data on bending angles for 20 segments in one dish takes 3-4 minutes. All experiments were performed at 25 $\pm$ 0.5 ^{0}C.

The value of the bioeffect induced by 60 Hz magnetic field was expressed as the relative difference between the average angle of bending in the experiment, $\alpha_{\exp}$, and in the control, α_{con}, according to the equation: $\frac{(\alpha_{\exp} - \alpha_{con}) \pm (\delta_{\exp} + \delta_{con})}{\alpha_{con}} 100\%$, where $\delta_{\exp}$ and δ_{con} - standard errors of the means.

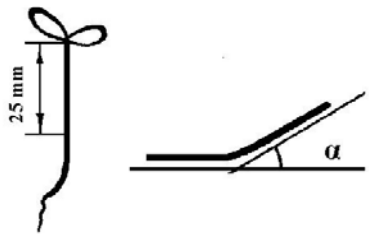

Figure 2. The scheme of measurements of the gravitropic bending angle in a segment of flax stem.

3. Results and discussion.

Earlier we have shown, that the value of bioeffects, ***I***, induced by EW AMF can be described by the expression:

$$I = kJ_1(\gamma B_{AC} / f) \times [J_2(\gamma B_{AC} / f) - J_0(\gamma B_{AC} / f)] \quad (1),$$

where k - constant, $\gamma B_{AC} / f$ - argument of Bessel's functions, γ = 42.578 Hz/μT – gyromagnetic ratio of the nuclear spin of hydrogen atom, B_{AC} and f_{AC} - magnetic induction and a frequency of an alternating component of the EW AMF [19]. As it may be seen (Fig. 3 and Fig. 4), the expression (1) reasonably well approximates the experimentally observed dependence of bioeffects on the amplitude of the 60 Hz magnetic field: the maximal values of bioeffects (i.e. activation of the rate of regeneration in planarians and activation of the gravitropic bending in the stem segments of flax) appear at the values of $\gamma B_{AC} / f$ equal to 0.9 and 2.75, while at $\gamma B_{AC} / f$ equal to 1.8 and 3.8 the effect of the field is absent. These results confirm our earlier conclusion, according to which the nuclear spins of hydrogen atoms are the primary targets in the the interaction of EW AMF with biosystems [19]. It should be noticed, that according to expression (1) at standart experimental conditions the value of bioeffects of EW AMF for the particular type of magnetic moment is completely defined by the amplitude/frequency - ratio of the alternating component and practically does not depend on the exact value of a static magnetic field.

An increase of the amplitude of the 60 Hz magnetic field up to 8-10 μT is accompanied by a change in a sign of the bioeffect - activation of planarian's regeneration is replaced by its inhibition. In Fig. 3 we have given only one experimental point. In fact, the inhibition of regeneration, characterized by a decrease in the regeneration index, s/S, by 20-30 % was observed with an increase of the amplitude in the range from 10 μT to at least 140 μT. Apparently a change of a sign of effect is caused by the induction of eddy currents in the vessels with planarians at relatively high amplitudes of the 60 Hz magnetic field.

It seems quite instructive to compare the results and conclusions represented in this paper with those of another study devoted to the influence of sinusoidal 60 Hz magnetic fields with amplitude ranging from 1 μT to 20 μT on the enzymatic activity of ornithine decarboxylase (ODC) in cultured fibroblast cells, exposed to the field during 4 hours [20]. The authors came to the following conclusions: 1) the enchancement of ODC activity induced by exposure of culture cells to a 60 Hz magnetic field suggested a sigmoidal relationship to magnetic field amplitude; an approximate doubling of the ODC activity was observed at field amplitude of 7 μT or higher; 2) the observed bioeffects are caused by the induced electric fields in a test-system, which is a function of the orientation of the magnetic field relative to the exposed sample, and the geometry and electrical properties of the sample; therefore, the threshold amplitude - value of the 60 Hz magnetic field may substantially differ for the different test-systems.

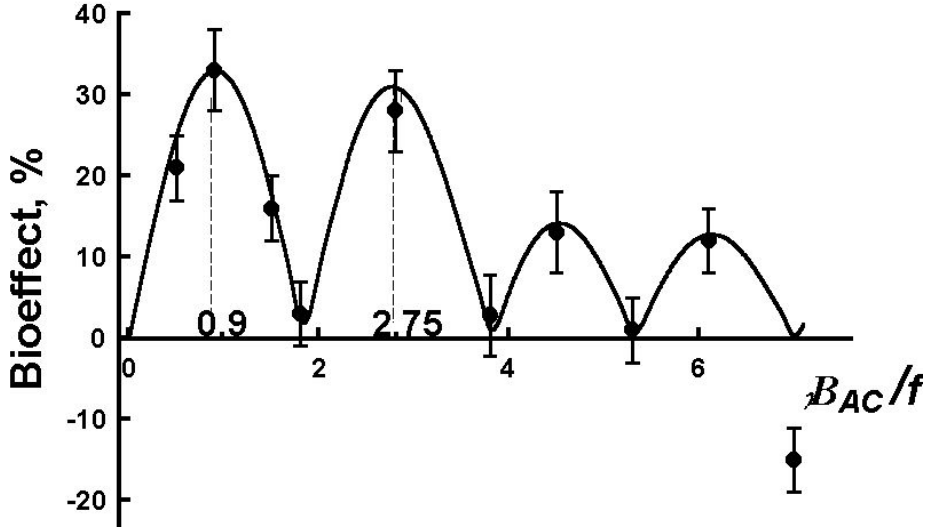

Figure 3. The dependence of the rate of planarian regeneration on value of $\gamma B_{AC}/f$ - parameter. The solid curve represents theoretically expected dependence. The parameters of combined magnetic field: B_{DC} = 42 μT, f_{AC} = 60 Hz B_{AC} = 0.7; 1.3; 2.1; 2.5; 3.9; 5.4; 6.3; 7.4; 8.6; 9.8 μT corresponding to $\gamma B_{AC}/f$ = 0.5; 0.9; 1.5; 1.8; 2.75; 3.8; 4.5; 5.3; 6.1; 7.0.

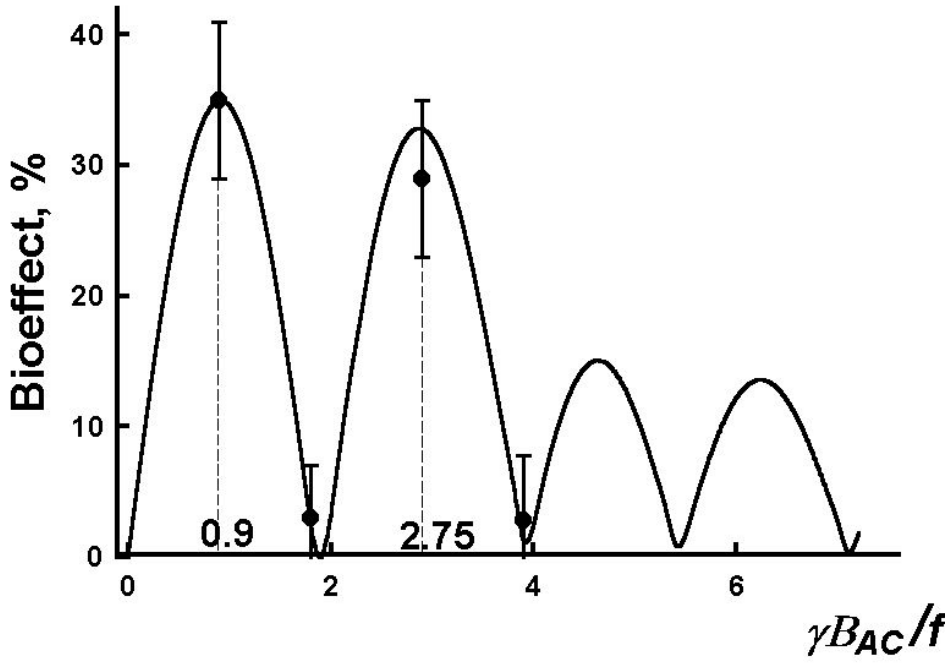

Figure 4. The dependence of the value of gravitropic bending in the segments of flax stem on value $\gamma B_{AC}/f$ - parameter. The solid curve represents theoretically expected dependence. The parameters of the combined magnetic field: B_{DC} = 42 μT, f_{AC} = 60 Hz B_{AC} = 1.3; 2.5; 3.9; 5.4 μT corresponding to the values $\gamma B_{AC}/f$ = 0.9; 1.8; 2.75; 3.8.

As it can be seen, the experimental results and conclusions presented by Mullins et al. [20] seem to be drastically different from those obtained in this paper. However, it is nesessary to point out that the experimental results published by Mullins et al. [20] and by some other groops [6, 7, 14, 15] were obtained with the use of μ - metal shielded Helmholtz coil pairs, so that the amplitude of a residual static Earth's magnetic field at the location of the test-systems was not exceeding 0.1-0.2 μT. It means that in these studies the test-systems were exposed to very weak sinusoidal 60 Hz magnetic field in the practical absence of a static magnetic field. It is known, the effects of AMF in the presence and in the absence of a static magnetic component may be essentially different [21, 22]. Obviously, in the real enviroument and work places both EW AMF and geomagnetic static field are pesent. Therefore, the experimental data obtained with a shielded Earth's magnetic field do not seem to be directly related to the effects of power – frequency magnetic fields, which may occur at real environmental conditions.

4. Conclusions.

The experimental results presented in this paper and earlier [18, 19] show, that the combined magnetic fields with the extremely weak amplitudes of the alternating component are capable to influence substantially the properties of biological test-systems derived from the animal's and plant's sourses (regenerating planarians and gravitropically responding stems of flax). Our data clearly show that the dependence of biological effects on the amplitude of the 60 Hz magnetic field ranging from 0.5 to 8 μT is polyextremal. In particular, the maxima of effects is observed at B_{AC} = 1.3 and 3.9 μT, while at B_{AC} = 2.5 and 5.4 μT the value of bioeffects are close to zero. The experimental points can be reasonably well approximated by the theoretical expression, which we obtained earlier [19]. These results confirm our earlier conclusion, according to which the nuclear spins of hydrogen atoms are the primary targets in the the interaction of some types of EW AMF with biosystems. At the values of B_{AC} >8-10 μT the bioeffect changes its sign – in particular an activation of planarian's regeneration starts to be replaced by its inhibition. The inhibition takes place for the range of the amplitudes from 10 to 140 μT. The change in the sign of the effect may appear due to the prevalence of the effect caused by the induction of the alternating currents in the test-system at relatively high B_{AC} – amplitudes. These results allow to clarify the interaction mechanism of the weak power-frequency magnetic fields with biosystems and provide the basis for planning of the epidemiological studies and interpretation of the corresponding results.

This study was supported by the Russian Foundation for Basic Research (grant № 04-04-97324) and by the Programm " Fundamental sciences in medicine".

5. References.

1. Hansson Mild K. IEEE Transactions on Instrumentation and Measurement. 1996, Vol. 45, №3, 710-714.
2. Juutilainen J., Laara E., Saali K. // International Journal Radiation Biology & Relat. Stud. Physical Chemistry Medicine 1987. Vol. 52, № 5, 787-793.
3. Berman E., Chacon L., House D. // Bioelectromagnetics. 1990. Vol. 11, №2. P. 169-187.
4. Martin A.H. // Bioelectromagnetics. 1992. Vol. 13, №3, 223-230.
5. Liburdy R.P., Sloma T.R., Sokolic R., Yaswen P. // Journal Pineal Research 1993. Vol. 14, 89-97.
6. Luben R.A., Saraiya S., Morgan A.P. // Abstract A-1. Annual Review of Research on Biological Effects of Electric and Magnetic Fields from the Generation, Delivery & Use of Electricity. San Antonio, TX, 1996, Nov. 19-21.
7. Harland J.D., Liburdy R.P. // Bioelectromagnetics. 1997. Vol. 18, №8, 555-562.
8. Valberg P.A., Kavet R., Rafferty C.N. // Radiation Research. 1997. Vol. 148, №1, 2-21.
9. Harland J., Eugstrom S., Liburdy R. // Cell Biochemistry and Biophysics 1999. Vol. 31, №3 295-306.
10. Persinger M.A., Cook L.L., Koren S.A. // International Journal of Neuroscience. 1999. Vol. 100, №1/4, 107-116.
11. Cook L.L., Persinger M.A. // Neuroscience Letters. 2000. 13/292, №3, 171-174.
12. Belova N.A. & Lednev V.V. // Biofizika 2001, v. 46, № 1, 122-125 (in Russian).
13. Novoselova E.G., Ogay V.B., Sorokina O.B. et al. // Biofizika. 2001. Vol. 46, № 1, 131-135 (in Russian).
14. Blackman C.F., Benane S.G., House D.E. // Bioelectromagnetics. 2001. Vol. 22, №2, 122-128.
15. Ishido M., Kabuto M. // Carciogenesis. 2001. Vol. 22, №7, 1043-1048.

16. Lednev V.V. & Malyshev S.L. // Abstract Collection Bioelectromagnetics Society Annual Meeting, St Paul, Minnesota, USA. 2001, 3-4.
17. Adair R.K. // Physical Review. A. 1991. Vol. 43, 1039-1040.
18. Lednev V.V., Belova N.A., Rojdestvenskaya Z. Ye., Tiras Kh. P. // Geophysical processes and biosphere. 2003. Vol. 2, № 1, 3-11 (in Russian).
19. Lednev V.V. // In a book "Modelling of geophysical processis. 2003, 130-136 (in Russian)
20. Mullins J.M., Penafiel L.M., Juutilainen J., Litovitz T.A. // Bioelectrochemistry and Bioenergetics. 1999. Vol. 48, 193-199.
21. Alexandrov Ye.B., Konstantinov O.B., Perel V.I., Khodovoy V.A. // Journal experimental and theoretical physics. 1963. Vol. 45, iss. 3. № 9, 503-510 (in Russian).
22. Lednev V.V. // Biofizika. 1996., Vol. 41, № 1, 224-232 (in Russian).

MAGNETIC FIELD ZONING IN THE FRAMEWORK OF THE DUTCH POWER LINE POLICY

GERT KELFKENS, MATHIEU PRUPPERS

RIVM, NATIONAL INSTITUTE FOR PUBLIC HEALTH AND THE ENVIRONMENT, P.O. BOX 1, 3720 BA BILTHOVEN, THE NETHERLANDS, E-MAIL: GERT.KELFKENS@RIVM.NL

Abstract

The possibility of a greater risk of childhood leukaemia due to magnetic fields caused by overhead power lines is currently a matter of scientific and public debate. However, a causal relationship has not been proven and it is not obvious whether the magnetic fields are the cause. In October 2005 the Dutch government issued a power-line policy based on the precautionary principle aimed at avoiding new situations in which children undergo prolonged exposure to magnetic fields exceeding 0.4 microtesla. For this purpose, a 0.4 microtesla magnetic field zone in the vicinity of overhead power lines would have to be established. However, defining such a zone is complicated, firstly, because the width of the zone varies continuously with the actual line load and, secondly, because the width of the magnetic field zone should account for future growth in the use of electricity.

The Ministry of Housing, Spatial Planning and the Environment has succeeded, nevertheless, in developing magnetic field zoning in consultation with the grid companies. This paper describes the choices made in establishing the 0.4 microtesla zone. The approach used has led to a guideline for calculating the width of the 0.4 microtesla zone. The calculations are based on a line load equivalent to a fixed fraction of the maximum allowable line load, where the fixed fraction is deduced from an analysis of the line loads during 2003.

Introduction

Modern society benefits greatly from electricity, but generation, transport and use of electricity create electric and magnetic fields with extremely low frequencies (ELF-fields). In 1979 Wertheimer and Leeper [1] demonstrated an increased cancer risk for children living near electric wiring configurations. Since then the adverse health effects possibly induced by ELF-fields have been a matter of scientific and social debate. The scientific investigations focused on the possibility of an increased risk for childhood leukaemia associated with transport and distribution of electricity. Initially, not all studies met solid scientific standards and the scientific evidence was inconclusive and contradictory, but over the years the number and quality of the investigations improved. From the aggregate of the epidemiological evidence in the year 2000, the Health Council of the Netherlands – an advisory council to the Dutch government - inferred a consistent statistical association between the occurrence of childhood leukaemia and living near overhead power lines, although a causal relationship between childhood leukaemia and ELF-fields could not be proven [2]. Two pooled analyses published in 2000 (Ahlbom *et al.* [3] and Greenland *et al.* [4]) support the statistical association between childhood leukaemia and exposure to ELF magnetic fields. From these pooled analyses the Netherlands National Institute for Public Health and the Environment (RIVM) concluded that there is a possibly elevated risk of childhood leukaemia at magnetic field strengths above a value somewhere between 0.2 and 0.5 microtesla [5]. On the assumption of a causal relationship between exposure to magnetic fields and development of childhood leukaemia, which is not proven, and the relative risks observed by both Ahlbom and Greenland, RIVM calculated the number of additional cases of childhood leukaemia due to overhead power lines [6]. In the Netherlands, with a childhood leukaemia incidence of 110 new cases every year, approximately 0.5 cases may be attributable to the magnetic fields due to overhead

power lines. In 2002 the International Agency on the Research of Cancer (IARC), which is related to the World Health Organisation, also concluded a consistent statistical association between ELF magnetic fields and childhood leukaemia, and designated the ELF magnetic fields as 'possibly carcinogenic to humans' [7]. A recent investigation yielded a statistical association between childhood leukaemia and living in the vicinity of overhead power lines in Great Britain [8].

Because of the public concern and the inconclusive scientific evidence the Dutch government indicated, in the Fourth National Environmental Policy Plan (NMP4), that the present evidence formed sufficient reason for further research and for taking appropriate precautionary measures in relation to social costs and benefits [9]. Studies were started into the actual number of dwellings in the vicinity of the overhead power lines [10], into the expected rise in the number of 'exposed' dwellings during the next 25 years due to realisation of plans for new dwellings [11, 12] and into the costs of the reduction of magnetic field strengths [13].

Finally, in 2004 the State Secretary of Housing, Spatial Planning and the Environment, P.L.B.A. van Geel, stated his policy aim with respect to overhead power lines in the policy document 'Nuchter omgaan met risico's' [1] [14]. The objective of this policy is to prevent the development of new situations in which children are exposed to magnetic fields near overhead power lines whenever possible. The policy to achieve this goal was designed in consultation with stakeholders (municipalities, provinces, grid companies). On October 3, 2005 this policy was issued in a policy letter [15]. The policy letter is addressed to stakeholders with 'recommendations with regard to overhead high-voltage power lines'.

Overhead power lines

In the Netherlands overhead high-voltage power lines have five voltage levels: 380, 220, 150, 110 and 50 kilovolts (kV). Occasionally circuits of different voltages are attached to the same pylon, the so-called combi-lines (380 and 220 kV circuits, 380 and 110 kV circuits, 220 and 110 kV circuits). In the framework of a previous study [10] the Dutch network of overhead power lines was digitised from topographic maps (1:25,000) by KEMA (a technical consultancy with expertise in the energy sector). The map of the high-voltage power grid in the Netherlands is depicted in Figure 1.

The total length of overhead high-voltage power lines amounts to nearly 4000 km (Table 1). The regional grid of 150 kV has the highest share in this total, approximately 45%.

Table 1 Summary of the overhead power lines in the Netherlands

voltage level (kV)	total line length (km)
50	164
110	778
150	1781
220	249
380	840
combi	159
total	3971

[1] English translation: Coping Rationally with Risks

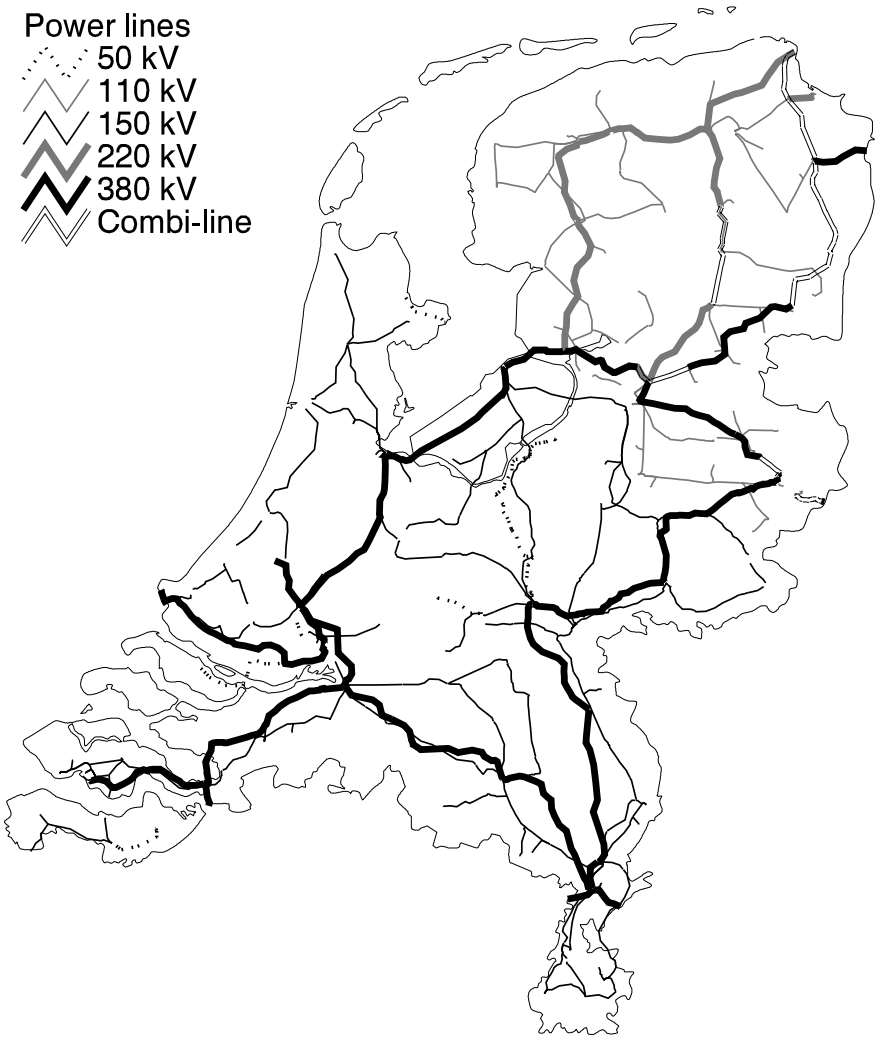

Figure 1 Overhead power lines in the Netherlands (2002)

Children living near overhead power lines

As a first step to calculating the number of children living in the vicinity of overhead power lines RIVM analysed the number of dwellings close to overhead power lines [11, 12]. A total number of 45,000 dwellings are located within 100 m (on both sides) of the overhead power lines. About 23,000 dwellings are situated within the 0.4 microtesla zone.

The average Dutch dwelling is inhabited by 2.6 persons, including 0.49 children aged 0-15 years [6]. As a result the number of children living within the 0.4 microtesla zone is estimated at 11,000.

For the next 25 years 800,000 new dwellings have been planned for the Netherlands. In a 'business-as-usual' scenario 10,000 of these dwellings will be built within the 0.4 microtesla zone. Consequently the number of children living within this zone may increase by 5,000 over the next 25 years.

Outline of the Dutch power line policy

Legal status

The Dutch power line policy was sent on October 3, 2005 as a policy letter by the State Secretary. The policy letter is addressed to stakeholders (municipalities, provinces, grid companies) with 'recommendations with regard to overhead high-voltage power lines'. Stakeholders are advised to act in accordance with this advice whenever this is reasonably possible, but the recommendations have no force of law. As a consequence stakeholders have no obligation to act according to the proposed policy.

New situations versus old situations

The Dutch power line policy is based on the observed statistical association between ELF magnetic fields and childhood leukaemia and the social concern on possible health effects, and follows the precautionary principle. The State Secretary has limited his policy to new situations, because the effects on health are unclear and because measures in existing situations often have substantial social consequences, and are expensive. In new situations prevention is possible at lower costs. With regard to the power line policy there are two types of 'new situations':

- new spatial plans (or changes in existing ones) in the vicinity of an existing overhead power line
- new overhead power lines (or changes in existing ones) in the vicinity of existing buildings

Sensitive designated uses

The statistical association between ELF magnetic fields and childhood leukaemia is observed in children living near overhead power lines. As a precaution the Dutch power line policy is not restricted to dwellings only. Some other places where children may undergo long-term exposure to the ELF magnetic field are indicated as 'sensitive uses'. The Dutch policy defines dwellings, schools, crèches and day-care centres as sensitive uses. The restrictions formulated in the Dutch overhead power line policy only apply to these sensitive uses. Other locations where children spend shorter periods in comparison to how long they spend at home, like sports centres, playgrounds, swimming pools etc. are not indicated as sensitive use. The Dutch policy does not apply to these locations. The purpose of the policy is to prevent the realisation of new sensitive uses within the magnetic field zone.

Magnetic field zones

Specific zone

In an Annex to the recommendations by the State Secretary the magnetic field zone is characterised as being:

… the area which extends along both sides of the overhead high-voltage power line and within which the magnetic field is, on average over a year, higher than 0.4 microtesla or can become so in the future.

This magnetic field zone is referred to as 'specific zone'. The value of 0.4 microtesla is a somewhat arbitrary choice in the range of 0.2 – 0.5 microtesla, the range where the childhood leukaemia risk possibly begins to be elevated [5]. The value of 0.4 was firstly mentioned with respect to overhead power lines in a letter from the former Minister of Housing, Spatial Planning and the Environment, J.P. Pronk, in 2001 [16]. The value of 0.4 microtesla was advocated by the Ministry and acceptable to the grid companies. The specific zone is calculated at a given location with the actual parameters (representative line load, pylon type, number of circuits, phase conductor geometry and earthing) for the specific section of the power line. RIVM has developed 'Guidelines for the calculation of the specific 0.4 microtesla zone in the vicinity of overhead high-voltage power lines'.

At the launching of the Dutch power line policy in 2005 no specific zones were known. To facilitate municipalities in the implementation of the policy the indicative zone was introduced in addition to the specific zone.

Indicative zone

Prior to the launching of the power line policy the indicative zone was established for all overhead power lines in the Netherlands [17]. The indicative zone is meant as an indication of the width of the specific 0.4 microtesla zone. In establishing the indicative zone, typical parameters for power lines at a given high-voltage level were used. Based on these typical parameters, zone widths were calculated for all power lines with the same voltage level. The 90th percentile of these zone widths was chosen as the indicative zone for that voltage level. Table 2 gives the values calculated for the indicative zone widths. The width of the indicative zone is not location-specific. Because the choice for the 90th percentile and due to the fact that for some of the parameters the 'worst-case' value was chosen, the specific zone is expected to be smaller than the indicative zone in most cases.

Table 2 Indicative 0.4 microtesla zone widths used in the Dutch power line policy: zone widths are rounded off to the nearest multiple of five

voltage level (kV)	zone width (m)
50	2 x 40
110	2 x 50
150	2 x 80
220	2 x 150
380	2 x 125
combi	2 x 200

TenneT, the operator of the national grid of 220 kV and 380 kV lines, was not satisfied with the established indicative zone in [17], because it gave only a rough indication of the specific zone. Consequently, TenneT recalculated the magnetic field zones for all 220 kV and 380 kV power lines. For line load, number of circuits, phase conductor geometry and earthing, TenneT used power line specific values in the calculation. One type of pylon was chosen for the entire power line. The zone from this recalculation is referred to as the 'improved indicative zone'.

The indicative (or the improved indicative) zone is used as a first check for a new spatial plan. If the plan does not overlap the indicative zone, the power line policy has no further consequences for the planning procedure. If the new spatial plan and the indicative zone overlap, it is advised to calculate the specific zone.

As a service to municipalities and provinces the indicative zone for every power line is given on a clickable Gridmap. This Gridmap is part of an internet site [18], developed by RIVM, to support implementation of the power line policy.

Establishing the specific zone

The definition of the specific zone is the result of a series of discussions between the Ministry and the grid companies. The discussions focused on two aspects of the calculation of the specific zone. The first problem to tackle was establishing which load of the power line best accounted for the actual line loads and for the expected future growth in electricity use. The second topic was how to average the magnetic field over time.

Estimating power line load

Power line loads during 2003

As a first step to estimating the line loads RIVM analysed the load of the power lines during the year 2003. Because not enough detailed information is available for the regional grid (150 kV, 110 kV, 50 kV) analyses had to be restricted to the 220 kV and 380 kV lines. The grid operator (TenneT) kindly provided RIVM with measurements of the 5-minute averaged current flowing through the circuits during 2003. Line loads vary over the day, over the days of the week and during the seasons. Figure 2 shows the variation of the line load over the day and Figure 3 over the year for a typical 380 kV power line. As the current through the power line changes the width of the actual 0.4 microtesla zone will change too. Figure 4 shows the variations of the distance of the 0.4 microtesla contour to the heart of this typical power line.

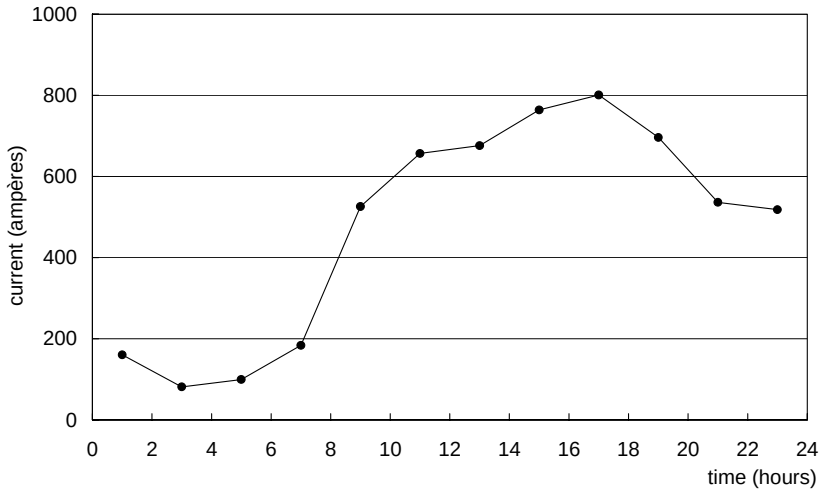

Figure 2 *Line load (two-hourly averaged current) of a typical 380 kV circuit on a typical day (July 7, 2003)*

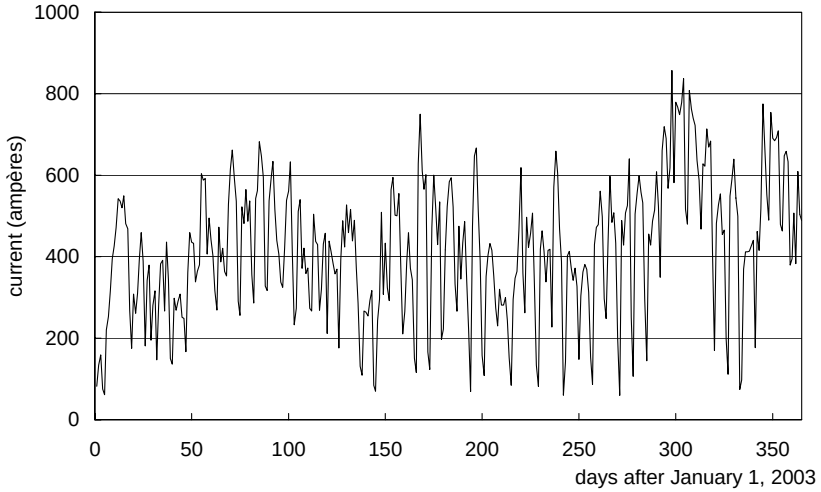

Figure 3 *Line load (daily averaged current) of a typical 380 kV circuit during 2003*

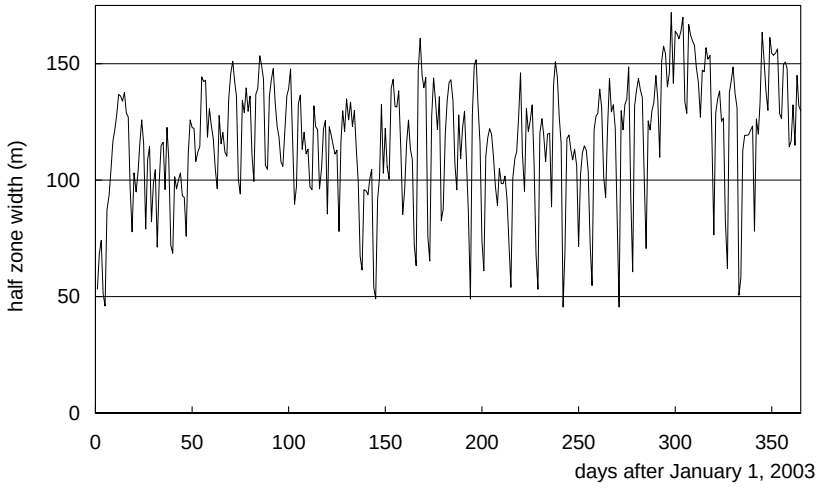

Figure 4 *Variation of the zone width for a typical 380 kV power line over the year 2003; the distance of the 0.4 microtesla contour to the heart of the power line was calculated based on the daily averaged current*

Estimating the representative current

A last, but crucial step, is to estimate the current used for the calculations of the magnetic field zone. In principle the actual yearly averaged current over the year 2003 could be used in this calculation for every power line. However, this approach does not account for the growing use of electricity, and the heavier line loads for the power lines expected in the coming decades. Calculating the width of the 0.4 microtesla zone on basis of the 2003 line load data would underestimate the width of the zone in the near future. Accounting for this growing use of electricity is one of the explicit requirements, as can be judged from the wording 'can become so in the future' added to the definition of the specific zone. In fact most power lines in the Netherlands are designed for heavier line loads than observed in 2003, and are likely to get loaded more heavily in the near future. All power lines have been designed for a maximum allowable line load, the so-called 'maximum design load'. This maximum design load is mainly determined by the cross-section of the conductors, the material (aluminium, copper) of the conductors, the surface treatment of the conductors, the ambient temperature and the wind speed. The maximum design load for a power line sets an absolute maximum to the width of the 0.4 microtesla zone. However, deriving the 0.4 microtesla zone directly from this maximum design load places a strain on the available land. Moreover, from the viewpoint of operational safety the maximum allowable yearly averaged load must be below the maximum design load.

To get an insight into the relationship between the yearly averaged load and the maximum design load the 'load fraction', defined as the yearly averaged line load divided by the maximum design load, was calculated for the year 2003. Load fractions for the 220 kV and 380 kV lines are plotted in Figure 5.

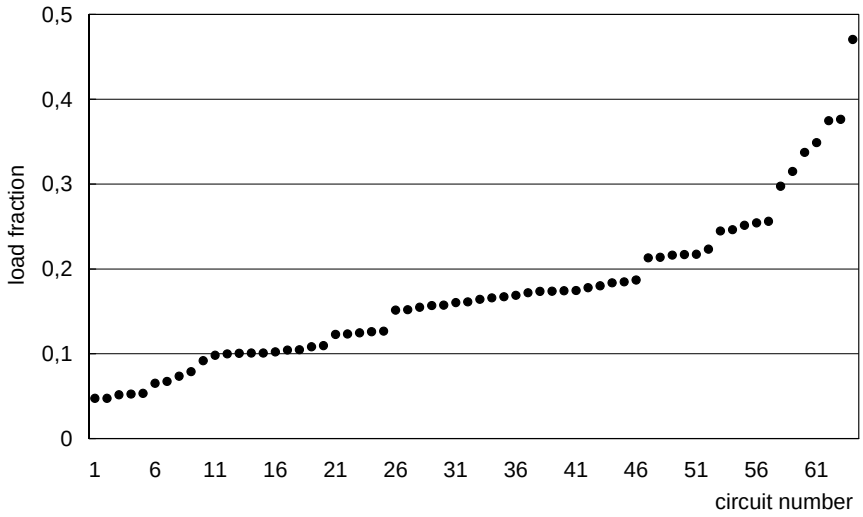

Figure 5 *Relative load of all 380 kV and 220 kV power lines: the load fraction is defined as the yearly averaged load (over 2003) divided by the maximum design load*

From Figure 5 it is evident that in 2003 these power lines were not heavily loaded. Averaged over all the 220 kV and 380 kV circuits the relative load is 0.17, and 90% of the circuits have a load fraction below 0.3. Based on this analysis the grid companies and the Ministry agreed to use a fraction of 30% of the maximum design load for the 220 kV and 380 kV power lines as yearly averaged load for the calculation of the specific 0.4 microtesla zone. For most power lines a load fraction of 30% will not be reached in the near future, and the calculated specific zone will maintain its validity during the next decades.

For the regional power lines (150 kV, 110 kV, 50 kV) a similar analysis could not be done because of the lack of sufficient data. For these lines a load fraction of 50% of the maximum design load was chosen as a 'worst case' estimate.

Time averaging the magnetic field

The epidemiological studies showing an association between the magnetic field and an increased risk for childhood leukaemia relate the leukaemia risk to magnetic field strength averaged over relatively long periods of time [3, 4]. Most studies measure the magnetic field in the dwelling, typically over a period of 24 hours. Other studies calculate the magnetic field in the dwelling, based on the yearly averaged current. From Figure 4, it can be concluded that averaging over a relatively short period may

lead to erroneous and divergent values for the magnetic field zone. For instance, averaging over a twenty-four-hour period in the beginning of January would result in a full zone width of 2 x 50 metres, whereas averaging over the same period in the beginning of November would yield a full zone width of 2 x 160 metres. In view of the epidemiological studies and the strong variation of the line load and zone width over the year the Ministry decided to base the power line policy on the yearly averaged magnetic field.

For practical purposes in calculating the width of the 0.4 microtesla zone, the yearly averaged current through the power line is estimated and with this current the width of the specific zone is calculated with one of the available software packages. For this calculation commercially-available software packages may be used. Although no comparative research into these software packages has been carried out yet, the packages used in the Netherlands[2] are regarded to yield equivalent results.

Comparison with the Swiss situation

In Switzerland precautionary emission limitations, so-called installation-limit values must be respected at places of sensitive use. For high-voltage power lines the installation limit value is 1 microtesla at the maximum rated current for the power line. In practical terms the 0.4 microtesla zone calculated at 30% of the maximum load (380 kV, 220 kV) or at 50% of the maximum load (150 kV, 110 kV, 50 kV) according to the Dutch guidelines leads to widths for the magnetic field zone that are nearly the same. For a typical 380 kV power line the 'Swiss' 1 microtesla zone is 2 x 77 metres, whereas the 'Dutch' 0.4 microtesla is 2 x 70 metres. For a typical 150 kV the 'Swiss'1 microtesla zone is 2 x 57 metres and the 'Dutch' 0.4 microtesla zone 2 x 65 metres. Starting from quite different viewpoints the Dutch and the Swiss policies lead to comparable magnetic-field zoning. Apart from this similarity there are a number of differences between the Swiss and the Dutch policies. The most striking are:

- the Swiss installation limit values have power of law and must be respected[3], whereas the Dutch policy only advises stakeholders to abandon certain activities in the 0.4 microtesla zone;
- the Dutch policy only applies to overhead power lines as sources of magnetic fields; in Switzerland the installation limit value of 1 microtesla also applies to magnetic fields generated by transformer stations, substations and switchyards; and
- the Swiss policy applies to a larger number of sensitive uses; in the Netherlands only dwellings, schools, crèches and day-care centres are designated as sensitive uses. The Swiss list of 'places of sensitive use' encompasses dwellings, schools, hospitals, playgrounds and permanent workplaces.

Discussion

Several European countries are considering a precautionary policy for overhead power lines. The basis for such a policy is the observed statistical association between childhood leukaemia and living near overhead power lines. The epidemiological studies suggest that the association holds for childhood leukaemia and long-term exposure to magnetic fields, although a causal relationship between leukaemia and magnetic fields has not been proven. According to the epidemiological data, a possibly elevated risk is observed at magnetic field strengths above a value somewhere between 0.2 and 0.5 microtesla. The Ministry of developed a precautionary power line policy. This policy is founded on a 0.4 microtesla zone, the value of 0.4 microtesla being a somewhat arbitrary choice within this 0.2 - 0.5 range. This value of 0.4 microtesla is often compared to the exposure limit of 100 microtesla for 50 Hz recommended by the European Union [19]. But in fact these two magnetic-field strengths are incommensurable. The recommendations of the European Union are derived from the International Commission on Non-Ionizing Radiation Protection and based on well-established short-term effects.

[2] In the Netherlands magnetic field calculations are based on EFC-400 (Program package developed by Forschungsgesellschaft für Energie und Umwelttechnologie: FGEU, GmbH, Berlin, Germany), CDEGS (Current Distribution, Electromagnetic Fields, Grounding and Soil Structure Analysis Program package developed by Safe Engineering Services & technologies ltd., Quebec, Canada) and ATP (Alternative Transient Program European EMTP-ATP Users Group (EEUG), Osnabrück, Germany). These software packages cannot directly calculate the width of the 0.4 microtesla zone, but calculate profiles for the magnetic field as a function of distance to the heart of the power line. To calculate the actual zone width these profiles need to be exported for further processing.

[3] Exemptions are granted if the line operator shows that all measures to limit radiation that are technically and operationally possible and economically acceptable have been taken.

The 0.4 microtesla, on the other hand comes from epidemiological evidence for a possible long-term effect.

Summary

In the Netherlands, a policy has been implemented to prevent new situations where children are exposed to magnetic fields due to overhead power lines. To achieve this goal municipalities and provinces are advised to avoid realisation of new sensitive uses (dwellings, schools, crèches and day-care centres) within the specific 0.4 microtesla zone. RIVM developed guidelines for the calculation of the 0.4 microtesla zone. This paper describes the choices that have been made in dialogue between the Ministry of Housing, Spatial Planning and the Environment, and the grid companies for the calculations of this specific 0.4 microtesla zone.

In accordance with the epidemiological studies, the specific 0.4 microtesla zone is based on a yearly averaged magnetic field. To calculate this yearly averaged magnetic field a ‘representative’ yearly averaged current through the power line has to be estimated. This representative current should reflect the present load of the power lines as well as the growth of the load expected during the coming decades. The growth potential for the load of a power line is set by the maximum design load and operational safety criteria. Analysis of the line loads during 2003 led, after careful consideration between the Ministry and the grid companies, to a choice for the representative load. For 380 kV and 220 kV the yearly averaged load is estimated as 30% of the maximum design load. For lack of data on the 150 kV, 110 kV and 50 kV overhead power lines, a ‘worst case’ estimate of the yearly averaged load is used: 50% of the maximum design load. Based on this representative load and location specific data on the power line section (type of pylons, number of circuits, phase conductor geometry and earthing) the specific 0.4 microtesla zone at a specific location can be calculated with commercially-available software.

References

1 Wertheimer N and Leeper E. Electrical wiring configurations and childhood cancer. Am. J. Epidemiol. 1979; 109(3):273-84.

2 Health Council of the Netherlands. ELF Electromagnetic Fields Committee. Exposure to electromagnetic fields (0 Hz - 10 MHz). The Hague: Health Council of the Netherlands. 2000; publication no. 2000/6 (in Dutch).

3 Ahlbom A, Day N, Feychting M et al. A pooled analysis of magnetic fields and childhood leukaemia. Br. J. Cancer. 2000; 83(5):692-8.

4 Greenland S, Sheppard AR, Kaune WT, Poole C, Kelsh MA. A pooled analysis of magnetic fields, wire codes, and childhood leukemia. Epidemiology. 2000; 11(6):624-34.

5 Van der Plas M, Houthuijs DJM, Dusseldorp A, Pennders RMJ and Pruppers MJM. Magnetic fields due to overhead power lines and leukaemia in children. RIVM report 610050007. RIVM, Bilthoven, 2001 (in Dutch with English abstract).

6 Pruppers MJM. 'Blootstelling aan extreem laag frequente elektromagnetische velden van hoogspanningslijnen' - Herberekening naar aanleiding van het KEMA/RIVM-onderzoek naar de kosten en baten van maatregelen ter beperking van magnetische velden bij hoogspanningslijnen. RIVM-briefrapport 032/2003. RIVM, Bilthoven, 2003 (in Dutch).

7 IARC Monographs on the Evaluation of Carcinogenic Risks to Humans Static and Extremely Low-Frequency Electric and Magnetic Fields, Vol. 80. IARC Press, Lyon, France 2002.

8 Draper G, Vincent T, Kroll ME and Swanson J. Childhood cancer in relation to distance from high voltage power lines in England and Wales: a case-control study. British Medical Journal. June 2005. Vol. 330 (7503): 1290-1295.

9 National environmental policy plan (NMP4). Chapter 10.1. Ministry of Housing, Spatial Planning and the Environment (VROM). The Hague, 2001 (in Dutch).

10 Kelfkens G, Pennders RMJ and Pruppers MJM. Dwellings near overhead power lines in the Netherlands. RIVM report 610150001. RIVM, Bilthoven, 2002 (in Dutch with English abstract).

11 Kelfkens G, Pennders R and Pruppers MJM. Planning new dwellings near overhead power lines, presented at the 6th International Congress of the European Bioelectromagnetics Association (EBEA), November 13-15 2003, Budapest, Hungary.

12 Kelfkens G, Pennders RMJ and Pruppers MJM. Planning new dwellings near overhead power lines. RIVM report 610150004 RIVM, Bilthoven, 2003 (in Dutch with English abstract).

13 Kelfkens G, Van Wolven J, Pennders RMJ, Stuurman C, Van Aernsbergen L, Delfini G and Pruppers M. Costs and benefits of the reduction of magnetic fields due to overhead power lines. Proceedings of the 2nd International Workshop on Biological Effects of Electromagnetic Fields, October 7 - 11 2002, Aldemar Paradise Royal Mare Hotel, Rhodes, Greece.

14 Ministry of Housing, Spatial Planning and the Environment (VROM). Nuchter omgaan met risico's. Beslissen met gevoel voor onzekerheden. (Coping Rationally with Risks) Document number 4016. The Hague, 2004 (in Dutch).

15 Policy letter with annexes sent by State Secretary of Housing, Spatial Planning and the Environment, P.L.B.A. van Geel, to Provincial and Municipal Executives and grid companies, October 3, 2005, reference SAS/2005183118

16 Letter from the Minister of Housing, Spatial Planning and the Environment, J.P. Pronk, to Mayor and Alderman of the city of Utrecht, November 13, 2001, reference SAS/2001140036.

17 Stuurman CS and Van Wolven JF. Kostenanalyse van de technische maatregelen ter beperking magnetische velden nabij bovengrondse hoogspanningslijnen (vooronderzoek), Deel 1: samenvatting, KEMA T&D consulting report no. 40130074-TDC 02-25766A, October 2002 (in Dutch).

18 Internet site: www.rivm.nl/hoogspanningslijnen (general site in Dutch) and http://milntj34.rivm.nl/website/lso/hoogspanningsnet/viewer.htm (Gridmap, with Dutch annotation).

19 Council Recommendation 1999/519/EC of 12 July 1999 on the limitation of exposure of the general public to electromagnetic fields (0 Hz to 300 GHz). Official Journal of the European Communities, L 197 of 30 July 1999; 59-70.

IMPLICATIONS OF THE NEW POLICY ON MAGNETIC FIELDS IN THE VICINITY OF HIGH-VOLTAGE POWER LINES IN THE NETHERLANDS

M.A.M. Beerlage, e-mail: monique.beerlage@kema.com
C.S. Stuurman, e-mail: claudi.stuurman@kema.com
J.F. van Wolven, e-mail: jos.vanwolven@kema.com

KEMA Nederland BV, PO Box 9035, 6800 ET, Arnhem, The Netherlands

ABSTRACT

The Council of the European Union has made recommendations to its member states regarding specific actions on magnetic field exposure of the general public [1]. These recommendations are based on the reference values by ICNIRP, published in 1998 [2].

In the year 2000 two pooled analyses were published, both dedicated to epidemiological studies on the incidence of leukaemia among children living in the vicinity of overhead power lines. Especially the paper by Ahlbom c.s. [3] was and still is giving rise to a lot of concern for governments, as well as for many people living close to overhead power lines.

In the past few years, the Dutch government has initiated additional research, based on the assumption (consistent with the conclusion of Ahlbom c.s. [3]) that the leukaemia risk indeed increases twofold for children with a long-term mean exposure to magnetic field strengths higher than 0,4 μT, originating from overhead high-voltage power lines [4]. This research contained investigations of e.g.:

- the number of "extra" children that may develop leukaemia due to the presence of overhead high-voltage power lines each year in The Netherlands (i.e. 0.5 per year)
- the number of Dutch dwellings situated within the zones around high-voltage power lines with long-term magnetic field strengths > 0,4 μT, at present (i.e. 23.000 in 2003) and in the future (i.e. 33.000 in 2028)
- implementation costs of field reducing measures, on a national scale.

Consequentially, the Dutch government has published new recommendations for municipal executives, other local authorities and grid operators in October 2005 [5]. This advice is based on the recommendations of the European Council as mentioned above, but with the addition of some important precautionary measures: for new situations in the vicinity of overhead high-voltage power lines the government recommends to prevent that children experience long-term exposure to magnetic fields, with annually averaged field strengths higher than 0,4 μT.

As an aid to local authorities and grid operators, magnetic field zoning around high-voltage power lines has been introduced. Two types of zones have been defined:

- an indicative magnetic field zone: a rough estimate of the zone, based on known indicators for Dutch high-voltage power lines in general
- a specific zone: a more accurate calculated estimate of the zone, based on actual phase configurations and electrical current of the high-voltage power line.

The recommendations are accompanied by a set of guidelines to calculate the specific magnetic field zone, as a surrogate for the "long-term mean magnetic field" of a Dutch high-voltage power line [6].

During the past few months, municipal executives, local authorities and grid operators have been managing this new Dutch policy on power lines. They have initiated or already performed several practical solutions to meet the recommendations. These solutions can be based mainly on two principles:

- reduction of the magnetic field by technical measures
- reduction of the exposure by revision of new housing development plans.

During the presentation, several implications and consequences of the Dutch recommendations for local authorities, grid operators, as well as for the general public will be discussed. This will be illustrated by presenting some examples of practical solutions.

References

[1] The Council of the European Union (1999). Council recommendation of 12 july 1999 on the limitation of exposure of the general public to electromagnetic fields (0 Hz to 300 GHz). In: Official Journal of the European Communities, L 199/59 (1999/519/EC)

[2] ICNIRP (1998). Guidelines for Limiting Exposure to Time-Varying Electric, Magnetic, and Electromagnetic Fields (up to 300 GHz). In: Health Physics, vol. 74, pp. 494-522

[3] A. Ahlbom et al (2000). A pooled analysis of magnetic fields and childhood leukaemia. In: British Journal of Cancer, vol. 83, pp. 692-698

[4] Several reports are available (in Dutch language) on the website of the Dutch Ministry of Spatial Planning, Housing and the Environment: www.vrom.nl

[5] P.B.L.A. van Geel (State Secretary of Housing, Spatial Planning and the Environment) (2005). Recommendations with regard to overhead high-voltage power lines. Letter dated on October 3rd, SAS/2005183118 (also on www.vrom.nl)

[6] G. Kelfkens and M.J.M. Pruppers (2005). Guidelines for the calculation of the specific 0.4 microtesla zone in the vicinity of overhead high-voltage power lines. RIVM, appendix to [5] (also on www.vrom.nl)

The German Mobile Telecommunication Research Programme (DMF)

Cornelia Baldermann [(1)], Gunde Ziegelberger [(1)] , Blanka Pophof [(1)]

[(1)] Federal Office for Radiation Protection
Ingolstädter Landstraße 1, D-85764 Oberschleißheim, Germany, cbaldermann@bfs.de

Abstract

The purpose of this paper is to introduce the current state of the German Mobile Telecommunication Research Programme (DMF). The Programme was initiated by the German Federal Ministry for the Environment, Nature Conservation and Nuclear Safety (BMU) and is performed by the Federal Office for Radiation Protection (BfS). In the period from 2002 to 2007 a total of 51 research projects in mobile telecommunications are proceeded in four fields: biology, dosimetry, epidemiology and risk communication. The total financial volume of the program is 17 million €. Final results of the programme are expected at the end of 2007.

Keywords: high frequency electromagnetic fields; mobile communication, health impact, research programme, Germany

1 Introduction

High frequency electromagnetic fields such as those found, for example, near transmitters (e.g. radio frequency towers and mobile telephone base stations) or when using mobile end devices (cell phones) are often suspected by the public of having adverse health effects on human. There is some indication that such electromagnetic fields can cause biological or physiological effects at levels below international limit values. In which extent they pose a health risk to the general public can´t be completely determined at this time.
The German Mobile Telecommunication Research Programme (DMF) was initiated by the German Federal Ministry for the Environment, Nature Conservation and Nuclear Safety (BMU) and the Federal Office for Radiation Protection (BfS) to take part in the international efforts clarifying the above question. The total financial volume of the program is 17 million €, appropriated half by half by the BMU and the network providers. Coordination and implementation is carried out by the BfS. The research projects chosen for the program are based on the findings of two expert workshops in 2001 and 2003 in Berlin and additional comments expressed by the general public. The first preliminary results were presented in April 2005 at a public expert workshop.
Detailed information on the single projects can be found on the DMF website http://www.emf-forschungsprogramm.de/. Project descriptions, current results and workshop results are presented. Regular reports on the state of the research projects can be found on this web-site. The researcher's Final Report together with an evaluative statement by the BfS will be made available to the public at the conclusion of every project. Further general information on electromagnetic fields and cellular telecommunication can be found on the BfS websites under http://www.bfs.de/.

2 Research Projects

In the period from 2002 to 2007 51 research projects in mobile telecommunications are realized in four scientific fields: biology, dosimetry, epidemiology and risk communication. With state of Oktober 2006 23 of them are already finished, the remaining will be completed within 2006 and 2007. The topics cover a broad spectrum, reaching beyond current GSM and UMTS standards. One objective, among others, is to clarify fundamental effects and mechanisms. Another will be to delve into the possible causes of electromagnetic sensitivity. The programme will seek results pertinent not only to existing mobile telecommunications but in order to make statements on future developments as well.

2.1 Biology

The 23 projects investigating possible biological and effect and health consequences of high frequency electromagnetic fields cover about 56 % of the financial volume of the DMF. Four projects are already completed. It could be shown, that a life-long exposure with GSM and UMTS signals does not influence the survival and the incidence of lymphoma in a genetically modified mice stock especially susceptible to lymphoma (AKR-mice). Though, the hypothesis, that chronic exposure to high frequency electromagnetic fields promote neoplastic development in the hematopoietic system in genetically predisposed mice was not supported. The "melatonin hypothesis", claiming that ELF as well as HF electromagnetic fields result in decreased melatonin levels, could not be confirmed during investigations on explanted pineal organs of hamster. A feasibility studies was successfully finished and made it possible to start investigations on the age dependence of the action of HF EMF. A study on the sleep quality of population living close to mobile phone base stations started as well.

2.2 Dosimetry

13 projects, covering about 14 % of the total financial volume of the DMF, are concerned with dosimetry and exposure assessment, eleven of them are already finished. The topics cover on the one hand the field distribution around transmitters and far-field exposure of the population by mobile phone base stations, WLAN transmitters, transmitters of the digital TV, etc. On the other hand, near-field scenarios are investigated predominantly by modelling the indoor field distribution in homes, offices, shielded rooms, etc. SAR and temperature variations in the heads and trunks of persons using mobile communication devices are determined. The SAR distribution in experimental animals was investigated as well. Investigations of the real exposure due to daily use of mobile phones have shown, that GSM-mobile phones regulate quite often to the maximum transmission power, predominantly as a result of frequent handovers and poor signal quality, and cause therefore correspondingly high SAR-values in the heads of the user. The different regulatory mode of UMTS-mobiles results in drastically reduced exposure of the user by a factor of about 1000. Determination of human exposure caused by indoor wireless communication technologies applied in homes and offices showed that in general the exposure values lay far below the prescriptive limits. Another study analysed the exposure from transmitters worn near the trunk of the body. In generic and anatomical models was revealed that under far-field-like conditions standing waves can develop, and a rise of the SAR value specifically in the skin was determined. The limit values were not exceeded. In near-field-like conditions standing waves do not arise. Although the temperature rise due to HF exposure was calculated. With free convection a maximum of 0.8 ^{o}C was determined. Using anatomical models the values determined are up to 0.31 ^{o}C at the body surface. The temperature rise determined under these conditions for the internal organs is negligible as long as the SAR limit values are kept. A project concerning the exposure of the head has shown that the temperature increase in the skin. This is caused more by the heat accumulation under the phone than by the radiation. The temperature increase within the skull (brain, pineal, inner ear) was up to 0.01 °C. One project concerned determination of exposure to the population living near digital radio and television transmitters. The measurements in Bavaria before and after introduction of the digital transmitters showed an increasing of mean exposure in the areas with "portable indoor" coverage around the transmitter sites caused by the introduction of DVB-T.

2.3 Epidemiology

Eight epidemiological projects are performed covering about 19 % of the financial volume of the DMF. Four projects are already finished. A feasibility study has shown, that an occupational cohort study on persons highly exposed to HF EMFs cannot be performed due to a lack of a highly exposed cohort of an acceptable size and without conflicting confounders. Furthermore, the feasibility of a prospective cohort study on handy users failed because of a response rate of only 5 %. The effort necessary to recruit a sufficient number of participants would be enormous and is not practicable within the DMF. The German part of INTERPHONE study is finished, the results of the evaluation of the internationally pooled data are expected in 2006. According to preliminary national results, there seems to be no increased risk for brain cancer due to a regular handy usage for up to 10 years. Two epidemiological studies on children are just starting – one investigating childhood leukemia around powerful radio and TV transmitters, another concentrating on health effects in the vicinity of mobile phone base stations. In the later one, personal dosimeters will be used to assess the exposure.

2.4 Risk Communication

Seven projects are concerned with risk perception and some other social aspects of mobile communications, covering about 9 % of the financial volume of the DMF. Yet, four projects are already finished. The analysis of target groups for differentiated information showed, that different population groups are differentially worried about possible health effects of electromagnetic fields. The results of the project “Examination of the knowledge and effects of information activities in the field of mobile telecommunications and determination of further approaches to improve information of different population groups” gained from the focus groups and the mobile phone survey in 2005 illustrate the importance of differentiating between target groups. The essential differences but also potential similarities between the views of the different citizens’ groups and the experts have become apparent. The quantitative and qualitative survey performed in the framework of the project “Supplementary information about electromagnetic hypersensitive persons” provide more detailed findings of persons who see the origin of certain physical disorders in the existence of electric, magnetic or electromagnetic fields (EMF). According to the working definition, this group is considered as electrosensitive persons. The study also reveals, however, that only a small part of this group declares themselves to be "electrosensitive". The important factor is rather their handling and/or the significance of "radiation" in the context of their everyday lives, irrespective of terms and definitions. The findings obtained are an important basis for improving the communication with people who feel impaired. They also help to adapt the way information is offered to the particular needs of this group of people.

3 Summery

A large portion of the projects will be finished in 2006 and 2007. To provide a scientific evaluation of all results of the German Mobile Telecommunication Research Programme (DMF) in the international context, single thematic topics will be presented internationally in scientific workshops and discussed with national and international experts. First, the workshop with the topic “dosimetry” was proceeded in July 2006. The next workshop with the topic “risk communication” will take place at October 2006. The biological and epidemiological projects are combined in three workshops with the topics “Acute health effects” (December 2006) as well as “Action mechanism” and “Long-time health effects” in 2007.
A final evaluation of the combined national and international research on the health effects of high frequency electromagnetic fields within and outside of DMF is planned in the form of an international scientific conference, together with international experts and the WHO. The results will be presented in a final national expert workshop at the end of 2007 and will be the base for a re-evaluation of the limits.

4 Appendix: Projects of the DMF

4.1 Biology

Completed

- Feasibility study on age dependent effects of RF electromagnetic fields on the basis of relevant biophysical and biological parameters
- Investigation of mechanisms of action in cells exposed to the high frequency electromagnetic fields of mobile telephone technology. B. Pineal gland
- Influence of low and high frequency electromagnetic fields on spontaneous leukaemia in AKR/J mice
- *in vivo* experiments on exposure to the high frequency electromagnetic fields of mobile telecommunication. B. carcinogenesis

Assigned – results in 2006 and 2007

- Investigation of mechanisms of action in cells exposed to the high frequency electromagnetic fields of mobile telephone technology. A. Demodulation / communication
- Investigation of mechanisms of action in cells exposed to the high frequency electromagnetic fields of mobile telephone technology. C. Functions
- *in vivo* experiments on exposure to the high frequency fields of mobile telecommunication. A. Long-term study
- *in vitro* experiments on exposure to the high frequency fields of mobile telecommunications. C. Blood-brain barrier
- Influence of mobile telecommunication fields on the permeability of the blood-brain barrier in laboratory rodents (*in vivo*)
- Influence of high frequency electromagnetic fields of mobile telecommunications on sensory organs. A. The auditory system
- Possible influence of high frequency electromagnetic fields of mobile communication systems on the induction and course of phantom auditory experience (tinnitus)
- Influence of high frequency electromagnetic fields of mobile telecommunications on sensory organs. B. The visual system
- Possible genotoxic effects of GSM signals on isolated human blood
- Influence of GSM signals on isolated human blood. B. differential gene expression
- Long-term study on the effects of UMTS signals on laboratory rodents
- Influence of high frequency electromagnetic fields of mobile telecommunications on the metabolic rate in laboratory rodents
- Investigation of age-dependent effects of high frequency electromagnetic fields based on relevant biophysical and biological parameters
- Investigation of sleep quality in persons living near a mobile base station - Experimental study on the evaluation of possible psychological and physiological effects under residential conditions
- Investigation of sleep quality of electrohypersensitive persons living near base stations under residential conditions
- Studies of the effects of exposure to electromagnetic fields emitted from mobile phones on volunteers
- Investigation of the phenomenon of 'electromagnetic hypersensitivity' using an epidemiological study on 'electrosensitive' patients including the determination of clinical parameters
- Investigation of electrosensitive persons with regard to accompanying factors or diseases, such as allergies and increased exposure or sensitivity to heavy metals and chemicals
- Influence of HF-EMF of mobile communications on the metabolic rate in an animal model (laboratory rodents)

4.2 Dosimetry

Completed

- Investigation of SAR distribution in laboratory animals exposed to electromagnetic fields
- Development of measurement and calculation methods for the determination of the public exposure due to electromagnetic fields in the vicinity of mobile phone base stations
- Determination of the exposure of groups of people that will be investigated within the scope of the project 'Cross-sectional study for ascertainment and assessment of possible adverse effects by the fields of mobile phone base stations'
- Determination of human exposure caused by indoor wireless communication technologies applied in homes and offices
- Determination of the specific absorption rate (SAR values) occurring during day-to-day mobile phone use
- Exposure from transmitters worn near the trunk of the body
- Determination of exposure distribution from high frequency fields in the human body with regard to small structures and relevant thermo-physiological parameters
- Determination of the real field distribution of high frequency electromagnetic fields near wireless LAN installations (WLAN) in inner cities
- Determination of the real field distribution from high frequency electromagnetic fields near UMTS transmitters
- Determination of the real exposure from using mobile phones in partially shielded rooms as compared to exposure under optimal conditions outdoors
- Determination of exposure to the population living near digital radio and television transmitters

Assigned – results in 2006

- Investigation of the validity of macroscopic dielectric tissue properties at cellular and subcellular level
- Determination of exposure by ultra-wideband-technolgies

4.3 Epidemiology

Completed

- Feasibility study for a cohort study: the cohort study should investigate highly exposed (occupational) groups to estimate the risk associated with high frequency electromagnetic fields.
- Feasibility study for a prospective cohort study on mobile phone users
- Extension of an international epidemiological study on the association between high-frequency electromagnetic fields and the risk of brain cancer (INTERPHONE)
- Addendum to a case control study on uveal melanoma and radio frequency radiation (RIFA Study)

Assigned – results in 2006 and 2007

- Cross-sectional study to record and evaluate possible adverse health effects due to electromagnetic fields from cell-phone base stations
- Addendum to the cross-sectional study on acute health effects caused by fields of mobile phone base stations
- Epidemiological study on childhood cancer and proximity to radio and television transmitters
- Acute health effects by mobile telecommunication among children

4.4 Risk Communication

Completed

- Knowledge-based database of literature describing the effects of electromagnetic fields on the organism and implants
- Analysis of target groups for differentiated information
- Supplementary information about electromagnetic hypersensitive persons
- Examination of the knowledge and effects of information activities in the field of mobile telecommunications and determination of further approaches to improve information of different population groups

Assigned – results in 2006

- Identifying the general public's fears and anxieties with regard to the possible risks of high frequency electromagnetic fields of mobile telecommunications (annual survey)
- Innovative methods of conflict mediation when determining the location for mobile phone base stations
- Support of the cooperation of the mobile telecommunication players by the local agenda 21

Reflection and Absorption Characteristics of Human body at Millimeter Wave

Naoyuki YAMADA[†] **Masahiro HANAZAWA**[††] **Soichi WATANABE**[††]

Koji SUZUKI[†††] **Setsuo TOKORO**[†††]

[†]*Toyota Central Research and Development Laboratories, Inc.*
[††]*National Institute of Information and Communications Technology*
[†††]*Toyota Motor Corporation*

E-mail: [†]yamada@mosk.tytlabs.co.jp, [††]hana@nict.go.jp, [††]wata@nict.go.jp,
[†††]koji@suzuki.tec.toyota.co.jp, [†††]tokoro@setsuo.tec.toyota.co.jp

Abstract

A traffic accident by a car becomes a social problem all over the world. Therefore, the requirement for safety system of a car is increasing. In Japan, there are many car accidents with pedestrian, a performance enhancement of the pedestrian detection with an in-vehicle sensor such as millimeter wave radars is demanded. In this report, we were aimed for construction of a human body electromagnetic phantom for millimeter wave, we derived a reflection and an absorption characteristic in the human body by an experiment. As a result, the reflection coefficient (S11) when we irradiated a millimeter wave on the human body surface was about -5dB. In addition, we measured a transmission coefficient (S21) of meat for the purpose of evaluating an absorption characteristic in the human body of millimeter wave. As a result, we understood that most of electricity was absorbed within around 2mm by the surface. Based on these results, we developed a human body phantom for automotive radar designs.

1. Introduction

A traffic accident by a car becomes a social problem all over the world. Therefore, the requirement for safety system, such as the Forward Collision Avoidance Assistance System (FCAAS), has been increasing. The radar sensor of such a safety system has to be capable of detecting not only other vehicles but also pedestrians, bicycles, and roadside objects [1]. Furthermore, such a safety system should be able to make a decision without any mistake as to whether a collision occurs. Therefore, the radar sensor must be capable of detecting objects immediately before a collision would otherwise occur. The development of a radar sensor for safety system requires that we know the radio wave reflection characteristics, such as the average value of the radio wave reflection intensity, of an object relatively close to the sensor, as well as the range of fluctuation. That is, if the radio wave reflection characteristics of objects are known, the performance of a safety system using a radar sensor can be refined.

In this paper, we evaluated a reflection and an absorption characteristic when a millimeter wave was irradiated by the human body by an experiment. In addition, we evaluated a reflection and an absorption characteristic for the wearing cloths quantitatively.

2. Measurement method

2.1 Reflection characteristic

We measured a millimeter wave reflection characteristic in the human body surface by free space method (figure 1). In this method, we set a calibration plane in the back side of the acrylic board which is fixed at a position of 0.27m by a lens antenna. Then, a reflection characteristic of a forearm part is measured by a network

analyzer accurately. When it measures a millimeter wave reflection from the human body, it is a problem to suppress a fluctuation of the reflection depended on movement of a body. However, the high precision measurement is possible by pushing an arm to an acrylic board. This measurement frequency range is 75GHz - 110GHz.

2.2 Absorption characteristic

It is difficult to measure a millimeter wave absorption characteristic in a body tissue directly, so we measured it by the following method. At first, we measure a complex permittivity of the human body surface by a coaxial probe method. Then, we measure the complex permittivity of meat (chicken, a chicken cuticle, pork, etc.) of some thickness. We measure a transmission characteristic of meat by free space method. So, the absorption characteristic of millimeter wave in the human body is derived equivalently.

3. Measurement result

3.1 Reflection characteristic

Figure 2 shows a millimeter wave reflection characteristic of a forearm part of four persons (30-40 generations). Although there was some difference in a value by frequency, the reflection characteristic was almost -5dB to -4dB. The difference by a person was small with less than 1dB. From this result, It understand that 30% of millimeter wave incidence energy reflect in an incidence direction in the human body surface

3.2 Absorption characteristic

Figure 3 shows the complex permittivity of the human body surface by a coaxial probe method. In this coaxial probe method, only a characteristic up to 50GHz is provided precisely, so the complex permittivity more than 50GHz estimated by extrapolation. As a result, the complex permittivity (real part) of the human body surface at 70GHz was 3 to 4. Figure 4 shows the complex permittivity of the meat (pork) by a coaxial probe method. The complex permittivity of a fat and a muscle at 70GHz was 4 and 7 respectively. In addition, compare with the complex permittivity of the human body surface, fat characteristic was near to the human body surface one. Transmission characteristics of several kinds of meat are shown in figure 5. The transmission characteristic was about -10dB at thickness 0.3mm, and it was about -60dB more than thickness 3mm. When a millimeter wave was irradiated by the human body, about 30% of electric power was reflected and other electric power was absorbed at less than 2mm by the surface of human body. From these results, it is thought that a millimeter wave reflection in the human body has little influence of inside composition. In addition, this experiment result accords with an analysis result by FD-TD method very well.

4. Reflection and transmission characteristic of clothes

It is thought that a millimeter wave reflection and absorption characteristic of the person who wore clothes is different from the state that does not wear clothes. In this chapter, we evaluated a millimeter wave reflection and transmission characteristic of clothes by an experiment. Same as the measurement of a reflection and transmission characteristic of the human body and meat, we applied free space method. Table 1 shows measurement results. Average values of reflection and transmission characteristics from 75GHz to 110GHz are shown in this table. From these results, the reflection characteristics were -13dB to -30dB, and the transmission characteristics were -0.1dB to -0.8dB. The transmission losses in one piece of cloth were less than 1dB. There were less transmission losses of chemical fiber materials such as polyester than a loss of cotton materials.

Furthermore, we performed the measurement that assumed wearing clothes one over another. As a result of three pieces of cloth (No.2, No.3 and No.4), the reflection and transmission characteristics were -13.2dB, -1.51dB respectively. A reflection characteristic depends on cloth of large reflectance, and a transmission characteristic is almost a total of each transmission characteristic. When we examine a millimeter wave reflection and absorption characteristic of pedestrian of a wearing clothes, we have to consider these influence.

5. Conclusion

We evaluated a reflection and absorption characteristic experimentally when a millimeter wave was irradiated by the human body. In addition, we evaluated a reflection and transmission characteristic of cloth used for

wearing clothes in the same way.

When a millimeter wave was irradiated by the human body, about 30% of electric power was reflected and other electric power was absorbed at less than 2mm by the surface of human body. Furthermore, the reflection characteristics of clothes were -13dB to -30dB, and the transmission characteristics were -0.1dB to -0.8dB. Based on these results, we developed a human body phantom for automotive radar designs and development of millimeter wave radar for pedestrian detection.

REFERENCES

[1] S. Ohshima, Y. Asano and K. Nishikawa, "A Method for Accomplishing Accurate RCS Image in Compact Range", IEICE Trans. Commun., E79-B-12(1996), 1799-1805

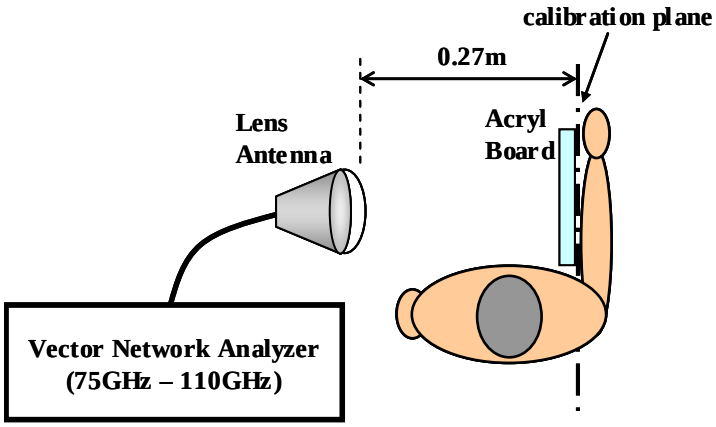

Fig. 1 reflection characteristic measurement method (A human body forearm part)

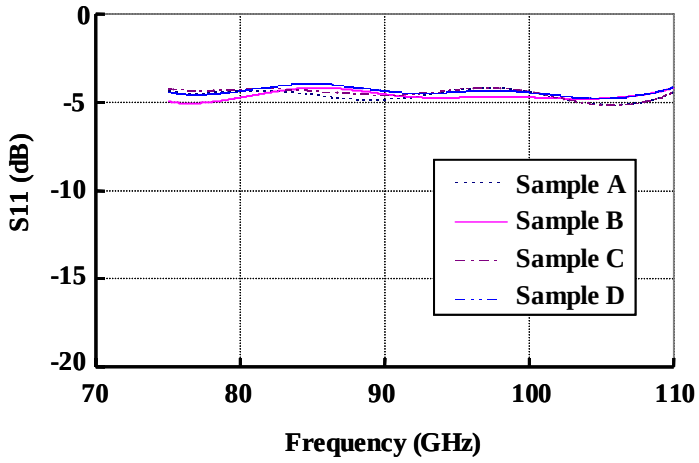

Fig. 2 reflection characteristic measurement result (A human body forearm part)

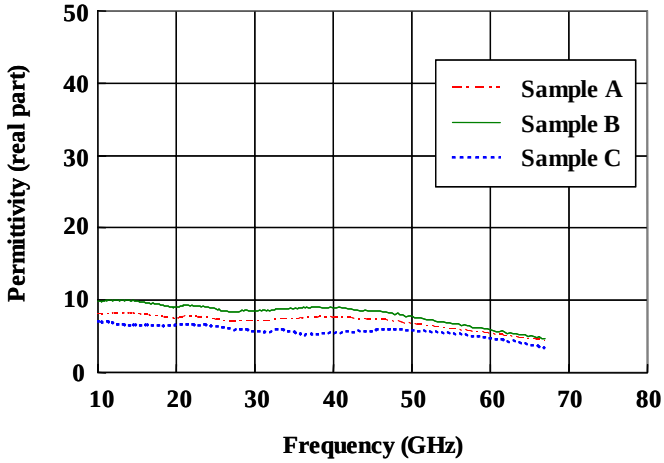

Fig. 3 permittivity of the human body surface

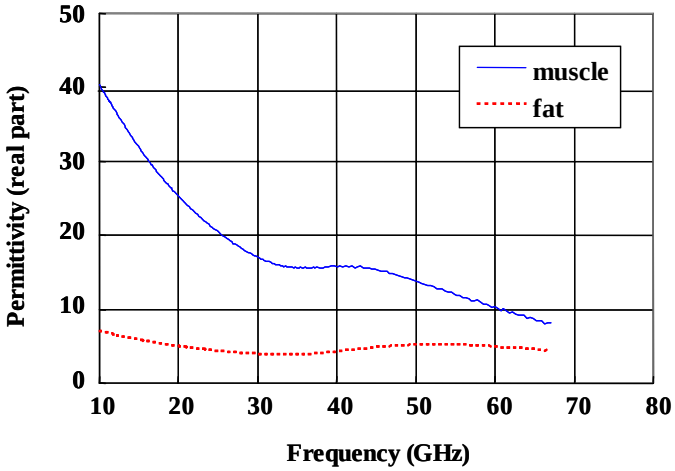

Fig. 4 permittivity of the pork

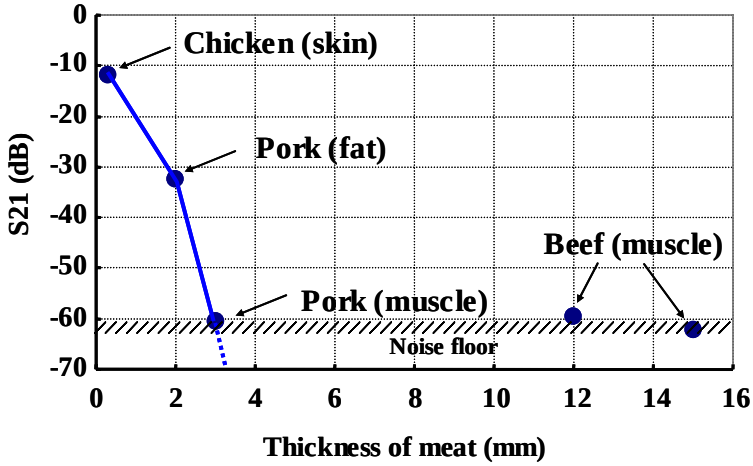

Fig. 5 transmission characteristic for thickness of meat

Table.1 reflection and transmission characteristic measurement result of various cloth

	material	s11(dB)	s21(dB)
No.1	polyester:50%, acryl:30%, cotton:20%	-26.5	-0.18
No.2	polyester:65%, cotton:35%	-18.3	-0.36
No.3	cotton:100%	-17.2	-0.77
No.4	cotton:95%, polyurethane:5%	-13.8	-0.79
No.5	polyester:100%	-27.4	-0.46
No.6	acryl:80%, nylon:20%	-30.1	-0.28
No.7	polyester:100%	-22.9	-0.21
No.8	polyester:100%	-17.8	-0.26
No.9	polyester:100%	-23.7	-0.11
No.10	acryl:85%, wool:15%	-23.3	-0.3
No.11	cotton:98%, polyurethane:2%	-19.4	-0.79

ELECTROMAGNETIC INDUCTION THROUGH THE BIOLOGICAL TISSUE

N. M. SALEM

DEPT. OF ENGINEERING PHYSICS, FACULTY OF ENGINEERING, CAIRO UNIVERSITY, EGYPT

Abstract

The study of the BIA has firstly been introduced as an effective tool to assess many of the biological and biochemical activities of the body. Due to the ubiquitous exposure to electromagnetic waves in our environment and the recent extensive use of mobile handsets, another trend appeared to exploit the BIA, namely its relation to electromagnetic absorption of the body especially in terms of its frequency dependence and the possible ability of power attenuation. In the present study we concentrate on the biological impedance of the body when subjected to high frequency and low energy microwaves. Full mathematical analysis is introduced to examine the fraction of power transmitted via the body impedance and the possible wave shape delay or distortion of the incident wave.

Introduction

Perhaps the term bioelectrical impedance analysis (BIA) was first introduced in 1940's [1], to assess the induced changes in hydration status as it is related to the total body changes in resistance and capacitive reactance. BIA was also associated with the dynamic changes in pulsatile blood flow to organs, arterial pulse waveforms and respiration [2]. The applications of impedance plethysmography, to detect dynamic blood volume changes, have been widely confirmed by numerous research workers [3-6].

The significant correlation between total body water (TBW) and the BIA has been reported by hundreds of peer reviewed papers [4,7,8].

Measurement of the electrical impedance of biological tissue in vitro and in vivo has entered into several prominent classes of biological research and biomedical applications. More than half a century ago, Fricke [9], then followed by Cole and Curtis [10], have measured the electrical self-impedance of a variety of cell and tissue systems; these measurements were made across a large spectrum of frequencies ranging from the audio to the high radio frequencies. Their results were studied in the usual impedance domain of resistance and reactance rather than in the electrically equivalent admittance domain of conductance and susceptance, thus a series of organized circuit models were obtained.

Most of the body tissue contains large amounts of water and conducting electrolytes, and represents a low resistance electrical pathway; hence the resistance is indirectly related to the extracellular mass. This equivalent electric resistance has conductivity σ. Also the body tissue has an equivalent electric capacitance which reflects the ability of the tissue to store electrical energy. This reactance originates from the cell membrane that consists of two conductive layers of protein molecules having a nonconductive lipid material of relative permittivity ε_r . The dielectric constant of the biological tissue is anisotropic and frequency dependent. The reactance is a measure of the volume of cell membrane capacitance and an indirect measure of the intracellular volume or body cell mass.

In the present work the emphasis is on the dependence of the BIA on the frequency particularly in the microwave region. Moreover, the power attenuation through a biological tissue is examined.

Models for the equivalent biological circuit

Different models have been put forward to describe the human body. As of yet, there is no consensus on the equivalent biological circuit that will serve all purposes.

The basic concept of the proposed models depends on the assumption that human tissues can be treated as a set of resistors and capacitors connected together in series or in parallel. Two effective simple models of the skin barrier will be assumed. Firstly, Model A consists of a capacitor and resistor connected together in series, where the resistor represents the input ohmic impedance of the rest of the body. Secondly, Model B consists of a capacitor and a resistor connected in parallel, and all the rest of the human body may be represented by an ohmic resistor, R_2, which represents the input impedance of the body. The electromagnetic wave enters as V_{in} and the induced wave is represented by V_{out}. The capacitor in Model A, and the parallel combination in Model B represent the skin barrier.

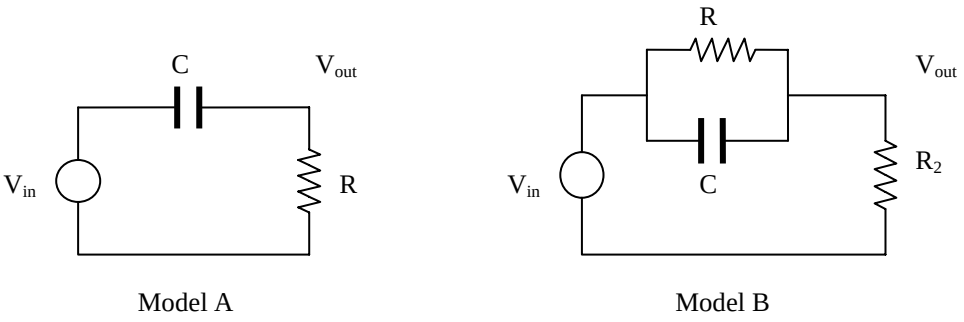

Fig. 1. Two bioelectric equivalent circuits, Models A and B, respectively.

We investigate two assumptions: firstly that the dielectric constant of either model is frequency independent and secondly, as it should, a function of the incident frequency. The particular treatment in the present work considers that the tissue is subjected to pulsating microwaves that are emitted from sources like mobile network antenna or mobile handsets.

Mathematical Analysis

Typically, for mobile communication, the incident wave comprises pulses of sinusoidal waves. The frequency of the pulses is around 100 KHz, while that of the sinusoidal waves is of the order of GHz. The pulses may be considered as square waves of periodic time *T*. For the first period the square wave is nonzero in the region $-T_1 \le t \le T_1$ where its value is unity. The sinusoidal wave may be simply represented by $V_o \cos(m\omega_o t)$, where $\omega_0 = \dfrac{2\pi}{T}$ is the angular frequency of the square wave, while $m\omega_0$ is the angular frequency of the sinusoidal wave; V_o is the amplitude of the incident signal. Therefore the input signal may be considered as the direct multiplication of the square and sinusoidal functions and is given by

$$V_{in}(t) = \begin{cases} V_o \cos(m\omega_o t) & -T_1 \le t \le T_1 \\ 0 & T_1 \le t \le T - T_1 \end{cases}$$

The input signal is illustrated in Fig. 2. $V_{\text{in}}(t)$ is then represented as a Fourier series [11] such that

$$V_{\text{in}}(t) = \sum_{k=-\infty}^{\infty} c_k \, \mathrm{e}^{jk\omega_0 t}$$

The Fourier coefficients c_k are evaluated; to elaborate

$$c_k = \frac{1}{T}\int_T V_{in}(t)\mathrm{e}^{-jk\omega_0 t}dt = \frac{V_0}{T\omega_0}\left\{\frac{\sin(k+m)\omega_0 T_1}{(k+m)} + \frac{\sin(k-m)\omega_0 T_1}{(k-m)}\right\}$$

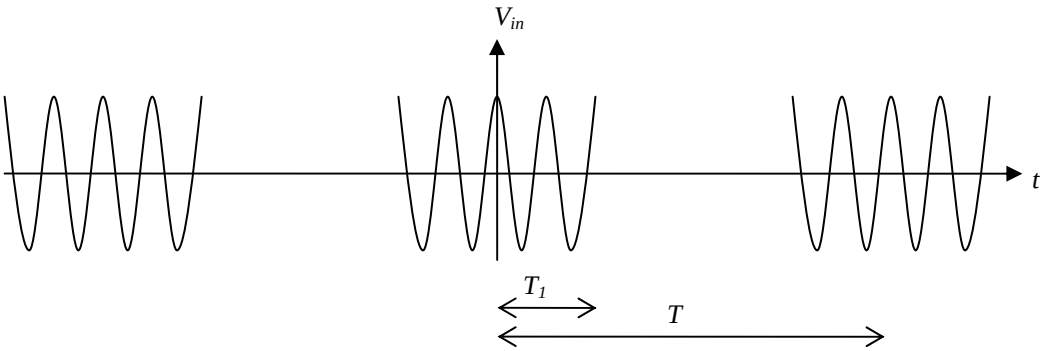

Fig. 2. The input singnal.

As soon as the signal is converted into its Fourier series and the coefficients are obtained for each harmonic component, each frequency may be treated separately such that $V_{\text{in}}(k\,\omega_0) = c_k$. The output signal, V_{out}, is calculated by standard circuit analysis; namely

$$V_{\text{out}}(\omega) = \frac{R}{Z(\omega)} V_{\text{in}}(\omega); \qquad Z(\omega) = R + \frac{1}{j\,\omega C} \qquad \text{(Model A)}$$

$$V_{\text{out}}(\omega) = \frac{R_2}{Z(\omega)} V_{\text{in}}(\omega); \qquad Z(\omega) = \frac{R}{1 + j\,\omega CR} + R_2 \qquad \text{(Model B)}$$

where $\omega = k\,\omega_0$. The total output signal as a function of time is given by

$$V_{\text{out}}(t) = \sum_{k=-\infty}^{\infty} V_{\text{out}}(k\,\omega_0) \mathrm{e}^{jk\,\omega_0 t} = \sum_{k=-\infty}^{\infty} d_k\, \mathrm{e}^{jk\,\omega_0 t}$$

The average power of a signal that is dissipated in a resistor is given by Parseval's relation and is proportional to

$$V_{\text{rms}}^2 = \frac{1}{T} \int_T |V(t)|^2\, dt = \sum_{k=-\infty}^{\infty} |a_k|^2$$

where a_k are the Fourier series coefficients of $V(t)$.

Results

The dielectric characteristics, permittivity and conductivity, of the human tissues have been subject to a great research [12,13]. As of yet there is no agreement among research workers regarding their values. In this work the values used for the specific absorption rate (SAR) calculations according to the IEEE 1528-200x [14] are used as a guideline. A summary of these values is given in Table 1. The extrapolated values [13] from Hartsgrove's *et al.* [15] formula for simulating body tissues at higher frequencies are supplied as well

Table 1. The permittivity and conductivity as a function of frequency.

Frequency MHz	ε_r	σ S/m	Reference
900	41.5	0.97	IEEE 1528-200x [14]
1800	40	1.4	
2100	39.8	1.49	
2450	39.2	1.8	
3000	38.5	2.4	
8000	26	9	Hartsgrove *et al.* [15]
10000	23	11	

Two calculations for each of Models A and B were conducted. The first one explicitly considers the frequency dependence of the permittivity and conductivity and, by curve fitting, relations are obtained that satisfy the above data. The fitted relation for the permittivity as a function of frequency is:

$$\varepsilon_r(f) = 10^4 \times \left(0.8871 f^{-8} - 4.5381 f^{-6} + 6.544 f^{-5} - 3.9988 f^{-4} + 1.2852 f^{-3} - 0.2507 f^{-2} + 0.0376 f^{-1} + 0.0001\right)$$

Whereas the fitted relation for the conductivity as a function of frequency is:

$$\sigma(f) = \left(0.0002 f^{8} - 0.01 f^{7} + 0.163 f^{6} - 1.2121 f^{5} + 4.2548 f^{4} - 6.1646 f^{3} + 8.1443 f - 4.0236\right)$$

For the sake of simplicity and the lack of experimental data, it is assumed that the above equations hold for the other frequency values that are not included in the table. In the second approach constant average values were taken, namely $\varepsilon_r = 40$ and $\sigma = 2$ S/m. As usual, $C = \frac{\varepsilon_0 \varepsilon_r A}{d}$ and $R = \frac{d}{\sigma A}$. The length d and area A are taken to be unity in SI units, thus our results are for unit length and unit area. The obtained results are summarized in Tables 2 and 3.

Table 2. Summary of the results for Model A.

Frequency	Frequency dependent dielectric parameters		Frequency independent dielectric parameters	
	$\frac{V^2_{\text{out, rms}}}{V^2_{\text{in, rms}}}$	$20\log\frac{V_{\text{out, rms}}}{V_{\text{in, rms}}}$ dB	$\frac{V^2_{\text{out, rms}}}{V^2_{\text{in, rms}}}$	$20\log\frac{V_{\text{out, rms}}}{V_{\text{in, rms}}}$ dB
10^7	0.999986	-0.00006	0.000219	-36.6
10^8	0.999981	-0.00008	0.0123	-19.1
10^9	0.99617	-0.0167	0.553	-2.57
2×10^9	0.9053	-0.432	0.832	-0.799
5×10^9	0.1925	-0.716	0.969	-0.138
8×10^9	0.001803	-27.4	0.988	-0.0545
10^{10}	0.000054	-42.7	0.992	-0.0349

Table 3. Summary of the results for Model B. $R_2 = 100\ \Omega$.

Frequency	Frequency dependent dielectric parameters		Frequency independent dielectric parameters	
	$\frac{V^2_{\text{out, rms}}}{V^2_{\text{in, rms}}}$	$20\log\frac{V_{\text{out, rms}}}{V_{\text{in, rms}}}$ dB	$\frac{V^2_{\text{out, rms}}}{V^2_{\text{in, rms}}}$	$20\log\frac{V_{\text{out, rms}}}{V_{\text{in, rms}}}$ dB
10^7	0.99993	-0.00029	0.99008	-0.0433
10^8	1	0	0.9902	-0.0428
10^9	1	0	0.996	-0.0194
10^{10}	1	0	0.9999	-0.000349

Conclusion

The main objective of the present work is to demonstrate the behaviour of the BIA as a power attenuator at different values of modulated high frequency. Comparison was set out between two simplified models of the skin barrier of a body. This is considered under the two assumptions that firstly the dielectric constant is sensitively dependent on the frequency or, secondly, its variation with the frequency is insignificantly small within the given frequency range.

Regarding the frequency dependent assumption, the results show that for both models the input induced voltage is slowly attenuated at frequencies below 10^7 Hz, but over this frequency Model B shows no attenuation while Model A indicates that as the frequency increases a considerable amount of energy is absorbed within the skin.

On the other hand when the dielectric constant is insensitive to frequency variation, Model A shows large attenuation at low frequencies which decreases gradually as the frequency increases, whereas Model B displays an opposite behaviour such that the attenuation is very poor almost at all frequencies in the range from 10^7 to 10^{10} Hz. This seems reasonable since according to the first model the skin behaves as a high pass filter, while the second model shows insensitivity to the variation of frequency.

We believe that the problem is more sophisticated than the proposed two models, which can only be considered as a first order approximation of the problem. There are other important factors that should be considered such as the multilayered structure of biological tissues, the effect of blood circulation, as well as the active elements incorporated in living tissues.

References

[1] Barnett, A., *Electrical method for studying water metabolism and translocation in body segments.* Proc. Soc. Exp. Biol. Med., 44: 142, 1940.
[2] Nyboer, J., Bango, S., Barnett, A. and Halsey, R.H.: *Radiocardiograms - the electrical impedance changes of the heart in relation to electrocardiograms and heart sounds.* J. Clin. Invest., 19: 963, 1940.
[3] Kubicek, W.G.: *Development and Evaluation of an Impedance Cardiographic System to Measure Cardiac Output and Other Cardiac Parameters*. National Aeronautics and Space Administration (NASA). July 1, 1968 to June 30, 1969. Contract No. NAS 9-4500.
[4] Nyboer, J.: *Electrical Impedance Plethysmography.* Second Edition. Charles C. Thomas, Springfield, IL, 1970.
[5] Nyboer, J.: *Workable volume and flow concepts of biosegments by electrical impedance plethysmography.* T.I.T. Journal of Life Sciences (2): 1-13, 1972.
[6] Thomasett, A.: *Bioelectrical properties of tissue impedance.* Lyon Med. 207: 107-118, 1962.
[7] Hoffer, E.C., Meador, C.K. and Simpson, D.C.: *Correlation of whole body impedance with total body water volume.* J. Appl. Physiol., **27**, 531, 1969.
[8] Nyboer, J., Liedtke, R.J., Reid, K.A. and Gessert, W.A.: *Nontraumatic electrical detection of total body water and density in man.* Proceedings of VIth ICEBI, 381-384, 1983.
[9] Fricke, H., *The theory of electrolyte polarization*, Phil. Mag., **14**, 310-318, 1931.
[10] Cole, K. S. and Curtis,H. J., Electric impedance of the giant squid axon during activity. Journal of general Physiology, **22**, 649–670, 1939.
[11] V. Oppenheim, A. S. Willsky, and S. Hamid Nawab, *Signals and Systems*, Second Edition, Prentice-Hall International, Inc., 1997.
[12] Martinsen, Ø. G., Grimnes, S., Schwan, H. P., Interface phenomena and dielectric properties of biological tissues, Encyclopedia Surface and Colloid Science, Marcel Dekker, New York, pp. 2643-2652, 2002.
[13] Ping Liu, Rappaport, C.M., Yan-zhen Wei, and Sridhar, S**.,** *Simulated Biological Materials at Microwave Frequencies for the Study of Electromagnetic Hyperthermia***,** Engineering in Medicine and Biology Society, Proceedings of the Annual International Conference of the IEEE**, 14**, 1992.
[14] IEEE Standard P1528-200x. Recommended Practice for Determining the Spatial-Peak Specific Absorption Rate (SAR) I the Human Body Due to Wireless Communications Devices: Experimental Techniques.
[15] G.Hartsgrove, A. Kraszewski, and A. Surowiec, *Simulated Biological Materials for Electromagnetic Radiation Absorption Studies*, Bioelectromagnetics, **8**, pp. 29-36, 1987

ARTIFICIAL AND NATURAL NEAR-INFRARED RADIATION EFFECTS UPON THE CELL MOTILITY. BIOLOGICAL HYPOTHESE

Gérard DUBOST
Institut d'Electronique et de Télécommunications de Rennes
UMR CNRS 6164, UNIVERSITE DE RENNES 1
Avenue du Général Leclerc, Campus de Beaulieu, 35042 – Rennes Cedex – France

André BELLOSSI
Villa Gabrielle, Chemin du Goh Vras, 56730 – Saint Gildas de Rhuys – France

ABSTRACT

We proved that the centrioles were the device used for the detection of an artificial infrared source external to 3T3 fibroblast and epithelial CV1 cells. The fundamental contribution of the cytoskeleton explains the cell motility. In effect the strain due to the physical pressure on the plasma cell membrane is a sufficient stress to activate Hsp 27 which results in actin polymerization and motility of the cell. We calculate the diffracted field inside the cell due to the current induced along the centriole equivalent to a cylindrical dipole. We deduced the centriole bistatic area function of the directions of the incident and diffracted fields. Some idea of the theoretical pressure equal to several $nN/\mu m^2$ is in good agreement with recent experiments. About the two centrioles in orthogonal positions 100 % of the space is covered, while during the experiments 88 % of 3T3 and 50 % of CV1 cells were put in motion in presence of a near infrared source. So we must consider than the strain due to the pressure on the membrane can be transmitted to the side facing the light source throughout the actin cyto-skeleton. The stress fibers serve as force transmitters in fast mecanotransduction and act as mechano-sensors with direction sensitivity on slow mechanotransduction. We determine the spectral emission power of a single cell from the black-body one. Finally a cell scatters a weak ambient black-body theoretical power radiation. The cellular agregate radiation is able to be detected by one cell located at a certain distance following recent measurements.

INTRODUCTION

Albrecht-Buehler showed that 3T3 mouse fibroblast cells and epithelial CV1 cells could react to a near-infrared light by moving either towards or away from the light source. The type of response depended on the cell type and on the temporal pattern of the emission of the light. He also proved that the centrioles were the detection device for the direction of the infrared source [1] - [4].

CONTRIBUTION OF THE CYTOSKELETON CONCERNING THE CELL MOTILITY (fig. 1)

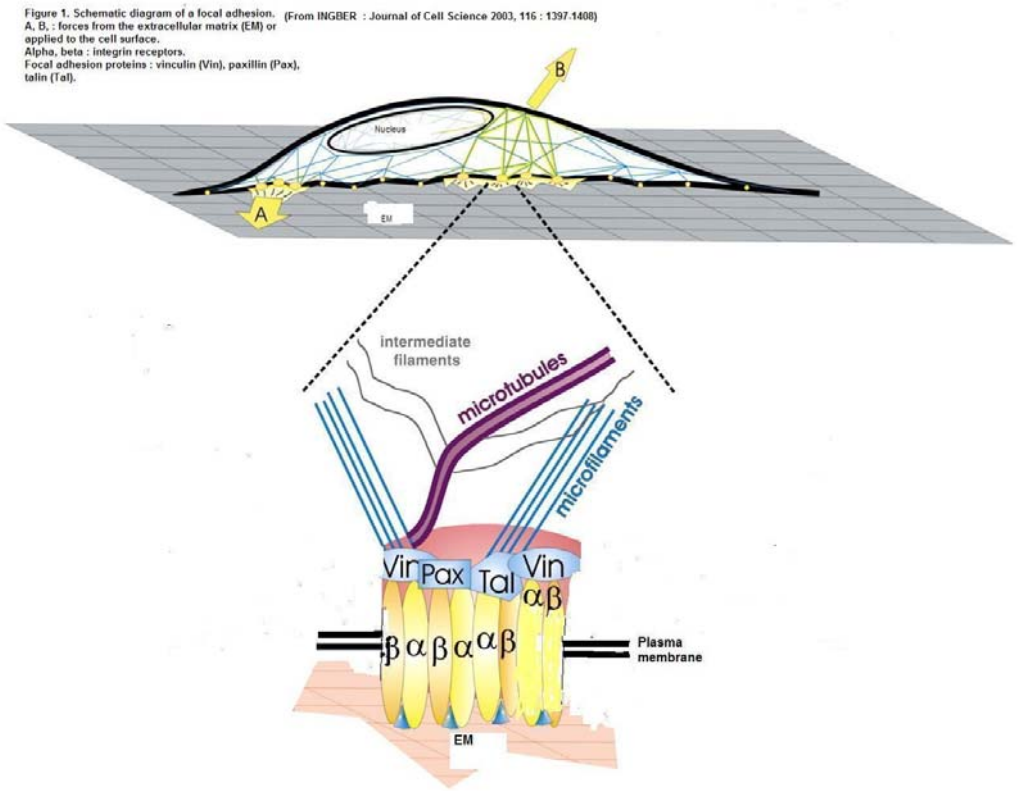

Fig. 1 : Schematic diagram of a focal adhesion.
(From INGBER : Journal of Cell Science 2003, 116 : 1397-1408)
A, B : forces from the extracellular matrix (EM) or applied to the cell surface
Alpha, beta : integrin receptors.
Focal adhesion proteins : vinculin (Vin), paxillin (Pax), talin (Tal).

The plasma membrane is an assembling of various proteins inserted in the fluid matrix of a lipid bilayer. In non muscle cells integrins receptors are membrane spanning proteins that ligate extracellular matrix proteins and link to actin skeleton on the inside of the cells [5] providing a great degree of mechanical coupling across the cell surface. The cytoskeleton is composed of microtubules, actin microfilaments and intermediate filaments. Application of forces to integrins receptors and associated focal adhesion proteins results in physical distorsion of the membrane surface and repositionning of the cytoskeletal filaments along applied field lines within the cytoplasm [6]. Among the three filament systems that form the cytoskeleton, the actin network plays the principal role in determining the cell dynamic response [7]. The cell motility is driven by the sum of asymmetric traction forces exerted on the substrate through adhesion foci that interface with the actin skeleton [8] stimulating polymerization of monomeric globular actin to filamentous actin [9]. Polymerization of actin filaments is necessary for the extension of membrane structures, creating a propulsive force that pushes forward the lamellipodia at the front of migrating cell [10], [11]. Stress proteins, called heat shock proteins (Hsps), are synthesized by cells in case of stress. In the small heat shock protein family, Hsp27 participed in regulating the organization of the actin cytoskeleton in both control and stress conditions. When Hsp27 is phosphorylated, its stimulates actin polymerization and modulates the rate of polymerization, therefore determining the motility of the cell [10], [12], [13], [14], [15]. So we could assume that the strain due to the pressure on the plasma

membrane, resulting from the near infrared radiation, constituted a sufficient stress to activate Hsp27 which resulted in actin polymerization and motility of the cell.

INFLUENCE OF A FLUCTUATING NEAR-INFRARED EXTERNAL SOURCE ABOUT THE CENTRIOLE DIFFRACTION INSIDE THE CELL

Albrecht-Buehler G. showed [1], [4], that a pair of centrioles is able to detect the direction of a near-infrared pulsed source of a 0.8 µm wavelength. Recently [16] we introduced the theoretical selective transparence of the cell membrane deduced from experimental results in the range stretched from 0.2 to 1µm. It was called the transmission coefficient T_{13} . Then from an isotropic radiated power of 4 µW of the light source located at 60 µm, we calculated, inside the cell, an electric field E_i equal to 40 V/m. The wave attenuation along the path and the transmission through the membrane (T_{13}) were taken into account. Inside the cell the mean incident power per unit of area is equal to :

$$p_i = \frac{1}{2}\sqrt{\frac{\varepsilon_o}{\mu_o}}\left|\vec{E}_i\right|^2 \qquad (1)$$

We compare each protofilament of the centriole to a cylindrical dipole of length 2h and diameter 2a, which is equivalent to an opened transmission line of characteristic impedance Z_c and linear propagation constant : $\gamma = \alpha + jk$ [17].
We use the following parameters without dimension :

$$\left.\begin{aligned} K = kh = 2\pi h/\lambda, \qquad \Omega = 2\log_e(2h/a), \\ A = \alpha h = (kh)^2 \big/ 2(\Omega - 3.4) \end{aligned}\right\} \qquad (2)$$

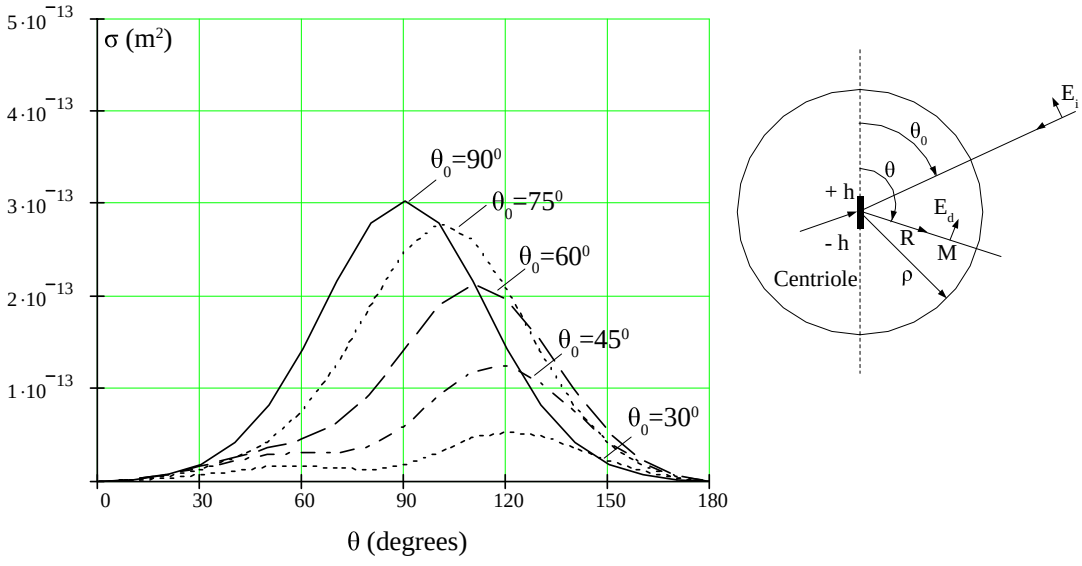

Fig. 2. Cell bistatic area σ (θ, θ_0)

The figure 2 shows the centriole lighted by a plane-wave from the θ_o direction with an electric field $\vec{E}_i(\theta_o)$. The diffracted field at point M : $\vec{E}_d(\theta,\phi,\theta_o,R)$ $(0 \le \phi \le 2\pi)$, inside the cell is due to the current $I(z,\theta_o)$ induced along the centriole. The distance between the center of the centriole and M is R. The bistatic area of the centriole related to the two directions θ_o and θ is given by the following expression :

$$\sigma(\theta,\theta_o) = \frac{\lambda^2}{\pi}|S(\theta,\theta_o)|^2 \qquad (3)$$

$$\text{with :} \quad \left|\frac{\vec{E}_d(\theta,\theta_o,R)}{\vec{E}_i(\theta_o)}\right|^2 = \frac{|S(\theta,\theta_o)|^2}{(kR)^2} = \frac{\sigma(\theta,\theta_o)}{4\pi R^2} \qquad (4)$$

The expressions (3) and (4) are valid when $R \ge 8h^2/\lambda$ (5), that is when the diffracted field is associated with an electromagnetic plane-wave.

$I(z,\theta_o)$ and $S(\theta,\theta_o)$, which depend on A, K and Ω parameters are given in the annex of calculation.
The whole power P_d diffracted inside the cell by the centriole is :

$$P_d(\theta_o) = \frac{1}{2}\sqrt{\frac{\varepsilon_o}{\mu_o}}\int|\vec{E}_d|^2 ds = \frac{1}{2}\sqrt{\frac{\varepsilon_o}{\mu_o}}|\vec{E}_i|^2 \int\frac{\sigma(\theta,\theta_o)\,ds}{4\pi R^2} = \frac{p_i}{2}\int_o^\pi \sigma(\theta,\theta_o)\sin\theta\, d\theta \qquad (6)$$

with $ds = R^2 \sin\theta\, d\theta\, d\phi$.

For the pulse light emission the form factor is the product of the length of time τ by the frequency f_r.
In a corresponding stochastic way the energy is stored inside the cell of radius ρ, where it is trapped because its transmission through the membrane is lower than 10 percent [16].

The stored energy during a length of time Δt will be equal to :

$$W_S = P_d(\theta_o)\Delta t\, \tau\, f_r \qquad (7)$$

The density of energy u_S and the mean pressure P applied on the membrane are then :

$$u_S = \frac{W_S}{(4/3)\pi\rho^3} \qquad (8) \qquad\qquad P = \frac{u_S}{3} \qquad (9)$$

In the fig. 2 we present the bistatic area (3) in terms of θ for several θ_o values with the following parameters given in (2) :

$$2h = \lambda = 0.8\,\mu m, \quad 2a = 40\,nm, \quad \Omega = 7.38, \quad K = \pi, \quad A = 1.24$$

The validity condition (5) is fulfiled when : $R \ge 1.6\,\mu m$. Whatever, the chosen incident angle θ_o, the max of σ and P_d occur for $\theta \ge 90°$. The active diffracted beam draws an asymmetrical cone-shaped zone around the centriole axis so that the diffracted light propagation goes away from the light source.
The Table I shows P_d, W_S, u_S and P with $p_i = 2W/m^2$ (1), $\tau f_r = 1/2$,

$\rho = 11\mu m$ and $\Delta t = 600\,s$.

θ_o (degrees)	90	75	60	45	30
P_d (watts) (6)	3.10^{-13}	3.10^{-13}	$2.6\,10^{-13}$	$1.4\,10^{-13}$	$7\,10^{-14}$
W_S (Joules) (7)	9.10^{-11}	9.10^{-11}	8.10^{-11}	4.10^{-11}	2.10^{-11}
u_S (Joules/m^3) (8)	$1.6\,10^4$	$1.6\,10^4$	$1.4\,10^4$	$7.4\,10^3$	$4\,10^3$
P(nN/μm^2)	5.0	5.0	4.6	2.3	1.2

Table I : Power and energy diffracted by a 3T3 cell.
Pressure applied on the membrane

Some idea of the size of the pressure P has been obtained in recent experiments [18]. In the abstract we can read: "we measure dynamic traction forces applied by epithelial cells (monolayer) on a substrate. The force sensor is a high-density array of elastomeric microfabricated pillars that supports the cells. Traction forces induced by cell migration are deduced from the measurements of the bending of these pillars and are correlated with actin localization by fluorescence microscopy". Each post or pillar is a cylinder of radius r and length L. The deflection Δx of the free end of the post is due to a force F exerted by the cell on its underlying substrate given by :

$$F = \left(\frac{3}{4}\pi E \frac{r^4}{L^3}\right)\Delta x \qquad (10)$$

E is the Young's modulus of the pillar.

With $\Delta x = 0.1\mu m$, $r = 1.5\ \mu m$, $L = 5\ \mu m$, $E = 2\ 10^6\ P_a$, we find : F = 19 nN.

This force applied to the area of the pillar $\pi r^2 = 7.07\ \mu m^2$ corresponds to a pressure of 2.7 nN/μm^2.
This pressure is in good agreement with our theoretical results shown in Table I.
Previous analysis (2001, 1999), related in [18], have indicated a 5.5 nN/μm^2 value relating force and contact area.

Note : Albrecht-Buehler said (April 23, 2003) : *"The cells used were always moving. The first sign of changing direction, i.e the extension of a new lamellipodium in the direction of the light source, was usually visible after 5-10 min (factor 2) since the beginning of the lighting"*. This explains the choice of $\Delta t = 600$ s in W_S (7).

Then the radiation by one centriole is the most efficient when $45° \le \theta_o \le 135°$ which correspond to a diffraction zone : $60° \le \theta \le 120°$ (fig 2) for a variation of σ and P_d by a same factor 2. If the two centrioles are in orthogonal positions 100 % of the space is covered. According to Albrecht-Buehler about 88 % of 3T3 cells and 50 % of CV1 cells were put in motion in presence of near-infrared source. This information is related in [19].

CELL SCATTERING OF A NEAR-INFRARED FRACTION OF THE BLACK-BODY RADIATION

Recently Albrecht-Buehler G. explains that a cell can scatter the near-infrared portion of the ambiant black-body radiation to become a light source, as a result of the experiments [20]. The present purpose is to justify a

such hypothesis giving some theoretical development. We are sure that the scattered light of the black-body radiation for one cell in the near-infrared range is very small and cannot be detected, but may be by a group of aggregated cells.

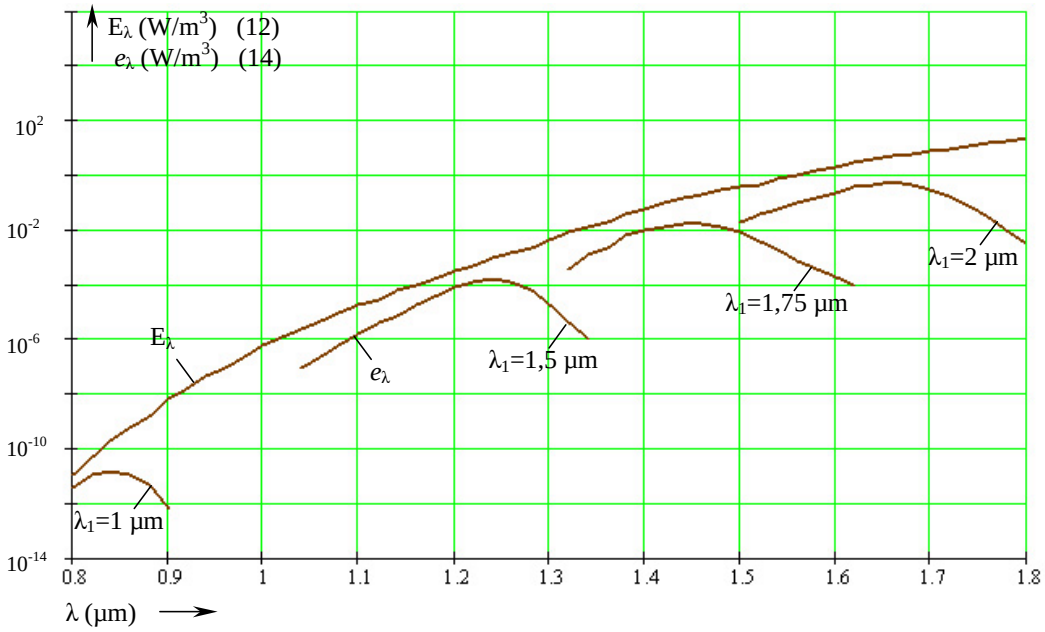

Fig. 3. Spectral emission powers E_λ and e_λ (for T=310°K).

The spectral-emission power E_λ is given by :

$$E_\lambda = \frac{2hc^2}{\lambda^5}.\frac{1}{\exp\left(\frac{h\nu}{kT}\right)-1} \qquad (11)$$

In international units it is expressed in W/m^3 :

$$E_\lambda = \frac{1.19\,10^{-16}}{\lambda^5}.\frac{1}{\exp\left(\frac{14.4\,10^{-3}}{\lambda T}\right)-1} \qquad (12)$$

The whole specific intensity E_T of the black-body expressed in W/m^2 is :

$$E_T(\lambda,T) = \int_0^\infty E_\lambda \, d\lambda \qquad (13)$$

The spectral-emission power of one cell is equal to :

$$e_\lambda = \alpha_\lambda E_\lambda = |T_{13}|^2 . E_\lambda \qquad (14)$$

$\alpha_\lambda < 1$ is the absorption coefficient, and T_{13} the transmission coefficient through the cell membrane given in [16] by :

$$|T_{13}|^2 = 1 \Big/ \left[ch^2(\Gamma_2 d) + k_2^2 sh^2(\Gamma_2 d) \Big/ 4n_1^2 \right] \qquad (15)$$

d is the membrane thickness and $\Gamma_2 d = 2\pi k_2 d/\lambda$. k_2 is the index of absorption of the membrane and n_1 is the index of refraction of the interstitial medium. We present in fig. 3 the spectral-emission powers E_λ and e_λ in terms of λ for T = 310° K. The parameter λ_1 is the maximal wavelength which limits the near-infrared absorption range. The max of E_λ is equal to $10^7\,W/m^3$ for $\lambda = 9.3\,\mu m$.
The whole specific intensity e_T of the cell is then given by :

$$e_T = \int_0^{\lambda_1} e_\lambda d\lambda \qquad (16)$$

It appears in the table II :

$\lambda_1(\mu m)$	1	1.5	1.75	2
$e_T\left(\mu W/cm^2\right)$ (16)	10^{-16}	10^{-9}	2.10^{-7}	8.10^{-6}

Table II (valid for T = 310 °K)

According to the second principle of thermodynamics, at $T = 310°K$, the power radiated by a cell of radius ρ is : $P_d = 4\pi\rho^2 e_T$ (17)

For a 3T3 cell with : $\rho = 11\,\mu m$, P_d is shown in Table III.

$\lambda_1(\mu m)$	1	1.5	1.75	2
P_d (watts) (17)	$1.5\,10^{-27}$	$1.5\,10^{-20}$	3.10^{-18}	$1.2\,10^{-16}$

Table III – Power radiation by a 3T3 cell

We note the great importance of the limit of the membrane cell transparence upon its natural radiation power. So a cell scatters a weak ambient black-body radiation. Only aggregate cells is able to be detected by one cell located at a certain distance as recently measured [20].

BIOLOGICAL HYPOTHESE

Could the pressure P calculated in (9) be the cause of the displacement of the cell to protect the overall integrity of the membrane ?

The strain (fig. 1, A) due to the pressure P, is received in focal adhesion proteins and integrins activate the signaling pathway leading to actin polymerization and motility of the cell towards the light source. However Albrecht-Buehler observed more cells were going forward than backward. So we must consider that the strain on the membrane can be transmitted to the side facing the light source. Externally applied forces (fig. 1, A) are transmitted throughout the actin cytoskeleton and result in immediate repositionning of cytoskeletal filaments along applied tension field lines within the cytoplasm [6], [21]. Stress fibers, composed of actin filaments, myosin and α-actinin, are anchored at focal adhesions at one side of the cell, and at focal adhesions on the other side of the cell. They serve as force transmitters in fast mechanotransduction and act as mechanosensors with direction sensitivity on slow mechanotransduction [22]. So the strain due to the pressure could be transmitted to the opposite side of the cell where it would determine the moving of the cell away the light source. This can be akin to the transmission of tension due to fluid shear stress from the apical surface of endothelial cells through the cytoskeleton to the integrins which then change in tension (23). Moreover, in the Albrecht-Buehler's experiments, the percentages of cells that were either attracted or pushed away from the light source depended on the pulsing frequencies of the light source. Were the threshold between a fast and a slow mechanotransduction linked to the difference in frequency ?

SUMMARY

The 3T3 fibroblast and epithelial CV1 cells motility has been explained :

- firstly by their centrioles diffraction under the influence of a fluctuating near-infrared artificial external pulsed source. The diffraction light propagation is such that, due to the physical pressure on the plasma cell membrane, the cell goes towards the light source.
- secondly when a sufficient strain, transmitted along the cytoskeleton, can move the cell away the light pulsed source.

On the other hand, we show that a cell scatters a weak part of the natural near infrared ambient black body radiation.
All these theoretical results are in good agreement with recent published measurements.

REFERENCES

[1] Albrecht-Buehler G., Surface extension of 3T3 cells towards distant infrared sources. J. Cell. Biol. 1991, 114 : 493-502.
[2] Albrecht-Buehler G., Changes of cell behavior by near-infrared signals. Cell Mobility and the Cytoskeleton 1995, 32 : 299-304.
[3] Albrecht-Buehler G., Does the geometric design of centrioles imply their function ? Cell Motility 1981, 1 : 237-265.
[4] Albrecht-Buehler G., The cellular infrared detector appears to be contained in the centrosome. Cell Motility and the Cytosketelon 1994, 27 : 262-271.
[5] W.T. Gerthoffer, S.J. Gunst, Signal transduction in smooth muscle. Invited review : focal adhesion and small heat shock proteins in the regulation of actin remodeling and contractility in smooth muscle. J. Appl. Physiol. 2001, 91 : 963-972.
[6] D.E. Ingber Tensegrity I., Cell structure and hierarchical system biology. Journal of Cell Science 2003, 116 : 1157-1173.
[7] D. Stamenovic, Z. Liang, J. Chen, N. Wang, Effect of the cytoskeleton prestress on the mechanical impedance of culture airway smooth muscle cells. J. Appl. Physiol. 2002, 92 : 1443-1450.
[8] I. Kaverina, O. Kryliskina, K. Beningo, K. Anderson, Y-L Wang, J.V. Small : Tensile stress stimulates microtubule outgrowth in living cells. Journal of Cell Science 2002, 115 : 2283-2291.

[9] D. Mehta, S.T. Gunst, Actin polymerization stimulates by contractil activation regulates force development in canine tracheal smooth muscle. The Journal of Physiology, 1999, 519, 3 : 820-840.
[10] D.A. Schafer, M.T. Welch, L.M. Machessky, P.C. Bridgman, S.M. Meyer, J.A. Cooper, Vizualisation and molecular analysis of actin assembly in living cells. J. Cell Biol. 1998, 143, 7 : 1919-1930.
[11] Dynamique de la membrane et du cytosquelette. Compartimentation et dynamique cellulaire. UMR 144 CNRS/IC. Avril 2004.
[12] Histologie de la peau. Collection Mémoires et thèses électroniques, R. Benndorf., Université de Laval (Québec).
[13] J. Landry, J. Huot, Modulation of actin dynamics during stress and physiological stimulation by a signaling pathway involving p38MAP kinase and heat shock protein 27. Biochem. Cell Biol. 1995, 73, 9-10 : 703-707.
[14] C. Schäfer, P. Clapp, M.J. Welsh, J.A. Williams HSP 27 expression regulates CCK-induced changes of the actin cytoskeleton in CHO-CCK-A cells. Am. J. Physiol. Cell. Physiol. 1999, 227 : 1032-1043.
[15] S. Hirano, E.A. Shelden, R.R. Glimont Hsp 27 regulates fibroblast adhesion, motility and matrix contraction. Cell Stress and Chaperones 2004, 9, 1 : 29-37.
[16] G. Dubost, A. Bellossi, Cell membrane physical model in near-infrared, visible and near-ultraviolet spectra. Biological Effects of EMFS, 3rd International Workshop KOS, Greece 2004, October : 492-500.
[17] G. Dubost, S. Desclos, Y. Commault, G. Debionne, Calcul en mode TEM du courant et de la section efficace bistatique d'une antenne filaire chargée éclairée par une onde plane. Ann. Télécommun. 44, n°7-8, 1989, pages 374 to 380.
[18] O. du Roure, A. Saez and all, communicated by Pierre-Gilles de Gennes, Collège de France. Force mapping in epithelial cell migration. PNAS, February 15, 2005, vol. 102, n° 7, 2390-2395.
[19] C. Lowry, Comment les cellules se voient-elles ? Fusion 2001, 87 : 20-25.
[20] G. Albrecht-Buehler, A long-range attraction between aggregating 3T3 cells irrediated by near-infrared light scattering. PNAS 2005, 102, 14, 5050-5055.
[21] M.F. Coughlin, D. Stamenovic, A prestress cable network model of the adherent cytoskeleton. Biophysical Journal 2003, 84 : 1328-1336.
[22] M. Sokabe, K. Hayakawa, H. Tatsumi, Varieties of mechanotransduction : the cytoskeletal stress fiber as a force transmitter and mechanosensor. http://www.aups.org.au/Proceedings/36/95P.
[23] A. Katsumi, A.W. Orr, E. Tzima, M.A. Schwartz, Integrins in mechanotransduction. J. Biol. Chem. 2004, 279, 3 : 12001-12004.

APPENDIX

Induced current along the centriole due to the incident electric field $\vec{E}_i(\theta_o)$ (figure 1)

It is given by the following equation [17] :

$$I(z,\theta_o) = C\left\{-j\frac{\sin(K\cos\theta_o)}{sh(A+jK)}sh\left[\frac{z}{h}(A+jK)\right]-\right.$$

$$\left.-\frac{\cos(K\cos\theta_o)}{ch(A+jK)}ch\left[\frac{z}{h}(A+jK)\right]+\exp(jKz\cos\theta_o)\right\}$$

with : $C = \frac{2hE_i}{Z_c} \frac{(A + jK)\sin\theta_o}{\left[(A + jK)^2 + K^2 \cos^2\theta_o\right]}$, $Z_c = \frac{Z_o}{2\pi}\left(1 - j\,2\frac{A}{K}\right)^{1/2} (\Omega - 3,4)$

With the previous parameters, $E_i = 40\,V/m$, and $Z_o = 377$ ohms , the module of the current $\frac{2\,h\,E_i}{Z_c}$ is equal to 0.12 µA.

Bistatic area of the centriole

The function $S(\theta,\theta_o)$ is extracted from [17] : $S(\theta,\theta_o) = j\frac{K\,Z_o}{2\pi\,Z_c} F(\theta,\theta_o)$

$$\text{with} \qquad F(\theta,\theta_o) = (p + q + r).\frac{s}{u}$$

and $p = K\frac{shx}{x}\left[\frac{-z}{ch(A + jK)} + j\frac{t}{sh(A + jK)}\right]$ $q = -\left(K\frac{sh\,y}{y}\right)\left[\frac{z}{ch(A + jK)} + j\frac{t}{sh(A + jK)}\right]$

$$r = 2\frac{\sin(Kv)}{v} \qquad s = (A + jK)\sin\theta\sin\theta_o$$

$$u = (A + jK)^2 + K^2\cos^2\theta_o \qquad x = A + jK(1 - \cos\theta)$$

$y = A + jK(1 + \cos\theta)$, $z = \cos(K\cos\theta_o)$, $t = \sin(K\cos\theta_o)$, $v = \cos\theta + \cos\theta_o$

Hypersensitivity to Electricity: The effect of the current waveform on the perception level.

B. Mattivi, V. Beauvois, P. Dular, J.L. Lilien, R. Lorphèvre, R. V. Sabariego

University of Liège - Dept. of Electrical Engineering and Computer Science
Institut Montefiore – Sart Tilman Bât 28 – B-4000 Liège (Belgium)
Contact email : JL.Lilien@ulg.ac.be

Abstract - Hypersensitivity to electricity has been reported many times in the literature. From another point of view, numerous measurements have been performed on perception level. Even if it appears that part of the population has a lower perception level of current, there is no clear link with the so called "hypersensitivity to electricity" which is more related to declared physiological disorders in part of the population (sleeping problem, headache …). Such declared hypersensitivity is currently not yet related to any biological parameter.

Our research team is currently trying to determine a relationship between hypersensitive declared people and the perception level when injecting current in the low frequency range 50-1000 Hz.
We have performed current perception tests with individuals under different conditions (different wave shapes, frequencies, influence of external electric field, male and female…) using a particular protocol and our own designed system for current injection.

This paper will present our test system design (current injector, wave shape converter, safety aspects) and our first results based on both sine wave (different frequencies) and wideband signal.

I. Introduction

Hypersensitivity to electricity, i.e. non-specific health symptoms such as headache, sleep disturbance, nervousness, concentration disturbances or skin arousal, attributed by the patient to the "electromagnetic pollution", has been frequently reported in the literature (Hilert et al, 2002, Leitgeb, 1998) but until now, no clear link has been shown between the electromagnetic field and the symptoms of these persons.

In (Leitgeb and Schrötner, 2003), a subgroup of people with significantly increased electrosensibility was detected. Herein, the electromagnetic sensibility is described as the ability to perceive electric and electromagnetic exposure, and electromagnetic hypersensitivity, developing health symptoms due to exposure to environmental field. The measurements showed a clear difference between men and women. A log-normal law was proved to fit fairy well to their results (see fig 1).

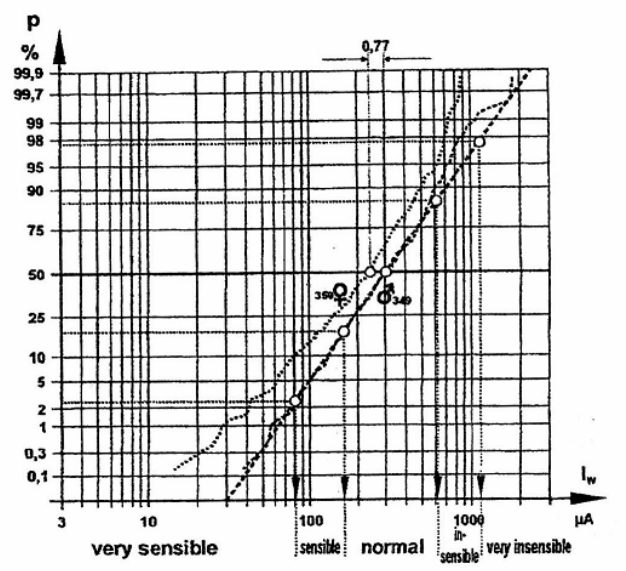

Fig1: Distribution of the cumulative probability perception Threshold current I_w (following Leitgeb-2003)

The existence of the very "electrosensible" subgroup can be seen as the second log-normal distribution on the fig 2.

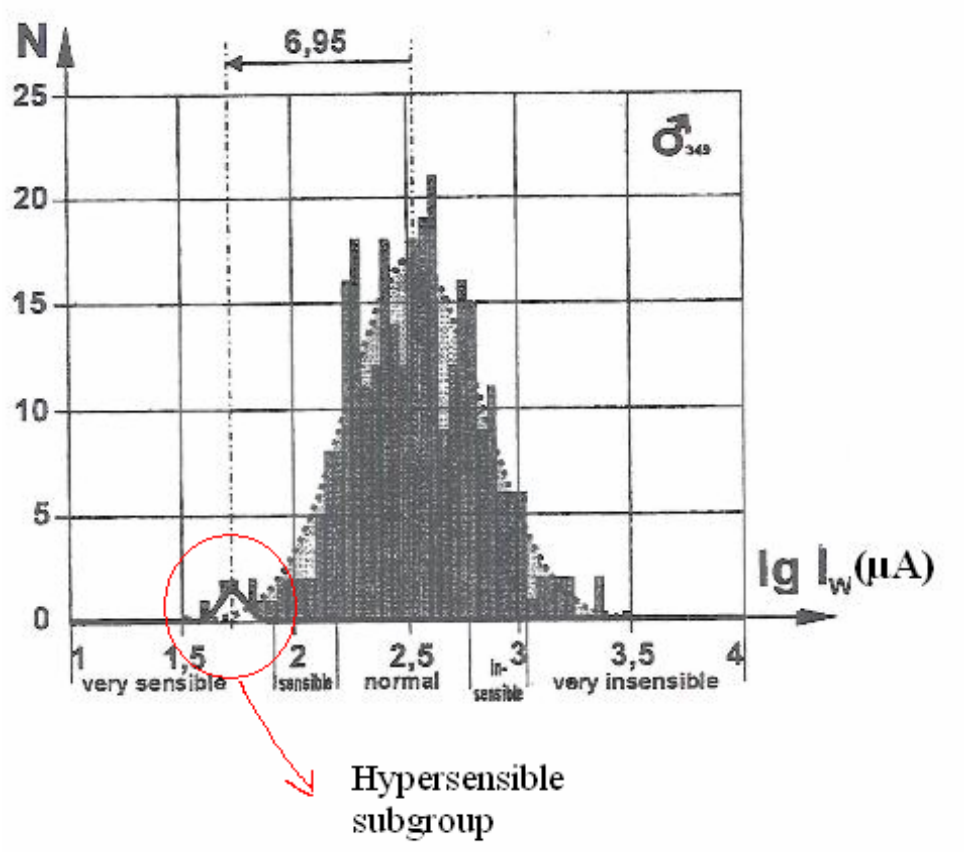

Fig 2: Best least square fit of two ideal log-normal distributions with the frequency distribution of measured electric current perception thresholds of men (following Leitgeb-2003.

Similarly to the work in (Leitgeb and Schrötner, 2003), but in a wide band of frequency, and signal shape, we try to determine a link between the "hypersensitivity to electromagnetism" and the sensibility to electricity. Our aim is to measure the smallest current intensity that a given person can feel when electrical current is flowing between two electrodes placed on the forearm of this person.

A home-made device, that allows injecting any waveform current within the frequency range 50Hz-1kHz, has been designed. This injector will be described in detail hereafter.

This paper will be focused on the sensitivity to electricity of a person according to the frequency. The first results of measurements will be shown for two different frequencies (50Hz and 1 kHz).

II. Measurements method

The developed experimental system is composed of a computer, a current injector and an external supply (see fig 3).

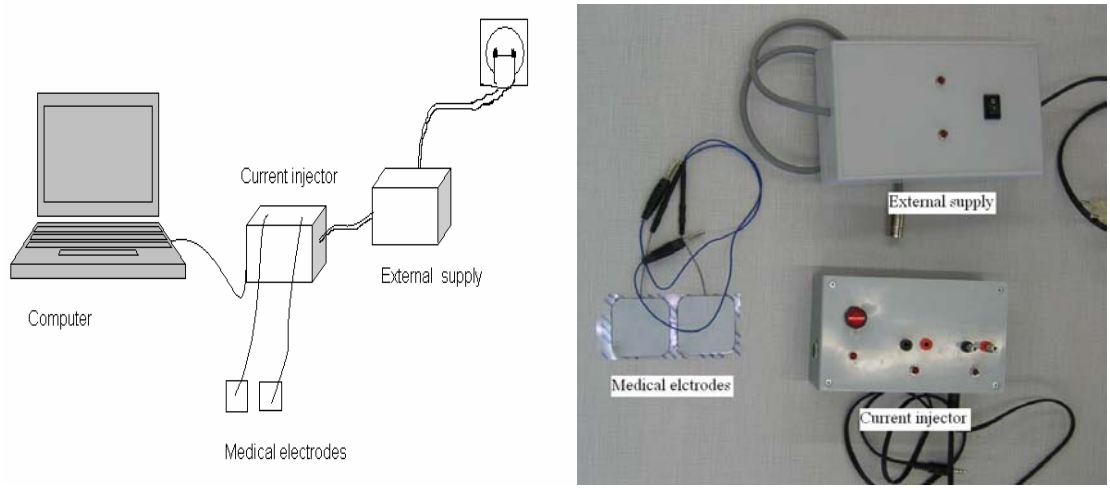

Fig3: Experimental System

A home-made program creates an audio signal (wave file) which is transmitted via the sound card to the current injector. The latter converts the voltage in a stable current flowing between the two electrodes through the body of the volunteer. For safety reasons and to prevent any electric current pathways across the heart, the investigations were done on the forearms on the volunteers. The complete description of the current injector can be found on the Section 3.

The sinusoidal current is applied by trains of constant rms (root mean square) value with dead time of 5 ms between each of them. Between two sequences, the rms current level is increased following a given law, which has been chosen in these experiments as exponential. Our system can easily handle any dead time or increasing law at a given frequency. Currents were increased by step until the program was interrupted by the volunteer's push of the computer's space bar (or any other computer's button) when perceiving the current flow. To minimize random influences, measurements were performed six times with 5 seconds break between each. The mean value of this first test was considered as the first evaluation of the perception level. After 30 sec, the measurements were performed six more times, but with a more precise range of current, according to the first evaluation. The tests evaluated the sensitivity to a 50 Hz sinusoidal wave and 1 kHz sinusoidal wave. The value of 1 kHz was arbitrary chosen to compare the sensibility at two different frequencies. Recruitment method of volunteer was done essentially on the student of the University of Liège; they were informed about the procedure and explicitly expressed their consent to the measurements.

III. Technical specification and safety aspect

The electronic scheme of the current injector is shown on the Fig.4. It is composed of seven "blocks".

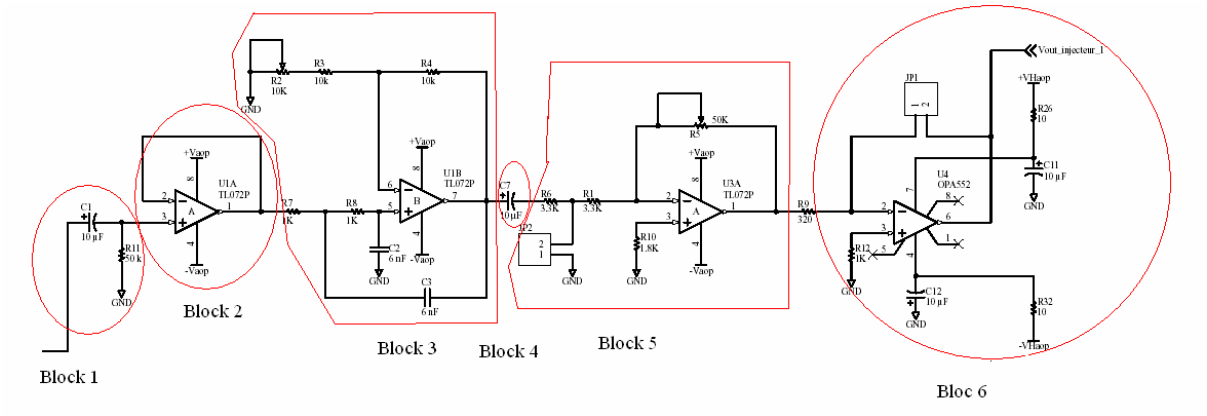

Fig4: Scheme of the current injector

- *Block 1: RC high pass filter:*

Its role is to eliminate the DC component of the signal. The value of the cut down frequency is 0.3 Hz. The DC part has to be eliminated because it could damage the tissues of the volunteer.

- *Block 2:Follower circuit*

It makes sure that there is no interference between the part one and the part three of the circuit.

- *Block 3: Butterworth low pass filter*,

This block eliminates the high frequency parasites. Its cut down frequency is 25 kHz

- *Block 4: RC high pass filter*:

It serves to eliminate the DC component of the signal. Indeed, the signal can have been perturbed by the precedent part of the circuit and have again a DC component. Its cut down frequency is the same than the block 1's : 0.3 Hz.

- *Block 5:Amplifier with variable gain*:

This part of the circuit is used to adjust the output (calibration) of the device.

- *Block 6: Current injector circuit* :

This part of the circuit is the current injector itself; it uses the human body resistance as feedback resistance.

We have characterized the bandwidth of the device in order to be sure that our signals are not altered (attenuated). The results are shown on the following figure (voltage peak to peak taken on the output of the device in function of frequency). The results measurements showed that in the range of our experiment, i.e. 50 Hz to 1 kHz, the signals are not altered.

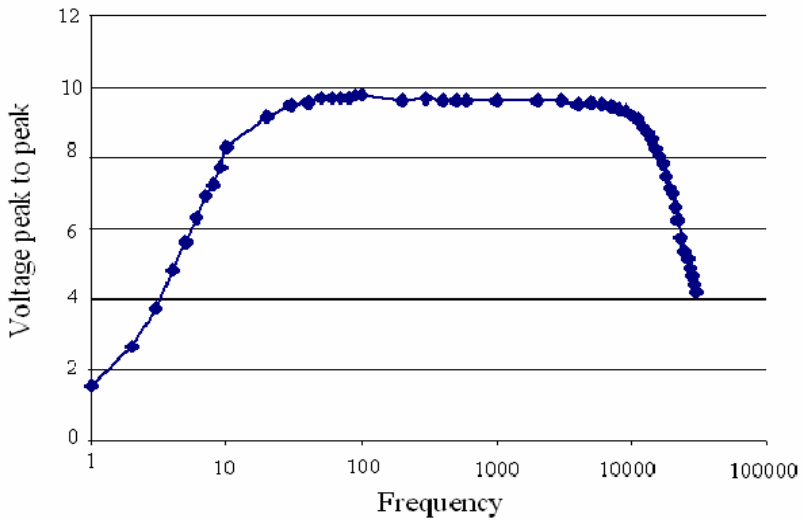

Fig 5: Frequency response of the current injector

On such a kind of device, the safety aspect is crucial. In order to be sure that any perturbation of the electric network is rejected, a system of low pass filter, in the external supply, has been designed to eliminate the high frequency component, as the perturbation can be seen as a high frequency signal, it is thus eliminated. The device is also limited with a maximum output current of 5mA.

As already mentioned, we have ensured, by a system of high pass filter, that the signal injected in the body does not have a continuous (DC) component, as a DC component would be dangerous for the tissues.

The last feature that guarantees the security of the person tested is a stop button that disconnects immediately the person from the current injector. When the user pushes the button, the entry of the amplifier (Block 5) is forced to the mass, so the entry of the amplifier is zero.

IV Results and discussion

It was possible to perform measurement on 150 persons. These persons were aged between 17 and 60 years, in order to avoid bias by including possibly more sensitive children or less sensitive elderly. As the persons were generally students of the university, almost all of them were under 25 years old.

Our first data clearly show a difference to the perception level at 50 Hz and 1 kHz. It has already been shown that the sensitivity to electricity varies according with the frequency (Dalziel & Manfield, 1950) of the signal; but our study is focused on the low frequency range.

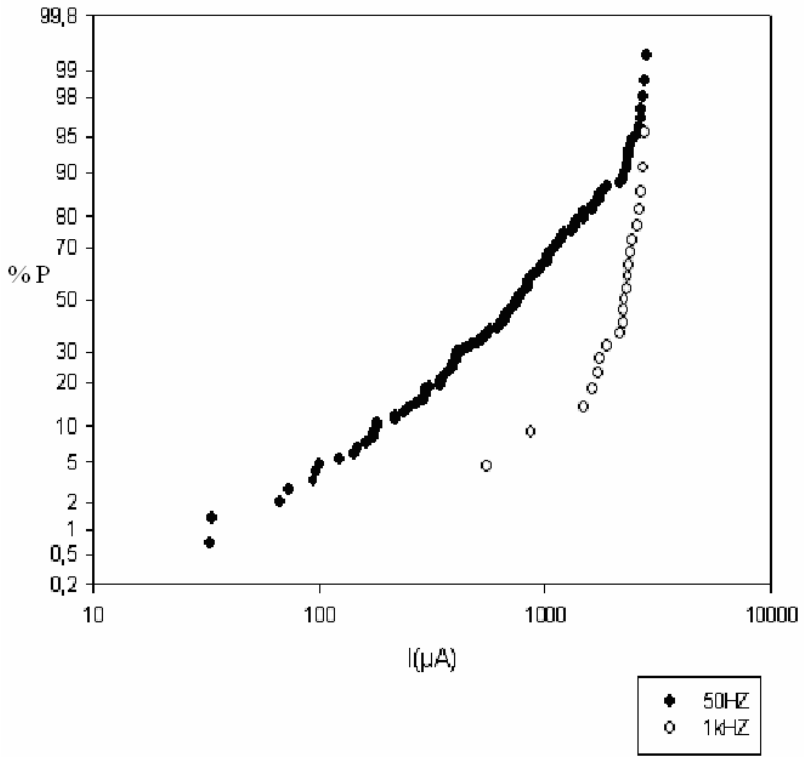

Fig 6: distribution of the cumulative frequency

We have compared our data concerning the 50Hz sinusoidal current to Leitgeb's results (Leitgeb and Schrötner, 2003). Our results superpose to their results are shown on the Fig 7. The mean value of the perception threshold in our study (760.23 µA) is higher than the mean value they found (for men, near 300µA). Nevertheless the mean value we found is still lower than the related mean value (Reilly, 1998). It seems also that the mathematical law is different; the kind of frequency distribution of perception level was analyzed by Kolmogorov-Smirnov testing. The null hypothesis of log-normal distribution data was rejected by a significance $P<0.01$. Until now, we hadn't found a proper law to fit our results. The histogram of the frequency distribution of measured electric current perception threshold is shown on the Fig 7

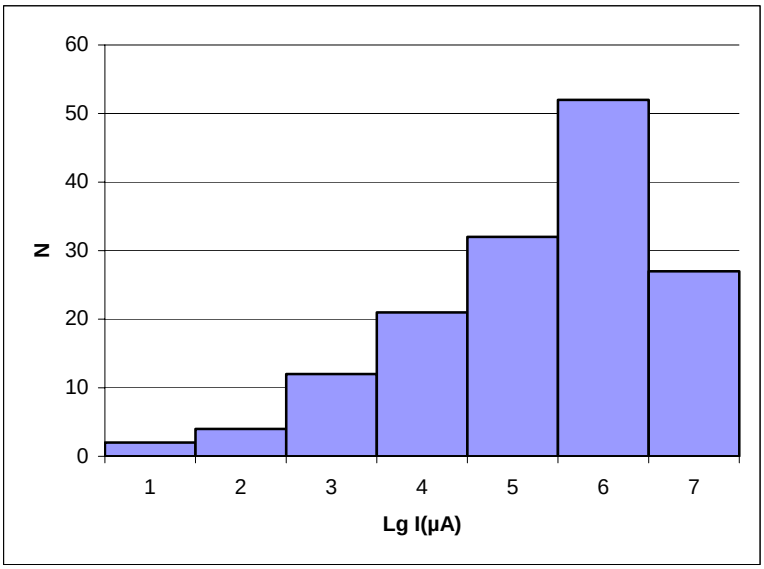

Fig 7: histogram of the frequency distribution of measured electric current perception threshold

It is possible that the observed differences are due to the differences in the measurements protocol, Leitgeb (Leitgeb and Schrötner, 2003) increased their current linearly, but we increased it exponentially, they also took six measurements, but did not proceed to a refining like us and take a break of 3min after each measurement whereas we took only 5sec. Two other differences are the facts that our volunteers were almost all under 25 years old. The results are not separated between male and female because we had only 19 percent of female volunteers. It has to be said that the two "weak perception volunteers" were male.

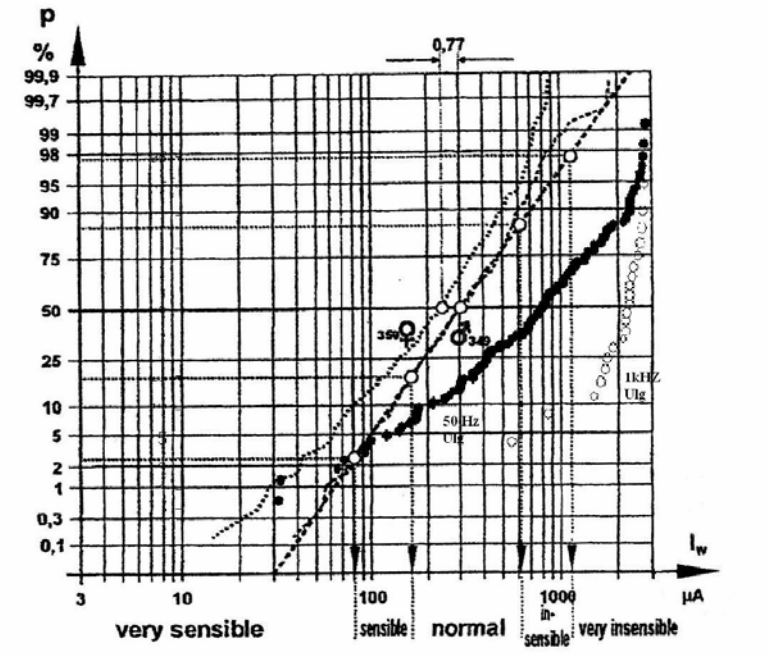

Fig 8: Our results superposed to Leitgeb's data

The current injector and its program can be used to generate a more complex waveform than a sinus. The Fig 8 and 9 show a typical waveform used during the last year in our study. Even if our device is now able to generate any whished waveform, the problem is to have a comparison point between two waveforms. Up to now, we have chosen to compare the RMS (Root Mean Square) value, but we have doubts about the validity of this approach. A value linked to a biological characteristic such as the Action Potential of the nervous cells would certainly be more suitable.

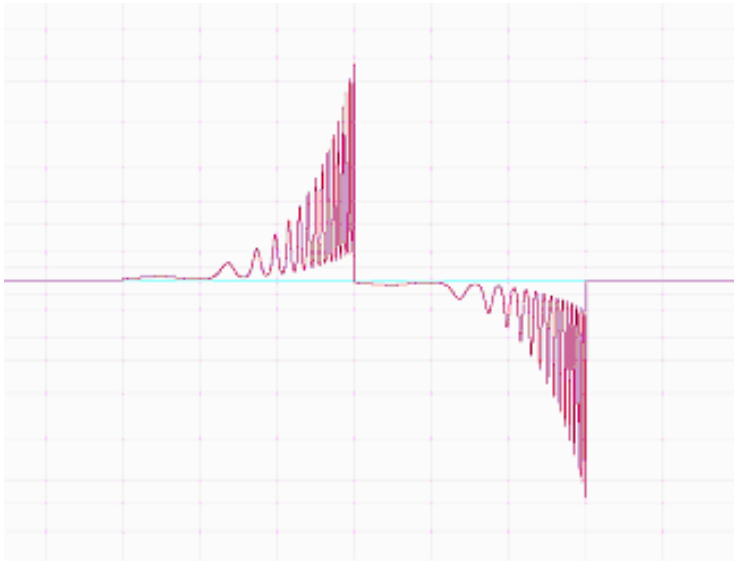

Fig 9: Wideband signal

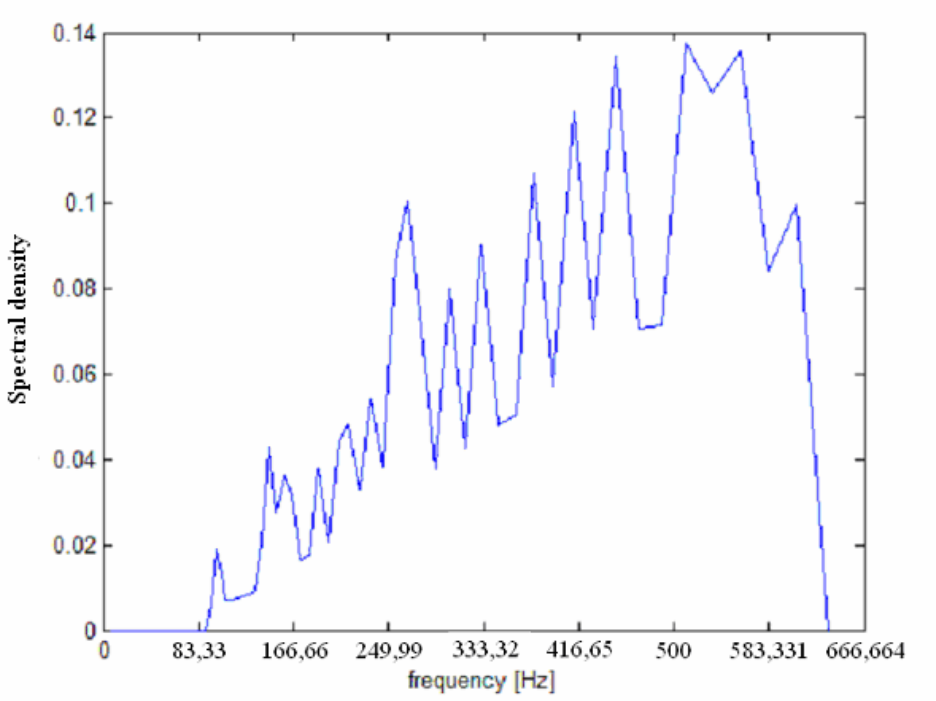

Fig10. Frequential analysis by the wavelet method of the wideband signal.

V. Conclusion

We have designed a device that has shown to be a useful tool to study the human sensibility to electricity. One of our priorities was to ensure the security of the volunteers.

The measurements obtained with our device were quite different from those published in a similar work. We concluded that the protocol chosen influences considerably the results.

A study on the effects of the frequency and the waveform on the perception level has begun. The first results, even if few measurements have been done, clearly show that the human sensibility decreases with the frequency. This effect is maybe due to a “relaxation effect” of the neurons. Our device is able to generate any waveform, but the problem is to have or select a comparison magnitude between two waveforms. This magnitude could maybe be linked to a biological characteristic like the Action Potential of the nervous cell.

Acknowledgments

This research has been supported by Elia, the Belgium's transmission system operator. We would like to thanks Pascal Harmeling for the realisation of the electronic part of this work and David Lilien for the implementation of the wave-generating software.

References

Hillert L, Berglind N, Arnetz BB, Bellander T. Prevalence of self-reported hypersensitivity to electric or magnetic field in a population based questionnary survey. Scand J work Environ Health. 2002; 28:33-41.

Leitgeb N, Schrötner J, Electrosensibility and Electromagnetic hypersensitivity, Bioelectromagnetics 2003;24: 387-394.

Lyskov E, Sandström M, Hansson Mild K. 2001.b, Neurophysiology study of patients with perceived hypersensitivity. Int J. Psychophysiol 42: 223-241.

Reilly JP. 1998. From electrical stimulation to electropathology. New York: Springer Verlag.

Appendix I: Results (table)

Person number	Sensibility(µA)	Person number	Sensibility(µA)	Person number	Sensibility (µA)	Person number	Sensibility (µA)	Person number	Sensibility (µA)
1	32,98	31	348,03	61	644,38	91	918,47	121	1496,1
2	33,76	32	349,17	62	665,58	92	952,13	122	1501,41
3	67,68	33	358,22	63	669,33	93	957,31	123	1633,51
4	74,22	34	372,24	64	672,67	94	963,44	124	1641,22
5	94,8	35	379,69	65	673,03	95	969,53	125	1658,06
6	96,79	36	382,21	66	680,98	96	996,15	126	1716,69
7	101,82	37	388,82	67	689,03	97	1031,19	127	1741,75
8	124,12	38	392,52	68	696,02	98	1033,52	128	1761,12
9	143,2	39	402,25	69	699,17	99	1036,11	129	1766,01
10	147,57	40	404,86	70	717,8	100	1037,6	130	1838,65
11	162,86	41	409,32	71	723,5	101	1044,95	131	1895,77
12	174,75	42	410,17	72	738,21	102	1047,75	132	2141
13	176,58	43	413,25	73	744,01	103	1081,14	133	2219,56
14	177,48	44	415	74	760,14	104	1097,02	134	2230,09
15	181,05	45	416,23	75	760,23	105	1109,5	135	2251,5
16	181,35	46	438,42	76	765,18	106	1125,08	136	2323,71
17	216,51	47	451,58	77	774,43	107	1136,47	137	2328,3
18	218,93	48	471,99	78	781,19	108	1158,31	138	2332,96
19	240,99	49	477,37	79	805,99	109	1178,81	139	2336,15
20	248,03	50	502,34	80	813,27	110	1185,21	140	2360,27
21	258,5	51	529,54	81	823,39	111	1200,55	141	2401,14
22	270,14	52	532,75	82	837,5	112	1207,93	142	2432,56
23	292,25	53	538,85	83	840,67	113	1320,73	143	2578,9
24	293,9	54	552,89	84	840,67	114	1331,47	144	2642,4
25	295,99	55	553,71	85	848,9	115	1341,86	145	2664,78
26	298,27	56	562,55	86	850,2	116	1354,68	146	2700
27	298,71	57	579,62	87	853,4	117	1361,42	147	2743,05
28	309,97	58	615,64	88	855,8	118	1381,65	148	2783,27
29	345,11	59	636,58	89	870	119	1489,26	149	2820,93
30	345,55	60	637,53	90	895,29	120	1495,92	150	3000

Table1: electrical sensibility to a 50Hz sinusoidal current.

Person number	Sensibility (µA)	Person number	Sensibility
1	552,89	12	2328,3
2	870	13	2332,96
3	1495,92	14	2336,15
4	1633,51	15	2401,14
5	1716,69	16	2432,56
6	1761,12	17	2578,9
7	1895,77	18	2642,4
8	2141	19	2700
9	2219,56	20	2743,05
10	2230,09	21	2783,27
11	2251,5	22	3000

Table 2: Electrical sensibility to a 1 kHz current.

MOBILE TELECOMMUNICATIONS RISK PERCEPTION AND COMMUNICATION IN EGYPT

HAMDY ELLAITHY, EBI ELOMBI

VODAFONE EGYPT

Abstract

Health concern of mobile telecommunications is widespread and found in all countries with the technology. The level of perceived risk varies among countries depending on a number of factors. In developing countries such as Egypt, the level of concern and perceived risk is heightened mainly due to the overall average lower level of education, lack of understanding of the technology as well as the natural fears of an invading and extensively used technology.

This paper discusses the current level of concern and risk perception in Egypt and how various factors have contributed to their changes over the past three years. Various risk communication strategies are discussed; in particular a project to address the public's concerns regarding emissions from mobile telecommunications base stations.

This project, called HORUS, continuously measures the electric field levels from GSM base stations across Egypt with the use of solar-powered GSM EMF monitoring stations. The 24-hour a day measured field readings are compared with national and international limits and published on a dedicated website.

Introduction

In 2003, an EMF perception survey, commissioned by Vodafone, was carried out in several countries including Egypt by an independent marketing research company - MORI. The main aim of the survey was to assess the level of concern among the public and to assess how this could be addressed. This survey provided Vodafone with an objective view of how the mobile telecommunications industry and technology is perceived in terms of health concerns and how this public concern differs from that in other countries [1, 2]. The results of this survey guided communication strategies to address the public's concern and attempt to reduce the level of concern.

Another survey carried out by the same company in 2005 in Egypt, showed the current level of public concern and highlighted areas where there have been significant changes. It is clear that several factors including communications programs put in place after the 2003 EMF perception survey may have had an impact in the way the public perceives the technology.

I. The Ipsos-MORI EMF Perception survey

A total of 1,000 interviews were conducted in Egypt, among the general public, using CATI (Computer Assisted Telephone Interviewing). This was in contrast to the 2003 survey when the interviews were conducted face-to-face [2]. Respondents were aged 18+ and were from across the whole of Egypt. Quotas were set on age, gender and region. The results are weighted to reflect the population of Egypt.

The main aim of the survey was to assess the nature and level of concern among the Egyptian public and to determine what impact this concern may have for the telecommunications business.

II. Key Findings of the 2005 EMF survey in Egypt

The results of the 2005 survey summarised below is taken from the independent Ipsos-MORI report [3].

Mobile phones, masts and health were not a major top-of-mind concern; ranking 8th amongst the issues mentioned such as air pollution, smoking or cancer. On prompting, mobile phones and masts rose in importance to 4th place.

Concern appeared to be caused largely by the respondent having read or heard information on this issue, as opposed to direct personal experience. Only 10% of all respondents were concerned about mobile phones and masts with 79% of those concerned (8% of the population) because of information read or heard, see Figure 1.

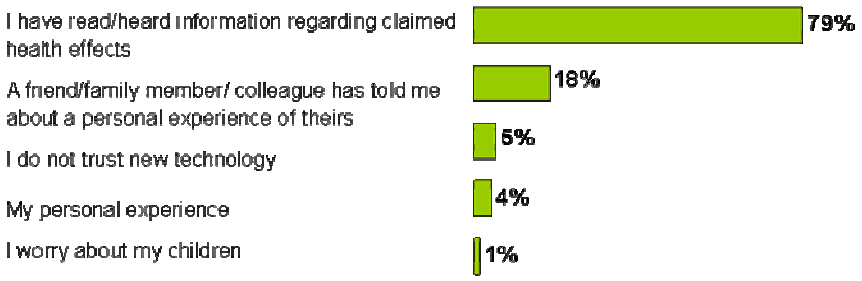

Figure 1: Causes of Concern

Despite this initial low level of concern, 36% of the Egyptian population surveyed, thought that mobile phones were not safe to use, with about 50% believing that masts were worse for health than mobile phones. However, the majority (90%) agreed that they have more important things to worry about. This reiterates the observation obtained from the initial concern result, that is that mobile phones, masts and health are an issue for some, but when put in context other health problems are of a greater priority.

Many believed that mobile phones cause some kind of physical effect, whether that be headaches, a warming of the ear or, more seriously, cancer – Figure 2.

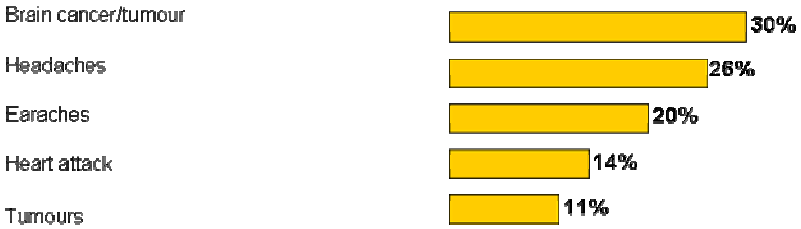

Figure 2: Claimed health problems

Knowledge of the role of masts in mobile operation was still an issue. 17% did not understand the necessity for masts in the operation of mobile phones, stating that they believed a mobile phone could work without being near to a mast.

49% of respondents were aware of a mast anywhere e.g. neighbourhood, work, other locality. However, the majority of mobile phone users were indifferent, with a small minority (6%) actively objecting.

62% of respondents believed that there was no conclusive information on mobile phones, masts and health, whilst 81% stated that they did not know whom to believe. Despite this reservation, 77% believed the benefits of using a mobile phone outweighed any potential risks involved.

13% stated on an unprompted basis that they required information on how mobile masts work. On prompting, the information sought ranged from information on how mobile phones work through to the relative safety of a mobile phone in comparison to other items.

The study revealed a lack of trust, with 72% of the public believing that the industry was withholding

information on this issue, whilst large numbers did not know whether the industry takes this issue seriously or not.

40% would speak more highly of an operator who supplied information on this issue. 3% would be less inclined to trust their operator should they do this.

III. Changes in attitude and concern between 2003 and 2005

The most significant changes in the attitude of the Egyptian public has been in the level of concern and the understanding of the role of masts or base stations in the operation of mobile phones. Some of the key changes are illustrated in Figure 3.

Issue	2003	2005
Prompted concern on Mobile Phones/Masts	43%	10%
Percentages who do not believe mobile phones are safe to use.	71%	36%
Percentages who believe benefits outweigh the risk	68%	77%
Percentages who do not understand the necessity of masts in the operation of mobile phones.	41%	17%

Figure 3: Comparison of attitudes between 2003 and 2005

The general level of concern dropped by more than 70% to 10% in 2005 while concern regarding the safety of mobile phones was halved to 36% in 2005. The level of knowledge and understanding of the technology has also increased with significantly more people understanding the relationship between masts and mobile phone operation.

These changes could be attributed to some communication initiatives implemented by Vodafone after the 2003 survey as well as to changes in the technological environment.

Over this period, Vodafone organised and sponsored several seminars on mobile phones, masts and health across Egypt, targeting various segments of the public. Providing material for and speaking to local councils, landlords and the press as well as leaflets made available to customers. One of Vodafone Egypt's key initiatives has been the implementation of a project called Project HORUS, which continuously monitors field levels from GSM base stations in selected locations across the country and makes the readings available to the public through a dedicated website.

Other influencing factors include the fact that the penetration level moved from 8% in 2003 to 18% in 2005; increased familiarity with the technology over time; government support for a third operator into the market as well as ongoing coverage campaigns by the existing operators.

IV. The project HORUS

This project was an initiative to inform the general public about Radio Frequency (RF) Radiation, through the continuous (24-hour) monitoring of RF field levels in selected locations. Through Project HORUS the public are able to monitor RF radiation levels in several locations across Egypt 24 hours a day.

Vodafone Egypt has deployed over 54 electro-magnetic radiation probes across Egypt. The probes measure radio frequency field levels emitted in the GSM frequency bands at 900 MHz and 1800 MHz, and are powered by solar cells Figure 4. This makes it easy to relocate the units to monitor new areas where there is public concern.

Figure 4: A PMM8055S EMF monitoring station deployed on a rooftop

The readings from each probe are downloaded daily to a web server, which then displays readings on a dedicated website. These readings are displayed on graphs, which can be viewed in comparison with the maximum allowable levels set by the Egyptian authorities and the ICNIRP (International Commission on Non-Ionizing Radiation Protection). Typical readings are hundreds of times below standards as illustrated in Figure 5. More details on the project can be found on the project's website www.projecthorus.com.

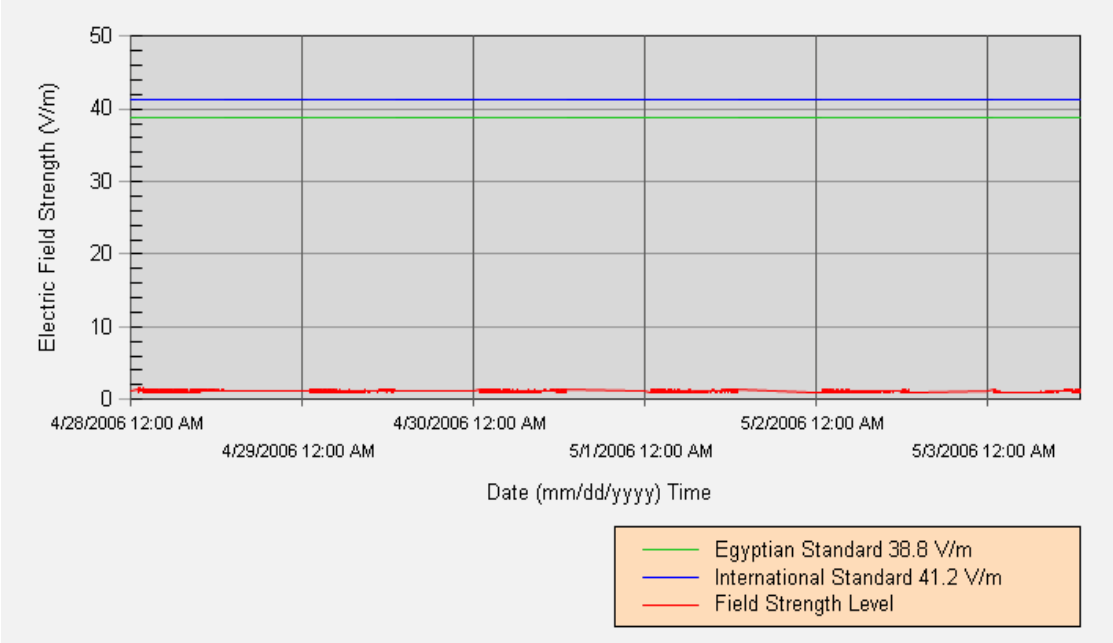

Figure 5: Readings from a monitoring station in the Alexandria governorate

The average reading during this period was 1.15V/m, which is less than 3% of national or international safety limits.

The project was a direct result of the 2003 survey which showed that a significant proportion of the public was concerned about emissions from base stations. Vodafone Egypt first launched Project HORUS in early 2005 across 13 governorates and has expanded the project to cover all 27 governorates. The project has been a useful tool in communication with the public as it demonstrates compliance with standards and an openness and transparency on Vodafone's part which seems to have a positive impact on the public's level of concern.

V. Conclusion

Mobile phones, masts and health is an important issue, but not a primary health concern. This low level of concern mirrors the findings of MORI's research for Vodafone in 2003. The majority of the population are more concerned about other health issues. However, the industry as a whole needs to respond to concerns that important information is being withheld.

The principal trigger leading to concern is information on health effects that people have heard or read, not their personal experience. Lack of understanding, especially on the need for masts, is also fuelling concern. Many people would like to receive more information, including explanations of how the technology works. Communication material will need to be tailored to specific requirements, as different people would like to receive information on a variety of topics.

Open and transparent communication on the issue seems to have an effect on reducing concern, with the continuos EMF monitoring project HORUS, serving to reduce both concern and build operator trust and confidence.

References

1. H. Ellaithy, "Microwave Risk Perception In Egypt", 3rd International Workshop on Biological Effects of EMF, Oct. 4-8, 2004, Kos, Greece.
2. H. Ellaithy, "RF Exposure Health Risk Perception – A Field Study On The Egyptian Public", The Environmentalist, November 2005.
3. Ipsos MORI report, "Understanding Public Perceptions of Mobile Phones, Masts and Health", 2006.

DESIGN, DEVELOPMENT AND OPERATION OF AN ELECTROMAGNETIC RADIATION MONITORING NETWORK IN GREECE: "HERMES" PROJECT

D. KOMNAKOS, A. GOTSIS, N. KOUTSIANAS, A. YALOFAS, P. CONSTANTINOU

NATIONAL TECHNICAL UNIVERSITY OF ATHENS
MOBILE RADIO-COMMUNICATIONS LABORATORY
9, HEROON POLYTECHNEIOU ST., 15773, ATHENS, GREECE
Tel: +30 210 7724196, Fax: +30 210 7723851
E-mail: {dkomna, gotsis, nkout, yalofas, fkonst}@mobile.ntua.gr

T. GANATSOS, A. BOURSIANIS, G. TSANIDIS, T. SAMARAS, J. SAHALOS

ARISTOTLE UNIVERSITY OF THESSALONIKI
RADIOCOMMUNICATIONS LABORATORY, DEPT. of PHYSICS,
GR-54124 THESSALONIKI, GREECE
E-mail: {teogan, ampoursi, theosama, sahalos}@auth.gr

E.CHERA, C.TYRAKIS, G. BELESIOTIS, M. PETKARIS, K.VASILIOU

VODAFONE-PANAFON S.A.
1 – 3 TZAVELA ST., GR-15231, HALANDRI, GREECE
E–mail: { Charilaos.Tyrakis, georgios.belesiotis, marios.petkaris }@vodafone.com

Abstract

A network for the monitoring of the non-ionizing electromagnetic radiation levels in several areas of Greece is presented in this paper. During its 4-year operation more than 4,000,000 measurements of the electric field strength have been performed and recorded. The results aided by useful scientific information are open to the public through a devoted web site. The network measurement results have shown that the field values are several times below the EC recommended and Greek law safety values.

I. Introduction

During the last decade, the installation and operation of several wireless networks, such as the GSM, UMTS and TETRA system has led to increasing public concerns about the exposure to electromagnetic radiation emitted from these sources. In conjunction with traditional broadcasting systems such as FM Radio and TV services, RADAR systems etc. these concerns call for the continuous information of the public regarding their exposure to EM radiation levels. The conduction of repetitive, on site, "ad-hoc" measurements is a first step for estimating the exposure levels. Nevertheless, ad-hoc measurements refer to a specific time period (usually 1-2 hours). On the other hand the notion of continuous measurement of EM radiation levels on a 24-hour basis is more appealing to the concerned public. This is due to the fact that the recorded values can be compared to the public exposure safety values, called reference levels, which are set by the relevant organisations, such as the EC [5] and government authorities [6].

Therefore, a network for the measurement and recording of non-ionizing Electromagnetic Radiation (EMR) emissions on several sites and on a 24-hour basis is one of the best solutions for keeping the public informed. Another important parameter of such a network is the possibility to present the results via a public accessible and user-friendly web site.

As described above, monitoring networks are a valuable tool in attempting to deal with public concerns about the

potential health effects of non-ionizing radiation of electromagnetic radiation. As a result, several monitoring networks are implemented all over Europe and Africa (Italy, Spain, Portugal, United Kingdom, Malta, Egypt etc.) [1]-[4]. Moreover network deployment entails a number of challenges, in terms of hardware certification, network control and daily maintenance. With all the above considerations in mind an Electromagnetic Radiation Monitoring System was developed in Greece. It is known as the "Hermes" project [7], and it is fully operational since November 2002 and currently expanding in several areas around the country.

The paper below is structured as follows: Section II gives a general technical description of a monitoring network, as well as a framework which may be applied in any similar system. Section III presents the system developed for the "Project Hermes" and the measurement results to date. Finally, Section IV presents the current project phase and future planning.

II. Design Aspects of the Monitoring Network

The system architecture is depicted in Figure 1.

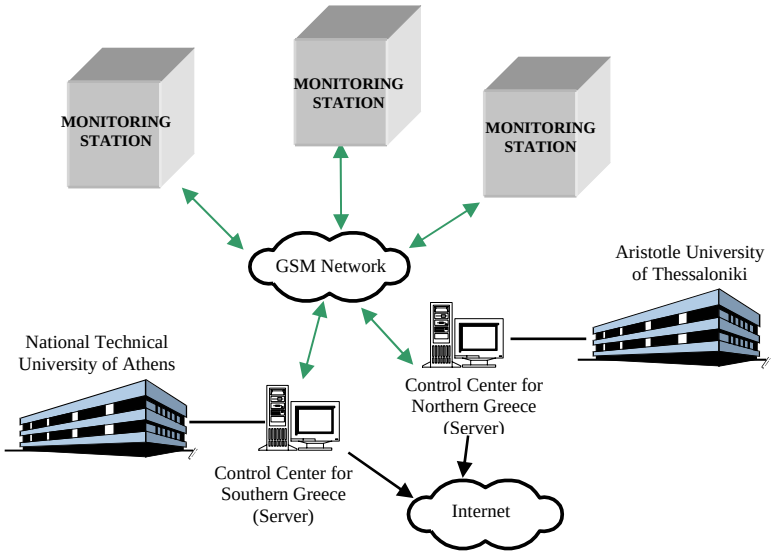

Figure 1: *Block diagram of the monitoring network.*

The system consists of:

(a) The remote monitoring stations, which are located on the desired sites and perform continuous measurements of the Radio frequency (RF) radiation levels and,

(b) The two central control stations (one for Southern and one for Northern Greece), which are located at the corresponding administrative authorities. The control units are responsible for the control of the monitoring stations and the publication of the measurement results on the web site.

a. The Measuring Equipment

The Measuring Equipment must be able to: (a) operate continuously (24 hours per day) (b) perform Electromagnetic Radiation measurements in the frequency range of interest covering the main sources that contribute to the total electromagnetic pollution, (c) store the measurements in its internal memory and transmit them to the Control Centre via a wireless interface for further elaborations, (d) supplied either by the main power supply or a solar panel (preferable), (e) be fully remotely controlled, which means that after their installation no human presence is needed on site and (f) detect abnormal operation of any kind (self diagnostics such as power loss and overheating problems) and inform the central control stations of the problem. To fulfil these requirements, the remote monitoring station consists of a broadband isotropic and triaxial electric field sensor, a module containing the necessary electronics, a GSM modem, as well as temperature and humidity sensors. A major problem encountered in this system is the periodic calibration of the monitoring stations. The calibration procedure requires the deinstallation of the stations, which means the interruption of the measurements, unless a spare station is available for the replacement.

Regarding the measurement quantities, either broadband or narrow-band measurements can be conducted. Broadband Measuring Stations record the Electric Field Strength for a given frequency range. A range of 100 KHz - 3 GHz is usually enough in order to take into account the multitude of the sources. Other possible ranges are for example 880 - 960 MHz (the GSM900 band), 1880 - 2100 MHz (GSM-1800 + UMTS bands), etc. In [8], [9] and [10] the interested reader could find a plethora of such monitoring units. Recently, selective (spectrum analysers) monitoring systems became commercially available. The referred stations are fully autonomous and can be remotely controlled via the GSM/GPRS protocol.

The main drawback of broadband stations is that they cannot estimate the radiation level from each source; rather they estimate the total exposure. Equipment such as a spectrum analyser is capable of measuring and quantifying the contribution of each electromagnetic radiation source to the total exposure level. Nevertheless, this equipment is not designed for continuous operation. If selective monitoring stations are not installed, the best solution is the use of a continuous broadband monitoring station for 24-hour recording and conducting "ad-hoc" narrow band measurements with a period of 3 - 6 months for every measurement site.

b. The Control Centre

The Control Centre is equipped with a Server Station, a wireless modem and the necessary software applications and it is responsible for: (a) controlling the remote monitoring stations and configuring the operational parameters, (b) downloading the measurement data via the wireless interface (e.g. GSM network), (c) storing the data in its hard disk and (d) processing the measurement results and publishing them to the corresponding web site.

The measurement data is stored in a Database (such as MS Access, SQL Server or MySQL) after their checking and processing. Therefore the full historical record for every measurement site is kept on the Server. In addition, a Web Server (such as MS IIS or Apache) hosts the web site.

c. The Web Site

The Web Site contains both static and dynamic pages and it aims at presenting the measurement results for every monitored site. It also provides thorough information concerning the electromagnetic radiation issue. Through the web site the user may view electric field strength graphs with custom time interval selection and statistical quantities about the measurements. Furthermore, a comparison of the measured quantity with the Greek legislation reference levels is presented. A feedback form can be also available to the public in order for them to express questions or comments to the administrators of the system.

III. The "Hermes" Monitoring Network

a. General Description

A monitoring network based on the principles described above has been developed and operating since November 2002. The system at its present state (April 2006) comprises 27 remote monitoring stations spread all over Greece (23 active and 4 inactive) and two control units located in two University laboratories (National Technical University of Athens – NTUA and Aristotle University of Thessaloniki – AUTH). The stations are located at schools, universities, public authorities' buildings and private flats. The following figure depicts the spreading of the monitoring stations.

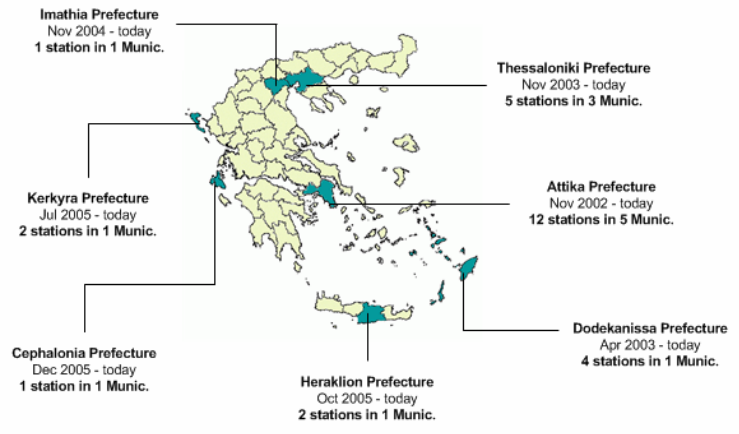

Figure 2 : *"Hermes" Monitoring Network*

The measuring devices record the broadband electric field strength quantity for the range 100 KHz - 3 GHz [10]. Three slightly different monitoring units' models are used.

- EE4070 - WB model which records the Electromagnetic Field Strength in the band 100 KHz - 3 GHz
- EE4070 - SL which records the field strength for three bands: 100 KHz - 3 GHz, GSM-900 Band and GSM1800 + UMTS band.
- MCE410 - SL, which records the field strength for two bands: 100 KHz - 3 GHz and 900 MHz - 3 GHz.

A detailed description of the specific units and the measurement procedure can be found in [11]. In the following figures several measurement sites are presented.

Figure 3: *EE4070-WB Station at Koskinou, Rhodes*

Figure 4: *EE4070-SL Station at Menemeni, Thessaloniki*

Figure 5: *MCE410-SL station at Heraklion, Crete*

Regarding the "ad-hoc" measurements, the guidelines proposed in the ECC recommendation [12] serve as the basis for our measurement procedure. A set of directional antennas covering the frequency range of 20 MHz – 3 GHz and a Spectrum Analyzer for measuring the received RF Power comprise the measurement apparatus (see Figure 6*)*. Each frequency band is scanned and the power of each RF source, such as a FM or TV radio stations, a GSM channel etc is recorded. After the needed processing the total exposure levels and the contribution of each frequency band are estimated. A similar procedure is performed if we substitute the Spectrum Analyser with a Selective Radiation Meter such as the one presented in [13] and the directional antennas with broadband isotropic triaxial E-field probes (see Figure 7).

Figure 6: *"Ad-Hoc" Measurement Apparatus (Spectrum Analyser based)*

Figure 7: *"Ad-Hoc" Measurement Apparatus (SRM based)*

b. Measurement results

On the Web Site, both broadband and narrow-band measurement results are presented. The broadband measurements are updated on a daily base. Below, at first a table containing the most significant information about the monitoring stations is given. Afterwards in the following figures sample diagrams from the web site are drawn (Figure 8 - Figure 11). Finally, cumulative results regarding all the stations are presented (Figure 12 - Figure 13).

Table 1 *: Stations informative table*

Station ID	Site Name	Activation date	Mean 6-min Average value of electric field	Standard deviation of electric field	Maximum 6-min Average value of electric field	Number of recorded measurements	Status
1	1st & 6th Pr. Schools at Holargos	November 18, 2002	1.6	0.1	2.7	77,603	Inactive
2	2nd & 3rd Pr. Schools at Holargos	November 18, 2002	1.9	0.1	2.3	77,609	Inactive
3	5th Primary School at Holargos	November 22, 2002	2.6	0.2	3.2	72,726	Inactive
4	1st Primary School at Zefiri	March 31, 2003	1.7	0.2	2.5	263,276	Active
5	High School at Zefiri	April 1, 2003	1.7	0.6	8.9	250,005	Active
6	Municipal Office of Psinthos	April 23, 2003	0.9	0.8	5.8	209,517	Active
7	Municipal Office of Koskinou	April 23, 2003	1.5	0.3	4.0	209,808	Active
8	First Aid Station of Faliraki	April 23, 2003	0.0	0.1	1.5	91,620	Inactive
9	Building of E.C.E. School	November 6, 2003	2.9	0.2	4.6	172,585	Active
10	5th Primary School at Renti	November 10, 2003	0.7	0.1	1.0	209,315	Active
11	Kindergarten at Renti	November 10, 2003	1.5	0.3	2.1	206,892	Active
12	1st Primary School at Renti	November 10, 2003	1.1	0.5	4.3	193,026	Active
13	Kalithies, DEYAK	May 11, 2004	0.1	0.2	1.1	155,210	Active
14	1st Primary School at N. Erithrea	July 7, 2004	2.5	0.3	3.5	129,941	Active
15	2nd & 3rd Pr. Schools at N. Erithrea	July 7, 2004	2.5	0.2	3.1	132,297	Active
16	Esperia Build. - Town Planning Build.	October 5, 2005	1.6	1.0	3.5	45,115	Active
17	Dimokratias Avenue	October 5, 2005	2.1	1.0	7.8	44,061	Active
18	1st Primary School at Ilion	November 21, 2005	2.2	0.1	2.9	33,872	Active
19	3rd High School of Argostoli	December 21, 2005	0.1	0.4	6.5	18,336	Active
20	A.U.TH., Building of School of Science	November 1, 2003	1.3	0.2	3.5	206,279	Active
21	A.U.TH., Rectorate Building	February 27, 2004	3.7	1.4	17.7	173,067	Active
22	City Hall of Menemeni	June 12, 2004	2.7	0.5	7.7	155,283	Active
23	City Hall of N. Michaniona	June 9, 2004	0.9	0.2	1.8	153,406	Active
24	High School of N. Michaniona	June 4, 2004	1.8	0.4	3.4	163,964	Active
25	1st and 2nd High Schools of Naoussa	November 16, 2004	0.7	0.2	2.1	123,851	Active
26	City Hall of Lefkimi	July 22, 2005	1.7	0.3	3.0	57,957	Active
27	2nd Primary School of Lefkimi	July 22, 2005	0.8	0.2	1.7	63,977	Active

In Figure 8 the measured points correspond to 6-minute average electric field (E-field) values as is proposed in [5]. An immediate comparison with the reference levels can be done based on this diagram. Moreover the

variation of the field during one day or a longer period is distinguishable. The time span can vary from 1 hour to the whole measurement period (several years). In Figure 9(a) and 9(b), the mean and the maximum of the total set of 6-min average E-field values are presented and compared with the corresponding reference levels, for both EE4070 – SL and MCE410 – SL models.

Sample measurement results from two "ad-hoc" measurements are depicted in Figure 10. Specifically, one can see how many times below the safety values were the measured field values, in terms of the Power Flux Density (Watt/m^2) (Figure 10(a)) and in terms of the Electric Field Strength (V/m) (Figure 10(b)), for each frequency band such as FM, TV, GSM900, UMTS etc. The total exposure level is also evaluated and presented. The comparison between the results of Figures 9(b) and 10(b) (which correspond to the same measurement site) shows that the values of the monitoring station measurements are close to the "ad-hoc" measurement values. In addition, Figure 11 illustrates the percentage contribution of each frequency band to the total EMR exposure level.

Finally, the last two diagrams (Figure 12 and Figure 13) present cumulative results regarding the mean 6-min average E-field strength (continuous measurements) and the exposure level in terms of the Power Flux Density extracted by "ad-hoc" measurements.

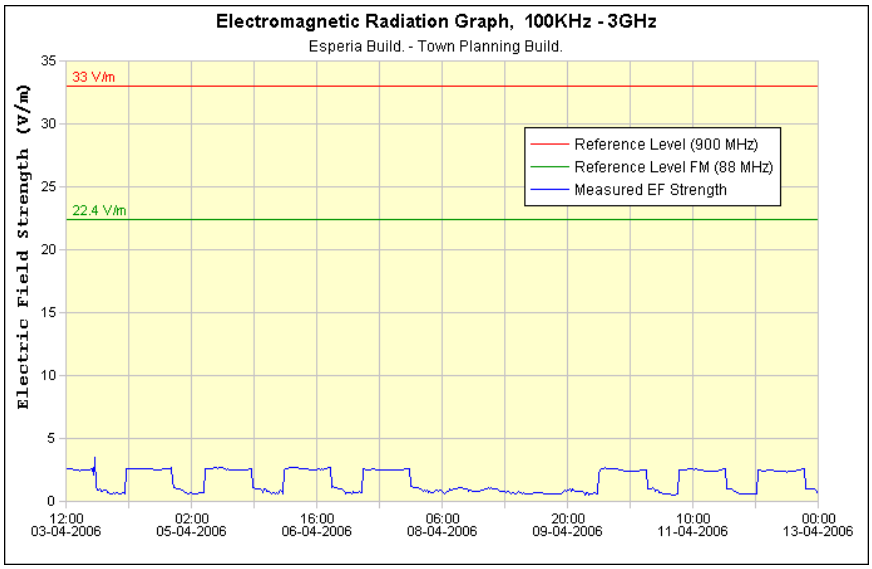

Figure 8: *Sample Electric Field Strength Diagram (Broadband)*

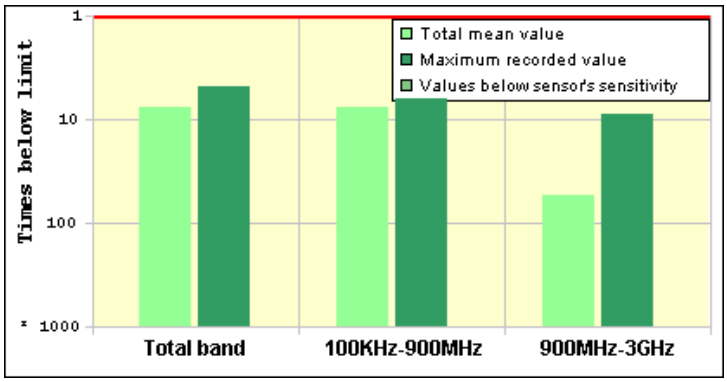

(a)

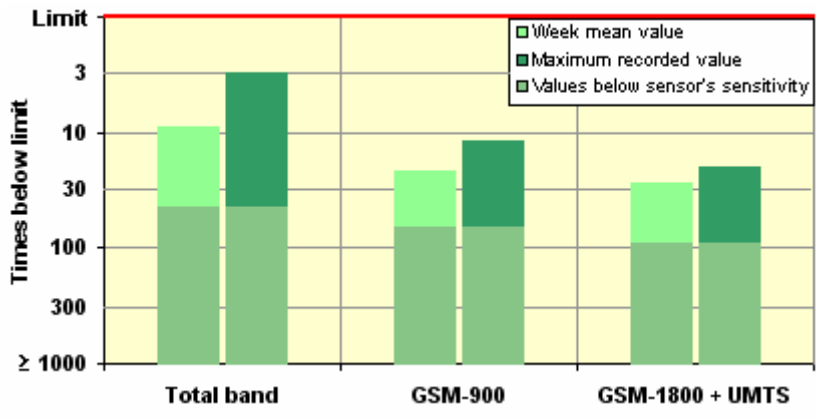

(b)

Figure 9. *(a) Sample Mean Electric Field Strength Diagram for Selective Stations (MCE410 – SL model). (b) Sample Mean Electric Field Strength Diagram for Selective Stations (EE4070 – SL model)*

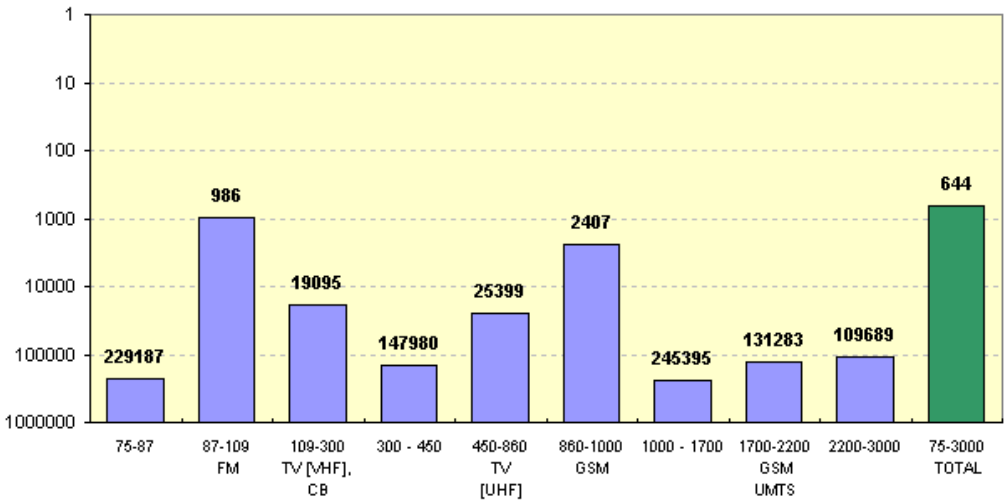

(a)

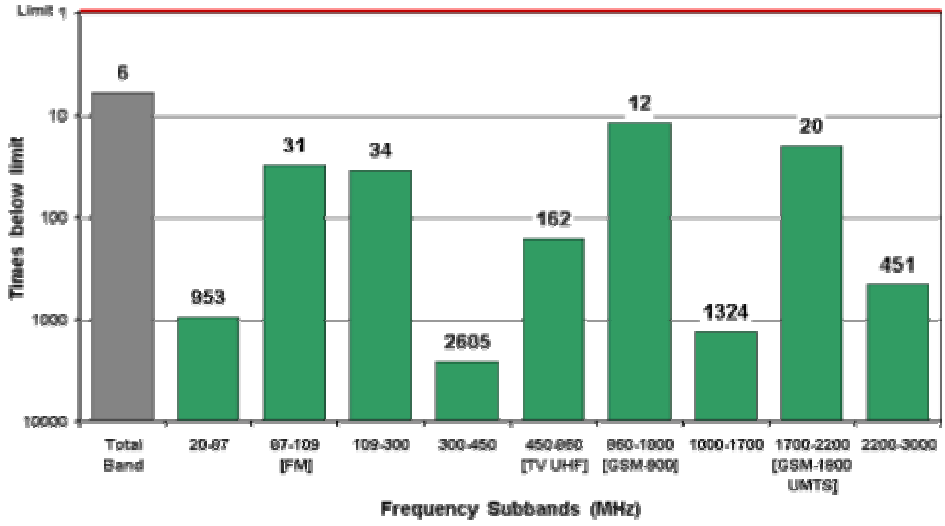

(b)

Figure 10: *(a) Sample of Power Density Measurement Results conducted with SRM (Narrow-Band). (b) Sample Equivalent Electric Field Strength Measurement Results conducted with Spectrum Analyzer (Narrow-Band)*

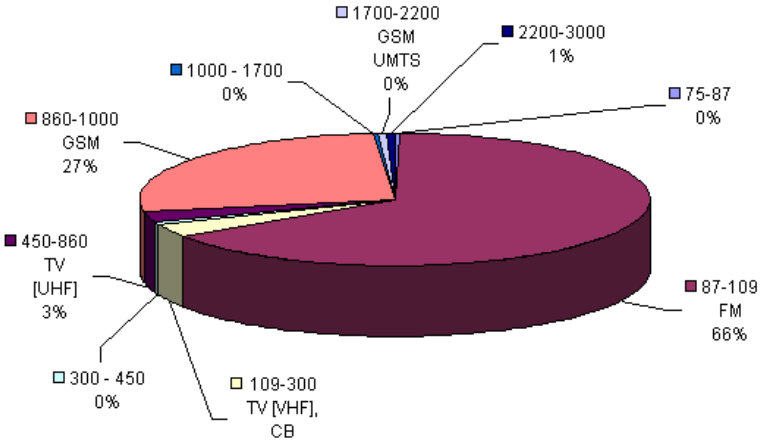

Figure 11: *Sample of Contribution of each band to the total electromagnetic radiation, calculated by SRM measurements (Narrow-Band)*

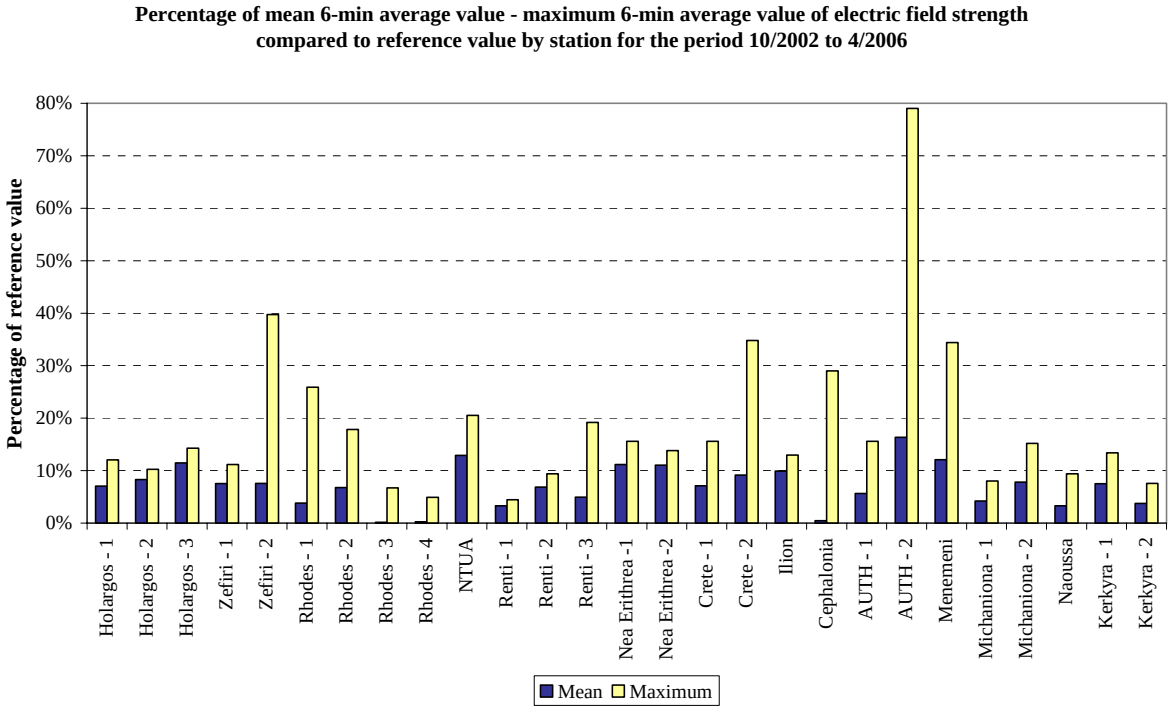

Figure 12 : *Percentages of electric field strength compared to reference value (overall)*

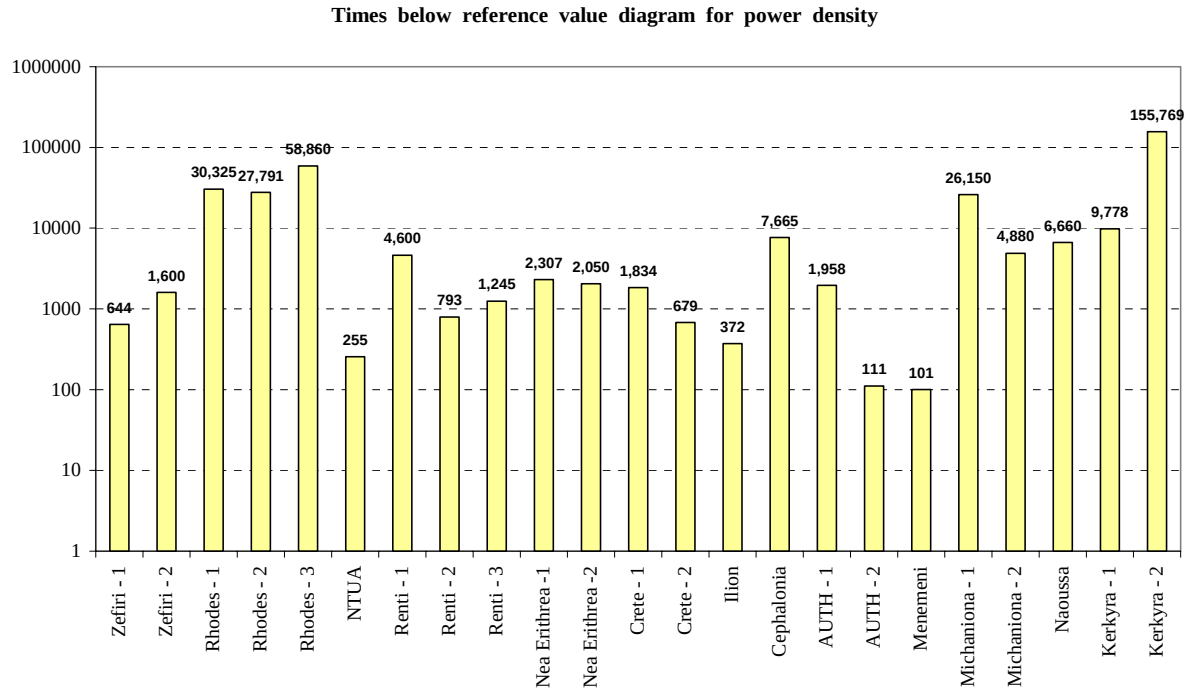

Figure 13: *Comparison of monitored power densities to reference value (overall)*

c. Comments on the Measurement results

Based on the above diagrams and the cumulative results from our measurement database, several general conclusions could be drawn:

- The electric field strength / power flux density values are several times lower than the safety reference levels, even on sites close to antennas (see Figure 4). As far as the mean E-field, the higher values have been recorded at the National Technical University of Athens (Table 1– Station ID 9) and at Aristotle University of Thessaloniki (Table 1– Station ID 21). The first is located near the Imittos Mountain hosting the Antenna Park of Attica (FM and TV broadcasting stations, Radars, etc.). The second measurement site is on the roof of the 9-floor Rectorate building, almost at the maximum of the main lobes of the antennas located at the Antenna Park of Hortiatis Mountain. Still, the mean values are respectively 2.9 V/m and 3.7 V/m, that is, 13% and 16.5% of the adopted reference level (22.4 V/m).
- The variation of the E-field on each site is negligible except for the two stations located in Heraklion, Crete. The standard deviation computed over the whole measurement period varies between 0.1 – 0.3 V/m for the majority of the sites.
- The measured E-field depends on the relative position between the site and the antennas, that is, the distance between them and the radiation pattern of the transmitting antenna(s).
- The recorded values to date indicate that in general higher E-fields are present on urban and dense urban sites in comparison with rural areas. Nevertheless, the contribution of mobile telephony cellular emissions to the total exposure is higher in rural areas.

IV. Summary - Future work

An automated nationwide monitoring network of the electric field strength in the RF spectrum was presented. The system uses reliable hardware based on electric field strength probes and the measured data is presented openly to the public using the Web. More than 4,000,000 E-field strength values have been recorded in our database and 63 “ad-hoc” measurements have been conducted in the context of “Hermes” Project. Since the commencement of operation the measured EM Radiation levels are significantly below the safety reference levels.

We are currently planning the installation of more remote stations in dense urban and rural environments. Our

intention is to extend the network of the monitoring stations. In the long-run and in conjunction with repetitive "ad-hoc" measurements using a Spectrum Analyser or a Selective Radiation Meter, a more detailed statistical analysis of the RF radiation levels in urban and rural areas is going to be performed. Our interest will be focused mainly in the proximity of cellular base stations.

References

[1] "monIT Project": Electromagnetic Radiation Monitoring in Mobile Communications http://www.lx.it.pt/monit/

[2] "Cassiopea Project": http://www.stroud.gov.uk/docs/cassiopea/cassiopea.asp

[3] "Progett Gardjola": http://gardjola.eng.um.edu.mt/emr

[4] "Project Horus": http://www.projecthorus.com/EMF/

[5] European Commission (EC), "Council Recommendation 1999/519/EC of 12 July 1999 on the limitation of exposure of the general public to electromagnetic fields (0 Hz to 300 GHz)", *Off. J. Eur. Comm.*, L 199, 59, 30 July 1999.

[6] Hellenic Republic Law No. 3431, About Electronic Communications and other Provisions, Government Gazette, FEK No. 13 A'/ 03.02.2006.

[7] "Hermes" Project: A Project for Systematic Measurements of the Electromagnetic Radiation, http://www.hermes-program.gr

[8] Narda Area Monitor System 2600, "Narda Safety Test Solutions": http://www.narda-sts.com/en/produkte/2600.htm

[9] PMM 8055S Electric and Magnetic Field Monitoring Station, "PMM Safety Products", http://www.pmm.it/main/safetyproducts.asp

[10] EE4070, EE4070S,MCE Monitoring System, "E.I.T. s.r.l", http://www.eitsrl.it/iMCE.htm

[11] A. Yalofas, A. Gotsis, C. Veranopoulos, P. Constantinou, G. Belesiotis, M. Petkaris, N. Babalis, *"A Fully Automated and Geographically Distributed Network for the Continuous Measurement of the RF Radiation – "Hermes" Project"*, TELSICS, IEEE 6th International Conference on Telecommunications in Modern Satellite, Cable and Broadcasting Services, Niš, Yugoslavia, October 2003.

[12] Electronic Communications Committee (ECC) within the European Conference of Postal and Telecommunications Administrations (CEPT) : ECC RECOMMENDATION (02)04 "MEASURING NON-IONISING ELECTROMAGNETIC RADIATION (9 kHz – 300 GHz)"

[13] Narda Selective Radiation Meter SRM-3000, "Narda Safety Test Solutions": http://www.narda-sts.com/en/produkte/srm.htm

THE NEW EMF PROTECTION FRAMEWORK REGARDING ANTENNA STATIONS IN GREECE

E. KARABETSOS G. FILIPPOPOULOS

NON IONIZING RADIATION OFFICE
GREEK ATOMIC ENERGY COMMISSION
P. O. BOX 60092, 15310 AGIA PARASKEVI, GREECE

Abstract
In February 2006, the Greek Parliament passed a Law setting new standards for siting antenna stations. According to this Law, the permissible general public exposure levels for EMF in the vicinity of all kinds of antenna stations are set in general to 70% of the EU Recommendation and ICNIRP's limits, and to 60% of them for stations located closer than 300 meters from the perimeter of schools, kindergartens, hospitals or eldercare facilities. Installation of mobile phone base stations at the premises of these facilities is now prohibited. Furthermore, it is not allowed to build a new antenna station before the approval by the Greek Atomic Energy Commission of a technical study showing that the EMF levels in the vicinity of the station will be lower than the aforementioned limits. The Greek Atomic Energy Commission will be monitoring EMF exposure levels by performing in situ measurements, ex officio or within 20 working days after request of any interested party. These measurements should, on an annual basis, concern at least 20% of all the antenna stations installed in urban areas and their results will be announced on the web site of the Greek Atomic Energy Commission. The provisions and ramifications of this new Law are presented in this paper.

Introduction

In 2000 Greece implemented legally binding measures for the protection of the public from exposure to electromagnetic fields by putting into force a national legislative act concerning all kinds of land-based antenna stations, [1]. In this legislative act, the basic restrictions and the reference levels set in the Council Recommendation, [2], and ICNIRP's guidelines, [3], for general public protection have been implemented. However, the Greek legislation applied additional safety parameters to the allowed EMF exposure levels. Hence, the safety limits for the exposure of the general public to all land based antenna installations were set to 80% of the EU values. Also, with this legislation the Greek Atomic Energy Commission is set as the national authority, responsible for the protection of the environment and the general public against man-made electromagnetic radiation.

In February 2006, the Greek Parliament passed a Law, [4], setting new standards for siting antenna stations. According to this Law, the permissible general public exposure levels for EMF in the vicinity of all kinds of antenna stations are now set, in general, to 70% of the EU Recommendation and ICNIRP's limits, and to 60% of them for stations located closer than 300 meters from the perimeter of schools, kindergartens, hospitals or eldercare facilities. It must also be noted that installation of mobile phone base stations at the premises of these facilities is now strictly prohibited. The Greek Atomic Energy Commission will be monitoring EMF exposure levels by performing in situ measurements, ex officio or within 20 working days after request of any interested party. These measurements should, on an annual basis, concern at least 20% of all the antenna stations installed in urban areas and their results will be announced on the web site of the Greek Atomic Energy Commission.

In the next paragraphs the EMF protection in Greece, after the introduction of the new Law is analysed.

Competent Authorities in Greece

The competent national authority for the protection of the general public and the environment against artificially produced non-ionising radiation is the Greek Atomic Energy Commission (EEAE, www.eeae.gr), which lies under the Ministry of Development. Specifically the EEAE:

- Publishes prototype technical studies-notes for all kinds of antennas (such technical notes have been

published for mobile phone base stations, earth satellite stations and microwave antennas, http://www.eeae.gr/el/services/templates/)
- Defines the measurements protocol based on international standards
- Organises educational programs for the personnel of all public sector and all interested groups concerning the protection of the general public to electromagnetic fields, informs and replies to requests from the public authorities and citizens about the possible health hazards induced by non- ionising radiation.
- Provides all details concerning the authorisation of teams that perform measurements in all non-ionising radiation installations and controls the measurements procedure.

Measurements in antenna stations according to the legislation, may also be performed by the Ministry for the Environment, Physical Planning and Public Works, the Ministry of Health and Welfare and the Ministry of Transport and Communications or other, authorised by the EEAE, laboratories (e.g. University laboratories).

Public Information

The EEAE is responsible for providing information to all interested public groups for matters concerning the health effects of electromagnetic fields. To this end, the EEAE published in 2001 a 16-page informative brochure entitled: “Non-ionising radiations: Mobile phones and base stations” (also available at www.eeae.gr), distributed freely to all interested parties. Recently (after the new Law) EEAE has published a new updated 36-page brochure entitled “Mobile telephony and health” that is also freely distributed (also available at www.eeae.gr).

The EEAE also organises or participates in lectures; courses and workshops open to the local authorities, the public and the media. Some major risk communication events have been the organisation of 5 one-day workshops, in the years 2001-2003, entitled: “Exposure of the general public from mobile phones base stations” open to the local authorities, the public and the media, organised by the Ministry of Transport and Communications, the National Committee of Post and Telecommunications, the EEAE and/or the municipal authorities (proceedings from some of these workshops have been published as booklets and are freely distributed from the National Telecommunications and Post Commission, EETT).

It must be also stated that the EEAE was recently financed by the General Secretariat of Research and Technology of the Ministry of Development in order to produce informative material in electronic and paper format (cd-roms and brochures) and to organise workshops for specially selected target groups (representatives of the ministries, the local authorities and the media) for matters concerning EMFs and Health. The scope of organising such workshops is to inform and train persons able to form a “critical mass” necessary for further dissemination of this information to the general public.

Exposure Limits

In 2000 legislative act [1], the basic restrictions and the reference levels set in the Council Recommendation, [2], and ICNIRP’s guidelines for general public protection, [3], have been implemented. However, this legislation applied additional safety parameters to the allowed EMF-exposure levels. Hence, the safety limits for the exposure of the general public to all land based antenna installations were set to 80% of the EU values.

In accordance with the new Greek Law, the limits for general public exposure to electromagnetic fields are set to 70% of EU Recommendation Values. In case that an antenna is sited at a distance lower than 300m from the perimeter of the premises of kindergartens, schools, hospitals or eldercare facilities the Greek limits are set to 60% of EU Values. Furthermore, it is not allowed to install mobile phone antenna stations at these premises. All existing installations at the above mentioned premises must be removed in 6 months from the publication of the new Law.

Technical Studies

According to the Greek Legislation, [1], before the construction and the operation of an antenna station a special license must be issued by the National Telecommunications and Post Commission, (EETT). The EEAE is involved in the license issuing process since a technical study of electromagnetic emissions is mandatory to be submitted to EEAE before the antenna station owner submits the application to the competent authority for issuing a license for an antenna station in a particular location. These studies include architectural blueprints and

topographical charts of the station as well as technical information about the operation of station's antenna system. The intensity of the incident electromagnetic radiation is calculated in places accessible to general public. The existence of any other antenna station at a distance lower than 50 meters from the examined antenna station is also taken into account.

Through these calculations it must be proven that the intensity of the electromagnetic radiation is lower than the established limits in the Greek Legislation at any place that is freely accessible to the public in the vicinity of the station. Of course, very close to the antenna systems (for example for mobile phones base stations usually till 4 to 8 meters), at the directions of maximum emission and at the height where the antennas are located it is possible that the radiation exceeds the established limits. If there is public access to these places the study foresees that it will be forbidden. The EEAE after the examination of the study sends its expert opinion (given that the study is not deficient or inadequate or mistaken) to the competent authority in order to issue license for installing the antenna.

It is noteworthy that these studies are composed on the basis of the very strict technical prototype studies that have been issued by the non ionizing radiation office of EEAE. These prototype studies adopt worst case considerations and assumptions, due to which the intensity of the electromagnetic radiation is overestimated in relation to the actual intensity in the vicinity of the station. This has been confirmed through the comparison of the calculated values in the studies with the results of measurements at areas close to antenna stations.

In accordance with the existing legislation [1], if the process of checking the technical study by EEAE took over 1 month the license by EETT for this installation could be issued without EEAE's positive expert opinion. However, with the new legislation [4], it is no longer allowed to build a new antenna station before the approval by the Greek Atomic Energy Commission of a technical study showing that the EMF levels in the vicinity of the station will be lower than the aforementioned limits. Also, due to the change of exposure limits the owners of all the installed antenna stations are obliged to submit new technical studies to EEAE showing that their stations adhere to the new limits.

Audits

In accordance with the existing legislation, the levels of the emitted electromagnetic fields from all kind of antenna stations are regularly monitored, in order to ensure compliance with the safety limits for the public or, if this is not the case, to ensure that all necessary protection measures around an antenna base station, are being taken in every case. To that end, the EEAE also carries out measurements in all kinds of antenna stations in order to monitor whether the general public exposure limits are being adhered to. It must be stated here that from the year 2000 until today, the non - ionising radiation office of the EEAE has performed over 1700 inspections and measurements at various sites in Greece, where all kinds of antenna stations are installed. Concerning cellular phone base stations, the EEAE has conducted measurements in the vicinity of 1200 such stations. The major part of this information is in the form of written measurement reports that have already been delivered to the authorities or persons who asked for these measurements, but are also available to everyone interested.

The non ionising radiation office of GAEC has expert personnel and suitable measuring equipment and is accredited in accordance with the requirements of the EN IS0/IEC 17025 standard by the Hellenic Accreditation Council (ESYD - the Greek National Accreditation Body) for performing measurements of low and high frequency fields, as it is determined in the accreditation certificate No. 117 (22-01-2003) for tests.

With the new legislation, [4], the audits of the electromagnetic fields in the vicinity of antenna stations are drastically intensified. To this end, the EEAE or other laboratories authorized by it, performs inspections and measurements in the vicinity of antenna stations either:

a) ex officio, through a sampling process and annually in the vicinity of 20% of all antennas installed in urban areas, or,
b) after the request of any interested party, in 20 working days

The results of these inspections are immediately published at EEAE's web site and collectively per year. Soon all this information about the already measured sites as long as the results for every new measured antenna station will be posted to the web page of EEAE

Penalties

In case EEAE finds trough measurements an excess of the limits, it informs the competent license-issuing authority, which then notifies the antenna owner in order to do the following:

• immediately cease the operation of the responsible equipment and then inform about this the competent license-issuing authority;

• clear the causes of malfunction before resuming operation

• inform the competent license-issuing authority about the operation resumption, providing explanations about the causes of the malfunction.

If, at any time after the initial notification, an irregular operation of the same equipment is found again, then the license is permanently recalled for this location.

Environmental aspects

According with the new Law, [4], the approval concerning all environmental aspects related to each antenna installation foreruns the license for the construction of this installation issued by EETT. Hence, a technical study examining the environmental impact of a new antenna station should be submitted to the General Secretariat of each District, which in 10 days sends it to EEAE asking its expert opinion. The General Secretariat of each District has to answer for each technical study, after a positive opinion by EEAE. However, the content and the process of these environmental studies are to be defined in a new decision by the Minister of Environment and Public Works. All the existing antenna stations that have not an environmental permission have to acquire one in 12 months from the publication of this ministerial decision.

Funding

According with the new Law, [4], the owners of all antenna stations are billed annually by EETT the sum of 200€ for each station and the total amount is transferred to EEAE. In this way, EEAE will have the necessary funds to achieve its duties.

Conclusions

The existing legislation in Greece imposed a strict framework for the protection of the general public from the electromagnetic fields emitted by antenna stations. It sets exposure limits based on the well-established limits of the EU recommendation and ICNIRP Guidelines. Furthermore, it established a mechanism for checking compliance with these limits before and after the installation of antenna stations. The new legislation reduced the exposure limits (towards the safe side) and made the control mechanisms stricter and intense.

References

[1] Greek legislation: Common Ministerial Decision, Protection measures for the exposure of the general public to all land based antenna stations, Act No.1105/Vol. B/6-9-2000.
[2] European Union Council Recommendation of 12th July 1999 on the limitation of exposure of the general public to electromagnetic fields (0Hz to 300 GHz) (1999/519/EC).
[3] International Commission on Non Ionizing Radiation Protection (ICNIRP), Guidelines for limiting exposure to time – varying electric, magnetic and electromagnetic fields (up to 300 GHz), Health Physics, Vol. 74, No 4, April 1998, pp 494 – 522.
[4] Greek legislation: Law No 3431 About electronic communications and other provisions, Act No. 13/A/03-02-2006.

NON-IONISING ELECTROMAGNETIC FIELD EXPOSURE MONITORING AND MEASUREMENT CAMPAIGNS IN MALTA

CHARLES V SAMMUT

DEPARTMENT OF PHYSICS, UNIVERSITY OF MALTA, MSIDA, MSD 06, MALTA

charles.v.sammut@um.edu.mt

ABSTRACT

This paper reports first on a completed three-year campaign to assess exposure of the public to electromagnetic fields from mobile phone base station antennas. The project was commissioned by the Malta Communications Authority (MCA) and consisted of information gathering and construction of a comprehensive database, field simulation at all sites in operation and detailed measurements at over half the base station sites installed on Malta.

The measurement results were analysed to supply useful information of a statistical nature. Measurement techniques are also described in the light of a recent preliminary standard (prEN 50413). Correlation exists between measured and calculated field intensities, although absolute values are not in good agreement. This occurs mainly on account of fluctuating power output from base stations, multiple reflections and diffraction effects due to surrounding structures. Field calculation is, however, useful for worst-case site assessment.

The paper proceeds by outlining the present non-ionising radiation monitoring and measurement campaign, which now includes all broadcast frequencies, and gives a brief account of a recent extensive survey conducted around the leading telecommunications tower situated in a village. Recent measurements show that, notwithstanding the proximity of some residences, radiation levels in publicly accessible areas rarely exceed much above 5% of ICNIRP reference levels for public exposure.

1. INTRODUCTION

The advent of mobile telephony and liberalisation of the telecommunications market in Malta brought about a proliferation of radio antenna sites. There are currently two companies operating mobile telephone networks in Malta, Vodafone-Malta (GSM900) and Mobisle Communications (GSM1800). Together they have about 300 base stations in operation and are developing UMTS networks, due to start operating later this year.

The country's high population density and restricted land area necessitate location of base station antennas predominantly within a densely built environment. An initial lack of public information and rapidity of base station deployment in response to increasing consumer demands have contributed to public concern that the perceived increase in exposure to radio frequency electromagnetic fields could be harmful to health. This concern was also fuelled by reports from various sources of possible exposure-related health effects. In this respect, the Stewart Report [1] has unwittingly contributed to this concern, as some of the recommendations made therein were based on the precautionary principle, which has often been misunderstood and misinterpreted by the media and the general public.

Public concern has led to some court cases instituted locally against the operators in order to prevent them from setting up new antenna sites. Some individuals living close to base station sites claimed they were suffering form adverse health effects and radio interference linked to radiation from these antennas. In some instances, adverse effects were reported soon after the installation of the base station hardware and even before its coming into operation.

In order to allay such fears and to ensure that the local mobile phone companies operate within the national guidelines [2], the MCA, which is the regulatory agency for electronic communications, post and e-Commerce, commissioned the Malta National Laboratory (MNL), as an independent provider of testing services, to conduct an extensive survey. Some preliminary results appeared in [3] and [4].

This project constituted the first phase and is followed by an ongoing programme of monitoring and measurement of emissions from all radiofrequency sources in use for telecommunications. This paper proceeds by outlining the elements of the first phase project and discussing the subsequent results. An outline of the present monitoring and field measurement activities then follows.

2. PHASE I: SURVEY OF MOBILE PHONE BASE STATION SITES

This project was spread over three years and consisted of three distinct tasks:

1. compilation of a detailed database of all base stations;
2. calculation/simulation of electromagnetic field exposure based on the transmission specifications contained in the database for each base station site;
3. measurement of electromagnetic fields at a sample of 150 of the transmission sites.

To the author's knowledge, the survey element of this project is relatively one of the most extensive yet reported in Europe, in that the measurement campaign involved over half of the licensed sites. This section describes each task, discusses calculations/simulations of electromagnetic field power density and the survey methodology, as well as analysing the measurement results.

2.1 Mobile phone base station database

The database was designed so as to enable easy record maintenance and update, as well as providing for easy access to site details, including antenna types, physical layout and transmission characteristics, as required for field calculations. The records are searchable through a number of fields and the user can retrieve associated information, such as polar plots of the antenna gain profiles in the vertical and horizontal planes and copies of field survey reports in the case of audited sites.

2.2 Field calculations and simulations

Field calculations are useful in cases where certification of site compliance is required as a precondition to granting of permits for transmission. Given maximum output power, field calculation and simulation results could generate worst case exposure scenarios. This is also useful in the case of operational transmitting stations, especially those, such as GSM, which are characterised by a fluctuating power output depending on network use. Field measurements will only reveal the prevailing emissions at the time of measurement and rarely result in registering maximum possible values.

Field simulation was an integral part of the project. Two-dimensional field intensity plots were generated for all the base station sites on the Maltese islands over planes containing publicly accessible areas. Both commercially available and in-house field calculation and simulation software were used. In both cases, far field strengths were calculated using manufacturer-supplied antenna gain profiles in the vertical and horizontal planes, and utilising height, vertical tilt, azimuth and power input information provided by the operators [3].

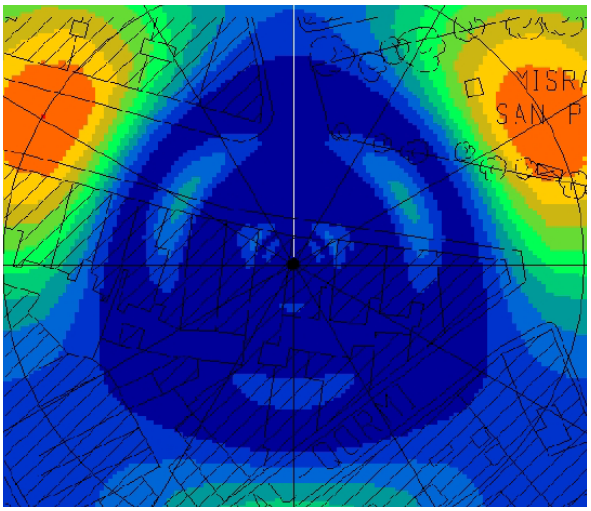

Figure 1: A typical two-dimensional field plot generated by MBSFIP™. A three-sector antenna is situated at the centre.

The commercial software used was Telstra's Mobile Base Station Field Intensity Plotter (MBSFIP™). This enabled two-dimensional colour mapping of field intensity which could be overlaid on the site plan (Figure 1). MBSFIP allows the user to select either a direct or a two-ray path model for the RF propagation loss calculations and if the two-ray model is selected, then calculations assume flat ground with ground constants (relative permittivity and conductivity) that have to be specified by the user. The program calculates reflection for vertical, horizontal or slant polarization. Information about the transmit antenna polarisation is obtained from an antenna pattern library. Thus, in the two-ray path model, the program combines the field intensity calculated along the direct path and combines this with the two ray path calculation.

Comparison between measured and calculated fields at some locations showed moderate agreement in absolute terms but high correlation [3, 10], suggesting

a systematic error, thought to be mostly due to fluctuating output power determined by network use. However, there are other factors, such as multiple reflections and diffraction effects due to surrounding structures.

2.2 Field measurement

The central and most publicly visible element of the project was the field measurement campaign which aimed to carry out audit measurements of electromagnetic field emissions at half the base station sites in operation. In fact, 151 base station sites were surveyed out of a total of 271. The sites can be classified as single operator GSM900 or GSM1800, shared (by the two GSM operators) and shared multiple technologies (GSM and other RF transmission technologies).

The aims of the base station emissions audit were to:

1. ascertain compliance of base station emissions with the ICNIRP guideline reference levels for exposure of the general public;
2. establish a baseline for typical emission scenarios which would help in deciding if and where to grant permission to operate base stations;
3. address public concerns in respect of perceived hazards of radiofrequency emissions from base stations;
4. inform and educate the public in matters concerning radiofrequency emissions.

At the beginning of the project, public concern about the possible hazard from mobile phone base station antennas was high. Selection of sites for audit was therefore a delicate task as we had to balance technical considerations with the need to allay public concerns. A broad representation of audit sites based on type and geographical location was sought. Sites were therefore selected roughly on the basis of the number of base stations installed per locality, which is indicative of population density and frequency of use. Within each locality, base station sites close to schools were audited and in all such cases the adjacent school premises were also surveyed carefully. The bulk of the base stations selected for the audit survey were sited over commercial buildings and private homes within or in the vicinity of densely built residential areas. In general, and wherever possible, measurements were taken over properties neighbouring the selected base station sites. Surveyed areas included accessible recreational open spaces situated in the vicinity of base station sites selected for audit. Table 1 lists the base station sites by type. Commercial buildings included hotels, shopping outlets of varying sizes, showrooms, stores and industrial units.

Table 1: Base station sites classified by type

SITE TYPE	Number of base stations	Number surveyed
Commercial buildings	105	61
Private residences	94	41
Social clubs	15	10
Churches	11	9
Public buildings	9	4
Transmission stations	6	1
Old people's homes	5	5
Hospitals	2	2
Schools	2	2
Other	22	16
TOTAL	271	151

Owing to expected higher power density levels and for reasons of greater public concern, 80% of shared sites were audited, compared to 62% and 45% respectively of single operator GSM900 and GSM1800 base stations. Broad representation on the basis of geographical location and population density was also achieved.

2.3 Field survey methodology

The project started when European measurement standards for non-ionising radiation safety assessment were still in a state of flux. The methods adopted were inspired by Canadian [5] and US [6] recommendations and developed by the author in the light of his own research and local experience. However, the methods subsequently described in the CENELEC preliminary standard prEN 50413 [7] and the ECC Recommendation [8] are similar and additional techniques were shown to generate useful data for assessing exposure realistically at most transmission sites [3, 4, 9, 10].

Measurement procedures and subsequent analysis were geared principally toward assessment of the extent of human exposure arising from operation of the sources present at the investigated sites. Each survey started with a visual inspection of the antenna site and all transmitting antennas were photographed for the records. The antenna locations were marked on the site plan and notes were taken describing the site, access restrictions and antenna configurations.

The field survey equipment used consisted of the Narda 8718B survey meter in conjunction with the models 8760D and the D8722D broadband, isotropic electric field probes. Summary specifications of these isotropic probes are listed in Table 2. The field survey started with a preliminary scan of the site conducted by meandering within areas where exposure was expected to be relatively higher, i.e. along the transmission directions facing the antenna panels. This procedure allowed the surveyor to establish a set of measurement points that included regions of maximum exposure. However, measurement points were also chosen on grounds of site use by the public or authorised personnel, in cases where the site was not accessible to the public.

Table 2: Broadband isotropic field probes used during the phase field surveys

Model No.	Frequency Range	Nominal Measurement Range		Frequency Response	Sensor Type
		Power Density	*E* [Vm^{-1}]		
8760D	300kHz – 3.0GHz	5.0×10^{-2} – 1.0 Wm^{-2}	0.5 – 19.4	Flat	Compensated Diode
D8722D	300kHz – 50GHz	0.3 – 300% of Standard*	–	Weighted	Compensated Diode and Thermocouple

* Referenced to ICNIRP guideline levels for occupational exposure

Three main measurement modes were used, depending on site-specific suitability:

Time averaging (TAV) – measurement of field intensity at a given point over a pre-defined time interval, the survey meter storing average and maximum field strengths during the process. About 1,500 such measurements were made during the course of the survey. The intervals varied between 10 and 120 seconds, depending on signal variability. At none of the sites investigated was it found necessary to take six-minute time averages because the power density levels recorded were below the ICNIRP reference levels for exposure of the public, as recommended in [7] and [8].

Spatial averaging over the human body area (BAV) – vertical scan with the probe moved at a slow, steady speed between points distant 10 and 200cm above ground level [3] while the survey meter stores the average and maximum field strengths. Over 1,500 such measurements were made during the course of the project. This allowed a more extensive exposure assessment than would have been possible with the more laborious procedures described in [5], [7] and [8].

Extended spatial averaging (ESA) over a defined three-dimensional region – a scan of a defined region with the probe raised and lowered at a steady speed while zigzagging systematically through the designated area, the survey meter storing average and maximum field strengths during the process. This technique was reported in [3] and further validated in [4]. In all, 277 ESA measurements were conducted at various sites throughout the project.

2.4 Field survey results

A total of about 3,300 field strength measurements were made during the course of the project at 151 sites. Summary values are represented in Figure 2. These values represent site average and maximum recorded field strengths. More than half the surveyed sites were found to have average exposure levels between 0.08 and 0.47% of the ICNIRP public exposure level (PEL), while the maximum exposure level at over half the sites ranged between 0.27 and 2.14%.

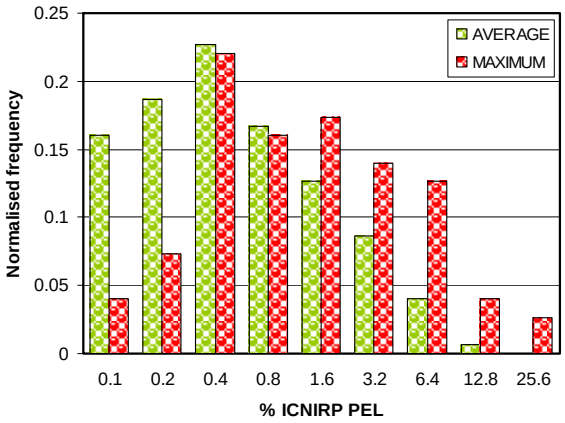

Figure 2: Normalised frequency distribution of measured site average and maximum field strengths.

At two sites the 25% ICNIRP PEL mark was exceeded but at locations that were not easily accessible to the general public. At one particular shared site, GSM900 and 1800 base stations were collocated on the roof of a hotel only accessible to authorised personnel for maintenance purposes. Broadcast radio and TV antennas were also in operation at that site. The maximum measured field strength recorded from the GSM base stations was 29.3%. A BAV of 61% and a maximum of 382% of ICNIRP PEL were also recorded at the same site with all sources operating together. It was possible to identify the GSM component by collaboration with the operators, who kindly switched off the relevant transmitting antennas during part of the

survey to allow measurement of the non-GSM component.

Figure 3 shows the normalised frequency distribution of time average field strengths (TAV), along with the maxima recorded during these measurements. The data included all measurements recorded during the project at all the sites investigated, except for the extreme values mentioned in the preceding paragraph. The distribution indicates predominantly low field strengths. Half the time average field strengths measured were between 0.04 and 0.42% of ICNIRP PEL (Table 3), while half the maxima were between 0.05 and 0.51%.

Table 3: Statistical summary of measured field intensity in % of ICNIRP PEL

	TAV-AV	TAV-MAX	BAV-AV	BAV-MAX	ESA-AV	ESA-MAX
Lower quartile	0.04	0.05	0.03	0.06	0.04	0.16
Median	0.14	0.17	0.08	0.19	0.09	0.34
Upper quartile	0.42	0.51	0.28	0.55	0.30	1.05

The measured BAV field strengths show similar overall characteristics, in that they are predominantly low, as can be seen from Figure 4, which shows the frequency distribution, along with maxima recorded during the averaging process. This analysis also included all the BAV measurements made throughout the course of the project at all the sites investigated, except for the mentioned extreme values. As indicated in Table 3, half the values obtained were between 0.03 and 0.28% of ICNIRP PEL, while half the recorded maxima were between 0.06 and 0.55%.

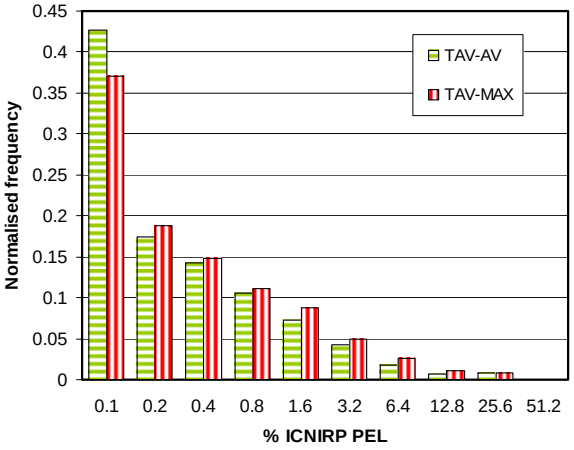

Figure 3: Normalised frequency distribution of measured time average (TAV-AV) and maximum (TAV-MAX) field strengths.

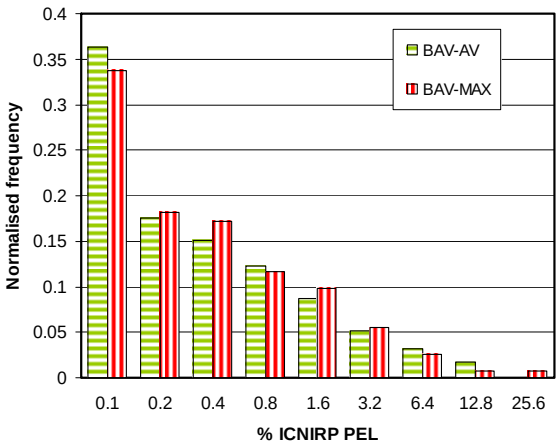

Figure 4: Normalised frequency distribution of measured body average (BAV-AV) and maximum (BAV-MAX) field strengths.

The ESA field strength values obtained are represented in Figure 5, which shows the frequency distribution of measured extended spatial average field strengths and maxima obtained during the averaging process. Some of these measurements were made in areas not accessible to the public and in close proximity to radiating antennas and this explains the relatively higher ESA-MAX median and quartiles given in Table 2. The TAV-MAX and BAV-MAX statistics are close. This is explained when considering that, during the BAV scans, the maximum field strength was recorded predominantly at about 2m above ground level, where most TAV measurements were made close to the same spot. Measurements at this level tend to be higher in the vicinity of a transmitting antenna, which would typically have its main beam directed well above accessible heights.

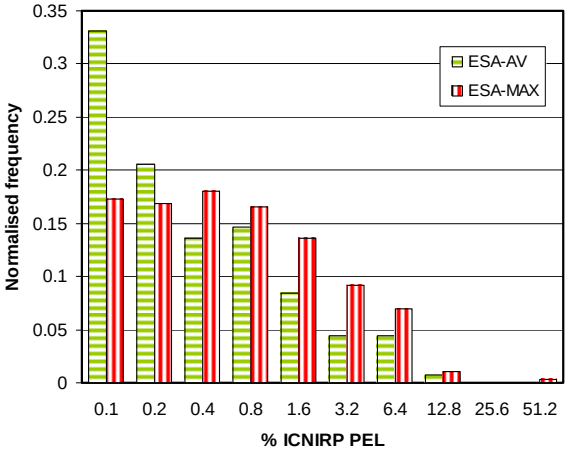

Figure 5: Normalised frequency distribution of measured extended spatial average (ESA-AV) and maximum (ESA-MAX) field strengths.

The BAV measurement records (about 1500) were analysed for possible variation with weekday and time of day. From Figures 6 and 7, it is not possible to draw suitable conclusions, when one considers the large standard deviation in the data, ranging from 0.4 to 1.3 %

ICNIRP over the week days Monday to Friday (Table 3). Such variation arises as a consequence of the fact that field measurements were conducted at many different locations and heights with respect to the transmitting antennas and were not intended to monitor diurnal fluctuations at specific locations.

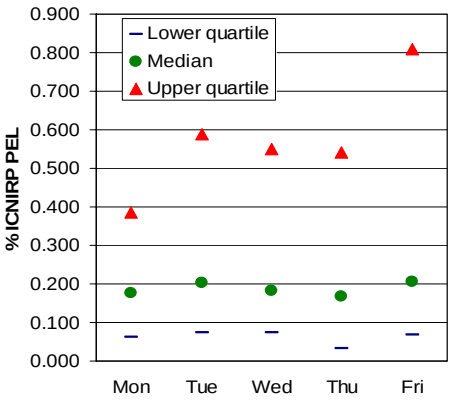

Figure 6: Variation of BAV-MAX by weekday.

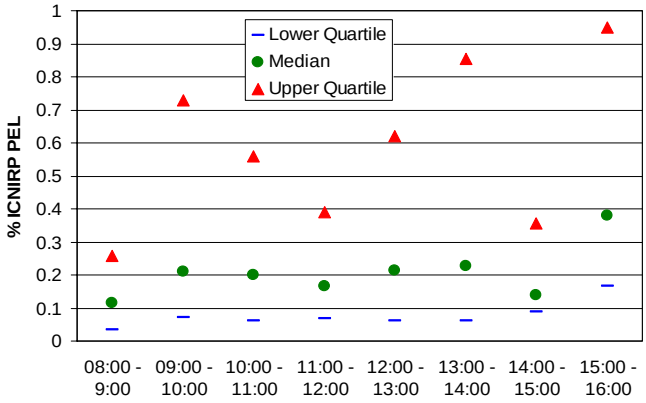

Figure 7: Diurnal variation of BAV-MAX (all weekdays).

3. PHASE II: ONGOING PROGRAMME OF AUDIT SURVEYS

At some shared radio sites, non GSM sources were present that had been set up before the present guidelines [2] came into force. It had been clear from the outset that at such transmission sites, field intensity apportionment and careful assessment of the antenna layout and transmission equipment were required. Having completed the first phase, the scope of the audit surveys was therefore widened in 2004 to include all telecommunications sources within the remit of the MCA. Monitoring compliance is now the major objective, since increased awareness of the general public, partly resulting from the phase I project, has somewhat succeeded in allaying public apprehension toward mobile phone base station emissions.

MCA now has an ongoing programme to verify compliance of radio transmission sites with ICNIRP reference levels for exposure of the general public. MCA technicians were trained by the author to conduct RF emissions using frequency selective and broadband techniques based on those outlined in [7] and [8]. Most transmission sites have by now been audited at least once.

The main instrument being used for the frequency selective measurements is the Narda SRM 3000 in conjunction with an isotropic electric field probe, covering the range 75MHz to 3GHz. Conventional spectrum analysers in conjunction with single axis antennas are also used for more accurate measurements when required.

One of the most sensitive sites investigated extensively during the second phase was the area surrounding the island's main telecommunications tower installed at the village of Gharghur. The tower, which for some years has been a source of concern to the residents, is situated about 400m from a primary school and close to private residences. It is host to the main broadcast TV and radio station repeaters, GSM and other communications antennas, as well as microwave links (Figure 8). Six-minute frequency selective time average field strength measurements were made at 15 carefully chosen locations in this village, including two inside the neighbouring school and several within private residences. Figure 9 represents the summary results including all emissions within the frequency range 75 MHz to 3 GHz. Again, the measured field intensities were relatively low, even within the tower precincts. The highest level recorded was 10% of ICNIRP PEL on a first floor terrace at a nearby residence.

Figure 8: The Gharghur telecoms tower.

Measurements conducted so far have rarely resulted in field strengths higher than about 5% of ICNIRP PEL. More accurate measurement techniques than those afforded by isotropic probes place an additional burden not required for the purpose of site compliance certification.

Field calculations will soon form part of the ongoing programme of radiation hazard assessment. The database will incorporate all licensed transmission sources and shall include technical details sufficient to permit field calculations. These will be used to generate worst-case

exposure scenarios in support of the measurement campaigns and should serve as an important tool in educating the general public, apart from helping to dispel misconceptions concerning emission levels.

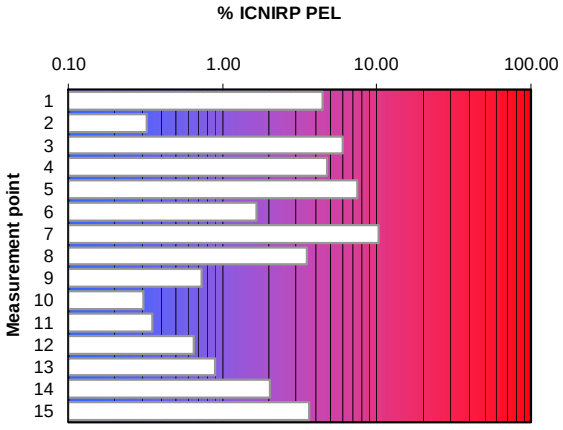

Figure 9: Summary of Gharghur survey results, indicating total field intensity from all sources obtained by taking six-minute time averages at 15 different locations in the village.

3. SUMMARY

A three-year national survey of emissions from GSM base stations in Malta started during 2002. This project was concluded and showed that the emissions in all areas accessible to the general public were well below the ICNIRP reference levels for exposure of the general population.

As part of this project, a detailed database containing relevant information on each operational base station was constructed and field simulations made on the basis of the data supplied by the operators. Although specific values of calculated and measured fields only concur moderately because of the variability of network use and clutter occurring within built environments, field calculation is a valuable tool that can be used to establish worst-case exposure to electromagnetic fields and is useful in cases where certification of site compliance is required as a precondition to granting of transmission permits.

Recently, MCA has updated measurement and survey techniques in line with the preliminary CENELEC standard prEN 50413 [7] and a Recommendation of the ECC [8]. All telecommunications sources are now being targeted in this second phase, which aims to survey fixed transmission sites periodically.

Finally, it is observed that broadband field measurement techniques used during the first phase resulted in many more measurements than were feasible with narrowband techniques, especially when conducting six-minute averaging. The case for narrowband measurements when conducting compliance-oriented field surveys can only really be justified at sites found close to the prevalent limit level as this would allow apportionment by source. Furthermore, although taking a six-minute time average is better than averaging over shorter time intervals, in the latter case more such measurements may be made with minimal additional effort. This could give a better picture of the prevailing exposure scenario at the site under investigation since, in the case of cellular networks, the power output fluctuates significantly over short time spans. Supporting such field surveys with reliable worst-case field calculations provides an economical and reliable means of examining site compliance.

ACKNOWLEDGMENTS

The author wishes to acknowledge the support of MNL, for providing the test equipment and logistics during phase I of the project and MCA for financing this phase and assisting in the often complicated logistical arrangements required during the measurement campaigns.

The author is indebted to John Bugeja (MNL) for assisting in the audit surveys conducted during phase I and acknowledges the support of Joanna Formosa Borg, Brian Sghendo and Kevin Aquilina from MCA, who have conducted most of the work during phase II.

REFERENCES

[1] S Steward, *Mobile Phones and Health*. A report from the Independent Expert Group on Mobile Phones. Independent Expert Group on Mobile Phones Secretariat.

[2] *Report on Recommendations for Limiting Human Exposure to Time Varying Electric, Magnetic and Electromagnetic Fields in the Frequency Range from 0 Hz to 300 GHz*, Ministry of Transport and Communications, Ministry of Health and Ministry for Social Policy, Malta.

[3] C V Sammut and A Micallef, *A An Extensive RF Emissions Survey at Cellular Mobile Phone Base Station Sites in Malta*, Proceedings of the 2nd International Workshop On Biological Effects of Electromagnetic Fields, 7-11 October 2002, Rhodes, Greece, 977-986.

[4] C V Sammut and A Micallef, *Analysis of a simple technique for measuring the average exposure to electromagnetic fields over an extended region of space*, 3rd International Workshop On Biological Effects of Electromagnetic Fields, 4-8 October 2004, Kos, Greece, 832-836.

[5] *Limits of Human Exposure to Radiofrequency Electromagnetic Fields in the Frequency Range from 3 kHz to 300 GHz*, Safety Code 6, Environmental Health Directorate, Minister of Public Works and Government Services, Canada 1999.

[6] *Evaluating Compliance with FCC Guidelines for Human Exposure to Radiofrequency Electromagnetic Fields*, OET Bulletin 65, Edition 97-01, Federal Communications Commission, Office of Engineering & Technology, August 1997.

[7] prEN 50413: *Basic Standard on measurement and calculation procedures for human exposure to electric, magnetic and electromagnetic fields (0 Hz – 300 GHz)*, CENELEC, 2006.

[8] ECC/REC/(02)04, *Measuring non-ionising electromagnetic radiation (9kHz – 300 GHz)*, Revised ECC Recommendation (02)04, Electronic Communications Committee within the European Conference of Postal and Telecommunications Administrations, October 2003.

[9] C V Sammut and A Camilleri, *An Extensive Survey of RF Emissions at Cellular Mobile Phone Base station sites in Malta and Gozo: First Year*, XII Annual Engineering Conference: Engineering the Environment, 21 May 2003, St. George's Bay, Malta.

[10] C V Sammut, *Exposure to electromagnetic fields from cellular phone base stations in Malta: Final report of the three-year national survey*, Malta Communications Authority, 2006.

THE ETIOLOGY OF MELANOMA

ÖRJAN HALLBERG

HALLBERG INDEPENDENT RESEARCH
POLKAVÄGEN 14B, 142 65 TRÅNGSUND, SWEDEN
http://hir.nu

Abstract
The main purpose of this project was to find a possible explanation for the steadily increasing incidence of melanoma in Western countries since the mid-20th century. A secondary purpose was to develop models with predictive value in order to estimate future melanoma trends. Results indicate that the immune defense system for cell repair and apoptosis was disrupted by body-resonant broadcasting radiation from FM towers, and that this disturbance can fully explain both local and temporal variations in melanoma incidence and mortality.

Introduction
In May 1998 the author became aware that at the end of the 1950's, there was a sudden increase in melanoma incidence in Sweden; this coincided with a time when the country was in the midst of the process of gradually becoming covered with FM and TV broadcasting towers. This realization led to a study comparing Nordic countries with the USA to see if there was any association between melanoma incidence and the appearance of large numbers of FM broadcasting towers. A second, later study investigated the geographical variation of melanoma incidence in Sweden and its possible correlation with the geographical variation of other cancers. In a third study, melanoma incidence over time was compared with the advent of FM broadcasting in Swedish counties and with increasing habits of taking charter travels to sunnier resorts. A fourth study investigated if melanoma incidence could successfully be modeled as a response to sudden changes in environmental stress. A theory and model to explain the increased incidence of melanoma were then developed, and the model was then refined to take into account the observation that UV radiation-induced cell damage is cumulative but normally compensated for by a cell repair process that was assumed to have become less efficient from a specific point in time.

Summary
An initial study showed that Nordic countries and the USA both appeared to have the same exposure-time-specific incidence of melanoma, despite the fact that the advent and subsequent spread of FM transmitter appearance differed among the different countries [1]. A second study showed that the incidence of some cancers correlated with variations in melanoma incidence across the Swedish counties, while others (e.g. leukemia) did not [2]. Melanoma also appeared to persist at a low and stable incidence in the counties as long as FM transmitters had not yet been substantially introduced. Mortality from existing cases of melanoma showed an immediate increase that correlated with the introduction of FM broadcasting towers, and the incidence of new cases started to increase a few years after the spread of FM towers [3]. Melanoma incidence appeared to be significantly correlated with the number of main FM towers simultaneously covering an area [4]. A model for melanoma incidence was developed based on a statistical distribution of the time from the introduction of FM broadcasting until the onset of melanoma [4, 5]. Finally, it was also shown that a model based on a precipitous decrease in the efficiency of the immune defense system (presumably caused by FM broadcasting towers) was able to accurately predict the reported age-standardized incidence and age-specific incidence of melanoma for all birth cohorts during the 20th century [6].

The project concluded that body-resonant radiation from FM broadcasting towers may disturb cell repair and apoptosis processes and that this may be one of the most important factors behind the observed increase in melanoma rates in the Nordic countries. Normal broadcasting radiation is not likely to be able to cause cellular damage *de novo*, but may be able to weaken defenses against cellular damage that may be caused by pervasive "natural" sources such as UV exposure etc. It would seem logical to extend this study to similarly review lung cancer and breast cancer to examine the possibility of a correlation between these cancers and FM broadcasting radiation.

Acknowledgements
The author thanks assoc. prof. Olle Johansson at the Experimental Dermatology Unit, Department of Neuroscience, the Karolinska Institute, Stockholm, Sweden, for co-operation in several papers related to this project.

References

1. Hallberg Ö, Johansson O. Melanoma incidence and frequency modulation (FM) broadcasting. Arch Environ Health 2002; 57: 32-40
2. Hallberg Ö, Johansson O. Cancer trends during the 20th century. ACNEM Journal 2002; 21: 3-8
3. Hallberg Ö. and Johansson O. Malignant Melanoma of Skin - Not a Sunshine Story!, Med Sci Monit, 2004; 10: CR336-340
4. Hallberg Ö, Johansson O. FM broadcasting exposure time and malignant melanoma incidence. Electromagnetic Biology and Medicine 2005; 24: 1-8
5. Hallberg Ö. Increasing incidence of malignant melanoma of the skin can be modeled as a response to suddenly imposed environmental stress. Med Sci Monit, 2005; 11: CR457-461
6. Hallberg Ö. A theory and model to explain the skin melanoma epidemic. Melanoma Research, 2006; 16: 115-118

FORCE CALIBRATION OF OPTICAL TRAP BY DIELECTROPHORESIS

T. SAVOPOL*, E. PAPAGIAKOUMOU**, M. CHIRILA*, M. MAKROPOULOU**, A. SERAFETINIDES**, M. RADU*, D. PIETREANU*, G. MARTÍNEZ-LOPEZ***, M. SANCHO RUIZ***, E. KOVÁCS*

**CAROL DAVILA MEDICAL UNIVERISTY, P.O.Box 35-43, BUCHAREST, ROMANIA*
***NATIONAL TECHNICAL UNIVERSITY OF ATHENS , GREECE*
****COMPLUTENSE UNIVERSITY OF MADRID, SPAIN*

Abstract

A calibration method for optical tweezers, based on equilibration with a dielectrophoretic force, is presented. The analytical method for the computation of the dielectrophoretic force is based on a mathematical model using Green's theorem. The dependence of the optical force profile on the particle position between the electrodes and on the vertical axis is rigorously analysed and the best operating conditions are determined.

In order to have an experimental validation of the model, we used a dielectrophoretic chamber with planar electrodes and a laser diode optical tweezers (800 nm). A suspension of red blood cells was placed between the electrodes of the dielectrophoretic chamber and the optical trapping force was measured under different conditions.

We show that by applying simultaneously dielectrophoretic and optical forces on a cell, the evaluation of intracellular dielectric parameters (i.e. cytoplasmic and membrane conductivity in normal and/or pathological states) at a single cell level is possible.

Introduction

Micromanipulation of cells has become in the last years an important tool for the fundamental research as well as for some clinical applications. There are different techniques to do this, including micropipettes, microelectrodes, optical and magnetic traps. When comparing these techniques, there are of course, for each of them, advantages and disadvantages, but, the most important and decisive advantage of optical and magnetic traps is the minimal mechanic contact with the cell, optical and magnetic trapping being nowadays considered to be the less invasive micromanipulation methods.

For research purposes, the method can be used to put cells into contact, to measure interaction forces between cells and / or molecules (e.g. ligand – receptor interaction forces). The main problem in pursuing such experiments is to calibrate the trapping force. In the following we will focus our attention only on optical trap force, but the rationale can be used as well for the magnetic trap.

We will show that one can use the dielectrophoretic force as a quite simple and reliable tool to calibrate the optical trap force, and, based on this, we'll show interesting possibilities to determine some physical properties of cells in relation with their physiological state.

Principles of the optical trap

Optical traps (or tweezers) were first described by Ashkin [1 – 3] and are based on the interaction of light with a particle. In this interaction different regimes of theoretical approach can be distinguished based on the ratio of the incident light wavelength λ to the diameter d of the irradiated particle: Rayleigh Regime ($\lambda/20 >> d$), Lorenz-Mie Regime ($\lambda \approx d$) and Ray Optics Regime ($\lambda/20 << d$).The net force is the result of a combination of two different components: scattering force and gradient force. In the Rayleigh Regime the particle is acting like an induced dipole in the electric field of the laser beam. The expressions of the forces are:

$$\vec{F}_{scatt}(\vec{r}) = \vec{z} n_m \frac{\sigma(S)_T}{c} \tag{1}$$

$$\vec{F}_{grad}(\vec{r}) = \frac{1}{2}\alpha\vec{\nabla}\vec{E}(\vec{r},t)^2 \tag{2}$$

where $(S)_T$ is the temporal average of the Poynting vector, which defines the intensity of the laser beam, $\sigma = \frac{8}{3}\pi(ka)^4 a^2\left(\frac{n^2-1}{n^2+2}\right)^2$ is the cross section of the particle, $\vec{z}$ is the laser beam direction, n_m is the relative refractive index, a is the radius of the particle, $k = 2\pi/\lambda$ is the wave number, c represents the light speed in vacuum, $\vec{E}$ is the electric field and n is the absolute refractive index of the particle.

For a spherical particle in Ray Optic Regime, Ashkin established formulae for these two forces as a function of the Fresnel coefficients [1]. The expressions can be deduced based on geometrical optics laws, their scalar form being:

$$F_{scat} = \frac{n_1 P}{c}\left\{1 + R\cos(2\theta) - \frac{T^2\left[\cos(2\theta - 2r) + R\cos(2\theta)\right]}{1 + R^2 + 2R\cos(2R)}\right\} \tag{3}$$

$$Fgrad = \frac{n_1 P}{c}\left\{R\sin(2\theta) - \frac{T^2\left[\sin(2\theta - 2r) + R\sin(2\theta)\right]}{1 + R^2 + 2R\cos(2R)}\right\} \tag{4}$$

where *P* is the power of the incident beam, n_1 is refractive index of the particle, R and T are the reflectance and transmittance coefficients, θ and r are the incident and refracted angles. The expressions (3) and (4) are true for a "normal" light ray. The laser beam, being a bundle of rays, has a specific profile which has a significant contribution to the gradient force.

Finally, the net force exerted on the particle is given by the expression

$$F_{optic} = Q\frac{n_{med} P}{c} \tag{5}$$

where Q is a scaling constant which depends on the size of the particle and the refractive index difference between the particle and the surrounding medium, P is the power of incident laser beam, n_{med} is the refractive index of the medium and c is the light speed in vacuum.

Summarizing, one can say that the optical force is proportional to the power of the laser beam, and depends on some physical properties of the particle. To calibrate the laser trap means to determine this scaling factor, Q.

Calibration methods

There are two main calibration methods which are presently used for optical traps:

- Brownian movement analysis: this method is based on the statistical analysis of the Brownian movement of a trapped particle, from which one can learn about the trapping force. The method implies an extremely rigorous temperature control of the microscope stage, which is not technically trivial considering that the laser beam itself provoke some local heating of the sample, and sophisticated mathematics for image analysis;
- Viscous drag of the trapped particle: the particle is placed in a capillary tube with a constant known diameter through which the suspension buffer flows with a constant speed. A particle is trapped, and the flowing speed is increased until the particle escapes. Assuming that the flow is Newtonian, one can calculate the viscous force, which, at that moment, equals the optical force. The major problem with this method is to ensure a real Newtonian flow through the capillary.

In this paper we describe a calibration method based on the dielectrophoretic force exerted on the trapped particle.

The dielectrophoretic force exerted on a particle depends on the induced dipole moment and is unaffected by the direction of the electric field, responding only to the field gradient. Accordint to Pohl [4], the dielectrophoretic force is given by the expression:

$$\vec{F}_{DEP} = \left(\vec{P}_{eff}\cdot\vec{\nabla}\right)\vec{E}_0 \tag{6}$$

For a spherical particle of radius r, the dielectrophoretic force is given by the expression:

$$\vec{F}(\omega) = 2\pi r^3 \varepsilon_m \,\mathrm{Re}\left[K(\omega)\right]\vec{\nabla}E^2 \tag{7}$$

with

$$K(\omega) = \frac{\left(\varepsilon_p^* - \varepsilon_m^*\right)}{\left(\varepsilon_p^* + 2\varepsilon_m^*\right)} \tag{8}$$

and

$$\varepsilon^* = \varepsilon - j\frac{\sigma}{\omega} \tag{9}$$

where ε_m^*, ε_p^* are the complex permitivities of the medium and the particle respectively and ω is the angular frequency of the applied field. For a particle with shell, the expression of the complex permitiviy becomes:

$$\varepsilon_p^* = \frac{\left[\frac{r}{r-d}\right]^3 + 2\left[\frac{\varepsilon_{\mathrm{int}}^* - \varepsilon_{mem}^*}{\varepsilon_{\mathrm{int}}^* + 2\varepsilon_{mem}^*}\right]}{\left[\frac{r}{r-d}\right]^3 - \left[\frac{\varepsilon_{\mathrm{int}}^* - \varepsilon_{mem}^*}{\varepsilon_{\mathrm{int}}^* + 2\varepsilon_{mem}^*}\right]} \tag{10}$$

The computation of the root mean square of the electric field at a specified point between and over the electrodes is made using the second Green's identity:

$$\int_V dV\left(\Phi\nabla^2\Psi - \Psi\nabla^2\Phi\right) = \oint_A dA\left(\Phi\frac{\partial\Psi}{\partial n} - \Psi\frac{\partial\Phi}{\partial n}\right) \tag{11}$$

One of the function (Φ) is choosen to be the potential between electrodes ($z = 0$), $\nabla^2\Phi = 0$ and the other (Ψ) is a Green function given by $\nabla^2\Psi\left(\vec{r},\vec{r}_0\right) = -4\pi\delta\left(\vec{r} - \vec{r}_0\right)$. Determination of the Green function is made using the mirror-image method.

$$\begin{aligned}\Psi &= \frac{1}{\left|\vec{r} - \vec{r}_0\right|} + \frac{-1}{\left|\vec{r} - \vec{r}_0'\right|} \\ &= \frac{1}{\sqrt{\left(x - x_0\right)^2 + \left(y - y_0\right)^2 + \left(z - z_0\right)^2}} \\ &+ \frac{-1}{\sqrt{\left(x - x_0\right)^2 + \left(y - y_0\right)^2 + \left(z - z_0\right)^2}}\end{aligned} \tag{12}$$

The first order approximation (assuming that the potential varies linearly between the two electrodes) is used, so that the boundary conditions are given by:

$$\Phi\left(x, y, z = 0\right) = \begin{cases} \frac{V}{2}\cos\left(\omega t\right), & -l_x - \Delta\langle x\langle -\Delta \\ -\frac{V}{2}\cos\left(\omega t\right)\frac{x}{\Delta}, & -\Delta \le x \le +\Delta \\ 0 & -\infty\langle x \le l_x - \Delta, l_x + \Delta\langle x\langle\infty \end{cases} \tag{13}$$

Where Δ is half distance between the electrodes.
The expression for the electrical field is then:

$$\Phi(x, y, z) = \frac{-V}{2\pi}\cos(\omega t)\left[\frac{z}{\Delta}\ln\sqrt{\frac{(x+\Delta)^2 + z^2}{(x-\Delta)^2 + z^2}} - \arctan\left(\frac{2xz}{z^2 + \Delta^2 - x^2}\right) + \frac{x}{\Delta}\arctan\left(\frac{2\Delta z}{z^2 - \Delta^2 + x^2}\right)\right] \tag{14}$$

After an algebric calculation, the root mean square of E^2 becomes, as it was shown by [5]:

$$E_{rms}^2 = \frac{V^2}{8\pi^2\Delta^2}\left[\frac{-8x^2z\Delta+\left[x^4+2x^2\left(z^2-\Delta^2\right)+\left(z^2+\Delta^2\right)^2\right]\arctan\left(\frac{2x\Delta}{x^2+z^2-\Delta^2}\right)}{\left[(x-\Delta)^2+z^2\right]\left[(x+\Delta)^2+z^2\right]}\right]^2 \quad (15)$$

$$+\frac{V^2}{8\pi^2\Delta^2}\left[\frac{4x\Delta\left(x^2-z^2-\Delta^2\right)+\left[x^4+2x^2\left(z^2-\Delta^2\right)+\left(z^2+\Delta^2\right)^2\right]\ln\sqrt{\frac{(x+\Delta)^2+z^2}{(x-\Delta)^2+z^2}}}{\left[(x-\Delta)^2+z^2\right]\left[(x+\Delta)^2+z^2\right]}\right]^2$$

For the particular case of our dielectrophoretic cell, the root mean square of E^2 has the profile shown in Fig. 1.

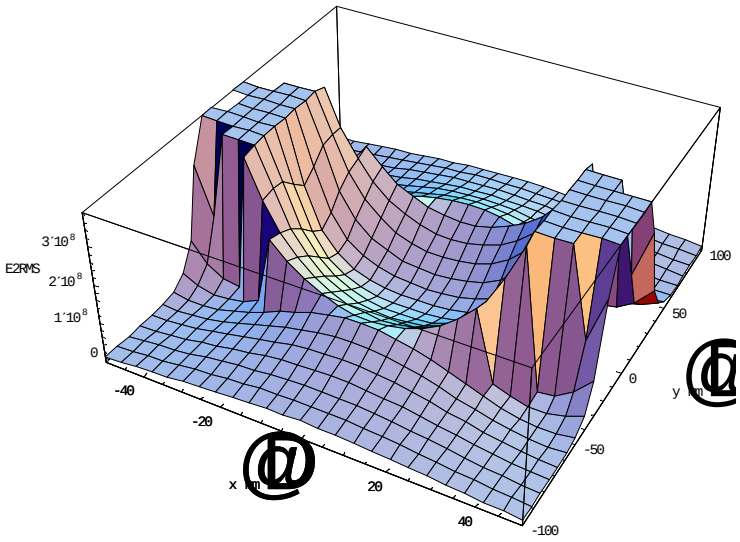

Figure 1: *Distribution of root mean square of E^2 between the electrodes of the dielectrophoretic chamber. The x axis is along a direction within the plane of the cell and perpendicular to the electrodes, while the y axis is perpendicular to the plane of the cell and along the optical axis of the microscope.*

The value of the dielectrophoretic force can thus be calculated by introducing this last equation in (7).
As an example, we give the profile of the horizontal (x) component of the force in the case of our experimental setup, at two different constant heights (5 μm and 35 μm) above the plane of the cell, as a function of the position of the particle between the electrodes (Fig. 2). In this case the distance between electrodes is 100 μm (Δ = 50 μm) , and the voltage is $V = \pm 1.5\,V$

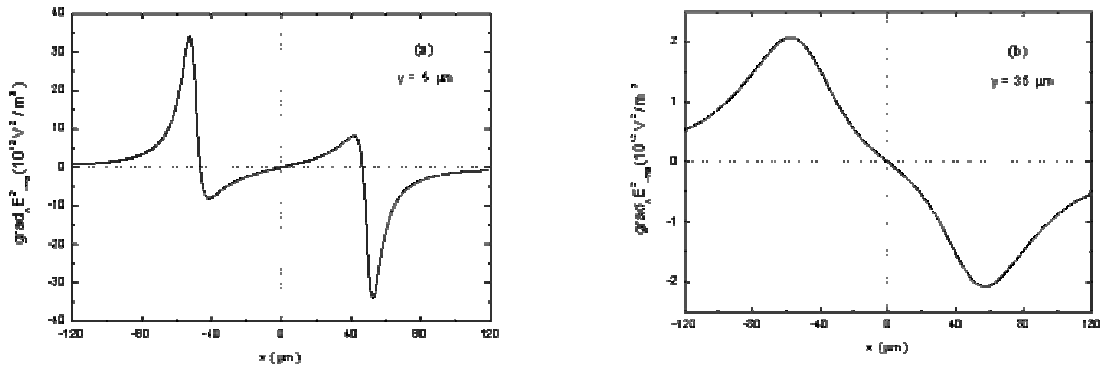

Figure 2: *The x-component force profile computed as a gradient of E_{rms}^2 at two different heights above the plane of the dielectrophoretic cell : (a) y = 5 5 μm and (b) y = 35 μm. The gap between the electrodes lays from*

-50 μm to 50 μm along the x axis.

The vertical component of the force can be also computed, but it is less important for our purposes.

Experimental protocol and results

The optical tweezers we used was built on a normal optical microscope (IOR MC9) on which a laser diode of 830 nm wavelegth and 40 mW maximum power was mounted. Maximum 27 mW power was getting out of the lens in the focal plane, as measured by a power-meter. The diode was connected to a variable power supply which allows adjustment of the laser beam output power.

The dielectrophoretic chamber consisted of two thin planar electrodes deposited on a microscope slide at a distance of $2\Delta = 100\mu m$. The electric field was applied by a computer controlled function generator (PC Generator PCG10/K8016 Welleman Instruments). For calibration, red blood cells with dielectric parameters, $\varepsilon_{\text{int}} = 50\varepsilon_0$ and $\sigma_{\text{int}} = 0.5\ S \cdot m^{-1}$, $\varepsilon_{mem} = 11.3\varepsilon_0$ and $\sigma_{\text{int}} = 10^{-7}\ S \cdot m^{-1}$ were used. The suspension buffer was a 0.3 M Mannitol solution at $pH = 7.4$ and dielectric parameters: $\varepsilon_{med} = 80\varepsilon_0$ and $\sigma_{med} = 235\ \mu S \cdot cm^{-1}$.

All measurements were performed using a 100X microscope lens with 1.25 numerical aperture.

The first step is to determine the output force of hte laser beam at the focal point as a function of the applied voltage on the diode. This is done by using an appropriate power-meter and measuring the emitted power at different voltages. The results can be seen in Fig. 3.

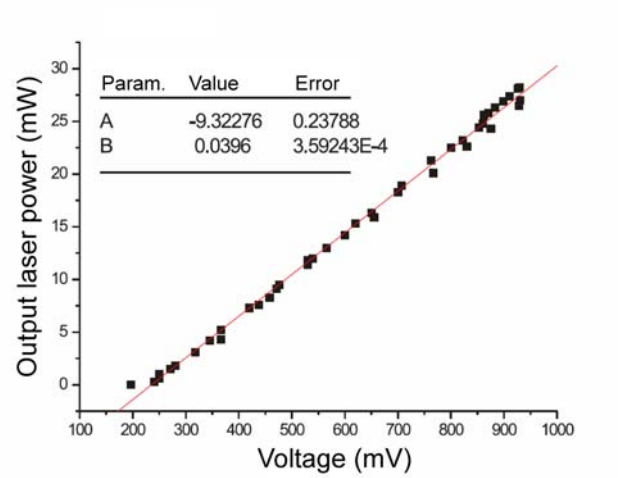

Figure 3: *Laser beam power calibration, as a function of the electric power applied to the laser diode.*

After this first step, we used a standard procedure which consists in the following:

- a cellular suspension is placed on the dielectrophoretic chamber and mounted on the microscope;
- a cell which lays between the electrodes, but closer to one of them is trapped in the laser beam using the maximum laser power;
- then an AC field of 1 MHz frequency and very low voltage amplitude is applied on the electrodes. As a result, a dielectrophoretic force will act on the trapped cell, which depends on the cell diameter and its position between the electrodes (the *x* position) and along the vertical (*y*) axis;
- the voltage is then increased until the cell escapes the trap (at this moment the dielectrophoretic force equals the optical force); introducing this last value of the voltage in equations (15) and (7), one can compute the optical force exerted by the laser on the cell.

We measured these forces for red blood cells at different intervals after the blood colllection and different times after withdrawal of the sample from the refrigerator.

Some representative results can be seen in Figs. 4 and 5.

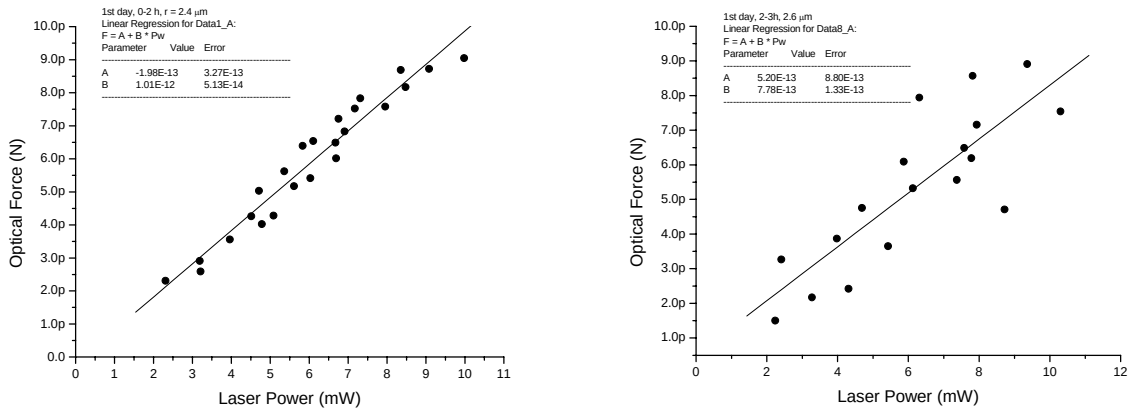

(a) (b)

Figure 4: *Optical trap force as a function of the applied laser power, measured soon after the sample was taken out of the refrigerator(a) and 2 h later (b) .*

Inspecting Fig. 4 it can be seen that the dependence is linear. It can also be seen that in similar conditions, cells which were kept for longer periods at the room temperature (Fig. 4b) present a much higher dispersion than samples measured immediately after they were taken out of the refrigerator.
In Fig. 5 we present results obtained on cells with the same diameter (2.6 μm), at different storage times (1st day after blood collection (a) and 5th day after (b)).

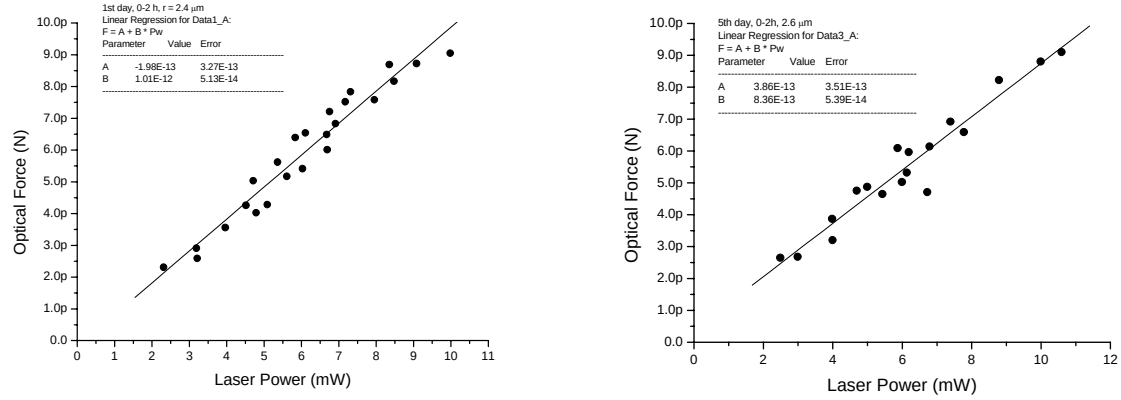

(a) (b)

Figure 5: *Optical trap force as a function of the applied laser power, measured at two different blood storage periods (a)- 1st day after blood collection and (b) – 5th day after blood collection .*

It can be seen that at the same laser power, the resulting optical force is lower as the sample becomes older, although the dispersion of the data remains almost unchanged (e.g. for 6 mW laser power, the optical force is 5.5 pN in Fig. 5a, and 6.5 pN in Fig. 5b).

Discussions

We have shown that dielectrophoretic force can be used to calibrate an optical trap force using an adequate model. On the other hand, analysing the behaviour of the cells in an optical trap combined with dielectrophoresis, we were able to detect significant differences in the cell's response, depending on their metabolic state.
Considering that the optical trap force depends essentially on the cell surface and the cytoplasmic refractive index, it is obvious that biochemical modifications associated with different states of the cell will influence its

behaviour in the optical trap.

References

1. Ashkin, J.M. Dziedzici, J.E.Bjorkholm and S. Chu, Observation of a single-beam gradient trap for dielectric particles, Opt. Lett., **11**, 288 – 290 (1986)
2. Ashkin, J.M. Dziedzici and T. and T. amane, Optical trapping and manipulation of single cells using infrared laser beams, Nature (London), **330**, 769 – 771 (1987)
3. Ashkin, K. Schultze, J.M. Dziedzici, U. Euteneuer and M. Schliwa, Force generation of organelle transport measured in vivo by an infrared laser trap, Nature (London), **348**, 346 – 348 (1990)
4. H.A. Pohl, Dielectrophoresis: the behaviour of neutral matter in nonuniform electric fields, Cambridge Univ. Press, London, 1978
5. E. Papagiakoumou, D. Pietreanu, M.I. Makropoulou, E. Kovacs, A.A. Serafetinides, Evaluation of trapping efficiency of optical tweezers by dielectrophoresis, J. Biomed. Opt., **11**, 1 – 8 (2006)

MULTIPLE ANTENNA SYSTEMS IN MOBILE PHONES AND THEIR PERFORMANCE IN TERMS OF EMF EXPOSURE

MICHAEL A. BALDAUF, CHRISTIANE KUHNERT, STEPHAN SCHULTEIS, AND WERNER WIESBECK

INSTITUT FÜR HÖCHSTFREQUENZTECHNIK UND ELEKTRONIK, UNIVERSITÄT KARLSRUHE (TH), KAISERSTR. 12, 76131 KARLSRUHE, GERMANY

Abstract

Communication systems with several antennas at the transmitting and receiving end are called multiple input multiple output (MIMO) systems. In a first approach it is shown that demanding a certain capacity expressed as information per bandwidth and time (in bit/Hz/s) MIMO systems permit a significant reduction of transmit power. Therefore, also the specific absorption rate (SAR) in the human head decreases. In a second approach the total transmit power is held constant. In this case the increased capacity of a MIMO system leads to a performance increase by which the time of the data transmission can be reduced. There exist different MIMO schemes: systems without channel state information available at the transmitter or systems having full channel knowledge at the transmitter. Comparing these schemes we show that MIMO systems show a better performance in terms of exposure than classical single antenna systems. The exposure efficiency of a system as quotient of capacity and SAR is suggested as a measure of the exposure.

Introduction

There are limit values concerning the human exposure to electromagnetic fields (EMF). A lot of countries refer to the ICNIRP Guidelines [1]. For the far field exposure due to base stations the exposure can be conveniently described by the electric field strength (E) or the power density (S). For the human head held close to a mobile phone there is a strongly varying near field over different tissue types. Therefore, a determination of the specific absorption rate (SAR) is necessary. The exposures which encounter in real life due to base and mobile stations are very different compared to the limit values. Safety distances to base stations based on the ICNIRP Guidelines [1] are typically just a few meters [2]. Thus, the exposures due to base stations are usually well below the limits. However, concerning the exposure to mobile phones some phones are quite close to the SAR limit [3].

Classical systems consist of one antenna at the transmitter and one antenna at the receiver. These are named Single Input Single Output (SISO) systems. Recently, wireless communication systems with multiple transmit and multiple receive antennas are subject to many research activities. In these Multiple Input Multiple Output (MIMO) systems, smart antenna techniques are exploited on both sides of the link. Simple MIMO systems have got no information about the propagation channel at the transmitter. In systems with channel knowledge the antenna arrays are adapted to the spatial properties of the propagation channel. The increased performance of MIMO systems in terms of capacity can be used to lower the transmit power leading to a lower exposure. The first approach to examine the exposure of MIMO systems presented in this paper is based on the decrease of the transmit power to achieve the same capacity as in SISO systems. On the other hand in a second approach presented in this paper the transmit power is held constant for SISO and MIMO. The increase in capacity is set into a relation with the SAR. Therefore, this approach shows that MIMO systems will result in lower doses.

Since the propagation channel is non-static the capacity is a random variable. In the investigations done here the term capacity refers to an outage capacity of 10 %. I.e. the calculated capacities are not reached in 10 % and exceeded in 90 % of the realizations.

Handy Model

The simulation model of the handheld device consists of a metallic block, representing the battery and the display of the device, and a PVC housing (cf. Fig. 1). The size of the housing is 55 x 115 x 27 mm^3. The metallic block is 40 x 80 x 10 mm^3 in size. A standard type of miniaturized antennas (Inverted-F) is built in the mobile phone. One, three or four Inverted-F antennas are mounted onto the metallic block spatially separated and with different orientations to exploit different diversity techniques, such as spatial, pattern and polarization diversity. Usually Inverted-F antennas require an infinite ground plane, which is not available in the small hand-held device. Thus the metallic block, representing the ground plane, acts as a part of the antennas and influences the shape of the patterns and the mutual coupling impedances. Detailed results on design and performance of these MIMO hand-held models can be found in [4].

An operating frequency of 2 GHz and a bandwidth of 3.84 MHz are considered for all the simulations performed. The maximum value of the localized SAR is averaged over any 10 g tissue SAR_{10g}. The calculation is done numerically with FEKO [5].

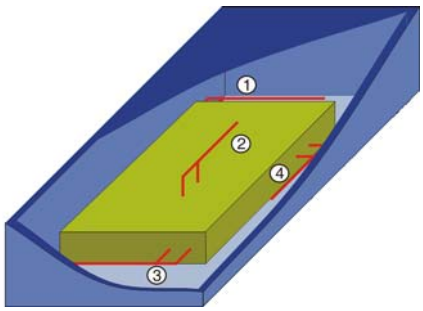

Fig. 1: Model of a hand-held device equipped with four Inverted-F antennas.

The hand-held device is attached to a phantom head, which has the size and the shape of an adult human head (density 1000 kg/m^3) and adequate dielectric properties ($\varepsilon_r = 40$, $\sigma = 1.4$ S/m) (cf. Fig. 2).

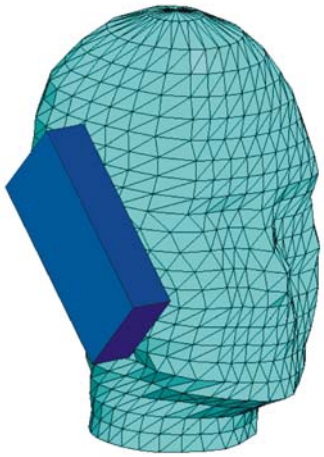

Fig. 2: Model of the user's head where the mobile phone is attached.

Model for the Propagation Channel

The campus of the University of Karlsruhe was modeled. Therefore, an outdoor scenario is considered for the wave propagation channel. The base station is mounted 3 m above the roof top of one of the highest buildings of the campus. The mobile phone is located at about 1000 randomly chosen positions on street level. By a ray-tracing technique the waves between the mobile and the base station are calculated [6].

Base Station Antennas

The base station is equipped with one antenna for the SISO case and three antennas with spacings of 1 m for the MIMO cases. The commercially available base station antenna Kathrein type 735147 is used and modeled [2]. The radiation pattern illuminates a 120° sector in the azimuth plane. The elevation pattern is tilted down by 5°, see Fig. 3.

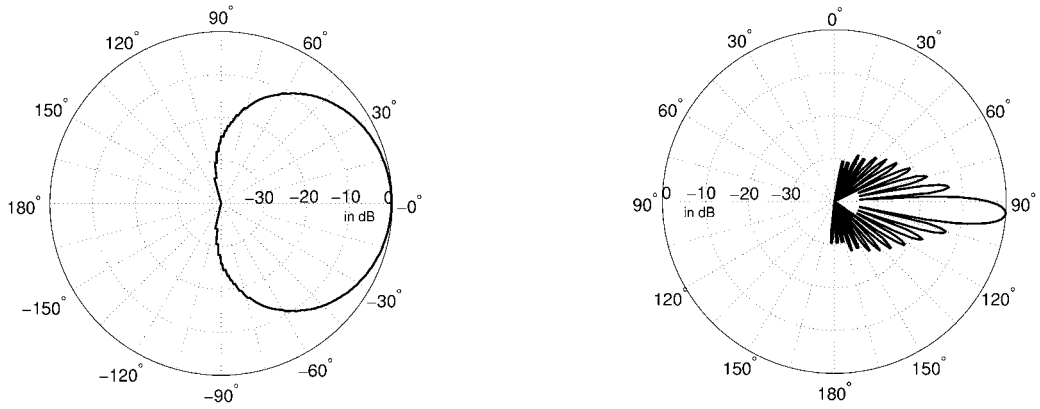

(a) azimuth pattern (b) elevation pattern

Fig. 3: Radiation pattern of a base station antenna in azimuth and elevation.

MIMO schemes

MIMO systems can be classified by the transmission scheme applied. It is important to distinguish between MIMO systems with and without channel state information (CSI) at the transmitter. In other words, it has to be distinguished between transmitters that do know or do not know the channel. The channel can only be estimated by the receiver. To supply the transmitter with the channel knowledge, it has to be transmitted back to the transmitter. (For time division duplex systems reciprocity may be applied). This back transmission of the channel state information is difficult to realize and reduces the data rate available for the user of the link. Therefore, MIMO systems which do not need to know the channel at the transmitter are very attractive. On the other hand, the optimal capacity of a MIMO system is only reached with perfect channel knowledge at the transmitter. Thus, to reach very high data rates, the transmitter must be informed about the channel. To reduce the complexity of MIMO systems, systems that do only beamforming on both sides of the link, are an attractive option. Those systems do not (except for a very small signal to noise ratio) reach the capacity of normal MIMO systems, because only one data stream is transmitted at one time – in contrast to the spatial multiplexing systems described before.

The following three MIMO schemes are considered:

- MIMO without CSI at the transmitter
- MIMO with CSI at the transmitter
- Beamforming-based MIMO

The capacity and the SAR are calculated and compared for several antenna configurations.

Excitation of the Antennas at the Transmitter

In general, an excitation voltage excites an antenna. Hence, the electric field strength and therewith the SAR in the human head depend also on the excitation voltages of each antenna element. In a SISO system, this voltage is directly related to the transmit power. In a MIMO system the transmit power is distributed over all antennas. Each antenna in the mobile phone can be excited by an individual excitation voltage. The distribution of the transmit power is dependent on the MIMO scheme applied. In the case of MIMO without CSI the transmit power is distributed uniformly. In the case of MIMO with CSI or MIMO-based beamforming the excitation voltages are adjusted to obtain a high capacity. Therefore, the propagation channel has to be taken into account. The model given in [7] is applied. It describes the propagation channel for a MIMO system including the transmit and the receive antennas. It is based on a scattering parameter description.

Investigated Antenna Systems

The following antenna configurations are considered:

- SISO: the handheld with one antenna next to a human head, transmitting to a base station with one antenna
- SIMO 1x3: the single antenna handheld next to a human head, transmitting to a base station with three antennas
- MISO 3x1: the three-antenna handheld next to a human head, transmitting to a base station with one antenna
- MISO 4x1: the four-antenna handheld next to a human head, transmitting to a base station with one antenna
- MIMO 3x3: the three-antenna handheld next to a human head, transmitting to a base station with three antennas
- MIMO 4x3: the four-antenna handheld next to a head, transmitting to a base station with three antennas

For the case of MIMO without CSI it is assumed that via each antenna an independent subchannel is transmitted. At the receiving end the transmitted signal has to be reconstructed. For a system without CSI only configurations are possible were the number of transmit antennas is smaller or equal to the number of receiving antennas.

Approach 1: Constant Capacity

To show the performance of MIMO systems a constant capacity C = 0.25 bit/s/Hz is considered. For simplicity a MIMO scheme without CSI at the mobile phone is regarded. I.e. only systems were the number of transmit antennas is smaller or equal to the number of receiving antennas are taken into account.

A classical SISO system will need a transmit power P_T = 19.9 dBm to reach the demanded capacity, resulting in a SAR_{10g} = 0.46 W/kg (cf. Fig. 4). Increasing the number of antennas at the receiving base station will lower the required transmit power to P_T = 10.2 dBm. Since the transmit power can be decreased by almost 10 dB by just adding more antennas at the base station, while using the same antenna at the mobile phone, there is a decrease in the SAR by the same amount to 0.049 W/kg. Further on, adding two antennas to the mobile phone will allow a further decrease of the transmit power (P_T = 4.9 dBm) yielding a SAR_{10g} = 0.018 W/kg.

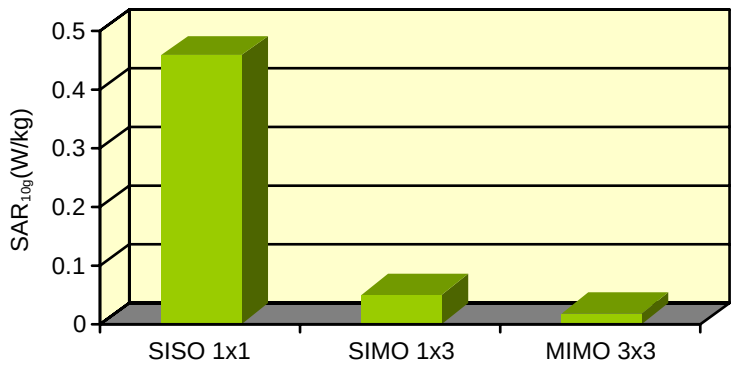

Fig. 4: SAR_{10g} for systems without CSI. Constant capacity C = 0.25 bit/s/Hz.

Approach 2: Constant Transmit Power

Since there is an increasing demand for higher capacities the transmit power of the mobile phone was fixed to P_T = 20 dBm, which is 1 dB below the maximum transmit power of a UMTS class 4 mobile phone [8]. As a rule of thumb: The more antennas there are the higher will be the achievable capacity. This capacity increase can be used to transmit the same information in a shorter time interval. The product of the SAR multiplied by the time of the exposure duration will give a dose.

Therefore, for different antenna configurations and the three mentioned MIMO schemes the SAR_{10g} (exposure) and capacities C are evaluated.

Systems without CSI

The cumulative distribution function (cdf) of the MIMO capacity is given in Fig. 5 for the case of MIMO without CSI at the transmitter. Shown is the probability P that the capacity is smaller than the value on the x-axis. The run of the curves demonstrates that adding further antennas tremendously increases the achievable capacity while keeping the total transmit power constant.

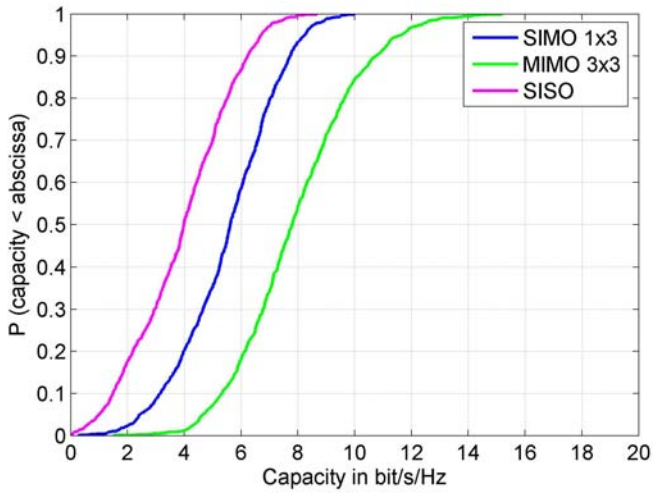

Fig. 5: Capacity for SISO and MIMO systems without CSI at the transmitter. Constant transmit power P_T = 20 dBm.

The calculation of the SAR is independent of the channel matrix in this case, because the excitation voltages are kept constant due to the lack of the channel knowledge at the transmitter. There is only one SAR_{10g} value for all channel realizations. This SAR_{10g} value is shown in Fig. 6 for different antenna configurations. SISO A1 and SISO A4 correspond to SISO systems were different transmit antennas are excited. Since the show very similar capacities there is just one line in Fig. 5.

The antenna configurations with only one antenna at the mobile station lead to the largest SAR_{10g}. Especially if the antenna is close to the head as in the case of SISO A4 the SAR_{10g} is close to 1.4 W/kg. The SAR_{10g} can be decreased by using an antenna position which is more optimized in terms of exposure. The configuration SISO A1 and SIMO 1x3 use the same transmit antenna at the mobile phone. For the MIMO case the SAR_{10g} is reduced to a value of 0.36 W/kg, although the transmit power is the same as in the single antenna cases and the capacity is remarkably higher.

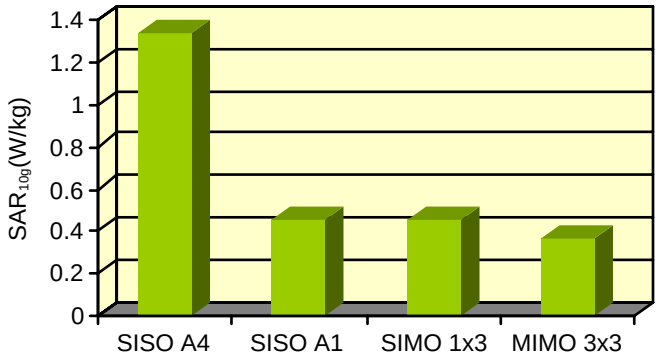

Fig. 6: SAR_{10g} for SISO and MIMO systems without CSI at the transmitter. Constant transmit power P_T = 20 dBm.

Systems with CSI

Figure 7 shows the cdf of the capacity for the optimum MIMO scheme with channel state information (CSI) at the transmitter. These MIMO systems by far exceed the other MIMO schemes in terms of capacity – keeping in mind that the total transmit power is kept constant for all systems.

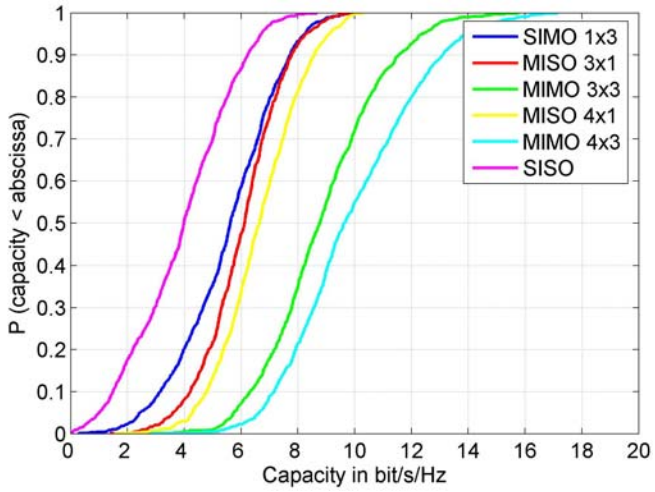

Fig. 7: Capacity for SISO and MIMO systems with CSI at the transmitter. Constant transmit power P_T = 20 dBm.

The localized SAR_{10g} are shown in Fig. 8. Since the channel changes with time the mean value of 100 SAR values is considered. For the MIMO cases, the scheme with CSI at the transmitter leads to larger SAR values than the scheme without CSI at the transmitter. For the SISO systems, the SAR values do not depend on the scheme applied, because the amplitude of the excitation voltage is held constant and its phase does not influence the SAR due to a lack of interfering signals.

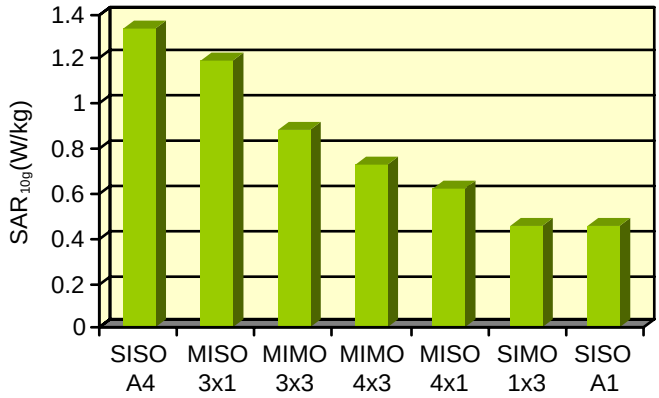

Fig. 8: SAR_{10g} for SISO and MIMO systems with CSI at the transmitter. Constant transmit power P_T = 20 dBm.

Systems with beamforming-based MIMO

Beamforming-based MIMO uses only the best subchannel, i.e. there is only one data stream transmitted. Fig. 9 shows that in this case the lowest capacities are obtained. Due to beamforming at both ends, the capacity is still enhanced by increasing the number of antennas.

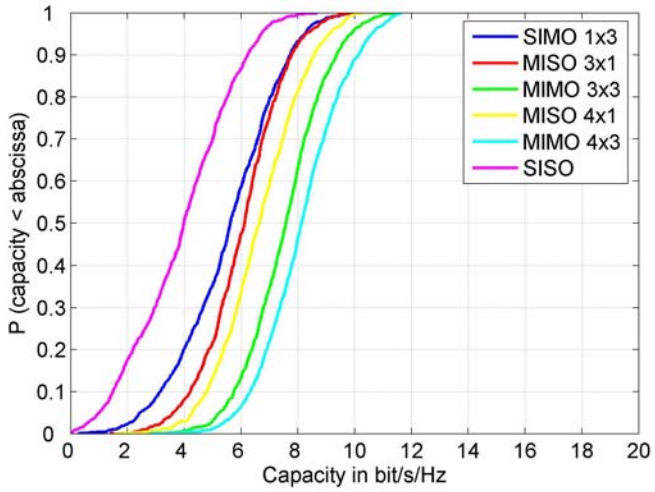

Fig. 9: Capacity for SISO and beamforming-based MIMO. Constant transmit power P_T = 20 dBm.

The results for the SAR_{10g} are given in Fig. 10. In systems where the minimum number of transmit and receive antennas equals one there exists only one subchannel. Therefore, there is no difference between MIMO with channel state information at the transmitter and beamforming-based MIMO in these cases and the SAR values are the same. For the MIMO 3x3 configuration the SAR values are quite similar, 0.88 W/kg with CSI and 0.86 W/kg for beamforming-based MIMO. For the MIMO 4x3 case, the SAR values are also similar.

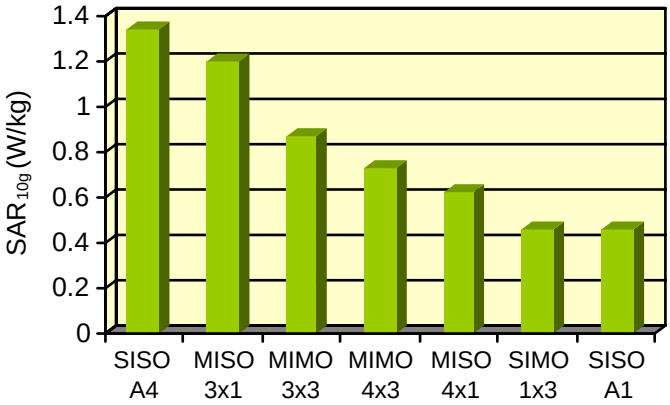

Fig. 10: SAR_{10g} for SISO and beamforming-based MIMO. Constant transmit power P_T = 20 dBm.

Exposure Efficiency

The total transmit power has been kept constant for all MIMO schemes and all antenna configurations in the second approach. But the capacity differs remarkably for the different cases.

For a further evaluation of the MIMO schemes and antenna configurations the quotient of 10% outage capacity *C* and the specific absorption rate SAR is computed. The result is given as exposure efficiency EE of the system:

$$\mathrm{EE} = \frac{10\%\ \text{outage capacity}}{\text{max. localized SAR averaged over 10g tissue}} = \frac{C}{\mathrm{SAR}_{10g}}$$

An exposure-optimized system exhibits a high capacity and low SAR_{10g}. I.e. for an exposure-optimized system the value of EP is larger compared to a system with poorer exposure efficiency. The higher the value of EE the smaller is the exposure integrated over time experienced by the operator of the mobile to transmit a certain amount of information.

Fig. 11 shows the exposure efficiency EE for all antenna configurations and MIMO transmission schemes. No results are shown for the case of a system without CSI at the transmitter if the number of transmit antennas is larger than the number of receiving antennas since the receiver can't reconstruct the transmitted data streams without a channel knowledge.

The exposure efficiency EE for configurations where there is only one transmit antenna is the same for all MIMO schemes since the fixed transmit power is radiated by the single antenna. Adding antennas at the receiving or transmitting end will yield a higher EE. The MIMO 3x3 system without channel knowledge shows the best EE. If channel knowledge is available for this configuration the antenna weightings are adjusted to increase the capacity. Howecer, this adjustment leads also to a higher SAR value. The increase in SAR is larger than the increase in capacity. The considered SISO systems show the worst exposure efficiency EE.

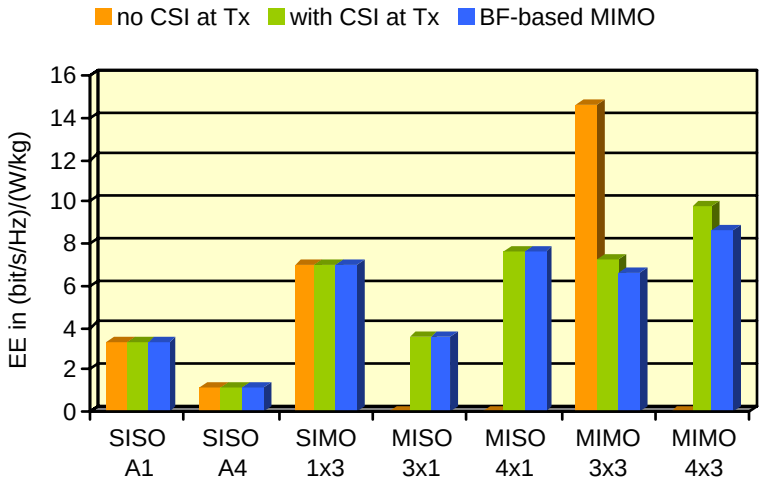

Fig. 12: Exposure efficiency for the investigated MIMO schemes.

Conclusion

It is shown that multiple antenna systems outperform classical single antenna systems by allowing higher capacities. To reach a demanded capacity the transmit power of a MIMO system can be clearly lowered compared to a SISO system. This leads to a tremendous decrease in exposure. Keeping the transmit power constant shows that MIMO systems with channel knowledge give the highest capacities. However, the exposure efficiency might be lower than in a system without channel knowledge. The MIMO scheme allowing the highest capacity is not necessarily optimized in terms of exposure.

References

[1] ICNIRP, "Guidelines for limiting exposure to time-varying electric, magnetic, and electromagnetic fields (up to 300 GHz)", *Health Physics*, vol. 74, no. 4, pp. 494-522, 1998

[2] M.A. Baldauf, A. Herschlein, W. Sörgel, W. Wiesbeck, "Safety Distances in Mobile Communications", *Proceedings of 2nd International Workshop on Biological Effects of Elektromagnetic Fields*, pp. 148-156, Rhodes, Greece, Oct. 2002

[3] http://www.mobile-phones-uk.org.uk/sar.htm

[4] C. Waldschmidt, C. Kuhnert, M. Pauli, W. Wiesbeck, "Integration of MIMO antenna arrays into hand-helds", *IEE Int. Conf. on 3G Mobile Communication Technologies*, London, UK, Sept. 2004

[5] FEKO. http://www.feko.info

[6] J. Maurer, C. Waldschmidt, T. Kayser, W. Wiesbeck, "Characterisation of the time-dependent urban MIMO channel in FDD communication systems", *Proc. IEEE Vehicular Technology Conference VTC-Spring*, April 2003, pp. 544-548

[7] C. Waldschmidt, S. Schulteis, W. Wiesbeck, "Complete RF system model for the analysis of compact MIMO arrays", *IEEE Transactions on Vehicular Technology*, vol. 53, pp. 579-586, May 2004

[8] *3rd Generation Partnership Project; Technical Specification Group Radio Access Networks; User Equipment (UE) radio transmission and reception (FDD) (Release 4)*, 3GPP TS 25.101, 2004

THE EFFECT OF 1800 MHZ ELECTROMAGNETIC RADIATION EXPOSURE ON CORTICAL AND HIPPOCAMPAL ELECTROGENY IN NEURODEFECTIVE AND HEALTHY BRAIN

JAN BARCAL[1], JAN VRBA[2], FRANTIŠEK VOŽEH[1]

[1]Charles University in Prague, Faculty of Medicine Pilsen, Department of Pathophysiology; Czech Republic
[2]Czech Technical University in Prague, Faculty of Electrical Engineering, Department of Electromagnetic Field; Czech Republic

Abstract

In this study a simultaneous registration of the brain cortical and hippocampal activity during a high-frequency electromagnetic field (HF EMF) exposure was performed. All procedures were done under urethane anaesthesia (20%, 2g/kg i.p.) in Lurcher mutant mice (LMM) which serve as an excellent model of neurodegeneration. Healthy wild type mice (WTM) were used as controls. The animals were exposed to 1800 MHz HF EMF corresponding with the mobile phone frequency. We used gel electrodes (silicon tubes or glass microcapillaries filled with agar) where the connection with metallic electrodes is located out of HF EMF space. The evaluation of electrocorticograms and spontaneous hippocampal rhythmicity showed a distinct shift in main components of frequency spectra but clear effect has been observed only in WTM. Mice with inborn neurodegeneration (LMM) exhibited only gentle differences. The comparison of cortical and hippocampal electrogeny suggest an opposite effect of HF EMF on the brain cortex and hippocampal neuronal circuits. These findings support ideas about possible influencing the central nervous system by HF EMF exposure and support also some recent results about hidden health risks resulting from the mobile phones use.

Introduction

Each electromagnetic source localized near the biological object produces electromagnetic field which may cause **both thermal and non-thermal biological effects.**

A basic principle of **thermal effects** is the rise of temperature produced by the energy absorbed from oscillating electric fields. The force produced by an electric field on charged objects, such as the mobile ions present in the body, causes them to move, resulting in electric currents, and the electrical resistance of the material in which the currents are flowing results in heating. This heat input causes the temperature to rise and it continues to do so until the heat input is balanced by the rate at which it is removed, mostly by blood flowing to and from other parts of the body. Theoretical studies are fosussed to the computation of specific absorption rate (SAR). The relationship between the SAR and the resulting temperature rise is complex, and significantly dependent on antenna configuration, location and frequency. The most problematic feature of a temperature calculation is modelling the effect of blood flow on heat transfer. Van Leeuwen et al. [1] published that heat deposition within the head was computed by coupling a finite difference time domain model for SAR with a new thermal model. T'he thermal model includes the convective effects of discrete blood vessels, whose anatomy was determined using magnetic resonance angiography of a healthy volunteer. For a 915 MHz dipole antenna with a time-averaged power output of 0.25 W (equivalent to a typical mobile phone), this study results in an SAR of about 1.6 W/kg and predicts a maximum brain temperature rise of 0.11 °C in the steady state.

An explanation of **non-thermal effects** seems to be more complicated and also controversial. The energy quanta of radiation at 0.9 and 1.8 GHz equal 4 and 7 μeV, respectively. Both these values are extremely small compared with the energy of around 1 eV needed to break the weakest chemical bonds in genetic molecules (DNA). Detectable changes can arise only if the effect of the electric field within the biological system exposed to RF fields is not masked by thermal noise. Thermal noise or random motion, also known as Brownian motion, is due to the thermal energy that all objects possess at temperatures above absolute zero. In solids, the atoms vibrate and in gases and liquids they move erratically to and fro following very frequent collisions with other atoms. So all components of biological tissue - ions, molecules and cells - are in

constant motion. Another mechanism involving cells concerns the attraction between them in the presence of an electric field [2], [3]. The electric field polarises the cell, that is to say charges in the cell move so that one side of it becomes positive with respect to the other. The cell is then an electric dipole (like a tiny torch battery) and attracts similarly polarised cells. For typical cells and frequencies below about 100 MHz, the energies involved are calculated to become comparable to thermal noise in electric fields of E=300 V/m. The energies are calculated to become appreciably less for RF fields, but Adair [3] suggests that, since these values would depend on the detailed structure of the biological elements involved, the possibility of biological effects for fields of this size cannot be excluded. Other possible biological effects are associated with cell membranes and the movement of currents through the membrane in either direction. Membranes are known to have strongly non-linear electric properties [4]. When a voltage is applied across the membrane, the current that flows is not always proportional to the voltage. Part of this non-linearity may, in fact, be due to the effect of the electric field on the proteins in the membrane or nearby, which assist the flow of the product currents through the membrane. The membrane also acts as a rectifier. If a voltage is connected across the ends of a wire, the size of the current that flows depends solely on the magnitude of the voltage: if the polarity of the voltage is reversed, the current changes direction but its size is unchanged. However, if the polarity of the voltage applied across a rectifier is reversed, the current changes direction but now its size also changes. So, if an oscillating voltage (electric field) is applied across a rectifier, the total current that flows when the field is in one direction is not balanced by the current when the field is in the other: an AC field produces a net DC current and hence a net flow of products through the membrane. However, the response times of the ion gates are very much slower than the period of microwave frequencies and, using data obtained from measurements on membranes [4], it has been shown that, for electric fields of 200 V/m, the relative change in the membrane potential is very small [3]. Another hypothesis is that the interaction with biological tissue depends on the coherence of the electromagnetic fields [5].

Possible effects on the brain and behaviour during acute exposure to RF fields are permanently discussed - mobile phones are conventionally held close to the head. Many results are about effects of RF fields on isolated nerve cells (neurons), on cultured nervous tissue, on living brain slices, on brain function in experimental animals, on the blood-brain barrier and on behavioural measures of brain function [6,7,8,9]. The behaviour of animals can be a very sensitive indicator of adverse health consequences. Early signs of potential insult are often behavioural rather than anatomical [10].

RF fields, continuous or pulsed, can affect membrane channels [11]. Experiments of Cleary [12,13] suggest that the flux of positively charged sodium and potassium ions across cell membranes can also be affected by RF exposure, over a wide range of frequencies (27 MHz to 10 GHz). Philippova [14] found that 900 MHz radiation, at SARs of 1 and 100 W/kg, specifically affects the binding of odorant molecules to receptor protein in the membranes of olfactory receptor neurons in the rat. Liburdy and Vanek [15] have also reported protein shedding from membranes as a result of RF exposure. A radiation at very low power can affect the ion channels associated with transmitter receptors: experiments of D'Inzeo et al. [16] suggest decrease in the frequency of opening of sodium channels associated with acetylcholine receptors in muscle membranes as a result of exposure to 9.75 GHz radiation at only 10-20 $\mu W/m^2$, which might cause a decrease in the excitability of the muscle. An increase in membrane conductance and a decrease in the spontaneous firing of impulses in neurons of the snail *Helix aspersa* when exposed for an hour to continuous and amplitude modulated 2.45 GHz radiation was described by Arber and Lin [17,18]. The effects were abolished by the application of ethylenediamine tetraacetic acid (EDTA), which chelates kalcium. Another studies also described a decrease in the electrical amplitude of impulses and a reduction in the excitability of the frog sciatic nerve when exposed to 2.45 GHz radiation [19], and a decrease in spontaneous activity of neurons isolated from the marine gastropod *Aplysia* at relatively high intensities [20, 21].

The main aim of the presented study was a electrophysiological investigation of an influence of high-frequency electromagnetic field (HF EMF) on brain functions in Lurcher mutant mice, which represent an excellent model of neurodegenerative disease, and healthy animals.

Animals and Methods

Lurcher mutant mice (Lurchers) represent a natural model of genetically determined olivocerebellar degeneration [22]. Heterozygote individuals (+/Lc) are characterized by the postnatal complete loss of cerebellar Purkinje cells (excitotoxic apoptosis) and by the decreased number of granule cells and inferior olivary neurons (secondary to the loss of Purkinje cells). Affected homozygots (Lc/Lc) are not viable. Unaffected homozygots, wild type mice (+/+) are completely healthy and serve as controls. Our previous results suggest that in Lurchers some cognitive functions are changed - in series of experiments studying the development of spatial learning in Lc/+ and +/+ during the first month of life using the standard Morris water maze [23, 24]. Some neurons of Lurchers are more sensitive to neurotoxic substances [25] and other experiments discovered a higher degree of the CNS excitability in Lc/+ when compared with +/+ using a metod of audiogennic epilepsy [26]. Similar

findings were obtained in experiments which measured brain cortical activity after previous electrical and drug stimulation [27, 28]. Also significant changes of hippocampal activity (LTP) were found in anesthetized Lc/+ in comparison with +/+ [29].

We expect that some brain structures in Lurchers would be more sensitive (i.e. with lower treshold) to different kind of stimulation and neuronal injury. It is possible to assume a higher effect of other types of stimulation on such neurons, including HF EMF. A direct registration of brain cortical and hippocampal activity during exposure to high-frequency electromagnetic field (HF EMF) and a depiction of possible changes in the hippocampal rhythmicity were performed. All experimental procedures were done under urethane anaesthesia (20%, 2g/kg i.p.) in adult (10-12 weeks) Lurcher mutant mice (n=20) and wild-type (healthy littermates) which served as controls (n=20). Experimental animals were exposed to HF EMF with frequency of 1800 MHz, similar to the range used by mobile phones. As a source of the HF EMF a high-frequency generátor was used; the power output was approximately 1 W. The radiation was directed by a waveguide to a space with the animals placed (modified stereotaxic frame in the Faraday's chamber). The area of the orifice was 150 cm^2.

An important problem in the use of classical EEG technology is the presence of conductive (contact) electrodes in brain tissue resulting to discontinuity of HF EMF and possible electrolytical processes caused by the nonhomogeneity on the boundary line of metal-tissue. Our original method [30] is based on the use of gel electrodes (silicon or glass capillary tubes filled with agar). The corresponding conductivity is achieved by supplementation of saline and final biophysical quality is adequate to the brain tissue. The connection with classical (wire) electrodes is performed out of HF EMF space. Spontaneous electrocorticogram (ECoG) was measured as 2 min segments from continously recorded activity either without HF EMF exposure or with it. Final calculation with Fourier analysis and averaging were performed off-line on DISYS-system (Software for data acquisition and analysis). Hippocampal activity was recorded by glass capillary filled with agar (used as a registration electrode), grounding electrode was a silicon tube filled with agar located on the neck. Stereotactic coordinates [31] - ref. point bregma: AP: 2.0; L: 1.5; V: 1.3 (CA1) – 2.0 (hilus DG). DISYS-system for a final averaging according to Fourier analysis with emphasis on a theta-oscillation especially was used.

Results

The experiments confirmed a possibility of direct EEG registration during exposure to HF EMF. Recording time for each experimental animal was aproximately 30 minutes and DISYS system was able to describe spontaneous activity either before influencing by the HF EMF or during it. Examples of five seconds recording in wild type mouse (Fig. 1, 2) and in Lurcher mutant mouse (Fig. 3, 4) are shown bellow.

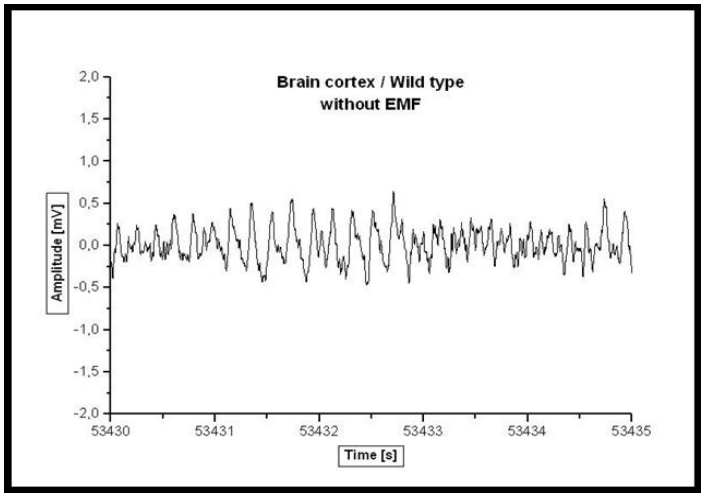

Fig. 1 – Spontaneous brain cortical activity (ECoG) in wild type mouse without HF EMF exposure

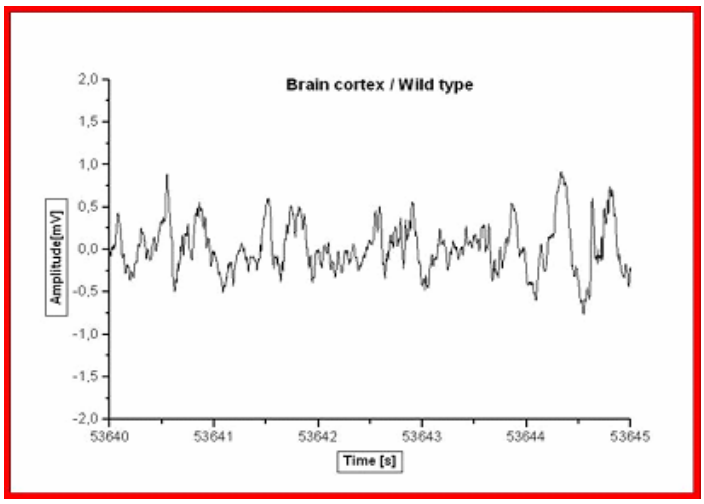

Fig. 2 – Spontaneous ECoG in wild type mouse during exposure to HF EMF

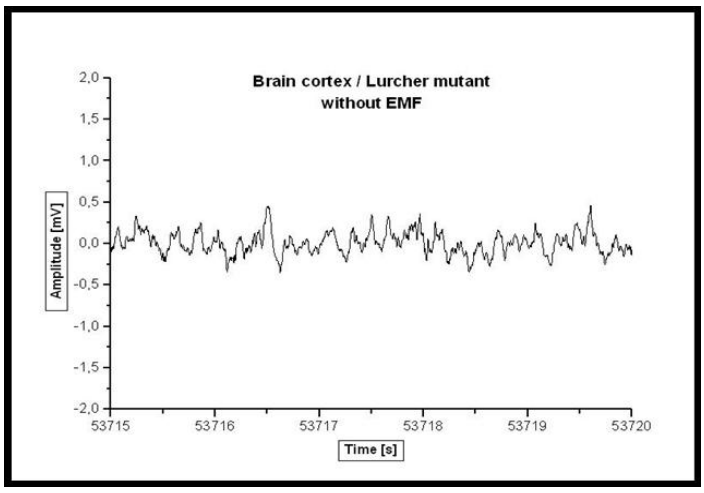

Fig. 3 – Spontaneous brain cortical activity (ECoG) in Lurcher mutant mouse without HF EMF exposure

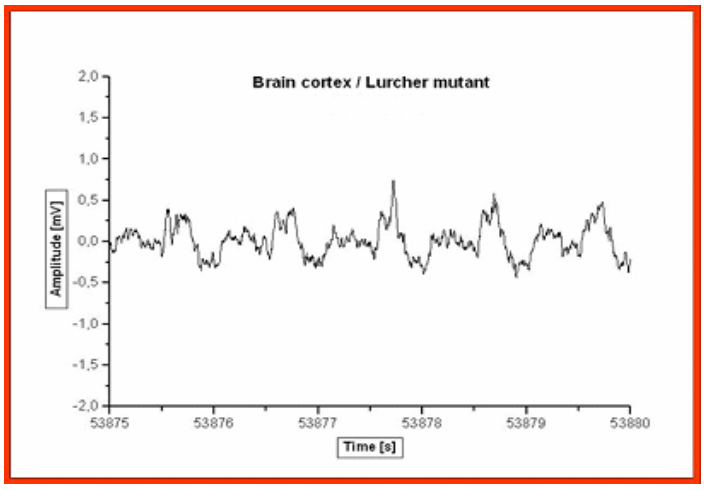

Fig. 4 – Spontaneous ECoG in Lurcher mutant mouse during exposure to HF EMF

The final evaluation and averaging of cortical activity showed a distinct shift to lower frequency components. These findings are in accordance with older and recent results but clear effect only in wild type

(healthy littermates) was observed (Fig. 5) whereas in Lurcher mutant mice only gentle differences between frequency spectra were found (Fig. 6).

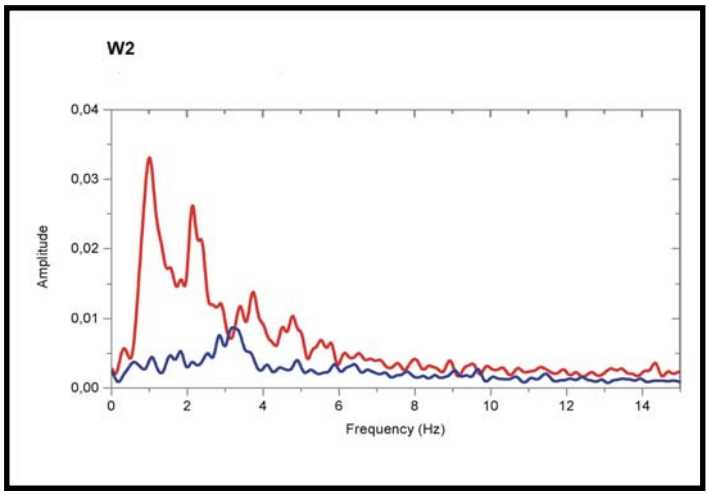

Fig. 5 – Fourier analysis of ECoG in wild type mice group before (blue line) and during (red line) exposure to HF EMF

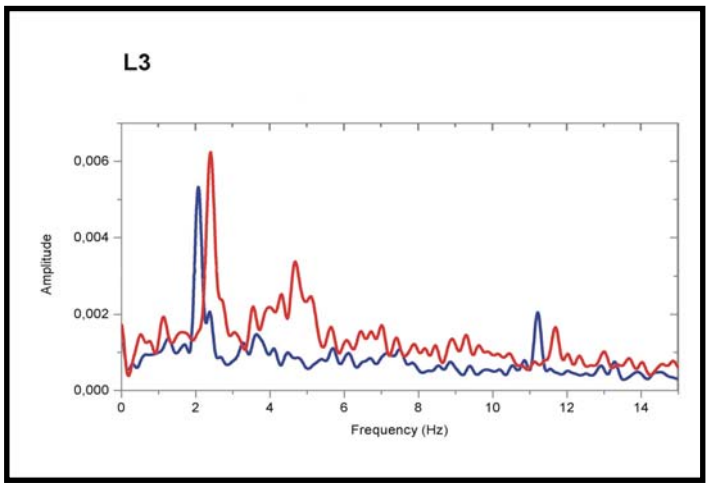

Fig. 6 – Fourier analysis of ECoG in Lurcher mutant mice group mice before (blue line) and during (red line) exposure to HF EMF

On the other hand, changes of hippocampal activity and shift towards higher frequencies in both types of animals (healthy and mutant) were observed (Fig. 7, 8).

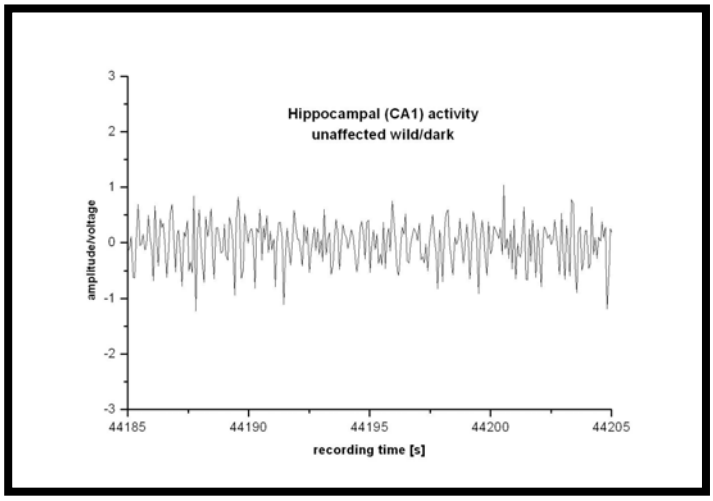

Fig. 7 – Hippocampal activity in wild type mouse before exposure to HF EMF

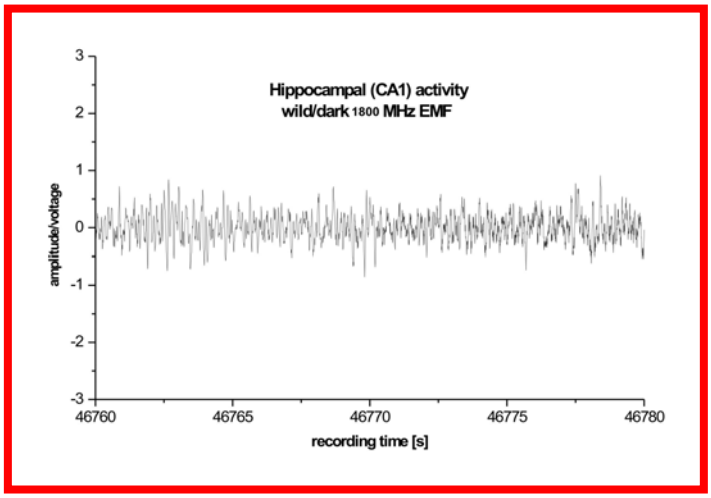

Fig. 8 - Hippocampal activity in wild type mouse during exposure to HF EMF

The serious problem is depiction of SAR which is generally accepted as a indicator of the energy absorption by different kinds of living tissue. In our experiments we used mathematical modelling of SAR calculation. In the figures 9 and 10 examples of SAR calculation were shown (both using 900 MHz HF generator, where power output was approximately 10 W). We expect a similar distribution of SAR corresponding to the lower power output at one side but higher concentration of HF EMF resulting from less area of waveguide orifice.

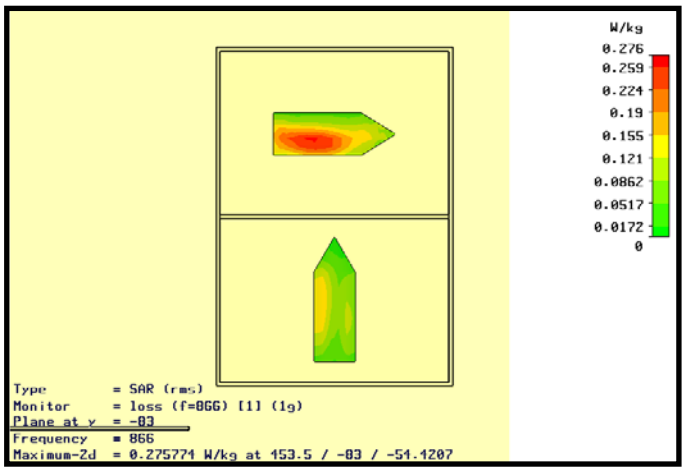

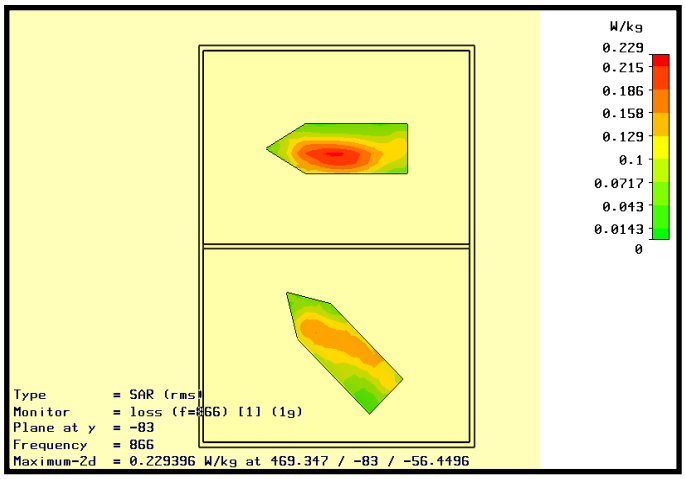

Figs 9 and 10 – mathematical model of SAR in two different mice position

Discussion

An arteficial source of HF EMF used in our experimental paradigm influenced spontaneous cortical activity. A shift towards lower frequencies was observed with gentle differences between Lurcher mutant mice and wild type mice. Our main working hypothesis was that some brain structures in Lurchers should be more sensitive (i.e. they have lower treshold) to different kind of stimulation and neuronal injury. We suppose that thermal gradient arising between lipo- and hydrophylic structures influences ion movement through membranes of neurons and/or glial cells. However, possible delicate changes were identified rather in the brain of healthy animals. These relatively ambiguous findings support our idea about a different vulnerability of the CNS in mice with neurodefective brain to some physical and chemical factors in comparison with controls. The higher CNS excitability in Lurcher mutant mice and its possible supression or masking effect on the HF EMF influence may be used as an explanation of unsignificant differences between healthy and mice with inborn neurodegeneration. Newertheless, our general findings are in accordance with previously published investigations of Bawin et al. [32, 33] that exposed cats, which had been previously conditioned to produce selected EEG rhythms in response to a light flash, to low level RF fields. The changes were reported in the performance of the conditioned EEG response task and in various other behavioural parameters. It was argued that the fields acted directly on brain tissue causing a minute release of calcium, resulting in changes in membrane excitability, which could possibly affect EEG rhythms. Takashima et al. [34] reported changes in EEG of rabbits following exposure to a modulated RF field of 1-10 MHz, a frequency range outside the main interest but Shandala et al.[35]; Thuroczy et al.[36] reported about subtle effects on the EEG in rats and rabbits exposed to RF fields within the frequency range of interest. McRee et al. [37] described experiments performed by Rosensteig of the US Environmental Protection Agency, who exposed rats to RF from late fetal life until adult. He saw no changes in either the spontaneous EEG or the electrical responses evoked by flashes of light (visual evoked responses). Mitchell et al. [38] reported the findings of a joint project on the same subject carried out in the USA and the former Soviet Union. Both groups exposed rats to fairly intense continuous-wave RF fields for seven hours. Interestingly, both

teams found small but statistically significant reduction of power in the EEG, but in different parts of the frequency spectrum.

Laboratory studies investigating the effects of mobile phone signals on the spontaneous EEG in awake subjects have produced somewhat mixed results. Reiser et al. [39] reported that exposure to GSM signals was associated with increases some 15 minutes later in the power of EEG frequencies of about 10 Hz and higher, Roschke and Mann [40] were unable to detect any differences in EEG spectra related to exposure to GSM signals. A similar inconsistency appears to hold for the study of sleep EEG. Mann and Roschke [41] reported that exposure to GSM-like signals reduced latency to sleep onset, and altered spectral characteristics of REM sleep, although a subsequent study by the same group [42] failed to replicate these findings. In other study [43], exposure to a "pseudo-GSM signal" (15 minute on/off cycles, 900 MHz, duty cycle of 87.5 % rather than the 12.5 % used in phone signals, and an estimated whole-body SAR of 1 W/kg) was associated with reduced waking after sleep onset and changes in EEG power spectra during the first of the night's episodes of non-REM sleep. In three studies „event-related potentials“ (ERPs) were investigated during exposure to GSM-like signals. In the first [44] visual sensory responses to checkerboard reversal were found to be unaffected during exposure. In two other studies [45, 46] positive effects were reported. In a recent study in Czech Recublic, Jech and colleagues [47] also found changes of visual event related potentials during exposure to HF EMF.

Taken together, main importance of this study was that neurodefective animals and their healthy littermates (as ideal controls) were used. Despite our experimental paradigm (i.e. whole-body HF EMF exposure characterised by lower amount of absorbed energy in comparison with human brain during cellular phone use), presented results suggest that some neuronal populations (cortical and subcortical) react on this type of radiation. Current WHO recommendation published by Repacholi [48] consists of basic principles of safety for individuals. The limiting of the lenght of calls or using „hands-free“ device has probably higher importance in children in which possible thermal effect on the developing brain may be connected with higher healthy risks.

References

1. Van Leeuwen G. M. J., Lagendijk J. J. W., Van Leersum B. J. A. M., Zwamborn A. P. M., Hornsleth S. N., Kotte A. N. T. J.: Calculation of brain temperatures due to exposure to a mobile phone. Phys. Med. Biol. 44: 2367-2379, 1999.
2. Schwan H. P.: EM-field induced force effects. In: Interactions between Electromagnetic Fields and Cells (A. Chiabrera, C. Nicolini and H. P. Schwan, Eds). New York, Plenum Press, 1985.
3. Adair R. K.: Effects of weak high-frequency electromagnetic fields on biological systems. In: Radiofrequency Radiation Standards (B. J. Klauenberg, M. Grandolfo and D. N. Erwin, Eds). New York, Plenum Press, p. 207-211, 1994.
4. Montaigne K., Pickard W. F.: Offset of the vacuolar potential of Characean cells in response to electromagnetic radiation over the range 250 Hz - 250 kHz. Bioelectromagnetics 5: 31–38, 1984.
5. Litovitz T. A., Penafiel L. M., Farrel J. M., Krause D., Meister R., Mullins J. M.: Bioeffects induced by exposure to microwaves are mitigated by superposition of ELF noise. Bioelectromagnetics 18: 422–430, 1997.
6. UNEP/WHO/IRPA: Electromagnetic Fields (300 Hz-300 GHz). Geneva, World Health Organization, Environmental Health Criteria 137, 1993.
7. Cleary S. F.: Effects of radiofrequency radiation on mammalian cells and biomolecules in vitro. In: Electromagnetic Fields: Biological Interactions and Mechanisms (M Blank, Ed). Washington, American Chemical Society, p 467, 1995.
8. Hermann D. M., Hossman K.-A.: Neurologic effects of microwave exposure related to mobile communication. J. Neurol. Sci. 152: 1, 1997.
9. Royal Society of Canada Expert Panel Report: A review of the potential health risks of radiofrequency fields from wireless telecommunication devices. An Expert Panel Report prepared at the request of the Royal Society of Canada for Health Canada. Ottawa, Royal Society of Canada, RSC.EPR 99-1, 1999.
10. Salzinger K.: Behavioral effects of electromagnetic fields in animals. In: Biological Effects of Electric and Magnetic Fields, Volume 1, Sources and Mechanisms (D. O. Carpenter and S. Ayrapetyan, Eds). New York, Academic Press, p 315, 1994.
11. Repacholi M. H.: Low level exposure to radiofrequency electromagnetic fields: health effects and research needs. Bioelectromagnetics 19: 1-19, 1998.
12. Cleary S. F.: Cellular effects of radiofrequency electromagnetic fields. In: Biological Effects and Medical Applicatians of Electromagnetic Energy (O. P. Gandhi, Ed.). Englewood Cliffs, New Jersey, Prentice-Hall, p 339, 1990.

13. Cleary S. F.: Effects of radiofrequency radiation on mammalian cells and biomolecules in vitro. In: Electromagnetic Fields: Biological Interactions and Mechanisms (M. Blank, Ed). Washington, American Chemical Society, p 467, 1995.
14. Philippova T. M., Novoselov V. I., Alekseev S. I.: Influence of microwaves on different types of receptors and the role of peroxidation of lipids on receptor-protein shedding. Bioelectromagnetics 15: 183-192, 1994.
15. Liburdy R. P., Vanek P. F., Jr.: Microwaves and the cell membrane. III. Protein shedding is oxygen and temperature dependent: evidence for cation bridge involvement. Radiat. Res. 109: 382-395, 1987.
16. D'Inzeo G., Bernardi P., Eusebi F., Grassi F., Tamburello C., Zani B.M. Microwave effects on acetylcholineinduced channels in cultured chick myotubes. Bioelectromagnetics 9: 363-372, 1988.
17. Arber S. L., Lin J. C. Microwave enhancement of membrane conductance: effects of EDTA, caffeine and tetracaine. Physiol. Chem. Phys. Med. NMR 16: 469-475, 1984.
18. Arber S. L., Lin J. C.: Microwave induced changes in nerve cells: effects of modulation and temperature. Bioelectromagnetics 6: 257-270, 1985.
19. McRee D. I., Wachtel H.: The effects of microwave radiation on the vitality of isolated frog sciatic nerves. Radiat. Res. 82: 536-546, 1980.
20. Wachtel H, Seaman R., Joines W: Effects of low-intensity microwaves on isolated neurons. Ann. N.Y. Acad. Sci. 247: 46-62, 1975.
21. Seaman R. L., Wachtel H.: Slow and rapid responses to CW and pulsed microwave radiation by individual Aplysia pacemakers. J. Microwave Power 13: 77-86, 1978.
22. Zuo J., Philip L., De Jager P. L., Takahashi K. A., Jiang,W., Linden D. J., Heintz N.: Neurodegeneration in Lurcher mice caused by mutation in δ-2 glutamate receptor gene. Nature 388: 769-773, 1997.
23. Vožeh F., Cendelín J., Motáňová A.: The development of different types of learning in cerebellar degeneration model. Homeostasis 39: 248-250, 1999.
24. Cendelín J., Barcal J., Korelusová I., Vožeh F.: The effect of various levels of dopaminergic transmission influencing the spatial learning process in healthy and neurodefective Lurcher mutant mice (C57B1/7). Homeostasis 42: 239-241, 2003.
25. Caddy K. W. T., Vožeh F.: The effect of 3-acetylpyridine on inferior olivary neuron degeneration in Lurcher mutant and wild type mice. Europ. J. Pharmacol. 330: 139-142, 1997.
26. Cendelín J., Vožeh F.: Assessment of CNS excitability in natural model of cerebellar degeneration. Homeostasis 39: 115-116, 1999.
27. Barcal J., Ježek K., Vožeh F., Žalud V.: Changes of excitability in the cerebellar degeneration model (Lurcher mutant mice). Physiol. Res. 49: 38P, 2000.
28. Sobotka P., Barcal J., Žalud V., Vožeh F.: The effect of caffeine on the heart activity of mice with inborn cerebellar degeneration. Homeostasis 40: 128-129, 2000.
29. Barcal J., Vožeh F., Štenglová V., Žalud V.: The effect of nitric oxide on hippocampal potentiation in the cerebellar degeneration model. Homeostasis 41: 67-69, 2001.
30. Žalud V., Barcal J., Cendelín J., Vožeh F.: EEG recording in mice during exposure to high-frequency electromagnetic field. Homeostasis 41: 203-206, 2001.
31. Franklin, K. B. J., Paxinos, G.: The mouse brain in stereotaxic coordinates. Academic Press, San Diego, 1997.
32. Bawin S. M., Gavalas-Medici R. J., Adey W. R.: Effects of modulated very high frequency fields on specific brain rhythms in cats. Brain Res. 58: 365–380, 1973.
33. Bawin S. M., Gavalas-Medici R. J. , Adey W. R.: Reinforcement of transient brain rhythms by amplitude-modulated VHF fields. In: Biological and Clinical Effects of Low Frequency Magnetic and Electric Fields (J. G. Llaurado, A. Sances and H. Battocletti, Eds). Springfield, Charles C. Thomas, p. 172–177, 1974.
34. Takashima S., Onaral B., Schwan H. P.: Effects of modulated RF energy on the EEG of mammalian brains. Radiat Environ. Biophys. 16: 15–27, 1979.
35. Shandala M. G., Dumanskii U. D., Rudnev M. I., Ershova L. K., Los I. P.: Study of nonionizing microwave radiation effects upon the central nervous system and behavior reactions. Environ. Health Perspect. 30: 115–121, 1979.
36. Thuroczy G., Kubinyi G., Bodo M., Bakos J., Szabo L. D.: Simultaneous response of brain electrical activity (EEG) and cerebral circulation (REG) to microwave exposure in rats. Rev. Environ. Health 10: 135–148, 1994.
37. McRee D. I., Elder J. A., Gage M. I., Reiter L. W., Rosenstein L. S., Shore M. L., Galloway W. D., Adey W. R., Guy A. W.: Effects of nonionizing radiation on the central nervous system, behavior and blood: a progress report. Environ. Health Perspect. 30: p. 123–131, 1979.
38. Mitchell C. L., McRee D. I., Peterson N. J., Tildin H. A., Shandala M.G., Rudnev M. V., Varetskii V.V., Navakatkyan M. I.: Results of a United States and Soviet Union point project on nervous system effects of microwave radiation. Environ. Health Perspect. 81: 201-209, 1989.
39. Reiser H , Dimpfel W., Schober F.: The influence of electromagnetic fields on human brain activity. Eur. J. Med. Res. 1: 27–32, 1995.

40. Roschke J., Mann K.: No short-term effects of digital mobile radio telephone on the awake human electroencephalogram. Bioelectromagnetics 18: 172–176, 1997.
41. Mann K., Roschke J.: Effects of pulsed high-frequency electromagnetic fields on human sleep. Neuropsychobiology 33: 41–47, 1996.
42. Wagner P., Roschke J., Mann K., Hiller W., Frank C.: Human sleep under the influence of pulsed radiofrequency electromagnetic fields: a polysomnographic study using standardized conditions. Bioelectromagnetics 19: 199–202, 1998.
43. Borbely A. A., Huber R., Graf T., Fuchs B., Gallmann E., Achermann P.: Pulsed high-frequency electromagnetic field affects human sleep and sleep electroencephalogram. Neurosci. Lett. 275: 207–210, 1999.
44. Urban P., Lukas E., Roth Z.: Does acute exposure to the electromagnetic field emitted by a mobile phone influence visual evoked potentials? A pilot study. Centr. Eur. J. Public Health 6: 288–290, 1998.
45. Eulitz C., Ullsperger P., Freude G., Elbert T.: Mobile phones modulate response patterns of human brain activity. NeuroReport 9: 3229–3232, 1998.
46. Freude G., Ullsperger P., Eggert S., Ruppe I.: Effects of microwaves emitted by cellular phones on human slow brain potentials. Bioelectromagnetics 19: 384–387, 1998.
47. Jech R., Šonka K., Růžička E., Nebuzelský A., Bohm J., Juklíčková M., Nevšímalová S: Electromagnetic field of mobile phones affects visual event related potential in patiens with narcolepsy. Bioelectromagnetics 22: 519–528, 2001.
48. Repacholi M. J.: Health risks from the use of mobile phones. Toxicol. Lett. 120: 323-331, 2001.

Acknowlledgments

This work was supported by the COST Action 281 „Electromagnetic fields and health emerging information and communication technologies“ and Research Program Project No. MSM ČR 021620816.

EEG BIOEFFECTS ON COCHLEAR DEAF FROM CELLULAR PHONES, (FIRST TESTS).

J.L. Bardasano
Department of Medical Specialities, University of Alcalá, Madrid, Spain
Corresponding author: E-mail: joseluis.bardasano@uah.es

J. Álvarez-Ude
Department of Physics, University of Alcalá, Madrid, Spain

I. Gutiérrez
Department of Medical Specialities, University of Alcalá, Madrid, Spain

M. Raposo
Department of Physics, University of Alcalá, Madrid, Spain

R. Goya
Department of Physics, University of Alcalá, Madrid, Spain

Abstract

- Objectives:

This work aims to provide evidence of an inductive electromagnetic bio-effect on the human brain, which is independent from sound waves and produced by mobile phones, in proximal field, through correlating the EEG data obtained from electrodes placed on both normal and cochlear deaf individuals.

- Methods

Two groups of four subjects are placed under controlled electromagnetic conditions inside a Faraday chamber, (two healthy and another two suffering from cochlear deafness). Each is sitting on a chair, fitted with additional support, and holding a cellular phone 2 cm away form the right auricular, in order to avoid a thermal effect as much as possible. All of them, relaxed and with their eyes closed, are EEG recorded in a basal state with their mobile phones off.

Then, each of them is again recorded under the same conditions but with the mobile on and listening to the same conversation. In order to assess the EEG changes so observed, a statistical analysis by means of the FFT (Fast Fourier Transform) was carried out.

- Results

For both, healthy and cochlear deaf, assimilation or integration of the mobile phone signal by some electrodes is to be found. This is due to the increase of amplitudes for alpha and theta waves, whereas the signal is not integrated in other electrodes. By correlating the spectra of frequencies of corresponding EEG records for the same brain areas, we have not observed significative differences for both groups.

- Conclusion

A possible electromagnetic direct inductive, non-thermal, bio-effect on the human brain is observed. This effect is produced by the use of mobile phones and it bears no relation to the sound waves.

Keywords: electromagnetic field, bio-effects, electroencephalogram, mobile phone, cochlear deaf.

Introduction

Recent technological advances in telecommunications have led to the use of electromagnetic fields (EMF) to man's own convenience, such as in Telemedicine, in the field of Medicine (Ramos and Monteagudo, 2006) or for diagnosis and treatment as well, within the field of medical specialities (Bardasano and Elorrieta, 2000, Rosch and Markov, 2004).

Nevertheless, electromagnetic fields from GSM mobile phones (Global System Mobile Communication) and from their base stations can have an effect on living beings and man, in particular, in different ways. More and more often we find proof from different fields of knowledge of this environmental electromagnetic pollution, which might involve the health of human and other living beings, (Navarro *et al*., 2003, Santini *et al*., 2003, Balmori, 2004, 2005, Hutter *et al*., 2006).

Neurons can respond to electromagnetic fields, (Beasond and Semm, 2002) and different degrees of neurological and other kinds of alterations, which may change the physiology of the brain, can also be found and are associated to mobile phone radiofrequencies, (Hossmann and Hermann, 2003, Westerman *et al*., 2004, Huber *et al*., 2005, Maby *et al*., 2005, Szyjkowska *et al*., 2005, Papageorgiou *et al*., 2006).

Evidence of alterations in the permeability of the hematoencephalic barrier in rats from mobile phones has been presented (Fritze *et al*., 1997) as well as histological changes due to neural damage in the cortex, hippocampus and basal ganglia in the brain of exposed rats (Salford *et al*., 2003) and changes in the EEG of the rabbit (Marino *et al*., 2003).

We also have evidence of alterations in the brain of rats not only at the biochemical level but also at that of the glial cells. There is evidence of molecular alterations in the rat's brain due to GSM mobile phones after an acute exposure to high power 900 MHz micro waves. (Mausset-Bonnefont *et al*., 2004).

Also, the effects of 900 MHz electromagnetic exposure on cochlear cell functionality in rats are evaluated as a distortion product due to otoacoustic emissions by Galloni *et al*., 2005. In this work, in order to evaluate the influence of mobile phones on the human brain, we give the EEG recording an essential role as a working tool, (Krause *et al*., 2004, Lin, 2004, Curcio *et al*., 2005, Loughran *et al*., 2006).

The EEG is a representative signal containing information about the condition of the brain. The shape of the wave may contain useful information, hence Croft *et al*., 2002, found that EMF exposure decreased 1 Hz – 4 Hz activity in right hemisphere sites, and was associated with increasing 8 Hz – 12 Hz activity as a function of exposure duration in the midline posterior sites.

Along the same lines, Kramarenko *et al*., 2003, used a telemetric EEG, and found that within 20 s – .40 s of exposure to a 900 MHz phone signal subjects showed slow-wave activity in the contralateral, frontal and temporal areas. They lasted for one second and were repeated every 15 s – 20 s. When the signal stopped the slow waves progressively disappeared in the next 10 minutes.

Furthermore, Cook *et al*., 2004, suggested that 30% of the variation in alpha activity seen in their study were due to the pulsed magnetic field exposure and also, Papageorgiou *et al*., 2004, found that baseline EEG energy was greater in males, while exposure to EMF decreased EEG energy of males and increased that of females. There were not statistically significant differences in memory performance between men and women, nor was there any difference between exposed and non-exposed states.

Additionally, in a small pilot study, Hamblin, *et al*., 2004, found some evidence of neural activity as a result of mobile phone exposure during an auditory task.

Moreover, the effects of EMF emitted by mobile phones on human EEG were studied during an auditory memory task. The energy was found concentrated at the four basic bands. The results show evidence of a strong gender radiation interaction effect on the EEG energy and on the peak amplitudes within each of the four rhythms (Nanou *et al*., 2005).

The EEG analysis performed with three different methods showed that statistically significant changes occur in the EEG rhythms, energy and dynamics between 12% and 30% of subjects. The results suggest that microwave exposure affects part of the population and can have an impact on health. (Hinrikus *et al*., 2006).

This research is aimed at providing evidence of electromagnetic induction from mobile phones, in proximal field, to the human brain by comparing the EEG of healthy normal individuals with that of cochlear deaf, regardless of sound stimulus (sound waves).

- **Materials and Methods**

We have followed the protocol (patterns), as in previous experiences in our laboratory, as to the subjects, procedures, materials (Faraday screen, mobile phones, electroencephalograph and recording), etc. For more details, see Bardasano *et al*., 2005.

Subjects

We have carried out this study on four individuals in two groups, (two healthy individuals and two suffering from cochlear deafness).

Procedure

Each subject is placed inside the Faraday chamber and comfortably seated on a plastic chair. The mobile phone is held over the right ear by an insulated device 2 cm from the auricular to avoid a thermal effect as much as possible. By means of the EEG, we tested the effects of the mobile phone on the subjects as follows: basal EEG activity, with eyes closed, for 5 min; each subject was recorded while listening to a five minute conversation with the phone placed on the right ear.

Materials

Mobile phone

Technical specifications: Global System Mobile Communication (GSM) class 4 (2 W), 880 MHz –960 MHz frequency band, which is a proximal field in relation to the subject. Specific Absorption Rate (SAR), highest value, 0.955 W/kg.

Electroencephalograph and recording

A digital EEG, with system plus software, model: SAM 32 FOFC I (latest version) by Micromed®, which incorporates amplitude and frequency maps, was employed. EEG signals were collected from 18 channels and filtered with a band filter.

Statistical Analysis

In order to assess our EEG results, we have applied the FFT (Fast Fourier Transform) mathematical analysis.

- **Results**

In healthy and cochlear deaf individuals, we find assimilation or integration of the mobile phone signal in some electrodes. This is due to the increase of the amplitudes of alpha and theta waves. By correlating the spectra of frequencies of corresponding EEG records for the same areas, significative differences for both groups are not observed (see Appendix, Fig. 1 and Fig. 2).

- **Discussion**

Our discussion focuses on physiological interpretation and on methodological observation.

Physiological interpretation

During transduction of external signals, FFT analysis shows that a healthy subject's brain behaves in two ways to the signal from the mobile phone. It rejects the incoming signal or integrates it by making it its own, and generates another signal as a response. This is done by increasing the spectral power density of the incoming signal which implies an increase of energy without altering the frequencies. This means that a larger number of neurons are being activated underneath than at the basal phase for the same activated frequencies.

In short, the brain responds by yielding signals which lead to the generation of alpha and theta rhythms. The EEG response of the cochlear deaf is similar to that of the healthy subject with the phones on. For both groups, the behaviour of the EEG towards the signal from the mobile shows that it can either be integrated in the brain or it appears in the spectrum of frequencies of the typical peaks of mobile phones which overwhelm the normal brain signal, on the same recording electrode and for the same subject at a given time.

Let us call *integration* the capacity for assimilating, processing an incoming signal, and for emitting another signal as a response. Given that, the sound waves do not seem to affect the integration of such a signal in the brain.

Methodological observation

Research on the harmful bioeffects of mobile phones on the brain faces one of its challenges; that is, to avoid suffering, lesion, and death of the neurons. Neuroprotection is a way of guarding neurons which, for different reasons, have their death scheduled. We find several programs in the central nervous system which schedule the death of mobiles, which are activated by internal alterations (genetic features of the patient) or external (biological, chemical, such as exposure to toxins, heavy metals in drinking water, pesticides, and others, and physical elements such as artificial and uncontrolled electromagnetic fields. (Bardasano *et al*., 2005)

The EEG shows the influence of mobile phones on man. In the field of Biomedical Engineering, research should contemplate at least the following aspects:

a. The General Adaptation Syndrome to changes in the state of mater and energy. Those changes take place in the environment of living beings, bearing in mind the threesome 'oppressor, depressor, stressor', adverse hypersensitive reactions and the microwave syndrome.

b. Electromagnetic Compatibility. In the field of the modern theory of the signal, the task is to observe machines or systems in good working condition and the human body, itself as a system, (the inductive influence of electromagnetism from a mobile phone and the bioelectromagnetism of the human brain).

c. The Physiology of Regulatory Systems and Chronobiology. To avoid alterations in the permeability of the hematoencephalic barrier or chronopathologies due to alteration of circadian rhythms, (waking and sleeping states), among others, due to this inductive influence.

Summary

By comparing the EEG data from mobile phones, independent from sound, through the electrodes glued onto normal and cochlear deaf subjects, we have tried to find evidence of an inductive electromagnetic bio-effect on the human brain.

We found that the signal is not integrated in some electrodes and we have not found significant differences for either group of healthy and cochlear deaf subjects, which, on the other hand, show assimilation or integration of the mobile phone in other electrodes because of the increase of amplitude of the alpha and theta waves. By comparing the spectrum of frequencies of the corresponding EEG for the same areas, we have not observed significant differences in both groups, either.

The effect, observed in the brain, is produced by the mobile phones.

Acknowledgements

This project was carried out thanks to the collaboration of Bioelectromagnetism European Foundation (BEF), BIOECODEFENSA 7, L.S. and sponsored by SIEMENS, AG.

References

Bardasano, J.L. and Elorrieta, J.L.: 2000, *Bioelectromagnetism, Science and Health*, McGraw-Hill, edit. Madrid, (In Spanish).

Bardasano, J.L., Álvarez-Ude, J., Gutiérrez, I. and Goya, R.: 2005, New Device against non-thermal Effects from Mobile Telephones, *The Environmentalist* **25**, 257-263.

Balmori, A.: 2004, Posibles Efectos de las Ondas Electromagnéticas utilizadas en la Telefonía Inalámbrica sobre los Seres vivos, *Ardeola* **51**(2), 477-490.

Balmori, A.: 2005, Possible Effects of Electromagnetic Fields from Phone Masts on a Population of white Storks, *Electromagn. Biol. Med.* **24**,109-119.

Beasond, R.C. and Semm, P.: 2002, Responses of Neurons to an Amplitude modulated Microwave Stimulus, *Neurosci. Lett.* **33**, 175-178.

Cook, C.M., Thomas, A.W. and Prato, F.S.: 2004, Resting EEG is affected by Exposure to a pulsed ELF Magnetic Field, *Bioelectromagn.* **25**, 196-203.

Croft, R., Chandler, J.L., Burgess, A.P., Barry, R.J. *et al*.: 2002, Acute Mobile Phone Operation affects Neural Function in Humans, *Clin. Neurophysiol.* **113**, 1623-1632.

Curcio, G., Ferrara, M., Moroni, F., D'Inzeo, G., Bertini, M. and De Gennaro, L.: 2005, Is the Brain influenced by a Phone Call? An EEG Study of Resting Wakefulness, *Neurosci. Res*. **53**(3), 265-70.

Fritze, K., Wiessner, C., Custer, N., Sommer, C., *et al*..:1997, Effect of global System for Mobile Communication (GSM) Microwave Exposure in Blood Brain Barrier Permeability in Rat, *Acta Neuropathol. (Berl)* **94**, 465-470.

Galloni, P, Lovisolo, G.A., Mancini, S., Parazzini, M. *et al*.: 2005, Effects of 900 MHz Electromagnetic Fields Exposure on Cochlear Cells' Functionality in Rats: Evaluation of Distortion Product Otoacoustic Emissions, *Bioelectromagn.* **26**(7), 536-47.

Hamblin, D.L., Wood, A.W., Croft, R.J. and Stough, C.: 2004. Examining the Effects of Electromagnetic Fields emitted by GSM Phones on Human Event-Related Potentials and Performance during an Auditory Task, *Clin. Neurophysiol.* **115**, 171-178.

Hinrikus, H., Bachmann, M., Lass, J., Tomson, R and Tuulik,V.: 2006, Changes caused by Microwave in Human EEG of Individuals. In Action COST-281, *Potential Health Effects of Mobile Communication Systems. Graz*, 20-21 april.

Hossmann, K.A. and Hermann, D.M.: 2003, Effects of Electromagnetic Radiation of Mobile Phones on the Central Nervous System, *Bioelectromagn.* **24**, 49-62.

Huber, R., Treyer,V., Borbely, A.A., Schuderer, J., Gottselig, J.M. *et al* : 2002, Electromagnetic Fields, such as those from Mobile Phones, alter regional Cerebral Blood Flow and Sleep and Waking EEG, *J. Sleep Res*.**11**, 289-295.

Hutter, H.P., Moshammer, H., Wallner, P. and Kundi, M.: 2006, Subjetive Symptoms, sleeping Problems, and Cognitive Performance in Subjects living near Mobile Phone Base Stations, *Occup. Environ. Med*. **63**, 307-313.

Kramarenko, A.V. and Tan, U.: 2003, Effects of High-Frequency Electromagnetic Fields on Human EEG: A Brain Mapping Study, *Int. J. Nurosci.* **113**, 1007-1019.

Krause, C.M., Haarala, C., Sillanmaki, L., Koivisto, M. *et al*.: 2004, Effects of Electromagnetic Field emitted by Cellular Phones on the EEG during an auditory Memory Task: A Double Blind Replication Study, *Bioelectromagn.* **25**, 33-40.

Lin, J.C.: 2004, Human Electroencephalograms (EEG) and Mobile-Phone Radiation, *Radio Sci. Bull.* **308**, 52-54.

Loughran, S.P., Wood, A.W., Barton, J.M., Croft, R.J. *et al*.: 2005, The Effect of Electromagnetic Fields emitted by mobile Phones, *Neuroreport* **16**, 1973-1976.

Maby, E., Jaenés, R.L., Faucon, G., Liegeois-Chauvel, C. and De Seze, R.: 2005, Effects of GSM Signals on Auditory Evoked Responses, *Bioelectromagn.* **26**(5), 341-350.

Mausset-Bonnefont, A.L., Hirbec, H., Bonnefont, X., Privat, A. *et al*.: 2004, Acute Exposure to GSM-900 MHz Electromagnetic Fields induces Glial Reactivity and Biochemical Modifications in the Rat Brain, *Neurobiol. Dis.* **17**, 445-454.

Nanou, E., Tsiafakis, V., Kapareliotis, E., Papageorgiou, C., Rabavilas, A. and Capsalis, C.: 2005, Influence of the Interaction of a 900 MHz Signal with Gender on EEG Energy: Experimental Study on the Influence of 900 MHz Radiation on EEG, *The Environmentalist* **26**, 173-179.

Navarro, E.A., Segura, J., Portolés, M. and Gómez-Perretta, C.: 2003, The Microwave Syndrome: A preliminary Study in Spain, *Electromagn. in Biol. Med.* **22**, 181-171.

Papageorgiou, C.C., Nanou, E.D., Tsiafakis, V.G., Capsalis, C.N. and Rabavilas, A.D.: 2004, Gender related Differences on the EEG during a simulated Mobile Phone Signal, *Neuroreport*. **15**(16), 2557-2560.

Papageorgiou, C.C., Nanou, E.D., Tsiafakis, V.G., Kapareliotis, E *et al*.: 2006, Acute Mobile Phone Effects on Pre-attentive Operation, *Neurosci. Lett*. **397**(1-2), 99-103.

Ramos, V. and Monteagudo, J.L.: 2006, Assessment of EM Environment for Home Telemedicine. In International Conference and COST 281 *Workshop on Emerging EMF Technologies, Potential Sensitive Groups and Health. Graz*, April 20/21.

Rosch, P.J. and Markov, M.S.: 2004, *Bioelectromagnetic Medicine*, Marcel Dekker, Inc., edit. New York and Basel.

Salford, L.G., Brun, A.E., Eberhardt, J.L., Malmgren, L. and Person, B.R.: 2003, Nerve Cell Damage in Mammalian Brain after Exposure to Microwave from GSM Mobile Phones, *Environ. Health Perspect*. **111**, 881-883.

Santini, R., Santini, P., Danze, J.M., LeRuz , P. and Seigne, M.: 2003, Survey Study of People living in the Vecinity of Cellular Phone Base Stations, *Electromagn. Biol. Med*. **22**(1), 41.

Szyjkowska, A., Bortkiewicz, A., Szymczak, W. and Makowiec-Dabrowska, T.: 2005, Subjective Symptoms related to Mobile Phone Use, *Pol. Merkuriusz. Lek*. **19**(112), 529-532.

Westerman, R. and Hocking, B.: 2004, Diseases of Modern Living; Neurological Changes associated with Mobile Phones and Radiofrequency Radiation in Humans, *Neurosci. Lett.* **361**, 13-16.

Appendix

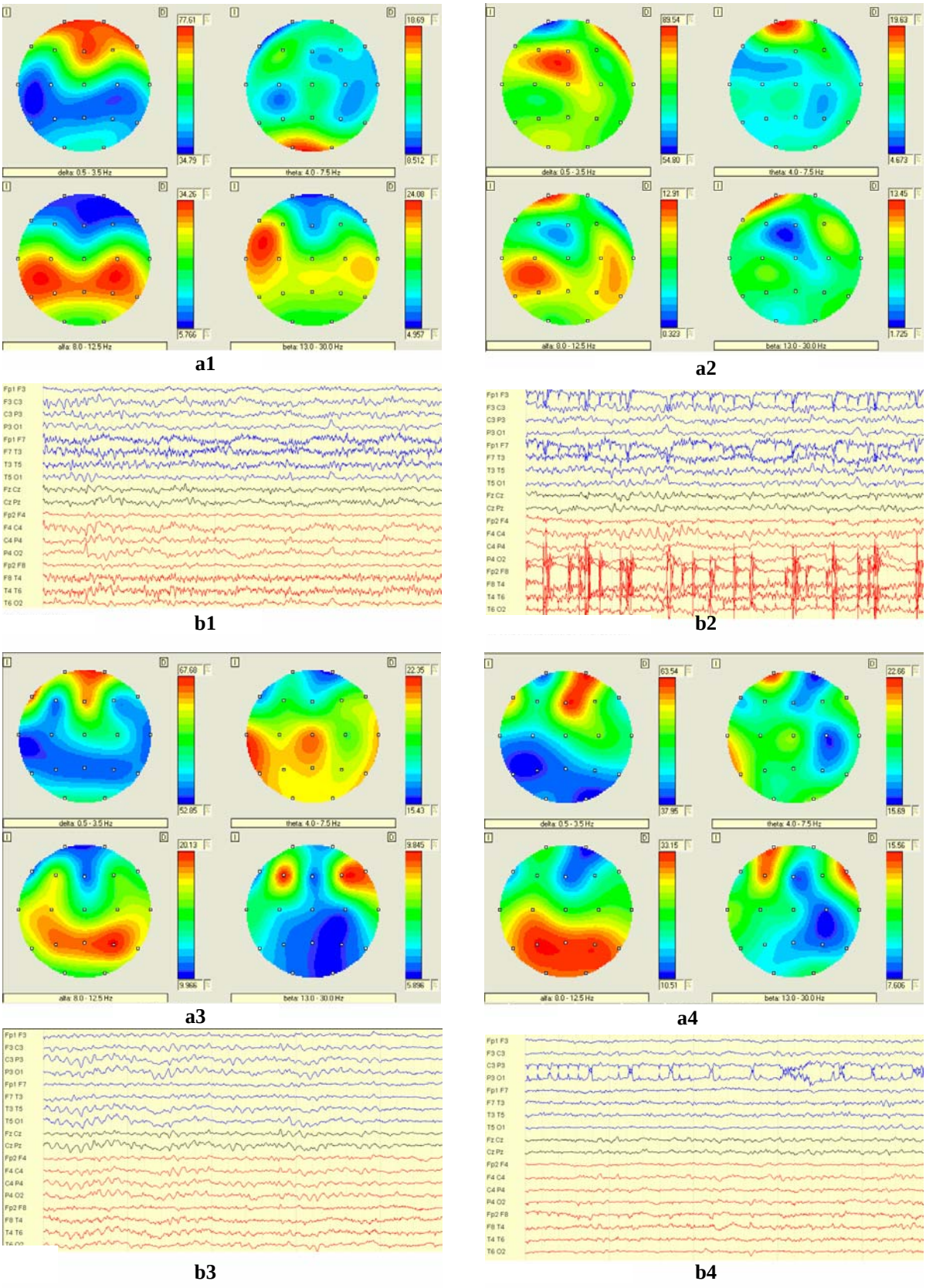

Fig. 1. Mapping of: **a1–** basal non-deaf, **a2–** non deaf with mobile on and listening, **a3–** basal deaf and **a4–** deaf with mobile on and listening.
EEG of: **b1–** basal non-deaf, **b2–** non deaf with mobile on and listening; **b3–** basal deaf and **b4–** deaf with mobile on and listening

NON DEAF

BASAL

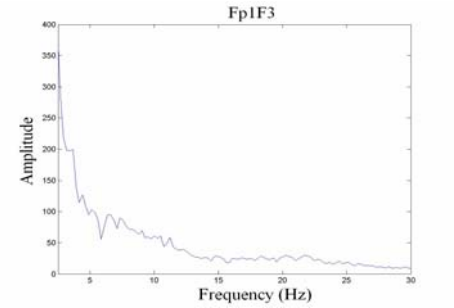

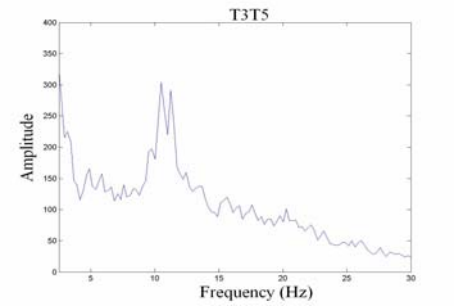

MOBILE

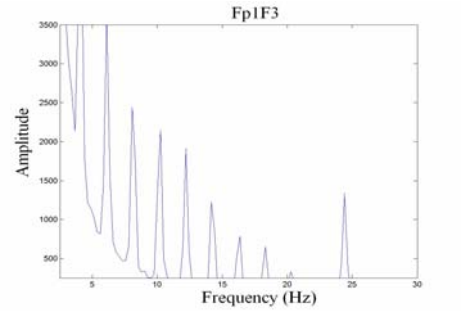

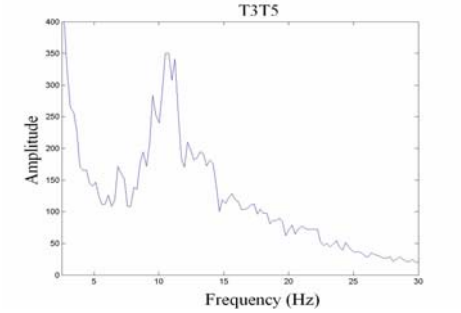

DEAF

BASAL

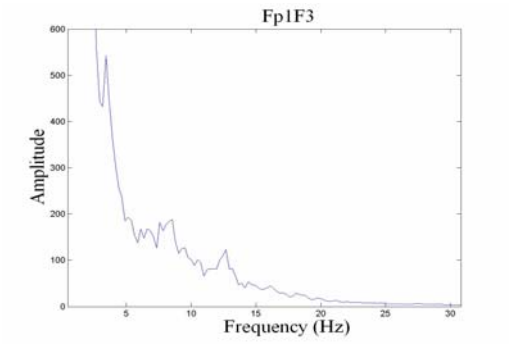

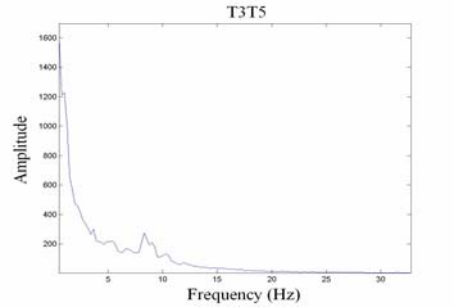

MOBILE

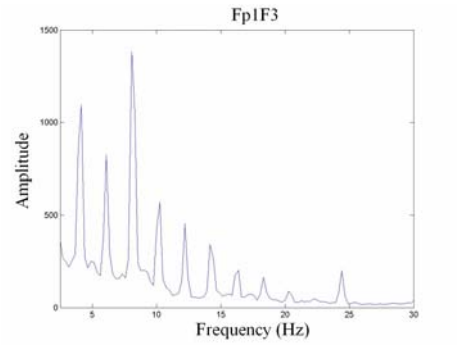

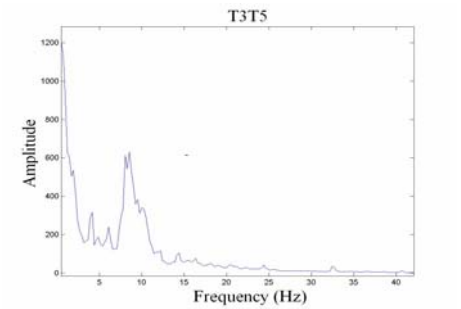

Fig 2: Spectrum of EEG frequencies obtained: **BASAL**– in basal position (electrodes Fp1F3 and T3T5) **MOBILE–**with the mobile on and listening (electrodes Fp1F3 y T3T5), for both, deaf and non-deaf.

EEG EFFECTS OF TRANSCRANIAL MAGNETIC STIMULATION AT pT RANGE

J.L. Bardasano
Department of Medical Specialities, University of Alcalá, Madrid, Spain
Corresponding author: E-mail: joseluis.bardasano@uah.es

J. Álvarez-Ude
Department of Physics, University of Alcalá, Madrid, Spain

I. Gutiérrez
Department of Medical Specialities, University of Alcalá, Madrid, Spain

M. Raposo
Department of Physics, University of Alcalá, Madrid, Spain

R. Goya
Department of Physics, University of Alcalá, Madrid, Spain

Abstract

- **Objectives**.

We aim to obtain a model or pattern among normal subjects. Thus, we are subsuming a diagnostic method (digital EEG) and a therapeutic one, which is the physiological TMS (Transcranial Magnetic Stimulation), into a new technique, pending validation. This new technique will be able to obtain an electroencephalographic response and to quantitatively evaluate the alteration of cerebral rhythms in healthy subjects, (pattern for normality), employing physiological TMS at 10 pT (picotesla) and 8 Hz, simulating the alpha rhythm. The study is single blind and the subjects do not know when they are being stimulated.

- **Material and Methods**

We have employed digital EEG, mod. SAM 32 FOFC 1, with System PLUS Software by Micromed, latest version, and spectral analysis by FFT (Fast Fourier Transform). The sample was made up of 16 healthy subjects with their eyes open, half males and half females. The recording cap, which is elastic has twenty Ag/AgCl electrodes (SIEMENS) placed bilaterally and is electrode-glued onto the scalp of the subject. The 10/20 IS (International System) of electrode placement is used. EEG signals are collected from 18 channels, filtered through a 0.5 Hz – 70.0 Hz band filter and sampled at 128 Hz. We have also used a TMS prototype stimulator, mod. MG28TR10, which incorporates a timer for the EEG recorder to control the stimulation periods and pauses (1.5 min followed by a 1 min pause). Twenty magnetic stimulation coils are placed on the EEG recording elastic cap at a distance of 2 cm between them and the recording electrodes. This way, stimulation and recording can be carried out without interference.

- **Results**

A global increase in the alpha and beta rhythms has been observed as well as a decrease in delta and theta. Alpha and delta register the highest increase and decrease, respectively. A 17.5% increase in alpha rhythm and a 4.5 % in beta are performed at the expense of a decrease in delta and theta rhythms.

The most relevant increase in alpha rhythm, as the stimulation was going on, was registered at the Fp1, Fp2, F3 and F4 frontal electrodes, as well as at the central Cz.

- **Conclusions**

By means of the TMS at 10 pT and 8 Hz, we obtain a mimetic global bioelectrical neuronal response, as the alpha rhythm magnetic field is simulated and the brain is timed to it. We also find an alpha rhythm displacement towards frontal and central areas of the brain.

Keywords: magnetic stimulation, EEG, brain rhythms.

Introduction

Research on 500 µT weak magnetic fields, extremely low frequencies (ELF) (between 0 Hz and 300 Hz), and their exposure to humans has yielded incomplete and contradictory evidence, (stemming mainly from clinical results) (Sandyk, 1992, Sandyk and Derpapas, 1993, Bardasano *et al*., 1997a, Ramírez *et al*., 1997, Anninos *et al*., 2003).

This may be due to the scarce number of studies conducted under EEG, MEG (Magnetoencephalography) examination conditions or evoked potentials and how they affect the perceptual and cognitive processes in human beings. It must also be added that most bioelectromagnetic results in the different studies have been inconsistent with one another. The most important explanations, which may account for those inconsistencies are those aimed to clarify how different the features of the applied field may be (different intensity and frequency, waveform, and duration of exposure). We also find differences among the disparate protocols employed, which can be more or less precise regarding the elimination of artefacts or elements that bring about confusion in the electrophysiological recording (Cook *et al*., 2002).

Most studies on low-power fields carried out inside Helmholtz coils generate a homogenous and continuous field, (Lyskov *et al*.,1993, Marino *et al*.,1996 and Heusser *et al*.,1997), in which the subject has electrodes placed on both his first and second fingers of his non-dominant hand and on his scalp. The former measures skin conductance and the latter cerebral electric activity. A computer controlled system allows us to change the type of field generated by the coils at desired intervals, in either a random or pre-determined pattern and to register the ongoing physiological changes.

Most EEG studies so far, which observe the effects after applying a weak magnetic field, have been using this magnetic fields generation model and have been comparing the differences so obtained.

As regards to physiological stimulation, the simultaneous registry between stimulator and EEG does not allow us to categorically state the effect it has on the brain because a signal under possible electromagnetic pollution leads to doubtful interpretations. To sort out that problem a new biomedical engineered prototype must be designed. That prototype will allow for evaluation of the electrical response of the brain, as a response to an electromagnetic stimulus, under the best conditions, free of pollution and interference.

We have studied and evaluated the physiological low field TMS (Transcranial Magnetic Stimulation) at pT (picotesla) with a new stimulation system whereas other authors used a high field TMS (Pascual-Leone *et al*. 1998, Iramina, *et al*. 2002). This technique also applies to the treatment of neurodegenerative diseases, (Parkinson's disease, Alzheimer's, multiple sclerosis), psychiatric, etc. (Bardasano *et al*., 1997a, b, Ramírez *et al*., 1997, Wassermann and Lisanby, 2001, Bardasano *et al*., 2005a, b, Bardasano *et al*., 2006).

Material and Methods

- **Subjects**

The sample is made up of sixteen healthy voluntary subjects, (an average of 35 years of age; 8 male and 8 female), properly and ethically informed, and the readings are registered inside a Faraday chamber (For details, see Bardasano *et al*., 2005c).

- **Electroencephalograph and recording**

We have employed digital EEG, mod. SAM 32 FOFC 1, with System PLUS Software by Micromed, latest version, and spectral analysis by FFT (Fast Fourier Transform). An elastic recording cap, glued to the scalp on both sides, holds twenty Ag /Ag Cl electrodes (SIEMENS) which are placed on both sides of the cap. The 10/20 IS (International System) of electrode placement is used and the actual placement has a common reference electrode placed at the frontotemporal intersection point and is grounded to the ear lobules. EEG signals are collected from 18 channels, filtered through a 0.5 Hz –70.0 Hz band filter and sampled at 128 Hz.

- **Stimulator**

Stimulating and recording can be carried out without interference using a TMS prototype mod. MG28TR10 at 10 pT and 8 Hz, which has a timer for the EEG recorder to control stimulation periods and pauses (1.5 min followed by a 1 min pause). Twenty magnetic stimulation coils are placed on the EEG recording elastic cap at a distance of 2 cm between them and the recording electrodes (Bardasano *et al*., 2006) (Fig.1).

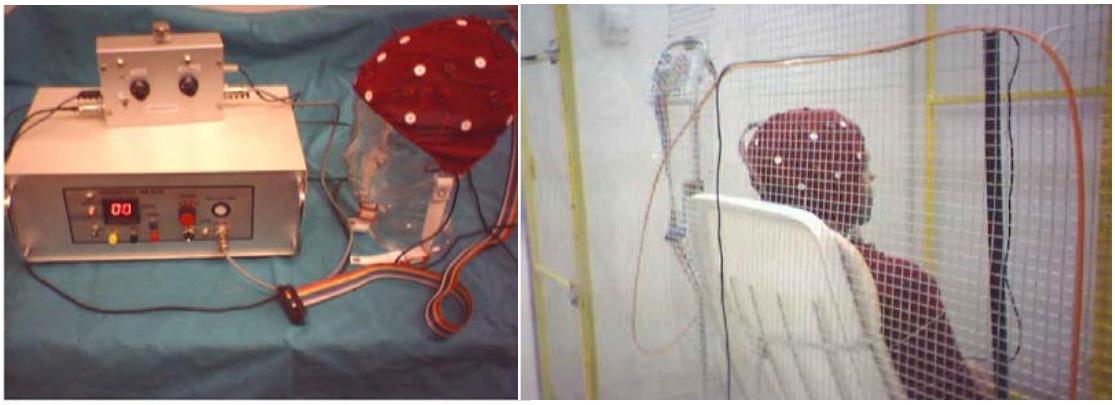

Fig. 1. TMS stimulator, mod. MG28TR10 (left). Subject sitting inside the Faraday chamber. Recording cap and amplifier are also shown here, (right).

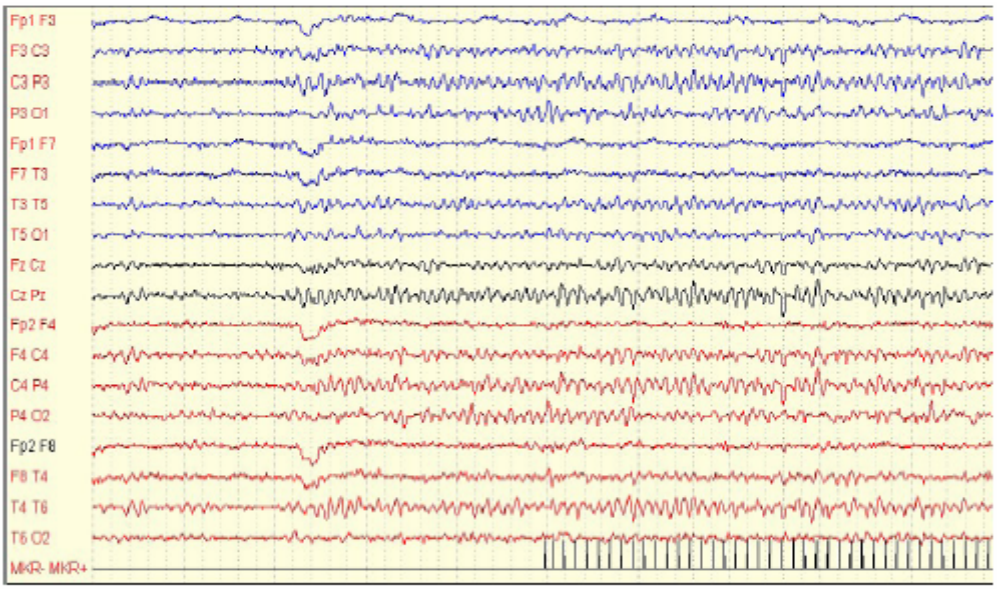

Fig 2. Beginning of the stimulation process. We can see a lower channel designed to observe the morphology and frequency of the stimulus. The stimulus-pause sequence allows for both he ulterior elimination of traces of stimulus and analysis of the pause tracks as though it had been done with a non-stop recording.

- **Procedure**

The subjects are comfortably seated (Fig 1) with their eyes open and without outside stimulation. A basal EEG is first done for 5 min and then a long 10 min sequence stimulation (Fig 2). The subjects are single blind, as they do not know when they are being stimulated.

- **Statistical analysis**

The data have been computed, analysed and interpreted by means of the statistical set SAS System Release 8.02 by SAS Institute Inc. Cary, N.C., USA.

In the frequency tables, (in ASCII format for the 19 electrodes applied), the comparison between groups was evaluated by differential pairing and contrast with the paired T-Student. The p-values are given for up to 4 decimal figures.

- **Results**

An important increase in the alpha and beta rhythms has been observed as well as a decrease in delta and theta. alpha and delta record the highest increase and decrease, respectively, (a 17.5% increase in alpha rhythm and a 4.5 % in beta rhythms, repeatedly, at the expense of a decrease in delta and theta (see Fig 3 and Appendix, Fig. 4).

The most significant increase in alpha rhythm, at the same time as the stimulation was being carried out, was registered at the Fp1, Fp2, F3 and F4 frontal electrodes and at the central Cz.

This leads us to believe that there is a displacement towards anterior brain areas of the physiological alpha rhythm, under stimulation.
Below, find bar graphs of mentioned electrodes where the basal state is the first bar, the second bar stands for stimulation and the third for the difference.

As soon as the recording was over, each subject was asked how he felt as a whole; 84% mentioned they experienced a pleasing and soothing sensation; the remaining did not mention any particular feeling, (indifference) and 3 cases felt their hands going numb.

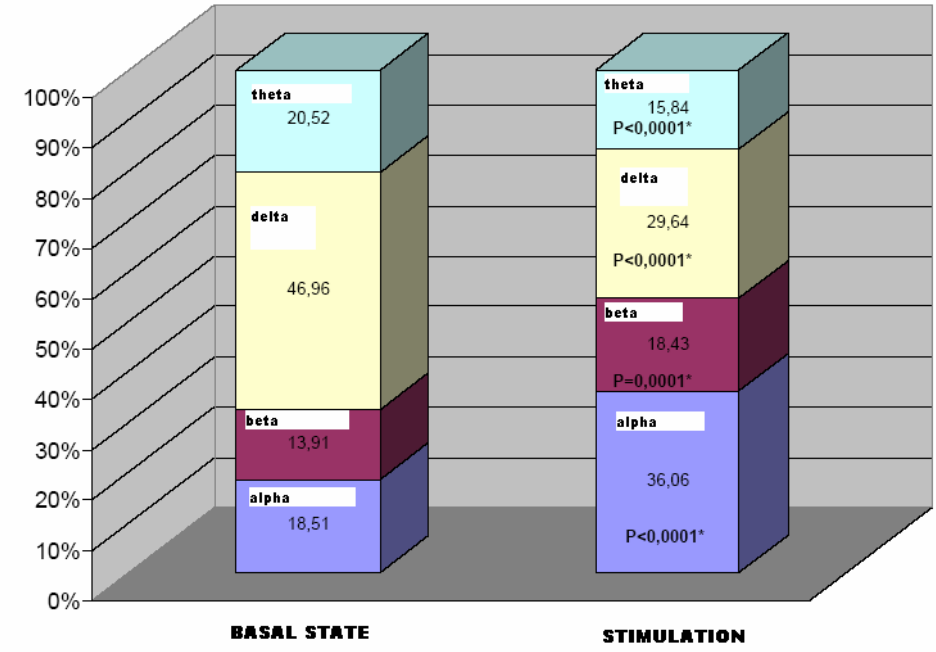

Fig 3. Comparison of frequency-percentage histogram. Redistribution of brain rhythms (alpha, beta, delta and theta), mean value of all the electrodes.

- **Discussion**

The systems usually employed for TMS have high intensity field-generating coils with a current peak of between 2 kA and 8 kA. This way, the different resulting potential, which is needed to induce functional stimulation or inhibition in the cortical area, can be achieved and it can be done with a 600 ms single-pulse field or with a 200 ms – 300 ms double-pulse field. These field intensities induce currents a lot higher than needed to obtain a selective effect. Furthermore, they expand over too large areas of the cortex to stimulate a target area round a few square millimetres. There is no reliable evidence found as yet to prove that the way to standardise the useful stimulation intensity may be based on the evoked muscular potentials obtained after stimulation. However, the fact that low intensity does not yield evoked muscular potentials does not imply there is not any effect. There are other effects, yet subclinical, that can be more relevant than the evoked motor responses.

Therefore, localization and selective stimulation objectives are not guaranteed with the high-power field systems which, additionally, provide undesirable thermal effects, preventing stimulation for long periods of time. The stimulated cerebral areas selected as objectives are not the only ones receiving this induced current. Besides the target area, there are stimulations in subcortical areas where their effect is yet unknown, or where undesirable effects are found, with hard to control collateral consequences.

Conversely, the intensity that flows through our coils is in µA, which allows for stimulations for as long a duration as desired without adverse effects on the patient. We should bear in mind that the intensity of the current is so high as it flows through the high-power field coils that there is a noise to be taken into consideration as we interpret the results (Nikouline *et al*., 1999). However, our subject can not hear a thing and, therefore, does not know whether the current is flowing; it is a single blind experiment.

High-power field stimulation is not physiological which is conceptually different from low-power field stimulation. The latter tries to simulate neuronal biophysics in that it works within the same ranks of frequency

and intensity, whereas a high-power field is quite a few ranks more intense than natural bioelectromagnetism and works with antiphysiological frequencies (Gutiérrez, 2004).

After a decade of experimentation, high-power field transcranial magnetic stimulation has not yet come up with a treatment for relief from any illnesses (Wassermann and Lisanby, 2001). However, studies on low-power field research have been fewer, isolated, inhomogenous, and contradictory. If we only focus on the physiological transcranial stimulation (at pT rank), the Sandyk, Anninos's team stands out alone in the world in the field of therapeutics as they aim to simulate the physiological cerebral magnetic field during stimulation (Sandyk *et al*., 1993, Anninos *et al*., 2003).

We must remark that all the studies we have analysed use the same methodology; firstly, they carry out a basal registry, then they stimulate a given field and, finally, they record EEG post-stimulation; the results are then compared and the "before-after" differences are observed. We, on the other hand, apply the stimulation and pause it serially. This allows us to see what goes on at consecutive moments, immediately after the moment of stimulation. This way, we do not need to observe a given effect much later. Furthermore, we use direct application coils on the skull, which generate small fields round it and does not require surrounding the subject with a large field.

By using pT magnetic field, the rank of physiological stimulation is never reached as opposed to those other studies which usually work at the μT rank.

Summary

We aim to obtain a model or pattern among normal subjects. We have used a new technique, the physiological TMS, (validation pending), which is a therapeutic method and a digital EEG, a diagnostic method. Thus, we are subsuming two methods. This new technique allows us to obtain an electroencephalographic response and also to measure changes in the rhythms of a healthy subject's brain, (pattern for normality). Physiological TMS at 10 pT and 8 Hz, simulating the alpha rhythm, were employed. The subject does not know when stimulation is taking place, so this study is single blind.

This way, we obtain a mimetic global bioelectrical neuronal response, as the alpha rhythm magnetic field is stimulated and the brain is timed to it. An alpha rhythm displacement towards frontal and central areas of the brain was also observed.

Acknowledgements

This project was carried out thanks to the collaboration of Bioelectromagnetism European Foundation (BEF) and sponsored by SIEMENS, A.G.

References

Anninos, P., Kotini, A., Adamopoulos, A. and Tsagas, N.: 2003, Magnetic Stimulation can modulate Seizures in Epileptic Patients, *Brain Topogr.* **16** (1), 57-64.

Bardasano, J.L., Ramos, J.L. and Picazo, M.L.: 1997a, Device for a non-invasive Treatment with ELF Electromagnetic Fields (pT Intensity). In *Bioelectromagnetismo y Salud Pública*, I.B.A.S.C., edit. Alcalá de Henares (University), 395-400, (In Spanish).

Bardasano, J.L., Ramírez, E., De la Hoz, J., Ramos, J.L. and Picazo, M.L.: 1997b, Extracranial Device for Noninvasive Neurological Treatments with pulsating ELF Magnetic Fields. Second World Congress for Electricity and Magnetism in Biology and Medicine, 8-13 June, Bologna.

Bardasano, J.L., Gutiérrez, I., Goya, R., Montiel, I., and Álvarez-Ude, J.: 2005a, Transcranial Magnetic Stimulation at pT and Synchronization of the alpha Rhythm, The First International Congress of applied Chronobiology and Chronomedicine, Antalya, June 1-5, Abstract Book, 43-44.

Bardasano, J.L., Carrillo, G.L., Gutiérrez, I., Goya, R. and Álvarez-Ude, J.: 2005b, Transcranial Magnetic Stimulation and EEG Changes in Multiple Sclerosis. Preliminary Results. First International Congress of Histology and Tissue Engineering. Alcalá de Henares, Sept.14-17. Item.: *Histol. Histopathol*. *Suppl.* **1**, 140-141.

Bardasano, J.L., Álvarez-Ude, J., Gutiérrez, I., Goya, R.: 2005c, New Device against non-thermal Effects from Mobile Telephones, *The Environmentalist* **25**, 257-263.

Bardasano *et al*.: 2006, Equipment for Magnetic Field Treatment for Neurodegenerative Illnesses. *Bol. Ofic. Prop. Industr*.1780, (In Spanish).

Cook, C.M., Thomas, A.W.and Prato, F.S.: 2002, Human Electrophysiological and Cognitive Effects of Exposure to ELF Magnetic and ELF modulated RF and Microwave Fields: A Review of recent Studies, *Bioelectromagnetics* **23**, 14-157.

Gutiérrez, I.: 2004, Electroencephalographic (EEG) Evaluation of Physiological Transcranial Magnetic

Stimulation Technique. New Application Device. Doctoral Thesis, Medical Specialities Department, School of Medicine, University of Alcalá, (In Spanish).

Heusser, K., Tellschaft, D. and Thoss, F.: 997, Influence of an Alternating 3 Hz Magnetic Field with an Induction of 0,1 Millitesla on Chosen Parameters on the Human Occipital EEG, *Neurosci. Lett.* **239**, 57-60.

Iramina, K., Maeno, T., Kowatari, Y. and Ueno, S.: 2002, Effects of Transcranial Magnetic Stimulation on EEG Activity, *IEEE Transactions on Magnetics* **38(**5), 3347–3349.

Lyskov, E.B., Juutilainen, J., Jousmäki,V., Hänninen, O., *et al.*: 1993, Influence of Short-term Exposure of Magnetic Field on the Bioelectrical Processes of the Brain and Performance, *Int. J. Psychophysiol*. **14**(3), 27-231.

Marino, A.A., Bell, G.B. and Chesson, A.: 1996, Low-level EMFs are traduced like other Stimuli, *J. Neurol. Sci.* **144**, 99-106.

Nikouline,V., Ruohonen, J. and Ilmoniemi, R.J.: 1999, The Role of the Coil Click in TMS assessed with simultaneous EEG, *Clinical Neurophysiol*. **110**, 1325-1328.

Pascual-Leone, A., Tormos, J.M., Keenan, J., Tarazona, F., Cañete, C. and Catalá, M.D.: 1998, Study and Modulation of Human Cortical Excitability with Transacranial Magnetic Stimulation, *J. Clin. Neurophysiol*. **15**, 333–343.

Ramírez, E., Bardasano, J.L., De la Hoz, J., Ramos, J. and Picazo, M.L.: 1997, Non invasive Treatment of some Neurodegenerative Illnesses with ELF (pT Intensity) Magnetic Fields. In *Bioelectromagnetismo y Salud Pública*, I.B.A.S.C., edit. Alcalá de Henares (University), 349-354, (In Spanish).

Sandyk, R.: 1992, Magnetic Fields in the Therapy of Parkinsonism, *Int. J. Neurosci*. **66,** 209-235.

Sandyk, R. and Derpapas, K.: 1993, The Effects of external Picoteslas Range Magnetic Fields on the EEG in Parkinson´s Disease, *Int. J. Neurosci*. **70**, 85-96.

Wassermann, E.M. and Lisanby, S.H.: 2001, Therapeutic Application of Repetitive Transcranial Magnetic Stimulation: a Review. *Clin. Neurophysiol.* **112**, 1367-1377.

Appendix

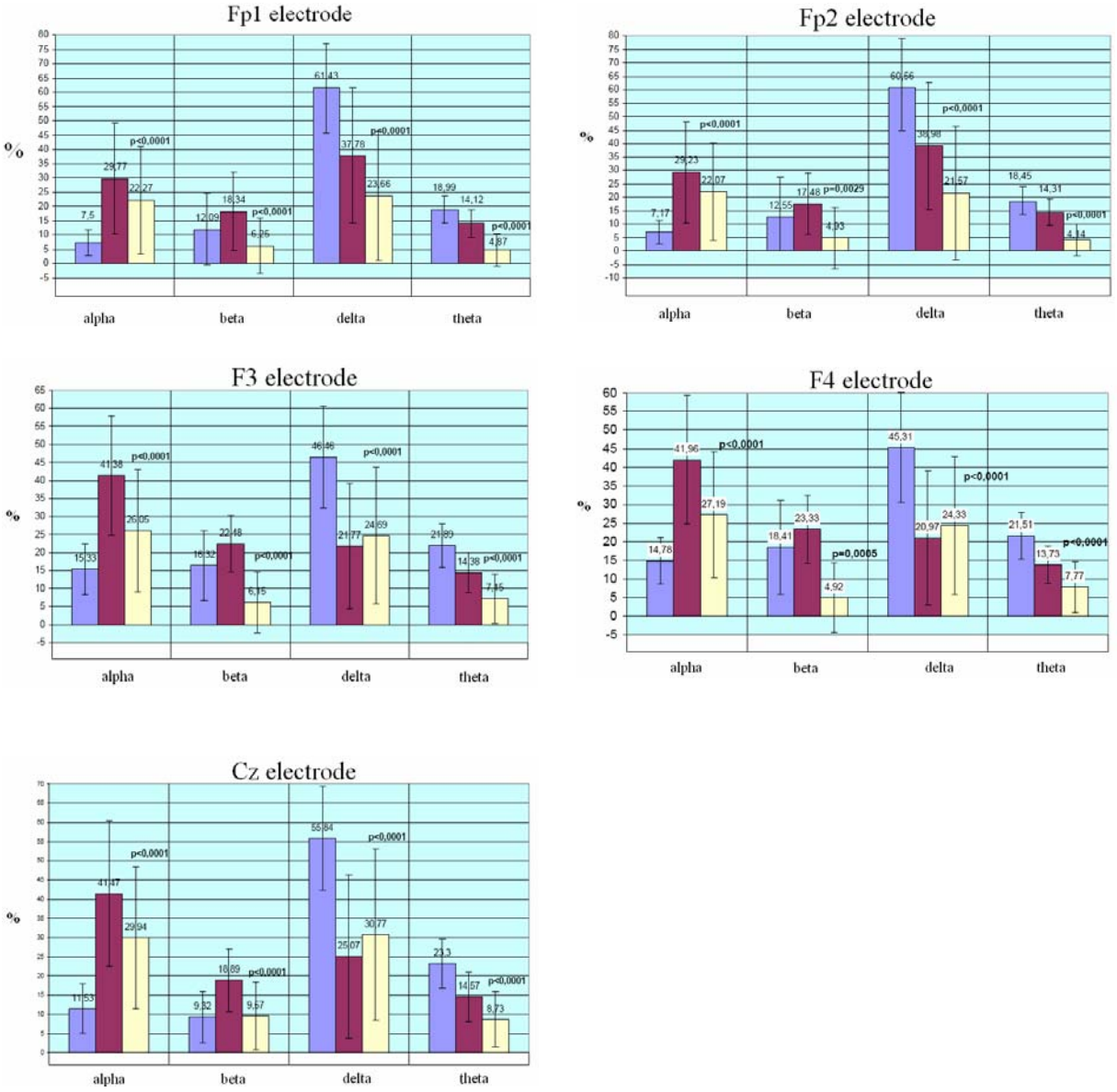

Fig 4. Diagrams of Fp1, Fp2, F3, F4 and Cz electrodes, where the four brain rhythms (alpha, beta, delta and theta) are analysed. For each rhythm, the left column stands for the basal state data; the central column, at 10 pT stimulation, and the right column stands for the difference between the other two.

TAMMEF (THERAPEUTIC APPLICATION OF MUSICALLY MODULATED ELECTROMAGNETIC FIELDS) THERAPY IN THE TREATMENT OF CHRONIC LOW BACK PAIN.

Battisti E.°, Albanese A.°, Bianciardi L.°, Piazza E.°, Rigato M.°, Vittoria A.*, Messa G.L.*, Giordano N.^.

°TAMMEF Centre - University of Siena, Italy.
*** Department of Clinical Medicine and Immunological Science - University of Siena, Italy.**
^ Department of Internal Medicine - University of Siena, Italy

Dr. Battisti Emilio
TAMMEF Centre – Ospedale S. Maria alle Scotte-
Strada delle Scotte,1
53100 Siena- ITALY
e-mail: battistie@unisi.it

ABSTRACT

Background: Numerous studies have demonstrated the utility of extremely low frequencies (ELF) electromagnetic fields in the treatment of pain. Moreover, the effects of these fields seems to depend on their respective codes (frequency, intensity, waveform).
Purpose of the study: In our study we want to value the effects of the TAMMEF (Therapeutic Application of a Musically Modulated Electromagnetic Field) system, which field is piloted by a musical signal and its parameters (frequency, intensity, waveform) are modified in time, randomly varying within the respective ranges, so that all possible codes can occur during a single application.
Ninety subjects, affected by chronic low back pain, were enrolled in the study and randomly divided into three groups of 30 patients each: A exposed to TAMMEF, B exposed to ELF, C exposed to a simulated field. All subjects underwent a cycle of 15 daily sessions of 30 minutes each and a clinical examination upon enrolment, after 7 days of therapy, at the end of the cycle and at a follow-up 30 days later.
Results: All the patients of groups A and B completed the therapy without the appearance of side effects: they presented a significant improvement of the subjective pain and the functional limitation, which remained stable at the follow-up examination. In group C, there was no improvement of the pain symptoms or articular functionality.
Conclusions: This study suggests that the TAMMEF system is efficacious in the control of pain symptoms and in the reduction of functional limitation in patients with chronic low back pain. Moreover, the effects of the TAMMEF system cover those produced by the ELF field.
Key words: electromagnetic fields, therapy, low back pain, TAMMEF.

INTRODUCTION

The effects of the various types of low frequency electromagnetic fields used in clinical practice depend on their codes (frequency, intensity, waveform, the number of impulses per train and the interval between one train and another). The electromotor forces induced at a given point of a biological system act on the electric charges present which respond, causing functional modifications in the cellular microenvironment (1-3).

The overall biophysical effect can be appreciated only by observation, since the level of complexity of the system does not allow one to predict what mechanisms of action will predominate. However, it is possible to

compare the effects of a certain field with those of an all-inclusive reference field whose parameters continually change in time so that all possible codes can occur in a single application.
Our group has already shown the efficacy and tolerability of the extremely low frequency (ELF) field in patients affected by osteoporosis (4), rheumatoid arthritis (5) and osteoarthritis (6,7). Recently to evaluate the utility of applying the widest possible magnetic field, we introduced the new TAMMEF (Therapeutic Application of a Musically Modulated Electromagnetic Field) system. The field is obtained from recorded musical passages; thus its parameters (frequency, intensity, waveform) are modified in time, randomly varying within the respective ranges, so that all possible codes can occur during a single application (6,7).
The aim of this study is to evaluate the efficacy of the TAMMEF system in the treatment of chronic low back pain. In particular, we wished to ascertain if the effects of the field piloted by a musical signal are comparable with those of field with frequency of 100 Hz and a sinusoidal waveform. Both fields are generated by an opposing pair of heteronomous polar expansions and thus present the characteristic spatial conformation.

METHODS AND PATIENTS

Methods
The instruments used to generate the ELF and TAMMEF fields are similar.
An audiotape player sends the relative monochannel-microphone signal to two low frequency amplifiers A and B, both with adjustable gain. The current from amplifier A, modulated according to the recorded signal, feeds two electromagnets with iron-silicon cores joined posteriorly by a ferromagnetic arc. The anatomical region to be treated is placed between the opposing faces (3x4 cm) of the polar expansions. The current from amplifier B feeds a loudspeaker that plays the pilot musical passage. The music can also be heard through headphones, with automatic exclusion of the loudspeaker. The gain of amplifier A is regulated so that when the audiotape contains a sinusoidal signal with frequency of 100 Hz, the electromagnetic field is equal to the ELF field used (about 3 gauss midway between the poles when this distance is 30 cm). This set-up is then left unchanged whatever the contents of the audiotape used subsequently. The patient is allowed to regulate the gain of amplifier B, with the volume preferred, whether the music is being transmitted over a loudspeaker or into a headset.

Patients
Ninety subjects (63 females and 27 males), between 59 and 76 years old, affected by chronic low back pain, were enrolled in the study (table 1a) and randomly divided into three groups: A = 30 patients subjected to TAMMEF, B = 30 patients subjected to ELF and C = 30 patients subjected to a simulated field**.** Group C was introduced because of the possibility that the TAMMEF effects would be indistinguishable from those of the ELF, and thus to test for the presence of a substantial placebo effect. All the patients including in group C listened to the music. Evaluation of the stage of the disease was based on the radiographic system of Kellegren and Lawrence (8). The clinical examination was based on the Million Instrument test (9), a validated questionnaire specific for back pain. On the basis of the point of the score of the test, the patients were divided into three subgroups, as shown in Table 1b.
All the subjects were out-patients and, correctly informed of the experimental plan, gave their written consent. All the patients underwent a cycle of 15 daily sessions of 30 minutes each, with application of the magnets in contact with the lumbar spine. In the past, all the patients had been treated occasionally or cyclically with analgesic (paracetamol) or non-steroidal anti-inflammatory drugs (diclofenac, or piroxicam, or celecoxib, or rofecoxib), but they had suspended any drug at least 15 days before the beginning of the cycle. The clinical examination was performed when the patients were enrolled in the study, after 7 days of therapy, at the end of the cycle and at a follow-up, 30 days later (10).
The evaluation of the possible therapeutic effects has been effectuated using the Million Instrument test as modified by the authors: we have divided the evaluation of pain from the evaluation of articular function because of the well-known subjectivity of pain to the placebo effect (11).

Statistical analysis
The differences between the means of the various parameters at 0, 15 and 45 days were tested by Student's t test or Mann-Whitney-U test as appropriate.

RESULTS

Above all, we specified that no significant differences were found between the three groups of patients, concerning private data and their degree of disease. All the patients of group A and B completed the therapeutic cycle, without side-effects that might have required suspension of the treatment. With regard to the efficacy of the therapy, it should be underlined that none of these patients had to take analgesic-

antiinflammatory drugs during the cycle and that all the patients presented a significant improvement of both subjective pain and regional functional limitation. In particular, in the TAMMEF group, the subjective pain progressively decreased in all subjects even after the first week and regressed completely at the end of treatment in 24 (80%) of the 30 patients. In the remaining 6 patients (20%), the pain symptoms, albeit not totally regressed, decreased significantly with respect to the basal values and to those recorded after the first week (Figure 1a). In the ELF group, the time course of subjective pain was equivalent to that of the TAMMEF group, with complete regression in 23 patients (76.6%) and a significant reduction in the remaining 7 patients (23.4%) (Figure 1b). With regard to the evaluation of articular functionality, there was a significant partial recovery of mobility in all patients, starting from the first week (thus concomitant with the improvement of subjective pain). At the end of the cycle, in the TAMMEF group, 21 patients (70%) manifested a total recovery of the partially compromised articular functionality, while 9 patients (30%) showed a significant further improvement with respect to the already positive trend recorded after the first week of therapy, although they did not achieve a total functional recovery (Figure 2a). In the ELF group, there was a total functional recovery in 19 patients (63.3%), while in 11 patients (36.7%) the change was similar to that of the TAMMEF group (Figure 2b). The clinical follow-up, one month after the end of the cycle, revealed that in 28 group A patients (93.3%), there was no appreciable variation in the regression or improvement of pain symptoms from what was recorded at the end of the magnetotherapy; in the other 2 subjects (6.7%), there was a clear relapse of pain. However, this was not accompanied by a concomitant worsening of articular functionality, which continued to show the same recovery as recorded at the end of the therapy one month previously. There was a very similar pattern in group B: in 27 patients (90%), there was no change from the situation at the end of therapy, whereas 3 subjects (10%) reported a relapse of the pain symptoms. The time course of the articular pathology was clearly different in the 30 subjects of group C. Only 3 of them (10%) presented a slight subjective improvement of the symptoms in the first 5 days of the cycle, while the other 27 patients (90%) reported no significant pain reduction. After the first week, application of the simulated magnetic field had to be suspended in 12 group C patients (40%) because of its ineffectiveness, while the remaining 18 patients (60%) completed the cycle. At the end of treatment and at the clinical follow-up one month later, all the patients who completed the cycle reported no improvement of pain symptoms or articular functionality; indeed, there was a slight worsening of pain (Figures 1c-2c).

DISCUSSION

All the patients treated with TAMMEF or ELF completed the therapeutic cycle and manifested a significant improvement of the clinical picture. The two electromagnetic fields had equivalent effects and produced a so-called “tail effect", continuing after the suspension of therapy, as if the biophysical action interfered with the pathogenetic mechanisms of the disease, probably by inhibition of the inflammatory process (4,5). The lack of efficacy in the group C patients confirms the therapeutic effects of the two fields. Indeed, considering the known relationship between the pain pathways and the psychic habitus of the patient (12-14), only the slight improvement of pain symptoms initially shown by the group C subjects could be attributed to the placebo effect. It should be mentioned that all the patients subjected to TAMMEF applications stated that they enjoyed listening to the music and they manifested a psychological attitude of trust and satisfaction. It also seems that these patients showed more evident and quicker responses, although this was not statistically significant and is reported only as an impression and a possible topic for future research.Our results confirm the efficacy and tolerability of low frequency magnetic fields as previously reported (4-7,10,15), also support the hypothesis that the effects of magnetic fields with parameters that change in time, like those produced by the music-piloted TAMMEF system, are equivalent to the effects of the ELF field (6,7).Moreover, in relation to current studies on interactions between the nervous, endocrine and immune systems (16,17), it may be possible to combine the electromagnetic stimulus with the corresponding acoustic stimulus, i.e. listening to the pilot musical passage. In fact, the two mechanisms, triggered in different sites and acting by different but simultaneous and coherent channels, might produce responses that reinforce one another (18).

Acknowledgement: Work supported in part by a contribution of the “Fondazione del Monte dei Paschi di Siena”, Siena, Italy.

REFERENCES

1. KATSIR G, BARAM SC, PAROLA AH: Effect of sinusoidally varing magnetic fields on cell proliferation and adenosine deaminase specific activity. *Bioelectromagnetics* 1998;1:46-52.
2. MACRI MA, DI LUZIO S: Biological effects of electromagnetic fields. *Int J Immunopathol Pharmacol* 2002; 15: 95-105.
3. VOLPE P: Interaction of zero-frequency and oscillating magnetic field biostructures and biosystems. *Photochem Photobiol Sci* 2003; 2: 673-48.
4. GIORDANO N, BATTISTI E, GERACI S *et al.*: Effect of electromagnetic fields on bone density and biochemical markers of bone turnover in osteoporosis: a single blind, randomized pilot study. *Current Therapeutic Research* 2001; 62: 187-93.
5. GIORDANO N, BATTISTI E, GERACI S *et al.*: Analgesic-antiinflammatory effect of 100 Hz variable magnetic field in R.A. *Clin Exp Rheumatol* 2000; 18: 263.
6. RIGATO M, BATTISTI E, FORTUNATO M, GIORDANO N.: Comparison between the analgesic and therapeutic effects of a musically modulated electromagnetic field (TAMMEF) and those of a 100Hz electromagnetic field: blind experiment on patients suffering from cervical spondylosis or shoulder periarthritis. *Journal of Medical Engineering & Technology* 2002; 26: 253-8.
7. BATTISTI E, PIAZZA E, RIGATO M, NUTI R, BIANCIARDI L, SCRIBANO A, GIORDANO N: Efficacy and safety of a musically modulated field (TAMMEF) in patients affected by Knee osteoarthitis. *Clin Exp Rheumatol* 2004; in press.
8. KELLGREN JK, LAWRENCE JS: Radiological assessment of osteoarthritis. *Ann Rheum Dis* 1957; 16: 494-501.
9. MILLION R, HALL W, NILSEN KH, BAKER RD, JAYSON MI: Assessment of the progress of the back-pain patients. *Spinel* 1982; 7 : 204-12.
10. TROCK DH, BOLLET AJ, MARKOLL R : The effect of pulsed electromagnetic fields in the treatment of osteoarthritis of the knee and cervical spine. Report of randomized, double blind, placebo controlled trials. *J Rheumatol 1994*; 21: 1903-11.
11. WAGER TD, RILLING JK, SMITH EE *et al* : Placebo-induced changes in FMRI in the anticipation and experience of pain. *Science* 2004; 303:1162-7.
12. GRUBB BD: Peripheral and central mechanisms of pain. *Br J Anaesth* 1998; 81: 8-11.
13. SCHAFER M: Physiology and pathophysiology of pain. *Ther Umsch* 1999; 56: 426-30.
14. QUITTAN M, SCHUHFRIED O, WIESINGER GF, FIALKA-MOSER V: Clinical effectiveness of magnetic field therapy- a review of literature. *Acta Med Austriaca* 2000; 27: 61-8.
15. JACOBSON JI, GORMAN R, YAMANASHI WS *et al* : Low amplitude, extremely low frequency magnetic fields for the treatment of osteoarthritis knees: a double blind clinical study. *Altern Ther Health Med* 2001; 7: 54-64.
16. YANG EV, GLASER R: Stress-induced immunomodulation and the implications for health. *Int Immunopharmacol* 2002, 2: 315-24.
17. HARBUZ M: Neuroendocrinology of autoimmunity. *Int Rev Neurobiol* 2002; 52:133-61.
18. ESKANDARY F, STERNBERG EM: Neural-immune interactions in health and disease. *Ann N Y Acad Sci* 2002; 966: 20-7.

Figure 1 Evaluation of pain

FIGURE 1A - Evaluation of pain at the start of the treatment, after 7, 15 (at the end of the treatment) and 45 days, in A group

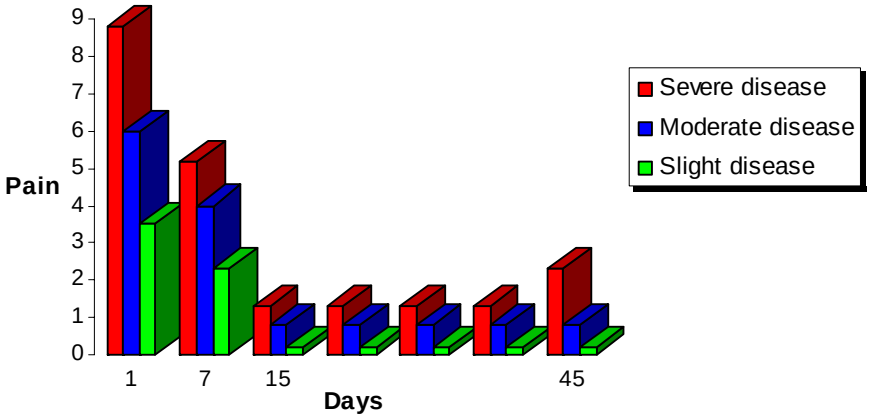

Statistical significance between the start of the treatment and the end of the treatment (15 days):
- p < 0,05
- p < 0,001
- p < 0,001

Statistical significance between the start of the treatment and the final control (45 days):
- p < 0,01
- p < 0,001
- p < 0,001

FIGURE 1B - Evaluation of pain at the start of the treatment, after 7, 15 (at the end of the treatment) and 45 days, in B group

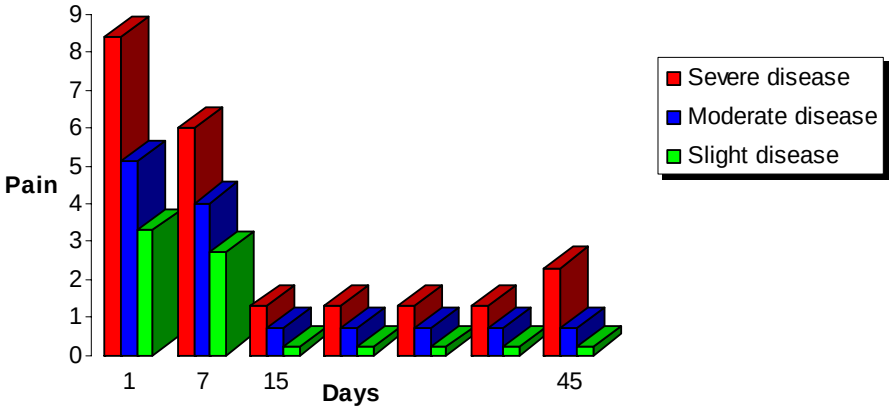

Statistical significance between the start of the treatment and the end of the treatment (15 days):
- p < 0,05
- p < 0,001
- p < 0,001

Statistical significance between the start of the treatment and the final control (45 days):
- p < 0,01
- p < 0,001
- p < 0,001

FIGURE 1C - Evaluation of pain at the start of the treatment, after 7, 15 (at the end of the treatment) and 45 days, in C group

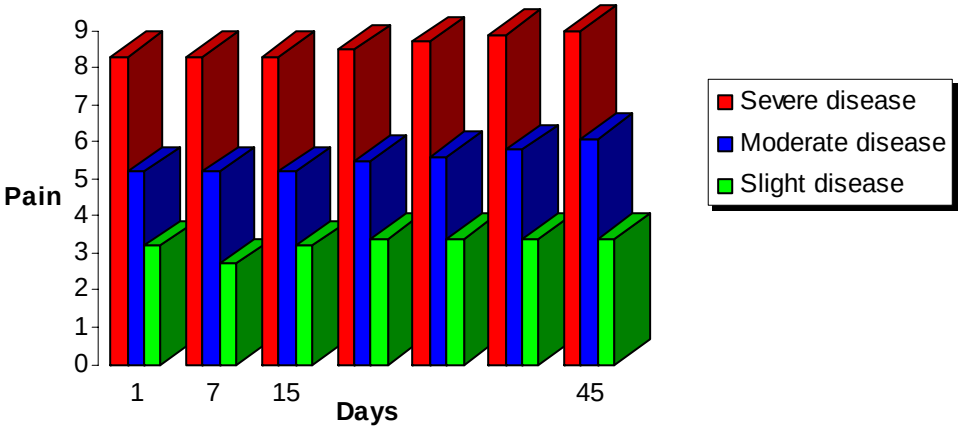

Statistical significance between the start of the treatment and the end of the treatment (15 days):
- no significant
- no significant
- no significant

Statistical significance between the start of the treatment and the final control (45 days):
- no significant
- no significant
- no significant

Figure 2 Evaluation of functionality

FIGURE 2A - Evaluation of functionality at the start of the treatment, after 7, 15 (at the end of the treatment) and 15 days, in A group

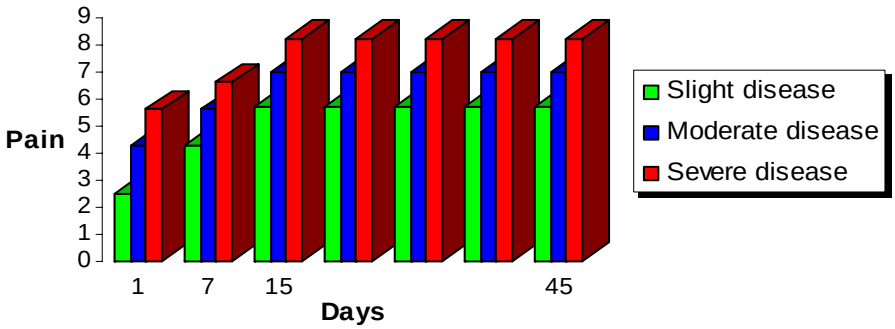

Statistical significance between the start of the treatment and the end of the treatment (15 days):
- $p < 0,05$
- $p < 0,01$
- $p < 0,01$

Statistical significance between the start of the treatment and the final control (45 days):
- $p < 0,01$
- $p < 0,01$
- $p < 0,01$

FIGURE 2B - Evaluation of functionality at the start of the treatment, after 7, 15 (at the end of the treatment) and 45 days, in B group

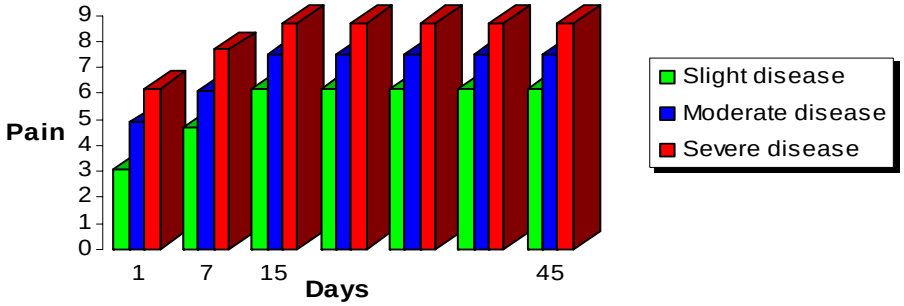

Statistical significance between the start of the treatment and the end of the treatment (15 days):
- $p < 0,05$
- $p < 0,01$
- $p < 0,01$

Statistical significance between the start of the treatment and the final control (45 days):
- $p < 0,01$
- $p < 0,01$
- $p < 0,01$

FIGURE 2C - Evaluation of functionality at the start of the treatment, after 7, 15 (at the end of the treatment) and 45 days, in C group

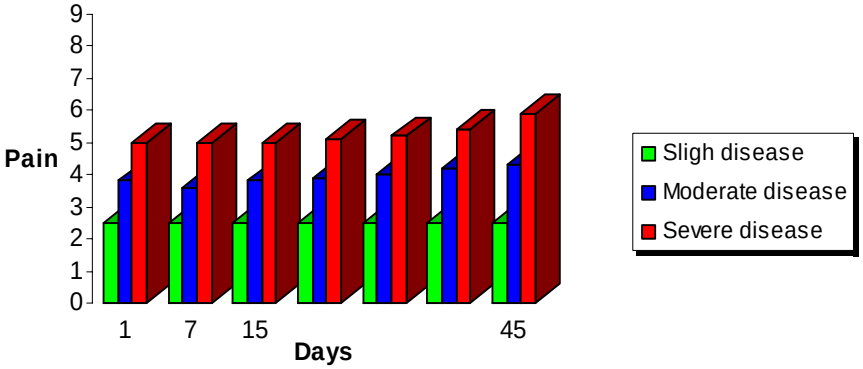

Statistical significance between the start of the treatment and the end of the treatment (15 days):
- no significant
- no significant
- no significant

Statistical significance between the start of the treatment and the final control (45 days):
- no significant
- no significant
- no significant

Table 1a Personal and clinical characteristics of the examined patiens (Pts)

Sex	Pts's number (%)	Mean age (years)	Duration of the disease (years)
M	27 (30 %)	54,3 ± 7,4	10,6 ± 2,2
F	63 (70 %)	58,6 ± 7,2	11 ± 3,3
Total	90 (100 %)	57,6 ± 7,3	10,9 ± 2,9

Table 1b Clinical characteristics of the examined patiens (Pts)

	Pts number (%) A B C	Slight disease (%) A B C	Moderate disease (%) A B C	Severe disease (%) A B C
Pts with low back pain (%)	30 30 30 100% 100% 100%	24 22 24 48% 44% 48%	20 22 20 40% 44% 40%	6 6 6 12% 12% 12%

EFFECTS OF VIDEO DISPLAY TERMINALS ELECTROMAGNETIC FIELDS INFLUENCE ON THE HEALTH OF THEIR USERS

Eleonora Bydianskaya
Kharkov Scientific Research Institute of Hygiene of Labour and Industrial Diseases
Trinklera st., 6, 61022, Kharkov, Ukraine

Eugeney Nikolenko
Kharkov Scientific Research Institute of Hygiene of Labour and Industrial Diseases
Trinklera st., 6, 61022, Kharkov, Ukraine

Abstract

A great experience of investigation of the EMF influence on the personal computers users' health has been accumulated. Carried out long-term observations of the health condition of the VDT users have shown that stress of their main life support systems: central nervous, cardiovascular, immune has been observed. Clinical-laboratory data have been obtained by the results of the profound medical examination of 1052 investigated users; from them 467 men and 585 women. The total number of factors, which have been put into database, is about 150000. Statistical processing of multivariate data was used for revealing early signs of negative influence of the factors of professional activity amongst VDT users. It is shown that reduction of the adaptation capacities of an organism is noted already in the first years of work at VDT. It causes breaches of the adaptation processes: decline of the functional activity of the antioxidant systems and activation of the processes free radicals oxidations, oppression of the immunological reactivity. Modification of the immunological and biochemical indices were considered and analysed with regard of the professional seniority and age. Such approach has allowed revealing the symptoms of fore-pathology of some part of working with VDT and referring them to the defined group of risk.

MODELING AND GIS SOFTWARE APPLICATIONS FOR EMF ENVIRONMENTAL MONITORING IN SICILY

S. CALDARA, P. COSTANZA, G. LISCIANDRELLO

REGIONAL AGENCY FOR ENVIRONMENTAL PROTECTION OF SICILY (ARPA SICILIA)

Via U. La Malfa, 169 90146 Palermo Italy

scaldara@arpa.sicilia.it, piero.costanza@gmail.it, glisciandrello@arpa.sicilia.it

Abstract

Regional Agency for Environmental Protection has been operating for 5 years in Sicily to ensure environment and consequently public health protection from EMF exposure.

This paper deals with EMF monitoring in all county territory.

In order to increase the knowledge of sources and their impact on environment, a register of telecommunication devices has been implemented; technical items have been used as inputs for modeling tools and simulation outcomes are compared with measurement results.

All these data are collected in GIS software.

In particular mobile phone networks and broadcasting systems have been studied. A complex site for TV and Radio broadcasting is reported as an example.

Moreover some comparison between two different simulation software has been developed.

GIS register show that whole Sicilian territory is covered by mobile phone base stations with high concentration in big cities (Palermo and Catania). Simulations have been used to determine measurements and monitoring policy according to particular needs related to special places like schools, hospital, etc.

Introduction

The development of new telecommunication systems, as mobile phone base stations and broadcasting antennas, as well as electric power plants and power delivery lines, even if has contributed to improve life quality, is also responsible of the increasing human exposure to electromagnetic fields (EMF) from manmade sources which are to be added to natural electromagnetic irradiation.

Italian national law n. 36 of 2001, separately regulates both extremely low-frequency (ELF) and radio-frequency (RF) electromagnetics fields and makes a difference between acute (thermal) and chronic (non thermal) adverse health consequences.

Acute exposures are associated with thermal hazards and are characterized by threshold exposures below which no health effects occur.

In case of long term exposure to low (non thermal) levels of EMF there are no threshold exposures significant for human health. In this case health risk is thought to be of probabilistic nature: if the time exposure increases not the magnitude of adverse health consequence but the probability to have consequences increases.

According to the A.L.A.R.A. caution principle of keeping the exposure to lower possible level, “attention values” and “quality aims” have been fixed; they are not safety threshold exposures but an operational reference for prevention and public health protection.

In particular, the Italian “DPCM July 8th 2003” law arranges “threshold exposures” (Tab. 1) and “attention values” (Tab. 2) to prevent short term and possible long term health effects due to exposure to EMF generated by RF fixed source in the range 100 kHZ up to 300 GHz; it also arranges “quality aims” to minimize, in a progressive way, people exposure to EMF and measurement standards.

The Regional Agency for Environmental Protection of Sicily has been operating for 5 years in Sicily to ensure environment and consequently public health protection from EMF exposure.

The Agency has an important role of technical support to local councils by giving preventive opinions about the installation of new TLC systems based on existing systems emission evaluation compared with threshold exposures and attention values.

Table 1 – Threshold exposures (DPCM July 8th 2003)

Frequency range (MHz)	RMS e. f. E (V/m)	RMS m. f. H (A/m)	Power density S (W/m^2)
0,1 - 3	60	0,20	-
>3 – 3.000	20	0,05	1
>3.000 – 300.000	40	0,10	4

Table 2 – Attention values (DPCM July 8th 2003)

Frequency range (MHz)	RMS e. f. E (V/m)	RMS m. f. H (A/m)	Power density S (W/m^2)
0,1 – 300.000	6	0,016	0,10

Register of TLC fixed EMF sources

Mobile phone base stations

In order to carriy out the register of TLC fixed EMF sources, which complies with the Italian law n. 36/2001, the Regional Agency for Environmental Protection of Sicily, in February 2003, has stipulated an agreement with the TLC Companies which periodically transfer data about their system.

All mobile phone base stations of the regional area have been then geo-mapped (Fig. 1 and 2). In particular, each point of the chart represents a site with several antennas of base stations. Of each site Gauss-Boaga co-ordinate, number and model of the antennas, the power (W), the gain (dB), the frequency and the eight of the electrical center are known.

As we can see from figures 1 and 2 and from table 3 the overall regional area is covered by mobile phone base stations. The highest concentrations are specially in big cities (Palermo and Catania) and near the coastline. Table 4 highlights the lower specific power of 3G (UMTS) systems compared with GSM technology based ones.

Table 3 – Base stations distribution

Town	n. of sites	n. of antennas	Total power (W)
Palermo	442	1960	46189
Catania	239	1044	22691
Messina	179	650	13696
Trapani	66	264	7735
Siracusa	72	268	6143
Ragusa	61	93	6226
Agrigento	25	86	2691
Caltanissetta	26	93	2183
Enna	12	36	835

Table 4 – Base stations characteristics

Frequency	n. of antennas	Power (W)	Specific power (W)
GSM - 900	4110	134925	32,82
GSM - 1800	2233	52482	23,50
UMTS	2878	55712	19,35

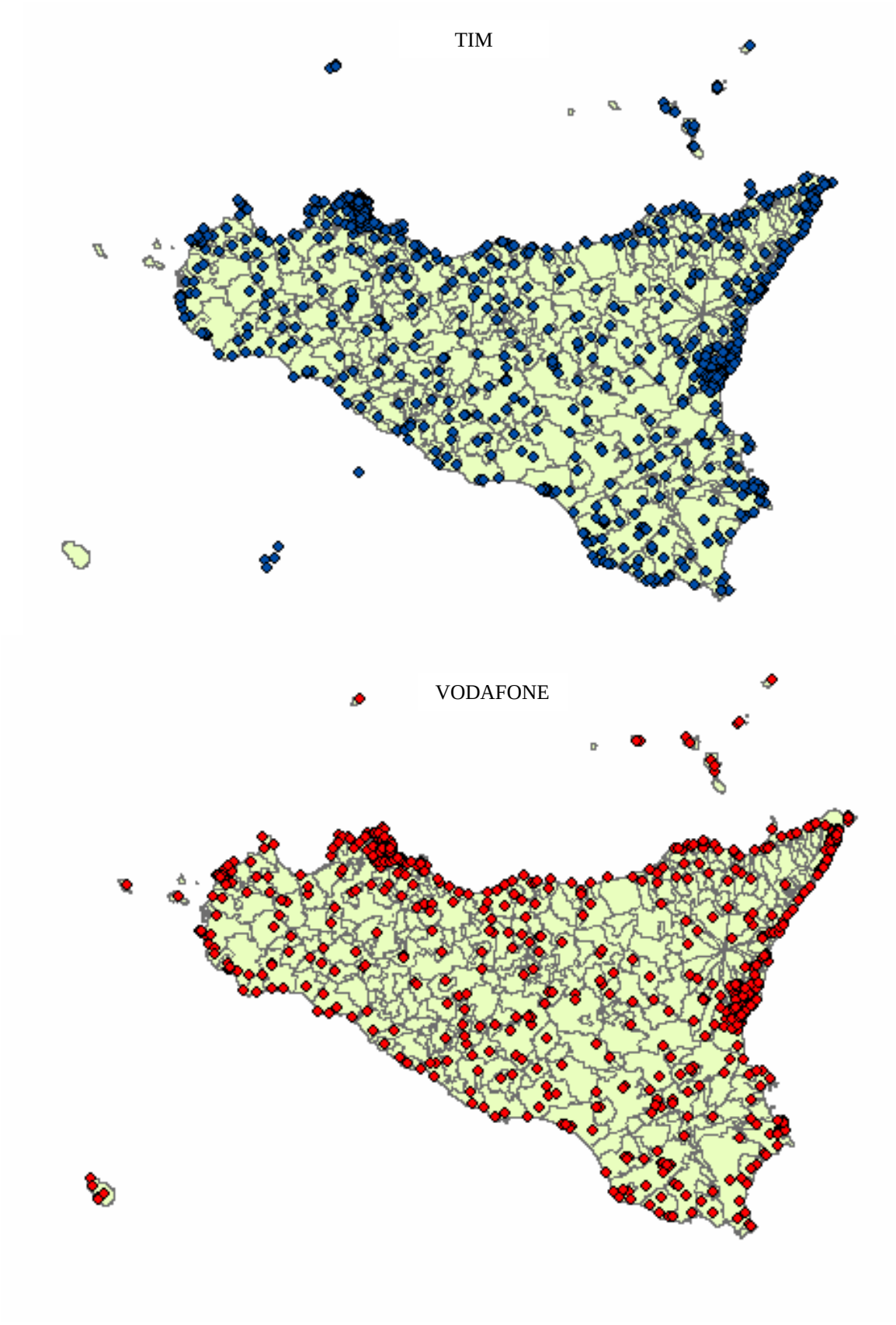

Figure 1 – GIS representation of mobile phone base stations distinguished per company

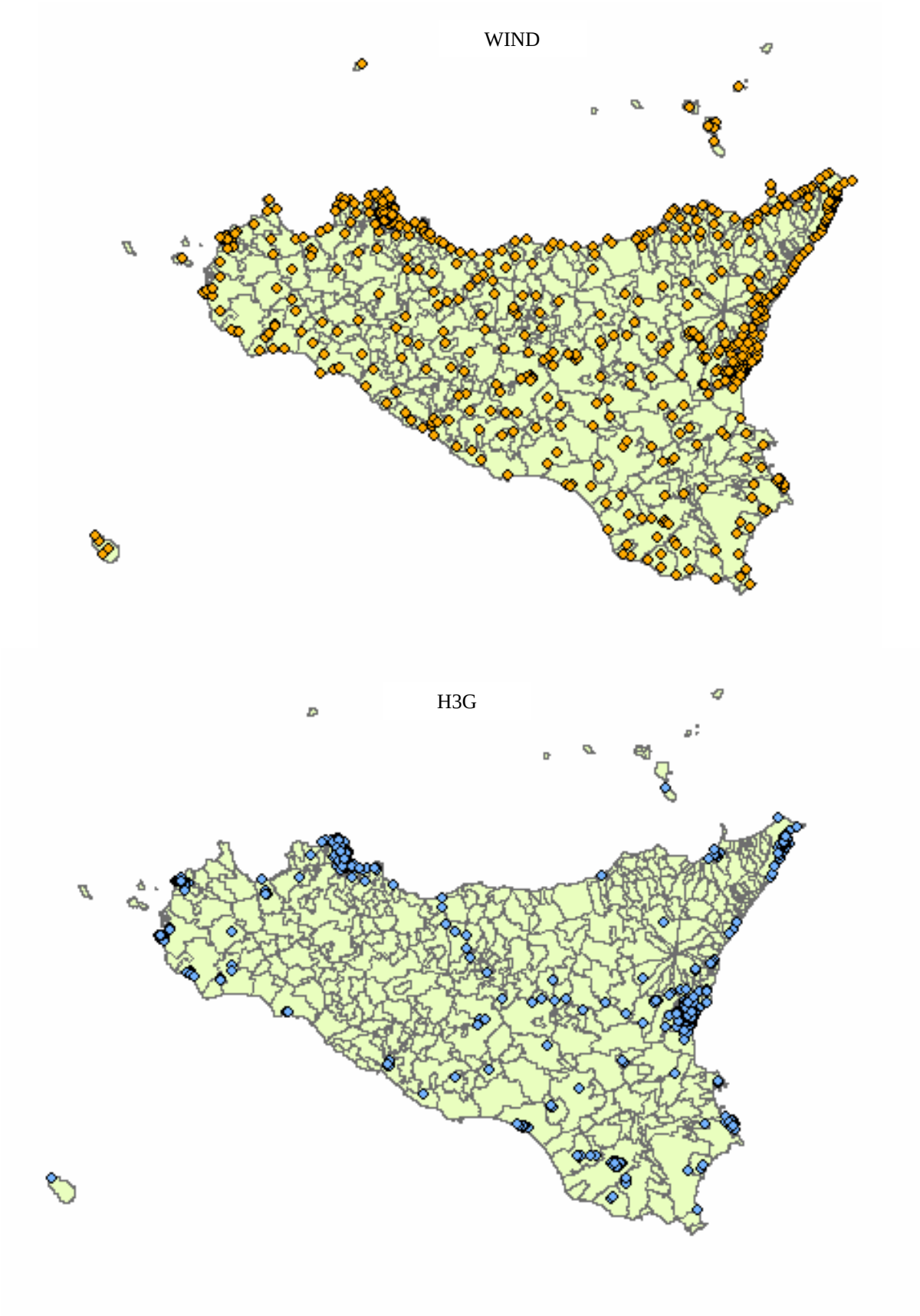

Figure 2 – GIS representation of mobile phone base stations distinguished per company

TV and Radio broadcasting

Data concerning Radio and TV supplied by the Telcomunication Regional Department were not complete so that all Radio and TV company in the regional area were directly asked to transfer information about broadcasting systems.

Such action brought to identify eleven crowded multiple antenna sites in the regional area (Fig. 3)

Figure 3 – RTV crowded multiple antenna sites

In particular, the features of broadcasting multiple antenna site of Caltanissetta are listed below:

Mount S. Anna

- Total power 20950 W
- Intersted Area 1,8 km^2
- Specific power 11 mW/m^2
- N. of antennas 9 RTV antennas (one of which with a power of 20000W)

Mount S. Giuliano

- Total power 6160 W
- Intersted Area 1,25 km^2
- Specific power 5 mW/m^2
- N. of antennas 19 RTV antennas (one of which with a power of 2000W)

Modeling and GIS software

The Geographical Information System (GIS) is based on a relational database containing all technical information of EMF sources, a cartography managing software and a model based software which, starting from geo-mapped and technical information, is able to simulate the EMF distribution in a given area.

The GIS returns the following informations:

1. number and positioning of geo-mapped sistems (Fig 1 e 2)
2. technical data-sheets
3. photographic documentation (Fig. 4)
4. EMF simulation based on “Radmap 8.0” 2D modelling software (Fig. 5).
5. EMF simulation based on “VICREM” 2D and 3D modelling software (Fig. 6).

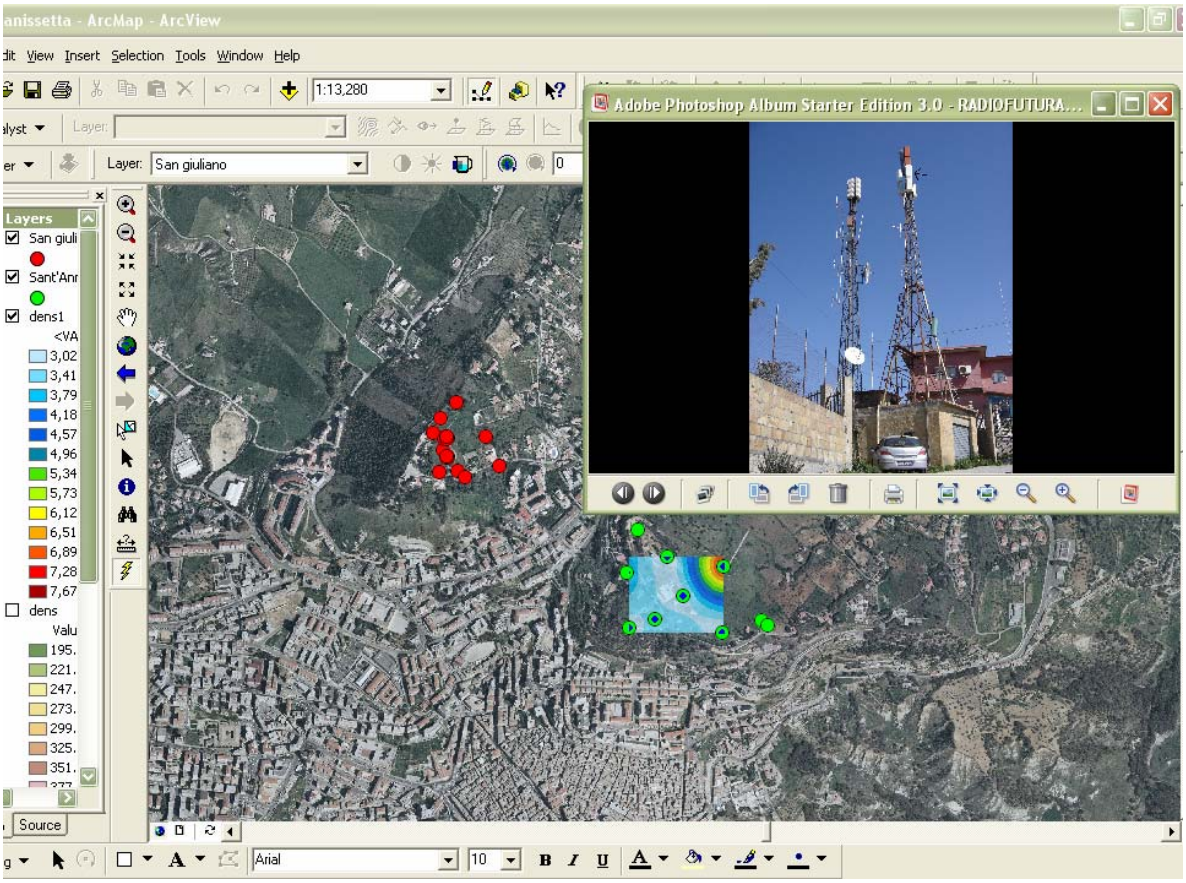

Figure 4 – Example of GIS informations (Caltanissetta)

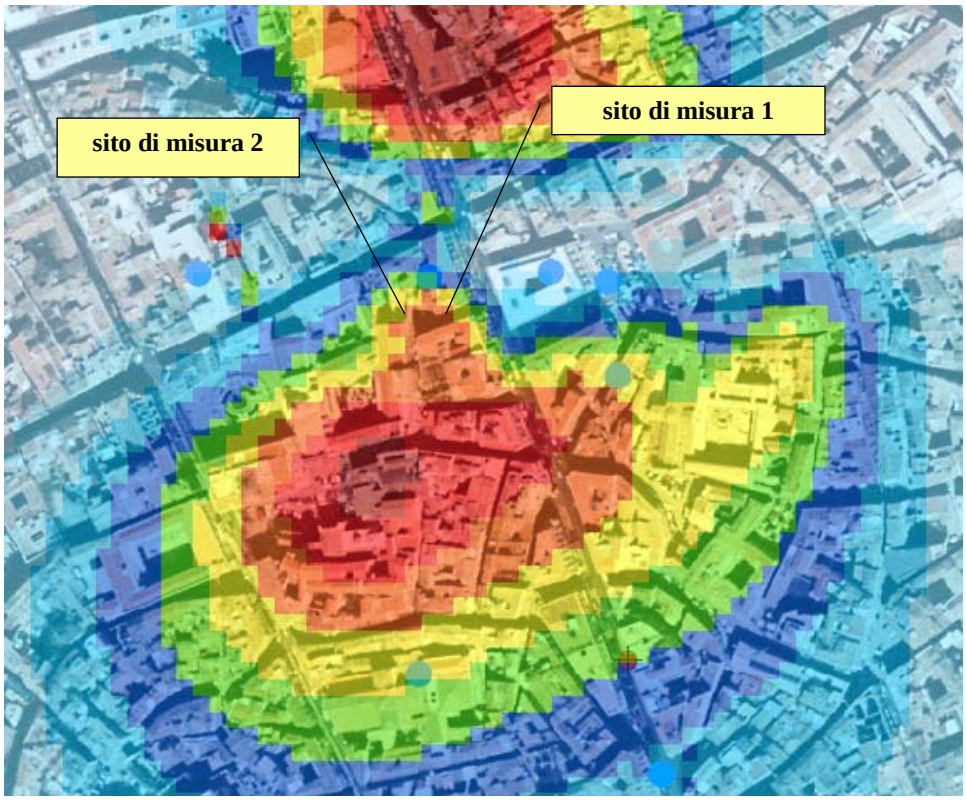

Figure 5 – Example of Radmap 2D simultation in Palermo

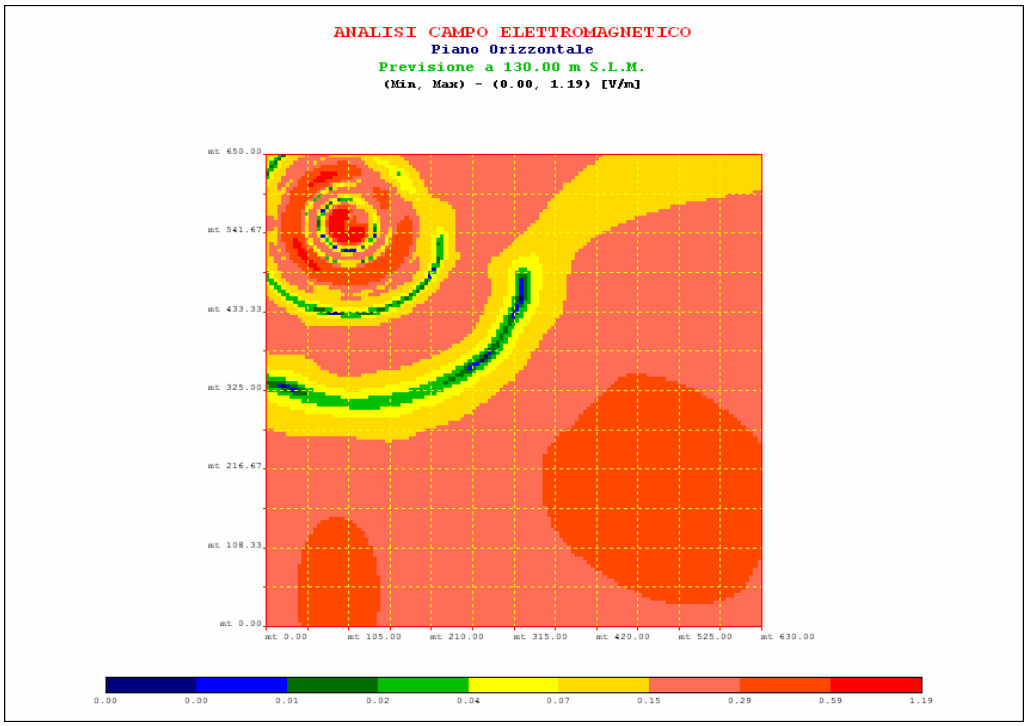

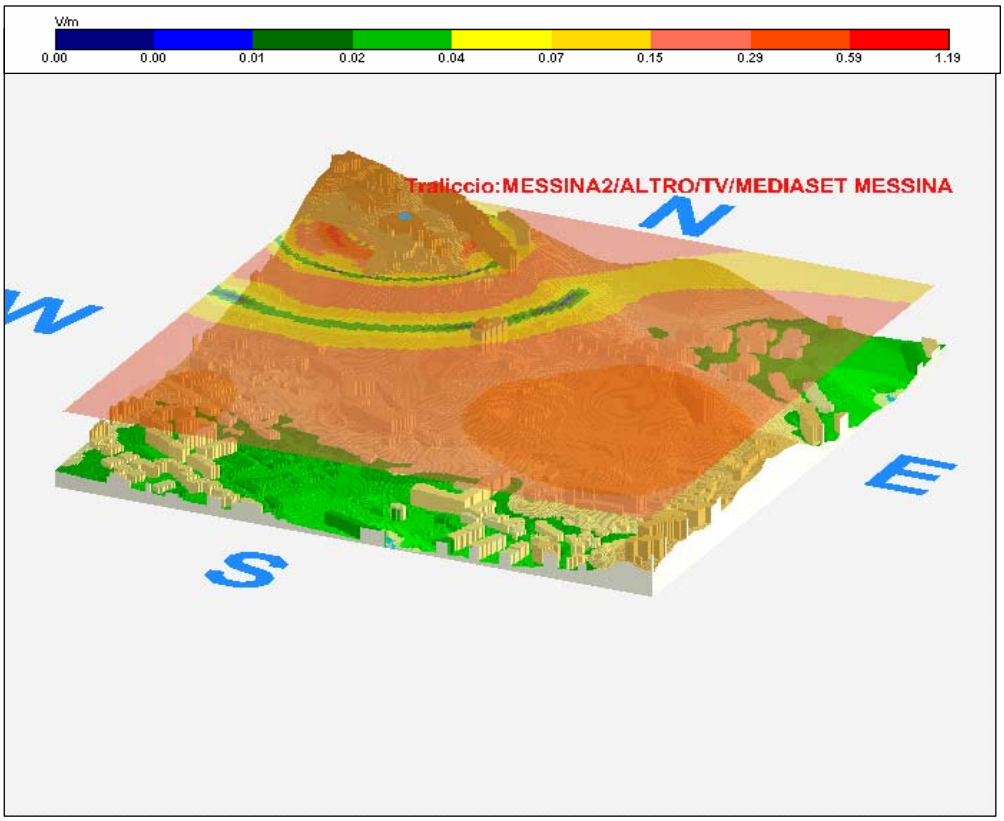

Figure 6 – Example of VICREM 2D and 3D simultation in Messina

Monitoring network

Continuous EMF monitoring is thought to be a suitable answer to the strong citizens' expectations of environmental controls which could give warranty threshold exposures respect 24 hours a day.

This measurement method is particularly significant because it takes into account the time history of the EMF level.

The ARPA Sicilia EMF monitoring network is based on 182 mobile monitoring devices, 102 of which have been supplied by the Ugo Bordoni Foundation for a national monitoring project.

The selection of monitoring sites has been based upon the following criterions:

- Analysis of already known sources generating EMF levels higher than threshold exposures;
- Analysis of particular sites in order to deal with the public concerns about potential health effects (schools, hospitals, etc.);
- Specific claims by local councils or citizens.

In Tab. 5 RF EMF (100 kHz – 3 GHz) monitoring results in Sicily in 2004 and 2005 are reported.

Table 5 – Continuous EMF monitoring results (2004-2005)

PROV.	N. town 2004	N. town 2005	N. town 04/05	N. sites 2004	N. sites 2005	N. sites 04/05	N. hours 2004	N. hours 2005	N. hours 2004 +2005
AG	4	5	7	15	11	26	12416	16962	29378
CL	1	5	5	2	30	32	839	11260	12099
CT	3	9	10	40	115	155	27182	81480	108662
EN	0	2	2	0	6	6	0	3856	3856
ME	5	2	7	13	15	28	6955	5891	12846
PA	6	18	19	34	157	191	14463	72049	86512
RG	1	3	3	1	13	14	186	7920	8106
SR	1	2	2	1	7	8	250	5769	6019
TP	5	1	5	8	1	9	8246	411	8657
TOTAL	**26**	**47**	**60**	**114**	**355**	**469**	**70537**	**205598**	**276135**

Monitoring results can be collected in the GIS. In Fig. 8 the GIS representation of monitoring activity in the city of Palermo is shown.

Monitoring results have been compared with the simulation software outcomes in order to setup the models and, at the same time, to check measurement procedures. The correlation between measurement results and simulations is good (Fig. 7 and Tab. 6) although simulations are lower than measurements.

Figure 7 – Simulations Vs Measurements correlation

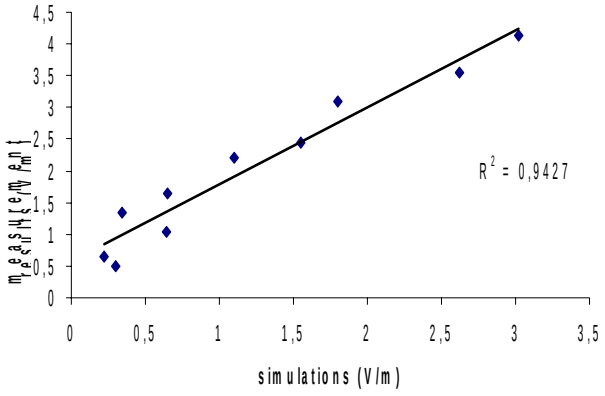

Table 6 – Difference between measurements and simulations (V/m)

simulations	measurements	difference
1.55	2.44	0.89
0.34	1.34	1
1.8	3.1	1.3
0.65	1.65	1
0.3	0.5	0.2
1.1	2.2	1.1
2.62	3.54	0.92
3.02	4.14	1.12
0.22	0.64	0.42
0.64	1.03	0.39
	average	**0.834**

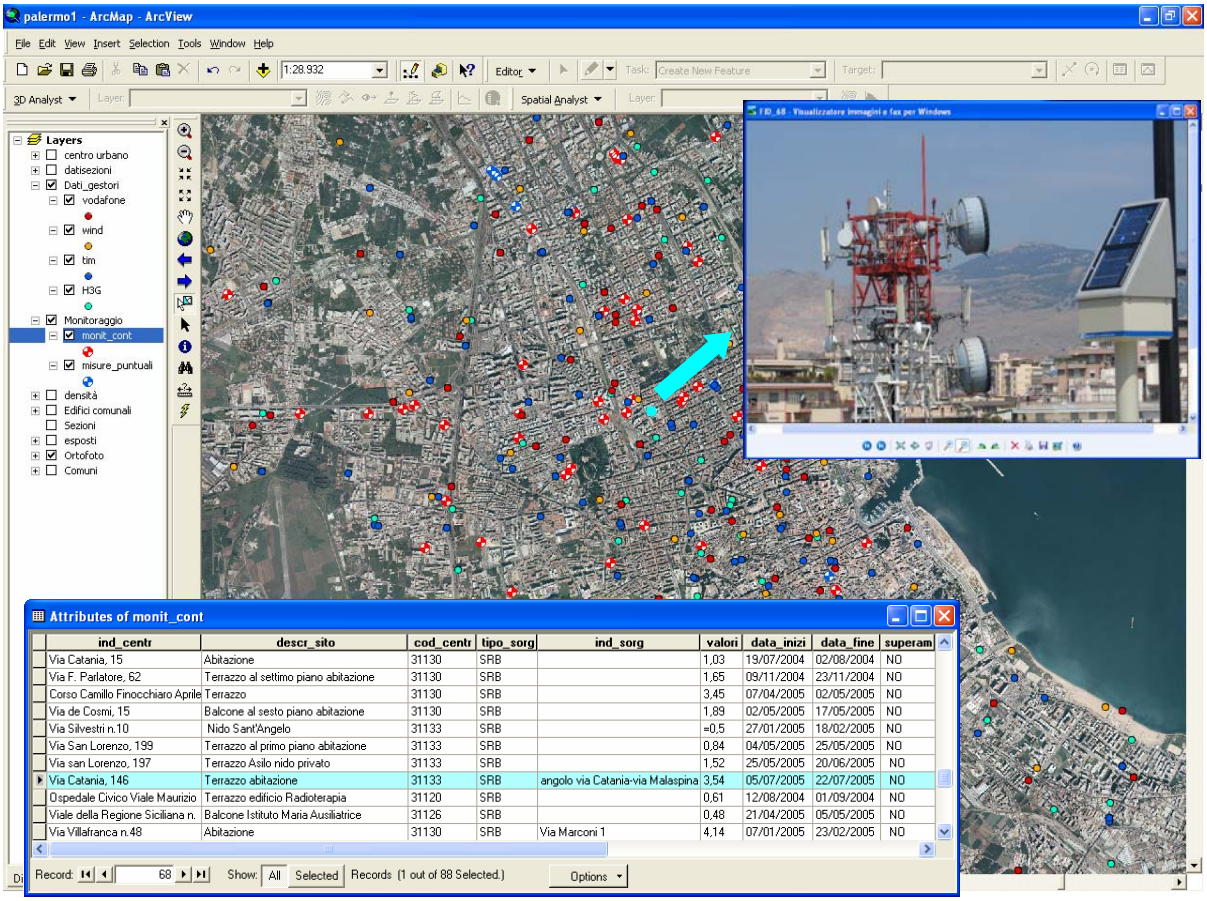

Figure 8 – EMF Monitoring metadata in Palermo

Summary

In this paper ARPA Sicilia register of TLC fixed EMF sources is presented. The Geographical Information System (GIS) which all these data are collected in is presented as well. In particular mobile phone networks and broadcasting systems have been studied and a complex site for TV and Radio broadcasting is reported as an example.
Register data contain the technical items which have been used as inputs for modeling tools; simulation outcomes have been compared with measurement results showing an high correlation.
GIS register show that whole Sicilian territory is covered by mobile phone base stations with high concentration in big cities (Palermo and Catania).
Moreover the results of RF EMF continuous monitoring in Sicily and, in particular, graphical GIS data of Palermo have been reported.

Acknowledgments
The authors want to acknowledge the support from the “Ugo Bordoni Foundation” for the continuous monitoring devices availability.

References

[1] Guidelines on Limits of Exposure to Electromagnetic Fields in the Frequency Range from 1 Hz to 300 GHz, ICNIRP, 1998
[2] Non-Ionizing Radiation, Part 1: Static and extremely low frequency (ELF) electric and magnetic fields, WHO – IARC Press, Lyon, 2002

RESULTS OF EMF MODELLING AND GIS SOFTWARE APPLICATIONS FOR RISK COMMUNICATION AND MANAGEMENT IN SICILY

S. CALDARA, P. COSTANZA, G. LISCIANDRELLO

REGIONAL AGENCY FOR ENVIRONMENTAL PROTECTION OF SICILY (ARPA SICILIA)

Via U. La Malfa, 169 90146 Palermo Italy

scaldara@arpa.sicilia.it, piero.costanza@gmail.it, glisciandrello@arpa.sicilia.it

Abstract

Regional Agency for Environmental Protection has been operating for 5 years in Sicily to ensure environment and consequently public health protection from EMF exposure.

Another task of ARPA Sicilia is the correct EMF exposure risk communication to citizens.

ARPA Sicilia is already partner of a national monitoring program which gives information by web only for mobile phone b.s. generated emf.

This paper deals with the use of EMF modeling and GIS software results as possible tools for a clear risk communication.

In order to increase the knowledge of sources and their impact on environment, a register of telecommunication devices has been implemented; technical items have been used as inputs for modeling tools and simulation outcomes are compared with measurement results.

All these data are collected in GIS software and processed to generate charts which gives graphical information about base stations, TV and Radio broadcasting systems and power lines territorial distribution, simulations of EMF level, monitoring activity results and petitions. These charts, published in the Agency web site, can be a user-friendly instrument which allows people to get a correct perception of risk better than tables or numbers.

Introduction

In the societies with a high rate of industrialization Citizens' restlessness is increasing for the possible consequences of technological development. Such worries derive also from the changed image of science, than in general terms, it is not anylonger more perceived as caretaker of "sure knowledge", also because of the inability demonstrated by the scientific world in the last few decades to preview, to manage and to interpret some catastrophic events.

The risk is diffusely perceived and it invests multiple aspects of our life, the fear of unexpected events, of personal or collectives risks is so intense that it has made our society defined as "the society of risk". Particularly, regarding electromagnetic fields, the worries are magnified by the electromagnetic fields potential risks evaluation uncertainty.

The majority of the papers written on the topic have often been of dubious interpretation, moreover, some of them present methodological inaccuracies and it is quite difficult to make comparisons between different studies as the data seem to be strictly related to the various methodologies applied.

In ICNIRP's 1998 guidelines we read that: the results of epidemiological studies on exposure to electromagnetic fields and neoplastic pathologies do not allow the creation of a scientific base on which basing the guidelines for the exposure.

Even the definition of possible cancerogenous for the 50 - 60 Hz EMF, given from IARC, takes into consideration the fact that epidemiological tests so far carried out are limited and the tests on animals limited or inadequate. In this situation of uncertainty, mass media's tendency of emphasising such kind of news, surely contributes to instil worries to citiziten up to the point of transforming such worries in a real society issue

In the past, these worries were looked at as irrational and due to people's inability to understand scientific data

that, through probability theory, demonstrated how the risk related to a given technology (for example in terms of human life losses) was insignificant.
They have been later on analyzed, in a comprehensive way, the complex interactions between the factors that contribute to create in the citizen the perception of the risk and the consequent behaviours.
In particular, fears and worries on the risk deriving electromagnetic fields are inexplicable if the risk is only defined through statistical calculation.
The results of such studies have highlighted some persisting aspects which contribute to expand risks' perception from electromagnetic fields. Such aspects can be summarized as follows:

- Lack of confidence, the risk is more feared as it is caused by an immaterial and imperceptible physical agent;
- Uncontrollability, the subject exposed to the risk by not being able to control exposure feels incapable of dealing with the risk;
- Uncertainty, there are no realiable evidences about consequences, the apprehension is augmented by the fact that the risk could actuall be greater for children and that the possible effects could manifest themselves even after a long period;

The World Health Organisation launched in 1996 an international programme on electromagnetic fields, suggesting the evalution of health and environment risks with the aim of defining research protocols to be carried out following standards compatible and comparable among them. This project will be ended by 2006.
In July 2003, when the first block of activities was over, ARPA Sicilia organised a conference on the topic which marked the beginning of a new path. All the stakeholders, which are involved, in the field , have been invited to participate from TLC companies to environmental association not forgetting the institutional stakeholders involved in the overall managing of the problem.
Such occasion has been useful in order to start a dialogue, an essential premise to establish a climate of mutual confidence needed to be able to manage the problem effectively.

Risk communication

ARPA Sicilia's plan for the communication of the risk due to electromagnetic fields exposure previews two articulations: on one hand, the essencial "usual" communication, even if accompanied by the use of the Internet, on the other hand, the new approach of communicating the results of monitoring activities aimed at encouraging and promoting citizens' involvement.
Taking into account these premise, a study on health implications deriving from the exposure to the electromagnetic fields has been commissioned the Department of Biotechnologies of the Medicine Faculty of the University of Palermo. The results of this research are avalaible on the Internet (www.arpa.sicilia.it).
Starting from a preliminary analysis of potential users' characteristics, the documents have been drawn up modelling the type of information to the different targets.
The preferred approach was based on divulgation, in fact, the adoption of a winning graphic and animated images, allowed not only to render basic concepts of physics easily comprehensible (an example could be the difference between an electric field, a magnetic field and electromagnetic field or between direct current and alternating current), but also epidemiology fundamental principles and base terminology.
The opportunity of getting deeper on the subject has also been guaranteed (links to specialized sites and a list of downloadable epidemiological studies)
Beside the communication of "usual" type, the plan currently being developed aims at the diminution of "uncontrollability of the risk" feeling and at responding adequately to the citizen steadily increasing need of involvement through the adoption of GIS.

The GIS software

The system, in ArcMap environment, allows the geo-mapping of electromagnetic fields sources of all types, from radio frequency (RF) and low frequency (ELF) collecting all the data in a database containing all the physical parameter that allow, by using ad-hoc models of calculation, to make forecasts about the distribution of a electric or magnetic field in a given area. Such simulations can be carried out on horizontal and vertical plans and to be overlapped to the cartography (orthophotographs and/or technical charts) for a correct understanding of the results in their context. It is also possible to relate the distribution of field with the buildings's height in order to characterize possible critical situation.
In order to obtain a structured and versatile communication a multi-steps and multi-phases procedural approach needs to be followed. The different phases are summarized in the following diagram:

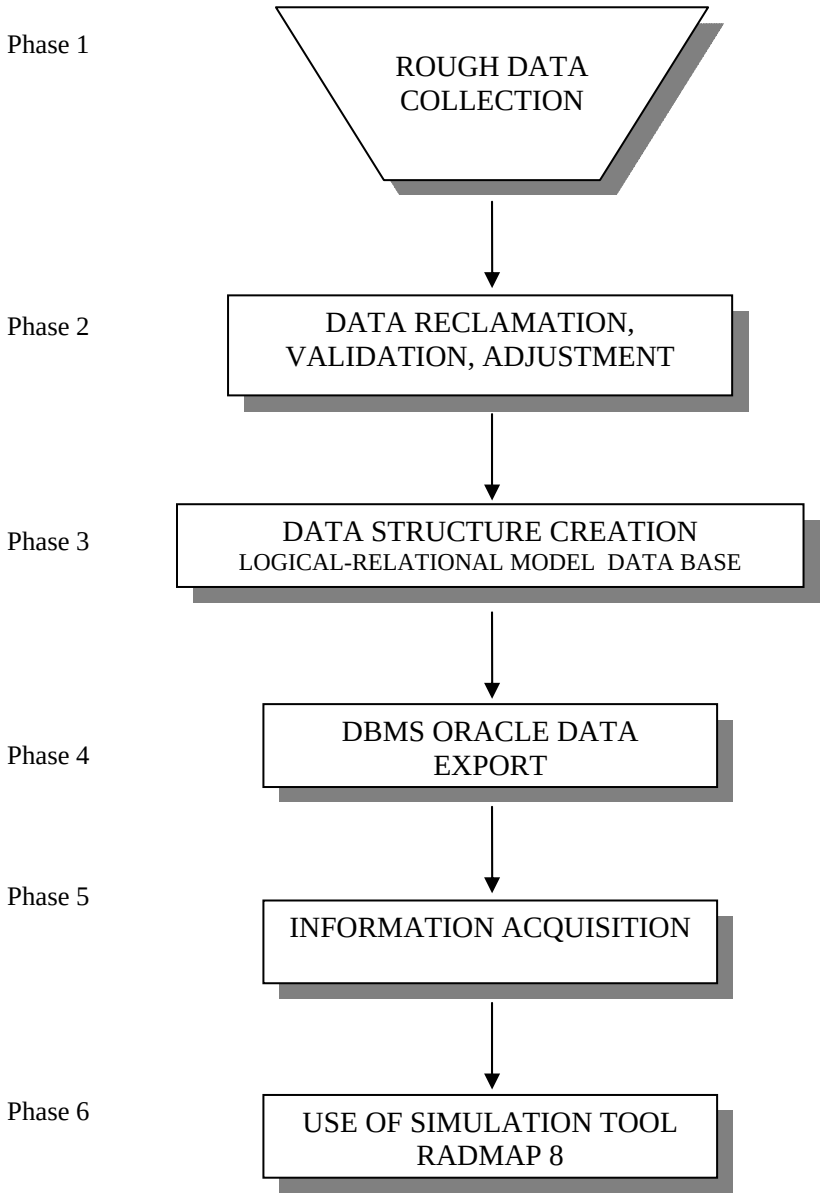

Phase 1

In this phase the elementary information is received in the form of a electronic sheet in a classic tabular structure.

Phase 2

The rough data (radioelectric parameters, geographic coordinates, etc) are carefully examined, corrected if imprecise or incongruous, and once validated, manipulated in order to take the most suitable format for the successive elaborations (e.g. a file text information containing the attenuations in dB of the diagram of radiation of a given antenna , needs to be converted in a numerical format, or still it is necessary to execute the conversion of co-ordinates for a corrected geo-mapping). This often is the most laborious phase due to the various kinds of adjustments needed.

Phase 3

In this phase the data are organized, subdivided and correlated among them in order to reflect the logical relational model of the date base (already pre-existing) on which the tool of simulation is based. Congruency controls are carried out and the original electronic sheet format is abandoned in favour of a most suitable one such as MsAccess.

Phase 4

At this point, usually by means of specific queries, data are exported into DBMS Oracle as implied by the simulation tool and essential for its correct functioning.

Phase 5

To complete the supply of input data and to improbe the output data, it can be useful to collect additional information such as cartography, orthofotographies, raster images. Particular attention needs to be paid to cartographic data nearly always subordinate to procedures of adaptation (e.g poly-lines in polygons, creation of shapefiles, etc) and of conversion of coordinates.

Phase 6

The epilogue of this sequence of activities is the creation of a visual environment rich of details, able of producing visual and analytical reliable results for an immediate perception of the informative message derived from the analyses.

The informative system also allows to geo-map, by collecting the relevant information (meta data), not only the control activity carried out by ARPA's Provincial Laboratories but also the continuous monitoring activities and the state of claims and demands of the population resident on the territory.

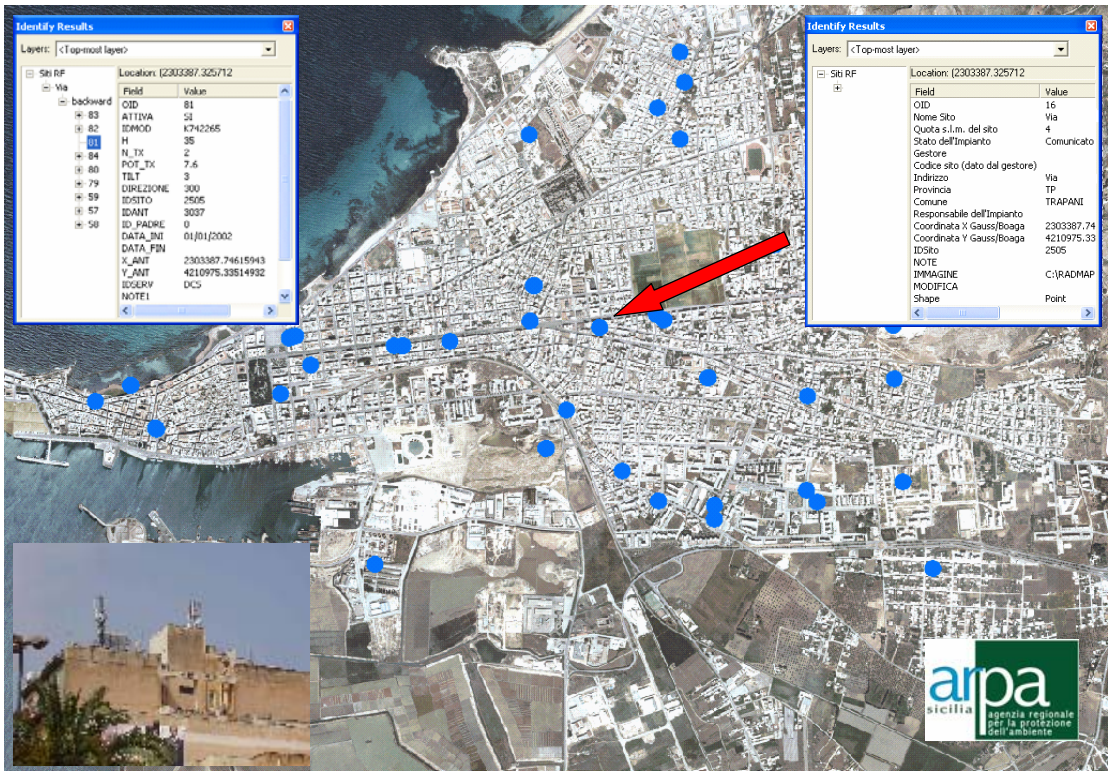

Fig. 1 GeoMapping of Mobile Phones Basic Radio Station in the City of Trapani

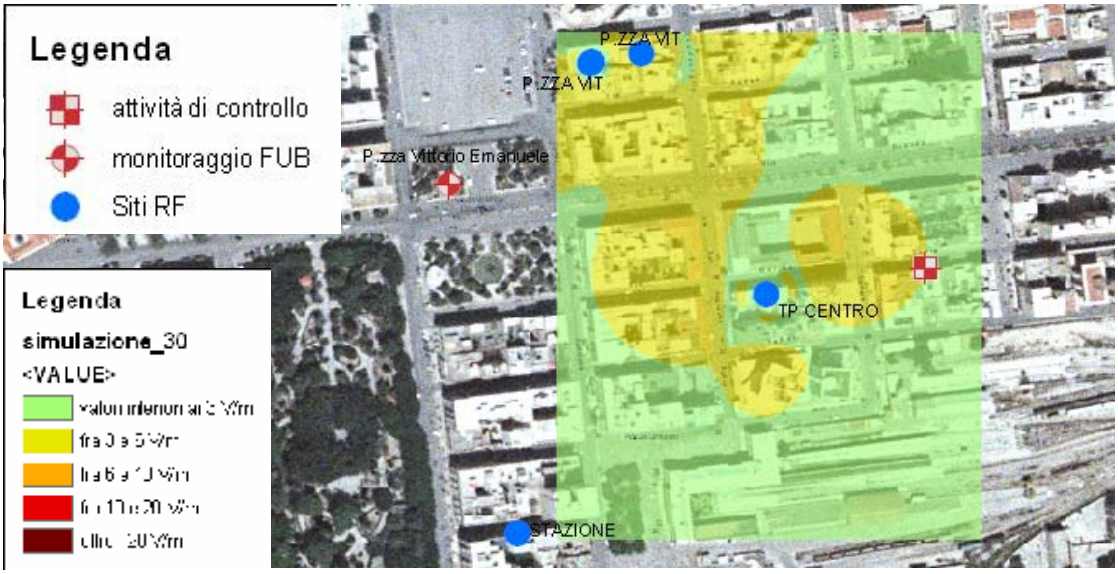

Fig. 2 Example of simulation of the distribution of electromagnetic field from RF source

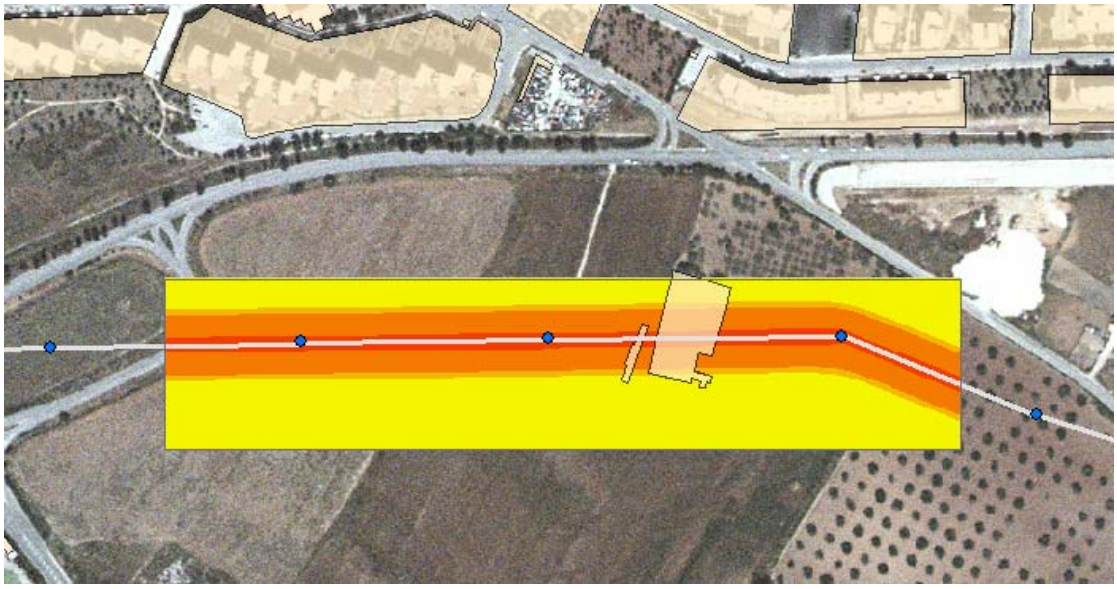

Fig. 3 Example of simulation of the distribution of electromagnetic field from ELF source

In this way, the Agency monitoring activities will be available on the Internet.
The customer will be able to interact with the digital thematic chart obtained through the elaboration of the data already supplied by the companies; such elaborations, even with the approximations tied to the intrinsic simplifications of every model, will concur, intercrossed with the data of citizens' demands, to spot on the

territory the situations on which the worries of the population are mainly concentrated.
Following the identification of such areas, it will be possible to define "the sensitive" areas from the point of view of the emotional impact on the population, even if in such zones an overcoming of the limits of exposure or the values of attention (as defined in Italian law) is not found or expectable.

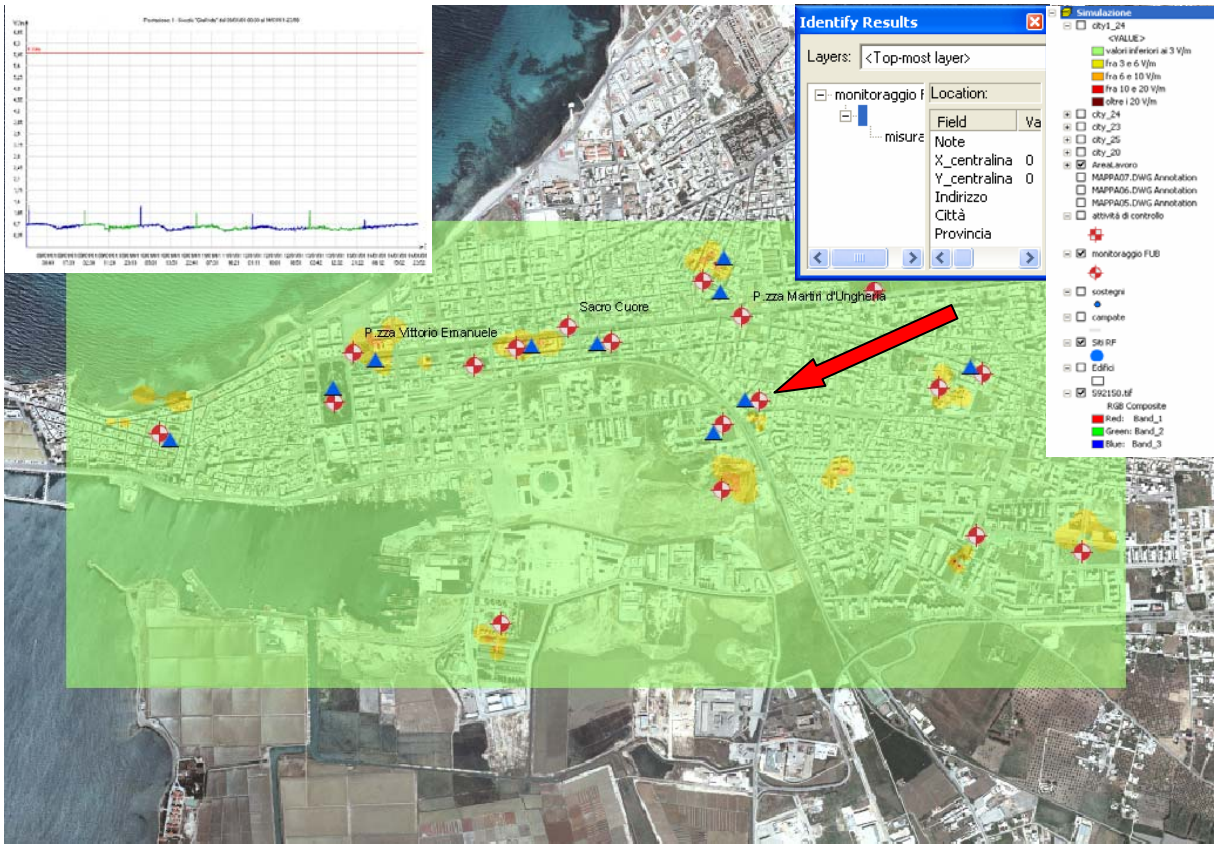

Fig. 3 Example of simulation chart, citizens' claims and demands theme and monitoring results.

The graphical reppresentetion, containing all the themes synthesizing all the informational elements used , will contribute to plan the monitoring activity let alone to communicate such programming by taking into account two elements: the quantitative data (the estimated value of the levels of electromagnetic field) and the population's perception level towards the problem manifested through claims, petitions, activity of civil society association etc.. In such identified areas, by applying a priority order determined trough the analysis of the quantitative element (outcomes of measures or provisional calculations) monitoring devices will be put in place and the collected data will be made available directly to the customer on the net.
The addressee of the information, will be able to interact with the thematic charts, on which they will be highlighted: the forecasted distribution of the levels of electromagnetic field, the claims, the monitoring-devices position. Connected to the theme of monitoring-devices, measure outcomes and graphs on the monitoring activity will also be displayed.

Conclusions
With such procedure that does not have a conclusion, but it is under continuous update, it will be possible for the citizen to follow the monitoring in all its phases, from the planning to the communication of the validated data.
It is believed that this way of transmitting the information, which supplies contextualized data on the territory which the customer can interact with, can be more effective as compared to a sterile communication of numbers or diagrams of difficult reading and comprehension and that it can contribute to clear the legitimate doubts of people and to supply to citizens the instruments needed to acquire an effective knowledge of the problem.

GENOMIC INSTABILITY IN BLOOD SAMPLES SUBMITTED TO CONTROLLED CELL PHONE RADIATION LEVELS

HEINRICH, JKR[1]; CAMPANHOL, CL[1]; RODRIGUES, RM[1]; FRANCO, VCO[1]; SANTOS, BP[1]; ALMEIDA, AM[2].

1. CYTOGENETICS LABORATORY – CAISM / UNICAMP – STATE UNIVERSITY OF CAMPINAS, BRAZIL 2. CPQD FOUNDATION, CAMPINAS, BRAZIL

Mailing Address: Dr. Juliana Heinrich
CAISM UNICAMP – Universidade Estadual de Campinas
Laboratórios Clínicos Especializados – Citogenética
Rua Alexandre Fleming, 101 Campinas – SP – CEP 13.083-881
Phone: +55 19 3788-9524 FAX: +55 19 3788-9395
Email: julianah@unicamp.br

ABSTRACT

Genomic instability is characterized by genetic alterations such as chromosomal rearrangements, aneuploidy, micronuclei frequency increase, microsatellite instability, mutations, gene amplification, gene transcription changes, transformation and cell death in the first and following generations of cells after the first insult. We have investigated the effect of AMPS and CDMA radiation in cultured blood samples from 10 donors in 200 replicates after 72hs exposure in a specially designed exposition set up (TEM CELL) at SAR levels from 0,8 to 10W/kg. The genome was investigated for structural chromosomal abnormalities, micronuclei frequency and aneuploidy of chromosomes 8 and 17 through both conventional and molecular cytogenetics (FISH) techniques. Genomic changes such as chromosomal breaks, translocations, marker chromosomes and aneuploidy, when compared to the controls, were detected in SAR levels above 5W/kg as well as the increase of micronuclei frequency above 10W/kg. As genomic instability and chromosome damage are frequently related to tumorigenesis, our findings support the hypothesis of a positive effect of RF radiation on the genome of cultured blood cells and also give further evidence to suggest continuous cytogenetic investigation of occupationally exposed individuals to SAR levels above the accepted international limits.

INTRODUCTION

In vitro studies are important to delineate possible damage mechanisms caused by non-ionizing radiation or radiofrequency (RF) fields and its interaction with biological systems such as cells, tissues and organisms. The main advantage of these studies are the possibility to control almost all variables and test conditions to discard interferences and also to delineate investigation targets to be explored through *in vivo* and clinical-epidemiological studies.

Genomic instability (GI) has been identified mostly in tumor cells and is characterized by the accumulation of multiple changes that converts the genome of a normal cell into an instable genome [1]. This instability is characterized by genetic alterations such as chromosomal rearrangements, aneuploidy, micronuclei frequency increase, microsatellite instability, mutations, gene amplification, gene transcription changes, transformation and cell death in the first and following generations of cells after the first insult [2].

In vitro investigations in different cell systems have shown both a positive and negative association of cell damage leading to GI after RF exposure although most of them were attributed to thermal effects. These groups suggested that RF is not mutagenic by itself and that the adverse effects of such exposition would be due to hyperthermia caused by cell exposition in high frequencies or high intensity fields [3,4,5,6].

By the other hand, aneuploidy of chromosome 17 was observed in a dose-dependent way along with alterations related to chromosome segregation suggesting that RF can interfere in the cell cycle and cause chromosome damage and genomic instability in temperature controlled exposition environments [7]. Other events were observed and associated with RF dose-dependent exposition such as transmembrane efflux of molecules, transcription errors, cell transformation, enzyme activity changes, fosforilation of hsp27 (heat shock protein 27) and increase of mRNA levels of the FOS gene [8,9,10,11,12].

Since there is a major concern regarding the association of RF exposition and tumorigenesis and as genomic instability is one of the first events for tumor onset we investigated the frequency of chromosome damage, micronuclei formation and aneuploidy in lymphocytes submitted to RF fields in a controlled and highly monitored exposition set-up.

MATHERIALS AND METHODS

The study population consisted of 10 healthy, non-smokers male and female subjects that were not X-rayed in the last 12 months. The study was approved by the University's and by the National Ethical Committee (CONEP). Participants were informed of the study aims and asked to sign consent. Venous blood samples were collected in coded heparinized tubes and divided to be used in different assay as both test, sham-exposed and control samples.

1. Cytogenetics: short-term lymphocytes cultures were established using 0,5 ml of blood added to HAM F-10 medium (NUTRICELL) supplemented with phytohaemagglutinin (INVITROGEN) and 10% of fetal bovine serum (NUTRICELL). Cells were harvested after 72 hours of stimulation and colcemid (INVITROGEN) was added 1 hour before harvesting. Cultures were submitted to hypotonic shock for 10 min with 0,075 M KCl at 37o.C and then fixed in methanol-acetic acid (3:1) washes 3 times. For conventional cytogenetics analysis, after being air-dried and dropped onto glass slides in a humidified chamber, lymphocytes were stained with 5% Giemsa-Wright solution for 6 minutes. Structural aberrations such as chromatid and chromosome gaps and breaks, acentric and dicentric fragments, double minutes, satellite increase were evaluated. Each abnormality was scored as an event. Mean frequencies were obtained for each exposition type. For each donor, 200 cells were analyzed. For aneuploidy analysis, centromere probes for chromosomes 8 and 17 (QBIOGENE) were hybridized through mini-preps FISH assays according to the manufacturer's instructions. Mini-preps were obtained dropping 10 μl of cell suspension onto glass slides. For each probe, 200 cells were analyzed, per donor. Cells containing less and more than 2 hybridization signals were scored as aneuploidy. Mean frequencies were obtained for each exposition type.
2. Micronuclei: lymphocytes cultures were established as described previously for the cytogenetics assays but Cytochalasin B (SIGMA) was added after 44 h of estimulation. Cells were also submitted to hypotony but fixed only in methanol, 3 times. Cells were stained with 5% Giemsa-Wright solution for 6 minutes. For each donor, 1000 cells were analyzed and the mean frequencies for each exposition type were obtained. Micronuclei were evaluated only with SAR values of 0,8 and 10W/kg using AMPS technology.

The exposition set up was especially designed for this project. A transverse electromagnetic cell (TEM CELL) was used to irradiate the samples inside an incubator at 37oC (Figure 1A) for 72 hours that is the current standard time to obtain metaphases for cytogenetic analysis. Temperature was corrected by air insufflations, when necessary, especially in high SAR levels. All exposition parameters were controlled and the conditions to obtain the desired SAR levels were measured and established before the experiments through the robotic device DASY4 (Figure 1B). Cell cultures were submitted to 0,8; 2,0; 5,0 and 10,0 W/kg SAR levels in AMPS and CDMA technologies. Sham exposed (all transportation conditions and no exposition) and control samples (patient control, no transportation conditions, no exposition) were also analyzed.

Figure 1: Exposition set up. A. Diagram of the exposition system. B. DASY4 robotic device for set up characterization and calibration.

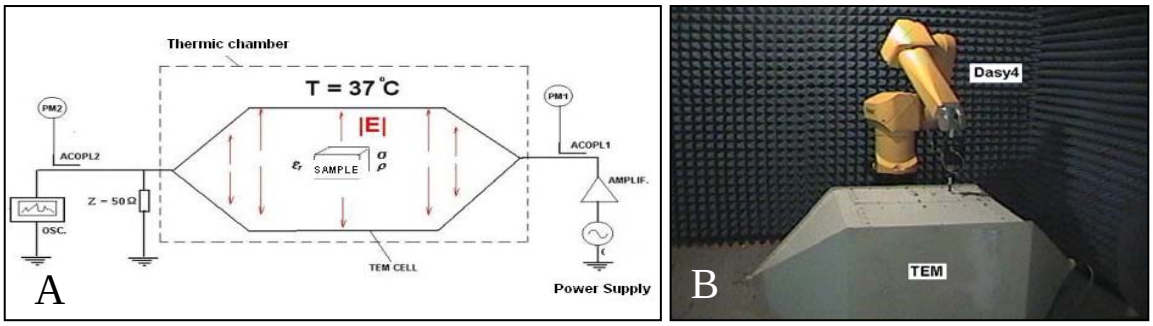

RESULTS

The results for chromosome abnormalities, aneuploidy of chromosomes 8 and 17 and micronuclei frequency are summarized in Table 1.

Table 1. Summarized results of the genomic imbalances

Type	*SAR*	Chromosome Ab.		Aneup 17		Aneup 8		Micronuclei Freq (%)	
		Mean	Range	Mean	Range	Mean	Range	Mean	Range
CDMA	**2**	0,019	0-0,058	0,48	0,96-1,92	0	0-0		
	5	0,021	0-0,070	0,13	0-0,95	2,15	1,96-6,14		
	10	0,039	0-0,079	2,91	0-5,56	4,44	4,0-9,84		
AMPS	**0,8**							8,93	(7,39-10,76)
	2	0,006	0-0,035	0,53	0,97-1,79	1,26	0,98-2,91		
	5	0,016	0-0,043	0,54	0,94-1,92	2,4	0,81-4,50		
	10	0,025	0-0,055	6,1	3,17-10,62	4,19	1,47-7,38	13,36	(6,06-19,44)
Control		0	0-0	1,04	0,65-2,80	0,375	0-1	4,07	(2,30-6,56)
SHAM		0,006	0-0,035	1,31	0,99-1,96	0,492	0-1,96	8,74	(7,50-11,24)

A dose dependent effect was clearly noted for all the evaluated patterns as the abnormalities were shown to be more frequent as higher were the SAR levels of exposition despite of CDMA and AMPS technologies.

The most frequent observed chromosome abnormalities were chromosome and chromatid breaks although other events such as fragment deletions and amplifications as well as ring chromosomes were also found as shown in Figure 2.

Figure 2: Chromosome Abnormalities A. Satellite length increase. B/C. Chromosome breaks. D. Chromatid gap. E. Deletion. F. Ring Chromosome G. Acentric Fragment. H. Amplification

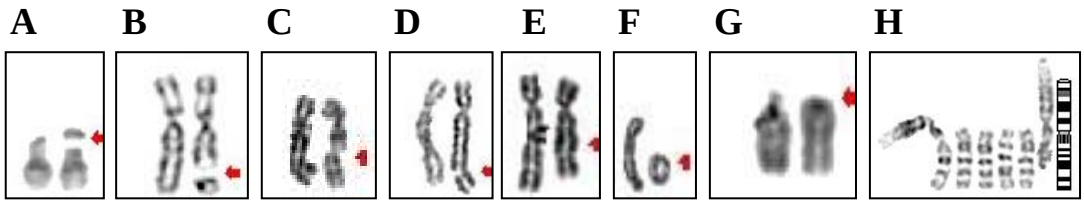

The micronuclei frequency has increased with SAR levels of 10W/kg and the results obtained with a SAR level of 0,8 W/kg, which is close to what a person might be exposed realistically, was very similar to the frequency obtained in the sham-exposed samples. Aneuploidy of chromosome 17 was considered relevant only with SAR levels of 10W/kg, when compared to the mean frequencies of the control and sham exposed samples. Aneuploidy of chromosome 8 was considered relevant, when compared to the controls only with SAR levels of 5 and 10W/kg.

DISCUSSION

A general concern for people that are exposed to RF fields, especially with the increasing number of cell phone users, is the connection between radiation and cancer. Genomic instability is largely found in tumor cells and there is a strong evidence that high SAR levels, above the international regulation limits, may have a genotoxic effect and induce DNA damage at some level.

It is interesting to note that aneuploidy and chromosome damage have been considered two of the most notorious transformation-related events in tumorigenesis because it precedes malignant transformation in many tumors. Cancer aneuploidy and other imbalances affect gene dosage and a large number of proteins including those involved in the mitotic spindle apparatus resulting in a self-perpetuating chromosomal instability [13]. As we detect genomic imbalances in blood cells submitted to increasing SAR levels we remain to understand if these instable cells are still capable to escape to an apoptotic via in order to exterminate the imbalanced clones and preserve tissue integrity. We have observed much more translocations and marker chromosomes, yet to be identified through SKY (spectral karyotyping) than dicentrics, acentrics and rings which are considered much more unstable aberrations with fast disappearance *in vivo* [14,15].

In response to genotoxic such as RF, various chemicals and reactive cellular metabolites, cell cycle checkpoints that slow down or arrest cell cycle progression can be activated, allowing the cell to repair or prevent the transmission of damaged or incompletely replicated chromosomes. The balance between cell cycle arrest, damage repair and initiation of cell death could determine if cellular or DNA damage is compatible with cell survival or requires cell elimination by apoptosis. Defects in these processes may lead to hypersensitivity to cellular stress, and susceptibility to DNA damage, genomic defects, and resistance to apoptosis, which characterize cancer cells. This is the main issue to justify chromosomal studies in *in vitro* models [16]. Molecular chromosome techniques such as CGH – Comparative Genomic Hybridization [17] and SKY – Spectral Karyotyping [18] can add more information to conventional cytogenetics reports and indicate hot spots for chromosome structural abnormalities.

When individuals exposed to RF in a work environment were evaluated it was shown that other factors might potentiate the clastogenic effects of RF radiation such as light deprivation resulting in a disturbance of melatonin secretion [19]. Such observations may explain the fact that our sham-exposed samples have always shown higher mean frequencies of abnormalities when compared with the controls alone. It is necessary to consider that epigenetic and environmental factors may play an important role to potentiate the radiation effect on the DNA.

Our findings support other groups' results as we were able to demonstrate a dose-dependent effect against the genome particularly with SAR levels above 5W/kg [20].

The set up system used for the expositions was carefully designed to meet the needs described at the WHO´S EMF International Project. Parameters such as temperature, power input and output, TEM CELL characterization prior to the experiments and experimental dosimetry tests were developed and taken into account to achieve reliable results in isothermal conditions.

Our results have shown the importance of genomic analysis especially through conventional and molecular cytogenetics techniques and suggest the use of continuous cytogenetics analysis especially for occupationally exposed professionals who are the ones that might be exposed to higher SAR levels [15].

We are yet to describe the effect of RF in different systems and exposition parameters specially with regard to an intermittent mode of radiation exposure.

ACKNOWLEDGEMENTS

The authors would like to thank Mauro Lins, M.Sc for the initial technical support for the exposition set up. This research was supported by FUNTTEL.

REFERENCES

1. Smith, LE; Nagar,S; Kim,GJ; Morgan,WF. Radiation-induced genomic instability:radiation quality and dose response. Health Phys 2003. 85(1):23-9.
2. Huang, L; Snyder, AR; Morgan, WF. Radiation-induced genomic instability and its implications for radiation carcinogenesis. Oncogene, 2003; 22: 5848-5854.
3. Ivaschuk, OL; Jones, RA; Jones, TI; Haggren, W; Adey, WR; Phillips, JL. Exposure of nerve growth factor-treated PC12 rat pheochromacytoma cells to a modulated radiofrequency field at 836.55 MHz: effects on c-jun and c-fos expression. Bioelectromagnetics, 1997; 18:223-229.
4. Brusick, D; Chairman; Albertini, R; McRee, D; Peterson, D; Williams, G; Hanawalt, P; Preston, J. Genotoxicity of radiofrequency radiation. Environmental and Molecular Mutagenesis, 1998; 32: 1-16.
5. Moulder, JE; Erdreich, LS; Malyapa, RS; Merritt, J; Pickard, WE; Vijayalaxmi. Cell phones and cancer: what is the evidence for a connection?. Radiation Research, 1999; 151: 513-531.
6. Blettner, M; Berg, G. Are mobile phones harmful?. Acta Oncologica, 2000; 39(8): 927-930.
7. Mashevich, M; Folkman, D; Kesar, A; Barbul, A; Korenstein,R; Jerby, E; Avivi, L. Exposure of human peripheral blood lymphocytes to electromagnetic fields associated with cellular phones leads to chromosomal instability. Bioelectromagnetics, 2003; 24:82-90.
8. Goswani, PC; Albee, LD; Parsian, AJ; Baty, JD; Moros, EG; Pickard, WF; Roti, JLR; Hunt, CR. Proto-oncogene mRNA levels and activities of multiple transcription factors in C3H 10T1/2 murine embryonic fibroblasts exposed to 835.62 and 847.74 MHZ cellular phone communication frequency radiation. Radiation Research, 1999; 151:300-309.
9. Velizarov,S ; Raskmark,P; Kwee,S. The effects of radiofrequency fields on cell proliferation are non-thermal. Bioelectrochemistry and Bioenergetics 1999. 48:177-180.
10. French, PW; Penny, R; Laurence, JÁ; Mckenzie, DR. Mobile phones, heat shock proteins and cancer. Differentiation, 2000; 67:93-97.
11. Leszczynski, D; Joenväärä, S; Reivinen, J; Kuokka, R. Non-thermal activation of the hsp27/p38MAPK stress pathway by mobile phone radiation in human endothelial cells: molecular mechanism for cancer and blood-brain barrier-related effects. Differentiation, 2002; 70:120-129.
12. Di Carlo, A; White,N; Guo,F; Garrett, P; Litovitz,P. Chronic electromagnetic field exposure decreases HSP70 levels and lowers cytoprotection. J Cell Biochem 2002. 84(3): 447-54.
13. Bialy, H. Aneuploidy and cancer – the vintage wine revisited. Nature Biotechnology, 2001; 19: 22-23.
14. Johnson,KL; Tucker, JD; Nath, J. Frequency, distribution and clonality of chromosome damage in human lymphocytes by multi-color FISH. Mutagenesis, 1998; 13:217-227.
15. Lalic, H; Lekic, A; Radosevic-Stasic, B. Comparison of chromosome aberrations in peripheral blood lymphocytes from people occupationally exposed to ionizing and radiofrequency radiation. Acta Medica Okayama, 2001; 55 (2):117-127.
16. Ishikawa,K; Ishii,H; Saito,T. DNA damage-dependent cell cycle checkpoints and genomic stability. DNA Cell Biol 2006. 25(7):406-11.
17. Kallioniemi,A; Kallioniemi,OP;Sudar, D; Rutovitz,D; Gray, JW; Waldman,F; Pinkel,D. Comparative genomic hybridization for molecular cytogenetic analysis of solid tumors. Science, 1992. 258(5083):818-21.
18. Schrock E; Veldman, T; Padilla-Nash,H; Ning, Y; Spurbeck,J; Jalal,S; Shaffer,LG; Papenhausen,P; Kozma, C; Phelan, MC; Kjeldsen,E; Schonberg,AS; O´Brien,P; Biesecker,L; DuManoir,S; Ried,T. Spectral karyotyping refines cytogenetic diagnostics of constitutional chromosomal abnormalities. Hum Genet 1997. 101(3):255-62.
19. Cassone,VM; Warren,WS; Brooks,DS; Lu,J. Melatonin, the pineal gland and circadian rhythms. J Biol Rhythms, 1993. 8:S-73-S78.
20. Tice,RR; Hook,GG; Donner,M; McRee,DI; Guy,AW. Genotoxicity of radiofrequency signals. I. Investigation of DNA damage and micronuclei induction in cultured human blood cells. Bioelectromagnetics 2002. 23(2):113-26.

ANALYTICAL STUDY OF THE IRRADIATION OF A HUMAN HEAD MODEL BY AN ACTIVE IMPLANT

ANGELA P. MONEDA

ARISTOTLE UNIVERSITY OF THESSALONIKI
E-MAIL ADDRESS: apmoneda@egnatia.ee.auth.gr

DIMITRIOS P.CHRISSOULIDIS

ARISTOTLE UNIVERSITY OF THESSALONIKI
E-MAIL ADDRESS: dpchriss@auth.gr

P.O. BOX: 1562, ZIP CODE: 54124, THESSALONIKI, GREECE

Abstract
An exact, analytical solution has been used to calculate the electromagnetic (EM) radiation emitted by an active implant within an eccentric-spheres, human head model and variations thereof. The EM field is determined by use of Green's dyadic for a lossy, dielectric sphere containing any number of lossy, dielectric, spherical inclusions. The inclusions can be placed anywhere within the host sphere. The source is a point dipole encapsulated within a tiny, lossless, dielectric sphere. In theory, this implant can be placed anywhere within the head model; calculations have been made with the implant inside the scull, either at the side, near a temple, or at the side of the jaw. Numerical results have been obtained for frequencies ranging from 400 *MHz* to 4 *GHz*. The effect of the orientation of the dipole source has been investigated. The radiation absorbed by the head model has been studied by use of plots of the total absorbed power per tissue against the frequency as well as by use of maps of the Specific Absorption Rate (SAR) on cross sections of the head.

I. Introduction

The growing interest of the scientific community in the implantation of active antennas inside the human body has been related to communication and monitoring purposes. In this paper the operation of an active implant, which radiates in the RF or microwave band, from within the human head has been examined. Applications of this study may include (a) comparisons of SAR calculations with the guidelines of international standards, (b) controlled absorption, aimed at therapeutic interventions, and (c) diagnosis of anatomical abnormalities through measurements of near- or far-field radiation escaping from the head.

The analytical solutions that have been made available over the years treat the human head as a multilayered, lossy, dielectric sphere [1]-[3]. Herein, an eccentric-spheres model of the human head and two simplified versions thereof have been considered. The implanted antenna is an infinitesimal, electric dipole encapsulated within an acrylic sphere, which immunes the source dipole from the surrounding tissue, which may be conductive.

From the point of view of eventual health hazards of communication devices, the focus is on the power absorbed by the brain, the appearance of hot spots, and the peak SAR values. Furthermore, the characteristics of the implant are investigated by calculations of the delivered power, maps of the electric-field intensity around the head, and far-field radiation diagrams.

II. Head Model and Implant

All three head models, which are of interest in this paper, can be obtained from the geometry shown in Fig. 1. Model 1 comprises a spherical bone shell (host sphere), which represents the scull, and three inclusions; the latter are a major, spherical core, representing the brain and a pair of small eyeballs, all properly placed within the bone shell. The (outer) radius of the scull is $\alpha_0 = 9\,cm$, the radius of the brain is $\alpha_1 = 7\,cm$ and those of the eyes are $\alpha_2 = \alpha_3 = 1\,cm$. The center of the brain, O_1, is vertically displaced by $d_{01} = 1.5\,cm$ from the center of the scull, O_0. The eyes are centered at O_2, O_3, which are horizontally displaced by $d_{02} = d_{03} = 7.95\,cm$ from O_0; the left-hand eye is in the meridian plane $\varphi = 23^\circ$ (Fig. 1a), whereas the right-hand eye is in the meridian plane $\varphi = (360 - 23)^\circ = 337^\circ$. Thus, the eyes are symmetrically placed with respect to the coordinate plane

xO_0z . Model 2 is obtained from model 1 by omission of the eyeballs and model 3 is obtained from model 2 by the substitution $d_{01}=0$. The brain volume is $1436.75cm^3$, this value being in the range $[1400-1500\,cm^3]$ of normal, human brain volumes. The electrical properties assigned to bone, brain, and eye tissue as well as the corresponding density of each tissue, are shown in Table I for two frequencies which are of special interest [4].

The active implant is an infinitesimal, electric dipole, placed at the center of an acrylic sphere of radius $\alpha_4=0.5cm$ and refractive index $n_4=n_{acr}=1.61+j0$. The lossless capsule immunes the source from the conductive bony shell [5]. The implant is positioned at distance $d_{04}=8cm$ from O_0 , either on the *y*-axis (position 1) or on the yO_0z plane at $\theta=145°$ declination from the *z*-axis (position 2). The first position of the source is supposed to be inside the left auricular and the second in the mouth, where the lower left, 3rd molar (tooth #38) is found.

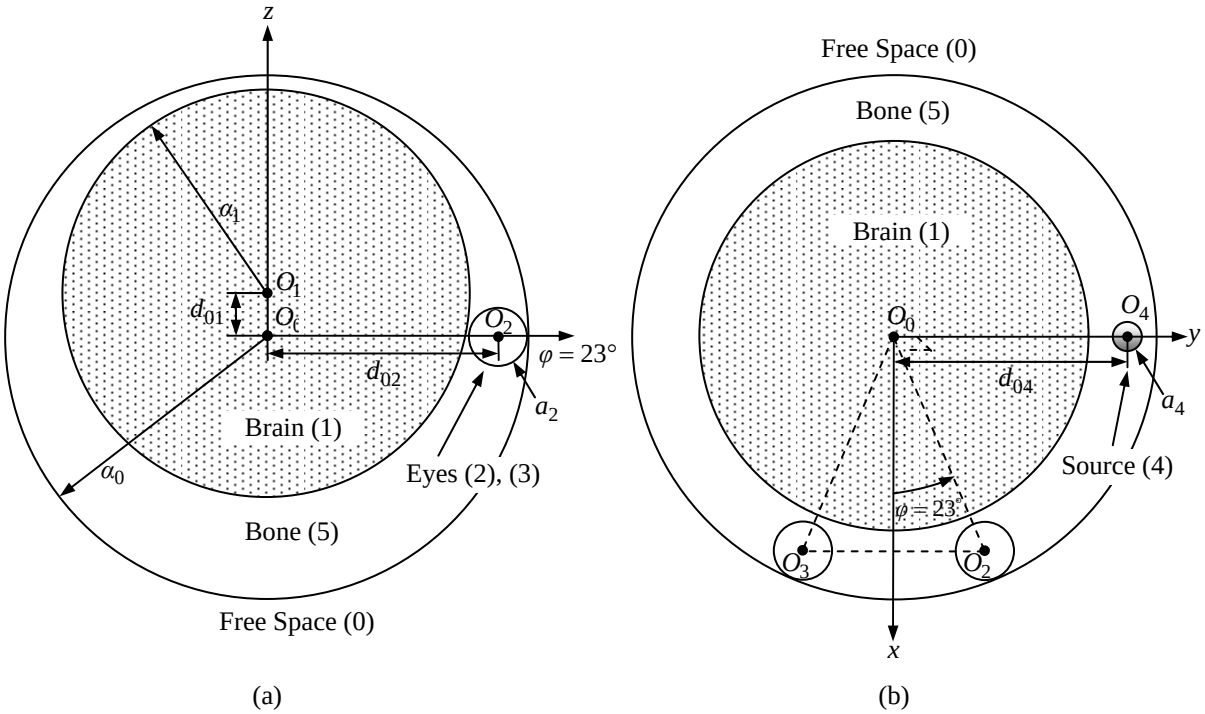

Figure 1. (a) Vertical ($\varphi=23°$) and (b) horizontal ($\theta=90°$) cross-sections of head model 1; the point source, encapsulated in an acrylic sphere of radius α_4 , is shown in position 1 (left auricular); position 2 is also in the meridian plane $\varphi=90°$, but below the xO_0y plane, at $\theta=145°$.

Table I. Relative, dielectric constant ε_r , conductivity $\sigma(mhos/m)$, and density $\rho(kg/m^3)$ of human head tissue layers

Frequency (MHz)	**Bone** $(1850\,kg/m^3)$		**Brain** $(1030\,kg/m^3)$		**Eyes** $(1010\,kg/m^3)$	
	ε_r	σ	ε_r	σ	ε_r	σ
1500	11.98	0.22	45.99	1.12	68.70	1.87
2400	11.41	0.38	44.33	1.62	68.24	2.44

III. Analytical Determination of the Electric-Field Intensity

The electric-field intensity anywhere within, as well as outside, the aforesaid head model is determined by use of the dyadic Green's function (dGf) $\overline{\overline{G_e}}(\vec{r},\vec{r}')$ of a dielectric sphere with several, eccentric, spherical, dielectric inclusions; all dielectrics may be lossy. The position vectors $\vec{r}$, $\vec{r}'$ correspond to the field and source points. The point source can be placed anywhere, but, in this study it has been placed in the bone shell, which is denoted as region 5 (Fig. 1); the generality of the analysis is not impaired otherwise. The analytical determination of $\overline{\overline{G_e}}(\vec{r},\vec{r}')$ is an intricate task which has been undertaken by the authors elsewhere [6]. Still, it

might be convenient to state that the analysis begins by consideration of the dGf of an unbounded space with electrical properties identical to those of the acrylic inclusion; that dGf is given by [7]

$$\bar{\bar{G}}_{e0}(\vec{r},\vec{r}') = -\frac{1}{k_4^2}\hat{r}\hat{r}\delta(\vec{r}-\vec{r}') + \\ + j\frac{k_4}{4\pi}\sum_{mn}(-1)^m\frac{2n+1}{n(n+1)}\begin{cases}\left[\vec{M}_{mn}^{(1)}(k_4\vec{r})\vec{M}_{-mn}^{(3)}(k_4\vec{r}')+\vec{N}_{mn}^{(1)}(k_4\vec{r})\vec{N}_{-mn}^{(3)}(k_4\vec{r}')\right] & r<r' \\ \left[\vec{M}_{mn}^{(3)}(k_4\vec{r})\vec{M}_{-mn}^{(1)}(k_4\vec{r}')+\vec{N}_{mn}^{(3)}(k_4\vec{r})\vec{N}_{-mn}^{(1)}(k_4\vec{r}')\right] & r>r'\end{cases} \quad (1)$$

where $k_4 = k_0\sqrt{\varepsilon_{r,4}}$ is the wavenumber within region 4 of the nonspherical body, which accommodates the source; $k_0 = \omega/c_0$ is the wavenumber of free-space, i.e. region 0, and $\varepsilon_{r,4}$ is the relative permittivity of the acrylic sphere; $\vec{M}_{mn}^{(1)}$, $\vec{N}_{mn}^{(1)}$ and $\vec{M}_{mn}^{(3)}$, $\vec{N}_{mn}^{(3)}$ are vector, spherical harmonics of an unbounded acrylic medium; the former pair comprises wavefunctions that remain bounded at the origin of coordinates, whereas the latter pair of wavefunctions are bounded at infinity. By application of the boundary conditions on every spherical interface of the nonspherical body, $\overline{\overline{G_e}}(\vec{r},\vec{r}')$ is ultimately obtained, but neither further details about that analytical formulation nor the resulting, cumbersome expression for $\overline{\overline{G_e}}(\vec{r},\vec{r}')$ are needed in this paper, which is focused on numerical results. The validity of the solution has been checked numerically through reciprocity and energy-conservation checks as well as analytically by simplifying the geometry and comparing the resulting solution to those of articles published before [8], [9].

The point source is represented by the current distribution

$$J(\vec{r}') = I_0 l\frac{\delta(r'-r_0)\delta(\theta'-\theta_0)\delta(\phi'-\phi_0)}{r'\sin\theta}\hat{e}, \quad (2)$$

wherein $I_0 l$ is the dipole moment and $\hat{e}$ is the orientation, i.e. polarization, vector. The electric-field intensity due to this dipole source can be determined anywhere in space by integration of the posterior scalar product of $\overline{\overline{G_e}}(\vec{r},\vec{r}')$ with the aforesaid current [10]:

$$\vec{E}(\vec{r}) = j\omega\mu_0\int_{\vec{r}'}\bar{\bar{G}}_e(\vec{r},\vec{r}')\cdot\vec{J}(\vec{r}')d^3\vec{r}' \quad (3)$$

IV. Numerical Results

The effect of the implant on the head has been investigated first by use of diagrams of the absorbed power versus the operating frequency of the implant, which is in the range $400MHz$ - $4GHz$, for both positions of the implant. The aforesaid frequency range is associated with ISM, TETRA, GSM, UMTS, WLAN, and Bluetooth devices. Moreover, these diagrams display lucidly which fraction of the radiated power is absorbed by each tissue at anyone of those frequencies. Absorption by the brain and the bone is shown in Figs. 2 and 3 as percentage of the total radiated power, respectively, for head models 1, 2 and 3. The dipole orientation is in every case along the *z*-axis.

The first remark yielding from the aforementioned diagrams is that the brain absorption is maximized at about $1500MHz$ when the dipole is placed in the ear and at $1700MHz$ when the implant is placed at the tooth. At the very same frequencies absorption by the bone shell is minimal.

When the eccentric-brain, head model, i.e. model 1 or 2, is under consideration it is obvious that there is strong dependence of the absorbed power on the dipole position. Absorption by the brain with the implant in the ear exceeds that with the implant in the tooth, and the opposite is true for absorption by the scull. This outcome can be justified by the different distance of the source from the brain in the aforesaid positions.

The remark made above does not apply to the concentric-brain, head model, i.e. model 3, because the source is equidistant from the brain for both the positions examined. In that model, the difference in the frequency, whereby absorption is maximized, can be justified by the different angle by which the dipole is aimed at the brain.

The overall absorption by the left eye, which in every case is closer to the implanted antenna, in model 1, is less than 0.05% and it is not shown. Finally, for all three models, a very small percentage of the radiated power escapes from the head into the free-space surrounding. That percentage is less than 3% for position 1 of the implant, with the maximum value occurring at $2700MHz$, and it does not exceed 1% of the radiated power for position 2, the maximum value being at $2200MHz$.

Next, the effect of the dipole orientation on the power absorbed by the brain, the bone and the eyes is investigated. In Figs. 4 and 5 the overall absorbed power by the brain and the bone, respectively, is plotted against the declination angle θ of the polarization vector of the point dipole; θ is measured from the *z*-axis. The operating frequency is $1500MHz$.

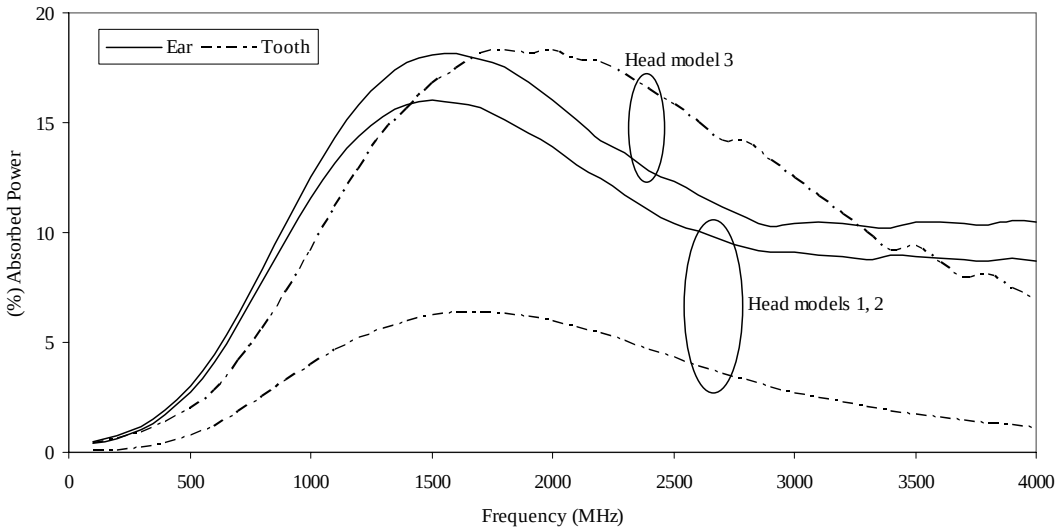

Figure 2. Absorption by the brain vs. frequency for head models 1, 2 and 3.

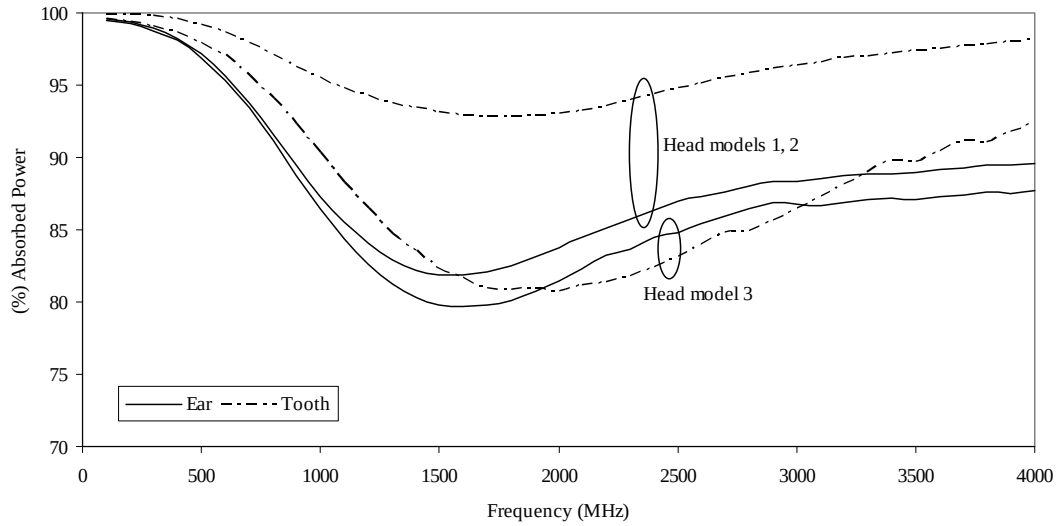

Figure 3. Absorption by the bone vs. frequency for head models 1, 2 and 3.

It is clear that absorption by the brain and the bone is practically unaffected by the orientation of the dipole when the latter is placed inside the ear. A slight increase in the absorption by the brain and a corresponding decrease in the absorption by the bone are observed when the dipole is placed at the tooth for all three head models.

The effect of dipole orientation on the absorption by the eyes is far more significant. As shown in Fig. 6, absorption by the left eye, which is closer to the radiating implant, increases as the main radiation lobe of the dipole rotates so as to include the eye, and decreases as that lobe points elsewhere. However, the overall power absorbed by the eyes remains a small percentage of the total radiated power

Subsequently, numerical results are shown for the SAR anywhere within the nonspherical head model; the SAR has been determined by use of the definition

$$SAR = \frac{\sigma |E|^2}{2\rho}, \tag{4}$$

wherein σ is the conductivity and ρ is the density of tissue.

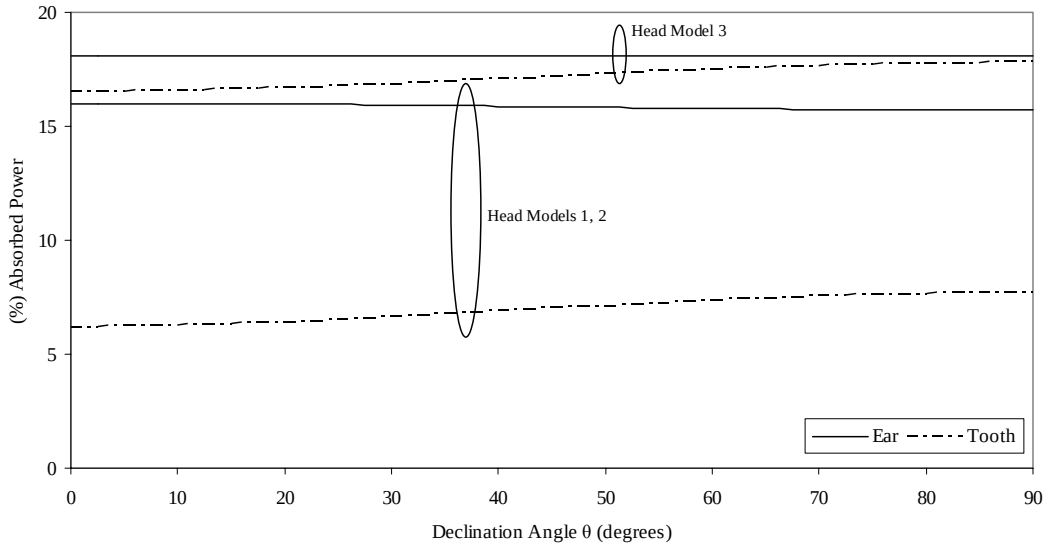

Figure 4. Absorption by the brain vs. dipole orientation (i.e. declination angle) for head models 1, 2 and 3

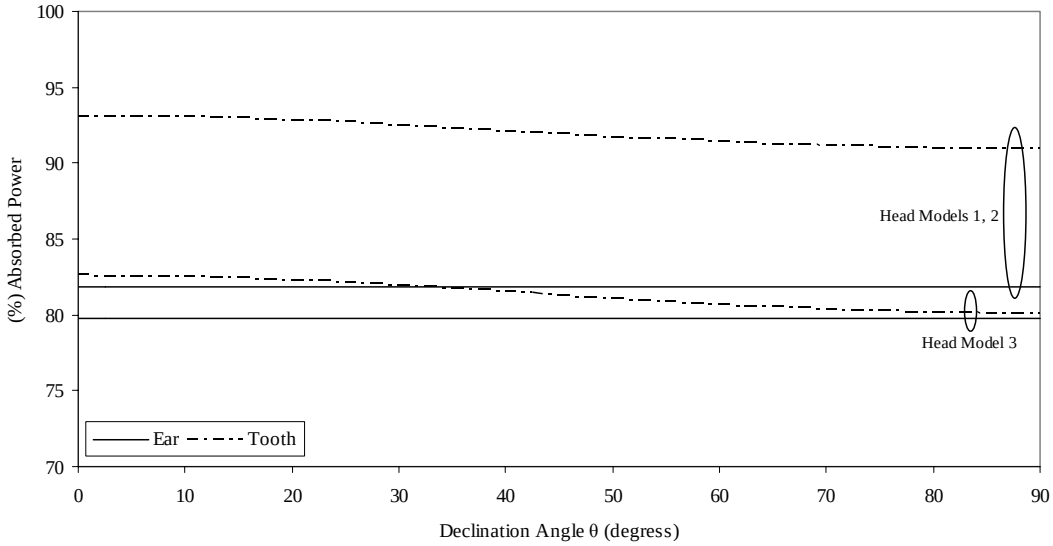

Figure 5. Absorption by the bone vs. dipole orientation (i.e. declination angle) for head models 1, 2 and 3

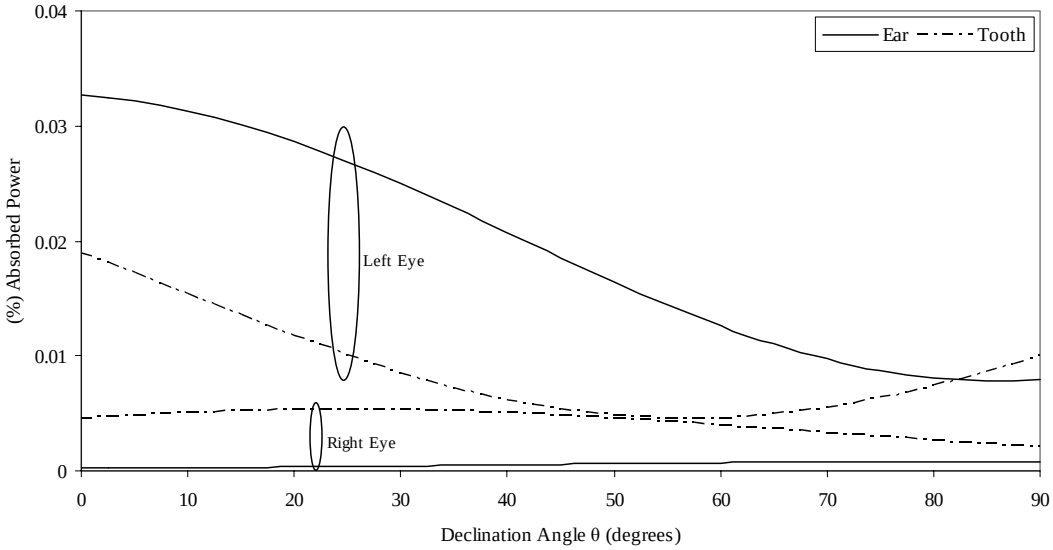

Figure 6. Absorption by the eyes vs. dipole orientation (i.e. declination angle) for head model 1

SAR maps are shown for characteristic cross-sections of the human head. The SAR maps of Figs. 7 and 8 correspond (a) to a horizontal cross section of the head through the centers of the scull and the eyes and (b) to a vertical cross section of the head through the centers of the scull, the brain and the acrylic capsule. The brain core in Figs. 7(a) and 8(a) seems smaller because it is somewhat raised above that cross section, i.e. the xO_0y plane. The active implant is inside the left ear and the operating frequency is $1500MHz$ in Fig. 7 and $2400MHz$ in Fig. 8. The radiated power is $1W$ for all the cases examined.

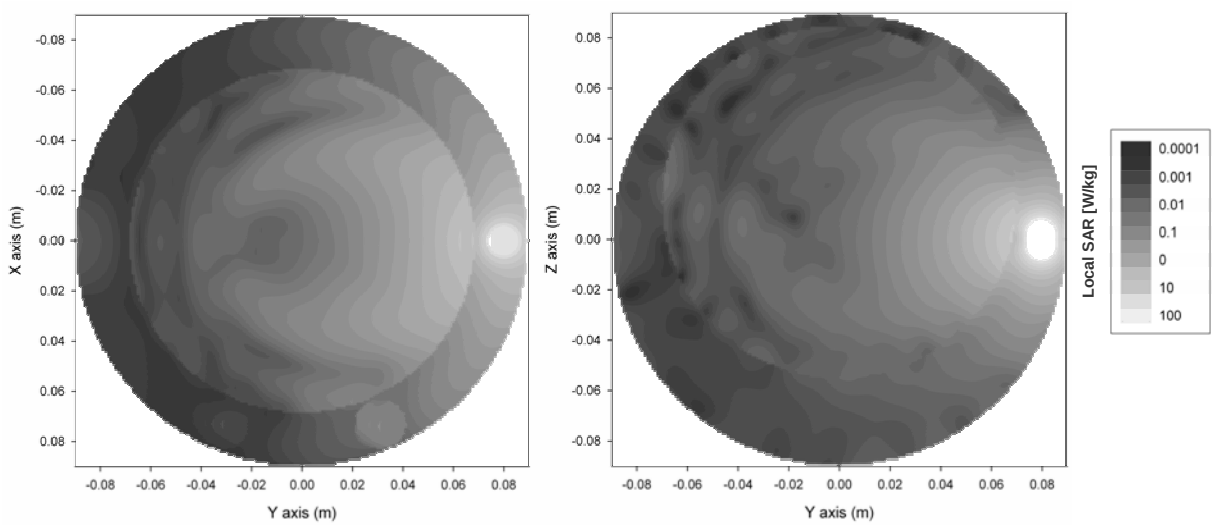

(a) (b)

Figure 7. SAR maps on (a) xO_0y and (b) yO_0z planes; the implant is inside the left ear and the frequency is 1500 *MHz*.

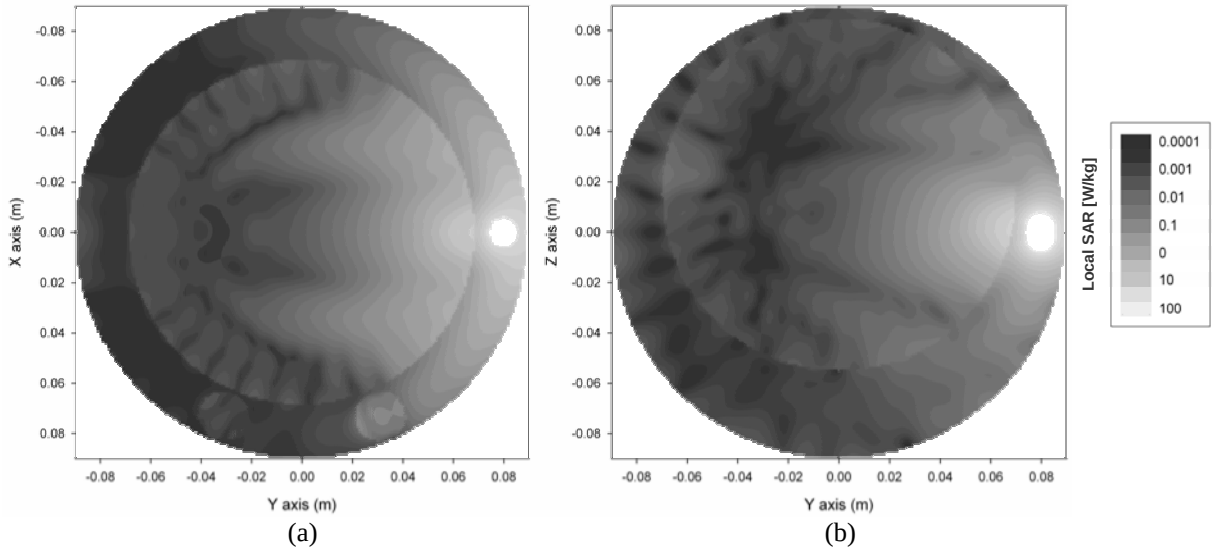

(a) (b)

Figure 8. As Fig. 7 at 2400 *MHz*.

A cursory look at the above SAR maps suggests that the higher the frequency the more superficial is the penetration of the EM radiation inside the brain and the eyes. The maximum SAR in the brain is found at the cortex, directly in front of the implant, where the radiation is most intense. The maximum SAR in the brain is $10.8W/kg$, when the frequency is $1500MHz$, and it reaches $21.0W/kg$ at $2400MHz$.

Finally, local SAR evaluations have been made with the implant inside the tooth. Figs. 9 and 10 are SAR maps for the same cross-sections of the eccentric-brain head model as Figs. 7,8 and for the same frequencies. The aforesaid remark about the dependence of the penetration depth of the EM radiation on the operating frequency of the implant is reconfirmed. However, the importance of the distance of the implant from the brain on the power absorbed by the brain is now made evident, since the maximum local SAR in the brain in these cases is $1.6W/kg$ at $1500MHz$ and $2.4W/kg$ at $2400MHz$.

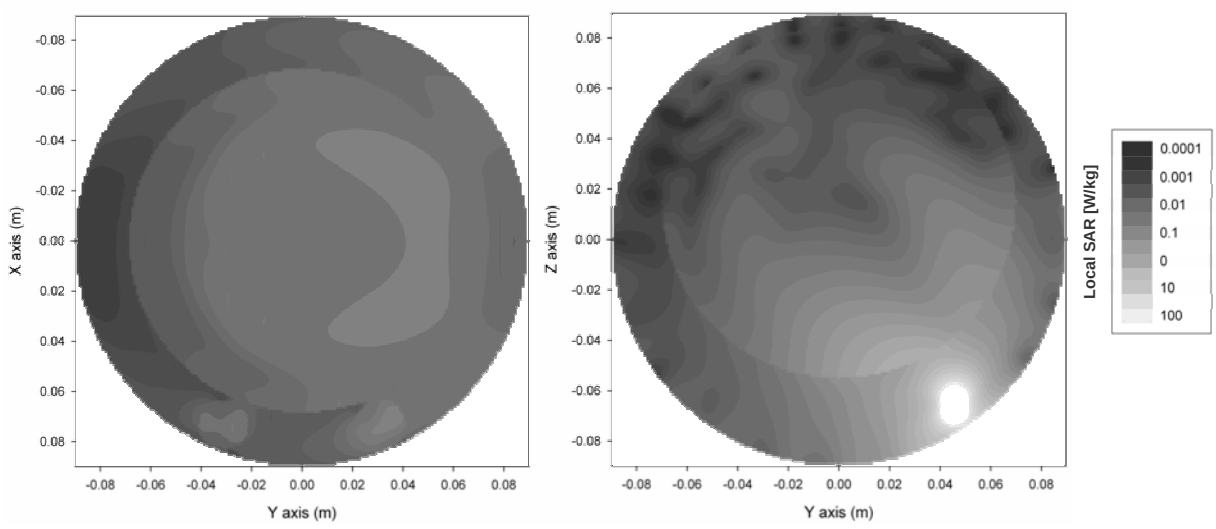

(a) (b)

Figure 9. SAR maps on (a) xO_0y and (b) yO_0z planes; the implant is inside a tooth and the frequency is 1500 *MHz*.

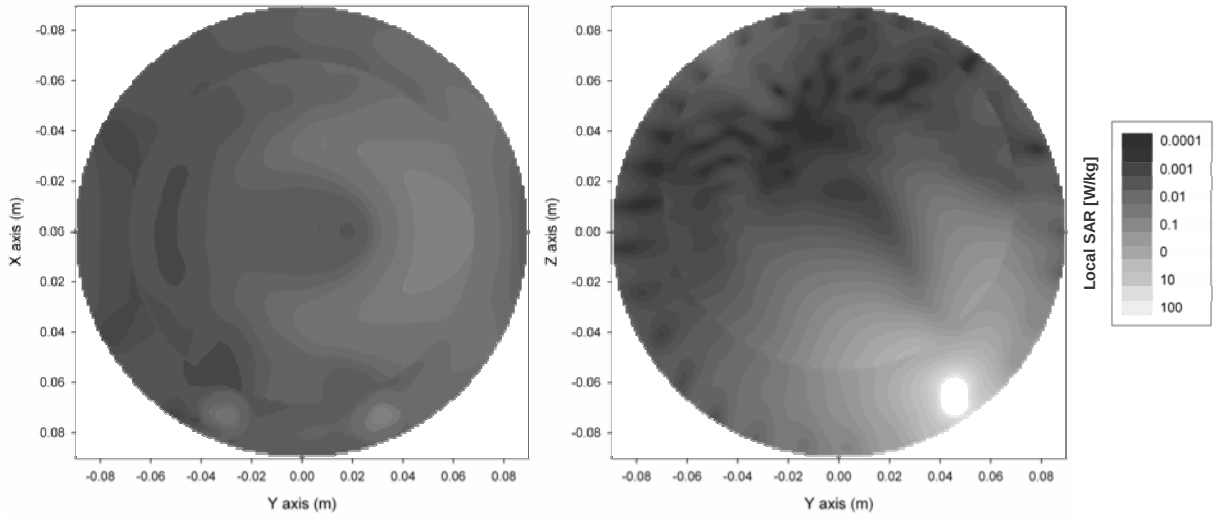

(a) (b)

Figure 10. As Fig. 9 at 2400 *MHz*.

When the implant is intended for telecommunication or monitoring purposes the field outside the head is important for the appliance that receives the transmitted data. The EM field outside the head is shown in Figs. 11 and 12 as maps of the amplitude of the electric-field intensity up to distance $90\,cm$ from the center of the head. Those maps correspond to the coordinate plane xO_0y with the implant inside the ear or in a tooth. The operating frequency is either $1500MHz$ or $2400MHz$ and the power radiated by the implant power is $1W$. It is clear from those maps that the presence of the head orients the EM radiation in directions opposite to the head and this effect is stronger at the higher frequency, i.e. at $2400MHz$, for both positions of the implant examined. Finally, it is noted that, the average electric-field intensity on that plane is stronger with the implant in the ear than with the implant in the tooth. This, last remark holds even when the electric-field intensity is mapped on a horizontal plane through the tooth.

The study of the EM field outside the head model is completed by the radiation patterns shown in Figs. 13-16. Radiation patterns are plotted on all three coordinate planes, i.e. xO_0z (a), yO_0z (b), and xO_0y (c). The electric-field intensity in all those patterns has been normalized with respect to the maximum value of the electric-field intensity generated by the encapsulated dipole in free space. The comments incited by Figs. 11 and 12 about the re-orientation of the EM radiation due to the presence of the head and about the dependence of the electric-field intensity on the frequency and the position of the implant are compatible with Figs. 13-16.

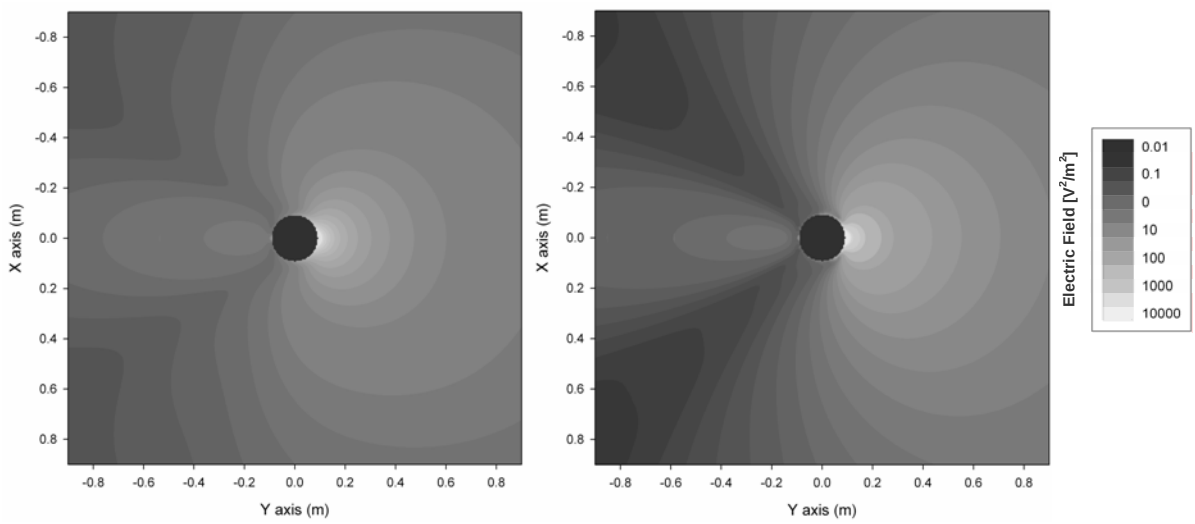

(a) (b)

Figure 11. Field maps around head model 1; the implant is in the left ear and the frequency is (a) 1500 *MHz*, (b) 2400 *MHz*

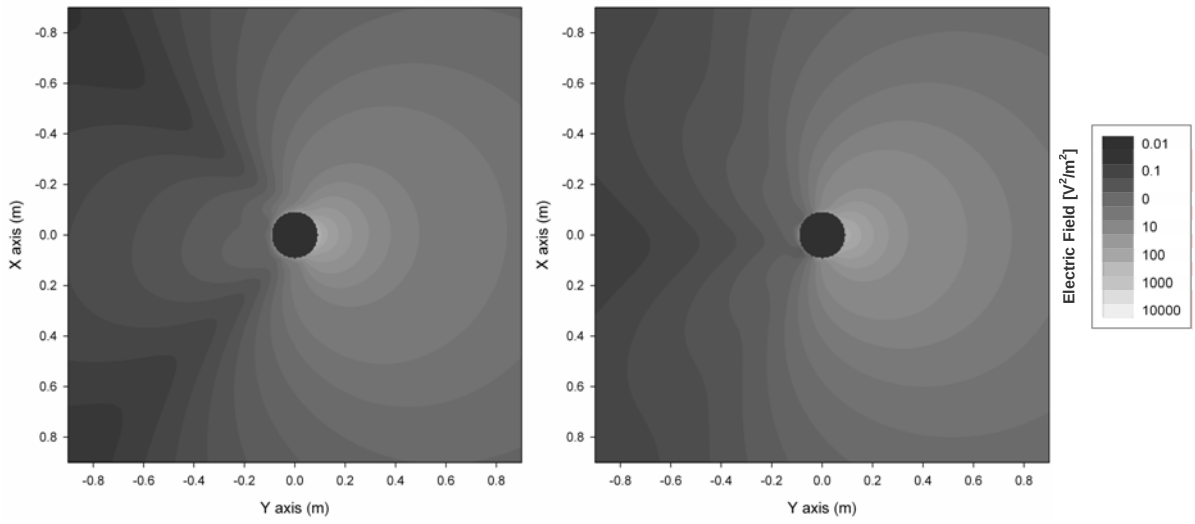

(a) (b)

Figure 12. As Fig. 11 with the implant in a tooth

The radiation characteristics of the dipole itself are strongly affected by the electrical and geometrical features of the head model. Comparisons with radiation patterns corresponding to models 2 and 3 suggest that the position of the brain in the scull strongly affects the radiation patterns, whereas the effect of the eyes can hardly be noticed.

The final part of this investigation on the effect of the human head on the radiation characteristics of the implant, concerns the variation of the radiated power crossing the surface of the acrylic capsule with the operating frequency; that plot is shown in Fig. 17 across the frequency range $400MHz - 4GHz$. Since the acrylic medium has been considered lossless, the aforesaid radiated power is equal to power delivered by a tiny transmitter to the dipole, provided that matching between them is possible even though the current flowing along the dipole is modified by the presence of the head. The continuous line in Fig. 17 corresponds to power radiated by the dipole from within the acrylic sphere in free space; that power has been normalized with respect to the power radiated by the very same dipole in free space at every frequency; the dashed line corresponds to the power radiated by the implanted antenna and it has been normalized by the power radiated by the encapsulated dipole in free space. It can easily be seen from Fig. 17 that when the radius of the acrylic capsule is greater that 40 wavelengths, i.e. for frequencies above $1500MHz$, the power radiated by the implanted antenna varies periodically with the frequency and the effect of the head is minimal.

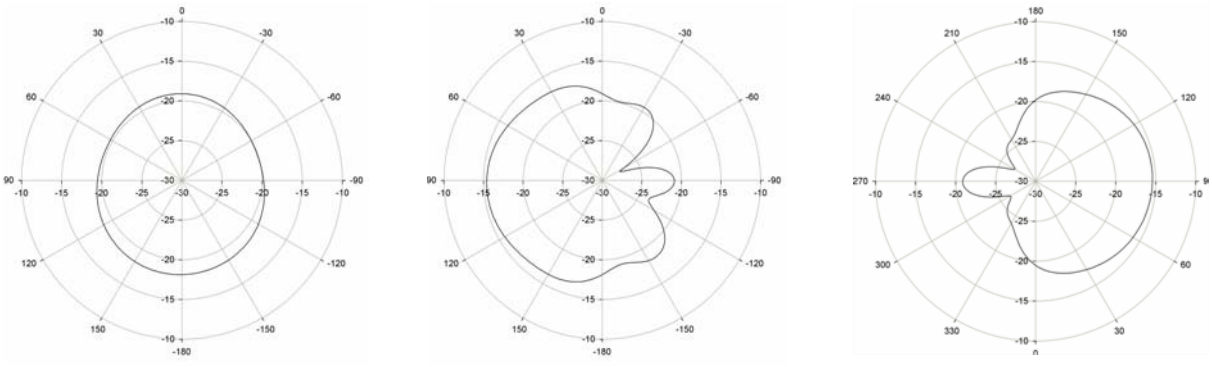

(a) (b) (c)

Figure 13. Radiation Patterns on xO_0z (a), yO_0z (b), and xO_0y (c) plane around head model 1; the implant is inside the left ear and the frequency is 1500 *MHz*

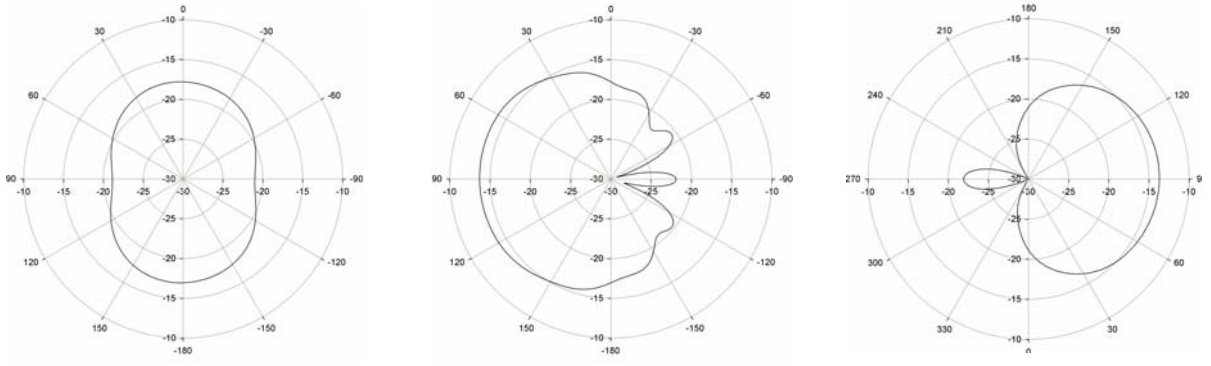

(a) (b) (c)

Figure 14. As Fig. 13 at 2400 *MHz*

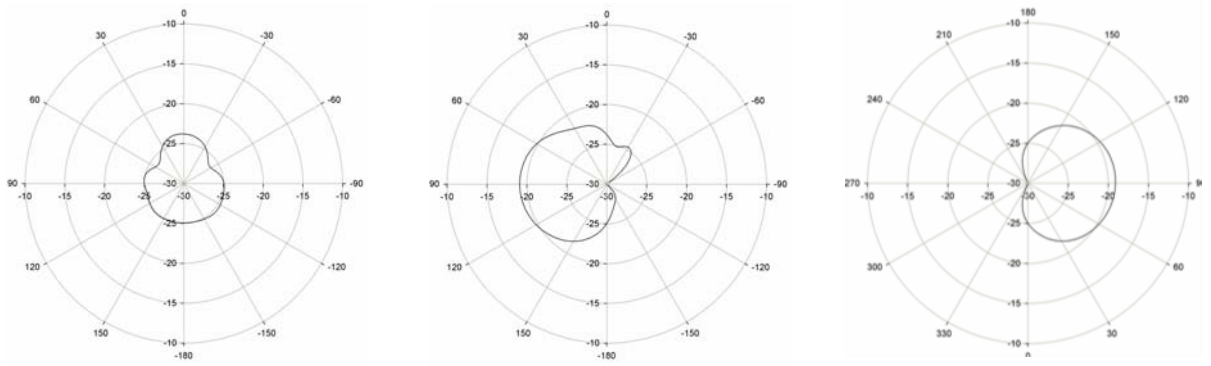

(a) (b) (c)

Figure 15. As Fig. 13 with the implant in a tooth

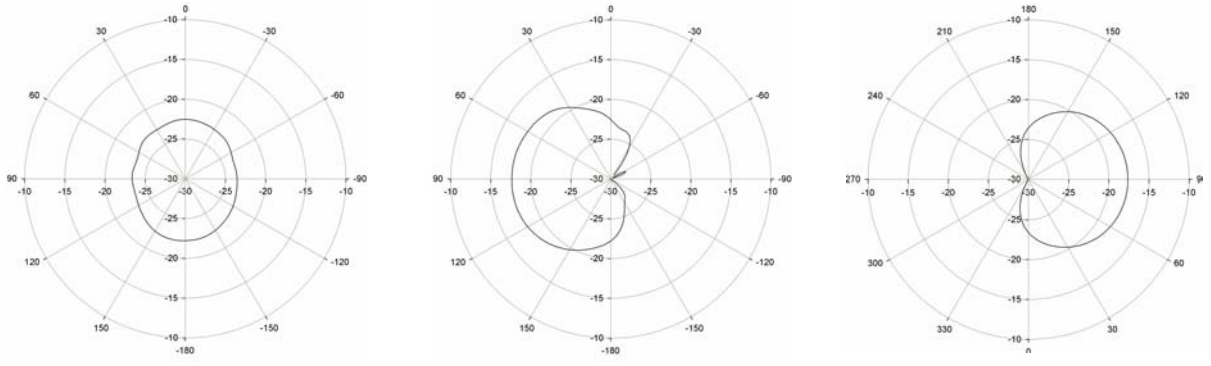

(a) (b) (c)

Figure 16. As Fig. 14 with the implant in a tooth

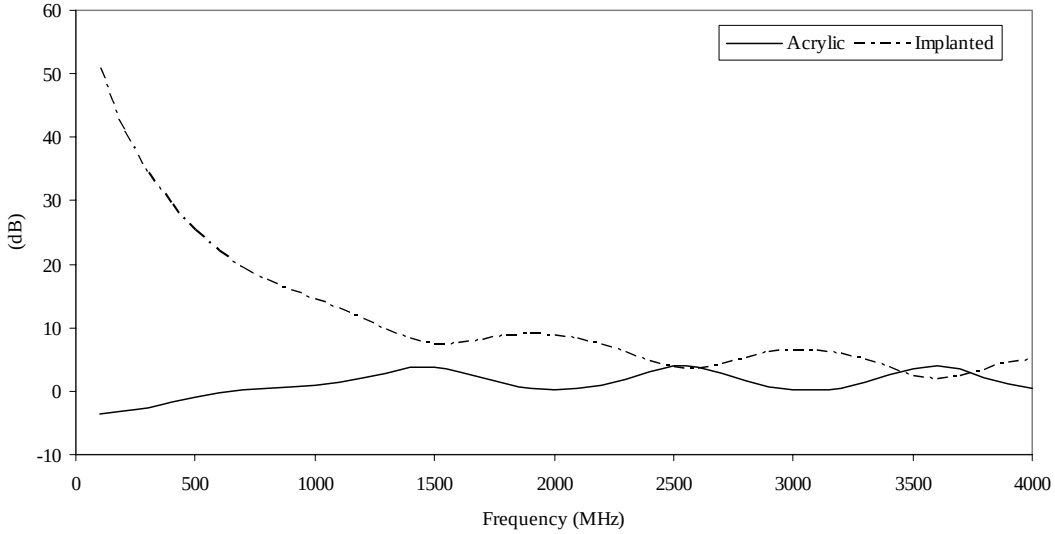

Figure 17. The power radiated by the encapsulated dipole against the frequency

V. Summary

The effects of an infinitesimal electric dipole placed at the centre of an acrylic sphere and implanted inside the human head have been studied by use of three head models. On the one hand, the absorbed power and the SAR in any part of the head models, have been evaluated and the importance of the operating frequency, the position and the orientation of the dipole have been established; the EM radiation escaping the head as well as the effects of the head on the characteristics of the implant have been examined. On the other hand, the importance of some anatomical details of the head models, within the framework of analytical methods, has been assessed, thus allowing for the appropriate head model to be used for the application at hand.

References

[1] S.M.S Reyhani and R.J. Glover, "Electromagnetic dyadic Green's function for a multilayered homogeneous lossy dielectric spherical head model for numerical EMC investigation," *Electromagnetics*, vol. 20, pp. 141-153, 2000.

[2] J. Kim and Y. Rahmat-Samii, "Implanted antennas inside a human body: Simulations, design, and characterizations," *IEEE Trans. Microwave Theory Tech.*, vol. 52, pp. 1934-1943, Aug. 2004.

[3] F. Liu and S. Crozier, "Electromagnetic fields inside a lossy, multilayered spherical head phantom excited by MRI coils: models and methods," *IOP Publishing, Phys. Med. Biol.*, vol. 49, pp. 1835-1851, 2004.

[4] C. Gabriel, "Compilation of the dielectric properties of body tissues at RF and microwave frequencies," Occupational and Environmental Health Directorate, RFR Division, Brooks AFB, TX, Final Tech. Rep. AL/OE-TR-1996-0037, 1996.

[5] C.T. Tai and R.E. Collin, "Radiation of a Hertzian dipole immersed in a dissipative medium," *IEEE Trans. Ant. Prop.*, vol. 48, no. 10, pp. 1501-1506, Oct. 2000.

[6] A.P. Moneda and D.P. Chrissoulidis, "Dyadic Green's function of a dielectric sphere with an eccentric inclusion," submitted to *J. Opt. Soc. Am. A.*

[7] K.S. Nikitia, G.S. Stamatakos, N.K. Uzunoglu, and A. Karafotias, "Analysis of the interaction between a layered spherical human head model and a finite-length dipole," *IEEE Trans. Microwave Theory Tech.*, vol. 48, no. 11, pp. 2003-2013, Nov. 2000.

[8] L.W. Li, P.S. Kooi, M.S. Leong, and T.S Yeo, "Electromagnetic dyadic Green's function in spherically multilayered media," *IEEE Trans. Microwave Theory Tech.*, vol. 42, no. 12, pp. 2302-2310, Dec. 1994.

[9] A.P. Moneda, M.P. Ioannidou, and D.P. Chrissoulidis, "Radio-wave exposure of the human head: analytical study based on a versatile eccentric spheres model including a brain core and a pair of eyeballs," *IEEE Trans. Biomed. Eng.*, vol. 50, no. 6, pp. 667-676, June 2003.

[10] C.T. Tai, *Dyadic Green Functions in Electromagnetic Theory*, 2nd Edition, New York, IEEE Press, 1993.

EFFECTS OF MELATONIN AND 50 Hz MAGNETIC FIELDS ON GAP JUNCTIONAL INTERCELLULAR COMMUNICATION IN HEPG2

M.A.CID, M.L. HERNÁNDEZ-BULE, M.A. MARTÍNEZ, A. ÚBEDA, J. LEAL AND M.A. TRILLO

DEPT. INVESTIGACIÓN-BEM, HOSPITAL RAMÓN Y CAJAL, 28034 MADRID, SPAIN
mariancid@yahoo.es; angeles.trillo@hrc.es

ABSTRACT

Experimental evidence exists suggesting that Extremely Low Frequency Magnetic Fields (ELF-MF) and Melatonin (MEL) can exert antagonistic effects on different cellular responses. However, the nature of such an interaction remains unknown. Our previous studies have shown that MEL significantly reduces proliferation and stimulates cytodifferentiation in HepG2 human hepatocarcinoma cells, these effects being antagonized by the exposure to 50 Hz, 10 µT MF. Conversely, the MF increases the growth rate of HepG2 when administered alone, but not in the presence of MEL. The present work investigates whether gap junctional intercellular communication (GJIC) could be involved in the described MF/MEL responses. Connexin32 (Cx32) expression (Immunocytochemistry - Image analysis) and functional GJIC (Parachute technique) have been analyzed in cultures exposed to the following conditions: Control, MEL (10 nM), MF (50 Hz, 10 µT) and MEL + MF. The results show that MEL stimulates dye transfer and induces expression of Cx32. Both effects are inhibited by the simultaneous exposure to MF. Therefore, the results suggest that previously reported antagonistic effects of MEL/MF in the proliferation and/or differentiation of HepG2 could be mediated by modulation of Cx32 expression and functional GJIC.

INTRODUCTION

There is mounting evidence that the pineal gland's hormone melatonin (MEL) intervenes in the control of neoplastic processes in cells, animals and humans (Blask *et al.*, 1993; Stevens, 2005). Melatonin has been reported to inhibit cell proliferation in different tumor types, such as hepatoma and colon cancer from rodents (She *et al.*, 2004; Dakshayani *et al.*, 2005; Mei *et al.*, 2005) and to reduce the incidence and growth of chemically induced mammary tumors (Melancon *et al.*, 2005; Cos *et al.*, 2006a). Also, several studies addressing oncostatic effects of MEL in the human breast cancer cell line MCF-7 have shown that MEL can inhibit proliferation and the metastatic behavior in these cells (Cos *et al.*, 2006b). Although different mechanisms have been proposed to explain the potential ability of MEL to suppress tumor promotion and progression, the actual mechanisms responsible for the oncostatic capacities of this hormone remain unidentified. Recent experimental evidence suggests that MEL could also influence proliferative processes due to its oxidative function and free radical scavenging properties (reviewed by Vijayalaxmi *et al.*, 2004). In addition, MEL has been reported to affect processes involved in cell differentiation (Radio *et al.*, 2006), including the establishment of cell adhesion and cell contacts, (Cos and Fernández 2000). In previous works we have reported that MEL enhances junctional transfer in normal C3H/10t1/2 cells and in primary cultures of mouse hepatocytes (Úbeda *et al.*, 1995a; Blackman *et al.*, 2001a). These results suggest that melatonin could exert its antitumoral action, at least in part, by modulating the levels of gap junctional intercellular communication (GJIC).

On the other hand, a number of *in vivo* studies have shown that extremely low frequency (ELF) magnetic fields (MF) can influence the development of tumor-promoting processes (reviewed by Loscher and Mevissen, 1994; Fedrowitz *et al.*, 2004) and alter MEL secretion by the pineal gland (reviewed by Reiter, 1994; Henshaw and Reiter 2005). The results of different studies suggest that ELF MF-induced reduction of MEL levels in the circulating blood could be determinant to the tumor promoting action of these fields. In vitro, 60/50 Hz MF have been reported to block Melatonin-induced inhibition of cell proliferation in human breast cancer MCF-7 cells (Liburdy 1993; Blackman *et al.*, 2001b; Ishido *et al.*, 2001). The HepG2 cell line has been extensively used for studying the mechanisms of action of a wide spectrum of potential carcinogens including ELF MF, which have been shown to promote proliferation in these cells (Trillo *et al.*, 2001). Moreover, previous studies by our group have shown that MEL significantly reduces proliferation and stimulates cytodifferentiation in HepG2 cells, these effects being antagonized by the exposure to 50 Hz, 10 µT MF. Conversely, when administered alone, the MF increased the growth rate in HepG2, whereas the presence of

MEL in the medium blocked such a cellular response (Cid *et al.,* 2004; Cid *et al.,* 2005). The present work investigates whether gap junctional intercellular communication could be involved in the previously described MF/MEL antagonistic responses on the proliferation or differentiation of HepG2. For that purpose the functionality of GJIC and the expression of connexin32 (Cx32) were analyzed on samples exposed to 50 Hz, 10 µT MF and/or treated with 10 nM MEL.

MATERIAL AND METHODS

Cell culture

HepG2 human hepatocarcinoma cells (ECACC, TDI S. A., Madrid) were cultured in Dulbecco's-Eagle modified medium (DMEM; Bio-Whittaker) supplemented with 5% heat-inactivated Fetal Bovine Serum (FBS, GIBCO), 10% Glutamine, and 10% penicillin/streptomycin (GIBCO), in water-jacket incubators (Forma Scientific) at 5% CO_2, 37 ºC and 100% RH atmosphere.

MF exposure

The exposure set-up used in these experiments was reproduced from that described by Blackman *et al.,* (1993). Each exposure system consisted of two identical sets of two 1000-turn, 20-cm-diameter coils of enameled wire, aligned coaxially 10 cm apart, in a Helmholtz configuration, and oriented to produce vertically polarized magnetic fields. Each set of coils was kept inside a magnetically shielded chamber (co-netic metal; Amuneal Corp., Philadelphia, PA) placed inside a CO_2 incubator (Forma Scientific). The generating (Newtronic Model 200MSTPC, Madrid, Spain) and monitoring (Hewlet Packard, 974A, Loveland CO) equipment was connected to the coils. The flux density and electromagnetic background in the exposure area were measured and recorded before and after the experiment with a fluxgate magnetometer (EFA-3, Wandel & Golterman GMW & Co. Germany). The background MF inside the shielded chambers was AC: 0.04 ± 0.03 µT, DC: 0.05 ± 0.04. In each experimental run only one of the two sets of coils was energized. The samples in the unenergized set were considered sham-exposed controls. Both incubators were used, in a random sequence, alternatively for MF exposure and sham-exposure. The MF exposure parameters were chosen on the basis of our previous observations (Trillo *et al.,* 2001; Trillo *et al.,* 2003; Martínez et al., 2006), which revealed that a 42-h exposure to a sinus wave 50 Hz intermittent (3-h On/3-h Off) MF at 10 µT significantly stimulates cell growth in both, the HepG2 human hepatocarcinoma cell line and the NB69 human neuroblastoma cell line.

GJIC assay: Parachute and Flow cytometry techniques

The GJIC was examined through a two-dye method based on the parachute technique, previously described by Goldberg *et al*. (1995). This technique is currently used to detect and quantify GJIC functionality in different cellular systems (Czyz *et al.,* 2000; reviewed by Fonseca *et al.,* 2006). The high sensitivity of this method allows for detection of small changes in functionality of GJIC by examining a large number of cells in a single experimental run. In our experiments, the samples were seeded at a density of 10 x 10^4 cells/ml. After allowing for cell attachment (4 hours post-plating) the dishes were distributed in two groups and an initial dose of Melatonin (N-acetyl-5-methoxy-tryptamine, Sigma) was added to one of the two groups. At the end of day 3 postplating the medium was renewed and a second dose of MEL was administered to the previously treated group. At this time both groups, with or without MEL, were divided in sham-exposed and MF-exposed samples. The cells were subjected to: a) no treatment: controls, b) treatment with MEL, c) exposure to MF, and d) MF exposure imposed upon MEL treatment. The MF-exposed samples were treated intermittently, 3h On/3h Off, with a 50 Hz, 10 µT MF for 24 h. At the end of day 4, when cells were close to confluence, all the samples were distributed into two groups: the recipient and the donor group. The group of recipient cells was pre-stained with a permanent, non-toxic lipophilic dye that binds to membranes irreversibly, DiI (1-1´dioctadecyl-3,3,3´,3´-tetramethylindocarbocyanine perchlorate; Molecular Probes). The donor population was treated with a gap junction-permeable dye Calcein, a derivative of Calcein acetoxymethyl ester (Calcein-AM, Molecular Probes). After seeding the donor cells on the corresponding recipient samples under conditions promoting gap junction (GJ) formation, the four experimental groups were exposed and/or incubated for an additional 18 h lapse. At the end of this period the samples, two per experimental condition: Control, MEL, MF and MEL + MF, were analyzed by flow cytometry (Cell Quest software) and the percent of cells showing both dyes (Cal+ / DiI+ events) vs. the total Cal+ events, were determined. A total of 20,000 events per sample were recorded. Two additional samples were used to establish the basal level of fluorescence.

Cx32 expression assay

The Cx32 expression was estimated as the percent of Cx32 positive cells by immunochemistry and Computer-Assisted Image-Analysis. The methodology used for treatments with MEL and/or MF has been described previously by Cid *et al*. (2004). In short, cells were seeded at a density of 9.5 x 10^4 cells/ml on 12 mm ∅

coverslips sited into the Petri dishes. Additional Petri dishes were used to test viability and cell proliferation. A total of 12 or 20 dishes, to obtain 3 or 5 plates, per experimental condition: Control, Melatonin, MF and Melatonin + MF, were assayed. After allowing for cell attachment to the coverslips (4 hours post-plating) the dishes were distributed in two groups and an initial dose of Melatonin was added to one of the two groups. At day 3 post-plating the medium was renewed, and a second treatment with MEL was administered in the previously treated group. Each of the two groups, treated with MEL or untreated, was distributed in sham-exposed and MF-exposed samples. The MF-exposed samples were treated intermittently, 3h On/3h Off, with a 50 Hz, 10 μT MF for 42 h. At the end of this period the cells were tested for appropriate viability and cell proliferation before being processed for analysis of connexin32. Cells on coverslips were fixed with periodate-lysine-paraformaldehyde (PLP). After washing with PBS, cells were permeabilized, (acetone 50%) and the endogen peroxidase was inactivated (H_2O_2 3%.) The non-reactive sites were blocked (FCSi 10%, Triton X-100 0.05% in PBS) for 1 h at room temperature. Then, the samples were incubated for 24 h at 4 ºC with a monoclonal antibody against the central cytoplasmic loop of human Cx32 (IgG clone M12.13; Chemicon Int.), dilution 1:200, in FCSi 5% / Triton X-100, 0.15% / PBS. Immunostaining was enhanced through the ABC method (Vectastain ABC Elite kit, Vector Laboratory, Burlingame CA), and revealed with the peroxidase substrate, diaminobenzidine tetrahydrochloride (DAB). The nuclei were counterstained with Hematoxiline. Background controls without the primary antibody were also included in the study. The samples were visualized and evaluated through a photomicroscope. Two coverslips per experimental condition were randomly chosen and a total of 20 microscope fields per coverslip were analyzed. The quantification of the immunolabeling was carried out through Computer Assisted Image-Analysis (IPWin and AnalySIS software). The ratio of Cx32 positive cells vs. total cells per microscope field was determined. Additional analysis taking into account the total immunostaining area of Cx32 vs. total cells per microscope field was carried out.

RESULTS

GJIC functionality in samples exposed to MF in the presence or the absence of MEL

Previous studies by our group showed that a dose of 10 nM MEL was effective inducing decreases in cell proliferation and in the promotion of differentiation in HepG2. These effects were antagonized by the exposure to 50 Hz, 10 μT MF (Cid *et al.*, 2004; Cid *et al*., 2005). On that basis, in the present study the concentration 10 nM MEL was assayed to study the functional GJIC in cells exposed to 50 Hz 10 μT MF in the presence or absence of MEL. The parachute technique revealed that untreated HepG2 cells (control condition) exhibit a low degree of junctional activity. However, the presence of 10 nM MEL in the medium increases significantly the coupling rate (17.7 ± 0.4 % over controls $p<0.01$) in these cells (Fig. 1). In contrast, the coupling response to the MF exposure did not differ significantly from that in controls, both in the presence and in the absence of MEL; which reveals that the 10 μT MF, per se, does not change the functional GJIC in HepG2, but can block the MEL-induced coupling in these cells.

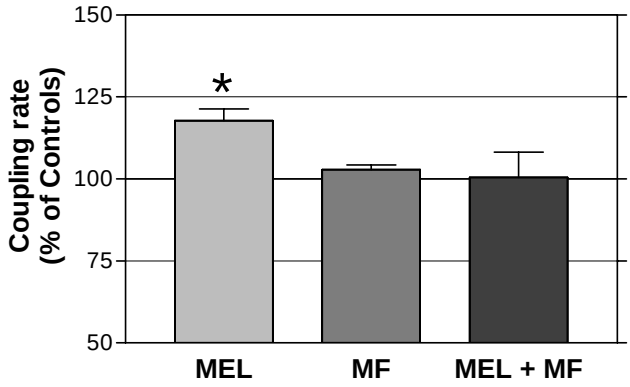

Fig. 1. The functional GJIC was measured as the percent of cells showing both dyes (Cal+ / DiI+ events) over the total Cal+ events. Coupling rate in the different conditions tested, Control, MEL, MF and the combined treatment, MEL + MF. The MEL-induced coupling was antagonized by the exposure to MF. Data normalized over controls N = 4 experiments. Mean ± SEM *, $p< 0.05$ (ANOVA followed by Student's T test).

Cx 32 expression in samples exposed to MF in the presence or the absence of MEL

The effect of the treatments with MEL and/or MF on the Cx32 expression and on its subcellular distribution was determined through Computer Assisted Image-Analysis. The analysis was focused on the expression of Cx32 because changes in both, the amount and distribution of this connexin have been suggested to be implicated in human hepatocarcinogenesis (Nakashima *et al.,* 2004), and increases in Cx32 expression induce phenotypic normalization in HepG2 (Yang *et al.,* 2003), whereas decreases in Cx32 seem to be linked to cell proliferation and progression in rodent hepatocarcinomas (Temme *et al.,* 1997). In the untreated cells the Cx32 expression presents an abnormal localization and distribution when compared to normal hepatocytes (data not shown). This abnormal pattern of expression consists on an increased cytoplasmic accumulation, either distributed in vesicular structures or presenting a diffuse appearance located generally in the perinuclear zone. The cytoplasmic membrane presents little expression of Cx32, with no immunoreactive gap junctional plaques. This aberrant pattern of Cx32 expression in HepG2 cells was not modified by the exposure to MF or by the MEL treatment. However, in MEL treated samples a significant increase (32.9 ± 0.9 % over controls, p< 005) in the percent of cells expressing cytoplasmic Cx32 immunostaining was observed at day 5 of treatment (Fig 2). In contrast, the response to MF alone or to the combined treatment (Mel + MF) was similar to that observed in controls. These data reveal that, when applied alone, the MF did not exert significant effects on Cx32 expression or on functional GJIC. However, when applied on MEL treated samples, the MF exposure antagonized the MEL-induced responses. Preliminary data (not shown) on immunoblot for Cx32 confirm these results.

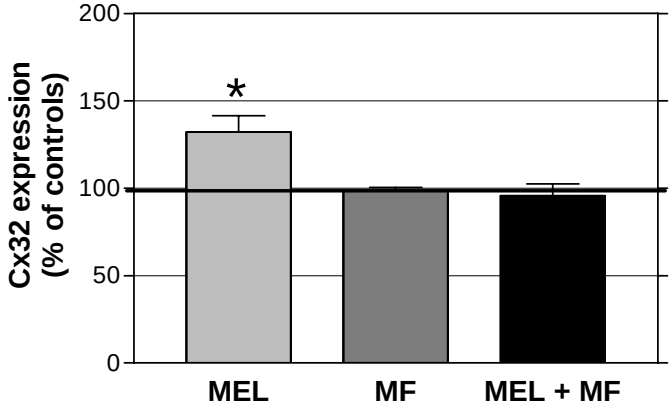

Fig. 2. Percent of Cx32 positive cells, quantified by the Image Analysis software IPWin, in the different experimental conditions tested. The treatment with 10 nM MEL increased significantly the percent of cells expressing Cx32. This response was counteracted by the exposure to 50 Hz, 10 µT MF. Data normalized over controls, Mean ± SEM of 4 experimental replicates; *, p< 0.05 (ANOVA followed by Student's T test.)

DISCUSSION

Previously reported results by our group have shown that MEL significantly reduces proliferation and stimulates cytodifferentiation in HepG2 human hepatocarcinoma cells; these effects being antagonized by the exposure to sinusoidal 50 Hz, 10 µT MF. Conversely, the MF increases the growth rate of HepG2 when administered alone, but not when in the presence of MEL (Cid *et al.,* 2004; Cid *et al*., 2005). It is currently believed that a tight regulation of gap junctional intercellular communication mediated by connexins may contribute to cell growth and differentiation by keeping important signals, such as those involved in growth control, at equilibrium among gap junction-connected cells. The present work investigates whether gap junctional intercellular communication could be involved in the MF/MEL responses described before. The results of the present work show that untreated, control HepG2 cells have a low degree of junctional activity and an aberrant expression of Cx32. However, the treatment with MEL increases the functional GJIC and the percent of cells that express the gap-junctional protein Cx32 in HepG2. On the other hand, although the exposure to MF alone does not exert any significant influence on these junctional processes, when applied on MEL-treated cells the MEL-induced responses on the functionality of GJIC and on Cx32 expression were abolished.

The stimulating effect of MEL on GJIC functionality has been well described in a variety of cell lines. Úbeda *et al.* (1995a) reported that physiological concentrations of MEL between 0.01 and 0.1 nM, induce significant increases in the junctional transfer of mouse normal fibroblast C3H/10T1/2. Blackman *et al.* (2001a)

found similar results in primary cultures of mouse hepatocytes treated with MEL at the physiological doses of 0.2 and 0.4 nM. In the present study, the HepG2 human hepatocarcinoma line also responded with significant increases of the coupling rate (parachute technique) when treated with a concentration (10 nM) higher than the above described as effective in normal, non-cancer cells. Even higher, pharmacological concentrations of MEL (10 µM) have been reported to efficiently increase GJIC functionality in the breast cancer cell line MCF-7 (Cos and Fernandez 2000). Taken together, these results are consistent with the hypothesis that cancer lines are, in general terms, less sensitive to MEL than normal cells.

It has been well established that the restoration of connexin expression in tumor cells often leads to a partial reversion of the tumoral phenotypes and to increased growth control (King and Lampe 2004). Like reported by other authors working with poorly differentiated hepatocarcinomas (Krutovskikh *et al*., 1994), an aberrant pattern of Cx32, mainly cytoplasmic and diffuse, was observed in the present study in the HepG2 line. This may represent a general pattern in hepatocarcinoma cells, potentially due to the presence of abnormalities in the intracellular transport of Cx32, in the exportation of this connexin to the cell membrane, in the process of formation of GJIC plaques or in the recycling of the connexons. All these alterations would provoke the retention of the Cx32 in compartments of the endoplasmic reticulum, Golgy or lysosomes (Segretain and Falk 2004). In the present study, the MEL treatment stimulated the Cx32 expression. However, the connexin remained in the cytoplasm and did not stimulate the formation of GJ plaques in cell membranes. Moreover, growing experimental evidence supports the hypothesis that connexins can exert by themselves anti-proliferative effects that are independent of their functionality in intercellular communication. Such effects have been observed in a number cellular types including, glioma C6 (Bond *et al.*, 1994), bladder carcinoma BC31, (Krutovskikh *et al*., 2000) and the breast cancer line MDA-MB-231 (Qin *et al*., 2002). Although the mechanism responsible for the described effect remains unknown, some authors have suggested that interactions with transcription factors and regulation of gene expression of specific proteins, like the cell cycle regulator p27 could be involved in the effect (review, Jiang and Gu 2005). Consequently, the effects of MEL in the GJIC functionality and in the expression of Cx32 observed in the present work could be responsible, at least in part, for the antiproliferative and differentiating actions exerted by MEL in the same, HepG2 cell line (Cid *et al.*, 2004; Cid *et al*., 2005.)

Although a number of in vivo and in vitro studies have described MEL/MF interactions on the growth and/or differentiation, the mechanisms responsible for the these interactions remain unknown. In the present study, the exposure to a 50 Hz, 10 µT MF did not influence significantly the functionality of the GJIC or the Cx32 expression in the absence of MEL. However, in MEL-treated samples, the exposure to the MF abolished the stimulating effect of MEL on the gap junctional activity and on the expression of Cx32. These results are consistent with those previously reported by our group (Úbeda *et al.*, 1995b) showing that a 30-minute exposure to a 50 Hz, 1.6 mT MF blocks MEL-induced increase in GJIC in C3H/10T1/2 cells. Úbeda and coworkers proposed that the MF could influence the regulation of the permeability of the GJ channels and/or the channels' renovation. Other authors have suggested that the MF could exert an influence on signal transduction pathways that regulate the cell cycle, through modifications in the functionality of cell membrane receptors, including the MEL receptors (Ishido *et al.*, 2001). Thus, in the present study, the antagonistic effects exerted by MF on the cellular responses to MEL could be due to a blocking of the MEL's stimulatory actions at different levels including GJIC regulation and signal transduction pathways that regulate the cell cycle.

SUMMARY

In the present work we studied the effects of a 50 Hz 10 µT magnetic field on melatonin-induced responses on GJIC. The HepG2 human hepatocarcinoma cell line has been previously shown by our group to be responsive to a 50 Hz, 10 µT MF, which acts on these cells as a promoter of proliferation when administered alone, but not in the presence of MEL. Conversely, MEL reduces the growth rate of HepG2 and the field antagonizes such a response. The present results show that at a 10 nM concentration the neurohormon melatonin stimulates GJIC and Cx32 expression in HepG2, a cell line that exhibit a low degree of functional GJIC and an aberrant expression of Cx32. On the other hand, the exposure to MF alone does not influence the GJIC parameters, but blocks the MEL-induced responses on GJIC. Consequently, the herein reported effects of MEL in the GJIC functionality and in the expression of Cx32 could be responsible, at least in part, for the antiproliferative and differentiating actions exerted by MEL in the same HepG2 cell line (Cid *et al*., 2004*; Cid et al*., 2005). Besides, the antagonistic effects exerted by MF on the cellular responses to MEL could be due to a blocking of the MEL's stimulatory actions at different levels including GJIC regulation and signal transduction pathways that regulate the cell cycle.

Supported by FISS-03/0806 and Project I+T under agreement MOU EUROPA, ERG 101.013.

REFERENCES

Blackman C.F., Benane S.G., House D.E. and Pollock M.M. 1993. Action of 50 Hz magnetic fields on neurite outgrowth in pheochromocytoma cells. Bioelectromagnetics 14(3): 273-86.

Blackman C.F., Andrews P.W., Úbeda A., Wang X., Trillo M.A. and Pimentel M.E. 2001a. Physiological levels of melatonin enhance gap junction communication in primary cultures of mouse hepatocytes. Cell Biology and Toxicology. 17: 1-9.

Blackman C.F., Benane S.G. and House D.E. 2001b. The influence of 1.2 microT, 60 Hz magnetic fields on melatonin- and tamoxifen-induced inhibition of MCF-7 cell growth. Bioelectromagnetics. 22(2): 122-8.

Blask, D.E. 1993. Melatonin in oncology. In Yu, H.-S. and Reiter, R.J. (eds.) Melatonin, Biosynthesis, Physiological Effects and Clinical Applications. CRC Press, Boca Raton, pp. 448-475.

Bond S.L., Bechberger J.F., Khoo N.K. and Naus C.C. 1994. Transfection of C6 glioma cells with connexin 32. The effects of a non endogenous gap junction protein. Cell Growth Differ 5: 179-186.

Cid M.A., Martínez M.A., Úbeda A., Chacón L., Leal J. and Trillo M.A. 2004. Melatonin at a physiological concentration inhibits power frequency magnetic field-induced growth in human hepatocarcinoma cells. 11th International Congress of the International Radiation Protection Association (IRPA), 23-28 May Madrid, Spain. Abstract Book: 310.

Cid M.A., Úbeda A., Henández-Bule M.L., Martínez M.A., Díaz-Enriquez M., Leal, J. and Trillo M.A. 2005. Power frequency magnetic fields block melatonin-induced changes in alpha-fetoprotein and albumin in human hepatocarcinoma cells. Meeting of The Bioelectromagnetics Society and The European BioElectromagnetics Association. June 19 – 24; University College. Dublin, Ireland. Abstract Book: 316.

Cos S. and Fernandez R. 2000. Melatonin effects on intercellular junctional communication in MCF-7 human breast cancer cells. J Pineal Res 29: 166-171.

Cos S., González A., Guezmes A., Mediavilla M.D., Martínez-Campa C., Alonso-González C. and Sánchez-Barceló E.J. 2006a. Melatonin inhibits the growth of DMBA-induced mammary tumors by decreasing the local biosynthesis of estrogens through the modulation of aromatase activity. Int J Cancer 118(2): 274-8.

Cos S., González A., Martines-Campa C., Mediavilla M.D., Alonso-González C. and Sánchez-Barceló E.J. 2006b. Estrogen-signaling pathway: A link between breast cancer and melatonin oncostatic actions. Cancer Detect Prev 30(2): 118-28.

Czyz J., Irmer U., Schulz G., Mindermann A. and Hulser D.F. 2000. Gap-junctional coupling measured by flow cytometry. Exp Cell Res 255(1): 40-6.

Dakshayani K.B., Subramanian P., Manivasagam T., Essa M.M. and Manoharan S. 2005. Melatonin modulates the oxidant-antioxidant imbalance during N-nitrosodiethylamine induced hepatocarcinogenesis in rats. J Pharm Pharm Sci 8(2): 316-21.

Fedrowitz M., Kamino K. and Loscher W. 2004. Significant differences in the effects of magnetic field exposure on 7,12-dimethylbenz(a)anthracene-induced mammary carcinogenesis in two substrains of Sprague-Dawley rats. Cancer Res 64(1): 243-51.

Fonseca P.C., Nihei O.K., Savino W., Spray D.C. and Alves L.A. 2006. Flow cytometry analysis of gap junction-mediated cell-cell communication: advantages and pitfalls. Cytometry A 69(6): 487-93.

Goldberg G.S., Bechberger J.F. and. Naus C.C. 1995. A pre-loading method of evaluating gap junctional communication by fluorescent dye transfer. Biotechniques 18: 490-497.

Henshaw D.L. and Reiter R.J. 2005. Do magnetic fields cause increased risk of childhood leukemia via melatonin disruption? Bioelectromagnetics (Suppl 7): S86-97.

Ishido M. Nitta H, and Kabuto M. 2001. Magnetic fields (MF) of 50 Hz at 1.2 μT as well as 100 μT cause uncoupling of inhibitory pathways of adenylyl cyclase mediated by melatonin 1a receptor in MF-sensitive MCF-7 cells. Carcinogenesis 22: 1043-1048.

Jiang J.X. and Gu S. 2005. Gap junction- and hemichanel-independent actions of connexins. Biochim Biophys Acta 1711: 208-214.

King T.J. and Lampe P.D. 2004. Mice deficient for the gap junction protein Connexin32 exhibit increased radiation-induced tumorigenesis associated with elevated mitogen-activated protein kinase (p44/Erk1, p42/Erk2) activation. Carcinogenesis 25(5):669-80.

Krutovskikh V., Mazzoleni G., Mironov N., Omori Y., Aguelon A-M., Mesnil M., Berger F., Partensky C. and Yamasaki H. 1994. Altered Homologous And Heterologous Gap-Junctional Intercellular Communication In Primary Human Liver Tumors Associated With Aberrant Protein Localization But Not Gene Mutation Of Connexin 32. Int. J. Cancer 56: 87-94.

Krutovskikh V.A., Troyanovsky S.M.,Piccoli C., Tsuda H., Asamoto M. and Yamasaki H.. 2000. Differential effect of subcellular localization of communication impairing gap junction protein connexin43 on tumor cell growth in vivo. Oncogene 19: 505-513.

Liburdy,R.P. (1993) ELF magnetic fields, breast cancer and melatonin: 60 Hz fields block melatonin's

oncostatic action on ER+ breast cancer cell proliferation. J Pineal Res 14, 89–97.
Loscher W. and Mevissen M. 1994. Animal studies on the role of 50/60-Hertz magnetic fields in carcinogenesis. Life Sci 54(21): 1531-43.
Martínez M.A., Cid M. A., Úbeda A.,. García V. J., Leal J., and Trillo M.A. 2006. A role of ERK signaling in the proliferative effects of 50 Hz magnetic fields on human neuroblastoma cells. The 4th International Workshop on Biological Effects of Electromagnetic Fields. 16-20 October, Crete, Greece.
Mei Q., Xu J.M., Xiang L., Hu Y.M., Hu X.P. and Xu Z.W. 2005. Change of nitric oxide in experimental colitis and its inhibition by melatonin in vivo and in vitro. Postgrad Med J 81(960): 667-72.
Melancon K., Cheng Q., Kiefer T.L., Dai J., Lai L., Dong C., Yuan L., Collins A., Thiyagarajah A., Long S., and Hill S.M. 2005. Regression of NMU-induced mammary tumors with the combination of melatonin and 9-cis-retinoic acid. Cancer Lett 227(1): 39-48.
Nakashima Y., Ono T., Yamanoi A., El-Assal O.N., Kohno H. and Nagasue N. 2004. Expression of gap junction protein connexin32 in chronic hepatitis, liver cirrhosis, and hepatocellular carcinoma. J Gastroenterol 39(8): 763-8.
Qin H., Shao Q., Curtis H., Galipeau J., Delliveau D.J., Wang T., Alaoui-Jamali M.A. and Laird D.W. 2002 Retroviral delivery of connexin genes t human breast tumor cells inhibits in vivo tumor growth by a mechanism that is independent of significant gap junctional intercellular communication. J. Biol Chem 277: 29132-29138.
Radio N.M., Doctor J.S. and Witt-Enderby P.A. 2006. Melatonin enhances alkaline phosphatase activity in differentiating human adult mesenchymal stem cells grown in osteogenic medium via MT2 melatonin receptors and the MEK/ERK (1/2) signaling cascade. J Pineal Res 40(4): 332-42.
Reiter R.J. 1994. Melatonin suppression by static and extremely low frequency electromagnetic fields: relationship to the reported increased incidence of cancer. Rev Environ Health 10(3-4): 171-86.
Segretain D. and Falk M.N. 2004. Regulation of connexin biosynthesis, assembly, gap junction formation and removal. Biochim Biophys Acta 1662: 3-21.
She M.H., Chen B.B., Wang X.M. and He S.S. 2004. p53-dependent antiproliferation and apoptosis of H22 cell induced by melatonin. Ai Zheng 23(7): 803-7.
Stevens R.G. 2005. Circadian disruption and breast cancer: from melatonin to clock genes. Epidemiology 16(2): 254-8.
Temme A., Buchmann A., Gabriel H.D., Nelles E., Schwarz M. and Willecke K. 1997. High incidence of spontaneous and chemically induced liver tumors in mice deficient for connexin32. Curr Biol 7(9): 713-6.
Trillo M.A., Martínez M.A., Cid M.A., Úbeda A., García V.J., Chacón L. and Leal J. 2001. Influence of 50 Hz magnetic fields on the proliferation of human hepatocarcinoma cells in vitro. BEMS, Twenty-Third Annual Meeting, St. Paul, Minnesota, June 10-14, Abstract Book: 211.
Trillo M.A., Martínez M.A., Cid M.A., García V.J., Ubeda, A. and Leal, J. 2003. Action of 50 Hz magnetic fields on the growth of human neuroblastoma cells. 25th BEMS Meeting, Maui, Hawaii, Abstract Book: 287.
Úbeda A., Trillo M.A., House D.E., and Blackman C.F. 1995a. Melatonin enhances junctional transfer in normal C3H/10T1/2 cells. Cancer Lett 91: 241-245.
Úbeda A., Trillo M.A., House D.E., and Blackman C.F. 1995b. A 50 Hz magnetic field blocks melatonin-induced enhancement of junctional transfer in normal C3H/10T1/2 cells. Carcinogenesis 16: 2945-2949.
Vijayalaxmi, Reiter R.J., Tan D.X., Herman T.S. and Thomas C.R. Jr. 2004. Melatonin as a radioprotective agent: a review. Int J Radiat Oncol Biol Phys 59(3): 639-53.
Yang J., Ichikawa A., and Tsuchiya T. 2003. A novel function of connexin 32: marked enhancement of liver function in a hepatoma cell line. Biochem Biophys Res Commun 307: 80-85.

A DETAILED ANALYSIS OF THE ELECTRICAL DYNAMICS OF THE HODGKIN-HUXLEY CELLULAR MODEL INCLUDING ELECTROPORATION

N. CITRO[*], V. TUCCI [**]

[*] DEPT. OF ELECTRICAL AND INFORMATION ENGINEERING, UNIVERSITY OF SALERNO NCITRO@UNISA.IT

[**] DEPT. OF ELECTRICAL AND INFORMATION ENGINEERING, UNIVERSITY OF SALERNO VTUCCI@UNISA.IT

Abstract

Electro-permeabilization of biological cells has been proposed as a very efficient method in medicine for gene therapy, cancer chemotherapy, and drug delivery. Although the molecular processes involved in the permeabilization mechanisms are very complex, the formation of "pores" in the plasma membrane, under the influence of an electric field, is deemed responsible of the cellular responses. The model accuracy is crucial to understanding the behaviour of the cell. It must include the majority physical phenomena in order to obtain realistic results from the numerical scheme approximating the theoretical model (circuital or field based). In this work an improved electrical model of the cellular membrane is presented taking into account the electro-permeabilization phenomena occurring under the action of electrical impulses. In particular, the presented model consists of a modified Hodgkin-Huxley–type non linear equivalent circuit for the cell membrane. The electroporation phenomena are considered by introducing a controlled current source in the basic model. The global cellular dynamics is examined for different characteristics (amplitudes, duration, rise and fall time) of the applied electrical pulses. The trans-membrane voltage and the conduction dynamics of the ionic channels are evaluated through an efficient simulation procedure.

Introduction

Since its introduction the conceptually simple model of the cell membrane behaviour, firstly proposed by Hodgkin and Huxley (HH) [1], has been widely studied in order to describe a wide class of biological phenomena associated to the transmission of information in excitable cells systems (see for example [2-3]. The HH approach has been employed to model electrical activation in a range of cell types including neurons [4], [5], ventricular myocytes [6], smooth muscles [7], etc. Although several studies have put in evidence that the HH model needs some improvements, its simplicity and efficiency in describing significant properties of the biological processes still motivate its use in medicine, biology, bioengineering etc.

The physical mechanisms allowing the development of excitable cell signal dynamics are based on the mutual interactions among ionic currents flowing through the membrane. The flux of the different ionic species taking place through channels across the cellular membrane is considered as a time continuous, deterministic and voltage-dependent phenomenon driven by the potential difference across the membrane (Trans-Membrane Voltage, TMV).

From an electrical point of view the cell membrane can be effectively modelled as a lumped parameter circuit, as shown in fig. 1. The membrane is represented by a capacitance, the ionic channels as linear or nonlinear conductances and the voltage generators are linked to the so called Nernst equilibrium potential, determined by the ratio of the specific ionic concentrations inside and outside the cell.

The TMV dynamics in response to electrical stimuli has been extensively analyzed in the literature on the basis of such a circuit model, thus allowing to infer or verify many interesting properties of the cell behaviour. In some cases the applied

electrical pulses are such that the number and dimensions of the pores on the membrane may be affected giving rise to the so called phenomenon electroporation [8-10]. The increased pore density on the cell surface determines an additional current path which has been traditionally modelled by a current generator characterised by a constant value. However, since the modification of the pores number and dimensions is dependent on the instantaneous value of the TMV, a more accurate model can be envisaged in which the current injection associated to electroporation is taken into account by considering a voltage dependent instead of a constant current generator.
Therefore, in this paper an accurate analysis of the electrical dynamics of the Hodgkin-Huxley cellular model is performed. The modifications induced by the voltage dependent electroporation generator is studied for different values of the amplitude, duration, rise and fall time of the applied electrical stimulus applied to a cell. The dynamics of trans-membrane voltage and conduction currents associated to the ionic channels are evaluated through an efficient simulation procedure. It is worth remarking that the aim of this first work is exclusively oriented to the numerical analysis of the modified HH circuit. The biological implications on the cell behaviour due to the obtained numerical results, which require complex and multidisciplinary research efforts, will be developed in future works.

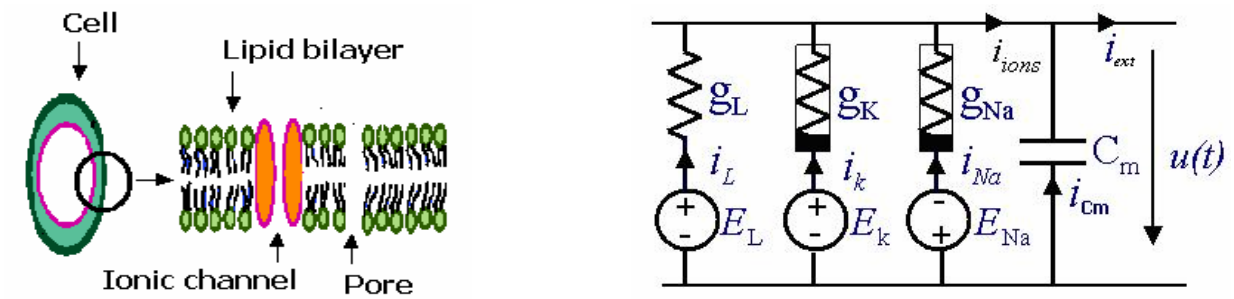

Fig. 1 Cell membrane and associated Hodgkin-Huxley circuit model.

Proposed circuit model including electroporation

In the electric circuit of Fig. 1, the total ionic currents $i_{ions}(u,t)$ can be expressed as:

$$i_{ions}(u,t) = i_{Na}(u,t) + i_K(u,t) + i_L(u,t) = \\ [g_{Na}^{\max} \cdot m^3(u,t) \cdot h(u,t) \cdot (u - E_{Na})] + [g_K^{\max} \cdot n^4(u,t) \cdot (u - E_K)] + [g_L^{\max} \cdot (u - E_L)] \quad (1)$$

where $g_c^{\max}$ (c=K, Na, L) is the maximum value of the conductance corresponding to the largest aperture of the channel, m (or n) and h are two nonlinear variables describing the activation or inactivation of the channel and p and q are suitable exponents depending on the ion type, E_c is the Nernst voltage and $u(t)$ is the trans-membrane voltage. The Nernst voltage is linked to the ratio of the external and internal ionic concentrations [C]: $E_c \propto \ln \frac{[C]_{ext}}{[C]_{int}}$. In Tab. 1 the values of the typical parameters are reported.
It has to be noted that all voltages are referred to the value E_R assumed at rest across the membrane.

Tab. 1

C_m [µF/cm^2]	E_R [mV]	E_{Na} [mV]	E_K [mV]	E_L [mV]	g_{Na}^{max} [mS/cm^2]	g_K^{max} [mS/cm^2]	g_L [mS/cm^2]
1.0	-75.0	E_R+15.0	E_R- 2.0	E_R+0.613	120.0	36.0	0.3

In order to describe the electroporation phenomenon, a voltage controlled current generator is introduced through a branch in parallel as shown in Fig. 2. It accounts for the ions exchange between an external cleft space around the cell where charge build-up and depletion occurs, and the cell interior.
Its influence in the charge dynamics across the cell can be particularly remarkable when the TMV assumes high values and for quasi static variation.

The charge flow, governed by the ions concentration gradient, can be modelled by a current I_{ep} given by:

$$I_{ep}=N\cdot i_{ep}= \quad N\cdot\left\{\frac{\pi\cdot r_m^2\cdot\sigma\cdot\upsilon_m\cdot R\cdot T}{F\cdot h}\cdot\frac{e^{\upsilon_m-1}}{\frac{w_0\cdot e^{w_0-n\upsilon_m}-n\cdot\upsilon_m}{w_0-n\cdot\upsilon_m}e^{\upsilon_m}-\frac{w_0\cdot e^{w_0+n\upsilon_m}+n\cdot\upsilon_m}{w_0+n\cdot\upsilon_m}}\right\} \tag{2}$$

where N is the pore density, r_m is the radius of the pore, σ is the conductivity of the fluid solution, F is the Faraday constant, R is the gas universal constant, T is the absolute temperature, h is the thickness of the cell membrane, w_0 and n are the energy gap and the length of the pore. $\upsilon_m = u(t)\left(\frac{F}{RT}\right)$ is the adimensional TMV. The pore density $N(t)$ is governed by a firs order differential equation:

$$\frac{dN(t)}{dt}=\alpha e^{\left(u(t)/V_{ep}\right)^2}\left(1-\frac{N(t)}{N_0}e^{-q\left(u(t)/V_{ep}\right)^2}\right) \tag{3}$$

where N_0 is the pore density for $u(t)$=0 and α, V_{ep} and q are suitable constants. In Tab. 2 the values adopted for the different quantities appearing in (2) and (3) are reported together with the initial condition considered for the integration of eq. (3).

Tab. 2

r_m [nm]	**h** [nm]	**s** [mS/cm]	**R** [mJ/molK]	**T** [°K]	**n**	**w_o**	**q**	**a** [$cm^{-2}s^{-1}$]	**V_{ep}** [mV]	**N_0** [cm^{-2}]	**N(t=0)** [cm^{-2}]	**F** [Coulomb/mol]
0.76	50.	13.0	8314.0	279.3	0.15	2.65	2.46	100.0	258.0	$1.5\text{x}10^5$	$1.7\text{x}10^5$	$9.6487\text{x}10^4$

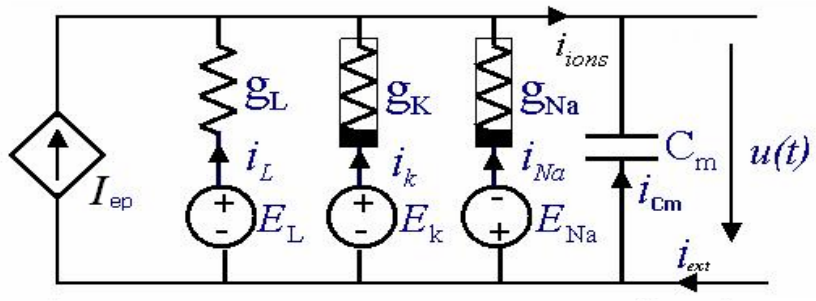

Fig. 2 Proposed circuit model including the electroporation generator

Numerical experiments and results

Kirchhoff current law applied to the circuit of Fig. 2 gives:

$$C_m\frac{du(t)}{dt}= \quad i_{ext}-[I_{ep}+i_L+i_{Na}+i_k]$$

The dynamic evolution of the TMV and the different current can be determined by evaluating at each time step the unknowns the 5 unknowns *u, m, n, h, N:*

$$\mathbf{Y} = [m(u,t),\, h(u,t),\, n(u,t),\, u(t),\, N(t)]^{\mathrm{T}}$$

$$\begin{cases} \dfrac{d\,\mathbf{Y}}{dt} = \mathbf{f}(t, m, n, h, u, N) = \mathbf{f}(t, \mathbf{Y}) \\ \mathbf{Y}\big|_{t=0} = \mathbf{Y}_0 \end{cases} \tag{4}$$

$$\mathbf{Y}|_{\mathrm{t=0}} = \begin{bmatrix} m(u,0) \\ h(u,0) \\ n(u,0) \\ u(0) \\ N(0) \end{bmatrix} \qquad \mathbf{Y}_0 = \begin{bmatrix} m_\infty(E_r) \\ h_\infty(E_r) \\ n_\infty(E_r) \\ E_r \\ N(t=0) \end{bmatrix}$$

In order to solve the nonlinear equation system (4) a Runga-Kutta scheme has been implemented in a suitable numerical procedure written in C language. The effectiveness of such a numerical scheme has been proven in a previous work concerning a range analysis on a simpler circuit based on the HH model [11]

In order to envisage the influence of the electroporation generator on the TMV and different current components dynamics, the most relevant quantities appearing in the model have been calculated either with the classic HH model (i.e. the circuit of fig. 1) or with the modified one (i.e. the circuit of fig. 2). In particular, the different current components have been evaluated as a response to an applied external rectangular pulse i_{ext} characterised by a duration Δt=1ms and by variable amplitudes (I= 5, 7.5, 10, 15,20, 25, 30, 40 e 50μA).

The effects of the electroporation generator is described by the plots of Figs 4, where the difference between the time evolution of the current components obtained in presence of such a generator (characterised by the suffix *ep*) or with the classic HH model are reported for the different values of the external current pulse.

As can be noted by the analysis of the presented simulation results, the greater influence of the electroporation generator is obtained for an applied pulse of 10μA where a very strong variation appears for ionic currents, especially those associated to Na and K channels, and for the displacement current i_{Cm} through the membrane. For greater values of the external pulse amplitude the presence electroporation current becomes weaker as it concerns all the considered variables. In fact the pulse of about 100 μA for i_{Cm} and i_{Na} corresponding to an external pulse of 10μA reduces of about one tenth for an applied current of 50μA. This findings are also summarised in Fig. 5, where the absolute value of the max discrepancies between the currents values obtained with or without the electroporation generator are presented.

A similar influence can also be noted for the TMV, as can be evinced from the results shown in Fig. 6. Even for this variable the more sensible effect of the presence of the electroporation in limited to applied current pulses of about 10-15μA.

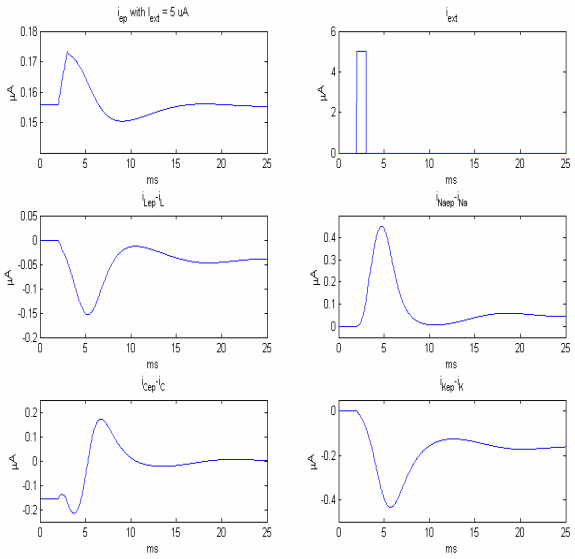

i_{ext}^{max} =5μA

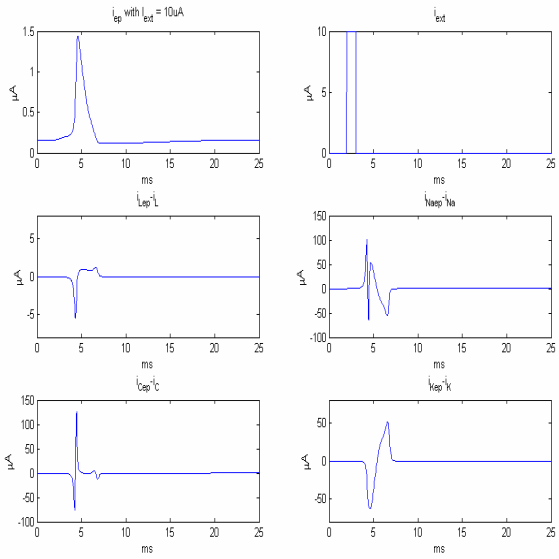

i_{ext}^{max} =10μA

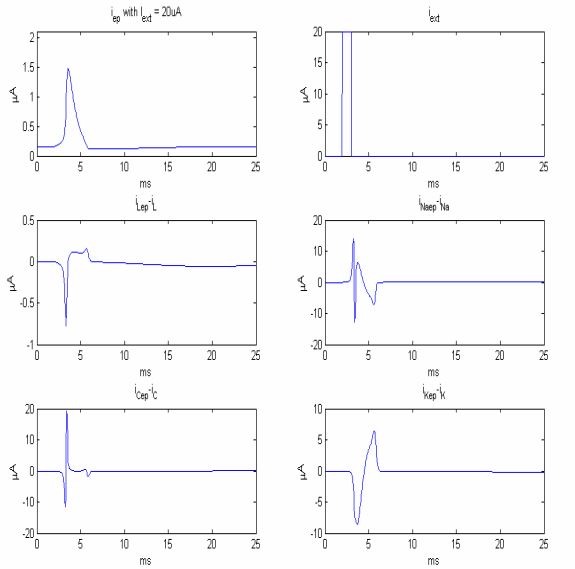

i_{ext}^{max} =20μA

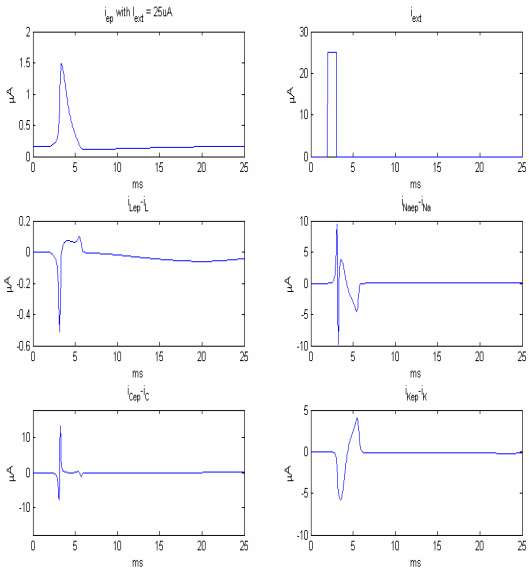

i_{ext}^{max} =25μA

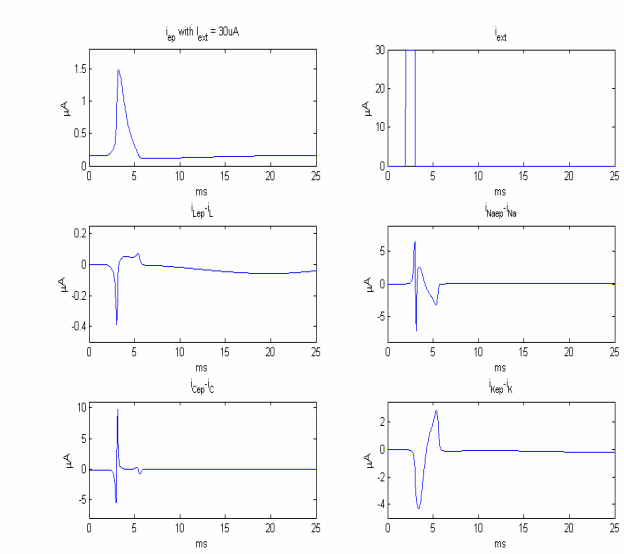

i_{ext}^{max} =30μA

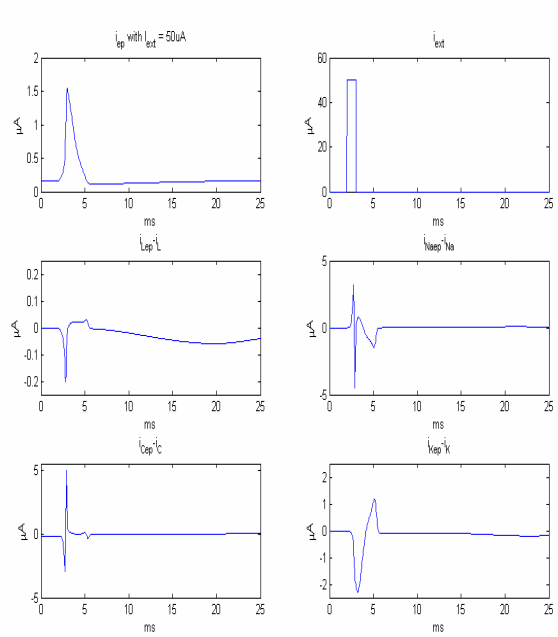

i_{ext}^{max} =50μA

Fig. 4: Difference between the time evolution of the ecurrent components induced by the presence of the electroporation generator for the different values of the external current pulse.

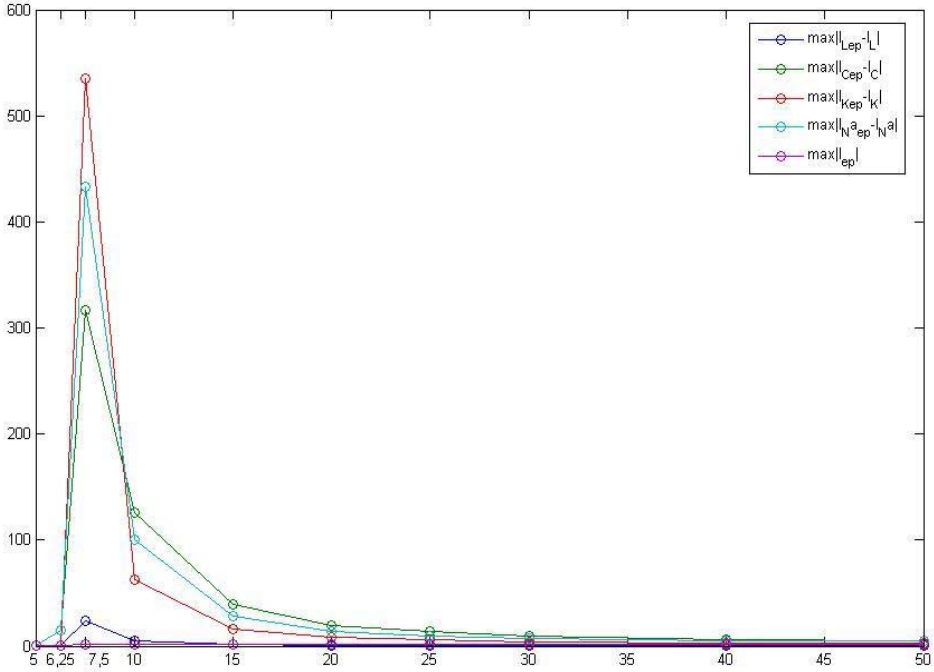

Fig. 5 Max discrepancies between the absolute values of the different currents obtained with and without the electroporation generator

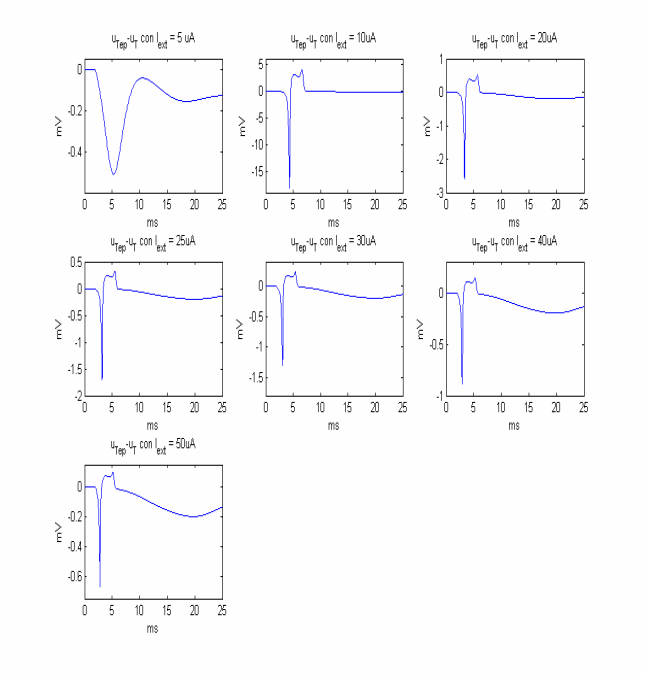

Fig. 6 Differences between the time evolution of the TMV induced by the presence of the electroporation generator for the different values of the external current pulse.

Conclusions

In this paper an analysis of the electrical dynamics of a modified Hodgkin-Huxley cellular model which takes into account the electroporation phenomenon has been performed. The modifications induced by a voltage dependent current generator emulating the electroporation has been studied for different values of the amplitude, of the applied electrical stimulus applied to a cell.

The dynamics of trans-membrane voltage and conduction currents associated to the ionic channels obtained by adopting an efficient simulation procedure put in evidence that the electroporation phenomenon is effective for moderate values of the applied current stimulus. The peak effect is obtained for an external pulse of about 10-15 μA. Greater values of the applied pulse induce a masking effect on the electroporation phenomenon: the dynamics of either the trans membrane voltage and the ionic currents become increasingly governed by the external pulse rather than the electroporation generator.

References

[1] A. L. Hodgkin, A. F. Huxley: "A quantitative description of ion currents and its applications to conduction and excitation in nerve membranes", J. Physiol., (1952), 117, pp. 500-544.

[2] B. Hille, "Ion channels of excitable membranes", Sinauer Associates Inc., Sunderland, (MA) 2001.

[3] Gerstner and Kistler: "Spiking Neuron Models. Single Neurons, Populations, Plasticity", Cambridge University Press, 2002.

[4] R. E. Plant, M. Kim: "Mathematical description of a bursting pacemaker neuron by a modification of the Hodgkin-Huxley equations", Biophys J. 1976 March; 16(3): 227–244.

[5] P. R. Shorten, D.J.N. Wall: "A Hodgkin–Huxley model exhibiting bursting oscillations" Bull. Math. Biol., 2000, 62, pp. 695–715.

[6] G. W. Beeler, H. Reuter: “Reconstruction of the action potential of ventricular myocardial fibers”. J Physiol, 1977; 268, pp. 177-210.
[7] R. J. Lang, C. A. Rattray-Wood: “A simple mathematical model of the spontaneous electrical activity in a single smooth muscle myocyte”, in Smooth Muscle Excitation, eds. T. B. Bolton, T. Tomita, London, Academic, pp. 391– 402.
[8] K. A. DeBruin, W. Krassowska, “Modeling Electroporation in a Single Cell. I. Effects of Field Strength and Rest Potential”, Biophysical Journal Volume 77 September 1999, pp. 1213-1224
[9] Y. A. Chizmadzhev, J. C. Weaver, “Theory of electroporation: A review” Bioelectrochemistry and Bioenergetics, Volume 41, No. 2, Dec. 1996, pp. 135-160 (26).
[10] R. P. Joshi, Q. Hu, H. P. Hjalmarson, K. H. Schoenbach: “Improved energy model for membrane electroporation in biological cells subjected to electrical pulses”, Phys. Rev. E 65, 041920 1-8 (2002).
[11] N. Citro, B. De Vivo, G. Spagnolo, V. Tucci: ““Range Analysis of Biological Cells Subjected to Pulsed Electric Fields” Proc. Of the Conference on Electrical Insulation and Dielectric Phenomena. October 2005, pp. 511-514.

IMMUNE STIMULATION EFFECTS IN CHICKEN BROILERS WITH COCCIDIA INFECTION THROUGH WEAK LOW FREQUENCY ELECTROMAGNETIC FIELDS

J.J.M. Cuppen[1], M.A. Elmusharaf[2], A.C. Beynen[2], H.N.A. Grooten[3], W. Smink[3]

1: Immunent BV, 2: Utrecht University, 3: FIS BV, The Netherlands

Abstract

A series of experiments was designed to determine the potential of EMF exposure to stimulate the immune system of chicken against infections that are common in farm practice.

In a first experiment 32 groups of six one-week old chicken were either (8) or not exposed (8) to *campylobacter* infection and exposed (16) to both infection and EMF treatment with an LF alternating field (Immunent BV, 30 minutes per day, 6,5 µT). Fresh excrement samples were taken on 6 different time points during the trial and were analyzed for the quantitative presence of *Campylobacter jejuni*. No difference in the course of this infection was observed between the non-treated and EMF treated groups.

Birds were weighed individually on day of arrival and subsequently on days 7, 14, 21, 28, 35 and 42. Feed intake is measured per cage on a weekly basis. A large and significant difference ($p<0.0005$) in feed conversion (feed intake divided by growth) was observed between the EMF group (1.61) and the non treated group (1.75).

In a second and third experiment 32 groups of eight chickens were either (8+8) or not (8+8) exposed to infections with *Eimeria* parasite (coccidiosis) and either (8+8) or not (8+8) given the same EMF treatment as above. Thus all combinations of treatment and/or infection were given to 8 groups of eight chickens.

Feed conversion was determined as above. Infection course was determined by counting oocysts in excrement as above. Moreover intestinal lesions were scored (blind) as caused by the different *Eimeria* after the chickens were slaughtered after the growth period.

Feed conversion was equally good between the negative control and both EMF groups. For the EMF treated infected chicken feed conversion was better (1.52) than the non-treated infected chicken (1.62).

In both experiments a significant reduction ($p<0.01$) in intestinal lesions caused by the different subspecies of the parasite was observed in the EMF treated group.

Introduction

For chicken farmers infectious disease poses the biggest problem both for animal welfare as economically.

Preventive antibiotics have been used as a growth promoter in animal production. These could eliminate infectious disease early, before the animals had to spend energy on the disease. In general up to 5% increase of growth could be achieved with preventive antibiotics. However, preventive antibiotics have been banned in Europe from animal feed since 2006, because of development of microbial resistance in humans.

In chicken farming, hygiene and waiting periods between production cycles are measures that help against infectious disease for pathogens that cannot survive outside the host. However in particular Coccidia parasites with their long surviving spores are an infection that cannot in practice be avoided. Chemical/pharmaceutical agents against coccidia infection will be banned in the EU from 2012 onwards. This has led to a cessation of development of such agents. The farming community has the impression that the existing agents already increasingly lose their effectiveness due to development of resistance in the coccidia parasites.

Coccidiosis is a common infectious disease in poultry, causing major economic losses. The protozoan parasite of the genus *Eimeria* explosively multiplies in the intestinal tract of poultry and produces tissue damage, resulting in interruption of feeding and digestive process or nutrient absorption, reduced body-weight gain, dehydration and blood loss, and increase susceptibility to other diseases agents (McDougald, 2003) such as *Clostridium perfringens*, leading to necrotic enteritis (Helmond and Bryant, 1971; Maxy and Page, 1977; Shane et al., 1985).

Economically the damage due to coccidia infection is estimated at 10 points feed conversion (100 grammes more feed necessary for 1 kg weight growth), which translates into a result loss of 5 euro cts per chicken.

Immunent has designed a technology in which low field strength (around 5 micro Tesla) LF EMF is applied for the treatment of chicken. In (Cuppen et al. 2006a) , it is proposed that the working mechanism of this treatment is that LF EMF induces positive stress at cell level, which causes an increased production of cytokines (called

danger signals) that put the immune system in a higher state of alertness and activity.

Figure 1. Our Hypothesis

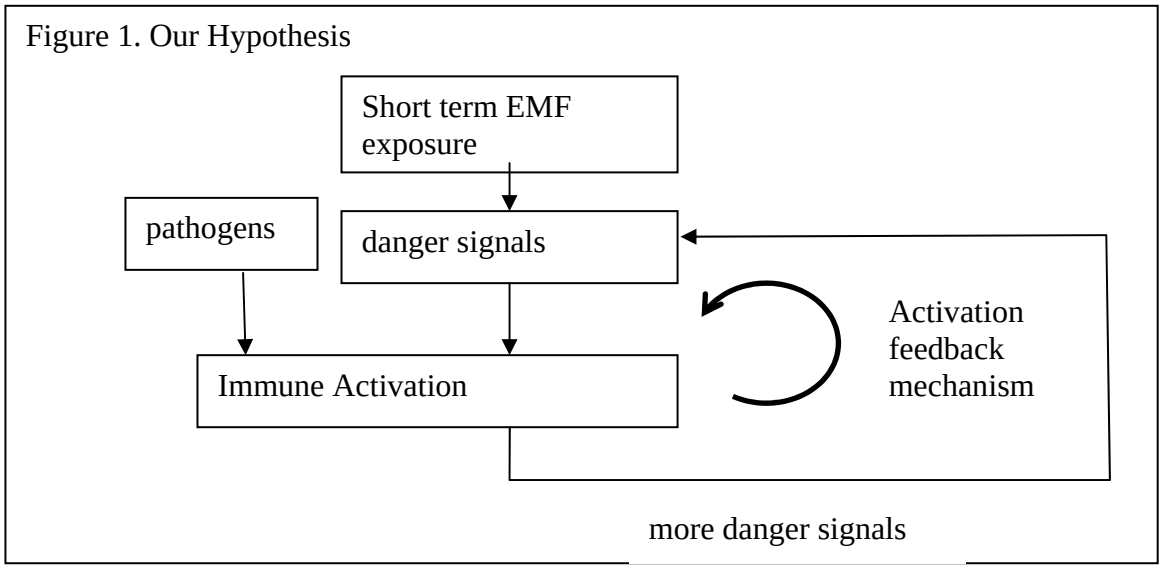

This reduces the time that it takes for a self sustained immune reaction to pathogens to be established. Therefore pathogens have less time to multiply and damage is reduced.
Many studies have suggested that the immune response to *Eimeria* infection in part is mediated through the release of cytokines. Breed et al. (1997) reported that chicken peripheral blood leucocytes of *E. tenella* infected chickens produce interferon-γ after in vitro re-stimulation. Moreover, it has been shown that treatment of chickens with interferon-γ preceding infection with *E. acervulina* decrease the negative effect of infection on weight gain (Lowenthal et al., 1997).

The aim of this study is to determine the potential of the treatment with the Immunent LF EMF signal as a weapon against infections in chicken that are common in practice.

Experiment design
Three experiments have been done, with 1) campylobacter infection, 2) coccidia infection with high infection pressure and 3) coccidia infection with lower, more practical infection pressure.
For the three subsequent experiments 192, 288 and 272 one-day old female broilers (Ross 308) are purchased from the hatchery. On day of arrival, they are wing-banded, weighed and randomly housed in wire-floor, suspended cages. Each cage is provided with thick foil and litter. Each test cage was provided with a 16 loop coil under the floor through which LF EMF treatment was administered for 30 minutes per day. No attempt was made to create a uniform field since in another experiment it was determined that effective field strengths lie between 0.1 and 50 micro Tesla. Moreover the practical application that is our goal will also not allow uniform field strengths. The field strength (rms) in the middle of the cage was set at 6,5 micro Tesla, measured with a F.W.Bell 5180 Tesla meter with sensitive probe. Dosimetry control during the experiment was ensured by constantly monitoring the (rms) current through the coil. The applied signal was designed by Immunent, which contains several LF components with frequencies between 100 and 10.000 Hz.
Continuous lighting is provided throughout the experiment. The temperature in the cage at arrival is 32°C as required by one day chicken and is gradually decreased to ambient temperatures during the experiment.
Two different basal diets are produced for this experiment by Research Diet Services BV in Wijk bij Duurstede, The Netherlands: a starter diet (week 1 – 2) and a grower/finisher diet (week 3 – 6).
Feed and water were available ad libitum.

Treatment and control groups for the three experiments are indicated in Table 1.

Table 1. Test groups in 3 experiments.
-/+camp indicates without/with campylobacter infection; -/+cocc indicates without/with coccidia infection.

A	B	C	D
Experiment 1, 42 days, each replicate starts with 6 chicken, of which 2 are removed at random and analyzed on day 12. Infection pressure at day 6 with *Campylobacter jejuni* (indicated as +camp)			
Negative control, -camp 8 replicates	Positive control, +camp 8 replicates		EMF, +camp 16 replicates
Experiment 2, 35 days, each replicate starts with 8 chicken, 2 are removed and analyzed at day 21, 2 at day 28, 2 at day 36. Infection pressure (high) at day 15 with Coccidia (+cocc)			
Negative control, -cocc 8 replicates	Positive control, +cocc 8 replicates	EMF, -cocc 8 replicates	EMF, +cocc 8 replicates
Experiment 3, 35 days, each replicate starts with 8 chicken, 2 are removed and analyzed at day 21, 2 at day 28 and 2 at day 36. Infection pressure (low) at day 15 with Coccidia (+cocc)			
Negative control, -cocc 8 replicates	Positive control, +cocc 8 replicates	EMF, -cocc 8 replicates	EMF, +cocc 8 replicates

Measurements
Chickens are weighed individually on day of arrival and subsequently on days 7, 14, 21, 28, 35 and 42 in experiment 1, on day 13 in experiment 2 and day 8 in experiment 3, and on days 21, 29 and 36 in experiment 2 and 3. Feed intake is measured per cage on a weekly basis. Feed intake per broiler is calculated as feed intake per cage divided by number of broiler days. Mortality is registered on a daily basis, but rates are only calculated for the total period.

Statistical analysis
The oocyst values were logarithmically transformed (log10 (X + 1)) to create a normal distribution before being analyzed, and lesion scores were transformed using multinomial transformation.
All performance data for each variable are subjected to an analysis of variance, in which the treatment (control vs. EMF) and infection (positive or negative) were the independent factors with the statistical program SAS.
The level of statistical significance is set at $P< 0.05$.

Infection with *Campylobacter jejuni* in experiment 1
On day 7, after collection of control excrement samples, water infected with *Campylobacter jejuni* C356 (ASG-Lelystad) (~$1*10^5$ per ml) is offered to the broilers in a separate drinking cup. For infection, broilers need to drink only 1 ml of this infected water. The birds had access to drinking water for 1 hour.

Collection of excrements in experiment 1
On days 7, 12, 19, 26, 33 and 40 plastic foil is placed on top of the litter in each cage in order to collect fresh excrements. After 2 hours, plastic is removed, fresh excrements are scraped of the foil and stored in plastic jars. Samples are sent to the laboratory the same day. Analysis of the excrements starts within 24 hours after collection according to the method of Jacobs-Reitsema et al. (1995).

Inocula and contamination procedure experiment 2
Sporulated oocysts of *E. acervulina* (W119, Weybridge), *E. maxima* (Weybridge), and *E. tenella* (Houghton) laboratory strains were obtained from the Animal Health Service, Poultry Health Centre (Deventer, The Netherlands). The number of oocysts per milliliter of suspension was counted with a hemocytometer (Fuchs-Rosenthal counting chamber). A volume containing sporulated oocysts ($1.76x10^4$ E. acervulina, $1.25x10^4$ E. maxima, and $7.5x10^3$ E. tenella) in K2Cr2O7 was transferred into a scaled plastic tube and the K2Cr2O7 was washed out by centrifugation. On day 15 of the experiment birds in 18 cages (144 birds) were individually infected. The sporulated oocysts were administered with 1 ml of tap water via a scaled 1-ml syringe directly into the crop.

Inocula and contamination procedure experiment 3

In this experiment a natural simulation of a coccidial infection within the broilers' test facility was developed. This was accomplished by seeding a portion of the litter with coccidial oocysts prior to broiler placement on new litter on day 15 of the trial. A similar dose of *Eimeria* species was used as in experiment 2, e.g. E. acervulina, E. maxima and E. tenella. Equal amounts of each species was mixed into the wood shaving and spread evenly across the back half of each contaminated group pens. The broilers picked up the oocysts from the seeded litter, mimicking a natural infection, as all birds do not pick up oocysts at the same time, which led to a progression of the infection as in the field. The non-infected broiler groups were reared in clean litter.

Infection measurements experiments 2 and 3

Oocyst Count (OPG)

The oocyst per gram faeces (OPG) counting were performed on fresh faeces collected on days 15, 29, and 36 (days 6, 14, and 21 post infection). Oocyst shedding was assessed on one sample of homogenized faeces material collected from each cage. Modified MacMaster counting chamber techniques of Hodgson (1970) was used to determine the OPG in the homogenized faeces. A 10% (w/v) faeces suspension in a salt solution (1.1%) was made. After shaking vigorously, 1 ml of the suspension was pipetted into 9 ml-saturated sodium chloride (1.2%). After mixing again, a portion of the later suspension was run into the MacMaster chamber and the oocysts per gram faeces were counted.

Caecal lesions

Intestinal lesion scorings were performed blindly to the treatment modality on days 15, 29, and 36 (days 6, 14, and 21 PI). Two birds per cage (36 cages) were euthanized by cervical dislocation, dissected and different coccidial lesions were scored. The 0-4 scoring system described by Johnson and Reid (1970) was used. The scores for the individual birds of the same treatment group were summed up to arrive at a treatment value.

Results and discussion

Feed intake and feed conversion

Daily feed intake per broiler is calculated as weekly feed intake per cage divided by so-called 'broiler days', which is the number of broilers per cage times the number of days corrected for drop outs. Data show that the feed intake of broilers of the EM group was significantly lower than the negative control group for all three experiments.

Feed conversion is calculated as the growth [g] divided by the feed intake [g] over the total period. The results of the feed conversion are shown in Table 2. Feed conversion of the broilers of the EM group with infection (as in practice) was significantly lower than controls for all three experiments.

Table 2: Feed conversion of broilers

Total period	Negative control	Positive control	EMF no infection	EMF w infection
Experiment 1	1.78 ± 0.02	1.73 ± 0.04		1.61± 0.03*
Experiment 2	1.58 ± 0.04	1.63 ± 0.04	1.57 ± 0.05	1.52 ± 0.06 *
Experiment 3	1.83 ± 0.03	1.84 ± 0.05	1.73 ± 0.03*	1.72 ± 0.03*

∗ significant ($p<0.05$)

Comparing negative control with EMF no infection, and positive control with EMF with infection results it turns out that in 4 out of 5 cases a significant and economically highly relevant improvement in feed conversion is achieved by EMF treatment. In chickens, one explanation for less feed uptake indicates could be less energy spent on developing infections. Given a certain amount of meat consumption this also translates in the corresponding 8% decrease in resource usage for meat production. Assuming that manure production is proportional to feed conversion minus 1 (the amount of feed *not* transformed into live weight) and assuming that digestion of phosphates in feed is 60%, this corresponds to a reduction in phosphate load, for equal end weight of the animals, to the environment of about 16%.

The calculation is as follows: Feed contains X per kg. The animal takes up Y = X * 60% * 1.84. Excretion is (X * 40% * 1,84) without EMF and (X * 1.72 – Y) in the second case. Reduction is ((X * 0.4 * 1.84 – (X * 1.72 – X * 0.6 * 1.84))/ (X * 0.4 * 1.84) = 16%.

Moreover it should be noted that the reduction in feed conversion achieved rivals the best results achieved in comparable trials with preventive antibiotics (now illegal in animal feed in the EU). This indicates that EM treatment is as effective in suppressing infections and the resulting productive loss in chicken as preventive antibiotics were.

Microbiological analysis of excrements

Fresh excrement samples were taken on different time points during the trial and were analyzed for the quantitative presence of *Campylobacter jejuni* in experiment 1 and OPG count (oocyst shedding – parasite spores) in experiments 2 and 3.. The results are presented in Table 3.

Despite proper hygienic conditions the negative control group and negative EMF groups were also infected during the course of the experiment. Thus they became also infected groups, though there is no control of the level of infection.

Table 3:

	Negative control	Positive control	EM not infected	EM infected
Experiment 1, Amounts of colony forming units (cfu) of *Campylobacter jejuni* in excrements of broilers (expressed as 10 log CFU per g of excrement)				
Day 6	negative	negative		negative
Day 12	3.24 ± 0.61*	6.05 ± 0.15		5.78 ± 0.14
Day 19	5.71 ± 0.24	6.55 ± 0.08		6.37 ± 0.15
Day 26	5.25 ± 0.65	6.16 ± 0.23		6.60 ± 0.21
Day 33	4.58 ± 0.54	5.66 ± 0.24		5.88 ± 0.21
Day 40	6.20 ± 0.26	5.98 ± 0.17		5.53 ± 0.19
Experiment 2, OPG counts (oocysts per gram faeces, expressed as log10 (X+1))				
Day 21	0.00 ± 0.00	5.70 ± 0.35	0.00 ± 0.00	5.96 ± 0.06
Day 29	2.10 ± 0.69	4.02 ± 0.34	2.89 ± 0.66	3.86 ± 0.17
Day 36	4.10 ± 0.20	2.24 ± 0.52	3.87 ± 0.58	1.93 ± 0.59
Experiment 3, OPG counts (oocysts per gram faeces, expressed as log10 (X+1))				
Day 21	1.72 ± 0.87	4.03 ± 0.12	2.17 ± 0.83	4.11 ± 0.10
Day 29	3.26 ± 0.71	4.58 ± 0.18	2.05 ± 0.78	4.35 ± 0.27
Day 36	4.04 ± 0.27	3.82 ± 0.13	2.36 ± 0.71*	3.66 ± 0.23*

Results show that the infection with *Campylobacter* was significantly lower in the negative control group than in the other two groups on day 12. One week later, on day 19, infection with *Campylobacter jejuni* was similar for all three groups. Applying the EM field under the cages of the broilers had no effect on the infection rate of *Campylobacter* throughout the experiment in terms of bacteria excretion.

Also during experiments 2 and 3 cross-contamination occurred again in both uninfected groups despite proper hygienic conditions, which indicates that *Campylobacter* and *Coccidiosis* are both very infectious in practical circumstances.

OPG counts on day 29 and day 36 are numerically lower for infected EMF group compared to the infected control group and only in experiment 3 on day 36 this difference is statistically significant. More investigations are required to determine whether the EMF treatment can contribute to a diminished outbreak of a coccidiosis contamination.

Coccidial lesion scores in experiment 2 of intestines due to E. acervulina and E. maxima were significantly lower in the positive EMF group compared to the positive control group on day 21 (Table 4a). On day 14 of the experiment cross contamination was detected, but still lesion due to E. maxima of the EMF positive group was significantly lower than that of the positive control group. This might suggest that the EMF treatment counteracts the onset of a coccidiosis infection.

Table 4a: Mean lesion scores of intestines for experiment 2

	Control		EMF	
	- cocc	+ cocc	- cocc	+ cocc
E. acervulina				
Day 21	0.00 ± 0.00	1.95 ± 0.15	0.00 ± 0.00	1.19 ± 0.10*
Day 29	0.30 ± 0.11	0.90 ± 0.10	0.50 ± 0.13	0.63 ± 0.13*
E. maxima				
Day 21	0.00 ± 0.00	2.30 ± 0.15	0.00 ± 0.00	1.50 ± 0.13*
Day 29	0.45 ± 0.17	1.55 ± 0.20	0.63 ± 0.18	0.81 ± 0.19*
E. tenella				
Day 21	0.00 ± 0.00	2.65 ± 0.13	0.00 ± 0.00	2.00 ± 0.20*
Day 29	0.30 ± 0.12	1.00 ± 0.16	0.56 ± 0.18	0.69 ± 0.15*

During experiment 3lesions scores of intestines were also determined (see Table 4b) due to the same *Eimeria spp*. These results show that the EMF treatment caused significantly lower lesions scores for all species investigated during the whole trial for both infected as well as uninfected groups, except for E. acervulina and E. tenella on day 21 (numerically lower).

Lesions scores of both infected groups in experiment 1 started at a similar level compared to the individual contamination of experiment 2, although lesions due E. acervulina were higher and lesions due to E. tenella were lower. Results further show that lesions scores decreased during the trial for both infected groups, which showed that the contamination by seeded litter is a good contamination method in order to study immunity against coccidiosis during natural contamination. Lesion scoring of both uninfected (control and EMF) groups increased during the trial, which shows that these broilers did not yet reach immunity against coccidiosis.

Table 4b: Mean lesion scores of intestines for experiment 3

	Control		EMF	
	- cocc	+ cocc	- cocc	+ cocc
E. acervulina				
Day 21	0.44 ± 0.22	2.44 ± 0.15	0.44 ± 0.18	2.00 ± 0.16*
Day 29	1.06 ± 0.27	1.69 ± 0.09	0.31 ± 0.13*	1.50 ± 0.15*
Day 36	1.38 ± 0.26	1.75 ± 0.19	0.94 ± 0.24*	1.22 ± 0.10*
E. maxima				
Day 21	0.13 ± 0.08	2.25 ± 0.19	0.06 ± 0.06*	1.67 ± 0.13*
Day 29	0.56 ± 0.20	1.63 ± 0.08	0.00 ± 0.00*	1.33 ± 0.21*
Day 36	1.50 ± 0.38	2.10 ± 0.12	0.50 ± 0.25*	1.22 ± 0.21*
E. tenella				
Day 21	0.13 ± 0.08	1.50 ± 0.09	0.06 ± 0.06	1.42 ± 0.11
Day 29	0.19 ± 0.09	1.31 ± 0.13	0.06 ± 0.06*	1.00 ± 0.11*
Day 36	0.56 ± 0.15	1.42 ± 0.15	0.13 ± 0.08*	1.17 ± 0.11*

It is unlikely that there is a direct effect of EMF on the *Eimeria* parasites. In literature there are no indications that organisms are directly and seriously damaged by EMF without an extremely high energy content. In our experiments, the energy levels are extremely low. On the other hand, cytokine production has been reported, as well as oxygen burst, both of which are instrumental in immune activation. It is therefore not unlikely that the reduction in pathology found is caused by a more effective immune reaction in the animal.
Mortality was almost equal between EMF and corresponding control groups in all experiments (11 vs. 12%, 7 vs. 7% and 16 vs. 14% total mortality respectively for experiments 1, 2 and 3).

Conclusions

The study indicates that

- LF EMF treatment does not seem to reduce a *Campylobacter* infection in broilers, which is in agreement with our hypothesis since this bacteria is a commensal for chicken and an enhanced immune system cannot be expected to fight it.
- LF EMF treatment reduces the damage, in terms of intestinal lesions of Coccidiosis infection in broilers. This supports the hypothesis that LF EMF can enhance the immune response.
- LF EMF treatment was shown in 4 out of 5 measurements to improve feed conversion up to 12 points. This is highly interesting to farmers economically, but also to society as a whole since it represents a decrease in resource usage of 8% and a decrease in phosphate load on the environment of 16%.
- Since feed conversion improvement is not restricted to the experiments where the chickens were actually suffering from (for them) relevant infections it seems that LF EMF improves the immune competence of the animals, independent of one particular infection.

References

Breed D.G., Dorrestein J., Schetters T. P., Waart L. V., Rijke E., and Vermeulen A. N.. (1997). Peripheral blood lymphocytes from Eimeria infected chicken produce gamma-interferon after stimulation in vitro. Parasite Immunol. 19:127-135.

Cuppen J.J.M., Parmentier H.K. and Savelkoul H.F.J. (2006a): Immune Stimulation In Fish And Farm Animals Through Weak Low Frequency Electromagnetic Fields, A. Hypothesis, this proceedings.

Helmboldt, C.F., and E.S. Bryant. 1971. The pathology of necrotic enteritis in domestic fowl. Avian Dis. 15:775-780.

Hodgson J.N. (1970) Anticoccidial drugs: lesion scoring techniques in battery and floor-pen experiments with chickens. Exp. Parasitol. 28: 30-36.

Jacobs-Reitsma W.F., Giessen A.W. van de, Bolder N.M. and Mulder R.W. (1995) Epidemiology of Camplyobacter spp. at two Dutch broiler farms. Epidemiology and Infection 114(3): 413-421.

Johnson, J. and Reid W.M. (1970). Anticoccidial drugs: Lesion scoring techniques in battery and floor-pen experiments with chickens. Exp. Parasitol., 28:30-36.

Lowenthal J.W., York J.J.,. O'Neill T.E, Rhodes S., Prowse S. J., Strom D.G., and Digby M.R.. (1997). In vivo effects of chicken interferon-gamma during infection with Eimeria. J. Interferon Cytokine Res. 17:551-558.

Maxey B.W and Page R.K. (1977) Efficacy of lincomycin feed medication for the control of necrotic enteritis in broiler-type chickens. Poult Sci., 56: 1909-13.

McDougald L.R. (2003) Coccidiosis. In: Saif et al. (Eds.), Poultry Diseases. Iowa State Press, Iowa, pp: 947-991.

Shane S.M., Gyimah J.E., Harrington K. S. and Snider III T.G. (1985). Etiology and pathogenesis of necrotic enteritis. Vet. Res. Commun. 9: 269-287.

Acknowledgements

Messrs Van Kraaij, Brock, Berghs, and Bloo provided indispensible services in creating the hardware and software that supported these experiments.

IMMUNE STIMULATION EFFECTS IN FISH AND FISH IMMUNE CELLS THROUGH WEAK LOW FREQUENCY ELECTROMAGNETIC FIELDS WITH VARIABLE FIELD STRENGTH

J.J.M. Cuppen[1], G.F. Wiegertjes[2], M. Molenaar[2], J. Geervliet[3], W. Smink[3]

1: Immunent BV, 2: Wageningen University, 3: FIS BV, The Netherlands

Abstract

A series of experiments (n=14) was designed to determine the potential of LF EMF exposure to stimulate the immune system of fish.

Common carp head kidney-derived phagocytes were used to determine respiratory burst activity as a measure for immune activation. Exposure to the Immunent LF EMF signal at 5 µT or 1,5 mT led to 42% or 33% increase in immune activity, respectively, compared to negative control values. EMF could also additionally stimulate chemically pre-stimulated samples up to 18% (5 µT) or 22% (1,5 mT). Statistical analysis was carried out with SAS via a meta-analysis of the 14 datasets. A significant ($p<0.0001$) increase on the response of the EMF exposed cells was found.

Subsequently, a series of experiments were performed using live goldfish. During transport from the grower commercial goldfish suffer from heavy parasitic and microbial infections to such an extent that without treatment high mortality will be observed over a period of a few weeks.

Groups of fish were housed under equal conditions in at least 4 control tanks and 8 to 16 EMF-exposed tanks. Exposure was done at field strengths between 0,15 and 50 µT by coils positioned around the outside of the fish tanks, creating a predominantly vertical field.

In the experiments without treatment mortality was about 50% after 18 days, while the treatment at 5 µT reduced it to 20%.

In a third experiment the treatment field strength was varied between 0,05 µT and 50 µT in 6 steps. The decrease in mortality after EMF exposure was equally strong between 0,15 and 50 µT and only slightly less strong at 0,05 µT. In a fourth experiment the field strength was further reduced to 0,01 and 0,003 µT. The effect is gone at 0,001 µT and below, while the situation between 0,003 and 0,06 µT an increasing dose response is visible.

Introduction

Immunent has designed a proprietary low field strength (around 5 micro Tesla) LF EMF treatment, aimed at stimulating the immune system. In another paper in this proceedings (Cuppen et al. 2006a), it is proposed (see Fig. 1.) that the working mechanism of this treatment is that LF EMF induces stress at cell level, which causes an increased production of cytokines (called danger signals) that put the immune system in a higher state of alertness and activity. This reduces the time that it takes for a self sustained immune reaction to pathogens to be established. Therefore pathogens have less time to multiply and damage is reduced.

In aquaculture and farming, infectious disease is one of the biggest, if not the biggest problem and challenge, economically as well as in terms of animal welfare and environmental pressure. "Disease is the biggest single impediment to aquaculture development," said Rohana Subasinghe, Senior Fisheries Research Officer at the United Nations' Food and Agriculture Organization (FAO). Total damage in aquaculture of infectious disease is estimated at 9 billion $ yearly. In Equador in 1999 70% of the crop of farmed shrimp was lost due to a single virus infection, that led to a national crisis and a loss of 150.000 jobs. Environmentally, infectious disease causes a lot of pressure: by the chemicals and pharmaceuticals used, by the pathogens that multiply in farms and increase disease pressure on the surrounding wildlife, and by the pressure on farmers to abandon farms with disease and start new farms in nature areas.

Figure 1. Our Hypothesis

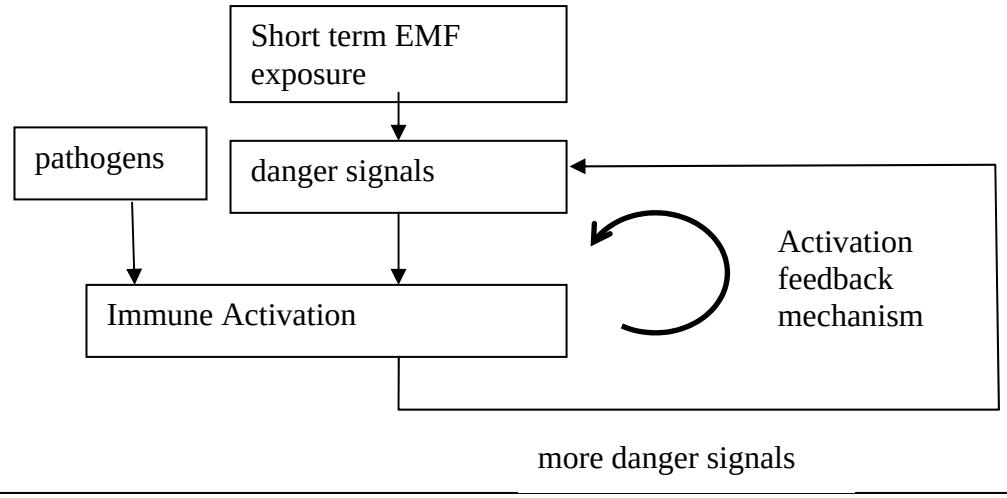

Fish and other aquatic animals such as shrimps are particularly vulnerable to infectious disease because they have no, or much less adaptive immune system and have no transferred immunity from the mother.

Simkó, Droste, Kriehuber and Weiss (2001) and Lupke, Rollwitz and Simkó (2004), have demonstrated that human and murine macrophages can be stimulated to higher activity through LF EMF. In this research we will likewise determine the effect of the Immunent signal at cell level by measuring oxygen burst, and then proceed to in vivo experiments aimed at demonstrating, and then optimizing the effectiveness of Immunent treatment on fish.

Materials and methods

In vitro experiments

Common carp head kidney-derived phagocytes were used to measure oxygen burst activity as a measure for immune activation.

Oxygen burst causes a marked increase in oxygen uptake, which is mainly channeled to a pathway initiated by the reduction of oxygen to super oxide anion (O2-), using NADPH or NADH as the electron donor. The O2- is subsequently converted to hydrogen peroxide (H2O2) with the aid of the enzyme super oxide dismutase (SOD).

$$202 + NADPH \xrightarrow{\quad} 202^- + NADP^+ + H^+$$

$$202^- + 2H^+ \xrightarrow{\text{SOD}} H_2O_2 + O_2$$

The objective of this test is to measure the modulation of the oxygen burst activity in macrophages and neutrophilic granulocytes of the carp pronephros, or head-kidney.

The measurement is based on the reduction of a salt: Nitro Blue Tetrazolium NBT by O2-. This results in a blue color, which is measured spectrophotometrically.

Biochemical Materials

Phorbol 12-myristate 13-acetate (PMA), 0.01 µg/µl, a standard chemical stimulant of Oxygen burst in leukocytes known to give a high response as a positive control

RPMI without phenol red: washing and culture media (the red indicator dye disturbs the final reading on the spectrophotometer)

Nitro Blue Tetrazolium in RPMI without phenol red. (NBT; grade III) 1 mg/ml final concentration

2N KOH (Potassiumhydroxid)

100% and 70% methanol

Dimethylsulfoxide (DMSO)

flat bottomed 96-well microtiterplate (sterile) coated with adherent cells

spectrophotometer with filter at 690 nm

Biochemical Methods

Leukocytes are collected from the head kidney and placed at 4 degrees Celcius overnight. Next, they are plated

out in 96 well trays with 100 µl in each well. The cells are allowed to adhere for 30 mins at 27 oC (5 % CO2, humidity 100 %). After inspection, non-adherent cells are washed away by rinsing twice with 100 µl of RPMI-phenol red culture medium (one row at a time).
The NBT assay is started by removing the supernatant and by adding 150 µl of NBT and subsequently the stimulators (10 µl of PMA and/or 30 mins EMF), followed by or, in case of EMF, in parallel to incubation of the cells for 90-120 minutes at 27 oC (5 % CO2, humidity 100 %).
After the incubation, the NBT solutions are removed and the cells are washed once by rinsing with RPMI medium without phenol red. The remaining cells are fixated for 5 minutes with 100 µl 100 % methanol, then washed twice with 100 µl 70 % methanol to remove possible NBT-rests. The plate is left to dry.
The blue formazan inside the cells is solubilized in 100 µl 2N KOH to which 100 µl DMSO is added. The content of the well is mixed thoroughly.
The optical density is measured at 690 nm (ref. filter at 414 nm) in a spectrophotometer.

EMF materials
An exposure magnet was designed for exposing one or two rows of a 96 well plate simultaneously. Since earlier experience indicated cross talk to controls at enormously low field strengths we aimed for the lowest fringe fields possible. Based on experience from MRI magnets, eight Ferrite C arm units were built (six used), each for exposing one or two rows of a 96 well plate to a uniform AC magnetic field. The “C” of the magnet was built of 16 mm2 Ferrite 3C90, the pole shoes were 99x30x8 mm. above and below the pole shoes, coils with 600 turns each were placed around the C arm. Saturation in the ferrite occurs above 170 mT, therefore this setup allowed a field strength of 5 mT to be achieved in the exposure gap without saturation effects in the C. A uniformity of 10% or better was achieved at the well positions.
Side ways, the fringe field was measured to decrease by at least a factor 2 every 2 cm. Thus at a distance of 5 meters (which was kept for the controls) one may safely assume the fringe field to be below 1 pT. It was no longer measurable with our equipment at 1 m distance.
Signals were generated by an Immunent signal generator, capable of generating field strengths between 0,15 µT and 1.5 mT in the exposure area, with a proprietary signal consisting of several LF components with frequencies between 100 and 10.000 Hz.
The signal generator monitored currents through the coils during the experiment, which were calibrated to correspond to the desired field strength using an F.W.Bell 7000 Tesla Meter with sensitive probe.

Experiment design
Each run measured 48 samples, in six groups of 8 samples. Half of the groups were not chemically pre-stimulated (negative) and half were pre-stimulated with PMA (positive). Two groups were taken as controls, while EMF stimulation was done on four groups, two at 5 µT field strength and two at 1,5 mT field strength.
Exactly those runs were included in the results where the positive control average exceeded the negative control average by at least 50%, independent of the measurements for the EMF exposed cells. If that is not the case it must be assumed that the cell isolation was not properly done. This led to the exclusion of 6 runs out of a total of 20 runs executed.

In vivo experiments
Subsequently, a series of experiments were performed using fantail goldfish (*Carrassius auratus spp*.), heavily infected with ecto parasites (gill parasites) such as *dactylogyrus/ gyrodactylus, trichodina, chilodinella* and *costia*. Infection with those parasites occurs consistently at the grower and increases during storage, packing and international transport due to crowding. This and subsequent secondary bacterial infections cause high mortality if not treated. The progress of the diseases can be measured by daily counting and removing dead fish over a period of a few weeks. Fish were randomly allotted over the tanks. Individual fish weight was 2.5 (± 0.5 g)
Daily, the fish were checked for health. Dead fish were counted, removed and discarded.
The number of fish per replicate tank varied between the experiments, 12 in the first and second experiment, 21 in the third, and 30 in the fourth.
Fish were housed in PVC tanks with a content of 30 liter. Aeration of water and daily change of 20 % of the water maintained water quality. |Fish were fed commercial feed ad libitum.

Groups of fish were housed under equal conditions in at least 4 control tanks and 8 to 16 EMF-exposed tanks. Exposure was done at field strengths between 0,15 and 50 µT by coils positioned around the outside of the fish tanks, creating a predominantly vertical field. Lower field strength exposures were achieved by placing additional tanks in the stray field of a tank with a coil, calibrating that stray field to the current in the coil, and then controlling the current.

The tanks were standard PVC tubs of 50 cm height, 30 cm diameter, around which standard isolated 1.5 mm2 electricity wire was tightly wound in 160 turns. At the lower end a spiral end cap of 12 turns over the outer half of the diameter and at the top flange 20 additional turns were wound to optimize uniformity in the tub. Thus inside the tubs a practical, but close approximation was achieved of the field of a long solenoid coil. The deviation of the theoretically uniform field of the solenoid was calculated using Vector Fields software by dr. Johan Overweg of Philips Research, MRI section, and is better than 5% in the water volume further than 4 cm from the lower outside circumference of the tub, and better than 20% further than 2 cm from that outside circle. The signal generator was as described above for the in vitro experiments.

Results and discussion

In vitro experiments

Oxygen burst measurements were averaged over the 8 samples available in each group. Averages of the measurements without pre-stimulation and of the positive control group (with pre-stimulation) were divided by the negative control average in the corresponding run. The averages of pre stimulated measurements were divided by the corresponding positive control average. The resulting data, with standard deviation estimates derived from the data in each group, are given in Table 1.

Table 1. Oxygen burst results of 14 runs with 6 times 8 samples each

			% average normalized to negative control average						% average normalized to positive control average			
	neg contr		neg, 5 µT		neg, 1,5 mT		pos contr		pos, 5 µT		pos,1,5 mT	
	gem	stdev	gem	stdev	gem	stdev	gem	stdev	gem	stdev	gem	stdev
v50131	100%	8%	109%	6%	95%	7%	223%	41%	99%	13%	87%	10%
v50202	100%	6%	131%	23%	108%	8%	162%	30%	117%	19%	103%	30%
v50209	100%	24%	138%	36%	142%	23%	418%	73%	115%	9%	190%	17%
v50215	100%	54%	278%	120%	176%	131%	788%	118%	98%	17%	113%	46%
v50222	100%	24%	118%	41%	115%	50%	319%	59%	130%	25%	144%	32%
v50223	100%	50%	75%	17%	151%	32%	235%	90%	136%	22%	104%	24%
v50315	100%	10%	120%	25%	62%	18%	166%	28%	131%	34%	106%	21%
v50405	100%	15%	128%	29%	112%	31%	162%	23%	141%	42%	141%	31%
v50406a	100%	17%	142%	25%	152%	23%	179%	37%	143%	26%	126%	16%
v50406b	100%	31%	206%	119%	322%	70%	230%	33%	143%	54%	175%	26%
v50419a	100%	28%	93%	27%	66%	11%	201%	48%	92%	20%	101%	14%
v50419b	100%	10%	212%	50%	138%	40%	259%	54%	133%	26%	110%	17%
v50420	100%	15%	112%	27%	118%	21%	205%	38%	86%	17%	122%	14%
v50426	100%	55%	126%	89%	112%	67%	323%	86%	82%	13%	92%	19%
average	100%		142%		133%		276%		118%		122%	

Oxygen burst was increased in 12 out of 14 cases after 5 µT treatment, in 11 out of 14 cases after 1,5 mT treatment. With pre stimulation, oxygen burst was further increased in 9 out of 14 cases at 5 µT, and in 12 out of 14 cases at 1,5 mT.

On average, exposure to 5 µT or 1,5 mT led to 42% or 33% increase in immune activity, respectively, compared to negative control values. EMF could also additionally stimulate PMA-stimulated samples up to 18% (5 µT) or 22% (1,5 mT). Statistical analysis was carried out with SAS via a meta-analysis of the 14 datasets. A significant ($p<0.0001$) increase on the response of the EMF exposed cells was found.

These data are in line with those reported for 50 Hz, sinusoidal, 1 mT fields in murine and human macrophages in Simkó et al. 2001 and Lupke et al. 2004.

In vivo experiments

The subsequent series of experiments with diseased goldfish returned the following results. In each graph mortality is indicated in % of the total number of fish in each test group, as it develops over the course of the experiment. As can be seen the horizontal mortality lines after day 20 in experiment 3 (no further mortality), after 18 to 20 days usually the surviving fish had recovered from the diseases both in the control and the test groups, as was confirmed by visual inspection. Most test groups consisted of at least 4 replicates, in which the number of fish initially was gradually increased after more experience was gained. For some experiments

however with gradually varying parameters 2 replicates were taken.
Please note that in each experiment a new batch of fish was procured from the importer of the fish. Fish from groups heavily infected with parasites were selected. However the initial disease/health level of the fish varies between experiments. The absolute levels of survival between experiments are therefore not comparable. Within one experiment the fish had comparable health so the comparisons within one experiments are valid.

The first experiment compared survival in 4 control groups with 8 groups treated at 5 µT. Each group contained 12 fish.

Figure 2. Experiment 1.

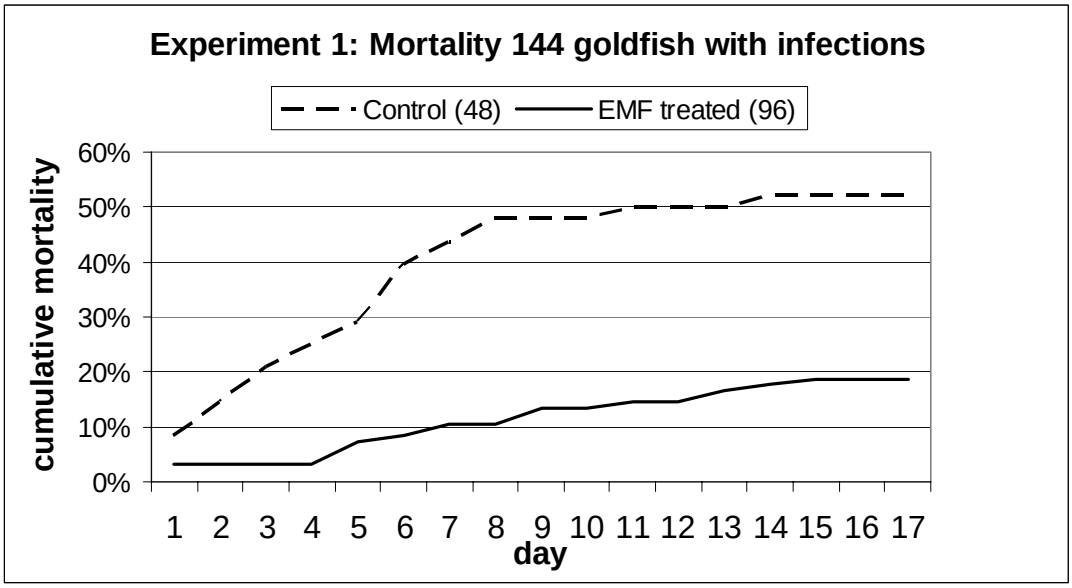

As can be seen there is a large difference in the survival, which was consistently more than 80 % better in the treated group over the course of the experiment. The end values were 52% ± 14% untreated and 19% ± 10% treated. The experiment was repeated, this time with 12 treatment groups of 12 fish each.

Figure 3.

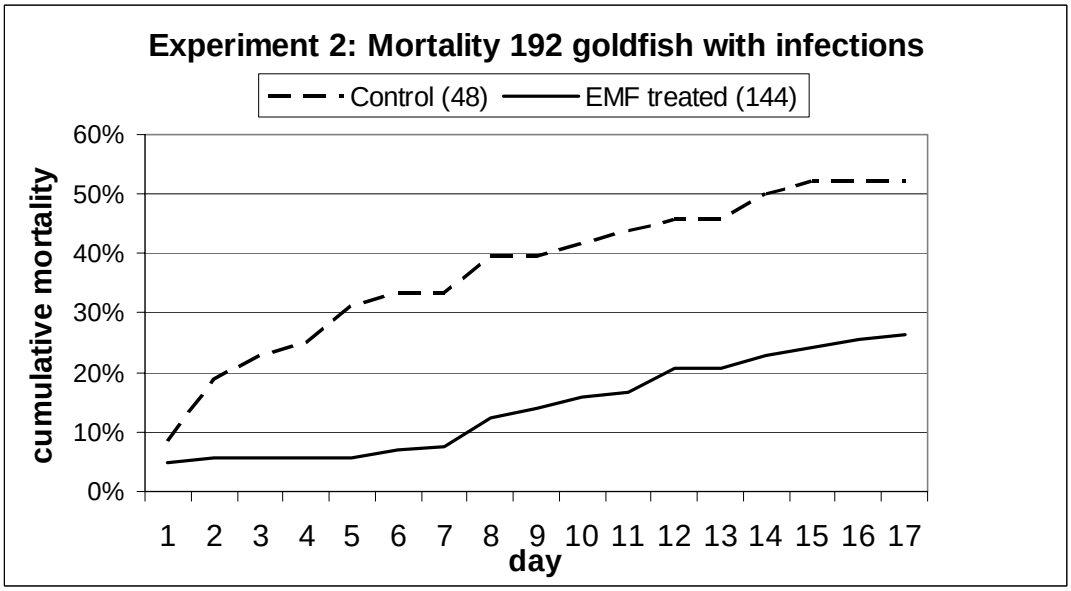

This time the improvement was again a factor 2. The end values were 52% ± 8% untreated and 26% ± 19% treated.
In order to find out more about the field strength dependency of the effect and to determine the required distance between tubs for parameter variation experiments, a next experiment was done with varying field strength. There

were 4 control groups and 2 test groups for 6 different field strengths varying from 0.15 to 50 µT. Each group contained 21 fish initially.

Figure 4.

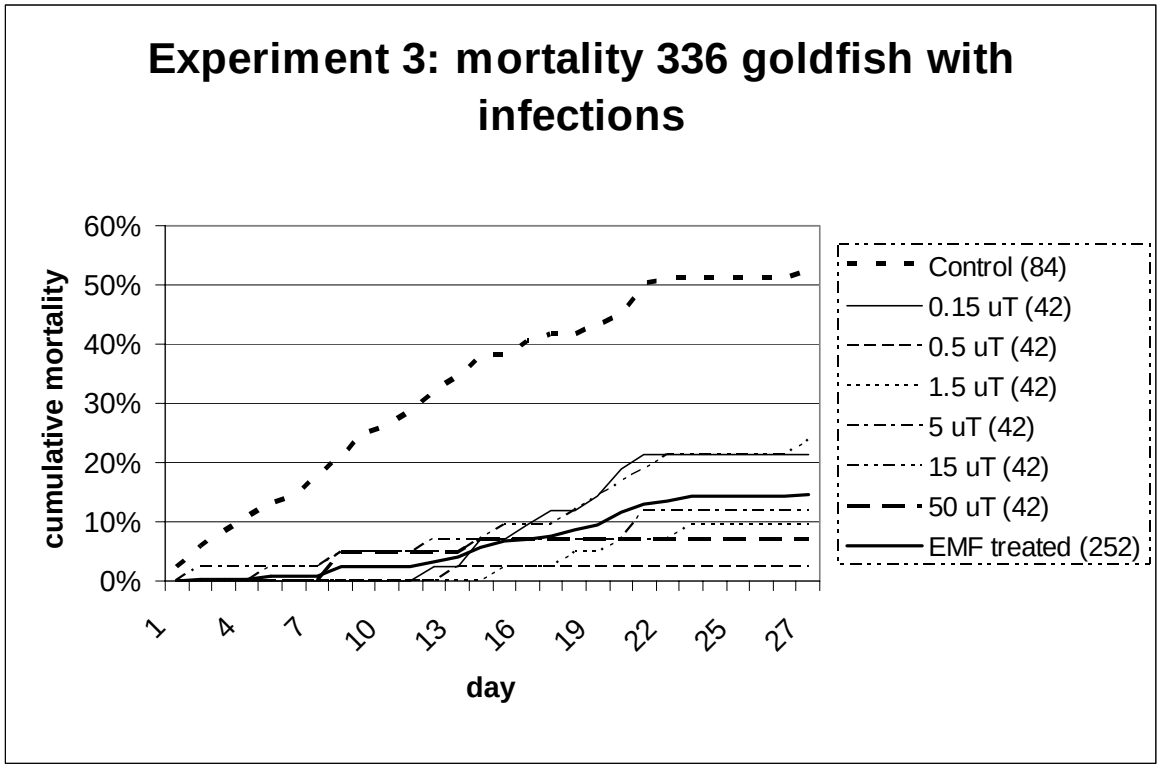

In this figure for 6 different field strength, ranging from 0.15 µT (thin solid line) to 50 µT (thick, long dashed line) the mortality development is given as before. Again, the control groups suffered mortality increasing to 52% on day 28 (upper, thick short dashed line). The average of all treatment groups is also given (thick solid line), this increases to 15% at day 28. The end values were 52% ± 29% untreated and 15% ± 11% treated (all together). Again, the treatment resulted in a strong decrease in mortality at all field strength levels. The final percentages at day 28 are given for clarity also in Figure 5.

Figure 5.

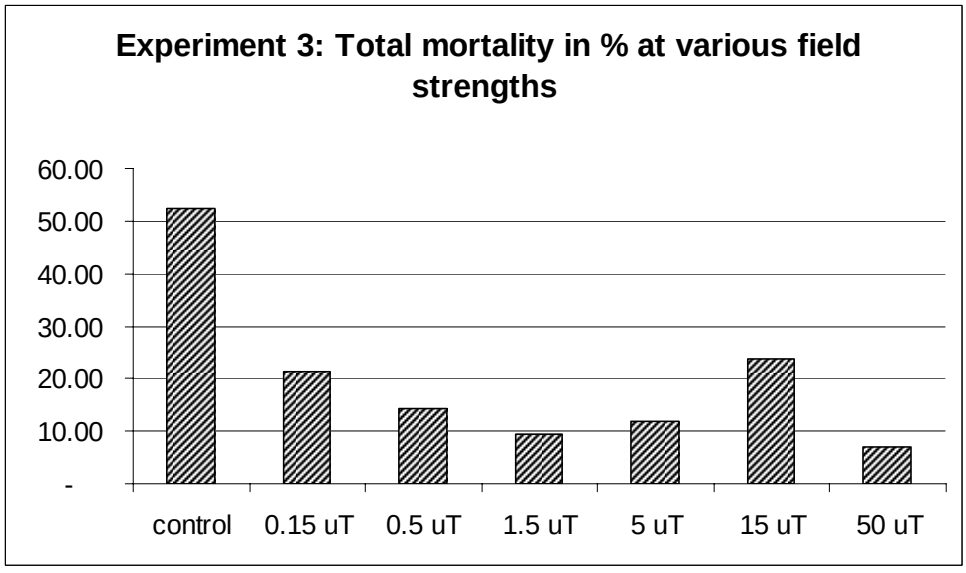

The result indicated that the decrease in mortality after EMF exposure was equally strong between 0,15 and 50 µT, except at 15 µT. There seems to be a decease in effectiveness from 0,05 µT downwards which becomes noticeable at 0,015 µT.

Since for our application especially the lowest field strength range is important a follow up experiment was performed that simulated lower field strength than 0,15 µT by placing test tubs in the stray field of a 5 µT tub. This was done because the voltages and currents needed to create such small fields are so low that electronic noise became too high. The 5 µT tub is built as a solenoid coil along the complete height of the tub. Such a solenoid coil has a small but rather uniform stray field that is suitable for the analysis that we wished to perform. The result is given in Figure 6.

Figure 6.

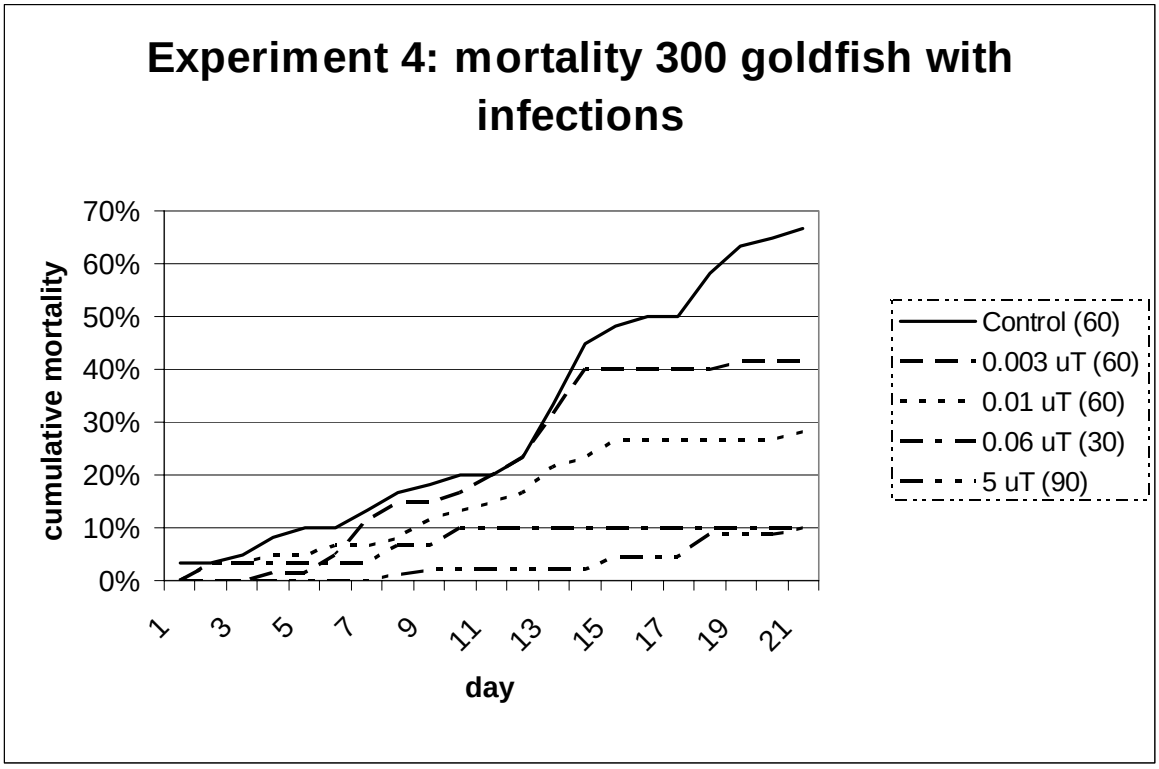

From the .06 µT group in Fig. 6 one replicate was lost due to a technical problem.
It can be observed that over the whole period mortality is highest in the control group and lowest in the group treated at 5 µT. From day 7 onwards mortality is strictly increasing with decreasing field strength.
Even at 0.003 µT (3 nT) these results indicate that there still is an effect of the treatment.
These results indicate that in order to be reasonably confident that there is no influence of EMF on control groups one must go to field strength levels of 1 nT or lower.

Conclusions

This research shows that the ELF EMF treatment as used by Immunent is capable of stimulating the immune system. On a cell level phagocyting cells have been shown to become more active after treatment. This result was obtained at 1,5 mT as well as at 5 µT.

On the level of the whole organism it was shown that at and around 5 µT the survival of diseased fish could be greatly improved by the treatment. In the light of the cell experiments also reported on, it is likely that this is based on an increased immune activity of the fish. The effect is present in a large window of field strengths around 5 µT, and one must go to the level of 1 nT or lower to be confident that the effect is no longer present. Proper distances between controls and test tubs are therefore important.

Because of the low field strengths required, and the surprisingly large effects on animal health, the results indicate that practical application with important economic advantages for farmers is possible. Moreover, the new experimental model used in this study can be important for bioeffects studies for EMF in general.

References

Simkó M., Droste S., Kriehuber R. and Weiss D.G. (2001): Stimulation of phagocytosis in murine macrophages by 50 Hz electromagnetic fields. Eur. J. Cell Biol. 80, 562-566

Lupke M., Rollwitz J. and Simkó M. (2004) 50 Hz magnetic fields induce reactive oxigen intermediates in human monocytes and in Mono Mac 6 cells. Free Radic. Res. 38, 985-993

Matzinger P. (2002): The danger model: a renewed sense of self. Science 2002;296:301-5.

Cuppen J.J.M., Parmentier H.K. and Savelkoul H.F.J. (2006a): Immune Stimulation In Fish And Farm Animals Through Weak Low Frequency Electromagnetic Fields, A. Hypothesis, this proceedings.

Acknowledgements

Messrs Van Kraaij, Brock, Berghs, and Bloo provided indispensible services in creating the hardware and software that supported these experiments.

ENVIRONMENTAL ANALYSIS OF THE ELECTRIC FIELD DUE TO MV OVERHEAD LINES SUPPORTED BY CONCRETE POLES

D. DESIDERI, A. MASCHIO, E. POLI

UNIVERSITY OF PADOVA, DEPARTMENT OF ELECTRICAL ENGINEERING
VIA GRADENIGO 6/A, I-35131 PADOVA (ITALY)

Abstract
This paper presents an environmental analysis of the electric field due to MV overhead lines supported by concrete poles with a pole-top-pin construction. A three-phase system of voltages has been applied to an electric model of the configuration and a three-dimensional numerical analysis has been done by using the charge simulation method. The time variation of the electric fields at the frequency of 50 Hz has been numerically computed and the obtained results have been experimentally validated by means of an extensive campaign of measurements. The preliminary set-up checks in order to minimize the perturbation error due to the measurement instrument are described. The rms values of the three components of the electric field have been measured and the data obtained around a MV line, at different heights (up to 2 m from the ground), far and near a supporting concrete pole are reported. A significant result is that the electric field at the pole surface at the height of 2 m is greater than the one at the same level under the line in the midpoint of the span.

Introduction
A three-phase MV overhead power line is relevant to an environmental analysis of the electromagnetic field in the ELF range. Poles made in reinforced concrete are extensively used as line supporting structure [1, 2], but their inclusion in the electric field evaluation is not easy. In fact, the electric field analysis far from the concrete poles, e.g. in the midpoint of the span, is a well-known case, and a bi-dimensional (2-D) model can be used obtaining good results [3, 4]. On the contrary, the inclusion of a supporting conductive structure is complicated, requiring the use of a three-dimensional (3-D) model [5].
In the following the results of an analysis on a pole-top-pin configuration used in MV overhead lines are referred. The paper is split in three sections; the first section reports the numerical analysis of the configuration, starting from an electric model, and then describing the numerical method and the obtained results. The second section reports the extensive campaign of measurements performed, whose data have been used for the validation of the numerical results. The third section presents a discussion of the results. The conclusive remarks have been reported in a final short summary.

Numerical analysis

a) Electric model of the pole-top-pin construction
The simplified structure of the analyzed MV overhead line supported by concrete poles with a pole-top-pin construction is shown in fig. 1. The three wires are represented by three straight cylindrical conductors; each one of them will be referred to in the remainder as "overhead conductor"; the axes of the conductors are parallel to each other and to the ground. The diameters of the overhead conductors (*Ø*) are the same. A three-phase system of voltages is applied to the overhead conductors.
The supporting concrete pole (referred to in the remainder as "pole") is assumed to be a cylindrical conductor, with vertical axis and radius *R* of the cross-section. The pole is assumed equipotential with the ground.
A Cartesian coordinate system has been adopted, where z is the vertical pole axis and x is the direction of the central overhead conductor (fig. 1).
The height of the pole is *a*. The axis of the central top overhead conductor (marked with 2 in fig. 1) is high *b* over the top of the pole, while the axes of the two lateral overhead conductors (marked with 1 and 3 in fig. 1) are high *a* over the ground and distant *c* from the pole axis.
In MV overhead lines with a pole-top-pin construction different values are used for the geometry, i.e. for the pole height, the pole diameter, the spacing of the overhead conductors, or the wire diameter. Among all the cases, for the numerical analysis an average value for *a* and typical values for the other parameters have been

chosen. The following values have been taken: a = 10.5 m, b = 0.8 m, c = 0.76 m, R = 0.1 m, and $Ø$ = 0.01 m [1, 2].

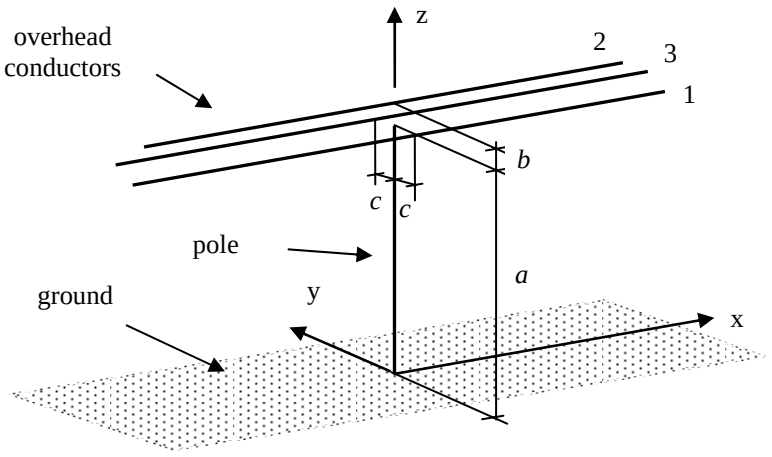

Fig. 1 Three-phase MV power line: overhead conductors, pole and ground.

b) The charge simulation method

The electric field around the MV power line was computed by using the charge simulation method (CSM). In this method conductors and their surface charges are replaced by simulating charges placed inside the equipotential contours of the conductors [6-9]. The presence of the ground plane is taken into account by a corresponding set of image charges. The charge density is initially unknown but is readily calculated when potentials are set on a number of points of the contours. Then potentials and electric field can be computed everywhere. The accuracy of the method is tested, by determining potentials and fields on control points of the conductors different from those at fixed potential.

In this study, uniformly charged segments have been used. A section of the MV line, extending 30 m apart from the pole on both sides, was considered: the equipotential contour of each overhead conductor was simulated by means of 60 couples of segments, symmetrically placed close to the axis and parallel to it, one twentieth of the radius apart from the axis. Other 70 couples of segment charges were arranged in the same way to simulate the pole equipotential contour. These 70 couples were placed on two axes, parallel to the pole axis and at opposite sides to it along y.

The accuracy was tested following two different, widely used, criteria, on potentials and on fields [7]. With 1 kV applied on one phase and 0 V on the other two, an electric potential difference generally lower than 0.2 V was found on control points. Furthermore, the ratio between tangential and normal components of the electric field on control points on the surface of the conductors was calculated, and resulted to be generally lower than 0.01 (i.e. a deviation of less than one degree of the direction of the computed field from the normal to the surface of conductors).

It is worth noting that the charge simulation method was chosen in this study because it allows to compute the electric field with a very small number of simulating charges: for the calculation, a matrix of only 500x500 elements shall be solved. Consequently, each computation run requires about 5 seconds on a PC with 256 MB RAM, 1.8 GHz Pentium IV.

c) Electric field computations

It is well known [1, 2] that the electric field around a three-phase transmission line is generally a vector rotating in a plane, where it draws an ellipsis. In order to get the complete description of the ellipsis, in this research the field was computed by means of the CSM at different times along the whole cycle: the direction and magnitude of the electric field at its maximum and minimum were recorded, giving the major and minor axes of the ellipsis and the plane where it lies.

In order to achieve this result, the three contributions to the electric field due to each conductor at unit potential, while the two others are at zero potential (with the pole always at zero potential), were computed.

Indicated with $\mathbf{E}(x, y, z, V_1, V_2, V_3)$ the vector of the electric field in a point x, y, z due to the potentials V_1, V_2, V_3 applied to the three overhead conductors 1, 2 and 3, the contributions are:

$$\begin{aligned}\mathbf{E}_1(x, y, z) &= \mathbf{E}(x, y, z, 1, 0, 0)\\ \mathbf{E}_2(x, y, z) &= \mathbf{E}(x, y, z, 0, 1, 0)\\ \mathbf{E}_3(x, y, z) &= \mathbf{E}(x, y, z, 0, 0, 1)\end{aligned} \quad (1)$$

and the total electric field is:

$$\mathbf{E}(x, y, z, V_1, V_2, V_3) = \mathbf{E}_1(x, y, z)\, V_1 + \mathbf{E}_2(x, y, z)\, V_2 + \mathbf{E}_3(x, y, z)\, V_3 \quad (2)$$

The potentials V_1, V_2, V_3 have been set with reference to a three-phase line voltage of 20 kV rms: 3600 values have been computed with an iteration process, by increasing the phase of 0.1° each step, in order to cover the whole cycle of 360°.
Recording the maximum of E_x, E_y and E_z, their rms value can be computed simply dividing the maximum by $\sqrt{2}$. Moreover the rms value of the intensity of the total electric field results as the root sum square of the three rms values of E_x, E_y and E_z.
Finally, the major and minor axes of the ellipsis are found by recording the maximum and minimum of the magnitude of $\mathbf{E}(x, y, z, V_1, V_2, V_3)$, while the values of the three components E_x, E_y and E_z at the maximum and the minimum give the direction of the axes.

d) Numerical results

As a first analysis, the rms values of E_x, E_y and E_z on the plane y = 0 have been considered up to z = 2 m. The numerical results of E_x, E_y and E_z at z = 1 m and at z = 2 m are reported in fig. 2, respectively on the left, at the centre and on the right. The data are reported up to 10 m from the pole.

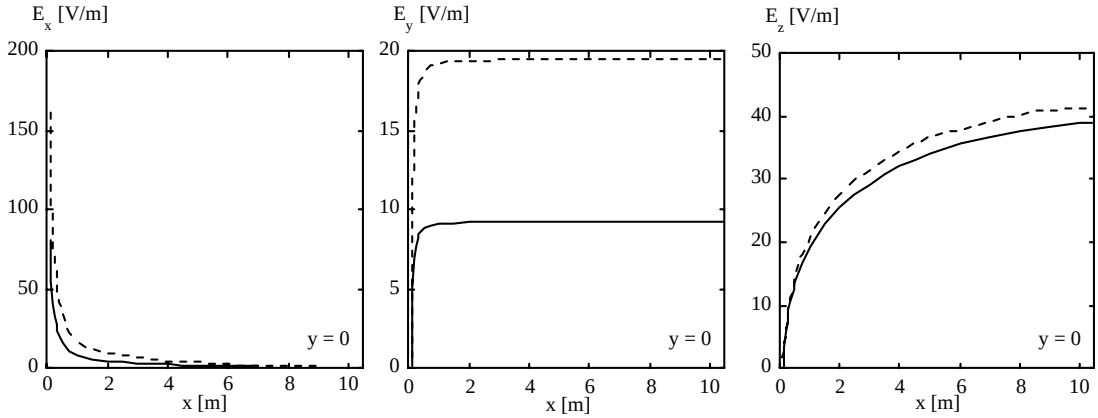

Fig. 2 Numerical results of E_x (left), E_y (centre), E_z (right) at y = 0, z = 1 m (continuous lines) and at y = 0, z = 2 m (dashed lines).

The effect of the pole is clear. At the pole, the electric field is normal to the pole surface. E_x is large, while E_y and E_z are null.
Moving from the pole in the x direction, from fig. 2 it can be seen that E_y quickly reaches the same value that is found far from the pole, i.e. at the midpoint of the span at y = 0. In particular the effect of the pole for E_y is extremely localized. E_x and E_z reach the same value found far from the pole approximately after a few meters. Increasing x, at y = 0, E_x tends to zero, while E_z increases its value at the one expected at the midpoint of the span.
It can be noticed that the reinforced concrete pole makes E_x at the pole even higher than the values of E_y and E_z evaluated at the midpoint of the span.
A second analysis has been performed at x = 0 and at x = 5 m and the rms values of E_x, E_y and E_z have been considered again up to z = 2 m. The values at x = 5 m are assumed not affected by the pole, as indicated by the data reported in fig. 2. On the other hand, the data at x = 0 are reported to analyze the effect of the pole in the y direction.
The numerical results of E_y and E_z at z = 1 m and at z = 2 m are reported in fig. 3 and fig. 4 respectively, showing on the left the value at x = 0 and on the right the value at x = 5 m. The data are reported up to y = 10 m.
Again, at the pole, the electric field is normal to the pole surface. At x = 0, on the pole surface, E_y is large, while

E_x and E_z are null. It is worth noting that the value of E_y at the pole surface is equal to E_x, at the pole at y = 0, as shown in fig. 2.
At a few meters from the pole E_y has the same value at x = 0 and at x = 5 m, and E_z behaves in the same way. It is again confirmed that at this distance the pole effect is negligible.
From the numerical analysis it results that E_x is null at x = 0, as expected from the symmetry of the configuration, and quite small (only few volts per meter) at x = 5 m and z not greater than 2 m.

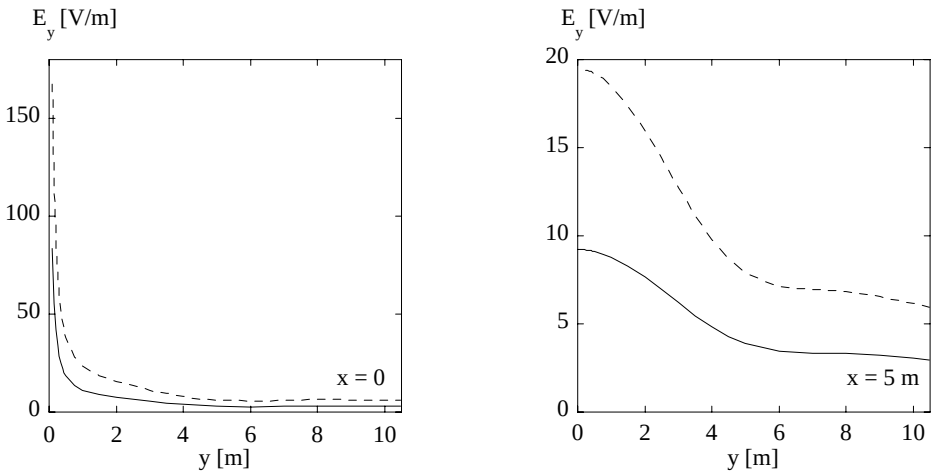

Fig. 3 Numerical results of E_y on the left at x = 0, z = 1 m (continuous line) and at x = 0, z = 2 m (dashed line); on the right at x = 5 m, z = 1 m (continuous line) and at x = 5 m, z = 2 m (dashed line).

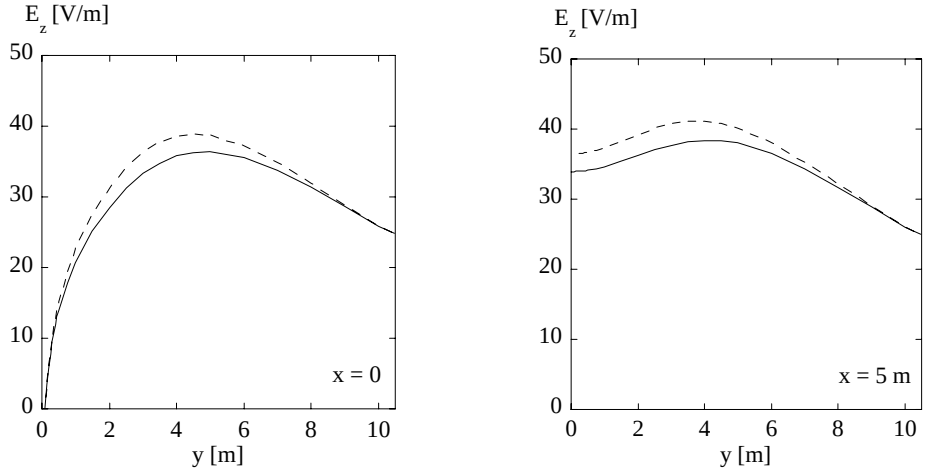

Fig. 4 Numerical results of E_z on the left at x = 0, z = 1 m (continuous line) and at x = 0, z = 2 m (dashed line); on the right at x = 5 m, z = 1 m (continuous line) and at x = 5 m, z = 2 m (dashed line).

A third analysis was done on the magnitude and on the direction of **E** at its maximum and minimum, thus identifying the axes of the ellipsis drawn by the field. The direction can be indicated by means of the angles of the vector of the field with the three coordinate axes. As an example, in the plane z = 2 m and on x = 0, 0.5, 1 and 5 m, the magnitude of the field vector and its minor angle (0 ÷ 90°) with the vertical axis z, as a function of y up to 10 m, are reported in fig. 5, on the left and on the right respectively.
About the angle with the z direction, at x = 0, it is noticed that on the pole surface only a field at 90° with z is allowed, while, increasing the distance from the pole, the angle is reduced to 20° at y = 2 m, is almost null at y = 5 m, and is about only 10° for greater distances. Near y = 0, at x = 0.5 m the influence of the pole gives still a deviation of about 70° from the perpendicular, while at x = 1 m the angle is reduced to 40°. Finally, for x = 5 m the angle with the z direction is generally equal or less than 10° for any y up to 10 m.
It is interesting to note that also the data reported in fig. 5 show that the influence of the pole tends to vanish at a distance of a few meters, in agreement with the observations done on the electric field components.

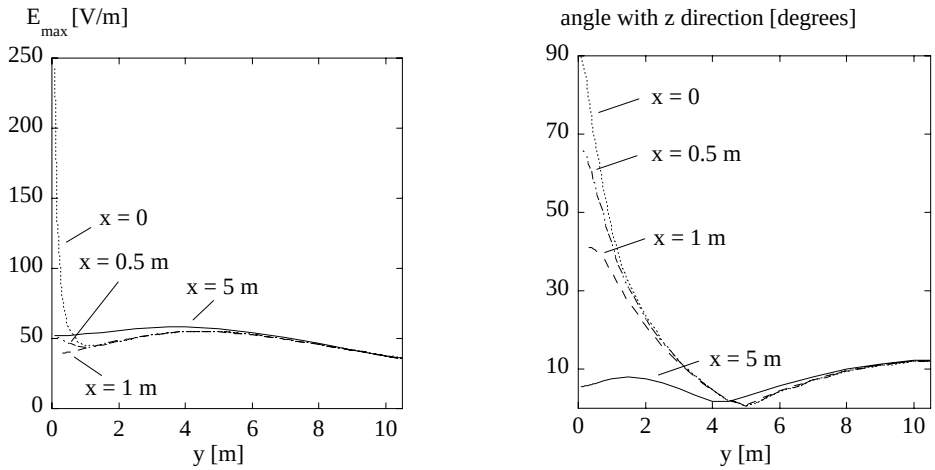

Fig. 5 Numerical results of E_{max} and the angle with the z direction versus y at different values of x.

Experimental results

a) Instrumentation and perturbation error

The instrumentation used for the electric field measurement consisted in a PMM EHP-50C probe, connected via an optical fibre to a PMM 8053 portable field meter.

The probe is approximately a cube with 8 cm side. The experimental data are referred to the barycentre of the probe: therefore with the probe placed on the ground, the z quote is 0.04 m.

The probe was taken at a distance of at least five meters from the PMM 8053 and the operator. The PMM 8053 unit was set to measure electric fields in the frequency range 6 ÷ 500 Hz; the display showed the rms value of the total electric field, together with the rms values of the three field components along the probe axes. The system allows the analysis resolved in frequency of the measured signal and the measure of the rms value of the electric field at a specific frequency (among those allowed).

For the measurements at different heights, the probe is installed on an insulating rod and then connected to a supporting structure, mainly a wooden tripod with a limited metallic parts, e.g. at the connection between the insulated rod and the wooden tripod.

The effect of these metallic parts on the measurements was investigated. It was considered that if a local variation was due to these metallic parts and the probe was near to them, the probe should have measured a distorted electric field, so affecting the data. In this respect a few measurements have been taken with different distances *d* between the EHP-50C probe and the metallic parts of the tripod. The data have been taken under a MV power line, with the two configurations planned for the experimental campaign. The most critical was the configuration for the measurements at z = 1 m, where *d* might be taken very small. At z = 1 m, a clear variation on the measurements have been obtained with *d* set at a few centimetres, while the effect became negligible when *d* was kept greater than about 0.3 m. For the experimental campaign it has been decided to keep *d* greater than 0.4 m, for the measurements taken at z = 1 m. For the measurements at z = 2 m, *d* was always about 0.7 m.

b) System description

Fig. 6 shows the place where the measurement campaign has been performed. No objects of any kind (trees, fences, etc,) are present at a distance less than 20 m from the pole.

Measurements of the geometry have been done by a laser meter (Bosch, mod. DLE 150). The height *a* of the pole was about 10.5 m; the spacing of the overhead wires at the pole were in good agreement with the *b* and *c* values used for the numerical analysis. The pole radius was about 0.15 m at the ground level, and was reducing its value of about 0.075 m per meter of increase along the pole height.

Small ground irregularities and few centimetres of grass and brushwood, evenly distributed, have given local perturbations to the electric field at ground level.

On the side where the measurements have been done, the increase of the ground level was of about 0.1 m at a distance of 10 m from the pole under the overhead wires. By using a rough estimate of the sag in the midpoint of the span, combined with the catenary curve, at 10 m from the pole the overhead wires lowering was estimated to be about 0.3 m.

A Cartesian system was used, the same indicated in fig. 1.

Fig. 6 The MV power line.

During the experimental campaign, the measurements were performed with the PMM EHP-50C probe at three different distances from the ground: 0.04 m, 1 m and 2 m respectively. Preliminary measurements have been done to check the contribution of harmonics to the electric field. As they have shown to be negligible, the data have been obtained with the range 6 ÷ 500 Hz and assumed to be due only to the main component, at 50 Hz.
The measurements have been performed in three days of fine and dry weather, with a temperature between 18°C and 24°C. About the measurement uncertainties, from the certificate of calibration of the instrument, the expanded uncertainty [10] at 50 Hz is 3% on the magnitude of the electric field at 23±3°C. Moreover a temperature effect of 0.05 dB/°C, obtained from the probe technical data sheets, has also been considered. With a temperature between 18°C and 24°C, a maximum value of 0.4 dB has been considered due to the temperature effect. Without considering further components of uncertainties, with a normal distribution for the uncertainty reported on the certificate of calibration, and a rectangular distribution for the temperature, a combined standard uncertainty has been calculated and a coverage factor of two has been used for obtaining the expanded uncertainty [10]. In this way the uncertainty results 6% of the total electric field value.
The rms value of the line voltage was 20 kV.

c) Experimental results and validation of the numerical analysis
A first set of experimental results is reported in fig. 7. The data are taken at y = 0.

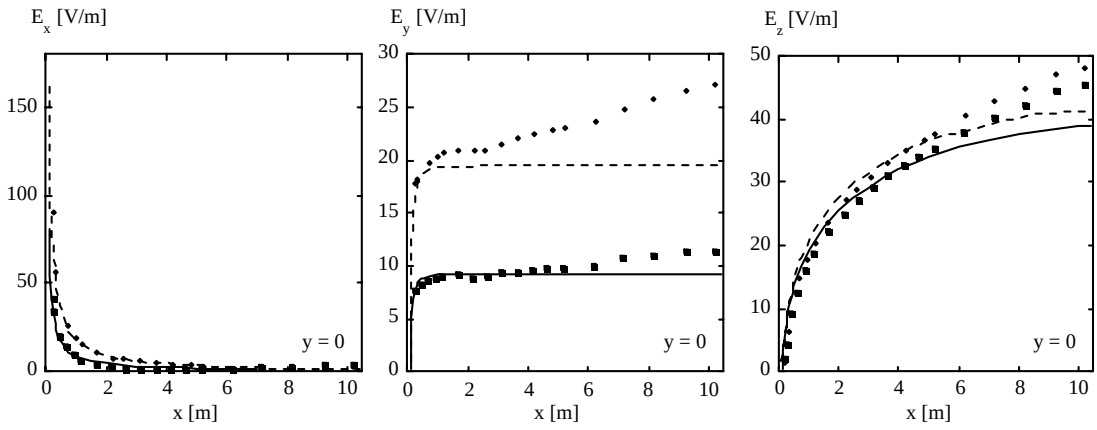

Fig. 7 Comparison between numerical and experimental data. Numerical results of E_x (left), E_y (centre), E_z (right) at y = 0, z = 1 m (continuous lines) and at y = 0, z = 2 m (dashed lines). Experimental data of E_x (left), E_y (centre), E_z (right) at y = 0, z = 1 m (full squares) and at y = 0, z =2 m (full diamonds).

The rms values of E_x, E_y and E_z at z = 1 m and at z = 2 m are reported respectively on the left, the centre and the right of fig. 7: full squares show the experimental data at z = 1 m, and full diamonds show the experimental data at z = 2 m. For comparison, also the numerical data at y = 0 are reported: continuous lines show the numerical results at z = 1 m, dashed lines show the numerical results at z = 2 m. The numerical data are those already reported in fig. 2, which are repeated here for a simpler comparison between numerical and experimental data.
It can be noticed a good agreement between the results obtained from the CSM and the experimental data. Moreover the lowering of the overhead wires, combined with the variation of the ground level, agrees with the increase in the experimental data of E_y and E_z at distances greater than about 4 m from the pole.

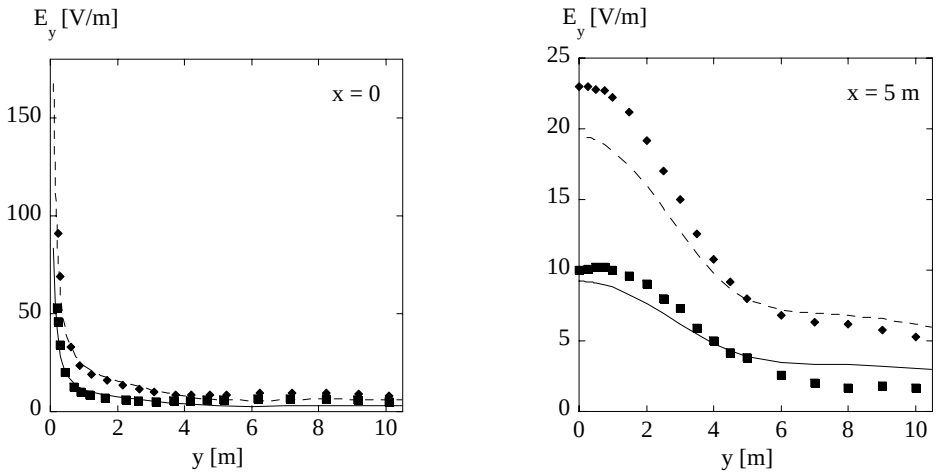

Fig. 8 Comparison between numerical and experimental data. Numerical results of E_y on the left at x = 0, z = 1 m (continuous line) and at x = 0, z = 2 m (dashed line), on the right at x = 5 m, z = 1 m (continuous line) and at x = 5 m, z = 2 m (dashed line). Experimental data of E_y on the left at x = 0, z = 1 m (full squares) and at x = 0, z = 2 m (full diamonds), on the right at x = 5 m, z = 1 m (full squares) and at x = 5 m, z = 2 m (full diamonds).

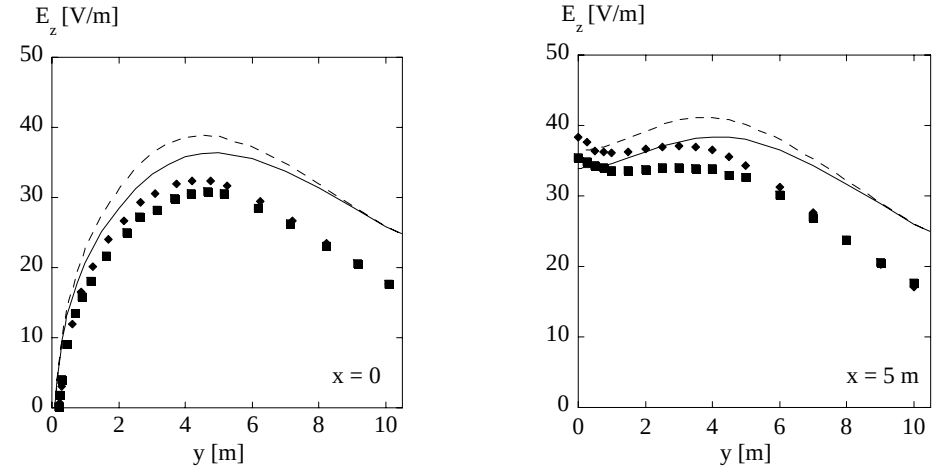

Fig. 9 Comparison between numerical and experimental data. Numerical results of E_z on the left at x = 0, z = 1 m (continuous line) and at x = 0, z = 2 m (dashed line), on the right at x = 5 m, z = 1 m (continuous line) and at x = 5 m, z = 2 m (dashed line). Experimental data of E_z on the left at x = 0, z = 1 m (full squares) and at x = 0, z = 2 m (full diamonds), on the right at x = 5 m, z = 1 m (full squares) and at x = 5 m, z = 2 m (full diamonds).

A second analysis has been performed at x = 0 and at x = 5 m. The rms values of E_y and E_z at z = 1 m and at z = 2 m are reported in fig. 8 and fig. 9 respectively, showing on the left the values at x = 0 and on the right the values at x = 5 m. In both figures numerical and experimental data are reported: continuous lines show numerical results at z = 1 m, dashed lines show numerical results at z = 2 m, full squares show experimental data at z = 1 m, and finally full diamonds show experimental data at z = 2 m. The numerical data are those already

reported in fig. 3 and fig. 4.
Numerical and experimental data are in good agreement, with in general a difference of about 20% for E_z and a lower difference for E_y. Therefore the validation of the numerical analysis previously reported has been obtained.

Discussion

The analysis performed up to z = 2 m, has shown that a reinforced concrete pole used in a MV power line, with a pole-top-pin construction, and with a height of 10.5 m, extends its effects in the electric field configuration around the pole up to a few meters.
At the pole, at the quote z = 2 m, the value of the electric field normal to the pole equipotential surface is higher than the value of its main component at the midpoint of the span. This result appears from the values of E_x, E_y and E_z under the line (y = 0) reported in fig. 7, and the values at x = 0 and at x = 5 m reported in fig. 8 and fig. 9.
Therefore, the usual analysis performed at the midpoint of the span is not able to give an evaluation of the maximum exposure to the electric field with a MV power line supported by reinforced concrete poles, at least with reference to a maximum quote of z = 2 m.

Summary

The electric field due to a MV power line with a pole-top-pin construction has been analyzed in this paper.
A numerical analysis has been performed, based on an electric model equivalent to the configuration. The numerical results have been validated by an extensive experimental campaign of measurements, performed after checks on the measurement equipment, in order to minimize the perturbation errors.
At z = 2 m, at the pole surface, the maximum rms value of the electric field has been obtained: this value is greater than the one calculated far from the pole at the midpoint of the span.

References

[1] *Standard Handbook for Electrical engineers*, 10th ed., D. G. Fink and J. M. Carroll, Eds. McGraw-Hill, 1968
[2] V. Cataliotti, *Impianti elettrici*, vol. I, Italy: Flaccovio Editore, 2005.
[3] CEI 211-4, Guide to calculation methods of electric and magnetic fields generated by power-lines, Comitato Elettrotecnico Italiano, Milano 1996.
[4] CIGRE WG 36-01, Electric and magnetic fields produced by transmission systems. Description of phenomena - practical guide for calculation, Paris 1980.
[5] D. Desideri, M. Guarnieri, and E. Poli, "MV line electric field evaluation near a concrete pole," *IEEE Trans. Magn.*, vol. 40, pp. 718-721, Mar. 2004.
[6] H. Singer, H. Steinbigler, and P. Weiss, "A charge simulation method for the calculation of high voltage fields, " *IEEE Trans. Power App. Syst*., vol. 93, pp. 1660-1668, Sept. 1974.
[7] N. H. Malik, "A review of the charge simulation method and its applications," *IEEE Trans. Electr. Insulation*, vol. 24, pp. 3-20, Feb. 1989.
[8] E. Poli, "The use of image charges in the charge simulation method: a parallel-plane dielectric plate covering a conductor," *IEEE Trans. Magn.*, vol. 28, pp. 1076-1079, Mar. 1992.
[9] P. N. Nikolopoulos, "On the accurate evaluation of the electric field and of the field-lines of three-phase overhead lines with smooth or stranded conductors," 4th Int. Symp. on High Voltage Engineering, paper 12.10, Athens 1983.
[10] *NIS 3003 - The expression of uncertainty and confidence in measurement for calibrations*, NAMAS, England, edition 8, May 1995.

DEVELOPMENT OF A SIMPLE AND LOW COST MAGNETIC FIELD MEASUREMENT EQUIPMENT UP TO 400 kHZ

D. DESIDERI, A. MASCHIO

UNIVERSITY OF PADOVA, DEPARTMENT OF ELECTRICAL ENGINEERING
VIA GRADENIGO 6/A, I-35131 PADOVA (ITALY)

Abstract

In this paper the design, realization and operative ratings of a new simple and low cost magnetic field measurement equipment in the frequency range from 10 Hz to 400 kHz are reported. The design specifications of this device have been chosen following the indications given for the magnetic field reference sensor in Standard EN 50366, concerning emissions of household and similar electrical appliances with reference to human exposure to electromagnetic fields. The developed equipment consists of three mutually perpendicular concentric coils, each one of two turns, for magnetic field analysis up to 400 kHz. By using operational amplifiers, an electronic elaboration of the coil signals has been done and is described. The characterization of the equipment has been performed by using a laboratory set-up, where the test magnetic field configuration has been obtained with a single layer solenoid in house developed.

Introduction

Quantitative determinations of the magnetic field emissions from equipments in the Extremely Low Frequency (ELF) range have been performed and reported [1, 2]. The analysis of electric appliances, relevant to the evaluation of the human exposure to electromagnetic fields, is in particular required by Standard EN 50366, that in general considers for the magnetic fields a frequency range from 10 Hz to 400 kHz [3].

Purpose of this work is to develop a new simple and low cost instrument able to measure the magnetic field in the above mentioned frequency range.

The paper is divided in two main sections. In the first part, the design and realization of the measurement equipment are reported. In the second section, the laboratory set-up used for the characterization of the system is depicted, and the obtained operative ratings of the developed device are reported.

Finally, in the summary, the conclusive remarks are given.

Design and realization of the measurement equipment

a) *Coils*

For the measurement of the magnetic flux density, Standard EN 50366 indicates a reference sensor that consists of three mutually perpendicular concentric coils, with a total measuring area for each coil of 100 ± 5 cm^2. The outside diameter of the reference sensor must be lower than 13 cm.

Following the specifications given in Standard EN 50366 for the magnetic field reference sensor, a simple and low cost probe has been developed.

It consists of three mutually perpendicular concentric coils. Three two turns coils have been built by using a transformer wire with a cross-section area of 0.3 mm^2. Two of the three coils are almost rectangular in shape, with dimensions for each turn of 65 mm x 76 mm and 64 mm x 78 mm respectively; the third coil has a circular cross section, with diameter of each turn of 79 mm. In such a way a measuring area of about 100 cm^2 is obtained for each coil.

For supporting the three mutually perpendicular coils a PVC cylindrical structure has been built, 68 mm height and 80 mm diameter, on which three grooves have been drawn for placing the coils. Each coil ends with a twisted pair 0.6 m long.

The cylindrical PVC structure is mounted on a PVC base.

For the wires a fixing structure has been set, in order to make the system stable during operation.

In fig. 1 a picture of the three coils probe is shown.

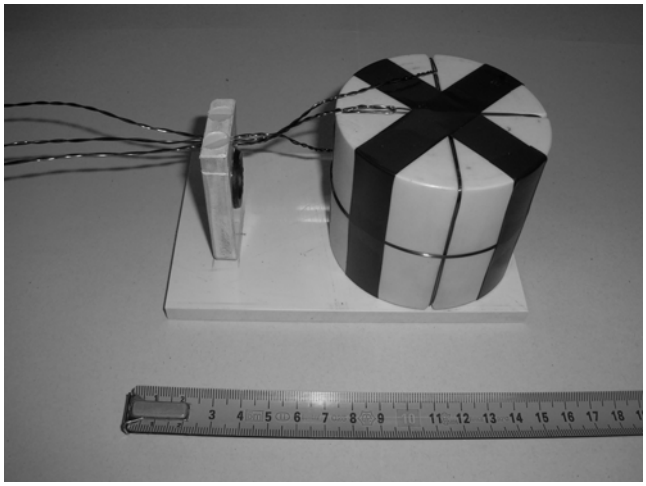

Fig.1 Picture of the three-coils probe

b) *Equivalent electrical parameters for a coil*

The frequency range of interest for the system is the one indicated in the Standard EN 50366, i.e. from 10 Hz to 400 kHz. Related to it, an electrical analysis of each coil has been performed.

The length of the wires of the three coils is almost equal for all of them; so their electric resistance R can be considered the same, and it is about 0.12 Ω in DC. When the frequency f increases, the resistance increases due to the skin effect. The parameter involved is the penetration depth δ that is:

$$\delta = \frac{1}{\sqrt{\pi f \mu_0 \sigma}} \tag{1}$$

with the permeability of free space $\mu_0 = 4\ \pi\ 10^{-7}$ H/m and the conductivity of the copper $\sigma = 5.8\ 10^7$ S/m. At 400 kHz, δ is about 0.1 mm, and assuming a current evenly distributed near the surface on a depth equal to δ, it results an estimated value for R of 0.22 Ω, in agreement with the value obtained by an LCR meter (Agilent 4285A) that has been of about 0.25 Ω at 400 kHz.

As far as the calculation of the inductance L is concerned, being the coils made up of only two turns, the concept of total inductance L_{tot} of a circuit split in two parts has been used:

$$L_{tot} = L_1 + L_2 + 2M \tag{2}$$

where $L_1 = L_2 = L$ is the self inductance of one turn and M is the mutual inductance between the two turns. For the evaluation of L and M, the two rectangular coils have been approximated with a square one (side length 71 mm); according to [4], the corresponding value of L_{tot} is 1 μH when the current is evenly distributed inside the coil conductor. Increasing the frequency, a correction due to the skin effect could be introduced as the current tends to concentrate on the outer part of the conductor, but is quite small and can be neglected: in fact, with the current concentrated on the conductor surface, the inductance decreases down to 0.97 μH. In a similar way, for the circular coil, a value of 0.92 μH for the current evenly distributed and 0.90 μH for the current concentrated in the outer part of the conductor have been estimated. Finally, an additional term of about 0.15 μH, due to the length of the twisted pair connection, must be added to the previous values. By using an LCR meter (Agilent 4285A) a value of about 1.2 μH for L was measured for the three coils (with their connections) up to a few MHz, in good agreement with the estimation above reported.

A coil, without load, has an output voltage $v_0(t)$ equal to:

$$v_0(t) = -\frac{d\Phi(t)}{dt} = -\frac{d}{dt}\int_{A_p} \mathbf{B}(t) \bullet \mathbf{n} dA = -A_p \frac{d}{dt} B_{\perp av}(t) \tag{3}$$

where A_p is the coil area and $B_{\perp av}$ is the average value on A_p of the component of **B** perpendicular to the coil area.

In the frequency range from 10 Hz to 400 kHz, an equivalent electrical scheme of the probe, shown in fig. 2, is

therefore given by an ideal voltage source in series with a resistance *R* and an inductance *L*, with *R* and *L* above reported; with $v_1(t)$ it has been indicated the coil output voltage.

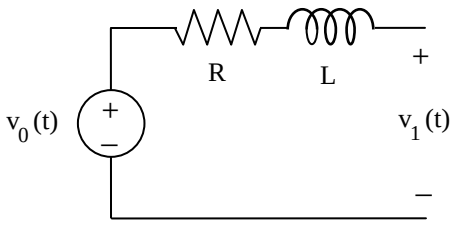

Fig.2 Equivalent electrical parameter for a coil.

Finally, in the frequency domain, by using phasors, (3) becomes:

$$\overline{V}_0 = -j\omega A_p \overline{B}_{\perp av} \tag{4}$$

where $\omega = 2\pi f$; j is the imaginary unit, and $\overline{V}_0$ and $\overline{B}_{\perp av}$ are the phasors of $v_0(t)$ and $B_{\perp av}(t)$ respectively.

c) *Electronics*

An integration of the coil output signal is required in order to obtain the value of $B_{\perp av}$, as derives from (3). Therefore the electronic circuit is basically an integrator, combined with a low pass filter, as schematically indicated in fig. 3.

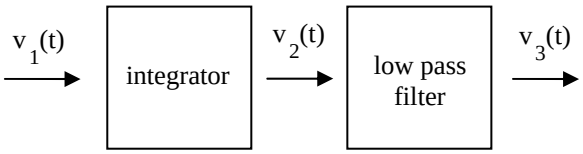

Fig.3 Schematic of the electronic circuit.

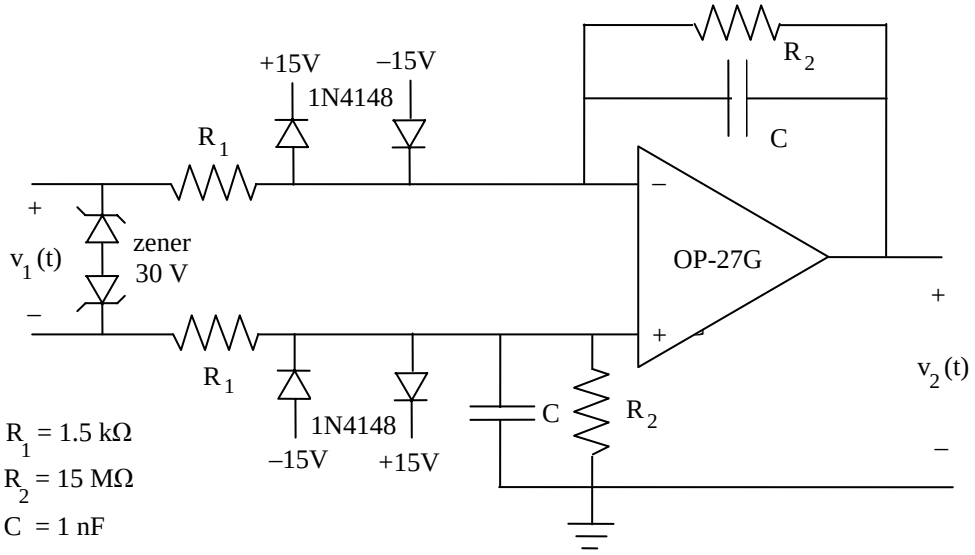

Fig.4 The integrator.

For the integrator, the basic circuit is the one commonly used for magnetic field coil, depicted in [5]. The detailed circuit is reported in fig. 4. An OP-27G has been used as operational amplifier. In the input, zener diodes and 1N4148 diodes are placed for protection. The input of the integrator has two resistances (R_1) each one of

1.5 kΩ: when the coil is connected to the integrator, it results that the resistance R and the inductance L, equivalent of the coil, are in series with R_1, and, on considering their values and the frequency range of interest, R and L can be neglected in the analysis. Therefore, in the frequency domain and using (4) it results that:

$$\overline{V}_1 = \overline{V}_0 = -j\omega A_p \overline{B}_{\perp av} \tag{5}$$

In the frequency domain, with $\overline{V}_2$ phasor of the integrator output voltage, the transfer function $A_1(j\omega)$ of the integrator is:

$$A_1(j\omega) = \frac{\overline{V}_2}{\overline{V}_1} = -\frac{R_2}{R_1}\frac{1}{1+j\omega C R_2} \tag{6}$$

with R_1, R_2, and C indicated in fig. 4. The DC gain of the integrator is 80dB (i.e. 10000), and a pole is set at 10 Hz.
An active filter has been placed after the integrator: it is a second order Butterworth low-pass filter [6]. In the frequency domain, with $\overline{V}_3$ phasor of the low-pass filter output voltage, the transfer function $A_2(j\omega)$ of this filter is:

$$A_2(j\omega) = \frac{\overline{V}_3}{\overline{V}_2} = K_1 \frac{1}{1+j\omega R_3 C_3 (3-K_1) - (\omega R_3 C_3)^2} \tag{7}$$

C_3 has been set at 1 nF, R_3 at 390 Ω, and therefore the cutoff frequency has been set at 400 kHz, in order to filter the noise at frequencies higher than those of interest. The DC gain K_1 is equal to 4dB, i.e. 1.586.

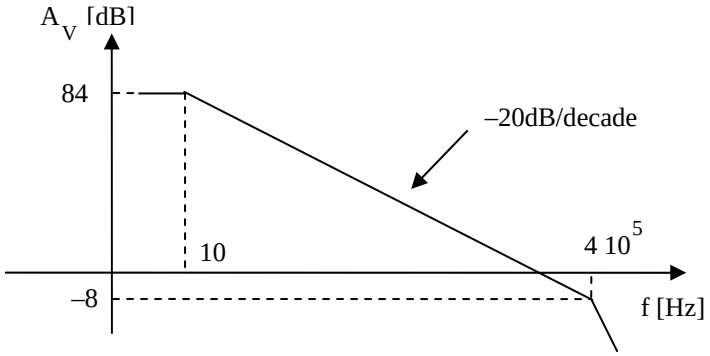

Fig.5 Bode diagram of the amplitude of $A_V(j\omega)$.

Combining the two electronic stages, a voltage transfer function in the frequency domain $A_V(j\omega)$ results, that is given by the product of (6), and (7):

$$A_V(j\omega) = A_1(j\omega)\, A_2(j\omega) = \frac{\overline{V}_3}{\overline{V}_1} \tag{8}$$

The Bode diagram of the amplitude of $A_V(j\omega)$ is reported in fig. 5.
In the frequency range from 10 Hz to 400 kHz, the amplitude of the voltage transfer function of the electronics has a slope of –20dB/decade, from 84dB at 10 Hz down to –8dB at 400 kHz.

d) *Coil function transfer*
Considering the coil, from (5) and (8), the function transfer $H(j\omega)$ of the system results:

$$H(j\omega) = \frac{\overline{V}_3}{\overline{B}_{\perp av}} = \frac{\overline{V}_1}{\overline{B}_{\perp av}}\frac{\overline{V}_3}{\overline{V}_1} = -j\omega A_p\ A_V(j\omega) \tag{9}$$

The coil therefore adds a zero to the transfer function $A_V(j\omega)$, resulting a Bode diagram of the amplitude of

H(jω) that has been reported in fig. 6.

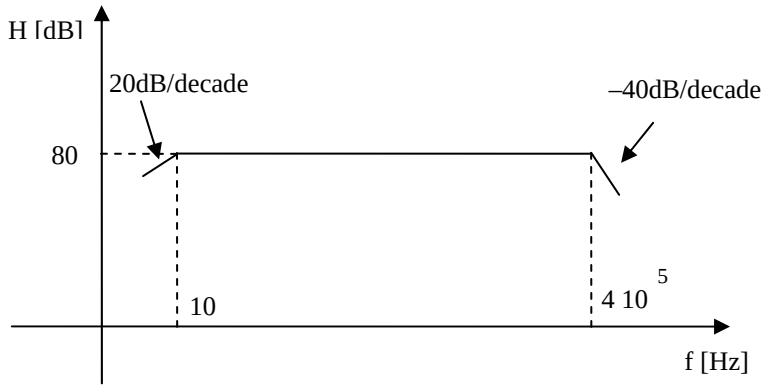

Fig.6 Bode diagram of the amplitude of the function transfer of the system H(jω).

Therefore, in the frequency range from 10 Hz to 400 kHz, the integrator stage and the coil (that makes the derivative of $B_{\perp av}$) give an output voltage proportional to $B_{\perp av}$; a constant gain of 80dB (i.e. 10000) results, i.e. at 100 μT of average perpendicular magnetic flux density corresponds an output voltage of 1 V. Frequency components out of the considered frequency range are filtered.
As the output voltage can vary from ± 10 V, a maximum rating of 1 mT results. It must be noticed that, due to the slew rate (typically of 2.8 V/μs) of the OP-27G that has been used in all the electronic stages [7], a distortion of the signal occurs with the maximum output signal at the highest frequencies of the considered frequency range.

Characterization of the measurement equipment
An experimental laboratory set-up has been performed for the characterization of the measurement equipment. It consisted of a large solenoid, inside which the three coils have been placed during the tests.

a) *Test solenoid*
A single layer cylindrical solenoid, with the characteristics given in Table I, has been realized. The solenoid ends with a twisted pair 4.5 m long. The solenoid has been built on a polypropylene tube, 5 mm thick and with nominal minor diameter of 305 mm. The turns have been realized by using a conductor with a section of 2.5 mm^2.

Table I. Construction data of the test solenoid.

Number of turns	N	187
Internal diameter	Φ	0.305 m
Length	a	0.67 m
Section of the conductor	S_{cond}	2.5 mm^2
Diameter of the conductor (including insulation)	Φ_{cond}	3.6 mm

Two LCR meters (a Metrix IX 3131 at 120 Hz and 1 kHz, and an Agilent 4285A from 75 kHz up to 30 MHz) were used for evaluating the parameters of the solenoid. The equivalent circuit consisted of a capacitance *C* in parallel to the series of a resistance *R* and an inductance *L*.

Table II. Electrical parameters of the test solenoid.

Inductance	L	4.3 mH
Capacitance	C	220 pF
Resistance (DC)	R	1.6 Ω

The parameters found for the solenoid are reported in Table II; L and C values hold up to a few MHz. With reference to the measured inductance value, it is well in agreement with the one estimated from the geometry: in fact, the short solenoid approximation gives for *L* an estimated value of 4.1 mH. From the short solenoid

approximation also results that the calculated magnetic flux density in the centre of the solenoid is 316 μT (directed along the axis of the cylinder) for 1 A of current in the solenoid turns.
A check of this value has been performed by measuring the current in the solenoid turns with a LEM PR50 (DC-50 MHz bandwidth) current probe and the magnetic flux density with a PMM EHP-50C (DC-100kHz bandwidth) probe connected via an optical fibre to a PMM 8053 portable field meter. Tests have been performed at 50 Hz, 100 Hz, 1 kHz, and 10 kHz, and the magnetic flux density directed along the axis of the cylinder was between 330 and 340 μT for 1 A of current in the solenoid turns. This values are in good agreement with the estimated one.

b) *Test circuit*
Two power supplies have been used for the solenoid: a Kepco BOP-100-4D and an Agilent 33120A function generator. The output signal from the electronic circuit has been acquired by a Yogokawa DL1540L digital oscilloscope. The block scheme of the test circuit is shown in fig. 7.

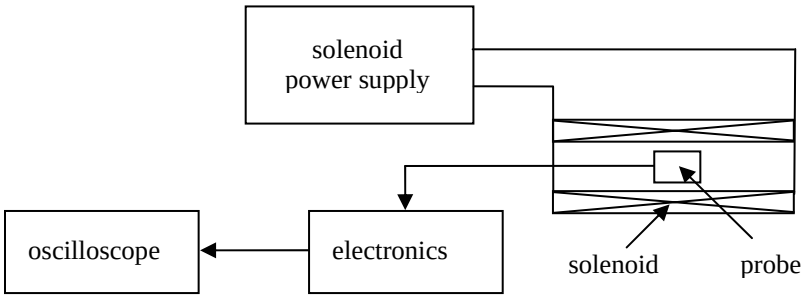

Fig.7 Block scheme of the test circuit for the probe characterization

The probe has been placed in the centre of the solenoid, with the coil under test with the area perpendicular to the solenoid axis. The solenoid has been connected to the Kepco BOP-100-4D power supply, driven by the Agilent 33120A function generator.

c) *System ratings*
An offset was present at the output of the electronics, and was eliminated by selecting the AC signal input coupling of the oscilloscope: a less than 10 Hz cutoff frequency is introduced in this way.
An output voltage noise of about ± 2 mV has been measured, that is 0.02% of the output maximum voltage.

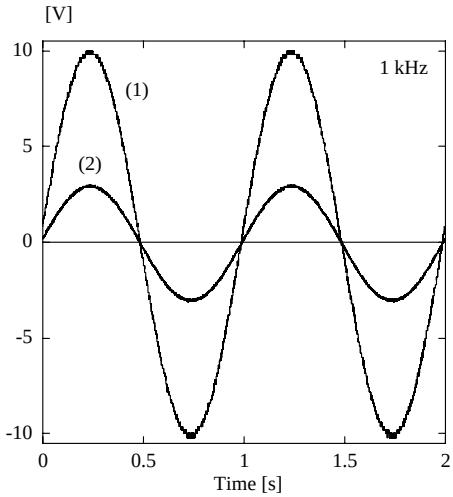

Fig.8 Test at 1 kHz: (1) electronics output voltage $v_3(t)$ and (2) solenoid turns current (1 V corresponds to 1 A).

By using the test circuit previously described, tests have been performed at 10 Hz, 1 kHz, 10 kHz and 100 kHz.
At 10 Hz and 1 kHz, the maximum of the magnetic flux density was 1 mT (i.e. 707 μT rms value), obtained with a maximum current in the solenoid turns of 3 A (i.e. 2.12 A rms value); the electronics output voltage $v_3(t)$ was

measured and the rms value is reported in Table III. As an example, at 1 kHz, in fig. 8, the electronics output voltage $v_3(t)$ and the solenoid turns current (1 V corresponds to 1 A) are reported, indicated with (1) and (2) respectively.
The test circuit could not test the system at the maximum ratings at 10 kHz and 100 kHz, and therefore at these frequencies the tests have been performed at the reduced ratings shown in Table III. The solenoid turns current has been measured directly at the output of the solenoid, in order to avoid the capacitance effect of the connections.
The results are in good agreement with the design ratings.

Table III. System ratings

Frequency [kHz]	B [μT] rms	I [A] rms	V_3 [V] rms
0.01	707	2.12	5.00
1	707	2.12	7.07
10	70.7	0.212	0.723
100	1.5	0.0045	0.015

c) *Analysis at 400 kHz*
At 400 kHz the analysis has been performed by using a simple equivalent model of the system.
The power supply has been modelled with an ideal voltage source, and the solenoid has been considered an ideal inductor (with L = 4.3 mH), magnetically coupled with the coil. The ratio between the ideal voltage source and the coil output voltage results of about 1300.
For the test, the Agilent 33120A function generator has been used as solenoid power supply. Its 50 Ω equivalent output resistance is in effect negligible compared with the equivalent impedance of the test solenoid at 400 kHz. With a 7 V rms value of power supply voltage and the test circuit of fig. 7, the electronics output voltage was about 2 mV rms value. This value is in agreement with the value expected from the system, even if it is close to the noise of the electronics output voltage.

Summary
A new simple and low cost magnetic field measurement equipment in the frequency range from 10 Hz to 400 kHz has been developed.
The design and realization of the equipment has been reported. The function transfer of the system has a constant 80dB gain in the above mentioned frequency range.
The characterization of the system has been performed at maximum ratings from 10 Hz up to a few kHz. At the higher frequencies, the characterization has been performed only at small signals.
The results are all well in agreement with the design ratings.

References
[1] M. Addari, F. Bessi, O. Bottauscio, G. Crotti, G. D'Amore, I. Gallimberti, G. Molinari, M. Repetto, S. Tofani, and U. Tromboni, “Household ELF environment assessment,” in *Proc. EMC '94 International Symposium on Electromagnetic Compatibility*, Roma, 1994, pp. 21-26.
[2] *CEI 211-6 - Guide for the measurement and the evaluation of electric and magnetic fields in the frequency range 0 Hz - 10 kHz, with reference to the human exposure*, Comitato Elettrotecnico Italiano, Milano 2001.
[3] *Household and similar electrical appliances - Electromagnetic fields - Methods for evaluation and measurement*, European Standard EN 50366: 2003-05.
[4] F. Glover, *Inductances calculations – Working formulas and tables*, Instruments Society of America, Research Triangle Park, NC, 1973.
[5] I. Hutchinson, *Principles of Plasma Diagnostics*, Cambridge University Press, Cambridge, 1987.
[6] P. Horowitz, and W. Hill, *The art of electronics*, Cambridge University Press, 2nd ed., 1989.
[7] *Analog Devices data sheets.* Available: http://www.analog.com

EFFECT OF MOBILE PHONE (GSM-900) FIELD ON KINDLED SEIZURES (AS AN INDEX OF NEURAL EXCITABILITY) IN RATS

A. BAYAT

DEPARTMENT OF MEDICAL PHYSICS, TARBIAT MODARES UNIVERSITY, TEHRAN, IRAN
agbayat@gmail.com

S. M. P. FIROOZABADI

DEPARTMENT OF MEDICAL PHYSICS, TARBIAT MODARES UNIVERSITY, TEHRAN, IRAN
Pourmir@Modares.ac.ir

J. MIRNAJAFI-ZADEH

DEPARTMENT OF PHYSIOLOGY, TARBIAT MODARES UNIVERSITY, TEHRAN, IRAN
mirnajafi@yahoo.com

M.E. REZVANI

DEPARTMENT OF PHYSIOLOGY, TARBIAT MODARES UNIVERSITY, TEHRAN, IRAN

Abstract

The rapid expansion of mobile communication has generated intense interest, but has also fuelled ongoing concerns. Radiofrequency radiations are suspected to affect cognitive functions in both humans and animals. Previous studies have suggested that biological parameters of central nervous system can be impaired by "Global System for Mobile Communication" (GSM) exposure in animals.

In this study, the effect of GSM radiation on kindled seizures (as an index of neural excitability) was investigated. All the animals were implanted with a tripolar (stimulating and recording) electrode in the amygdala and were kindled by daily electrical stimulating of amygdala. Different groups of full kindled rats exposed by radiofrequency fields emitted from GSM (950 MHz, Band with: 200 kHz, pulsed at 217 Hz) mobile phone simulator (output power of antenna: 3 and 5 W, power density: 1.8 mW/cm^2) for 2 and/or 4 hours and at different times after the last kindling seizure (24, 48 and 72 h) and their seizure parameters (afterdischarge duration, latency to stage 4 seizure, stage 5 seizure duration and seizure stage) were measured immediately after radiation. The exposed rats were compared to those of sham-exposed and cage-control rats. There was no difference between exposed, sham, and cage-control rats. Therefore, the data indicates that GSM radiation with the mentioned parameters had no effect on seizure severity in kindling model of epilepsy.

Keywords: GSM, mobile phone, neural excitability, seizure, kindling

Introduction

The increasing use of mobile communication has raised serious concerns among people and governments about possible health hazard effects. Radiofrequency waves emitted by GSM mobile phones have a frequency band between 890 MHz and 960 MHz. Mobile phones in operation emit a pulsed radiofrequency electromagnetic field (EMF), a large part of which is absorbed into the user's head [1]. Some EEG and ECG studies have reported that GSM-EMF affects brain electrical activity [2, 3, 4, 5, 6, 7, 8], specially during cognitive performance [9, 10]. Also other investigators that have worked on this issue believe that mobile phones exposure modifies biological parameters of excitable tissues and disturbs performance of neural systems [11, 12, 13, 14, 15, 16, 17]. In a recent study it has been suggested that the EMF emitted by a commercial GSM mobile phone affects regional cerebral blood flow (rCBF) in human [18].

On the contrary, some of the studies have revealed that mobile phones EMF have no significant effects on human health (19, 20, 21, 22, 23). These results have remained controversial yet. In this study we tried to investigate the effect of GSM EMF on neural excitability. Using kindling model of epilepsy, we created seizure conditions in rats. In this situation the excitability of the CNS was high enough to study if the GSM field had any effects on this excitability. Chronic exposure of kindled rats by magnetic field (50 Hz, 100 micro tesla) exerts weak inhibitory effects on some seizure parameters [24]. However there is no report concerning effect of mobile phone (GSM-900) field on neural excitability in kindling model of epilepsy.

Materials and Methods

Surgical and kindling procedure

Male Sprague–Dawley rats weighing 330–360 g, under ketamin and rampoune anaesthesia (50 mg/kg) were stereotaxically implanted with bipolar stimulating and monopolar recording electrodes (twisted into a tripolar configuration) terminating in the basolateral amygdala of the right hemisphere (coordinates: A, 2.5 mm; L, 4.8 mm and 7.5 mm below dura). Electrodes (stainless steel, Teflon coated, A-M Systems, Inc., USA) were insulated except at their tips. Two other electrodes were connected to skull screws, placed above the left cortical surface, as earth and differential electrodes. One week after surgery, afterdischarge (AD) threshold was determined in the amygdala by a 2 s., 60 Hz monophasic square wave stimulus of 1 ms per wave. The stimulations were initially delivered at $10\,\mu A$ and then at 5 min intervals increasing stimulus intensity in increments of $10\,\mu A$ until at least 5s of AD were recorded as previously described [25]. Then, animals were stimulated daily at the AD threshold intensity until five consecutive stage 5 seizures (according to Racine, 1972) were elicited [26]. The recorded parameters were: a) seizure stage (SS) which was measured by observing the behaviour of the animal; b) AD duration (ADD) which was measured from starting of stimulation to the end of AD recording; c) the latency to the onset of bilateral forelimb clonus (S4L) which was measured from starting of stimulation to starting of stage 4 seizure; d) the duration of stage 5 seizure (S5D) which was started with loss of balance and stopped after acquisition of balance; and e) seizure duration (SD) which was measured from starting of stimulation to the end of seizure behaviours.

Radiation procedure

The EMF was provided by a GSM simulator in two level 3 and 5 mean power. When the GSM system was on, the antenna emitted a 950 MHz EMF with mean field strength 1.8 mW/cm^2 pulsed at a frequency of 217 Hz with a pulse width of 0.577 ms. According to the measurements that achieved by Iranian atomic energy organization experts, field strength was 1.78 m mW/cm^2 and 1.82 mW/cm^2 for 3 w and 5 w mean power of antenna, respectively. Thus mean field strength of this EMF is double of workers permissible limits [27].

Exposure chamber that we employed for radiation procedure was a cylindrical shape with 30 cm height and 30 cm diameter of base circle. It was made of special hard transparent PVC. The Simulator antenna with 15 cm height was placed in the centre of base circle (Fig. 1).

Exposure chamber was placed in a greater space (we call it radiation box) with dimensions of 1.1 m×1.1m×1.1m. For protection intentions the external sidewalls of the box covered with aluminium sheets. Long time EMF radiation generates hot and cavity spots throughout the radiation space. Hot spot have high density of field lines and energy and cavity spots have no field lines or energy. Avoiding to this phenomena and creation a uniform RF field around the chamber, we used conical shape absorbers that were made of graphite dyed spongy matters in internal sidewall of the radiation box. Fig. 2 shows these electromagnetic absorbers dimensions. Reflection Coefficient for these electromagnetic absorbers in 950 MHz is -40 dB approximately [28]. Obviously, in this condition we would have a uniform field throughout the exposure chamber. Fig. 3 shows a rat in near field of the antenna within the exposure chamber and radiation box, respectively. During radiation, for eliminating the external stress, animal was released in the chamber. So average distance from antenna was 10 cm that is equal with near field of GSM antenna [29]. Mean field strength was measured in this distance.

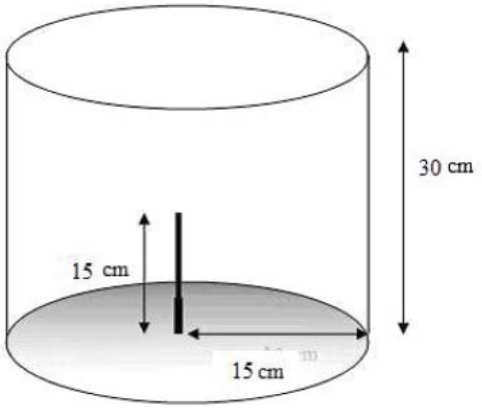

Fig. 1. The exposure chamber and the position of the antenna.

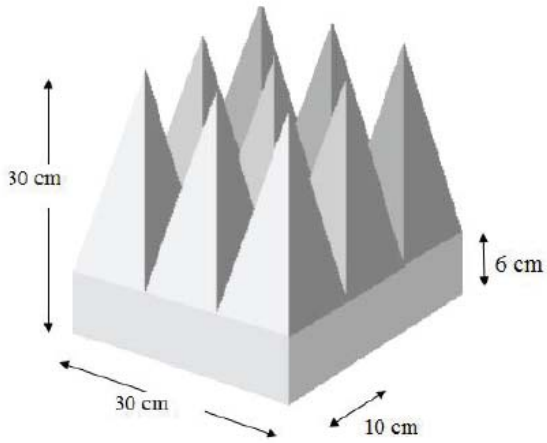

Fig. 2. Electromagnetic absorbers

Fig. 3. A rat is released in near field of the antenna within the exposure chamber. The black shapes are electromagnetic absorbers in internal sidewall of the radiation box.

We only considered non-permanently effects of GSM exposure on kindling parameters. In this way, we used four radiation paradigm and a different group of full-kindled animals (n=6) were employed in each experiment. The results were expressed as the mean ± S.E.M. for each test groups. The comparison between last fully kindling (control) values and sham exposure or GSM radiation values was done by paired t-test. A P-value of less than 0.05 was considered to represent a significant difference.

Results

The assessment of probable effect of radiation chamber and its dark environment on seizure severity was an essential note for research accuracy. Therefore, 24 h after the last kindling seizure, rats were affected by muted GSM generator (sham exposure) for 2 hours. This work was repeated at 48 and 72 h after full kindling creation for each subject, similarly. Immediately after each radiation animals were stimulated and their seizure parameters were measured and were compared with the last kindling or control values. Obtained results showed no significant differences between data (Table 1).

The above method was performed similarly, except that GSM exposure had a mean power of 3 watt and field strength of 1.78 mW/cm^2 (experiment 2) or a mean power of 5 watt and field strength of 1.82 mW/cm^2 (experiment 3). Statistical analysis showed no significant affect of GSM on seizure parameters (Tables 2, 3). In experiment 4, at 24 h after the last kindling seizure animals affected by GSM generator with a mean power of 5 watt and field strength of 1.82 mW/cm^2 for 4 hours and seizure parameters were measured immediately after radiation. Again, no significant difference was observed in compared to pre-exposure data (Table 4).

Discussion and Conclusion

In this study we found that, a GSM simulator with field strength of 1.8 mW/cm^2 and mean power of 3 and 5 watt doesn't create any considerable effect on amygdala kindled seizure parameters and there is no evidence for predicting reduction or increasing in neural excitability. Radiation time for 2 and 4 hours had no sensible or measurable effects too. Therefore these results confirm that radiation time and mean power of GSM antenna have no essential effects on seizure parameters in kindling model of epilepsy. This conclusion is in adjusted with several studies that have indicated mobile phone and radiofrequency fields have no effect on neural excitability [21, 22, 30, 31]. It is specially in adjusted with a coincident study that has showed a 900 MHz exposure with SAR of 0.25, 1, 2, 4 W/kg, has no effect on hippocampus parameters of free rats in cage [32].

However, this study doesn't confirm EMF field effects on epileptiform activity induced by amino pyridine in hippocampal slices [33, 34]. Additionally, according to this study, GSM EMF field, hadn't any inhibitory effects on seizure parameters in kindling model of epilepsy such as low frequency magnetic field [24, 35].

Also these results are differing with another research that has investigated effects of GSM-900 field (SAR less than 2 W/kg) on neural lesion possibility in rats [36].

Compatibility, some studies have suggested that GSM field couldn't change EEG parameters (that shows normal function of neural activity) in volunteers. Therefore GSM mobile phones exposure (according to this study conditions) couldn't modify seizure parameters in an excited neural system and have no significant effects on seizure biological parameters in kindling model of epilepsy. Obviously, this conclusion is exceptionally fastened to above conditions, experimental setup and methodologies.

Acknowledgement

We thank the Iran Telecommunication Research Center (ITRC) for its financial support in this project (grant No. 500/6639).

Table 1. Effect of sham exposure of animals in radiation box on seizure parameters

	Control	24 h	48 h	72 h
S4L	24.68 ±2.86	25.36±2.57	23.50±1.80	24.55±2.35
S5D	45.57±3.20	43.74±4.80	46.25±3.64	44.63±5.43
ADD	86.29±9.16	89.82±6.86	83.52±8.52	88.40±6.65
SD	103.00±7.78	100.5±2.57	104.0±7.60	99.60±8.46

Animals were exposed at 24, 48 and 72 h after the last kindling seizure and their parameters were compared with pre-exposure (control) values. Mean power and sham radiation time were 0 watt and 2 hours, respectively. Values (s) are mean±SEM. No significant difference was observed with compared to control data.

Table 2. Effect of GSM (3 watt, 2 h) exposure of animals on seizure parameters

	Control	24 h	48 h	72 h
S4L	16.66± 3.46	15.90±3.05	16.10±3.33	14.53±3.93
S5D	33.41±3.15	34.02±3.55	30.58±3.63	35.70±5.63
ADD	89.53±11.2	83.20±9.73	87.18±10.2	84.74±12.4
SD	93.50±7.55	92.50±7.73	93.00±6.06	99.00±2.20

Animals were exposed at 24, 48 and 72 h after the last kindling seizure and their parameters were compared with pre-exposure (control) values. Values (s) are mean±SEM. No significant difference was observed with compared to control data.

Table 3. Effect of GSM (5 watt, 2 h) exposure of animals on seizure parameters

	Control	24 h	48 h	72 h
S4L	22.93±1.91	22.18±1.85	20.40±1.49	19.98±1.05
S5D	42.37±2.00	41.63±1.62	43.37±2.7	43.10±3.07
ADD	96.71±9.16	91.82±7.66	92.52±7.22	90.96±6.44
SD	113.0±7.78	105.0±3.96	109.0±7.98	102.0±3.66

Animals were exposed at 24, 48 and 72 h after the last kindling seizure and their parameters were compared with pre-exposure (control) values. Values (s) are mean±SEM. No significant difference was observed with compared to control data.

Table 4. Effect of GSM (5 watt, 4 h) exposure of animals on seizure parameters

	Control	24 h
S4L	19.50±1.48	17.88±1.24
S5D	39.86±3.20	42.53±2.93
ADD	85.40±6.80	83.30±5.40
SD	89.25±5.60	92.50±4.54

Animals were exposed at 24 h after the last kindling seizure and their parameters were compared with pre-exposure (control) values. Values (s) are mean±SEM. No significant difference was observed with compared to control data.

References

1- Schonborn F, Burkhardt M, Kuster N. Differences in energy absorption between heads of adults and children in the near field of sources. Health Phys 1998; 74:160–8

2- Röschke J, Mann K. The Effects of Digital Mobile Radio Telephones on the Electroencephalogram of Humans. In Proceeding of the International workshop on electromagnetic fields and non-specific health symptoms; 1998 Sep 19 – 20; Graz, Austria. p. 69-79.

3- Borbely AA, Huber R, Graf T, Fuchs B, Gallmann E, Achermann P. Pulsed high-frequency electromagnetic field affects human sleep and sleep electroencephalogram. Neuroscience Letters 1999; 275:207-210.

4- Freude G, Ullsperger P, Eggert S, Ruppe I, Effects of microwaves emitted by cellular phones on slow brain potentials. Bioelectromagnetics 1998; 19:384-7.

5- Fritze K, Wiessner C, Kuster N, Sommer C, Gass P, Hermann DM, Kiessling M, Hossmann KA. Effect of global system for mobile communication microwave exposure on the genomic response of the rat brain. Neurosience 1997; 81(3): 627-39.

6- Mausset AL, de Seze R, Montpeyroux F, Privat A. Effects of radiofrequency exposure on the GABAergic system in the rat cerebellum. Brain Res 2001; 912(1):33-46.

7- Reiser HP, Dimpfel W, Schrober F. The influence of electromagnetic fields on human brain activity. Eur J Med Res 1995; 1:27–32.

8- Croft RJ, Chandler JS, Burgess AP, Barry RJ, Williams JD, Clarke AR. Acute mobile phone operation affects neural function in humans. Clin Neurophysiol 2002; 113:1623–32.

9- Eulitz C, Ullsperger P, Freude G, Elbert T. Mobile phones modulate response patterns of human brain activity. Neuro Report 1998; 9:3229–32.

10- Freude G, Ullsperger P, Eggert S, Ruppe I. Microwaves emitted by cellular telephones affect human slow brain potentials. Eur J Appl Physiol 2000; 81:18–27.

11- Kavaliers M, Eckel L A, Ossenkopp K P. Brief exposure to 60 Hz magnetic fields improves sexually dimorphic spatial learning in the meadow vole, Microtus pennsylvanicus. J Comp Physiol 1993; 173: 241–48.

12- Lovely RH, Creim JA, Bushbom RL, Miller DL, Anderson LE. Changes in rat's error rates in a radial arm maze during exposure to magnetic fields may have a chronological basis. Sixteenth Annual Meeting of the Bioelectromagnetics Society; 1994; p.62.

13- Lai H, Carino MA, Ushijima I. Acute exposure to a 60 Hz magnetic field affects rats water-maze performance. Bioelectromagnetics 1998; 19: 117–22.
14- Lai H, Singh NP, Melatonin and a spin-trap compound block radiofrequency electromagnetic radiation-induced DNA strand breaks in rat brain cells. Bioelectromagnetics 1997;18(6): 446-5.
15- Koivisto M, Krause CM, Revonsuo A, Laine M, Hamalainen H,The effects of electromagnetic field emitted by GSM phones on working memory. Neuro report 2000;11: 1641–3.
16- Tattersall JEH, Scott IR, The effects of radiofrequency radiation on hippocampal long potentiation in vitro. In Proc. Of International conference and exhibition on Electromagnetic compability; (EMC York 99)1999; p. 26-9.
17- Hamblin DL, Wood AW, Croft RJ, Stough C. Examining the effects of electromagnetic fields emitted by GSM mobile phones on human event-related potentials and performance during an auditory task. Clinical Neurophysiology 2004; 115:171–8.
18- Sargo Aalto, Christian Haarala, Anna Bruck, Hannu Sipila, Heikki Ha¨ma¨la¨inen and Juha O Rinne, Mobile phone affects cerebral blood flow in humans, Journal of Cerebral Blood Flow & Metabolism 2006; Pp: 1–6.
19- Hietanen M, et al. Human brain activity during exposure to radio frequency fields by cellular phones. Scandinan journal of work, Enviroment and health 2000; 26(2):87-92.
20- Wagner P, Röschke J, Mann K, Hiller W, Frank C. Human sleep under the influence of pulsed radiofrequency electromagnetic fields: A polysomnographic study using standarized conditions. Bioelectromagnetics 1998; 18:199-202.
21- Johansen C, Olsen JH. Cellular telephones, magnetic field exposure, risk of brain tumors and cancer at other sites: a cohort study. Radiate Prot Dosim 1999; 83: 155.
22- Morrissey JJ, Elder J, Swicord ML, Joyner KH. A Review of Completed and Ongoing RF Bioeffects Research Relevant To Cancer Risk Assessment. In Proceedings of the International Conference on Non-Ionizing Radiation at UNITEN: Electromagnetic Fields and Our Health (ICNIR 2003); 2003 Oct. p.20- 22.
23- Wagner P, Roschke J, Mann K, Fell J, Hiller W, Frank C, Grozinger M, Human sleep EEG influenced of pulsed radiofrequency electromagnetic fields. Neuropsychobiology 2000; 42:207-212.
24- Potschka H, Thun-Battersby S, Wolfgang Loscher. Effect of low-intensity 50-Hz magnetic fields on kindling acquisition and fully kindled seizures in rats. Brain Research 1998; 809:269–276.
25- Pourgholami MH, Mirnajafi-Zadeh J, Behzadi J. Effect of intraperitoneal and intrahippocampal 2-chloroadenosine in amygdaloid kindled rats. Brain Res. 1997; 751: 259–264.
26- Racine RJ. Modification of seizure activity by electrical stimulation: 2. Motor seizure. Electroencephalogr. Clin. Neurophysiol. 1972; 32: 281–294.
27- Trzaska H. SAR? In the proceedings of 3rd International workshop on biological effects of electromagnetic fields; 2004 Oct 4-8; Greece.
28- www.emctest.com
29- Zervos T, Alexandridis AA, Petrovic VV, Dangakis K, Kolundzija BM, Dordevic AR, Soras C.Comparison between helical and monopole antennas regarding mobile handset and human head interaction.In proceedings of the 3rd International workshop on biological effects of electromagnetic fields; 2004 Oct 4-8; Greece.
30- Dubreuil D, Jay T, Edeline JM. Head-only exposure to GSM 900-MHz electromagnetic fields does not alter rat's memory in spatial and non-spatial tasks. Behav Brain Res 2003; 145:51–61.
31- Dubreuil D, Jay T, Edeline JM, Dose head only exposure to GSM 900-MHz electromagnetic fields affect the performance of rats in spatial learning task?. Behav Brain Res 2002; 129:203-210.
32- Finnie J, Gebski V. Neuronal changes produced in mouse brain after short and long term exposure to global system for mobile communication (GSM)- link radiofrequency fields. In proceedings of the 3rd International workshop on biological effects of electromagnetic fields; 2004 Oct 4-8; Greece.
33- Tattersall JE, Scott IR, Wood SJ, Nettell JJ, Bevir MK, Wang Z, Somasiri NP, Chen X. Effects of low intensity radiofrequency electromagnetic fields on electrical activity in rat hippocampal slices. Brain Res 2001; 904:43–53.
34- Bawin SM, Satmary WM, Jones RA, Adey WR, Zimmerman G. Extremely-low-frequency magnetic fields disrupt rhythmic slow activity in rat hippocampal slices. Bioelectromagnetics 1996; 17:388–395.
35- Ossenkopp KP, Cain DP. Inhibitory effects of acute exposure to low- intensity 60- Hz magnetic fields on electrically kindled seizures in rats. Brain Res 1988; 442: 255-260.
36- Eberhardt J. L., Persson B., Brun A., Salford L. G., Effect of microwaves from GSM mobile phones on the rat brain, in proceedings of 3rd International workshop on biological effects of electromagnetic fields; 2004 Oct 4-8; Greece.

50 HZ MAGNETIC FIELD EFFECT ON THE MORPHOLOGY OF BACTERIA

LUKÁŠ FOJT[1,2], PETR KLAPETEK[3], LUDĚK STRAŠÁK [1,2], VLADIMÍR VETTERL[1,2]

1 INSTITUTE OF BIOPHYSICS, CZECH ACADEMY OF SCIENCES, KRÁLOVOPOLSKÁ 135, 612 65 BRNO, CZECH REPUBLIC
2 DENTAL RESEARCH CENTRE, MASARYK UNIVERSITY, VINAŘSKÁ 6, 603 00 BRNO, CZECH REPUBLIC
3 CZECH METROLOGICAL INSTITUTE, OKRUŽNÍ 31, 638 00 BRNO, CZECH REPUBLIC

Abstract

In our previous works we found that different strains of bacteria are affected by the magnetic field exposure. The decrease of CFU number (colony forming units) was observed in cultures of different bacterial strains after 12 minutes exposure to 10 mT 50 Hz magnetic field. This effect was strain dependent and the relative decrease was from 30% (*Escherichia coli*) to 12% (*Staphylococcus aureus*). We observed that rod-like bacteria (*Escherichia, Leclercia*) are more affected than spherical ones (*Staphylococcus, Paracoccus*). We carried out AFM study to determinate surface changes of bacteria after 60 minutes of 50 Hz 10mT magnetic field exposure of *Escherichia coli* and *Paracoccus denitrificans*. We have not observed any change in bacterial morphology of both used bacterial strains. Magnetic field did not influence the surface and shape of bacteria.

Introduction

Investigation of effects of electromagnetic fields on living organisms is needed in our community. It is important to know, how biological objects react to exposure of external electromagnetic field. According to this knowledge, we will be able to estimate health and economical aspects of using of many electrical and magnetic devices. Recently, there have been a lot of studies concerning these problems. We can found many studies of magnetic and microwave effects on DNA (1-3), enzymatic activity (4,5), proliferation control (6,7) and many others (8,9).

In our previous studies we have found, that effect of 50 Hz magnetic fields on different types of bacteria is strain-dependent (10-13). This effect was even shape dependent. We used CFU – colony forming units – method to determinate proliferation of bacteria after magnetic field exposure. Rod-like bacteria (*Escherichia coli* and *Leclercia adecarboxylata* - decrease of CFU number after 12 minute exposure to 10 mT 50 Hz magnetic field was about 40%, respectively 30% - survived in lower number than spherical ones (*Paracoccus denitrificans* and *Staphylococcus aureus* - decrease of CFU number after 12 minute in 10 mT 50 Hz magnetic field was about 14%, respectively 21%). Thus, we decided to measure surface characteristics of *Escherichia coli* and *Paracoccus denitrificans* with AFM technique to estimate possible morphological change after magnetic field exposure.

Material and Methods

Bacteria *Escherichia coli* was obtained from Biological department of Masaryk university Brno (strain K12, Row, genotype 58–161 *metB1rpsL* 1+ F^{def}P.Fredericq), *Paracoccus denitrificans* CCM 982 (NCIB 8944) was obtained from the Czech Collection of Microorganisms. For AFM measurements was used Explorer AFM (Veeco). Cylindrical coil parameters are given in our previous papers (10-12).

For morphological changes determination we used this procedure: bacteria were placed on thin glass surface. After evaporating, we take control samples measurements. Than were the bacteria placed to center of the coil and kept here for 60 minutes in 10 mT 50 Hz magnetic field. After this exposition we took another AFM pictures. Thus, we were able to detect the same bacteria before and after exposure.

Results and Discussion

On Fig.1 an Fig. 2 we can see the AFM pictures of control and exposed samples of bacteria. We have done some correlation data processing (for x,y and z position of every pixel on AFM picture). We have found, that the bacteria had not changed their morphology. There were only small changes on edges of samples, but these could be satisfactory explained by AFM head drift. Every experiment was at last 3 times repeated in high-resolution scans (area around 5x5μm) and 3 times in low resolution (area around 50x50 μm).

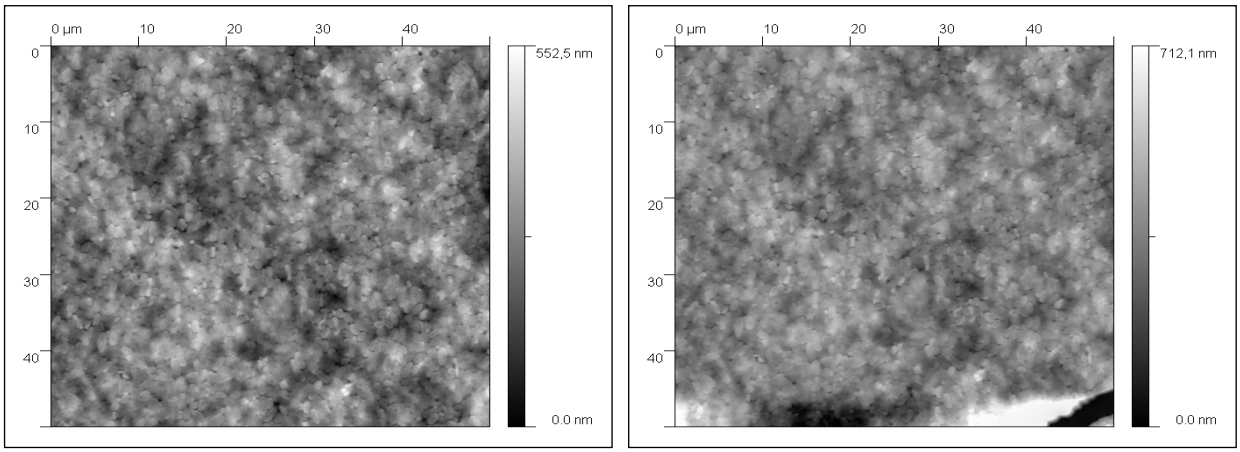

Fig. 1 Escherichia coli, sample before exposure (left), and exposed sample (1 hour 10 mT, 50 Hz) – (right)

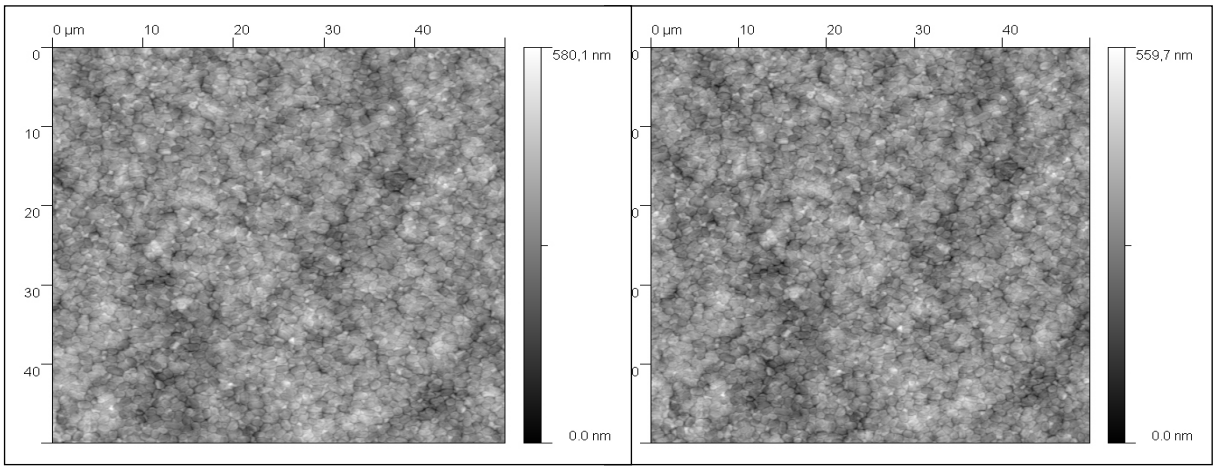

Fig. 2 Paracoccus denitrificans, sample before exposure (left), and exposed sample (1 hour 10 mT, 50 Hz) – (right)

We have found, that both types of used bacteria - *Escherichia coli* and *Paracoccus denitrificans* did not change their shapes after 1 hour exposure to 50 Hz magnetic field, B_m=10 mT. We used AFM method for bacterial surface monitoring.

Reference

1. Federica I. Wolf , Angela Torsello, Beatrice Tedesco, Silvia Fasanella, Alma Boninsegna, Marcello D'Ascenzo, Claudio Grassi, Gian Battista Azzena, Achille Cittadini. 50-Hz extremely low frequency electromagnetic fields enhance cell proliferation and DNA damage: Possible involvement of a redox mechanism, Biochimica et Biophysica Acta 1743 (2005) 120– 129

2. Maciej Lopucki, Ivo Schmerold, Agnes Dadak, Henryk Wiktor, Hans Niedermüller, Marta Kankofer. Low dose magnetic fields do not cause oxidative DNA damane in human placental cotyledons in vitro, Virchows Arch 446 (2005) 634–639

3. C. Schmitz, E. Keller, T. Freuding, J. Silny, H. Korr. 50-Hz magnetic field exposure influences DNA repair and mitochondrial DNA synthesis of distinct cell types in brain and kidney of adult mice, Acta Neuropathol 107 (2004) 257–264

4. Tomonori Sakurai, Shin Koyama, Yoshiki Komatsubara, Wang Jin, Junji Miyakoshi. Decrease in glucose-stimulated insulin secretion following exposure to magnetic fields, Biochemical and Biophysical Research Communications 332 (2005) 28–32

5. Maria Piera Piacentini, Elena Piatti, Daniele Fraternale, Donata Ricci, Maria Cristina Albertini, Augusto Accorsi. Phospholipase C-dependent phosphoinositide breakdown induced by ELF-EMF in *Peganum harmala* calli, Biochimie 86 (2004) 343–349

6. Masakazu Iwasaka, Masateru Ikehata, Junji Miyakoshi, Shoogo Ueno. Strong static magnetic field effects on yeast proliferation and distribution, Bioelectrochemistry 65 (2004) 59– 68

7. Strašák L, Vetterl V, Fojt L., Effects of 50 Hz magnetic fields on the viability of different bacterial strains,ELECTROMAGNETIC BIOLOGY AND MEDICINE,24, 293-300, 2005

8. H. Berg. Possibilities and problems of low frequency weak electromagnetic fields in cell biology, Bioelectrochem. and Bioenerg. 38 (1995) 153-159

9. C Polk.Physical mechanism for biological effects of low field intensity ELF magnetic fields, Biological Effects of Magnetic and ElectromagneticFields, Plenum Press, New York, 1996, 63-83.

10. L. Strašák, V. Vetterl, J. Šmarda. Effects of low-frequency magnetic fields on the bacteria Escherichia coli, Bioelectrochem. Bioenerg. 55 (2002) 161– 164.

11. L. Fojt, L. Strašák, V. Vetterl, J. Šmarda. Comparison of the low-frequency magnetic field effects on bakteria Escherichia coli, Leclercia adecarboxylata and Staphylococcus aureus, Bioelectrochemistry 63 (2004) 337– 341.

12. L. Fojt, L. Strašák, V. Vetterl,Effect of electromagnetic fields on the denitrification activity of *Paracoccus denitrificans*, Bioelectrochemistry, in press

13.L.Strašák, V.Vetterl, L.Fojt, Effects of 50 Hz magnetic fields on the viability of different bacterial strains, Electromagnetic Biology and Medicine, 24(2005) 293-300

SUBJECTIVE SYMPTOMS IN GSM NETWORK WORKERS

GADZICKA E., BORTKIEWICZ A., SZYJKOWSKA A., SZYMCZAK W., SIŃCZUK-WALCZAK H.

NOFER INSTITUTE OF OCCUPATIONAL MEDICINE, 91-348 LODZ, 8 TERESY ST., POLAND, E-MAIL: ela@imp.lodz.pl

Abstract

The aim of the study was to investigate the effect of EMF from mobile phones and stress perception on general health condition. The subjects were 208 GSM communication workers who responded to a 53-item questionnaire. Most of them (57%) assessed their health condition as good, 14.% as very good and 18% as fair. The level of stress was assessed in 89 workers (mean age 30.3±7.7, employment duration 4.1±1.7 years) using the Perceived Stress Scale (PSS) by Cohen and the Subjective Assessment of Work Characteristics Questionnaire (SAWCQ). EMF exposure was calculated as daily call duration (CT). The study population was divided into two groups (similar in age and employment duration): I with CT below 60 min., mean 23 min., II with CT above 60 min., mean 158 min. Group II more frequently reported headache (58% vs. 78.4%, p=0.045), dizziness (10% vs. 32.4%; p.=0.009), impaired concentration (2% vs. 13.5% p.=0.05), and heat sensation in the auricular area (30% vs. 51.4%, p.=0.044). The score on SAWCQ was higher in group II (p=0.05). The risk of a headache was significantly dependent both on CT (OR=3, p=0.0044) and PSS (OR=1.12, p=0.043). EMF exposure and stress significantly contributed to an increased rate of subjective symptoms reported by GSM workers.

Introduction

The professional group of mobile communication workers who can experience simultaneous exposure to EMF and work-related stress has developed as a result of the dynamically growing mobile communication systems and the increasing demand for mobile phone services. Mobile communication workers are exposed at work to stress related to a high pace of work performance (time pressure), high responsibility and continuous contact with customers; the level of stress depending on a given workpost. When evaluating the impact of work environment on the workers' health, one should take into account the factors related to job characteristics. Relevant literature reports on the significance of psychosocial factors such as work-related stress, effort-reward imbalance, shift work, sedentary work and other work-related stressors [1]. It seems then, that apart from the 'hard' parameters of work environment, such as EMF, one should also consider the potential influence of the psychosocial factors. Therefore, our study focused on the assessment of the level of stress related to work and everyday activities. Stress at work is associated not only with some objective factors but depends on the subjective assessment of working conditions and job requirements. This assessment evokes emotions that in turn trigger different physiological processes and mechanisms that can lead to adverse health effects if such activity is long-term or too intensive [2,3,4]. The health impact of prolonged experience of stress combined with EMF exposure may concern large communities because most of the executive staff and administration, whose duties can be perceived as highly stressful, can also be subjected to EMF exposure, as a result of a common use of mobile communication both at work and at home.

The aim of the study was to investigate the combined effect of EMF from mobile phones and stress perception on the health condition of GSM workers.

Material and Methods

Study population

The study was performed on a population of Polish workers of GSM network who are occupationally exposed to EMF from mobile phones. For this population it was possible to precisely determine the level of EMF exposure through analysis of billing and work history documentation to elicit call duration and time of EMF exposure. Some of the workers performed their duties using a stationary telephone (Call Centre operators), while others (sale dept. workers and individual and company service workers) used mobile phones. We could thus ensure study groups with

varying type and level of exposure for our investigation. In total, 208 workers were qualified for the survey. Of this number, 89 persons responded to the psychological questionnaire.

Exposure to EMF evaluation
Since most of the workers used the same type of mobile phone in their job, exposure assessment could be limited to analyzing the parameters regarding the intensity of phone use. The level of occupational exposure to EMF was calculated based on the time and frequency of mobile phone calls, SAR, and an output for a given phone used.

Each worker had the following parameters calculated:
- total period of mobile phone use
- mean daily number of calls
- mean duration of a single call
- mean daily exposure (call) duration (mean call time x daily number of calls)

Questionnaire on subjective symptoms related to mobile phone use
The questionnaire was designed specifically for this study and focused on general health condition and health complaints as well as the frequency of mobile phone use. It was tested on a group of 600 individuals using mobile communication. When developing the questionnaire, the authors consulted Scandinavian and Australian researchers about similar surveys conducted in their countries. Finally, some items from a Swedish and an Australian questionnaire were included to facilitate comparison with their findings [5,6].

The questionnaire comprises 53 items regarding (a) personal data: age, gender, education, history of work under EMF exposure; (b) self-assessment of health condition, and specific symptoms: headache, dizziness, tinnitus, visual impairments, skin symptoms of the head and neck area, sleep disturbances, and present or past diseases; (c) mobile phone use: type of phone (handsets, hands-free kits), and (d) habits related to phone use: frequency and duration of calls; (d) subjective symptoms related to mobile phone use.

Stress evaluation:
- Subjective Assessment of Work Characteristics Questionnaire (SAWCQ). The questionnaire has been developed and validated at the Nofer Institute of Occupational Medicine, Lodz, Poland. It consists of 50 items inquiring about different psychosocial stressors (factors) related to work [7]. Each subject is asked to assess whether a given factor occurs at his/her workpost and if so, to what extent it accounts for his/her irritation, fatigue, anger, stress, etc. A five-point scale is used to assess the impact of every potential stressor. The individual index of job stressfulness is calculated as a total score on all questionnaire items indicated by the subject. SAWCQ proved to be a reliable measuring instrument: r_{tt}= 0.87 an Cronbach α= 0.84. Raw scores can be transformed into normalized scores on a 10-point scale. The questionnaire was positively validated on a large sample (N = 2570) of Polish working population
  - low level of stress - score 65-80 points
  - medium level of stress - score 81-101 points
  - high level of stress - score about 102 points

- Perceived Stress Scale (PSS) developed by Cohen [1983]. The Scale is used for measuring the perceived stress, both related to everyday life situations and work performance [8]. The Scale consists of 14 questions on the frequency of recent stressful conditions that the person could or could not cope with. The recipients answer the questions using a five-point scale, with '0' denoting the absence of such a situation and '4' a high frequency of stressful events. The higher the total score, the more a given individual perceives his life course as unpredictable and beyond his/her control.

Statistical analysis
The following methods were used for the statistical analysis: Student's t-Test or F-Snedecor test to compare mean values of parameters in the study groups; chi^2 test or Fisher exact test for comparing frequency of the analysed parameters in the study groups; uni- and multivariate logistic regression for quantitative risk assessment of symptoms in relation to exposure level, after adjusting for confounders.

Results
The study population was homogenous with regard to the occupation, educational level, lifestyle, health status etc., while it differed with respect to the level of EMF exposure and work-related stress.

Mean age of the examined workers was 30.3 ± 7.7 years (21-62 years). The study group included 41 female workers aged 23-45 years (mean 27.8±4.5) and 48 male workers aged 21-62 years (mean 32.4±9.2). The mean age of female workers was significantly lower (p=0.0089).

Mean employment duration was 4.1 ± 1.7 years (2 month-8 years) and did not differ significantly in relation to gender: 3.5±1.7 years (from 2 months to 6.5 years) for female workers and 4.6±1.7 years (from 2 months to 8 years) for male workers.

The mean daily duration of phone calls was 80.4±105.1 min. (2 min.- 600 min.) and was similar in both groups: 75.8±97.5 min. (2 min.-400 min) for females and 84.1±111.8 min (2 min.- 600 min) for males (table 1).

Most of the subjects (75.4%) had university education and 24.6% of workers presented secondary/college level education.

Table 1. Exposure characteristics for the total study population

Exposure parameters	Mean value ±SD
period of mobile phone use (years)	4.1±1.8
mean daily call duration [min]	80.4±105.1

Self-assessment of general health condition and subjective symptoms
Most of the examined people (57%) assessed their health condition as good, 14% as very good and 18% as fair. Nobody reported bad or very bad condition of health and no significant differences in the health status could be found between male and female workers.

67,5% subjects complained of headache; this symptom was significantly (p=0.05) more frequent in female workers (78% vs. 58%) but only 10% of female workers related this symptom to using a mobile phone. 19% of the total subjects reported dizziness; it was more prevalent among females (27% vs. 12.5%) but the difference was statistically insignificant. Other symptoms, like tinnitus, visual impairments etc., were reported by 12.5% of the subjects, with roughly similar prevalence in the groups of female and male workers (17.1 % vs. 10.4%) Impaired concentration occurred in 37.1% of respondents, prevailing among females (41.5% vs. 33.3%). Sleep disturbances occurred in 30.3% of the subjects; they were more frequent among males (33.3% vs. 26.8%) but the difference was statistically non-significant. Facial dermatitis was reported by 12.6% of the subjects. The most prevalent symptom related to mobile phone use was the thermal sensation within the auricle and behind/around the ear. This was reported by more women than men (43.9% vs. 33.3%). 15.7% of the subjects reported fatigue after the call, even if the conversation was a pleasant one, and 6.7% impaired concentration. 11.2% reported difficulties in recalling what they had been doing before they answered the phone call (short-term memory impairments). This symptom was significantly more prevalent among male workers (18.8% vs. 2.4%).

Stress assessment
In the study population, the level of general stress was estimated at 22.1±6.9 and was significantly (p=0.0089) higher among female workers (24.2±6.6 vs. 20.3±6.7). The work-related stress was assessed at 95.3±19.1 and a higher level was found among male workers (96.8±20.2 vs. 93.5±17.8) but the difference was not statistically significant. Although in the study group, the level of stress, according to the classification adopted in earlier studies, assumed medium values (81-101), some individual workers presented very high values (134-145).

Analysis of relationship between reported symptoms and occupational factors (EMF from mobile phone, and stress)
The study population was divided into two groups according to EMF exposure calculated as daily call duration (CT):

- Group I (50 subjects): CT below 60 min., mean 23 min (2-50 min).
- Group II (39 subjects): CT above 60 min., mean 158 min (60-600 min).

These groups were similar with respect to age and employment duration.

The prevalence of the symptoms depended on the total daily duration of calls: the subjects with CT of more than 60 min. more frequently reported symptoms than the subjects with shorter CT (Table 2).

Table 2. Prevalence of symptoms in relation to call duration

Symptoms	Group 1	Group 2	p
Headache	58%	78.4%	0.045
Dizziness	10%	32.4%	0.009
Headache related to mobile phone use	4%	16%	0.05
Impaired concentration	2%	13.5%	0.05
Impaired short-term memory	4%	21.6%	0.01
Thermal sensation in the auricular area	30%	51.4%	0.044
Thermal sensation in the auricle	26%	51.4%	0.015

The level of stress was assessed in the study group with different exposure levels (table 3)

Table 3. General and work-related stress in relation to exposure level

Study groups	General stress (Cohen)	Work-related stress
(I)	21.2±7.3	92.0±18.2
(II)	23.1±6.5	100.2±19.9
(p)	ns	0.05

Analysis by exposure and stress parameters
The analysis was made using logistic regression model including EMF exposure parameters and level of stress.

After adjusting for stress, in group I (with CT of more than 60 min), the risk for headache related to mobile phone use was four times as high as in group II with CT of up to 60 min (Table 4).

Table 4. The risk for headache related to mobile phone use

Parameters	Regression coefficient (B)	Standard error (SE)	p	Odds ratio (OR)
Stress after Cohen	011	0.062	0.059	1.1
CT	1.44	0.87	0.075	4.2

The risk for headache as a symptom that was not associated with mobile phone use was also significantly higher in group II than in group I (OR=3).

Apart from the duration of the call, also stress perception significantly contributed to an increased risk for headache (Table 5).

Table 5. The risk for headache not related to mobile phone use

Parameters	Regression coefficient (B)	Standard error (SE)	p	Odds ratio (OR)
Stress (Cohen)	0.11	0.04	0.0044	1.12
CT	1.10	0.54	0.043	2.97

The risk for dizziness unrelated to mobile phone use was significantly higher (OR =6.8) in group II in comparison with group I (Table 6).

Table 6. The risk for dizziness unrelated to mobile phone use

Parameters	Regression coefficient (B)	Standard error (SE)	p	Odds ratio (OR)
Stress (Cohen)	0.17	0.07	0.0084	1.19
CT	1.91	0.70	0.0058	6.81

As regards concentration impairments, both related and unrelated to mobile phone use, the risk for this symptom was higher among the workers with a high level of work-related stress but was not dependent on the intensity of the calls (tables 7, 8).

Table 7. Risk for concentration impairments related to mobile phone use

Parameters	Regression coefficient (B)	Standard error (SE)	p	Odds ratio (OR)
Work-related stress	0.15	0.05	0.0044	1.17

Table 8. The risk for concentration impairments unrelated to mobile phone use

Parameters	Regression coefficient (B)	Standard error (SE)	p	Odds ratio (OR)
Work-related stress	0.04	0.014	0.0026	1.049

At the next stage of the analysis, we investigated whether including the duration of daily calls in the model describing stress and exposure parameters had influence on the risk for a given symptom. The daily call duration did significantly increase the risk for headache related and unrelated to mobile phone use ($p=0.0063$ and $p=0.02$, respectively), after adjusting for other parameters. Likewise, the risk for dizziness significantly increased with an increasing duration of daily calls ($p=0.0041$). No relationship was found between sleep disturbances and the level of stress.

Summary

The findings of the present study revealed that EMF exposure from mobile phone combined with parallel stress perception significantly increased the prevalence of symptoms reported by GSM workers. This referred to headache, dizziness and sleep disturbances that were much more frequent among workers who reported intensive use of mobile communication (frequent and long calls) and had a high level of stress perception. Concentration impairments were significantly related to the level of occupational stress. It seems that the best parameter to assess EMF exposure was the daily call duration, for it significantly correlated with the prevalence of the reported symptoms.

The study demonstrated that parallel activity of these factors: EMF from mobile phone and a high level of stress, both of the general and work-related stress, produce negative health consequences and increase the prevalence of subjective symptoms among workers. No research has been performed that could explain whether this effect is additive, duplicate or potentiating.

The results of our previous studies indicated that exposure to EMF from mobile phone might increase arterial blood pressure, have influence on melatonin level resulting in sleep disturbances, produce concentration and short-term memory impairments [9,10]. Similar physiological reactions (increased blood pressure, heart rate, headache, sleep disturbances) have been associated with stress.

Surveys on subjective symptoms from mobile phone use conducted in Sweden, Norway, UK, US, New Zealand and Australia revealed headache as the most frequently reported symptom [6,11,12,13]. The Australian study demonstrated that headache (including cluster headache and migraine) appeared during or shortly after the phone call and often turned more intense during the day. About 50% of the subjects reported that they had receded within one hour after the call was over and the rest of the subjects complained they could persist throughout the whole day and recede no earlier than in the evening or even on the day after [6]. The first reports on headache following exposure to microwave and radiofrequency EMF were published about 30 years ago but at that time EMF exposure at these frequencies was not common and the findings had little if any response [14]. Apart from headache, the persons using mobile phone reported malaise and fatigue, muscle pain, nausea, and thermoregulation impairments [15].

Seeking explanation to the concomitant activity of electromagnetic fields emitted by mobile phones and stress needs further studies.

References

1. Kristensen T.S., Kronitzer M., Alfedsson L.: Social factors, work, stress, and cardiovascular disease prevention. Brussels, The European Heart Network, 1998

2. Hanke W., Dudek B.: The effect of stress in the workplace on the risk of ischemic heart diseases--the role of epidemiologic studies. Med. Pr., XLVIII, 6, 1997.
3. Hammar N., Alfredsson L., Johnson J.V.: Job strain, social support at work, and incidence of myocardiel infarction. Occupational and Environmental Medicine 55 (8), 548-553, 1998.
4. Schnall PL., Landsbergis PA, Schwartz J, et al.: A longitudinal study of job strain and ambulatory blood pressure: Results from 3-year follow-up. Psychosom Med. 60, 697-706, 1998.
5. Oftedal G., Wilen J., Sandstrom M., Mild K.H.: Symptoms experienced in connection with mobile phone: Occup. Med. 50 (4), 237-245, 2000.
6. Hocking B. Preliminary report: Symptoms associated with mobile phone use. Occup. Med. 48, 357-360, 1998.
7. Dudek B., Waszkowska M., Hanke W.:. Workers protection against health effects of work-related stress IMP, Łódź 1999.
8. Cohen S., Kamarck T., Mermelstein R.A.: A global measure of perceived stress. Journal of Health and Social Behavior 24, 385-396, 1983.
9. Bortkiewicz A., Jarupat S., Kawabata A., Tokura H., Szymczak W., Gadzicka E.: Heart rate and blood pressure during exposure to cellular phone-an experimental study in: Environmental Ergonomics IX. Eds. J. Werner & M. Hexamer, 227-230, Aachen, 2000.
10. Bortkiewicz A., Piłacik B., Gadzicka E., Szymczak W.: The excretion of 6-hydroxymelatonin sulfate in healthy young men exposed to electromagnetic fields emitted by cellular phone-an experimental study. Neuroendocrinol. Lett 23 (suppl. 1), 88-91, 2002.
11. Sandstrom M., Wilen J., Oftedal G., Hansson Mild K.: Mobile phone use and subjective symptoms. Comparison of symptoms experienced by users of analogue and digital mobile phones. Occup. Med. 51 (1), 25 – 35, 2001.
12. Lundgren K.: GSM phones-no more symptoms than NMT. Working Life, Research and Development News, Newsletter 3, 1998.
13. Royal Society of Canada: A review of the potential health risks of radiofrequency fields from wireless telecommunication devices. Royal Society of Canada, Ottawa, Ont, 1999.
14. Frey A.: Headaches from cellular Telephones: Are they real and what are the implications. Environ Health Perspect 106, 101-103, 1998.
15. Repacholi M.H.: Low level exposure to radiofrequency electromagnetic fields. Health effects and research needs. Bioelectromagnetics 19, 1-19, 1998

EFFECT OF ELF-EMF ON APOPTOSIS OF K562 CELL LINE INDUCED WITH QUERCETIN AND OXIDATIVE STRESS

AKAN ZAFER,[1] TULUNAY AYSIN,[2] İNHAN GARIP AYŞE[1]

[1] Marmara University, School of Medicine, Biophysics Dept. İstanbul
[2] Marmara University, School of Medicine, Immunology Dept. İstanbul

Correspondence to : Ayşe İnhan Garip, e-mail: aysein9@yahoo.com

Abstract

This work aimed to determine the effect of ELF-EMF (50Hz,1mT) on 1-apoptosis of cells induced with the hydrogen peroxide and 2- quercetin on K562 cells. Quercetin is a flavonoid, a group of polyphenolic phytochemicals known for their beneficial effects. Quercetin has been shown to induce apoptosis. Oxidative stress is well known for its apoptosis or necrosis inducing effect. Recent work has shown that ELF-EMF affects the free radical levels probably by increasing their life-time. K562 cells were induced with quercetin or H_2O_2 and ELF-EMF (1mT,50 Hz) was applied for three hours. ELF-EMF decreased the number of viable cells in H_2O_2 induced cells. ROS levels were increased with ELF-EMF application implying the free radical stabilizing effect of ELF-EMF on free radicals and were well correlated with the viability of cells. When quercetin was used to induce cells to apoptosis it was observed that ELF-EMF abolished the apoptotic effect, increasing viability to control levels suggesting that ELF-EMF interfered with apoptotic pathway. In conclusion we showed that ELF-EMF affected the viability of cells induced with quercetin or oxidative stress and that a free radical stabilizing effect of ELF-EMF may be involved.

INTRODUCTION

The extremely low electromagnetic fields have been found to produce a variety of biological effects. It has been shown that ELF-EMF can cause changes in cell proliferation, cell differentiation, cell cycle, apoptosis, DNA replication and expression [1,2].

Flavonoids are a large group (5000 flavonoids described) of low molecular weight naturally occurring polyphenolic compounds distributed in vascular plants and are important constituents of human diet. They have a broad range of biological functions in plants and also in animal cells since they have co-existed for over a billion years [3]. They regulate the activity of many enzymes and cell cycle progression they can alter gene expression and have anti-oxidative properties. Quercetin (3,3',4',5,7-pentahydroxyflavone) is a plant flavonoid that occurs naturally in a wide range of fruits and vegetables. It is the most studied flavonoid. It has been observed that Quercetin interferes with regulatory pathway of apoptosis [4] and causes cell cycle arrest [5].

ROS including H_2O_2, O_2 .- and OH-, are endogenously generated inside cells by a variety of enzymes and through the mitochondrial respiratory chain. ROS levels are balanced by the intracellular

antioxidative defense which consists of enzymatic (superoxide dismutase which reduces O_2 .- to H_2O_2, catalase, and glutathione peroxidase which reduce H_2O_2 to H_2O) and nonenzymatic components (the vitamins C, A, E, lipoate, thiols, urate, ubiquinone, glutathione (GSH), thioredoxin, and glutaredoxin) [6]. However exogenous H_2O_2 can cause cellular injury by both apoptosis and necrosis.[7]

Extremely low frequency electromagnetic fields are considered to be weak stressors and it is thought that they may act as costressors in the presence of a stress factor [8]. And since membrane poses a barrier to these weak fields the interaction must involve a physicochemical change in the membrane leading to changes in the signal transduction system of the cell [2] and/or as Myrtill proposed cause deleterious effects by stabilizing the metabolically formed free radical [9]

Taking these facts into consideration we aimed to determine the effect of ELF-EMF on viability of K562 induced with the two above mentioned stressors. The results were correlated with ROS levels.

1. Materials and Methods

a. Cell Culture

K562 cells were cultured at 37°C in suspension in RPMI 1640 (Sigma-Aldrich Chemie GmbH, Taufkirchen, Germany) containing 10% FCS (Gibco-Invitrogen Ltd. , Paisley, Scotland) in a humidified 5% CO_2 atmosphere. Cell count was made with trypan blue. Viability was 85-90%. Quercetin (Sigma-Aldrich QO125) was added by the indicated concentrations. K562 cells were induced to apoptosis with 150, 300 µM H_2O_2 (Riedel Dehaen D3016)

b. Exposure System

Electromagnetic field was generated with two solenoids (25 cm diameter and 10 cm height) serially connected each having 400 turns of copper wire. During exposure the cells (control and ELF-EMF applied) were kept in a water bath (37° ± 0.5°C) . The magnetic field, obtained with 20V 1 mA was measured to be 1mT. Field intensity varied for ± 0.1mT during exposure. For the measurement a Hall Effect Teslameter of Leybold Heraous 54 050 model was used.
1mT, 50Hz ELF EMF was applied for three hours.

c. Apoptosis detection and Annexin V Staining Protocol

After induction with quercetin or H_2O_2 and /or application of ELF-EMF cells were washed twice with PBS and suspended in 1x binding buffer at a concentration of approx. 1 x 10^6 cells/ml. 5 µl of Annexin V-FITC and 10 µl of propidium iodide was added to each cell suspension (control and induced). After incubation at room temperature for 10 minutes the fluorescence of the cells was determined immediately with a flow cytometer (Becton-Dickinson FACSCalibur).

d. ROS determination

After washing with PBS, cells were plated in 96-well plates (10^4cells/well). Cells were incubated for 45 min with PBS supplemented with 1 mM p-nitro blue tetrazolium (NBT, Molecular Probes),1 mM $CaCl_2$. Measurements were made in the absence or presence of EMF exposure. $O2^-$ generation reduces NBT to blue formazan within the cells, which was measured using a microplate reader (Thermo Multiscan EX) at 550 nm. Intracellular formazan crystals were solubilized in 100 ml DMSO prior to reading.

SUMMARY

1. Results

a. Viability of cells induced with different concentrations of quercetin.

The viability of K562 cells were determined starting from 5µM quercetin to 500µM quercetin to be able to obtain a concentration response. Indicated concentrations of quercetin were added for three hours and viability measured with flow-cytometer using Annexin V Flow kit taking into consideration apoptotic

and necrotic cells. As can be seen from Figure 1(A.B) viability decreased starting from 200μM quercetin. After having determined the breaking point, several concentrations were chosen and viability measured after 24 hours of quercetin induction (Figure 1.).

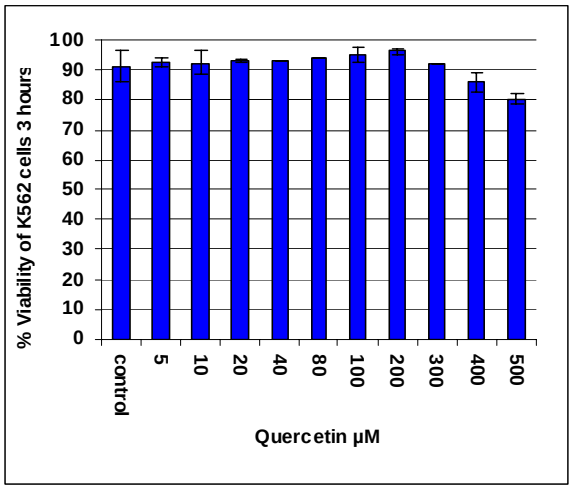

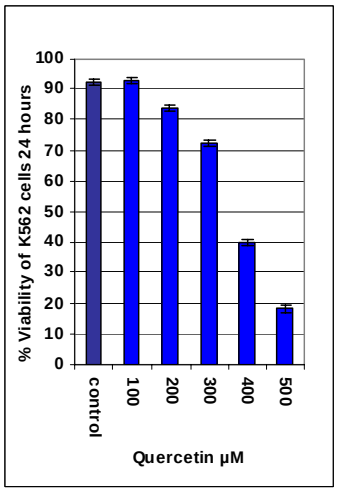

Fig.1 (A) Viability of K562 cells induced with quercetin. Quercetin concentrations from 50μM to 500μM were applied for three hours and viability was determined using Annexin V Flow kit. Concentrations greater than 200μM started to decrease viability.

(B) Several concentrations were chosen and viability measurements were made after 24 hours. It was observed that the decrease in viability was concentration dependent as expected. Results are mean ± S.E.M .n= 4.

b. Effect of ELF-EMF on quercetin induced apoptosis of K562 cell line.

300μM quercetin was chosen to determine the effect of ELF-EMF on quercetin induced apoptosis of K562 cells. Cells were induced with quercetin for three hours and ELF-EMF (1mT, 50Hz) applied at the onset of induction for the same duration. Measurements of viability were made at the end of ELF-EMF application and 24 hours later with Annexin as indicated in Methods. (Fig.2)

Quercetin decreased the number of viable cells (about 12% decreases in 24 hours) as expected. ELF-EMF alone did not change the viability of K562 cells although a slight increase which did not seem to be significant, in the number of cells was observed. When ELF-EMF was applied together with quercetin it was seen that ELF-EMF increased % of viable cells indicating that it blocked the apoptotic pathway induced by quercetin.

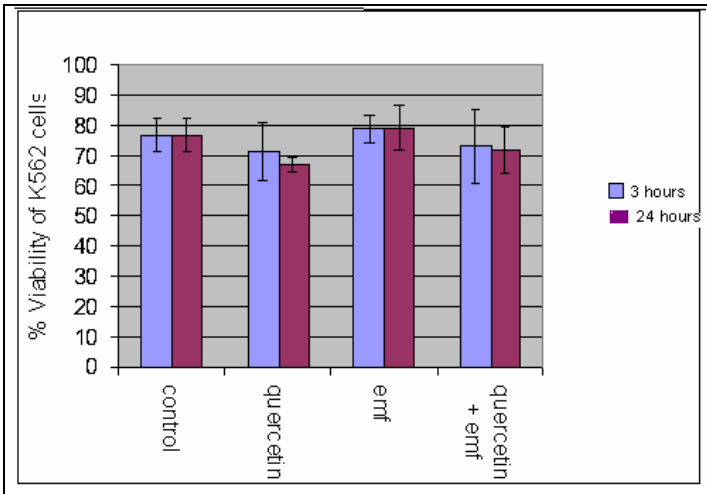

Fig.2 Effect of ELF-EMF on viability of K562 cells induced with quercetin.

Measurements were made at the end of incubation and ELF-EMF application period (3 hours) and 24 hours later. Quercetin decreased the viability as expected. ELF-EMF alone had no significant effect on the viability of K562 cells. However when ELF-EMF (1mT, 50Hz) was applied the viability of quercetin induced cells increased when measured 24 hours later. Results are mean ± S.E.M .n= 4.

c. Effect of ELF-EMF on viability of K562 cells induced with H2O2

Two H_2O_2 concentrations (150µM and 300µM) were used to determine the effect of ELF-EMF on the viability of K562 cells. Cells were induced with H_2O_2 for three hours and ELF-EMF applied during induction. Viability was determined at the end of three hours using Annexin. As expected H_2O_2 decreased viability. Application of ELF-EMF decreased viability which was seen to be more pronounced for 150µM H_2O_2 . (Fig.3).

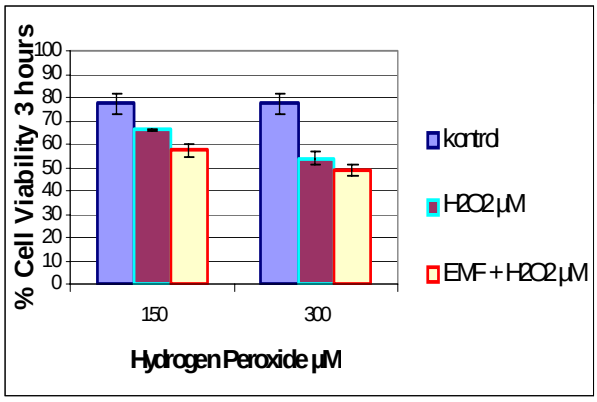

Fig.3. Effect of ELF-EMF on viability of K562 cells induced with H_2O_2.
Cells were incubated with the indicated concentrations of H_2O_2 and ELF-EMF applied for three hours during the incubation period. Measurements were made at the end of incubation and ELF-EMF application period and 24 hours later with flow cytometer. ELF-EMF decreased the viability indicating it's stabilizing effect on free radicals. Results are mean ± S.E.M .n= 4.

d. Effect of ELF-EMF on ROS levels in K562 cells with or without H2O2 induction.

Cells were kept for three hours under ELF-EMF (1mT, 50Hz). In case of H_2O_2 induction, ELF-EMF was applied immediately after induction. As can be seen from Fig.4 ELF-EMF increased ROS levels either with or without H_2O_2 induction. When cells were induced with H_2O_2 the increase was more pronounced with 150µM H_2O_2. The results indicate the stabilizing effect of ELF-EMF on free radicals.

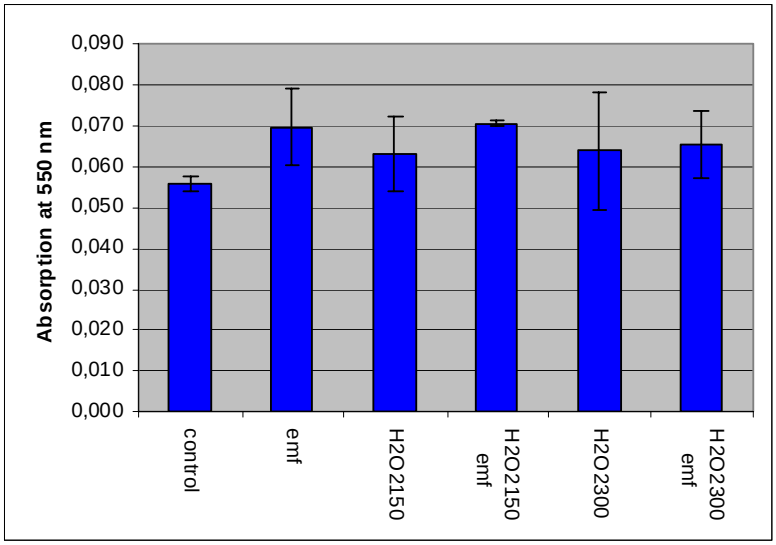

Fig.4 Effect of ELF-EMF on ROS levels in K562 cells with or without H2O2 induction.

Cells were induced with or without H_2O_2 for three hours and ROS levels were determined with NBT assay. ELF-EMF increased ROS levels in both cases. Results are mean ±S.E.M, n=4

2. Discussion

We observed that the concentration of quercetin that caused a decrease in viability, through apoptotic pathways, was 200μM to 300μM (Fig1). This is in contrast with the observation of Kothan et al [10]. They found that much lower concentrations of quercetin caused early apoptosis. On the contrary we found that low concentrations of quercetin protected the cell from oxidative stress (data not shown). As expected viability decreased with increasing concentrations of quercetin.

300μM quercetin, which was the concentration that initiated a decrease in viability, was chosen to determine the effect of ELF-EMF. The reason for this choice was that since ELF-EMF is weak stressor [8] higher concentrations of quercetin would suppress the effect of ELF-EMF. ELF-EMF caused a small increase in the viability of cells in 24 hours indicating that it interfered in the apoptotic pathway of quercetin (Fig2). There may be two reasons for this. It has been shown that quercetin modifies the membrane via reaction with lipids and proteins and thus may cause alterations in lipid transduction pathway [11]. ELF-EMF might have interfered with this modification by altering the electrical properties of the membrane. Or the reason may be a change in the expression of heat-shock proteins. It has also been observed that Quercetin and other flavonoids inhibited the induction of heat shock proteins [12]. However Goodman et al has shown that ELF-EMF increases heat shock protein levels that were exposed to short term 60 Hz. magnetic field [13] ELF-EMF may have increased hsp levels thus protecting the cell from quercetin induced apoptosis.

Reactive oxygen species are known to cause apoptosis and necrosis in many cell types [14]. This cytotoxicity is mediated by an oxidative event that produces the hydroxy radical. We first measured the concentration dependence of the viability of K562 cells induced with 150μM, 300μM and 600μM H_2O_2 which as expected decreased with increasing concentration (data not shown).

To be able to detect the effect of ELF-EMF two H_2O_2 concentrations (150μM, 300μM) were chosen. As can be seen from Fig.3. ELF-EMF caused a small but significant decrease in viability. These results were correlated with ROS measurements. It was observed that when ELF-EMF was applied to H_2O_2 induced K562 cells ROS levels increased for both of the concentrations used. This correlated very well with the decreased viability of these cells under the same conditions (Fig.4). Application of ELF-EMF alone without any H_2O_2 induction was also seen to increase ROS level which is another indication of the free radical stabilizing effect of ELF-EMF.

References

[1] Nie, K., Micic-Vasovic, A., Henderson, A.S. Molecular and cellular response to EMF exposure; a review of studies of EMF and the relationship to signal transduction. In *Biological Effects of Electromagnetic Fields* ; Stavroulakis P.,Ed; Springer-Verlag,2003.

[2] Lacy-Hulbert, A., Metcalfe, J.C., Hesketh, R. Biological responses to electromagnetic fields. FASEB J. 12, 395-42, 1998

{3] Middleton, JR E., Chithan , K., Theoharides C.T. The Effects of Plant Flavonoids on Mammalian Cells:Implications for Inflammation, Heart Disease, and Cancer Pharmacological Reviews Vol. 52, 4, 673-751. 2000

[4] Xianming Zhang, Qiang Xu and Ikuo Saiki. Quercetin Inhibits the Invasion and Mobility of Murine Melanoma B16-BL6 Cells through Inducing Apoptosis via Decreasing Bcl-2 Expression. Clin Exp. Metastasis.; 18(5): 415-421. 2001

[5] Choi, J.A., KimJ.Y., Lee,J.Y.,Kang,C.M., Kwon,H.J., Yoo,Y.D.,Kim,T.W., Lee,Y.S.Induction of cell cycle arrest and apoptosis in human breast cancer cells by quercetin. Int J Oncol. Oct;19(4):837-44.2001

[6] Heinrich Sauer, Maria Wartenberg and Jórgen Hescheler. Reactive Oxygen Species as Intracellular Messengers During Cell Growth and Differentiation. Cell Physiol Biochem 2001;11:173-186 Accepted: June 13, 2001

[7] Bladier C, Wolvetang EJ, Hutchinson P, deHaan JB, Kola I: Response of a primary human fibroblast cell line to H_2O_2: senescence- like growth arrest or apoptosis? Cell Growth Differ;8:589-598. 1997

[8] Gutzeit, H.O. Interaction of stressors and the limits of cellular homeostasis.Biochem Biophys Res Commun., 283(4), 721-5. 2001

[9] Myrtill S. Induction of cell activation processes by low frequency electromagnetic fields. The Scientific World Journal, 4(S2), 4-22. 2004

[10] Kothan, S., Dechsupa, S., Leger,G., Moretti, J.L., Vergote,J., Mankhetkorn,S. Spontaneous mitochondrial membrane potential change during apoptotic induction by quercetin in K562 and K562/adr cells. Ca. J. Physiol. Pharmacol. 82;1084-1090. 2004

[11] Pawlikowska-Pawlega,B., Gruszecki,W.I., Misiak, L.E., Gawron, A. The study of the quercetin action on human erythrocyte membranes. Biochem Pharmacol. 15;66:605-12. 2003

[12] Rusak,G., Gutzeit,H.O., Ludwig-Móller,J. Effects of strycturaly related flavonoids on hsp gene expression in human promyeloid leukemia cells. Food Technol. Biotechnol.,40,4, 267-73. 2002.

[13] Goodman, R., Lin, H., Blank, M. The mechanism of magnetic field stimulation of the stress response is similar to other environmental stresses. In *Electricity and Magnetism in Biology* ; Bersani F.,Ed.; Kluwer Academic/Plenum Publishers: New York, 1999.179-182.

[14] Lennon, S V; Martin, S J; Cotter, T G. Dose-dependent induction of apoptosis in human tumor cell lines by widely diverging stimuli. Cell Proliferation Volume 24, Issue 2 , pp.203-214.1991

EFFECT OF MAGNETIC FIELD ON SOME PHYSIOLOGICAL AND BIOCHEMICAL ASPECTS OF GROWTH OF PEA (CICER ARIENTINUM)

FAEZEH GHANATI, PARVIZ ABDOLMALEKI, MOHAMMAD YAZDANI
DEPT. BIOL. FAC. SCI. TARBIAT MODARES UNIV (TMU), POB: 14115-175, TEHRAN -IRAN

Abstract
Magnetic fields (MF) are widely distributed in the environment and their effects are increasing by the development of electrical machines. Moreover, many investigators are studying the effect of MF on the various functions or living organisms. In the present study, we tested the influence of exposure to 30 mT static magnetic field (SMF) on seed germination, growth and some physiological and biochemical aspects in roots and shoots of intact pea plants (*Cicer arientinum*). The results showed that under SMF with 30 mT intensity, seed germination was increased. The root growth was inhibited but shoot length partially increased. Furthermore, a significant increase was observed in the activity of amylase and peroxidase enzymes probably due to the oxidative stress in both roots and shoots. In addition, lignin content was increased in both roots and shoots but the level of increase of lignin in shoots was not significant.

Introduction
With the increased extent of urbanization application of electrical appliances are increasing and living organisms are inevitably subjected to the frequent exposure to low electric and magnetic fields (Patterson, 1992; Breysse et al., 1994; Frey, 1994; Merchant et al., 1994). The magnetic fields (MF) generated by electrical equipment are many times higher than those occurring naturally, and their prevalence is a consequence of technological developments in the second half of the 20th century (Jackson, 1992). However, the role of MF and its influence on organisms' functioning are still insufficiently investigated (Belyavskaya 2001). There have been several studies on the effects of MF on plants (Kato et al., 1989; Phirke et al., 1996; Ruzic & Jerman, 2002). Smith et al. (1993) found that using different field combinations, one could separately alter the root mass, leaf size and stems thickness. Roots seem much more susceptible to the magnetic than shoots (Kato, 1988; Kato et al., 1989). The 15-min treatment of wheat seeds by MF (30 mT) followed by 17-h imbibitions, when they initiated root growth, increased the root formation (Aksyonov et al., 2001). Singh et al. (1994) found that MF with a magnetic flux density of 3000 gauss applied from a permanent magnet for l-6 h inhibited the growth of *Anabaena doliolum*. Takahashi et al. (1985) investigated the effect of MF on the growth of *Chlorella* using MF with magnetic flux densities of 60-580 gauss, and have identified facilitation of growth below 400 gauss and inhibition of growth at 580 gauss. The mechanisms of facilitation or inhibition of the growth of microorganisms by MF still remain to be elucidated. It has also been found that such fields cause an increase in the free radicals activity in living organisms (Savitz, 1995; Kula et al., 2002) which results in the formation of excessive amounts of reactive oxygen species (ROS). In the present study, in order to obtain more insights into the effects of a MF on plants, we investigated the influence of 30 mT SMF on the growth and certain physiological and biochemical aspects of the growth of pea plant (*Cicer arientinum*).
Seeds of uniform size were selected and surface sterilized with 0.1% sodium hypochlorite solution for 10 min and then germinated between wet filter paper at 25˚C in the dark for 4 days, with or without exposure to magnetic field. The seedlings of uniform size were then transferred to sand culture in plastic pots in growth chamber providing white fluorescent light with an irradiance of 150 µ mol m^{-2} s^{-1}, 25±3 ˚C and 60 (± 5) % relative humidity, for 20 days.
Exposure to SMF was performed by a locally designed SMF generator. The electrical power was provided using a 220 V AC power supply equipped with variable transformer as well as a single-phase full-wave rectifier. The maximum power and passing current were 1 KW and 50 A DC, respectively. This system designed to generate SMF in range of 0.5 µT – 30 mT with stable conditions. It consisted of two coil (each 3000 turns of 3 mm copper wire) equipped with a U-shaped laminated iron core (to prevent eddy current losses). Using two vertical connectors, the arms of the U-shaped iron core were terminated to four circular iron plates covered with thin layer of Nickel (each 23 mm thickness, 260 cm in diameter). An electronic board was used to stabilize the system so that we always got a uniform SMF. A water circulation system around the coils was employed to avoid the increase of the temperature.

The temperature between the circular iron plates (where the samples were located), was measured by a thermometer and was almost the same as other parts of the room (e.g., the location site of the control cells) ±1°C. Since no other electric appliance was working, the control samples were only exposed to the extremely low MF of the earth, as the treatment group was too. Moreover, the control cells were kept far enough from the EMF producing apparatus, to avoid any potential exposure to the magnetic field.Calibration of the system as well as tests for the accuracy and uniformity of the magnetic fields were performed by a Teslameter (PHYWE, Germany) with a probe type of Hall Sound. The accuracy of the system was ±0.1% for static field and the range of measurements was 3 μT – 30 mT 20-day old pea plants were treated with 30 mT, discontinuously for 5 days, each 5 h. After treatments, the roots and shoots of pea were harvested and frozen in liquid N_2 and kept at – 80 °C until used for biochemical measurements.

Iodometric method was used to determine the endo-amylase activities (Lecker & Khan, 1996). The starch solution (1.5 g/L) was made by dissolving starch in 2 M NaOH solution at room temperature, followed by the addition of an equal volume of 2 M HCl. The resulting solution was then heated to a clear solution before its pH was adjusted to desired value by addition of 2 M NaOH. Final solutions were made by dilution with buffer at the desired pH. A solution (126.9 mg/L), containing the same volume of 0.1 M iodine and 5 g/100 mL potassium iodide, was diluted with cold distilled water to obtain a cold iodine solution (around 2 °C). Activity values were determined at 25 °C by allowing the enzyme solution in buffer (0.5 mL) to react with the starch solution (5 mL) for 2 min. The reaction was then stopped by adding 2.5 mL of cold iodine solution, which converts the nonhydrolyzed starch to starch-iodine blue complex. The resulting solution was afterwards placed in a thermostatic bath at 25 °C for 10 min and its absorbance was measured at 615 nm.

Peroxidase (PO) was extracted and determine in three fractions; the soluble-(SPO), ionically-(IPO) and covalently-(CPO) bound fractions, using guaiacol as an electron donor, as described previously (Ghanati et al. 2004). The activity of SPO and IPO was expressed as the increase in absorbance per min per mg protein and of CPO was expressed as the increase in absorbance against cell wall dry weight The protein content was determined by the method of Bradford (1976) using bovine serum albumin (BSA) as a standard.

Total sugar content was measured by the anthrone-sulfuric acid method (Dubois et al., 1956).

Lignin content was measured via a modified acetyl bromide procedure (Iiyama & Wallis, 1990). In brief, 6 mg of fine-powdered wall preparation was treated with a mixture (total of 2.5 ml) of 25% (w/w) AcBr in HOAc and 0.1 ml of 70% $HClO_4$ at 70 °C for 30 min with shaking at 10 min intervals. After cooling with ice, the digestion mixture was transferred to a 25 ml volumetric flask containing 5 ml of 2 M NaOH and 6 ml HOAc and made up to 25 ml. The lignin content was determined by measuring the absorbance at 280 nm using a specific absorption of 20.0 g^{-1} L cm^{-1}. All of the experiments were carried out with at least three independent repetitions in triplicate. All values are shown as the mean ± SD. Statistical analysis was performed using Student t.Test and the differences at level of p <0.05 were considered significant.

Exposure to 30 mT SMF had a positive effect on germination of pea seeds but it inhibited elongation of those seedlings that had not been treated with MF during their germination (data not shown).

The sugar content of roots and shoots of pea was affected greatly by SMF and a significant increase was observed at 30 mT (Fig. 1).

The starch content of roots and shoots was considered as the activity of amylase enzyme. Compared to the controls, we found that the starch content of roots and shoots of pea plant reduced significantly after exposure to 30 mT SMF (Fig. 2).

Our experiments showed that the activity of SPO in roots of pea plant was significantly increased by exposing to 30 mT SMF (Fig.3 A,D). Moreover, the activity of IPO and CPO increased substantially compared to those in control plants (Fig.3 B,C,E,F).

The lignin content of roots of pea plant treated with 30 mT SMF was significantly higher than non-treated roots (Fig. 4). Compared to the control, an increasing in the lignin content was also observed in shoots of pea plant treated with 30 mT SMF, although it was not statistically significant (Fig.4).

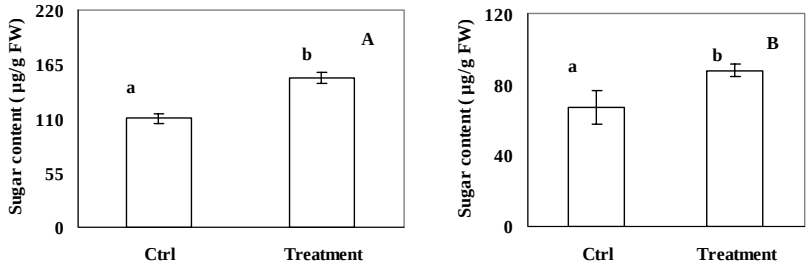

Fig.1 Effect of SMF on sugar content of shoot (A) and roots (B) of pea. Data are means of at least three different experiments in triplicate ±SD. Signs with different letters indicate significant differences at $P < 0.05$ according to Student's t-Test.

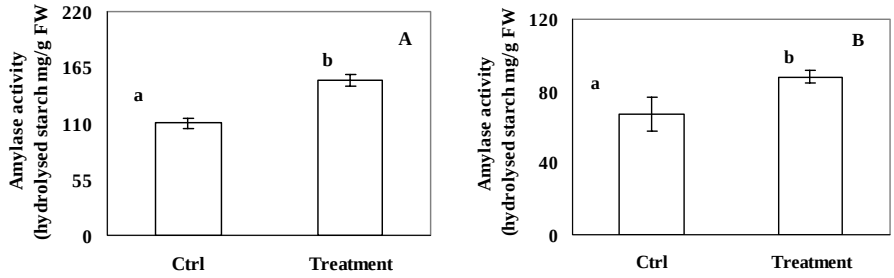

Fig.2 Effect of SMF on the activity of amylase in pea shoots (A) and roots (B). Data are means obtained from at least three different experiments in triplicate ±SD. Signs with different letters indicate significant differences at $P < 0.05$ according to Student's t-Test.

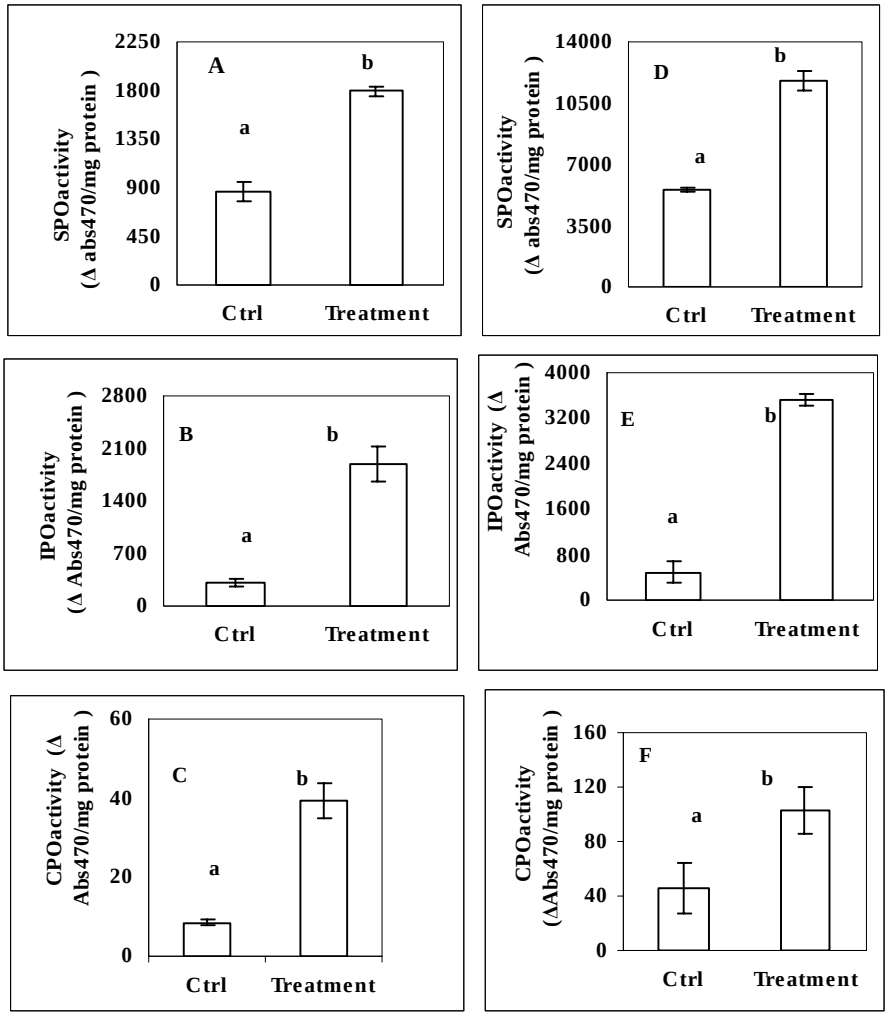

Fig 3. Effect of SMF on different fractions of PO in pea shoots (A-C) and roots (D-F). Data are means of at least three different experiments in triplicate ±SD. Signs with different letters indicate significant differences at $P < 0.05$ according to Student's t-Test.

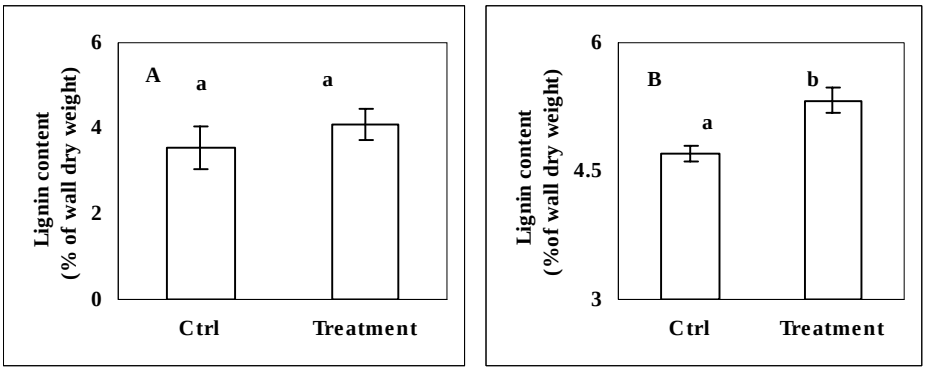

Fig.4 Effect of SMF on lignin content of pea shoots (A) and roots (B). Data are means obtained from at least three different experiments in triplicate ±SD. Signs with different letters indicate significant differences at $P < 0.05$ according to Student's t-Test.

Summary

Investigations of many authors showed that treatment of plants seed by MF increases their germination. In our study, germination of pea seeds increased by 30 mT SMF. Similar results were obtained by the effect of MF on rice, wheat, barley and soybean seeds (Cho et al., 1992). The studies show that this increasing in germination is probably due to the alteration of water relations in seeds by MF (Reina et al., 2001). Root growth reduction may be related to a reduced extensibility of the cell wall. Such effect could result from the stiffening of the wall, partly regulated by PO responsible for the polymerization of monolignins (Fry, 1986). In shoots, we have seen a slight increasing on the length of two latest internodes. This increasing was probably due to the lower synthesis of lignin in shoots than roots under 30 mT SMF, resulted in enhancement of cellular turgor and cell enlargement. Negishi et al. (1999) were observed the epicotyle elongation in pea seedlings exposed to MF. They suggested that the promotion of cell elongation under MF may relate to an increase of osmotic pressure in the cells. The effects of MF on photosynthesis in plants have not been studied in detail. In our study, the sugar content in roots and shoots of pea plant increased at 30 mT SMF. These results suggest that MF probably promote the photosynthetic processes. The similar results were obtained at the study of the effect of MF (100 gauss) on photosynthesis of the *Spirulina platensis* (Hirano et al., 1998). The authors suggested that MF accelerate the light excitation of chlorophyll, reactions of electron transfer and the conversion of light energy to chemical energy.

It has been proposed that α-amylase may be a regulatory enzyme of starch breakdown since this enzyme, unlike β- amylase, can attack and degrade intact starch granules (Dunn, 1974; Manners, 1985), while β-amylase is thought to hydrolyse oligosaccharide products of α-amylase activity and play a secondary role in the regulation of starch hydrolysis (Gallagher et al., 1997). In this research, increased soluble sugar content and also decreased starch in MF-exposed roots and shoots suggest that the hydrolysis of starch under 30 mT SMF is mainly attributed to the enhanced amylase activity. This enhancement was probably due to the increasing of ROS production under MF stress. Similar to our observations, enhanced amylase activity have been reported under water stress in barley leaves (Jacobsen et al., 1986) and cucumber cotyledons (Todaka et al., 2000). Furthermore, Mishra et al. (2005) reported significant increase in activity of amylase by increase in the level of ROS in *Bacillus subtilis*. These authors showed that the increase in enzyme activity was result of adaptive responses induced under oxidative stress.

POs are heme containing proteins that utilize H_2O_2 in the oxidation of various organic and inorganic substrates (Asada, 1994). These enzymes participate in developmental processes, ethylene biosynthesis, defense, wound healing, etc. (Asada, 1992). POs are widely accepted as stress enzymes (Asada, 1992). Induction in PO activity has been documented under a variety of stressful conditions such as water stress (Zhang & Kirkham, 1994), salinity (Mittal & Dubey, 1991), chilling (Prasad et al., 1995) and γ-radiation (Wada et al., 1998). In plants, POs have been mainly detected in cell walls, endoplasmic reticulum, Golgi apparatus and vacuoles, and this distribution is presumably related to different physiological functions (Pandolfini et al., 1992). It has also an important role in the lignification (Asada, 1992; Castillo et al., 1984) and the formation of cross-links between extension and feruloylated polysaccharides, resulting in the

increase of wall stiffening and reduction of cell expansion (Castillo et al., 1984). Our results indicated an enhancement in the activity of SPO in both roots and shoots of pea plants when compared to controls.
It is demonstrated that the activity of SPO is related to the stress conditions (Pandolfini et al., 1992). Furthermore, in the present study an increased activity was seen in IPO and CPO in both roots and shoots. In some cases, the increased activity is mainly due to the extracellular POs (cell-wall-bound) which are known to play an important role in the lignification and the formation of cross-links between extension and feruloylated polysaccharides (Castillo & Greppin, 1986; Fry, 1986). The enhanced PO activity in the intercellular spaces, involved in cell wall lignification might represent a mechanical defense under biotic and abiotic stress conditions (Gaspar et al., 1985; Castillo, 1986).

References

Aksyonov S I, Bulychev A A, Grunina T Yu, Goryachev S N, Turovetsky V B. 2001. Effects of ELF–EMF treatment on wheat seeds at different stages of germination and possible mechanisms of their origin. *Electromagnetic Biology and Medicine* 20:231–253.

Asada K. 1994. Production and action of active oxygen species in photosynthetic tissues, in: C.H. Foyer, P. Mullineaux (Eds.), Causes of photo-oxidative stress and amelioration of defense systems in plants. CRC Press, Boca Raton, FL. pp. 77 - 104.

Asada K. 1992. Ascorbate peroxidase- a hydrogen peroxide scavenging enzyme in plants. *Plant Physiology* 85:235-241.

Belyavskaya N A. 2001. Ultrastructure and calcium balance in meristem cells of pea roots exposed to extremely low magnetic fields. *Advances in Space Research* 28:645-650.

Bradford M M. 1976. A rapid and sensitive method for the quantitation of microgram quantities of protein utilizing the principle of protein-dye binding. *Analytical Biochemistry* 72:248-254.

Breysse P, Less P S, Mc Diamid M A, Curbow B. 1994. ELF magnetic field exposures in an office environment. *American Journal of Indastrial Medicine* 25:177-185.

Castillo F J, Greppin H. 1986. Balance between anionic and cationic extracellular peroxidase activities of *Sedum album* leaves after ozone exposure. Analysis by high-performance liquid chromatography. *Physiologia Plantarum* 68:201-208.

Castillo F J, Penel C, Greppin H. 1984. Peroxidase release induced by ozone in *Sedum album* leaves: involvement of Ca^{+2}. *Plant Physiology* 74:846-851.

Cho E G, Kweon S J, Suh D Y, Suh S H, Lee S K, Sohn J K, Oh J F. 1992. Studies of utilization of magnetic force in agricultural genetic engineering. *Research Reports of the Rural Development Administration Biotechnology* (Korea Republic), 34: 10-14.

Dubois M, Gilles K A, Hamilton J K, Rebers P A, Smith F. 1956. Colorimetric method for determination of sugars and related substances. *Analytical chemistry* 28:350-356.

Dunn G. 1974. A model for starch breakdown in higher plants. *Phytochemistry* 13:1341-1346.

Frey A H (Ed.). 1994. On the nature of electromagnetic field interactions with biological systems. R. G. Landes, Austin TX.

Fry S C. 1986. Polymer-bound phenols as natural substrates of peroxidases. In Molecular and Physiological Aspects of Plant Peroxidases (eds H Greppin, C Penel & Th Gaspar), University of Geneva, Geneva, pp.169-182.

Gallagher J A, Volence J J, Turner L B, Pollock C J. 1997. Starch hydrolytic enzyme activities following defoliation of white clover. *Crop Science* 37:1812-1818.

Gaspar T, Penel C, Castillo F J, Greppin H. 1985. A two step control of basic and acidic peroxidases and its significance for growth and development. *Physiologia Plantarum* 64:418-423.

Ghanati F, Morita A, Yokota H. 2004. Deposition of Suberin in roots of soybean by Excess Boron Plant Sci., 168: 397-405.

Hirano M, Ohta A, Abe K. 1998. Magnetic field effects on photosynthesis and growth of the cyanobacterium *Spirulina platensis*. *Journal of Fermentation and Bioengineering* 86: 313-316.

Iiyama K, Wallis A F A. 1990. Determination of lignin in herbaceous plants by an improved acetyl bromide procedure. *Journal of the Science of Food and Agriculture* 51: 145-161.

Jacobsen J V, Hanson A D, Chandler P C. 1986. Water stress enhances expression of an α–amylase gene in barley leaves. *Plant Physiology* 80:350-359.
Jackson J D. 1992. Are the stray 60 Hz electromagnetic fields associated with the distribution and use of electric power a significant cause of cancer? *Proceedings of the National Academy of Sciences*.USA. 89:3508-3510.
Kato R. 1988. Effects of magnetic fields on the growth of primary roots of *Zea mays*. *Plant and Cell Physiology* 29:1215–1219.
Kato R, Kamada H, Asashma M. 1989. Effects of high and very low magnetic fields on the growth of hairy roots of *Daucus carotta* and *Atropa belladonna*. *Plant and Cell Physiology* 30:605–608.
Kula B, Sobczak A, Kuska R A. 2002. study of the effects of static and extremely low frequency magnetic fields on lipid peroxidation products in subcellular fibroblasts fractions. *Electromagnetic Biology and Medicine* 21:173-180.
Lecker D N, Khan A. 1996. Theoretical and Experimental Studies of the Effects of Heat, EDTA, and Enzyme Concentration on the Inactivation Rate of π-Amylase from *Bacillus* sp. *Biotechnology Progress* 12:713–717.
Manners D J. 1985. Starch. In: Dey P M, Dixon R A, eds. Biochemistry of storage carbohydrates in green plants. London: Academic Press, pp. 149-203.
Merchant C J, Renew D C, Swanson J. 1994. Exposure to power-frequency magnetic fields in the home. J. Radiol. Protect. 14:77-87.
Mishra S, Noronha S B, Suraishkumar G K. 2005. Increase in enzyme productivity by induced oxidative stress in *Bacillus subtilis* cultures and analysis of its mechanism using microarray data. *Process Biochemistry* 40:1863–1870.
Mittal R, Dubey R S. 1991. Behaviour of peroxidases in rice: changes in enzyme activity and isoforms in relation to salt tolerance. *Plant Physiology and Biochemistry* 29: 31- 40.
Moore R L. 1979. Biological effects of magnetic fields: studies with microorganisms. *Canadian Journal of Microbiology* 25:1145-1151.
Negishi Y, Hashimoto A, Tsushima M, Dobrota C, Yamashita M, Nakamura T. 1999. Growth of pea epicotyl in low magnetic field: implication for space research. *Advances in Space Research* 23:2029–2032.
Pandolfini T, Gabbrielli R, Comparini C. 1992. Nickel toxicity and peroxidase activity in seedlings of Triticum aestivum L. *Plant, Cell and Environment* 15:719-725.
Patterson R M. 1992. Exposure assessment for electric and magnetic fields. *Journal of Exposure Analysis and Environmental Epidemiology* **2**:159-176.
Phirke P S, Kubde A B, Umbarkar S P. 1996. The influence of magnetic field on plant growth. *Seed Science and Technology* 24:375–392.
Prasad T K, Anderson M D, Stewart C R. 1995. Localization and characterization of peroxidases in the mitochondria of chilling acclimated maize seedlings. *Plant Physiology* 108:1597-1605.
Reina F G, Pascual L A, Fundora I A. 2001. Influence of a stationary magnetic field on water relations in lettuce seeds. Part II: experimental results. *Bioelectromagnetics* 22:596–602.
Ruzic R, Jerman I. 2002. Weak magnetic field decreases heat stress in cress seedlings. *Electromagnetic Biology and Medicine* 21:69–80.
Savitz D A. 1995. Overview of occupational exposure to electric and magnetic fields and cancer: Advancements in exposure assessment. *Environmental Health Perspectives* 69:103-108.
Singh S S, Tiwari S P, Abraham J, Rai S, Rai A K. 1994. Magnetobiological effects on a cyanobacterium, *Anabena doliolum. Electro and Magnetobiology* 13:227-235.
Smith S D, McLeod B R, Liboff A R. 1993. Effects of CR-tuned 60-Hz magnetic fields on sprouting and early growth of *Raphanus sativus*. *Bioelectrochemistry and Bioenergetic* 32:67–76.
Takahashi F, Kamezaki T. 1985. Effect of magnetism of growth of *Chlorella. Hakkokogaku* 63:71-74.
Todaka D, Matsushima H, Morohashi Y. 2000. Water stress enhances β–amylase activity in cucumber cotyledons. *Journal of Experimental Botany* 51:739-745.
Wada H, Koshiba T, Matsui T, Sato M. 1998. Involvement of peroxidase in differential sensitivity to γ - radiation in seedlings of two Nicotiana species. *Plant Science* 132:109- 119.
Zhang J, Kirkham M B. 1994. Drought-stress induced changes in activities of superoxide dismutase, catalase and peroxidase in wheat species. *Plant and Cell Physiology* 35:785- 791.

DISCUSSION ON THE INFLUENCE OF THE ELECTRIC CHARGE OF AEROSOL PARTICLES ON THEIR DEPOSITION IN HUMAN RESPIRATORY SYSTEM

ZYGMUNT J. GRABARCZYK

CENTRAL INSTITUTE FOR LABOUR PROTECTION – NATIONAL RESEARCH INSTITUTE, ul. Czerniakowska 16, 00-701 Warszawa, POLAND

Abstract

Aerosol particle deposition in human respiratory system is a complex function of the size and geometry of the particles. There are distinguished three main mechanisms of the deposition of the particles during the breathing – inertial force, Brownian motion and gravitational force. Depending on the size, the significance of that mechanisms and the region of respiratory system the efficiency of them is different. The fourth mechanism – electrostatic forces – because of the theoretical predictions (mainly the works of Yu) is neglected usually. The theoretical analysis of the electric forces is limited to passive mechanisms of electrostatic dispersion and the image force in tubes and bulbs of smooth, grounded surfaces and the viscous gas medium. The experimental work of Cohen made with the cast of human air ducts shows that deposition can be significantly higher than that theoretically predicted. The analysis of the influence of the image forces acting at the distance lower than free length and hypothetical non-zero potential of the parts of inner duct surfaces on the particle settlement shows that it can be more efficient for nano-particles than the previous theoretical and experimental works showed.

Key words: aerosol, electric charge, respiratory system, particle deposition, image force

Introduction

The influence of the electric charge on the aerosol particles on the efficiency of their deposition in human airways is usually neglected. A lot of theoretical and experimental work has proved that the deposition of uncharged aerosol particles in airways is governed by following mechanisms:

- diffusion towards the inner surfaces of the respiratory ducts,
- gravitational sedimentation,
- inertial impaction,
- interception.

The deposition efficiency of individual mechanisms depends on particle size and shape and on the considered part of the airways. Diffusion dominates for small particles, especially for nano-particles, and sedimentation dominates in case of coarse particles (larger than 1 μm). The efficiency of deposition in different parts of human respiratory system was shown in Fig. 1. This picture was obtained by NRBP on the basis of calculations using HRTM model (2004). The other authors report the similar deposition curves, so this one can be treated as a representative view. The experimental and analytical research work during the years has shown that the electrical charge of the particle increases its deposition. Those research works could be divided into few groups:

- measurements of the dust retention in exposed animals,
- measurements of the dust retention in exposed humans (very rare),
- measurements and calculations of the deposition in the surrogates of parts of the air ducts,
- measurements of the particle deposition in the hollow airway cast of the human lungs.

The data from the human studies made in *vivo* are rare and difficult to obtain, especially concerning the values of regional depositions. For that very important are studies with hollow casts of human airways, which seem to be the closest to the real conditions and can be useful for verify calculations.

Cohen et al. (1995) gave the detailed review of research results up to 1995. Generally, she contrasted theoretical and experimental results. They showed that the real increase of the deposition of charged particles in airways surrogates or casts (especially in her own experiments) is higher than that predicted theoretically (e.g. *Yu*, *Yu* and *Chandra*). There is general agreement, that the dominating electrical mechanism for the typical particle concentrations is the image force attracting the charge toward the conducting surface.

The new impact to the scientific interest of the share of the image forces in the particle deposition, brought the hypothesis of *Fews, Henshaw et al*. (1999 a, b) for the explanation for the increase number of some cancer cases (especially childhood leukaemia) among the populations living in the vicinity of very high voltage AC powerlines, shown in epidemiological studies. There is a common believe that the very weak AC magnetic fields (about 0.5 to few hundred of nT) could promote the development of some rare kind of cancers, but still the mechanisms of that are not understood. According to *Henshaw, Fews, et al.*, the corona discharge in HV powerlines could charge the particles of aerosol pollutants passing with the wind through the corona region. This could cause the increased deposition of charged pollutants, including cancerigenic substances existing in the air, in human respiratory system, and increase the risk of developing of some pulmonary and cancer diseases. They experimentally confirmed the existence of the cloud of ions on the leeward side of the HV AC powerlines on the basis of measurements of the vertical component of the electrostatic field at the ground level, up and down the wind. In 2005, *Grabarczyk et al*. (2005) confirmed the existence of increase in the concentration of the space charge carried by the particles sized 2 - 22 nm, down the wind of the 110 and 400 kV AC powerlines. This hypothesis was analysed carefully by the *ad hock* group of experts, and the results were published by National Radiological Protection Board (2004). They concluded that the probability of the adverse health effects of pollutants charged by HV AC powerlines is not high, but many questions need the answer before the conclusions.

The main problem, which still is not clear, is the difference between the calculated and measured deposition of charged particles in the respiratory system. It seems that this is important only near processes, which can generate the high fractions of charged nano-particles or charge fine and coarse particles close to their charge saturation.

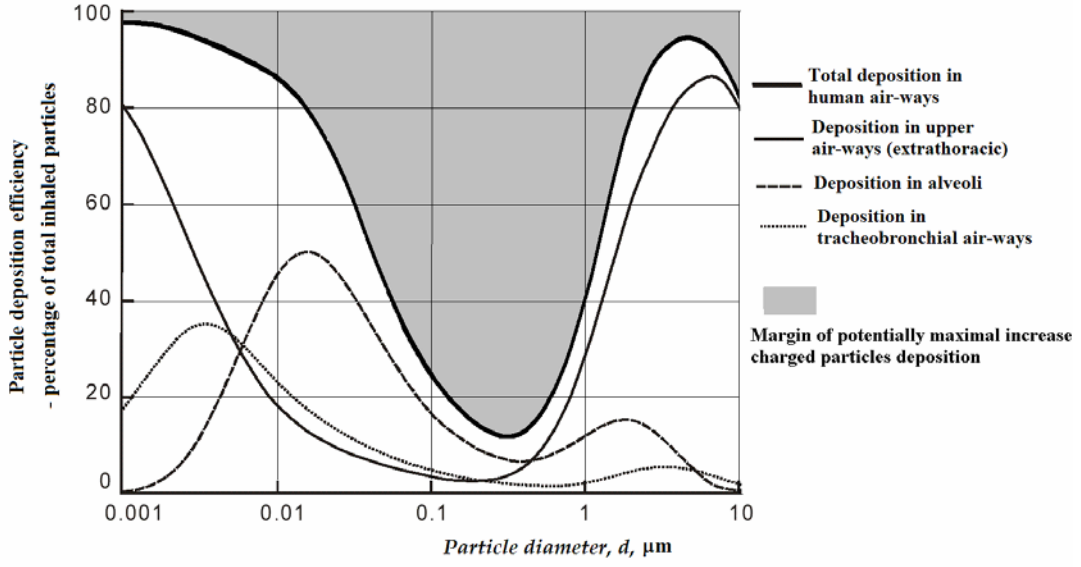

Figure 1. Total and regional deposition efficiency of spherical, uncharged particles in human respiratory system, after NRPB calculations using HRTM model (2004)

Discussion

There are the crucial points of the discussion on the significance for human health of the inhalation of the charged aerosol particles:

1) the potential margin for the possible increase of the deposition by any active factor, other than diffusion, gravitation impaction or interception,
2) the real values of deposition enhancement by the image forces,
3) the influence of image forces on the regional increase of deposition,
4) the health effects of the deposition increased by image forces,
5) the way in which image forces can enhance the efficiency of the other, mentioned above, mechanisms:

Ad 1. The potential, theoretically possible increase of the deposition is shown in Fig 1 (the grey area over the total deposition curve). It can be seen well, that for the particles sized below 10 nm and above 5 μm, the margin is very low, about a few percent. However, in the size range 0.1 – 1 μm the margin is very wide, and at about 0.3 – 0.4 μm ten-fold increase of deposition is theoretically possible. In this range, all the local depositions are low, so they could be potentially increased.

Ad 2. The real values of deposition efficiency can be calculated for all airways generations and then be summed, or total deposition can be measured with hollow cast model. Those data are not complete now and need further studies. Especially the reason for which the experimental exposition is higher than theoretically predicted, should

be explained. *Yu* et al have done most of the theoretical calculations. He derived formulas for calculating the deposition efficiency at different generation of air ducts, for parabolic and for slug airflow, and some calculations for bend pipes and some calculations for simultaneous electric effect and diffusion or gravitation.
Ad 3. As the image forces are "short distant" they can be effective rather in the narrow air tubes (e.g. bronchial region or alveoli). They should be active in similar region as the diffusion deposition dominates.
Ad. 4. The health effects of deposition depend on the kind and amount inhaled material rather than on the mechanism of deposition. So the electrostatic deposition potentially could be biologically active it could significantly increase the amount of deposited pollutants or move the deposition to the more sensitive region. The last one not seems very likely. On the other hand if image forces enhanced the deposition, they should in obvious way to cause earlier deposition, that means in lower (in sense of the number) generations.
Ad. 5. This not clear if the electrical and mechanical forces responsible for deposition can enhance or weak each other. The simplest way is to treat them as the additive factors, but likely they are not. *Chen* and *Yu* (1993) proposed the formula for the combined efficiency $\eta = \mathrm{sqrt}(\eta_1^2 + \eta_2^2 - 2\eta_1\eta_2)$ where η_x - individual efficiencies by factor 1 and factor 2.

This should be noticed that in the atmospheric conditions the aerosol particles are in thermodynamic equilibrium, and the charge carried by particles is rather low (see Fig. 2.), especially in the case of free molecular regime particles (very small particles), so probably the health effect could be small or negligible. However, if compare the atmospheric aerosol to the industrial one, especially to the particles being atomized mechanically or charged electrically (e.g. electrostatic painting), their charge could be closer to the possible maximum (limited by the electric breakdown of the air – about $3 \cdot 10^6$ V/m) and the image effect could be significant.

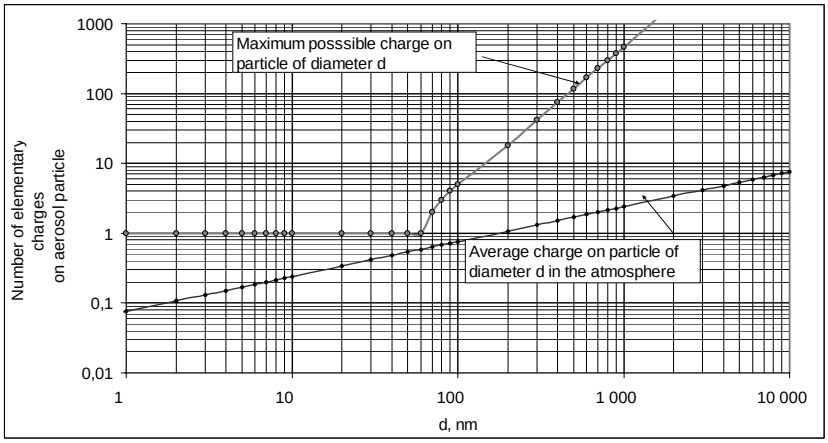

Figure 2. Number of elementary charge carried by aerosol particles seized 1 nm – 10 μm. Grey line – maximum values limited by electric breakdown of the air, black line – the average values typical for the thermodynamic equilibrium in the atmospheric conditions.

The calculations made by *Yu*, were based on the simplifying assumptions of smooth inner surfaces of analysed pipe like surrogates of the airway, the ideal conductivity, and bioelectrical passivity (no biomechanical or bioelectrical activity of epithelial cells was concerned).

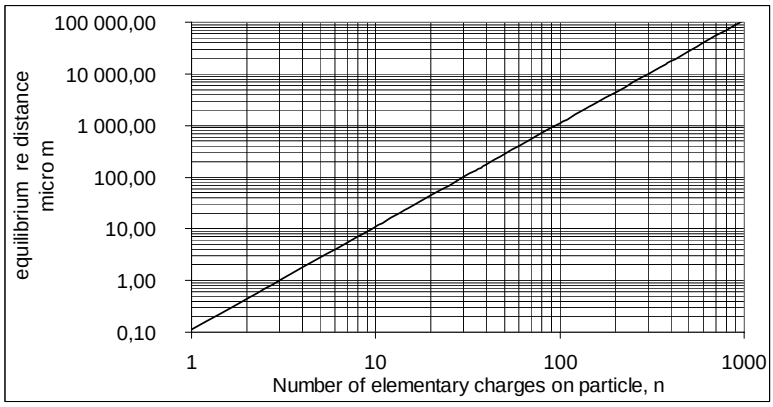

Figure 3. Critical distance from the conducting surface for which the thermal and electric energy (image force energy) are equal, versus number of elementary charge carried by particle.

Diffusion and image force are "short distance" mechanisms of deposition. Potential energy of image force of

charged particle is proportional to the second power of the particle charge. If neglect the other forces acting on the particle, every particle with energy of image force greater than thermal energy, should achieve the conducting surface. The relation between the particle charge and the border distance at which both kinds of energy are equal, is shown in Fig. 3. Particles below the curve in Fig. 3 theoretically, should settle on the conducting surface. However, for the longest distances and coarse particles, this could take a long time, probably longer than sedimentation for large particles. For that, the more effective is to compare the time of flight *T* of the air along the considered airway (e.g. pipe model) with the time τ of the drift of the particle from the point placed at the input cross section to the inner surface of the pipe. Practically the task is to find the minimum radius of the cylinder coaxial with the pipe, above which all the particles carrying charge *q* are deposited, it means for which $T \geq \tau$. The profile of the airflow in the pipe is complex. Usually there have been analysed two modes of the laminar airflow – the mode without the boundary layer at the inner surface of the pipe (air speed is constant at the all cross section area –slug flow), and with boundary layer (parabolic flow). The choice of the model depends on the length of the pipe, sharpness of the surface, and air speed, usually for short airways there is no enough time for developing full parabolic flow. According to the calculations by *Yu* and *Chandra* (1978), the deposition by the image forces is more effective for slug than for parabolic flow.

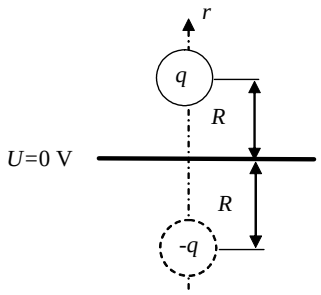

Figure 3. The simplified model of image effect of charge *q* over the conducting plane (*U* = 0V)
R - the distance between the charge and the conducting, grounded plane, (-*q*) – image of the charge (*q*).

For the analysis of the image, force effect there can be used the model shown in Fig. 3. This is the exact model for plane, conducting and grounded material. In case of the respiratory system the cylindrical pipes or spherical conducting cavities are used, where (-*q*) = *K*·*q*, where *K* is a function of the shape of the conducting material and distance of the charge *q* to the conducting surface. In the atmospheric air, there is the most important, and usually correct the common assumption that the charged particle moves along the electric field line, with the average speed:

$$\overline{\mathbf{v}(\mathbf{r})} = \mu\, \mathbf{E}(\mathbf{r}), \tag{1}$$

where, μ is the mobility of the charged particle.

In geometry case shown in Fig. 3, in the atmospheric air, which is viscous, the particle movement forced by the image force can be described by the following differential equation:

$$\frac{dr}{dt} = -\mu E = -\frac{\mu q}{16\pi\varepsilon_0 r^2}, \tag{2}$$

with the initial condition for the particle drift $r(t = 0) = R$.

That relation is only statistically true. If the distance *R* is enough small, comparable with the particle free path, the particle movement can be described by the following equation:

$$m\frac{d^2 r}{dt^2} = qE = \frac{q^2}{16\pi\varepsilon_0 r^2}, \tag{3}$$

and the initial conditions are: $r(t = 0) = R$ and $v(t = 0) = 0$, where *m* is the particle mass.

Solution of the Eq. 2 is:

$$\tau = \left(R^3 - r^3\right)\frac{16\pi\varepsilon_0}{3\mu q}, \qquad \text{or} \qquad r = \sqrt[3]{R^3 - \frac{3\mu q}{16\pi\varepsilon_0}\tau}, \tag{4}$$

and, solution of Eq. 3 is:

$$\tau = \sqrt{\frac{32\pi\varepsilon_0 m}{3q^2}\left(R^3 - r^3\right)}, \qquad \text{or} \qquad r = \sqrt[3]{R^3 - \frac{3q^2}{32\pi\varepsilon_0 m}\tau^2}, \tag{5}$$

where $d/2 \leq r \leq R$, and *d* is the particle diameter.

The ratio of the time of flight τ_2 of the distance *R* in case without collisions (Eq. 5) to the time τ_2 with collisions

(Eq. 4) is:

$$\frac{\tau_2}{\tau_1} = \sqrt{\frac{\gamma\mu^2}{2\varepsilon_0}}, \tag{6}$$

where γ is the particle material density. This ratio is always less then one, and for the fine particles τ_2 is a few orders of magnitude smaller than τ_1.

The free path l of aerosol particle of diameter d and density γ can be calculated from the Eqs 6, 7, after *Friedlaner* (2000):

$$l = \frac{\sqrt{(mkT)}}{3\pi\eta d}\left(1+\frac{2\lambda}{d}\left(A_1 + A_2\exp\left(\frac{-A_3 d}{\lambda}\right)\right)\right), \tag{7}$$

where, A_1=1.257, A_2=0.400, A_3=0.55, η - dynamic viscosity of air, λ - mean free path of the air particles (about 0.065 μm), and

$$m = \frac{4}{3}\pi\left(\frac{d}{2}\right)^3\gamma\,. \tag{8}$$

The relation (Eq. 7) is shown in Fig. 4.

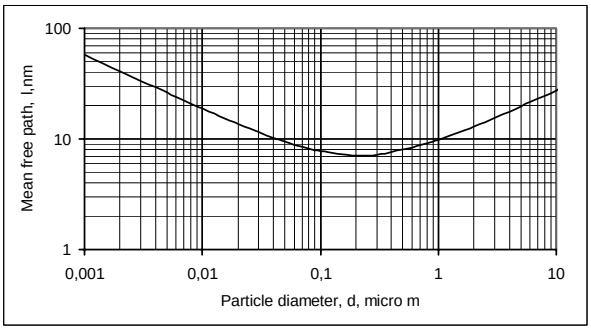

Figure 4. The mean value of the free path l of the aerosol particle of density for $\gamma = 10^3$ kg/m^3 and diameter d

The fraction of the particles for which the ratio (a) of a free path to the mean free path is inside the range $<a_1; a2>$, can be calculated as difference of probabilities $p(a_1)$ - $p(a_2)$. The probability function $p(a) = \exp(-a)$ is shown in Fig.5.

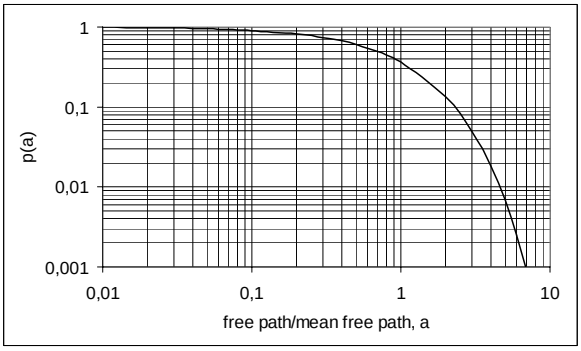

Figure 5. Probability $p(a)$ that the free path of the particle is a – folds of the mean free path.

It can be seen that the free path is larger than mean free path for about 37% of the particle population and larger than twice mean free path for 13,5%. So the image force effect without particle collisions is effective only at a distance from few tenth to few hundred of nanometres, but at such distance it is very strong and all charged particles (even with one elementary charge) would be deposited onto the airway surface. In this case the charged particles which are attracted toward the conducting surface by image force, achieve the surface much sooner than 1 ms if not collide with air particles. This effect can increase the deposition efficiency in smaller airways and if turbulent flow takes place. The effect should by studied more precisely and it seems that it was not concerned before.

Generally, because of *Yu* calculations, there exists general opinion that the image forces do not influence the

deposition in significant level. To verify that opinion the following simple case study, based on the *Yu* and *Chandra* (1978) example of 1 μm charged particles, was carried.

This is put the assumption, that the efficiency of the deposition by image force, in generation number *n* is equal $\eta_{i\,n}$. If the image force would be the only active mechanism in the airway, the deposition in generations from *m*=0 to *m* = *n*≠0 could be expressed as follows:

$$\eta_{i\,0\text{-}n} = \eta_{i\,0} + \sum_{m=1}^{n} \eta_{i\,m}\left(1-\eta_{i\,m-1}\right) \tag{9}$$

That should be noticed that Eq. 9 concerns only the population of the particles of defined diameter and charge, for which the values $\eta_{i\,m}$ were calculated before. As the number of generation is 24, even at the
According to *Yu* and *Chandra*, the deposition efficiency at the chosen generation pipe of the inner radius *R* of inner hole, can be presented for laminar flow, as:

$$P = 1-\left(\frac{r_c}{R}\right)^2, \tag{10}$$

for slug airflow, or:

$$P = \left[1-\left(\frac{r_c}{R}\right)^2\right]^2, \tag{11}$$

for parabolic airflow (with boundary layer), where r_c is the critical radius coaxial with the tested pipe, outside of which all particles are deposited.

The relation between r_c and the characteristics of the particle, pipe and airflow is:

$$\tau = 4\left(\frac{R}{r_c} + 2\ln\frac{r_c}{R} - \frac{r_c}{R}\right) \text{ for slug airflow, and} \tag{12}$$

$$\tau = 4\left(\frac{R}{r_c} + 2\ln\frac{r_c}{R} - \left(\frac{r_c}{R}\right)^2 + \frac{1}{3}\left(\frac{r_c}{R}\right)^3 - \frac{1}{3}\right) \text{ for the parabolic airflow,} \tag{13}$$

where, dimensionless time of residence was defined by *Yu* and *Chandra* (1978) as follows:

$$\tau = \frac{\mu q^2 L}{4\pi\varepsilon_0 R^3 u_0}, \tag{14}$$

where, *L* is the length of the pipe and u_0 the velocity of slug airflow.

On the basis of Eqs. 11-14, *Yu* and *Chandra* (1978) calculated the deposition for each of twenty four generations of the human respiratory system, for the particles of diameter 1 μm and density 1g/cm^3, carrying 100e charge, for breathing at 1000 cm^3 tidal volume, 12 respirations/minute. Those calculations are presented in Figs. 5 and 6 for the parabolic and slug airflows. Additionally, at those Figures, the total efficiencies calculated according to the Eq. 9, are shown also. For chosen particles, the deposition efficiency is between 30% and 70%. To get the more exact results, the airflow profile in specified generation should be known. Theoretically, there is possible to deposit 100% of highly charged particles, including four mentioned before active mechanisms also.

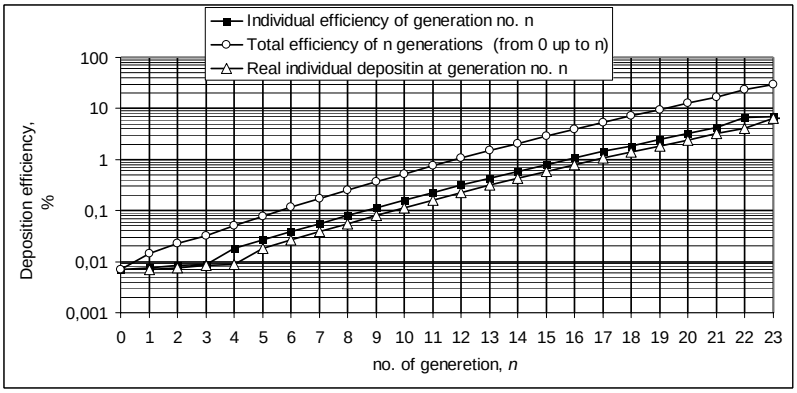

Figure 5. The efficiency of deposition by image forces at the individual generations of human respiratory system, calculated by Yu and Chandra, and ascending cumulative efficiency of the first *n* generations, calculated in this paper, and real cumulative deposition in individual generations. Calculations are made at the parabolic airflow.

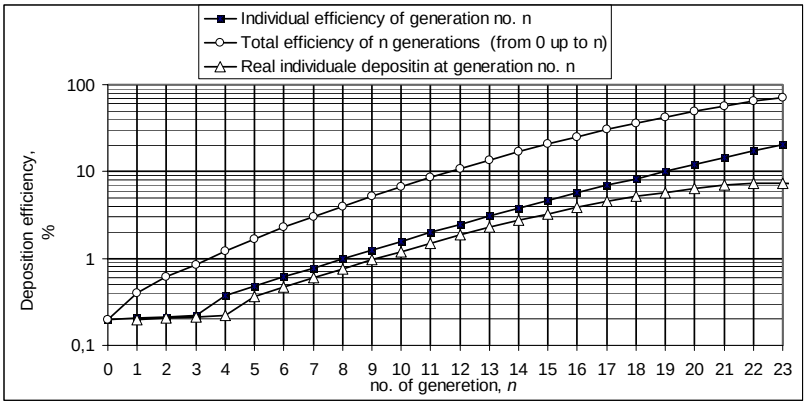

Figure 6. The efficiency of deposition by image forces at the individual generations of human respiratory system, calculated by *Yu* and *Chandra*, and ascending cumulative efficiency of the first *n* generations, calculated in this paper, and real cumulative deposition in individual generations. Calculations are made at the slug airflow.

The experiments of *Cohen et al*. (1995), mentioned before, with the deposition of charged particles in the hollow, conducting cast of human respiratory system showed, that the possible deposition of charged particles can be much higher than theoretically expected. There was measured the deposition of neutral particles, charged with 1e and neutralized particles. The studies with 20 and 125 nm particles were done; their results are shown in the Tab. 1.

Table 1. Deposition efficiency of the charged, neutralized and uncharged fluorescein particles in conducting hollow cast of human airways, at average airflow 5000 ccm/min, measured by *Cohen et al*. (1995)

Electrification of particles	**Particle diameter d = 20 nm**	**Particle diameter d = 125 nm**
	Mean value of deposition, %, ±2σ	Mean value of deposition, %, ±2σ
Single elementary charge (*q*=1e)	6.62±0,70	1.61±0.08
Charge neutralized	1.96±0,29	0.70±0.16
Neutral (*q*=0)	1.24±0,09	0.26±0.06

Those data show that the image force is an important factor enhancing the deposition of charged particles (5.3 folds for 20 nm and 6.2 for 125 nm). The model had to be different from the human respiratory system (e.g. lack of extrathoracic region), so the obtained deposition of neutral particles is significantly lower than that obtained by calculations (see Fig. 1). In case of particles sized above 0.1 μm, which can carry much higher number of elementary charges than only one, there can be expected significantly higher efficiency, which was shown above (see Figs. 5 and 6).

In the cited studies, there were not considered electrical activity of the cells in air ducts. At this moment, there is no data for assessment the significance of bioelectric potentials in deposition of charged particles and the influence of the particles charge on the cilia activity.

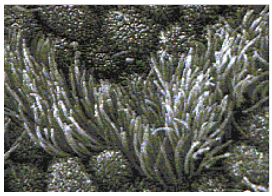

Figure 7. Example of the ciliated cells from the trachea.
Cilia's dimensions are about 10 μm length and 0.3 μm diameter.
After*: Kenneth S. Saladin, Anatomy and Physiology, the Unit of Form and Function,* WBC/McGraw Hill, 1998, p. 116.

The cilia on epithelial cells (see Fig. 7) move the mucus along a surface layer of saline. This is very likely that the cilia, beating with the frequency about few tenth of Hertz, generate some evoke potentials which should be different during power and recovery strokes. Mucus and saline layers separate the inner space of the airway duct from them, but those layers are not ideal conductors and are not continuous, so there is possible the penetration of electrostatic field of them into the airway duct space. If consider the sizes of cilia and surrounding cells and typical bioelectrical potential, it can be expected the electric field strength of order several to few tenths of kV/m. Such potentials can be compared with electrostatic potentials induced by charged particles between them and the mucus layer or cilia. The potential distribution between the charged particle and conducting surface (as in the Fig. 3) can be expressed as:

$$U(r) = \frac{q}{2\pi\varepsilon_0 R}\frac{r}{\left(R^2 - r^2\right)}, \tag{15}$$

and is illustrated for q = 1e at the Fig. 8. The change of the potential conducting surface from zero up to U, in rough modelling, can be concern as a virtual change of the distance R. The result of approximate calculations of this change dr related to the distance R, are shown in Fig. 8. This is the case of the particle charge q = 1e, for which the sensitivity of the particle to the changes of the conducting surface potential is the highest. The sign of virtual dr is positive if the signs of the surface and particle are opposite, and negative if both signs are the same, respectively. For typical membrane potential about 20 mV, the influence of bioelectric potential is very effective compare to the image forces if R>1 μm (dr/R > 0.9).

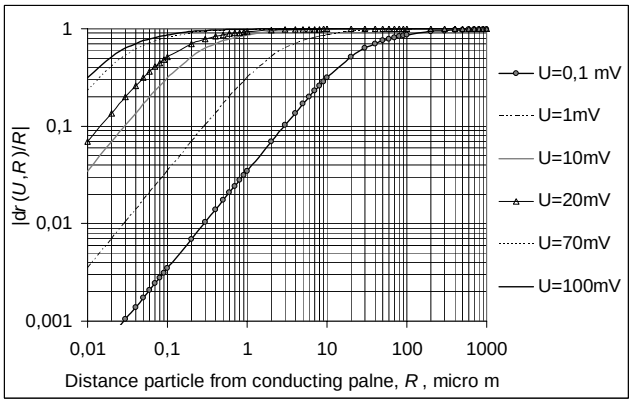

Figure 8. The virtual change |dr/R| of the distance R between the conducting plane and charge particle (q=1e), when change the conducting plane potential from zero to U.

Summary

The efficiency of charged particles deposition in human airways can significant, especially for highly charged aerosol particles. The above analysis made on the example of individual deposition efficiency of 24 generations of airway ducts, using calculation by *Yu* and *Chandra*, has shown that image forces acting alone are able to deposit up to 30-70% of highly charged particles. If include mechanical deposition factors, that efficiency could arise even more. Especially important can be increase of the deposition particles sized 0.1 - 1μm, where the deposition spare margin is very large, up to ten folds. As the experiments of *Cohen et al*. showed, the deposition of charge 125 nm particles, can be about six folds higher than those of zero charged, potentially this margin can be filled. The analysis of the example of 1 μm and 100e charged particles showed that not only the total deposition increase, but the individual deposition in all generation also. So it seems unlikely, that charging of aerosol particles could cause stopping them in upper parts of airways and significantly prevent the deposition in bronchioli and alveoli, which could positive health effect.

The significant increase of charged particle deposition, on the theoretical basis seems to be very probable if the particles charge is close to their saturation charge, and the most of the particle population is highly charged. Such cases are very rare in practice, excluding some very special conditions like particles charge in electrostatic precipitators or portable electrostatic air cleaners, paint powder particles at the electrostatic painting, and some other technologies. In the processes of particle atomization, young particles which did not achieve the state of thermodynamic equilibrium, could be electrified highly also, and the almost whole population of them can be charged.

The attention should paid to bacteria, especially water born, which charge can be very high, in some cases even up to 10^4e (*Mainelis*, 2001), but always much higher than that of the non-biological particles in the same environment. For such biological objects, the deposition in human airways can be very effective.

Real efficiency of the image forces can be enhanced also, as it was shown above, by very fast non-collision drift of the particles to the duct surface from the distance close to the free path of the particles. In this case the most effective could be attracting of nano-particles (see Fig. 4) and the least effective of 0,3-0,4 μm particles. This hypothetical effect could enhance the deposition during turbulent airflow much more than during laminar flow.

Other proposed hypothesis is that the deposition of charged particles can be enhanced if some bioelectric potential differences occur on the inner surface of the air-ducts. This effect could modulate the virtual distance of the particles to the inner surface of air duct and could be significantly stronger, especially for small charge on the particles, than the image force effect. These hypotheses should be tested experimentally, but it seems very difficult in the latest case.

Acknowledgements

This paper has been prepared on the basis of the results of a task carried out within the scope the second stage of the National Programme "Adaptation of Working Conditions in Poland to European Union Standards", partly supported - within the scope of research - in 2005–2005 by the Ministry of Science and Higher Education. The

Central Institute for Labour Protection – National Research Institute has been the Programme's main co-ordinator.

References

1. Chen, Y.K., Yu, C.P. (1993), Particle deposition from duct flows by combined mechanisms, *Aerosol Sci. Technol.,* 19, 389-395
2. Cohen, B.S., Xiong, J.Q., Fang Ching-Ping, Li, W., (1998), Deposition of charged particles on lung airways, *Health Physics*, vol. 74, no. 5, 554-560
3. Cohen, B.S., Xiong, J.Q., Li, W. (1995). The influence of charge on the deposition behavior of aerosol particles with emphasis on singly charged nanometer sized particles. 153-164 w: Ed. Marijnissen, J.C.M., Gradoń, L. *Aerosol inhalation: Recent research frontiers*. Kluwer Academic Publishers
4. Fews, A.P., Henshaw, D.L., Keitch, P.A., Close, J.J., Wilding, R.J (1999a). Increased exposure to pollutant aerosols under high voltage power lines. *Int. J. Radiat. Biology,* vol. 75, no. 12, 1505-1521
5. Fews, A.P., Henshaw, D.L. Wilding, R.J. & Keitch, P.A. (1999b). Corona ions from powerlines and increased exposure to pollutant aerosols. *Int. J. Radiation Biology,* 75(12), 1523–1531
6. Friedlander, S.K., Smoke, Dust and Haze. Fundamentals of Aerosol Dynamics. Oxford University Press
7. Grabarczyk, Z., J., Berliński, J., (2005), Charging of atmosphere aerosols by AC HV power lines, *Journal of Electrostatics*, 63, 755–759
8. Henshaw, D.,I., *et al*. (1996). Enhanced deposition of radon daughter nuclei in the vicinity of power frequency electromagnetic fields. *Int. J. Radiat. Biol.* 69(1), 25-38.
9. Mainelis, G. *et al*., Electrical charges on airborne microorganisms, *Aerosol Science,* 32, 2001, 1087-1110
10. NRPB (2004). Particle deposition in the vicinity of power lines and possible effects on health. Report of an independent Advisory Group on Non-ionising Radiation and its Ad Hoc Group on Corona Ions. National Radiological Protection board. *Documents of NRPB. vol. 15, No. 1. 2004*.
11. Yu, C.P., Chandra, K. (1978). Deposition of charged particles from laminar flows in rectangular and cylindrical channels by image force, *J. Aerosol Sci.* (9), 175-180

EXTREMELY LOW FREQUENCY MAGNETIC FIELD PROMOTES DIFFERENTIATION OF THE EX VIVO EXPANDED HUMAN CARDIAC STEM CELLS

POZZI D.[1], LISI A.[2], MESSINA E.[1], LEDDA M.[2], GAETANI R.[1], D`EMILIO E.[3], GIULIANI L.[3],BERTANI F.[1], CHIMENTI I.[1], ROSOLA E.[2], BARILE L.[1], GIACOMELLO A.[1], GRIMALDI S.[2]

[1]DEPARTMENT OF EXPERIMENTAL MEDICINE AND PATHOLOGY UNIVERSITY OF ROME "LA SAPIENZA", ITALY;
[2] INSTITUT OF NEUROBIOLOGY AND MOLECULAR MEDICINE CNR ROME, ITALY; [3] ISPESL DIPIA ROME, ITALY.

Abstract

Studies for the identification of suitable stem cells culture and differentiating conditions that are devoid of xenogenic growth supplements is actually considered an important issue for the clinical applicability of cell therapy for heart failure. We have recently demonstrated the possibility to obtain Cardiac Stem Cells (CSCs), from human endomyocardial biopsy specimens. CSCs self-assemble into multi-cellular clusters known as cardiospheres (CSps) that engraft and partially regenerate infarcted myocardium.

CSps were exposed for five days in an incubator inside a solenoid system with temperature and humidity and CO_2 regulated. This exposure system were placed in an a-magnetic shielded room in the simultaneous presence of a static MF and a low-alternating-frequency-MF, close to the cyclotron frequency corresponding to the charge/mass ratio of Ca^{++} ion. In this exposure conditions CSps modulate their differentiation turning on cardiogenesis and turning off vasculogenesis. Cardiac markers such as Troponin I (TnI) or Myosin Heavy Chain (MHC) were up-regulated, conversely angiogenic markers such as Vascular Endothelial Growth Factor (VEGF) or Kinase Domain Receptor (KDR) were down-regulated as evidenced by immunocytochemistry. The improvement in the cardiogenic differentiation was confirmed by Real-Time PCR and Western Blotting analysis. Interestingly, an increase in the proliferation was observed and evidenced by Brd-U incorporation (ELISA) and cell counting kit-8 (WST-8) analysis.

Exposure to Extremely Low Frequence Magnetic Field (ELF-*MF)* can modulates the cardiogenic *versus* angiogenic differentiation process of *ex vivo* expanded CSCs.This may pave the way for novel approaches in tissue engineering and cell therapy.

Introduction

In order to increase the reliability and the clinical feasibility of the CSCs employment for cardiac cell therapy we need new methods that allow a modulation of the differentiation process with a minimal cell manipulation.

CSCs can be clonally expanded from myocardial biopsies; these cells are spontaneously shed from human surgical specimens and murine heart samples in primary culture. This heterogeneous population of cells expresses c-kit. These cells are self-renewing, clonogenic and multipotent giving rise spontaneously to cardiomyocytes, smooth muscle cells and endothelial cells. In suspension culture they form multicellular clusters dubbed Cardiospheres (CSps).[1]

Recently spontaneous differentiation of ES cells into cardiac myocytes by exposure to ELF-MF has been reported[2]. We assessed the hypothesis that the exposure of CSps to defined Magnetic Field could modulate the cardiac differentiation process with a minimal cell manipulation.

Methods and results

Human biopsy specimens were obtained from patients undergoing clinically-indicated percutaneous endomyocardial biopsy and processed. Samples were stored on ice in high potassium cardioplegic solution and processed within two hours. Briefly, samples were cut into fragments, washed, partially enzymatically digested, and the single cells discarded. The remaining tissue fragments were cultured as explants on dishes.

A lawn of flat cells spreads from the biopsy and covers the bottom of the dish in 14-20 days. Cells can be seen budding off from the main explant and then seeding the dish, a process which is robust by 12-18 days. The cells surrounding the explant are harvested, initially after 5-7 days, and then every 4-5 days (for a total of 4 harvests). When grown in suspension, the cells form CSps within 12-20 days. On the basis of our previous results obtained with other cellular model (cheratinocytes, neuronal cells) [3-5], CSps were exposed for five days in the a-magnetic room with simultaneous presence of a static Magnetic Field and a ELF-MF, close to the cyclotron frequency corresponding to the charge/mass ratio of Ca^{++} ion.

The equipment for electro-magnetic field (solenoid) production is installed in a-magnetic room. This equipment include cellular incubator made to a-magnetic material were temperature regulation (37± 0.1°C) and atmosphere (5% CO2) and humidity were provided and continuously controlled and recorded by a lab view program embedded computer.

The main body of the solenoid is a cylinder in PVC 5 mm thick and has a diameter of 33 cm and a height of 3 m. It is made of 3,300 turns of 1 mm diameter copper wire. It is driven from three amplifiers and a signal generator that generated static and alternate current for electromagnetic field production. This equipment is able to produce 0.01Hz to 1 KHz frequency and 10 nT to 1mT of electromagnetic field and induction respectively at 33 mV RMS drove.

Under these conditions an increase in cell metabolism was observed and evidenced by cell counting kit-8 (WST-8) analysis (Fig. 1). Moreover, cardiac markers such as Troponin I (TnI) or Myosin Heavy Chain (MHC) were up-regulated. Conversely angiogenic markers such as Vascular Endothelial Growth Factor (VEGF) or Kinase Domain Receptor (KDR) were down-regulated as evidenced by immunocytochemistry (Fig. 2) and by RT-PCR (Fig. 3).

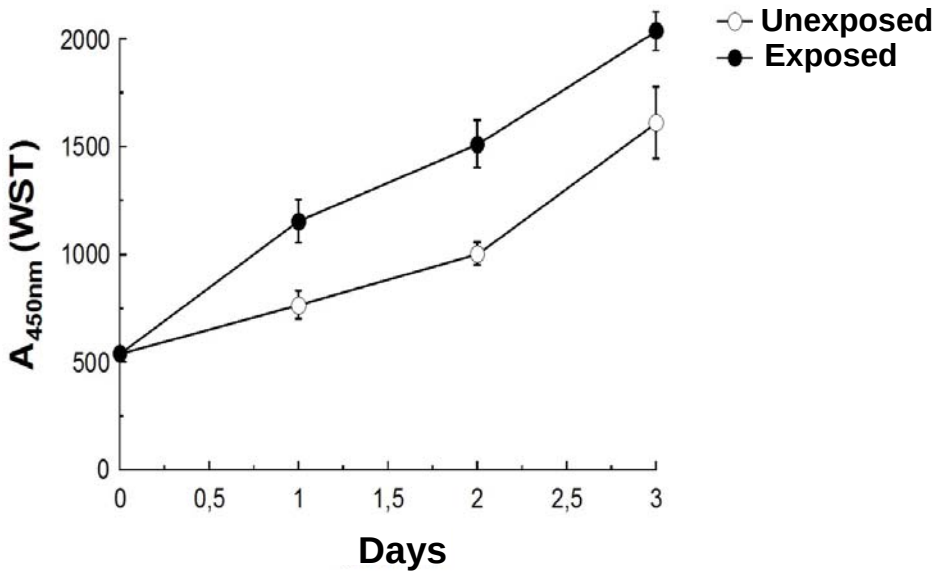

Figure 1: ***Metabolic activity***

Evaluation of cell metabolism by utilizing sensitive colorimetric assays. WST-8 is reduced by dehydrogenases in cells to give a yellow colored product (formazan), which is soluble in the tissue culture medium. The amount of the formazan dye generated by the activity of dehydrogenases in cells is directly proportional to the number of living cells. Figure shows that cells exposed to ELF-MF (●) have higher metabolic activity then the unexposed cells (○).

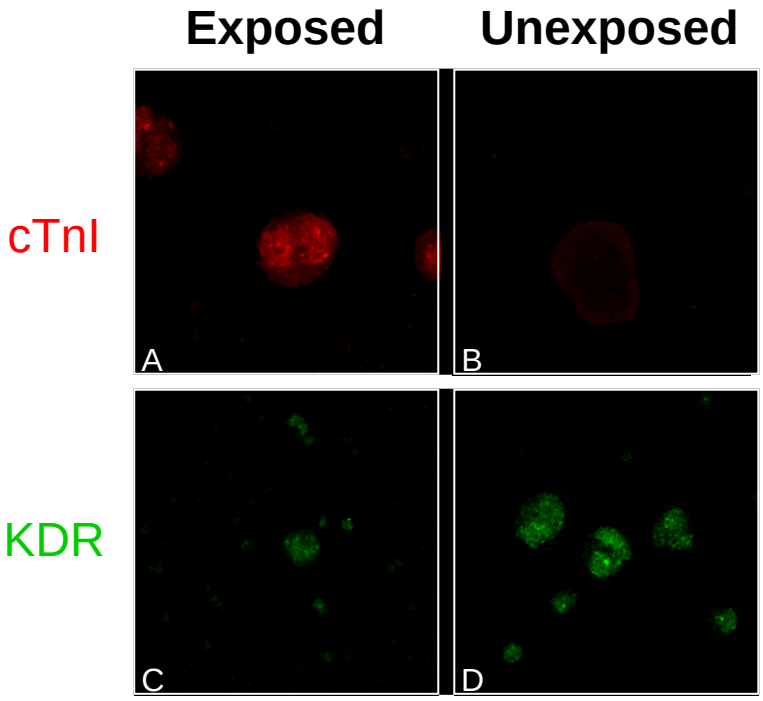

Figure 2: ***Cardiosphere and CDC Phenotypes***

A) Cardiospheres expressing cardiac TnI after exposure to the ELF-MF for 5 days. C-D) The exposure to the magnetic field seems to down-regulate the vasculogenesis

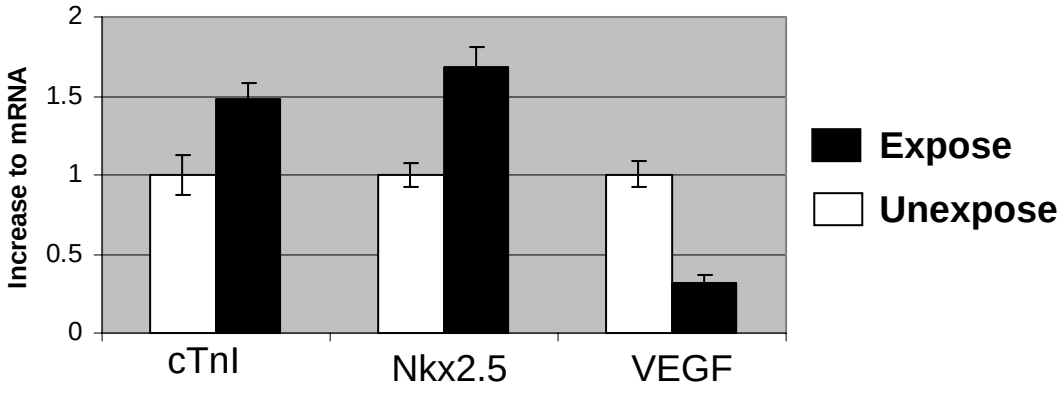

Figure 3: ***Real Time PCR***

Effect of field exposure on expression of cardiac markers such as cTnI,Nkx 2.5 and angiogenic markers such as VEGEF after five days. The column diagram shows the differences in mRNA production of exposed (■) and unexposed (□) CSps.

Discussion

One hundred years ago the humans were exposed only to natural electromagnetic field (EMF). With technical and industrial growth, the EMF generated by human activities became several times higher than the field found in nature.

Because most of the physiological processes of the eukaryotic cell are voltage regulated, in the last 20 years underwent a strong increase of the interest to investigate the effect of extremely low frequency electric and magnetic fields [6-8].

Some of this studies reported changes induced in calcium efflux from chicken brain hemispheres [9], nerve regeneration [10], alteration gene transcription [11], and they may also play a synergic role in cellular processes that are already activated, such as cell proliferation and cell differentiation.

The possible mechanisms of the induced effects are not known, although a number of theoretical models have been proposed) [12-14]. Studies focusing on the role of Calcium signalling in the mechanisms of the ELF-MF-induced differentiation are ongoing in our laboratory.

We have obtained data showing that exposure of the *ex vivo* expanded CSps to ELF-MF modulates their differentiation turning on cardiogenesis and turning off vasculogenesis. Interestingly this effect was accompanied by increase of cellular metabolism and proliferation.

If confirmed, these results should increase the reliability and the clinical feasibility of the CSCs employment for cardiac cell therapy.

References

1. Messina E., et al. (2004) Isolation and expansion of adult cardiac stem cells from human and murine heart. *Circ Res.;95(9):911-21*
2. Ventura C. et al. (2004) Turning on stem cell cardiogenesis with extremely low frequency magnetic fields**.** *The FASEB Journal* 2004 19(1):155-7
3. Lisi A., et al. (2005) Exposure to 50Hz electro-magnetic radiation promote early maturation and differentiation in newborn rat cerebellar granule neurons. *J. Cell. Physiology, 204, 532-538*
4. Manni V., et al. (2002) Effect of extremely low frequency (50 Hz) magnetic field on morphological and biochemical properties of human keratinocytes. *Bioelectromagnetics .23:298–305.*
5. Manni V., (2004) Effect of low frequency (50 Hz) non ionising radiation on primary human oral keratinocytes (HOK). *Bioelectromagnetics 25:118–126.*
6. Blank M., et al. (1987) Mechanistic approaches to interactions of electromagnetic field with living systems. *New York: B. Plenum.*
7. Tenforde TS. (1995) Interaction of extremely low frequency electric and magnetic fields with humans. *In: Polk C, Postow E, editors. Handbook of biological effects of electro-magnetic fields, 2nd edition. Boca Raton: CRC Press, pp 185–230.*
8. Zhadin MN., (2001) Review of Russian literature on biological action of DC and low-frequency AC magnetic fields. *Bioelectromagnetics 22(1):27–45.*
9. Blackman C.F., (1988) Stimulation of brain tissue in vitro by extremely low frequency, low intensity, sinusoidal electromagnetic field. *Prog Clin Biol Res 257: 107-117;*
10. Rusovan A, et al. (1992) Magnetic fields stimulate peripheral nerve regeneration hypophyctiomia rats. *Neuroreport 3(12):1039–1041.*
11. Phillips JL., et al. (1992) Magnetic fieldinduced changes in specific gene transcription. *Biochimica Biophysica Acta1132:140–144.*
12. Glaser R., et al. (1992) Current concepts of the interaction of of weak electro-magnetic fields with cells. *Bioelectrochem Bioener 27:255–268.*
13. Liburdy RP., et al. (1992) Calcium signalling in lymphocytes and ELF fields: Evidence for an electric field metric and a site of interaction involving calcium ion channels. *FEBS Lett 301(1):53–59.*
14. Barnes PS., et al.(1996) Effect of electro-magnetic field on the rate of chemical reactions. *Biophysics 41:801–880.*

OCCUPATIONAL ELECTROMAGNETIC FIELD EXPOSURE AND INDUCED CURRENT'S HAZARDS FROM ELECTROSURGERY DEVICES

KRZYSZTOF GRYZ, JOLANTA KARPOWICZ

CENTRAL INSTITUTE FOR LABOUR PROTECTION – NATIONAL RESEARCH INSTITUTE, WARSZAWA, POLAND, e-mail: krgry@ciop.pl

Abstract

The investigations concerning medical staff exposure to electromagnetic fields and induced currents hazards from electrosurgery devices have been completed. The exposure has been evaluated following the European Directive 2004/40/EC and national occupational safety and health regulations. The main sources of workers exposure are powered electrode and cables. Electromagnetic fields from electrosurgery devices are pulsed modulated and have heterogeneous spatial distribution. It has been found that in the vicinity of electrosurgical devices, the area of electromagnetic fields to which only workers operating the source of field should be exposed can exist up to the distance of tens of centimetres from the active electrode and supplying cables. In the case when the cables are placed directly on the surgeon's body the overexposure of workers can appear. The current flowing through the arm of surgeon keeping the electrode emitting electric field of the maximum strength (app. 1000 V/m or higher) can exceed the permissible value of 40 mA established by the Directive 2004/40/EC for contact current. The obtained results of measurements and suggestions for reduction of the surgeon's exposure are presented.

Keywords: electromagnetic fields, occupational exposure, induced currents, electrosurgery.

Introduction

Electrosurgery is used for various surgical treatments - to cut or to coagulate a patient's tissues. Electromagnetic hazards produced by these apparatus are essential for a big group of medical staff given a common use of electrosurgery devices. Electrosurgery devices consist of a generator (with output power of up to 500 W, but usually the output power used during surgical treatment is of 50-150 W), an active (powered) electrode connected with the generator by long cable and a passive electrode, fixed at a patient's body and connected by long cable with "0" electric potential of the generator.

Controllable surgical effect is a result of the flow of radiofrequency (RF) currents through the tissues of the body and local heating them. This current is the result of capacitive coupling of powered electrode with a patient's body. Current can flow with or without a direct contact between the active electrode and the body of patient if the potential of the electrode is higher than 200 V in the relation to potential of the tissues. Electric arc can be burned under the active electrode in the case of a higher potential of the electrode.

Currents of frequency above 300 kHz (up to approx. MHz) are used to avoid electrical stimulation of tissues. The waveforms of electric potential and current (and in consequences, electromagnetic field (EMF) produced in the vicinity of cables) depend on a type of a device and it's selected mode of a device operation. As a result, the EMF waveform changes from sinusoidal (usually exists during cut mode) to pulsed modulated (during different coagulation modes) – fig. 1, and additionally it is always pulsed modulated by the switch-on and switch-off actions of surgeon which are taking following surgical treatment needs.

The sources of the occupational exposure are mainly [2]:

- the active electrode at a high electric potential from which the RF current penetrates the tissue
- the cables connecting the generator with the active electrode, kept in the hand by a surgeon, and with the passive electrode (grounded plate), mounted to the patient's body.

The additional sources of EMF can be:

- the generator in the case of not leakproof housing (without electromagnetic shield),
- metallic objects located in the vicinity of the electrodes cables (for example, surgical or instrumentation's tables) and which can become secondary sources of EMF.

The EMF is produced from the moment of activation of an electrosurgery device. It may be operated by foot-control or through a button-control on the handle of the active electrode.

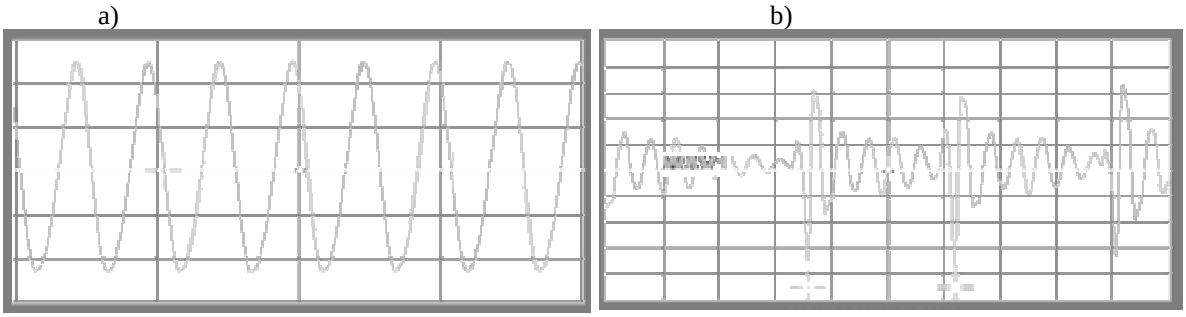

Fig. 1. Examples of EMF waveform registered in the vicinity of electrosurgery devices: a) pure cut mode; b) coagulation “spray” mode.

Electrodes and supplying cables are sources of strong electric field because of radiofrequency (RF) high voltage between electrodes. The exposure to EMF of a surgeon and medical staff depends on the selected mode of device operation, the kind of active electrode used and the location of cables connecting electrodes with generator.

During patient’s treatment, generator and cables can be located in various places against to the surgical table and medical staff bodies. It is crucial for the level of exposure to electric field and capacitive coupling between elements of electrosurgery device and the worker’s body and it determines the level of current flowing through the worker’s body, similarly to currents through the patient’s tissues. If the cables create loops, an increased magnetic field exists also in their vicinity.

The surgeon, who keeps the active electrode in hand, is usually the most exposed person from the team. The hand's exposure always exists, but other parts of the body can be also exposed as a result of the contact with cables, e.g. head's or torso's EMF exposure.

Methods

The EMF measurements have been performed to assess the medical staff exposure to EMF during the use electrosurgery devices [2]. The measurements of RMS electric and magnetic field strength have been conducted according to the Polish Standard PN-T-06580:2002 [6]. Broadband electric and magnetic field strength meter EMR 300 from Wandel & Goltermann with H-field probe type 13 (0.02-250 A/m; 300 kHz – 30 MHz) and E-field probe type 8 (1-800 V/m; 100 kHz – 3 GHz) has been used. The obtained results have been evaluated according to the Polish national regulations concerning the limitation of occupational exposure to EMF of 0 Hz - 300 GHz frequency range [5, 7]. This regulation stated that the worker’s exposure assessment should be performed on the results of the spot measurements of RMS value of unperturbed (it means existing in the workplace during the absence of workers) electric and magnetic field strength (the maximum result of measurements over the worker’s body position in the workplace).

Additionally, the investigated EMF exposure of medical staff has been analysed following the internationally published limitations [5], European Directive 2004/40/EC [1], ICNIRP's guidelines [3] and IEEE standard [4]. According to the European Directive, workers' exposure assessment should be performed on the results of measurements of RMS value of unperturbed (existing in the workplace during the absence of workers) electric and magnetic field strength averaged over the workers body position and averaged for particular time, which depends on the frequency of assessed fields. For example, for the EMF of the frequency 100 kHz - 10 GHz, E and H should be averaged within any 6 minutes of worker's exposure and E^2 and H^2 should be averaged over the worker's body position. Electric field strength (E) and magnetic field strength (H) were included into the set of the Directive’s “action values”, which were defined as the set of external measures, which can be used to describe the EMF exposure for testing and roughly assessing environmental conditions in the workplace. The exposure results inside exposed body, which were taken as “exposure limit values” (internal measures) refer to

the physical quantities as current density (J) and specific energy absorption rate (SAR) should be considered in the case of environmental exposure conditions exceeding above-mentioned "action values". Additionally, Directive's provisions refer to contact current (I_C) and limb induced current (I_L), which can be also used for testing the compliance with "exposure limit values".

Exposure limitation in the frequency range of EMF produced by electrosurgery devices established by Polish national regulations and European Directive is shown in table 1.

Table 1.

Electric and magnetic field strength – exposure limitation established in Poland [6] and by European Directive's "action values" [1].

Frequency range	Exposure limitation in Poland				Directive 2004/40/EC	
	Electric field strength, E [V/m]		Magnetic field strength, H [A/m]		Electric field strength, E [V/m]	Magnetic field strength, H [A/m]
	prohibited exposure	8-hours exposure	prohibited exposure	8-hours exposure		
300 kHz $< f \leq$ 800 kHz	1000	100	100	10	610	1.6/f
0.8 MHz $< f \leq$ 1 MHz	1000	100	80/f	8/f	610	1.6/f
1 MHz $< f \leq$ 3 MHz	1000	100	80/f	8/f	610/f	1.6/f

f - frequency in MHz

Measurements of RMS current flowing through surgeon's hand (fig. 2) keeping the active electrode (Holaday HI-3702 clamp-on meter) and through feet (Narda 8850 stand-on meter) have been also conducted. These currents are the results of coupling between element with high electric potential (active electrode or cable) and workers body. This current should be considered rather as induced current than contact current.

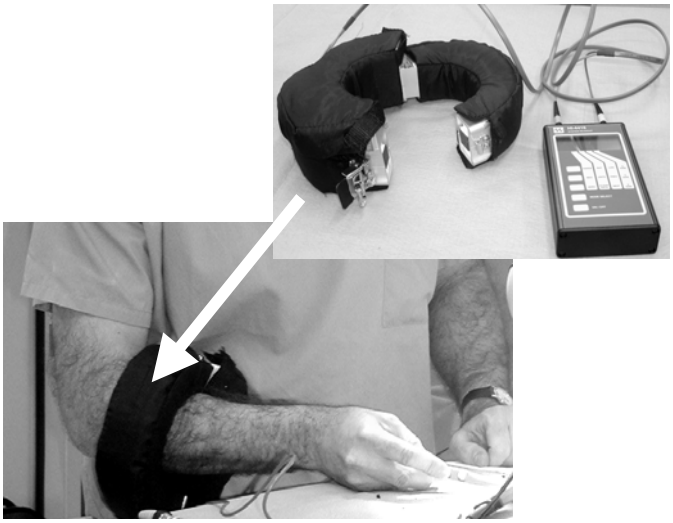

Fig. 2. The clamp-on meter measurements of the current in surgeon's hand.

The assessment of these quantities may be carried out following the permissible values as specified in Directive 2004/40/EC [1] and in ICNIRP guidelines [3] for contact current or permissible values for induced current in the feet specified in IEEE standard [4]. The Directive's criteria for induced current in limbs are not given for frequency below 10 MHz. Polish regulations don't refer directly to current inside workers body. Exposure limitation of contact and induced current in the frequency range of EMF produced by electrosurgery devices established by European Directive and IEEE standard is shown in table 2.

Table 2.

Contact and induced current – exposure limitation established by European Directive [1] and by IEEE [4].

Frequency range	Directive 2004/40/EC		IEEE			
	Contact current, I_C [mA]	Limb induced current, I_L [mA]	Contact current, I_C [mA]		Induced current in feet, I_L [mA]	
			for touch	for grasp	each foot	both feet
100 kHz $< f \leq$ 10 MHz	40	not specified	50	100	100	200
10 MHz $< f \leq$ 110 MHz	40	100	50	100	100	200

Measurements were performed for more than 30 types of common-used electrosurgery devices: various types of ERBE, Aesculap, Bovie, Valleylab and Olympus operated in the various modes. The output power during investigations (approx. 100-150 W) was a little higher than during normal work to obtain results representing the worst case of workers exposure conditions.

For the technical reasons, measurements have been performed during a simulated operation - absorbent cotton with saline has been used as phantom equivalent to the patient's body.

Results

The results obtained have shown that the surgeon is usually exposed to non-homogenous electric field. Metallic objects, which are in the operating theatre influence on spatial distribution of electric field. The level of exposure of medical staff can be changed by 2-3- fold depending on the location of these objects.

In the worst case implying the use of a monopolar electrode and non-shielded cables surgeon's hand keeping this electrode can be exposed to electric field exceeding 1000 V/m, head and torso up to a few tens V/m (fig. 3). When the cables touch the surgeon's body then the torso exposure is stronger, up to the level of the exposure of hand keeping electrode.

Near electrosurgical devices, the area of electric field strength exceeding 10 V/m can exist up to the distance of 70-100 cm from the active electrode and supplying cables.

Magnetic field in the nearest distance of electrodes and cables (5-10 cm) is usually below 1 A/m.

For the operation with output power less than 50 W or with the use of bipolar electrode, electric field exposing the hand is less than 80 V/m and less than 30 V/m in the case of head and torso exposure.

Electric field around the housing of the generator with effective EMF shielding is below 30 V/m during the use of both kinds of electrodes.

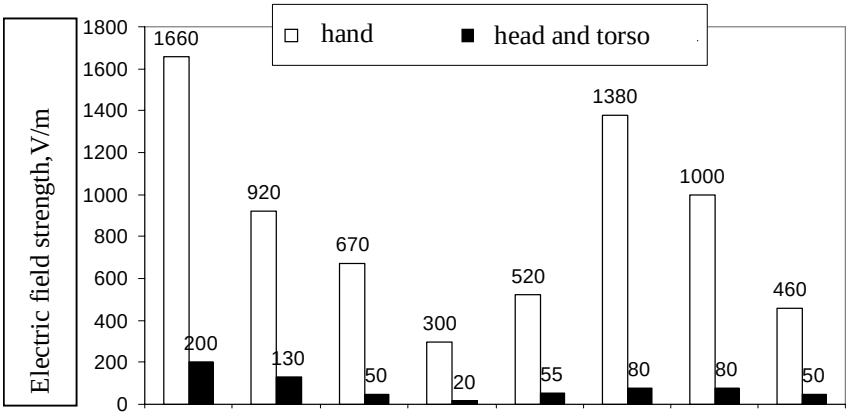

Fig 3. The examples of surgeon's exposure to electric field during the use of various electrosurgery devices (output power 100-150 W, a monopolar active electrode, cables far from the torso and head).

The execution of electrosurgical treatment with an electric arc burned under the active electrode lead to significant increase of electric field affecting on medical staff. The level of exposure during electric arc-surgery can be 4-fold higher in comparison to the operation without arc (fig. 4).

Waveform of EMF as well as the level of exposure in the vicinity of active electrode and supplying cables depend on the mode of electrosurgery devices operation. Figure 5 illustrates how electric field strength from the same electrosurgical device depends on it's selected mode.

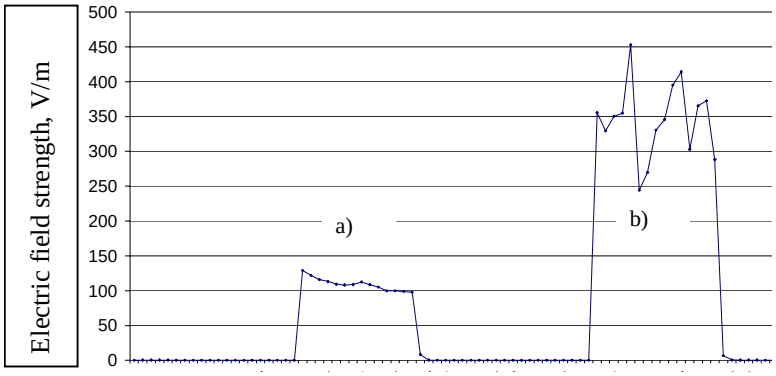

Fig. 4. The examples of registration of electric field strength in the vicinity of active electrode: a) cut mode without burned electric arc; b) cut mode with burned electric arc.

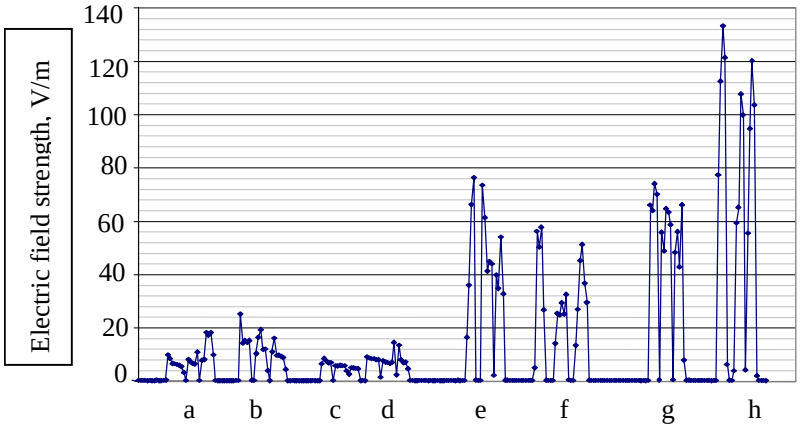

Fig 5. Examples of registration of electric field strength in the vicinity of electrosurgery device - various modes of operation: a) cut ”pure”; b) cut “blend”; c) coagulation „desicate”; d) coagulation „fulgurate”; e) coagulation „spray”; f) cut „pure” with argon; g) cut „blend” with argon; h) coagulation „spray” with argon.

The results presented indicate the possibility of a high exposure of the surgeon’s hand in the case of keeping the active electrode or touching the cable to forearm. Measurements of current in surgeon’s body may be used for additional assessment of exposure conditions and internal results in exposed body. The investigations carried out show, for example, that current in the hand keeping the active electrode can be of order 5 - 18 mA in the case of electric field strength of approx. 70 V/m in the distance of 5-10 cm from a monopolar active electrode (fig. 6), and significantly depends on the location of cable towards the hand.

Current in the feet of surgeon, insulated by shoes from ground and without direct contact with cables, is below 20 mA when electric field strength in the vicinity of monopolar active electrode is approx. 250 V/m. Taking into account the possibility of exposure to a stronger field (app. 1000 V/m or even higher) or a contact of the body with the cables, the current flowing through the arm of surgeon keeping the electrode can exceed the permissible values established in the Directive 2004/40/EC for contact current (40 mA).

The results obtained also indicate that current measured by clamp-on meter in the hand keeping the active electrode is approx. 2-fold higher than current measured by stand-on meter in the feet.

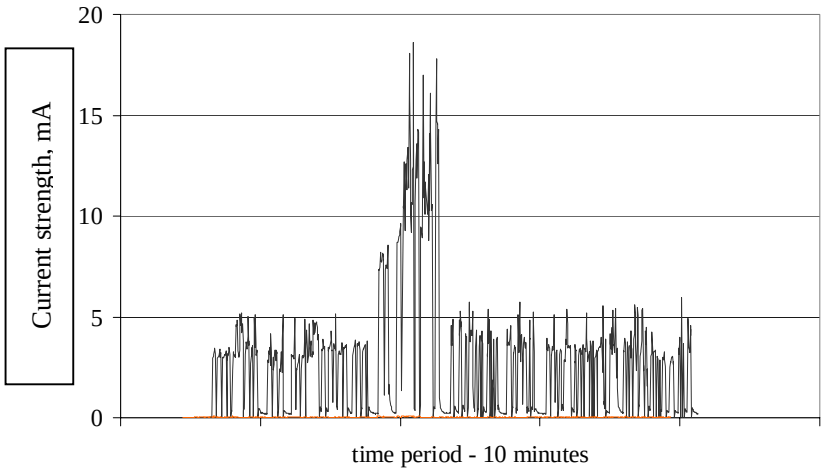

Fig 6. The examples of registration of current in surgeon’s hand exposed to EMF from the electrode's cable.

The conclusive assessment of surgeons exposure to EMF, presenting compliance with European Directive provisions concerning internal measures (“exposure limit values”), will be possible after publishing harmonised European standards. These standards should fixed in details the protocol for measurements or calculations, necessary for such exposure assessment. The numerical simulations for the verification of the compliance of particular EMF exposure scenarios with the Directive provisions need the use of a high resolution of the worker’s body models and an adequate representation of the workplace environment. For the electro-surgeon's EMF exposure, the conditions such as calculations for particular exposure situations need high professional skills, specialised software and they are very often time-consuming. The basic problems identified during pilot calculations are: the representation of the realistic posture of worker's body, the adequate representation of the electrical grounding conditions at the workplace and the adequate representation of realistic impedance of near-field produced by electrosurgery devices, as well as it's dynamic changes in the course of surgery treatment.

The additional problem with assessment of measurements results can appear for highly modulated EMF, when the properties of the used EMF meters calibrated in harmonic field cannot be relevant to such field's measurements and then the use of correction's factors taking into consideration the waveform of incident fields should be recommended. It was analysed for various kinds of modulations of EMF produced by various devices examined that the value of the measurement's uncertainty component coming in consequences of measurements of modulated fields in the case of common electrosurgery devices can be on the level of 50%. It is possible to find both effects, overestimation and underestimation in the EMF strength measurement's results.

Conclusion

In consideration of a necessity to keep the active electrode in the hand, complete elimination of surgeon's exposure to strong electric field is impossible. The reduction of the surgeon's exposure can be reached by the proper positioning of the cables supplying a monopolar electrode. The exposure of others persons from medical staff is relatively weak if they don’t have a direct contact with cables. In the worst case of cable's location and electrosurgery devicee's output power, the EMF overexposure can occur. The surgeon’s EMF exposure assessment for the case of the use of a monopolar electrode should be completed with measurements or calculation of currents flowing through the body.

The results of the investigations presented show that the effective reduction of the surgeon exposure can be obtained by keeping cables between the generator and the surgeon’s hand without a contact with the bodies of workers. Cables located at the surgical table decrease the surgeon’s exposure but increase the influence of electric field on other medical workers (e.g. nurses). A compromise is indispensable in that situation. A radical reduction of the EMF exposure level is possible by the use of the bipolar electrode if a kind of surgical treatment allows for that. Avoiding work with burned electric arc under the electrode reduces the exposure of personnel, too.

If weak electric field near the electrode is found (usually in the case when output power is approx. 50 W or less, the use of bipolar electrodes or shielded cables) measurements of electric field strength can be considered as

sufficient to confirm a low level of exposure there. The measurements uncertainty and the consequences of a high modulation of EMF from electrosurgery devices for the measurement's results should be analysed very carefully in every case when a relatively high level of exposure is found at the workplace.

Acknowledgments

The investigations supported by the State Committee for Scientific Research of Poland and Poland's Ministry of Economy, Labour and Social Policy (grant 1.A.03)

References

1. Directive 2004/40/EC of the European Parliament and of the Council of on the minimum health and safety requirements regarding the exposure of workers to the risks arising from physical agents (electromagnetic fields) (18th individual Directive within the meaning of Article 16(1) of Directive 89/391/EEC), O.J. Nr L-184, 2004.
2. Gryz K. Karpowicz J.; Electromagnetic hazards from electrosurgery – assessment of occupational exposure to electromagnetic field and currents induced in the body, Roczniki PZH, (in Polish)
3. ICNIRP Guidelines for Limiting Exposure to Time-Varying Electric, Magnetic, and Electromagnetic Fields (up to 300 GHz), Health Physics, 1998, 74, 4 (April), 494-522.
4. IEEE Std C95.1, Standard for Safety Levels with Respect to Human Exposure to Radio Frequency Electromagnetic Fields, 3 kHz to 300 GHz. 2005 Edition Published by the Institute of Electrical and Electronics Engineers, New York, USA, 2006.
5. Karpowicz J., Hietanen M., Gryz K. - EU Directive, ICNIRP Guidelines and Polish Legislations on Electromagnetic Fields - International Journal of Occupational Safety and Ergonomics (JOSE), 2006, vol. 12, No. 2, 125-136
6. Polish Standard PN-T-06580:2002. Labour protection in electromagnetic fields and radiation of the frequency range from 0 Hz to 300 GHz. Part 1: Terminology. Part 3. Methods of measurement and evaluation of the field on the work stands (in Polish).
7. Regulation of the Minister of Labour and Social Policy of 29 November 2002 on the maximum admissible concentrations and intensities for agents harmful to health in the working environment. Dz. U. 2002;217(item 1833):13614–60 (In Polish)

-Measurement of Complex Permittivities of Biomedial tissue at Millimeter Wave Band

Masahiro Hanazawa*, Atsuhiro Nishikata* ** and Soichi Watanabe*

****National Institute of Information and Communications Technologies***
*****Tokyo Institute of Technologies***

Abstract

For this paper, we directed our attention to the free-space method using a dielectric lens antenna, using this method to measure the permittivity of a cow's blood in the millimeter-wave band. We confirmed that measurement results under this method were in agreement with measurement results obtained by the coaxial probe method; here we report on the measurement results up to 65 GHz.

Introduction

Recently, utilized frequency band has been extended to higher frequency region including millimeter-wave band. The electromagnetic dosimetory is therefore required in the millimeter-wave band. This area of study deals with a simulation of exposure and a calculation of internal field within an exposed human body. A permittivity of a tissue is required for electromagnetic dosimetry and it well known that the permittivities of the biological tissues have frequency dispersion. Under these backgrounds, a great number of measurement methods of dielectric constants have been studied in various frequency bands [1]-[3]. However, few studies on permittivities of biological tissues have been reported in millimeter-wave band. Therefore strong demands for measurement of the dielectric constants of biological tissues in the millimeter-wave band exist.
In this study, we gave attention to a free space method using a lens antenna [4] and measured dielectric constants of cow's whole-blood samples from 33 GHz to 65 GHz. As a result, these were in good agreement with those measured by an alternative method (coaxial probe method). The result suggests that the proposed method can be used for permittivity measurement of a biological tissue in millimeter-wave band even higher than 65 GHz.

Measurement theory

We used the multi-line model for determining a complex coefficient of a surface of a liquid. We defined a measured cascade matrix of the glass of measured scattering parameter.

$$[T_g] = \frac{1}{S_{21}} \begin{bmatrix} (S_{21}S_{21} - S_{11}S_{22}) & S_{11} \\ -S_{22} & 1 \end{bmatrix} \quad (1)$$

The measured cascade matrix can be also be written as

$$[R_T] = [T_g][R_s] \quad (2)$$

Where cascade matrix $[R_T]$ and $[R_S]$ represent reflection coefficient of the glass and of the sample. If we neglect the reflection wave from the bottom of the holder, we can relate the complex permittivity of a liquid to the complex reflection coefficient. So from scattering parameter measurements, we determine the complex permittivity of the sample within the holder.

Measurement method

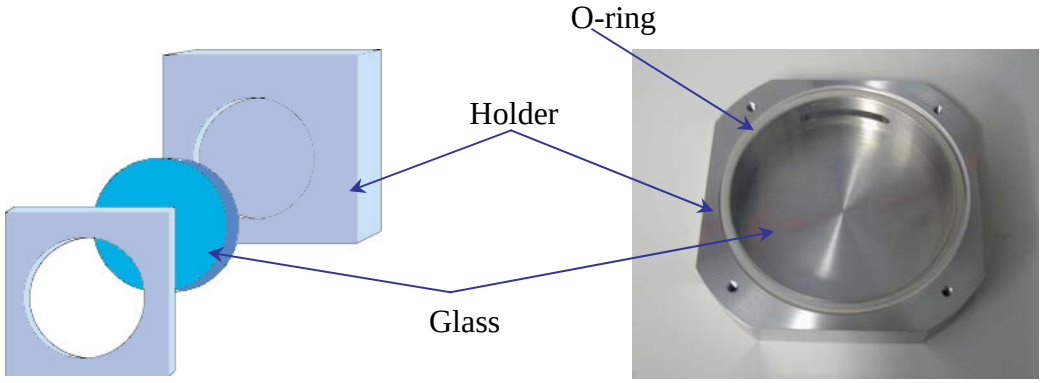

(a) Composition (b) picture

Fig.1. Composition and picture of sample holder.

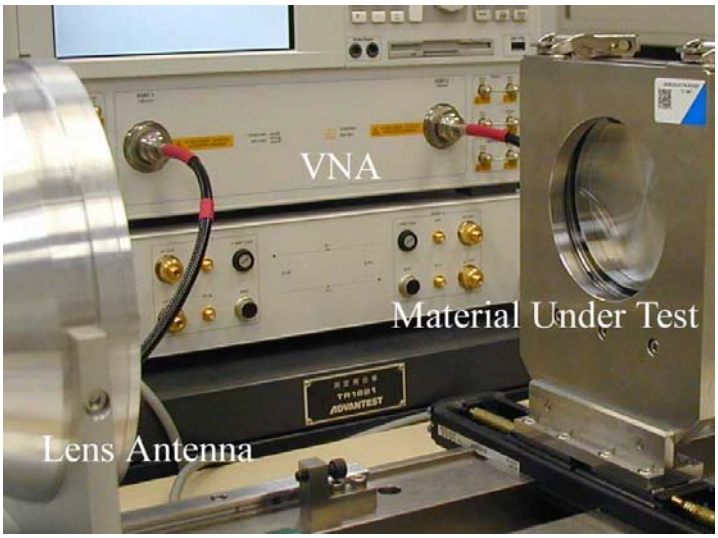

Fig.2. Picture of measurement set-up.

Figures 1 and 2 show a measurement set up and a sample holder, respectively. As shown in Fig.2, a liquid agent is hold with an optical glass and a tank made from a stainless steel. This measurement, as shown in Fig. 1, an electromagnetic wave generated by a VNA (Vector Network Analyser) is transmitted from the lens antenna to a test sample held by the sample holder. The lens antenna then receives a reflected wave (S_{11}) from the sample. These waves and T-parameter of the optical glass are then used to calculate the complex permittivity of the sample. Since in this measurement the metal plate of the holder and deformation of the liquid surface on the top surface of the holder may result in measurement errors, a high-directivity lens antenna [4] was used, as well as a 65-cm^2 holder (sufficiently large for the test irradiation area). Calibration was carried out via TRL (Through-Reflection-Line), which does not require any open and load standards [5]. The room temperature and the temperature of the blood during measurement were approximately 24°C and 22°C, respectively.

Measurement results

The permittivity of the blood of a cow was measured using the sample holder and the measurement set-up mentioned above. Fig. 3 shows the measurement results using the above set-up as well as measurement results using the coaxial probe method. Note that although the lens antenna used in measurement is functional in the frequency range from 18 GHz to 110 GHz, it features a cut-off frequency because it is connected to the VNA through a coaxial waveguide converter. Measurement was therefore performed using two types of waveguide, the WR22 and the WR15.
The measurement results using the WR22 and those using the probe method showed agreement, confirming that the measuring method proposed in this paper enables millimetre-wave band measurement of the permittivity of a biological tissue. Moreover, permittivity in a range from 50 GHz to 65 GHz (difficult to measure with existing coaxial probes) was measured by changing to the WR15 waveguide. As a result, the measurement results agree with those of the above-mentioned WR22 (with a difference of approximately 5%); we thus concluded that the experiment successfully demonstrated the possibility of measuring the permittivity of a biological tissue using a wide range of frequencies. We inferred that the difference noted above was most likely brought about due to factors such as variation in liquid temperature and absorption of water in the liquid agent.

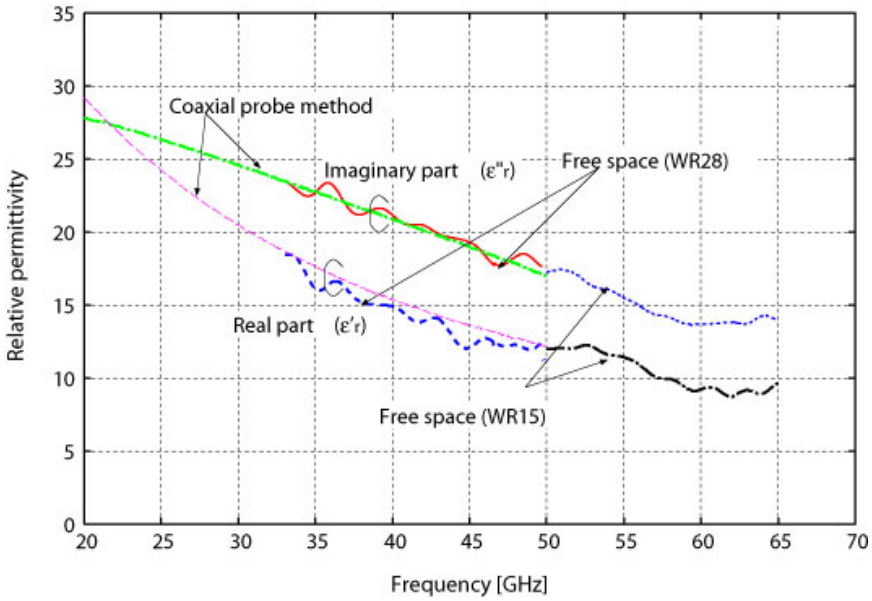

Fig.3. Measurement result (blood).

Conclusion

For this paper, we directed our attention to the free-space method using a dielectric lens antenna, using this method to measure the permittivity of the blood in millimeter-wave band. Based on our results, we confirmed that the measurement values obtained under this method were in agreement with the measured values obtained by the coaxial probe method, demonstrating that this method is appropriate for the measurement of permittivity of a biological tissue in the millimeter-wave band. Investigation of changes in liquid temperature remains as issues to be resolved in the future.

Acknowledgements

We are thankful to Mr. Noda of OSHIMA PROTOTYPE EMGINEERING Co., Ltd, who manufactured the sample holder.

Reference

[1] C Gabriel, R W Lau and C Gabriel "The dielectric properties of biological tissue : II Measurement in the frequency range 10 Hz to 20 GHz," Physics Medicine and Biology Vol.42, pp.2251-2269 (1996).
[2] J M Alison and R J Sheppard "Dielectric properties of human blood at microwave frequencies," Physics Medicine and Biology Vol.38, pp.971-978 (1998).
[3] C.M Alabaster "Permittivity of human skin in millimetre wave band," Electronics letter, Vol.39, No.21 (2003).
[4] K. Ghodgaonker, V. V. Varadan and V. K. Varadan, ``A Free-Space Method for Measurement of Dielectric Constant and Loss Tangents at Microwave Frequencies, `` IEEE Trans. IM-38, pp. 789 -793, (1989).
[5]R.B.Marls "A Multiline Method of Network Analyzer Calibration," IEEE Trans. MTT Vol.39, No.7, pp.1205-1215, (1991).

UMTS MOBILE PHONE BASE STATION AND HEALTH EFFECTS

SABINE HEINRICH[1], SABINE SCHLITTMEIER[2] , JÜRGEN HELLBRÜCK[2]

[1] INSTITUTE FOR OCCUPATIONAL AND ENVIRONMENTAL MEDICINE, UNIT FOR OCCUPATIONAL AND ENVIRONMENTAL EPIDEMIOLOGY & NETTEACHING, ZIEMSSENSTR. 1; 80336 MUNICH, GERMANY

E-MAIL: SABINE.HEINRICH@MED.UNI-MUENCHEN.DE

[2] WORK, ENVIRONMENTAL AND HEALTH PSYCHOLOGY, CATHOLIC UNIVERSITY OF EICHSTÄTT-INGOLSTADT, OSTENSTRAßE 26-28, 85072 EICHSTÄTT, GERMANY

Abstract

The increasing number of mobile phone base stations in Germany is associated with concerns in the population that the electromagnetic fields (EMF) could have adverse effects on health and well-being. The aim of the study was to investigate the association between EMFs of a UMTS-mobile phone base station and health of office workers.
A newly installed UMTS (Universal Mobile Telecommunications System) - base station was in a double blind fashion randomly turned on and off for 24-hours over a period of three months. Using an online questionnaire participants (n = 95) indicated their health at the beginning and the end of each working day. In addition, participants assessed whether the base station was turned on or off.
No evidence for an association between the exposure of the mobile phone base station and health of the participants was found. However, when the participants thought that the base station was turned on they indicated statistically significant more health complaints.
On the basis of the results of the study no association between the exposure to an UMTS base station and health could be shown. A follow-up study with a larger sample of the general population and personal dosimetry would be desirable.

Introduction

Proliferation of mobile phone base stations enables more and more people worldwide to use new telecommunication systems. However, many people are concerned about possible adverse health effects of the electromagnetic fields emitted by cellular phones and mobile phone base stations, even if exposure levels are far below those recommended. (Bavarian State Ministry of the Environment, Public Health and Consumer Protection, 2003). In Germany, introduction of UMTS (Universal Mobile Telecommunications System) requires installation of 15.000 new base stations. One reason for the concern about health effects of mobile phone base stations is the inability of neighbouring residents to regulate the duration and timing of these electromagnetic fields (Revermann 2003).

Despite the concerns, few studies of the effects of exposure to mobile phone base stations have been published. Published studies – e.g. by Santini et al. (2002) and Navarro et al. (2003) - have numerous methodological problems, so that their results are likely to be biased. The main issue is the valid exposure assessment, and it was not fully resolved in the pilot study of Hutter et al. (2002), who measured exposure to the base stations in the participants` bedrooms. Level of electromagnetic emissions of a mobile phone base station varies over time, making it difficult to capture accurately. To date, specific variation of the exposure over time has only been possible in laboratory studies.

Thus, the effects of UMTS exposure on human health and well-being have only been investigated in laboratory settings. Zwamborn et al. (2003) exposed people who reported sensitivity to radio-frequency waves (electrosensitive group) and a control group to a 1 V/m field at 900 MHz and 1800 MHz by replicating GSM fields, and also 2100 MHz UMTS fields. The study found a statistically significant association between the UMTS fields and well-being for both groups. By contrast, no effect was seen for the GSM frequencies at 900 and 1800 MHz. However, a Swiss follow-up study did not confirm these results (Regel et al. 2006). In a double blind provocation study (900 MHZ GSM mobile phone signal), Rubin et al. (2006) tested persons reporting electrosensitivity and controls but found no evidence either for the ability of electrosensitive people to detect such signals or of any increased symptom severity among them.

Within the feasibility study presented here, a newly installed UMTS mobile phone base station could be used for study purposes over a period of three months. The aim of this double-blind experiment was to investigate whether the electromagnetic fields of a UMTS base station influence the well-being of office employees working in its proximity. In addition, it should be taken into consideration in what way psychological factors like causal attribution are involved.

Material and Methods

The study took place from September to December 2003.

Participants

Overall 104 employees of the Bavarian Environmental Agency participated in the study. Of them, 95 participants (67 male and 28 female), age between 26 and 62 years (median = 40), answered the questionnaire in the morning and in the evening on at least 25 percent of the 70 days of the study and could thus be included in the analyses. Of these 95 participants, 71 (75 %) completed the daily questionnaires on at least 42 out of the 70 working days (60 %). Reasons for questionnaire non-completion were holidays, work outside the agency or sickness leaves. Most of the participants had a high level of education (university degree or doctoral level). All subjects gave their written informed consent to the participation.

Study design

The UMTS-mobile phone base station was installed in summer 2003 on the roof of the Bavarian Environmental Protection Agency. The mobile phone base station was switched on or off (control days) for one, two or three consecutive business days. The number of exposure and control days was equal (n = 35 each). We thus created six different exposure conditions, which differed by operating status (on, off) and duration (one to three days). Differing duration of the UMTS-exposure would enable to assess its potential cumulative effects on health.

Double-blinding

Several measures were taken to ensure the double-blind design. The operating status of the base station was chosen randomly from three possible versions. The power of the base station was recorded over the study period, with notebook and record located in a closed room. A modification on the software of the base station guaranteed that the operating status of the base station could not be received by a mobile phone. In addition, the base station had its own electricity.

Exposures

The mobile phone base station manufactured by Kathrein (type K742 212) transmitted the UMTS signal with a mean frequency of 2167,1 MHz, 5 MHz frequency range und a transmitting power of 20 W. With the downward tilt of the antenna of 8° it was possible to achieve maximum exposure level in the office building.

The UMTS exposure of the participants differed by the location of their offices in the building. Exposure measurements were carried out in the empty offices of all participants on weekends with base station turned on. Measurements were done by a physicist of the Bavarian Environmental Agency. The UMTS exposure in the offices ranged from 0.05 V/m (detection limit) to 0.53 V/m. The mean level was 0.10 V/m (standard deviation 0.09 V/m).

Questionnaire

Using an online questionnaire, participants indicated their health condition at the beginning and the end of each working day. The questionnaire contained items on health complaints that were used in connection with electromagnetic fields in several publications (Berg et al. 2004, David et al. 2002, Frick et al. 2002, Hietanen et al. 2002, Hillert et al. 1999, Röösli et al. 2004). A summary of the items is shown in table 1. In addition, participants were asked to guess whether the base station was on or off.

Table 1: Online-questionnaire used to evaluate health symptoms and the mean scores (M) and standard deviations (SD) of the score differences between morning and afternoon score, listed by operating status of the mobile phone base station (on or off)

Question: „How intensively did you experience the following health complaints today since you started working this morning? “

Answer categories: rarely–slightly–somewhat –strong–very strong

	M (SD)		
	MBS switched off	MBS switched on	p
concentration problems	0.090 (0.217)	0.138 (0.211)	0.680
lack of energy	0.037 (0.566)	0.065 (0.230)	0.161
headache	0.128 (0.274)	0.152 (0.214)	0.187
neck and shoulder pain	0.044 (0.194)	0.067 (0.182)	0.219
strong perspiration	0.008 (0.143)	0.029 (0.138)	0.181
dejection	0.002 (0.179)	0.018 (0.129)	0.172
feeling of pressure at the ear	0.010 (0.135)	0.022 (0.134)	0.616
tinnitus	0.020 (0.126)	0.032 (0.151)	0.075
breathing difficulties	-0.004 (0.077)	0.007 (0.039)	0.165
lack of appetite	0.000 (0.084)	0.003 (0.075)	0.563
paraesthesia	0.015 (0.120)	0.017 (0.106)	0.978
dry skin	0.006 (0.143)	0.008 (0.128)	0.685
allergic disorders	-0.005 (0.055)	-0.003 (0.055)	0.782
restlessness	0.020 (0.327)	0.021 (0.143)	0.371
cardiac symptoms	-0.001 (0.056)	0.000 (0.064)	0.699
nervousness	0.020 (0.206)	0.020 (0.129)	0.674
irritability	0.022 (0.245)	0.021 (0.123)	0.448
dizziness	0.018 (0.058)	0.015 (0.066)	0.604
feeling of anxiety	-0.005 (0.220)	-0.009 (0.075)	0.237
limb pain	0.012 (0.101)	0.003 (0.098)	0.202
back pain	0.051 (0.171)	0.042 (0.186)	0.494

Statistical analyses

Complaints were assessed on a five-point Likert scale: “rarely” = 1, “slightly” = 2, “somewhat” = 3, “strong” = 4, “very strong” = 5. In order to assess the change in well-being during the day, the score difference between morning and afternoon was calculated. The overall level of well-being was calculated as the sum of answers to the 21 questionnaire items. Higher score indicated worse well-being. The absolute change in the overall score over the working day was calculated as the difference between morning and afternoon score.

We used two sided t-tests for paired samples and ANOVA to examine the research questions of this study. Statistical analyses were carried out using SPSS 11.5.

Results

On average, the well-being decreased slightly, but not significantly, over the course of the working day. As shown in table 1, the mean symptom score did not differ statistically significantly over the working day between exposure and control days. In order to study a potential accumulation of effects, the mean change in symptom scores over a series of 1, 2 or 3 days with exposure was compared with sham-exposure (table 2). The ANOVA did not indicate statistically significant differences between the exposure conditions. (operating status: $F = 1,36$, $p = 0,35$; duration: $F = 0,66$, $p = 0,52$; interaction: $F = 0,37$, $p = 0,69$).

In contrast, the mean symptom score was significantly higher if the participants considered the base station to be switched on ($M = 1,93$; $SD = 2,49$) than on days they considered unexposed ($M = 0,16$; $SD = 0,95$; $T(77) = -6,66$, $p < 0,01$).

Table 1: Mean scores (M) und standard deviations (SD) of the overall score differences from all participants dependant on the exposure of the mobile phone base station (MBS)

(n = 90 due to missing values)

	MBS switched off			**MBS switched on**		
	1 day	**2 days**	**3 days**	**1 day**	**2 days**	**3 days**
M	0,54	0,47	0,64	0,77	0,56	0,65
SD	(1,48)	(1,19)	(2,14)	(1,26)	(1,37)	(1,63)

Discussion

We aimed to investigate the association between electromagnetic fields of a UMTS mobile phone base station and health complaints reported by office workers. A newly installed base station was in a double blind design randomly turned on and off for 24-hours over a period of three months. 95 office workers participated in this field experiment and reported health status daily using an online questionnaire.

No evidence for an association between UMTS mobile phone base station exposure and self-reported health complaints was found. In general, the reported complaints increased over of the working day. This increase was associated neither with exposure presence nor with its duration. These findings are in agreement with previous provocation studies, which used different frequencies (Andersson et al. 1996, David et al. 2002, Hietanen et al. 2002, Koivisto et al. 2001, Lyskov et al. 2001, Radon and Maschke 1998, Regel et al. 2006, Rubin et al. 2006). As this was a pilot study including a relatively small sample the results can not be generalized.

Only the association of perceived exposure condition with health was statistically significant. This might be interpreted as an incorrect attribution, which strongly emphasises the importance of using (double-) blind designs in corresponding research. This effect has also been shown in studies on EMF and health complaints (Andersson et al. 1996, Bergqvist et al. 1998, Harlacher und Schahn 1998, Hillert und Kolmodin-Hedman 1997).

One advantage of our study was the objective exposure assessment. However, as only exposure in the workplace was taken into account exposure assessment was incomplete. This problem might only be overcome with personal dosimetry (Radon et al. 2006). Overall exposure levels in our study were comparable to those found in other studies (Schüz and Mann 2000, Bernkopf 2004).

The results of this pilot study show feasibility of using online questionnaire. However, an investigation with online questionnaire is only possible in a specific Internet-using population, like office workers. In a follow-up study it could be useful to employ a CAPI (computer assisted personal interview). Also the use of a PDA (Personal Digital Assistant) and Handheld-computer might be feasible as recently shown by Schreckenberg and Guski (2005).

Overall, the results of this study show that the online questionnaire developed is practicable. The questionnaire instrument is capable to register health complaints. No evidence for an association between exposure to mobile phone base station and self-reported health complaints was found. However, well-being depended on the self-reported exposure condition. This might indicate an incorrect attribution, which strongly emphasises the importance of using (double-) blind designs in corresponding research. A follow-up study with a larger sample of the general population and personal dosimetry would be desirable.

Acknowledgements

The study was supported by the Bavarian Environmental Agency.

References

Andersson B, Berg M, Arnetz BB, et al. (1996): A cognitive-behavioral treatment of patients suffering from "Electric Hypersensitivity". Journal of Occupational and Environmental Medicine 38(8), 752-758.

Bavarian State Ministry of the Environment, Public Health and Consumer Protectio (2003). Stichwort Mobilfunk. München

Berg G, Breckenkamp J, Schlehofer B, et al. (2004). Querschnittstudie zur Erfassung und Bewertung möglicher gesundheitlicher Beeinträchtigungen durch die Felder von Mobilfunkbasisstationen - Zwischenbericht zum Abschluss der Pilotphase. Bielefeld, Heidelberg, Mainz, München, http:/www.emf-forschungsprogramm.de/forschung/epidemiologie_verg/epi_020_Zwie_01.pdf.

Bernkopf J (2004). EMF-Monitoring in Bayern - Messungen der elektromagnetischen Felder in Wohngebieten. Augsburg, Bayerisches Landesamt für Umweltschutz (LfU); www.bayern.de/lfu/wir/.

David E, Reißenweber J, Wojtysiak A, Pfotenhauer M (2002): Das Phänomen der Elektrosensibilität. Umweltmedizin in Forschung und Praxis 7(1), 7-16.

Frick U, Rehm J, Eichhammer P (2002): Risk perception, somatization and self report of complaints related to electromagnetic fields - A randomized survey study. International Journal of Hygiene and Environmental Health 205, 353-360.

Hietanen M, Hämäläinen A-M, Husman T (2002): Hypersensitivity symptoms associated with exposure to cellular telephones: no causal link. Bioelectromagnetics 23, 264-270.

Hillert L, Kolmodin-Hedman B, Söderman E, Arnetz BB (1999): Hypersensitivity to electricity: Working definition and additional characterization of the syndrom. Journal of Psychosomatic Research 47(5), 429-438.

Hutter H-P, Moshammer H, Kundi M (2002): Mobilfunk-Basisstationen: Erste Ergebnisse von zwei Feldstudien. Umweltmedizin in Forschung und Praxis 7(4), 213-213.

Koivisto M, Haarala C, Krause CM, et al. (2001): GSM phone signal does not produce subjektive symptoms. Bioelectromagnetics 22(3), 212-215.

Lyskov E, Sandström M, Hansson Mild K (2001): Provocation study of persons with perceived electrical hypersensitivity and controls using magnetic field exposure and recording of electrophysiological characteristics. Bioelectromagnetics 22, 457-462.

Navarro EA, Segura J, Portoles M, Gomez-Perretta C (2003): The microwave syndrom: a preliminary study in spain. Electromagnetic Biology and Medicine 22, 161-169.

Radon K, Maschke C (1998): Gibt es Elektrosensibilität im D-Netzbereich? Umweltmedizin in Forschung und Praxis 3, 125-129.

Radon K, Spegel H, Meyer N, et al. (2006): Personal Dosimetry of Exposure to Mobile Phone Base Stations? An Epidemiologic Feasability Study Comparing the Maschek Dosimeter Prototype and the Antennessa DSP-090 System. Bioelectromagnetics 27, 77-81.

Regel SJ, Negovetic S, Röösli M, et al. (2006): UMTS Base Station-Like Exposure, -Being and Cognitive Performance. Environmental Health Perspectives online: http://dx.doi.org with doi adresse: 10.1289/ehp.8934.

Revermann C (2003). Risiko Mobilfunk. Berlin, edition sigma.

Röösli M, Moser M, Baldinini Y, Braun-Fahrländer C (2004): Symptoms of ill health ascribed to electromagnetic field exposure - a questionnaire survey. International Journal of Hygiene and Environmental Health 207(2), 141-150.

Rubin GJ, Hahn G, Everitt BS, Cleare AJ, Wessely S (2006): Are some people sensitive to mobile phone signals? Within participants double blind randomised provocation study. Britisch medical Journal 332(7546), 886-891

Santini R, Santini P, Danze JM, Le Ruz P, Seigne M (2002): Study of the health of people living in the vicinity of mobile phone base stations: 1. Influences of distance and sex. Pathologie Biologie 50(6), 369-373.

Schreckenberg D, Guski R (2005): Lärmbelästigung
durch Straßen- und Schienenverkehr zu unterschiedlichen Tageszeiten. Umweltmed Forsch Prax 10(2), 67-76.

Schüz J, Mann S (2000): A discussion of potential exposure metrics for use in epidemiological studies on human exposure to radiowaves from mobile phone base stations. Journal of Exposure Analysis and Environmental Epidemiology 10(6), 600-605.

Zwamborn APM, Vossen SHJA, van Leersum BJAM, Ouwens MA, Mäkel WN (2003). Effects of global communication system radio-frequency field on well being and cognitive functions of human subjects with and without subjective complaints, Netherlands Organisation for Applied Scientific Research (TNO).

EXPERIMENTAL INVESTIGATIONS ON THE BIOLOGICAL FREE RADICAL PRODUCTION IN HUMAN BLOOD CELLS DUE TO MICROWAVE EXPOSURE

M. ENDO, T. HIKAGE, T. MANABE AND T. NOJIMA

GRADUATE SCHOOL OF INFORMATION SCIENCE AND TECHNOLOGY,
HOKKAIDO UNIVERSITY
KITA 14, NISHI 9, KITA-KU, SAPPORO, HOKKAIDO, 060-0814 JAPAN
E-MAIL: endo@emwtinfo.ice.eng.hokudai.ac.jp, {hikage, nojima}@wtemc.ist.hokudai.ac.jp

Abstract

The purpose of this study is to investigate the effects of microwave exposure on biological free radical production, focusing especially on mobile radio frequencies. In vitro experiments for the hydroxyl radical production on human white blood cells after exposure to modulated or non-modulated 900 MHz and 2.45 GHz microwave were performed. Several signals were used: continuous-wave (CW), several typical modulations of the GSM, PDC, cdma2000, and non-modulated pulse-wave. Developed 900 MHz ridged-waveguide exposure equipment and 2.45 GHz open-type equipment were used for high intensity irradiation, and the specific absorption rates (SARs) were estimated by numerical simulations. The fluorescence probe method was adopted to estimate the radical production. Furthermore heat (20°C-39°C) was used for the purpose of controlling the hydroxyl radical excitation.

The exposure experiments were carried out by using about six hundred tissues, and the free radical production was estimated with the fluorescence images. Some irradiations produced a difference in free radical production. However, this difference disappeared when data was compared to the heat controls.

As a result, any free radical production due to non-thermal effect of microwave exposure was not detected.

Introduction

It has been already suggested that the microwave EMF interactions with biomolecules, or with portions of biological structure, are unlikely at the frequencies below the high gigahertz spectral regions [1]. However, to the best of the authors' knowledge, there have not been any investigations conducted so far concerning the possibility of biological interactions due to the microwave EMF, which may result in the production of free radicals.

A free radical is an atom or a molecule with an unpaired electron and has a high chemical reactivity. There are various kinds of free radicals. If the radical production occurs in living tissues, it can trigger a chain reaction resulting in various influences on important cellular components such as DNA, or the cell membrane in the worst case [2,3,4]. Thus, in the discussion on the adverse health effect issues due to microwave irradiation, it is very important to obtain reliable experimental evidences revealing the fact that microwave EMF irradiation might not affect free radical production directly.

It is known that white blood cells (WBCs) generate free radicals to destroy bacteria and viruses. In order to investigate the biological free radical production in human WBC, experiments of 900 MHz and 2.45 GHz microwave exposure are conducted in this study.

Materials and Methods

The procedure for preparing the WBC sample is shown Figure 1. Firstly, dextran is added to whole blood taken from a healthy person. After letting it stand for 30 minutes, the supernatant fluid is obtained. Secondly, in order to separate into an upper plasma layer and a lower WBC layer, the blood samples are centrifuged at 400 g for 6 minutes. The plasma layer is removed and then 2 ml calcium, magnesium free phosphate buffered saline (CMF-PBS) is added to the settlement cell. Finally, 1950 μl CMF-PBS and 100 μl 2',7'-dichlorodihydrofluorescein diacetate (DCFH) are added to this 50 μl settlement cell. This WBC sample is used for this experiment.

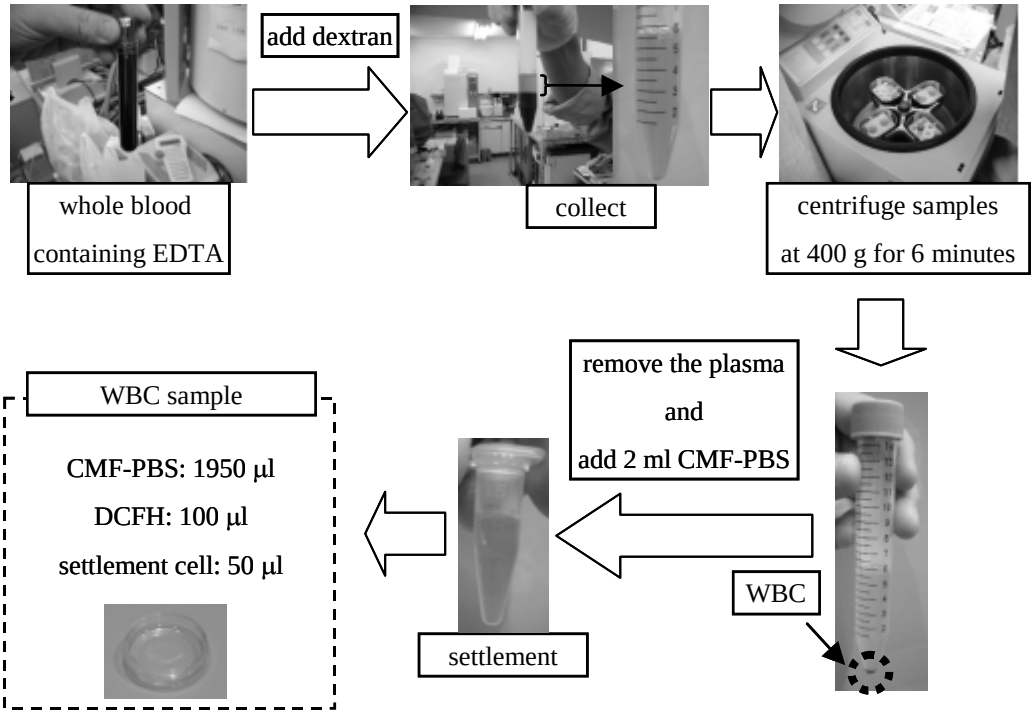

Figure 1. The procedure for preparing WBC sample

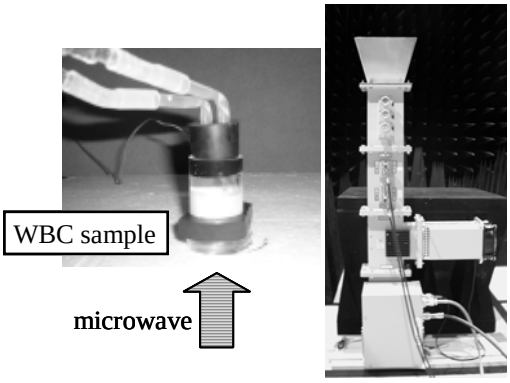

Irradiation Parameters

Frequency	2450 MHz
Modulations	CW, Pulse modulation (pulse width: 1 msec, duty ratio: 1/10)
Output Powers	CW: 57 dBm Pulse modulation: 49 dBm
Exposure time	5 minutes

Figure 2. Open-type exposure equipment of 2.45 GHz

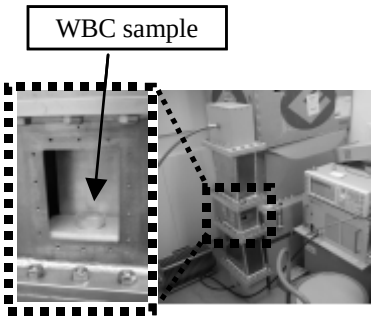

Irradiation Parameters

Frequency	900 MHz
Modulations	CW, GSM, PDC, cdma2000 Pulse modulation (pulse width: 1 msec, duty ratio: 1/10)
Output Powers	CW, PDC, cdma2000: 44 dBm Pulse modulation, GSM: 50 dBm
Exposure time	5 minutes

Figure 3. Ridged-waveguide exposure equipment of 900 MHz

Figure 2 and Figure 3 show the developed 2.45 GHz open-type exposure equipment and 900 MHz ridged-waveguide exposure equipment [5,6,7]. These exposure equipments can achieve high intensity and a uniform exposure on the WBC sample and they are available at the same time without special degradation of the impedance matching caused by the scattering waves from the WBC sample.

In the case of exposure to 2.45 GHz microwave, we carry out the irradiations for five minutes with continuous-wave (CW) or high power pulse modulated wave that provided the pulse width and duty ratio of 1 msec and 1/10, respectively. Figure 4 (a) shows the exposure plane on which the WBC sample is located. This plane is positioned at a distance of 205 mm from the centre of the horn antenna. Figure 4 (b) shows the electric field distribution of CW measured in this area. In addition, Figure 4 (c) shows the electric field distribution of CW obtained in this area by using numerical analysis. The FDTD based commercial software, SEMCAD [8] is used for the estimation. From these Figures, the computed result agrees well with measured ones. Furthermore, the thermostatic device shown in Figure 5 is adopted to maintain the temperature of the WBC sample at less than 39 degrees Celsius. The SAR of the WBC sample exposed on the petri dish is obtained by measurement and calculation. The increase in temperature during the exposure is used for estimation of SAR. FDTD analysis is used for SAR calculation as well. When we measure the SAR, the PBS does not touch the thermostatic device. Figure 6 shows the FDTD model. Figure 7 and Table 1 show these results as well.

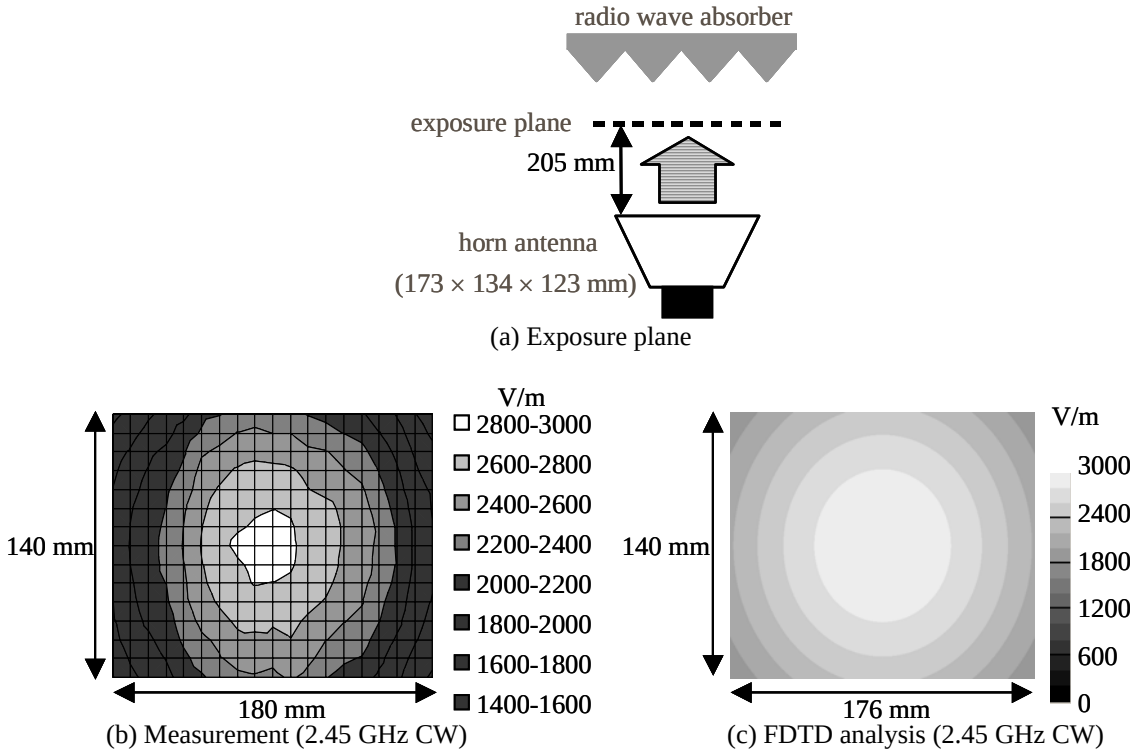

Figure 4. Electric field distributions on exposure plane

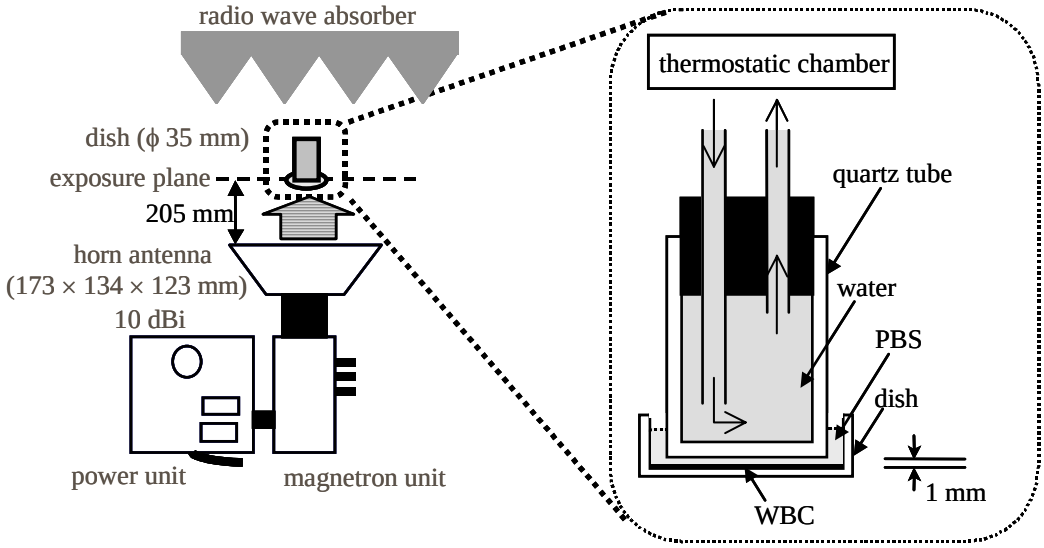

Figure 5. Exposure equipment of 2.45 GHz

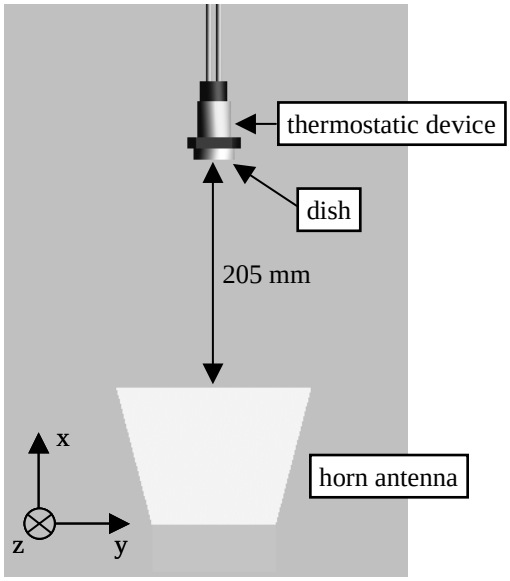

Figure 6. FDTD model (2.45 GHz)

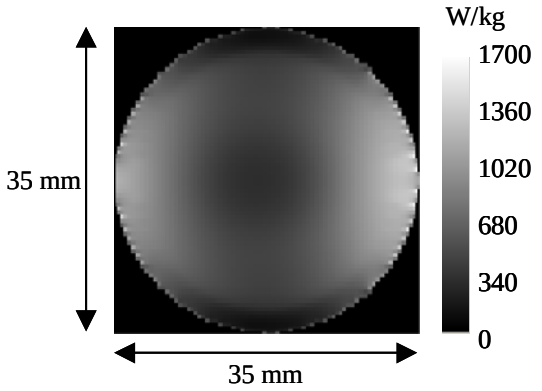

Figure 7. SAR distribution (2.45 GHz)

	measurement	FDTD analysis
Ave. SAR [W/kg]	725	632

Table 1. Measurement and analysis results of SAR (2.45 GHz)

In the case of exposure to 900 MHz microwave, the duration of exposure is 5 minutes. Moreover, several signals are used: CW, GSM, PDC (half rate), cdma2000 and pulse waves. During exposure, the temperature of the cells never exceeded 39 degrees Celsius. Table 2 shows both measured and calculated electric field strengths at the point that the WBC sample is located. In addition, the SAR of the WBC sample exposed on the petri dish is obtained by both measurement and calculation. In order to estimate the SAR of the WBC sample, the waveguide's output powers are measured. Then, the output power with or without the WBC sample in the waveguide are compared to estimate the SAR. Figure 8 shows the FDTD model. Figure 9 and Table 3 show these results.

	measurements					FDTD analysis
Modulations	CW	Pulse	GSM	PDC	cdma2000	CW
E-field strengths [V/m]	1140	615	960	1140	1160	1730

Table 2. E-field strengths central axis of the exposure plane (900 MHz)

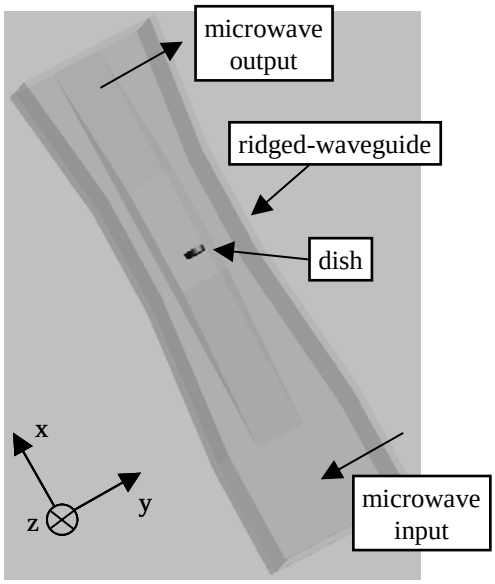

Figure 8. FDTD model (900 MHz)

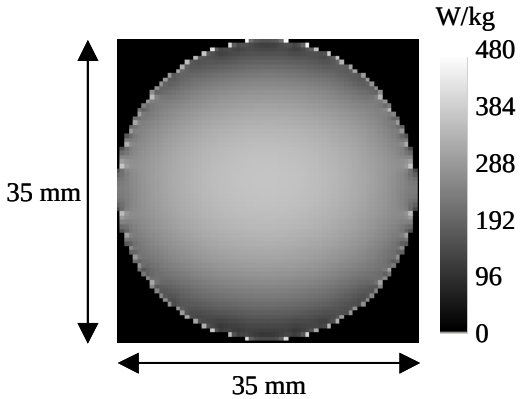

Figure 9. SAR distribution (900 MHz)

	measurement	FDTD analysis
Ave. SAR [W/kg]	150	276

Table 3. Measurements and analysis results of SAR (900 MHz)

The fluorescence probe method is adopted to estimate free radical production. First, DCFH which is used for fluorescence probe of hydroxyl radical production is added to the WBC sample. Secondly, the WBC sample is exposed to RF microwave for 5 minutes. Finally, fluorescence intensity is measured.

Results

Figure 10 and Figure 11 show the fluorescence intensities of WBCs after exposure to 2.45 GHz and 900 MHz microwaves respectively. The control (sham exposure) is defined as the WBC sample that was not exposed to microwaves and increased in temperature by thermostatic device. In the case of 2.45 GHz exposures, there are no obvious differences between the control and the WBC exposed by CW or pulse modulated microwave. In addition, in the case of 900MHz exposures, no significant differences in radical production are detected after any modulated microwave exposures. At both frequencies, no radical excitation is observed in the WBC after irradiation by microwaves, provided that the temperatures of target samples did not exceed 39 degrees Celsius.

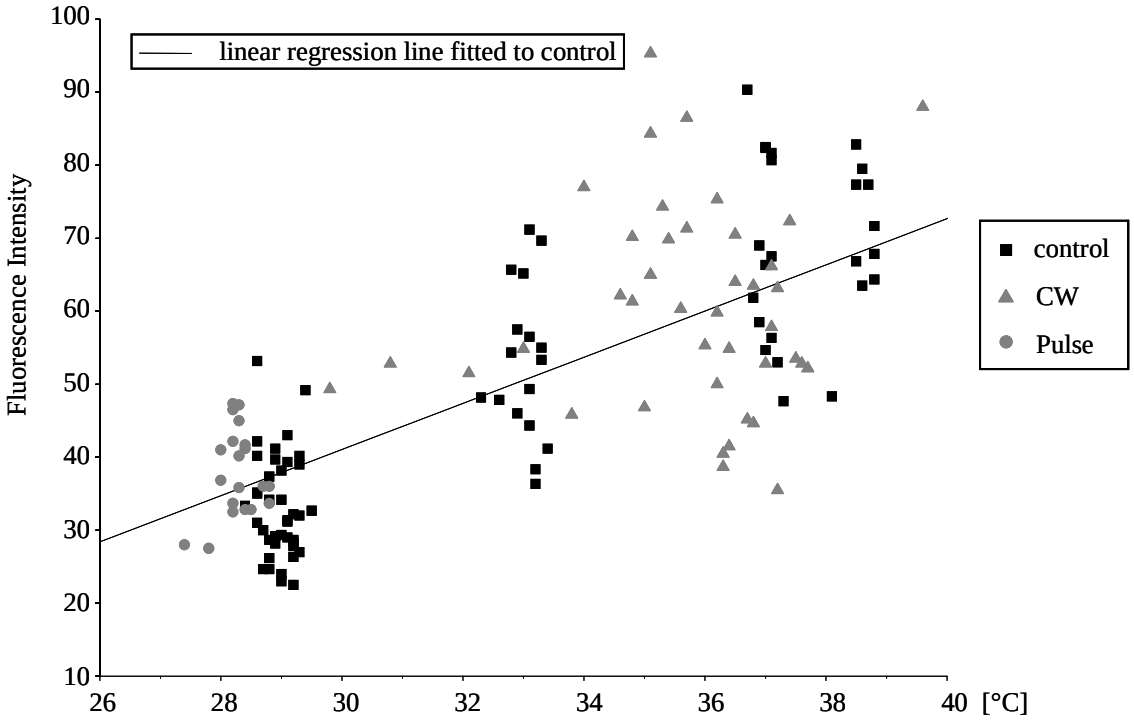

Figure 10. Fluorescence intensities of WBCs after exposure to 2.45 GHz microwave

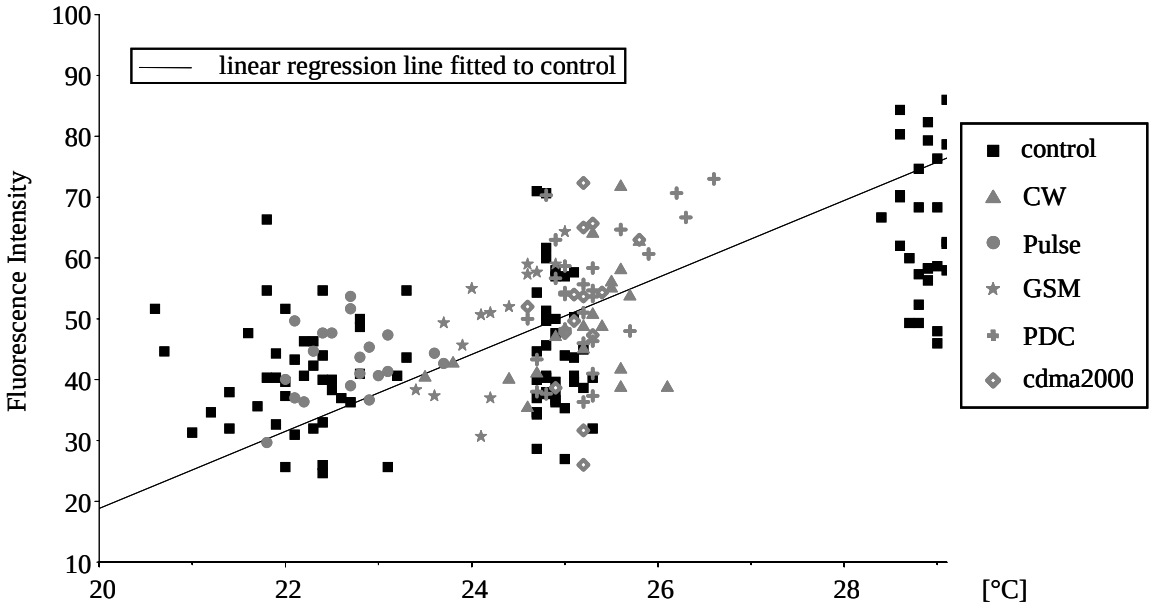

Figure 11. Fluorescence intensities of WBCs after exposure to 900 MHz microwave

Summary
Experiments for the biological free radical that treats human WBCs were performed. In the experiments, both modulated and non-modulated 900 MHz and 2.45 GHz microwaves were irradiated. Furthermore, the electric field strengths on the exposure plane and SARs of the WBCs were estimated by using measurement and FDTD simulation. The differences due to biological uncertainty in experimental results obtained under the same conditions (cell temperature, exposure condition) could not be negligible, and therefore, our experiments were carried out by using many WBC samples.
From our experiments, there was no difference in fluorescence intensities estimated by the fluorescence images of between the control (sham exposure) and the exposed samples. In addition, the intensities of the samples after exposure to modulated microwaves agreed with those after exposure to non-modulated microwaves. The fluorescence intensities which are proportional to radical production in WBCs depended on the temperatures of the samples. As a result, any free radical production due to non-thermal effects of 2.45 GHz or 900 MHz microwave exposure was not detected.
More precise SARs calculations and a statistical analysis of the fluorescence intensities data obtained by many of our experiments will be conducted.

Acknowledgements
This work is supported by Grant-in-Aid from the Ministry of Internal Affairs and Communications (MIC) of Japan.

References
[1] R.K. Adair, “Biophysical limits on A thermal effects of RF and microwave radiation”, Bioelectromagnetics Vol24, No.1, pp.39-48, (2003)
[2] W.Ross Adey, “Potential Therapeutic Applications of Nonthermal Electromagnetic Fields: Ensemble Organization of Cells in Tissue as a Factor in Biological Field Sensing”, Bioelectromagnetic Medicine, New York:Mercel Dekker Inc. (2004)
[3] M.H. Repacholi and B. Greenebaum, “Interaction of Static and Extremely Low Frequency Electric and Mgnetic Fields With Living Systems: Health Effects and Research Needs”, Bioelectromagnetics, 20, pp.133-160 (1999)
[4] H. Kamada and H. Ohya, “Overview of Laboratory Technology on Bioradicals”, Journal of IEICE, vol.81, No.2, pp.146-153
[5] T. Hikage, T. Manabe, and T. Nojima, “Microwave Exposure Effects on the Biological Free Radical Production –2.45 GHz exposure system desigh and estimation with ESR –”, BIOLOGICAL EFFECTS of EMFs 3rd International Workshop, pp. 82-86, (2004).
[6] T. Manabe, T. Hikage and T. Nojima, “Experimental investigations on the Biological Free Radical Production – 2.45 GHz & 900 MHz exposure systems design and estimation with ESR –”, XXVIIIth URSI General Assembly at New Delhi, India on October 23-29, (2005)
[7] T. Hikage, T. Manabe, M Endo and T. Nojima, “EXPERIMENTAL INVESTIGATIONS ON THE BIOLOGICAL FREE RADICAL PRODUCTION IN HUMAN FIBROBLASTS DUE TO MICROWAVE EXPOSURE”, The Bioelectromagnetics Society the 28th Annual Meeting at Cancun, Mexico on June 11-15, P-B-78, (2006)
[8] SEMCAD: Schmid & Partner Engineering AG, Zurich, Switzerland

Mobile radio base station-emitted radiation does not induce phosphorylation of hsp27 or cellular stress response.

M. Sekijima[1], H. Hirose[1], N. Sakuma[1], N. Kaji[1], K. Nakayama[1], T. Nojima[2], J. Miyakoshi[3]

[1]Research division for advanced technology, Kashima Laboratory, Mitsubishi Chemical Safety Institute Ltd., 14 Sunayama, Kamisu 314-0255, Japan. [2]Division of Electronics and Information Engineering, Graduate School of Hokkaido University, N-13, W-8, Kita-ku, Sapporo 060-8628, Japan. [3]Department of Radiological Technology School of Health Sciences, Faculty of Medicine, Hirosaki University, 66-1 Hon-cho, Hirosaki 036-8564, Japan.

ABSTRACT

The objective was to assess any signs of stress or apoptosis induced by radiofrequency (RF) fields, which corresponds to the limit of the average whole body SAR for general public exposure defined as a basic restriction in the ICNIRP guidelines. We investigated if continuous wave (CW) and Wide band Code Division Multiple Access (W-CDMA) RF fields at 2.1425 GHz, which corresponded to the middle frequency allocated to the downlink band of the IMT-2000 from mobile radio base stations, induce activation of hsp27 and p53. All levels and types of the investigated RF fields did not result in a statistically significant increase or decrease in hsp27[pS82] protein or p53[pS15] protein of each sample. No noticeable differences were observed between any of the RF field exposure groups and the sham exposed controls in the gene expression profile, including hsp or p53 related genes, in either the RF field experiments. These results confirm that RF exposure to W-CDMA and CW at 2.1425 GHz cannot be associated with apoptosis or cancer via induction of the p53 pathway or hsp response at the limit of the average whole-body SAR level (80 mW/kg) as defined by the ICNIRP guidelines.

INTRODUCTION

The rapid introduction of mobile telecommunication services over the last decade has drastically increased the amount of radiofrequency (RF) field irradiation frequencies and energies in our living environment. In order to continue stable growth and expansion of RF utilizations, it is necessary to investigate the possibility of any biological health effects of RF fields and to obtain reliable confirmation data with respect to safety. It is important to examine the possible biological effects and to obtain reliable data for 2-GHz band RF irradiation to facilitate the smooth deployment of the International Mobile Telecommunication 2000 (IMT-2000) cellular system. We conducted a study focusing on the effects of a practical modulated signal for Wideband Code Division Multiple Access (W-CDMA) as well as a continuous wave (CW) at 2.1425 GHz, which corresponds to the middle frequency allocated to the downlink band of IMT-2000 from mobile radio base stations.

French et al [2001] proposed that repeated exposure to mobile phone radiation acts as a repetitive stress leading to continuous expression of hsps in exposed cells and tissues, which in turn affects their normal regulation, and cancer results. Hsp27 phosphorylation in the human endothelial cell line EA.hy926 showed a transient increase by 1 h of non-thermal exposure to 900 MHz GSM mobile phone radiations [Leszczynski et al., 2002]. They proposed a hypothetical mechanism whereby RF exposure could be associated with cancer. We examined the induction of hsp27 phosphorylation and other cellular stress response that activate the p53 or the p53 signaling pathway using cultures of the human tumor A172 cells and untransformed IMR-90 cells. The results suggest that RF radiation at a SAR of the mobile radio base station level does not affect the stress response pathways following hsp27 phosphorylation.

METHODS

Exposure System

A detailed description of the exposure system has been published by Iyama et al. [2004]. Briefly, two identical RF field exposure incubators, one for RF field exposure and the other for sham exposure, were established in separate anechoic chambers, and a mechanical switch in a dummy box allows the selection of RF field exposure or sham exposure (Fig.1). This system allowed simultaneous exposure of 49 (7 x 7 array), 35 mm culture dishes to a 2.1425 GHz RF electromagnetic field, which corresponds to the center frequency of the IMT-2000 down link band, with a uniform SAR distribution in the medium of all 49 culture dishes. The main unit for the cell exposure provides identical air to the two culture units through sealed ducts at the appropriate temperature (37.0°C), CO_2 (5.0 %), and humidity (>90 %). The mean SAR of the culture fluid at the bottom of the inner 25 culture dishes (5 x 5 array) used in the in vitro experiments was 139 mW/kg for an antenna input power of 1 W, and the standard deviation of the SAR distribution was 47%. The W-CDMA cellular system is one of the component systems of the IMT-2000 cellular system, and its frequency spectrum is shown in Figure 2. W-CDMA adopts Direct Sequence CDMA (DS-CDMA) and Frequency Division Duplex (FDD) as a multiple access and duplex scheme, respectively. The chip rate of the spread code of this system is 3.84 Mcps. A beam-formed RF exposure incubator employing a horn antenna, a dielectric lens, and a culture case in an anechoic chamber was developed for large-scale *in vitro* studies.

Cells

Human glioblastoma A172 cells and human IMR-90 fibroblasts from fetal lungs were obtained from the American Type Culture Collection (ATCC, Rockville, MD). A172 cells were cultured in Dulbecco's Modified Eagle Medium (Invitrogen, Tokyo, Japan) supplemented with 10% heat-inactivated fetal calf serum (FCS; Invitrogen), 100 U/ml penicillin and 100 μg/ml streptomycin, and IMR-90 fibroblasts were grown in Eagle's minimal essential medium with Earle's balanced salts (Invitrogen) supplemented with 0.1 mM non-essential amino acids, 1.0 mM sodium pyruvate, 10% heat-inactivated FCS, 100 U/ml penicillin, and 100 μg/ml streptomycin. The both cells have been previously used in RF field research [Sakuma et al., 2006].

Experimental Design

The experimental design has been described by Hirose et al. [2006a,b]. A172 cells were exposed to W-CDMA radiation at SARs of 80, 250, and 800 mW/kg, and to CW radiation at 80 mW/kg for 24 or 48 h, which equates to one or two doubling times of the cell. IMR-90 cells were exposed to W-CDMA at 80 and 800 mW/kg, and CW at 80 mW/kg for 28 h, which is one doubling time of the cell. The cells were also exposed to W-CDMA radiation at SARs of 80 and 800 mW/kg for 2 h. The RF field exposure was processed in a blind manner. Exposure to W-CDMA signals in the study was 80 mW/kg, which corresponds to the limit of the average whole-body SAR for general public exposure defined as a basic restriction by the ICNIRP guidelines [1998]. The air temperature was monitored for all cultures during the course of the sham and RF field exposure, resulting in 37.0±0.3°C, 37.0±0.1°C, and 37.0±0.1°C at SARs of 800, 250 and 80 mW/kg for W-CDMA radiation, respectively.

Detection of Hsp27 and p53 Phosphorylation

To determine changes in hsp27[pS82] or p53[pS15], HSP27[pS82] and Total HSP27 or p53[pS15] and Total p53 Antibody Bead Kits (BioSource, Camarillo, CA) were used according to the manufacturer's instruction. The specific proteins were detected using the bead-based multiplex assay [Carson and Vignali, 1999], which is similar to a capture sandwich immunoassay.

Microarray hybridization

Human genome HG-U133 Plus2.0 (Affymetrix, Santa Clara, CA) was used for the analysis of heat shock and p53 related gene expressions in cells exposed to RF fields. Data were analyzed using Affymetrix®

Microarray Suite 5.0 software.

RT-PCR analysis

The pairs of primers and the TaqMan probes [tumor protein 53 (TP53), TP53 binding protein 2 (TP53BP2), apoptotic protease activating factor (APAF1), and caspase 9 (CASP9)] for the target mRNAs were purchased from Applied Biosystems (Foster City, CA). The TaqMan OneStep RT-PCR Master Mix Reagents Kit (Applied Biosystems) was used for the RT-PCR reaction. Amplification and detection were performed using the ABI PRISM 7700 Sequence Detector System (Applied Biosystems).

Indirect Immunofluorescence Analysis

For visualization, cells were incubated with anti-hsp27 (diluted at 10 μg/ml) or anti-hsp70 (diluted at 5 μg/ml) antibodies (Stressgen, BC, Canada) for 1 h, and then incubated with Alexa Fluor 488-labeled goat anti-mouse IgG antibody (Molecular Probes, Eugene, OR) diluted at 10 μg/ml for 30 min.

Detection of Apoptosis

Apoptosis was evaluated using the annexin V affinity assay [Koopman et al., 1994]. The procedure using the fluorescein-conjugated annexin V (annexin V-FITC; BD Biosciences, Franklin Lakes, NJ) was carried out according to the manufacturer's technical protocol. The cell samples were analyzed by flow cytometry (EPICS ALTRA, Beckman Coulter, Tokyo, Japan).

Statistical Analysis

The gene expression levels obtained with GeneChip expression analysis were analyzed by Welch's t-test using the data for the sham-exposed samples and the RF field-exposed samples in either the 2.1425 GHz W-CDMA at a SAR of 80, 250 or 800 mW/kg or CW at 80 mW/kg RF field experiments. The multiplicity problem was controlled by the Benjamini and Hochberg false discovery rate [Benjamini and Hochberg, 1995]. A p-value of less than 0.05 was considered statistically significant.

RESULTS

Expression of phosphorylated hsp27 at serine 82

As shown in Figures 3-1 and -2, the exposure to W-CDMA or CW radiations at a SAR of 80, 250 or 800 mW/kg for 2-48 h resulted in similar measurements of hsp27[pS82] compared to sham exposed controls. The exposure to all of the presented RF fields did not result in a statistically significant change in hsp27[pS82]. The exposure to W-CDMA at a SAR of 80 or 800 mW/kg for 2-48 h did not noticeably change the total hsp27 level in either cell. Moreover, there were no significant changes in total hsp27 expression levels in the cells exposed to W-CDMA signal at 250 mW/kg or CW signal at 80 mW/kg.

Heat shock gene expression

In the RF field exposure experiments, 18,041-24,119 and 18,971-23,180 genes were "present" or "marginal" in A172 and IMR-90 cells, respectively, of 54,675 gene probe sets. We evaluated the changes in gene expression by RF field exposure on their genes that were "present" or "marginal" in A172 or IMR-90 cells. No significant differences were observed between any of the RF field exposure groups and the sham-exposed controls in the gene expression profile, including hsp related genes in either experiments of exposure to W-CDMA or CW signal for 2-48 h.

Cellular localization of hsp27 and hsp70

There was no remarkable effect on the induction of translocation or expression of hsp27 or hsp70 after exposure to W-CDMA or CW signal at a SAR of 80, 250 or 800 mW/kg for 2-48 h. Immunofluorescence staining revealed that some of A172 cells in sham culture expressed a high level of hsp27 and some of IMR-90 cells in sham culture expressed a low level of hsp27. It was found that some of A172 and IMR-90 cells in sham cultures expressed a very low level of hsp70.

Expression of phosphorylated p53 at serine 15

The exposure to W-CDMA or CW radiations resulted in similar measurements of p53[pS15] compared to sham-exposed controls, and resulted in similar values of total p53 compared with sham-exposed controls. The exposure to all of the presented RF fields did not result in statistically significant changes in p53[pS15] (Fig. 4), or the total p53 in each sample. All of the measurements of p53[pS15] protein in the RF field exposure samples were close to the lower limit of the analytical sensitivity of the assay, and almost equal to those in sham-exposed and non-treated samples, or could not be detected with the used p53[pS15] Antibody Bead Kit.

p53-related Gene Expression

There were no noticeable changes of p53 related gene expression levels in A172 or IMR-90 cells exposed to W-CDMA radiation (SARs of 80, 250 or 800 mW/kg) or CW radiation (80 mW/kg). We analyzed the gene expression of TP53, TP53BP2, APAF1, and CASP9 to reconfirm the change of the p53-dependent apoptosis signal cascade on a molecular level by the exposure to RF signals, using a real-time RT-PCR analysis. Relative gene expression was determined based on the threshold cycles of the RF field or sham exposed samples. No noticeable effect on TP53, TP53BP2, APAF1, and CASP9 gene expression was observed after exposure to W-CDMA or CW radiation, as expression ratios were below 2-fold and over 0.5-fold in two independent experiments performed with triplicate RNA samples.

Induction of Apoptosis

The exposure to W-CDMA or CW radiations resulted in a similar percentage of apoptotic cells compared to sham-exposed controls (1.1-3.7 % compared to 1.2-3.0 % in the case of A172 cells, and 2.4 or 4.1 % to 2.4 or 4.7 % in the case of IMR-90 cells). No statistically significant differences were observed between any of the RF field exposure groups and the sham-exposed controls in percentage of apoptotic cells, in either the 2.1425 GHz W-CDMA or CW radiation exposure experiments.

CONCLUSION

Hsp27 and p53 phosphorylation in A172 cells and IMR-90 fibroblasts are not induced by exposure to W-CDMA or CW RF radiation. Furthermore, changes in gene expression levels of hsp family and p53-related genes, and the frequency of apoptotic cell death were not induced by any of the RF exposure.

The results confirm that RF exposure to W-CDMA and CW at 2.1425 GHz cannot be associated with apoptosis or cancer via induction of the p53 pathway or hsp response at the limit of the average whole-body SAR level (80 mW/kg) as defined by the ICNIRP guidelines.

ACKNOWLEDGEMENT

This work was supported by NTT DoCoMo Inc., Japan.

REFERENCES

Benjamini, Hochberg, 1995. Controlling the false discovery rate: a practical and powerful approach to multiple testing. J R Statist Soc B 57, 289-300.

Carson R, Vignali D. 1999. Simultaneous question of fifteen cytokines using a multiplexed flow cytometric assay. J Immunol Meth 227, 41-52.

French PW, Penny R, Laurence JA, McKenzie DR. 2001. Mobile phones, heat shock proteins and cancer. Differentiation 67: 93-97.

Hirose H., Sakuma N., Kaji N., Suhara T., Sekijima M., Nojima T., Miyakoshi J. 2006a. Phosphorylation and gene expression of p53 are not affected in human cells exposed to 2.1425 GHz band CW or W-CDMA modulated radiation allocated to mobile radio base stations. Bioelectromagnetics 27: in press.

Hirose H., Sakuma N., Kaji N., Nakayama K., Inoue K., Sekijima M., Nojima T., Miyakoshi J. 2006b. Mobile Phone Base Station-Emitted Radiation Does Not Induce Phosphorylation of Hsp27. Bioelectromagnetics: accepted.

ICNIRP. 1998. Guidelines for limiting exposure to time varying electric, magnetic and electromagnetic fields (up to 300 GHz). Health Phys 74: 494-522.

Iyama T, Ebara H, Tarusawa Y, Uebayashi S, Sekijima M, Nojima T, Miyakoshi J. 2004. Large-scale i*n vitro e*xperiment system for 2 GHz-exposure. Bioelectromagnetics 25: 599-606.

Koopman G, Reutelingsperger CP, Kuijten GA, Keehnen RM, Pals ST, van Oers MH. 1994. Annexin V for flow cytometric detection of phosphatidylserine expression on B cells undergoing apoptosis. Blood 84: 1415-1420.

Leszczynski D, Joenvaara S, Reivinen J, Kuokka R. 2002. Non-thermal activation of the hsp27/p38MAPK stress pathway by mobile phone radiation in human endothelial cells: Molecular mechanism for cancer- and blood-brain barrier-related effects. Differentiation 70: 120-129.

Sakuma N, Komatsubara Y, Takeda H, Hirose H, Sekijima M, Nojima T, Miyakoshi J. 2006. DNA strand breaks are not induced in human cells exposed to 2.1425 GHz band CW and W-CDMA modulated radiofrequency fields allocated to mobile radio base stations. Bioelectromagnetics 27: 51-57.

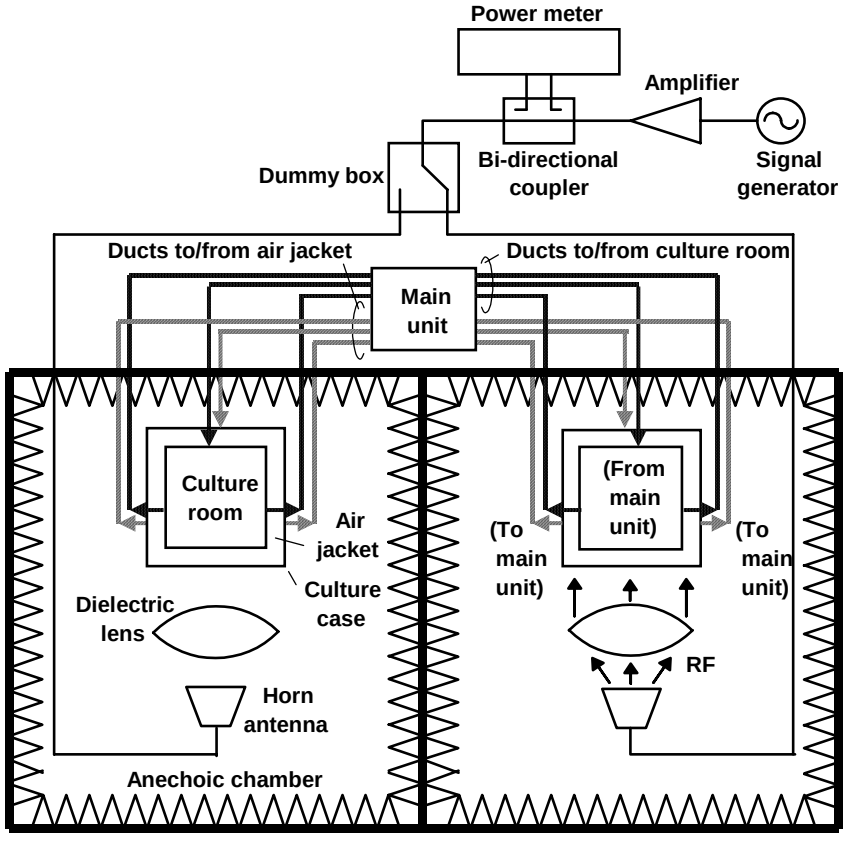

Figure 1. RF exposure system for *in vitro* experiments [Iyama et al., 2004]. Arrows from the horn antenna indicate the direction in which the RF travels. Schematic diagram of the electrical design and the air circulation in the RF exposure system. In this figure, the system on the right is for RF exposure and that on the left is for sham exposure.

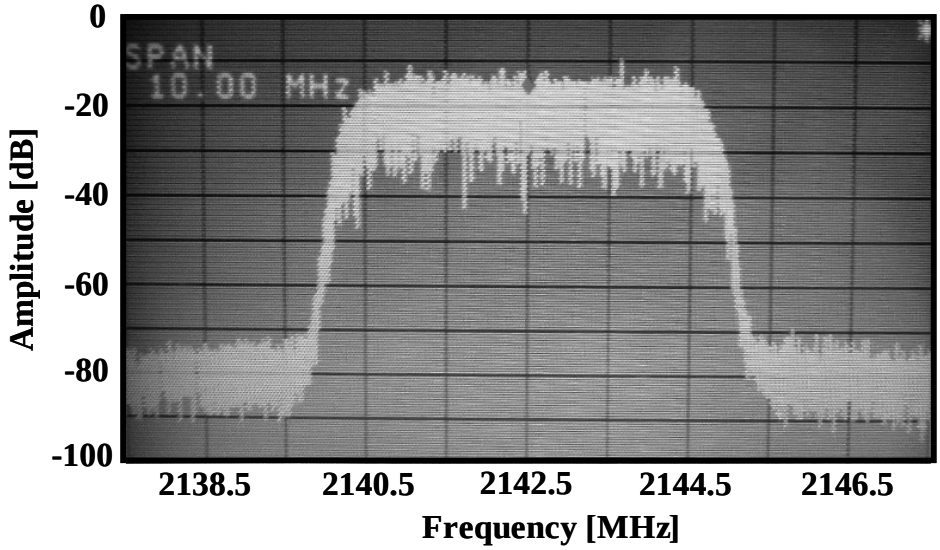

Figure 2. W-CDMA frequency spectrum.

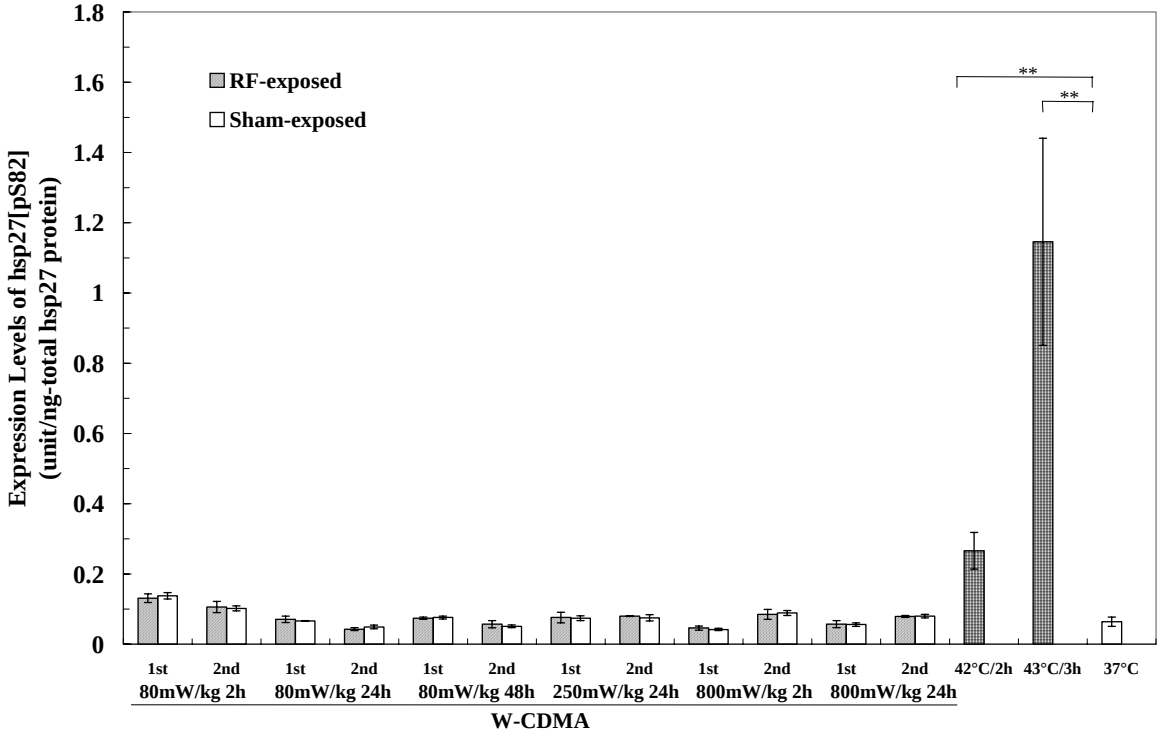

Figure 3-1. Expression levels of phosphorylated hsp27 in A172 cells exposed to W-CDMA RF field. Experiments under the same RF field exposure conditions were repeat twice, and 3 different cultures were used in each experiment. No statistically significant differences were observed between any of the RF field exposure groups and the sham-exposed controls in either the 2.1425 GHz W-CDMA RF field experiments. Other cultures were treated with heat at 42 or 43°C in a temperature-controlled water bath and at 37°C in a conventional incubator. **; $p<0.01$

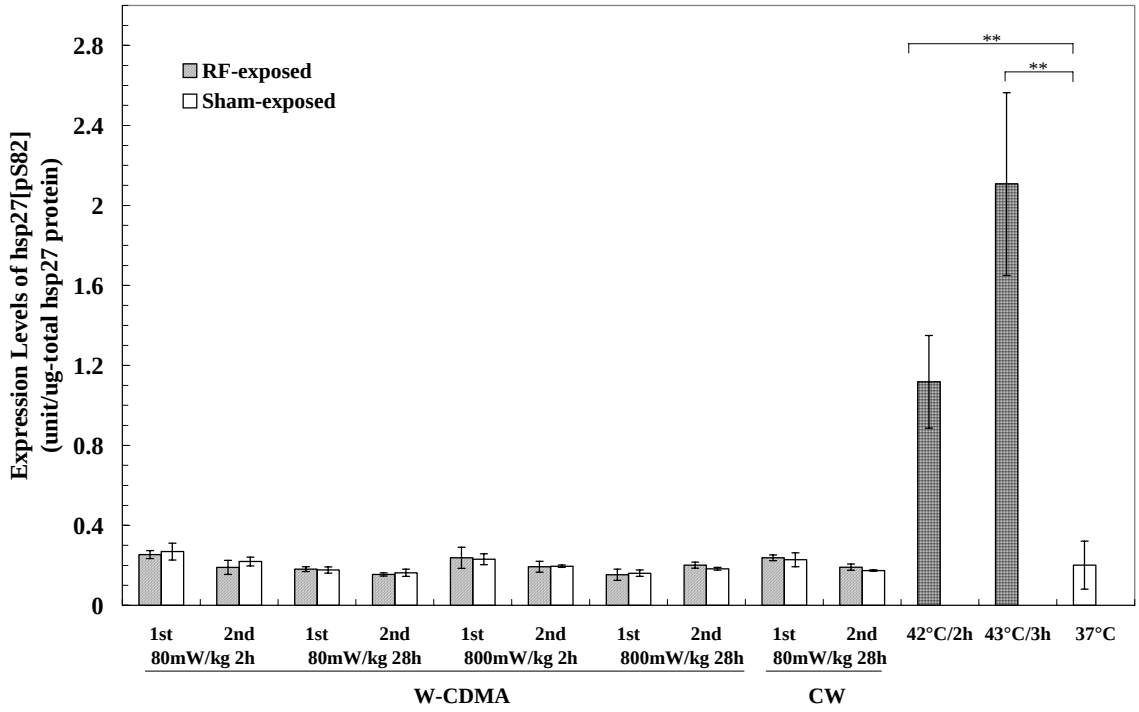

Figure 3-2. Expression levels of phosphorylated hsp27 in IMR-90 cells exposed to W-CDMA and CW RF fields. Experiments under the same RF field exposure conditions were repeat twice, and 3 different cultures were used in each experiment. No statistically significant differences were observed between any of the RF field exposure groups and the sham-exposed controls in either the 2.1425 GHz W-CDMA or CW RF field experiments. Other cultures were treated with heat at 42 or 43°C in a temperature-controlled water bath and at 37°C in a conventional incubator. **; $p<0.01$

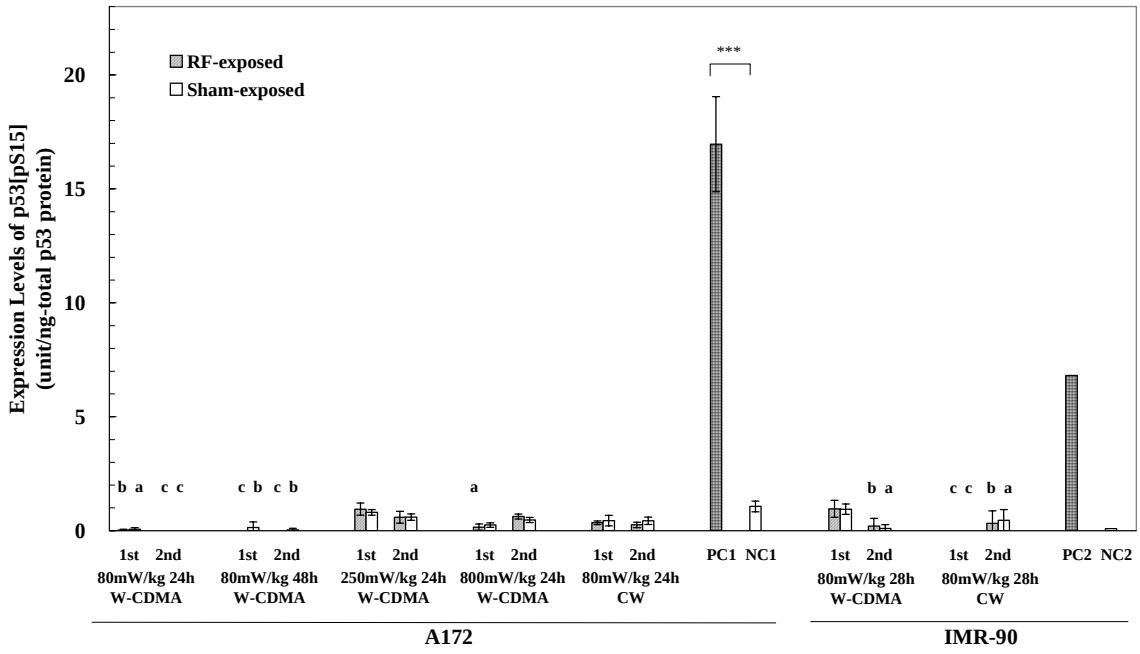

Figure 4. Expression levels of phosphorylated p53 at serine 15. Experiments under the same RF field exposure conditions were repeated twice, and 3 different cultures were used in each experiment. Undetectable samples (presented to zero) were one (a), two (b) or three (c) in 3 different culture samples. Treatment of A172 cells with 1.7 μmol/l (1.0 μg/ml) Dox (positive control; PC1) resulted in a statistically significant increase ($^{***}p<0.001$, n=5) compared to RF field- and sham-exposed samples, and non-treated samples (negative control; NC1). Treatment of IMR-90 fibroblasts to heat shock at 42°C (positive control; PC2) resulted in a remarkable increase (n=2) compared to RF field- and sham-exposed samples, and the non-treated samples (negative control; NC2).

REAL-TIME MEASUREMENT OF BRAIN MICROCIRCULATION DURING RF-EMF EXPOSURE USING AN "8"-SHAPED LOOP ANTENNA.

HIROTA S.[1], MASUDA H. [1], USHIYAMA A. [1], TAKAHASHI M. [1], TANAKA S. [2], KAWAI H. [2], WAKE K. [2], WATANABE S. [2], TAKI M. [3] and OHKUBO C. [4]

[1]Dept. of Environmental Health, National Institute of Public Health, 2-3-6 Minimi, Wako-shi, Saitama 351-0197, JAPAN. [2] Electromagnetic compatibility group, applied electromagnetic research center, National Institute of Information and Communications Technology, 4-2-1 nukui-kitamachi, koganei, Tokyo 184-8795, Japan. [3]Dept. of Electrical and electronic Engineering, Tokyo Metropolitan University, 1-1 minami-osawa, hachioji, Tokyo 192-0397, Japan. [4]RAD, World Health Organization, Geneva CH1211, Switzerland.

Abstract

Few studies have directly observed brain microcirculation during exposure to radio frequency electromagnetic fields (RF-EMF). The aim of present study was to investigate whether RF-EMF exposure induces acute effects on brain microcirculation being transiently observed only during RF-EMF radiation period. Male Sprague-Dawley rats (8 weeks old) were subjected to cranial window implantation prior to the exposure experiments and fluorescent intravital-microscopic observation under anesthesia. To simultaneously perform a microcirculatory observation and RF-EMF exposure, we developed and used an ''8''-shaped loop antenna. Rat's head was locally exposed to 1,457MHz electromagnetic near-field TDMA signal for PDC systems by the ''8''-shaped loop antenna. RF-EMF exposure intensity was maintained at 2.0 W/kg of the averaged SAR in parietal targeted area. During experimental period including RF-EMF exposure, four microcirculatory parameters (BBB-function, plasma velocities, leukocyte behaviours, and arterial vasomotion) were measured. No changes in any of the four microcirculatory parameters were elicited by RF-EMF exposure. The results revealed that there were no RF-EMF exposure effects on brain microcirculatory parameters, at least on BBB-function, plasma velocities, leukocyte behaviours, or arteriolar vasomotion under the present exposure conditions.

Introduction

Few studies have directly observed brain microcirculation during exposure to radio frequency electromagnetic fields (RF-EMF). Our previous study showed no effects of RF-EMF exposure on blood-brain barrier (BBB), plasma velocity or vessel diameter, as microcirculatory parameters in rat brain using a cranial window method [1]. However, the changes in these parameters were measured just after RF-EMF exposure, but not during exposure. To simultaneously perform measurements of rat brain microcirculation and RF-EMF exposure to a local cerebral region just under the cranial window, we developed a new type of antenna, ''8''-shaped loop antenna [2]. The aim of present study was to investigate whether RF-EMF exposure induces acute effects on brain microcirculation being transiently observed only during RF-EMF radiation period.

Male Sprague-Dawley rats (8 weeks old) were used. The rats were divided into two groups: RF group was exposed to RF-EMF and Sham group was not exposed to any RF-EMF. All rats were subjected to cranial window implantation and intravital-microscopic observation under pentobarbital anesthesia with a cocktail of ketamine and xylazine. The pial microcirculation within cranial windows was observed using a fluorescent microscope equipped with an EBCCD camera. In order to measure four microcirculatory parameters, BBB function, plasma velocities, leukocyte behaviours, and arteriole vasomotion, we used rhodamine 6G for leukocyte behaviours and FITC-Dx (70k or 2000k) for the other three parameters.

Rat heads were locally exposed to 1,457MHz electromagnetic near-field TDMA (time division multiple access) signal for PDC (Personal Digital Cellular, Japanese cellular telephone standard) systems by the ''8''-shaped loop antenna placed 4 mm upward to the cranial window. RF-EMF exposure was maintained at 2.0 W/kg of the averaged SAR in parietal targeted area.

Arteriolar vasomotion was observed during 12 min experimental period including 3 min RF-EMF exposure. The other three microcirculatory parameters, BBB-function, plasma velocity, and leukocyte behaviour in pial venules were measured every 10 min during 80 min experimental period including 50 min RF-EMF exposure. The results were compared between RF and Sham group. The statistical analysis was performed by Student's t-test or ANOVA.

Using an intravital fluorescence microscopy and the ''8''-shaped loop antenna enable us to observe rat pial microcirculation directly, and expose RF-EMF to rat, simultaneously (Fig. 1). Plasma image flowing in microvessels of the pia mater was visualized by FITC-Dx injected into vein.

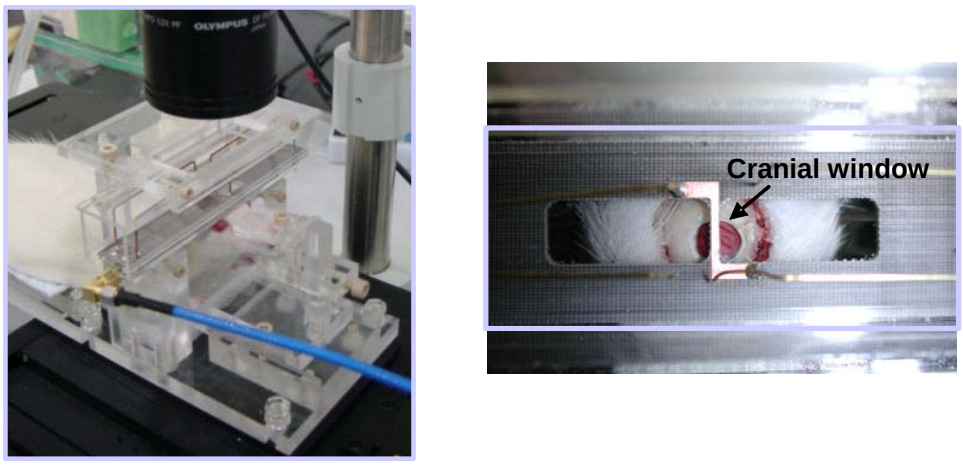

Fig. 1. Real-time measurement system

Blood-brain barrier permeability was evaluated by extravasation of FITC-Dx (70k) molecules injected into a rat venule. Although fluorescence intensity of pia mater area decreased through an experimental period, there were no significant difference in the fluorescence intensity between sham and RF group.

Velocities of plasma flowing in pial venules were measured by a dual-slit method and indicated as a relative (%) velocity of initial value. No significant difference in the percent velocities between two groups were showed until the end of experiment.

Leukocyte behaviours were evaluated by the numbers of rolling and sticking leukocytes stained with rhodamine 6G at 0, 10, 20, 40 min after beginning of the exposure. No significant difference in these numbers was found between two groups.

The arteriole vasomotions were monitored pre-, during, and post- RF exposure (Fig. 2). As an index for dynamic changes in the vasomotion, we calculated the mean value of arteriolar diameter for each experimental period and showed them as a relative (%) diameter of pre-exposure. As a result, no significant difference in the arteriolar diameter was found between two groups.

Summary

Our developed new type of loop antenna, the ''8''-shamped loop antenna succeeded to concentrate SAR distribution into the target area just under the cranial window. This was convenience to evaluate dynamic changes in microcirculatory parameters in the target area during RF-EMF exposure. In present experiment, we focused on four microcirculatory parameters, BBB-function, plasma velocities, leukocyte behaviours, and arterial vasomotion. However, no significant differences of these parameters were recognized between sham and exposed group even in during exposure period. The results revealed that there were no RF-EMF exposure effects on brain microcirculatory parameters, at least on BBB-function, plasma velocities, leukocyte behaviours, or arterial vasomotion under the present exposure conditions.

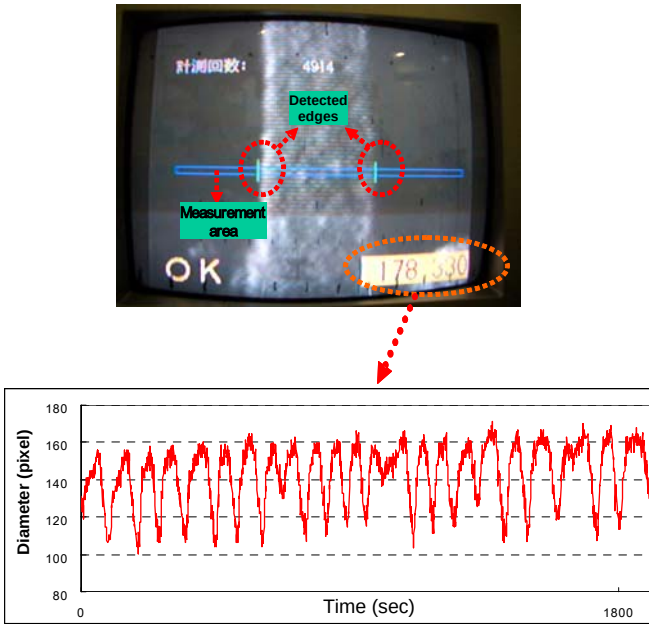

Fig. 2. The changes in pial ateriole diameter were measured using an automatically edge detection camera.

Acknowledgments

This study was financially supported by The Committee to Promote Research on the Possible Biological Effects of Electromagnetic Fields, Ministry of Internal Affairs and Communications, Japan.

References

[1] H. Masuda, K. Wake, S. Watanabe, M. Taki, and C. Ohkubo, "Acute effects of local exposure to radio-frequency electromagnetic fields on the cerebral microcirculation in rats," BEMS 2001 Abstract book, pp.139-140, June 2001.

[2] H. Watanabe, K. Wake, M. Hanazawa, S. Watanabe, H. Masuda, C. Ohkubo, M. Taki, Y. Yamanaka, and T. Uno. "Dosimetry of rat-head SAR caused by a high-performance ''8''-shaped loop antenna." BEMS 2004 Abstract book, pp.52-53, June 2004.

DEVELOPMENT OF CALCULATION PROGRAM 16MAGEXPO ON 24-HOUR PERSONAL MAGNETIC FIELD EXPOSURE UNDER HIGH SCHOOL STUDENTS

MUNNO JU[1], KWANGHO YANG[1], SUNGHO MYUNG[1], GIHYUN HWANG[2], JAEJOON KIM[3], SEUNGDO BAIK[3]

1. KOREA ELECTROTECHNOLOGY RESEARCH INS., CHANGWON, KOREA
2. DONGSEO UNIVERSITY, BUSAN, KOREA
3. KOREA ELECTRIC POWER CO., SEOUL, KOREA

Abstract

Currently, a number of scientific researches are conducted on potential health hazards of electric and magnetic fields. There is a non-objective and psychological belief that they are harmful. However, no scientific and objective proof exists. The ELF magnetic field (MF) has become one of the Korea's social issues due to MF's possible harmful health effect, especially for children under 17 years of age. Therefore, in order to evaluate the magnetic field exposure levels of those children in their general living environment, personal MF exposures of 347 subjects were measured in 2005 with government funding. This study developed the calculation program 16MAGEXPO based on the above measured database to predict personal MF exposure. This program can serve as a valuable tool in estimating 24-hour personal MF exposure without directly measuring the exposure. Three types of personal MF exposure estimation formulas - a formula for infants and preschool children from 1 to 7 years of age, a formula for elementary school children from 8 to 13 years of age and a formula for junior high school students from 14 to 16 years of age - were developed by applying evolutionary computation method to the measured database. Genetic algorithm (GA) and genetic programming (GP) were used among evolutionary computations. After tuning the database with the above methods, final three formulas with the smallest estimation error were selected. The target estimation error was approximately 0.3 mG. The seven parameters of each formula included gender (G), age (A), house type (H), house size (HS), distance between residence and power line (RD), power line voltage class (KV) and the usage and condition of electrical appliances (RULE).

I. Introduction

There is an increasing concern on possible health hazard caused by exposure to power frequency EMF, a part of electro-magnetic interference that is considered the 4th environmental pollution. The concerns over potentially negative biological effects produced by power lines and other sources began in 1979 when Wertheimer and Leeper reported that children living in the vicinity of high-voltage transmission lines had an increasing risk for developing cancer than other children. Although a number of researches were conducted on this subject, biological effects of EMF still remain a heated technological and medical controversy.[1, 2, 3] Therefore, this research developed a method to indirectly estimate the EMF level generated by using electrical energy for participants under 17 years of age. Exposure estimation formulas and calculation program (16MAGEXPO) will provide a method of epidemiological survey for the EMF's biological effects. The 347 participants, ranging from infants to junior high students, were divided into three age brackets to establish EMF exposure estimation formulas. The evolutionary computation was used as an optimization method.

II. Participant Database

The measured personal MF exposure database could be secured by participants who resided near transmission lines up to 345kV. These participants were categorized by the radial distance from the power line and age groups. The subjects included 62 infants to preschool children (1-7 years old), 261 elementary school children (8-13 years old) and 24 junior high students (14-16 years old). In Figure 1, junior high students and preschool children wore a MF measurement meter (Model EMDEX-Lite, Enertech, USA).

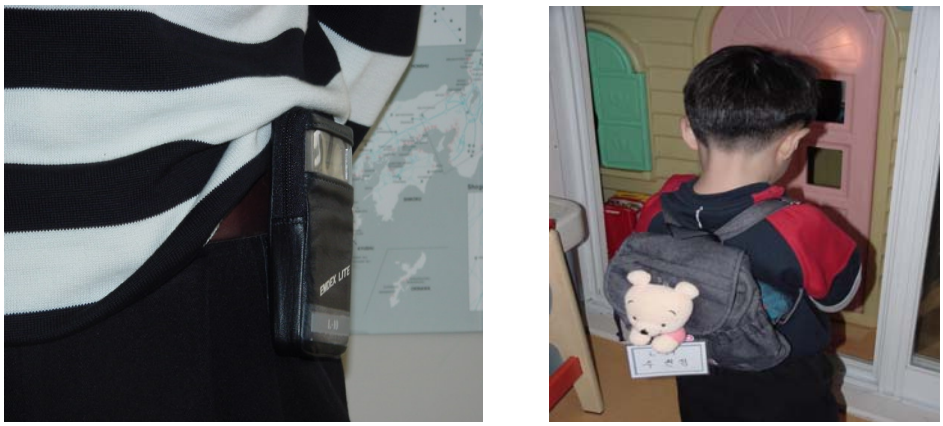

Fig. 1 Surveying personal MF exposure for junior high students and preschool children

III. Evolutionary Computations as Optimization Method

A. Evolutionary Computations

Evolutionary computations (ECs) have received significant attention during the last decade, although ECs were originally introduced in the late 1950's [4, 5]. ECs are search algorithms based on the mechanics of genetics and natural selection. ECs combine the survival of the fittest mechanism among string structures with a structured, yet randomized, information exchange to form a search algorithm. ECs efficiently exploit historical information to speculate on new search points with improved performance. In another words, ECs are search methods combining elements of directed and stochastic search, which can strike a remarkable balance between exploration and exploitation of global and local search capability. This research describes the GA and GP application procedures in developing personal MF exposure estimation formulas. The GA was developed by John Holland in the early 1970's. It finds the best solution for the environment by searching the solution space with a probability method and a hierarchical exchange of information between each individual (string or chromosome). GA does not use real parameters but uses chromosomes composed of string coded genotype. GA simulates crossover and mutation of natural systems, thus giving it a global searching capability. GP follows the trend of the GA paradigm but uses trees to represent genotypes. Trees provide a flexible representation for creating and manipulating programs. GP starts with an initial population of randomly generated computer programs (S-expressions) composed of functions and terminals appropriate to the problem domain. Each individual computer program in the population is measured in terms of how well it performs in the particular problem environment. This measure is called the fitness measure. [5, 6]

B. Applications to Develope Formulas

The ECs optimization method was applied to the measured database to develop personal MF exposure estimation formulas. During the development, the following key techniques were employed

1) Types and characteristics of parameters

The 6 main parameters included Gender (G), Age (A), House Type (H), House Size (HS), Radial Distance (RD), and Power Line Voltage (KV). However, occupation was excluded from the parameter. We also added a supplemental parameter called the 'RULE' to increase the estimation accuracy. This RULE represents the length and pattern of electrical appliances usage such as PC and electric heat mat. On the other hand, variables with negligible effects such as sleep, school, commute to and from school and TV watching have not been included in the rules.

2) Radial distance

In order to measure the distance between the power line and the residence, Radial Distance (RD-1), which is considered the real distance, was used instead of Lateral Distance (LD). A digital laser distance meter was used to measure the distance. If distance is difficult to measure, distance RD-2 between tower and the residence was applied.

3) Power line voltage

This research used transmission and distribution line voltage as a parameter instead of load current that directly decides MF level of the power line. The voltage was chosen because the load current fluctuates tremendously by day and season. This research also revealed that there is a significant similarity between increase in transmission line voltage and increase in average MF.

4) Code table of main parameters

Table 1 outlines the main parameter codes and input values during database (DB) tuning.

Table 1. Codes and input values of main parameters

Gender **(G)**	Age **(A)**	House Type **(H)**	House Size **(HS)**	Radial Distance **(RD)**	Power Line Voltage **(KV)**
·Male: 10 ·Female: 20	·1~16	·Apt.: 10 ·Etc.: 20	·the square footage of the unit	·0~30m: 10 ·31~50m: 20 ·51m or more: 30	·Line Voltage

5) Applications of ECs

Table 2 describes the DB tuning parameters of each method based on ECs. Equation 1 illustrates the general objective function for genetic algorithm.

Table 2. Tuning parameters of genetic optimizations

ECs	Generations	Population Size	Crossover Probability	Mutation Probability
GA	2,000	100	0.95	0.05
GP	200,000	1,000	0.8	0.08

$$MFExposure = k1\log(G) + k2\log(A) + k3\log(H) + k4\log(HS) + k5\log(RD) + k6\log(KV) + Rule \quad (1)$$

IV. The Results of Formulas Development

A. Development Conditions

The conditional criteria and functional evaluation characteristics for developing MF exposure estimation formula are as follows:

1) Six parameters: G, A, H, HS, RD and KV
2) Supplementary rules were applied to reduce estimation error.
3) Target error value: mean absolute estimation error below 0.3mG, or tuning and verification errors below 30%.
4) KV: Actual power line voltage. However, if RD is over 100m, '1' is inputted to bring KV term to '0'.
5) Database was tuned with GA and GP first. Then, formulas with the smallest estimation error or ones that incorporated the most parameters were chosen for each case.
6) When the formula produced a negative value due to a peculiar problem between the formula parameters under normal condition, a penalty was issued to the fitness of string (chromosome) during DB tuning.
7) HS: For apartments, the square footage of the unit was used. For houses and villas, the square footage of the floor which the participants live was used.

B. Resulting Formulas and Their Applicable Conditions

1) Types of formulas

This research developed six types of formulas as below.

◦ Formula for infants and preschool children: 1 type (Equation 2)
◦ Formula for elementary school children: 1 type
◦ Formulas for junior high school students: 2 types
◦ Supplementary formulas for elementary school children and junior high school students : 2 types

2) Sample result of personal MF exposure estimation formula for infants and preschool children and their applicable conditions

$$\#1MFExp = -0.002\log(G) + 0.003\log(A) + 0.94\log(H) - 0.24\log(HS) - 1.22\log(RD) + 1.09\log(KV) + Rule \quad (2)$$

• Applicable condition
- A: Ages between 1 and 7
- KV: 22.9~345 kV

C. Estimation Error

Table 3 combined the estimation errors of each formula; thus, displaying the reliability of each formula. Most estimation errors satisfy the target error of approximately 0.3mG (~30%). Yet, supplementary formulas exceeded

the target error due to their DB characteristics. The supplementary formulas are applicable only if participants' powre line voltage (KV) does not meet the criteria. Figure 2 is the graphic representation of the DB tuning and verification trend in case of elementary school children.

Table 3. Collection of MF exposure estimation formula errors

Formula type	Tuning percentage error (Tuning error/ average measurement value)	Verification percentage error (Validation error/ average measurement value		
Formula for infants & preschool children	32.1 % (0.36/1.12 mG)	29.6 % (0.37/1.25 mG)		
Formula for elementary school children	26.2 % (0.43/1.64 mG)	22.8 % (0.45/1.97 mG)		
Formulas for junior high school student	25.0 % (0.28/1.12 mG)	27.9 % (0.29/1.04 mG)		
Supplementary formulas for elementary school children & junior high school student	41.3 % (0.66/1.60 mG)	Elementary school children & junior high school students 39.7 % (0.71/1.79 mG)	Elementary school children 40.6 % (0.8/1.97 mG)	Junior high school students 33.7 % (0.35/1.04 mG)

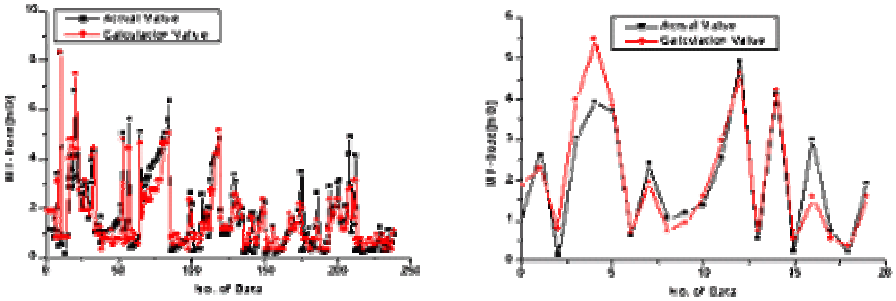

(a) DB tuning trend (b) DB verification trend

Fig. 2 Example of DB tuning and verification trends in elementary student database

V. MF Exposure Calculation Program 16MAGEXPO

A. 16MAGEXPO Features

The measurement of MF exposure is rather complicated, and it may be impossible according to circumstances,. 16MAGEXPO allows accurate estimation of the personal MF exposure level without directly measuring. The following is the main features of 16MAGEXPO.

1) Calculates personal MF exposure level by incorporating all MF sources commonly found in daily living environment.
2) Applies to children younger than 17 years old, including infants.
3) Any person, including non-experts, can predict personal MF exposure level if six personal parameters such as gender, age, house type, house size, distance between the residence and power line, and power line voltage and daily lifestyle of rules are known.
4) Rules are variables decided by electrical appliances usage such as PC and electric heat mat. Rules are introduced to enhance the prediction accuracy.
5) This program contains 6 types of personal MF exposure estimation formulas, and the prediction can be made as accurate as mean absolute error below 0.4mG.
6) This program will serve as a valuable tool in surveying and evaluating ELF MF's epidemiological effects.

B. Calculation Modules of 16MAGEXPO

16MAGEXPO has three calculation modules, infants and preschool children, elementary school children and junior high school students as shown in Figure 3. Figure 4 is the screen shot of the main menu. When you select a module button (for example: Infant and preschool child), a detailed calculation screen appears as shown in Figure 5. In the calculation screen, enter the calculation condition first and execute to display the 24-hour personal MF exposure result. If calculating multiple computation cases, use the output files as described in Table 4.

C. Main Calculation Functions of 16MAGEXPO

The following is the main calculation functions of 16MAGEXPO.

1) Calculates personal MF exposure level based on personal traits such as gender and age and living environment conditions such as house size, residence condition, and power line voltage.
2) Enhances the estimation accuracy by integrating daily usage pattern of electrical appliances such as electric heat mat that generate high magnetic field.
3) The user maintains the input file by entering above parameters in a menu-driven method.
4) Personal traits, rules, and calculation results are stored and maintained as an output file of Table 4.

Fig. 3 Diagram of 16MAGEXPO calculation module

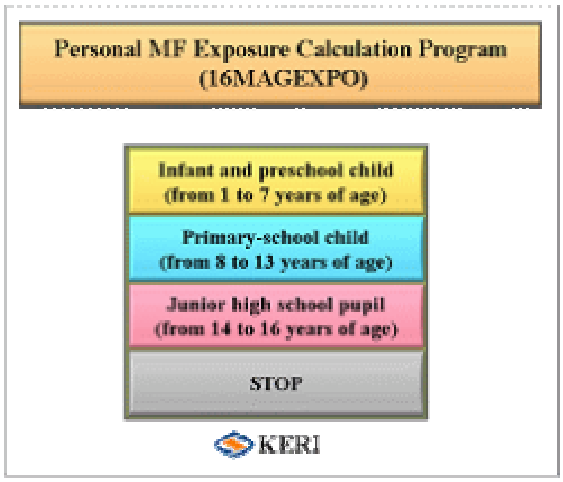

Fig. 4 Main menu of 16MAGEXPO

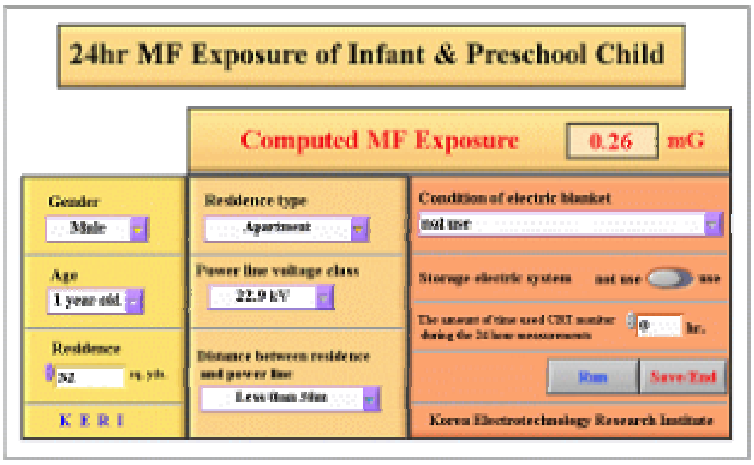

Fig. 5 A 24-hour personal MF exposure calculation sample for infants and preschool children

Table 4. A sample of output file about 24-hour personal MF exposure

G	A	HS [yard^2]	H	RD [m]	KV [kV]	k1	k2	k3 [hr]	MF [mG]
20.00	11.0	142.3	20.00	30.00	345.0	0.00	0.00	0.00	1.33
10.00	13.0	142.3	20.00	30.00	345.0	0.00	0.00	0.00	1.33
10.00	8.00	87.00	20.00	30.00	345.0	0.00	0.00	0.00	1.33
10.00	8.00	261.0	10.00	30.00	345.0	0.00	0.00	0.00	1.17
10.00	8.00	261.0	10.00	10.00	345.0	0.00	0.00	0.00	3.82
10.00	8.00	261.0	10.00	30.01	345.0	0.00	0.00	0.00	1.17
10.00	8.00	261.0	10.00	20.00	345.0	0.00	0.00	0.00	1.93
10.00	8.00	261.0	10.00	20.00	22.90	0.00	0.00	0.00	1.16
10.00	8.00	261.0	10.00	20.00	22.90	1.00	1.00	0.00	3.66
10.00	8.00	261.0	10.00	20.00	22.90	2.00	1.00	0.00	7.66
10.00	8.00	261.0	10.00	20.00	22.90	3.00	1.00	0.00	4.16
10.00	8.00	261.0	10.00	20.00	22.90	3.00	1.00	1.00	4.56
10.00	8.00	261.0	10.00	20.00	22.90	3.00	0.00	1.00	3.56

VI. Conclusions

The human health problem caused by ELF magnetic field has become one of Korea's most debated social issues. The possible health effect on children less than 17 years of age is especially a matter of primary concern. Therefore, this paper proposed the 16MAGEXPO software that can estimate personal MF exposure levels of the above children in their general living environment. The key features and significance of this software development are as follows:

1) The data used to develop estimation formulas were collected from 347 participants.
2) Since the program was designed to estimate the effects of MF near power lines, participants living close to power lines were selected. As a result, as much as 24% of the participants lived within 50m from power lines.
3) Total of six formulas was developed, including a formula for infants and preschool children.
4) The program chose gender, age, house type, house size (square footage), radial distance between residence and power lines and line voltage as parameters. This research revealed that the voltage, distance, and age parameters are highly relative to the MF exposure level.
5) First time in the world, the evolutionary computation suitable for this problem was used as an optimization method. This computation showed that these estimation formulas yielded approximately 0.4mG mean average errors. However, the supplementary formulas, which have limited use, resulted in higher estimation errors. The target estimation error was approximately 0.3 mG.
6) This research developed the personal MF exposure estimation program, 16MAGEXPO, by utilizing the previously mentioned estimation formulas and daily living patterns (rules). The program based on LabView can be used to calculate personal MF exposure for children less than 17 years of age.
7) 16MAGEXPO can serve as a valuable tool in estimating 24-hour personal MF exposure in children without directly measuring.
8) This software marks the suggestion of a new MF exposure estimation method since the introduction of the wire code in late 1970's. In addition, this software will provide an effective and practical means to study MF's effects on human health, especially the epidemiological study on correlation between magnetic field and childhood cancer.

REFERENCES

[1] Zaffanella L.E., Kalton, G.W., “Survey of Personal Magnetic Field Exposure, Phase Ⅱ: 1000-Person Survey”. EMF RAPID Engineering Project #6, Enertech Consultant, 1998

[2] ICNIRP Guidelines, “ICNIRP (International Commission on Non-Ionizing Radiation Protection), Guidelines for Limiting Exposure to Time-Varying Electric Magnetic, and Electromagnetic Fields (up to 300GHz), Preprint scheduled to appear in Health Physics”, Vol. 74, No. 4, 1998, pp. 494-522

[3] Christopher J. Portier, Mary S. Wolfe, "Assessment of Health Effects from Exposure to Power-Line Frequency Electric and Magnetic Fields", NIEHS Working Group Report, June 1998

[4] D. E. Goldberg, *Genetic Algorithms in Search, Optimization, and Machine Learning*, Reading, MA: Addison-Wesley, 1989.

[5] J. R. Koza, *Genetic Programming*, MIT, London, England, 1993, pp. 162-169.

[6] J. A. Miller, W. D. Potter, et al., "An Evaluation of Local Improvement Operators for Genetic Algorithms", *IEEE Transactions on Systems, Man, and Cybernetics*, Vol. 23, No. 5, Sep./Oct. 1993, pp. 1340-1351.

Calculation of Induced Current Inside a Human Body near an IH Cooker by SPFD Method

Yoshitsugu KAMIMURA, Kunihiko ITO and Yoshifumi YAMADA

Utsunomiya University, 7-1-2 Yoto, Utsunomiya 321-8585 Japan
(*gami@is.utsunomiya-u.ac.jp*)

Abstract

In this study, magnetic field exposure of human body near an induction heating (IH) cooker is numerically evaluated using Scalar Potential Finite Difference (SPFD) method. The maximum induced current densities are compared among three kinds of anatomical human body models of the Japanese adult male/female and the American adult male. The induced current densities are averaged over one square centimeter in the area, and they are compared with the guideline of International Commission on Non-Ionized Radiation Protection (ICNIRP). As a result, it is found that the maximum induced current densities are considerably different among these three models of the human body, and the induced current exceeding the guideline of ICNIRP may not flow inside human body in the case with a portable type IH cooker and a pan designed for the IH cooker. In addition, reducing the computation load and the computer resource by dividing the model is considered. As a result, the difference of calculation result by dividing the model is almost negligible, and computation load is decreased.

Introduction

Recently, people have been concerned about the effect of the electromagnetic field on the human body. Because the IH cooker is widespread in Japan, the Japanese especially has the interest of influence on health by the leakage magnetic field. The basic restrictions for exposure to electromagnetic fields in each frequency band are determined by ICNIRP. At the frequency of 20 kHz (internal frequency of the IH cooker used in this study), the basic restriction for the exposure to the induced current density is 40 mA/m^2 (for the general public exposure) and 200 mA/m^2 (for the occupational exposure)[1].

In this study, we use the small loop as a magnetic source equivalent to the IH cooker. We calculate the potential and the induced current density inside the body by SPFD method which is useful for the low frequency magnetic field exposure problem. We use the male and the female models of National Institute of Information and Communications Technology (NICT) as Japanese standard human models[2], and the male model of the Air Force Research Laboratory (AFRL) of Brooks City-Base as a reference[3]. We calculate the induced current density distribution for these models, average them over a cross-section of 1 cm^2 perpendicular to the each direction of axes, and compare those magnitude with the guideline of ICNIRP.

Methods

SPFD method:

The SPFD method is a numerical technique used for calculating potential and the induced current inside conductor under the low frequency magnetic field[4]. At first, we digitize the subject to three dimension cells. The edge conductance s is posited to the each edge of the cell. The scalar potential Ψ is assumed to each node. A simple finite difference equation is given as

$$\left(\sum_{r=1}^{6} s_r\right)\psi_0 - \sum_{r=1}^{6} s_r\psi_r = i\omega\sum_{r=1}^{6}(-1)^{r+1} s_r l\vec{A}_r \,, \qquad (1)$$

where r is the local node index (1~6) and target node is labeled 0. The symbol l denotes the length of the edge, and A_r is the magnetic vector potential tangent to the r-th edge. The set of equations are arranged to the simultaneous equations of unknown Ψ, and solved by SOR method or conjugate gradient method.

Numerical models and source:

In this study, we use three kinds of anatomical human models (Figs.1-3). Figs.1 and 2 are the Japanese male and female models, respectively, developed by NICT. The cell size is 2 mm. Fig.3 shows the male model developed by AFRL. The cell size of the model which we used is 3 mm. The conductivities of the tissues in all models are obtained from Gabriel's report[4].

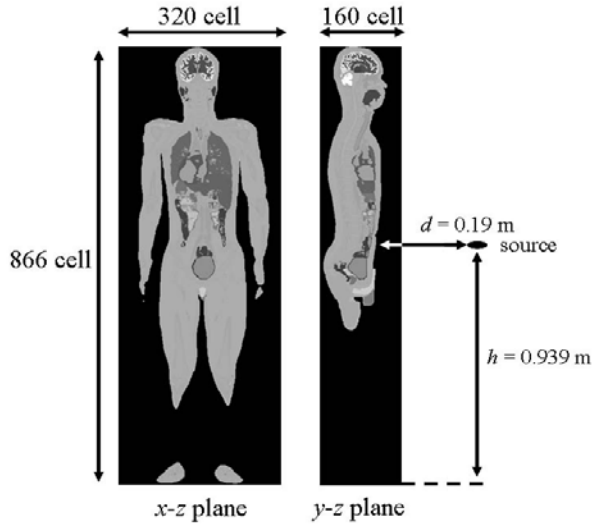

Fig.1 NICT male model and magnetic source.

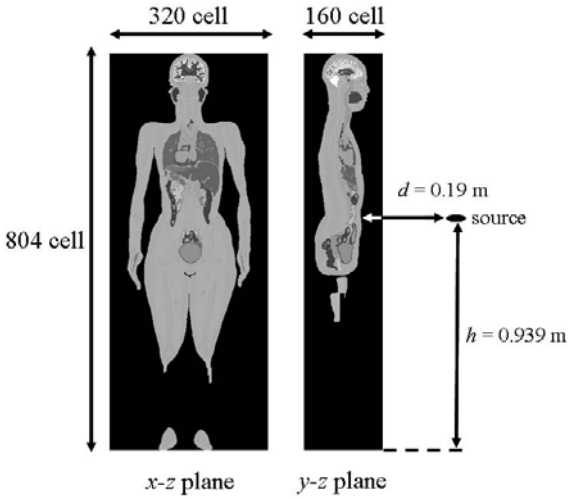

Fig.2 NICT female model and magnetic source.

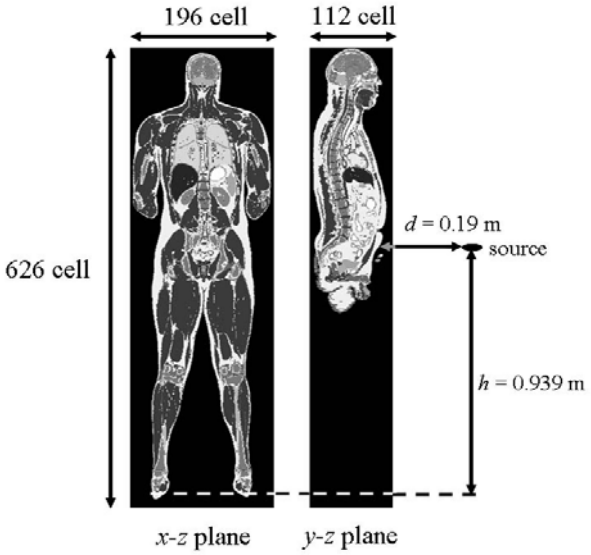

Fig.3 AFRL male model and magnetic source.

A small loop is posited to 0.939 m in height and the distance 0.19 m as a magnetic source equivalent to the IH cooker. The axis of the loop is *z*-direction. The magnetic moment is 1.07×10^6 wbm when we use a portable IH cooker and a pan designed for the IH cooker, and the frequency is 20 kHz.

Averaging filter:

According to the guideline of ICNIRP, the current densities should be averaged over a cross-section of 1 cm^2 perpendicular to the current direction[1]. We calculate the running average using 2D filter like Fig. 4 in the perpendicular plane for each component of current. The cell at the center of the filter represents the tissue after averaging. When the cell size of the model is 3 mm, an equivalent area is adjusted to 1 cm^2 by weighting as shown in Fig. 5.

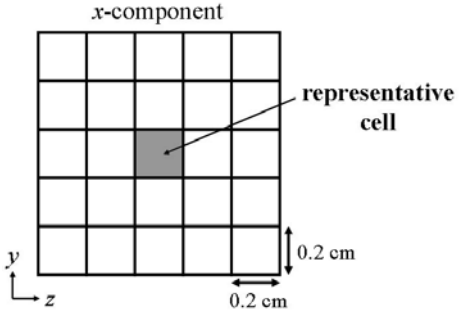

Fig.4 Averaging filter for 2 mm model.

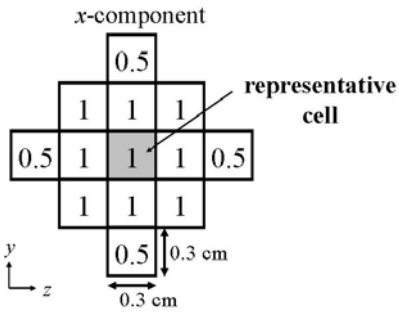

Fig.5 Averaging filter for 3 mm model.

Dividing of models:

When a magnetic source is replaced with small dipole, the current doesn't have *z* component in the *x*-*y* plane including the source since the external magnetic field has only *z* component in that plane. Therefore, we can calculate the induced current density independently by dividing the body into the upper and the lower half by that plane. The saving of the computer resource is expected by dividing the models. We investigate whether the computation load can be reduced by dividing as shown in Fig. 6.

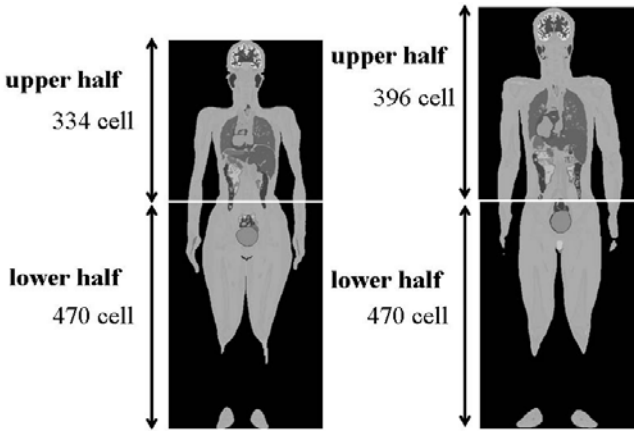

Fig.6 Dividing of the models of NICT.

Results

NICT male model:

Figure 7 shows the comparison between the raw value and averaged value, concerning the maxumum induced current density in each tissue for NICT male model. Figure 8 shows the distribution of averaged current densities in the cross section of the same height as the source.

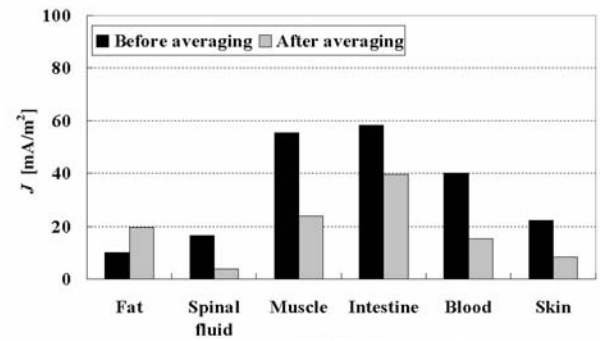

Fig.7 Comparison of induced current density for NICT male model.

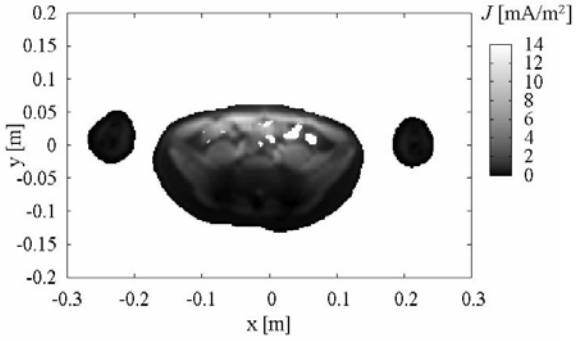

Fig.8 The distribution of averaged current density for NICT male model.

NICT female model:

Figure 9 shows the comparison between the raw value and averaged value, concerning the maxumum induced current density in each tissue for NICT female model. Figure 10 shows the distribution of averaged current densities in the cross section of the same height as the source.

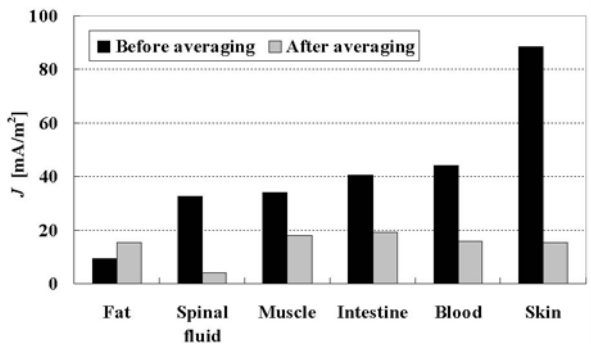

Fig.9 Comparison of induced current density for NICT female model.

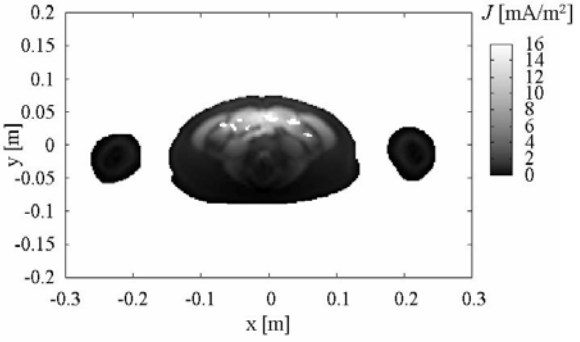

Fig.10 The distribution of averaged current density for NICT female model.

AFRL male model:

Figure 11 shows the comparison between the raw value and averaged value, concerning the maximum induced current density in each tissue for AFRL male model. Figure 12 shows the distribution of averaged current densities in the cross section of the same height as the source.

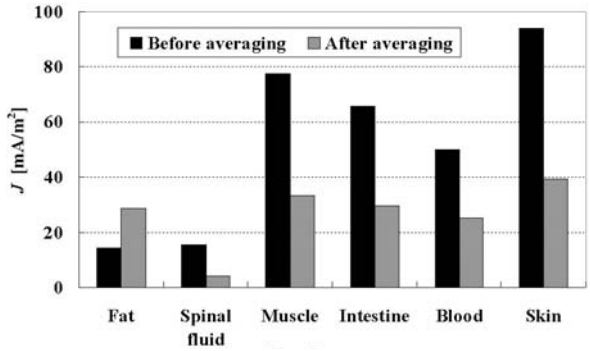

Fig.11 Comparison of induced current density for AFRL male model.

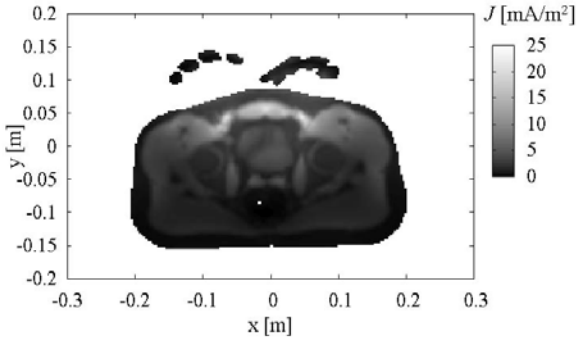

Fig.12 The distribution of averaged current density for AFRL male model.

According to Figs. 7, 9, and 11, the averaged current densities do not exceed the basic restriction 40 mA/m^2 of ICNIRP for the general public. Generally, the model with a fat body has the trend with large averaged current density.

Reduction of computation load by dividing of models:

Comparing the maximum value of the division model with the value of the whole body model, they are almost corresponding (Figs. 13, 14). Tables 1 and 2 show the required computer resource in our computation of the induced current densities. The computing time is proportional to the multiplication of the memory usage with the number of repetitions. Convergence in the upper half model has quickened due to dividing of the model, and the computing time could be saved

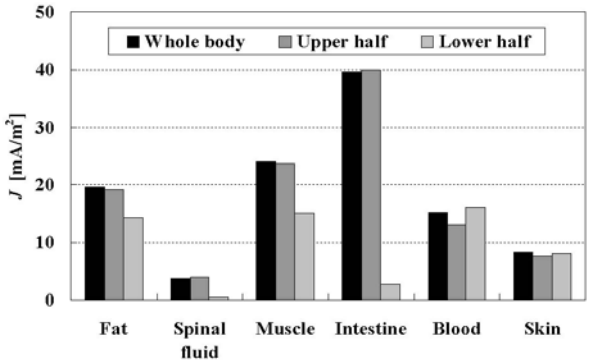

Fig.13 Maximum of averaged current density for divided NICT male model.

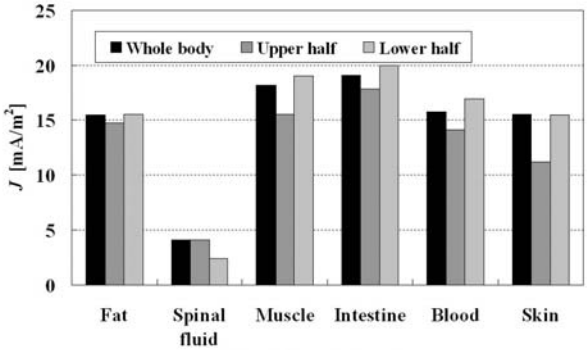

Fig. 14 Maximum of averaged current density for divided NICT female model.

Table 1 Reduction of computor load by dividing of the NICT male model.

	No. of reputation N	Memory usage M (MB)	Load ratio of N*M (%)
Whole body	24466	1532	100
Upper half	9311	707	17.6
Lower half	21664	837	48.4
Division model			66.0

Table 2 Reduction of computor load by dividing of the NICT female model.

	No. of reputation N	Memory usage M (MB)	Load ratio of N*M (%)
Whole body	17797	1423	100
Upper half	6812	598	16.1
Lower half	17727	836	58.5
Division model			74.6

Summary

We have replaced the IH cooker by the small loop, and provided the magnetic vector potential required by the SPFD method theoretically. The induced current densities have been obtained using Japanese anatomically models and the SPFD methods. As a result, it is found that the averaged current densities of them is lower than that of the American male model. The induced current exceeding the guideline of ICNIRP may not flow inside human body in the case with a portable type IH cooker and a pan designed for the IH cooker.

Acknowledgments

This study has been sponsored by Grants-in-Aid for Scientific Research (C) No.17560246 of JSPS.

References

[1] ICNIRP, "Guidelines for limiting exposure to time-varying electric, magnetic and electromagnetic fields (up to 300 GHz)," Health Physics, vol.41, no.4, pp.449-522 (1998).

[2] T. Nagaoka, et al., "Development of realistic high-resolution whole-body voxel models of Japanese adult males and females of average height and weight, and application of models to radio-frequency electromagnetic-field dosimetry," Phisics in Medicine and Biology, 49, pp.1-15 (2004).

[3] Air Force Research Laboratory/ The Human Effectiveness Directorate/ Directed Energy Bioeffects Division, "Dosimetry Models," http://www.brooks.af.mil/AFRL/hed/hedr/HEDR_modeling_irt-temp.htm

[4] T. W. Dawson, J. D. Moerloose and M. A. Stuchly, "Comparison of magnetically induced ELF fields in humans computed by FDTD and scalar potential FD codes," ACES Journal, 11(3), pp.63-71 (1996).

[5] C. Gabriel, "Compilation of the Dielectric Properties of Body Tissues at RF and Microwave Frequencies," Brooks Air Force Base, Report No.AL/ OE-TR-1996-0037, 1996.

SOURCES AND LEVELS OF ELF ELECTRIC AND MAGNETIC FIELDS IN GREECE

E. KARABETSOS G. FILIPPOPOULOS D. KOUTOUNIDIS CH. GOVARI N. SKAMNAKIS

NON IONIZING RADIATION OFFICE
GREEK ATOMIC ENERGY COMMISSION
P. O. BOX 60092, 15310 AGIA PARASKEVI, GREECE

Abstract
The Greek Atomic Energy Commission (EEAE) is the competent national authority for the protection of the general public and the environment from artificially produced non-ionizing radiation. To this end, EEAE carries out measurements in the vicinity of all kinds of sources emitting ELF electric and magnetic fields (e.g. power lines and substations), in order to monitor whether the general public exposure limits are being adhered to. The limit values for the ELF fields in Greece are set exactly the same as those in ICNIRP's guidelines. EEAE has conducted many measurements regarding the levels of ELF electric and magnetic fields in Greece around the elements of the electric power grid where the main interest of the public is focused. Theoretical estimations and typical values based on actual measurements of the fields in the vicinity of all the power lines used in Greece are presented. Measurement results in the vicinity of substations are also presented. In general, the levels of the magnetic field in the vicinity of the power grid elements are well below the established limits; whereas the levels of the electric field may reach values comparable to the safety limits very close to extremely high voltage lines. However, there is no case where the measured values of electric or magnetic fields were higher than the safety limits.

Introduction
Extremely low frequency or ELF electric and magnetic fields are omnipresent in modern societies. The possibility that long-term exposure to these fields might cause adverse health effects is a source for concern, especially for those people residing or working nearby high voltage lines or substations. Competent international scientific committees are watching the scientific developments in order to reach general conclusions about the health effects of these fields, [1].

In 2002, Greece put into force a legislative act, [2], implementing the recommendation, [3], of the Council of the European Union, adopting ICNIRP's limit values, [4], for the protection of the general public. The competent national authority for the protection of the general public and the environment from artificially produced non-ionizing radiation in Greece is the Greek Atomic Energy Commission (EEAE). To this end, the EEAE carries out measurements in the vicinity of all kinds of facilities emitting ELF electric and magnetic fields (e.g. power lines, high voltage substations) in order to monitor whether the general public exposure limits are being adhered to. The EEAE has been accredited in accordance with the requirements of the EN IS0/IEC 17025 standard for performing this kind of measurements. Figure 1 shows the number of annual audits conducted by the Non Ionizing Radiation Office of EEAE in the vicinity of ELF sources. There is an incremental tendency in these measurements reflecting the increasing interest for them.

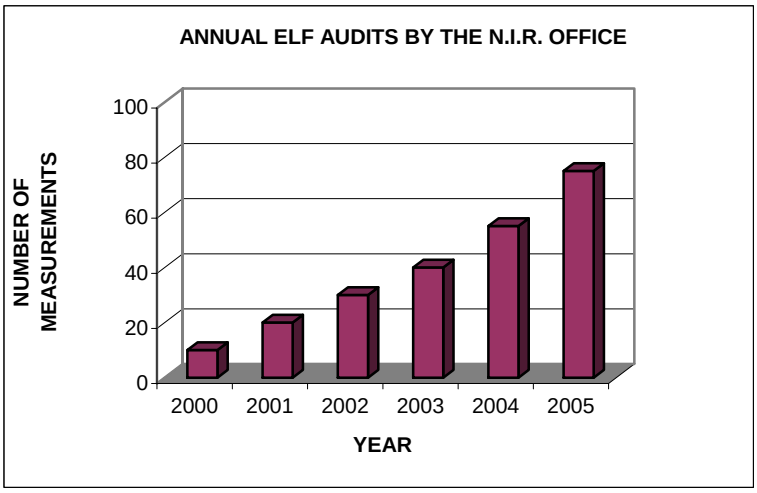

Fig. 1. Annual audits conducted by the Non Ionizing Radiation office of EEAE concerning ELF sources.

In the next paragraphs the main sources of ELF electric and magnetic field exposure of the general public are presented. Domestic sources as the electrical appliances, internal wiring and currents on large grounded metallic objects as water pipes, drains and rails are presented. Also, the exposure resulted from the electric power transmission and distribution system is examined. Special emphasis is given to the situation in Greece and its particularities in relation to other parts of the world. That is because the levels of the electric and magnetic fields are to an important extent depending on the practices applied at electrical installations and on the electric power grid construction and operation, which might be quite different from country to country, [5].

Domestic Sources

In domestic environments the most common sources of ELF fields are the electric appliances, the internal wiring as well as the currents in large grounded objects as water pipes, drains and rails. These sources mainly create magnetic fields in their vicinity, because the created electric field is small due to the low voltage and is further attenuated by closures, walls etc.

The magnetic fields produced by appliances are rapidly attenuated with increasing distance from them and are noteworthy at distances much lower than 1 meter. The field at the surface of the appliance might be very strong, reaching values of hundreds μT. However, in most practical cases the human exposure takes place at much greater distances. Exceptions to this are devices that require their operator to be in close vicinity as electric shavers and hair driers. However, these devises are usually used for short time-periods each day and so the exposure of their operators is limited. Furthermore, exposure from these devises is locally focused in a small area of the body and the coupling of the field with the human body is weak. Taking into account these special exposure situations it is rather impossible that exposure from these sources might be capable to stimulate the neural or muscle cells.

The internal electrical wiring usually does not create important magnetic field levels in its vicinity. The involved practices applied at the construction of these installations are described in the electrical safety codes for the avoidance of the electrocution and other dangers. According to the safety code in Greece, [6], but also in many other parts of the world, the currents at the internal wirings create magnetic fields that at a great extent cancel each other. However, in the rare cases of installations not complying with the terms of the safety code, it is possible to find unusually strong magnetic fields, due to faulty connections or leakage currents. The existence of strong magnetic fields from the internal wiring might be an indication of an installation not complying with electrical safety codes and even hiding risks for electrocution or other dangers (as initiation of a fire).

It is noteworthy that in Greece the main supply is 50Hz and 220V ac voltage (as in the rest of Europe). That means that the currents used in electric appliances and the magnetic fields associated with them are roughly half of those that are used in other parts of the world (as the North America) where 110V are used. Furthermore the 50Hz magnetic fields in Europe induce 20% less internal fields and currents in the body of an exposed individual in relation to the 60Hz used in North America.

Another important source of domestic ELF magnetic fields might be the existence of ground currents at large grounded objects as water pipes, drains and rails. These currents create elevated levels of background magnetic

fields, i.e. fields that decay relatively slowly with the distance from their source. These currents are actually a portion of the returning currents normally located at the neutral conductor. However, the multiple ground connections of the neutral conductor allow alternative paths for the flow of the returning currents back to the power grid through large grounded metallic objects as water pipes, figure 2. Ground currents typically flow if there is a fault on the power system or they can be a normal condition, if there are many connections of the neutral conductor to the ground. However, the use of non-conductive parts at the water supply system significantly reduces the levels of the return currents.

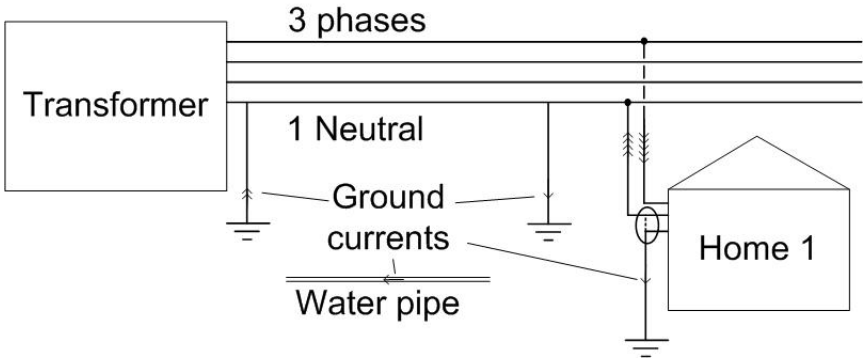

Fig. 2. Mechanisms for the creation of ground return currents. The connection of the neutral conductor with the protective earth (ground) at the beginning of each consumer installation is either prohibited or imperative in Greece, depending on the geographic area.

Electric power distribution

The electric power distribution network is consisted of the low and medium voltage network used for the delivery of the electric power as well as the medium to low voltage substations. In Greece the low voltage is at the nominal level of 220/380V. The medium voltage is at various nominal levels but the last years it is being standardized to 20kV.

The low voltage network is the final piece of the electric network used for the delivery of the electric power at home level. This network consists of overhead and underground lines. These lines create mainly magnetic fields in their vicinity. The created magnetic fields may reach values up to a few μT close to the conductors and attenuate at much lower levels a few meters away from the lines. However, the low voltage loads are usually not well balanced on the three phases of the system and that causes the appearance of currents on the line neutral conductor. A portion of this current might flow on large grounded metallic objects in the vicinity of the line but in special circumstances also far from it, with the results described in the previous paragraph. That also means that there is a net current on the line producing magnetic fields that decay relatively slow with the distance from it.

The medium voltage network is used for the power supply of the substations feeding the low voltage network as well as for the immediate supply of large consumers. The voltage in this network is many times higher than that in low voltage network and so the currents are many times lower for the same amount of transferred power. Table 1 includes typical EMF values found in the vicinity of medium voltage lines in Greece. It is noteworthy that the medium voltage lines do not suffer from the unbalances mentioned for low voltage lines, because the medium voltage loads are usually well balanced and the medium to low voltage substations act as barriers not allowing the low voltage unbalance to pass on the medium voltage side.

The medium to low voltage substations are usually sources of public concern. The attention is mistakenly focused on the transformer, which is used for power transmission from one voltage level to another. However, the transformer itself is not producing any significant levels of electric and magnetic fields in its vicinity. It is the medium and low voltage conductors connected to the transformer that create the electric and magnetic fields. Typically, the medium voltage equipment is the dominant source of the electric fields and the low voltage one is the dominant source for the magnetic fields close to a substation. The electric and magnetic fields produced by these substations does not extent further than a few meters from it. However, the current on the low voltage lines, which are fed by the substation, is higher close to the substation than far from it, as the electric power is dispatched to the various consumers along the line's way.

Electric power transmission

High and extremely high voltage lines are used to carry vast amounts of electric power. In Greece the main centers for electric power generation are located at the north part of the country; whereas the main consumption is occurring at the south part nearby Athens metropolitan area. Three double circuit 400kV (extremely high voltage) power lines are used to carry the electric power from the north to the south. Also, 400kV power lines are used for the interconnections with the neighbour countries at the north. The rest of the transmission is mainly accomplished with 150kV (high voltage) single or double circuit power lines.

Figure 3 shows typical levels of the electric and magnetic fields in the vicinity of the 150kV overhead power lines used in Greece. The magnetic field calculations refer to 50MVA apparent transferred power, which is considered typical for this level of voltage. The capacity for power transmission of these lines reaches 202MVA per three-phase circuit. In the 3rd row of this figure the fields in the vicinity of compact single circuit line are shown. This line creates the least field levels in its vicinity as it was also shown in [7].

Similarly, figure 4 shows typical levels of the electric and magnetic fields in the vicinity of 400kV power lines used in Greece. For these lines the magnetic field calculations refer to a typical level of apparent transferred power of 350MVA (typical capacity is 1400MVA per three-phase circuit). In the 2nd and 3rd row of this figure the fields in the vicinity of a double circuit line with different phase arrangements are shown. The double circuit 400kV power lines in Greece used to be constructed with the symmetrical phase arrangement on the two circuits (2nd row). However, for the barrel type double circuit lines used in Greece, this phase arrangement is not the optimum for the reduction of the produced electric and magnetic fields (actually for the parallel operation of the two circuits this phase arrangement is the worst one) and this led to elevated levels of electric and magnetic fields. The new 400kV double circuit lines are now constructed with opposite phase sequence on the two circuits, which is the optimum phase arrangement (3rd row) for this type of lines and leads to reduced electric and magnetic fields, [7]. Also, the phase sequence on the existing power lines of this kind were switched to the optimum one causing significant reduction of the produced fields,[8].

In Greece there are about 10000km of overhead high voltage power lines (400kV and 150kV) as well as 200km of underground high voltage power lines (150kV). The later are used for transferring high voltage power in the dense populated urban areas. Underground cables do not produce any electric field above the ground. Comparing the magnetic fields produced by an overhead and an underground high voltage line, carrying the same power, the underground cable produces a higher magnetic field value in a narrow area right above it (figure 5).

Table 2 shows worst-case values (based on theoretical estimations) and typical values (based on actual measurements) of electric and magnetic fields in the vicinity of the power lines used in Greece. The levels of the magnetic field are, as a rule, much lower than ICNIRP's reference level for general public exposure to 50Hz magnetic fields (100μT), [4]. The levels of the electric field can reach values close to 5kV/m (ICNIRP's reference level for general public exposure to 50Hz electric fields) under 400kV lines and under worst-case considerations. However, in no case the measured values for the electric field were higher than ICNIRP's reference level.

High Voltage Substations

Regarding the electric and magnetic fields produced in the vicinity of high voltage substations the measurements conducted by EEAE have shown that the equipment installed into the substation does not produce any significant values of electric and magnetic fields outside the substation. It is the power lines connected to it, that produce the levels of electric and magnetic fields measured in the vicinity of the substations. Figure 6 shows a satellite photo of Agios Stefanos 400kV substation of the Greek power transmission system. EEAE was called upon to examine the levels of the produced fields outside this substation and performed measurements around the perimeter of it. The routes of the power lines connected to the substation as well as the measurement points are indicated in figure 6. These measurements verified that far from the power lines there are insignificant levels of fields, whereas close to the power lines the typical electric and magnetic field levels in the vicinity of the corresponding lines are found.

Table 1. Electric and magnetic field levels at the vicinity of the power lines used in Greece. The values refer at a distance of 2m above ground level in the vicinity of overhead lines and at ground surface in the vicinity of underground cables.

Arrangement		**Magnetic field (μT)**	**Electric field (V/m)**
400 kV lines	Worst-case scenario Typical (underneath the conductors) Typical (25m aside from line)	25 1 – 4 0.5 – 2	5000 2000 – 4000 200 – 500
150 kV lines with lattice towers	Worst case scenario Typical (underneath the conductors) Typical (25m aside from line)	15 0.5 – 2 0.1 – 0.2	2000 1000 – 2000 100 – 300
150 kV compact lines on poles	Worst case scenario Typical (underneath the conductors) Typical (25m aside from line)	10 0.3 – 1.5 0.05 – 0.2	1200 500 – 1000 50 – 100
150 kV underground cables	Worst case scenario Typical (above the cable) Typical (25m aside from cable)	20 3 – 6 < 0,01	-
20 kV overhead lines (medium voltage network)	Worst case scenario Typical (underneath the conductors) Typical (25m aside from line)	5 0.2 – 0.5 0.01 – 0.05	700 50 – 200 10 – 20

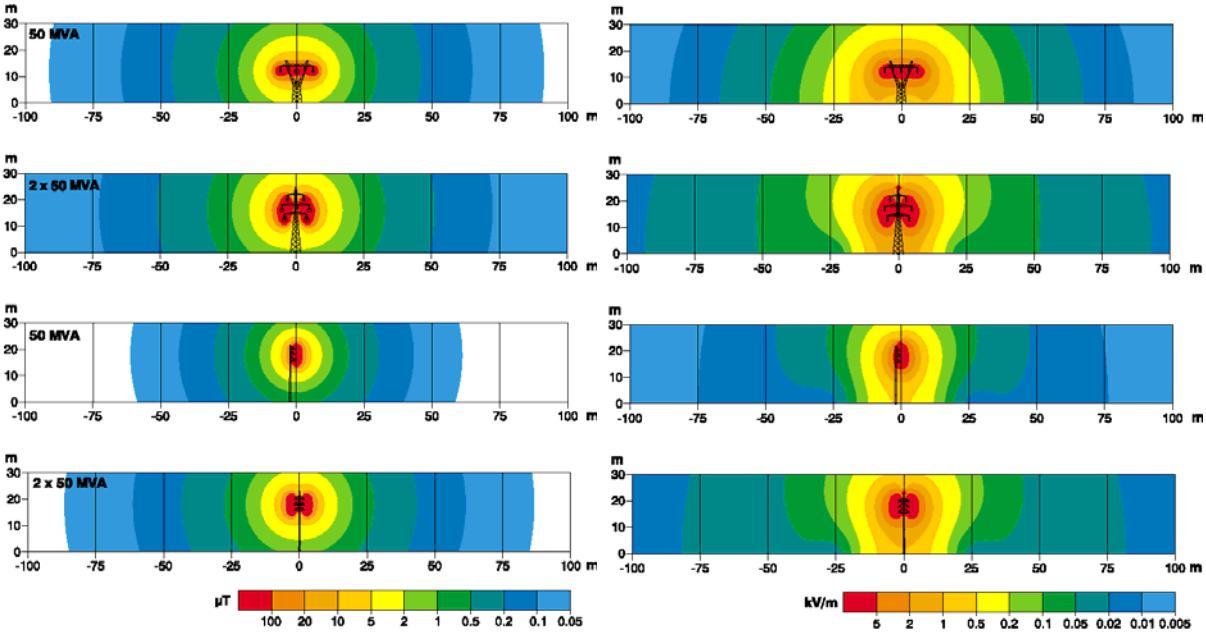

Fig 3. Typical levels for the magnetic field (on the left) and electric field (on the right) in the vicinity of the 150kV overhead power lines used in Greece. The considered clearance of the conductors to the ground was 12m and the indicated power line types are:
1st row: single circuit line on steel lattice towers
2nd row: double circuit line on steel lattice towers
3rd row: compact single circuit line on poles
4th row: compact double circuit line on poles

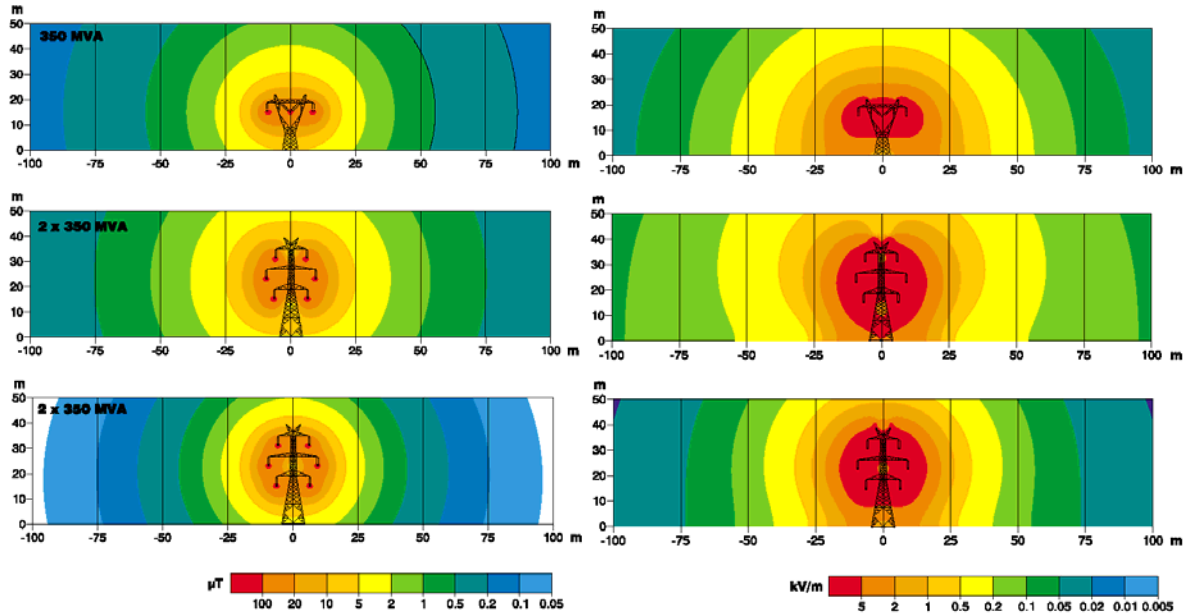

Fig 4. Magnetic field (on the left) and electric field (on the right) in the vicinity of the 400kV overhead power lines used in Greece. The considered clearance of the conductors to the ground was 15m and the indicated power line types are:
1st row: single circuit line
2nd row: double circuit line with the symmetrical phase arrangement
3rd row: double circuit line with the optimum phase arrangement

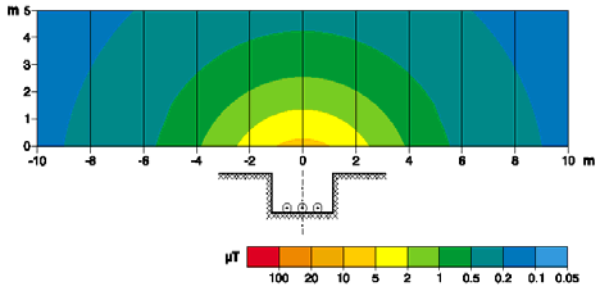

Fig. 5. Magnetic field in the vicinity of a 150kV underground cable carrying 50MVA. The considered cable is buried at 1.5m depth and the distance between the neighbor pole centers is 25cm.

Fig. 6. Satellite photo of Agios Stefanos 400kV substation (Greece) where the routes of 150kV and the 400kV power lines connected to it and the locations where EEAE have conducted measurements outside its perimeter are indicated.

Conclusion

The main sources of ELF magnetic field exposure of the general public in domestic environments are the electrical appliances, the internal wiring and the return currents on large grounded metallic objects as water pipes, drains and rails. The electrical appliances produce fast decreasing fields with distance that typically are considered important only for those devises where the operator must be in the close vicinity of them. The internal wiring normally does not produce any significant levels of magnetic fields, unless there is a faulty connection or a leakage current. The return currents on large grounded metallic objects as water pipes, drains and rails cause elevated levels of background magnetic fields.

Unbalanced loads at low voltage lines might cause net currents on them creating magnetic fields that decay relatively slowly with the distance. The medium voltage network does not suffer from these unbalances. The medium to low voltage transformer does not actually produce any fields in its environment. It is the lines connected to it that produce the electric and magnetic fields in its vicinity.

The electric and magnetic fields in the vicinity of high and extremely high voltage power lines depend on the type of line, its load and the distance from it. In Greece the application of the optimum phase arrangement at double circuit 400kV power lines caused a significant reduction of EMF levels around them. Furthermore, the use of compact lines also reduces the produced fields in relation to lines with normal dimensions. Underground cables create magnetic fields that decay very fast with distance from them. However, the magnetic field might be higher than that of an overhead line in a narrow zone above the cables.

References

[1] G. Filippopoulos, E. Karabetsos, D. Koutounides, Ch. Govari: Health effects of ELF electric and magnetic fields – WHO/IARC evaluation and other recent reviews, Second International Workshop on Biological Effects of Electromagnetic Fields, Rhodes, Greece, October 7-11, 2002.

[2] Greek legislation: Common Ministerial Decision, Protection measures for the exposure of the general public to all low frequency electric and magnetic fields emitting devices, Act No.512/Vol. B/25-4-2002.

[3] European Union Council Recommendation of 12th July 1999 on the limitation of exposure of the general public to electromagnetic fields (0Hz to 300 GHz) (1999/519/EC).
[4] International Commission on Non Ionizing Radiation Protection (ICNIRP), Guidelines for limiting exposure to time – varying electric, magnetic and electromagnetic fields (up to 300 GHz), Health Physics, Vol. 74, No 4, April 1998, pp 494 – 522.
[5] J. Swanson, W.T. Kaune: Comparison of residential power-frequency magnetic fields away from appliances in different countries, Bioelectromagnetics, Vol 20, No 4, pp 244-254, 1999.
[6] Hellenic Organization for Standardization, Requirements for electrical installations, ΕΛΟΤ HD 384, 2004.
[7] D. Tsanakas, G. Filippopoulos, J. Voyazakis, G. Kouvarakis: Compact and optimum phase conductor arrangement for the reduction of electric and magnetic fields, CIGRE Symposium Report 36 – 103, Paris 2000.
[8] E. Mimos, D. Tsanakas, G. Filippopoulos: Measurements of electric and magnetic fields produced by 400kV overhead power lines during the symmetrical and the optimum phase conductor arrangement, 3rd International Workshop on Biological Effects of Electromagnetic Fields, Kos, Greece, October 4-8, 2004.

SOURCES AND LEVELS OF RF ELECTROMAGNETIC FIELDS IN GREECE

E. KARABETSOS G. FILIPPOPOULOS D. KOUTOUNIDIS CH. GOVARI N. SKAMNAKIS

NON IONIZING RADIATION OFFICE
GREEK ATOMIC ENERGY COMMISSION
P. O. BOX 60092, 15310 AGIA PARASKEVI, GREECE

Abstract
The Greek Atomic Energy Commission (EEAE) is the competent national authority for the protection of the general public and the environment from artificially produced non-ionizing radiation. To this end, EEAE carries out measurements in the vicinity of all kinds of sources emitting RF electromagnetic fields (e.g. audio, radio and television antennas, mobile phone base stations, radar and satellite earth stations and other microwave communication systems), in order to monitor whether the general public exposure limits are being adhered to. The safety limits in Greek legislation for the electromagnetic fields emitted by antenna stations, were recently set to 70% of the ICNIRP's values and to 60% of them if the antenna station is closer than 300m from the perimeter of kindergartens, schools, hospitals or eldercare facilities. There are a few exceptional cases where measurements of RF fields conducted by EEAE in the vicinity of radio and TV broadcasting antennas have revealed excess of ICNIRP's reference levels. The results of one such case are presented. About 70% of the RF measurements conducted by EEAE concern cellular phone base stations. EEAE has conducted measurements in the vicinity of 1200 such stations and virtually in all measurements the results are from tens to thousands times below ICNIRP's reference levels for general public protection.

Introduction
The proliferation of wireless communication technologies caused a radical change on the modern society. In Greece the penetration of cell phones is about 80% that is close to the average of the developed world. At the same time there is an increasing concern among people residing nearby cell phone base stations about adverse health effects caused by the presence of the station.

In order to protect against known effects of the exposure to electromagnetic fields, competent committees as ICNIRP have developed exposure guidelines, [1]. In the recommendation, [2], issued in 1999, the EU Council adopted ICNIRP's guidelines for the protection of the general public. Implementing this recommendation, Greece put into force a national legislative act concerning the protection of the public from exposure to electromagnetic fields emitted by all kinds of land-based antenna stations, [3] in 2000. The limits in Greek legislation were set to 80% of the European Recommendation values. Recently, however, the Greek Parliament has voted the Law [4] setting the Greek limit values at 70% of the European Recommendation values, in general, and 60% of them, if the antenna station is closer than 300m from kindergartens, schools, hospitals or elder-care facilities.

The competent national authority for the protection of the general public and the environment from artificially produced non-ionizing radiation in Greece is the Greek Atomic Energy Commission (EEAE). To this end, the EEAE carries out measurements in the vicinity of all kinds of facilities emitting RF electromagnetic fields (e.g. audio, radio and television antennas, mobile phone base stations, radar and satellite earth stations and other microwave communication systems), in order to monitor whether the general public exposure limits are being adhered to. The EEAE has been accredited in accordance with the requirements of the EN IS0/IEC 17025 standard for performing this kind of measurements. Figure 1 shows the number of annual audits conducted by the Non Ionizing Radiation Office of EEAE regarding RF sources. There is an incremental tendency in these measurements reflecting the increasing interest for them.

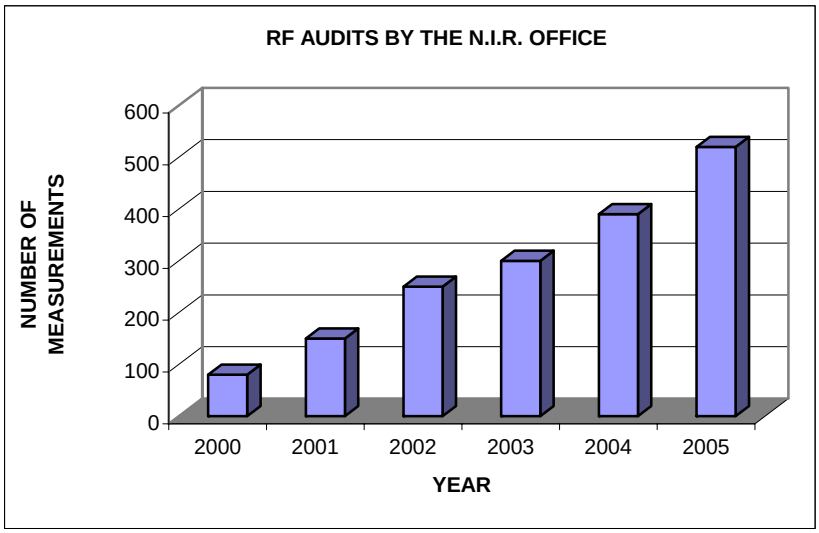

Fig. 1. Annual audits conducted by the Non Ionizing Radiation office of EEAE concerning RF sources.

In the next paragraphs results of measurements conducted by EEAE in the vicinity of the most common types of antenna stations are presented. Though the use of mobile phones is the major source of exposure to RF electromagnetic fields, mobile phones are not treated in this paper. That is because the measurements conducted by EEAE generally concern fixed antenna stations as mobile phone base stations, radio and TV broadcasting stations radar and satellite earth stations and other microwave communication systems. The purpose of these measurements is to check compliance with the limits set in the Greek legislation. Figure 2 shows the percentage of the measurements conducted in the vicinity of mobile phone base stations, radio and TV broadcasting antennas as well as radar facilities. The majority of measurements concern mobile phone base stations. This big ratio is due to the constantly increasing relevant requests from municipal authorities, individual citizens and even the mobile phone network operators.

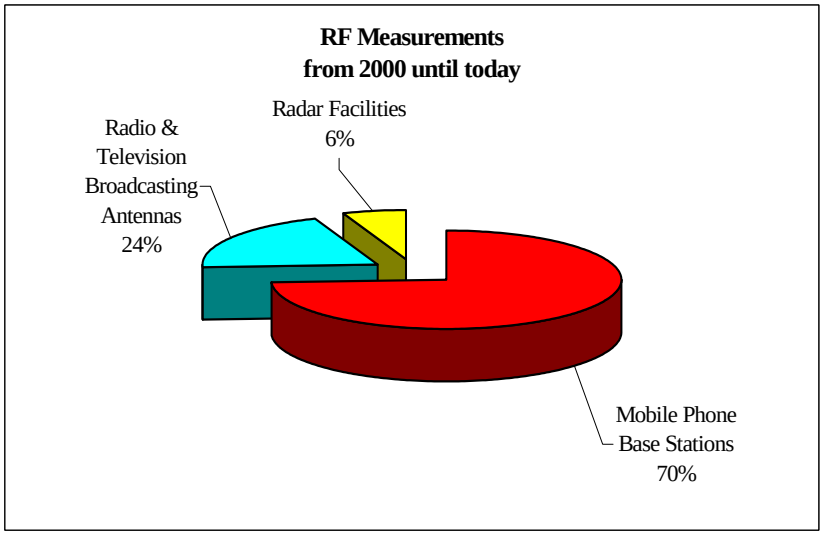

Fig. 2. Percentage of the measurements conducted by EEAE regarding mobile phone base stations, radio and TV broadcasting antennas and radar facilities.

Mobile phone base stations

Mobile phone base station antennas in Greece are, as everywhere else, placed either on top of large metal pylons (in rural places) or on poles on top of buildings (in urban areas). Nowadays, it is also common to find micro antennas in the interior of big buildings such as airports, metro stations, stadiums, etc, where a lot of people are assembled. Throughout the country there are about 6000 base stations installed until now, including the new UMTS stations. The EEAE has conducted measurements in the vicinity of almost 1250 such stations and practically in all cases the results were found to be from tens to thousands times below ICNIRP's reference levels for general public exposure. Table 1 shows typical maximum levels of the electromagnetic fields measured in the vicinity of mobile phone base stations in Greece. It is noted that these values refer to the maximum value at worst-case selected areas in the vicinity of the base station. These areas are usually on the roofs of nearby tall buildings in the main lobe directions of the base station's antennas. The levels of the electromagnetic fields caused by these stations at areas where people normally dwell or work are, as a rule, much lower.

Table 1. Typical maximum values of electromagnetic radiation in the vicinity of mobile phone base stations and the reference levels imposed by the Greek legislation for the frequencies used in mobile phone systems.

		Electric field (V/m)	**Magnetic field (A/m)**	**Equiv. Power Density (W/m^2)**
Typical maximum values		0.25 – 5	0.0005 – 0.01	0.0002 – 0.05
Reference levels for GSM-900*	70%	34.5	0.0929	3.1
	60%	31.9	0.0860	2.7
Reference levels for GSM-1800*	70%	48.8	0.1313	6.3
	60%	45.2	0.1216	5.4
Reference levels for UMTS* (2100MHz)	70%	51	0.1339	7
	60%	47.2	0.1239	6

* The Greek limits are set to 70% of ICNIRP's values for the electromagnetic fields in the vicinity of antenna systems further than 300m from the perimeter of day nurseries, schools, hospitals or elder-care facilities and to 60% of ICNIRP's values closer than 300m from these facilities. The Greek reference levels are calculated from corresponding basic restrictions set to 70% and 60% per case of ICNIRP's basic restrictions.

Radio and TV broadcast stations

In many cases, a great number of powerful radio and TV broadcasting installations have been assembled in one place forming an antenna park. In some of these places, measurements conducted by EEAE have revealed excess of ICNIRP's reference levels. Usually, the excess is limited a few meters away from the antenna installations. In a specific and exceptional case, the side lobe of a powerful installation in an antenna park near Herakleion, Crete Island radiates a nearby, elevated area where an army camp is situated, causing excess of ICNIRP's reference levels in almost half of the camp (see figure 3).

EEAE was called upon to examine the levels of the electromagnetic radiation caused by this antenna park. The measurements performed by EEAE revealed levels of electromagnetic fields much in excess of Greek reference levels (and ICNIRP reference levels as well). After that, the area where the excess occurs was defined and special signs were temporally set in order to warn the personnel of the high EMF levels, until the competent authorities take all the appropriate remedial actions. Figure 3 indicates the area where the electromagnetic fields exceed the Greek reference levels and the points where measurements have been taken. Besides measuring the levels of the electromagnetic fields spectral analyses were also performed in order to specify the contribution of each source to the measured levels. Figures 4 and 5 show the results of spectral analyses per service and per FM radio station, respectively, conducted at point M1 (a typical point). These analyses revealed that the major contribution at the measured fields came from FM radio stations and particularly from a single radio station operating at 97.5MHz.

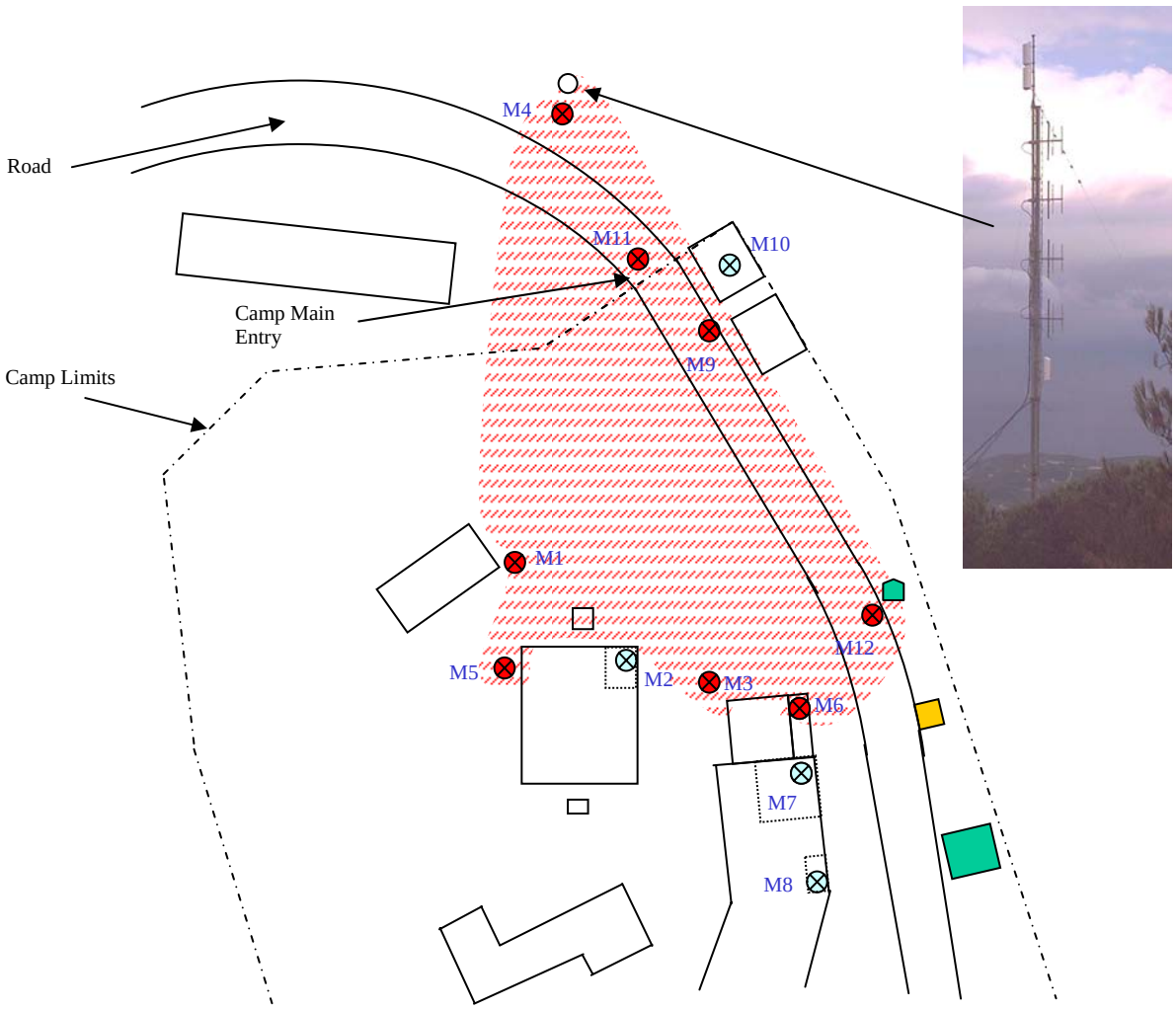

Fig 3. A sketch of the camp and the surrounding area showing the points of measurement (M1- 12) and the area in red where the RF radiation exceeds the Greek reference levels. The photo shows the radio station antenna causing the high radiation levels.

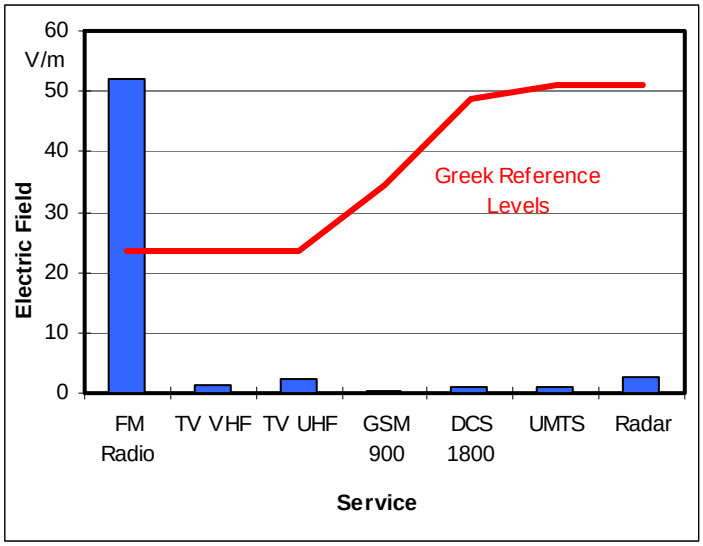

Fig. 4. Spectral analysis per service for the electromagnetic radiation at point M1.

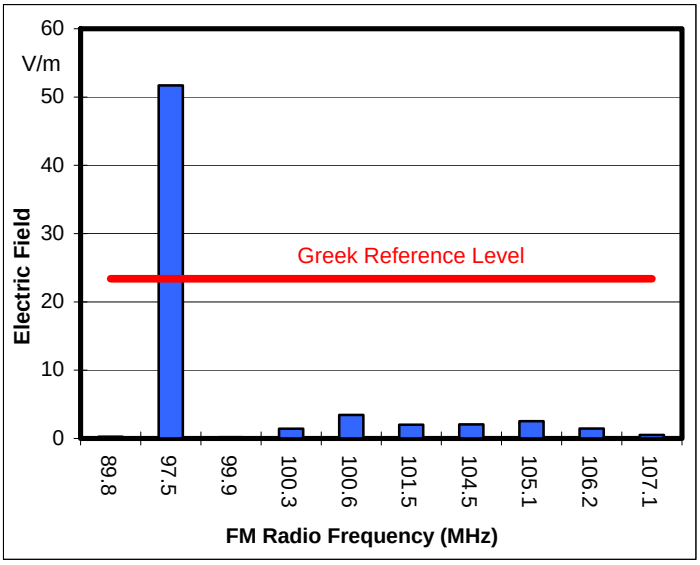

Fig. 5. Spectral analysis per FM radio station for the electromagnetic radiation at point M1.

Radar Stations

EEAE has also conducted measurements in the vicinity of radar installations. Despite the powerful emitted pulses the exposure in the vicinity of these installations is in general some hundreds to thousand times lower than ICNIRP's reference values for general public protection. It is noteworthy that the measurement process in these cases is much more difficult and time requiring because the instrument's response to pulsed modulated fields has to be taken into account and the peak and average exposure has to be calculated.

Conclusions

EEAE carries out measurements in the vicinity of all devices emitting RF electromagnetic fields throughout Greece in order to check compliance with the limits imposed by the Greek Legislation. To that end over one and a half thousand audits have been performed. It is noted that the Greek limits were recently set to 70% of ICNIRP's values in general, and 60% of ICNIRP's values for exposure caused by antenna station at a distance lower than 300m from the perimeter of day nurseries, schools, hospitals or elder-care facilities.

The results of RF electromagnetic field measurements show that there might be cases where powerful radio or TV broadcasting antennas cause levels of these fields greater than the established reference values for human exposure, if proper care were not shown during their design and installation phases. Regarding the electromagnetic field levels in the vicinity of mobile phone base stations, the measurements conducted by EEAE show that the maximum values of electromagnetic fields are typically hundreds to thousand times lower than ICNIRP's reference levels.

References

[1] International Commission on Non Ionizing Radiation Protection (ICNIRP), Guidelines for limiting exposure to time – varying electric, magnetic and electromagnetic fields (up to 300 GHz), Health Physics, Vol. 74, No 4, April 1998, pp 494 – 522.
[2] European Union Council Recommendation of 12th July 1999 on the limitation of exposure of the general public to electromagnetic fields (0Hz to 300 GHz) (1999/519/EC).
[3] Greek legislation: Common Ministerial Decision, Protection measures for the exposure of the general public to all land based antenna stations, Act No.1105/Vol. B/6-9-2000.
[4] Greek legislation: Law No 3431 About electronic communications and other provisions, Act No.13/A/03-02-2006.

DEVELOPMENT OF MOTOR AND PSYCHOLOGICAL FUNCTION ON CHILDREN AND ELECTROMAGNETIC FIELD

ANTON KOLODYNSKI & VALDA KOLODYNSKA

Institute of Biology University of Latvia,

3 Miera str., Salaspils, LV- 2269, Latvia

Email: anton.kolodynski@email.lubi.edu.lv

ABSTRACT

The use of mobile connection that relates to electromagnetic satiation is rapidly increasing during the recent 10 years in Latvia. People who carry mobile phones constantly subject themselves to the action of an electromagnetic field (EMF). And in the process of talking the mobile phone EMF exceeds the standards admissible by a factor of 10 times.

The number of children who always use mobile phones rapidly augments too. According to our data (2005) every tenth pupil of the first form has a mobile phone. Moreover, at the age of the secondary school nearly every pupil has a mobile phone.

The main tasks of the studies were the EMF influence on the development of the children motor and psychological function. The intensity of the EMF influence determined on the children neuropsychic development peculiarities was studied.

A complex of motor and psychological parameters was found.

The studies were performed every year on 112 children in 2 schools of Riga from 1996 and will be finished in 2008. Tests were carried out with every child determining their motor functions (taping-test, reaction time on sound stimuli were given binaurally or bilaterally with stereo earphones and light stimuli presented at the centre of table and on the left or right sides), psychological IQ—by Raven's test, capacity for attention switching was tested according to a modified Shulte's procedure, stability and capacity to focus attention were studied using an "entangled line" test, and memory was tested by the capacity to remember numbers functions.

The paper presents the preliminary results of experiments on a possible interdependence between EMF and children motor and psychological functions development.

Key words: children, development, mobile phone, IQ, attention, reaction time, tapping-test.

INTRODUCTION

Children, like adults, are subjected to the effect of harmful environmental factors, including also those generated by electromagnetic fields (EMF) of modern communication systems. At the same time, recent reviews demonstrate that there has been little research on the EMF effects on children.

The literature data available contain no common opinion on the mechanism of EMF effect on human health. There are studies on the heat effect of high frequency EMF on human health (Maier *et al*., 2000; Kumar, 2001; Liesenkotter, 2002; Lin *et al*., 2002; Walton, 2002; Evans-Pughe, 2003; Hocking, 2003), human body (Schonborn *et al*., 1998; Nesse *et al*., 2001; Lin, 2003; Toropainen, 2003), nervous system (Croft *et al*., 2002; Hamblin and Wood, 2002; Hietanen *et al*., 2002; Hossmann and Hermann, 2003; Huber *et al*., 2003; Salford *et al*., 2003), and psychological function (Lee *et al*., 2001; Edelstyn and Oldershaw, 2002; Haarala *et al*., 2003;); however, the data available are on contradictory. The number of children who persistently use mobile phones has rapidly increased as well. The studies were performed with a psychophysiological diagnostic system "Polytest-8802 (Produced by Engineering Center of Latvian Academy of Science, Latvia). The "Polytest-8802" is a specialized computer that uses psychophysiological reactions to determine human functional state. In total, 11 tests were made for each child. A rest break was included and the test duration was 70 minutes. Each test included twenty measurements that were used to obtain the arithmetical mean, standard deviation, and standard error of the mean (Kolodynski and Kolodynska, 1996, 2006). The studies were performed on 112 children (57 boys and 55 girls) in 2 schools of Riga in 1996–2003 (Table 1).

Tapping-test. To evaluate the functional state of the neuromuscular system, a tapping-test was used. The children examined had to press two keys with their right and left hands at maximum rate for 30 seconds. The rate of key pressing per second was registered for each hand separately.

Reaction time Red light diodes were used to present light stimuli at the centre of the table and on the left and right sides. The visible diameter of the light was 2.5 mm and the stimulus duration was 40 ms. Sound stimuli were given with stereo earphones (intensity, 60 dB; stimulus duration, 100 ms; frequency, 1 kHz). The interval between both light and sound stimuli was randomized (2.5–4 s). Children had to rapidly press and release keys after stimuli. Presentations of stimuli from the table centre or binaurally required the child to press both keys simultaneously. When the stimulus was presented from the side of the table, or in one earphone, the subject had to press the key on the side corresponding to the stimulus. In the cross variant of the test, the subject had press the key at the side opposite that of the stimulus. The response time, duration of press contact, and the number of errors were registered.

Attention. The capacity for attention switching was tested according to a modified Shulte's procedure. The procedure used a double-colored table of 64 squares. Each square consisted of two numbers: large black and small red colors (index), as well as a response button. At the beginning of the test the monitor displayed a number which the child was required to find among the black numbers. When the required black number was found, the child was required to press the appropriate key and memorized the associated red number. This new number was then searched for among the black numbers and the process was repeated 20 times.

The stability and capacity to focus attention were studied with the "entangled lines" test. The test table was covered with entangled lines. Each line began with a number on the left side and finishes with another number on the right side. The child was required to rapidly follow each line visually and press the key at its finish. The time taken to follow every line and the number of errors were registered.

Memory. Memory was tested by the capacity to remember numbers. During the experiment, a series of numbers of increasing complexity was presented, beginning with three digits and ending with nine. White digits of 6 x 10 mm, on a dark-grey background were presented on the computer monitor. During one test, three numbers were displayed on a monitor at 1 second intervals. The child then entered the three numbers on the keyboard. This was repeated seven times, progressively increasing the number of numbers displayed from three to nine. One volume of operative memory was determined according to the formula $V = A + (m/n)$ where A is the largest numbers of digits in the operation which was successfully reproduced by the child in all experiments, n is the number of experiments, m is the number of correctly reproduced number series.

Test of Raven's (Q I). The data obtained were transferred to the Wexler's scale, where the mean parameter value was equated to 100 points and a deviation from the mean value for one standard deviation – to 15 points.

Statistics**. S**tatistically significant differences were evaluated by Student's criteria for quantitative variables and Pearson's coefficient was used for analysis of correlations.

Results. In each age group were tested 55 girls and 57 boys (Table 1). The duration of talks using mobile phone increased with age from 3 min/day (7 years old children's) to 21 min/day (14 years old children's). Mean power of mobile phone 0.6 W (GSM-900).

Table 1

MEAN AGE±STANDARD ERROR (YEARS) IN FEMALE AND MALE CHILDREN

Forms	Sex	Mean age ± SE, years
1st form	Female	7.3±0.04
	Male	7.4±0.03
2nd form	Female	8.2±0.02
	Male	8.5±0.03
3rd form	Female	9.4±0.03
	Male	9.6±0.05
4th form	Female	10.3±0.03
	Male	10.5±0.04
5th form	Female	11.5±0.03
	Male	11.6±0.02
6th form	Female	123±0.04
	Male	12.4±0.03
7th form	Female	13.5±0.05
	Male	13.6±0.03
8th form	Female	14.4±0.03
	Male	14.5±0.03

The rates of all motor reaction (tapping-test end reaction time) tests in boys were better then in girls Table 2 and Table 3).

The rates of all attention (attention switching and attention concentration) tests in girls were better then in boys.

No differences in the volume of operative memory and the time required to fulfil the test for the rate of the attention switching were detected (Table 4).

A weak negative correlation dependence was observed between the duration of daily conversations using MT and intellect $r = 0.37$ ($P < 0.01$) and concentration of attention $r = 0.29$ ($P < 0.05$).

The pupils began to use mobile telephones at different time. Therefore, the analysis of the data obtained was started from the analysis of separated cases. In example, the testing results of one girl aged 7 to 14 (Fiig.1 and Fig.2) during eight years. The start of the persistently MT use – in the 5th form. Figures 1 and 2 demonstrate a worsening of some motor and psychological parameters during the first year of using MT, later these parameters gradually become more equable. On the basis of this observation 2 groups of pupils were chosen for the analysis: those who use MT during the first year and those who use MT during more than one year.

It turned out that the highest worsening of the parameters is observed during the first year of MT use, and the parameters improve more quickly in the children who started to use MT later (Fig.3 and Fig.4.).

Table 2

MEAN±STANDARD ERROR OF THE RESPONS REACTION TIMES USING LEFT HAND TO LATERILIZED LIGHT (RTL) AND MONAAURAL SOUND (RTS) STIMULI AND RETENTION TIME OF KEYS IN THE PRESSED STATE FOR LGHT (RTLP) AND SOUND (RTSP) STIMULI IN FEMALE AND MALE CHILDREN

Forms	Sex	Light stimuli		Sound stimuli	
		RTL, ms	RTLP, ms	RTS, ms	RTSP, ms
1st form	Female	500±12	286±1`1	595±32	279±13
	Male	476±11	295±10	483±27	305±21
2nd form	Female	457±7	269±10	523±21	287±14
	Male	438±10	256±8	518±20	266±11
3rd form	Female	435±9	241±6	558±15	245±7
	Male	401±8	227±7	475±25	234±8
4th form	Female	388±5	230±5	467±11	264±6
	Male	370±5	225±4	432±10	245±5
5th form	Female	373±5	223±5	457±11	259±6
	Male	348±4	231±5	389±9	241±7
6th form	Female	360±5	224±5	451±10	263±7
	Male	323±4	200±5	371±8	228±6
7th form	Female	338±4	211±4	377±8	250±7
	Male	313±5	185±4	343±6	207±5
8th form	Female	330±3	215±4	363±6	235±4
	Male	304±3	178±4	324±5	194±4

Table 3

MEAN±STANDARD ERROR OF THE TAPPING TEST FREQUENCES FOR LEFT (TTL) AND RIGHT (TTR) HANDS AND RETENTION TIME OF KEYS IN THE PRESSED STATE FOR LEFT (TTLP) AND RIGHT (TTRP) HANDS IN FEMALE AND MALE CHILDREN

Forms	Sex	Left hand		Right hand	
		TTL, Hz	TTLP, ms	TTR, Hz	TTRP, ms
1st form	Female	4.02±0.09	125±6	4.21±0.10	105±6
	Male	3.91±0.15	132±7	4.15±0.14	108±6
2nd form	Female	4.14±0.10	118±6	4.23±0.10	108±5
	Male	4.28±0.10	108±6	4.63±0.09	87±5
3rd form	Female	4.39±0.08	108±4	4.68±0.07	88±3
	Male	4.71±0.07	93±3	8.88±0.07	78±2
4th form	Female	4.85±0.07	98±3	5.01±0.06	85±3
	Male	4.90±0.06	91±3	5.17±0.06	76±1
5th form	Female	4.92±0.05	90±2	5.19±0.06	75±2
	Male	5.09±0.05	87±2	5.37±0.06	74±2
6th form	Female	5.15±0.05	88±2	5.38±0.06	75±2
	Male	5.29±0.05	84±2	5.59±0.06	71±2
7th form	Female	5.36±0.05	85±2	5.60±0.05	71±2
	Male	5.45±0.05	81±2	5.72±0.05	68±2
8th form	Female	5.38±0.05	88±2	5.61±0.04	78±2
	Male	5.71±0.06	80±1	5.92±0.06	67±1

Table 4

MEAN±STANDARD ERROR OF THE ATTENTION SWICHING (A1), CAPACITY TO FOCUS ATTENTION (A2) TESTS AND THE CAPACITY OF OPERATVE MEMORY (MEM) IN FEMALE AND MALE CHILDREN

Forms	Sex	A1, s	A2, s	MEM
1st form	Female	19.1±3.0	17.6±3.0	5.5±0.7
	Male	24.8±3.0	16.5±1.0	5.4±0.3
2nd form	Female	21.0±1.1	13.9±0.5	5.9±0.2
	Male	21.5±1.0	14.0±0.7	5.4±0.2
3rd form	Female	16.7±0.6	11.7±0.4	6.2±0.2
	Male	17.4±0.7	12.3±0.4	6.0±0.2
4th form	Female	12.3±0.3	10.0±0.3	7.6±0.2
	Male	14.0±0.4	10.3±0.3	6.8±0.2
5th form	Female	11.2±0.4	9.4±0.2	7.8±0.2
	Male	11.9±0.3	9.1±0.2	7.9±0.2
6th form	Female	10.1±0.3	8.8±0.2	8.6±0.2
	Male	11.3±0.3	8.9±0.2	7.9±0/2
7th form	Female	8.8±0.2	8.4±0.2	9.1±0.2
	Male	10.4±0.2	8.4±0.1	8.8±0.2
8th form	Female	8.6±0.1	8.3±0.1	9.5±0.1
	Male	9.4±0.1	8.1±0.1	9.4±0.1

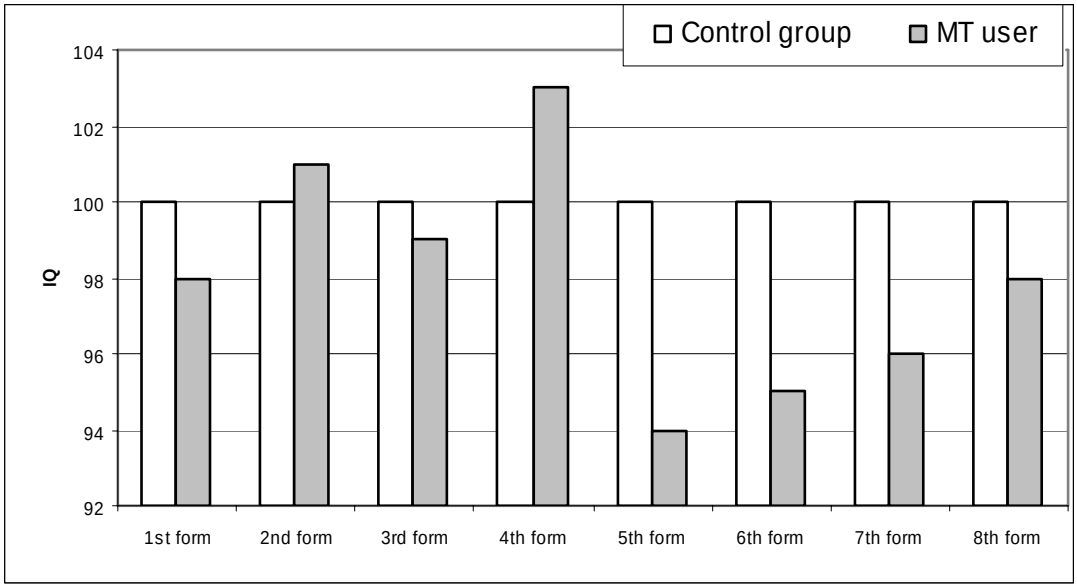

Fig.1. Mean ± SE time to perform the test for IQ. The development of IQ in girl was testing.

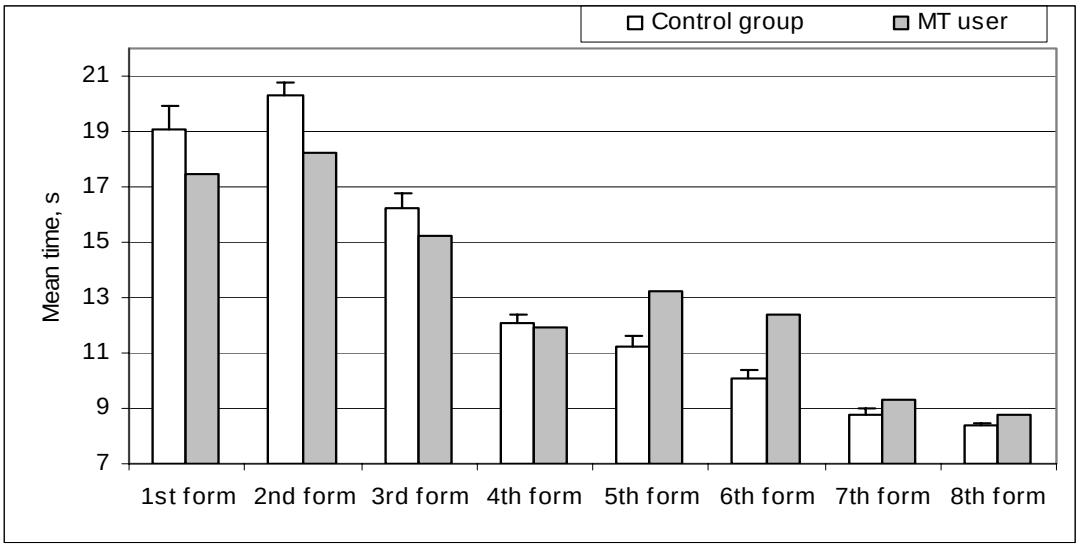

Fig.2. Mean ± SE time to perform the test for attention concentration. The development of attention in girl was testing.

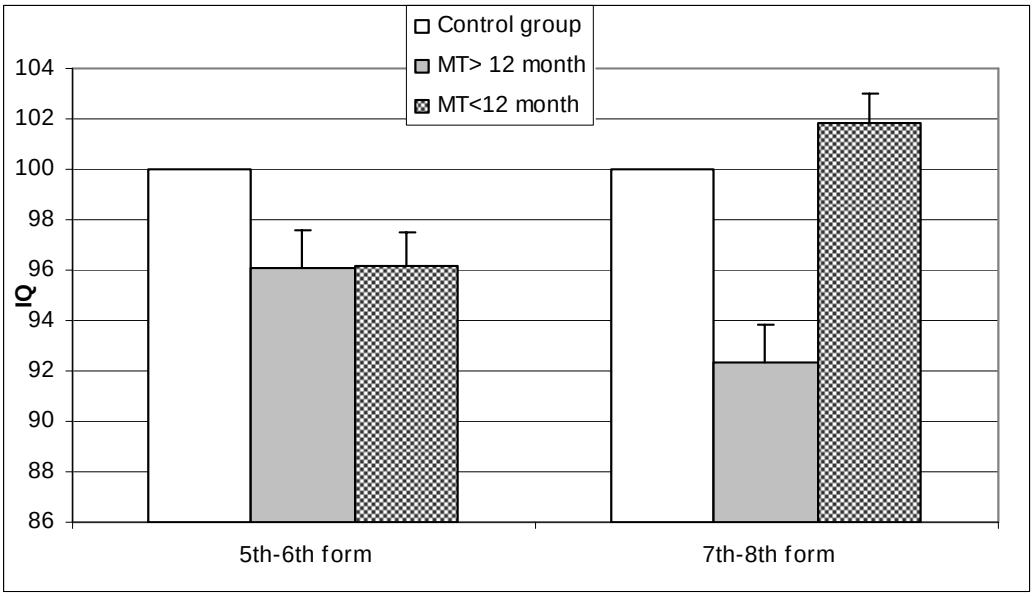

Fig.3. Mean±SE of IQ. The differences are significant ($P < 0.05$) between the mobile phone users and control groups in children of 5th-6th forms and ($P < 0.01$) in children of 7th-8th form for MT >12 month group with control..

Unexpectedly, IQ differences were found between the mobile phone users and control groups in children of 5th-6th forms and in children of 7th-8th form for "MT >12 month" group with control..

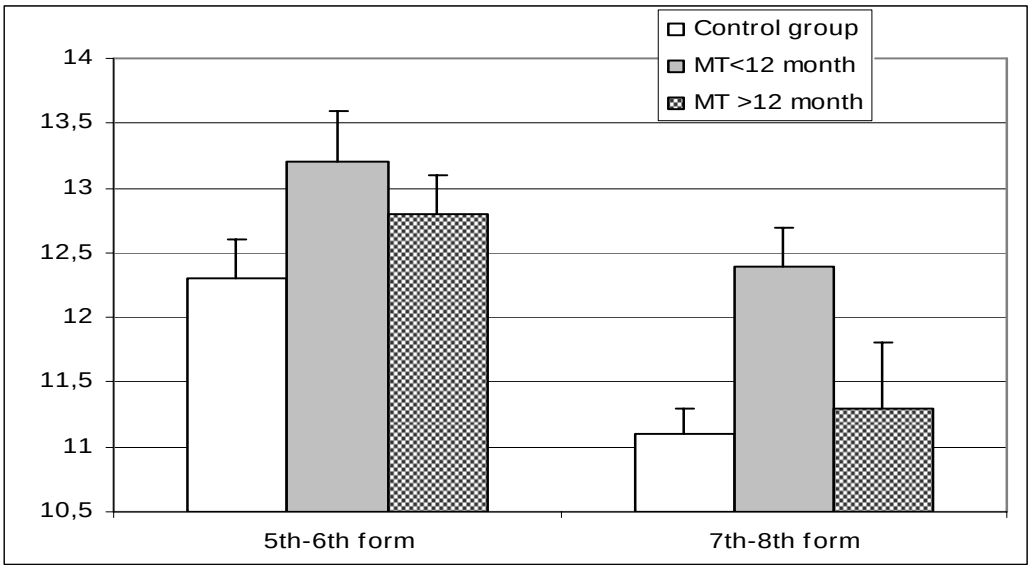

Fig.4. Mean ± SE time (s) to perform the test for attention concentration. The differences are significant ($P < 0.05$) between the mobile phone users of 5th-6th forms and ($P < 0.01$) in children of 7th-8th form for MT >12 month group.

Younger children using mobile phone are more sensitive to the EMF radiation than oldest and have worse results to IQ and attention tests (Fig.3. and Fig.4).

SUMMARY

The highest shifts in motor and psychological parameters are detected during the first year of MT use, and later they gradually improve.

The improvement of parameters proceeds more rapidly in the children who started to constantly use MT at an elder age.

The improvement of parameters proceeds more rapidly in the children who started to constantly use MT at an elder age.

The analysis of the data obtained will be continued basing on the working hypothesis on that the oldest children organism, being adapted to the EMF chronic influence better, responses by the increase in the IQ and attention after 12 month of mobile phone using..

Children are more sensitive to the EMF radiation than adults, and on the basis of the data available, the Independent Expert Group on Mobile Phones (IEGMP) in the United Kingdom came to the conclusion that children may be more vulnerable because they have a developing nervous system, children's brain tissue is more conductive than that of adults since is has a higher water content and ion concentrations, children have a greater absorption of RF energy at mobile telephone frequencies in the tissues of the head, and that children would have a longer lifetime of exposure. The IEGMP also recommended that, as a precautionary approach, mobile phone use by children should be for non-essential calls only, and that the mobile phone industry should refrain from promoting mobile phones to children.

The authors of the paper support the point of view of the IEGMP.

The research should be continued in this direction, including the individual dosimetry and analysis of each separate case.

.

ACKNOWLEDGEMENTS

This study was supported by a grant No 1429 from the Latvian Council of Science

REFERENCES

Croft, R. J., Chandler, J. S., Burgess, A. P., Barry, R. J. (2002) Acute mobile phone operation affects neural function in humans. *Clin. Neurophysiol*., **113** (10), pp. 1623–1632.

Edelstyn, N., Oldershaw, A. (2002) The acute effects of exposure to the electromagnetic field emitted by mobile phones on human attention. *NeuroReport*, **13** (1), pp. 119–121.

Evans-Pughe, C. (2003). Phones and health—the science. *IEE Rev.*, **49** (5), pp. 16–17.

Haarala, C., Bjornberg, L., Ek, M., Laine, M., Revonsuo, A., Koivisto, M., Hamalainen, H. (2003) Effect of a 902 MHz electromagnetic field emitted by mobile phones on human cognitive function: A replication study. *Bioelectromagnetics*, **24** (4), p. 283–288.

Hamblin, D. L., Wood, A. W. (2002) Effects of mobile phone emissions on human brain activity and sleep variables. *Int. J. Radiat. Biol*., **78** (8), pp. 659–669.

Hietanen, M., Hamalainen, A.-M., Husman, T. (2002) Hypersensitivity symptoms associated with exposure to cellular telephones: No causal link. *Bioelectromagnetics*, **23** (4), p. 264–270.

Hocking, B. (2003) Update on mobile phones and health. *Int. Med. J*., **33** (5/6), p. 235.

Hossmann, K.-A., Hermann, D. M. (2003) Effects of electromagnetic radiation of mobile phones on the central nervous system. *Bioelectromagnetics*, **24** (1), pp. 49–62.

Huber, R., Schuderer, J., Graf, T., Jutz, K. (2003) Radio frequency electromagnetic field exposure in humans: Estimation of SAR distribution in the brain, effects on sleep and heart rate. *Bioelectromagnetics*, **24** (4), pp. 262–276.

Kolodynski, A., Kolodynska, V. (1996) Motor and psychological function of school children living in the area of the Skrunda Radio Location Station in Latvia. *Sci. Total Environ*., **180** (1), pp. 87–93.

Kolodynski, A., Kolodynska, V. (2006) Differences between the motor and psychological functions of children who persistently use mobile phone. Proceeding of the Latvian Academy of Science. Section B, Vol. 60,No 1 (642), pp 16-19.

Kumar, A. (2001) Electromagnetic radiation and biological effects. *International Symposium on Electromagnetic Compatibility, Vol. 2, Piscataway, NJ, USA.* Institute of Electrical and Electronical Engineers Inc., **NJ,** pp. 1048–1053.

Lee, T., Ho, S., Tsang, L., Yang, S., Li, L., Chan, C. (2001) Effect on human attention of exposure to the electromagnetic field emitted by mobile phones. *NeuroReport*, 12 (4), pp. 729–31.

Liesenkotter, B. (2002) Analysis of the contended health risks due to digitally modulated mobile phone radiation. *Ztschr. Med. Phys*., **12** (3), p. 198–203.

Lin, J. C. (2002) Health effects: Scientific research and mobile phone testing. *IEEE Microwave Magazine*, **3** (4), pp. 26–30.

Lin, J. C. (2003) Risks to children from cellular telephone radiation. *IEEE Microwave Magazine*, **4** (1), pp. 20–26.

Maier, M., Blakemore, C., Koivisto, M. (2000) The health hazards of mobile phones. *Brit. Med. J*., **320**, Issue 7245, p. 1288-1289.

Maier, R. (2001) Do pulsed electromagnetic fields impair CNS activity? *Biomedizinische Technik*, **46** (1–2), p. 18–23.

Nesse, R., Nikookar, H., Ligthart, L. P. (2001) An overview of the effects of mobile phone radiation on the human body. In: *2001 European Conference on Wireless Technology: Conference Proceedings.* Microwave Engineering European, London, p. 73–76.

Pandere, D., Andaburska, M. (eds.) (2001) *Rīgas pašvaldību izglītības iestāžu audzēkņu veselības stāvoklis laika posmā no 1995. mācību gada līdz 2001. mācību gadam* [Health of Pupils from Rīga Municipal Educational Institutions during 1995–2001 School Years]. Rīga, Rīgas domes Izglītības, jaunatnes un sporta departaments, 177 lpp. (in Latvian).

Salford, L. G., Brun, A. E., Eberhardt, J. L., Malmgren, L., Persson, B. (2003). Nerve cell damage in mammalian brain after exposure to microwaves from GSM mobile phones. *Environ. Health Perspectives*, **III** (7), p. 881-883.

Schonborn, F., Burkhardt, M., Kuster, N. (1998) Differences in energy absorption between heads of adults and children in the near field of sources. *Health Phys*., **74** (2), pp. 160–168.

Toropainen, A. (2003) Human exposure by mobile phones in enclosed areas. *Bioelectromagnetics*, 24 (1), pp. 63–65.

DNA-damaging effects of UMTS electromagnetic fields in human cells *in vitro*

Elisabeth Kratochvil[1], Claudia Schwarz[1], Petra Hartbauer[1], Marietta Weninger[1], Alexander Pilger[1], Franz Adlkofer[2], Hugo W. Rüdiger[1]

[1] Medical University of Vienna, Division of Occupational Medicine, Vienna, Austria
[2] Verum Foundation, Munich, Germany

Our previous research demonstrated that radiofrequency electrsignals have genotoxic properties *in vitro*[1]; there are no corresponding data concerning the recently introduced European mobile communication standard UMTS (Universal Mobile Telecommunication Standard) as yet. A putative genotoxic potential of UMTS signals was investigated in cultured human cells using the alkaline comet assay and the cytokinesis-blocked micronucleus assay.

Materials and Methods

Cultured human fibroblasts (diploid fibroblasts obtained from a male 6 year old healthy donor) were continuously exposed to UMTS test signals (carrier frequency 1950 MHz) in a temperature-controlled exposure setup[2] specially designed for blind *in vitro* exposures of cell monolayers and provided by the IT'IS foundation (Zurich, Switzerland). Various exposure conditions (specific absorption rate SAR: 1 and 2 W/kg; exposure time: 4, 16 and 24 hours) were tested. Each exposure condition was tested in duplicate. Positive (comet assay: 5 min UV light/254 nm, which equals 0,6 kJ/m^2; micronucleus assay: 3 µg Bleomycin/ml - time corresponding to the exposure time) and negative controls were included in each set of experiments to check for effective operation of the method.DNA damage was assessed in terms of DNA strand breaks (alkaline comet assay, evaluated by visual classification[3]) and micronuclei (cytokinesis-blocked micronucleus assay[4]).

Summary

Exposure to UMTS signals resulted in a twofold increase in DNA strand breaks after 16 and 24 hours for both SAR investigated. In addition, a corresponding doubling in micronuclei frequency was detected.
Preliminary experiments using peripheral blood lymphocytes showed no increase in DNA strand breaks after UMTS exposure (not shown).
In conclusion, UMTS signals may have genotoxic effects in certain cell systems *in vitro* below and at the current European safety limit (2 W/kg).

References

[1]Diem, E., Schwarz, C., Adlkofer, F., Jahn, O. & Rüdiger, H. (2005). Non-thermal DNA breakage by mobile phone radiation (1800 MHz) in human fibroblasts and transformed GFSH-R17 rat granulosa cells in vitro. *Mutat Res* **583:** 178-183.

[2]Schonborn, F., Pokovic, K., Burkhard, M. & Kuster, N. (2001). Basis for optimization of in vitro exposure apparatus for health hazard evaluations of mobile communications. *Bioelectromagnetics* **22:** 547-559.

[3]Ivancsits, S., Diem, E., Jahn, O. & Rüdiger, H. (2003). Intermittent extremely low frequency electromagnetic fields cause DNA damage in a dose-dependent way. *Int Arch Occup Environ Health* **76:** 431-436.

[4]Fenech, M. (1993). The cytokinesis-block micronucleus technique: a detailed description of the method and its application to genotoxicity studies in human populations. *Mutat Res* **285:** 35-44.

LOW-FREQUENCY ELECTROMAGNETIC FIELD PROMOTE THE EXPRESSION OF DIFFERENTIATION MARKERS IN PLURIPOTENT HUMAN MESENCHIMAL STEM CELLS (hMSC).

LEDDA M.●., ROSOLA E.●., PATTI A.M.♦., VULCANO A.♦ D' EMILIA E.© GILIBERTI C. ©., GIULIANI L. ©., POZZI D.±., GRIMALDI S.●. and LISI A. ●

●Istituto di Neurobiologia e Medicina Molecolare C.N.R. Rome Italy

♦Dipartimento di Scienze di Sanità Pubblica G. Sanarelli Università "La Sapienza" Rome Italy

© ISPESL-DIPIA Rome Italy

± Dipartimento di medicina sperimentale e patologia Università La Sapienza Roma Italy

ABSTRACT

Reports of biological effects of low-energy electromagnetic field (EMF) have increased in recent years. Particularly debated is the question of the epidemiological evidence of adverse effects of an extremely low frequency magnetic field (ELF-MF) generated by 50-60 Hz high voltage power transmission lines, video display terminals, electric blankets and other home appliances, which raise the possibility of deleterious health effects from exposure to radio frequency or low frequency fields. A valid objection is that field intensity is many orders of magnitude below the noise threshold so that selective, cooperative, or amplifying mechanisms must be postulated. The therapeutic potential of magnetic field can be seen in the proven efficacy of low-energy, pulsed magnetic fields in non-union bone fracture healing (Bassett, 1993), confirming that under certain conditions non-ionizing electromagnetic energy can influence physiological processes in organisms. Low frequency magnetic fields at 50 or 60 Hz are also reported to stimulate nerve regeneration (Rusovan and Kanje, 1992) alteration gene transcription (Phillips et al., 1992), and they may also play a synergic role in cellular processes that are already activated, such as cell proliferation and cell differentiation (Walleczeck, 1992; Manni et al., 2002., Lisi et al 2005).

The possible mechanisms of the induced effects are not known, although a number of theoretical models have been proposed (Glaser, 1992., Liburdy, 1992., Barnes,1996).

In this work we have studied the effect of EMF radiations on human mesenchymal Stem Cells (hMSC) differentiation

In litterature is well described that this cells are able to differentiate to osteoblast following treatment with chemical agents such as dexamethasone. Regulation of osteoblast differentiation its an important fenomena that must occur to mantain the continuos supply of mature osteoblast needed for bone growth, remodelling, and in particular for bone repair.

INTRODUCTION

Culture and differentiation of mesenchymal stem cells. Height- ten ml of bone marrow, obtained from iliac crest, was mixed with one volume of phosphate-buffered saline and nucleated cell fraction was enriched for mesenchymal stem cells by density-gradient centrifugation over Lympholyte-H cushion. The cells at the medium- Lympholyte-H interface were collected, washed three times with culture medium and seeded into culture flask. Confluent monolayers of adherent cells were obtained about one week after the start of cell division. Subcultivation was performed by replating at $6x10^3$ cells per cm^2 flasks. To promote osteogenic differentiation

cells were stimulated during subpassages by cultivation in standard medium supplemented with 100nM dexamethasone or by exposure to extremely low frequency electromagnetic field (50Hz 1mT)under controlled condition.

Cells were continuously exposed to a sinusoidal 50 Hz magnetic field at a flux density of 1 mT (10 G) (rms) in a temperature regulated solenoid. Temperature regulation (37 ± 0.2 °C) and 5% CO_2 was provided. Temperature was continuously recorded by a Hanna HI 9274 OC printing thermometer, within the centre of the solenoid and was in the 37°C ± 0.2 range. In a control experiment the sample was placed in an identical cell incubator containing the solenoid with no field, in the same conditions as the exposed one. All experiments were under blind conditions. The solenoid manufacture has been published elsewhere (Santoro et al, 1997; Lisi et al, 2000; Manni et al, 2004, Lisi et al, 2005).

The main body of the solenoid is a cylinder in concrete-asbestos 2 cm thick and has a diameter of 20 cm and a height of 40 cm. It is made of 1200 turns of 2 mm diameter copper wire wound in three layers in continuous forward-backward fashion. It is driven from the 50 Hz power mains through a variable autotransformer and generates a flux density of 1 mT (rms) for an applied voltage of 6 Volts (rms).The solenoid is then placed into a cell incubator with its centre ventilated by the fan for appropriate air circulation. The modest heat due to Joule effect is efficiently dispersed by the continuous forced ventilation in the total mass of the CO_2 incubator. Field density measured with a calibrated Hall probe, is within – 5% of centre value inside the cylindrical exposure volume of 11 cm by 17 cm along the solenoid axis. The measured geomagnetic ambient field is 32 μT (vertical component) and 16μ T (horizontal component). Stray ambient ac fields are below 0.1 μT. An often overlooked fact related to solenoids is the presence of an almost homogeneous electric field oriented parallel to the magnetic field (Chute et al., 1981) unless adequate electric shielding is used (Stauffer et al., 1994). An approximate estimate of this field may be obtained from the voltage across the extremes of the inner of the six layers and its length. The corresponding field induced by capacity coupling in the culture medium will be in the order of 0.01 μV/cm (Foster et al., 1995).

SUMMARY

Exposure to low frequency electromagnetic field for 5 days resulted in a change in plasma membrane morphology and this modification were also accompanied by a rearrangement in actin filaments as showed by confocal miscroscopy analysis after cells labeling with FITC-phalloidin.
In particular, mesenchimal cells exposed to the field showed the same actin organization found in cells after treatement with dexamethasone. The differentiating effect of dexamethasone were potentiate by exposure to the field.
After 5 days of exposure, the mRNA expression for osteoblast markers differentiation such as Alkaline Phosfatase (AP), Osteocalcin (OCL) and Osteopontin (OPN) increase (Fig.1) this result were further confirmed by indirect immunofluorescence assay for osteopontin Osteopontin showed an increase in exposed and dexamethasone-esposed cells with respect to control (Fig. 2).
In conclusion our finding demonstrated that exposure to ELF can act as a differentiating agent on mesenchymal human cells outlining the relevance of low frequency electro-magnetic field as a terapeutical agent suggesting a possible use of ELF as support in medicine for different pathologies therapy.

Aknowledgements

This work as been partially supported by grant ISPESL B1/42/DIPIA/04 and B1/45-a/DIPIA/04

REFERENCES

Barnes PS. 1996. Effect of electro-magnetic field on the rate of chemical reactions.Biophysics 41:801–880.

Basset CAL. 1993. Beneficial effects of electro-magnetic fields. J Cell Biochem. 51:387–393.

Foster KR, Schwan H. 1995. Dielectric properties of tissues. In: Polk C, Postow E, editors. Handbook of biological effects of electro-magnetic fields, 2nd edition.Boca Raton, FL: CRC Press, pp 27–96.

Glaser R. 1992. Current concepts of the interaction of of weak electro-magnetic fields with cells. Bioelectrochem Bioener 27:255–268.

Liburdy RP. 1992. Calcium signalling in lymphocytes and ELF fields: Evidence for an electric field metric and a site of interaction involving calcium ion channels. FEBS Lett 301(1):53–59.

Lisi A, Pozzi D, Pasquali E, Rieti S, Girasole M, Cricenti A, Generosi R, Serafino AL, Congiu-Castellano A, Ravagnan G, Grimaldi S. 2000. Three dimensional (3D) analysis of the morphological changes induced by 50 Hz magnetic field exposure on human lymphoblastoid cells (Raji). Bioelectromagnetics 21:46–51.

Lisi, A., Ciotti, M.T., Ledda, M., Pieri, M., Zona, C., Mercanti, D., Rieti, S., Giuliani, L., Grimaldi, S. (2005). Exposure to 50Hz electro-magnetic radiation promote early maturation and differentiation in newborn rat cerebellar granule neurons. J. Cell. Physiology, 204, 532-538

Manni V, Lisi A, Pozzi D, Rieti S, Serafino AL, Ledda M, Giuliani L, Grimaldi S.2002. Effect of extremely low frequency (50 Hz) magnetic field on morphological and biochemical properties of human keratinocytes. Bioelectromagnetics.23:298–305.

Phillips JL, Haggren W, Thomas WJ, Jones TI, Adey W. 1992. Magnetic fieldinduced changes in specific gene transcription. Biochimica Biophysica Acta1132:140–144.

Rusovan A, Kanje M. 1992. Magnetic fields stimulate peripheral nerve regeneration hypophyctiomia rats. Neuroreport 3(12):1039–1041.

Santoro N, Lisi A, Pozzi D, Pasquali E, Serafino A, Grimaldi S. 1997. Effect of extremely low frequency magnetic field exposure on morphological and biophysical properties of human lymphoid cell line (Raji). Biochim Biophys Acta 1357:281–290.

Walleczeck J. 1992. Electro-magnetic field effect on cells of the immune system:The role of calcium signalling. Faseb J 6:3177–3185.

Fig.1

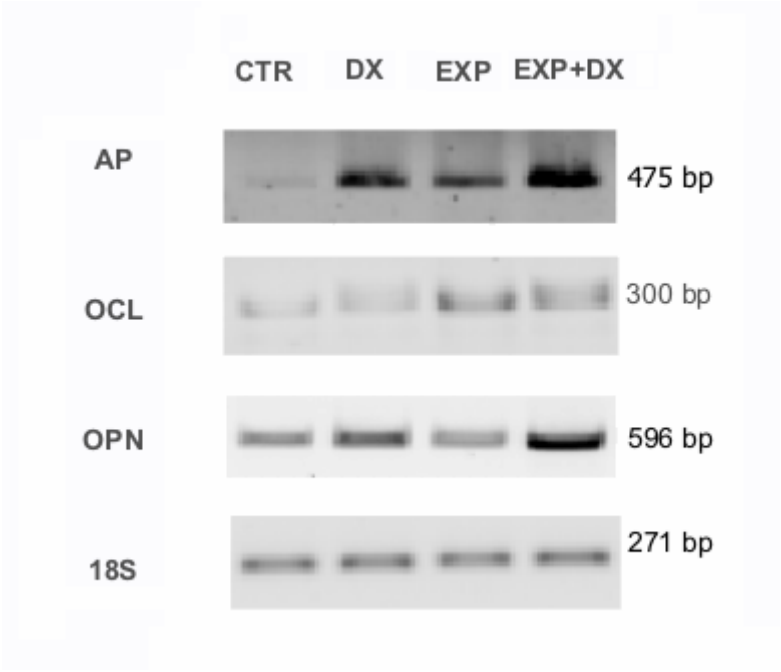

Fig. 1 - RT-PCR analysis. Total mRNA was extracted from Control (CTR), Dexamethasone (DX), Exposed (EXP) and Exposed+Dexamethasone-treated stem cells (EXP-DX). RT-PCR analysis was used for osteoblast differentiation markers detection with specific primers: Alkaline Phosfatase (AP), Osteocalcin (OCL) and Osteopontin (OPN). Dexamethasone treatment is the positive control. The amount of template and the number of amplification cycles were preliminarily optimized for each PCR reaction to avoid conditions of saturation.

Low-frequency electromagnetic field promote the expression of differentiation markers in pluripotent human mesenchimal stem cells (hMSC).

Fig.2

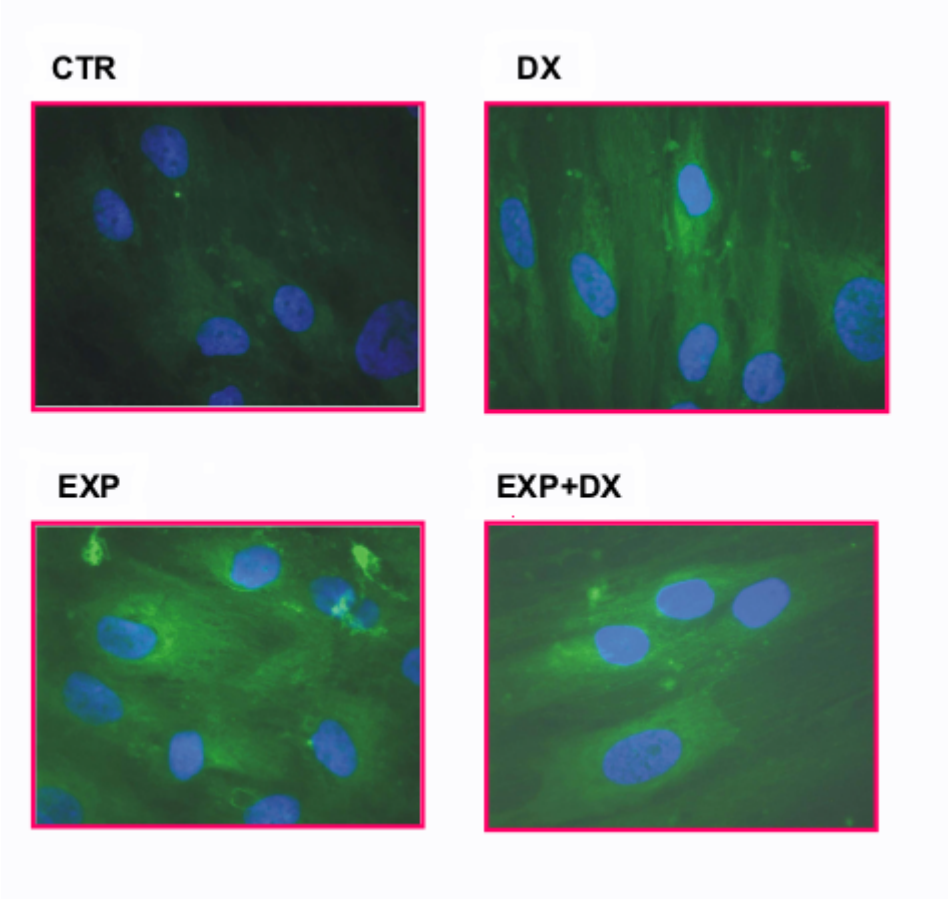

Fig. 2 ELF-MF (50Hz) modulation Osteopontin
differentiation marker expression see by indirect immunofluorescence microscopy.
Images show modulation of Osteopontin expression in control (CTR), Dexamethasone (DX), Exposed (EX) and Exposed+ Dexamethasone-trated (EXP+DX) stem cells. Figures were executed with 100x objective.

THE NATIONAL REGISTER OF RF WORKERS (UK): A LONG-TERM FOLLOW-UP STUDY

Ian Litchfield, Tom Sorahan.

The Institute of Occupational and Environmental Health, The University of Birmingham, Edgbaston, Birmingham, England B15 2TT

AIMS AND OBJECTIVES: In 1999, the Minister of Public Health asked the Radiation Protection Division of the Health Protection Agency (formerly the National Radiological Protection Board (NRPB)) to set up an independent expert group to examine the possible effects on health from the use of mobile phone telecommunication technologies. The group, under the chairmanship of Sir William Stewart, published its report in May 2000 [1]. One of the main conclusions was that there was no evidence to suggest that exposures to radiofrequency (RF) radiation below the guidelines of the NRPB and the International Commission on Non-Ionising Radiation Protection (ICNIRP) cause adverse health effects. Nevertheless, a key recommendation was that a register of occupationally exposed workers be established to facilitate studies into cancer incidence, mortality or other potentially harmful effects.

The Health and Safety Executive (HSE) responded to this recommendation by holding a consultation meeting on 9 January 2001 in Birmingham to which independent experts and those with an interest in telecommunications were invited. At this meeting, a decision was made to establish a Working Group to discuss how the recommendation should be implemented. In an attempt to ensure involvement across the whole industrial sector, representatives from the broadcast companies, mobile phone operators (FEI), contractors, the Ministry of Defence, National Grid, Trade Unions, and HSE were included.

The Working Group agreed to set up a register of exposed workers with a potential for exposure to radio-frequency radiation, and that the register would be confined to people whose work brings them in close proximity to transmitting antennas on telecommunication, broadcasting masts or other similar structures. Information about the workers would be retained and maintained in a centralised database or register. The Institute of Occupational and Environmental Medicine (IOEM) was contracted to administer the database. Now in its second phase, the register is guided by a Steering Group consisting of representatives from the HSE, the Institute of Occupational and Environmental Medicine and industry.

The study described here seeks to obtain important new information on the topic of long-term health effects of occupational RF exposure by examining data from the on-going National Register of RF workers.

MATERIALS AND METHODS: Analyses will be based on data from the on-going National Register of RF workers. The Register was first supported by the Health and Safety Executive (HSE) for the two-year period 2003-2004. It was always the intention of the HSE to support the start-up costs but then seek industry support for later years of data collection and analysis. Industry support is currently in place for the three-year period 2005-2007.

STUDY POPULATION

The cohort available for analysis currently comprises 604 male employees. All employees have some period of employment working in close proximity to transmitting antennas on telecommunication, broadcasting masts or other similar structures in the period 1961-2004. Work continues on increasing the size of the Register and in the next twelve months it is estimated that the Register will comprise some 2000 employees.

In order to account for the variation in exposure between different occupationally exposed jobs the participants are asked to supply their job title. This is then placed in one of five job categories (Antenna Support, General Maintenance Worker, Occasional Climber, Rigger and Satellite Support). The level of exposure typically experienced by each job category is informed by the five-year study carried out

by the Institute of Occupational and Environmental Medicine in conjunction with the Radiation Protection Division of the Health Protection Agency. This work, titled 'A Feasibility Study for an Epidemiological Investigation into the Health Effects of Radiofrequency Fields and Radiation' [2] produced a job exposure matrix for job titles relevant to the Register.

The National Register of RF Workers follow-up study will seek the approval of the Office for National Statistics (ONS) to receive follow-up particulars (copies of death certificates and cancer registration (incidence) details from the National Health Service Central Register (NHSCR) of the ONS). Underlying cause and multiple-cause coding will be supplied by the ONS for all deaths according to the tenth revision of the International Classification of Diseases (ICD-10).

STANDARDISED MORTALITY RATIOS AND STANDARDISED REGISTRATION RATIOS

The mortality experience of the cohort will be compared with that which might have been expected to occur if rates of mortality for the general population of England and Wales had been operating on the study cohort, having due regard to the composition of the study cohort by sex, age (five-year age groups), and calendar year (five-year calendar periods). Expectations based on person-years-at-risk (pyr) will be calculated using the PERSONYEARS computer program.[3] Individuals enter the pyr on the date of consenting to join the National Register. Individuals leave the pyr on the date of death, date of emigration, date last known alive or the closing date of the study, whichever is the earlier. Individuals will be "censored" on reaching their 85th birthday - that is, they will make no further contributions to expected or observed numbers past this age. Standardised mortality ratios (SMRs) will be calculated as the ratio of observed to expected numbers of deaths expressed as a percentage. In calculating P-values and confidence intervals, it will be assumed that deaths occur as a Poisson process [4]. Any significance tests will be two-tailed. Similar analyses will be performed on the cancer registration data to calculate standardized registration ratios (SRRs). Overall SMRs and SRRs will be calculated for individual sites of cancer (3-digit IICD codes) as well as SMRs for broader non-cancer causes (ICD chapters). Causes of special interest will be selected on the basis of significantly elevated SMRs or SRRs obtained either from this study or from similar studies of RF workers in other parts of the world. For causes of special interest, SMRs and SRRs will also be calculated by industry sector (telecommunications or broadcast), job type (1-5 names) and period from first RF work (ten-year intervals). In addition SMRs and SRRs for causes of special interest will also be calculated separately for workers reporting any high exposure incidents.

COLLABORATION: The National Register of RF Workers seeks to collaborate with international bodies undertaking similar research with the aim of contributing data and expertise and increasing understanding of the issue for the benefit of those occupationally exposed to RF radiation.

REFERENCES

1. Independent Expert Group on Mobile Phones; Mobile Phones and Health, 2000 (IEGMP pub)

2. A Feasibility Study for an Epidemiological Investigation into the Health Effects of Radiofrequency Fields and Radiation (University of Birmingham, unpublished)

3. Coleman M, Douglas A, Hermon C, Peto J. Cohort study analysis with a Fortran computer program. *Int J Epidemiol* 1986;**15**:134-7.

4. Breslow NE, Day NE. *Statistical methods in cancer research. Vol II - The design and analysis of cohort studies.* Lyon: International Agency for Research on Cancer, 1987. (IARC sci pub No 82.)

NUMERICAL CHARACTERIZATION OF AN EXPOSURE SET UP FOR 900 MHz AND 1800 MHz *in vitro* EXPERIMENTS

ROSARIA FALSAPERLA, SERGIO LO MEO, PAOLO ROSSI

National Institute of Occupational Safety and Prevention - Occupational Hygiene Dept. (ISPESL) Rome, Italy
Via Fontana Candida, 1 - 00040 Monte Porzio Catone (Rome)
Tel. +39 0694181440 - Fax +39 0694181419
E-mail: rosaria.falsaperla@ispesl.it, sergio.lomeo@ispesl.it, paolo.rossi@ispesl.it

Abstract

The aim of this study is to evaluate the efficiency of two exposure set up realized for *in vitro* experiments purposes. Maximum dimensions of these systems are 198x99x27 mm, with an exposure zone of 80x99x27 mm in order to allow the simultaneous insertion of four Petri dishes 35 mm of diameter, or other shape flasks. The set up efficiency was been evaluated at the frequency of 900 MHz and 1820 MHz by means of SAR calculations (local and average) on cell cultures. To this scope a commercial software package (CST Microwave Studio) based on Finite Integration Technique (FIT) was used. Cad drawing tools allowed the parameterization of the structure made up of culture medium thickness contained in plexiglas dishes or flasks inserted between two metallic plates fed by 1 W power.

All materials employed were electromagnetically characterized by appropriate values of dielectric permittivity and conductivity. SAR calculation accuracy was improved by defining a refining mesh in the cell culture volume. SAR distributions on the exposed samples were investigated, and several SAR calculations were made employing flasks of various forms and with different quantity of culture medium.

The study was developed in the frame of activities referring to the European Project EMF-NET, Main Task 2, Work Package 12 (focused on numerical calculations for occupational exposure).

I. Introduction

The study of the effects of radio frequency radiation on biological systems is a topic of great concern due to the rapid spreading of mobile communication systems in the recent years and the identification of the mobile phone as a potential source of risk for people. Then a wide number of research has been and is presently carried out with particular reference to the frequencies employed by the Global System for Mobile Communications (GSM) standard, that is frequencies near 900 MHz and 1800 MHz.

This paper presents a numerical efficiency evaluation of two exposure set up designed in such scenario for *in vitro* experiments purposes.
The efficiency of the systems was investigated through numerical SAR evaluation inside cell cultures, performing *in vitro* tests based on the employ of flasks and dishes of different size and culture medium content. The effects of the number of samples exposed at the same time on SAR were also investigated.
Basing on the equipment present in our laboratory, an experimental characterization of the efficiency of the two set up were also performed by means of the ratio between direct and reflected power. The results of measurements indicated that the frequencies giving the best performance of the two systems (minimum reflected power) are centred respectively at 900 MHz and 1820 MHz.
These frequencies were then selected for the simulations.
Both experimental and numerical characterization was carried out at the ISPESL Research Centre in Monte Porzio Catone (Rome).

II. Exposure set up

The exposure set up under test consisted of two parallel metallic plates T-modelled as shown in Figure 1.

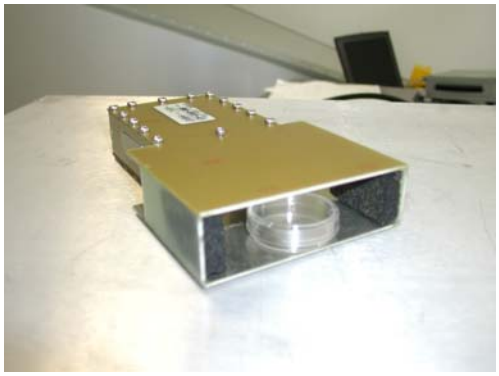

Figure 1 – Exposure set up operating near 1800 MHz

Both set up were designed to generate an RF electric field, one at 900 MHz and the other one at 1800 MHz, as much as possible uniform between the two metallic plates and orthogonal to them.
To this aim the systems consisted of two contiguous zones. The first one (the basis of the T), the so called adaptive section, was designed in order to maximize the power transfer from the feed to the exposure zone by means of a gradual change of the wave impedance. A coaxial connection allowed to feed the systems.
The second zone (the head of the T), the so called exposure zone, was the volume available for the exposure of the biological samples. In this regard the final part of this zone was open (see Figure 1), while the side walls were closed by two layers of absorbing material covered by thin plastic sheets.

The dimensions of the exposure zone were the same for both set up, that is about 80×99×27 mm, inside of which 80×80×27 mm were available for exposure (between the two panels of absorbing material). On the opposite, due to the different working frequencies, the dimensions of the adaptive sections were different for the two systems and are the following:

- 118×69×27 mm for 900 MHz set up
- 80×99×27 mm for 1800 MHz set up

III. Numerical method and SAR evaluation

Computational simulations have been carried out by employing the electromagnetic commercial simulator Microwave Studio (MWS) by CST-Germany [1], based on the Finite Integration Technique (FIT) [2]. This numerical method, developed by Weiland in 1977, provides a discrete reformulation of Maxwell's equations in their integral form suitable for computers and it allows simulating real-world electromagnetic field problems with complex geometry. In order to numerically solve Maxwell's equations, a finite calculation domain is defined. By creating a suitable mesh system, this domain is split up into small cubes, so-called grid cells.
In combination with the FIT, MWS employs the Perfect Boundary Approximation (PBA) for the spatial discretization of the simulated structure that allows an accurate modelling of bend-shaped structures also [3].

In order to simulate *in vitro* tests, the exposure set up were simplified. In fact in the numerical model only the exposure zone of the two set up was modelled, presuming that the detailed description of the adaptive section was not relevant for SAR evaluation purposes. Each exposure set up was then represented as two parallel metallic plates of (80 × 99) mm size, at 27 mm of distance.

Figures 2 show the various simulations performed inserting different Petri dishes or flasks between the plates. In particular Figure 2 a) refers to exposure to 900 MHz electromagnetic field of one plexiglas dish of 54 mm diameter, height of 11 mm and of 1 mm of thickness. Culture medium was then parameterized as dish of 52 mm of diameter, height of 2.4 mm for a total liquid volume of 5 ml.
Figure 2 b) refers to simultaneous exposure to 900 MHz electromagnetic field of four plexiglas dishes of 35 mm of diameter, height of 8 mm and 1 mm of thickness. Each culture medium was then parameterized as dish of 33 mm of diameter and 3.5 mm of height for a total liquid volume of 3 ml.
Figure 2 c) refers to simultaneous exposure to 1820 MHz electromagnetic field of two plexiglas flasks. Each flask was represented by means of a plexiglas parallelepiped of (35 x 35 x 20) mm size and of 1 mm thickness for each wall. Consequently each culture medium was parameterized as a parallelepiped of (33 x 33 x 3.7) mm size, for a total liquid volume of 5 ml.

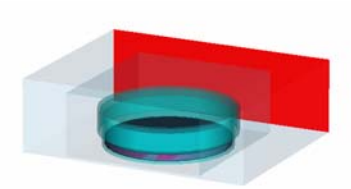

Fig 2 a

Fig 2 b

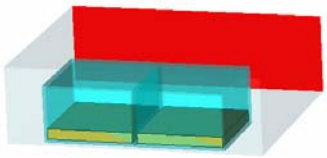

Fig 2 c

All simulations have been carried out feeding exposure systems through an electromagnetic pulse of 1 W.
All materials were characterized, on the basis of data literature, with their particular values of dielectric permittivity (ε_r), conductivity (σ) and density (ρ) at the frequency of 900 MHz and 1820 MHz as shown in Table 1.

Table 1 - Properties of materials used in the simulations

	frequency 900 MHz		
Materials	ε_r	ρ [kg/m^3]	σ [S/m]
Plexiglas	2.6	1200	neglectable
Cell Culture (culture medium)	80.5	1000	1.55
	frequency 1820 MHz		
Plexiglas	2.6	1200	neglectable
Cell Culture (culture medium)	76.8	1000	2.21

To perform dosimetric evaluation with better accuracy, a refined mesh in the culture medium volume was adopted. This involved a not uniform spatial discretization of the calculation domain ensuring a good compromise between the need of accuracy in the volume of interest and the simulation time.

As MWS evaluates both local and total average SAR through closed routines, in order to be sure regarding the mass involved in the calculation, we adopted a suitable numerical procedure made up of two steps [4].
The first one was aimed to produce electric field peak values on the whole domain by MWS, with higher accuracy in the sample volume. As second step, a mesh refinement limited in the cell cultures volumes was carried out, and the electric field values were recalculated. In this way the volume of each culture medium was discretized with spatial resolution of about (0.5 x 0.05 x 0.5) mm corresponding to 157248 mesh nodes. Finally, the electric field values were exported to commercial SW and post-processed to compute local spatial SAR (W/kg) values according to the relation**:**

$$SAR = \frac{\sigma E_{(i)}^2}{2\rho} \qquad \text{(Eq. 1)}$$

where:

$E_{(i)}$	:	internal electric field in an elementary volume of the cell culture (peak value) [V/m]
σ	:	conductivity of culture medium [S/m]
ρ	:	density of culture medium [kg/m^3]

The total average SAR was evaluated by summing every SAR spatial contribution on the basis of relation:

$$\langle SAR \rangle = \frac{1}{N} \frac{\sigma}{2\rho} \sum_{k=1}^{N} E_{(i)k}^2 \qquad \text{(Eq. 2)}$$

where:

$E_{(i)k}$	:	internal electric field in an elementary volume (k-elementary cell) of the cell culture (peak value) [V/m]
σ	:	conductivity of culture medium [S/m]
ρ	:	density of culture medium [kg/m^3]

IV Results

<u>900 MHz</u>

Figures show the most relevant results for electric field calculations. Figures 2 (a) e (b) show a chromatic 3D scalar representation of the absolute value of electric field distribution (peak values) in the exposure set-up and in the culture medium, as calculated by MWS.

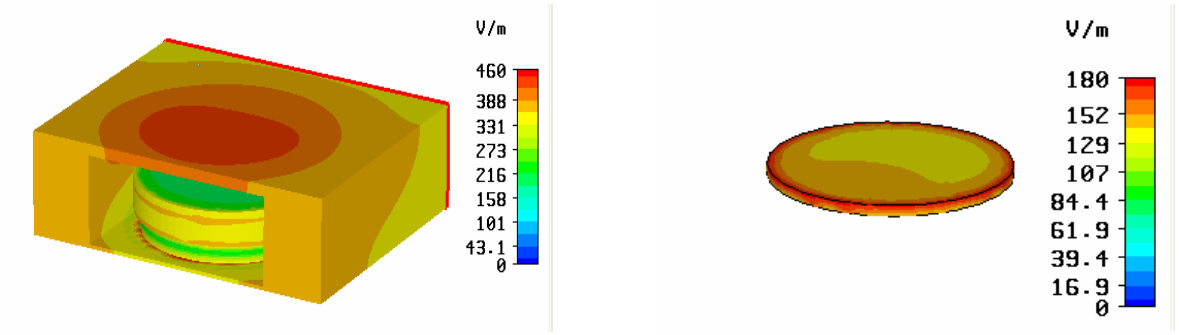

(a) E field in exposure set-up (b) E field in culture medium

Fig.2 - 3D scalar representation of the electric field inside the structure (peak values)

Figures 3 show the SAR distribution histogram inside the culture medium and a chromatic power loss density (PLD) distribution inside the cell cultures. The local spatial SAR values inside the cell culture as calculated from our numerical procedure previously described. The total average SAR calculated from these distributions is 0.1 W/kg .

Power Loss Density is supplied by MWS and it is related to the electromagnetic power locally delivered into the sample. PLD is described by

$$PLD = \frac{d}{dt}\left(\frac{dU}{dV}\right) \qquad \text{(Eq. 3)}$$

where dU is the incremental energy dissipated in an a volume element dV. The PLD values are expressed in units of W/m^3.

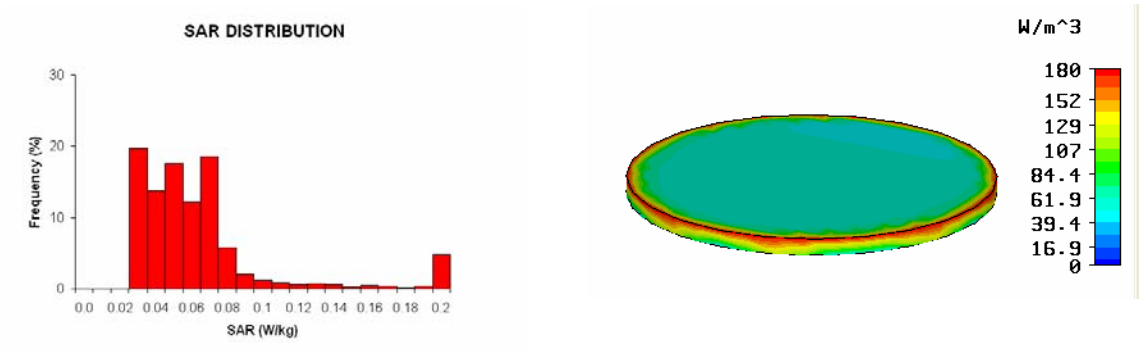

(a) – SAR (b) – Power Lost

Fig. 3 -SAR and Power loss density distribution histogram in the culture medium

Figures from 4 to 7 show the most relevant results of the 4 disks case.

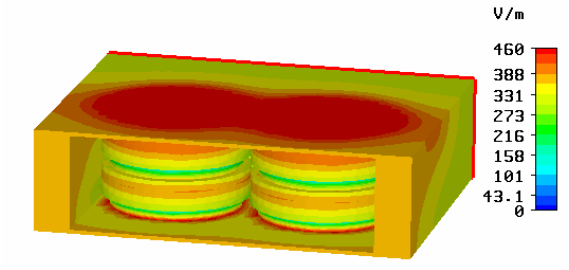

(a) E field in exposure set-up

Fig 4

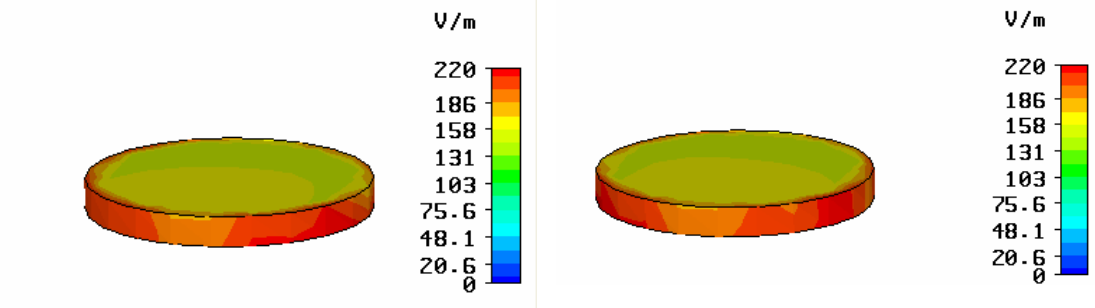

(a) – E field (up left culture) (b) E field (up right culture)

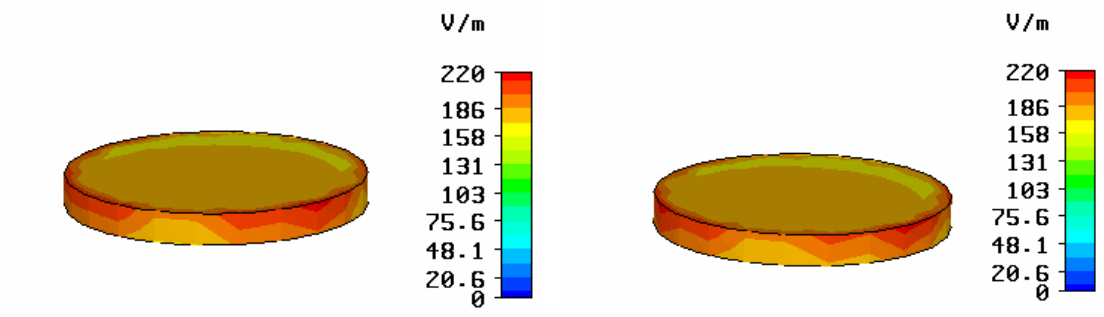

(c) –E field (down left culture) (d) E field (down right culture)

Fig 5

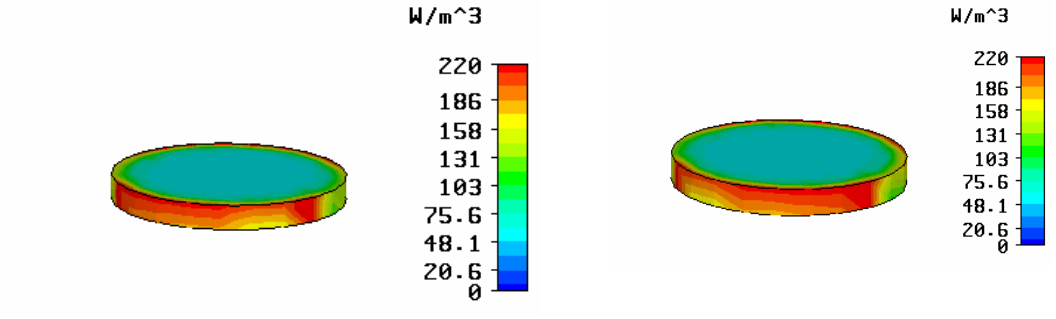

(a) – PLD (up left culture) (b) PLD (up right culture)

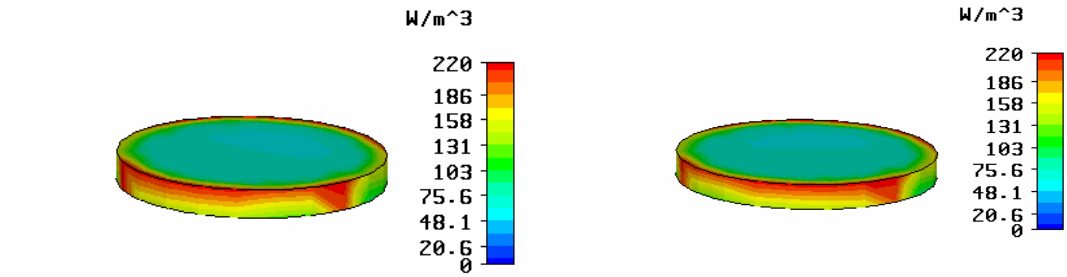

(c) –PLD (down left culture) (d) PLD (down right culture)

Fig 6

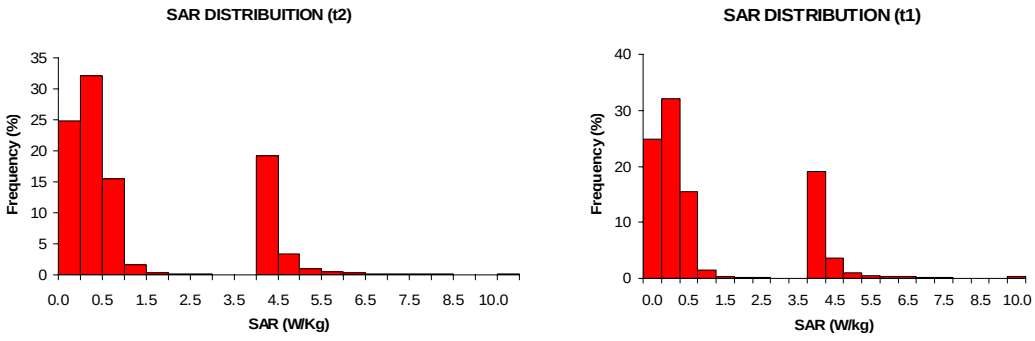

(a) – SAR histogram (up left culture) (b) SAR histogram (up right culture)

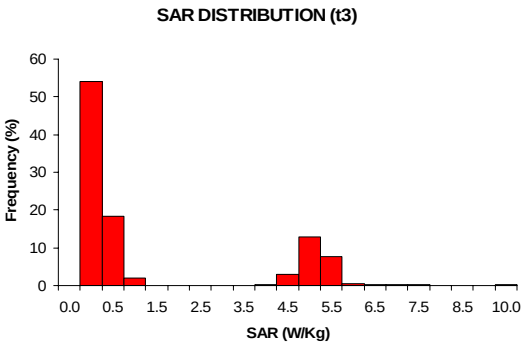

(c) – SAR histogram (down left culture)

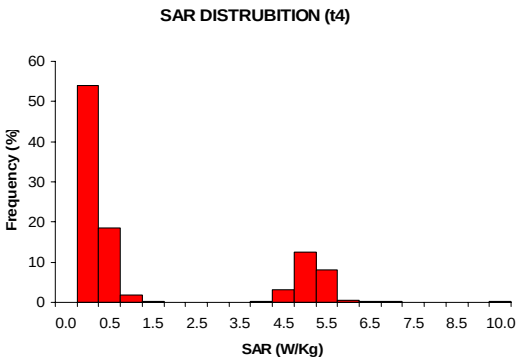

(d) SAR histogram (down right culture)

Fig 7

The total average SAR calculated from these distributions is:

CULTURE POSITION	SAR (W/kg)
up left	1.1
up right	1.1
down left	1.4
down right	1.4

1820 MHz

Figures from 8 to 11 show the most relevant results, as calculated by MWS at the frequency of 1820 MHz. At this frequency, there are some modes of field propagation. For each mode, we have calculated SAR contribution. Only first an second mode have a significant value. However, in our calculations, we have considered ten modes.

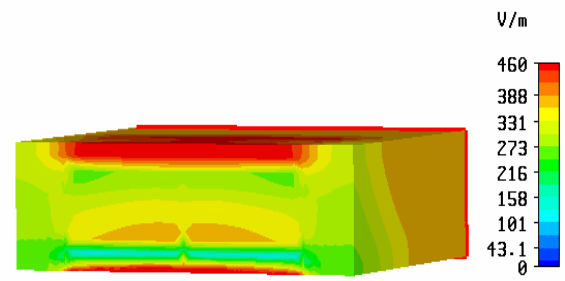

(a) E field in exposure set-up

Fig 8

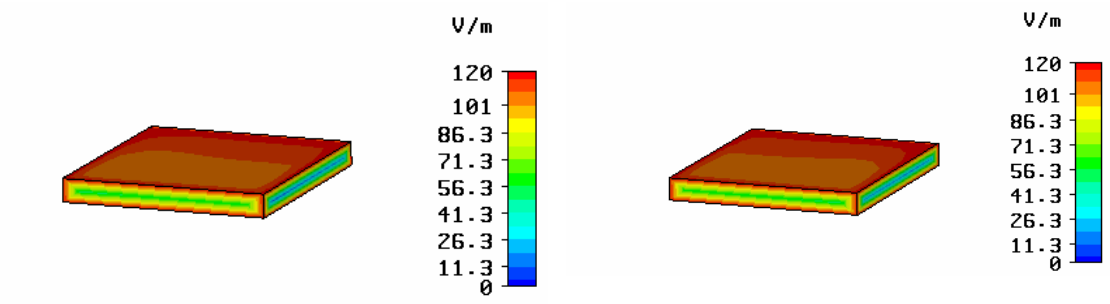

(a) – E field left culture (b) E field right culture

Fig 9

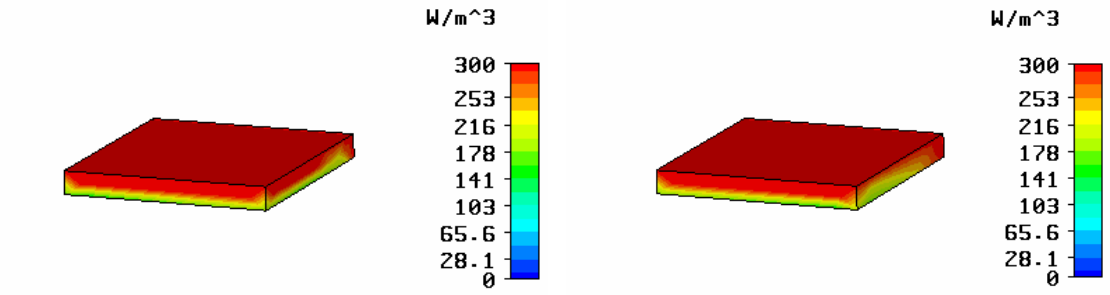

(a) – PLD left culture (b) PLD right culture

Fig 10

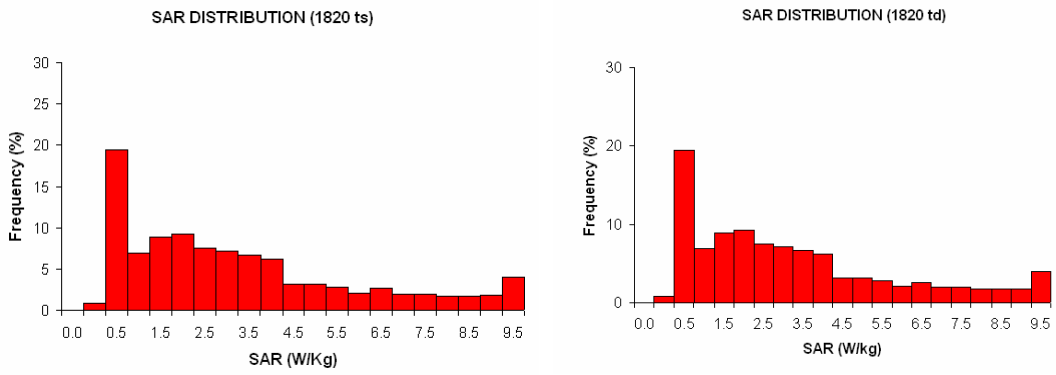

(a) – SAR histogram left culture (b) SAR histogram right culture

Fig 11

The total average SAR calculated is 3.5 W/Kg for the left culture and the right culture

V Concluding Remarks

This study was carried out in the frame of activities referring to the European Project EMF-NET, Main Task 2. In fact our group is leader of the Work Package 12 focused on numerical calculations for occupational exposure.

Variability of the efficiency depending of the shape of terrain culture container (flask o dish), number of samples exposed at the same time, their positions, has been investigated.

Separately, for the various numerical calculations performed, the results can be summarized as follows:

- 900 MHz average SAR and distribution depend on quantity of culture medium (3 o 5 ml) and depend on number of culture exposed.
- 900 MHz average SAR and distribution depend on positions of the culture medium
- 1820 MHz average SAR doesn't depend on positions, because we have a symmetry in our set up.
- All simulations show that the spatial distribution of SAR inside each sample is not homogeneous, and local SAR values may be highly variable

Acknowledgments

The authors would like to thank Vincenzo Brugaletta for his precious support in experimental characterization of the exposure set up.

References

[1]	Microwave Studio, User's Manuals 5.02 2004, CST Computer Simulation Technology, D-64289 Darmstadt, Germany.
[2]	T. Weiland, "A discretization method for the solution of Maxwell's equations for six-component field", *Electronics and Communications AEÜ*, vol.31, no.3, pp.116-120, 1977.
[3]	B. Krietenstein, R. Schuhmann, P. Thoma, T. Weiland, "The Perfect Boundary Approximation technique facing the challenge of high precision field computation", *Proc. of the XIX International Linear Accelerator Conference (LINAC '98)*, Chicago, USA, pp. 860-862, 1998.
[4]	Cannelli V., Falsaperla R., "Numerical SAR evaluation for cell culture exposed to 900 MHz continuous waves", Third International Workshop on ElectroMagnetic Fields; 4-8 October 2004,Kos, Greece.

EFFECT OF SIGNAL MODULATION ON THE LINEAR RESPONSE OF ELECTRIC FIELD PROBES USED TO DETERMINE SPECIFIC ABSORPTION RATE

BENJAMIN LOADER, DANIEL BOWNDS.
NATIONAL PHYSICAL LABORATORY,
HAMPTON ROAD, TEDDINGTON MIDDLESEX, UK, TW11 0LW

Abstract
Electric field probes used to assess the specific absorption rate (SAR) of energy in human tissues due to radio transmitters are largely based on diode detectors. To determine the accuracy of SAR measurements, it is necessary to characterise the effect of the signal modulation on the linear response of these probes. This paper describes the system developed at the National Physical Laboratory to assess the linearity of SAR probes to different signal modulations, and gives results for four commercially available SAR probes. There was a wide variation in the linearity of the probes to pulse modulated signals, and this highlights the need to assess the linearity to the signal modulation to be measured. The results show that the tests in the IEEE 1528-2003 [1] give a conservative estimate for the linearity error in most cases.

Introduction
SAR is the specific absorption rate of radio frequency energy in a material and has the unit watts per kilogram. SAR forms part of the basic restriction limiting exposure of humans to radio-frequency fields over the frequency range 100 kHz to 10 GHz. The SAR resulting from the use of mobile radio transmitters is assessed by measuring the electric field in a liquid phantom that approximates the electrical properties of the biological material of interest. For a dielectric, SAR is then calculated by

$$SAR = \frac{E^2 \sigma}{\rho} \tag{1}$$

where E is the electric field in the liquid, σ its conductivity and ρ its density. The electric field probes used to assess SAR contain three orthogonal electric field sensors, and these commonly use Schottky diode detectors. Below the diode compression point the output voltage from the diode is proportional to the average power during the measurement (square law region). At high powers the output voltage is proportional to the r.m.s voltage during the measurement period (linear region). There is a transition region between the linear and square law region. Since the diodes are operated beyond the square law region, the output voltage (V) must be corrected to obtain a linear response (V_{LIN}), using

$$V_{LIN} = V\left(1 + \frac{V}{DCP}\right) \tag{2}$$

where DCP is the diode compression point. For pulse-modulated signals, the sample rate of the probe may be too slow to correctly sample the modulation, and in this case the V_{LIN} is obtained using

$$V_{LIN} = V\left(1 + \frac{CF \times V}{DCP}\right) \tag{3}$$

where CF is the crest factor of the signal. Linearity is defined as the maximum deviation over the measurement range of the measured quantity from the closest linear reference curve defined over a given interval [2]. The linearity of each sensor in the probe must be assessed to determine the uncertainty for SAR measurements. This paper describes the system developed at NPL for testing the linearity of SAR probes, and gives the measurement results for probes from three manufacturers to a range of communications signals.

Description of the measurement system
Linearity is measured by placing the sensor in an electric field and recording the diode output voltage as a function of input power to the system used to generate the field. This can be done with the sensor in air or liquid, but air is preferable since the conductivity of liquids will change with temperature, introducing non-linearity to the field generating system. Figure 1 shows a schematic of the system used. The probe is placed into IEC-R22 (UK WG8) waveguide through an aperture in the broad-wall with its axis at an angle of 54.7° to the axis of the waveguide, so that rotation of the probe about its axis allows each sensor in turn to be aligned with the polarisation of the field. This is necessary to avoid over-range errors occurring. The signals were generated using an Agilent ESG vector signal generator, which can produce a wide range of communications signals. A 5 W low noise linear amplifier allowed sensors to be tested up to a sensor output voltage that is equivalent to 100 Wkg^{-1}.

A power sensor monitors the input power to the system via a high directivity coupler and step attenuator. The step attenuator was adjusted to keep the burst average power readings in the range –20 dBm to 0 dBm, as this limits the uncertainty due to the linearity of the power sensor. Note that changing the attenuation step does not alter the power transfer between the signal generator and the waveguide, and this is an important requirement for such a system.

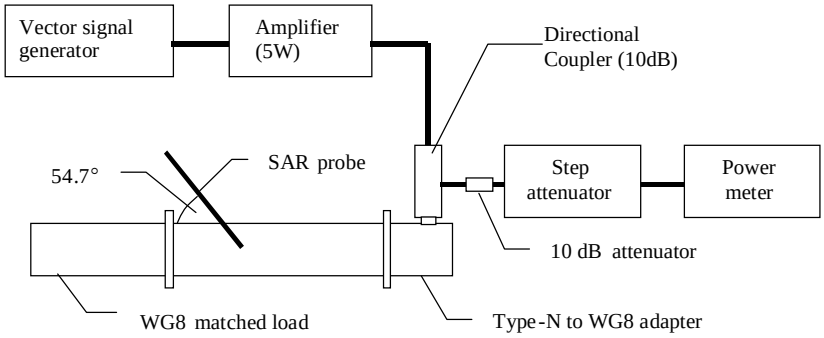

Figure 1: Schematic of linearity measurement system.

The linearity measurements were made at 1800 MHz. Table 1 lists the modulation frequency and crest factor for the signals used. UMTS 1 has a single carrier (5 MHz bandwidth), and UMTS 4 has four carriers (20 MHz bandwidth). Pulse 1 and Pulse 2 correspond to the linearity tests specified in [1].

Table 1. Signal characteristics

Signal type	Crest factor	Modulation frequency
CW	1	0 Hz
GSM	8	217 Hz
DECT	12	100 Hz
TETRA	4	17.6 Hz
Bluetooth	3.25	(625μs per slot)
WCDMA-1	1	0 Hz
WCDMA-4	1	0 Hz
Pulse 1	10	11 Hz
Pulse 2	25	1 kHz

Measurement results

The linearity of the probes was measured for peak SAR readings over the range 0.02 Wkg^{-1} to 100 Wkg^{-1}. Table 2 gives the maximum linearity error of the probes over this range. Figures 2 to 5 show the SAR reading against the ratio of average input power to the system. All of the probes over-read at high SAR levels when measuring pulse-modulated signals. The extent of the linearity error varies considerable between probes from different manufacturers. The linearity error for UMTS signals is similar to that for CW signals. Table 3 gives the maximum change in the relative sensitivity of the three sensors in each probe over the range 0.02 Wkg^{-1} to 100 Wkg^{-1}. This corresponds to the change in isotropy due to differences in linearity of the three sensors in the probe.

Table 2: Linearity over the peak SAR range 0.02 Wkg^{-1} to 100 Wkg^{-1}.

Signal type	Maximum linearity error (± dB)				
	Power sensor	Probe A	Probe B[1]	Probe C	Probe D
CW	0.05	0.12	0.51	0.82	0.93
GSM	0.07	0.68	1.71	4.39	1.45
DECT	0.06	0.51	1.98	4.00	2.80
TETRA	0.06	0.69	3.74	4.90	3.33
Bluetooth	0.07	1.04	0.52	4.60	1.13
WCDMA 1	0.05	0.12	0.25	0.55	0.91
WCDMA 4	0.05	0.20	0.18	0.41	1.31
Pulse 1	0.05	0.58	0.97	3.11	1.81
Pulse 2	0.25	1.81	0.57	4.76	2.41

[1] Quoted over the range 0.1 Wkg^{-1} to 100 Wkg^{-1}, as this probe has limited sensitivity.

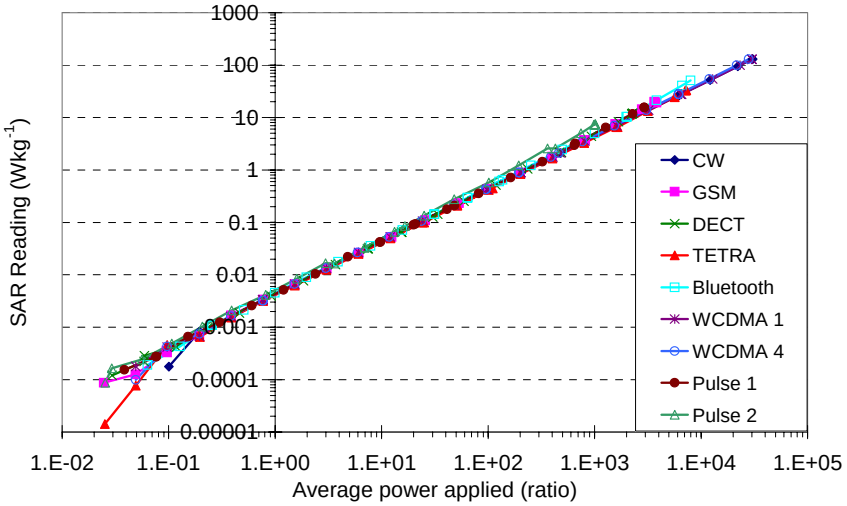

Figure 2. Probe A: SAR reading against average applied power.

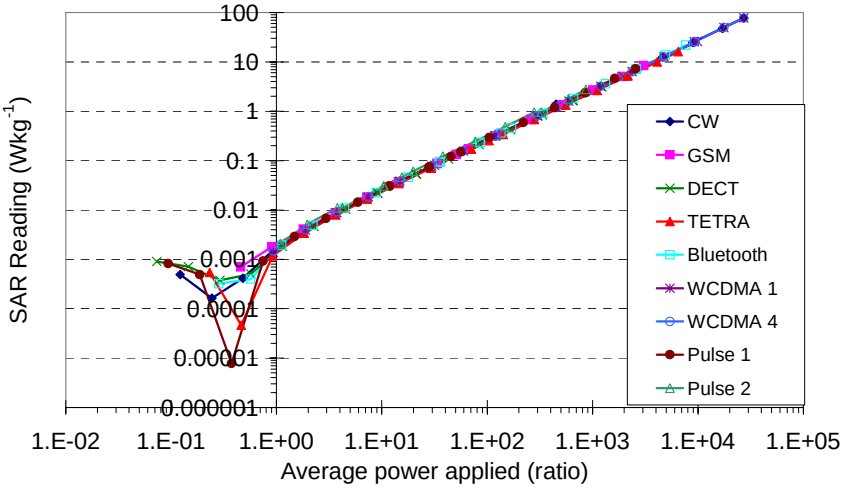

Figure 3. Probe B: SAR reading against average applied power.

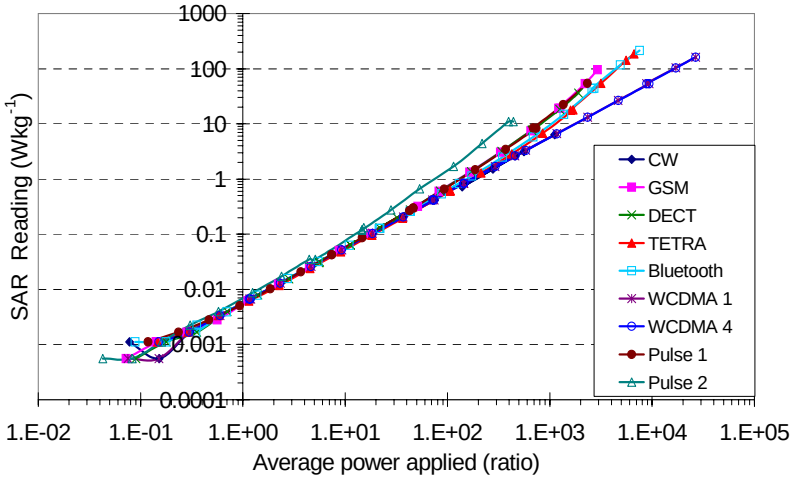

Figure 4. Probe C: SAR reading against average applied power.

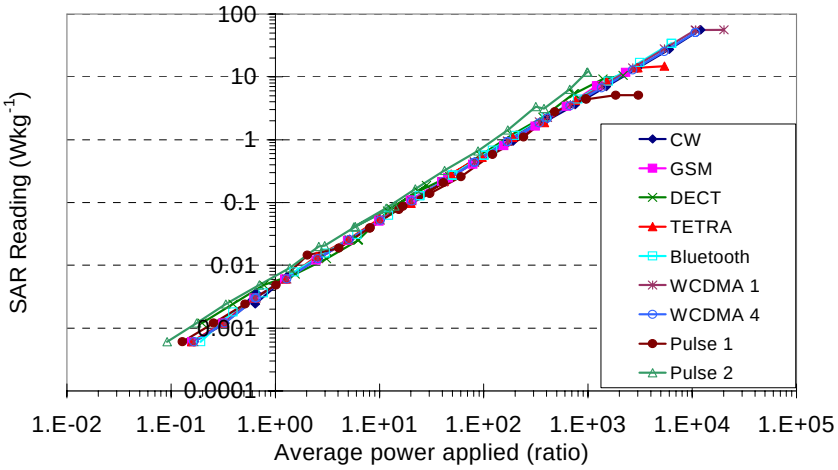

Figure 5. Probe D: SAR reading against average applied power.

Table 3: Change in isotropy over the peak SAR range 0.02 Wkg^{-1} to 100 Wkg^{-1}.

Signal Type	Maximum change in relative sensitivity of the three sensors (dB)			
	Probe A	Probe B	Probe C	Probe D
CW	0.30	0.30	0.39	0.25
GSM	0.16	0.57	0.39	0.31
DECT	0.24	0.68	2.13	0.76
TETRA	0.29	2.42	0.47	0.69
Bluetooth	0.05	0.22	0.59	0.23
WCDMA 1	0.03	0.03	0.24	0.27
WCDMA 4	0.03	0.06	0.02	0.31
Pulse 1	0.28	0.69	0.33	0.94
Pulse 2	0.14	0.44	2.53	1.21

Conclusions

The linearity performance of four commercially available probes for measuring SAR was tested for a variety of communications signals over the range 0.02 Wkg^{-1} to 100 Wkg^{-1}. The linearity performance of the probes to CW signals and UMTS signals was found to be good. The low-level detection limit of one probe was limited to around 0.05 Wkg^{-1}. For pulse-modulated signals, the equation used to compensate for diode compression (Eq 3) was found to cause the probes to over-read at high peak SAR levels. The extent of this error varied considerably between the probes tested. For one probe, this correction did not give a linear response for pulse-modulated signals. Differences between the linear responses of the three sensors in the probes were also observed. It is therefore essential to characterise the linear performance of SAR probes to determine the measurement uncertainty. Each sensor should be tested separately, as differences in linear response between the sensors change the isotropy of the probe. In most cases, the tests specified in the [1] gives a conservative estimate for the linearity error for the range of pulse modulation schemes, but will over-estimate the measurement uncertainty for many real signals. Ideally, the linearity should be tested to the actual signal modulation to be measured.

Acknowledgement.

The Department for Trade and Industry (DTI) funded this work for the National Measurement System (NMS) of the UK.

References

[1] IEEE Standard 1528-2003 "Recommended Practice for Determining the Peak Spatial-Averaged Specific Absorption Rate (SAR) in the Human Head from Wireless Communications Devices: Measurement Techniques".

[2] British Standard BS EN 503361:2001. “Basic standard for the measurement of specific absorption rate related to human exposure to electromagnetic fields from mobile phones (300 MHz – 3 GHz)”.

C-FOS EXPRESSION ON BRAIN AFTER ACUTE EXPOSURE TO 900 MHz GSM RADIATION OF PICROTOXIN MODEL OF EPILEPTIC RATS IS RECOVERING AFTER 3 DAYS.

LÓPEZ-MARTÍN E.[(1)], CARBALLO QUINTÁ M. [(1)], RELOVA QUINTEIRO JL[(2)], SEBASTIAN FRANCO JL[(3)], JORGE BARREIRO[(1)] ARES F.J [(4)]

[(1)] *MORPHOLOGICAL SCIENCES DEPARMENT, UNIVERSITY OF SANTIAGO DE COMPOSTELA, 15782 SANTIAGO DE COMPOSTELA, SPAIN.*
Emails: cmelena@usc.es (Lopez–Martin); cmjorge@usc.es (Jorge–Barreiro)

[(2)] *PHYSIOLOGY DEPARMENT, UNIVERSITY OF SANTIAGO DE COMPOSTELA, 15782 SANTIAGO DE COMPOSTELA, SPAIN.*
Email: fsrelova@usc.es (Relova–Quinteiro)

[(3)] *DEPARMENT OF APPLIED PHYSICS III, UNIVERSITY COMPLUTENSE OF MADRID, 28040, MADRID, SPAIN.*
Email: jlsf@fis.ucm.es (Sebastian–Franco)

[(4)] *RADIATING SYSTEM GROUP, APPLIED PHYSICS, UNIVERSITY OF SANTIAGO DE COMPOSTELA, 15782 SANTIAGO DE COMPOSTELA, SPAIN.*
Email: faares@usc.es (Ares–Pena)

Abstract

Acute effect of electromagnetic fields (EMFs) and induction of genes, with no thermal stress, have been reported but remain controversial. In previous studies we have found neuronal activation markers (c–fos) in the brain of rats pre–treated with subconvulsive doses of picrotoxin, after 2hs exposure to 900 MHz GSM radiation, at intensities similar to those emitted by mobile phones. In this study we analyzed in 50 adult male Sprague-Dawley rats the time course effects of induction of c–fos immunochemical testing of relevant anatomical areas with acute experimentally model induced by picrotoxin, after 60 minutes, 24 hours and 3 days of exposure to EMF radiation. C-Fos positives cells were counted in cortical and hippocampal areas, using a morphometric software, having expressed counts per field as means ± s.e m.. 60 m and 24 hs after the radiation (AR), the c-Fos positive cells were increase on cortical and hippocampal areas; after 3 days the counts were similar in the same areas of the exposed–and–treated and non–exposed–and–treated animals. After 3 days, none of them showed differences. The time course of the effects after the GSM radiation on the CNS showed to be recovered after 3 days.

1. Introduction

The modulation of gene expression can be initiated by external events, acting through intracellular signalling pathways triggers changes in differentiation of cells, cell growth and programmed cell death. It

is well know that the induction and up-regulation of immediate–early genes (IEGs) precede degenerative process of central nervous system (CNS). Induction of c-fos has been associated with cellular injury and even cellular death (1, 2) c-fos is also easly induced under non-pathogenic environmental conditions and can be used as a sensitive marker of neuronal activation (3, 4). The expression of genes called proto-oncogenes can be increased by tumor-promoting agents, ultraviolet radiation and X-rays.
In relation with gene activation by exposure to non-ionizing radiofrequency electromagnetic radiation on CNS is controversial topic that normally it is explain normally by thermal influence. The results of studies of gene expression in mammals have been variable and generally negative (5). Studies of changes in the expression of the early response gen c-fos (6, 7, 8, 9) in the brain of rats and mice exposed to RF radiation and in vitro exposure (10,11) generally find no effects following at thermally insignificant levels. In any case, c-fos expression is known to increase enter sham and exposure animals of the expression levels proto-oncogene c-fos after exposure to RF and suggest the acute genomic response detected was due to immobilisation (12) of an animal or to increase simply as a result of stress (13). In previous study in rats that have been made seizure-prone by subconvulsive doses of picrotoxin, GSM radiation can trigger seizures and induce changes in cerebral activity reflected by high levels of c-Fos-positive neurons in certain brain areas (14). The brain tissue of seizure proneness can be especially sensitive to the effects of mobile-phone type radiation (15).In this paper the time course of the effects of radiation were evaluated by immunochemical testing of relevant brain areas for a marker of neuronal activation c-Fos expression at 60m 24 hs and 3 days after 2h of GSM-modulated 900 MHz radiation at intensity similar to that emitted by mobile phones.

2. Material and Methods

2.1. Animals and experimental procedure

72 adult male Sprague-Dawley rats weighing 230-270 g were housed during exposure under standard environmental conditions (12:12 h light/dark cycle, 22°C) with food and water available *ad libitum*. Twelve groups of eight rats were given the following treatments:

EXPERIMENTAL GROUPS	
Group 1:	**Picrotoxin Treated (PT)+ irradiated (IR) studied to 60m**
Group 2:	**PT+ Non-Irradiated (NIR) studied to 60m**
Group 3:	**PT+ IR studied to 24hs**
Group 4:	**PT+ NIR studied to 24hs**
Group 5	**PT+ IR studied to 3 ds**
Group 6	**PT+ NIR studied to 3ds**
Group 7	**Non-Treated with Picrotoxin (NTP) + IR studied to 60m**
Group 8	**NTP + NIR studied to 60m**
Group 9	**NTP + IR studied to 24hs**
Group 10	**NTP + NIR studied to 24hs**
Group 11	**NTP + IR studied to 3 ds**
Group 12	**NTP + NIR studied to 3 ds**

Table 1. This table showed experimental groups used in this experiment

Immediately following intraperitoneal administration of 2 mg/kg of picrotoxin (Sigma), used in groups 1-6, each animal was immobilized in a methacrylate tube and placed in a $150 \times 46 \times 70\,cm^3$ radiation cage that had previously been calibrated to enable measurement of the radiation absorbed by the animal.

2.2. Determination of exposure

Animals belonging to groups 1 and 4 (2 and 5) were irradiated with GSM-modulated (non-modulated) 900 MHz radiation, and the power absorbed by the animal was correspondingly determined (see [14]). The irradiation power level ± 1000 MW, was chosen to be somewhat lower than the average power radiated by a GSM mobile phone. In the metallic cage all the animals were videotaped to record their behaviours while radiated; after 2 h they were removed from the cage and sedated with pentobarbital to transfer them to the histochemistry laboratory. In the radiation cage, the experimental animal in its methacrylate tube was located between a radiating antenna and a receiving antenna with its head at an electromagnetic field maximum (as calculated by finite-difference time domain (FTDT) calculations [16] for the cage plus radiating antenna set up).

2.3. Immunohistochemistry, quantification and statistical analysis of immunohistochemical findings

Approximately 1 h after removal from the radiation cage, the rats were given an overdose of pentobarbital, as said above, and prefixed by transcardial perfusion with physiological saline followed by formaldehyde in phosphate buffer (pH 7.4). Their brains were immediately removed and processed in sections of 40µ. The free-floating sections were used for polyclonal sheep anti-Fos antibody immunochemistry tests (from Cambridge Research Biochemicals, Billingham, UK).
For each rat, c-Fos positivity was evaluated in cerebral cortex (frontal motor, parietal motor, piriform olfactory and entorhinal olfactory areas), in hippocampal structures (dentate gyrus, CA1 and CA3). For each area, three or four sections were examined. c-Fos-positive cells were counted in a 0.30 mm^2 field magnified 20×. Counts per field were reported for each group of rats as means ± SEMs. The significance of between-group differences was estimated by two-way analysis of variance (*picrotoxin status*: PT *vs* NTP × *radiation status*: IGSM *vs* INM *vs* NI). *Post hoc* comparisons were made using Scheffé-type tests. Differences with $p > 0.05$ were considered not to be statistically significant.

3. Results and Discussion

3.1. SAR Results

The parameters of radiation absorbed power, incident power, for the calculus of average SAR $_{exp}$, Peak SAR values calculated for picrotoxin-treated and untreated irradiated rats are listed in Table 1. Every values are lower thermal level (5 W/kg)

	Absorbed Power (AP)	**Incident Power (IP)**	**Efficiency= Mean Abs. Power / Incident Power (η)**	**Mean Weight**	**Mean SAR (experim.) in Brain**	**Mean SAR (experim.) in Body**	**Peak SAR (experim.) averaged in 1g brain**	**Peak SAR (experim.) averaged in 1g body**
	(mW)		**(%)**	**(g)**	**(W/kg)**			
Group 1	178.37	956.72	19.00	209.95	1.32379	0.74551	1.48858	4.09329
Group 3	192.67	710.83	27.16	225.07	1.32961	0.74879	1.49512	4.11127
Group 5	186.17	717.50	26.10	199.98	1.44819	0.81556	1.62846	4.47793
Group 7	189.41	1060.64	17.84	211.83	1.38628	0.7807	1.55884	4.28651
Group 9	202.33	744.17	27.28	228.65	1.37498	0.77434	1.54613	4.25156
Group 11	201.60	801.88	25.10	230.66	1.35739	0.76443	1.52636	4.19719

Table1. SAR values (W/kg) of picrotoxin-treated and untreated rats during irradiation with GSM-modulated 900MHz radiation (means of 7 or 8 rats) Rat group whole body Brain Mean Peak 1-g-averaged Mean Peak 1-g

3.2. Morphological Results

In picrotoxin-treated animals, c-Fos-positive neurons appeared systematically in the thalamus and cortical areas, and some animals also showed more-or less scattered c-Fos positivity in the hippocampus, amygdale, or putamen–caudate complex, and/or in hypothalamic and pontomesencephalic nuclei c-Fos-positive neuron counts.

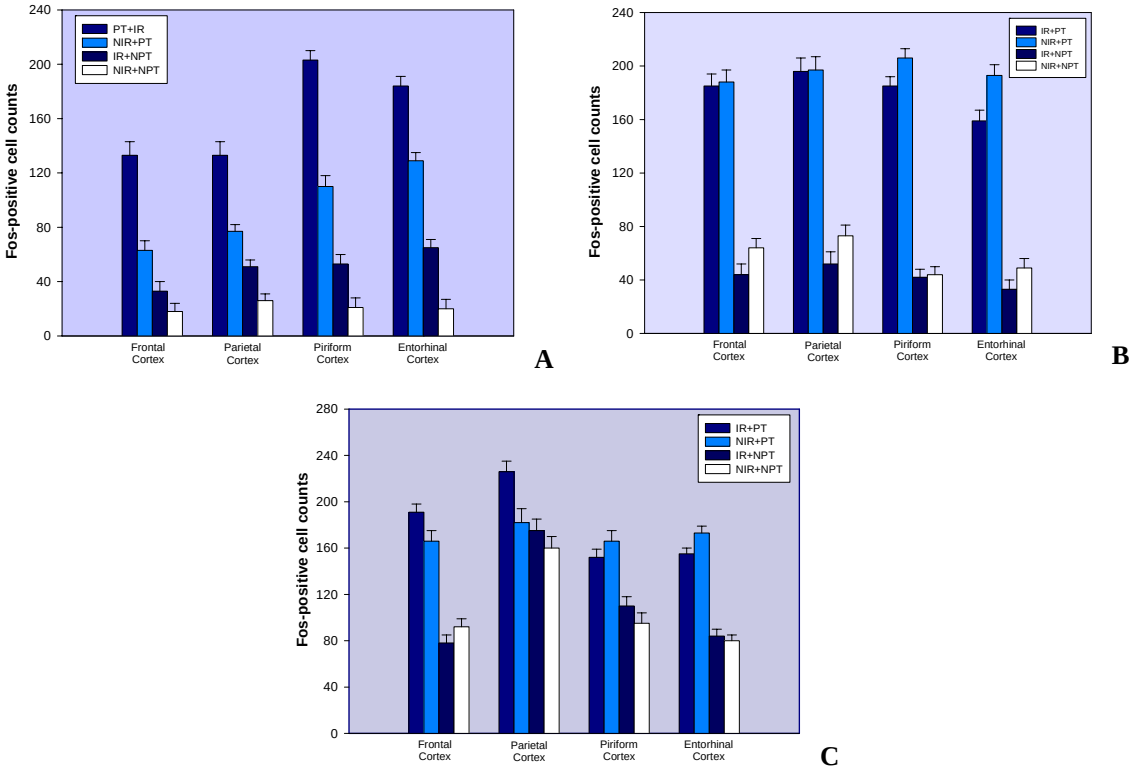

Figure 1. C-fos-positive cell counts in the frontal, parietal, piriform and entorhinal cortex (**A**) 60 minutes (**B**) 24 hours (**C**) 3 days after irradiation. (means of seven or eight rat groups; whiskers indicate SEMs).

3.2.1. Cortical Areas:

- Sixty minutes after radiation neuron counts in irradiated picrotoxin-treated rats were almost double those found in non-irradiated picrotoxin-treated rats. In rats without picrotoxin treatment, counts were lower than in picrotoxin-treated animals and may were in relation with cortical area. In almost all the areas examined analysis of variance showed that both picrotoxin and radiation had statistically significant effects on counts, and that the effect of each was significantly modified by the other.

Irradiated picrotoxin-treated animals had significantly higher counts than non-irradiated picrotoxin-treated animals in both the frontal cortex ($p < 0.001$) and the parietal cortex ($p < 0.004$). There were no significant differences for counts in frontal cortex but in parietal cortex we found significant differences ($p < 0.05$) between irradiated and non-irradiated rats that had not received picrotoxin. In the piriform cortex there is statistically significant difference in picrotoxin-treated irradiated and non irradiated ($p < 0.001$) and non treated irradiated and non irradiated animals ($p < 0.003$), in this area there is important interaction between radiation and treatment ($p= 0.002$). In entorhinal cortex did radiation per se have a statistically significant influence on counts ($p < 0.001$) and in this area it significantly modified the effect of picrotoxin ($p < 0.01$) but there is not a statistically significant interaction between both variables; In both areas there was a statistically significant difference in counts between irradiated and non-irradiated rats that had not received picrotoxin ($p < 0.05$).

Twenty-four hours after radiation neuron counts in irradiated picrotoxin-treated rats values were similar found in non-irradiated picrotoxin-treated rats. In cortical areas examined analysis of variance showed that picrotoxin had statistically significant effects on neuron counts. However both variables picrotoxin and radiation had statistically significant effects on counts alone in Entorhinal cortex ($p < 0.001$). In neither the frontal, parietal and piriform cortex did radiation per se have a statistically significant influence on counts, but in this areas the

counts it significantly modified for the effect of picrotoxin**.** In neither cortical area was there a statistically significant difference in counts between irradiated and non-irradiated rats that had not received picrotoxin.

Three days after radiation in cortical areas there are a statistically significant effects on counts in relation with treatment picrotoxin but the statistically significant interaction effects between radiation x picrotoxin it happen on frontal cortex alone. C–fos positive neurons in irradiated-treated rats showed statistically significant difference in non-irradiated picrotoxin-treated rats on frontal ($p < 0.026$) and parietal ($p < 0.05$) cortex. In neither cortical areas there were a statistically significant difference in counts between irradiated and non-irradiated rats that had not received picrotoxin.

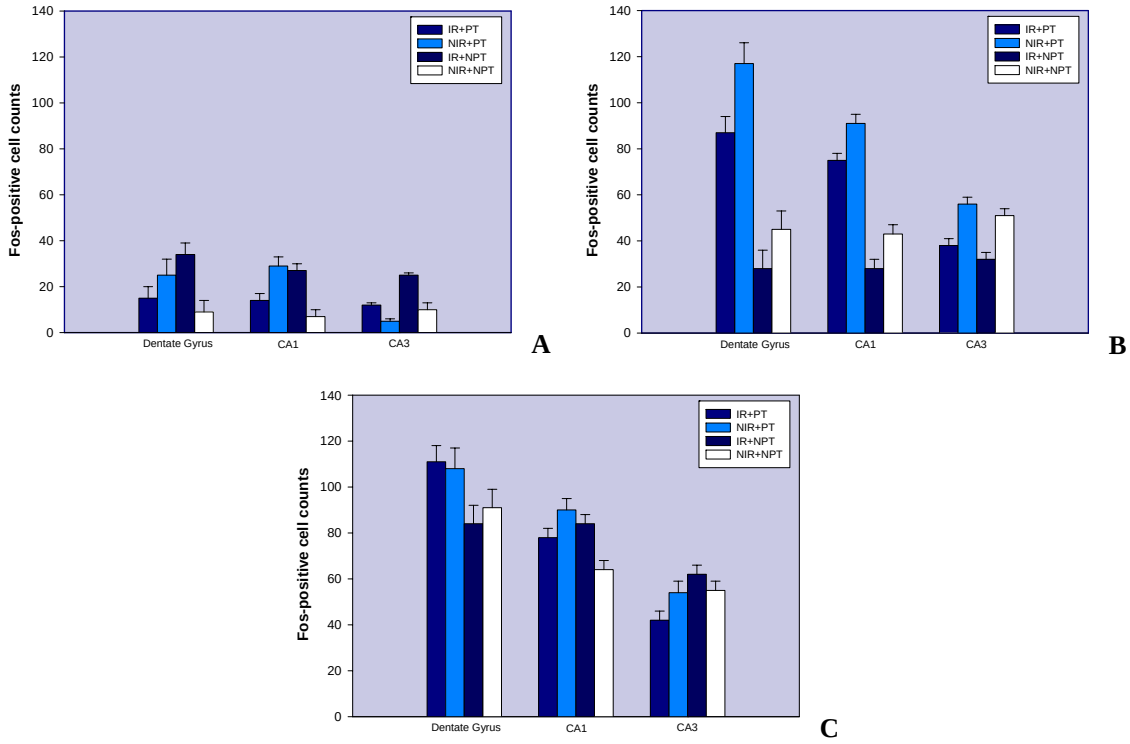

Figure 2. C-fos-positive cell counts in Gyrus dentate,CA1 and CA3 in Hippocampal areas (**A**) 60 minutes (**B**) 24hous (**C**) 3 days after irradiation. (means of seven or eight rat groups; whiskers indicate SEMs).

3.2.2. Hippocampal Areas:

-Sixty minutes after radiation neuron counts in hippocampal areas showed the highest levels c-Fos in rats without picrotoxin treatment and irradiated. The two way analysis of variance showed that there is a statistically significant interaction between radiation and treatment in hippocampal areas and generally a major effect of radiation in untreated animals. In Gyrus dentate untreated and radiated animals showed significance differences with treated and radiated animals ($p < 0.013$) and untreated and non radiated animals ($p < 0.002$). C-Fos positive neuron counts in non picrotoxin treated and irradiated animals had statistically significant difference with picrotoxin treated and irradiated animals in CA1 ($p < 0.009$) and CA3 ($p < 0.013$). Irradiated and untreated animals and non-irradiated and untreated animals showed significance differences in both areas CA1 ($p < 0.001$) and CA3 ($p < 0.001$).Treated animal irradiated and non irradiated showed significant differences in CA1 alone ($p < 0.012$).

- Twenty-four hours after radiation neuron counts in the most animals unirradiated showed higher levels of c-fos positives neurons than irradiated animals. The same way picrotoxin treatment animals showed important levels in the counts neurons respect to animals without treatment. Non-irradiated picrotoxin-treated animals had significantly higher counts than irradiated picrotoxin-treated animals in GD, CA1 and CA3 ($p < 0.05$, $p < 0.05$, $p < 0.001$). Non irradiated animals without picrotoxin showed significance differences with in irradiated animals in three cortical areas.

-Three days after radiation disappear the major differences in the counts in picrotoxin treated and irradiated animals and non picrotoxin treated and non-irradiated animals except in CA3 area where there is a significance differences in counts enter two groups ($p < 0.05$). The animals without picrotoxin treatment showed significant differences in irradiated and unradiated animals in CA1 hippocampal area alone.

3.3. Discussion

We have studied the time course of effects of RF radiation on the CNS in two relevant anatomical areas: cerebral cortex and hippocampal areas. Within the CNS, the cerebral cortex is the part of the brain that is most vulnerable to the electromagnetic field (EMF) [17] exposure as it is a peripheral anatomical structure that received most of SAR of microwave radiation at non thermal levels (see table). However, a very low level of radiation may produce effects due to the vulnerability of cerebral cortex, altering the activity of the nervous system [18]. Hippocampal areas are in the middle of the brain and the low level SAR did not explain the direct effect of GSM radiation in this area. The radiation seems to act as a periodic peripheral stimulus that increases the vulnerability of neuronal circuits that, in the case of GABA-ergic circuits, have already been weakened by picrotoxin [14]. Sixty minutes after radiation there is high expression of c-Fos in cortical areas. Neuronal changes are not persistent and 24 hs after irradiation both groups, picrotoxin-treated rat irradiated and picrotoxin-treated and non radiated, had similar levels. Finally 3days after irradiation there was a compensation in most of the groups. The progressive time course recovering of c-fos levels in this acute model of seizure-proneness indicate no altered functionally physiological normal mechanism after acute radiation.

4. Conclusions

The time course of the effects after the GSM radiation in rats that have been treated by subconvulsive doses of picrotoxin showed induced changes in cerebral activity. These are reflected by high levels of c-Fos-positive neurons in certain brain areas after 60m. The differences between the irradiated and non irradiated groups are shown to be minor after 24 hs from radiation and finally they be recovered after 3 days.

5. Acknowledgements

This work was supported by the Secretariat General for Research and Development of the Xunta de Galicia under project PGIDIT02BTF2060

6. References

[1] Smeyne R. J., Vendrell M., Hayward M., Baker S.J., Miao J., Schilling K., Robertson L.M., Curran T. and Morgan J.I. Continous c-fos expression precedes programmed cell death in vivo. *Nature*.363, 166-169. (1993).

[2] Schreiber S. S and Baudry M, Selective neuronal vulnerability in the hippocampus –a role for gene expression, Trends Neurosci.,18, (1995) 446-451.

[3] Morgan J.I. and Curran T. Stimulus-transcription coupling in the nervous system: involvement of the inducible proto-oncogenes fos and jun. *A. Rev. Neurosci.* 14, 421-451. (1991)

[4] J. I. Morgan and T. Curran, Proto-oncogene transcription factors and epilepsy, *Trends Pharmacology Science* 12 (9) 343-349. (1991)

[5] Whitehead TD, Brownstein BH, Parry JJ, Thompson D, Cha BA, Moros EG, Rogers BE, Roti Roti JL. Expression of proto-oncogene Fos after exposure to radiofrequency radiation relevant to wireless communications *Radiat Res* 164 (4 pt 1);420-30. (2005)

[6] Mickley G.A. Mickley, B.L. Cobb, P.A. Mason, S. Farrell, Disruption of putative working memory task and selective expression of brain c-fos following microwave-induced hyperthermia, *Physiol. Behav.* 55 1029 (1994).

[7] Walters TJ, Mason PA, Sherry CJ, Stevens C and Merritt JH, No detectable bioe-effects following acute exposure to high peak power ultra-wide band electromagnetic radiation in rats. *Aviat Space Environ Med* 66 (6), 562 (1995)

[8] K. Fritze, C. Wiessner, N. Kuster, C. Sommer, P. Gass, D.M. Hermann,M. Kiessling, K.A. Hossmann, Effect of global system for mobile communication microwave exposure on the genomic response of the rat brain, *Neuroscience* 81 (3) 627–63(1997)

[9] R.W. Morrissey, S. Raney, E. Heasley, P. Rathinavelu, M. Dauphinee, J.H. Fallon, IRIDIUM exposure increases c-fos expression in the brain only at levels which likely result in tissue heating, *Neuroscience* 92, 1539–1546 (1999).

[10] Oleg I. Ivaschuk, Robert A. Jones, Tamako Ishida-Jones, Wendy Haggren, W. Ross Adey and Jerry L. Phillips Exposure of nerve growth factor treated PC12 rat pheochro mocytoma cells a modulated radiofrequency field at 836.55 MHz: effects on c-jun and c-fos expression. *Bioelectromagnetics* 18: 223-229 (1997)

[11] Goswami PC, Albee L.D, Parsian A.J, Baty J.D, Moros E.G, Pickard W.F, Roti Roti JL, Hunt C.R, Proto-oncogene mRNA levels and activities of multiple transcription factors in C3H 10T ½ murine embryonic fibroblast exposed to 835.62 and 847.74 MHz cellular phone communications frequency radiation, *Rad Res* 151(3):300-9.(1999)

[12] w.E. Cullinan, J.P. Herman, D.F. Battaglia, H. Akil, S.J. Watson, Pattern and time course of immediate early gene expression in rat brain following acute stress, *Neuroscience* 64 (2) 477–505. (1995)

[13]Finnie JW, Expression of immediate early gene, c-fos, in mouse brain after acute global system for mobile communication microwave exposure, *Pathology* 37(3):231-3 (2005)

[14] López-Martín. E., Relova –Quinteiro José Gallego-Gómez Rosalía, Peleteiro-Fernández Manuel, Jorge-Barreiro Francisco J, Ares-Pena Francisco J, GSM radiation triggers seizures and increases cerebral c-Fos positivity in rats pretreated with subconvulsive doses of picrotoxin, *Neuroscience Letters*, 398, 139-144 (2006)

[15] K.A. Hossmann and Hermann, Effects of electromagnetic radiation of mobile phones on the central nervous system, *Bioelectromagnetics* 24:49-62 (2003).

[16] Schmid & Partner Engineering AG, Reference manual for the SEMCAD Simulation Platform for Electromagnetic Compatibility, Antenna Design and Dosimetry, vilable from: http://www.semcad.com.

[17] Huber R., Treyer V., Schuderer J., Berthold T., Buck A., Kuster N., Landolt H.P., Achermann P. 2002 Exposure to pulse-modulated radiofrequency electromagnetic fields affects regional cerebral blood flow *European Journal of Neuroscience* 21, 1000-1009

[18] James C. Lin, 2003. Cellular telephone radiation and electroencephalograms (EEG) of the human brain. *IEEE Antennas and Propagation Magazine*, 45 (5)150-153.

EXPOSURE OF RAT THYROID GLAND TO 2450 MHZ MICROWAVE INDUCES CHANGES IN EXPRESSION OF HSP-90.

MISA AGUSTIÑO M. J. [(1)], JORGE MORA M. T. [(1)], MORENO PIQUEIRO E. [(2)], ARES PENA F. J. [(2)], JORGE BARREIRO F. J. [(3)], LÓPEZ MARTÍN E. [(3)].

[(1)] PHYSICAL MEDICINE AND REHABILITATION, UNIVERSITY HOSPITAL COMPLEX OF SANTIAGO DE COMPOSTELA, SPAIN.
Email: mjmisa73@hotmail.com (Misa–Agustiño)

[(2)] RADIATING SYSTEMS GROUP, DEPARTMENT OF APPLIED PHYISCS, UNIVERSITY OF SANTIAGO DE COMPOSTELA, 15782, SANTIAGO DE COMPOSTELA, SPAIN.
Email: faares@usc.es (Ares–Pena)

[(3)] MORPHOLOGIC SCIENCE DEPARTMENT OF MEDICINE FACULTY OF SANTIAGO DE COMPOSTELA, SPAIN.
Email: cmelena@usc.es (López–Martín)

Abstract

Rat thyroid gland was exposed in vivo to 2.450 MHz microwave fields using a commercial set up (GTEM). Heat shock protein Hsp90 is constitutively expressed in most cells under normal physiological conditions and is induced in cells upon cellular stress. The purpose of this work is to explore the expression of chaperone Hsp-90 as a biological marker that determines the sensitivity of thyroid gland to whether acute or repeated microwave exposures.

Twenty-six female Sprague-Dawley rats were studied with an irradiating microwave experimental system subject to: 1) 30 minutes acute exposure to whether 1,5 or 3,0 W and 2) Repeated exposure of 30 minutes per day during 10 days to 3,0 W. Rats were perfused with 4% paraformaldehyde, and thyroid gland removed 90 min and 24 hours post-exposure. Finally the thyroid glands were studied with histochemestry techniques: Hematoxylin-Eosin and inmunocytochemical analysis of Hsp90

These results suggest that microwave radiation provokes a stress stimulus for thyroid gland with both thermal and non-thermal mechanisms. In acute exposures they showed response to functional activity changes, but with chronic exposure the physiological mechanism of the gland suffered a certain degree of adaptation to this type of stress.

1. Introduction

The heat shock proteins (Hsps) are a cytoprotective cellular system which has different physiologic functions for homeostatic cellular balance and in response to cellular stress. Hsps have been shown to function in protein maturation events such as protein folding, unfolding and translocation across membranes [1] [2]. There are two cytoplasmic isoforms mains: Hsp90α (inducible form/major form) and Hsp90ß (constitutive form/ minor form) [3][4].

Hsp90 is an abundant and highly conserved molecular chaperone that is essential for viability in eukaryotes [5], comprises as much as 1%-2% of total cellular protein under basal conditions and increase to 4%-6% of cellular

proteins under stress [4]. Therefore, it is constitutively expressed in most cells under normal physiological conditions and is induced in cells upon exposure to elevated temperatures or other forms of cellular stress [6] as hypoxic/anoxic injury, radiations, heavy metals, viral infections, drugs … Then Hsp90 is a main functional component of an important cytosol chaperone complex, and is involved in different cellular processes, such as cell proliferation, differentiation and apoptosis. It is also associated with various cellular proteins such as steroid-hormone receptors, aryl hydrocarbon receptor, MyoD, oncogen tyrosine kinases, haem-regulated aukariotic initiation factor 2α kinase, casein kinase II, actin and tubulin [7]. Hsp90 expression is higher in proliferative cellular process than in normal tissues [8] and allow tumor cells to tolerate alterations that would be lethal.
A lot of years before ionizing radiation has been proven to cause genetic damage, which can lead to cancer and thyroid gland is one of the organs most sensitive to radiation [9][10]. In the last years the investigation of anti-cancer therapy is direct to specific proteins as Hsp90 [11][12][13].
Heat shock protein is released after exposure to microwave at levels causing, or not, heating [14][15]. And thyroid gland function change in response to environmental temperature and can be directly stimulated by microwave heating changed the activity [15].
Although non-ionizing radiation like microwaves have not been established as a cancer-causing agent, we like to explore the expression of chaperone, Hsp90 as a biological marker that determines the sensitivity of thyroid gland to whether acute or repeated microwave exposures. And we like to check if existed differences between thyroid gland exposed to microwaves and non exposed (controls).

2. Material and Methods

2.1. Animal exposure

Twenty-six female Sprague-Dawley rats, weighting between 168,7 and 248,5 gr. were exposed in vivo to 2.450 MHz microwave fields using a commercial set up GTEM 250: twenty-two rats were exposed during 30 minutes one day, acute exposure to 1,5 or 3,0 W and four rats were exposed during 30 minutes/day for 10 days, chronic exposure to 3,0 W. Radiation was direct to left front leg. During exposure, rats were housed in transparent cylindrical perspex jigs that did not allow them to move.

GROUP	TIME EXPOSURE -MICROWAVE POWER - PERFUSION		
1	EXPOSURE 30´ ,	P= 1,5 w ,	PERFUSION 90´
2	EXPOSURE 30´ ,	P= 1,5 w ,	PERFUSION 24 h
3	EXPOSURE 30´,	P= 3 w,	PERFUSION 90´
4	EXPOSURE 30´,	P= 3 w,	PERFUSION 24 h
5	EXPOSURE 30´/10 days,	P=3 W,	PERFUSION 10 d

TABLE 1. Exposure groups relative to time of exposure, microwave power applied and time elapsed until perfusion with 4% paraformaldehyde.

2.2. Tissue processed

Rats were anesthetized with dose of pentobarbital 40 mg/Kg and sacrificed 90 minutes or 24 hours after exposure. Were perfused with 4% paraformaldehyde in phosphate buffer during 20 minutes through transcardiac cannula and thyroid glands removed 90 minutes and 24 hours post-exposure and were introduced in post-fixed (10% paraformaldehyde) during 12-24 hours.
The tissues were passed for different alcohols for dehydrate (OH 70º one hour, OH 96º two hours, OH 100º two hours, and finally Toluol two hours), following paraffin embedding during six hours and 4 µ sections were taken for Hematoxylin-Eosin and inmunocytochemical analysis of Hsp90.
The same process was realized regarding to control groups.
All tissues were observed with optical microscope for different magnification (20x, 40x and 100x) of the constitutive structures and a quantitative model was established between exposure rats and control rats.

3. Morphological Results

In thyroid glands the structures studied were: connective tissue of capsular membrane; interlobule connective tissue; follicular cell and parafollicular cell.
In acute microwave exposure of thyroid glands, Hsp90 proteins expressed increase at all structures respect to controls and this increase was greater with high potency. But this increase was lesser in thyroid removed 24 hours respect to 90 minutes post-exposure. In chronic microwave exposure we observed a decreased of Hsp90 expression respect to the control in all structures studied.
In table 2 we can see the representation of data. Results concerning SAR will be presented in the poster.

ACUTE EXPOSURE 1,5 W		**ACUTE EXPOSURE 3,0 W**		**CHRONIC EXPOSURE 3,0 W**	
PERFUSION		**PERFUSION**		**PERFUSION**	
90 minutes	**24 hours**	**90 minutes**	**24 hours**	**90 minutes**	
+ + +	+ + +	+ + +	+	+	**CONNECTIVE TISSUE CAPSULAR MEMBRANE**
+ +	+ +	+ + +	+ +	+	**CONNECTIVE TISSUE INTERLOBULE**
+	+	+ +	+	-	**FOLLICULAR CELL**
+	+	+ +	+	-	**PARAFOLLICULAR CELL**

TABLE 2. In this table we group the results about all types of radiation (acute and chronic) power, exposure time and perfusion time after radiation.

- \- Without expression
- \+ Poor expression
- + + Moderate expression
- + + + High expression

The Hsp90 expression in different structures of thyroid gland respect corresponding controls:

- **Capsular membrane:** Hsp90 expression is high whether for 3.0W or 1.5W, for the animals sacrificed 90 minutes after exposure. But for animals sacrificed 24 hours after exposure there is a decrease in the Hsp90 expression, and such a decrease is more pronounced in animals exposed to 3.0W including expressed levels below the control group. For exposures chronics the Hsp90 expression were poor for all samples with respect to the control group.

- **Interlobule:** The levels Hsp90 expression are higher with 3.0W than with 1.5W for animals sacrificed 90 minutes after exposure. With 3.0W Hsp90 expression was higher than with 1.5W. But when animals were sacrificed 24 hours after exposure the expression is equal for both 1.5W and

3.0W. And for chronic exposed animals Hsp90 presented a decrease with respect to the control group with a poor expression at the same mode than capsular membrane.

- **Follicular cell:** Hsp90 expression was higher for groups exposed to 3.0W (moderate expression) than for groups exposed to 1.5W (poor expression), all of them sacrificed 90 minutes after exposure. The expression was very marked at the periphery follicular cells. 24 hours after exposure, to whether 3.0 W or 1.5W, a poor expression persisted (with respect to control group). And in the other hand in follicular cells of thyroid glands exposed with chronic radiation did not express Hsp90, while the control group presented a minimal expression.

- **Parafollicular cell:** The expression of these cells is similar to that of follicular cells. In thyroid gland removed 90 minutes after exposure, the group exposed to 3.0W presented a higher Hsp90 expression compared to the group exposed to 1.5W, respect to control group. When thyroid glands were removed 24 hours after exposure, Hsp90 expression was the same for two groups (3.0W and 1.5W). And in contrast to chronic exposure control (minimal expression of Hsp90) the chronic exposure group did not present Hsp90 expression.

PHOTOS

CONTROL **ACUTE EX. (3.0W)**

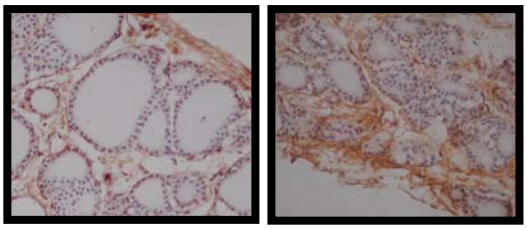

Figure 1. In thyroid glands exposed to acute radiation, the HSP90 expression increase in cellular membrane and intracellular structures with respect to control.

CONTROL **CHRONIC EX. (3.0W)**

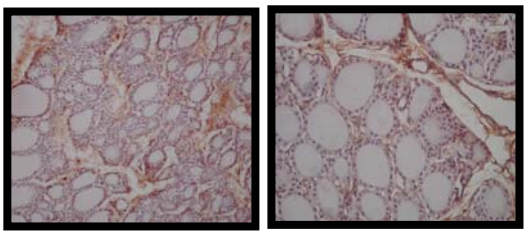

Figure 2. In thyroid glands exposed to chronic radiation, the HSP90 expression in chronic exposure is is lower than in control.

4. Discussion

With these results we can observe that the use of microwave power at whether 1.5w or 3.0W stimulated Hsp90 production, compared to control groups, because this radiation constitutes a stressing factor for thyroid gland, in acute exposure. In chronic exposure Hsp90 expression decreased, perhaps due to adaptation of the cells to this type of stress. M. Brennan and colleagues observed the effects of body temperature during exercise training on myocardial, and they described that Hsp90 increases with exercise in cold run; and at the end of 9 weeks training Hsp90 levels were no longer significantly increased, which may indicate that a certain degree of adaptation to this type of stress occurs [17]. By contrast, in animals adapted to some stressor, such as anoxia, Hsp90 expression does increase after acute stress exposure; and in chronic exposure Hsp90 experiment a rapid increase. It is possible that such an increase in the expression of stress proteins is part of a rescue mechanism, triggered at the survival limit, similar to a behaviour observed in the experiment with the western painted turtle Chrysemys picta belli, which is the most anoxia-tolerant vertebrate known [18].

5. Conclusions

These results suggest that microwave radiation is a stressful stimulus for thyroid gland in acute exposure with power of 1.5 and 3.0 watts. Nevertheless, with chronic exposure the gland suffers a certain degree of adaptation to this type of stress revealed by the Hsp90 expression decrease.

6. References

[1] J. Biochem (1994) 219: 11-23. Heat shock proteins as molecular chaperones. J. Becker, EA Craig.
[2] Cell prolif (2000) 33: 341-365. Chaperones in cell cycle regulation and mitogen signal transduction: a review. K. Helmbrecht, E. Zeise, L. Rensing.
[3] FEBS Letters (2004) 562 11-15. Hsp90 isoforms: functions, expression and clinical importance. Amere Subbarao Sreedhar, Eva Kalmar, Peter Csermeley Yu-Fei Shen.
[4] Pharmacol. Ther. (1998); 79: 129-68. The 90 Kda molecular chaperone family: structure, function and clinical applications. Csemeley P et al.
[5] Cell.Mol. Life Sci. (2002) 59 1640-1648.
Heat-shock protein 90, a chaperone for folding and regulation CMLS, D Picard. [7] Little JB. Ionizing Radiation. In: Kufe DF, Pollock RE, Weischelbaum RR, et al., eds. Cancer Medicine e. 6. Hamilton, London: B.C. Decker, Inc. 2003: 289-302.
[6] Cell Stress and Chaperones (1998) 3 (3), 188-199. Constitutive expression of heat shock proteins Hsp90, Hsc70, Hsp70 and Hsp60 in neural and non-neural tissues of the rat during postnatal development. Sandra M. D´Souza and Ian R. Brown.
[7] Biochem J. (1996) 314, 205-213. The 90 KDa heat-shock protein (hsp90) modulates the binding of the oestrogen receptor to its cognate DNA. Michèle Sabbah et al.
[8] Jpn J Cancer Res (1996) 87: 908-915. Expression and roles of heat shock proteins in human breast cancer. Yano M, Naito Z, Takana S, Asano G.
[9] Little JB. Ionizing Radiation. (2003): 289-302.
In: Kufe DF, Pollock RE, Weischelbaum RR, et al., eds. Cancer Medicine e. 6. Hamilton, London: B.C. Decker, Inc.
[10] j. Clin Endocrinol Metab (1950); 10: 1296-1308. Thyroid cancer in chilshood and adolescence. Report of 28 cases.Duffy BJ, Fitzgerald P.
[11]The Journal of Clinical Endocrinology and Metabolism (2003) 88 (7):3346-3353. The Heat Shock protein 90-Binding Geldanamycin Inhibits Cancer Cell Proliferation, Down-Regulates Oncoproteins, and Inhibits Epidermal Grow Factor-Induced Invasion in Thyroid Cancer Cell Lines. Jin-Woo Park et al.
[12] Molecular Cancer Therapeutics (2004); 3 (8) Minireview. Altered Hsp90 function in cancer: A unique therapeutic opportunity. Rouchelle Bagatell and Luke Whitesell.
[13]Annals of Oncology (2003) 14:1169-1176. The Hsp90 chaperone complex as a novel target for cancer therapy. M. P. Goetz, D. O. Toft, M. M. Ames and C. Erlichman.
[14] Generation of Heat shock proteins by EMF. Sianette Kwee. Institute of Medical Biochemistry Denmark, Helsinki 2004. AARHUS UNIVERSITY.
[15] Mutat. Research (1997) 399,55. Transgenic nematodes as biomotors of microwave–induced stress. Danniells J. A., Device I., Thomas D., Sewell P., Tatterstall J. and De Pomerai.
[16] IEEE Transaction on Biomedical Engineering, Vol BME-24, Nº 6, November 1977. Microwave Heating Effect on the Dog Thyroid Gland. Richard L Magin, Shin-Tsu Lu, Sol M. Michaelson.
[17] Am J Physios Heart Circ Physiol (2001) 280: H2271-H2280. Effects of body temperature during exercice training on myocardial adaptations. M. Brennan Harris and Joseph W. Starnes.
[18] The Journal of Experimental Biology (2004) 207, 3775-3784. Time-dependent expression of heat shock proteins 70 and 90 in tissues of the anoxic western painted turtle. Valeria Ramaglia and Leslie T. Buck.

MICROWAVE EXPOSURE OF RATS TO THERMAL AND NON-THERMAL 2450 MHz RADIATION PRODUCES CHANGES IN NEURONAL EXPRESSION OF HEAT SHOCK PROTEIN (HSP-90).

JORGE-MORA M. T. [(1)], MISA-AGUSTIÑO M. J. [(1)], BREGAINS J. C. [(2)], ARES-PENA F. J. [(2)], JORGE-BARREIRO F. J [(3)], LÓPEZ-MARTÍN E. [(3)]

[(1)] PHYSICAL MEDICINE AND REHABILITATION, UNIVERSITY HOSPITAL OF SANTIAGO DE COMPOSTELA. SPAIN.
Email: mjmisa73@hotmail.com (Misa–Agustiño)

[(2)] RADIATING SYSTEMS GROUP, APPLIED PHYSICS, UNIVERSITY OF SANTIAGO DE COMPOSTELA, 15782, SPAIN.
Emails: fares@usc.es (Ares–Pena); fajulio@usc.es (Brégains)

[(3)] DEPARTMENT OF MORPHOLOGIC SCIENCE, FACULTY OF MEDICINE, UNIVERSITY OF SANTIAGO DE COMPOSTELA, 15782, SPAIN.
Emails: cmelena@usc.es (Lopez–Martin); cmjorge@usc.es (Jorge–Barreiro)

Abstract

Microwave radiation can switch certain genes in response to stressful challenges to the cell. Heat shock protein 90 (HSP-90) are immediately expressed as marker of stress injury and play a protective role on central nervous system. Moreover, HSP-90 is preferentially expressed in neuronal cell populations in the unstressed mammalian brain. We explore the expression of molecular chaperone HSP-90 on brain neuronal circuits of rats using high-power microwaves with no-thermal or thermal radiation.
Twenty adult males Spragüe-Dawley were exposure to radiation (1.5 and 3 W at 2.45 GHz) using a commercial set up GTEM-250. (1) In acute exposures during 30´; (2) Repeated acute exposures (30´) during ten days. Control-rats were immobilized in set up considering the same elapse time but with no exposure to microwave.
Approximately 90´and 24 h after removal from the radiation cage, the rats were prefixed by transcardial perfusion saline followed by formaldehyde (4%). Their brains were cut with a vibrotome in transverse 40 µm sections. Finally, the sections were processed with blue toulidine and were tested with HSP-90 immunochemistry on hypothalamus, thalamus, hippocampus and cortical areas.
Acute exposure to microwave increases the HSP-90 expression in subregions of hypothalamus, thalamus, hippocampus and cortical areas; and these changes persist with repeated exposure.

1. Introduction

In the last years a great social and scientific concern has arisen for the possible adverse effects of the electromagnetic fields in the living organisms, in short of the radiofrequency, given the great technological advance of the last years, mainly in the field of the mobile telephones. However, already for many years that one comes applying the radiofrequency, in short the microwave, in the human being. A clear example is the medical-therapeutic application of high frequency radiation microwave (2,45 GHz)

in processes ostheoarticulars (diathermy for microwave) at different powers, usually between 25 and 200 watts (w). Microwave treatment is applying in humans directly over the anatomical treatment part about 15-30 minuts during 10-20 sessions. There is recently experimental evidence that the interaction of the radiofrequency with the living organism could produce effects not cause by heating biological tissue (D. Pomerai, 2003; E.Diem, 2005). There by, there are describe two types of biological effects: thermal and not thermal. Thermal effects make reference to secondary effects of energy deposited in the organism which cause an increase of temperature in the biological body and secondarily stimulates the thermoregulation mechanisms; and non-thermal effects are caused by the microwave radiation which does not increase the temperature in the organism (J. L. Franco and cols, 2006).

Heat shock proteins are constitutively expressed under normal conditions in cells and they intervene in a routine way in the metabolic processes essentials for the cell, like the "novo" proteins folding (D. Picard, 2002). But it is also known that under stressful conditions these proteins are overexpressed (induced HSP) to have a protective role in cells (D. S. Latchman, 2004), and even several studies showed that HSP synthesis is responsible for the protective effect of preconditioning by mild stressful stimuli (V. Amin et al, 1995). Recent studies have demonstrated than heat shock protein 90 (HSP-90) is expressed under physiologic conditions in more quantity in neural tissue that not neural (P. Gass, 1994; S. M. D´Souza and I. R. Brown, 1998), and that overexpression of HSP-90 plays an important role in the maintenance of the survival neuronal (G.S. Jeon and cols, 2004; R.G. Ahmed, 2005), for what we conclude that HSP-90 constitutes a biomarker that will help us to know the effects at level neuronal of different types of cellular stress, in this case of the radiation microwave.

The aim of this study was to explore the expression of molecular chaperone HSP-90 on brain neural circuits of rats, using whether thermal and non-thermal acute high-powered microwave (HPM) radiations (2,45 GHz) at 3.0 and 1.5 W respectively, and also after repeated-acute radiation exposure.

2. Material and Methods

2.1. Animals and Experimental Procedure

16 female Spragüe-Dawley rats were exposed to a HPM radiation (2.45 GHz) by using a GTEM250 commercial chamber. Rats were assigned to one of this two treatment groups: Acute and Chronic. "Acute group" rats were radiated, only one time, at 1.5 w or 3.0 w, for 30 minutes, and "Chronic group" rats were exposed to repeated acute HPM at 3.0 w for 30 minutes during 10 sessions (1 per/day) (see Table 1).

Table 1. Radiated Experimental Groups

Group	Microwave Power (watts)	Time Exposure (minuts)	Time Postradiation	Repeated Sesions (days)
Acute (n=16)	1,5 (n=8)	30	90 m	–
		30	24 h	–
	3 (n=8)	30	90 m	–
		30	24 h	–
Chronic (n=4)	3 (n=4)	30	90 m	10

The issuing field of the radiation was directed toward the upper left leg. Besides, control-rats were inmobilized during 30 minutes similar that radiation animals, but not exposured to radiation, in set up the same time (see Table 2).

Table 2. Non Radiated Control Groups

Group	Time post-inmovilization	N
Control Acute	90 m	5
	24 h	5
Control Chronic	90 m, 10 days	4

2.2- Tissue Preparation and Immunohistochemistry

Rats were deeply anesthetized with pentobarbital sodium and then, they were perfused transcardially with heparinized physiological saline followed by a solution of 4% parafolmaldehide in fosfate buffer, 90 minutes (m) and 24 hours (h) postradiation in acute group, and 90 m post radiation in chronic group. Following, rats were sacrificed, their brains were immediately removed and cryoprotected in sucrose for

approximately 24 hours. Subsequently, brains were frozen and cut into 40 µ coronal sections using a cryostat. These sections were processed using immunohystochemical techniques for demonstrating HSP-90 expression.

Finally, we evaluated HSP-90 positivity under an optic microscope Nikon Eclipse E2000 in 12 selected encephalic anatomical areas which nomenclature are from Paxinos and Watson: Hypothalamus (nucleus periventricular, PV; nucleus paraventricular, Pa; Lateral of Hypothalamus, LH and nucleus Arcuate, Arc), Hippocampus (Dentaty Gyrus, DG; CA1, CA2 and CA3) and Cortex (frontal, Fr; parietal, Parl; piriform, Pir and entorhinal, Ent). We compared acute and chronic radiated groups with their respective control-rats.

3. Results and Discussion

3.1 HSP-90 Expression in Acute 1.5 W Group

90 minutes after HPM exposure resulted in increases HSP-90 expression in all studies anatomical rat brain areas respect control, except PV of hypothalamus, where expression was similar to controls-rats. This expression still remained high after 24 hours microwave exposure in the same areas except in LH where the expression was similar to controls (see Table 3). HSP-90 expression was similar in hippocampus and cortex after 24 hours than after 90 minutes post radiation. Several studies have been observed that heat shock stress produced upregulation throughout the brain (Tynell M, 1993; Goldbaum O. & Ritchter-Landsberg, 2001), however, heat shock response depends on different factors, such as stress stimulus, and little is known about HSP-90 response to microwave at 2.45 GHz in the brain of rats, thereby we cannot compare our results.

3.2 HSP-90 Expression in Acute 3.0 W Group

HSP-90 expression in 90´postradiation group was greater than control-rats in subregions of hypothalamus (Pa and Arc) and hippocampus (CA1, CA2, CA3). The PV and LH expression were decrease and there were not different with controls in GD and cortex. After 24 hours, hsp-90 expression increase in more areas (nucleus arcuatus, hippocampus, and cortex), however, there were not significant changes in PV, Pa and LH (see Table 3).

Tabla 3. Expression of HSP-90 following exposure acute power (1.5 and 3 W) microwave radiations compared with control groups.

Anatomical Areas	1.5 W		3.0 W	
	Post–irradiation time		Post–irradiation time	
	90 m	24 h	90 m	24h
Hypothalamus				
PV	—	—/↑	↓	—
Pa	↑	↑	↑	—
LH	↑	—	↓	—
Arc	↑	↑	↑	↑
Hippocampus				
DG	↑↑	↑↑	—	↑
CA1	↑↑	↑↑	↑	↑
CA2	↑↑	↑↑	↑	↑
CA3	↑↑	↑↑	↑	↑
Cortex				
Fr	↑↑	↑↑	—	↑↑
Parl	↑↑	↑↑	—	↑↑
Pir	↑↑	↑↑	—	↑↑
Ent	↑↑	↑↑	—	↑↑

PV, periventricular nucleus; Pa, paraventricular hypothalamic nucleus; LH, lateral hypothalamus; Arc, arcuate nucleus; DG, dentate gyrus; Fr, frontal cortex; Par1, parietal cortex; Pir, piriform cortex; Ent, entorhinal cortex.

We observed than brain areas exposed to 3.0 W power microwave radiation are as much stimulated as brain areas exposed to 1.5 W; and HSP-90 expression at 3 W even was decreased with respect to 1.5 W acute group in some areas, such as hypothalamus and cortex.

3.3 HSP-90 Expression in Chronic Group

We observed that HSP-90 expression decreased in DG of hippocampus, hypothalamus (PV, Pa and LH) and piriform and entorhinal cortex (see Table 4). There were not differences in Arc, CA1, CA2, CA3 and frontal and parietal cortex.

Table 4. Expression of HSP-90 following repeated acute exposure to high-power microwave radiations (3 W, during 10 days) compare with controls.

Anatomical Areas	
Hypothalamus	
PV	↓↓
Pa	↓
LH	↓↓
Arc	–
Hippocampus	
DG	↓
CA1	–
CA2	–
CA3	–
Cortex	
Fr	–
Parl	–
Pir	↓
Ent	↓

PV, periventricular nucleus; Pa, paraventricular hypothalamic nucleus; LH, lateral hypothalamus; Arc, arcuate nucleus; DG, dentate gyrus; Fr, frontal cortex; Par1, parietal cortex; Pir, piriform cortex; Ent, entorhinal cortex.

We noted that the less stimulated area in all the groups corresponds to hypothalamus, and even in chronic group the expression in this area spreads to diminish. Loones and cols. (2000) have shown that HSP90 is most abundant in hypothalamus, preoptic areas, pons and medulla in the central nervous system of unstressed mouse.
Both the SAR values and the morphological thermal–SAR results will be presented on the poster, at the Symposium.

4. Conclusions

Acute high power (1.5 and 3.0 Watts) 2.45 GHz microwave radiation produces an upregulation heat shock response in subregions of central nervous system. Moreover, we observe that HSP–90 expression decrease when the delivered power increases in animals that are subject to acute exposure. Nevertheless, the repeated acute exposure causes decrease of the HSP–90 expression in hypothalamus and limbic areas, whereas keeps unchanged (compared to control groups) in several cortex and hyppocampal areas.

5. References

Ahmed R. G. *Heat stress induced histopathology and pathophysiology of the central nervous system.* Int. J. Devl. Neuroscience 23 (2005) 549-557.

Amin V, Cumming D , Coffin R, Latchman D. The degree of protection provided to neuronal cells by a pre-conditioning stress correlates with the amount of heat shock protein 70 it induces and not with the similarity of the subsequent stress. Neuroscience Letters 200 (1995) 85-88.

D´Souza S. M., Brown I. R. *Constitutive expression of heat shock proteins Hsp90, Hsc70 and Hsp60 in neural and non-neural tissues of the rat during postnatal development.* Cell stress and Chaperones (1998) 3 (3), 188-199.

Diem E., Schwarz C., Adlkofer F., Jahn O., Rüdiger H. Non-thermal DNA breakage bu mobile-phone radiation (1800 MHz) in human fibroblast and in transformed GFSH-R17 rat granulosa cells in vitro. Mutation Research 583 (2005) 178-183.

Gass P. , Schröder H. , Prior P., Kiessling M. Constitutive expression of heat shock protein 90 (HSP90) in neurons of the rat brain. Neuroscience Letters 182 (1994) 188-192.

Goldbaum O. and Richter-Landsberg. Stress proteins in oligodendrocytes: differential effects of heat shock and oxidative stress. Journal of Neurochemistry, 2001, 78, 1233-1242.

Jeon GS, Park SW, Kim DW, Seo JH, Cho J, Lim SY, Kim SD and Cho SS. Glial expression of the 90-kDa heat shock protein (HSP90) and the 94-kDa glucose-regulated protein (GRP94) following an excitotoxic lesion in the mouse hippocampus. Glia 48:250-258 (2004).

Latchman D. *Protective effect of heat shock proteins in the nervous system.* Current Neurovascular Research, 2004, 1, 21-27.

Loones MT, Chang Y, Morange M. The distribution of heat shock proteins in the nervous system of the unstressed mouse embryo suggest a role in neuronal and non-neuronal differenciation. Cell Stress & Chaperones (2000) 5 (4), 291-305.

Paxinos G., Watson C., The rat brain in steretaxic coordinates. 2nd ed. Sydney: Academic Press; 1986.
Picard D. *Heat-shock protein 90, a chaperone for folding and regulation*. CMLS Cellular and Molecular Life Science. 59 (2002) 1640-1648.

Pomerai D. Smith B. Dawe A., North K., Smith T., Archer D., Duce I. R., Jones D. and Candido P. M. Microwave radiation can alter protein conformation without bulk heating. FEBS Letter 543 (2003) 93-97.

Sebastian Franco JL, Muñoz San-Martín S, Sancho Ruíz M and Miranda Pantoja, JM. Medición de radiación en seres vivos. Investigación y Ciencia, Febrero, 2006, 46-55.

Tynell M., Barbe m. F. and Brown I. R. Stress (heat shock) protein accumulation in the central nervous system. Its relationship to cell stress and damage. Advances in Neurology. Vol 59

ANALYSIS OF MICROWAVE EXPOSURE TO A METEOROLOGICAL RADAR

C. MALACARNE, R. PONTALTI, A. VACCARI, L. CRISTOFORETTI

ITC-IRST - CENTRO PER LA RICERCA SCIENTIFICA E TECNOLOGICA

VIA SOMMARIVE, 18 - 38050 POVO, TRENTO – ITALY

Abstract

Exposure evaluation to radiofrequency and microwave non-ionizing radiation of both general public and workers is considered an emerging sector in environmental and safety work surveys. Nevertheless, radars are typically rarely analyzed, due to difficulties in measuring such kind of source, but also inaccessibility or even secrecy of some installations.

Aim of this study was to analyze the emissions of a meteorological doppler radar, placed in the Province of Trento (North Italy), working in C band, with a wavelength of about 5 cm and nominal peak power of 250 kW.

The survey involved: i) electric field monitoring around the radar, to assess the general public and operators exposure, and ii) test measurements on radar functioning, such as evaluation of the antenna's radiation pattern.

In the first case measurements were performed with electric field probe and spectrum analyzer, while in the second case only with spectrum analyzer in far field conditions. The signal was characterized both in frequency domain, to analyze operating frequency and frequency stability, and time domain, to acquire radiation patterns in the principal planes as well as pulse duration and duty cycle.

The obtained results are compared to standard limits, with particular reference to the EU Directive 2004/40/CE.

Introduction

Starting from the 1980s radar networks have become extensively used in meteorology for determining the location of rain and storm activity. The radar under analysis is one of the North–Italian network and consists of a DSWR-2500C (EEC) pulsed-doppler radar, which means that it is not only capable of detecting target's location (bearing, range, and altitude), but also measuring its velocity. In particular, velocity is determined by transmitting many radar pulses towards each target (hydrometeor in this specific case) over a very short period of time, and thus measuring relative target movement between each pulse. The frequency in which the pulses are emitted are usually referred to as Pulse Repetition Frequency (PRF). The radar operates at 5.8 GHz (C–band), with a wavelength of 5.5 cm; its nominal peak power is 250 kW, thus guaranteeing a coverage range of about 120 km.

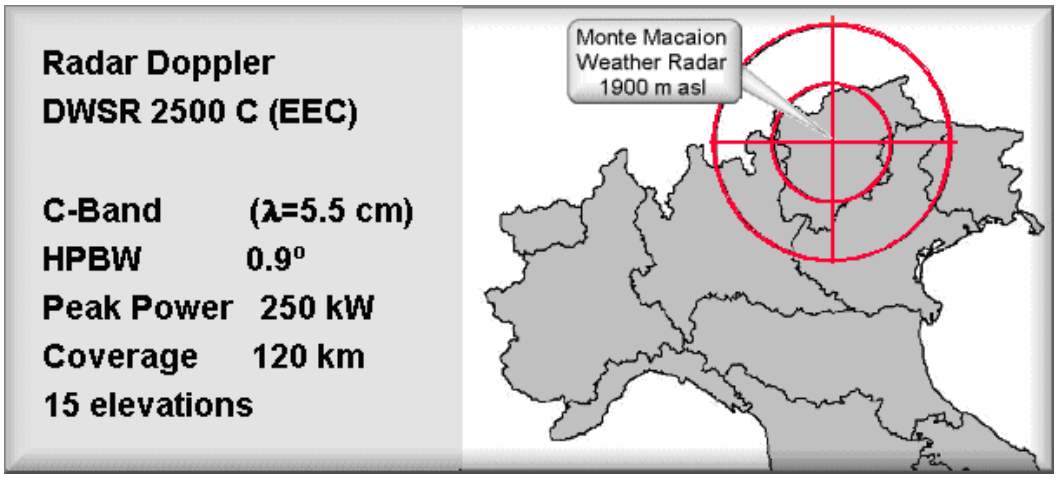

Figure 1: Location and main technical specifications of the weather radar system under analysis (Northern Italy).

The weather radar systems are generally designed and located to ensure that power densities that humans could be exposed to, fulfil the exposure limits. In order to assess this, measurements have to be carried out when the system is installed and operating in fully functioning conditions.
In particular, the two principal aspects investigated in this work were:

- the electric field values monitoring in the proximity of the radar (in near field conditions), in order to assess the exposure of both population and maintenance workers. Besides the radar personnel, exposed people could be only hikers, considering that in the area neither residential buildings nor commercial concerns are present.
- the measurement of the antenna's radiation pattern, being this latter crucial to predict the far field exposure. It is worth noting that the radar is located at a high altitude (1900 m a.s.l.), which permits a good extension of its horizons, otherwise limited by the mountainous orography. Therefore, the closest built-up areas are out of the radar's optical visibility, whilst those areas satisfying this condition are several kilometres far form the source, and at a significantly lower altitude.

In the first case, both the broadband electric field sensor and the spectrum analyser were used in proximity of the radar. Conversely, in the second case measurements were performed on a mountain 15 km south of the radar's location, since this ensured at the same time the fulfilling of the far field conditions (at a distance from the emitter larger than 700 meters), the good optical visibility, as well as a higher altitude (necessary for the characterisation of the antenna's lobe along the vertical direction). In this case only the spectrum analyser with the suitable antenna was used.
Afterwards, the results of the radioprotectional survey were compared to the limits provided by the EU Directive 2004/40/CE on workers' exposure to electromagnetic fields [1], to the thresholds reported by the ICNIRP [2] referred both to general public and workers, and also with the limits imposed by the national Italian law concerning general public exposure [3].

Site Description

The site housing the radar system lies on the top of a mountain (Monte Macaion, 1865.5 m a.s.l.; longitude WGS84: 11º12'32.6", latitude WGS84: 46º29'35.7"), characterised by a ridge gently descending towards west and by a rocky vertical front in east direction. The radar is mounted on a metallic tower 10 m high, with, at its bottom, two shelters housing the electronic equipment connected to the antenna. The radiating system consists of a 4.27 m diameter paraboloid antenna installed on a motorised pedestal, which enables orientations along whatever azimuth angles and elevations from -2º and 90º. Moreover, the antenna is covered by a 6.25 m diameter glass–reinforced plastic radome (Figure 2).

Figure 2:
The Monte Macaion summit, housing the weather radar. Measurement points 2 and 3 are also indicated.

In east direction with respect to the radar's tower there are some ruins and a redoubt, whose roof represented the highest measurement point of the area. Proceeding a few tens of meters in north-east direction, the terrain is

gently descending and without trees, forming a panoramic site rather frequented by hikers, especially during the summertime. About 350 m in 160º north direction there is another hill, at the same level of Monte Macaion, housing several broadcast antennas which contribute to the overall RF exposure level in this area.

Measurement points, instruments and technique

The measurement points for radioprotectional purposes were chosen at ground level and providing that optical visibility of the source was satisfied. In the absence of such a condition–even when the sight was obstructed only by leafy branch–a so considerable attenuation of the field was indeed registered, that exposure levels became insignificant from a radioprotectional point of view. The reason of such behaviour could be easily found in the highly absorptive character of high water content media in the microwaves frequency range.
Four different measurement points were chosen:

1. The radar equipment room, where personnel stands occasionally. The measurements were carried out with the radar in operating conditions, in order to assess possible dispersions from the cases containing the generation apparatuses.
2. The roof of the redoubt visible in Figure 2, as it is an interesting and comfortable place to stay for hikers, which also corresponds to the closest approaching point to the emission beam of the paraboloid antenna. During the measurements the most conservative conditions for the exposure were reproduced, by choosing an elevation of -2º and keeping an azimuth angle fixed along the receiving antenna direction. It is worth mentioning that such angle choices are not likely in normal operating conditions. In particular, the chosen elevation value produces images highly disturbed by orography and the fix azimuth angle is meaningless for meteorological purposes, even though manually selectable. In correspondence of this point the difference in height between the electric centres of the antennas (receiving antenna and radar) was 7 m, their distance was 30 m in 30º north direction, and the radar observation angle was +10º.
3. The panoramic site (see Figure 2) in north-east direction from the radar. In this case the difference in height between the electric centres of the antennas was 13 m, their distance was about 80 m in 40º north direction, and the radar observation angle was +9º.
4. The summit of the mountain Monte Roen, 14.9 km far from the radar. Its altitude is 2065.5 m a.s.l., that is 200 m higher than the Monte Macaion; its longitude WGS84 is 11º11’12.6”, its latitude WGS84 46º21’41.8”. The receiving antenna was placed 3 m above the ground, thus resulting in a difference in height of about 195 m between the electric centres of the antennas. The radar could see this point setting a theoretical azimuth value of 185.1º north with an elevation equals to +0.75º.

The measurements were performed by using:

- a spectrum analyser Agilent Technologies ESA–E4407B, which operates in the frequency range 100 Hz–26 GHz;
- a doubled ridge horn antenna EMCO 3115, linearly polarised and operating in the frequency range 1–18 GHz;
- a power density sensor General Microwave RAHAM (RAdiation HAzard Meter), Model 495. It features a six minute power density averaging function which automatically computes and displays the average exposure measurement over the six minute period as required by safety standards;
- an isotropic E-field probe General Microwave Model 94, operating in the frequency range 200 kHz–40 GHz and characterised by a wide dynamic range of 46 dB (from 0.005 to 200 W/m^2, or correspondingly from 1.37 to 274 V/m).

Being the radar signal composed by a succession of pulses, each of which lasts about 1/1000 of the time occurring between one pulse and the successive, the linearity of the response of the broadband sensors was initially checked. This was performed at the ITC-irst laboratory, before any measurement on site. The instruments used in this case were:

- a pulse generator (Philips PM5705) 0.1 Hz–10 MHz;
- a voltage variable attenuator (Mini Circuits ZFAS–15);
- a synthesised RF generator (HP8660C) from 10 kHz to 2600 MHz;
- a high power RF amplifier (PST–BHE, 500W);
- a biconical antenna (EMCO 3109);

In particular, the attenuator received the signal from the two generators (RF and pulse), mixing them into a new “composed” signal which was then amplified and used to feed the biconical antenna, placed in an anechoic chamber (Siemens–Matsushita). In this way, in the proximity of the antenna, pulses with E–field peak values of hundreds of V/m and a duty cycle typical of the radar (1/1000) were obtained. In these conditions, the satisfactory linearity of the sensor RAHAM 495 with its probe 94 was verified, at least up to values of about 10 V/m, corresponding to E peak values of 320 V/m. This led to the conclusion that, in the aforesaid E field range, the displayed value actually corresponded to the time-averaged field and the sensor was hence suitable for on-site radar signal measurements.

The electric field measurements for radioprotectional purposes were generally performed by the only use of the broadband sensor, with the exception of point 2, which was analysed also in narrow band with spectrum analyser and horn antenna. In correspondence of point 4 (far field) the only narrow band characterisation was instead performed.
While operating with the broadband sensor, it was placed at the three different heights (1.1, 1.5 and 1.9 m above the ground) prescribed by the Italian CEI 211-7 guide [4]. Considering the fact that the radar was remotely controlled, pointing the antenna towards the measurement point and keeping constant the signal emission conditions, the results obtained with the two operational modes 'Normal' (for direct reading of power density) and 'Average' (for computing the average power density over a six minute period) were equivalent. In fact, this assumption neglected the possible magnetron power fluctuations, but these were found to be insignificant with respect to those characteristic of the measurement point itself, such as the unpredictable signal scattering due to the foliage waving in the breeze. Consequently, the 'Normal' mode was used, which refreshed the power density values every 1.5 s.
The measurements with spectrum analyser were carried out in time domain (zero span), in peak detection mode and selecting a resolution bandwidth of 5 MHz, in order to filter as little as possible the impulsive nature of the signal. Furthermore, the chosen sweep time (20 μs) was the shortest selectable for the acquired points number. The signal was acquired in max-hold mode, which provides the envelope of all the maxima observed during the acquisition time, so that the snapshot of each pulse was frozen on the display as soon as it appeared in the measurement time window.
The horn antenna was placed with its electric centre at 1.5 m above the ground, in conformity with the CEI 211-7 guide [4] prescriptions. The polarisation of the antenna was horizontal, like that of the radar. During the measurements, the neglectability of the vertical component of the signal was also assessed: while in optical visibility of the radar, it always remained 15–20 dB lower than the horizontal.
Finally, the measurements performed in correspondence of point 4 (Monte Roen, 14.9 km far from the radar) were carried out with the only use of the spectrum analyser, following the same set-up just described, with some variations/additions. In particular:

- the horn antenna was placed at the highest possible height (3 m) on the roof of an off-road vehicle, in order to minimise the contribution of signals scattered from the ground;
- measurements were carried out also in the frequency domain, setting a 10 MHz span, in order to characterise the magnetron frequency as well as the pulse duration;
- some measurements were devoted to the assessment of the PRF (Pulse Repetition Frequency), by using the same settings described before (zero span), but with longer sweep times (up to 10 ms);
- the radiation pattern measurements were performed with the same settings, but making use of much longer sweep times (up to 100 s), in order to cover the complete azimuth revolution time. Consequently, the number of acquired points per sweep was much higher than before (up to 3600 points), in order to obtain a good angular resolution;
- the radiation pattern in the vertical plane was determined in a similar way. In this case, the radar azimuth angle was set as that maximising the radiation in correspondence of the measurement point; afterwards, the radar was made scan vertically, covering an overall amplitude of 27º (from -1º to +26º).

Results

It is well known that regulations in general define different limit for general public and occupational exposure. Moreover, some of them refer explicitly to only one of these categories: either the general public (like for example the Italian law DPCM 8 July 2003 [3]) or the workers (like for example the European Directive 2004/40/EC [1]). Regarding the general population, both the Italian law and the ICNIRP [2] limits were taken into account in the present work. In the first case, the E-field limit imposed in the frequency range under analysis is 40 V/m, expressed as rms value, which must not be exceeded in any case. The same law, as a cautionary measure to protect against any possible long-term effects, adopts a more conservative 'attention value' of 6 V/m in correspondence of children's playgrounds, residential dwellings, school premises and in general in those areas where people could stay for 4 hours or more per day, as well as in outdoor annexes that may be used as residential environments, such as balconies, terraces, courtyards, but excluding roof pavings. Therefore, this second limit was suitable only for residential buildings, far from the radar source. Both these values must be averaged over any six-minute period in an area equivalent to the vertical cross-section of the human body
Yet while the Italian Law does not discriminate between pulsed and not-pulsed sources, the ICNIRP guide establishes a peak value limit for the pulse, which must not exceed–in the considered spectrum range–1000 times its average value in terms of density power (S). Another aspect, which is taken into account in the ICNIRP guide while is lacking in Italian regulation, concerns the safeguard from annoying auditory effects, possibly caused by a thermoelastic interaction in the auditory cortex of the brain [5, 6, 7]. In order to avoid the onset of such kind of effect, the ICNIRP guide fixes a limit on the Specific Absorption (SA–energy per mass unit), which is however impossible to assess directly, being it related to quantities internal to the body. In addition, the guide indicates a

threshold for perception of about 100–400 mJ m^{-2} for pulses of duration less than 30 μs at 2.45 GHz (corresponding to an SA of 4–16 mJ kg^{-1}). However, other publications identify more conservative values: a threshold of 20 mJ m^{-2}, always for pulses of duration less than 30 μs, is stated in [8], while in [9] RF hearing has been reported also for energy density per pulse values lower than 90 mJ m^{-2} for pulse widths from 3 to 5000 μs. Furthermore, the Australian Radiation Protection and Nuclear Safety Agency in its Standard [10] establishes, on the basis of the considerations exposed in [11], a limit for the spatial peak SA of 2 mJ kg^{-1} (for general public) and 10 mJ kg^{-1} (for workers) in the head within any 50 μs interval.
On the other side, regarding the occupational exposure, there is not a specific Italian regulation, so that the normative reference has been the European Directive 2004/40/EC, which assumes in its turn the same limits established by the ICNIRP guideline for the workers.
Summing it up, the limits taken into account in this work were:

- Electric field: 40 V/m (averaged) for the general public–DPCM 8 July 2003;
  1952 V/m (61 V/m × 32), as peak value, for the general public–ICNIRP;
  137 V/m (averaged), for the workers–ICNIRP and 2004/40/EC;
  4384 V/m (137 V/m × 32), as peak value, for the workers–ICNIRP and 2004/40/EC
- Energy density per pulse: 20 mJ m^{-2}

Finally, the compliance with the 'attention value' of 6 V/m of the DPCM 8 July 2003 were also verified, in correspondence of the residential places at far distance from the radar but in optical visibility of it. Considering the minimum elevation of the radar (equals to -2º), at least 10 km are necessary to the radar beam for reaching the altitude of the closest villages (1500 m a.s.l).

In evaluating the electric field values, conservative hypotheses were applied, in order to eventually overestimate the field. Similarly, during the measurements, conservative parameters were adopted. For instance, it is customary to estimate the electric field in the antenna boresight (which extends up to $0.2\ D^2/\lambda = 70$ m) with its time-averaged value, without taking count of its angular-averaged value due to its rotation. Assuming this, it is:

$$E = \sqrt{\frac{Z_0\ P\ dc}{\pi\ D^2/4}} = 78.6\ \text{V/m}$$

where Z_0 (377 Ω) is the free space characteristic impedance, *dc* is the duty cycle (conservatively chosen as 0.00094), D is the paraboloid diameter (4.27 m) and P is the nominal peak power (250 kW). This averaged E-field intensity corresponds to a peak value of 2563 V/m. The energy density per pulse values are equal to 6.9, 13.9 and 34.8 mJ/m^2 for the three considered kinds of pulses, corresponding to the 'velocity' mode the first two and to the 'intensity' mode the last one.
From these results it follows that in the antenna boresight (cylinder which base corresponds to the paraboloid aperture and with an height of 70 m) a worker could occasionally stay in safety conditions according to the Directive 2004/40/EC and the ICNIRP, but with a possible auditory effect (perceived as a noise at 250 Hz) in the 'intensity' mode. Furthermore, no site in the antenna boresight is accessible to the general public, whilst the only site accessible to the workers is the platform (with parapet) surrounding the antenna radome.
Considering the first kilometre from the radar, only the broadcast towers in south direction could be interested by considerable exposure levels. However, owing to the minimum elevation value of -2º, the radar beam could only approach them from above, so that only maintenance workers who should climb them could be exposed to the radar primary radiation lobe. In this condition, neglecting again the radar rotation (thus representing the conservative but unlikely condition of fixed azimuth at 160ºN and elevation of -2º), the electric field can be estimated as:

$$E = \frac{\sqrt{30\ P\ dc\ G_n}}{d} = 41.5\ \text{V/m}$$

where $30 = 377/(4\pi)$, G_n represents the numeric antenna gain that is about 30000, d is the distance (radar–broadcast towers) equals to 350 m. Should the angular average be taken into account, this would introduce a further multiplying factor of $360^{-1/2} = 0.053$, which would make decrease the obtained value to about 2.2 V/m.
Therefore, even maintenance personnel potentially working on the towers facing the radar would operate in safety conditions accordingly to ICNIRP and EU Directive.
While these exposure points were characterised only from a theoretical point of view, those accessible to general public, as well as the equipment room (as described in the third paragraph), were instead actually measured. In particular, Table 1 refers to the results obtained in correspondence of point 2, where measurements were carried out both in broad- and narrow-band. Taking into account the different measurement techniques (in the first case three values at different heights were acquired, each of which represented the 6-minute average value; in the

second case one only intermediate height was considered and the acquisition was detected in peak mode), the difference between the two obtained values (1.2 dB) is widely justified.

<table>
<tr><th>POINT 2 (broadband)</th><th colspan="2">POINT 2 (narrow band)</th></tr>
<tr><td>Height 110 cm: E = 8.68 V/m</td><td rowspan="2"> 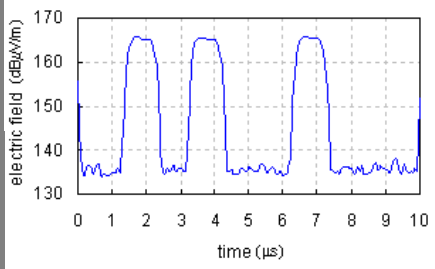
</td><td rowspan="2">Height 150 cm:
E (peak value) = 165.65 dBµV/m</td></tr>
<tr><td>Height 150 cm: E = 5.12 V/m</td></tr>
<tr><td>Height 190 cm: E = 5.82 V/m</td><td></td><td></td></tr>
<tr><td>Spatial average:
$E = \sqrt{\frac{8.68^2 + 5.12^2 + 5.82^2}{3}} = 6.72\,V/m$</td><td></td><td>Mean value with duty cycle:
$E = 10^{-6} \cdot 10^{\frac{165.65}{20}} \sqrt{9.4 \times 10^{-4}} = 5.87\,V/m$</td></tr>
</table>

Table 1: Electric field measurements in correspondence of point 2 (redoubt's roof). On the left the results obtained averaging the values acquired for the three heights, by using the broadband RAHAM sensor, are presented, while on the right, those obtained with the spectrum analyser. The picture in the middle displays the acquired spectrum: the three different peaks are due to the max-hold operating mode, and refer to different repetitions of the radar signal.

In correspondence of the remaining measurement points, the sensitivity limit (0.5 µW/cm^2) of the sensor was never reached, which means that the electric field kept lower than 1.37 V/m

The other set of measurements performed were devoted to the characterisation of the radar antenna radiation pattern in far field conditions. The horizontal plane pattern (alongside the azimuth angle) was acquired by making the antenna rotate with an angular velocity of 5°/s and by setting the spectrum analyser in zero span mode with a sweep time suitable to cover a complete turn. Figure 3 shows the part of the diagram concerning the angular range from -40° to +40° from the radiation maximum, acquired at 1.1° of elevation. In the remaining part of the diagram, the electric field level kept about 40 dB under the maximum and did not rise in correspondence of either the back lobe or possible spillovers.

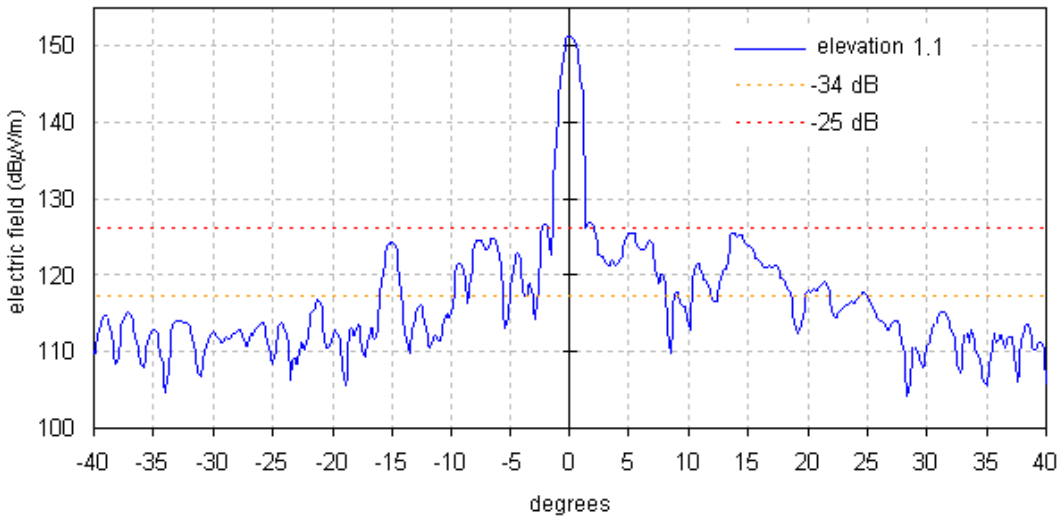

Figure 3: Electric field diagram by varying azimuth angle (horizontal plane), centred in the main lobe.

Finally, further measurements were carried out to better characterise the main lobe, in particular determining its amplitude in both the azimuth and elevation directions. The knowledge of these quantities (θ e φ, expressed in radiant and calculated at -3 dB from the maximum) enables to determine the antenna gain (Gn), on the basis of the formula:

$$Gn = \pi^2/(\theta\varphi)$$

which assumes a gaussian profile of the main lobe. The data acquired for different elevation values are shown in Figure 4 together with the parabola, which represents the fit using a quadratic regression. Being the ordinate axis in logarithmic scale, the curve would correspond to a gaussian trend in linear scale, thus confirming the suitability of the previous formula in determining the antenna gain.
The θ e φ angles obtained from the diagrams are 0.93º (azimuth) and 1.14º (elevation), thus giving a Gn=44.85 dB. This value is very close to that provided by the manufacturer: 45 dB.

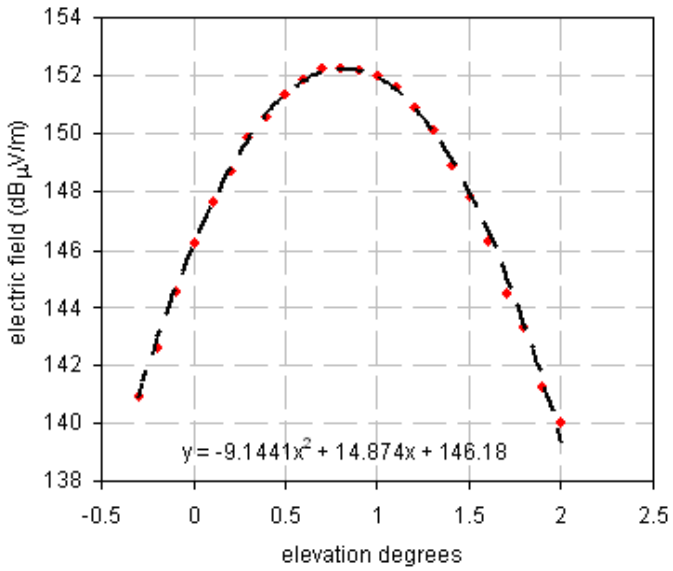

Figure 4:
Characterisation of the main lobe by varying the elevation (vertical plane). Points represent the acquired data, while the parabola is the fit obtained by using a quadratic regression.

Furthermore, the peak amplitude is verifiable by means of the following analytical formula, valid in far field condition:

$$E\,[\mathrm{dB\mu V/m}] = 120 + 20\log_{10}\frac{\sqrt{30\,P\,G_n}}{d} = 150.28\ \mathrm{dB\mu V/m}$$

where P is the nominal peak power ($2.5\ 10^5$ W), G_n is the numerical gain of the antenna and d is the distance ($1.49\ 10^4$ m). The comparison between this result and the actually measured value (with spectrum analyser, in peak mode detection) shows a discrepancy of 2 dB, with measured values exceeding those estimated. However, some considerations have to be taken into account:

- the directivity of the radar antenna is so high that, even at a long distance, the electric field peak values are important. For instance, at 15 km distance E=30 V/m, which however corresponds to 1 V/m provided it is time-averaged;
- also in this case the radar beam was intentionally pointing the measuring point, without rotating. In realistic operating conditions, the radar is continuously rotating, so that further reduction factors representing its movement both in the horizontal and vertical planes should be added.

As a consequence, it is possible to confirm that, even in correspondence of the residential places satisfying the optical visibility requirement and considering direct pointing of the radar beam over them, also the 'attention value' (6 V/m) of the Italian law would be fulfilled.

Conclusions

Regarding both the measurements and the theoretical estimation of electric field for radioprotectional purposes, all sites taken into consideration in the present work met the requirements of the Italian law DPCM 8 July 2003 (only concerning the general public), even considering the unlikely and highly conservative operating conditions of the radar, directly and constantly pointing to the measurement point. Moreover, no significant RF dispersion was found inside the equipment room. Also the exposure conditions of the maintenance personnel who could

access on broadcast towers facing the radar were assessed–through theoretical estimations–to comply the safety standards for the workers (ICNIRP and Directive 2004/40/CE), even in case of direct pointing of the radar beam towards their direction. The peak exposure thresholds of the ICNIRP and Directive 2004/40/CE are fulfilled as well, as the multiplying factor to introduce for the continuous exposure corresponds to the inverse of the radar duty cycle. Even the possible access on the platform surrounding the radar radome would comply the occupational limits. The only effect which could be observed in such condition (within the antenna boresight), as reported in literature [8, 9], is the onset of annoying auditory effects, as long as the 'intensity' pulse mode had been used. The antenna boresight is reachable by workers in this only situation, while it is never accessible to the general public.

References

[1] Directive 2004/40/EC of the European Parliament and of the Council on the minimum health and safety requirements regarding the exposure of workers to the risks arising from physical agents (electromagnetic fields) (18th individual Directive within the meaning of Article 16(1) of Directive 89/391/EEC), 29 April 2004.

[2] International Commission on Non Ionizing Radiation Protection (ICNIRP), "Guidelines for Limiting Exposure to Time-varying Electric, Magnetic, and Electromagnetic Fields (up to 300 GHz)". Health Physics 74: 494-522, 1998.

[3] DPCM 8 luglio 2003, "Fissazione dei limiti di esposizione, dei valori di attenzione e degli obiettivi di qualità per la protezione della popolazione dalle esposizioni a campi elettrici, magnetici ed elettromagnetici generati a frequenze comprese tra 100 kHz e 300 GHz", GU n. 199 del 28 agosto 2003.

[4] CEI 211-7, Fascicolo 5909: "Guida per la misura e per la valutazione dei campi elettromagnetici nell'intervallo di frequenza 10 kHz – 300 GHz, con riferimento all'esposizione umana", 2001.
CEI (Comitato Elettrotecnico Italiano) is the Italian Electrotechnical Committee. CEI is member of CENELEC, and CEI Standards are often endorsement of CENELEC Standards, designated by the same number.

[5] JC Lin. "Hearing microwaves: The microwave auditory phenomenon." IEEE Antennas Propagation Mag 43:166–168, 2001.

[6] J.A. Elder and C.K. Chou. "Auditory Responses to Pulsed Radiofrequency Energy", Bioelectromagnetics Suppl 6: S162-73, 2003.

[7] Louis N. Heynick, Peter Polson, "Human Exposure to Radiofrequency Radiation: a Comprehensive Review of the Literature Pertinent to Air Force Operations", United States Air Force Research Laboratory Technical Report AL/OE-TR-1996-0035, Brooks Air Force Base, Texas USA, 1996.

[8] Martin Röösli, Regula Rapp and Ursula Ackermann-Liebrich, "Hochfrequente Strahlung und Gesundheit", Bundesamt für Umwelt, Wald and Landshaft (BUWAL), 2003.

[9] Röschmann P. "Human auditory system response to pulsed radiofrequency energy in RF coils for magnetic resonance at 2.4 to 179 MHz." Magn Reson Med 21:197–215, 1991.

[10] Australian Radiation Protection and Nuclear Safety Agency, "Radiation Protection Standard for Maximum exposure levels to radiofrequency fields - 3kHz to 300GHz", Radiation Protection Series No. 3, 8 May 2003.

[11] Australian Radiation Protection and Nuclear Safety Agency, "Human auditory perception resulting from exposure to high power pulsed or modulated microwave radiation–specification of appropriate safety limits", 10 December 2004 (http://www.arpansa.gov.au/aud_perc.htm)

EXTREMELY LOW FREQUENCY ELECTROMAGNETIC FIELDS AND OXIDATIVE STRESS IN EXCITABLE CELL LINES

MARIA A. MARIGGIÒ[▲●], FERNANDA AMICARELLI[*], MARIA R. GROSSI[*], STEFANO FALONE[*], CATERINA MORABITO[▲●], ENZO TETTAMANTI[■], GIORGIO FANÒ[▲●], FRANCO CUCCURULLO[▲], CARMINE DI ILIO[▲]

LAB. FISIOLOGIA -[•]ISTITUTO INTERUNIVERSITARIO DI MIOLOGIA (IIM), [▲]CENTRO DI STUDI DELL'INVECCHIAMENTO (CESI) – UNIVERSITÀ "G.D'ANNUNZIO" CHIETI-PESCARA ", VIA COLLE DELL'ARA, I-66013 CHIETI)
***LAB DI BIOLOGIA APPLICATA, DIP. BIOLOGIA DI BASE ED APPLICATA, UNIVERSITÀ DEGLI STUDI DELL'AQUILA VIA VETOIO, COPPITO, I-67100 L'AQUILA**
[■]*DIP. DI SCIENZE BIOMEDICHE COMPARATE – FACOLTÀ DI MEDICINA VETERINARIA - UNIVERSITÀ DI TERAMO*

Corresponding Author: Prof. Maria A. Mariggiò Lab Fisiologia, Centro di Studi dell'Invecchiamento – Università "G.d'Annunzio"-Chieti-Pescara
via Colle dell'Ara
Chieti 66013, Italy
Tel +39 0871 3554048 Fax +39 0871 3554043
e-mail: mariggio@unich.it

M.A. MARIGGIÒ, F. AMICARELLI, M.R. GROSSI, S. FALONE, C. MORABITO, E. TETTAMANTI, G. FANÒ, F. CUCCURULLO, C. DI ILIO

Abstract

Recently, epidemiological studies and researches have proposed a relation between exposure to electromagnetic fields (extremely low frequency, ELF) and the development of several neurodegenerative diseases (WHO and NRPT progress reports 12-4-2004). This has stimulated scientific interest to verify ELF effects on different life forms (Repacholi MH, 2003).

We have analysed the effects of ELF on neuron-like cell lines (PC12 and SH-SY5Y), glioblastoma GL15 as glial model and C2C12 myocytes as muscle model, focusing our attention on the cellular oxidative stress machinery.

We exposed cell cultures to 50Hz ELF (0-1mT) generated by a solenoid or Helmholtz coils adapted to a confocal microscope, and investigated cell proliferation, ROS production, mitochondrial membrane potential, antioxidant enzymatic activities (SOD, Catalase, GSH-Px, etc).

The growth curves of tested cells did not show any differences between ELF-treated cells towards controls. The presence of ELF influenced ROS production in dependence of cell phenotype and of field intensity. Also mitochondrial potential as well as antioxidant enzymatic activities were altered by ELF.

These results show that ELF modified oxidative stress status in excitable cells. These were able, in different way depending on their biological activity, to counteract ELF effects and to adapt themselves without altering their proliferation rate.

Introduction

In 1996, the World Health Organization (WHO) decided to start a world program named "International Electromagnetic Fields (EMF) Project" regarding potential dangerous health effects of the exposure to electric and magnetic fields at extremely low frequencies (ELF-EMF). Such exposures arise mainly from the transmission and use of electrical energy at power frequencies of 50/60 Hz. The International EMF Project is scheduled to complete its health risk assessments of EMF in 2007, since it is likely that current and proposed research should provide sufficient results within this time frame to allow more definitive health risk assessments.

While the enormous benefits of using electricity in every day life and health care are unquestioned, the presence of possible inappropriate effects, or health consequence, needs to be clearly identified. The results of research currently available are often contradictory and this adds to people confusion and lack of confidence that supportable conclusions about safety can be reached.

The biological effects in cell lines derived from different modalities of ELF-EMF exposures have been frequently noted but the basic interaction mechanism(s) between such fields and living matter is unknown (Kavet et al., 2001; Foster KR, 2003). Even if some hypotheses have been suggested, none of these is adequately supported by experimental data (Repacholi and Greenebaum, 1999; Preece et al., 2000). Various cellular components, processes, and systems can be affected by ELF-EMF exposure, e.g. cell membrane (both internal and external) and signal transduction pathways (Czyz et al., 2004), cell cycle regulation and cell proliferation and/or differentiation (Simko and Mattsson, 2004; Frahm et al., 2006). Also direct or indirect DNA damage can be measured in different substrates but this does not directly lead to genotoxic effects (Villarini et al., 2006; Stronati et al., 2004). If the biological effects induced by ELF-EMF exposures are not easy to understand, the possible physiological effect of power frequency fields is still a hotly debated issue. In living organisms, above all in vertebrates, some tissue constituted by excitable cells (neurons and muscle fibres) are more sensible to the presence of perturbation of electric fields present around their cell membranes (Sieron et al., 2004). Some recent papers seem to confirm this assumption, in fact short-time exposure (5 days) to ELF-EMF radiations showed, by the cytotoxic glutamate (Glu) pulse test, a 30% decrease of cell survival in primary neurons, prepared from newborn rat cerebellum (Nikolova et al., 2005) and ELF-EMF exposure of neural progenitor cells transiently affects the transcript level of genes related to apoptosis and cell cycle control (Blackman et al., 1993). Also "in vivo" experiments seem to confirm the peculiar responsiveness of this particular cell typology to ELF-EMF presence. It has been found, in fact, that ELF-EMF exposure for 14 days (1 h daily) did not influence the level of the biogenic amines and their metabolites, but increased the rate of synthesis of DA and 5-HT in rat frontal cortex as compared to control (Jenrow et al., 1998). Several investigations have revealed that electrical activity within the central nervous system (CNS) can be affected by exposure to ELF-EMF. Many of these studies have concerned CNS structures exhibiting endogenous oscillations and synchrony as optimal sites for field coupling. In this regard, a particularly well characterized structure is the rat hippocampus whose rhythmic slow activities (necessary to some pathways of memory procedures) are exclusively susceptible to field-mediated perturbation suggesting that the sensitivity of these networks to ELF-EMF exposure may be really significant (Wolf et al., 2005).

In conclusion, the various modifications measured in several laboratories utilizing different substrates showed the presence of real biological effects (acute and chronic) derived from ELF-EMF exposure even if not without troublesome questions, these responses can be associated with detectable changes in cell physiology. This last consideration suggests that somehow, compensatory mechanisms at the translational and posttranslational level could exist.

Also for this reason, it is necessary to suggest the hypothesis regarding a possible initial cellular event affected

by exposure to ELF-EMF, an event which is present in a large number of effects observed as consequence of ELF-EMF exposure. Based on an extensive reviewed literature, Simko and Mattsson (2004) recently suggested that ELF-EMF exposure is able to perform such activation by means of increasing levels of free radicals. Such a general activation is compatible with the diverse nature of observed effects. Free radicals are intermediates in natural processes and they could be the stimulus to induce an "activated state" of the cell which then enhances the release of free radicals, in turn leading to biological events such as, in the CNS, an inhibition of the effects of the melatonin release and, as consequence of this, an alteration of biological rhythms or the deregulation of the neurotransmitter synthesis. In general, reactions in which radicals are involved become more frequent, increasing the possibility of DNA damage and therefore, to an increased risk of tumour development.
The purpose of this paper is to provide information about the effects of ELF-EMF applied to excitable cell lines. In particular, we focused our attention on the generation of radical oxygen species (ROS) and on the antioxidant system correlated with “in vitro” cell exposure to ELF-EMF having different intensities and duration using pheocromocytoma- and neuroblastoma-derived cell lines (PC12 and SH-SY5Y respectively) as neuronal models, glioblastoma GL15 as glial model and C2C12 myocytes as muscle substrates.
Results. To verify if the “in vitro” cell exposure to ELF-EMF influences cell proliferation rate, the cells were grown for 4-7 days in absence (control) or in presence of ELF-EMF (0.1, 0.5, 1.0mT). In fig. 1 a representative proliferation curve of the muscle cell line C2C12 is shown. At every considered intensities the proliferation rate didn’t show any significant difference in regard to control cells.

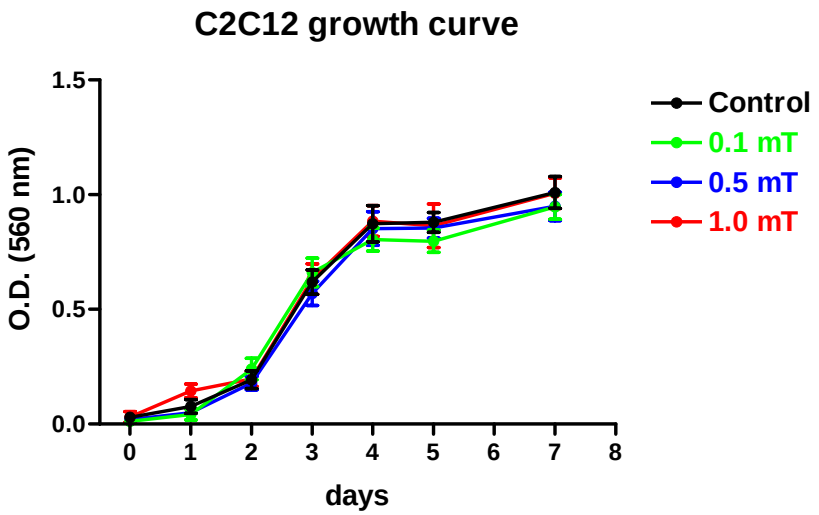

Fig. 1: Proliferation rate in C2C12 cell line exposed 0-7 days at different ELF-EMF intensities (0.1, 0.5 and 1 mT). The data are means±SEM, n=8.

In Tab.I we have reported the mean values of cell number/1000 ± SEM after 4 exposure days in the other tested cell lines. The PC12 cells showed a very slight dose-dependent increase of cell number (529.2±22.6 in the controls and 579.2±19.0 in the cell exposed to 1.0 mT), while the SH-SY5Y cell line didn't show any modification and the GL15 cells seemed to suffer a very slight decrease after 4 days at 1.0 mT ELF-EMF.

Proliferating cells (mean of the cell number/1000 ± SEM after 4 exposure days in growth medium, n=5)				
	Control	0.1 mT	0.5 mT	1.0 mT
PC12	529.2±22.6	547.2±25.6	569.0±27.6	579.2±19.0
SH-SY5Y	887.0±49.6	897.0±39.0	857.5±33.6	877.0±40.3
GL15	580.4±31.6	550.7±47.8	563.5±33.8	504.5±43.8

Tab. I: Cell proliferation of three cell lines (PC12, GL15 and SH-SY5Y) after 4 days exposure to ELF-EMF of different intensities (0.1, 0.5 and 1 mT).

To summarize, under these experimental conditions, the ELF-EMF exposure didn't show a single significant effect on cell proliferation rate.
A possible effect of the exposure to electric and magnetic fields at extremely low frequencies could be an

increase of ROS production and, as one consequence of this, a modification of mitochondrial membrane potential. To check if the exposure to ELF-EMF could induce ROS production, SH-SY5Y and GL15 cells were exposed to ELF-EMF (10-60 min) and ROS production was assayed (fig. 2). The data obtained show that in both cell lines and at each ELF-EMF intensity tested, there is a significant increase of ROS production at 20 min even with a quantitative and qualitative different time-course.

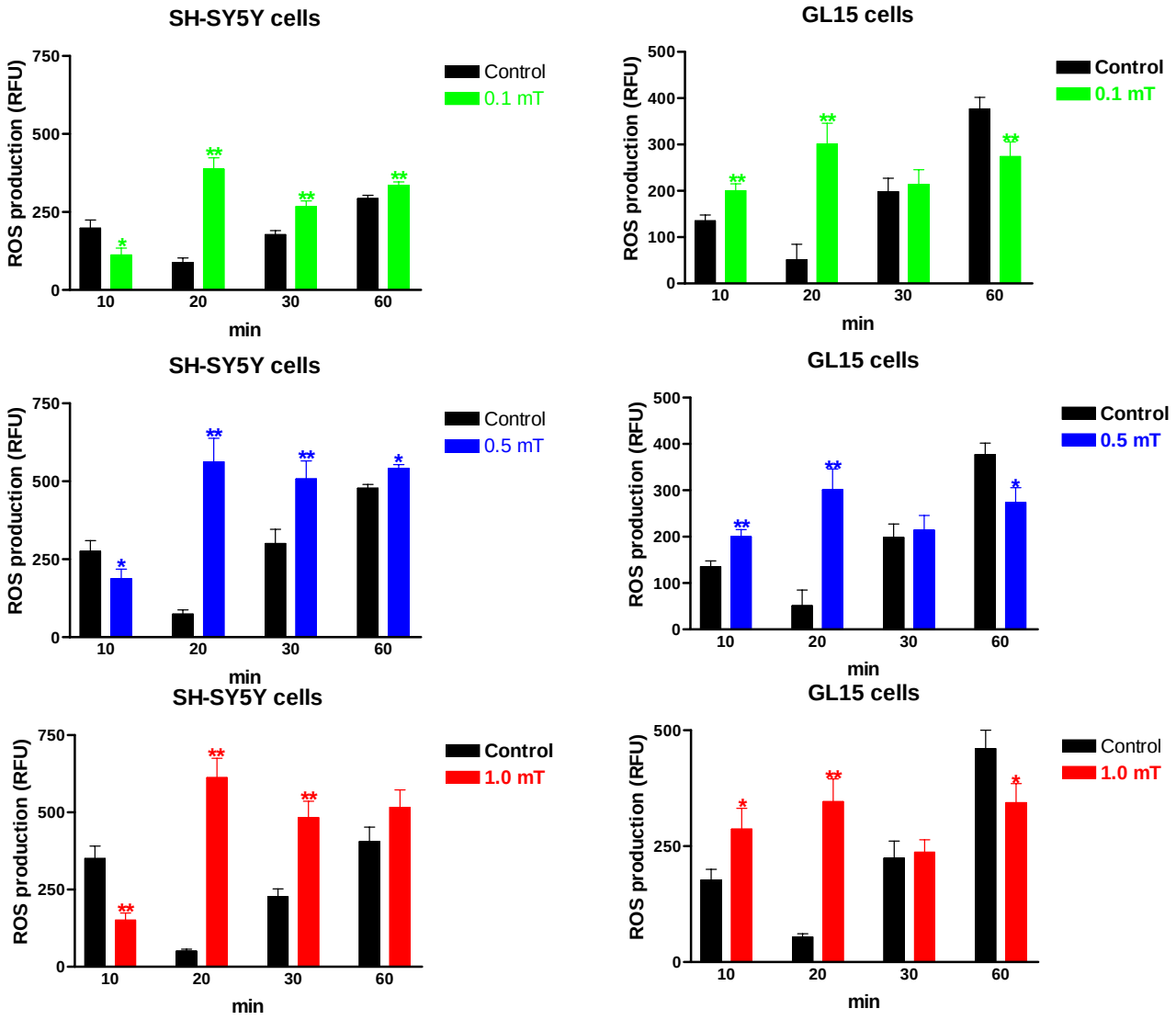

Fig. 2: ROS production analysed on cell populations. The ROS production was measured using DCF fluorescence emission assayed at different exposure times (10′, 20′, 30′, 60′) and different ELF-EMF intensities (0,1, 0,5 e 1mT). Data are mean ±SEM, n=4; *p<0.05, **p<0.01 vs control.

Using a single cell approach and a specific fluorescent dye (JC-1), we monitored mitochondrial membrane potential during ELF-EMF exposures utilizing a confocal microscope equipped by Helmholtz coils. Preliminary data suggested that mitochondrial membrane potential was affected by 1.0mT ELF-EMF on the cell lines tested.
The undaubted increase of ROS production could induce, as response, an activation of endogenous antioxidant system. For this reason, in PC12 and GL15, we tested the antioxidant enzymatic activities (superoxide dismutase: SOD, glutathione reductase: GSSG-Rx, catalase: CAT, glutathione transferase: GST, glutathione peroxidase/Se-dependent: GSH-Px/Se^{+}, γ-glutamylcysteine synthetase: γGCS) after 3 days 1.0mT ELF-EMF exposure. As shown in Fig. 3, these activities varied depending on the cellular typology and on the considered enzyme. Each cell line showed a peculiar pattern of enzymatic activities probably depending on their biological activity.

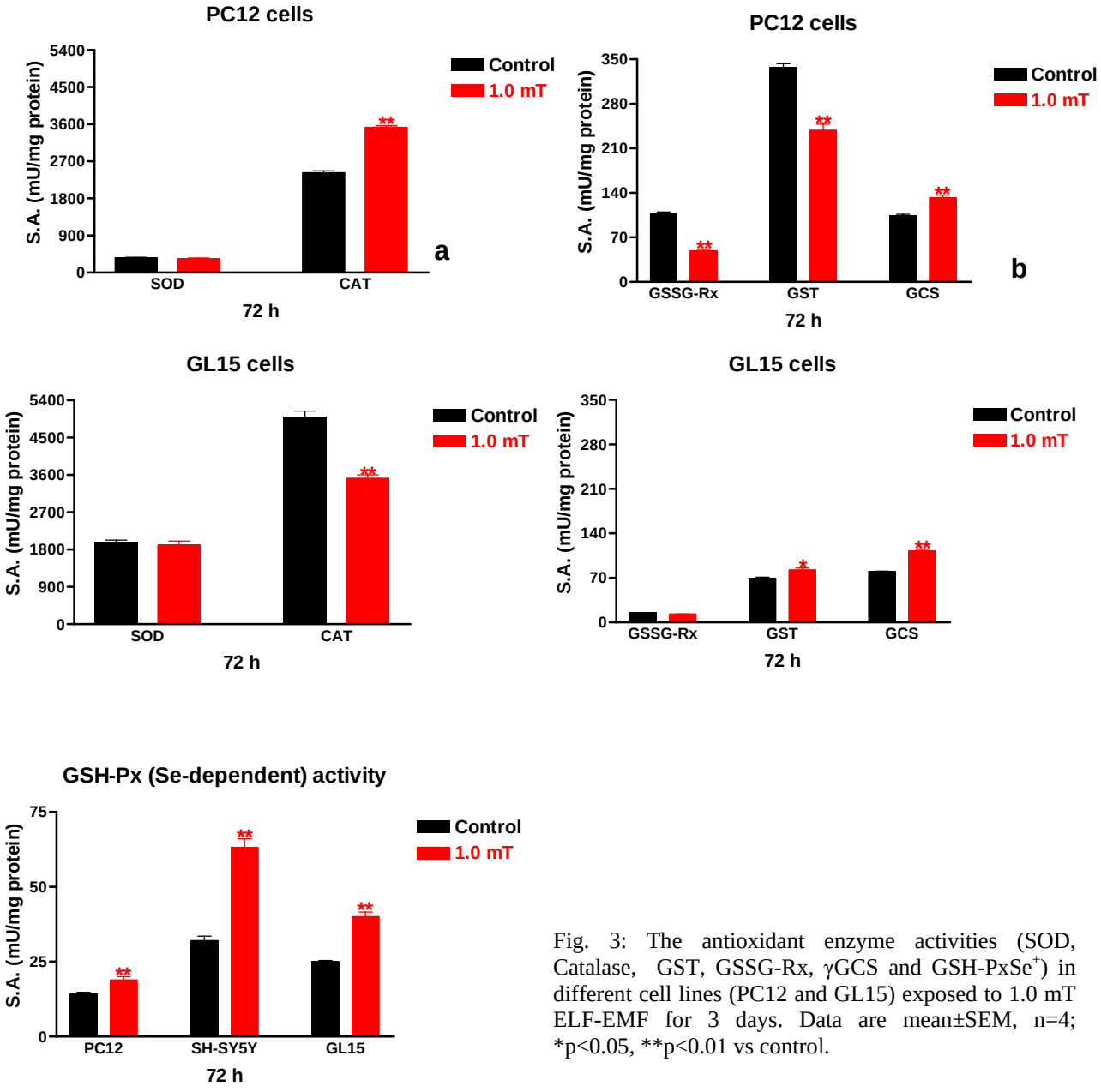

Fig. 3: The antioxidant enzyme activities (SOD, Catalase, GST, GSSG-Rx, γGCS and GSH-PxSe^{+}) in different cell lines (PC12 and GL15) exposed to 1.0 mT ELF-EMF for 3 days. Data are mean±SEM, n=4; *p<0.05, **p<0.01 vs control.

To complete the picture of the antioxidant system in GL15 cells, the levels of GSH, an endogenous antioxidant source, were measured. The levels of this molecule increased in GL15 cell line in the presence of ELF-EMF (fig. 4).

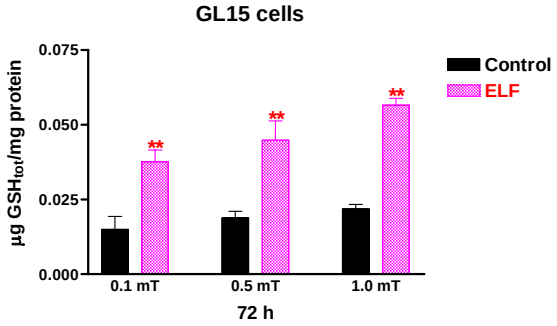

Fig. 4: The GSH total levels measured in GL15 cell line. Data are means±SEM, n=4; ** p<0,001.

In conclusion, depending on their intensity (mT), ELF-EMF affected the oxidative status, but the cells counteracted the induced increase of ROS production modifying their antioxidant ability.

Discussion. One mechanism through which ELF-EMF could influence neoplastic development is the deregulation of cancer-related genes and, in particular those related to different cyclins and cyclin-dependent kinases which are deputy to control cell cycle progression and cellular proliferation. The results of our experiments show that a slight, but dose-dependent, increase of proliferation rate was observed only in PC12 cells after exposure to ELF-EMF with graduated intensities (0.1-1.0 mT). This result is only apparently contradictory compared to those already published by McFarlane et al (2000) which reported no effect on cell proliferation of PC12 cells exposed to 4.5-15.8 microT ELF-EMF. In addition, during our experiments, if the intensity of ELF-EMF was lower than 0.5 mT, no modification in cell proliferation was noted. In the other cell types no variations (SH-5YSY) nor a significant slight decrease (GL15) after 4 days of exposure to the highest ELF-EMF intensity (1.0 mT) occurred. From these results, an initial consideration comes out: the effect of ELF-EMF on cell proliferation is dependent on the phenotype of cell model rather than on a direct action of ELF-EMF on some steps of cell cycle progression. As previously demonstrated by Ross in the 90's, markedly different effects, ranging from inhibition to stimulation of proliferation, were obtained, depending on the signal parameters (amplitude and frequency of ELF-EMF) as well as the types of utilized cell substrate (Ross SM, 1994). This fact is also supported by somewhat unclear results on the effect of the ELF-EMF on stromal stem cell proliferation (CFU-f); in fact, CFU-f from female mice showed a reduction, while CFU-f from male mice no decrease in cell proliferation (Van Den Heuvel et al., 2001).

More recently Wolf et al (2005) showed that the stimulation of proliferation, as well as the presence of DNA damage, was noted in HL-60 leukemia cells, Rat-1 fibroblasts and WI-38 diploid fibroblasts exposed for 24-72 h to 0.5-1.0-mT ELF-EMF. These effects were prevented by pre-treatment of cells with an antioxidant like alpha-tocopherol, suggesting that redox reactions were involved. Accordingly, the cells after exposure to 1.0 mT ELF-EMF exhibited a significant increase in ROS accumulation which was decreased by addition in the culture medium of an adequate scavenger (Wolf et al., 2005). Also under our experimental condition it was possible to note a significant increase of ROS production in all the tested cell lines even with a different qualitative and quantitative time-course. Moreover, also "in vivo" experiments seem to confirm that the chronic exposure to ELF-EMF is able to generate a stress oxidative status (Regoli et al., 2005; Harakawa et al., 2005; Yokus et al., 2005). In addition, the presence of an increase of ROS production is also indirectly demonstrated by the analysis of the enzymatic pathways involved in the catalytic removal of reactive oxygen species accumulated as an effect of ELF-EMF exposure. The "in vitro" experiments reported here, as well as the results derived from "in vivo" techniques (Lee et al., 2004) in mouse, show that the presence of ELF-EMF can induce a variable and specie-specific alteration of the stress oxidative pathway.

Summary

In vitro experiments performed in excitable cell lines: SY-SY5Y, GL15, PC12 and C2C12, seem to indicate that the biological response (proliferation rate) to ELF-EMF (0.1- 1.0 mT) exposure strictly depends on cell model than on the utilized ELF-EMF intensity or time of exposure. However, in both neuronal-like and glial-like cell lines, a significant increase of ROS production, with a different time-course in each cell line, was detected. This caused the enzymatic detoxification pathway involvement. In conclusion, even if further studies are necessary to identify the kind of ROS produced by the exposure to ELF-EMF, we propose that this biochemical substrate could be the candidate as the cellular "primum movens" of ELF-EMF induced effect on biological systems.

Acknowledgments

This study was supported by grants from MATT (5379/2002/SIAR; DSA/2004/0026774)

References

1. Blackman CF, Benane SG, House DE Evidence for direct effect of magnetic fields on neurite outgrowth FASEB J. 7(9):801-6; 1993.
2. Czyz J, Nikolova T, Schuderer J, Kuster N, Wobus AM. Non-thermal effects of power-line magnetic fields (50 Hz) on gene expression levels of pluripotent embryonic stem cells-the role of tumour suppressor p53. Mutat Res. 557(1):63-74; 2004.
3. Foster KR Mechanisms of interaction of extremely low frequency electric fields and biological systems. Radiat Prot Dosimetry. 106(4):301-10; 2003.
4. Frahm J, Lantow M, Lupke M, Weiss DG, Simko M. Alteration in cellular functions in mouse macrophages after exposure to 50 Hz magnetic fields. J Cell Biochem. Apr 5; 2006.
5. Harakawa S, Inoue N, Hori T, Tochio K, Kariya T, Takahashi K, Doge F, Suzuki H, Nagasawa H. Effects of a 50 Hz electric field on plasma lipid peroxide level and antioxidant activity in rats. Bioelectromagnetics. 26(7):589-94; 2005.
6. Jenrow KA, Zhang X, Renehan WE, Liboff AR. Weak ELF magnetic field effects on hippocampal rhythmic slow activity. Exp Neurol. 153(2):328-34; 1998.
7. Kavet R, Stuchly MA, Bailey WH, Bracken TD. Evaluation of biological effects, dosimetric models, and exposure assessment related to ELF electric- and magnetic-field guidelines. Appl Occup Environ Hyg. 16(12):1118-38; 2001.
8. Lee BC, Johng HM, Lim JK, Jeong JH, Baik KY, Nam TJ, Lee JH, Kim J, Sohn UD, Yoon G, Shin S, Soh KS. Effects of extremely low frequency magnetic field on the antioxidant defense system in mouse brain: a chemiluminescence study. J Photochem Photobiol B.73(1-2):43-8; 2004.
9. McFarlane EH, Dawe GS, Marks M, Campbell IC. Changes in neurite outgrowth but not in cell division induced by low EMF exposure: influence of field strength and culture conditions on responses in rat PC12 pheochromocytoma cells. Bioelectrochemistry. 52(1):23-8; 2000.
10. Nikolova T, Czyz J, Rolletschek A, Blyszczuk P, Fuchs J, Jovtchev G, Schuderer J, Kuster N, Wobus AM. Electromagnetic fields affect transcript levels of apoptosis-related genes in embryonic stem cell-derived neural progenitor cells. FASEB J. 19(12):1686-8; 2005.
11. Preece AW, Hand JW, Clarke RN, Stewart A. Power frequency electromagnetic fields and health. Where's the evidence? Phys Med Biol. 45(9):R139-54; 2000.
12. Regoli F, Gorbi S, Machella N, Tedesco S, Benedetti M, Bocchetti R, Notti A, Fattorini D, Piva F, Principato G. Pro-oxidant effects of extremely low frequency electromagnetic fields in the land snail Helix aspersa. Free Radic Biol Med. 39(12):1620-8; 2005
13. Repacholi MH, Greenebaum B. Interaction of static and extremely low frequency electric and magnetic fields with living systems: health effects and research needs. Bioelectromagnetics. 20(3):133-60; 1999.
14. Repacholi MH. WHO's health risk assessment of ELF fields. Radiat Prot Dosimetry.106(4):297-9; 2003.
15. Ross SM. Combined DC and ELF magnetic fields can alter cell proliferation. Bioelectromagnetics. 15(5):493; 1994.
16. Sieron A, Labus L, Nowak P, Cieslar G, Brus H, Durczok A, Zagzil T, Kostrzewa RM, Brus R. Alternating extremely low frequency magnetic field increases turnover of dopamine and serotonin in rat frontal cortex. Bioelectromagnetics. 25(6):426-30; 2004.
17. Simko M, Mattsson MO. Extremely low frequency electromagnetic fields as effectors of cellular responses in vitro: possible immune cell activation. J Cell Biochem. 93(1):83-92; 2004.
18. Stronati L, Testa A, Villani P, Marino C, Lovisolo GA, Conti D, Russo F, Fresegna AM, Cordelli E. Absence of genotoxicity in human blood cells exposed to 50 Hz magnetic fields as assessed by comet assay, chromosome aberration, micronucleus, and sister chromatid exchange analyses. Bioelectromagnetics. 25(1):41-8; 2004.
19. Van Den Heuvel R, Leppens H, Nemethova G, Verschaeve L. Haemopoietic cell proliferation in murine bone marrow cells exposed to extreme low frequency (ELF) electromagnetic fields. Toxicol In Vitro. 15(4-5):351-5; 2001.
20. Villarini M, Moretti M, Scassellati-Sforzolini G, Boccioli B, Pasquini R. Effects of co-exposure to extremely low frequency (50 Hz) magnetic fields and xenobiotics determined in vitro by the alkaline comet assay. Sci Total Environ. 361(1-3):208-19; 2006.
21. Wolf FI, Torsello A, Tedesco B, Fasanella S, Boninsegna A, D'Ascenzo M, Grassi C, Azzena GB, Cittadini A. 50-Hz extremely low frequency electromagnetic fields enhance cell proliferation and DNA damage: possible involvement of a redox mechanism. Biochim Biophys Acta. 1743(1-2):120-9; 2005.
22. Yokus B, Cakir DU, Akdag MZ, Sert C, Mete N. Oxidative DNA damage in rats exposed to extremely low frequency electro magnetic fields. Free Radic Res. 39(3):317-23; 2005.

Appendix

Instrumentation. The 50Hz ELF-EMF were generated by two different devices: a solenoid and a pair of

Helmholtz coils. These devices were planned and built to deliver variable, homogeneous, sine-wave alternate current magnetic fields with 50 Hz frequency and intensities ranging between 0.1-1.0 mT±2%. The horizontal cylindrical solenoid (length=340mm, diameter=113mm), on a supporting base, was supplied by a power supply Elgar Electronics (mod. CW-801P). The solenoid was used in an incubator (5% CO_2 and 37°C) for continuous long time cells exposures during which the solenoid's eventual added temperature was negligible. The pair of Helmholtz coils (r=445mm, distance between coils=400mm), producing homogeneous magnetic field over the specified volume-under-test corresponding to the cell chamber , were located in the working zone of a confocal microscope and connected to a power supply Elgar Electronics (mod. CW-1251P).

Cell culture. C2C12 and PC12 (American Culture Collection) and GL15 (functionally characterized in our lab, Mariggiò et al BMC Physiology 1:4, 2001) were cultured as exponentially growing cells in growth medium (GM). The GM for C2C12, SH-SY5Y and GL15 contains Dulbecco's modified Eagle's medium (DMEM), 10-20% foetal calf serum (FCS), 2-4 mM L-glutamine and 100 UI mL^{-1}-100 μg mL^{-1} Penicillin-Streptomycin. The GM for PC12 cells contains RPMI 1640 with 5% FCS and 10% horse serum, glutamine and antibiotics as mentioned above. Reagents for cellular culture were purchased from Gibco (Paisley, Scotland, UK). The cells were seeded on Petri dishes in GM and sub-cultured every 3 days (C2C12 and GL15) or weekly (SH-SY5Y and PC12) (Mariggiò et al, BMC Physiology 1:4, 2001; Guarnieri et al, Neuroscience 128:697–712, 2004; Pietrangelo et al., J Physiol.572(3):721-733, 2006). We exposed cell cultures to 50Hz ELF-EMF (0-1mT) generated by a solenoid or Helmholtz coils for different times according to the experimental plane.

Cellular proliferation was tested during 7 days in C2C12 and 4 culture days in the other cell lines, using the colorimetric assay of 3-[4,5-dimethylthiazol-2-yl]-2,5 diphenyltetrazolium bromide (MTT) as described by Pietrangelo et al. (J Physiol.572.3:721-733, 2006).

Mitochondrial membrane potential measurements. These were determined using a carbocyanine dye JC-1 (Molecular Probes, Eugene, Oregon, USA) which is taken up by the mitochondria. When the transmembrane potential is high, like in normal cells, JC-1 forms red fluorescence dimers (J-aggregate), while when it is low the red fluorescence disappears and green fluorescence emission appears (monomer). Briefly, the cells on coverslips were incubated in growth medium containing 5 mM of JC-1 for 10 min. After being rinsed three times with PBS, each coverslip was observed and images were recorded with or without the ELF-EMF generated by Helmholtz coils applied to a confocal microscope (excitation was fixed at 488 nm and emission was set to either 522 nm, for green monomer, or 605 nm, for red J-aggregate, using a bandpass filter). To estimate the modification of fluorescence in mitochondria, the change in green and red areas was calculated for the whole image using Scion Image ver. beta 3b (Scion Corporation, Frederick, Maryland, USA). The red/green area ratio, resulting from each single image of the experiment was plotted against time (Castellano et al., Arch. Pharm. Pharm. Med. Chem. 333:373–380; 2000).

ROS production. After different exposure times (10′, 20′, 30′, 60′) at different ELF-EMF intensities (0,1, 0,5 e 1mT), the cells, plated on 96 multiwell, were incubated at 37°C with dichlorodihydrofluorescin-diacetate (H_2DCF-DA) for 30'. After incubation the cells were washed and the ROS production was revealed by the fluorescence emission of oxidized 2',7'-dichlorofluorescein (DCF) read on a multiwell fluorimeter (excitation at 485 nm and emission at 530 nm).

Antioxidant enzyme activities. The enzymatic activities were measured on cell extracts using spectrophotometric assays according to Sun and Zigman (Anal. Biochem. 90: 81-89; 1978) for SOD1; Aebi HE (Methods in enzymatic analysis. New York: Academic Press; pp.:673-684; 1974) for CAT; Paglia and Valentine (J. Lab. Clin. Med. 70:158-169; 1967) for GSH-Px Se^{+}; Habig and Jacoby (Methods Enzymol. 77:398-405; 1981) for GSSG-Rx; Di Ilio et al. (Bioch. Med. 29:143-148; 1983) for GST; Volohonsky et al. (Chem. Biol. Interact. 140:49-65; 2002) for γ-GCS. The extracts were obtained through homogenization of $1x10^7$ cells and centrifugation at 12,000 rpm for 45 min.

GSH total levels. The total glutathione levels were determined using a kinetic assay in which catalytic amounts of GSH or GSSG derived from the continuous reduction of 5'5'-dithiobis (2-nitrobenzoic acid) (DTNB) by NADPH. The reaction rate is directly related to the concentration of glutathione at values up to about 2 mM. The formation of 5-thio-2-nitrobenzoate (TNB) was measured spectrophotometrically at 405 or 414 nm.

A ROLE OF ERK SIGNALING IN THE PROLIFERATIVE EFFECTS OF 50 Hz MAGNETIC FIELDS ON HUMAN NEUROBLASTOMA CELLS

M. A. MARTÍNEZ, M. A. CID, A. ÚBEDA, V. J. GARCÍA, J. LEAL, AND M.A. TRILLO

DEPT. INVESTIGACIÓN-BEM, HOSPITAL RAMÓN Y CAJAL, 28034-MADRID, SPAIN (m.antonia.martínez@hrc.es)

ABSTRACT

OBJECTIVE. We have reported before that 42 or 63 h intermittent exposure to 50 Hz, 100 μT magnetic field (MF) can induce cell proliferation in the NB69 line, from a human neuroblastoma (REFLEX Project, Final Report 2004). Evidence exist that mitogen-activated protein kinases can be involved in the MF- induced bioeffects. We have used a MAPK-specific inhibitor (PD98059) to investigate whether the activation of extracellular signal-regulated kinase (ERK1/2) is involved in the proliferative response elicited by MF.
METHODS. The growth response was analyzed through haemocytometer counting after 63 h of exposure to four conditions: control; PD98059 (20 μM); MF alone and MF + PD98059. In short-term studies, the expression of phosphoryled MAPK/ERK (p-ERK1/2) was analyzed (Immunocytochemistry - Image analysis) at 15, 30, 60 and 120 min of exposure.
RESULTS AND CONCLUSIONS. The results confirm that a 63 h, intermittent exposure to 50 Hz, 100 μT increases the growth rate of NB69 cells. This effect was blocked by the MAPK-specific inhibitor PD98059. In the short term, the MF induced a transitory significant increase of p-ERK1/2 expression peaking at 30 min (63.4%; p= 0.0010), such an effect was also negated by the inhibitor. These results indicate that the proliferative effects induced by the MF-exposure in NB69 cells could be mediated by a repeated (intermittent) transitory activation of the MAPK/ERK pathway.

INTRODUCTION

A number of epidemiological data have raised concerns about the relationship between exposure to power frequency magnetic fields (MF) and cancer promotion (Ahlbom *et al.* 2001) and on the potential contribution of the occupational exposure to power frequency fields to the pathogenesis of neurodegenerative diseases such as Alzheimer's or Parkinson's diseases (Feychting *et al.* 2003; Park *et al* 2005). Cellular studies are needed to reveal the cellular and molecular mechanisms underlying the biological effects and possible health implications of the exposure to power frequency MF.

In previous studies on NB69 human neuroblastoma cell line, we have reported that power frequency fields at 10 or 100 μT increase proliferation through activation of DNA synthesis (Trillo *et* al 2003; REFLEX-Project, Final Report 2004). Numerous studies have investigated the influence of power frequency magnetic fields with magnetic flux densities (MFD) in the mT range on cell proliferation (Katsir and Parola 1998; Wei *et al.* 2000; Wolf *et al.* 2005). However, there is limited evidence on the effects of MFD ≤ 100 μT, which corresponds to the ICNIRP recommended threshold for short-term exposure of the general public to 50-Hz MF. Since it is unlike that EMF can induce DNA damage directly, most studies have examined EMF effects at the cell membrane level, on general and specific gene expression, and on signal transduction pathways. Among the cellular processes proposed as implicated in the MF growth-promoting activity, signaling and regulatory cycle proteins have been reported altered, though this effect did not result in apparent changes in routine physiological processes such as cell growth or division (Korzh-Sleptsova *et al.* 1995; Richard *et al.* 2002; Lange *et al.* 2004). However, the type, the age and the state of the cell as well as the physical parameters of ELF-MF can affect in a different degree the reported MF bioresponses.

The aim of the present work is to explore the signaling and the regulatory proteins involved in the proliferative action exerted by a 50 Hz, 100 μT MF on the NB69 human neuroblastoma cell line, investigating whether mitogen-activated protein kinases (MAPK) could be involved in such a proliferative response. MAPK kinase pathways are signaling pathways that enable cells to respond to external stressors and stimuli (Kolch, 2000) and play a key role in a variety of cellular responses including proliferation, differentiation, and death. MAPK have been implicated in the cellular responses to magnetic fields (Jin *et al* 2000, Nie and Henderson,

2003). The MAPK family includes the extracellular signal–regulated kinases (ERK1/2). This ERK signaling pathway, also called the MEK-ERK cascade, is one of the principal cytoplasmic signal transduction systems that regulate processes of proliferation and survival in eukaryotic cells. Besides, up-regulation of ERK1/2 has been proposed to be implicated in tumor progression and metastasis in different cancer types (de Melo *et al.* 2006; Suthiphongchai *et al.* 2006; Cuevas *et al.* 2006). In the nervous system ERK1/2 has been connected to neuronal responses both, to functional (modulating neuronal survival, neuronal differentiation, and plasticity) and pathologic stimuli (such as Alzheimer or Parkinson disease, Chu *et al.* 2004; Webster *et al.* 2006). The results of the present study indicate that the activation of the extracellular, signal-regulated kinase, ERK1/2, is involved in the proliferative response of NB69 cells to the exposure to 50 Hz 100 μT MF.

MATERIAL AND METHODS

Cell growth assays. NB69 human neuroblastoma cells were maintained in Dulbecco's Minimum Essential Medium (D-MEM, Biowhittaker) supplemented with 15% heat inactivated fetal bovine serum, 4 mM L-Glutamine and 100 U/ml penicillin and 100U/ml streptomycin (Gibco BRL, Invitrogen, Spain). Cells were cultured at 37 ºC in a humidified incubator under an atmosphere of 5% CO_2. Cells were seeded, at a density of 4.5 x 10^4 cells/ml, into 60 mm Ø plastic Petri dishes (Nunc) or on circular 12 mm Ø coverslips placed into the Petri dishes, and cultured under standard conditions for three days. When needed, media were supplemented with the ERK1/2 kinase inhibitor, PD98059 (2'-amino-3'-methoxyflavone, Biosource). PD98059 was dissolved in dimethyl sulfoxide (DMSO). An equal dose of DMSO was added to the control dishes. The final concentration of DMSO in the medium was 0.1%. The mean value of the number of cells in controls with or without the vehicle, DMSO, was 649.0 ± 114.9 (x 10^4) and 647.2 ± 83.2 (x 10^4), respectively.

Magnetic field exposure. NB69 cells were exposed to a 50 Hz, sinus wave, linearly polarized magnetic field, at 100 μT. The MF was generated by a wave generator Newtronic Model 200MSTPC connected to a pair of coils set in a Helmholtz configuration. Currents in the coils were monitored using a multimeter (Hewlett Packart, model 974A, Loveland, CO) and measured with fluxgate magnetometers (EFA-3, Model BN 2245/90.20 Wandel and Goltermann S.A, EMDEX II, Enertech Consultants, Campbell CA). Two pairs of coils were placed inside two magnetically shielded chambers (co-netic metal; Amuneal Corp., Philadelphia, PA) kept in identical CO_2 incubators (Forma Scientific) with a 5% CO_2, 37 ºC and 100% humidity atmosphere. The background MF inside the shielded chambers was AC: 0.04 ± 0.03 μT; DC: 0.05 ± 0.04. In each experiment only one set of coils was energized. The samples in the unenergized set were considered sham-exposed controls. Both incubators were used, in a random sequence, alternatively for MF exposure and sham-exposure.

Study of the growth response at the end of a 63-hour lapse of intermittent exposure in the presence or absence of the MAPK inhibitor PD98059. NB69 cells were cultured under standard conditions for three days. At this time medium was renewed and 20 μM PD98059 was added to the culture media 60 min prior to the MF exposure. Ten Petri dishes, 5 with and 5 without PD98059 were placed in each exposure set up inside the incubators. The exposed group was treated intermittently, 3h On/3h Off, to 50 Hz MF at a 100 μT magnetic flux density for 63 h. The cells were subjected to: a) no treatment: controls, b) treatment with PD98059, c) exposure to MF, and d) MF exposure imposed upon PD98059 treatment. At the end of the exposure and or treatment, on day 6 post-plating (pp), the cellular viability and growth were determined through Trypan blue exclusion. All assays and analysis were performed in the blind for experimental condition.

Studies of the phosphoryled ERK1/2 expression in response to short-term MF exposure or PD98059 treatment. NB69 cells were exposed for 15, 30, 60 and 120 min at day 4 pp. The percent of phosphoryled ERK1/2 (p-ERK1/2) positive cells was analyzed by immunocytochemistry. At the end of the magnetic field exposure, the cells were fixed with 4% paraformaldehyde for 20 min at 4 ºC and permeabilized with 5% ethanol/acetic acid. The non-reactive sites were blocked (10% goat serum in PBS) for 1 hour at room temperature. Immunostaining was performed by incubating cells overnight at 4 ºC with primary antibody antiphospho –specific ERK1/2 (1:100) rabbit polyclonal antibody (44 -480G, Biosource) and a secondary, goat antirabbit IgG, antibody (1:500) conjugated with the fluorophore Alexa Fluor 488 (Molecular Probes) for 1 hour at room temperature. Hoechst 33342 (Bisbenzimide, Sigma) was included in the mounting medium as a counterstain for nuclei and was visualized and evaluated by photomicroscope. In each experiment 3 coverslips were studied per experimental group (Control; Inhibitor; MF; Inhibitor + MF). In each coverslip 15 random microscope-fields were analyzed and in each microscope-field the total nuclei (Hoechst fluorescent dye) and the percent of p-ERK1/2 positive cells were recorded. A total of about 4500-5000 cells per experimental group was evaluated. The statistical study applied the ANOVA test followed by the Student's T test.

RESULTS

1. Growth response at the end of a 63-hour lapse of intermittent exposure in the presence or absence of the MAPK inhibitor PD98059. The effects of 100 μT MF on the cell growth in the presence or absence of PD98059 at 20 μM are represented in Figure 1. The exposure to the MF induced a significant increase in the number of cells (9.1% over controls, $p< 0.01$), which confirms previously reported observations by our group (Trillo *et al*., 2003; REFLEX-Project, Final Report 2004). In contrast to that, the treatment with PD98059 provoked equivalent, significant decreases in the number of cells of MF-exposed (16.7% below controls, $p< 0.001$) or unexposed samples (16.7 % below controls; $p< 0.001$). The latest indicates that the MAPK inhibitor PD98059 inhibits cell growth in the NB69 line and blocks the MF-induced growing effect on these cells.

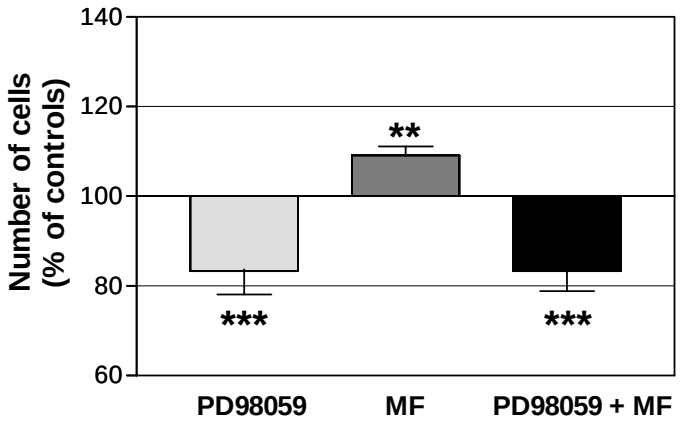

Figure 1. Effects of a 63 hours exposure to 100 μT MF and/or of treatment to 20 μM PD98059 on the number of cells. Data from 4 experimental replicates normalized with respect to controls (Mean ± SEM). **: $p< 0.01$; ***: $p< 0.001$ (ANOVA followed by Student's T-test.)

2. Phosphoryled ERK1/2 expression in response to short-term MF exposure or PD98059 treatment. Figure 2 shows the results of short-term treatment with MF or MAPK inhibitor on day 4 pp. The MF exposure provoked a transitory increase in the percent of cells that express p-ERK1/2, peaking at 30 min of exposure (63.4% over controls $p< 0.01$), the effect being prevented by PD98059. However, at 120 min of exposure a significant decrease in the p-ERK 1/2 expression (19.0% below controls; $p< 0.001$) was obtained. This response was similar to that induced by the inhibitor alone and by the combined treatment (27.6%; $p< 0.05$ and 28.8%, $p< 0.05$ below controls, respectively). As can be observed, the MAPK inhibitor PD98059 only provoked a significant reduction in ERK1/2 activation after 120 min of treatment, although it was able to prevent the MF induced ERK1/2 expression at 30 and 60 min of treatment. Taken together, these results indicate that the MF can induce transitory activation of the MAPK/ERK pathway in NB69 cells and suggest that the proliferative response induced by the exposure to 50 Hz 100 μT MF could be mediated by this transitory activation of MAPK, ERK1/2 transduction pathway, in each of the 3-hour On periods of the intermittent exposure cycle.

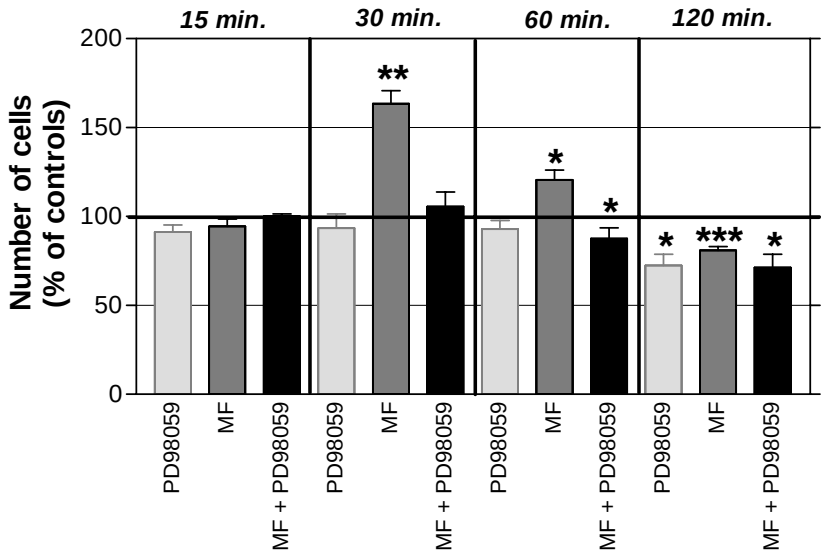

Figure 2. p-ERK 1/2 expression in response to short-term MF exposure or PD98059 treatment. Transitory effect of the MF exposure, peaking at 30 min. The MAPK-specific inhibitor, PD98059, blocks the MF effect. N = 4 independent replicates, data normalized with respect to controls (Mean ± SEM). *: $p< 0.05$; **: $p< 0.01$; ***: $p< 0.001$, Student's T- test.

DISCUSSION:

The effect of the MAPK-specific inhibitor PD98059 on MF-induced cell growth and on ERK1/2 phosphorylation was examined to determine whether ERK1/2 is involved in the proliferative effects of 50 Hz MF on NB69 human neuroblastoma cells. The ERK1/2 signaling pathway is a major determinant in the control of diverse cellular processes such as proliferation, survival, differentiation and motility. This pathway is often up regulated in human tumors (de Melo *et al.* 2006; Kohno and Pouyssegur 2006), and play an essential role in cell cycle progression, through induction of cell cycle regulatory proteins and transcription factors (Chang *et al.* 2003).

The present data confirm that a 63-hour intermittent exposure to 50 Hz, sinus wave MF at 100 μT promotes cell growth in the NB69 cell line. This increased growth was prevented when the specific inhibitor of the ERK1/2 activation, PD98059, was present. Besides, the field provoked a transitory increase in the activated, extracellular signal regulated kinase, p-ERK1/2, peaking at 30 min of exposure. The presence of PD98059 blocked this transitory activation of ERK1/2. At 120 min of MF exposure a significant decline in the expression of p-ERK1/2 occurred, both in the presence or in the absence of PD98059. Three other human cell lines (HTB 124, MCF7 and HL60), known to respond to MF with a 2 - 3-fold induction of HSP70 expression (Goodman *et al.* 1998), have also been reported to be responsive to a 30 min MF exposure (60 Hz, 8.0 and 80 μT) and induce ERK1/2 phosphorylation (Jin *et al.* 2000). The level of MAPK activation in MCF7 and HL60 cells exposed to the MF (60 Hz, 100 μT) was approximately equivalent to that in cells treated with 0.1 - 0.5 ng/ml of 12-O-tetradecanoylphorbal-13-acetate, TPA, (Nie and Henderson, 2003). Moreover, a cooperative effect on PKC activity has been observed when exposure to TPA and MF (50 Hz, 1 mT) were applied simultaneously on human amniotic cells (Richard *et al.* 2002), which is suggestive of a role for protein kinase C in the process leading to MAPK activation in MF exposed cells. It is currently believed that power frequency fields initiate the activation of the stress response when the signal affect receptors in the plasma membrane and that this subsequently triggers the specific signal transduction pathway that regulates different cell processes. In our study, the question whether the MF-activation of EKR1/2 in NB69 cells is a consequence of the conventional extracellular stress-activated signaling to the nucleus remains unanswered. However, like in the work by Jin *et al.* (2000), in the present study a MF activation of ERK1/2 was obtained, this activation being associated to the MF-induced promotion of proliferation in NB69 cells.

Different authors have reported effects of power frequency MF on cell proliferation in neuroblastoma lines; however, the molecular regulatory mechanisms underlying these MF-induced bioeffects remain unidentified. Namely, proliferation induction was obtained in neuroblastoma cells (LAN-5) after seven days of

continuous exposure to 50 Hz, 1 mT; this effect being associated to transitory increases of the proto-oncogen B-myb (Pirozzoli *et al.* 2003). Also, Tonini *et al.* (2001) reported inhibition of proliferation in NG108-15 cells treated with the differentiating agent BT2cAMP. This chemically-induced inhibition of cell proliferation was relieved by exposure to a 50 Hz MF at 120 or 240 μT. Our present results suggest that the proliferative response induced by the exposure to 50 Hz 100 μT magnetic fields could be mediated by a repeated transitory activation of MAPK, ERK1/2 transduction pathway, in each of the 3-hour On periods of the intermittent exposure cycle. Recently Ebisuya *et al* (2005) have reported that differences in the duration, magnitude and compartmentalization of ERK activity can generate variations in the signaling output that determine the cellular outcome. Furthermore, in the study by Ebisuya and coworkers several molecules have been identified as spatial, temporal or strength-controlling regulators of ERK activity. Consistent with that, a potential induced modulation by the MF exposure of these regulators of ERK activity could represent one of the mechanisms implicated in the MF-induced proliferation observed by us in NB69 cells.

SUMMARY

The purpose of the present work is to determine whether the mitogen-activated protein kinases MAPK, ERK1/2 is potentially involved in previously reported effects of the intermittent exposure to a 50 Hz, 10 or 100 μT magnetic field on the proliferation of the NB69 human neuroblastoma cell line. The influence of the MAPK-specific inhibitor PD98059 on MF-induced effects on cell growth and on ERK1/2 phosphorylation was examined. The obtained results show that the MF-induced growth response is prevented when the ERK1/2 activation was chemically inhibited. Besides, the MF provoked a time course significant, transitory increase in the p-ERK1/2 expression, peaking at 30 min of exposure. That transitory effect was also prevented by the MAPK specific inhibitor. Taken together, the present data indicate that the increase in cell proliferation induced by a 50 Hz, 100 μT MF in the NB69 line could be the result of a consecutive, transitory activation of the MAPK, ERK1/2 transduction pathway, during the On periods of intermittent exposure to the field.

Supported by EU Commission REFLEX-Project QLK4-1999-01574, FISS-03/0806 and Project I+T under agreement MOU EUROPA, ERG 101.013.

REFERENCES

Ahlbom A, Cardis E, Green A, Linet M, Savitz D, Swerdlow A. 2001. Review of the epidemiologic literature on EMF and Health. Environ. Health Perspect. 109: 911-933.

Chu CT, Levinthal DJ, Kulich SM, Chalovic EM, DeFranco DB. 2004. Oxidative neuronal injury. The dark side of ERK1/2. Eur.J.Biochem. 271: 2060-2066.

Chang F, Steelman LS, Shelton JG, Lee JT, Navolanic PM, Blalock WL,Franklin R, McCubrey JA. 2003. Regulation of cell cycle progression and apoptosis by Ras/Raf/MEK/ERK pathway (Review). Int. J. Oncol. 22:469-480.

Cuevas P, Diaz-Gonzalez D, Garcia-Martin-Cordova C, Sanchez I, Lozano RM, Gimenez-Gallego G, Dujovny M. 2006. Dobesilate diminishes activation of the mitogen-activated protein kinase ERK1/2 in glioma cells. J. Cell. Mol. Med. 10: 225-230.

de Melo M, Gerbasse MW, Curran J, Pache JC. 2006. Phosphorilated extracellular signal-regulated kinases are significantly increased in malignant mesothelioma. J. Histochem. Cytochem. Available: http://www.jhc.org/cgi/

Ebisuya M, Kondoh K, Nishida E. 2005. The duration, magnitude and compartmentalization of ERK MAP kinase activity: mechanisms for providing signal specificity. J. Cell. Sci. 118: 2997-3002.

Feychting M, Jonsson F, Pedersen NL, Ahlbom A. 2003. Occupational magnetic field exposure and neurodegenerative disease. Epidemiology 14(4):413-419.

Goodman R, Blank M. 1998. Magnetic field stress induces expression of hsp70. Cell Stress Chaperones, 3 : 79-88.

Jin M, Blank M, Goodman R. 2000. ERK1/2 phosphorylation, induced by electromagnetic fields, dismishes during neoplastic transformation. J. Cell. Biochem., 78 : 371-379.

Katsir G, Parola AH. 1998. Enhanced proliferation caused by a low frequency weak magnetic field in chick embryo fibroblasts is suppressed by radical scavengers. Biochem. Biophys. Res. Commun. 252 :753-756.

Kohno M, Pouyssegur J. 2006. Targeting the ERK signaling pathway in cancer therapy. Ann. Med. 38 : 200-211.

Kolch W. 2000. Meaningful relationships: the regulation of ras/raf/MEK/ERK pathway by protein interactions. Biochem J. 351: 289-305.

Korzh-Sleptsova IL, Lindstrom E, Mild KH, Berglund A, Lundgren E. 1995. Low frequency MFs increased inositol 1,4,5-trisphosphate levels in the Jurkat cell line. FEBS Lett. 359 : 151-154.

Lange S, Viergutz T, Simkó M. 2004. Modifications in cell cycle kinetics and in expression of G1 phase-regulating proteins in human amniotic cells after exposure to electromagnetic fields and ionizing radiation. Cell Prolif 37: 337-349

Nie K, Henderson A. 2003. MAP Kinase activation in cells exposed to a 60 Hz electromagnetic fields. J. Cell. Biochem. 90: 1197-1206.

Park RM, Schulte PA, Bowman JD, Walker JT, Bondy SC, Yost MG, Touchstone JA, Dosimeci M. 2005. Potential occupational risk for neurodegenerative diseases. Am J Ind Med 48: 63-77

Pirozzoli MC, Marino C, Lovisolo GA, Laconi C, Mosiello L, Negroni A. 2003. Effects of 50 Hz electromagnetic field exposure on apoptotic and differentiation in a Neuroblastoma cell line. Bioelectromagnetics 24 : 510-516.

REFLEX-Project 2004. Risk evaluation of potential environmental hazards from low energy electromagnetic field exposure using sensitive in vitro methods. Report Final, pp 274.
Available: http://www.verum-foundation.de/apopis

Richard D, Lange S, Viergutz T, Kriehuber R, Weiss DG and Simko M. 2002. Influence of 50 Hz electromagnetic fields in combination with a tumor promoting phorbol ester on protein Kinase C and cell cycle in human cells. Mol. Cell. Biochem. 232 (1-2): 133-141.

Suthiphongchai T, Phimsen S, Sakulkhu U, Tohtong R. 2006. PD98059-inhibited invasion of Dunning rat prostate cancer cells involves suppression of motility but not MMP-2 or uPA secretion. Oncol. Rep. 15: 1605-1610.

Tonini R Baroni MD, Masala E, Micheletti M, Ferroni A and Mazzanti M. 2001. Calcium protects differentiating neuroblastoma cells during 50 Hz electromagnetic Radiation. Biophys. J. 81 :2580-2589.

Trillo MA, Martínez MA, Cid MA, García VJ, Ubeda, A and Leal, J. 2003. Action of 50 Hz magnetic fields on the growth of human neuroblastoma cells., 25th BEMS Meeting, Maui, Hawaii, Abstract Book: 287

Wei M, Guizzetti M, Yost M, Costa LG. 2000. Exposure to 60-Hz magnetic fields and proliferation of human astrocytoma cells in vitro. Toxicol Appl Pharmacol. 162(3):166-176.

Webster B, Hansen L, Adame A, Crews L, Torrance M, Thal L, Masliah E. 2006. Astroglial activation of extracellular-regulated kinase in early stages of Alzheimer disease. J. Neuropathol. Exp. Neurol. 65: 142-151.

Wolf FI, Torsello A, Tedesco B, Fasanella S, Boninsegna A, Ascenzo MD, Grassi C, Azzena GB, Cittadini A. 2005. 50-Hz extremely low frequency electromagnetic fields enhance cell proliferation and DNA damage: Possible involvement of a redox mechanism. Biochim Biophys Acta 1743: 120-129.

GUIDELINES COMPLIANCE IN HUMAN EXPOSURE TO ELECTROMAGNETIC FIELDS FROM WLAN DEVICES

MERCEDES MARTÍNEZ-BÚRDALO, AGUSTÍN MARTÍN,
VÍCTOR PIZARRO, RAIMUNDO VILLAR

INSTITUTO DE FÍSICA APLICADA. CONSEJO SUPERIOR DE INVESTIGACIONES CIENTÍFICAS (CSIC)
C/ SERRANO 144. 28006 - MADRID. SPAIN

Abstract

Human exposure to electromagnetic fields from mobile communications (base-stations and mobile phones) has been widely studied in the last years. Nevertheless, the increasing use of wireless technology for short range data transfer (DECT, Bluetooth and WLAN) in home and office has enhanced the social concern about potential adverse health effects of electromagnetic fields from those technologies. Moreover, epidemiological studies and assessments of electromagnetic environments make necessary to know the influence that the electromagnetic field from a certain new technology source has in the total exposure level of a person.

The aim of this work is to assess, by using the finite-difference time-domain method (FDTD), the human exposure to electromagnetic fields from the antennas of wireless devices such as those of wireless local area networks (WLAN) access points. Several geometrical configurations are considered to simulate the exposure of the head of a person, as a worst case, to the fields from a WiFi antenna operating at 2400 MHz in home or office environments, calculating both, field values to be compared with reference levels and maximum specific absorption rate (SAR) values to be compared with basic restrictions. The situation of short-distance exposure to the bluetooth antenna of a personal digital assistant (PDA) in front of the eye of the user is also studied by calculating the SAR. Results are presented.

Introduction

In the last years, there has been a social concern about the possible harmful effects on the human health derived from people exposure to radiofrequency electromagnetic fields, specially those produced by mobile telephony (base-station antennas and mobile phones). Nevertheless, the rapid introduction in home and office environments of new emerging wireless technologies, such as the wireless local area networks (WLAN of WiFi) and Bluetooth, is motivating the users to worry about possible negative effects on their health caused by these technologies.

The human exposure to radiofrequency electromagnetic fields is regulated by national and international guidelines [1,2] which limit the exposure of general public to those fields, based on the guidelines from the International Commission on Non Ionizing Radiation Protection [3]. In the same way, the European Union has defined a specific directive for the protection of workers from the exposure to those fields [4].

Measurements of the WLAN signals in different environments have been made by several authors considering access points only, with client card enabled, uploading or downloading large files [5], or access points and mobile terminals with a maximum power of 100 mW [6], having found a strong dependence with distance and measured values far below the limits of the international guidelines. Measurements of the electric field near a WiFi 802.11b router so as numerical simulations of the electric field surrounding a wireless laptop computer with two hands over the keyboard have been made in [7], with a theoretical estimation of the channel occupation as a means of knowing the real emitted power of the system and an experimental assessment of compliance with safety limits of several short-range wireless devices used in home and office environments has been made in [8], by means of E-fields measurements in a semi-anechoic chamber and SAR measurements in a body-emulating phantom, concluding that, in the very near future, the background exposure in everyday life situations will exceed exposures from base stations and broadcast stations, so that it is necessary to assess the simultaneous exposure of people to multiple sources in its surrounding environment.

In this work the FDTD technique, which has demonstrated to be very useful for dosimetry studies of human exposure to electromagnetic fields, is used to analyze the field distribution in the vicinity of a person during the use of several radiofrequency devices. Two different situations will be considered, trying to simulate actual operating conditions in exposure to wireless access points antennas (based on the standard IEEE802.11b) in home or office environments and use of a WiFi or bluetooth PDA at several distances in front of the user's eye. In all cases, the SAR in the head of the user will be calculated to be compared with basic restrictions from the guidelines.

Models and Results

A. Exposure to wireless access points antennas.

Several situations of possible exposure to the antenna of a wireless access point in a domestic or office environment have been studied. In the simulations, brick walls and metalic cabinets are included to consider the influence of the environment in the SAR calculated in the head of the exposed person. Figure 1 shows the schematic geometries of four studied configurations: (a) a person working in a table where a desktop antenna in located, near the brick walls of the room, at a distance of 40 cm of the person head; (b) the worst-case of a person with the antenna in front of its eyes at a distance of 20 cm, with a reflecting plate behind the antenna at a distance of 4 cm; (c) a person in front of an antenna which is on the opposite side of a 12 cm thick brick wall, the antenna-eye distance being 20 cm or (d) a person exposed to the radiation of two desktop antennas at 15 and 20 cm from the head, respectively, with metalic cabinets behind the antennas at 15 and 25 cm (fig. 1d).

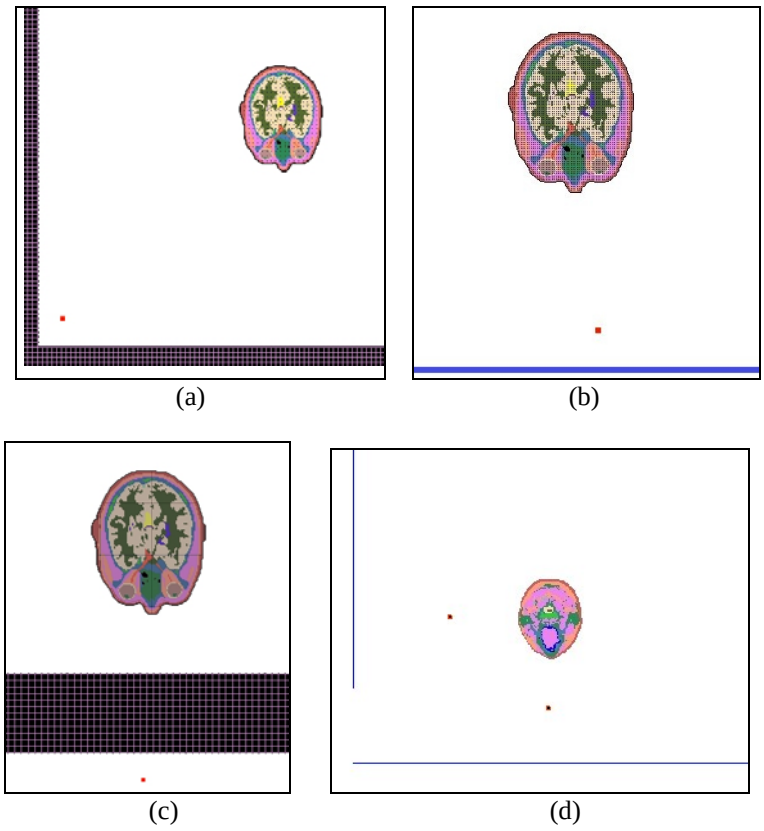

Figure 1. Schematic view of the analyzed exposure situations: (a) Head at 40 cm from the antenna which is at 4 cm of both walls. (b) Head at 20 cm from the antenna and at 24 cm of a metalic wall. (c) Head at 20 cm from the antenna, which is 4 cm on the opposite side of the brick wall. (d) Head in presence of two antennas, surrounded by metalic cabinets.

The antennas have been simulated, in all cases, as half-wavelength dipoles, operating at a frequency of 2400 MHz with a radiated power of 100 mW. To simulate the user, a high-resolution head and shoulders mesh,

developed from nuclear magnetic resonance by REMCOM Inc. and the Hershey Medical Center, Hershey, PA, USA, has been used. The model has 2 x 2 x 2,5 mm cells and includes 17 different biological tissues which corresponding densities and dielectric characteristics at the operating frequency (2400 MHz) are sumarized in table 1 [9].

The walls have been modeled by rectangular plates with a width of 12 cm, by using a material which simulates the dielectric characteristics of brick, with a relative permitivity of $\varepsilon_r = 5.1$ and a conductivity of $\sigma = 0.028$ S/m, assumming they are similar to those corresponding to 1800 and 2140 MHz [10].

Tissue	ε_r (S/m)	σ (S/m)	ρ (kg/m^3)
Skin	37.63	1.29	1125
Tendon	44.03	1.80	1151
Fat, yellow marrow	4.4	0.08	943
Cortical bone	11.67	0.41	1850
Cancellous bone	17.47	0.60	1080
Blood	53.31	2.68	1057
Muscle	55.84	2.32	1059
Grey matter	46.47	2.10	1035.5
White matter	35.80	1.36	1027.4
Cerebro-spinal-fluid	66.87	3.22	1000
Sclera/cornea	51.77	2.11	1151
Vitreous humor	66.80	2.48	1000
Nerve	31.61	1.10	1112
Cartilage	37.18	1.57	1171
Tongue, thyroid	53.14	2.05	1059
Cerebellum	47.31	1.79	1035.5
Esophagus	36.10	1.47	1126

Table 1. Relative permitivities, conductivities and densities of the tissues in the head model for 2400 MHz.

By using the FDTD method, we have calculated the electric field values in the proximity of the antennas when there is no exposed person, to be compared with the limits stablished in the exposure guidelines (reference levels). Moreover, the SAR values inside the human head model have been calculated to be compared with basic restrictions. Figure 2 shows contour plots of the calculated fields in absence of the head model for, respectively, the four exposure situations described in the first paragraph.

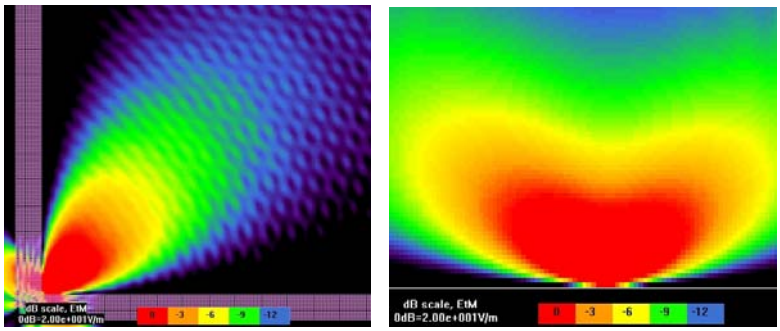

(a) (b)

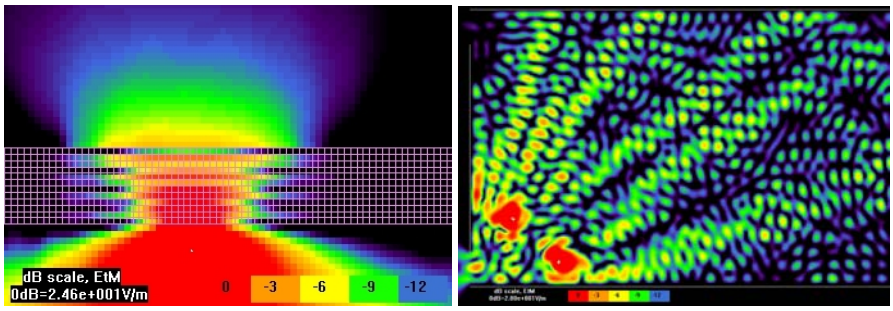

(c) (d)

Figure 2. Contour plots of the calculated fields in absence of the head model for the four exposure situations shown in figure 1.

In all the studied configurations, it can be observed that local field values in the position where the person is to be located are below the reference level for this frequency (61 V/m for the electric field). Spatially averaged values are obviously lower. As it is well known, guidelines compliance based on reference levels ensures the fullfilment of guidelines based on basic restrictions. Nevertheless, in exposure situations at short distances from the antennas, it is interesting the assessment of the SAR. The calculated values of SAR averaged over the whole exposed object (SAR_{wb}), so as the maximum local SAR values, averaged over 10 grams of contiguous tissue (SAR_{10g}), are shown in table 2.

	Geometry (a)	Geometry (b)	Geometry (c)	Geometry (d)
SAR_{wb} (W/kg)	0.00044	0.00054	0.00012	0.0006
SAR_{10g} (W/kg)	0.008	0.019	0.008	0.027

Table 2. SAR_{wb} and SAR_{10g} for the four simulated exposure situations.

It can be appreciated that SAR_{wb} and SAR_{10g} values are far below the corresponding basic restrictions for all geometries.

B. Use of a PDA device close to the user's face.

The study of the SAR produced by the use of PDA devices is interesting because, due to the reduced screen size, the distance from the antenna to the eye of the person (which is known to be a critical organ) can be very short. For that reason, we have modeled a 2400 MHz antenna in front of the eye of the head and shoulders model at several distances, from 5 to 30 cm, trying to simulate a worst-case exposure situation. The electrical and geometrical models of the antenna and the person are the same than those used in the previous section. Results for the calculated maximum SAR_{10g} as a function of the antenna-aye distance are presented in figure 3 for different antenna radiated powers.

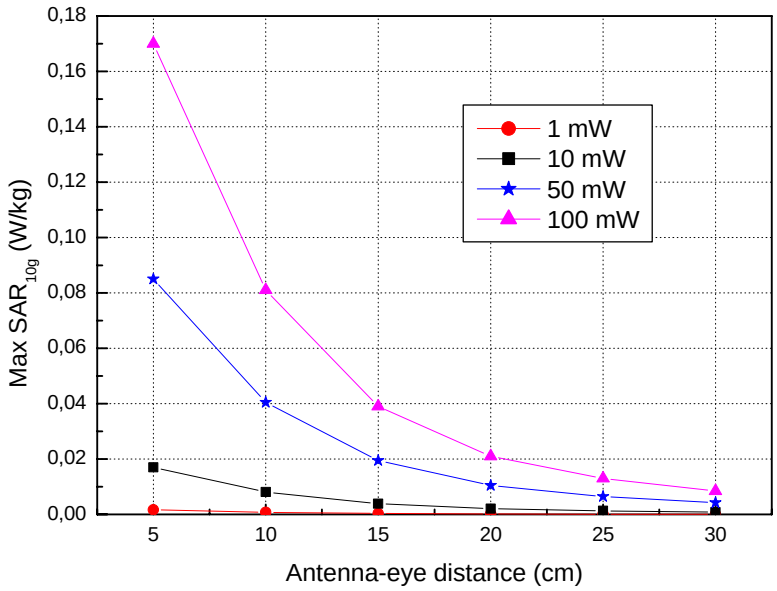

Figure 3.- Maximum SAR_{10g} as a function of antenna-eye distance for different radiated powers.

It can be seen that SAR values increase strongly as the antenna-eye distance becomes shorter, although the maximum value of 0.18 W/kg, obtained for the lowest (unusual) considered distance, corresponding to a radiated power of 100 mW (the maximum expected with WiFi or Bluetooth standards), clearly fulfills safety guidelines.

Conclusions

In this work, the human exposure to the electromagnetic fields from the antennas of wireless devices such as those of WLAN access points or WiFi or bluetooth personal digital assistants has been analyzed by using the FDTD method. Several exposure situations have been considered, assessing field levels and SAR in the exposure to access point antennas, to be compared with reference levels and basic restrictions, respectively, or max SAR_{10g} in short-distance exposure to a PDA device.

Results show that the exposure levels, even in worst case situations, as can be the case of WiFi access point or blueooth antennas at a short distance in front of the eye of a person, are lower than those obtained when analyzing the exposure to mobile phones, the SAR_{10g} values being far below the basic restrictions from the guidelines.

Acknowledgements

This work has been supported by the PN I+D+I of the Spanish Ministry of Science and Education, State Secretariat for Universities and Research, project TIC 2003-00130.

References

[1] Real Decreto 1066/2001, de 28 de septiembre, por el que aprueba el Reglamento que establece condiciones de protección del dominio público radioeléctrico, restricciones a las emisiones radioeléctricas y medidas de protección sanitaria frente a emisiones radioeléctricas, B.O.E. de 29 de septiembre de 2001.

[2] European Commission 1999 Council Recommendation (1999/519/EC) of 12 July 1999 on the Limitation of Exposure of the General Public to Electromagnetic Fields (0 Hz to 300 GHz). *Official Journal of the European Communities* **L199** 59-70.

[3] ICNIRP (International Commission on Non-ionizing Radiation Protection) Guidelines for limiting exposure to time-varying electric, magnetic and electromagnetic fields (up to 300 GHz) Health Phys 74 pp 494-522, 1998.

[4] European Union 2004 DIRECTIVE 2004/40/EC of the European Parliament and of the Council of 29 April 2004 on the minimum health and safety requirements regarding the exposure of workers to the risks arising from physical agents (electromagnetic fields) *Official Journal of the European Communities* **L 159** 47 1-26.

[5] K. R. Foster, "Dosimetric Studies on Wireless LANs," COST 281 Workshop, Graz, Austria, April 20-21, 2006.

[6] Chr. Bornkessel and M. Wuschek, "Exposure Measurements in Different WLAN-Scenarios," COST 281 Workshop, Graz, Austria, April 20-21, 2006.

[7] A. Cortel-Carrasco, A. Gati, M- Wong and J. Wiart, "WiFi Exposure Assessment", Abstracts of the XXVIII Annual Meeting of the Bioelectromagnetics Society (BEMS' 03), Cancun, Mexico, pp 49-51, June 2006.

[8] S. Kuehn, A. Kramer, U. Lott and N. Kuster, "Assessment Methods for Demonstrating Compliance with Safety Limits of Wireless Devices Used in Home and Office Environments," CD Proceedings of the XXVIIIth General Assembly of the International Union of Radio Science (URSI), New Delhi (India), October 2005.

[9] C Gabriel C. Gabriel and S. Gabriel, Compilation of the dielectric properties of body tissues at RF and microwave frequencies, *Technical Report* AL/OE-TR-1996-0037, King's College, Physics Department, London, 1996, available http://www.brooks.af.mil/AFRL/HED/hedr/reports/dielectric/home.html.

[10] P. Bernardi, M. Cavagnaro, R. Cicchetti, S. Pisa, E. Piuzzi and O. Testa, "A UTD/FDTD Investigation on Procedures to Assess Compliance of Cellular Base-Station Antennas With Human-Exposure Limits in a Realistic Urban Environment," IEEE Trans. Microwave Theory Tech., vol. 51, pp. 2409-2417, December 2003.

ELECTROMAGNETIC FIELD PREVISION AND EXPERIMENTAL VALIDATIONS IN INDOOR ENVIRONMENTS

MARINA BARBIROLI[1], MARIA LUCIA CALABRESE[2], GABRIELE FALCIASECCA[1], RITA MASSA[2]

[1]DEIS, UNIVERSITY OF BOLOGNA, ITALY
VIALE RISORGIMENTO, 2 - 40136 – BOLOGNA, ITALY
GFALCIASECCA@DEIS.UNIBO.IT
[2] DIET, UNIVERSITY OF NAPLES FEDRICO II, ITALY
VIA CLAUDIO, 21 - 80125 – NAPOLI, ITALY
MASSA@UNINA.IT

Abstract
The aim of this study was to provide an optimization procedure in order to experimentally evaluate RF exposure levels due to wireless devices, other than phones, used in home and office environments. To this end, several measurements were carried out at UMTS and Wi-Fi frequencies and the results were then compared with simulations provided by the ray tracing prediction model ARMONICA. The comparison between measurement and numerical results showed a satisfactory agreement and suggest that, in order to avoid time consuming measurements for monitoring the electromagnetic field levels due to wireless communications in indoor environments, the use of a ray tracing prevision model is a valid support allowing to perform experimental validations only in that points where the simulator has shown some critical aspect.

Introduction
In the last years the enormous growth of mobile telecommunications leads to the necessity of developing effective and accurate techniques to calculate and measure the electromagnetic field (EMF) levels in indoor environments. To determine the EMF levels and to assure population against excesive exposure according to the international standards [1], [2], that have specified the exposure limits, measurements must be done in the place under test, using appropriated procedures for the new types of radio communications signals. However, the use of experimental valuations in order to determine the EM fields levels in indoor settings could give rise to high costs and long times; for this reason an EMF prevision software could represent an advantageous opportunity to reach the purpose. The computation of electromagnetic field propagation in real environments is a complex problem for the difficulty to describe with sufficient precision the antenna system, the geometry, the electromagnetic properties of present objects, the morphology and the ground characteristics.
Besides, the zone interested by the field computation could be extremely extensive compared with the wave lengths of the typical mobile communication frequencies, so that the computation resources could become an excessive load. It is for these reasons, that the classical numerical techniques for the resolution of Maxwell equations such as the finite elements method (FEM) or the finite difference time domain technique (FDTD) are inapplicable. So many studies were carried out about this argument and empiric and semiempiric models were developed to solve the problem [3-6], but in the two last decade the ray tracing techniques [7-9] were applied to the EMF prediction since it is proved the more appropriate, although there are still some unsolved questions.
The aim of this study is to provide a methodology for characterizing realistic electric-field exposures in home, office and occupational settings and suggests an approach for evaluating compliance with guideline limits in such settings. To this end, several measurements were carried out at UMTS and Wi-Fi frequencies and the results were then compared with simulations provided by a ray tracing prediction model.
Materials and methods.
Simulations. The program used for the EMF prevision was ARMONICA; it was developed by DEIS (Dipartimento di Elettronica, Informatica e Sistemistica) at the University of Bologna in a joint work with A.R.P.A. Emilia Romagna (Italy). In particular, we used the "mray" module; it calculates the EM field in the analysis point as the vectorial sum of all contributions corresponding to all main rays that reach the receiving

point after a number of interactions with the possible obstacles. The adopted program implements a three dimensional spatial ray tracing model involving both reflection and rifraction contributions but negleting the diffraction ones. The program requires in input 5 files in order to:

- describe the radiative characteristics of the trasmitting antenna;
- describe the geometrical characteristics of environment:
- specify the electromagnetics properties of the materials;
- set up opportune boolean values in order to have an output file with the description of the various rays which contribute to the electromagnetic field value in each analysis point;
- define the irradiated signal frequency, the maximum number of reflected rays, positioning and orientation of the transmitting antenna, power supply, analysis domain and the type of output quantity.

The program provides in output:

- the amplitude of the electric field components: |Ex| [V/m]; |Ey| [V/m]; |Ez| [V/m];
- the amplitude of the electric field |E| [V/m];
- the received power [dB].

Measurements. A large number of measurements were carried out in different environments and configurations. Several analysis domains were considered: the microwave laboratory room (fig. 1), an office room (fig. 2) and a hall way out of the DIET (Department of Electronic and Telecommunication Engeneering at the University of Naples Federico II). The WiFi or UMTS signal was transmitted by either a WLAN antenna (Cisco Aironet Yagi 1949) or a ridged horn (Schwarzbeck BBHA 9120D). The measurements were performed using either a spectrum analyzer (R&S FSH3) connected to the receiving antenna (precision conical dipole PCD 8250, Austrian Research Centers, Seibersdorf), or a vector network analyzer (Anritsu 37247C) connected to the receiving (PCD 8250) and transmitting antennas. In the latter, several positions of the transmitting antenna, working at 2.0 GHz frequency, were adopted, while the receiving antenna was mounted on an automated planar scanning system (fig.3). In this way a planar distribution of the electric field was obtained [10] as shown in fig. 4. Then we analyzed the predictive potentality of the ray tracing technique in indoor environments by comparing the numerical results with those observed in the several measurements carried out in different settings.

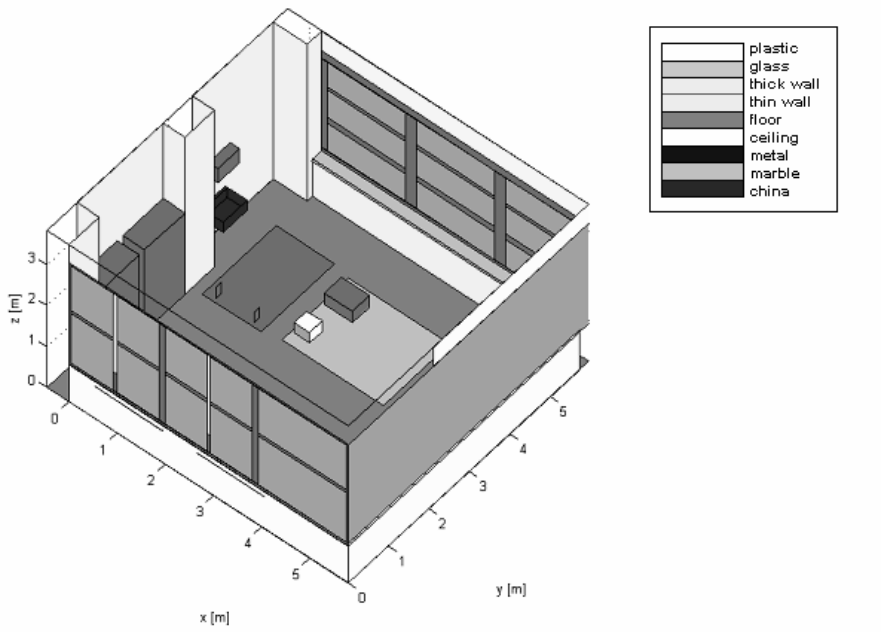

Fig. 1. Matlab three-dimensional reconstruction of the microwave laboratory at DIET, Un.of Naples Federico II.

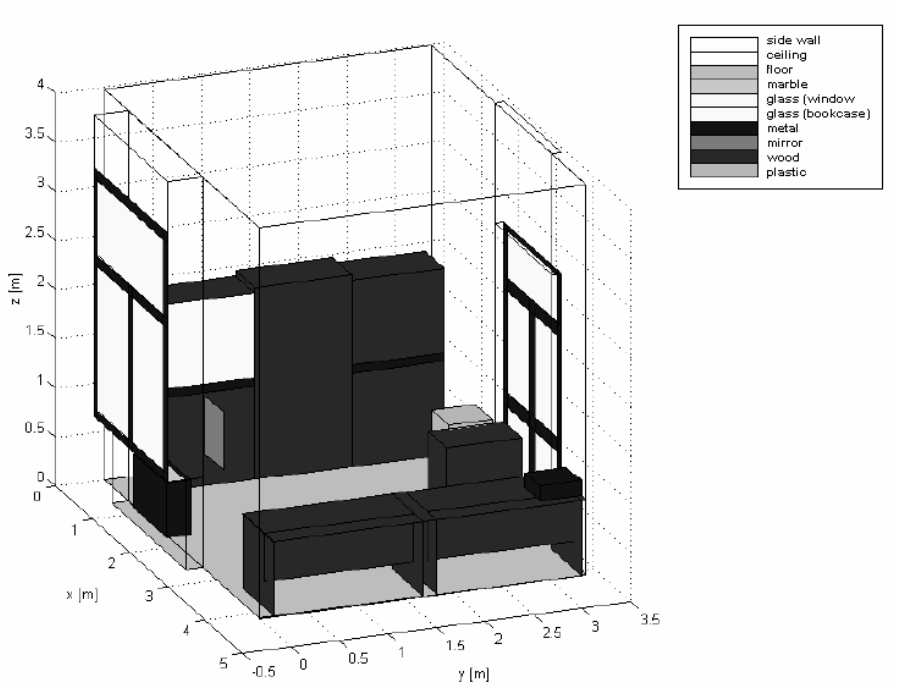

Fig. 2. Matlab three-dimensional reconstruction of the office room at DIET, Un.of Naples Federico II.

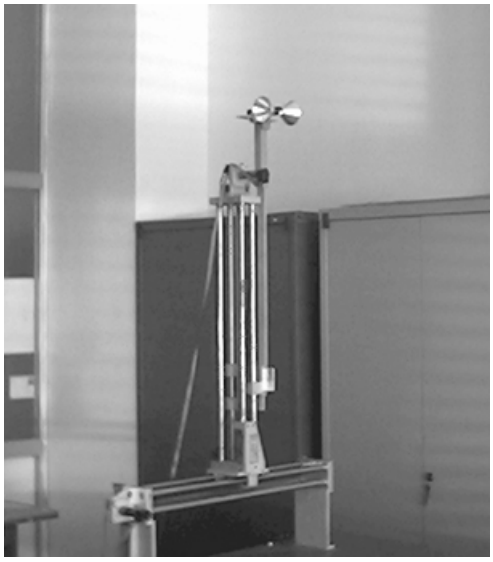

Fig. 3. Precision conical dipole receiving antenna mountated on planar scanning system.

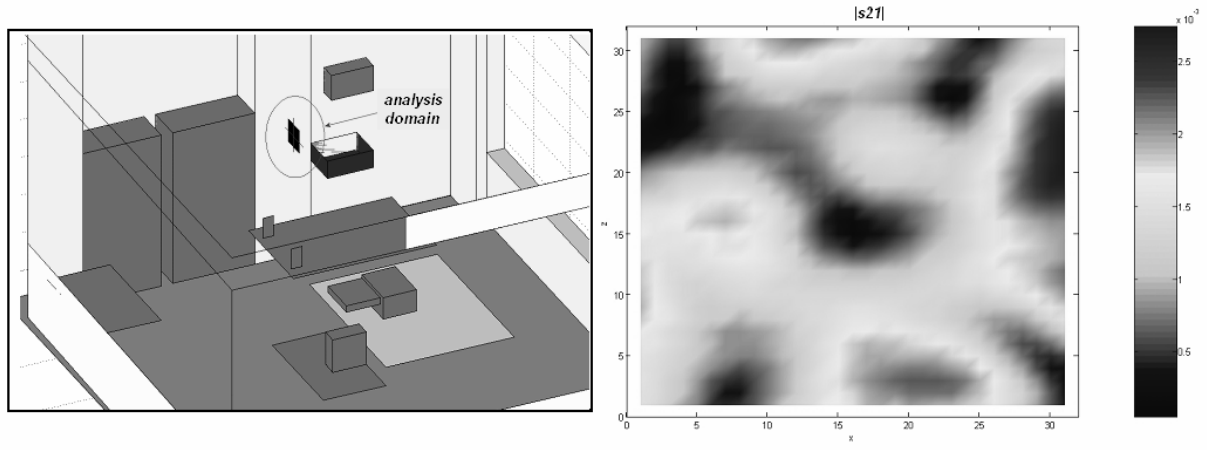

a) b)

Fig.4.a) Microwave laboratory. Analysis domain; b) planar distribution (0.3 x 0.3 m^2) of the measured |s21| values.

Results. The comparison between measurement and numerical results showed a satisfactory agreement (figg. 5, 6). Although, due to the complexity of the analysis domain, some critical aspects were evidentiated: a not accurate geometric description of the environment can strongly affect the prevision model results; the addition of diffraction contributes can improve the numerical results; in indoor environments it isn't always simple to guarantee the far field conditions at the wireless working frequencies; a very accurate technical decription of the instrumentation is necessary.

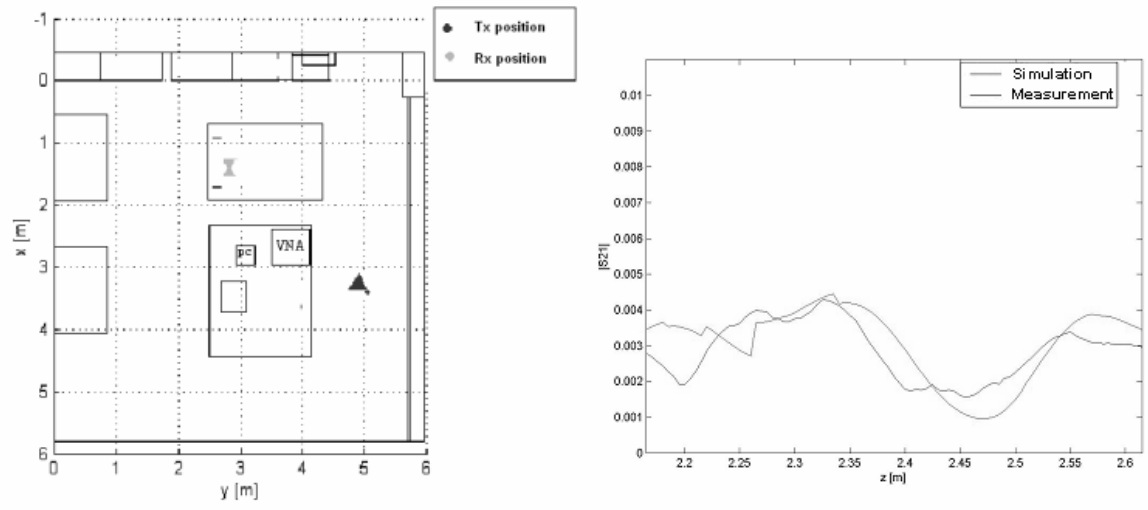

Fig. 5. Measured and calculated |s21| values and the corresponding scenario

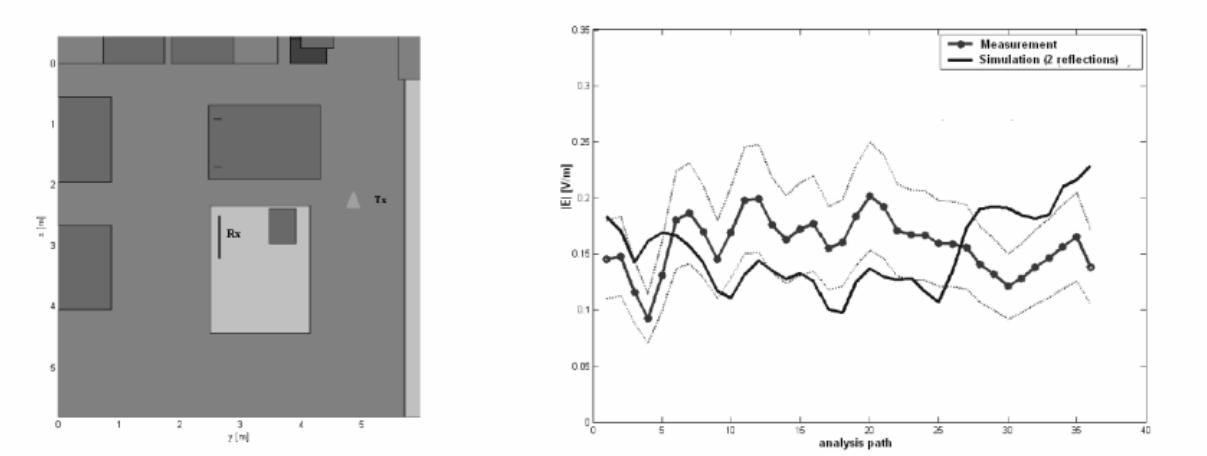

Fig. 6. Calculated and measured electric field levels, with estimated uncertainity, and the corresponding scenario.

SUMMARY

The aim of this study was to provide an optimization procedure for evaluating RF exposure levels due to wireless devices other than phones used in home and office environments. To this end several measurements were carried out in different settings; the results were then compared with those calculated by means of a ray tracing prediction model.

A satisfactory agreement between the experimental and calculated results suggest that, in order to avoid time consuming measurements for monitoring the electromagnetic field levels due to wireless communications in indoor environments, the use of a ray tracing prevision model is a valid support allowing to perform experimental validations only in that points where the simulator has shown some critical aspect.

AKNOWLEDGMENTS

The authors would like to remember professor Guglielmo d'Ambrosio for his constructive and helpful suggestions. The work was supported by CdC-ICT Campania Region Italy.

REFERENCES

[1] International Commission on Non-Ionizing Radiation Protection (ICNIRP), *Guidelines for Limiting Exposure to Time-Varying Electric, Magnetic, and Electromagnetic Fields (up to 300 GHz)*, Health Physics, no. 4, vol. 74, pp. 494-522, April 1998;

[2] American National Standards Institute (ANSI), *IEEE C95.1-1991: IEEE Standard for safety Levels with Respect to Human Exposure to Radio Frequency Electromagnetic Fields, 3kHz to 300 GHz*, IEEE Inc., 345 East 47 Street, New York, NY 10017-2394, USA;

[3] M. Barbiroli, C. Carciofi, M. Frullone, P. Grazioso, *A measurement-based methodology for the identification of validity domains of prediction models in urban environmen*t, IEEE Trans. Vehicular Tech., Vol 49, No. 5, pp. 1508-1515, Sept. 2000;

[4] M. Hata, *Empirical Formula for Propagation Loss in Land Mobile Services*, IEEE Trans. Vehicular. Tech., Vol. 29, No. 3, Aug. 1980;

[5] J. Walfish, H. Bertoni, *A theoretical model of UHF propagation in urban environments*, IEEE Trans. Ant. and Prop., Vol. 36, No. 12, pp. 1788-1796, Dec. 1988;

[6] H. H. Xia, H. Bertoni *et al.*, *Radio Propagation Characteristics for Lineof- Sight Microcellular and Personal Communication*, IEEE Trans. Ant. And Prop., Vol. 41, No. 10, pp. 1439-1446, Oct. 1993;

[7] Vittorio Degli-Esposti, Giancarlo Lombardi, Cristiano Passerini, and Guido Riva, *Wide-Band Measurement and Ray-Tracing Simulation of the 1900-MHz Indoor Propagation Channel: Comparison Criteria and Results,*

IEEE Transactions on Antennas and Propagation, vol. 49, no. 7, july 2001;
[8] G.E. Athanasiadou, A.R. Nix, *A Novel 3-D Indoor Ray-Tracing Propagation Model:The Path Generator and Evaluation of Narrow-Band and Wide-Band Predictions,* IEEE Transactions on Vehicular Technology, Vol. 49, no. 4, july 2000;
[9] M. Barbiroli, C.Carciofi, V. Degli-Esposti, G. Falciasecca, *Evaluation of Exposure Levels Generated by Cellular Systems: Methodology and Results*, IEEE Transactions on Vehicular Technology, vol. 51, no. 6, november 2002;
[10] M. Barbiroli, M. L. Calabrese, G. Falciasecca, R. Massa, *Electromagnetic Field Measurements and Simulations at UMTS and Wi-Fi Frequencies in Indoor Settings*, The Bioelectromagnetics Society 28th Annual Meeting, June 11-15, 2006, Cancun, Mexico.

A FAMILY OF RF EXPOSURE SISTEMS FOR MONITORING CONFORMATIONAL CHANGES OF BIOMOLECULES INDUCED BY ELECTROMAGNETIC FIELDS

Enrico M. Bucci[1], Ovidio M. Bucci[2,3], Maria Lucia Calabrese[2], Rita Massa[2]

[1] *IBB, CNR- NAPLES*
VIA MEZZOCANNONE 16, NAPOLI, ITALY
bucci@chemistry.unina.it
[2] *DIET, UNIVERSITY OF NAPLES FEDRICO II, ITALY*
VIA CLAUDIO, 21 - 80125 – NAPOLI, ITALY
MASSA@UNINA.IT
[3] *IREA, CNR-NAPLES*
VIA DIOCLEZIANO 328, NAPOLI, ITALY
bucci@unina.it

Abstract.
A set of different devices for "*in vitro*" exposures of biological samples (DNA, proteins) to electromagnetic field (300 MHz – 2.45 GHz) and the contemporary control of conformational changes of the exposed biostructure was designed and tested. To this end all the RF applicators were provided of a non perturbative optical apparatus, which allows the continuous monitoring, during the exposure, either the absorption spectra or the absorbance at a given wavelenght in order to observe reversible effects induced by the electromagnetic field.

Introduction

In vitro studies performed on simple but fundamental components of biological systems, i.e., biomolecules, in particular proteins and nucleic acid and artificial or isolated fragments of membranes, can provide important insights into fundamental mechanisms for biological effects due to electromagnetic field action. Proteins possess usually a net charge at pH corresponding to the native condition; moreover a large number of charge aminoacid residues are distributed in their structure. Protein structures are intrinsically flexible structures and can assume multiple conformations (in some cases called "open" and "closed"forms). During the course of their biological function, proteins undergo different types of structural rearrangements ranging from local to large-scale conformational changes. Since protein machines are flexible structures having own electric charges, such motions involved in many basic functions such as catalysis, regulation, transportation, and aggregation could be triggered by their interactions with electromagnetic field.

Since many years our research group is involved in the study of interaction mechanisms between the electromagnetic fields and biomolecules. An irreversible time dependent inactivation was observed in thermophilic enzymes exposed at 10.4 GHz. The percentage of deactivation depended on the temperature (60 – 90°C) , SAR (0.8 – 3.1 W/g), and microenvironment (enzyme concentration or influence of salts). Conformational changes detected by fluorescence and circular dichroism techniques suggested that microwaves induced in this cases protein structural rearrangements not related to temperature [1,2,3]. Non thermal effects induced by exposure to 1.95 GHz, a typical frequency used in mobile communication, have been observed on the kinetic of reconstitution of the heme binding site from acidic tuna myoglobin solution [4]. More recently our attention was focussed on the possibility that electromagnetic field can remotely control these nano-biomachines [5,6].

The possibility of evidencing possible reverse effects (effects that fade away when the field is turn off)

is particularly attractive, to this end a family of applicator working in the 300 MHz – 2.45 GHz frequency band was designed and tested in order to expose macromolecules to microwaves and contemporary control the conformational change of the structure during the exposure. In all the devices is possible to insert two fibre optics connected, from one end, to the spectophotometer Lambda 25 (Perkin Helmer, Wellesley, USA) while the other end was in contact with the quartz cuvette containing the sample.

Device design

At low frequencies (300 MHz – 900 MHz) the applicator was a coil similar to that used in [7]. It consisted of 35 turns with a cross section of ~1 cm^2 and with an open structure in the middle in order to allow the insertion, perpendicularly to the axis coil, of two teflon cilinders that facilitate accurate placement of the fibre optics for absorbance measurements (fig.1). The sample, a DNA solution, was contained in a 3mm x 3mm x 22 mm quartz cuvette axially inserted into the coil. Being the coil an open structure it was possible to follow both the increase of temperature and the temperature distribution on the sample surface by means of an infrared thermocamera (ThermoVision A40M, Flir System, North Billerica, Boston, USA).

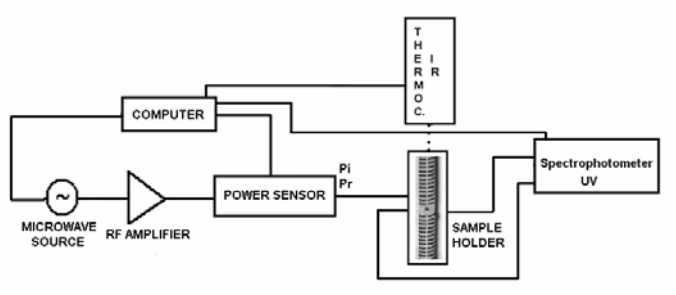

Fig.1 Exposure setup at 300 MHz and 900 MHz

Another applicator was designed in order to expose samples at 1.95 GHz, which is an up-link frequency of universal mobile telecommunication systems (UMTS). It was a rectangular thermostated waveguide (WR 430: 109.2 mm x 54.6 mm). The feeding end of the waveguide was a coax waveguide adapter Maury Microwave R213A2 (VSWR < 1.05) while on the other side a fixed short circuit (SC) termination was adopted. The sample was positioned in a maximum of the unperturbed field and inserted into a teflon support which allowed the fibre optics (fig.2) insertion.

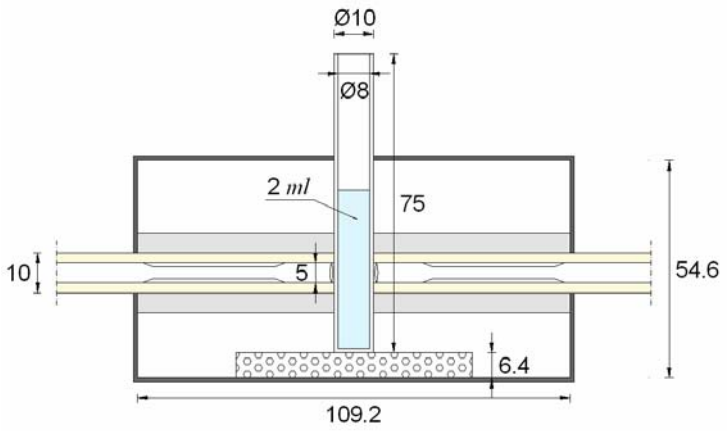

Fig.2 Cuvette inserted into a WR430 waveguide and fibre optics holder

Finally a thermostated rectangular waveguide cavity (72 mm x 33.8 mm x 340 mm), coupled to the coax-adapter waveguide by means an inductive diaphragm and excited by a 2.47 GHz radiation (fig.3), allowed the exposure of the samples to the only magnetic field. In fact, sample size (35 mm x 10 mm x 1 mm) and position (in contact with the short circuit) ensured a minimum interaction with the electric field and a satisfactory homogeneity of the magnetic field.

Dosimetry

Numerical and experimenatal dosimetry was carried out in order to assess efficiency and field uniformity into the sample. The efficiency of the system (the ratio between the absorbed power, P_a,and the incident power, P_0 , $\eta = P_a/P_0$) and the absorbed power distribution inside the samples were numerically and experimentally evaluated.

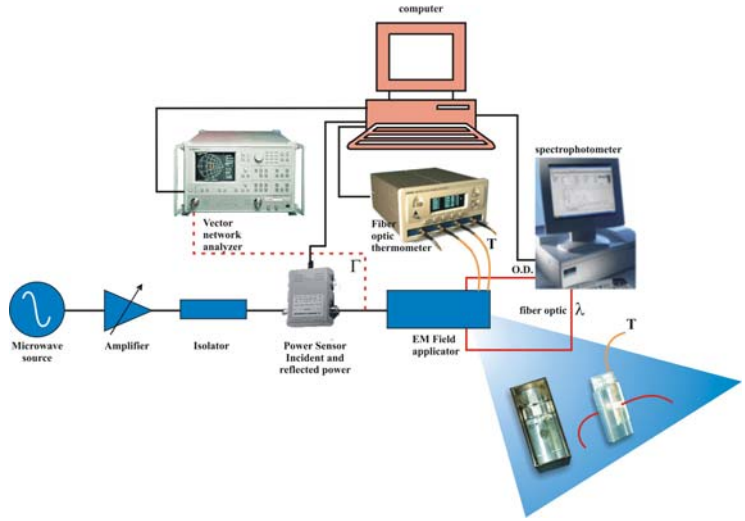

Fig.3 Exposure setup at 2.47 Ghz for magnetic field sample exposures.

In particular the following parameters were calculated [8]:

• $|E^1(x,y,z)|$: the local electric field amplitude per unit incident power [(V/m)/W]. This was evaluated at each node of the computing domain.

• $SAR^1(x,y,z) = \sigma |E^1|^2 / 2\rho$: the local absorbed power per unit mass and per unit incident power [(W/kg)/W]. This is also the local specific efficiency, and it is zero outside the sample ($\sigma = 0$).

• AV^1: the average $SAR^1(x,y,z)$ over the sample [(W/kg)/W].

• SD^1: the standard deviation of $SAR^1(x,y,z)$ values

• $CV = SD^1/AV^1$: the coefficient of variation [9] is usually taken [10] as the "nonuniformity degree"of the SAR^1 (P_0 = 1 W) values. The SAR (any P_0) nonuniformity degree, SD/AV, is the same as $CV = SD^1/AV^1$.

The local SAR values were calculated from the slope of the heating curves [11], T(t), at t = 0, as: $SAR = c\, dT/dt|_{t=0}$ (c being the sample specific heat; t=0 is the starting time of radiofrequency radiation).

The efficiency, $\eta = P_a/P_0$, was evaluated by measuring the reflection coefficient (s_{11}) [12] of the exposure chamber loaded by the samples by means of a microwave vector network analyzer (Wiltron-Anritsu 37269B, Japan) over the working band, being $\eta = 1 - |s_{11}|^2$. In the case of the cavity the power absorbed by the samples was calculated by means of the measurements of the unloaded and loaded Quality factor [12].

Results

The efficiency simulated was successfully verified through measurements of the scattering parameters; as well as the nonuniformity degree was checked and confirmed by means of local temperature measurements using both the infrared thermocamera and the fibre optic thermometer.
The possibility of following the conformational change of the molecule was obtained. In particular we observed as [7] that a DNA double helix, with a gold nanocrystal covalently attached, was opened up and closed back upon exposition to an oscillating RF signal (~1 GHz), i.e., the electromagnetic field denaturated and renaturated the double-helical DNA. The extreme simplicity of assembly and operation of our devices, which resulted to be low cost and with an optical equipment that is commonly used in bio-chemical laboratory, makes them easily available and particularly interesting for studies about interaction mechanisms between biological structures and electromagnetic fields.

References

[1] La Cara F., Scarfì M.R., D'Auria S., Massa R., d'Ambrosio G., Franceschetti G., Rossi M., De Rosa M.: "Different effects of microwave energy and conventional heat on the activity of a thermophilic β-Galactosidase from *Bacillus acidocaldarius*", Bioelectromagnetics, 20, N.3, pag.172-176, 1999

[2] La Cara F., Scarfì M.R., D'Auria S., Zeni O., Massa R., d'Ambrosio G., Franceschetti G., De Rosa M., Rossi M.: "Microwave exposure effect on a thermophilic alcohol dehydrogenase", in press on Protein and Polipeptide Letters.

[3] Porcelli M., Cacciapuoti G., Fusco S., Massa R., d'Ambrosio G., Bertoldo C., De Rosa M., Zappia V.: "Non-thermal effects of microwaves on proteins: thermophilic enzymes as model system", FEBS Letters 402 (1997) 102-106.

[4] F. Mancinelli, M. Canaglia, A. Abbruzzese, G. d'Ambrosio, R. Massa, E. Bismuto: "Non thermal effects of electromagnetic fields at mobile phone frequency on the refolding of an intracellular protein: myoglobin" J. of Cellular Biochemistry, 93, pp.188-196, 2004.

[5] E.M. Bucci, O.M. Bucci, M.L. Calabrese, G. d'Ambrosio, R. Massa, A. Messere, G. Milano, D. Musumeci, G. Petraglia, G. Roviello, "Preliminary Report on a Radiofrequency Controlled Biosensor", The Bioelectromagnetics Society 27th Annual Meeting, June 19-24, 2005, Dublin, Ireland.

[6] E.M. Bucci, G. Bellizzi, O.M. Bucci, M.L. Calabrese, A. Capozzoli, A. Messere, G. Milano, D. Musumeci, G. Petraglia, G. Roviello and R. Massa: "Remote Control of Biomolecules by Radiofrequency: a test study". The Bioelectromagnetics Society 28th Annual Meeting, June 19-24, 2006, Cancun, Mexico.

[7] K. Hamad-Schifferli, J.J. Schwartz, A.T. Santos., S. Zhang, and J.M. Jacobson: " Remote electronic control of DNA hybridization through inductive coupling to an attached metal nanocrystal antenna". *Nature*, 415, 152-155, 2002.

[8] M.L. Calabrese, G. d'Ambrosio, R. Massa, G. Petraglia: "A High-Efficiency Waveguide Applicator for In Vitro Exposure of Mammalian Cells at 1.95 GHz", IEEE Trans. Microwave Theory and Techniques vol. 54,no. 5, pp. 2256-2264, May 2006.

[9] R. R. Sokal, F. J. Rohlf, "Biometry", 1st ed., San Francisco, California, USA: W. H. Freeman and Co., 1969, Chapter 4, pp. 50-63.

[10] N.Kuster, F. Schonbörn, "Recommended minimal requirements and development guidelines for exposure setups of bio-experiments addressing the health risk concern of wireless communications", *Bioelectromagnetics*, vol. 21, issue 7, pp. 508-514, 2000.

[11] J.W. Allis, C.F. Blackman, M.L. Fromme, S.G. Benane, “Measurement of microwave radiation absorbed by biological systems. Analysis of heating and cooling data”, Radio Sci., vol. 12, issue 6(s), pp. 1-8, 1977.

[12] D. M. Pozar, “Microwave Engineering”, 1st ed., New York, USA: Addison-Wesley Publising Co. Inc., 1993.

EFFECTS OF 915 MHZ ELECTROMAGNETIC FIELD IRRADIATED IN TEM-CELL ON BLOOD-BRAIN BARRIER AND NEURONS IN THE RAT BRAIN.

MASUDA H. [1], USHIYAMA A. [1], TAKAHASHI M. [1], WANG J. [2], FUJIWARA O. [3], HIKAGE T. [4], NOJIMA T. [4], FUJITA K. [5], KUDO M. [5] AND OHKUBO C. [6]

[1]Dept. of Environmental Health, National Institute of Public Health, 2-3-6 Minami, Wako-shi, Saitama 351-0197, Japan. [2]Dept. of Computer Science and Engineering, Graduate School of Engineering, Nagoya Institute of Technology, Gokiso-cho, Showa-ku, Nagoya 466-8555, Japan. [3]Dept. of Electrical and Computer Engineering, Nagoya Institute of Technology, Gokiso-Cho, Showa-ku, Nagoya 466-8555, Japan. [4]Graduate School of Information Science and Technology, Hokkaido University, Kita-ku, Sapporo, 060-0814, Japan. [5]Dept. of Pathology, Tokyo Medical University, 6-1-1 Shinjuku, Shinjuku-ku, Tokyo 160-8402, Japan. 6RAD, World Health Organization, Geneva CH1211, Switzerland.

Abstract

This study was carried out to evaluate whether or not albumin leakage and degenerated dark neurons were indeed present in rat brains of 50 days after a single 2 hour-exposure to 915MHz electromagnetic field (EMF) as reported earlier by Salford et al. Thirty two male F344 rats (12 weeks old) were used in the present study and they were exposed to 915MHz EMF at 0, 0.02, 0.2 and 2.0 W/Kg of whole body averaged SAR in a TEM cell for two hours as protocols described by Salford et al. The rats were killed 50 days later by a trans-cardiac perfusion technique with 4% PFA fixative solution under a deep anesthetic condition. The brains were examined histologically and immunohistochemically. As results, degenerated dark neurons, which were studied by Cresyl violet, HE and Fluoro Jade B stainings were only rarely present in small numbers with no statistically significant difference between exposed and sham exposed animals. In addition, no albumin immunoreactivity was observed anywhere even in any exposed groups. We must conclude thus that the data reported by Salford et al can not be confirmed by the present confirmation study.

Introduction

Since Salford et al. found that albumin leakage sites and increase in appearance of degenerated neurons presented in the rat brain 50 days after a single 2 hours-exposure to radiofrequency electromagnetic field (RF-EMF), many research groups have tried to confirm Salford's results. However, there were few confirmation studies performed using the same exposure system, endpoints, and experimental schedule. Therefore, the aim of present study was to confirm their reported results using a similar experimental design they used.

Thirty two male F344 rats (12 weeks old) were used in the present study. The rat placed in an acrylic box was set only on the upper side of the TEM-cell (Fig. 1) and was exposed to 915MHz EMF at 0, 0.02, 0.2 and 2.0 W/Kg of whole body averaged SAR for two hours as protocols described by Salford et al.. To know the whole body averaged SAR value that actually irradiated to the rat, we measured input, output, and reflected power using a power meter.

The rats were killed 50 days later by a trans-cardiac perfusion technique with 4% PFA fixative solution under a deep anesthetic condition. In the three selected sections of the brain (Fig. 2), albumin leakage sites were examined using immunohistochemistry of albumin. Furthermore, the appearance of degenerated neurons was evaluated using Cresyl violet, HE and Fluoro Jade B staining. We used a cold injury method for making positive control. A piece of dry ice was put on the skull of the rat for 5 min. Brown stained area was observed in positive control.

Degenerated dark neurons, which were studied by Cresyl violet, HE and Fluoro Jade B staining were only

rarely present in small numbers with no statistically significant difference between exposed and sham exposed animals. In addition, no albumin immunoreactivity was observed anywhere even in any exposed groups (Fig. 3).

Summary

We must conclude thus that the data reported by Salford et al can not be confirmed by the present confirmation study.

Acknowledgments

This study was financially supported by Association of Radio Industries and Businesses in Japan. We would like to thank Patrick A. Mason, PhD and Air Force Research Laboratory, Human Effectiveness Directorate, Directed Energy Bioeffects Division, Radio Frequency Radiation Branch, for lending us the TEM-cell.

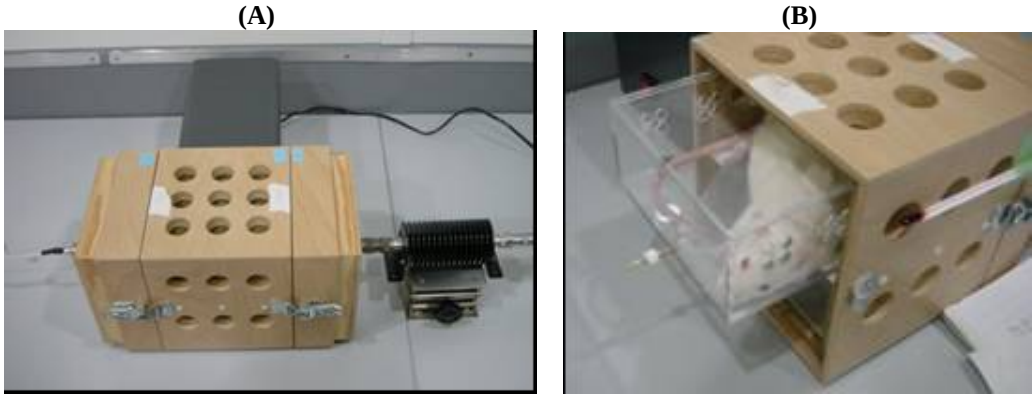

Fig. 1. Exposure system (A)TEM-cell was used in the present experiment. Input, output, and reflected power were measured by a power meter through RF exposure. Whole body averaged SAR values were calculated these measured powers and rat body weights. (B)Rat placed in an acrylic box was set only on the upper side of the TEM-cell.

Fig. 2. Evaluated brain section. Three regions of the brain were selected for histological evaluation. Section 1, 2, and 3 are typical region including third ventricule, hippocampus, and pineal body, respectively.

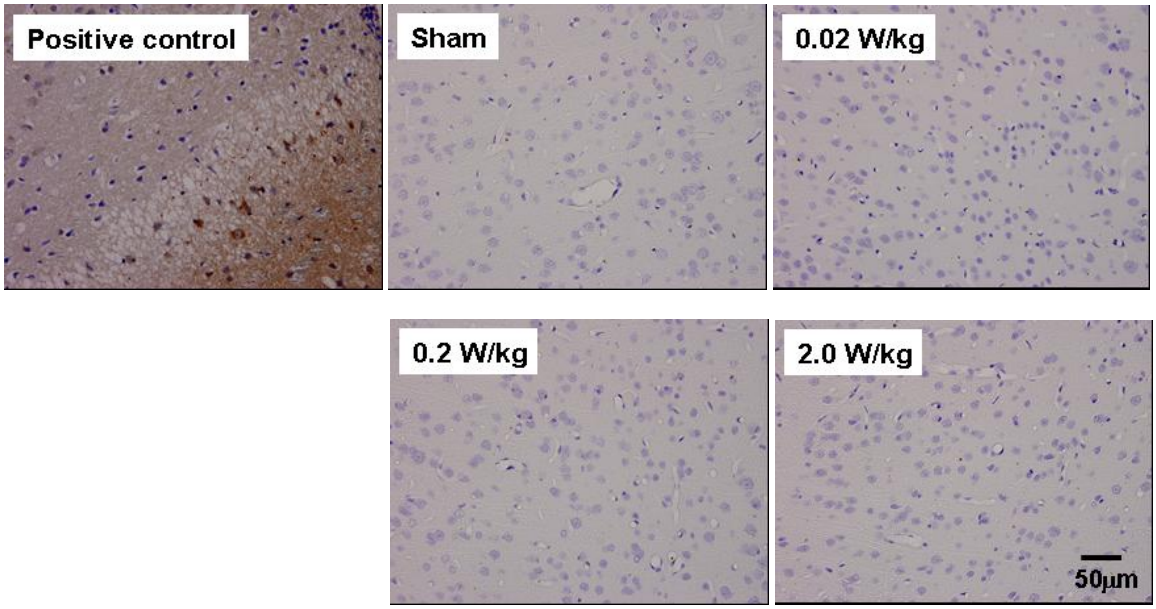

Fig. 3. Typical photographs of albumin immunohistochemistry. Albumin leakage sites were examined using anti-albumin antibody in the brain 50 days after RF exposure. Positive control was made by a cold injury method. A piece of dry ice was put on the skull of the rat for 5 min. Brown stained area was observed in Positive control. On the other hand, no stained area was seen in any exposed groups.

ASPECTS REGARDING RADIOFREQUENCY RADIATION EXPOSURE OF POPULATION IN ROMANIA

MICLAUS SIMONA[1], BECHET PAUL[2]

LAND FORCES ACADEMY, 3-5 REVOLUTIEI ST., 550170 – SIBIU, ROMANIA
miclaus@armyacademy.ro
COMMUNICATION AND INFORMATICS CENTER, 1-3 V. MILEA ST., 550325 – SIBIU, ROMANIA

Abstract
On the background of an accentuated risk perception of Romanian citizens to the radiofrequency (RF) radiation emitted by GSM base station antennas, we present the general situation in our country and results of a little scale measurement campaign we made for RF exposure assessment. The frequency selective method was used, the refinement of the methodology is discussed and results are presented and commented. All measurements showed that urban outdoor and indoor RF exposure is low comparative to the limits given in the ICNIRP guidelines that are applied in our country. We suggest for good quality exposure assessment and the need for a possibility to select between different RF sources radiation contribution in connection to further health impact studies.

Keywords: RF exposure, frequency selective method, measurement methodology, risk assessment

Introduction

Passed years in bioelectromagnetics research show that scientists cannot yet exclude the possibility that electromagnetic fields (EMFs), especially radiofrequency (RF) and microwaves (MW) can cause health problems, even for exposure levels lower than the ones stipulated in present exposure standards. One of the challenges of RF bioelectromagnetics remains the clear demonstration of the existence of athermal or nonthermal effects of RF/MW, since safety standards consider only the thermal biological effects as hazardous, when they give the basic restrictions and the reference levels in conformity [1], [2].

Exposure standards harmonization is not yet accomplished at international level, as with the efforts supported by the International EMF Project of World Health Organization. In the two most known regulations, i.e. ICNIRP guidelines [1] and IEEE standard C95.1-2005 [2], the establishment of the maximum permissible exposure limits is given in different ways: IEEE limits are based on spatial averaging of the incident field over the standing person's projection area, while ICNIRP refers to peak-field limits instead. A sensible aspect is that standard recommendations are based on short-term exposure. Of a special interest in present standardization are the problems concerning mobile and wireless communication systems, due to the rapid and huge spreading of this kind of RF radiation sources in the environment. In Europe there are countries that didn't adopted the ICNIRP reference levels for human exposure, but more stricter ones, as for example Italy and Switzerland, with specific rules for the base station transceivers (BTS) in mobile telephony systems. China and Russia are similar examples, which didn't adopted international guidelines, but due to a different rationale of the limits calculation. A debate is still going on from years, in many countries, on the application of the precautionary principle [3], regarding the sensitive problem of BTS sitting and only some local authorities in Italy, Switzerland and Belgium really apply it. Coming to citizens and media level, the situation is even more complicated, since, for example, neither can people be involved in BTS sitting decision, nor have they the right to be informed of the (expected) EMF exposure.

In Romania, the adopted limits for human exposure are those given in the ICNIRP guidelines [1]. European regulations [4],[5], were applied starting with 2002. That year the Romanian Health Ministry issued the Order no. 1007/13.12.2002 referring to the regulations on admissible exposure limits and the measurement

methodology, order that follows the European Directive no. 199/519/EC. General norms for work safety no. 880/06.12.2002 offer supplementary rules on working places in electromagnetic environment.

In the present, in Romania there are four public mobile communication operators: Vodafone (GSM 900MHz and 3G-UMTS 2GHz), Orange (GSM 900MHz and 3G-EDGE 2GHz), Telemobil - Zapp (CDMA and EV-DO 450 MHz) and Cosmote (DCS 1800MHz). 3G UMTS services were recently launched in Romania by Vodafone – April 2006 and Orange – June 2006. The present number of mobile telephone users in Romania is about 12 million, for a total population of 22 million people (approx. 55% of the population).

Mobile phone BTS antennas debate have become of unprecedented intense public health concern in Romania in the last period, starting with the end of 2005. Numerous journals at central and local level published articles on the issue under the pressure of citizens [6]. Numerous population complaints were received at Local Consumer Protection Agencies, Environmental Agencies and Guards. As a result, some local authorities adopted decisions for national budget financial support of EMF measurements campaigns in 2006 (first one in Cluj county, March 2006 [7]). Most of the newspaper articles and media news were published/broadcasted starting with January 2006 and focused on reported health state impair (even cancer-related cases – one in Oradea city, the second in Sibiu city) and complaints on BTS sitting on the blocks and private gardens (population protests in 2 counties: Sibiu and Zalau). At least 2 titles in newspapers refer to BTS antennas as a second "Tchernobil", by comparison to the nuclear threat. Two private judicial processes are mentioned in media, won by the complaining persons against mobile telephony operators. One hospital (County Hospital Salaj) cancelled its contract to a mobile phone operator in order to renounce to the antenna mounted on the hospital's roof. The National Consumers Protection Agency, which received tens of protests and complaints in 2006, decided to demand the Town (Local) Councils in the country to adopt decisions that forbid further BTS sitting on residential buildings. The Agency is preparing a well documented file on the issue. On the other hand, Romanian Government recognised the potential hazard of BTS antenna sitting (even mounted on its own building), by issuing the Ordinance no. 2/12.01.2006, on supplementary financial rights for hazardous workplace conditions (specific RF emissions) of public functionary, in a quote of 10% from the base salary. The authorised institutions for measurements of EMF emissions in Romania are: the Public Health Direction with its local institutions, Ministry of Defence Health Direction and Ministry of Transportation Health Direction. Measurements made till the end of 2005 in our country were done in the majority by using wideband survey meters type EMR-300 and Narda-8718. Relevant information on GSM topic is available to the public via the ACER Bulletin and ACER website (ACER is the Romanian Electromagnetic Compatibility Association - http://www.acero.ro), GSM Magazine, mobile telephony company websites and the press (which features related international press reports).

On this background, our study aimed to prepare for a reliable measurement campaign of residential exposure. This is needed from at least two essential perspectives: a) compliance testing of BTS antennas and other RF emission sources and in situ measurements, according to present methodology [5], [8] and standards; b) accurate assessment of frequency-selective RF exposure, that should be considered from the view of the finding that biological effects depend on the carrier frequency, as recently proved in the mobile communication band [9].

We had two principal objectives: a) refinement of the measurement methodology in accordance to the aim of the measurement; b) exposure assessment due to RF sources, especially GSM BTS antennas and comparison between quotients afferent to different sources.

The measurements were made by using the frequency-selective method (spectrum analyser with isotropic antenna) in a number of outdoor and indoor locations, urban and extra-urban places, for different settings of the measurement system.

Materials and methods

As for ICNIRP guidelines requirements, the principal need is that the measurement system be a frequency selective one. The equipment must also be sensitive enough, must allow averaging the values over any 6 minutes in time and averaging in space, considering the volume of the human body respectively the interesting areas of it. It is essential to use procedures that allow measurements with low uncertainty and good reproducibility [10], [11].

The equipment we used for most of the measurements was the TS-EMF system by Rohde & Schwarz, Germany. At some point we also used the Field Nose System by Austrian Research Centre in Seibersdorf, which

also helped in comparison of the same measurement results during one session. The TS-EMF system is composed by the R&S FSH3 spectrum analyser, an isotropic sensor (30MHz to 3GHz) and the computer software R&S RFEX for data acquisition and settings management. The tri-axis sensor has got an isotropic characteristic so the measurement is done independent from direction or polarization of the emitter. This makes measurements easier. In contrast to directional antennas, it is no longer necessary to move the antenna for covering all directions and polarization. The Field Nose System uses the proven Add3D technique to conduct precise measurements and is composed by an Anritsu M2711D spectrum analyzer with a broadband omnidirectional precision conical dipole PCD8250 as measurement antenna (80MHz to 2.5GHz), driven by Nose Basic software. The antenna is consecutively positioned in three orthogonal directions during the measurement, by a software-driven rotor. A picture of the two measurement systems is presented in fig.1.

Figure 1 –TS-EMF system by Rohde&Schwarz (left, “spherical antenna”) and Field Nose System by ARCS Seibersdorf, (right, “biconical dipole”).

Reproducible time averaging method with well known uncertainty estimation can be performed on one single point in the area of interest. Different measurement modes were possible and applied: a) single measurement; b) average and peak (e.g. 6 minutes average); c) long term (e.g. determination of time variations of the signals). The most used was the average & peak measurements. To increase the sensitivity of the TS-EMF system, the function Threshold-Calibration can be introduced, and in all measurements this was applied.

The measurement protocol took into account the objectives of the research which was either compliance verification, or in situ measurements [10]-[12]. We followed the measurement methods described in [5] and [8]. No a-priori knowledge was available regarding sources emissions or the environment. The general scheme for compliance verification was not completely followed, since no simulation was made prior to measurements and no measurement with broadband field probe was prior made. The measurements were executed by means of the frequency-selective system, in urban and extra-urban locations, either outdoor or indoor. The choice of measurement points (location and number of points) was in accordance with the general considerations in [5]. Refinement of the measurements by settings modification was made in most locations, in order to consider the “worst case” exposure. Processing of measured data and final report followed each measurement.

For the major services, the TS-EMF system offers pre-defined measurement packets. This should insure optimum settings for evaluation according to single frequencies, complete services and total emission. However, at least in the case of GSM measurements, personally defined packets/settings were also prepared, since we need to refine the measurements. Comparison between results obtained with different settings will be presented and discussed. Data presentation of the measured emissions (field strength, power density or exposure ratio - ‰ of

ICNIRP limit) was possible as a sum value and can be split into frequency bands if necessary. Detected signal spectrum and histograms may be represented.
All measurements were made fully-automatic using the R&S software RFEX and they were performed inside macrocells and mostly outdoor. The ten locations chosen for measurements were situated in intra-urban highly populated areas, and only in two cases it was situated remote from the city. All were positioned in the vicinity of the transmitter sites, the distance between the measurement system and the base stations being from 40 to 500m.

Results and Discussion

A. Refinement of the measurement methodology:
Residential exposure assessment, if highly accurate, is a complex task. It should take into account:

- position of the spot measurement;
- signal characteristics and variations in time and space;
- environment impact thru physical influences (fast fading, etc.)

However, since in the great majority the population partial exposure quotients due to various RF signals proved to be much lower than that stipulated in standards (for example, for BTS antennas generally the measured power density levels are <<10% from the reference levels, [13]), the question of optimum settings of a measurement system may be not so important. But if one is more sceptical regarding fundaments that conducted to present "safe" reference levels in standards, than he might always keep in mind that:

- not only RF/MW heating may be responsible for health hazards, but also athermal/nonthermal mechanisms of interaction could trigger a biological response;
- long term exposure was not the basis of standard value considerations;
- "frequency windows" were proved to exist in connection to specific biological responses,

and then the optimum settings of a system may crucially influence the results of the exposure assessments and further epidemiological findings.

In this respect, it is of big importance to correctly set the resolution bandwidth (RBW), sweep rate (SR) and detector type (DT) [14], in function of the measured signal. Secondary, in the case of GSM signal for example, the resolution of adjacent channels and the effect of number of active time slots should be attentively considered. We made measurements to compare results, while modifying different setting parameters. As an example, we show here the consequences of modification of "Trace mode" (TM) and "Detector type" (DT) on the results obtained in the case of a GSM 900MHz signal measured in one indoor location, with conserving all the interior environmental conditions the same, and all other system settings. The results are showed in table I and were obtained for a series of 10 consecutively measurements for each setting. For these measurements, the commune settings of TS-EMF system were: RBW=200kHz; Span=30MHz; Reference level=91 dBµV; Dwell time=5s.

Table I : Influence of trace mode (TM) and detector type (DT) of the measurement settings on the results

	TM = Clear/Write DT = RMS		**TM = Max hold DT = Positive peak**		**TM = Max hold DT = RMS**	
	Average	***Peak***	***Average***	***Peak***	***Average***	***Peak***
Total field strength, RMS, (V/m)	**0.141** ± 0.005	**0.190** ± 0.004	**0.510** ± 0.004	**0.720** ± 0.003	**0.091** ± 0.003	**0.110** ± 0.006
Max single value (V/m)	**0.050** ± 0.003	**0.050** ± 0.002	**0.082** ± 0.002	**0.111** ± 0.003	**0.051** ± 0.002	**0.050** ± 0.004

"Max hold" setting is generally used for worst case when time variations of the signal are present. "Positive peak detector" represents also a worst case, but it may give over-rated values. "RMS" detector is usually used for non-sinusoidal signals to correctly derive the average signal power (it is especially used for UMTS mobile signals). As one can observe in the table above, the combination "Max hold" + "Positive peak detector" will give the worst case assessment possible. The values in this case are approximately 5 times larger in the case of total field strength then the ones obtained with the setting "Max hold" + "RMS detector" and about 3.5 times higher than the ones with the setting "Clear/Write" + "RMS detector". However, these values may be overestimated. The results repeated as well for measurements on GSM 1800 signals. We could then conclude about the "worst case" settings. Due to these observations, most of the compliance testing or in situ measurements made by us for GSM900 and GSM1800 signals were done by using the intermediary setting, "Clear/Write" + "RMS detector".

Moreover, we were able to observe that a lower RBW, for example one of 30kHz, is a better choice for "worst case" measurement. This setting should be completed by a sufficiently low sweep rate (long dwell time, thousands of milliseconds), or even better, multiple sweeps, so that the independence of the result upon the instantaneous traffic on a GSM signal to be assured.

As a result of lots of GSM measurement sessions, we were able to conclude that it is practically impossible to predict positions in space where hot spots of field distribution will appear, either outdoor or indoor. Time evolution of the field level is only predictable on the basis of traffic diminution in the late time hours, but otherwise is low-predictable also. Special aspects for further refinement of measurement methodology should focus on frequency hopping and power control of BTS.

B. Compliance testing and in situ measurement results:

Peak values measured in some outdoor locations for GSM900 signals are given bellow. Locations 1 and 2 are urban locations, while location 3 is extra-urban. In figure 2 – a,b,c one can visualise these locations. The settings of the TS-EMF system were: Trace Mode:Clear/Write; Detector: RMS; RBW=200kHz, span=30 MHz, Dwell time=5000ms. Power density (S) peak values measured in the 3 locations exampled in fig. 2 are:

$S_1^{peak}=(9.66 \pm 2.73)x10^{-5}$ W/m^2

$S_2^{peak}=(23.00 \pm 5.51)x10^{-5}$ W/m^2

$S_3^{peak}=(62.00 \pm 13.54)x10^{-5}$ W/m^2

a – Loc. 1

b – Loc. 2

c – Loc. 3

Figure 2 – Locations of outdoor measurements for GSM900 signals

The maximum peak value measured outdoor during the campaign either for GSM 900 or for GSM 1800, was $S_{max}^{peak}= 100x10^{-5}$ W/m^2, which is also far beyond ICNIRP reference levels. The reference levels are: for

GSM900, S_{ref}=4.5 W/m^2 and for GSM1800, S_{ref}=9 W/m^2. They are equivalent, for the E-field RMS value, to E_{ref}=42 V/m for GSM900 and E_{ref}=58 V/m for GSM1800.
Average values for GSM packets measured in location 2 (fig.1), at a later date, are given in table II. The location of the measurement is very central in the city. In table II, ER is the exposure ratio (=E^2/L^2 where L is the E-field limit given in standard). The values were obtained by "peak/average" menu of RFEX software, the averaging being made on 6 minutes of continuous scan. The scans alternatively changed from packet GSM900 to packet GSM1800. One can see from table II that the field levels are very low comparative to the reference levels. In figure 3 – a,b, a sample of the spectrum of measured GSM signals is given. Figure 4a shows a comparison of the prevalence of the two RF signals measured in location no. 2 as average exposure quotients (‰ of ICNIRP limits). In figure 4b, exposure quotients are represented for all significant RF signals present in the environment at the position of location no. 2. We used the prefigured packets with afferent settings offered by RFEX software itself for the measured bands. From fig. 4 one can outline that GSM 900 contribution is not much higher than "UKW" band or than "All 200M" band. In fact "UKW band" and "All 200M" band are the same, but have different analysis settings. "UKW band" covers frequencies between 87.6 – 106.3 MHz, with the following settings: Trace Mode / Detector: Max Hold / RMS, RBW=100kHz, Span=7.5 MHz, Dwell time=1000ms, while "All 200M" band covers emissions in the 88-106 MHz band, with the following settings: Trace Mode / Detector: Max Hold / RMS, RBW=300kHz, Span=45MHz, Dwell time=250ms. From histograms corresponding to the two similar packets, it is obvious how important the settings are, concerning field level assessment.

Table II: Values of average E-field RMS values for GSM signals in location no.2 from fig.1 and afferent exposure ratios:

Packet	Total Field (RMS) [V/m]	Total ER * 1000 [‰]
FSH3 GSM1800 bis	0,1224	0,0044
FSH3 GSM900	0,2815	0,0443
Sum	0,3070	0,0486

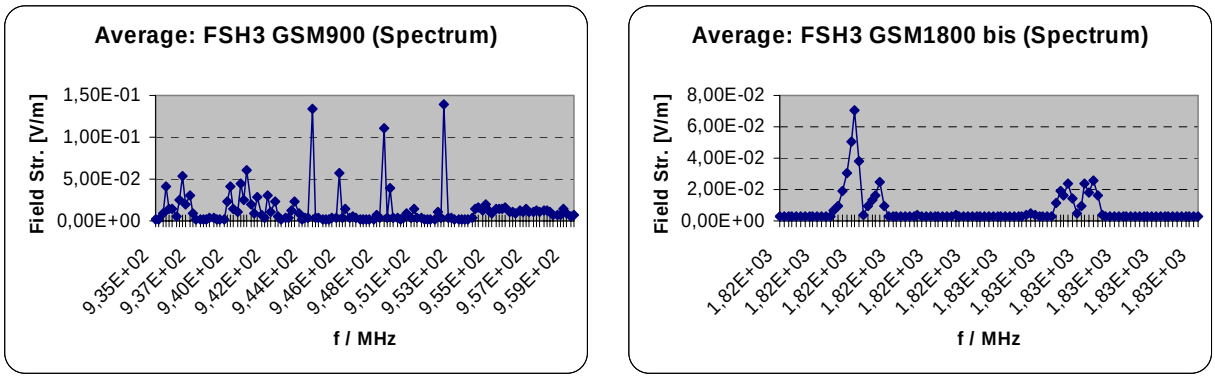

a) GSM 900 b) GSM 1800

Figure 3 – Spectrum of averaged values of GSM signals measured in location no. 2

Average values of total field and total exposure ratios for measured packets from above are given in table III. Here one observes a significant difference of the values corresponding to first and last line of the table respectively, which is solely due to system settings, and once more outlines the findings presented in part A of current section of the paper.

Generally, the existence of a large number of scatterers and absorbing objects around leads to a highly non-uniform field distribution in the environment of BTS antennas, due to shadowing and fast fading effects. Houses, trees, cars and other objects lead to field variations that can only be determined by very large measurement campaigns. The buildings cause a strong shadowing effect so the field distribution is very heterogeneous [15] – [17].

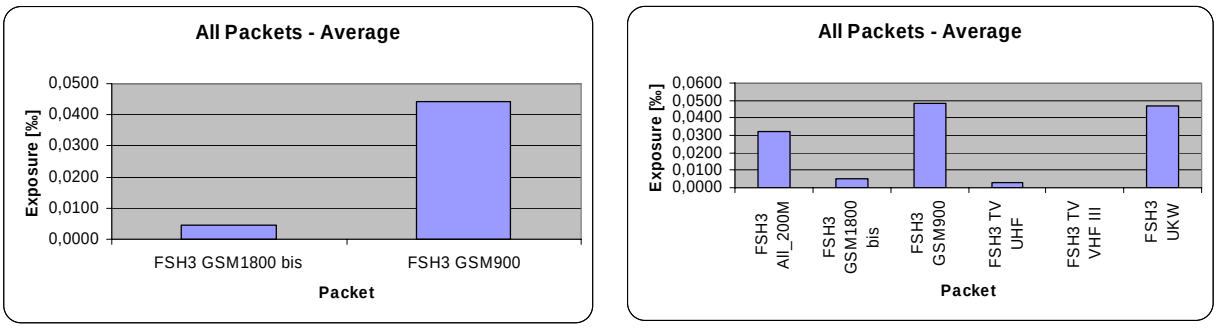

a) GSM bands comparison b) all RF signals comparison

Figure 4 – Histogram with exposure quotients (‰ of ICNIRP limits) corresponding to different RF signals measured in location no. 2

Table III: Values of average E-field RMS values for various RF signals measured in location no.2 and afferent exposure ratios:

Packet	Total Field (RMS) [V/m]	Total ER * 1000 [‰]
FSH3 All_200M	0,1568	0,0325
FSH3 GSM1800 bis	0,1309	0,0050
FSH3 GSM900	0,2941	0,0483
FSH3 TV UHF	0,0615	0,0028
FSH3 TV VHF III	0,0000	0,0000
FSH3 UKW	0,1876	0,0466
Sum	0,4089	0,1351

Time evolution of radiated GSM signals was also studied (long term measurements). Two examples are illustrated in figure 5 a,b, where traffic variations and trend in daytime, as a function of hour, can be seen for two indoor sites, situated between 300-500m distance from BTS antennas. For fig. 4a, the measuring location was location no. 2 from fig. 1. The field values are again far beyond ICNIRP references.

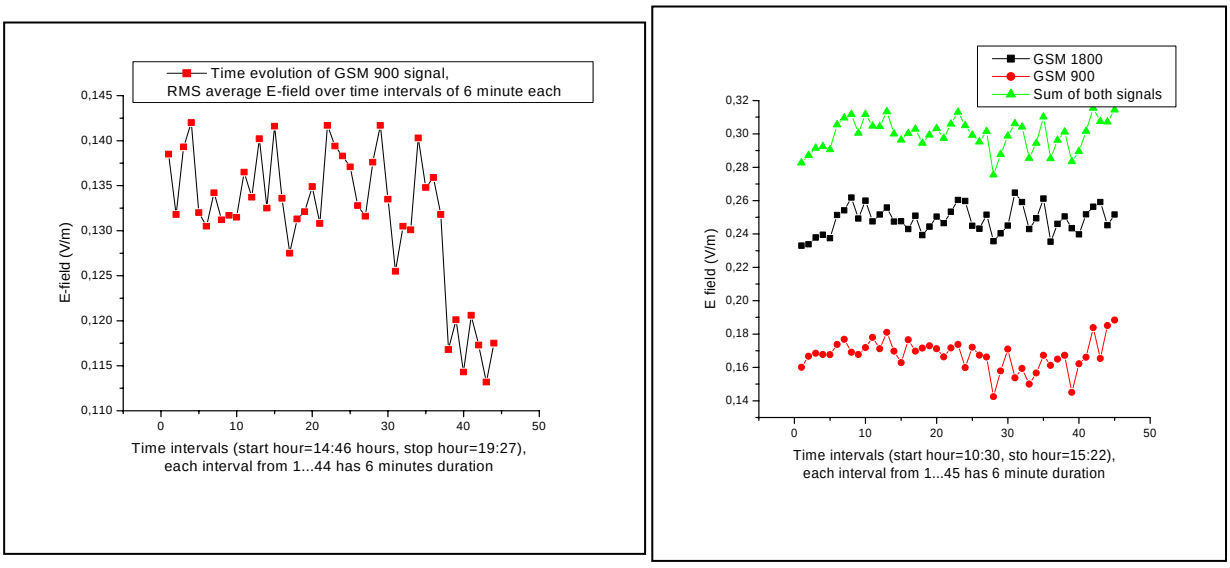

a) GSM 900 signal trend during afternoon hours; b) GSM 900 and 1800 signal trends during morning hours

Figure 5 – Time evolution of GSM signals: a) GSM900, measured between hours 14:46 and 19:27 in one indoor location; b) GSM900, GSM1800 and sum of them, measured between hours 10:30-15:22, in a second indoor location

Other indoor measurements were made in some sensitive sites, for both GSM signals and also for other RF signals in the environment. In indoor conditions (inside buildings), the field distribution is even more complicated. It may happen that inside a room volume, the E-field strength of a GSM broadcast channel (BCCH) alone, which operates permanently and on the same power, to vary from point to point inside the room as much as +8 to – 10 dB from the average value. So a single measurement is completely non-representative for the exposure scenario. Field variations versus time caused by changes of the power of traffic channels, the stability of BCCH's or moving scatterers have to be taken into account in order to determine their contribution to the uncertainty of exposure assessment [18]. The search for maximum field level is a very crucial point, because of the need of comparison to the limits given in exposure standards. The reproducibility of identified maxima is one of the largest problems, due to field variations in time and space. In this context it is important to say that the selection of the location for performing measurements is very important.

A challenging vista with regard to human exposure is nowadays the wireless devices technologies used in homes and offices. Several new wireless connectivity standards and technologies, e.g., DECT, Bluetooth, IEEE 802.11, may be interesting to be evaluated from human safety point of view. In present paper we assessed a DWL-2100AP 2.4GHz (802.11g) Wireless Access Point connected to the ANT24-1201 Outdoor antenna (figure 6). The antenna is mounted on the window frame of an educational institution, as seen in figure 6 and has a peak output power of 100mW. We measured the field level in the far field of the antenna, indoor, starting at a distance of 2 m of it. As in other cases, a non-predictable distribution of the E-field was achieved inside the classroom, all the values complying with the ICNIRP reference levels. At distance d=2m from antenna, average field value over 12 minutes was E=0.21V/m, representing an ER=0.01‰. A measurement sample spectrum for the antenna is presented in figure 7, in a position at a distance d=3m. The settings for these measurements were: Trace Mode / Detector: Max Hold / Max peak, RBW=1000kHz, Span=150 MHz, Dwell time=1000ms. Total field strength for the single measurement in fig. 7 was 0.29V/m, and ER=0.02 ‰.

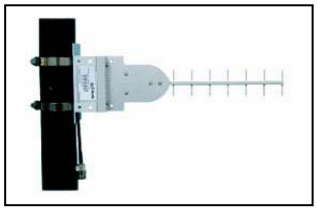

ANT24-1201 Outdoor antenna,
12dBi , H50/V50, 2.4 GHz

DWL-2100AP High Speed
2.4GHz (802.11g) Wireless 108Mbps
Access Point

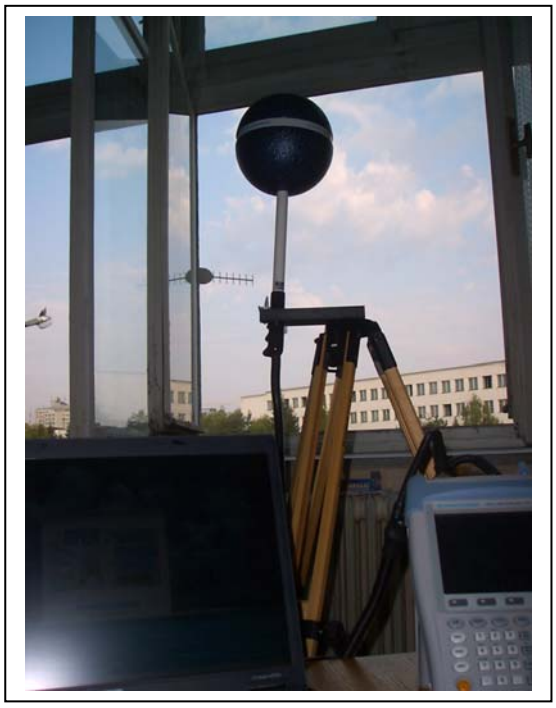

Figure 6 – Measurement of indoor field emitted by a 8011.g technology wireless access point antenna type ANT 24-1201.

A local radio broadcasting antenna radiation, placed in a residential zone, was measured in the neighbourhood zone, as seen in figure 8a. The Field Nose system was used this time. FM broadcasting antenna was placed on a tower at about 30m above the ground. The emitted frequency was f=103.2 MHz. The system settings were: frequency band=80 to 120 MHz; max peak detector; RBW = 100KHz; sweep rate= 40MHz/s; reference level=-20 dBm. Measurements were made at 2 different heights above the ground, at 1.7 and 1.2 m respectively, at a distance of about 50m from broadcasting antenna. E-field strength value for the two positions were: E_1=2.2 V/m and E_2=2.6 V/m respectively. Spectrum of the total field at 1.7 m height is represented in fig. 8b. The reference

level in ICNIRP guideline for this frequency is E=28V/m. In these conditions ER ≈ 10% and we can conlude that this case represents one of the highest exposures measured during present session. Cumulating with other RF sources emissions could conduct to non-neglijible exposure but still considerably under ICNIRP limits.

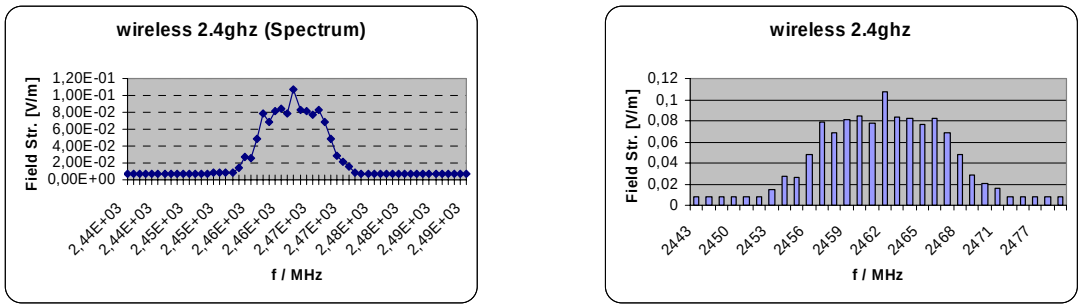

Figure 7 – Spectrum and histogram of E-field strength for wireless point outdoor antenna

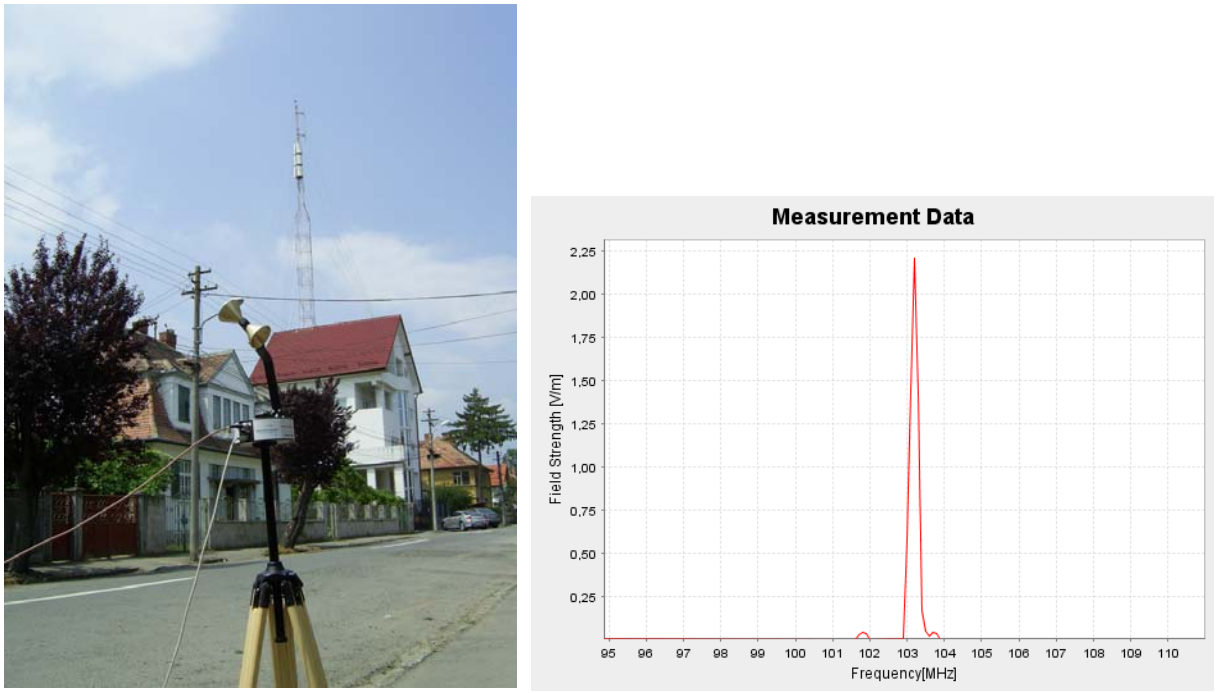

(a) (b)

Figure 8 – RF broadcasting antenna measured by Field nose system: a) position in respect to emissive antenna; b) total E-field spectrum in a position at approx. d=50m, and at 1.7 m above the ground.

Conclusion

Risk perception accentuated in the last period in Romania in connection to RF sources emissions, and especially to BTS antennas. We consider that perceived risk differs from the assessed risk, in that it may more readily be manipulated. On this basis, at the level of accredited institutions it became obvious the need for measurement campaigns. Systematic studies to evaluate individual exposure of different parts of the population are needed. In this regard, at the level of each county, specific measures were taken, starting with financial support of measurement campaigns and ending to risk communication. However, fears exist that precautionary measures may undermine the scientific basis for the established exposure limits. In this view, precautionary measures for EMFs should be adopted only with great care. The national Agency for Consumer's Protection demanded all Local Town Councils to refuse further sitting of BTS antennas on blocks or residential roofs. The same agency prepares a well documented file on the issue and the Public Health Direction and Institutes were designated to apply specific measures for exposure assessment and reduction.

Results of present study showed the importance of a refined measurement methodology from the perspective that frequency and/or signal specific exposure recently turned out to be relevant, so exposure due to base stations might be important. Biological relevant exposure circumstances are of great interest in our opinion. Contributions from other RF sources have also to be taken into account. The reduce-scale campaign we developed in and around one single town in Romania, showed that RF exposure of citizens is reduced reported to regulations limits. A key concern across the epidemiological or health-related studies should be the quality of assessment of RF exposure. Despite the ubiquity of new technologies using RF, little is known about population exposure from RF sources and even less about the relative importance of different sources.

Acknowledgement: Present research was funded by the Romanian Ministry of Education and Research by the CEEX Programme 2005 / CERES, under the Contract CEx 05-D11-54/10.10.2005 with Land Forces Academy, Sibiu, Romania.

References

[1] ICNIRP, Guidelines for limiting exposure to time-varying electric, magnetic, and electromagnetic fields (up to 300 GHz), Health Physics 74 (4), pp. 494 – 522, 1998.
[2]. IEEE Standard for Safety Levels with Respect to Human Exposure to RF Electromagnetic Fields, 3kHz to 300GHz, IEEE Std. C95.1-2005.
[3] Wiedemann P.M., SchützH., The Precautionary Principle and Risk Perception: Experimental Studies in the EMF Area, Environmental Health Perspectives VOLUME 113 | NUMBER 4, 402-405, April 2005
4] EUR-OP: Council Recommendation of 12 July 1999 on the limitation of exposure of the general public to electromagnetic fields (0 Hz to 300 GHz) 1999/519/EC, Official J. European Communities, Luxembourg, 1999.
[5] ECC RECOMMENDATION (02)04 revised, Measuring non-ionising electromagnetic radiation (9kHz-300GHz), October 2003.
[6] Personal collection of newspapers articles (in Romanian): "Ziua" newspaper (issue 30 May 2006, issue 31 May 2006, issue 5 June 2006, issue 8 June 2006, issue 20 July 2006), "Jurnalul National" (issue 8 June 2006, issue 20 July 2006), "Ziarul" (issue 8 June 2006, issue 22 July 2006), "Tribuna Sibiului" (issue 18 January 2006, issue 20 July 2006, issue 21 July 2006).
[7] Hotararea nr. 234 din 28 martie 2006 a Consiliului Local Cluj Napoca (in romanian)
[8] Agence Nationale de Frequences, Protocole de mesure in situ, Visant à vérifier pour les stations émettrices fixes, le respect des limitations, en terme de niveaux de référence, de l'exposition du public aux champs électromagnétiques prévues par le décret n° 2002-775 du 3 mai 2002.
[9] Markova E., Hillert E., Malmgren L., Persson B.R.R., Belyaev I.Y., Microwaves from GSM Mobile Telephones Affect 53BP1 and -H2AX Foci in Human Lymphocytes from Hypersensitive and Healthy Persons, Environmental Health Perspectives VOLUME 113 | NUMBER 9 , 1172 -1177, September 2005
[10] Mann S.M., Cooper T.G., Allen S.G., Blackwell R.P., Lowe A.J.: Exposure to Radio Waves near Mobile Phone Base Stations, Chilton, Natl. Rad. Protect. Board Report-321, 2000.
[11] G. Neubauer, D. Papameletiou, T. Samaras, Y. Hamnerius, J. Wiart,K. Lamedschwandner, Methods to assess exposure of the population next to mobile communication base stations, 27th triennial General Assembly of the International Union of Radio Science, Maastricht, 2002.
[12] Müllner W., Neubauer G., Haider H., Add3D, a new technique for precise power flux density measurements at mobile communications base stations, 10th Internat. Fachmesse und Kongress für EMV, Düsseldorf, pp 305–312. 2002.
[13] Miclaus S., Bechet P., Goiceanu C., Olariu O.V., Demeter S., Practical issues concerning cellular base station emissions and population exposure in Romania, 3rd European Medical & Biological Engineering Conference, Prague, Czech Republic, 20-25 Nov. 2005, IFMBE Proceedings 11 (1), 2005.
[14] C. Olivier, L. Martens, Optimal Settings for Narrow-Band Signal Measurements Used for Exposure Assessment Around GSM Base Stations IEEE Trans. on Instrumentation and Measurement, vol. 54, No. 1, pp.311-317, Febr. 2005.
[15] Preiner P., Überbacher R., Kaczmarczyk A., Neubauer G.: Evaluation of Electromagnetic Field Distributions near Mobile Communication Base Stations, Proc. COST 281 Workshop: STM Base Station Monitoring, Vienna, 26-27 August 2003.
[16] C. Olivier, L. Martens, EMF measurements around base stations: Some issues, COST 281-STM Base Station Monitoring Workshop, Vienna, 26-27 Aug. 2003.
[17] G. Neubauer, H. Haider, K. Lamedschwandner, M. Riederer, R. Coray, Measurement Methods and Legal Requirements for Exposure Assessment Next to GSM Base Stations, International Zürich Symposium on EMC, pp 143 – 147, February 2003.
[18] H. Lehmann, B. Eicher, P. Fritschi, Indoor measurements of the electrical field close to mobile phone base stations, 27th triennial General Assembly of the International Union of Radio Science, Maastricht, 2002.

LOW POWER MICROWAVE RADIATION EFFECTS ON MAIZE SEEDS

RĂCUCIU MIHAELA[1*], MICLĂUŞ SIMONA[2]

[1] "Lucian Blaga" University, Faculty of Sciences, Dr. I. Ratiu Street, No.5-7, 550012, Sibiu, Romania, mracuciu@yahoo.com
[2] Land Forces Academy "N. Balcescu", 3-5 Revolutiei Street, 550170, Sibiu, Romania

Abstract
In this study young plantlets, obtained from the control and microwave irradiated seeds, were studied in laboratory experiments. The electromagnetic radiation with the frequency of 10.8GHz was generated by a microwave generator, based on a rectangular waveguide. The effective incident power was measured to be of 5.2mW. The *maize* seeds with uniform genophond were irradiated one at a time inside the irradiation waveguide, by means a Teflon cuvette, with different exposure times. After germination the young plantlets growing was conducted in the same controlled laboratory conditions and the culture medium of young plantlets was daily the same amount of deionized water. The length of the 12 days plantlets was measured as well and statistical analysis was performed on the data. Assimilatory pigments and average nucleic acid level were assayed of 12 days old plantlets, by spectrophotometric methods and using a Perkin - Elmer UV-VIS spectrophotometer. The data provided by the chlorophylls ratio (chlorophyll **a** / chlorophyll **b**) measurement offered the main insight into the photosynthesis complex processes since they revealed the response of the LHC II system (Light Harvesting Complex II), associated to the photosynthetic system II from the tylakoidal membranes, to the external stress. For chlorophylls ratio a slight stimulatory effect was noticed for shorter time exposures, suggesting putative stimulation of photosynthesis process. The same effect was registered to average nucleic acid level.

Keywords: low power microwave, *maize*, plants growth, photoassimilatory pigments, nucleic acids.

Introduction

The effect of electromagnetic microwave irradiation on agricultural crops has scarcely been studied yet. For decades a great variety of living beings have been used by researchers in order to detect possible changes in ecosystems. Thirty years ago two Canadian researchers observed a deterioration that was unpredictable on the plants subjected to microwaves (Tanner and Romero-Sierra) [1].

Some studies on the effect of microwave irradiation (2.45 GHz) on seeds were conducted and detected an enhanced rate of germination [2-4]. Bhaskara Reddy *et al.* [3-4] used the microwave range (2.45 GHz) on seeds of charlock, wheat, soybeans, peas and rice with the aim of pre-storage destroying. Yoshida *et al.* [5-7] used microwave radiations (2.45 GHz) on soybean, peanut and sunflower seeds for improving the triglycerides distribution in the seed. Studies on the effect of electromagnetic irradiation of the microwave range on seeds have also been conducted by Aladjadjiyan *et.al.* [8] and Kalinin *et.al.* [9].

Recent experiments have shown that exposure to radiation emitted from a global system for mobile communication (GSM) telephone followed by calcium deprivation, leads to meristem production in flax seedlings [10]. To investigate the possibility that plants may be affected by exposure to a frequency in this range some investigators used radiation with 105 GHz frequency at non-thermal levels by a Gunn oscillator [11].

[*] Corresponding author: E-mail: mracuciu@yahoo.com

As well known, photosynthesis is a very complex phenomenon resulting in the transformation of solar electromagnetic energy into chemical energy, stored in organic compounds, synthesized from inorganic carbon and water. The study of assimilatory pigments from plant green tissue is able to provide information upon the capacity of solar energy conversion at the level of chloroplast membranes, during photosynthesis.

In this paper the authors present some quantitative observations of microwave radiations exposure influence of seeds on the growth of *Zea mays* (*maize*) agrotechnical plants.

Materials and methods

Young plants, obtained from the control and microwave irradiated seeds, were studied in laboratory experiments. The electromagnetic radiation was generated by a microwave generator, based on a rectangular short-ended waveguide. The microwaves were generated as 10.8 GHz continuous waves modulated by rectangular pulses with a duty factor of ½ at a repetition frequency of 1.75 kHz. The effective incident power was measured to be of 5.2 mW. The absorbed microwave power inside the cuvette was estimated at 0.20 mW, corresponding to an average specific absorption rate of 1.33 W/kg. The *maize* seeds (plant species with major role in people life) with uniform genophond were irradiated one at a time inside the irradiation waveguide, by means a Teflon cuvette, with different exposure times. Batches of 30 seeds were irradiated for 5, 10, 15, 20, 40, 60 and 120 minutes. The irradiated seeds germinated in deionized water on porous paper support, in darkness and closed Petri dishes. After germination the young plantlets growing was conducted in the same controlled laboratory conditions (temperature (24^{o}C), illumination (10 h: 14 h light/dark cycle) and 90% humidity) and the culture medium of all young plantlets groups was daily the same amount (10ml) of deionized water.

The length of the 12 days plantlets was measured with 0.1 cm precision as well and statistical analysis was performed on the data.

After 12 days of plantlets growth, spectrophotometric assays were accomplished: the content of chlorophyll a and chlorophyll b and total carotenoid pigments (Meyer-Berthenrath's method modified by Ştirban [12]) and the average content of nucleic acids (Spirin's method [13]). The spectral device was a Perkin-Elmer spectrophotometer UV-VIS provided with quartz cells.

Green tissue harvested, from each exposed and control sample (mixture of green tissue picked up from all the 30 plantlets), was weighted, crushed and mixed with the same volumes, of 85% acetone in deionized water for the assimilatory pigments extraction [12] and 6% perchloric acid for nucleic acid extraction [13], being further quantitatively transferred into quoted glass tubes.

The levels of chlorophyll a, chlorophyll b and total carotenoid pigments may be calculated with the next formulae according to [12]:

$$\text{chla} = \frac{12{,}3\cdot \text{A}(663) - 0{,}86\cdot \text{A}(645)}{1000\cdot \text{d}\cdot \text{w}}\cdot \text{V},$$

$$\text{chlb} = \frac{19{,}3\cdot \text{A}(645) - 3{,}6\cdot \text{A}(663)}{1000\cdot \text{d}\cdot \text{w}}\cdot \text{V},$$

$$\text{t.c.} = \frac{10\cdot \text{A}(472)}{2485\cdot \text{d}\cdot \text{w}}\cdot \text{V},$$

while the average content of DNA and RNA is given by the relation [13]:

$$[\text{AN}] = \frac{\text{E}(270) - \text{E}(290)}{0.19}\frac{\text{V}}{\text{w}}$$

where: w-the fresh vegetal sample mass, V-the extract volume; A(λ)-the light absorption to the wavelength λ; d-the quartz cell width.

Three repetitions of each spectrophotometric assay have been accomplished. Statistic analysis was accomplished by means of average values, standard deviations and *t*-test (two tails, pair type) considering the significance criterion of 0.05.

Results and discussions

The average lengths and the standard deviations were calculated for each batch of test seeds. The confidence interval was calculated for every batch of plantlets using the Student test, for the confidence level P = 90%. In Fig. 1 average plantlets length for control and microwave exposure samples is presented.

The average values of plants length are enhanced proportionally to the microwave exposure time – a linear regression curve with correlation coefficients R^2 about 0.9561 was found.

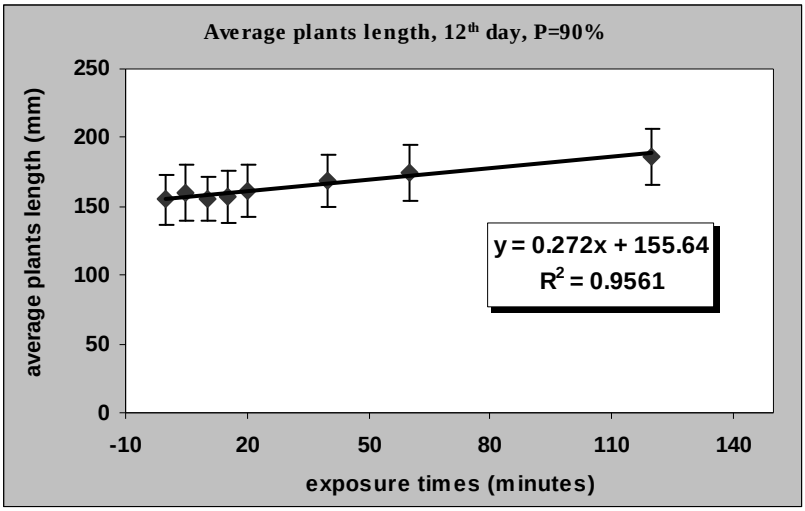

Fig.1. The average length versus microwave exposure time

The contents of photosynthesis pigments (**a** and **b** chlorophylls and total carotenoids) in the green tissue of young maize plantlets (aged of 12 days) for experimental samples in Fig.2 are presented. For all exposure times all three pigments present averaged values ranging around control values, i.e. small enhancements or small diminutions, with statistical significance for short exposure times (5; 10 and 15 minutes) while for longer exposure times (15; 20; 40; 60 and 120 minutes) the statistical analysis no revealed statistic significance. Similar response at microwave irradiation of seeds was get for the all three assimilatory pigments analyzed.

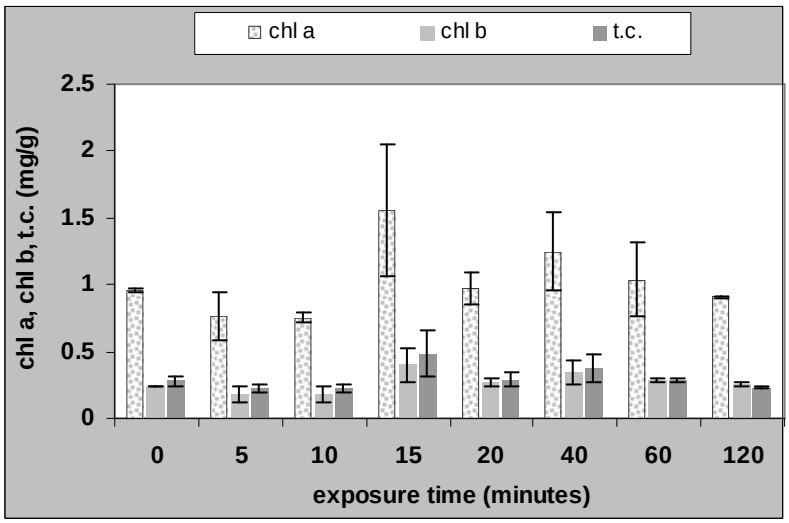

Fig.2. Assimilatory pigments level in *maize* plantlets versus microwave exposure time
(chl a –the content of chlorophyll a, chl b-the content of chlorophyll b,
t.c.-the content of total carotenoid pigments)

The total assimilatory pigments contents have the same variation to the increase of the microwave exposure time that was observed for chlorophyll **a** level. Very good linear correlations were revealed between pairs of pigments level (Fig.3). These results can be taken as an indication upon the correlated influences of microwave radiation in the all: chlorophyll **a**, chlorophyll **b** and the secondary carotenoids like pigments. As known chlorophyll **a** molecules represent the main photosynthesis pigment, able to control directly the solar energy conversion into chemical form while carotenoids are playing very important role in the sustaining of photosynthesis efficiency, by indirect energetic transfer of the absorbed energy to chlorophyll **a** molecules. Concluding on these results, all analyzed assimilatory pigments had similar variations versus microwave irradiation times.

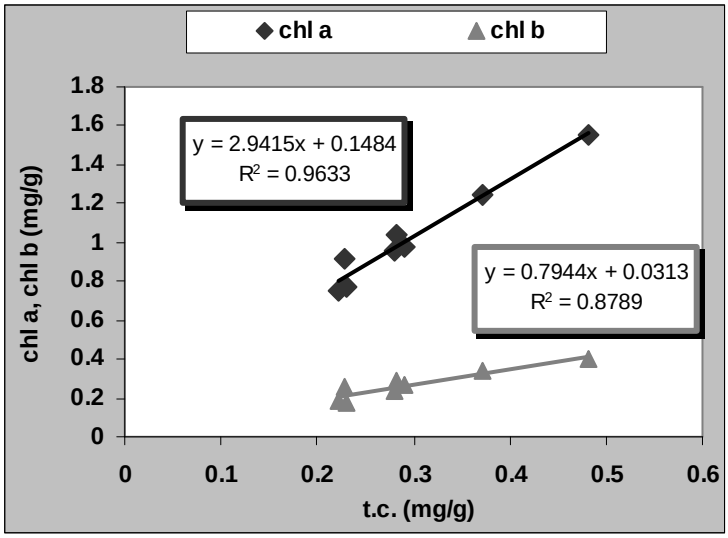

Fig.3. Linear correlation between chlorophyll a, chlorophyll b and total carotenoid pigments levels
(chl a –the content of chlorophyll a, chl b-the content of chlorophyll b,
t.c.-the content of total carotenoid pigments)

The best indicator upon the photosynthesis process efficiency is considered the chlorophylls ratio (chlorophyll **a** / chlorophyll **b**) [14] which provides indirect information on the enzymatic aggregates of the **L**ight **H**arvesting **C**omplex II (**LHC II**) from the photosynthetic system II located in the chloroplasts membranes. In Fig.4 a slight stimulatory effect can be seen for shorter microwave exposure time to photosynthesis process, as suggested by chlorophyll **a** and **b** ratio; inhibitory effect is obvious for the highest microwave exposure time. The ratio chlorophyll **a** / chlorophyll **b** was enhanced with 6% for shorter microwave exposure time sample and diminished with 15% for higher microwave exposure time.

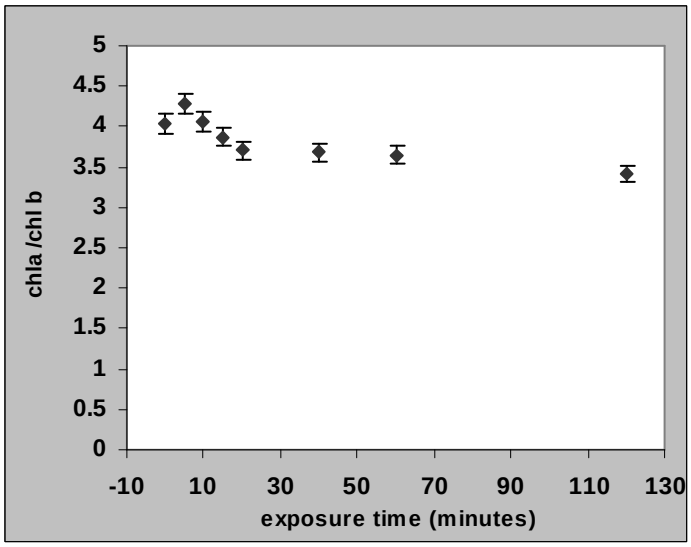

Fig.4. The effects of microwave exposure of seeds on chlorophylls ratio in 12 days old plantlets

The average content of nucleic acids (DNA and RNA) in young *maize* plantlets provided by microwave irradiated seeds, after 12 days of grown is presented in Fig.5. A stimulatory influence of microwave exposure on the biosynthesis of nucleic acids was revealed for low exposure times (to 14% for 20 minutes microwave exposure sample) while for the higher microwave exposure time an inhibitory effect (35%) than control was observed. Applying the *t*-test to compare control and test sample, data for the average nucleic acid level have revealed statistic significance ($p<0.05$) for all exposed samples.

Thermal as well as non-thermal effects of microwaves interaction with seeds are supposed to underlay these modifications.

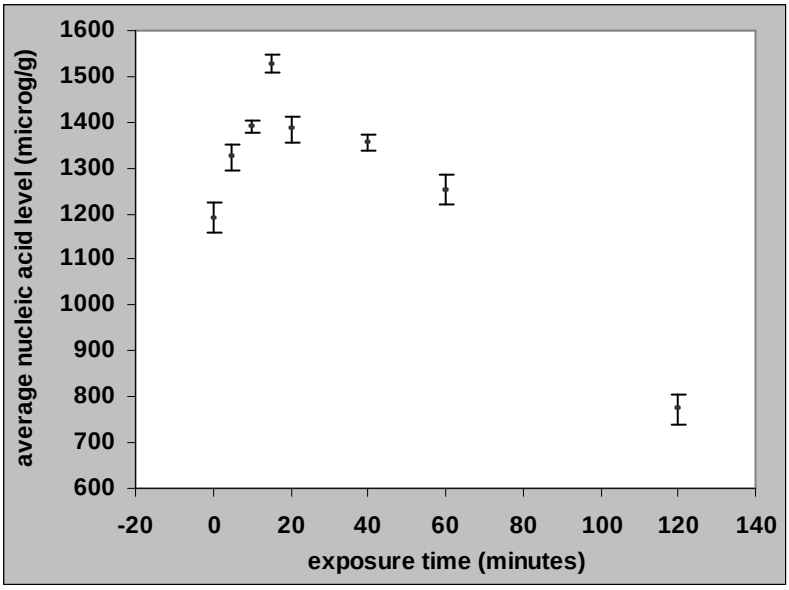

Fig.5. The average nucleic acid levels in *maize* plantlets provided by irradiated seeds

The electromagnetic energy of the microwave absorbed photon is six orders of magnitude lower than that of chemical or even hydrogen bonds needed to break down. So, the absorption of a microwave photon cannot break these bonds [15]. But, more complex indirect phenomena, possible within cellular complex structures may occur, that finally can lead to the plants growth disturbing. Maybe the accumulation of oxygen radicals is the primary cause, as they are suspected for dissociating the covalent bonds of DNA [16] when water molecules are adsorbed on the surface of large bio-molecules within cellular medium.

Summary

In summary, in this experimental study regarding microwave radiation with 10.8 GHz frequency influences upon maize seeds, observed on the 12 days old plantlets derived by irradiated seeds, a very slight stimulation of the photosynthesis process was revealed by means of chlorophylls ratio (to 6% increasing) in the case of shorter microwave exposure time. For the higher microwave exposure time the chlorophylls ratio was diminished with 15% than control. Also, a stimulatory influence of microwave exposure on the biosynthesis of nucleic acids was revealed for low exposure times (to 14%) while for the higher microwave exposure time an inhibitory effect (to 35%) than control was evidenced. The low power microwave treatment of seeds has revealed that *maize* young plantlets development may be slightly affected during their first twelve days of growth.

In fact the complexity of plant growth phenomena can not be evaluated only by means of the chlorophylls and carotenoids or nucleic acids behavior but also by considering the enzymes activity, the capacity of water accumulation and so on. It is designed that our further experimental projects to be focused on the diversification of the investigation methods able to provide data regarding the plant electromagnetic sensitivity in the range of microwave exposure parameters tested inhere.

Based on the fact that such microwave exposure can often occur in natural plant populations but no phenotypic changes are reported regarding the perturbation of the main biological patterns, the presumption that the recover mechanisms are also activated following the microwave exposure is a challenging issue.

References

[1] J.A. Tanner, C. Remero-Sierra, Beneficial and harmful growth induced by the action of nonionizing radiation, Annals of the New York Academy of Sciences, 238: 171-175 (1974).
[2] V. Nguyen Tran, Effects of Microwave Energy on the Strophiole, Seed Coat and Germination of Acacia Seeds, Australian Journal of Plant Physiology, 6(3): 277 - 287 (1979).

[3] M.V. Bhaskara Reddy, A.C. Kushalappa, G.S.V. Raghavan, M.M.P. Stevenson, Eradication of seedborne Diaporthe phaseolorum in soybean by microwave treatment, 66th Annual meeting of the Canadian Phytopathological Society, June 25-28, Toronto, (1995).
[4] M.V. Bhaskara Reddy, G.S.V. Raghavan, A.C. Kushalappa, T.C. Paulitz, Effect of microwave treatment on quality of wheat seeds infected with *Fusarium graminearum*, Journal of Agric.Engin.Res., 71:2 (1998).
[5]H. Yoshida, S. Takagi, Y. Hirakawa, Molecular species of triacylglycerols in the seed coats of soybeans following microwave treatment, Food Chemistry, 70:63-69 (2000).
[6] H. Yoshida, Y. Hirakawa, Y. Tomiyamaa, Y. Mizushina, Effects of microwave treatment on the oxidative stability of peanut (*Arachis hypogaea*) oils and the molecular species of their triacylglycerols, European Journal of Lipid Science and Technology, 105(7): 351 – 358 (2003).
[7] H. Yoshida, Y. Hirakawa, Y. Mizushina, T. Tanaka, Molecular species of triacylglycerols in the hulls of sunflower seeds (*Helianthus annuus L.*) following microwave treatment, European Journal of Lipid Science and Technology, 104(6): 347 – 352 (2002).
[8] A. Aladjadjian, D. Svetleva, Influence of Magnetron Irradiation on Common Bean (Phaseolus vulgaris L.) Seeds, Bulg. J. Agr. Science, 3: 741-747 (1997).
[9] L. G. Kalinin, I. L. Boshkova, G. I. Panchenko, S. G. Kolomiichuk, Influence of Low-Frequency and Microwave Electromagnetic Fields on Seeds, Biophysics, 50(2): 334-337 (2005).
[10] M. Tafforeau, M.C. Verdus, V. Norris, G. White, M. Demarty, M. Thellier, C. Ripoll, SIMS study of the calcium-deprivation step related to epidermal meristem production induced in flax by cold shock or radiation from a GSM telephone, J Trace Microprobe Techn., 20: 611–623 (2002).
[11] M. Tafforeau, M.C. Verdus, V. Norris, G. J. White, M. Cole, M. Demarty, M. Thellier, C. Ripoll, Plant sensitivity to low intensity 105 GHz electromagnetic radiation, Bioelectromagnetics, 00: 1-5 (2003).
[12] M. Stirban, *Procese primare în fotosinteza*, Ed. did. si ped., Bucharest, 1985, 229.
[13] A. Spirin, *Biochimia*, Ed. Mir , Moscow, 1958, 656.
[14] D. Ort, J. Whitmarsh, *Photosynthesis.Encyclopedia of Life, Sciences*, Macmillan, London, 2001.
[15] H. Fujikawa, H. Ushioda, Y. Kudo, Kinetics of Escherichia coli destruction by microwave irradiation, Applied and Environ. Microbiol., 58: 920-924 (1992).
[16] Y. Kakita, M. Funatso, F. Miake, K. Watanabe, Effects of microwave irradiation on bacteria attached to the hospiral white coats, International J. of Occup. Med. & Environ. Health, 12(2): 123-126 (1999).
[17] C. Polk, E. Postow, *Handbook of Biological Effects of Electromagnetic Fields*, CRC Press Ltd., Boca Raton, New York (1996).

PRELIMINARY DOSE-FINDING EXPERIMENT FOR THE STUDY OF THE PROMOTIONAL EFFECTS OF POWER FREQUENCY MAGNETIC FIELDS ON RAT LEUKEMIA

T. NEGISHI[1], I. NISHIMURA[1], K. SHIBUYA[2], M. ITABASHI[2] AND S. IMAI[1]

[1]Biological Environment Sector (Risk Assessment Group), Environmental Research Laboratory
Central Research Institute of Electric Power Industry
1646 Abiko, Abiko, Chiba 270-1194, Japan.
[2]Contract Testing Department, Nippon Institute for Biological Science
2221-1 Shin-machi 9, Ome, Tokyo 198-0024, Japan.

Abstract

A total of 200 female Donryu rats at 11 weeks of age were randomly divided into 10 groups of 20 rats. Animals in 8 groups were given 0 (olive oil: vehicle only), 10, 20, 30, 40, 50, 60 or 70 mg/kg body weight of 1-propyl-1-nitrosourea (PNU) by oral administration, 5 days a week for 5 weeks. Animals in other 2 groups were given 300 or 350 mg/kg body weight of PNU, once a week for 5 weeks. They were observed for 30 weeks after PNU administration. Except for dead animals due to acute PNU toxicity during PNU injection period and the first 2 weeks of observation period, the cumulative proportions of dead animals and animals with leukemia in 0, 10, 20, 30, 40, 50, 60, 70, 300 or 350 mg/kg of PNU-injected groups were 0.0, 0.0, 0.0, 10.5, 40.0, 47.4, 73.7, 80.0, 22.2, 27.8% and 0.0, 0.0, 5.0, 10.5, 10.0, 21.1, 63.2, 80.0, 27.8, 27.8%, respectively. Main cause of death was erythrocytic leukemia. The incidence of myelocytic leukemia, which we intended to induce mainly, was low and 5.0, 16.7, 22.2% in 20, 300 and 350 mg/kg of PNU-injected groups, respectively. Body weight gain during observation period showed that PNU toxicity was lower in 300 mg/kg group than 350 mg/kg group. Based on these results, administration of 300 mg/kg body weight of PNU, once a week for 5 weeks was selected for initiation method. 50Hz magnetic field exposure study of up to 350μTrms is now in progress.

INFLUENCE OF LOW-FREQUENCY MAGNETIC FIELD ON ENZYME ACTIVITIES OF STREPTOZOTOCIN-INDUCED DIABETIC RATS

Işıl Öcal[1], Gülen Atilla[2] and İsmail Günay[1]

[1]Cukurova University, Medical Faculty, Department of Biophysics, 01330 Balcalı/Adana, TURKIYE

[2]Cukurova University, Medical Faculty, Department of Biochemistry, 01330 Balcalı/Adana, TURKIYE

Tel:+90-322-3386060/3472

iocal@cu.edu.tr

The effects of magnetic fields seem to depend on their respective codes (frequency, intensity, and waveform). The aim of the present study is to examine the effects of magnetic field on changes of glucose, lipid levels and activations of alpha-amylase and lipase enzymes in diabetic rats that were different exposed durations to magnetic field. The rats were first divided into two groups. The first group (30 rats) was made up diabetic control group ((D_I, D_{VII} and D_{XIV}), the second group was comprised of rats described as diabetic-exposed to magnetic field groups (DMF_I, DMF_{VII} and DMF_{XIV}). Diabetic (D) and diabetic-exposed to magnetic field (DMF) groups were made up adult male Wistar Albino rats (60 rats). DMF groups (30 rats) were exposed to magnetic field for thirty minutes per one, seven and fourteen days. The combinations: of alternating modulated magnetic fields were set up 5 mT intensity, 50 Hz frequency and oriented north-south direction. Also, diabetic groups of adult male Wistar Albino rats (30 rats) were treated in identical fashion to the exposed rats, except that the magnetic field was switched off.

The end of first, seventh and fourteen days, blood of rats in diabetic-exposed to magnetic field and diabetic groups was collected under ether anesthesia for biochemical parameters, activations of enzymes and ion concentrations. The end of 1 st day that in diabetic-exposed to alternative magnetic field groups, while serum glucose and lipid levels were changed, changes of ion concentrations were changed end of seventh and fourteen day; increased serum K^+ and decreased serum Ca^{2+} concentrations.. In addition, activations of enzymes were no changed in diabetic rats exposed to 14 days magnetic field. Data are significantly ($p<0.05$). The effects of magnetic field in diabetic rats depend on exposed-duration to magnetic field. The changes of activations of enzymes of ion concentrations were depended on combinations of magnetic fields as exposure duration, intensity and directions. We observed different affected activations of enzymes and ion concentrations in diabetic-exposed to magnetic field according to exposed duration of magnetic field. The results indicate that an alternative magnetic field may positively affect diabetic rats in respect of blood serum parameters, depending on exposed duration of magnetic field

Key Words: Diabetic rats, alpha-amylase enzyme, Magnetic field, exposure duration to magnetic field.

Introduction

Numerous experimental findings suggest that exposure to extremely low-frequency (ELF) magnetic fields (MFs) affects various cell functions via actions exerted on intracellular and membrane proteins; including ion channels, membrane receptors and enzymes (1,2).

Diabetes has profound effects on the metabolism of various tissues, including vascular smooth muscle. Both glycolysis and glucose oxidation are decreased in diabetic animals and there is an overall decrease in ATP production (3). One mechanism that may contribute to this disturbance in tissue metabolism is the elevation of long-chain fatty acid levels (4,5). Recent investigations revealing that after exposure to magnetic fields, insulin release and glycogen levels are increased in diabetic rats and the blood glucose level is decreased provided the stimulus for the current studies. (6,7). Similar results were recorded in other studies (8-10). Goodman et al has been suggested that an electromagnetic field affects the movement of Ca^{2+} ions across membranes and has

effects at the gene level, but the mechanism of the MF effect is not yet clear (11,12). A recent study revealed ultrastuctural changes in β cells, with indications of extension of the rough endoplasmatic reticulum and significant expansion of the Golgi apparatus, in a group of rats exposed to a magnetic field (13). The rats used in this research had body weights of 284.4 ± 12.6 g: 35 were put into a sinusoidal magnetic field with frequency 10 Hz and intensity 1.8-3.8 mT; 35 were put into a sinusoidal magnetic field with frequency 40 Hz and intensity 1.3-2.7 mT for 30 minutes per day for 1, 3, 6, 9 and 14 days. It was thought that the expansion of the Golgi apparatus might relate to storage of increased amount of proinsulin in the form of small vesicles (14). The special granules around the site might indicate insulin storage by the β cells; they are affected by the magnetic field. On the other hand, electron-transparent vesicles in the β cells may indicate an intensification of hormone secretion after the oscillation of the insulin granules (13, 14). Finally, the reversible structural changes in β cells that occur depending on the magnetic parameters may increase insulin oscillation and synthesis.
A low intensity magnetic field has been used to treat late complications of diabetes such as diabetic retinopathy, diabetic angioplasty and peripheral neuropathy (15). In almost all the patients receiving this treatment, complaints of intestinal motor activities and pain disappeared and laboratory markers were normalized; magnetic therapy was further suggested for the treatment of juvenile diabetes (16,17). These studies on the effects of electromagnetic fields on living systems led us to investigate whether such fields may be used for treatment. For these reasons, we undertook this study to determine the effects of exposure to alternating modulated magnetic fields on blood parameters and activation of enzymes in diabetic rats.

Material and Method

Experiments were conducted on 60 male Wistar albino rats aged 5 months, weighing 245-300g. The experimental protocol was approved by the Animal Ethics Committee at Cukurova University. Firstly, animals were divided into two groups: control diabetic (D_I, D_{VII} and D_{XIV}) and diabetic-exposed to magnetic field groups ($D\text{-}MF_I$, $D\text{-}MF_{VII}$ and $D\text{-}MF_{XIV}$). We injected 45 mg/kg streptozotocin (STZ) in citrate buffer (CB) (pH 4.5) into the tail veins to induce diabetes (D group). A similar volume of CB solution without STZ was injected into control rats (S group). Then, animals were exposed to magnetic field between 09:00 and 09:30 or 13:00 and 13:30 h for one, seven and fourteen days to control for possible circadian variations in response. Rats in the D-MF groups were exposed for thirty minutes per day to alternating modulated magnetic fields of frequency 50 Hz, intensity 5 mT

Rats in the control or sham diabetic groups were treated in exactly the same fashion as the exposed rats, except that the magnetic field was switched off. The rats in each group were allowed to roam freely in the cage irrespective of exposure to the MF. They were fed a standard rat chow and tap water *ad libitum* and kept in an environmentally controlled room at 21-23°C, relative humidity 40-60%, with a light/dark cycle of 12/12 h.

The end of exposure period of one, seven and fourteen days, serum glucose and lipid levels were determined to indicate any relationship with diabetes mellitus. The serum was used to determine levels of glucose and lipids K^+ and Ca^{2+} concentrations, activations of alpha-amylase and lipase enzymes.

All values were expressed as means ± SEM. Levels of glucose, K^+ and Ca^{2+} ion concentrations and activations of enzymes were compared between diabetic and diabetic-exposed to magnetic field groups by 2-way ANOVA. Statistical significance was assumed at $p< 0.05$.

Results

The mean values of serum glucose and lipid levels of rats in three groups were significantly decreased after diabetic rats were exposed to magnetic field during one, seven and fourteen days, compared to those of the rats (glucose: D_I 259.8±5.1 mg/dl, DMF_I 257.2±7,1 mg/dl, D_{VII} 240.6 ±10,1, DMF_{VII} 190.2 ± 2.7 mg/dl, D_{XIV} 239.4± 3.8 mg/dl; DMF_{XIV} 176.6 ± 1.2 mg/dl) The mean values ± SEM of the other lipid levels were shown in Table1. When K^+ and Ca^{2+} ion concentration in serum of rats in diabetic-exposed to magnetic field groups were compared to control diabetic rats, we were measured decreased Ca^{2+} ion concentration in end of the fourteen days and increased K^+ ion concentration in end of the seven days according to intensity or density of diabetic (Table 2, Fig1,2).
There were no significant difference activations of α-amylase or lipase enzymes of rats between diabetic and diabetic-exposed to the magnetic field groups. (Table 2, Fig3,4).

Table 1. Serum parameters (glucose, cholesterol, triglyceride, HDL and LDL (mg/dl)) of rats were measured by enzymatic techniques in diabetic and diabetic-exposed to magnetic field groups (mean ± SEM).

	Groups					
Serum Parameters	**D_I**	**D-MF_I**	**D_{VII}**	**D-MF_{VII}**	**D_{XIV}**	**D-MF_{XIV}**
Glucose (mg/dL)	259.8±5.1	257.2±7.1	240.6±10.1	190.2±2.7	239.4 ± 3.8	176.6 ± 1.2
Cholesterol (mg/dL)	67.6±3.0	43.4±1.8	66.2±1.2	41.4±2.0	76.4±1.4	47.8±2.3
Trygliceride (mg/dL)	86±1.1	73.6±1.7	115.4±4.6	76.4±9.9	141,8±2.5	73.0±5.7
LDL (mg/dL)	1.2±0.2	1.2±0.1	1.4±0.4	1.2±0.4	2.7±0.6	1.3±0.9
HDL (mg/dL)	34.4±1.0	44.8±2.7	36.2±0.9	44.8±1.5	32.6±0.5	44.6±1.3

Table 2. Ion concentrations (K^+ and Ca^{2+}) and activations of enzymes (alpha-amylase and lipase) of rats were measured in diabetic and diabetic-exposed to magnetic field groups (mean ± SEM).

	Groups					
Serum Parameters	**D_I**	**D-MF_I**	**D_{VII}**	**D-MF_{VII}**	**D_{XIV}**	**D-MF_{XIV}**
Lipase (U/L)	13.2±0.6	12.6±0.8	12.0±0.8	11.6±0.7	13.0 ± 0.7	14.2 ± 0.9
α-amylase (U/L)	2107.4 ± 26.7	2077.8 ± 34.4	2232 ± 31.6	2229.8 ± 26.6	2111.0 ± 38.7	2111.8 ± 40.3
Ca2+ (mg/dL)	11.6±0.7	11.6±1.3	11.7±0.8	11.7±1.02	13.2±0.4	12.4 ± 0.9
K+ (mmol/L)	4.5±0.7	4.8±0.5	4.5±1.2	5.5±1.6	4.6±0.4	6.4 ± 1.2

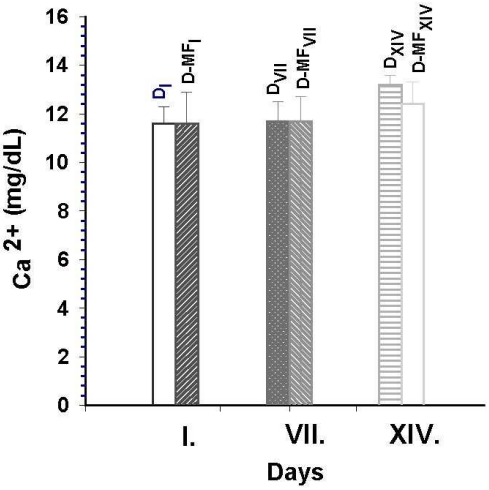

Fig1. Serum Ca^{2+} concentration of rats in D and DMF groups.

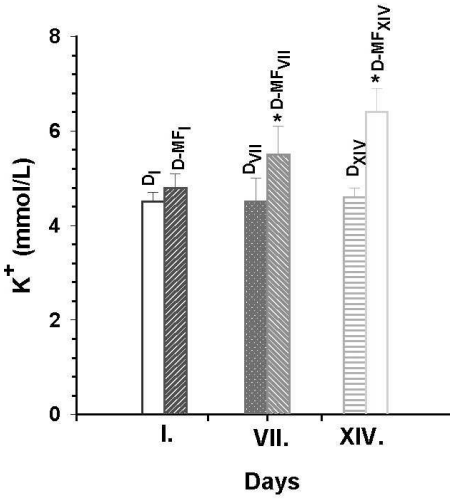

Fig2.Serum K^+ concentrations of rats in D and DMF groups

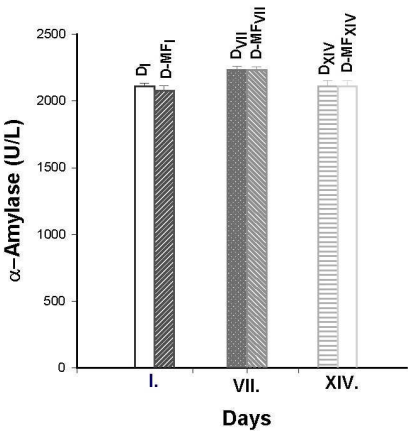

Fig3. Activation of serum α-amylase enzyme of rats in D and DMF groups

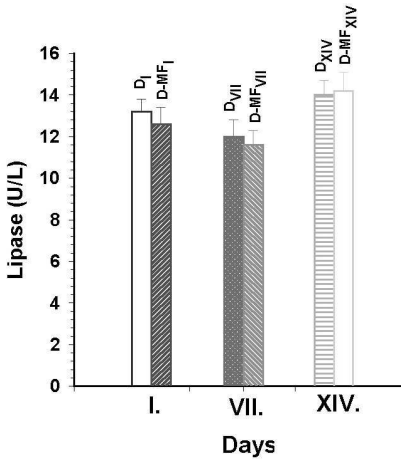

Fig4. Activation of serum lipase enzyme of rats in D and DMF groups

Discussion

Data from this study show that exposure duration of magnetic field can interact. In diabetic-exposed magnetic field one day, no significant change in blood parameters was observed in glucose, lipid and enzymes activities. The plasma glucose, lipid and cholesterol levels were slightly decreased in the D-MF group compared with the D group. These results might indicate a transiently healthy response by rats to the alternating modulated magnetic field. The decrease in plasma glucose was statistically significant ($p<0.05$). The MF may cause an increased synthesis and oscillation of insulin. Therefore, MF is expected to decrease the glucose level and increase the glycogen level (7,18-21) Oroza et al. 1987 found similar results. They suggested that the magnetic field slowed down the fat metabolism of the rats and so decreased the levels of glucose and lipid. If the magnetic field increases the synthesis and oscillation of insulin, as Laiti-Kobierska et al. 2002 suggested, then there may be a decrease in the blood glucose level in the diabetic rats. Epidemiological studies have indicated that MFs can also induce adverse health effects. Other studies have yielded important clues to the interaction between MF and cellular systems, particularly at the molecular level. Laiti-Kobierska et al. 2002 identified granules in the β cells of rats exposed or not exposed to a magnetic field; these granules were called special granules. On the other hand, there were inflated mitochondria and expanded endoplasmic tubules in the pancreatic acinar cells. These authors suggested that the observed changes occurred because of the magnetic field and were related to increased

synthesis and oscillation of insulin (13). If the special granules stimulate insulin synthesis, then decreased lipid and glucose levels are to be expected.
Chernysheva suggested that if the rats were exposed to an alternating magnetic field for 5 hours a day, the concentrations of cholesterol esters, triglycerides and free fatty acids decreased, so there was an increase in lipid catabolism and energy production (10). In addition, they observed that magnetic fields change the velocity, flow and direction of particles in biological systems, with impacts on the transport/charge system depending on shape, frequency, intensity and exposed duration (10). The decrease in plasma glucose, total cholesterol and triglyceride levels may be attributed to the retardation of lipid metabolism as suggested by Hefco et al , or to the increased synthesis and oscillation of insulin in the β cells as Laiti-Kobierska et al. 2002 suggested (13,22). Byus et al. and Blank et al. realized that there was an increase in the concentration of Na^{+}-K^{+}ATPase, effected through changes in intracellular Ca^{2+}. One of the most obvious candidates is the calcium ion. Changes in calcium concentration may influence the interaction with calmodulin, activate the protein kinase C, or act directly on the activity of intracellular enzymes. Other signal transductive candidates may membrane receptors whose interactions with G-proteins are modified by MF stimulation or ligand-gated channels that are acted upon by the fields. These findings might be attributed to complicated mechanisms. Further studies are required to show the effect of MF on intracellular Ca^{2+} ions and their movements, and on enzyme levels. Diabetes affects many mechanisms causing different complications at different stages of the disease. The apparently healthy response of the exposed rats might be consequent on a temporary recovery in hormonal regulation caused by the magnetic field, which may be a stress-generating factor. Therefore, we need to identify the mechanisms affected by the diabetes and the magnetic field and further studies are needed for this purpose. The mechanism of action of alternating magnetic fields on biological systems at the cellular level is under investigation.

References

1. C. Polk, E. Postow, Handbook of Biological Effects of Electromagnetic Fields, CRC Press, New York, 1996.

2. A. Lacy-Hulbert, J.C. Metcalfe, R. Hesketh, Biological responses to electromagnetic fields, FASEB J. 12 (1998) 395–420.

3. Behari J and Mathur R (1997). Exposure effects of static magnetic field on some physiological parameters of developing rats**.** *Indian Journal of Experimental Biology*, **35:**894-897.

4. Chen G, Suzuki H and Weston AH (1988). Acetylcholine releases endothelium-derived hyperpolarizing factor and EDRF from rat blood vessels. *Br J Pharmacol*, **95:**1165-1174.

5. Mayhan WG. Idvire SD, Sharpe GM (1999). Constrictor responses of resistance arterioles during diabetes mellitus. *Diabetes Research and Clinical Practice*), **44:**147-156.

6. Byus CV, Kartun K, Pieper S, Adey WR (1988). Increased ornithine decarboxylase activity in cultured cells exposed to low energy modulated microwave fields and phorbol ester tumor promoters. *Cancer Res*, 48:4222–4226.

7. Blank M, Soo I (1998). Enhancement of cytochrome oxidase activity in 60 Hz magnetic fields. *Bioelectrochem Bioenerg*, 45:253–259.

8. Beisher DE, Brehl RJ. (1975) Search for effects of 45 Hz magnetic field on liver triglycerides in mice. *Res Rep NU NAMRL*,1197.

9. Beisher DE, Grisett JD, Mitchell RE (1972). Exposure of man to magnetic fields alternating at extremely low frequency. *Naval Aerospace Medical Research Laboratory*,

10. Cherysheva ON (1987). Effect of alternating magnetic field of industrial frequency on the lipid composition of the rat liver. *Ukrainskii Biokhmicheskii Zhurnal*, 59:91-4.

11. Goodman EM, Greenebaum B, Marron MT (1993). Altered protein synthesis in a cell-free system exposed to a sinusoidal magnetic field. *Biochim Biophys Acta*, 1202:107–112.

12. Goodman EM, Greenebaum B, Marron MT (1995). Effects of electromagnetic fields on molecules and cells. *Int Rev Cytol*, 158:238–279.

13. Laiti-Kobierska A, Cieslar G, Sieron A and Grzybek H (2002). Influence of alternating extremely low frequency ELF magnetic field on structure and function of pancreas in rats. *Bioelectromagnetics*, 23;49-58.

14. Tartakoff AM (1980). The Golgi complex: crossroads for vesicular traffic. *Int Rev Exp Pathol*, 22:227-251.

15. Bassett C (1993). Beneficial effects of electromagnetic fields. *Cell Biochem,* 51(4):387-93.

16. Bassett C (1989). Fundamental and practical aspects of therapeutic uses of pulsed electromagnetic fields (PEMFs). [Review] [330 refs]. *Crit Rev Biomed Eng*, 17(5):451-529.

17. Navratil L, Hlavaty V, Landsingerova E (1993). Possible therapeutic applications of pulsed magnetic fields. *Cas Lek Cesk*, 132(19):11 PP. 590-4.

18. Iwasaka M, Miyakoshi J and Ueno S (2003). Magnetic field effects on assembly pattern of smooth cells. *In vitro Cell Dev Biol Anım,* **Mar;** 39(3):120-123.

19. Blank M, Goodman R (2001). Electromagnetic initiation of transcription at specific DNA sites. *J Cell Biochem,* 81:689–692.

20. Ovenchkina ZA, Martyniuk VS, Martyniuk SB and Kuchina NB (2001). Effects of the variable magnetic field of the extremely low frequency on metabolic processes in the liver of animals with various individual and typological characteristics. *Biofizika,* Sep-Oct**;** 46(5):915-

21. Oroza MA, Calcice L, Sanchez-Fkanco F, Rivas L (1987). Hormonal, hematological and serum chemistry effects of weak pulsed electromagnetic fields on rats. *Journal of Bioelectricity***;** 6(2):139-151.

22. Hefco V, Hefco E, Birca C (1969). Influence of the magnetic field on glycemia, pyruvic acid and lactic acid in white rat blood. *Rev Roum Biol-Zoologie*, 14:79-85.

CHANGES IN MEMBRANE POTENTIALS OF AORTA IN STREPTOZOTOCIN-INDUCED RATS EXPOSED TO LOW FREQUENCY MAGNETIC FIELD

Işıl Öcal[1], Mustafa Emre[1], Ufuk Mete[2] and İsmail Günay[1]

[1]Cukurova University, Medical Faculty, Department of Biophysics 01330 Balcalı/Adana, TURKIYE

[2]Cukurova University, Medical Faculty, Department of Histology 01330 Balcalı/Adana, TURKIYE

Tel:+90-322-3386060/3472

iocal@cu.edu.tr

Abstract

Endothelium-dependent and independent derived responses are diminish in some diseases, including hypertension, preclampsia and some models of diabetes. A study of the effects of weak, modulated sinusoidal low frequency electromagnetic field stimulation in changes in membrane potentials of the rat aorta in diabetes was carried out. Forty rats (n=40, Wistar albino spp) weighing between 220-300g were used in this study. The rats were first divided into four groups. The first group was made up of the citrated rats or sham (S, n=10), the second group was comprised of rats described as sham or citrated+magnetic field group (S-MF, n=10), third group contained experimental diabetic rats (D, n=10), and the fourth group was comprised of both experimental diabetic+magnetic field group (D-MF, n=10). Magnetic fields of 5 mT intensity and 50 Hz frequency oriented in the north-south direction was applied to the S-MF and D-MF groups for 2 hours and 45 minutes at each day during one month.

After one month, Rats were killed by decapitation. After the thoracic aorta preparation isolated, excess fats and/or connective tissues were removed. For measurement of smooth muscle membrane potential, arter was cut open longitudinally and pinned to the bottom, endothelial surface uppermost. Tissues were maintained at 37 °C and constantly perfused with Krebs buffer at a rate of 2 ml min^{-1}. Measurements of membrane potential were made sharp glass microelectrodes, back-filled with 3 M KCl and with resistances of 60-100 M Ω. All data were recorded through a Nihon Kohden instruments.

The negative of membrane potential of aorta in diabetes was significantly increased compared to control animals. One of the most obvious candidates is the calcium ion. Changes in calcium concentration may influence the interaction with calmodulin, activate the protein kinase C, or act directly on the activity of intracellular enzymes. Other signal transductive candidates are membrane receptors whose interactions with G-proteins are modified by EMF stimulation or ligand-gated channels that are acted upon by the fields. This knowledge could provide the basis of novel therapeutic inventions in the amelioration or prevention of vascular complications of these diseases.

Key words: Magnetic field, diabetes rat, rat aorta, resting membrane potential

Introduction

Macro and microvascular disease are currently the principal causes of morbidity and mortality in patients with type I and type II diabetes mellitus. Loss of the modulatory role of the endothelium may be a critical and initiating factor in the development of diabetic vascular disease. Microvascular disease is the main cause of morbidity and mortality in patients with diabetes Mellitus (DM). Endothelial dysfunction may be a critical and initiating factor to develop diabetic vascular disease (1). Mechanisms that participate in the reduced vasodilatory

responses in endothelial dysfunction include reduced nitric oxide generation, oxidative excess, and reduced production of hyperpolarizing factor.

Vascular smooth muscle relaxation in response to a signal initiated by stimulation of overlying endothelium is known as endothelium-dependent relaxation and involves the release of at least endothelium-derived relaxing factor /EDRF). There appear to be several important EDRFs the most well understood of these being NO and prostacyclin. It is now well established that endothelium-dependent vascular relaxation is often accompanied by K^+ channel-meditated hyperpolarization of the vascular smooth muscle. Because both NO and prostacyclin are known to be able to elicit vascular relaxation, at least in part, through activation of K^+ channels, endothelium-dependent hyperpolarization may often simply reflect part of the mechanism of relaxation produced by NO and prostacyclin.

An important function of all cells is their ability to regulate the movement of ions and macromolecules between the cell interior and its environment using membrane bound protein channels. If (K^+) channel opens in the vascular smooth muscle cell membrane, K^+ efflux increases, causing membrane potential hyperpolarization, closure of voltage-activated calcium (Ca^{2+}) channels, decreased Ca^{2+} entry, and vasodilatation. Biological effects of magnetic fields can be mobility or movement or induce variety of ions of effects in cells and tissues. These biological effects include nerve regeneration, influences on cell calcium levels and bone healing.

The release of endothelium-derived NO by agonists, such as acetylcholine (ACh), is dependent on a rise in intracellular calcium levels ([Ca^{2+}]i) within endothelial cells and activation of NO synthase (NOS). The entry of Ca^{2+} from the extracellular space is required to maintain production of NO (2,3) and several lines of evidence indicate that endothelial cell membrane potential plays a critical role in the regulation of Ca^{2+} entry (4). Ca $^{2+}$ entry is not dependent on voltage-gated Ca^{2+} channel activity, rather it occurs via a nonselective cation pathway and is dependent on membrane hyperpolarization to provide an inwardly directed electrochemical driving force for Ca^{2+} movement (4-7) Ocal et al magnetic field was supported to cause the changing movement of Ca^{2+} ions and direction in aorta rings of diabetic rats (8).

In the present study, we attempted to combine the beneficial properties of MF, which have been proved to be ion flows according to measure resting and 10^{-7} M phenylephrine (PE), 10^{-6}M acetylcholine (ACh) and 10^{-6} M sodiumnitroprusside (SNP)-induced membrane potentials.

Material and Methods

Approval for this study was obtained from local Institution's Animal Care and Ethics Committee. Forty adult white Wistar rats weighing 220 to 300 g were used in this study. The rats were first divided into four groups. The first group was made up of the citrated or sham rats (S, n=10), the second group was comprised of rats described as sham or citrated+magnetic field group (S-MF, n=10), third group contained experimental diabetic rats (D, n=10), and the fourth group was comprised of both experimental diabetic + magnetic field group (D-MF, n=10).

We injected 45 mg/kg streptozotocin (STZ) in citrate buffer (CB) (pH 4.5) into the tail veins to induce diabetes (D group). A similar volume of CB solution without STZ was injected into control rats (S group). Then, magnetic fields of 5 mT intensity and 50 Hz frequency oriented in the north-south direction was applied to the S-MF and D-MF groups for 2 hours and 45 minutes at each day during one month.

After the one-month study period, the rats under ether anesthesia before rats were killed by decapitation. After the thoracic aorta preparation isolated, excess fats and/or connective tissues were removed. For measurement of smooth muscle membrane potential, arter was cut open longitudinally and pinned to the bottom, endothelial surface uppermost. Tissues were maintained at 37°C and constantly perfused with Krebs buffer at a rate of 2 ml min^{-1}. Measurements of membrane potential were made sharp glass microelectrodes, back-filled with 3 M KCl and with resistances of 60-100 M Ω. A vessel sample was pinned to the bottom of the recording chamber. Modified Krebs solution had the following composition (mM): 119,: NaCl, 4.6 KCl, 1.5 $CaCl_2$, 1.2 $MgCl_2$ 15 $NaHCO_3$, 1.2 $NaHPO_4$ and 11 Glucose. All data were recorded through a Nihon Kohden instruments.

After the resting membrane potentials of rat aorta in each group were measured, ACh, PE and SNP-induced membrane potentials of aorta preparations were.measured. ACh, PE and SNP-induced membrane potentials were recorded though a Nihon Kohden instruments.

The negative of membrane potential of aorta in D group was significantly decreased compared to S group. While 10^{-7} M PE-induced negative of membrane potential were decreased in each group, 10^{-6} M-induced membrane potential in D-MF group was enclosed resting membrane potential of D group. Results were significantly ($p<0.05$).

Ultrastructure of thoracic aorta preparation

For histopathology of thoracic aorta preparations of rats, of citrated or sham, sham-exposed to magnetic field, diabetic and diabetic-exposed to magnetic field groups were examined. After opening the abdominal cavity,

samples of the thoracic aorta were taken, and after appropriate fixation and preparation were examined ultrastructurally in an electron microscope.

Solutions and chemicals

All drugs were obtained from Sigma Chemical Co. (St. Louis, MO,USA). Stock solutions of phenylephrine hydrochloride (PE), acetylcholine bromide (ACh) and sodium nitroprusside (SNP) were dissolved in distilled water. Streptozotocin was freshly dissolved in 0.1 M citrate buffer (pH 4.5) immediately before use at a concentration of 45 mg/kg; all drugs were obtained from Sigma Chemical Co.

Statistics

All data were expressed as means ± S.E.M. The statistical significance of all differences between mean values was calculated using Student's paired *t* test or repeated measures ANOVA followed by Tukeys *post hoc* test. A level of $P<0.05$ was considered to be statistically significant.

Results

Table 1. The mean ± SEM of 10^{-7} M phenylephrine (PE), 10^{-6} M acetylcholine (ACh) and 10^{-6} M sodium nitroprusside (SNP)-induced membrane potentials.

Experimental Groups	Membrane Potential (mV)			
	Resting	**10^{-7} M PE**	**10^{-6} M ACh**	**10^{-6} M SNP**
S	-56,2 ± 1,0	-51,1 ± 0,9	-59,2 ± 0,9	-56,1 ± 1,2
S-MF	-53,6 ± 0.6	-48 ± 0,6*	-57,8 ± 0,9	-51,8 ± 0,6
D	-47,5 ± 0,6*	-42,8 ±0,8*	-43,1 ± 1,7	-46,7 ± 0,8
D-MF)	-43,4 ± 0,7	-36 ± 0,3*	-43,7 ± 0,7	-44,4 ± 0,4

The mean values of negative of resting membrane potential of aorta preparations were significantly decreased in both groups of rats after sham-exposed and diabetic-exposed to the alternating modulated magnetic field groups for four weeks, compared to those of sham and diabetic groups (Table 1, Fig 1). The negative of 10^{-7} M PE-induced membrane potential of aorta in S, S-MF, D and D-MF groups were decreased (Table 1, Fig 2), while negative of the 10^{-6} M ACh-induced membrane potential in S, S-MF, D and D-MF groups were increased (Fig 3). Data were significant ($p<0.05$).

There was no significant difference between the membrane potentials of aorta preparation of rats in D or S and in SMF or DMF groups that the aorta induced by 10^{-6} M sodium nitroprusside (Fig 4).
Electron micrographs of the thoracic aorta preparations from the S-MF group showed only minimal ultrastructural changes (Fig 5,6). In the D-MF group, however, a decreased density of elastic tissues compared to the D group was apparent after 30 days (Fig 7,8).

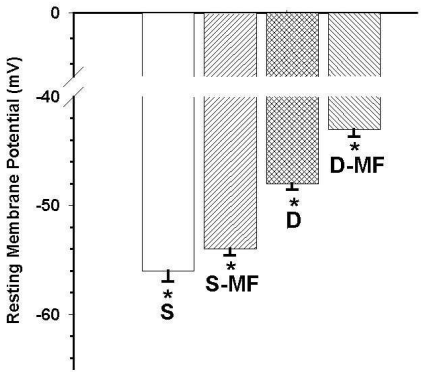

Fig1. Resting membrane potentials of aorta preparation of rats in citrated (S), citrated-magnetic field, diabetic and diabetic-magnetic field groups

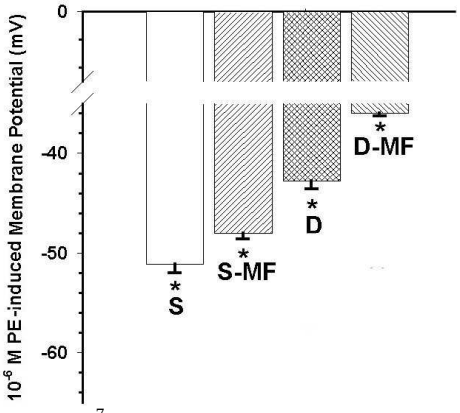

Fig2. 10^{-7} M PE-induced membrane potentials of aorta preparation of rats in citrated (S), citrated-magnetic field, diabetic and diabetic-magnetic field groups

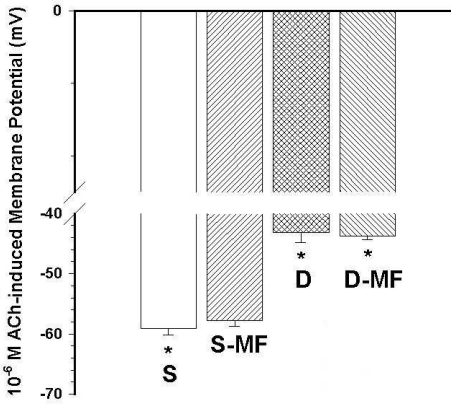

Fig3. 10^{-6} M ACh-induced membrane potentials of aorta preparation of rats in citrated (S), sitrated-magnetic field, diabetic and diabetic-magnetic field groups

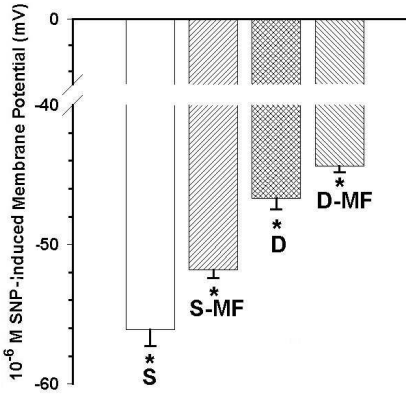

Fig4. 10^{-6}M SNP-induced membrane potentials of aorta of rats in citrated (S), citrated-magnetic field, diabetic and diabetic-magnetic field groups.

Fig 5. Electron micrograph of thoracic aorta from rats in the S group; el-elastic fibers, sm-smooth muscle.

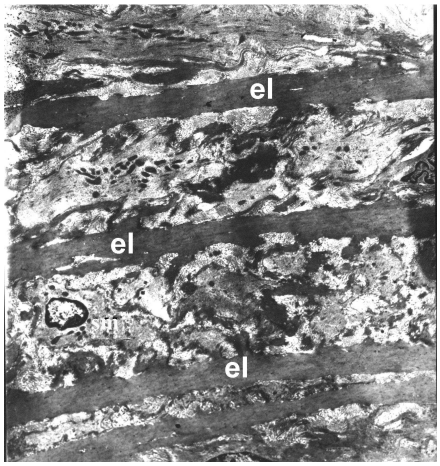

Fig 6. Electron micrograph of thoracic aorta from rats in the S-MF group; el-elastic fibers, sm-smooth muscle.

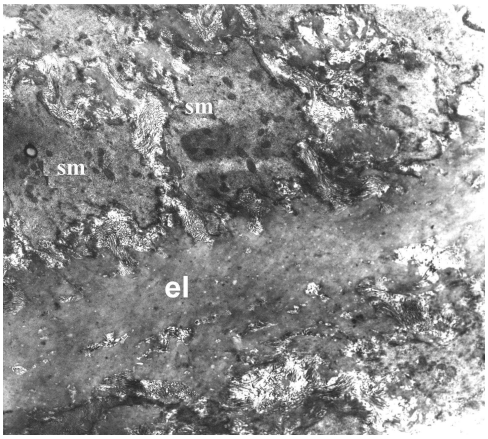

Fig 7. Electron micrograph of thoracic aorta from rats in D group; el-elastic fibers, sm-smooth muscle.

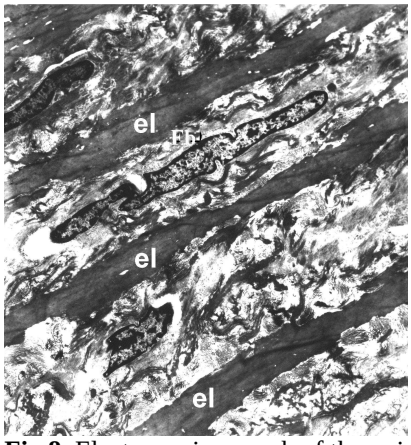

Fig 8..Electron micrograph of thoracic aorta from rats in the D-MF group; el-elastic fibers, sm-smooth muscle.

Discussion

Changes in EDRF in diabetes have been studied in most detail in streptozotocin (STZ)-induced diabetes in rats. In the rat aorta vessel, negative of resting membrane potentials were significantly diminished compared with membrane potentials of aorta preparations of rats in S group. The mechanisms underlying disease-associated impairment of EDHF-attributed hyper polarization and relaxation are far from clear and require further studies to determine whether the dysfunction arises in the smooth muscle cells and/or the endothelial cells and/or myoendothelial communication. This knowledge could provide the basis of novel therapeutic inventions in the amelioration or prevention of vascular complications of these diseases.

In the resting membrane potential of the rat aorta, negative of resting membrane potential in S group was decreased from-56.2 ±1.0 mV to -53.6± 0.6 mV compared with resting membrane potential of S-MF group. But there was no significant difference between the S and S-MF groups. When the resting membrane potentials of rat aorta in S group (-56.2 ± 1.0 mV) were compared with D groups (-47.5 ± 0.6 mV), negative of resting membrane potentials were increased (Table 1). Data were significantly. Also, negative of resting membrane potentials in D-MF groups were decreased from -47.5 ± 0.6 mV to 43.4 ± 0.7 mV too. Ocal et al were observed the positive effects of low frequency magnetic field on mechanical activities in diabetic rats (8). Magnetic fields may affect movement ions and directions in biological tissues. K^+ channels are critical in maintaining the normal resting membrane potential in a variety of excitable cells. But mechanism of relaxation is no only affected K^+ ion or K^+ ion movements.

In this study, we observed only minimal ultrastructural changes in electron micrographs of thoracic aorta preparations from rats in the S-MF group (Fig 5, 6). However, by the end of the 30th day, ultrastructural changes related to decreased elastic tissue density were seen in the D-MF group compared to the D group (Fig 7,8). Laiti-Kobierska et al. 2002 identified granules in the β cells of rats exposed or not exposed to a magnetic field; these granules were called special granules. On the other hand, there were inflated mitochondria and expanded endoplasmic tubules in the pancreatic acinar cells. These authors suggested that the observed changes occurred because of the magnetic field and were related to increased synthesis and oscillation of insulin (Laiti-Kobierska et al. 2002). Numerous experimental findings suggest that exposure to extremely low-frequency (ELF) magnetic fields (MFs) affects various cell functions via actions exerted on intracellular and membrane proteins, including ion channels, membrane receptors and enzymes (9,10).For these reason, enzymes activities and membrane receptors and as Ca^{2+} the other ions have to examine. One of the most obvious candidates is the calcium ion. Changes in calcium concentration may influence the interaction with calmodulin, activate the protein kinase C, or act directly on the activity of intracellular enzymes. Other signal transductive candidates may membrane receptors whose interactions with G-proteins are modified by MF stimulation or ligand-gated channels that are acted upon by the fields.

References

1- Pomilio M, Mohn A, Verrotti A, Chiarelli F (2002). Endothelial dysfunction in children with type 1 diabetes mellitus. J Pediatr Endocrinol Metab; 15: 343-61.

2. Lückhoff, A., Pohl, U., Mülsch, A. & Busse, R. (1988). Differential role of extra- and intracellular calcium in the release of EDRF and prostacyclin from cultured endothelial cells. *British Journal of Pharmacology* **95**, 189–196.

3. Kruse, H. J., Grunberg, B., Sıess, W. & Weber, P. C. (1994). Formation of biologically active autacoids is regulated by calcium influx in endothelial cells. *Arteriosclerosis Thrombosis* **14**, 1821–1828.

4. Nılıus, B. & Droogmans, G. (2001). Ion channels and their functional role in vascular endothelium. *Physiological Reviews* **81**, 1415–1459.

5. Busse, R., Fıchtner, H., Lückhoff, A. & Kohlhardt, M. (1988). Hyperpolarization and increased free calcium in acetylcholinestimulated endothelial cells. *American Journal of Physiology* **255**, H965–969.

6. Lückhoff, A. & Busse, R. (1990*a*). Activators of potassium channels enhance calcium influx into endothelial cells as a consequence of potassium currents. *Naunyn-Schmiedebergs Archives of Pharmacology* **342**, 94–99.

7. Kamouchı, M., Droogmans, G. & Nılıus, B. (1999). Membrane potential as a modulator of the free intracellular Ca2+ concentration in agonist-activated endothelial cells. *General Physiology and Biophysics* **18**, 199–208.

8. Öcal I, Günay İ: The effects of chronic ac magnetic field on contraction and relaxation of isolated thoracic aorta rings of healthy and diabetic rats. Brazilian Archives of Biology and Technology, 47(5), 2004.

9 C. Polk, E. Postow, Handbook of Biological Effects of Electromagnetic Fields, CRC Press, New York, 1996.

10 A. Lacy-Hulbert, J.C. Metcalfe, R. Hesketh, Biological responses to electromagnetic fields, FASEB J. 12 (1998) 395–420.

Temperature Increase and SAR in a Phantom Model of the Human Head Exposed to 1800 MHz Non-Ionizing Radiation

[1]Şükrü Özen, [1]Selçuk Helhel, [2]Ömer H.Çolak

[1]Akdeniz University, Department of Electrical and Electronics Engineering, Antalya, Turkey
[2]Akdeniz University, TBMYO, Department of Biomedical, Antalya, Turkey

sukruozen@akdeniz.edu.tr, selcukhelhel@akdeniz.edu.tr, omercol@akdeniz.edu.tr

Abstract

In this study, temperature rise and Specific Absorption Rate (SAR) induced by 1800MHz microwave (MW) frequency non-ionizing radiation in human brain tissue has been investigated by using brain equivalent liquid. Brain equivalent tissue was exposed to MW radiation of 1800MHz for various time duration within a system allowed positions. As a radiation source, 1800MHz MW generator was used. The brain tissue phantom model was placed in a near field of half wave dipole antenna. A temperature rise in a brain tissue which's equivalent model was exposed to 1800 MHz was measured for investigating a SAR absorbed in brain tissue of human head.

Keywords: MW, Cellular Phone, Brain-equivalent phantom, Temperature Rise, SAR.

INTRODUCTION

During the last years, wireless data and phone networks have become widely used. And especially, adverse health effects of cellular phones and base stations have been discussed. Many international organizations have defined safety limits for exposure to these type communication devices. Adverse health effects of the cellular phones used close to the human body have been especially interested, because of complexity of interaction of RF (Radio Frequency) radiation and human body, and EM (Electromagnetic) fields induced in human head difficulty determinations. Recently, it is possible to find a lot of investigations on this subject in the literature. Whole body SAR (Specific Absorption Rate) limit of 4 W/kg is recommended by international organizations [1]. After applying the safety standards, maximum SAR limits are 0.4 W/kg and 0.08 W/kg for controlled and uncontrolled environment, respectively. European standard of ENV50166-2 is determined SAR limit of 2 W/kg for 10g tissue and 6 minute period in a controlled environment [2]. Heat transfer mechanisms of human body are limited temperature rise for the SAR limit. For general public in Turkey, power density limits of f/200 W/m^2, 10 W/m^2 and $6.67x10^{-5}f$ are approved in the frequency ranges 0.4-2 GHz, 2-150 GHz and 150-300 GHz, respectively [3].

While theories on the biological effects of EM fields have not been exactly established, there are still insufficient treatments have not been exactly understood, yet. The interdisciplinary investigations have been continued. One of the known basic experimental method was used to investigate thermal effects of EM radiation in tissue equivalent liquids[4]. In this study, the temperature rise in human brain and SAR are investigated by using an equivalent model.

SPECIFIC ABSORPTION RATE (SAR)

SAR is an important quantity in dosimetry which indicates the temperature rise and the absorbed energy by tissue, and other biological events that occur in the tissue depended on internal fields. SAR varies depending on frequency and tissue properties. The effects in the biological tissues depend on the penetrated fields not to the external fields. To determine the SAR in human body and laboratory animals is so important to explain biological effects. There are two basic methods are used to evaluate SAR. They are calculation and measurement of absorbed energy in phantom models. Experimentally, SAR is determined measuring electric field $\left|\vec{E}\right|$ induced in tissue or temperature rise $\partial T/\partial t$.

$$SAR = \frac{\sigma}{2\rho}\left|\vec{E}\right| = C\frac{\partial T}{\partial t} \qquad (1)$$

Where; σ (S/m) is tissue conductivity, ρ (kg/m^3) is tissue density, *C* (j/kg°C) is the heat capacity of tissue (or phantom material) and E (V/m) is the rms value of intensity of the electric field induced in tissue. If the heating time is sufficiently short so that the effect of thermal conduction in the phantom can be neglected, the SAR can be derived form the measured temperature rise as follows[5]. If the temperature rise in tissue is measured, (1) can be arranged as

$$SAR = C\frac{\Delta T}{\Delta t} \quad [\text{W/kg}] \qquad (2)$$

Where; ΔT is the temperature rise in °C for Δt second period and *C* (j/kg°C) is the heat capacity of tissue (or phantom material). From the above, it is found that a temperature rise sufficient for SAR observation can be obtained by low power illumination for a short time if the specific heat of the phantom is small to a certain degree to an advantage in the measurement[6].

MEASUREMENTS

In this study, the brain equivalent tissue suggested by [7, 8] has been prepared and used. The human brain tissue equivalent mixture contains water of 54.90%, salt of 0.18% and Glycol (Diethylene Glycol Butyl Ether) of 44.92%. Electrical parameters of the equivalent tissue have been measured as ε_r=40.3 and σ=1.35(S/m) using HP4194A Impedance/Gain-Phase Analyzer. The measurement set-up of the temperature rise is shown in Figure 1. Prepared brain tissue equivalent liquid has been put into a spherical pyrex glass bowl that has an outer diameter of 224 ± 0.5 mm and glass thickness 5 ± 0.5 mm. Glycol provides a big easiness to prepare brain equivalent tissue. Evaporation of phantom liquid has been prevented from taking precautions in the measurement period and the measurements have been completed in one week.

The expected temperature rises in the liquid have been measured depending on the parameters of antenna-tissue distance, deepness, exposure time and signal generator output power and logged on a computer. PT-104 Platinum Resistance Thermometer Data Logger measurement system has been used. The system has sensitivity of 0.001^{0}C and accuracy of 0.01 ^{0}C. RF signal generator has adjustable output power level in the range of 0-2W and frequency in the range of 1800-1900MHz. 1800MHz half-wave dipole antennas has been used in the measurements. The liquid level was equal to 160 mm during all measurement.

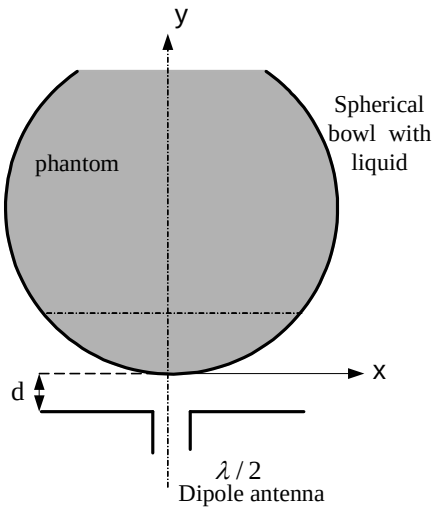

Figure 1. The measurement set-up of the temperature rise in the brain equivalent tissue

Measurements have been realized in the isolated box where the change in temperature approaches to zero. The temperature variation in the box has been continuously measured, and it has been logged when its value is approximately 22^{0}C±0.2^{0}C. Considering the radiation characteristics of the half wave dipole antenna, maximum field intensity is expected on the feed point direction. Because of this, temperature rise in the tissue that is on the feed point direction has been measured considering various exposure probabilities.

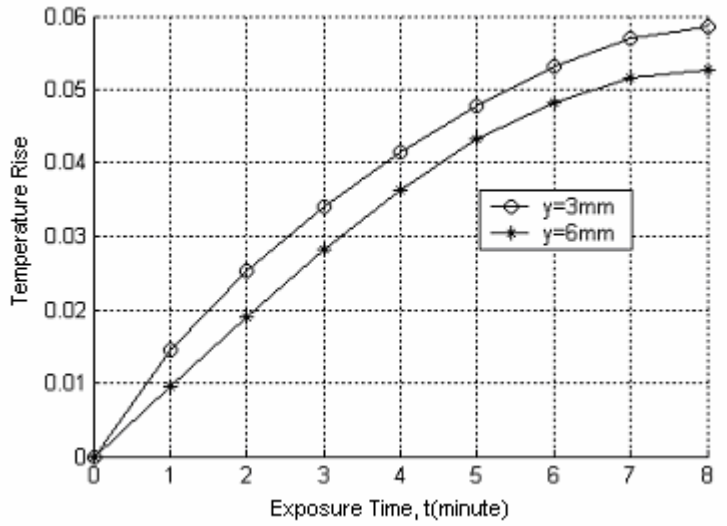

Figure 2. Varying in the temperature rise (^{o}C) in the brain equivalent liquid at 1800MHz depending on the exposure time period and deepness (d=13mm and p=1.5w)

The distance to the tissue surface has been adjusted to d=13mm and the temperature rise generated in the tissue at the distances of y=3mm and y=6mm has been measured depending on the exposure time period, as shown in Figure 2. The temperature rise decreases depending on the deepness.

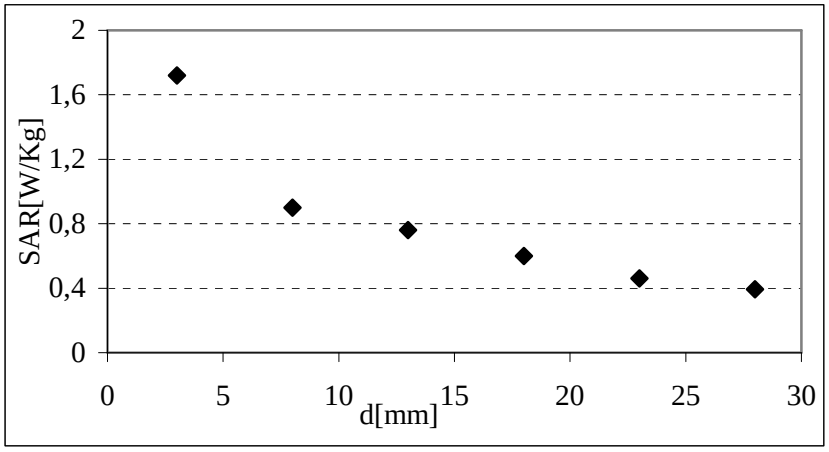

Figure 3. Changing in SAR depending on the distance between the antenna and the tissue at 1800 MHz (y=1mm, p=1.5w, Δt=120sn)

Absorbed SAR has been calculated by Equation 2. with the measured temperature rises in the brain equivalent tissue. The SAR calculated at the deepness of y=1mm at 1800MHz versus the distance between the dipole and the tissue is shown in Figure 3. The specific heat capacity has been chosen as C=4000 (W sec/kg °C) for the SAR calculation. As shown in Figure 3, the SAR absorbed by tissue decreases depending on the distance between the dipole and the tissue like the change of the temperature rise. The temperature rises depending on the various distances, d and exposure time at 1800MHz is shown in Figure 4.

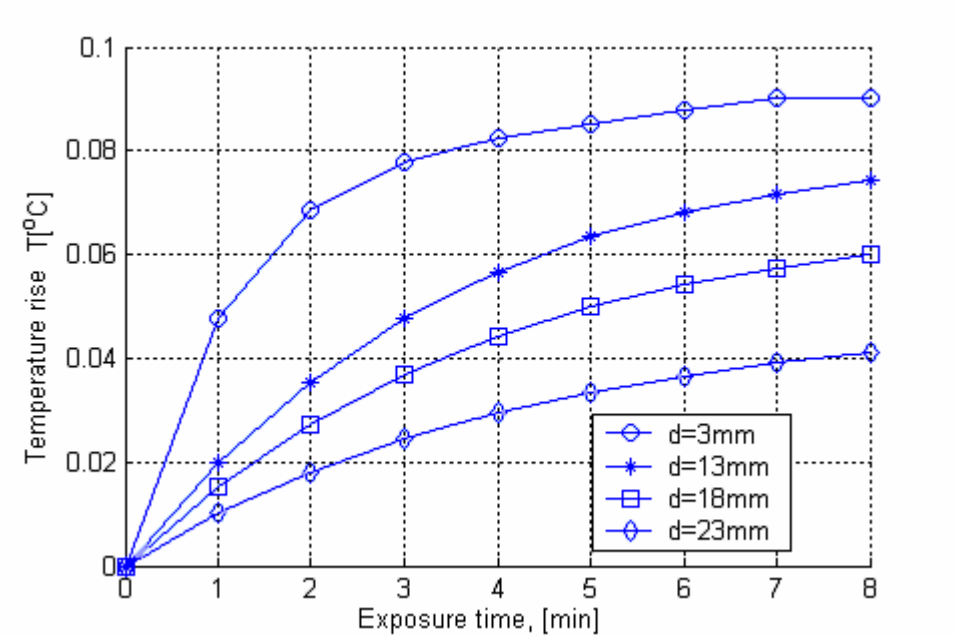

Figure 4. Shows the temperature rises depending on the various distances, d and exposure time at 1800MHz (y=1mm and p=2w)

CONCLUSIONS

The temperature rise generated in the brain tissue does not exceed 0.1 °C at 1800 MHz cellular phone frequency. The cellular phones operated at 1800 MHz cause the temperature rise less than the lower limit value 1°C. The temperature rise curves formed using measurement data are exponential function of the exposure time period. The SAR estimation has also been done depending on the temperature rise in the equivalent tissue using the model in this study. The cellular phones used in close body situation especially the head close usage causes absorbing the high level SAR. An investigations with laboratory animals present an indirect data for human being, and it is clear that the experimental investigations realized using biologic tissue equivalent phantom models provide big easiness. Further investigations on the other biological effects of the cellular phones are required considering thermal effects. Since the knowledge of biological structure and dielectric properties of children have not been exactly revealed, further investigations need to be focused on children.

REFERENCES

[1] IEEE Standard Board, IEEE-C95.1, Safety Levels With Respect to Human Exposure to Radio Frequency Electromagnetic Field, 3 kHz to 300 GHz, IEEE Standard Department, Piscataway, New Jersey, 1991.

[2] European Communities Prestandard, ENV 50166-2, Human Exposure to Electromagnetic Fields High Frequency (10 kHz to 300 GHz), 1995.

[3] TS ENV 50116 Türk Standardı, İnsanların Elektromagnetik Alanlara Maruz Kalması–Yüksek Frekanslar (10kHz-300GHz), TS ENV 50116 – 2, 1996.

[4] Ozen, S., Onural A.Ş., Çömlekçi S., Çerezci O., "Experimental Determination of Heat Rise and SAR Occurred by 900 MHz EM Radiation on Human Brain by Using Brain Phantom Model", G.U Journal of Science. 17(3):127-132, 2004

[5] Guy AW, Analyses of electromagnetic fields induced in biological tissues by thermographic studies on equivalent phantom models IEEE Trans MTT 1971; 19:205-214

[6] Koichi I., Katsumi F., Yoshinobu O., and Lira H., "Development and Characteristics of a Biological Tissue-equivalent Phantom for Microwave, Electronics and Communications in Japan, Part 1, Vol. 84, No.4, 2001

[7] Ozen S., Theoretical and Experimental Study on Thermal Analysis in Biological Tissue Which Under Exposure of MW Frequency EM Radiation, PhD, Thesis, Sakarya University, Science Institute, 2003.

[8] Ozen S., Köylü H., " Phantom Model Of Human Brain Tissue For Cellular Phone Frequencies in Electromagnetic Field Radiation Absorption Studies", G.U Journal of Science. 18(2):193-200, 2005

Acknowledgments- This study was supported by Scientific Research Projects Department of Akdeniz University

NO EFFECT OF 1800 MHZ RFR TO COLLAGEN SYNTHESIS TO GUINEA PIG LIVER TISSUE

ELCIN OZGUR, GOKNUR GULER

BIOPHYSICS DEPARTMENT, GAZI UNIVERSITY MEDICAL FACULTY
GAZI UNIVERSITESI TIP FAKULTESI BIYOFIZIK ANABILIM DALI
06510 BESEVLER ANKARA TURKEY
elcinozgur@gazi.edu.tr, gozturk@gazi.edu.tr

Abstract
RF radiation values generated Nokia 3210 mobile phone operating 1800 MHz frequency band measured by Electromagnetic (EM) radiation meter during experiment. Male Guinea pigs were exposed to operating mobile phone for 10 minute-periods in 7 days of a week. Average external Electric (E) field measured during exposure was 11.2 V/m. Effects of whole body exposure of 11.2 V/m to collagen synthesis in liver tissue were determined by using three different hydroxyproline level designation methods named H. Stegemann-K. Stalder, I.S. Jamall, V.N. Finell and ISO 3496.
It was observed that the increment found hydroxyproline level due to mobile phone radiation in liver was statistically insignificant. It was detected statistically that the hydroxyproline level designation methods of ISO 3496 is the most accurate way of measuring hydroxyproline level in between the methods used in this research.

Introduction
Since time began until about hundred years ago living beings had to deal with naturally occurring radiation, which somehow was balanced or life was shielded from detrimental parts of that radiation such as certain cosmic radiation. When people began to harness electricity, generate and transport it over long distances a different kind of energy was introduced to our life: AC (Alternating Current) electric, AC magnetic fields and radiofrequency radiation. The superimposition of electromagnetic fields caused by all kinds of electromagnetic radiation that arise in the human environment is known as electromagnetic pollution. Not only is electromagnetic pollution responsible for interference between electrical devices, but it is also affects the human body. The organism reacts to the electrical, magnetic and electromagnetic fields around it. The biological effects depend on the type, frequency and strength of these fields. The boom in the use of the cellular phone has led to a very evident increase in this kind of stress.
Many in vivo and in vitro studies have been performed to investigate the biological consequences and to assess health risks of RFR (Radio Frequency Radiation) generated from cellular phones. Relation between RFR and protein synthesis is still unclear mechanism continuing to investigate.
The connective tissue protein, collagen, is the most abundant protein in higher animals . Collagen also provides the framework for parenchymal organs such as the liver, kidney, and spleen, either in its fibrous form or organized in basement membranes. The rate of hydroxyproline formation is therefore considered to be a good indication of the rate of collagen biosynthesis. The collagen content of a tissue is determined by measuring the content of protein bound hydroxyproline. Hydroxyproline is necessary for collagen helix formation, and in its absence collagen is unable to be properly secreted from fibroblasts (Irvin, 1981; Craig et al, 1975; Takahashi and Lee, 1987).
The connective tissue protein, collagen, is not only abundant but also significant protein in higher animals since it is charged molecule tend to be directed trough electric field applied.. In this research, effects of RFR generated by mobile phones on liver tissue collagen examined by using tree different hydroxyproline detection methods.

Material and Method
In this investigation, 3 month-old guinea pigs were exposed to RFR radiated from Nokia 3210 mobile phone operated in GSM DCS 1800 MHz. During the exposure of every Guinea pig, external E fields were measured by NARDA EMR 300 and type 8.3 probe. Measurements were taken for duration of 10 minutes per 2 seconds and the data saved to the computer connected to device via fiber optic cable. The whole data were averaged before statistical analysis.
Guinea pigs were exposed to RFR averaged as 11.2 V/m for 10 minutes a day during 7 days and analyzed for the effects on liver tissue collagen level. Changes of collagen level were analyzed biochemically by three different

hydroxyproline determination method named as “H. Stegemann-K. Stalder”(Stegemann, 1958; Stegemann et al, 1963; Stegemann et al, 1964; Stegemann and Stalder, 1967a; Stegemann and Stalder, 1967b), “I.S. Jamall-V.N. Finell” (Jamall et al, 1981) and “ISO 3496” (TS 6236 ISO 3496, 1997). Also, histological analyzes were accomplished.

Result

The outcome of the biochemical analysis pointed out that hydroxyproline level increased with respect to control but this increase was not statistically significant for all methods ($p>0.05$). On the contrary, histological analyses showed that RF exposure makes fibrosis in liver tissue increase significantly. In addition to this, difference in hydroxyproline determination accuracy of ISO 3496 method with respect to other two methods was found as statistically significant ($p<0.05$) (Table 1- Figure 1).

Discussion

In this study, effects of RFR generated by mobile phones on liver tissue collagen examined by using hydroxyproline detection methods. Hydroxyproline is characteristic amino acid whose tissue level is used to determine the tissue collagen level (Dahl and Persson, 1963; Edwards and O’brien, 1980; Bondjers and Bjorkerud, 1973; James et al, 1990; Neuman and Logan, 1963; Stegemann, 1958; Stegemann et al, 1963; Stegemann et al, 1964; Stegemann and Stalder, 1967a; Stegemann and Stalder, 1967b; Mommersteeg etal, 1993; Reddy and Enwemeka, 1996; Switzer and Summer, 1971; Wood et al, 1990).

Biological effect mechanisms of RFR were analysed as thermally and non-thermally also the cumulative effects which are not clear yet. Increase of the molecular activities when matter interactions with EMF can cause thermal effects’ arises. Electrically charged particles as ion, molecular dipole and colloidal particles are always in motion in the unstable fields. Electromagnetic fields affect collagen since it is charged particle. If a low current is applied to the collagen solution in acid solvent, a concave band is formed around cathode which shows that collagen behaves like cation under the effect of electric field. Effects of electric field on hydroxyproline can be explained as collagen consists of hydroxyproline with the ratio of 1/10(Gustavson, 1956; Ramachandran, 1967a; Ramachandran, 1967b). The physical phenomenon which states that low frequency RFR can penetrate into more internal tissues than high frequency RFR can be active mechanism on which can explain why RF radiation is non-effective on liver tissue collagen. Also, wavelength changes with respect to electrical qualifications of the medium. Certain systems with ionic conductivity can have high dielectric constant in the range of several thousands. For this reason, it is considered that macro molecules can have comparable dimensions with the wavelength of microwaves which express spatial resonances. But, if the frequency increases, resonance of the large dipolar molecules like proteins gets harder with the field. Resonance frequency matching may be the reason why 1800 MHz RFR is not effective on collagen in liver tissue. Besides this study, the evidences in the earlier studies expressed that static and extremely low frequency (ELF) 50 Hz electric fields and magnetic fields applied in different direction and strength affected the hydroxyproline level in liver and some other tissues like kidney, lung, skin and wound (Güler, etal, 1996; Güler and Atalay Seyhan, 1996; Güler and Seyhan , 2001; Canseven and Seyhan, 2005; Canseven and Atalay Seyhan, 1995; Canseven and Atalay Seyhan, 1996; Canseven and Seyhan, 2000, Seyhan et al, 2006)

It is possible to determine the collagen level in tissue by applying hydroxyproline determination methods which should be very accurate since liver tissue collagen level is less than other tissues like skin or bone. In this study, “H. Stegemann-K. Stalder”, “I.S. Jamall-V.N. Finell” and “ISO 3496” were chosen as biochemical methods of liver tissue hydroxyproline level determination after literature search. In each of tree methods, tissue hydrolysis hydroxyproline measured by spectrometry after adding Cloramin-T reactive which stains the solution. The wavelength for measuring optic density of solution for “H. Stegemann-K. Stalder” and “I.S. Jamall-V.N. Finell” is 560 nm, but for the method called “ISO 3496” is 558 nm. One of the method named as “ISO 3496” was found as the most accurate method with respect to the other two ($p<0.05$). This method is nowadays used for determining the absolute value of hydroxyproline in the meat and meat product industry which should be very little collagen content in order to be fine product.

RFR radiated by mobile phones which are daily components of our daily lives, exposed to male guinea pigs 10 minutes daily for 7 days and the increase of hydroxyproline level in liver tissue was found as statistically insignificant with respect to controls. However, although not significant, this increase make a question be asked that what the consequence will be if the exposure period is prolonged because people use their mobile phones more than 1 week and also may use them more than 10 minutes daily.

For this reason, prolonged researches should be done in order to determine the biological effects of RFR.

Table 1: Comparison of liver tissue hydroxyproline level measured by tree different methods of 10 minutes exposure group with controls

H. Stegemann-K. Stalder		**I.S. Jamall-V.N. Finell**		**ISO 3496**	
Control –HP level	**Exposure- HP level**	**Control –HP level**	**Exposure- HP level**	**Control –HP level**	**Exposure- HP level**
0.2686	0.3260	0.1845	0.2902	0.2851	0.3419
0.3045	0.3003	0.2706	0.2882	0.2914	0.3302
0.2479	0.2418	0.3198	0.2872	0.2987	0.3158
0.2606	0.2551	0.3690	0.2671	0.3041	0.2849
0.3225	0.2710	0.2706	0.2730	0.3057	0.2861
0.2985	0.2911	0.3075	0.3171	0.3117	0.3044
0.2427	0.2729	0.3321	0.3029	0.3209	0.3006
0.2460	0.2913	0.2828	0.2652	0.3301	0.2910
0.2553	0.2692	0.3819	0.3152	0.3012	0.2994
0.2433	0.2547	0.2706	0.3006	0.3034	0.3037
0.2979		0.1968	-	0.3075	-
0.2716 ± 0.0289	**0.2773 ± 0.0251**	**0.2897±0.0622**	**0.2907±0.0185**	**0.3054 ± 0,0125**	**0.3058 ± 0.0186**

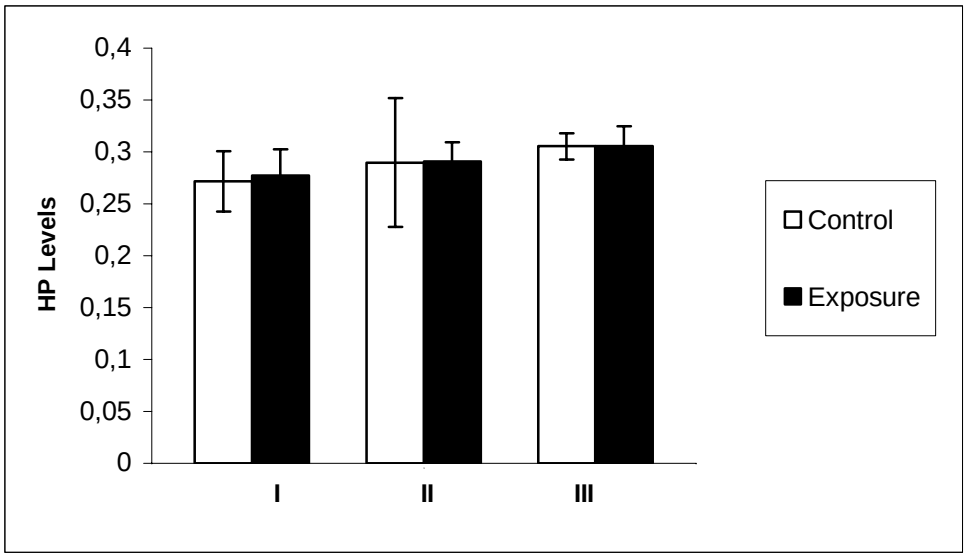

Figure 1: Liver tissue hydroxyproline level determination by using tree different biochemical methods I: H. Stegemann-K. Stalder's method, II: I.S. Jamall-V.N. Finell's method and III: Method of ISO 3496.

References

Bondjers G., Bjorkerud S. (1973). Spectrophotometric Determination of Hydroxyproline in Connective Tissue on the Nanogram Level, *Anal. Biochem*, 52, 496-504,.

Canseven, A.G., Atalay Seyhan, N. (1995). Electric Current – Collagen Synthesis Interaction in Wound Healing I. *Turkish Med J* 2:71-77 (Turkish)

Canseven, A.G., Atalay Seyhan, N. (1996). Is It Possible to Trigger the Collagen Synthesis by Electric Current in Skin Wounds?. *Indian J Biochem. Biophys* 33: 223-227.

Canseven, A.G., Seyhan, N. (2000). Changes in Skin Hydroxyproline Levels Under the Effect of Magnetic Fields. World Congress on Medical Physics and Biomedical Engineering. 23-28 July 2000, Navy Pier, Chicago (from CD/TU-B205-04)

Canseven, A.G., Seyhan, N. (2005). Effects of Ambient ELF Magnetic Fields: Variations in Collagen Synthesis of Guinea Pigs' Skin and Scaling From Animals to Human. *Gazi Medical Journal* 16:160-165 (Turkish)

Craig, RDP, Schofield, JD, Jackson, D. (1975).Collagen biosynthesis in normal and hypertrophic scars and keloid as a function of the duration of the scar. *Br. J. Surg*. 62 : 741-744.

Dahl, O., Persson, K (1963). Hydroxyproline, Methodological Studies of Analysis, *Act. Chem. Sc*., 17, 2499-2503,

Edwards C.A., O'brien W.D. Jr. (1980). Modified Assay for Determination of Hydroxyproline in a Tissue Hydrolyzate, *Clin Chim Acta*, 7: 104, 161

Güler G., Seyhan Atalay N., Özoğul C., Erdoğan D. (1996). Biochemical and structural approach to collagen synthesis under electric fields. *Gen. Physiol. Biophys*. 15: 429-440.

Güler, G., Atalay Seyhan, N. (1996). Changes in Hydroxyproline Levels in Electric Field Tissue Interaction. *Indian Journal of Biochemistry and Biophysics* 33: 531-533.

Guler, G.; Seyhan, N. (2001). The effects of electric fields on biological systems. Engineering in Medicine and Biology Society, 2001. Proceedings of the 23rd Annual International Conference of the IEEE , Volume 2, 25-28 Oct. 2001 Page(s):1023 - 1025 vol.2

Gustavson K.H. (1956). *The Chemistry and Reactivity of Collagen*, Academic Pres Inc., Publishers, New York.

Hutterer, F. , Singer, E.J. (1960). A Modified Method for Hydroxyproline Determination, *Anal. Chem.*, 32: 556-558

Irvin, T. (1981): *Wound Healing Principles and Practice*. Cambrige: Chapman and Hall Ltd., pp 2-6.

Jamall I.S., Finelli V.N., Que Hee S.S. (1981 Mar 15). A simple method to determine nanogram levels of 4-hydroxyproline in biological tissues, *Anal Biochem*. 112(1):70-75

James J., Bosch K.S., Aronson D.C., Houkooper J.M. (1990). Sirius Red Histophometry and Spectrophoometry of Sections in the Assessment of the Collagen Content of Liver Tissue and its Application in Growing Rat Liver, *Liver*,10: 1-5.

Mommersteeg T.J.A., Kauer J.M.G., Huiskes R.,Blankevoort L. (1993). Method to Determine Collagen Density Distributions in Fibrous Tissues, *Journal of Orthopaedic Reseach*, 11: 612-616.

Neuman, R.E., Logan, M. (1963). The Determination of Hydroxyproline, *J. Biol. Chem*., 184, 299-306.

Ramachandran G.N. (1967a).*Treatise on Collagen*, Volume 1, Chemistry of Collagen, Academic Pres, London and New York.

Ramachandran G.N. (1967b). *Treatise on Collagen*, Volume 2, Biology of Collagen, Academic Pres, London and New York.

Reddy G.K., Enwemeka C.S. (1996). A Simplified method fort he Analysis of Hydroxyproline in Biological Tissues, *Clinical Biochemistry*, 29: 225-229.

Seyhan, N., Canseven, A., Güler, G. (2006). Animal Studies on the Effects of ELF and Static EMF, in Bioelectromagnetics Current Concepts, The Mechanisms of the Biological Effect of Extremely High Power Pulses (Ayrapetyan S.N., Markov M.S., eds), NATO Security through Science Series B: Physics and Biophysics, Vol. 5, Springer Press, the Netherlands, pp: 195-212 ISBN: 1-4020-4277-9

Stegemann, H., Fuchs, G., Eger, W. Der Transplantierte Knochenspan und Seine Qualitat Nach Partieller und Vollstandiger Enteiweibung Bei Erhaltener Anorganischer Substanz, Arch., Klin. Chir., 303,240-60.

Stegemann, H., Stalder K., Bernhard, G. (1964). Über die Isomerisierung von Hydroxyprolin, *Hoppe- Seyler's Z. Physiol. Chem.*, 337: 179-185.

Stegemann, H., Stalder K. (1967a). Determination of Hydroxyproline, *Clin. Chim. Acta*., 18: 267-273.

Stegemann, H., Stalder K. (1967b). Zur Ausscheidung von Hydroxyprolin im Harn, *Hoppe- Seyler's Z. Physiol. Chem.*, 348: ,242-3.

Stegemann, H. (1958). Mikrobestimmung von Hydroxyprolin Mit Chloramin- T und p-Dimethylaminobenzaldehyd, *Hoppe-Seyler's Z. Physiol. Chem*.,311: 41-5,

Switzer B.R., Summer G.K. (1971). Improved Method for Hydroxyproline Analysis in Tissue Hydrolyzates, *Anal. Biochem*, 39: 487-491,

Takahashi, S., Lee, J. (1987). Quantitative study of tissue collagen metabolism. *Ana l Biochem* 162: 553-561.

TS 6236 ISO 3496 , (April, 1997). Meat and meat products -- Determination of hydroxyproline content, Turkish Standards Institude, First Publication, ANKARA

Wood, D.D., Mclaurin J., Moscarello M.A. (1990). A Hydroxyproline- contining Protein from Shark Brain that is Related to Myelin Basic Protein, *Journal of Neurochemistry*, 55: 1697-702.

CELLULAR AND INTRACELLULAR RESPONSE TO ELECTROMAGNETIC FIELD OF ULTRA HIGH FREQUENCY RADIATION

IVAN PAVICIC
IVANCICA TROSIC

INSTITUTE FOR MEDICAL RESEARCH AND OCCUPATIONAL HEALTH
KSAVERSKA CESTA 2. POB 291. HR-10001 ZAGREB, CROATIA
e-mail: ipavicic@imi.hr, phone: ++ (385 1) 4673 188

Abstract

The aim of this study was to evaluate whether low-level, ultra high frequency (UHF) irradiation of 935 MHz influences the cytoskeleton and the cell growth of V79 cells. UHF field was generated inside a Gigahertz Transversal Electromagnetic Mode cell (GTEM-cell) equipped with a Hewlett Packard signal generator. The electric field strength was 8.2±0.3 V/cm, and the average specific absorption rate (SAR) was calculated to be 0.12 W/kg. Cell samples were cultivated in a humid atmosphere at 37 °C in 5% CO_2. Prepared cell samples were exposed to the 935 MHz continuous wave frequency field for 1, 2 and 3 hours. The structure of microtubule proteins was determined using the immunocytochemical method. Cell growth was determined by counting cells for each hour of exposure during five post-exposure days. The experimental procedure included exposed V79 and unexposed control cells. In comparison to the control cells, the microtubule structure of the exposed cells significantly altered after 3 hours of irradiation ($p<0.05$). Cell growth of the cells exposed for three hours significant dropped 72 hours after exposure ($p<0.05$). It could be concluded that the 935 MHz low-level UHF radiation affected microtubule proteins, consequently influencing the cell growth.

Introduction

Common concern about biological effects of ultra high frequency (UHF) electromagnetic (EM) fields in the range from 300 MHz to 3 GHz grows with development of telecommunications systems. So far, many reported biological effects of UHF are considered to be simply indeterminate with respect to their significance to health [1]. Therefore, it is important that biological effects of UHF fields be understood at least on cellular level. Numerous *in vitro* biological effects caused by low-level UHF irradiation have been reported, and a number of studies conducted to assess changes at the cellular level reported adverse effects on cell proliferation and cell membrane structure [2, 3]. It was also suggested that UHF could interact with different apoptosis pathways [4]. No other effects have been observed on the cell cycle, enzyme activity, gene expression or DNA and chromosome damage [5-12]. A wide range of studies *in vivo* showed that rat blood-forming system could be affected by low-level UHF fields [13, 14, 15]. In addition, a number of biological effects were observed in animals during non-thermal exposure to the UHF field [16, 17, 18]. It is apparent that studies of mobile phone frequencies often present conflicting results. Accordingly, there is a permanent need for independent and objective research of the UHF biological potency. In addition, Repacholi in 1998, has recommended that the time course of effects should be investigated to determine if they are chronic, acute, or whether the effects disappear after cessation of exposure [19].
The aim of this study was to evaluate whether low-level UHF of 935 MHz frequency field affects the cytoskeleton microtubule structure and cell growth in the continuous line of V79 cells after 1, 2 and 3 hours of exposure.

Material and methods

A continuous cell line of Chinese hamster V79 lung fibroblasts was routinely grown in nutrient medium supplemented with antibiotics and fetal calf serum, (RPMI 1640, SIGMA Chemical CO, St. Louis, USA). The cells were maintained in a humid atmosphere at 37 ^{0}C in 5% CO_2, and incubated for 24 hour prior to the beginning of the assay. Electromagnetic field frequency of 935 MHz was generated by a certified Gigahertz Transversal Electromagnetic Mode Cell (GTEM-cell) equipped with a signal generator (Mod. 5402, ETS^{TM}

Lindgren, USA and Hewlett Packard HP8657, Pablo Alto, USA) [20]. Cell samples were exposed to UHF EM radiation in triplicate for one, two and three hours. Control cells were kept in the same experimental conditions, but were not exposed to UHF EM radiation. Positive control cells treated with 0.1 mM colchicine (SIGMA Chemical CO, St. Louis, USA) were also included into the study. The specific absorption rate (SAR) was averaged to be 0.12 W kg^{-1} for a single cell. SAR was calculated by averaging the individual parameters of the cell substance in accordance with their volume fraction in the live cell according to the Steffensen's mathematical model [21, 22]. Temperature inside the GTEM-cell was measured at 10-minute intervals in order to preserve steady temperature of 37 ^{0}C during irradiation. Indirect immunocytochemical method was used to determine microtubule proteins in irradiated and control cells [23]. Cell culture samples were initially seeded in total volume of 5 ml in Permanox Lab-Tek Chamber Slides (Nunc, Roskilde, Denmark) at a concentration of $2.5x10^4$ cells/ml. After irradiation the cell culture samples were washed in 0.5% triton X-100 and permeabilized with calf albumin (Imunološki zavod, Zagreb, Croatia). Subsequently, cells were fixed in a 4% paraformaldehyde. Microtubule proteins were marked by a primary antibody (IgG anti-β-tubulin, SIGMA Chemical CO, St. Louis, USA). The secondary antibody was represented by a conjugate of anti-mouse IgG and fluorescein isothiocyanate (FITC, Imunološki zavod, Zagreb, Croatia). The smears of cells were mounted on a fluorescent medium. To determine cell proliferation, V79 cells were plated in the concentration of $1x10^4$cells/ml in 24-well plates (TPP, Switzerland). For each hour of exposure, cell proliferation was determined microscopically by cell counts on post-exposure hours 24, 48, 72, 96 and 120 [24]. Collected data were analyzed using Statistica 7.0 (StatSoft Inc., USA). Results were presented as mean values and standard deviations or errors (SD/SE). Pairwise comparisons between groups of data were performed using the analysis of variance ANOVA/MANOVA. Statistical difference was determined at $p<0.05$.

Results

Figures 1a and 1b show marked microtubule proteins in control and positive control samples V79 cells. Compared to controls, the exposed V79 cells showed time-dependent susceptibility to UHF irradiation associated with microtubule activity. Irregularities were also observed in cell morphology and microtubule protein structure. The observed phenotype changes in irradiated cells were characterized by cytoplasm membrane knobs and cytoplasm bubbles. After one and two hours of exposure, most microtubules were normally developed and their features did not essentially differ from control samples (Figure 2a, 2b). The structure of mitotic spindle remained regular (Figure 3). After the three-hour UHF exposure, the microtubule proteins started to significantly differ from matched control samples ($p<0.05$). After three irradiation hours cellular microtubule structure changed to more grainy (Figure 2c). Irregularity in microtubule structure was defined by distinct grainy clusters of proteins. These findings suggested that microtubule fiber organization could be acutely dissipated by the 935 MHz UHF irradiation. Figures 4, 5 and 6 show the growth of V79 cells after one, two and three hours of 935 MHz microwave irradiation and the growth of control cells. In comparison to control cells, cells exposed for three hours showed a significant drop ($p<0.05$) in cell growth 72 hours after irradiation (Fig. 6). The fall in the cell number on the fifth day (120 hours) after exposure seems to be the consequence of cell culture confluence and depletion of medium ingredients, which is confirmed by a decrease in the cell number of matched controls. Each data point at the curves represents the mean value obtained from six separate cell samples.

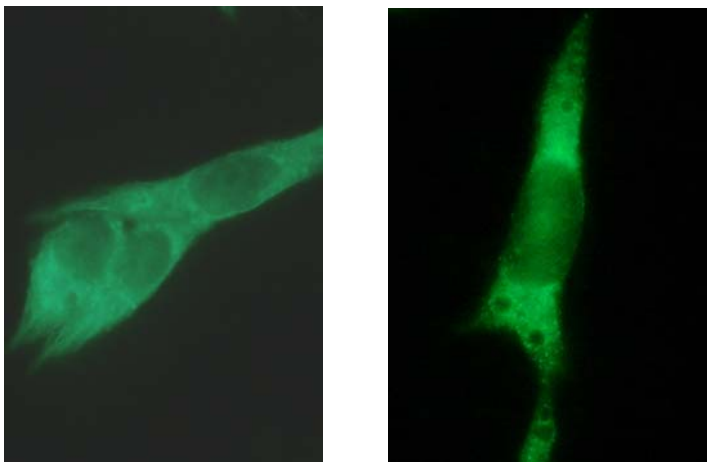

(a) (b)

Figure 1. Appearance of microtubules structure in control cells (a) and positive control cells (b)

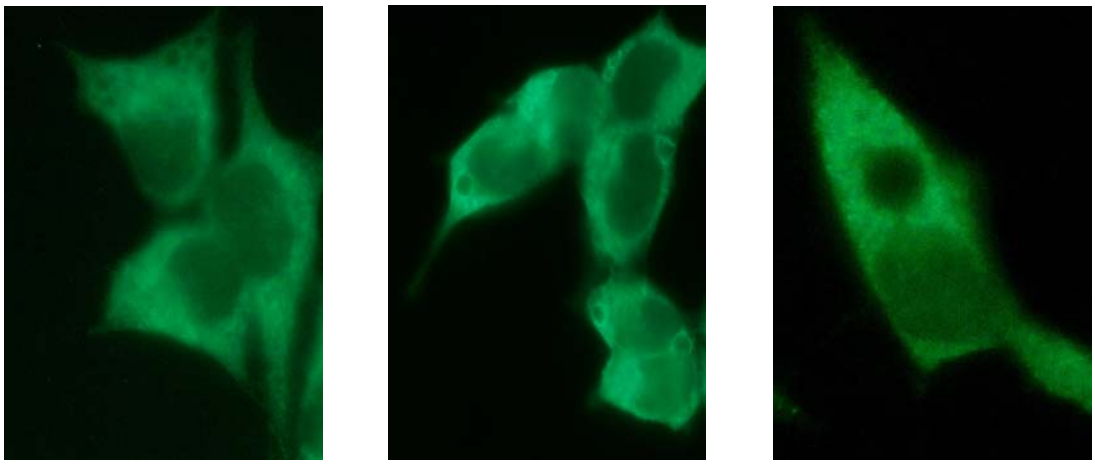

(a) (b) (c)

Figure 2. Appearance of microtubules structure in V79 cells after 1(a), 2(b) and 3(c) hours of UHF exposure

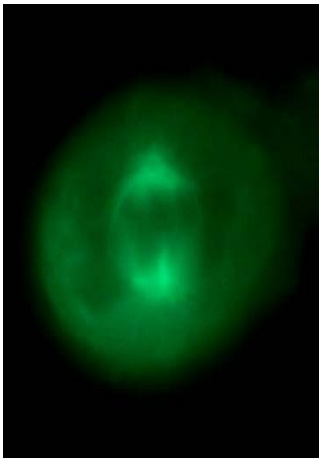

Figure 3. Mitotic spindle structure in V79 cell after two hours of UHF exposure

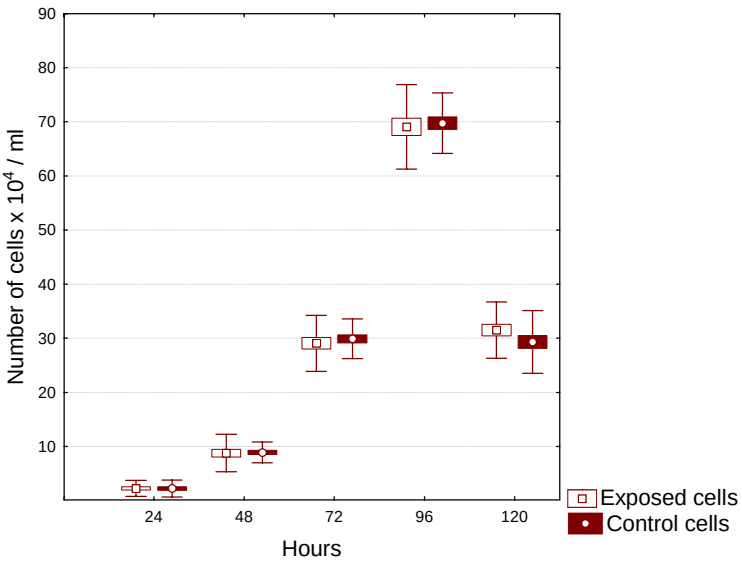

Figure 4. Growth of V79 cell culture after one-hour of UHF exposure and of matched control culture

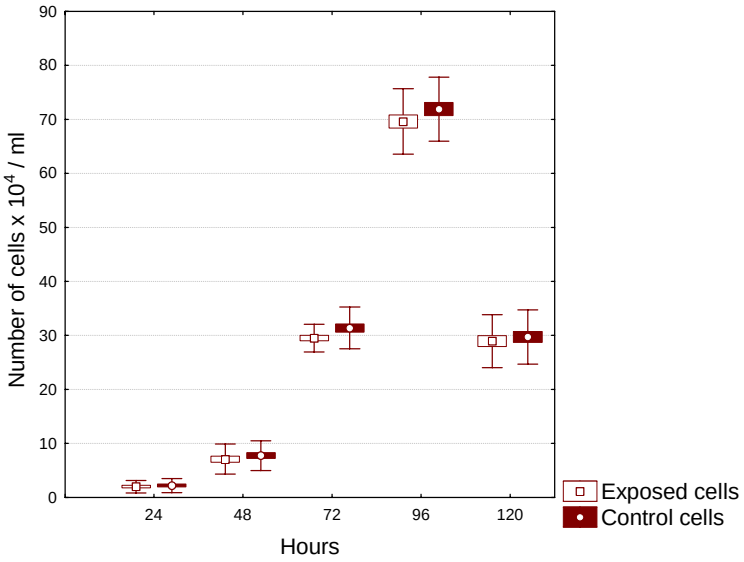

Figure 5. Growth of V79 cell culture after two-hour of UHF exposure and of matched control culture

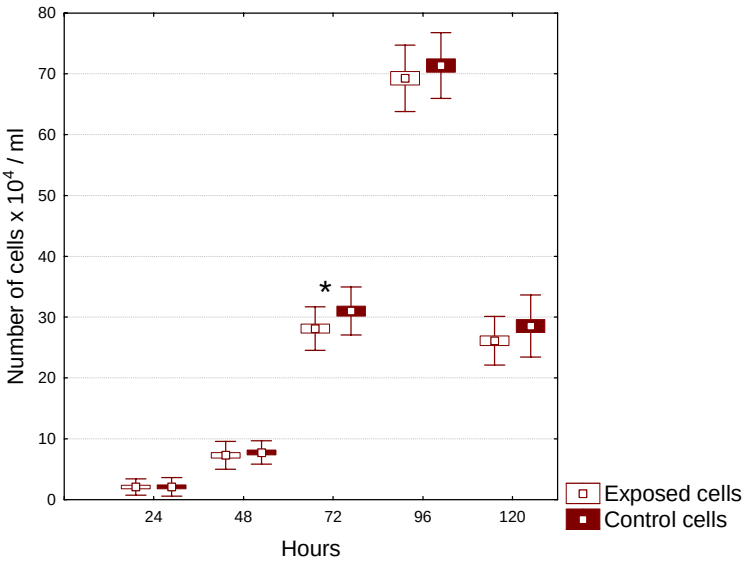

Figure 6. Growth of V79 cell culture after three-hours of UHF exposure and of matched control culture (* significance $p<0.05$)

Discussion

An experiment with whole-body exposure of rats showed that UHF EM irradiation had an effect on the proliferation and maturation of heamotopoietic cells [14]. Although the authors propose a reasonable explanation of the UHF EM action *in vivo*, we believe that a precise insight into the mechanism requires an *in vitro* approach to the problem. Microtubule protein fibers are extremely dynamical structures whose function depends on dynamic instability, i.e. on continuous binding of free tubulin proteins in microtubules and their degradation to basic protein units. It is believed that internal electrostatic forces and microtubule dynamic instability can be disturbed by outside electrostatic forces. Depending on the dipole momentum, an external electric field could affect the dynamic instability of microtubules and increase the number of free tubulin proteins in cytoplasm [25]. In our study the 935 MHz UHF exposure seems to have led to time-dependent increases of visible fluorescent grain structures or free cytoplasmatic tubulin proteins. The observed grain

structures revealed noticeable destruction of microtubule fibers. Pacini et al., demonstrated that exposure of cultured human cells to cellular phone radiofrequencies caused massive morphological and functional changes. After one hour of exposure to 902.4 MHz frequency field with the SAR of 0.6 W/kg, a significant increase was reported in gene expression related to the stress response proteins, cell cycle regulators, nuclear receptors, cytoskeleton and proteins of extracellular matrix [26]. The alteration of cytoskletetal actin protein structure in human astrocytoma cell line caused by 835 MHz irradiation and field power density of 40 mW/cm^2 was reported as well. In the same frequency field an alteration of cell proliferation was observed at 8.1 mW/cm^2 [27]. Neither Stagg's no Higashikubo's group observed any other changes through the G1, G2 and S phase, and cell division, immediately after exposure up to modulated 835.62 MHz frequency wave, SAR 0.6 W/kg [28, 29] for 100 hours. According Bohr & Bohr, UHF field affects the kinetics of conformational changes of the protein β-lactoglobulin. Exposure accelerates changes towards the equilibrium state by excitation of collective intrinsic modes in the protein [30]. Electric dipole momentum of microtubule proteins complies with the basic condition for vibration excitation and creation of internal oscillated electric field [31]. It becomes clear that internal oscillated electric field might interfere with outside electromagnetic forces which could finally lead to a measurable biological effect. It could be concluded that under the applied conditions, 935 MHz low-level UHF radiation affects microtubule protein structure, followed by disturbances in cell growth kinetics in a time-dependent manner.

Acknowledgements

Research described in this paper was supported by the Ministry of Science, Education and Sports, Republic of Croatia, Grant No. 0022005.

References

[1] Elwood, J.M. Epidemiological studies of radio frequency exposures and human cancer. Bioelectromagnetics. S6: 63-73(2003)

[2] Grundler,W., Keilmann F. Nonthermal effects of millimeter microwaves on yeast growth. Z. Naturforsch. 33(1-2):15-22(1978)

[3] Phelan, A.M. Lange, D.G. Kues, H.A. Lutty, G.A. Modification of fluidity in melanin-containing cells by low level microwave radiations. Bioelectromagnetics. 12: 131-146. (1992)

[4] Peinnequin, A., Piriou, A., Matheiu, J., Dabouis, V., Sdebbah, C., Malabiau, F., Debouzy, J.C. Non-thermal effects of continuous 2.45 GHz microwave on Fas-induced apoptosis in human Jurkat T-cell line. Bioelectrochemistry. 51: 157-161(2000)

[5] Cleary, S.F., Cao G.H., Liu L.M. Effect of isothermal 2.45 GHz microwave radiation on the mammalian cell cycle: comparison with effects of isothermal 27 MHz radiofrequency radiation exposure. Bioelectrochem. Bioenerg. 39: 167-173 (1996)

[6] Dutta, S.K., Das, K., Gosh, B., Blackman, C.F. Dose dependence of acetylcholinesterase activity in neuroblastoma cells exposed to modulated radio-frequency electromagnetic radiation. Bioelectromagnetics. 13(4): 317-322(1992)

[7] Pentafield L.M, Litovitz T, Krause D, Desta A, Mullins JM.. Role of modulation on the effect of microwaves on ornithine decarboxylase activity in L929 cells. Bioelectromagnetics. 18: 132-41.

[8] Fritze, K., Wiessner, C., Kuster, N., Sommer, C., Gass, P., Hermann, D.M., Klessing, M., Hossmann, K.A. 1997. Effect of GSM microwave exposure on the genomic response of the rat brain. Neuroscience. 81: 627-639(1997)

[9] Goswami, P.C., Albee L.D., Parsian, A.J., Baty, J.D., Moros, E.G., Pickard W.F., Roti Roti, J.L., Hunt, C.R. Proto-oncogene mRNA levels and activities of multiple transcription factors in C3H 10 T ½ murine embryonic fibroblasts exposed to 835.62 and 847.74 MHz cellular phone communication frequency radiation. Radiat Res. 151(3): 300-309(1999)

[10] Malyapa, R.S., Ahern, E.W., Straube, W.L., Moros, E.G.,Pickard W.F., Roti Roti J.L., Measurement of DNA damage after exposure to electromagnetic radiation in the cellular phone communication frequency band (835.62 and 847.74 MHz). Radiat Res. 148: 618-627(1997)

[11] Zeni, O., Chiavoni, A.S., Sannino, A., Antolini, A., Forgio, D., Bersani, F. Lack of genotoxic effects (micronucleus induction) in human lymphocytes exposed *In vitro* to 900 MHz electromagnetic fields. Radiat Res. 160: 152-158(2003)

[12] Bisht, K.S., Moros, E.G., Straube W.l., Baty J.D., Roti Roti j.l. The Effect of 835.62 MHz FDMA or 847.74 MHz CDMA Modulated radiofrequency radiation on the induction of Micronuclei in C3H $10T^1/_2$ Cells. Radiat Res. 157: 506-515(2002)

[13] Trosic, I., Busljeta, I., Kasuba, V., Rozgaj, R. Micronucleus induction after whole-body microwave irradiation of rats. Mutat Res. 521: 73-79(2002)
[14] Trosic, I., Busljeta, I., Modlic, B. Investigation of the genotoxic effect of microwave irradiation in rat bone marrow cells: *in vivo* exposure. Mutagenesis. 19(5): 361-364(2004)
[15] Trosic, I., Busljeta, I., Pavicic I. Blood-forming system in rats after whole-body microwave exposure; reference to the lymphocytes. Toxicol Lett. 154(1-2): 125-132(2004)
[16] Repacholi M.H., Basten, A., Gebski, V., Noonan, D., Finnie, J., Harris A.W. Lymphomas in Eμ-*Pim1* transgenic mice exposed to pulsed 900 MHz electromagnetic fields. Radiat Res. 147: 631-640(1997)
[17] Busljeta, I., Trosic, I., Milkovic-Kraus, S.. Erythropoietic changes in rats after 2.45 GHz nonthermal irradiation. Intl J Hyg Env Health. 207: 549-554(2004)
[18] Trosic, I. Multinucleated giant cell appearance after whole body microwave irradiation of rats. Int J Hyg Environ Health. 204: 133-138(2001)
[19] Repacholi M.H.. Low-level exposure to radiofrequency electromagnetic fields: health effects and research needs. Bioelectromagnetics. 19(1): 1-19(1998)
[20] Operating manual Gigazertz Transverse Electromagnetic cell (GTEM). Model 5400 Series. ETS test systems , LP. –ESCO Company EMCO. Austin, SAD (1999)
[21] Steffensen, K.V., Raskmark, P., Penersen, G.F. FDTD calculations of the EM-field distribution in a microtiter suspension well, COST 244: Biomedical Effects of Electromagnetic fields. Kuopio. 80-87(1995)
[22] World health organization. Electromagnetic Fields (300 Hz to 300 GHz), Environmental Health Criteria 137, World Health Organization, Geneva, pp.79. (1993)
[23] Bell PB, Safiejko-Mroczka B. Improved methods for preserving macromolecular structures and visualizing them by fluorescence and scaning elektron microcroscopy. Scanning Microscopy;9 (3):843-60(1995)
[24] Freshney, R.I. Culture of animal cells, A manual of basic technique.4th Ed. Wiley-Liss Publication, New York, 329 pp. (2000)
[25] Ortner MJ, Galvin MJ, Irwin RD. The effect of 2450-Mhz Microwave radiation during microtubular polymerization in Vitro. Radiation Res;93:353-63 (1983)
[26] Pacini, S., Ruggiero, M., Iacopo, S., Aterini, S., Gulisano, F., Gulisano, M. Exposure to global system for mobile communication (GSM) cellular phone radiofrequency alters gene expression, proliferation, and morphology of human skin fibroblasts. Oncol. Res./Anticancer Drug Des. 13: 19-24(2002)
[27] French, P.W., Donnellan, M., McKenzie, D.R. Electromagnetic radiation at 835 MHz changes morphology and inhibits proliferation of a human astrocytoma cell line. Bioelectrochem. Bioenerg. 43: 13-18(1997)
[28] Stagg, R.B., Thomas, W.J., Jones, R.A., Adey, W.R. DNA synthesis and cell proliferation in C6 glioma and primary glial cells exposed to a 836.55 MHz modulated radiofrequency field. Bioelectromagnetics. 18: 230-236(1997)
[29] Higashikubo, R., Ragouzis, M., Moros,EG, Straube, WL., Roti Roti, JL. Radiofrequency electromagnetic fields do not alter the cell cycle progression of C3H 10T1/2 and U87MG cells. Radiat Res. 156: 786-795(2000)
[30] Bohr, H., Bohr, J. Microwave enhanced kinetics observed in ORD studies of a protein. Bioelectromagnetics. 21: 68-72R(2000)
[31] Pokorný J, Jelínek F, Trkal V, Šrobár F. Vibration in microtubules. In: Bersam F, Ed. Electricity and magnetism in biology and medicine; Bologna; Kluwer Academic/Plenum Publishers; 967-70(1999)

INNOVATIVE MICROWAVE SYSTEM FOR THE CYTOLOGY DIAGNOSIS

G. BONGALLINO, M. BOZZETTI, G. CALO', A. D'ORAZIO, M. DE SARIO, L. MESCIA, V. PETRUZZELLI, F. PRUDENZANO*, F. TRISOLINI**

DEE – DIPARTIMENTO DI ELETTROTECNICA ED ELETTRONICA - POLITECNICO DI BARI

Via Re David, 200 – 70125 – Bari - Italy

***DIASS - DIPARTIMENTO DI INGEGNERIA DELL'AMBIENTE E PER LO SVILUPPO SOSTENIBILE – II FACOLTA' DI INGEGNERIA**

Viale del Turismo, 8 – 74100 – Taranto - Italy

****HOSPITEX DIAGOSTICS**

Via Provinciale Lucchese, 145 – Sesto Fiorentino (Florence) – Italy

Abstract

This paper proposes an innovative microwave system for the preparation of cytological slides. The system exploits an electromagnetic field to allow the cellular deposition thus reducing the use of the centrifuge. The analysis of the electromagnetic field effects on the cells in solution is of primary importance. In fact, to perform a uniform cell deposition, the generated electric field must not induce deformation of the cell structure and, in particular, the sizes of its nucleus.

A new version of GTEM cell able to generate a uniform and well controlled electromagnetic field has been designed. The cellular solution is inserted inside the GTEM cell by using a container, on the bottom of which the slide is placed. The electric and magnetic field strengths, that best fit the process requirements, have been evaluated by using a commercial computer code able to model the electromagnetic propagation inside the GTEM cell together with the cytological sample. The distribution of the electric and magnetic field modulus has been evaluated to verify the electromagnetic uniformity conditions.

Introduction

The conventional technique for the cytological tests is manual and based on the smear of vaginal cells (PAP TEST). The transfer of the material, captured by a small brush, on the glass is a complex practice. In most cases the smeared cells are not representative of the entire population of captured cells. In fact, all species must be present in reasonable quantities such to be able to represents the whole sample. Moreover, the cellular overlap and the casual disposition of mucus make difficult the PAP TEST preparation.

The most important parameter which is needed to evaluate the cell malignancy is the ratio between its total volume and the volume of its nucleus. In tumoral cells the nucleus, compared with the cell dimensions in its complex, appears enlarged. It is possible to distinguish two types of intraepithelial lesions: HSIL (High Grade Squamous Intraepithelial Lesion) and LSIL (Low Grade Squamous Intraepithelial Lesion). Therefore, the fixing effect can affect the correct interpretation of the cytological solution. In order to overcome this problem, that can compromise the diagnosis, the cytology market evolves in the direction of monolayer-based technologies [1-3]. At present, these technologies are not much spread, because of the required complex techniques, such as filtration and centrifuge steps, for cellular deposition on slide. In fact, because of the filtration step [4] some species, such as bacterium and little particles, could be not present on the slide. On the other hand, because of the centrifuge step, strong forces are involved, that might change the cellular nucleus sizes.

In this paper an innovative system for the preparation of the cytological slides is proposed. This system exploits the electromagnetic (EM) field in order to facilitate the cellular deposition thus reducing or avoiding the

centrifuge step.
Because of to the innovativeness of this technology, the analysis of the electromagnetic field effects on the cells in solutions is of primary importance. We propose a new version of the GTEM (Gigahertz Transverse Electro-Magnetic) cell to be used for the cytology slide preparation able to generate a uniform and well controlled electromagnetic field. The electric field polarization and strength, that best fit the process requirements, have been evaluated. In fact, to perform a uniform cell deposition and to increase the cell mobility, the electric field must not deform the cell structure and, in particular, the nucleus sizes. It is important to assure the uniformity of EM field in the sample. Therefore, the design of the GTEM cell has been aimed to achieve a uniform distribution of electromagnetic field in the test region. For this purpose, the requirement of the 50 Ω impedance matching condition along the propagation direction and at the terminal sections, must be satisfied.

GTEM cell prototype design

The GTEM cell is a tapered coaxial waveguide commonly used in Electromagnetic Compatibility (EMC) tests to simulate free-space radiation conditions in a shielded and restricted, environment. Accurate and repeatable measures can be performed for operating frequencies up to a few GHz. Additionally, a uniform EM field distribution can be guaranteed in the test region of the shielded overall volume. In absence of resonance and reflection phenomena inside the GTEM cell, a good EM field uniformity can be reached. This implies that the impedance matching condition must be satisfied both along the propagation direction and at the terminal sections by an appropriate design of the GTEM cell as regards its sizes and the absorbing load.
A GTEM cell can actually be considered as a tapered stripline with an offset inner conductor, here referred to as septum, that allows the only TEM mode propagates. Such a cell behaves as a transmission line with an associated characteristic impedance depending on the geometrical parameters of the structure. These have been chosen in order to maximize the test volume [5]: cell length L = 45 cm (pyramid height), aspect ratio $(b+d)/a$ = 2/3 (in the terminal section we have a = 24 cm, b = 4 cm and d = 12 cm), angles θ = 5°, γ = 10° and α = 15°. These parameters are shown in Fig. 1. The characteristic impedance of the GTEM cell have been evaluated with the use of a code based on the singular integral technique [6]. A 50 Ω characteristic impedance occurs in the case of the septum width w to the cell width a ratio equal to w/a = 0.7. This impedance is constant because the tapered shape of the GTEM cell allows to hold the same aspect ratio throughout the propagation direction. In Fig.2 the fabricated GTEM cell prototype is shown.
The GTEM cell has been designed by using a full-wave commercially computer code (CST MW Studio), based on the Finite Integration Technique (FIT). Figs. 3 and 4 illustrate the used CST model of the GTEM cell without and with the sample, respectively. A few simplifications are introduced in order to reduce its complexity and the related computation time. The SMA connector, where the signal generator is connected, together with its transition to the GTEM cell septum, have been neglected. According to the CST specifications, a waveguide port has been defined by cutting the GTEM cell pyramidal shape in correspondence of the SMA-connector to the septum transition. A second waveguide port has similarly been defined at the terminal section of the GTEM cell, thus allowing an optimal impedance matching condition at both the input/output load sections.

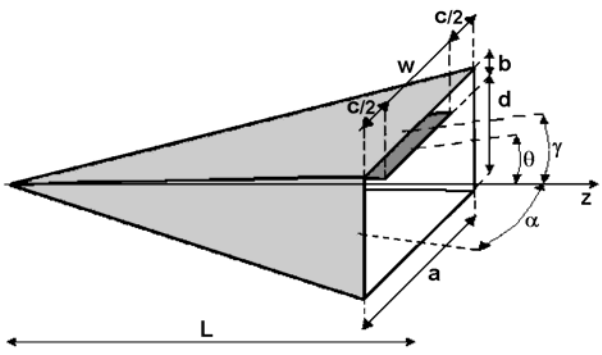

Fig. 1: Geometric parameters of the GTEM cell.

Fig. 2: Photo of the GTEM cell prototype.

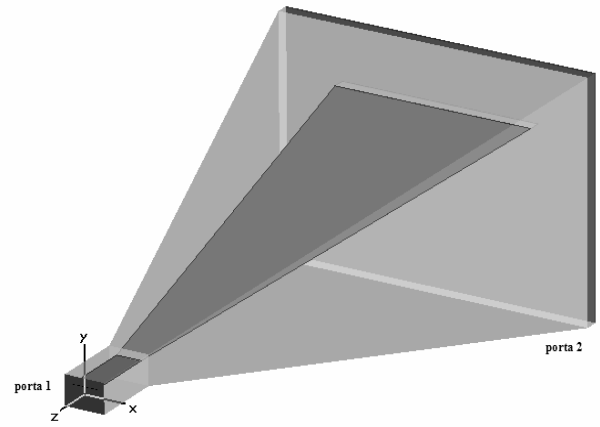

Fig. 3: CST model of the GTEM cell without sample.

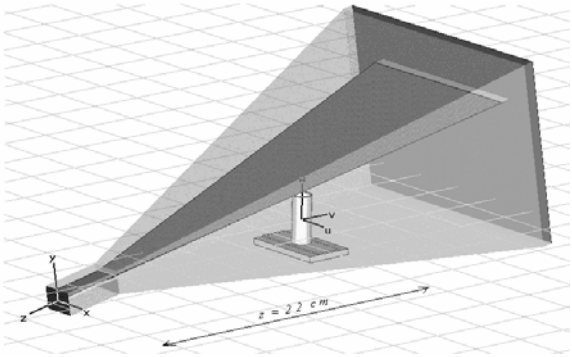

Fig. 4: CST model of the GTEM cell with the chamber.

Electromagnetic analysis

The electromagnetic analysis in the transversal section of the GTEM cell has been carried out by means of a home-made computer code based on the Transverse Resonance Diffraction (TRD) method [7]. In the region under the septum the E-field exhibits an almost uniform pattern along the propagation direction z. However, the tapered shape of the GTEM cell allows the propagation of a few higher-order modes. They can be originated only in correspondence of the larger sections and are responsible for a possible perturbation of the electromagnetic field distribution and uniformity. Further modes can be originated either by cross-sectional discontinuities or by the presence of the biological sample, that introduces inhomogeneous conditions along the propagation direction. These higher-order modes can be neglected, due to their low associated power. Moreover, the contribution of higher-order modes to the whole electromagnetic field can be minimized by suitably choosing the position of the sample in the GTEM cell. Therefore, the optimal position of the cytologic sample must be chosen in order to reduce the number of propagating modes and the induced electromagnetic field perturbation. In fact, the presence of higher-order modes reduces the extension of the test region in the GTEM cell. By means of the TRD method we have verified that for the frequency f = 0.9 GHz the monomodality is ensured from z = 0 m to z = 0.30 m. In fact, the first higher-order mode starts to propagate exactly from z = 0.295 m. On the other hand, for f = 1.8 GHz the monomodality is ensured only for z < 0.150 m. Therefore the best operating frequency is f = 0.9 GHz, for which two modes appear at the end section of the GTEM cell, that are the TEM and the TE_{p1} modes. The latter can be neglected , it being excited at the bottom of the GTEM cell and the energy exchange between the two modes being very low. Then, we can consider the only TEM mode without an valuable error. In order to confirm this result, the scattering parameters have been calculated. Fig. 5 reports the S_{11} and S_{21} parameters as a function of the frequency in the range from 0 Hz and 3 GHz. In particular, the S_{11} parameter is everywhere low, thus putting in evidence that the signal reflection is low. On the other hand, the S_{21} parameter assumes unitary value that is equivalent to total power transfer at the terminal section.
Moreover, the scattering parameters assume an almost flat behaviour for the frequencies around 1 GHz. Vice versa, for f > 1 GHz the scattering parameters assume an oscillating trend, with peaks more and more increasing. In conclusion, for f < 900 MHz the reflection phenomena inside the simulated GTEM cell model can be neglected.
The described ideal behaviour modifies by the introduction of the sample into the GTEM cell. To this aim the cellular solution is inserted into the GTEM cell by using a suitably designed holder, shown in Fig. 6, on the bottom of which the slide, devoted to collect the cells, is placed.
The holder has the following geometric parameters: basement of sizes 7.5 cm x 4.4 cm x 0.5 cm; slide of sizes 7.5 cm x 2.5 cm x 0.1 cm; cylinder extern diameter 1.8 cm; cylinder internal diameter 1.6 cm; cylinder height 4 cm. The basement and the cylinder, made of plastic, are characterized by the following electromagnetic parameters: $\varepsilon_r = 2.55$ and $\mu_r = 1$; the slide, made of Glass Pyrex by $\varepsilon_r = 4.82$ and $\mu_r = 1$. The cylinder has been simulated by considering the presence of cells in watery solution. This solution fills for half height the cylinder and is identified by $\varepsilon_r = 49.779$, $\mu_r = 1$ and dielectric tangent $\delta = 0.38$.
Figs. 7 and 8 show the S_{11} and S_{21} parameters as a function of the frequency in the range from 0 Hz to 3 GHz, calculated in the presence of the sample. Fig. 7 shows that the S_{11} parameter assumes low values, while Fig. 8 shows the S_{21} values equal to about 1 for f < 900 MHz.

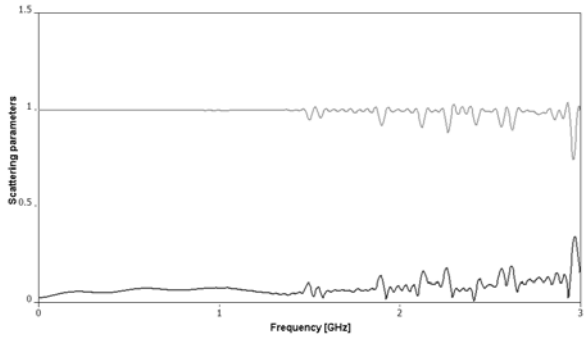

Fig. 5: Scattering parameters vs frequency for the GTEM cell without sample: S_{11} (red line) and S_{21} (green line).

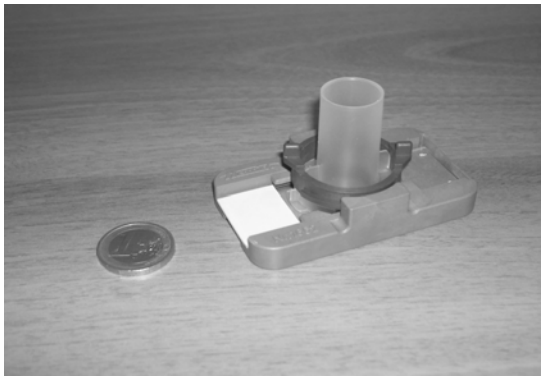

Fig. 6: Chamber for cytological vaginal samples.

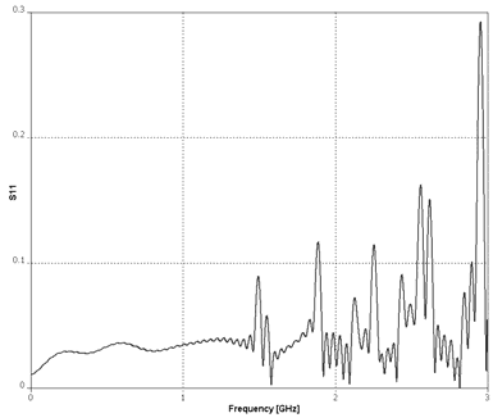

Fig. 7: S_{11} parameter vs frequency for the GTEM cell in presence of the cytological sample.

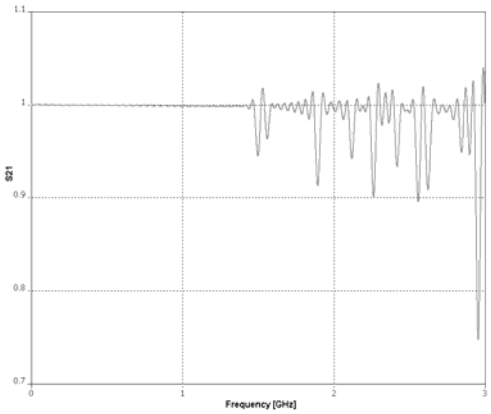

Fig. 8: S_{21} parameter vs frequency for the GTEM cell in presence of the cytological sample.

Electromagnetic field evaluation

Several simulations of the EM field have been carried out by changing the position of the holder in the GTEM cell. The monomodality is ensured from z = 0 m to z = 0.30 m, but the geometrical sizes of the holder do not allow to place the sample anywhere in the GTEM cell, owing to the presence of the septum. The sample has been placed in seven positions: z = 0.172 m, z = 0.182 m, z = 0.204 cm, z = 0.220 m, z = 0.236 m, z = 0.252 m, z = 0.262 m. The distance between two adjacent positions is 1.6 cm, equal to the diameter of the cylinder. For each position the average strength of the electric field components has been calculated in a circular section of the sample placed at a height of 1.5 cm from the bottom of the GTEM cell, having a thickness equal to 1 mm. Fig. 9 reports the average strength of the three E_x, E_y, E_z components of the electric field as a function of the seven positions. The most important electric field component for the cell deposition on the slide is E_y. In fact, in order to deposit the cells on slide without deforming its nucleus, the E_x and E_z components must be negligible with respect to E_y to avoid the deposition of the cells on the walls of the holder. Fig. 10 shows the variance V_E of the average components of the electric field. We can see that the dominant E_y component assumes an almost constant variance in dependence of the z position.

The same analysis has been carried out for the magnetic field and the results are shown in Figs. 11 and 12. The strength of the magnetic field must be very low in order to not give a rotational moment to the cells. On the basis of the obtained results, the sample inside the GTEM cell must be inserted in correspondence of the region within z = 0.23 m and z = 0.25 m.

In Figs. 13 and 14 the distribution of the electric and the magnetic field modulus is shown in the case of sample placed inside the GTEM cell at z = 0.236 m, where the best uniformity condition takes place.

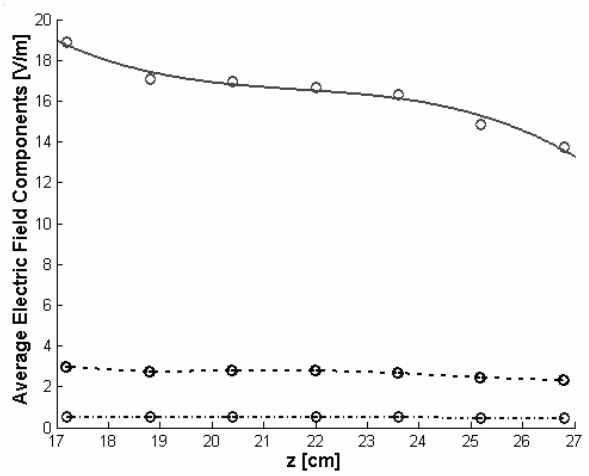

Fig. 9: Average electric field components vs z position: E_x (dash-dot curve); E_y (solid curve); E_z (dashed curve).

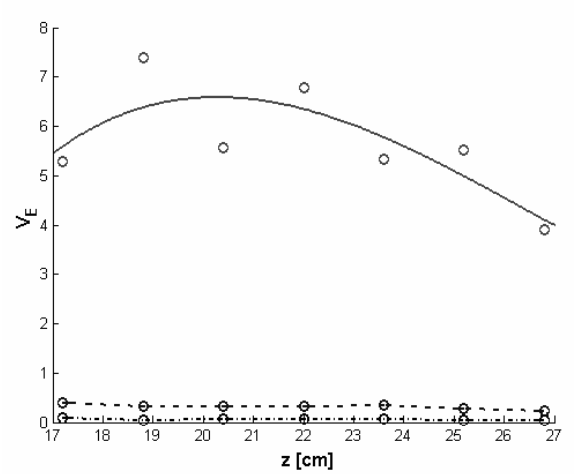

Fig. 10: Variance V_E of the average electric field components vs z position: E_x (dashed curve); E_y (solid curve); E_z (dash-dot curve).

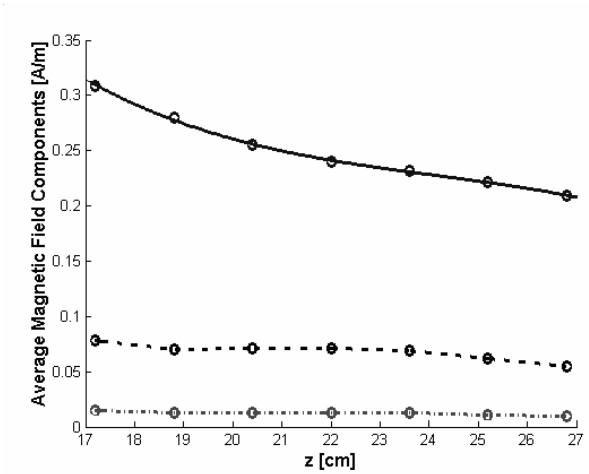

Fig. 11: Average magnetic field components vs z position: H_x (solid curve); H_y (dash-dot curve); H_z (dashed curve).

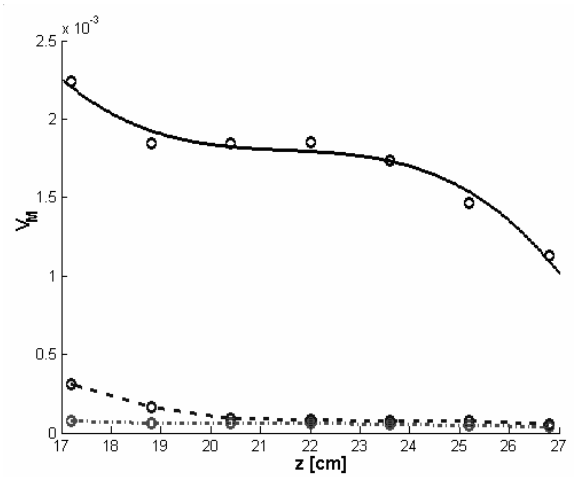

Fig. 12: Variance V_M of the average magnetic field components vs z position: H_x (dashed curve); H_y (dash-dot curve); H_z (solid curve).

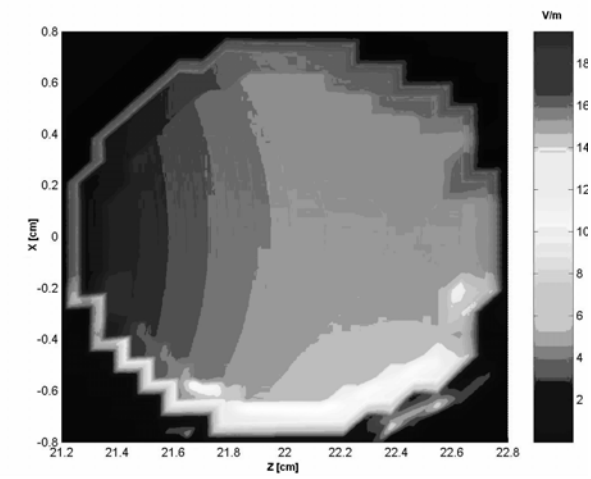

Fig. 13: Distribution of the electric field modulus with the sample positioned at z = 0.236 m.

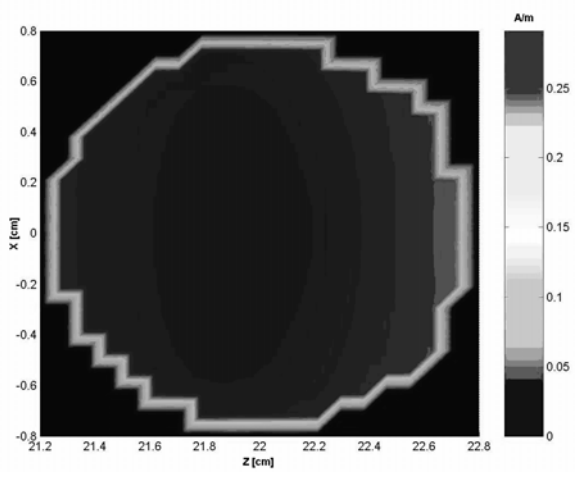

Fig. 14: Distribution of the magnetic field modulus with the sample positioned at z = 0.236 m.

Conclusions

An innovative system for the preparation of cytological slides has been studied. It exploits the electromagnetic field in order to allow the cellular deposition on slides. A new version of GTEM cell, able to generate a uniform and well controlled electromagnetic field, has been proposed and designed. A prototype has been realized by taking into account special test requirements. 50 Ω characteristic impedance has been found by adequately choosing the geometrical parameters. The electromagnetic analysis has been carried out by a Transverse Resonance Diffraction method and by a commercial computer code (CST MWS). The cellular solution has been inserted inside the GTEM cell by using an apposite holder, on the bottom of which the slide has been placed. At the best operating frequency f = 0.9 GHz, two modes propagate along the GTEM cell: the TEM and the TE_{p1} modes. This latter can be neglected because the energy exchange between the two modes is practically null.
By considering the average electric field at different positions along the GTEM cell, we have evaluated that the best position where the sample must be placed during the deposition is in the region within z = 0.23 m and z = 0.25 m. In fact, in those section both the electric and magnetic fields are uniform.

References

[1] Venancio Avancini Ferreira Alves, Marluce Bibbo, Fernando Carlos Landèr Schmitt, Fernanda Milanezi, and Adhemar Longatto Filho, M.Sc: "Comparison of Manual and Automated Methods of Liquid-Based Cytology: A Morphologic Study", Acta Cytol 2004; 48:187-193.

[2] Maurice Fremont-Smith, James Marino, Bryan Griffin, Lynn Spencer, David Bolick: "Comparison of SurePath™ Liquid-Based Papanicolau Smear with the Conventional Papanicolau Smear in a Multisite Direct-to-Vial Study", Cancer Cytopathology, Volume 102, No. 5, October 2004.

[3] Sandra M. Sulik, Karin Kroeger, Jennifer K. Schultz, Jennie L. Brown, Lorne A. Becker William D. Grant:: "Are Fluid-Based Cytologies Superior to the Conventional Papanicolaou Test? A Systematic Review", The Journal of Family Practice, Vol. 50, No. 12, December 2001.

[4] P.Trempat, R.C. Zenou, P. Brousset: "Evaluation de la Conservation de l'AND et de l'ARN Dans Les Milieux de cytology Liquides", Molecular Pathology, vol 55, No. 2, p. 125, April 2002.

[5] M. Bozzetti, G. Calò, A. D'Orazio, M. De Sario, L. Mescia, V. Petruzzelli, F. Prudenzano, G. Cibelli, R. Zefferino : "A Novel GTEM Cell for in vitro Dosimetric Experiments" , 3rd International Workshop on Biological Effects of ElectroMagnetic Fields, Kos, Greece, ISBN 960-233-151-8, vol. I, pp. 11-17, October 2004.

[6] J. Tippet, D. Chang : "Characteristic impedance of a rectangular coaxial line with offset inner conductor", IEEE Trans. on Microwave Theory and Technique, vol. MTT-26, pp. 876-883, November 1976.

[7] R. De Leo, T. Rozzi, C. Svara, L. Zappelli, "Rigorous Analysis of the GTEM Cell", IEEE Transaction on Microwave Theory and Technique, vol. MTT-39, n. 3, pp 488-499, 1991.

HANDS FREE KITS DOSIMETRY PROTOCOL AND RESULTS

D. PICARD
DRE - SUPELEC - 3 RUE JOLIOT CURIE - 91192 GIF SUR YVETTE CEDEX - FRANCE
TEL : 33 1 69 85 15 55 - dominique.picard@supelec.fr

Abstract
This study is the analysis of Hands Free Kits SAR measurement results corresponding to 124 different mobile phones. The mobile phones are measured following EN50361 protocol and the Hands Free Kits following a new specific protocol. The comparison between phone SAR and Hands Free Kits SAR is made and we introduce the SAR reduction factor, which is the ratio of the phone and the Hands Free Kits SAR values. The mean value of the SAR reduction factor is about 11 for GSM900 frequency band and 18 for DCS1800, which are very consistent values. The lower values of SAR reduction factor correspond to lower values of phone SAR. Finally, the use of Hands Free Kits decreases statically significantly the SAR value in the user head but the obtained SAR values are not absolutely negligible and it is necessary to study Hands Free Kits SAR.

Introduction
Since a few years the use of Hands Free Kits (HFK) with mobile phones is increasing. The distance between the phone antenna and the user head is larger with HFK and one can think that the RF power deposited in the user head is significantly reduced. However the wire of HFK is metallic and the RF currents induced on this wire can be the sources of power deposition is the user head [1] Supélec carries out dosimetry measurements for HFK since a few years, by the mean of its high sensitivity own dosimetry measurement system [2] (figure 1), and a large data base has been constituted from 2002 to 2004. 124 different mobile phones and HFK, corresponding to 20 different marks, have been tested, 100 of which are classical phones, 21 are clamshells and 3 are PDA. The number of monopole antenna handsets is 37 and the number of integrated antennas is 87.

Measurement protocols
The 124 different mobile phones and their HFK have been measured following EN50361 protocol for the handset and the following described protocol for HFK. There are 6 different measurements for each frequency band, corresponding to 2 different HFK wire configurations and 3 different frequencies: lower, center and upper frequencies. The 2 different wire configurations are 1) tensed wire (figure 2.a), 2) wire with two three cm diameter loops near the phone antenna (figure 2.b), the exact position of which corresponding to an obtained maximum SAR value at the center frequency. The tensed wire configuration corresponds to a ‘’natural’’ situation and the wire with loops to a worst case. The end of the wire near the earpiece is applied to the SAM phantom head surface close to the ear. The wire length in contact with the phantom is 2cm. The HFK Specific Absorption Rate (SAR) in each frequency band is the maximum obtained value for the 6 measurements.

Measurement results analysis
Phone and HFK SAR
The results of these measurements are shown in figure 3.a for GSM900 frequency band and b for DCS1800 band. The SAR values are very smaller in the case of HFK than for mobile phones for the two frequency band.

Figure 1: Supélec dosimetry facility.

Figure 2.a: Tensed HFK wire configuration.

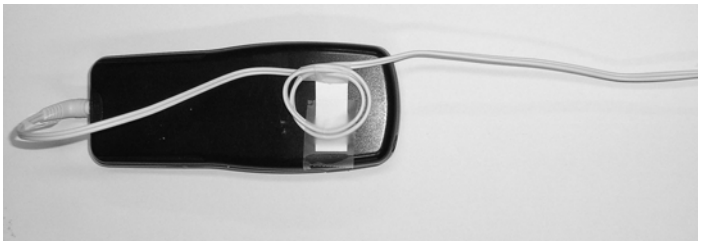

Figure 2.b: Two loops HFK wire configuration.

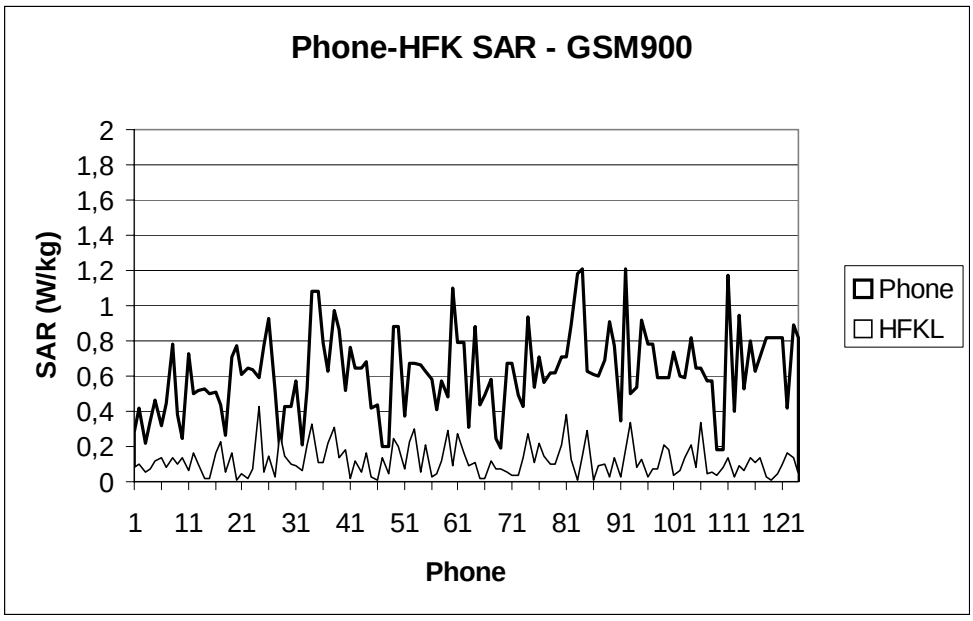

Figure 3.a: Maximum SAR values obtained in GSM900 frequency band function of mobile phone number.

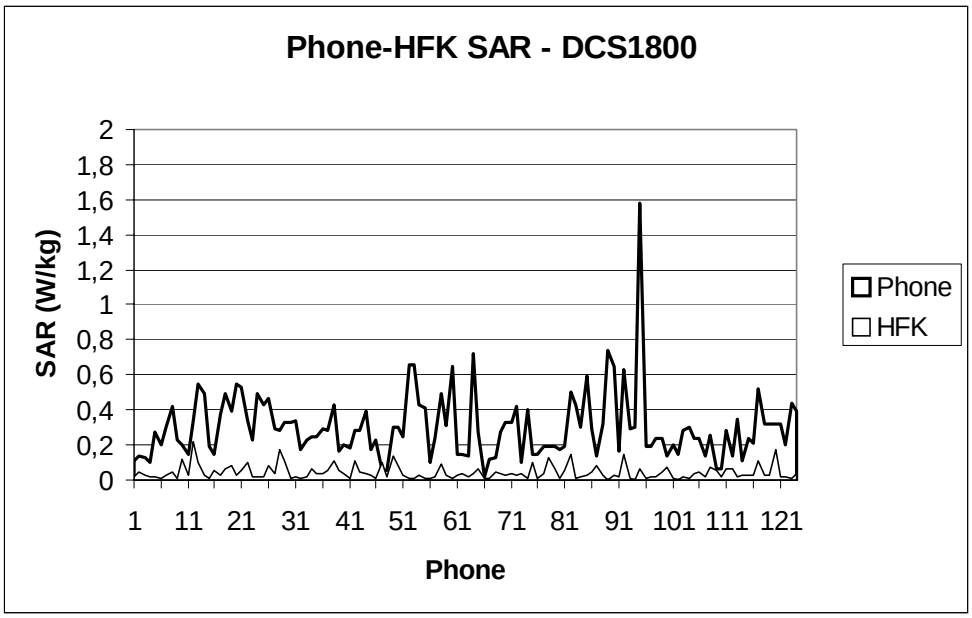

Figure 3.b: Maximum SAR values obtained in DCS1800 frequency band function of mobile phone number.

The measurement results have been analysed. Table 1 and fig 4.a and b show the repartition of the SAR values obtained for GSM900 and DCS1800 frequency bands.

	Handset		HFK	
Freq.band	GSM900	DCS1800	GSM900	DCS1800
Mean value	0.62	0.30	0.12	0.044
Standard deviation	0.23	0.19	0.088	0.041
Max.value	1.2	1.6	0.43	0.22
Min.value	0.17	0.018	0.006	0.001

Table 1: Maximum, minimum and mean value for SAR measurement results (W/kg). These values are taken on the different mobile phones.

For the handset SAR, GSM900 frequency band values are larger than DCS1800 frequency band values, in about a 2 to 1 ratio (the emitted power ratio). Phone SAR values are hardly larger than HFK SAR values with a ratio larger than 10.
The table 2 presents the phone proportion giving the maximum phone or HFK SAR value in the GSM900 or DCS1800 frequency band.

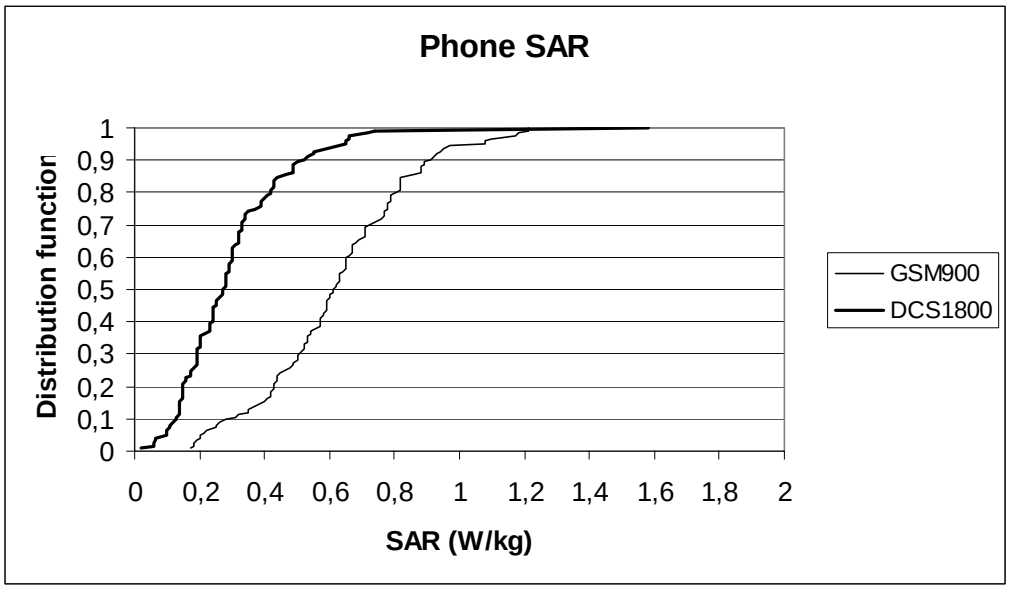

Fig. 4.a. Mobile phones SAR distribution function.

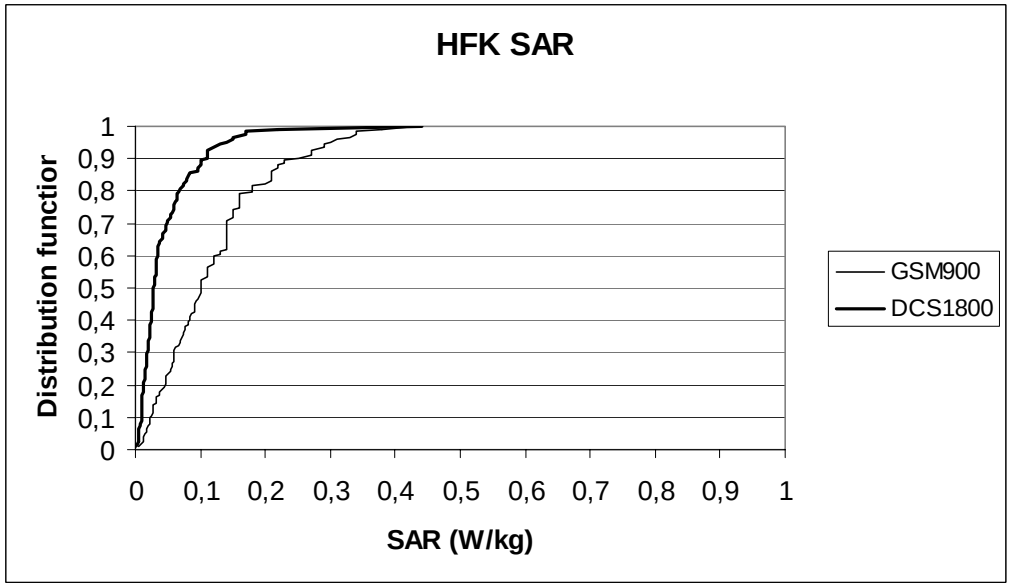

Figure 4.b: HFK SAR distribution function.

Freq. band	GSM900	DCS1800
Max. phone SAR	96%	4%
Max.HFK SAR	84%	16%

Table 2: Phones and HFK percentage giving the maximum phone or HFK SAR value in the corresponding frequency band.

A large majority of phones have their maximum phone and HFK SAR values for the GSM900 band, due to the two time higher emitted power.

SAR Reduction factor due to HFK

To evaluate the impact of HFK use on user head exposition, we have calculated the SAR reduction factor, which is the ratio of the handset SAR value and the HFK SAR value for a given frequency band. Table 3 and figure 5 present the SAR reduction factor value repartition obtained from the measurements.

The SAR reduction factor is very significant: the mean value is 11.2 for GSM900 frequency band and 17.4 for DCS1800 band. It can reach 103 and 300 respectively for GSM900 and DCS1800. For one handset, a PDA one, there is no SAR reduction and the SAR reduction factor is 0.63 for GSM900 and 0.36 for DCS1800.

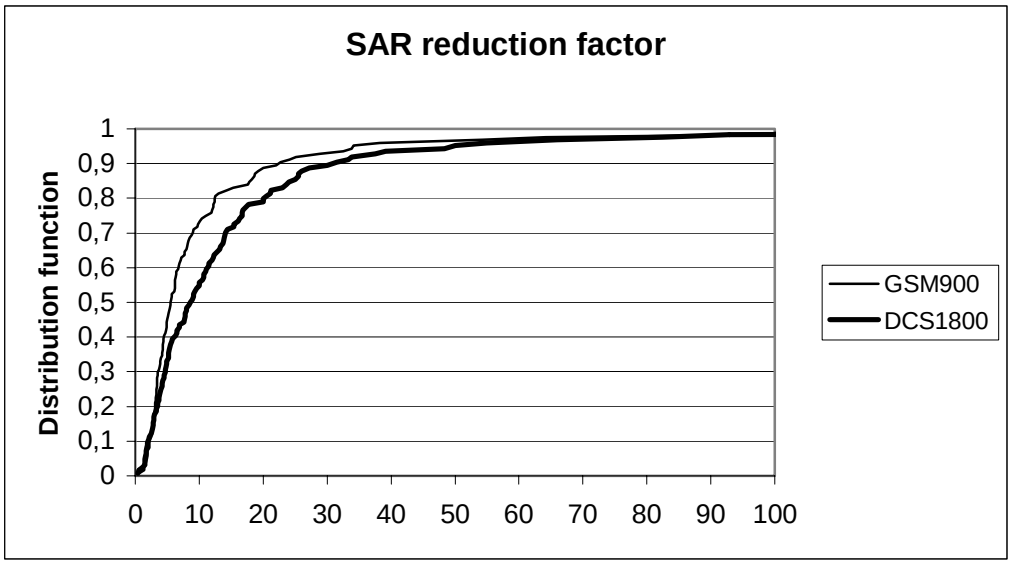

Figure 5: SAR reduction factor distribution function.

Freq. band	GSM900	DCS1800
Mean value	11.2	17.5
Standard deviation	17.2	36.2
Max. value	102	300
Min. value	0.63	0.57

Table 4: Maximum, minimum and mean value for SAR reduction factor. These values are taken on the different mobile phones.

Relation between Handset SAR and HFK SAR

For HFK SAR interpretation we have compared handset and HFK SAR values for each mobile phone. This comparison is done in figures 6.a and b.

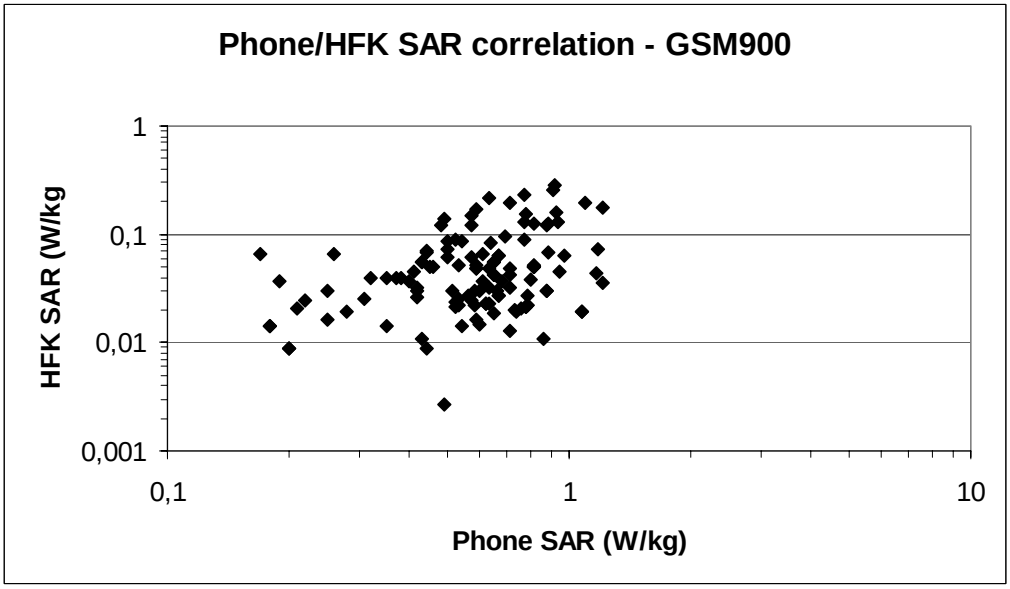

Fig. 6.a. Correlation between phone and HFK SAR values for GSM900 frequency band.

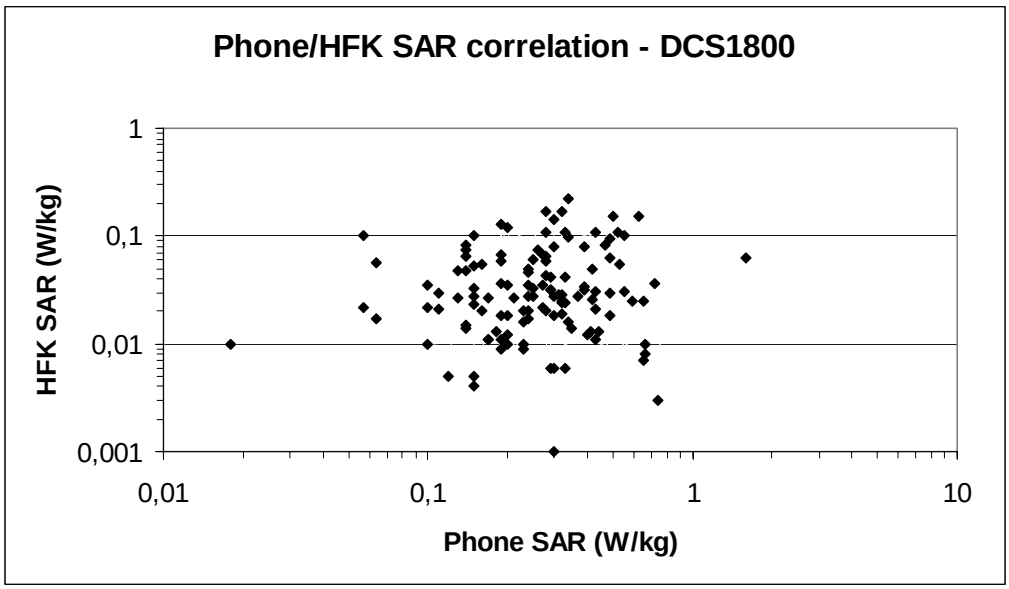

Fig. 6.b. Correlation between phone and HFK SAR values for DCS1800 frequency band.

The correlation between phone and HFK SAR values are low, especially for DCS1800 frequency band.

Relation between Handset SAR and SAR reduction factor

The same method has been applied to handset and HFK SAR reduction factor comparison. The figures 7a and b show this comparison.

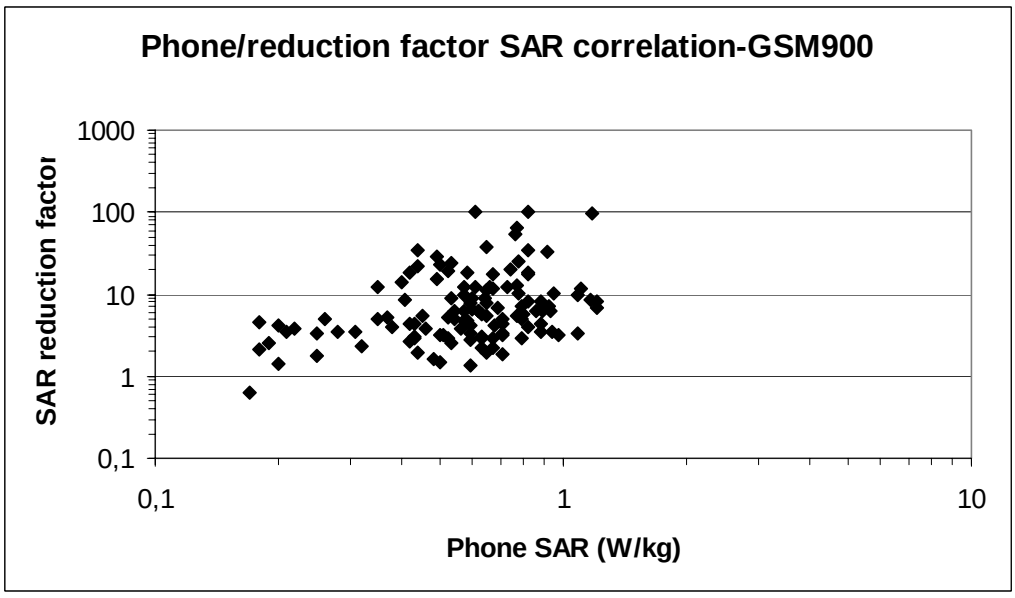

Figure 7a: Correlation between phone SAR and SAR reduction factor values for GSM900 frequency band.

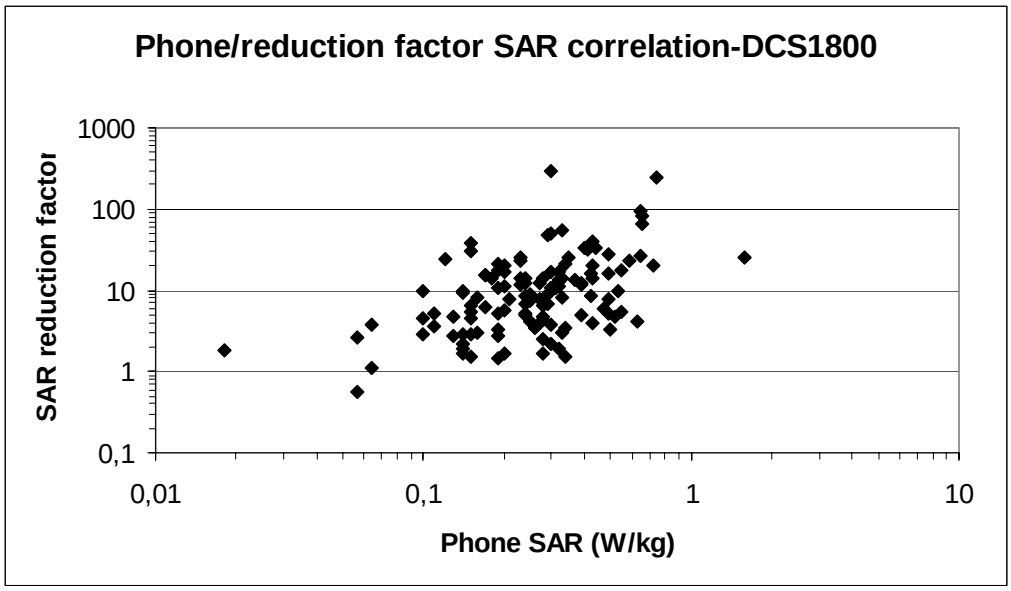

Figure 7b: Correlation between phone SAR and SAR reduction factor values for DCS1800 frequency band.

SAR reduction factor and phone SAR are also moderately correlated, but the lower values of SAR reduction factor corresponds to lower value of SAR phone values and higher values of SAR reduction factor corresponds to higher value of SAR phone values.

Conclusion

The use of HFK decreases significantly the phone user head exposition with a factor larger than 11 for GSM900 frequency band and 17 for DCS1800. There is quite no correlation between the phone SAR and the HFK SAR. HFK SAR are relatively low but not absolutely negligible. Consequently, it is interesting to measure systematically HFK SAR and to study it. We are now working to a new HFK dosimetry protocol in the french RNRT research program Adonis. Mobile phones manufacturers have also to consider this problem for HFK SAR reduction.

This research was sponsored by the french operator Bouygues Telecom.

References

1. S. E. Troulis, W. G. Scanlon, N. E. Evans, 2003, 'Effect of a hands-free wire on SAR for a waist-mounted 1.8GHz cellular telephone handset', Phys. Med. Biol., Vol.48, pp1675-1684.
2. D. Picard, A. Ziyyat, J. Ch. Bolomey, September 2001, 'Improvement of SAR measurement sensitivity on TDMA phones with detected E-field probes', 5th EBEA Conferences, Helsinki Finland.

SARMETER: AN EFFICIENT TOOL FOR MOBILE PHONE REAL EXPOSURE OF THE USER HEAD EVALUATION

D. PICARD[(1)] , S. CHAUVIN[(2)]

(1) DRE - SUPELEC- 3 RUE JOLIOT CURIE - 91192 GIF SUR YVETTE - FRANCE - dominique.picard@supelec.fr

(2) DIRECTION FREQUENCES ET PROTECTION - BOUYGUES TELECOM - 1, PLACE ABEL GANCE - 92640 BOULOGNE BILLANCOURT - FRANCE - sechauvi@bouyguestelecom.fr

Abstract

The real exposure to the RF radiation of a given mobile phone depends upon several parameters: emitted power level, TDMA pulses density, position of the handset, frequency bandwidth... The normative value for the SAR corresponds only to a given configuration at maximum power. The emitted power of a mobile phone can vary over a 30dB dynamic range due to Power Control (PWC). For GSM, when no information has to be transmitted, the TDMA pulses density can decrease with a factor 10 or more. The result of this is the potential variation of the mean emitted power of a mobile phone over a dynamic range larger than 40dB. Then the real SAR value can be significantly lower than the normative value.

The SAR meter performs real time in situ measurements of mobile phone radiated power, allowing the evaluation of the real exposure of the user head. This set up is portable and consists of a sensor, a receiver and a laptop microcomputer which performs data acquisition, signal processing and results visualization. A lot of measurements have been made and the order of magnitude of the real emitted power of mobile phones has been evaluated.

Introduction

The real exposure to the RF radiation of a given mobile phone depends upon several parameters: emitted power, TDMA pulses density, position of the handset, frequency bandwidth... The normative value for the SAR (EN50361) corresponds only to a given configuration at maximum power. The emitted power of a mobile phone can vary over a 30dB dynamic range due to Power Control (PWC). For GSM when no information has to be transmitted, the TDMA pulses density can decrease with a factor 10 or more. The result of this is the potential variation of mean emitted power of a mobile phone over a dynamic range larger than 40dB.

Real exposure

This paper describes a device allowing the evaluation of real mobile phones exposure of the user head. The principle of this device is to analyse the signal transmitted by the phone antenna by the mean of a low perturbing reception antenna. The received power is proportional to the phone emitted power. At the beginning of the communication the power is maximum (P_{max}), and we can use this value to normalize the emitted power (P) at a given time. Then, we obtain a reduction coefficient on the emitted power (C_{rp}).

$$C_{rp} = P/P_{max}$$

When all the TDMA pulses are present, their frequency is F_{max}=209Hz. This value allows the normalisation of the real frequency (F) of the TDMA pulses leading to the density (D) of the TDMA pulses.

$$D = F/F_{max}$$

In these conditions the mean emitted power (P_m) is decreased with a factor C_{rmp} in comparison with the maximum mean emitted power (P_{mmax})

$$C_{rmp} = P_m/P_{mmax} = C_{rp}\, D$$

The SAR is proportional to the mean emitted power and C_{rmp} is also the reduction coefficient on the SAR.

The device

The device consists in the low perturbation antenna, a specific receiver and a laptop micro computer [1]. The weight of the receiver and the antenna is about 1kg. The receiver uses 4 different channels: one wideband channel and 3 selective channels corresponding to GSM900, DCS1800 and UMTS frequency bands (figure 1). Each channel uses a detector followed by a low noise and high stability amplifier. The receiver dynamic range is

larger than 45dB. The antenna is a resistive loaded dipole. The sensitivity variation of this antenna in function of frequency is about 3dB. The figure 2 shows the antenna output signal corresponding to 11 different mobile phones emitting at the maximum power level in the GSM900 and DCS1800 frequency bands. The power variation of this signal in function of mobile phones is less than 10dB for each frequency band and less than 15dB for the two frequency bands.

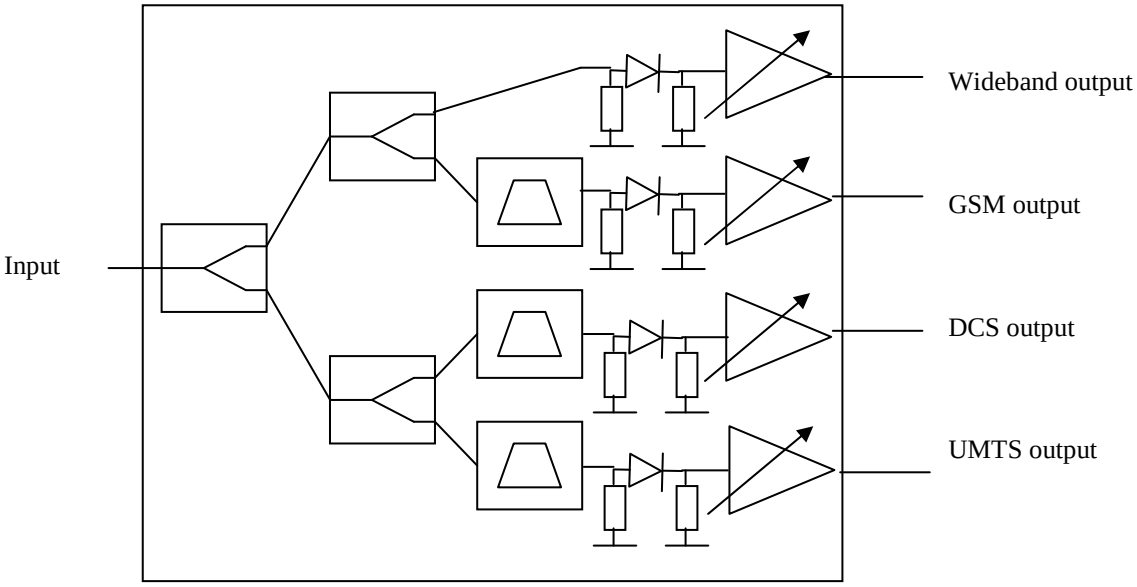

Figure 1: Receiver: overview with its four ways..

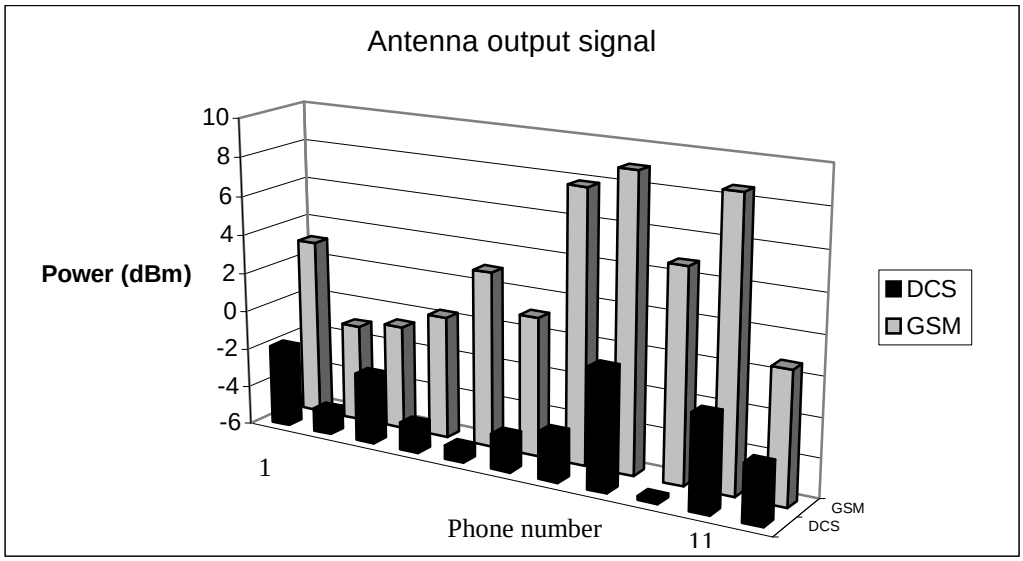

Figure 2: Antenna output signal corresponding to 11 different mobile phones for the GSM900 and DCS1800 frequency bands.

The laptop micro computer performs data acquisition and processing, with a specific software which has been developed with National Instrument Labview development system (figure 3). The power is measured on the broadband channel. Then, the reduction coefficient on the emitted power, the pulse density and the reduction coefficient on the mean emitted power, for a given duration are calculated. These three coefficients are displayed in real time during the measurement. The comparison between the different selective channels signals allows the determination of the used frequency band. The measured power and the frequency band are written in a file for each TDMA period for all the measurement duration. The figure 4 presents the entire SARmeter.

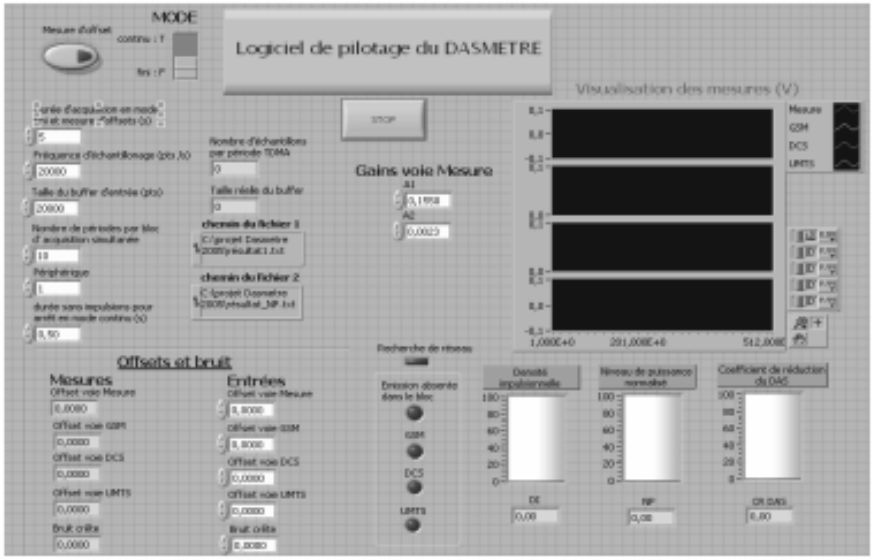

Figure 3 : Window of the SARmeter software.

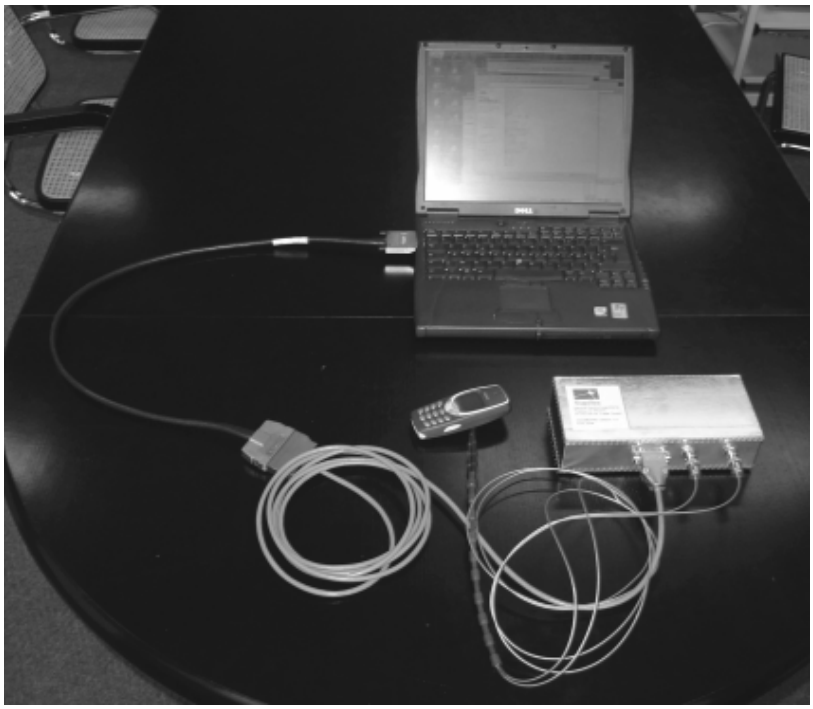

Figure 4: The SARmeter.

Result example

The figure 5 shows the variation of the emitted power in function of time for a pedestrian user on the Montparnasse Street in Paris [2]. The dynamic range of the emitted power is about 30dB and it is possible to see the different used power levels.

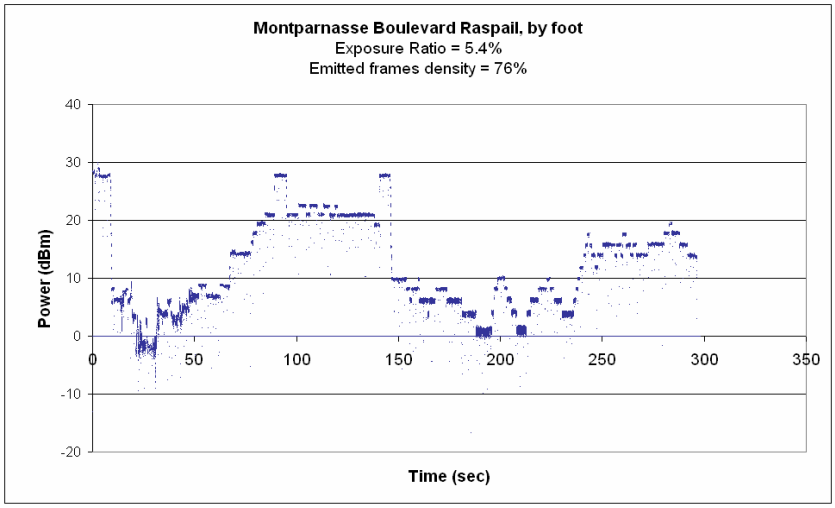

Figure 5: Example of measurement result: variation of emitted power in function of time.

Conclusion

Real exposure to RF radiation of mobile phone may hardly differ from normative SAR value. The SARmeter constitutes an efficient portable tool to determine in situ real exposure. Its use allows especially the real exposure comparison between several different networks or mobiles phones.

This research was sponsored by the french operator Bouygues Telecom.

References

[1] R. Veysset, D. Picard, S. Chauvin, 'Dispositif de determination des variations du DAS (Débit d'Absorption Spécifique) d'un mobile en communication', European Patent n°04292037.1-2411, 11.08.2004

[2] P. Le Duigou, S. Chauvin, D. Picard, R. Veysset, 'Assessment of user's exposure to GSM mobile phones emissions with the SARmeter, *BEMS 2005*, Bioelectromagnetics Society, Dublin, June 2005.

ELECTROMAGNETIC COMPATIBILITY BETWEEN SIMULATED GSM BASE STATION AT 1800 MHZ AND EEG SIGNALS.

PRAGIATIS LAZAROS[1], SOTIRIOU APOSTOLOS[1], NANOU ELENA[1], KAPARELIOTIS EVANGELOS[1], TSIAFAKIS VASILEIOS[1], PAPAGEORGIOU CHARALABOS[2], CAPSALIS CHRISTOS[1]

[1] NATIONAL TECHNICAL UNIVERSITY OF ATHENS, DEPARTMENT OF ELECTRICAL ENGINEERING, DIVISION OF INFORMATION TRANSMISSION SYSTEMS AND MATERIAL TECHNOLOGY, GREECE

[2] DEPARTMENT OF PSYCHIATRY, EGINITION HOSPITAL, UNIVERSITY OF ATHENS, GREECE

9 IROON POLYTECNEIOY STR., ATHENS, GREECE, 15773, Tel: ++30210-7722574, Fax: ++30210-7723520, email:laz_pra@mail.ntua.gr

Abstract

The current experiment studies the EMC issue that occurs when a simulated GSM base station is situated in the area where an electroencefalographer is functioning.

The experimental setup was situated in an anechoic chamber so that no electromagnetic interference would affect the measurements. The amplifier room, outside the anechoic room, situated the other part of the experimental apparatus. 32 electrodes entered a low-pass filter placed at the boundary wall of the Faraday screen room. The signal was amplified, before entering a 32-bit analogue to digital converter. The recording frequency was at 1 kHz.

The simulated GSM base station operated at the frequency of 1800 MHz emitting a GSM signal at the EIRP of 17dbm. The used piece of equipment is generally called DAS (Distributed Antenna Signal) and is used to simulate the signal emitted by one of the antennas of a GSM base station or for indoor coverage.

The results showed that the measured signals are significantly different both in frequency and in energy context.

Introduction

Issues regarding electromagnetic interference and medical devices continue to be popular topics in the technical world of electromagnetic interference. Reports of medical device failure from electromagnetic interference have increased [1, 2, 3]. This is due to the increasing number of electronically controlled medical devices in hospitals as well as the increasing number of the radiofrequency (RF) sources of radiation. The modern instruments are often more sensitive to electromagnetic interference (EMI) because they incorporate low power integrated electronic circuitry that can be much more sensitive to electromagnetic fields than their electrical and electromechanical predecessors. Digital wireless communications systems often utilize pulsed amplitude modulation, a type of modulation that can enhance the potential for EMI.

The European Union has gotten much of attention with regard to the regulation of electromagnetic compatibility (EMC) and medical electronics. Today, most medical EMC regulations originate within the International Electro technical Commission (IEC). The standard EN60601-1-2 [4] defines limits for emissions and levels of immunity and was updated to encompass the frequencies used by mobile. The IEC standard states that electronic medical equipment must operate normally in electric field intensity of 3 V/m and at a 10 V/m threshold for life – sustaining equipment.

The Electroencephalograph (EEG) is a recording equipment of brain signals with typical voltage of 100 μV and frequency range (EEG bands) beginning from 0.5 Hz up to several hundreds Hz. The EEG is connected directly to the patient in order to detect these small physiological signals which are then amplified. The EEG is known to be very sensitive to EMI due to the fact that the pulsed RF signals maybe demodulated by non-linear elements in amplifier circuits. [5].

The most recent problems of electromagnetic interference (EMI) with medical equipment arise from the widespread use of GSM signals in the hospitals [6]. Global System for Mobile communications (GSM) is an open, digital cellular technology used for transmitting mobile voice and data services in the 900MHz (890 MHz - 960 MHz) and 1.8GHz bands in Europe and Asia and the 1.9GHz PCS (Personal Communications Services) band in the US[7]. GSM uses digital technology and time division multiple access transmission methods (TDMA), which utilize schemes that produce 100% amplitude modulated pulses of the RF carrier at frequencies within the EEG frequency range. Recently, warnings have been published concerning the use of wireless communications equipment in the clinical environment. Morrisey et al. reported distortion of EEG bands throughout the 0-70 Hz range during full power exposure to CDMA and GSM signals for both frequencies of 1.800 and 1900 MHz at distances of between 0.25 to 0.5 m. [8]. Also a study by Tri et al. of Mayo Clinic revealed increase of the noise of the EEG waveform measured in the presence of a GSM signal [9].

Taking into account the above considerations, in our current work, we study the EMC status that involves the usage of an electroencephalograph in an environment infested with electromagnetic radiation produced by a GSM base station. The purpose is to observe the effects of the GSM signal on the EEG signal.

Materials and Methods

The experimental setup (Fig 1) was situated in a Faraday chamber so that no electromagnetic interference would affect the measurements. A head phantom was placed in the chamber and the signals were recorded from thirty two electrodes (Fp1, Fp2, Fpz, AFz, F2, F3, F4, F7, F8, FC1, FC2, FC5, FC6, C2, C3, C4, A1, A2, CP1, CP2, CP5, CP6, P3, P4, Pz, T3, T4, T5, T6, O1, O2,Oz) with a surface of Ag/ AgCl, which were placed on the scalp of the model-head. The electrodes were positioned according to the International 10-20 system of electroencephalography [10]. The measured magnitude was the voltage at the edges of a 2 kΩ resistance placed between each electrode and a common ground. The total electrode impedances were below 5 kΩ. The amplifier room, outside the Faraday room, situated the other part of the experimental apparatus. The electrodes entered a low-pass filter placed at the boundary wall of the Faraday screen room. The filter cut frequencies over 35 Hz so that the signal of the power supply network which is at 50 Hz would not interfere with the signal. The signal was amplified by a Braintronics DIFF/ISO-1032 amplifier, before entering a 32- bit analogue to digital converter which has a GPIB output. The digitized signal comprises an input for a Data Acquisition Card. The PC with the DAQ Card ran a LabView program for the recording of the signals, which can be monitored by an on-screen graphical representation. The recording frequency was at 1 kHz. Another PC, connected with the one described above, ran a program which triggered the other PC to save the brain signals

whenever the user wanted .The recording time was 1.5 sec so the saved signal consisted of 1500 values. The total task consisted of 55 repetitions.

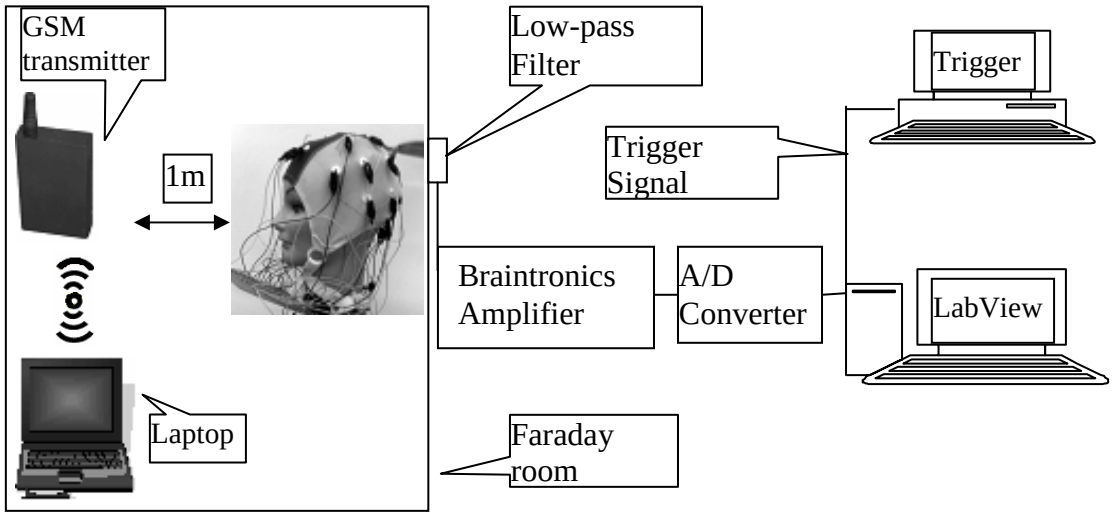

Figure 1. Experimental setup

A GSM TEMS Transmitter was placed at a distance of 1m from the head phantom. The GSM TEMS Transmitter was used to simulate the indoor coverage of a GSM base station within a cellular network. The GSM TEMS Transmitter sends out Frequency Correction Channel (FCCH), Synchronisation Channel (SCH) and optionally Broadcast Control Channel (BCCH) and Paging Channel (PCH) signaling, on a GSM carrier of human voice (900 MHz or 1800 MHz band). Prior to taking a measurement, the instrument was calibrated and adjusted. Scanning of the radio spectrum was performed in order to find a channel suitable for transmission. The Transmitter was equipped with four attenuators (3dB, 6dB, 10dB and 20 dB) suitable to connect between the Transmitter and an external antenna used with it. By combining the attenuators in all possible ways, output power levels from 17 dBm down to -22 dBm can be achieved. At the experiment the power level of 17dBm and frequency 1812,8 MHz (Absolute Radio Frequency Channel Number 550) was applied.

The electromagnetic field strength at the point where the head phantom was situated was 1,6 V/m.

The experimental procedure was done twice. The first time the GSM base station was off and practically the noise of the device was measured and the second time the GSM base station was functioning.

Finally in order to optimize the signal to noise ratio (SNR) the grand average across the 55 repetitions for each channel was calculated according to the following equation:

$$\overline{V_t} = \frac{1}{55} * \sum_{j=1}^{55} V_{jt}$$

Where Vjt is the value that results after the subtraction of the amplification and the average referencing and corresponds at the time t of the trial j .This SNR optimization procedure is considered a standard practice when it comes to brain signal measurements, which are generally considered to be quite noisy [11].

The final data for analysis for each radiation condition consisted of 1500 amplitude values for each electrode, expressed in μVolts corresponding to the 1500 msec of the time period as described above.
For each electrode, the following magnitudes were also calculated:

- the energy E of the recorded signals ($E=V_t^2$)
- the amplitude in the frequency domain by using the Fourier Transform (FFT).

Statistical analysis

The amplitudes at the thirty two electrodes were subjected to Independent Samples t-test for the two radiation conditions (GSM off – GSM on). The mean values of the amplitudes for each electrode and radiation condition were also calculated. Statistical significance was set at 0.05.

Results

The data analysis showed that the energy of the recorded signals was significantly increased when the GSM Transmitter was operating. Figure 2 shows this increase at all electrodes except the C3 electrode. The white bars denote the calculated energy in the absence of the GSM signal while the black bars denote the signal energy in the presence of the GSM signal.

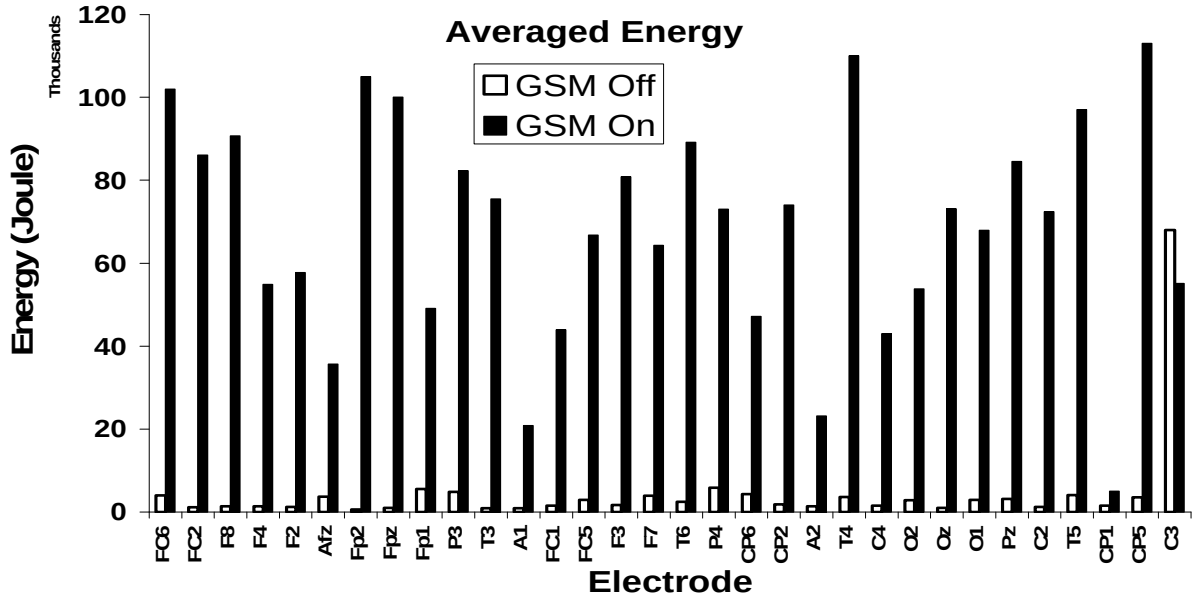

Figure 2. Averaged Energy at each electrode and each radiation condition. . The white bars denote the calculated energy in the absence of the GSM signal while the black bars denote the signal energy in the presence of the GSM signal.

The statistical analysis revealed that the presence of the GSM signal had significant effect on the amplitudes of the signals at the thirty two leads. Table 1 is quite helpful in explaining this effect, showing the mean values of the recorded signals at each electrode for the two radiation conditions.

Electrodes		**Mean Values**	
Number	**Name**	**GSM off**	**GSM on**
1	FC6	-1.61	8.25
2	FC2	-0.85	7.57
3	F8	-0.95	7.77
4	F4	-0.95	6.05
5	F2	-0.90	6.20
6	AFz	-1.55	4.87
7	Fp2	-0.59	8.38
8	Fpz	-0.78	8.18
9	Fp1	-1.90	5.72
10	P3	-1.78	7.41
11	T3	-0.76	7.09
12	A1	-0.77	3.72
13	FC1	-0.99	5.41
14	FC5	-1.36	6.67
15	F3	-1.03	7.34
16	F7	-1.59	6.55
17	T6	-1.27	7.71
18	P4	-1.94	6.97
19	CP6	-1.68	5.60
20	CP2	-1.07	7.02
21	A2	-0.95	3.92

22	T4	-1.54	8.57
23	C4	-0.99	5.35
24	O2	-1.35	5.99
25	Oz	-0.79	6.98
26	O1	-1.38	6.73
27	Pz	-1.42	7.50
28	C2	-0.89	6.95
29	T5	-1.63	8.04
30	CP1	-0.99	-1.73
31	CP5	-1.50	8.69
32	C3	-6.72	6.06

Table 1. Mean values of the amplitudes of the recorded signals for each electrode for the two radiation conditions.

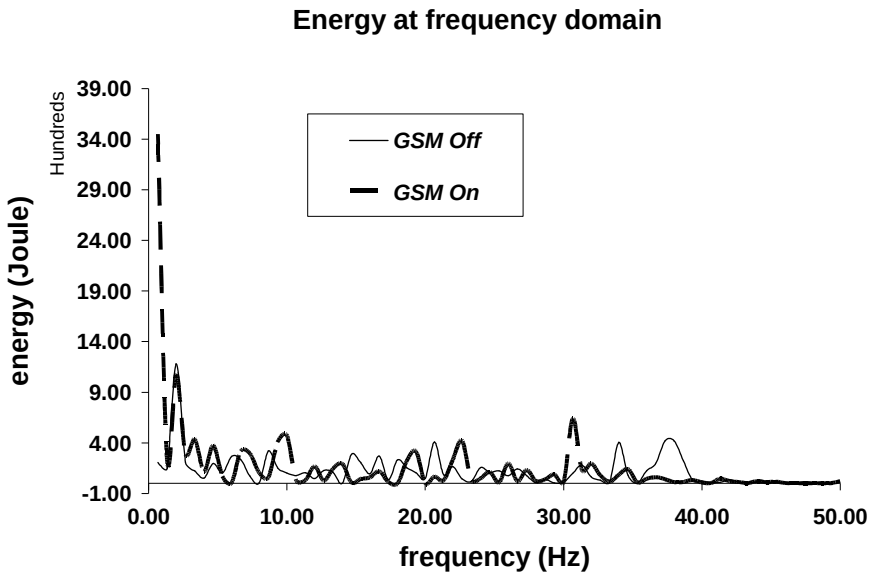

Figure 3. Calculated Energy of F8 electrode at frequency domain. The thin continuous black line denotes the calculated energy in the absence of the GSM signal while the discontinuous denotes the signal energy in the presence of the GSM signal.

Except the regarded increase of the amplitudes of the recorded signals in the time domain, the FFT calculation revealed that there was also a change in the frequency domain. A spike of the energy at the span of 1-2 Hz is observed in all electrodes. Figure 3 shows indicatory this fact at one of the 32 electrodes

Discussion

In the present study we focused on the electromagnetic interference of a GSM base station might on an electroencephalograph. The results of this study revealed that in the presence of radiation of the GSM transmitter the energy of the recorded signals was in average 38 times higher than the energy calculated in the absence of radiation. Also an alteration at the frequency domain was observed at the presence of GSM signal.

These effects are very important in view of the fact that the EEG energy as well as the frequency bands are magnitudes evaluated by doctors and related to brain activity [12, 13, 14, 15] so it is absolutely necessary to be measured accurately in order to achieve the right diagnosis.

These findings are similar to those reported by Morrisey et al [8] where distortion of EEG bands was observed. Also the studies of Sibakov and Appelqvist (1998) [16], Barbaro et al. (2000) [17], and Hietanen et al. (2000) [18] referred device sensitivity. However these findings were observed at the presence of GSM signals with higher power and at closer distance than this applied to our experiment. This is rather worrying, because EMI problems occurred even with less electromagnetic field strength.

It should be noted that although the testing was performed in a shielded environment, this doesn't exclude the influence of the measurements by some factors, such as coupling between electrodes and the presence of radiation reflecting or absorbing objects in the neighbouring area.

Moreover the source of radiation had constantly 17dBm power. This factor has to be taken into account in studies about EMI of GSM signals on Medical Equipment because most studies refer to GSM cell phones which are designed to quickly reduce their power when the channel paging stops.

According to our findings it seems that the distance of 1m and the 17dBm signal power are not sufficient to protect an electroencephalograph from EMI of GSM signals. The indoor GSM base stations are necessary inside buildings as relay stations. However before installing such a communication system an EMI study is essential in order to ensure the immunity of the medical equipment. The efficient distances of the base stations from the devices must be kept so that the electromagnetic field (EMF) power and field levels would be under the recommended values [19]. Technology does exist to protect or "harden" medical devices from radiation emissions including shielding, grounding, and filtering. These modifications are not always costly and are even less problematic if incorporated by the manufacturer during assembly.

EMC is a concern not just for manufacturers, but also for those who install, use, modify or maintain medical equipment. The existence of directives and standards has encouraged good EMC design practices, but should not be relied on to prevent EMI problems owing to the nature of the hospital electromagnetic environment. Mobile telecommunication systems are very convenient and useful to doctors, nurses and patients and studies must be done to promote awareness of EMI and its underlying coupling mechanisms.

References

1. Silberberg JL: Performance degradation of electronic medical devices due to electromagnetic interference. Compliance Eng 10(5):25-39, 1993.

2. Joyner K, Anderson V, Wood M: Interference and energy deposition rates from digital mobile phones. In: Abstracts Annual Meeting of the Bioelectromagnetics Society 16:67-68, 1994

3. Silberberg JL: Medical device electromagnetic interference issues, problem reports, standards, and recommendations. In: Proc Health Canada Medical Devices Bureau Round-Table Discussion on Electromagnetic Compatibility in Health Care, Ottawa, Canada, pp. 11-20, 1994.

4. International Electrotechnical Commission, "IEC 60601-1-2, Medical Electrical Equipment Part 1: General Requirements for Safety, Amendment No. 2. Collateral Standard: Electromagnetic Compatibility—Requirements and Tests," 1st ed., Geneva, 1993.

5. M P Robinson, D Bozec and C A Marshman, "Healthcare Engineering and Electromagnetic Compatibility", Healthcare Engineering: Latest Developments and Applications; I Mech E, London, 25-26 Nov 2003

6. Kok-Swang Tan Hinberg, "I.Radiofrequency susceptibility tests on medical equipment. Engineering in Medicine and Biology Society", 1994.

7. Wireless Intelligence 06/07/06. Also available at http://www.gsmworld.com/technology/what.shtml

8. Morrissey, Joseph James; Swicord, Mays; Balzano, Quirino, "CHARACTERIZATION OF ELECTROMAGNETIC INTERFERENCE OF MEDICAL DEVICES IN THE HOSPITAL DUE TO CELL PHONES", Health Physics. 82(1):45-51, January 2002

9. Jeffrey L. Tri, Rodney P. Severson, Allen R. Firl, David L. Hayes, and John P. Abenstein, "Cellular telephone interference with medical equipment" mayo clinic proceedings, October 005;80(10):1286-1290, 2005

10. Jasper H. The ten-twenty electrode system of the international federation. Electroencephalogr Clin

Neurophysiol, 1958

11. Roth, W.T., Ford, J.M., Pfefferbaum, A. and Elbert, T.R. Methodological issues in event-related potential and magnetic field studies. Chapter 78 in Psychopharmacology: The Fourth Generation of Progress, F.E. Bloom and D.J. Kupfer (Eds.), pp. 895-910. New York, NY: Raven Press, 1995

12. Chang PF, Arendt-Nielsen L and Chen AC. "Dynamic changes and spatial correlation of EEG activities during cold pressor test in man." Brain Res Bull 57:667–675, 2002

13. Fisch B.J.: "Fisch & Spehlmann's EEG Primer", Elsevier, 148pp, 1999

14. Epstein C.M.: "Introduction to EEG and Evoked Potentials", Lippincot Williams & Wilkins, 1983

15. Hughes J.R.: "EEG in Clinical Practise", Butterworth-Heinemann, Newton,15pp, 1994

16. Sibakov, V.; Appelqvist, M. "Immunity of medical electronic devices to electromagnetic field of cellular mobile hones."Helsinki, Finland: VTT Technical Research Center; VTT Tiedotteit Research Bulletin; 1998.

17. Barbaro, V.; Bartolini, P.; Benassi, M.; Di Nallo, A. M.; Reali, L.; Valsecchi, S. "Electromagnetic interference by GSM cellular phones and UHF radios with intensive care and operating room ventilators." Biomedical Instrum. Tech. 34:361–369; 2000.

18. Hietanen, M.; Sibakov, V.; Hallfors, S.; von Nandelstadh, P. "Safe use of mobile phones in hospitals." Health Phys. 79(Suppl. 2):S77–S84; 2000.

19. D Davis, B Segal, and T Pavlasek, "Can Minimum Separation Ensure Electromagnetic Compatibility in Hospitals? An Experimental Study," Biomedical Instrumentation and Technology/Association for the Advancement of Medical Instrumentation 33, no. 5: 411- 416, 1999

NUMERICAL DETERMINATION OF TRANSMEMBRANE VOLTAGE INDUCED ON IRREGULARLY SHAPED CELLS

GORAZD PUCIHAR, TADEJ KOTNIK, BLAŽ VALIČ, DAMIJAN MIKLAVČIČ

Faculty of Electrical Engineering, University of Ljubljana, Tržaška 25, SI-1000, Ljubljana, Slovenia.

e-mail: gorazd.pucihar@fe.uni-lj.si, tadej.kotnik@fe.uni-lj.si, blaz.valic@fe.uni-lj.si, damijan.miklavcic@fe.uni-lj.si

Abstract

The paper presents an approach that reduces several difficulties related to the determination of induced transmembrane voltage (ITV) on irregularly shaped cells. We first describe a method for constructing realistic models of irregularly shaped cells based on microscopic imaging. This provides a possibility to determine the ITV on the same cells on which an experiment is carried out, and can be of considerable importance in understanding and interpretation of the data. We also show how the finite-thickness, nonzero-conductivity membrane can be replaced by a boundary condition in which a specific surface conductivity is assigned to the interface between the cell interior (the cytoplasm) and the exterior. We verify the results obtained using this method by a comparison with the analytical solution for an isolated spherical cell, obtaining a very good agreement. In addition, we compare the ITV computed for a model of an irregularly shaped CHO cell with the ITV measured on the same cell by means of a potentiometric fluorescent dye. Finally we confirm that electropermeabilization occurs in those areas of cell membrane, where the absolute value of ITV is the highest.

1. Introduction

Induced transmembrane voltage (ITV) forms on the cell membrane when the cell is exposed to the external electric field [1-3]. The ITV is proportional to the amplitude of electric field and with a sufficiently strong field, a sudden increase in membrane permeability occurs, a phenomenon termed electropermeabilization. During the state of high permeability it is possible to deliver membrane impermeant ions and molecules into the cell.

In many applications of electropermeabilization an efficient and at the same time reversible permeabilization is essential (e.g. DNA electrotransfer [4-6]). Thus, a careful planning of the experiment, which involves the estimation of the amplitude of ITV leading to cell permeabilization, is required. It was demonstrated experimentally that ITV determines the regions of the membrane where electropermeabilization occurs [1, 2]. Namely, increased permeability is observed only in regions of the membrane where ITV exceeds a critical value. As already stated ITV is proportional to the electric field, varies with the position on the cell membrane, and is influenced by cell geometry and physiological characteristics of the medium surrounding the cell [3, 7-10]. For an isolated cell of simple shape, such as a cylinder, a sphere, or an ellipsoid, ITV can be described analytically [3, 8, 11 – 14]. However, when cell geometry is more complicated (e.g. cells in tissues) an analytical description is in general not attainable and ITV can be determined either experimentally [15-20] or numerically [21-28].

Usually, numerical models are constructed using simple geometrical shapes, e.g. hemi-spheres, hemi-ellipsoids or combination of simple shapes [22, 23, 28, 29]. These models can be realistic for cells in suspensions, but cells growing in a dish or in tissues typically have profoundly irregular shapes, and combinations of several simple geometrical objects are not usable anymore. In this study, we present a method for construction of more realistic models of irregularly shaped cells from their cross-section images. We also present a method to replace a cell membrane in the model with a boundary condition. We then calculate the ITV on the model of an irregularly shaped cell and compare it to the ITV determined experimentally by means of fluorescent dye. In addition, the course of permeabilization of this cell is monitored and regions of membrane where permeabilization occurred are determined.

2. Methods

2.1 Construction of a three-dimensional model of a cell

Three-dimensional models of irregularly shaped cells were constructed from a sequence of microscopic fluorescence images representing cross-sections of a cell attached to the cover glass. The models presented in the study were built from CHO cells, but the method can also be applied to other cell types. Fluorescence images were obtained by staining the cell with a fluorescent dye di-8-ANEPPS. The dye emits a strong fluorescence when it binds to the membrane, therefore making the cell edges visible. The cross-sections were obtained by shifting the focus on a fluorescence microscope (Zeiss AxioVert 200, objective ×100, oil immersion, Zeiss, Germany) in constant steps of 2 μm from the bottom to the top of the cell (Figure 1A). The images were acquired using a cooled CCD camera (VisiCam 1280, Visitron, Germany) and MetaMorph 5.0 software (Visitron, Germany), and converted from grayscale (8 bit) to black and white (1 bit, Figure 1B) in Corel PhotoPaint 11.0 (Corel Corp., Ottawa, Canada). Using FEMLAB 3.1 package (COMSOL Inc., Burlington, MA, USA) with MATLAB 6.5 (MathWorks Inc., Natick, MA, USA), the contours of the cell were detected using *flim2curve* (Figure 1C), transformed to solid planes with 35 edges with *solid2*, and the planes were connected into a 3D object using *loft* to obtain the model of the cell. This model was then imported to the FEMLAB workspace, where it was positioned to the bottom of a rectangular block, thereby mimicking the cell attached with its bottom to the cover glass (Figure 1D). To construct a model of several cells, or a cell cluster, this procedure is repeated for each cell separately [30]. In case of a cell cluster, individual cells are, after they are imported to FEMLAB, merged together to form a cluster.

2.2 Modeling the cell membrane

Direct incorporation of a realistic cell membrane (i.e. a layer of very small, yet non-zero thickness surrounding the cell) into the model is technically very problematic. Unless the distribution of the electric field, current density, and/or electric potential within the membrane is of interest, this can be avoided. Namely, the effect of the membrane on these electric quantities in the cell interior and exterior is equivalent to the effect of a corresponding surface conductivity assigned to the interface between the interior and the exterior. More precisely, as the specific conductivity of the membrane – typically about 5×10^{-7} S/m [31] – is at least five orders of magnitude lower than the specific conductivities of the media surrounding it, the current flows through the membrane practically orthogonally to its surface. Consequently, in the membrane the total current density is virtually equal to its normal component alone (J), which is given by:

$$J = \frac{\sigma_m (V_o - V_i)}{d}, \tag{1}$$

where σ_m is the specific membrane conductivity, d is the membrane thickness and V_o, V_i are the electric potentials at the outer and inner surface of the membrane, respectively. Here J, V_o, and V_i are functions varying with the position on the membrane, while σ_m and d are constants. For the purpose of determining ITV, the events inside the membrane layer are not relevant, and the ratio σ_m/d can be treated as a single entity — the specific surface conductivity, $\kappa_m = \sigma_m/d$. The interface between the cell interior (the cytoplasm) and the cell exterior is then characterized by

$$J = \kappa_m (V_o - V_i). \tag{2}$$

Despite the membrane as such being absent from the model, the drop of electric potential at such an interface is equivalent to ITV on a membrane with a specific conductivity σ_m and thickness d. In models constructed in this way, the mesh of finite elements is generated without difficulty, as very small elements corresponding to the membrane itself are avoided [30].

2.3 Settings of the model and subsequent computations of induced transmembrane voltage

The computation of the functions J, V_o and V_i was performed in FEMLAB by introducing two application modes, the cell exterior (extracellular medium) being active in the first, and the cell interior (cytoplasm) in the second mode. Both application modes were of a static current density type. For models containing several cells, an additional application mode active in the cytoplasm of each cell must be introduced, and the functions J_1, J_2, ... and V_o, V_{i1}, V_{i2}, ... are then computed.

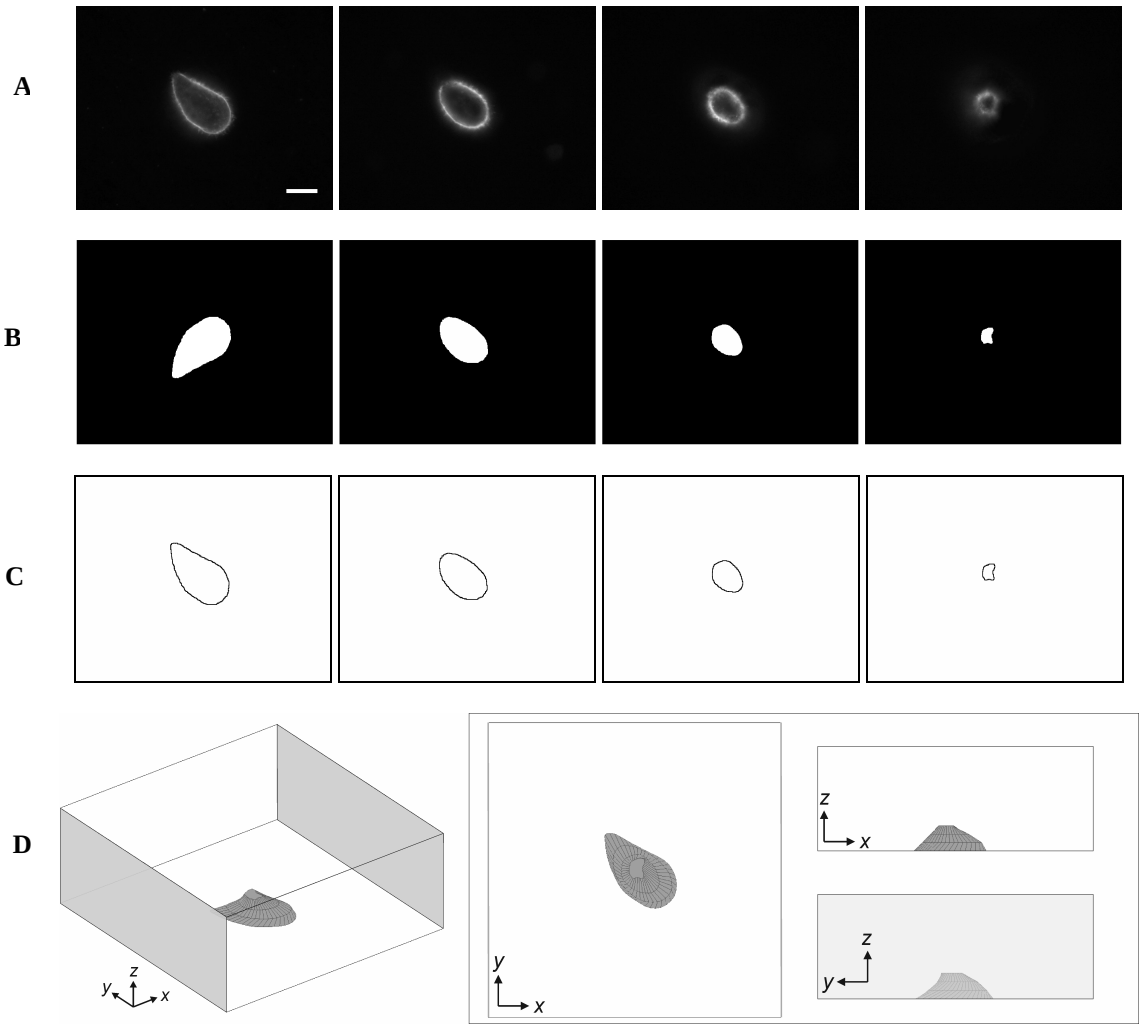

Figure 1. Construction of a 3D model of an irregularly shaped CHO cell. (A) Fluorescence images (8 bit) of an irregularly shaped CHO cell stained with di-8-ANEPPS. The images represent four cross-sections of the cell, acquired from bottom to the top of the cell in 2 µm steps. Bar represents 10 µm. (B) Black and white (1 bit) images. (C) The corresponding contour of the cell edge for a given cross-section. (D) The three-dimensional geometry of the cell model constructed from the cross-sections. The interior of the rectangular block represents the extracellular medium, the grey-shaded faces are the electrodes, and the other four faces are insulating.

The specific conductivity of the cell interior was set to 0.3 S/m [32], and the specific conductivity of the rest of the block (the cell exterior) to 0.14 S/m [33]. Two of the opposite vertical faces of the block were modeled as electrodes, which was done by assigning fixed electric potentials to both electrodes (one was usually set to ground) to obtain the voltage-to-distance ratio of 100 V/cm. The remaining four faces of the block were modeled as insulating surfaces, the bottom one representing the cover glass. At the boundary surface between the cell interior and exterior, the normal component of the current density was set corresponding to Eq. 2 with a negative sign (-*J*) in the mode corresponding to the cell exterior, and with a positive sign in the mode corresponding to the cytoplasm (or, with several cells, in all such modes). The specific surface conductivity was set at κ_m = 100 S/m^2, which is the ratio between a specific membrane conductivity of 5×10^{-7} S/m and a membrane thickness of 5 nm [34].

After the mesh was generated, the electric potential was computed using finite elements method with FEMLAB's stationary nonlinear Conjugate gradients solver with Algebraic multigrid preconditioner. ITV was calculated as the difference between electric potentials on the two sides of the boundary surface separating the inside and outside of the cell, i.e. as ITV = V_i - V_o. ITV was then plotted as a function of relative arc length.

2.4 Measurements of induced transmembrane voltage

To experimentally determine ITV we used di-8-ANEPPS, a fast potentiometric fluorescent dye. The dye binds to the cell membrane, which causes a considerable increase in its fluorescence. With the change in ITV, the fluorescence of the dye then varies linearly [15-17]. CHO K1 cells were grown on cover glasses in culture medium. Six to eight hours latter the culture medium was replaced with SMEM medium containing 30 µM of di-8-ANEPPS and 0.05% of Pluronic. After staining for 12 min at 4°C, the cells were washed thoroughly with pure SMEM to remove the excess dye. Before the experiments, SMEM was replaced with an isoosmotic pulsing buffer (10 mM K_2HPO_4/KH_2PO_4, 250 mM sucrose, 1 mM $MgCl_2$, [33]). Cells were then exposed to a voltage of 40 V applied for duration of 100 ms on two parallel wire electrodes with a 4 mm distance between them (voltage-to-distance ratio 100 V/cm). Before and during the pulse, the fluorescence image of the lowermost level of a cell or a cell cluster was acquired, with excitation at 490 nm and emission detected at 605 nm. The procedure was repeated five times, with a 2 s delay between pulses. The control image was then subtracted from the corresponding pulse image and the corrected images were averaged to increase the signal-to-noise ratio. The changes in fluorescence of the dye in the membrane were quantified by measurements of grey levels along the region of interest, which was a 5 pixel wide line encircling the cell at the site of the membrane. Using a calibration curve obtained in a separate experiment (6% of fluorescence change per 100 mV, not shown [30]), fluorescence changes were transformed to the values of ITV, which were plotted on a graph as a function of the normalized arc length. The images were acquired using the same imaging system as described in Section 2.1.

2.5. Monitoring the course of electropermeabilization

Cells (CHO K1) were grown and prepared as described in Section 2.4. Prior to experiments, the culture medium was replaced with pulsing buffer, which contained 100 µM of fluorescent dye Propidium Iodide (PI, Sigma, Saint Louis, USA). The dye is essentially membrane impermeant, but can enter the electropermeabilized cells, where its fluorescence increases significantly, making it suitable to detect electropermeabilization of cells. The electrodes were positioned to the bottom of cover glass. A 400 V, 200 µs pulse was delivered to the electrodes, and fluorescence from cells was monitored in 100 ms time steps. The imaging system was the same as described in Section 2.1.

3. Results and discussion

3.1 Validation of the model by comparison with analytical solution for a spherical cell

The method introduced in Section 2.1 was first verified by comparing the calculations of ITV on a model of a spherical cell with the analytically derived ITV for the same cell. Under physiological conditions, the ITV induced by an electric field E on a spherical cell with outer radius R is given by Schwan's equation [3]:

$$ITV = f_s E R \cos\varphi \tag{3}$$

where φ is the angle between the direction of the field and the line connecting the center of the cell to the point of interest and f_s is a function reflecting the electric and dimensional properties of the cell and the surrounding medium [8]:

$$f_s = \frac{3\lambda_o\left[3dR^2\lambda_i + \left(3d^2R - d^3\right)\left(\lambda_m - \lambda_i\right)\right]}{2R^3\left(\lambda_m + 2\lambda_o\right)\left(\lambda_m + \frac{1}{2}\lambda_i\right) - 2\left(R-d\right)^3\left(\lambda_o - \lambda_m\right)\left(\lambda_i - \lambda_m\right)} \tag{4}$$

In Eq. 4, λ_o, λ_i, and λ_m are the specific conductivities of the extracellular medium, cytoplasm and the membrane, respectively, and d is the thickness of the membrane. Schwan's equation provides a precise description of the ITV on a single spherical cell, and was as such used as the first test of the method of numerical determination of the ITV described in this paper. Figure 2B shows the ITV computed using this method and Figure 2C shows the error with respect to Schwan's equation (note that the y-scale is much smaller than in 2B). On the basis of these results we can conclude that the numerical computation of ITV using our method is sufficiently accurate for any practical purpose. Both the analytical and the numerical solution were determined for a spherical cell with R = 10 µm, λ_o = 1 S/m, λ_i = 0.2 S/m, $\lambda_m = 5 \times 10^{-7}$ S/m, and d = 5 nm. The cell was exposed to an electric field of 100 V/cm, which was, in the numerical solution, generated by applying 1 V to a pair of rectangular parallel plate electrodes 0.01 cm apart.

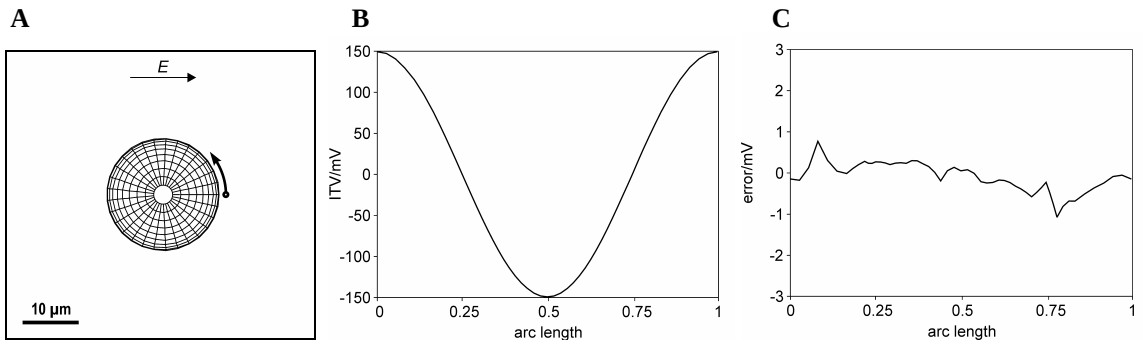

Figure 2. (A) Geometry of a spherical cell. The arrow denotes the start and the direction of the path along which the normalized arc length is measured. (B) Computed ITV for a spherical cell with a membrane modeled as a boundary condition. (C) The difference between the computed and analytically derived ITV. The calculations were performed for a spherical cell with R = 10 µm, λ_o = 1 S/m, λ_i = 0.2 S/m, $\lambda_m = 5 \times 10^{-7}$ S/m, d = 5 nm, and E = 100 V/cm.

The main advantage of replacing the cell membrane with a boundary condition is that the mesh elements corresponding to the membrane are avoided. This efficiently reduces the time for mesh generation and time needed to solve the problem. If the membrane is instead modeled explicitly, its thickness must typically be exaggerated by an order of magnitude or more, otherwise the number of mesh elements is far too large to be handled by a computer. To compensate for this, the membrane can be assigned a correspondingly higher specific conductivity [30].

3.2 Comparison with fluorescence measurements

The model of an irregularly shaped cell was constructed from four cross-sections of the cell photographed under a microscope, as described in detail in Section 2 (Figures 1A-1D). The distribution of electric potential was first computed (Figure 4A) and the ITV was than calculated as the difference between the electric potential in the cell interior and exterior. The results are, for the lowermost layer of the cell, shown in Figure 3C with dashed curve. Figure 4B shows the areas of the cell where the absolute value of ITV is the highest (within arbitrarily chosen range of 15% of the maximal value). The calculations of ITV were then compared with measurements of ITV on the same cell using a potentiometric fluorescent dye di-8-ANEPPS. The changes in fluorescence of dye upon exposure of cell to the electric field are presented in Figure 3A and are hardly noticeable. They become visible after subtraction from the control image (without electric field) as shown in Figure 3B. In this figure, the side of the cell colored in white represents an increase in fluorescence, and the side of the cell colored in black, a decrease in fluorescence. Fluorescence changes were transformed to ITV using a calibration curve (see Materials and Methods) and are presented with solid curve in Figure 3C as a function of the normalized arc length. The results are shown for two opposing orientations of external electric field (100 V/cm). For the investigated cell, ITV changes along the cell membrane between approximately 75 mV and -65 mV for electric field directed from left to right and between -80 mV and 55 mV for the opposite direction of the field (Figure 3C) and is in qualitative agreement with the calculated ITV. Small differences between the amplitudes could be attributed to the variations of the slope of calibration curve between different cells, the differences between the actual and implemented parameters of the model (especially the membrane permeability), and the experimental setup.

3.3 Monitoring the course of electropermeabilization

In the presence of the membrane-impermeant fluorescent dye Propidium Iodide, the same cell was then exposed to a single unipolar rectangular 400 V pulse (1000 V/cm) with 200 µs duration. The changes in fluorescence of the cell were observed 100 ms after the pulse application on both sides of the membrane, denoting the regions where permeabilization occurred. With time, cell interior becomes more fluorescent indicating continuous dye uptake into cell after permeabilization. The fluorescence regions of the membrane on the first image (100 ms) were compared with calculations of ITV (shown in Figure 4B). A good agreement between the observed fluorescence increase and the regions where the absolute value of ITV was the highest was obtained (cf. Figure 4B and Figure 5A).

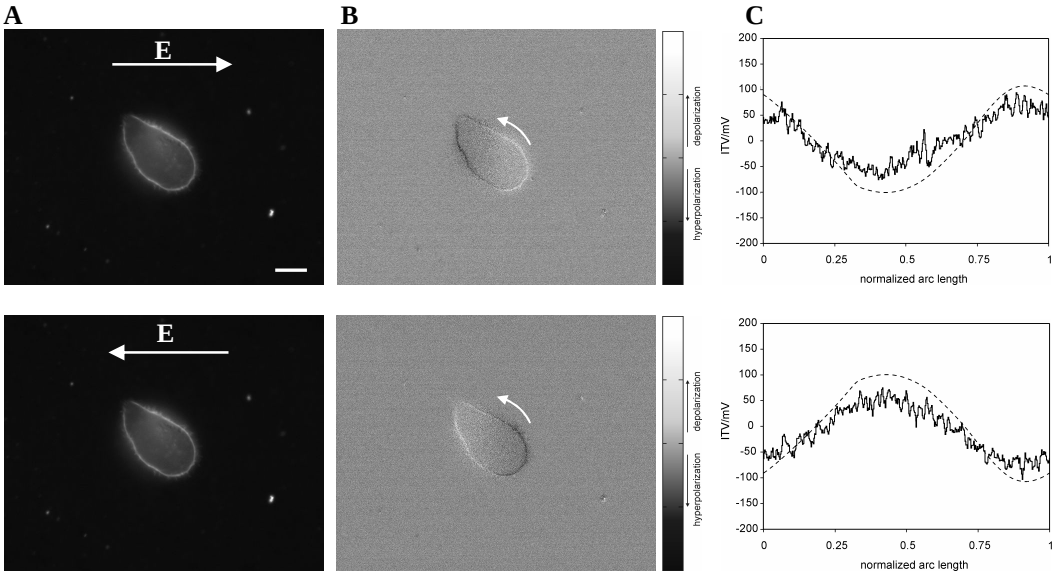

Figure 3. Measurements of ITV on an irregularly shaped CHO cell. First row shows the results for the electric field *E* directed to the right and the second row for the opposite direction. (A) The 8-bit fluorescence images of a cell stained with di-8-ANEPPS and acquired during the exposure to 40 V (100 V/cm), 100 ms rectangular pulse. Bar represents 10 µm. (B) Changes in fluorescence of cell obtained by subtracting the control image (not shown) from the image with pulse and shifting the grayscale range by 50%. White arrow shows the path along which ITV was measured. (C) ITV as a function of normalized arc length. Solid curve – measured values, dashed curve – numerically calculated values. The changes in fluorescence were transformed to ITV by using a 6%/100mV calibration curve.

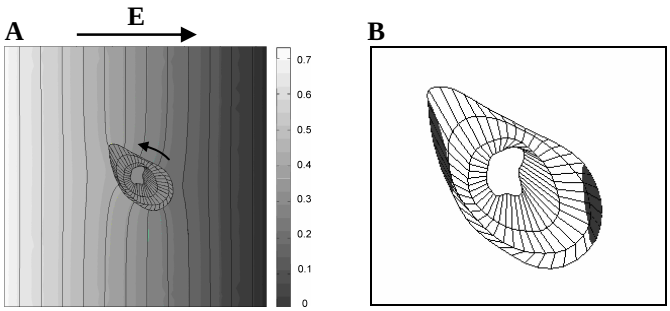

Figure 4. (A) The calculated distribution of the electric potential around and inside the cell in the lowermost x-y plane of the cell. The black curves represent the equipotentials and the arrow marks the path along which the potential was measured. The scale is in volts. (B) Regions of the membrane where the absolute value of ITV, calculated as a difference between the potentials on both sides of the membrane ($ITV = V_i - V_o$), is the highest (within arbitrarily chosen range of 15% of the maximal value).

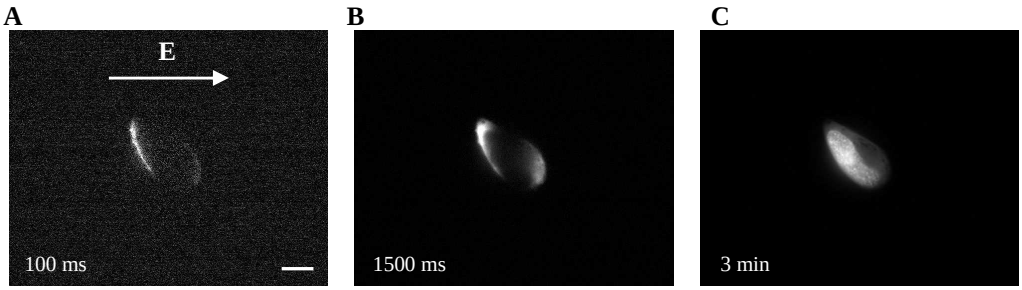

Figure 5. Monitoring of cell electropermeabilization. (A) Fluorescence of the cell 100 ms, (B) 1500 ms, and (C) 3 min after pulse delivery. The images were corrected for the background fluorescence and the brightness was automatically enhanced. The cell was exposed to a 1×400V, 200 µs (1000 V/cm) rectangular pulse. Propidium Iodide was added to suspension before the pulse was applied to visualize the permeabilized regions. Bar represents 10 µm.

4. Summary

We demonstrated how to construct realistic models of irregularly shaped cells from their cross-section images. This allows determination of the ITV on the same cells on which the experiment is carried out, and can be of considerable importance in understanding and interpretation of the data. We also presented a method to replace a cell membrane in the model with a boundary condition. Such replacement efficiently eliminates the number of elements of the mesh and consequently time needed to solve the problem. To validate the method, the computed ITV for a spherical cell was compared with the analytical expression describing the ITV for the same cell, showing a very good agreement between both solutions. This can be considered as the evidence that this method is a reliable and accurate one. We then showed that the ITV computed for a model of an irregularly shaped cell is comparable to the ITV measured on the same cell. Finally, we confirmed that electropermeabilization occurs in those areas of cell membrane, where the absolute value of ITV is the highest. The presented methods of model construction from cross-section images and replacement of the membrane by a boundary condition can also be used to study more complicated cell geometries, such as several cells in contact, which represent a simple model of a tissue.

5. Acknowledgements

This work was supported by the Ministry of Higher Education, Science and Technology of the Republic of Slovenia. The authors wish to thank dr. Marko Puc for building the switcher device for delivery of electric pulses in the experiments.

6. References

1. Hibino M., et al. *Biophys. J.* 59:209-220, 1991.
2. Hibino M., et al. *Biophys. J.* 64:1789-1800, 1993.
3. Schwan H. P. *Adv. Biol. Med. Phys.* 5:147-209, 1957.
4. Golzio M., et al. *Gene Therapy.* 12: 246-251, 2005.
5. Somiari S., et al. *Mol. Ther.* 2:178-187, 2000.
6. Šatkauskas S., et al. *Mol. Ther.* 5:133-140, 2002.
7. Gabriel B. and Teissié J. *Eur. Biophys. J.* 27:291-298, 1998.
8. Kotnik T., et al. *Bioelectrochem. Bioenerg.* 43:285-291, 1997.
9. Lojewska Z., et al. *Biophys. J.* 56:121-128, 1989.
10. Pucihar G., et al. *Bioelectrochemistry* 54:107-115, 2001.
11. Kotnik T. and Miklavčič D. *Biophys. J.* 79:670-679, 2000a.
12. Kotnik, T. and Miklavčič D. *IEEE T. Bio- Med. Eng.* 47:1074-1081, 2000b.
13. Gimsa J. and Wachner D. *Biophys. J.* 81:1888-1896, 2001.
14. Gimsa J. and Wachner D. *Eur. Biophys. J.* 30:463-466, 2001.
15. Gross D., et al. *Biophys. J.* 50:339-348, 1986.
16. Montana V., et al. *Biochemistry* 28:4536-4539, 1989.
17. Loew L. M. *Bioelectromagnetics.* 1:179-189, 1992.
18. Knisley S. B., et al. *Circ. Res.* 72:255-268, 1993.
19. Bedlack R. S., et al. *Neuron.* 13:1187-1193, 1994.
20. Hassan N., et al. *IEEE T. Plasma Sci.* 30:1516-1524, 2002.
21. Miller C. E. and Henriquez C. S. *IEEE T. Bio-Med. Eng.* 35:712-718, 1988.
22. Fear E. C. and Stuchly M. A. *IEEE T. Bio-Med. Eng.* 45:856-866, 1998a.
23. Fear E. C. and Stuchly M. A. *IEEE T. Bio-Med. Eng.* 45:1259-1271, 1998b.
24. Susil R., et al. *Electro. Magnetobiol.* 17:391-399, 1998.
25. Pavlin M., et al. *IEEE T. Bio-Med. Eng.* 49:605-612, 2002.
26. Valič B., et al. *Bioelectrochem.* 63:311-315, 2004.
27. Gowrishankar T. R. and Weaver J. C. *Proc. Natl. Acad. Sci. USA.* 100:3203-3208, 2003.
28. Buitenweg J. R., et al. *IEEE Trans. Biomed. Eng.* 50:501-509, 2003.
29. Valič B., et al. *Eur. Biophys. J.* 32:519-528, 2003.
30. Pucihar G., et al. *Ann. Biomed. Eng.*, 34:642-652, 2006.
31. Gascoyne P. R. C., et al. *Biochim. Biophys. Acta.* 1146:119-126, 1993.
32. Harris C. M. and Kell D. B. *Bioelectrochem. Bioenerg.* 11:15-28, 1983.
33. Rols M. P., et al. *Eur. J. Biochem.* 254:382-388, 1998.
34. Alberts B., et al. Biology of the Cell, 3rd ed., Garland Publishing, New York, 1994.

MODULATION OF *IN VITRO* EMF-INDUCED EFFECTS ON HUMAN KERATINOCYTES (HaCaT) BY Ca^{2+}-DEPLETION

[††]DURANTI G., [*]BARTOLETTI C., [††]ERDEMBILEG T., [**]FALSAPERLA R., [††]FAZIO G., [††]PAGNOTTA S., [††]ROSATO N., [††]ROSSI A., [**]ROSSI P., [*]SACERDOTI G., [†]SUPINO R.

[*]University of Rome "La Sapienza" – Italy;
[**]National Institute of Occupational Safety and Prevention (ISPESL) – Rome – Italy;
[††]University of Rome "Tor Vergata" – Rome – Italy; [†]Istituto Nazionale Tumori – Milano – Italy.

Abstract

Effects of 900 MHz CW on human immortalized keratinocytes (HaCaT) were investigated. Cells kept in a CO_2 independent medium were exposed inside a cell-culture incubator at 37 °C. Sham samples were in the same environmental conditions. Exposure durations ranged from 2 up to 18 hours, and dose-response investigation was performed at average SAR levels of 0.7 mW/kg and 3 mW/kg.

The inhibition of proliferation and viability reached its maximum for exposures of 2^h15^m duration (21% at lower SAR level and 12% at highest one), and for exposures of 18^h duration (40% at lower SAR level and 20% at highest one). Less marked effects were observed with exposures of 4 and 9 hours to the SAR level of 3 mW/kg.

To test the dependence on calcium of the effect, experiments were performed in Ca-depleted medium (KCl 1mM was added to keep the right ionic strength). Exposure to EMF for 18 hours in these experimental conditions caused a further 10% increase in cell growth inhibition, regardless SAR levels.

Moreover we studied the effect of EMF on the structure of tissue Transglutaminase (tTG), a calcium-dependent enzyme involved in wound healing and epithelial differentiation. Indeed, after 2 hours exposure at the SAR level of 0.7 mW/kg, the fluorescence spectrum of tTG (excited at 293 nm) was differentially modulated in comparison to sham samples. EMF treatment seems to induce a conformational change similar to that observed during its activation which occurs upon calcium addition.

Introduction

Several authors reported about the alteration of cell membrane surface charges exposed to low frequency electromagnetic fields (EMF) and conflicting results have been reported on the probably consequent mobilization of intracellular calcium. However only little studies have been reported on the effects of radiofrequencies (900 MHz) on calcium metabolism in normal human cells. The role of calcium ions in several biological pathways has been supported. In the case of EMF it could be hypothetized that EMF exposure, by disturbing intracellular calcium availability and fluxes, can interfere with biological cellular pathways. Additional mechanism of interaction of EMF with biological tissue could be traced to the different permeability of certain ions, like calcium, through the canals of the membranes that permit the passage of salts (called ionic canals); today of fundamental importance for the study of brain cells and of other neurological diseases (Marchionni et al., 2006). Moreover, exposure to EMF is able to change *in vitro* protein conformation and enzyme activity suggesting a great influence in cellular metabolism (Barteri et al., 2005). It has been reported also that 900 MHz do not modulate the signal transmission in the peripheral nervous system, whereas 50/60 Hz are effective. Moreover biphasic actions depending on frequencies and intensities have been reported (Marchionni *et al.*, 2006).

Following the previuos results assessing that exposure to 900 MHz could trigger a differentiation program in HaCaT cells (Duranti et al, 2004; Duranti et al., 2005), in the present work, we investigated *in vitro* the EMF-induced effects in relation to calcium concentration. We choose a human normal immortalized keratinocytes cell line (HaCaT), since keratinocytes are naturally exposed to both mechanical and thermal stimuli, and skin is usually exposed to electromagnetic radiation at considered frequency more than inner tissues. We examined the cell proliferation at different times of EMF exposure in the presence or absence of calcium and at different SAR exposures. Moreover we observed, by spectrophotometric determination, a modification in the structure of tissue transglutaminase (tTG) a calcium-dependent enzyme involved in wound healing and epithelial differentiation.

Altogether, our results suggest an involvement of the intracellular Ca^{2+} availability in the cell response to 900 MHz EMF exposure.

Materials and Methods

Reagents

Cell culture media (Dulbecco's MEM mix F-12 and CO_2-independent media) were obtained from Invitrogen, Carlsbad, CA, USA; heat-inactivated fetal bovine serum FBS and trypsin were obtained from HyClone, Oud-Beijerland, Holland. Tris (hydroxymethyl)-aminomethane, HCl, were obtained from Fluka (Buchs, Switzerland), Calcium-free keratinocyte growth medium from Cambrex-Clonetics (Baltimore USA). Primary and secondary antibodies were obtained from Santa Cruz (Santa Cruz, CA USA). All the other reagents, unless otherwise specified, were from Sigma Chemical (St. Louis, MO, USA).

SAR determination

Computational simulations have been carried out by employing the electromagnetic commercial simulator Microwave Studio (MWS) by CST-Germany, based on the Finite Integration Technique (FIT). This numerical method, developed by Weiland in 1977, provides a discrete reformulation of Maxwell's equations in their integral form suitable for computers and it allows simulating real-world EMF problems with complex geometry. In order to numerically solve Maxwell's equations, a finite calculation domain is defined. By creating a suitable mesh system, this domain is splitted up into small cubes, so-called grid cells. In combination with the FIT, MWS employs the Perfect Boundary Approximation (PBA) for the spatial discretization of the simulated structure that allows an accurate modelling of bend-shaped structures.

In order to simulate in vitro tests, the exposure set up was represented as two parallel metallic plates of (80 x 99) mm size, at 27 mm of distance and 4 Petri dishes or 2 flasks were inserted between the plates. In simulation for exposure to 900 MHz EMF, the plexiglas dishes were of 35 mm of diameter, height of 8 mm and 1 mm of thickness. Each culture medium was then parameterized as dish of 33 mm of diameter and 3.5 mm of height for a total liquid volume of 3 ml. In the simulation of exposure to 1.8 GHz EMF the flasks were represented by means of a plexiglas parallelepiped of (35 x 35 x 20) mm size and of 1 mm thickness for each wall. Consequently each culture medium was parameterized as a parallelepiped of (33 x 33 x 3.7) mm size, for a total liquid volume of 5 ml.

Cell cultures and EMF exposure

Human keratinocytes (HaCaT) were grown in T25 cell colture flask (SARSTEDT) in a 1:1 mixture of minimal essential medium (Dulbecco's MEM) and Ham's F-12 medium supplemented with 10% (v/v) heat-inactivated foetal calf serum, 1% non-essential amino acids, at 37°C with 5% CO2 in a humidified atmosphere. No antibiotics were used. Cells were split 1:6 twice weekly and fed 24 hours before each experiment.

Cells were seeded (8.000 cells/cm^2) in culture medium and allowed to recover physiological growth conditions in a 5% CO_2 atmosphere at 37°C for 24h. Then medium was replaced with calcium-free keratinocyte growth medium and KCl (1mM) was added to keep the right ionic strength, then samples were transferred in a 37°C incubator without CO_2 and exposed to EMF for different times.

Shame samples prepared exactly as the exposed were in the same incubator out of radiation field. All samples were in duplicate. All the results are the mean with standard deviation of at least 3 independent experiments.

Cell proliferation

HaCaT cells, were exposed to an EMF of 900 MHz with different intensities ranging between 1.5 and 12V/m for different times (2h-72h). To assess HaCaT viability and proliferation, cells were counted at 72h after EMF exposure by a Burker chamber and viability was evaluated by trypan blue exclusion assay. Briefly, cells were trypsinized, collected in 1 ml PBS and mixed 1:1 with trypan blue solution (0.8 mM in PBS). Viable cells exclude trypan blue while dead cells stain blue due to trypan blue uptake.

Spectroscopic Assays

tTG from guinea pig liver was dissolved in Tris-HCl 50 mM buffer, pH 7.5, containing 5 mM EDTA. Steady-state fluorescence was measured with a ISS-K2 fluorometer (ISS, Champaign, IL) thermostating the sample at 20°C by an external bath circulator. The emission spectra was detected through a WG 305 cut-off filter to suppress scattered light.

Protein expression level

10-20 µg of cellular proteins (in 25 mM Tris-HCl pH 8, 0.5% SDS, 0.05% mercaptoethanol, 2.5% glycerol and 0.001% bromephenol blue) were denaturated at 100°C for 5 minutes, subjected to SDS-PAGE on a 10% polyacrylamide gel and then electroblotted onto a PVDF membrane at 130 V for 1 hour. Blots were blocked with 5% non-fat dry milk (Biorad, Hercules, CA) and then incubated with specific primary antibodies, p-ERK (Santa Cruz CA USA) and β-tubulin (Santa Cruz CA USA). After washing and incubation with the horseradish peroxidase-conjugated secondary antibody, detection was carried out with ECL (Amersham).

Results and Discussion

Effects of 900 MHz CW on HaCaT cells were investigated. Exposure for 18 h to 900 MHz at different intensities in a range between 1.5 and 12 V/m corresponding to a maximal SAR of 3 mW/kg caused a cell growth inhibition not directly related to the intensity (Table 1).

Table 1. HaCaT proliferation after exposure for 18 h to 900 MHz at different intensities

	V/m (SAR:mW/kg)			
	1.5	3	6 (0.7)	12 (3)
Sham	1	1	1	1
Exposed	0.95±0.04	1.0±0.1	0.73±0.04	0.82±0.08

The antiproliferative effect of EMF was evaluated at 72h after different times of exposure ranging from 2 up to 72 hours. As shown in table 2, maximal effects were found for short exposure times, whereas at 72h of exposure, no cell growth inhibition could be detected.

Table 2. HaCaT proliferation after exposure to 900 MHz for different times

	Time of exposure (hours)					
	2.15	4.30	9	18	24	72
Sham	1	1	1	1	1	1
Exposed (0.7 mW/kg)	0.79±0.12	n.d.	n.d.	0.80±0.1	n.d.	n.d.
Exposed (3 mW/kg)	0.74±0.1	0.86±0.03	1.05±0.04	0.82±0.08	0.84	0.97

The inhibition of proliferation and viability reached its maximum for exposures of 2h15m duration (21% at the lower SAR level and 26% at the highest one), and for exposures of 18h duration (20% at the lower SAR level and 18% at the highest one) (Table 2). Less marked effects were observed with exposures of 4 and 9 hours to the SAR level of 3 mW/kg (Table 2).

Since it has been reported an involvement of ion channels in the effects of EMF exposure on biological materials, we investigated the dependence on calcium of the effects of EMF at SAR level of 3 mW/kg as above reported. Thus we performed some experiments in Ca-depleted medium. Exposure to EMF for 18 hours in these experimental conditions caused a further 10% increase in cell growth inhibition (Table 3).

Table 3. Cell proliferation after exposure to 900 MHz EMF (3 mW/kg) for 18h in the presence or absence of Ca^{2+}. Cell number was determined at 72h after the end of exposure.

	Cell number x 10^3	
	+ Ca^{2+}	- Ca^{2+}
Sham	520±26	407±32
Exposed	467±28	313±19

This result suggests that a modification of intracellular calcium concentration would affect the antiproliferative activity of 900 MHz EMF. Ca^{2+} modulates several signaling pathways. In epidermal growth factor receptor stimulation, calcium is required for the activation of the extracellular signal-regulated kinases (ERK) (Pusl *et al*., 2002). ERKs, in turn, phosphorylate the transcription factor Elk-1 which becomes active. Activation of Elk-1 leads to the transcription of growth-related genes (Sharrocks, 2001) (Fig.1). We therefore examined the level of phospho-ERK expression by western blot analysis. A barely detectable decrease of phospho-ERK expression was found immediately after EMF exposure with respect to the control sham cells. This effect was more evident for exposures performed in the absence of Ca^{2+} , supporting a role for calcium in keratinocytes proliferation and differentiation. After 72h recovery, p-ERK expression in exposed cells rise to sham level suggesting that the decrease in ERK phosphorylation was due to the presence of the EMF (Fig. 2). Additional experiments are required to determine the role of EMF in such process.

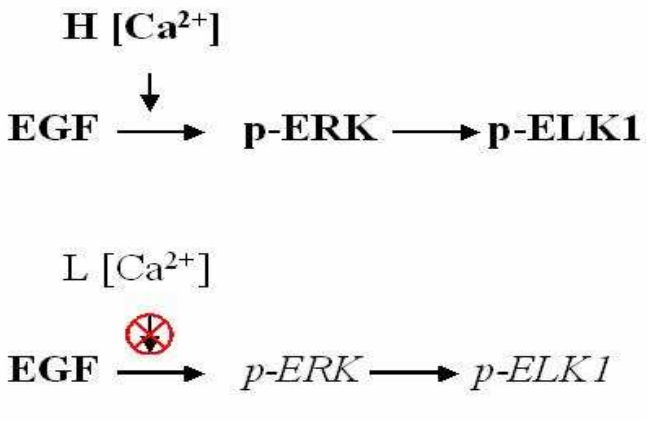

Fig.1 Effect of High (H) and Low (L) calcium concentration on ERK phosphorylation.

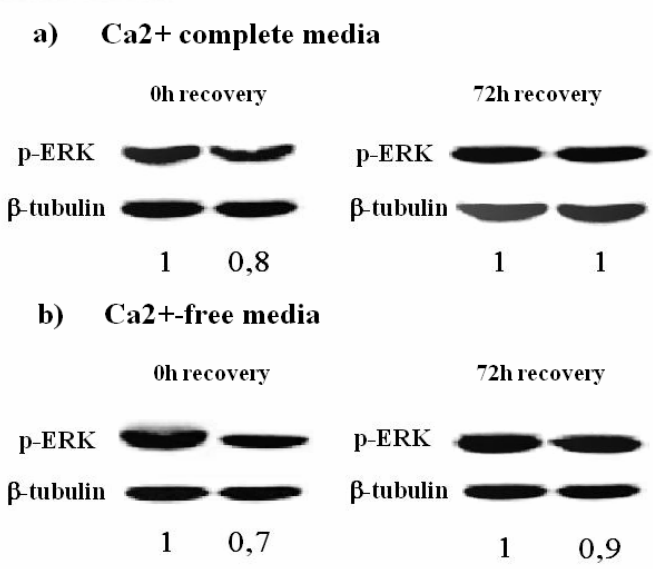

Fig. 2 – Phospho-ERK expression after exposure to 900 MHz EMF for 18h in the presence or absence of Ca^{2+}. Western blot analysis was performed immediately after exposure and 72h after exposure in Ca^{2+} complete medium (a) or in Ca^{2+} free medium (b). Tubulin is reported as control of loading. Numbers indicate the normalization of p-ERK band in exposed samples versus sham samples.

Transglutaminases are a class of enzymes that induce cross-link between proteins by catalyzing the formation of an isopeptidyl bond. They are involved in processes like apoptosis, differentiation, wound healing. Tissue transglutaminase (tTG) is activated by a conformational change induced by calcium which is necessary for its activation (Folk *et al*., 1967). It has been reported that calcium binding to tTG can be monitored because it alters the steady-state protein fluorescence spectra (Di Venere *et al*., 2000). We found that after 2 hours exposure at the SAR level of 0.7 mW/kg, the fluorescence spectra of tTG was altered in comparison to sham samples in a way resembling calcium binding to the enzyme. Therefore EMF treatment seems to induce a conformational protein change similar to that observed during its activation. It is interesting to note that EMF could exerts this effect in absence of calcium. Further studies are needed to clarify the mechanism and the effects on cell metabolism.

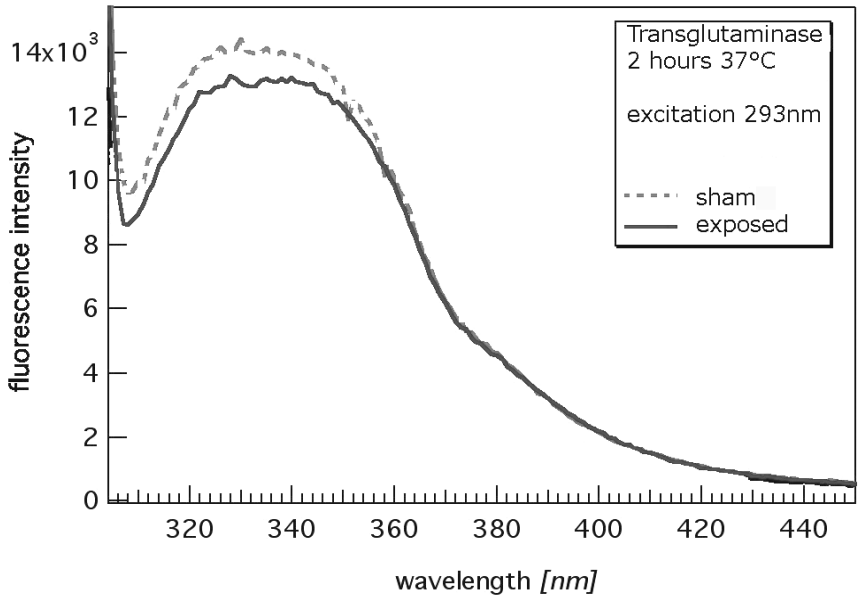

Fig. 3 – Steady state fluorescence spectra of tTG exposed at 900 MHz EMF for two hours (solid line) compared to sham (dotted line). Excitation wavelenght at 293 nm.

Altogether, our results suggest that the cellular response to EMF could be mediated by intracellular Ca^{2+} availability.

References

Barteri M., Pala A., Rotella S. Structural and kinetic effects of mobile phone microwaves on acetylcholinesterase activity. Biophys Chem. 2005 Mar 1;113(3):245-53.

Duranti G, Rossi A, Rosato N, Fazio G, Sacerdoti G, Rossi P, Supino R. In vitro evaluation of biological effects on human keratinocytes exposed to 900 MHZ electromagnetic field. Proceedings of the 3rd International Workshop Biological Effects of EMFS, Kos, Greece 4-8 october, 2004.

Duranti G, Rossi A, Rosato N, Fazio G, Sacerdoti G, Rossi P, Falsaperla R, Cannelli V, Supino R. In vitro evaluation of biological effects on human keratinocytes exposed to 900 MHz electromagnetic field. The Environmentalist 2005; 25:113-119.

Di Venere, A., Rossi, A., De Matteis, F., Rosato, N., Finazzi Agro', A. and Mei, G.: 2000,'Opposite effects of Ca(2+) and GTP binding on tissue transglutaminase tertiary structure' *J. Biol. Chem.* **275**, 3915-3921.

Folk, J.E., Mullooly, J.P. and Cole, P.W.: 1967, 'Mechanism of action of guinea pig transglutaminase. II. The role of metal ion in enzyme activation' *J. Biol. Chem.* **242**, 1838-1844

Marchionni, I., Paffi, A., Pellegrino, M., Liberti, M., Apollonio, F., Abeti, R., Fontana, F., D'Inzeo, G. and Mazzanti, M.: 2006, 'Comparison between low-level 50 Hz and 900 Mhz electromagnetic stimulation on single channel ionic currents and on firing frequency in dorsal root ganglion isolated neurons' *Biochim. Biophys. Acta* **1758**, 597-605.

Pusl, T., Wu, J.J., Zimmermann, T.L., Zhang, L., Ehrlich, B.E., Berchtold, M.W., Hoek, J.B., Karpen, S.J., Nathanson, M.H. and Bennett, A.M.: 2002, 'Epidermal Growth Factor-mediated Activation of the ETS Domain Transcription Factor Elk-1 Requires Nuclear Calcium' *J. Biol. Chem.* **277**, 27517-27527.

Sharrocks, A.D.: 2001, 'The ETS-domain transcription factor family' *Nat. Rev. Mol. Cell. Biol.* **2**, 827-837.

HIGH FREQUENCY EMFs ON HUMAN KERATINOCYTES IN VITRO: DIFFERENT TIME EXPOSURE EFFECTS

[†]SUPINO R., [*]BARTOLETTI C., [*]CAPUTO G., [††]DURANTI G., [#]ESPOSITO G. ,[**]FALSAPERLA R., [†]FAVINI E., [††]ROSATO N., [**]ROSSI P., [*] SACERDOTI G., [†]ZUNINO F.

[†]Istituto Nazionale Tumori – Milano – Italy; e.mail rosanna.supino@istitutotumori.mi.it
[*]University of Rome "La Sapienza" – Italy
[**]National Institute of Occupational Safety and Prevention (ISPESL) – Rome – Italy
[††]University of Rome "Tor Vergata" – Italy
[#] Politecnico di Milano - Italy

Abstract

The effects of ultra high frequency EMFs with biological systems were investigated by *in vitro* studies in human immortalized keratinocytes (HaCaT). Cells were exposed to 900 MHz CW at average SAR level of about 1-5 mW/kg, and 1.8 GHz CW at average SAR level of about 10 mW/kg, for different periods of time. Exposures to 900 MHz CW, at durations of 2^h15^m and 18^h caused a reduction in the cell growth, whereas same duration exposures to 1.8 GHz CW caused an increase of cell proliferation. Cell cycle perturbations were observed in both cases, with a decrease of G1 phase after 18^h exposure. Longer exposure durations (72^h) were ineffective, suggesting a cellular adaptation to these stress conditions.
Preliminary studies showed that the effects of 900 MHz exposure were independent of temperature (34°C or 38°C), but dependent on calcium concentration in the medium. The effects of exposure on the redox balance were examined. Short time (2^h15^m) 900 MHz exposure evidenced a decrease of Total Antioxidant Status (TAS) values, whereas 1.8 GHz was ineffective, regardless the higher SAR level. Our results suggest that exposure to different frequencies and SAR levels caused different effects on biological systems. Cell cycle perturbations and oxido-reductive response seem to be involved.

Introduction

Electromagnetic field (EMF) exposure from sources such as power lines, mobile phones, TV and radio transmitters, and from new and emerging technologies, is frequently seen as a potential source of risk for people and environment. While significant EMF research has been conducted over the past years, technological changes have been so rapid that science has been unable to sufficiently assess potential health risks in a timely manner [1]. The effect of extremely low-frequency electromagnetic field (ELF/EMF) exposure on human health has been widely debated. A number of epidemiological studies have pointed to a slight increase in malignant diseases in populations exposed to electromagnetic fields through the vicinity of power lines. A significant positive association was observed between childhood leukemia and exposure of children to magnetic fields during the night [2-4]. Our previous studies showed a low but reproducible antiproliferative effect of 50 Hz magnetic field on human leukemia cells [5] while no long term effects were found in human breast carcinoma cells [6]. The increasing number of epidemiological observations prompted us to a study on the impact of electromagnetic fields on biological parameters of a human normal keratinocytes cell line, to verify whether there exist significant effects induced by the exposure to high frequency EMF in a controlled and reproducible experimental condition (biological and physical). HaCaT (human keratinocytes) cell line has been chosen as an excellent model to study the biological effect of radiations since they are cells which receive, in the first line, the energy associated to radiations. We already reported that exposure to 900 MHz could trigger a differentiation program in HaCaT cells [7,8]. We examined the eventual effects of two different high frequencies (900 MHz and 1.8 GHz) on cell proliferation, cell cycle progression and oxidative response of these cells after different times and intensities exposures. The aim was to examine the biological effects of exposures to a wide range of SAR values. Thus, we started the study by exposing cells to very low levels of SAR such as 1mW/kg at 900 MHz and 10mW/kg at 1.8 GHz.

Interestingly we observed an increase in cell growth after exposures to 1.8 GHz and an inhibition of cell growth after exposures to 900 MHz. Exposures till 24 h caused differences in the considered biological parameters whereas after longer times of exposure a kind of adaptation and a decrease of the effects, which revert to control values, was found. The involvement of temperature and of calcium concentration was also examined.

Materials and Methods

SAR determination

Computational simulations have been carried out by employing the electromagnetic commercial simulator Microwave Studio (MWS) by CST-Germany [9], based on the Finite Integration Technique (FIT) [10]. This numerical method, developed by Weiland in 1977, provides a discrete reformulation of Maxwell's equations in their integral form suitable for computers and it allows simulating real-world EMF problems with complex geometry. In order to numerically solve Maxwell's equations, a finite calculation domain is defined. By creating a suitable mesh system, this domain is splitted up into small cubes, so-called grid cells. In combination with the FIT, MWS employs the Perfect Boundary Approximation (PBA) for the spatial discretization of the simulated structure that allows an accurate modelling of bend-shaped structures [11].

In order to simulate *in vitro* tests, the exposure set up was simplified. In fact in the numerical model only the exposure zone of the two set up was modelled, presuming that the detailed description of the adaptive section was not relevant for SAR evaluation purposes. Each exposure set up was then represented as two parallel metallic plates of (80 × 99) mm size, at 27 mm of distance and Petri dishes or flasks were inserted between the plates. In simulation for exposure to 900 MHz EMF we have four plexiglas dishes of 35 mm of diameter, height of 8 mm and 1 mm of thickness. Each culture medium was then parameterized as dish of 33 mm of diameter and 3.5mm of height for a total liquid volume of 3 ml. In the simulation of exposure to 1.8 GHz electromagnetic field we have two polystyrene flasks. Each flask was represented by means of a plexiglas parallelepiped of (35 x 35 x 20) mm size and of 1 mm thickness for each wall. Consequently each culture medium was parameterized as a parallelepiped of (33 x 33 x 3.7) mm size, for a total liquid volume of 5 ml.

Cell cultures and EMF exposure

Human keratinocytes (HaCaT) were grown in D-MEM/F-12 medium (Invitrogen, Carlsbad, CA, USA), supplemented with 10% (v/v) heat-inactivated foetal calf serum (HyClone, Oud-Beijerland, Holland) and non-essential aminoacids 1%, at 37°C in a 5% CO_2 humidified atmosphere. No antibiotics were used. Cells were seeded (8.000 cells/cm^2) in culture medium and allowed to grow in physiological conditions in a 5% CO_2 atmosphere at 37°C for 24 h. Then medium was replaced with CO_2-independent medium (Invitrogen) to maintain the correct pH and samples were transferred in a 37°C incubator without CO_2 and exposed to EMF for different times.

Sham samples, prepared exactly as the exposed, were in the same incubator out of radiation field. All samples were in duplicate. The results are the mean with standard deviation of at least 3 independent experiments.

Cell proliferation and Cell cycle analysis

HaCaT cells, were exposed to an electromagnetic field of 900 MHz with different intensities ranging between 1.5 and 12 V/m or 1.8 GHz at 25 V/m for different times (2 h-72 h).

Cell proliferation was evaluated at 72 h after EMF exposure by counting, in a Burker chamber, trypan blu excluding cells (alive cells).

For cell cycle analysis, samples were washed in PBS (phosphate buffered solution) and stained with a solution of propidium iodide (PI) (20 µg/ml) (Sigma-Aldrich, St. Louis, MO, USA) e RNase (Sigma) 1 mg/ml in PBS. Cell cycle distribution was analyzed by a FACScan cytofluorimeter equipped with an argon laser for fluorescence excitation at 488 nm (Becton Dickinson, Mountain View, CA, USA) after 30-60 min of incubation. Analysis of the percentage of cells in each phase of the cell cycle was performed by means of Cellfit software (Becton Dickinson).

Total Antoxidant Status

Total antioxidant status (TAS), including enzymatic and non-enzymatic cellular systems, was measured in cells homogenates as Trolox Equivalent Antioxidant Capacity (TEAC), with the modification of ABTS-cation radical method [12].

After exposure, cells were trypsinized, centrifuged, and the cell pellets were resuspended in 100 µl PBS with 1 mM PMSF. After sonication, 10 µl of cellular homogenates was immediately tested.

Briefly, 300 µl ABTS (500 µM), 36 µl metamyoglobin(70 µM), 487 µl PBS, 10 µl sample (0.6 mg of proteins) were mixed and then the reaction was started by adding 167 µl H_2O_2 (450 µM). This method is based on the reactivity of intracellular antioxidant compounds relative to a 1 mM Trolox (vitamin E analogue) standard. A Trolox-calibration

curve by three concentrations was performed during each esperiment. The reaction was followed specrophotometrically at 734 nm for 15 minutes. All compounds were from Sigma-Aldrich.

Protein level expression

10-20 µg of cellular proteins (in 25 mM Tris-HCl pH 8, 0.5% SDS, 0.05% mercaptoethanol, 2.5 % glycerol and 0.001 % bromephenol blue) were denaturated at 100°C for 5 minutes, subjected to SDS-PAGE on a 10% polyacrylamide gel and then electroblotted onto a PVDF membrane at 130 V for 1 hour. Blots were blocked with 5% non-fat dry milk (Biorad, Hercules, CA) and then incubated with specific primary antibodies, HSP-70 (Chemicon International) and β-tubulin (Abcam plc, Cambridge,UK). After washing and incubation with the horseradish peroxidase-conjugated secondary antibody, detection was carried out with ECL (Amersham-GE Healthcare).

Results and discussion

SAR determination

By applying the above reported computational simulation for SAR determination, we verified that with an EMF at 900 MHz with an electric field between 1.5 and 12 V/m, the mean value of SAR in our samples was between 1 and 5 mW/kg. In samples exposed to 1.8 GHz at an electric field of 25 V/m, the mean value of SAR was 10 mW/kg.

Cell growth

HaCaT cell growth was determined by cell counting at 72 h after different times of EMF exposure. As shown in Fig. 1 (panel A) exposures to 900 MHz caused a reduction in cell growth at least till 24 h, whereas exposures to 1.8 GHz caused an increase of cell proliferation. In both cases longer times of exposition to EMF were ineffective on cell proliferation. Moreover (Fig.1, panel B), exposures to 900 MHz to different intensities were ineffective till 3 V/m, whereas 6 and 12 V/m caused a marked decrease in cell growth.

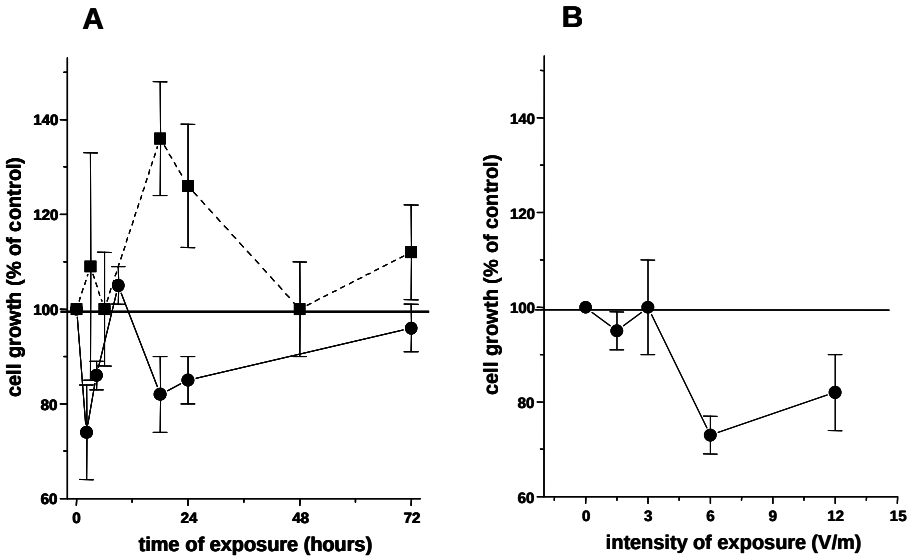

Fig. 1 HaCaT cell growth at different times of exposure to EMF 1.8 GHz 25 V/m (dotted line) or 900 MHz 12 V/m (solid line) (panel A), or 900 MHz and different intensities for 18 h (panel B).

Thus next experiments were performed after short time exposures (2.15 or 18 h) and at 12 V/m (SAR = 5 mW/kg) of intensity for 900 MHz and 24h of exposure to 25 V/m (SAR = 10 mW/kg) for 1.8 GHz.

As shown in table 1, exposure to EMFs of 900 MHz or 1.8 GHz caused a modification in S phase, immediately after exposure to 900 MHz for 18 h. The decrease in S phase after 900 MHz exposition and increase in the same phase after

1.8 GHz are in agreement with the respective decrease and increase in cell proliferation. At longer times of exposure (not shown) or of recovery after a 18 h exposure, values similar to sham control samples were found in all experimental conditions.

Table 1. Effect of 18 h EMF exposure on cell cycle distribution after different times of recovery. The percentage of cells in each phase is reported.

	0 h of recovery			24 h of recovery			48 h of recovery		
	G1	S	G2	G1	S	G2	G1	S	G2
Sham	44	41	15	44	41	14	48	40	12
900 MHz (5mW/kg)	50	31	19	46	42	14	49	40	11
1.8 GHz (10mW/kg)	38	46	16	43	42	15			

Since modification of temperature induced by EMFs could be involved in the observed modification in cell proliferation and cell cycle progression, cell growth after incubation for 18 h at 34°C or 38°C was evaluated. As shown in table 2, no modifications in cell cycle distribution were observed nor at 34°C nor at 38°C, indicating that the EMF effects were not related to the temperature.

Table 2. Effect of EMF on cell cycle distribution at different times of recovery after 18 h of exposure to different temperatures. The percentage of cells in each phase is reported.

		% of cells		
		G1	S	G2
0 h of recovery	37°C	44	41	15
	34°C	38	43	19
	38°C	40	41	19
24 h of recovery	37°C	44	41	14
	34°C	45	40	15
48 h of recovery	37°C	48	40	12
	34°C	44	43	13

Results are from one of two independent experiments.

A dependence of EMF antiproliferative effect on Ca^{++} was found. Indeed in the absence of Calcium (replaced by K^{+}) a higher reduction of cell growth in comparison to that of cells exposed in normal culture conditions was observed (Fig 2). This result suggests that an inhibition of calcium-dependent enzymes could synergize with the antiproliferative effect of EMF.

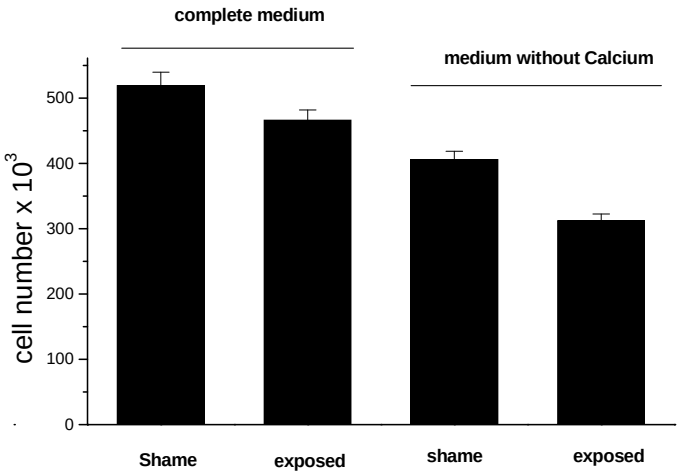

Fig. 2 – Cell proliferation after exposure to 900 MHz EMF for 18 h in the presence or absence of Ca^{++}. Cell number was determined at 72 h after exposure.

To deeply understand the mechanism of the induction of the cellular response observed in EMF exposed cells, we examined the redox balance after 2.15 h and 18 h of 900 MHz exposure. As shown in Fig. 3 a decrease in the total antioxidant status was found mainly after 2.15 h of exposure. At longer times (18 h of exposure) a less marked reduction was observed.

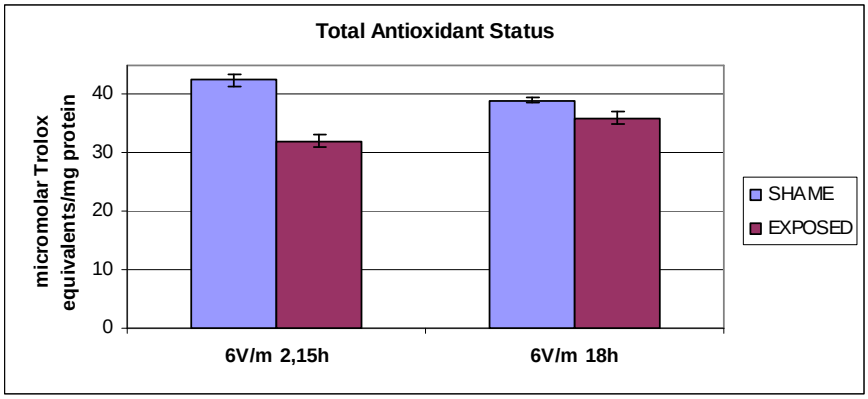

Fig. 3 – Total Antioxidant Status of HaCaT cells after exposure to 900 MHz EMF for 2.15 h or 18 h.

Then the expression level of HSP-70, a stress induced protein, was detected. In agreement with the above reported results an increase in HSP-70 expression was found in cells exposed for 2.15 h to 900 MHz (Fig. 4). Again, after 18 h of cell exposure to EMFs, the expression level of this protein was similar to sham samples.

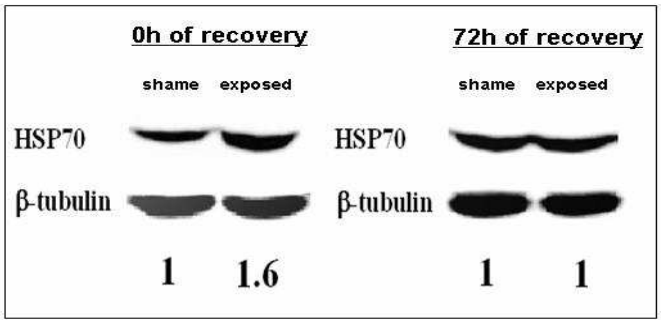

Fig. 4 – HSP-70 protein expression. Protein level was determined at 0 h and 72 h after 18 h of EMF exposure. Tubulin is reported as control of loading. Numbers indicate the normalization of HSP-70 band in exposed samples versus sham samples.

In conclusion the biological effects of the two different high frequencies (900 MHz and 1.8 GHz) examined in the human normal cell line HaCaT after exposures for different times and to different intensities were quite different. Indeed, we observed an increase in cell growth after exposures to 1.8 GHz and an inhibition of cell growth after exposures to 900 MHz. These modulations were reduced (10-25 %) but reproducible. Temperature, often reported as the cause of biological effects of EMF [13] was ineffective, in range between 34°C and 38°C on this cell system suggesting the lack of its involvement in the response of HaCaT cells. On the contrary, an increase EMF antiproliferative effect was found in the absence of calcium, suggesting a dependence of biological effects of EMF on calcium concentration.

Moreover the inhibition observed after 900 MHz exposure was related to an increase in the expression of HSP-70 a protein related to the cellular stress and to the antioxidant status of the cell. The observation that these parameters reverted to control levels after longer times of exposure or of recovery after exposure to EMFs support the hypothesis of other authors of an “adaptation” of cells to the effects produced by electromagnetic energy on the biological matter.

From this study it emerges that an interaction between EMF and cell systems exists even at very low levels of exposure. Moreover they confirm that frequency, intensity, and time of EMF exposure are parameters markedly affecting the biological response for which is not easy to find a model of correlation.

References

1. Repacholi MH. WHO's health risk assessment of ELF fields. Radiat Prot Dosimetry. 2003; 106(4):297-9.
2. Dockerty JD, Elwood JM, Skegg DC, Herbison GP. Electromagnetic field exposures and childhood leukaemia in New Zealand. Lancet 1999; 354:1967-8.
3. Hocking B. Pulsed electromagnetic fields and cancer. Occup Environ Med. 1998; 55:288.
4. Repacholi MH, Ahlbom A.Link between electromagnetic fields and childhood cancer unresolved. Lancet 1999 Dec 4; 354:1918-9.
5. Supino R, Dal Bo L, Favini E, Zunino F, Bartoletti C, Sacerdoti G, Rossi P, Caputo G, Rosato N. In vitro evaluation of biological effects on human cell lines exposed to elf and static electric and magnetic fields. Proceedings of the 3rd International Workshop Biological Effects of EMFS, Kos, Greece 4-8 october, 2004.
6. Supino R, Bottone MG, Pellicciari C, Caserini C, Bottiroli G, Belleri M, Veicsteinas A. Sinusoidal 50 Hz magnetic fields do not affect structural morphology and proliferation of human cells in vitro. Histol Histopathol. 2001; 16(3): 719-26.
7. Duranti G, Rossi A, Rosato N, Fazio G, Sacerdoti G, Rossi P, Supino R. In vitro evaluation of biological effects on human keratinocytes exposed to 900 MHZ electromagnetic field. Proceedings of the 3rd International Workshop Biological Effects of EMFS, Kos, Greece 4-8 october, 2004.

8. Duranti G, Rossi A, Rosato N, Fazio G, Sacerdoti G, Rossi P, Falsaperla R, Cannelli V, Supino R. In vitro evaluation of biological effects on human keratinocytes exposed to 900 MHz electromagnetic field. The Environmentalist 2005; 25:113-119.

9. Microwave Studio, User's Manuals 5.02 2004, CST Computer Simulation Technology, D-64289 Darmstadt, Germany.

10. T. Weiland T. A discretization method for the solution of Maxwell's equations for six-component field, Electronics and Communications AEÜ 1977, 31:116-20.

11. Krietenstein B, Schuhmann R, Thoma P, Weiland T. The Perfect Boundary Approximation technique facing the challenge of high precision field computation. Proc. of the XIX International Linear Accelerator Conference (LINAC '98), 1998, Chicago, USA, pp. 860-862.

12. Miller NJ, Rice-Evans C, Davies MJ, Gopinathan V, Milner A. A novel method for measuring antioxidant capacity and its application to monitoring the antioxidant status in premature neonates. Clin Sci (Lond). 1993 Apr;84(4):407-12.

13. Sukhotina I, Streckert JR, Bitz AK, Hansen VW, Lerchi A. 1800 mHz electromagnetic field effects on melatonin release from isolated pineal glands. J. Pineal Res. 2006, 40:86-91.

\

MODELLING SURFACE ROUGHNESS EFFECTS IN THE INTERACTION OF EM FIELDS WITH BIOLOGICAL CELLS

A. SANCHIS

G. MARTÍNEZ

M. SANCHO

J.L. SEBASTIÁN

S. MUÑOZ

DPT. DE FÍSICA APLICADA III, FACULTAD DE CIENCIAS FÍSICAS
UNIVERSIDAD COMPLUTENSE, 28040 MADRID, SPAIN

Abstract

Standard models of cells for studying their interaction with electromagnetic fields are based on shelled spheres or ellipsoids with characteristic electrical parameters –permittivity and conductivity– for each homogeneous region. However, many biological cells present a complex surface structure with microvilli, blebs, folds, etc., that make these models inadequate to correctly describe the field effects.

In this work we examine the dielectric response of 2D dielectric particle models with surface roughness in quasi-static approximation, using a BEM method based on the integral formulation for the induced polarization charges on the interfaces. Different mathematical surface morphologies are considered: sinusoidal or fractal corrugations, characterized by their corresponding height and correlation length. Results are interpreted by comparing with the standard BEM approach for the electrostatic potential.

Introduction

The dielectric behavior of materials depends sensitively on the characteristics of their surfaces. These characteristics have influence on important phenomena and applications, such as the dielectric breakdown of insulating materials, the development of capacitors with very high capacitance using fractal surfaces or the electrorheological response of particle suspensions [Klingenberg and Cooper 1995]. On the other hand, it is well established that most examples of surfaces exhibit certain degree of roughness. The inclusion of the surface structure in the models that describe the electrical response of colloidal suspensions, can be of help in the characterization of particles using dielectric spectroscopy or electrokinetic measurements, as well as for designing purposes in the development of new applications in these or related fields. In the high frequency range, scattering by rough surfaces have been extensively investigated using Kirchhoff theory, based on a local application of Fresnel laws, using the tangent plane approximation [Caron et al. 2002]. At lower frequencies, where the roughness size is comparable or greater than the field wavelength, the incorporation of the detailed morphology of surfaces in the numerical treatment of the electromagnetic field at dielectric interfaces poses a great challenge for the capability of existing computational methods. This is probably the main reason behind the fact that there are very few studies that consider realistic rough surfaces in the dielectric modeling of particles in spite of its obvious interest.

Methods

In order to investigate the dielectric response of particles with complex surface structure, we have applied two approaches with complementary characteristics. They consist of boundary element (BE) formulations that give information on the potential and charge density distributions. For the sake of clarity, a brief account of the basis of these methods is given below. The interested reader is referred to publications for more details.

i) BEM for the quasi-static potential

This method is based on the following integral equation [Poljak and Brebbia 2005]

$$\frac{\varepsilon_i+\varepsilon_j}{2}\phi(\boldsymbol{r}) = \phi_0(\boldsymbol{r}) + \left(\varepsilon_i-\varepsilon_j\right)\int_L \phi(\boldsymbol{r}')\frac{\partial G(\boldsymbol{r},\boldsymbol{r}')}{\partial n'}dl' \tag{1}$$

where ϕ is the electric potential at a point of a dielectric interface between media of complex permittivities ε_i and ε_j, immersed in an external potential ϕ_0 and the integral extends to the interface contour. $G(\boldsymbol{r},\boldsymbol{r}')$ is the Green's function, defined by $\nabla^2 G = \delta(\boldsymbol{r},\boldsymbol{r}')$. For a 2D problem, $G(\boldsymbol{r},\boldsymbol{r}') = \ln\left|\boldsymbol{r}-\boldsymbol{r}'\right|/2\pi$. The singularity in the integrand when $\boldsymbol{r} = \boldsymbol{r}'$ has been integrated and the integral in the r.h.s. of (1) is to be interpreted in the sense of Cauchy principal part. The formulation can be easily extended to the case of several dielectric interfaces.

The problem is discretized by dividing the contour into N sub-elements of length Δ and equation (1) correspondingly converted to an algebraic equation. The coefficients A_{ij} have a simple analytical expression,

$$A_{ij} = \int_\Delta \frac{d}{dn}(\ln|\boldsymbol{r}-\boldsymbol{r}'|) = \int_\Delta \frac{\cos\theta}{|\boldsymbol{r}-\boldsymbol{r}'|}dl' = \varphi \tag{2}$$

where φ is the angle subtended by the element j from the center of the element i. The algebraic system of equations for the potentials at the N points on the contour is solved by a triangulation method.

ii) BEM for the charge density on the interfaces

For certain types of applications, especially those related to ponderomotive effects produced by electromagnetic fields, we have shown that a BEM formulation based on the charge density induced by the external field can be advantageous. The corresponding integral equation is in that case [Sancho et al. 2003]

$$\frac{\varepsilon_i+\varepsilon_j}{2}\sigma(\boldsymbol{r}) = \left(\varepsilon_i-\varepsilon_j\right)\sigma^0(\boldsymbol{r}) + \left(\varepsilon_i-\varepsilon_j\right)\int_L \sigma(\boldsymbol{r}')\frac{\partial G(\boldsymbol{r},\boldsymbol{r}')}{\partial n}dl' \tag{3}$$

where $\sigma(\boldsymbol{r})$ is the complex charge density at the point $\boldsymbol{r}$ of a dielectric interface and $\sigma^0(\boldsymbol{r}) = \varepsilon_0 E_{ij}^0(\boldsymbol{r})$, $E_{ij}^0(\boldsymbol{r})$ is the normal component of the electric field, pointing from medium i to medium j. The complex character of the permittivity of each medium, depending on the magnitudes of their real permittivity and conductivity, gives rise to complex charge densities, phase shifted with respect to the applied field. As in equation (1), the integral in (2) is interpreted in the sense of the Cauchy principal value.

Results

A measure of the response of a dielectric particle to an external electric field is given by its complex polarizability $\tilde{\alpha}$. This property is related to the dipole moment induced on the particle by means of the expression:

$$\tilde{\boldsymbol{p}}_{eff} = \tilde{\alpha}(\omega)\,\tilde{\boldsymbol{E}} \tag{4}$$

where $\tilde{\boldsymbol{p}}_{eff}$ is the effective dipole moment of the particle, $\tilde{\boldsymbol{E}} = \boldsymbol{E}_0 e^{-i\omega t}$ is the external electric field applied and $\boldsymbol{\omega}$ the angular frequency of the field. These magnitudes are frequency dependent, so they are complex quantities. In this work we deal with the response of a particle to a field strength of 1V/m at a fixed frequency of 10^5 Hz, in order to pay attention to the effects of surface roughness, a question hardly taken into account in previous studies about dielectric particles under electric fields.

The polarizability of 2D circular dielectric objects in an external field is representative of very long dielectric circular cylinders with the electric field applied perpendicularly to the cylinder axis.

As a first approach to this problem, we have investigated how the polarizability of the particle is dependent on the depth of a sinusoidal roughness all around the cylinder surface. We have first considered the case of a lossless particle with a permittivity $\varepsilon_1 = 10\varepsilon_0$ immersed in the vacuum. As indicated in the cross section of the

schematic draw in Figure 1, the particle is characterized by a radius $a = 1$ μm and a roughness extent given by the parameter *h*. The figure also shows the results of the transverse polarizability of the cylindrical particle when two different numbers of undulations are considered. We can observe that when the roughness is getting smaller with respect to the radius, the results are becoming similar in both cases, and tend to the value for a circular particle.

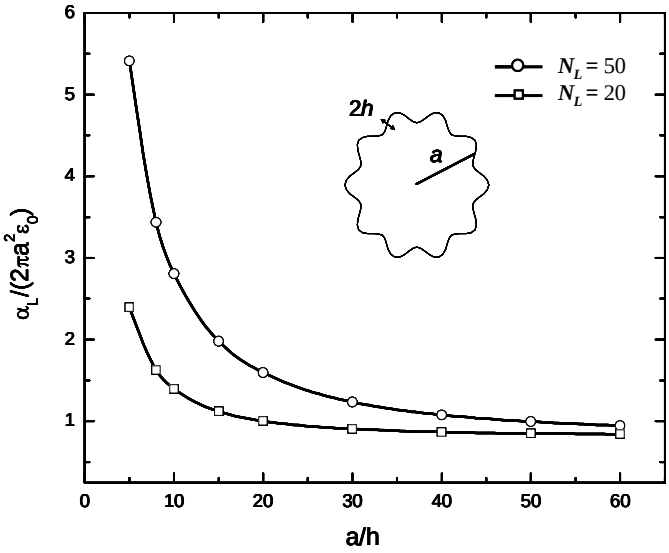

Figure 1. Transverse polarizability of a dielectric circular cylinder with sinusoidal surface roughness. Cylinder permittivity ε =10ε$_o$; N_L is the number of undulations.

For the sake of comparison, we have analyzed the induced superficial charge and potential over both a soft and a rough surface of the particle. The results are given in Figure 2(a) and (b), respectively.

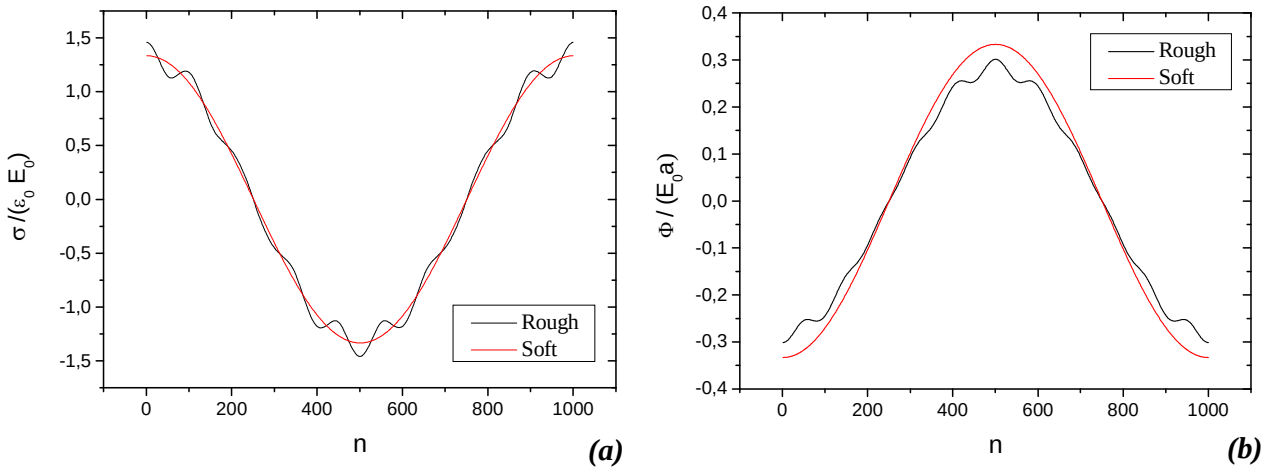

Figure 2. Induced surface charge (a) and induced potential (b) along the surface points by an electric field of 1V/m on both soft and rough dielectric surfaces; the number of undulations is N_L = 10, the total number of points *N = 1000* and the ratio a/h = 20.

The next step for the 2D analysis of the roughness surface effects consists on the study of the polarizability of a layered particle, as a typical biological cell. The cell has been modeled as a particle of 1 μm of radius

surrounded by an undulating shell –the membrane– with 10 nm of thickness. This characterization of the cell membrane as a roughness surface is a first improvement in the approach to the reality of the complex cell envelope. The cell is considered immersed in an external continuous medium formed by electrolytes in free water with the dielectric properties of physiological saline. All the results presented in this work have been obtained by using typical values for the electric properties of the internal layer, membrane and external medium. These values are based on interpolations of impedance measurements on tissues and theoretical calculations [Gabriel et al. 1996]. Table 1 shows the electrical parameters for the non conductive membrane and the highly polarizable internal layer considered for the cell as well as those for the external medium. In Figure 3 the obtained polarizability of a particle as a function of the roughness relative height, *a/h*, is shown.

Layer	Parameter	Value
Internal Layer	**ε**	50
	σ	0.5
Membrane Uniform shell d = 10 nm	**ε**	10
	σ	$1x10^{-6}$
External Medium	**ε**	80
	σ	$1.5x10^{-3}$

Table 1. Electrical parameters for the different layers of the cell model: relative permittivity ε and conductivity σ (S m^{-1}).

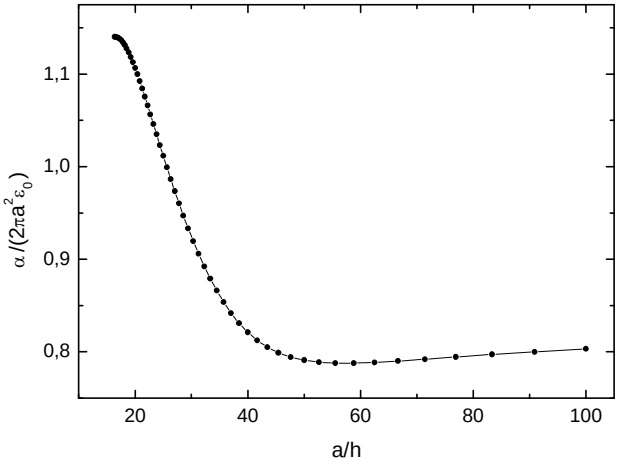

Figure 3. Variation of the polarizability of a shelled particle with sinusoidal undulated membrane as a function of *a/h*; the number of undulations is $N_L = 80$.

Further improvement in the approach to the real, highly irregular surface of a cell with different protrusions and microvilli, has been realized by means of a different morphology based on fractal surfaces. The fractal description provides a very general, scale-invariant, characterization of the electrical response of a biological membrane. It has been applied to the analysis of impedance measurements of human lymphocytes by Bordi et al. [1990]. A fractal surface topography can be generated using a modified (truncated) Weierstrass-Mandelbrot function that can be written as [Yan and Komvopoulus 1998]

$$f(r) = \sum_{n=-n_{\max}}^{n_{\max}} b^{-n(2-D)}[1 - k\cos(b^n r + \varphi)] \tag{5}$$

In this equation *f(r)* is the rough profile, *b* is a frequency multiplier factor (with a typical value between 1.1 and 3), φ is a randomly generated phase, *D* is the fractal dimension (it has a non integer value between 1 and 2), and *k* is a form factor used to modify the profile.

The dielectric response of a cell with fractal surface has been analyzed using the BEM for surface charge. Average results, obtained using five different random phases, for typical membrane topography are shown in figure 4.Variable *h* is the square mean value of the roughness height.

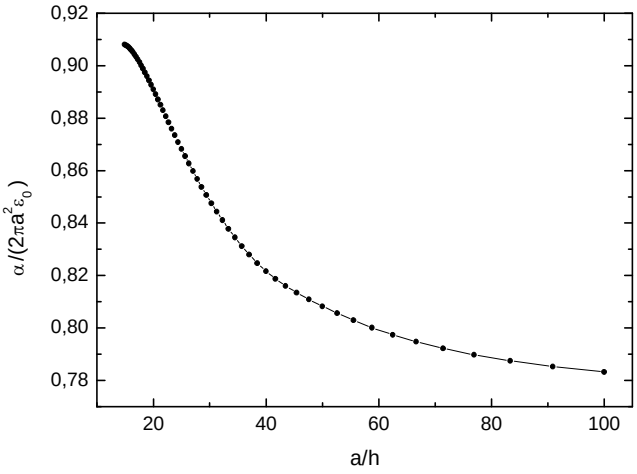

Figure 4. Variation of the polarizability of a shelled particle with a fractal membrane of fractal dimension D = 1.5 as a function of *a/h*. Form factor *k* = 1.9.

Discussion and Summary

We have analyzed the electrical response of plain and coated particles characterized by a rough surface using a superficial 2D model. Sinusoidal and fractal surfaces have been generated and their electrical characteristics have been studied using BE methods. We have found that both the potential and the induced charge experience changes following the surface topography. As a consequence, the polarizability is in general markedly enhanced as the roughness height increases. The trends for sinusoidal and fractal topography are similar, except in the region of intermediate roughness height, where the polarizability for the sinusoidal case is lower, probably due to correlations in the induced charges on neighbor undulations. Although the results have been obtained for 2D models, similar conclusions can be expected for globular cells such as lymphocytes or spiculated red blood cells. In fact, it has commonly been obtained that the specific capacitance of these cells derived from electrorotation (ER) data, is greater than the typical cell membrane value of 1 mF/m^2. Work on full 3D models that allows to interpret these ER studies is in progress.

References

Bordi F., Cametti C. and Di Biasio A., Determination of cell membrane passive electrical properties using domain dielectric spectroscopy technique. A new approach, BBA-BIOMEMBRANES 1028 (1990): 201-204.

Caron J., Lafait J. and Andraud C., Scalar Kirchoff´s model for light scattering from dielectric random rough surfaces, Optics Communications 207 (2002): 17-28.

Gabriel S., Lau R.W. and Gabriel C., The dielectric properties of biological tissues: III. Parametric models for the dielectric spectrum of tissues, Phys. Med. Biol. **41 (**1996): 2271-2293.

Klingenberg D.J. and Cooper S.L, Electrostatics at Rough Interfaces, J. Electrostatics, **35** (1995): 339-348.

Poljak D. and Brebbia C.A., Boundary Element Methods for Electrical Engineers (WitPress, Southampton, Boston, 2005)

Sancho M., Martínez G. and Martín C., Accurate modelling of shelled particles and cells, J. Electrostatics 57 (2003): 143-156.

Yan W. and Komvopoulus K., Contact analysis of elastic-plastic fractal surfaces, J. Appl. Phys. 84 (1998): 3617-3624.

ACUTE EXPOSURE TO WEAK, 800 HZ MAGNETIC FIELD DOES NOT ALTER SKIN MICROCIRCULATION OR PRESSURE PAIN THRESHOLD IN HEALTHY VOLUNTEERS

VEIT SCHNABEL AND LARS ARENDT-NIELSEN

DEPARTMENT OF HEALTH SCIENCE AND TECHNOLOGY,
AALBORG UNIVERSITY, FREDRIK BAJERSVEJ 7 D3, 9220 AALBORG, DENMARK
EMAIL VS@HST.AAU.DK

Abstract

The therapeutic application of weak electromagnetic fields (EMF) is often targeted at improving circulation or alleviating pain. This double-blind, cross-over study was aimed at quantifying the effects of acute exposure to a weak EMF in healthy volunteers.

20 healthy volunteers participated in the experiment in two sessions (at one week interval). Two coils, 4 cm in diameter, where placed laterally on both ankles (device manufacturer Actera A/S, Denmark). The frequency was 800 Hz (monopolar, triangular waveform). The flux density ranged from 0.2 mT, at the center between the coils, to 6 mT directly underneath the coils (RMS values). There were three placebo devices and one active device. The subjects were treated with two devices (one at each ankle) in each session, and the order and position of the devices was randomised. Pain thresholds to pressure were determined before and after 30 minutes exposure. Cutaneous microcirculation was monitored with thermography and laser-Doppler-flowmetry.

The repeated measures ANOVA test showed no effect of the device treatment factor for either pain thresholds or cutaneous microcirculation.

This study demonstrates that, in healthy volunteers, acute exposure to a weak (below 6 mT), 800 Hz magnetic field has no effect on cutaneous microcirculation or pressure pain thresholds.

Introduction

The therapeutic application of magnetic or electromagnetic fields is gaining in popularity and the range of treated ailments is increasing (Shupak et al., 2003). By the year 2004, more than 2 million patients had been treated worldwide for a large variety of injuries, pathologies and diseases, with an 80% success rate and practically absent side effects (Markov, 2004). Despite this high success rate, electromagnetic therapy is still not fully accepted as standard clinical practice. This is partly because some of the clinical trials are based on small sample sizes or have methodological shortcomings (Podd et al., 1998; Cullum et al., 2001), and partly because there is no consensus as to which biophysical or biochemical mechanisms are involved (Polk et al., 1996; Stavroulakis, 2003; Swanson et al., 2006). It has been shown theoretically and experimentally that strong magnetic fields (over about 1.5 T) can have direct cardiovascular effects in humans (Jauchem, 1997). For magnetohydrodynamic interactions, even stronger fields are required, about 5 to 10 T (Kinouchi et al., 1996). Exposure to an electromagnetic field, that induces currents in the body that are about 25 to 40 times stronger than those used in the present study, evokes a pain sensation with muscle contraction, accompanied by a reduction in skin blood flow in the fingertips (Ueno et al., 1986).

The beneficial effects of electromagnetic therapy are often explained by improving blood circulation, thereby reducing pain and inflammation, and enhancing soft tissue repair (McMeeken, 1992). This study seeks to quantify, in healthy volunteers, the acute effects of a weak (below 6 mT) magnetic field.

Methods

Study Design. The study was performed as a double-blind, randomised, placebo controlled trial with cross-over. The experiment had been approved by the local ethics committee "Den Videnskabsetiske Komité for Viborg og Nordjyllands Amter", case number VN 2005/62.

a) b)

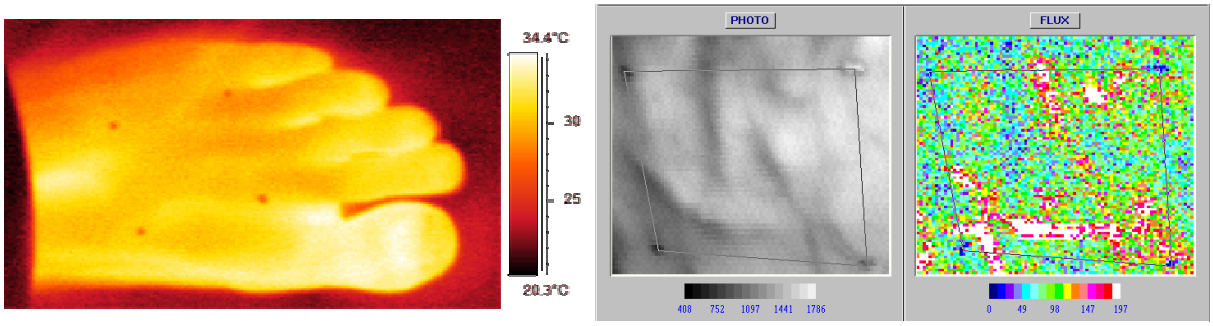

Fig. 1 Examples of pictures as recorded with thermography, a), and laser-Doppler-flowmetry, b). The corners of a 4×4 cm square were marked with a silver pen, visible on both pictures. Mean values of temperature and blood perfusion over this area were calculated and stored for analysis. The cork shield, used for covering the coils, is visible on the left side of a).

Subjects. 20 healthy volunteers (14 male, 6 female) were recruited through on-campus advertisements. The mean age was 24 years (range 22–30 years), mean BMI was 22.2 ± 2.9 kg/m². Subjects were only admitted to the experiment if they were healthy, not pregnant, and not taking any form of medication. None of the participants had tried any form of magnetic or electromagnetic therapy before. None of the participants were heavy smokers or had excessive use of tea/coffe/alcohol. The subjects were instructed not to drink tea/coffee/alcohol, nor to smoke, for a period of 2 hours prior to the experiment. All subjects gave signed written informed consent before conducting the study. All subjects received a compensation (600 DKK) for their participation in the experiment.

Magnetic Field Exposure Condition. The devices used for this study were Actera ELMS-3 stimulators (Actera A/S, Aalborg, Denmark). These devices consist of two applicator coils, approximately 4 cm in diameter, and a control unit. The positions "high" intensity, 800 Hz frequency, and 30 min duration were chosen, resulting in a non-uniform magnetic field with flux densities ranging from 0.2 mT, at the centre between the coils, to 6 mT directly underneath the coils (RMS values). The produced magnetic field was monopolar (about 20% static offset) and had an asymmetric, saw-tooth like waveform repeated at 800 Hz (duty cycle 100%). There was one active device and three placebo devices, with labels A–D. The placebo devices looked and behaved exactly like the active device, but did not produce any magnetic field. It was not possible to see, hear, feel, or sense in any other way which of the devices was active or placebo. The devices were provided by Actera A/S, and only their Chief Technology Officer knew which of the devices the active one was. The blinding was maintained until after the experiment had been concluded and the statistical analyses had been completed.

Assessment of Blood Flow. Skin temperature and cutaneous microcirculation were measured with thermography (Thermovision, Scanner 900 SW-TE, AGEMA Infrared System, Sweden) and laser-Doppler-flowmetry (LDI, Moor Instruments, Devon, UK), respectively, on a predefined area (4×4 cm), proximal and centred to the base of the middle toe. The thermography camera records the infrared emission of the skin as a measure of the skin temperature, which is affected by both cutaneous and deeper lying (muscular) structures as a result of blood perfusion and metabolic processes. A temperature-coded colour picture of the foot was taken, and the mean temperature over the predefined area was calculated and stored. Cork shields were used to cover the magnetic coils when taking the thermographic pictures, because the electrical current flowing through the active device slightly heats up the coils (by about 2°C after 30 minutes), which could not be felt by the subjects but might have unveiled the active device on the thermographic pictures. Laser-Doppler-flowmetry uses a low power laser beam to scan the skin in a raster pattern. Moving blood in the microvasculature causes a Doppler shift in the laser beam, which is processed to build up a colour coded image of blood flow in relative perfusion units (PU). Laser-Doppler-flowmetry measures the cutaneous microcirculation in the superficial layers of the skin within a depth of a few hundred of microns, as a product of number and velocity of the erythrocytes. The mean perfusion value over the predefined area was calculated and stored. Both measurements were non-contact at about 40 cm distance. In Fig. 1, examples of pictures as recorded with thermography and laser-Doppler-flowmetry are shown.

Assessment of Pressure Pain Threshold (PPT). PPT measurements were performed with a hand-held electronic algometer (Somedic AB, Stockholm, Sweden) mounted with a 1-cm diameter circular rubber probe calibrated in kilopascals. To assess the PPT, the probe was held perpendicularly and pressure increased at a constant rate of 30 kPa/s. The PPT, defined as the value where the subject felt the first change from pressure sensation to pain, was recorded. When PPT was reached the volunteers were instructed to press a button that froze the actual pressure on a digital display. The median of three measurements on each point was recorded as

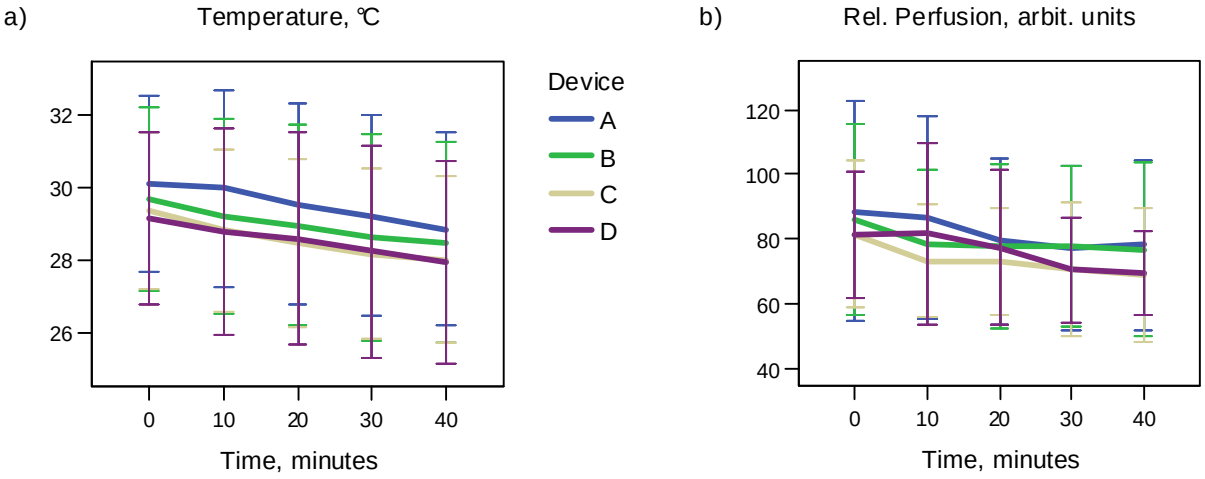

Fig. 2 Profiles of skin temperature and blood perfusion in the dorsum of the foot, at baseline (0 min), 10 and 20 min after start of stimulation, at the end of stimulation (30 min), and 10 minutes post-stimulation (40 min). Values are means ± standard deviation (n = 20).

threshold value. PPT values were measured on the top of both feet (mostly skin and bone) and on the centres of the tibialis anterior muscles.

Assessment of Vaso-Motoric Reaction to Mild Heat. A small (approximately 1 cm^2) metal plate was heated up to 41°C (computer-controlled) and was applied to the skin for 30 seconds, 4 cm medial to the centre of the tibia. Cutaneous microcirculation was measured in a predefined area (4×4 cm) around the heat stimulation site, both before and after the heat impulse, with thermography and laser-Doppler-flowmetry (see above). The heat impulse resulted in vasodilatation in the superficial layers of the skin, increasing the blood perfusion. The increase of the mean temperature and flux profiles due to the heat impulse was recorded (difference post-pre impulse).

Experimental Procedures. Each subject participated in two sessions with one week interval (on the same time of the day). In each session, the subjects received stimulation (active and/or placebo) from two devices, one for each ankle. The order and position of the four devices was randomised according to a random permutation table, prepared with a computer programme (MATLAB 7, The MathWorks Inc., Natick, MA, USA). The room temperature in the laboratory ranged from 21 to 23°C, and all experiments were performed under normal illumination conditions (fluorescent light). The subjects were in supine position, with bare legs and feet, throughout the experiment. The vaso-motoric reaction to mild heat was measured on the right and left leg, followed by determination of the PPT on right foot, right leg, left foot, and left leg. After a 10 minute rest period, the coils were placed laterally on both ankles, and baseline values for the blood flow (temperature and blood perfusion) in the right and left foot were determined. Then, the electromagnetic therapy devices were switched on. After 10, 20, 30 (end of stimulation), and 40 minutes (10 minutes post-exposure), temperature and blood perfusion were measured in the right and left foot. Finally, vaso-motoric reaction to mild heat and PPT were determined as mentioned before. One experimental session lasted in total between 1.5 to 2 hours.

Statistical analysis. The results were expressed as means and standard deviation (means ± SD) in the text and figures. The statistical procedures performed, for the analysis of the blood flow, were multivariate (skin temperature and blood perfusion) repeated measures ANOVA, with within-subject factors “device” (4 levels) and “time” (5 levels). For the analysis of PPT values and vaso-motoric reaction to mild heat, multivariate (foot PPT, leg PPT, increase in skin temperature, and increase in blood perfusion) repeated measures ANOVA was applied, with within-subject factors “device” (4 levels) and “time” (2 levels).
The software used for the statistical analysis was SPSS 14.0 (SPSS Inc., Chicago, IL, USA). A value of $P < 0.05$ was considered as significant.

Results and Discussion

There were no drop-outs in this study, and complete measurement sets were obtained for all 20 subjects. No side effects were observed in this study. None of the participants felt any discomfort, paresthesia, or pain during or after the magnetic field exposure. Only three participants felt warmth in one of the legs after the exposure, but the indicated leg was receiving placebo stimulation in all three cases. None of the participants guessed the active

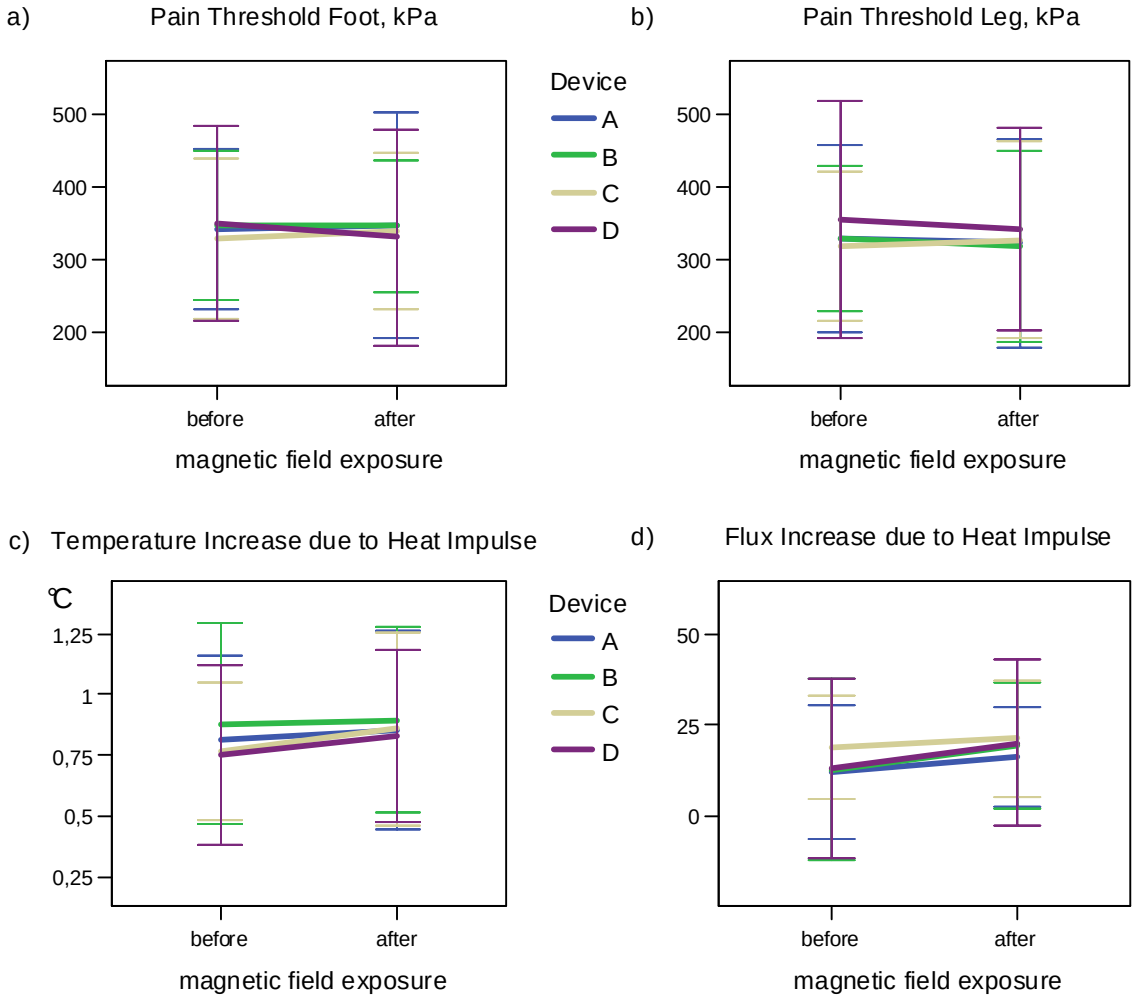

Fig. 3 Profiles of pain thresholds: on dorsum of foot, a), and on the centre of the tibialis anterior muscle, b). Profiles of vaso-motoric reaction to mild heat: temperature and blood perfusion increase caused by a 41°C heat impulse, c) and d). Measurements were done 15 minutes before and 15 minutes after magnetic field exposure. Values are means ± standard deviation (n = 20).

device correctly (only three of the participants tried to identify the active device). A few of the participants became sleepy, and four of them fell asleep during the experiment.

Skin Temperature and Blood Microcirculation (Fig. 2). At baseline, the mean value (averaged over all four devices and all 20 subjects) of the foot temperature was 29.6 ± 2.3°C (mean ± SD, n = 80), and the mean value of the foot blood perfusion was 84.3 ± 26.6 arbitrary units. At the end of the experiment, the mean values decreased to 28.3 ± 2.6°C and 73.4 ± 22.4, respectively. Profiles of the mean values for the four devices at each time point are shown in Fig. 2. The multivariate (dependent variables temperature and blood perfusion) within-subject repeated measures (factors time and device) ANOVA test showed a statistically significant effect for the time factor ($p < 10^{-8}$; partial $\eta^2 = 0.36$), but failed to reach statistical significance for the device factor ($p = 0.40$; partial $\eta^2 = 0.053$; observed power = 0.40) and the time×device interaction ($p = 0.44$; partial $\eta^2 = 0.051$; observed power = 0.82). The univariate tests confirmed the statistically significant effect ($p < 0.001$) of the time factor on both dependent variables, temperature (partial $\eta^2 = 0.56$) and blood perfusion (partial $\eta^2 = 0.36$).

Pain Thresholds and Reaction to Mild Heat (Fig. 3). Before magnetic field exposure, the mean value (averaged over all four devices and all 20 subjects) of the pain threshold in the foot was 342 ± 112 kPa (mean ± SD, n = 80), mean pain thresholds in the leg was 332 ± 124 kPa, mean temperature increase due to mild heat stimulation was 0.80 ± 0.35°C, and mean blood perfusion increase due to mild heat stimulation was 14.25 ± 20.74 arbitrary units. The post-exposure values of the means were 342 ± 126 kPa, 327 ± 135 kPa, 0.86 ± 0.38°C, and 19.24 ± 17.57 arbitrary units, respectively. The corresponding mean values for the four devices are shown in Fig. 3. The multivariate (dependent variables foot PPT, leg PPT, temperature increase, and

increase in blood perfusion) within-subject repeated measures (factors time and device) ANOVA test did not reach statistical significance, neither for the factors time ($p = 0.22$; partial $\eta^2 = 0.29$; observed power = 0.39) or device ($p = 0.30$; partial $\eta^2 = 0.08$; observed power = 0.66), nor for the time×device interaction ($p = 0.89$; partial $\eta^2 = 0.04$; observed power = 0.30).

Unblinding. Device A was the active device.

Discussion. The only statistically significant effect in this study was observed for the time factor. This means, that over time both the temperature and the blood perfusion changed. Since the subjects were in a passive supine position for 40 minutes with bare legs and feet, it was expected that the temperature would decrease over time. The results show that this was indeed what happened (see Fig. 2). This is consistent with other studies (Schuhfried et al., 2005). There are other forms of application of electromagnetic fields where either the intensity or the frequency is high enough to heat body tissue due to eddy currents (Ueno et al., 1986; Alekseev et al., 2005). But the magnetic field used in the present study is too weak to evoke eddy currents in the body of the required amplitude. Direct heating of the skin with the magnetic field device might also occur due to ohmic heating of the applicator coils (McMeeken, 1992). McMeeken (1992) observed a temperature increase of the applicator coil of 3.7°C after 15 minutes of operation, which led to a temperature increase of 0.5°C in the skin underneath the applicator (due to infrared radiation), without affecting the blood flow. In the present study, we observed a temperature increase of the applicator of 2°C after 30 minutes of operation.

There was no statistically significant effect of the device factor in the present study. If there were an effect of the device factor, then baseline values would have to be different for the different devices (different intercepts in Fig. 2 and 3). However, this is not a reasonable assumption.

It would be reasonable to assume different slopes of the profiles, e.g. if the leg treated with the active device cooled less than the leg treated with the placebo device. This is tested by the time×device interaction, which did not reach statistical significance. The observed power of this test was 82%. Therefore it is concluded that a magnetic field (only present in the active device) of strength and frequency as used in the present study does not change temperature and blood flow in healthy volunteers. This is consistent with other studies (McMeeken, 1992; Schuhfried et al., 2005; Wenzel et al., 2005).

Summary

This study shows that, in healthy volunteers, acute exposure to a weak (below 6mT) magnetic field with a specific waveform, repeated at 800 Hz, does not change skin blood flow and temperature, nor pressure pain thresholds.

Acute exposure of healthy volunteers was chosen in this study in order to detect (and quantify) a possible basic, direct effect of magnetic fields. Prolonged or repeated exposure might show different effects. Patients receiving the magnetic field stimulation might show different effects, because the biological response to electromagnetic field exposure depends on the state of the biological target tissue (Mayrovitz et al., 2001). It was shown that patients react differently than healthy people to electromagnetic therapy (Giordano et al., 2000).

The results of the present study do not allow drawing conclusions about the possible effects of electromagnetic therapy in patients. Therefore, this study can not answer the question whether enhanced microcirculation might or might not be an effect of electromagnetic therapy in patients. However, this study shows that there is no direct (acute) effect of exposure to a magnetic field, of strength and frequency as used in this study, on microcirculation in healthy subjects.

Acknowledgements

This project was financially supported by Actera A/S, Denmark, and the Faculty of Engineering, Science and Medicine, Aalborg University. The authors thank Parisa Gazerani for her kind help in the preparation of the experiment.

References

Alekseev SI, Radzievsky AA, Szabo I, Ziskin MC. 2005. Local heating of human skin by millimeter waves: effect of blood flow. *Bioelectromagnetics* 26(6):489–501.

Cullum N, Nelson EA, Flemming K, Sheldon T. 2001. Systematic reviews of wound care management: (5) beds; (6) compression; (7) laser therapy, therapeutic ultrasound, electrotherapy and electromagnetic therapy. *Health Technology Assessment* 5:1-221.

Giordano N, Battisti E, Geraci S, Santacroce C, Lucani B, Fortunato M, Mattii G, Gennari C. 2000. Analgesic-antiinflammatory effect of a 100 Hz variable magnetic field in RA. *Clin Exp Rheumatol* 18(2):263.

Jauchem JR. 1997. Exposure to extremely-low-frequency electromagnetic fields and radiofrequency radiation: cardiovascular effects in humans. *Int Arch Occup Environ Health* 70:9–21.

Kinouchi Y, Yamaguchi H, Tenforde TS. 1996. Theoretical analysis of magnetic field interactions with aortic blood flow. *Bioelectromagnetics* 17(1):21–32.

Markov MS. 2004. Magnetic and electromagnetic field therapy: Basic principles of application for pain relief. In: Rosch PJ, Markov MS, editors. *Bioelectromagnetic Medicine*. Marcel Dekker, p 251–264.

Mayrovitz HN, Groseclose EE, Markov M, Pilla AA. 2001. Effects of permanent magnets on resting skin blood perfusion in healthy persons assessed by laser Doppler flowmetry and imaging. *Bioelectromagnetics* 22(7):494–502.

McMeeken JM. 1992. Magnetic fields: effects on blood flow in human subjects. *Physiotherapy Theory and Practice* 8:3–9.

Podd J, Page W, Rapley B, Beale I. 1998. Bioelectromagnetic research and statistical power. *Proceedings of the 2nd International Conference on Bioelectromagnetism*, p 197-198.

Polk C, Postow E. 1996. *Handbook of biological effects of electromagnetic fields*. 2nd edition, CRC Press, Boca Raton, New York, London, Tokyo.

Schuhfried O, Vacariu G, Rochowanski H, Serek M, Fialka-Moser V. 2005. The effects of low-dosed and high-dosed low-frequency electromagnetic fields on microcirculation and skin temperature in healthy subjects. *Int J Sports Med* 26(10):886–90.

Shupak NM, Prato FS, Thomas AW. 2003. Therapeutic uses of pulsed magnetic-field exposure: A review. *The Radio Science Bulletin* 307:9–32. www.ursi.org/RSBissues/RSBdecember2003.pdf (retrieved June 2006).

Stavroulakis P. 2003. *Biological effects of electromagnetic fields*. Springer, Germany.

Swanson J, Kheifets L. 2006. Biophysical mechanisms: a component in the weight of evidence for health effects of power-frequency electric and magnetic fields. *Radiat Res* 165(4):470-8.

Ueno S, Lövsund P, Öberg PÅ. 1986. Effects of alternating magnetic fields and low-frequency electric currents on human skin blood flow. *Med Biol Eng Comput* 24(1):57–61.

Wenzel F, Reissenweber J, David E. 2005. Cutaneous microcirculation is not altered by a weak 50 Hz magnetic field. *Biomed Tech (Berl)* 50(1-2):14-8.

INFLUENCE OF MICROWAVE RADIATION ON SERUM ALKALINE PHOSPHATASE IN RAT

M.SEDEHI ESFAHANI, S.KHADIVI F.RASHID NAJAFI, J.GOODARZI , A.KOHBODI

Biological research center of institute of standard and industrial research Of Iran. P.o.box:31585-163

Email address:mansoureh_sedehi@yahoo.com

Abstract

The level of serum alkaline phosphatase(alp),as a a possible promoter of bone or tumor disease was studied in 80 rats exposed to microwave radiation(2450 mh with power density of 1 and 10mw/cm²), for a period of one year.
The animals were devided to 5 groups of 16 each(8males and 8 females), 4 for treatment and one for control group. First two treated groups were exposed to microwave radiation at power density of 1mw/cm² in different period (30 minutes for one group and 5 minutes for another one), daily. Next two treated groups were exposed to microwave radiation at power density of 10 mw/cm² in different period (30 minutes for one and 5 minutes for another group), daily. Control group were kept under the normal condition without any microwave exposure.
Animals were observed daily and body weight and food and water consumption was assessed weekly too.
In the end of study the blood sample were taken from the heart of animals under ether anesthesia and alp analysis was performed on blood serum of animals.
According to the test result and statistical analysis the level of alp in groups exposed To microwave radiation at power density of 10 mw/cm² was significantly increased ($p<0/011$), but in other treated groups,the statistical resuts has not been significant in comparison with control group.

Introduction :

Alkaline phosphatase is a group of enzymes found primarily in the liver and in bone.It also is produced by the placenta and to a lesser extent by the intestines and kidney.
In this study, the gole of measuring alkaline phosphatase is to check the possibility of bone or liver disease in rat after a period of one year exposure to 2450 mh microwave radiation at incident power densities of 1and 10 mw/cm2 for 5 and 30 minutes daily.

Method of study :

Animals

80 sprague Dawley rats with 5 week age were used in this investigation for a period of one year. The animals were housed individually in polycarbonate cages under standard conditions with free access to tap water and standard food (1,2,3,4,5). the rats were devided to 5 group , each containing 16 rats (8 male and 8 females) , as follows :

Group D and E : exposed to microwave radiation with power density of 1 mw/cm2 for 30 minutes daily for group D and 5 minutes daily for group E .

Group F and G : exposed to microwave radiation with power density of 10 mw/cm2 for 30 minutes daily for group F and 5 minutes daily for group G .

Group H : as a control group were kept under the same condition without any microwave exposure .

Records and Control :

The rats were weighed before experiment and weekly and recorded. Any clinical abnormality were noted and recorded .

Food and water consumption were controlled weekly too .

Method of ALP Measurment :

In the and of study the blood sample were taken from the heart of animals after 12 howrs fasting under ether anesthesia .

The level of alp was measured by enzymatic method. the enzyme splits off the phosphate group from 4-NPP to form free 4-mitrophenol. Thus the rate of formation of 4-NP by the action of the enzyme on 4-NPP at 37oC can be monitored with a recording spectrophotometer(6,7,8):

4-nitrophenylphosphate+h2o---ALP-------→-phosphate+4-nithrophenol

Statistical analysis :

Statistical evaluation of data for comparison of treated and control group were made by using one way analysis of variance (anova) technique , followed by a multiple comparison , the one way anova was applied using the F distribution to assess significance at the level of 0/05

Results and discussion :

Clinical observation :there was one death related to group E.

Body weight and food and water consumption : according to the results , the percentage of body weight and food consumption was reduced in treated groups in comparison with control(9), but the *percentage of* water intake was increased in treated groups especially in group F in comparison with control.

Serum ALP Level :

As illustrated in fig 1-3 , the level of ALP in group male of G and mixed group male and female of G that were exposed to microwave radiation at power density of 10 mw/cm2 for 5 minutes daily was significantly increased ($P < 0/01$) , but as statistical analysis is showed in table1-3 increasing of ALP in other treated groups was not significant in the level of 0/05 , in which microwave exposure at 10 mw/cm2 is suspected as a possible promoter of bone or tumor disease that should be considered (6,10,11,12)

Fig 1- Mean content of ALP in male groups

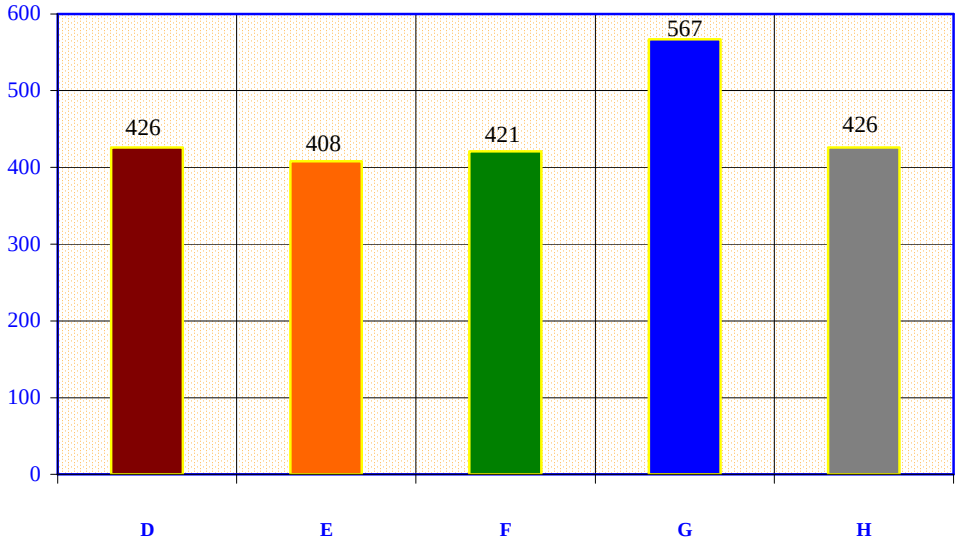

Fig 2- Mean content of ALP in female groups

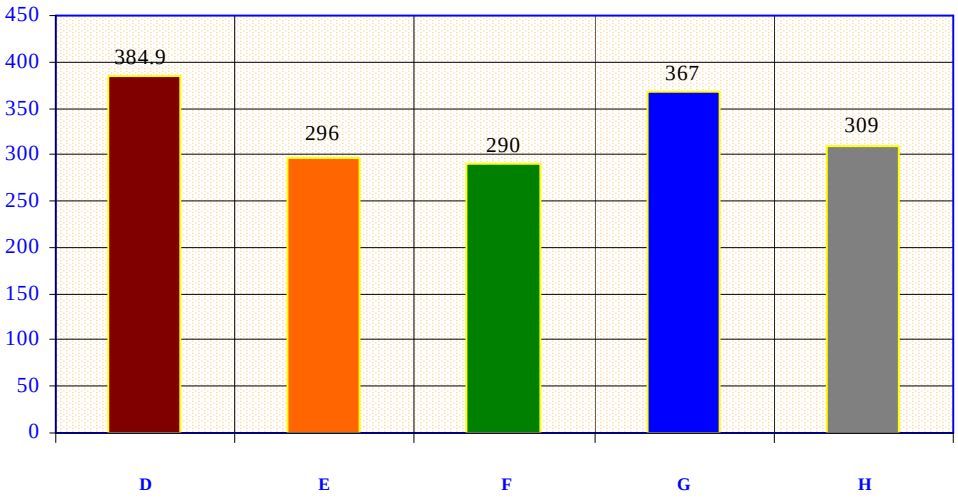

Fig 3- Mean content of ALP in Mixed groups (males and females)

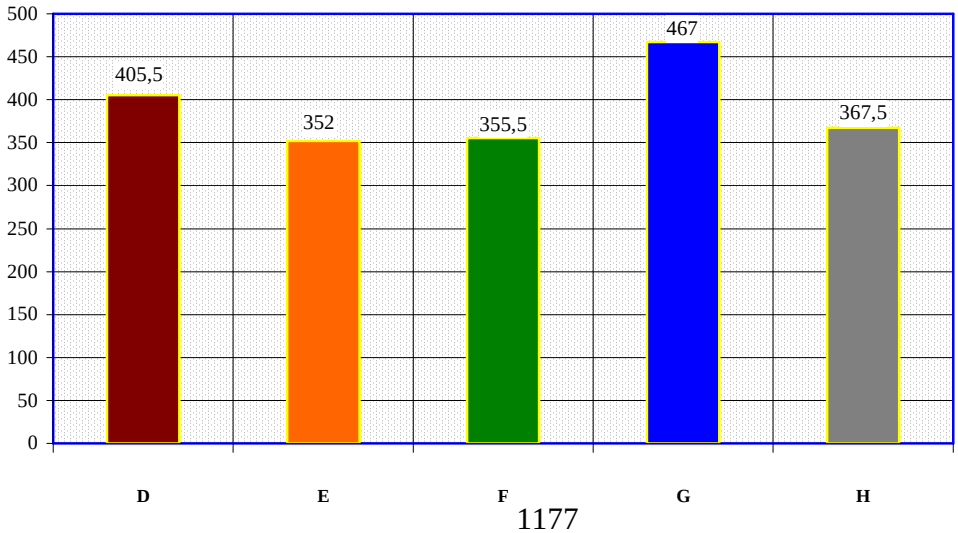

Table 1- Comparison of Statistical analysis of ALP in treated female groups with control group

Dependent Variable	(I) V14	(J) V14	Mean Difference (I-J)	Std. Error	Sig.	95% Confidence Interval	
						Lower Bound	Upper Bound
ALP	H	D	-75.13	41.41	075	-158.08	7.83
		E	13.50	41.41	.746	-69.45	96.45
		F	19.50	41.41	.640	-63.45	102.45
		G	-70.25*	41.41	095	-153.20	12.70

*. The mean difference is significant at the 05 level .

Table 2- Comparison of Statistical analysis of ALP in treated male groups with control group

Dependent Variable	(I) V14	(J) V14	Mean Difference (I-J)	Std. Error	Sig.	95% Confidence Interval	
						Lower Bound	Upper Bound
ALP	H	D	-17.00	53.55	.752	-124.28	90.28
		E	18.13	53.55	.736	-89.15	125.40
		F	5.38	53.55	.920	-101.90	112.65
		G	-141.38*	53.55	011	-248.65	-34.10

*. The mean difference is significant at the 05 level .

Table 3- Comparison of Statistical analysis of ALP in treated both male and female groups with control group

Dependent Variable	(I) V14	(J) V14	Mean Difference (I-J)	Std. Error	Sig.	95% Confidence Interval	
						Lower Bound	Upper Bound
ALP	H	D	-46.06	41.12	.265	-127.49	35.36
		E	15.81	41.12	.701	-65.61	97.24
		F	12.44	41.12	.763	-68.99	93.86
		G	-105.81*	41.12	011	-187.24	-24.39

*. The mean difference is significant at the 05 level .

Summary :

In conclusion , the results shown here confirm that , the level of ALP was increased in serum of rats exposed to microwave radiation at power density of 10 mw/cm2 is suspected as a possible promoter of bone or tumor disease , that should be considered. our data also indicate that the measure of ALP in other treated groups has not been significantly increased in the level of 0/05 in comparison with control group .

Acknowledgment :

We wish to thank to miss T.Niavarani for technical assistance and also grateful to Mr Sh. Kasgeh for statistical analysis of data, and research center of pars azmoon for supporting this work .

References :

1- Presented pursuant to act Eliz “code of practice for the housing and care of animals used in scientific procedures” , C.14 section 21 , 1986 .

2- Clarke , HE. Coates Meeva . JK, Ford “Dietary standards for laboratory animals” report of the lac diets advisory committee. Lab.11 1-28 , 1977 .

3- Royal society / UFAW “Guidelines on the care of laboratory animals and their use for scientific purposes” , 1987 .

4- Ivan Bartosek et al “Animals in toxicological research” Raven press , 1981 .

5- Wallach , Boever “Diseases of animals, medical and surgical management” W.B saunders company 1983 , P 132-195 .

6- Carl A . Burtis Tiets textbook of chemical chemistry 2th , 1994 .

7- Weisshaar , D. Grossau , EU. Faderl B.med. welt 26 , 387-390 , 1975 .

8- Bowers , GM , JR , McComb , RB : A continuous spectrophotometric method for measuring the activity of serum alkaline phosphatase clin chem. , 12 : 70-89 , 1966 .

9- Ray 5 , Behari J “Physiological changes in rats after exposure to low level of microwaves” Radiat Res 123 (2) : 199-202 Aug 1990 .

10- Gorczynska E , wegrzynowicz R , “Effect of static magnetic field on some enzymes activities in rats” . J Hyg Epidemol Microbiol Immunol 33 (2) : 149-55 , 1989 .

11- Pashovkina Ms, Akoev IG.“Effect of low intensity pulse modulated electromagnetic radiation on activity of alkaline phosphatase in blood serum” , Radiats Biol Radioecol . 41 (1) : 62-6 , 2001 .

12- Schmitto, “The influence of the electromagnetic filed on the activity of alkaline phosphatase in immobilised children” . Arch orthop trauma surg 93 (1) : 21-4 , 1978 .

EFFECT OF MICROWAVE EXPOSURE ON SOME HEMATOLOGICAL PARAMETERS IN RAT

M.SEDEHI ESFAHANI,A.KOHBODI,S.KHADIVI,

Biological research center of institute of standard and industrial research of Iran.P.o.box:31585-163

Email address:mansoureh_sedehi@yahoo.com

Abstract

80 sprague Dawley rats were exposed to 2450 mhz microwave field for a period of one year. The experiment groups were devided to 5 groups,each 16(8 males and 8 female), 4 for treatment,and one,for control(D,E,F,G,H).

The incident power density of the first two experiment groups was 1mw/cm^2,and, for next two grours,was 10mw/cm^2.The daily exposure time,was5 minutes for groups F and G,and 30 minutes for groups,D and F. The animals in control group(H) were under normal condition without any microwave exposure.

In the end of the study the blood samples were taken from the heart of animals under ether anesthesia,and determination of blood parameters were performed by cell counter auto analyser.

Accrrding to the statistical results the level of RBC in male groups of F and G,and percentage of PCVin female and male groups of F,and content of HB,in female groups of F,in comparison with control group were significantly increased and variation of results in other groups were not significant.

Introduction :

The aim of this study was to investigate and check the possibility altration of some blood parameters in rats after a period of one year exposure to 2450 Mh microwave radiation at power density of 1 and 10 mw/cm^2 for 5 and 30 minutes daily and also to compare the treated groups with that of control group .

Method of study :

Animals

80 sprague dawley (SD) rats with 5 weeks age were used this study for a period of one year. The animals were housed individually in polycarbonate cages under standard condition with free access to tap water and standard food (1,2,3,4,5).the rats were devided into 5 groups (4 treated and 1 control) of eight male and eight female rats each .Two first experimental groups were exposed to 2450 mh microwave radiation with field powers density of 1mw/cm^2 for 30 minutes daily for group (D) and 5 minutes daily for group (E) .

Next two treated groups were exposed to 2450 mh microwave radiation with filed power density of 10 mw/cm^2 for 30 minutes for group (F) and 5 minutes for groups (G) daily.Control group(H) were under normal condition without any microwave radiation exposure.

Records and control :

The animals were weighed before experiment and weekly and recorded .

Any clinical abnormality were cared and recorded. Food and water consumption were also weekly controlled .

Blood analysis :

In the end of study the blood samples were taken from the heart of animals under ether anesthesia and the blood samples were mixed with ethylenediamine tetraacetic acid (EDTA) and then analysed by auto analyser of cell counter .

Statistical analysis :

The differences between groups were analysed using appropriate one way analysis of variance (anova) technique , followed by a multiple comparison .

The one way anova was applied using the F distribution to assess significance in the level of 0/05 .

Fig 1- mean difference of R B C in female groups

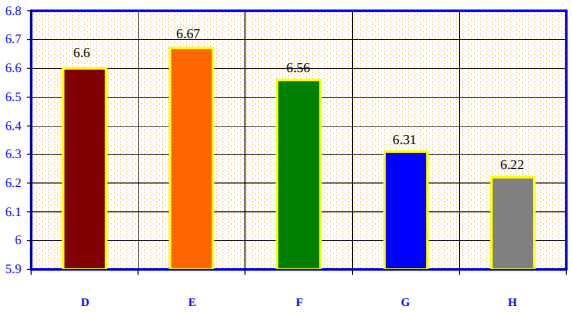

Fig 2- mean difference of R B C in male groups

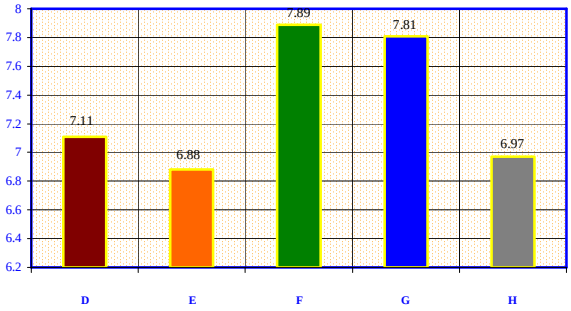

Fig 3- mean difference of P V C in female groups (%)

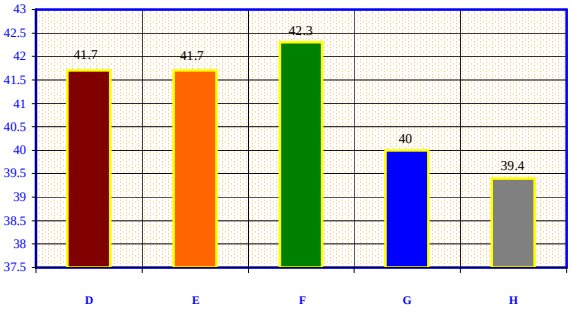

Fig 4- mean difference of P V C in male groups (%)

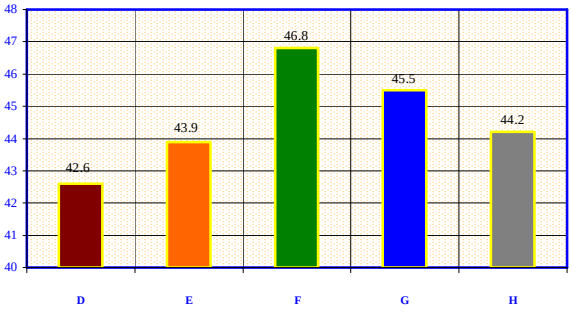

Fig 5- mean difference of Hb in male groups (g/dl)

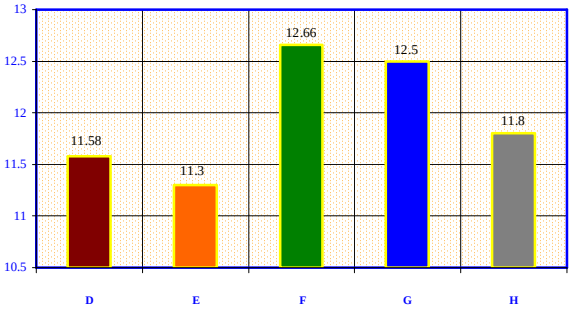

Fig 6- mean difference of Hb in female groups (g/dl)

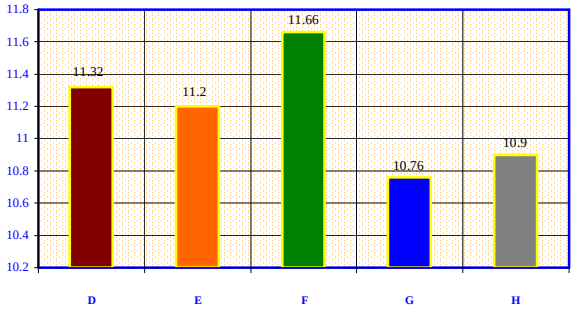

Summary :

The data presented in this study indicate that there is increasing of blood parameters of RBC , PVC and Hb in treated groups exposed to microwave radiation at power density of 10 mw/cm^{2,} in

which microwave exposure in this field is a probable agent for stimulation of proliferation processes in red bone marrow,may be due to hypoxia and releasing of erythropoietin hormon, that can be considered. Our data also indicate that the test results of same blood parameters in treated rats exposed to microwave radiation at 1 mw/cm^2 powers density has not been significant in comparison with that of control group.

Acknowledgment :

We wish to thank to Dr Z. Maleki for her advice and comments, and also grateful to Miss T.Niavarani, Miss F.Najafi for technical assistance and Mr Sh.kasgeh for assistance with the data analysis and statistical evaluation.

References :

1- Clarke , HE. Coats , Meeva. JK , Ford "Dietary standards for laboratory animals" report of the lac diets advisory committee , lab .11 1-28 , 1977 .
2- Presented pursuant to act Eliz"code of practice for the housing and care of animals used in scientific procedures" C.14 section 21 , 1986 .
3- Royal society / UFAW "Guidelines on the care of laboratory animals and their use for scicntific purposes" , 1987 .
4- Ivan Bartosek et al "Animals in toxicological research" Raven press , 1981 .
5- Wallach , Boever "Diseases of animals,medical and surgical management" W.B saunders company p 132-195 , 1983 .
6- Ragan .HA, Phillips RD et al"Hematologic and immunologic effects on pulsed microwaves in mice" Bioelectromagnetics ; 4 (4) : 383-96, 1983.
7- Koveshnikova IV. Antipenke EN. "Changes in body weight of rats during irradiation with microwave of nonthermal intensity" Radiobiologiia . 28 (4) : 561-3 , 1988 .
8- D , Andrea JA , Gandhi op, et al "Physiological and behavioral effects of chronic exposure to 2450 Mh microwaves" J Micro power;14(4):351-62,1979
9- Human exposure to radio frequency radiation : A Comprehensive review pertinet to air force operations .
http://www.brooks.af.mil/AFRL/HED/hedr/reports/human_exosure/htmfile 13.html .
10-The associated bioelectromagnetics technologists http://emfbioeffects. Org, 4/15/04 .
11- Ray – S , Behari –J"Physiological changes in rats after exposure to low level of microwaves" Radiat – Res 123 (2) 199-202 , Aug 1990 .
12-cleary Sf et al"Effects of x-band microwave exposure on rabbit erythrocytes"Bioelectromagnetics;3(4):453-66,1982.
13-Alex O Sonnenwirth,Leonard Jarett"clinical laboratory methods and diagnosis"8th 1980.
14-Carl A,Burtis tiets"textbook of clinical chemistry",2th,1994.

EFFECT OF EXTREMELY LOW FREQUENCY ELECTROMAGNETIC FIELDS ON MOUSE THYMUS AND TESTIS

FUMIO SHIMAMOTO,
DEPARTMENT OF HEALTH AND SCIENCE, PREFECTURAL UNIVERSITY OF HIROSHIMA
e-mail:simamoto@pu-hiroshima.ac.jp

HANDAN TUNCEL,
DEPARTMENT OF BIOPHYSICS, CERRAHPASA MEDICAL FACULTY ISTANBUL UNIVERSITY

TAKASHI TAKATA, KOUEI SAI
DERPATMENT OF ORAL PATHOLOGY, HIROSHIMA UNIVERSITY

MASAAKI TATUKA,
DEPARTMENT OF MOLECULAR RADIOLOGY, RESEARCH INSUTITUTE FOR RADIATION BIOLOGY AND MEDICINE, HIROSHIMA UNIVERSITY

Abstract

PURPOSE: We examined the apoptotic effects of extremely low-frequency electromagnetic fields (EMFs) on murine thymus gland and testis after whole-body irradiation.

METHODS: Thymus gland and testis are highly susceptible to ionizing irradiation (IR). When suffered to apoposis by IR, the apoptosis-related signal molecules including nuclear transcription factors and cytoplasmic caspases are activated. Here, we measured the expression levels of nuclear transcription factors such as ATF-3 and p53 and a caspase-3-cleaved product LyGDI/GDI-D4/RhoGDI2/RhoGDIβ in thymus gland and testis after whole-body EMFs irradiation.

RESULT: Both transcription factors, ATF-3 and p53, were not up-regulated according to time course and dose-response of EMFs. The caspase-3-cleaved product, N-terminal deleted 21-kDa fragment of LyGDI (ΔN(1-19)LyGDI), was also not induced by EMFs. Besides, in immunoblotting of ΔN(1-19)LyGDI, we noticed an unexpected 55-kDa band which was disappeared by EMFs although this epitope has not been identified. CONCLUSION: Apoptotic signals mediated by DNA strand breaks are not generated in whole-body irradiation of EMFs. Instead of this, an unknown intracellular signalling may possibly be provoked in EMFs-irradiated thymic gland and testis.

Introduction

An association between residential extremely low-frequency electronic and magnetic fields (EMF) and childhood leukemia was first reported in 1979 by Wertheimer and Leeper[1)]. In Japan also epidemiologic studies recently showed that residential power-frequency magnetic fields levels above 0.4 micro T exposure was associated with a higher risk of childhood leukemia (acute lymphoblastic leukemia)[2)]. Experimentally, we found that the offspring mice coming from late pregnant mice exposed to a 500mG 50Hz developed chronic

myelogenic leukemia with chronic exposure[3]. Exposure to a 60-Hz magnetic field at 0.001mT for 24 hr was reported to cause a significant increase in DNA single-and double-strand breaks in the brain cells of rats[4].

As a general mechanism, apoptotic cell death is triggered by DNA strand breaks. When apoptotic signalling caused by ionizing radiation (IR) is generated in the cells, transcription factors such as ATF-3 and p53 are up-regulated. Subsequently, as post-mitochondrial signals, caspases are activated to execute apoptosis. LyGDI, also known as GDI-D4/RhoGDI2/RhoGDIβ, is a substrate of caspase-3 and is cleaved by activated forms of this during IR-induced thymic apoptosis[5]. Therefore, the cleaved product, N-terminal deleted ΔN(1-19)LyGDI, becomes a marker for the activation of caspase-3. To examine whether EMFs provoke such an apoptotic signalling, we measured the expression levels of either transcription factors and ΔN(1-19)LyGDI in thymic gland and testis from whole-body irradiation of EMFs. The presented data clearly indicate that EMFs do not induce the apoptotic signalling in both thymic gland and testis. Besides, an unidentified immunoblot band, which is reactive to N-terminus of ΔN(1-19)LyGDI, has been found to respond to EMFs in both organs.

Materials and Methods

Animal: C57BL/6NCrlCrlj male mice were purchased from Charles River Japan Inc. at 6 weeks of age.

EMF exposure: The exposure facility was produced by Chugoku electronics (Hiroshima, Japan). Magnetic fields were provided by electromagnet which has air gap of 10cm cubic and exciting coli of 1400 turns. Sixty Hz magnetic fields of 100mG, 500mG, 1G, 5G and 10G were generated for exposure. Animals in the air gap were kept under constant conditions of temperature(24±2℃) and humidity(50± 10%).

Experimental procedure:

1) To investigate expression of ΔN (1-19) LyGDI and full-length LyGDI in the exposed cells, mice were exposed to 60Hz field 5G for 6 hours. Then thymus and testis were aseptically taken out from sacrified mice.
2) Time-dependent p53 and ATF-3 were studied with 60Hz field of 10G, at 0, 3 and 6hr, respectively.
3) Dose-dependent p53 and ATF-3 were examined with 60Hz field of 0, 0.1, 0.5, 1, 5 and 10 G, respectively for 6hr.

Mouse thymus irradiated with 5 Gy was used as positive control in expression of ATF-3 and p53.

Antibodies:

Primary antibodies used in the present study is summarized in Table 1.

Table 1. Primary antibodies used in the present study

Recognized molelcule	antibody	Source	Type number
Full length LyGDI	goat polyclonal antibody	Santa Cruz	sc-6047G
N-terminal deleted form of LyGDI	monoclonal antibody	Active Motif	40941
p53	goat polyclonal antibody monoclonal antibody	Santa Cruz Cell Signaling	sc-6243G 2524
ATF-3	rabbit polyclonal antibody	Santa Cruz	sc-188
α-tubulin	monoclonal antibody	Cederlane	L9002T

Protein analysis:

To extract total protein, thymus and testis was homogenized with ice-cold sodium dodecyl sulfate(SDS) sample buffer (pH 6.8) consisting of 25mM Tris-HCl, 5% glycerol and 1% SDS. The homogenized solution was sonicated five times for 5 s on ice and centrifuged at 15,000 rpm for 1min at 4℃. The supernatant was then used for Western blot analysis. After extraction, the protein concentration was determined using a BioRad protein assay Kit. Then Protein of 20 micro gr per lane were applied to a 12% SDS-polyacrylamino gel, after which whole cell lysate and the fractionated samples were resolved by electrophoresis and transferred to Immobilon-P membrane. The gels were probed with primary antibodies, followed by secondary antibodies. Horseradish peroxidase-conjugated anti-goat rabbit antibody and horseradish peroxidase-conjugated anti-mouse or anti-rabbit donkey antibodies were used as secondary antibodies. Proteins were visualized on X-ray film using ECL Western Blotting Detection Reagent.

Results and discussion

To elucidate the apoptosis-inducing signal of exposed thymus and testis cells, we first investigated the cleavage of LyGDI. In mouse LyGDI, cleavage by caspase 3 and caspase 1 occurs after the Asp^{18} and Asp^{54} residues, respectively, resulting in the production of two truncated protein, 21-kDa and 17-kDa products. Thus the products of truncated LyGDI indicates which caspase are activated in exposed cells. But as Figure 1 shows, truncated LyDGI was not detected in both of thymus and testis with 5 G exposure for 6hr. Interestingly, unknown substance (55kDa) reactive antibody recognized the N-terminal amino acids of the deleted ΔN (1-19) LyGDI, was detected in thymus and testis cells and indicated decrease in exposed both the cells(Figure 1-B).

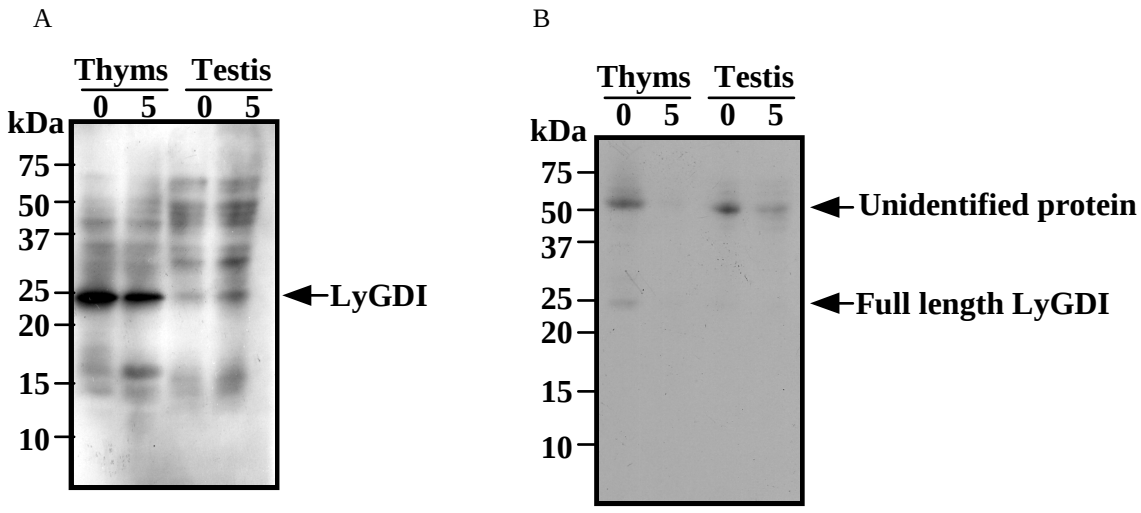

Figure1. Truncation of LyGDI and full-LyGDI after magnetic irradiation for 6hr. Panel A: Full-LyGDI was detected in both of thymus and testeis with 0 and 5 G. Panel B: Truncation of LyGDI was not found in both of thymus and testis with 0 and 5 G, respectively. Unknown substance was detected in about 55KDa with antibody of delta19-LyGDI.

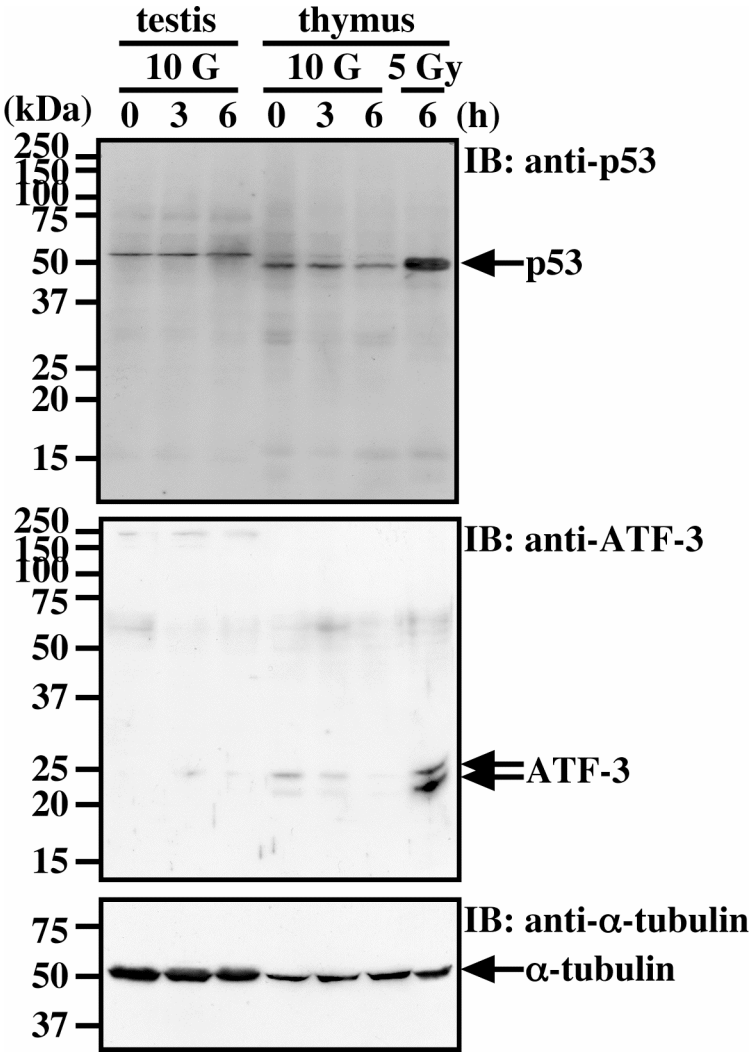

Figure 2. Variation in the protein level of p53 and ATF-3 in thymus and testis with time after exposure with 10 G.

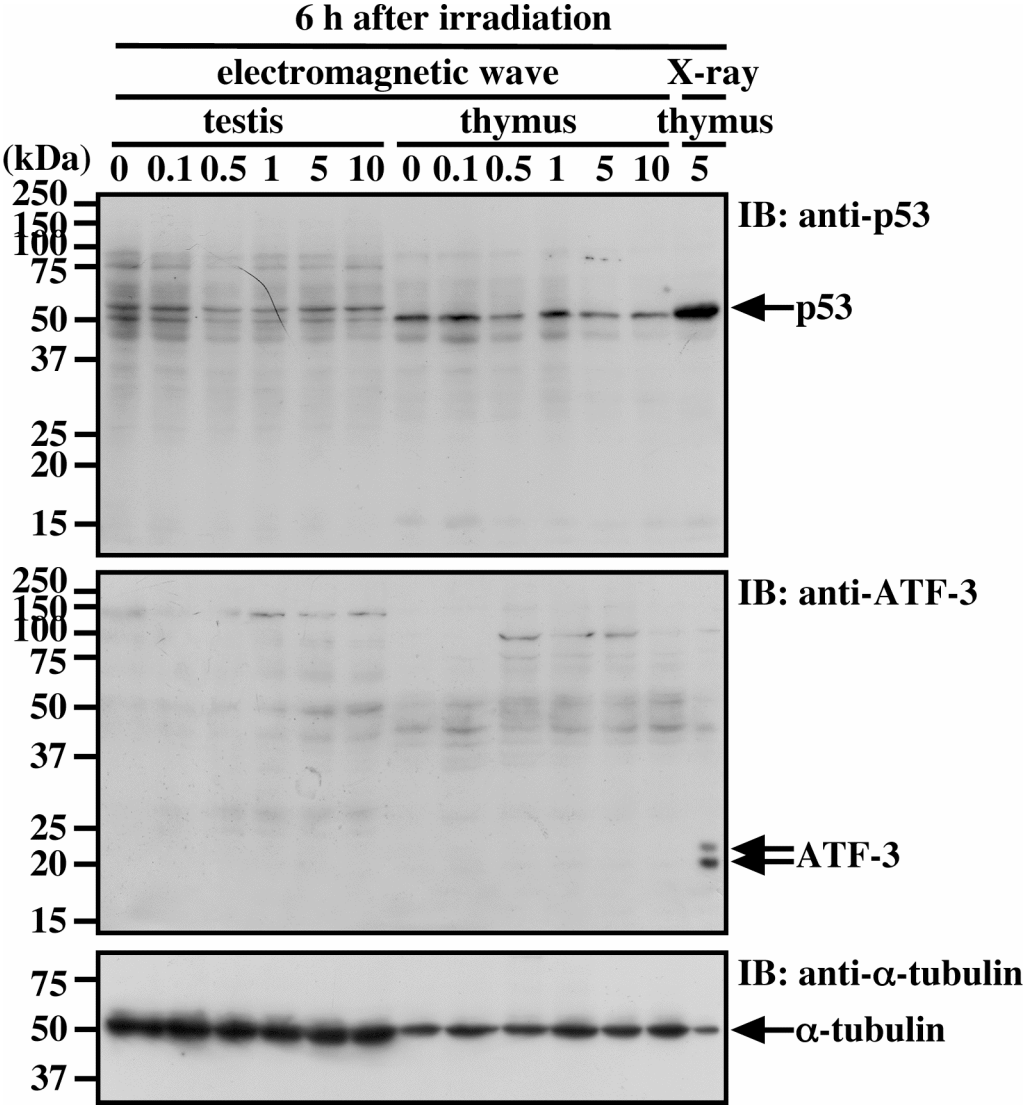

Figure 3. Effect of the exposed dose on activation of p53 and ATF-3 of thymus and testis in 6hr after exposure.

ATF3(activating transcription factor 3)is a member of the ATF/CREB subfamily of basic-region leucine zipper(bZIP) protein and is induced in response to endoplasmic reticulum stress or amino acid starvation[6]. ATF3 is a novel stress-activated regulator of p53 protein stability/function providing the cell with a means of responding to a wide range of environmental insult[7]. It is also reported that regulation of ATF3 induction after DNA damage utilizes both the p53-dependent and-independent pathways, and may also involve MAP kinase signalling pathway[8]. In this study we could not detected significant expression of AFT3 and p53 of thymus and testis in time- and dose-dependent variation. The important role of ions, particularly of Ca^{2+}, in the apoptotic process of the exposed cells is considered[9], and then there may be another p53-independent pathway in magnetic field action on apoptosis.

Those result indicated that that there may be another signaling pathway to produce the effects of EMF, although EMF-induced signaling cascade that mediates apoptosis was not found.

Acknowledgements

We would like to thank Emeritus Prof. S.Keitoku, Miss Sakiie and Miss Suto for help of animal experiment and molecular analysis. This work was supported by the Research Fund of Prefectural University of Hiroshima, H16(2003).

Reference

[1] Wertheimer N, Leeper E. Electrical wiring configurations and childhood cancer. Am J Epdemiol. 1979, 109: 273-84

[2] Kabuto M, Nitta H, Yamamoto S, Yamaguchi N, Akiba S, Honda Y, Hagihara J, Isaka K, Saito T, Ojima T, Nakamura Y, Mizoue T, Ito S, Eboshida A, Yamazaki S, Sokejima S, Kurokawa Y and Kubo O. Childhood leukemia and maginetic fields in Japan: A case-control study of childhood leukemia and residential power-frequency magnetic fields in Japan. Int J Cancer. 2006, 119: 643-650

[3] Shimamoto F, Tuncel H, Takada T, Aoki E, Sai K, Watanabe M, Keitoku S. Effect of extremely low frequency electromagnetic fields on pregnant mice. Biological effects of EMFs 3rd International Workshop Proceedings, 2004, 939-943

[4] Lai H and Singh NP. Magnetic-Field-Induced DNA strand breaks in brain cells of the rat. Environmental Health Perspectives. 2004,112,687-693

[5] Xinwen Zhou, Shiho Suto, Takahide Ota, and Masaaki Tatuka.: Nuclear Translocation of cleaved LyGDI dissociated from Rho and Rac during Trp53-dependent ionizing radiation-induced apoptosis of thymus cell in vitro. Radiation research 162,287-295(2004)

[6] Jiang Hy, Wek S A, MuGrath BC, LuD, Hai, Harding HP, Wang X, Ron D, Cavener DR.: Activating transcription factor 3 is integral to the eukaryotic initiation factor 2 kinase stress response. Mol Cell Biol. 2004 Feb;24(3):1365-77.

[7]Yan C, Lu D, Hai T, Boyd DD.: Activating transcription factor 3, a stress sensor, activates p53 by blocking its ubiquitination EMBO J. 2005 Jul 6;24(13):2425-35. Epub 2005 Jun 2.

[8] Fan F,Jin S, Amundson SA, Tong T, Fan W, Zhao H, Zhu X, et al.: ATF3 induction following DNA damage is regulated by distinct signaling pathways and over-expression of ATF3 protein suppresses cells growth. Oncogene. 2002 Oct 24;21(49):7488-96.

[9] Santini MT, Ferrante A, Rainaldi G, Indovina P, Indovina PL.:Extremely low frequency (ELF) magnetic fields and apoptosis. Int J Radiat Biol. 2005 Jan;81(1):1-11

EFFECTS OF RF ELECTROMAGNETIC FIELDS ON MICROORGANISMS

LUDĚK STRAŠÁK[1,3], LUKÁŠ FOJT[1,3], VÁCLAV ŽALUD[2], JAN NOVÁK[1], FRANTIŠEK VOŽEH[2], VLADIMÍR VETTERL[1,3]

1 INSTITUTE OF BIOPHYSICS, CZECH ACADEMY OF SCIENCES, KRÁLOVOPOLSKÁ 135, 612 65 BRNO, CZECH REPUBLIC
2 CHARLES UNIVERSITY IN PRAGUE, FACULTY OF MEDICINE IN PILSEN, DEPARTMENT OF PATOPHYSIOLOGY, LIDICKÁ 1, 301 66 PLZEŇ, CZECH REPUBLIC
3 DENTAL RESEARCH CENTER, MASARYK UNIVERSITY, VINAŘSKÁ 6, 603 00 BRNO, CZECH REPUBLIC

Abstract

We examined the viability of bacteria Escherichia coli and yeast Saccharomyces cerevisiae after their exposure to radio-frequency electromagnetic field. The frequency of the field was f=867 MHz, the maximal power was 10W and the maximal duration of irradiation was 48min. The exposure took place at laboratory temperature. We measured the viability using optical spectrography of microbial culture in broth and we also used the CFU (colony forming units) counting on agar plate. We observed the decrease of viability both for bacteria and yeasts. According to our previous results for ELF-EMF the electromagnetic field effect showed the saturation and the viability decrease of bacteria was bigger compared to decrease in viability of yeasts.

Introduction

High frequency electromagnetic fields (HF-EMF), very often called as radio-frequency (RF), are electromagnetic fields with frequency in the range of GHz. It consists of GSM range (0.9-2.1 Ghz) and microwaves (up to 3000 GHz) The wave length in vacuum is from 0.33m – 0.1 mm.
The effect of high frequency electromagnetic fields on living organisms is subjected to research. The importance of investigation growths with increasing use of different high-frequency devices, mainly cell phones, that produce potentially harmful radiation. Controversy and contradiction still surround the question whether HF-EMF cause any detectable biological effects. In spite of great deal of results it is necessary to observe that it is often difficult to obtain a good repeatability of data among different laboratories, thus generating conflicting results about possible effects. It is important to perform all experiments in well-defined experimental conditions. Searching in the databases we must have on mind that the results depend on the power of electromagnetic field, on the examined cells or tissue, on the duration of exposure and on the other parameters. We can bring in works showing the HF-EMF effects (1-3), or showing no EMF effect (4,5) on living organisms.

Electromagnetic fields can have negative effects on human. International Commission on Non-Ionizing Radiation Protection, part of WHO, estimated on the base of plenty scientific studies the exposure limit for HF-EMF SAR=0.4W/kg (6). There are not clear evidences whether long-term exposures under the limit are harmful for health. The mechanism of acting is not still clarified. The possible way to understand it could be experiments on microorganisms in vivo.

Microorganisms – bacteria and yeasts seem to be good biological objects to study electromagnetic fields effects. Bacteria, their life cycle and metabolic paths are well-examined and described. Short replication time enable us

to study more bacterial generations. Similar properties have also yeasts. They are the simplest eucaryotic organisms. Using microorganisms we study effects both on cell level and the reaction of the whole organisms. The EMF effects on bacteria has been studied for many years (7-10).

In our previous studies we applied low-frequency electromagnetic fields (50 Hz, Bm=10mT, duration of exposure till 1h) on different bacterial strains (for example *Escherichia coli, Leclercia adecarboxylata, Staphylococcus aureus...*) and on the yeasts (S*accharomyces cerevisiae*). We observed the decrease of viability of exposed bacteria and yeasts. The decrease was strain-dependent, the effect was higher for rod-like bacteria, spherical bacteria were more resistant to electromagnetic field exposure (11-15).

In this work we used HF-EMF on the same microorganisms. The electromagnetic field was the same as was for exposure of neurodefective C3H mices. The acute effect of HF EMF on the central nervous system excitation and inhibition and some histochemical (NADPH diaphorase) and immunohistochemical (c- Fos) characteristics were investigated. The acute exposure to HF EMF had no significant effect on these parameters but the long-term irradiation (3hours daily, 1-2 months, 880MHz) had. (16). The exposure induced the difference in NADPH-diaphorase activity in hippocampus in C57B1/7 mice and shifted spontaneous cortical and LTH hippocampal activities to lower frequencies (17).

Experimental

Bacteria

Bacteria *Escherichia coli* K12 Row, genotype 58-161 *metB1*rpsL 1^{+} F^{def}(P.Fredericq) from Department of biology of Faculty of Medicine of Masaryk University Brno (Czech Republic) were used. Bacteria were cultivated in TY broth (8 g tryptone, 5 g yeast extract – HiMedia Lab, Bombay; 5 g NaCl –Lachema Brno/ 1 l water). The growth in closed system took place in laboratory temperature (25°C)

Yeasts

The prototrophic tetraploid strain *α/A* of yeast *Saccharomyces .cerevisiae* CCY 21-4-59 (yeast collection, Institute of Chemistry, Slovak Academy of Science, Bratislava) was used. Yeast cultures were grown in Malt extract Broth (2% Malt extract broth – Fluka, 2% Glukose – Lachema Brno) laboratory temperature (25°C). Number of microorganisms was determined using spectrophotometry.

For all experiments fresh yeasts and bacteria cultures were used.

Spectrophotometry

Spectrophotometer Libra S 22(Biochrom) was used to measure optical density (OD) at the wavelenghts 570 and 620nm. As a reference sample the distilled water was used. The calibration curve was repeatedly measured by taking values of OD_{570} or OD_{620}. and counting of corresponding number of CFU (see bellow). The logarithmic calibration curves were calculated by the method of minimal squares from 36 measured data.

HF-EMF Exposure

Electromagnetic field was generated by HF generator with HF amplifier. Frequency of the field was 867 Hz (close to the frequencies used in mobile phones). The wave (TEM 111) was directed by a waveguide to the place of exposure). The power output was 10W. The system microorganisms in broth were exposed 4.5-5h since its inoculation to field with SAR=2W/kg. The density of cells during the exposure was approximately 10^6 cells/ml.

Statistics

The data are collected from 5 experiments. Each experiment consists of 3 measurements. The Student's statistics (P=0.95) and t-test were used to analyse.

Results and discussion

Bacteria *E.coli* were exposed to electromagnetic field for 12min, 24min and 48 min. Fig. 1 shows the growth curve of bacteria. The number of bacteria is expressed in units optical density (OD), it means relative absorbance of bacterial culture compared with the absorbance of reference (water). Time T=0 h marks the beginning of exposure. The decrease of number of bacteria in solution was observed for all exposed samples. The decrease of viability is adequate to duration of exposure.
Yeasts *S.cerrevisiae* were exposed to electromagnetic field by the same way as bacteria. The growth curves are presented on Fig. 2. Comparing growth curves *E.coli* and *S.cerevisiae* we can observe smaller effect of EMF on yeasts. The significant changes in growth curve were observed for 24 min and 48 min exposures.

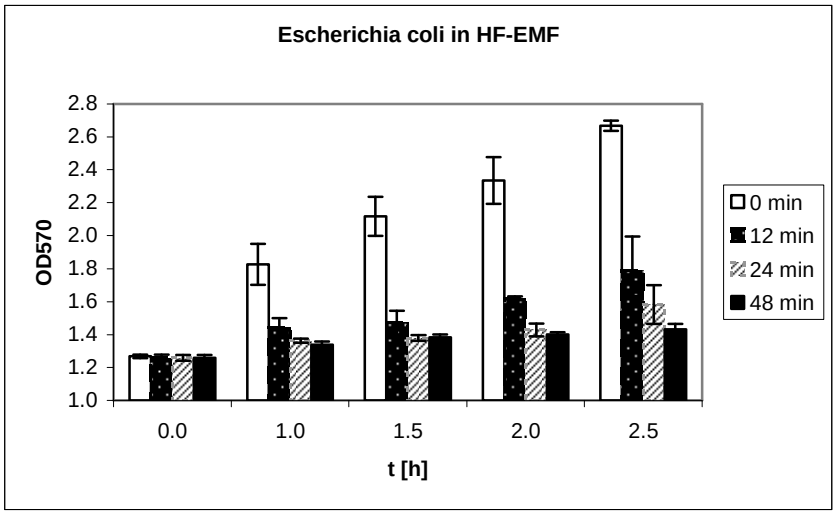

Fig.1. *Growth curves of bacteria E.coli after magnetic field exposures.*

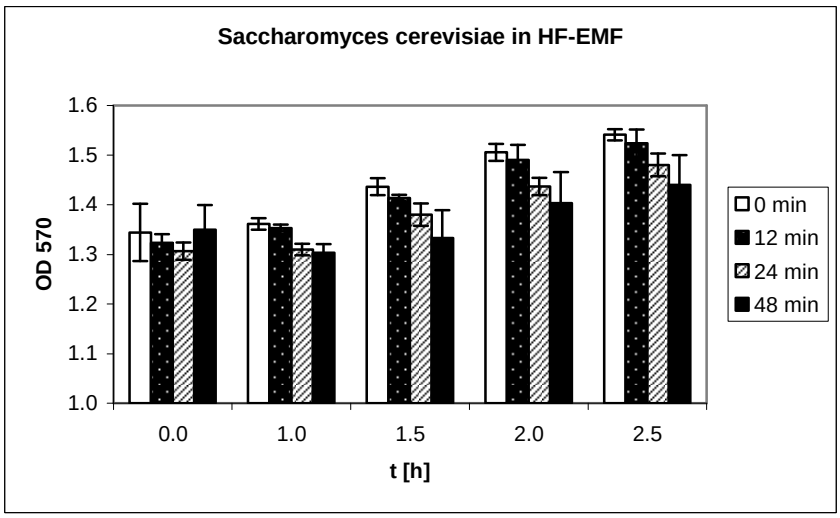

Fig.1. *Growth curves of yeast S.cerevisiae after magnetic field exposures.*

These results show that
a) EMF decreases the number of cells in broth.
b) EMF effect is stronger in bacteria cells
c) the decrease of the number of cells is apparent in the first serie of measurement after exposure.
d) the number of cells in affected cultures is growing with time, but the growth is slower than in control culture.
e) the effect of HF-EMF on the observed parameters is similar to the effect of ELF-EMF (11-13)

From the results it seems that EMF kill part of cells in broth. The growth of affected cultures is retarded by the smaller initial number of cells continuing to division process. The next progress of exposed cultures continues by the normal way, with the same rate of division.

It would be useful to perform the experiments measuring the number of cells during the EMF action.

References

1) M.H. Repacholi, A. Basten, V. Gebski, D. Noonan, J. Finnie and A.W. Harris, Lymphomas in Eμ-Pim1 transgenic mice exposed to pulsed 900 MHz electromagnetic fields, Radiat Res 147 (1997), 631–640.
2) B. Junkersdorf, H. Bauer and H.O. Gutzeit, Electromagnetic fields enhance the stress response at elevated temperatures in the nematode Caenorhabditis elegans, Bioelectromagnetics 21 (2000), 100–106.
3) T. Miyakawa, S. Yamada, S.-I. Harada, T. Ishimori, H. Yamamoto and R. Hosono, Exposure of Caenorhabditis elegans to extremely low frequency high magnetic fields induces stress responses, Bioelectromagnetics 22 (2001), 333–339.
4) T.D. Utteridge, V. Gebski, J.W. Finnie, B. Vernon-Roberts and T.R. Kuchel, Long-term exposure of Eμ-Pim1 transgenic mice to 898.4 MHz microwaves does not increase lymphoma incidence, Radiat Res 158 (2002), 357–364.
5) .D. Utteridge, V. Gebski, J.W. Finnie, B. Vernon-Roberts and T.R. Kuchel, Long-term exposure of Eμ-Pim1 transgenic mice to 898.4 MHz microwaves does not increase lymphoma incidence, Radiat Res 158 (2002), 357–364.
6) ICNIRP Guidelines, Guidelines for limitting exposure to time-varying electric, magnetic, and electromagnetic fields, ICNIRP, Health Physics, 74(1998), 494-522
7) Goldblith S.A., Wang D.I.C. Effect of microwaves on Escherichia coli and bacillus subtilis. Appl. Microbiol. 15(6) (1967), 1371-1375.
8) Belyaev Y., Alipov Y.D., Shcheglov V.S., Lystsov V.N. Resonance effect of microwaves on the genome conformational state of E.coli cells. Z. Naturforsch. 47C (1992), 621-627.
9) Atmaca S., Akdag Z., Dasdag S., Celik S. Effect of microwaves on survival of some bacterial strains. Acta Micr. Immun. Hungarica 43(4) (1996), 371-378.
10) Yeo C.B.A., Watson I.A., Stewart-Tull D.E.S., Koh V.H.H. Heat transfer of Staphylococcus aureus on stainless steel with microwave radiation. Journal of Applied Microbiology 87 (1999), 396-401.
11) Strašák L., Vetterl V., Šmarda J., Effects of low-frequency magnetic fields on bacteria Escherichia coli, Bioelectrochemistry and Bioenergetics 55(2002)161-164
12) Fojt L., Strašák L., Vetterl V., Šmarda J., Comparison of the low-frequency magnetic field effects on bacteria Escherichia coli, Leclercia adecarboxylata and Staphylococcus aureus, Bioelectrochemistry 63 (2004), 337-341
13) Strašák, L, Fojt L., Vetterl, V, Šmarda, J., Effects of low-frequency magnetic fields on the living organisms, Proceedings of Biological effects of EMFs, 3rd International workshop, Kos, Greece, 4.-.8.10.2004, Ed: P.Kostarakis, p.944-949.
14) Strašák L, Vetterl V, Fojt L., Effects of 50 Hz magnetic fields on the viability of different bacterial strains,ELECTROMAGNETIC BIOLOGY AND MEDICINE,24, 293-300, 2005
15) Novák J., Strašák L., Fojt L. , Slaninová I.Vetterl V.,Effects of low-frequency magnetic fields on the viability of yeast Saccharomyces cerevisiae, Bioelectromagnetic, in press 2006
16) Cendelín J., Schmidtmayerová B., Štenglová V., Vožeh F., CNS excitability in normal and neurodefective C3H mices exposed to high-frequency electromagnetic field, Proceedings of Biological effects of EMFs, 3rd International workshop, Kos, Greece, 4.-.8.10.2004, Ed. P.Kostarakis, p.866-871
17) Vožeh F., Barcal J., Cendelín J., Korelusová I., Štenglová V., Žalud V., The effect of high-frequency electromagnetic field on some brain function in healthy and neurodefective mice, Proceedings of Biological effects of EMFs, 3rd International workshop, Kos, Greece, 4.-.8.10.2004, Ed. P.Kostarakis, p.1113-1120

MAGNETIC FIELDS IN PUBLIC TRANSPORTATION IN CZECH REPUBLIC

JAN NOVÁK[1] , LUDĚK STRAŠÁK[1,2], LUKÁŠ FOJT[1,2], VLADIMÍR VETTERL[1,2]

1 INSTITUTE OF BIOPHYSICS, CZECH ACADEMY OF SCIENCES, KRÁLOVOPOLSKÁ 135, 612 65 BRNO, CZECH REPUBLIC
2 DENTAL RESEARCH CENTER, MASARYK UNIVERSITY, VINAŘSKÁ 6, 603 00 BRNO, CZECH REPUBLIC

Abstract

There is a lot of epidemiological studies showing possible effects of magnetic fields on the living systems. The ICNIRP limit for maximal magnetic field exposure was established by WHO to protect people before not-fully understood and not-fully proved harmful magnetic field effect on human. The public transportation is a place where we meet magnetic fields.

We measured magnetic fields in tramways, trolleys and buses in Brno city, tramways, trolley and buses in Ostrava city and subway and tramways in Prague. In addition the magnetic fields in intercity trains were measured.

Our results stated that the measured values do not exceed the ICNIRPs limit.

Introduction

Man-made low-frequency magnetic fields became an important part of our environment. They occur in our biosystem everywhere where low-frequency electric field is produced. Magnetic field exposure is in vicinity of electric equipments including electric engines in means of public transport. The passenger are exposed to magnetic fields. The ICNIRP (International Committee for Non Ionising Radiation Protection) limits of magnetic field exposure are highly protective and are based on all the available scientific evidence. For 50 Hz field is limit ICNIRP 100 μT (1).
The passenger's magnetic field exposures were studied in London *(2)* and in Toronto *(3)*. Our study shows the results from public transportation in three cities in Czech Republic to determine whether the ICNIRP limit is fulfilled and to compare magnetic fields in different means of transport.

Experimental

The EnviroMentor Magnetic Field Meter BMM-3000 (produced by EnviroMentor AB, Sweden) was used for used for measurement of magnetic induction.
The device is able to measure magnetic field in low-frequency range 5 - 2000 Hz and five induction ranges (200 nT-2 mT).

Tramways:

T3 (m=16 000 kg, P= 4 x 40 kW, capacity 110 passengers, 1961-1990, produced by Tatra ČKD Smíchov, Czech Republic, measured in Brno, line 1),

K2 (m=21 800 kg, P= 4 x 40 kW, capacity 157 passengers, 1966-1989, produced by Tatra ČKD Smíchov, Czech Republic, measured in Brno, line 1, 4),

KT8D5 (m=38 000 kg, P= 8 x 45 kW, capacity 231 passengers, 1999 –, produced by Tatra ČKD

Smíchov, Czech Republic, Brno, measured in line 1) and

Anitra (m=24 200 kg, P= 4 x 90 kW, capacity 155 passengers, 2000-present, produced by Škoda Plzeň, Czech Republic, measured in Brno, Ostrava, lines 1).

Trolleys:

14Tr and 14TrM (m= 10 000 kg, P= 2x100 kW, capacity 145 passengers, 1974-1984, produced by Škoda Ostrov, Czech Republic, measured in Brno, line 30),

15 Tr (m= 15 900 kg, P= 100 kW, capacity 80 passengers, 1983, produced by Škoda Ostrov, Czech Republic, measured in Brno line 26 and Ostrava line 104) and

22 Tr (m= 18 000 kg, P= 2x132 kW, capacity 140 passengers, 2002, produced by Škoda Ostrov, Czech Republic, measured in Brno line 26).

Metro trains:

81-717.1 (m= 33 500 kg, P= 4x110 kW, capacity 260 passengers, 1977-1990, produced by Mitishchinsky engineering factory, Soviet Union, measured in Prague lines A, B)

2MT (m= 31 000 kg, P= 110 kW, capacity 262 passengers, 1996-present, produced by Škoda Plzeň, Czech Republic, measured in Prague lines A, B)

M1 – Siemens (m= 27 900 kg, P= 141.5 kW, capacity 284 passengers, 2000-present, produced by Siemens AdTranz,, Czech Republic, measured in Prague line C)

Intercity train:

Pendolino 680 (m= 385 000 kg, P= 4000 kW, capacity 333 passengers, 2003, produced by Alstom Ferroviaria, Italy, route Prague – Děčín - Prague).

Results

Tramways

Totally 12 600 values, 3012 during stops, 9588 operating. The maximal value of magnetic induction was 7.23 μT (operating) or 1.16 μT (standing).

Trolleys

4369 data, 1030 – standing, 3339 – operating. The maximal value was 3.23 μT (operating) or 1.03 μT (standing).

Metro

10136 data, 2269 – standing, 7867 – operating. The maximal value was 8.17 μT (operating) or 0.09 μT (standing).

Train

6648 measured values. The maximal value was 0.14μT (operating) or 0.002 μT (standing).

The comparison of all used means of public transport is summarized in Fig.1. The maximum peak value was measured in metro (8.17 μT), then it decreased in order tramway>trolley>train (0.139 μT). The different order is if we take in the account average value. In that case trolleys have the biggest induction (3.18 μT) and than tramway>metro>train (0.002 μT).

The average values of different means of transportation differ depending on the type of tram, trolley or metro. It depends also on the external sources of magnetic fields, on the driver's style and on the profile of track. The engine draws maximal electric energy during acceleration or during breaking. In other cases the train uses inertia. The maximal values of magnetic induction are reached in a very short time just before changes in its velocity.

As for magnetic field exposure, the public transportation in Czech Republic is safe. All data are below ICNIRP limit, which is 100 μT for 50Hz fields.

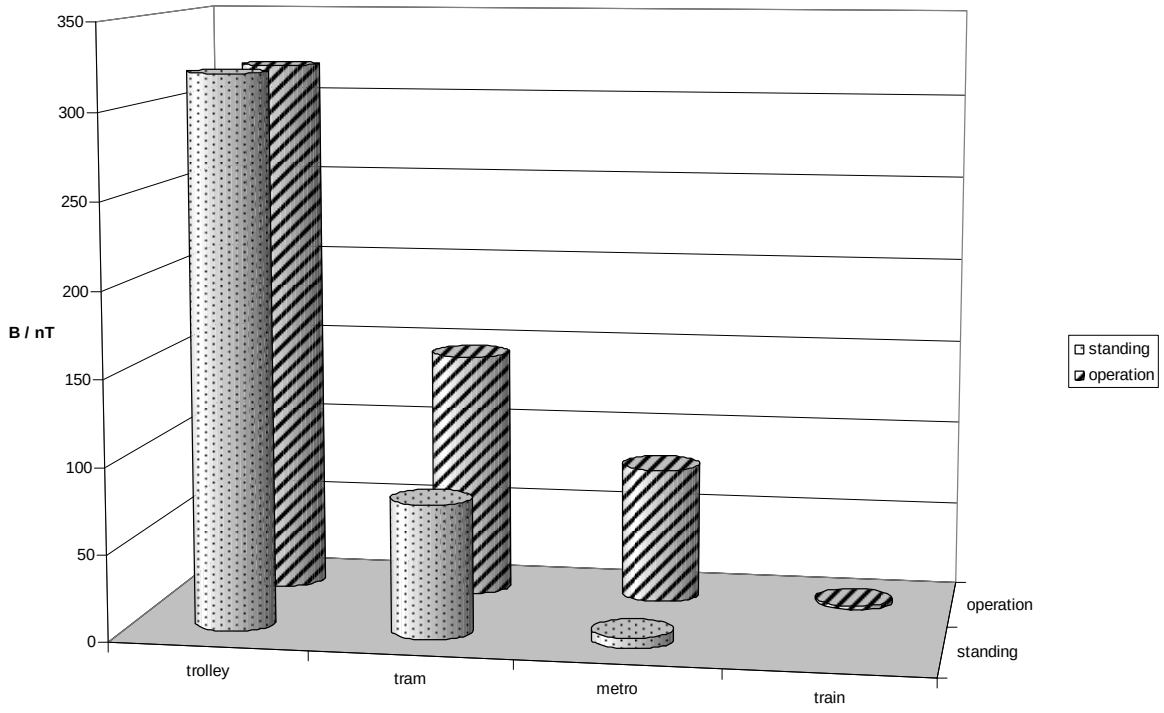

Fig.1 *Comparision of average values of magnetic induction in different means of public transport.*

		Number of data	Max (nT)	Min (nT)	Median (nT)	Mode (nT)	Average (nT)	Stdev (nT)	Confidence (95%) (nT)
tram	stop	3012	1160	0	50.0	20.0	77.6	90.0	3.2
tram	operating	9588	7230	0	80.0	20.0	145.1	273.7	5.5
trolley	stop	1030	2230	0	220.0	0.0	319.6	334.7	20.4
trolley	operating	3339	3230	0	230.0	10.0	318.2	353.2	12.0
metro	stop	2269	90	0	2.0	0.0	6.4	11.1	0.5
metro	operating	7867	8170	0	20.0	10.0	80.1	242.6	5.4
trains	operating	6680	139	0	0.3	0.2	1.7	5.8	0.1

Tab.1:Review of all measurements. Mode = the most often measured value, Stdev= standard deviations, Confidence = The error of measurement (Student's distribution)

References

1) ICNIRP Guidelines, Guidelines for limitting exposure to time-varying electric, magnetic, and electromagnetic fields, ICNIRP, Health Physics, 74(1998), 494-522

2) Chadwick F., Lowes F., Magnetic fields on British Trains. Annual Hygienic Occupational 1998;42: 331-335

3) Havas M., Shum S., Dhalla R., Passenger exposure to magnetic fields on go-trains and on buses, streetcars, and subways run by the Toronto transit comission. In: Proceedings of Biological effects of EMFs, 3rd International workshop, Kos, Greece, 4.-.8.10.2004, Editor P.Kostarakis, p.1065-1071

TRANSIENT EFFECTS OF RF-EMF EXPOSURE ON THE BRAIN MICROCIRCULATION IN EITHER JUVENILE OR ADULT RATS.

TAKAHASHI M. [1], HIROTA S.[1], MASUDA H. [1], USHIYAMA A. [1], TANAKA S. [2], KAWAI H. [2], WAKE K. [2], WATANABE S. [2], TAKI M. [3] and OHKUBO C. [4]

[1]Dept. of Environmental Health, National Institute of Public Health, 2-3-6 Minimi, Wako-shi, Saitama 351-0197, Japan. [2] Electromagnetic compatibility group, applied electromagnetic research center, National Institute of Information and Communications Technology, 4-2-1 nukui-kitamachi, koganei, Tokyo 184-8795, Japan. [3]Dept. of Electrical and electronic Engineering, Tokyo Metropolitan University, 1-1 minami-osawa, hachioji, Tokyo 192-0397, Japan. [4]RAD, World Health Organization, Geneva CH1211, Switzerland.

Abstract

The aim of the present study is to investigate whether radio frequency electromagnetic fields (RF-EMF) exposure induces acute effects on brain microcirculation being transiently observed only during RF-EMF radiation period in juvenile rats. As a model of juvenile and adult rats, we used 4 and 8 weeks old male Sprague-Dawley rats, respectively. All rats were subjected to cranial window implantation prior to the experiments and intravital-microscopic observation under anesthesia. Rat's head in RF group was locally exposed to 1,457MHz electromagnetic near-field by an ‘‘8’’-shaped loop antenna. RF-EMF exposure intensity was maintained at an averaged SAR (2.0W/kg) in parietal targeted area. Three microcirculatory parameters (BBB-function, plasma velocities, and vessel diameters) in pial venules were measured every 10 min for 50min exposure period. In 4 weeks juvenile rats, no changes in any of the three microcirculatory parameters were elicited by the RF-EMF exposure. No statistical changes were recognized between those values obtained from RF group and sham exposed group. These negative effects in juvenile rats were also confirmed in adult rats. The results reveal that there were no RF-EMF exposure effects at least on our measured brain microcirculatory parameters in either juvenile or adult rats under the present exposure conditions.

Introduction

Possible adverse health effects of radiofrequency electromagnetic field (RF-EMF) exposure during mobile phone uses on the brain are one of the public health concerns, especially, the effects on the developing brain in the children. However, few studies have evaluated this possible effect using juvenile animals. Our previous studies focused on the brain microcirculation during RF-EMF exposure, and showed no noticeable change in parameters including blood-brain barrier function, vessel diameters or plasma velocities was found in adult rats. The aim of the present study is to investigate whether RF-EMF radiation affects the brain microcirculation in juveniles or not.

We used 4-week-old male Sprague-Dawley rats as juvenile animals. The rats were divided into two groups: RF group was exposed to RF-EMF and Sham group was not exposed to any RF-EMF. All rats were subjected to cranial window implantation prior to the exposure experiments and intravital-microscopic observation under anesthetic. To compare the results of juvenile animals with those of adult animals, we also performed the same preparation and experiments in 8-week-old SD rats.

Rat heads were locally exposed to 1,457MHz electromagnetic near-field TDMA (time division multiple access) signal for PDC (Personal Digital Cellular, Japanese cellular telephone standard) systems by the ‘‘8’’-shaped loop antenna placed 4 mm upward to the cranial window. RF-EMF exposure was maintained at 2.0 W/kg of the averaged SAR in parietal targeted area (Table 1).

Table 1 Averaged SAR (W/kg)

Age	Target area	Whole brain	Whole body
4-week-old	2.0	0.59	0.057
8-week-old	2.0	0.54	0.032

The pial microcirculation within cranial windows was observed using a fluorescent microscope equipped with an EBCCD camera. In order to measure four microcirculatory parameters, BBB function, plasma velocities, leukocyte behaviours, and arteriole vasomotion, we used rhodamine 6G for leukocyte behaviours and FITC-Dx (70k or 2000k) for the other three parameters.

We prepared two experimental protocols. Arteriole vasomotion was observed for 12 min experimental period including 3 min RF-EMF exposure. The other three microcirculatory parameters, BBB-function, plasma velocities, and leukocyte behaviours in pial venules were measured every 10 min during 80 min experimental period including 50 min RF-EMF exposure. The results were compared between RF and Sham group. The statistical analysis was performed by Student's t-test or ANOVA.

BBB permeability was evaluated by extravasation of FITC-Dx (70kDa) from pial microvessels. After intravenous injection of FITC-Dx, the fluorescence intensities of brain surface area (0.74 mm^2) were measured every 10 min during pre- and during RF exposure period. As a result, there was no significant difference in the intensity changes between sham and exposed group in either juvenile or adult rats (Figure 1).

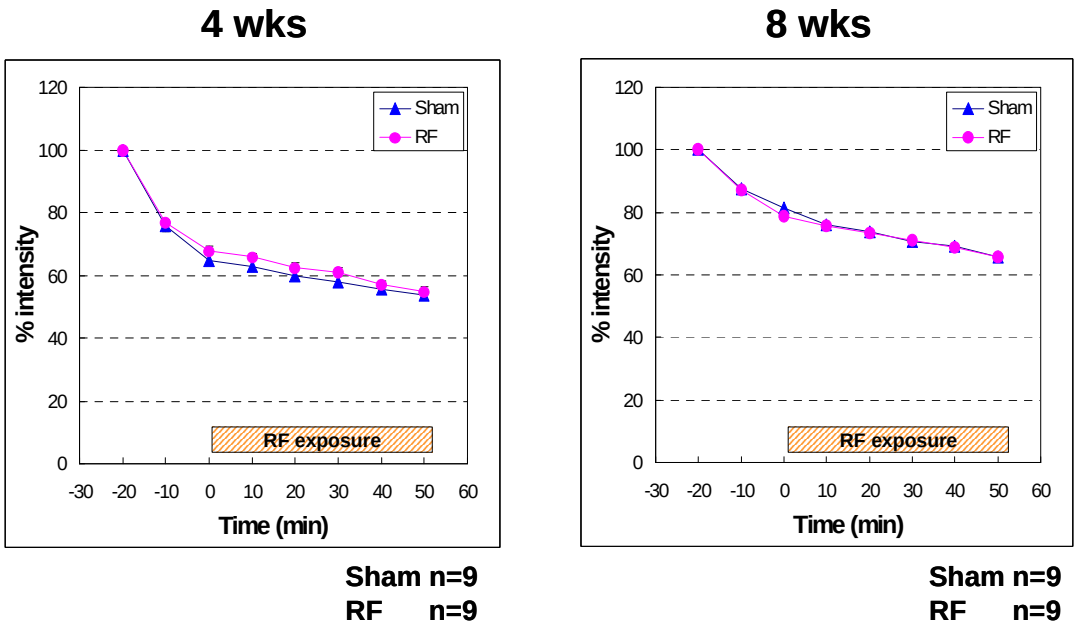

Figure 1 BBB permeability changes during RF-EMF exposure

The numbers of rolling and sticking leukocytes stained with rhodamine 6G were counted at 0, 10, 20, 40 min after RF exposure. As a result, no significant difference in these counts was found between sham and exposed group even in juvenile rats.

The velocities of plasma flowing in the pial venules were measured using Dual-Slit technique. We compared the velocities of each period with those of 20 min before RF exposure. But there was no significant difference in the plasma velocity between sham and exposed group even in juvenile rats.

The arteriolar vasomotion was monitored pre-, during, and post- RF exposure. As a index for dynamic changes in the vasomotion, we calculated the mean values of arteriolar diameter for each experimental period and showed them as a relative (%) diameter of pre-exposure. As a result, no significant difference in the arteriole diameter was found between two groups even in juvenile rats.

Conclusions

The results reveal that there were no effects of RF-EMF exposure on brain microcirculatory parameters, at least on BBB-function, leukocyte behaviours, blood flow or arteriolar vasomotion, in either juvenile or adult rats under present exposure conditions.

Acknowledgments

This study was financially supported by The Committee to Promote Research on the Possible Biological Effects of Electromagnetic Fields, Ministry of Internal Affairs and Communications, Japan.

INFLUENCE ON THE TRANSIENT EVOKED OTOACOUSTIC EMISSION BY GSM 915 MHZ ELECTROMAGNETIC FIELDS: COMPARATIVE ANALYSIS BETWEEN CONTROL AND EXPOSED GROUPS

MARTINES F.[(1)], MARTINES E.[(2)], TINE' G.[(3)], *Member IEEE*

(1), (2): UNIVERSITY OF PALERMO – DIPARTIMENTO DI BIOTECNOLOGIE MEDICHE E MEDICINA LEGALE – SEZ. DI AUDIOLOGIA, PIAZZALE DELLE CLINICHE 5 – 90126 PALERMO, ITALY
(3): COUNCIL NATIONAL RESEARCH (CNR), – ISTITUTO DI STUDI SUI SISTEMI INTELLIGENTI PER L'AUTOMAZIONE, VIA DANTE 12 – 90141 PALERMO, ITALY

Abstract
To evaluate the possible alterations of the human cochlear activity to the GSM 915 MHz electromagnetic fields (EMF) exposition in a significant statistically human subjects group, the transient evoked otoacoustic emissions (TEOAEs) have been measured.
130 volunteers took part in the experiment; they were randomly divided into two groups (group X, exposure to EMF consisting of 85 people; group Y, control consisting of 45 people) and underwent TEOAEs measurements two times. Participants were healthy young adults (18–40 years old) without any evidence of hearing or ear disorder. In group X the TEOAEs were recorded before and throughout 6 minutes EMF exposition (average power irradiated: 1Watt), while for group Y the TEOAEs were recorded for two consecutive intervals of six minutes without EMF.
The TEOAEs were measured in the time domain while the corresponding analysis have been carried out by the estimate of the density power spectrum relating to each waveform using the Welch's method. Comparing the results obtained in the case-control groups the variations of the density power spectrum found in the exposed subjects are not significant statistically respect to ones in the control group. Therefore the external hair cells activity is not modified by GSM cellular phones.

Introduction
The explosive increase in the use of mobile phones during the last years has aroused suspicions about their adverse effects on human health. Normally the cellular phone antenna is positioned near the human head and in particular close the ear causing a part of the electromagnetic energy emitted from the antenna to be absorbed by the auditory apparatus. Some authors studied the interaction between the electromagnetic fields (EMF) generated by cellular phone and inner ear, in particular the cochlear outer hair cells measuring the otoacoustic emission in humans [1], [2] [3]. Sometimes significant variations on the otoacoustic emission due to the presence of the electromagnetic fields have been reported while in other cases any variations has been noticed. In addition to these conflicting results must be considered that in the studies above reported the number of subjects examined was very low.
In this paper the study of the effects of the electromagnetic fields generated by 915 MHz GSM cellular phones on the otoacoustic emission in a statistically significant number of subjects is reported. The volunteers that took part at the study were divided randomly in two groups: control and exposed group. All the subjects underwent transient evoked otoacoustic emission (TEOAE) measurements. The TEOAE signals are generated by the movement of the outer hair cells on the Corti's organ when the auditory periphery is stimulated by an acoustic click. The TEOAEs are present in 100% of normal hearing subjects and constitute an expression of a normal cochlear functionality. To evaluate the alterations brought on by the EMF on the auditory responses the power spectral density (PSD) estimation of each TEOAE have been calculated. Since these signals are noise corrupted the classic FFT algorithm is not indicated for the PSD estimation but it is advisable to apply the periodogram method and in particular the Welch method. Finally in order to evaluate the presence of statistically significant variations in the exposed group respect to the control group the Chi square test has been carried out.

Experimental procedure and set-up

The OAE are stimulated by the application of a sound stimulus in the ear channel. A rectangular stimulus (click) has been chosen because it is very brief and has a broad-range frequency spectrum, so that a complete and simultaneous stimulation of the Corti's organ can be obtained down its entire length.
The experimental activity was performed using the ILO88 system by Otodynamics. It is composed of analog-to-digital converter, a preamplifier, an acoustic probe (microphone) and software to manage the stimulus and to collect and elaborate data. As the probe position can modify the stimulus' shape, checking the noise floor level, shape, spectrum and intensity level of the stimulus is compulsory. The probe fit was evaluated by measuring the adequacy of stimuli, i.e., flat acoustic spectrum across the frequency range of 0.5 – 5 kHz. The OAEs were obtained with stimuli consisting of clicks of 80 μs duration. The stimulus level in the outer ear was set at 80 ± 3 dB SPL. The click rate was 50 click per second and post-stimulus analysis was in the range of 2 to 20 ms. A total of 700 sweeps, corresponding about 6 minutes, was averaged above the noise rejection level of 47 dB.
The responses were filtered with the use of a II order high pass filter, with cutoff at 500 Hz, and a low pass IV order filter with cutoff at 5 kHz and sample rate of 25000 samples/s for a total of 512 samples. A response is valid if its amplitude is higher than noise floor level plus 3 dB.
The TEOAE was recorded in ASCII files and analysed later with a suitable Matlab® computer programme [4].
The exposition system was composed by: a vector signal generator SMIQ02B by Rohde&Schwarz for the generation of the TDMA mobile radio standard signals as GSM, GSM-EGDE etc., operating in the 300 kHz - 2.2 GHz frequency range; to amplifier the signal generated at the desired level a 5 W linear amplifier, operating in the frequency range 860 MHz – 960 MHz, it was cascade connected to the signal generator; to measure the transmission and reflection power from the antenna a mobile power measurement, with NRT sensor and PC card adapter NRT-Z4 by Rohde&Schwarz, it was interposed between the amplifier and the antenna; at the end of the generation and transmission chain a short dipole antenna to radiate the signal was connected. The positioning of the antenna near the ear was realized by a suitable plastic support mounted on an modified earphones.
The average power at the antenna input was fixed to 1 Watt and the exposition frequency at 915 MHz.

Subjects

130 subjects volunteers took part in the investigation; they were informed in detail about the purpose and procedures of the study and a written informed consent was obtained. Participants were healthy young adults (18–40 years old) without any evidence of hearing or ear disorder, corresponding to the ISO standard definition of otologically normal to exclude middle ear pathology that may impair OAE measurements.
The rationale was to test a group that was representative of the population of young otologically normal people. Absence of pre-existing hearing or ear disorder maximizes the sensitivity of the study to detect small changes that may occur. Acceptance as participants was based on otoscopy, audiometry by air conduction (0.5, 1, 2, 3, 4, 6, 8 kHz) and bone conduction (0.5, 1, 2 kHz), tympanometry and acoustic reflex testing, and a simple screening questionnaire concerning medical and otological history.
The subjects were randomly divided into two groups (group X, exposure to EMF consisting of 85 people; group Y, control consisting of 45 people) and underwent TEOAEs measurements twice. In group X the TEOAEs were recorded before and throughout 6 minutes EMF exposition (average power irradiated: 1Watt), while for group Y the TEOAEs were recorded for two consecutive intervals of six minutes .

Signal detection

To analyse TEOAEs, the signals revealed by the microphone are averaged by time-locking to the transient stimuli and alternatively storing them into two separate buffers (A and B). Thus each of the two waveform A and B (see Fig.1) corresponds to an average of 700 accumulated responses without any intervening time lag.
The two waveforms of each signal collected in separate buffers were cross correlated by means of a product moment correlation coefficient. The entity of correlation is considered as a measure of the response reliability and hence as a score of the functional efficiency of the auditory system. In the ILO88 test, an correlation index, called "Repro", between two waveforms of an OAE signal is considered. An index value > 70 % is considered as physiological, therefore if this condition should not occur the examination would not have considered.
In Fig. 1 two waveforms related to TEOAE response with "Repro"=90% is shown. Each waveform is composed by 512 points graphically interpolated and the differences among the waveforms A and B are due to the noise overlapped to the signals.

Power spectrum density estimation

In order to quantify the TEOAE response alterations the power spectral density (PSD) estimate associated with

each TEOAE has been calculated. There are several approaches to calculate PSD estimates; the most widely used PSD method analysis it is based on the application of the well know FFT algorithm while other use the periodogram method which is know as classic way to estimate PSD.
Widely, the PSD estimate of a time varying signal is obtained by computing first the frequency spectrum of the sampled data through the Discrete Fourier Transform (DFT) then the square module amplitude of the frequency spectrum. In case of signal corrupted by noise it is appropriate to compute power spectral density estimate of the signal using the Bartlett and Welch periodogram methods [5]. These methods make no assumption about how data was generated and, hence, are called nonparametric [6].

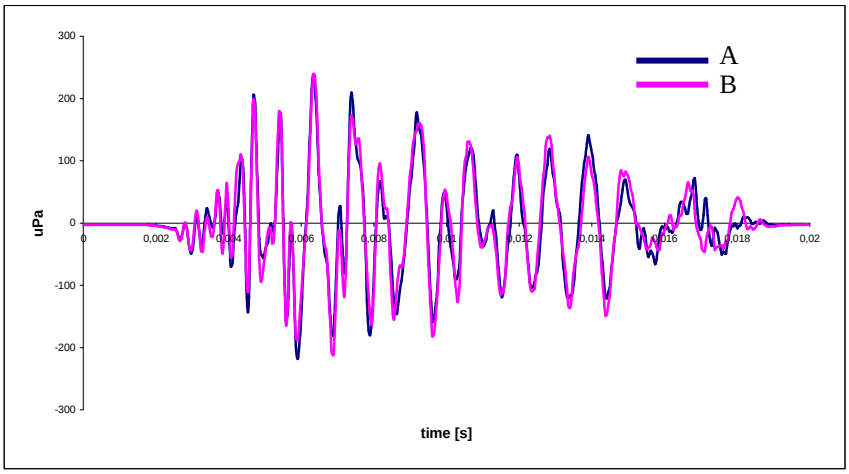

Fig. 1. Waveforms of a click evoked otoacoustic emission signal: A and B are two waveforms of a typical TEOAE signal recorded by the ILO88 system.

In the Bartlett method the N-point time domain sequence x(0), x(1), x(2),……, x(N-1) is divided into P no overlapping segments, where each segment has length D.
For each segment, the periodogram is computed and the Bartlett power spectral density estimate is obtained by averaging the periodograms for the P segments, as in the following formula:

$$S_B(f)=\frac{1}{P}\sum_{p=0}^{P-1}\frac{1}{DT}\left|T\sum_{n=0}^{D-1}x^{(p)}[n]\exp(-j2\pi fnT)\right|^2 \qquad (1)$$

By this averaging of the spectrum the variance of the spectrum estimation is reduced by a factor P, however at the expense of a reduction of the frequency resolution by a factor P.
Welch has modified Bartlett's method by using windowed data segments overlapping in time. The overlapping is used for further reducing the periodogram variance while the windowing is applied to reduce the spectral leakage associated with finite observation intervals. The frequency spectrum calculated by the Welch periodogram is given by:

$$S_w(f)=\frac{1}{P}\sum_{p=0}^{P-1}\frac{1}{UDT}\left|T\sum_{n=0}^{D-1}w[n]x^{(p)}[n]\exp(-j2\pi fnT)\right|^2 \qquad (2)$$

U is the discrete-time window energy of the used window function w[n] as defined as follow:

$$U=T\sum_{n=0}^{D-1}w^2[n] \qquad (3)$$

In our case the Welch method has been applied with a 50% overlapping and Hamming window selected.
In Fig.2 an example of PSD estimate computed by the Welch's method is shown. It has been calculated using a Matlab® software toolbox with A and B TEOAE signals as input data. The numerical computation output are two column vectors called [$P_x^{(A)}$ (f)] and [$P_x^{(B)}$ (f)] with dimension 256x1. The elements of [$P_x^{(A)}$ (f)] and [$P_x^{(B)}$ (f)] represent the power spectrum density estimates calculated for each frequency value of the column vector [f] of same dimension.

The example reported in Fig.2 shows the Power Spectrum Density (PSD) estimates in Watt/Hertz (W/Hz) vs. frequency (f) in Hertz (Hz) of the TEOAE signals reproduced in Fig.1.

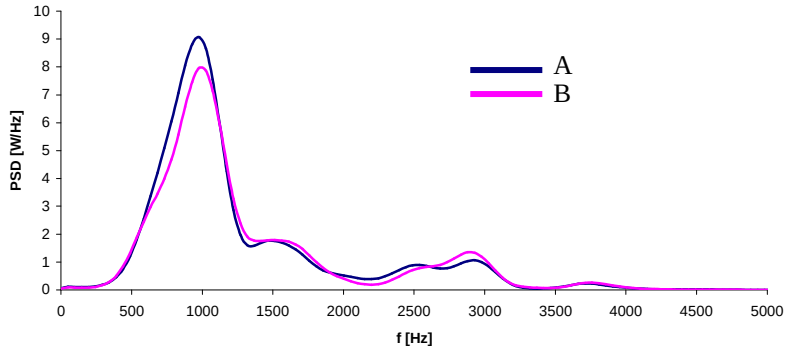

Fig.2. Example of Power Spectral Density estimate computed by Welch's method: these curves are relative to the TEOAE waveforms shown in Fig.1

Data analysis procedure

The data analysis for the exposed group has been carried out following the below procedure:

1. Estimation of the PSD using the Welch's function available on Matlab® software for the A and B TEOAE signals;
2. Evaluation of the average power associated to each signal by numerical integration of $[P_x^{(A)}(f)]$ and $[P_x^{(B)}(f)]$ above the frequency range 500 Hz – 5 kHz;
3. Calculation of the mean between the two power values determined in the previous step and evaluation of the mean relative deviation;
4. Repetition of the steps 1 – 3 considering the TEOAE registered in presence of electromagnetic fields;
5. Comparison between the means calculated with and without EMF;
6. The difference computed in the 5 step is defined "Significant" when its absolute value is greater than the addition of the relative deviations calculated in the two cases with and without EMF.

As regard the data analysis of the control group the procedure is the same of the exposed group with the only difference that the subjects are not exposed to EMF.

Results

In Tab.I an example of the numerical result obtained applying the first 5 steps of the above procedure is reported. In particular the average power for the two TEOAE signals relative to a single subject in both the exposition and no exposition conditions are calculated. Moreover the mean and the mean relative deviation it is also computed for both conditions. All the power values are expressed in decibel (dB).

Tab.I – Example of average power calculated for a single subject with and without EMF

Subject XXX	Average power signal A [dB]	Average power signal B [dB]	Mean [dB]	Mean relative deviation [dB]
No exposed	37,47	37,73	37,60	± 0,13
Exposed	37,98	37,72	37,85	± 0,13

In order to compare the results obtained in the two conditions the difference between the means has been calculated and the result is shown in Tab.II, where "Mean (NoEx)" indicates the mean of the average powers in the 'no exposed' condition while "Mean (Ex)" indicates the mean of the average powers in 'exposed' condition.

Tab.II – Difference of the means and "Significant" variation test

Subject XXX	Absolute value difference [dB]	"Significant" variation
Mean (NoEx) – Mean (Ex)	0,24	NO

In the same table the result of the "Significant" variation test is also reported. In the test, the absolute value of the

difference is compared with the addition of the relative deviations respect to the corresponding means obtained in the two condition above mentioned. The result of the test is a Boolean variable which value is "YES" when the difference absolute value is greater than the addition of the relative deviations. In the example shown in Tab.I the addition of the relative deviations is 0,26 dB while the difference absolute value is 0,24 dB, thus in this case the test response is "NO".
Repeating the procedure for all the subjects included in the exposed and control groups the results obtained are summarized in Tab.III and Tab.IV respectively.

Tab. III – Exposed group: summary sheet	
Subjects number	85
"Significant" differences number	58 (68,2%)
"No Significant" differences number	27 (31,8%)

Tab. IV – Control group: summary sheet	
Subjects number	45
"Significant" differences number	25 (55,6%)
"No Significant" differences number	20 (44,4%)

Analysing the above results an greater cases number with TEOAE response alterations in the exposed group (68%) respect to control group (55,6%) it has been obtained. Besides in the control group, in absence of EMF, more than 50% presents a "Significant difference" probably due to the random noise overlapped to the TEOAE signal.

Statistical analysis

The results do not clear up if the TEOAE alterations founded in the exposed group was really in correlation to the typical GSM electromagnetic field, so a statistical comparison of the results obtained in the two group it is necessary.
In our case the Chi square test is indicated. Chi square is a non-parametric test of statistical significance for bivariate tabular analysis. Any appropriately performed test of statistical significance lets us know the degree of confidence we can have in accepting or rejecting an hypothesis. Typically, the hypothesis tested with Chi square is the null hypothesis [7]. In our case it establish that the two groups (exposed and control groups) are not different enough respect to their behaviour in presence of EMF.
The first step in the building the Chi square test is the data summary in a table (as shown in Tab.V) where in the rows the independent variables and in the columns the dependent variables are reported. In this analysis the two groups are considered the independent variables while the results of the computation analysis on the TEOAE responses are considered the dependent variables

Tab.V – Data summary of the experimental results			
	"Significant" differences	No "Significant" differences	Total
Exposed group	58	27	85
Control group	25	20	45
Total	83	47	130

The expected frequencies for the above data are calculated multiplying the total number of each row for the total number of each column and dividing the result by the subjects total number. The results are shown in Tab. VI.

Tab.VI – Data summary of the experimental results			
	"Significant" differences	No "Significant" differences	Total
Exposed group (**observed**)	58	27	85
Exposed group (**expected**)	54,26	30,73	
Control group (**observed**)	25	20	45
Control group (**expected**)	28,73	16,26	
Total	83	47	130

Before to calculate the Chi square value it is necessary to determine the threshold of tolerance for error. For our purposes we set a probability of error threshold of 1 on 20, or $p < 0.05$. Applying the following formula (4) the Chi square value has been computed:

$$\chi^2 = \sum_{i=1}^{4} \frac{(O_i - E_i)^2}{E_i} \qquad (4)$$

where O_i represent the observed values while E_i the expected values. On the basis of the data reported in Tab.VI the Chi square value is:

$$\chi^2 = 0{,}257 + 0{,}452 + 0{,}484 + 0{,}86 = 2{,}05$$

For significance at the 0,05 level and degree of freedom equal to one, the Chi square should be greater than or equal to 3,84.
Therefore the distribution is not significant and the null hypothesis is not rejected. In other words, the difference between the two groups is not statistically significant respect to their TEOAE responses in presence or not of EMF, so the variations are not ascribable at the electromagnetic fields emitted by the GSM cellular phones but probably to the random noise overlapped to the TEOAE signals.

Summary

A study of the GSM 915 MHz electromagnetic fields effects on the auditory system has been carried out. For the first time the subjects number that taken part in a study of this matter has been statistically significant. 130 healthy young adults volunteers randomly divided into two groups have been considered: group (X) exposed to EMF consisting of 85 people and group (Y), control, consisting of 45 people.
All the subjects have been underwent TEOAEs measurements two times. In particular for the group (X) the TEOAEs were recorded before and throughout 6 minutes EMF exposition (average power irradiated: 1Watt), while for the group (Y) the TEOAEs were recorded for two consecutive intervals of six minutes without EMF.
The TEOAEs measured are composed by two slightly different signals in the time domain. The difference is due at the randomly overlapped noise to the signal. The analysis of the signals have been carried out by the density power spectrum estimate related to each waveform using the Welch periodogram method.
The results shown an greater cases number with TEOAE response alterations in the exposed group (68%) respect to control group (55,6%). Besides in the control group, in absence of EMF, more than 50% of the subjects present TEOAE response alterations probably due to the random noise overlapped at the TEOAE signal
Therefore a statistic analysis has been conducted in order to establish whether the alterations found in the exposed group are correlated with the EMF exposition. Applying the Chi square test the null hypothesis has been tested: the two groups, exposed and control, are not different in their behaviour in presence of EMF.
The test result indicates that the distribution is not significant and the null hypothesis is not rejected. In other words, the difference between the two groups is not statistically significant respect to their TEOAE responses in presence or not of EMF, so the variations are not ascribable at the electromagnetic fields emitted by the GSM cellular phones but probably to the random noise overlapped to the TEOAE signals

References

[1] Grisanti G., Parlapiano C., Tamburello C., Tinè G., Zanforlin L.: "Cellular phones effects on otoacoustic emissions", Microwave Symp. Digest IEEE MTT-S Int. 2, pp. 771-774, 1998.
[2] Ozturan O., Erdem T., Miman M.C., Kalcioglu M.T., Oncel S. : "Effects of electromagnetic field of mobile thelephones on hearing", Otolaryngology 122, pp. 289-293, 2002.
[3] Parazzini M., Bell S., Thuroczy G., Molnar F., Tognola G., Lutman M.E., Ravazzani P. : "Influence on the mechanisms of generation of distorsion product otoacoustic emision of mobile phone exposure", Hearing Research 208, pp. 68-78, 2005
[4] Matlab Editor, Version 7.0.0, The Mathworks, Inc.
[5] Marple S.L. : "Digital spectral analysis with applications", Prentice-Hall, ISBN 0-8493-7892-3, 1987.
[6] Proakis J.G., Manolakis D.G. :" Digital signal processing principles, algorithms and application", 3rd ed., New Delhi, India, Prentice-Hall, 2002.
[7] Papoulis A., Pillai U.S.: "Probability, random variables and stochastic processes", McGraw Hill, 2002.

EPIDEMIOLOGICAL STUDY TO ASSESS THE RISK OF RF-EMFS FROM MOBILE TELEPHONY

RAVINDRA TIWARI[1*], AHUJA YR[2], BHARGAVA SC[3], LAKSHMI NK[1]

[1] Bhavans New Science College, Narayanguda, Hyderabad, Andhra Pradesh, India.
[2] Director, Department of Genetics and Molecular Medicine, Vasavi Medical and Research Center, Khairthabad, Hyderabad, Andhra Pradesh, India.
[3] Head, Dept of Electrical and Electronic Engineering, MGIT, Gandipet, Hyderabad, Andhra Pradesh, India.
*** Corresponding Author**

Abstract

Modernization has led to increased proliferation of various electronic and electrical equipment in all fields of human life including domestic, industrial, the fast expanding information technology sector and above all wireless telecommunication. The increasing use of mobile telephony in our society has brought focus and great concern on the health effects of EMFs. A number of epidemiological, *in vitro*, *in vivo* studies have shown conflicting, inconclusive and controversial reports. Considering the scientific evidence from the current scenario, the objective of this epidemiological study was planned to assess the genotoxic potential of RF-EMF exposure from mobile telephony (800-900MHz). 100 subjects using mobile telephones for more than three years, were compared with 80 age and sex matched controls. The statistical data indicated in our study, involving Comet assay showed a lesser significance in exposed subjects compared to controls. The hormonal profile of melatonin is supportive to our study, possibly envisaging the role of the hormone in EMFs stress. Lipid Peroxidation assay also substantiated the DNA damage via oxidative stress. The comparatively lesser significance reported from our findings may have large implications with chronic exposure, emphasising the need for health concern, amidst the environmental hazard of this invisible electromagnetic pollution.

Introduction

The radiofrequency (RF) signals emitted from mobile phones are considered as a type of non-ionizing electromagnetic radiation and are perceived as health risk. More focus has been brought on the potential effect of RF-EMFs to elicit biological response, in association with its detrimental effects on widespread application and long-term induction. The biological effects as a result of RF exposure include changes in cell membrane function, metabolism, cellular signal communication, activation of protooncogenes and cell death. There are scientific evidences on the health hazards due to RF-EMFs, like neurodegenerative disorders, brain tumors and cancer. Most of these reports are inconclusive and no convincing data has been established on causal relation between RF and health risk.

Mobile phone has become the fastest selling consumer product with about 1.6 billion users worldwide and 76 million users in India, contributing to 8% of the population. To date, few epidemiological studies have directly examined the relationship of mobile phones to genomic instability. With a need to arrive at a scientific consensus, an attempt has been made to study the genomic instability on human subjects exposed to mobile phones operating at 800-900MHz.The subjects using mobile phones for more than 2 years were screened with age and sex matched controls with similar socioeconomic status (non-smokers, non-alcoholics). The frequency and duration of mobile phone use along with the model and type of phone with specific absorption rate (SAR) were taken into account.

The whole body exposure of mobile phone radiation is hypothesized to result in structural rearrangement of DNA and increase in number of single-strand and double strand DNA breaks. The DNA damage was observed using

single cell gel electrophoresis SCGE (comet assay) in which the leukocytes were isolated, placed on a microscope slide, lysed, eventually electrophoresed and silver stained. The DNA fragmentation was assessed from the DNA migration path length or comet tail length.

The potentially hazardous effects of electromagnetic fields on melatonin rhythm disturbances remain to be elucidated. The physiological relevance of melatonin could be important in the explanation of the RF-EMFs effect via oxidative stress. The RF fields may induce oxidative stress that has been implicated with increase in free radicals, which mainly enhance lipid peroxidation. To substantiate lipid peroxidation, the level of malonyl dialdehyde (MDA) in plasma and RBCs was measured.

Methodology

DNA Integrity

Single cell gel electrophoresis or Comet assay (Singh *et al*, 1998) was used to study DNA damage. Leukocytes suspended in low-melting agarose were embedded on to a pre-coated layer of normal melting agarose and layered again with low-melting agarose. The cells were treated in lysing solution for overnight and then incubated in alkaline electrophoresis buffer for 20 minutes to facilitate DNA unwinding and expression of alkali labile sites. Electrophoresis was carried out for 30minutes at 300mA at 0.67V/cm and then neutralized using Tris buffer. Silver stain technique was followed to visualize and measure migration path length. 200 cells per treatment was measured in duplicates. Mean$\pm$SD of DNA damage was calculated.

Melatonin Levels

Competitive enzyme immunoassay was performed for the quantitative determination of melatonin in plasma (IBL kit. Germany). The sealed ELISA plate consisting of equal proportion of sample (standard, subject and controls), melatonin-biotin and antiserum was incubated overnight at 2-8˚C. The plates washed thrice with assay buffer and enzyme conjugate was added (1:5) and incubated for 2 hours at room temperature. After incubation, washing step was repeated and substrate p-nitrophenyl phosphate (PNPP) added to incubate for 20 minutes. Stopping solution was then added to end the substrate reaction. Optical density was read at 405nm.

Lipid peroxidation assay

Lipid peroxidation was estimated by measuring the stable end product, malondialdehyde(MDA) in plasma (Lef'evre *et al*, 1998) and RBCs (Armstrong and Browne, 1994). The protein free plasma was treated with thiobarbituric acid that forms a 1:2 adduct measured at 535nm with spectrophotometer. Mean and ± SD or SE was established for the samples. The concentration of MDA equivalents in nmol/ml in samples were interpolated from the standard curve.

Results & Discussion

The findings from our epidemiological study show, some statistical significance in the DNA migration path lengths, of the exposed subjects when compared with the controls. The SCGE (Comet assay) demonstrated a mean of comet tail length for control group as 6.63 $\pm$ 0.120 and for the subjects as 8.26 $\pm$ 0.092. Phillips (1998) reported, DNA single strand breaks exposed to cellular telephone frequency at 813.5 MHz and 836.5 MHz. The protocol and findings for evaluating the DNA breaks is similar and supportive to the present study. Similarly, Gandhi and Anita (2005) employed SCGE assay for assessing genetic damage in mobile phone users being exposed to 800-2000 MHz and reported a significant increase in DNA tail length and micronuclei. The Swedish-Norwegian epidemiological study concluded a statistical significance between mobile phone users and prevalence of certain bioeffects (Mild *et al* 1998). The *in vitro* study performed by Diem *et al* 2006 indicated a stronger non-thermal DNA breakage effect, in intermittent exposure by mobile phone radiation at 1800MHz. A dose dependent increase in DNA strand breaks from microwave RF at low intensity levels as evaluated by Lai and Singh (1995, 1996) indicate a casual relationship between RF exposure and genetic damage. Many controversial findings report on non-cooperative action between the RF-EMF exposure and induced DNA damage (Annemarie *et al* 2006).

Few epidemiological studies reported an increased risk of brain tumors among analogue cellular phone users (Hardell *et al* 2003). Repacholi *et al* (1997), conducted mice studies using 900 MHz mobile phone frequency radiation and found a statistically significant 2.4 fold increase in lymphoma. On the contrary, Heynick's (2003) report on epidemiological studies showed no indication of *in vivo* and *in vitro* exposure of RF field and cancer.

Currently, there is insufficient evidence to assess an association between RF exposure and brain cancer, leukaemia, or lymphoma (ICNIRP, 2004).

The sleep disruption related to radiofrequency radiation hypothesized from our findings for melatonin relevance has been reported in several scientific studies (Lai and Singh 1998, Burch *et al* 2002). Mann *et al* (1996) and Loughran *et al* (2005) observed that a radiofrequency radiation, similar to digital mobile phones reduced sleep in humans altering the EEG (brain wave) signals.

The increase in free radical production for LPO activity shows a statistical significance (Table 1) in the exposed population compared to those unexposed. This observation is similar to the data published by Stopczyk *et al* 2005.

Despite both negative and positive findings about the biological effects of radiofrequencies, certain more long term studies, better conceived and supported by, *in vitro* experimentations would envisage the possible cumulative effects on general health. Further, the lag periods that have been examined are short, where if a longer lag period of about 10 years is required for a health effect to occur, it would not be possible in short exposures and the results will be difficult to interpret.

Table 1: RBC and Plasma markers of Oxidative stress for Lipid Peroxidation (MDA)

MDA (nm/mL)	Control Group	Exposed Population
RBC	0.20 $\pm$ 0.07	0.28 $\pm$ 0.10
Plasma	0.21 $\pm$ 0.1	0.42 $\pm$ 0.2

Data in terms of Mean $\pm$ SD; Significant * $P<0.001$

Summary

Mobile telephony, the integral unit of modern telecommunication and third generation wireless technology, relays information with RF signals. The extensive use of mobile telephones has given rise to public concern about the possible health effects that the whole-body exposure to RF signals may have. There is a wide spread conviction that electromagnetic emissions from mobile phones were capable of significant biological tissue interactions. The temperature increase is insignificant to cause direct effect but certain scientific reports document increase in DNA strand breaks and chromosomal damage in cells. The non-thermal resultant effects do include increased free radical production, cell stress and premature aging, changing in brain function, neurodegenerative conditions, reduction in melatonin secretion and cancer.

This epidemiological study, assesses the long-term human health risk from RF-EMF exposure for genomic instability. Some individuals have reported to experience certain non-specific symptoms such as sleeplessness, fatigue and headache. The levels of melatonin and the oxidative stress marker, MDA could substantiate in hypothesizing the correlation of non-specific symptoms and whole body exposure to mobile phones. The effects of the RF-EMFs on genomic instability determined by SCGE assay in our study showed lesser statistical significance from the control population. The results are expressed in terms of an estimate of relative risk, ie the multiplier by which risk is higher in people exposed to the RF-EMF of mobile telephony than in unexposed group. However, the findings and scientific interpretations drawn from this epidemiological study about the potential risk from mobile telephony might not be sufficient to arrive at a consensus. But possible implications on long term and chronic exposure to mobile phone use could be made.

Acknowledgement

The authors acknowledge the generosity of the UGC, New Delhi, India for the sanction of Major Project without which this attempt would not have been completed.

Reference

1. Annemarie Maes, Urbain Van Gorp and Luc Verschaeve. Cytogenetic investigation of subjects professionally exposed to radiofrequency radiation Mutagenesis. 2006, 21(2):139-142.
2. Armstrong, D. and Browne, R. The analysis of free radicals, lipid peroxidases, antioxidant enzymes and compounds related to oxidative stress as applied to the clinical chemistry laboratory. Free Radicals in Diagnostic Medicine, 1994, 366:46.
3. Burch JB, Reif JS, Noonan CW et al. Melatonin metabolite excretion among cellular telephone users. Int J Radiat Biol 2002, 78:1029–1036.
4. Diem E, Schwarz C, Adlkofer F, Jahn O, Rudiger H Non-thermal DNA breakage by mobile-phone radiation (1800 MHz) in human fibroblasts and in transformed GFSH-R17 rat granulosa cells in vitro. Mutat Res. 2006, 603(1):104 -106.
5. Gandhi Gursatej, Anita. Genetic damage in mobile phone users: some preliminary findings. Indian Journal of Human Genetics. 2005, 11 (2): 99-104.
6. Hardell L, Mild KH, Carlberg M. Further aspects on cellular and cordless telephones and brain tumors. Int J Oncol. 2003, 22: 399-407.
7. Heynick LN, Johnston SA, Patrick A, Mason PA. Radio frequency electromagnetic fields: Cancer, mutagenesis, genotoxicity. Bioelectromagnetic. 2003,24: 74-100.
8. ICNIRP Report. Epidemiology of health effects of radiofrequency. Environ Health Perspect. 2004, 112 (17): 1741-1754.
9. Lai H and Singh NP. Acute low intensity microwave exposure increases DNA single-strand breaks in rat brain cells. Bioelectromagnetics. 1995,16:207-210.
10. Lai H and Singh NP. Single-and double-strand DNA breaks in rat brain cells after acute exposure to radiofrequency electromagnetic radiation. International Journal of Radiation Biology. 1996, 69:513-521.
11. Lai H, Singh NP. Melatonin and a spin-trap compound block radiofrequency electromagnetic radiation-induced DNA strand breaks in rat brain cells. Bioelectromagnetics. 1998, 18(6): 446 – 454.
12. Lef'evre G., et.al. Evaluation of lipid peroxidation by measuring thiobarbituric acid reactive substances. Annals de Biologie Clinique. 1998, 56(3): 305-319.
13. Loughran, Sarah P, Wood, Andrew W., Barton, Julie M., Croft, Rodney J., Thompson, Bruce b, Stough, Con. The effect of electromagnetic fields emitted by mobile phones on human sleep. SLEEP Neuroreport. 2005, 16(17): 1973-1976.
14. Mann K and Roschke J. Effects of pulsed high-frequency electromagnetic fields on human sleep. Neuropsychobiology. 1996, 33: 41-47.
15. Mild KH Oftedal G Sandstrom M Wilen J Tynes T Haugsdal B and Hauger E, 1998. Comparison of symptoms experienced by users of analugue and digital mobile phones. A Swedish-Norwegian epidemiological study. National Institute for Working Life. 1998, 23. Umea, Sweden.
16. Oktem F, Ozguner F, Mollaoglu H, Koyu A, Uz E. Oxidative Damage in the Kidney Induced by 900-MHz-Emitted Mobile Phone: Protection by Melatonin. Arch Med Res. 2005, 36(4): 350-355.
17. Phillips J, Ivaschuk Ishida-Jones T, Jones R, Campbell-Beachler M, Haggren W. DNA damage in Molt-4 T-lymphoblastoid cells exposed to cellular telephone radiofrequency fields in vitro. Bioelectrochemistry and Bioenergetics. 1998, 45: 103-110.
18. Repacholi MH Basten A Gebski V Noonan D Finnie J and Harris AW. Lymphomas in Eμ-Pim 1 transgenic mice exposed to pulsed 900 MHz electromagnetic fields. Radiation Research. 1997, 147: 631-640.
19. Singh NT, Mc Coy NT, Tice RR, Schneider A. A simple technique for quantification of low levels of DNA in individual cells. Experimental cell research. 1998, 517: 184-191.
20. Stopczyk D, Gnitecki W, Buczynski A, Markuszewski L, Buczynski J.Effect of electromagnetic field produced by mobile phones on the activity of superoxide dismutase (SOD-1) and the level of malonyldialdehyde (MDA)--*in vitro* study Med Pr. 2002, 53(4): 311-314.

THE EFFECT OF RF FIELDS ON GERMINATION AND GROWTH OF *LACTUCA SATIVA, LYCOPERSICUM ESCULENTUM* AND *ALLIUM CEPA*

MIRTA TKALEC[1], KREŠIMIR MALARIĆ[2], ŽELJKA VIDAKOVIĆ-CIFREK[1], BRANKA PEVALEK-KOZLINA[1]

[1]UNIVERSITY OF ZAGREB, FACULTY OF SCIENCE, DEPARTMENT OF BIOLOGY, ROOSEVELTOV TRG 6, HR-10000 ZAGREB, CROATIA
[2]UNIVERSITY OF ZAGREB, FACULTY OF ELECTRICAL ENGINEERING AND COMPUTING, UNSKA 3, HR-10000 ZAGREB, CROATIA

Abstract

The effects of exposure to radiofrequency fields on germination and seedlings growth were investigated in lettuce (*Lactuca sativa* L.), tomato (*Lycopersicum esculentum* L.) and onion (*Allium cepa* L.). Seeds were exposed to continuous EMF (23 V m^{-1}) at 400 and 900 MHz for 2 and 4 h as well as to modulated field (80% AM 1 kHz sinus) for 2 h in GTEM-cell. At 400 MHz, inhibition of lettuce germination was noticed after 2 h of exposure to continuous RF-EMF while the growth of lettuce and tomato was decreased after 4 and 2 h of exposure, respectively. Contrary, the growth of onion was increased after 2 h of exposure to continuous RF-EMF. At 900 MHz, increased germination of tomato was observed after exposure to modulated field. At this frequency, the growth of lettuce increased after 4 h of exposure to continuous RF-EMF while the growth of onion increased also after exposure to modulated field. On the other hand, the growth of tomato decreased after 2 and 4 h of exposure to continuous RF-EMF. Results indicate that seedlings growth was more sensitive to RF-EMF exposure than germination and that the effects depended on field and exposure characteristics as well as plant species.

INTRODUCTION

Various kinds of radiofrequency electromagnetic fields (RF-EMF) from 30 kHz to 300 GHz are used to transmit information (TV, radio, mobile phones and satellite communications). Although classified as nonionizing, these fields can have various biological effects including changes in the cell membrane's permeability and interferences with ions and molecules like DNA and proteins (Kwee & Raskmark 1998, Kwee *et al.* 2001, Banik *et al.* 2003).
Germinating seeds and seedlings subjected to environmental stresses could failure to cope with the adverse effects which results in poor germination, disturbed seedling development, and eventually reduced crop yields. Only few investigations about effects of RF-EMF exposure on seed germination and early plant growth have been reported so far with various results (Jonas 1952, Nelson & Walker 1961).
In this work the effects of exposure to EMF at 400 and 900 MHz on germination of lettuce (*Lactuca sativa*), tomato (*Lycopersicum esculentum*) and onion (*Allium cepa*) seeds as well as some parameters of seedlings early growth were investigated.

Determination of germination and early growth

Seeds of *Lactuca sativa* L. ("Unicum"), *Lycopersicum esculentum* L. ("Marglobe") and *Allium cepa* L. ("Srebrnjak") were placed in plastic Petri dish on filter paper wetted with distilled water. The Petri dishes were maintained for 12 h at 24 ± 2 ºC in the darkness and then subjected to EMF. During exposure control was kept in the same growth conditions (24 ± 2 ºC, darkness) as seeds exposed to EMF but in the field-free environment. Three replicates of 15 seeds were used in each treatment. Protrusion of the radicle was the criterion used for germinated seed. After germination seedlings were watered every day and their root and shoot length as well as fresh weight was measured after four days (lettuce) or seven days (tomato and onion). All results were expressed as means followed by the

corresponding standard errors. Significant differences between means ($P \leq 0.05$) were established by one-way ANOVA followed by Duncan's multiple range test (STATISTICA 6.0) and presented in the Figures with asterisks (*).

Exposure to radiofrequencies fields

For generation of RF-EMFs Gigahertz Transversal Electromagnetic (GTEM) cell (Fig. 1.) was used (Tkalec *et al.* 2005). In GTEM-cell, electric and magnetic field exist at the same time and they are perpendicular to the wave propagation direction. Besides the GTEM-cell, a signal generator with continuous wave and an amplifier was also needed.
Seeds in plastic Petri dishes were exposed in GTEM cell to the continuous EMFs of 400 and 900 MHz at field strengths of 23 V m^{-1} for 2 and 4 hours as well as modulated EMF (80% AM 1 kHz sinus) for 2 h. Petri dishes were placed in parallel, perpendicular to the electric field, in the area where field was uniform with required field levels (Fig. 2).

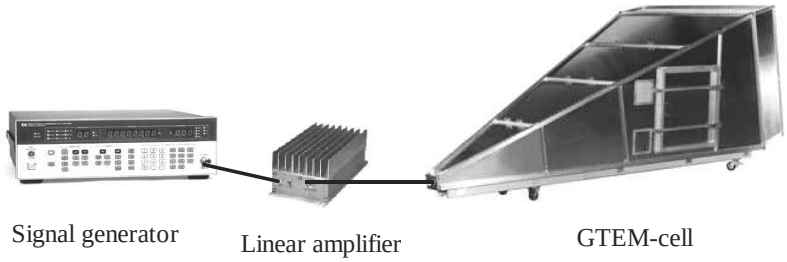

Figure 1. Instruments used for the exposure to RF-EMF: GTEM-cell, HP 8657A signal generator and 5 W MiniCircuits amplifier.

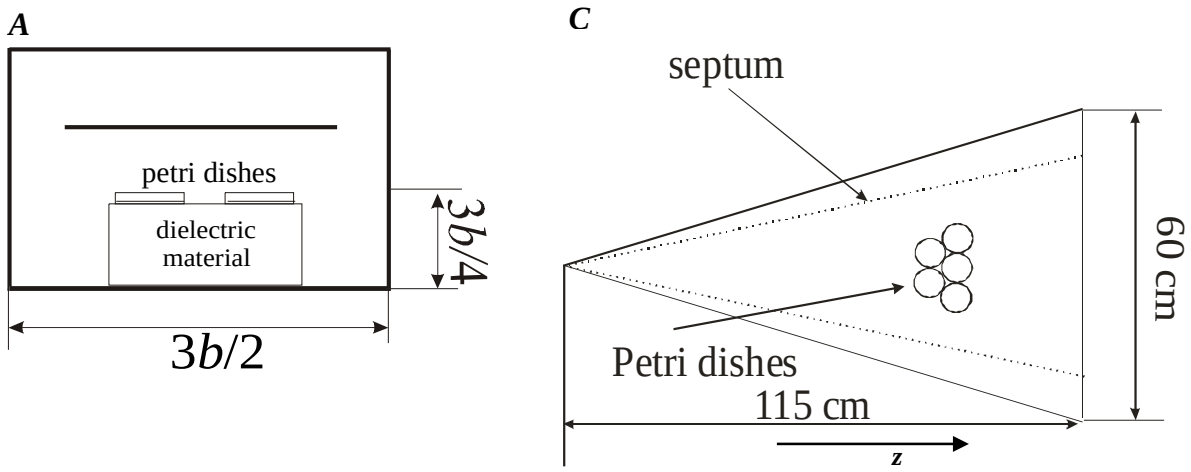

Figure 2. Position of Petri dishes (*d*=9 cm, *h*=1.5 cm) in GTEM-cell: below the septum (A), in respect to the direction of wave propagation, *z* (B).

RESULTS

Seed germination

The exposure of seeds to continuous EMF at field frequency of 400 MHz and strength of 23 V m^{-1} for 4 h as well as to modulated field at the same frequency and strength for 2 h did not have significant effect on germination of lettuce (*Lactuca sativa*), tomato (*Lycopersicum esculentum*) and onion (*Allium cepa*) seeds in comparison with non-exposed seeds. On the other hand, exposure to continuous field at 400 MHz and 23 V m^{-1} for 2 h inhibited lettuce germination (Figure 3A).
The exposure of seeds to continuous EMF at field frequency of 900 MHz and strength of 23 V m^{-1} for 4 h as well as to modulated field at the same frequency and strength for 2 h also did not have significant effect on germination of seeds. The exception was stimulation of tomato germination noticed after exposure to modulated field at 23 V m^{-1} for 2 h (Figure 3B).

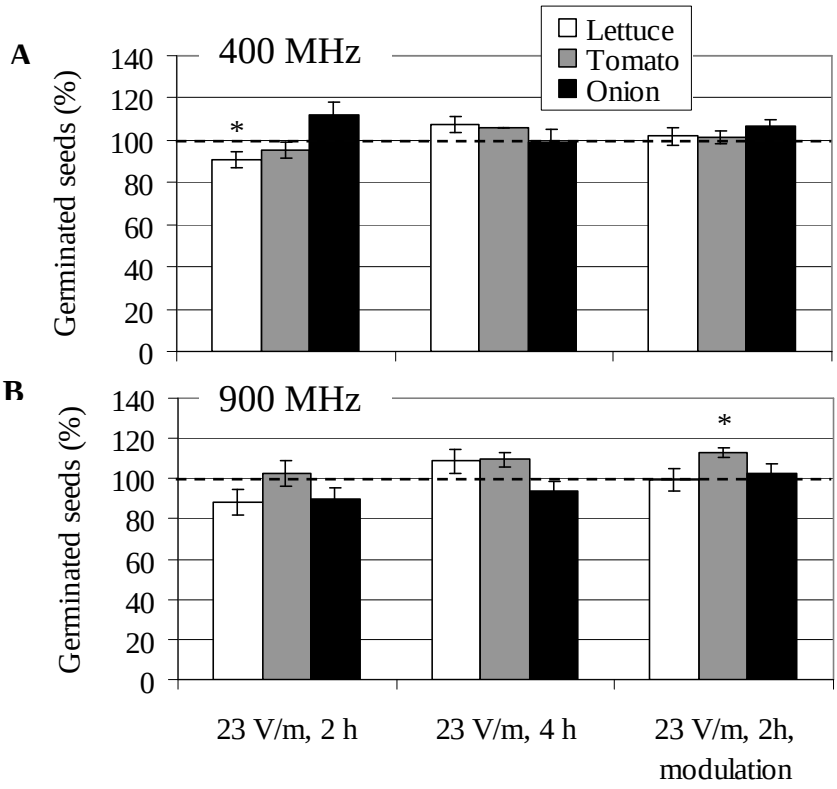

Figure 3. Germinated seeds (%) of lettuce (*Lactuca sativa*), tomato (*Lycopersicum esculentum*) and onion (*Allium cepa*) seeds after exposure at 400 and 900 MHz to continuous field at 23 V m^{-1} for 2 and 4 h and to modulated field for 2 h. Data represent means ± SE (n = 45). Control (non-exposed seeds) is expressed as 100 %. Significant differences between exposed and non-exposed seeds at $P \leq 0.05$ are marked with asterisk (*).

Early growth of seedlings

The growth of lettuce seedlings measured as root and shoots length and seedling fresh weight was neither affected by exposure for 2 h to continuous nor modulated EMF at 400 MHz and 23 V m^{-1}. But, lettuce root length and fresh weight decreased after exposure for 4 h to continuous EMF at the same frequency and strength (Fig 4A).

Root and shoot length and fresh weight of tomato seedlings decreased after exposure for 2 h to the continuous field at 400 MHz and 23 V m^{-1} while exposure to the modulated field and longer exposure to the continuous field at the same frequency and strength did not affect tomato growth significantly (Fig. 4B).

The growth of onion seedlings was not significantly impaired after exposure to EMFs at 400 MHz except increase of shoot length noticed after exposure for 2 h to the continuous field at 23 V m^{-1} (Fig. 4C).

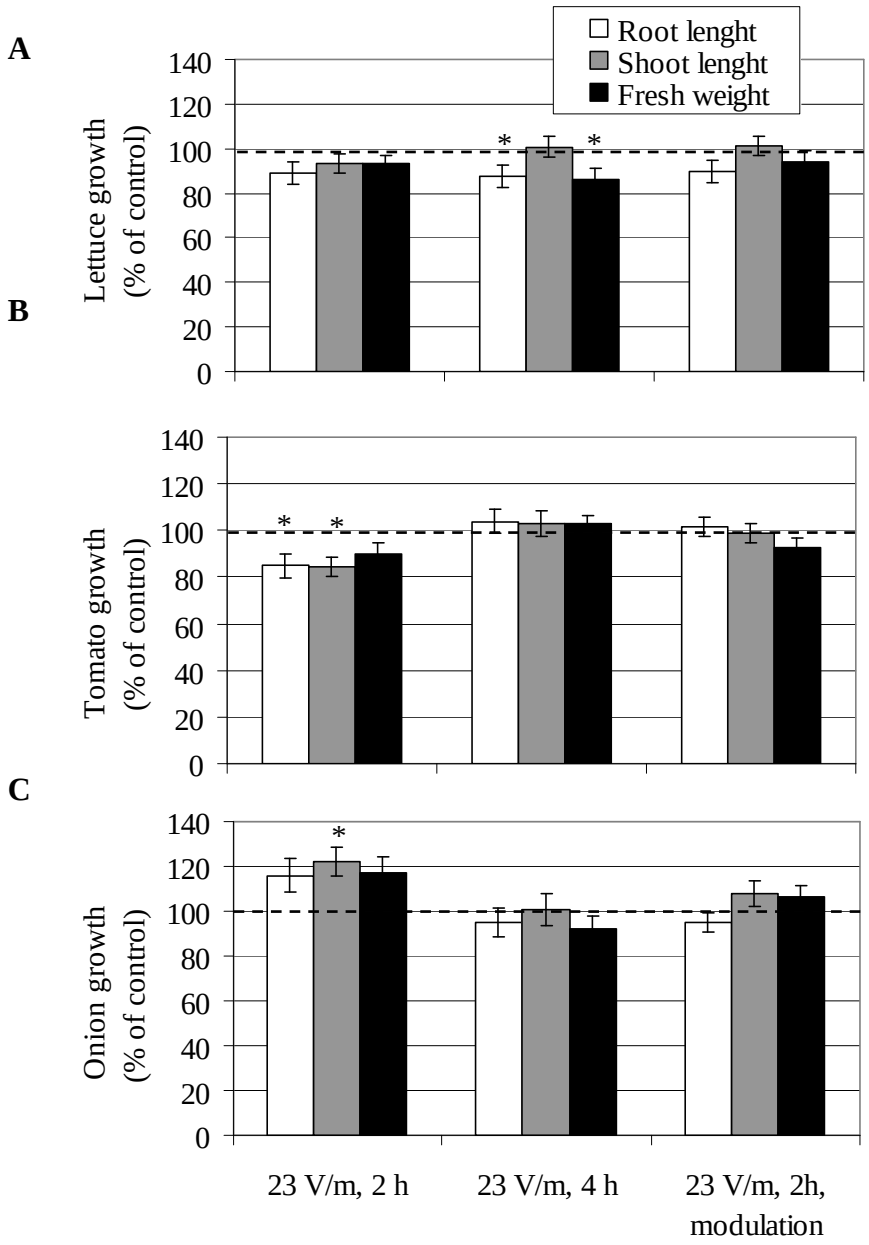

Figure 4. Root and shoot length as well as fresh weight of lettuce (A), tomato (B) and onion (C) seedlings after exposure at 400 MHz to continuous field at 23 V m^{-1} for 2 and 4 h and to modulated field for 2 h. Data represent means ± SE (n = 45). Control (non-exposed seeds) is expressed as 100 %. Significant differences between exposed and non-exposed seeds at $P \leq 0.05$ are marked with asterisk (*).

At 900 MHz the early growth of lettuce seedlings, similarly as at 400 MHz, was neither affected by exposure to continuous nor modulated field at 23 V m^{-1} for 2 h. However, at this frequency, lettuce shoot length and fresh weight significantly increased after exposure for 4 h to continuous EMF (Fig 5A).

The growth of tomato seedlings measured as fresh weight significantly decreased after exposure for 2 h to continuous field at 900 MHz and 23 V m^{-1}, similarly as after exposure at 400 MHz, but at this frequency longer exposure to the field had the same effect (Fig. 5B).

The growth of onion seedlings at 900 MHz, like lettuce growth, significantly increased after exposure for 4 h to the continuous field at 23 V m^{-1} as well as after exposure to modulated field (Fig. 5C).

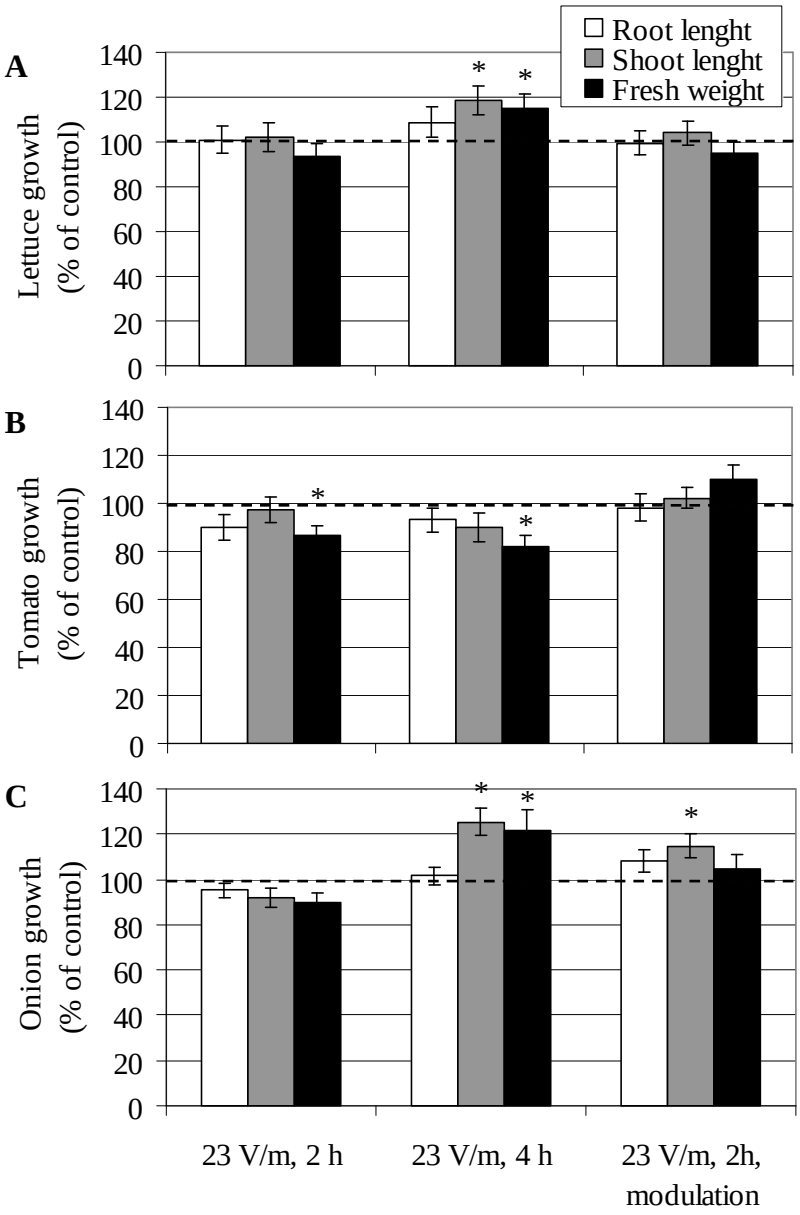

Figure 5. Root and shoot length as well as fresh weight of lettuce (A), tomato (B) and onion (C) seedlings after exposure at 900 MHz to continuous field at 23 V m^{-1} for 2 and 4 h and to modulated field for 2 h. Data represent means ± SE (n = 45). Control (non-exposed seeds) is expressed as 100 %. Significant differences between exposed and non-exposed seeds at $P \leq 0.05$ are marked with asterisk (*).

Summary

The effect of radiofrequency electromagnetic fields (RF-EMF) on seeds germination and early plant growth has been investigated. At 400 MHz, the exposure to continuous field at 23 V m^{-1} for 2 h inhibited the lettuce germination while longer exposure decreased the growth of lettuce seedlings. At this frequency after 2 h of exposure to the continuous field growth of tomato seedlings was decreased, but the growth of onion seedlings significantly increased. At 900 MHz, germination of tomato seeds was increased after exposure to modulated field at 23 V m^{-1} as well as the growth of onion seedlings. The growth of lettuce and onion seedlings significantly increased after 4 h of exposure to continuous field at this frequency while, on the other hand, the tomato growth decreased after 2 and 4 h of exposure. Obtained results indicated that seedlings growth was more sensitive to RF-EMF exposure than germination and that the effects of RF exposure on plant germination and growth could be positive as well as negative depending not only on field and exposure characteristics but on plant species as well.

References

Banik S, Bandyopadhyay S, Ganguly S. 2003. Bioeffects of microwave-a brief review. Bioresource Technol. 87:155-159.

Jonas H. 1952. Some effects of radio frequency irradiations on small oilbearing seeds. Physiol. Plant. 5:41-51.

Kwee S, Raskmark P. 1998. Changes in cell proliferation due to environmental non-ionizing radiation 2. Microwave radiation. Bioelectrochem. Bioenerg. 44:251-255.

Kwee S, Raskmark P, Velizarov S. 2001. Changes in cellular proteins due to environmental non ionizing radiation. I. Heat-shock proteins. Electro Magnetobiol. 20:141-152.

Nelson SO, Walker ER. 1961. Effects of radio-frequency electrical seed treatment. Agric. Eng. December:688-691.

Repacholi MH. 2001. Health risk from the use of mobile phones. Toxicol. Lett. 120:323-331.

Tkalec M, Malarić K, Pevalek-Kozlina B. 2005. Influence of 400, 900 and 1900 MHz electromagnetic fields on Lemna minor growth and peroxidase activity. Bioelectromagnetics 26:185-193.

ACUTE EFFECTS ON OXIDATIVE STRESS MARKERS OF HIGH FREQUENCY ELECTROMAGNETIC FIELD 900 AND 1800 MHz IN RATS- PRELIMINARY EXPERIMENTS

L.Traikov[1], G.Lawlor[3], A.Bocheva[2], V.Hajimitova[1], C.Shalamanova[4], M.Israel[4], H.Koshimizu[5], M.Markov[6]

1- Department of Medical Physics and Biophysics, Faculty of Medicine, Medical University-Sofia , Sofia-1431, Bulgaria

2- Dept. Pathophysiology, Faculty of Medicine, Medical University-Sofia, Sofia-1431, Bulgaria

3-Department of Environmental Health; National Institute of Public Health,

Tokyo-108-8638, Japan

4- Dept. Physical Factors, National Institute of Public Health, Sofia-1431, Bulgaria

5- Department of Human Living System Design, Kyushu University, Fukuoka-815-8540, Japan

6- Research International, Buffalo Office, 135 Arielle Court Apt E, Williamsville NY 14221, USA

Abstract

Over the past 3 decades the actions of Radio-frequency EMF (RF) on biological systems have been examined extensively, concurrently with investigations into the generation of free radicals and reactive oxygen species under stress conditions. Biological systems endure complex environments where countless interactions among myriad different factors are important to our understanding the pathophysiological mechanisms and events by which RF may induce the activation or suppression of natural occurring antioxidant systems.

A total of 75 rats were exposed to 2 frequencies of RF (SAR=0.5 W/kg): (n=25, sham exposure; n=25, 900 MHz; n=25, 1800 MHz). After a 30 min exposure period, blood plasma levels showed increased levels of both catalase (CAT) and superoxide dismutase (SOD) and total glutathione peroxidase (GSH-Px). After initiating RF exposures at 900 MHz and 1800 MHz, animals at each 5 min interval (5min (n=5); 10min (n=5); 15min(n=5); 20min (n=5); 25min (n=5)), showed increasing levels of malondialdehyde (MDA) (lipid peroxidation product). After 10-th minute from the beginning of exposure simultaneous increasing of SOD, CAT and GSH-Px concentrations in rat blood plasma appear. No statistically significant differences in these blood plasma products were observed between the 2 RF exposures used. Our results are in good agreement with previous investigations examining free radical generation in the early stages of EMF exposure. Radio-frequency EMF may affect biological systems by increasing the lifespan of reactive oxygen species.

Introduction

Studies of electromagnetic field promotion of free radical formation are provided widely and significant effects are obtained in low frequencies of electromagnetic field spectrum, which are predominant. According Bordiushkov,IuN, et al. 2000 low frequency EMF, increase 2 fold SOD activity. Katsir,G. and Parola,A.H. 2002 showed indirectly changes of catalase activity by low frequency EMF.

High frequency EMF may affect biological systems by increasing free radicals, which appear mainly to enhance lipid peroxidation, and by changing the antioxidase activities of human blood which leading to oxidative stress.

ACUTE EFFECTS ON OXIDATIVE STRESS MARKERS OF HIGH FREQUENCY ELECTROMAGNETIC FIELD 900 AND 1800 MHz IN RATS- PRELIMINARY EXPERIMENTS

Influence of high frequency EMF on Antioxidant enzymes activity at model systems in vitro correlative analysis of SOD activity and MDA concentration in human blood platelets at 900 MHz exposure for different time intervals have been investigated by Stopczyk,D. [Stopczyk,D. et al 2002; Stopczyk,D. et al. 2005], they obtained significant increase of both levels of MDA and SOD after 7 min exposure.
Again at in vitro experiments Hook,G.J et al. 2004 find out that the levels of activities of superoxide dismutase (SOD), total glutathione peroxidase (GSH-Px) are increased by 847.74 MHz (CDMA) RF EMF.
Other investigations of RF EMF action at systems in vivo with healthy volunteers showed that, after RF EMF exposure lipid peroxide and the activities of superoxide dismutase (SOD), total glutathione peroxidase (GSH-Px) and catalase levels are measured. The results obtained showed that the plasma level of lipid peroxide was significantly increased after 1, 2 and 4 h of exposure to RF EMF. Moreover, the activities of SOD and GSH-Px in human erythrocytes showed significant reduction while the activity of catalase in human erythrocytes did not decrease significantly. These results indicate that acute exposure to RF EMF of commercially available cellular phones may modulate the oxidative stress of free radicals by enhancing lipid peroxidation and reducing the activation of SOD and GSH-Px, which are free radical scavengers. Therefore, these results support the interaction of radiofrequency fields of cellular phones with biological systems [Moustafa,Y.M. et al 2001]

Free radical processes in living organism could be impact by exogenic way as follow:

- direct reducing of abnormal production of ROS by means of antioxidant molecules;
- by inactivation of already formed prooxidants;
- by means of phagocyte inhibitors or by COX inhibitors.

In our experiments we divided experimental animals by groups according time intervals each interval has a 5 min by three investigated groups (Sham, Exposed 900, Exposed 1800 MHz) and estimate four parameters MDA concentration and SOD, CAT, and GSH-Px enzyme activity.

Exposure Mean Enzyme activity Rel.U.	Sham exposed	900 [MHz]	1800 [MHz]
SOD	2.31±0.201	2.66±0.495	3.56±0.172
CAT	2.03±0.201	2.49±0.436	2.56±0.432
GSH-Px	2.42±0.201	2.19±0.695	2.48±0.373

Anti-oxidative activity
Fluorescent analysis were applied for investigation of concentrations of antioxidant enzymes (SOD, CAT, and total GSH) when their concentration where measured we calculated their activity per protein concentration and velocity of substrate catalysis.

TBARS-test (Thiobarbituric Acid Reactive Substances) was applied for in vivo registration of MDA derivates. The influence on the ROS formation in liposome suspensions was investigated by measurement of MDA (malondialdehyde), which is the final product of lipid peroxidation in the same model systems. The sensitivity of TBARS has made this assay the method of choice for screening and monitoring lipid peroxidation, a major indicator of oxidative stress [Armstrong, D. and Browne, R. 1994; Yagi, K, 1998]. Some modifications made possible the application of this rapid procedure at animal biological tissues [Janero, D. 1998]. Despite of some controversy regarding the specificity of TBARS toward compounds other than MDA, the test remains the most widely employed assay used to determine lipid peroxidation [Armstrong, D. and Browne, R. 1994].

According to TBARS-test, MDA is captured by thiobarbituric acid in a colored product comprising 532 nm chromophore by means of condensation presented in Figure 3:

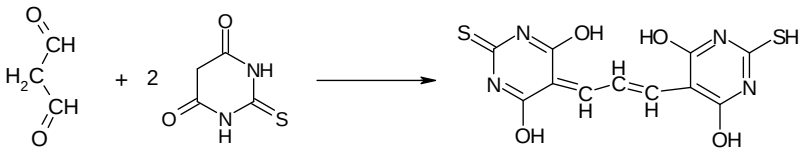

Figure 3. Condensation of TBA with MDA and creation of 532 nm chromophore

The concentration of MDA as a product of lipid peroxidation is calculated from the molar extinction coefficient (E) as specified below.

The samples were centrifuged at 3000 rpm for 10 min, the supernatant was taken off and 1.8 ml of 0.5% thiobarbituric acid was added to 2 ml of supernatant. The resulted solution was incubated at 90°C for 40 min to obtain pink color with λ_{max} = 532 nm [Asakawa, T. and Matsushita, S. 1980]. The molar extinction coefficient (E) was measured at 532 nm with spectrophotometer (Cecile-3000) with polystyrene quvettes.

ANOVA statistical method for evaluation of significance of the present results were applied, Bonferoni test for statistical significance in the range P>0.05 were applied and results are presented as ±S.D.

Results

We obtained time dependence of high frequency EMF action at in vivo systems by means consequence measurements of concentration of oxidative stress marker (MDA) and antioxidant enzymes activity

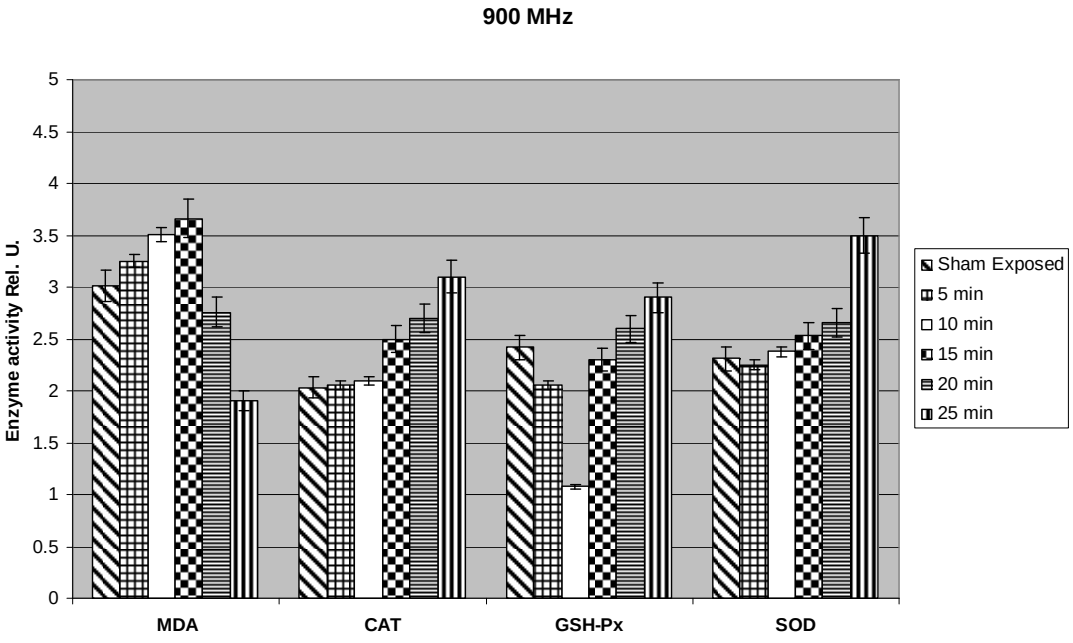

For 900 MHz exposure we obtained significant changes at MDA concentration at 15 min. after beginning of exposure and for 25-th minutes we obtained maximum of SOD concentration.

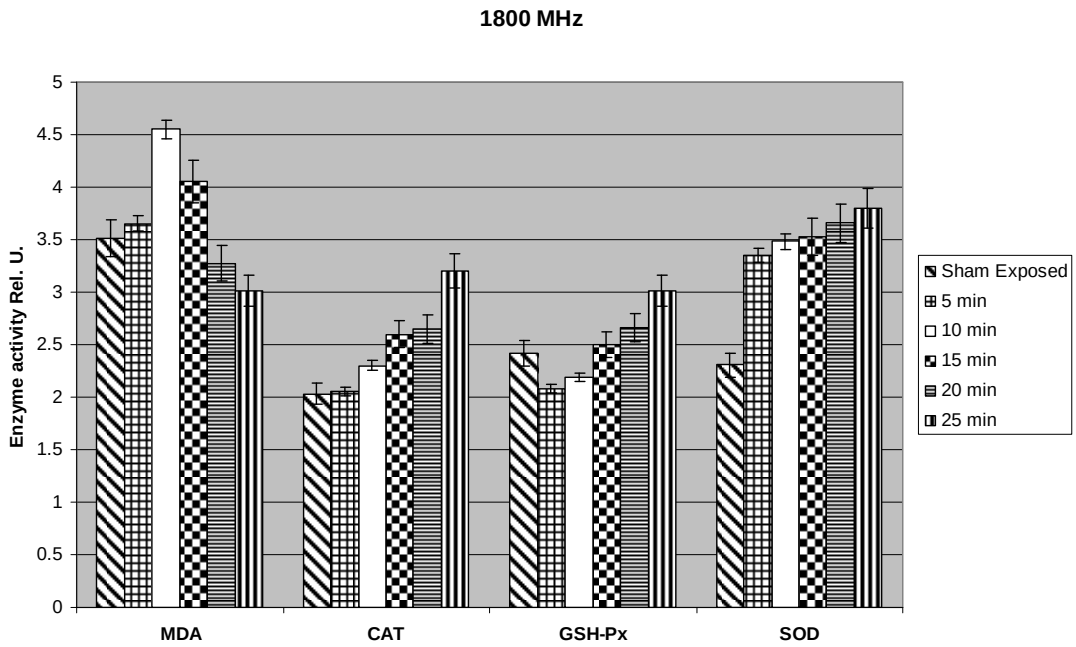

For 1800 MHz exposure we obtained significant changes at MDA concentration at 10 min. after beginning of exposure and for 25-th minutes we obtained maximum of SOD concentration. Other enzymes CAT and GSH-Px, have smaller but also significant increase of their concentrations in comparison with sham exposed group. Between two exposed groups have no significant differences therefore we can claim for any frequency dependence of RF EMF action.
It have been measured tendency for increasing of life span of ROS formation and in parallel with that increasing of concentration of anti-oxidant enzymes, but with significant time-delay.

Summary

On the base of our results we can conclude that oxidative stress after exposure to RF EMF may be the reason for many adverse changes in cells and may cause a number of systemic disturbances in the human body

References

[1] Armstrong, D.; Browne, R. The analysis of free radicals, lipid peroxidases, antioxidant enzymes and compounds related to oxidative stress as applied to the clinical chemistry laboratory. Free Radic. Biol. Med. 366(1):43-58; 1994.

[2] Asakawa, T. and Matsushita S. Coloring conditions of thiobarbituric acid test for detecting lipid peroxides. Lipids 15[1], 137-140. 1-1-1980.
Ref Type: Magazine Article

[3] Bordiushkov, I.; Goroshinskaia, I. A.; Frantsiiants, E. M.; Tkacheva, G. N.; Gorlo, E. I.; Neskubina, I. V. [Structural-functional changes in lymphocyte ans erythrocyte membranes after exposure to alternating magnetic field]. *Vopr. Med Khim.* **46**:72-80; 2000.

[4] Bordiushkov, I.; Goroshinskaia, I. A.; Frantsiiants, E. M.; Tkacheva, G. N.; Gorlo, E. I.; Neskubina, I. V. [Structural-functional changes in lymphocyte ans erythrocyte membranes after exposure to alternating magnetic field]. *Vopr. Med Khim.* **46**:72-80; 2000.

[5] Cotgreave, I. A. Biological stress responses to radio frequency electromagnetic radiation: are mobile phones really so (heat) shocking? *Arch Biochem Biophys* **435**:227-240; 2005.

[6] Hook, G. J.; Spitz, D. R.; Sim, J. E.; Higashikubo, R.; Baty, J. D.; Moros, E. G.; Roti Roti, J. L. Evaluation of parameters of oxidative stress after in vitro exposure to. *Radiat Res* **162**:497-504; 2004.

[7] Janero, D. Malondialdehyde and thiobarbituric acid-reactivity as diagnostic indices of lipid peroxidation and peroxidative tissue injury. Free Radic. Biol. Med. 9(1): 515-540; 1998.

[8] Katsir, G.; Parola, A. H. Enhanced proliferation caused by a low frequency weak magnetic field in chick embryo fibroblasts is suppressed by radical scavengers. *Biochem Biophys Res Commun.* **252**:753-756; 1998.

[9] Moustafa, Y. M.; Moustafa, R. M.; Belacy, A.; Abou-El-Ela, S. H.; Ali, F. M. Effects of acute exposure to the radiofrequency fields of cellular phones on plasma lipid peroxide and antioxidase activities in human erythrocytes. *J Pharm. Biomed Anal.* **26**:605-608; 2001.

[10] Musaev, A. V.; Ismailova, L. F.; Shabanova, A. B.; Magerramov, A. A.; Iusifov, E. I.; Gadzhiev, A. M. [Pro- and antioxidant effect of electromagnetic fields of extremely high frequency (460 MHz) on brain tissues in experiment]. *Vopr. Kurortol. Fizioter. Lech. Fiz Kult.* 19-23; 2004.

[11] Yagi, K. Simple procedure for specific assay of lipid hydroperoxides in serum or plasma. Free Radical and Antioxidant Protocols 108(1):101-106; 1998.

URINARY 6-SULFATOXYMELATONIN EXCRETION IN RATS AFTER MICROWAVE IRRADIATION

IVANCICA TROSIC
IVANA BUSLJETA
IVAN PAVICIC
LJILJANA ZANINOVIC[1]
SANJA MILKOVIC-KRAUS

INSTITUTE FOR MEDICAL RESEARCH AND OCCUPATIONAL HEALTH
KSAVERSKA CESTA 2. POB 291. HR-10001 ZAGREB, CROATIA
e-mail: itrosic@imi.hr, phone: ++ (385 1) 4673 188
[1]ENDOCRINOLOGY LABORATORY, CLINICAL HOSPITAL CENTER, ZAGREB, CROATIA

Abstract

Aim of this study was to examine whether 2.45 GHz irradiation has effects on rats' nocturnal urinary 6-sulfatoxymelatonin (6SM) excretion. Urinalysis parameters after whole-body exposure of two hours per day, five days a week, throughout fifteen days lasting experiment was followed-up. The average specific absorption rate (SAR) was calculated to 1.25 (±0.36) W/kg. The concentration of 6SM in urine samples was determined by direct radioimmunoassay kit (Stockgrand Ltd., Guildford, UK). Urinary glucose, bilirubin, ketones, specific gravity, blood, pH, protein, urobilinogen, nitrite and leukocytes appearance has been accomplished by means of multiple reagent strips (N-Multistix® Bayer Diagnostic, UK). In comparison to the sham-exposed group, no significant changes in body temperature or food and water intake were observed. Delayed significant decline in 6SM of irradiated rats has been obtained between days eight and eleven. Until the end of experiment 6SM level remained low. The results of urinary pH, glucose, bilirubin, ketones, specific gravity, blood, protein, urobilinogen, nitrite, leukocyte appearance in the urine indicated no significant differences between treated and control group. In conclusion: it is likely that applied microwave field poses capacity to affect the hormone melatonin balance in rats after repeated exposure.

Introduction

Current scientific effort is based on the growing recognition that low-intensity radiofrequency microwave (RF/MW) exposure can be detected in living tissues and result in well-defined bioeffects. Because mechanisms involved into the complexity of RF/MW biological activity are multiple, animal studies play an important role in evaluating the complex reactions of various body systems. Systems like nervous, haematopoietic or immune are largely responsible for homeostasis – the essential maintenance of the internal environment. Co-coordinated, interdependent response of these systems when challenged by potentially damaging stimuli could be easier reproduced in contrast to a human study [1, 2]. One of straightforward approach with comprehensive output of possible elucidation how RF/MW affects living organisms, certainly could be covered by melatonin hypothesis [3]. Hypothesis that melatonin as oncostatic, or inhibitor of cancer cell growth or it is effect on immune system, along with the report that EMF could alter its oncostatic properties [4]. There are three postulates how EMF could be acting through the melatonin pathway. EMF could lower melatonin concentration, resulting in increased estrogen and prolactin levels, and consequently increase hormonally-mediated cancers. Further, lower melatonin levels, with melatonin acting as an antioxidant, could result in increased susceptibility to DNA damage. This may result in a general increase in risk for a variety of cancers. Finally, EMF may affect the effectiveness of melatonin for inhibiting cell proliferation. This mechanism could be relevant to cancer in general [3]. Several studies show that EMF across the spectrum from extremely low

frequencies (ELF) to RF/MW reduces melatonin in animals and people [5]. Light going through our eyes passes a message to the pineal glands in the brain which slows down the production of melatonin during the day time. At night the production of melatonin is speeded up. Melatonin is considered to scavenge cancer cells and impurities in our bodies and boost the immune system. Non-ionizing radiation is supposed to act on the pineal gland and suppress the night-time melatonin to daytime levels; hence the good work of the melatonin at night will be restricted leading to suppression of the immune system [6]. Otherwise, melatonin circadian profile was not been disrupted in 37 young male volunteers submitted to the EMFs of 900 and 1800 MHz frequency field [7]. Additionally, both continuous and/or pulsed 900 MHz field exposure for 15 min to 6 hours at day or night had no notable effect on pineal melatonin synthesis in rodents [8].

There has been insufficient research on the effects of RF/MW on melatonin excretion level, and the few existing studies do not provide clear information about such effects. As urinary 6-sulfatoxymelatonin (6SM) appears to be the main metabolic end product of pineal melatonin hormone, the aim of this investigation was to examine whether 2.45 GHz exposure has effects on rats' nocturnal urinary 6SM along with. Urinalysis parameters after exposure were also studied.

Materials and Methods

Male Wistar rats (13 week old, approximate body weight 450 g) had passed through a week accommodation period. Both sham-exposed control (n=10) and exposed animal group (n=10) were kept in steady-state microenvironment conditions (22 ^{o}C ± 1 ^{o}C), receiving standard laboratory food and water from 7:00 AM till 7:00 PM, with alternating 12-hours light and dark cycles. The animals were exposed to 2.45 GHz continuous waves two hours daily, five days a week every day between 8:00 AM and 10:00 AM. The animals were exposed to RF/MW source (modified Micro-Chef Moulinex generator, 900 W, 2.45 GHz) in individual Plexiglas cages. Rats were irradiated separately at the same time. The field power density within the cages was measured by EM Radiation Monitor, EMR-20 and 8.2, Wandel & Golterman GmbH & Co. Germany, at "average mode". The exposures were conducted with a field power density of 5-10 mW/cm^2. Specific absorption rate (SAR) was estimated according to radiation dosimetry handbook [9]. The average whole-body SAR value was calculated to be 1.25 (±0.36 SE) W/kg. According to recent literature calculated SAR of this range excludes thermal stress in rats [10]. The animals did not receive food or water during exposure sessions. The experiment lasted fifteen days. The rectal body temperature was measured by Thermo Scan thermometer (Braun GmbH, Germany) before and after the treatment. No significant changes in body temperature were observed. Control animals were handled as the treated ones, but without RF irradiation. In order to collect nocturnal urine, both, control and exposed animals were held individually in metabolic cages every night, from 7:00 PM till 7:00 AM next day. The volume of collected urine was measured. The concentration of 6SM in rat urine samples was determined by direct radioimmunoassay kit (Stockgrand Ltd., Guildford, UK). To get a quick overview into the urinary biochemical parameters, a rapid screening test has been performed. Nocturnal urinary glucose, bilirubin, ketones, specific gravity, blood, pH, protein, urobilinogen, nitrite and leucocyte manifestation has been accomplished by multiple reagent strips (N-Multistix® Bayer Diagnostic, UK). During or after exposure procedure no changes were observed neither in food/water intake or behavioral pattern. The results were statistically evaluated using Mann-Whitney and Kruskal-Wallis tests [11].

Results

When we conducted the 6SM test after 2.45 GHz rats' whole-body microwave irradiation, samples of urine were collected every morning at the same time during the fifteen days lasted experiment. The time-course of nocturnal 6SM in rat urine samples during the 2.45 GHz exposure of 2 hours a day, 5 days a week is presented at Figure 1. In comparison with sham-control animal group the significant decline in 6SM of irradiated rats has been obtained between experimental days eight and eleven ($p<0.05$). Reduced metabolic end product of melatonin appears to be consequence of cumulative RF/MW irradiation. The 6SM level in urine of exposed animal group remained low until the end of the experiment, but it has not significantly differed in comparison with the sham-control ones.

The semi-quantitative biochemical findings in nocturnal urine samples during the 2.45 GHz exposure of 2 hours a day, 5 days a week is presented at Figure 2. The results of urinary pH, glucose, bilirubin, ketones, specific gravity, blood, protein, urobilinogen, nitrite, leukocyte appearance in the nocturnal urine indicated no significant differences between treated and control animal group.

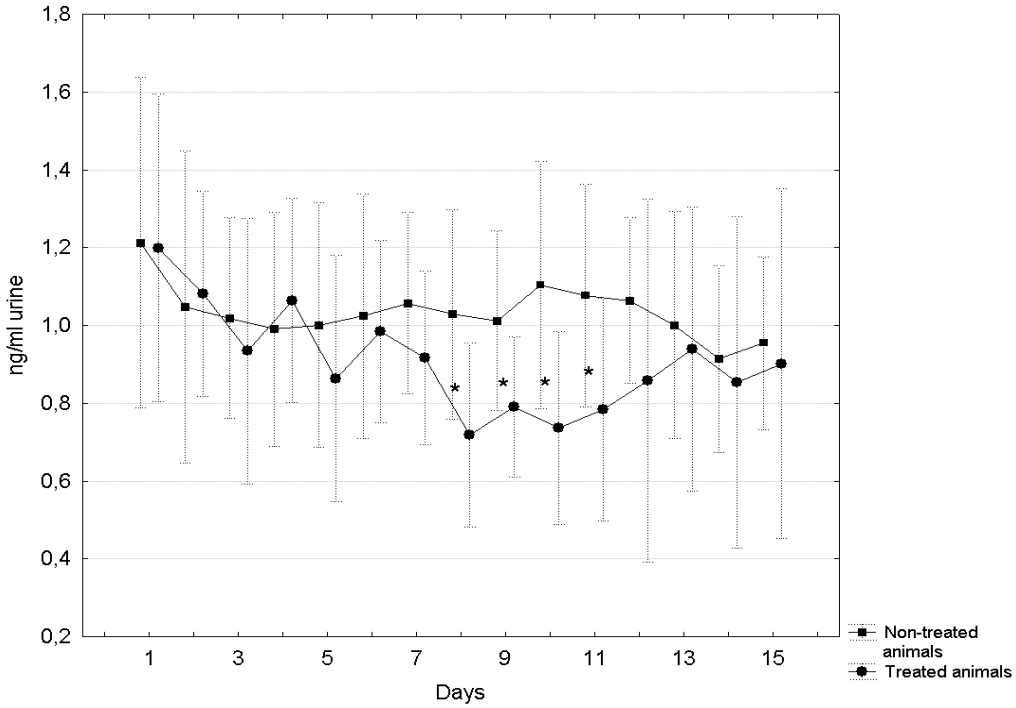

Figure 1. The time-course of nocturnal melatonin metabolite; 6-sulphaxymelatonin (6SM) in rat urine samples during the 2.45 GHz exposure and matched sham-controls (*significant difference $p<0.05$)

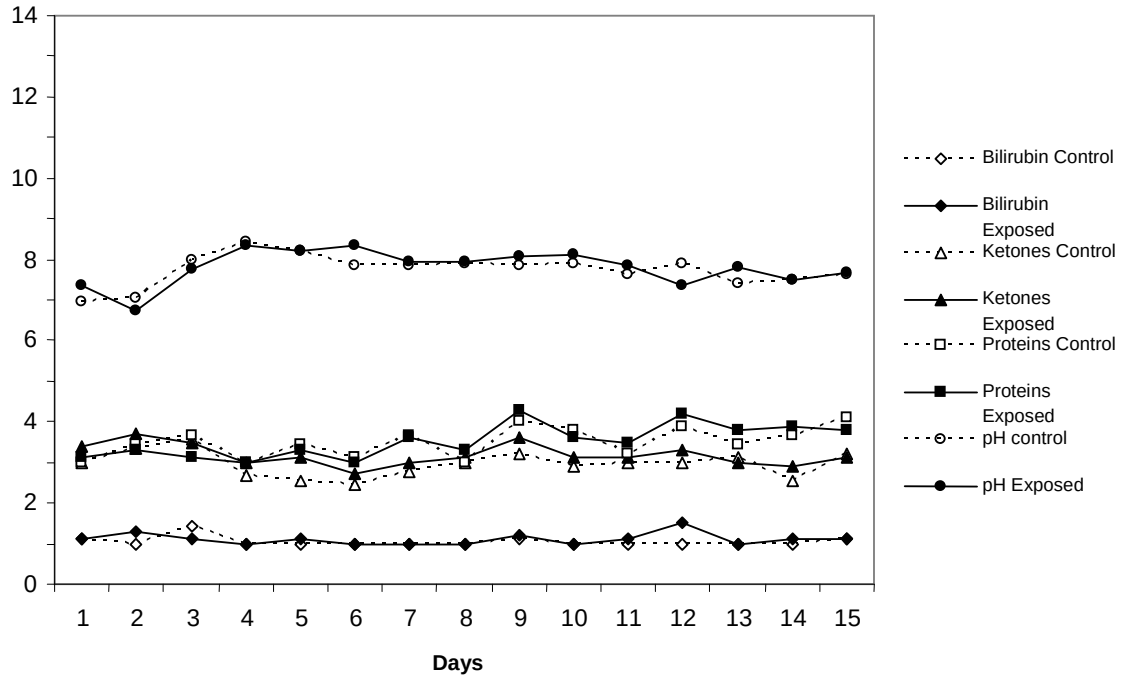

Figure 2. Semi-quantitative biochemical findings (urinary pH, bilirubin, ketones, protein) in nocturnal urine samples during the 2.45 GHz irradiated and sham-exposed control rats

Discussion

Interest in melatonin is that it could help explain results of some studies on unsafe EMF biological potency across the spectrum from ELF to RF/ MW by means of the reasonable underlying mechanisms of action. Melatonin has been reported to block RF/EM radiation-induced DNA strand breaks in rat brain cells and slow the growth of some preneoplastic lesions in rats in relation to the influence of EM exposure [12, 13]. Studies on small animals provide the strongest data supporting the hypothesis that EM field suppresses melatonin. It gives the impression that EMF suppresses different elements of melatonin biosynthesis, specifically secretion and metabolism [4, 14, 15, 16]. On the other hand, chronic exposure of lambs to the environmental electric and magnetic fields revealed that EMF does not affect the mechanism underlying the generation of the circadian pattern of melatonin secretion [17]. Additionally, Stärk et al., call attention to the absence of chronic RF exposure effect on salivary melatonin concentrations in cattle, along with Vollrath's group who found no short-term effect of high frequency RF exposure on the mammalian pineal gland and melatonin synthesis [18, 8]. Recent investigations suggest that short term exposure to 1439 MHz field does not alter melatonin synthesis in rats, and two hours daily exposure to the 900 and 1800 MHz during 14 day period achieve no effect on 6SM excretion in rats [19, 20]. We studied whether 2.45 GHz frequency field has demonstrable effects on nocturnal urinary 6SM level and urinalysis parameters in rats after exposure of two hours a day, five days a week exposure. The animals were not irradiated for two days on weekends. Major decline in 6SM excretion in microwave exposed rats has been obtained between experimental days eight and eleven ($p<0.05$). Reduction in melatonin metabolite levels seems to be consequence of increasing RF/MW irradiation over the time. Obtained effects appeared after repeated exposure, but apparently not leading into the irreparable damage. Recovery of 6SM urinary excretion is likely related to absence of irradiation on experimental day thirteen and fourteen. The findings reveal that urinary melatonin metabolite could be a sensitive marker of RF/MW biological potency (Figure 1). Accordingly, it is in agreement with Lai's statement that: "Existing results indicate changes in the response characteristics of the nervous system with repeated exposure suggesting that the effects are not "forgotten" after each episode of exposure" [21]. The semi-quantitative biochemical findings in nocturnal urine indicated that applied 2.45 GHz exposure does not influence glucose, bilirubin, ketones, blood, protein, urobilinogen, nitrite, leukocyte appearance as well as urinary pH and specific gravity (Figure 2). The behavioral pattern of the animals was not altered during the course of the experiment. It can be concluded that 2.45 GHz microwave field has a capacity to affect the hormone melatonin balance in rats after repeated exposure.

Acknowledgements

The research was supported by Ministry of Science, Education and Sports, Croatia, Grant No. 0022005.

References

[1] Trošić I, Mataušić-Pišl M, Radalj Ž, Prlić I. Animal study on Electromagnetic field biological potency. Arh. Hig. Rada Toksikol. 50: 5-11 (1999)

[2] Trosic I, Busljeta I, Modlic B. Investigation of the genotoxic effects of microwave irradiation in rat bone marrow cells: *in vivo* exposure. Mutagenesis 1:361-364 (2004)

[3] Stevens RG, Davis, S. The melatonin hypothesis: electric power and breast cancer. Environ. Health Perspect. 104: (Suppl 1), 135-140 (1996)

[4] Brainardet GC, Kavet R, Kheifets LI. The relationship between electromagnetic field and light exposure to melatonin and breast cancer risk: A review of the relevant literature. J. Pineal. Res. 26: 65-100 (1999)

[5] Cherry, N. EMR Reduces Melatonin in Animals and People. Available from: http://www.feb.se/EMFguru/Research/emf-emr.htm (2000a)

[6] Cherry N. Probable Health Effects Associated with Base Station in Communities: The Need for Health Surveys. In: Oberfeld G. (Ed.), Proceedings of International Conference on Cell Tower Sitting. Printing Office Salzburg, Austria, p.p. 192-233 (2000b)

[7] deSeze R, Ayoub J, Peray P, Miro L, Touitou Y. Evaluation in humans of the effects of radiocellular telephones on the circadian patterns of melatonin secretion, a chronobiological rhythm marker. J. Pineal. Res. 27: 237-242 (1999)

[8] Vollrath L, Spessert R, Kratzsch T, Keiner M, Hollmann H, No Short-Term Effects of High-Frequency Electromagnetic Fields on the Mammalian Pineal Gland. Bioelectromagnetics 18:376-387 (1997)

[9] Durney CH, Iskander MF, Massoudy H, Allen BS, Stewart J, Mitchell BS, John C. Radiofrequency Radiation Dosimetry Handbook, 3rd Ed, USAF School of Aerospace Medicine, Texas (1980)
[10] IEGMP (Independent Expert Group on Mobile Phones): Mobile phones and Health, Available from: http://www.iegmp.org.uk (2000)
[11] Willemsen EW. Understanding statistical reasoning. Freeman WH & Company, San Francisco (1974)
[12] Lai H, Singh NP. Melatonin and a Spin-Trap Compound Block Radiofrequency Electromagnetic Radiation-Induced DNA Strand Breaks in Rat Brain Cells. Bioelectromagnetics 18: 446-454 (1997)
[13] Imaida K, Hagiwara A, Yoshino H, Tamano S, Sano M, Futakuchi M, Ogawa K, Asamoto M, Shirai T. Inhibitory effects of low doses of melatonin on induction of preneoplastic liver lesions in a medium-term liver bioassay in F344 rats: relation to the influence of electromagnetic near field exposure. Cancer Letters 155:105-114 (2000)
[14] Brendel H, Niehaus M, Lerchl A. Direct suppressive effects of weak magnetic fields (50Hz and $16^{2/3}$ Hz) on melatonin synthesis in the pineal gland of Djungarian hamsters (*Phodopus sungorus*). J. Pineal. Res. 29:28-33 (2000)
[15] Fernie KJ, Bird DJ, Petitclerc D. Effects of Electromagnetic Fields on Photophasic Circulating Melatonin Levels In American Kestrels. Environ. Health Perspect. 107:901-904 (1999)
[16] Grota LJ, Reiter RJ, Keng P, Michaelson S. Electric field exposure alters serum melatonin but not pineal melatonin synthesis in male rats. Bioelectromagnetics 15:427-437 (1994)
[17] Lee JM, Stormshak F, Thompson JM, Thinesen P, Painter LJ, Olenchek EG, Hess DL, Forbes R, Foster DL. Melatonin Secretion and Puberty in Female Lambs Exposed to Environmental Electric and Magnetic Fields. Biology of Reproduction 49:857-864 (1993)
[18] Stärk KDC, Krebs T, Altpeter E, Manz B, Griot C, Abelin, T. Absence of chronic effect of exposure to short-wave radio broadcast signal on salivary melatonin concentrations in dairy cattle. J. Pineal. Res. 22:171-176 (1997)
[19] Hata K, Yamaguchi H, Tsurita G, Watanabe S, Wake K, Taki M, Ueno S, Nagawa H. Short Term Exposure to 1439 MHz Pulsed TDMA Field Does Not Alter Melatonin Synthesis in Rats. Bioelectromagnetics 26:49-53 (2005)
[20] Bakos J, Kubinyi G, Sinay H, Thuróczy G, GSM Modulated Radiofrequency Radiation Does Not Affect 6-Sulfatoxymelatonin Excretion of Rats. Bioelectromagnetics 24:531-34 (2003)
[21] Lai H. Neurological effects of radiofrequency electromagnetic radiation. Workshop on Possible Biological and Health Effects of RF Electromagnetic Fields Vienna, Austria p.p. 1-13 (1998)

THE EFFECT OF EMF ON THE EARLY COMPONENTS OF ERPS IS DEPENDENT ON THE KIND OF STIMULUS USED.

TSIAFAKIS VASILEIOS[1], NANOU ELENA[1], KAPARELIOTIS EVANGELOS[1], PRAGIATIS LAZAROS[1], PAPAGEORGIOU CHARALAMBOS[2], SOLDATOS KONSTANTINOS[2], RABAVILAS ANDREAS[3], CAPSALIS CHRISTOS[1]

[1] NATIONAL TECHNICAL UNIVERSITY OF ATHENS, DEPARTMENT OF ELECTRICAL ENGINEERING, DIVISION OF INFORMATION TRANSMISSION SYSTEMS AND MATERIAL TECHNOLOGY, GREECE

9 IROON POLYTECNEIOY STR., ATHENS ,GREECE, 15773, Tel: (+30)210 7722574, Fax: (+30)210 7723520, email:vtsiaf@mail.ntua.gr

[2] DEPARTMENT OF PSYCHIATRY, EGINITION HOSPITAL, UNIVERSITY OF ATHENS, GREECE
email: cpapage@eginitio.uoa.gr

[3] UNIVERSITY MENTAL HEALTH RESEARCH INSTITUTE, ATHENS, GREECE.

Abstract

Probable alterations of human cognitive functions, caused by electromagnetic fields (EMF) emitted by cellular phones, are still under investigation. The present study focused on the effect of a 900MHz signal on the early components of event related potentials (ERPs) recorded during an auditory memory task.

Nineteen normal subjects (10 women and 9 men) were examined with and without radiation in a random order. Measurements included the recording at 16 scalp electrodes of the P50 and N100 components which were evoked by two warning stimuli which differed in frequency (low=500 Hz, high=3000Hz).

Results showed that for the low frequency stimulus radiation caused a statistically significant positive shift on the waveform of the early components while for the high frequency stimulus there was a significant negative shift at the Fp1 electrode. The affected area of the left prefrontal cortex (Fp1 electrode site) plays a key role in working memory operation.

These findings provide further evidence that both the P50 and N100 components of the ERPs, which reflect pre-attentive and attentive information processing respectively, are modality specific. Furthermore the amplitudes of the two components for the two modalities are influenced by EMF in opposite ways.

Introduction

Cellular (GSM) telephones are widely used throughout the world. Although there is no clear evidence of possible effects of the electromagnetic field (EMF) on brain physiology, there is common concern about this matter. In this context, some reports suggested that the exposure to mobile phone (MP) EMF exerts facilitating effects on these brain operations [1, 2, 3, 4] while other studies did not find any changes in these functions in relation to the applied MP-EMF [5, 6]. Thus, it has been proposed that 'the inability to replicate previous findings could have been caused by lack of actual EMF effects or the magnitude of effects being at the sensitivity threshold of the test used. [5].

Event related potentials (ERPs) due to their high resolution properties can be of significant use in studying EMF effects on brain activity [7]. It should be noted that the earlier components of the ERPs are thought to represent the activity of the sensory pathways that transmit the signal generated at peripheral receptors to central processing systems. These components are 'modality specific', that is they are influenced primarily by the stimulus parameters such as intensity and frequency. In this respect, given that both attention and WM are associated with the P50 and N100 components of ERPs [8, 9, 10] it seems reasonable to review the effects of MP-EMF on these components taking also into account the kind of stimulus that provokes them.

The analysis of the patterns of N100 waveforms of ERPs during MP-EMF exposure revealed conflicting results. Urban et al., [11] did not find changes to the visual evoked N100 components of ERPs (amplitude and latency) following 5 min exposure to EMFs. A recent study by Maby et al. [12], based on the investigation of auditory evoked potentials recorded from healthy volunteers and epileptic patients revealed that the exposure to MP-EMF induced decreased N100 amplitude in both assessed groups, and decreased N100 latency for the healthy subjects. The authors drew the conclusion that these effects are attributable to the 'mild, localized heating' evoked by MP-EMF. It is possible that some of the inconsistencies just mentioned may be related to the different modalities involved (i.e. auditory versus visual) and complexity of the tasks employed

Taking into account the above considerations, we hypothesized that the electrophysiological brain activity as indexed by P50 and N100, in relation to WM operation, could be of value in detecting possible psychophysiological mechanisms underlying alterations evoked by MP-EMF. Thus, the present study was designed to assess the effect of the exposure of MP-EMF on the patterns of P50 and N100 ERP components elicited during a WMtest.

Methods

Participants

Nineteen healthy individuals (9 men and 10 women, mean age = 23.3 ± 2.23 years, mean education = 16.9 ± 1.82 years) participated in the experiment. The male and female subgroups were homogeneous with regards to age and educational level. All participants were right-handed and had no history of any hearing problem. Informed consent was obtained from all subjects.

Stimuli and procedure

The subjects were evaluated with the digit span Wechsler Auditory test [13, 14]. A warning stimulus of either high (3000 Hz) or low frequency (500 Hz) was presented through earphones to the subjects, who were asked to memorize the numbers that followed. The warning stimulus lasted 100msec. A one second interval followed the onset of the warning stimulus and then the numbers to be memorized were presented by a male voice. At the end of the number sequence presentation, the same signal tone was repeated. If the frequency of the signal tone was low the subjects had to recall the numbers in the same order with that presented, else, if the frequency was high, the subjects had to recall the numbers in the opposite order.

Before any ERPs' recording, practice trials were administered until the subjects could clearly discriminate the warning stimuli (tones). After completion of the above-mentioned process, a rest period of five minutes followed, before the recording of the ERPs.

The experimental setup included a Faraday room, which screened any electromagnetic interference that could affect the measurements. The subjects sat in an anatomical chair and a certified dipole antenna was fixed near their right ear. Care was taken so that the distance between telephone and ear (about 20 cm) was constant during the whole session. The antenna was driven by a signal generator, which could be switched on or off. In the on mode the antenna emitted a 900 MHz electromagnetic field with mean power at 64 mWatt [13].

ERPs were recorded during 1 sec between the onset of the warning stimulus and the onset of the first

administered number. The electrophysiological signals were recorded with Ag/AgCl electrodes. Electrode resistance was kept constantly below 5 kΩ. EEG activity was recorded from 15 scalp electrodes based on the International 10-20 system of Electroencephalography [15], referred to both earlobes. An electrode placed on the subject's forehead served as ground. The bandwidth of the amplifiers was set at 0.05 Hz to 35Hz. During the administration of stimuli, the subjects had their eyes closed in order to minimize eye movements and blinks. Eye movements were recorded through electro-oculogram (EOG) and recordings with EEG higher than 75mV were rejected. Warning stimuli, as well as learning material, i.e. the numbers to recall, were presented binaurally via earphones at an intensity of 65dB sound pressure level. The evoked biopotential signal was submitted to an analogue-to-digital conversion, at a sampling rate of 1 KHz, and was averaged by a computerized system. Each recording session consisted of 52 repetitions of the trial.

Because the P50 and N100 components are included in the array of early-endogenous ERPs components, which normally are modality specific, the ERPs induced by the two modal stimuli were averaged separately [7]. In particular, two varieties of waveforms for each component were obtained, one (low P50 and low N100) evoked by the low frequency modality (26 trials) for each lead in all subjects and another (high P50 and high N100) evoked by the high frequency modality (26 trials) for each lead in all subjects .

The following parameters were calculated. ERPs were recorded for each subject at EEG leads Fp1, Fp2, F3, F4, C3, C4, C5, C6, P3, P4, O1, O2, Pz, Cz, and Fz. Recordings with acceptable EEG level were averaged for each lead by a computerized system. An algorithm was used, which identified the P50 as the most positive peak in each averaged lead curve, between 30 and 80 msec and the N100 as the most negative peak in each averaged lead curve, between 70 and 150 msec, after the onset of the warning stimulus. Peak amplitudes were measured relative to the mean amplitude of the 100-msec prestimulus baseline period and latency measurements were computed relative to stimulus onset.

Statistical analysis

The values of the P50 and N100 amplitudes and latencies at the fifteen leads were subjected to multivariate analysis of variance with the two frequency tones and the two radiation conditions as the between subjects factors. The frequency X radiation interaction was also taken into consideration. Post-hoc pairwise comparisons (with the necessary corrections for multiple comparisons) were carried out between the two frequencies in the absence and presence of radiation, as well as between the two radiation conditions at the low and high frequencies for both components. Statistical significance was set at 0.05.

Results

The multivariate analysis revealed that neither frequency, nor radiation by themselves had any significant effect on P50 and N100 amplitudes of the entire group of subjects taken as a whole. There was, however, a significant frequency X radiation interaction effect (p value of Pillai's trace=0.013).

Figure 1 and figure 2 are quite helpful in explaining this interaction effect. In the absence of radiation the following findings were observed: The low frequency tone induces higher negative peak amplitude values of the N100 component than the high frequency one at all the fifteen leads under consideration. This difference achieves statistical significance at nine leads (Fp1, C3, Fp2, C6, O1, O2, P3, Pz, Fz). The high frequency tone induces higher positive peak amplitude values of the P50 component than the low frequency one at all the fifteen leads under consideration. This difference achieves statistical significance at eleven leads (Fp1, C5, C3, Fp2, C6, C4, O1, O2, P3, Pz, Fz).

The application of EMF radiation demotes these differences, since in the case of this application statistically significant differences of the P50 amplitudes for the two frequency tones are observed only in three leads while no statistically significant differences of the N100 amplitudes for the two frequency tones are observed.

This is accomplished by a slight increase of the negative values of the N100 amplitudes together with a slight decrease of the positive values of the P50 amplitudes at the high frequencies. These differences achieve statistical significance at lead Fp1 for both N100 and P50. Also a slight decrease of the N100 amplitudes together with a slight increase of the P50 amplitudes was observed at the low frequencies. In P50 the increase achieves statistical significance at two leads (Fp1 and O1) while in N100 the decrease achieves statistical significance at lead Fp1

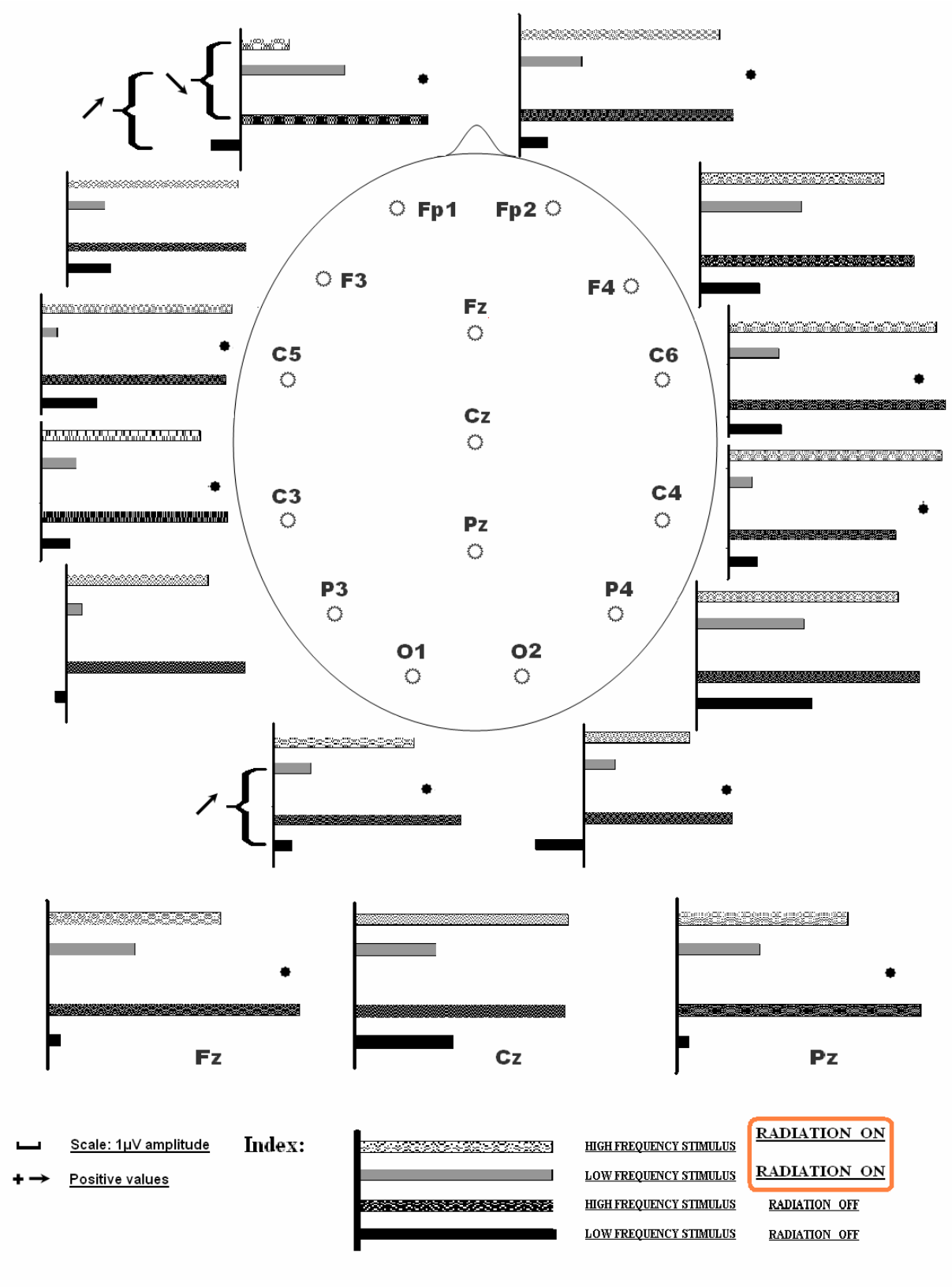

Figure1: P50 amplitudes at 15 leads for high and low frequency stimuli, with and without EMF exposure.

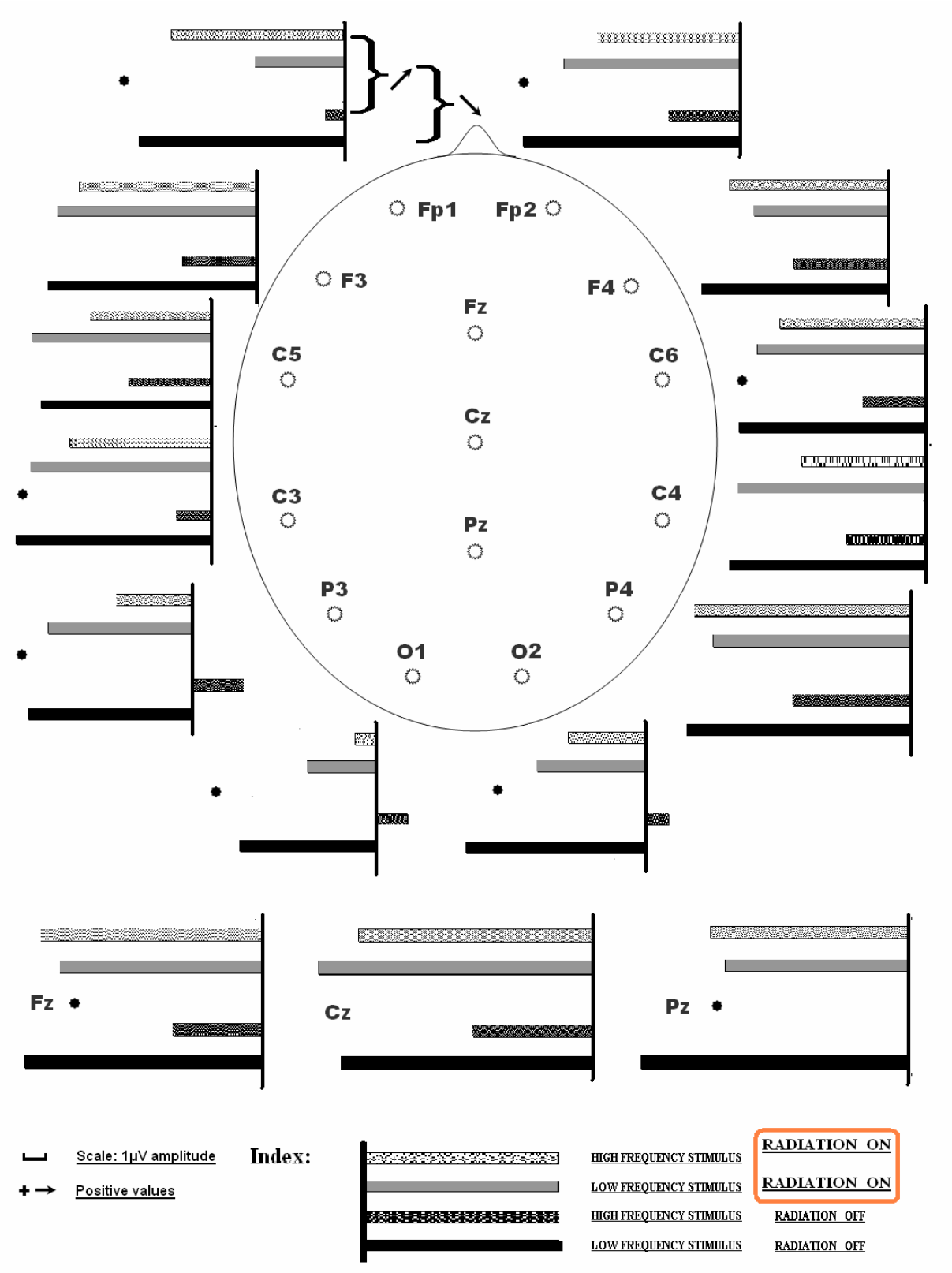

Figure2: N100 amplitudes at 15 lead for high and low frequency stimuli, with and without EMF exposure

The crossover effect of these changes results in the fact that Fp1 stands as the only lead, at which in the presence of radiation the N100 amplitudes are lower at the low frequency than at the high frequency tone while the P50 amplitudes are higher at the low frequency than at the high frequency tone. This is the main reason for the appearance of a significant overall frequency X radiation interaction effect.

Neither radiation, nor frequency, nor their interaction had any significant effect on the N100 and P50 latencies. Memory performance did not differ, in both cases, between the two frequency modalities (58.4±26.5 for the low frequency tone, and 54.9±24.6 for the high frequency tone, *t*-test, p=0.552). It also did not seem to depend on radiation, and sex.

Discussion

The findings of the present study indicate that MP-EMF may alter the patterns of the auditory P50 and N100 components of ERPs elicited in a working memory task. More precisely, the results showed that the presence of MP-EMFs, when high frequency stimulus was applied, induced statistically significant decrease in the amplitude of P50, while there was a statistically significant increase in the amplitude of N100 at Fp1 electrode site, as compared to themselves without MP-EMF exposure. In contrast, the exposure to EMF when low frequency stimulus was applied, revealed statistically significant increase of the amplitude of P50 at Fp1 and O1 electrode site while there was a statistically significant decrease of the amplitude of N100 at Fp1 only electrode site, as compared to themselves without EMF exposure. Also the amplitude of P50 without radiation appeared significantly higher in the high frequency warning stimulation as compared with those of low frequency stimulation while the opposite situation appeared for the N100 (smaller values of N100 for the high than these for low frequency stimulus)

The observed differences of the amplitudes of P50 and N100 without radiation may be explained considering the fact that these components belong to the earlier components of ERPs which are sensitive to physical parameters of the stimuli [7]. The dissociation observed for the P50 and N100 potentials with reference to the modality of the warning stimuli just mentioned, suggests that an alternative explanation must be considered in connection with the effects of EMF upon these peaks evoked by high frequency and the peaks evoked by low frequency warning stimuli.

In line with this point of view, the obtained changes concerning N100 waveforms evoked by low frequency warning stimuli seem to be in accordance with those reported by Maby et al.[12] and Hamblin et al.[11], as mentioned earlier. On the other hand, the patterns of results concerning the N100 evoked by the high frequency warning stimuli appears to be consistent to those reported by Koivisto et al.[3] who reported that the exposure to the EMF has a facilitating effect of attentive processing involving left frontal area during the manipulation of information in WM.

Taken together, the obtained results provide evidence that the EMF emitted by mobile phone affect differentially the attentive information processing, as it is reflected by the N100 component of ERPs. This differential effect might be explained considering that the N100 arises from multiple sources [17, 18]. An alternative explanation can be conceived in terms of attentional demands: Eulitz et al. [19] reported that 30 min EMF exposure altered the beta frequency band of the brain electrical response to acoustic stimuli in an oddball paradigm. More precisely, this effect appeared when subjects processed task-relevant target stimuli but it was not present for irrelevant standard stimuli. Another group of investigators observed reduced slow brain potentials as an effect of exposure to EMF during a demanding experimental condition, whereas they did not observe any alteration when the exposure occurred during a not demanding experimental condition [20]. Thus, a possible explanation of the finding concerning the N100 evoked by the high frequency warning stimuli may be due to the fact that in this condition the subjects had to recall the administered numbers in the opposite order (see experimental procedure), consequently, the subjects faced a rather demanding experimental condition.

The findings of P50 amplitudes in relation to the MP-EMF radiation cannot be compared with those of other studies, because to our knowledge there are no previous reports assessing this ERP component in relation to MP-EMF radiation. An exception appears to be the study by **Arai** et al. [21], which reported no effects on mid latency evoked brain potentials in 15 healthy controls using the Japanese mobile phone emitting 800MHz. But there are important differences in methodology that make a direct comparison difficult, for instance, in the present study the obtained findings would likely have occurred immediately upon presentation of the MP-EMF and lasted throughout its presence, whereas, in the study by Arai et al., [21] the reported effects referred to evoked brain response before and after using a mobile phone for 30 min. The main difference is that in the present study the evoked potentials were recorded during the presence of the radiation and without the presence of the radiation, while in the study of Arai the ERPs were studied before and after the expose to the MP-EMF. However, it may be easier to understand the importance of the pattens in P50 amplitude during MP-EMF radiation reported here in the light of psychophysiological indices concerning the meaning of the P50 potential on the one hand, and on the other considering the proposed influence of MP-EMF on brain function. The P50 potential is a subcomponent of the γ EEG activity reflecting the transient synchronization of thalamocortical

activity in response to sensory stimulation [22, 23]. In keeping with this suggestion, concerning the low frequency amplitude of P50 waveforms, the present findings, seem to be compatible with a recent study by Croft et al.,[24] focusing on the effects of mobile phone on EEG as a function of time, which show 'an increase in the γ response at midline frontal and lateral posterior sites'. Further, since the MP-EMF is observed to enhance the enzymatic activity of the cholinergic system [25, 26, 27], and on the other hand the augmentation in P50 amplitude is thought to reflect increased cholinergic activation during arousal [28, 29], thus it is reasonable to suppose that this mechanism could account for the observed increase in the amplitude of P50 evoked by the low frequency stimuli, in association with MP-EMF radiation. The obtained results provide evidence that the MP-EMF emitted by mobile phone affect pre-attentive information processing; however, the underlying mechanisms of such influence are still unclear, although several possibilities exist, calling for potential directions of future research. These highly complex physical and biological phenomena necessitate the development of new experimental, measuring and observation procedures.

A further point for discussion is the location of the observed changes with regard to the N100 amplitude. The affected area of the left prefrontal cortex (Fp1 electrode site) plays a key role in working memory operation [30, 31]. Moreover, comparable effects on this brain area after PM-EMF exposure has been reported by other researchers. Specifically, Huber et al. [32] using positron emission tomography scans showed that exposure to MP-EMF alters the cerebral blood flow of 12 healthy young men in the left dorsolateral brain region. In line with this, it is noteworthy that brain imaging studies suggest that attention and working memory generally engage left frontal areas of the brain cortex [33, 34].

In conclusion, the findings of the present study support the view that MP-EMF during the performance of a WM task, affect pre-attentive and attentive operation, possibly mediated by the left frontal brain networks. However, before drawing any final conclusions, the present results advocate the need for more follow-up studies in order to evaluate not only the short-term but also the long-term effects of MP-EMF use in pre-attentive, attentive and WM operation.

The findings of the present study indicate that MP-EMF may alter the patterns of the auditory P50 and N100 of ERPs elicited during a working memory task. More precisely, the results showed that the presence of MP-EMFs, when high frequency stimulus was applied, induced statistically significant decrease in the amplitude of P50, while there was a statistically significant increase in the amplitude of N100 at Fp1 electrode site, as compared to themselves without MP-EMF exposure. In contrast, the exposure to EMF when high frequency stimulus was applied, revealed statistically significant increase of the amplitude of P50 at Fp1 and O1 electrode site while there was a statistically significant decrease of the amplitude of N100 at Fp1 only electrode site, as compared to themselves without EMF exposure.

References

[1] N. Edelstyn , A. Oldershaw, The acute effects of exposure to the electromagnetic field emitted by mobile phones on human attention, Neuroreport 21;13(1) (2002) 119-21.
[2] M. Koivisto, A. Revonsuo, C. Krause, C. Haarala, L. Sillanmaki, M. Laine, H. Hamalainen, Effects of 902 MHz electromagnetic field emitted by cellular telephones on response times in humans, Neuroreport 11 (2000) 413-415.
[3] M. Koivisto, M.C. Krause, A.Revonsuo, M. Laine, H. Hamalainen, The effects of electromagnetic field emitted by GSM phones on working memory, Neuroreport 11 (2000) 1641-1643.
[4] T.M. Lee, P.K. Lam, L.T. Yee, C.C. Chan, The effect of the duration of exposure to the electromagnetic field emitted by mobile phones on human attention, Neuroreport 14(10) (2003)1361-4.
[5] C Haarala , M. Ek, L. Bjornberg, M. Laine, A. Revonsuo, M. Koivisto, H . Hamalainen, 902 MHz mobile phone does not affect short term memory in humans, Bioelectromagnetics 25(6) (2004) 452-6.
[6] M.C. Krause, C. Haarala, L. Sillanmaki, M. Koivisto, K. Alanko, A. Revonsuo, M. Laine, H. Hamalainen, Effects of electromagnetic field emitted by cellular phones on the EEG during an auditory memory task: a double blind replication study, Bioelectromagnetics 25(1) (2004) 33-40.
[7] M.Fabiani, G. Gratton, M. Coles, Event-related potentials: methods, theory, and applications. In: Cacioppo J, Tassinary L, Bernston G, eds. Handbook of psychophysiology, Cambridge University Press, New York, 2000, pp. 53–84.
[8] EM Conley , HJ Michalewski, A. Starr, The N100 auditory cortical evoked potential indexes scanning of auditory short-term memory, Clin Neurophysiol. 110(12) (1999) 2086-93.
[9] JT. Coull, Neural correlates of attention and arousal: insights from electrophysiology, functional neuroimaging and psychopharmacology, Prog Neurobiol 55(4) (1998) 343-61.
[10] E.J. Golob , A. Starr, Serial position effects in auditory event-related potentials during working memory retrieval, J Cogn Neurosci. 16(1) (2004) 40-52.
[11] P. Urban, E. Lukas, Z. Roth, Does acute exposure to the electromagnetic field emitted by a mobile phone influence visual evoked potentials? A pilot study, Eur J. Public Health 6(1998) 288-290.
[12] E.Maby , R. Le Bouquin Jeannes, C. Liegeois-Chauvel, B. Gourevitch, G. Faucon, Analysis of auditory evoked potential parameters in the presence of radiofrequency fields using a support vector machines method, Med Biol Eng Comput. 42(4) (2004) 562-8.
[13] C. Papageorgiou, E. Nanou, V. G. Tsiafakis, C. Capsalis, A. D. Rabavilas, Gender related differences on the EEG during a simulated mobile phone signal, Neuroreport, 15 (2004) 2557-2560.
[14] D. Wechsler, Manual for the Wechsler adult intelligence scale. New York: Psychological Corporation, 1955.
[15] H. Jasper, The ten-twenty electrode system of the international federation, Electroencephalogr Clin Neurophysiol. 10 (1958) 371–375.
[16] D.L. Hamblin, A.W. Wood, R.J. Croft, C. Stough, Examining the effects of electromagnetic fields emitted by GSM mobile phones on human event-related potentials and performance during an auditory task, Clin Neurophysiol. 115(1) (2004) 171-178.
[17] B.Godey , D. Schwartz , J.B. de Graaf , P. Chauvel , C. Liegeois-Chauvel, Neuromagnetic source localization of auditory evoked fields and intracerebral evoked potentials: a comparison of data in the same patients, Clin Neurophysiol. 112(10) (2001) 1850-1859.
[18] Yvert B, Fischer C, Bertrand O, Pernier J. Localization of human supratemporal auditory areas from intracerebral auditory evoked potentials using distributed source models. Neuroimage 28(1) (2005) 140-53.
[19] C. Eulitz, P. Ullsperger, G. Freude, T. Elbert, Mobile phones modulate response brain activity, Neuroreport 9 (1998) 3229-3232.
[20] G. Freude, P. Ullsperger, S. Eggert, I. Ruppe, Effects of microwaves emitted by cellular phones on human slow brain potentials, Bioelectromagnetics 19 (1998)384-387.
[21] N. Arai, H. Enomoto, S. Okabe, K. Yuasa, Y. Kamimura, Y. Ugawa, Thirty minutes mobile phone use has no short-term adverse effects on central auditory pathways, Clin. Neurophysiol. 114 (2003)1390-1394.
[22] A.B.Clementz, D.L. Blumenfeld, S. Cobb, The gamma band response may account for poor P50 suppression in schizophrenia. Neuroreport. 8(18) (1997)3889-3893.
[23] G. Zouridakis, N.N. Boutros, H.B. Jansen, A fuzzy clustering approach to study the auditory P50 component in schizophrenia. Psychiat. Res. 69 (1997) 169-181.
[24] R. J. Croft, J.S. Chandler, A.P.Burgess, R.J.Barry, J.D.Williams, A.R.Clarke, Acute mobile phone operation affects neural function in humans, Clin. Neurophysiol. 113(2002)1623-1632.
[25] M. Barteri, A. Pala, S. Rotella, Structural and kinetic effects of mobile phone microwaves on acetylcholinesterase activity, Biophys. Chem. 113 (2005) 245-253.
[26] H. Lai, A. Horita, A.-W. Guy, Acute low-level microwave exposure and central cholinergic activity: studies

on irradiation parameters. Bioelectromagnetics 9 (1988)355-362.
[27] H. Lai, M.-A. Carino, A. Horita, A.-W. Guy, Acute low-level microwave exposure and central cholinergic activity: a dose-response study. Bioelectromagnetics 10 (1989), 203-209.
[28] M. J. Griffth, E.J. O'Neill, F. Petty, D. Garver, D. Young, R. Freedman, Nicotinic receptor desensitization and sensory gating deficits in schizophrenia Biol Psychiat., 44(1998) 98-106.
[29] K.F. Stevens, J. Meltzer, G. M. Rose, Nicotinic cholinergic normalization of amphetamine-induced loss of auditory gating in freely moving rats, Psychopharmacology, 119(1995)163-170.
[30] L.A. Dade , R.J. Zatorre , A.C. Evans , M. Jones-Gotman, Working memory in another dimension: functional imaging of human olfactory working memory, Neuroimage 14(3) (2001) 650-60.
[31] A.D. Wagner , A. Maril , R.A. Bjork , D.L. Schacter, Prefrontal contributions to executive control: fMRI evidence for functional distinctions within lateral Prefrontal cortex, Neuroimage 14(6) (2001) 1337-1347.
[32] R. Huber, V. Treyer, J. Schuderer, T. Berthold, A. Buck, N. Kuster, H.P. Landolt, P. Achermann, Exposure to pulse-modulated radio frequency electromagnetic fields affects regional cerebral blood flow, Eur J Neurosci. 21(4) (2005) 1000-6.
[33] H.R.Naghavi, L. Nyberg, Common fronto-parietal activity in attention, memory, and consciousness: shared demands on integration? Conscious Cogn 14(2) (2005) 390-425.
[34] B.R. Postle, L.N. Brush, The neural bases of the effects of item-nonspecific proactive interference in working memory, Cogn Affect Behav Neurosci 4(3) (2004) 379-92.

P-SELECTIN EXPRESSION IN A COLON TUMOR MODEL EXPOSED BY SINUSOIDAL ELECTROMAGNETIC FIELDS

HANDAN TUNCEL, ASSOC.PROF.DR.,
ISTANBUL UNIVERSITY, CERRAHPAŞA MEDICAL FACULTY,
DEPARTMENT OF BIOPHYSICS, TÜRKİYE
handantun@superonline.com

FUMIO SHIMAMOTO, PROF.DR.,
PREFECTURAL UNIVERSITY OF HIROSHIMA, JAPAN
simamoto@pu-hiroshima.ac.jp

MEHMET ALI KORPINAR, PROF.DR.,
ISTANBUL UNIVERSITY, CERRAHPAŞA MEDICAL FACULTY,
DEPARTMENT OF BIOPHYSICS, TÜRKİYE
korpinar@istanbul.edu.tr

MUSTAFA TUNAYA KALKAN, PROF.DR.,
ISTANBUL UNIVERSITY, CERRAHPAŞA MEDICAL FACULTY,
DEPARTMENT OF BIOPHYSICS, TÜRKİYE
tunaya@istanbul.edu.tr

Abstract:

P-selectin plays roles mainly in the initial process of tumor cell adhesion to platelets. The object of present work was to determine the expression level of P-selectin in a colon tumor model that was affected by sinusoidal electromagnetic fields (SMF).

We used male Wistar albino rats 2-2.5 months age. Animals were divided into 4 groups: I (MNU), II (SMF+MNU), III (SMF) and IV (CONTROL). Rats were housed five per polycarbonate cage. 60 mg MNU was dissolved in 6 ml sterile 0.9% NaCl. Prepared solutions were given i.r. to the 1st and 3rd groups as 0.2 ml /per animal. The same procedure was applied to the 2nd and 4th groups but 0.2 ml /per animal sterile isotonic solution was administrated instead. This procedure was repeated once a week for 10 weeks. After administered at MNU, 2nd and 3rd groups were exposed to a sinusoidal magnetic field (SMF, 50 Hz, 5mT) for 6 hours/day for 8 months. The expression of P-Selectin in four groups of rat colon tissues by immunohistochemistry on paraffin sections. The labeled streptavidin biotin method was performed.

Fisher's exact test was used for differences between proportions. There was no statistically significant ($p>0.05$) change in expression level of P-selectin.

Keywords:
P-selectin, carcinogenesis, electromagnetic fields

P-SELECTIN EXPRESSION IN A COLON TUMOR MODEL EXPOSED BY SINUSOIDAL ELECTROMAGNTIC FIELDS

Introduction:

One of the major man-induced environmental changes, which occurred in the last century, is the continued use of oscillating electromagnetic fields (EMF). These fields are generated for communication (*via* radio, television, cellular telephones), as by products of the technology set up for the visualizing on computer and television screens, or from power lines. It has been long believed that electromagnetic radiation in this wavelength range were harmless, and for sure, their inconvenience as pollutants were extremely small when compared to the health dangers associated with, for instance, smog-generating fuel. Yet, now that the major sources of environmental pollution have been identified and are being taken care of, the question about the biological effects of these electromagnetic fields becomes relevant (1).

In fact, some investigators have seen variations in cell proliferation and apoptosis after exposure to ELF fields (2), while others have not observed such changes. Thus, from a careful examination of the literature in this field, it is apparent that further studies examining the role of ELF fields in cancer are necessary. Cancer cell proliferation, apoptosis, invasion, and metastasis are complex phenomena controlled by an even more complex series of pathways, which communicate with each other through a myriad of signaling cascades. In this scenario, a pivotal role is played by cell adhesion molecules (CAMs). CAMs and their receptors mediate cell–cell and cell–matrix interactions and also play a fundamental role in tumor growth, death, metastasis, and invasion. The CAMs principally involved in these processes are those directed against important components of the extracellularmatrix (ECM) such as fibronectin, collagen, laminin, hyaluronan, heparan sulfate, and elastin. Although the number of studies examining the effects of magnetic fields on cell adhesion is rather limited, nonetheless, several studies have provided important insights into this important question (3).

Stimulated endothelial cells and activated platelets express P-selectin (CD62P), a member of the selectin family of cell adhesion molecules, which interacts with P-selectin glycoprotein ligand-1 (PSGL-1, CD162) for leukocyte rolling on stimulated endothelial cells and heterotypic aggregation of activated platelets onto leukocytes. Cross-linking of PSGL-1 by P-selectin also primes leukocytes intracellularly for cytokine and chemoattractant-induced integrin activation for firm adhesion of leukocytes. Furthermore, P-selectin mediates heterotypic aggregation of activated platelets to cancer cells and adhesion of cancer cells to stimulated endothelial cells. There is an increasing body of *in vivo* experimental evidence indicating that P-selectin can play important roles in the growth and metastasis of cancers.In this regard, the elucidation of the molecular mechanisms responsible for the regulation of the expressions of these different P-selectin ligand molecules in various human cancer cells will be an important and very interesting future task (4).

The object of present work was to determine the expression level of P-selectin in a colon tumor model that was affected by sinusoidal electromagnetic fields (SMF).

Material and Methods:

Animals

Healthy male Wistar albino rats, 2-2.5 months age, were employed in the present study. A duration of one week before the experimental period was held for the compliance and controls of experimental animals. Animals were divided into 4 groups as shown in Table 1.

TABLE 1.

Experimental groups with number of animals.

1-MNU 7
2-SMF+MNU 7
3-SMF 9
4-Control 5

Rats were housed five per polycarbonate cage (cages standard for all groups were cleaned twice a week). Water and pelleted diet were available ad libitum. The animal room was checked for temperature, humidity and light status (12:12 light-dark cycle). Temperature was maintained between 23 and 25 °C and relative humidity between 35 and 65 %.

Carcinogen administration

60 mg MNU (N-Methyl-N-Nitrosurea) (Sigma Chemical Co., Dorset, England) was dissolved in 6 ml sterile isotonic solution (0.9% NaCl). Prepared solutions were given i.r. (intra-rectal) to the MNU and SMF+MNU

groups as 0.2 ml /per animal. In the procedure a number 8 feeding tube was inserted 6 cm into the rectum and solution was administered. The same procedure was applied to the SMF and Control groups but 0.2 ml /per animal sterile isotonic solution was administrated instead. This procedure was repeated once a week for 10 weeks.

Application of magnetic field

12 serially connected copper solenoid coils generated the magnetic fields, each having 560 turns. The cores of the coils were filled with soft iron rods and they were tightened to increase the magnetic flux intensity. Plastic cages were used so that the magnetic field strength and distribution would not be affected. The coils were placed vertically and the cages were held 1.2 cm above the coils to hinder them from probable vibration. To protect the cages from heat of the coils, 1 cm thick wooden plates were placed between the coils and the cages. The coils were connected to the 220 V 50 Hz sinusoidal city electric systems. When current passed through the coils, the magnetic flux intensities were measured at five different places inside the cages to be 5 mT. For measurement, we used a Leybold Heraeus 54050 model Hall effect teslameter.

Histological processing

The animals from all groups were killed 8 months after the first i.r. injections of MNU. Immediately after the sacrifice, colons were removed, cut open along its longitudinal axis, and fixed flat in 10% buffered formalin for 24 hours at room temperature. We photographed and/or checked the aberration of the surface of colon mucosa.

Immunohistochemistry and evaluation

For immunohistochemical analysis, the labeled streptavidin biotin method was performed using a Vectastain Universal Quick Kit (Vector Laboratories, Burlingame, CA, USA) with microwave accentuation. The paraffin-embedded sections were heated for 30 minutes at 65°C, deparaffinized in xylene, and rehydrated through graded alcohols at room temperature. A 0.05 M Tris-HCl buffer (pH 7.6) was used to prepare solutions and for washes between various steps. Incubations were performed in a humidified chamber. Four-µm-thick sections were treated for 20 minutes at room temperature with 5% BSA and incubated overnight at 4°C with primary antibodies against P-selectin (BD PharMingen, San Diego, CA, USA). For each case, negative controls were performed on serial sections. On the control section, incubation with the primary antibody was omitted. Horseradish peroxidase activity was visualized by treatment with H_2O_2 and diaminobenzidine for 5 minutes. At the last step, the sections were weakly counterstained with hematoxylin.

A semiquantitative analysis of the immunohistochemistry was performed to determine the approximate percentage of cells expressing P-selectin as follows: absent (-), 0% expression; slight (+), up to 20% of cells positive; moderate (++), 21% to 50% of cells positive; and strong (+++), more than 50% of cells positive.

Histopathological examination

Histological evaluation was performed by routine procedures with H&E staining. The stained sections were examined for grade of histological abnormality.

Results

No appreciable change in food consumption was observed among different groups of rats. Fisher's exact test was used for differences between proportions. There was no statistically significant ($p>0.05$) change in expression level of P-selectin.

Discussion:

Electric and magnetic fields associated with the production, transmission, and use of electricity are ubiquitous in industrialized society. These electric and magnetic fields are predominantly of low frequency (60 Hz in the US, 50 Hz in Europe and Japan) and generally of low intensity. Electric fields exist when there is electric potential in a line, while magnetic fields exist only when there is current flow (5). Since both electric and magnetic fields often occur together and are interactive, these fields have often been referred to as electric and magnetic fields or EMFs.

More recent research has focused on potential adverse biological effects of exposure to magnetic fields. The residential exposures in most homes are to magnetic field intensities of <2 milligauss (mG), which is equivalent to 0.2 microtesla (µT) although some areas in homes may exceed this field intensity. In certain industrial settings, mean workplace magnetic field exposure may exceed 10 mG (6).

Metastasis is a cascade of cellular events by which cancer cells establish new colonies at distant sites in the

body (7,8). It comprises multiple, consecutive steps. Several cell adhesion molecules are involved in the various stages of cancer metastasis (9). P-selectin has been shown to bind to several human cancers and human cancer-derived cell lines, such as colon cancer, lung cancer including small-cell lung cancer, breast cancer, malignant melanoma, gastric cancer, neuroblastoma, and adenoid cystic carcinoma of the salivary gland. There is an increasing body of *in vivo* experimental evidence indicating that P-selectin can play important roles in the growth and metastasis of cancers. In this regard, the elucidation of the molecular mechanisms responsible for the regulation of the expressions of these different P-selectin ligand molecules in various human cancer cells will be an important and very interesting future task (10,11,12).

The expression of P-selectin is regulated at both the transcriptional and cellular levels. At the transcriptional level, tumor necrosis factor-á induces P-selectin expression in mouse and bovine endothelial cells (13,14) whereas interleukin-4 and oncostatin M induce P-selectin expression in human umbilical vein endothelial cells, which can last up to 72 h (15).There is still a long way to go to elucidate the details regarding this pathway (12).

Immunohistochemical studies of P-selectin expression in this model demonstrated no statistically significant ($p>0.05$) differences between the groups. Our results suggest that this study needs confirmation by repetitive experiments, including new methods for P-selectin detection in-vivo and in-vitro. Further work is required to determine the relative effect of the magnetic fields on this molecule and relation with metastasis phenomena.

Acknowledgements

We thank thank Katsunari Ogawa and Miyo Oda for their excellent technical assistance.
This study was supported in part by Tsuchiya Hospital, Japan.
This study was supported by the Research Fund of the University of Istanbul.

References

1-Paolo U. Giacomoni,. & Glen Rein, 2001. Factors of skin ageing share common mechanisms Biogerontology 2: 219–229

2-Tofani,S., Barone, D., Cintorino, M., De Santi, M.M., Ferrara, A., Orlassino, R., Ossola, P.,Peroglio, F., Rolfo,K., and Ronchetto, F. 2001. Static and ELFMagnetic Fields InduceTumor Growth Inhibition and Apoptosis. Bioelectromagnetics 22:419-428.

3-Maria Teresa Santini, Gabriella Rainaldi, Antonella Ferrante, Pietro Luigi Indovina, Paolo Vecchia, and Gianfranco Donelli, 2003. Effects of a 50 Hz SinusoidalMagnetic Field on Cell Adhesion Molecule Expression in Two Human Osteosarcoma Cell Lines (MG-63 and Saos-2). Bioelectromagnetics 24:327-338.

4-Ming Chen and Jian-Guo Geng ,2006. P-selectin mediates adhesion of leukocytes, platelets, and cancer cells in inflammation, thrombosis, and cancer growth and metastasis.Arch. Immunol. Ther. Exp., 54, 75–84.

5-Miller,F.J. and Schroeer,D. (1987) College Physics. 6th edn. Harcourt Brace Jananovich, San Diego, CA.

6-Theriault,G., Goldberg,M., Miller,A.B., Armstrong,B., Guenel P., Deadman,J., Imbernon,E., To,T., Chevalier,A., Cyr,D. and Wall,C. (1994) Cancer risks associated with occupational exposure to magnetic fields among electric utility workers in Ontario and Quebec, Canada, and France: 1970–1989. Am. J. Epidemiol., 139, 550–572.[Abstract]

7- Albelda S. M. and Buck C. A. (1990): Integrins and other cell adhesion molecules. FASEB J., **4**, 2868–2880.

8-Miyasaka M. (1995): Cancer metastasis and adhesion molecules. Clin. Orthop. Relat. Res., **312**, 10–18.

9-Huang Y. W., Baluna R. and Vitetta E. S. (1997): Adhesion molecules as targets for cancer therapy. Histol. Histopathol., **12**, 467–477.

10-Aruffo A., Dietsch M. T., Wan H., Hellstrom K. E. And Hellstrom I. (1992): Granule membrane protein 140 (GMP140) binds to carcinomas and carcinoma-derived cell lines. Proc. Natl. Acad. Sci. USA, **89**, 2292–2296.

11-Mannori G., Crottet P., Cecconi O., Hanasaki K., Aruffo A., Nelson R. M., Varki A. and Bevilacqua M. P. (1995): Differential colon cancer cell adhesion to E, P, and L-selectin: role of mucin-type glycoproteins. Cancer Res., **55**, 4425–4431.

12-Ming Chen and Jian-Guo Geng, 2006. P-selectin mediates adhesion of leukocytes, platelets, and cancer cells in inflammation, thrombosis, and cancer growth and metastasisArch. Immunol. Ther. Exp., 54, 75–84

13-Hahne M., Jager U., Isenmann S., Hallmann R. And Vestweber D. (1993): Five TNF-inducible cell adhesion mechanism on the surface of mouse endothelioma cells mediate the binding of leukocytes. J. Cell. Biol., **121,** 655–664.,

14-Sanders W. E., Wilson R. W., Ballantyne C. M. And Beaudet A. L. (1992): Molecular cloning and analysis of *in vivo* expression of murine P-selectin. Blood, **80,** 795–800.

15-Yao L., Pan J., Setiadi H., Patel K. D. and McEver R. P. (1996): Interleukin 4 or oncostatin M induces a prolonged increase in P-selectin mRNA and protein in human endothelial cells. J. Exp. Med., **184**, 81–92.

BIOLOGICAL EFFECT ON BLOOD-CEREBROSPINAL FLUID BARRIER DUE TO RADIO FREQUENCY ELECTROMAGNETIC FIELDS EXPOSURE OF THE RAT BRAIN IN VIVO

USHIYAMA A.[1], MASUDA H.[1], HIROTA S.[1], KAWAI H.[2], TANAKA S.[2], WAKE K.[2], WATANABE S.[2], SUZUKI Y.[3], TAKI M.[3] and OHKUBO C.[4]

[1]Dept. of Environmental Health, National Institute of Public Health, 2-3-6 Minimi, Wako-shi, Saitama 351-0197, Japan. [2] Electromagnetic compatibility group, applied electromagnetic research center, National Institute of Information and Communications Technology, 4-2-1 nukui-kitamachi, koganei, Tokyo 184-8795, Japan. [3]Dept. of Electrical and electronic Engineering, Tokyo Metropolitan University, 1-1 minami-osawa, hachioji, Tokyo 192-0397, Japan. [4]RAD, World Health Organization, Geneva CH1211, Switzerland.

Abstract

In this study, we explored the subchronic effect of RF-EMF on blood-cerebrospinal fluid barrier (BCB) function, which defined as one of the blood-brain barrier functions. To attain the purpose, we used the micro-perfusion method, which makes it possible to quantify BCB function in vivo with high sensitivity, and evaluate the effect on barrier function during RF-EMF exposure to rat. Using a custom-made "8"-shaped loop antenna, which optimized for RF-EMF exposure to rat's head locally, we exposed 1.5 GHz RF-EMF with PDC modulation to the head of juvenile rats. A 30 minutes exposure was repeated everyday for 6 successive days, and on the 6th day, BCB function was quantified by using micro-perfusion method. The fluorescence intensity in collected cerebrospinal fluid did not increase indicating BCB did not affected by RF exposure at the brain average SARs of 0.5, 2.0 and 10 W/kg. These results suggest that the daily exposure of 1.5 GHz RF-EMF did not affect the BCB function in juvenile rats under our experimental conditions.

Introduction

Possible health effects of weak RF-EMF have been discussed worldwide. However, further scientific evidences are needed for better health risk assessment, particularly; the effects on the blood-brain barrier (BBB) which are still not clear due to the variety of experimental designs. One of the main problems on BBB study is that there are few methods which are able to monitor the barrier function on real time in vivo. In this study, we developed a real-time measuring system for blood-cerebrospinal fluid barrier (BCB) function which defined same as BBB in a broad sense. To collect CSF continuously, we employed micro-perfusion method to the measuring system. By using this method, we explored the subchronic effects on the BCB when RF-EMF was exposed to the head of animal.

Animals and surgical procedure We used male Sprague-Dawley rats (Tokyo Laboratory Animals Science Co., Japan) aged 5 weeks. Rats were anesthetized by i.m. injection of a cocktail of ketamine hydrochloride (90 mg/kg body weight, Sigma Chemical Co., St. Louis, MO) and xylazine hydrochloride (10 mg/ kg body weight, Sigma Chemical Co.), and a guide cannula (Eicom Co., Kyoto, Japan) was introduced to one of the lateral ventricles through the hole and secured to the skull with dental cement. Assembly of push-pull cannula including guide cannula was shown in Fig 1.

Exposure conditions Rats for exposure groups were divided into three groups. Each exposure condition was at 0.5, 2.0, 10W/kg (brain averaged SAR) for 30 minutes per day for 6 consecutive days. We applied RF-EMF (1,439 MHz) with PDC modulation which generated by an 8-shaped loop antenna (Fig.2). During exposure, the antenna was located at 4 mm above the rat head by using the stereotaxic apparatus. In the sham exposure group, rats were also anesthetized and kept on the stereotaxic apparatus without RF-EMF exposure. On the 6th day of exposure, a push pull cannula (Fig.1) was inserted into a guide cannula. The inlet and the outlet of the cannula

were connected to the push-pull micro perfusion pump unit (EP-70, Eicom Co.) which enabled the collection of CSF continuously. At the beginning of RF-EMF exposure, FITC-labeled albumin (FITC-albumin) was injected into caudal vein and CSF perfusion was started at a rate of 1 µl/min. Fluorescence intensity of FITC-albumin in perfusate was monitored by using spectrofluorometry under the condition of excitation /emission wave length at 490/515nm .Fluorescence intensity in perfusate was monitored for 180 minutes from the beginning of the exposure. Experimental setup was summarized in Fig. 3.
All experimental procedures are approved by the animal experiment committee in National Institute of Public Health.

Results No statistical difference on BCB function was detected among each exposure condition (Fig.4).

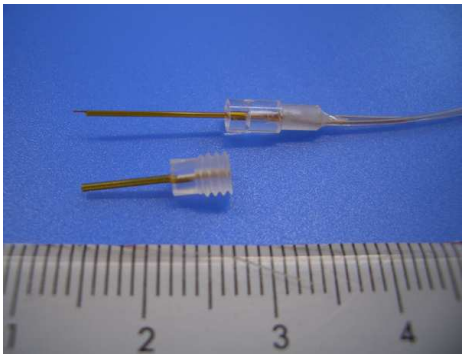

Fig 1 Assembly of push-pull cannula for rat
Upper is an inner cannula which includes in/out route and lower is a guide cannula

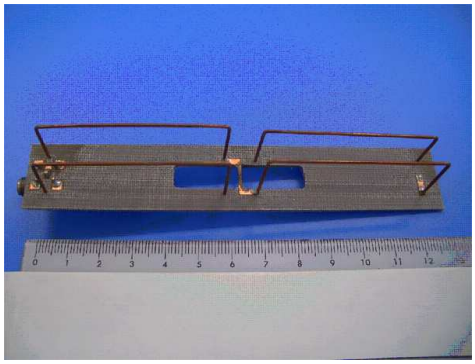

Fig 2 Overview of an "8-shaped" loop antenna for RF-EMF exposure

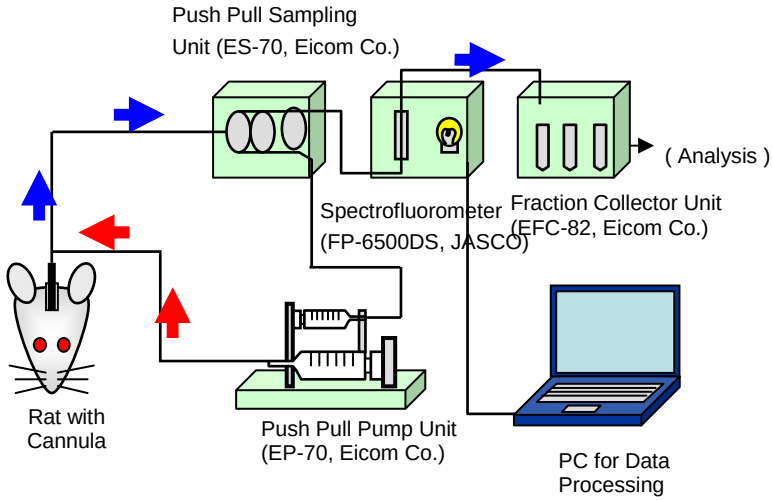

Fig.3 Schematic diagram of developed system for real- time monitoring of blood barrier function
Artificial CSF flow into the lateral ventricle via inlet of cannula (red arrow) and perfusate flow out via outlet of cannula (blue arrow).

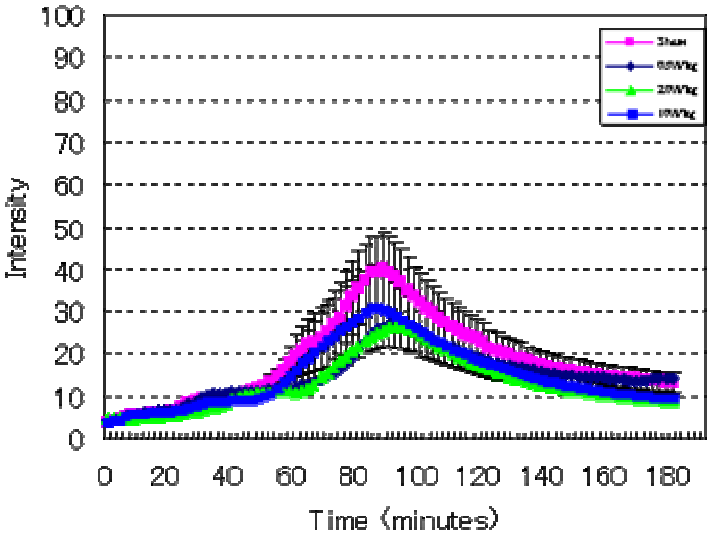

Fig.4 Fluorescent profiles of sham and RF-EMF exposed group
Fluorescence intensity was emitted by fluoro-spectrometer which connected to the outlet of the push-pull cannula. Due to the dead-volume of the connection tubes, changes of fluorescence intensity in cerebrospinal fluid were reflected to this profile with some time delay. There is no statistical difference among each group.

Summary

In the previous studies, we have already reported that acute exposure to RF-EMF does not induce the effect on the blood-cerebrospinal fluid barrier (BCB) [1, 2]. In this study, we explored the subchronic effect on BCB by RF-EMF exposure. To attain the purpose, we used the micro-perfusion method, which makes us possible to quantify the barrier function in vivo with high sensitivity, and can be applied during exposure. After 6 consecutive days exposure for 30 minutes/day to 1.5GHz RF-EMF using an "8"-shaped loop antenna, the fluorescence intensity in collected fluid did not increase in any group. These results indicate blood-cerebrospinal fluid barrier did not affected by the RF exposure. As a conclusion, sub-chronic RF-EMF exposure under this experimental condition was not affect blood-cerebrospinal fluid barrier function in rats.

Acknowledgements

This study was financially supported by the Ministry of Health, Labour and Welfare, Japan.

References

[1] Ushiyama A, Masuda H, Hirota. S, Watanabe. H, Wake K, Watanabe S, Yamanaka. Y, Taki M, Ohkubo C. Acute effects on blood barrier function by RF-EMF exposure to rat brain in vivo. In: Abstract book of the 28th General Assembly of International Union of Radio Science; 2005 Oct 23-29; New Delhi, India. 2005. KP.6(01436) in CD-ROM.

[2] Ushiyama A, Masuda H, Hirota S, Takahashi M, Kawai H, Tanaka S, Wake K, Watanabe S, Suzuki Y, Taki M, Ohkubo C. Blood-Cerebrospinal barrier in rats is not affected by 1.5 GHz RF-EMF exposure at non thermal level. In: Abstract Collection of the 28th Annual meeting of Bioelectromagnetics Society; 2006 Jun 11-15; Cancun, Mexico. 2006. p.384-385

THE EFFECT OF HIGH-FREQUENCY ELECTROMAGNETIC FIELD ON SOME SOMATIC AND NERVOUS CHARACTERISTICS IN HEALTHY AND NEURODEFECTIVE MICE

[1]FRANTIŠEK VOŽEH, [1]ANTONÍN DONĚK, [1]JAN CENDELÍN, [1]IVANA KORELUSOVÁ, [2]JAN VRBA

[1]CHARLES UNIVERSITY IN PRAGUE, FACULTY OF MEDICINE IN PILSEN, DEPARTMENT OF PATHOPHYSIOLOGY, LIDICKÁ 1, 301 66 PLZEŇ, CZECH REPUBLIC

[2]CZECH TECHNICAL UNIVERSITY IN PRAGUE, FACULTY OF ELECTRICAL ENGINEERING, DEPARTMENT OF ELECTROMAGNETIC FIELD, TECHNICKÁ 2, 166 27 PRAHA 6, CZECH REPUBLIC

e-mail: frantisek.vozeh@lfp.cuni.cz

Abstract

The effect of long-term exposure to high frequency electromagnetic field (HF EMF) on some somatic and neural characteristics was studied in neurodefective Lurcher mutant (+/Lc) and normal wild type mice (+/+). Both newborn and young adult (3 months) animals derived from two strains (C3H, C57Bl/7) were exposed to HF EMF (870 MHz) from 1st to 21st day or from 91st to 120th day respectively. In animals of both groups and controls we observed the development of body weight. Moreover, in the HF EMF exposed adult C57Bl/7 animals we studied spatial learning ability, motor functions and the CNS excitability. To investigate specific energy absorption rate (SAR) in experimental animals we have done the basic 3D calculations of the electromagnetic energy distribution in the simplified model of the mouse. The HF EMF exposed animals exhibited a mild increase of body weight with small strain differences. The long-term exposure to HF EMF did not significantly influence the ability to learn in the Morris water maze. However, lower swimming speed was found in the irradiated +/Lc as well as lower motor activity of +/+ in the open field when compared to controls. No significant differences were found between HF EMF irradiated animals and controls in examination of the CNS excitability and motor functions.

Introduction

Increasing use of different devices (mobile phones) and other ones (radars, radio transmitters) that emit potentially harmful radiofrequency (RF) radiation is the reason why the effect of high frequency electromagnetic field (HF EMF) on human (and/or animal) body and especially on the brain, is subjected to a concentrated research. Despite this effort there is e.g. no unambiguous evidence about broadly discussed promoting effect of RF EMF on the brain cancer growth. Some results have indicated increased risk (Repacholi et al., 1997; Hardell et al., 2002) while other studies have shown no effect (Salford et al., 1997a) or even decreased risk (Adey et al., 1999). On the other hand, the clear effect of RF radiation - including that from global system for mobile communication (GSM) microwaves (MWs) - increase in blood-brain barrier (BBB) permeability in rats for their own albumin has been found (Persson and Salford, 1996; Fritze et al., 1997; Persson et al., 1997; Malmgren, 1998; Salford et al., 2001; Töre et al., 2001). Furthermore, it was observed, that the albumin leakage over the BBB caused neuronal damage in both the cortex, the hippocampus and the basal ganglia in the brains of rats exposed acutely two hours to GSM mobile phone EMF of different strengths (Salford et al., 2003). Recently, rats exposed also for 2h to GSM MWs (915 MHz, SAR 0.4 mW/g) exhibited affected expression of genes in cerebellar cells (Belyaev 2006).

Behavioral experiments in animals showed performance deficits in spatial learning in rats (Lai, 1996; Lai et al., 1998) and in mice (Sienkiewicz et al., 1998) exposed to low-frequency EMF (50 and 60 Hz). Affected learning process was also described in rats exposed to HF EMF (2450 Hz) and examined in the radial and the

Morris water maze (Lai et al., 1994; Wang et al., 2000). On the contrary, no significant effect on spatial learning was described in rats influenced by head only exposure system emitting a 900-MHz GSM EMF (Dubreuil et al., 2002).

In human, changes of working memory and evoked potentials were found as a consequence of mobile phone use (Koivisto et al., 2000; Jech et al., 2001). Except for influence of EMF on membrane ion transport (Bawin, Adey, 1976; Blackman et al., 1982; Dutta et al., 1989; Liu et al., 1990; Cleary 1990a,b, 1995) and neurotransmitter system (Merritt et al., 1977; Modak, et al., 1981; Inaba et al., 1992) the reason of the effect can be also, that mobile phones broadcast specifically at frequencies at which the head serves as an antenna and brain tissue serves as a demodulating radio receiver (Weinberger and Richter, 2002).

In previous works we described the results of our research dealing with some functional and morphological characteristics of the brain in normal and neurodefective mice exposed to both acute and chronic influence of HF EMF (Vožeh et al. 2004, Cendelín et al. 2004). The aim of this work was to survey further results of experiments concentrated on somatic and neurobehavioral characteristic in the same types of mice chronically influenced by HF EMF in two phases of their life.

Animals and methods

Experimental animals we used were Lurcher mutant and wild type mice of both sexes derived from two strains (C3H, C57B1/7). Mice were kept on a 12:12 hour light:dark cycle with constant temperature (21± 1^{o} C) and humidity (60±10%). Water and food were available ad libitum. All these experiments have been done in full agreement with the law of the Czech Republic dealing with the right treatment of experimental animals.

The mutants suffer from genetically determined olivocerebellar degeneration due to mutation of the δ2 glutamate receptor gene. The δ2 glutamate receptor is especially expressed by cerebellar Purkinje cells (Zuo et al., 1997) and this is a reason why Lurcher mutants (heterozygotes, +/Lc) are characterized by complete progressive extinction (a type of excitotoxic apoptosis) of Purkinje cells and by a substantial decrease in number of cerebellar granule cells and inferior olive neurons (Caddy and Biscoe, 1979). The mutants exhibit signs of cerebellar ataxia, deterioration of cognitive function and higher sensitivity to some neurotoxic agents (Caddy and Vožeh, 1997; Vožeh et al., 1999). Their littermates - wild-type mice (homozygotes +/+) are healthy. One half of experimental animals (+/Lc and +/+) was subjected to chronic exposure to HF EMF, the unexposed animals of the second half were controls. The whole body exposition was performed using HF generator with HF amplifier and antenna. Frequency of HF EMF was 870 MHz (close to mobile phones frequency) and power output of the apparatus was 10 W. The radiation was directed by a wave guide to a plastic box with the animals placed just in front of it (Fig.1).

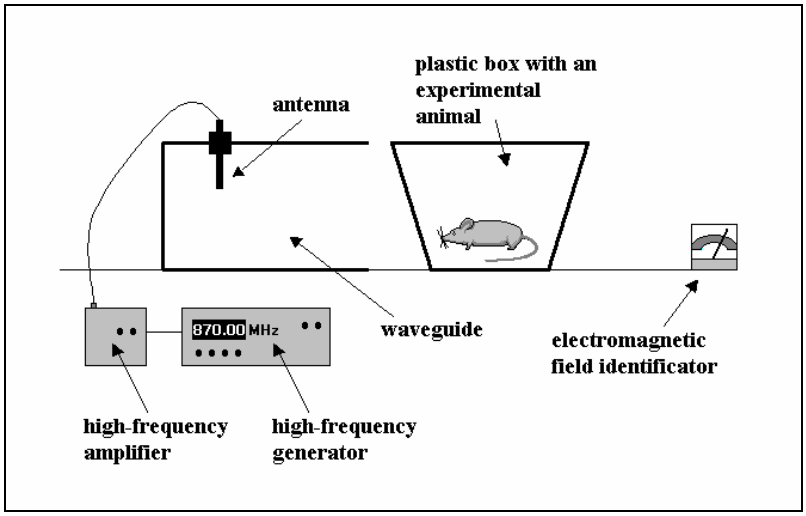

Fig. 1: Scheme of HF EMF exposure

The animals of two developmental periods were exposed to HF EMF:

1) newborns (irradiated from 1st to 21st day of life, 2.5 h daily, together 162 animals of both strains),

2) young adults (irradiated from 91st to 120^{ies} day of life, 3 h daily, together 94 animals of both strains).

To estimate SAR in experimental animals we have done basic 3D calculation of electromagnetic energy distribution in a simplified dielectric model of an adult mouse. The model consists of a homogenous lossy dielectric material mimicking muscle tissue and has shape of a cylinder (radius 3 cm and high 9 cm terminated to cone) with dielectric properties $e_r = 54$, conductivity s = 0.8 S/m, density r = 1000 kg/m^3 (Fig. 2).

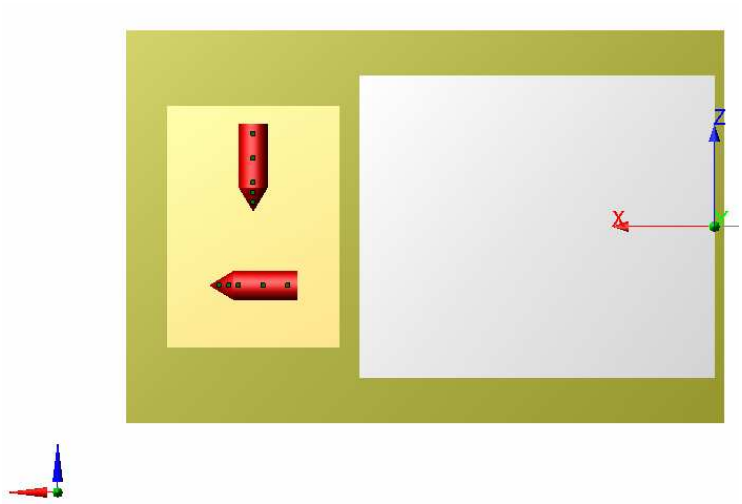

Fig. 2: Scheme of the simplified dielectric model of an adult mouse during SAR measurement (bird´s-eye view).

The calculations were done with the aid of 3D electromagnetic field simulator SEMCAD which used FDTD (Finite Different Time Domain). The method is based on the fact that original continuous function is replaced by the set of discrete function´s values. Maxwell's equations are discretized using a 2nd order finite-difference approximation both in space and in time in an equidistantly spaced mesh. Several simulations for different positions of mice were done. Input power during simulations was normalized to 1 watt.

Both HF EMF exposed and unexposed animals (C3H and C57B1/7 newborns and young adults) were subjected to examination of the body weight development during the irradiation periods. Spatial learning ability, passive avoidance learning, CNS excitability and behavioral activity as well as topical motor skills were tested in young adult C57B1/7 mice only.

The topical body weight in individual animals was investigated every day during the irradiation period. Data obtained in individual days we used for calculation of the relative body weight increase which represented the ratio of the values in individual days to the value received on the first day of the HF EMF exposure.

Spatial learning was tested using Morris water maze. It consists of round plastic pool with a small round platform hidden under the water surface, permanently at the same place. The mouse had to locate the platform only by its relationship to distant landmarks (window, laboratory furniture, tube lights). Four swimming trials daily were performed during 6 days long examination period (D1 – D5 and D8). If the mouse did not find platform within 60 s, it was placed there. The mouse stayed on the platform always for 30 s. Mean latencies of reaching platform, swimming speed and the length of trajectory were compared in HF EMF exposed animals and controls.

For examination of discriminative learning we used "step down" method of the passive avoidance inhibitory reaction. In this test the mouse is positioned on a small platform (bench), the size of which is dependent on the age of the animal, 5 mm above an electrified grid floor of the plastic box (200 x 250 x 200 mm high). The animal is trained until the chosen criterion (100 s on the bench without descent) is met. Four parameters are measured: latency to the first descent, number of descents, time to criterion and time of stay on the grid. The same procedure is repeated 24 hours later and evaluation of each parameter is obtained by dividing the values of the retention test by those obtained in the learning (1st day) test.

CNS excitability was tested with the audiogenic epilepsy method. The mouse was placed into a plastic box covered with a transparent lid. Inside the box was an electric doorbell which served as a source of a sound stimulus of intensity of 90 dB. The sound was switched on for 60 s and the reaction of the animal was observed. The reactions were divided into 5 degrees: 1. no reaction, or exploration, 2. running, 3. fast running and

jumping, 4. convulsions, 5. death of the animal as a consequence of the convulsions. Mean reaction degree was compared.

Behavioral and spontaneous motor activity were studied using the open-field test. The open-field chamber was rectangular plastic box (400 x 400 x 450 mm high), open at the top. The box was cleaned using dilute alcohol before each trial to eliminate odorous cues. Behavior of mice and their activity were coded by a simple computer program and time spent in the central zone or in individual corners of the box as well as the length of locomotion trajectory were evaluated.

The topical complex motor skills were tested using four methods:

1) Fall - releasing the mouse (the right hand grips the mouse tail, the left hand the skinfold behind) from the height of 30 cm and evaluation of the drop to the cushioned table either to four extremities or to the flank.
2) Wire suspension - evaluation of the mouse ability to hang on a horizontal wire (diameter 1 mm, 40 cm above a cushioned table) after its front paws were placed on it. The criterion for success: 1 min.
3) Slanting ladder - evaluation of the mouse ability to stay on or climb up the ladder (length 35cm, width 4 cm, distance of 1 cm, inclination from horizontal 60^{o}) after being positioned in the middle of it with head upwards.
4) Rotating cylinder - evaluation of the mouse ability to stay on a slowly rotating cylinder (diameter 15 cm, length 20 cm, after being positioned there with its head in the direction of the rotation.The criterion for success: 1 min.

Results

The animals exposed to HF EMF from 1^{st} to 21^{st} day exhibited body weight differences between them and controls only in C3H wild type mice females. They revealed statistically significant body weight increase mainly between 7^{th} and 18^{th} day of irradiation (Fig. 3).

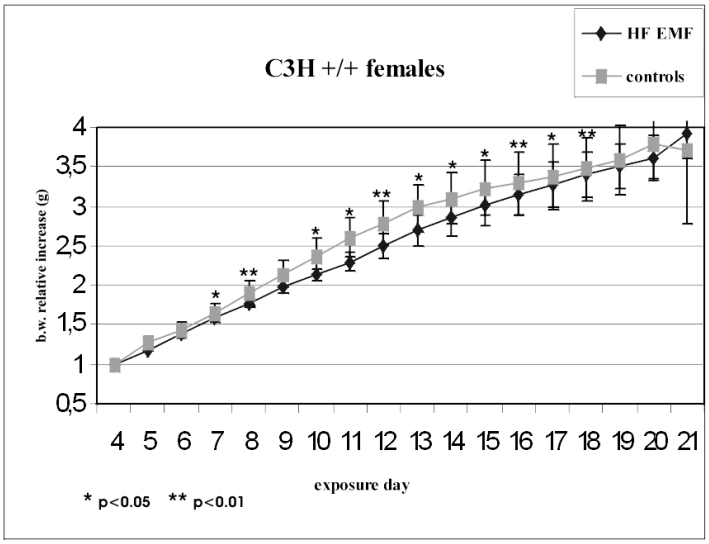

Fig. 3: Relative body weight (b.w.) increase (in grams) in C3H wild type HF EMF irradiated females and controls during the postnatal period 1 - 21 days.

The animals exposed to HF EMF between days 91 and 120 of their life exhibited most significant body weight differences also in females but in some cases in males too. In C3H neurodefective females the significant body weight increase was found 7 times during the 30 days irradiation period (Fig. 4).

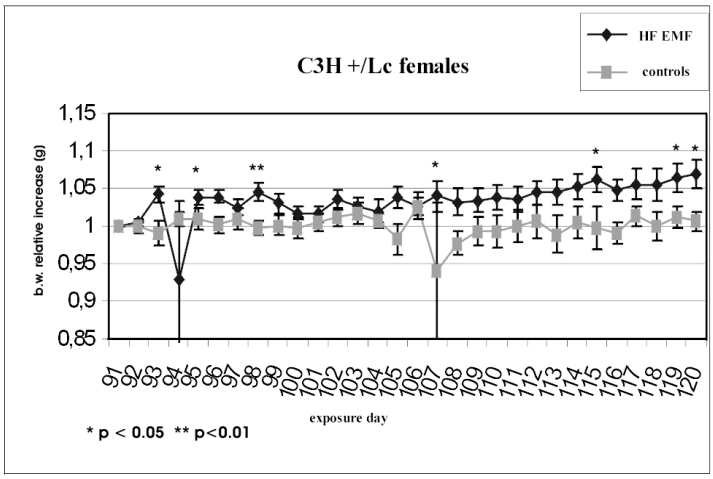

Fig. 4: Relative body weight (b.w.) increase (in grams) in C3H Lurcher mutant HF EMF irradiated females and controls during the postnatal period 91- 120 days.

In C57B1/7 neurodefective females were no significant differences between HF EMF exposed animals and controls while the HM EMF irradiated neurodefective males revealed significant body weight increase 3 times during the first half of the irradiation period (Fig. 5).

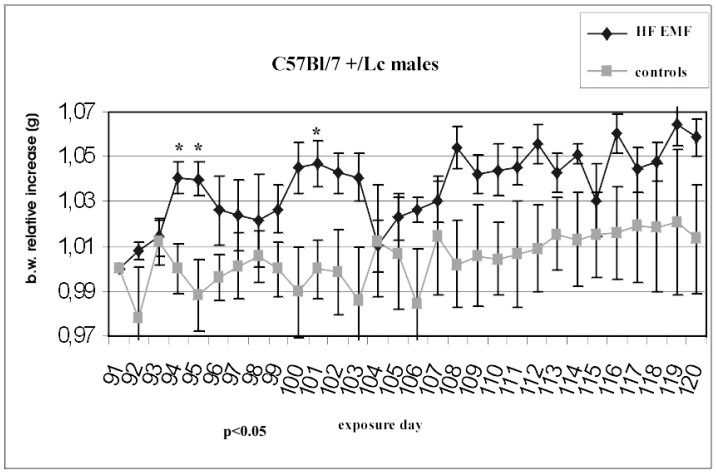

Fig. 5: Relative body weight (b.w.) increase (in grams) in C57Bl/7 Lurcher mutant HF EMF irradiated males and controls during the postnatal period 91- 120 days.

Investigation of spatial learning ability showed no statistically significant differences in latencies of climbing the platform and the lengths of trajectories between HM EMF exposed animals and unexposed controls of both types (+/+, +/Lc). However, HF EMF exposed Lurcher mutant mice revealed significantly lower swimming speed (in D1 and D2, $p<0.01$ and $p<0.02$ respectively) in comparison with controls (Fig. 6).

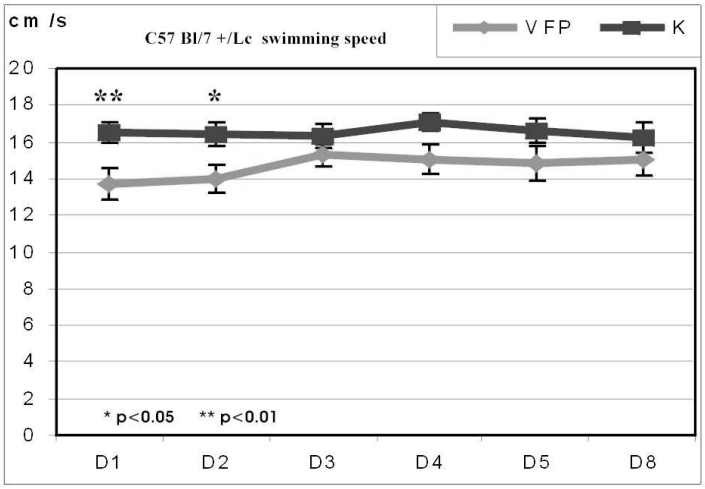

Fig. 6: Average swimming speed in C57Bl/7 HF EMF irradiated Lurcher mutants and controls in individual days of the spatial learning process examination.

Results of inhibitory reaction of passive avoidance learning showed no significant differences between HF EMF exposed animals and unexposed controls of both types (+/+, +/Lc). Any significant differences were found between experimental (irradiated) animals and controls neither in investigation of open field activity nor in the examination of CNS excitability by the method of audiogenic epilepsy. Nevertheless, HF EMF irradiated wild type mice exhibited mildly lower motor activity (on the margin of statistical significancy) in the open field testing when compared to controls.

Also tests of complex topical motor skills did not show any statistically significant differences between animals exposed to HF EMF and unexposed controls. On the other hand there are visible clear differences in the graphs between performances of healthy wild type mice a neurodefective Lurcher mutants (Figs. 7A, B).

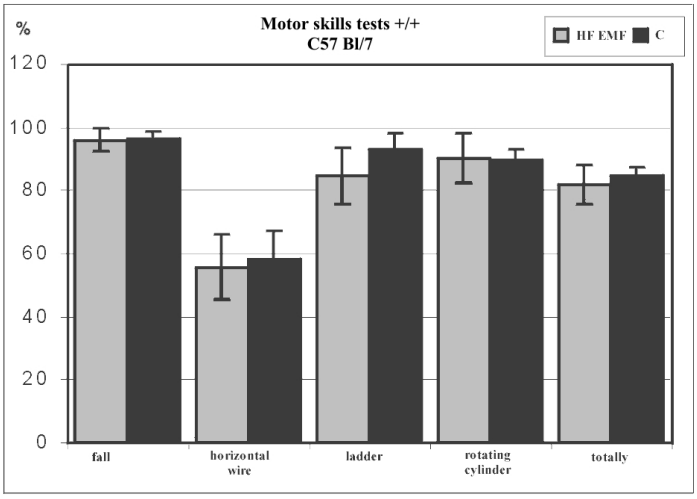

Fig. 7A: Meeting criteria in individual topical motor skills tests and in total expressed as percentage in C57Bl/7 HF EMF irradiated wild type mice and controls.

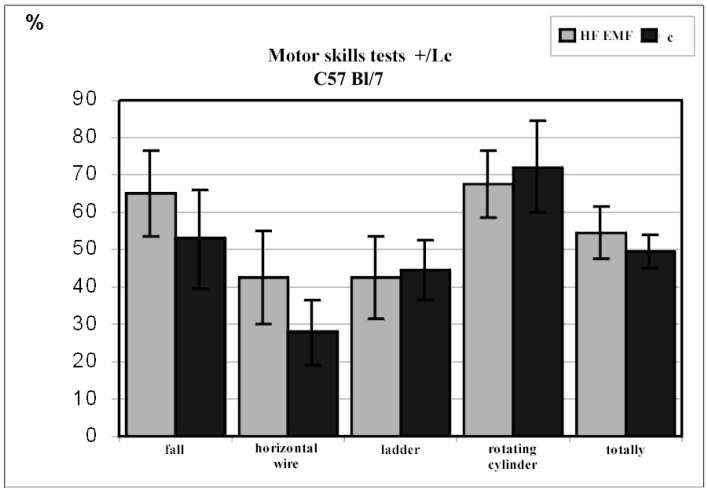

Fig. 7B: Meeting criteria in individual topical motor skills tests and in total expressed as percentage in C57Bl/7 HF EMF irradiated Lurcher mutant mice and controls.

Calculations of SAR performed in connection with the simulation of absorption electromagnetic energy by experimental animals using the artificial dielectric model showed the dependence of the absorption on the real topical position of the mouse against the waveguide and was in the range of 0.05 to 1.44 mW/g (Fig. 8).

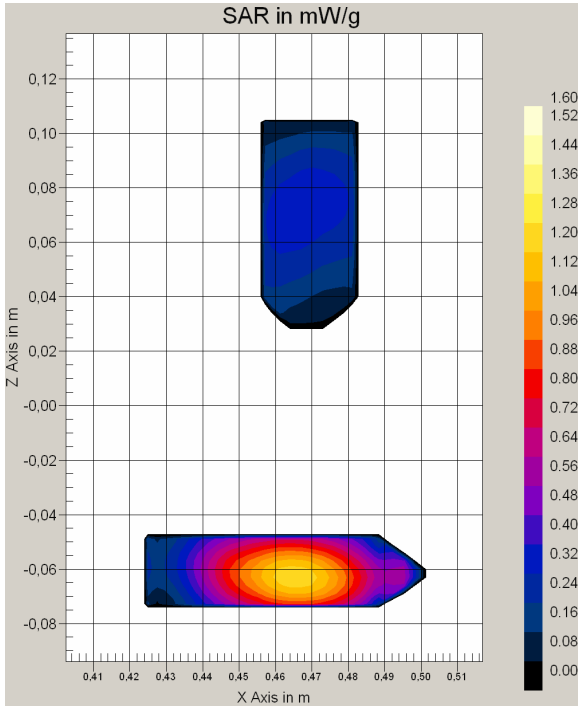

Fig. 8: SAR value (in mW/g) expressed as different hues in dependence on position of the dielectric mouse model.

Summary

Similarly as in our previous works the results were obtained in healthy and partly neurodefective mice in two developmental periods chronically exposed to HF EMF which corresponded to that used in GSM mobile phones.

Both healthy and partly neurodefective animals were used and some of experiments were realized in both types of mice derived from two different strains. The fact that the chronical exposure of mice to HF EMF was performed in their early ontogeny (during the first 3 weeks of life) which involved "the brain growth spurt" period and later (from 3 to 4 month of life) enabled us to investigate the effect of HF EMF in complex and more detailed way.

First of all, the results of our experiments showed the positive effect of chronic HF EMF exposure on gentle but in some cases significant body weight increase mainly in females of both strains. In addition, on days (D1, D2) HF EMF irradiated C57Bl/7 Lurcher mutants exhibited significantly lower swimming speed in the Morris water maze when compared with HF EMF unexposed animals.

Despite other examinations didn´t show any further significant differences between HF EMF irradiated animals and HF EMF unexposed controls it is possible to say: in agreement with our previous results the HF EMF revealed the indubitable effect on some somatic and neuro-behavioral characteristics in newborn and young adult animals. This is the reason why the problem of the biological effect of HF EMF on living beings needs to be further studied.

Acknowledgement

The work was supported by the Research Program Project MSM CR 021620816

References

1. Adey, W., Byus, C., Cain, C., Higgins, R., Jones, R., Kean, C. et al.: Spontaneous and Nitrosourea-induced Primary Tumors of the Central Nervous System in Fisher 344 rats exposed to 836 MHz Modulated Microwaves. Radiat Res. 152: 293-302, 1999.
2. Bawin, S.M., Adey, W.R.: Sensitivity of calcium binding in cerebral tissue to weak environmental electrical fields oscillating at low frequency. Proc. Natl. Acad. Sci., USA 73(6): 1999-2003, 1976.
3. Belyaev, I.Y., Koch, C.B., Terenius, O., Roxtrom- Lindquist, K., Malmgren, L.O., H. Sommer, W., Salford, L.G., Persson, B.R.: Exposure of rat brain to 915 MHz GSM microwawes induces changes in gene expressuion but not double stranded DNA breaks or effects on chromatin conformation.
4. Blackman, C.F., Benane, S.G., Rabinowitz, D.E., House, D.E., Joines, W.T.: Effects of ELF fields on calcium-ion efflux from brain tissue in vitro. Radiation Res. 92: 510-520, 1982.
5. Caddy, K.W.T., Biscoe, T.J.: Structural and quantitative studies on the normal C3H and Lurcher mutant mouse. Phil. Trans. Roy. So. Lond. B. 287: 167-201, 1979.
6. Caddy, K.W.T., Vožeh, F.: The effect of 3-acetylpyridine on the inferior olivary degeneration in the Lurcher mutant and wild type mice. Europ. J. Pharmacol. 330: 137-142, 1997.
7. Cendelín J., Schmidtmayerová B., Štenglová V., Vožeh F., CNS excitability in normal and neurodefective C3H mice exposed to high-frequency electromagnetic field, Proceedings of Biological effects of EMFs, 3rd International workshop, Kos, Greece, 4.-.8.10.2004, Ed. P.Kostarakis, p.866-871.
8. Cleary, S.F.: Cellular effects of radiofrequency electromagnetic fields. In: Biological Effects and Medical Applications of Electromagnetic Energy (O. P. Gandhi, Ed.). Engelewood Cliffs, New Jersey, Prentice-Hall, p 339, 1990a.
9. Cleary, S.F.: Biological effects of radiofrequency electromagnetic fields. In: Biological Effects and Medical Applications of Electromagnetic Energy (O.P. Gandhi, Ed.). Englewood Cliffs, New Jersey, Prentice-Hall, p 236, 1990b.
10. Cleary, S.F.: Effects of radiofrequency radiation on mammalian cells and biomolecules in vitro. In: Electromagnetic Fields: Biological Interactions and Mechanisms (M. Blank, Ed.). Washington, American Chemical Society, p 467, 1995.
11. Dubreuil, D., Jay, T., Edeline, J.M.: Does head-only exposure to GSM-900 electromagnetic fields affect the performance of rats in spatial learning tasks? Behav. Brain Res. 129: 203-210, 2002.
12. Dutta, S.K., Ghosh, B., Blackman, C.F.: Radiofrequency radiation-induced calcium-ion-effux enhancement from human and other neuroblastoma cells in culture. Bioelectromagnetics 10: 197-202, 1989.
13. Fritze, K., Sommer, C., Schmitz, B., Mies, G., Hossman, K., Kiessling, M. et al.: Effect of global system for mobile communication (GSM) microwave exposure on blood-brain barrier permeability in rat. Acta Neuropathol. (Berlín) 94: 465-470, 1997.
14. Hardell, L., Hallquist, A., Hansson, Mild, K., Carlberg, M., Pählson, A., Lilja, A.: Cellular and Cordless telephones and the risk for brain tumours. Europ. J. of Cancer Prevention 11: 377-386, 2002.
15. Inaba, R., Shishido, K., Okada, A., Moroji, T.: Effects of whole body microwave exposure on the rat brain contents of biogenic amines. Eur. J. Appl. Physiol. 65: 124, 1992.

16. Jech, R., Sonka, K., Ruzicka, E., Nebuzelsky, A., Bohm, J., Juklickova, M., Nevsimalova, S.: Electromagnetic field of mobile phones affects visual event related potential in patiens with narcolepsy. Bioelectromagnetics 22 (7): 519-28, 2001.
17. Koivisto, M., Krause, C.M., Revonsuo, A., Laine, M., Hamalainen, H.: The effects of electromagnetic field emitted by GSM phones on working memory. Neuroreport 11: 1641-3, 2000.
18. Lai, H., Horita, A., Guy, A.W.: Microwave irradiation affects radial-arm maze performance in the rat. Bioelectromagnetics 15: 95-104,1994.
19. Lai, H.: Spatial learning deficit in the rat after exposure to a 60 Hz magnetic field. Bioelectromagnetics 17: 494-496, 1996.
20. Lai, H., Carino, M.A., Ushijima, I.: Acute exposure to a 60 Hz magnetic field affects rats´ water- maze performance. Bioelectromagnetics 19: 117-122, 1998.
21. Liu, D.S., Astumian, R., Tsong, T.: Activation of Na^+ and K^+ pumping modes of NA/K-ATPase by an oscillating electric field. J. Biol. Chem. 265: 7260, 1990.
22. Malmgren, L.: Radio frequency systems for NMR-imaging-Coil development and studies of non-thermal biological Effects. Series of Licentiate and Doctoral These, No. 6, Department of Applied Electronics, Lund University, Lund, Sweden. 1998.
23. Merritt, J.H., Chamness, A.F., Hartzell, R.H., Allen, S.J.: Orientation effects on microwave-induced hyperthermia and neurochemical correlates. J. Microwave Power 12: 167, 1977.
24. Modak, A.T., Stavinoha, W.B., Dean, U.P.: Effect of short electromagnetic pulses on brain acetylcholine content and spontaneous motor activity in mice. Bioelectromagnetics 2: 89, 1981.
25. Persson, B., Salford, L.: Permeability of the blood-brain barrier in rats induced by continuous wave and pulse-modulated 915 MHz electromagnetic radiation exposure in TEM-cells. (Chiabrera A, Juutilainen J, eds). Brussel: EU DG XIII, 66-72, 1996.
26. Persson, B., Salford, L., Brun, A.: Blood- brain barrier permeability in rats exposed to electromagnetic fields used in wireless communication. Wireless Networks 3: 455-461, 1997.
27. Repacholi, M., Basten, A., Gebski, V., Noonan, D., Finni, J., Harris, A.W.: Lymphomas in Eμ-Pim 1 transgenic mice exposed to pulsed 900 MHz electromagnetic fields. Rad. Res. 147: 631-640, 1997.
28. Salford, L.G., Brun, A., Persson, B.: Brain tumour development in rats exposed to electromagnetic fields used in wireless communication. Wireless Networks 3: 463-469, 1997a.
29. Salford, L.G., Person, B., Malmgren, L., Brun, A.: Téléphonie Mobile et Barriére Sang-Cerveau. In: Téléphonie Mobile-Effets Potentiels sur la Santé des Ondes Électromagnétiques de Haute Fréquence. (Pietteur Marco, ed.) Embourg, Belgium, 141-152, 2001.
30. Salford, L.G., Brun, A.E., Eberhardt, J.L., Malmgren, L., Persso, B.R.: Nerve cell damage in mammalian brain after exposure to microwaves from GSM mobile phones. Environ Health Perspect 111 (7): 8813, 2003.
31. Sienkiewicz, Z.J., Haylock, R.G., Saunders, R.D.: Deficits in spatial learning after exposure of mice to a 50 Hz magnetic field. Bioelectromagnetics 19: 79-84, 1998.
32. Töre, F., Dulou, P.E., Haro, E., Veyret, B., Aubineau, P.: Two-hour Exposure to 2 W/kg, 900 MHz GSM microwaves induces Plasma Protein Extravasation in Rat Brain. In: Proceedings from the 5th International Congress of the European Bioelectromagnetics Association, 6 September 2001 (Hietanen, M, Jokela, K, Juutilainen, J, eds.). Finnish Institute of Occupational Health, Helsinki, 43-45, 2001.
33. Vožeh, F., Cendelín, J., Motáňová, A.: The development of different types of learning in cerebellar degeneration model. Homeostasis 39: 248-250, 1999.
34. Vožeh, F., Barcal, J., Cendelín, J., Korelusová, I., Štenglová, V., Žalud, V.: The effect of high-frequency electromagnetic field on some brain function in healthy and neurodefective mice, Proceedings of Biological effects of EMFs, 3rd International workshop, Kos, Greece, 4.-.8.10.2004, Ed. P.Kostarakis, p.1113-1120.
35. Wang, B., Lai, H.: Acute exposure to pulsed 2450-MHz microwaves affects water-maze performance of rats. Bioelectromagnetics 21: 52-56, 2000.
36. Weinberger, Z., Richter, E.D.: Cellular telephones and effects on the brain: The head as an antenna and brain tissue as a radio receiver. Med. Hypotheses 59: 703-705, 2002.
37. Zuo, J., De Jager, P.L., Takahasi, K.J., Jiang, E., Linden, D. J., Heintz, H.: Neurodegeneration in Lurcher mice caused by mutation of δ2 glutamate receptor gene. Nature 388: 769-773, 1997.

FAST MICRODOSIMETRY

Z. WANG, Y. ALFADHL, X. CHEN

DEPARTMENT OF ELECTRONIC ENGINEERING, QUEEN MARY, UNIVERSITY OF LONDON,
MILE END ROAD, LONDON, E1 4NS, UK

Abstract

Microdosimetry has emerged as an interesting area in the electromagnetic studies at cellular level. However, it is confronted with the difficulty of the treatment of the thin cell membrane, which often leads to extremely large memory usage and long running time in simulation. In this paper, we have introduced a technique for fast microdosimetry in the RF band. A simple double layer spherical cell model has been set up with given dielectric properties. Under the quasi-static approximation, the E field of the cell model can be evaluated by solving Laplace's equation. This simple cell model was solved by using Finite Element Method (FEM), verified with analytical solution and MIE theory. Next, the FEM with quasi-static approximation has been applied to evaluate the EM field interaction with the cells in various shapes, such as ellipsoidal, cylindrical and erythrocyte. It is demonstrated that, under the same meshing scheme, the FEM with quasi-static approximation runs much faster than the FEM solving full-wave Maxwell's equations.

I. Introduction

Recently, microdosimetry, i.e. the numerical study of EM fields interacting with the cellular and sub-cellular substances has received considerable interest. However, microdosimetry is confronted with a major difficulty, that is, the treatment of the thin cell membrane, which quite often leads to extremely large memory usage and long running time in simulation. In the previous work [1], FEM (Finite Element Method) with adaptive meshing has been used to solve the Maxwell's equations to evaluate the electric field distribution within cells. In the literature [2], quasi-static approximation was introduced to simplify the problem, i.e., the electric field distribution being approximately evaluated by solving Laplace's equation.

In this paper, a quantitative evaluation of the quasi-static approximation has been performed on a simple double layer spherical cell model at first. It is demonstrated that, under the same meshing scheme, the FEM with quasi-static approximation runs much faster than the FEM solving full-wave Maxwell's equations. The FEM with quasi-static approximation has been applied to evaluate the EM field interaction with the cells in various shapes, such as ellipsoid, cylinder and erythrocyte.

II. The models

The initial cell model in this study is a rigid particle rounded by a thin shell, representing a cell with membrane, with homogeneous, lossy and dispersive dielectric properties for each layer, as shown in figure 1. The cell radius is normally 10 μm and membrane thickness is 10 nm. The cell is exposed to a linear polarized plane wave with the electric field E_0 of 1V/m in the external medium. Due to the axial symmetry; a 2D model is adopted to evaluate the electric field distribution within the cell.

The frequency-dependent dielectric properties of the cytoplasm, membrane and external medium vary according to the Debye 1st order relaxation model, which will be further discussed in section 3.1. The values at 2.45GHz are listed in table 1.

	Cytoplasm (Ω_1)	Membrane (Ω_2)	External (Ω_3)
Permittivity (ε)	55.6	11.3	75.3
Conductivity (σ)	1.43	0	2.04

Table 1 Dielectric properties of cell compartments at 2.45 GHz

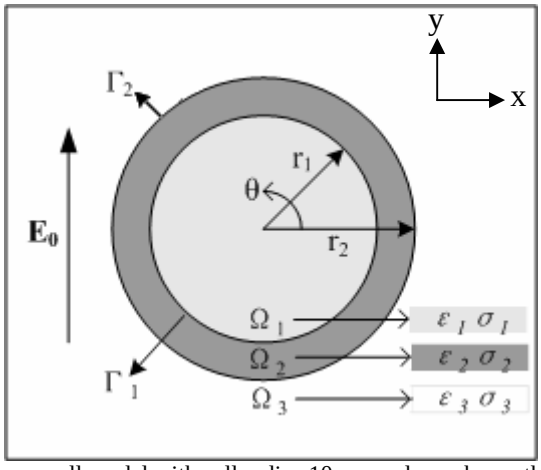

Fig. 1 Double layer cell model with cell radius 10 μm and membrane thickness 10 nm.

2.1 Quasi-static analysis by solving Laplace's equation

The wavelength at the studying frequency band (100MHz ~ 100GHz) is much larger than the cell dimension, so the quasi-static approximation applies in this study. Therefore, Laplace's equation together with the boundary conditions on the interfaces is sufficient to define the problem.

$$\nabla^2\Phi = 0 \qquad \text{In } \Omega_1\ \Omega_2\ \Omega_3 \qquad (1)$$

$$\left(\varepsilon_2\vec{E}_2 - \varepsilon_1\vec{E}_1\right)\cdot\hat{n} = 0 \qquad \text{On } \Gamma_1$$

$$\left(\varepsilon_3\vec{E}_3 - \varepsilon_2\vec{E}_2\right)\cdot\hat{n} = 0 \qquad \text{On } \Gamma_2$$

The analytical solutions of the Laplace's equation in a spherical cell model can be solved as follows.

$$E_{1n} = \frac{3\varepsilon_2\varepsilon_3}{\varepsilon_2(\varepsilon_1+2\varepsilon_3)+2\alpha(\varepsilon_1-\varepsilon_2)(\varepsilon_3-\varepsilon_2)}E_0 \qquad \text{In } \Omega_1 \qquad (2a)$$

$$E_{2n} = \frac{\varepsilon_3(\varepsilon_1+2\varepsilon_2)}{\varepsilon_2(\varepsilon_1+2\varepsilon_3)+2\alpha(\varepsilon_1-\varepsilon_2)(\varepsilon_3-\varepsilon_2)}E_0 + \frac{(1+\cos^2\theta)r_1^3}{r^3}\frac{\varepsilon_3(\varepsilon_1-\varepsilon_2)}{\varepsilon_2(\varepsilon_1+2\varepsilon_3)+2\alpha(\varepsilon_1-\varepsilon_2)(\varepsilon_3-\varepsilon_2)}E_0 \qquad \text{In } \Omega_2 \qquad (2b)$$

$$E_{3n} = E_0 + \frac{(1+\cos^2\theta)r_1^3}{r^3}\frac{\varepsilon_2(\varepsilon_1-\varepsilon_3)-\alpha(\varepsilon_1-\varepsilon_2)(\varepsilon_3-\varepsilon_2)}{\varepsilon_2(\varepsilon_1+2\varepsilon_3)+2\alpha(\varepsilon_1-\varepsilon_2)(\varepsilon_3-\varepsilon_2)}E_0 \qquad \text{In } \Omega_3 \qquad (2c)$$

where $\alpha = \dfrac{1-\left(r_1/r_2\right)^3}{3}$.

In addition to the analytical solution, the Laplace's equation (Equation 1) can also be solved numerically. The numerical solution was performed in the trial version v3.2b of Comsol Multiphysics (FEMLAB) based on FEM (Finite Element Method). Meshing scheme of a quarter of the cell model and the zoom-in view of mesh on the membrane are shown in figure 2.

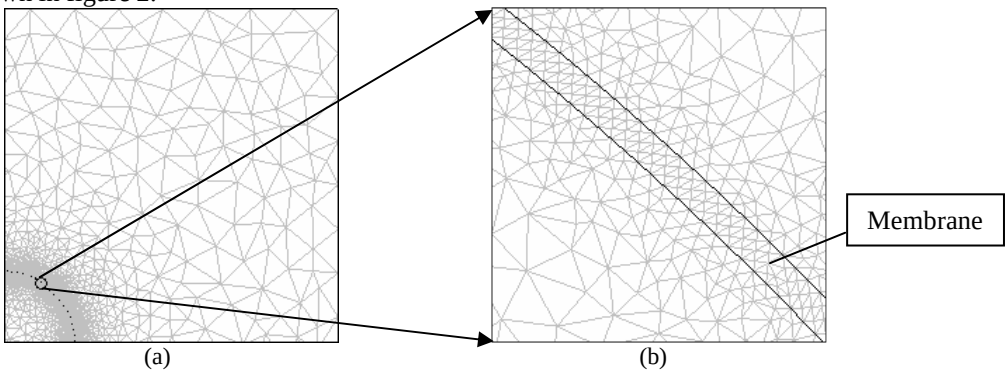

Figure 2 Meshing schemes of the cell model: (a) mesh on a quarter of a cell; (b) the zoom-in view of mesh on the membrane

2.2 Full-wave analysis by solving Maxwell's equations

On the other hand, the full wave equation, i.e. Maxwell's equations is a complete description of the problem. The theoretical solution of Maxwell's equations is obtained based on the Mie theory, which solves the Helmholtz's equations in the studying regions. Boundary conditions at the interfaces Γ_1 and Γ_2 are involved with the electric and magnetic fields of the incident wave.

$$\nabla^2\vec{E} + k^2\vec{E} = 0 \qquad \text{In } \Omega_1\ \Omega_2\ \Omega_3 \qquad (3a)$$

$$\nabla^2\vec{H} + k^2\vec{H} = 0 \qquad (3b)$$

$$\left(\vec{E}_2 - \vec{E}_1\right)\times\hat{e}_r = 0; \quad \left(\vec{H}_2 - \vec{H}_1\right)\times\hat{e}_r = 0; \qquad \text{On } \Gamma_1$$

$$\left(\vec{E}_i + \vec{E}_3 - \vec{E}_2\right)\times\hat{e}_r = 0; \quad \left(\vec{H}_i + \vec{H}_3 - \vec{H}_2\right)\times\hat{e}_r = 0; \qquad \text{On } \Gamma_2$$

The calculated electric and magnetic fields are expressed by the vector harmonics $\boldsymbol{M}_{o1n}$, $\boldsymbol{M}_{e1n}$, $\boldsymbol{N}_{o1n}$, $\boldsymbol{N}_{e1n}$ (products of cosine, Legendre and Bessel functions of corresponding parameters in spherical coordinate system) in equation 4. The coefficients a_n, b_n, c_n, d_n, f_n, g_n, v_n and w_n are solved by the wave expressions together with the boundary conditions. The summation of infinite elements in the following equations provides the accurate result, which is not applicable in practical calculation, so the element-summation truncation number N is selected as 12 to balance the accuracy and computation overheads.

$$\vec{E}_1 = E_0\sum_{n=1}^{N} i^n\,\frac{2n+1}{n(n+1)}\left(c_n\vec{M}_{o1n}^{(1)} - id_n\vec{N}_{e1n}^{(1)}\right) \qquad (4a)$$

$$\vec{H}_1 = \frac{-k_1}{\omega\mu_1}E_0\sum_{n=1}^{N} i^n\,\frac{2n+1}{n(n+1)}\left(d_n\vec{M}_{e1n}^{(1)} + ic_n\vec{N}_{o1n}^{(1)}\right) \qquad (4b)$$

$$\vec{E}_2 = E_0\sum_{n=1}^{N} i^n\,\frac{2n+1}{n(n+1)}\left(f_n\vec{M}_{o1n}^{(1)} - ig_n\vec{N}_{e1n}^{(1)} + v_n\vec{M}_{o1n}^{(2)} - iw_n\vec{N}_{e1n}^{(2)}\right) \qquad (4c)$$

$$\vec{H}_2 = \frac{-k_2}{\omega\mu_2}E_0\sum_{n=1}^{N} i^n\,\frac{2n+1}{n(n+1)}\left(g_n\vec{M}_{e1n}^{(1)} + if_n\vec{N}_{o1n}^{(1)} + w_n\vec{M}_{e1n}^{(2)} + iv_n\vec{N}_{o1n}^{(2)}\right) \qquad (4d)$$

$$\vec{E}_3 = E_0\sum_{n=1}^{N} i^n\,\frac{2n+1}{n(n+1)}\left(-b_n\vec{M}_{o1n}^{(3)} + ia_n\vec{N}_{e1n}^{(3)}\right) \qquad (4e)$$

$$\vec{H}_3 = \frac{k}{\omega\mu}E_0\sum_{n=1}^{N} i^n\,\frac{2n+1}{n(n+1)}\left(a_n\vec{M}_{e1n}^{(3)} + ib_n\vec{N}_{o1n}^{(3)}\right) \qquad (4f)$$

The Maxwell's equations are also solved by FEM in the Comsol Multiphysics (FEMLAB) as the full-wave analysis, using the same meshing scheme as the quasi-static method, as shown in figure 2. The scattering boundary conditions are used assuming the boundary is transparent for the scattered wave.

2.3 Results

Figure 3 shows the calculated E-fields by using Mie theory (red dotted line) and the Laplace's solution (red solid line), compared with the numerical calculated results of full-wave (blue dotted line) and quasi-static FEM (blue solid line). It is observed that the two dotted lines (Mie theory and FEM with full-wave) agree with each other quite well, presenting a more accurate evaluation than the other two methods based on the quasi-static approximation (Laplace's solution and FEM with quasi-static). However, the largest discrepancy between them is no more than 5%, which is acceptable in the estimation of the field distribution in cell modelling.

The left part of the separator symbol ('//') on figure 3 shown the electric field distribution near the membrane of the cell. The field inside the cell is slightly higher than the external field strength (1V/m), and the field outside the cell is lower than the external field. The right part (right of '//') showed that the electric field increases while leaving the edge of the cell, and approaches the external field strength gradually.

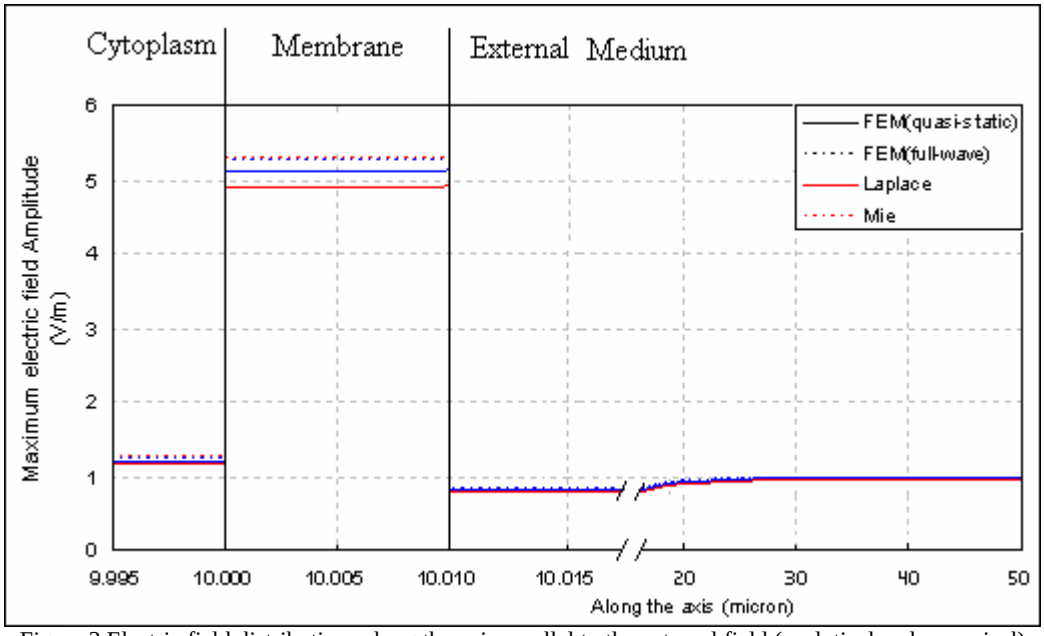

Figure 3 Electric field distributions along the axis parallel to the external field (analytical and numerical)

Solving the 2D cell model with quasi-static approximation took 2 minutes 27 seconds in the simulation software FEMLAB, whereas the full-wave analysis of the same cell model and meshing scheme took 26 hours 48 minutes, both on a 2.80GHz PC with 512M memory. Therefore, the fast microdosimetry based on quasi-static approximation is much more efficient than the traditional full-wave analysis while maintaining acceptable accuracy (<5% error). All the simulations in next two sections use the models based on the quasi-static approximation.

III. Analyses

3.1 Influences of dielectric properties

The cytoplasm was modelled as physiological saline (0.07N) containing a protein volume fraction of 0.262, so the relative permittivity and the conductivity were obtained in literature [3]. As a protein solution, the major dispersion at microwave frequencies is dominated by the water relaxation near 20GHz, and diminished a little due to the proteins' displacement of a corresponding volume of water. The membrane, as a phospholipid bilayer, has a frequency-independent relative permittivity of 11.3 (membrane capacity 1.0μF/cm^2) and conductivity of 0 [4]. The external medium is assumed to have the frequency-dependent dielectric properties of physiological saline (0.15N) [4] with a static and infinite frequency permittivity values of 76 and 5, respectively. There is no apparent difference between the relaxation frequency of the medium and that of the pure water, which is 20GHz at room temperature. The characteristic values of the dielectric properties on the three sub-domains are listed in table 2.

	Cytoplasm (Ω_1)	Membrane (Ω_2)	External (Ω_3)
ε_s	57	11.3	76
ε_{in}	5	0	5
f_c (Hz)	15e9	-	20e9
σ_s (S/m)	0.3	0	1.1

Table 2 Dielectric properties of double layer cell model

The parameters illustrated in table 2 are static relative permittivity, infinite frequency relative permittivity, relaxation frequency and static conductivity, respectively. The frequency dependent permittivities are plotted in figure 4. The electric fields inside and outside the cell are almost uniform, whereas the field concentrated on the membrane varies according to the theta angle in the polar coordinate. The maximum value of the field intensity happens at the zenith angle (90^0), and depends on the frequency, as plotted in figure 5.

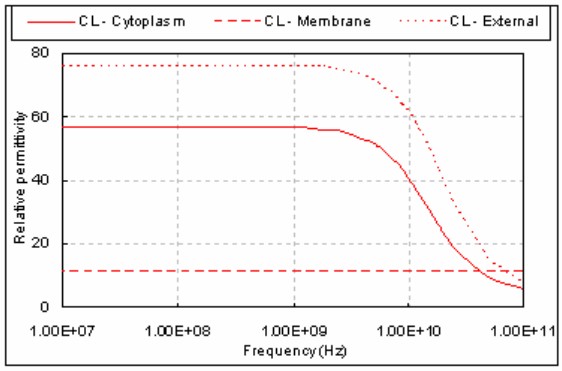

Figure 4 Debye 1st order relaxation properties of cell model (Relative permittivity)

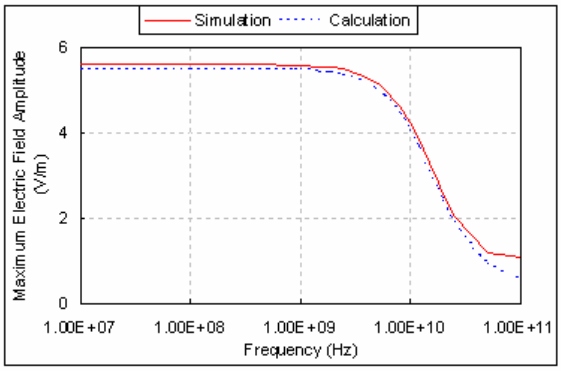

Figure 5 Maximum E fields on the membrane of the spherical cell model

Figure 5 displays the electric field simulated by FEM with quasi-static approximation and calculated by directly solving Laplace's equation. The two curves agree with each other very well. With the logarithm scaled axes, figure 5 illustrates that at the lower frequency band, the E-fields are not significantly dependent on the dielectric model. While at the higher frequency range the maximum electric field is strongly dependent on the frequency, which agrees well with the trends shown in figure 4 of the dielectric properties.

3.2 Elliptical cells

One of the most common cells shapes is ellipsoid, which has one more dimensional variable than the spherical model, axial ratio (the ratio between major and minor axes). When the cell is exposed to the plane wave illumination, the electric field also concentrates on the membrane and the maximum electric field appears at the zenith angle of the cell. The dielectric properties used in the simulations in this section are the same values as listed in table 1. Amplitudes of the maximum electric fields of the cell model with different axial ratios are plotted in figure 6.

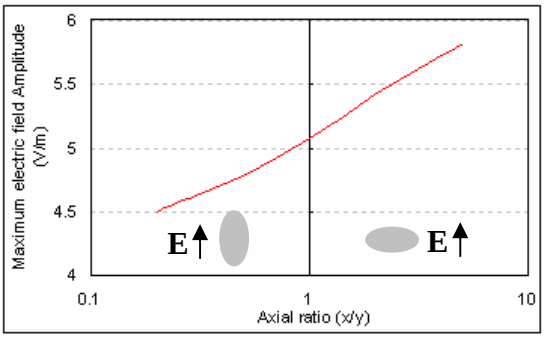

Figure 6 Maximum E fields on the membrane of the ellipsoidal cell (according to different axial ratio)

Figure 6 presents that the maximum electric field is higher when the major axis of the ellipsoidal cell is perpendicular to the external field, and the value decreases while the minor axis increasing. When the major axis is parallel to the external field, the E field value increases with the increasing of the minor axis. Plotting the E field amplitude according to the axial ratio in logarithm scale, this relationship is approximately linear.

The ellipsoid exposed to external electric fields with different polarisations as illustrated in Figure 7 has also been investigated. The maximum value of electric field presents at the frontier of the structure. Figure 8 shows the maximum electric field on the membrane decreasing when the external electric field polarisation changing from 0 degree to 90 degree.

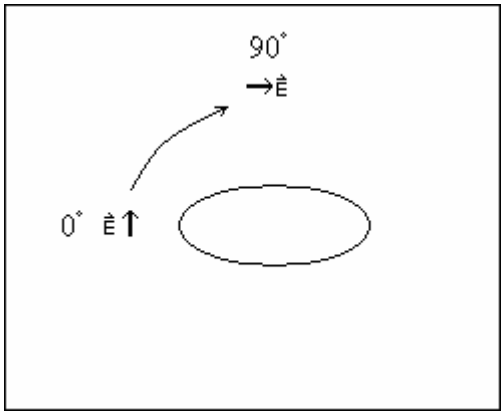

Figure 7 Ellipsoidal cell exposed to electric field with different polarisation

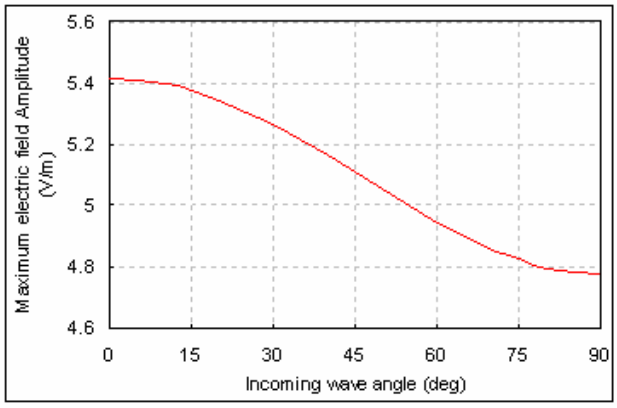

Figure 8 Maximum eelectric fields on the membrane of the ellipsoidal cell (according to different polarisation of external electric field)

3.3 Other shapes of models

The geometric shape of the structure also influences the maximum electric field on the membrane. For a cell model with length 10 microns and width 5 micros, the maximum E fields of the ellipsoids, rods and erythrocytes are compared in Table 3. The "vertical (↑0°)" and "horizontal (→90°)" in Table 3 indicates the directions of external electric field as shown in Figure 4. The location of maximum electric field is labelled by the red circles in Table 3.

		E field (external E_0: horizontal → 90°)		E field (external E_0: vertical ↑0°)	
Ellipsoid		4.776		5.415	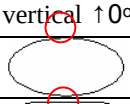
Rod		4.762		5.492	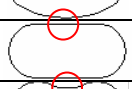
Erythrocyte		4.779	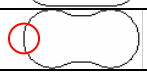	5.780	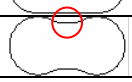

Table 3 E fields on the membrane (according to different cell shapes)

IV. Summaries

In this paper, a fast microdosimetry technique based on the quasi-static approximation has been studied. It is demonstrated that the fast microdosimetry technique runs much faster than the one working with full-wave analysis, while maintaining acceptable accuracy. The following analyses of frequency-dependent dielectric properties of the simple cell model have revealed their influences on the electric field concentration on the membrane. In addition, the effects of the various shapes of cell models have been also been investigated. In the future, the fast microdosimetry can be performed on more realistic cell models, in order to study the field distribution and transmembrane potential of the cell.

References

[1] S Munoz San Martin, J L Sebastian, M Sancho and J M Miranda, "*A study of the electric field distribution in erythrocyte and rod shape cells from direct RF exposure*", Phys. Med. Biol. vol.48, 1649-1659, 2003

[2] C Merla, M Liberti, G d'Inzeo, "*Dielectric models of biological cells and quasi-static EM analysis at radio and microwave frequencies: A microdosimetric study*", Proceeding of BEMS Annual meeting, Ireland, 2006

[3] G P Drago, S Ridella, "*Evaluation of electrical fields inside a biological structure*", Br J Cancer (Suppl V), 45: 215-219, 1982.

[4] H P Schwan, K R Foster, "*RF-field interactions with biological systems: Electrical properties and biophysical mechanisms*", Proceedings of IEEE, 68(1): 104 – 113, 1999.

Directional Effects of a Moderate-Intensity Static Magnetic Field on Anomalous Chemical Wave Propagation

Daisuke Akai[a], Hideyuki Okano[b], Hiroyuki Kitahata[c], Kenichi Yoshikawa[c] and Naohide Tomita[a,b]

[a]Department of Mechanical Engineering, Graduate School of Engineering, Kyoto University, Japan
[b]International Innovation Center, Kyoto University, Japan
[c]Department of Physics, Graduate School of Science, Kyoto University, Japan

Abstract
The effect of the spatial magnetic gradient in static magnetic field (SMF) exposure on the velocity of chemical wave in Belousov-Zhabotinsky (BZ) reaction was examined. The BZ medium was exposed to SMF of maximum magnetic flux density 210 mT and maximum spatial gradient 37 mT/mm for a period of up to 20 min at room temperature. The SMF was generated by a parallel pair of attracting rectangular NdFeB magnets positioned opposite to each other. The results suggested three characteristics for the alternation of BZ chemical wave formation: (1) the magnetic gradient could be the dominant factor for the alternation of the chemical wave; (2) the direction of accelerated velocity of chemical wave was vertical to the direction of magnetic gradient; (3) the effect was symmetry to the gradient direction and our experiments demonstrate clearly that The effect of SMF on the chemical wave propagation was affected by the thickness of the BZ medium.

1. Introduction

It has been reported that static magnetic field (SMF) can influence physicochemical reactions [Boga et al., 1990; He et al., 1994] and biochemical reactions [Harkins and Grissom, 1994], and therefore it has been predicted that SMF might affect auto-oscillations in the nonequilibrium system. We used the Belousov-Zhabotinsky (BZ) reaction known as nonequiriblium system and one of the simplest chemical oscillators in order to test this hypothesis. The steady oscillations of BZ reaction can be easily observed for a long period. The present study shows that the spatial magnetic gradient in the SMF exposure affects the velocity of chemical wave propagation. This phenomenon could be attributed primarily to the magnetic force acting the iron ion complexes in the BZ solution.

2. Experiment

The BZ medium of 20 ml contains the following solutions: (1) 7 ml H_2O, (2) 3 ml $NaBrO_3$ (1 M), (3) 2 ml H_2SO_4 (3 M), (4) 2 ml $CH_2(COOH)_2$ (1 M), (5) 2 ml NaBr (3 M), and (6) 4 ml $Fe[(phen)_3]^{2+}$ (20 mM). Every solution from (1) to (5) was added in number order. After these 5 solutions were mixed in a glass vessel, the solution turned yellowish, started to fade and became colorless in some minutes. In the end, solution (6) ferroin was added into the previous solution.

The magnetic device is constructed using a pair of rectangular neodymium magnets (Fig.1). The opposite magnets attracting each other through a 26 mm air gap are fixed parallel to both sides of the stainless frame. The maximum magnetic flux density was measured to be approximately 210 mT at the bottom center of the Petri dish by using a gaussmeter (Model 4048, Hall probe A-4048-002; Bell Technologies, Orlando, FL, USA).

(1) The BZ medium was put into a petri dish with a diameter 140 mm (3030-150; Iwaki Glass Co, Japan), which was put on a magnetic device (Fig.1). BZ reaction was initiated at the center of the Petri dish using a silver wire. The images were taken by a digital video camera (DIGICAM, NV-GS250-S, Panasonic, Japan) from above. The pictures were quantified by using Scion software (Scion Image; Scion, Frederick, MD, USA). All the experiments were carried out at a room temperature. Four independent experiments were averaged per data point. All values are expressed as mean ± SD.

(2) To examine the effect of the thickness of BZ medium on the chemical wave propagation, the thickness of BZ medium was controlled from 0.5 to 0.9 mm at 0.2 mm intervals by slipping some cover glasses with a thickness 0.1 mm in between two square plates. These plates were put on one side of the magnetic device with the edges of the plates parallel to the inner line of the magnet. The BZ medium was poured in between two plates. BZ reaction was initiated from the edge of plates using a silver wire to observe chemical wave propagation from the center of the device. The images were taken by a digital video camera in the same way as

the previous experiment.

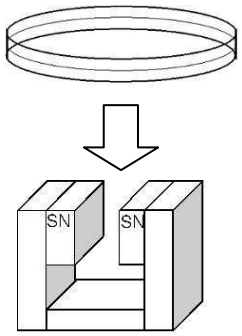

Fig.1. Experimental device
A Petri dish with a diameter 140 mm was put on the magnetic table where, two parallel rectangular magnets (NdFeB, L. 80 × W. 18 × H. 55 mm, TDK Corporation, Japan) attract each other.

3. Results and discussions

The concentric propagation of chemical wave was observed in the BZ medium when sham exposure was performed without magnet (the background geomagnetic field intensity at our laboratory is ~50 μT) (Fig.2A). On the other hand, the different propagation from concentric pattern of chemical wave was observed when the BZ medium was exposed to SMF (Fig.2B). The thickness of BZ medium in the petri dish was 1.3 mm.

These results suggested three characteristics for the alternation of BZ chemical wave formation: (1) the magnetic gradient could be the dominant factor for the alternation of the chemical wave; (2) the direction of accelerated velocity of chemical wave was vertical to the direction of magnetic gradient; (3) the effect was symmetry to the gradient direction.

The velocity of chemical wave of BZ reaction to Y direction was accelerated on the inner line of the magnet where the magnetic gradient to X direction was maximum (Fig.2). This result indicates that the BZ chemical reaction was accelerated to one direction by the magnetic gradient, and that the direction was perpendicular to the gradient. The chemical wave can be visualized by the oxidation-reduction reaction of ferroin. However, BZ reaction is induced by the complicated combination of several chemical reaction steps. Ions produced in the chemical reaction could be affected by the inhomogeneous magnetic field. The alternation of the chemical wave propagation in BZ reaction could be caused by the different orientation of iron ions under SMF exposure from that of sham exposure (no magnet).

In order to quantify the alternation of chemical wave, the angles θ of tangent line of the chemical wave front to the inner line of the magnet defined in Fig.3 were measured under the both conditions of sham exposure (no magnet) and SMF exposure (Fig.4). The deformation rates of chemical wave in SMF exposure were significantly larger and reached their maximum levels earlier than those in sham exposure.

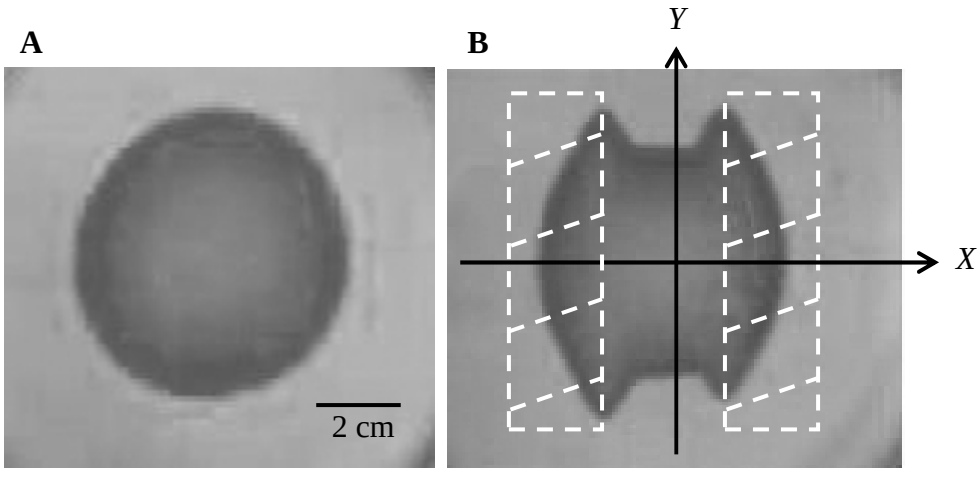

Fig.2. (A) Chemical wave not exposed to magnets (sham exposure) (B) Chemical wave exposed to magnets (SMF exposure; white dashed lines correspond to the position of magnets)

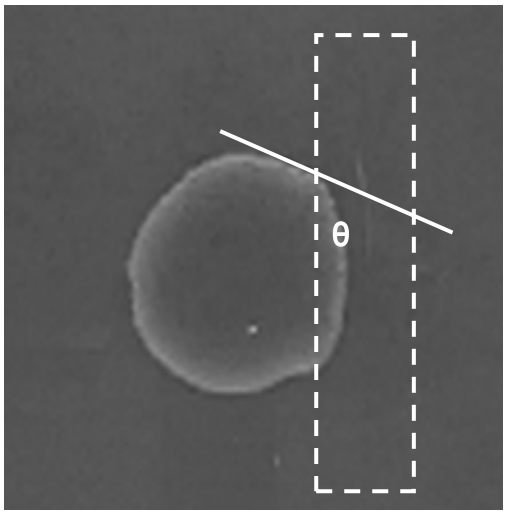

Fig.3. Angle θ of tangent line of the chemical-wave front to an inner line of the magnet (dashed line corresponds to the position of magnet)

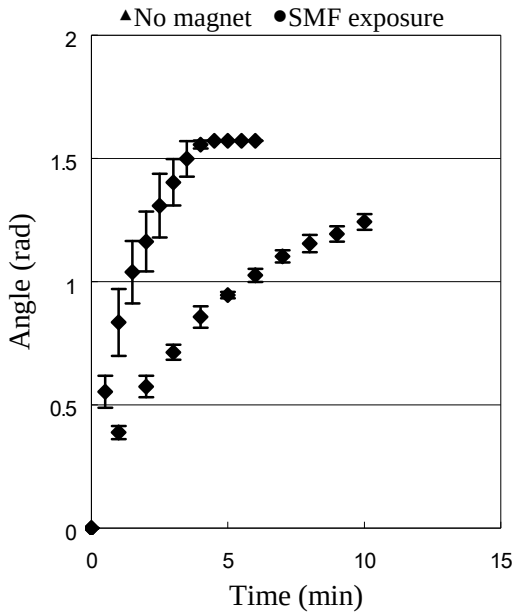

Fig.4. Angles defined in Fig.3 measured per data point in the case of no magnet and SMF exposure

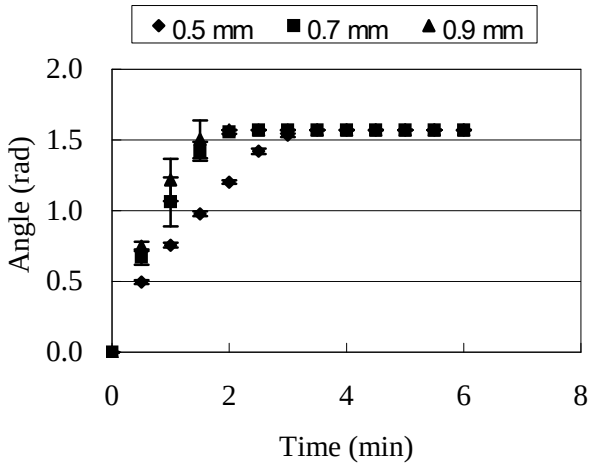

Fig.5. Angles defined in the same way as Fig.3 per data point of BZ reaction of several thickness 0.5, 0.7, 0.9 mm of BZ medium

The effect of SMF on the chemical wave propagation was affected by the thickness of the BZ medium as shown in Fig.5. When the thickness of BZ medium was different, the velocity of reaction front varied. Therefore, the forms of chemical wave propagation were different among three conditions. The thicker the BZ medium was, the larger the deformation rate of chemical wave was. However, there was no significant difference per data point between the thickness 0.7 and 0.9 mm. It is conceivable that the degree of the chemical wave propagation would not change in the case of both more than constant thickness and less than the threshold of thinner thickness. This means that there is a window effect of SMF on the deformation rate of chemical wave depending on the thickness of the BZ medium. The result given in Fig.5 includes the factor of the velocity of the reaction front on the inner line of the magnet. The elements of the distance of reaction front should be taken into account in order to quantify the anomalous propagation in detail.

References

Boga E, Kádár S, Peintler G, Nagypál I. 1990. Effect of magnetic fields on a propagating reaction front. Nature 347:749–751.

Harkins TT, Grissom CB. 1994. Magnetic field effects on B_{12} ethanolamine ammonia lyase: evidence for a radical mechanism. Science 263:958–960.

He X, Kustin K, Nagypál I, Peintler G. 1994. A family of magnetic field dependent chemical waves. Inorg Chem. 33:2077–2078.

COMPARATIVE STUDY OF THE EFFECTS OF EMF-TREATED AND HYDROGEN PEROXIDE-CONTAINING SOLUTIONS ON NEUROMEMBRANE CHEMOSENSITIVITY

SINERIK AYRAPETYAN, ARSEN HUNANYAN

UNESCO CHAIR- LIFE SCIENCES INTERNATIONAL POSTGRADUATE EDUCATIONAL CENTER
31 ACHARYAN ST., YEREVAN, 375040 ARMENIA, LIFE@ARMINCO.COM

Abstract

The hydrogen peroxide (H_2O_2) which is formed in cell bathing aqueous solution upon Electromagnetic Fields (EMF) exposure is very often considered as the most reliable messenger through which the biological effect of EMF is realized. To check this hypothesis the comparative study of the effects of 4Hz EMF-treated and H_2O_2 - containing physiological solutions (PS) on Ach sensitivity of snail neuron as well as on the nerve tissue hydration were studied. The 4 Hz EMF-treated and H_2O_2-containing PS at room temperature (23^0C) had depressing effects on Ach-induced current, while in cold medium (12^0C) these effects disappeared. The EMF-treated ouabain-containing and K-free PS elevated the amplitude of Ach-induced current, while the H_2O_2 – containing PS has inhibitory effect on it. The both, EMF-treated and H_2O_2 -containing PS have dehydration effects on cell hydration in nerve ganglia. It is suggested that the ELF EMF-induced H_2O_2 formation could serve as one of the metabolic pathways through which the depressing effect of ELF EMF on membrane chemosensitivity is realized.

Key words: EMF, H_2O_2,, neuron, acetylcholin -sensitivity, membrane, cell volume.

Introduction

Although, the abundance of experimental data on the biological effect of magnetized water and water solutions on different cells and organisms are available (Klassen, 1982; Ayrapetyan et al., 1994a; Ayrapetyan, 2006), the nature of the messenger transferring the signal of magnetic and electromagnetic fields-induced water structural changes to cell metabolic cascade is not clear yet. As the water molecule dissociation is the most variable water property, it is suggested that the EMF-induced vibration of water dipoles could change water dissociation and its products could serve as possible messengers through which the biological effect of EMF is realized (Ayrapetyan 1994). By privies our work the depressing effect of extremely low frequency (ELF) EMF on specific electrical conductivity (SEC) of water and water solutions (which is marker for its dissociation) was documented (Ayrapetyan et al., 1994). It was also shown that the depressing effect of LF EMF on water SEC as well as its biological effects on various cells are most pronounced at frequency of 4 Hz (Stepanian et al. 1999; Ayrapetyan 2006).

The fact that the vibration of water dipoles in presence of oxygen could generate the H_2O_2, which could initiate the modulation of a number of metabolic pathways in the cell, makes it as one of the most reliable candidates for the messenger able to transfer the ELF EMF-induced water structure changes to cell metabolic cascades (Klassen, 1982). As the acetylcholine (Ach) sensitivity of neuronal membrane is sensitive to the effect of magnetized physiological solutions (MPS) (Ayrapetyan et al., 1994a; Ayrapetyan et al., 2004), it was chosen as an experimental model for testing the above-mentioned hypothesis.

The overall aim of the present review is to present the results of the comparative study of 4 Hz EMF-treated and H_2O_2 –containing PS on snail neuromembrane chemosensitivity, as well as on the nerve tissue hydration which has a crucial role in metabolic regulation of membrane chemosensitivity (Ayrapetyan & Arvanov, 1979).

Method

The experiments were carried out on non-selected giant neurons of the right parietal ganglion of Helix pomatia. The standard Voltage-Clamp method was used to record the Ach-induced current through the neuronal membrane (Ayrapetyan and Arvanov, 1988). The normal physiological solution contains (in mM): NaCl-80,

KCl-4, CaCl2-7, MgCl2-13, Tris-HCl (pH 7.8)-10, glucose-10. In K-free solution 4mM KCI was replaced by 4mM NaCI. Different concentrations of acetylcholine (10^{-4}-10^{-6} M) and H_2O_2 (10^{-4}-10^{-11} M) were prepared from Ach and H_2O_2 stock solution (10^{-2} M) before the experiments. The transient application (less than 30 sec) of Ach was performed by thin (diameter ~1mm) polyethylene tube placed near the investigated neuron. The H_2O_2 was added to the perfusion solution to a final concentration from 10^{-4} to 10^{-11} M and applied to the cells at a rate of 2-3 ml/min. The time of pre-incubation of neurons in tested physiological solution before the Ach application was 3 min.

The tested physiological solution was preliminary exposed to 4Hz EMF with the intensity of 2,5 mT for 30 minutes. The experimental setup consisted of a glass test tube with diameter of 10 mm and volume of 10 ml., EMF generator with low-noise amplifier and a coil. The coil has the cylindrical form with diameter of 154 mm. and height of 106 mm. The coil consists of Helmholtz rings that generate the homogeneous magnetic field. Rings of Helmholtz are formed by two equal ring coils located coaxially and in a parallel way. The distance between ring coils is equal to their radius of 77 mm. The magnetic field created by these rings has high homogeneity. For example, on distance of 0.25R from the center of an axis strength differs from computed by formula only on 0.5 % $H = 71.6 \cdot \omega \cdot \frac{I}{R}$. Herewith, the intensity of generated EMF is equal to 2.5 mT and 4 Hz frequencies. The instrument used for measurement of magnetic field intensity was a Teslometer W1-8 (Armenian Radiophysical Institute). This instrument measures magnetic fields in the range 10^{-3} to 1.6 T (±5%). The magnetic induction converter was a crystal, type X511-1, 1.5 X 0.2 mm^2 and was fixed on non-magnetized material (PX13-1). During the experiment the neurons were perfused with normal and 4Hz EMF treated solutions. The physiological solution treated by 4Hz EMF for 30min. and immediately (interval from the end of the treatment and till the beginning of perfusion was no longer than 1-2 min.) used for perfusion of neuronal ganglia. The control (unexposed) PS taken from the same reservoir of PS (Vol: 1-2 l) also was placed in the same test tube for 30min in an inactive coil system, i.e. the background field was the same for the control (sham exposed) and tested PS. The background of magnetic field in the area of experimental setup in the laboratory, supplied by 60 Hz electricity, was less than 0,001 mT. The holder of the exposure tube and the coil holder were placed in two neighboring tables to excluded the vibration during the exposure.

For determination of tissue hydration, the wet samples of the nerve ganglia were weighted and dried in thermostat at 105^0C, during 24 hours. After determination of dry weight the quantity of water on 1 g. of dry weight was determined by the equation: (A - B) / B , where A- wet weight of the tissue, B- weight of the tissue after drying.

The procedure of measuring a single cell volume has been previously described in Ayrapetyan et al., 1994a. Briefly, single neurons were dissected and isolated from the ganglion under a dissecting microscope (Lomo, B-14, Russian production) on which was mounted a digital video camera (WPI, USA) connected to PC. The system had the sensitivity such that changes of ±0.1 µm could be detected. These neurons had diameters of 50-100 µm.

The mean value, standard deviations, and the statistical probability, determined by Student Test were calculated with the help of computer program Sigma Plot (Version 8.02A).

Results

It is known that three types of neurons can be distinguished according their sensitivity to Ach: (a) insensitive, (b) depolarizing (D), and (c) hyperpolarizing (H) (Shakarov et al., 1969). The present experiments were carried on 22 neurons having D-responses and 20 neurons having H-responses. The membrane potential (MP) of neurons was clamped on the level of resting potential (-40 to -60 mV). After recording the control Ach-induced currents in normal physiological solution (control) the cells were perfused with magnetized PS (MPS) or by different concentrations of hydrogen peroxide- containing PS during 7 minutes and the end of 7-th minutes the application of Ach was performed.

By previous our work was shown that the normal MPS has a reversible depressing effect on Ach-induced membrane current and this effect of MPS was absent in cold (12^oC) medium. The typical record of such responses presented on Figure 1. (Ayrapetyan et al., 2004).

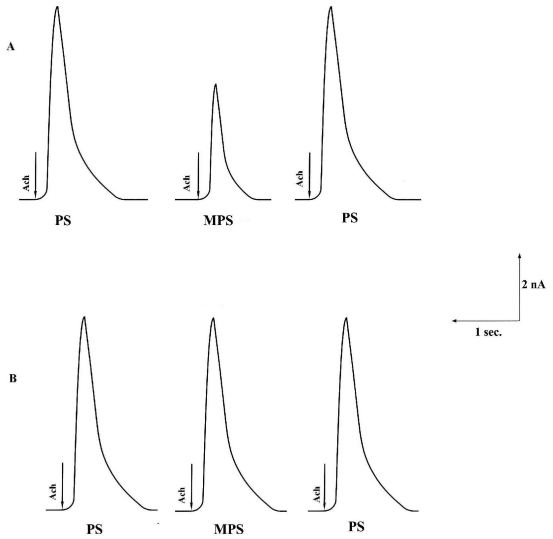

Figure 1. *The effect of magnetized physiological solution (MPS) on Ach-induced current in D type neuron in voltage-clump experiments, where the clumping potential (E_c) was equal to the resting membrane potential (E_r = -50 mV).*
A- at room temperature (23^0C), B- in cold medium (12^0C).
The rows show the transit (30 msec) application of 10^{-4} M Ach containing PS. The time of pre-incubation of neurons in tested physiological solution (PS and MPS), before the application of Ach was 3 min. The intervals between Ach applications was 5 min.

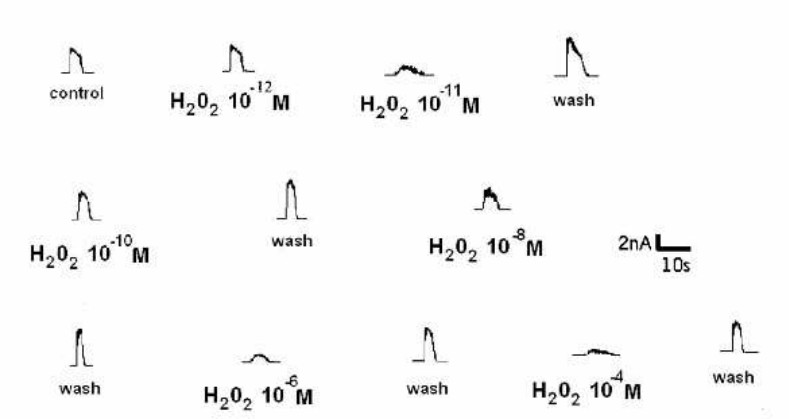

Figure 2. *The typical record of dose-dependent effect of H_2O_2 on Ach-induced current in D-type neuron in voltage-clamp experiments, where the clamping potential (E_c) was equal to the resting membrane potential (E_r = -60mV). Ach concentration was 10^{-4}M. The time of pre-incubation of neurons in H_2O_2 containing physiological solution (PS) was 7 min. All presented data were taken from one neuron. The intervals between Ach application was 5 min.*

As shown in Figure 2, the H_2O_2 at concentrations of 10^{-11}-10^{-4} M also has a depressing effect on Ach (10^{-4} M)-induced ionic currents in D-type neurons. After removing of H_2O_2 from extracellular medium the amplitudes of Ach-induced currents were recovered to their initial level within 5 minutes. The maximum depressing effect of H_2O_2 on Ach-induced current appeared at concentration of 10^{-4} M (75±1.2%), while the threshold of H_2O_2 concentration, unable to change the amplitude of Ach-responses of the membrane during 7 min. pre-incubation, was 10^{-12} M . The character of H_2O_2-induced inhibition of Ach-responses in both, H-and D- types neurons was the same (Figure 3, n=5), which could serve as indicator of potential independence of inhibitory effect of H_2O_2 on Ach responses.

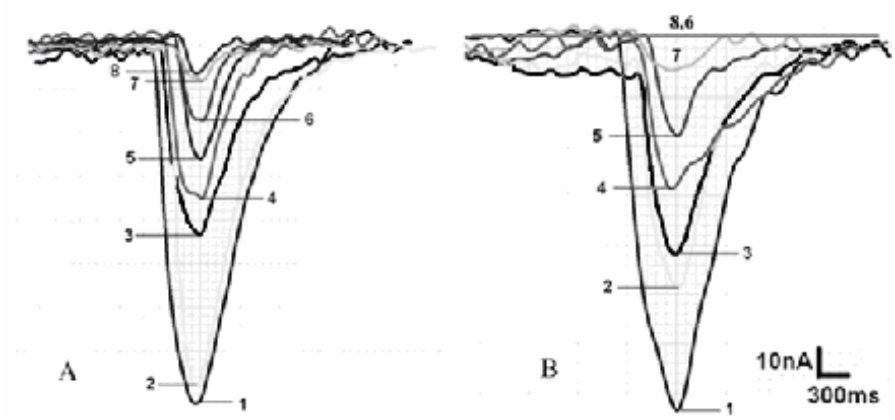

Figure 3. *The dose-dependent effect of H_2O_2 on Ach-induced current in H-type neurons in PS (A) and in K-free solution (B), where the clamping potential (E_c) was equal to the resting membrane potential (E_r = -52mV).*
1- Ach 5 × 10^{-4} M; 2- Ach 10^{-4} M; 3- H_2O_2, Ach 5 × 10^{-4} M; 4- H_2O_2, Ach 10^{-4} M; 5- Ach 10^{-5} M; 6- H_2O_2, Ach 10^{-5} M; 7- Ach 10^{-6} M; 8- H_2O_2, Ach 10^{-6} M.
The data are taken from one neuron. The presented data are typical for all 10 studied neurons. The H_2O_2 concentration was 10^{-6} M. The time of pre-incubation of neurons in H_2O_2 containing PS was 7 min.

This suggestion was confirmed by studying the potential-dependency of inhibitory effect of H_2O_2 on Ach responses, by clamping MP at different levels (Figure 4).

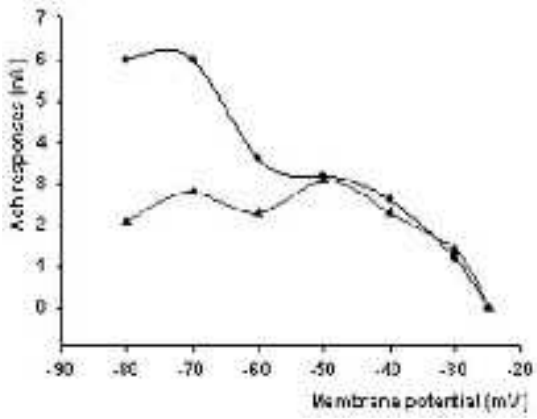

Figure 4. *The Ach-responses (nA) in D-type neuron in voltage-clamp experiments in normal (circles) and 10^{-6} M H_2O_2- containing (triangles) PS, when the membrane potential was clamped on different levels (n=5).*

The study of the potential-dependence of Ach-induced outward currents in normal and H_2O_2 (10^{-6} M) containing solution showed that the Ach-induced currents in presence of H_2O_2 became potential independent in the range of MP= - 50 – - 80 mV (Figure 4, n=5). These data could serve as additional evidence that H_2O_2 – induced depression of Ach-responses could not be explained by modulation of ionic channel activity, determining the Ach-responses. As shown in Figure 5, the depressing effect of H_2O_2 on Ach-responses as in case of MPS (Figure 1B), disappeared in cold medium (5^0C) (Figure 5, n=5), which could be considered as an evidence on the metabolic nature of H_2O_2-induced depression of Ach-responses of the membrane. The low temperature (12^0C) -induced slight elevation of Ach-induced current (Figure 1B) could be interpreted as the increase of the lifetime of agonist-activated ionic channels (Bregetovski et al., 1979).

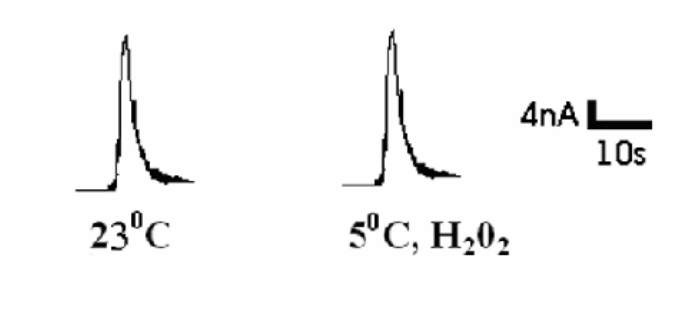

Figure 5. *The absence of depressing effect of H_2O_2 on Ach (10^{-4}M)-induced ionic currents in cold medium (5^0C). H_2O_2 concentration was 10^{-4} M, (n=5).*

The data on temperature sensitivity of the EMF-treated and H_2O_2 –containing PS-induced depressing effects on Ach membrane responses allow us to speculate on their metabolic nature. As shown in our early works the electrogenic Na^+-K^+ pump serves as one of the powerful metabolic mechanism through which the metabolic regulation of membrane chemosensitivity is realized (Ayraperyan and Arvanov, 1988). As shown by the obtained data, these factors have opposite effects on Ach-induced membrane currents in K-free medium, when Na^+-K^+ pump was in inactive state (Thomas 1972): the K-free -induced pump inactivation reversed the effect of EMF-treated PS on Ach-induced membrane current (Figure 6), while the H_2O_2 had more pronounced inhibitory effect in K-free medium than in normal K-containing PS.

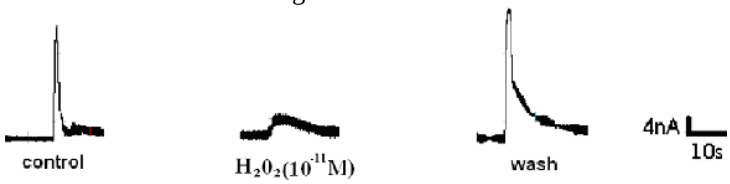

Figure 6. *The depressing effect of 10^{-11} M H_2O_2 in K-free solution on Ach-induced current in D-type neuron in voltage-clamp experiments. Neuron was clamped E_c = -55mV. The data are taken from one neuron. The presented data are typical for all 5 studied neurons.*

As shown in Figure 6, the H_2O_2 at 10^{-11} M in K-free solution has strong (reversible) depressing effect on Ach-induced current amplitude (80±2.5%, n=5) in D-type neurons. No significant differences were observed between H_2O_2 –sensitivity of Ach-responses in D and H-type neurons. These data allow as to conclude that from one side, the both MPS and H_2O_2 -induced modulations of Ach-responses could not be explained by the activation of Na^+-K^+ pump, and from another side, the nature of metabolic pathways through which they modulate the membrane chemosensitivity in K-free medium is different. Therefore, the elucidation of the nature of mechanism of H_2O_2 effect on membrane chemosensitivity would be the subject for the next series of experiments.

It is known that the agonist-induced membrane current changes could be the result of modification of ionic channel properties or the process of interaction between receptors and agonists. As the above-mentioned data on potential independence of the H_2O_2 effect on membrane chemo-sensitivity excluded the role of channel mechanism in this process, the main reliable mechanism through which the H_2O_2-induced depression of Ach-responses is realized is the process of modification of interaction between Ach and its receptors: the changes of the number of functionally active receptors or their affinity to agonist. Therefore, the effect of H_2O_2 on kinetic curve of doze-dependent Ach-induced membrane response was studied.

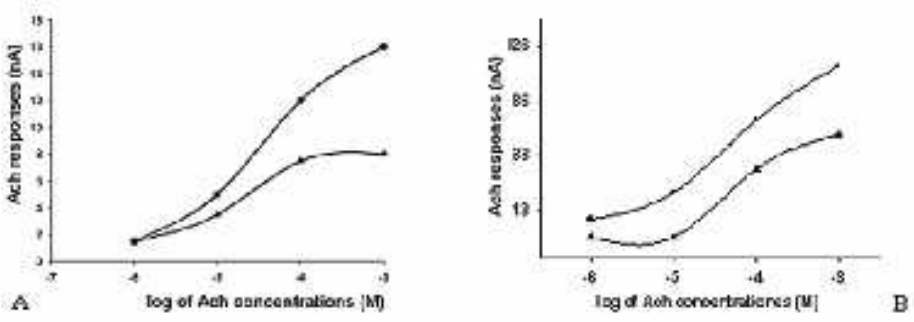

Figure 7. *The effect of 10^{-6} M H_2O_2 on dose-dependent curve of Ach-response in K-containing (A) and K-free (B) mediums in H-type neuron. Circles show the control, the triangles - in the presence of H_2O_2, (n=10).*

As shown in Figure 7A, in H_2O_2-containing solutions the Ach-induced responses reached of their maximum values at 10^{-4} M concentration, while in normal physiological solution the curve wasn't saturated even at 10^{-3} M Ach concentration. Such pronounced depressing effect of H_2O_2 on "maximums" of the doze-dependent curves of Ach could serve as evidence on the decreasing effect of H_2O_2 on the number of functionally active Ach-receptors in the membrane. It is worth to note that, although, in K-free solution the H_2O_2 also has depressing effect on number of receptors involving in generation of Ach-responses, there are significant differences between the kinetics of dose-dependent curves of Ach-responses in K-free and K-containing solutions (Figure 7B), which could be the subject for more detailed investigation.

Thus, it is important to clarify, which metabolic pathways could be responsible for H_2O_2 –induced decrease of number of functionally active receptors interacting with the agonists. It is suggested that the actinolike protein phosphorilation-induced contraction of cytoskeleton could serve as one of such mechanism through which the H_2O_2 could decrease the number of membrane receptors. As the citosceleton (cell) shrinkage is accompanied by the increase of membrane electrical resistance (Carpenter et al., 1992), for testing the above-mentioned suggestion the effect of H_2O_2 on I-V characteristics of membrane was studied (Figure 8).

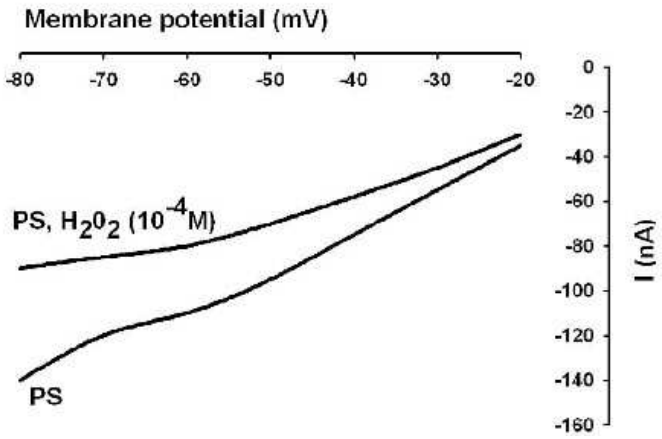

Figure 8. *The effect of H_2O_2 on current-voltage (I-V) characteristic of D-type neurons. The I-V curves in normal and 10^{-4} M H_2O_2-containing solutions were obtained by changing the holding potential from -20 to -80mV. Pre-incubation time in H_2O_2-containing solution was 7min. (n=5).*

As shown in Figure 8 there are significant increase of membrane resistance upon the effect of H_2O_2 and this effect has pronounced elevation tendency by increasing the cell membrane polarization. If the H_2O_2–induced increase of membrane resistance could be explained by the possible decrease of cell volume, the mechanism responsible for potential-dependence of such effect of H_2O_2 is not clear and needs more detailed investigation.

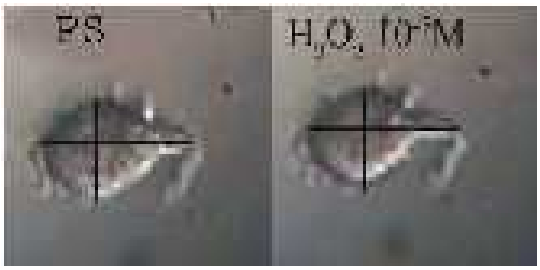

Figure 9. *The effect of 10^{-9} M H_2O_2 on neuronal volume. Scale bar 10μm. (n=5)*

For testing the above mentioned conclusion on H_2O_2 –induced cell volume (shrinkage), which leads to the decrease of membrane active surface (number of receptors in the membrane), in the next series of experiments the effect of H_2O_2 on cell volume was studied by means of light microscopy. Figure 9 shows that H_2O_2 in nM concentrations has shrinking effect on the cell.

Discussion

Although the hypothesis on the role of H_2O_2 as a possible messenger through which the biological effect of magnetized aqueous solutions is realized has long history (Klassen, 1982), its role in biological effect of SMF and ELF EMF is not elaborated yet. This difficulty is due to the absence of reliable theory explaining the cellular and molecular mechanisms of biological effects of ELF EMF from one side, and multisided metabolic effect of the H_2O_2 from the other side. Previous works of our laboratory have shown a crucial role of intracellular messenger-dependent Na^+/Ca^{2+} exchanger in realization of biological effect of magnetized solution (Ayrapetyan et al., 1994b, 2005). As the Na^+/Ca^{2+} exchanger serves as one of powerful mechanisms regulating the intracellular Ca^{2+} homeostasis (Dipolo and Beauge, 2006), which determines the membrane chemo-sensitivity (Bregestovski et al., 1979], the latter could serve as a convenient experimental model for studying the role of H_2O_2 as a potential messenger in realization of biological effect of magnetized solution on cell membrane.

The presented data on similar inhibitory effect of MPS (Figure 1) and H_2O_2 (Figure 2) on Ach-induced current and their temperature dependence, from the first face could be considered as an evidence of their synergic influences on membrane chemosensitivity. In previous our works the following metabolic cascade through which ELF EMF-treated PS can modulate the membrane chemosensitivity was suggested: the MPS-induced activation of cGMP-dependant Na^+/Ca^{2+} exchanger leads to the removal of the intracellular Ca-induced inhibition of Na^+-K^+- ATPase as a result of reactivation of Na^+-K^+ pump, which causes the decrease of a number of receptors in the membrane due to the pump-induced cell shrinkage. While the pump is in inactive state (when the pump-induced cell volume changes are excluded), the ELF EMF-induced elevating effect can be explained by the decrease of intracellular Ca concentration (Ayrapetyan et al., 2004). The fact that in K-free solution the H_2O_2 has more pronounced inhibitory effect on Ach-induced current compared to its effect in normal PS could not be explained from the point of the mentioned metabolic cascades and serves as evidence on different nature of metabolic pathways through which the inhibitory effects of MPS and H_2O_2 are realized.

It is known that the agonist-induced membrane responses could be changed as a result of modification of ionic channel properties and (or) interaction processes between membrane receptors and agonists. The obtained data on potential independence of H_2O_2–induced inhibition of Ach-responses (Figure 4) allow us to exclude the role of ionic channels in this inhibition and it could be explained by the depression of the process of interaction between receptors and agonists. The H_2O_2 –induced depression of the "maximum" in Ach doze-dependent curve serves as evidence on the changes of number of functionally active receptors in the membrane interacting with the agonist molecules (Figure 7). Early our works showed that the Na^+-K^+ pump-induced activation caused the similar inhibition of membrane Ach-sensitivity in result of cell shrinkage (Ayrapetyan and Arvanov, 1979), however the data obtained in present experiments on elevation of H_2O_2–induced depression on Ach- responses in K-free solution (when Na^+-K^+ pump is inactive) (Figures 3B, 7B), excludes the role of Na^+-K^+ pump in this process. The disappearance of such inhibitory effect of H_2O_2 on membrane chemo-sensitivity in cold (5^0C) medium (Figure 5) indicates its metabolic nature. Therefore, it is suggested that the H_2O_2 leads to the decrease of the number of functionally active receptors in the membrane by unknown metabolic mechanisms (not by Na^+-K^+ pump). Previous our works showed the close correlation between membrane active surface (cell volume) and number of functioning chemo-receptors in the membrane (Ayrapetyan and Arvanov, 1979). It is predicted that the H_2O_2–induced depression of membrane Ach-sensitivity could be the result of cell shrinkage. The microscopic study of the H_2O_2 effect on cell volume (Figure 9) proved this suggestion.

Summary

The data obtained in the present work clearly showed that the H_2O_2 in nM concentrations depressed the membrane chemosensitivity by decreasing the number of functioning receptors in the membrane as a result of cell shrinkage (probably by cytoskeleton phosphorylation). We came to the same conclusions in previous our work on studying the effect of magnetized solutions on Ach-induced responses of the membrane (Ayrapetyan et al., 2004). It was shown that the MPS caused the depression of membrane Ach-responses at room temperature (23 ^{0}C), while in cold medium (5 ^{0}C) it had no effect (Ayrapetyan et al., 2004, Figure 1). These effects were explained by MPS-induced cell dehydration which led to the decrease the number of chemo-receptors in the membrane (Danielyan et al., 1999).

Thus, the comparison of the physiological data obtained in the present work on the influences of H_2O_2 with the previous results on the effects of magnetized solution on membrane sensitivity to Ach demonstrates the close synergism between the effects of these two factors on Ach responses in normal PS which are the result of cell dehydration. However, opposite dependence of their effects on Na^+-K^+ pump activity allow us to suggest that H_2O_{2-} -dependent metabolic pathway could serve as one of the metabolic pathways through which the biological effect of ELF EMF is realized.

References

Ayrapetyan SN, Arvanov VL. 1979. On The Mechanism of The Electrogenic Sodium Pump Dependence of Membrane Chemosensitivity. *Comp. Biochem. Physiol.*, **64A**: 601-604.

Ayrapetyan SN, Arvanov VL. 1988. The Metabolic Regulation of Membrane Chemosensitivity. In Salanki (ed): Neurobiology of Invertebrates, Budapest, 36:669-684.

Ayrapetyan SN, Grigorian CV, Avanesian AS. 1994a. On a mechanism of action of magnetic field on the electrical conductivity of water solutions and some properties of Helix neurons. *Bioelectromagnetics*, **15**: 133-142.

Ayrapetyan SN, Avanesian AS, Avetisian TH, Majinian SB. 1994b. Effects of incubation of snail ganglia in physiological solutions exposed to magnetics fields on levels of intracellular cyclic nucleotides. In: *Biological effects of electric and magnetic fields* (Ayrapetyan & Carpenter, eds), Academic press, INC, pp: 185-186.

Ayrapetyan SN, Hunanyan ASh, Hakobyan SN. 2004. 4Hz EMF–treated physiological solution depresses Ach-induced neuromembrane current. *Bioelectromagnetics*. **25**(5): 397-399.

Ayrapetyan GS, Papanyan AV, Hayrapetyan HV, Ayrapetyan SN. 2005. Metabolic pathway of magnetized fluid-induced relaxation effects on heart muscle. *Bioelectromagnetics*. **26**(8): 624-30.

Ayrapetyan SN. 2006. Cell aqua medium as a preliminary target for the effect of electromagnetic fields. In: *Bioelectromagnetics: Current Concepts*, S. Ayrapetyan and M. Markov, eds., NATO Science Series, Springer Press, The Netherlands, pp: 31-64

Bregestovski PD, Bukharaeva EA, Iljin I. 1979. Volotage clamp analysis of acetylcholine receptor desensitization in isolated mollusk neurons. Nature, **279**: 581- 595.

Carpenter DO, Fejtl M, Ayrapetyan SN, Szarowski DH, Turner JN. 1992. Dynamic changes in neuronal volume resulting from osmotic and sodium transport manipulations. Acta Biologica Hungarica, 43: 39-48.

Danielian AA, Ayrapetyan SN. 1999. Changes of Hydration of Rats' Tissues after in Vivo Exposure to 0.2 Tesla Steady Magnetic Field. *Bioelectromagnetics*, **20**(2): 123-128.

Dipolo R, Beauge L. 2006. Sodium/Calcium exchanger: Influence of metabolic regulation on ion carrier interactions. *Physion. Rev*. **86**: 155-203

Klassen 1982; in: *Magnetized Water Systems*. "Chemistry" Press, 296 p (in Russian), English translation: *European Biology and Bioelectromagnetics*, 2006, **1**(2): 201-220

Sakharov DA, Salanki J. 1969. Physiological and pharmacological identification of the neurons in the central nervous system of helix pomatia. *Acta Sci. Hungar*., **35**: 19-30.

Stepanyan R., Ayrapetyan G., Arakelyan A., Ayrapetyan S. 1999. Effect of Mechanical Oscillations on Electrical Conductivity of Water Biophysics, **44**: 197-202.

Thomas RC. 1972. Intracellular sodium activity and the sodium pump in snail neurons. J. Physiol. 220:55-71.

Simulations of ELF Magnetic Shields

Josef Pekar Moshe Netzer Yekutiel Pekar
EMC Engineering & Safety
Haifa, Israel

Abstract
This paper describes a multi-stage algorithm for efficient calculation of magnetic flux contours, for optimizing the design of structural magnetic shielding. The multi-stage algorithm enables albeit medium-power computer system to calculate the effect of shielding materials with a given geometry, in a reasonable timeframe without compromising precision. The outcome results are a large number of electrical utility models and the best cost-effective shielding materials and geometries for ELF magnetic flux reduction per Authority regulations and requirements.
This paper attempts to review methods and principles for calculation of an extremely low frequency (50/60 Hz) electromagnetic field originating from power utilities and power lines, for the purpose of constructing efficient magnetic shielding. The paper points out difficulties in existing methods and proposes a new algorithm for analysis and construction of magnetic shielding.

Introduction

Magnetic field of extremely low frequency (ELF) is produced by utility and industrial electric lines, machines and cables, and various electrical fixtures, devices, and apparatuses all of which are surrounding us and deployed everywhere. Often, the level of the magnetic fields exceed the permissible exposure limits setup by international[1] and national agencies for non-ionizing radiation protection, thus need to be reduce at locations where people dwell. It can be achieved by several cost effective methods, such as: relocation of strong magnetic field emitters; reduction of electrical current; reconstruction of the electrical circuits to reduce the loop areas generating magnetic fields. If any of the above outlined relative simple solutions do not provide the desired results, it might be necessary to install structural magnetic shielding made of various metal types some of which might be very expensive such as μ-metal, co-netic and other metals with great permeability.

Before the actual building of structural magnetic shielding starts, one needs to determinate the magnitude of the magnetic field exposure problem. It can be performed by actual field measurements, or if the electrical utilities are still unavailable or none operational it entails modeling the utilities and solving electro-magnetic equations[3], all of which enables the prediction of magnetic flux contours with and without magnetic shielding buriers.

To determine the best engineering solutions for structural shielding, one needs to employ very complex analysis. The analog approach is impractical because of the uniqueness of each problem and the associated difficult level. Also, the digital approach is still too difficult for the most of today's personal computer systems. Subsequently, the calculation is less accurate and time-consuming. It can take from tens to hundreds of man-hours to prepare models and to solve a single problem.

Strategies and Stages in Planning Magnetic Field Reduction

To first stage in planning the shielding effectiveness required for magnetic field reduction is to obtain the overall worst-case intensity of the ELF magnetic flux in locations where people may reside. This can be doe using two methods – the analytical method (also good for the design stage), and/or field measurements when construction is completed and populated). These two strategies to determine the magnetic field is summarized as follows:

1. **Analytical Prediction:** given the geometry of the structure and the current sources producing the ELF magnetic fields, including the geometry of these magnetic sources, the integrated cumulated field levels in every relevant place (places where there may be people residing) can be predicted.
2. **Measurements:** conducting field level measurements where people work and reside could provide a general picture of the magnetic field including evaluation of maximal loads in maximal power consumption, hence, worst-case magnetic flux contours.
   The decision for the need for magnetic shielding is best taken based on results obtained by strategy 2 – measurements. However, the structural shielding design must use strategy 1 – analytical prediction. It facilitates cost-effective shielding design, placement, barrier dimensions, shielding materials, and installation methods. It enables theoretical examination of the shielding effectiveness elsewhere in the facility. If shielding is insufficient based on phase I of the analytical design effort, it is modified by reselecting of:
   - shielding materials;
   - barrier dimensions;
   - placement

   Phase II of the shielding design commences to obtain the shielding effectiveness of the modified design. Phase II might yield an insufficient engineering solution and go into Phase III, etc., until a best engineering solution is obtained.

Availability of Analytical Methods

The analysis methods available for determining the electromagnetic field levels are many and vary in complexity, accuracy and easiness of pre and post processing. Some of the most known numerical methods are:

- Finite Difference Methods
- Variation Methods
- The Methods of Moments (MoM)
- Finite Element Method[4,5]
- Transmission-line-matrix Method
- Monte Carlo Methods
- Method of Lines

The **Finite Difference Method** requires the performance of the following steps:

1. Divide the region of interest into a grid of nodes (common rectangular, skew, triangular or circular type of grids)
2. Approximate the given differential equation by finite difference. (To relate the dependent variable at a point in the region of interest to its values at the neighboring points)
3. Solve the difference equations subject to the boundary and initial condition.

This method is very intuitive and fairly easy for numeric realization. It is not clear which grid is preferable in every case. A problem arises in cases where the point for which the value is calculated is not exactly on the grid. The ease or programming "balances" in extensive calculation time.
For simple enough problems, when one arrives at a collection of equations (both integral and differential), the problem can be solved by finding functions that give the integrals a minimum value[6]. Problems of this type are called *variational problems.*
This method is limited to theoretical problems, requires a high level of mathematics and seldom used to solve practical problems.

The **MoM** requires the performance of the following steps:

1. Derivation of the appropriate integral equation.
2. Conversion this set of equation into a matrix equation (the process called discretization that is based on using basic functions (kernels) and weighting (or testing) functions.
3. Evaluation of the matrix elements.
4. Solving the matrix equation and obtaining the parameters of interest.

This is a sturdy method that turns problems containing integral equations into matrix equations (of course, accurate calculation requires an extensive calculation power and a large amount of memory). Many of today's solutions are based on this method.

The **Finite Element Method** comes from the area of materials strengthening and has been used for calculating electromagnetic fields since the 1970s.

The **Finite Element Method** requires the performance of the following steps:

1. Discretizing the solution region into a finite number of subregions (called elements). These elements may be one, two or three-dimensional.
2. Deriving governing equations for a typical element.
3. Assembling all elements in the solution region.
4. Solving the system of equations obtained.

Among the method's advantages, it can be used with almost no changes for different areas of problems. The most accepted areas are mechanics and electricity, but lately it has also been used for image processing. It is difficult to match an appropriate element for every problem, and the method required extensive calculation time.

Other methods are more theoretical or methods suitable for solving specific problem types not related to our goals.

It is customary to imagine shielding as an infinite surface or a closed sphere. Only in these cases may accurate analytic methods be obtained. All analysis of other models is semi- empirical. The accuracy of the results decreases as we increase the practical details of the shielding.
The analytical solution for calculating shielding cannot take the form of a method as we must solve a different problem each time (this includes building a new model with range, limit conditions, sources, new geometry etc.).

Solving the problem using a computer somewhat reduces the complexity of the mathematical solution, but adds the problem of a model that is very resource consuming for most existing computers. The problem lies in both memory size and calculation power.

As a result, any calculation (construction of a mathematical or digital model, inputting the problem's data, calculation and examination of probability of the received results) requires hundreds of man hours and dozens of computer hours. It is clear that under these limitations it is impossible to perform a large number of attempts (analysis phases as described above) in order to reach an appropriate solution. The desire to examine a single problem for several shielding solutions, in order to select the best one, often seems as "mission impossible".

Practical Methods Combined with Analysis

The problem we face is: to calculate the electromagnetic field in defined areas generated by known sources with the presence of a given specific shielding burrier design to reduce the EM fields.
There are no analytical systems and algorithms that we know for writing a program that enables inputting of entry data (such as range, sources, shielding location, shielding materials etc.), followed by the required targeted field level in a certain area, let one or more parameters acting as the unknown ones and perform calculations (assuming convergence) that solve the unknown parameters.
Presently, all we can do is as follows: place shielding (using previous practical experience) in places that seems most logical using materials that were suitable in similar cases, calculating the field levels in questioned areas, comparing the results to the values we aim for, and if the results are unsatisfactory, slightly change the shielding size, geometry, location and/or materials.
The form of shielding accepted today is a rectangular plate, inserted between the source and the area in which field level should be reduced. Magnetic shielding includes 3 different effects: reflection, absorption, and fringe radiation (that usually reduces the shielding effectiveness). The theoretical basis for high frequency (radiofrequency) shielding for distant EM field is relatively well developed and has accelerated in recent years. In the case of ELF fields and for an adjacent source – these theories cannot be straightforward adopted. In the case of high impedance, the source if electric field is dominant; in the case of low impedance – the source is a magnetic field is dominant. In this case a separate approach for shielding against the magnetic part and from the electric part of the EM field is the correct approach.
An alternating electromagnetic field, originating from 50 Hz electrical facilities is an "adjacent source" field. The characteristic impedance of the magnetic component is very low while the characteristic impedance of the electric component is high. Therefore, currents in low voltage electric facilities generate dominant magnetic field components; the associated electric field component is negligible. A source of a solely magnetic field does not cause electromagnetic waves. Therefore a 50Hz magnetic field is quasi- static in nature. This field is "static" because it acts as a static field, but is called "quasi" as it is not completely static due its source (alternating field).

Two phenomena exist in magnetic shielding for a quasi- static field – static shielding and dynamic shielding.
Static shielding is independent of the field frequency and works in the same way for both the earth's static magnetic field and for sources of 50 Hz or more. The shielding quality depends on the material's relative permeability (μ) and its geometrical dimensions. The higher the permeability (μ) and the thicker the plate, the more effective is the shielding.
Dynamic shielding depends on the frequency of the primary field and the shielding material's electric conductivity. At 50 Hz the effect is well pronounced. The phenomenon is based on Foucault currents (eddy currents) and Lentz laws. The higher the conductivity and the higher the frequency – the more effective is the shielding.
There are no materials that combine both phenomena well, and so it is customary to use two plates or more for constructing shielding to reduce quasi- static magnetic field. In many cases shielding construction is attempted using no analysis, based only on instinct, experience or luck. In many cases this might not only not decrease field levels, but even raise its intensity in undesirable locations.
The principle of magnetic shielding is based on two phenomena of decrease of the electromagnetic field intensity in different materials: absorption of a magnetic field (absorption loss) and reflection of the field back to the source (reflection loss).

The above discussion is highlighted with a real problem description and shielding planning demonstration.

The field level in an area adjacent to a transformation substation inside a residential building is analyzed.

The area of interest is only the residential area as shown in Figure 1. Analysis show that the level is higher than desirable and shielding must be constructed.
A simplistic calculation with substitution of a plate of finite dimensions with an infinite surface does not give correct results. In this case substitution of the plate creates distortions in the plate ends, and as a result the field level would not only decrease, but may increase. It is clear that in this case the attempt to build magnetic shielding without proper planning might causes more damage than benefit.
Three dimensional shielding against the magnetic field from the transformation substation could be done by covering parts of the walls, ceiling and floor adjacent to the location of the transformers. Walls, ceiling and floor covering is obtained by using special materials that decrease the magnetic flux density caused by the transformer's secondary terminal (low voltage) phase lines and neutral line loops.

Field sources are often having a complex geometry which makes it analysis difficult to solve. It is much more difficult to solve the problem of the shielding effect on the magnetic source flux lines as it is in our example. It is important to note that for our specific problem, the source is 3 currents in the same frequency and different phases, and at every point the field vector is a complex vector value (as are all the matrix analysis).
"Absorption" of a static magnetic field can be done using magnetic materials with a high magnetic permeability. Plates of this material are used for construction of static shielding. The efficiency of the static shielding depends on several factors, as follows:

- Relative magnetic permeability (μ_r) of the plate material.
- Plate width.
- Angle between the direction of the magnetic flux vector and the plane of the plate.

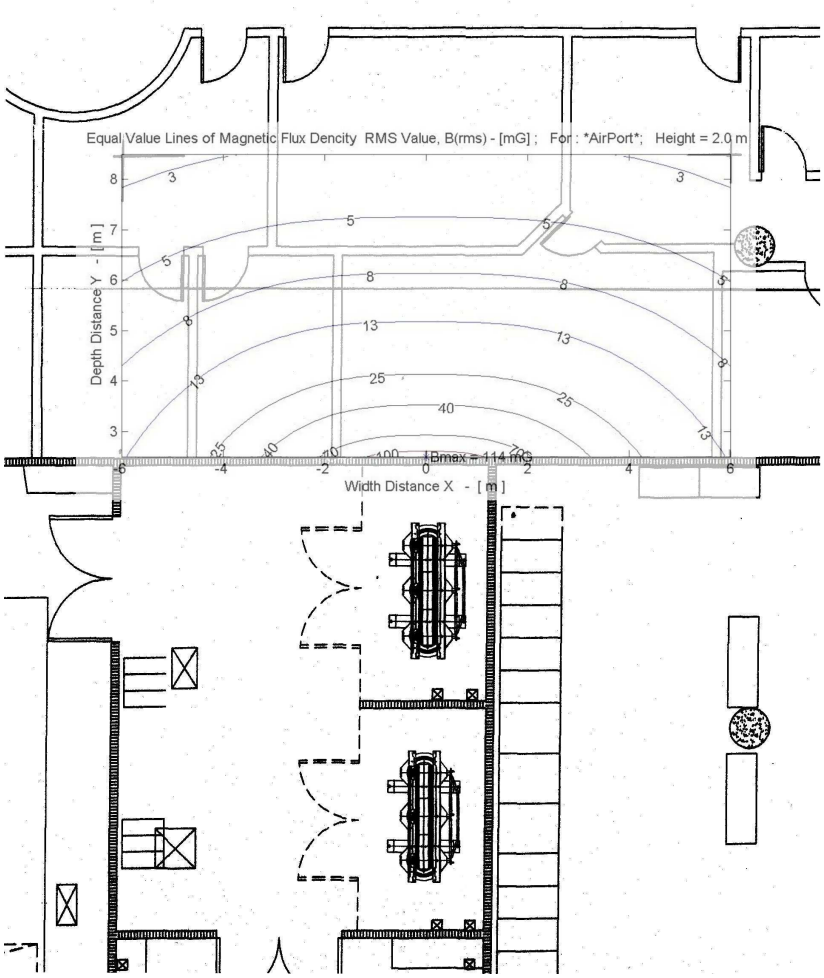

Figure 1: Primary Magnetic Flux Analysis near an Internal Transformation Station

There is no "reflection" phenomenon of a static magnetic field. The reflection phenomenon exists only in an alternating electromagnetic field. The flux of an alternating magnetic field that permeates plates made of a material with electric conductivity creates induced currents known as eddy currents. These currents create a secondary magnetic flux at a direction opposed to the direction of the original magnetic field flux and thus reduce the magnetic field flux. This is known as Lenz's law.

Plates made of metals with high electric conductivity are used for building dynamic shielding. The efficiency of the dynamic shielding depends on several factors, as follows:

- The plate material's electric conductivity σ.
- Frequency of the alternating magnetic field.
- Plate width (up to a certain width).
- Angle between the direction of the magnetic flux vector and the plate's perpendicular.

The efficiency of static and dynamic shielding, as a rule, is a different and non linear dependence on the parameters outlined above. The main difference, in terms of shielding efficiency, is in the inverse effect on efficiency of the incident angle of the magnetic flux lines on the shielding plate:

- When the direction of the magnetic flux vector is closer to that of the shielding plate's normal direction, the efficiency of dynamic shielding increases while that of static shielding decreases.
- When the direction of the magnetic flux vector is closer to that of the tangent to the shielding plate, the efficiency of dynamic shielding decreases while that of static shielding increases.

As the magnetic flux adjacent to electric facilities is not uniform in size and direction, the highest efficiency in reducing the magnetic flux density in the entire shielded space is accomplished by a combination of static and dynamic shielding.

New Algorithm for Shielding Analysis

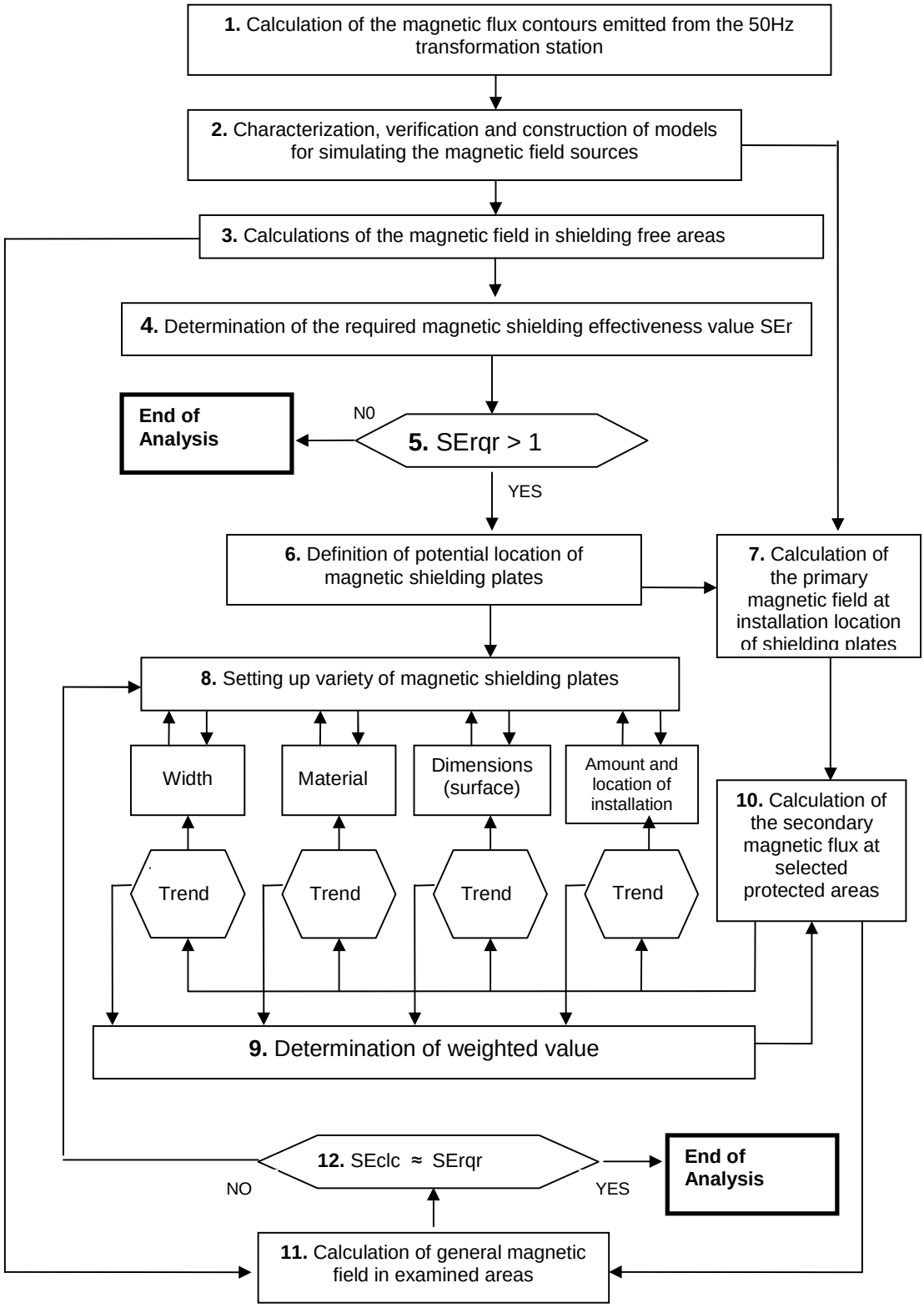

The first step is the calculation of the magnetic flux density in the entire space, especially the area we wish to protect and the apace in which we wish to introduce the shielding barrier. Analysis of the **primary field** is done using the laws of Faraday and Ampere. This analysis affords a comprehensive picture of the entire area, and a decision on whether shielding is in fact necessary or can be substituted by simpler less-costly measures, such as relocation of power utilities or personnel.
There are many analysis methods, most popular of which is the finite elements method discussed above. Using this method, the shielding burrier is divided into subcomponents so that lack of uniformity can be neglected and the field is perceived as uniform. This is the second step of the analysis.
In the third step, each point in the shielded area is analyzed as a sum of the effects of each shielding element. This is the **secondary field** reduced from the primary field by the shielding.
Now, as a picture of the effect of the shielding is formed, one can decided on the continuation (or termination) of the process.
Using this method there is no need for difficult neither complex analysis for the entire problem, only for the shielding effect on the secondary field intensity in the examined area. This analysis method greatly reduces analysis complexity, gives accurate results and reduces calculation time by an order of magnitude. The finite elements method enables to perform sufficient iterations in order to obtain the best results among several different shielding barriers from different materials and dimensions and compare the outcome results to select the best solution. The time required for the entire process is equal to the time it would have taken to calculate a single iteration using one of the old methods.

The course of the analysis is presented in the algorithm flow chart.

1. Analysis of 50 Hz magnetic field contours caused by the transformation substation – step 1 of this project is defining the problem and possible solution subset.
2. Construction, verification and determination of models for simulating the magnetic field source. These models can be used to calculate magnetic flux densities in all areas adjacent to the field source.
3. Analysis of the magnetic field in the areas that are examined without any shielding. Analysis is carried out using a computer program based on integrals of complex magnetic moment methods.
4. Determination of the required magnetic shielding effectiveness value SErqr. This action is taken and is presented in table 3 of step 1 of the project (reference 2). The SErqr value is determined by comparing the results of the analysis to the exposure threshold recommended by the Ministry of the Environment or other requirements of the client, using the following formula:

   $$SErqr = Bmax / Brcm$$

   Where:
   - Bmax – the maximal value of the magnetic flux density analyzed in the examined area based on a model of magnetic field source simulation at its typical current, as coordinated with the client.
   - Brcm – the value of magnetic flux density coordinated with and determined by the client based on recommendations set by the Ministry of the Environment for general public magnetic field exposure at 50/60 Hz.
5. Existence of a condition SErqr > 1 (YES) causes the continuation of the project for design and magnetic shielding burrier required, while the (NO) response ends the analysis and the project.
6. Selection of potential locations for installation of magnetic shielding plates. As a rule, it is accepted to cover walls and/or ceilings and/or floors within the area in which the magnetic field source is located. In transformation substation with two transformers, these areas are: the TR01 and TR02 transformer cells and/or the entire transformer room.

The possibility to install shielding around a whole transformer cell is not feasible, as complete and continuous shielding in the cell might hinder the maintenance and natural ventilation of the transformers. Opening ventilation hatches and/or installation of forced ventilation might reduce shielding effectiveness to below requirements.
The feasible shielding practice is to cover all or part of the walls, ceiling and floor of the transformer room.

7. Analysis of the magnetic field in some locations of the shielding plates. As an auxiliary action for calculating shielding effectiveness, the complex vector of the magnetic flux density in the walls, ceiling and floor of the transformer room is analyzed, meaning – primary magnetic field with no shielding, similar to the primary magnetic field in the examined areas (step 3 above).
8. Setting up variety of magnetic shielding plates. This step determines shielding parameters as follows:
   A. Amount and location of shielding plate installation, static and dynamic separately.
   B. Plate size (surface area) for static and dynamic shielding separately.
   C. Static shielding plate's material – magnetic permeability value; dynamic shielding plate's material – electric conductivity value.
   D. Plate width for static and dynamic shielding separately.
9. Determination of weighted value. In this step we prepare the parameter matrix for static and dynamic shielding for the analysis following in step 10.
10. Analysis of the secondary magnetic field created by the shielding plates in the examined area. The analysis is carried out by a computer program based on a Numerical finite element method.

The starting data for analysis are the results of the primary magnetic field analysis described in step 7 above and the data of the shielding plates described in step 8.
At the beginning of the analysis the shielding plate areas are divided into elements in order to reach a state wherein in most separate elements there is a uniform magnetic field incident the single element. The data of the complex vector of the magnetic flux density, $\vec{\mathbf{B}}$ that permeates through the shielding area element, we receive from the primary magnetic field analysis (7).
The elements of the high magnetic permeability shielding material are forced to become magnetic moments under the effect of the primary magnetic field. The magnetic flux density Bmag in the area of these elements increases according to the formula:

$$Bmag = \mu_r \times B_0$$

Where:

B_0 – primary magnetic flux density

μ_r – relative magnetic permeability through the static shielding material.

The main direction of the moment vectors from the static shielding plates is tangential to the plane of the plates. Magnetic moments of the static shielding material elements emanate a secondary magnetic field, and thus affect the overall magnetic flux density in the examined areas. Alternating magnetic flux creates eddy currents of elements in the dynamic shielding material with the high electric conductivity. These currents create a secondary magnetic field. The direction of the secondary magnetic field flux is opposed to the direction of the primary magnetic flux, known in physics as Lenz's law. Eddy currents in the dynamic shielding elements are considered to be magnetic moments. The main direction of the moment vectors from the dynamic shielding plates are normal to the plane of the plates. These moments emanate a secondary magnetic field. And thus affect overall magnetic flux density in the examined areas.

11. Analysis of overall magnetic field in the examined areas. The analysis is carried out using a computer program based on a complex vector superposition method.
12. The realization of the SEclc ≈ SErqr (YES) condition ends the analysis, while (NO) causes the continuation of the analysis in a loop including stages 8 – 11. SEclc – the analyzed value of the shielding effectiveness.

Back to the practical example – an analysis is performed based on this algorithm. The following results were obtained:
Primary flux density analysis (without the shielding plates):

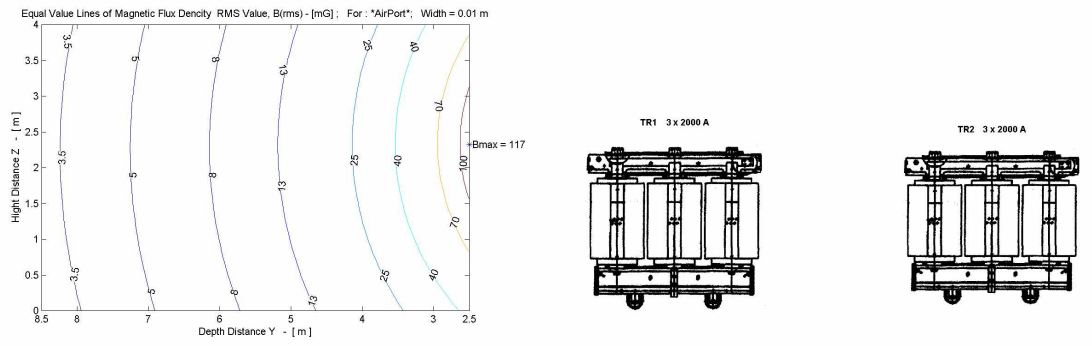

Based on the results tt was decided to shield only the transformer adjacent to the residential area.

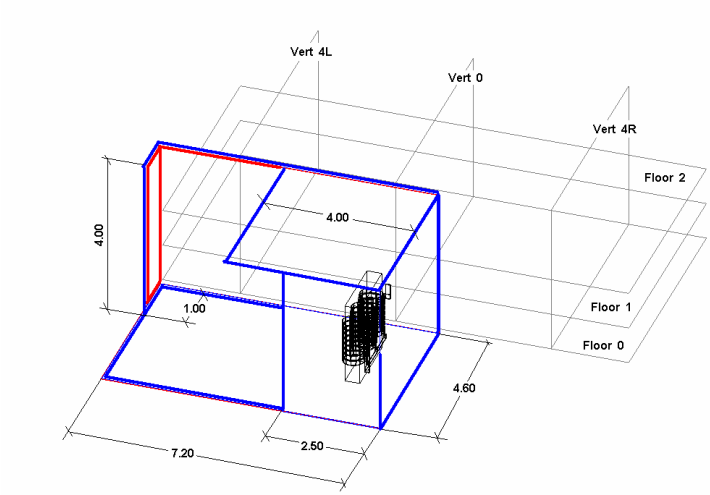

Analysis show that the field level decreased to the following levels:

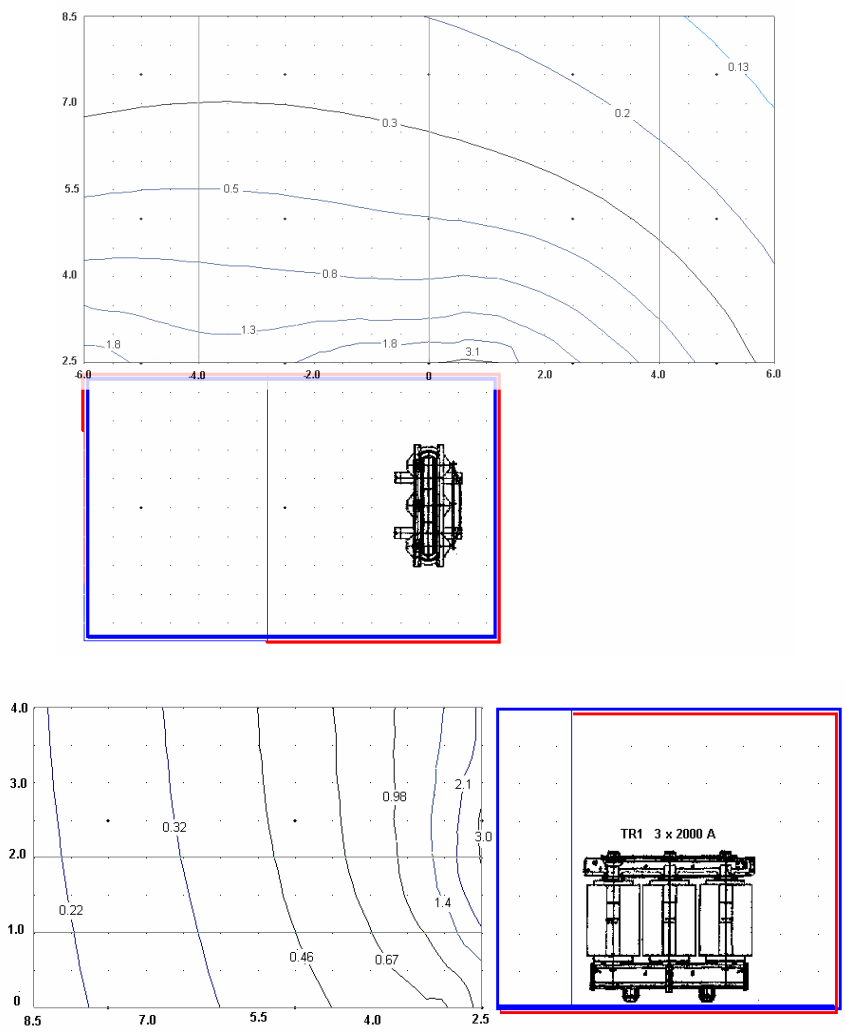

Conclusions

The question of potential adverse effects due to ELF magnetic fields exposure has been discussed and hypnotized in the past years. The potential magnetic field adverse effects on the human body are still under ongoing studies; nevertheless, the adoption of the precautionary principal by many countries and environmental conservation offices owes to minimize personnel exposure[2]. Many countries have already established regulations and limitations for the maximal magnetic field allowed at the workplace and residential areas which is much lower than the WHO ICNIRP[1] guidelines. The best situation exists when a building design (both architecture and infrastructure) considers magnetic flux reduction design. In reality, this does not happen often. At best, magnetic field surveys and shielding design (if needed), is the very last stage before construction is completed. In many cases, construction is completed; inhabited and only thereafter magnetic flux reduction is taken care by the building management. This paper describes a multi-stage algorithm for efficient analysis of magnetic flux contours, for optimizing the design of structural magnetic shielding. The multi-stage algorithm enables albeit medium-power computer system to calculate the effect of shielding materials with a given geometry, in a reasonable timeframe without compromising precision. The outcome results are a large number of electrical utility models and the best cost-effective shielding materials and geometries for ELF magnetic flux reduction per Authority regulations and requirements.

References

[1] "Guidelines on Limits of Exposure to Electromagnetic Fields in the Frequency Range from 1Hz to 300GHz", ICNIRP, 1998
[2] Josef Pekar and M. Netzer, "Graphical Presentation of 50/60 Hz Magnetic Field Contours as an Engineering Tool for Minimizing ELF Fields", Kos Workshop, 2004
[3] Edward M. Purcell, "Electricity and Magnetism", Berkeley Physics Course –Volume 2, McGraw-Hill Book Company, 1970
[4] K.H. Huebner and E.A. Thornton, "*The Finite Element Method for Engineers*", New York: John Wiley and Sons, 1982
[5] P.P. Silvester and R.L. Ferrari, "Finite Elements for Electrical Engineers", Cambridge University Press, 3rd ed., 1996
[6] N. Morita et al., "Integral Equation Methods for Electromagnetics", Boston, MA, Artech House, 1990

A NEW TECHNIQUE FOR REDUCING EXTREMELY LOW FREQUENCY MAGNETIC FIELD EMISSIONS AFFECTING LARGE BUILDING STRUCTURES

[(1)]E. SALINAS, [(2)]J. ATALAYA, [(2)]Y. HAMNERIUS, [(3)]J. SOLANO, [(3)]D. GONZALES, [(3)]C. CONTRERAS, [(3)]C. CHINCHAY, [(3)]M. A. SUMARI, [(1)]S. DIMITRIOU and [(4)]M. REZINKINA

[(1)] CENTRE OF PHYSICAL ELECTRONICS AND MATERIALS, (PEM) FACULTY OF ENGINEERING, SCIENCE AND THE BUILT ENVIRONMENT, LONDON SOUTH BANK UNIVERSITY, 103 BOROUGH ROAD, LONDON SE1 0AA, UK

[(2)] CHALMERS UNIVERSITY OF TECHNOLOGY, GOTHENBURG, SWEDEN

[(3)] UNIVERSIDAD NACIONAL DE INGENIERÍA, LIMA, PERU

[(4)] NATIONAL POLYTECHNIC UNIVERSITY, KIEV, UKRAINE

Abstract

When large structures such as residential compounds or public buildings are under the influence of extremely low frequency (ELF) magnetic fields, such as the one generated by a system of railways fed by 16 ⅔ Hz, standard methods of designing shielding structures by numerical methods usually fail. The latter can be explained by the difficulty posed in the computing process by the large aspect ratios involved due to thin layers of metal (a few millimetres or centimetres) in contrast to the large dimensions of the affected structure (several tens of meters). In some cases one has to utilize special approximations such as surface conductivity, which are not easy to handle when the designed shielding structure is clearly 3-dimensional. Other alternatives such as experimentation *in-situ* are very costly. Here, a new technique is presented of mitigating the field by using 3-dimensional propagation of induced currents optimizing the field reduction factors and minimizing the cost of shielding material. The particular designing method is a hybrid of numerical simulations combined with lab experimentation using scaled models of the large structure. The method is rather cost-effective and flexible as various designs can be easily tested. Results are presented in the form of magnetic field values, at various locations in the buildings, *before* and *after* this mitigation technique is applied.

Introduction

There are two major sources of extremely low frequency magnetic fields (ELF/MF) which are able to affect large scale areas in their extended vicinity (i.e. tens or in some cases even hundreds of metres). One of them is overhead power lines and the other is AC powered railway systems. Mitigation techniques for the first source have been extensively studied for more than two decades and there are a manifold of references in the literature. On the other hand, although some studies related to magnetic fields originated in rail systems have been published [1-6], there is a lack of literature on mitigation techniques of magnetic fields originated from AC railway sources. In this investigation, the magnetic field produced by a system of trains operating at 16 ⅔ Hz (~16.67 Hz) is analyzed and mitigated using a combined technique, i.e. designing a structure able to redirect induced currents improving their effectiveness and performing cost-effective experimental settings at reduced scale. The present study was made before starting the construction of the

buildings. Fig. 1 shows the location of the railway system in the central area of the city of Stockholm. The configuration of the buildings is also shown, which is "L"-shaped formed by two type of buildings, namely: "A+B" and "C" or correspondingly *Frontal and Lateral* the first notation is from the architectural map while the second notation is related to the ways the trains pass with respect to the buildings. Two reasons motivated this study. Firstly, there is a growing concern on suspected harmful effects of ELF/MF on human health. Although several epidemiological studies suggest that long-term exposure to fields in excess of 0.2-1 μT (depending on the study) can explain some bias in the statistics of some deceases. The issue is still not resolved at the moment and there is no clear indication that there will be a conclusive answer in a near future. Some countries are adopting some policies upon limits in residential and public buildings, as low as 1 μT, while others subscribe to ICNIRP recommendations of 100 μT for 50 Hz, limit based on effects of induced currents in the human body [7], [8]. Secondly, this type of field is able to produce interference on electronic equipment driven by electron beams such as TV and computer screens, oscilloscopes and electron microscopes. This interference becomes evident at field values over 0.5-1 μT, depending on the device. For the present study, we have chosen to aim at averaged (per floor) after-mitigation field values not exceeding 0.5 μT while trying to keep peak values at the sub-microtesla level. The feasibility of achieving these values will be explained in the next sections.

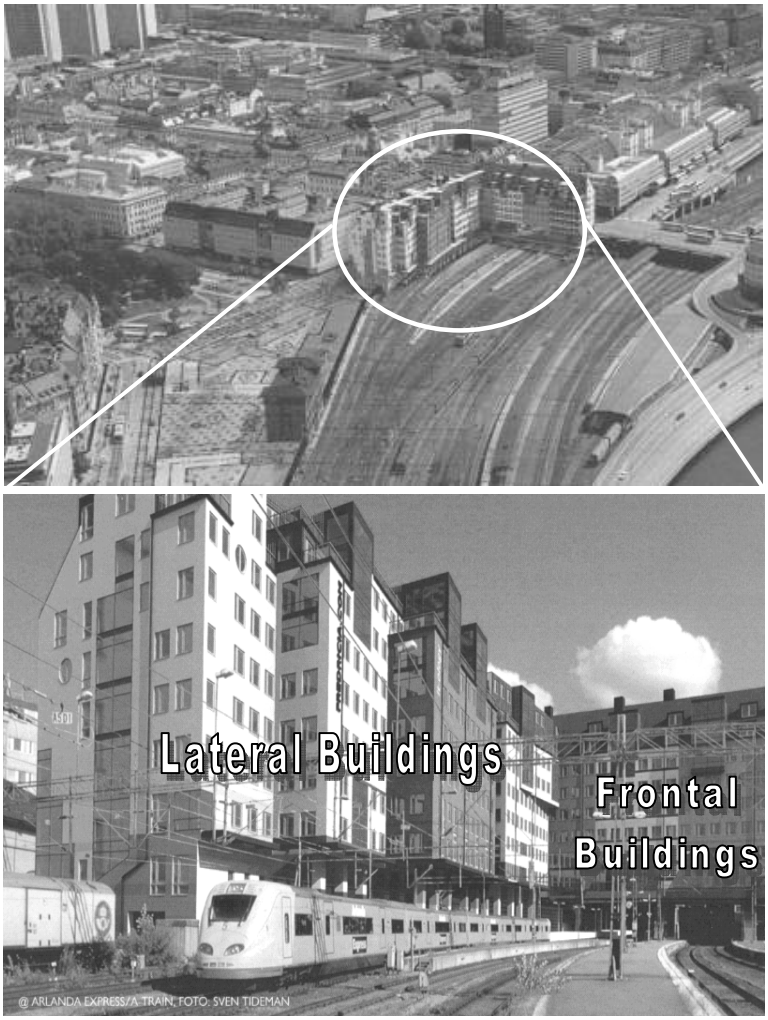

Fig. 1 Location of the buildings in the central part of the city of Stockholm; the pictures are virtual as the study was performed before the buildings were constructed. The lower picture shows the way the trains would pass with respect to the buildings.

The Sources of the Field

Power is supplied to the train system by the overhead wires of 15 kV carrying an average current of 200A (rms). The current's return path follows the rail track (Fig. 2). In fact, the amount of traction current depends on the power consumption of the engine needed to accelerate these trains; which reverts in a complex time-variability. The magnetic field rms values against time are shown in Fig. 3. The measurements shown were taken during 1-hour at a high traffic time. In spite of the short duration of the pulses, these are still rather long compared with the period corresponding to 16.67 Hz. Therefore, this study is concern only with the influence of the periodic signal. The number of trains considered is 10. Two of them, the closest to the lateral buildings, will stop before reaching the frontal buildings. The other eight trains will either not stop or stop for a few minutes and then continue to the next station crossing the frontal buildings.

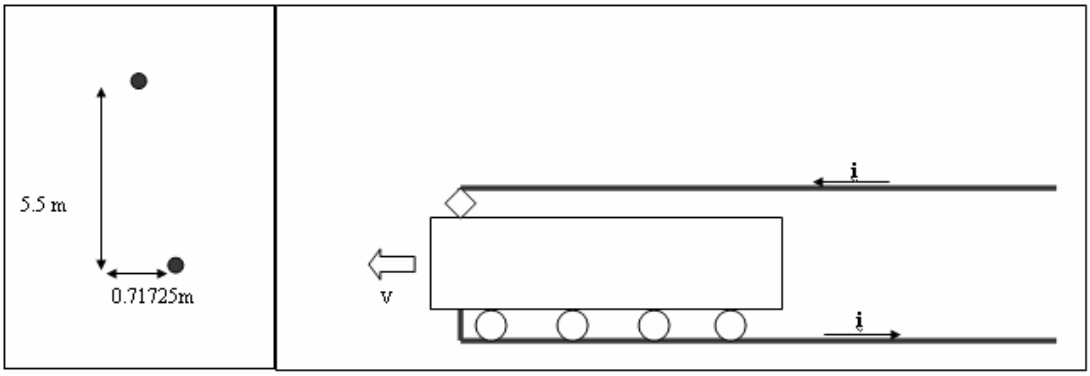

Fig. 2 A simplified diagram of the source of magnetic field. The train is powered by an overhead wire carrying an average current of 200 A. The return path is by one of the rail tracks.

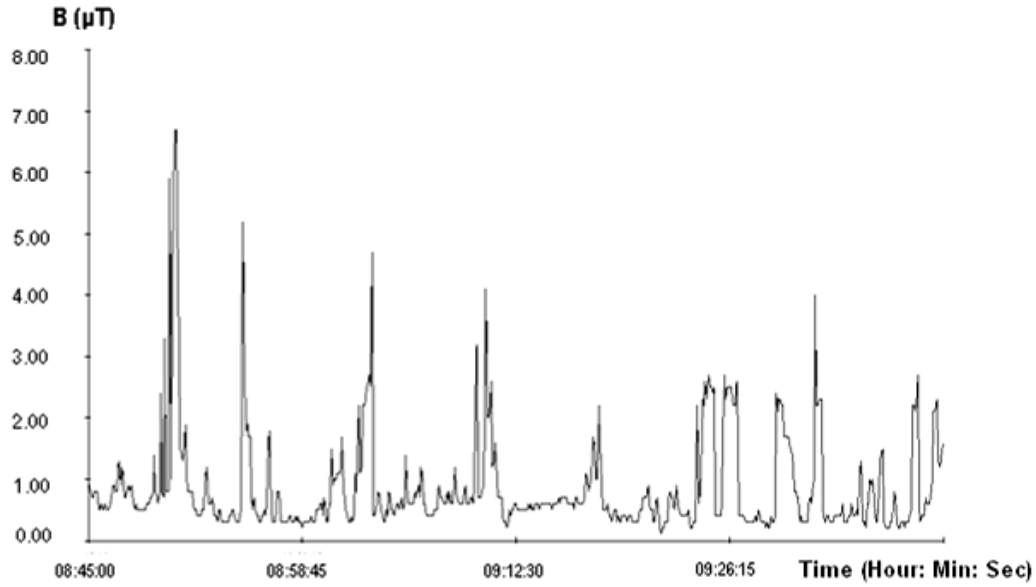

Fig.3 Time variability of the magnetic field. The values were taken at the nearest floor to the rails, near the intersection of the lateral buildings with the frontal buildings. Although the short duration of the pulses; these are still rather long compared with the period of the feeding current

The Shielding Challenges

The dimensions of the building are, for the lateral buildings: (20-30)m x 100m; and for the frontal buildings:18mx65m. The height of both buildings is 34 m. Traditional methods of mitigating magnetic fields suggest placing a metallic plate (shield) between the source of magnetic fields and the affected area. The most commonly used materials for the shield are steel (ferromagnetic), or aluminium (pure conductive). Because of the large dimensions of the building, iron would be excessively heavy, thus aluminium seems to be the obvious choice. However, when an aluminium shield is applied to the **frontal buildings**, some issues arise. The nearest floor (5^{th} floor) to the railway track has an average distance of 1 m to the upper cable of the feeding source; the extreme proximity of the cable poses a challenge to the shielding properties, for most of the eddy currents will be behaving as if they were induced by a homopolar (single cable) source. Fig. 4 shows the similarity of the eddy current pattern on a shield placed on the floor in close proximity to the upper cable of the railway dipole and a single cable in the same location. In the same figure one can also observe that eddy currents try to generate a cancellation field to the source that originated the effect (by Faraday and Lenz laws) with a concentration in the middle of the plate. At the same time they also go towards the edges as they try to reach for a return path. Thus, the result is that an aluminium plate *alone* would not be very effective shield when a train is passing through just under and in close proximity to the shield. The simulations were performed using 3d software Opera and its solver ELEKTRA [9].

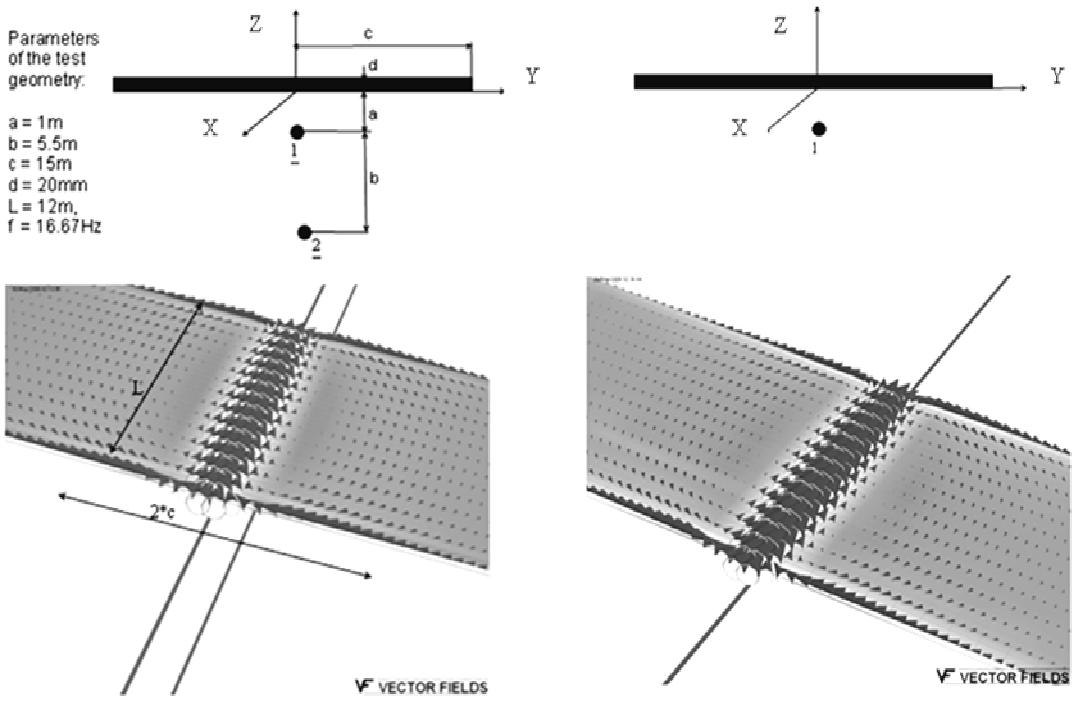

Fig. 4 Comparison between a railway feeding-dipole and a homopolar source; both sources behave similarly in the proximity of an aluminium conducting plate.

A proposed solution to this issue is to redirect the induced currents in a spatial configuration such that the returning paths will become useful to mitigate the field inside the enclosed area. This can be achieved by conductive ribbons joining two plates. The upper plate is used as part of the currents' returning path, thus it can be thinner than the bottom plate (Fig. 5). In some designs the upper plate or even both plates can be replaced by a set of ribbons providing further cost reduction. Yet, as different shielding configurations will yield different results, balance between material cost and mitigation factors has to be considered.

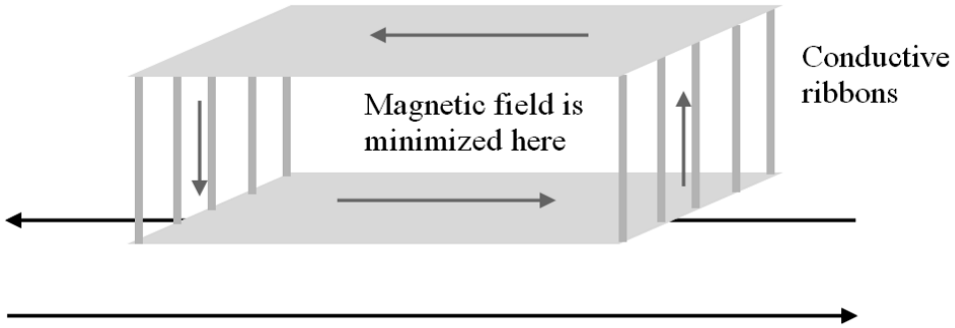

Fig. 5 extended shielding structure that redirects the induced currents creating effective current loops resulting in a minimization the field inside the enclosed region. In some designs, the upper conductive plate (or even both plates) can be replaced by ribbons resulting in further cost reduction.

Considering the **lateral buildings** we note that the sources pass alongside the buildings at different distances, some even under the building, such as the one shown in Fig.1. An aluminium shield alone, even if thick relatively to the skin depth (δ), will neither be optimal nor cost effective. The solution is a combination of optimally positioned system of loops and shields. Because the lateral region is 100m long with a cross-section area 20m(width)x34m(height), such a section can be modelled approximately assuming YZ symmetry (fields do not change in the X direction). Such a simplification can be considered accurate for the central part of the lateral buildings, but it does not model its ends, which are in fact interconnected. From the latter, is noticed that the total eddy current (at the cross section) must be zero. This condition comes from the fact that the eddy currents must find a return path when they meet the physical ends of the longitudinal extension. After performing numerical 2d simulations for the cross section (see Fig. 6), it was found that the results depend on the kind of boundary condition assumed (the total domain boundary is far from the region of interest).

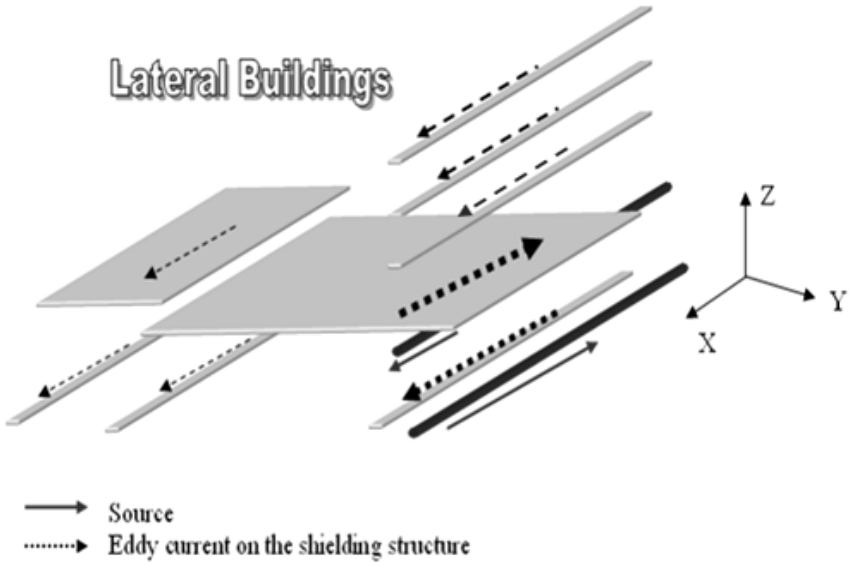

Fig. 6 The lateral shielding structure is shown which can be modelled using YZ symmetry (the field does not depend on the x coordinate). The eddy currents (dotted arrows) on the shielding structure are shown as well as the source (continuous arrows). This simplification can be considered accurate for the central part of the lateral buildings, but it does not model the endings.

It is observed that the boundary condition: $A_x = 0$ at $\partial\,\Omega$ (A_x is the x- component of the magnetic vector potential and Ω is the problem domain) allows a net eddy current flowing at the shielding structure. If the total domain boundary $\partial\,\Omega$ is far from the region of interest, we can assume the magnetic field intensity **H** = **0** at $\partial\,\Omega$ as the boundary condition. This boundary condition makes the net eddy current be zero because its circulation on $\partial\,\Omega$ is zero. Figure 7 shows 2d numerical results using both boundary conditions; the 2d simulations were performed using the code Femlab 3.1 [10]. A line L was added for comparison reference between the two conditions; this will be plotted later when contrasted with experimental validation.

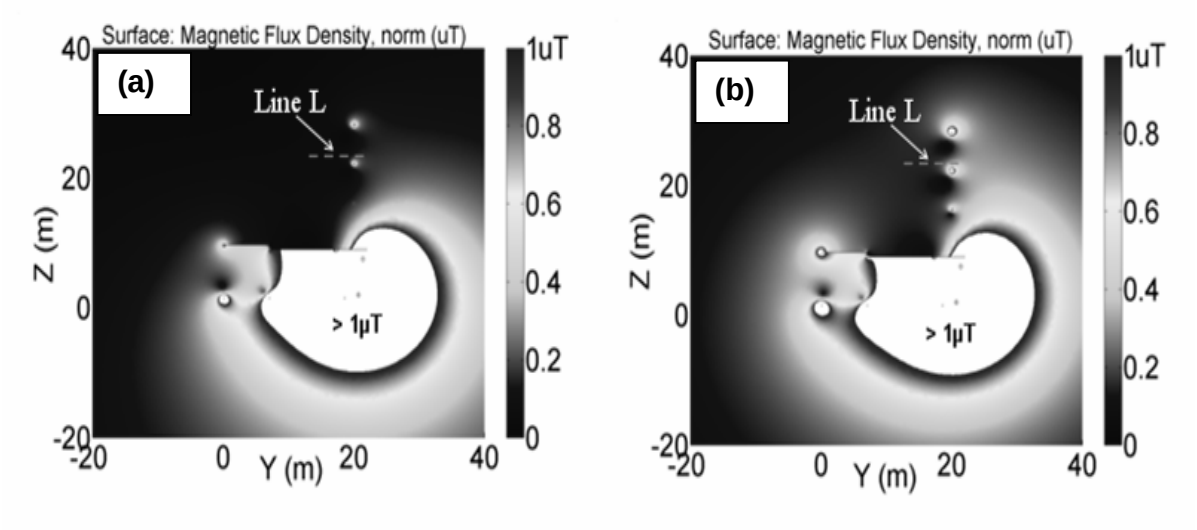

Fig. 7 Numerical results are shown for the two boundary conditions discussed above. In (a) the boundary condition is assumed $A_x = 0$ at $\partial\,\Omega$, while in (b) it was assumed **H** = **0** at $\partial\,\Omega$. The line L is added as comparison reference when contrasted with experimental validation.

Scaling rules

The computation of shielding factors for the frontal structure (which is evidently 3-dimensional) by numerical simulations, is rather complicated as a result of the large aspect ratios involved. Something similar can be said for a fully 3d numerical simulation of the lateral structure, since the 2d- simulations presented can only represent accurately the central region. Here an experimental technique, based on scaling rules, is combined with the suggested 3d structures which are the paths of the induced currents. This technique will make it possible to experiment in a lab with various shielding designs and to predict shielding factors of 3dimensional structures more accurately.

Let the scaling factor between two shielding systems M and M' be k then length, surface and volume scale as $L' = k\,L$; $A' = k^2 A$; $V' = k^3 V$ respectively. A current I is scaled assuming a homogeneous scale-invariant current density J. Then: $J' = J$, $I'/A' = I/A$, and $I'/(k^2 A) = I/A$, therefore: $I' = k^2 I$. Having units of length, the *skin depth* δ scales linearly: $\delta' = k\,\delta$. This expression allows the computation of the scaling rule for the frequency: $(2\mu\pi'\sigma' f')^{-1/2} = k\,(2\sigma\mu\pi f)^{-1/2}$. Assuming scale-invariance and homogeneity of the materials ($\mu = \mu'$, $\sigma = \sigma'$), then the frequency scales as: $f' = (1/k)^2 f$. The application of Ampere law yields the scaling rule for the magnetic field: $B' = k\,B$, i.e. it is linear with respect to scaling. Finally the shielding factors (SF) which are relative comparisons between the magnetic field before and after mitigation become invariant with respect to scaling, i.e. SF' = SF. When applying this method [11], [12] to our study we will adopt a scaling factor k = 1/10. Therefore the frequency for the small system is 1667 Hz. These settings were implemented in a laboratory where the frontal and lateral structures were built and tested independently. Figures 8, 9 and 10 show details of this structure and Fig. 11 shows values obtained, before and after mitigation procedures were applied, for one of the floors (level two stories above the train tracks).

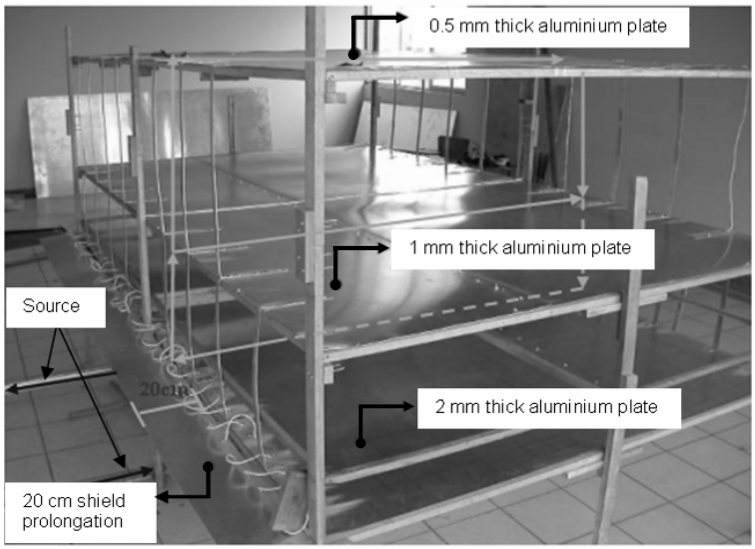

Fig. 8 Scale model ten times reduced (k = 1/10) of the shielding structure for the frontal buildings. The model was built in an electronic laboratory and low power was used to feed the source, which represented the effect of the current loop and the corresponding magnetic field generated by it. Different location of the loop represented different trains.

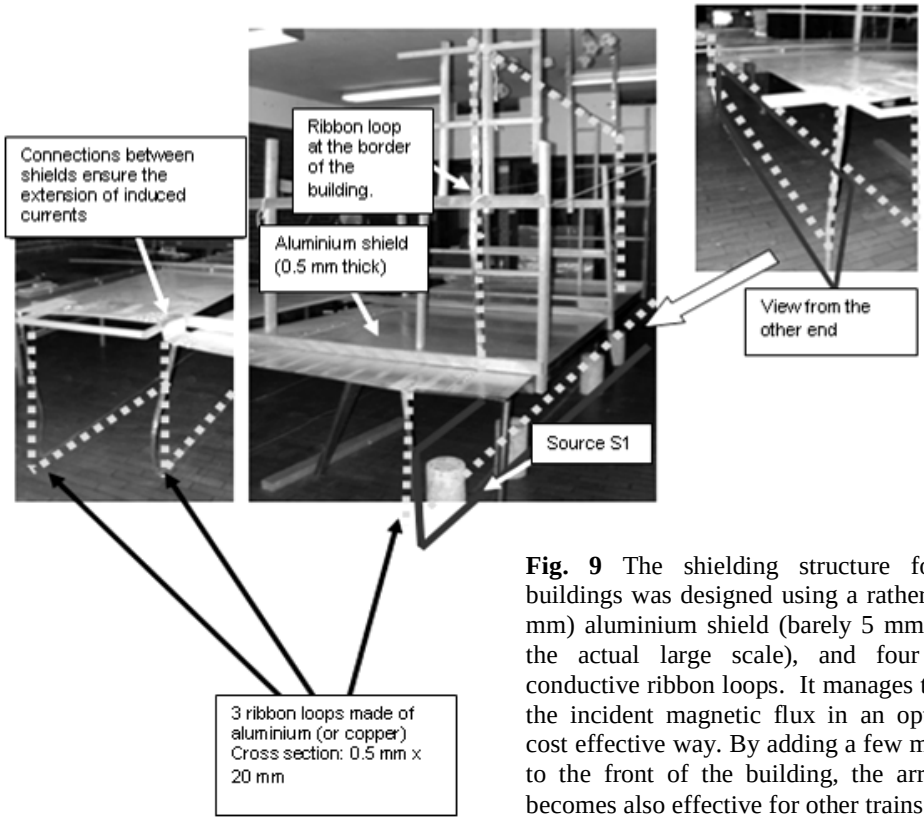

Fig. 9 The shielding structure for lateral buildings was designed using a rather thin (0.5 mm) aluminium shield (barely 5 mm thick for the actual large scale), and four attached conductive ribbon loops. It manages to restrain the incident magnetic flux in an optimal and cost effective way. By adding a few more loops to the front of the building, the arrangement becomes also effective for other trains.

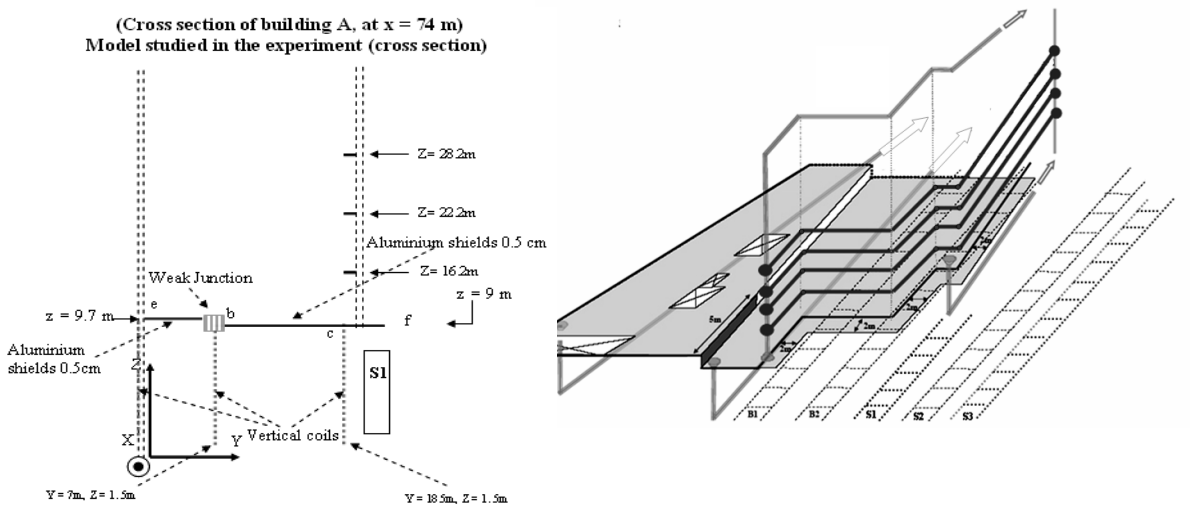

Fig. 10 Cross section (left) and a 3D picture (right) are shown of the final shielding structure for the lateral buildings. The extra loops have been added to consider the influence of any of the 10 trains, namely, B1, B2, S1, S2…or S8.

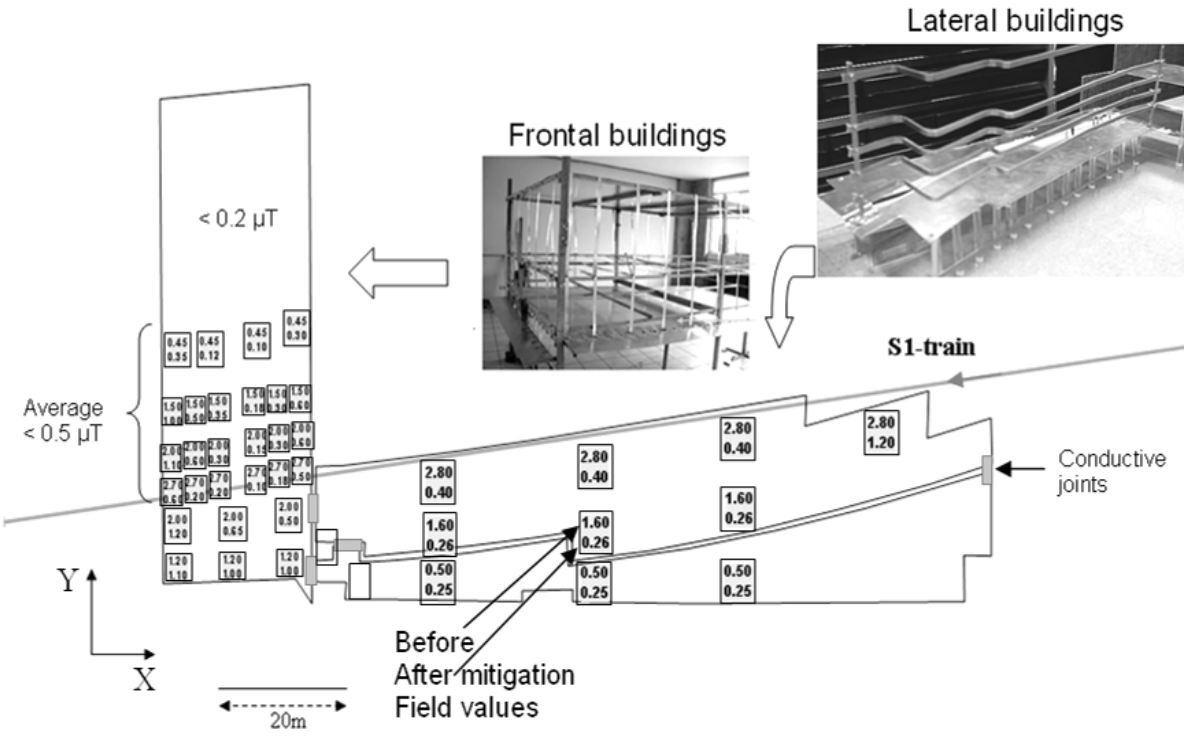

Fig. 11 Before and after mitigation field values are shown for the level located two floors above the train tracks. The resulting average magnetic field levels in each floor were kept below 0.5 μT.

Returning to the shielding issues and numerical modelling, a comparison was made (Fig. 12) between the experimental results and the two results applying two different boundary conditions mentioned in the two-dimensional modelling (see Fig. 7). The line L was taken at z = 22.7 m . The result is that the condition H = 0 fits the obtained data more accurately than $A_x = 0$. This boundary condition is also physically more realistic as it makes the net eddy current be zero; which is demanded in the experiments due to the connecting paths of the shielding loops.

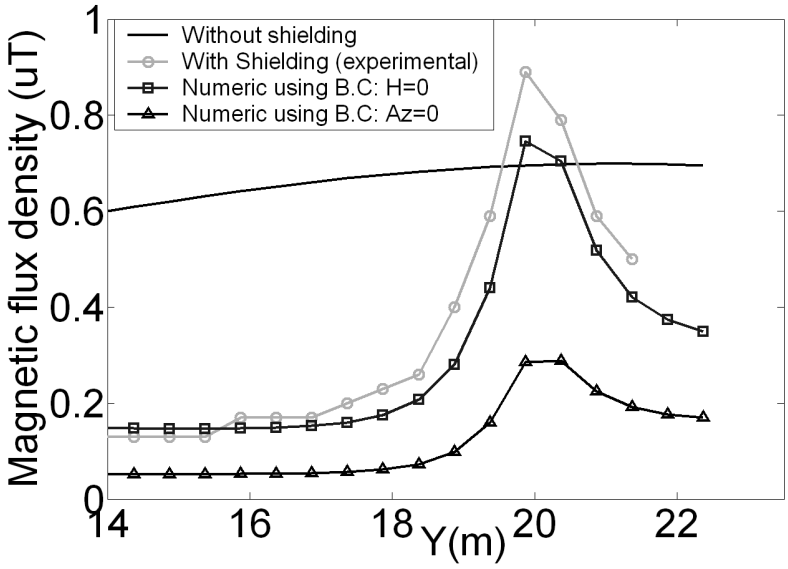

Fig. 12 Comparison between numerical results and experimental data is shown. The values taken over the line L at z = 22.7m (see Fig. 7). Notice that the boundary condition H = 0 agrees more with experimental data. The experimental data is obtained by using the scale model described in this article.

Conclusions

The problem of shielding extremely low frequency magnetic fields of 16.67 Hz that affect large buildings certainly poses several challenges to standard field mitigation schemes and to modern numerical modelling methods too. A new technique was used based on re-directing eddy currents towards ribbon paths that effectively contributed to reduce the magnetic field inside the buildings. Due to the 3-dimensional character of the proposed models the design was elaborated using scaling rules and performing tests in a low-power laboratory. The scaling factor for the experiment was 1/10 and the frequency 1.67 kHz. The division of lateral and frontal buildings proved to be useful in the design of shielding structures. Complex but cost-effective structures based on conductive material consisting on plates and ribbons were built. Good mitigation factors (up to SF=10) were achieved. After shielding averages field values were measured under 0.5 microtesla and peak values were kept (with a few localized exceptions) under 1 microtesla.

Acknowledgements

The authors are grateful to the representatives of the Swedish company *NCC AB* for proposing the problem. We would like to thank the Faculty of Science of the *Universidad Nacional de Ingeniería,* in Lima Peru, for allowing us to use of their lab facilities. Our gratitude also goes to ELFORSK for the grant N° 3950, which enabled us the development of some the methods used in this study.

References

[1] C. Buccella, M. Feliziani, F. Maradei, and G. Manzi, Evaluation of the Magnetic Field Levels Produced by a Railway Line, Proceedings of conf. Environmental Modelling and Simulation – 2004, ref. 432.

[2] P. Chadwick et al: Magnetic fields on British trains. *Ann Occup Hyg* 5:331-335, 1998.

[3] M. Röösli, M. Lörtscher, D. Pfluger, N. Schreier: ELF (16.7 Hz) magnetic field exposure assessment in Swiss railway engineers. Bioelectromagnetics 2005, Dublin, Ireland - Book of abstracts pp. 41-42.

[4] P. Rossi, R. Falsaperla, V. Brugaletta, P. Betti e A. Gaggelli: Occupational exposure to static and ELF magnetic fields on railway engines. VI International Congress of the European BioElectromagnetics Association, EBEA 2003. Budapest Nov. 13-15, 2003, p.31.

[5] Minder, C. E.; Pfluger, D.H., Leukemia, Brain Tumors and Exposure to Extremely Low Frequency of Electromagnetic fields in Swiss Railway Employees, Am J Epidemiol 153(9):825-835.

[6] Information Ventures, Inc. Electromagnetic Fields and Rail Maintenance Workers: Final Report of an Exposure Survey and Feasibility Investigation. Exposure Assessment, http://infoventures.com, 1999.

[7] International Commission on Non-Ionizing Radiation Protection (ICNIRP): Guidance on determining compliance of exposure to pulsed and complex non-sinusoidal waveforms below 100 kHz with ICNIRP guidelines, 2003; 84: pp. 383-387.

[8] ICNIRP. Guidelines for limiting exposure to time-varying electric, magnetic and electromagnetic fields (up to 300 GHz). *Health Phys.*, 74, No. 4, 494–522 (1998).

[9] Opera 3d User manual; solver ELEKTRA, Vector Fields Ltd. 1996.

[10] Comsol AB, Femlab 3.1, *Electromagnetics Module User's Guide*, Sweden, 2004.

[11] E. Salinas, Y. Q. Liu , P. Souza Jr. , J. Atalaya, , P. Cruz , J. Daalder. "Design and Validation of Power-Frequency Magnetic field Conductive Shielding for Underground Cables" *Proceedings of CIRED'2005, 18th International Conference and on Electricity Distribution*, IEE Technical Report, Technical Theme 2, Power Quality and EMC, paper 97 pp 1-4, Turin, 2005.

[12] Ener Salinas, Per Pettersson, Jaap Daalder, Yueqiang Liu, Juan Atalaya, Diego Gonzales, Munish Jassi, Cynthia Contreras, Carlos Leon. Minimization of Power-Frequency Magnetic Fields in Confined Regions Using 3-Dimensional Physical Processes; with Applications to Currently Active Electrical Substations, *ELFORSK Report, project 3950, 2006.*

DAILY PULSED ELECTROMAGNETIC FIELD (PEMF) THERAPY INHIBITS TUMOR ANGIOGENESIS VIA THE HYPOXIA DRIVEN PATHWAY: THERAPEUTIC IMPLICATIONS

IVAN L. CAMERON, NICOLAS J. SHORT, MARKO S. MARKOV

University of Texas Health Science Center at San Antonio, Department of Cellular and Structural Biology, San Antonio, Texas 78229 [I.L.C., N.J.S.], Research International, 135 Arielle Ct, Suite E, Williamsville NY, 14221 [M.M.]

Abstract

Ten minute daily PEMF inhibits hypoxia driven angiogenesis and tumor growth (Williams et *al*. 2001, Cameron et *al*. 2005a) but does not inhibit angiogenesis that normally occurs during embryogenesis and tail fin regeneration in zebrafish (Short et *al*. 2006). As discussed, the reason for this difference may be due to the hypoxic state of the tissues. Daily pulsed electromagnetic field (PEMF) was found to retard angiogenesis and growth of a human breast cancer xenograft, causing the tumor to develop proportionately larger areas of necrosis and hypoxia and smaller areas of proliferatively active cancer cells. It was also demonstrated that the daily PEMF therapy continued to inhibit tumor angiogenesis and tumor regrowth for two weeks following a standard course of ionizing radiation (IR) therapy (Cameron et *al*. 2005a). However, this PEMF therapy renders large areas of the tumor hypoxic and therefore is expected to lessen susceptibility to oxidative damage caused by further IR treatments or by oxidative dependent chemotherapy. The need for a 2-4 day recovery from the anti-angiogenic effects of PEMF prior to the next round of oxidative IR therapy is discussed.

Introduction

There appears to be only two previously published original research reports on use of pulsating electromagnetic field (PEMF) to reduce tumor angiogenesis and tumor growth (Williams et *al*. 2001, Cameron et *al*. 2005a). These two previous reports both indicated that a 15 mT PEMF given for 10 minutes per day safely reduces tumor growth and tumor vascularization. In an accompanying report in these proceedings the effects of the exact same PEMF exposure condition on zebrafish development and tail fin regeneration was reported to be ineffective in retarding fish embryonic development or fin regeneration or to retard the vascularization accompanying these processes (Short et *al*. 2006). What factor or factors might be responsible for the difference in response to the same PEMF exposure conditions between the transplantable tumors in mice and the development and fin regeneration in the fish? Thus, an aim of the current report is to briefly reexamine the results of these two prior reports on growth of a transplantable tumor and on fish development and tail fin regeneration and to explore possible differences in responsiveness to the same PEMF exposure conditions.

It seems likely that clinical oncologists might not be inclined to use PEMF as the sole method of cancer therapy. Thus, it was decided to combine a commonly used form of cancer therapy, specifically a standard course of ionizing radiation (IR) with PEMF therapy in hopes of finding additive or synergistic benefits. The therapeutic implications of the results of the IR and PEMF study are presented and discussed.

Materials and Methods

EMF on Tumor Growth/Angiogenesis—Green fluorescent protein transfected with MDA-MB 231 breast cancer cells were injected into the mammary fat pad of young female athymic mice. Six weeks later, mice were randomly divided into four treatment groups: untreated controls; 10 minute daily PEMF; 200 cGy of IR every other day (total of 800 cGy); IR plus daily PEMF. Detail of the PEMF method and the IR method are given in Cameron et *al.* (2005a). Tumor size and body weight measurements were made

throughout the course of treatment. Some mice in each group were euthanized 24 hours after the end of the IR treatment. PEMF treatment continued for three additional weeks. Tumor sections were stained for: endothelial cells with CD31 and PAS or hypoxia inducible factor 1α (HIF). Tumors were scored for angiogenesis, for metaphase index and for lung metastases.

EMF on Zebrafish Embryonic Development—Newly fertilized zebrafish embryos were given daily PEMF and developmental stages were scored versus untreated control embryos based on developmental designations made my Kimmel et *al*. (1995). Details of the methods are given in accompanying report in these proceedings (Short et *al*. 2006).

Results

Whole body IR and PEMF therapy suppressed tumor growth (Fig. 1), cell proliferation (Fig. 2), lung metastases (Fig. 3) and angiogenesis (Fig. 4).

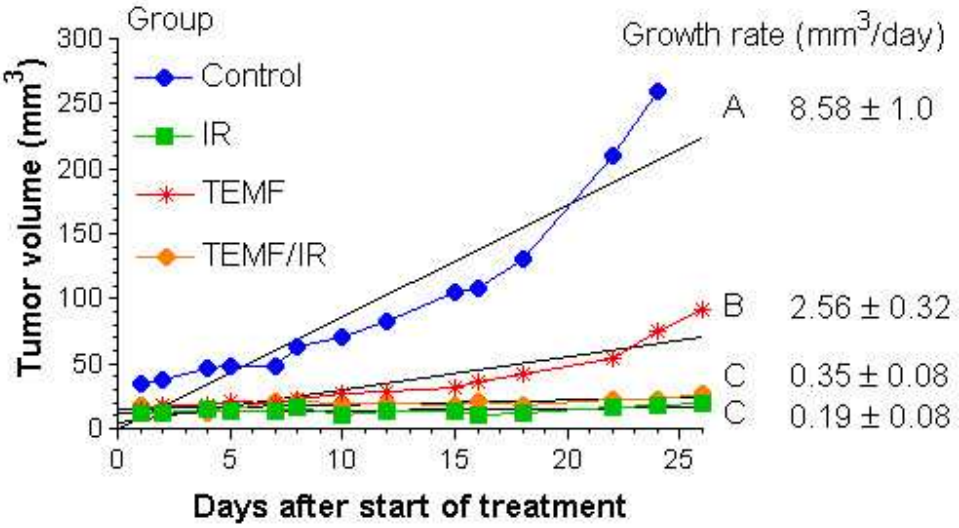

Figure 1. Illustrates the effect on tumor growth of: the 8-day course of gamma irradiation therapy (IR), the daily exposure to the TEMF therapy (TEMF), a combination of gamma irradiation and TEMF therapy (TEMF/IR), and no treatment (Control). The tumors were all 35mm^3 or less at the start of treatment.

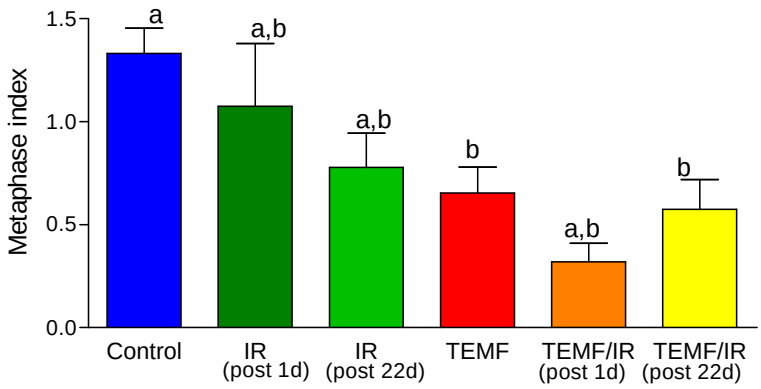

Figure 2. Number of metaphase figures per midaxial histological section of tumor. Column height indicates mean ± SEM. The columns that do not share a common letter are significantly different ($p<0.01$). TEMF significantly suppresses metaphase index in the tumor. Data from the untreated mice (Control) and the TEMF treated mice were pooled from mice of the early and the late sacrifice because there were no significant time of sacrifice differences within these groups. Not shown are data on number of metaphase figures per midaxial histological section of duodenal crypts from mice sacrificed one day after last IR exposure. The data reveal significant decreases in IR treatment. Treatment with IR but not TEMF caused a significant decrease in metaphase index in the intestinal crypts.

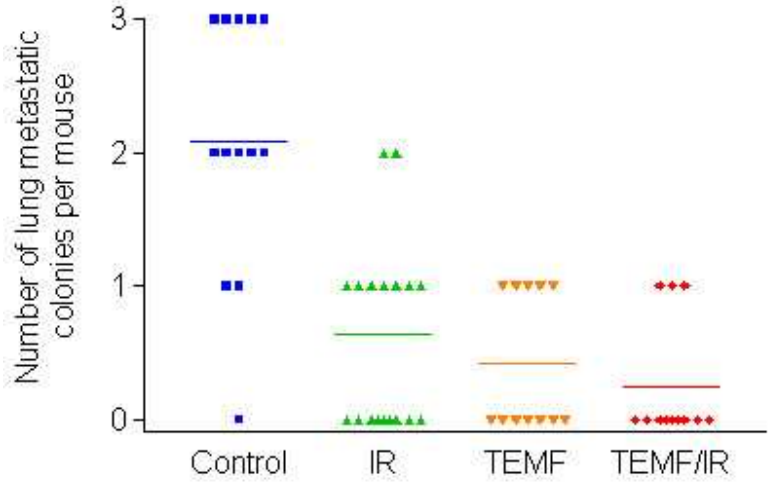

Figure 3. Metastasis of GFP-expressing human breast MDA MB231 cells from the site of inoculation in the inguinal mammary fat pad to lodge in the lungs of mice in each of the four treatment groups. The lungs were removed and smashed between microscopic slides and microcolonies of GFP cells were observed by epilumination using blue light and detected by presence of green fluorescence microcolonies observed using both 3.5× and 10× objective lens. The untreated mice had a significantly higher number of GFP positive microcolonies than the groups of mice that received gamma irradiation therapy or those mice that received EMF therapy. There were no other significant differences between groups in either mean number of microcolonies per lung or in incidence. Horizontal lines indicate mean values for each treatment group.

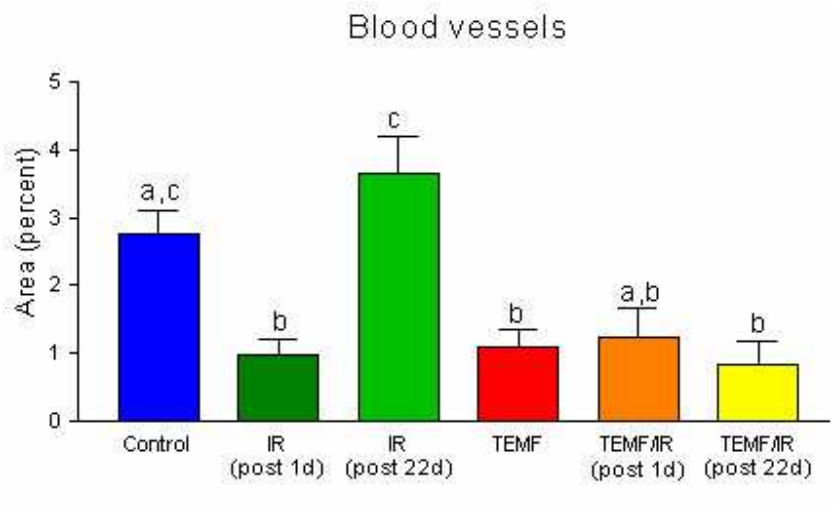

Figure 4. Quantification of changes in tumor vascularization between treatment groups. The percent of area (volume density) of blood vessels was determined using an ocular grid intercept counting method. The mean ± SEM of each treatment group is graphed. Columns that do not share a common letter within a graph are significantly different ($p < 0.01$). The data indicate that gamma irradiation and EMF alone or in combination decreased the total area of blood vessels and increased the total area of pseudopods compared to the control. Data from the untreated mice (Control) and the EMF treated mice (TEMF) were pooled from mice from the early and from the late sacrifice because there was no significant time of sacrifice difference within these groups.

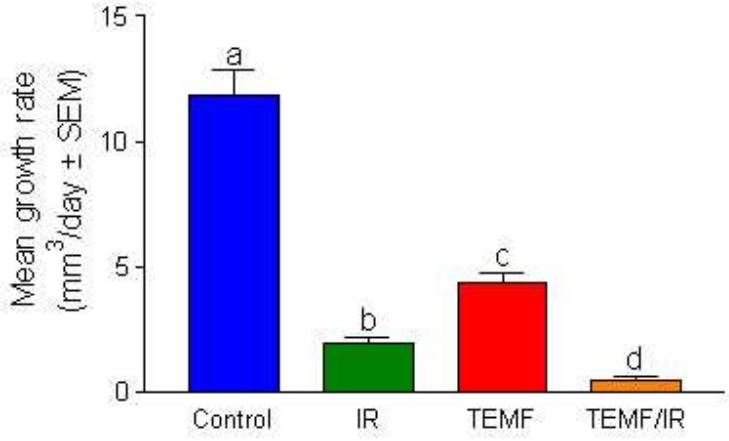

Figure 5. Mean ± SEM tumor growth rate data from day 7 to day 15 post IR therapy in each treatment group. ANOVA was used to determine any statistical differences in growth rates between treatment groups. Different letters demonstrate significant differences. Tumors in the untreated control group grew significantly faster than did tumors in the other three groups. Tumors in the IR/TEMF group had a growth rate significantly lower than that of the other three groups.

Continued daily PEMF therapy following IR treatment prevented angiogenesis and tumor regrowth (Fig. 4-5). PEMF therapy did not result in the body weight decreases nor the decreases in blood elements that IR did (not shown). Embryogenesis was not inhibited by daily PEMF therapy (Fig. 6).

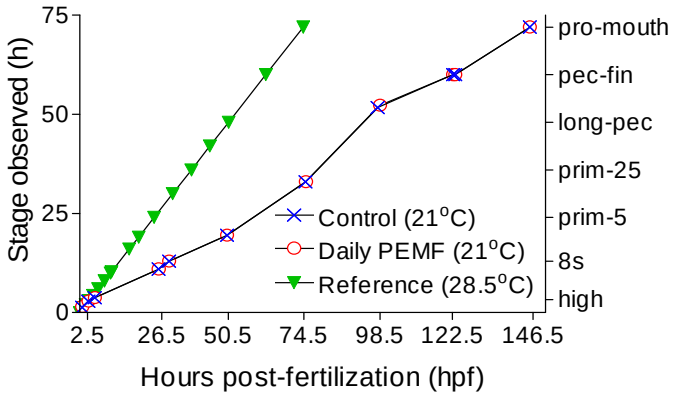

Figure 6. Temperature and 10 minute daily exposure to PEMF on development. The time post-fertilization to reach each stage at 28.5°C (from Kimmel et *al*., 1995) is plotted on the left y-axis. Corresponding morphological stages are listed along the right y-axis. Stage abbreviations used are 8 somite (8s) and protruding mouth (pro-mouth). Times of PEMF exposures are labeled on the x-axis.

Discussion

Angiogenesis in the tumor was hypoxia driven. (see Fig. 7 that summarizes a model of human MDA MB231 breast cancer tumor). Continued daily PEMF therapy following IR treatment prevented tumor angiogenesis and regrowth. However, it did not suppress metaphase index in intestinal crypts. This suggests that PEMF works selectively on hypoxia driven angiogenesis such as that in growing tumors. Angiogenesis during embryogenesis in fish was not inhibited by daily PEMF treatment. Had hypoxia occurred in fish development then developmental retardation or arrest has been demonstrated to occur (Padilla and Roth 2001). Lack of effect of angiogenesis in the fish versus the tumor suggests the difference in response to PEMF is because PEMF interferes with hypoxia driven angiogenesis that occurs in tumors but not in normal fish embryogenesis.

PEMF is an effective adjunct therapy following IR therapy but the continued daily PEMF therapy should be stopped sometime (2-4 days) prior to a second round of IR therapy. The temporary cessation of PEMF prior to the second round of IR is necessary for resumption of angiogenesis, decrease of hypoxic areas and increase in proliferative activity in well oxygenated areas within the tumor, all of which are needed for an effective second round of IR treatment.

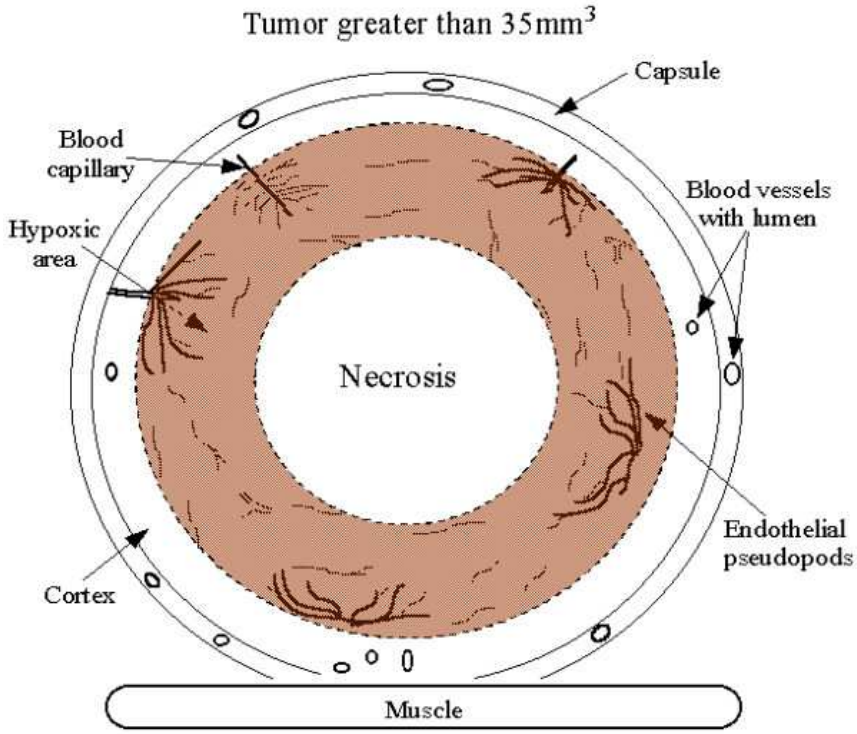

Figure 7. Model of vascularization as observed in the human MDA MB231 breast cancer cell tumor grown as a xenograph in a female nude mouse. The well vascularized tumor capsule overlies the tumor cortex. The cortex extends between 100 and 150 μm beneath the capsule. The HIF-α positive region is located in the subcortical region, at distances greater than 150 μm of the capsule. More endothelial pseudopods are located in this subcortical region than are located in the cortical region of the tumor. Even further away from the vascularized capsule is the region of tumor necrosis which contains no blood vessels or endothelial cell pseudopods. This model is consistent with the conclusion that the hypoxic regions of the tumor produce HIF leading to production of vascular endothelial growth factors and sprouting of endothelial cell pseudopods (Cameron et *al.* 2005b).

Acknowledgements

This work was supported by EMF Therapeutics, Inc. and NIH grant CA 75253. Figures 1-6 are from Cameron et *al.* 2005a, and figure 7 is from Cameron et *al.* 2005b. Cancer Cell International is gratefully acknowledged. The authors wish to thank Matt Cykowski for help with animal handling and photography.

References

Cameron IL, Sun LZ, Short N, Hardman WE, Williams CD. 2005a. Therapeutic electromagnetic field (TEMF) and gamma irradiation on human breast cancer xenograft growth, angiogenesis and metastasis. *Cancer Cell International* 5:23.

Cameron IL, Short N, Sun LZ, Hardman WE. 2005b. Endothelial pseudopods and angiogenesis of breast cancer tumors. *Cancer Cell International* 5:17.

Kimmel CB, Ballard WW, Kimmel SR, Ullmann B, Schilling TF. 1995. Stages of embryonic development of the zebrafish. *Developmental Dynamics* 203:253-310.

Padilla PA, Roth MB. 2001. Oxygen deprivation causes suspended animation in the zebrafish embryo. *PNAS* 98:7331-7335.

Short N, Miera KL, Markov M, Cameron IL. 2006. A pulsed electromagnetic field that inhibits tumor growth fails to delay zebrafish embryonic development and tail fin regeneration. These proceedings.

Williams CD, Markov MS, Hardman WE, Cameron IL. 2001. Therapeutic electromagnetic field effects on aniogenesis and tumor growth. *Anticancer Research* 21:3887-3892.

A PULSED ELECTROMAGNETIC FIELD THAT INHIBITS TUMOR GROWTH FAILS TO DELAY ZEBRAFISH EMBRYONIC DEVELOPMENT AND TAIL FIN REGENERATION

N. SHORT, K. L. MIERA, M. MARKOV[2], P. JAGADEESWARAN, I. L. CAMERON[3]

University of Texas Health Science Center at San Antonio, Department of Cellular and Structural Biology, San Antonio, Texas 78229 [N.S., K.M., P.J., I.L.C.], [2]Research International, 135 Arielle Ct, Suite E, Williamsville NY, 14221 [M.M.]

This work was supported by EMF Therapeutics, Inc. and by National Institutes of Health grants HL63792 and AG20863

[3]To whom requests for reprints should be addressed, at Department of Cellular and Structural Biology, University of Texas Health Science Center, 7703 Floyd Curl Drive, Mail Code 7762, San Antonio, TX 78229-3900. Phone: (210)567-3817; Fax: (210)567-3803; E-mail: cameron@uthscsa.edu.

Abstract

A rectified semi-sinewave signal with an amplitude of 15mT and a frequency of 120 pulses per second (PEMF) given as a 10 minute daily session has proven to be a safe means for retarding tumor growth and angiogenesis in a transplantable tumor in mice. The experiments reported here were designed to test the same PEMF exposure on embryonic development and on caudal fin (tail) regeneration in zebrafish. The results of single and multiple exposures to PEMF at different times during embryonic development and tail fin regeneration demonstrated no significant delay in either embryo development or in tail fin regeneration. Possible difference between the inhibitory effect of PEMF on tumors compared to the lack of effect of the PEMF on embryo development and on tail fin regeneration is discussed.

Background

It has been reported that a 10 minutes per day exposure to a 15mT pulsed electromagnetic field (PEMF) given at 120 pulses per second reduced tumor growth and vascularization and resulted in increased survival time in mice with a breast cancer xenograft [Williams et *al*., 2001, Cameron et *al*., 2005]. The study reported here was designed to investigate the potential effects of the same PEMF on embryonic development and tail fin regeneration of zebrafish (*Danio rerio*).

In the present study it was decided to exactly repeat the PEMF exposure conditions used in the previous breast cancer xenograph experiments. No attempt was made to increase the dose of exposure (time or intensity). Thus, no claims are made to any possible effects outside the dosage range used in the present fish study.

Zebrafish are excellent organisms for the study of embryonic development. A single mating pair can provide 200 newly fertilized eggs that progress through development in synchrony. The zebrafish is a leading model for studies of vertebrate development because one can obtain a large number of transparent, externally and rapidly developing embryos [Kimmel et *al*., 1995]. Thus, even modest experimental perturbations can influence the rate of sequential development in a subset of these fertilized embryos.

The caudal tail fin is an excellent model organ for studying regeneration. It has a comparatively simple architecture, consisting of several segmented, bony fin rays composed of concave hemirays, which are surrounded by connective tissue, nerves, and blood vessels [Ferretti and Géraudie, 1998]. Hundreds of amputations per hour may be performed. Regeneration is rapid and reliable, with most structures replaced within 1 to 3 weeks. Zebrafish survive their amputation wound, allowing for study of formation of new blood vessels and nerve regeneration [Johnson and Weston, 1995].

Because of the critical events associated with blood vessel formation and circularization between the 21 and 26 somite stages of embryogenesis [Stainier et *al*., 1993] and the need for angiogenesis during tail regeneration as well as the past report that PEMF has anti-angiogenic action in rapidly growing mammalian tumors [Williams et *al*. 2001, Cameron et *al*. 2004], it was decided that exposure of fish embryos and regenerating fish fins to the PEMF at known times of angiogenesis might shed light on the mechanism of action the PEMF on suppression of tumor growth and angiogenesis.

Materials and Methods

A pulsed electromagnetic field (PEMF) system having a proprietary signal designed by EMF Therapeutics, Inc. (Chattanooga, TN, USA) was used (Figure 1). The system generates a pulsating half sinewave magnetic field with a frequency of 120 pulses per second. An ellipsoidal coil with 21" large diameter and 14" small diameter is used to deliver the signal to the target. In the experiment reported here, the magnetic flux density measured in the exposure chamber was 15 mT. This value of magnetic field flux density was chosen based upon our previous dose response experience and data (Williams and Markov 2001 and Williams et al. 2001). A thorough 3-D mapping of the magnetic field was performed for the entire space covered by the coil.

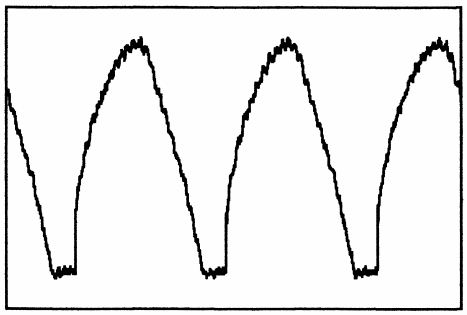

Pulsed (120 pps) rectified semi-sine wave

Figure 1. Photograph of the EMF device and a separately suspended exposure table that was used to avoid vibration of the exposure chamber (left). An illustration of the fully rectified 60Hz signal transferred to 120 pulses per second pulsating magnetic field (right).

The flux density of the magnetic field in the exposure chamber (25 cm long, 10 cm wide and 13 cm high) was consistent within the entire volume of the chamber. The same type chamber was used on sham controls. The temperature inside the exposure chamber before and at the end of the PEMF treatment was the same. The exposure chamber is suspended separately from the EMF device and no vibrations were detected in the chamber during

operation of the EMF device.Zebrafish (4 months old) were purchased from Ekkwill Waterlife Resources (Gibsonton, FL). Zebrafish were cultured according to Westerfield [1989]. Developmental times were determined from the morphological features of the embryos under a dissecting microscope. All experiments were conducted at 21^{o}C. A time point for a particular stage as judged by the morphological staging of each individual embryo in the cohort was assessed and the corresponding time value from Kimmel et *al*., 1995 was then used for statistical analysis. Linear regression analyses of all data obtained revealed a significant linear fit between hours post-fertilization (hpf) from this study and hpf from Kimmel et *al*., 1995 when plotted against one another at various morphological stages. This indicates that the method of scoring development in numerical hours, as done in this study, is justified.

In an attempt to determine an action of the PEMF on embryogenesis, fertilized zebrafish eggs were exposed to the PEMF at designated stages of development. A first group was exposed daily to the PEMF beginning at the 64 cell stage (2.5 hpf) for a total of 7 daily pulses. A second group of fertilized eggs was exposed at either the 8 cell stage (1.6 hpf) or at the 64 cell stage (2.5 hpf), both at times during synchronous cell divisions. The third group was exposed to the PEMF pulse at the sphere/blastula stage (7 hpf), shortly after the initiation of embryonic mRNA transcription [Zamir et al., 1997]. The fourth group was divided into four subgroups: embryos not exposed to the PEMF (controls), embryos exposed to the PEMF at the 4 somite stage (27 hpf), embryos exposed to the PEMF at the 13 somite stage (31 hpf), and embryos exposed to the PEMF at the 25 somite stage (48 hpf). The timing of exposure to the PEMF pulses of these four subgroups was designed to coincide with the time of cardiovascular development in zebrafish (between the 21 and the 26 somite stages) [Stainier et *al*., 1993].

For the caudal fin regeneration study, adult zebrafish were anesthetized in a 10µmol Tricaine solution and the distal one-half of each fish's caudal fin was amputated. Afterwards, the fish were returned to tanks of distilled water and fed brine shrimp every third day. To assess regeneration at 2 days, 7 days and 13 days post-amputation, the fish were anesthetized in 10µmol solution at these times and the amputated fin regeneration areas were determined by assessment of the ratio of the tail fin area regeneration to the tail fin area remaining after amputation. Tail regeneration was observed using images captured using a Nikon CoolPix 995 CCD camera mounted on a Nikon Optiphot microscope using a 4x objective.

To further assess tail fin regeneration, the number of new bone centers per fin ray of the middle five rays from each fish was scored. Finally, the number of fin rays with bifurcated bone segments at the distal end was scored.

Statistical analyses consisted of one- and two-way ANOVA followed by Student Newman Keuls multiple range test. Linear regression analyses were used to assess correlations.

Results

Figure 2 summarizes the results of daily exposure of zebrafish embryos to the 10 minute PEMF. Both the PEMF and the no PEMF controls each had at least 20 embryos. There were no significant differences at any of the times of scoring and the variance from the mean values was so small as not to be visible within the experimental points on the figure. No significant differences were found between the two groups at any time post-fertilization. Linear regression analysis gives a significant linear fit of data.

The slope of the mean rate of embryo development was 0.4983 ± 0.0142 for the control embryos and was 0.4985 ± 0.0147 for the embryos exposed to the daily PEMF. These slope values are not significantly different. The slopes of both the control and the daily PEMF groups, both at 21^{o}C, differed significantly from the reference values at 28.5^{o}C ($p<0.001$).

When embryos were exposed to a single pulse of the PEMF at either the 8 cell stage (1.6 hpf), the 64 cell stage (2.5 hpf), or the sphere/blastula stage (7 hpf) and were followed to the 4 somite stage (26 hpf), no significant differences in development were detected compared to the untreated controls (data not shown).

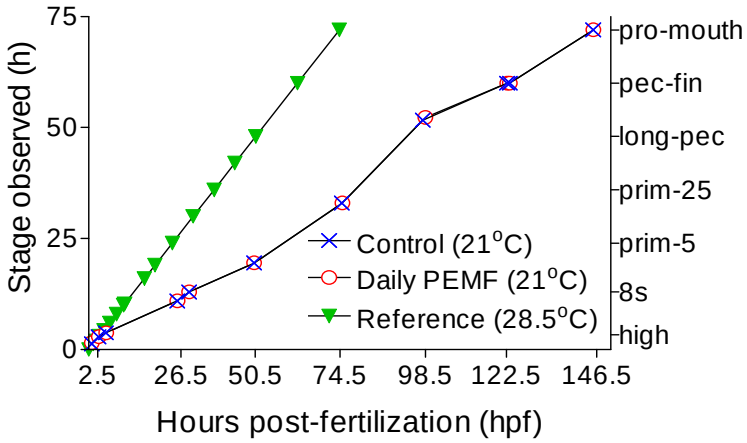

Figure 2 Temperature and 10 minute daily exposure to PEMF on development. The time post-fertilization to reach each stage at 28.5°C (from Kimmel et *al*., 1995) is plotted on the left y-axis. Corresponding morphological stages are listed along the right y-axis. Stage abbreviations used are 8 somite (8s) and protruding mouth (pro-mouth). Times of PEMF exposures are labeled on the x-axis.

In an attempt to bracket PEMF pulse exposure to the time of cardiovascular development in the fish embryo, a single pulse of PEMF was given to subgroups of embryos at: the 4 somite stage (27 hpf), the 13 somite stage (31 hpf), and the 25 somite stage (48 hpf). The results are illustrated in Fig. 3.

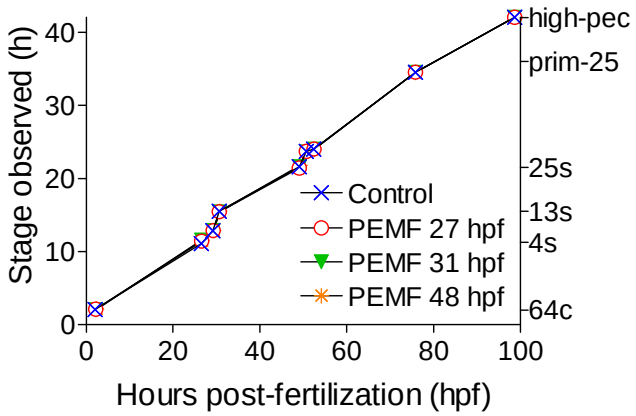

Figure 3 Effect of the PEMF exposure before (4 somite stage, 27 hpf) just prior to (13 somite stage, 31 hpf) and at the end of (25 somite stage, 48 hpf) development of a functional cardiovascular system in the zebrafish embryo (21 to 26 somite stage) [Stainier et *al*., 1993] on rate of embryonic development. The time post-fertilization to reach each stage at 28.5°C (from Kimmel et *al*., 1995) is plotted on the left y-axis. Corresponding morphological stages are listed along the right y-axis. Stage abbreviations used are 64 cell (64c), 4 somite (4s), 13 somite (13s) and 25 somite (25s). Linear regression analyses of the slopes of each of the four groups of embryos from the time of the first PEMF exposure (27 hpf) to the conclusion of the experiment (100 hpf) revealed no significant differences in the rate of development due to PEMF exposure compared to the untreated controls (see text for slope statistics).

There were no significant differences between the four groups at any time after treatment. Variance around the mean values was so small as not to be visible within the points in Fig. 3. Statistical analyses of mean rate of development slopes of each of the four embryo groups yielded the following linear regression slopes: 0.445 ± 0.0075 for the control embryos, 0.4441 ± 0.0073 for the embryos exposed to TEMF 27 hpf, 0.4443 ± 0.0070 for the embryos exposed to the PEMF 31 hpf, and 0.4449 ± 0.0072 for the embryos exposed to the PEMF 48 hpf. These mean slope values are not significantly different.

Table 1 summarizes the results of zebrafish caudal fin regeneration with and without a 10 minutes per day exposure to the PEMF. The ratio of the area regenerated to the area remaining after amputation is presented at 2, 7 and 13 days post-amputation. Statistical analysis reveals a significant increase with time post-amputation but no significant difference between the fish that were exposed to the PEMF and the fish that were not exposed to the PEMF. Likewise, the scoring of newly forming bone centers per fin ray reveals differences with time after amputation but no significant differences between fish with or without the daily PEMF. As fin rays increased in length, they were each observed to have a centrally located artery with veins on each side. Capillaries with circulating blood cells were observed between adjacent rays, indicating return of normal blood vessel morphology by 19 days post-amputation.

Table 1 Analysis of Zebrafish Caudal Fin Regeneration With and Without Daily PEMF Treatments Mean $\pm$ SEM (n=5 fish per group)[a]

Time after amputation in day	Area regenerated / Area remaining after amputation	New bone centers/fin ray[b]
Day 2 - PEMF	.042 $\pm$ .008	0
Day 2 + PEMF	.045 $\pm$ .010	0
Day 7 - PEMF	.739 $\pm$ .140	.600 $\pm$ .167
Day 7 + PEMF	.536 $\pm$ .087	.320 $\pm$ .136
Day 13 - PEMF	1.279 $\pm$ .247	4.320 $\pm$ .361
Day 13 + PEMF	1.258 $\pm$ .168	4.320 $\pm$ .382

[a] Results of two-way ANOVA: Significant increases with time ($p<0.001$) but no significant differences between the group receiving daily PEMF exposure and the group not receiving daily PEMF exposure.

[b] Five middle fin rays were scored in each fish.

Another measurable indicator of fin regeneration is bifurcation of fin rays. As time of regeneration increased, the number of fin rays demonstrating bifurcation increased. The mean percentage of fin rays demonstrating bifurcation did not differ significantly between the control and the PEMF treated experimental groups. For instance, at 13 days post-amputation the PEMF group had (21.0 ± 5.6) % of rays with bifurcation while the control group had (18.8 ± 7.3)% of rays with bifurcation. At 19 days post-amputation, the PEMF group had (70.2 ± 9.4) % of rays with bifurcation while the control group had (68.3 ± 19.0) of rays with bifurcation. Adults whose tails were not amputated and all of the fish in this study with tail amputation demonstrated 100% of the fin rays with bifurcation by 24 days post-amputation.

Discussion

It was shown that a single 10 minute exposure to the PEMF given at either the 8 cell stage (1.6 hpf) or at the 64 cell stage (2.5 hpf) did not delay development indicates that the PEMF is not acting to slow or to interfere with nuclear DNA synthesis, mitosis, or cytokinesis, all of which take place during these synchronous cell division stages. A single 10 minute exposure to the PEMF at the sphere/blastula stage (7 hpf) did not delay development indicates that the PEMF did not interfere with production of zygotic mRNA synthesis known to be needed for continued embryonic development at this stage of development [Zamir et *al*., 1997].

The timing of a pulse of the PEMF at the 4 somite (27 hpf), the 13 somite (31 hpf) or the 25 somite (48 hpf) stages (at times before, just prior to and just after initiation of heart tube formation, respectively)

suggests that the PEMF exposure at these stages of development did not delay normal cardiovascular development known to occur between the 21 and 26 somite stages [Stainier et *al*., 1993]. Clearly, use of the PEMF did not delay embryonic development using any of the experimental conditions tested.

Zebrafish continue to grow throughout life, and fin ray growth occurs by distal addition of bony segments [Iovine and Johnson, 2000]. The caudal fin is a usable model for studying genetics of regeneration [Poss et al., 2002, Akinemko et *al*., 1995] and also as a tool for evaluation of the effects of drugs and natural products [White et *al*., 1994, Santos-Ruiz et *al*., 2001, Zodrow and Tanguay, 2003]. The regeneration process involves: blastema formation, bone formation, nerve regeneration, and formation of new blood vessels (angiogenesis). Because of the usefulness of the regenerating tail fin model for the evaluation of the action of drugs and natural products, it was decided to evaluate the effects of a 10 minutes per day pulse of the PEMF on tail fin regeneration. The question was would a daily 10 minute pulse of PEMF treatment suppress regeneration of the caudal fin of adult zebrafish following partial amputation of the fin? Based on the experimental data in this report, the answer is no.

The failure of daily PEMF to delay development of fish embryogenesis and to delay fin regeneration indicates that daily exposure to the PEMF is without measurable effect. However, the same daily PEMF exposure was effective at slowing growth and angiogenesis of a rapidly growing transplantable tumor in mice [Williams et *al*., 2001, Cameron et *al*., 2005]. What might account for a lack of effect of PEMF on fish development and on wound repair as well as the report that the PEMF inhibits growth and angiogenesis of a transplantable breast cancer in nude mice. One possible explanation may be differences in angiogenesis in the different experimental systems. In the rapidly growing tumor, the cancer cells proliferate so rapidly that development of the needed vascular supply cannot keep pace, thus resulting in hypoxic regions within the tumor. The hypoxic cancer cells respond by production of hypoxia inducible factor, leading to release of vascular endothelial growth factor, which stimulates the subsequent sprouting of new endothelial cell pseudopods into the hypoxic areas of the tumor [Wachsberger et *al*., 2003, Cameron et *al*., 2005]. This eventually leads to formation of new capillaries and blood vessels. Clearly, the angiogenesis process in this tumor system is hypoxia driven. On the other hand, angiogenesis during normal fish development and tail fin regeneration appears not to be hypoxia driven, perhaps because diffusion of oxygen to the embryo and to the regenerating tail fin is adequate enough to avoid hypoxic conditions during normal embryonic development and tail fin regeneration. Thus, angiogenesis in the fish embryo and in fin regeneration may not be hypoxia driven whereas angiogenesis in the rapidly growing tumor is hypoxia driven. This difference between systems may account for the observed differences in response to PEMF. It seems unlikely that zebrafish embryos and adults experienced hypoxia under the experimental conditions based on the fact that induced oxygen deprivation does cause arrest of zebrafish development and heartbeat until returned to normoxia (Padilla and Roth, 2001). A testing of this hypothesis is planned by the authors.

References

1. Akimenko M-A, Johnson SL, Westerfield M, Ekker M. 1995. Differential induction of four *msx* homeobox genes during fin development and regeneration in zebrafish. Development 121:347-357.
2. Cameron IL, Sun LZ, Short N, Hardman WE, Williams CD. 2005. Therapeutic electromagnetic field (TEMF) and gamma irradiation on human breast cancer xenograph growth, angiogenesis and metastasis. Can Cell Int. 5:23.
3. Ferretti P, Géraudie J. 1998. *Cellular and Molecular Basis of Regeneration: From Invertebrates to Humans*. New York: Wiley Press.
4. Iovine MK, Johnson SL. 2000. Genetic analysis of isometric growth control mechanisms in the zebrafish caudal fin. Genetics 155:1321-1329
5. .Johnson SL and Weston JA. 1995. Temperature-sensitive mutations that cause stage specific defects in zebrafish fin regeneration. Genetics 141:1583-1595.
6. Kimmel CB, Ballard WW, Kimmel SR, Ullmann B, Schilling TF. 1995. Stages of embryonic development of the zebrafish. Developmental Dynamics 203:253-310.
7. Padilla PA, Roth MB. 2001. Oxygen deprivation causes suspended animation in the zebrafish embryo. PNAS 98:7331-7335.
8. Poss KD, Nechiporuk A, Hillam AM, Johnson SL, Keating MT. 2002. Mps1 defines a proximal blasternal proliferative compartment essential for zebrafish fin regeneration. Development 129:5141-5149.
9. Santos-Ruiz L, Santamaría JA, Becerra J. 2001. Differential expression of FGF receptors during zebrafish fin regeneration. Int J Dev Biol 45(S1):S131-S132.

10. Stainier DYR, Lee RK, Fishman MC. 1993. Cardiovascular development in the zebrafish. Development 119:31-40.
11. Wachsberger P, Burd R., Dicken AP. 2003. Tumor response to ionizing radiation combined with antiangiogenesis or vascular targeting agents: exploring mechanisms of interaction. Clin Can Res 9: 1957-1971.
12. Westerfield M. 1989. *The Zebrafish Book.* Oregon: University of Oregon Press.
13. White JA, Boffa MB, Jones B, Petkovich M. 1994. A zebrafish retinoic acid receptor expressed in the regeneration caudal fin. Development 120:1861-1872.
14. Williams CD, Markov MS, Hardman WE, Cameron IL. 2001. Therapeutic electromagnetic field effects on angiogenesis and tumor growth. Anticancer Res 21:3887-3892.
15. Williams CD, Markov MS. 2001. Therapeutic electromagnetic field effects on angiogenesis during tumor growth: a pilot study in mice. Electro-and magnetobiology 20:323-329.
16. Zamir E, Kam Z, Yarden A. 1997. Transcription-dependent induction of G1 phase during the zebra fish midblastula transition. Mol Cell Biol 17(2):529-536.
17. Zodrow JM, Tanguay RL. 2003. 2,3,7,8-tetrachlorodibenzo-p-dioxin inhibits zebrafish caudal fin regeneration. Toxicol Sci 76(1):151-161

Acknowledgements

The authors wish to thank Matt Cykowski for help with animal handling and photography.

EMF RISK FOR OPERATORS MOUNTING, ADJUSTING AND MAINTAINING BASE STATIONS

Ts. Shalamanova, I. Iliev, M. Ivanova, M. Israel

National Center of Public Health Protection, Sofia, Bulgaria

ABSTRACT

There are many publications in the last years about the risk of radiofrequency (RF) exposure to the general population from base stations for mobile communication. Unfortunately, very few of them concern the risk to the personnel mounting and maintaining these systems.

Here, we present a pilot study of the exposure to the personnel in selected objects with different types of antennae mounting.

The exposure assessment is made according to the typical work positions corresponding to the operations of the personnel. Calculations of the energetic load are made on the basis of the Bulgarian national legislation.

The data show that the maximal values of power density measured at distances up to 50 cm in front of the antennae reach to 2.5 mW/cm^2. In other locations of the worker: behind, aside and under the antenna, measured values are logically much lower, and corresponding to the exposure limits of ICNIRP Guidelines.

Basing on the results, we recommend future studies in this fields and a special attention to this personnel because of the possible risk of RF overexposure

We propose special protective measures for this particular work group.

INTRODUCTION

There are a lot of recent publications dealing with the emission of mobile communication antennae in settlements affecting the population health. Unfortunately, the results are contradictory and more evidences are needed for the possible effect of electromagnetic fields (EMF) at frequency 900 MHz and 1800 MHz which provokes diseases like cancer, cardiovascular disorders and other health consequences among the population.

Furthermore, little attention was paid to the risk of RF exposure on service staff of base stations and mobile communication antennae up to now. There is evidence that despite the special requirement of the manufacturers that service operations should be performed when antennae are switched off, the personnel frequently works when the antennae emit, i.e. without interrupting the emission, and very close to them. Mild (1) reports similar practice among the service staff of base stations and antennae in Sweden.

AIM AND SCOPE

This study is aimed at assessing the risk of the microwave EMF radiation for the service staff of base stations and mobile communication antennae.

For this purpose typical antennae systems were investigated on routine operations of the personnel which they perform close proximity and around antennae. EMF values were measured and exposure assessment is made for each particular operation. Energetic loading of the organism and whole body SAR were calculated as well. The scenario, technological operations and their average duration were presented by the mobile operator.

The object of investigation is personnel working on base stations antennae emitting EMF with frequencies about 900 MHz, and UMTS systems with 2100 MHz.

On pictures No. 1, 2 and 3 are presented various technological operations in the close proximity of a single antennae for which were made corresponding measurements and evaluations.

Pic. 1
Operation aside and in front of emitting antenna

Pic. 2
Operation behind the antenna

Pic. 3
Operation close to the connectors (lower edge)

On pictures No. 4 and 5 are presented various technological operations in the close proximity of more than one antennae (mounted a pole) for which were made corresponding measurements and evaluations.

Pic. 4
Operation between antennae

Pic. 5
Operation close to lower edges of antennae

This study does not deal with the exposure close to antennae, mounted on telecommunication masts.

The study covers temporary workplaces for adjustment, maintenance and repair of antennae, mounted on base stations. The selected sites cover all possible working conditions, under which the respective service tasks are performed by the staff.

EXPOSURE ASSESSMENT

The evaluation of electromagnetic effects was performed at two stages:

1. Measurement of EMF for various procedures performed by the personnel and evaluation of the compliance with the respective exposure limits

2. Evaluation of the energetic loading (exposure assessment) for various processes, activities and shifts and its compliance with the respective limit values of Bulgarian and European standards.
3. Calculation of Specific Absorption Rate, SAR W/kg.

METHOD AND MATERIALS

Measurement equipment:

Power - meter 'NARDA', model EMR-21C of "NARDA Safety Test Solutions'

The evaluation was performed according to national [2,3], and international standards. [4,5]

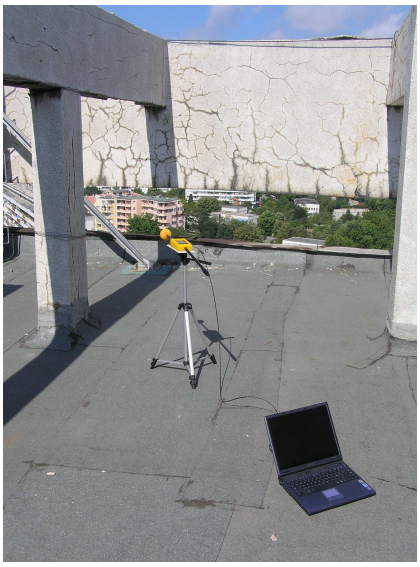

Pic. 6
Measurement equipment

Table 1. shows the limit values according to the normative documents listed above.

Table 1

Standard	Power density S, μW/cm^2	Average time t, h	SAR W/kg	Energetic loading W, μW.h/cm^2
ICNIRP				
900 MHz	2250	0.1	0.4	-
1800 MHz	4500	0.1	0.4	-
2100 MHz	5000	0.1	0.4	-
BSS 17137-90				
900 MHz	1000	1	-	200
1800 MHz	1000	1	-	200
2100 MHz	1000	1	-	200

MEASUREMENT METHOD

Measurements were made in wide frequency range by nonselective method.

All measurements were made in few selected typical sites. Measuring device was chosen with probe sensitive to electrical component of EMF.

To avoid human influence on the measurement process handle and optical cable connected to the device. Data were collected using Narda EMR-21C software, installed on laptop. In cases when the height of antenna mounting allows performing measurements from the rooftop level the equipment was mounted on tripod.

Data were collected considering the typical work positions of base station service workers. The average (averaged over 1.5 min) and maximum power densities were measured. The average values for 1.5 min were measured in order to assess the compliance with the international guidelines (ICNIRP), which require determining the (measured) 'reference' values for 6-minute period (0.1 h). This facilitates also the further determination of the energetic loading performed for 1 h. It was calculated with respect to the mean time for performing the above-mentioned work tasks.

In the far field zone, the values of SAR and energetic loading coincide for external exposure to radiation of a 'human equivalent antenna' (receiving antennae equipment corresponding to the resonance and subresonance absorption of incident energy by an average human body size).

Energetic loading of the organism was calculated considering average time duration for performing the described above operations.

On pictures No. 7 to 11 are shown spots where measurements were performed according to the technological operations of the personnel.

Pic. 7

Pic. 8

Pic. 9

Pic. 10

Pic. 11

RESULTS OF MEASUREMENTS AND CALCULATIONS

The results of measurements are shown according to the tasks performed by the service staff of mobile communication antennae and base stations. The measurement points correspond to the location of the subjects at work with respect to the antennae.

In Table 2 are shown the measured values of power density, calculated values of energetic loading of the organism, permissible time duration and whole body SAR values as well.

Table 2

No	Point of measurement according to working position	Measured values		Permissible time duration, t_{max},	Energetic loading of the organism		Operation duration	SAR, W/kg
		S_{avg}, $\mu W/cm^2$	S_{max}, $\mu W/cm^2$		W_{avg}, $\mu W.h/cm^2$	W_{max}, $\mu W.h/cm^2$		
1	2	3	4	6	7	8	9	10
CDMA antennae								
1	Operation on changing the position of the antenna	62.00	180.00	1h7min	31.00	90.00	30min	0.012
2	Single Antennae							
2.1	Operation in a close proximity of antennae							
2.1.1	Operation behind antennae	12.00	47.00	4h15min	24.00	94.00	2h	0.002
2.1.2	Operation in front of antennae	1240.00	2500.00	Not permissible	2480.00	5000.00	2h	0.242
2.1.3	Operation close to the lower edge of antennae	227.00	403.00	30min	454.00	806.00	2h	0.044
2.2	Operation near emitting antennae (distance up to 2 m)	390.00	820.00	15min	780.00	1640.00	2h	0.076
2.3	Operation along the feeder line	-	6.40	>8h	-	25.60	4h	0.001
3	Antennae mounted on a pole (wrist type)							
3.1	Operation in a close proximity of more than one antenna							
3.1.1	Operation in the area among antennae, on a pole	20.10	27.60	7h15min	120.60	165.60	6h	0.004
3.1.2	Operation between side edges of antennae	39.30	73.10	2h44min	235.80	438.60	6h	0.007
3.1.3	Operation close to the lower edge of antennae	235.60	620.90	19min	1413.60	3725.40	6h	0.046
3.1.4	Operation on new near emitting antennae	331.00	1223.00	Not permissible	1986.00	7338.00	6h	0.064

1	2	3	4	6	7	8	9	10
UMTS antennae								
2	**Single Antennae**							
2.1	**Operation in a close proximity of antennae**							
2.1.1	**Operation behind antennae**	45.00	86.50	Not permissible	888.00	2694.00	2h	0.006
2.1.2	**Operation in front of antennae**	444.00	1347.00	2h19min	90.00	173.00	2h	0.062
2.1.3	**Operation close to the lower edge of antennae**	29.00	60.00	3h20min	58.00	120.00	2h	0..004
2.2	**Operation on new near emitting antennae**	72.80	117.30	1h42min	145.60	234.60	2h	0.010
2.3	**Operation along the feeder line**	-	4.30	>8h	-	17.20	4h	0.001

ANALYSIS OF RESULTS AND CONCLUSIONS

The average and maximum power density S measured at the temporary workplaces for adjustment, maintenance and repair works exceed the limit values of both Bulgarian and European standards. The same is true for all works performed close to antennae at a distance up to 1 m during radiation. Even for short-duration tasks (for up to 2 h) the EMF values exceed the limits. When they are below them, the calculated energetic loading is above the limit.

The energetic loading is within the permissible limits only during works done behind the antennae or along the antenna-feeder lines.

Nevertheless high measured values of power density and calculated values of energetic loading of the organism calculated whole body SAR values correspond to the ICNIRP guidelines basic restriction for occupational exposure. Our legislation is stringent and in some operations forbids stay in such conditions. Although compliance of SAR values to the guidelines we consider that the personnel exposure especially on particular operations is significant.Therefore employers should take the following measures in order to protect the workers' health:

- technological operations in the close proximity of antennae should be performed after switching off emitters;
- use of personal protective equipment (clothes, glasses, etc.) when it is not possible to switch antennae off,
- when protective equipment is not used, combinations of technological operations should be made respecting the following limitation of the exposure:

$$\frac{\Sigma W_i}{W_н} \leq 1,$$

where Wi is the total energetic loading of the organism resulting from the "i" - technological operation;
Wlim is the maximum permissible energetic loading of the body according to the national standards.

Others not less important recommendations for the operators' safety work are the followings:

- permissible time duration specified in Bulgarian regulations should be kept;
- workers should use personal dosimeters, which provide data about the cumulated dose;
- periodical training of the staff about the risks of EMF and protection;

In conclusion, a high risk for EMF exposure is found for workers mounting and maintaining base stations for mobile communication. Hence, measures should be taken to improve the working conditions with respect to EMF by decreasing radiation, carrying administrative and organizational measures, ensuring continuous monitoring and personal protection. The energetic loading should be regularly assessed, while the field should be currently monitored by personal dosimeters. Periodical medical check-ups done by neurologist, cardiologist, therapist and ophthalmologist should be included into the prophylaxis program. Last but not least, the qualification of the staff in standards, biological effect, methods of measurement and protection against microwave fields should be currently maintained. Special attention should be paid to workers with active implants.

Bibliography

1.Mild, K. H., *et.al*, Occupational RF exposure from base stations antennae on roof-tops and buildings, Workshop, Base stations and wireless networks, 15-16 June, 2005, WHO, Geneva.

2. **Ordinance No 7 of 23.09.1999** of the MLSP and the MH on the minimum requirements for healthy and safe working conditions in workplaces and in the use of working equipment (SG No 88/1999.)[2]

3. **Bulgarian State Standard (BSS)17137-90**. Occupational hygiene. Electromagnetic microwave fields. Allowable values and control requirements [3].

4.Guidelines for limiting exposure to time varying electric, magnetic, and electromagnetic fields (up to 300 GHz), ICNIRP, Health Physics, April 1998, Vol.74, No.4.

5.Directive 2004/40/EC of the European parliament and of the council of 29 April 2004 on the minimum health and safety requirements regarding the exposure of workers to the risks arising from physical agents (electromagnetic fields) (18^{th} individual Directive within the meaning of Article 16(1) of Directive 89/391/EEC).

DIRECT AND MEDIATED EFFECTS OF THE EXTREMELY HIGH FREQUENCY COHERENT ELECTROMAGNETIC RADIATION (MILLIMETER WAVES) WITH LOW INTENSITY ON BACTERIA

TADEVOSYAN H.[1], KALANTARYAN V.[2], TRCHOUNIAN A.[1*]

Departments of Biophysics[1] and of High Frequencies Radiophysics and Telecommunication[2] of the Yerevan State University,
1 Alex Manoukian Str., 0025 Yerevan, Armenia
[*]E-mail: Trchounian@ysu.am

Abstract

In addition to bactericidal effect of "noise" electromagnetic irradiation (EMI) of extremely high frequencies [1-2], the coherent EMI of such frequency (the range of frequencies from 45 to 53 GHz) or millimeter waves (the wavelength of 5.6 to 6.7 mm), with low intensity (the flux capacity of 0.06 mW/sm^2), upon direct irradiation (during 30 min or 1 h), affected *Escherichia coli* K12, wild-type, grown under anaerobic conditions with fermentation of sugar (glucose): it caused a decrease in bacterial growth rate, maximal inhibitory effect was achieved at the frequency of 51.8 or 53 GHz. This effect depended on medium pH, the maximal one was at pH 7.5. The noticeable changes in membrane proton conductance, membrane potential, proton fluxes through the membrane of whole cells and total and *N,N'*-dicyclohexylcarbodiimide (DCCD)-inhibited ATPase activity of membrane vesicles were determined. These membranous effects might be accounted in action of EMI. A decrease in sensitivity to reagents (DCCD) by cells was also determined. Moreover, EMI had mediated effects on bacteria. Separate irradiation (the frequency of 51.8 and 53 GHz) of doubly distilled water or some inorganic ions containing Tris-phosphate buffer (pH 7.5), into which grown cells were transferred, during 30 min or 1 h, had changed further growth of these bacteria in different, opposite directions; irradiation of water only caused inhibitory effect. These might point out a role of water in the effects of EMI of extremely high frequency on bacteria. A significant action disappeared upon repeated irradiation at the frequency of 51.8 and 53 GHz during 1 h and with interruption for 2 h. This result indicates some compensatory mechanisms within bacteria.

The *keywords*: coherent electromagnetic radiation of extremely high frequency, bacterial growth, membranous effects, resonant frequencies, water.

INTRODUCTION

The bacterial effects of the electromagnetic irradiation (EMI) of extremely high frequencies, or millimeter waves, with low (low-energetic) intensity and with non-thermal action, are of interest because of two reasons, at least. First of all, bacteria and other cells can interact with each other through EMI (for reviews, see [3-4]). It has been shown, for instance, that bacteria possess the ultrasonic radiation [5-7] or reemission of secondary photons in sub-millimeter frequency range [8]. However radiation of extremely high frequency is not clearly registered in spite of the fact that fine methods have been developed and enough sensitive instruments have been already constructed for last years [9-10]. Secondly, EMI of extremely high frequency is widely used in telecommunication technology and therapeutic practice [2, 11] although low-orbital systems of cosmic communication and different elements of mobile one, and in addition, low-energetic devices used in therapeutic practice radiate EMI of this frequency, small and very small doses of which (low flux capacity of 0.005 mW/sm^2) might affect cells.

The coherent and so named "noise" (with broadband frequencies and accidentally changing phases) EMI of extremely high frequencies with low intensity have been shown to cause different, including bactericidal effects on *Escherichia coli* and the other bacteria [10-14]. Such effects depend on phase and anaerobic or aerobic conditions of

the bacterial growth, composition of growth media, genetic features and peculiarities of the metabolism in bacterial strains. Together with these, coherent and noise EMI of extremely high frequencies can render the different bacterial effects depending on frequency and intensity of EMI, duration of the irradiation and the other parameters [1-2]. Moreover, studies on repeated and mediated action of noise EMI on *E coli* [2] have allowed expecting compensatory mechanisms and role of other factors.

Among cellular mechanisms of bacterial effects of EMI of extremely high frequencies, the membranous changes connected with surface characteristics of plasma membrane, ion and other substances transport across the membrane and energy-conversing processes [1-2, 12-13] are of significance. Action of EMI of extremely high frequency is offered also on structure and properties of water [14-16] leading, for instance, to increase in chemical activity of water or hydration of proteins and other cellular structures. These could also relate to modifications of structure, properties and function of membrane, especially membrane proteins. On the other side, conformational changes in bacterial genome or DNA are also suggested [17]. Bactericidal effect might be determined by transition of bacterial pro-phages from lysogenic to lytic state [18-19].

Finally, effects of such EMI can be a result of the resonant interaction, when in case with *E coli* it is shown that, regardless of intensities of EMI of extremely high frequency, resonance is at the frequencies of 41.5, 51.8 or 70.6 GHz [17-19]; other resonant frequencies are not ruled out. However, effects of EMI on these and other bacteria and cells in generally, especially primary cellular mechanisms of these effects, require the further study.

In the present report with fermenting *E coli*, grown in anaerobic conditions, it is shown that maximal inhibitory effect of coherent EMI of extremely high frequency on bacterial growth rate was observed at the frequencies in 51.8 or 53 GHz. The changes in membrane properties and functions have been determined. The certain effects might be mediated by the other factors and changed by repeated irradiation.

MATERIALS AND METHODS

E coli K12, wild type strain, was used in the study.

The methods for bacterial growth in peptone medium (0.2 % peptone, 0.5 % NaCl and 0.2 % K_2HPO_4) at slightly alkaline (pH 7.4) or the other (specified in text) pH in anaerobic conditions upon fermentation of sugar (glucose, 0.2 %) [1, 20] and determination of bacterial specific growth rate (μ) [1, 21] were described elsewhere. The methods for preparation of whole cells for assays and isolation of membrane vesicles [21-22], for determination of membrane proton conductance (G_m^{H+}) [23], membrane potential ($\Delta\Psi$) [24] and energy-dependent proton efflux (J_H^+) [1, 23-24] from whole cells as well as of ATPase activity of membrane vesicles [21-22], and, in addition, for data processing [25] did not differ from widely described.

The pH of growth medium and assay solutions was measured by using a fine pH-potentiometer with selective (pH) electrode and adjusted by means of HCl and NaOH, although pH of doubly distilled water was 6.5 and did not changed when kept during 2 days at 4 ^{0}C in spite of its less-buffering capacity. The dry weight of bacteria and protein were determined by the method described by Trchounian and Vassilian [21] and Lowry et al. [26], correspondingly. Bacterial titer was calculated by counting colonies grown on solid media with glucose after plating of diluted bacterial suspension.

The irradiation of *E coli*, water or the other solution was produced by means of generator G4-141 (radiating the coherent electromagnetic waves with frequency within the range of 45 to 53 GHz, wavelength of 5.6 to 6.7 mm, correspondingly; the flux capacity was of 0.6 mW/sm^2). The generator was assembled in the Institute of Radiophysics and Electronics of the National Academy of Sciences of Armenia (Ashtarak City). For the others, the conditions of the irradiation of bacteria were similar to those described previously [1]. After direct irradiation of bacterial suspension (grown cells concentrated by centrifugation in water), cells were immediately transferred into the fresh growth (with glucose, 0.2 %) or assay medium.

At determination of the mediated influence of EMI of extremely high frequency on *E coli*, grown cells were transferred into the distilled water or buffer (Tris-phosphate, pH 7.4) containing 0.4 mM $MgSO_4$, 1 mM KCl and 1 mM NaCl, and then, after incubation of 10 min, growth or other assays were carried out immediately. Water or buffer was irradiated during 30 min or 1 h as specified in text. The repeated influence of EMI of extremely high frequency was conducted with interruption of 2 h.

The data processed to be statistical with determination of the standard error and of the Student's validity criteria (p) [26].

RESULTS AND DISCUSSION

Inhibitory effect of coherent EMI of extremely high frequency on bacterial growth

Bactericidal effect of "noise" EMI with frequencies of 53.5 to 68 GHz on *E coli* was installed earlier [1-2]. If such effect is conditioned resonant interaction of EMI of extremely high frequency with bacteria, the range of frequencies of "noise" EMI used does not include the resonant frequencies in 41.5, 51.8 or 70.6 GHz shown for *E coli* [17-19]; the other resonant frequencies may be allowed. Therefore a study of bacterial effects of the coherent EMI with resonance frequency in 51.8 GHz, which is radiated by the generator used (see Materials and methods) was done. Together with this, effects of EMI of extremely high frequency hang from conditions of the growing bacteria [1-2, 11-13] and they can differ in anaerobic conditions, favorable for the majority of pathogenic and conditionally pathogenic bacteria, therefore studies conducted with *E coli*, grown in anaerobic conditions under fermentation of sugar.

Irradiation of *E coli* K12 by coherent EMI with the coherent frequency of 45 to 53 GHz during 30 min (not shown) or 1 h (Fig. 1) brings a gradual decrease in the specific rate of bacterial growth for the frequency of 49 GHz, moreover maximal inhibitory effect was observed at the frequency of 51.8 or 53.0 GHz. Such result complies with those the frequency of 51.8 GHz is resonant for *E coli* [17-19] and, on the other side, the exposition of 1 h is effective to inhibit bacterial growth [11]. The resonances in which proteins and other macromolecules can be entered probably are the basis of membranous and the other mechanisms of the action on bacteria and define bactericidal effect of EMI of extremely high frequency.

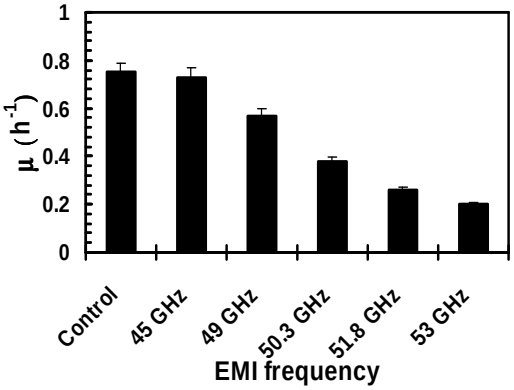

Fig. 1. The changes in the growth rate of *E coli* K12 after direct irradiation with coherent EMI of extremely high frequency. The specific growth rate (μ) was defined as 0,693/time of the reduplication to absorbance (OD) in bacterial suspension (when logarithm of OD linearly increased at time) [10-11]; in checking control, bacteria without irradiation. For the others, see Materials and methods. The average values are from not less than three independent experiments with standard errors.

Note that the inhibitory effect of coherent EMI of extremely high frequency on bacterial growth depends on duration of the irradiation: increase in time of the direct irradiation from 30 min to 1 h at the frequency of 51.8 or 53.0 GHz brings about reinforcement of the effect in 2.2- or 1.6-fold, respectively.

A dependence of the action of EMI of extremely high frequency on *E coli* from pH is of interest: under pH 6.0 and 8.0 in contrast with pH 7.5, inhibitory effect noticeably decreased (Tabl. 1.). Since the specific growth rate practically does not depend on medium pH in noted range (not shown), the change in this rate after irradiation can be indicative of some process as in cells themselves, so and in water medium with determined reaction (pH), in which bacteria grow. Probably, a slightly alkaline medium (pH 7.3-7.5) is chosen not accidentally as the most optimal for growing *E coli* (neutrophilic bacteria) [27].

Table 1. The specific growth rate of *E. coli* K12 irradiated by EMI of extremely high frequency at different pH.

pH*	Growth rate (h^{-1})		
	Control	51.8 GHz	53.0 GHz
6.0	0.86 ± 0.05 (100 %)	0.63 ± 0.03 (73.3 %) ($p<0.05$)**	0.60 ± 0.03 (69.8 %) ($p<0.05$)
7.5	0.82 ± 0.03 (100 %)	0.52 ± 0.02 (34.7 %) ($p<0.01$)	0.34 ± 0.02 (26.7 %) ($p<0.002$)
8.0	0.77 ± 0.03 (100 %)	0.70 ± 0.05 (91.0 %) ($p<0.05$)	0.50 ± 0.02 (64.9 %) ($p<0.05$)

* irradiation time was 1 h, for the other conditions, see Materials and methods and the legends to Fig. 1.

** p is calculated for the difference between the values in checking control and obtained ones; percentage is determined in relation to checking control (100 %).

On mechanisms of bacterial effects of EMI

Determination of some properties and of activity of some key membrane-associated enzymes having a key role in ion and the other substances transport and energy conversation could be of much interest to reveal mechanisms of bacterial effects of EMI. The marked changes in G_m^{H+} (Fig. 2A), $\Delta\Psi$ (Fig. 3) and energy-dependent proton efflux (Fig. 2B) were shown followed irradiation of *E coli* K12 by EMI with the resonant frequency of 51.8 [17-19] or 53 GHz. It is possible to suggest some relationship between these properties of the membrane since the changes in the values of G_m^{H+} and $\Delta\Psi$ were in opposite directions and moreover J_H^+ decreased upon irradiation. Such relationship between G_m^{H+} and $\Delta\Psi$ has been proposed by Akopyan et al. [23] requiring a further study. These changes in the properties of the bacterial membrane might be of significance and could be accounted for decrease in bacterial growth rate.

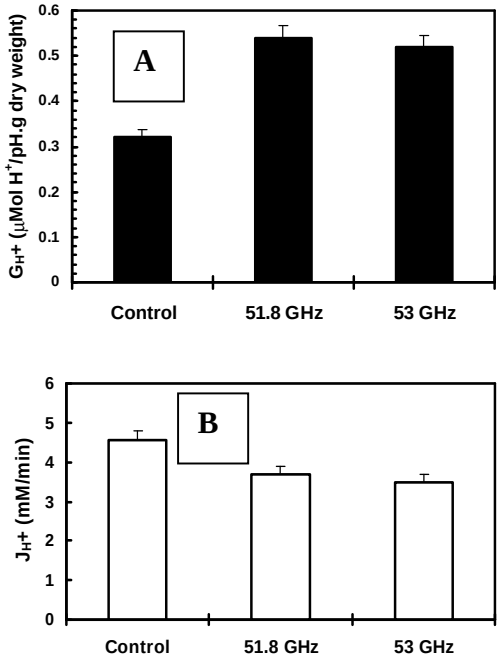

Fig. 2. Changes in membrane proton conductance (G_m^{H+}, A) and energy-dependent proton fluxes (J_H^+, B) of of *E coli* K12 after direct irradiation with coherent EMI of extremely high frequency. The irradiation time was 1 h, the frequency was shown. G_m^{H+} was determined by an acid-pulse technique used before [23]. Energy-dependent ion fluxes were determined by using selective (pH) electrode upon glucose (22 mM) adding; the values represented are for bacterial count of 10^{12} cells [23-24]. For the others, see Materials and methods and the legends to Fig. 1.

Furthermore, total and DCCD-sensitive ATPase activity was inhibited significantly by irradiation with coherent EMI of the frequency of 51.8 or 53 GHz although ATPase activity in the presence of DCCD (0.1 mM) has no changes or, in opposite, is increased a little (Fig. 4). Taken into consideration the fact that DCCD is inhibiting the F_0F_1-ATPase in *E. coli* under fermentation [28], the results obtained indicate that this ATPase may be a target for action of EMI of extremely high frequency.

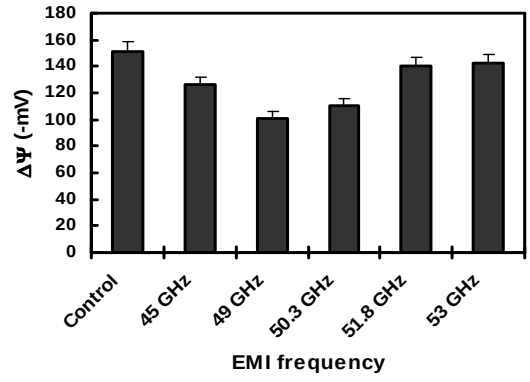

Fig. 3. *E. coli* K12 membrane potential ($\Delta\Psi$) values after irradiation with coherent EMI of extremely high frequency. The irradiation time was 1 h. $\Delta\Psi$ was calculated from distribution of tetraphenyl-phosphonium cation (initial external concentration of 1 μM) between the cytoplasm and the external medium determined with appropriate selective electrode [24]. For the others, see the legends to Fig. 1.

In addition, it should be noted that, in the K^+-less assay medium (concomitant K^+ was of 0.02 mM [21]), total ATPase activity was of lower values close to those in the presence of DCCD (see Fig. 4) having no any marked changes by irradiation with the frequency used (not shown). This is of importance since K^+-sensitive and DCCD-inhibited ATPase activity in *E. coli* has been shown clearly be the F_0F_1-ATPase activity that is associated with K^+ uptake TrkA system [21, 29-30]. Therefore, EMI of extremely high frequency affected K^+-sensitive and DCCD-inhibited ATPase activity suggesting that the F_0F_1-ATPase could be a target for EMI.

Moreover, inhibitory effect of DCCD (in different concentrations of 0.1 to 1 mM) on J_H^+ markedly decreased after irradiation with EMI at the frequency of 51.8 or 53 GHz (Fig. 5) in sprite of different proton fluxes (comp. with Fig. 2B) suggesting that sensitivity of bacteria to inhibitors (DCCD) may be also affected by irradiation with coherent EMI of extremely high frequency. Such an effect was determined with "noise" EMI before [1]. A less sensitivity to DCCD could result from conformational changes in subunits of the F_0F_1-ATPase [31] having a key role in effects of EMI on bacteria. This seems to be in accordance with results reported by Bulgakova et al. [13] that EMI of extremely high frequency with non-thermal intensity could change the sensitivity of *Staphylococcus* to various antibiotics having membranotropic properties. The irradiation (during up to 1 h) is of importance can result in opposite changes inhibiting and stimulating bacterial growth [13]. In all cases, these results might be extrapolated to different reagents and drugs and should be accounted in therapeutic practice. Moreover, this would lead to further study to reveal primary cellular mechanisms for bacterial effects of EMI of extremely high frequency.

Fig. 4. The ATPase activity of membrane vesicles isolated from *E. coli* K12 after irradiation with coherent EMI of extremely high frequency. The irradiation time was 1 h. ATPase activity was calculated by colorimetric determination of liberation of inorganic phosphate (P_i) per time and protein [21-22] upon ATP (3 mM) adding. DCCD was added in final concentration of 0.05 mM in parallel assays. For the others, see Materials and methods and the legends to Fig. 1.

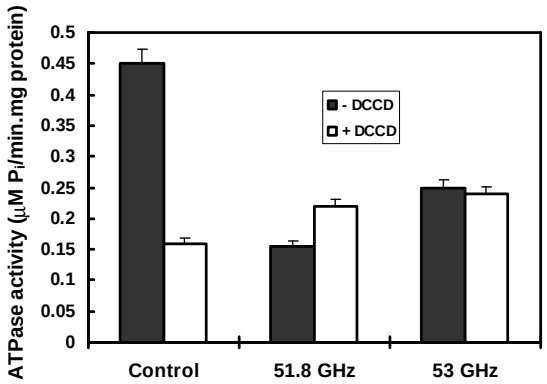

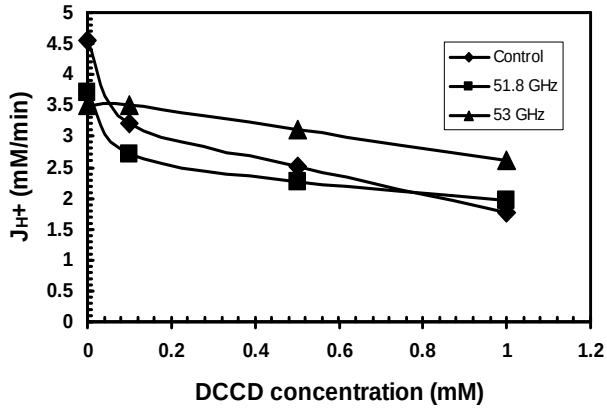

Fig. 5. The changes in inhibitory effect of DCCD on J_H^+ from *E. coli* K12 after direct irradiation with coherent EMI of extremely high frequency. The irradiation time was 1 h, for the others see Materials and methods and the legends to Fig. 1.

Mediated action of EMI on bacteria

The action of EMI of extremely high frequency on bacteria studied under separate irradiation of water or buffers containing different ions (see Materials and methods), in which bacteria are kept under assays [2, 12].

Table 2. Mediated action of EMI of extremely high frequency on the following growth rate of *E. coli* K12.

Conditions*	Growth rate (h^{-1})		
	Control	51.8 GHz	53.0 GHz
Doubly distilled water	0.82 ± 0.03 (100 %)	0.52 ± 0.02 (63.4 %) ($p<0.01$)**	0.34 ± 0.02 (41.5 %) ($p<0.002$)
Assay medium	0.78 ± 0.03 (100 %)	1.22 ± 0.05 (156.4 %) ($p<0.01$)	1.41 ± 0.08 (180.8 %) ($p<0.01$)

* irradiation time was 1 h, for the other conditions, see Materials and methods and the legends to Fig. 1.
** see the legends to Table 1.

When irradiation by the duration of 30 min (not shown) or 1 h (Table 1) and with the frequency of 51.8 or 53.0 GHz was subjected to water, the specific growth rate for *E coli* K12 (after premises in such water during 10 min and then their moving into growth medium with glucose, see Materials and methods) decreased on more than 35 % in comparison with control (Tabl. 2.). But this mediated action was with less effects than direct irradiation of bacteria in the water (comp. with Fig. 1 and Tabl. 1). When irradiation was subjected to the buffer, the growth rate, on the contrary, increased on more than 56 % (Tabl. 2). Evidently, cells may be affected by Tris (hydroximethilaminomethane) or the other buffer components, but data are very poor [2, 32].

Note that water has acidic reaction and transferring cells from slightly acidic medium or slightly alkaline medium could affect growing bacteria. In addition, osmotic shock should be also taken into consideration, since cells are transferring into the medium with greater osmolarity. However, such procedures were shown before do not affect growing *E coli* [33].

Thereby, mediated action of coherent EMI of extremely high frequency on *E coli* might be of different nature. This was observed earlier with "noise" EMI depending on bacterial growth phases and other factors [2]. The results point out a role of water and medium composition in effects of EMI of extremely high frequency on bacteria.

Repeated action of EMI on bacteria

If bacteria have any compensatory mechanisms [2], then these mechanisms possibly become to be important under the repeated irradiation with coherent or "noise" EMI of extremely high frequency. Indeed, the repeated action of coherent EMI with the frequencies in 51.8 or 53.0 GHz on *E coli* K12 (irradiation during 1 h with interruption of 2 h, in checking control repeated irradiation was absent but bacteria were kept with the same time) reduced considerably an inhibitory effect (in 1.7- or 1.9-fold for the frequency of 51.8 or 53.0 GHz, correspondingly; $p<0.01$).

Certainly, compensatory mechanisms in bacteria have not studied, although miscellaneous defensive proteins like those discovered in animal cells [34] might play a role.

Thereby, the results obtained are indicative of negative action of coherent EMI of extremely high frequency on bacteria, when maximal effect is observed at the frequency in 51.8 and 53.0 GHz. The frequency of 51.8 GHz in studied range of EMI (see Materials and methods) is probably a resonant frequency causing maximal effect.

Concluding remarks

The study done defines the bacterial effects of coherent EMI of extremely high frequency with low intensity causing changes in *E. coli* growth and points out some membranous aspects of the mechanisms of such an action. The effects of coherent EMI of the frequency of 51.8 or 53.0 GHz on bacterial growth rate and some properties of the bacterial membrane (see Results and discussion) should be noted to be much stronger than appropriate effects of "noise" EMI of extremely high frequency reported [1-2].

Bacterial effects of "noise" and coherent EMI of extremely high frequency with low intensity shown in the present paper and by different groups [1-6, 10-13, 17-19] are of significance to understand distinguishing role of bacteria in biosphere nowadays leading to changed metabolic pathways and, for instance, to antibiotics resistance (for review, see [35]).

The present results are principal to the further study of mechanisms of biological effects of EMI, on the one hand, and in the same time, for determination of the allowed doses of the long irradiation of the persons and the

other organisms by means of EMI of extremely high frequency to manage appropriate preventive ways. Moreover, it should be necessary to improve using EMI of extremely high frequency in therapeutic purpose, when repeated action can turn out to be inefficient. It is also possible to use EMI for product protection from bacteria. In addition, the results are important for construction of new generators of EMI of extremely high frequency and facilities for telecommunications.

The authors thank L. Arutyunyan and K. Akopyan for help in undertaking some experiments. This study was done within the framework supported by Ministry of Education and Science of the Republic Armenia (Grant # 54).

REFERENCES

1. Trchounian A., Ogandzhanyan E., Sarkisyan E., Gonyan S., Oganesyan A., Oganesyan S. // *Biophysics*. 2001. V 46. P. 69-76.

2. Isakhanyan V., Trchounian A. // *Biophysics.* 2005. V. 50. P. 604-606.

3. Kaprelyants A., Kell D.B // *Trends Microbiol.* 1996. V. 4. P. 237-242.

4. Trushin M.V // *J. Microbiol. Immunol. Infect.* 2003. V. 36. P. 153-160.

5. Matsuhashi M., Pankrushina A.N., Endoh K., Watanabe H., Mano Y., Hyodo M., Fujita T., Kugunita K., Kaneko T., Otani S // *J. Bacteriol.* 1995. V. 177. P. 688-693.

6. Matsuhashi M., Pankrushina A.N., Takeuchi S., Ohshima H., Miyoi H., Endoh K., Murayama K., Watanabe H., Endo S., Tobi M., Mano Y., Hyodo M., Kobayashi H., Kaneko T., Otani S., Yoshimira S., Harata A., Sawada T // *J. Gen. Appl. Microbiol.* 1998. V. 44. P. 49-55.

7. Norris V., Hyland G.J // *Mol. Microbiol.* 1997. V. 24. P. 879-880.

8. Alipov E.D., Scheglov V.S., Sarimov R.M., Belyaev I.Ya. // *Radiats. Biol. Radioecol*. 2003. V. 43. P. 167-171.

9. Alekseev S.I., Ziskin M.C. // *Bioelectromagnetics.* 2000. V. 21. P. 264-271.

10. Chen W.S., Ma P.M., Liu H.L., Yeh C.K., Chen M.S., Chang C.W. // *J. Acoust. Soc. Am.* 2005. V. 117. P. 3740-3749.

11. Akyel Y., Pakhomova O.N., Stuck B.E., Murphy M.R // *Bioelectromagnetics.* 1998. V. 19. P. 393-413.

12. Gub N.M., Luneva I.O., Denisova S.N., Ostrovsky N.V. // *Millimeter waves in medicine and biology*. 10th Russian Symp. with intern. participation. Moscow, 1995. P. 96 (in Russian).

13. Bulgakova V.G., Grishina V.A., Orlova T.I., Petryakina Z.M., Polin A.N., Noks P.P., Kononenko A.A., Rubin A.B. // *Biophysics.* 1996. V. 41. P. 1289-1293.

14. Bechkii O.V., Devytakov N.D., Kislov V.V. // *Crit Rev. Biomed. Eng.* 2000. V. 28. P. 247-268.

15. Fesenko E.E., Geletyuk V.I., Kazachenko V.N., Chemeris N.K // *FEBS Lett.* 1995. V. 366. P. 49-52.

16. Gapeyev A.B., Safronova V.G., Chemeris N.K., Fesenko E.E // *Bioelectrochem. Bioenerg*. 1997. V. 43. P. 217-220.

17. Belyaev I.Ya., Alipov Y.D., Scheglov V.S., Lystsov V.N. // *Z. Naturforsch*. 1992. V. 47. P. 621-627.

18. Lukashevsky K.V., Belyaev I.Ya // *Med. Sci. Res.* 1990. V. 18. P. 955-957.

19. Belyaev I.Ya., Shcheglov V.S., Alipov Y.D., Polunin V.A // *Bioelectromagnetics.* 1996. V. 17. P. 312-321.

20. Trchounian A., Kobayashi H. // *FEBS Lett.* 1999. V. 447. P. 144-148.

21. Trchounian A., Vassilian A. // *J. Bioenerg. Biomembr*. 1994. V. P. 563-571.

22. Bagramyan K., Mnatsakanyan N., Trchounian A. // *Biochem. Biophys. Res. Commun.* 2003. V. 306. P. 361-365.

23. Akopyan K., Zakharyan E., Kirakosian G., Mnatsakanyan N., Bagramyan K., Trchounian A. // *Biophysics.* 2002. V. 47. P. 985-988.

24. Martirosov S.M., Trchounian A., Petrosian L., Vardanyan A. // *Bioelectrochem. Bioenerg*. 1981. V. 8. P. 513-520.

25. Lakin G.F. Biometriya. M.: High School. 1992 (in Russian).

26. Lowry O.H., Rosenbrough N.J., Farr A.C., Randall R.J. // *J. Biol. Chem.* 1951. V. 193. P. 265-275.

27. Kobayashi H // *Recent Res. Devel. Bioenerg*. 2000. V. 1. P. 33-43.

28. Trchounian A., Ohandjanyan E., Bagramyan K., Vardanyan V., Zakharyan E., Vassilian A., Davtian M. // *Biosci. Rep.* 1998. V. 18. P. 143-154.

29. Bagramyan K., Mnatsakanyan N., Poladian A., Vassilian A., Trchounian A // *FEBS Lett.* 2002. V. 516. P. 172-178.

30. Trchounian A. // *Biochem. Biophys. Res. Commun.* 2004. V.315. P. 1051-1057.

31. Nakamoto R.K., Ketchum C.J., Kuo P.H., Al-Shawi M. // *Biochim. Biophys. Acta.* 2000. V. 1458. P. 289-299.

32. Dosch D.C., Helmer G.L., Sutton S.H., Epstein W. // *J. Bacteriol.* 1991. V. 173. P. 687-694.

33. Trchounian A.A., Ogandjanian E.S., Vanian P.A // *Curr. Microbiol.* 1994. V. 27. P. 187-191.

34. Novoselova E.G., Glushkova O.V., Sinotova O.A., Fesenko E.E. // *Dokl. Russ. Acad. Sci.* 2005. V. 401. P. 117-119 (in Russian).

35. *Bacterial Stress Responses*. Storz G., Hengge-Aronis R. (Eds.). ASM Press. Washington DC. 2000. 502 p.

MICROWAVE IONOSPHERIC EMISSION AS A NEW FACTOR OF SOLAR-BIOSPHERE RELATIONS

SERGEI V. AVAKYAN

S.I. VAVILOV STATE OPTICAL INSTITUTE, Tuchkov lane 1, 199034, St. Petersburg, Russia, avak2@mail.ru

Abstract

This paper proposes and provides substantiation for a hypothesis concerning the mechanism by which solar and geomagnetic activity (mainly of solar flares and magnetic storms) affects the biosphere, including man. The hypothesis, including a physical mechanism introduced by the author and new for aeronomy, is that high-lying (Rydberg) states of all gases of the earth's upper atmosphere are excited by ionospheric electrons. Rydberg atoms, molecules and ions of all atmospheric gases emit characteristic radio emission in the spectral range from decimeters to millimeters. This radiation can easily penetrate to low atmosphere and biosphere carrying complete information about power and duration of solar flare and geomagnetic storms to biosphere. The microwave radioemission have the resonances at the spectral range $10^9 \div 10^{12}$ Hz at the biological cells and membranes, DNA and RNA, molecules of hemoglobin, human erythrocytes, and this fact can explain the extremely small threshold for influence of ionospheric radioemission at the monochromatic (characteristic) Rydberg transitions on biological objects, including the viscosity of blood.

The energy estimates of the flux intensity of microwave radiation of the ionosphere from Rydberg states are used to prove for the first time that the values of this flux agree with the experimental data. A method is proposed for distinguishing the contributions of microwave radiation and magnetic perturbation in the geobiocorrelations, taking into account the effect that the magnetic-field variations are not in phase with the flux of corpuscles from the radiation belts in the ionosphere during the period of a geomagnetic storm.

There are several problems in ionospheric and atmospheric physics, biophysics and medicine concerning the investigations of Rydberg excitation role:

- determination of the real spectral distributions for Rydberg ionospheric emission at all transparency windows;
- determination of the perception threshold for the characteristic sharp-resonance microwave Rydberg emission for healthy and sick persons;
- modelling investigations of negative influence of cell telephone. The sporadic increase for the microwave ionospheric Rydberg radioemissions during power solar flares and principal magnetic storms will be taken into account for consideration of the stochastic resonance.

Introduction

One of the fundamental problems of modern natural science is the search for biophysical mechanisms by which solar and geomagnetic activity, and especially solar flares and magnetic storms, affect people and the biosphere as a whole. The accumulated experimental material is mainly evidence, at least in indirect form, of the presence of heliogeobiocorrelations. It is obvious that such correlations are very complex because of their multifactorial nature. At the same time, they indicate that there is some physical mechanism responsible for the transport of the energy given off into the thickness of the lower atmosphere and biosphere when the solar and geomagnetic activity increases. In fact, the main energy flows that vary when there are variations of the solar and geomagnetic activity do not reach the lower atmosphere but are completely absorbed in the earth's upper and middle atmosphere (above 20 km). The chief variations in the electromagnetic radiation flux from the sun actually occur in the region of far- and extreme-UV radiation and soft x rays, which is completely absorbed in the upper atmosphere. It is well known that the radiation flux which ionizes the earth's upper atmosphere in the range from soft x rays to the vacuum UV (with wavelengths from 0.1 to 134 nm) increases most strongly (by a factor of several thousand and sometimes by tens of thousands) in the periods of solar flares. The energy of this flux is 6–7 orders of magnitude higher than that of solar rf radiation in the periods of strong flares.

Corpuscular solar radiation (the solar wind, energetic solar protons and electrons) also do not penetrate into the lower atmosphere. When the geomagnetic activity increases—magnetic storms and substorms, there is a sporadic precipitation of electrons and protons from the earth's radiation belts into the ionosphere, but these flows also completely dissipate at higher altitudes (above 40 km).

The fluxes of charged particles, mainly electrons, as well as protons, that precipitate into the earth's upper atmosphere from the overlying radiation belts also increase by several orders of magnitude during strong

magnetic storms. In periods of solar flares and during magnetic storms, the very first process of complete dissipation of the energy of particle fluxes intruding into the earth's upper atmosphere is the ionization of all the atmospheric gases with the formation of photoelectrons, secondary electrons, and Auger electrons.

The energetics of the variations during the period of geomagnetic perturbations of the geomagnetic field itself with respect to the mean value and even more in absolute magnitudes are insignificant. Therefore, the "*kT* problem" in magnetobiological effects1 is continually being discussed in the literature [1].

In this connection, there is interest in discussing the arguments in favor of the hypothesis of [2, 3] on the importance in heliogeobiospheric correlations of the contribution of the microwave radiation of the earth's ionosphere, detected as sporadic rf radiation when the solar and geomagnetic activity increases [4-6].

Microwave Rydberg radiation of the ionosphere as a factor of the action of solar and geomagnetic perturbations on the biosphere

In 1994, we were the first to propose [7] that the fact that the plasma of the earth's upper atmosphere (and of other planetary atmospheres) unconditionally contains highly excited Rydberg states of atoms, molecules, and their ions should be taken into account in aeronomy and ionospheric physics.. Rydberg states correspond to strong excitation of a valence electron that had been in orbit with high principal quantum number $n>10$. In practice, this is a state of an atomic-molecular particle of any gas of the upper atmosphere close to its ionization potential. The corresponding atomic spectra were experimentally studied for the first time by the Swedish physicist Johannes Robert Rydberg (1854– 1919). These Rydberg states are metastable (long-lived), since most radiative quantum transitions from them have low probability. Transitions from the Rydberg states fill virtually the entire region of the electromagnetic spectrum of the upper atmospheric emissions, beginning from the extreme UV radiation. According to the selection rules for electric dipole transitions, the allowed transitions will be those for which the orbital-momentum quantum number change by an amount $l=\pm1$. Therefore, because of the high values of n and hence of l ($l=n-1$ and below), transitions from high l can occur only between adjacent Rydberg states and consequently lie in the rf region [8].

It should be emphasized that there has been no monitoring of the variations of the absolute magnitude of the fluxes of solar ionizing (soft x rays and EUV) radiation and their spectral composition. There are no experimental data on the spectra or increments of the fluxes in the periods of flares on the sun of various levels and classes. And the only experiment that carries out the tasks involving the total monitoring of solar shortwavelength activity is the Permanent Space Solar Patrol that we proposed. This experiment includes measurements in the entire spectral interval with the spectral resolution needed for solar-terrestrial physics of about 1 nm in the constant regime with continuous scanning of the spectrum every 72 sec, which is close to the duration of subflares and to the pulse phase of powerful flares [9, 10].

In [2, 3, 7, 8] for the physical mechanism of the generation of microwave radiation of the ionosphere, using the process of excitation by electron impact (by ionospheric photoelectrons, auroral and secondary electrons, and also Auger electrons) of the Rydberg states of the components of the upper atmosphere and ionosphere. Specific emissions from Rydberg levels are constantly recorded when the optical radiation of the upper atmosphere is observed [11] as well as in active experiments [12]. These experiments consisted of heating the ionosphere with powerful pulses of radio waves at frequencies of 4.7–6.8 MHz. In response, the ionosphere generated microwave decimeter radiation from the altitude interval from 185 to 240 km, as well as additional emission of the red lines of the oxygen atom. The analysis given in [12] of various ways to generate the detected microwave radiation includes the following: scattering of the earth's thermal radiation at artificial inhomogeneities of the electron concentration, bremsstrahlung of electrons accelerated by high-frequency plasma turbulence to energies of the order of 10–15 eV, and transitions of the electrons between high Rydberg levels of the molecules of the neutral components of the ionospheric plasma excited when they collide with accelerated electrons, showed that the last of the three enumerated mechanisms is the most probable. It was also emphasized in [12] that the region of artificial generation of microwave radiation coincides in altitude (about 200 km) with the position of the maxima of the altitude profiles of the excitation rates of the Rydberg states, calculated in [8] for the ionosphere under natural conditions. Thus, [12] is the first experimental proof of the excitation mechanism of Rydberg levels by energetic ionospheric electrons proposed in [8].

In this investigation the results of calibration for excitation rates of Rydberg states at the altitudes of 95 to 360 km are presented. The main process of this excitation at ionosphere is electron impact, by photoelectrons at the low and middle latitudes and by precipitating from magnitosphereelectron at auroral zones. In the upper atmosphere and ionosphere there are three types of electrons with energies up to several tens and hundreds of electronvolts for which the Rydberg excitation cross sections are maximal:

- photoelectrons, which arise when gases are ionized by the sun's x radiation and extreme UV radiation;
- secondary electrons, formed during ionization by corpuscles (electrons and protons from the radiation belts) precipiteted into the upper atmosphere during geomagnetic storms and substorms;
- Auger electrons, formed both during photoionization and during corpuscular ionization.

The Auger effect in all its manifestations in the ionospheres of the planets also was considered for the first time in our papers [13]. All these ionization electrons in their flux intensity directly track any variations of the solar and geomagnetic activity – from quiet periods to the strongest solar flares and geomagnetic storms and substorms. The Rydberg rf radiation of the ionosphere excited by these electrons accordingly carries full spatiotemporal information concerning all the variations of the ionizing fluxes; i.e., it scans all forms of heliogeophysical activity.

The excitation rate increases with the growth of geomagnetic and solar activities in particular during the solar flares (up to 10 times and more) and during the principal magnetic storms (up to 100 times and more). Unlike the auroral zone, where the excitation rate as a rule shows only one main maximum at the altitude about 100 km, during the solar flare there are usually two maximuma. The first maximum, connected with EUV solar radiation, occurs at the altitude near 200 km and its value increases during a flare by several tens per cents. The second maximum at the altitude above 100 km becomes the main one the large flare. Its increase comes up to ten times and resulted from the X-ray solar radiation. During the quiet Sun the excitation rate of sum of the Rydberg states exceeds the value 10 $cm^{-3}s^{-1}$ for atoms and molecules of oxygen and 100 $cm^{-3}s^{-1}$ for molecules of nitrogen. During solar flare 2B the integral intensity in vertical column is 10^9 photons cm^{-2} s^{-1}. It is important that the increase of excitation rates of the non-Rydberg states in the visual and UV spectral range (for example the LBH system of bands of nitrogen) at the same flare is smaller by factor of three. The centimeter radioemission results from transition with changing the orbital quantum number on 1, for example in atomic oxygen at n = 10 − 20, and the decimeter radioemission occurs at n = 20 − 40, if n is constant. If $\Delta n > 1$ and $n > 10$, there are the millimeter emissions of ionosphere. In the experiments, which registrated sporadic ionospheric radioemission in the range from 3 cm to 2 m with intensity increase of several times during solar flares, particularly when there were sudden ionospheric disturbances (SID), associated with X-ray flux of solar flare [5, 6, 14-17].

It should thus be assumed that a direct information channel from the lowest layers of the atmosphere and the biosphere itself concerning variations of the solar and geomagnetic activity has been determined [2, 3, 8]. For the biosphere and in particular for the human organism, this information, in the form of flux variations of the microwave radiation, can be just the Agent X that was postulated by A.L. Tchijevsky. It should be emphasized that the sun itself emits in the rf region, but this radiation does not directly correlate with the main flare flux—the flux of geoeffective short-wavelength (extreme UV and x-ray) radiation, whose energy is seven orders of magnitude greater than the solar rf flux. The main thing, however, is that the rf radiation of the sun is not monochromatic and consists not of separate lines and bands but has a continuous spectrum.

The latter circumstance can be decisive in demonstrating that the microwave radiation of the ionosphere is biologically effective. In fact, numerous experimental and theoretical papers on studies of the mechanisms by which millimeter and centimeter radiation acts on a living organism emphasize the resonance character of the response of biological cells and erythrocytes to such irradiation. So, there are several works about the theoretical and experimental resonance of living systems: biological cell at the $f = 41.782 \cdot 10^9$ Hz (λ = 7.2 mm) and f = 83.564 10^9 Hz (λ = 3.6 mm) [20]; DNA-spirale at the $f = 4\ 10^{10}$ Hz (λ = 7.5 mm) [21]; molecule DNA at the f = 10^9 Hz (λ = 3 dm) [22], molecule RNA at the $f = 10^9$ Hz (λ = 3 dm) [22], cellular membrane at the $f = 10^{10}$–10^{11} Hz (λ = 3 cm – 3 mm) [22], human erythrocytes at the $f = 10^{10}$ Hz (λ = 3 cm) [23]. It is very important that experimental Δf less than $10^{-3} \div 10^{-4}$ f [21]. Consequently, not only cells of the human organism, but also the blood, have resonance microwave frequencies at which the Rydberg ionosphere excited by flares and magnetic storms radiates. The explanation of how flares and storms act on cardiovascular patients follows from this. Thus, the influence of geomagnetic perturbations on the capillary circulation in patients of ischemic disease of the heart [24] on the day of a magnetic storm and the influence of solar flares and magnetic storms on patients with vascular pathology of the heart and brain [25]. are directly explained by the action of Rydberg rf radiations on the blood, including an increase of the viscosity and deformability of the erythrocytes.

The influence on the blood of a hypothetical signal associated with solar activity and manifested in the period of a flare on the sun and during the subsequent geomagnetic storm (in terms of the statistics of cardiovascular diseases) was discussed in [26]. Of course, these questions were discussed earlier by A. L. Tchijevsky. He proposed in this case that Agent X is (among other things) ‘‘electric vibrations of a definite frequency’’ [27]. and later that the agent of the action of solar activity “is in particular millimeter radiation” [28]. Recently Russian scientists [25] have discovered that the reason that flares on the Sun and following geomagnetic storms have influence the cardiovascular system lies in the change to the physical attributes of the blood. During solar flares changes are experienced in human blood viscosity, red corpuscle proportion in the blood, in the concentration of fibrinogen and the aggregation of blood corpuscles and platelets. These processes take place differently in healthy and meteo-dependent people with cardiovascular problems. In the latter, the blood thickens when magnetic disturbance on the Sun reach the Earth. In the case of healthy people, the organism prepares for the event two days before its advent, immediately after a solar flare. The microwave radioemission have the resonances at the spectral range 10^9 – 10^{12} Hz at the biological cells and membranes, DNA and RNA, human erythrocytes, and this fact can explain the extremely small threshold for influence of

ionospheric radioemission at the monochromatic (characteristic) Rydberg transitions on biological objects. We propose the next scheme of the heliogeobiocorrelations: see Fig. During of high solar activity specially flares at the Sun and also large geomagnetic activity (magnetic storms) there are increased fluxes of EUV and X-rays and precipitating particles from geomagnetosphere, during magnetic storms, which generate the additional ionization of terrestrial ionosphere. This ionization results in production of photoelectrons and secondary electrons and especially Auger electrons. Rydberg excitation of atoms and molecules by these electrons generate microwave monochromatic radiation: (mm, cm, dm), which can produce the resonance reaction of living systems [20-23] during "unfavorable days" for sick people. It is important that microwave radiation in the system that we proposed is capable of acting as the carrier frequency, with modulation by infrasound and internal acoustic-gravity waves of the upper atmosphere, as well as by vibrations of the background electromagnetic field (Alfven and Schuman resonances at the terrestrial ionosphere), including in the region of biorhythms. This amplifies the influence of low-frequency vibrations of the background electromagnetic field, with its high biological efficiency but low energetics of its action [29]. especially because of the surprisingly strong action on biological objects from the side of microwave radiation [1].

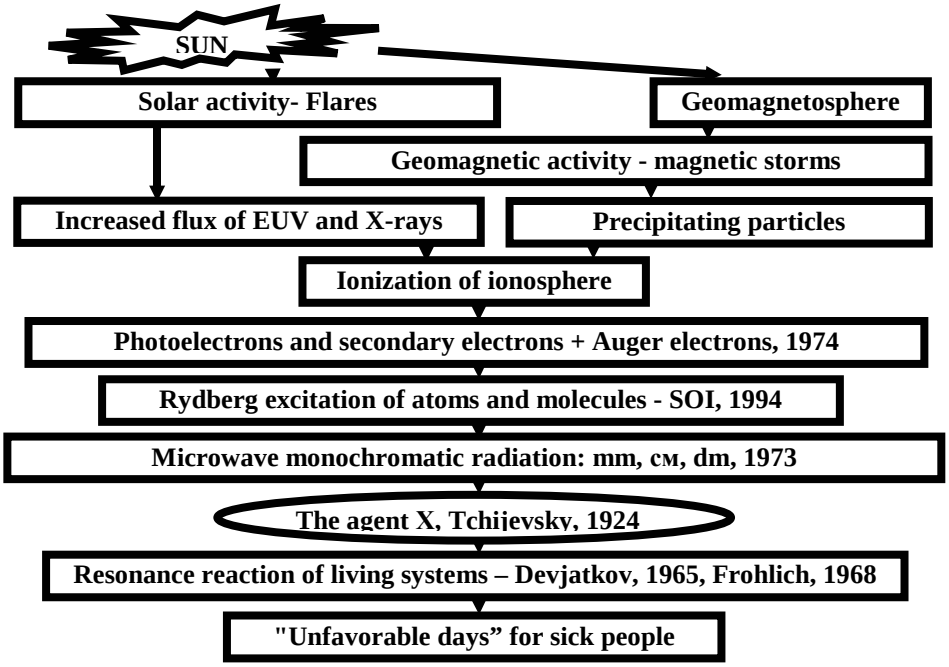

Fig. Biological effects of solar activity and Rydberg states.

There are numerous experimental confirmations that microwave radiation has a biological effect. From the aggregate of such studies, it is possible to expect uniquely low levels of threshold action, all the way to 10^{-15} W/cm2, which is close to the thresholds of perception of vision and hearing [1]. There are a number of considerations in favor of the reliability of such anomalously low threshold levels:

• Fixed action through acupuncture points makes it possible to speak of the possibility of reducing the threshold in actual laboratory experiments.

• Low-frequency modulation of microwave radiation (including in the range of biorhythms) can reduce the action threshold of this radiation.

• When determining spectral resonances, a contribution of the inaccuracy of the resonance is possible when laboratory sources of microwaves are used.

• The contribution of a synergetic effect when several factors are combined (for example, in the period of a geomagnetic storm, microwave radiation of the ionosphere and storm-induced variations of the geomagnetic field become active).

• The appearance of a synergetic effect from the reaction to an external stimulus (for example, a solar flare or magnetic storm) simultaneously of several individuals associating with each other in this case and influencing each other (including via biomagnetism [30]) under the action (in the case under discussion) of sporadic microwave radiation of the ionosphere.

There is an extremely nontrivial effect for the case of a geomagnetic storm, and taking this into account can fundamentally alter the technique and treatment of numerous experiments on magnetobiology. Actually, unlike the standard understanding of the changes of the geomagnetic field during a storm (with a maximum at

the center of the main phase), the precipitation of particles from the radiation belts that accompany these changes experience sharp attenuations (to the recording threshold in the course of 1.5–3 h) at the beginning and end of the main phase. Only at the center of the main phase at middle latitudes in 2–4 h do they actually reach the maximum values – to the level of auroral precipitations [31, 32].

Thus, the mapping of a biophysical experiment on magnetobiology to the values of the generally used indices of geomagnetic activity that semi-quantitatively describe the variation of the earth's magnetic field (*Kp*, *Ap*, or *Dst*), as it is usually done, does not perfectly reflect the intensity of the corpuscular precipitation into the ionosphere in the period of a magnetic storm and hence does not correspond to the intensity level of sporadic microwave radiation of the ionosphere. This may be associated with the appearance of null results when modelling the conditions of a magnetic storm in laboratory experiments on biological objects. The papers [2, 3]. showed that it is the microwave radiation of the ionosphere that must play the main role in the biospheric effect of a magnetic storm. This is confirmed by the increase of the probability of phenomena detected in various statistical studies of the effects of a magnetic storm in medical indices among people [33-35] concurrent with the period of the storm and also for 24–48 h after the storm, when variations in the geomagnetic field no longer exist. At the same time, the experimental fact is well established that the fluxes of corpuscles that pour out in just this time period increase after a storm ([32], p. 290). Incidentally, it is noteworthy in a number of such papers on the statistics of medical cases that the maximum of the effect occurs two days before the storm. [33, 35]. A flare occurs on the sun at just this time [2, 3, 32], and sporadic microwave radiation of the ionosphere also is observed [4-6, 14-17]. A direct correlation has been recorded [36] with solar x-ray flares in the statistics of medical events.

We will discuss more closely at the energy aspect of the problem of how the sporadic microwave (Rydberg) radiation of the ionosphere affects the biosphere and the lower atmosphere. Radiant energy from the sun with a flux density of 1367 W/m^2 reaches the earth's surface, and about 10^{-2} W/m^2 (all of the solar flux of soft x rays and UV radiation with a wavelength of $\lambda<134$ nm, including the L_α line of the hydrogen atom) is absorbed in the ionosphere under quiet heliogeophysical conditions. However, the ratio of the value of absorbed energy per unit mass of atmospheric gas is substantially different: 10^{-3} W/g in the ionosphere, and $7\ 10^{-5}$ W/g at the bottom of the troposphere. Thus, per unit mass of atmospheric gas or per one atomic-molecular particle of this gas, an order of magnitude more electromagnetic energy reaches the ionosphere from the sun than reaches the lower layers of the atmosphere. This ratio is still greater in periods of solar flares and geomagnetic storms. The greater part of the energy of the solar EUV radiation and soft x rays with wavelength $\lambda<50$ nm (capable of producing energetic photoelectrons) generates microwave radiation of the ionosphere from the Rydberg levels of all the atmospheric gases, including the minor components. This generation is supplemented by the action of fluxes of charged particles in the auroral zone under virtually any conditions of heliogeophysical activity. The fluxes of short-wavelength solar radiation double (in the spectral region $\lambda<120$ nm) during periods of flares on the sun, and the fluxes of precipitated electrons increase by a factor of 100 or more during geomagnetic storms, not only at high but at middle latitudes. The energy of the electron fluxes precipitated into the upper atmosphere in this case is about a factor of 50 greater than the energy of the ionizing radiation of the quiet sun. It is important that the energy flux of the microwave radiation of the ionosphere completely reaches the earth's surface. We can estimate the energy flux of the sporadic microwave radiation of the ionosphere recorded in [5]. It is important that the radiation signal of the ionosphere exceeded the intensity of the rf flux from the quiet sun by a factor of 2–40 (at a wavelength of $\lambda=50$ cm), where the latter equals (4–6) 10^{-21} W cm^{-2} m^{-1} ([32], p. 13). The width of the surge reached 1 GHz. The flux of ionospheric microwave radiation of the ionosphere at $\lambda=50$ cm in the period of a solar flare is then (according to the data of the measurements of [5]) (3–70) 10^{-16} W cm^{-2}.

This is orders of magnitude greater than the sensitivity threshold of biological objects to microwaves [1] Thus the "Porog" generator [37] for medical purposes, which works efficiently in a wide range of microwaves from superhigh to extremely high frequencies, provides a spectral power density level of 10^{-16} – 10^{-18} W cm^{-2} Hz^{-1}, i.e., an even smaller value. At the same time, a further decrease of the output power of devices with a monochromatic signal (we recall that, according to [2, 3], the microwave radiation of the ionosphere in Rydberg transitions has indeed a monochromatic character) all the way to 10^{-10} – 10^{-12} W, and noise to 10^{-18} – 10^{-20} W cm^{-2} Hz [1], does not reduce the efficiency of the treatment. Moreover, such radical reductions of the output power to the level of counted quanta even increase this efficiency. In [37] pointed out that an explanation of this effect can be found by using a quantum-mechanical approach. When the energy of the entire spectrum of sporadic rf radiation of the ionosphere is taken into account, the threshold value for biological objects (10^{-16} – 10^{-17} W cm^{-2} [1] can be exceeded even by a factor of 10–100. The ratio of the energies dissipated in the ionosphere when there is a medium solar flare and during a geomagnetic storm shows that the flux of microwave radiation can be factor of 10–100 greater in intensity in the period of a magnetic storm. In this case, the radiation in the centimeter and decimeter ranges can now exceed 10^{-11} – 10^{-12} W cm^{-2}.On the other hand, a calculation of the excitation rates of the Rydberg states of the oxygen atom [8] gave a value of about 10^9 particles cm^{-2} sec^{-1} in a column of the ionosphere during the period of a medium class-2B solar flare. Then, for values of the quantum energy in the centimeter range of $2\ 10^{-23}$ (for $\lambda=1$ cm) – $2\ 10^{-24}$ J (for $\lambda=10$ cm) in this

column in ten allowed transitions, we have a flux density of microwave radiation of $2\ 10^{-13} - 2\ 10^{-14}$ W cm^{-2}. This flux density is the lower limit for transitions with $\Delta n=1$ (only for $\Delta l=1$), i.e., those of the type n', $l'=n'-1 \rightarrow n'-1$, $l'=n'-2$, where $n'=11–20$ for an oxygen atom. This value increases to $10^{-11} - 10^{-12}$ W cm^{-2} during a magnetic storm. Because the densities of oxygen atoms and nitrogen molecules are about equal at an altitude of about 200 km, where, according to [8], there is a maximum of the altitude profiles of the Rydberg excitation rates, and recalling the identical character of the allowed radiative transitions in highly excited (hydrogen-like) atoms and diatomic molecules, it should be expected that the total flux of sporadic rf radiation, taking into account the nitrogen molecules, is approximately doubled [38].

Our energy estimates, without claiming to be complete, show that the experimentally observed sporadic rf radiation of the ionosphere in the period of solar flares and geomagnetic storms is well explained by the energetics of the allowed microwave transitions from the Rydberg excited states of the main gases of the upper atmosphere at altitudes of about 200 km – the oxygen atom and the nitrogen molecule. Thus, the resulting energies of the microwave radiation flux of the ionosphere make it possible to regard this radiation as the main agent in heliogeobiocorrelation effects. According to [2, 39], the microwave radiation itself mainly provides the energy component of the effect, and its modulation by low-frequency oscillations of the electromagnetic and infrasound geomagnetic fields provides the information component. Laboratory experiments in which modulated microwave radiation acts on biological objects show that it is substantially stronger than microwaves with constant intensity. The effect of modulation is most pronounced at lower intensity levels of the microwave flux and also depends on the initial state of the biological system.

Conclusion

Ways of experimentally checking the possible role of the microwave radiation of the earth's ionosphere in heliogeobiocorrelations have been considered, taking into account the variability of its intensity at the different phases of a geomagnetic storm. Energy estimates are presented for the density of such a flux during periods of a moderate solar flare and a magnetic storm, reaching values of 10^{-11} W cm^{-2}. It follows from what has been said that it is necessary to provide constant monitoring of the intensity and spectrum of the microwave radiation of the earth's ionosphere, not only in terms of a methodological improvement of biophysical experiments under conditions of elevated solar and especially geomagnetic activity but also possibly for recording the level of "unfavorability" of the heliogeophysical situation. The medical and biological mechanisms of this problem should be considered, taking into account the phenomenon of stochastic resonance [1], where the background microwave radiation of the ionosphere (before a storm and a flare) plays the role of the noise component. The same phenomenon can be significant in studies of the influence of the microwave frequencies of cellular telephones [38]. Here the role of the noise signal, which sharply increases in the period of solar flares and magnetic storms, will be played by the ionospheric microwave radiation. Since it is very variable, the possible resulting medical effect from cellular telephones and ionospheric sporadic radiations significantly varies in magnitude, and this creates indeterminacy when it is studied. The phenomenon of dissipative resonance can also be relevant to the study of these problems.

There are also other problems in ionospheric and atmospheric physics, biophysics and medicine concerning the investigations of the ionospheric Rydberg excitation role:

- determination of the real spectral distributions for Rydberg ionospheric emission at all transparency windows;
- determination of the perception threshold for the characteristic sharp-resonance microwave Rydberg emission for healthy and sick persons.

These problems can be solved at several Russian institutes by support of the International Science and Technology Center [9, 10, 39].

References

1. Bingi V.N., Magnetobiology. Experiments and Models, IOF RAN, Moscow, 2002.

2. Avakyan S.V., "Microwave Emission of Rydberg States as a New Factor of Solar–Biosphere Relations," in Proceedings of the Fifth International Conference on Problems of Geocosmos, St. Petersburg, 2004, pp. 335–338.

3. Avakyan S.V., "Microwave radiation of the ionosphere as a factor in the way solar flares and geomagnetic storms act on biological systems," Opt. Zh. 72, No. 8, 41 (2005)", [J. Opt. Technol. 72, 608 (2005)].

4. Forsyth P.A., Petrie W., Currie B.W., On the origin of ten centimeter radiation from the polar aurora, Can. J. of Res., 28, ser. A, 3, 324-335, 1950.

5. Troitskii V.S., Starodubtsev A.M., Bondar L.N., et al., "The search for sporadic rf radiation from space at centimeter and decimeter waves," Izv. Vyssh. Uchebn. Zaved., Radiofiz. 16, 323 (1973).

6. Musatenko S.I., “Radio-frequency radiation of near-earth space as a result of the action of solar flares on the earth’s magnetosphere and ionosphere,” Geomag. Aeronom. 20, 884 (1980).

7. Avakyan S.V., ‘‘New factors in the physics of solar-terrestrial relationships—Rydberg states of atoms and molecules,’’ in Abstracts of Reports of the International Conference on the Physics of Solar- Terrestrial Relationships, Almaty, 1994, pp. 3–5.

8. Avakyan S.V., Voronin N.A., and Serova A.E., “The role of Rydberg atoms and molecules in the upper atmosphere,” Geomag. Aeronom. 37, No. 3, 99 (1997).

9. Avakyan S.V., E.P. Andreev, I.M. Afanas’ev, N.B. Leonov, A.V. Savushkin, A.E. Serova, N.A. Voronin; "Creating of the permanent Space Patrol of ionizing solar radiation", In: "Innovative Telescopes and Instrumentation for Solar Astrophysics", USA, Eds. S.L. Keil (NSO, USA), S.V. Avakyan (SOI, Russia), Proc. SPIE, v. 4853, pp. 600-611, 2002.

10. Avakyan S.V. Space Solar Patrol: Absolute measurements of ionizing solar radiation, Advances in Space Research, v. 37, pp. 297-302, 2006.

11. Slanger T.G., Huestis D.L., Cosby P.C., Oxygen atom Rydberg emissions in the equatorial ionosphere from radiative recombination, J. Geophys. Res. 109, A10309, 2004.

12. Grach S.M., Fridman V.M., Lifshits L.M., Podstrigach T.S., Sergeev E.N., and Snegirev S.D., “UHF electromagnetic emission stimulated by HF pumping of the ionosphere,” Ann. Geophys., 20, 1687 (2002).

13. Avakyan S.V., ‘‘Auger processes in the optics of the upper atmosphere,’’ Opt. Zh. 65, No. 11, 4 (1998) [J. Opt. Technol. 65, 870 (1998)].

14. Troitsky V.S., Bondar’ L.N., Starodubtsev A.M., A new type of radio noise. Sporadic radio emission of the near-Earth medium at centimeter and decimeter waves, Dokl. Akad. Nauk SSSR, 212, 3, 607–610, 1973.

15. Bondar’ L.N., Starodubtsev A.M., Troitsky V.S., A search of sporadic radio emission from space, Usp. Fiz. Nauk, 113, 4, 719–723, 1974.

16. Bondar’ L.N., Strezhneva K.M., Troitskiy V.S., Sporadic background radio emission, solar activity and aurorae, Astron. Vestnik, 9, 4, 210–217, 1975.

17. Musatenko S.I. Solar phenomena and the ionospheric UHF radio emission, Solar Data, 8, 92, 1984.

18. Avakyan S.V., ‘‘New processes in aeronomy: the Auger effect - 30 years later, multiple photoionization - 25 years later, Rydberg excitation - 10 years later,’’ in Proceedings of the Fifth International Conference on Problems of Geocosmos, St. Petersburg, 2004, pp. 190–195.

19. Avakyan S.V., ‘‘Biological effects of solar activity and Rydberg states,’’ in the Interdisciplinary Seminar on Biological Effects of Solar Activity: IKI RAN, ITEB RAN, 2004, Pushchino-na-Oke, pp. 45–47.

20. Sevastyanova, L.A., Vilenskaya R.L., A study of the effects of millimeter microwaves on the bone marrow of mice, Sov. Phys. Usp. (Engl. Transl.), 16, 570, 1974.

21. Devyatkov, N.D., Golant M.B., Bezkiy O.B., Millimeter waves and its role in processes of vitalfunctions, M., “Radio i svjaz”, 1991.

22. Frohlich H. The biological effects in microwaves and related questions, in Adv. Electronics and Electron Phys., 53, 85–152, 1980.

23. Pohl H.A., Natural Oscillating fields of cells. In Coherent excitations in biological Systems, eds. H. Frohlich, F. Kremer, Springer, Berlin, p. 198–210, 1983.

24. Gurkinfel Yu.I., Lyubimov V.V., Oraevskii V.N., et al., ‘‘The effect of geomagnetic excitations on capillary circulation,’’ Preprint IZMIRAN, 1994.

25. Ionova V.G., Sazonova E.A., Sergienko N.P., et al., ‘‘The reaction of the human organism to heliogeophysical perturbations,’’ Biofizika 48, No. 2, 380 (2003).

26. Vladimirskii B.M., ‘‘On possible factors of solar activity that affect processes in the biosphere,’’ in The Effect of Solar Activity on the Earth’s Atmosphere and Biosphere (Nauka, Moscow, 1971), pp. 126–141.

27. Tchijevsky A.L., The Cosmic Pulse of Life (Mysl’, Moscow, 1995), pp. 646–647.

28. Tchijevsky A.L., Terrestrial Echo of Solar Storms (Mysl’, Moscow, 1976), p. 327.

29. Temur’yants N.A., Vladimirskii B.M., and Tishkin O.G., Low-Frequency Electromagnetic Signals in the Biological World (Naukova Dumka, Kiev, 1992).

30. Vvedenskii V.L., and Ozhogin V.I., Supersensitive Magnetometry and Biomagnetism, series on Modern Problems of Physics (Nauka, Moscow, 1986).

31. Avakyan S.V., et al., “Electron flows during the magnetic storm of 14–15, December, 1970, from the data of the Kosmos-381 satellite,” Issled. Geomag. Aeron. Fiz. Solntsa 32, 158 (1974).

32. Avakyan S.V., Vdovin A.I., and Pustarnikov V.F., Near-Earth space ionizing and penetrating radiations. Handbook, Gidrometeoizdat, St. Petersburg, 501 pp., 1994.

33. Gurfinkel’ Yu.I., and Lyubimov V.V., “Screened ward in a clinic to protect patients with ischemic heart disease from the action of geomagnetic perturbations,” Med. Phys. 23, No. 3, 34 (2004).

34. Samsonov S.N., Sokolov V.D., Strekalovskaya A.A., and Petrova P.G., “On the relationship of cardiovascular disease exacerbation to heliogeophysical disturbances,” in Proceedings of the Twenty-seventh Annual Seminar, Apatity, 2004, pp. 134–137.

35. Breus T.K., Chibisov S.M., Baevskii R.M., and Shebzukhov K.V., The Chronostructure of the Biorhythms of the Heart and Factors of the External Medium (RUDN, Moscow, 2002).

36. Bobko N.A., Lychak M.M., Il'in V.N., Zelyk Ya.I., Vershigova A.V., Erigina V.T., and Chernyuk S.V., "The effect of heliogeomagnetic perturbations on the appearance of illnesses that require rapid medical treatment," in Transactions of the Russian–European Scientific Conference on Space Weather, Its Influence on Biological Objects and Man, Moscow, 17–18, February, 2005.

37. Sit'ko S.P., Skripnik Yu.A., and Yanenko O.F., "Reaction of the human organism to superlow doses of millimeter radiation," in Abstracts of Reports of the Sixth International Crimean Conference on Space and the Biosphere, Ukraine, 2005, p. 13.

38. Avakyan S.V., Voronin N.A., "Possible mechanisms for the influence of heliogeophysical activity on the biosphere and the weather", Opt. Zh. 73, No. 4, 281-285 (2006) ," [J. Opt. Technol. 73, 78-83 (2006)].

39. Avakyan S.V., "About microwave emissions of the ionosphere and its influence at the biosphere", Proceedings of an International Scientific Workshop "Space weather effects on biological systems and human health" held in Moscow, Russia, February 17-18, 2005, Eds . O.Yu.Atkov, Yu.I.Gurfinkel; Moscow, Reprocenter, 2006, pp. 80-81.

THE HYDROGEN PEROXIDE AS A POSSIBLE MESSENGER FOR MAGNETIZED PHYSIOLOGICAL SOLUTION-INDUCED STIMULATION OF HEART MUSCLE CONTRACTILITY

GAYANE AYRAPETYAN, ANAHIT GRIGORYAN, HOVIK HYRAPETYAN, ERNA DADASYAN

UNESCO CHAIR- LIFE SCIENCES INTERNATIONAL POSTGRADUATE EDUCATIONAL CENTER
31 ACHARYAN ST., YEREVAN, 375040 ARMENIA, LIFE@ARMINCO.COM

Abstract

Previous our works have shown that magnetized physiological solution (MPS) has dual effect on heart muscle contractility: from one hand it leads to muscle relaxation, from the other hand- it stimulates the frequency of heart contractility. If the first effect is explained by the activation of Na^+/Ca^{2+} exchanger, then the mechanism of the second effect is still unclear. It is known that the magnetization of aqua solutions leads to the elevation of the concentration of hydrogen peroxide (H_2O_2) and the later is suggested as one of the possible candidates through which the biological effect of MPS is realized. The purpose of our work was to check this hypothesis for which the comparative study of the effects of MPS and H_2O_2 on isolated and intra-cordially perfused snail heart muscle contractility and intracellular messenger contents were performed.

It was shown that MPS and H_2O_2 have the following synergic effects: it depresses the Na^+-K^+ pump-induced relaxation, intracellular cAMP/cGMP contents and ^{45}Ca-uptake and leads to cell dehydration. It is suggested that the H_2O_2-induced activation of cyclic nucleotide-dependent Na^+/Ca^{2+} exchanger has pivotal role in MPS–induced stimulation of heart contractility; however, the nature of this mechanism could be the subject for future investigations.

Introduction

At present the biological effect of magnetized physiological solution (MPS) on different cells and organisms can be considered as proven fact (Klassen 1982; Ayrapetyan 2006). But the nature of the messenger transferring the signal of EMF-induced water structural changes to the metabolic cascade is not clear yet. By previous our works have shown that MPS has dual effect on heart muscle contractility: from one hand it leads to muscle relaxation, from the other hand- it stimulates the frequency of heart contractility. If the relaxing effect of MPS on heart muscle could be explained by the activation of cGMP-dependant Ca efflux bringing to the deflection of intracellular Ca ions and reactivation of Na^+-K^+ pump (Ayrapetyan et al., 2005), the stimulatory mechanism of the MPS on heart beating is still unclear. As the water molecule dissociation is the most variable water property, it is suggested that the magnetization of water could change the quantity and quality of its dissociation products which are potential messengers through which the biological effect of SMF and EMF on cells could be realized (Ayrapetyan et al. 1994). By previous our study was shown that SMF and ELF EMF has depressing effect on specific electrical conductivity (SEC), It was also shown that the depressing effect of LF EMF on water SEC as well as its biological effects on various cells are most pronounced at frequency of 4 Hz (Stepanian et al. 1999; Ayrapetyan 2006).

Therefore, it is suggesting that the H_2O_2 could serve as one of the most reliable candidate for the messenger transferring EMF-induced water structure changes to cell metabolic cascades (Klassen 1982; Bistolfi 1991). For testing this hypothesis the comparative study of the effects of magnetized and H_2O_2 containing physiological solution (PS) on heart muscle contractility and ^{45}Ca uptake by muscle was performed.

The isolated and intra cordially perfused snail heart muscles, which is able to contract *in vitro* state for more than 24 hours (Azatian et al., 1998), was chosen as an experimental model for the present study.

Methods

Removed snail (Helix pomatia) hearts were cannulated and suspended in bath with physiological solution (PS) for snails that contains (in mM): NaCl (80), KCl (4), CaCl2 (7), Tris-HCl (5), pH 7,5. Continuously intra- and extra-heart perfusion with PS was applied. The intra cordial pressure was controlled by keeping the perfusion solution in reservoirs vessel at a constant level.

The transducer was fixed to the bottom of the heart by a silk suture. To monitor the heart contraction with the electrical signals for subsequent recording with a computer a special setup was constructed, which is schematically presented in Figure 1.

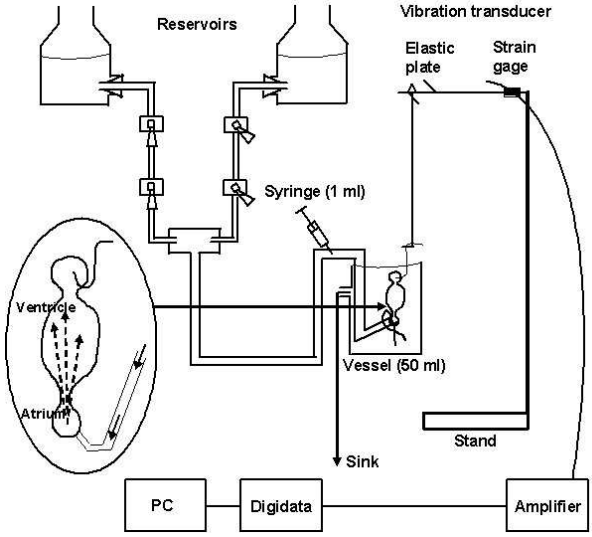

Figure 1. *The setup for the registration of heart muscle contractility. Heart contractions were recorded isotonically and displayed on PC through Digidata 1322A.*

The up and down movements of the baseline of records showed the heart contraction and relaxation, correspondingly. Usually, after heart isolation from the snail, its cannulation and suspension in bath with normal PS, its contraction stops in systole phase (which can be detected visually) or has irregular bursting with short amplitudes of contractions which sometimes could continue 1-2 hours, and then it is gradually relaxed and starts its regular contractions.

The PS treatment by Static Magnetic Field (SMF) was performed by the method described earlier (Ayrapetyan et al. 1994a). PS in a 20 ml glass chamber (50x30x15 mm) was exposed to SMF at intensities of 27 mT generated by a strong magnet for 60 minutes. The magnetic field was homogeneous within the gap in the centre of the magnet (the size of the gap varied from 0 to 15 cm, and at 50 mT the field varied by no more than 5% within a sphere with a diameter of 6 cm. Thus, the size of the vessel was small relative to the size of the homogeneous region). The background of magnetic field in the area of experimental setup in the laboratory, due to the 60 Hz electricity system, was less than 0.001 mT.

The magnetic field intensity was measured with a Teslometer W1-8 (Armenian Radiophysical Institute). This instrument measured magnetic fields in the range 10^{-3} to 1.6 T(±5%). This magnetic induction converter was a crystal type X511-1, 1.5 x 0,2 mm^2 and was fixed on nonmagnetized material (PX13-1).

The sham treatment of PS was performed on the same table and in a same 20 ml glass chamber located at same geometric place, i.e. the sham exposed PS was in the same environmental medium excluding SMF (the static magnet was moved away from the exposure table for ~10m). The both sham and SMF exposed solutions were taken from the same container of stock solution, which was preliminary kept in water bath with stable temperature (21±0,5^o C) during no less than one hour. The temperature of the heart incubated in the chamber was continuously recorded by needle-type thermometer having sensitivity of ±0,1 ^{0}C. The room temperature was 22^{o}C.

In physiological experiments only the reversible effect of MPS-induced changes of heart contractility (frequency, amplitudes and basic line) were considered as a reliable, i.e. when after replacing the MPS by sham exposed solutions, the initial activity of the heart muscle was restored. For each individual heart muscle the number of repetitions of such protocol was varied from 1 to 10 depending on the duration of stabile heart muscle contractility *in vitro*, which for some preparations could prolong until ~24 hours.

The stock solution (10^{-2} M) of H_2O_2 was prepared each day by diluting 3% H_2O_2 by physiological solution and protected it from light to minimize its photo-degradation. H_2O_2 was added to the intra-cordially perfused solution to a final concentration from 10^{-4} to 10^{-12} M. All the experiments were carried out at 18 ± 0.5°C.

^{45}Ca uptake by muscles incubated in normal and magnetized PS was measured by ^{45}Ca isotope having specific activity: 0.185-1.85GBq/mg Ca, 5-50mCi/mg Ca (Amersham Life Science production). Control and experimental groups contained per 10 hearts each(total n=.40) Isolated hearts were incubated in four plastic tubes with control and magnetized normal or K-free solutions containing ^{45}Ca isotopes (0,45 mCi/ml). Then hearts were washed three times per 5min with cold normal or K-free PS (where 4mM KCI was replaced by 4mM NaCl) to remove isotope from the extra cellular spaces. Radioactivity was measured using a liquid scintillation spectrometer (production of Packard TRI-CARB Canberra Cambridge Company) and calculated as pM/mg of wet weight. .

The mean value, standard deviations, and the statistical probability, determined by Student Test were calculated with the help of computer program Sigma Plot (Version 8.02A).

Results

For estimating the role of H_2O_2 in realization of biological effect of MPS on heart contractility the dose-dependent effect of H_2O_2 on heart contractility was studied in normal and K^+-free solution. As seen in Figure 2A the low concentrations (10^{-12}- 10^{-10} M) of H_2O_2 had elevation effect on amplitude of heart contractility, while at higher concentrations (>10^{-7} M) this amplitude was depressed.

In order to estimate the role of electrogenic Na^+-K^+ pump in H_2O_2-induced effect on heart contractility, similar experiments were repeated in K-free solutions, when Na^+-K^+ pump is in inactive state (Figure 2B). It was known that K ions removal from extra cellular medium led to the inactivation of Na^+-K^+ pump, and the restoration of K ions in the medium caused the reactivation of the pump leading to hyper polarization of the cell membrane (Thomas, 1972).

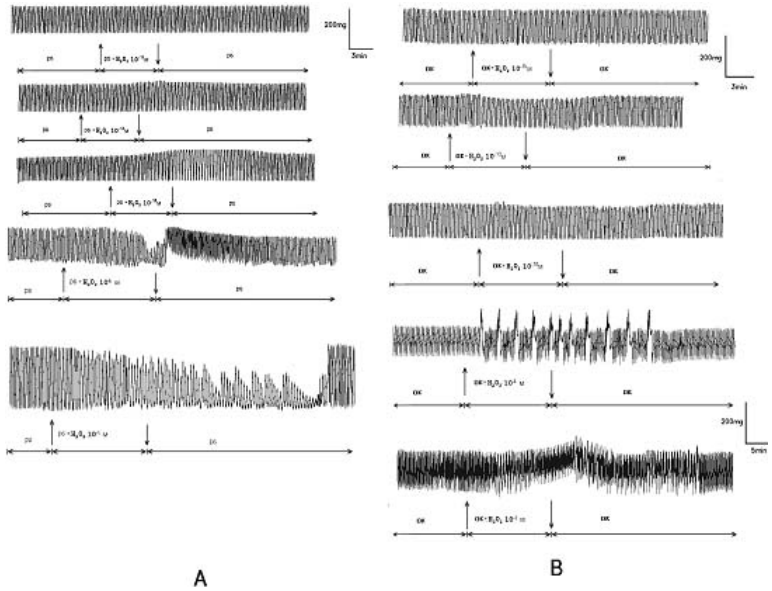

Figure 2. *The dose-dependent effect of H_2O_2 on heart muscle contractility in normal (A) and K-free (B) PS.*

In K-free medium the sensitivity of heart contractions to $H_2O_2$was increased compared to those in normal PS (Figure 2A). If the minimal concentration of H_2O_2 in normal PS able to modulate the heart contractility is 10^{-12} M, in K-free solution it was 10^{-13} M. Previously it was shown that Na^+-K^+ pump activation leads to the inhibition of heart beating (Azatyan et al., 1998). At the same time it was shown that this effect disappeared after perfusion of heart muscle by MPS (Ayrapetyan et al., 2005). In order to find out whether this effect is due to the H_2O_2 formation in MPS, the dose-dependent effect of H_2O_2-containing K-free PS on Na^+-K^+ pump-induced transit inhibition of heart beating was studied (Figure 3A).

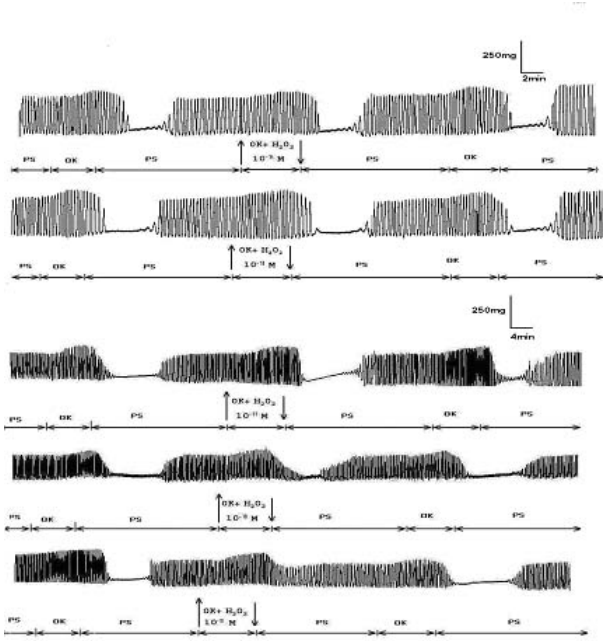

Figure 3. *The dose-dependent effect of hydrogen peroxide in K-free solution on Na-K pump-induced transient inhibition of heart muscle beating.*

It is known that the muscle incubation in K-free solution leads to the increase of intracellular Na ion concentration because of inactivation of Na^+-K^+ pump and its re-incubation in normal K-containing medium, the pump activation was accompanied by depression of heart contractility (Azatyan et al., 1998). As can be seen in Figure 3 the muscle incubation in 10^{-10} M H_2O_2 containing K-free medium in period of pump-induced inhibition of heart beating, the small amplitude of vibration of heart muscle appeared, while in case of 10^{-9} M H_2O_2 this pump-induced transit inhibition of heart beating fully disappeared. Similar effect was obtained when the Na enrichment of muscle was performed in normal K-free and then was re-incubated in H_2O_2-containing normal PS (Figure 4).

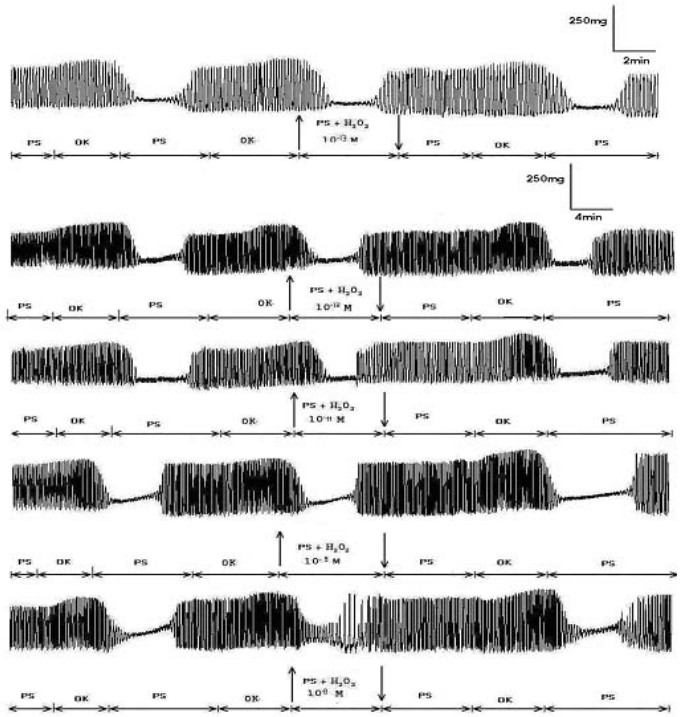

Figure 4*. The dose-dependent effect of hydrogen peroxide in normal PS on Na-K pump-induced transient inhibition of heart muscle beating.*

Thus, the H_2O_2-induced stimulation of heart muscle contractility in period of pump-induced transit inhibition of heart beating is very similar to the effect of MPS (Figure 5).

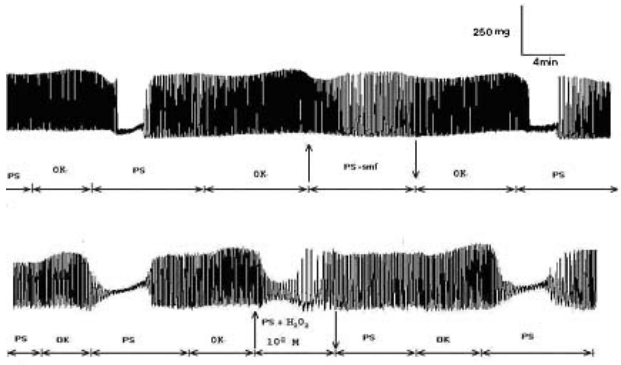

Figure 5. *The effects of magnetized PS (upper) and 10^{-8} M hydrogen peroxide (lower) on Na-K pump-induced transient inhibition of heart muscle beating.*

As intracellular Ca ions concentration has pivotal role in muscle contractility in the next series experiments the comparative study EMF –treated PS and H_2O_2 on ^{45}Ca uptake by muscle was study in Na^+-K^+ pump active (in normal PS) and inactive state (in K-free medium).

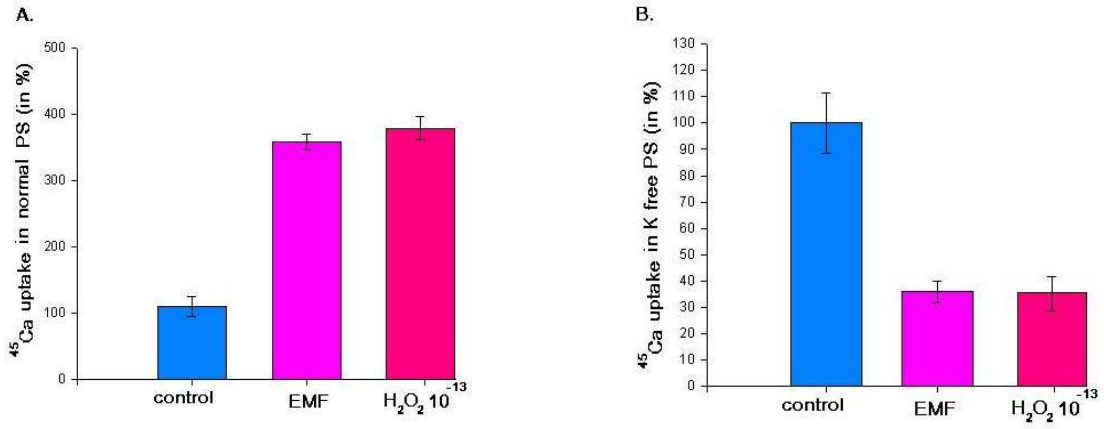

Figure 6. *The effect of MV- and EMF-treated PS (A) and K-free PS (B) in ^{45}Ca uptake by heart muscles (expressed in %, compared to their control value).*

As can be seen in Figure 6 the both EMF-treated and H_2O_2- containing solutions have activation effect on Ca uptake in normal PS, while in K-free solution this effect was reversed, i.d. the both factors have inhibitory effect on ^{45}Ca uptake.

Summary

Previously it was shown that MPS had dual effect on heart muscle contractility: relaxation and stimulation of pacemaker activity (Ayrapetyan et al., 2005). If the relaxation effect of MPS on heart muscle was explained by Ca-deflection of muscle in result of activation of cGMP-dependent Na^+/Ca^{2+} exchanger, the mechanism of MPS-induced stimulation of heart contractility in period of pump-induced inhibition of heart beating still remains unclear. At the same time in literature the experimental data showing the H_2O_2 generation in water medium upon the effect of magnetic fields are available (Klassen 1982). The obtained data on the synergic effects of H_2O_2 and MPS on Na^+-K^+ pump-induced muscle relaxation following the pre-incubation of the heart in K-free medium allow us to conclude that MPS-induced stimulation of heart contractility is due to the H_2O_2 formation in MPS. The data that the activation effects of H_2O_2 and MPS on Na^+-K^+ pump-induced muscle relaxation following the pre-incubation of the heart are present in both cases: in K-free medium or in case of heart re-incubation in K-containing solutions treated by EMF or containing H_2O_2, i.e. when the pump was in active and inactive states, correspondingly, could serve as an evidence on the pump-independent stimulation effects of MPS and H_2O_2 on heart. It is strange that this effect does not depend on Ca metabolisms: in spite that the MPS and H_2O_2 in normal PS have activation and in K-free solution- inactivation effects on Ca uptake, in

both cases MPS and H_2O_2 have stimulation effects on heart muscle contractility.

Thus, the main conclusion from the presented data is that H_2O_2 is one of important messenger through which the biological effect of ELF EMF on heart muscle contractility is realized.

References

Ayrapetyan SN, Grigorian CV, Avanesian AS. 1994a. On a mechanism of action of magnetic field on the electrical conductivity of water solutions and some properties of Helix neurons. *Bioelectromagnetics*, **15**: 133-142.

Ayrapetyan GS, Papanyan AV, Hayrapetyan HV, Ayrapetyan SN. 2005. Metabolic pathway of magnetized fluid-induced relaxation effects on heart muscle. *Bioelectromagnetics*. **26**(8): 624-30.

Ayrapetyan SN. 2006. Cell aqua medium as a preliminary target for the effect of electromagnetic fields. In: *Bioelectromagnetics: Current Concepts*, S. Ayrapetyan and M. Markov, eds., NATO Science Series, Springer Press, The Netherlands, pp: 31-64

Azatian KV, White AR, Walker RJ, Ayrapetyan SN. 1998. Cellular and Molecular Mechanisms of Nitric Oxide-Induced Heart Muscle Relaxation. Gen. Pharmac., **30**: 543-553.

Bistolfi F. 1991. Biostructures and Radiation Order Disorder, Edizioni Minerva Medica, Torino, Italy.

Klassen 1982; in: Magnetized Water Systems. "Chemistry" Press, 296 p (in Russian), English translation: European Biology and *Bioelectromagnetics*, 2006, **1**(2): 201-220

Stepanyan R., Ayrapetyan G., Arakelyan A., Ayrapetyan S. 1999. Effect of Mechanical Oscillations on Electrical Conductivity of Water Biophysics, **44**: 197-202.

EFFECTS OF SURFACE CHARGE AND DC EF FIELDS ON CELLS

RICHARD H.W. FUNK THOMAS K. MONSEES

DEPARTMENT OF ANATOMY, UNIVERSITY OF TECHNOLOGY, DRESDEN, GERMANY

Abstract

In this paper we will concentrate on the effects of surface charge patterns of surfaces which are the substrate for cell adhesion and migration as well as on the effects of static direct current electric (dc EF) fields. Findings in the literature and own results will be discussed.

Results and Discussion

In vitro, the application of static dc EF of physiological power causes directed movement and guiding of bone cells and various other cell types. This phenomenon is called electrotaxis (or galvanotaxis) [Zhao et al., 2002]. In vitro, at field strengths of 0.1–10 V/cm, cells often migrate to the cathode (neural crest cells, fibroblasts, keratinocytes, chondrocytes, rat prostate cancer cells and many epithelial cell types). Only few cell types move to the anode (corneal endothelial cells, bovine lens epithelium, human granulocytes and human vascular endothelial cells). Speed and direction of the movement are voltage dependent: human vascular endothelial cells migrate towards the anode, whereas bovine aortic endothelial cells move to the cathode. During movement, ruffled membranes, lamellipodia and filopodia are formed preferentially in the direction of the anticipated electrotaxis migration [Sulik et al., 1992; Zhao et al., 2002]. Several cell types changed their initial direction of movement by 180° when the current polarity was reversed [Soong et al., 1990; Brown and Loew, 1994; Chao et al., 2000; Wang et al., 2000b]. EF-induced cell migration can be modified by proteins of the ECM. For example, highest cathodal migration was noticed with keratinocytes plated on collagen and plastic, whereas lowest locomotion occurred on laminin. Cell response on fibronectin was in between the two. Similar results were observed for epithelial cell electrotaxis on laminin or fibronectin coatings. Sun et al. [2004] noticed directed movement of fibroblast migration at a field strength as low as 0.1 V/cm in 3-dimensional collagen gels, but not in conventional 2-dimensional cultures. Thus, 3-dimensional conditions seem to reflect the in vivo situation, where dc EF of 0.1 – 0.2 V/cm occur that are important for embryonic development [Nuccitelli, 2003]. Several steps are involved in cell migration: (1) due to their connection to several adaptor proteins, the growing of actin filaments will push the cell membrane in the direction of movement; (2) formation of focal contacts at the leading edge, i.e. specific bindings via membrane bound integrin receptors and ECM proteins, which will also influence several signaling pathways and structural elements of adhesion; (3) focalized proteolysis by recruitment of surface proteases to ECM contacts; (4) cell contraction driven by myosin II binding to actin filaments, and (5) disassembly of focal contacts and detachment of the trailing edge. Many of these events have also been observed in EF-induced cell movement.

If one looks at the level of a single cell in an EF, then elongation of the cell body and alignment of its long axis perpendicular to the field lines are striking phenomena. This behavior was first described for Xenopus myoblasts and thereafter observed in many other cell types including fibroblasts, osteoblasts, chondrocytes, keratinocytes, endothelial and epithelial cells. As dc EF trigger migration and orientation, cells must orchestrate cytoskeletal elements and shape in response to this trigger.

An accumulation of actin stress fibers was observed on the cathodal (leading) edge of several cell types [Sulik et al., 1992; Zhao et al., 2002]. Often, the total amount of filamentous actin transiently increased and became

selectively enriched in the leading lamellipodia. Here, focal contacts were also accumulated. Recent experiments showed that EF-mediated motility in fibroblasts can be halted by inhibition of microfilament dynamics, whereas inhibition of microtubules only reduced migration speed [Finkelstein et al., 2004]. Membrane extensions from the trailing edge of chondrocytes were concomitantly retracted [Chao et al., 2000]. Also osteoblasts and osteoblast-like cells undergo processes of retraction and elongation ultimately resulting in the realignment of the long cellular axis perpendicular to the EF [Curtze et al., 2004]. These authors presented a theory to explain the EF-induced perpendicular orientation of cells: cell attachment is made by the adhesive interaction of ECM proteins with a group of transmembrane adhesion receptors, the integrins. After binding to their specific ligands, integrins cluster within the membrane and recruit several adaptor and signaling proteins to form focal contacts (also called focal adhesions) that anchor the ends of intracellular actin filaments (stress fibers). Vinculin is one of these adaptor proteins and is frequently used as a marker for integrin-based focal contacts. As stated here and elsewhere [Jaffe, 1977; Poo, 1981], dc EF trigger the separation of charged membrane components. In order to achieve perpendicular elongation, a certain self-induced cytoskeletal tension is required along the axis. Assuming that all free integrin receptors drift towards an electrode and accumulate there, the cell is only able to connect to two focal adhesions and increase tension between them if they are on an axis perpendicular to the drift. Cell adhesion is a dynamic process, thus after some time, disassembly of focal contacts on the opposite side of the drift destination leads to another drift. Consequently, the cell is no longer able to maintain protrusions with the same orientation as the EF [Curtze et al., 2004].

Our experiments using corneal endothelial cells support this hypothesis: vinculin proteins, used as a marker for integrin receptors, are normally randomly distributed within the cell with a preference for the cell border. However, after dc EF application, they concentrate on two major spots of focal contacts oriented perpendicular to the EF vector. Mechanical load is also discussed as a possible transducer of EF. EF-induced effects such as dynamic changes in intracellular calcium concentration, cell traction and orientation are similar to the cellular response after mechanical stimulation [Curtze et al., 2004]. Converse flexoelectricity may thereby be a way for cells to sense small dc EF. Charged proteins in the lipid bilayer of the cell membrane repel each other, influencing membrane tension. If the charge on one side of the membrane is changed by dc EF, the membrane tension also changes, resulting in a modified curvature of the membrane. Such flexoelectric effects have already been demonstrated on voltage-clamped cells. Using traction force microscopy, Curtze et al. [2004] noticed a 5–30% increase in average traction force magnitude 10–30 s after dc EF exposure as the first detectable reaction of osteoblasts. The visible retraction phase started after 5–10 min, and then, cells subsequently elongated and oriented perpendicular to the EF lines. Traction forces at the margins tangential to the EF decreased 2–15 min after the start of EF exposure below their initial values. A mean delay of 85 s between EF application and first observable changes in Ca 2+ levels occurred, suggesting that stretch-activated Ca 2+ channels may be responsible for the Ca 2+ influx. Static MF (10 T) also oriented glioblastoma cells in the presence of collagen fibers possibly due to the rearrangement of microtubules [Hirose et al., 2003].

Studies of Erskine and McCaig [1997] and Ohgaki et al. [2001] as well as our own results showed that negatively charged surfaces are a sometimes better interface for cell adhesion and further cell function than positively charged ones. Using controlled surface charge induction on implants, it was shown that the above mentioned charge densities are sufficient to alter cell growth, adhesion and phenotypic. Moreover, specific effects can be observed when cells are plated onto substrates which have been exposed to ELF EMF before plating [McLeod and Rubin, 1994]. Together, these results strongly suggest that the observed effects are associated with an alteration in absorption of charged proteins, and change in the cellular response results from the altered ‘charge environment’.

Seen ‘with the eyes of a cell’, the surface of an implant is covered with water and ions (in vivo serum, in vitro cell culture medium). Then, amino acids and proteins (especially albumin, fibronectin and vitronectin) are absorbed to the surface due to unspecific charge interactions [Vroman, 1988]. At negatively polarized (e.g., glass) and negatively charged surfaces, inorganic cations like calcium and cationic amino acids and proteins may bind to the surface, making it a suitable interface for the negatively charged surface of the cell [Ohgaki et al., 2001]. Additionally, Ca 2+ ions are required for the formation of focal adhesions. Thus, a higher local concentration of Ca 2+ will accelerate specific integrin receptor-mediated binding. In the next step of the attachment sequence, the cell recognizes RGD motifs (a sequence of amino acids which is important for binding processes) of surface-bound proteins, and finally, specific binding occurs at focal adhesions via integrin receptors (early and late). As the ‘missing link’ between the patterns of surface charges and special adhesion proteins described above, Botti et al. [1998] described a class of adhesion proteins that, because of their common electrostatic and structural motif,

were called ‘electrotactins’. These proteins had a functional region common to cholinesterases and exhibitied a special pattern of electrostatical surface potentials.

Responding to extracellular cues like EMF involves a cascade of events, transducing signals from the cell surface to the cytoskeleton. Due to the high dielectric property of the lipid bilayer membrane, externally applied dc EF will be considerably attenuated. For example, a dc EF of 5 V/cm will produce an intracellular field of only 0.5 mV/cm, which is unlikely to produce significant effects [Poo, 1981].

What is the sensor for EF gradients? A suggested mechanism is the electrophoretic mobility of charged molecules in the cell membrane in a dc EF [Jaffe, 1977; Poo, 1981]. In this respect, electroosmosis (see also above) plays a role: the imposition of a dc EF on the negatively charged cell membrane produces a flow of positive counter ions, which will result in a flow of fluid towards the cathodal site of the membrane. By this flow, a negatively charged receptor will be swept to the cathodal side of the membrane if its _ potential is less negative than the potential of the cell surface; otherwise it will accumulate on the anodal site [Poo, 1981; McCaig et al., 2005]. The potential is the electric potential at the interface between a solid surface or membrane and a liquid. Such lateral movements and enrichments of membrane components towards the cathode have been observed in several cell types. Examples are concanavalin A and acetylcholine receptors or positively charged membrane lipids in Xenopus myotomal membrane [Poo, 1981], fibronectin receptor in fibroblasts [Brown and Loew, 1994], lipids and epidermal growth factor (EGF) receptor in keratinocytes [Song et al., 2002], membrane lipids or EGF and hepatocyte growth factor receptors in corneal epithelial cells [Zhao et al., 2002; McBain et al., 2003]. Thus, one can imagine that redistributed membrane molecules can be sensed inside the cell by components of the cytoskeleton and be used as an orientation cue. Some of these mechanisms have been explored in more detail. Finkelstein et al. [2004] recently demonstrated that microtubules are involved in EF-induced cell migration. Signaling molecules such as Rho GTPases and protein kinases interact with microtubules and can effectively hitchhike microtubule-based transport. In this way, they pass signals from the leading edge of the cell via the nucleus to the trailing edge. An EF induces redistribution of hepatocyte growth factor receptors and triggers the mitogen-activated protein kinase pathway downstream that is involved in epithelial cell migration [McBain et al., 2003]. Similarly, EGF receptor kinase activity and redistribution in the cell membrane are necessary for electrotaxis in keratinocytes. In chondrocytes, antagonists of the inositol phospholipid pathway were able to inhibit cathodal migration [Chao et al., 2000]. In contrast to the arising weak internal field, the externally applied dc EF can induce substantial alterations of the membrane potential. The resting potential of a nonexcitable cell is approximately –45 to –75 mV. A usual dc EF of 1–10 V/cm applied to a cell of 10 _ m in radius will hyperpolarize the membrane facing the anode by 1.5– 15 mV and depolarize the cathodal site by the same amount. This is sufficient to induce several physiological effects such as changes in the levels of calcium ions [Poo, 1981; Mycielska and Djamgoz, 2004; Robinson, 1985]. In many cells, dc EF-induced migration depends on changes in intracellular Ca 2+ concentration. Since the cytoplasm on the anode-facing site became more negative, the inward driving force of Ca 2+ was increased at the anode, whereas that on the cathodal site decreased (passive influx). Increasing [Ca 2+] often activates myosin light chain kinase that phosphorylates the regulatory light chain of myosin II. This in turn triggers the actin-activated myosin ATPase, a major regulator in cell contraction. In consequence, the anodal site contracts and the cell will be propelled towards the cathode. If voltage-gated Ca 2+ channels are present, a cathode-faced membrane depolarization should open them, and the Ca 2+ influx following this opening will cause cell migration towards the anode. The calcium waves measured were fast (22.5–50 _ m/s, i.e. faster than electroosmosis) which could possibly explain the very fast cell reactions reported in other EMF studies. However, the net movement (and direction of cell migration) depends on the balance of passive influx and voltage-gated influx of Ca 2+. Calcium ions are also essential for the coupling of other forms of EMF to a biological system.

In conclusion, the cell-guiding effects of static EF have a good explanation with the observations of the electrophoretic mobility of charged cell membrane molecules. However, a cascade of events must be initiated for this effect to be linked to classical biochemical pathways.

Literature

Botti, S.A., C.E. Felder, J.L. Sussman, I. Silman
(1998) Electrotactins: a class of adhesion proteins
with conserved electrostatic and structural
motifs. Protein Eng *11:* 415–420.

Brown MJ, Loew LM: Electric field-directed fibroblast locomotion involves cell surface molecular reorganization and is calcium independent. J Cell Biol 127:117-28, 1994

Chao PHG, Roy R, Mauck RL, Valhmu WB, Hung CT: Chondrocyte translocation response to direct current electric fields.
J Biomech Engineering 122:261-267, 2000

Curtze S, Dembo M, Miron M, Jones B: Dynamic changes in traction forces with DC electric field in osteoblast-like cells. J Cell Sci 117:2721-9, 2004

Erskine L, McCaig CD: Integrated interactions between chondroitin sulphate proteoglycans and weak dc electric fields regulate nerve growth cone guidance in vitro. J Cell Science 110:1957-1965, 1997

Fang K. S., Ionides E., Oster G., Nuccitelli, Isseroff R. R.: Epidermal growth factor receptor relocalization and kinase activity are necessary for directional migration of keratinocytes in DC electric fields. J Cell Sci 112:1967-1978, 1999

Finkelstein E., Chang W., Chao P. H. G., Gruber D., Minden A., Hung C. T., Bulinski J. C.: Roles of microtubules, cell polarity and adhesion in electric-field-mediated motility of 3T3 fibroblasts. J Cell Sci 117:1533-1545, 2004

Hirose H., Nakahara T., Zhang Q. M., Yonei S., Miyakoshi J.: Static magnetic field with a strong magnetic field gradient (41.7 T/m) induces c-Jun expression in HL-60 cells. In Vitro Cell Dev Biol Anim. 39:348-52, 2003

Jaffe L. F.: Electrophoresis along cell membranes. Nature 265: 600-602, 1977

MacBain V. A., Forrester J. V., McCaig C. D.: HGF, MAPK, and a small physiological electric field interact during corneal epithelial cell migration. Invest Ophthalmol Vis Sci 44:540-547, 2003

McCaig, C.D., A.M. Rajnicek, B. Song, M. Zhao
(2005) Controlling cell behavior electrically:
current views and future potential. Physiol Rev
85: 943–978.

McLeod K. J., Rubin C. T.: Regulation of Cell Growth Rates in Vitro by Alteration of Induced Charge Density. The Annual Review of Research on Biological Effects of Electric and Magnetic Fields From the Generation, Delivery and Use of Electricity, Frederick, MD, W/L Associates, Ltd 80:65, 1994

Mu-ming Poo: In situ electrophoresis of membrane components. Ann. Rev. Biophys Bioeng 10:245-76, 1981

Nuccitelli R.: A role for endogenous electric fields in wound healing. Curr Top Dev Biol. 58:1-26, 2003

Ohgaki M., Kizuki T., Katsura M., Yamashita K.: Manipulation of selective cell adhesion and growth by surface charges of electrically polarizes hydroxyapatite. J Biomed mater Res 57:366-373, 2001

Soong H. K., Parkinson W. C., Bafna S., Sulik G. L., Huang S. C. M.: Movements of cultured corneal epithelial cells and stromal fibroblasts in electric fields. Invest Opthalmol Vis Sci 31:2278-2282, 1990

Sulik G. L., Soong H. K., Chang P. C., Parkinson W. C., Elner S. G., Elner V. M.: Effects of steady electric fields on human retinal pigment epithelial cell orientation and migration in culture. Acta Ophthalmol (Copenh) 70:115-122, 1992

Sun, S., J. Wise, M. Cho (2004) Human fi broblast migration in three-dimensional collagen gel in response to noninvasive electrical stimulus. 1. Characterization of induced three-dimensional cell movement. Tissue Eng *10:* 1548–1557.

Vroman, L. (1988) The life of an artifi cial device in contact with blood: initial events and their effect on its fi nal state. Bull N Y Acad Med *64:* 352–357.

Wang E., Zaho M., Forrester J. V., McCaig C. D.: Re-orientation and faster, directed migration of lens epithelial cells in a physiological electric field. Exp Eye Res, 71; 91- 98, 2000b

Zhao M., Pu J., Forrester J. V., McCaig C. D.: Membrane lipids, EGF receptors, and intracellular signals colocalize and are polarized in epithelial cells moving directionally in a physiological electric field. FASEB J (April 10) 10.1096/fj.01-0811fje, 2002.

RETINAL SCANNING OF CRITICAL FUSION FREQUENCY (CFF) OF THE HUMAN EYE

MAGDY S. IBRAHIM

DEPARTMENT OF ENGINEERING MATHEMATICS AND PHYSICS
FACULITY OF ENGINEERING, CAIRO UNIVERSITY, 12211
GIZA, EGYPT

Abstract:

The aim of the present study is to introduce an electronic experimental setting for measuring of critical time (CT) and corresponding critical fusion frequency (CFF) for healthy subjects at different wavelengths and different acuities. The work introduces a simple measuring setting that utilizes an electronic device capable of controlling the frequency of illuminated monochromatic light source.

The investigation considered the size of the stimulus, its luminance, the distance from the eye to the fixed and movable light sources. Particular interest was given to scanning the retina for various CFF responses. The results show that , CFF has a maximum value at fovea and this value decreases nonlinearly as we move to the periphery, explanation of this results is introduced and related to cone and rod distribution at different retinal visual angle as well as the different response of cones to color .

Introduction:

Critical flicker frequency (CFF) is the transition point of an intermittent light source where the flickering light ceases and appears as a continuous light. Accordingly, it is the minimum frequency of a pulsating light source at which the light appears to be fused into continuous, rather than flickering, stimulus. There are a multitude of factors that determine our perception of flicker such as the intensity and size of the test stimulus[1].

Researches in this field are important in diagnosing by the measurements of fusion of the human eye. Braunstein[2] was one of the first to investigate CFF in cases of optic atrophy, optic neuritis and glaucoma. Since then measurements have shown to be sensitive to the presence of retinal or optic nerve diseases when other clinical tests remain unaffected[3, 4].

Several factors such as the light intensity, the target size, and the luminance contrast[5] are affecting on the CFF. Keesey[6] , illustrated that the visual target size affects flicker perception at frequencies higher than 20 Hz , CFF is known to increase with increasing target stimulus size ; under 20 Hz, the sensitivity decrease with increasing target size. Delange[7] demonstrated that for visual stimulus with a fixed temporal frequency; sensitivity to flicker increases as the amplitude of the luminance is increased.

At high frequencies, flicker sensitivity curves for different size of visual stimuli have similar shapes, Kelly[8]. This indicates the visual system responds the temporal characteristics of stimuli in a consistent fashion. At frequency higher than 20 Hz CFF thresholds decreased as target size increases. The age plays an important role, Kim[9], showed that young people in general have higher CFF than older ones. In addition, women enjoy higher CFF than men[10].

CFF is significantly higher than at the fovea when the image is projected at the fovea, also the flicker depends of the background illumination, for dark background, the CFF is lower than that for background at 50 lux[11]. Wolfgang[12], studies the effects of the CFF at the accommodation, convergence and pupil diameter of the human eye. Toshiyuki[13], studied the effects of illumination, distance between the eye and the light source and age on the CFF.

However, very little attention is given to the study of flickering at different point on the retina. Most of the reported literature is concerned with CFF when the image is received at the fovea. In the present work, the CFF at different locations in the visual field for different wavelengths is examined. It employs a device, which enable the researchers to obtain accurate data concerning the effect of the both locations and wavelengths on the CFF value.

Apparatus used:

An electronic device was designed so that light of several wavelengths can produced and jittered from different LEDs. The light pulses are supplied from a square wave function generator. The wave generator produces square pulse, which is differentiated electronically, and then the edge of the pulse was used to initial a rectangular wave using a monostable oscillator. This stage is necessary to control both the pulse duration (T_1) and the time interval between the successive pulses (T_2). At the end, the output of the monostable vibrator is sent to a movable LED 2 light source. The light is filtered so that only the concerned wavelengths are obtained purely.

The pulse is observed using an oscilloscope and fed to PC to record the results. The pulse duration was kept constant while the time interval between pulses varied electronically. The block diagram of electronic circuit can be shown in Figure 1.

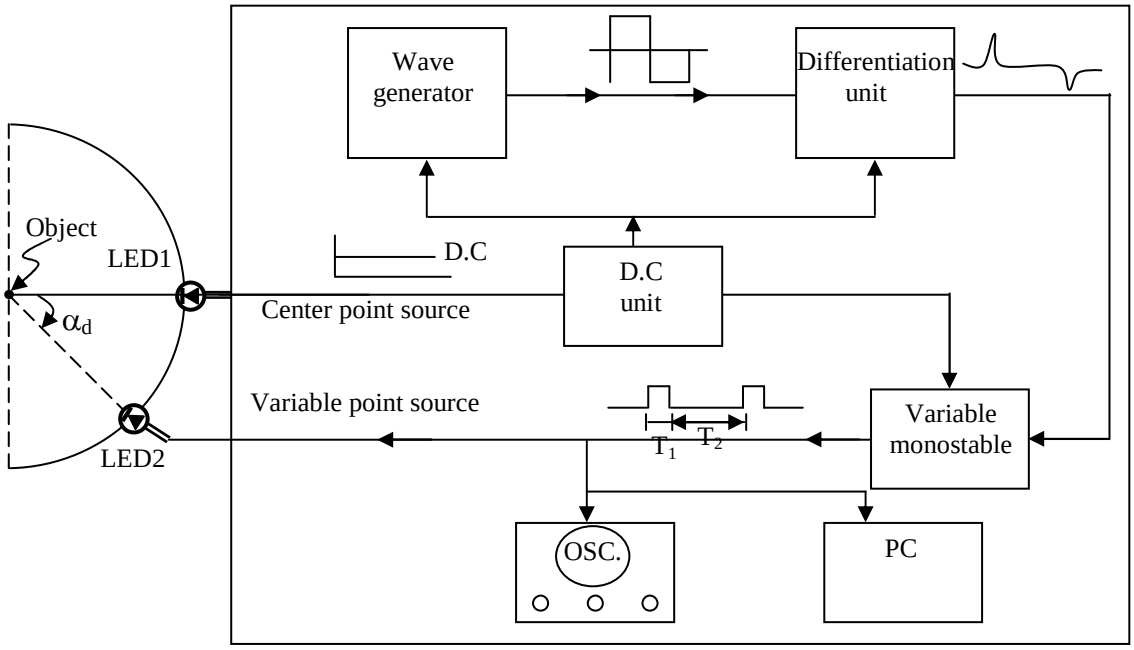

Figure 1

The mechanical device consists of two stand and semi-circular arc of radius 49 cm , the length of the arc is calibrated such that the distance from the center of fixation point to any point on the arc (d) corresponds to an angle α d which is called retinal visual angle at the center of the arc as shown in Figures 2 (a , b) .

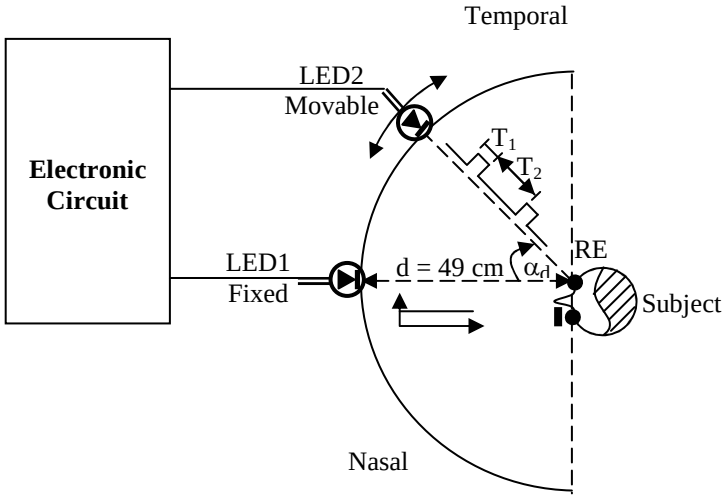

Experimental setting for measurement of critical time
Figure 2-a Nasal and Temporal Vision of R.E

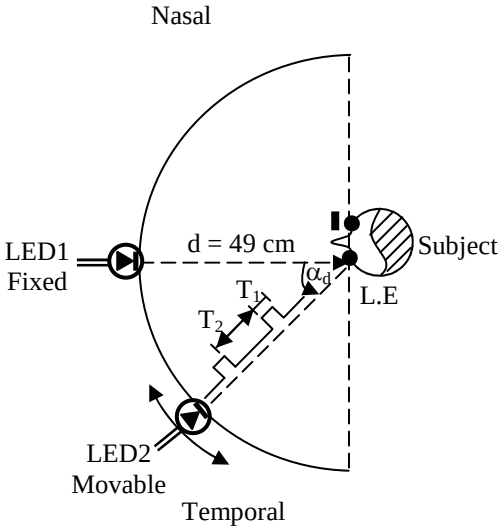

R.E
Figure 2-b Nasal and Temporal Vision of L.E

Procedure:

Ten subjects (mean age 30 ± 5 years) were examined for CFF , the visual acuity , sex ,weight , occupation and the state of the health are recorded . The experimental setting is kept under dark conditions. Measurements were taken for each eye separately for each subject. The subject was asked to keep focusing on the center of the arc where a fixed light source LED 1 at the fixed wavelength is located. As the subject is focusing on this source, another source LED 2 of the same wavelength was made to slide slowly on the arc at different positions.

For each position, the light controlled from the second source is made to fluctuate electronically at different frequency, the subject was asked to tell when he sees the light continuously. At that time, the frequency of the light was determined using an oscilloscope. The value of the CFF is obtained an average value for more than six repetitions of the CFF thresholds were obtained.

The procedure was repeated for different wavelengths of λ_1 = 540 nm , λ_2 = 580 nm and λ_3 = 660 nm at different locations on the retinal visual field for each subject. In addition, the effect of the visual acuity was investigated on the CFF thresholds.

Results:

The effects of the different wavelengths on the Critical Time (CT) are measured as shown in Figures 3 and 4. CT has a minimum value at the fovea for all wavelengths; this is because the fovea is the most region of the retina, which contains the maximum concentration of the receptors of, cons (337×10^3 cones). At the temporal side of the eye, CT increases due to the decreasing of the concentration of the cons. CT is higher throughout the periphery than the fovea CT for λ_1 = 540 nm is less than CT for λ_2 = 580 nm and for less than λ_3 = 660 nm .

Fig . 3 - a Critical Time for R.E (Temporal)

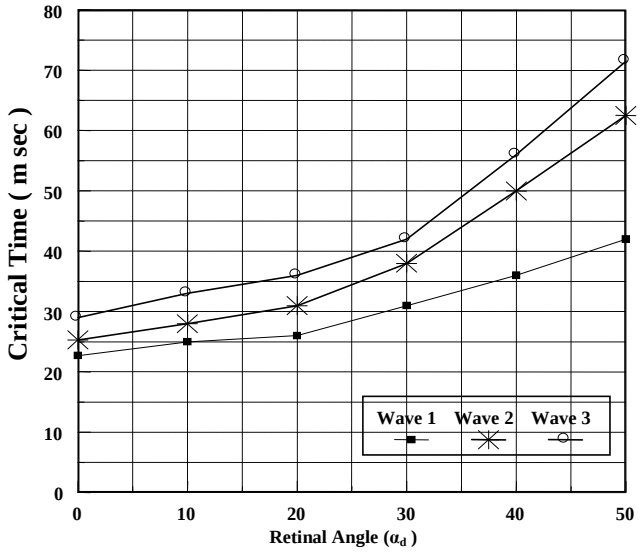

Fig . 3 - b Critical Time for R.E (Nasal)

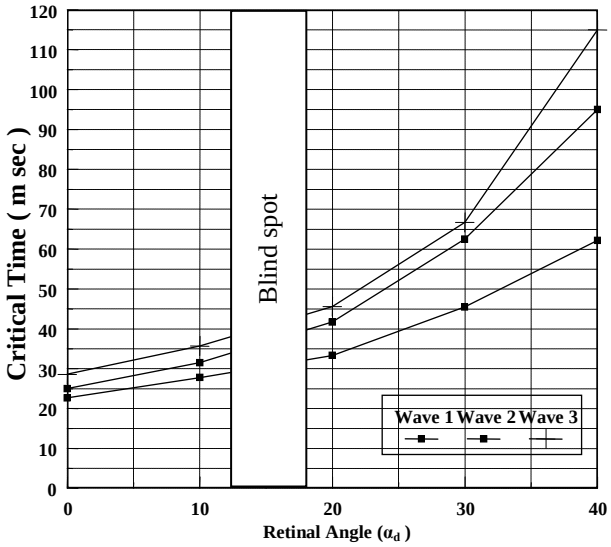

Fig . 4 - a Critical Time for L.E (Temporal)

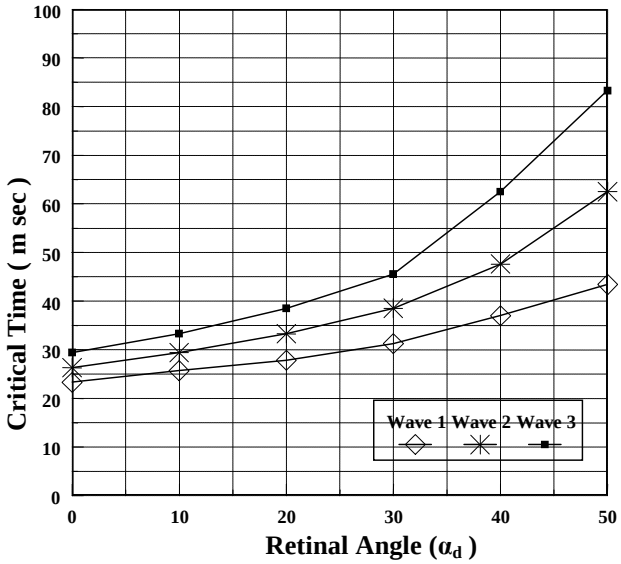

Fig . 4 - b Critical Time for L.E (Nasal)

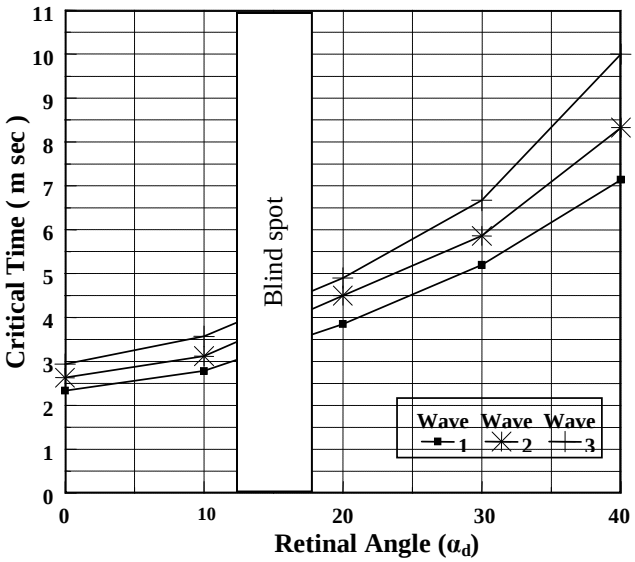

CFF has a maximum value at fovea (± 2.5º from the visual axis) and this value decreases in the periphery, the reason of this return to the existing of different pathways long (SC) & short (LGN) CFF has a maximum value than in periphery. Also , the different rates , low (blue cone) & high (red and green cones) of neural signal causes that the CFF has a different value at different retinal visual angle, and at different wavelengths of light sources , the values of CFF at different locations of the retina for different wavelengths for right and left eyes respectively are shown in Tables 1,2.

Table 1: CFF values at different locations of visual retinal angle (α_d°) for different wavelengths. (R.E)

Retinal angle (α_d°)	CFF (Hz) Temporal Side		
	Wave 1 λ_1 **= 540 nm**	**Wave 2** λ_2 **= 580 nm**	**Wave 3** λ_3 **= 660 nm**
0º	44	40	35
10º	40	35	30
20º	38	32	28
30º	32	26	24
40º	28	20	18
50º	24	16	14

Table 1-a Temporal side

Retinal angle (α_d°)	CFF (Hz) Nasal Side		
	Wave 1 λ_1 **= 540 nm**	**Wave 2** λ_2 **= 580 nm**	**Wave 3** λ_3 **= 660 nm**
0º	44	40	35
10º	36	32	28
20º	30	24	22
30º	22	16	15
40º	18	10	8

Table 1-b Nasal side

Table 2: CFF values at different locations of visual retinal angle (α_d°) for different wavelengths. (L.E)

Retinal angle (α_d°)	CFF (Hz) Temporal Side		
	Wave 1 λ_1 **= 540 nm**	**Wave 2** λ_2 **= 580 nm**	**Wave 3** λ_3 **= 660 nm**
0º	43	38	34
10º	39	34	30
20º	36	30	26
30º	32	36	22
40º	27	21	16
50º	23	16	12

Table 2-a Temporal side

Retinal angle (α_d°)	CFF (Hz) Nasal Side		
	Wave 1 λ_1 = 540 nm	Wave 2 λ_2 = 580 nm	Wave 3 λ_3 = 660 nm
0º	43	38	34
10º	36	32	28
20º	28	26	24
30º	18	17	15
40º	14	12	8

Table 2-b Nasal side

Figure 5 shows the variation of the Critical Time (CT) with the different visual acuities at different locations of the retina. Critical Time has a minimum value at the fovea and this value is increasing at outside of the fovea. For good visual acuity (20/20), CT is minimum (CFF is maximum) than for low visual acuity (20/120). The values of CFF at different locations of visual angle for different visual acuities are shown in Table 3. In periphery, CFF values did not change almostely for different acuities.

Fig . 5 Critical Time for different visual acuities

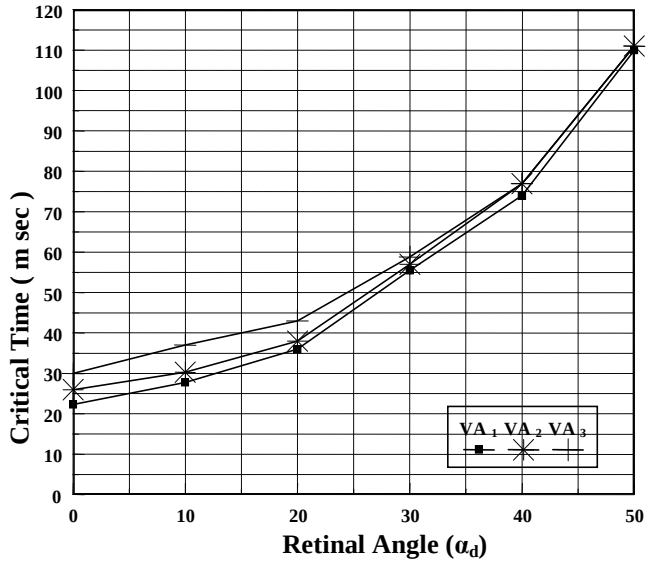

Table 3: CFF values at different locations of visual retinal angle (α_d°) for different acuities. (V.A)

Retinal angle (α_d°)	CFF (Hz)		
	VA_1 20/20	VA_2 20/30	VA_3 20/120
0º	43	42	35
10º	36	33	27
20º	26	25	22
30º	18	17	17
40º	14	13	13
50º	10	9	9

Figures 6 (a , b) Show the visual field of right and left eyes at different wavelengths respectively, the visual field for smallest wavelength is largest area than for largest wavelength .

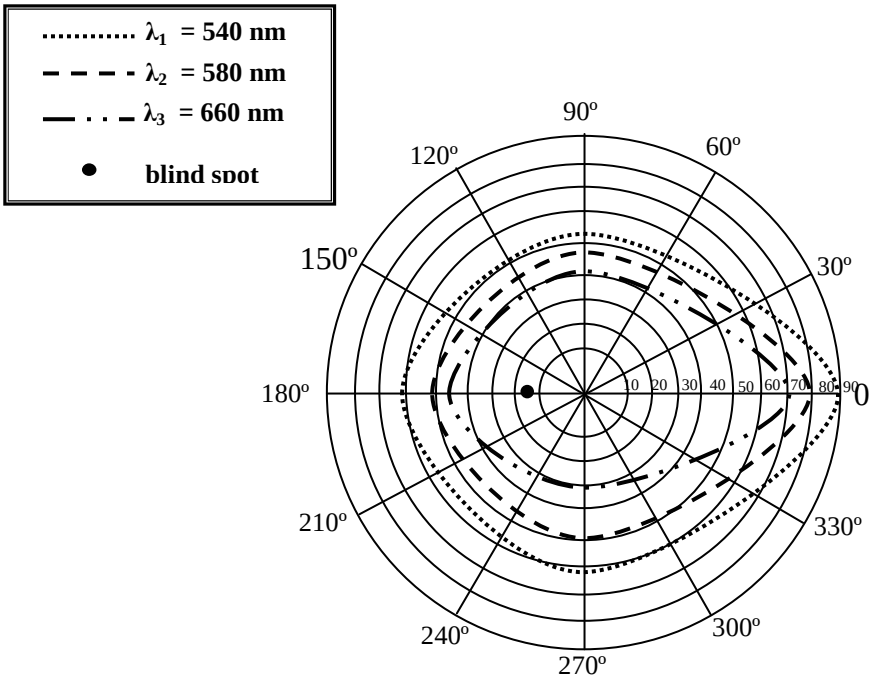

Figure (6 – a) Visual field of R.E

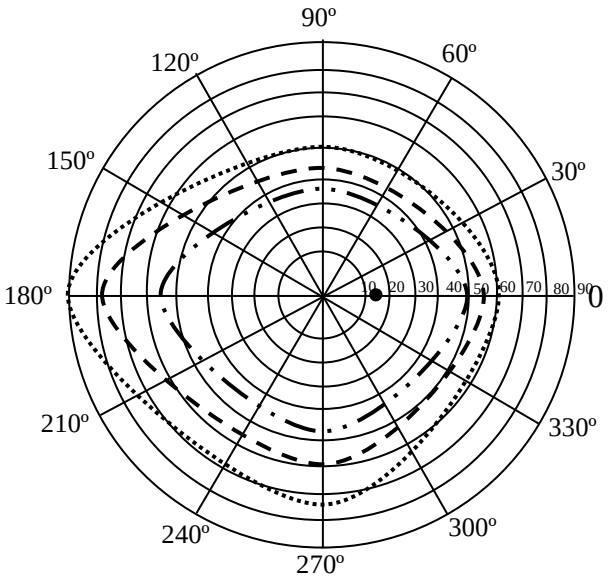

Figure (6 – b) Visual field of L.E

The critical flicker frequency is often used as a measure of the current state of the optical nervous system. As such, it may be affected by several factors; internal as well as external. Internal factors concerned with the subject characteristics, such as stimulus, modulation, luminance (Intensity and area), and wavelength. There are two possible routes for the neural signal from the receptors across the optic nerve to the brain, via the lateral geniculate nuclei (LGN) or via the superior colliculus (SC) as shown in Figure 7. The presence of different pathways {long (SC) & short (LGN)} and different rates {low (Blue cone) & high (Red and Green cones)} of neural signal causes that the CFF has a different value at different retinal visual angle, and its maximum value at fovea.

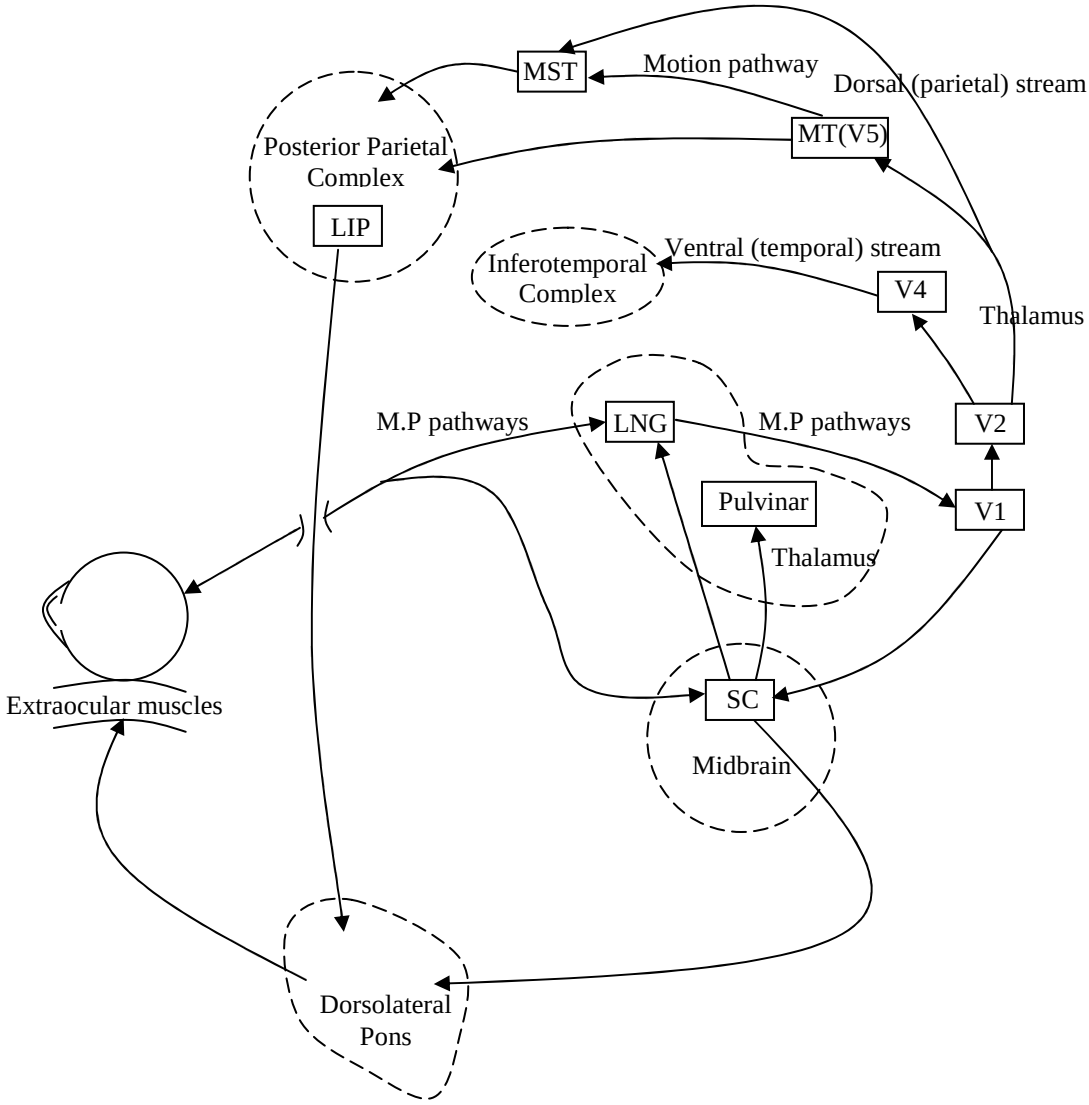

Fig. 7: The brain and the visual pathways

From the pervious results, it is clear that the retina and the occipital cortex synchronize with the flicker, and then CFF is regarded as a function of activity of both the eye and the cerebral cortex. The highest degree of cortical response that is registered when a subject is exposed to flicker is found in the occipital lobe.

Conclusion:

The precedence enables as to examine the variation of CFF with location on the retina as whole. The spatial approach overcomes the pervious literature, which concentrate on the measurement of CFF on the fovea itself. The work also examines the effect of light wavelength on the CFF at different spatial location on the retina and shows that for away from the fovea the CFF decreases.

Also the proposed electronic and mechanical setting have the advantage of simplicity and accuracy for the future work, varying wavelength may be examined and related to know diseases.

References:

1- Martavianya E., William A., Konrad P., " Development of a Critical Flicker/ Fusion Frequency Test for Potential Vision Testing in Media Opacities " Optometry and vision Science, Vol.81, No. 12, December 2004.

2- Braunstein EF : Beitrag Zur lehre des intermittierendem Lichreizes der gesunden and Kranken.Z Psychol. 1903; 33 : 241-88 .

3- Han DP, Thompson Hs , Folk JC. Differentiation between recently resolved optic neuritis and central serous retinopathy . Use of tests of visual function. Arch Ophthalmol 1985 ; 103 : 394 - 6 .

4- Nakamura M, Yamamoto M. Variable pattern of visual recovery of Lebers hereditary optic neuropathy . Br J Ophthalmol 2000 ; 84: 534- 5 .

5- Lachenmayr B J, Gleissner M . Flicker perimetry resists retinal image degradation Invest Ophthalmol Vis Sci 1992; 33 ; 3539- 42 .

6- Keesey U.T. " Flicker and pattern detection " A comparision of thresholds . Journal of the optical society of American , 62 , 446 – 448 , 1972 .

7- Delange H. "Research into the dynamic nature of the human fovea – cortex systems with intermittent and modulated light. Journal of the optical society of American, 48, 777 – 789, 1958.

8- Kelly , D.H. " Flicker , In the Handbook of sensory physiology " vo111/4 ; visual psychophysics D. Jameson and L.M. Hurvich (Eds) New York , spring Verlag , 1972 .

9- Kim , C.B.Y. and mayer , M.J. " Foveal flicker sensitivity in healthy aging eyes Journal of the optical society of American , 11 (7) , 1994 .

10- Amir , T. and Ali , M . R " Critical Flicker Frequency , personality , and sex of Subjects. Perceptual and motor skills , 69 , 1019 – 1026 , 1989 .

11- Jones, M. "Effects of luminance, luminance, viewing angle, and screen test pattern on the perception of flicker in CRT display. Virginia Polytechnic institute and state university, Blacksburg , VA . 1996.

12- Wolfgang J., Matthias B., Edald A., "Accommodation, convergence, pupil diameter and eye blinks at a CRT display flickering near fusion limit" Ergonomics, 1996, Vol. 39 , No. 1 , 152 - 164.

13- Toshiyuki H., Kohki M., Kazuo S., " Basic study of the portable fatigue meter : effects of illumination distance from eyes and age " Ergonomics , 1997, Vol. 40 , No. 9, 887 – 894 .

PLANAR ELLIPTICAL RING BANDPASS FILTER WITH CONTROLLED BANDWIDTH AND OPTIMAL SIZE

MAGDY. S. IBRAHIM

DEPARTMENT OF ENGINEERING MATHEMATICS AND PHYSICS
FACULITY OF ENGINEERING , CAIRO UNIVERSITY, 12211
GIZA, EGYPT

Abstract:

A design of a bandpass filter is presented in this paper and tuned at 2.4 GHz. The resonating element in this design is an elliptical ring with a specific width. The microstrip line is directly connected to the ring. Both the ring and the microstrip line are placed on one side of a dielectric substrate. The slotline is connected to the substrate below the ring. The slotline is electromagnetically coupled to the ring resonator.

A detailed parameter study has been performed for the proposed filter. The results show that both the bandwidth and the surface area of the filter can be controlled via controlling the width and the aspect ratio of the ring.

Introduction:

Bandpass filters play an important role in radio front-end systems. For example a bandpass filter is put immediately after the receiving antenna to reduce the susceptibility of the receiver to unwanted frequencies. Superheterodyne receivers make use of one or more intermediate frequencies with image reject bandpass filters on every intermediate frequency. A passive bandpass filter can be constructed by combining a number of elements [1]. These elements can be either lumped components (such as inductors, capacitors, resistors) or distributed transmission lines [2]. For the bandpass filter based on distributed transmission lines, any type of lines can be used (such as microstrips, coplanar waveguides, slotlines …). Different topologies can be used to achieve the required frequency selection function of the bandpass filter. For example, parallel coupled lines [3] and hairpin resonator [4, 5].

In this paper, a new design of a bandpass filter is presented. The design is based on distributed transmission lines of the microstrip type. The resonator used takes the shape of an elliptical ring of a specific width. Two lines are coupled to this ring. The first line is of microstrip type and directly connected to the ring. The second one is of slot type and coupled electromagnetically, through the substrate, to the ring. Hence, the proposed design is perfectly planar and consists of two metal layers and one dielectric layer.

Section 2 introduces the proposed geometry of the filter. The method used for analysis is mentioned in Section 3. The steps to be followed in order to tune the proposed filter are given in Section 4. A detailed parameter study is performed in Section 5. The important conclusions are stated in Section 6.

Filter Configuration:

Figure 1 shows the proposed design for the bandpass filter. It consists of two planar metallic layers placed on both sides of a dielectric substrate. Without loss of generality, a glass substrate with dielectric constant of 6.2 and thickness of 0.7 mm is selected. This substrate is identical to that used in the multichip module with deposited thin films, MCM-D, technology [6]. The first metal layer is placed on top of the substrate. It includes a microstrip line connected to an elliptical ring resonator. Port 1 is assigned to the microstrip line. The second metal layer is placed on the other side of the substrate. Within this layer, a slotline is etched and connected to port 2. Both metal layers are assumed made up of copper with conductivity of 58×10^6 1/Ωm and thickness of 5 μm.

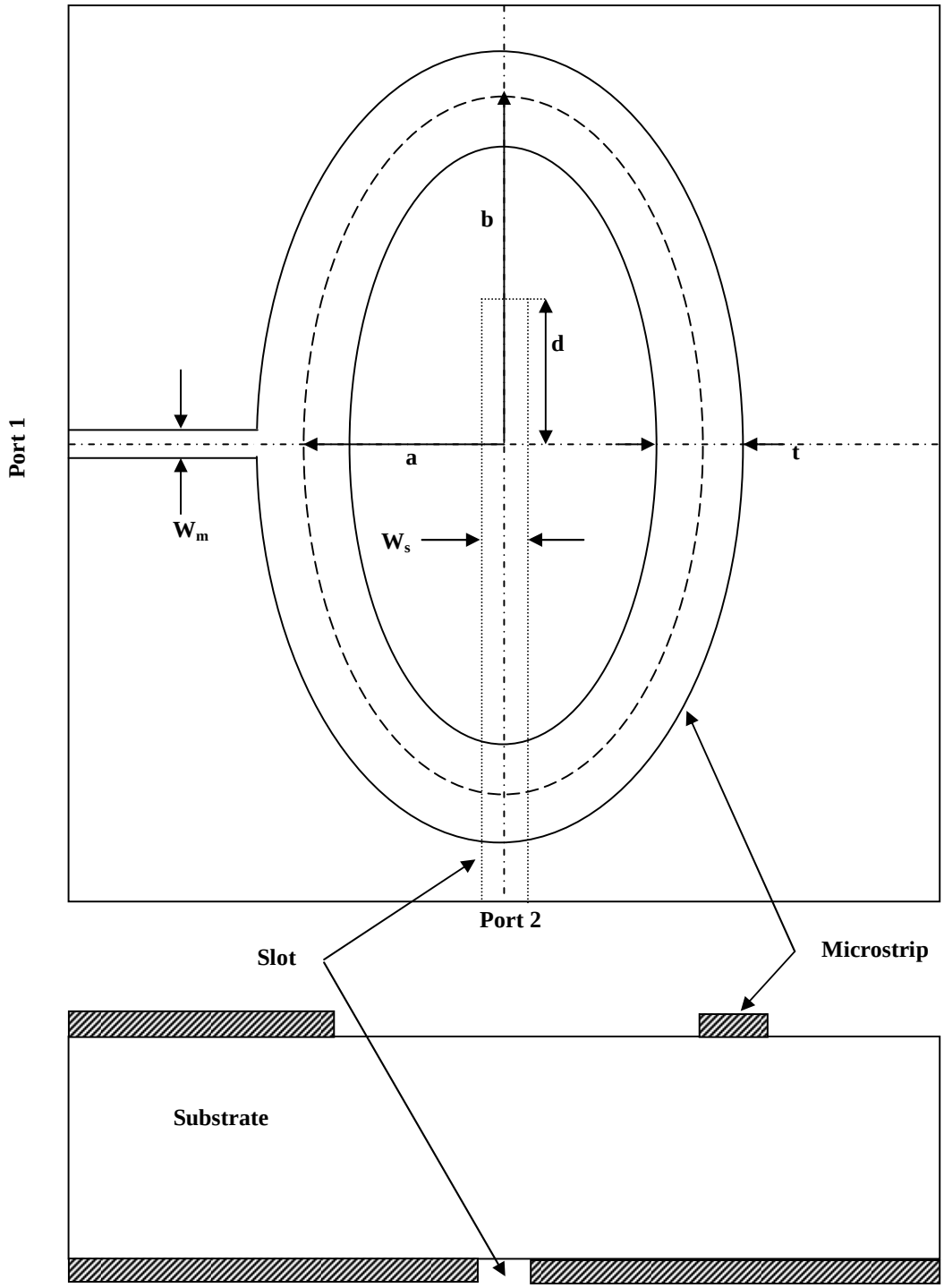

Figure 1 Geometry of the elliptical ring resonator bandpass filter

The proposed filter design has the advantage of allowing the antenna to be of microstrip type, and the rest of the transceiver circuit to be of slot type. This combination is attractive for many practical situations. Being of microstrip type, the integrated antenna, which will be connected to port 1, provides radiation from one side only of the substrate. This feature is desired in several wireless systems. On the other hand, the preferable technology for the rest of the system is either the slotline or the coplanar waveguide (CPW). This is due to the fact that in these technologies both the signal and the ground terminal(s) are brought in the same plane.
This simplifies the integration of shunt lumped elements and active devices and avoids the necessity of drilling via holes through the substrate. It is clear from Fig. 1 that the proposed filter design has 6 feature dimensions. These dimensions are: the minor and major radii of the elliptical ring resonator (*a* and *b*, respectively), the width of the ring *t*, the distance between the edge of the slotline and the center of the ring *d*, the width of the microstrip line W_m, and the width of the slotline W_s. Practically, the last two dimensions are adjusted to achieve specific values for the characteristic impedances of the feeding lines. Knowing the substrate properties and the resonance frequency, 2.4 GHz, the widths which correspond to 100 Ω for both lines are: W_m = 0.21 mm and W_s = 0.8 mm.

The theory of operation of the proposed bandpass filter is that at resonance, the electrical circumference of the elliptical ring equals one guided wavelength λ_g. The width of the microstrip line forming the ring, *t*, defines the corresponding value of the guided wavelength. The satisfaction of this condition, forces the two signal components excited from one port to travel distances of $\lambda_g/4$ and $3\lambda_g/4$ in the two branches of the ring to reach the other port. The resulting 180^0 phase shift is compensated by the 180^0 spatial opposition of the two arms at the other port, which results in an in-phase addition.

Method of Analysis:

The analysis of the proposed bandpass filter is carried out using Agilent-Momentum [7]. Momentum is a 2.5D full-wave solver based on the integral equation formulation solved using the Method of Moments. Since it is a well-known full-wave simulator validated many times in literature, it is possible to rely on its simulation results. For meshing the filter under development, mixed rectangular and triangular segments are used. Twenty five cells per wavelength combined with a narrow edge mesh are adopted.

Filter Design:

As stated in Section 2, the remaining 4 dimensions of the filter to be determined are: *a*, *b*, *t*, and *d*. The first two dimensions can be combined into one parameter called the aspect ratio of the elliptical ring resonator. This new parameter is defined as the ratio between *b* and *a*, i.e. (*b*/*a*). Knowing *b*/*a* and *t*, the last dimension *d* is determined via optimization such that the best impedance matching with the slotline is obtained. This leaves only two independent design parameters, namely *b*/*a* and *t*. Consequently, the design space is a 2D space. The selected range for *b*/*a* starts from 1 up to 5, while the selected range for *t* starts from 0.25 mm up to 0.75 mm. Outside these ranges it has been observed that the response of the filter is unsatisfactory.

The frequency response of the filter at the central point of the design space, *b*/*a* = 3 and *t* = 0.5 mm, is shown in Figure 2. As desired, the resonance frequency of the filter is 2.4 GHz. There are several criteria for defining the percentage bandwidth of a bandpass filter. The selected definition in this paper is $\Delta f / f_0$, where f_0 is the resonance frequency and Δf is the common frequency band which satisfies the following conditions: $|S_{11}| < -10\,\text{dB}$, $|S_{21}| > -1\,\text{dB}$, and $|S_{22}| < -10\,\text{dB}$.
As mentioned in Section 2, once the width of the ring is defined, its circumference become available and equals to the guided wavelength of the microstrip line forming it. However, experimental iterations have shown that the ring circumference is slightly smaller than the corresponding theoretical value. This deviation is mainly due to the excitation of higher order modes around the feeding lines. For the selected width of the ring *t* = 0.5 mm and at *f* = 2.4 GHz, the guided wavelength is 60.62 mm, while the circumference of the ring is found to be 55.83 mm. Since the circumference of the elliptical ring equals $\pi(a + b)$, the specification of the aspect ratio *b*/*a*, results in determining the corresponding values for the minor and major radii, *a* and *b*, respectively.

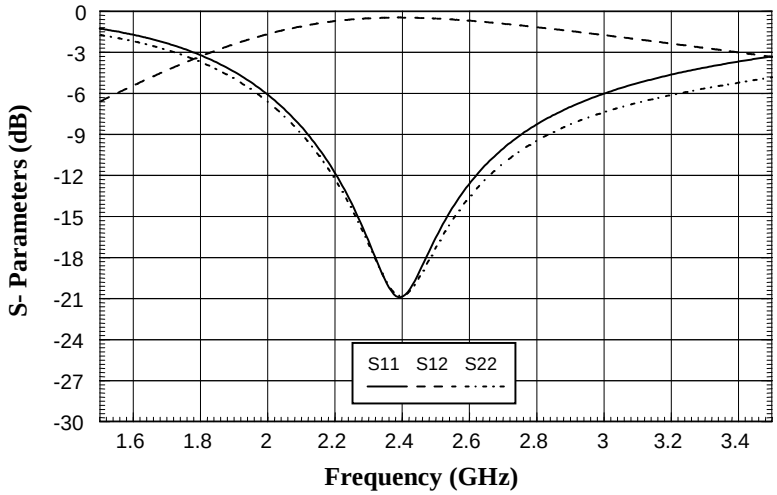

Figure 2 S-parameters versus frequency of the proposed bandpass filter.

Parameter Study:

In this section the effect of varying the independent design parameters on the filter's geometry and response is studied. As mentioned is the previous section, the proposed filter has two independent design parameters, namely the aspect ratio *b*/*a* and the width of the elliptical ring resonator *t*. Of particular interest to many modern wireless systems, is the surface area occupied by the filter. There is a definite trend toward specifying severe restriction on the surface area. For our proposed design the surface area occupied by the filter can be defined as the area of the rectangular which entirely contains the ring. Referring to Figure1, the surface area equals $(2a + t)$ $(2b + t)$. The response of the filter is characterized by its percentage bandwidth, which is defined in Section 4.

Variation of b/a:

In this subsection the aspect ratio of the elliptical ring is continuously varied from 1 to 5. The other independent parameter *t*, takes three discrete values: 0.25 mm, 0.5 mm, and 0.75 mm. Figure 3 shows both the minor radius *a*, and the major radius *b*, versus the aspect ratio. It is clear from the figure that *a* decreases as *b*/*a* increases, while *b* increases. This behavior allows *a* and *b* to provide the required aspect ratio, while keeping their summation approximately constant. The approximately constant summation results in an approximately constant circumference for the ring at the corresponding value of its width. Both *a* and *b* decreases as *t* increases. The reason for that is the guided wavelength, and also the circumference, decreases as *t* increases.

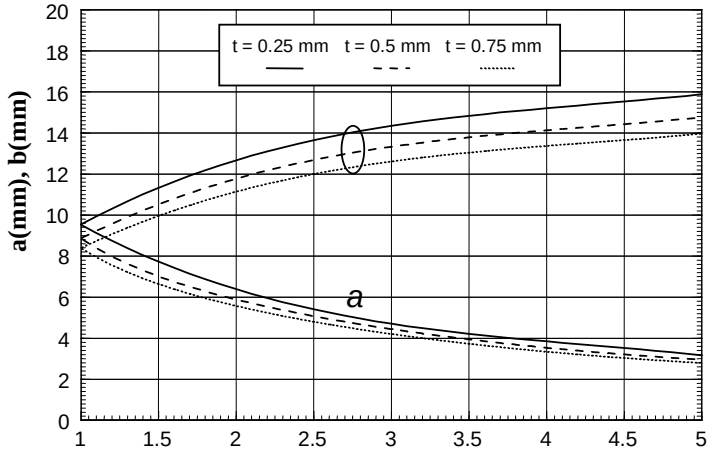

Figure 3 Minor and major radii of the ring versus its aspect ratio

The surface area occupied by the filter is plotted in Figure 4 versus *b*/*a* at three different values of *t*. The figure shows that increasing the aspect ratio *b*/*a*, results in decreasing the surface area. The decrease in the surface area with the increase of the width *t* is expected, because of the decrease of the guided wavelength. Figure 5 shows the optimized values of *d* versus *b*/*a* at the selected values of *t*. The optimization is based on obtaining the best possible match with the slotline of port 2. It is clear from Figure 5 that as *b*/*a* increases the edge of the slotline moves continuously downward. The percentage bandwidth of the filter is plotted versus *b*/*a*, at different values of *t*, in Figure 6. The figure shows that the percentage bandwidth decreases as either *b*/*a* or *t* increases. However, the effect of varying *t* is more pronounced. Based on the surface area and bandwidth specifications, the designer can use Figures 3, 4, 5, and 6 to specify the corresponding values of *a*, *b*, *t*, and *d*.

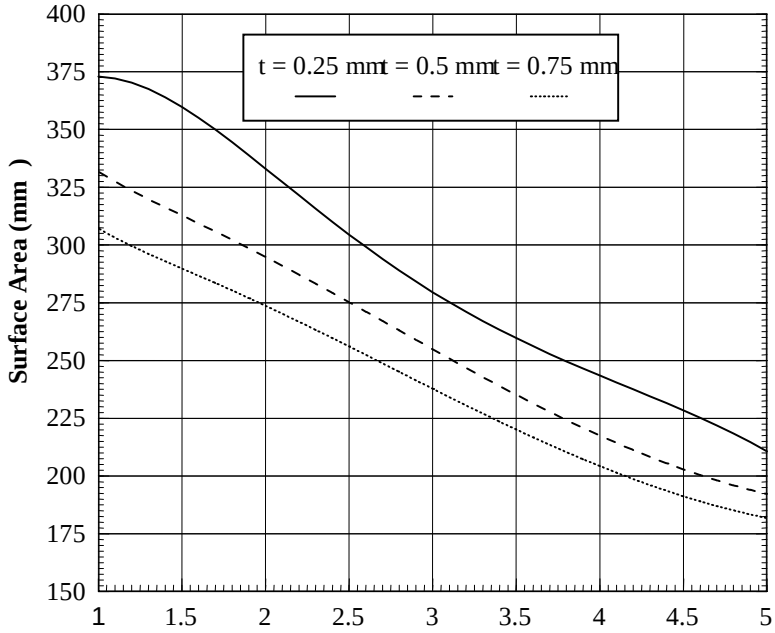

Figure 4 Surface area occupied by filter versus the aspect ratio of its ring

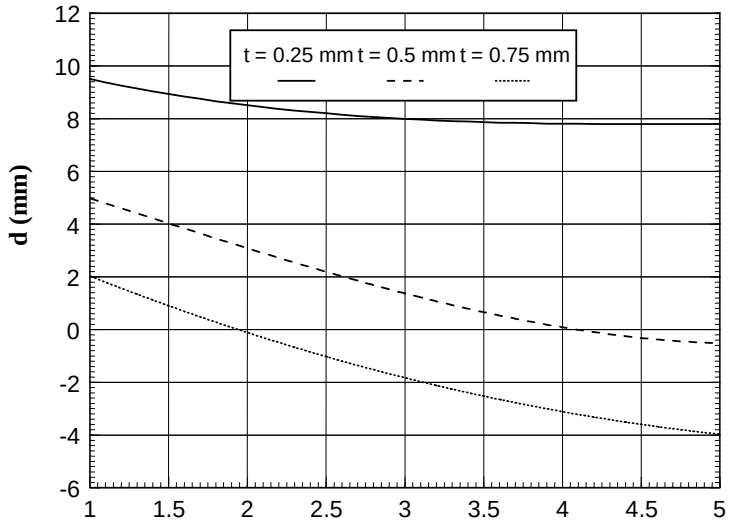

Figure 5 Distance between the edge of the slotline and the center of the ring versus its aspect ratio

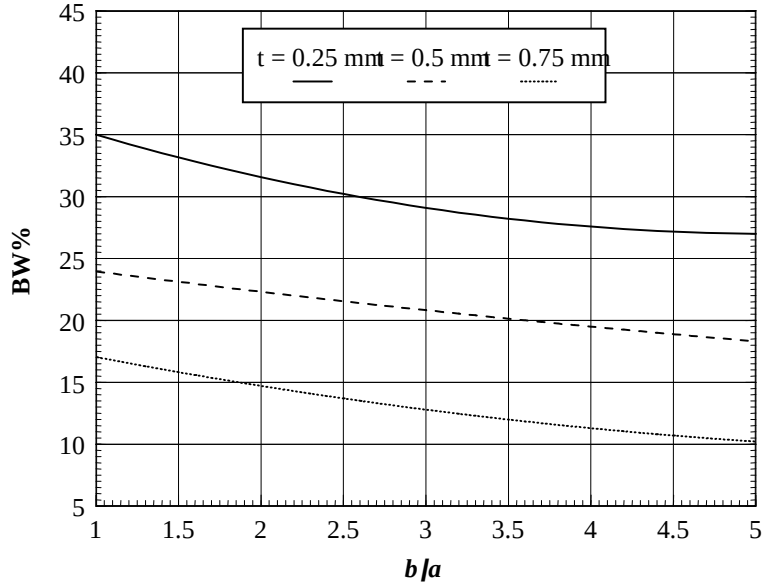

Figure 6 Percentage bandwidth of the proposed filter versus the aspect ratio of its ring

Variation of t

In order to examine the design space in the orthogonal direction, the width *t* of the ring is going to be varied continuously, from 0.25 mm to 0.75 mm, in this subsection. The aspect ratio *b*/*a* will be fixed at three discrete values: 1, 3, and 5. Figure 7 shows both the minor radius *a* and the major radius *b* versus *t*. As *t* increases, both *a* and *b* decreases. This is a result of the reduction of the guided wavelength as well as the circumference of the ring as *t* increases. It is also clear that as *b*/*a* increases *a* decreases, while *b* increases. This behavior allow *a* and *b* to preserve the required aspect ratio while keeping their summation approximately constant at a specific value of *t*.

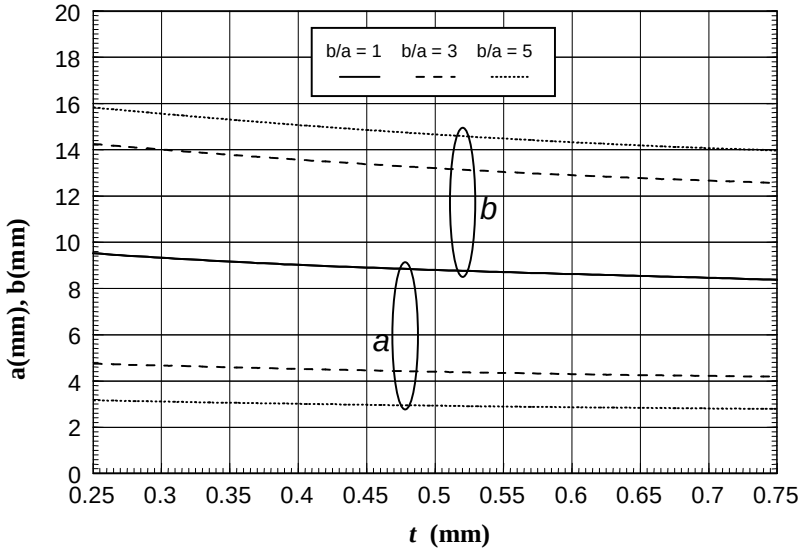

Figure 7 Minor and major radii of the ring versus its width

Knowing *a* and *b*, the surface area occupied by the filter can be calculated. In Figure 8, the surface area is plotted versus *t* at three different values of *b*/*a*. The surface area decreases as either *t* or *b*/*a* increases. The parameter *b*/*a* has more impact on the surface area than that of *t*. After obtaining the radii of the ring, the value of *d* should be optimized in order to achieve the best matching between the slotline and the elliptical ring resonator. The optimum value for *d* is plotted in Figure 9. It is clear from this figure that the distance between the edge of the slot line and the center of the ring decreases as either *t* or *b*/*a* increases.

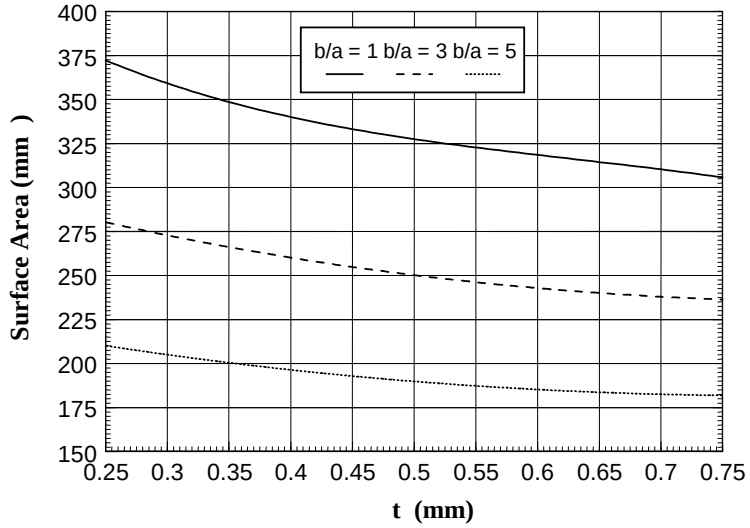

Figure 8 Surface area occupied by the filter versus the width of its ring

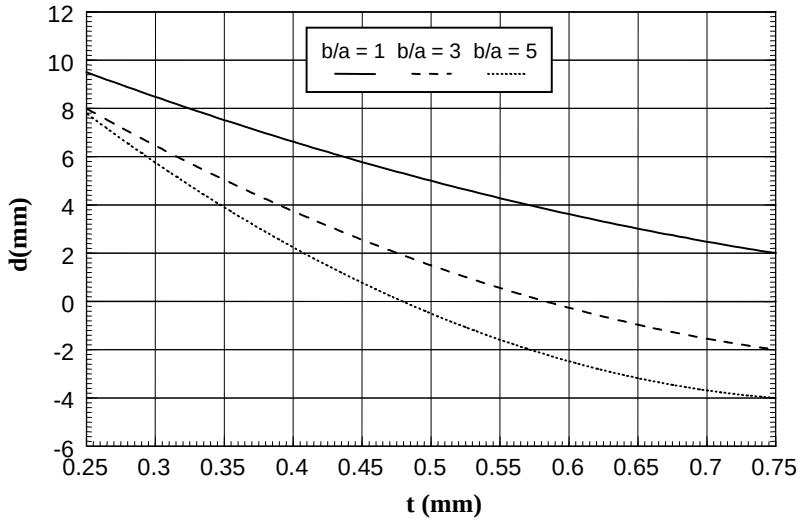

Figure 9 Distance between the edge of the slotline and the center of the ring versus its width

Finally, the percentage bandwidth is presented in Figure 10 versus *t* at the same three values of *b*/*a*. The figure shows that the percentage bandwidth decreases as either *t* or *b*/*a* increases. In consistence with Figure 6, the variation of *t* has stronger effect on the percentage bandwidth than that of *b*/*a*. It is clear from both Figures 6 and 10 that the proposed bandpass filter offers a wide range of bandwidth variation. For the selected ranges of *b*/*a* and *t*, the percentage bandwidth varies from 10% up to 35%.

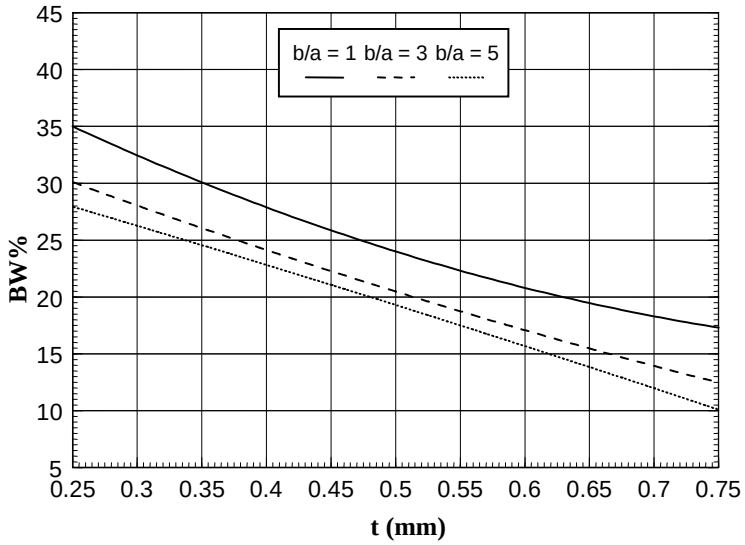

Figure 10 Percentage bandwidth of the proposed filter versus the width of its ring

Conclusion :

This paper presents a new bandpass filter design. The proposed filter is of planar nature which makes it consistent with the modern microwave systems. A rigorous parameter study for the proposed design has been performed via a reliable full-wave commercial software. It has been found that two independent parameters are affecting the performance of the filter. Varying these parameters, it has been demonstrated that the percentage bandwidth of the filter can be controlled within the range from 10% up to 35%. This makes the proposed filter suitable for a wide range of microwave applications. At the selected resonance frequency of 2.4 GHz, it has been also found that changing the independent parameters of the filter results in controlling the surface area of the filter from 373mm^2 down to 182mm^2. This feature indicates that the proposed design is able to satisfy the size reduction requirement of some wireless applications.

References :

1- K. Chang, I. Bahl, and V. Nair, RF and microwave circuit and component design for wireless systems, Wiley, New York, 2002.

2- P. Pieters, K. Vaesen, W. Diels, G. Carchon, S. Brebels, W. De Raedt, E. Beyne, and R.P. Mertens, High-Q integrated spiral inductors for high performance wireless front-end systems, IEEE Radio and Wireless Conference, Denver, Colorado, 11-13, Sept. 2000.

3- E.A. Soliman, M.H. Bakr, and N.K. Nikolova, Accelerated gradient-based optimization of planar circuits, IEEE Trans. Antennas Propagat 53 (2005), 880-883.

4- S.Y. Lee and C.-M. Tsai, New cross-coupled filter design using improved hairpin resonators, IEEE Trans. Microwave Theory Tech 48 (2000), 2482-2490.

5- J.S. Hong and M.J. Lancaster, Cross-coupled microstrip hairpin resonator filters, IEEE Trans. Microwave Theory Tech 46 (1998), 118-122.

6- S. Mestdagh, W. De Raedt, and G.A.E. Vandenbosch, CPW-fed stacked microstrip antennas," IEEE Trans. Antennas Propagat 52 (2004), 74-83.

7- Momentum, version 4.8, Agilent Technologies, 2003.

MULTIPHOTON ABSORPTION IN CHIRAL BRAIN UNDER MICROWAVE RADIATION FROM WLAN'S SYSTEMS

H. TORRES-SILVA* AND M. ZAMORANO

***Instituto de Alta Investigación**
Departamento de Electrónica, Universidad de Tarapacá,
18 de Septiembre 2222, Arica, Chile
E-mail: **htorres@uta.cl**

Abstract
A model formed by chiral bioplasma with a set of macromolecules of DNA, which represents the human head inner structure, makes possible to analyze its behavior, when it is radiated by a microwave electromagnetic field WLAN's. The finite difference time domain, FDTD is used under multiphoton regime deduced from Maxwell equations. The numerical results of the Specific Absorption Rate, SAR, show the SAR behavior in function of the chirality factor. The main conclusions of our work is that the microwave absorption from WLAN's systems is enhanced, compared with classical models, when values of the normalized chiral factor are of order of one. This absorption appears under multiphoton regime in the brain region. To illustrate this effect in our simulations we considerer electromagnetic waves at frequencies of 5.2 and 5.8 GHz.

Keywords: chirality; brain tissue; Maxwell; FDTD; SAR

PACS: 41.20Jb; 02.70.Bf; 52.35; 87.15.Aa

1. Introduction

Even though a lot of work has been done there is still no complete assessed knowledge about the interaction between electromagnetic fields and biological systems . However, there is a general agreement about the relevance of the correct evaluation of the real mechanism. It seems clear that RF fields can have some effects on tissue and it still remains to be determined whether these effects are functionally and pathologically significant.
Different models of human head range from simple models, such as homogeneous sphere to heterogeneous anatomically correct models based on magnetic resonance (MR) imaging. In this paper a FDTD method to determine the absorption of RF waves emitted by WLAN`s is presented. We use a simple model, which takes into account the main interaction between the bioplasma of the brain neurons and the microwave radiation of WLAN's systems. To address the problem and on the basis of our previous approach [1-2], our method have three main steps: 1) modelling of human head through MRI, 2) evaluation of the electromagnetic fields distribution inside the biological target, considering the brain tissue as chiral bioplasmatic media, and 3) SAR simulation for to evaluate both the thermal effect and resonant absorption under multiphoton regime. A explanation of the theoretical base of the technique used and description of the models are given in section 2. Results comparing the computed SAR values in the different models are shown and discussed in the section 3. Finally, conclusions are presented.

2. Fundamentals and models

By looking a special natural chiroplasma like a citoplasma in the human brain the multiphoton mechanism can provide a new approach of the problem of absorption in the human brain. Here the eigenfrequency of collective twist excitation in proteins, DNA and other biological chain molecules can be in the gigahertz range [3-5].
Here, we assume that the electrons within chiral molecules oscillate along a helix and from the averaged electric current [1] we can find the polarization (P) and the magnetization (M) which in a helical geometry may be proportional to $\nabla\times\boldsymbol{E}$ ($\nabla\times\boldsymbol{H}$) respectively. For typical double helices, giving the moment of inertia per unit length, the

torsional factor and the length of a typical chain (I, tor, L), and following [3], For double stranded DNA we estimate I = 300 auA°, torsion constant of 0.8 ev/A°, and L between 200 A° and 2000 A° the frequency falls in the interval between 1 GHz and 10 GHz [4]-[5]. Similar results we can obtain using the Ford's model [7].
In this work we propose that when the multiphoton effect is considered, this microscopic problem is reflected at macroscopic level as thermal absorption combined with resonant absorption. Here, besides the tissue conductivity and dielectric permittivity we considerer the chiral effect caused by the interaction of microwaves and biomolecules of DNA. The chiral wave propagation in bounded helical structures may support mode excitation, mode interactions, mode conversion and amplification of molecular chirality by eigenwaves in a bioplasma [6]

This chiral effect in the brain is considered in this work as a macroscopic mechanism where the typical cell membrane of brain is a fluid bilipid layer with a lot big chiral protein molecules embedded in it. Every protein molecule is polar and will tend to align itself with an electric field and often helical rotate in its socket, so any volume of brain tissue must have a lot of cells bearing protein molecules that happen to resonate at its eigenfrequency which can be similar to the microwave frequency f or when there are n- multiphoton interaction the eigenfrequency can resonate with nf. By contrast with ionizing radiation which damage to genetic structures of cells, microwave may span thousands of cells with a single wavelength. Microwaves set up current in tissue, and any noticeable effect of such current would involve many, many of the relatively weak microwave photons, damage, if any, would be all over the path of the current and would be numerous cells in extend, so damage to general cytoplasm, mitochondria, and so forth would seem likely to be more salient than damage to genetic structure.
Accordingly with the above discussion, we apply the Maxwell´s equations to sets of microtubules and helical molecules embedded in a substrate, characterized by a global chirality factor, T, (equation 1). Chiral media can be characterized by a generalized set of constitutive relations in which the electric and magnetic fields are coupled. In this paper, we consider the Born-Fedorov approach

$$D_{x,y,z} = \varepsilon_0 \varepsilon_r E_{x,y,z} + \varepsilon_0 \varepsilon_r T \left[\frac{\partial E_{z,x,y}}{\partial y, z, x} - \frac{\partial E_{y,z,x}}{\partial z, x, y} \right]; B_{x,y,z} = \mu_0 H_{x,y,z} + \mu_0 T \left[\frac{\partial H_{z,x,y}}{\partial y, z, x} - \frac{\partial H_{y,z,x}}{\partial z, x, y} \right] \quad (1)$$

where ε, μ and T (meter) are the permittivity, permeabilitty and the chiral scalar respectively. Solving Maxwell` equations for a plane electromagnetic wave of frequency ω ($\omega = k_t v = 2\pi f$, k_t is the tissue wavenumber and v is the phase velocity) propagating in a chiral medium, it can be shown that the left- and right hand circularly polarized waves have different wavenumbers, $k = k_t/(1 + k_t T)$, $k = k_t/(1 - k_t T)$ respectively [2]. The chiral parameter T has the dimension of a length, which in an exactly solvable two helical model for a set of oriented handed molecules, is proportional to $\beta N h^2 a \rho$. Here, β is some coefficient determined by the internal elasticity of a molecule, N is the number density of molecules of radius and a pitch h with the charge ρ per unit length of each [1].
Using the MKS system of units, the following system of scalar equations is the set of Maxwell's equations in the rectangular coordinate system (x, y, z):

$$\frac{\partial H_{x,y}}{\partial t} = \mp \frac{1}{\mu} \frac{\partial E_z}{\partial y, x} \pm T \frac{\partial^2 H_z}{\partial y, x \partial t}; \frac{\partial H_z}{\partial t} = \frac{1}{\mu} \left(\frac{\partial E_x}{\partial y} - \frac{\partial E_y}{\partial x} \right) + T \left(\frac{\partial^2 H_y}{\partial x \partial t} - \frac{\partial^2 H_x}{\partial y \partial t} \right) \quad (2)$$

$$\frac{\partial E_{x,y}}{\partial t} = \pm \frac{1}{\varepsilon} \frac{\partial H_z}{\partial y, x} \pm T \frac{\partial^2 E_z}{\partial y, x \partial t} - \sigma E_{x,y}; \frac{\partial E_z}{\partial t} = \frac{1}{\varepsilon} \left(\frac{\partial H_y}{\partial x} - \frac{\partial H_x}{\partial y} \right) + T \left(\frac{\partial^2 E_y}{\partial x \partial t} - \frac{\partial^2 E_x}{\partial y \partial t} \right) - \sigma E_z \quad (3)$$

where σ (mho/m) is the tissue electrical conductivity. The main difficulty for an analytic treatment of this system is in the partial derivatives of space and time in which the chiral parameter T is present. For this reason, equations (2)-(3) can't be reduced to a typical differential equation with known solution. In our formulation, the second order approximation of Mur is used for the near-field irradiation problems in an achiral-chiral interface case. After calculation of the induced chiral electric field by the FDTD method, the local specific absorption rate SAR, is

calculated as

$$SAR_{i,j}(T) = \frac{\sigma_{i,j}\, E_T^2\big|_{i,j}}{2\rho_{i,j}}; with\, E_T\big|_{i,j}(T) = \sqrt{\frac{1}{n}\sum_{1}^{n}\left(E_y^2\big|_{i,j}^{n} + E_x^2\big|_{i,j}^{n} + E_z^2\big|_{i,j}^{n} \right)} \qquad (4)$$

3. SAR simulation and analysis of results

For the numerical calculation we normalize the chiral factor as kT where k is the wave number in the tissue layer, in some case it may be $k_t = nk_0$, ($k_0 = \omega / c$ is the vacuum wave number), with n = 1, 2, 3…n. It is necessary to take into account the multiphoton absorption when the resonance absorption at macromolecular level become important. For the brain we considerer $k = k_b /(1 - k_b T)$ because, the clusters of DNA molecules have eigenwaves like right hand circularly polarized waves and for the rest of tissues we considerer $kT = k_t T = 0$. The values for kT are choose by considering $T \approx \beta N h^2 a \rho \approx 1 - 10 \mu m$, $k = k_b /(1 - k_b T) >> k_b \approx k_0 \sqrt{\varepsilon_b}$, $k_0 T$ is of the order of $10^{-4} - 10^{-3}$ so when the multiphoton effect appears, $k_b T \approx n k_0 T$, $1 - n k_0 T \le 1$ and then kT is of order of one and this effect increases when kT increases Here we suppose that the macromolecules vibrations of the helical structures inside typical brain cells are likely to lead to reasonably absorption enhanced by the proteinic water in which these molecules are immersed (induced chirality).

Stages of the bioplasmatic model for SAR determination are shown in reference [1]. Using the linear FDTD algorithm with chirality, obtained from equations (4) simulations for the mobile phones microwave spectrum are made. The model of human head was constructed with 540,000 cubic cells of 2.5 mm side each. The total number of layers, counted from the bottom of head, used in this model was 54. Here we choose the layers 34, 35 and 36, because there are great concentrations of brain tissue. The figure 1 shows these layers in digitalized version (matrix of 100x100), likewise is exhibited the antenna position. Both, the dielectric constant and the conductivity of the brain were obtained from literature [9-10]. In order to study and isolate the chiral effect, calculations are made for plane wave assumption, powers of 0.1 W were used, at frequencies of 5.2 and 5.8 GHz respectively. Four types of tissues (skin, bone, blood and brain) are considered. Simulations were made in a systematic way, in order to determine the effect that the variation of the chiral coefficient have over the absorption of coefficient SAR and results, for layer 35th, are shown in figures 2-3. Owing to the different electromagnetic properties of the tissues the power absorption is not a monotonically decreasing function of depth. For kT = 0, absorption is highest in the skin, low in the skull, but higher again in the brain. These curves were obtained performing similar simulations and then obtaining a statistical average of the SAR. As the wave penetrates the head, it traverses the different parts of which the head model is made and the value of the SAR is attenuated quickly due to the change in medium and the increase of the distance from the emitting source (antenna). SAR maximum (hot point) is in outer part (skin). After passing through the bone level, the SAR is much attenuated (between cells 5 and 10) and around cell 10, the SAR increases at brain level. Here, starting on cell 10 approximately is important to analyze the performance of our bioplasmatic model.

The profile of the SAR for 35th layer, at 5.2 GHz, as function of distance for different values of chiral factor kT, is showed in figure 2, where the variation is observed for $0 < kT \le 3.0$ values of chiral factor. A SAR of 0,48 W/kg, is observed in the brain region, for a null chiral factor (kT = 0). For kT = 1 the SAR found was 0,65 W/kg, an increase of 35% with respect to the achiral case (kT = 0) and a SAR of 0.75 W/kg was found for kT = 3.0, with an increase 56%. This increase corresponds to the power absorbed by the brain region.

Figures 3 shows the distribution of the SAR for 35th layer, as function of distance, for different values of the chiral factor when the work frequency is 5.8 GHz. The maximum SAR found, in the blood-brain region, was 0.6 W/kg for to kT = 0 and 0.8 W/kg for kT = 1, i.e. an increase of 33% with respect to the achiral case. For a high value of chiral factor, kT = 3.0, the maximum SAR found was 0.93 W/kg with an increase of 55%. Also, this increase corresponds to the power absorbed by the brain region. Following the same procedure, similar results for the layers 34 and 36 are obtained. Here with kT=3 we have an enhanced multiphoton effect which is reflected in strong absorption, SAR=0.93 (5.8GHz).

Apparently the SAR appears to increase as the square root of the power, because in the numerical calculation as initial condition we start with an initial varying electric field $E_i = (V/\Delta)\sin \omega t$ where the voltage is proportional to the square root of the power with constant impedance [5]. Important results are the values of SAR obtained for 5.2 and 5.8 GHz, where a remarkable characteristic is found: at higher frequency the absorption is bigger in the brain

tissue where a lower absorption by skin effect was expected.

The classical skin effect does not occur in our simulation, because the effective induced current penetrate inside the head where the multiphoton resonance is active.

This "inverse skin effect" phenomenon is verified in the brain layers, as shown in figures 2 and 3, where it is possible to observe that in all cases, for any chiral factor and input power values, the maximum SAR at 5.8 GHz is larger than at 5.2 GHz.

4. Conclusions

A bioplasmatic chiral model of the human head has been presented that allows determination and evaluation of the absorption induced by the radiation of cellular phone. After having obtained the digitalized layers of correspondent MR images, the electromagnetic fields radiated were determined firstly by means of the FDTD technique and then the specific absorption coefficient (SAR). It is shown that the use of a more realistic model of the human head, derived from the magnetic resonance of images allows for improved determination of the chiral near fields induced in the head.

Using the proposed bioplasmatic chiral model, the simulation of SAR distribution in layers with high quantity of brain tissue (layers 34, 35 and 36) was made. These results shows that the power absorbed by the head increases with the chiral factor. Other important result found is that the absorption at 5.8 GHz, in the brain tissue, is larger that at 5.2 GHz, therefore there is an effect like an "inverse skin effect" phenomenon. In this calculation it is not possible that chain molecule can alter their conformation and a breaking of the chain can result having in mind the restricting forces which are higher than the EM forces.

Here we are studied a more elaborated model of the head (with chiral effect), but with a simple model for the antenna. For real antennas the proximity of tissue clearly alter the radiation pattern, the antenna gain and the input impedance a more general numerical simulation techniques and an accurate model have to be developed. However for left-hand circular, right-hand circular and helical antennas, now available for isotropic and omni-directional radiation, our analysis on SAR have correct conclusions regarding the chiral effect. Certainly for systems to greater frequencies (wireless LANs) the chiral effect will be more pronounced. This makes it worth to check the first results by means of still more advanced models.

Acknowledgments

The authors thank the University of Tarapacá Projects: 8721-06 and 8722-06.

References

[1] Torres-Silva H and Zamorano M. 2003. SAR simulation for chiral waves in head model. *Revista Facultad de Ingeniería* UTA, Vol. 11, pp. 3-11.

[2] Torres-Silva H and Zamorano M. 2003. Chiral Effect on Optical Soliton, *The Journal Mathematics and Computers in Simulation*, Vol. 62, pp. 149-161.

[3] Bhor H. 1997. Molecular wring resonances in chain molecules, *Bioelectromagnetics*, Vol. 18, pp. 187-189.

[4] Davis C C and Swicird M L, 1982. Microwaves absorption of DNA between 8 and 12 GHz, *Biopolymers* Vol. 21, pp. 2453.

[5] Edwards G S et al, 1984. Resonant of selected DNA molecules, *Physical review letters* 53, pp. 1248-1287.

[6] Nina P. et al, 1996. Dynamic control and amplification of molecular chirality by circular polarized light, *Science*, Vol. 273, pp. 1686-1688

[7] Ford L H. 2003. An estimate of the vibrational frequencies of spherical virus particles, *arXiv:physics/0303089*, Vol. 1.

[8] Belyaev Y I et al, 2000. Nonthermal Effects of Extremely High-Frequency Microwaves on Chromatin Conformation in Cells *in vitro* - Dependence on Physical, Physiological, and Genetic Factors, *IEEE Transactions on Microwave Theory and techniques*, Vol. 48, pp. 2172-2179.

[9] Bernardi P. Cavagnaro and Pisa S. 1997. Assessment of the potential risk exposed to millimeter-wave wireless LANs *Wireless networks* Vol. 3, pp. 511-517.

[10] Taflove A and Hagness SC, Ed. 2000. C*omputational Electrodynamics: The Finite-Difference Time Domain Method*, Artech House, pp. 35-171.

figures caption

Fig. 1a,b,c The structure of layer 34th, 35th and 36th.

Fig. 2 SAR variation as function of the transverse distance, for $0 < kT \leq 3.0$ at 5.2 GHz. Layer 35th.

Fig. 3 SAR variation, as function of the transverse distance, for $0 < kT \leq 3.0$ at 5.8 GHz. Layer 35th.

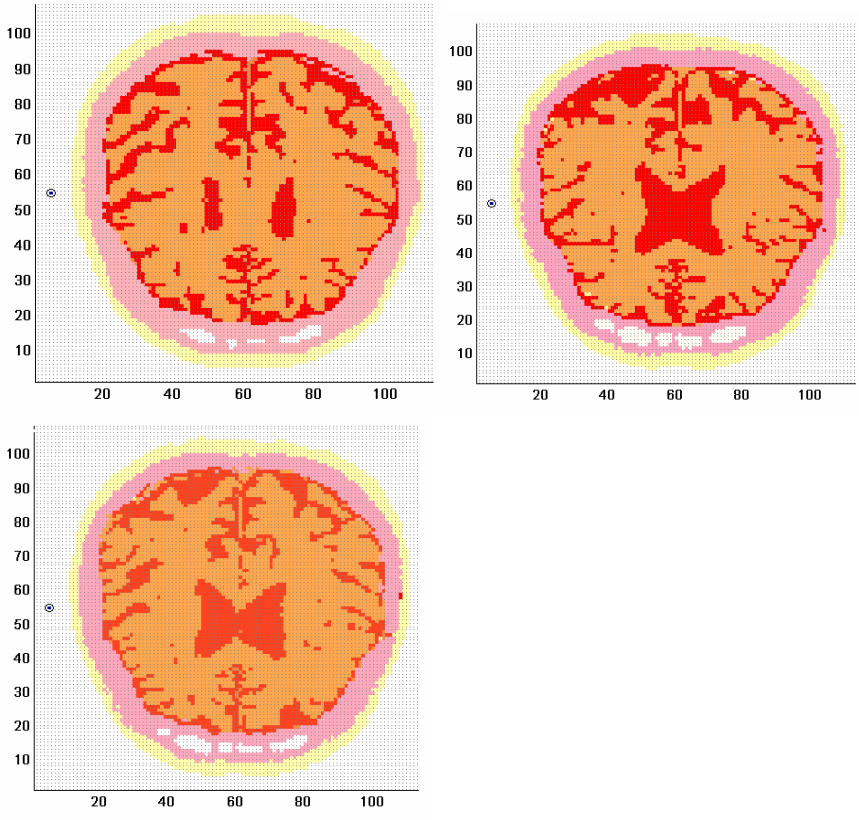

Fig 1

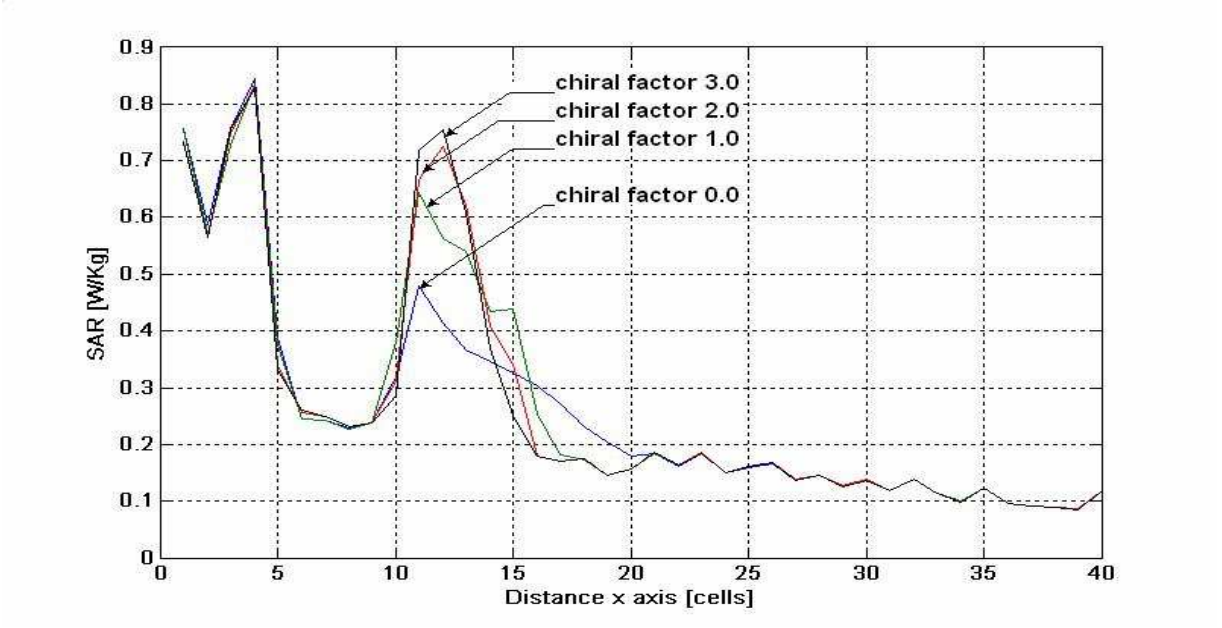

figure2

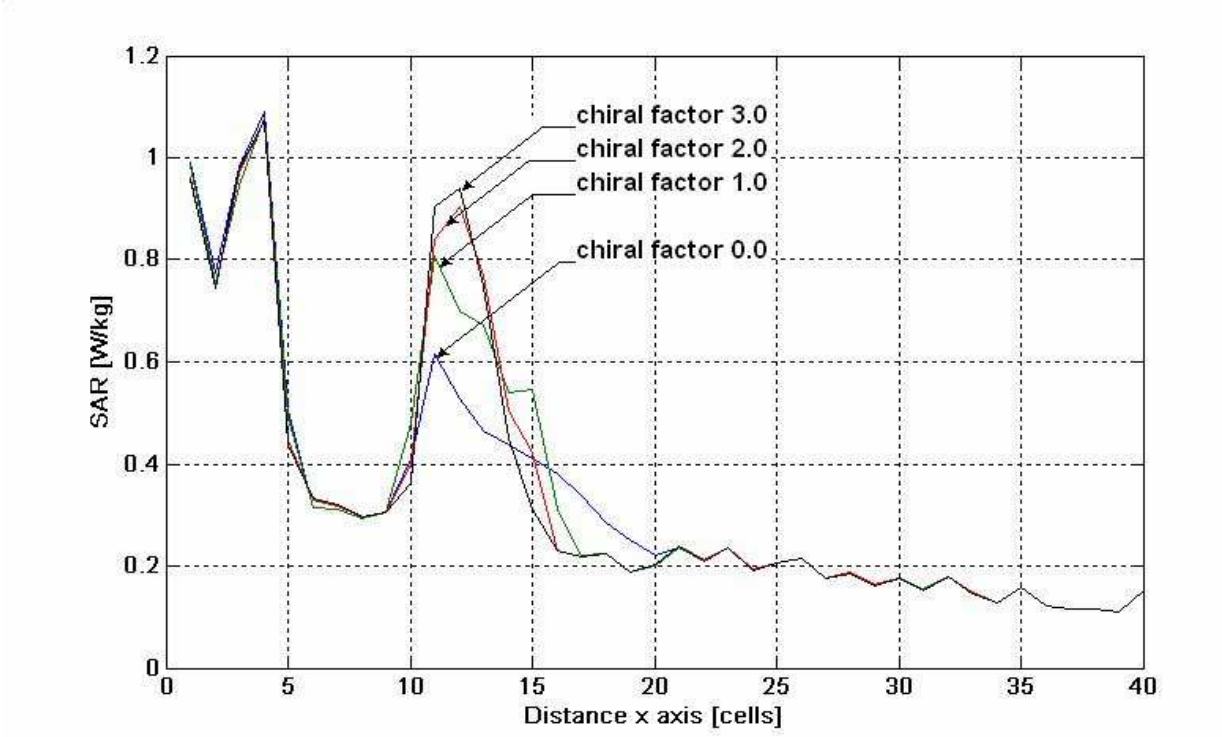

figure 3

INCREASE OF CELL DEATH IN SUSPENTION-CULTURED TOBACCO CELLS FOLLOWING EXPOSURE TO STATIC MAGNETIC FIELD

PARVIZ ABDOLMALEKI, FAEZEH GHANATI

FACULTY OF SCIENCE, TARBIAT MODARES UNIVERSITY, P.O. BOX 14115/175, TEHRAN, IRAN.

Despite to studies demonstrating the effect of static magnetic field (SMS) on animal and/or human cell death fewer studies have been conducted on plant cells. In the present study suspension cultures of tobacco cell in the exponential phase of the growth were exposed continuously for 5 days each 5 hours to SMF of 10 and 30 mT. The viability, lipid proxidation as well as morphological features of the cells were then studied and compared to those of the control cells. The level of peroxidation of membrane lipids in the treated cells was significantly increased compared to those of non-exposed (control) cells while the viability of the treated cells was decreased. In addition, certain characteristics of programmed cell death (PCD) or necrosis e.g., vacuolization and fragmentation of nucleus were remarkably visible in the treated cells, compared to the control cells which had intact nuclei with clear nucleoli. The control cells also excluded ethidium bromide from their walls, whereas most of the treated cells allowed ethidium bromide to penetrate into the cells, emphasizing induction of cell death by magnetic field. Our result suggests that SMF can increase the rate of death in tobacco cells.

Introduction

Electromagnetic fields (EMF) are widely distributed in the environment and their effects are increasing with the burgeoning development of electrical machines [1, 2]. This make the concern about the possible risk of functional disorders in biological systems being growing. Results of the numerous experimental, epidemiological and theoretical studies are rather controversial, and in all areas so far, no unanimous conclusions have been reached [1-3]. Several studies on bacterial and animal cells have shown that EMF exert influence on a large variety of cellular functions, nevertheless the exact mechanism of the interaction with living cells are still unclear [4, 5].

Considering the cell as an electrical system provide a framework to investigate the exact mechanisms of the effect of the electric, magnetic and electromagnetic fields in the physiological behavior of the cell. Taking into consideration the previous reports on the presence of window effect this question raised whether or not a cell absorbed the energy in EMF like a receiver which work in a special band of frequency. If it is positive these fields can therefore act like primary messengers such as hormones. Then it is justified to say that the cells respond to physical stimulus (like EMF) in the same way that they respond to the hormones. Also, it would be helpful to understand whether the exposure of cells to the magnetic fields has any effect on the apoptosis. In the other words the magnetic field works as pro-apoptosis factor or as anti-apoptosis factor. If the MF had a pro-apoptosis role it will be useful in cancer treatment because one possible mechanism through which cells are prompted to develop cancer is the disruption of the equilibrium between the processes of proliferation and apoptosis [6,7. However, apoptosis is a part of normal cell physiology which includes both proliferation and differentiation. It is a major component of both normal cell development and disease. The morphological demonstration of apoptosis is characterized by rapid condensation of the cytoplasm and nuclear chromatin, resulting in DNA fragmentation and membrane blebbing followed by fragmentation of the cells into apoptotic bodies, made up of condensed cytoplasm, nuclear material and/or whole organelles surrounded by intact plasma membranes. [7-9].

There are reports about the short-term EMF exposure that elicited an immune response [10]. A potential link between EMF and its effects on living organisms is the fact that EMF causes an oxidative stress i.e., increase in the activity, concentration, and life time of free radicals [11-13]. Oxidative stress is a function of oxidative metabolites, free radicals and reactive oxygen species (ROS) which are highly reactive by-products of normal metabolism and immune defense [11-13]. It brings changes in enzyme activity, gene expression, and release of

calcium from intracellular storage sites. Oxidative stress also affects membrane structure, cell growth, and cell death, thereby contribute to cancers and leukemia [11-14].

Less studies of this kind have been conducted on plant cells and few available literatures, have particularly directed their attention to the effects of magnetic fields on the germination of seeds, pollen germination and plant growth and development [15, 16].

The goal of the present study was to determine a potential relationship between viability, lipid proxidation as well as morphological features of the suspension-cultured tobacco cells which exposed to static magnetic fields. It may help us to improve the general knowledge about mechanism(s) of the responses of the living systems to EMF.

Suspension cultures established from calli of tobacco cells (Nicotiana tabacum L. cv. Burley 21) that had been maintained in our laboratory for 52 subcultures. Both calli and subsequent suspensions were grown in a modified Murashige and Skoog medium without glycine and containing 3% sucrose. The medium was containing: (NH4)NO3 20.61 mM; KH2PO4, 1.25 mM; CaCl2, 2.99 mM; MgSO4, 1.50 mM; MnSO4, 0.1 mM; Fe-EDTA, 0.1 mM; H3BO3, 0.1 mM; CoCl2, 0.11 μM ; CuSO4, 0.1 μM;; Na2MoO4 μM, 1.03; ZnSO4, 29.91 μM , KI, 5 μM . pH was adjusted to 5.8. All chemicals were purchased from Sigma, Japan. Suspension-cultured cells were grown at 25 °C in darkness on an orbital shaker at 120 rpm and were sub-cultured every 7 day, when they were still in their logarithmic growth phase [17]. Frequent subcultures provided us homogenous and undifferentiated batches of tobacco cells that no longer have kept their original properties and their physiological response to EMF could resemble physiological response of plant cells regardless of their species.

Exposure to EMF was performed by a locally designed EMF generator The electrical power was provided using a 220 V AC power supply equipped with variable transformer as well as a single-phase full-wave rectifier. The maximum power and passing current were 1 KW and 50 A DC, respectively. This system was designed to generate EMF in range of 0.5 μT – 30 mT with stable conditions. It consisted of two coils (each 3000 turns of 3 mm copper wire) equipped with a U-shaped laminated iron core (to prevent eddy current losses). Using two vertical connectors, the arms of the U-shaped iron core were terminated to four circular iron plates covered with thin layer of Nickel (each 23 mm thickness, 260 cm in diameter). A water circulation system around the coils was employed to avoid the increase of the temperature. The temperature between the circular iron plates (exposure sites of samples) ,measured by a thermometer, was almost the same as other parts of the room (e.g., the site of the control cells) ±1°C. Nevertheless, the control cells were kept far enough from the apparatus, to avoid any potential exposure to the magnetic field from aforesaid generator. Since no other appliance was working, the control samples were only exposed to the extremely low MF of the earth, as the treatment group was too.

An electronic board was used to stabilize the system so that we always got a uniform MF. Calibration of the system as well as tests for the accuracy and uniformity of the magnetic fields were performed by a teslameter (PHYWE, Germany) with a probe type of Hall Sound. The accuracy of the system was ±0.1% for static field and the range of measurements was 3 μT – 30 mT.

It is generally accepted that household and office levels of magnetic fields vary between 0.01 to 0.1 mT and levels near a power transmission line are between 10-30mT and much higher levels are expected in occupational exposures [18]. A magnetic field of 30mT is also a limit requiring controlled access - being a level at which magnetic materials may move under the influence of a field. Therefore, the present study was undertaken to test the effects of 10 and 30 mT on plant cells. The cells in their exponential growth phase were continuously exposed to EMF by magnitudes of 10 or 30mT, for 5 days (from day 3 to 7). After the period of treatment the cells were harvested and frozen in liquid N2 and kept at – 80 °C until used for biochemical analysis.

Viability of both treated and control samples of the suspension-cultured tobacco cells was obtained by staining the cells with 0.1% aqueous solution of Evans Blue for 3 min and washed with deionized water. Then it was observed using a light microscope (Olympus, BH2, Japan) with different magnifications. The cells with complete blue color was considered dead and the ones in which the membrane inhibited insertion of the blue dye was considered live. Consequently by counting the live and dead cells the viability of both treated as well as the control cells was obtained.

Level of damage of membranes was determined by measuring malonyldealdehyde (MDA) as the end product of peroxidation of membrane lipids [19]. In brief, samples were homogenized in an aqueous solution of trichloroacetic acid (TCA) (10% w/v) and aliquots of the filtrates were heated in 0.25% thiobarbituric acid (TBA). The amount of MDA was determined from the absorbance at 532 nm followed by correction for the nonspecific absorbance at 600 nm. The amount of MDA-TBA complex was calculated from the extinction coefficient 155mM-1cm-1and expressed against mg of protein.

Cell wall preparations were obtained by homogenization of frozen samples in water with a mortar and pestle followed by centrifugation at 1000g and sequential washing of the pellet with EtOH, CHCl3-MeOH (2: 1) and acetone and then drying in air. Lignin content of wall preparations was measured via a modified acetyl bromide

procedure. The lignin content was determined by measuring of absorbance at 280 nm using specific absorption coefficient value 20.0 g-1 liter cm -1.

Cells were stained with acridine orange (10µg/mL distilled water) or ethidium bromide (10µg/mL distilled water) to extract the morphological features of both treated and control cells. Observations were made with an Olympus BH2 fluorescence microscope equipped with filter combinations WU (330-385-nm excitation and 420-nm barrier filters) and WBV (400- to 440-nm excitation and 475-nm barrier filters).

All of the experiments were carried out with at least three independent repetitions, each three samples, and all data were expressed as the mean values ± standard deviation (SD). Statistical analysis was performed using Student's t- Test and the differences between treatments were expressed as significant at level of $P<0.05$.

The tobacco cells in suspension culture were seen in different shapes such as round, cylindrical as well as ellipse (Figure 1). As mentioned in material and method we exposed the prepared cells in exponential phase which started from day 3 - 8 (Figure 2). The dimension of these cells is presented in table 1. Our results showed that the average size of the treated cells with both 10 and 30 mT SMF was significantly decreased compared to the control cells. Although, the growth rate of the treated cells decreased compared to the control cells by measuring the weight of cells, but it was not significant (Table 1). Exposure to SMF significantly increased the level of the peroxidation of membrane lipids of suspension-cultured tobacco cells, compared to those of non-exposed (control) cells. The MDA level did not show a noticeable difference in both 10 and 30 mT.

Figure 3 shows the MDA level in treated cells compared with the control cells. The obtained average for MDA level on treatment group (10 mT) was 1.16 ± 0.03 (MDA/g Fw) while the obtained average for MDA level on control group was 0.89±0.02 (MDA/g Fw). Similarly, the obtained average for MDA level on treatment group (30 mT) was 1.13±0.04 (MDA/g Fw) while the obtained average for MDA level on control group was 0.84±0.12 (MDA/g Fw). However, there was not significant difference between the levels of lipid peroxidation of 10 and 30 mT of SMF-exposed cells.

Figure 4 shows the lignin content of wall in treated cells compared with the control cells. The results showed that the exposure of the magnetic field caused a significant increase in the lignin content of wall in treated cells (n=24) compared with the controls (n=24). However the lignin content did not show a noticeable difference in both 10 and 30 mT. The obtained average for lignin content on treated groups (10 and 30 mT) were 7.09 ± 0.45 and 6.96 ± 0.08, respectively. While the obtained average for lignin content on control groups were 6.17±0.26 and 5.7 ±0.06, respectively.

The viability of the treated cells as well as control cells using Evans Blue and ethidium bromide were presented in figure 5 and 6. These results showed that the viability of the treated cell (30 mT) was approximately 68% while the viability of treated cells (10 mT) was 72%. The viability of the control cells was 84%.

Certain characteristics of programmed cell death (PCD) or necrosis e.g., nuclear vacuolization and fragmentation were observed in tobacco cells exposed to the static magnetic fields (Figure 7A, Figure 7B), compared to the control cells who had intact nuclei with clearly visible nucleoli (Fig.7D). The latter also excluded ethidium bromide in their walls (Figure 6), whereas most of the magnetic field-exposed cells allowed ethidium bromide to penetrate into the cells, emphasizing induction of cell death by magnetic field (Figure 7)

Table 1: demonstrating the obtained average diementions and weight of treated cells compared with control cells.

SMF(mT)	Diameter(μ_m)		Weight(g/flask)
	Width	Length	
0	48.2±13[a]	40.5±12.5[a]	13.3±.22[a]
10	37.8±10.8[b]	33.6±8.3[b]	12.1±1.01[a]
0	41.8±17.9[a]	49.2±10.8[a]	11.6±1.07[a]
30	29.3±5.9[b]	37.2±10.2[b]	10.9±1.06[a]

Different letters refer to significant differences at the level of $p\leq0.05$ according to student t-test.

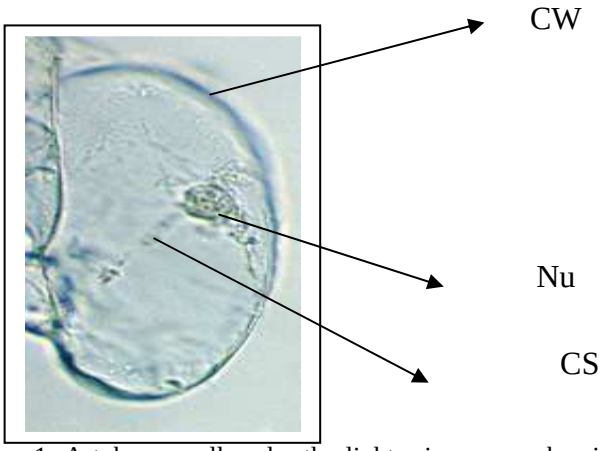

Figure 1: A tobacco cell under the light microscope showing cell wall (CW), nucleus (Nu), and Cytoplasmic strands (CS), X660.

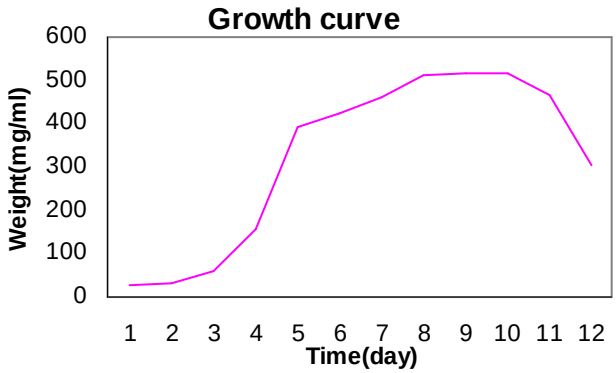

Figure 2: Growth curve of suspension-cultured tobacco cells.

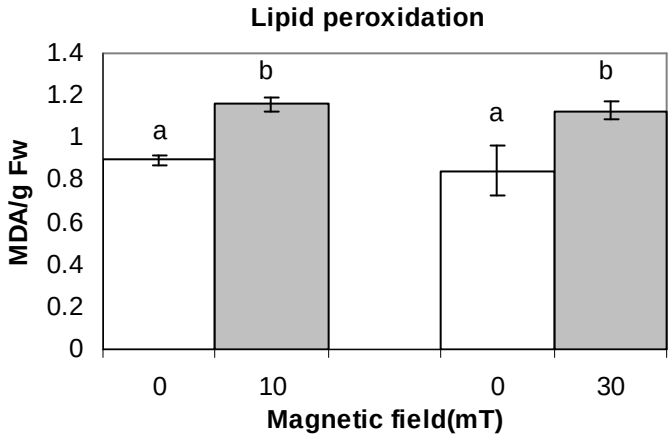

Figure 3. Effect of SMF on the rate of lipid peroxidation of suspension-cultured tobacco cells. Data are means ± SD, n=3. Signs with different letters in each group indicate significant differences at $P < 0.05$ according to Student's t-Test.

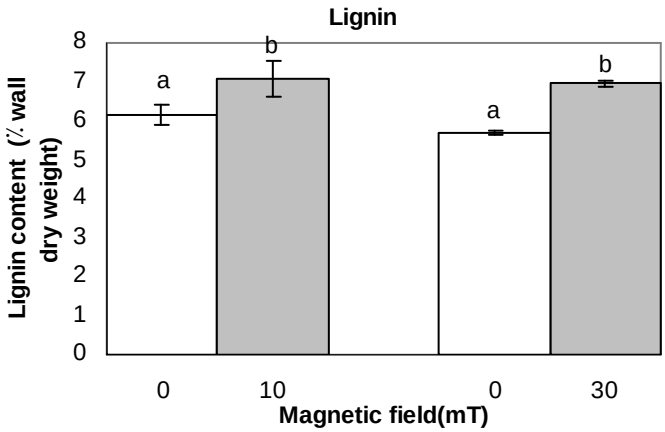

Figure 4.Effects of 10mTand 30mT SMF 5h for 5day on lignin content in tobacco cell. Each column indicates the mean ± SD, n=3.

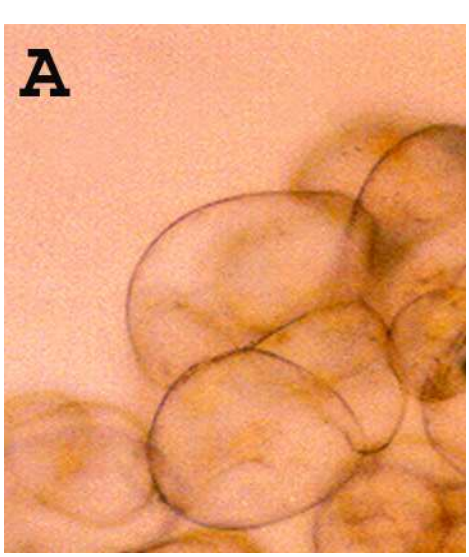

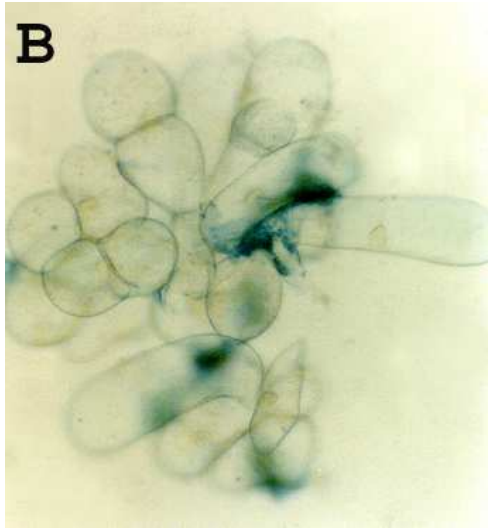

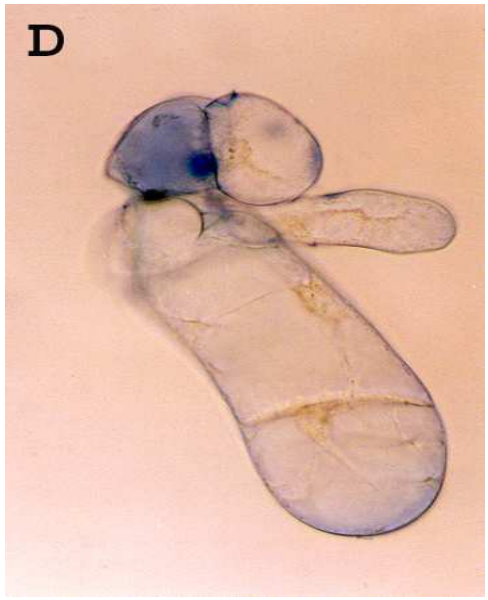

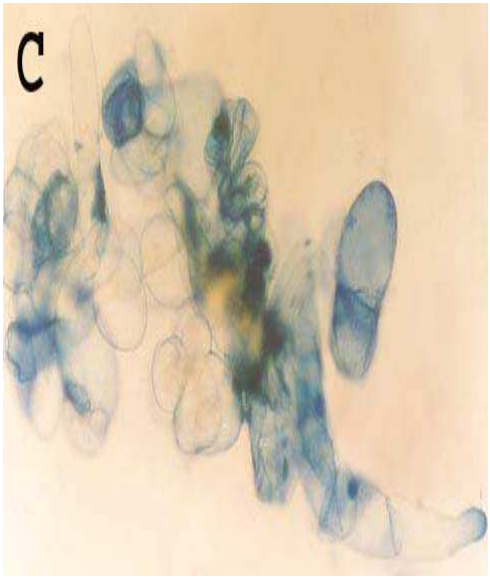

Figure 5: Showing the viability of treated cells (C and D) compared with the control cells (A and B), A-C, X330; D, X660.

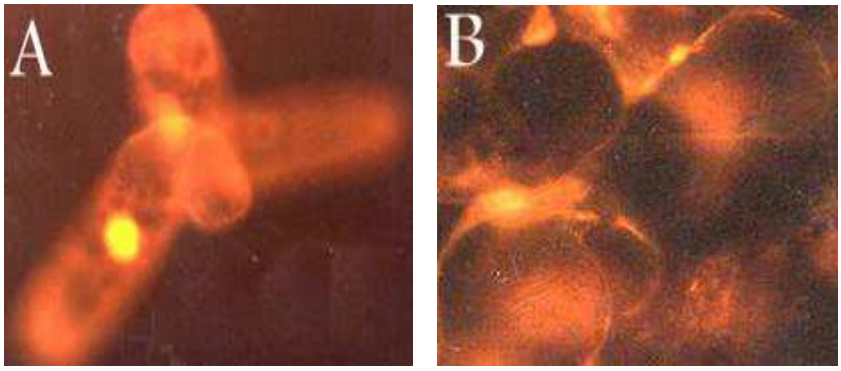

Figure 6. Penetration of ethidium bromide in dead cells after exposure to magnetic field (A), compared to the control cells where excluded dye in their walls (B). Magnifications of both X 660.

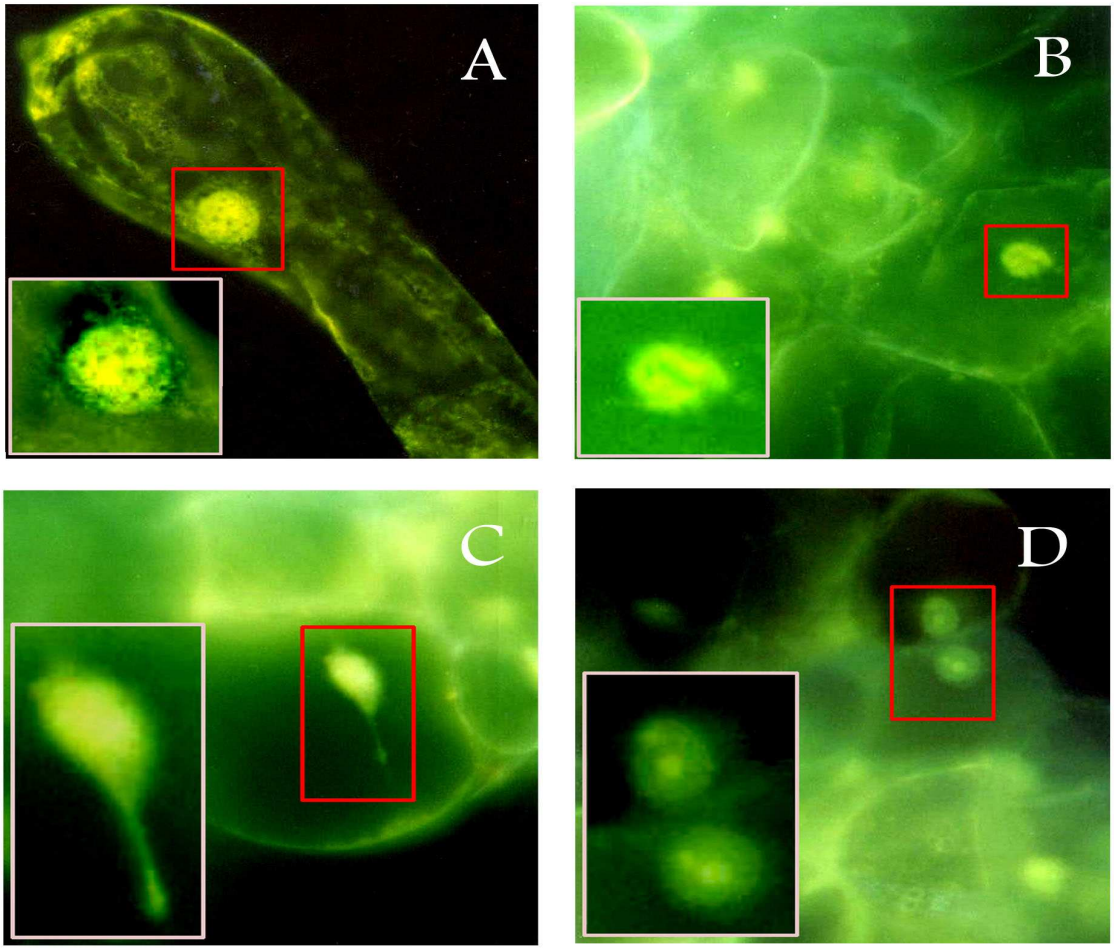

Figure 7. Morphological features of suspension-cultured tobacco cells exposed to static magnetic fields. Cleavage of nucleus of tobacco cells exposed to 10 (A) and 30 mT static magnetic fields (B, C), compared to the control cells with intact nuclei and clearly visible nucleoli (D). Cells were stained with acridine orange and observed under epifluorescence microscope. Magnifications of A, X1320 and of B, C, and D, X660.

Summary

Electromagnetic fields for many years were considered as an absolutely neutral form of radiation, but epidemiological data and results of experimental in vivo studies have attracted more attention to the biological effects of EMF. Primary action of SMF in biological systems is the induction of electrical charges and currents [18]. One of the major molecular effects of magnetic fields is their influence on nuclear spins of paramagnetic molecules. This mechanism plays an important role when in the course of a chemical reaction the chemical bound is disrupted and two molecules with unpaired electrons are formed (a pair of radicals). Depending on their spin orientations, radical recombination or diffusion and formation of free radicals (e.g., Oxygen radicals) may take place [20]. The radical pairs may be affected for a long and continuous time interval by the static magnetic field [21]. This may extend the life time of the free radical and its potential damage could be exaggerated. Although formed in normal cell metabolism, free radicals are potentially damaging and can initiate chain reactions to form new free radicals. A main protective role against free radicals is attributed to SOD in catalyzing and dismutation of superoxide anions to O_2 and H_2O_2 [22]. We showed somewhere else that the exposure to SMF increased the activity of SOD in tobacco cells compared to those corresponding control groups. It implies the first step of the increased production of free radicals by SMF in tobacco cells. An increase in SOD activity might enhance cytotoxicity by active oxygen species likely owing to the accelerated H_2 O_2 generation and subsequent $OH^{\bullet}$ overproduction by the metal catalyzed Haber-Weiss reaction [23]. Scavenging and detoxification of H_2O_2 that is produced by SOD, can be achieved by either non-enzymatic antioxidants or scavenging enzymes, e.g., CAT. Likewise, the activity of CAT was also reduced by SMF.

Accumulation of H_2O_2 and other reactive species of oxygen in SMF-exposed tobacco cells may subsequently result in peroxidation of membrane lipids as well as damage of DNA [24]. Ishisaka and his colleagues (2000) showed H_2O_2 -induced rapid fragmentation of DNA and a slow decrease in the viability of human cancer cell line HL-60[25]. In the same cell line, Robison and his colleagues presented data demonstrating that a decrease in the DNA repair may occur following oxidative burst induced by EMF [26]. Although morphological features of programmed cell death and necrosis of plant cells, to some extent, differ from those in animal cells, however some of these features, e.g., cleavage of DNA to internucleosomal fragments and increase of lipid peroxidation (membrane lysis) were observed more in SMF-exposed cells, compared to the control cells.

MDA measurement also indicates that 10, 30mT SMF exposure induces lipid peroxidative stress. This implies that SMF is somehow involved with free radical reaction in tobacco cells. It means that increase in lipid peroxidation can be another proof for the accumulation of H2O2 in treated tobacco cells compared to the controls. These results indicate that exposing to the SMF can induse oxidative stress due to activity of the free radicals and it will therefore caser more lipid peroxidation. Increase in the lipid peroxidation of the membrane in both 10 and 30 mT SMF also showed that the failure of the antioxidant defence system of treated cells against the free radicals. The results presented in table 1 indicated that the treated cells become smaller in size and less prolifrative compared to the control cells. This could be explained by this suggestion that the SMF shortened the cell cycle and it also inhibitated the extention of the cell membrane. Exposing to the SMF was the main reason for Increase in SOD activity may represent a compensatory reaction against oxidative stress. Increase in lignin content of treated cells (7.09 ± 0.45 and 6.96 ± 0.08 for 10 and 30mT) compared to the control (6.17 ± 0.26 and 5.7 ± 0.06) demonstrating the wall loosening through increasing the wall stiffening. This can possibly decrease the cellular growth.

Taken all together, the results presented here reveal that SMF can cause an inconsistency in the function of antioxidant enzymes in suspension-cultured tobacco cells thereby, lead to oxidative burst and cell death.

References

[1] Patterson RM, Exposure assessment for electric and magnetic field ,J.Expo. Am.Environ.Epidemial 2 (1992)159-176.

[2] Breysse P, Lees PS, McDiamid MA, curbow B., ELF magnetic field exposure in an office environment, Am.J.Ind.Med.25 (1994)177-185.

[3] Ilulbert Al, Metcalfc J, Ilesketh R, Biological response to electromagnetic fields, FASEB.J.12 (1998)395-420.

[4] Lai H, Singh NP, Melatonin and N-tert-butyl-alpha-phenylnitrone block 60-Hz magnetic field –induced DNA single and double strand breaks in rat brain cells, J.Pineal Res.22 (1997)152-162.

[5] Potschka H, Thun-Battersby S, Lioscher W, Effect of low –intensity 50-Hz magnetic fields on kinding acquisition and fully kindled seizures in rats, Brain Res 809(1998)269-276.

[6] Dini L, Abbro L. Bioeffects of moderate-intensity static magnetic fields on cell cultures. Micron 36 (2005) 195–217.

[7] Liu MC, Marshall JL, Pestell RG, 2004. Novel strategies in cancer therapeutics: targeting enzymes involved in cell cycle regulation and cellular proliferation. Current Cancer Drug Targets 4, 403–424.

[8] Alenzi FQ, 2004. Links between apoptosis, proliferation and the cell cycle. British Journal of Biomedical Science 61, 99–102.
[9] Dini L., Coppola, S., Ruzittu, M., Ghibelli, L., 1996. Multiple pathways for apoptotic nuclear fragmentation. Experimental Cell Research 223, 340–347.
[10] Repacholi MH, Greenebaum B. 1999. Interaction of static and extremely low frequency electric and magnetic fields with living systems: Health effects and research needs. Bioelectromagnetics 20: 133-160.
[11] Scaiano JC, Cozens FL, Mclean J. 1994. Model for the rationalization of magnetic field In vivo. Application of the radical-pair mechanism to biological systems. Photochemistry and Photobiology 59: 585-589.
[12] Sobczak A, Kula B, Dancii A. 2002. Effects of electromagnetic field on free-radical processes in steelworkers. Part II: Magnetic field influence on vitamin A, E and selenium concentrations in plasma .J Occup Health 44: 230-233.
[13] Dat JF, Van Montagu M, Inze D, Van Breusegem F. 2001. Catalase-deficient tobacco plants: tools for in planta studies on the role of hydrogen peroxide. Redox Report 6: 37-42.
[14] Green LM, Miller AB, Agnew DA, Greenberg ML, Li J, Villeneuve JP, Tibshirani R. 1999. Childhood leukemia and personal monitoring of residential exposures to electric and magnetic fields in Ontario. Canada. Cancer Causes Control 10: 233-243.
[15] Yano A, Hidaka E, Fujiwara K, Iimoto M. 2001. Induction of primary root curvature in radish seedlings in a static magnetic field. Bioelectromagnetics 22:194-199.
[16] Rakosy-Tican L, Aurori CM, Morariu VV. 2005. Influence of near null magnetic field on in vitro growth of potato and wild solanum species. Bioelectromagnetics 26: 548-557.
[17] Ghanati F, Morit A, Yokota H. 2001. Selection and partial characterization of a boron-tolerant tobacco cell line, Soil Science and Plant Nutrition 47: 405-410.
[18] Roy C, Repacholi M. 2005. Electromagnetic field and Health, A WHO perspective, World Health Organization, Geneva, Switzerland, Available from: http://www.world-aluminium.org/news/ montreal/roy.htm.
[19] De Vos CHR, Schat H, De Waal MAD, Vooijs R, Ernst WHO. 1991. Increased resistance to copper-induced damage of the root plasma membrane in copper tolerant Silene cucubalus. Physiol Plant 82: 523-528
[20] Kula A. Sobczak, Kuska R. 2002. Effects of electromagnetic field on free-radical processes in steelworkers. Part I: Magnetic field influence on the antioxidant activity in red blood cells and plasma. J Occup Health 44: 226-229.
[21] Zmyslony M, Palus J, Jajte J, Dziubaltowska E, Rajkowska E. 2000. DNA damage in rat lymphocytes treated in vitro with iron cations and exposed to 7mT magnetic fields (static or 50HZ). Mutation Res 453: 89-96.
[22] Sreenivasulu N, Grimm B, Wobus U, Weschke W. 2000. Differential response of antioxidant compounds to salinity stress in salt-tolerant and salt-sensitive seedlings of foxtail millet (Setaria italica), Physiol. Plant. 109: 435-442.
[23] Piacentini MP, Fraternale D, Piatti E, Ricci D, Vetrano F. 2001. Senescence delay and change of antioxidant enzyme levels in Cucumis sativus L.etiolated seedling by ELF magnetic fields. Plant Science 161: 45-53.
[24] Jajte J, Grzegorczyk J, Zmyslony M, Rajkowska E, Kowalska MS, Kowalski ML. 2001. Influence of a 7mT static magnetic field and irons on apoptosis and necrosis in rat blood lymphocytes. J Occup Health 43: 379-381.
[25] Ishisaka R, Kanno T, Inai Y, Nakahara H, Akiyama J, Yoshioka T, Utsumi K. 2000, Effects of a magnetic fields on the various functions of subcellular organelles and cells. Pathophysiology 7: 149-152.
[26] Robison JG, Pendleton AR, Monson KO, Murray BK, O'Neill KL. 2002. Decreased DNA repair rates and protection from heat induced apoptosis mediated by electromagnetic field exposure. Bioelectromagnetics 23: 106-112.

IMPLICIT FDTD METHODS AND THE SAMPLING THEOREM

ĽUBOMÍR ŠUMICHRAST

INSTITUTE OF ELECTROMAGNETIC THEORY, SLOVAK UNIVERSITY OF TECHNOLOGY, ILKOVIČOVA 3, SK-81219 BRATISLAVA, SLOVAKIA

Abstract

The numerical properties of two factorized implicit formulations of the method of Finite-Differences-in-Time-Domain (FDTD) for the simulation of electromagnetic wave propagation are investigated and compared with explicit Yee-FDTD and full Crank-Nicolson FDTD formulation. It is shown that the ADI-FDTD factorization approaches asymptotically the Nyquist limit and can be used with arbitrarily large time steps. Also from the point of view of numerical dispersion gives acceptably small deviations from the full Crank-Nicolson FDTD formulation. On the other hand the CNSS-FDTD factorization does not fulfill Nyquist limit for arbitrarily large time steps.

Introduction

Numerical simulations are routinely used for modeling electromagnetic wave propagation problems in the area of high frequency electromagnetics and photonics. The finite-difference time-domain (FDTD) method of explicit type designed by Yee [1] was for long years the preferred numerical technique for such simulations due to its flexibility, since it allows the inclusion of arbitrarily heterogeneous objects in the region to be simulated. In the course of numerical computations artificial artifacts are introduced, such as numerical amplification of the wave power-flow-density (stability issues) as well as the numerical dispersion. For the explicit-type methods the well-known Courant-Friedrichs-Levy (CFL) condition concerning the stability of the calculations must be met, limiting thus the step-length of the in-time-forward-marching algorithm. The extent of literature in this area is huge, including several book publications, e.g. [2].

Recently the implicit types of FDTD methods has been constructed - the "Alternating Directions Implicit" (ADI) FDTD method [3], [4] and the "Crank-Nicholson Split-Step" (CNSS) FDTD method [5], [6]. Both are implicit procedures requiring inversion of tridiagonal matrices in two half steps. Both are theoretically unconditionally stable, i.e. they enable one to avoid the severe CFL condition and use the unlimited length of the time step in the course of calculation. However, another kind of bounds on the length of the time step, due to aliasing effects with growing time step, is imposed on both these methods.

Explicit and implicit FDTD formulations

The Maxwell equations

$$\operatorname{curl} \boldsymbol{H} = \varepsilon \frac{\partial \boldsymbol{E}}{\partial t}, \qquad \operatorname{curl} \boldsymbol{E} = -\mu \frac{\partial \boldsymbol{H}}{\partial t} \tag{1}$$

are for the simplicity taken in the simple form for lossless isotropic homogeneous linear medium without external sources, i.e. the permeability μ and the permittivity ε are constants. Here $\boldsymbol{E}(\boldsymbol{r},t)$ and $\boldsymbol{H}(\boldsymbol{r},t)$ are the electromagnetic field intensities for arbitrary time dependence.

In the Yee-FDTD method are Maxwell equations (1) discretised taking so called staggered grids [1] on all three spatial axes and in time with equidistant intervals $\{\Delta_x, \Delta_y, \Delta_z, \Delta_t\}$ (denoted by the serial indexes $\{i, j, m, n,\}$, i.e.

$$E_x\left([i+\tfrac{1}{2}]\Delta_x, j\Delta_y, m\Delta_z, [n+\tfrac{1}{2}]\Delta_t\right) = E_x\big|_{i+\frac{1}{2},j,m}^{n+\frac{1}{2}} \qquad H_x\left(i\Delta_x, [j+\tfrac{1}{2}]\Delta_y, [m+\tfrac{1}{2}]\Delta_z, n\Delta_t\right) = H_x\big|_{i,j+\frac{1}{2},m+\frac{1}{2}}^{n}$$
$$E_y\left(i\Delta_x, [j+\tfrac{1}{2}]\Delta_y, m\Delta_z, [n+\tfrac{1}{2}]\Delta_t\right) = E_y\big|_{i,j+\frac{1}{2},m}^{n+\frac{1}{2}}, \qquad H_y\left([i+\tfrac{1}{2}]\Delta_x, j\Delta_y, [m+\tfrac{1}{2}]\Delta_z, n\Delta_t\right) = H_y\big|_{i+\frac{1}{2},j,m+\frac{1}{2}}^{n} \tag{2}$$
$$E_z\left(i\Delta_x, j\Delta_y, [m+\tfrac{1}{2}]\Delta_z, [n+\tfrac{1}{2}]\Delta_t\right) = E_z\big|_{i,j,m+\frac{1}{2}}^{n+\frac{1}{2}} \qquad H_z\left([i+\tfrac{1}{2}]\Delta_x, [j+\tfrac{1}{2}]\Delta_y, m\Delta_z, n\Delta_t\right) = H_z\big|_{i+\frac{1}{2},j+\frac{1}{2},m}^{n}$$

Discretised Maxwell equations (only the E_x and H_x are considered bellow) take the form

$$\varepsilon\frac{E_x\big|_{i+\frac{1}{2},j,m}^{n+\frac{1}{2}} - E_x\big|_{i+\frac{1}{2},j,m}^{n-\frac{1}{2}}}{\Delta_t} = \frac{H_z\big|_{i+\frac{1}{2},j+\frac{1}{2},m}^{n} - H_z\big|_{i+\frac{1}{2},j-\frac{1}{2},m}^{n}}{\Delta_y} - \frac{H_y\big|_{i+\frac{1}{2},j,m+\frac{1}{2}}^{n} - H_y\big|_{i+\frac{1}{2},j,m-\frac{1}{2}}^{n}}{\Delta_z}, \tag{3}$$

$$\mu\frac{H_x\big|_{i,j+\frac{1}{2},m+\frac{1}{2}}^{n+1} - H_x\big|_{i,j+\frac{1}{2},m+\frac{1}{2}}^{n}}{\Delta_t} = \frac{E_y\big|_{i,j+\frac{1}{2},m+1}^{n+\frac{1}{2}} - E_y\big|_{i,j+\frac{1}{2},m}^{n+\frac{1}{2}}}{\Delta_z} - \frac{E_z\big|_{i,j+1,m+\frac{1}{2}}^{n+\frac{1}{2}} - E_z\big|_{i,j,m+\frac{1}{2}}^{n+\frac{1}{2}}}{\Delta_y}. \tag{4}$$

Yee-FDTD method as represented by the equations (3) and (4) is the explicit method: the values $E_x\big|_{i+\frac{1}{2},j,m}^{n+\frac{1}{2}}$ in (3) in the "new" time layer $n+\frac{1}{2}$ are directly calculated from the "old" known values in layers $n-\frac{1}{2}$ and n. Similar holds for $H_x\big|_{i,j+\frac{1}{2},m+\frac{1}{2}}^{n+1}$ in (4). The main drawback of the Yee-FDTD explicit method is its conditional stability. In order to have conserved the wave-power-flow-density in the computational window, the CFL-condition

$$c\Delta_t\sqrt{\Delta_x^{-2}+\Delta_y^{-2}+\Delta_z^{-2}} < 1 \tag{5}$$

where $c = (\mu\varepsilon)^{-1/2}$ is the phase velocity in the lossless medium, has to be met, limiting thus severely the permissible length of the time steps Δ_t.

In the matrix notation (1) reads

$$\varepsilon\frac{\partial}{\partial t}\boldsymbol{E} = \boldsymbol{\Delta}\cdot\boldsymbol{H} \qquad -\mu\frac{\partial}{\partial t}\boldsymbol{H} = \boldsymbol{\Delta}\cdot\boldsymbol{E} \tag{6}$$

where $\boldsymbol{E} = \left[E_x, E_y, E_z\right]^T$ and $\boldsymbol{H} = \left[H_x, H_y, H_z\right]^T$ are column vectors of field components and $\boldsymbol{\Delta}$ is given as

$$\boldsymbol{\Delta} = \boldsymbol{\Delta}_1 - \boldsymbol{\Delta}_2 = \begin{bmatrix} 0 & -\partial/\partial z & \partial/\partial y \\ \partial/\partial z & 0 & -\partial/\partial x \\ -\partial/\partial y & \partial/\partial x & 0 \end{bmatrix}, \quad \boldsymbol{\Delta}_1 = \begin{bmatrix} 0 & 0 & \partial/\partial y \\ \partial/\partial z & 0 & 0 \\ 0 & \partial/\partial x & 0 \end{bmatrix}, \quad \boldsymbol{\Delta}_2 = \begin{bmatrix} 0 & \partial/\partial z & 0 \\ 0 & 0 & \partial/\partial x \\ \partial/\partial y & 0 & 0 \end{bmatrix}. \tag{7}$$

Combining $\boldsymbol{E}$ and $\boldsymbol{H}$ into one vector $\boldsymbol{F}$

$$\boldsymbol{F} = \begin{bmatrix} \boldsymbol{E}/\sqrt{Z} \\ \boldsymbol{H}\sqrt{Z} \end{bmatrix}, \tag{8}$$

where $Z = \sqrt{\mu/\varepsilon}$ is the wave impedance of the lossless medium, one arrives to the equation

$$c^{-1}\frac{\partial}{\partial t}\boldsymbol{F} = \boldsymbol{D}\cdot\boldsymbol{F}, \tag{9}$$

where

$$\boldsymbol{D} = \begin{bmatrix} \boldsymbol{0} & \boldsymbol{\Delta}_1 - \boldsymbol{\Delta}_2 \\ \boldsymbol{\Delta}_2 - \boldsymbol{\Delta}_1 & \boldsymbol{0} \end{bmatrix}, \quad \boldsymbol{D} = \boldsymbol{D}_1 + \boldsymbol{D}_2 = \boldsymbol{D}_{12} - \boldsymbol{D}_{21}, \tag{10}$$

$$\boldsymbol{D}_1 = \begin{bmatrix} 0 & \boldsymbol{\Delta}_1 \\ -\boldsymbol{\Delta}_1 & 0 \end{bmatrix}, \quad \boldsymbol{D}_2 = \begin{bmatrix} 0 & -\boldsymbol{\Delta}_2 \\ \boldsymbol{\Delta}_2 & 0 \end{bmatrix}, \quad \boldsymbol{D}_{12} = \begin{bmatrix} 0 & \boldsymbol{\Delta}_1 \\ \boldsymbol{\Delta}_2 & 0 \end{bmatrix}, \quad \boldsymbol{D}_{21} = \begin{bmatrix} 0 & \boldsymbol{\Delta}_2 \\ \boldsymbol{\Delta}_1 & 0 \end{bmatrix}. \tag{11}$$

Crank-Nicolson formulation of discretisation of differential equation is known to be unconditionally stable. For (9) with respect to the time derivative it yields

$$\frac{\boldsymbol{F}^{n+1} - \boldsymbol{F}^n}{c\Delta_t} = \boldsymbol{D}\cdot\frac{\boldsymbol{F}^{n+1} + \boldsymbol{F}^n}{2}, \tag{12}$$

Equation (12) can be put in the following form

$$\left\{\boldsymbol{I}-\frac{2}{c\Delta_t}\left(\boldsymbol{D}_1+\boldsymbol{D}_2\right)\right\}\cdot\boldsymbol{F}^{n+1}=\left\{\boldsymbol{I}+\frac{2}{c\Delta_t}\left(\boldsymbol{D}_1+\boldsymbol{D}_2\right)\right\}\cdot\boldsymbol{F}^{n}, \tag{13}$$

which can after some calculation be re-cast into the following form (see e.g. [7])

$$\left\{\boldsymbol{I}-\frac{2}{c\Delta_t}\boldsymbol{D}_1\right\}\cdot\left\{\boldsymbol{I}-\frac{2}{c\Delta_t}\boldsymbol{D}_2\right\}\cdot\boldsymbol{F}^{n+1}-\frac{4}{c^2\Delta_t^2}\boldsymbol{D}_1\cdot\boldsymbol{D}_2\cdot\boldsymbol{F}^{n+1}=$$

$$=\left\{\boldsymbol{I}+\frac{2}{c\Delta_t}\boldsymbol{D}_2\right\}\cdot\left\{\boldsymbol{I}+\frac{2}{c\Delta_t}\boldsymbol{D}_1\right\}\cdot\boldsymbol{F}^{n}-\frac{4}{c^2\Delta_t^2}\boldsymbol{D}_2\cdot\boldsymbol{D}_1\cdot\boldsymbol{F}^{n}. \tag{14}$$

Solving the full system of implicit equations (13), (14) is far beyond the capabilities of common computational machinery. Therefore after having neglected last terms on the RHS and LHS of (14), one can split the approximate equation

$$\left\{\boldsymbol{I}-\frac{2}{c\Delta_t}\boldsymbol{D}_1\right\}\cdot\left\{\boldsymbol{I}-\frac{2}{c\Delta_t}\boldsymbol{D}_2\right\}\cdot\boldsymbol{F}^{n+1}=\left\{\boldsymbol{I}+\frac{2}{c\Delta_t}\boldsymbol{D}_2\right\}\cdot\left\{\boldsymbol{I}+\frac{2}{c\Delta_t}\boldsymbol{D}_1\right\}\cdot\boldsymbol{F}^{n} \tag{15}$$

into two subsequent steps

$$\left\{\boldsymbol{I}-\frac{2}{c\Delta_t}\boldsymbol{D}_2\right\}\cdot\boldsymbol{F}^{n+1/2}=\left\{\boldsymbol{I}+\frac{2}{c\Delta_t}\boldsymbol{D}_1\right\}\cdot\boldsymbol{F}^{n},\qquad\left\{\boldsymbol{I}-\frac{2}{c\Delta_t}\boldsymbol{D}_1\right\}\cdot\boldsymbol{F}^{n+1}=\left\{\boldsymbol{I}+\frac{2}{c\Delta_t}\boldsymbol{D}_2\right\}\cdot\boldsymbol{F}^{n+1/2}. \tag{16}$$

where $\boldsymbol{F}^{n+1/2}$ denotes the intermediate value after the first sub step. This procedure is called Alternating-Directions-Implicit (ADI)-FDTD method. If there are N spatial discretisation points along each axis x, y, and z, then the algorithm for (16) can be organized in such a way that it requires six inversions of the tri-diagonal $(N\times N)$ matrices. The original problem (13) requires inversion of the $\left(6N^3\times 6N^3\right)$ sparse matrix. This is already for moderate number of sampling points N an unrealizable task.

Alternatively can (12) be expressed in the following way

$$\left\{\boldsymbol{I}-\frac{2}{c\Delta_t}\left(\boldsymbol{D}_{12}-\boldsymbol{D}_{21}\right)\right\}\cdot\boldsymbol{F}^{n+1}=\left\{\boldsymbol{I}+\frac{2}{c\Delta_t}\left(\boldsymbol{D}_{12}-\boldsymbol{D}_{21}\right)\right\}\cdot\boldsymbol{F}^{n} \tag{17}$$

and then similarly recast into the form

$$\left\{\boldsymbol{I}-\frac{2}{c\Delta_t}\boldsymbol{D}_{12}\right\}\cdot\left\{\boldsymbol{I}+\frac{2}{c\Delta_t}\boldsymbol{D}_{21}\right\}\cdot\boldsymbol{F}^{n+1}+\frac{4}{c^2\Delta_t^2}\boldsymbol{D}_{12}\cdot\boldsymbol{D}_{21}\cdot\boldsymbol{F}^{n+1}=$$

$$=\left\{\boldsymbol{I}+\frac{2}{c\Delta_t}\boldsymbol{D}_{12}\right\}\cdot\left\{\boldsymbol{I}-\frac{2}{c\Delta_t}\boldsymbol{D}_{21}\right\}\cdot\boldsymbol{F}^{n}+\frac{4}{c^2\Delta_t^2}\boldsymbol{D}_{12}\cdot\boldsymbol{D}_{21}\cdot\boldsymbol{F}^{n}. \tag{18}$$

After having neglected last terms on RHS and LHS of (18) one again arrives to analogous equation as (15)

$$\left\{\boldsymbol{I}-\frac{2}{c\Delta_t}\boldsymbol{D}_{12}\right\}\cdot\left\{\boldsymbol{I}+\frac{2}{c\Delta_t}\boldsymbol{D}_{21}\right\}\cdot\boldsymbol{F}^{n+1}=\left\{\boldsymbol{I}+\frac{2}{c\Delta_t}\boldsymbol{D}_{12}\right\}\cdot\left\{\boldsymbol{I}-\frac{2}{c\Delta_t}\boldsymbol{D}_{21}\right\}\cdot\boldsymbol{F}^{n}. \tag{19}$$

which can again be splitted into two subsequent sub steps

$$\left\{\boldsymbol{I}+\frac{2}{c\Delta_t}\boldsymbol{D}_{21}\right\}\cdot\boldsymbol{F}^{n+1/2}=\left\{\boldsymbol{I}-\frac{2}{c\Delta_t}\boldsymbol{D}_{21}\right\}\cdot\boldsymbol{F}^{n},\qquad\left\{\boldsymbol{I}-\frac{2}{c\Delta_t}\boldsymbol{D}_{12}\right\}\cdot\boldsymbol{F}^{n+1}=\left\{\boldsymbol{I}+\frac{2}{c\Delta_t}\boldsymbol{D}_{12}\right\}\cdot\boldsymbol{F}^{n+1/2}. \tag{20}$$

This procedure is called Crank-Nicolson-Split-Step (CNSS)-FDTD method. In both methods are the terms of the second order on the RHS and the LHS of (14) and (18) neglected. Therefore both are in Δ_t second order approximate in comparison with the full Crank-Nicolson formulation (13) or (17).

Numerical dispersion

For the sake of simplicity let us consider the two-dimensional case only. Waves of any temporal and/or spatial shape can be Fourier expanded into the angular spectrum of either TM or TE monochromatic plane waves. Propagation of a spatio-temporal spectral TM component having the vectorial components

$\{E_y, H_x, H_z\}$ in the direction given by the k_x, k_z components of the wave vector $\boldsymbol{k}$, $|\boldsymbol{k}| = k = \sqrt{k_x^2 + k_z^2}$, is described in two dimensions *x* and *z* by

$$E_y = E_0 \exp(j\omega t)\exp(-jk_x x)\exp(-jk_z z), \tag{21}$$

where the angular frequency ω is given as $\omega = kc = c\sqrt{k_x^2 + k_z^2}$, and *c* is the "physical" phase velocity in the given medium.

The FDTD discretisation is performed on the so-called staggered grids [1]. The discretised TM plane wave using (21) is then given by

$$E_y\big|_{i,m}^{n} \approx \xi^n \exp(-jk_x\Delta_x i)\exp(-jk_z\Delta_z m), \tag{22}$$

and similarly for $H_x\big|_{i,m+\frac{1}{2}}^{n}$ and $H_z\big|_{i+\frac{1}{2},m}^{n}$, where $\xi = \exp(j\omega\Delta_t)$ should hold. However, during the numerical simulation of the wave propagation instead of differential equations the difference equations are being solved. Therefore, instead of the above correct terms for ω and *c*, one obtains different values ω_A and v_p from the formula $\xi = \exp(j\omega_A\Delta_t) = \exp(jkv_p\Delta_t)$, where $v_p = \text{phase}(\xi)/k\Delta_t$ is the numerical phase velocity different from the "physical" phase velocity *c* due to the numerical dispersion. The numerical dispersion, i.e. the differences between *c* and v_p are artifacts stemming from the nature of the numerical procedure itself. To avoid aliasing effects for all discretisations the sampling theorem must be fulfilled, i.e.

$$k_x\Delta_x \le \pi, \quad k_z\Delta_z \le \pi, \quad \omega_A\Delta_t = \text{phase}(\xi) \le \pi. \tag{23}$$

For the full Crank Nicolson formulation of the FDTD method using discretised Maxwell equations one obtains the result

$$\xi = \left\{1 - A_x^2 - A_z^2 + j2\sqrt{A_x^2 + A_z^2}\right\} \Big/ \left(1 + A_x^2 + A_z^2\right) \tag{24}$$

where

$$A_x = (c\Delta_t/\Delta_x)\sin(k_x\Delta_x/2), \quad A_z = (c\Delta_t/\Delta_z)\sin(k_z\Delta_z/2). \tag{25}$$

For the ADI-FDTD for each of two simulation-half-steps $\Delta_t/2$ the result

$$\sqrt{\xi_{1,2}} = \left\{1 + j\sqrt{\left(1 + A_{x,z}^2\right)\left(1 + A_{z,x}^2\right) - 1}\right\} \Big/ \left(1 + A_{x,z}^2\right), \tag{26}$$

. For the CNSS-FDTD method one similarly obtains the formula

$$\sqrt{\xi_{1,2}} = \left(2 - A_{x,z}^2 + j2\sqrt{2}A_{x,z}\right) \Big/ \left(2 + A_{x,z}^2\right). \tag{27}$$

The power-flow-density for the full step Δ_t is in all cases unconditionally conserved since either in (24) $|\xi| = 1$, or in (26) and (27) $|\xi| = \left|\sqrt{\xi_1}\right|\left|\sqrt{\xi_2}\right| = 1$, holds. The dispersion characteristics are fully determined by the phase of ξ in the case of full Crank-Nicolson formulation (24)

$$\text{phase}(\xi) = \arctan\frac{2\sqrt{A_x^2 + A_z^2}}{1 - A_x^2 - A_z^2} \tag{28}$$

or by the phase of $\xi = \sqrt{\xi_1}\sqrt{\xi_2}$ using (26) and (27)

$$\text{phase}\left(\sqrt{\xi_1\xi_2}\right) = 2\arctan\sqrt{\left(1 + A_x^2\right)\left(1 + A_z^2\right) - 1}, \quad \text{phase}\left(\sqrt{\xi_1\xi_2}\right) = \arctan\frac{2\sqrt{2}A_x}{2 - A_x^2} + \arctan\frac{2\sqrt{2}A_z}{2 - A_z^2}. \tag{29}$$

For the sake of comparison we show the result for the classical explicit Yee-FDTD. Here one obtains

$$\xi = 1 - 2\left(A_x^2 + A_z^2\right) \pm j\sqrt{1 - \left\{1 - 2\left(A_x^2 + A_z^2\right)\right\}^2} \tag{30}$$

In order to have the stability condition fulfilled the term under the square root must be positive, therefore $\left(A_x^2 + A_z^2\right) < 1$, or

$$c\Delta_t\left\{\frac{\sin^2(k_x\Delta_x/2)}{\Delta_x^2} + \frac{\sin^2(k_z\Delta_z/2)}{\Delta_z^2}\right\} < 1 \tag{31}$$

Since the spatial harmonics due to the sampling theorem (Nyquist limit) can have maximum wave numbers equal to $k_x = 2/\Delta_x$, $k_z = 2/\Delta_z$, i.e. the sine functions in (31) are equal to one and the ultimate CFL-limit

$$c\Delta_t \sqrt{\Delta_x^{-2} + \Delta_z^{-2}} < 1 \tag{32}$$

is obtained. Depending on the actual length of Δ_t the formula (32) defines so-called Courant number that cannot be in case of explicit Yee-FDTD larger than one. For the unconditionally stable methods such as CN-FDTD, ADI-FDTD, or CNSS- FDTD can however reach any values larger than one.

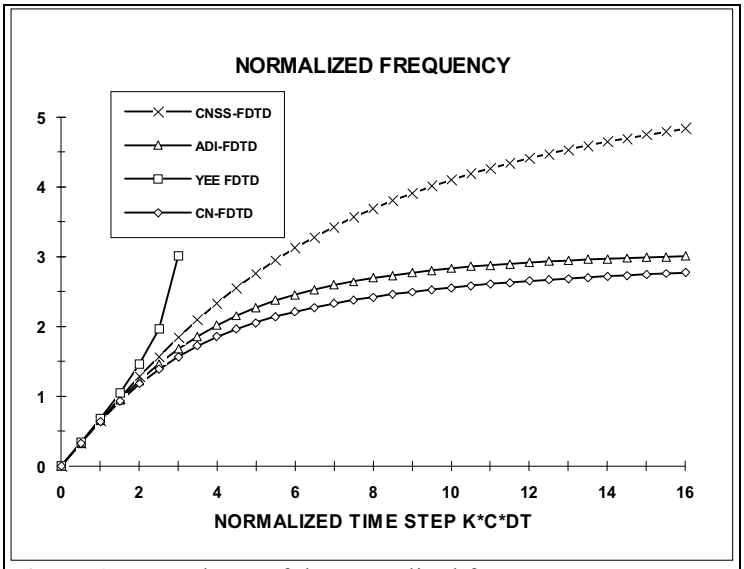

Figure 1. Dependance of the normalised frequency $\omega_A \Delta_t \le \pi$ on the normalised time step $kc\Delta_t$ for $k_x\Delta_x = 3$, $k_z\Delta_z = 3$.

Conclusions

Wave propagation characteristics using the ADI-FDTD and CNSS-FDTD methods are illustrated in Fig.1. For the explicit Yee-FDTD the values can be calculated until the Courant limit is reached. Here the normalized frequency arrives at the Nyquist limit $\omega_A \Delta_t = \pi$. For CN-FDTD and ADI-FDTD it seems that the Nyquist limit $\omega_A \Delta_t = \pi$ is approached asymptotically with increasing Δ_t . Thus, it is inferred that the sampling theorem criteria are fulfilled for any step length for the CN-FDTD and the ADI-FDTD method. As seen from the comparison of curves for CN-FDTD and ADI-FDTD neglecting the second order terms in ADI-FDTD factorization (16) does not cause any substantial error as compared with the "exact" Crank-Nicolson formulation. As it can be easily seen the condition (23), i.e. $\omega_A \Delta_t \le \pi$, is fulfilled for CNSS-FDTD only until the normalized time step value reaches $kc\Delta_t \approx 6$ .This is a substantial not yet published difference between ADI-FDTD and CNSS-FDTD. Moreover, the possibility of the arbitrarily large Δ_t steps in the ADI-FDTD method does not necessarily mean any advantage, since with growing Δ_t the phase velocity $v_p = \text{phase}(\xi)/k\Delta_t$ decreases, i.e. the simulated spatial propagation path pertaining to increased time step remains effectively the same.

Acknowledgment: This work has been supported by the Slovak government grant agency under the VEGA Grant No. 1/1056/04.

References:

[1] K. S. Yee, "Numerical solution of initial boundary value problems involving Maxwell's equations in isotropic media", *IEEE Trans. Antennas & Propagation*, **AP-14**(1966), pp. 302–307.

[2] A. Taflove, S. C. Hagness, Computational Electrodynamics: The Finite-Difference Time-Domain Method, 2nd ed. Boston, MA: Artech, 2000.

[3] F. Zheng, Z. Chen, J. Zhang, "A finite-difference time-domain method without the Courant stability conditions", *IEEE Microwave & Guided Wave Lett.*, **9**(1999), pp. 441–443.

[4] F. Zheng, Z. Chen, J. Zhang, "Toward the Development of a Three-Dimensional Unconditionally Stable Finite-Difference Time-Domain Method", *IEEE Trans. Microwave Theory & Techn.*, **MTT-48**(2000), No. 9, pp. 1550-1558.

[5] J. Lee, B. Fornberg, "A split step approach for the 3-D Maxwell's equations", *J. Comp. Appl. Math.*, **158**(2003), pp. 185-505.

[6] J. Lee, B. Fornberg, "Some unconditionally stable time stepping methods for the 3D Maxwell's equations", *J. Comp. & Appl. Math*., **166**(2004), pp. 497-523.
[7] S. G. Garcia, R. G. Rubio, A. R. Bretones, R. G. Martin, "On the Dispersion Relation of ADI -FDTD, *IEEE Microwave & Wireless Comp. Lett.*, **16**(2006), pp. 354–356.

SIMULATION OF A BIOPLASMATIC CHIRAL MODEL FOR HUMAN HEAD RADIATED BY MICROWAVES BETWEEN 1 TO 100 GHZ

M. ZAMORANO[(1)] AND H. TORRES-SILVA[(2)]

[(1)] Escuela de Electricidad y Electrónica - [(2)] Instituto de Alta Investigación
Universidad de Tarapacá, 18 de Septiembre 2222, Arica, Chile
E-mail: mhzlucero@uta.cl : htorres@uta.cl

Abstract
A bioplasmatic chiral model of the human head, constructed with 540,000 cubic cells in 54 layers derived of MR images, that allows us to simulate and to evaluate the absorption induced by the radiation microwaves wireless systems between 1 to 100 GHz is presented. The procedure to determine the absorption of microwaves waves emitted by wireless systems consisting of the following three main steps: 1) evaluation of the electromagnetic fields distribution inside the biological target, 2) modeling of human head, and 3) SAR simulation by including chirality effects. The simulations were developed by means of the FDTD technique and the specific absorption coefficient (SAR) was determined for a layer with great concentrations of brain tissue (layer 35). The results show the evolution of SAR coefficient, as function of input power and chiral factor.

Keywords: chirality; brain tissue; Maxwell; FDTD; SAR
PACS: 41.20Jb; 02.70.Bf; 52.35; 87.15.Aa

1. Introduction

In recent years, there has been a continuing explosion in the growth of microwave and radio frequency communications, particularly a dramatic acceleration in the use of cellular phones and wireless local area networks (WLANs).This has resulted in public concern about the health hazards of microwave electromagnetic fields emitted by these systems. This growth has raised the research on the effects of microwave interaction with biological tissues. Cellular phones use low-speed data transmission (e.g., voice data) over wide geographical areas, while WLANs and wireless Internet are adopted in services requiring high-speed data transmission over small confined areas (e.g., inside a building). It is important to assess the risk, if any, of the wireless revolution and determine if need exists for the establishment of new regulations for evaluation of the mechanisms of interaction between electromagnetic fields and biological systems. [1]

To transmit data, wireless LAN systems use a directive antenna placed at a mobile personal terminal (computer, telephone, camera, etc.) and a wide beam antenna placed at a fixed site (the base station) usually located on the room ceiling. In this arrangement, the user can find him self in close proximity to the radiating mobile antenna, where the EMF assumes its highest values. As a consequence, it is important to consider the possible health hazard due to such systems. Specifically, the heads of many users are exposed to a sequence of microwave fields modulated in substantially different ways [2]. When the cellular phone is close to the head, background levels are sharply distorted, with 40 to 50 percent of radiated phone energy absorbed in the hand and the head of an user [3]. Its emission at the head surface is typically 10,000 times stronger than fields reaching the head of a user standing within 30 m of the base of a typical mobile phone relay transponder mounted on a tower 30m above ground.

In a technical perspective, the carrier wave remains constant in amplitude throughout the transmission epoch, all data information being transmitted in the frequency domain, where systems generally transmit at 900, 1800 MHz and 2.4 GHz. When the antenna is close to the head, background levels are sharply distorted, with 40 to 50 percent of radiated phone energy absorbed in the hand and the head of a user [4].

In this paper, we propose to use a simple chiro-electrodynamical model, which takes into account the main interaction between the bioplasma of the brain neurons and the microwave radiation of mobile phone or wireless systems. To address the problem and on the basis of our previous experience [2][6], our method consists of the following three main steps: (1) modelling of human head through MRI, (2) evaluation of the EM distribution inside the biological target, considering the brain tissue as chiral bioplasmatic media, and (3) SAR simulation to evaluate the thermal effect. A brief explanation of the theoretical base of the technique used and description of the models are given in section 2. Results comparing the computed SAR values in the different models are shown and discussed in section 3. Finally, conclusions are presented.

2. Electrodynamic point of view.

To characterize the microwave absorption by the brain tissue, radiated by cellular phones, it is assumed that the brain tissue media is chiral. This chiral effect is due to a microscopic mechanism where the typical cell membrane of brain is a fluid bilipid layer with a lot big chiral protein molecules embedded in it. Every protein molecule is polar and will tend to align itself with an electric field and often helical rotate in its socket, so any volume of brain tissue must have a lot of cells bearing protein molecules that happen to resonate at its rotation frequency.

Studies on DNA have shown that large electron flows are possible with the stacked base pairs of the double helix and a collective interaction of large ionic ensembles where the electromagnetic field is assumed in aqueous solutions of amino acids. Also when the twisted DNA molecule is a right-handed helix is transcribed into RNA, the DNA molecule can be unwound. And it is possible that signaling inside neurons can have two twists. Here, we propose the hypothesis that all these features can be explained in a unified manner, namely the chiral-electrodynamics model, where the bioplasma is divided into two very thin layers separated by a permeable membrane, having cylindrical microtubules or helical structures. The dimmers α and β can exist in two different geometric configurations which correspond to the electric polarization states of dimmers, whose helicoidal structure can be right (R) or left (L). Then, since the protein medium is chiral, an electromagnetic wave in this medium necessarily will rotate its polarization plane in accordance with the dominant biological structure. Preliminary calculus show that the medium frequencies are between 10 and 20 GHz (microwave radiation). The eigenfrequencies, for typical proteins become between 10 GHz -12 GHz and for cluster DNA molecules the interval is between 1 GHz to 12 GHz. These frequencies are typical for microwave radiation. Accordingly with the above discussion, we consider the brain tissue as a chiral bioplasma immersed in a low magnetic field, characterized by a global chirality factor, T, so the Born-Fedorov constitutive equations are

$$\boldsymbol{D} = \varepsilon\left(\boldsymbol{E} + T\nabla\times\boldsymbol{E}\right),...\boldsymbol{B} = \mu\left(\boldsymbol{H} + T\nabla\times\boldsymbol{H}\right) \tag{1}$$

where ε, μ and T are the permittivity, the permeability and the chiral scalar, respectively. Solving Maxwell`s equations for a plane electromagnetic wave of frequency ω ($\omega = k_t v = 2\pi f$, k_t is the tissue wave number and v is the phase velocity) propagating in a chiral medium, it can be shown that the left- and right-hand circularly polarized waves have different wave numbers, $k = k_t/(1+k_t T)$ and $k = k_t/(1-k_t T)$, respectively. The chiral parameter T has the dimension of a length. Here, the rotor of polarization plane can be predicted from Maxwell´s equations, considering that the $\boldsymbol{P}$ or $\boldsymbol{M}$ vector has a proportional additional term to rotor $\boldsymbol{E}$ or rotor $\boldsymbol{H}$, respectively. If it is assumed that the medium is isotropic, non-permeable and non-dispersive, the Cartesian field components are [7]

$$D_{x,y,z} = \varepsilon_0\varepsilon_r E_{x,y,z} + \varepsilon_0\varepsilon_r T\left[\frac{\partial E_{z,x,y}}{\partial y,z,x} - \frac{\partial E_{y,z,x}}{\partial z,x,y}\right],..B_{x,y,z} = \mu_0 H_{x,y,z} + \mu_0 T\left[\frac{\partial H_{z,x,y}}{\partial y,z,x} - \frac{\partial H_{y,z,x}}{\partial z,x,y}\right] \tag{2}$$

Using the MKS system of units, the following system of scalar equations is the set of Maxwell's equations in the rectangular coordinate system (x, y, z)

$$\frac{\partial H_{x,y}}{\partial t} = \mp\frac{1}{\mu}\frac{\partial E_z}{\partial y,x} \pm T\frac{\partial^2 H_z}{\partial y,x\partial t},..\frac{\partial H_z}{\partial t} = \frac{1}{\mu}\left(\frac{\partial E_x}{\partial y} - \frac{\partial E_y}{\partial x}\right) + T\left(\frac{\partial^2 H_y}{\partial x\partial t} - \frac{\partial^2 H_x}{\partial y\partial t}\right) \tag{3}$$

$$\frac{\partial E_{x,y}}{\partial t} = \pm\frac{1}{\varepsilon}\frac{\partial H_z}{\partial y,x} \pm T\frac{\partial^2 E_z}{\partial y,x\partial t} - \sigma E_{x,y},..\frac{\partial E_z}{\partial t} = \frac{1}{\varepsilon}\left(\frac{\partial H_y}{\partial x} - \frac{\partial H_x}{\partial y}\right) + T\left(\frac{\partial^2 E_y}{\partial x\partial t} - \frac{\partial^2 E_x}{\partial y\partial t}\right) - \sigma E_z \tag{4}$$

where σ (S m^{-1}) is the tissue electrical conductivity. After calculation of the induced chiral electric field by the FDTD method, the local specific absorption rate SAR is obtained as

$$SAR_{i,j}(T) = \frac{\sigma_{i,j}\left.E_T^2\right|_{i,j}}{2\rho_{i,j}} \tag{5}$$

where

$$\left.E_T\right|_{i,j}(T) = \sqrt{\frac{1}{n}\sum_1^n\left(\left.E_y^2\right|_{i,j}^n + \left.E_x^2\right|_{i,j}^n + \left.E_z^2\right|_{i,j}^n\right)} \tag{6}$$

In these equations, the electric (magnetic) fields depend not only on $\boldsymbol{E}$ (resp. $\boldsymbol{H}$) but also on the transverse components.

3. SAR simulation and analysis of results

For the numerical calculation, the chiral factor is normalized as *kT*, where *k* is the wave number in the tissue layer, in some cases it may be $k_t = nk_0$ ($k_0 = \omega / c$ is the vacuum wave number), with *n* = 1, 2, 3…, taking into account the multiphoton absorption when the resonance absorption at macromolecular level becomes important. For the brain, we considered $k = k_b /(1 - k_b T)$ because the clusters of DNA molecules have eigenwaves representing right-hand circularly polarized waves and for the rest of the tissues we considered $kT = k_t T = 0$. Calculation stages of the bioplasmatic model for SAR determination are shown in figure 1. Using the linear FDTD algorithm with chirality, obtained from equations (3)-(6), simulations for microwave spectrum are made. The model of human head was constructed with 540000 cubic cells of 2.5 mm side each. The total number of layers, counted from the bottom of head, used in this model was 54. Here we choose layer 35, because it has a large concentrations of brain tissue. Figure 2 shows these layers in digitalized version (matrix of 100 × 100), likewise is exhibited the antenna position. Both, the dielectric constant and the conductivity of the brain were obtained from literature. In order to study and isolate the chiral effect, calculations are made for plane wave assumption, powers of 1.25, 12.5 and 125 mW were used, at frequencies of 0.9, 1.8. 2.4, 5.2, 5.8, 30, 60 and 100 GHz, respectively, having the cellular phone antenna an impedance of 180 Ω. Four types of tissues (skin, bone, blood and brain) are considered. Simulations were made in a systematic way, in order to determine the effect that the variation of the chiral coefficient had over the absorption of coefficient SAR, and results, for layer 35, are shown in figures 3-9. Owing to the different electromagnetic properties of the tissues, the power absorption is not a monotonically decreasing function of depth. For $kT = 0$, absorption is highest in the skin, low in the skull, but higher again in the brain. These curves were obtained performing similar simulations and then obtaining a statistical average of the SAR. In all curves, as the wave penetrates the head, it traverses the different parts of which the head model is made and the value of the SAR is attenuated quickly due to the change in medium and the increase of the distance from the emitting source (antenna). It is important to say that the SAR maximum (hot point) is in the outer part (skin). After passing through the bone level, the SAR is much attenuated (between cells 5 and 10) and around cell 10 the SAR increases at brain level. Here, starting from cell 10 approximately it is important to analyze the performance of our bioplasmatic model.

The profile of the SAR for 35th layer, at 0.9 GHz as function of distance for different values of chiral factor *kT*, is shown in figure 3, where the variation is observed for values of chiral factor $0 < kT \leq 3$. A SAR of 0.032 W kg^{-1}, is observed in the brain region, for a null chiral factor ($kT = 0$). For $kT = 1$, the SAR found was 0.036 W kg^{-1}, an increase of 12.5% with respect to the achiral case ($kT = 0$), and a SAR of 0.043 W kg^{-1} was found for $kT = 3$, with an increase 34%. This increase corresponds to the power absorbed by the head. Figure 4 shows the distribution of the SAR for 35th layer, as a function of distance, for different values of the chiral factor when the work frequency is 1.8 GHz. The maximum SAR found, in the blood-brain region, was 0.08 W kg^{-1} for to $kT = 0$ and 0.116 W kg^{-1} for $kT = 1$, i.e. an increase of 45% with respect to the achiral case. For a high value of chiral factor, $kT = 3$, the maximum SAR found was 0.12 W kg^{-1} with an increase of 50%. Again, this increase corresponds to the power absorbed by the head. Figure 5 shows the distribution of the SAR for 35th layer, as a function of distance, for different values of the chiral factor when the work frequency is 2.4 GHz. The maximum SAR found, in the blood-brain region, was 0.09 W kg^{-1} for to kT = 0 and 0.13 W kg^{-1} for $kT = 1$, i.e. an increase of 44% with respect to the achiral case. For a high value of chiral factor, $kT = 3$, the maximum SAR found was 0.16 W kg^{-1} with an increase of 77%.

Figures 6-8 show the distribution of the SAR, for 35th layer as a function of distance, for different values of the chiral factor, when the work frequency is 30, 60 and 100 GHz. The SAR found in the blood-brain region increase when the power get higher also for chiral factor 0, 1, and 2, the SAR is barely increase, for each power simulated. Figure 9 show the distribution of the SAR maximums in the blood-brain region, as a function of frequency, for different powers and chiral factors as summary of all the simulations made it. The consequence of being at such frequency is the fact that the human tissue (especially brain tissue) absorptivity of microwave radiation increase with frequency in this spectrum region. Theses must be verified by using more advanced models. The results of figure 9 are similar to those of Curry [8].

4. Conclusions

A bioplasmatic chiral model of the human head has been presented that allows determination and evaluation of the absorption induced by the radiation of cellular phone and wireless systems. Electromagnetic fields radiated were determined firstly by means of the FDTD technique and then the specific absorption coefficient (SAR). It is shown that the use of a cell model, combined with a real model of the human head, derived from the magnetic resonance of images allows exact determination of the near fields induced in the head when the brain chirality is considered. The simulations are made for the 35th layer. The results also show the evolution of the specific

absorption rate, (SAR coefficient), as function of input power and chiral factor. The more importants conclusion of our work are: 1) with the chiral electrodynamics model the head absorption of microwave fields, produced by cellular phones and wireless systems, is bigger that the results obtained for classical models, and 2) the absorption of microwave radiation increase with frequency.

Acknowledgments
The authors thank the University of Tarapacá Project Nº 8721-06 and 8722-06. Also, we greatly appreciate the help received from M. Sc. Enrique Fuentes H.

References

[1] Lang S., "Recents advances in Bioelectromagnetics Research on Mobile Telephony and Health" *Progress in Electromagnetics Research Symposium*, Cambridge, USA, March, 29-29, 2006.
[2] Torres-Silva H. et al. "Los campos electromagnéticos en la telefonía celular, su interacción con el sustrato neuronal". *Revista Facultad de Ingeniería* UTA, Vol. 9, pp. 3-19, 2001.
[3] Torres-Silva H. and Zamorano M. "Chiral Effect on Optical Soliton". *The Journal Mathematics and Computers in Simulation*, Vol. 62, pp. 149-161, 2003.
[4] Torres-Silva H. and Zamorano M. "SAR Simulation for Chiral Waves in Head Model". *Revista Facultad de Ingeniería* UTA, Vol. 11, pp. 3-11, 2003.
[5] Zamorano M. and Torres-Silva H. "Ecuación de Schrödinger para una Fibra Óptica Quiral". *Revista Mexicana de Física*, 46(1), pp. 62-66, 2000.
[6] Zamorano M. and Torres-Silva H. "Efecto de la Quiralidad sobre Solitones Polarizados en un Medio Anisotrópico". *Revista Mexicana de Física*, Vol. 49(1), pp. 20-27, 2003.
[7] Taflove A and Hagness SC, Ed. C*omputational Electrodynamics: The Finite-Difference Time Domain Method*, Artech House, pp. 35-171., 2000.
[8] Curry B. Ph.D. Consulting Physicist; http://www.emrnetwork.org/schools/curry_broward.pdf

FIGURES CAPTION

Fig. 1 Stages of the bioplasmatic model for SAR determination.
Fig. 2 The structure of layer 35.
Fig. 3 SAR variation, as function of the transverse distance, for $0 < kT \leq 3$ at 900 MHz. Layer 35.
Fig. 4 SAR variation, as function of the transverse distance, for $0 < kT \leq 3$ at 1800 MHz. Layer 35.
Fig. 5 SAR variation, as function of the transverse distance, for $0 < kT \leq 3$ at 2400 MHz. Layer 35.
Fig. 6 SAR variation, as function of the transverse distance, for $0 < kT \leq 2$ at 30 GHz. Layer 35.
Fig. 7 SAR variation, as function of the transverse distance, for $0 < kT \leq 2$ at 60 GHz. Layer 35.
Fig. 8 SAR variation, as function of the transverse distance, for $0 < kT \leq 2$ at 100 GHz. Layer 35
Fig. 9 SARmax variation in the blood-brain region, as function of frequency for $0 < kT \leq 2$ and different power. Layer 35.

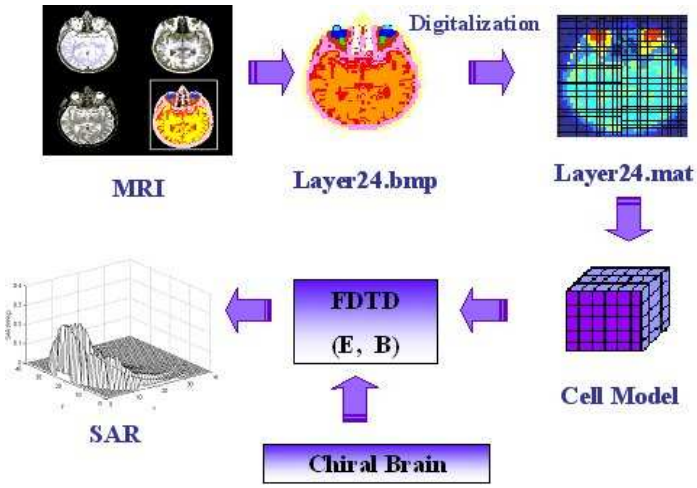

Figure 1

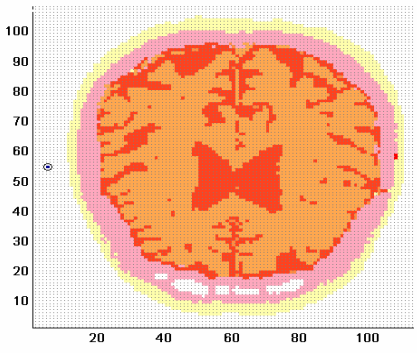

Figure 2

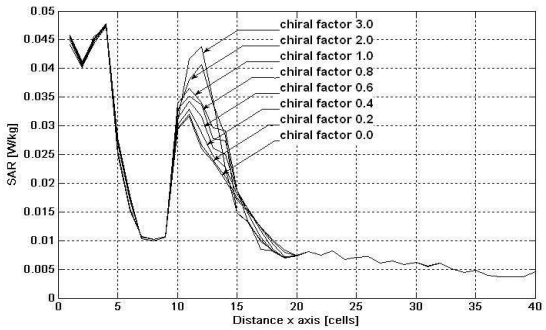

Figure 3

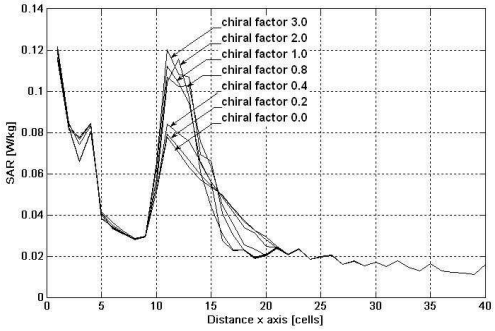

Figure 4

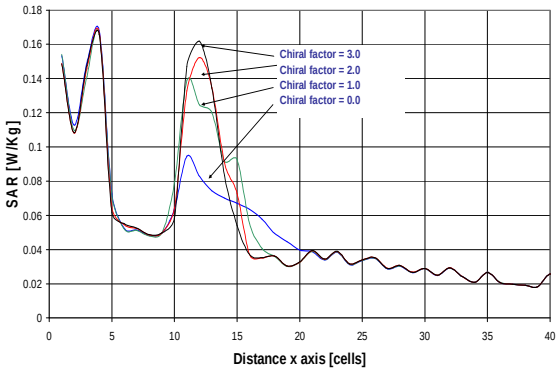

Figure 5

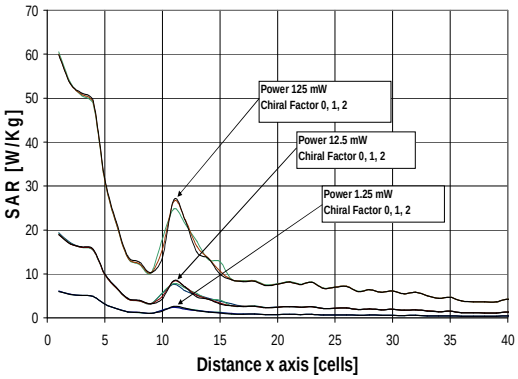

Figure 6

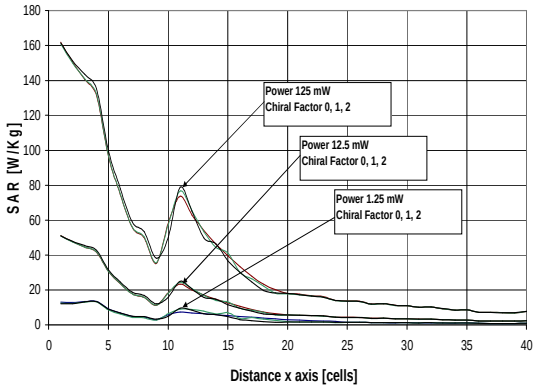

Figure 7

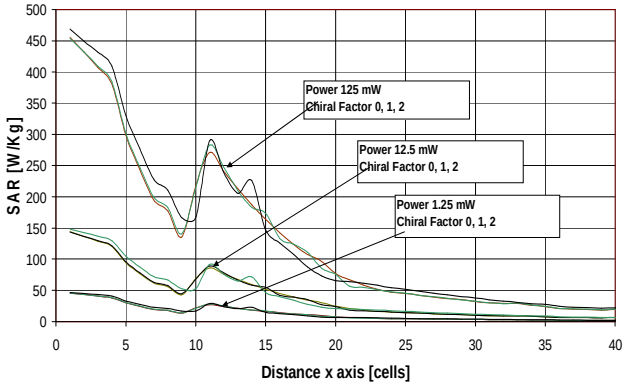

Figure 8

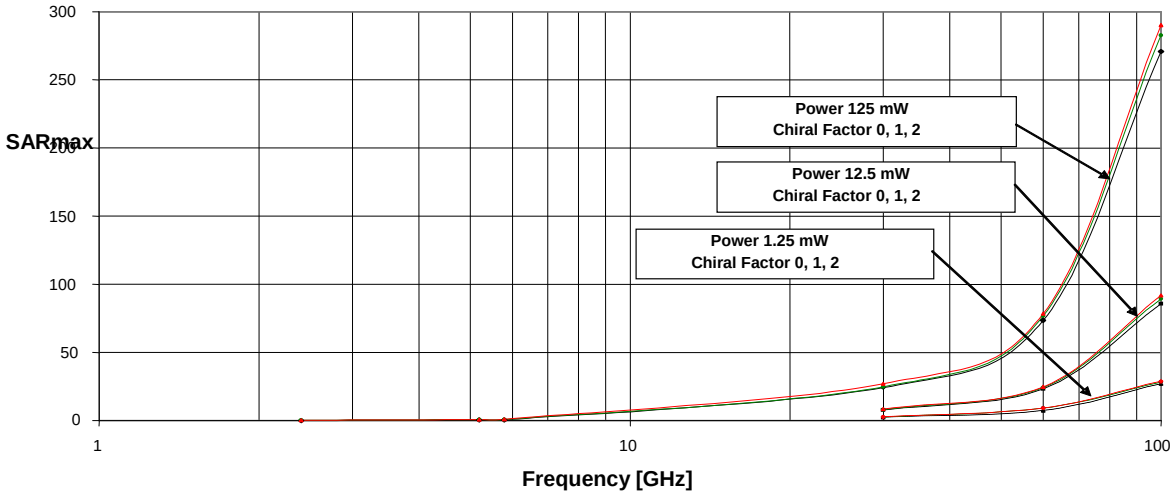

Figure 9

ELECTROMAGNETIC FIELD LEVELS IN THE WORKING ENVIRONMENT IN RADIO AND TV STATIONS. PROGRAM FOR HEALTH PROMOTION

Ivanova, M., V. Zaryabova, Ts. Shalamanova, M. Israel

National Center of Public Health Protection, Sofia, Bulgaria

Abstract

Electromagnetic field sources used for communication always are subject of serious interest. There are many publications concerning exposure and risk assessment of the working in such environment. Results of epidemiological study performed in Bulgaria in 90s (Varna, Proceedings 2001) show exceeding of the maximal permissible values especially in radio stations for the personnel in 24 h working shift.

In the last years the situation is strongly influenced by the development of the technology which leads to changes in equipment in radio and TV stations, using lower power, facilitate the working regime.

Paper presents data of exposure assessment of different professional groups in selected radio and TV stations. Assessment is being performed on basis of EMF parameters values and energetic load calculations according to the national legislation. Data are compared with the results of previous investigation to evaluate the new situation in this branch. Exposure levels are much lower than those in the last study, and lower compared to the exposure limits, as well.

INTRODUCTION

The policy of the World Health Organization (WHO) after its establishment incorporates occupational health issues. Numerous important WHO documents, such as the Constitution, Alma Ata Declaration, "Health for All" Strategy, working programs and certain resolutions of the World Health Assembly underline the necessity to protect and strengthen health and safety at work through prevention and control of workplace hazardous factors and promotion of workers' health and work ability.

The transition during the past two decades experienced by European socioeconomic communities contributed to accelerated changes in labor conditions and market. Many European countries show a tendency to re-orienting the occupational health and safety policy towards improved workers' work ability and significant reduction of increasing social costs for work-related health disorders, injuries and disability.

The new global strategy of the EU Commission and International Labor Organization (ILO) is fully focused on improving the activities on health and safety at work (HSW) at enterprise and national level. The developed systems for HSW control are a successful approach to fulfillment of the responsibilities and gaining maximal benefits through their incorporation in company and national policy, moreover, these systems are implemented in many countries, including a number of Bulgarian companies. They are built on the belief that good work management and reduction of workplace risk are based on self-control, self-assessment and adequate measures for improved safety. Such management is much more effective and with better results than just observing the regulations, moreover, ILO methodological guidelines for systems for control of health and safety at work are not mandatory. They are recommendations to the employer on achievement of better prevention level; reduction of risk for work accidents and occupational diseases and following costs and company losses; reduction of occupational risk and hence – improvement of the company image; improved work quality leading to elevated company competence; last, but not least – functional social dialogue.

The employer has to present his HSW policy as a written program, after consultations with the employees and their representatives.

A very interesting professional group exposed to high levels EMF is those of operators working in radio and TV stations. Electromagnetic field sources used for communication always are subject of serious interest. A wide-spread set of communication systems exists in each country and its types and number is ever increasing.

An epidemiological study carried out in Bulgaria in 90 [5] showed exposure to the personnel of such stations above the permissible levels accepted in the country, especially in the cases of 24-hour working shifts. The results showed that the long-term service of emitting systems results in serious health problems for operating staff, charged with broadcasting.

The present study is a continuation of the previous epidemiological study [5] and one of its goals is to assess how the development of the technology which leads to changes in equipment in radio and TV stations, using lower power, facilitation of the working regime affects the exposure of the operators. The investigation

covers a part of previously studied stations, which gives an opportunity for direct comparison of the results for the personnel's' exposure.

MATERIAL AND METHODS

Objects of study

This study was performed on radio broadcasting system of short waves (SW), television (TV), and on satellite systems. The study covers the following stations:

- ***Radio broadcasting*** station on short waves (SW) - from 6 to 25 MHz;
- ***TV station 1 with sources emitting EMF with frequencies from*** 66 MHz (UHF) to microwaves up to 6 GHz;
- ***TV station 2 with sources emitting EMF with frequencies*** 101 MHz (UHF) to microwaves up to 6 GHz;
- ***TV station 3 with sources emitting EMF with frequencies*** UHF и microwaves;
- ***Satellite station*** – frequencies from 5 GHz to 7 GHz.

We found 5 types of work shifts - A, B, C, D и G as follows:

- A – 5 days a week, 8 h per day – ordinary shift. The rest of the time the personnel is outside the station;
- B – one twenty-four hour period (24 h) in the working environment being followed three subsequent twenty-four hour periods of rest at home;
- C – four subsequent twenty-four hour periods in working environment being followed by three subsequent twenty-four hour periods of rest at home; During its stay in the station the personnel is 10 hours on shift (active working) and 14 h on disposal;
- D –7 days in the working environment followed by 14 days outside (rest at home). During its stay in the station the personnel 5 days is 12 hours on shift (active working) and 12 h on disposal and the other two days are resting in the station;
- G – two subsequent twenty-four hour periods in working environment being followed by two subsequent twenty-four hour periods of rest at home.

The following jobs were characterized: radio engineer, engineer (both with master degrees), mechanic, technician, fitter, sound-technician, radio technician, power engineer, electric fitter, electrician, electric technician, mast operator. Every station depending on its type, equipment, geographical position, etc. has different professionals. Here, we present the results for the next groups: operator on duty, chief of station, power engineer.

Additionally results for a group "other staff" being not directly engaged in the transmitters' service is presented. It includes: cleaners (other assistant jobs) and canteen managers.

Measurement equipment

The measurements of the EMF exposures were made using the following equipment:

N F M - 1 (made in Germany):

- measuring values: E = 2 to 40 kV/m for f = 50 Hz
  E = 2 to 1500 V/m for f = 0.06-350 MHz
  H = 0.1 to 10 A/m for f = 0.06-10 MHz
- uncertainty: $\sigma = \pm 20$ %;
- probes - dipole and frame.

RAHAM 495, model 40, "General Microwave Corporation"(USA).

- Frequency range: 200 kHz - 40 GHz;
- Measurement ranges – 0.02, 0.2, 2 and 20 mW/cm^2;
- Uncertainty ± 20 %;
- Minimal measured value – 0.5 μW/cm^2
- Probe – isotropic.

The devices measure the EMF values in a wide frequency range so specific methods for exposure assessment are used.

Measurement procedure

The measurements were made for typical permanent and temporary work places:

In closed premises: transmission's halls, in front of the transmitters, central desks and central control desks, central control rooms, in front of the final cascades of multipliers, near the antenna control boards, etc. All measurements were made on three levels above the ground (floor) - on the levels of head, chest and genitals of the operator, and the hygienic assessment was formed according to the maximum measured value.

On the antennae's field area we measured the field strength both under the feeder lines (feeders) at the same three levels, and along the roots of the antennas, at different depending on the area. In case of TV towers measurements were made on some of the platforms with antennae as well.

In living rooms only the maximum values of EMF measured have been taken for hygienic assessment.

All measurements were made while the transmitters worked at maximum power of radiation.

On the time of measurements the serving operators stayed on minimal distance of 5 to 10 meters behind the measurer.

The hygienic assessment of the measured values of EMF in the living rooms was made according to Ordinance No:9 for exposure to the general population (Table 3) as the personnel staying in this rooms should not be considered as performing its work tasks. The measured values of EMF in living rooms were added to the common assessment for the energetic loading of the organisms of the workers for 24 hours.

Table 3. Maximum permissible levels (MPL) according to the Bulgarian standards

STANDARD	**FREQUENCY RANGE**	$\mathbf{E_{max}}$, V/m	$\mathbf{H_{max}}$, A/m	$\mathbf{S_{max}}$, μW/cm²	$\mathbf{W_E}=E^2.T$, $(V/m)^2.h$	$\mathbf{W_H}=H^2.T$, $(A/m)^2.h$	$\mathbf{W_S}$=S.T, μW.h/cm
BNS 14525-90	60kHz - 3MHz	500	50	-	20000	200	-
	3MHz - 30MHz	200	50	-	3200	200	-
	30MHz-300MHz	60	-	-	800	-	-
BNS 17137-90	300MHz -300GHz	-	-	1000	-	-	200
Ordinance No.9 - 1991	3MHz - 30MHz	10	-	-	-	-	-
	30MHz-300 MHz	3	-	-	-	-	-
	300MHz – 30GHz	-	-	10	-	-	-

Parameters for exposure assessment

For exposure assessment the following parameters were used:

- *energetic loading of organism*:

$$W_E = \sum_i E_i^2.t_i \text{ , V}^2\text{.h/m}^2; \qquad W_S = \sum_i S_{,i}.t_i \text{ , μW.h/cm}^2;$$

Energetic loading of the organism was calculated for the average and maximal measured values on “i” measurement point (place of stay or premise) respectively for electric field strength (V/m) and power density (μW/cm^2), depending on the frequency of emitted EMF;

- *Time weighted average (TWA) values* of electric field strength and power density, TWA:

$$TWA = \frac{\sum_i E_i.t_i}{T} \text{ , V/m} \qquad TWA = \frac{\sum_i S_i.t_i}{T} \text{ , μW/cm}^2$$

where E_i and S_i are the measured values on the “i” workplace; t_i is the time duration of exposure on the same place, i = 1,...n; $T = \sum_{i=1}^{n} t_i$.

For the described stations TWA of electric field strength and power density are calculated for the average and maximal measured value of EMF on the corresponding places of stay of the personnel. Calculations for two averaging periods were made:

- for one working day – 8h, 10 h, 12 h and 24 h corresponding to the work shift duration and work cycle. Here, the real working time, time on disposal, time of rest in the station, time of rest outside the station were taken into account.
- For 120 h (5 twenty-four hour periods – one working week), taking into account the shift type (A, B, C, D и G).

Energetic loading of the organism is considered for zero for the stay outside the station.

Calculated TWA values for SW range (V/m) are presented in units μW/cm^2 “equivalent power density” for plane wave.

The real time of exposure was determined in the following ways:

- "script or scenario" method - an expert method, based on repeated measurements and for long findings of the working process. It was applied for the three groups of personnel (those, working for 24 h in a shift, others working for 8 h - normal shift, and for the "other" workers) at all studied sites, namely radio stations, TV stations and radio relay stations.

- calculating the maximum permissible time duration. The requirements of the Bulgarian National Standards (BNS) were used when determining the limits of the energetic loading of the organism. Maximum permissible time duration of every working place was calculated according to the average values of EMF by using the formulae:

$$T_{\max} = \frac{W_E}{E^2}, \qquad T_{\max} = \frac{W_S}{S}$$

where W_E , W_H and W_S are values of the energetic loading of organism for corresponding frequency range according to national legislation (Table 3).

RESULTS AND DISCUSSION

Measured EMF values in relative units compared to the limits for corresponding frequency range are presented in Table No.4.

Table No.4.

Station	Average values	Maximal values
Radio station		
transmission's halls	0.02	0.09
antennae field	0,15	0.95
TV station 1		
transmission's halls	0.003	0.05
antennae field	0.20	0.06
TV station 2		
transmission's halls	0.0075	0.0196
antennae field	0.38	0.085
TV station 3		
transmission's halls	0.0045	0.00305
antennae field	0.002	0.00175
Satelite station		
transmission's halls	0.004	0.0163
antennae field	-	

Calculated TWA values are presented in Table No.5.

Table No.5

Professional groups	Radio station		TV station 1		TV station 2		TV station 3		Satelite station	
	$TWA_{avg.}$ $\mu W/cm^2$	TWA_{max} $\mu W/cm^2$	$TWA_{avg.}$ $\mu W/cm^2$	TWA_{max} $\mu W/cm^2$	$TWA_{avg.}$ $\mu W/cm^2$	TWA_{max} $\mu W/cm^2$	$TWA_{avg.}$ $\mu W/cm^2$	TWA_{max} $\mu W/cm^2$	$TWA_{avg.}$ $\mu W/cm^2$	TWA_{max} $\mu W/cm^2$

For one working shift										
Operator on duty	3.10 (B)	137.0 (B)	1.89 (B)	5.24 (B)	1.49 (D)	3.63 (D)	1.19 (G)	1.28 (G)	1.60 (B)	3.57 (B)
Chief of station	3.96	66.90	2.56 (C)	15.41 (C)	0.96 (C)	2.38 (C)	1.57 (A)	2.22 (A)	1.88 (B)	3.67 (B)
Power engineer	0.74 (B)	6.19 (B)	1.69 (B)	4.89 (B)	-	-	-	-	1.43 (B)	3.22 (B)
Worker/ cleaner	2.40 (A)	26.56 (A)	2.12 (A)	17.22 (A)	1.03 (D)	2.18 (D)	0.96 (A)	1.2 (A)	1.83 (A)	3.65 (A)
Canteen manager	0.34 (A)	0.99 (A)	0.80 (A)	1.44 (A)	0.64 (C)	1.40 (C)	0.82 (A)	0.91 (A)	0.79 (A)	1.28 (A)
For 1 working week – 120 h										
Operator on duty	0.30 (B)	1.40 (B)	0.76 (B)	2.09 (B)	0.42 (D)	1.01 (D)	0.52 (G)	0.57 (G)	0.69 (B)	1.51 (B)
Chief of station	0.44 (B)	7.42 (B)	1.03 (C)	6.16 (C)	0.77 (C)	1.81 (C)	0.52 (A)	0.74 (A)	0.75 (B)	1.53 (B)
Power engineer	0.15 (B)	1.53 (B)	0.56 (B)	1.40 (B)	-	-	-	-	0.66 (B)	1.44 (B)
Worker cleaner	0.27 (A)	2.94 (A)	0.71 (A)	5.74 (A)	0.31 (D)	0.66 (D)	0.34 (A)	0.43 (A)	0.61 (A)	1.22 (A)
Canteen manager	0.04 (A)	0.11 (A)	0.27 (A)	0.48 (A)	0.12 (C)	0.26 (C)	0.27 (A)	0.30 (A)	0.26 (A)	0.43 (A)

Calculated values of the energetic loading of organism are presented in Table No. 6

Table No.6

Professional groups	Radio station		TV station 1		TV station 2		TV station 3		Satelite station	
	$W_{avg.}$ $(V/m)^2.h$	W_{max} $(V/m)^2.h$	$W_{avg.}$ $\mu W.h/cm^2$	W_{max} $\mu W.h/cm^2$	$W_{avg.}$ $\mu W.h/cm^2$	W_{max} $\mu W.h/cm^2$	$W_{avg.}$ $\mu W.h/cm^2$	W_{max} $\mu W.h/cm^2$	$W_{avg.}$ $\mu W.h/cm^2$	W_{max} $\mu W.h/cm^2$
For one working shift										
Operator on duty	342.79 (B)	1644.00 (B)	45.30 (B)	125.75 (B)	35.86 (D)	87.20 (D)	14.27 (G)	15.38 (G)	19.25 (B)	42.88 (B)
Chief of station	332.73 (A)	10336.0 (A)	61.98 (C)	369.75 (C)	23.12 (C)	57.38 (C)	12.53 (A)	17.75 (A)	22.61 (B)	44.00 (B)
Power engineer	121.79 (B)	1610.0 (B)	19.69 (B)	58.75 (B)	-	-	-	-	17.21 (B)	38.75 (B)
Worker/ cleaner	83.68 (A)	1312.00 (A)	16.96 (A)	137.75 (A)	24.73 (D)	52.20 (D)	8.18 (A)	10.25 (A)	14.65 (A)	29.25 (A)
Canteen manager	13.03 (A)	32.0 (A)	6.43 (A)	11.50 (A)	15.43 (C)	33.70 (C)	6.56 (A)	7.25 (A)	6.32 (A)	10.25 (A)
For 1 working week – 120 h										
Operator on duty	738.26 (B)	3392.0 (B)	90.60 (B)	251.50 (B)	49.83 (D)	120.95 (D)	61.94 (G)	68.63 (G)	83.40 (B)	181.76 (B)
Chief of station	1663.65 (B)	51680 (B)	180.80 (C)	1287.00 (C)	92.48 (C)	229.52 (C)	62.63 (A)	88.75 (A)	89.92 (B)	184.00 (B)
Power engineer	243.58	3220.0	67.50 (B)	167.50 (B)	-	-	-	-	79.12 (B)	173.50 (B)
Worker cleaner	418.40 (A)	6560.00 (A)	84.80 (A)	688.75 (A)	36.58 (D)	79.28 (D)	40.90 (A)	51.25 (A)	73.25 (A)	146.25 (A)
Canteen manager	65.15 (A)	160.0 (A)	32.15 (A)	57.50 (A)	14.69 (C)	32.09 (C)	32.80 (A)	36.25 (A)	31.60 (A)	51.25 (A)

*The types of shifts are mentioned in brackets

The investigation showed the highest exposure for the personnel in radio station.

The highest values of EMF for every station are measured near the final cascades of the amplifiers, when setting up or repairs are carried out, in the antenna's field (around the irradiating antenna), near the feeders or antenna control board. For these places maximal permissible time of stay was calculated. By professional groups the highest energetic loading of the organism values were found for the professional groups which tasks require prolonged work in antennae field and comutator premises, namely operator on duty and chief of station.

The average values of the energetic loading of the organism in relative units compared to the limit values are between 0.003 и 0.31 depending on the professional group and the working shift type. The calculation for the maximal values (worst case) gives ratio of 3.23 for the SW radio station. In the previous study 3,58 times

exceeding of the energetic loading limit value was established for the 24 h shifts for SW transmitters and up to 0,7 of the limit value for the 24 h shift in the TV stations.

The previous study had shown exceeding of the energetic loading values for 28.1% and 43 % of the working places in the SW stations for 8 h and 24 h shift respectively, exceeding of EMF values was found in 14,3 % of working places in TV stations.

In the present study the exceeding of the maximal permissible values was found only for single cases in antennae field.

There were not measured EMF values above the limits for the general public in the living rooms in stations. Previously, in 67,4% of the studied living rooms EMF values exceeded the limits for the general public.

On the basis of conducted study and estimated exposure to the personnel we propose a risk communication and management program following requirements of WHO and the Precautionary Principle.

Activities concerning risk communication

An acting, addressed towards workers in EMF conditions program demands adhering to WHO requirements for informing the workers, training and limiting the risk to minimal levels. The effectiveness of the program is specified as from the permanent analysis of the taken measures as from the traceability of the actions and from the back link with the management and the group developed the program furthermore.

In this case we recommend outlining the following main actions:

1. Towards EMF levels:
   - adhering to the maximal permissible levels in the current hygienic standards.
   - observing the permissible time duration of stay in sites, where the electric field strength and/or power density exceed the maximal permissible level for corresponding frequency;
2. Control (dosemeters, measurements etc.,)
   - regular check of EMF values, considering different powers or changes in the equipment.
   - each station should be equipped with at least one control measuring instrument (dosemeter), especially for performing tasks in antenna field;
3. Prophylaxis (technical, medical)
   - Periodical control of the technical equipment;
   - periodical check up of the health status of the staff including specialized surveillance: cardiovascular, nervous system, analysers, blood cells, germinative functions.
4. Collective and personal means for protection:
   - use and control of the protection measures and equipment
5. Compensations (nutrition, vitamines, etc.)

In cases when other prophylaxis is impossible or insufficient compensations could be applied. This approach is very extreme, and is applied only when all other possibilities are spent.

6. Training

There is necessity for topical courses on the main activities. The staff is well qualified concerning labour safety. The idea is to widen the training in the field of their specialities, work conditions, and the influence of the factors in the working environment.

7. Living conditions; resting rooms

It is clear that this is very important issue, and takes a special place in the risk communication and management. It ensures special attitude in workers.

8. Precautions (labels and fences, briefings, informational sheets and newsletters)

It is necessary precautionary labels, signs and fences (with bright and reflection colours), briefings, informational sheets and newsletters to be developed, and placed on appropriate places to show areas for stay and crossing, to warn for a possible accidents. Boards indicating the limited stay in the antenna field to be placed.

The materials prepared by the management concerning information about the communication program both for activities and results of the control, prophylaxis measures, preventive actions for health protection of the workers, news about the company organization, cases of accidents, etc., should be distributed on appropriate areas (working places, restrooms, dining rooms) aiming to inform the whole personnel.

Special attention should be paid to pregnant women and persons wearing active implants.

Mechanisms for back link

This part is fundamental for realizing the program. This could be performed by the management through an Occupational Health Service, Labour Committee, and Human Resources Department.

CONCLUSIONS

The comparison of results of the two considered studies shows decreasing of EMF exposure to the specific group of operators working in radio and TV stations. This result could be associated with the development of the technology which leads to changes in equipment in radio and TV stations, using lower power, using better shielding in the control rooms, facilitating the working regime.

REFERENCES

1. BNS 14525-90 Labour protection. Electromagnetic fields - Radiofrequency range. Permissible Exposure Levels and Requirements for Safety
2. BNS 17137-90. Labour protection. Electromagnetic fields - Microwaves. Permissible Exposure Levels and Requirements for Safety.
3. Dobrev B., D. Dimitrov, M. Israel, G. Dimitrov. Hygienic assessment of RF EMF as a factor of the working environment in radio and TV stations. Annals, No. 6, 1978.(in Bulgarian)
4. Electromagnetic Fields in the Frequency Range from 100 kHz to 300 GHz, Health Physics,54,115-123.
5. Israel M., P. Tomov: Epidemiological study of the effects of radiofrequency radiation on operators in radio, TV and relay stations, Proceeding of the Eastern European Regional Meeting and Workshop “Measurements and Criteria for Standard Harmonization in the field of EMF Exposure” and WHO EMF Standards Harmonization Meeting, Varna, Bulgaria, 28 April – 3 May, 2001, pp.145-153
6. Ordinance No.9, for maximal permissible levels of electromagnetic fields in populated areas and determining hygienic safety zones around objects emitting EMR, Ministry of Health, Ministry of Environment, State gazette 35, 1991
7. Report No.2.1/01 NCHMEN, 2004. Assessment of the effect of low-level radiofrequency electromagnetic radiation on the secretion of melatonin, the level of stress hormones and cardiovascular system, NCHMEN, Sofia (in Bulgarian)
8.Tzenova B., M. Israel, M. Topalova – Well-being and Biochemical Correlates of Non-24-Hour Sleep Schedule in Communication, Shiftwork International Newsletter, 1995, vol.12, N:1, p.103
9.WHO Environmental Health Criteria 137,1991,Geneva,Regional Office for Europe.

Biological Effects and Potential Hazards of Microwaves used in Cellular Phone System on Infertility

***Farzaneh Ahmadi*[1]**
***S. Hamed Rohani*[2]**

1. MSc. Communication Engineering; University of Tehran.
2. General Physician; Azad University of Tehran; Member of Young Researchers Club

ABSTRACT
Although recent researches approved that EM waves cause harm to CNS and bone marrow systems [1-6], they are not studied to have health effects on other systems of human body, Nevertheless possible health effects of EM waves on genitalia system is also a question as this system has also dividing cells (like CNS and bone marrow) in males and females. In this case possible effects of E-M waves on infertility is a matter of concern.

This research is done to investigate infertile couples about possession and usage methods of mobile handsets and also to discuss the role of the proximity of housing/occupation to BTSs of GSM (900, 1800) mobile phone network as a means of possible cellular phone exposure and so having possible influence on infertility.
The research has been done by questionnaires and as cross-sectional. Collected data then was analyzed using SPSS software.

The results of the study show that these variables have correlation with infertility:

1. duration which these patients use cellular phone for speech
2. place of holding cellular phone regarding body
3. model of cellular phone
4. Proximity of the handset regarding body

1. INTORDUCTION
Although recent researches have approved that E-M waves may cause harm to CNS and bone marrow systems [1-4], they are not studied to have health effects on other systems of human body. As CNS and bone marrow systems are made of dividing cells in all individuals and are proved to be affected by E-M waves of power lines and Radio frequency which have resulted Brain Cancers and different kinds of Leukemia, this idea is formed that E-M waves may have possible effects on genitalia system also as this system has dividing cells in males and females.

Indeed, a large segment of the world's population is now exposed to RF and microwave radiation. We need a better understanding of the biological effects of RF electromagnetic field so that we can safeguard against possible harms to the general population and increase its beneficial medical uses.

We have chosen the Microwaves used in cellular phone system as a course of study for possible effects on urogenital system. There are many usages of Microwaves in urban lives like satellites, point to point links, and cellular phones. The last one has a higher energy regarding its frequency and also higher amplitude regarding its usage and also is more globally used. Other forms of RF waves do not have remarkable values regarding microwaves used in cellular phone systems. With the widespread use of mobile phones, the question of cellular phone health hazards should be answered. That’s why this research is focused mainly on the study of possible effects of cell phone microwaves on infertility.

2. BIOLOGICAL EFFECTS CAUSED BY MICROWAVES

Our knowledge regarding the biological effects of RF radiation have increased for many decades. It has become a focus of attention because of the accelerated use of RF radiation for wireless communication over the past few years. It is fairly well established that at sufficiently high power levels, RF and microwave energy can produce deleterious biological effects. Wireless communication systems use low power modulated forms of RF and microwave radiation that were not investigated extensively in the past.

Nevertheless, available data do not suggest any immediate cause for concern of an impending threat to the health of the population from acute or short term exposure to low level RF radiation. Investigations to answer some of the questions have already begun. Many of them are designed to study the effects of long term exposure. When considering repeated, low level radiation, the possibility of cumulative effects has been raised. While there is presently few confirmed evidence for cumulative effect, there is little information to the contrary.

Large scale epidemiological investigations should also be undertaken among the mobile telecommunication and cellular telephone users who may be exposed to varying levels of RF radiation over time. Better understanding is needed of the mechanisms of interaction between RF and microwave radiation and biological systems, and the significance of any observed effects. Enormous progress has been made in the difficult area of dosimetry. However, measurement of energy distribution in and around a subject for exposure assessment remains a challenge, more so for large numbers of people. This type of quantitative information is also required for extrapolation from animal experimentation to human response.

3. CHARACTERISTICS OF CELLULAR COMMUNICATION SYSTEMS

The research is focused on the health effects of cellular telephones. Cellular telephones operate at frequencies close to 850 and 1900 MHz in GSM[1] systems (these frequencies may vary for different countries.) The cellular phone system mainly consists of Base Transceiver Stations (BTS) and handsets for signal transmission. So studying the radiations of this system should be focused on these two parts.

Handsets transmit at low power levels. 0.6 watts for hand-held units in the first generation mobile telephones which were based on analog technology. Digital communication systems have made digital mobile technology competitive at power consumption as low as 10 mW. But, while in use, are located very close to the user's head. They are also to be used as placed on the belt or heart other locations near body for long hours when are on but not used for speech. They may also be in places near the body while sleeping. This has naturally led to concerns about potential health effects of handset radiations.

Returning to the BTS, the total MW power that could be transmitted from each BTS antenna at a cell site depends on the number of radio channels (transmitters) that have been authorized and the power of each transmitter. Typically, for a cellular base station, a maximum of 21 channels per sector (depending on the system) could be used. Thus, for a typical cell site utilizing sector antennas, each of the three transmitting antennas could be connected to up to 21 transmitters for a total of 63 transmitters per site. When omni directional antennas are used, up to 96 transmitters could be implemented at a cell site, but this would be unusual. While a typical base station could have as many as 63 transmitters, not all of the transmitters would be expected to operate simultaneously thus reducing overall emission levels.

Although an ***effective radiated power*** (ERP) of up to 500 watts per channel (depending on the tower height) is permitted, the majority of cellular base stations in urban and suburban areas operate at an ERP of 100 watts per channel or less. An ERP of 100 watts corresponds to an ***actual*** radiated power of about 5-10 watts, depending on the type of antenna used (ERP is not equivalent to the power that is radiated but, rather, is a quantity that takes into consideration transmitter power and antenna directivity). As the capacity of a system is expanded by dividing cells, i.e., adding additional base stations, lower ERPs are normally used. In urban areas, an ERP of 10 watts per channel (corresponding to a radiated power of 0.5 - 1 watt) or less is commonly used.

The signal from a cellular base station antenna is essentially directed toward the horizon in a relatively narrow pattern in the vertical plane. The radiation pattern for an omni-directional antenna might be compared to a thin doughnut or pancake centered around the antenna while the pattern for a sector antenna is fan-shaped, like a wedge cut from a pie. As with all forms of electromagnetic energy, the power density from a cellular or PCS transmitter decreases rapidly (according to an inverse square law) as one moves away from the antenna. Consequently, normal ground-level exposure is much less than exposures that might be encountered if one were very close to the antenna and in its main transmitted beam.

Measurements made near typical cellular installations, especially those with tower-mounted antennas, have shown that ground-level power densities are well below limits recommended by RF/microwave safety standards [7-9]. For example, for a base-station transmitting frequency of 869 MHz the RF exposure guidelines recommend a Maximum Permissible Exposure level for the public ("general population/uncontrolled" exposure) of about 580 microwatts per square centimeter (μW/cm2).

[1] Global Service Mobile system

This limit is many times greater than MW levels found near the base of typical cellular towers or in the vicinity of lower-powered cellular base station transmitters, such as might be mounted on rooftops or sides of buildings. Measurement data obtained from various sources have consistently indicated that "worst-case" ground-level power densities near typical cellular towers are on the order of 1 µW/cm2 or less (usually significantly less). Calculations corresponding to a "worst-case" situation (all transmitters operating simultaneously and continuously at the maximum licensed power) show that in order to be exposed to levels near limits for cellular frequencies, an individual would essentially have to remain in the main transmitting beam (at the height of the antenna) and within a few feet from the antenna.

This makes it extremely unlikely that a member of the general public could be exposed to MW levels in excess of these guidelines due to cellular base station transmitters. When cellular antennas are mounted at rooftop locations it is possible that ambient MW levels greater than 1 µW/cm2 could be present on the rooftop itself. However, exposures approaching or exceeding the safety guidelines are only likely to be encountered very close to or directly in front of the antennas. For sector-type antennas MW levels to the side and in back of these antennas are insignificant.

Even if MW levels were higher than desirable on a rooftop, appropriate restrictions could be placed on access. Factoring in the time-averaging aspects of safety standards could also be used to reduce potential exposure of workers who might have to access a rooftop for maintenance tasks or other reasons. The fact that rooftop cellular and PCS antennas usually operate at lower power levels than antennas on free-standing towers makes excessive exposure conditions on rooftops unlikely. In addition, the significant signal attenuation of a building's roof minimizes any chance for persons living or working within the building itself to be exposed to RF levels that could approach or exceed applicable safety limits. With this deduction, we have focused mainly on the radiation of the handsets while considering health effects on infertility.

4. MATERIAL AND METHOD

Isfahan is regarded to be Iran's second big city which has a vast cellular phone system. The population of infertile couples in Isfahan is rather high. Isfahan Fertility and Infertility Center (IFIC) is a place for the study of infertility and thus possible effects of microwaves used in cell phones on infertility.

This project is done as a cross-sectional research using questioners. As it was stated before, in lack of quantitative data about the exposure effects of microwave frequency band used in cellular phone system, the questioner based method will be useful to analyze situation. The questioner was designed to gather information about the usage and brand of mobile handsets and also the proximity of housing/occupation to BTSs of cellular phone network. The questioner was to get information of infertile couples that have visited the IFIC in a specific period of time. Our inclusion criteria was (1) visiting the IFIC in the interval of Sep. 2004 – Feb. 2005 (2) Owning a cellular phone.

As to omit the mixture results of Ionizing radiations and power frequencies, our exclusion criteria was (1) proximity of houses to nuclear equipments, (2) occupation in them and (3) occupation and living by power line frequencies sources, (4) power plants, (5) radio stations, and (6) Broadcast, satellite stations, so these cases were omitted of the study set. Data was gathered by interviewing and ask questions to fill the questionnaire. In this period, 209 cases who had the two inclusion criteria and did not have the exclusion criteria included in the study. Table 1 shows some inquiries made by the questioner.

The collected data was then analyzed by SPSS 11.5 and these to summarize data these types of charts used:

- ✔ Pie chart to summarize data of a nominal variable
- ✔ Histogram chart to summarize data of a scale variable

Table 1 shows the most significant inquiries made by the questioner.

Table 1. The inquiries made by the questioner

Personal Information
Name , Home address, Work address, Occupation
Date of infertility notice
Distance between Home and nearest BTS
Distance between work place and nearest BTS
Brand and model of hand set
Hours using handsets a day
Hours having the phone turned on near the body (less than one meter)
Place holding the phone when turned on (by body side)
Place holding the phone when turned on (while speaking)
How long is the phone turned on while sleeping?
How long do you speak with your phone a day
Do you use hands free? Wireless or wired?

5. Results and Findings

The measurement of duration which each case has used cell phone shows that the mean of this time is 4.05 years.

Table 2. Duration which each case has used cell

Duration which each case has used cell	N	Min	Max	Mean	Std. Dev.
Cell Phone Duration	**209**	**1**	**11**	**4.05**	**2.122**
Valid N (listwise)	**209**				

We measured the mean amount of time in which the cell phone is on and in a distance less than one meter regarding the body in each day. 77.9% of them have their cellular within this distance more than 10 hours (including near bed when sleeping).

Table 3. The mean amount of time more is than 10 hours

The mean amount of time more is than 10 hours		Frequency	Percent
Valid answer	**yes**	**163**	**77.**9
	no	**45**	22.1
Total		209	100.0

The study of cellular phones' model performed and the results below were achieved:

Table 4. Cellular phones' model

Cellular phones' model		Freq.	Valid Percent
Valid	**Samsung**	**63**	**30.1**
	Nokia	**101**	**48.3**
	Siemens	**12**	**5.7**
	Sonyericsson	**18**	**8.6**
	Panasonic	**14**	**6.7**
	LG	**1**	**0.5**
Total		209	100.0

The next Pie chart summarizes data above:

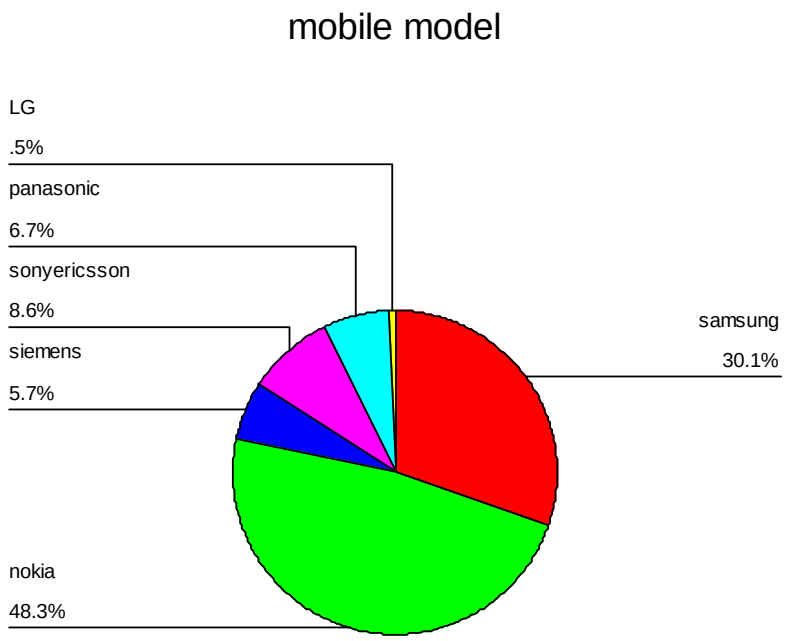

We also studied where each patient holds the cellular phone when it is on but not in use, so the results below achieved:

Table 5. Where does each patient hold the cellular phone?

Where does each patient hold the cellular phone		Frequency	Percent
Valid Answer	**Belt**	101	48.3
	Shirt pocket	43	20.6
	Slacks pocket	22	10.5
	In bag	17	8.1
	Tied from neck	26	12.4
Total		**209**	**100.0**

This Pie chart shows the latter data:

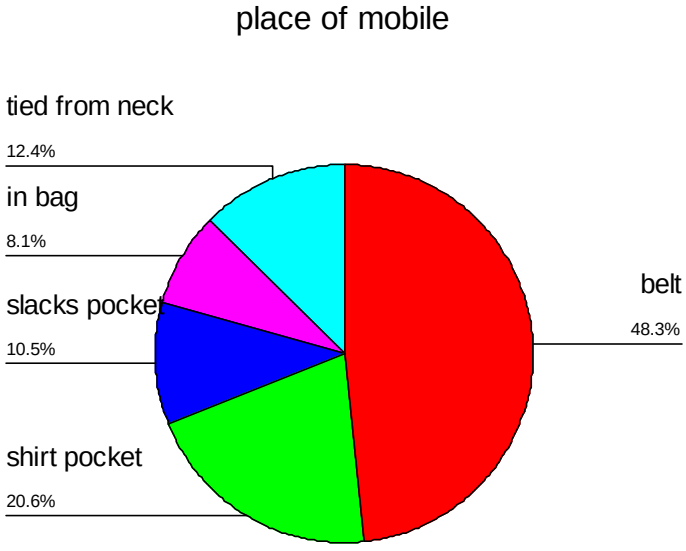

The measurement of the time which each patient calls with cellular phone each day was asked and showed that the mean of this time is 62.61 minutes/day for them. This table shows the data collected:

Table 6. The time each patient calls with cellular phone a day

The time each patient calls with cellular phone a day	N	Range	Min	Max	Mean	Std. Dev.
speech time	**209**	**100**	**10**	**110**	**62.61**	**7.093**
Valid N (listwise)	**209**					

This graph represents the number of cases which calls with cellular phone in each specific duration:

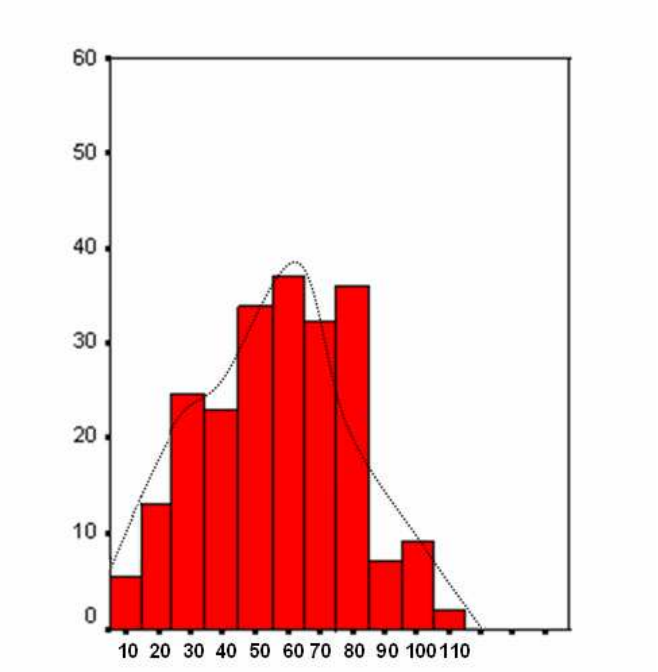

Figure 1. The number of people (vertical) regarding their speech time a day (horizontal)

The study of relation between the duration which these patients uses cellular phone and the duration of infertility shows a relation with correlation coefficient of P= 0.345 (ρ =0.037). This study performed by Bivariate Correlation and usage of Spearman coefficient[1].

---

[1] In statistics, ***Spearman's rank correlation coefficient,*** ρ (rho), is a non-parametric measure of correlation, it does not require the assumption that the relationship between the variables is linear,

In principle, ρ is simply a special case of the Pearson product-moment coefficient in which the data are converted to ranks before calculating the coefficient. In practice, however, a simpler procedure is normally used to calculate ρ. The raw scores are converted to ranks, and the differences *D* between the ranks of each observation on the two variables are calculated. ρ is then given by:

$$\rho = 1 - \frac{6 \sum D^2}{N(N^2 - 1)}$$

where:

D = the difference between the ranks of corresponding values of *X* and *Y*, and
N = the number of pairs of values.

The study of duration of infertility and distance between job/living place and the distance to the closest electric communication antenna shows a relation with correlation coefficient of P=0.0261 (ρ =0.0046). which shows weak correlation between the two variable. This study performed by Bivariate Correlation and usage of Spearman coefficient.

6. CONCLUSION

In this research, we investigated the possible effect of cellular phone system radiations on infertility. The result of our studies shows possible influences of cell phone handsets on the cases that have been sampled. The study shows that these variables have correlation with infertility:

5. duration which these patients use cellular phone for speech
   So that the increase of usage of mobile phone from 10 to 60 minutes a day yields to an increase of infertile couples
6. place of holding cellular phone regarding body
   48.3% of the cased hold their headsets on their belts
7. model of cellular phone
   48.3% of the cased used Nokia brand
8. Proximity of the handset regarding body
   77.9 of the cases had their handsets on and near the body more than 10 hours in 24 hours.

The study of relation between the duration which these patients uses cellular phone and the duration of infertility shows a relation with correlation coefficient of P = 0.345 (ρ =0.037) which shows a slight linear correlation.

The study of duration of infertility and distance between job/living place and the distance to the closest electric communication antenna shows a relation with correlation coefficient of P = 0.0261 (ρ =0.0046) which shows little correspondence between the two variables so the parameter: Distance between living/job place and the closest electric communication antenna, did not show any meaningful relationship with the infertility date, as was presumed by the discussion presented in section 2.

7. ACKNOWLEDGEMENT

The Authors wish to thank Dr. M. Ahmadi, member of IFIC, for his kindest cooperation in the research. They are also grateful of Mr. E and F. Ahmadi for spreading and gathering up the questioners.

8. REFERENCES

1. Savitz DA et al. Magnetic field exposure in relation to leukemia and brain cancer mortality and electric utility workers. *American Journal of Epidemiology*. 1995; 141: 1-12.
2. Theriault G et al. Cancer risk associated with occupational exposure to magnetic fields among utility workers in Ontario and Quebec, Canada and France. *American Journal of Epidemiology*. 1994; 139: 550-572.
3. National Institute of Environmental Health Sciences. Health effects from exposure to power-line frequency electric and magnetic fields. *NIEH Final Report of Congress.* 1998.
4.
a) Coleman Metal. Leukaemia and residence near electricity transmission equipment: A case-control study. *British Journal of Cancer*. 1989; 60:793-98.
b) London SJ et al. Exposure to residential electric and magnetic fields and risk of childhood leukemia. *American Journal of Epidemiology*. 1991; 134:923-37.
c) Feychting M. et al. Magnetic fields and cancer in children residing near Swedish high-voltage power lines. *American Journal of Epidemiology*. 1993; 138:467-81.

5. Sahl JD et al. Cohort and nested case-control studies of hematopoietic cancers and brain cancer among electric utility workers. *Epidemiology*. 1993; 4: 104-114.
6. National Institute of Environmental Health Sciences. Assessment of health effects from exposure to power-line frequency electric and magnetic fields. *NIEH Working Group Report.* 1998.
7. U.S. Federal Communications Commission (FCC), Guidelines for Evaluating the Environmental Effects of Radiofrequency Radiation, *Report and Order*, ET Docket 93-62, FCC 96-326, adopted August 1, 1996, 61 Federal Register 41006 (1996).

8. U.S. Federal Communications Commission (FCC), Guidelines for Evaluating the Environmental Effects of Radiofrequency Radiation, *Second Memorandum Opinion and Order and Notice of Proposed Rule Making*, ET Docket 93-62 (WT Docket 97-192), FCC 97- 303, adopted August 25, 1997, 62 Federal Register 47,960, 49,557 and 61,447 (1997).
9. Klauenberg, B.J., Grandolfo, M. and D.N. Erwin (eds.), *Radiofrequency Radiation Standards, Biological Effects, Dosimetry, Epidemiology and Public Health Policy*. NATO ASI Series A: Life Sciences, Plenum Press (1994).

10. List of web sited where one can gather more information

American National Standards Institute: www.ansi.org
Bioelectromagnetics Society: www.bioelectromagnetics.org
European Bioelectromagnetics Association: www.ebea.org
Electromagnetic Energy Association: www.elecenergy.com
US Federal Communications Commission: www.fcc.gov/oet/rfsafety
ICNIRP (Europe): www.icnirp.de
IEEE Committee on Man & Radiation: www.seas.upenn.edu/~kfoster/comar.htm
International Microwave Power Institute: www.impi.org
Microwave News: www.microwavenews.com
US National Council on Radiation Protection & Measurements: www.ncrp.com
US OSHA: www.osha-slc.gov/SLTC
Wireless Industry (CTIA): www.wow-com.com
Wireless Industry (PCIA): www.pcia.com
World Health Organization EMF Project: www.who.ch/peh-emf

IN VIVO EFFECTS OF ELF MAGNETIC FIELDS ON ANTIOXIDANT DEFENSE SYSTEM IN KIDNEY

AYSE G. CANSEVEN[*], SULE COSKUN[**], NESRIN SEYHAN[*]

[*] DEPARTMENT OF BIOPHYSICS, GAZI UNIVERSITY, FACULTY OF MEDICINE, 06510 BESEVLER ANKARA, TURKEY
[**] DEPARTMENT OF BIOLOGY, GAZI UNIVERSITY, FACULTY OF ART AND SCIENCE, 06500 TEKNIKOKULLAR ANKARA, TURKEY
canseven@gazi.edu.tr

Abstract

Electromagnetic Fields (EMF) can affect biological systems by increasing the amount of free oxygen radicals. Antioxidants are able to reduce the effects of free radicals formed in body. Glutathione (GSH) is one of the important antioxidants in body defense system for free radical. In this study, we examined the effects of 50 Hz magnetic fields on GSH level in kidney. A total of 56 male guinea pigs were used. Forty-nine guinea pigs were exposed to 50 Hz, 1 mT, 2 mT and 3 mT fields with the exposure periods of 4 and 8 hours/day for 5 days. Seven subjects were handled in an identical manner with the exposed animals in the same laboratory. They were used as control without being exposed to any magnetic fields. The GSH levels were determined spectrophotometrically by modified Aykaç et al. method. Increased GSH levels were found in kidneys of guinea pigs exposed to 1 mT magnetic field for the exposure periods of 4 hours. For the magnetic fields of 2 mT and 3 mT applied with the period of 8 hours, increased levels of GSH were also found. It seems that ELF magnetic fields promote the levels of GSH which has a protective role against the oxidative damage.

Deleted: it was

Deleted: w

Introduction

Exposure of human bodies to extremely low frequency electromagnetic fields (ELF EMF) have been increased by growing use of electrical devices, which emit EMF. It has been showed that EMF influence enzymatic activity in biological systems (Noda, 2000). Several studies on effects of EMF have shown that EMF can induce cell proliferation, variations of calcium concentrations, alteration of DNA integrity, changes in transcription of immediate early genes and protein synthesis (Boland, 2002; Ishisaka, 2000; Gold, 1994; Kenneth, 1987; Guler, 1996a; Guler, 1996b; Guler, 1999; Seyhan, 2006; Canseven, 1996; Canseven, 1999, Canseven, 2005a; Canseven 2005b; Liboff, 1987; Liburdy, 1993) and perturbations of central nervous system (Ilhan, 2004; Jelenkovic, 2006; Jin, 1998; Lai, 1996; Lai, 2004). It is known that ELF magnetic fields (MFs) may cause an increase in free radicals activity in living organisms (Boland, 2002; Kula, 2002; Kula, 2000; Roy, 1995; Khadir, 1999; Simko, 2001; Seyhan, 2006; Guler, 2006). Free radicals are very reactive and unstable molecules that can initiate chain reactions to form new free radicals. Antioxidants are able to reduce the effects of free radicals formed in body. Cells are also equipped with the enzymatic antioxidant mechanisms that play an important role in the elimination of free radicals (Gorenek, 2006; Guler 2006; Ozgur, 2006; Seyhan, 2006) Glutathione (GSH), the most abundant non-enzymatic antioxidant present in the cell, plays an important role in the defense against oxidative-stress-induced cell injury.

Deleted: has

Deleted: been

Deleted: molecular species

It has been showed that exposures of magnetic fields with various frequency and intensity can change the antioxidant activity of human and animal bodies (Harakawa, 2005; Kashalda, 1995; Fiorani, 1997; Ozguner, 2005; Canseven et al., 2005c).

This study was designed to find the effects of exposure to 1 mT, 2 mT and 3 mT of 50 Hz magnetic fields on GSH levels in kidneys of guinea pigs in various exposure periods.

Materials and Methods

Animals

The experimental protocol was reviewed and approved by the Laboratory Animal Care Committee of Gazi University (Report no: 36-7838). A total of 56 male, 250-300 g weighted guinea pigs were used in this experiment. All animals were kept under laboratory conditions and fed standard pellet food.

Magnetic Field Exposure

The system used to generate the magnetic fields was Helmholtz coils' system which was specially designed by Bioelectromagnetic Laboratory at Biophysics Department of Medical Faculty of Gazi University (Canseven, 2005d). This system consisted of two parallel horizontal flat circular coils of 42.75 cm diameter, with a common axis, and separated by 21.375 cm. Each coil has 154 turns and was constructed by insulated copper wire. Sinusoidal current of frequency 50 Hz was generated by the specially designed variable transformer, 2.7 kVA in power. The intensity of MF was modulated by the transformer. The magnetic field generated by the coils is classified as vertical field since the field lines perpendicular to the bottom plane of the animal's cage.

Forty nine guinea pigs were housed in the centre of the Helmholtz coils, 2 per plexiglas cage and were exposed to 50 Hz, 1 mT, 2 mT and 3 mT fields with the exposure period of 4 hours/day or 8 hours/day over 5 days. Seven subjects were handled in an identical manner without being exposed to any magnetic field and studied as controls.

The temperature of laboratory was held constant at 23° C with day and night cycle of 12 hours and ambient geomagnetic field of 30 μT. To eliminate possible variations due to circadian rhythm, the exposure periods of magnetic fields were chosen as 8:00 - 12:00 a.m for 4 hours of exposure periods and 8:00 a.m - 4:00 p.m for 8 hours of exposure periods.

Following 12 h of starvation, guinea pigs were injected intramuscularly with ketamine (30 mg/kg) and xylazine (2 mg/kg) and 250 IU/kg heparin. Kidneys were sampled immediately. They shocked by liquid nitrogen and stored in deep freezer at -80°C until performing analysis.

Determination of GSH levels

The GSH levels were determined by modified Aykaç et al. (Aykac, 1985) method. Tissues were homogenized in nine volumes of cold 10% TCA solution and the homogenate was centrifuged for 15 min. at 3000xg at 4°C. The supernatants were transferred to glass test tubes.0.5 ml of supernatant was added to the 2 ml of 0.3 M $Na_2HPO_4.2H_2O$ solution.a 0.2 ml solution of dithiobisnitrobenzoate (0.4 mg/ml 1% sodium citrate)was added and absorbance at 412 nm was measured immediately after mixing.The GSH levels were calculated using an extiction coefficient of 13.600 $mol^{-1}cm^{-1}$.

All experiments were run in a blind manner.

Statistics

Statistical analyses were carried out using SPSS software (SPSS 11.5 for windows, SPSS Inc., Chicago, USA).

The p value was considered significant at $p<0.05$.

Mann Whitney-U and Kruskal-Wallis tests were used in statistical analysis. Comparisons between exposed groups and controls were made by using Mann Whitney-U test while magnetic fields of 1mT, 2 mT and 3 mT were compared with Kruskal-Wallis test with respect to exposure periods of 4 hours and 8 hours.

Results

In this study, GSH levels were measured in kidney of guinea pigs, which were exposed to magnetic fields of 1 mT, 2 mT and 3 mT fields with the exposure periods of 4 and 8 hours/day for 5 days. For both of the exposure periods, GSH levels were found increased with respect to controls in kidney of guinea pigs exposed to the 50 Hz magnetic fields of 1 mT, 2 mT and 3 mT, except 1 mT, 8 hours. The increases in GSH levels were found statistically significant for 1 mT , 4 hours ($p=0.000$), 2 mT, 8 hours ($p=0.000$) and 3 mT, 8 hours ($p=0.021$) in kidneys by Mann-Whitney U test.

Field intensities were compared with respect to exposure periods by Kruskal-Wallis test. Significant differences were determined between field intensities of 1 mT, 2 mT and 3 mT in kidney tissues for both of the exposure periods ($p=0.001$ and $p=0.000$ for 4 hours and 8 hours respectively).

Discussion

Glutathione is a major non protein thiol in living organisms.It plays a crucial role in coordinating the body's antioxidant defense process. Several studies have reported the effects of 50 Hz magnetic fields on antioxidant defense system activity or GSH levels (Kashkalda, 1995; Harakawa, 2005; Fiorani, 1997; Canseven, 2005d). Fiorani et al. reported that the fields are able to potentiate the cellular damage induced in vitro by oxiding agents (Fiorani, 1997).

Table 1 . GSH (micromole/g tissue) levels in kidney tissues of 1 mT, 2 mT and 3 mT exposed and control guinea pigs. Exposure periods were 4 hours/day and 8 hours/day for 5 days.

GROUPS	n	GSH Level (micromol/g tissue) mean ± sem
Control	7	3.09±0.48
1 mT; 4 hours	8	6.44±0.42
1 mT; 8 hours	10	2.43±0.17
2 mT, 4 hours	6	3.40±0.32
2 mT, 8 hours	8	5.93±0.33
3 mT; 4 hours	9	4.63±0.41
3 mT; 8 hours	8	5.16±0.50

To evaluate the effects of magnetic fields on antioxidant defense system, GSH levels were measured on guinea pigs exposed to magnetic fields of 1 mT, 2 mT and 3 mT fields with the exposure periods of 4 hours/day and 8 hours/day for 5 days, in this study. Our data clearly showed that GSH levels increase with respect to controls under the lowest magnetic field intensity with the relatively short exposure period, i.e. 4 hours.
Although statistically significant increased GSH levels were found for the magnetic fields of 1 mT for 4 hours, 2mT and 3 mT for 8 hours in tissues, no matter what the exposure period was, kidney GSH level started to increase at and after 2 mT exposures.
Antioxidants are able to reduce the effects of free radicals formed in body. Our results indicate that chronic exposure to various ELF magnetic fields increase GSH levels, which are free radical scavengers in kidney.

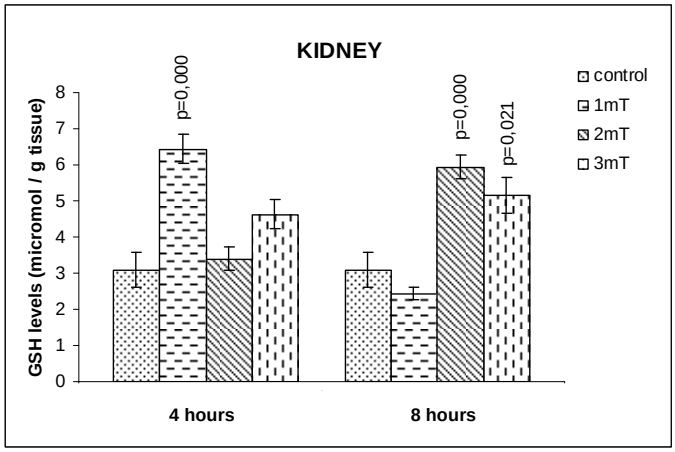

Figure 1. GSH levels in kidneys under effects of 50 Hz magnetic fields of 1 mT, 2 mT and 3 mT with the exposure periods of 4 hours and 8 hours.

References

Aykac G, Uysal M, Yalcin AS, Kocak-Toker N, Sivas A, Oz H. (1985). The effect of chronic ethanol ingestion on hepatic lipid peroxide, glutathione, glutathione peroxidase and glutathione transferase in rats. *Toxicology* 36: 71-76.

Canseven A.G., Seyhan N., Aydin, A., Cevik, C., Isimer, A. (2005a). Effects of Ambient ELF Magnetic Fields: Variations in Electrolytes Levels of Brain and Blood Plasma, Gazi Medical Journal, 16: 121 – 127.

Canseven, A.G., Atalay Seyhan, N. (1996). Is It Possible to Trigger the Collagen Synthesis by Electric Current in Skin Wounds?, *Indian J Biochem Biophys* 33, 223-227.

Canseven, A.G., Coskun S., Seyhan, N. (2005c): Magnetic fields have an effect on antioxidant defense system in heart tissue IFMBE Proceedings, Vol. 11. Prague: IFMBE, 2005. ISSN 1727-1983.Editors: Jiri Hozman, Peter Kneppo (Proceedings of the 3rd European Medical & Biological Engineering Conference - EMBEC´05. Prague, Czech Republic, 20-25.11.2005). pp: 2226-2228

Canseven, A.G., Coskun S., Seyhan, N. (2005e): Magnetic fields have an effect on antioxidant defense system in heart tissue IFMBE Proceedings, Vol. 11. Prague: IFMBE, 2005. ISSN 1727-1983.Editors: Jiri Hozman, Peter Kneppo (Proceedings of the 3rd European Medical & Biological Engineering Conference - EMBEC´05. Prague, Czech Republic, 20-25.11.2005). pp: 2226-2228

Canseven, A.G., Seyhan, N. (2005b). Effects of Ambient ELF Magnetic Fields: Variations In Collagen Synthesis of Guinea Pigs' Skin and Scaling From Animals To Human. *Gazi Medical Journal* 16 : 160 – 165 *(Turkish)*.

Canseven, A.G., Seyhan, N. (2005d). Design, installation and standardization of homogenous magnetic field systems for experimental animals IFMBE Proceedings, Vol. 11. Prague: IFMBE, 2005. ISSN 1727-1983. Editors: Jiri Hozman, Peter Kneppo (Proceedings of the 3rd European Medical&Biological Engineering Conference - EMBEC´05.Prague, Czech Republic, 20- 25.11.2005). pp: 2333-2338

Canseven, A.G., Seyhan, N., et al. (1999). Extremely Low Frequency Electromagnetic Field Effect on Brain Tissue and Blood Plasma Electrolytes, *Med & Biol Eng & Comput*., 37 (Suppl. 2): 1336-1337.

Fiorani, M., Biagiarelli, B., Vetrano, F., Guidi, G., Dacha, M., Stocchi, V. (1997). In vitro effects of 50 Hz Magnetic fields on oxidatively damaged rabbit red blood cells. *Bioelectromagnetics.* 18: 125-131.

Gold, S., Goodman, R., Henderson, A.S. (1994). Exposure of Simian Virus-40-Transformed Human Cells to Magnetic Fields Results in Increased Levels of T-Antigen mRNA and Protein. *Bioelectromagnetics.* 15 **:** 329-336.

Gorenek L., Acar A., Aydin A., Eyigun C. P., Cetinkaya A., Eken A., Sayal A. (2006). Oxidative stress and antioxidant defense in patients with chronic hepatitis C patients before and after pegylated interferon alfa-2b plus ribavirin Therapy. J Transl Med. Jun 20;4 (1) : 25.

Guler, G., Atalay Seyhan, N. (1996a). Changes in Hydroxyproline Levels in Electric Field Tissue Interaction. *Indian Journal Of Biochemistry and Biophysics* 33: 531-533.

Guler, G., Atalay Seyhan, N., Özoğul, C., Erdoğan, D. (1996b). Biochemical and Structural Approach to Collagen Synthesis Under Electric Fields. *Gen. Physiol. Biophys* 15: 429-440.

Guler, G., Atalay Seyhan, N. (1999). Extremely Low Frequency (ELF) Electric Field with Different Application Times Inhibits Protein Synthesis. *Med & Biol Eng & Comput* 37, (Suppl. 2) : 1338-1339.

Guler, G., Seyhan, N., Arıcıoglu, A. (2006). Effects of Static and 50 Hz Alternating Electric Fields on Superoxide Dismutase Activity and TBARS Levels in Guinea Pigs. *Gen. Physiol. Biophys* 25: 177-193.

Harakawa, S., Inoue, N., Hori, T., Tochio, K., Kariya, T., Takahashi, K., Doge, F., Suzuki, H., Nagasawa, H. (2005). Effects of 50 Hz electric field on plasma lipid peroxide level and antioxidant activity in rats. *Bioelectromagnetics.* 26: 589-594.

Ilhan, A., Gurel, A., Armutcu, F., Kamisli, S., Iraz, M., Akyol, O., Ozen, S. (2004). Ginkgo biloba prevents mobile phone-induced oxidative stress in rat brain. *Clin Chim Acta.* 340: 153-162.

Jelenkovic, A., Janac, B., Pesic, V., Jovanovic, D.M., Vasiljevic, I., Prolic, Z. (2006). Effects of extremely low-frequency magnetic field in the brain of rats. *Brain Research Bulletin*. 68: 355-360.

Jin, Y., Wang, H., Cheng, Y., Gu, H. (1998). Effects of static magnetic fields on free radical metabolism of human body. *Wei Sheng Yan Jiu*. 27: 97-99.

Kashkalda, D.A., Pashenko, E.A, Ziubanova, L.F. (1995). Effects of an impulse magnetic field on lipid peroxidation and the antioxidant system of the testes in animal experiments. *Med Tr Prom Ekol*. 10: 14-17.

Kenneth, J.M., Lee, R.C., Ehrlich, H.P. (1987). Frequency Dependence of Electric Field Modulation of Fibroblasts Protein Synthesis. *Science* 236 : 1465-1469.

Khadir, R., Morgan, J.L., Murray, J.J. (1999). Effects of 60 Hz magnetic field exposure on polymorphonuclear leukocyte activation, *Biochim Biophys Acta*, **1472** : 359-367.

Kula, B., Sobczak, A., Kuska, R. (2000). Effects of static and ELF magnetic fields on free- radical processes in rat liver and kidney, *Electro and Magnetobiology*, **19** : 99-105.

Kula, B., Sobczak, A., Kuska, R. (2002). Effects of electromagnetic field on free radical processes in steelworkers. Part I. Magnetic field influence on the antioxidant activity in red blood cells and plasma, *J. Occup Health*, **44** : 226-229.

Lai, H., Singh, N.P. (2004). Magnetic field-induced DNA strand breaks in brain cells of the rat, *Environmental Health perspectives*, **112** : 687-694 .

Liboff, A.R., Smith, S.D., Mc Leod, B.R. (1987). Experimental Evidence for Ion Cyclotron Resonance Mediation of Membrane Transport. In Blank, M., Findl, E., eds. *Mechanistic Approaches to Interactions of Electric and Electromagnetic Fields with Living Systems*. New York: Plenum Press; pp. 109-132.

Liburdy, R.P., Yost, M.G. (1993). Time Varying and Static Magnetic Fields Act in Combination to Alter Calcium Signal Transduction in the Lymphocyte. In Blank, M., ed. *Electricity and Magnetism in Biology and Medicine*. USA: San Francisco Press, Inc.; pp. 331-334.

Ozguner, F., Oktem, F., Ayata, A., Koyu, A., Yilmaz, H.R. (2005). A novel antioxidant agent caffeic acid phenethyl ester prevents long-term mobile phone exposure-induced renal impairment in rat. Prognostic value of malondialdehyde, N-acetyl-beta-D-glucosaminidase and nitric oxide determination. *Mol Cell Biochem*. 277: 73-80.

Ozgur, E., Guler, G., Seyhan, N. Effects Of Electromagnetıc Fıeld From Power Lines on the Oxidant and Antioxidant Levels in Guine pigs. *International Conference and COST 281 Workshop on Emerging EMF Technologies, Potential Sensitive Groups and Health*, April 20-21, 2006, Graz, Austria

Roy, S., Noda, Y., Eckert, V., Traber, M.G., Mori, A., Liburdy, R., Packer, L. (1995). The phorbol 12-myristate 13-acetate (PMA)-induced oxidative burst in rat peritoneal neutrophils is increased by a 0.1 mT (60 Hz) magnetic field, *FEBS Letters*, **376** : 164-166.

Seyhan N., Canseven A. G., Güler G. (2006). Animal Studies on the Effects of ELF and Static EMF. In Ayrapetyan S.N., Markov M.S., eds. *Bioelectromagnetics Current Concepts, The Mechanisms of the Biological Effect of Extremely High Power Pulses* . NATO Security through Science Series B: Physics and Biophysics, Vol. 5, pp: 195-212.

Simko, M., Droste, M., Kriehuber, R., Weiss D.G. (2001). Stimulation of phagocytosis and free radical production in murine macrophages by 50 Hz electromagnetic fields., *Eur J Cell Biol*, **80** : 562-566.

EFFECT OF INTERMITTENT AND CONTINUOUS EXPOSURE TO 50 Hz, 1.5 mT ON LIPID PEROXIDATION IN LIVER

AYSE G. CANSEVEN*, ARIN TOMRUK*, SULE COSKUN**, NESRIN SEYHAN*

**** DEPARTMENT OF BIOPHYSICS, GAZI UNIVERSITY, FACULTY OF MEDICINE, 06510 BESEVLER ANKARA, TURKEY***

*****DEPARTMENT OF BIOLOGY, GAZI UNIVERSITY, FACULTY OF ART AND SCIENCE, 06500 TEKNIKOKULLAR ANKARA, TURKEY***

canseven@gazi.edu.tr

Abstract

We investigated the effects of continuous and intermittent exposure to extremely low frequency (ELF) electromagnetic fields (EMF) on thiobarbituric acid reactive substances (TBARS) in liver. A total of 18 male, ten-twelve-weeks-old guinea pigs were used. Homogeneous magnetic fields were generated from a specially designed Helmholtz coil system. The subjects were divided into one control and two exposure groups which were exposed continuously (4 hours/day) or intermittently (2 hours on/ 2 hours off / 2 hours on) to 50 Hz magnetic field of 1.5 mT for 4 days. TBARS levels were determined by spectrophotometric method. Mann Whitney-U test was applied for statistical analysis. Increased TBARS levels were found in liver tissues for both of the continuous and intermittent exposures of 1.5 mT. These increases were found to be statistically significant ($p<0.05$). In conclusion, both types of the exposure to ELF electromagnetic fields (continuous or intermittent) could play a role in lipid peroxidation process.

Introduction

Although the development of technology provides people various facility, each of advanced technological devices are electromagnetic fields (EMF) sources. People are exposed to EMF seriously by wide usage of these devices. Most scientists have thought that EMF have adverse effects on people health. Several studies have been conducted on the effects of EMF as epidemiological and laboratory studies. It has been suggested that there is a link between ELF magnetic field exposure and the increased incidence of certain types of tumor, particularly in leukemia and brain cancer (Kheifets, 1995, 1997, 2004; Lin, 1985; Preston-Martin, 1989; Bastuji-Garin, 1990; Feychting, 1993; Wertheimer, 1979,1995; Hakansson, 2002; Savitz, 1988). Eextremely low frequency (ELF) electric and magnetic field exposure have recently been classified as a possible carcinogen class 3 and 2B respectively (NIEHS, 1998; IARC 2002). Electromagnetic field effects on protein synthesis (Canseven, 2005a; Guler, 1995) gene expression, signal transduction (Liburdy, 1992,1993), DNA damage (Lai, 2004; Jajte, 2001,2002), immune system functions (Canseven, 2006), apoptosis induction (Blumenthal, 1997), enzyme regulation (Canseven, 2003a,2003b,2004,2005b; Brocklehust, 1996; Khadir, 1999), free radical activity (Guler, 2004; Kula, 2000) have been investigated and reported in vivo and/or in vitro experiments. Studies conducted on free radical activities show that EMF Magnetic fields increase the activation of free radicals in tissues (Boland, 2002). The amounts and the activities of free radicals are important for tissue metabolism. Because free radicals are very reactive and unstable molecular species, they can initiate chain reactions to form new free radicals. Increased free radical activity in cellular levels can cause increase in lipid peroxidation which is known as a major factor in formation of the oxidative stress.

To answer the question “Can intermittent or continuous exposures to extremely low frequency magnetic field increase lipid peroxidation in liver?”, we examined the effect of continous or intermittently exposure of 1.5 mT magnetic field in this study. Guinea pigs were exposed to continuous and intermittent magnetic fields with the period of 4 hours/day for 4 days and lipid peroxidation was determined by measuring levels of TBARS in liver.

Materials and Methods

EMF System and Exposure

The experimental protocol was reviewed and approved by the Laboratory Animal Care Committee of Gazi University (Report no : 39-5858). A total of 18 male guinea pigs weighting between 250 and 300g were used in this study. All animals were kept under laboratory conditions and fed standard pellet food.

50 Hz magnetic field was produced by 42.75 cm diameter Helmholtz coil with winding embedded in an open wooden circular frame (Canseven, 2005c). Each coil was constructed by insulated copper wire with 154 turns. Sinusoidal current of frequency 50 Hz was supplied by a specially designed variable transformer (2.7 kilo Volt Amper-kVA) in power to feed the coils. A Hall-Effect Gaussmeter measured the magnetic field at the center of exposure system. Frequency and wave form of the magnetic field was monitored over an ossiloscope.The plexiglas animal cage was put at the center.

Animals were divided into three groups, controls and two magnetic field exposure groups. Exposure groups were exposed to continuously (4 hours/day) or intermittently (2 hours on/ 2 hours off/ 2 hours on) to 50 Hz MF of 1.5 mT with the exposure periods of for 4 days. Controls were handled in an identical manner without being exposed to any magnetic field.

Following 12 h of starvation, guinea pigs were injected intramuscularly with ketamine (30 mg/kg) and xylazine (2 mg/kg) combined with 250 IU/kg heparin. The liver was sampled immediately. They shocked by liquid nitrogen and stored in deep freezer at -80°C until performing analysis.

Determination of Lipid Peroxidation

Lipid peroxidation was quantified by measuring the formation of thiobarbituric acid reactive substances (TBARS). TBARS level of liver tissues was determined according to the Cassini et al.'s spectrophotometric method (Cassini, 1986). Tissues were homogenized in nine volumes of cold 10 % TCA solution and the homogenate was centrifuged for 15 min. At 3000xg at 4°C. The supernatants were transferred to glass test tubes containing 0.375 % (w/v) thiobarbituric acid and 0.02 % (w/v) butylated hydroxytoluene to prevent further peroxidation of lipids during subsequent steps. The samples were then heated for 15 min at 100°C in a boiling water bath, cooled and centrifuged to remove precipitant. The absorbance of each sample was determined at 532 nm. All experiments were run in a blind manner.

Statistics

Statistical analyses were carried out using SPSS software (SPSS 11.5 for windows, SPSS Inc., Chicago, USA). The p value was considered significant at $p<0.05$. Both comparisons between exposed groups and controls, and comparisons between intermittent and continuous exposed groups were made by using Mann Whitney-U test.

Results

In this study, TBARS level was investigated in liver tissues of guinea pigs which were continuously or intermittently exposed to 50 Hz magnetic field of 1.5 mT with the daily exposure of 4 hours for 4 days. Compared with the control TBARS levels were found significantly increased both continuous (p=0,009) and intermittent (p=0.016) exposures in liver tissues (Table1-Fig 1). Continuous and intermittent exposures were compared and found that there was no any statistical difference between them (p=0.093).

Table 1. Levels of TBARS (nmol/gr) in livers under 50 Hz magnetic field of 1.5 mT

GROUPS	n	TBARS (nmol/g tissue) mean ± sem
Control	6	79,32±3,65
Continuous Exposure	6	90,81±1,16
Intermittent Exposure	6	94,98±2,79

Discussion

Levels of TBARS were measured in livers to determine the lipid peroxidation which is one of the major factor in formation of oxidative stress.
We found significantly increased liver TBARS levels of guinea pigs which were exposed to 1.5 mT continuous (4 hours/day) and intermittent (2 hours on/ 2 hours off/ 2 hours on) exposures for 4 days compared with the control groups. This was in agrement with our previous studies in MDA (Coskun, 2006). We found statistically significant increases in liver MDA levels under the magnetic fields of 1mT (p=0.023) and 2 mT (p=0,027) with 4 hours of daily continuous exposure for 5 days These data reveal that increase of MDA levels as an indicator of lipid peroxidation may give rise to formation of oxidative stress in tissues.

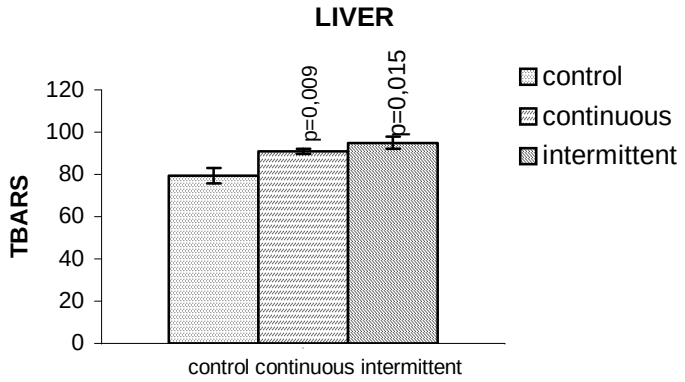

Figure 1. TBARS (nmol/g tissue) levels in liver of 1.5 mT exposed and control guinea pigs. Exposure was continous or intermittent for 4 days.

References

BASTUJI-GARİN S., RICHARDSON S., ZITTOUN R. (1990). Acute leukaemia in workers exposed to electromagnetic fields., *Eur. J. Cancer*., 26 : 1119-1120.

BOLAND A., DELAPIERRE D., MOSSAY D., DRESSE A., SEUTIN V. (2002). Effect of Intermittent and Contiuous Exposure to Electromagnetic Fields on Cultered Hippocampal Cells, Bioelectromagnetics, 23 : 97-105.

BROCKLEHURST B., MCLAUCHLAN KA. (1996). Free radical mechanism for the effects of environmental electromagnetic fields on biological systems., *Int. J. Radiat. Biol*., 69 : 3-24.

CANSEVEN, A.G., SEYHAN, N. (2005c). Design, installation and standardization of homogenous magnetic field systems for experimental animals IFMBE Proceedings, Vol. 11. Prague: IFMBE, 2005. ISSN 1727-1983. Editors: Jiri Hozman, Peter Kneppo (Proceedings of the 3rd European Medical&Biological Engineering Conference - EMBEC´05.Prague, Czech Republic, 20- 25.11.2005). pp: 2333-2338

CANSEVEN, A.G., OZEL U., BILGIHAN, A., SEYHAN, N. (2005b). Effects of environmental ELF magnetic fields on myeloperoxidase (MPO) activity. IFMBE Proceedings, Vol. 11. Prague: IFMBE, 2005. ISSN 1727-1983. Editors: Jiri Hozman, Peter Kneppo (Proceedings of the 3rd European Medical&Biological Engineering Conference - EMBEC´05. Prague, Czech Republic,20-25.11.2005). 2232-2236

CANSEVEN A. G., OZEL U., BILGIHAN A., SEYHAN N. (2004). Does ELF Magnetic Field Effect The Myeloperoxidase (MPO) Activity in the Lung., 11th International Congress of the International Radiation Protection Association, 23-28 May 2004, Madrid, Spain, ID 591

CANSEVEN, A.G., SEYHAN, N. (2005a). Effects of Ambient ELF Magnetic Fields: Variations In Collagen Synthesis of Guinea Pigs' Skin and Scaling From Animals To Human. *Gazi Medical Journal* 16 : 160 – 165 *(Turkish).*

CANSEVEN A. G., OZEL U., BILGIHAN A., SEYHAN N. (2003a). Myeloperoxidase (MPO) Activities in Brain, Lung and Renal Tissues After Exposure to Magnetic Fields of 50 Hz., 13th Balkan Biochemical Biophysical Days & Meeting on Metabolic Disorders, 12-15 October 2003, Kusadasi, TURKEY, P94

CANSEVEN A. G., OZEL U., BILGIHAN A., SEYHAN N. (2003a). The Effect of ELF Magnetic Field Exposure on Kidney Myeloperoxidase (MPO) Activity., 13th Balkan Biochemical Biophysical Days & Meeting on Metabolic Disorders, 12-15 October 2003, Kusadasi, TURKEY, 2003, P96

CANSEVEN, A.G., SEYHAN, N., MIRSHAHIDI, S., IMIR, T. (2006). Suppression of Natural Killer Cell Activity on *Candida Stellatoidea* by a 50 Hz Magnetic Field. *Electromagnetic Biology and Medicine,* 25 (2) : 79-85.

CASSINI A., F M, POMPELAM A, MAELLARO A, COMBORTI M. (1986). Lipid peroxidation and cellular damage in extrahepatic tissues of bromobenzene intoxicated mice., *Am J Pathol*; **123** : 520-31.

COSKUN, S., SEYHAN, N., CANSEVEN, A.G. (2006). Alterations induced in the lipid peroxidation levels of heart and liver tissues with ELF Magnetic Fields. International Conference and COST 281 Workshop on Emerging EMF Technologies, Potential Sensitive Groups and Health Graz, April 20/21.

FEYCHTING M., AHLBOM A. (1993). Magnetic fields and cancer in children residing near Swedish high-voltage power lines., *Am. J. Epidemiol*., 138 : 467-481.

GULER G., ATALAY SEYHAN N. (1995).The Interaction of Electric Field with Biological Systems I: Liver Hydroxyproline, *Gazi Medical Journal*, 6, 125-129.

GULER G., SEYHAN N., ARICIOGLU A. (2004). Effects of Electric Fields on Radical and Antioxidant Enzymes Levels in Spleen and Testis of Guinea Pigs, *Gazi Medical Journal* , 2, pp: 99-104.

HAKANSSON N., FLODERUS B., GUSTAVSSONB P., JOHANSEN C., OLSEN JH. (2002). Cancer incidence and magnetic field exposure in industries using resistance welding in welding in Sweden., *Occup. Environ. Med*., 59, pp: 481-486.

JAJTE J., ZMYSLONY M., PALUS J., DZIUBALTOWSKA, E., RAJKOWSKA, E. (2001). Protective effect of melatonin against in vitro iron ions and 7 mT 50 Hz magnetic field-induced DNA damage in rat lymphocytes., *Mutation Research*, 483, pp: 57-64.

JAJTE, J., GRZEGORCZYK J., ZMYSLONY, M., RAJKOWSKA (2002). Effect of 7 mT static magnetic field and iron ions on rat lymphocytes: apoptosis, necrosis and free radical processes., *Bioelectrochemistry*, 57, pp: 107-111.

KHADIR R., MORGAN JL., MURRAY JJ. (1999). Effects of 60 Hz magnetic field exposure on polymorphonuclear leukocyte activation., *Biochim Biophys Acta*, 1472, pp: 359-367.

KHEIFETS L. (2004). Childhood Leukemia and EMF, WHO EMF Project, Sensitivity of Children to EMF Exposure Workshop Proceedings, Istanbul.

KHEIFETS LI., AFIFI AA., BUFFLER PA., ZHANG ZW., MATKIN CC. (1997). Occupational electric and magnetic field exposure and leukemia. A meta-analysis., *J. Occup. Environ. Med*., 39, pp: 1074-1191.

KHEIFETS LI., AFIFI AA., BUFFLER PA., ZHANG ZW., MATKİN CC. (1995). Occupational electric and magnetic field exposure and brain cancer: a meta-analysis., *J. Occup. Environ. Med*., 37, pp: 1327-1341.

KULA B., SOBCZAK A., KUSKA R. (2000). Effects of static and ELF magnetic fields on free- radical processes in rat liver and kidney., *Electro and Magnetobiology*, 19 , pp: 99-105.

LAI H., SINGH NP. (2004). Magnetic field-induced DNA strand breaks in brain cells of the rat., *Environmental Health perspectives*, 112, 687-694.

LIBURDY, R.P. (1992). Biological interactions of cellular systems with time- varying magnetic fields. *Ann. N.Y. Acad. Sci*, 6, pp: 125-129.

LIBURDY, R.P., COLLAHAN DE., HASLAND J., DUNHAM E., SLOMA T. R., YASWEN P. (1993). Experimental evidence for 60 Hz magnetic fields operating through the signal transduction cascade. Effects on Calcium influx and C-MYC mRNA induction FEBS LETT. 334 pp:301-308.

LIN RS., DISCHINGER PC., CONDE J., FARRELL KP. (1985). Occupational exposure to electromagnetic fields and the occurrence of brain tumors. An analysis of possible associations., *J. Occup. Med*., 27, pp: 413-419.

PRESTON-MARTIN S., MACK W., HENDERSON BE. (1989). Risk factors for gliomas and meningiomas in males in Los Angeles County., *Cancer Res.*, 49, pp: 6137-6143.

SAVITZ DA., WACHTEL H., BARNES FA., JOHN EM., TVRDIK JG. (1988). Case-control study of childhood cancer and exposure to 60-Hz magnetic fields., *Am. J. Epidemiol*.,128, pp: 21-38.

WERTHEIMER N, SAVITZ DA, LEEPER E. (1995). Childhood cancer in relation to indicators of magnetic fields from ground current sources., *Bioelectromagnetics.*, 16, pp.:86-96.

WERTHEIMER N., LEEPER E. (1979). Electrical wiring configurations and childhood cancer., *Am. J. Epidemiol*., 109, pp:273-84.

INTERMITTENT EXPOSURE TO 50 HZ, 1.5 mT AND INCREASE IN NITRIC OXIDE (NO) LEVELS IN KIDNEY

AYSE G. CANSEVEN*, MEHMET Z. TUYSUZ*, SULE COSKUN** NESRIN SEYHAN*

DEPARTMENT OF BIOPHYSICS, GAZI UNIVERSITY, FACULTY OF MEDICINE,06510 BESEVLER ANKARA, TURKEY

**** DEPARTMENT OF BIOLOGY, GAZI UNIVERSITY, FACULTY OF ART AND SCIENCE, 06500 TEKNIKOKULLAR ANKARA, TURKEY***

canseven@gazi.edu.tr

Abstract

Reactive oxygen species (ROS) are constantly generated in small amounts during metabolic processes. Recent studies have demonstrated that electromagnetic fields (EMF) can cause increase in ROS formation and resulting oxidative stress. The aim of this study was to investigate the effects of continuous and intermittent exposure to a magnetic field (MF) on NOx levels in the kidneys in guinea pigs. A total of 18 male guinea pigs weighing 250-300 g were used. The subjects were divided into one control and two exposure groups which were continuously or intermittently exposed to 50 Hz MF of 1.5 mT with 4 hours daily exposure for 4 days. Determinations of NOx were performed by spectrophotometric methods. The Mann Whitney-U test was used in statistical analysis. Statistically significant increases in NOx level was found for the intermittent exposure to MF. These findings indicate that increased NOx levels may reflect formation of reactive nitrogen species following intermittent exposure to 50 Hz MF

Introduction

Recently, the concerns of people about the possible effects of the electromagnetic fields (EMF) on their health have been heightened with the increasing distribution and utilization of electrical machines, electronic equipments, broadcasting and telecommunication systems (Takebe, 1999). For this reason, most scientists have focused on the effects of EMF exposure on people's health and they have conducted several epidemiological and laboratory studies to define the risks of electromagnetic field exposures. Based on the results of these studies, there is growing evidence that electromagnetic fields, the power line frequency (50-60 Hz) and magnetic field (MF), may increase the risk of certain cancers, likely by a tumor-promoting / co – promoting effect. Long-term and as well as short-term electromagnetic field exposure can cause DNA damage and the risk of tumor development. Taking into consideration of the possible adverse effects of extremely low frequency (ELF) electric and magnetic field exposure, they have been recently classified as a possible carcinogens class 3 and 2B respectively, in NIEHS 1998 and IARC 2002 guidelines (Tuncel, 2003; Koifman, 1994; Parola, 1994).Especially, the cellular effects of ELF electric and magnetic field exposure have been investigated intensively. Studies have shown that EMF can induce cell proliferation, variations of calcium concentrations (Canseven, 1996; Canseven, 1999; Canseven, 2005a), alteration of DNA integrity, changes in transcription of immediate early genes and in protein synthesis (Boland, 2002; Ishisaka, 2000; Gold,1994; Canseven, 2005b) and perturbations of the central nervous system inducing behavioral disturbances in animals (Lai, 1996). In addition, EMF are also able to affect biological systems by increasing the level of free radicals produced by various oxidative stress (Boland, 2002). Oxidative stress is, a physiological condition characterized by an elevated level of oxygen free radical species that cause cellular damage and change vital functions and, is critically important for human health. Oxidative stress occurs due to increased production of reactive oxygen species (ROS) such as, super radical, hydrogen peroxide, and hydroxyl radical at the time of reperfusion, which in turn overwhelm the endogenous antioxidant defense (Narang, 2004). The increase in reactive oxygen species formation can cause the initiation of cumulative damage in the proteins, lipids and nucleic acids' structures. Actually, reactive oxygen species formations are related to the metabolic rate of an organism. In summary, there is a balance between reactive oxygen species formation and antioxidative defense which is important to maintain homeostasis within cells and tissues (Simko, 2004).

In the formation of Reactive Oxygen Species, one of the most important reactants is nitric oxide (NO). Nitric oxide (NO) can undergo numerous reactions as an endogenous mediator of numerous physiological processes. It has an important role in both oxidative stress and nitrosative stress. That is, NO can interact with ROS in many ways resulting in oxidative stress and it can also undergo many reactions that result in the formation of reactive nitrogen species (RNOS) which cause nitrosative stress. NO acts as biological messenger in many physiological processes and plays a role in pathogenesis of many disorders (Jelenkovic et al., 2006). It was suggested that nitric oxide synthase (NOS) activity or NO level could have a prognostic value, which may show the degree of EMF induced tissue damage (Noda et al., 2000; Ilhan et al., 2004; Ozguner et al., 2005).
In this study, the effect of continuous and intermittent exposure of 50 Hz, 1.5 mT magnetic field with the exposure period of 4 hours/day for 4 days on NOx levels was investigated.

Materials and Methods

Animals and Magnetic Field Exposure
The experimental protocol was reviewed and approved by the Laboratory Animal Care Committee of Gazi University (Report no : 39-5858). A total of 18 male, 250-300g weighted guinea pigs were used in this study. All animals were kept under laboratory conditions and fed standard pellet food.
Homogenous MF was generated by Helmholtz coils' system. The exposure system developed in our laboratory has been described in detail elsewhere (Canseven, 2005c).
Animals were divided into three groups, controls and two magnetic field exposure groups. Exposure groups were exposed to continuously (4 hours/day) or intermittently (2 hours on/ 2 hours off/ 2 hours on) to 50 Hz MF of 1.5 mT with the exposure periods of for 4 days. Controls were handled in an identical manner without being exposed to any magnetic field.
Following 12 h of starvation, guinea pigs were intramuscularly injected with combinations of ketamine (30 mg/kg), xylazine (2 mg/kg) and 250 IU/kg heparin. The kidney were sampled, shocked by liquid nitrogen and stored at -80°C until performing analysis. All experiments were run in a blinded manner.

Determination of NO Levels
NOx levels - stable end products of nitric oxide- in kidney tissues were measured by the Griess reaction (Green, 1982).
Tissue samples were homogenized in five volumes of phosphate buffer (pH= 7.5) and centrifuged at 2000x g for 5 min. to supernatants (0.5 ml) 0.25 ml of 0.3 M NaOH were added. After incubation for 5 min at room temperature, 0.25 ml of 10% (w/v) ZnSO4 was added for deproteinization. This mixture was then centrifuged at 14000x g for 5 min and supernatants were used for the Griess assay.
Nitrate levels in tissue homogenates were determined spectrophotometrically, based on the reduction of nitrate to nitrite by VaCI3 (Miranda, 2001). Nitrite levels were measured by the Griess reaction. Sodium nitrite and nitrate solutions (1, 10, 50, 100 μM) were used as standards.

Statistics
Statistical analyses were carried out using SPSS software (SPSS 11.5 for windows, SPSS Inc., Chicago, USA). The p value was considered significant at $p<0.05$. The Mann Whitney-U test was used in statistical analysis.
Both comparisons between exposed groups and controls, and comparisons between intermittent and continuous exposed groups were made by using Mann Whitney-U test.

Results

In this study, guinea pigs were continuously or intermittently exposed to magnetic field of 1.5 mT with 4 hours daily exposure for 4 days and levels of NOx in kidney were determined. An increased level of NOx was found in intermittent exposed animals (385.58± 18.79) with respect to controls (302.42± 6.18). This increase was statistically significant ($p=0.009$).
Continuous and intermittent exposures were also compared. Significant difference ($p=0.016$) was determined between continuous and intermittent exposed groups. Although both of the exposures increased the levels of NOx, intermittent exposure was more effective than continuous exposure in this study (Table 1- Figure 1)..

Table 1. NOx levels (µmol/g) in kidney of guinea pigs under 50 Hz magnetic fields of 1.5 mT

KIDNEY	Total (µmol/gr) mean±sem
Control	30.,42 ± 6.18
Continuous Exposure	314.30 ± 10.71
Intermittent Exposure	385.58 ± 18.79

Discussion

NO (Nitric oxide), one of the primary indicators of ROS (reactive oxygen species) production, may contribute to the pathophysiology of EMF - induced renal impairment. It can also undergo many reactions that result in the formation of reactive nitrogen species (RNOS), which cause nitrosative stress. Nitrogen derived species (RNOS), most notably the $ONOO^-$ (peroxynitrite) and peroxynitrous acid (ONOOH) are likely involved in renal damage during oxidative stress in all tissues (Wink, 2000; Ozguner, 2005).

In this study, we found significantly increased NOx levels in kidneys under intermittent exposure to 50 Hz magnetic field of 1.5 mT.

Our results indicate that, intermittent magnetic field exposure may cause the change in renal functions with the high levels of reactive oxygen species production.

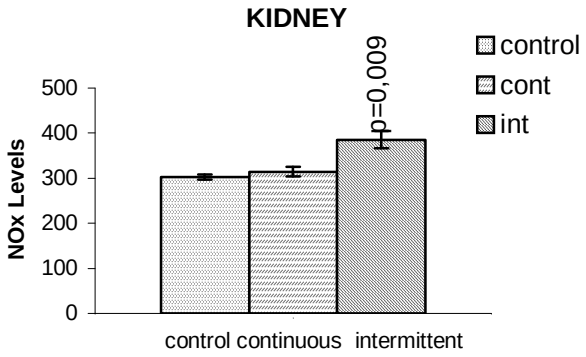

Figure 1. NOx levels (µmol/gr) in kidneys under 50 Hz magnetic fields of 1.5 mT.

References

Boland A., Delapierre D., Mossay D., Dresse A., Seutin V. (2002). Effect of Intermittent and Contiuous Exposure to Electromagnetic Fields on Cultered Hippocampal Cells., *Bioelectromagnetics*, 23:97-105.

Canseven A.G., Seyhan N., Aydin, A., Cevik, C., Isimer, A. (2005a). Effects of Ambient ELF Magnetic Fields: Variations in Electrolytes Levels of Brain and Blood Plasma, Gazi Medical Journal, 16: 121 – 127.

Canseven, A.G., Seyhan, N., Aydin, A., Isimer, A (1999). Extremely Low Frequency Electromagnetic Field Effect on Brain Tissue and Blood Plasma Electrolytes, *Med & Biol Eng & Comput.*, 37 (Suppl. 2): 1336-1337.

Canseven, A.G., Seyhan, N. (2005b). Effects of Ambient ELF Magnetic Fields: Variations In Collagen Synthesis of Guinea Pigs' Skin and Scaling From Animals To Human. *Gazi Medical Journal* 16 : 160 – 165 *(Turkish)*.

Canseven, A.G., Seyhan, N. (2005c). Design, installation and standardization of homogenous magnetic field systems for experimental animals IFMBE Proceedings, Vol. 11. Prague: IFMBE, 2005. ISSN 1727-1983. Editors: Jiri Hozman, Peter Kneppo (Proceedings of the 3rd European Medical&Biological Engineering Conference - EMBEC´05.Prague, Czech Republic, 20- 25.11.2005). pp: 2333-2338

Canseven A. G., Seyhan N. (1996). Is it Possible to Trigger Collagen Synthesis by Electric Current in Skin Wounds?., *Indian Journal of Biochemistry & Biophysics*, 33, pp:223-227.

Gold S., Goodman R., Shirley-Henderson A., (1994). Exposure of Simian virus-40-Transformed Human Cells to Magnetic Fields Results in Increased Levels of T-Antigen mRNA and Protein., *Bioelectromagnetics*, 15:329-336.

Green LC, Wagner DA, Glogowski J, Skipper PL, Wishnok JS, Tannenbaum SR. (1982). Analyses of nitrate, nitrite and [^{15}N] nitrate in biological fluids. *Anal Biochem*, **126**: 131-8.

Guler G., Canseven A.G., Seyhan N., (1994). DC Electric Field Effect on Tissues Hydroxyproline Level., *Physics in Medicine & Biology*, 39a, pp:767.

Guler G., Seyhan N. (1996). Changes in Hydroxyproline Levels in Electric Field Tissue interaction. , *Indian Journal of Biochemistry & Biophysics*, 33, pp: 531-533.

Guler G., Seyhan N., (1996). The Effect of Vertical and Horizontal Electric Fields on Collagen Synthesis., *Progress in Biophysics& Molecular Biology* , 65:1, pp: 215.

Ilhan, A., Gurel, A., Armutcu, F., Kamisli, S., Iraz, M., Akyol, O., Ozen, S. (2004). Ginkgo biloba prevents mobile phone-induced oxidative stress in rat brain., *Clin Chim Acta.* 340: 153-162.

Ishisaka R., Kanno T., Inai Y., Nakahara H., Akiyama J., Yoshioka T., Utsumi K., (2000). Effects of a magnetic fields on the various functions of subcellular organelles and cells., *Pathophysiology*, 7:149-152.

Jelenkovic, A., Janac, B., Pesic, V., Jovanovic, D.M., Vasiljevic, I., Prolic, Z. (2006). Effects of extremely low-frequency magnetic field in the brain of rats.. *Brain Research Bulletin*. 68: 355-360.

Koifman S., Theriault G. (1994). Electric and Magnetic Fields and Cancer:the Use of Field Exposure Measurements in Epidemiological Studies.,Eds:Carpenter D.O., Ayrapetyan S.,"Biological Effects of Electric and Magnetic fields:Beneficial and Harmful Effects", Academic Press Inc.,California, pp.201-231,

Lai H. (1996). Spatial learning deficit in the rat after exposure to a 60 Hz magnetic field, Bioelectromagnetics, 17: 494-496.

Miranda KM, Espey MG, Wink DA. (2001). A rapid simple spectrophotometric method for simultaneous detection of nitrate and nitrite. Nitric Oxide, 5: 67-71.

Narang D., Sood S., Thomas M. K., Dinda A. K., Maulik S. K., (2004). Effect of dietary palm olein oil on oxidative stress associated with ischemic-reperfusion injury in isolated rat heart., *BMC Pharmacology* , 4:29.

Noda, Y., Mori, A., Liburdy, R.P., Packer L. (2000). Pulsed magnetic fields enhance nitric oxide synthase activity in rat cerebellum. *Pathophysiology.* 7: 127-130.

Ozguner F., Oktem F., Ayata A., Koyu A., Yilmaz H. R. (2005). A novel antioxidant agent caffeic acid phenethyl ester prevents long-term mobile phone exposure-induced renal impairment in rat: Prognostic value of malondialdehyde, N-acetyl-β-D-glucosaminidase and nitric oxide determination, *Molecular and Cellular Biochemistry*; 277: 73-80.

Parola A. H., Markel A. (1994). Electric and Magnetic Fields and Carcinogenesis, Eds:Carpenter D.O., Ayrapetyan S.,"Biological Effects of Electric and Magnetic fields:Beneficial and Harmful Effects", Academic Press Inc.,California, pp:177-197.

Simko M., Mattson M.O., (2004). Extremely Low Frequency Electromagnetic Fields as Effectors of Cellular Response In Vıtro: Possible Immune Cell Activation. *Journal of Cellular Biochemistry*, 93: 83-92.

Takebe H., Shiga T., Kato M., Masada E. (1999). Biological and Health Effects from Exposure to Power- line Frequency Electromagnetic Fields: Confirmation of Absence of Any Effects at Environmental Field Strengths. Ohmsa Ltd., Japan, pp:76-113,.

Tuncel H. "Effects of Electromagnetic Fields on the Immune System", Eds:Stavroulakis P. "Biological Effects of Electromagnetic Fields", Springer-Verlag Berlin Heidelberg New York 2003 pp: 503-544.

Wink D.A., Miranda K.M., Espey M.G., Mitchell J.B., Grisham M.B., Fukuto J., Feelish M. (2000). The chemical Biology of Nitric Oxide, Balancing Nitric Oxide with Oxidative and Nitrosative Stress.,Eds:Mayer B., Handbook of Experimental Pharmacology, Springer , pp:7-29.

EFFECTS OF CONTINUOUS EXPOSURE TO 50 Hz MAGNETIC FIELDS ON NITRIC OXIDE LEVELS IN LUNG

AYSE G. CANSEVEN[*], SULE COSKUN[**], NESRIN SEYHAN[*]

[*] DEPARTMENT OF BIOPHYSICS, GAZI UNIVERSITY, FACULTY OF MEDICINE, 06510 BESEVLER ANKARA, TURKEY
[**] DEPARTMENT OF BIOLOGY, GAZI UNIVERSITY, FACULTY OF ART AND SCIENCE, 06500 TEKNIKOKULLAR ANKARA, TURKEY
canseven@gazi.edu.tr

Abstract

Interest in researches on the health effects of extremely low frequency electromagnetic fields (ELF EMF) is rapidly growing. ELF EMF has been classified as 2B, possibly carcinogenic to humans, by the International Agency for Research on Cancer. It is believed that ELF EMF prolongs the life of free radicals and can act as a promoter or co-promoter of cancer**.** It is also known that magnetic fields cause an increase in free radicals activity in living organisms. Free radicals are very reactive and unstable molecular species that can initiate chain reactions to form new free radicals. In the present study, we investigated the effect of various magnetic fields on lung tissue damage resulting from oxidative stress by measuring nitric oxide (NOx) levels. Twenty-three guinea pigs were exposed to 50 Hz, 1 mT and 3 mT fields with the exposure periods of 4 hours/day and 8 hours/day for 5 days. Control subjects (n=9) were handled in an identical manner with the exposed animals in the same laboratory. NOx levels - stable end products of nitric oxide - in lung tissues were determined spectrophotometrically using he Griess reaction. For both of the application periods, increases in NOx level were found by the effect of 3 mT MF whereas increased NOx level was determined only for groups of 1 mT, 4 hours. Nitric oxide (NO) has play an important role related to ELF magnetic fields' exposure in lung tissue.

Introduction

In recent years, scientists have focused on the effects of electromagnetic fields (EMF) on living organisms in cellular levels. These major interests have been born of the overexposure of people to extremely low frequency (ELF) electromagnetic fields (EMF) with the increase of wide use of technological devices in their daily life. In many epidemiological and laboratory studies, it has been suggested that there is a link between ELF magnetic field exposure and the increased incidence of certain types of tumor, particularly in leukemia and brain cancer (Lin, 1985; Preston-Martin, 1989; Bastuji-Garin, 1990; Feychting, 1993; Wertheimer, 1979, 1995; Savitz, 1988;). A variety of EMF effects on biological and biochemical responses such as protein synthesis (Kenneth, 1987; Gold, 1994; Canseven, 2005b), gene expression, signal transduction and DNA damage (Liburdy, 1992, 1993; Jajte, 2001; Lai, 2004), immune system functions (Canseven, 2006; Seyhan, 2006; Walleczek, 1992; De Seze, 1993; Blumenthal, 1997; House, 2000, 1996; Tremblay, 1996), apoptosis induction (Blumenthal, 1997; Jajte, 2002), enzyme regulation (Canseven, 2003a, Canseven, 2003b; Canseven, 2004; Canseven, 2005a, Brocklehurst, 1996), free radical activity (Kula, 2000; Kula, 2002; Roy, 1995; Khadir, 1999; Simko, 2001; Sboczak, 2002; Yokus, 2005; Watanabe, 1997; Fiorani, 1997; Mohtat, 1998; Kashkalda, 1995; Jin, 1998) have been described in the reports of many in vivo and/or in vitro experiments. Magnetic fields penetrate the cells and can alter cell membrane potential and the concentration of ions (Canseven, 1999; Canseven, 2005c; Garcia-Sancho, 1994). These alterations may affect free radical processes within the cell. EMF could be also able to affect biological systems by increasing the amount of free radical produced by various oxidative stress (Boland, 2002). ELF EMF has been thought to prolong the life of free radicals and can act as a promoter or co-promoter of cancer (Yokus, 2005). Free radicals, which are known as reactive oxygen species (ROS) are continuously formed in small amounts in biological systems. Depending on the oxygen consumption, the production of ROS increases; however there is a balance between ROS formation and antioxidant defense within cells and tissues. In the case of increase in the formation of ROS, it has been seen the initiation cumulative damage to proteins, lipids and nucleic acids and various physiological conditions, like oxidative stress has been observed. There are many factors, which cause the formation of oxidative stress; among them ROS production is one of the most important.
Nitric oxide (NO) can undergo numerous reactions as an endogenous mediator of numerous physiological

processes. NO plays an important role in both oxidative stress and nitrosative stress.
Taking into consideration the activation of free radicals in biological systems, the behavior of free radicals was investigated. NOx levels were measured in lung tissues of guinea pigs exposed to 50 Hz, 1 mT and 3 mT fields with the exposure periods of 4 hours/day and 8 hours/day for 5 days to determine the effects of electromagnetic fields on ROS production.

Materials and Methods

Animals

The experimental protocol was reviewed and approved by the Laboratory Animal Care Committee of Gazi University (Report no: 36-7838). A total of 32 male guinea pigs weighing between 250 and 300g were used in this study. All animals were kept under laboratory conditions and fed standard pellet food.

Magnetic Field Exposure

50 Hz magnetic field was produced by 42.75 cm diameter Helmholtz coil with winding embedded in an open wooden circular frame (Canseven, 2005d). Each coil was constructed by insulated copper wire and made of 154 turns. To feed the coils, sinusoidal current of frequency 50 Hz was supplied by a specially designed variable transformer, 2.7 kVA (kilo Volt Amper) in power. Magnetic field at the center of exposure system was measured by a Hall-Effect Gaussmeter. Frequency and wave form of the magnetic field were monitored over an ossiloscope. The animal cage without magnetic material was put at the center.
Twenty-three guinea pigs were exposed to 50 Hz, 1 mT and 3 mT fields with the exposure periods of 4 hours/day and 8 hours/day for 5 days. Control subjects (n=9) were handled in an identical manner with the exposed animals in the same laboratory.
Following 12 h of starvation, guinea pigs were injected intramuscularly with ketamine (30 mg/kg) and xylazine (2 mg/kg) combined with 250 IU/kg heparin. Lungs were sampled immediately. They shocked by liquid nitrogen and stored in deep freezer at -80°C until performing analysis. All experiments were run in a blind manner.

Determination of NO Levels

NOx levels - stable end products of nitric oxide- in lung tissues were determined by the Griess reaction (Green et al., 1982).
Tissue samples were homogenized in five volumes of phosphate buffer (pH= 7.5) and centrifuged at 2000 x *g* for 5 min. to supernatants (0.5 ml) 0.25 ml of 0.3 M NaOH were added. After incubation for 5 min at room temperature, 0.25 ml of 10% (w/v) $ZnSO_4$ was added for deproteinization. This mixture was then centrifuged at 14000 x *g* for 5 min and supernatants were used for the Griess assay.
Nitrate levels in tissue homogenates were determined spectrophotometrically, based on the reduction of nitrate to nitrite by $VaCI_3$ (Miranda et al., 2001). Nitrite levels were measured by the Griess reaction. Sodium nitrite and nitrate solutions (1, 10, 50, 100 μM) were used as standards.

Statistics

Statistical analyses were carried out using SPSS software (SPSS 11.5 for windows, SPSS Inc., Chicago, USA). The p value was considered significant at $p<0.05$.

Mann Whitney-U and Kruskal-Wallis tests were used in statistical analysis. Comparisons between exposed groups and controls were made by using Mann Whitney-U test while magnetic fields of 1mT and 3 mT were compared with Kruskal-Wallis test with respect to exposure periods of 4 hours and 8 hours.

Results

In this study, the NOx level was investigated in lung tissues of guinea pigs which were exposed to magnetic fields of 1mT and 3 mT with the exposure periods of 4 hours/day and 8 hours/day for 5 days. For both of the application periods, NOx levels were found increased with respect to controls in lung tissues of guinea pigs exposed to both of the magnetic fields (Table 1- Figure 1).
The increases in NOx levels were found statistically significant for 1 mT, 4 hours ($p=0.003$), 3 mT, 4 hours ($p=0.001$) and 3 mT, 8 hours ($p=0.000$) in lung tissues by Mann-Whitney U test.
Field intensities were compared with respect to exposure periods by Kruskal-Wallis test. Significant differences were determined between field intensities of 1 mT and 3 mT in lung tissues for only exposure period of 8 hours ($p=0.004$).

Table 1. Lung NOx levels of guinea pigs under the effects of 50 Hz magnetic fields of 1 mT and 3 mT with the exposure periods of 4 hours/day and 8 hours/day for 5 days.

GROUPS	n	NO_x Level (µmol/g tissue) (mean ± sem)
Control	9	103.61 ± 3.80
1 mT; 4 hours	4	141.65 ± 3.61
1 mT; 8 hours	4	110.78 ± 1.40
3 mT; 4 hours	7	133.31 ± 4.90
3 mT; 8 hours	8	131.99 ± 3.08

Discussion

For both of the exposure periods, significant increases in NOx levels were found by the effect of 3 mT magnetic field whereas increased NOx levels were found only for groups of 1 mT, 4 hours.
TBARS levels in the same tissue for the same exposure conditions were also investigated in our laboratory (Canseven 2005e). The increased NOx levels in lung for 1 mT, 4 hours and 3 mT, 4 hours was found consistent with the increases of TBARS in these tissues.
Further studies are required to better elucidate the mechanisms of the effect of ELF MFs on lipid peroxidation or oxidative stress in tissues.

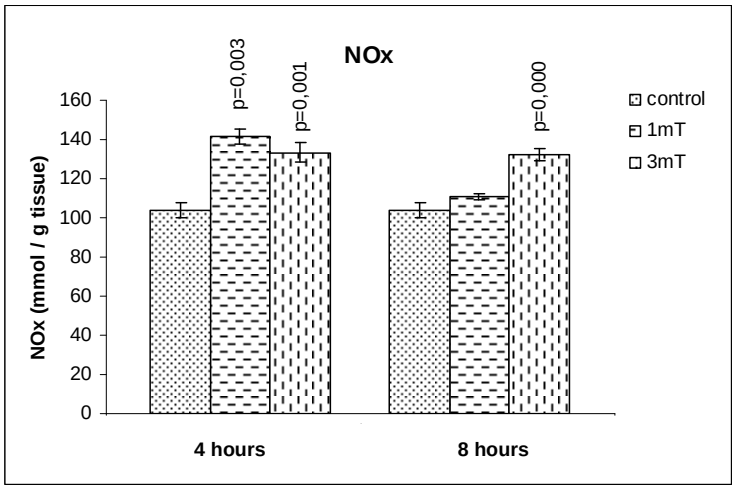

Figure 1. Lung NOx levels of 1 mT and 3 mT exposed and control guinea pigs.

References

BASTUJI-GARIN S., RICHARDSON S., ZITTOUN R. (1990). Acute leukaemia in workers exposed to electromagnetic fields, *Eur. J. Cancer*., 26 : 1119-1120.

BLUMENTHAL NC., RICCI J., BREGER L., ZYCHLINSKY A., SOLOMON H., CHEN GG., KUZNETSOV D., DORFMAN R. (1997). Effects of Low Intensity AC and/or DC Electromagnetic Fields on Cell Attechment and Induction of Apoptosis, *Bioelectromagnetics*, 18 : 264-272.

BOLAND A., DELAPIERRE D., MOSSAY D., DRESSE A., SEUTIN V. (2002). Effect of Intermittent and Contiuous Exposure to Electromagnetic Fields on Cultered Hippocampal Cells, Bioelectromagnetics, 23:97-105.

BROCKLEHURST B., MCLAUCHLAN KA. (1996). Free radical mechanism for the effects of environmental electromagnetic fields on biological systems., *Int. J. Radiat. Biol*., 69:. 3-24 .

CANSEVEN A.G., SEYHAN N., AYDIN, A., CEVIK, C., ISIMER, A. (2005c). Effects of Ambient ELF Magnetic Fields: Variations in Electrolytes Levels of Brain and Blood Plasma, *Gazi Medical Journal*, 16: 121 – 127.

CANSEVEN AG., OZEL U., BILGIHAN A., and SEYHAN N (2004). Does ELF Magnetic Field Effect The Myeloperoxidase (MPO) Activity in the Lung', 11th International Congress of the International Radiation Protection Association, 23-28 May 2004, Madrid, Spain, ID 591

CANSEVEN AG., SEYHAN N., AYDIN A., ISIMER A. (1999). Extremely Low Frequency Electromagnetic Field Effect on Brain Tissue and Blood Plasma Electrolytes., *Med & Biol Eng & Comput*, 37 : 1336-1337.

CANSEVEN, A.G., COSKUN, S., SEYHAN, N. (2005e). ELF magnetic fields' effecst on lipid peroxidation in lung and kidney. IFMBE Proceedings, Vol. 11. Prague: IFMBE, 2005. ISSN 1727-1983.Editors: Jiri Hozman, Peter Kneppo (Proceedings of the 3rd European Medical & Biological Engineering Conference - EMBEC´05. Prague, Czech Republic, 20-25.11.2005). pp: 4748-4752

CANSEVEN, A.G., OZEL U., BILGIHAN, A., SEYHAN, N. (2005a). Effects of environmental ELF magnetic fields on myeloperoxidase (MPO) activity. IFMBE Proceedings, Vol. 11. Prague: IFMBE, 2005. ISSN 1727-1983. Editors: Jiri Hozman, Peter Kneppo (Proceedings of the 3rd European Medical&Biological Engineering Conference - EMBEC´05. Prague, Czech Republic,20-25.11.2005). pp: 2232-2236

CANSEVEN, A.G., OZEL, U., BILGIHAN, A., SEYHAN, N. (2003a). Myeloperoxidase (MPO) Activities in Brain, Lung and Renal Tissues After Exposure to Magnetic Fields of 50 Hz. *13th Balkan Biochemical Biophysical Days & Meeting on Metabolic Disorders*, October 12-15, 2003, Kusadası, TURKEY, P94 (Abstract)

CANSEVEN, A.G., OZEL, U., BILGIHAN, A., SEYHAN, N. (2003b). The Effect of ELF Magnetic Field Exposure on Kidney Myeloperoxidase (MPO) Activity, *13th Balkan Biochemical Biophysical Days & Meeting on Metabolic Disorders*, October 12-15, 2003, Kusadası, TURKEY, P96 (Abstract)

CANSEVEN, A.G., SEYHAN, N. (2005b). Effects of Ambient ELF Magnetic Fields: Variations In Collagen Synthesis of Guinea Pigs' Skin and Scaling From Animals To Human. *Gazi Medical Journal* 16 : 160 – 165 *(Turkish)*.

CANSEVEN, A.G., SEYHAN, N. (2005d). Design, installation and standardization of homogenous magnetic field systems for experimental animals IFMBE Proceedings, Vol. 11. Prague: IFMBE, 2005. ISSN 1727-1983. Editors: Jiri Hozman, Peter Kneppo (Proceedings of the 3rd European Medical&Biological Engineering Conference - EMBEC´05.Prague, Czech Republic, 20- 25.11.2005). pp: 2333-2338.

CANSEVEN, A.G., SEYHAN, N., MIRSHAHIDI, S., IMIR, T. (2006). Suppression of Natural Killer Cell Activity on *Candida Stellatoidea* by a 50 Hz Magnetic Field. *Electromagnetic Biology and Medicine*, 25 (2) : 79-85.

DE SEZE R., BOUTHET C., TUFFET S., DESCHAUX P., CARISTAN A., MOREAU JM., VEYRET B. (1993). Effects of Time-Varying Uniform Magnetic Fields on Natural Killer Cell Activity and Antibody Response in Mice., *Bioelectromagnetics*, 14: 405-412.

FEYCHTING M., AHLBOM A. (1993). Magnetic fields and cancer in children residing near Swedish high-voltage power lines., *Am. J. Epidemiol*., 138 : 467-481.

FIORANI M., BIAGIARELLI B., VETRANO F., GUIDI G., DACHA M., STOCCHI V. (1997). In vitro effects of 50 Hz magnetic fields on oxidatively damaged rabbit red blood cells, *Bioelectromagnetics*.,18:. 125-131

GARCIA-SANCHO J., MONTERO M., ALVAREZ J., FONTERIZ RI., SANCHEZ A (1994). Effects of Extremely Low Frequency Electromagnetic Fields on Ion Transport in Several Mammalian Cells., *Bioelectromagnetics*, 15 : 579-588.

GOLD, S., GOODMAN R., HENDERSON, A.S. (1994). Exposure of Simian Virus-40-Transformed Human Cells to Magnetic Fields Results in Increased Levels of T-Antigen mRNA and Protein', *Bioelectromagnetics*, 15: 329-336.

GREEN LC, WAGNER DA, GLOGOWSKI J, SKIPPER PL, WISHNOK JS, TANNENBAUM SR. (1982). Analyses of nitrate, nitrite and [^{15}N] nitrate in biological fluids. *Anal Biochem* 126: 131-8.

HOUSE, R. V., MCCORMİCK, D. L. (2000). Modulation of natural killer cell function after exposure to 60Hz magnetic fields: confirmation of the effect in mature B6C3F1 mice. *Radiation Res.* 153:722–724.

HOUSE, R. V., RATAJCZAK, H. V., GAUGER, J. R., JOHNSON, T. R., THOMAS, P. T., MCCORMİCK, D. (1996). Immune function and host defense in rodents exposed to 60Hz magnetic fields. *Fund. Appl. Toxicol.* 34:228–239.

JAJTE J., ZMYSLONY M., PALUS J., DZIUBALTOWSKA, E., RAJKOWSKA, E (2001). Protective effect of melatonin against in vitro iron ions and 7 mT 50 Hz magnetic field-induced DNA damage in rat lymphocytes, *Mutation Research*, 483 : 57-64.

JAJTE, J., GRZEGORCZYK J., ZMYSLONY, M., RAJKOWSKA (2002). E.Effect of 7 mT static magnetic field and iron ions on rat lymphocytes: apoptosis, necrosis and free radical processes, *Bioelectrochemistry*,

57, pp. 107-111

JIN Y., WANG H., CHENG Y., GU H (1998). Effects of static magnetic fields on free radical metabolism of human body., *Wei Sheng Yan Jiu*., 27: 97-99.

KASHKALDA DA., PASHENKO EA., ZİUBANOVA LF. (1995). Effects of an impulse magnetic field on lipid peroxidation and the antioxidant system of the testes in animal experiments, *Med Tr Prom Ekol*., 10: 14-17.

KENNETH JM., LEE RC., EHRLICH, HP. (1987). Frequency Dependence of Electric Field Modulation of Fibroblasts Protein Synthesis, *Science*, 236, pp. 1465-1469.

KHADIR R., MORGAN JL., and MURRAY JJ. (1999). Effects of 60 Hz magnetic field exposure on polymorphonuclear leukocyte activation, *Biochim Biophys Acta*, 1472: 359-367.

KULA B., SOBCZAK A., and KUSKA R. (2002). Effects of electromagnetic field on free radical processes in steelworkers.Part I. Magnetic field influence on the antioxidant activity in red blood cells and plasma, *J. Occup Health*, 44: 226-229.

KULA B., SOBCZAK A., KUSKA R. (2000). Effects of static and ELF magnetic fields on free- radical processes in rat liver and kidney., *Electro and Magnetobiology*, 19 : 99-105.

LAI H., SINGH NP (2004). Magnetic field-induced DNA strand breaks in brain cells of the rat, *Environmental Health perspectives*, 112 : 687-694.

LIBURDY RP., CALLAHAN DE., HARLAND J., DUNHAM E., SLOMA TR., YASWEN P. (1993). Experimental evidence for 60 Hz magnetic fields operating through the signal transduction cascade. Effects on calcium influx and c-MYC mRNA induction., *FEBS LETT*., 334: 301-308.

LIBURDY, R.P. (1992). Biological interactions of cellular systems with time-varying magnetic fields,, *Ann .N.Y. Acad. Sci*., 649: 74-94.

LIN RS., DISCHINGER PC., CONDE J., FARRELL KP. (1985). Occupational exposure to electromagnetic fields and the occurrence of brain tumors. An analysis of possible associations., *J. Occup. Med*., 27: 413-419.

MIRANDA KM, ESPEY MG, WINK DA. (2001). A rapid simple spectrophotometric method for simultaneous detection of nitrate and nitrite. *Nitric Oxide* 5: 67-71.

MOHTAT N., COZENS FL., HANCOCK-CHEN T., SCAİANO JC., MCLEAN J., KİM J. (1998). Magnetic field effects on the behavior of radicals in protein and DNA environments., *Photochem Photobiol*, 67 : 111-118.

PRESTON-MARTIN S., MACK W., HENDERSON BE. (1989). Risk factors for gliomas and meningiomas in males in Los Angeles County., *Cancer Res*., 49 : 6137-6143.

ROY S., NODA Y., ECKERT V., TRABER MG., MORI A., LIBURDY R., PACKER L. (1995). The phorbol 12-myristate 13-acetate (PMA)-induced oxidative burst in rat peritoneal neutrophils is increased by a 0.1 mT (60 Hz) magnetic field, *FEBS Letters*, 376 : 164-166.

SAVİTZ DA., WACHTEL H., BARNES FA., JOHN EM., TVRDİK JG. (1988). Case-control study of childhood cancer and exposure to 60-Hz magnetic fields., *Am. J. Epidemiol*.,128 : 21-38.

SBOCZAK A., KULA B., AND DANCH A (2002). Effects of electromagnetic field on free radical processes in steelworkers. Part II: Magnetic influence on vitamin A, E and Selenium concentrarions in plasma., *J. Occup health*., 44 : 230-233.

SEYHAN N., CANSEVEN A. G., GULER G. (2006). Animal Studies on the Effects of ELF and Static EMF. In Ayrapetyan S.N., Markov M.S., eds. *Bioelectromagnetics Current Concepts, The Mechanisms of the Biological Effect of Extremely High Power Pulses* . NATO Security through Science Series B: Physics and Biophysics, Vol. 5, pp: 195-212.

SIMKO M., DROSTE S., KRIEHUBER R., WEISS DG. (2001). Stimulation of phagocytosis and free radical production in murine macrophages by 50 Hz electromagnetic fields.', *Eur J Cell Biol*, 80 : 562-566.

TREMBLAY, L., HOUDE, M., MERCİER, G., GAGNON, J., MANDEVİLLE, R. (1996). Differential modulation of natural and adaptive immunity in Fisher rats exposed for 6 weeks to 60Hz linear sinusoidal continuous-wave magnetic fields. *Bioelectromagnetics* 17: 373–383.

WALLECZEK J. (1992). Electromagnetic field effects on cell of the immune system: the role of calcium signaling. *FASEB J.*, 6 : 3177-3185.

WATANABE Y., NAKAGAWA M., MİYAKOSHİ Y (1997). Enhancement of lipid peroxidation in the liver of mice exposed to magnetic fields, *Ind. Health*., 35 : 285-290.

WERTHEIMER N, SAVITZ DA, LEEPER E. (1995). Childhood cancer in relation to indicators of magnetic fields from ground current sources., *Bioelectromagnetics*., 16 : 86-96.

WERTHEIMER N., LEEPER E. (1979). Electrical wiring configurations and childhood cancer., Am. *J. Epidemiol*., 109 : 273-84.

YOKUS B., CAKIR DU., AKDAG MZ., SERT C., METE N (2005). Oxidative DNA damage in rats exposed to extremely low frequency electro magnetic fields, *Free. Radic. Res*., 39: 317-323.

A DOUBLE LAYER ARTERIAL WALL MODEL UNDER PULSATING BLOOD PRESSURE

MONA A. EL-NAGGAR

DEPT. OF ENGINEERING PHYSICS, FACULTY OF ENGINEERING, CAIRO UNIVERSITY, GIZA, EGYPT

Abstract

The behavior of a double layer arterial section of unit length is studied under the effect of radial pressure. The proposed model considers that the radial pressure follows an exponential rise exponential decay biphasic periodic function mathematically represented by a Fourier series. The dependence of the arterial strain response on viscoelastic properties of each layer is studied. The dissipated and stored power per unit length of the vessel, are computed. The stress-strain response is modeled for each layer. Storage and loss moduli are deduced as well**.**

Introduction

The study of the viscoelastic properties and response of the blood vessels have been one of the most important and biomechanical field of research for quite a while. This study represents an essential step towards controlling the efficiency of the blood pulse propagation process. The blood pulse propagates along the axis of the blood vessels, namely arteries, with a radial component pulsating on the inner wall. This propagation is similar to the propagation of waves in media. The arterial pulse is considered as a pressure wave travelling down the multilayer wall associated with a strain wave. The arterial strain response is the main issue here as it can be considered as an energy storage element that pushes the blood spurts forward down the artery. The rigidity or distensibility of the arteries causes the pressure to be very high during systole and it would fall to low values during diastole. The blood flow as a result of this would be intermittent. Furthermore, the reduced distensibility of the arterial wall has a direct effect on the efficiency of the heart markedly increasing its oxygen consumption making its attack more likely. It is thus extremely important to simulate the pressure wave propagation and its pulsating radial component. The problem is complicated not only because of the non-linearity in blood vessels elasticity, but because of the varying nature of the pulse wave as well. The anisotropic, multilayer and nonlinear viscoelastic properties of the arterial walls lead to certain mathematical complications when the radial dimensions are considered under the effect of pulsating pressure.

Previous work was concerned with mechanical and mathematical simulation to produce stress-strain relation for different soft tissues. Yu Q. et al. [1] evaluated the force-deformation relations for different layers of blood vessels by studying the non axis symmetric deformation of the vessel wall. This was done by imposing bending on the vessel. Young's modulus is given for the intima media and the adventitial layers of the thoracic artery. The circumferential stretch and axial stretch of abdominal arteries are given for different pressure values by Schulz-Bauer et al. [2] for both normal and hypertensive patients. They proposed a method to determine nonlinear constitutive models for human arteries from clinical data using a strain energy function. Mechanical properties are obtained by reliable experimental setups especially for different arterial layers, collagen and body tissues [3]. The degree of nonlinearity and blood vessel elasticity was studied by J. Zhou and Y. C. Fung [4] introducing a pseudo strain energy function and fitting experimental data to produce its parameters. Furthermore the relationship between wall shear stress and intimal thickening for the abdominal aorta was determined by Micheal Bonert et al. [5], who measured experimentally the wall shear stress using the laser photochromic dye tracer technique.

Imaging the mechanical properties of thrombosis, plaques and arterial wall can aid in the characterizing and understanding of the pathogenesis of the cardiovascular disease. Intravascular ultrasound is a widely used method of imaging the coronary arteries. Strain and elasticity images are generated to determine mechanical properties of arterial tissues [6], [7], [8]. Toshiaki Shishido *et al.* developed a new technique by applying minute vibrations at various frequencies to evaluate regional myocardial elastance and Young,s moduli at different

regions [9]. Blood flow and pressure in the larger systemic arteries are modelled by structuring a tree attached to the terminal branches in which the root impedance is estimated using an approach based on a linearization of the viscous axisymmetric Navier-Stokes equations[10].

In the present work, periodic pressure pulses are assumed to act in a radial direction on the inner wall of an arterial section. The periodic pulses are represented mathematically by a Fourier series. These pulses are considered to fluctuate between maximum values of a fraction of the mean arterial pressure. They approximately follow the known shape of the arterial pulse. Though the *in vivo* reported arterial pulses show faster rise than decay [11], we assume here that they are symmetric pulses. Biaxial symmetry of the artery is assumed as well. The radial pressure pulses are assumed to follow the heart beats with the same frequency. Some of the reported values concerning mechanical responses of arteries [1], [2], [3], [12] are adopted.

An R-L-C double section series circuit is proposed to simulate the double layer arterial wall. The flow of electric charge in the circuit is analogous to the strain fluctuations, the input voltage to the radial pressure pulses and the current is the pulse velocity. Parameters required to implement the mathematical model at hand are changed in appropriate ranges to show arterial stiffness, pulse damping, variation of the elasticity constant and heat loss.

The Model

A simplified model, introduced earlier [13], simulates the viscoelastic behaviour of a single layer blood vessel in response of the blood pulses acting in a radial direction on its inner wall. The proposed double layer arterial section is modelled as shown in Fig. 1.

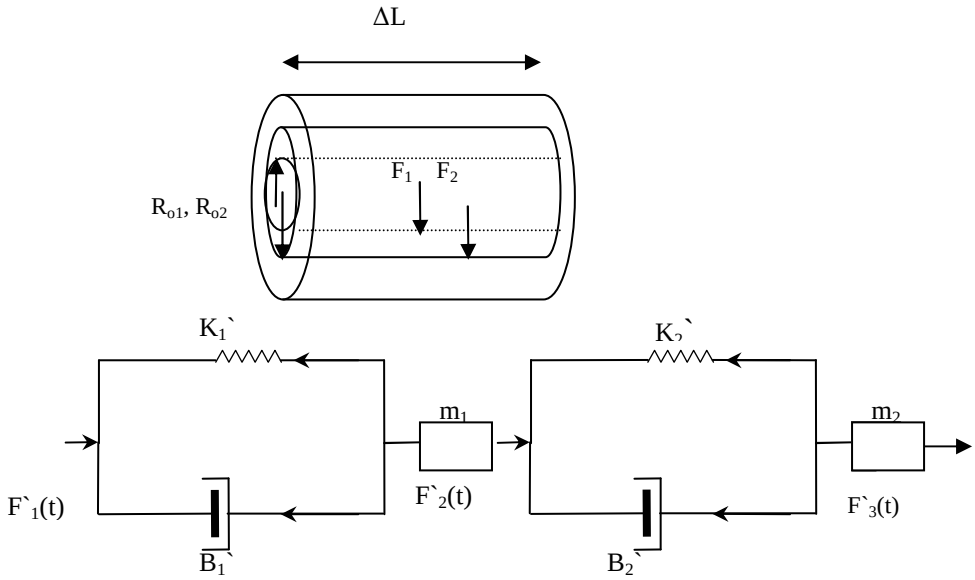

Fig.1. Double layer mechanical model

A section of unit length of the artery is assumed to be a double layer viscoelastic cylindrical tube. The inner layer is assumed to be the intima media layer with elasticity modulus, E_1, while the outer one is the adventitial layer with E_2 . The inner radii of the two layers are R_{01} and R_{02} .The elastic behaviour of the artery segment is represented by that of a spring with spring constants, K_1`and $K_2$` while its viscous component is represented by a dash pot of friction coefficients B_1` and $B_2$` for the first and second layers respectively.

The second degree differential equation that governs the strain functions, $\varepsilon_1(t)$ and $\varepsilon_2(t)$ of the interface of the two layers and the inertial forces on them is as follows:

$$\frac{d^2\varepsilon_1(t)}{dt^2} = F_1(t) - B_1\frac{d\varepsilon_1(t)}{dt} - K_1\varepsilon_1(t)$$
$$\frac{d^2\varepsilon_2(t)}{dt^2} = F_2(t) - B_2\frac{d\varepsilon_2(t)}{dt} - K_2\varepsilon_2(t) \qquad (1)$$

where $B_1=B_1`/\rho_{\ell 1}$ , $K_1=K_1`/\rho_{\ell 1}$, $B_2=B_2`/\rho_{\ell 2}$ , $K_2=K_2`/\rho_{\ell 2}$, are normalized viscosity and elasticity coefficients to the linear mass densities, $\rho_{\ell 1}$, $\rho_{\ell 2}$ for inner and outer layers respectively. $F_1(t)$ is defined as the normalized radial component of the force due to blood pressure pulses, $P_1(t)$, pulsating on the inner layer such that:

$$F_1(t) = 2\pi P_1(t) / \rho_{\ell 1} \qquad F_2(t) = 2\pi P_2(t) / \rho_{\ell 2} \tag{2}$$

Mathematical Analysis

Firstly, $P_1(t)$ is assumed to take the waveform of a biphasic exponential rise exponential decay periodic function, given below:

$$P_1(t) = \begin{cases} P_o(1-2e^{-t\pi/T}) & 0 \le t \ge T \\ P_o(2e^{-\pi(t-T)/T} - 1) & T \le t \ge 2T \end{cases} \tag{3}$$

The proposed model assumes the same time interval, T, for the rise and decay pulse components and hence equal decay constants. It is assumed that the pulses fluctuate between equal values $\pm P_o$.

A Fourier series is deduced to represent $P_1(t)$. The coefficients of the Fourier series, produced by integration on the two time intervals given in eq.(3), give a final form of:

$$P_r(t) = \frac{2}{\pi} P_0 \sum_{n=1}^{\infty} \begin{matrix} (e^{-\pi}(\cos n\pi - 1) - (\cos n\pi + 1))\cos\dfrac{n\pi t}{T} \\ + \dfrac{1}{n}(e^{-\pi}(\cos n\pi - 2) - (\cos n\pi + 1))\sin\dfrac{n\pi t}{T} - \dfrac{1}{n}e^{-\pi}\cos n\pi \end{matrix} \tag{4}$$

Fig. 2 shows the pressure periodic waveform. The maximum value P_0, is assumed to be a 10% of the mean arterial pressure in adults.

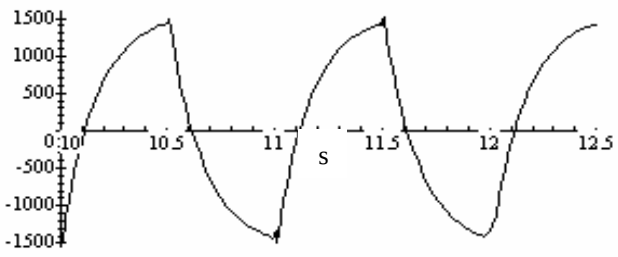

Fig. 2. The figure shows a simulation of the rise and fall of the radial pressure in Pa

An equivalent electrical model, introduced as a double R-L-C series circuit, is analogous to the mechanical model above. We give full analogy between the mechanical system and the equivalent electrical circuit in details in appendix 1. We should note that the stress on each layer is the difference in pressures on the lining interfaces. Thus the stress on the inner layer, T_1, is difference in pressure, P_1-P_2, and the stress, T_2, on the outer layer is P_2-P_3, where P_1 is the pressure on the inner wall, P_2 on the interface between the two layers and P_3 is that on the outer wall.

Consequently, the strain is calculated as:

$$\epsilon_1(t) = q_1 - q_2$$
$$\epsilon_2(t) = q_2 - q_3 \tag{5}$$

where q_1, q_2 and q_3 are related to the respective currents in the equivalent electric circuit as follows:

$$q_1(t) = \int_0^t i1(t)\,dt, \quad q_2(t) = \int_0^t i2(t)\,dt, \quad q3(t) = \int_0^t i3(t)\,dt \tag{6}$$

Since P_1, P_2 and P_3 are analogous with V_1, V_2 and V_3, thus we can deduce the involved quantities in the *s*-domain as follows:

$$I_1(s) = Y_{eq}(s) V_1(s) \tag{7}$$

where Y_{eq} represents the total admittance of the two circuit section.

$$V_2(s) = V_1(s) - I_1(s)(R_1 + \frac{1}{sc_1})$$
$$V_3(s) = V_2(s) - I_3(s)(R_2 + \frac{1}{sc_2}) \quad (8)$$

Results

The stress and the strain waveform for each layer can be produced by eqs.(5-8). Strain pulses follow those of the applied radial pressure having the same frequency with a time delay. They fluctuate between equal values of $\pm \epsilon_0$.

Taking the strain response to be the difference between strains of boundary interfaces, results are given for different parameter sets in Table 1. The periodic time for one pressure pulse is 1s.

The first parameter set, is a simulation of normal performance with elasticity constants close to those of intima media and advetitia layers of real arteries.

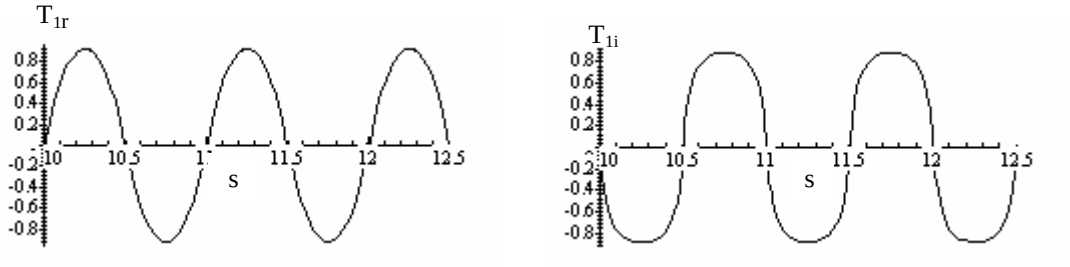

Fig.3. The stress waveform acting on the inner layer
real and imaginary components in kPa vs. time in s

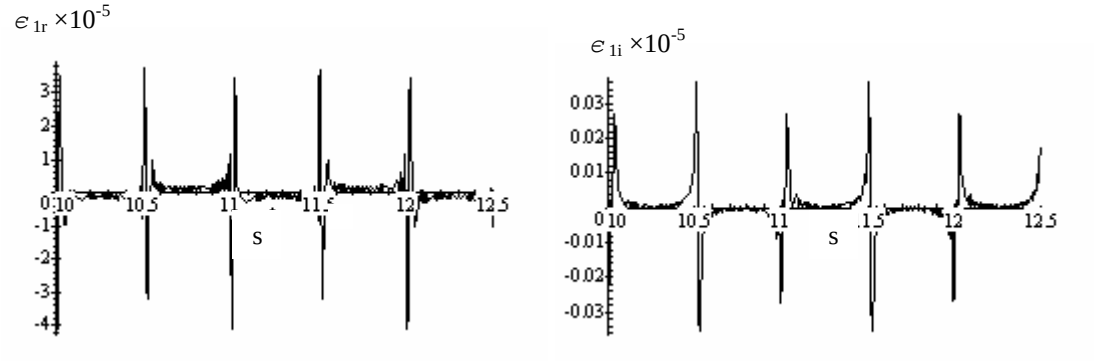

Fig.4. The strain waveform acting on the inner layer
real and imaginary components vs. time in s

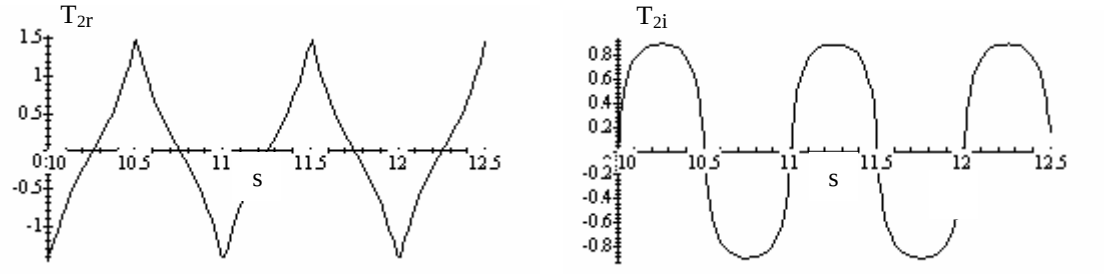

Fig.5. The stress waveform acting on the second layer,
real and imaginary components in kPa vs. time in s

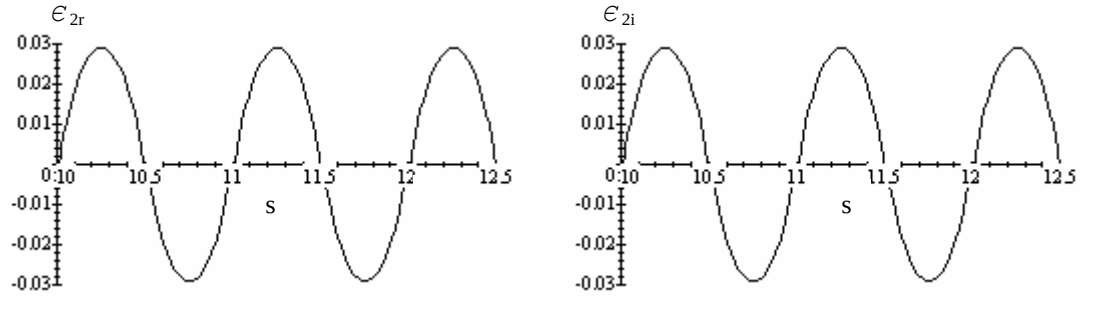

Fig.6. The strain waveform acting on the second layer, real and imaginary components vs. time in s

Figures 3 and 4 show the stress-strain response for the inner layer, intima media; whereas, Figs. 5 and 6 show the stress-strain response for the adventitia, outer layer. They show elastic response of about 3%, which is much higher than the inner layer. This is taken into account by parameters adjustment

Table 1. Normalized Parameter sets used as input for computer runs.

set	K_1 10^6 s^{-2}	K_2 10^6 s^{-2}	ϵ_{01r} 10^{-3}%	ϵ_{01i} 10^{-3}%	ϵ_{02r} %	ϵ_{02i} %	P_{diss} *w*/m	P_{str} *w*/m
1	8	0.05	3	0.03	3	2	83.850	101.640
2	4	0.8	0.5	0.008	0.4	0.4	13.775	19.7611
3	0.4	.02	0.1	8	6	6	1502.75	2486.04

For all sets P_0 and T are kept constant at 1.6 kPa and 0.5s respectively. $\rho_{\ell 1}$, $\rho_{\ell 2}$ are kept at 25*g/m* and 12*g/m* and B_1, B_2 have the values $0.4s^{-1}$ and $0.417s^{-1}$ respectively.

Fig. 7 shows the computed power versus time. The real component, P_{diss}, corresponds to the energy loss per second while the imaginary component represents the stored energy per second, P_{str}. The average values of the power dissipated and that stored, measured in *w/m*, computed over one pressure pulse for each set are given in Table 1.

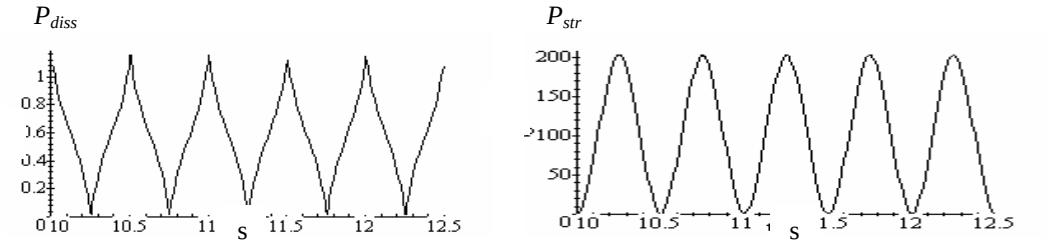

Fig.7. The power dissipated and that stored in *w*/m vs. time in s

The storage and loss moduli are computed using the above parameter sets. The average values calculated are shown in Table 2.

Table 2. Storage and loss moduli for a double layer section.

set	E_{loss1} 10^3 *kPa*	E_{str1} 10^3 *kPa*	E_{loss2} *kPa*	E_{str2} *kPa*
1	432.031	460.852	23.822	46.442
2	3744.905	4024.505	125.022	237.566
3	10.3577	11.0498	0.9822	1.8067

DISCUSSION:

Despite the enormous difficulties studying pulsating flow in an elastic tube of anisotropic material, the elastic analogy offers an adequate tool for approaching this case. The proposed model assumes linear stress-strain relationship and biaxial isotropy of the blood vessel. It offers a new perception towards the understanding of the mechanism of arterial pulsating nature. The elasticity modulus is computed using the stress and the strain complex functions for each layer.

The equivalent resistance, R_{eq}, is the component that is responsible for the dissipated energy per pulse per meter, e_{diss}. Whereas the equivalent reactance, X_{eq}, is the component that is responsible for the stored energy per pulse per meter, e_{st}. These can be deduced as follows:

$$e_{diss}(\mathrm{t}) = \frac{1}{T}\int_0^T i_1^2(t) R_{eq}\, dt, \quad e_{st}(\mathrm{t}) = \frac{1}{T}\int_0^T i_1^2(t) X_{eq}\, dt \qquad (9)$$

The results offer an understanding of how energy is stored and dissipated through a cyclic change of the radial pressure. Also the complex nature of the elasticity modulus is illustrated, in the absence of reliable experimental values for many biological constants of blood vessels. This work has to deal with hypothetical set of values that are believed to approach some previously reported values.

Accordingly the stress-strain pattern, the elasticity moduli, as well as the stored and dissipated power are dependant on the chosen set of values. The model proposed is valid to some extent according to reported experimental data. Furthermore, it shows that under all circumstances the strain developed, in both layers, lags the radial pressure and follows the pulsating wave shape. The elasticity, dissipated and stored power per unit length of both layers do as well.

References

[1] Yu Q,Zhou J, and Fung Y C, "Neutral axis location in bending and Young's modulus of different layers of arterial wall", Am J Physiol, H52-60, p 265, Jul 1993.

[2] Schulze-Bauer and Holzapfel, J.Biomechanics, 2003, Internet communications.

[3] Y. C. Fung, "Mechanical properties of living tissues", Springer, New York, second edition, 1993.

[4] J. Zhou. and Y. C. Fung, "The degree of nonlinearity and anisotropy of blood vessel elasticity", Proc. Natl. Acad. Sci. USA Vol. 94, pp. 14255-14260, Dec. 1997.

[5] Micheal Bonert, Richard L. Keask, Jagdish Butany, C. Ross Ethier, Jerry G. Myers, K. Wayne Johnston, and Matadial Ojha, "The relationship between wall shear stress distributions and intimal thickening in the human abdominal", Biomedical Engineering On Line, 2:18, doi:10.1186/1475-925x-2-18, 2003.

[6] Charles Choi, Biomedical Engineering Dept., Biomedical Ultrasonic lab., Univ. of Michigan, internet communication.

[7] Mingxi Wan, Yangamei Li, Junbo Li Yaoyao Cui, and Xiaodong Zhou, "Strain imaging and Elasticity Reconstruction of Arteries Based on Intravascular Ultrasound Video Images" IEEE Transactions on Biomedical Engineering, Vol. 48, No. 1, 2001.

[8]S. Cirovic, C. Walsh, W. D. Fraser, "A model of pulse transmission in the intracranial arteries", Intrnet communications.

[9] T.Shishido, M. Sugimachi, O. Kawaguchi, H.Miyano, T. Kawada, W. Matsuura, Y. Ikeda, T. Sato, J. Alexander Jr., and Kenji Sunagawa, "A new method to measure regional myocardial time-varying elastance using minute vibration", Am J Physiol Heart Circ Physiol, Vol. 274, issue 4, H1404-H1415, April 1998.

[10] Mette S. Olufsen, "Structured tree outflow condition for blood flow in larger systemic arteries. " Am J Physiol Heart Circ Physiol, Vol. 276, issue 1, H257-H268, January 1999.

[11] Harold J. Metcalf, " Topics in Classical Biophysics", Prentice-Hall, inc., New Jersey, May 1979.

[12] Ed VanBavel, Pier Siersma, and Jos A.E.Spaan, "Elasticity of Passive Blood Vessels: A New Concept", Am J Physiol Heart Circ Physiol, Vol.10, July 2003.

[13] M. A. El-Naggar, and M. A. El-Messiery, "The viscoelastic response of blood vessels under the effect of pulsating pressure", Proceedings of the biological effects of the EMFs, 3rd international workshop, Kos, Greece, Vol.11, Oct. 2004.

APPENDIX 1

The second order differential equation that governs the electrical charge Q with circuit components and input voltage V_0 is:

$$\frac{d^2Q(t)}{dt^2} = V_0(t)/L - \frac{R}{L}\frac{dQ(t)}{dt} - \frac{1}{LC}Q(t) \qquad (10)$$

By analogy between the two systems, mechanical and electrical, we note that:

$V_0(t) \leftrightarrow 2\pi P_1(t)$, $R/L \leftrightarrow B$, $1/LC \leftrightarrow K$, $L \leftrightarrow \rho_\ell$

THE ELECTROMAGNETIC WAVES OF 950 MHz, GSM MOBILE PHONE SYSTEM AND ACQUISITION PHASE OF SPATIAL MEMORY

MAJID JADIDI

PHYSIOLOGY RESEARCH CENTER, SEMNAN UNIVERSITY OF MEDICAL SCIENCES, SEMNAN, IRAN

Jadidim@Hotmail.com

S.M.P. FIROOZABADI

DEPARTMENT OF MEDICAL PHYSICS, TARBIAT MODARES UNIVERSITY, TEHRAN, IRAN

Pourmir@Modares.ac.ir

ALI RASHIDY-POUR

PHYSIOLOGY RESEARCH CENTER, SEMNAN UNIVERSITY OF MEDICAL SCIENCES, SEMNAN, IRAN

Rashidy-pour@Sem-ums.ac.ir

BAHRAM BOLOURI

DEPARTMENT OF MEDICAL PHYSICS, IRAN UNIVERSITY OF MEDICAL SCIENCES, TEHRAN, IRAN

BBolouri@Iums.ac.ir

YAGHOUB FATHOLLAHI

DEPARTMENT OF PHYSIOLOGY, TARBIAT MODARES UNIVERSITY, TEHRAN, IRAN

Fatolahi@modares.ac.ir

Abstract

With increasing in mobile communications, exposure to electromagnetic fields due to base station antenna has increased. This study was planned for evaluating the effects of whole-body exposure to 950 MHz GSM electromagnetic field on acquisition phase of spatial memory.

35 naive male Wistar Rats (3 month old, 220 $^{+}$15 g) randomly divided in three groups (control, sham-exposed and exposed) and were trained in a circular Morris water maze (3 days at 2 blocks, with 3 hours interval between blocks) to locate a submerged platform. The exposure program was planned for 10 session (45 min. and Power density = 0.835 mW/cm^2). According to water maze training, exposure was done just before each training session.

Performances of animals were tested 24 hours after the last training, by a 60 second probe test. Evaluation indexes were escape latency at target and opposite quadrants, swim speed and length.

Analysis of the probe data test showed no significant difference between control, sham and 950 MHz exposed groups.

Results of this study provide no evidence indicating that acquisition phase of spatial memory can be affected by the whole-body exposure to 950 MHz electromagnetic field.

Keywords: Electromagnetic field, Base station, Spatial memory, Morris water maze

Introduction

The RF radiations engage the spectrum of electromagnetic waves between 3 KHz - 300 GHz. This field can induce thermal or non-thermal effects on biological medium. Stimulation of excitable tissues will occur readily below 1 MHz, while thermal effects occur at higher frequencies [5].

In the last decade, many researches studied the effects of exposure to electromagnetic fields (EMF) on different nervous system functions such as memory in human and animals. Some of these studies have revealed deficits on memory due to EMF exposure [4; 8-21], whereas other studies did not [2, 3, 6, 7, 26, 31]. Nowadays, with increase in mobile communications, exposure to EMF due to mobile handset and base station antenna has increased. There are concerns about the effects of mobile phone electromagnetic waves on human body functions. These concerns emerge from results of epidemiological studies contributed to effects of mobile phone on human body. For example some of reports indicated that, mobile phone waves not only in regular power density but also in power density less than limited allowed (1 mW/cm^2), can produce headaches, warmth on ear, memory loss and fatigue.

These reports suggest that there is a significant association between calling time/number of calls per day and prevalence of these signs [10, 11, 12, 25, 29]. Although these results are important but in most of these studies the mobile phone handset frequency has been used and the effects of base station antenna waves have been less noticeable.

The GSM mobile phone system that is used in most of the countries has a frequency of either 900 or 1800 MHz (pulsed at 217 Hz, Band width of 200 KHz). The spectrum of 900 MHz has two band areas: 890-915 MHz that is specific for handset and 935-960 MHz that is specific for base station antenna.

To date, a few studies have evaluated the effects of EMF on memory functions in rodents. Studies performed by Wang and Lai [32] and Lai and Carino [18] reported deficits in two spatial learning tasks (Morris water maze and radial maze) after 45-min exposure to 2450 MHz EMF. On the other hand, studies reported by Cassel and colleagues failed to show any impairment of memory performance of rats in a radial maze after 45 min of whole-body exposure to a 2450- MHz EMF [2]. Findings of the last study were confirmed by recent studies showing no effect in spatial memory after daily 45 min of 900-MHz GSM exposure [6, 7]. The above findings indicate that the effects of GSM exposure on memory functions are still controversial. Moreover, to this date, we know no reports regarding the effects of exposure to 950 MHz waves, as a frequency in middle of base station band (935-960 MHz) on the memory function. There fore, the aim of this study was to examine the effects of exposure to 950 MHz waves, emitted by base station antenna, on acquisition phase of spatial memory in a Morris water maze.

Materials and methods

Subjects

35 naive male Wista rats (3 month old, 225 $^{+}$25 g) were divided randomly in to three groups: control (n=12), sham-exposed (n=11) and EMF exposed (n=12). Rats were maintained on a 12-h light-dark cycle and with an ambient temperature of 21^{o}C.They were housed in a maximum of six rats per breeding cage and allowed access to food and water ad libitum. All experiments were performed between 9:00 a.m and 13:00 p.m during the light cycle.

Morris Water Maze training

The behavioral training and testing was conducted in a water maze. The water maze was a blue circular pool (140 cm in diameter and 50 cm high) filled to a 25 cm depth with 22±2 ^{0}C water [27]. A circular glass platform (diameter: 11cm) was placed at the center of one quadrant (North-East quadrant) of the maze and submerged 3 cm below the surface of the water. The maze was located in a room containing several visual extra-maze cues.

Each animal was released into the water from the wall of the maze at arbitrarily defined east, south, west, and north points. The sequence of points of release into the water followed a random order. The animal was allowed to find the platform and land on it. If it could not find the platform within 1 minute, it was guided manually to the platform.

After finding the platform, it was allowed to stay there for 45 second before another trial. Performance in the maze was carried out and saved in a computer by an infrared receiver mounted on the roof.

The Morris water maze training program was planned for 3 days at 2 blocks, with 3 hours interval between blocks and 5 trials in each block. Performance of each rat was tested 24 hours after the final training day in a probe trial (60s) during which the platform was removed. Evaluation indexes were time spent in target quadrant, swim speed and total swim length during the probe test.

Electromagnetic field exposure

For whole body exposure to EMF, a 950 MHz GSM simulator (pulsed at 217 Hz and band width of 200 KHz, made by Khaje–Nasir Toosi University, Tehran, Iran) was used. It was connected to a 15 cm rod antenna fixed at the center of a circular plastic chamber (diameter = 30 cm). The animal could freely move inside the chamber. To prevent unknown exposure to reactive area of EMF, some of the near field restricted by a plastic mesh (radius = 5 cm). The power density inside the chamber was measured with RF meter (Narda 8716, USA) in different distances with 5 cm height from the base of antenna. With these records, the average value for power density was 0.835 mW/cm^2. The exposure program was consisted of ten 45 minute irradiation (as Lai et al., 1994). One day before running maze training, each animal exposed or sham-exposed to 4 sessions of 45 minute EMF with intervals of 1 hour. Subsequently, in 3 days, prior to each training session, animals were exposed to EMF or sham-exposed for 45 minute. The exposure room was adjacent to the experimental room.

Statistical analysis

The training data was analyzed with a one way analysis of variance (ANOVA) with trials as a repeated measure. Probe trial retention measures were analyzed with a two–way ANOVA. Tukey's *posthoc* test was performed to determine the source of detected significances. Values of $P<0.05$ were considered as significant

Results

All rats learned to locate the platform during training as indicated by decreasing escape latencies as training progressed (Fig.1). A two way ANOVA (group × block) with block as repeated measures showed significant effects of block ($P<0.001$), and no significant effects of groups [$F(3, 33) = 1.596$, $p=0.217$].

Fig.2, illustrates the retention performance as assessed by time spent in the four quadrants. A two way ANOVA (group × quadrant) showed significant effects of quadrants ($P<0.001$), and no significant effects of groups [$F(3, 33) = 1.02$, $p=0.368$].

Fig.3, illustrates the swim path data during the probe test. One- way ANOVA indicated no significant differences among the groups [$F(2, 31) = 2.334$, $p=0.114$].

Fig. 4 illustrates mean swim speed of rats during probe test. A one way ANOVA showed no significant differences between groups ($p>0.05$).

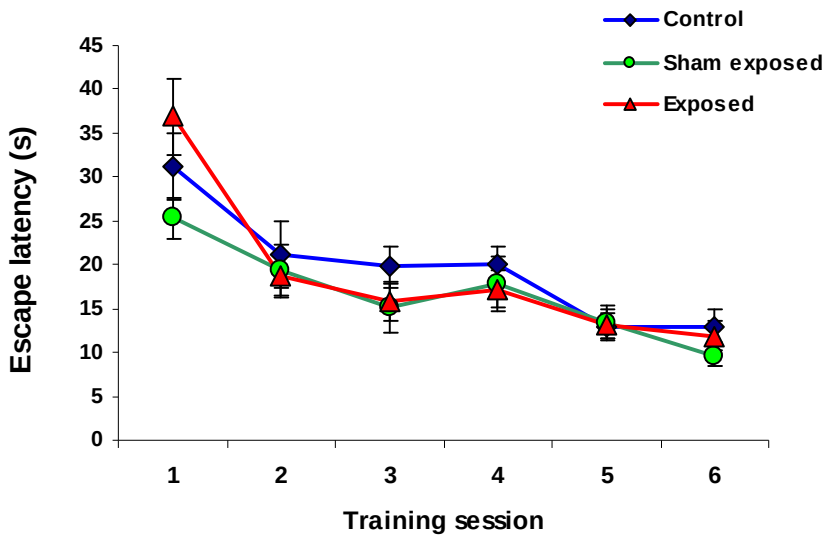

Fig. 1: Average escape time (Mean ± SEM); time to reach the platform after release into the water, during the trials.

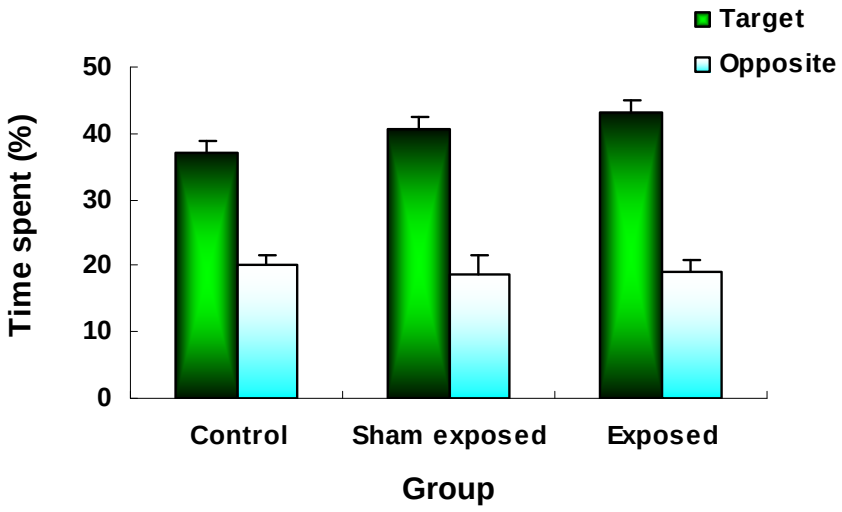

Fig 2: Average time spent (Mean + SEM) in three groups for target and opposite areas during probe trials.

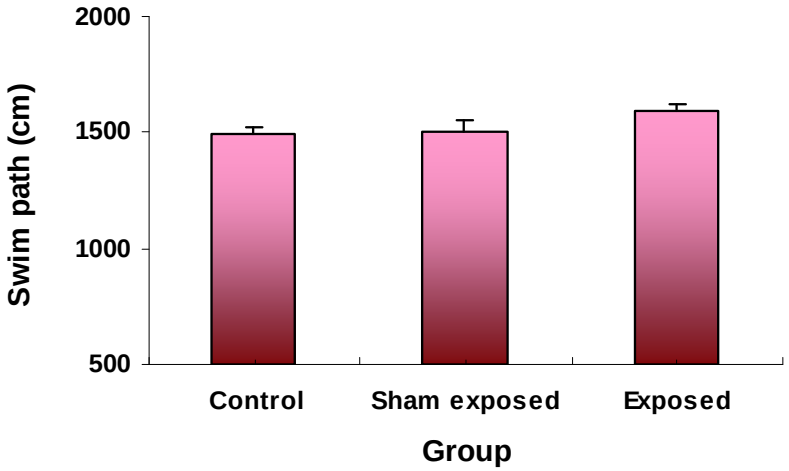

Fig. 3: Average swim path (Mean + SEM) in four groups during probe trials of acquisition phase.

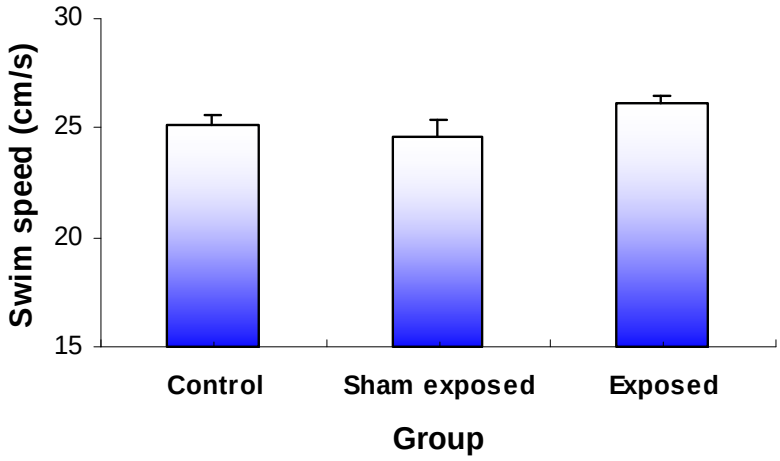

Fig. 4: Average swim speed (Mean + SEM) of the rats during probe trials in acquisition phase.

Discussion

The RF radiations engage the spectrum of electromagnetic waves between 3 KHz - 300 GHz. This field can induce thermal or non-thermal effects on biological medium. Stimulation of excitable tissues will occur readily below 1 MHz, while thermal effects occur at higher frequencies [5]. The mobile phones and their base station electromagnetic fields have low specific absorption rate that induce very low rise in brain temperature. Thus, the possible biological effects of mobile phone systems on brain would be expected to be the non-thermal effects [13]. Thus, the aim of this study was to examine the effect of exposure to 950 MHz waves, emitted by base station antenna, on spatial memory.

The findings of the present experiments indicate that acute whole body exposure to 950 MHz waves of GSM mobile phone system (pulsed at 217 Hz) dose not affect acquisition of spatial navigation in rat.

Our finding is in agreement with recent studies showing no effects of electromagnetic field on performance of rat or mice in an 8-arm radial-maze task [2, 17, 31]. Moreover, studies of Dubreuil et al., [6, 7] showed that head only exposure to GSM 900-MHz electromagnetic fields, did not alter rat's memory in spatial (radial maze) and non-spatial tasks. On the other hand the results of studies performed by Wang and Lai [32] and Lai and his colleagues [19] indicated that 45 min exposure to a 2450–MHZ electromagnetic fields induced deficits in spatial memory functions in Morris water maze and radial maze tasks.

Lai et al., [18] have shown that low level microwave irradiation could alter the cholinergic transmission in the hippocampus and cortex. Since cholinergic system plays an important role in memory processing, Lai et al., claimed that exposure to 2450–MHZ electromagnetic fields alter activity of this system in a way that produces impairment in spatial memory functions [17, 19].

The results of the present study are in contrast with the study of Wang and Lai indicting an impairment of spatial memory in a water maze induced by an acute exposure to electromagnetic fields. This discrepancy may be due to some subtle differences in the training paradigm (two blocks of five trials with a 3 min interval versus two blocks of 6 trials with a 3 h interval), time of probe test (24 h versus 1 h after the last training) or the characteristics of the used electromagnetic fields (950 MHz pulsed with 217 pulses/s, average power density 0.835 mW/cm^2 versus 2450-MHz pulsed with 500 pulses/s, average power density 2 mW/cm^2), and duration of exposure (45 min versus 1 h immediately before each training session). Moreover, previous studies have shown that hyperthermia can induce memory impairment [23], thus it is more likely that impairment reported by Wang and Lai can be due to consequences of a hyperthermia related to the whole body exposure [7].

The epidemiological studies were performed on human cases showed different results like animal experiments. Hocking et al., Oftedal et al. and Sandstrom et al., suggest that there is a direct relationship between the signs and calling time/number of calls per day [10, 11, 12, 25, 29]. In agreement with these results, studies on who lived in areas near the base station antenna showed irritability, depression, memory loss, concentration difficulties, vertigo, headache, sleep disturbances, feelings of discomfort and fatigue [2, 24, 28, 30]. The reported signs depend on duration of exposure, and the distance from antenna, and the antenna characteristics [2].

The results of the present study indicate that exposure to 950 MHz waves emitted by base station antenna had no effect on acquisition of rat's spatial memory in a water maze. Although this study was used as a model for understanding the effect of GSM electromagnetic field on acquisition phase of memory, further studies with a variety of intensities and durations of GSM electromagnetic fields are needed to test their effect on memory processing.

Acknowledgements

This study was supported by Iran Telecommunication Research Center, Tarbiat Modares University and Semnan University of Medical Sciences.

References

1] Bornkessel C, Stocker-Meier E. 2003. Results of a measurement programme concerning mobile phone base station emissions in North Rhine-Westphalia. Mobile Phone Base Station and Health. Dublin, May 15th and 16th, 2003.

2] Cassel JC, Cosquer B, Galiani R, Kuster N. 2004. Whole body exposure to 2.45 GHz electromagnetic fields does not alter radial-maze performance in rats. Behav Brain Res 155(1):37-43.

3] Cosquer B, Galini R, Kuster N, Cassel JC. 2005. Whole-body exposure to 2.45 GHz electromagnetic fields does not alter anxiety responses in rats: a plus-maze study including test validation. Behav Brain Res 156 (1):65-74.

4] Croft RJ, Chandler JS, Burgess AP, Barry RJ, Williams JD, Clarke AR. 2002. Acute mobile phone operation affects neural function in human. Clin Neurophysiol 113:1623-1632.

5] D'Andrea JA, Adair ER, Lorge JO. 2003. Behavioral and cognitive effects of microwave exposure. Bioelectromagnetics Supplement 6:S39-S62.

6] Dubreuil D, Jay T, Edeline JM. 2002. Does head-only exposure to GSM-900 electromagnetic fields effect the performance of rats in spatial learning tasks? Behav Brain Res 129:203-210.

7] Dubreuil D, Jay T, Edeline JM. 2003. Head only exposure to GSM 900 MHz electromagnetic fields does not alter rats memory in spatial and non-spatial tasks. Behav Brain Res 145:51-61.

8] Haarala C, Bjornberg L, Ek M, Laine M, Revonsuo A, Koivisto M, Hamalainen H. 2003. Effect of 902 MHz electromagnetic field emitted by mobile phone on human cognitive function: A replication study. Bioelectromagnetics 24(4):283-288.

9] Hermann DM, Hossmann KA. 1997. Neurological effects of microwave exposure related to mobile communication. J Neurol Sci 152:1-14.

10] Hocking B. 1998. Preliminary report: Symptoms associated with mobile phone use. Occup Med 48(6):357-360.
11] Hocking B, Westerman R. 2001. Neurological abnormalities associated with CDMA exposure. Occup Med 51(6):410-413.
12] Hocking B, Westerman R. 2003. Neurological effects of radiofrequency radiation. Occup Med 53:123-127.
13] Ilhan A, Gurel A, Armutcu F, Kamisli S, Iraz M, Akyol O, Ozen S. 2004. Ginkgo biloba prevents mobile phone-induced oxidative stress in rat brain. Clinica Chimica Acta 340:153-162.
14] Jadidi M, Firoozabadi SMP, Sajadi AA, Taherian AA. 2005. Acute exposure to 50 Hz, 8 mT Magnetic field can impair rat spatial memory. 3rd European Medical & Biological Engineering Conference. Prague, November 20th -25th, 2005.
15] Koivisto M, Krause CM, Revonsuo A, Laine M, Hamalainnen H. 2000a. The effects of electromagnetic field emitted by GSM phones on working memory. Neuroreport 11:1641-1643.
16] Koivisto M, Revonsvo A, Krause C, Haarola C, Sillanmaki L, Laine M, Hamalainen H. 2000b. Effects of 902 MHz electromagnetic field emitted by cellular telephones on response times in humans. Neuroreport 11:413-415.
17] Lai H. 2004. Interaction of microwaves and a temporally incoherent magnetic field on spatial learning in the rat. Physiology & Behavior 82:785-789.
18] Lai H, Carino M. 1999. 60 Hz magnetic fields and central cholinergic activity: effects of exposure intensity and duration. Bioelectromagnetics 20:284-289.
19] Lai H, Horita A, Guy AW. 1994. Microwave irradiation affects radial-arm maze performance in the Rat. Bioelectromagnetics 15:95-104.
20] Lass J, Tuulik V, Ferenets R, Riisalo R, Hinrikus H. 2002. Effects of 7 Hz-modulated 450 MHz electromagnetic radiation on human performance in visual memory tasks. Int J Radiat Biol 78(10):937-944.
21] Mann K, Roschke J. 1996. Effects of pulsed high-frequency electromagnetic fields on human sleep. Neuropsychology 33: 41-47.
22] McEwen BS, Sapolsky RM. 1995. Stress and cognitive function. Current Opinion in Neurobiology 5:205–216.
23] Mickley GA, Cobb BL, Mason PA, Farrell S. 1994. Disruption of a pulsative working memory task and selective expression of brain c-fos following microwave-induced hyperthermia. Physiol Behav 55:1029-1038.
24] Navarro EA, Segura J, Gomez-Perretta C, Portoles M, Maestu C, Bardasano JL. 2003. About the effects of microwave exposure from cellular phone base stations: A first approach. Mobile Phone Base Station and Health. Dublin, May 15th and 16th, 2003.
25] Oftedal G, Wilen J, Sandstrom M, Mild KH. 2000. Symptoms experienced in connection with mobile phone use. Occup Med 50(4):237-245.
26] Preece AW, Davies-smith A, Wesnes K, Butler S, Lim E, Varey A. 1999. Effect of 915 MHz simulated mobile phone signal on cognitive function in man. Int J Biol. 75(4):447-456.
27] Rashidy-Pour A, Motamedi F, Motaghed-Laijani, Z. 1996. Effects of reversible inactivation of the medial septal area on reference and working memory versions of the Morris water maze. Brain Res 709:131-40.
28] Roosli M, Moser M, Meier M, Braun-Fahlander C. 2003. Health symptoms associated with electromagnetic radiation – A questionnaire survey. Mobile Phone Base Station and Health. Dublin, May 15th and 16th, 2003.
29] Sandstrom M, Wilen J, Oftedal G, Hansson Mild K. 2001. Mobile phone use and subject symptoms.Comparision of symptoms experienced by users of analogue and digital mobile phones. Occup Med 51(1):25-35.
30] Santini R, Santini P, Danze JM, Le Ruz P, Seigne M. 2002. Study of the health of people living in the vicinity of mobile phone base stations: I. Influences of distance and sex. Pathol Biol 50:369-73.
31] Sienkiewicz ZJ, Blackwell RP, Haylock RG, Saunders RD, Cobb BL. 2000. Low-level exposure to pulsed 900 MHz microwave radiation does not cause deficits in the performance of a spatial learning task in mice. Bioelectromagnetics 21:151-158.
32] Wang B, Lai H. 2000. Acute exposure to pulsed 2450 MHz microwaves affects water-maze performance of rats. Bioelectromagnetics 21:52-56.

LOW-POWER DENSITY OF 950 MHz FIELD OF GSM MOBILE PHONE SYSTEM DOES NOT AFFECTS LONG-TERM POTENTIATION IN THE DENTATE GYRUS

MAJID JADIDI

DEPARTMENT OF MEDICAL PHYSICS, TARBIAT MODARES UNIVERSITY, TEHRAN, IRAN
Jadidi@modares.ac.ir

S. M.P. FIROOZABADI

DEPARTMENT OF MEDICAL PHYSICS, TARBIAT MODARES UNIVERSITY, TEHRAN, IRAN
Pourmir@Modares.ac.ir

ALI RASHIDY-POUR

PHYSIOLOGY RESEARCH CENTER, SEMNAN UNIVERSITY OF MEDICAL SCIENCES, SEMNAN, IRAN
Rashidy-pour@Sem-ums.ac.ir

BAHRAM BOLOURI

DEPARTMENT OF MEDICAL PHYSICS, IRAN UNIVERSITY OF MEDICAL SCIENCES, TEHRAN, IRAN
BBolouri@Iums.ac.ir

YAGHOUB FATHOLLAHI

DEPARTMENT OF PHYSIOLOGY, TARBIAT MODARES UNIVERSITY, TEHRAN, IRAN
Fatolahi@modares.ac.ir

Abstract

Over the last decade, exposure to electromagnetic field due to base station antenna has increased. This in vivo study was planned for evaluating the effects of whole-body exposure to 950 MHz field of GSM mobile phone system on dentate gyrus long-term potentiation.

24 naive male Wistar rats (3 month old, 225 $\pm$ 25 g) randomly divided in three groups (sham–exposed, GSM and continuous field exposed).

The exposure program was planned for 10 sessions at 3 days. Animals were exposed to electromagnetic field for 45-min in a circular plastic chamber (mean power density = 0.835 mW/cm^2). Immediately after end exposure, anesthesia was induced for LTP induction. Field potentials were recorded and analyzed using the population spike amplitude and EPSP slope for 60-min.

There were no significant differences in population spike amplitude, EPSP slope and EPSP slope maintenance among the three groups.

This experiment provides no evidence indicating that long-term potentiation can be affected by the whole-body exposure to low-power density of 950 MHz field of GSM mobile phone system.

Keywords: Electromagnetic field, Base station, Long-term Potentiation

Introduction

Nowadays, with increase in mobile communications, exposure to EMF due to mobile handset and base station antenna has increased. The GSM mobile phone system that is used in most of the countries has a frequency of either 900 or 1800 MHz (pulsed at 217 Hz, Band width of 200 KHz). The spectrum of 900 MHz has two band areas: 890-915 MHz that is specific for handset and 935-960 MHz that is specific for base station antenna.

In the last decade, many researches studied the effects of exposure to mobile phone electromagnetic fields (EMF) on different nervous system functions such as memory in human and animals. Some of these studies have revealed deficits on memory due to EMF exposure [5, 8-20, 23, 28], whereas other studies did not [3, 4, 6, 7, 31].

A number of studies have suggested that low frequency EMF may interact with learning and memory processes [18, 24]. Nevertheless, other studies have suggested that much higher frequency fields may also affect spatial memory [16, 18, 33]. Wang and Lai [18, 33] reported deficits in two spatial learning tasks (Morris water maze and radial maze) after 45-min exposure to continuous or pulsed, 2450 MHz EMF.

Since the spatial memory was accepted to have a substantial hippocampal involvement, these studies suggest that EMF may affect hippocampal function. This is supported by a report that exposure to 700 MHz continuous field can change electrical activity in the hippocampus of rat [32].

Long-term potentiation (LTP) is a long-lasting increase in synaptic efficacy resulting from the high-frequency stimulation of afferent fibers [1]. LTP in the hippocampus is thought to be a typical model of synaptic plasticity related to learning and memory [21].

To get insights into the cellular effects that 950 MHz exposure (as a frequency in middle of base station band) could induce on hippocampus, we decided to conduct a general study and investigated the consequences of exposure to continuous and pulsed (GSM) waves of 950 MHz EMF. Thus, the aim of this study was to examine the effects of exposure to 950 MHz fields on dentate gyrus (DG) long-term potentiation.

Materials and methods

Electromagnetic field exposure

For whole body exposure to EMF, a 950 MHz GSM simulator (made by Khaje–Nasir Toosi University, Tehran, Iran) was used to produce 950 MHz fields, in continuous (without any modulation) or GSM (217 Hz modulated and band width of 200 KHz) waveform. It was connected to a 15 cm rod antenna fixed at the center of a circular plastic chamber (diameter = 30 cm). The animal could freely move inside the chamber. To prevent unknown exposure to reactive area of EMF, some of the near field restricted by a plastic mesh (radius = 5 cm). The power density inside the chamber was measured with RF meter (Narda 8716, USA) in different distances with 5 cm height from the base of antenna. With these records, the average value for power density was 0.835 mW/cm^2. The exposure room was adjacent to the experimental room.

The exposure program was consisted of ten × 45-min irradiation, delivered at 3 days. In the first and second days, each animal's exposed or sham-exposed to 4 sessions of 45-min irradiation, with 1 hour interval. Subsequently, in the third day, animals had two irradiation sessions. Immediately after the end exposure, anesthesia was delivered for LTP induction.

Animals

.

24 naive male Wistar rats (3 month old, 225 $\pm$ 25 g) randomly divided in three groups: sham–exposed (n=8), GSM (n=8) and continuous field exposed (n=8). Rats were maintained on a 12-h light-dark cycle and with an ambient temperature of 21^{o}C. They were housed in a maximum of 8 rats per breeding cage and allowed access to food and water ad libitum. All experiments were performed between 9:00 a.m and 13:00 p.m during the light cycle.

Surgical method

Animals were food and water deprived for 1 hour prior to surgery. For electrophysiological recording, the rats were anesthetized with Urethane (1.5 g/Kg, i.p., with supplemental injections as required) and stereotaxically implanted with a bipolar Teflon-coated silver electrode (125 µm diameter) in the perforant pathway (coordinates: AP -6.8 mm, L -4.1 mm, DV -3 mm, from skull surface) and a recording electrode (glass micropipette, 1- 3 MΩ, filled with physiological saline) in the dentate gyrus granule cell layer (coordinates: AP -2.8 mm, L -1.8 mm, DV-3 mm, from skull surface).

Electrophysiological recordings

The stimulating and recording electrodes were adjusted to produce maximum field potentials by applying a single pulse stimulus (0.1 Hz, 200µs pulse width) and recording field potentials in the DG granule cell layer.

Test stimulus intensity, sufficient to produce population spike (PS) with approximately 50% of maximum amplitude, was selected. After the 15-min base line recording, for LTP induction, two high frequency stimulus (250 Hz, 1s, 30s interval) were delivered to the perforant pathway with test stimulus intensity. The field potentials were recorded at 10, 20, 30, 40, 50 and 60-min after the tetanic stimulations, with 0.1 Hz pulse stimulus. The evoked responses were amplified, filtered (band-pass: 5 Hz – 3 KHz), sampled at a rate of 20 KHz and stored.

Evaluation indexes were PS amplitude, excitatory postsynaptic potentiation (EPSP) slop and EPSP maintenance. The LTP signal parameters were extracted as shown in Fig. 1. For EPSP maintenance, the percent of changes in each recording time calculated as: (Last record value – first record value / first record value) × 100. Data were statistically analyzed by repeated measures of ANOVA.

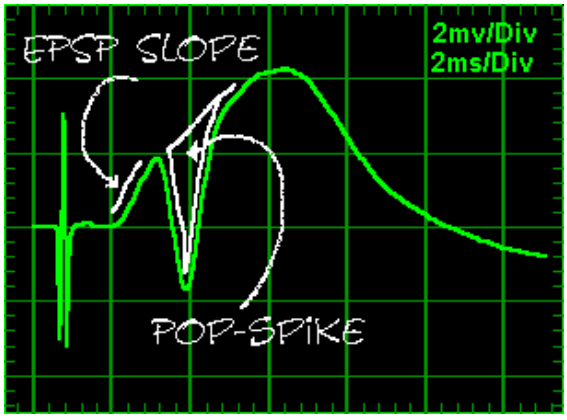

Fig.1: EPSP slope and PS amplitude that extracted from LTP signal.

Results

The results of EPSP slope of three groups, during the base line and 60-min recording are shown in fig.2. One-way ANOVA showed no significant differences among the groups.

Fig.3, illustrates the EPSP slope maintenance during the recording time. One-way ANOVA indicated no significant differences among the groups.

Results of the population spike amplitude are presented in fig.4. There were no significant differences between amplitudes of three groups during the base line recording and after LTP induction.

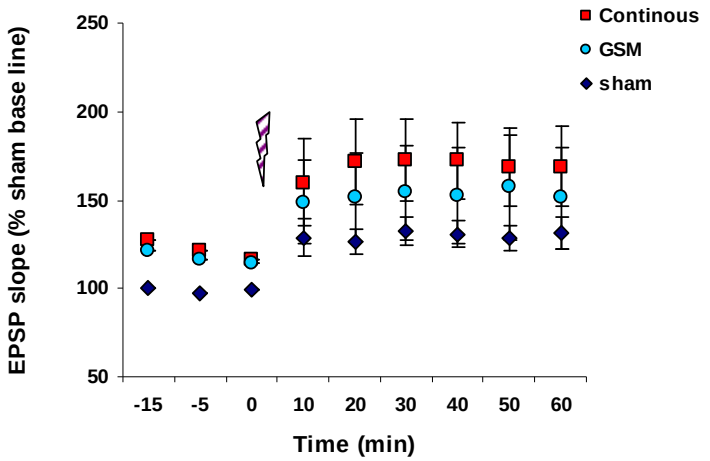

Fig.2: EPSP slope of three experimental groups (Mean ± SEM). Analysis of the data showed no significant differences between sham, continuous and GSM exposed groups.

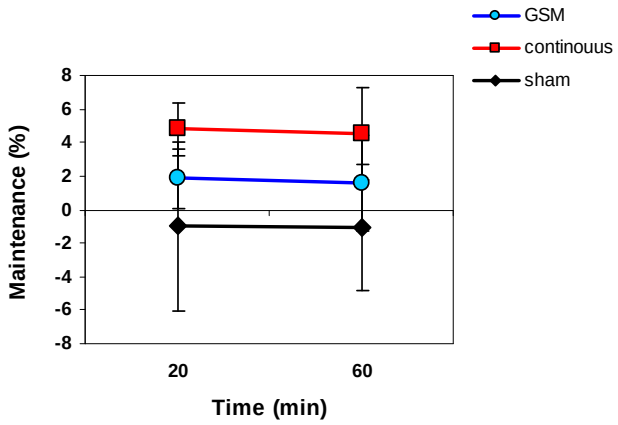

Fig.3: EPSP slope maintenance among the groups (Mean ± SEM). There was no significant difference between maintenance phase of the stimulated and sham exposed groups.

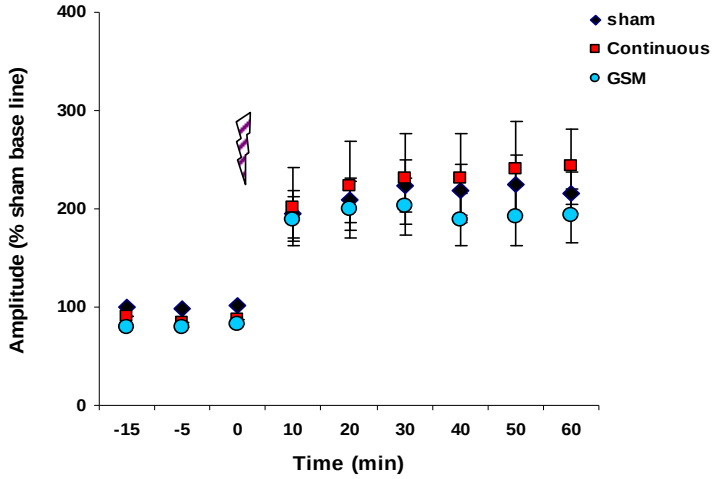

Fig.4: Population spike amplitude (Mean ± SEM). There were no significant differences between LTP induction and PS amplitude in the sham, continuous and GSM exposed groups.

Discussion

The mobile phones and their base station electromagnetic fields have low specific absorption rate that induce very low rise in brain temperature. Thus, the possible biological effects of mobile phone systems on brain would be expected to be the non-thermal effects [13]. This experiment results showed that exposure to continuous or GSM waves of 950 MHz EMF did not affect the LTP parameters. This is in agreement with recent studies showing that 900MHz EMF, in head-only exposure conditions, can not alter performances of rats in spatial memory and non-spatial memory tasks [7, 8]. Another study shows that 900MHz GSM EMF, dose not alter mice performance in an 8-arm radial-maze experiment [31].

On the other hand, Tattersall [32] indicated that exposure to 700 MHz continuous EMF for 5-15 minute reduced spontaneous epileptiform activity of rat hippocampus. Moreover, the results of Ogiue-Ikeda [26, 27] experiments signified the effect of low frequency magnetic field on EPSP slope of LTP.

Lai and Carino [18] found that low level microwave irradiations can alter the cholinergic functions in the rat hippocampus and cortex .This decrease in cholinergic activity in the brain can impair rat spatial memory [18].

Wang et al. and Lai [18, 33] showed that 45-min exposure to 2.45 GHz microwaves can alter spatial memory. But, Cassel et al. [3] could not access the same results, although their testing protocol was as similar as possible to that of the Lai et al. study.

The memory impairment reported by Lai et al and Wang and Lai [18, 33] can be related to a hyperthermia, because hyperthermia can produce amnesic effects [8].

Results of epidemiologic studies that performed on the effects of EMF, on who lived in areas near the base station antennas, showed that people's complaints (sleep disorders, headaches, concentration difficulties and fatigue) are due to EMF [25, 29] . These signs appeared after exposure and decreased slowly. Santini et al [30] suggest that the signs differ with increase of distance from antenna. In addition to distance, it seems that the antenna characteristics are important factors.

Bornkessel and Stocker-Meier [2] studies on 24 antennas showed that although electrical fields' intensities of these antennas are in standard limit, these results are time dependent and can differ with different antenna traffic along day. Although some of these studies suggest that exposure level is less than allowed level by ICNIRP in areas near the base station antenna, but the probability of long term exposure dangers of these waves for whom live in these areas are not rejected. In agreement with this point, Lai et al [17] showed, intensity and duration of exposure have interactions in effectiveness of the field on memory so that high-intensity/short-duration exposure and lower-intensity/longer-duration exposure have similar effects on frontal cortex and hippocampus cholinergic activity and memory. In addition, it is showed that chronic exposure to EMF can increase plasma corticosterone level [23]. This elevated level of corticosterone can induce time–dependent neuronal damage in hippocampus and impair cognitive function [22].

In the present research, the effect of exposure to 950 MHz waves emitted by base station antenna on electrical activity of hippocampus was investigated via the long-term potentiation. Although, this set of experiment provides no evidence indicating that LTP signal can be affected by the continuous or GSM waveform of 950 MHz EMF, further studies are needed to test other durations and intensities on brain activity. In addition, with

rapid increase of number of mobile phone users in the world and base station antenna in urban area, it seems that the knowledge about the effects of EMF on human body especially human brain is a necessity.

Acknowledgements

This study was supported by Iran Telecommunication Research Center, Tarbiat Modares University and Semnan University of Medical Sciences.

References

1] Bliss TVP, Lomo T. 1973. Long-lasting potentiation of synaptic transmission in the dentate area of the anaesthetized rabbit following stimulation of the perforant path. J Physiol. 232:357-374.
2] Bornkessel C, Stocker-Meier E. 2003. Results of a measurement programme concerning mobile phone base station emissions in North Rhine-Westphalia. Mobile Phone Base Station and Health. Dublin, May 15th and 16th, 2003.
3] Cassel JC, Cosquer B, Galiani R, Kuster N. 2004. Whole body exposure to 2.45 GHz electromagnetic fields does not alter radial-maze performance in rats. Behav Brain Res 155(1):37-43.
4] Cosquer B, Galini R, Kuster N, Cassel JC. 2005. Whole-body exposure to 2.45 GHz electromagnetic fields does not alter anxiety responses in rats: a plus-maze study including test validation. Behav Brain Res 156 (1):65-74.
5] Croft RJ, Chandler JS, Burgess AP, Barry RJ, Williams JD, Clarke AR. 2002. Acute mobile phone operation affects neural function in human. Clin Neurophysiol 113:1623-1632.
6] Dubreuil D, Jay T, Edeline JM. 2002. Does head-only exposure to GSM-900 electromagnetic fields effect the performance of rats in spatial learning tasks? Behav Brain Res 129:203-210.
7] Dubreuil D, Jay T, Edeline JM. 2003. Head only exposure to GSM 900 MHz electromagnetic fields does not alter rats memory in spatial and non-spatial tasks. Behav Brain Res 145:51-61.
8] Haarala C, Bjornberg L, Ek M, Laine M, Revonsuo A, Koivisto M, Hamalainen H. 2003. Effect of 902 MHz electromagnetic field emitted by mobile phone on human cognitive function: A replication study. Bioelectromagnetics 24(4):283-288.
9] Hermann DM, Hossmann KA. 1997. Neurological effects of microwave exposure related to mobile communication. J Neurol Sci 152:1-14.
10] Hocking B. 1998. Preliminary report: Symptoms associated with mobile phone use. Occup Med 48(6):357-360.
11] Hocking B, Westerman R. 2001. Neurological abnormalities associated with CDMA exposure. Occup Med 51(6):410-413.
12] Hocking B, Westerman R. 2003. Neurological effects of radiofrequency radiation. Occup Med 53:123-127.
13] Ilhan A, Gurel A, Armutcu F, Kamisli S, Iraz M, Akyol O, Ozen S. 2004. Ginkgo biloba prevents mobile phone-induced oxidative stress in rat brain. Clinica Chimica Acta 340:153-162.
14] Koivisto M, Krause CM, Revonsuo A, Laine M, Hamalainnen H. 2000a. The effects of electromagnetic field emitted by GSM phones on working memory. Neuroreport 11:1641-1643.
15] Koivisto M, Revonsvo A, Krause C, Haarola C, Sillanmaki L, Laine M, Hamalainen H. 2000b. Effects of 902 MHz electromagnetic field emitted by cellular telephones on response times in humans. Neuroreport 11:413-415.
16] Lai H. 2004. Interaction of microwaves and a temporally incoherent magnetic field on spatial learning in the rat. Physiology & Behavior 82:785-789.
17] Lai H, Carino M. 1999. 60 Hz magnetic fields and central cholinergic activity: effects of exposure intensity and duration. Bioelectromagnetics 20:284-289.
18] Lai H, Horita A, Guy AW. 1994. Microwave irradiation affects radial-arm maze performance in the Rat. Bioelectromagnetics 15:95-104.
19] Lass J, Tuulik V, Ferenets R, Riisalo R, Hinrikus H. 2002. Effects of 7 Hz-modulated 450 MHz electromagnetic radiation on human performance in visual memory tasks. Int J Radiat Biol 78(10):937-944.
20] Mann K, Roschke J. 1996. Effects of pulsed high-frequency electromagnetic fields on human sleep. Neuropsychology 33: 41-47.
21] Maren S, Baudry M. 1995. Properties and mechanisms of long-term synaptic plasticity in the mammalian brain: relationships to learning and memory. Neurobiol Learn Mem. 63:1-18.
22] McEwen BS, Sapolsky RM. 1995. Stress and cognitive function. Current Opinion in Neurobiology 5:205–216.
23] Mickley GA, Cobb BL, Mason PA, Farrell S. 1994. Disruption of a pulsative working memory task and selective expression of brain c-fos following microwave-induced hyperthermia. Physiol Behav 55:1029-1038.
24] Mostafa RM, Mostafa YM, Ennaceur A. 2002. Effects of exposure to extremely low-frequency magnetic field of 2 G intensity on memory and corticosterone level in rats. Physiology & Behavior 76:589- 595.

.

25] Navarro EA, Segura J, Gomez-Perretta C, Portoles M, Maestu C, Bardasano JL. 2003. About the effects of microwave exposure from cellular phone base stations: A first approach. Mobile Phone Base Station and Health. Dublin, May 15th and 16th, 2003.
26] Ogiue-Ikeda M, Kawato S, Ueno S. 2003. The effect of transcranial magnetic stimulation on long-term potentiation in rat hippocampus. IEEE Transactons on Magnetics 39(5):3390-3392.
27] Ogiue-Ikeda M, Kawato S, Ueno S. 2003. The effect of repetitive transcranial magnetic stimulation on long-term potentiation in rat hippocampus depends on stimulus intensity. Brain Res 993:222-226.
28] Preece AW, Davies-smith A, Wesnes K, Butler S, Lim E, Varey A. 1999. Effect of 915 MHz simulated mobile phone signal on cognitive function in man. Int J Biol. 75(4):447-456.
29] Roosli M., Moser M., Meier M., Braun-Fahlander C. Health symptoms associated with electromagnetic radiation – A questionnaire survey. Mobile Phone Base Station and Health. Dublin, May 15th and 16th, 2003.
30] Santini R, Santini P, Danze JM, Le Ruz P, Seigne M. 2002. Study of the health of people living in the vicinity of mobile phone base stations: I. Influences of distance and sex. Pathol Biol 50:369-373.
31] Sienkiewicz ZJ, Blackwell RP, Haylock RG, Saunders RD, Cobb BL. 2000. Low-level exposure to pulsed 900 MHz microwave radiation does not cause deficits in the performance of a spatial learning task in mice. Bioelectromagnetics 21:151-158.
32] Tattersall JEH, Scott IR, Wood SJ. 2001. Effects of low intensity radiofrequency electromagnetic fields on electrical activity in rat hypocampial slices. Brain Research 904:43-53.
33] Wang B, Lai H. 2000. Acute exposure to pulsed 2450 MHz microwaves affects water-maze performance of rats. Bioelectromagnetics 21:52-56.

INVESTIGATION ON THE CHANGES IN THE COMPOSITION OF AROMATIC COMPOUNDS OF RED CABBAGE IN RESPONSE TO STATIC MAGNETIC FIELD

MARYAM KHOSHSOKHAN MOZAFFAR[1], FAEZEH GHANATI[2], PARVIZ ABDOLMALEKI[2]

[1]DEPARTMENT OF BIOLOGY, FACULTY OF SCIENCE , AZAD UNIVERSITY OF QOM, QOM, IRAN
[2]DEPARTMENT OF BIOLOGY, FACULTY OF SCIENCE, TARBIAT MODARRES UNIVERSITY(TMU) , POB 14115-175, TEHRAN, IRAN.

Abstract
Treatment of Red cabbage (*Brassica oleracea* L. CV. Saccata) in vegetative growth phase with a 30 mT static magnetic field (SMF) resulted in altered content of lignin, anthocyanin and wall-bound phenolic compounds, compared with those of non-treated plants.
Exposure of red cabbage to the aforesaid static magnetic field during vegetative phase also induced the growth of the plants. The growth was accompanied by a delayed maturation and a lowered content of lignin in shoot and root system.

Introduction
During the past decade considerable evidence has been accumulated with regard to the biological effects of magnetic fields. Although several studies on bacterial and animal cells have shown that the magnetic fields influence a large variety of cellular functions, the mechanisms of its interaction with the living cells are still unclear and less studies have been conducted on plant cells. So far, many temporal and spatial electric phenomena occur during plant development (Moon 1999). Nevertheless, the magnetic field effects on the appearing of some cancers in human, embryogenesis in animals have been studied, seed germination and ion current and pollen-tube emergence in plants under MF also have been studied. The MF-induced inhibitory or stimulatory effects on the growth of plant tissues have seen to be species- specific, dependent on seasonal biological rhythms, field frequency and daily period of exposure (Moon 1999). In the present investigation the effect of static magnetic field on the growth and the metabolism of certain phenolic compounds of *Brassica oleracea* L. CV. saccata was subjected to study. It is well-known that phenolic compounds have various ecological and physiological roles and their contribution to defense system and UV protection have been studied. Phenolic compounds also inducible by different environmental stress and chemical stimuli (otto et al. 1999).
Brassica oleracea L. CV. saccata seeds were sterilized superficially with NaOCl and soaked in sterile Petri dishes on filter paper moisturized in distilled water. Seedlings were germinated and grown for 5 days at a constant temperature(25± 2°C) in a dark. after germination, the similar and entire seedlings were transferred to flower- pots and kept with a controlled condition at a constant temperature and light (25± 2°C and 6800 Luxe).
The plants were watered every day with ordinary water and every 15 days they were watered with Hoagland . after one month in the vegetative phase, the intact plants were selected and divided to treated and controlled groups. The treated groups were exposed to a 30 mT static magnetic field during 5 days and 5 hours in every day. The control group were maintained under a same environmental conditions as unexposed control. the samples were harvested in the end of treatment term.
Exposure to MF was performed by a locally designed MF generator. The electrical power was provided using a 220 V AC power supply equipped with variable transformer as well as a single-phase full wave rectifier. The maximum power and passing current were 1 KW and 50 A DC, respectively.
This system was designed to generate MF in range of 0.5 μT-30 mT. it consisted of two coils (each with 3000 turns of mm copper wire) on a U-shaped laminated iron core (to prevent eddy current losses). Using two vertical connectors, the arms of the U-shaped iron core were terminated in four circular iron plates covered with thin

layer of nickel (each 23 mm thickness, 260 cm in diameter). A water circulation system around the coils was employed to avoid the increase of the temperature. Without this system, the temperature of the coils increased, after the apparatus was working for 10 min, from 25 to 40 °C. Applying the water circulation system helped us to use apparatus for long exposures (5 h) as well as to keep the maintenance of the apparatus. The control cells were kept far enough from the MF producing apparatus, to avoid any potential exposure to the MF. Moreover, other electric appliances and laboratory facilities were not working; the control samples were therefore exposed only to the extremely low MF of the earth (60± 5 μT), as the treatment groups were too.

PPO was extracted from shoot and root systems, separately, in freshly prepared 200mM k-phosphate buffer (PH 6.8) followed by centrifugation at 12000x g . all these procedures were carried out at 2-4°C. Aliquots of supernatant were added to 200 mM k-phosphate buffer (PH 6.8) and freshly prepared 4-methylcatechol at a final concentration of 0.02 M. Enzyme activity was expressed as a change in absorbance at 410 nm per min per mg protein content of the homogenate. Protein concentration was determined by the method of Bradford (1976), using BSA as standard (Ghanati et al. 2002).

PO was extracted and the activity was determined in two fractions: the soluble PO fraction which is involved in the stress response(Pondolfini et al 1992) and the wall- bound PO fraction which is related to the lignification and suberization of cells(Fukuda and Komamine 1982 and Pando;fini et al 1992). The shoot and root systems , separately, were homogenized in 200 mM k-phosphate buffer (PH6.8) and centrifuged at 12000x g for 15 min at 2°C. the supernatant was used to assay soluble Po. The activity of wall- bound PO was determined in the ionically and covalently bound fractions, in turn. Pellets of the centrifugation were pooled, incubated with 0.2 M CaCl2 for 2h at room temperature, and centrifuged at was used to measure the activity of ionically wall- bound Po. The pellet was used directly for the assay of the covalently bound enzyme (Fukuda and Komamine 1982). The final reaction mixture (3 ml) was contained 200 mM k- phosphate buffer (PH 6.8) , 28 mM guaiacol and 5 mM H2O2. the enzyme activity of soluble and ionically fractions were expressed as the change in absorbance at 470 nm per min per mg protein content. The covalently enzyme activity was determined as the change in absorbance at 470 nm per min per cell wall dry weight (Ghanati et al. 2002).

The shoot and root systems, separately, were homogenized in ice- cold k-borate buffer (0.01 M, PH 8.8) containing 2 mM 2-mercaptoethanol and centrifuged at 16000x g for 10 min at 2°C. The supernatant was used as a crude enzyme solution. The reaction mixture (total 2ml) was composed of 0.5 ml of crude enzyme and 1 ml of extraction buffer (without 2-mercaptoethanol). The reaction started with addition of 0.5ml of 4mM phenylalanine and after 1 h incubation at 37°C, was stopped with 100 μl of 0.5 M HCl. The mixture was extracted three times with EtOAc. The EtOAc extract was air- dried, re- dissolved in 50% MeOH and analyzed by HPLC on an ODS-18 Ts column (15 cm x 6.0) at a flow rate of 0.5 ml min^{-1} with a linear gradient of 40-80% MeOH containing 0.1% HoAC and detected at 273 nm. The enzyme activity was expressed as the amounts of CA for 1h per mg of protein in the reaction mixture (Ghanati et al. 2002).

The shoot and root systems, separately, were homogenized in water after centrifugation at 1000x g, the pellet was sequentially washed with 10 volumes (v/w) of 0.5 mM CaCl2, EtOH, CHCl3- MeOH (2:1 v/v) and acetone followed by air- drying. Air-dried materials were desired as wall preparation. Phenolics were liberated from the wall preparations of samples with ammonium oxalate (20 mM, 70°C) and then with 0.1 M NaOH, under N2 for 24h. After acidification of both fractions to approximately PH 3.0 with HCl, phenolics were extracted three times with EtOAC, air- dried and re- dissolved in 50% MeOH before determination by HPLC as described for the determination of the PAL activity. Phenolics was detected at 280 nm (Ghanati et al. 2002; Liyama and Wallis 1990).

Isolation of cell walls was carried out as described for the determination of wall- bound phenolics. Lignin content was measured via a modified acetyl bromide procedure (Iiyama and Wallis 1990). In brief, 6 mg of fine-powdered wall preparation was treated with a mixture (total 2.5 ml) of 25% (w/w) AcBr in HOAC and 0.1 ml of 70% HClO4 at 70°C for 30 min with shaking at 10 min intervals. After cooling with ice, the digestion mixture was transferred to a 25 ml volumetric flask containing 5 ml of 2 M NaOH and 6 ml HOAC and made up to 25 ml. The lignin content was determined by measuring the absorbance at 273 nm using a specific absorption coefficient of 20.0g^{-1} L cm^{-1} (Ghanati et al. 2002; Liyama and Wallis 1990).

The anthocyanin of the shoot system tissues were extracted with cold methanol: water: acetic acid (11: 5: 1). The extraction was spun at 12000x g for 10 min. Anthocyanin concentration was determined by measuring optical absorption at 530 nm (Masakazu et al. 2003).

measurement of total sugar content in shoots and roots was based on phenol- sulfuric method, using glucose as standard (Duboise et al. 1956).

All experiments were repeated at least three times in triplicate. The data shown in the tables and figures are means ± SD. The significance of differences between treatments was evaluated by student's T- test.

PPO activity in shoot and root system were determined in both control and treatment groups. The activity PPO of root system of treated plants was higher than those of the control groups. The activity of PPO of shoot system of the treated plants was lower than that the control ones (Fig. 1).The activity of Po was measured in three fractions including soluble, ionically- and covalently-bound fractions (Table 1). The activity of three fractions

of PO increased in shoot system of treated plants under static magnetic field compared with those of the control groups. The results from measurement of PO activity in root system showed declining in treated plants in the three fractions relation to control ones. PAL enzyme was extracted from root and shoot system of red cabbage. PAL activity in the shoot and root system of treated plants was lower than those of the control ones (Fig. 2). The content of the phenols esterified to the wall polysaccharides of the shoot and root system under the control conditions and treatment with magnetic field, is shown in table 2.The content of these phenolics of root and shoot system under MF was significantly higher than those of the control ones. The lignin content of MF-treated shoot and root system decreased compared to control ones (Table 2).The results shown that the anthocyanin in shoot system has been increased in treated plants with 30 mT static magnetic field in comparison to the control groups (Fig. 3).
The total sugar were measured based on glucose standard curve in shoot and root system of samples. Compared to the samples under the control conditions, treatment samples significantly decreased total sugar (Fig. 4).

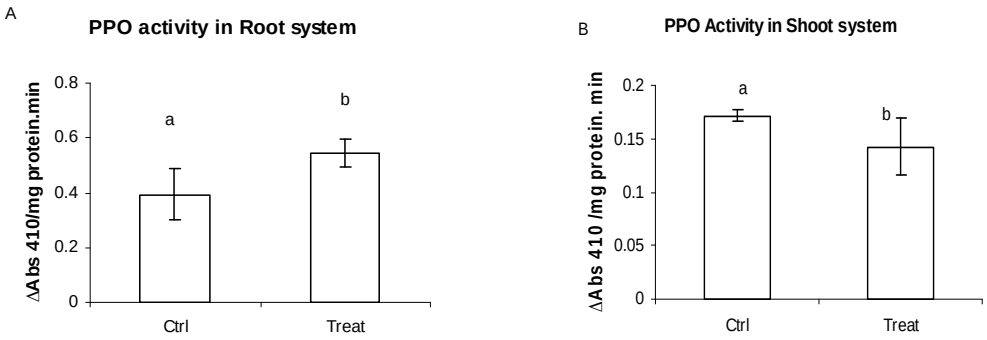

Fig. 1. Effect of Mf on the activity of PPO in root (A) and shoot (B) system of red cabbage. Data are means ± SD, n = 3. different characters refer to significant differences at P< 0.05 according to student' s T-test.

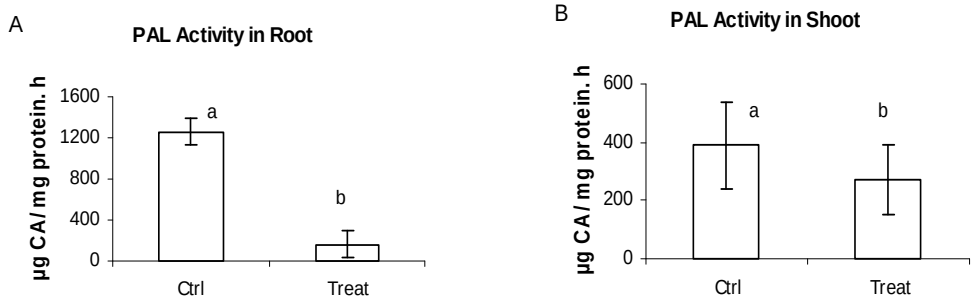

Fig. 2. Effect of MF on the activity of PAL in root (A) and shoot (B) system of red cabbage. Data are means ± SD, n = 3. different characters refer to significant differences at P< 0.05 according to student' s T-test.(CA: Cinnamic Acid)

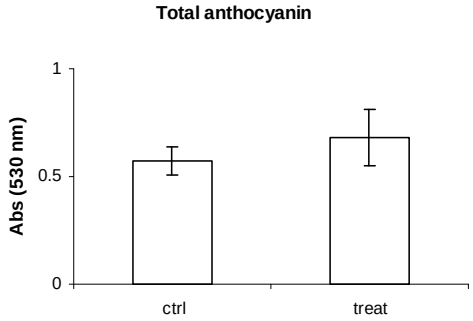

Fig. 3. Effect of Mf on total anthocyanin in aerial part of red cabbage. . Data are means ± SD, n = 3. different characters refer to significant differences at P< 0.05 according to student' s T-test.

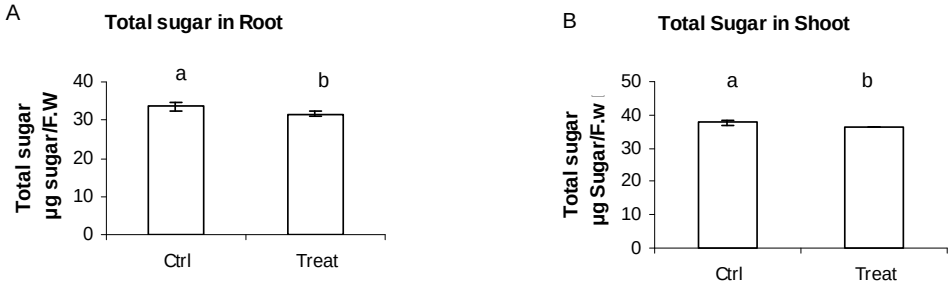

Fig. 4. Effect of MF on the lignin content of root (A) and shoot (B) system of red cabbage. Data are means ± SD, n = 3. different characters refer to significant differences at P< 0.05 according to student' s T-test.

Table. 1. Effect of MF on the activities of soluble, ionically and covalently bound cell fractions PO of root and shoot system of red cabbage

Peroxidase enzyme	Root		Shoot	
	Control	Treatment	Control	Treatment
Soluble PO Δ Abs 470 / mg protein.min	0.41± 0.2	0.4± 0.1	0.007± 0.0007	0.008± 0.001
Ionically bound PO Δ Abs 470 / mg protein.min	0.47± 0.05	0.41± 0.03	0.28± 0.03	0.54± 0.12
Covalently bound PO Δ Abs 470 / Cell Wall dry Weight.min	0.51± 0.01	0.44± 0.01	0.29± 0.009	0.55± 0.008

Data are means ± SD, n = 3.

Table. 2. Effect of MF on lignin content and cell wall phenolic compounds of root and shoot system of red cabbage.

Plant tissue	Lignin content (٪Lignin/ Cell Wall dry Weight)		Cell Wall Phenolic Compounds (µg phenol/ g Cell Wall dry Weight)	
	Control	Treat	Control	Treat
Root	4.1± 0.5	3.22± 0.7	3665.5± 282.7	7401.67± 2191.54
Shoot	5.04± 0.9	3.04± 0.46	2034.4± 594.8	4144.3± 968.43

Data are means ± SD, n = 3.

Summary

A magnetic field is an inescapable environmental factor for plants on the earth (Negishi et al. 1999). However, it´s impact on plant growth is not well understand(Negishi et al. 1999).In the current studies, contradictory results have been gained by scientists (Negishi et al. 1999). Static magnetic field, sometimes, has been received attention as a stress for beings (Aladjadjiyan 2002) and sometimes, it has been talked the co-operations of static MF with environmental factors, instance nourishing stresses, water deficit and heavy metals.

In the present paper the effect of SMF on the metabolism of certain phenolic compounds was investigated.

PPo is a bi-functional enzyme, that plays roles at both oxidation of phenols and conjugation of phenols to polyphenols. Increase of PPO activity in root system of treated plants can be related to accumulation of phenolic compounds. Also increase of PPO activity has been reported in tobacco cells affected by some nourishing stresses(Ghanati et al. 2002). Also the possibilities that the low PPO activity of the shoot system of treated plants can be due to the presence of an inhibitor, an in-activator or to factors degrading the enzyme (Kahn 1975).

Increased PO activity has been demonstrated to be a metabolic response under various stress conditions, including water stress, air pollution, and heavy metals (Pandolfini et al. 1992). Among the various forms of this enzyme , the wall-bound forms appear to be more efficient at catalyzing bound formation between extension and feruloylated polysaccharides and for the polymerization of phenolic monomers (Ghanati et al. 2002). Also Pandolfini (1992) reported the effects of nickel on peroxidases are always more marked in shoot than roots. Decrease of PO activity in the roots of treatment plants can be leading to stretch ability, wall-loosing and expansion in cell wall. Also, the percent of lignin content in treated roots can be help to this loosing. The lignin synthesis accomplishes from photosynthesis precursors .using of marked glucose showed relation between lignin synthesis and photosynthesis (Kollattukudy 1984). Decrease of lignin synthesis in the MF exposed plants, can be due to disorder in photosynthesis. According to Kazimov et al (1984) the magnetic fields results in decline in contents of photosynthetic pigments, chlorophyll a and b, in kidney bean leaves (Kazimov 1984). Also decrease of total sugar in treated plants with MF can be confirm this subject. it´s may be that MF was effected on lignin and sugar content from a common course.

PAL is a one of the main enzymes of metabolism of phenolic compounds that it catalyze changing of phenylalanine to cinnamic acid. The reaction catalyzed by phenylalanine ammonialyase. PAL is commonly regarded as akey step in the biosynthesis of phenols, and is affected by a number of factors (Ruiz et al 1998). This enzyme acts in the initial stages of lignin biosynthesis. rapid induction of the PAL activity (12 to 24 h) was observed during nourish stress and then decrease of PAL activity was reported in the next stages.(Ghanati et al. 2002,2004). In the present investigation, the activity of PAL in treated plants decreased after 10 days. Anthocyanins are another group of phenolic compounds belong to the flavonoids group. Anthocyanins in autumn leaves seem to prevent photo- oxidative irradiation.

The most important environmental cue in anthocyanin synthesis is light, which affects signal transduction and gene expression involved in anthocyanin biosynthesis. Other factors, such as sugar addition, phosphate limitation, and cold stress, can enhance anthocyanin accumulation induced by light. In the present research increase of anthocyanin and wall-bound phenlics may be resulted of phenols changing to anthocyanin and wall-bound phenolics and deviation from the lignin synthesis.

References

Aladjadjiyan A.; Study of the influence of magnetic field on some biological characteristics of Zea Mays . Journal of central European Agriculture; 2002; 3; 2: 89-94.

Belyavskaya N. A. ; Biological effects due to weak magnetic field on plants. Advances in space Research. 2003; 34: 1566- 1574.

Calzoni GL; Borghini F; Delgindice E. et al; Weak extremely high frequency microwaves affect pollen-tube emergence and growth Kiwifruit : Pollen grain irradiation and water- mediated effects; J Altern Complement Med; 2003; 9; 2: 217-228.

Daniel Otto; Meier Matthias Samuel; Schlatter Josef et al; Selected phenolic compounds in cultivated plants: Ecologic function; Health implications and Modulation by pesticides; 1999; 107: 109-114.

Dubois, M; Gilles, K; Hamilton, s; Rebes, P. and Smith F; Colorimetric method determination of sugars and related substances; Anal. Chem.; 1956; 28; 350-356.

Ghanati Faezeh; Morita Akio; Yokota Hiromi; Deposition of suberin in roots of Soybean induced by exess boron; Plant science; 2004. (Article in press).

Ghanati Faezeh; Morita Akio; Yokota Hiromi; Induction of suberin and increase of lignin content by excess Boron in Tobacco cells; Soil Sci. Plant Nutr. ; 2002; 48; 3; 357-364.

Hara Masakazu; Oki Karin; Hoshino Kyoko et al; Enhancement of anthocyanin biosynthesis by sugar in radish (Raphanus sativus) hypocotyl; 2003; 164; 2: 259-265.

Hirota Noriyuki; Nakagawa Jun and Kitazawa Koichi; Effects of a magnetic field on the germination of plants; Journal of Applied Physics; 1999; 85; 8: 5717-5719.

Iiyama Kenji and Wallis Adrian F. A. ; Determination of lignin in herbaceous plants by an improved Acetyl Bromide procedure; J Sci Food Agric; 1990; 51; 145-161.

Kahn Varda; Polyphenol oxidase activity and browning of tree Avocado varieties ; J. Sci. Fd Agric; 1975; 26; 1319-1324.

Kollattukudy P. E. ; Biochemistry and function o cutin and suberin. Can. J. Bot. ; 1984; 62; 2918-2933.

Mc Cann. J. ; Khiefts L; Rafferty C. ; Cancer risk assessment of Extremely Low Frequency Electric and Magnetic fields: a critical review of Methodology; Environmental Health Perspective; 1998; 6; 11.

Negeshi Y. ; Hashimoto A. ; Tsushima M. et al; Growth of pea epicotyl in low magnetic field implication eor space research; Adv. Space Res. ; 1999; 23; 12: 2029- 2032.

Pandolfini T; Gabbrielli R. and Comparini C. ; Nickel toxicity and peroxidase activity in seedlings of *Triticum aestivum* L. ; Plant cell and environment ; 1992; 15; 719-725.

Piera Piacentini Maria; Fraternale Daniel ; Piatti Elena et al; Senescence delay and change of antioxidant enzyme levels in Cucumis sativus L. etiolated seedlings by ELF magnetic fields; Plant science; 2001; 101; 45-53.

Ruiz Juan M. ; Bretones German; Baghour Mouurad et al; Relationship between Boron and phenolic metabolism in Tobacco leaves; 1998; 48; 2: 269- 272.

Ruiz R; Vodnic D; Jerman I; Influence of aluminum in biologic effects of ELF magnetic field stimulation; Electro- magnetobial; 2000; 19; 57- 68.

THE EFFECT OF ACUTE EXPOSURE TO 950 MHz WAVES OF GSM MOBILE PHONE SYSTEM ON CONSOLIDATION OF SPATIAL MEMORY IN RAT

MAJID JADIDI

PHYSIOLOGY RESEARCH CENTER, SEMNAN UNIVERSITY OF MEDICAL SCIENCES, SEMNAN, IRAN

Jadidim@Hotmail.com

S. MOHAMMAD P. FIROOZABADI

DEPARTMENT OF MEDICAL PHYSICS, TARBIAT MODARES UNIVERSITY, TEHRAN, IRAN

Pourmir@Modares.ac.ir

ALI RASHIDY-POUR

PHYSIOLOGY RESEARCH CENTER, SEMNAN UNIVERSITY OF MEDICAL SCIENCES, SEMNAN, IRAN

Rashidy-pour@Sem-ums.ac.ir

BAHRAM BOLOURI

DEPARTMENT OF MEDICAL PHYSICS, IRAN UNIVERSITY OF MEDICAL SCIENCES, TEHRAN, IRAN

BBolouri@Iums.ac.ir

YAGHOUB FATHOLLAHI

DEPARTMENT OF PHYSIOLOGY, TARBIAT MODARES UNIVERSITY, TEHRAN, IRAN

Fatolahi@modares.ac.ir

Abstract

With increasing in mobile communications, exposure to electromagnetic fields due to base station antenna has increased. This study was planned for evaluating the effects of short whole-body exposure to 950 MHz GSM electromagnetic field on consolidation phase of spatial memory.

33 naive male wistar rats (200 $^{+}$15 g) were trained (10 trials at 2 blocks, with 3 minutes interval between blocks for one day) to locate a submerged platform in a circular water maze. Immediately after training, animals randomly divided into three groups: control n= 11, sham-exposed n=11 and exposed n=11. The last group was exposed to 950 MHz electromagnetic waves (mean power density = 0.835 mW/cm^2) for 45 minutes in a circular plastic chamber. Performances of animals were tested 48 hours later by a 60 second probe test. Evaluation indexes were escape latency at target and opposite quadrants, swim speed and length.

Analysis of the probe data test indicated that, there were no significant difference between control, sham and 950 MHz exposed groups.

Results of this study provide no evidence indicating that consolidation phase of spatial memory can be affected by the 45 min whole-body exposure to 950 MHz electromagnetic waves.

Keywords: Electromagnetic field, Base station, Consolidation, Morris water maze

Introduction

Memory is defined as the capacity of brain to store and retrieve the information. It consists of three phases: encoding or acquisition phase, consolidation or stabilization phase that is a process by which new labile memories convert to more stable long-term memories, and retrieval phase in which memory is expressed.

In the last decade, many researches studied the effects of exposure to electromagnetic fields (EMF) on different nervous system functions such as memory in human and animals. Some of these studies have revealed deficits on memory due to EMF exposure [4; 7-20], whereas other studies did not [2, 3, 5, 6, 28, 33]. Nowadays, with increase in mobile communications, exposure to EMF due to mobile handset and base station antenna has increased. There are concerns about the effects of mobile phone electromagnetic waves on human body functions. These concerns emerge from results of epidemiological studies contributed to effects of mobile phone on human body. For example some of reported data indicated that mobile phone waves not only in regular power density but also in power density less than allowed limit (1 mW/cm^2) can produce headaches, warmth on ear, memory loss and fatigue. These reports suggest that there is a significant association between calling time/number of calls per day and prevalence of these signs [9, 10, 11, 27, 31]. Although these results are important but in most of these studies the mobile phone handset frequency has been used and the effects of base station antenna waves have been less noticeable.

The GSM mobile phone system that is used in most of the countries has a frequency of either 900 or 1800 MHz (pulsed at 217 Hz, Band width of 200 KHz). The spectrum of 900 MHz has two band areas: 890-915 MHz that is specific for handset and 935-960 MHz that is specific for base station antenna.

To date, we know no reports regarding the effects of acute exposure to 950 MHz waves, as a frequency in middle of base station band (935-960 MHz) on the memory processes. On the other hand, most of the experiments contribute to effects of exposure to mobile phone electromagnetic waves on acquisition phase of memory and few experiments are about the effects of these waves on consolidation phase. Thus, the aim of this study was to examine the effects of acute exposure to 950 MHz waves, emitted by base station antenna, on consolidation phase of spatial memory in a Morris water maze.

Materials and methods

Animals

Thirty three naive male Wistar rats (3 month old, 200 $^{+}$15 g) were used in three groups: control (n=11), sham-exposed (n=11) and EMF exposed (n=11). Rats were maintained on a 12-h light-dark cycle and with an ambient temperature of 21^{o}C.They were housed in a maximum of six rats per breeding cage and allowed access to food and water ad libitum. All experiments were performed between 9:00 a.m and 13:00 p.m during the light cycle.

Morris Water Maze training

The water maze was a blue circular pool (diameter: 140 cm, height: 50 cm) filled with water (22± 2°C) to a depth of 25 cm [29]. A circular glass platform (diameter: 11cm) was placed at the center of one quadrant (North-East quadrant) of the maze and submerged 3 cm below the surface of the water. The maze was located in a room containing several visual extra-maze cues. Each animal was released into the water from the wall of the maze at arbitrarily defined east, south, west, and north points. The sequence of points of release into the water

followed a random order. The animal was allowed to find the platform and land on it. If it could not find the platform within 1 minute, it was guided manually to the platform.

After finding the platform, it was allowed to stay there for 45 second before another trial. Performance in the maze was carried out and saved in a computer by an infrared receiver mounted on the roof. For spatial training, animals were given 10 trials (one training session) at 2 blocks, with 3 minutes interval between them for one day in Morris Water Maze. **Immediately after the last trial**, Rats were exposed to electromagnetic waves or sham exposed for a 45 minute.

Performance of each rat was tested 48 hours after the training session in a probe trial (60s), during which the platform was removed. Evaluation indexes were time spent in target quadrant, swim speed and total swim length during the probe test.

Electromagnetic field exposure

For whole body exposure to EMF, a 950 MHz GSM simulator (pulsed at 217 Hz and band width of 200 KHz, made by Khaje–Nasir Toosi University, Tehran, Iran) was used. It was connected to a 15 cm rod antenna fixed at the center of a circular plastic chamber (diameter = 30 cm). The animal could freely move inside the chamber. To prevent unknown exposure to reactive area of EMF, some of the near field restricted by a plastic mesh (radius = 5 cm). The power density inside the chamber was measured with RF meter (Narda 8716, USA) in different distances with 5 cm height from the base of antenna. With these records, the average value for power density was 0.835 mW/cm^2. The exposure room was adjacent to the experimental room.

Data analysis

The training data was analyzed with a one way analysis of variance (ANOVA) with trials as a repeated measure. Probe trial retention measures were analyzed with a two–way ANOVA. Tukey's *posthoc* test was performed to determine the source of detected significances. Values of $P<0.05$ were considered as significant

Results

The results of escape time during the 10 trials are shown in fig.1. Data analysis showed a significant trial effect (i.e., a significant decrease in escape time with training). There was no significant difference in time during the training session trials between three groups [F (2, 29) = 0.358, p=0.702].

Results of the probe trial are presented in fig.2, which shows the average time for the three groups of rats during the 1-minute probe trial period in the platform and opposite quadrants. There was no significant difference in time during the training session trials between three groups [F (2, 36) =1.03, p=0.364].

Fig.3, illustrates the swim path data during the probe test. One- way ANOVA indicated no significant differences among the groups [F (2, 27) =1.82, p=0.180]. Fig. 4, illustrates mean swim speed of rats during probe test. A one way ANOVA showed no significant differences between groups [F (2, 27) =1.72, p=0.198].

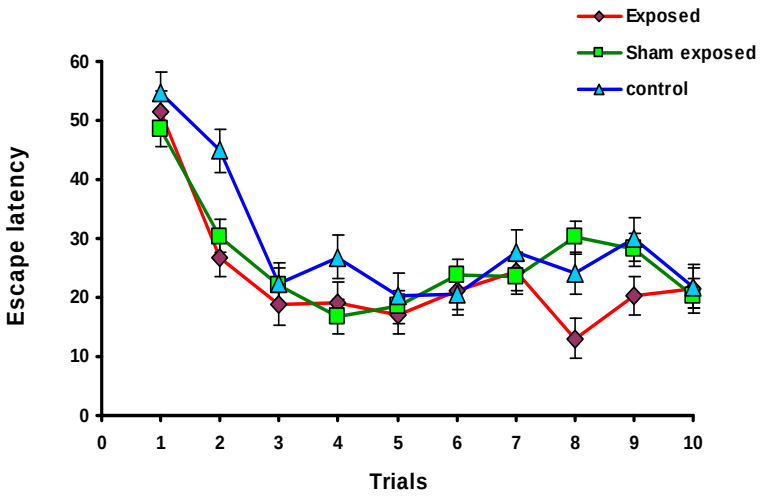

Fig. 1: Average escape time (Mean ± SEM); time to reach the platform after release into the water, during the trials.

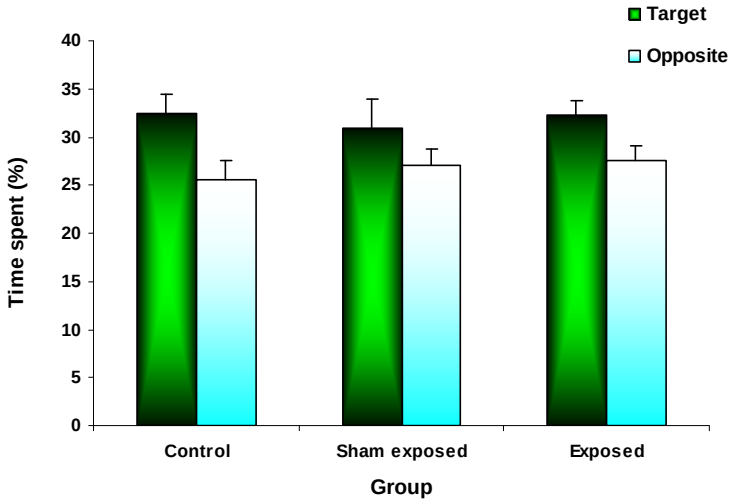

Fig 2: Average time spent (Mean + SEM) in three groups for target and opposite areas during probe trials.

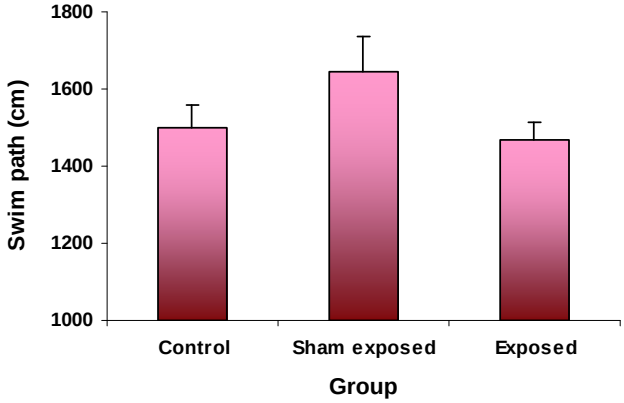

Fig. 3: Average swim path (Mean + SEM) in four groups during probe trials of consolidation experiment.

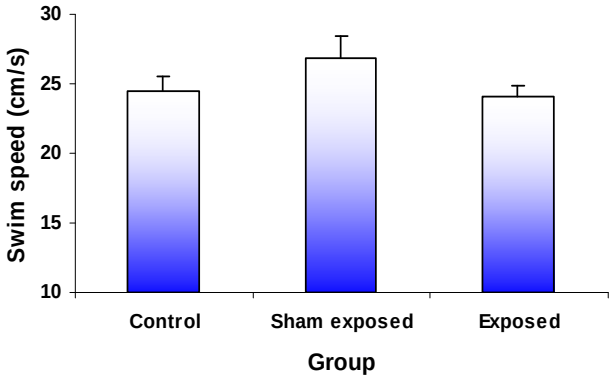

Fig. 4: Average swim speed (Mean + SEM) of the rats during probe trials in consolidation experiment.

Discussion

The mobile phones and their base station electromagnetic fields have low specific absorption rate that induce very low rise in brain temperature, thus, the possible biological effects of mobile phone systems on brain would be expected to be the non-thermal effects [12]. Data from this experiment showed that acute exposure (45 minute) of 950 MHz waves of GSM mobile phone system (pulsed at 217 Hz) does not affect the consolidation phase of rat spatial memory. This is in agreement with recent studies showing electromagnetic field dose not alter performance in an 8-arm radial-maze, either in mice [33] or in rats [16]. In addition, another study shows that 900MHz GSM electromagnetic field, in head-only exposure conditions, can not alter performances of rats in spatial memory and non-spatial memory tasks [5, 6].

On the other hand, Lai and Carino found that low level microwave irradiations can alter the cholinergic functions in the rat hippocampus and cortex [17]. This decrease in cholinergic activity in the brain can impair rat spatial memory [18]. Cassel et al. could not access the same results like the Lai et al findings, although their testing protocol was as similar as possible to that of the Lai et al. study [2]. Sienkiewicz et al. found similar results in radial-arm maze too [33]. But Wang and Lai showed that 45-minute exposure 2.45 GHz microwaves can alter spatial memory in Morris water maze [35]. Because it has showed that hyperthermia can produce amnesic effects, the memory impairment reported by Lai et al and Wang and Lai can be related to a hyperthermia due to the whole-body exposure [6].

McKay et al [23] indicated that exposure to magnetic field can impair memory consolidation of contextual conditioned fear rats. Consolidation is defined as a process by which new labile memories convert to more stable long-term memories. It is showed that consolidation requires RNA and protein synthesis [22, 25]. Sienkiewics et al [34] suggests that magnetic fields have no effects on the well-established long-term memories.

The epidemiological studies were performed on human cases showed different results like animal experiments. Hocking et al., Oftedal et al. and Sandstrom et al. reported that mobile phone waves can produce dizziness, headaches, discomfort, warmth on ear, memory loss, and fatigue not only in regular power density but also in power density less than allowed limit (1 mW/cm^2). They suggest that there is a direct relationship between these signs and calling time/number of calls per day [9, 10, 11, 27, 31]. In addition to studies performed on effects of waves emitted by phone handset, results of epidemiologic studies were done by Roosli et al and Navarro et al. on persons who lived in areas near the antenna, showed that 74% of people's complaints (sleep disorders, headaches, concentration difficulties and fatigue) are due to antenna. These signs appeared after exposure and decreased slowly [26, 30]. Santini et al suggest that the signs of persons, who live in areas near antenna, differ with increase of distance from antenna [32]. In addition to distance it seems that the antenna characteristics are important factors.

Bornkessel and Stocker-Meier studies on 24 antennas showed that although electrical fields' intensities of these antennas are in standard limit. These results are time dependent and can differ with different antenna traffic along day [1]. Although some of these studies suggest that exposure level is less than allowed level by ICNIRP in areas near the base station antenna, but the probability of long term exposure dangers of these waves for whom live in these areas are not rejected. In agreement with this point, Lai et al showed that intensity and duration of exposure have interactions in effectiveness of the field on memory so that high-intensity/short-duration exposure and lower-intensity/longer-duration exposure have similar effects on frontal cortex and hippocampus cholinergic activity and memory [17]. In addition, it is showed that chronic exposure to EMF can increase plasma corticosterone level [24]. This elevated level of corticosterone can induce time–dependent neuronal damage in hippocampus and impair cognitive function [21].

In the present research, the effect of acute exposure of 950 MHz waves emitted by base station antenna on the consolidation phase of spatial memory was investigated via the Morris water maze. This set of experiment provides no evidence indicating that spatial memory can be affected by the 45 minute whole-body exposure to 950 MHz electromagnetic field. Although this study was used as a model for understanding the effect of GSM electromagnetic field on consolidation phase of memory, further studies are needed to test other durations and intensities on this phase of memory.

Acknowledgements

This study was supported by Iran Telecommunication Research Center, Tarbiat Modares University and Semnan University of Medical Sciences.

References

1] Bornkessel C, Stocker-Meier E. 2003. Results of a measurement programme concerning mobile phone base station emissions in North Rhine-Westphalia. Mobile Phone Base Station and Health. Dublin, May 15th and 16th, 2003.

2] Cassel JC, Cosquer B, Galiani R, Kuster N. 2004. Whole body exposure to 2.45 GHz electromagnetic fields does not alter radial-maze performance in rats. Behav Brain Res 155(1):37-43.

3] Cosquer B, Galini R, Kuster N, Cassel JC. 2005. Whole-body exposure to 2.45 GHz electromagnetic fields does not alter anxiety responses in rats: a plus-maze study including test validation. Behav Brain Res 156 (1):65-74.

4] Croft RJ, Chandler JS, Burgess AP, Barry RJ, Williams JD, Clarke AR. 2002. Acute mobile phone operation affects neural function in human. Clin Neurophysiol 113:1623-1632.

5] Dubreuil D, Jay T, Edeline JM. 2002. Does head-only exposure to GSM-900 electromagnetic fields effect the performance of rats in spatial learning tasks? Behav Brain Res 129:203-210.

6] Dubreuil D, Jay T, Edeline JM. 2003. Head only exposure to GSM 900 MHz electromagnetic fields does not alter rats memory in spatial and non-spatial tasks. Behav Brain Res 145:51-61.

7] Haarala C, Bjornberg L, Ek M, Laine M, Revonsuo A, Koivisto M, Hamalainen H. 2003. Effect of 902 MHz electromagnetic field emitted by mobile phone on human cognitive function: A replication study. Bioelectromagnetics 24(4):283-288.

8] Hermann DM, Hossmann KA. 1997. Neurological effects of microwave exposure related to mobile communication. J Neurol Sci 152:1-14.

9] Hocking B. 1998. Preliminary report: Symptoms associated with mobile phone use. Occup Med 48(6):357-360.

10] Hocking B, Westerman R. 2001. Neurological abnormalities associated with CDMA exposure. Occup Med 51(6):410-413.1

11] Hocking B, Westerman R. 2003. Neurological effects of radiofrequency radiation. Occup Med 53:123-127.1

12] Ilhan A, Gurel A, Armutcu F, Kamisli S, Iraz M, Akyol O, Ozen S. 2004. Ginkgo biloba prevents mobile phone-induced oxidative stress in rat brain. Clinica Chimica Acta 340:153-162.

13] Jadidi M, Firoozabadi SMP, Sajadi AA, Taherian AA. 2005. Acute exposure to 50 Hz, 8 mT Magnetic field can impair rat spatial memory. 3rd European Medical & Biological Engineering Conference. Prague, November 20th -25th, 2005.

14] Koivisto M, Krause CM, Revonsuo A, Laine M, Hamalainnen H. 2000a. The effects of electromagnetic field emitted by GSM phones on working memory. Neuroreport 11:1641-1643.

15] Koivisto M, Revonsvo A, Krause C, Haarola C, Sillanmaki L, Laine M, Hamalainen H. 2000b. Effects of 902 MHz electromagnetic field emitted by cellular telephones on response times in humans. Neuroreport 11:413-415.

16] Lai H. 2004. Interaction of microwaves and a temporally incoherent magnetic field on spatial learning in the rat. Physiology & Behavior 82:785-789.

17] Lai H, Carino M. 1999. 60 Hz magnetic fields and central cholinergic activity: effects of exposure intensity and duration. Bioelectromagnetics 20:284-289.

18] Lai H, Horita A, Guy AW. 1994. Microwave irradiation affects radial-arm maze performance in the Rat. Bioelectromagnetics 15:95-104.

19] Lass J, Tuulik V, Ferenets R, Riisalo R, Hinrikus H. 2002. Effects of 7 Hz-modulated 450 MHz electromagnetic radiation on human performance in visual memory tasks. Int J Radiat Biol 78(10):937-944.

20] Mann K, Roschke J. 1996. Effects of pulsed high-frequency electromagnetic fields on human sleep. Neuropsychology 33: 41-47.

21] McEwen BS, Sapolsky RM. 1995. Stress and cognitive function. Current Opinion in Neurobiology 5:205–216.

22] McGaugh JL. 2000. Memory- A century of consolidation. Science 14:248-251.

23] McKay BE, Persinger MA. 2000. Application timing of complex magnetic fields delineates windows of posttraining- pretesting vulnerability for spatial and motivational behaviors in rats. Intern J Nuroscience 103:69-77.

24] Mickley GA, Cobb BL, Mason PA, Farrell S. 1994. Disruption of a pulsative working memory task and selective expression of brain c-fos following microwave-induced hyperthermia. Physiol Behav 55:1029-1038.

25] Nader K, Schafe GE, LE Doux JE. 2000,b. The labile nature of consolidation theory. Nat Rev Neurosci 1:216-219.

26] Navarro EA, Segura J, Gomez-Perretta C, Portoles M, Maestu C, Bardasano JL. 2003. About the effects of microwave exposure from cellular phone base stations: A first approach. Mobile Phone Base Station and Health. Dublin, May 15th and 16th, 2003.

27] Oftedal G, Wilen J, Sandstrom M, Mild KH. 2000. Symptoms experienced in connection with mobile phone use. Occup Med 50(4):237-245.
28] Preece AW, Davies-smith A, Wesnes K, Butler S, Lim E, Varey A. 1999. Effect of 915 MHz simulated mobile phone signal on cognitive function in man. Int J Biol. 75(4):447-456.
29] Rashidy-Pour A, Motamedi F, Motaghed-Laijani, Z. 1996. Effects of reversible inactivation of the medial septal area on reference and working memory versions of the Morris water maze. Brain Res 709:131-40.
30] Roosli M, Moser M, Meier M, Braun-Fahlander C. 2003. Health symptoms associated with electromagnetic radiation – A questionnaire survey. Mobile Phone Base Station and Health. Dublin, May 15th and 16th, 2003.
31] Sandstrom M, Wilen J, Oftedal G, Hansson Mild K. 2001. Mobile phone use and subject symptoms.Comparision of symptoms experienced by users of analogue and digital mobile phones. Occup Med 51(1):25-35.
32] Santini R, Santini P, Danze JM, Le Ruz P, Seigne M. 2002. Study of the health of people living in the vicinity of mobile phone base stations: I. Influences of distance and sex. Pathol Biol 50:369-73.
33] Sienkiewicz ZJ, Blackwell RP, Haylock RG, Saunders RD, Cobb BL. 2000. Low-level exposure to pulsed 900 MHz microwave radiation does not cause deficits in the performance of a spatial learning task in mice. Bioelectromagnetics 21:151-158.
34] Sienkiewicz ZJ, Haylock RG, Bartrum R, Saunders RD. 1998. 50 Hz magnetic field effects on the performance of a spatial learning task by mice. Bioelectromagnetics 19:486-493.
35] Wang B, Lai H. 2000. Acute exposure to pulsed 2450 MHz microwaves affects water-maze performance of rats. Bioelectromagnetics 21:52-56.

EXPOSURE OF MEDICAL STAFF TO STATIC MAGNETIC FIELDS FROM MAGNETIC RESONANCE IMAGING (MRI) SCANNERS

JOLANTA KARPOWICZ, MAILA HIETANEN*), KRZYSZTOF GRYZ

CENTRAL INSTITUTE FOR LABOUR PROTECTION – NATIONAL RESEARCH INSTITUTE, LABORATORY OF ELECTROMAGNETIC HAZARDS WARSZAWA, POLAND, e-mail: jokar@ciop.pl

**)FINNISH INSTITUTE OF OCCUPATIONAL HEALTH, HELSINKI, FINLAND, e-mail:maila.hietanen@ttl.fi*

Abstract

The health care staff operating MRI devices are exposed to static magnetic field of significant spatial heterogenity (dB/dx) and high level of flux density – usually existing permanently during the work shift. They can be also exposed to pulses of magnetic field of high rate of rise/fall dB/dt, so-called gradient fields - existing only during examination of patients. The level of the workers' exposure depends both on the type of the magnet and ergonomical design of the particular MRI device.

The paper presents current state of the art on the occupational exposure to static magnetic field health effects, gaps in scientific data, MRI workers' exposure characteristic, research needs and suggestions for the exposure assessment protocol for further investigations.

Keywords: MRI, occupational exposure, electromagnetic fields, exposure assessment

1. Introduction – MRI EMF and exposure results

Electromagnetic fields associated with Magnetic Resonance Imaging

Nuclear magnetic resonance (NMR) is research method which can be used for medical imaging or spectral analysis of chemical structure of samples. The basic physical phenomenon in NMR is resonant absorption and re-emission of radiofrequency (RF) radiation by protons in a strong static magnetic field. In the magnetic resonance imaging (MRI) scanners, magnetic field useful for medical examination is result of summation of 2 components: static field produced constantly by strong magnets (permanent, resistive or superconductive) and pulses of time-varying so-called gradient field produced by gradient coils placed inside the housing of the MRI scanner [10]. The dynamic changes of spatial distribution of field produced in the result enables 3D changes of RF resonating absorption by patients tissues and in consequences the 3D imaging of the internal structure of the patient's body. Diagnostic coils placed at the MRI table or directly on the body of examined patient produce pulses of RF radiation used for such imaging.

Magnets of magnetic flux density of 0.2 - 3 T are currently used as a source of static magnetic field. Higher field's (up to 8 T) MR imaging is under intensive pre-clinical investigations. Workers operating MRI scanners are one of the highest exposed group to static magnetic fields because usually superconductive or permanent magnets generate the field constantly. Only resistive magnets can be switched off when the shift is over. Exposure of workers to RF and gradient fields is not common among MRI workers because during patients' examination medical staff is usually far from the magnet, controlling examination by a computer-console.

Biological and health consequences of electromagnetic fields exposure

Biological and health consequences of RF and gradient fields, associated with thermal effects and electro-sensitive tissues excitations, are relatively well investigated. In contrary, health effects of static magnetic fields are still under question, especially in case of chronic exposure of high level. Recent World Health Organization (WHO) monograph 232 [6] concluded that there is not sufficient scientific data for establishing health risk of static magnetic field exposure.

Physical effects of static magnetic fields (translation and orientation of charged molecules) cause electrodynamic

forces on moving electrolytes, and effects on electron spin states of chemical reaction intermediates [7]. Translation and orientation of molecular and cellular substances such as retinal rods, and some living cells have been experimentally observed in vitro in static fields of high level (above 1 tesla (T)), in various materials - dia- and paramagnetic such as hemoglobin, collagen, fibrin, and also on ferromagnetic particles such as magnetite. Water distribution can be also affected by high-gradient magnetic fields of high flux density (e.g., 8 T, 50 T/m; Ueno and Iwasaka 1994, following [7]), producing the force directly proportional to the square of the magnetic field strength and inversely proportional to the radius of the magnet e.g. force up to 30% the force of gravity in above-mentioned 8 T magnetic field, but only about 1% of gravity in whole-body 4 T magnet.

Static magnetic fields exert electrodynamic forces on moving ions in blood vessels, generating an electric potential across the blood vessels (Hall effect) and theoretically a reduction of blood flow velocity (Tenforde 1992, following [7]) - a 5 and 10% reduction in blood flow in the aorta was predicted to occur in static fields of 10 and 15 T, respectively, due to magneto-hydrodynamic interactions (Kinouchi et al. 1996, following [7]). Related observations included a 0.2–3% change in blood velocity between 1–10 T (Dorfman; Keltner, following [9]). Experimental examination of the scale of biomedical effects associated with electrodynamic and magnetodynamic forces in exposed human body are still under examination, frequently using electrocardiogram (ECG) technique. In addition, vertigo and other sensations, as difficulty with balance, nausea, headaches, numbness and tingling, phosphenes, and unusual taste sensations, were recorded during movement in high field. The other investigated endpoint were: cognitive function, assessed during exposure using standard neuropsychological tests, effects of exposure to fields of up to 8 T on heart rate, respiratory rate, systolic and diastolic blood pressure, finger pulse oxygenation levels, and core body temperature [7]. The exposed volunteers moved very slowly in comparison with normal workers activities in the vicinity of magnets (one or two feet over a few seconds, followed by a 15–30 s pause, taking overall about 3–4 min) into the magnet bore in order to avoid the transient, movement-induced sensations described above. Nevertheless, nine subjects reported sensations of dizziness, and two reported a metallic taste, assumed to be due to electrolysis of metallic chemicals in the subjects' teeth fillings (Schenck et al. 1992, following [7]).

IARC (2002) [12] notes that two somewhat dated studies (Neurath 1968; Ueno et al. 1984) report that exposure to 1 T fields with high spatial gradients (10–1,000 T/m) can adversely effect the development of frogs and toads, but notes that most studies indicate a lack of effect of static field exposure.

With static magnetic fields, reactions under laboratory conditions include a 17% increase in human cardiac cycle length at 2 T (Jehesen et al., following [9]). The authors suggested that the observed effect is probably harmless in healthy subjects, but that its safety in dysrhythmic persons was not certain. Such question is very important in the case of health examination for workers, who are going to start or continue MRI scanners operation.

2. Pattern of occupational exposure during MRI scanners operation

For health care staff (nurses, technicians, radiologists), the static magnetic field from MRI units is of special concern as during the shift the field is permanently on. Inside the MRI's room, the highest exposure occurs in the direct proximity to the magnet's housing. The workers are exposed to the static magnetic field while attending patients before and after examination and also while operating the MRI unit by the console situated on the housing of the magnet. Exposure to gradient and RF pulses is possible only during the examination and affects workers only in special cases, e.g. during so-called dynamic examination, interventional MRI procedure or because of emerging needs (even inside the bore of magnet). During patient's examination, the attendants usually stay in front of the monitor of computer controlling the examination, outside the MRI room (which is usually electromagnetically shielded to screen MRI device from all kinds of outside electromagnetic radiation).

During MRI examination, examined subject (selected part of patient's body) lies at the MRI's table located within the area of static magnetic field of very high spatial distribution's homogeneity in the bore of magnet's housing (in the case of so-called close MRI device) or in the open space between magnet's legs (in the case of so-called open MRI device). Medical staff activities are carried out in the vicinity of magnet housing, in the static field of significant spatial heterogeneity. The standing with the patient before/after examination, usually at the distance of 0.3 - 1.5 m from the housing of the magnet, last in the most cases 2 - 15 minutes [9]. The basic activities are as follows (fig. 1):

- attending at the MRI room during patient's access and lay down on the MRI's table (area A + B)
- positioning of diagnostic's RF coils on the MRI's table or patient's body (area A + B)
- plugging-in/off the RF coils' cables into the supplying socket (area A + B or D or E)

- MRI table positioning for fixing its initial geometrical position and put in/out it into/from the area of uniform field (inside magnet's bore or within open space of open device) (area A + C)
- attending at the room while patient is getting off from the MRI table (area A + B).

In the case of certain types of examination, a patient is dosed with some pharmaceutical components, e.g. contrast, frequently when patient is placed inside the magnet. In the most of cases dosing/injection is made by nurses, even if the use of infusion pumps is technically possible. These activities last 1 - 2 minutes and is frequently the reason of high exposure of the staff within area D at fig. 1.

Cleaners can be also exposed to high level of static magnetic fields inside MRI room or inside the bore of magnet because permanent and superconductive magnets are permanently on.

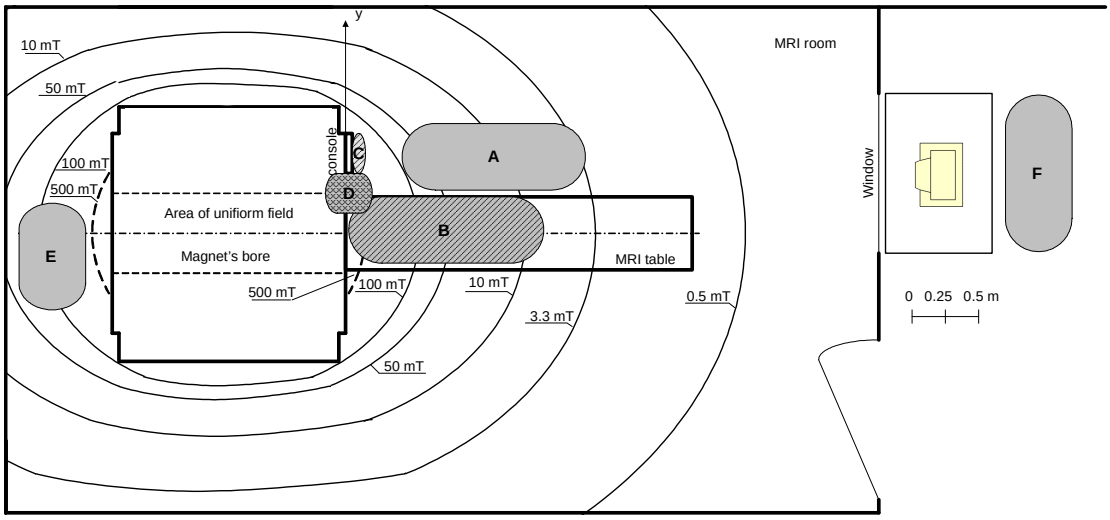

Fig. 1. Characteristic of the health care staff exposure while MRI examination attending: area A, E, F - whole body exposure; area B - hands exposure or head while worker is leaning towards the patient; C - hands exposure; D - hands or whole body exposure when worker have to approach very close to the area of uniform field (or is leaned against magnet housing) [9]

The exposure of medical staff to static magnetic fields while positioning the patient can be as high as the main field in the system, although locally and for limited periods of time. The trend towards the routine use of high field MRI systems (3–4 T) is increasing concern that exposure of workers and patients can exceed the existing recommended guidelines (tab. 1).

Table 1. Permissible occupational exposure to a static magnetic field.

Recommendations from	Whole body		Limbs		Cardiac stimulators and implanted electronically activated devices
	Whole working day	Ceiling value	Whole working day	Ceiling value	
ICNIRP guidelines, 1994 [7]	200 mT	2 T	not fixed	5 T	0.5 mT
EMF directive, 2004 [4]	200 mT	not fixed	not fixed	not fixed	mentioned but not fixed
IEEE standard, 2002 [8]	500 mT	500 mT	500 mT	500 mT	mentioned but not fixed
ACGIH, 2005 [1]	60 mT	2 T	600 mT	5 T	0.5 mT

Static field exposure levels must be quantified and controlled for medical staff safety. In the near future, ICNIRP is going to review its guidelines on limiting exposure to static magnetic fields [7]. Medical or paramedical staff may be exposed at low magnetic and electromagnetic fields around the device or outside the room for hours daily.

Concerning open or interventional MRI devices with magnetic field strength below 1.0 T, staff operating such devices are not exposed at levels higher than the currently recommended limits for occupational exposure. However, there are only limited data on the exposure of surgeons at open MRI devices.

Medical workers exposure to static fields from 20 various MRI devices of 0.2 - 2 T magnets, used for medical examination of various tissues (with head's examinations carried out the most frequently) presented by Karpowicz and Gryz [9] can be consider as the typical example of medical staff exposure pattern. The level of static magnetic field decreases rapidly with the distance from the magnet housing - app. 100-fold at a distance of about 2 m. In each of the cases, the area of controlled access for persons with cardiac pacemakers (B > 0.5 mT) exist, up to the distance no longer than approx. 5 m from magnet. Magnetic fields of B = 10 - 500 mT can be found in a distance up to approx. 1.5 m from the magnet. In the case of 0.5 - 2 T MRI units, the area of the high field, where occupational exposure limitations should be consider (B > 100 mT) can be found up to approx. 0.5 m from the border of the magnet's bore. The spatial distribution of the field levels are significantly non-isotropic around the bore magnets' housings - in front of and behind them much wider than sidelong. In the case of open MRI units, the spatial distribution of the field is isotropic around the magnet's housing.

Inside MRI rooms, the maximum exposure level in front of the magnet can reach 1 T. Exposure level in the area of workers' routine activities can reach 150 mT (for whole body exposure) and 600 mT (for hands exposure) (tab. 2). In the case of performing professional activities very close or inside the magnet's bore, workers can be exposed to higher fields. Exposure of hands to a static magnetic field up to 1,5 T was found. Exposure of workers outside the MRI room is lower, at a distance of 5 - 10 m, the magnetic field is normally less than 0.5 mT.

Table 2. Static magnetic field in the most possible places where health care staff attending patients before/after MRI examination [9].

Activities types	Health care staff exposure level, mT / MRI unit		
	0.2 T open	0.5 T bore	1.5 T bore
diagnostic RF coils positioning on the MRI table or patient's body - whole body exposure	3–50	5-100	50-150
diagnostic RF coils positioning on the MRI table or patient's body - hands exposure	5-100	20-250	100-600
plugging-in/off the RF coils cables into the supplying socket and console use - hands exposure	60-100	30-40	20-500 up to 1500*)
maximum field existing on the accessible for workers cover of magnet	200-270	80-300	250-600

*) - in case of location the supplying socket inside a magnet bore

3. Research needs concerning MRI exposure assessment

No serious adverse health effects from the whole-body exposure of healthy human subjects up to 8 T have been reported in the literature, but also no epidemiological studies have been performed yet to assess possible long term health effects in patients, workers, or volunteers. Only few informative studies have been performed using exposures above 2 T. This fact is very confusing against the growing up, the use of static magnetic fields in medicine, which lead to exposures of patients and workers to very high fields, even significantly exceeding the level of scientifically investigated exposure results (4 to 8 T). The main conclusions from WHO's health risk assessment of static magnetic fields [6], including the analysis of gaps in knowledge about possible health effects, indicated that, research carried out to date has not been systematic and has often been performed without appropriate methodology and exposure information. In consequences, no sufficient knowledge concerning safety conditions are available today for static magnetic fields exposure existing in the vicinity of MRI devices.

This lack of information resulted among others in the EU Directive 2004/40/EC provisions, which does not contain exposure limit value for static magnetic fields. To solve this serious problem for occupational safety and health engineering, further investigations concerning health risk assessments for static magnetic field exposure have been recently identified by international bodies [5, 6, 7, 14] as being of high priority for health risk assessment. The main areas identified for such research include:

- monitoring of occupational exposure, especially above 4 T, suitable to allow epidemiological studies

- epidemiological studies of possible long-term health effects in patients, volunteers, and staff with occupational exposure, particularly those with high levels of cumulative exposure

- epidemiological studies on pregnancy outcome, of high interest for patients as well as pregnant workers

- studies on biological effects of strong static magnetic fields, especially of chronic exposure on reproduction and development.

Further studies should be more systematic and coordinated. Appropriate dosimetry is important for all kind of research. There is a need to investigate the importance of physical parameters of exposure such as:

- field intensity

- exposure duration

- field gradient on biological outcome.

It means in practice the need of the use of investigations protocol, which allow the performance of the analysis of exposure level's distribution during the shift.

Epidemiological studies are of primary importance in health risk assessment [14]. The use of adequate estimates of exposure from all relevant sources and to establish real exposure pattern and it's variability among various countries is essential for quantitative analysis of research results and exposure's risk. High quality epidemiological studies, not executed yet, should focus on workers involved in high exposure areas and address endpoints such as cancer and pregnancy outcomes in occupational situations. Attention should be paid also to the important confounding variables, such as toxic fumes, vibration or other kinds of non-ionizing or ionizing radiation. Highly exposed occupational groups, as medical staff operating MRI scanners should be identified and followed over time with focus on common health outcomes with short latency periods (e.g. effects on CNS functions and cardiovascular effects). A health survey of surgeons, nurses and other workers using interventional MRI would provide useful information as to levels, durations and frequency of exposures of workers to static fields in these systems.

Experience with other frequencies has shown that obtaining reliable estimates of exposure to EMF for use in epidemiological studies can be very difficult, and surrogate measures of exposure, such as job title or distance from a particular source, may not always provide sufficiently accurate assessments. Investigations concerning low frequency exposure shown, that pocket-personal dosimeters would significantly improve exposure assessment for epidemiological studies and risk assessment. Adequate exposure assessment protocol for such method should be focused on:

- magnetic field strength
- magnetic field gradients
- exposure durations
- the rate of change of the magnetic due to motion.

Development of methods and tools for reliable assessment of human body exposure levels taking into account exposure metrics other than average field strength; criteria, improving exposure monitoring strategies both for static magnetic field and time-varying components, for complex and inhomogeneous exposure situations and for personal exposure assessment (personal dosimeters) is included in the high priority research needs [5] crucial for investigations on exposure risk for MRI technology. Numerical and experimental validation of the dosimeters is required and should consider technical properties of dosimeter coming from EMF sensor, its calibration, dynamic and frequency respond, spatial respond, sensitivity to human body, motion speed, sampling, etc. For the possibility of the use of monitoring results for various kind of analysis, it is very important to develop standardized exposure assessment protocol.

Studies in tissues, living cells and cell-free systems play a supporting role in health risk assessments [14]. Long-term and acute studies on experimental animals are needed using endpoints such as life-span, cancer, development, cardiovascular, immune system and CNS responses [5]. In vitro studies should investigate interaction mechanisms such as radical pair reactions and enzymatic activity, as well as effects on gene expression, mutagenicity and cell transformation.

Static magnetic fields may interact with biological systems in a number of ways, although the most likely means of causing health effects are via field-induced effects on charged molecules and alterations in the rate of biochemical reactions. Theoretical and computational studies are needed to investigate the magnitude and direction of induced currents and fields under various magnetic field exposure conditions.

Human laboratory studies on acute transient effects of exposure to static field effects studied in controlled exposure parameters can bring additional knowledge concerning thresholds of particular exposure effects and physical measures of exposure which should be monitored for exposure assessment in real situations. The priorities for such research [14] were identified including studies on field-induced vestibular dysfunction

including vertigo, head and eye coordination in a gradient and static magnetic field. Such investigations are focused on the MRI interventional procedures, when medical staff are in close proximity to patients within a magnet and are consequently exposed to relatively high fields. Further investigation of such mechanisms and intensity is considered of special interest because of the increasing likelihood that medical staff will be performing complicated tasks for extended periods of time within a magnetic field high exposure. Additional attention should be paid on cognitive and behavioral effects of static magnetic fields. Possible investigations could be executed as a battery of cognitive tasks that encompass standard tests of attention, reaction time and memory, as an initial work with exposed volunteers to find topics for further more focused work.

Proper design and interpretation of all types of above mentioned studies are not possible without expert dosimetric support. Computational dosimetry can provide the link between an external static magnetic field and the internal electric fields and induced currents caused by movement of living tissues in the field, taking into consideration specific tissues and organs. Precise investigations can be focused on the electric fields and currents associated with visual phosphenes and vertigo, fields and currents generated by head and eye movements in a static magnetic field, whole-body movement by staff around the interventional MRI system. Such investigations should be performed with the use of a very fine resolution head-and-shoulder phantom and are considered of particular relevance to interventional MRI procedures where reduced head movements of surgeons and other clinical staff may necessitate increased movement of the eyes.

The ability of non-error performing of such work can be of high importance for the patient’s safety, and should be also considered within occupational risk assessment.

4. Conclusion

There are many gaps in knowledge of biological effects and interaction mechanisms of MRI-related electromagnetic fields with tissues. High priority research needs cover the studies to fill important gaps in knowledge focused on health risk assessment that are needed to significantly reduce the uncertainty in the current scientific information. In the case of very specific occupational situation of medical staff operating MRI scanners, additional attention should take notice of the occupational risk assessment. Further investigations and exposure assessment should include the safety of patients from non-error work ability of medical staff and safety requirements preventing hazards from "flying metallic objects" (3 mT) and possible destroying of magnetic memories/cards (0.5 mT). Further investigations should provide knowledge for current scientific gaps, but also to allow verification of the protection level from exposure limitations published by various international and national bodies. Such needs indicate that exposure assessment should allow multi-level analysis of exposure pattern, harmonized with exposure limitations mentioned in Table 1. The most important topics for exposure assessment from MRI scanners should include static and gradient fields exposure, exposure results from workers movement in the area of spatially heterogeneous fields, medical staff, technicians, cleaners and other possible exposed workers groups, open and close magnets, low and high field magnets, diagnostic and interventional use, various types of medical procedures, availability of technical staff for the reduction exposure level and duration. In any case of further research, detailed exposure assessment protocol published with the biomedical research results will be of high importance for combined analysis of various studies and determination of the groups of highly exposed or at high risk groups of workers.

Acknowledgements

This paper was prepared as a part of the activities of European project EMF-NET (FP6 Co-ordination Action "EFFECTS OF THE EXPOSURE TO ELECTROMAGNETIC FIELDS: FROM SCIENCE TO PUBLIC HEALTH AND SAFER WORKPLACE", project No SSPE-CT-2004-502173)

References

1. ACGIH TLVs and BEIs. Based on the Documentations for Threshold Limit Values for Chemical Substances and Physical Agents & Biological Exposure Indices. American Conference Governmental and Industrial Hygienists, Cincinnati, OH, 2006.
2. Bassen H., Schaefer D. J., Zaremba L., Bushberg J., Ziskin M., Foster K. R., IEEE Committee on Man and Radiation (COMAR) Technical Information Statement “Exposure of Medical Personnel to Electromagnetic Fields from Open Magnetic Resonance Imaging Systems”, Health Physics, vol. 89, No. 6 (December), 684-689, 2005.

3. Cavin I. at all, Monitoring Occupational Exposure to MRI Static Magnetic Fields at 3T and & T, ICNIRP Workshop on EMF dosimetry, Berlin, March 2006 (poster)
4. Directive 2004/40/EC of the European Parliament and of the Council of 29 April 2004 on the minimum health and safety requirements regarding the exposure of workers to the risks arising from physical agents (electromagnetic fields) (18th individual Directive within the meaning of Article 16(1) of Directive 89/391/EEC), O.J. nr L-184 of 24 May 2004.
5. ENVIRONMENT AND HEALTH IMPLICATIONS OF ELECTROMAGNETIC FIELD EXPOSURE - Report on Research Needs, EMF-NET/WHO COMMITTEE on RESEARCH NEEDS - Elisabeth Cardis, Guglielmo D'Inzeo, Maria Feychting, Jukka Juutilainen, Jolanta Karpowicz, Norbert Leitgeb, Paolo Ravazzani (Chairman) , Mike Repacholi, Theo Samaras, Richard Saunders, Gyorgy Thuroczy, Emilie Van Deventer, Paolo Vecchia, and Bernard Veyret, sierpień, 2005 [http://www.jrc.cec.eu.int/emf-net/reports.cfm]
6. Environmental Health Criteria 232, Static Fields, World Health Organization, 2006
7. ICNIRP Statement on Medical Magnetic Resonance (MR) Procedures: Protection Of Patients. Health Physics 87(2): 197-216; 2004.
8. IEEE Standard for Safety Levels with Respect to Human Exposure to Electromagnetic Fields, 0-3 kHz, Std C.95.6, 2002.
9. Karpowicz J., Gryz K. - Health Risk Assessment of Occupational Exposure to a Magnetic Field From Magnetic Resonance Imaging Devices, International Journal of Occupational Safety and Ergonomics (JOSE), 2006, vol. 12, No. 2, 155-167.
10. Markisz J., Aquilia M., Technical Magnetic Resonance Imaging, Appleton&Lange, 1996.
11. Merkle E.M. et al – Safety, Compatibility, and Visualization Issues in Interventional MR Imaging, in: Practical MR Safety Considerations for Physicians, Physicists, and Technologists, ed. E. Kanal, Pittsburgh, USA, November 2001, pp 77-84.
12. Non-ionizing radiation, Part 1: Static and extremely low-frequency (ELF) electric and magnetic fields, IARC Monographs 80, IARC Press: Lyon, 2002.
13. Reilly P.J., Applied Bioelectricity. From Electrical Stimulation to Electropathology, Springer-Verlag New York, Inc., 1998.
14. WHO Research Agenda for Static Fields, World Health Organization, Geneva, 2006

CYTOTOXIC EFFECTS OF A SN MERCAPTONICOTINIC ACID COMPLEX ON WISTAR RAT LEIOMYOSARCOMA CELLS IN VITRO AND SIMULTANEOUS EXPOSURE AT LOW INTENSITY STATIC ELECTROMAGNETIC FIELDS: EVIDENCES OF A SYNERGY WITH STATIC ELECTROMAGNETIC FIELDS

IOANNIS VERGINADIS[1], IOANNIS ZELOVITIS[1], ANTONIOS AVDIKOS[1], TELEMACHOS DASKALOU[1], IOANNIS TOLIOPOULOS[1], IOANNIS SIMOS[1], MICHALIS BALLAS[1], SOTIRIS HADJIKAKOU[2], KONSTANTINOS HAVELAS[1], GEORGIOS HADZIAVAZIS[1], ANGELOS EVANGELOU[1], KONSTANTINOS CHARALABOPOULOS[1] AND SPYRIDON KARKABOUNAS[1]

[1]LABORATORY OF EXPERIMENTAL PHYSIOLOGY, DEPARTMENT OF MEDICINE, UNIVERSITY OF IOANNINA, GREECE,
[2]LABORATORY OF INORGANIC CHEMISTRY, DEPARTMENT OF CHEMISTRY, UNIVERSITY OF IOANNINA, GREECE

E-mail addresses: johnasterix20012001@yahoo.gr (Ioannis Verginadis), aevaggel@cc.uoi.gr (Angelos M. Evangelou), (Spyridon CH. Karkabounas).

Corresponding author: Dr Spyridon CH. Karkabounas, Lecturer of Physiology, Lab of Physiology, Dept of Medicine, University of Ioannina, Greece, Tel: 0030-26510-97576, Fax: 0030-26510-97850, E-mail : skarkabou@cc.uoi.gr.

Abstract

The aim of this study is to examine the possible synergistic action between the cytotoxic $Ph_3Sn(MNA)SnPh_3$ complex (SNMNA) and its electromagnetic resonance radiofrequencies on proliferation and viability of a cancer cell line. Leiomyosarcoma tumor cells (LMS cells) were isolated from cancer bearing Wistar rats and tested for their proliferation and viability after administration of the SNMNA complex in various concentrations. We used an appropriate system to take the resonance radiofrequencies spectrum of the SNMNA complex. Then the LMS cells were exposed to two groups of frequencies for 45 min every 24h to determinate their proliferation and viability. Lastly we studied the simultaneous administration of the SNMNA complex and exposure to two groups of its radiofrequencies. The data collected reveal that the SNMNA: 1) Is a very cytotoxic and antiproliferative agent against cancer cells and 2) In low concentrations exercises synergistic action with Electromagnetic Resonance Frequencies (ERFs) and promotes obvious cytotoxic and antiproliferative action. In conclusion, SNMNA complex presents a relatively strong anticarcinogenic and cytotoxic activity. The mechanism of SNMNA complex action on the LMS cells seems to be related with the inhibition of the glycolytic metabolism of the cancer cells. Possibly the SNMNA complex acts as an anti-metabolite competing nicotinic acid in energy production metabolic pathways in which it participates as a coenzyme. The cytotoxicity of the SNMNA complex can be modified with the use of electromagnetic fields which can result beneficial for its future therapeutic actions.

Introduction

LMS tumor is a type of cancer which presents great resistance to chemotherapy. Until, cis-platinum is the preferred therapeutic agent [1,2,3,4]. Due to its chemical characteristics and the ability to form bonds between DNA strands, the main intercellular target of cis-platinum is the cell's DNA [5] The Pt derivatives interpolate between DNA strands and provoke structural deformation to DNA molecules inhibiting the functional rotations around the histones resulting to DNA fragmentation. [5]. It is not really clear if cis-platinum as well as other forms of Pt complexes is metabolically activated by cell's microsomial system in order to react with DNA molecule [6]. Platinum is the preferred element used to construct metal complexes with antitumoral effects. Various Tin complexes are used in the same therapeutic approach as platinum, for cancer experimental therapy [7,8,9,10,11,12,13,14,15,16,17]. A restrict number of experimental studies indicated that Tin complexes may act with a different mechanism of cis-Pt [11,12,13,14,15,16,17]. The present project studies the cytotoxic and antiproliferative effects of SNMNA complex and the synergistic action between the SNMNA complex and its electromagnetic resonance radiofrequencies on cancer cells *in vitro*.

Material and Methods

Tumor cell line development: LMS cells were produced the following way: 3 male and 3 female Wistar rats were selected from a group of syngenic laboratory animals (7th generation). After anaesthetization with ketamine and midazolam, B[a]P was administered using the procedure described by Karkabounas et al [18,19,20,21,22]. 110 to 128 days late, all animals developed tumors. Biopsies were performed after anaesthetization with diethyl ether and a sample of malignant cells was attained using a bioptic needle. Tumors of 4 animals were histological identified as LMS tumors (65%). One of them developed fibromyosarcoma and another rhabdomyosarcoma. Aseptic samples of LMS tumors sizing about 0,5 cm^3 were placed into cold Ringer sterile solution. Then they were aseptically cut into smaller pieces (around 1mm^3) and placed in a sterilized glass beaker with 20 ml of Trypsin 0,25% solution. Incubation of the pieces was performed by a gently stir and every 15 minutes 20 ml of the supernatant were collected and placed into sterile plastic tubes (falcon) for further process. Before we commence the second round of trypsinisation 10ml of Dulbeco's Modified Eagles Medium (DMEM) were added to protect tumors from the trypsin action. Afterwards 10 ml of DMEM were rejected and 20 ml of trypsin 0,25% solution were added again and the same trypsinization process was repeated until the tumor pieces were dissolved in released tumor cells. In each tube with the collected tumor cells after trypsinization, we added 1 ml of Foetal Bovine Serum (FBS) in order to stop the action of trypsin. The tubes containing the initial trypsinised samples of the tumors centrifuged at 1200 rpm for 5 minutes in order to form a pellet all the remaining cells. Supernatant was rejected, 10ml of Phosphate Buffer Saline (PBS) were added and the cell suspension was gently mixed using pipette before the second centrifugation at 1200 rpm for 5 minutes. Supernatant was again rejected, 10 ml of DMEM with 10% FBS were added, mixed with the cells and a sample of 1 ml suspension was cultured in a Petri dish (9 ml DMEM, 1 ml FBS). Cells incubated at 37% ^oC, 95% O_2, 5% CO_2 and examined once a day by light microscopy. Cells were subcultured in order to obtain large numbers of tumor cells. The confluent tumor cells in each Petri dish washed with 10 ml of PBS to digress the dead cells, added 1 ml of trypsin 0,25% solution in order to be detached and 10 ml of DMEM to stop the trypsin action. The cell suspension from Petri dish transferred into sterilized plastic tubes and centrifuged at 3000 rpm for 5 minutes. The supernatant rejected and the pellet of cells resuspended in a cryopreservation solution of FBS and Dimethyl Sulfoxide (DMSO) at 9:1 ratio, placed in cryotubes (1ml of total volume) and stored in liquid nitrogen in order to be used again when needed. Examination the nature of these cells was performed using two techniques: 1) Classic diagnostic after Giemsa dyeing**,** 2) Biological testing. We used large numbers of viable tumor cells collected from a recent cell culture as described above. These cells were inoculated into Wistar rats, belonging to a homogenic line, to whom the initial tumor sample was taken (syngenic animals). Before the inoculation the rats anaesthetized with ketamine and midazolam (20mgr+6mgr per Kg BWt) followed by a 2 cm surgical incision performed aseptically on the left shoulder blade. The tissues removed and severed lightly until a small bleeding. $4x10^6$ LMS cells suspended in 1 ml of Hanke's solution and inoculated on the traumatized tissues by a gentle injection. The edges of the wound ascended και stitched so as the LMS cells to remain in the wound. Tumors were developed after a period of around 10-20 days. Small tumor pieces were cut for histopathological examination. All tumor samples were identified as Leiomyosarcomas. All the inoculated animals developed the characteristics of the neoplastic disease. Tumor's size at death was around 38-45% of the total animal weight.

SNMNA complex cytotoxicity and antiproliferative effects on LMS cells *in vitro*: For these experiments we used LMS cells taken from liquid nitrogen. The LMS cells were cultured in a Petri dish and incubated for 10 days in order to control the proliferation rate and viability. When the LMS cells become confluent, the DMEM rejected, washed with PBS and 1ml of trypsin 0,25% solution added. After five minutes incubation the LMS cells were detached and we added 10 ml of DMEM in Petri dish. We counted the LMS cells on a cymometer Newbauer and seeded in Petri dish containing 24 wells totally (25.000 LMS cells per well, total volume 1 ml). We seeded 3 Petri dishes for 24, 48 and 72 hours. After 24 hours incubation we renewed the DMEM in 12 wells of each Petri (control wells). At the remaining 12 wells of each Petri we rejected the DMEM and added the dissolved in DMEM SNMNA complex in various concentrations (test wells). The total volume was 1 ml per well. We examined the following concentrations of the SNMNA complex: $0,5x10^{-9}$ M, $0,75x10^{-9}$ M, $1x10^{-9}$ M, $5x10^{-9}$ M, $20x10^{-9}$ M, $50x10^{-9}$ M, $75x10^{-9}$ M, $100x10^{-9}$ M, $125x10^{-9}$ M, $150x10^{-9}$ M, 200 $x10^{-9}$ M, 250 $x10^{-9}$ M. After 24 hours incubation we rejected the DMEM, washed with 1 ml of PBS, added 0,25 ml of trypsin 0,25% solution and incubated again for 5 minutes. When the LMS cells were detached we added 0,25 ml of PBS and 0,5 ml of trypan blue 0,4% solution (total volume 1 ml). After 5 minutes we counted the LMS cells of each well on a cymometer Newbauer. The above procedure for 24 hours cell testing was repeated for 48 and 72 hours incubation.

Chemicals: DMEM, DMSO, PBS and Trypan Blue 0,4% were purchased from Sigma; Trypsin 0,25% and FBS were purchased from PAA (Cell culture company); Stereochemical formula of SNMNA complex is shown at photo 1.

Simultaneous administration of the tin complex and its electromagnetic resonance radio frequencies on LMS cells *in vitro*: This experiment included 5 different tests. Cell viability was the comparable parameter in every test. Cell viability was tested by using Trypan Blue 0,4% solution, counting only live cells. For all the 5 different tests, 25.000 LMS cells were cultured in each well of a Petri (24 wells totally), using 6 wells for each count at 24, 48 and 72 hours. Each test was performed as follows:
1st test line (control of the controls): The results of these tests were used to confirm the controls (double blinded) and were characterized as E1 test. Particularly, 24h after cell culture, DMEM was rejected, each well was washed with 1ml PBS and fresh DMEM was added to a final volume of 1ml. Cells were incubated for 24h at 37oC, 95% O_2, 5% CO_2. DMEM was again rejected in the first 6 wells which was washed using 1ml of PBS. 0,25 ml of trypsin solution 0,25%, was then added in each well and cells were incubated for 3 minutes in order to detach. After 3 minutes period 0,25ml of PBS and 0,5ml Trypan Blue (0,4%) solution were added. Following 5 minutes of incubation cell viability was measured using a microscope. This procedure was repeated at 48 and 72h.
2nd test line (control): The results of these experiments were used as controls (blind) and were characterized as E2 tests. LMS cell culture, 24h incubation, dead cell rejection, PBS wash, DMEM renewal was performed as descript above. The next step was to let the Petri outside the incubation chamber at RT (25 ^oC) and normal atmosphere (N_2 80% and O_2 20% approximately) under sterilized conditions for 45 minutes. LMS cell viability was measured after 24h incubation (Trypan Blue method described above). The same treatment was repeated at 48 and 72h in order to determinate the LMS cell viability.

3rd test line (substance activity): This line of experiments was characterized as E3 and was conducted the same way as E1 with the exception that before the first 24h incubation the SNMNA complex was dissolved in DMEM (1ml of total volume) and added in each well at various concentrations (1st group: 10^{-12} M, 10^{-15} M, 10^{-18} M and 2nd group: $5x10^{-9}$ M, $20x10^{-9}$ M, $50x10^{-9}$ M). LMS cell viability control was performed at the same time periods using the same methods as described above.

4th test line (electromagnetic field activity): This line of experiments was characterized as E4 and was performed in the same way as E2 with a simultaneous exposure of the Petri at a range EFRs of SNMNA complex for 45 minutes (1st group of exposure included 10 frequencies, 2nd 328 frequencies). LMS cell viability control was determinated at the same time periods using the same methods. The conditions of exposure were the same as E2.

5th test line (simultaneous activity of the SNMNA complex and the electromagnetic field): This line of experiments was characterized as E5 and included the simultaneous study of the SNMNA complex actions (2 groups of concentrations) and exposure to its ERFs (2 groups of frequencies) on the LMS cells. Experiments were performed by combining E3 and E4 test lines (addition of the SNMNA complex at known concentrations and exposure at known frequency groups of the LMS cells for 45min/24h). All cell lines experiments were repeated 5 times.

Equipment and used apparatus

Recording-storing-frequency broadcasting system: The used system is called Multi Channel Dynamic Exciter (MCDE) and it is composed of: a) the diagnostic system, b) the storing system and c) the field generator. The diagnostic system is based on Bohm-Aharonov effect, which was discovered by them in 1959 during a study involving experiments of recording beams of electrons (β rays) through a number of various solenoids [23,24]. A substance or a biological sample is put in a determinate part of the diagnostic apparatus in connection with a solenoid and the electromagnetic frequencies generator. The generator is activated and scan a broad spectrum of radiofrequencies from 0,1 Hz to 1 MHz. The frequencies in which observed resonance between electromagnetic radiofrequencies emitted by the sample (substance or biological material) and the generator's radiofrequencies are stored. In this manner is determinated a spectrum of resonating radiofrequencies that characterize the chemical substance or the biological material. This spectrum is called as the specific fingerprint of this chemical substance or biological material. This spectrum is registered at the memory of the storing system and transformed at different radiofrequencies by an appropriate algorithm. The transformed radiofrequencies can be used as input in the field generator and emitted back to the target to influence this chemical or biological material. The generator of electromagnetic fields used in the current study produce static electromagnetic fields with the following characteristics: the intensity of the electric field is 1,1-1,11±0,01 V/m and 0,0027-0,0029±0,00005 A/m for the magnetic field. The radiofrequencies broad ranged from 10Hz to 1MHz. The energy density of the MCDE system generated electromagnetic fields is approximately 100mW/cm^3. The MCDE system [photo 2] was examined for its safety application in animal and humans by the National (Greek) Center for Scientific Research «Demokritos» (Greek Department of the International Committee of Atomic Energy). The MCDE system was found safe for prolonging exposure humans, animals and other living systems. The MCDE system was placed inside a Faraday cage, in order not to be affected by external electromagnetic fields.

Results

Cytotoxicity of SNMNA complex: SNMNA complex is a very cytotoxic agent against LMS cells [figure 1-4]. The Inhibitory Concentration (IC_{50}) for this complex according to these figures is calculated between 5 and 20 nM for 24h, 48h and 72h. Minimal lethal concentration (MLC) of the complex at 24h ranges between 50-75nM, at 48h around 75nM and at 72h between 30-40nM. At all time points (24h, 48h, 72h) there was no significant different between the values of MLC. Thus, LMS cells seem sensitive to the SNMNA complex cytotoxic effects. The SNMNA complex presents a time depending cytotoxic action, and MLC reaches minimum value at 72h. At 48h MLC value is rather steady at 75nM which can be explained as a cell homeostasis adaptation for neutralize the SNMNA complex cytotoxic effects.

Synergistic activity of the complex and its ERFs:

Considering data from test lines E1, E2, E3, E4 and E5 we can conclude that: 1) LMS cell proliferation rate from 24h to 72h shows an increasing rate (control of controls E1). Thus, LMS cells present high viability during incubation without the presence of a substance or electromagnetic field [fig 1,2,3,4], [photo 3], 2) LMS cell proliferation rate (control E2) shows a slight decrease. Cells seem to be affective by stress when they are outside the incubating chamber (45minues/24h) although they continue to proliferate with increasing rates, 3) LMS cell proliferation rate at test line E3 is significantly lower compared with E1 and E2. Proliferation rate drop is smaller at low concentrations (10^{-12}, 10^{-15}, 10^{-18} M) [fig 5,7], [photo 4] and higher at high concentrations ($5x10^{-9}$, $20x10^{-9}$, $50x10^{-9}$ M) [fig 6,8],. These data imply the strong cytotoxic activity of the SNMNA complex, 4) LMS cell proliferation rate at test line E4 is lower compared with E1 and E2. Thus, even when the SNMNA complex is absent the exposure of the LMS cells to its resonance frequencies provokes the death of the cancer cells. The electromagnetic field exposure is more cytotoxic in comparison with the activity of the SNMNA complex at low concentrations (10^{-12}, 10^{-15}, 10^{-18} M) [fig 5,7]. At higher concentrations ($5x10^{-9}$, $20x10^{-9}$, $50x10^{-9}$ M) [fig 6,8] the fields shows smaller cytotoxic activity than the SNMNA complex, 5) LMS cell proliferation rate at test line E5 is significantly lower. The decrease of the proliferation rate is the highest among the test lines [fig 5,6,7,8] especially at 48h and 72h. In contrast a small increase is observed at 24h in relation with E2 test line and E1 (smaller than E2), [photo 5]. The decrease of the proliferation rate observed by simultaneous administration of the lowest SNMNA complex concentration (10^{-18} M) and the exposure to its electromagnetic radiofrequencies is the highest among the other low concentrations (10^{-12}, 10^{-15} M) with the presence of the electromagnetic field [Table 1,2]. There is a 54,79% (72h) [Table 1] decrease of the proliferation rate of E5 (C=10^{-18} and 10

radiofrequencies) and 51,35% (72h) [Table 1] decrease of the proliferation rate of E5 ($C=10^{-18}$ and 328 radiofrequencies), in comparison to E2. This result indicates a synergistic effect on LMS cells between the SNMNA complex and its electromagnetic radiofrequencies. The decrease of the LMS cell proliferation rate is related to the exposure time rather than the number of frequencies used in each group.

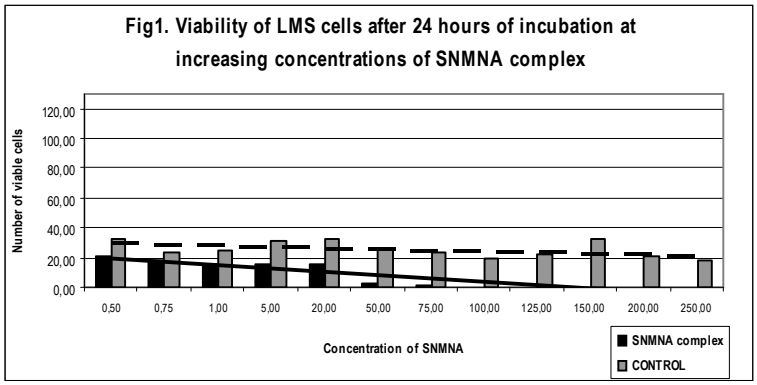

fig 1: We measure the viability of LMS cells after 24 hours of incubation at increasing concentrations ($0,5x10^{-9}$ M, $0,75x10^{-9}$ M, $1x10^{-9}$ M, $5x10^{-9}$ M, $20x10^{-9}$ M, $50x10^{-9}$ M, $75x10^{-9}$ M, $100x10^{-9}$ M, $125x10^{-9}$ M, $150x10^{-9}$ M, 200 $x10^{-9}$ M, 250 $x10^{-9}$ M) of SNMNA complex.

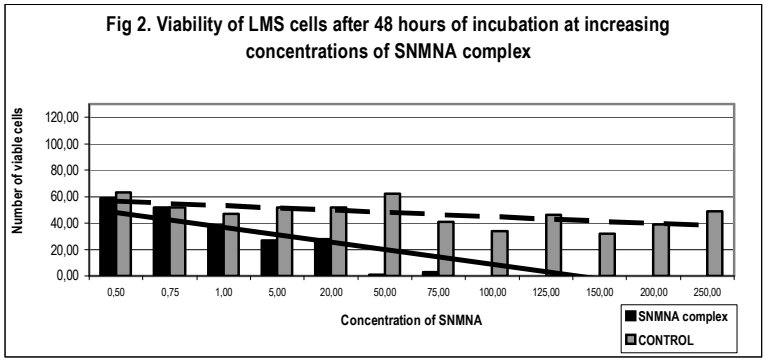

fig 2: We measure the viability of LMS cells after 48 hours of incubation at increasing concentrations ($0,5x10^{-9}$ M, $0,75x10^{-9}$ M, $1x10^{-9}$ M, $5x10^{-9}$ M, $20x10^{-9}$ M, $50x10^{-9}$ M, $75x10^{-9}$ M, $100x10^{-9}$ M, $125x10^{-9}$ M, $150x10^{-9}$ M, 200 $x10^{-9}$ M, 250 $x10^{-9}$ M) of SNMNA complex

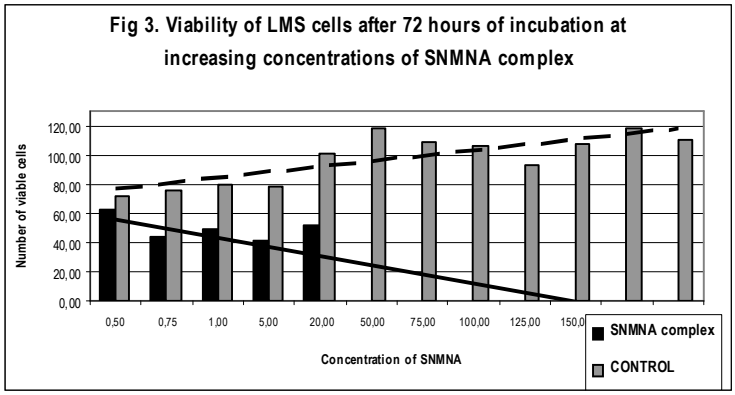

fig 3: We measure the viability of LMS cells after 72 hours of incubation at increasing concentrations ($0,5x10^{-9}$ M, $0,75x10^{-9}$ M, $1x10^{-9}$ M, $5x10^{-9}$ M, $20x10^{-9}$ M, $50x10^{-9}$ M, $75x10^{-9}$ M, $100x10^{-9}$ M, $125x10^{-9}$ M, $150x10^{-9}$ M, 200 $x10^{-9}$ M, 250 $x10^{-9}$ M) of SNMNA complex

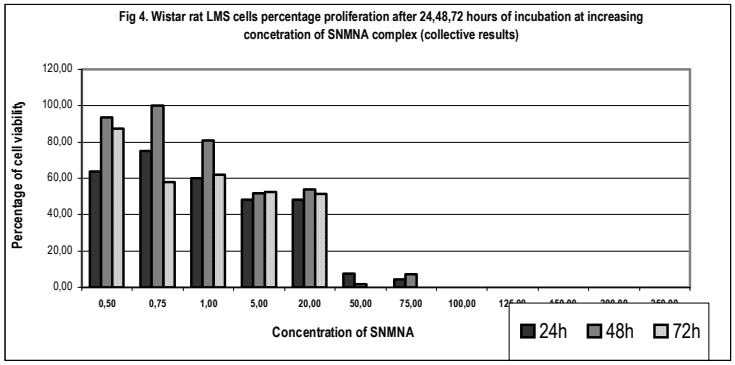

fig 4: Wistar rat LMS cells percentage proliferation after 24,48,72 hours of incubation at increasing concentrations (0,5x10^{-9} M, 0,75x10^{-9} M, 1x10^{-9} M, 5x10^{-9} M, 20x10^{-9} M, 50x10^{-9} M, 75x10^{-9} M, 100x10^{-9} M, 125x10^{-9} M, 150x10^{-9} M, 200 x10^{-9} M, 250 x10^{-9} M) of SNMNA complex (collective results)

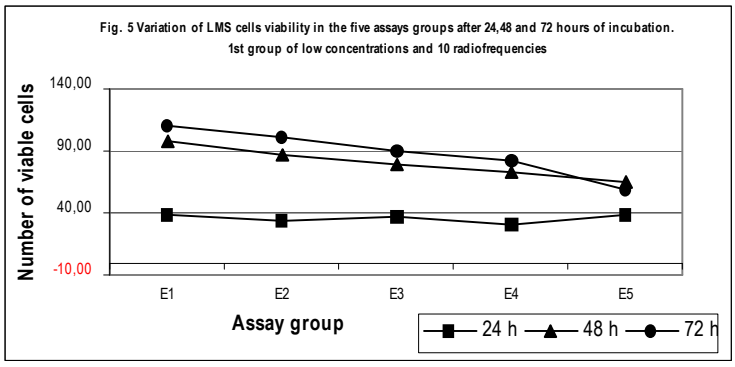

fig 5: In this one we measure the variation of LMS cells viability in the five assays groups (E1, E2, E3, E4, E5) after 24,48 and 72 hours of incubation. 1st group of low concentrations (10^{-12} M, 10^{-15} M, 10^{-18} M) and 10 radiofrequencies

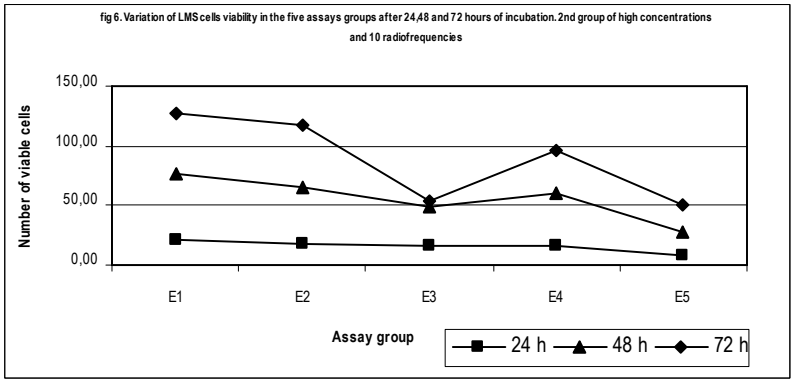

fig 6: We measure the variation of LMS cells viability in the five assays groups (E1, E2, E3, E4, E5) after 24,48 and 72 hours of incubation. 2nd group of high concentrations (5x10^{-9} M, 20x10^{-9} M, 50x10^{-9} M) and 10 radiofrequencies.

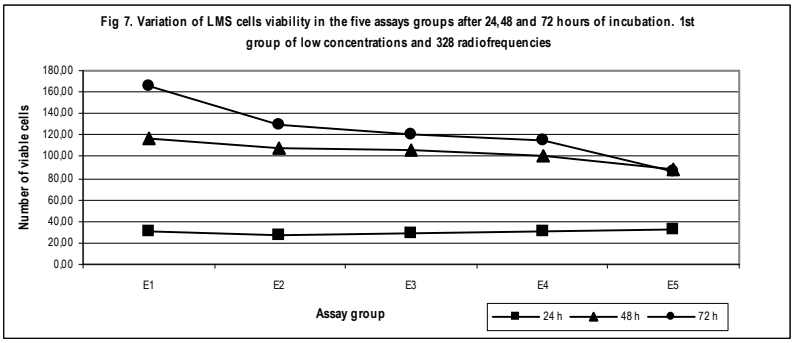

fig 7: We measure the variation of LMS cells viability in the five assays groups (E1, E2, E3, E4, E5) after 24,48 and 72 hours of incubation. 1st group of low concentrations (10^{-12} M, 10^{-15} M, 10^{-18} M) and 328 radiofrequencies

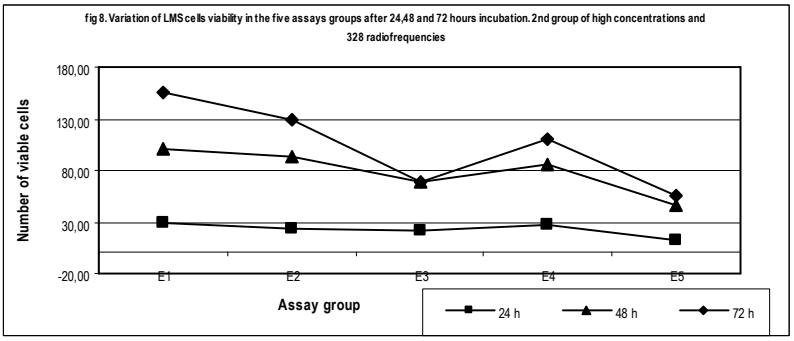

fig 8: We measure the variation of LMS cells viability in the five assays groups (E1, E2, E3, E4, E5) after 24,48 and 72 hours incubation. 2nd group of high concentrations ($5x10^{-9}$ M, $20x10^{-9}$ M, $50x10^{-9}$ M) and 328 radiofrequencies.

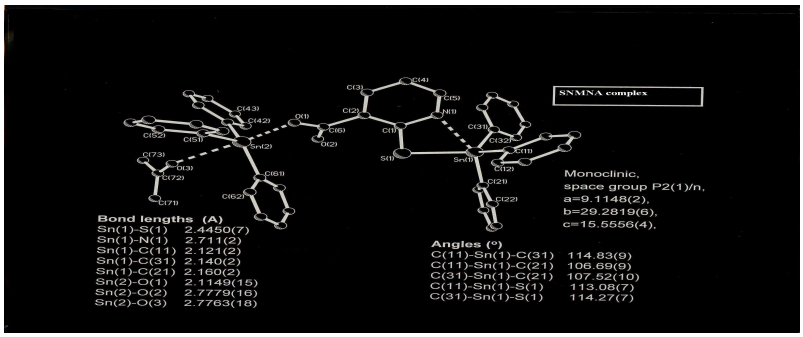

Photo 1: Formula and structural characteristics of the SNMNA complex.

Photo 2: The MCDE system in Faraday cage.

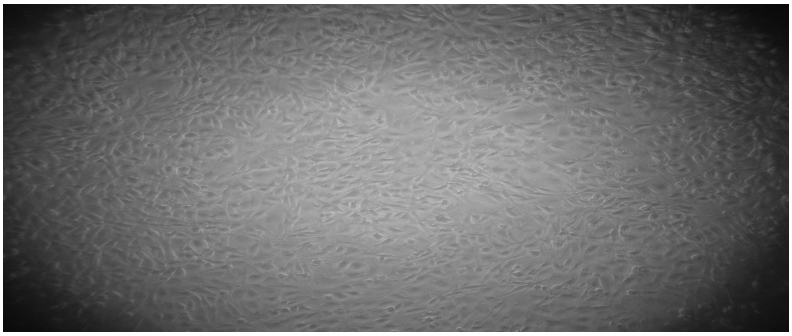

Photo 3: E1 assay (control of the controls). The LMS cells was confluent.

Photo 4: E3 assay (substance activity). Decrease of LMS cell population after 72 h incubation at 10^{-18} M of SNMNA complex.

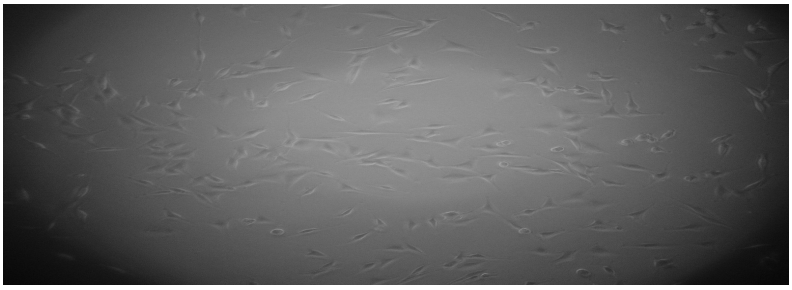

Photo 5: E5 assay (simultaneous activity of the SNMNA complex and the electromagnetic field). Synergistic decrease of LMS population after 72 h incubation at 10^{-18} M of SNMNA complex and 3x45 min total exposure at the electromagnetic field.

		(L+10)	
10^{-12} M	28,43	-15,96	-32,33
10^{-15} M	0,90	-31,19	-36,09
10^{-18} M	-5,68	-42,98	-54,79
		(L+328)	
10^{-12} M	18,32	2,99	-8,37
10^{-15} M	48,85	0,69	-50,13
10^{-18} M	1,15	-48,05	-51,35

Table 1: Shows the time dependent declination of LMS cell proliferation in low concentrations (10^{-12} M, 10^{-15} M, 10^{-18} M) of SNMNA complex. The decrease of the LMS cell proliferation is independent to the

number of radiofrequencies. The lowest concentration (10^{-18} M) shows the highest cell proliferation decrease. The table shows the percentage LMS cell proliferation (E5 in comparison with E2 assay).

		(H+10)	
5nM	-22,34	-35,44	-27,55
20nM	-41,08	-43,04	-44,60
50nM	-94,64	-100,00	-100,00
		(H+328)	
5nM	-25,98	-31,30	-27,02
20nM	-36,33	-39,23	-40,15
50nM	-91,63	-100,00	-100,00

Table 2: Shows the time dependent declination of LMS cell proliferation in high concentrations ($5x10^{-9}$ M, $20x10^{-9}$ M, $50x10^{-9}$ M) of SNMNA complex. The accumulative decrease (SNMNA complex+electromagnetic field) is minor in comparison with results in table 1. The prevalence of SNMNA complex concentration on the electromagnetic field effects is obvious. The table shows the percentage LMS cell proliferation (E5 in comparison with E2 assay).

Discussion

We have studied the effects of the SNMNA complex on a Wistar rat LMS cancer cell line. We also studied if it is possible to modify the cytotoxicity of the SNMNA complex using electromagnetic fields at radiofrequencies of the complex resonance spectrum. SNMNA complex is a strong cytotoxic agent on LMS cancer cells *in vitro* [11,12,13]. Mercaptonicotinic acid is an essential moiety of the complex and it is possible to act as anti-metabolite. Nicotinic acid participates in coenzymes (NAD^+, $NADP^+$), which take place as reduced equivalents carriers in glycolysis pathway and Krebs cycle in cancer cells [25]. Thus, nicotinic acid seems as a very important agent at energy production of tumors energetic metabolism [25]. Mercaptonicotinic acid of the SNMNA complex may compete nicotinic acid coenzymes in the above metabolic energy production pathways. The used LMS cells, such as other cancer cell types, seem to produce energy by glycolytic pathway [26,27,28,29,30,31,32]. This point has been shown by preliminary experiments in which the LMS cells are very sensitive to iodoacetic acid [31,32]. Iodoacetic acid is a strong inhibitor of the glyceraldehyde-3-phosphate dehydrogenase [29]. This enzyme plays a critical role for the whole glycolytic pathway and so the ATP glycolytic production stops by inhibiting this enzyme [33]. The SNMNA complex acts in very low concentrations lower than the iodoacetic acid. On the other hand the SNMNA complex is a strong inhibitor of the 5-lipoxygenase [13,14]. Generally the lipoxygenase, cyclooxygenase 1 and cyclooxygenase 2 inhibitors of synthetic or natural origins are still used as anti-cancer substances with target action [34,35]. It is possible that SNMNA complex acts as a non steroid antinflammation derivative (NSAID) inhibiting 5-lipoxygenase on LMS cells [13,14]. In a recently published work, we find that the SNMNA complex produces free radicals in aquatic solutions [13,14]. This is verified from the EPR spectrums of the SNMNA complex [13,14]. The energy of electromagnetic fields may activate the electrons of the SNMNA complex bonds causing electron excitation. Exposure of SNMNA complex aquatic solutions to UV radiation causes the immediate production of free radicals [13,14]. The chemical reactions can be accelerated when an external electromagnetic field influences a chemical system [36,37,38,39]. For example the Belluzov – Zhabotinsky (BZ) reaction of malic acid catalyzed by Fe^{+2} – Fe^{+3} ions (and not Ce) can be accelerated with the use of a low intensity external electromagnetic field (0,1 μT) [37]. Metal complexes such as SNMNA complex can be activated by external electromagnetic fields. The characteristic (fingerprint) resonance radiofrequencies spectrum of a substance can reduce the energy threshold activation of this substance and catalyse its chemical and biological effects.

Acknowledgements: We want to thank the Hellenic Hepirus Biotechnology R&D JS Company for the offer of many reagents.

References

1. K. Charalambopoulos , S. Karkabounas , E. Ioachim , V. Papalimneou , K. Sirigos , A. Evangelou , N. Agnantis and N. Hadjiliadis. Antitumour and toxic effects on Wistar rats of two new platinum complexes. European Journal of Clinical Investigation 2002;32(2):129-33

2. Pautier P, Rev A, Haie-Meder C, Kerbrat P, Dutel JL, Gesta P, Bryard F, Morice P, Duvillard P, Lhomme C. Adjuvant chemotherapy with cisplatin, ifosfamide, and doxorubicin followed by radiotherapy in localized uterine sarcomas: results of a case-control study with radiotherapy alone. Int J Gynecol Cancer. 2004;14(6):1112-7

3. Sagae S, Yamashita K, Ishioka S, Nishioka Y, Terasawa K, Mori M, Yamashiro K, Kanemoto T, Kudo R. Preoperative diagnosis and treatment results in 106 patients with uterine sarcoma in Hokkaido, Japan. Oncology. 2004;67(1):33-9

4. Resnik E, Chambers SK, Carcangiu ML, Kohorn EI, Schwartz PE, Chambers IT. Malignant uterine smooth muscle tumors: role of etoposide, cisplatin, and doxorubicin (EPA) chemotherapy. J Surg Oncol 1996;63(3):145-7

5. Ruiz J, Lorenzo J, Sanglas L, Cutillas N, Vicente C, Villa MD, Aviles FX, Lopez G, Moreno V, Perez J, Bautista D. Palladium(II) and Platinum(II) Organometallic Complexes with the Model Nucleobase Anions of Thymine, Uracil, and Cytosine: Antitumor Activity and Interactions with DNA of the Platinum Compounds. Inorg Chem. 2006;45(16):6347-60

6. LeBlanc GA, Sundseth SS, Weber GF, Waxman DJ. Platinum anticancer drugs modulate P-450 mRNA levels and differentially alter hepatic drug and steroid hormone metabolism in male and female rats. Cancer Res. 1992;52(3):540-7

7. Federica Barbieri, Fabio Sparatore, Monica Cagnoli, Cristina Bruzzo, Federica Novelli and Angela Alama. Antiproliferative activity and interactions with cell-cycle related proteins of the organotin compound triethyltin(IV)lupinylsulfide hydrochloride. Chem Biol Interact 2001;134(1): 27-39

8. Ruslan Sarimov, Eva Markova, Fredrick Johansson , Dag Jenssen, and Igor Belyaev. Exposure to ELF magnetic field tuned to Zn inhibits growth of cancer cells. Bioelectromagnetics 2005;26:631-638

9. Saxena A, Tandon JP. Antitumor activity of some diorganotin and tin(IV) complexes of Schiff bases. Cancer Lett 1983;19(1):73-6.

10. Martin Blank and Lily Soo. Electromagnetic acceleration of the Belousov–Zhabotinski reaction. Bioelectrochemistry 2003;61(1-2):93-97

11. Xanthopoulou M, Hadjikakou S, Hadjiliadis N, Schurmann M, Jurkschat K, Michaelidis A, Skoulika S, Bakas T, Binolis J, Karkabounas S and Charalabopoulos K. Synhesis, structural characterization and in vitro cytotoxicity of organotin[IV] derivatives of heterocyclic thioanides 2-mercapto-benzothiazole, 5-chloro-2-mercapto-benzothiazole, 3-methyl-2-mercapto-benzothiazole, and 2-mercaptonicotinic acid. Journal of Inorganic Biochemistry. 2003;96(2-3):425-34.

12. Xanthopoulou M, Hadjikakou S, Hadjiliadis N, Schurmann M, Jurkschat K, Binolis J, Karkabounas S, Charalabopoulos K. Synthesis of a novel triphenyltin[IV] derivative of 2-mercaptonicotinic acid with strong cytotoxicity in vitro. Bioinorganic Chemistry and Applications. 2003;1(3-4):227 – 231.

13. Xanthopoulou M, Hadjikakou S, Hadjiliadis N, Kubicki M, Karkabounas S, Charalabopoulos K, Kourkoumelis N, Bakas T. Synthesis and characterization of a new chloro – di – phenytin[IV] complex with 2-mercaptonicotinic acid : study of its influence upon a catalytic oxidation of linoleic acid to hydroperoxylinoleic acid by the enzyme lipoxygenase. Journal of Organometalic Chemistry, 2006;691:1780 – 1789.

14. Xanthopoulou M. Biomedical Applications of Thioamides. Synthesis and study of new organotin[IV] thioamides derivatives with biological actions. PhD Thesis, 2006, Department of Chemistry. University of Ioannina.

15. Li Q, da Silva MF, Pombeiro AJ. Diorganotin(IV) derivatives of substituted benzohydroxamic acids with high antitumor activity. Chemistry. 2004;10(6):1456-62

16. Han G, Yang P. Synthesis and characterization of water-insoluble and water-soluble dibutyltin(IV) porphinate complexes based on the tris(pyridinyl)porphyrin moiety, their anti-tumor activity in vitro and interaction with DNA.J Inorg Biochem. 2002;91(1):230-6

17. Syng-Ai C, Basu Baul TS, Chatterjee A. Inhibition of cell proliferation and antitumor activity of a novel organotin compound. J Environ Pathol Toxicol Oncol. 2001;20(4):333-42

18. Karkabounas S, Binolis J, Zelovitis J, Kotsis N, Charalabopoulos A, Avdilos A, Zuridakis A,, Liasko R, Giannakopoulos X, Charalabopoulos K. Inhibition and modification of benzo[a]pyrene induced chemical carcinogenesis of ascorbic acid alone or in combination wih a-tocopherol in Wistar rats .Experimental Oncology, 2002;24: 274-78

19. Karkabounas S, Kostoula O, Daskalou T, Veltsistas P, Karamouzis M, Zelovitis J, Metsios A, Lekkas P, Evangelou AM, Kotsis N, Skoufos I Anticarcinogenic and antiplatelet effects of carvacrol. Exp Oncol 2006;28(2):121-5

20. Karkabounas S., Assimakopoulos D., Malamas M.,. Skaltsounis A.L, Leonce S., Zelovitis J., Stefanou D. and Evangelou A.. Antiproliferative and anticarcinogenic effects of an aqueous preparation of Abies alba and Viscum album se abies , on a L-1210 malignant cell line and tumor-bearing Wistar rats. Anticancer Research 2000;20(6B)4391-5.

21. A. Charalabopoulos , S. Karkabounas , A. Charalampopoulos , V. Papalimneou , E. Ioachim , X. Giannakopoulos. Inhibition of benzo[a]pyrene induced carcinogenesis by vitamin C alone and by pairs of vitamin C –vitamin E and Selenium-Glutathion. Biol Trace Elem Res 2003;93(1-3):201-12

22. A Evangelou, S. Karkabounas, G. Kalpouzos, M. Malamas, R. Liasko, D. Stefanou, A. Vlahos, T. Kabanos. Comparison of the therapeutic effects of two Vanadium complexes administrated at low doses on benzo(a)-pyrene-induced malignant tumors in rats. Cancer Letters. 1997;119(2):221-5

23. Aharonov Y. and D. Bohm. Significance of electromagnetic potentials in quantum theory. Phys. Rev. 1959;115:485–491.

24. Peshkin M. and Tonomura A. The Aharonov-Bohm effect. Springer-Verlag: Berlin, 1989. ISBN 3-540-51567-4.

25. Muruganandham M, Alfieri AA, Matei C, Chen Y, Sukenick G, Schemainda I, Hasmann M, Saltz LB, Koutcher JA. Metabolic signatures associated with a NAD synthesis inhibitor-induced tumor apoptosis identified by 1H-decoupled-31P magnetic resonance spectroscopy. Clin Cancer Res. 2005;11(9):3503-13

26. Baggetto LG. Deviant energetic metabolism of glycolytic cancer cells. Biochimie 1992;74(11):959-74

27. Ristow M. Oxidative metabolism in cancer growth. Curr Opin Clin Nutr Metab Care 2006;9(4):339-45

28. Zu XL, Guppy M. Cancer metabolism: facts, fantasy, and fiction. Biochem Biophys Res Commun 2004;313(3):459-65

29. Tatton WG, Chalmers-Redman RM, Elstner M, Leesch W, Zagodzinski FB, Stupak DP, Sugrue MM, Tatton NA. Glyceraldehyde-3-phosphate dehydrogenase in neurodegeneration and apoptosis signaling. J Neural Transm Suppl 2000;(60):77-100

30. Mathupala SP, Rembel A, Pedersen PL. Aberrant glycolytic metabolism of cancer cells: a remarkable coordination of genetic, transcriptional, post-transcriptional, and mutational events that lead to a critical role for type II hexokinase. J Bioenerg Biomembr 1997;29(4):339-43

31. McKee RW, Parks ME, Dickey A. Influence of iodoacetate on glycolytic intermediates and on respiration in Ehrlich-Lettre ascites carcinoma cells. Arch Biochem Biophys 1968;124(1):450-5
32. Karkabounas S, Kartsiouni D, Stefanou A, Zelovitis J, Lekkas P, Theodosopoulou E, Yioti I, Batistatou A, and Evangelou A. Iodoacetic acid effects on Wistar rat leiomyosarcoma cells in vitro and on cancer bearing Wistar rats.2004, Nov 26 – 28. 5th Greek Congress on Tumor Markers and Target Therapy of Cancer. Book of Abstracts P-28, pg 82.

33. Foxall DL, Brindle KM, Campbell ID, Simpson RJ. The inhibition of erythrocyte glyceraldehyde-3-phosphate dehydrogenase. In situ PMR studies. Biochim Biophys Acta. 1984;804(2):209-15.

34. Matsuyama M, Yoshimura R, Mitsuhashi M, Tsuchida K, Takemoto Y, Kawahito Y, Sano H, Nakatani T. 5-Lipoxygenase inhibitors attenuate growth of human renal cell carcinoma and induce apoptosis through arachidonic acid pathway. Oncol Rep. 2005;14(1):73-9

35. Ye YN, Wu WK, Shin VY, Bruce IC, Wong BC, Cho CH. Dual inhibition of 5-LOX and COX-2 suppresses colon cancer formation promoted by cigarette smoke. Carcinogenesis 2005;26(4):827-34.

36. Kopf-Maier P, Janiak C, Schumann H.Antitumor properties of organometallic metallocene complexes of tin and germanium. J Cancer Res Clin Oncol 1988;114(5):502-6.

37. Kopf-Maier P. Complexes of metals other than platinum as antitumour agents. Eur J Clin Pharmacol 1994;47(1):1-16.

38. Blank M, Soo L. Electromagnetic acceleration of electron transfer reactions. J Cell Biochem. 2001;81(2):278-83

39. Blank M. Do electromagnetic fields interact with electrons in the Na,K-ATPase? Bioelectromagnetics 2005;26(8):677-83

EFFECTS OF LOW INTENSITY STATIC ELECTROMAGNETIC FIELDS ON LEIOMYOSARCOMA CELL LINES

SPYRIDON KARKABOUNAS[1], IOANNIS TOLIOPOULOS[1] , TELEMACHOS DASKALOU[1], KONSTANTINOS HAVELAS[1], OLGA KOSTOULA[1,2], PATRA VEZYRAKI[1], ANTONIOS AVDIKOS[1], JAYNE BINOLIS[1], GEORGE HADZIAVAZIS[1], APOSTOLOS METSIOS[1], IOANNIS VERGINADIS[1], ANGELOS EVANGELOU[1]

[1]Laboratory of Experimental Physiology, Faculty of Medicine, University of Ioannina, Greece
[2]Department of Applied Biology and Technology, University of Ioannina, Greece

Correspondence author: Spyridon Karkabounas, PhD, Lecturer of Experimental Physiology, Laboratory of Experimental Physiology, Faculty of Medicine, University of Ioannina, University Campus, 451 10 Greece. Tel: +30-26510-97751, +30-26510-97576, Fax: +30-26510-97850, E-mail: skarkabu@cc.uoi.gr

Abstract
In this study we investigated the effects of low intensity static electromagnetic field (EMF) causing no thermal effects, on leiomyosarcoma cells (LSC), isolated from tumors of Wistar rats. Electromagnetic resonance frequencies measurements and exposure of cells to static EMF's were performed by a device called Multi Channel Dynamic Exciter 100 V1 (MCDE). The tumors were developed in the rats via a 3,4-benzopyrene injection. The LSC were exposed to electromagnetic resonance frequencies (ERF's) between 10 kHz to 120 kHz, for 45 min. During a 24h period, after the exposure of the LSC to ERF's, there was no inhibition of cells proliferation. In contrast, at the end of a 48h incubation period, LSC proliferation dramatically decreased by more than 98%. At that time, the survived LSC were only 2% of the total cell population exposed to ERF's, and under the same culture conditions showed significant decrease of proliferation. These cells were exposed once again to ERF's for 45 min (totally 4 sessions of exposure, of 45 min duration each) and tested using a flow cytometer. It was found that 45% of these double exposed to ERF's, LSC (EMF cells) were apoptotic and only a small percentage 2%, underwent mitosis. In order to determinate their metastatic potential, these EMF cells were also counted and tested by an aggregometer for their ability to aggregate platelets and found to maintain this ability. They showed no difference in comparison to the LSC not exposed to ERF's (control cells). *In conclusion,* exposure of LSC to specific ERF's decreases dramatically their proliferation rate and induces a high rate of cell apoptosis. Also, the LSC that survived after exposed to ERF's, had a lower proliferation rate compared to the LSC controls but did not loose their potential for metastasis. The use of specific ERF's generated from the MCDE electronic device, is safe for humans and animals according to the international safety standards, and appropriate for the experimental treatment of cancer in vitro and in vivo.

Introduction
There are quite a few of data on the effects of electromagnetic field (EMF) on various kinds of malignant cells in experimental animals and in humans, some of them referring to the application of electromagnetic resonance principles [1,2]. The main concepts expressed so far referring to the effects of EMF on malignancies are: the intensity, frequency and duration of application of the electromagnetic waves. The EMF may act as co-carcinogen combined with the primary carcinogen, especially in experimental animals but can also exert anticarcinogenic effects, inhibiting the proliferation of malignant cells in vitro as well as decreasing the size of the experimental tumors in vivo [3-6]. Studies of the EMF pro-carcinogenic effects in experimental animals are not numerous and seem to have many uncertainties [3,4]. On the contrary, studies on the EMF anticancer effects are abundant and their methodology is well documented [7]. It has been also shown, that the cytostatic effects of the EMF on cancer cells are not related to their thermal effects but are temperature-

independent [8-10]. The purpose of the present study is to investigate the effects exerted by low intensity static electromagnetic field on a) the proliferation and the viability of the leiomyosarcoma cells line (LSC) and b) the cell cycle of LSC and c) the platelet's aggregation from a physiological agonist and LSC cells.

Materials and methods

Production of leiomyosarcoma cells (LSC) and smooth muscle cells (SMC): The malignant cells were isolated from selected leiomyosarcoma tumors of Wistar rats. Fifteen (7 male and 8 female) Wistar rats, of the fifth generation of a certain couple, 60 days old, were subcutaneously injected in their right scapula by 1 ml of 3,4-benzopyrene solution (B[a]P) in tricapryline in a dose of 10.08 mg/ml. The rat leiomyosarcomatic tumors B[a]P induced have the following characteristics: a) sensitivity to antioxidant substances and free radical scavengers indicating that their proliferation is related to the release of reactive oxygen species [11-13], b) their proliferation can be inhibited via the administration of cycloxygenase-2 (COX-2) and 5-lipoxygenase (5-LOX) inhibitors [14] and c) ability to induce leiomyosarcoma tumors when inoculated into Wistar rats. After 110 days (maximum 135 days) of B[a]P injection, all animals developed malignant tumors at the site of injection. All tumors were histologically identified as leiomyosarcomas. The tumors were surgically removed and cut under aseptic conditions into pieces of 0.5 cm^3 in volume. Each piece was placed immediately in cold Ringer's solution and sliced down again to smaller pieces (1 mm^3). All smaller pieces were inserted for 5 min into 5 ml of cold Dulbecco's modified Eagles medium (DMEM) solution which contained small quantities of trypsin and then these pieces were incubated in the same DMEM solution at 37º C for 4 h, with gentle mixing every 15 min. After incubation the DMEM solutions containing the tumor pieces were centrifuged at 900 rpm for 10 min and the supernatant was rejected. The remaining cells were resuspended in DMEM+10% fetal bovine serum (FBS) solution and seeded in plastic coated dishes of 52 mm in diameter. Tumor cells after been subcultured, were examined histologically and were characterized as leiomyosarcoma cells. In order to verify if these LSC were active and able to induce the same type of malignancy in rats, $4x10^6$ of them were suspended in Hanks salt solution and inoculated into every Wistar rat as follows: the animals were anaesthetized with midazolame and ketamine, and a surgical opening was made in their outer skin layer at the middle of their back. The tissue underneath was traumatized by lancing with a sharp blade in order to bring fresh blood to the surface. LSC were then aseptically infused into the operated area, and the incision was immediately sutured. The animals developed medium-sized malignant tumors approximately 12 cm^3 in volume, within the first 10 days after inoculation. Smooth muscle cells (SMC) were isolated from the aorta of Wistar rats and cultured again by the methods described above. The animal experimentation performed according to the European Community Directives and International Legacy for the animal protection. All the in vivo experiments were accomplished according to the European Union Directive for the Protection of Vertebrate Animals Used for Experimental and other Scientific Purposes (86/609/EEC, article 9 §§1,2).

Electromagnetic field equipment: Electromagnetic resonance frequencies measurement and exposure of cells to static EMF's were performed by a device called Multi Channel Dynamic Exciter 100 V1 (MCDE) invented by K. Havelas [17]. The MCDE has been certified by the Greek National Centre for Scientific Research "Democritos" and its Department of International Committee of Atomic Energy for its safe use in humans and animals. This device is consisted of two basic parts: A) an electromagnetic field generator of various intensities. The range intensities for the electrical field are 1.1 to 1.11 ± 0.01 V/m and for the magnetic field are 0.0027 to 0.0029 ± 0.00005 A/m. The radiofrequencies which generate from MCDE system range of 10 Hz to 1 MHz. The power density of the electromagnetic field is 100 mV/cm^3 approximately, B) an electron paramagnetic resonance spectrometer with specific characteristics. This spectrometer is a scanner-recorder of the ERF's emitted from biological systems (targets), such as localized tumors in experimental animal, or cultured cancer cells, exposed to EMF. It is well known that the normal function of any biological system produce electromagnetic waves of specific frequencies caused by cell electromagnetic properties (electric membrane potential, transport of ions charges etc). The specific ERF's emitted from an EMF excited biological system, is recorded as an electromagnetic resonance fingerprint of this system. This is due to the electromagnetic resonance taking part between ERF's produced by the generator and ERF's emitted from the biological system. The MCDE is supported by a sophisticated software easy to use (submitted for accreditation). First, it is necessary to record the electromagnetic resonance fingerprints emitted from the biological systems (targets). Then, by selecting the specific MCDE's programs of the software, the appropriate ERF's for the exposure of the target are calculated and then are emitted to the target.

Estimation of leiomyosarcoma cells and smooth muscle cells electromagnetic resonance frequencies: Electromagnetic resonance fringerprintings of LSC and SMC were recorded before and after their exposure to EMF (10 Hz-1 MHz). The ERF's of LSC electromagnetic resonance fingerprints are modulated using the software and after that, the cancer cells are exposed to these modulated

electromagnetic fingeprintings for 45 min. The cell proliferation and cell morphology were checked every 24 h. A total of 492 different frequencies emitted from LSC cells were recorded (fig 5).

Method of leiomyosarcoma cells and smooth muscle cells exposure to electromagnetic field

Leiomyosarcoma cells treatment: Twelve Petri dishes with 10 ml growth medium were seeded with $1x10^5$ LSC (zero time). The LSC cultures were incubated in 37º C at 95% O_2 + 5% CO_2 atmosphere for 48 h. Then the medium was replaced by 10 ml of new DMEM. At 72 h from zero time, six LSC cultures (EMF cells) were placed into a Faraday apparatus at room temperature (RT) and exposed to modulated electromagnetic fingerprints (from 10 kHz to 120 kHz and intensities from 1.1 to 1.11 +/- 0.01 V/m for the electric field and 0.0027 to 0.0029+/-0.00005 A/m for the magnetic field), for 45 min. A total of 492 frequencies were used for LSC exposure to EMF. The used frequencies were derived from a transformation of the 492 frequencies recorded as the LSC electromagnetic fingerprints (Fig 1) by an specific algorithm [$\sum f(r) + f(em) = c$, $f(r)$ = registrated frequence, $f(em)$= emitted frequence, c = a constant] The other six LSC cultures (control cells) remained at RT for the same time as EMF cells but without being exposed to EMF. The control and EMF cells were incubated once again at the same conditions as before, for about seven hours. At 79h and 96h from zero time, the cells of each culture were counted, subcultured at about $1x10^5$ cells per plate and incubated at the same as above conditions. At 120h from zero time, the EMF cells were re-exposed to EMF as before and 24 h later, both EMF and control cells in each plate were counted and examined microscopically. Then, to examine their proliferation rate in relation to time, both groups (EMF and control cells) were subcultured and incubated at the same described conditions, in order to estimate the time till cell confluence. The cells were then preserved in liquid nitrogen.

Smooth Muscle Cells treatment: The SMC isolated from Wistar rat aorta were subcultured in the same conditions as described above for LSC and exposed to EMF in the same manner and frequencies as rat LSC.

Leiomyosarcoma cells manipulations: The preserved in liquid nitrogen EMF and control cells were defrost and cultured again till cell confluence. Twelve plates were then seeded with the same number of LSC and incubated for 24 h. The EMF cells were again exposed to EMF for 45 min after 24 h and 48 h. Six hours after the last session, cell samples from each plate were taken for testing their cell cycle phases by a flow cytometer Bexton Dickinson system.

Estimation of platelet aggregation ability of leiomyosarcoma cells

The potential for metastasis of the **LSC** was determined from their ability to aggregate platelets before and after their exposure to EMF using the aggregometer CA-500, Cronolog, USA and the Cronolog kit for platelets aggregation. The Cronolog kit was used to verify the normal platelet responses. A total of 120 tests were performed on blood samples taken from six healthy volunteers who abstained from the use of drugs and alcohol for ten days before the tests. The tests were performed in platelet rich plasma (PRP) isolated from the blood samples and prepared according to the manual of the apparatus. The platelet aggregation tests were performed after the suspension of either $5X10^5$ EMF cells or of the same number of control cells, in PRP.

Statistics

Student's t-test was used for the statistical evaluation of the results and $P<0.05$ was considered statistically significant.

Results

Cell proliferation rate: Our results were as follows: a) Twenty-four hours after the first and second session of exposure to the EMF, the proliferation rate of the LSC was slightly decreased, in comparison to the control cells proliferation ($P<0.05$). Also the microscopic examination showed that the highest percentage of LSC was under stress, showing round-shaped cells with abortive pseudopodia and formation of nuclear membrane blebs. b) The multiplication rate of the EMF exposed LSC after 48 h of incubation was dramatically decreased at a percentage higher than 98%, ($P< 0,0001$ compared to the control cells) and most of the exposed malignant cells were found either dead (mainly apoptotic) or extremely stressed: round shaped cells, formation of bleeds in the outer cell membrane, absence of pseudopodia (fig 1) c) The survived LSC after one session of EMF exposure, showed a great difficulty in proliferating according to the time needed till cell confluence (6 days of incubation) in with comparison to the time needed till control cells confluence (3 days), (fig 2). Also, the survived LSC developed a remarkable resistance to EMF, showing only 20% decrease of cell proliferation rate compared to the much higher decrease in proliferation rate of 98%, shown after their first EMF exposure.

Leiomyosarcoma cells distribution in the cell cycle phases: Flow cytometry revealed that after the fourth cell exposure to EMF, 33% of the **LSC** were found to be in G0/G1, 9% in S phase, 2% in mitosis and 45% were undergoing apoptosis, while the control cells were found to be: 36% in G0/G1, 38% in S phase, 19% in mitosis and 2% undergoing apoptosis (Table 1).

SMC viability after exposure to EMF: The SMC seem not to be affected by electromagnetic fields exposure at 24 and 48 h (fig 3). The exposed SMC have a proliferation rate 10% lower than the non exposed SMC (control). This difference is not statistically significant (P<0,4).

Estimation of sarcoma cells " potential for metastasis" by platelet aggregation: The aggregation ability of the control as well as of the exposed to EMF cells, was 78%, and almost equal to the ability to aggregate of the ADP (82%). According to the above, LSC exposure to EMF did not affect significantly the "potential for metastasis" of LSC (fig 4).

Estimation of cell electromagnetic resonance – frequencies: Electromagnetic resonance frequencies of the: a) unexposed to EMF LSC were ranging between 10.5 to 120.5 kHz, b) exposed to EMF LSC, between 10 to 120 kHz and c) SMC between 10 to 120 kHz. Spectrum analysis of the above estimations revealed that the electromagnetic resonance frequencies of LSC exposed to EMF showed significant differences as compared to those of the unexposed LSC (control cells) presenting an almost 70% similarity to the electromagnetic resonance frequencies recorded from the SMC (data not shown).

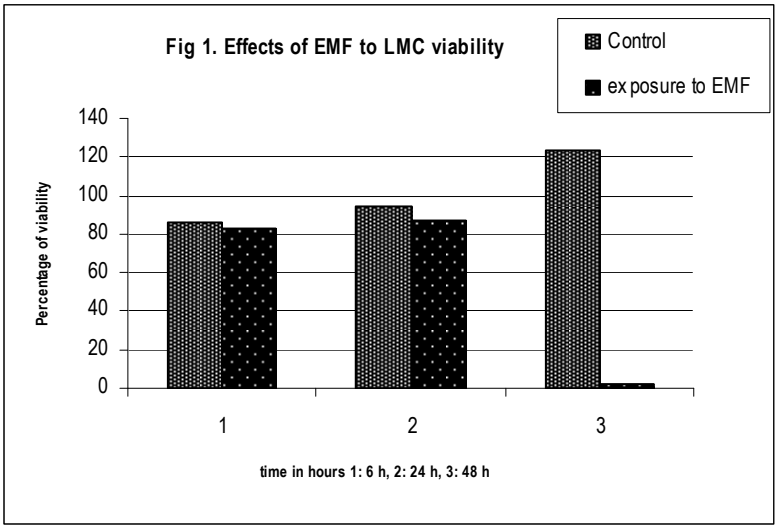

Fig 1. The viability of the EMF exposed LSC after 48 h of incubation was dramatically decreased at a percentage higher than 98%, (P< 0,0001 compared to the control cells)

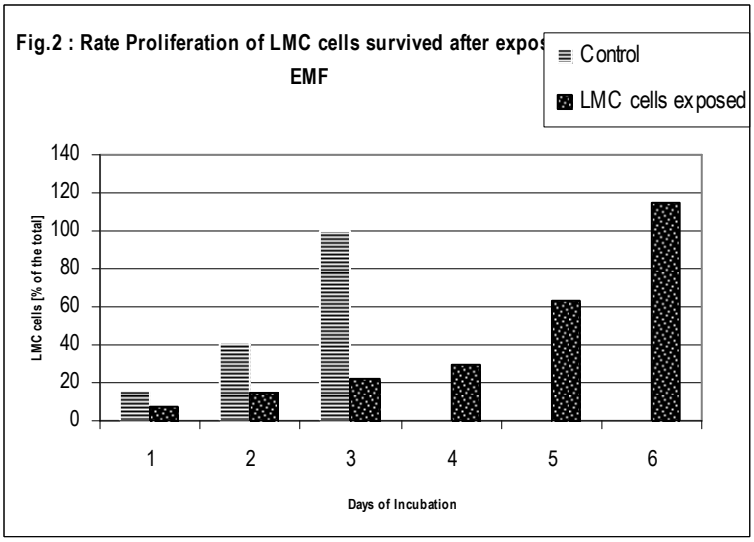

Fig 2. The survived LSC after one session of EMF exposure, showed a significant difficulty in proliferating according to the time needed till cell confluence (6 days of incubation) in with comparison to the time needed till control cells confluence (3 days)

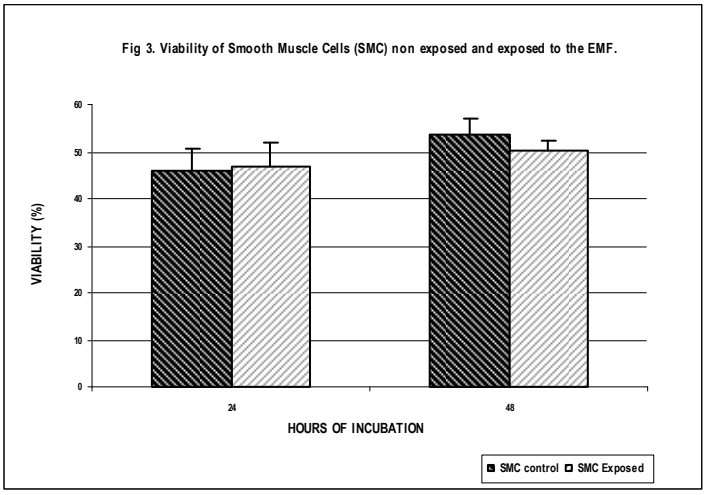

Fig.3 : Viability of Smooth Muscle Cells (SMC) not exposed and exposed to EMF. The non exposed SMC have a rate of growth 10% larger from the exposed ones [P< 0,4].

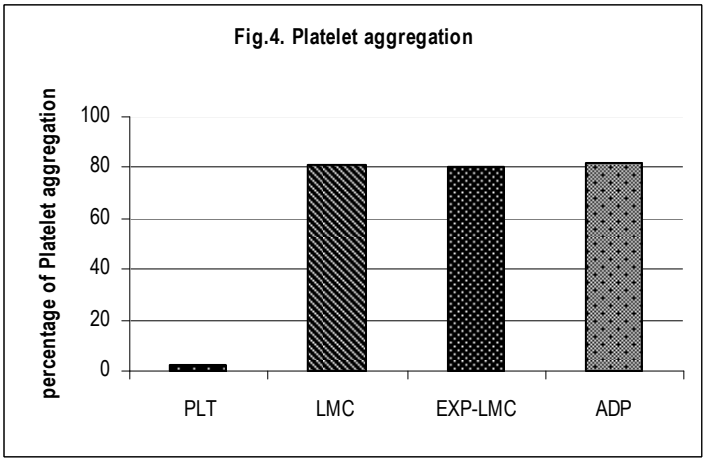

Fig 4. LSC exposure to EMF did not affect significantly the capacity of LSC to aggregate human platelets. PLT : resting platelets, LMC : platelet aggregation LMC induced, EXP-LMC: platelet aggregation induced by exposed LMC, ADP: control of platelet aggregation by ADP as agonist.

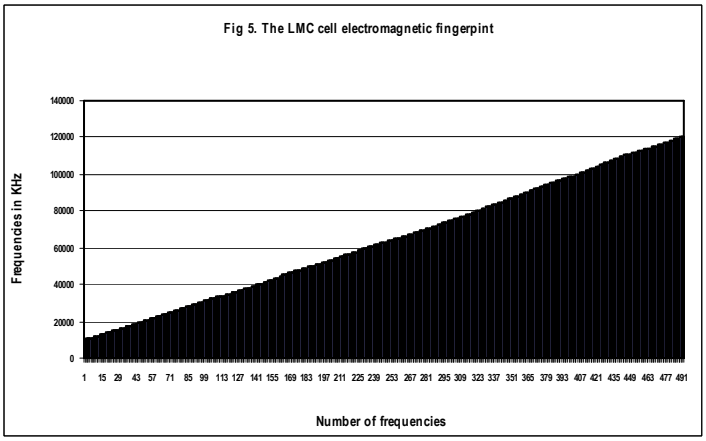

Fig 5. The fingerprint spectrum of 492 frequencies emitted from leiomyosarcoma cells of Wistar rat after an accurate registration by the resonating system of the MCDE apparatus

Table 1 : Flow cytometry for non exposed and exposed to EMF sarcoma cells .

The percentage of apoptotic nucleus in the group of control cells is very low (1,79 %) when the percentage of apoptotic nucleus in the group of exposed cells to EMF is much greater (45,34 %) .

Control (non exposed sarcoma cells)

Marker	Left	Right	Events	% Gated	Total
All	0	1023	9461	100.00	49,07
M1	26	149	169	1,79	0,88
M2	15	242	3366	35,58	17,46
M3	262	386	35,49	37,51	18,41
M4	391	565	1774	18,75	9,20

G0/G1 : 35,58%, S : 37,51% , G2/M : 18,75% , Apoptosis : 1,79%

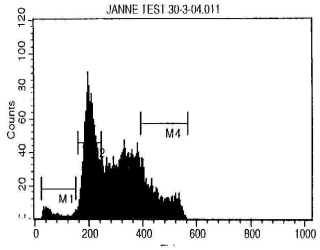

Exposed sarcoma cells to EMF

Marker	Left	Right	Events	% Gated	Total
All	0	1023	13232	100,00	17,89
M1	26	149	5999	45,34	8,11
M2	159	242	4396	33,22	5,94
M3	262	386	1232	9,31	1,67
M4	391	565	217	1,64	0,29

G0/G1 : 33,22%, S : 9,31%, G2/M : 1,61% , Apoptosis : 45,34%

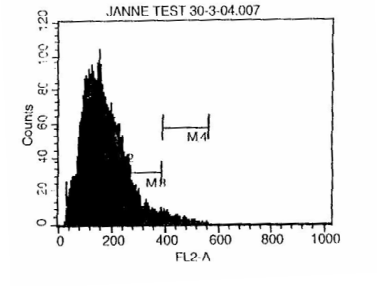

Exposed sarcoma cells to EMF

Marker	Left	Right	Events	% Gated	Total
All	0	1023	13232	100,00	17,89
M1	26	149	5999	45,34	8,11
M2	159	242	4396	33,22	5,94
M3	262	386	1232	9,31	1,67
M4	391	565	217	1,64	0,29

G0/G1 : 33,22%, S : 9,31%, G2/M : 1,61% , Apoptosis : 45,34%

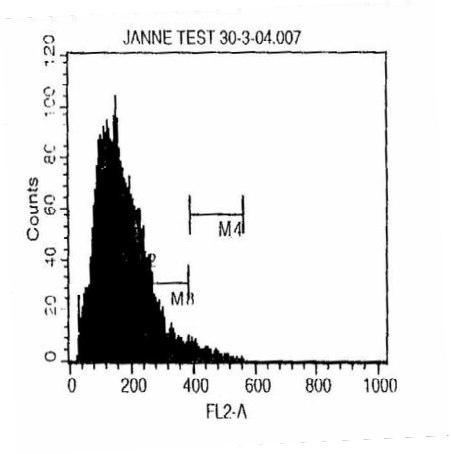

Discussion

Our findings indicate that high growth inhibition of LSC of more than 95% can be accomplished by the applying an EMF according to electromagnetic resonance principles. The results of this study reinforce the other authors findings on the proliferation inhibition and on the significant morphological alterations of human melanoma cell lines exposed to low power electromagnetic waves of 50-80 GHz [15] and also on the apoptotic effects of static EMF of 1.95 GHz on human epidermoid cancer cells [16]. In the present study antiproliferative and apoptotic effects have been achieved by exposing LSC to a static EMF of low energy waves and frequencies between 10 kHz to 120 kHz. This field is far lower in frequency and in power than the upper limit of permitted exposure (power: 200m Watt/cm^3), being thus, safe for use in animals and humans [17]. It is also evident from the literature, that the EMF effect is dependent on immediate interactions that affect the electronic spin of the atoms or molecules with uncoupled electrons in their external orbit, enhancing electron spin coupling; thus may help the neutralization of free radicals, especially those produced by the activation of arachidonic acid cascades [14,16,18-21]. It is also known that the EMF induce free radicals production that may act as activators of signal transduction pathways [10,19,20]. According to the above, it is possible that the effects of these EMF, could be similar to the effects of antioxidants and free radical scavengers on LSC lines. The high percentage of the exposed LSC found in apoptosis (45%) in comparison to that of the unexposed to EMF, control cells (2%), could be explained as the effect of the EMF's on cellular membranes activating signal transduction pathways leading to genes expression of cell apoptosis [5,7,16,22] or to inactivation of anti-apoptotic genes [15]. The low percentage of cells found in synthesis and in mitosis (9% and 2% respectively) compared to that of the control cells (38% and 19% respectively), indicates that radiofrequency of the EMF can act as cell cycle inhibitor, similarly to the effect of magnetic field on DNA synthesis [23,24,7]. There is also evidence that exposure to the EMF may reduce the immunoreactive p53 expression in tumor bearing mice [19], which has been found increased in BaP-induced leiomyosarcomas in Wistar rats [25]. The lower sensitivity of LSC after their fourth exposure to ERF's, compared to their higher sensitivity after the first exposure, indicates that LSC may have developed some type of resistance to EMF. Our finding, that the electromagnetic resonance fingerprints of LSC changed after their exposure to EMF and resembled to that of the SMC, may indicate that some differentiation in the LSC function has taken place. This differentiation is supported by our -yet unpublished- data indicating that the EMF treated LSC, after being inoculated to Wistar rats, retard the tumor development or even fail to develop tumor, in contrary to inoculated but unexposed to EMF LSC that develop tumors in a 100% of the experimental animals. There are also bibliographic references indicating that the EMF, specific or generalized is able to induce differentiation of cancer and non cancer cells [26,27]. Nevertheless, the LSC exposed to the EMF seem to retain their potential for metastasis as they can still aggregate platelets. It must be emphasized that for the first time a low intensity EMF has been used and it is essential that this EMF is carefully designed on the basis of the emitted electromagnetic frequencies from the target cells, in order to be effective. Also, the intensity of the electric field we used was 75 times lower and the intensity of the magnetic field was more than 1800 times lower than the average of the international safety standards according to the National Centre for Physical Sciences of Greece ("Demokritos", Athens Greece) [17]. Because of that, the use of this electronic device for the treatment of cancer cells seems to be safe. Unpublished data of ours, from the follow up of tumor-bearing animals and cancer patients treated with EMF by the above method, confirm the above. Our data, concerning the changes of LSC electromagnetic resonance fingerprints after repeated exposures to EMF, indicate that, in order to affect the cells functions, it is crucial to make regular readjustments of the electromagnetic resonance fingerprints, in order to differentiate the LSC phenotype to a phenotype with an electromagmetic resonance fingerprinting as close as possible to that of the normal cells (SMC). In this case, the LSC should loose their malignant phenotype, so that their inoculation to Wistar rats could not cause malignant disease. Experiments going on, in our lab, seem to confirm this hypothesis.

Acknowledgements: This research has been supported by funds of the Center for Energy Frequencies Studies in Physical and Mental Balance (Greece), through the Research Committee of the University of Ioannina. We thank Dr. Georgios Vartholomatos for his valuable assistance in flow cytometry and Nikos Papadopoulos for his contribution in the management and administration of this project.

References

1. Suss S. Bioresonace therapy in treatment of allergies. Every person has its own vibration pattern. *Fortschr Med* 1997; 115: 16-18.
2. Islamov BI, Balabanova RN, Funtikov VA, et al. Effect of bioresonance therapy on antioxidant system in lymphocytes in patients with rheumatoid arthritis. *Bull Exp Biol Med* 2002; 134: 248-250.

3. Foster KR, Repacholi MH. Biological effects of radiofrequency fields: does modulation matter? *Rad Res* 2004; 162: 219-225.
4. Heynick LN, Johnston SA, Mason PA. Radio frequency electromagnetic fields: cancer, mutagenesis and genotoxicity. *Bioelectromagnetics* 2003; Suppl 6: S 74-100.
5. Marinelli F, La Sala D, Cicciotti G, et al. Exposure to 900 MHz electromagnetic field induces an unbalance between pro-apoptotic and pro-survival signals in T-lymphoblastoid leukaemia CCRF-CEM cells. *J Cell Physiol* 2004; 198: 324-332.
6. Repacholi MH. Low-level exposure to radiofrequency electromagnetic fields: health effects and research needs. *Bioelectromagnetics* 1998; 19: 1-19.
7. Tofani S, Cintorino M, Barone D, et al. Increased mouse survival, tumor growth inhibition and decreased immunoreactive P53 after exposure to magnetic fields. *Bioelectromagnetics* 2002; 23: 230-238.
8. Han L, Lin H, Head M, et al. Application of magnetic fields induced heat shock protein 70 for presurgical cytoprotection. *J Cell Biochem* 1998; 78: 371-379.
9. Junkersdorf B, Bauer H, Gutzeit H.O. Electromagnetic fields enhance the stress response at elevated temperature in the nematode caenorabditis elegans. *Bioelectromagnetics* 2000; 21: 100-106.
10. Grundler W, Kaiser F, Keilmann F, Walleczek J. Mechanisms of electromagnetic interaction with cellular systems *Naturwissenschaften* 1992; 79: 551-559.
11. Kallistratos G, Evangelou A, Agnantis N, et al. Enhancement of the antineoplastic effect of anticarcinogens on benzo[a]pyrene treated Wistar rats, in relation of their number and biological activity. *Cancer Lett* 1994; 82: 153-165.
12. Evangelou A, Kalpouzos G, Karkabounas S, et al. Dose related preventive and therapeutic effects of antioxidants-anticarcinogens on experimentally induced malignant tumours in Wistar rats. *Cancer Lett* 1997; 115: 105-111.
13. Charalabopoulos K, Karkabounas S, Charalabopoulos AK, et al. Inhibition of benzo[a]pyrene-induced carcinogenesis by vitamin C alone and by vitamin C/ vitamin E and Selenium/glutathione. *Biol Trace Elem Res* 2003; 93: 201-212.
14. Xanthopoulou M, Hadjikakou S, Hadjiliadis N et al. Synthesis and characterization of a new chloro diphenyl (VI) complex with 2-mercapto nicotinic acid. A study of its influence upon the catalytic oxidation of linoleic acid to hydroperoxylinoleic acid by the enzyme lipoxygenase. *Organometal Chem 2006; 691: 1780-1789.*
15. Beneduci A, Chidichimo G, Rose R, et al. Frequency and irradiation time-dependant antiproliferative effects of low-power millimeter waves on RPMI 7932 human melanoma cell lines. *Anticancer Res* 2005; 25(2A): 1023-1028.
16. Caraglia M, Marra M, Mancinelli F, et al. Electromagnetic fields at mobile phone frequency induce apoptosis and inactivation of the multi-chaperone complex in human epidermoid cancer cells. *J Cellular Physiol* 2005; 204: 539-548.
17. Karabetsos E. Measurements report of electromagnetic radiation levels emitted from the device Multi Channel Dynamic Exciter 100 v.1 Report of ΕΕΑΕ: ΜΙΑ ΕΕΠ 2, 15-11-2000, Karabetsos E, ed, *Bulletin no 2, National Centre of Physics Research "Democritos"*publ, Athens, Greece, 2000.
18. Grudler W, Kaiser F, Keilmann F, Walleczek J. Mechanisms of electromagnetic interactions with cellular systems. *Naturwissenschaften* 1992; 79: 551-559.
19. Clejan S, Ide C, Walker C, et al. Electromagnetic fields induced changes in lipid second messengers. *J Lipid Mediat Cell Signal* 1996, 13: 301-324.
20. Lander M. An essential role of free radicals and derived species in signal transduction. *FASEB J* 1997; 11: 118-124.
21. Del Carratore R, Morichetti E, Della Croce C, Bronzelli G. Effect of magnetic fields on rodend monooxygenase enzymes. *Bioelectromagnetics* 1995; 16: 324-329.
22. Polyak K, Xia Y, Zweier JL, et al. A model for P53 induced apoptosis. *Nature* 1997; 389: 300-305.
23. Liboff AR, Wikkiams T Jr, Strong DM, Wistar R Jr. Time varying magnetic fields: effect on DNA synthesis. *Science* 1984; 223: 818-820.
24. Takahashi K, Kaneko I, Date M, Fukada E. Effects of pulsed electromagnetic fields on DNA synthesis in mammalian cells culture. *Experientia* 1986; 42:185-186.
25. Stefanou DG, Nonni AV, Kalpouzos G, et al. Immunophenotype ras oncogenes and p53 onco-suppressor genes on bezo(a)pyrene induced malignant soft tissue tumors in Wistar rats. *In Vivo* 1998; 12: 511-521.
26. Tao Q, Henderson A. EMF induces differentiation in HL-60 cells. *J Cell Biochem* 1999; 73: 212-217.
27. Rodenman HP, Peterson HP, Schwenke K, von Wangenheim KH. Terminal differentiation of human fibroblasts is induced by radiation. *Scanning Microscop* 1991; 5: 1135-1142.

CAN BE INCREASED EFFICIENCY OF ALA PHOTODYNAMIC THERAPY BY ELECTROPORATION?

F. CIOBANU, M.G. MOISESCU, I. STOIAN, M. RADU, E. KOVACS

CAROL DAVILA UNIVERSITY OF MEDICINE AND PHARMACY, PO BOX 35-43, BUCHAREST, 050461, ROMANIA, MRADU@NIPNE.RO

Abstract

One of the most used photosensitizer in photodynamic therapy of cancer is the aminolevulinic acid (ALA), a precursor in synthesis of protoporphyrin IX (PpIX). One of the disadvantages using this photosensitizer is the small rate of ALA uptake of the cells. Our work aim was to increase by electroporation the PpIX level in ALA treated cells. Electroinduced pores in membrane would facilitate an enhanced uptake rate of ALA forcing an increased level of PpIX and consequently a better efficiency of ALA photodynamic therapy. B16F10 melanocytes cultures were incubated with 1 mM ALA for 4 h and PpIX level was monitored by the fluorescent emission at 635 nm. The viability of cells was analysed by MTT test. The electroporation of cells in the presence of ALA was done with exponential decay electric pulses in the range of 500-4500 V/cm, 100 μs, 1-4 pulses. In the control experiment (without electroporation) a rate of PpIX production comparable with results in literature was obtained. Exposing the ALA treated cell cultures to light (633 nm) for various periods the apoptosis or necrosis of cells was triggered. This observation was confirmed by the results of cells viability tests. The electroporation of cells in the presence of ALA did not show significantly increase the cellular PpIX level. In conclusion our *in vitro* preliminary results did not supply evidences that the electroporation of cells can be a way to improve the ALA uptake of the cells and consequently to improve the efficiency of photodynamic therapy with ALA.

Introduction

Photodynamic therapy (PDT) concept is based on a combined effect of the light and chemicals. A photosensitive chemical species incorporated into cell and afterwards exposed to irradiation with light of appropriate wavelength produces very reactive chemical radicals which are able to trigger the apoptosis or necrosis of the cell. This type of therapy was proposed as an alternative to classical surgical techniques. The photosensitive molecules can be an exogenous (an appropriate techniques has to be used to uptake this molecules by the cell) or an endogenous one as protoporphyrin IX (PpIX). 5-aminolevulinic acid being a precursor of PpIX is one of the most used chemical in PDT. ALA is an endogenous precursor of PpIX. In normal conditions the rate of PpIX synthesis is regulated by means of a negative feedback loop limiting in this way the level of endogenous ALA. An enforced uptake of ALA allows overcoming this limiting mechanism resulting in an increased rate of PpIX production by the cells. PpIX absorption spectrum shows a high peak located 635 nm (Ma et al, 2001). Under the light irradiation the PpIX produces several photo-induced products having as final results an unbalanced oxidative status of the cell. As a consequence the cell triggers the apoptosis program. The technique was successfully used in *in vitro* and *in vivo* experiments.

The main disadvantage of this ALA-PDT method is the limiting step of ALA incorporation into the cell. ALA is a hydrophilic molecule and consequently has a very low diffusion coefficient through the membrane lipid bilayer. There are several reports concerning the mechanism of ALA uptake through the cell membrane. Mainly two paths are proposed: (i) the passive diffusion which would be important only during a short period of incubation, till 15 min (Bermudez Moretti et al, 2002) and (ii) an active mechanism mediated by a BETA family transporter (Rud et al, 2000; Bermudez Moretti et al, 2002).

An alternative proposed to improve the rate of ALA influx is the cell electroporation. The action of a short electric pulse of appropriate amplitude is able to produce a reversible permeabilisation of the membrane. During this state the exogenous molecules, for which normally the membrane is not permeable, can pass through the membrane barrier by diffusion. In cancer therapy the technique was successfully used to improve the efficiency of cytostatics (Orlowski, Belehradek et al.,1988). A derived method is the transdermal electroporation. The electric pulses are applied across the dermal layer increasing the diffusion of drugs through it. This method was proposed to improve the efficiency of ALA – PDT when ALA is topically applied (Johnson et al, 2002) and an increase of transdermal transport rate was reached.

In this report we present our preliminary results concerning the possibility to use the electroporation at the cell level in order to increase the uptake of ALA and consequently the production of PpIX.

Materials and Methods

B16F10 murine metastatic melanoma cells were used as biological experimental object. They were cultured in 3 cm Petri dishes, at 37°C, 5% CO_2, in Dulbecco's MEM (Gibco) supplemented with 10% foetal calf serum (Gibco), 100 units/ml of penicillin and 100 µg/ml of streptomycin (BioClone). The B16F10 cell line was kindly provided by Dr. L.M.Mir, Gustave-Roussy Institute (Villejuif), France.

1mM ALA (Sigma) was added in the fresh Dulbecco's MEM medium without foetal calf serum and without phenol red (Gibco) and the cells were incubated with at 37°C for 4 hours. A longer ALA incubation period did not increase the PpIX production (data not shown). After this incubation the ALA-treated cells were harvested by mild trypsination and the level of PpIX was measured by fluorescence. The PpIX excited at 510 nm has two emission peaks at 635 and 706 nm (Orenstein et al, 1997). The emission spectrum in the range of 600 – 750 nm was recorded in a SPEX spectrofluorometer. The intensity at 635 nm was considered as a measure of PpIX production.

In order to produce the photo-degradation of PpIX the cells attached to Petri dishes and incubated with ALA, were exposed to red He-Ne laser beam (power at the level of the dish surface was 16 mw) expanded by a simple lens system to cover the all dish surface. After different exposure durations (4-35 min) the cells were harvested by mild trypsination and the fluorescence spectrum recorded.

The level of toxic photo-induced products was evaluated using the MTT cell viability test after exposure to laser beam. The cells were seeded at appropriate concentration on a 96wells plate for 24h, than incubated for 4 h, at 37°C, with 0.5mg/ml thiazolyl blue tetrazolium bromide (TBTB, Sigma). The viable cells are transforming the TBTB into coloured formazan precipitate. The production of formazan was quantified using a spectrophotometer plate reader (Awarness).

The cell suspension electroporation was done using an Eppendorf electroporator. The suspension medium was the same as Eppendorf recommended. An exponential electric pulse (time constant of 100 µs) was applied between the electrodes of an electroporation cuvette (BioRad) where the cell suspension was introduced. The electric field intensity ranged from 0.5 to 6 kV/cm. In order to evaluate the efficiency of electroporation the uptake of a membrane impermeable molecule (ethidium bromide, EB) was followed. The dye was added to the cell suspension just before the electroporation. The labelled cells were counted under a fluorescence microscope (Zeiss Axiovert 200) equipped with an appropriate filter set and the percentage of the coloured cells was calculated. To evaluate the cells 'death' (at high electric field intensity a large number of cells die) the EB was added to the electroporated cell suspension after 10 min. It was considered that during this period the permeability membrane of surviving cells was recovered and only the irreversible permeabilized cells will uptake the dye.

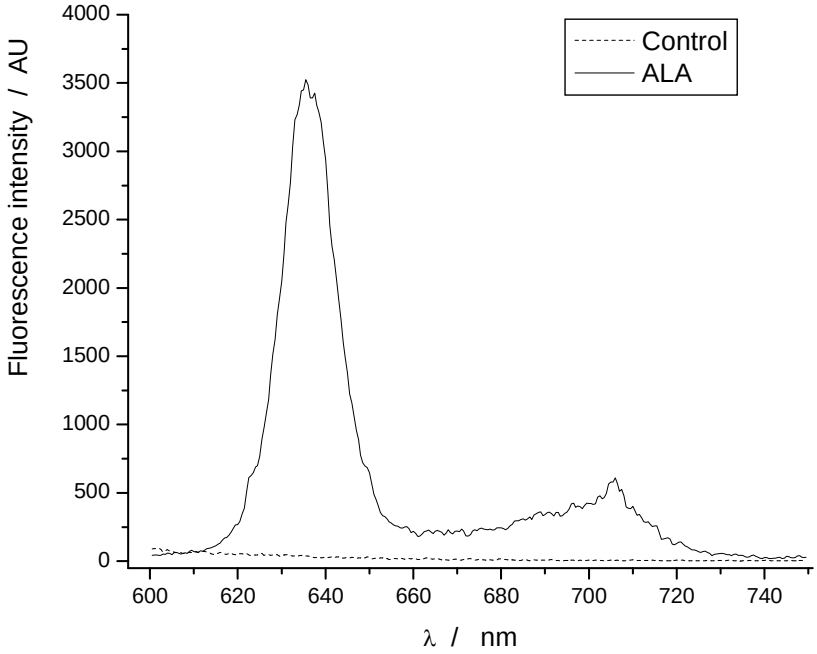

Figure 1. Fluorescence spectra of cells incubated with ALA, 1 mM, 4 hours (ALA) and without ALA (Control). λ_{ex} = 510 nm

Results and Discussions

The cells incubated with ALA, 1 mM, 4 hours, had a strongly increase of PpIX production (fig. 1). The spectrum is very similar with other reported results (Orenstein et al, 1997; Dysart and Patterson, 2006) and two peaks can be observed at 635 nm, the main one, and at 706 nm. In contrast, the control cells (without ALA) did not present observable levels of PpIX.

The effect of light irradiation on cells incubated with ALA was revealed by means of decrease of PpIX level in cells after irradiation (fig. 2). The PpIX level decreases with irradiation time confirming other results reported in the literature (Orenstein et al, 1997). Plotting the maximal intensity at 635 nm against irradiation time a linear decrease of PpIX level in irradiated cells can be observed (fig 3). Over 35 min of irradiation the fluorescence intensity at 635 decrease much slowly suggesting a saturation of the process (data not shown).

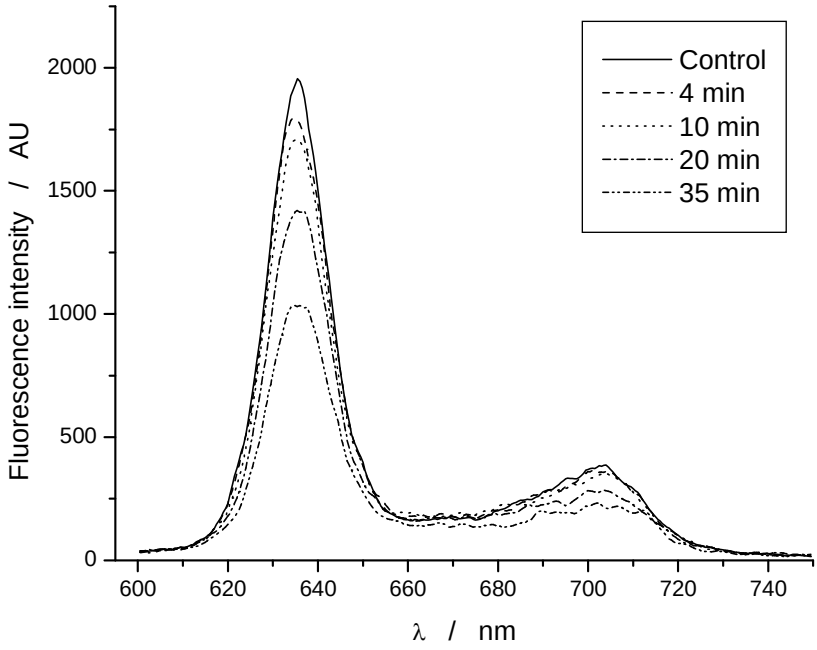

Figure 2. Fluorescence spectra of cells incubated with ALA, 1 mM, 4 hours (ALA) and irradiated with red laser light (633 nm) for different periods. λ_{ex} = 510 nm.

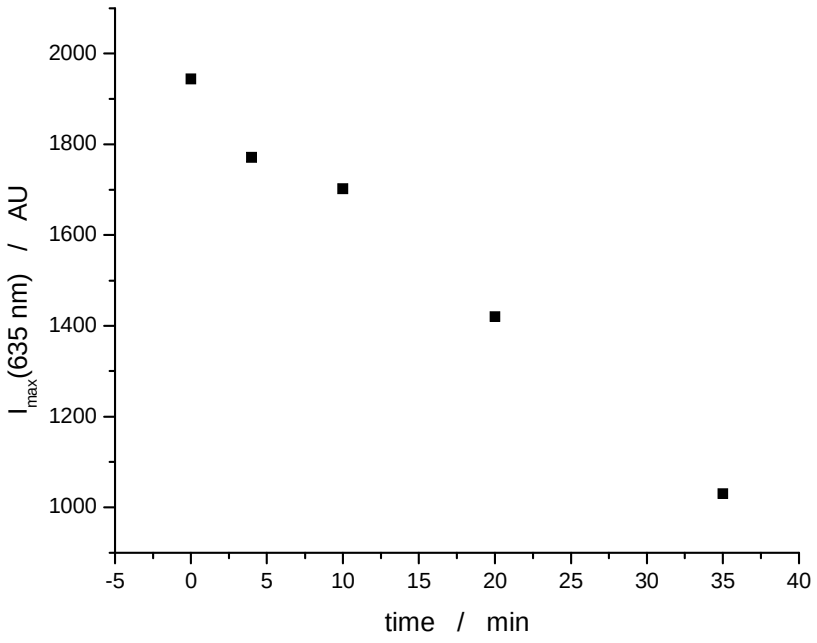

Figure 3. Fluorescence intensity at 635 nm (λ_{ex} = 510nm) of cells incubated with ALA, 1mM, 4 hours and irradiated with red laser light (633 nm) for different periods.

In order to check the effects of irradiation on the viability of the cells the MTT test was applied. Four variant of cell cultures were tested: a control consisting in cells without ALA, a second control without ALA but irradiated at 633 nm, a non-irradiated but ALA incubated culture cells and a culture cells incubated with ALA and irradiated with 633 nm laser light. The period of irradiation was 30 min. ALA incubation was performed as above. The results are in presented in Figure 4. The red light irradiation and ALA incubation did not affect the viability of cells with respect to the controls. Only the cells incubated with ALA and irradiated with red light show more than two times smaller viability. This experiment actually proves the fact that our experimental conditions are appropriate for an *in vitro* experiments revealing the presence of photo-induced products in ALA incubated cells and irradiated with red light.

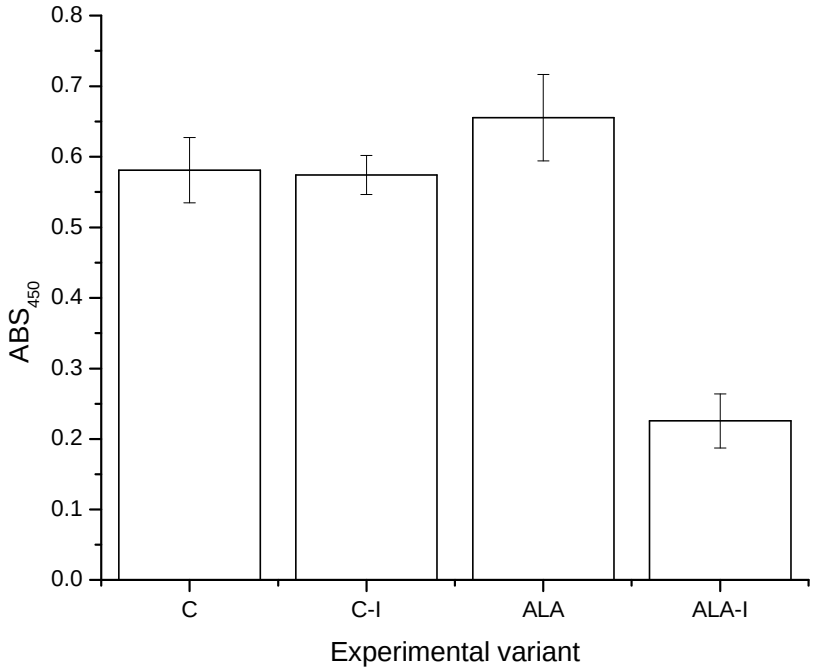

Figure 4. Viability of the cells evaluated by MTT test: C – control, C-I – control cells irradiated with red light, ALA – ALA incubated cells, ALA-I – ALA incubated cells and irradiated with red light.

In order to find out the optimal conditions for the electroporation a range from 0.5 to 6 kV/cm was used. One exponential pulse (time constant of 100 μs) was applied to the cell suspension with or without EB. The results are in Figure 5. At low level of electric field intensity a rapid increase of porated cells percentage is observed reaching a plateau for higher values of electric field. On the other hand, at low field intensity the viability of cells is very close to maximum (100%) and decreases when the electric field increases. For medium values of the field intensity (between 2 and 4 kV/cm) the cells have simultaneously a maximal level of poration and of viability. Considering the conditions of minimal stress for the cells we used in our experimental trials to increase the uptake of ALA in the cells by electroporation the following electric conditions: one exponential pulse of 2 kV/cm and 100 μs time constant.

After all these preparatory experiments which allow us to have proper conditions to reveal the photosensitizer effect and to have optimal electroporation parameters we performed experiments trying to find out an increase of PpIX production in cells electroporated in presence of ALA. The following conditions were used: ALA 1mM, one exponential pulse of 2 kV/cm and 100 μs time constant. 15 min after electroporation the cells were incubated in a fresh culture medium without ALA and after 1 h the cells PpIX level was recorded. For control cells the same experimental conditions were used without electroporation step but with a 4h incubation with ALA.

An unexpected result was obtained. In the electroporated cells no PpIX was revealed. The spectrum was very similar to the spectrum of control cells without ALA (data not shown).

In order to check if the electroporation step disturb or not the metabolism of cells a further control experiment was performed. Cells electroporated without ALA were incubated immediately after the electroporation in fresh medium with 1mM ALA for 4 hours. The level of PpIX was recorded by fluorescence spectrum and the PpIX value was similar to the control cells incubated with ALA for 4 h, without electroporation. This is an evidence for the fact that electroporated cells were able to develop the biochemical processes needed for PpIX synthesis.

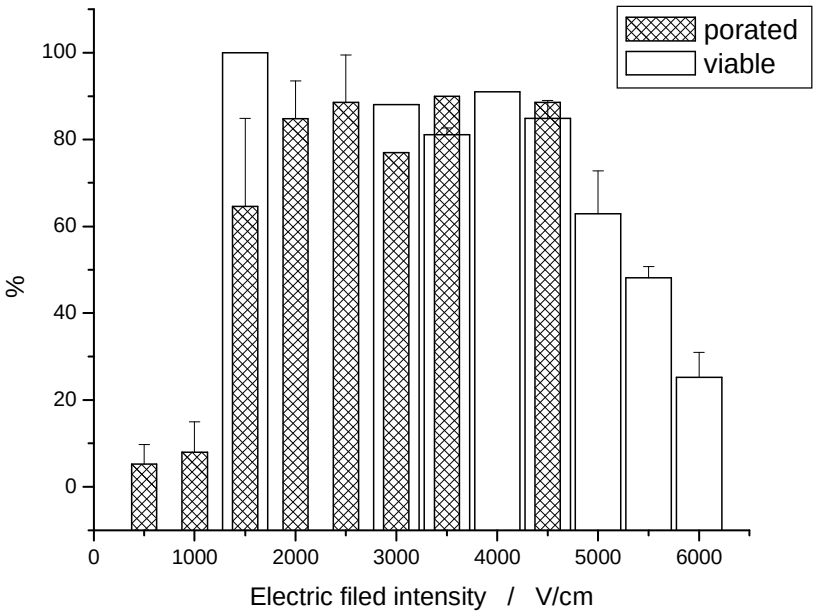

Figure 5. The electroporation yield and the viability of electroporated cells.

Summary

In this paper we report our preliminary results concerning the possibility to improve the efficiency of ALA – PDT method by electroporation. Our *in vitro* trials did not supply evidences that the electroporation of cells in suspension can be a way to increase the rate of ALA uptake of the cells. These results are apparently in contradiction with reports of other authors which successfully increase the transdermal transport rate of ALA and the level of PpIX production in *in vivo* experiments on mice (Johnson et al, 2002).

Refferences

Ma LW, Bagdonas S and Moan J, 2001 – The photosensitizing effect of the photoproduct of protoporphyrin IX – J Photochem Photobiol B, **60**: 108-113

Bermudez Moretti M, Correa Garcia S, Perotti C, and Casas A, 2002 – δ-aminolevulinic acid transport in murine mammary adenocarcinoma cells is mediated by BETA transporters – Br J Cancer, 87: 471-474

Rud E, Gederaas O, Hogset A, and Berg K, 2000 – 5-aminolevulinic acid, but not 5-aminolevulinic acid esters, is transported into adenocarcinoma cells by system BETA transporters – Photochem Photobiol, **73**:164-169

Johnson PG, Hui SW, Oseroff AR, 2002 - Electrically enhanced percutaneous delivery of delta-aminolevulinic acid using electric pulses and a DC potential - Photochem Photobiol., **75**: 534-40.

Dysart JS and Patterson MS, 2006 – Photobleaching kinetics, photoproduct formation, and dose estimation during ALA induced PpIX PDT of MLL cells uder well oxygenated and hypoxic conditions – Photochem Photobiol Sci, **5:** 73-81

Orenstein A, Kostenich G and Malik V, 1997 – The kinetics of protoporphyrin fluorescence during ALA-PDT in human malignant skin tumors – Cancer Lett, **120**: 229-234

Orlowski, S., J. Belehradek, Jr., et al.,1988 -- Transient electropermeabilization of cells in culture. Increase of the cytotoxicity of anticancer drugs -- Biochem Pharmacol, **37(24)**: 4727-33.

REGULATORY COMPLIANCE OF MOBILE PHONE BASE STATIONS IN AUSTRALIA

TANYA STOIANOFF BAgrEc MPS
EXECUTIVE DIRECTOR, MOBILE CARRIERS FORUM
L6, 46 MARKET STREET, SYDNEY 2000

Abstract

Mobile phone base stations in Australia are governed by a mix of regulatory and self-regulatory instruments ranging from how base stations are built, through to cumulative EME compliance on existing shared sites.

This paper explores various levels of regulatory compliance required of Australia's mobile phone carriers when it comes to siting, designing and operating mobile phone infrastructure.

The regulatory and self-regulatory mix aims to address both the science underlying human exposure safety and the public perception of health risks from mobile phone infrastructure - so there is a mix of both the ICNIRP standard for human exposure as well as the adoption of precautionary behaviours when carriers build base stations in Australia.

The ACIF Code for the Deployment of Mobile Phone Networks is the key instrument which has adopted precautionary behaviours requiring carriers to:

- Have written procedures for site selection;
- Improve notification and community consultation procedures;
- Design and operate base stations with the objective of minimizing electromagnetic emissions; and
- Provide electromagnetic radiation emission reports, or Environmental Reports for every site, as per the Federal Department of Health's requirements.

Australia's Mobile Carriers Forum (MCF) has played an important role in this regulatory/self-regulatory mix. It is an industry forum comprised of the four mobile phone carriers building networks in Australia, and was formed in 2000 to address a number of issues in the area of wireless infrastructure network operations and mobile base station deployment. Of particular relevance was responding to issues of community concern and improving inter-carrier cooperation.

The MCF has either contributed to the creation of the various regulatory and self-regulatory instruments discussed in this paper, or has developed operational programs and systems for the carriers to use in practice to ensure regulatory compliance. While it does not claim to be a complete analysis, this paper explores the main instruments and initiatives.

Introduction to the Australian Scene

Mobile phones have become an integral part of day to day life for individuals, businesses and the community at large. According to Credit Suisse First Boston 2005, the Australian mobile telecommunications industry today has approximately 19 million subscribers with various mobile technologies being used by about 95% of the Australian population. Although it may seem surprising, a penetration rate exceeding 100% has been achieved in a number of countries and research suggests that it will be achieved in Australia by the end of 2008.

The Allen Consulting Group states in its publication *Australian Mobile Telecommunications Industry – Economic Significance (2005*) that the mobile telecommunications industry is a high revenue, high cost industry that makes a substantial and growing contribution to the wider telecommunications industry and the Australian economy. Industry gross product for the financial year 2004/05 was $6.1 billion, up

from $5.3 billion in the previous year. Since 1997, capital expenditure by the industry on new networks has exceeded $10 billion. Revenue from the mobiles sector of the telecommunications industry was $9.9 billion in 2004/05 according to Credit Suisse First Boston 2005. Australia's mobile phone networks reach over 98 percent of the population and cover just over 20 percent of the Australian land mass.

Data such as industry gross product, mobiles revenue and capital expenditure figures are important in demonstrating the economic contribution of Australia's mobile phone industry, however those measures do not convey the many ways in which mobile telephony contributes to improvements in the quality of people's lives and increases in social equity.

For many people, mobile telecommunications is more than a tool to make voice calls; instead, the extensive coverage, array of services and information available mean that the mobile phone can "make life mobile". The accessibility and freedom for people on the move to maintain contact with other people is a significant benefit. From an emergency perspective, a third of all calls to emergency services in Australia are made from mobile phones. Furthermore, emerging technology such as 3G and video phones will help to increase social equity by expanding access to groups such as the hearing impaired. Mobile telephony is increasingly more affordable in Australia particularly through low-cost and capped plans, allowing more people to benefit from the connectivity of mobile telecommunications services.

The MCF found in its publication *Third Generation Mobile Networks in Australia, Broadband For Your Mobile Phone (2005)*, that 3G applications in the Australian business sector are also growing, ranging from video-calling to location based mobile data services and telecommuting for employees.

Regulatory Environment

In Australia, telecommunications facilities are primarily regulated under Commonwealth law. This is largely due to Section 51(V) of the Australian Constitution which reads:

"The Parliament shall, subject to this Constitution, have power to make laws for the peace, order and good government of the Commonwealth with respect to:…(V) postal, telephonic and other like services:…"

In 1991 the Commonwealth Parliament enacted the *Telecommunications Act 1991*. The *Telecommunications Act 1991* and subsequent Carrier licences obligated Carriers to provide mobile telecommunications services to a large percentage of the Australian population. To assist Carriers meet these obligations the *Telecommunications Act 1991* also provided broad ranging powers to Carriers to install all types of mobile telecommunications facilities by granting exemptions from State and Territory environmental planning laws. These exemptions allowed Carriers to build quite substantial structures such as, for example, 30-metre towers without regard to State and Territory planning law.

However in 1997 the telecommunications regulatory environment was reshaped with the introduction of the *Telecommunications Act 1997*. This Act significantly curtailed the carriers' powers to install telecommunications facilities by limiting those exemptions from State and Local planning laws. Carriers must now comply with State and Territory planning and environmental assessment laws in relation to the installation of certain types of telecommunications facilities.

The Australian Government recognised however, that there are some telecommunications facilities and activities that are "unlikely to cause significant community disruption or significant environmental disturbance". These are exempt from certain State and Territory laws. These new telecommunications facilities and activities are described in the *Telecommunications Act 1997 (as amended)*, (referred to as "the Act") and in a Ministerial determination made under the Act – the *Telecommunications (Low-impact Facilities) Determination 1997* (referred to as the "Low-impact Determination") as amended.

The Act and the Low-impact Determination define what low-impact installation activities may be undertaken in certain areas without reference to particular State and Territory laws. Low-impact facilities are those which are considered essential to maintaining telecommunications that cause minimal detrimental visual impacts. Common examples of low-impact facilities are smaller scale structures such as panel antennas on light poles, building facades and rooftop installations. The

Determination sets out performance criteria for certain types of facilities based on the proposed location (an area classification criteria) of the facility and the dimensions of the proposed facility (a dimension criteria).

Facilities that do not meet the performance criteria outlined in the Determination cannot be defined as low-impact facilities. Those activities which are not exempt require consent from the local council as they are subject to State planning laws which vary in each of the States of Australia. For the purposes of brevity, this paper will not outline each State's planning regime.

Mix of Regulation and Self-Regulation

The Australian Communications and Media Authority, the ACMA, (formerly known as the Australian Communications Authority) is the regulator of the Australian communications industry. Since 1997 it has regulated telecommunications consumer and technical matters, and manages radio-communications. Specifically, the ACMA is responsible for the issuing of carrier licenses, the regulation of service providers, the registration and enforcement of industry (including consumer, operations and technical) codes of practice and the setting of industry standards, to name a few of its responsibilities.

The issue of electro-magnetic radiation (EMR) is an important issue for consideration in the deployment of telecommunications infrastructure. Some members of the public perceive that exposure to this type of radiation from mobile telephony could be harmful to human health. For the purposes of this paper it is necessary to outline that in Australia, exposure to EMR is regulated by the ACMA. The applicable standard is the "Radiation Protection Standard – Maximum Exposure Levels to Radiofrequency Fields – 3kHz to 300 GHz. The standard prescribes "fundamental limits designed to ensure that known health effects do not arise from exposure to radio frequency fields".

The Australian Radiation Protection and Nuclear Safety Agency (ARPANSA) is an Australian Government agency under the Department of Health, charged with responsibility for protecting the health and safety of people, and the environment, from the harmful effects of ionizing and non-ionizing radiation. ARPANSA builds and maintains expertise in the measurement of radiation and assessment of health impacts, it advises Government and provides information to the public, on issues related to radiation protection and nuclear safety, and it leads in the development of standards, codes of practice, guidelines and other relevant material to support radiation protection and nuclear safety throughout Australia. For example, the ACMA changed its Radio-communications (Electromagnetic Radiation) Human Exposure Standard 2001 to incorporate the limits of the new radiation protection standard recommended by ARPANSA – harmonising Australia with the ICNIRP guidelines a few years ago.

The considered scientific opinion from ARPANSA about possible health effects from this type of infrastructure is that "the weight of national and international scientific opinion is that there is no substantiated evidence that RF emissions associated with living near a mobile phone base station of telecommunications tower poses a health risk". The Australian Government and its regulatory bodies commonly refer to the World Health Organisation's position on this issue. Comprehensive reviews of over 2200 research publications, including more than 410 studies specifically on mobile phones and base stations, by governments and health authorities continue, without exception, to find there is no substantiated scientific evidence of health effects.

The World Health Organisation (WHO) in May 2006 updated their fact sheet entitled "Electromagnetic Fields and Public Health – Base Stations and Wireless Technologies", saying:

> *"Considering the very low exposure levels and research results collected to date, there is no convincing scientific evidence that the weak RF signals from base stations and wireless networks cause adverse health effects"*

Only recently the WHO said that despite the feeling of some people that more research needs to be done, scientific knowledge in this area is now more extensive than for most chemicals.

The Australian Communications Industry Forum (ACIF) is an industry owned, resourced and operated company established by the telecommunications industry in 1997 to help implement and manage

communication self-regulation within Australia. ACIF develops Standards and Codes to support competition and protect consumers, and administer technical and operating arrangements.

ACIF developed an *Industry Code for the Deployment of Radio-communications Infrastructure* (referred to as "the Code") which was registered by the ACMA in 2002. The Code applies the precautionary approach to the siting, design and operation of mobile phone base station infrastructure in Australia. It requires carriers to:

- Have written procedures for site selection;
- Improve notification and community consultation procedures for low-impact sites;
- Design and operate base stations with the objective of minimizing electromagnetic emissions; and
- Provide electromagnetic radiation emission reports upon request, as per the Federal Department of Health's ARPANSA requirements.

The Code was developed in response to calls for greater council and community involvement and more information when mobile phone base stations are installed. It was developed and agreed to by carriers, local government, unions, community groups and the ACMA.

It is important to note that the Code was developed to increase the transparency and accountability of carriers and increase consultation with the community when low-impact mobile phone base stations are built. The Australian community now has rights of access to information about any proposed base station in their area.

Self-Regulatory Aspects to Code Implementation – Industry Activity

As the industry approached the introduction of the above mentioned Code, the MCF recognised that the industry needed to be well prepared for the significant changes the Code would make to Australia's traditional deployment processes. The Code introduced new notification and consultation requirements for low-impact sites that were not required previously by law. It requires carriers to provide certain EME information about all sites across the country and it requires carriers to demonstrate that they had investigated possible co-location opportunities in the first instance.

In order for the Code to succeed, the carriers needed an implementation program of proforma documentation and flowcharts which guided carrier staff to ensure industry compliance with the Code. The MCF created such documentation with the input and ownership of each carrier on the Code drafting committee. The implementation process was then transferred into an interactive web based system which each carrier utilises. The program has provided some industry consistency in what could have become a myriad of interpretations which may have resulted in poorer compliance and would have made it even more difficult for the regulator, the ACMA, to monitor. The ACMA records all legitimate complaints made to it about a carrier's compliance or lack of compliance with the Code and assesses whether in fact the Code has been breached. Fines of up to $250,000 per breach may be charged by the regulator.

Other countries have introduced similar industry policies to the Code, but none have been supported by industry-consistent implementation documentation and processes which provide a paper trail demonstrating industry compliance with such a regime.

As part of the implementation program it was important to engage with the key stakeholders in the Code. The MCF organised a series of National Workshops in partnership with each State Local Government Association (LGA), the ACA and ARPANSA, to improve council awareness of the new Code. The MCF also produced an Information Kit for councils, distributed via LGA channels.

One particular Council in Sydney even made a specific report to its full council on the MCF's Code Information Kit and Workshop and stated that "the Code appears to be a genuine attempt by the Carriers to gain some community and Council trust". This feedback was an important message confirming to the industry that its efforts had not gone unnoticed.

In addition to this work, the MCF embarked upon a project with State Local Government Associations in Australia, which resulted in the creation of *Guidelines for Local Government on the ACIF Code* in

2006. The Guidelines were created with extensive consultation with local councils and they provide a useful toolkit for local council staff to monitor carrier compliance with the Code, despite the fact that low-impact sites do not require local council consent.

Demonstrably, the MCF's promotional and operational activities have been world leading in that the adoption of the code was strengthened with the development of an implementation program for demonstrating industry compliance and process, as well as providing local government with enhanced awareness of required carrier processes. This has reinforced Australia's self-regulatory regime for telecommunications.

Coordinated Strategy for On-site Regulatory Compliance

The MCF has facilitated the creation of a regulatory compliance strategy for carriers to assist them in managing their cumulative EME exposure obligations at both carrier and non-carrier owned sites. This strategy involves inter-carrier data exchange as well as liaison with third party property owners and radio licensees.

The strategy, which is now known as the MCF EME Regulatory Compliance Strategy (MERCS) was first tested via a national trial of fifty rooftop sites each containing two or more carrier facilities. A process for inter-carrier information exchange, cumulative radio hazard assessment by accredited specialists and communicating compliance to the property owner through a standard form Radio-communications Site Management Book (RCSMB) was developed and tested. This strategy is now being used by the industry across the country.

The MCF Rooftop Trial, as it was known, was also transferred into an electronic repository or database of carrier sites by one of the MCF's members, Telstra. It is now being populated by all carriers. This database, known as the National Site Archive (NSA), facilitates an electronic information exchange amongst carriers. Each carrier site, as it is built, is uploaded onto the NSA and the public are provided access to each site's environmental EME report (ARPANSA report) and compliance certificate as part of the industry's objective of transparency and accountability.

During the Trial, a National Antenna Database (NAD) was developed as the centralised database of mobile carrier antenna data. The NAD is an essential system to ensure that consistent and standard antenna data is available to carriers for EME software applications. The NAD is also critical to further automation of the NSA e.g. producing automatic environmental reports from STAD tables.

The MCF Rooftop Trial created a system for ensuring cumulative assessment of EME at shared sites given the regulatory requirements placed on the carriers by the ACMA and ARPANSA which included occupational health and safety (OH&S) obligations for workers who would access such rooftop sites. It is not an overstatement to say that the MCF Rooftop Trial revolutionized how carriers ensured compliance with cumulative exposure standards and OH&S laws on non-carrier owned sites.

The resulting NSA is also linked to an electronic system for managing the afore mentioned ACIF Code. Australia's largest (majority Government owned) carrier, Telstra assisted the industry by taking the MCF's Code implementation documentation and transferring it into an electronic system for compliance, linked to the NSA. Carriers in Australia can now upload site data onto the NSA, record the required compliance documentation, upload the required site management book, and document the completion of their ACIF Code requirements through a linked MCF web based electronic system.

The efficiencies and benefits to the industry from these initiatives are significant. The MCF's ability to facilitate such a consistent industry owned and used system is laudable and is testimony to the growing maturity of the MCF's members - the Australian mobile telecommunications carriers.

Visual Impact of Mobile Phone Base Stations

As was outlined by Stoianoff (2004), when communities convey concerns over base station deployment, it usually arises in three areas, not in any particular order – firstly, EMR emissions and health, secondly, visual amenity concerns about infrastructure and thirdly, a perceived lack of community empowerment when base stations are being built.

In Australia, the third concern has somewhat been addressed via the previously described ACIF Code, however, this instrument, nor any other similar instrument, can ever fully satisfy every community member's desire to control development in their area.

The first concern in relation to emissions and health is a world-wide phenomenon and can only be managed with the assistance of ongoing replicated research and the communication of information and education to the community from independent expert bodies such as the World Health Organization and local authorities such as ARPANSA in Australia.

The second concern, visual amenity is a somewhat different issue in that it is influenced by a number of factors such as cost, technical RF requirements, topography and vegetation and land owner requirements. Given the varying range of issues, the most aesthetic design is not always an available option when building base stations, however, industry needed to make an effort wherever possible.

Early on in the MCF's formation, a set of Guidelines were created incorporating urban design principles with the requirements of the infrastructure regulatory regime in Australia. The *Guidelines for Better Visual Outcomes – Low-impact Mobile Facilities* book was published by the MCF in 2001. It was well received by planners, government and local councils. Some local councils even sought permission to extract sections of the Guidelines to insert into local government policies and planning schemes. A second edition of the Guidelines was produced in 2004 to include the ACIF Code in the chapter which outlines Australia's telecommunications regulatory regime.

More recently, with the imprimatur of the Australian Government, the MCF has convened a *Design and Innovation Taskforce* inviting key stakeholders to participate including the property sector, structural designers and engineers, local government, town planners and telecommunications industry representatives. This group of stakeholders was identified as those who are best placed to make either a technical contribution to the Taskforce or those who have a direct involvement in the siting and design component of mobile phone base station deployment.

The Taskforce's key objectives are to:

- help investigate the national and international scene for improving the visual amenity of infrastructure – what designs are in use globally,
- gain a better understanding of the real life impediments to the adoption of "aesthetic design options" in Australia; and
- identify practical methods or opportunities to improve the visual amenity of facilities in Australia - providing recommendations within the context of the Australian marketplace.

The MCF Taskforce intends to generate a technical paper drafted by a specialist planner which should focus on the above key objectives. The Technical paper will also focus on typical types of telecommunications sites including: building rooftops, base stations in parks and recreational space, and on telegraph/electricity poles and other utility structures.

Summary

This paper has outlined the main regulatory instruments which govern mobile phone base station deployment in Australia. It is clear to see that a balanced mix of regulatory and self-regulatory mechanisms are at play ranging from legislation and Codes of Practice through to industry initiatives geared towards ensuring compliance with regulatory expectations from Government and the community's perspective.

This paper has also outlined a summary of MCF initiatives from devising regulatory compliance programs to creating publications which assist in industry performance and stakeholder appreciation of the limitations in network deployment options. Each of the MCF's initiatives may assist other country's organisations in addressing similar issues of concern.

While the telecommunications industry is governed by a largely self regulatory regime, the industry must take a proactive and responsible approach to deployment in order to honour such a regime.

References

Australian Communications Media Authority, FSC 44 7/2001, *Mobile Base Stations and EMR* (www.aca.gov.au)

Australian Radiation Protection and Nuclear Safety Agency, (2002) *Prediction Methodologies for Radiated Electromagnetic Energy (EME) Exposure Levels from Mobile Phone Base Station Antennas - Technical Report,* Australia (www.arpansa.gov.au)

Credit Suisse First Boston (2005) *Australian Telecommunications 2005*, Equity Research.

Mobile Carriers Forum, (2002) *Your Right to Information about Mobile Phone Base Stations,* Sydney Australia (www.mcf.amta.org.au)

Mobile Carriers Forum, (2001) first and second edition (2004), *Guidelines for Better Visual Outcomes – Low-impact Mobile Facilities,* Sydney Australia (www.mcf.amta.org.au)

Mobile Carriers Forum, (2005) *Third Generation Mobile Networks in Australia, Broadband for Your Mobile Phone,* Sydney Australia (www.mcf.amta.org.au)

Stoianoff, T. (2004) *World Leading Activities of the Mobile Carriers Forum*, as presented at 3rd International Workshop Biological Effects of Electromagnetic Fields, Kos Greece

The Allen Consulting Group (2005) – research commissioned by AMTA, *Australian Mobile Telecommunications Industry – Economic Significance,* Canberra Australia

World Health Organisation (May 2006) Fact Sheet No. 304 *Electromagnetic Fields and Public Health, Base Stations and Wireless Technologies*, Geneva

NEUROPHYSIOLOGICAL AND BEHAVIORAL EFFECTS OF HUMAN ACUTE EXPOSURE TO A 60 HZ MAGNETIC FIELD UP TO 1800 µT: PRELIMINARY RESULTS

A. LEGROS[1], A. BEUTER[2], L. KEENLISIDE[1], D. GOULET[3], M. PLANTE[3], D. NGUYEN[3], F.S. PRATO[1], A.W. THOMAS[1]

[1] LAWSON HEALTH RESEARCH INSTITUTE AND UNIVERSITY OF WESTERN ONTARIO, ST JOSEPH HEALTH'S CARE, 268 GROSVENOR STREET, LONDON, ON, N6A 4V2, CANADA

[2] UNIVERSITE VICTOR SEGALEN BORDEAUX 2, INSTITUT DE COGNITIQUE, 146 RUE LEO SAIGNAT, 33076 BORDEAUX CEDEX, FRANCE

[3] HYDRO-QUEBEC, 800 BD DE MAISONNEUVE EST, 21^{E} ETAGE, MONTREAL, QC, H2L 4M8 CANADA

Abstract

For the past two decades, researchers have actively been studying the effects of time-varying magnetic fields (MF) on humans, principally examining the potential for the field to have acute effects on human physiology, neurophysiology and behaviour. The more consistent results reported in recent literature seem to show an increase in occipital alpha rhythm of resting electroencephalographic activity (EEG) with exposure (Cook et al., 2004; Ghione et al. 2005). Interestingly, other studies have demonstrated that human motor behavior can be modulated by exposure to an Extremely Low Frequency (ELF) MF, showing a reduction in anteroposterior standing balance oscillations (Thomas et al., 2001) and a decrease in physiological tremor intensity (Legros et al, 2006). However, to establish a connection between these observations would require a project that, in one procedure, investigates physiological, neurophysiological and behavioural parameters. Therefore, subject testing has begun, in a project approved by the University of Western Ontario (Health Sciences Research Ethics Board # 11956E), to investigate the effects of a 60 Hz, 1800 µT MF on heart rate (frequency and variability), peripheral blood perfusion, brain electrical activity (EEG), postural oscillations, voluntary motor functions, and physiological tremor. Preliminary results will be presented and should provide reliable information concerning human exposure to power-line frequency MF.

A. LEGROS, A. BEUTER, L. KEENLISIDE, D. GOULET, M. PLANTE, D. NGUYEN, F.S. PRATO, A.W. THOMAS

Introduction

Domestic electrical appliances, distribution and transport power-lines, and residential wiring are some of the numerous sources of magnetic field (MF) in our everyday environment. Over the past several years, studies have been conducted with the aim of characterizing the effects of Extremely Low Frequency (ELF, below 300Hz) MF on human health and performance. Despite the amount of work that has been done in this area, there remains no consensus as to the effects of ELF MF on humans.

From brain electrical activity to motor behaviour, a number of aspects of human physiology and behaviour have been examined in scientific literature in response to acute exposure to ELF MF. Among the potential effects, many studies detected neuropsychological changes induced by the exposure (Keetley *et al.* 2001; Preece *et al.* 1998). That these studies are still relatively rare, and often have conflicting findings prevents the confident characterization of the field's effects. Further, exposure protocol and neuropsychological evaluating tools differ between studies, and reported effects are tenuous or even absent. Nevertheless, the examination of these studies shows that any notable cognitive effects generally appear to affect high level cognitive processes such as attention mechanisms, learning and memory; and executive functions such as working memory, flexibility, categorization, deduction and problem solving (see Kazantzis *et al.* 1998; Podd *et al.* 2002; Preece *et al.* 1998; Stollery 1986). Moreover, authors have found that the changes influence the quality and the precision of high level cognitive mechanisms rather than the velocity of execution.

If such neuropsychological functions are effectively modulated by the exposure to ELF MF, effects should be detectable at a neurophysiological level. Several studies have shown effects of MF exposure on human electroencephalogram (EEG) or evoked potentials (Bell *et al.* 1992; Bell *et al.* 1994a; Bell *et al.* 1994b; Cook *et al.* 2005; Cook *et al.* 2004; Ghione *et al.* 2005; Heusser *et al.* 1997; Lyskov *et al.* 1993a; Lyskov *et al.* 1993b; Marino *et al.* 2004). Still, no consensus exists on the direction of these effects, though the most conspicuous results seem to suggest a higher resting EEG in the alpha rhythm after exposure (8-13 Hz, see for example Cook *et al.* 2004; Ghione *et al.* 2005).

Other studies analyzing the interaction between heart rate (HR) behavior and MF have shown that electrophysiological rhythms can also be modified at the peripheral level and that the exposure to 60 Hz MF could induce a slowing of the HR that may or may not be associated with changes in HR variability (Cook *et al.* 1992; Graham *et al.* 2000a; Maresh *et al.* 1988; Sastre *et al.* 1998; Sastre *et al.* 2000). Again, other works did not detect any exposure effect on HR (Graham *et al.* 2000b; Graham *et al.* 2000c; Kurokawa *et al.* 2003). For a better understanding of the mechanisms underlying observed changes in HR, electrophysiological data should be completed by the monitoring of hemodynamic parameters such as blood flow.

Another way to investigate the effects of MF on the human body in its entirety is to evaluate human motricity. A few studies have demonstrated an effect on human motor control resulting from exposure to time-varying MF. Thomas *et al.* 2001a, for example, explored human postural oscillations and reported significant decrease in anteroposterior balance using a pulsed MF at 200 µT. Legros *et al.* explored human physiological tremor (Legros and Beuter 2005; Legros and Beuter 2006; Legros *et al.* 2006). They did not report any significant effect of a 50 Hz, 1000 µT MF on physiological tremor occurring during a goal directed task. However, the analysis of tremor occurring during a postural task of the index finger suggested a relaxing effect induced by the exposure, decreasing tremor size. Interestingly, Cook et al. who, in 2004, showed an effect of a pulsed 200 µT MF on EEG alpha activity, also underlined the link between resting posterior alpha activity and the state of relaxed wakefulness (Niedermeyer 1999).

Reported results are subtle and often not replicated. These discrepancies defining the effect of an ELF MF on humans can be attributed to the heterogeneity in intensity, shape and frequency of the MF used, as well as the differences in exposure duration. Furthermore, results differ with continuous versus intermittent exposure, and depending on whether the testing of the subjects is performed during or after the exposure.

Objective

The main objective of this study is to evaluate subtle effects of a 60 Hz MF exposure up to 1800 µT on human physiology, neurophysiology and motor functions in a single procedure. This intensity has been chosen because the International Commission on Non-Ionizing Radiation Protection (ICNIRP) guidelines establishes that current density induced by MF occupational exposure "should be limited to fields that induce current densities less than 10mA/m2" (ICNIRP 1998), and this corresponds to computed MF value which can reach 1800 µT (Stuchly and Dawson 2002, http://www.emfs.info/sci_Numerical.asp). This global approach will then establish a better understanding of the effects of high intensity MF on these functions. Conclusions will be drawn from the examination of human blood perfusion, HR (frequency and variability), brain electrical activity (EEG), posturo-kinetic activity as postural sway, voluntary motor functions as rapidly alternating movements and involuntary movements through the measurement of postural tremor.

Based on results in the literature, we hypothesize that MF exposure will (1) not affect ECG or blood flow, (2) increase EEG power in alpha band activity, especially in the posterior regions of the brain, (3) decrease the quantity and the variability of anteroposterior displacements of postural sway, (4) increase the rapid voluntary movements' maximum frequency, and (5) decrease postural tremor amplitude. Effects should appear after several minutes of exposure. The results could be useful in the development of public policy regarding the safety of MF exposure.

Methods

This is a currently ongoing study. To date, 8 subjects have completed at least 1 of the 2 sessions of testing. All participants give their informed consent before participating (University of Western Ontario Health Sciences Research Ethics Board # 11956E). At term, 70 healthy adults between 18 and 55 years of age will have completed the full protocol consisting of 2 counterbalanced exposure sessions given on 2 separate days (with at least 2 days in between): 1 active exposure condition (real) and 1 control exposure condition (sham) as detailed in Figure 1a. None of the participants have ever experienced an epileptic seizure; have motor limitation; suffer from chronic illness (e.g., diabetes, severe psychiatric, cardiovascular or neurological diseases); or have a cardiac or cerebral pacemaker. They have no history of head, eye or thorax injury involving metal fragments; they do not wear metal braces on their teeth. Finally, women cannot be pregnant, nor have an intrauterine device. A double blind computer driven procedure controlling for variables is used such that neither the participant nor the experimenter know when the real or sham condition occurs. Each session lasts 1 hour and 45 minutes and is composed of four 15 minute blocks of testing with 15 minutes rest in between. 1 hour of MF exposure is given from minute 15 to minute 75 of the real exposure session. There is no MF exposure in the sham session.

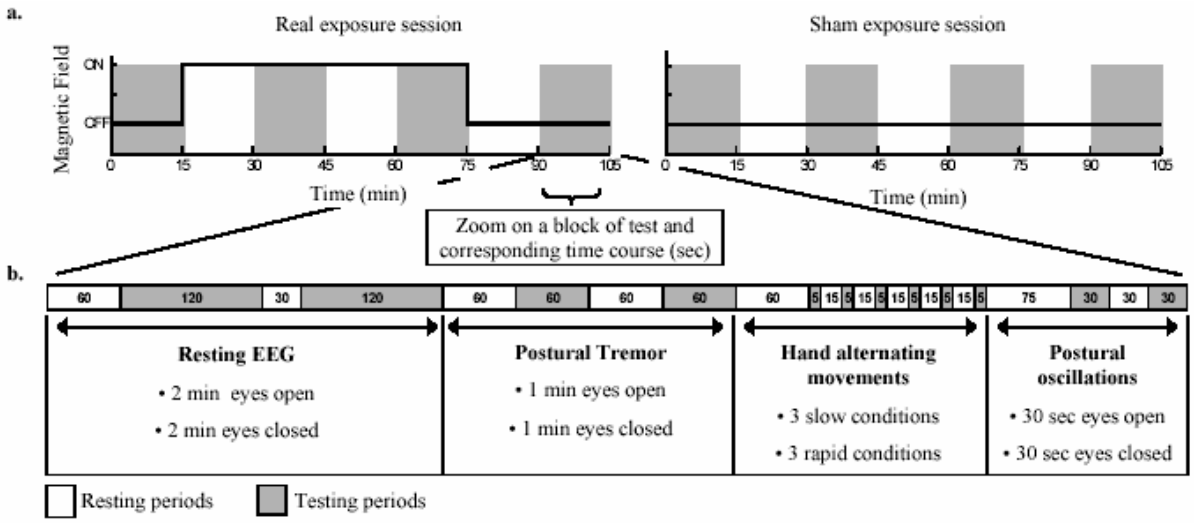

Figure 1: a. Time course of the 2 exposure sessions (real and sham). The horizontal black line represents the MF status (OFF when down, ON when up). Note that during the sham exposure session, the MF is never ON. Vertical grey bands represent the four 15-minute blocks of testing. **b.** Zoom on the time course of a block of testing (the same for each block). White cells represent resting periods and grey cells represent testing periods (duration is displayed in seconds inside the cells). The table below indicates the tests to which these periods correspond.

Each subject is equipped with the recording devices and his handedness is determined with the Oldfield questionnaire (Oldfield 1971). For the experiment, he is seated in an armchair in the exposure facility. The exposure system generating the MF has been designed for this experiment. It is composed of 2 octagonal coils, 1.6 meters in diameter, running parallel to each other 1.2 meters apart. Each coil contains 80 turns of AWG-10 wire mounted with a nonconductive cooling/heating tubing system. The system is configured to generate a homogenous 60 Hz field, up to 1800 µT, centred at the level of the head.

Prior to testing, the subject receives written directions, and is shown an audio-video demonstration of each task through a LCD screen and speakers, both positioned 1 meter in front of him. The room temperature is maintained at 23 °C. From the beginning of the testing session, both the subject and experimenter wear ear plugs to make it impossible to detect the subtle noise produced by the coils when the field is generated. The time course of the testing, as well as the MF generation and data acquisition, are entirely automated and computer driven (Labview 8.0 and Data acquisition card NI PCI-6289, National Instrument Inc., USA); except for recording of EEG, ECG and blood flow data. Automatic audio directions are given to the subject throughout the

duration of the experiment. He obtains visual information about the timing of the experiment through the screen in front of him.

Each of the 4 blocks of testing in each session follows the same time course (Figure 1b). The subject first relaxes for 1 min. Then his resting eyes-open-EEG is recorded for 2 min. After 30 sec of inactivity, his resting eyes-close-EEG is recorded for another 2 min. Baseline local blood perfusion (recorded at the tip of the non dominant index finger, PF 5010 Laser Doppler Perfusion Monitoring unit and probe 407-1, Perimed, Sweden) and ECG are recorded simultaneously. EEG and ECG are recorded at 512 Hz with a 32 channels ambulatory unit (Siesta unit, Compumedics Inc., USA). During the real exposure session, the MF is switched OFF during the second minute of both EEG recordings (eyes open and eyes closed) to keep 1 minute free of MF artefact in the data.

The subject is then asked to open his eyes, and after a resting period of 1 minute, his eyes-open postural tremor is recorded at the extremity of his dominant index finger for 1 minute. A Class II laser diode pointing toward the ground (Micro laser sensor LM10, series ARN11, Matsushita Electronic Work, Ltd., Osaka, Japan) and located 8 cm above the piece of white cardboard fixed on nail of the index finger enables 1000 Hz vertical displacement recording. A target horizontal line gives feedback about the index finger's vertical position, and is also displayed on the LCD screen. In this test, the subject must point the index finger (in extension at the level of the metacarpophalangeal joint) to keep the target line centred in the middle of the screen for 1 minute at the "zero position". After another 1 minute rest, he performs the same test with his eyes closed and therefore, with no visual feedback.

After another 1 min period, the subject is asked to extend his arms in front of him, parallel to the floor, and then to bend them to a 90 degree angle at the elbow, with hands open, palms facing each other. From this starting position, he has to execute alternating hand movements that involve rotating the hands at the wrist axis: (1) with the right hand at a natural rhythm; (2) with the left hand, natural rhythm; (3) with both hands, natural rhythm; (4) with the right hand at a higher frequency; (5) with the left hand, higher frequency; and (6) both hands, higher frequency. For the higher frequency condition, the subject is asked to rotate his hands "as fast and as far as possible". Recordings last 5 sec each, with a 15 sec rest between any two. Recordings are done with the liberty system (Polhemus inc., USA), with 2 transducers fixed like watches on the dorsal side of the wrists, allowing recording of movement kinematics with 6 degrees of freedom at 200 Hz in the used configuration (3D and 3 angles of rotation, accuracy of 0.03 RMS for X, Y, Z position and 0.15° RMS for orientation). The Liberty system is an electromagnetic tracking system and therefore, during MF exposure session, the field has to be turned OFF during each 5 sec recording periods so as not to affect data.

Finally, the subject has 75 sec to step onto a force plate (standardized socks, feet parallel, 1 cm apart) and to relax before his postural sway is recorded during 30 sec eyes open, and 30 sec eyes closed, with a 30 sec period in between. The 3-D force plate used in previous works (Thomas *et al.* 2001a; Thomas *et al.* 2001b, OR6-7-1000, AMTI, Watertown MA) is mounted on the floor in the centre of the MF exposure system, and measures the force and momentum applied by the subject's feet at a sampling rate of 1000 Hz. These measurements can be converted to centre of pressure (COP) values, i.e. the perpendicular projection of the centre of gravity through the force plate. Postural sway is then the change the COP over time.

As detailed in the Figure 1b, this block of testing is given 4 times over a session. During a real exposure session, this would mean that the testing begins: 15 minutes before the beginning of the exposure period, 15 minutes after the beginning of the MF exposure, 45 minutes after the beginning of the MF exposure, and 15 minutes after the end of the MF exposure. Skin temperature is monitored throughout the experiment. After each block, the subject has to answer the Field Status Questionnaire (FSQ, Cook *et al.* 1992) to assess his ability to detect the presence of the field.

Data processing and Analysis

As an ongoing study, data are still being collected and analysed. Therefore, given the advancement of the study and in a concern of clarity of the purpose, it has been chosen to focus here on a limited set of data, including EEG in the occipital region of the brain (O1, O2), postural tremor data, and postural sway data.

First, the ambulatory EEG data are recorded on a flash memory card, and then an averaged reference montage is used to import data in Matlab for processing (The MathWorks Inc., Natick, USA). Fast Fourier Transform (FFT) and inverse Fast Fourier Transform (iFFT) are used to extract time series in the theta (4-7 Hz), alpha (8-13 Hz), and beta (14-35 Hz) frequency bands. The average amplitude in each band is then computed for each electrode (O1, O2 here, see example in Figure 2).

Secondly, the laser system records vertical displacement with a resolution of 13 µm (i.e. 2σ, where σ is the standard deviation of a recording on a stationary target) which is effectively reduced to 5 µm after filtering out high frequencies (above 25 Hz, FFT, iFFT). Data are transferred to Matlab for A/D conversion to mm given a calibration constant (-3.97). Position and velocity data (obtained by differentiation of the raw displacement data) are used for indexes computation in time and frequency domains (Beuter and Edwards 1999; Edwards and

Beuter 2000) allowing the characterization and the examination of temporal, frequential and morphological components of the signals (see also Legros and Beuter 2005; Legros and Beuter 2006). Here, amplitude, drift, median frequency and frequency concentration are computed (see Appendix 1 for index definitions and Figure 3 for an example).

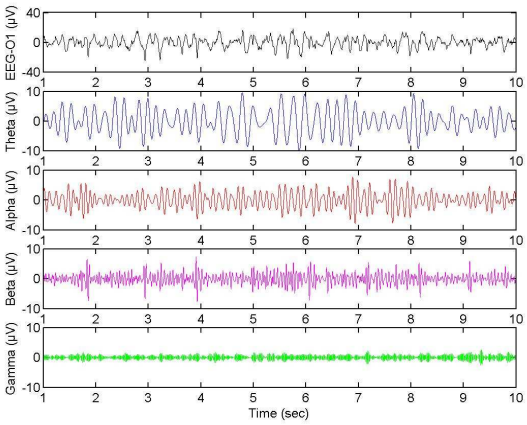

Figure 2: From the top to the bottom: 10 sec of O1 EEG trace and corresponding theta, alpha, beta and gamma components respectively extracted using FFT and iFFT. Averaged amplitude for this sample are: Theta = 3.909 µV, alpha = 2.485 µV, beta = 1.757 µV; gamma = 0.641 µV.

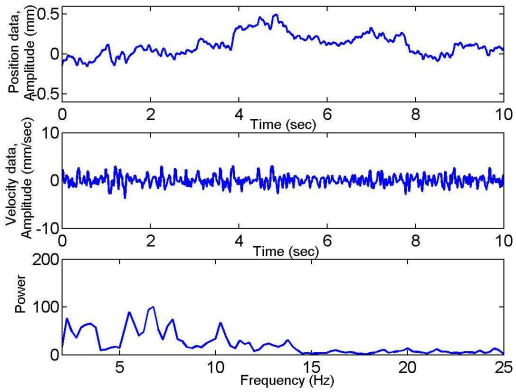

Figure 3: Position data (top), velocity data (middle) and corresponding power spectrum (bottom) for 10 sec of recording during MF exposure with eyes open (block 3). The computed values on this sample are: Amplitude = 0.032 mm; drift = 0.106 mm, median frequency = 7.04 Hz; and frequency concentration = 6.31 Hz.

Third, postural sway data are exported under Matlab and converted from volts to COP trajectories (in meters) using a calibration matrix. Through the inclusion of two dimensional trajectories (X vs. Y), the following validated characteristics have been computed (Despres *et al.* 2000; Thomas *et al.* 2001a): Mean sway, sway, velocity and sway area (see Appendix 1 for index definition and Figure 4 for an example).

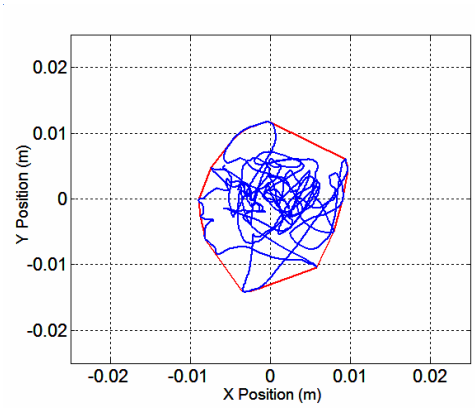

Figure 4: 30 sec of postural sway recording during MF exposure (block 3) with the eyes are closed. The smallest polygon including the entire trajectory is also displayed. The computed characteristics on this sample are: Mean sway = 0.53 cm; sway velocity = 1.62 cm/sec, sway area = 3.41 cm^2.

Preliminary results

For 3 of the 8 subjects who have completed at least 1 of the 2 sessions of testing, the first session was a real exposure condition. Therefore 3 subjects who have completed the sham session first have been chosen to afford a control group (i.e. the sham condition), which allowed providing a preliminary assessment of the exposure effects on their behaviour. According to the small sample size available at this step, a simplified statistical procedure has been chosen, focusing on the data acquired in the block 1 (before exposure) and the block 3 (during exposure, and after a 45 min period of continuous exposure, see Figure 1). A within-subject ANOVA including a between-subject factor (sham vs. real) have been conducted on each of the above

mentioned indexes: ANOVA 2 (eyes open vs. eyes closed) x 2 (block1 vs. block3) x 2 (sham vs. real). The level of significance has been set at $p < .05$ and no adjustment for multiple comparisons has been applied.

No Block main significant effect has been found either for EEG, postural tremor or postural sway recordings. However, with eyes closed, subjects had significantly higher EEG alpha activity in the occipital region (O1: $F = 24.85$, $p < .01$, $Eta^2 = .86$; O2: $F = 20.54$, $p < .05$, $Eta^2 = .83$), larger and faster postural oscillations (mean sway: $F = 17.38$, $p < .05$, $Eta^2 = .81$; sway velocity: $F = 51.47$, $p < .005$, $Eta^2 = .92$; sway area: $F = 35.14$, $p < .005$, $Eta^2 = .89$), and higher index finger drift ($F = 12.19$, $p < .05$, $Eta^2 = .75$) with eyes closed than with eyes open. No interaction effect was found.

Discussion-Conclusion

Preliminary results confirm that this experimental protocol is adapted to detect subtle changes in the neurophysiological characteristics investigated, despite the small number of subjects tested at this point. Indeed, as expected we observed significant differences between open and closed eyes conditions in EEG, tremor and postural sway. However due to the small number of subjects tested we did not detect a significant effect due to the presence of MF. This is why we performed a sample size analysis.

The sample size calculation for 2 independent samples with common variance was done on the sway velocity characteristic because this is the lowest p value for the interaction block x sham/real ($F = .509$, $p = .51$, $Eta^2 = .113$). In the present configuration, the decrease of .072 cm/sec observed for the real exposure group would be significant with two groups of 34 subjects (p fixed at .05, power = .80). We have planned to test a sample of $n = 70$ subjects which should be sufficient to detect the MF effects on the characteristics examined. We have to keep in mind that, at this stage of the study, 2 groups of subjects were evaluated. However in the final study all participants will have been tested under both MF conditions with a counterbalanced protocol. This should contribute to make the protocol more sensitive to subtle effects (reducing the impact of the between-subjects variability).

The results presented in this paper are only partial results on selected tests recorded. They will be completed by heart rate frequency and variability, blood flow perfusion, alternating movement performance. Finally data acquisition will be completed in 2007.

Acknowledgements

This research is funded in part by Hydro-Québec, Réseaux Transport Electricité (RTE), Electricitié de France (EDF), Ontario Research and Development Challenge Fund (ORDCF), Canadian Institutes of Health Research (CIHR) and Lawson Health Research Institute.

References

[1] Bell, GB, Marino, AA and Chesson, AL. 1992. "Alterations in brain electrical activity caused by magnetic fields: detecting the detection process." Electroencephalogr Clin Neurophysiol **83**(6): 389-97.

[2] Bell, GB, Marino, AA and Chesson, AL. 1994a. "Frequency-specific blocking in the human brain caused by electromagnetic fields." Neuroreport **5**(4): 510-2.

[3] Bell, GB, Marino, AA and Chesson, AL. 1994b. "Frequency-specific responses in the human brain caused by electromagnetic fields." J Neurol Sci **123**(1-2): 26-32.

[4] Beuter, A and Edwards, R. 1999. "Using frequency domain characteristics to discriminate physiologic and parkinsonian tremors." J Clin Neurophysiol **16**(5): 484-94.

[5] Cook, CM, Thomas, AW, Keenliside, L and Prato, FS. 2005. "Resting EEG effects during exposure to a pulsed ELF magnetic field." Bioelectromagnetics **26**(5): 367-76.

[6] Cook, CM, Thomas, AW and Prato, FS. 2004. "Resting EEG is affected by exposure to a pulsed ELF magnetic field." Bioelectromagnetics **25**(3): 196-203.

[7] Cook, MR, Graham, C, Cohen, HD and Gerkovich, MM. 1992. "A replication study of human exposure to 60-Hz fields: effects on neurobehavioral measures." Bioelectromagnetics **13**(4): 261-85.

[8] Despres, C, Lamoureux, D and Beuter, A. 2000. "Standardization of a neuromotor test battery: the CATSYS system." Neurotoxicology **21**(5): 725-35.

[9] Edwards, R and Beuter, A. 2000. "Using time domain characteristics to discriminate physiologic and parkinsonian tremors." J Clin Neurophysiol **17**(1): 87-100.

[10] Ghione, S, Seppia, CD, Mezzasalma, L and Bonfiglio, L. 2005. "Effects of 50 Hz electromagnetic fields on electroencephalographic alpha activity, dental pain threshold and cardiovascular parameters in humans." Neurosci Lett **382**(1-2): 112-7.

[11] Graham, C, Sastre, A, Cook, MR and Gerkovich, MM. 2000a. "Nocturnal magnetic field exposure: gender-specific effects on heart rate variability and sleep." Clin Neurophysiol **111**(11): 1936-41.

[12] Graham, C, Sastre, A, Cook, MR and Kavet, R. 2000b. "Heart rate variability and physiological arousal in men exposed to 60 Hz magnetic fields." Bioelectromagnetics **21**(6): 480-2.
[13] Graham, C, Sastre, A, Cook, MR, Kavet, R, Gerkovich, MM and Riffle, DW. 2000c. "Exposure to strong ELF magnetic fields does not alter cardiac autonomic control mechanisms." Bioelectromagnetics **21**(6): 413-21.
[14] Heusser, K, Tellschaft, D and Thoss, F. 1997. "Influence of an alternating 3 Hz magnetic field with an induction of 0.1 millitesla on chosen parameters of the human occipital EEG." Neurosci Lett **239**(2-3): 57-60.
[15] ICNIRP. 1998. "Guidelines for limiting exposure to time-varying electric, magnetic, and electromagnetic fields (up to 300 GHz). International Commission on Non-Ionizing Radiation Protection." Health Phys **74**(4): 494-522.
[16] Kazantzis, N, Podd, J and Whittington, C. 1998. "Acute effects of 50 Hz, 100 microT magnetic field exposure on visual duration discrimination at two different times of the day." Bioelectromagnetics **19**(5): 310-7.
[17] Keetley, V, Wood, A, Sadafi, H and Stough, C. 2001. "Neuropsychological sequelae of 50 Hz magnetic fields." Int J Radiat Biol **77**(6): 735-42.
[18] Kurokawa, Y, Nitta, H, Imai, H and Kabuto, M. 2003. "Can extremely low frequency alternating magnetic fields modulate heart rate or its variability in humans?" Auton Neurosci **105**(1): 53-61.
[19] Legros, A and Beuter, A. 2005. "Effect of a low intensity magnetic field on human motor behavior." Bioelectromagnetics **26**(8): 657-69.
[20] Legros, A and Beuter, A. 2006. "Individual subject sensitivity to extremely low frequency magnetic field." Neurotoxicology **27**(4): 534-46.
[21] Legros, A, Gaillot, P and Beuter, A. 2006. "Transient effect of low-intensity magnetic field on human motor control." Med Eng Phys **28**(8): 827-36.
[22] Lyskov, EB, Aleksanian, ZA, Iousmiaki, V, Medvedev, SV, Partanen, I, Safonova, TE, Khanninen, O and Iutilainen, I. 1993a. "[Neurophysiologic effects of short-term exposure to ultra-low-frequency magnetic field]." Fiziol Cheloveka **19**(6): 121-5.
[23] Lyskov, EB, Juutilainen, J, Jousmaki, V, Partanen, J, Medvedev, S and Hanninen, O. 1993b. "Effects of 45-Hz magnetic fields on the functional state of the human brain." Bioelectromagnetics **14**(2): 87-95.
[24] Maresh, CM, Cook, MR, Cohen, HD, Graham, C and Gunn, WS. 1988. "Exercise testing in the evaluation of human responses to powerline frequency fields." Aviat Space Environ Med **59**(12): 1139-45.
[25] Marino, AA, Nilsen, E, Chesson, AL, Jr. and Frilot, C. 2004. "Effect of low-frequency magnetic fields on brain electrical activity in human subjects." Clin Neurophysiol **115**(5): 1195-201.
[26] Niedermeyer, E (1999). The normal EEG of the waking adult. Electroencephalography.Basic principals, clinical applications, and related fields. ELdSF Niedermeyer. Baltimore, Williams and Willkins**:** 149–173.
[27] Oldfield, RC. 1971. "The assessment and analysis of handedness: the Edinburgh inventory." Neuropsychologia **9**(1): 97-113.
[28] Podd, J, Abbott, J, Kazantzis, N and Rowland, A. 2002. "Brief exposure to a 50 Hz, 100 microT magnetic field: effects on reaction time, accuracy, and recognition memory." Bioelectromagnetics **23**(3): 189-95.
[29] Preece, AW, Wesnes, KA and Iwi, GR. 1998. "The effect of a 50 Hz magnetic field on cognitive function in humans." Int J Radiat Biol **74**(4): 463-70.
[30] Sastre, A, Cook, MR and Graham, C. 1998. "Nocturnal exposure to intermittent 60 Hz magnetic fields alters human cardiac rhythm." Bioelectromagnetics **19**(2): 98-106.
[31] Sastre, A, Graham, C and Cook, MR. 2000. "Brain frequency magnetic fields alter cardiac autonomic control mechanisms." Clin Neurophysiol **111**(11): 1942-8.
[32] Stollery, BT. 1986. "Effects of 50 Hz electric currents on mood and verbal reasoning skills." Br J Ind Med **43**(5): 339-49.
[33] Stuchly, MA and Dawson, TW. 2002. "Human body exposure to power lines: relation of induced quantities to external magnetic fields." Health Phys **83**(3): 333-40.
[34] Thomas, AW, Drost, DJ and Prato, FS. 2001a. "Human subjects exposed to a specific pulsed (200 microT) magnetic field: effects on normal standing balance." Neurosci Lett **297**(2): 121-4.
[35] Thomas, AW, Drost, DJ and Prato, FS. 2001b. "Magnetic field exposure and behavioral monitoring system." Bioelectromagnetics **22**(6): 401-7.

Appendix 1

Postural tremor characteristics:

Amplitude: Root Mean Square (RMS) of position time series centered on their mean (highpass and lowpass filtered, between 2 and 25 Hz).

Drift: RMS of the low frequency component of the time series (below .01 Hz), quantifying slow movements of the finger.

Median frequency: Determines the value at which 50% of the power spectrum is below this frequency, and 50% is above. It is computed on the power spectrum between 2 and 25 Hz.

Frequency concentration: Quantifies the degree of organization of tremor by computing the width of the interval containing 68% of the power of the spectrum between 2 and 25 Hz.

Postural sway characteristics:

Mean Sway: Average distance between the geometric center of all recorded forces and each point visited by the Center of Pressure (COP) during a test.

Sway Velocity: Average velocity of the COP displacements.

Sway Area: Area of the smallest polygon including the entire trajectory of the COP.

ELECTROMAGNETIC FIELDS EFFECTS ON WITHDRAWAL SYNDROME SIGNS OF MORPHINE (WSSM)

A. SAFARI[1], H.JAFARI[2], H.JAHANI HASHEMI[3]

1. **Department of Occupational Health, Qazvin University of Medical Sciences.**
2. **Department of pharmacology, Qazvin University of Medical Sciences.**
3. **Department of Biostatics, Qazvin University of Medical Sciences.**

Abstract:

Background: Many studies have showed that electromagnetic field decreased WSSM.
Objectives: Effect of electromagnetic fields on WSSM investigated on rats.
Materials and methods: In this study 102 male rats with weight (225 ± 25) gr were classified in 17 groups (n = 6). They were addicted by morphine injection according to Pinelli Method. 16 groups of them exposed to electromagnetic fields with 25, 50, 75 and 100 Hz frequency and with magnetic field 0.5, 1.5, 2.5 and 3.5 G intensity. One group was chosen as control. WSSM jumping, climbing, rearing, diarrhea, weight loss, ptosis and yawning by naloxone injection in pretoon (5mg/kg) at all animals were investigated.
Findings: WSSM were obtained by counting the jumoing, wawing, alimbing, rearing and the ptosis, diarrhea were scrod from +1 to +4. Also weight losses were measured in all groups.
Results: This study showed that magnetic fields caused the significant decreased on waving, ptosis, weight loss and diarrhea at all of the exposure groups ($P<0.001$). Rearing and climbing decrease significantly in groups that exposed to electromagnetic fields and this fields with 25 Hz frequency and 0.5 G intensity have minimum and with 100 and 75 Hz frequency 3.5 G intensity have maximum effects on WSSM.
Keywords: Electromagnetic field, Withdrawal syndrome signs, Morphine, Rat.

Introduction:

About the role of electricity for curing addiction, some studies have been performed as bellow that about the laboratorial addicted animal has been used so that two metal electrodes have been touched around the two sides of its body, so that it would be done under special condition, and this action must be done daily for several times. This action is called Transcutanous Electrical Nerve Stimulation or TENS. And according to the Frequency and Voltage that is given two kinds of TENS can be done so that the low TENS and high TENS would have electrical changes in the epidictic system in this case this currency of addiction would be activated and then released. So if TENS be given to an addicted animal to morphine many of the signs in this field would be removed (1,2). In the recent years, the electromagnetic fields (EMF) in the medical sciences have many usages and they have indicated that the resulted energy from this field for curing the wound, reduction of all the kinds of pain can be effective, in a way that today the electromagnetic fields have found an important place as the alternative medicine and then they are mentioned like that.

Naturally the electromagnetic waves by high TENS would have some effects to the talent and focusing point and they would reduce the memory. Anyway in the animal tests it has been shown that the actions of electromagnetic fields in the addicted mice to morphine would cause the reduction of the signs of Syndrome especially for pain (3). The electromagnetic waves have some effects to the channels in the brain and also the environmental tissues would cause some changes in the physiological operation and the operation of these hormones, neurotransmitters, and some other medicine effects that strongly are related to the tissue of mind (4).

According to the last information of National Center for Complementary Alternative Medicine(NCCAM) National Institute of Health(NIH) the subsistent, electrical, magnetic, methods and electromagnetic fields and the electrical stimulations the nervous stimulation methods have been replaced(5). Some of the researchers about the role of electromagnetic in the addiction to morphine have provided some reports that would reduce the signs of dependency role,. They believe that the serotonin and triptophan surfaces and Hydroxide indol astic acid during the electromagnetism would be increased and following it some changes in some of the channels that are calcium in the brain (3). Some reports have been available that during electromagnetic therapy beta endorphins were increased. And this action will prevent the occurrence of syndrome in the body (3). It is possible that the increase of endorphin system and the increase of chemical materials in the brain be released (3). The last research of Magnet Therapy has caused the reduction of pain in the Post-Polio patients and this kind of therapy has little third effects (6). One of the usages of electromagnets is during the time of intensified pain. In the northern America the expenditures more than 10 to 15 thousands dollars for the reduction of pain for each person is used. 17 % of the population over 15 suffer from the pain that they get from the daily activities and in the United States of America about 93 millions dollars daily and more than 5 milliards dollars per year would be wasted for this purpose(7). Some evaluations would be done in the static and some channels that are similar to each other. Many researches about Pulsed Electromagnetic Filed have been done for reduction of pain and the provided results indicate the following effects:

1. Increase of pain field
2. Activation of anti-contagious system
3. Stimulation of producing aphetic points
4. Betterment of blood currency and the resulted effects of it including the increase of oxygen transferring and etc.
5. Improvement of blood thickness
6. Betterment of metabolism in the brain
7. Improvement of the movement of blood in body and brain

Pain is the important parameter that caused to become addicted patients. Some of researches showed that nerve systems affected by PEME curing (8).

Materials and methods

In this study 102 rat with 200-250g weight were divided in 17 group (n=6). That each group contains 6 muse. And these groups were Group one considers as the control group and the groups 2-17 as study groups that were expose to magnetic field as below detail.

Group2 (B= 0.5G, F = 100Hz), Group 3(B= 1.5G, F = 100Hz), group 4(B= 2.5G. F = 100Hz)
Group 5(B= 3.5G, F = 100Hz), Group 6 (B= 0.5G, F=75Hz), Group 7(B=1.5G.F= 75Hz)
Group 8(B=2.5G, F=75Hz), Group9 (B= 3.5G, F = 75Hz), Group 10 (B= 0.5G, F = 50Hz)
Group11 (B= 1.5G, F=50Hz), Group12 (B=2.5G, F = 50Hz), Group13 (B=3.5G, F = 50Hz)
Group14 (B= 0.5G, F = 25Hz), Group15 (B=1.5G, F=25Hz), Group16 (B=2.5G, F= 25Hz), Group 17 (B= 3.5G. F = 25Hz)

The animals were addicted according to Poinelli Method, and then animals of 16 groups as mention above condition were exposed to magnetic field for 30 minutes.

The syndrome signs of morphine stop were studied after Naloxone injection in pretoon. Jumping, Rearing, Climbing, yawning, diarrhea and ptosis, as syndrome signs were studied in this research after 2 hour naloxone injection. In this research we used the analyze variance, Dunnet and crouscal valis for data analyzing.

Findings

Seven signs for the stopping point of morphine in all the groups were considered. The most important sign was jumping, the number of Jumping in the groups 17, 16, 15, 12, 11 and 10 not only was not reduced but also ratio to other groups were more. In the groups 2, 6, 8, 13 and 14 the number of jumping was reduced but this reduction was not so much. In the groups 3, 4, 5, 7 and 9 the reduction of jumping was observed and it was so much in a way that in the groups 5 and 9 $P< 0.001$ was observed. In the groups 4^{th} and 7^{th} $P< 0.01$ and in the 3^{rd} group $P<0.05$ was seen. Except the group 14 and 15 which the reduction was so much. In the 9^{th} group more than other groups the reduction could be seen and it was as $p<0.001$. In all the groups the magnetic field except the group 4^{th} has an important

reduction which was P< 0.001. In the groups 9 and 12 the reduction was more than other groups. In the group 10, 14 and 15 there was not so much reduction but in the other 13 groups the reduction was so much. In way that other 14 groups had the weight reduction by p< 0.001. The little weight for reduction in the second and fourth groups is shown in the diagram 2. Generally it can be stated that the lesser response was in the groups 5^{th} and 9^{th} which had the best operation and the response would be provided.

Discussion

Present study showed that magnetic field with various intensity and frequency have affected on syndrome signs of morphine stop in rat magnetic field decrease jumping in exposure groups(3.4, 5 , 7 , 9) and also decries rearing in exposure groups (2-13 , 16 , 17) significantly (P<0.05).This study showed the magnetic field with various condition cause to reduce syndrome sings of morphine stop in rat such as climbing, yawning, Ptosis, diarrhea and weight significantly (P < 0.05).The magnetic field affected on the number of jumping depend on intensity, frequency and time exposure.

Morphine is an alkaline material and ionizes in body. The ionized form of morphine can't pass the Blood Brian Barrier (B.B.B), the magnetic field caused to ionizing the acidic and alkaline drug (9) for this reason the magnetic field can reduce the syndrome signs of morphine stop. The result of this study showed that the magnetic field with high frequency and high intensity reduce the syndrome signs of morphine in rat. This reduction can explain by this reason.

1- Increase the polarity of Naloxone
2- Alteration of receptors instruction
3- Reduction of morphine in brain cells

This study showed that rearing and climbing reduced significant in exposed groups (P<0.05).We think that these reduction is because of increase the induction and releasing the androgen peptides opiate and alteration of nerve mediator induction and releasing such as dopamine, glutamate, serotonin, Spartant.This nerve mediator affected to jumping, another study showed that Spartant system can increase the jumping in rat(10).Also other researcher showed that the electromagnetic field caused to induction and releasing the acetylcholine in animals cells(11).In this study we showed that magnetic field didn't have any effect on weight loss and this finding accompany with our result of previous study(1).The magnetic field with high frequency and high intensity decrease diarrhea but acetylcholine and piocarpin increase diarrhea(12). By considering the results of this study, we obtained that magnetic field reduce the cholinergic system and acetylcholine in brain cells and also other reports indicated dopamine has affected on climbing and yawning (13,14,15). According to results of others study we can guess the electromagnetic field increase serotonin and dinorphine and decrease dopamine and acetylcholine.

Reference

1. Jafari H., Vaez M. M., Gharebaghi R., Consideration the level of sufficiency of electrical stimulations as (IENS) and reasonable stress of (ICWS) against with the dependency to morphine in the desert mice and the comparison of these two methods. Daneshaver (Shahed collage) Vol.29, 2000, pp: 2-10.
2. Jafari H., Vaez M. M., Gharebaghi R., Study for the effect of TENS and ICWS in the reduction of syndrome signs of morphine in Rat, scientific magazine of medical sciences university of QazvinVol. 18, 2001, pp: 12- 16.
3. http:// www. Therrionresearch.com/learing-center-articles.html.(Drug addiction and brain. By Paul Tyler).
4. Albert E. Desantis M Microwaves alter nervous system structure? In: Tyler p. biological effect of non ionizing radiation. Proceeding of conferences. Ann New York Acad. Sci, 1975, 247: 87-108.
5. The first congress of paramedical therapy and traditional therapy from Islamic Azad university unit Qom 2001 and the introduction of replacement therapy.
6. Www. Therrionresearch.com/learing-center-articles.html. (Magnet Therapy Reduces pain in Post-polio Patients. By Carlos Vallbona).
7. Pawlo W. MD, MSC. Pain Management with Pulsed electromagnetic field. 2002, Black well Science, PP: 175-182.
8. Http//www. Rush star. Com/ health care/ magnetic therapy. Rush star magnetic therapeutic kit rush star health care.
9. Edward H. Microwave: Industrial, scientific and medical application (part IV- Biological affects and Medical application), pp: 445-450.
10. Nadia M. Pharmacology & Behavior Vol. 20. pp: 631-633.

11. Kalantari, Z., Jafari H., Riyahi, A., Using of electromagnet as the replacing therapy for using the medicine for addicted people. The collection of province conference for addiction by Islamic Azad University Unit Astara. pp. 227-229.
12. Clark, Barter, Janson, Goths Medical pharmacology.1992, Vol. (1):112-116.
13. Muore Na. Axton M. Production of climbing behavior in mice requires both D, Fe D2 receptors activation. Psychopharmacology. 94: 263-66.
14. Ramanda k. Tanaka M. Involvement of sepatel and stratal dopamine D2 receptors in yawning rats. J. Psychopharmacology. 1986, 90: 9-13.
15. Zarrindas Mr. Bromocriptine induced climbing behavior: possible D1 & D2 receptors J. psychopharmacology. 1990, 100: 275-280.

LEGISLATIVE NEEDS FOR COMPUTATIONAL EMF EXPOSURE ASSESSMENT THE EUROPEAN DIRECTIVE 2004/40/CE

PAOLO ROSSI, ROSARIA FALSAPERLA

National Institute of Occupational Safety and Prevention (ISPESL) – Rome – Italy
paolo.rossi@ispesl.it, rosaria.falsaperla@ispesl.it

Abstract

The European directive 2004/40/CE on the minimum health and safety requirements regarding the exposure of workers to the risks arising from electromagnetic fields, based on ICNIRP guidelines for occupational exposure, is presented and commented. The resulting needs for computational assessment of workers' exposure in terms of dosimetric quantities is considered and discussed.

I. The European Directive 2004/40/CE

The directive 2004/40/CE [1], on the minimum health and safety requirements regarding the exposure of workers to the risks arising from electromagnetic fields, has been issued in the European Official Journal on May 25, 2004, as the 18th individual directive within the meaning of framework directive on health and safety at work (391/89/EEC). The EMF directive follows the publication of directives on other physical agents, namely 2002/44/CE on vibration and 2003/10/CE on noise. The aim of the directive is the protection from established adverse effects caused by induced currents and by energy absorption, as well as by contact currents. Suggested long-term effects are not addressed, due to the lack of conclusive scientific evidence. The directive lays down minimum requirements giving EU member states the option of maintaining or adopting more favourable provisions for the protection of workers. Like in the previous directives on physical agents, the framework is based on the definition of "exposure limit values" and "action values". The exposure limit values can never be exceeded, whereas the action values are levels at which the employer must undertake technical or organizational measures to reduce exposure. The numerical definition of such values is based, respectively, on basic restrictions (dosimetric quantities) and reference levels (unperturbed fields) established for the workers in the relevant guidelines of the International Commission on Non-Ionizing Radiation Protection (ICNIRP) [2]. The directive claims the employer to give particular attention to any indirect effects, such as interference with medical devices like cardiac pacemakers, and adapt risk assessment and mitigation measures for workers at particular risk. Member states have to transpose the directive into national law within April 2008.

Directive 2004/40 CE claims the employer to a specific risk assessment, and to verify the respect of limits of exposure that are expressed in terms of dosimetric quantities, induction of current and Specific Absorption Rate (SAR). Such evaluation is achievable only by means of simulation computational methods, and in fact the directive often refers to calculations. Moreover, the directive shall be taken into account in the definition of product standards for special families of equipment emitting EMFs, to be used at the workplace. Compliance verification of the basic limits by calculations calls for the use of proper numerical methods able to solve Maxwell's equations, in combination with high resolution models of worker's body, and satisfactory representation of sources and workplace environment.

II. Computational exposure assessment for workers – Critical points

As information technology, numerical methods are increasing and developing very rapidly. Application to more and more complex problems is expectable, like multiple sources and complex environments, but the reliability of results critically depends on the representation of the real problem; any obtainable result refers in fact to the representation scenario and not to the actual problem, otherwise than *in situ* field measurements.

Many of the available numerical methods, that are listed in [3], are implemented on commercial SW packages mostly developed by research teams, provided with digital human body models and CAD tools able to realistically represent sources and environment. A lot of scientific work and applications have been developed, mostly addressed to relatively simply exposure evaluations, like in the case of mobile phones (head) or base

stations and broadcasting (whole body), and specific standards for calculations have been issued by CENELEC and IEC, but extensive application to more complex occupational exposures has not been carried out yet, due to lower public and authority concern.

All simulation packages and components are affected by limitations, advantages and disadvantages, so that the proper choice in a given situation may not be easy. The duration of calculation is one aspect to be considered in relation with the efficiency of the representation. Concerning human body models, the knowledge of dielectric properties of human tissues is still affected by gaps especially at low and intermediate frequencies range, and the available models only refer to very simple postures (erect), even if in occupational exposures the posture of the workers may be very complex. Methods have been introduced for scaling and obtain different body postures but results need to be carefully validated in a wide number of conditions.

III. Needs for computational exposure assessment - Discussion

The provisions from Directive 2004/40/CE pose the need to answer to some basic questions, and identify a logical pathway in order to manage the dosimetry problem. A basic question is to address when numerical dosimetry must be invoked in EMF occupational risk assessment. The first case is a condition where reference/action levels are exceeded, but basic/exposure limits are probably not. Such condition may occur for instance in the case of RF fields strictly confined close to the source, similarly to head exposure from a mobile phone. A second case, to be carefully considered, deals with compliance with local basic restrictions. Guidelines of ICINIRP [2] clearly states that: "*the reference levels are intended to be spatially averaged values over the entire body of the exposed individual, but with the important proviso that the basic restrictions on localized exposure are not exceeded"*. In other words, reference/action levels are able to guarantee compliance with body averaged SAR but don't assure compliance with restrictions on local SAR, which is however crucial when the source is very close to the worker and directly coupled to the body. In the frequency range 10 MHz - 110 MHz, where the electromagnetic energy is mostly absorbed inside legs and limbs, ICNIRP Guidelines [2] and Directive 2004/40/CE provide a reference/action level for feet current that is helpful in order to verify compliance with local SAR limits in the limbs. On the opposite hand, in the "hot spot" frequency range (400 MHz - 3 GHz) localized peaks of energy absorption may concern internal organs, and in such condition the assessment of local SAR by means of numerical dosimetry should be recommended even when the exposure levels (as spatially averaged values over the body) approach the reference/action levels.

Another critical point to be addressed is the accuracy, or approximation, of the representation of the exposure problem. This point needs consideration on sources characteristics, human model, but the surrounding work-place must be taken into account too, especially in the case of presence of metal objects or structures. The choice of proper resolution of the human model is crucial again; too low resolution could lead to unreliable results, but too high one could overload computational time and HW resources.

As a matter of fact occupational exposure assessments based on numerical methods are very complicated and require high level education, to-date available only in research centres or institutes. The possibility of practical use of numerical modeling by the employers for real cases in working environment seems to be very limited, in contrast to the relatively effective use of such technique for large scale manufacturing in standardized condition, bearing in mind however that occupational exposure patterns are much more complicated than general public ones (e.g. SAR in the head with mobile phones), and standardization bodies should carefully consider it.

Simplified models could be useful for performing rough assessment on occupational EMF sources and workers' exposure levels. Worst-case models could be used as intermediate step between field measurements and refined dosimetry. To such aim, extensive comparisons of standard case-studies should be carried out, analyzing the performance of simplified models compared to more sophisticated ones.

References

[1] Directive 2004/40/EC of the European Parliament and of the Council of 29 April 2004 on the minimum health and safety requirements regarding the exposure of workers to the risks arising from physical agents (electromagnetic fields) (18th individual Directive within the meaning of Article 16(1) of Directive 89/391/EEC), O.J. L-184 of 24 May 2004.

[2] INTERNATIONAL COMMISSION ON NON-IONIZING RADIATION PROTECTION (ICNIRP). Guidelines for Limiting Exposure to Time-Varying Electric, Magnetic, and Electromagnetic Fields (Up to 300 GHz). Health Physics 1998; 74: 494-522..

[3] EN 50392: 2004-01: Generic standard to demonstrate the compliance of electronic and electrical apparatus with the basis restrictions related to human exposure to electromagnetic fields (0 Hz – 300 GHz), CENELEC Standard.

EXISTING ELF, IF AND HF ELECTRICAL APPLIANCES AND TECHNOLOGIES PRODUCING HIGH EMF EXPOSURE

MONICA SANDSTRÖM, JONNA WILÉN, KJELL HANSSON MILD

NATIONAL INSTITUTE FOR WORKING LIFE, UMEÅ, SWEDEN

The new EU directive, 2004/40/EU, issued on occupational exposure to electromagnetic fields (EMF), calls for occupational risk assessment and implementation in the EU states national occupational safety and health regulations before April 2008. Commonly, workers are exposed to EMF with a mixture of different frequencies. In most cases the exposure levels are low and not in conflict with the new directive. However, some work situations or occupations need special attention due to risk of high exposure. Following the protocol in the directive, workers exposure to EMFs should be estimated, measured or calculated depending on type of workplace and possible risk of over exposure. One of the assigned issues in the EMF-NET MT2 group is to identify work situations that might be in conflict with the new EU directive. In this review, a number of work situations where there is a risk of high EMF levels will be presented and a few examples are listed below.

At electrolytic processes static magnetic field levels at the operator's location can be about 8-15 mT with an AC rectification's component about 30 %. The fundamental frequency is usually 50-300 Hz.

Magnetic resonance imaging systems use magnets typically from 0.05 T to about 3 T. In addition to static magnetic fields, RF fields (10-100 MHz) and rapidly changing gradient magnetic fields occur in pulse sequences within MRI equipment. The time derivatives of gradient fields (dB/dt) affecting patients vary typically from 1-3 T/s, and exposure of staff to EMF can be significant inside treatment rooms surrounding MRI equipment. The maximum exposure level is about 1 T in front of the magnet, and nurses/technicians staying with patients can be exposed to magnetic flux densities up to 0.2 T, approaching the protection guideline. In the case of performing professional activities very close or inside the magnet's tube, workers can be exposed to higher fields (up to 1-2 T), e.g. during adjutancy or plugging in RF cables of treatment coils, or device cleaning.

Transcranial magnetic stimulation or repetitive transcranial magnetic stimulation (TMS/rTMS) is currently being used in treatments of the central nervous system diseases, for instance, depressive states. During the treatment the therapeutic staff is exposed to a pulsed 100 kHz magnetic field that might exceed the reference values in the EU directive. The time derivative, in some of the measured tests, was in the order of kT/s!

Operators of induction furnaces and heaters are highly exposed to magnetic fields. At a distance of 1 meter from a 1-10 kHz heating equipment, flux densities typically range from 0.03 to 0.5 mT, and may reach 5 mT at 10 cm. Measurements of devices operating at 50 Hz, have shown that at a distance of 20 cm the flux density of the field might exceed 5 mT. At a distance of several meters 0.1 mT have been measured. The reference values in the EU directive (30.7 µT for 1-10 kHz and 500 µT for 50 Hz) are exceeded during work procedures close to furnaces.

Welders are one of the occupations that are highly exposed to EMF and thereby in conflict with the new EU directive. Arc welding uses high electric currents up to several hundreds of Amperes. The current, provided by the welding power source, flow through the torch-cable and torch to the welding arc, and into the workpiece and back to the power source via the ground cable. This provides a source for magnetic field to which the worker is exposed during the welding process as the cable can touch the welder or even be wrapped around the shoulder of the welder. Magnetic flux densities are about 1 mT at the surface of the welding cable and power supply, exposing the welders to strong ELF fields. (ref)

Glue dryers in the wood industry and plastic welders are using RF energi by applying a strong RF current between metal electrodes. The output powers range from 1 to 200 kW at the ISMfrequencies of 13.56, 27.12 or 40.68 MHz. Most plastic sealers are operated manually and require the presence of the operator close to the RF electrodes. In some applications, pieces of plastic materials to be heated must be held by hand, so that the operator's hands will be highly exposed to RF fields. Electric field strengths range in areas of operators typically from 1 to 300 V/m, and magnetic fields from 0.1 to 20 A/m, respectively.

Broadcast stations are using high RF energy intentionally radiated into the air. Typical maximum radio and TV transmitting powers fed to the antennas are about 500 kW for LF, MF and HF antennas and 10-50 kW for VHF and UHF antennas. Since the antennas are mounted near the top of a mast at the height of over 200 m, the exposure levels at the ground level are very low, but the occupational exposure can, however, be high during maintenance and installing work inside a mast, and special precautionary actions has to be taken.

A mobile phone base station emit RF fields in the range 450-2200 MHz. With a maximal output power of let say 50 W the EU directive might be exceed within a couple of dm in front of the antenna. In other positions or at a longer distance from the antenna there is no conflict with the directive.

References

Figueroa Karlström E., R. Lundström, O. Stensson, K. Hansson Mild. *Therapeutic staff exposure to magnetic field pulses during TMS/rTMS treatments*. Bioelectromagnetics, 2006, 27: 156-158.

International Journal of Occupational Safety and Ergonomics (JOSE) 2006, 12;2. *Special issue electromagnetic fields in the workplace*. http://www.ciop.pl/jose

Sandström M., K. Hansson Mild, O. Stensson. *Elektromagnetic fields associated with Arc welding - examples of measurements for compliance.* Workshop in welding, Mol, Belgium, 6 April 2006. http://www.vito.be/english/environment/pdf/welding_workshop.pdf

Wilén J., R. Hörnsten, M. Sandström, P. Bjerle, U. Wiklund, O. Stensson, E. Lyskov, and K. Hansson Mild, *Electromagnetic field exposure and health among RF plastic sealer operators.* Bioelectromagnetics, 2004. **25**(1): p. 5-15.

This project was partially funded by the Coordination Action EMF-NET "Effects of the Exposure to Electromagnetic Fields: from Science to Public Health and Safer Workplace" (European Commission FP6 Coordination Action, Thematic Priority 8, Policy support and anticipating scientific and technological needs, Contract N° SSPE-CT-2004-502173, 2004-2008)

THE FUNDAMENTALS OF OCCUPATIONAL EXPOSURE ASSESSMENT IN REAL LOW AND INTERMEDIATE FREQUENCY EMF ENVIRONMENT

JOLANTA KARPOWICZ, KRZYSZTOF GRYZ

CENTRAL INSTITUTE FOR LABOUR PROTECTION – NATIONAL RESEARCH INSTITUTE, LABORATORY OF ELECTROMAGNETIC HAZARDS WARSZAWA, POLAND, e-mail: jokar@ciop.pl

Abstract

The presentation is based on analysis of the fundamental problems defined for the use of numerical calculations for workers exposure assessment in real occupational situations. The examples of data from workplaces in the vicinity of LF or IF sources will be presented, focusing: space distribution of EMF, complex characteristics of the frequency content, workers activities/moving in the workplace, field impedance, etc., as well as discussion concerning situations when the use of calculations is required.

Keywords: EMF exposure, exposure assessment, numerical calculations, low frequency, intermediate frequency

1. Introduction

Electromagnetic field's (EMF's) exposure assessment adequate to the real exposure level is the crucial step towards appropriate risk assessment for occupational safety and health (OSH) engineering, epidemiological studies of EMF-exposed groups, environmental monitoring. The highest requirements concerning detailed EMF exposure assessment come from the legislations concerning mandatory control of occupational or environmental EMF exposure, e.g. European Directive on workers EMF exposure limitation.

The provisions of the Directive 2004/40/EC permit the employer to use exposure level (external measures of exposure like electric and magnetic field strength, *E* and *H*) or dosimetric quantities (internal measures of exposure results like induced current, *J*, and Specific Absorption Rate, *SAR*) for the mandatory risk assessment. In the case of EMF of low and intermediate frequencies (LF and IF) the basic internal measure used for exposure assessment is induced current density in head and torso. IEEE standards offer also the use of *E* field induced in exposed tissues. Both parameters can be used till low MHz frequencies. The use of internal measures require numerical calculations and detailed analysis and interpretation of data obtained from modeling.

EMF from LF and IF range, affecting workers are usually so-called near fields. The impedance of such fields (the ratio of electric fields strength to magnetic field strength) is defined by the technical properties of the EMF-source-worker-body system. Electric voltages and currents in the electric device, producing EMF play important role, but in many cases also the direct coupling between workers body and EMF source modify the exposure conditions. The sources of high level of EMF exposure to time-varying LF or IF fields are basically: high voltages power distribution systems, welding devices, industrial induction heating devices, electro surgery devices. In consequences the most important external measure of exposure is magnetic field strength (or magnetic flux density) assessed following the frequency-dependent exposure limitation in the case of very huge number of welding and induction heating devices. Significant exposure to electric component can be found in practice in the vicinity of high voltage electricity distribution systems. The most complicated situation can be found, when both components (*E* and *H*) should be consider, especially when the field impedance can varying significantly during the application, as in the case of electro surgery use.

For the practical EMF exposure assessment at workplace, first of all it should be discussed when it is acceptable to make the EMF exposure assessment by spot measurements with a broad-band RMS meter (i.e. the most convenient and less expensive method). For the other situations, it should be decided the use of more complicated (and more expensive) exposure assessment method: more detailed measurements or dosimetrical calculations.

2. Method

Professional activities of authors is focused on the detailed analysis of occupational EMF exposure characteristics in various enterprises and application of EMF measurements and/or numerical calculations

technique for workers exposure assessment. The presentation is based on analysis of the fundamental problems defined for the use of numerical calculations for workers exposure assessment in real occupational situations.

3. Results

Electromagnetic field (EMF) in the workplace has often very specific characteristics in comparison with the fields from general environment. In working conditions not only the locations of the EMF source and worker's body, but also the geometry of the source, frequency and level of produced EMF in its vicinity, can change significantly, exposure level can be high, even exceeding international safety guidelines.

The analysis of detailed data obtained from various work place and experience with the numerical calculations modeling realistic exposure scenarios for the assessment of the exposure following the internal measures' limitations have shown a number of practical problems, identified for the worker's exposure assessment.

In the most of cases of high level exposure of workers to LF or IF EMF, their professional activities need hand operation of the EMF sources. For the exposure assessment of such cases the modeling of realistic posture of worker's body and possible simplifications of it to reduce the complication and costs of exposure assessment process is of high priority. Important question is on the exposure assessment of hands, especially while hand-operating of EMF sources of high level. The use of calculations for exposure assessment in LF and IF band is more difficult, that RF (with huge experience obtained from mobile phones research) because of:

- the lack of models, transferable from one software to other one, representing realistic EMF occupational sources, already verified by reference data from workplaces and taken as standardized models

- the lack of well verified data on electrical properties of various elements of workplace, as shoes, floor cover, furniture's, etc.

- relatively small number of the scientific data concerning human body models, electrical properties of tissues, numerical calculations procedures, etc. for the assessment of IF fields.

For the wider use of numerical calculations for the assessment of workers EMF exposure, it is of high priority to obtained well verified scientific data concerning

- the possibility to use simplified numerical models of working places and EMF exposure conditions

- the uncertainty of exposure assessment for checking the compliance with the Directive

- the role of frequency components within the exposure assessment procedures

- the assessment of pulsed fields, especially in the case of hand-operated devices, when the repetition time of pulses is not fixed.

The practical use of numerical calculations for the EMF exposure assessment is also problematic because it was not defined when various software packages can be use, and non of currently available software is specialized for workers exposure. Additionally, a few commercial human body models are applicable for selected specialized software only. Separate problem is the calculations of induced and contacts currents, which can be also measured.

4. Conclusion

The use of internal measures of exposure results for risk evaluation is possible only by simulation computational methods, with the use of adequate representation of the workplace environment and worker’s body models. Such calculations for particular exposure situations require highly skilled professionals and specialized software. The modeling of real exposure scenario, validation of calculations result and interpretation of obtained data is usually very time-consuming and currently achievable by research centers only. These are reasons why, the possibility of practical use of numerical modeling by the particular employers, especially from SMEs is very limited in contrast to the relatively effective use of such technique for large series manufacturing (e.g. common use electrical devices, like mobile phones handsets). In this respect, the question arises if more simple models are powerful enough for performing roughly assessment of the occupational EMF sources and workers exposure level, while every day's occupational safety and health practice.

Acknowledgment
This review has been prepared from results obtained from the investigations supported by the State Committee for Scientific Research and Ministry of Economy, Labour and Social Policy of Poland (individual grants focused on occupational EMF exposure investigations).

ISSUES IN ACTUAL RF ENVIRONMENT OCCUPATIONAL EXPOSURE ASSESSMENT

DINA SIMUNIC

UNIVERSITY OF ZAGREB, FACULTY OF ELECTRICAL ENGINEERING AND COMPUTING, UNSKA 3, HR-10000 ZAGREB, CROATIA

Introduction

Exposure assessment of electromagnetic fields is a topic that gets more importance every day, especially related to Directive 2004/40/EC and EC Recommendation 1999/519. The complexity of interaction between electromagnetic fields and human body makes any kind of analysis (theoretical-analytical, numerical, experimental) difficult. In an actual multi-source radiofrequency environment situation is even worse, due to a consequent complex distribution of electromagnetic fields.

Method

Issues related to actual RF environment, specifically related to multi-frequency, multi-source environment require sound analysis. The number of issues is even bigger in the indoor environment, where a building structure influences the electromagnetic field distribution. In such environment a number of reflections exist, which forms a complex environment of standing waves. Thus, it is necessary to perform a detailed analysis of the field distribution.

The field distribution is the first step in performing exposimetry analysis, as well as dosimetry analysis.

Results

The results of exposimetry and dosimetry analysis indicate the issues addressed by the process, especially related to uncertainty of the analysis. The concerned sources are wireless communications devices, i.e., mobile telephony, Bluetooth and wireless LAN devices, which are located in the indoor and outdoor space. The devices in the outdoor space are treated by analytical methods, whereas in the indoor space, it is impossible to perform even exposimetry analysis without a numerical tool.

Conclusion

The complete dosimetric and exposimetric analysis of the human body in electromagnetic fields can be performed only by a numerical analysis. The needs and necessary requirements of the analysis for a full application for existing legislative acts, especially for Directive, are related to the complex electromagnetic environment which makes albeit difficult dosimetric analysis more complex.

NUMERICAL CODE VALIDATION WITH EMPIRICAL DATA

Dr. PETER GAJŠEK

INSTITUTE OF NON-IONIZING RADIATION, LJUBLJANA, SLOVENIA

Abstract

The development of mathematical dosimetry modeling techniques and powerful computer hardware has resulted in dosimetry modeling as a principle tool in determining EMF exposure. The results of any anatomical model are questionable if the model has not been validated with empirical data obtained from *in vivo* or *in vitro* experiments. Validation of the theoretical with empirical results and the subsequent refining of a model are essential in order to earn the credibility when using these models to establish or revise exposure standards. The increasing acceptance and use of FDTD modeling within the EMF community make it imperative that predictions be compared, and validated against experimental data. With the development of the Finite-Difference Time-Domain (FDTD) code, it is possible to predict whole body and localized SAR values under a wide range of exposure conditions in phantoms and laboratory animals, as well as humans.

In the past, FDTD predictions have been validated mainly for very simplistic geometric models. For far-field sources, simulation results have been compared with analytical results for square [Umashakar and Taflove, 1982], cylinders [Furse et al., 1990], spheres [Gandhi et al., 1992; Gandhi et al., 1999], and plates [Taflove et al., 1985]. Calculations of currents induced in a standing human have compared well with empirical data [Furse et al., 1997]. For near-field sources, simulation results have been compared with analytical, measured or method of moment results for dipole antennas in front of layered half-spaces, layered boxes and homogeneous spheres [Furse and Gandhi, 1998]. In addition, the FDTD method has been validated for near-field testing of realistic cellular telephones next to the human head [Dimbylow and Mann, 1994; Gandhi and Chen, 1995]. Agreement between FDTD code and experimental results (e.g. E-field measurements on simplistic canonical geometries such as box or sphere filled with tissue equivalent material) was excellent and generally within ±20 % (±1 dB) [Gandhi et al., 1999]. However, little direct comparison of empirical data obtained by actual type of organism with SAR values predicted by FDTD modeling exists in the published literature [Walters et al., 2000; Mason et al., 2000].

In this paper, we report on the use of the convergent technologies to validate the use of computational codes to predict SAR values in both, simplistic models (spheres) and actual biological organisms. Since experimental validation requires the implantation of thermal or e-field probes, it is not feasible to perform such studies in human subjects, therefore laboratory animals and phantoms were used. The brain of the rat offers an ideal organ for comparison, due to the reliability of stereotaxic probe placement, as well as the ability to easily confirm probe placements in tissue sections following experimentation [Walters et al., 1998].

Our predicted SAR values obtained by computer models based on FDTD code of spheres and Sprague-Dawley rat were compared to temperature measurements made with implanted probes and infrared thermography model [Gajsek et al., 2001].

The SAR values were determined thermally. Irradiation was performed at a high exposure level (above 700 mW/cm^2) and short exposure duration (30 seconds) to produce a measurable linear temperature rise. This was done to allow accurate quantification of the rate of temperature rise in the absence of any significant thermoregulatory effects. Good correlation between the predicted and empirical phantom and animal data would provide increased confidence in the results predicted by the man model [Mason et al., 2000].

REFERENCES:

Dimbylow PJ, and Mann SM (1994): SAR Calculations in an Anatomically Based Realistic Model of the Head for Mobile Communication Transceivers at 900 MHz and 1.8 GHz," Physics in Medicine and Biology, vol. 39, 1537-1553.

Furse CM, and Gandhi OP (1998): Calculation of Electric Fields and Currents Induced in a Milli mete r-Resolution Human Model at 60 Hz Using the FDTD Method, Bidelectromagnetics, Vol. 19, 293-299.

Furse CM, Mathur SP, and Gandhi OP (1990): Improvements in the FiniteDifference Time-Domain Method for Calculating the Radar Cross Section of a Perfectly Conducting Target, IEEE Transactions on Microwave Theory and Techniques, Vol. 38, no. 7, 919-927.

Furse CM, Yu SQ, Gandhi OP (1997): Improvements in the FDTD method for near field bioelectromagnetic simulations, Microwave and Optical Technology letters, Vol.16, 341-345.

Gajšek P, Ziriax JM, Hurt WD, Walters TJ, and Mason PA (2001): Predicted SAR in Sprague-Dawley rat as a function of permittivity values, Bioelectromagnetics 24, 1-17.

Gandhi OP, and Chen JY (1992): Numerical Dosimetry at Power-Line Frequencies using Anatomically Based Models, Bioelectromagnetics Supplement, 1, 43-60.

Gandhi OP, and Chen JY (1995): Electromagnetic Absorption in the Human Head from Experimental 6 GHz Hand-Held Transceivers, IEEE Transactions on Electromagnetic Compatibility, vol. EMC-37, 547-558.

Gandhi OP, Lazzi G, Tinniswood A, and Yu Q, (1999): Comparison of numerical and experimental Methods for determination of SAR and Radiation patterns of Handheld Wireless Telephones, Bioelectromagnetics, No. 20, 93-101.

Mason PA, Hurt WD, Walters TJ, D'Andrea JA, Gajšek P, Ryan KL, Nelson PA, and Ziriax JA (2000): Effects of frequency, permittivity, and voxel size on predicted specific absorption rate values in biological tissue during electromagnetic field exposure, IEEE Microw. Theory & Techn, Vol.48, No 11, 2050-2057.

Taflove A., Umashankar KR, and Jurgens TG (1985): Validation of FD-TD Modeling of the Radar Cross Section of Three-Dimensional Structures Spanning up to Nine Wavelengths, IEEE Transactions on Antennas and Propagation, pp. 662-666, June 1985.

Umashankar KR, and Taflove A (1982): A Novel Method to Analyze Electromagnetic Scattering of Complex Objects, IEEE Transactions on Electromagnetic Compatibility, vol. EMC-24, pp. 397-405.

Walters TJ, Blick DW, Johnson LR, Adair ER, and Foster KR (2000): Heating and pain sensation produced in human skin by millimeter waves. Health Phys., Vol. 78, No.3, 259-267.

Walters TJ, Ryan KL, Belcher JC, Doyle JM, Tehrany MR, and Mason PA (1998): Regional brain heating during microwave exposure (2.06 GHz), warm-water immersion, environmental heating and exercise, Bioelectromagnetics 19, 341-353.

SIMULATION OF ELECTROMAGNETIC FIELDS INCLUDING BIOLOGICAL MODELS WITH CST STUDIO SUITE

MONIKA BALK

CST – COMPUTER SIMULATION TECHNOLOGY

In our modern society technology and simultaneously electronics play an important role. It is almost impossible to avoid electromagnetic field exposure. When evaluation the human body field exposure the always occurring problem is: How to measure it. Most of the time it can't be measure in vivo. Thus, the interaction of electromagnetic fields and biological tissues is a topic of intense research. Therefore, 3D numerical EM simulations have been established as tool to analyse the effect of the electromagnetic fields caused by the environment on human beings. This effect is usually described by the Specific Absorption Rate (SAR).

The software package CST STUDIO SUITE™ is a specialised tool for evaluating 3D electromagnetic fields, which is based on the Finite Integration Technique (FIT). The software package offers the possibility to import data obtained by medical imaging. With this voxel import the characteristics of the biological tissues are translated in material information used by the simulation software to evaluate the electric and magnetic fields. Based on electric and magnetic field, the specific absorption rate can be calculated using a mass averaging approach compliant to the IEEE C95.3 standard. Alternatively, own procedures are offered that show improved consistency for structure rotations.

In this talk first of all the Finite Integration Technique fundamentals are described. Furthermore the simulation work flow within the software package is shown. Finally several examples concerning SAR calculations are shown

Dr. Monika Balk, Application Engineer

CST – Computer Simulation Technology

Bad Nauheimer Str. 19, 64289 Darmstadt, Germany

Tel: +49-6151-7303-0, Fax +49-6151-7303-100

Email: monika.balk@cst.com

BIOLOGICAL EFFECTS OF EXTREMELY LOW FREQUENCY ELECTRIC AND MAGNETIC FIELDS

AHMAD YOONESSI, ARASH MIRHASHEMI

KHAJE NASIR TOOSI UNIVERSITY OF TECHNOLOGY, TEHRAN,IRAN
AMIRKABIR UNIVERSITY OF TECHNOLOGY,TEHRAN,IRAN

Abstract- There has been numerous evidence that exposure to extremely low frequency magnetic and electric fields can produce biological effects. Many of these effects are not clearly understood so far. Most of these researches emphasize on power frequency (50 or 60Hz) and the biological effects at these frequencies. The following paper attempts to describe the current researches toward emphasizing the effects in the Extremely Low Frequency (ELF) range. Lab experiments regarding biological effects of ELF fields have been shown in various organs and the results have been discussed. There is presently no clear and convincing evidence from animal or cellular studies that demonstrates harmful effects of EMF. There are, however, some studies that are suggestive of potential health impacts. From the perspective of laboratory studies, this presentation will discuss biological responses to extremely low frequency electric and magnetic field exposures.

Introduction

With the ongoing advancement in electrical and electronic devices the odds of exposure to electrical and magnetic fields have raised dramatically. More and more people are exposed to electrical and magnetic fields daily. Therefore the need to understanding the effect that these fields have on the human body is significantly important. One of the areas that are often neglected is in the Extremely low Frequency Range (up to 300Hz). At the frequencies this low, the wavelength in air is very long (6000km at 50 Hz and 5000Km at 60Hz) The only area within this range that is on the main focus is the power frequency (50Hz or 60Hz) Since it is the widely found frequency in the environment. This paper tries to summarize the effect on the ELF range without focusing on any special frequency.

Biological effects may sometimes lead to adverse health effects. Biological effect is when exposure to an electromagnetic field produces a noticeable or detectable change in a biological system. An adverse health effect occurs when the biological effect is outside the normal range for the body to compensate and thus leads to some detrimental health conditions. [1], [9], [13]

The primary mechanism of interaction between elf fields and biological system is in the induction of electrical charge and current.

ELF electric fields exist whenever a voltage is present regardless of the current flowing. Almost none of the electric field penetrates into the human body. On the other hand ELF magnetic fields exist whenever a current is flowing. They can easily penetrate into the human body. [1], [9]

Circulatory System

Heart

There have been some studies suggesting that exposure to ELF electric and magnetic fields decreases heart rate [3]. While this studies report this incident, they often characterize it as temporary and within the normal physiological variation. The boundary for this effect is reported as low as 0.1μA/cm2.[3] There have been reports of effect on the blood pressure, Heart rate and electrocardiograph waveform but these studies are limited by uncertainties regarding exposure duration and subsequent control group.[3], [4], [5].

Endocrine system

Melatonin

Some studies suggest that exposure to ELF fields may suppress secretion of melatonin, a hormone related to human day-night rhythm [1], [6]. It has been suggested that melatonin is effective in the prevention of breast cancer and therefore suppressing it will result in an increased incident of breast cancer. Although there is some evidence in laboratory animals, human volunteer studies have not confirmed this report. [1], [7], [8]

Musculoskeletal System
Bone growth and fracture repair
Electrical and magnetic stimulation have been known to have effect on bone fracture repair since 1970. The mechanism which enables these fields to increase new bone formation is still not known. Effect of pulsed EMF on fracture healing have been proven in numerous clinical studies on human and animal subjects.[10],[11] However the mechanism that this interaction takes place is not clearly known so far. Some studies suggest that EMF can increase the secretion of growth hormone IGF-I and IGF-II and therefore increase the healing rate. [12], [14], [15]

Nervous System
Behavior
Many studies have been done to demonstrate the effect of elf magnetic and electric field on human and animal behavior Since nervous system plays a major role in function of all the body and since many of the nervous signals communicate in a form of electrical signal it can be predicted that the elf could alter the behavior.
There has been numerous studies showing the effect of E field on animals such as rats, mice, pigs and birds.[16] Most animals try to avoid exposure to E fields over 50-75kV/m. The exposure to B field shows little evidence on animal behavior in general. [13], [14]
In humans a phenomena known as phosphene is reported in the B fields as low as 20 mT. [13], [19]

Reproductive System
It is known that the developing system is more prone to various environmental hazards. Therefore it is assumed that a developing system is more sensitive in response to electrical and magnetic fields. Studies have been done mostly on animals such as chicken, rats and rabbits. Few studies have been done on human growing organisms such as hair follicles. [13], [16], [17]

Immune System
Cancer and Mutation
The EMF effects on promoting cancer have been studied more than anything else. However few life long studies have been reported. There have been some studies on the effect of 50 or 60 Hz B field on the male and female rats which showed that although the B field can increase the carcinogenic activity it is not effect is not significant.
Evidence of effect of ELF B and E fields on the DNA breaking and tumor initiation has been minimal. Since these frequencies do not possess enough energy to break bonds between molecules and damage DNA. [14], [15]

Summary
The health effects of extremely low frequency EMF still remains a controversial subject as the mechanism of interaction is not yet known. The biggest issue in various experiments regarding these fields is the lack of reproducibility of different outcomes. This will be the case until the clear mechanism of interaction between living systems and electric and magnetic fields

References:

[1] Electromagnetic fields and public health: extremely low frequency, WHO Fact sheet N205, Nov.1998
[2] Exposure to extremely low frequency electromagnetic fields and radiofrequency radiation: cardiovascular effects in humans, James R. Jauchem, Vol.70, No.1, Pages 9-21, 1997
[3] Effects of 50 Hz magnetic field exposure on human heart rate variability with passive tilting, Mardi L Sait, Andrew W wood, Richard L G Kirsner,Physiological Measurement, Vol 27, Pages 73-83, 2006
[4] Influence of exposure to electromagnetic field on the cardiovascular system.. Jeong J.H. Kim J.S. et all, Auton Autacoid Pharmacol, Vol 25, No1, Pages 17-23, Jan 2005

[5] Influence of 50 Hz electric and magnetic fields on the human heart, J. Korpinen, J. Partanen,A Uusitalo, Bioelectromagnetism , Vol 14 ,Issue 4, Pages 329 – 340, 1994
[6] Effects of extremely low frequency magnetic fields on pain thresholds in mice: roles of melatonin and opioids, J.H. Jeong, K.B. Choi et all,Journal of autonomic pharmacology, Vol 20, Issue 4, pages 259, 2000
[7] Static and extremely low frequency electromagnetic field exposure: reported effects on the circadian production of melatonin.. Reiter RJ, Journal Cell Biochemistry, Vol. 51, No.4 Pages 394-403, Apr 1993
[8] Human melatonin during continuous magnetic field exposure, Charles Graham, Mary R. Cook,Donald W. Riffle, Bioelectromagnetism, vol 18, issue 2, pages 166-171, 1998
[9] Biological Effects of low-level low frequency electric and magnetic fields, Charles Polk, IEEE transaction on education, Vol 34, NO 3, August 1991
[10] Effects of Pulsed Electromagnetic Fields on Bone Healing in a Rabbit Tibial Osteotomy Model.,Fredricks, Douglas C., Nepola, James V., Journal of orthopaedic trauma ,Vol. 14, No.2,Pages 93-100, February 2000
[11] Pulsing electromagnetic field treatment in ununited fractures and failed arthrodeses , Bassett C.A.L., S.N. Mitchell and S.R. Gaston, JAMA, Vol. 247, Pages 623-628, 1982
[12] Inhibition of gap junction intercellular communication by extremely low frequency electromagnetic fields in osteoblast like models is dependent on cell differentiation, Dean T. Yamaguchi, Jason Huang, Defang Ma, Paul K.C. Wang, Journal of cellular physiology, Vol. 190, Issue 2, Pages 180-188, 2002
[13] Biological effects of Magnetic Fields: Laboratory Studies, Larry E. Anderson, Proceeding of the 20th Annual International Conference of The IEEE Engineering in Medicine and Biology Society, Vol.20, No 6, 1998
[14] A Three generation animal study of the biological effects of very strong low frequency electromagnetic fields, W.Z. Fam, E.L, Mikhail, Engineering in Medicine and Biology Society, 1994. Engineering Advances: New Opportunities for Biomedical Engineers. Proceedings of the 16th Annual International Conference of the IEEE Volume 2, Page(s):756 – 757, 1994
[15] Where are the thresholds for biological effects of non-endogenous low frequency low intensity electric and magnetic fields?, Charles Polk, Engineering in Medicine and Biology Society, 1992. Vol.14. Proceedings of the Annual International Conference of the IEEE Volume 7, Issue , 29 Oct-1 Page(s):2879 – 2880, Nov 1992
[16] Biological effects of low frequency electric and magnetic fields: an overview, Charles Polk, Bioengineering Conference, 1992., Proceedings of the 1992 Eighteenth IEEE Annual Northeast Volume , Issue , 12-13 Page(s):55 – 57, Mar 1992
[17] Biological effects of electric and magnetic fields: what do we know?, Indira Nair, IEEE International Magnetics Conference, Stockholm, Sweden, April 13-16, 1993.
[18] Interaction of static and extremely low frequency electric and magnetic fields with living systems: health effects and research needs,Michael H. Repacholi, B. Greenebaum,Bioelectromagnetism, Vol 20, Issue 3, Pages 133-160, 1999
[19] Weak electric field interactions in the central nervous system, RD Saunders, JGR Jefferys, Health Physics, 83(3):366-375, 2002